MANIPULATING THE IMMUNOLOGICAL TUMOR MICROENVIRONMENT

EDITED BY: Peng Qu, Huanfa Yi and Keqiang Chen
PUBLISHED IN: Frontiers in Immunology and Frontiers in Oncology

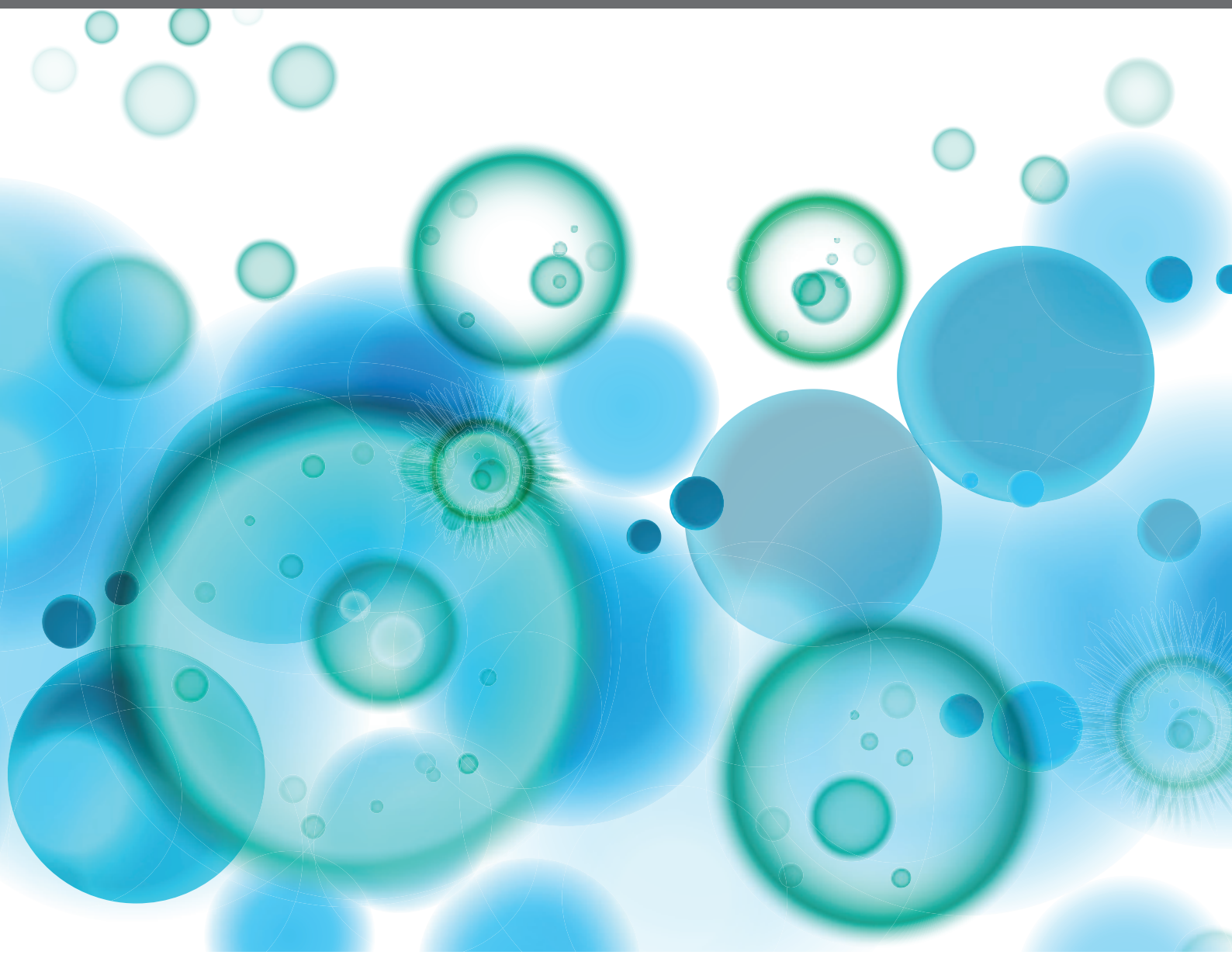

frontiers Research Topics

frontiers

Frontiers eBook Copyright Statement

The copyright in the text of individual articles in this eBook is the property of their respective authors or their respective institutions or funders. The copyright in graphics and images within each article may be subject to copyright of other parties. In both cases this is subject to a license granted to Frontiers.

The compilation of articles constituting this eBook is the property of Frontiers.

Each article within this eBook, and the eBook itself, are published under the most recent version of the Creative Commons CC-BY licence. The version current at the date of publication of this eBook is CC-BY 4.0. If the CC-BY licence is updated, the licence granted by Frontiers is automatically updated to the new version.

When exercising any right under the CC-BY licence, Frontiers must be attributed as the original publisher of the article or eBook, as applicable.

Authors have the responsibility of ensuring that any graphics or other materials which are the property of others may be included in the CC-BY licence, but this should be checked before relying on the CC-BY licence to reproduce those materials. Any copyright notices relating to those materials must be complied with.

Copyright and source acknowledgement notices may not be removed and must be displayed in any copy, derivative work or partial copy which includes the elements in question.

All copyright, and all rights therein, are protected by national and international copyright laws. The above represents a summary only. For further information please read Frontiers' Conditions for Website Use and Copyright Statement, and the applicable CC-BY licence.

ISSN 1664-8714
ISBN 978-2-88974-840-2
DOI 10.3389/978-2-88974-840-2

About Frontiers

Frontiers is more than just an open-access publisher of scholarly articles: it is a pioneering approach to the world of academia, radically improving the way scholarly research is managed. The grand vision of Frontiers is a world where all people have an equal opportunity to seek, share and generate knowledge. Frontiers provides immediate and permanent online open access to all its publications, but this alone is not enough to realize our grand goals.

Frontiers Journal Series

The Frontiers Journal Series is a multi-tier and interdisciplinary set of open-access, online journals, promising a paradigm shift from the current review, selection and dissemination processes in academic publishing. All Frontiers journals are driven by researchers for researchers; therefore, they constitute a service to the scholarly community. At the same time, the Frontiers Journal Series operates on a revolutionary invention, the tiered publishing system, initially addressing specific communities of scholars, and gradually climbing up to broader public understanding, thus serving the interests of the lay society, too.

Dedication to Quality

Each Frontiers article is a landmark of the highest quality, thanks to genuinely collaborative interactions between authors and review editors, who include some of the world's best academicians. Research must be certified by peers before entering a stream of knowledge that may eventually reach the public - and shape society; therefore, Frontiers only applies the most rigorous and unbiased reviews.
Frontiers revolutionizes research publishing by freely delivering the most outstanding research, evaluated with no bias from both the academic and social point of view. By applying the most advanced information technologies, Frontiers is catapulting scholarly publishing into a new generation.

What are Frontiers Research Topics?

Frontiers Research Topics are very popular trademarks of the Frontiers Journals Series: they are collections of at least ten articles, all centered on a particular subject. With their unique mix of varied contributions from Original Research to Review Articles, Frontiers Research Topics unify the most influential researchers, the latest key findings and historical advances in a hot research area! Find out more on how to host your own Frontiers Research Topic or contribute to one as an author by contacting the Frontiers Editorial Office: frontiersin.org/about/contact

MANIPULATING THE IMMUNOLOGICAL TUMOR MICROENVIRONMENT

Topic Editors:
Peng Qu, National Institutes of Health (NIH), United States
Huanfa Yi, Jilin University, China
Keqiang Chen, National Cancer Institute at Frederick (NIH), United States

Citation: Qu, P., Yi, H., Chen, K., eds. (2022). Manipulating the Immunological Tumor Microenvironment. Lausanne: Frontiers Media SA.
doi: 10.3389/978-2-88974-840-2

Table of Contents

08 ***Targeting Immunometabolism Mediated by CD73 Pathway in EGFR-Mutated Non-small Cell Lung Cancer: A New Hope for Overcoming Immune Resistance***
Anna Passarelli, Michele Aieta, Alessandro Sgambato and Cesare Gridelli

19 ***Immunogenomic Profiling and Classification of Prostate Cancer Based on HIF-1 Signaling Pathway***
Jukun Song, Weiming Chen, Guohua Zhu, Wei Wang, Fa Sun and Jianguo Zhu

35 ***Tumor-Secreted GRP78 Promotes the Establishment of a Pre-metastatic Niche in the Liver Microenvironment***
Lu Chen, Hao Zheng, Xiang Yu, Lei Liu, Heli Li, Huifen Zhu, Zhihong Zhang, Ping Lei and Guanxin Shen

48 ***Obesity-Associated Myeloid-Derived Suppressor Cells Promote Apoptosis of Tumor-Infiltrating CD8 T Cells and Immunotherapy Resistance in Breast Cancer***
Justin T. Gibson, Rachael M. Orlandella, William J. Turbitt, Michael Behring, Upender Manne, Robert E. Sorge and Lyse A. Norian

61 ***Emerging Blood-Based Biomarkers for Predicting Response to Checkpoint Immunotherapy in Non-Small-Cell Lung Cancer***
Shumin Li, Chengyan Zhang, Guanchao Pang and Pingli Wang

72 ***The Crosstalk Between Tumor-Associated Macrophages (TAMs) and Tumor Cells and the Corresponding Targeted Therapy***
Zhe Ge and Shuzhe Ding

95 ***Hyperthermia Targeting the Tumor Microenvironment Facilitates Immune Checkpoint Inhibitors***
Zihui Li, Jie Deng, Jianhai Sun and Yanling Ma

107 ***Tumor Derived SIGLEC Family Genes May Play Roles in Tumor Genesis, Progression, and Immune Microenvironment Regulation***
Zheng Chen, Mincheng Yu, Lei Guo, Bo Zhang, Shuang Liu, Wentao Zhang, Binghai Zhou, Jiuliang Yan, Qianni Ma, Zhangfu Yang, Yongsheng Xiao, Yongfeng Xu, Hui Li and Qinghai Ye

122 ***Identification of Interleukin-9 Producing Immune Cells in Endometrial Carcinoma and Establishment of a Prognostic Nomogram***
Huan Tong, Hao Feng, Xiang Hu, Meng-fei Wang, Yun-feng Song, Xiao-li Wen, Yi-ran Li and Xiao-ping Wan

134 ***Reconstruction of Immune Microenvironment and Signaling Pathways in Endometrioid Endometrial Adenocarcinoma During Formation of Lymphovascular Space Involvement and Lymph Node Metastasis***
Yuan Cheng, Xiaobo Zhang, Zhiqi Wang and Jianliu Wang

148 ***Identification and Verification of Immune-Related Gene Prognostic Signature Based on ssGSEA for Osteosarcoma***
Bo Xiao, Liyan Liu, Aoyu Li, Cheng Xiang, Pingxiao Wang, Hui Li and Tao Xiao

158 ***Myeloid-Derived Suppressor Cells: A New and Pivotal Player in Colorectal Cancer Progression***
Kai Yin, Xueli Xia, Ke Rui, Tingting Wang and Shengjun Wang

171 ***Tumor-Derived Extracellular Vesicles and the Immune System—Lessons From Immune-Competent Mouse-Tumor Models***
Marvin Droste, Basant K. Thakur and Brian P. Eliceiri

183 ***Anti-Cancer Nanomedicines: A Revolution of Tumor Immunotherapy***
Wei Li, Anghui Peng, Huajun Wu, Yingyao Quan, Yong Li, Ligong Lu and Min Cui

196 ***Exploring the Emerging Role of the Gut Microbiota and Tumor Microenvironment in Cancer Immunotherapy***
Qin Qiu, Yuqi Lin, Yucui Ma, Xiaoling Li, Juan Liang, Zhiyan Chen, Kaifeng Liu, Yuge Huang, Hui Luo, Riming Huang and Lianxiang Luo

211 ***GBP1 Facilitates Indoleamine 2,3-Dioxygenase Extracellular Secretion to Promote the Malignant Progression of Lung Cancer***
Yinnan Meng, Wei Wang, Meng Chen, Kuifei Chen, Xinhang Xia, Suna Zhou and Haihua Yang

222 ***Nocardia Rubra Cell Wall Skeleton Up-Regulates T Cell Subsets and Inhibits PD-1/PD-L1 Pathway to Promote Local Immune Status of Patients With High-Risk Human Papillomavirus Infection and Cervical Intraepithelial Neoplasia***
Wei Chen, Yi Zhang, Chunfang Zhao, Suxia Shao, Yanan Zhang, Xuehui Li, Xue Bai, Qianyu Guo, Qianwen Liu, Junmin Tang and Lei Zhang

234 ***Research Status and Molecular Mechanism of the Traditional Chinese Medicine and Antitumor Therapy Combined Strategy Based on Tumor Microenvironment***
Yang Zhang, Yanni Lou, Jingbin Wang, Cunguo Yu and Wenjuan Shen

247 ***Stereotactic Body Radiotherapy Is Effective in Modifying the Tumor Genome and Tumor Immune Microenvironment in Non-Small Cell Lung Cancer or Lung Metastatic Carcinoma***
Pu Zhou, Diangang Chen, Bo Zhu, Wei Chen, Qichao Xie, Yali Wang, Qiulin Tan, Bibo Yuan, Xuejiao Zuo, Changlin Huang, Hongfan Zhu and Guanghui Li

258 ***Advances in Hypofractionated Irradiation-Induced Immunosuppression of Tumor Microenvironment***
Yuxia Wang

266 ***CU06-1004-Induced Vascular Normalization Improves Immunotherapy by Modulating Tumor Microenvironment* via *Cytotoxic T Cells***
Songyi Park, Ji Hoon Oh, Dong Jin Park, Haiying Zhang, Minyoung Noh, Yeomyung Kim, Ye-Seul Kim, Hyejeong Kim, Young-Myeong Kim, Sang-Jun Ha and Young-Guen Kwon

281 ***Pan-Cancer Molecular Characterization of m^{6}A Regulators and Immunogenomic Perspective on the Tumor Microenvironment***
Jie Zhu, Jiani Xiao, Min Wang and Daixing Hu

303 ***Tumor Burden and Immunotherapy: Impact on Immune Infiltration and Therapeutic Outcomes***
Samuel I. Kim, Christopher R. Cassella and Katelyn T. Byrne

318 ***An Immune Cell Signature Is Associated With Disease-Free Survival and Adjuvant Chemosensitivity of Patients With Resectable Gastric Cancer***
Hongfei Yan, Yang Chen, Zichang Yang, Zhi Li, Xiaofang Che, Jiawen Xiao, Yunpeng Liu and Xiujuan Qu

331 ***Screening and Identification of Four Prognostic Genes Related to Immune Infiltration and G-Protein Coupled Receptors Pathway in Lung Adenocarcinoma***
Yan Wang, Liwei Qiu, Yu Chen, Xia Zhang, Peng Yang and Feng Xu

346 **CCR4*, CCR8, and* P2RY14 *as Prognostic Factors in Head and Neck Squamous Cell Carcinoma Are Involved in the Remodeling of the Tumor Microenvironment***
Liangliang Meng, Xiaoxi He, Quan Hong, Bo Qiao, Xiao Zhang, Bin Wu, Xiaobo Zhang, Yingtian Wei, Jing Li, Zhaoxiang Ye and Yueyong Xiao

363 ***Tryptophan: A Rheostat of Cancer Immune Escape Mediated by Immunosuppressive Enzymes IDO1 and TDO***
Minah Kim and Petr Tomek

372 ***Changes in the Peripheral Blood Treg Cell Proportion in Hepatocellular Carcinoma Patients After Transarterial Chemoembolization With Microparticles***
Zhizhong Ren, Yuanxun Yue, Yuewei Zhang, Jiahong Dong, Ying Liu, Xiaowei Yang, Xin Lin, Xueqiang Zhao, Zhanqi Wei, Yu Zheng and Tianxiao Wang

382 ***TRAF6 Regulates the Immunosuppressive Effects of Myeloid-Derived Suppressor Cells in Tumor-Bearing Host***
Ge Song, Yue Zhang, Jie Tian, Jie Ma, Kai Yin, Huaxi Xu and Shengjun Wang

393 ***Cyclooxygenase-2 Inhibitor: A Potential Combination Strategy With Immunotherapy in Cancer***
Dan Pu, Liyuan Yin, Lin Huang, Changlong Qin, Yuwen Zhou, Qiang Wu, Yan Li, Qinghua Zhou and Lu Li

400 ***Effects of Hypoxia in Intestinal Tumors on Immune Cell Behavior in the Tumor Microenvironment***
Luping Zhang, Shaokun Wang, Yachen Wang, Weidan Zhao, Yingli Zhang, Nan Zhang and Hong Xu

413 ***Analysis of m6A-Related Signatures in the Tumor Immune Microenvironment and Identification of Clinical Prognostic Regulators in Adrenocortical Carcinoma***
Yi Jin, Zhanwang Wang, Dong He, Yuxing Zhu, Xueying Hu, Lian Gong, Mengqing Xiao, Xingyu Chen, Yaxin Cheng and Ke Cao

430 ***Roles of the Dynamic Tumor Immune Microenvironment in the Individualized Treatment of Advanced Clear Cell Renal Cell Carcinoma***
Enyu Lin, Xuechao Liu, Yanjun Liu, Zedan Zhang, Lu Xie, Kaiwen Tian, Jiumin Liu and Yuming Yu

447 ***Deciphering the Prognostic Implications of the Components and Signatures in the Immune Microenvironment of Pancreatic Ductal Adenocarcinoma***
Rong Tang, Xiaomeng Liu, Chen Liang, Jie Hua, Jin Xu, Wei Wang, Qingcai Meng, Jiang Liu, Bo Zhang, Xianjun Yu and Si Shi

462 ***Fundamentals of T Cell Metabolism and Strategies to Enhance Cancer Immunotherapy***
Guillermo O. Rangel Rivera, Hannah M. Knochelmann, Connor J. Dwyer, Aubrey S. Smith, Megan M. Wyatt, Amalia M. Rivera-Reyes, Jessica E. Thaxton and Chrystal M. Paulos

479 ***Engineered TCR-T Cell Immunotherapy in Anticancer Precision Medicine: Pros and Cons***
Qijie Zhao, Yu Jiang, Shixin Xiang, Parham Jabbarzadeh Kaboli, Jing Shen, Yueshui Zhao, Xu Wu, Fukuan Du, Mingxing Li, Chi Hin Cho, Jing Li, Qinglian Wen, Tao Liu, Tao Yi and Zhangang Xiao

491 ***Interaction Networks Converging on Immunosuppressive Roles of Granzyme B: Special Niches Within the Tumor Microenvironment***
Weinan Wang, Rui Zou, Ye Qiu, Jishuang Liu, Yu Xin, Tianzhu He and Zhidong Qiu

505 ***Characterization of Immune Infiltration and Construction of a Prediction Model for Overall Survival in Melanoma Patients***
Gang Li, Xuran Zhu and Chao Liu

519 ***Identification of Prognostic Genes in the Tumor Microenvironment of Hepatocellular Carcinoma***
Shixin Xiang, Jing Li, Jing Shen, Yueshui Zhao, Xu Wu, Mingxing Li, Xiao Yang, Parham Jabbarzadeh Kaboli, Fukuan Du, Yuan Zheng, Qinglian Wen, Chi Hin Cho, Tao Yi and Zhangang Xiao

533 ***ATP2C2 Has Potential to Define Tumor Microenvironment in Breast Cancer***
Jiazhou Liu, Yuxian Wei, Yushen Wu, Jie Li, Jiazheng Sun, Guosheng Ren and Hongzhong Li

547 ***IDO1 Expression in Ovarian Cancer Induces PD-1 in T Cells* via *Aryl Hydrocarbon Receptor Activation***
Adaobi Amobi-McCloud, Ravikumar Muthuswamy, Sebastiano Battaglia, Han Yu, Tao Liu, Jianmin Wang, Vasanta Putluri, Prashant K. Singh, Feng Qian, Ruea-Yea Huang, Nagireddy Putluri, Takemasa Tsuji, Amit A. Lugade, Song Liu and Kunle Odunsi

562 ***Rapamycin Promotes ROS-Mediated Cell Death* via *Functional Inhibition of xCT Expression in Melanoma Under γ-Irradiation***
Yunseo Woo, Hyo-Ji Lee, Jeongyeon Kim, Seung Goo Kang, Sungjin Moon, Jeong A. Han, Young Mee Jung and Yu-Jin Jung

576 ***The Role of Tumor Necrosis Factor in Manipulating the Immunological Response of Tumor Microenvironment***
Dipranjan Laha, Robert Grant, Prachi Mishra and Naris Nilubol

588 ***Tumor Immune Microenvironment Characterization Identifies Prognosis and Immunotherapy-Related Gene Signatures in Melanoma***
Dan Liu, Xue Yang and Xiongzhi Wu

600 ***CXCL8 Associated Dendritic Cell Activation Marker Expression and Recruitment as Indicators of Favorable Outcomes in Colorectal Cancer***
Enhao Li, Xiaobao Yang, Yuzhang Du, Guanzheng Wang, David W. Chan, Di Wu, Peiqing Xu, Peihua Ni, Dakang Xu and Yiqun Hu

614 ***Immune Landscape of Gastric Carcinoma Tumor Microenvironment Identifies a Peritoneal Relapse Relevant Immune Signature***
Chuang Zhang, Danni Li, Ruoxi Yu, Ce Li, Yujia Song, Xi Chen, Yibo Fan, Yunpeng Liu and Xiujuan Qu

627 ***IL-35 Regulates the Function of Immune Cells in Tumor Microenvironment***
Kewei Liu, Ai Huang, Jun Nie, Jun Tan, Shijie Xing, Yue Qu and Ke Jiang

637 **Fusobacterium nucleatum** ***Facilitates M2 Macrophage Polarization and Colorectal Carcinoma Progression by Activating TLR4/NF-κB/S100A9 Cascade***
Lijun Hu, Yan Liu, Xuehua Kong, Rui Wu, Qi Peng, Yan Zhang, Lan Zhou and Liang Duan

650 ***Prognosis and Characterization of Immune Microenvironment in Acute Myeloid Leukemia Through Identification of an Autophagy-Related Signature***
Denggang Fu, Biyu Zhang, Shiyong Wu, Yinghua Zhang, Jingwu Xie, Wangbin Ning and Hua Jiang

666 ***CD58 Immunobiology at a Glance***
Yalu Zhang, Qiaofei Liu, Sen Yang and Quan Liao

686 ***Screening and Validation of the Hypoxia-Related Signature of Evaluating Tumor Immune Microenvironment and Predicting Prognosis in Gastric Cancer***
Jun-Peng Pei, Chun-Dong Zhang, Maimaitituusun Yusupu, Cheng Zhang and Dong-Qiu Dai

701 ***Follistatin-Like 3 Correlates With Lymph Node Metastasis and Serves as a Biomarker of Extracellular Matrix Remodeling in Colorectal Cancer***
Chao Yang, Fengyu Cao, Shuoyang Huang and Yongbin Zheng

715 ***Transferrin-Conjugated Erianin-Loaded Liposomes Suppress the Growth of Liver Cancer by Modulating Oxidative Stress***
Anhui Yang, Zhen Sun, Rui Liu, Xin Liu, Yue Zhang, Yulin Zhou, Ye Qiu and Xinrui Zhang

727 ***m^{6}A Methylation Modification Patterns and Tumor Microenvironment Infiltration Characterization in Pancreatic Cancer***
Mengyu Sun, Meng Xie, Tongyue Zhang, Yijun Wang, Wenjie Huang and Limin Xia

742 ***PTP4A3 Is a Prognostic Biomarker Correlated With Immune Infiltrates in Papillary Renal Cell Carcinoma***
Qian Song, Yutian Zheng, Junzhou Wu, Sheng Wang, Lin Meng, Qian Yao, Zhongwu Li and Shenyi Lian

756 ***From Cellular Infiltration Assessment to a Functional Gene Set-Based Prognostic Model for Breast Cancer***
Huamei Li, Yiting Huang, Amit Sharma, Wenglong Ming, Kun Luo, Zhongze Gu, Xiao Sun and Hongde Liu

771 ***Characterization of Interplay Between Autophagy and Ferroptosis and Their Synergistical Roles on Manipulating Immunological Tumor Microenvironment in Squamous Cell Carcinomas***
Lijie Chen, Xing Niu, Xue Qiao, Sai Liu, Hongmei Ma, Xueqing Shi, Xuemei He and Ming Zhong

frontiers in Immunology

REVIEW
published: 14 July 2020
doi: 10.3389/fimmu.2020.01479

Targeting Immunometabolism Mediated by CD73 Pathway in *EGFR*-Mutated Non-small Cell Lung Cancer: A New Hope for Overcoming Immune Resistance

Anna Passarelli[1*†], *Michele Aieta*[1†], *Alessandro Sgambato*[2] *and Cesare Gridelli*[3]

[1] Unit of Medical Oncology, Department of Onco-Hematology, Centro di Riferimento Oncologico della Basilicata (IRCCS-CROB), Rionero in Vulture, Italy, [2] Laboratory of Pre-clinical and Translational Research, Centro di Riferimento Oncologico della Basilicata (IRCCS-CROB), Rionero in Vulture, Italy, [3] Division of Medical Oncology, "S.G. Moscati" Hospital, Avellino, Italy

OPEN ACCESS

Edited by:
Peng Qu,
National Institutes of Health (NIH), United States

Reviewed by:
Hua Jiang,
Indiana University-Purdue University Indianapolis, United States
Jing Hao,
Shandong University, China

***Correspondence:**
Anna Passarelli
passarellian@libero.it;
anna.passarelli@crob.it

[†]These authors have contributed equally to this work

Specialty section:
This article was submitted to Cancer Immunity and Immunotherapy, a section of the journal Frontiers in Immunology

Received: 10 May 2020
Accepted: 08 June 2020
Published: 14 July 2020

Citation:
Passarelli A, Aieta M, Sgambato A and Gridelli C (2020) Targeting Immunometabolism Mediated by CD73 Pathway in EGFR-Mutated Non-small Cell Lung Cancer: A New Hope for Overcoming Immune Resistance. Front. Immunol. 11:1479. doi: 10.3389/fimmu.2020.01479

Despite the relevant antitumor efficacy of immunotherapy in advanced non-small cell lung cancer (NSCLC), the results in patients whose cancer harbors activating epidermal growth factor receptor (*EGFR*) mutations are disappointing. The biological mechanisms underlying immune escape and both unresponsiveness and resistance to immunotherapy in *EGFR*-mutant NSCLC patients have been partially investigated. To this regard, lung cancer immune escape largely involves high amounts of adenosine within the tumor milieu with broad immunosuppressive effects. Indeed, besides immune checkpoint receptors and their ligands, other mechanisms inducing immunosuppression and including adenosine produced by ecto-nucleotidases CD39 and CD73 contribute to lung tumorigenesis and progression. Here, we review the clinical results of immune checkpoint inhibitors in *EGFR*-mutant NSCLC, focusing on the dynamic immune composition of *EGFR*-mutant tumor microenvironment. The adenosine pathway-mediated dysregulation of energy metabolism in tumor microenvironment is suggested as a potential mechanism involved in the immune escape process. Finally, we report the strong rationale for planning strategies of combination therapy with immune checkpoints blockade and adenosine signaling inhibition to overcome immune escape and immunotherapy resistance in *EGFR*-mutated NSCLC.

Keywords: non-small cell lung cancer, epidermal growth factor receptor, immune metabolism, adenosine, CD73, immunotherapy, immune resistance

INTRODUCTION

Primary lung cancer is the most common malignant tumor and the main cause of cancer-related death in the world (1). Non-small cell lung cancer (NSCLC) accounts for 80–90% of lung cancers, while small cell lung cancer (SCLC) has decreased in terms of frequency over the past decades (2, 3). The World Health Organization (WHO) calculates that lung cancers cause 1.5 million deaths per years and about 70% of them are due to smoking. However, recent advances in the field of anti-cancer therapies and mutations in oncogenic drivers (4), such as Epidermal Growth Factor Receptor (*EGFR*) mutations and Anaplastic Lymphoma Kinase (ALK) gene translocation, have

improved the outlook in terms of both progression-free survival (PFS) and overall survival (OS), showing a promising future for advanced NSCLC therapy (5).

Tyrosine kinase inhibitors (TKIs) in oncogene-driven tumors and immunotherapy are the two major evolving strategies in the treatment of NSCLC (6, 7). To date, *EGFR*-TKIs are recommended by clinical guidelines as optimal first-line strategy in *EGFR*-mutated NSCLC (8). Despite initial responsiveness to *EGFR*-TKIs, acquired resistance within 9–18 months is almost inevitable (9). Therefore, the onset of acquired resistance to *EGFR*-TKIs has raised hopes of a role for immune checkpoint inhibitors (ICIs) characterized instead by durable response (10).

The use of immune checkpoint inhibitors (ICIs) has revolutionized the management of patients with non-oncogene addicted NSCLC in both first- and second-line settings, showing an unexpected long-term effectiveness and a good toxicity profile (11); on the other hand, to date the clinical outcomes of ICIs in oncogene-addicted NSCLC are disappointing.

To this regard, recent clinical studies have described limited efficacy of ICIs, targeting mainly cytotoxic T-lymphocyte antigen-4 (CTLA-4), programmed-cell death-1 (PD-1) or its ligand PD-L1, in NSCLC harboring *EGFR* mutations and TKIs naive (12). In addition, a recent work has suggested that the different molecular features of *EGFR* mutations in NSCLC may lead to a different responsiveness and outcomes to ICIs (13). It is noteworthy that *EGFR*-TKIs could modulate immune responsiveness to cancer by shaping the tumor microenvironment (TME) and enhancing ICIs benefit (14). Therefore, several clinical trials evaluating both efficacy and safety of immunotherapy combined with targeted therapy in patients *EGFR*-mutant NSCLC are currently ongoing (15, 16).

To date, several evidence have suggested that *EGFR*-mutated cancer cells represent a crucial hallmark of immunosuppression (17), actively establishing an immunosuppressive milieu and negatively influencing the quality of T-cell immune response.

Interestingly the immunosuppressive effects of *EGFR* mutations could also result in an immune metabolic dysfunction, in which an emerging role seems to be played by CD39/CD73 ectonucleotidases, catalyzing both over-production and release of extracellular adenosine (ADO), known as a powerful immunosuppressive nucleoside (18). In specific, the immune metabolic reprograming mediated by adenosine signaling in TME is reported as a further hallmark of *EGFR*-mutated NSCLC, with the precise aim to evade the immune surveillance and induce innate immune resistance to ICIs (19).

In this review, we discuss the role and features of TME in NSCLC harboring *EGFR*-mutation focusing on the involvement of immunometabolism mechanisms mediated by CD39/CD73—adenosine signaling. The potential application of targeting this pathway in the therapeutic strategy for overcoming the immunotherapy resistance is also evaluated.

IMMUNOTHERAPY IN THE MANAGEMENT OF *EGFR*-MUTATED LUNG CANCER

The relevant success of the immunotherapy associated with favorable safety profile in advanced lung cancer treatment (20–23) suggests that, similarly to other cancer types, escape, or immune evasion processes concur to lung cancer pathogenesis and progression as well (24, 25). Indeed, monoclonal antibodies (mAb)s targeting PD-1, PD-L1, and CTLA-4 immune checkpoints leading to increased anti-tumor response due to increased T-cell activity and proliferation, have received regulatory approval across a wide range of tumors, including NSCLC (26). Specifically, patients with PD-L1 tumor proportion score (TPS) $\geq$50% are typically offered monotherapy with the anti-PD-1 mAb (Pembrolizumab®) (27). For patients with PD-L1 expression <50%, the combination of a platinum-doublet chemotherapy and Pembrolizumab has been recently approved (28). In addition, the combination of carboplatin plus paclitaxel with anti-angiogenic drug (Bevacizumab®) and anti-PD-L1 mAb (Atezolizumab®) represents an alternative treatment for patients with non-squamous NSCLC, which just received EMA and FDA approval (FDA approval excludes patients with *EGFR* or *ALK* genomic tumor aberrations) (29). In the second-line setting, rather than single-agent chemotherapy, Pembrolizumab has been approved for tumors that express PD-L1 (30), while Nivolumab and Atezolizumab represent a standard option regardless of tumor PD-L1 expression (31–33).

Despite promising advances in immunotherapy, the role of ICIs in oncogene-addicted NSCLC remains unclear and conflicting. The majority of data come from subgroup analyses with low number of patients, therefore the use of ICIs, when permitted by regulatory agencies, should only be considered when other available therapies, including standard *EGFR*-TKIs, fail (34).

Unfortunately, after failure of first-line TKIs, patients with *EGFR* mutations have limited treatment options. Two meta-analysis covering several clinical trials observed relatively poor efficacy and low response rates to PD-1/PD-L1 inhibitors vs. standard second-line chemotherapy among patients with pre-treated *EGFR*-mutant lung cancer (35, 36). Based on molecular status, the OS improvement was confirmed for *EGFR* wild-type lung cancers (OS hazard ratio (HR): 0.67; $p < 0.001$], but not in those *EGFR* mutated (OS HR: 1.11; $p = 0.54$), although no clear conclusions can be drawn due to the limited number of patients as part of subgroup analyses.

Of most interest, Lisberg et al. reported the role of immunotherapy with Pembrolizumab as first-line for *EGFR*-mutant NSCLC patients with PD-L1 expression of at least 1%, confirming once again the failure of immunotherapy alone for *EGFR* mutant patients (12). Although this trial evaluated Pembrolizumab in only 10 *EGFR*-mutant, TKI naïve patients, the lack of efficacy in terms of objective response reported was striking, especially since 70% of these patients had PD-L1 expression $\geq$50% (12, 37). About this, an interesting retrospective analysis showed that among *EGFR*-mutated NSCLC patients with high PD-L1 expression (TPS $\geq$50%) the efficacy of PD-1 inhibitors tended to be lower as compared to *EGFR* wild-type patients (38). These disappointing results could be related, at least partly, to the genomic landscape of *EGFR*-mutant NSCLC (39). Indeed, this type of cancer shapes a typical "uninflamed" TME characterized by a lack of T-cell infiltration, a shrinking proportion of PD-L1$^+$/CD8$^+$ tumor infiltrating lymphocytes (TILs), an immune metabolic reprogramming process and a

lower mutation burden (17). Therefore, the limited benefit of immunotherapy in *EGFR*-mutant patients has led to alternative approaches or rather combination strategies targeting several pathways. These include ICIs plus an anti-angiogenic therapy or *EGFR*-TKIs (**Table 1**), as well as ICIs with chemotherapy to increase immunogenicity of *EGFR*-mutant tumors and responsiveness to ICIs (40).

Importantly, the IMpower150 trial reported that in *EGFR*-mutant NSCLC patients the addition of Atezolizumab to Bevacizumab plus carboplatin plus paclitaxel (ABCP) provided significant clinical benefit (41). In specific, in a subset analysis of *EGFR*-mutant patients treated after TKI failure, median OS was not estimable for patients treated with the addition of ABCP vs. 17.5 months for patients treated with Bevacizumab, carboplatin plus paclitaxel (BCP) (HR 0.31; 95% CI 0.11–0.83); median PFS was 10.3 months with ABCP vs. 6.1 months with BCP, associated with a similar and good safety profile (39). However, the subgroup analysis and the very low patients number (overall 114 patients) with activating *EGFR* mutation or *EML4-ALK* rearrangement status are important limitations.

Furthermore, preclinical studies reported an immune modulatory effect of *EGFR* signaling by regulating expression of MHC I/II and PD-L1 on tumor cells and the activity of T-cells. This suggests a potential synergistic effect for the use of immunotherapy in combination with *EGFR*-TKIs (42), according to the recent evidence of long-lasting antitumor responses of *BRAF/MEK* inhibitors with immunotherapy in the treatment of *BRAF*-mutated metastatic melanoma (43). However, this promising combination strategy remains controversial due to the significant toxicity observed in several clinical trials following administration of anti-PD-(L)1 mAbs in combination with *EGFR*-TKIs (44, 45) (see **Table 1**).

In conclusion, all these studies suggest that further and prospective clinical trials with different and less toxic drugs are required to better define if there is a role for ICIs strategy in the treatment of oncogene-addicted NSCLC.

THE IMMUNE MICROENVIRONMENT IN EGFR-MUTANT NSCLC

The TME composition plays a considerable role in tumor growth and progression (24). Surprisingly, the TME is able to act as either obstacle or facilitator of cancer proliferation and progression by affecting several biological mechanisms. During tumorigenesis, both immune and *EGFR*-mutant tumor cells are subjected to the immunoediting process consisting of dynamic and interconnected phases, including elimination, equilibrium, and finally immune evasion. Therefore, this complex interplay is essential to define appropriate strategies to target TME as part of the anti-cancer therapy.

To this regard, recently it has been reported that the TME of *EGFR*-mutated NSCLC concurs to create an immunosuppressive milieu, as represented in **Figure 1** (46). In fact, immunosuppressive effects of *EGFR* mutations shape both composition and function of TME by interfering with several intracellular pathways and modulating immune accessory cells such as tumor-infiltrating lymphocytes (TILs), natural killer (NK) cells, T-regulatory cells (Tregs), myeloid-derived suppressor cells (MDSCs), tumor-associated macrophages (TAMs), involved in the increased release of immunoregulatory soluble factors such as cytokines and exosomes, as summarized in **Table 2** (47, 48).

In NSCLC, several studies reported that highly infiltrating T-lymphocytes in TME are related to the efficacy of immunotherapy and thus good prognosis (49). Indeed, several studies found significantly reduced $CD8^+$ TILs in an *EGFR*-mutated NSCLC group compared with a wild-type *EGFR* group (17). In terms of

TABLE 1 | Clinical trials of immunotherapy combined with EGFR-TKi in EGFR-mutated NSCLC.

	Drugs Combination				Outcome	Safety	
Clinical trial	**TKi**	**ICI**	**Condition or disease**	**Phase**	**ORR (%)**	**AEs Grade 3-4**	**Trial Status**
NCT02088112	Gefitinib	Durvalumab	EGFRm NSCLC, TKi naive	I	63%	58%	Active, not recruiting
NCT02013219	Erlotinib	Atezolizumab	EGFRm NSCLC, TKi naïve or previously treated (without TKi)	I	75%	50%	Active, not recruiting
-	Erlotinib	Nivolumab	EGFRm NSCLC, TKi naïve or treated	I/II	15%	25%	Completed
NCT02143466 TATTON	Osimertinib	Durvalumab	EGFRm NSCLC, TKi naïve or treated	I	43%	48% (ILD-transaminitis)	Active, not recruiting
NCT02454933 CAURAL	Osimertinib	Durvalumab	EGFR-T790M NSCLC previously treated with TKi	III	64%	8%	Active, not recruiting
NCT02039674	Erlotinib/Gefitinib	Pembrolizumab	EGFRm NSCLC	I/II	-	-	Active, not recruiting

Source from ClinicalTrials.gov.

TKi, tyrosin-kinase inhibitor; ICI, immune checkpoint inhibitor; ORR, Overall Response Rate; AEs, Adverse Events; EGFR, epidermal growth factor receptor; NSCLC, Non-Small-Cell Lung Cancer; N/A, not available; ILD, Interstitial Lung Disease.

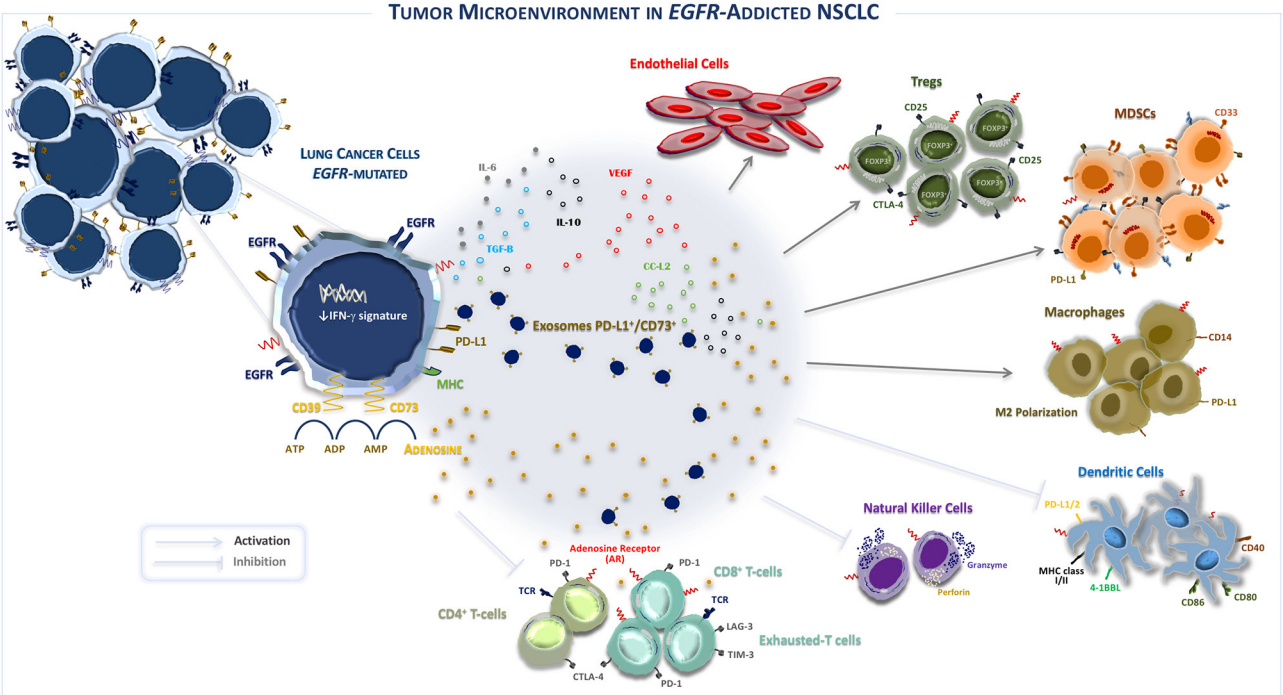

FIGURE 1 | The tumor microenvironment in EGFR-addicted NSCLC. *EGFR*-mutated NSCLC is typically characterized by an "uninflamed" tumor microenvironment, immunological tolerance, and weak immunogenicity. Recently, it was suggested that the over-expression of CD39/CD73—adenosine signaling also induces an immunosuppressive TME. Indeed, CD39/CD73 ectonucleotidases are widely expressed by lung cancer cells and induce the high extracellular production and release of immunosuppressive adenosine that shapes the activity of innate and adaptive immune system cells and endothelial cells in TME. Specifically, the activation of CD39 induces the de-phosphorylation of ATP to ADP and, subsequently, to AMP, while CD73 catalyzes the hydrolysis of AMP into adenosine and phosphate. By binding the A2A adenosine receptor A2AR, the most common receptor subtype expressed by both adaptive and innate immunity, extracellular adenosine induces inhibitory signals in TME that restrain the activity of immune system cells, promoting growth and survival of *EGFR*-mutated lung cancer cells. In addition, exosomes derived by tumor cells also contribute to modulate immunosuppression by influencing PD-L1^{+}/CD73^{+} expression and extracellular adenosine release. EGFR, Epidermal growth factor receptor; Tregs, T regulatory T-cells; MHC, Major histocompatibility complex; PD-1, Programmed cell death protein; CTLA-4, Cytotoxic T lymphocyte antigen-4; MDSCs, Myeloid-derived suppressor cells; TCR, T-cell receptor; VEGF, Vascular endothelial growth factor; IL, Interleukin; M2, Macrophages 2; ATP, Adenosine triphosphate; ADP, Adenosine diphosphate; AMP, Adenosine monophosphate; CCL2, C-C motif chemokine ligand 2; FoxP3, forkhead box P3.

EGFR mutation sites different immunological profiles have been reported with the prevalence of "inflamed" TME consisting of higher level of functional TILs in *EGFR*^{L858R} samples compared to *EGFR* exon 19 deletion tumor samples (50).

To support the evidence on the heterogeneity of *EGFR* mutations, Hastings et al. retrospectively analyzed clinical and molecular data on 171 cases of *EGFR*-mutant lung tumors treated with ICIs. Although *EGFR*-mutant tumors typically showed a low response to immunotherapy, clinical outcomes appear to vary by allele. In specific, *EGFR*^{L858R} tumors had a similar response rate and OS to an *EGFR* wild-type NSCLC population, while tumors harboring deletions in exon 19 cases did substantially worse (13).

Furthermore, it is noteworthy that the relationship between *EGFR* mutations and PD-L1 expression remains largely controversial, since pre-clinical data reported that the activation of *EGFR* signaling directly drives "intrinsic" PD-L1 up-regulation in a NSCLC model through several pathways such as PI3K/AKT/mTOR, Ras/RAF/MEK/ERK, JAK/STAT, and NF-kB (39). In addition, the activation of *EGFR* signaling may lead to the down-regulation of both class I and II antigens of the major histocompatibility complex (MHC) whose expression is regulated by the MEK/ERK pathway (51). Conversely, a large number of clinical trials reported that PD-L1 expression in *EGFR* wild-type tumors was significantly higher than in *EGFR* mutant NSCLC (52).

Regarding the field of predictive biomarkers research in NSCLC and other cancer types, tumor mutation burden (TMB) also emerged as a promising predictive biomarker of ICIs efficacy (53). TMB is the total number of insertion, deletion, and substitution mutations per megabase of the coding region of a tumor genome. Among patients with NSCLC treated with anti-PD-1 mAb, higher non-synonymous TMB seemed to be related with greater benefit, but a large phase III randomized trial did not confirm these preliminary observations (54). However, *EGFR*-addicted NSCLC were shown to have also low TMB (55).

Further, the activation of the *EGFR* oncogene pathway induces the release of several immunosuppressive factors to accomplish evasion of the host anti-cancer immune response. On the other hand, the inefficient killing of tumor cells is mostly due to a direct effect of *EGFR*-mutated lung cells through the over-production of negative modulators of immune cells including tumor necrosis factor-β (TGF-β), interleukin-10 (IL-10), vascular endothelial

TABLE 2 | The major hallmarks and mechanisms of Tumor Immune Escape in the TME of EGFR-mutated non-small cell lung cancer.

Mechanism of action	Population(s)/pathway(s)	Effect(s) on TME
Tumor-infiltrating lymphocytes (TIL)s	$CD3^+$ lymphocytes $CD8^+$ T-cells $CD4^+$ T-cells	Inefficacy tumor-cytotoxicity of T-cells
Over-expression of inhibitory immune checkpoints	↑ CTLA-4, PD-1, LAG3, TIM3, VISTA, TIGIT	Inhibition of T-cell function/T-cell anergy
Over-expression of immune checkpoint ligands	PD-L1 PD-L2	Activation of inhibitory immune checkpoints
Defective recognition of lung cancer cells	Downregulation, mutation or loss of MHC class I Lung cancer antigens Defective antigen presentation	↓ Initiation of the antigen-specific immune response, antigen processing and presentation, and the cross-priming processes Inefficacy activation of lung cancer infiltrating T-cells
Up-regulation of immune suppressive cells	MDSCs $CD4^+CD25^+FoxP3^+$ Tregs Macrophage infiltration (M2-TAM)	Inhibition of T-cell function Direct pro-tumorigenic effect (VEGF, TGF-β)
Release of pro-tumorigenic and pro-angiogenic factors by TME	TGF-β VEGF, IL-10, IL-6, MMP CCL-2 iNOS	Induction of both recruitment and accumulation of immunosuppressive cells Tumor angiogenesis and stroma remodeling Migration of MDSCs in the TME through STAT3 activation Inhibition of T-cell function
Intracellular activation of *EGFR* signaling	↑ JAK/STAT3 ↑ PI3K/AKT/mTOR ↑ Ras/RAF/MEK/ERK ↑ NF-kB	↓ Down-regulation of MHC I/II class - ↓ Inhibition of STAT1 activity ↑ MDSCs - ↓ DCs and APCs - ↑ TAM-M2 polarization ↑/↓ PD-L1; ↓ IFNγ signature ↑ Production and release of negative modulators (TGF-β, IDO, CCL-2)
Tumor mutational load and Neoantigens	↓ TMB	Low TMB may negatively influence the immune-mediated anti-tumor response
Dysregulation of the immunometabolism	↑ CD39/CD73 – adenosine signaling ↑ IDO ↑ ARG-1	↑ Immunosuppressive TME restraining anti-tumor immunity through A2AR ↑ Degradation of tryptophan into immunosuppressive kynurenines ↑ TAM-M2 polarization

TME, tumor microenvironment; mAb, monoclonal antibody; EGFR, epidermal growth factor receptor; NSCLC, Non-Small-Cell Lung Cancer; MHC, major histocompatibility complex; CTLA4, cytotoxic T-lymphocyte antigen 4; PD-1, programmed death 1; LAG3, lymphocyte activation gene-3; TIM3, T cell immunoglobulin and mucin domain 3; VISTA, V-domain immunoglobulin suppressor of T-cell activation; PDL1, programmed death ligand 1; PDL2, programmed death ligand 2; IFN, interferon; MDSCs, myeloid-derived suppressor cells; Tregs, regulatory T cells; TAM, tumor-associated macrophages; MMP, matrix metalloproteinase; CCL-2, CC chemokine ligand-2; TGF, tumor necrosis factor; VEGF, vascular endothelial growth factor; iNOS, inducible nitric oxide synthase; IDO, indoleamine 2,3 dioxygenase; IL, interleukin; TMB, tumor mutation burden; A2AR, adenosine 2A receptor; ARG, arginase.

growth factor (VEGF), indolamine 2,3-dioxygenase (IDO), C-C chemokine ligand 2 (CCL-2), arginase (ARG)-1, and adenosine. The abundant immunosuppressive environment promotes both conversion and proliferation of $CD3^+CD4^+CD25^-$ cells into $CD4^+CD25^+FoxP3^+$ Tregs population, leading to immune suppression mediated by tumor release of *EGFR*-containing exosomes (47). Similarly, the increased bioavailability of soluble factors, such as IL-10, TGF-β, and CCL2, induces both recruitment and accumulation of immunosuppressive cell populations, such as MDSCs, into the TME, resulting in the activation of the signal transducer and transcriptional activator-3 (STAT3) pathway. Furthermore, STAT3 induces the activation of MDSCs, exerting additional immunosuppressive functions, such as inducing impairment of the antigen processing machinery mediated by dendritic cells (DCs), compromising T-cell-mediated cytotoxicity, inducing angiogenesis process by VEGF and matrix metalloproteinase (MMP) release, and promoting macrophage phenotype polarization in TAMs. Thus, this TME composition strongly restrains T-cell effector functions through paracrine signals that promote cancer growth (40).

Finally, in addition to the avoiding immune destruction (56, 57), a major emerging "hallmark" of immune evasion in TME harboring *EGRF* mutations is the reprogramming of immunometabolism (58) through CD39/CD73 ectonucleotidases complex that quickly converts adenosine triphosphate (ATP) in adenosine (59), one of most powerful known immunosuppressive metabolite (18, 60). Therefore, it is likely that this impairment in the immune system expressed as "uninflamed" TME and characterized by immunological tolerance provokes a weak immunogenicity leading to a poor responsiveness to immunotherapy in patients with *EGFR*-mutant NSCLC.

IMMUNOMETABOLISM MEDIATED BY CD39/CD73 - ADENOSINE AXIS IN *EGFR*-MUTANT NSCLC

The hallmarks of cancer, defined as acquired functional capabilities allowing cancer cells to survive, proliferate, and spread, have been initially identified as modification in cells phenotype enabling replicative immortality, sustained proliferative signaling, evasion from growth suppressors, resistance to cell death, angiogenesis, invasion, and metastasis

(56). In the last few decades, further hallmarks have been added to this list, including tumor-promoting inflammation, genome instability and mutation, evasion from immune destruction, and reprogramming of energy metabolism (57). During the multi-step tumorigenesis process, the disruption of energy metabolism is proving to be a cardinal feature in lung cancer development and is characterized by the engagement of the aerobic glycolysis, a process where the conversion of glucose into lactate occurs even in presence of sufficient oxygen to support glucose catabolism (Warburg effect) (61).

The TME could alter the immunometabolism and provide immunosuppressive metabolic substrates, thereby modifying the function of immune cells. On the other hands, T-cell subsets need alternative energetic pathways to satisfy their immune response efficiency and to balance the immune system activity. In this context, adenosine signaling involving CD39/CD73 ectonucleotidases expressed on various tumor cells is a critical pathway in TME to evade the immune surveillance and generate an immunosuppressive milieu (18). Specifically, in addition to the pleiotropic effects on immune cells infiltrating tumor, hypoxia directly induces increased adenine nucleotide in TME. Adenosine is an intra- and extra-cellular nucleoside that shows several effects in different tissues depending on its interaction with the following four G-protein-coupled adenosine receptors: A1, A2A, A2B, and A3 (62). In specific, ATP is degraded to adenosine by the ectonucleotidases complexes such as CD39 (ectonucleoside triphosphate diphosphohydrolase-1, E-NTPDase1) and CD73 (ecto-5′-nucleotidase, Ecto5′NTase), which convert ATP to adenosine monophosphate (AMP) and AMP to adenosine and inorganic phosphate, respectively. Adenosine is irreversibly deamidated to inosine by the adenosine deaminase (ADA) enzyme, while extra-cellular adenosine binds to adenosine receptors differently expressed by stromal and immune cells surrounding tumor, thus contributing to immune cell dysfunction (60). Interestingly, A2AR (A2A adenosine receptor) expression has also been found in human lung cancer cells, mostly in adenocarcinoma, exerting a partially direct effect on tumor growth while its antagonism induces tumor growth inhibition through apoptosis activation. Moreover, A2AR is the high-affinity adenosine receptor and appears to have the highest prevalence across all immune cells within both the adaptive and innate systems.

CD73 is endogenously expressed on endothelial cells, epithelial cells, and some immune subsets, and its expression has also been observed in several cancer types, including melanoma, colon, breast, ovarian, and lung cancer (19). Notably, the main drivers of CD73 expression within TME include hypoxia, TGF-β, type I IFN, IL-1, and prostaglandin (63).

Contrarily, so far little is known about the expression levels of CD39 on intra-tumoral T-cells in NSCLC. Recently, an interesting study reported a consistent co-expression of CD39 and PD-1 receptor on tumor-infiltrating immune cells in NSCLC TME than immune cells from normal lung tissue. CD39 was found also upregulated on several immune cells, including $CD4^+$ and $CD8^+$ T-cells, $CD16^+$NK cells, macrophages, and B cells. Furthermore, $CD39^+FoxP3^+$ Tregs were highly enriched in the TME. Therefore, the CD39 upregulation on immune cells in TME suggests that the CD39 pathway may, in addition to PD-1 signaling, represent another relevant mechanism for tumor-induced immunosuppression in NSCLC (64). It is also demonstrated that tumor TGF-β induces CD39/CD73 over-expression on MDSCs in NSCLC TME via phosphorylation of mTOR, and subsequently activation of hypoxia-inducible factor-1 (HIF-1) signaling. Thus, TGF-β stimulating CD39/CD73 expression suppress both T-cells and NKs immunity (65). In addition, the increased expression of CD39 on cytotoxic T-cell induced by MDSCs correlated with poor prognosis in advanced NSCLC patients treated with anti-PD-1 mAbs (66).

Therefore, CD39/CD73 nucleotidases are not only involved in both purine and pyrimidine nucleotide synthesis but represents also a negative modulator of immune signaling through adenosine production in the TME (59). Accordingly, in TME the increased adenosine production mainly through A2AR activation on immune system cells impairs T-cell cytotoxicity, cytokine production, and T and NK cell function as well as induces suppression of antigen-presenting cells (APCs) (67). Indeed, in the myeloid compartment, adenosine skews the differentiation of DCs into tolerogenic and immunosuppressive DCs and enhances the immunosuppressive activity of TAM through macrophage M2 polarization. Adenosine release in TME also promotes Tregs and MDSCs proliferation (68) (see **Figure 1**). Moreover, recent studies have demonstrated that immunosuppressive populations including Tregs and MDSCs enhance their intrinsic suppressive activity also by direct CD73/CD39 upregulating on their cell surface. CD73 expression on $FoxP3^+$ Tregs mediates part of their pro-tumorigenic effect converting proinflammatory extracellular ATP into powerful immunosuppressive adenosine (69).

In addition to traditional pathways mediated by CD39/CD73, an alternative enzymatic cascade has been recently reported and includes ectoenzymes such as CD38 (NAD^+ nucleosidase), CD203α (ecto-nucleotide pyro-phosphatase phosphodiesterase 1) and CD73 (70, 71), thus participating to the composition of the so-called "purinergic milieu" (72). Indeed, in the search of a better understanding of the mechanisms involved in the acquired immunotherapy resistance, it has been reported that the unresponsiveness to PD-1/PD-L1 inhibition in lung murine models is probably mediated by the tumor up-regulation of CD38 enzyme, which is induced by all-trans retinoic acid and IFN-β in the TME. Therefore, CD38 represents an alternative ectoenzymatic pathway that limits the cytotoxic activity of $CD8^+$ T-cells through the activation of adenosine receptor signaling (73), suggesting a potential role of CD38 blockade to overcome immune resistance (74).

Regarding the clinical significance of adenosine signaling, tumor CD73 expression has been widely associated with poor prognosis in several types of cancer including melanoma, colorectal, and triple-negative breast cancers (75). Indeed, to better define the relevance of adenosine signaling in lung cancer, an interesting relationship between immunohistochemistry (IHC) expression of CD73 in tumor tissues and clinical outcome has been found in patients with advanced NSCLC (stage I-III) (76). Moreover, high CD73 expression was an independent factor

of poor prognosis in terms of OS and recurrence-free survival, thus exhibiting a remarkably worse prognostic meaning (76).

It is also noteworthy the relationship reported by Streicher et al. among the *EGFR* oncogene activation, the expression of CD73 and the reduced release of IFN-γ in NSCLC cell lines compared to wild-type cells. This exploratory analysis was conducted on tumor biopsies of advanced NSCLC patients from a non-randomized phase Ib/II clinical trial (NCT01693562) and from TGCA. According to these evidence, EGFR-mutant adenocarcinomas displayed >2-fold increased expression of CD73 compared to wild type, and this mechanism might, at least in part, explain their poor responsiveness to immunotherapy (19). Besides CD73 expression was induced by epidermal growth factor (EGF), and the pharmacological inhibition through *EGFR*-TKi induced its decrease in *EGFR*-mutated cancer cell lines.

A further study showed for the first time an inverse association between CD73 expression and activated tumor-infiltrating lymphocytes; in over 1,000 human lung cancer samples (77). It was demonstrated that high levels of CD73 significantly correlated with lower infiltration of activated $CD8^+$ T-cells compared to those tumor samples with low CD73 expression. Interestingly, CD73 expression was significantly increased in samples with *EGFR* mutations when compared with wild type tumors (77). To confirm this evidence, it has been recently reported that lower levels of baseline tumor adenosine are associated with a reduced efficacy of anti- PD-1/CTLA-4 mAbs in cohorts of ICI-treated patients (HR = 0.29, $P = 0.00012$) (78).

By contrast, Ishii et al. retrospectively showed that high CD73 expression correlated with favorable clinical efficacy of immunotherapy in patients with *EGFR*-mutated NSCLC who have developed resistance to *EGFR*-TKIs, although this study had some limitations such as the limited number of patients analyzed (63).

TARGETING IMMUNOSUPPRESSIVE CD73 - ADENOSINE AXIS IN LUNG CANCER: A NEW STRATEGY

The emerging role of CD39/CD73 - adenosine axis in *EGFR*-mutated NSCLC growth, progression, and ICI resistance has allowed to define a further immune checkpoint as a potential strategy to develop targeted treatments (79, 80).

Indeed, regarding the effect of adenosine signaling in the defective regulation of anti-tumor response observed in preclinical tumor models (81–83), different strategies targeting CD73 ectonucleotidase are currently under extensive clinical investigation also in advanced NSCLC (46). Given the broad expression of ectonucleotidases and adenosine receptors in the lung TME, a better understanding of their specific functions will be crucial to implement this new generation of immunological therapeutics (84).

In specific, the adenosine signaling inhibition is based on the use of either small molecule inhibitors or humanized mAbs in order to inhibit adenosine production in the TME or counteract adenosine pathway through targeting the adenosine receptors (85). Small molecules overcame mAbs in terms of both feasibility of administration and bioavailability. By contrast, anti-CD73 mAbs represent a valid alternative for their longer half-life and high specificity. In addition, both direct and indirect effects of mAbs on immune system cells as well as on target cells have been clearly demonstrated (86, 87).

Recent studies showed that the single A2AR blockade or the combination with either PD-1/PD-L1 or CTLA-4 mAbs induces T-cell proliferation, enhances the expression of IFNγ and granzyme B by tumor-infiltrating $CD8^+$ T-cells, thus restraining the tumor growth in preclinical models (82, 83). Therefore, the therapeutic effect of A2AR antagonists may be maximized in "inflamed" tumors characterized by infiltrating tumor-reactive T-cells that are otherwise rendered impotent by high adenosine levels in the TME. Interestingly, the A2AR antagonism could prevent negative signaling in T-cells and inhibit angiogenesis process, but also play a direct inhibitory effect on lung cancer cells themselves (88). Anyway, the safety and efficacy of several A2AR inhibitors await evaluation in many ongoing trials also in advanced NSCLC treatment, as summarized in **Table 3**. Preliminary data demonstrated that A2AR inhibitor (CPI-444), as a single agent and in combination with the anti-PD-L1 mAb (Atezolizumab®) is well-tolerated and shows anti-tumor activity in refractory renal cancer and NSCLC cohorts (89).

Finally, the current development of anti-CD73-based strategies and relative ongoing clinical trials in monotherapy or combination with immune checkpoint inhibitors as anti-PD-(L)1 mAbs or targeted therapies (*EGFR*-TKIs) in the treatment of advanced NSCLC are summarized in **Table 4**. The clinical results obtained from these trials might help to clarify the clinical relevance of CD73 as immune target in the treatment of patients with *EGFR*-mutated NSCLC.

To date, preliminary results suggest that anti-CD73 mAbs and PD-1 blockade represent a promising approach with an acceptable safety profile in several tumor subtypes such as metastatic melanoma (90), encouraging future therapeutic applications in the clinical practice.

CONCLUSIONS

Lung tumor remains the most aggressive and life-threatening cancer, although significant therapeutic improvements have been obtained in the last years. To this regard, immunotherapy combinations are promising strategies aimed at restoring the anti-cancer immunity as well as overcoming innate and adaptive resistance to ICIs. In the era of successful immunotherapy, while non-oncogene addicted advanced NSCLC obtains a great survival benefit, the effectiveness of immunotherapy in *EGFR*-mutated NSCLC appears disappointing. Indeed, the anti-PD-(L)1 monotherapy has been shown to have minimal activity in *EGFR*-mutant NSCLC and therefore should only be considered after all other therapies that have been shown to be more effective in this patient population, such as *EGFR*-TKIs, platinum-doublet chemotherapy, and probably docetaxel plus anti-angiogenic drug (Ramucirumab®), have been exhausted.

The identification of additional biomarkers that are predictive of benefit to anti-PD-1 mAbs would be an

TABLE 3 | Current development status of Adenosine Receptor Antagonists in advanced non-small cell lung cancer.

Clinical trial	Drug	Mechanism of action	Pharmaceutical company	Phase of development	Condition or disease	Drugs combination
NCT02503774	AZD4635	A2AR antagonist	MedImmune	I/II	*EGFR*m NSCLC	AZD4635; MEDI9447 (Oleclumab); Osimertinib
NCT02403193	PBF-509	A2AR antagonist	Palobiofarma SL/Novartis	I/II	Advanced NSCLC $EGFR^{L858R/Del19}$ mutations	PBF-509; PDR001
NCT03454451	CPI-444	A2AR antagonist	Corvus pharmaceuticals	I	Advanced solid tumors	CPI-444; CPI-006; Pembrolizumab
NCT03549000	NIR178	A2AR antagonist	Surface oncology, novartis	I	NSCLC; TNBC; PDAC; Colorectal Cancer MSS; Ovarian Cancer; RCC; mCRPC	NIR178; NZV930; Spartalizumab
NCT03274479	PBF-1129	A2AR antagonist	Palobiofarma SL	I	Locally advanced or metastatic NSCLC	PBF-1129
NCT02655822	CPI-444	A2AR antagonist	Corvus pharmaceuticals	I/Ib	Advanced cancers	CPI-444; anti-PD-1/PD-L1 mAb

Source from ClinicalTrials.gov.
mAb, monoclonal antibody; EGFR, epidermal growth factor receptor; NSCLC, Non-Small-Cell Lung Cancer; PDR001, anti-PD-1 mAb; CPI-006, anti-CD73 Fully mAb; TNBC, Triple Negative Breast Cancer; PDAC, Pancreatic Ductal Adenocarcinoma; MSS, Microsatellite Stable; RCC, Renal Cell Carcinoma; mCRPC, Metastatic Castration Resistant Prostate Cancer; NZV930, anti-CD73 Fully mAb.

TABLE 4 | Current development status of anti-CD73 strategies in advanced non-small cell lung cancer.

Clinical trial	Drug	Mechanism of action	Pharmaceutical company	Phase of development	Condition or disease	Drugs combination
NCT02503774	MEDI9447 (Oleclumab)	Fully mAb	MedImmune	I/II	*EGFR*m NSCLC	MEDI9447; Osimertinib; AZD4635
NCT03736473				I	Advanced solid tumors	
NCT03381274				I	Advanced solid tumors	MEDI9447; MEDI4736 MEDI9447
NCT02754141	BMS-986179	Fully mAb	Bristol-Myers Squibb	I/II	Advanced Solid Tumors	BMS-986179; Nivolumab
NCT03454451	CPI-006	Fully mAb	Corvus Pharmaceuticals	I	Advanced Solid Tumors	CPI-006; CPI-444; Pembrolizumab
NCT03549000	NZV930	Fully mAb	Surface Oncology, Novartis	I	NSCLC; TNBC; PDAC; Colorectal Cancer MSS; Ovarian Cancer; RCC; mCRPC	NZV930; NIR178; Spartalizumab
NCT04148937	LY3475070	CD73 inhibitor	Eli Lilly and Company	I	Advanced solid tumors	LY3475070; Pembrolizumab
NCT03835949	TJ004309 (TJD5)	Fully mAb	I-Mab Biopharma, TRACON Pharmaceuticals	I	Advanced solid tumors	TJD5; Atezolizumab
_	IPH5301	Fully mAb	Innate Pharma	Pre-clinical	_	_
_	AB680	CD73 inhibitor	Arcus	Pre-clinical	_	_

Source from ClinicalTrials.gov.
mAb, monoclonal antibody; EGFR, epidermal growth factor receptor; NSCLC, Non-Small-Cell Lung Cancer; AZD4635, oral adenosine A2A receptor antagonist; MEDI4736, Durvalumab; CPI-444, Adenosine A2A receptor antagonist; TNBC, Triple Negative Breast Cancer; PDAC, Pancreatic Ductal Adenocarcinoma; MSS, Microsatellite Stable; RCC, Renal Cell Carcinoma; mCRPC, Metastatic Castration Resistant Prostate Cancer; NIR178, oral adenosine A2A receptor antagonist.

important advance in our understanding, especially considering the potential lethal immune-toxicities and high cost of ICIs.

Therefore, a better understanding of biological mechanisms involved in tumor progression and immune evasion as well as of the dynamic hallmarks of *EGFR*-mutated NSCLC TME is required. The "uninflamed" TME and the low TMB are typical features of *EGFR*-mutated NSCLC, potentially explaining the impaired response to immunotherapies.

To this regard, an interesting hallmark of NSCLC-harboring oncogenic driver mutations, leading to immune escape, and conferring primary immune resistance, is the reprogramming of energy metabolism mediated by CD39/CD73—adenosine

signaling. In order to reinforce the critical role of adenosine signaling in tumorigenesis, several trials have demonstrated that CD73 over-expression by cancer cells correlated with poor prognosis in NSCLC patients. Furthermore, in advanced NSCLC recent findings identified a novel relationship between *EGFR* oncogene activation, over-expression of immunosuppressive molecule such as CD73 and reduced expression of IFNγ signature, and this may explain, at least in part, the limited responsiveness to immunotherapy in *EGFR*-mutated NSCLC. Despite these preliminary evidence, the exact relevance of CD73-adenosine signaling in both *EGFR*-mutated tumor cells and infiltrating immune cells to the efficacy of immune checkpoint inhibitors remains unclear. Anyway, in the preclinical studies the pharmacological antagonism of CD39/CD73—adenosine signaling potentiated anti-tumor responses in preclinical models that otherwise failed to respond to anti-PD-1/PD-L1 inhibition. These data agree with observations that blockade of other immune checkpoint inhibitors over-expressed in the TME, such as CTLA-4, TIM-3, TIGIT can enhancing IFNγ production by $CD8^+$ TILs following anti-PD-1 inhibition.

In conclusion, adenosinergic signaling is emerging as a powerful immune-metabolic checkpoint in advanced NSCLC. Hence, further pre-clinical data and clinical trials aiming at translating adenosine signaling inhibition strategies in *EGFR*-mutated NSCLC are needed to target the dysregulated immunometabolism in the TME, in order to overcome primary resistance to immunotherapy.

AUTHOR CONTRIBUTIONS

All authors listed have made a substantial, direct and intellectual contribution to the work, and approved it for publication.

REFERENCES

1. Siegel RL, Miller KD, Jemal A. Cancer statistics, 2018. *CA Cancer J Clin.* (2018) 68:7–30. doi: 10.3322/caac.21442
2. Jemal A, Bray F, Center MM, Ferlay J, Ward E, Forman D. Global cancer statistics. *Cancer J Clin.* (2011) 61:69–90. doi: 10.3322/caac.20107
3. Ferlay, J, Soerjomataram I, Dikshit R, Eser S, Mathers C, Rebelo M, et al. Cancer incidence and mortality worldwide: sources, methods and major patterns in GLOBOCAN 2012. *Int J Cancer.* (2015) 1:E359–86. doi: 10.1002/ijc.29210
4. Dong J, Lin B, Zhou Q, Huang D. Advances in targeted therapy and immunotherapy for non-small cell lung cancer based on accurate molecular typing. *Front Pharmacol.* (2019) 10:230. doi: 10.3389/fphar.2019.00230
5. Herbst, RS, Morgensztern D, Boshoff C. The biology and management of non-small cell lung cancer. *Nature.* (2018) 553:446–454. doi: 10.1038/nature25183
6. Takeda M, Nakagawa K. First- and second-generation EGFR-TKIs are all replaced to osimertinib in chemo-naïve EGFR mutation-positive non-small cell lung cancer? *Int J Mol Sci.* (2019) 20:146. doi: 10.3390/ijms20010146
7. De Marinis F, Barberis M, Barbieri V, Marchianò A, Gasperini S, Migliorino MR, et al. Diagnosis and first-line treatment of non-small cell lung cancer in the era of novel immunotherapy: recommendations for clinical practice. *Exp Rev Respirat Med.* (2019) 13:217–28. doi: 10.1080/17476348.2019.1569517
8. Planchard D, Popat S, Kerr K, Novello S, Smit EF, Faivre-Finn C, et al. Metastatic non-small cell lung cancer. *ESMO Ann Oncol.* (2019) 29(Suppl. 4):iv192–237. doi: 10.1093/annonc/mdy275
9. Ramalingam SS, Vansteenkiste J, Planchard D, Cho BC, Gray JE, Ohe Y, et al. Overall survival with osimertinib in untreated, EGFR-mutated advanced NSCLC. *N Engl J Med.* (2020) 382:41–50. doi: 10.1056/NEJMoa1913662
10. Gridelli C, Casaluce F. Immunotherapies in the management of epidermal growth factor receptor mutated non-small cell lung cancer: a role will be found? *Transl Lung Cancer Res.* (2018) 7(Suppl. 4):S370–2. doi: 10.21037/tlcr.2018.09.18
11. Ruiz-Patino A, Arrieta O, Cardona AF, Martin C, Raez LE, Zatarain-Barron ZL, et al. Immunotherapy at any line of treatment improves survival in patients with advanced metastatic non-small cell lung cancer (NSCLC) compared with chemotherapy (Quijote-CLICaP). *Thorac Cancer.* (2020) 11:353–61. doi: 10.1111/1759-7714.13272
12. Lisberg A, Cummings A, Goldman JW, Bornazyan K, Reese N, Wang T, et al. A phase II study of pembrolizumab in EGFR-mutant, PD-L1+, tyrosine kinase inhibitor naïve patients with advanced NSCLC. *J Thorac Oncol.* (2018) 13:1138–45. doi: 10.1016/j.jtho.2018.03.035
13. Hastings K, Yu HA, Wei W, Sanchez-Vega F, DeVeaux M, Choi J, et al. EGFR mutation subtypes and response to immune checkpoint blockade treatment in non-small-cell lung cancer. *Ann Oncol.* (2019) 30:1311–20. doi: 10.1093/annonc/mdz141
14. Jia Y, Li X, Jiang T, Zhao C, Zhang L, Liu X, et al. EGFR-targeted therapy alters the tumor microenvironment in EGFR-driven lung tumors: implications for combination therapies. *Int J Cancer.* (2019) 145:1432–44. doi: 10.1002/ijc.32191
15. Yang JC, Shepherd FA, Kim DW, Lee GW, Lee JS, Chang GC, et al. Osimertinib plus durvalumab versus osimertinib monotherapy in EGFR T790M-positive NSCLC following previous EGFR-TKI therapy: CAURAL brief report. *J Thorac Oncol.* (2019) 14:933–9. doi: 10.1016/j.jtho.2019.02.001
16. Yang JC, Gadgeel SM, Sequist LV, Wu CL, Papadimitrakopoulou VA, Su WC, et al. Pembrolizumab in combination with Erlotinib or Gefitinib as first-line therapy for advanced NSCLC with sensitizing EGFR mutation. *J Thorac Oncol.* (2019) 14:553–9. doi: 10.1016/j.jtho.2018.11.028
17. Dong ZY, Zhang JT, Liu SY, Su J, Zhang C, Xie Z, et al. EGFR mutation correlates with uninflamed phenotype and weak immunogenicity, causing impaired response to PD-1 blockade in non-small cell lung cancer. *Oncoimmunology.* (2017) 6:e1356145. doi: 10.1080/2162402X.2017.1356145
18. Passarelli A, Tucci M, Mannavola F, Felici C, Silvestris F. The metabolic milieu in melanoma: role of immune suppression by CD73/adenosine. *Tumour Biol.* (2019) 42:1010428319837138. doi: 10.1177/1010428319837138
19. Streicher K, Higgs BW, Wu S, Coffman K, Damera G, Durham N, et al. Increased CD73 and reduced IFNG signature expression in relation to response rates to anti-PD-1(L1) therapies in EGFR-mutant NSCLC. *J Clin Oncol.* (2017) 35:abstr 11505. doi: 10.1200/JCO.2017.35.15_suppl.11505
20. Martinez P, Peters S, Stammers T, Soria JC. Immunotherapy for the first-line treatment of patients with metastatic non-small cell lung cancer. *Clin Cancer Res.* (2019) 25:2691–8. doi: 10.1158/1078-0432.CCR-18-3904
21. Postow MA, Sidlow R, Hellmann MD. Immune-related adverse events associated with immune checkpoint blockade. *N Engl J Med.* (2018) 378:158–68. doi: 10.1056/NEJMra1703481
22. Stucci S, Palmirotta R, Passarelli A, Silvestris E, Argentiero A, Lanotte L, et al. Immune- related adverse events during anticancer immunotherapy: pathogenesis and management. *Oncol Lett.* (2017) 14:5671–80. doi: 10.3892/ol.2017.6919
23. Tucci M, Passarelli A, Todisco A, Mannavola F, Stucci LS, D'Oronzo S, et al. The mechanisms of acute interstitial nephritis in the era of immune checkpoint inhibitors in melanoma. *Ther Adv Med Oncol.* (2019) 11:1758835919875549. doi: 10.1177/1758835919875549
24. Passarelli A, Mannavola F, Stucci LS, Tucci M, Silvestris F. Immune system and melanoma biology: a balance between immuno- surveillance and immune escape. *Oncotarget.* (2017) 8:106132–42. doi: 10.18632/oncotarget.22190
25. Tucci M, Passarelli A, Mannavola F, Felici C, Stucci SL, Cives M, et al. Immune system evasion as hallmark of melanoma progression: the role of dendritic cells. *Front Oncol.* (2019) 9:1148. doi: 10.3389/fonc.2019.01148

26. Pardoll DM. The blockade of immune checkpoints in cancer immunotherapy. *Nat Rev Cancer.* (2012) 12:252–64. doi: 10.1038/nrc3239
27. Reck M, Rodriguez-Abreu D, Robinson AG, Hui R, Csoszi T, Fulop A, et al. Pembrolizumab versus chemotherapy for PD-L1-positive non-small-cell lung cancer. *N Engl J Med.* (2016) 375:1823–33. doi: 10.1056/NEJMoa1606774
28. Gandhi L, Rodriguez-Abreu D, Gadgeel S, Esteban E, Felip E, De Angelis F, et al. Pembrolizumab plus chemotherapy in metastatic non-small-cell lung cancer. *N Engl J Med.* (2018) 378:2078–92. doi: 10.1056/NEJMoa1801005
29. Socinsky MA, Jotte RM, Cappuzzo F, Orlandi F, Stroyakovskiy MD, Nogami N, et al. Atezolizumab for first-line treatment of metastatic nonsquamous NSCLC. *N Engl J Med.* (2018) 378:2288–301. doi: 10.1056/NEJMoa1716948
30. Herbst, RS, Baas P, Kim DW, Felip E, Pérez-Gracia JL, Han J-Y, et al. Pembrolizumab versus docetaxel for previously treated, PD-L1-positive, advanced non-small-cell lung cancer (KEYNOTE-010): a randomised controlled trial. *Lancet.* (2016) 387:1540–50. doi: 10.1016/S0140-6736(15)01281-7
31. Brahmer J, Reckamp KL, Baas P, Crinò L, Eberhart WE, Poddubskaya E, et al. Nivolumab versus docetaxel in advanced squamous-cell non-small-cell lung cancer. *N Engl J Med.* (2015) 373:1–13. doi: 10.1056/NEJMoa1504627
32. Rittmeyer A, Barlesi F, Waterkamp D, Park K, Ciardiello F, von Pawel J, et al. Atezolizumab versus docetaxel in patients with previously treated non-small-cell lung cancer (OAK): a phase 3, open-label, multicentre randomised controlled trial. *Lancet.* (2017) 389:255–65. doi: 10.1016/S0140-6736(16)32517-X
33. Borghaei H, Paz-Ares L, Horn L, Spigel DR, Steins M, Ready NE, et al. Nivolumab versus docetaxel in advanced nonsquamous non-small-cell lung cancer. *N Engl J Med.* (2015) 373:162739. doi: 10.1056/NEJMoa1507643
34. Berghoff AS, Bellosillo B, Caux C, de Langen A, Mazieres J, Normanno N, et al. Immune checkpoint inhibitor treatment in patients with oncogene-addicted non-small cell lung cancer (NSCLC): summary of a multidisciplinary round-table discussion. *ESMO Open.* (2019) 4:e000498. doi: 10.1136/esmoopen-2019-000498
35. Lee CK, Man J, Lord S, Links M, Gebski V, Mok T, et al. Checkpoint inhibitors in metastatic EGFR-mutated non-small cell lung cancer - a meta-analysis. *J Thoracic Oncol.* (2016) 12:403–7. doi: 10.1016/j.jtho.2016.10.007
36. Lee CK, Man J, Lords S, Cooper W, Links M, Gebski V, et al. Clinical and molecular characteristics associated with survival among patients treated with checkpoint inhibitors for advanced non–small cell lung carcinoma. a systematic review and meta-analysis. *JAMA Oncol.* (2018) 4:210–6. doi: 10.1001/jamaoncol.2017.4427
37. Lisberg A, Garon EB. Lack of clearly defined role for anti-programmed death-(ligand) 1 therapy in epidermal growth factor receptor mutated non-small cell lung cancer. *Transl Lung Cancer Res.* (2019) 8:195–7. doi: 10.21037/tlcr.2019.02.01
38. Masuda K, Horinouchi H, Tanaka M, Higashiyama R, Shinno Y, Sato J, et al. Efficacy of immune-checkpoint inhibitors and EGFR-TKIs in NSCLC patients with high PD-L1 expression. *J Thoracic Oncol.* (2019) 14:S292–3 doi: 10.1016/j.jtho.2019.08.588
39. Akbay EA, Koyama S, Carretero J, Altabef A, Tchaicha JH, Christensen CL, et al. Activation of the PD-1 pathway contributes to immune escape in EGFR-driven lung tumors. *Cancer Discov.* (2013) 3:1355–63. doi: 10.1158/1535-7163.TARG-13-B290
40. Lin A, Wei T, Meng H, Luo P, Zhang J. Role of the dynamic tumor microenvironment in controversies regarding immune checkpoint inhibitors for the treatment of non-small cell lung cancer (NSCLC) with EGFR mutations. *Mol Cancer.* (2019) 18:139. doi: 10.1186/s12943-019-1062-7
41. Reck M, Shankar G, Lee A, Coleman S, McCleland M, Papadimitrakopoulou VA, et al. Atezolizumab in combination with bevacizumab, paclitaxel and carboplatin for the first-line treatment of patients with metastatic non- squamous non-small cell lung cancer, including patients with EGFR mutations. *Expert Rev Respir Med.* (2019) 14:125–6. doi: 10.1080/17476348.2020.1701439
42. Im JS, Herrmann AC, Bernatchez C, Haymaker C, Molldrem JJ, Hong WK, et al. Immune-modulation by epidermal growth factor receptor inhibitors: implication on anti-tumor immunity in lung cancer. *PLoS ONE.* (2016) 11:e0160004. doi: 10.1371/journal.pone.0160004
43. Ribas A, Lawrence D, Atkinson V, Agarwal S, Miller WH, Carlino MS, et al. Combined BRAF and MEK inhibition with PD-1 blockade immunotherapy in BRAF-mutant melanoma. *Nat Med.* (2019) 25:936–940. doi: 10.1038/s41591-019-0476-5
44. Oxnard GR, Yang JC, Yu H, Kim SW, Saka H, Horn L, et al. TATTON: a multi-arm, phase Ib trial of osimertinib combined with selumetinib, savolitinib, or durvalumab in EGFR-mutant lung cancer. *Ann Oncol.* (2020) 31:507–16. doi: 10.1016/j.annonc.2020.01.013
45. Gibbons DL, Chow LQ, Kim DW, Kim TY, Song X, Jiang R, et al. Efficacy, safety and tolerability of MEDI4736 (durvalumab [D]), a human IgG1 anti-programmed cell death-ligand-1 (PD- L1) antibody, combined with gefitinib (G): a phase I expansion in TKI-naive patients (pts) with EGFR mutant NSCLC. *J Thorac Oncol.* (2016) 11:S79. doi: 10.1016/S1556-0864(16)30171-X
46. Santaniello A, Napolitano F, Servetto A, De Placido P, Silvestris N, Bianco C, et al. Tumour microenvironment and immune evasion in EGFR addicted NSCLC: hurdles and possibilities. *Cancers.* (2019) 11:E1419. doi: 10.3390/cancers11101419
47. Huang SH, Li Y, Zhang J, Rong J, Ye S. Epidermal growth factor receptor-containing exosomes induce tumor-specific regulatory T cells. *Cancer Investig.* (2013) 31:330–5. doi: 10.3109/07357907.2013.789905
48. Mannavola F, Tucci M, Felici C, Passarelli A, D'Oronzo S, Silvestris F. Tumor-derived exosomes promote the *in vitro* osteotropism of melanoma cells by activating the SDF1/CXCR4/CXCR7 axis. *J Transl Med.* (2019) 17:230. doi: 10.1186/s12967-019-1982-4
49. Teng MW, Ngiow SF, Ribas A, Smyth MJ. Classifying cancers based on T-cell infiltration and PD-L1. *Cancer Res.* (2015) 75:2139–45. doi: 10.1158/0008-5472.CAN-15-0255
50. Toki MI, Mani N, Smithy JW, Liu Y, Altan M, Wasserman B, et al. Immune marker profiling and programmed death ligand 1 expression across NSCLC mutations. *J Thorac Oncol.* (2018) 13:1884–96. doi: 10.1016/j.jtho.2018.09.012
51. Pollack BP, Sapkota B, Cartee TV. Epidermal growth factor receptor inhibition augments the expression of MHC class I and II genes. *Clin Cancer Res.* (2011) 17:4400–13. doi: 10.1158/1078-0432.CCR-10-3283
52. Takada K, Toyokawa G, Tagawa T, Kohashi K, Shimokawa M, Akamine T, et al. PD-L1 expression according to the EGFR status in primary lung adenocarcinoma. *Lung Cancer.* (2018) 116:1–6. doi: 10.1016/j.lungcan.2017.12.003
53. Rizvi H, Sanchez-Vega F, La K, Chatila W, Jonsson P, Halpenny D, et al. Molecular determinants of response to anti-programmed cell death (PD)-1 and anti-programmed death-ligand 1 (PD-L1) blockade in patients with non-small-cell lung cancer profiled with targeted next-generation sequencing. *J Clin Oncol.* (2018) 36:633–41. doi: 10.1200/JCO.2017.75.3384
54. *Update on the Phase III NEPTUNE trial of Imfinzi Plus Tremelimumab in Stage IV Non-Small Cell Lung Cancer [press release]*. AstraZeneca. (2019). Available online at: https://bit.ly/2Zdd5Zu (accessed August 21, 2019).
55. Spigel DR, Schrock AB, Fabrizio D, Frampton GM, Sun J, He J, et al. Total mutation burden (TMB) in lung cancer (LC) and relationship with response to PD-1/PD-L1 targeted therapies. *J Clin Oncol.* (2016) 34(Suppl. 15):9017. doi: 10.1200/JCO.2016.34.15_suppl.9017
56. Hanahan D, Weinberg RA. The hallmarks of cancer. *Cell.* (2000) 100:57–70. doi: 10.1016/S0092-8674(00)81683-9
57. Hanahan D, Weinberg RA. Hallmarks of cancer: the next generation. *Cell.* (2011) 144:646–74. doi: 10.1016/j.cell.2011.02.013
58. Chang C-H, Pearce EL. Emerging concepts of T cell metabolism as a target of immunotherapy. *Nat Immunol.* (2016) 17:364–8. doi: 10.1038/ni.3415
59. Allard B, Longhi MS, Robson SC, Stagg J. The ectonucleotidases CD39 and CD73: novel checkpoint inhibitor targets. *Immunol Rev.* (2017) 276:121–44. doi: 10.1111/imr.12528
60. Stagg J, Smyth MJ. Extracellular adenosine tripho- sphate and adenosine in cancer. *Oncogene.* (2010) 29:5346–58. doi: 10.1038/onc.2010.292
61. Singer K, Cheng WC, Kreutz M, Ho PC, Siska PJ. Immunometabolism in cancer at a glance. *Dis Model Mech.* (2018) 11:dmm034272. doi: 10.1242/dmm.034272
62. Fredholm BB, IJzerman AP, Jacobson KA, Linden J, Muller CE. International union of basic and clinical pharmacology. LXXXI. nomenclature and

classification of adenosine receptors – an update. *Pharmacol Rev.* (2011) 63:1–34. doi: 10.1124/pr.110.003285
63. Ishii H, Azuma K, Kawahara A, Kinoshita T, Matsuo N, Naito Y, et al. Predictive value of CD73 expression for the efficacy of immune checkpoint inhibitors in NSCLC. *Thoracic Cancer.* (2020) 11:950–5. doi: 10.1111/1759-7714.13346
64. Tøndell A, Wahl Freim SG, Sponaas A-M, Sorhaug S, Borset M, Haug M. Ectonucleotidase CD39 and checkpoint signalling receptor programmed death 1 are highly elevated in intratumoral immune cells in non–small-cell lung cancer. *Transl Oncol.* (2020) 13:17–24. doi: 10.1016/j.tranon.2019.09.003
65. Li J, Wang L, Chen X, Li L, Yu Li Y, Ping Y, et al. CD39/CD73 upregulation on myeloid-derived suppressor cells via TGF-β-mTOR-HIF-1 signaling in patients with non-small cell lung cancer. *Oncoimmunology.* (2017) 6:e1320011. doi: 10.1080/2162402X.2017.1320011
66. Koh J, Lee KY, Kim B, Kim MS, Cho HJ, Sun J-M, et al. Abstract A138: CD39 increase on cytotoxic T-cell induced by myeloid-derived suppressor cell correlated with poor prognosis in patients with non-small cell lung cancer. *Cancer Immunol Res.* (2019) 7(Suppl. 2):A138. doi: 10.1158/2326-6074.CRICIMTEATIAACR18-A138
67. Ohta A. A metabolic immune checkpoint: adenosine in tumor microenvironment. *Front Immunol.* (2016) 7:109. doi: 10.3389/fimmu.2016.00109
68. Antonioli L, Colucci R, La Motta C, Tuccori M, Awwad O, Da Settimo F, et al. Adenosine deaminase in the modulation of immune system and its potential as a novel target for treatment of inflammatory disorders. *Curr Drug Targets.* (2012) 13:842–62 doi: 10.2174/138945012800564095
69. Stagg J, Divisekera U, Duret H, Sparwasser T, Teng MWL, Darcy PK, et al. CD73-deficient mice have increased antitumor immunity and are resistant to experimental metastasis. *Cancer Res.* (2011) 71:2892–900. doi: 10.1158/0008-5472.CAN-10-4246
70. Horenstein AL, Chillemi A, Zaccarello G, Bruzzone S, Quarona V, Zito A, et al. A CD38/CD203a/CD73 ectoenzymatic pathway independent of CD39 drives a novel adenosinergic loop in human T lymphocytes. *Oncoimmunology.* (2013) 2:e26246. doi: 10.4161/onci.26246
71. Horenstein AL, Chillemi A, Zini R, Quarona V, Bianchi N, Manfredini R, et al. Cytokine-induced killer cells express CD39, CD38, CD203a, CD73 ectoenzymes and P1 adenosinergic receptors. *Front Pharmacol.* (2018) 9:196. doi: 10.3389/fphar.2018.00196
72. Wo YJ, Gan ASP, Lim X, Tay ISY, Lim S, Lim JCT et al. The roles of CD38 and CD157 in the solid tumor microenvironment and cancer immunotherapy. *Cells.* (2020) 9:26. doi: 10.3390/cells9010026
73. Chen L, Diao L, Yang Y, Yi X, Rodriguez BL, Li Y, et al. CD38-mediated immuno- suppression as a mechanism of tumor cell escape from PD-1/PD-L1 blockade. *Cancer Discov.* (2018) 8:1156–175. doi: 10.1158/2159-8290.CD-17-1033
74. Mittal D, Vijayan D, Smyth MJ. Overcoming acquired PD-1/PD-L1 resistance with CD38 blockade. *Cancer Discov.* (2018) 8:1066–8. doi: 10.1158/2159-8290.CD-18-0798
75. Monteiro I, Vigano S, Faouzi M, Treilleux I, Michielin O, Ménétrier-Caux C, et al. CD73 expression and clinical significance in human metastatic melanoma. *Oncotarget.* (2018) 9:26659–69. doi: 10.18632/oncotarget.25426
76. Inoue Y, Yoshimura K, Kurabe N, Kahyo T, Kawase A, Tanahashi M, et al. Prognostic impact of CD73 and A2A adenosine receptor expression in non-small-cell lung cancer. *Oncotarget.* (2017) 8:8738–51. doi: 10.18632/oncotarget.14434
77. Lee Chun P, Kyunghoon R, Won BK, Cho A, Song A, Anker JF, et al. Immunologic and clinical implications of CD73 expression in non-small cell lung cancer (NSCLC). *J Clin Oncol.* (2018) 36(Suppl. 15):12050. doi: 10.1200/JCO.2018.36.15_suppl.12050
78. Sidders B, Zhang P, Goodwin K, O'Connor G, Russel DL, Borodovsky A, et al. Adenosine signaling is prognostic for cancer outcome and has predictive utility for immunotherapeutic response. *Clin Cancer Res.* (2020) 26:2176–87. doi: 10.1158/1078-0432.CCR-19-2183
79. Prado-Garcia H, Sanchez-Garcia FJ. Editorial: immuno-metabolism in tumor microenvironment. *Front Immunol.* (2017) 8:374. doi: 10.3389/fimmu.2017.00374
80. Boison D, Yegutkin GG. Adenosine metabolism: emerging concepts for cancer therapy. *Cancer Cell.* (2019) 36:582–96. doi: 10.1016/j.ccell.2019.10.007
81. Willingham SB, Ho PY, Hotson A, Hill C, Piccione EC, Hsieh J, et al. A2AR antagonism with CPI-444 induces antitumor responses and augments efficacy to anti-PD-(L)1 and anti-CTLA-4 in preclinical models. *Cancer Immunol Res.* (2018) 6:1136–49. doi: 10.1158/2326-6066.CIR-18-0056
82. Beavis PA, Milenkovski N, Henderson MA, John LB, Allard B, Loi S, et al. Adenosine receptor 2A blockade increases the efficacy of anti-PD-1 through enhanced antitumor t-cell responses. *Cancer Immunol Res.* (2015) 3:506–17. doi: 10.1158/2326-6066.CIR-14-0211
83. Allard B, Pommey S, Smyth MJ, Stagg J. Targeting CD73 enhances the antitumor activity of anti-PD-1 and anti-CTLA-4 mAbs. *Clin Cancer Res.* (2013) 19:5626–35. doi: 10.1158/1078-0432.CCR-13-0545
84. Stagg J, Divisekera U, McLaughlin N, Sharkey J, Pommey S, Denoyer D, et al. Anti-CD73 antibody therapy inhibits breast tumor growth and metastasis. *Proc Natl Acad Sci USA.* (2010) 107:1547–52. doi: 10.1073/pnas.0908801107
85. Allard D, Chrobak P, Allard B, Messaoudi N, Stagg J. Targeting the CD73-adenosine axis in immuno-oncology. *Immunol Lett.* (2019) 205:31–9. doi: 10.1016/j.imlet.2018.05.001
86. Perrot I, Michaud HA, Giraudon-Paoli M, Augier S, Docquier A, Gros L, et al. Blocking antibodies targeting the CD39/CD73 immunosuppressive pathway unleash immune responses in combination cancer therapies. *Cell Rep.* (2019) 27:2411–25. doi: 10.1016/j.celrep.2019.04.091
87. Hay CM, Sult E, Huang Q, Mulgrew K, Fuhrmann SR, McGlinchey KA, et al. Targeting CD73 in the tumor microenvironment with MEDI9447. *Oncoimmunology.* (2016) 5:e1208875. doi: 10.1080/2162402X.2016.1208875
88. Mediavilla-Varela M, Luddy K, Noyes D, Khalil FK, Neuger AM, Soliman H, et al. Antagonism of adenosine A2A receptor expressed by lung adenocarcinoma tumor cells and cancer associated fibroblasts inhibits their growth. *Cancer Biol Ther.* (2013) 14:9:860–8. doi: 10.4161/cbt.25643
89. Fong L, Forde PM, Powderly JD, Goldman JW, Nemunaitis JJ, Luke JJ, et al. Safety and clinical activity of adenosine A2a receptor (A2aR) antagonist, CPI-444, in anti PD1/PDL1 treatment-refractory renal cell (RCC) and non-small cell lung cancer (NSCLC) patients. *J Clin Oncol.* (2017) 35:(Suppl. 15):3004. doi: 10.1200/JCO.2017.35.15_suppl.3004
90. Lannone R, Miele L, Maiolino P, Pinto A, Morello S. Adenosine limits the therapeutic effectiveness of anti-CTLA4 mAb in a mouse melanoma model. *Am J Cancer Res.* (2014) 4:172–81.

Conflict of Interest: CG received honoraria as speaker bureau and advisory board member from Astra Zeneca, BMS, MSD, and Roche.

The remaining authors declare that the research was conducted in the absence of any commercial or financial relationships that could be construed as a potential conflict of interest.

Copyright © 2020 Passarelli, Aieta, Sgambato and Gridelli. This is an open-access article distributed under the terms of the Creative Commons Attribution License (CC BY). The use, distribution or reproduction in other forums is permitted, provided the original author(s) and the copyright owner(s) are credited and that the original publication in this journal is cited, in accordance with accepted academic practice. No use, distribution or reproduction is permitted which does not comply with these terms.

frontiers in Oncology

ORIGINAL RESEARCH
published: 06 August 2020
doi: 10.3389/fonc.2020.01374

Immunogenomic Profiling and Classification of Prostate Cancer Based on HIF-1 Signaling Pathway

Jukun Song[1,2], *Weiming Chen*[3], *Guohua Zhu*[3], *Wei Wang*[3], *Fa Sun*[3] *and Jianguo Zhu*[1,3]*

[1] Medical College, Guizhou University, Guiyang, China, [2] Department of Oral and Maxillofacial Surgery, Guizhou Provincial People's Hospital, Guiyang, China, [3] Department of Urology, Guizhou Provincial People's Hospital, Guiyang, China

The HIF-1 signaling pathway plays an important role in the pathogenesis of cancer. Many studies have explored the progression of prostate cancer (PCa) under hypoxic conditions based on transcriptome data; few have uncovered the immunogenomic profiling and prostate cancer classification based on the HIF-1 signaling pathway. This pathway may help to identify the optimal subset of PCa patients responsive to immunotherapy/chemotherapy. The immunogenomic PCa subsets were classified based on profiling of the HIF-1 signaling pathway, using four publicly available PCa datasets. Three PCa subtypes that named as HIF-1 High (HIF-1_H), HIF-1 Medium (HIF-1_M), and HIF-1 Low (HIF-1_L) were identified. Functional enrichment was analyzed in each subtype. Several cancer-associated and immune-related pathways were hyperactivated in the HIF-1_H subtypes. In contrast, HIF-1_L subtypes were enriched in cell cycle and cell repair. Compared with other subtypes, HIF-1_H subtypes have greater immune cell infiltration, anti-tumor immune activity, and better survival prognosis. The submap and TIDE algorithm were used to predict the clinical response to immune checkpoint blockade, and GDSC was employed to screen potential chemotherapeutic targets for the treatment of PCa. Several chemotherapy drugs were identified in the GDSC dataset, including ABT 888, Temsirolimus, and EHT 1864. Meanwhile, HIF-1_H was defined as an early PCa marker, which is more likely to respond to immunotherapy. The identification of immunogenomic PCa subtypes based on the HIF-1 signaling pathway has potential clinical implications for PCa treatment. Immunopositive PCa subtypes will help to explore the reasons for the poor response of PCa to immunotherapy, and it is expected that immunotherapy will guide the personalized treatment of PCa patients.

Keywords: prostate cancer, tumor immunity, immunogenomic profiling, classification, HIF-1 signaling pathway

OPEN ACCESS

Edited by:
Peng Qu,
National Institutes of Health (NIH), United States

Reviewed by:
Guohao Wang,
National Institutes of Health (NIH), United States
Meng Xu,
National Institutes of Health (NIH), United States

***Correspondence:**
Jianguo Zhu
doctorzhujianguo@qq.com

Specialty section:
This article was submitted to Cancer Immunity and Immunotherapy, a section of the journal Frontiers in Oncology

Received: *09 May 2020*
Accepted: *30 June 2020*
Published: *06 August 2020*

Citation:
Song J, Chen W, Zhu G, Wang W, Sun F and Zhu J (2020) Immunogenomic Profiling and Classification of Prostate Cancer Based on HIF-1 Signaling Pathway. Front. Oncol. 10:1374. doi: 10.3389/fonc.2020.01374

INTRODUCTION

Prostate cancer (PCa) remains the most common malignancy in western countries. In America, PCa deaths ranked second to breast cancer (1). The American Cancer Society announced 174,650 new cases of PCa in 2019, ranking first at 20% of new male cancer cases, with 31,620 deaths accounting for 10% of total cancer deaths (2). Prostate cancer is the major tumor type in 28 European countries, and the second most prominent type in seven other countries (3). The ethnic differences in the incidence of prostate cancer are distinct. The incidence and mortality rate of PCa in China are lower than in Western countries, such as Europe and the United States.

However, with the advancement of society and changes in people's lifestyles, PCa has become a common tumor in the male urinary tract, and its incidence has increased annually (4). Prostate cancer is a heterogeneous disease that can vary greatly even within the same tumor (5). Early treatment of PCa using androgen deprivation therapy has achieved early satisfactory results, but ultimately inevitable to progress to hormone-dependent PCa, which causes clear clinical symptoms (6). The cancer phenotype is not only defined by the intrinsic activity of the tumor cells but also by immune cells recruited to its microenvironment. The role of immune cells in the tumor-associated microenvironment during tumor development has not been fully understood, especially in PCa.

Hypoxia-inducible factor-1 (HIF-1) is a major regulator of the cell's response to a hypoxic microenvironment, which is strictly controlled through synthesis, and degradation (7). Hypoxia and overexpression of HIF-1 may be related to radiotherapy and chemotherapy resistance, increased risk of tumor invasion and metastasis, and poor clinical prognosis of most solid tumors, especially PCa (8); therefore, the HIF_1 pathway is considered

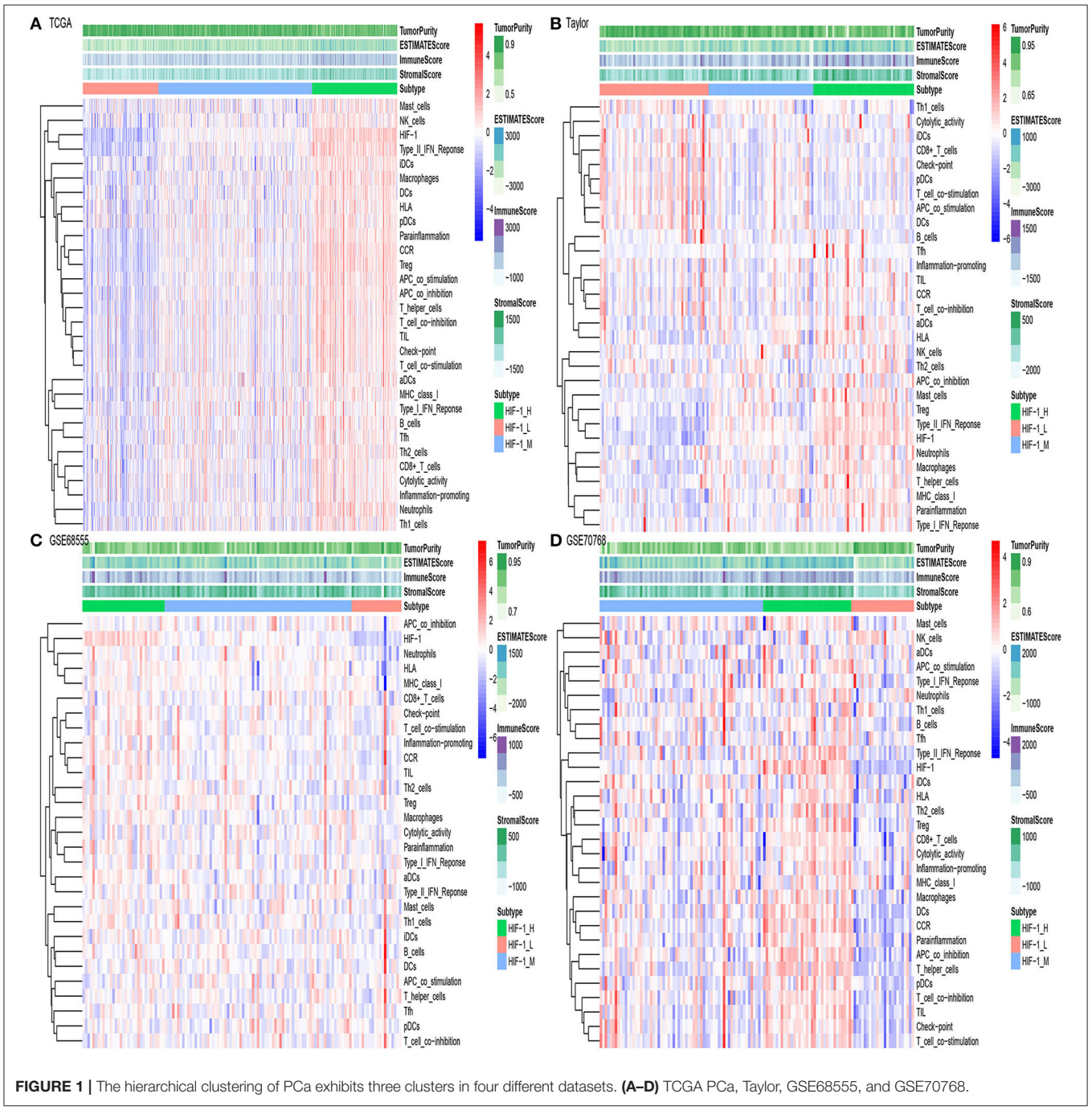

FIGURE 1 | The hierarchical clustering of PCa exhibits three clusters in four different datasets. **(A–D)** TCGA PCa, Taylor, GSE68555, and GSE70768.

as a viable pharmacological target in the treatment of solid tumors (9, 10). Hypoxia has been linked to cancer progression, recurrence, and metabolic reprogramming. Under hypoxic conditions, HIF-prolyl hydroxylases (PHDs) activity is inhibited, HIF-1a accumulates, and dimerizes with HIF-1b, thereby activating transcription of hundreds of genes. The prevalence

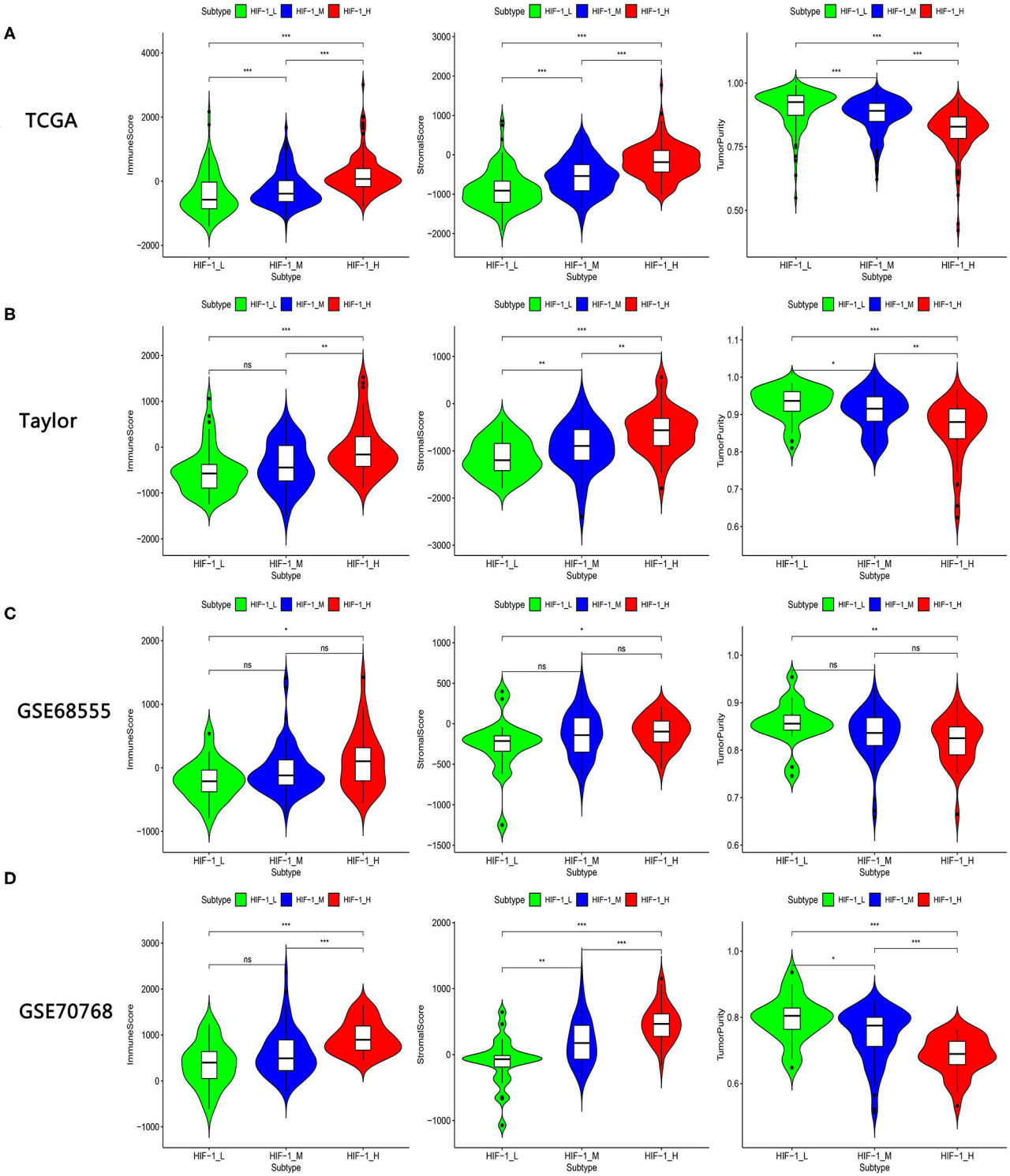

FIGURE 2 | Comparison of the Stromal Score, Immune Score, and Tumor Purity among four PCa subtypes. **(A–D)** TCGA PCa, Taylor, GSE68555, and GSE70768. (*$P < 0.05$, **$P < 0.01$; ***$P < 0.001$; ns, $P = 1$).

of hypoxia and the increase in HIF-1α have raised interest in targeting the HIF pathway for most solid tumors. Recent evidence from genetic and pharmacological research supports the view that inhibition of HIF-1 is beneficial for cancer treatment (11–13).

Cancer has gradually been recognized as an adaptive and complex system, and it is increasingly difficult to achieve the desired therapeutic effect using most single-target drugs. Immunotherapy is a promising therapeutic option for cancer, that also prevents drug resistance. It has achieved satisfactory results for some types of cancer, such as malignant melanoma, but is not effective in the treatment of PCa (14, 15). Specific genetic or genomic features, such as tumor mutation burden (TMB), neoantigen load, PD-L1 expression, and deficient DNA mismatch repair, have been associated with cancer immunotherapeutic response. Three immunogenomic PCa subtypes were classified based on HIF pathway enrichment scores by transcriptome data. The stability and reproducibility of this classification were validated in three other independent datasets. This study identified the subtype-specific molecular features, including genes, gene ontology, pathways, and networks. We found a subtype of immunopositive PCa subtype which will help to explore the reasons for the poor response of PCa to

TABLE 1 | Comparison of the stromal score, immune score, and tumor purity among three PCa subtypes in four datasets.

Dataset	Comparison	Immune score (*P*-value)	Stromal score (*P*-value)	Tumor purity (*P*-value)
TCGA	HIF-1_H vs. HIF-1_L	6.40E−15	2.22E−16	2.22E−16
	HIF-1_H vs. HIF-1_M	7.40E−14	5.90E−14	4.20E−16
	HIF-1_M vs. HIF-1_L	0.00058	2.80E−10	2.90E−07
Taylor	HIF-1_H vs. HIF-1_L	3.40E−06	3.90E−08	1.90E−07
	HIF-1_H vs. HIF-1_M	0.004	0.0014	0.0013
	HIF-1_M vs. HIF-1_L	0.13	0.0095	0.03
GSE70768	HIF-1_H vs. HIF-1_L	3.70E−06	1.80E−09	8.70E−09
	HIF-1_H vs. HIF-1_M	4.70E−05	0.00011	2.30E−05
	HIF-1_M vs. HIF-1_L	0.1	0.0013	0.011
GSE68555	HIF-1_H vs. HIF-1_L	0.013	0.035	0.0076
	HIF-1_H vs. HIF-1_M	0.085	0.51	0.083
	HIF-1_M vs. HIF-1_L	0.13	0.098	0.077

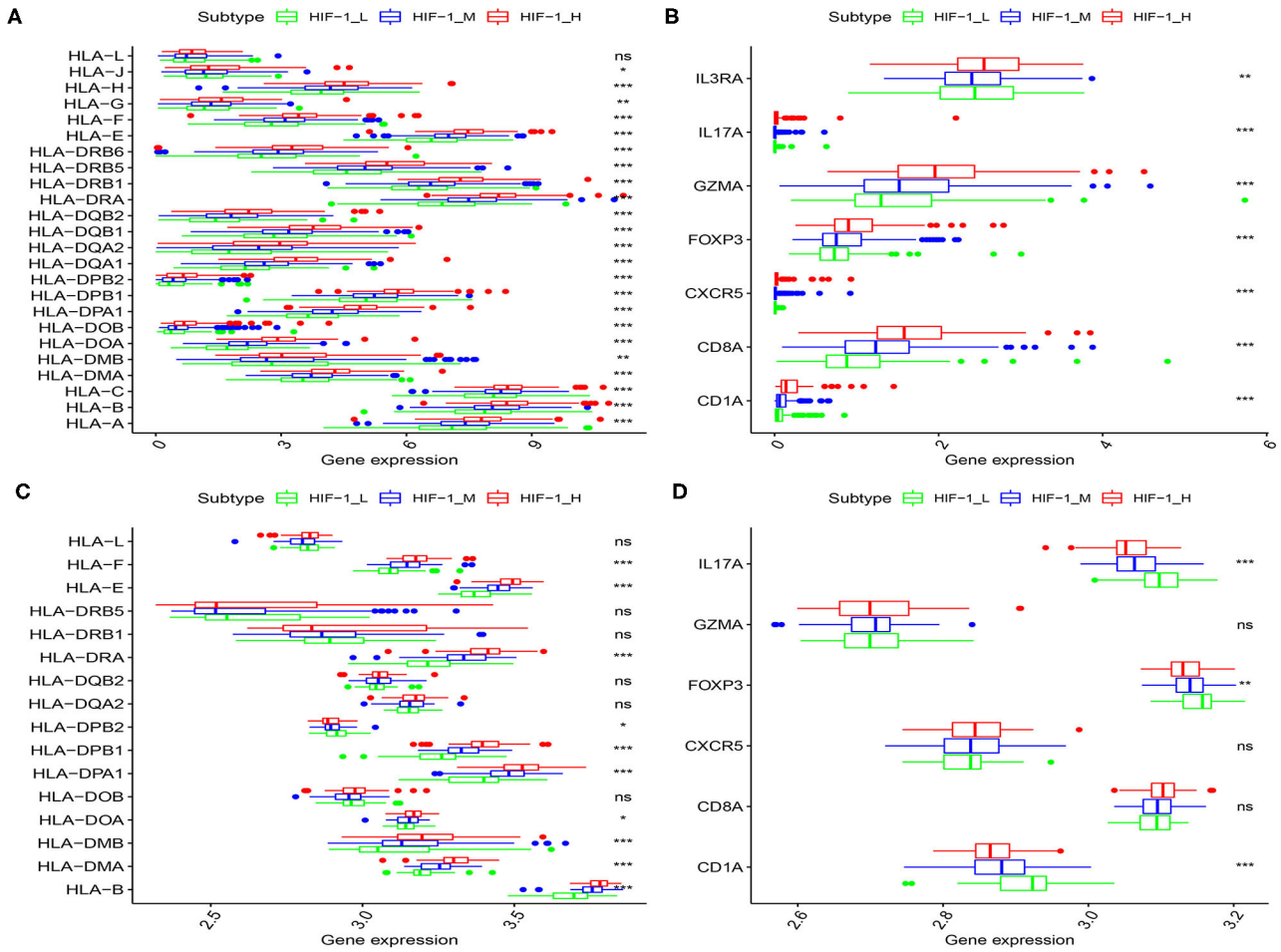

FIGURE 3 | Comparison of the expression of HLA genes (**A,C**: TCGA and Taylor) and immune cell subpopulation marker genes (**B,D**: TCGA, and Taylor) among three PCa subtypes. (*$P < 0.05$, **$P < 0.01$; ***$P < 0.001$; ns, $P = 1$).

immunotherapy; it is expected that immunotherapy will be used in the individualized treatment of PCa patients.

METHODS

Data Sources

Gene expression profiles were downloaded from three publicly available datasets: Taylor (16), TCGA (17), and two GEO datasets [GSE70768 (18) and GSE68555] (19). The TCGA dataset included 499 tumor samples, Taylor dataset enrolled 150 samples, and GSE70768 and GSE68555 datasets had 125 and 128 tumor samples, respectively. The RNA-seq profiles and phenotype data were downloaded. The expression matrix and clinical characteristics of each patient were collected manually. Patients with full clinical data and survival time of more than 30 days were included in the study.

Gene Set Variation Analysis (GSVA) and Unsupervised Clustering Analysis

The Gene set variation analysis (GSVA) was employed to derive the absolute enrichment scores, to calculate HIF-1 signaling pathway enrichment in PCa samples (20). First, the gene set of the HIF-1 signaling pathway (hsa04066) was downloaded from KE (Kyoto Encyclopedia of Genes and Genomes) dataset (http://www.genome.jp/kegg/) (**Supplementary Table 1**). Then, GSVA was used to analyze the enrichment scores based on the HIF-1 signaling pathway in different PCa samples. The hierarchical clustering of PCa samples was done based on the enrichment scores of the HIF-1 signaling pathway.

Implementation of Single-Sample Gene Set Enrichment Analysis (ssGSEA)

The ssGSEA predicted 29 immune cells that are involved in innate and adaptive immunity, using gene signatures expressed by immune cell populations of individual PCa samples (21, 22). The enrichment scores of the 29 immune signatures were quantified by ssGSEA for each PCa dataset.

Assessment of Immune Cell Infiltration Level, Tumor Purity, and Stromal Content in PCa

The ESTIMATE method was used to assess the immune cell infiltration level, including immune score, tumor purity, and stromal content (stromal score) for each PCa sample in four datasets (23). The ABSOLUTE algorithm (24) was also used to evaluate the ploidy and purity score of each PCa sample in the

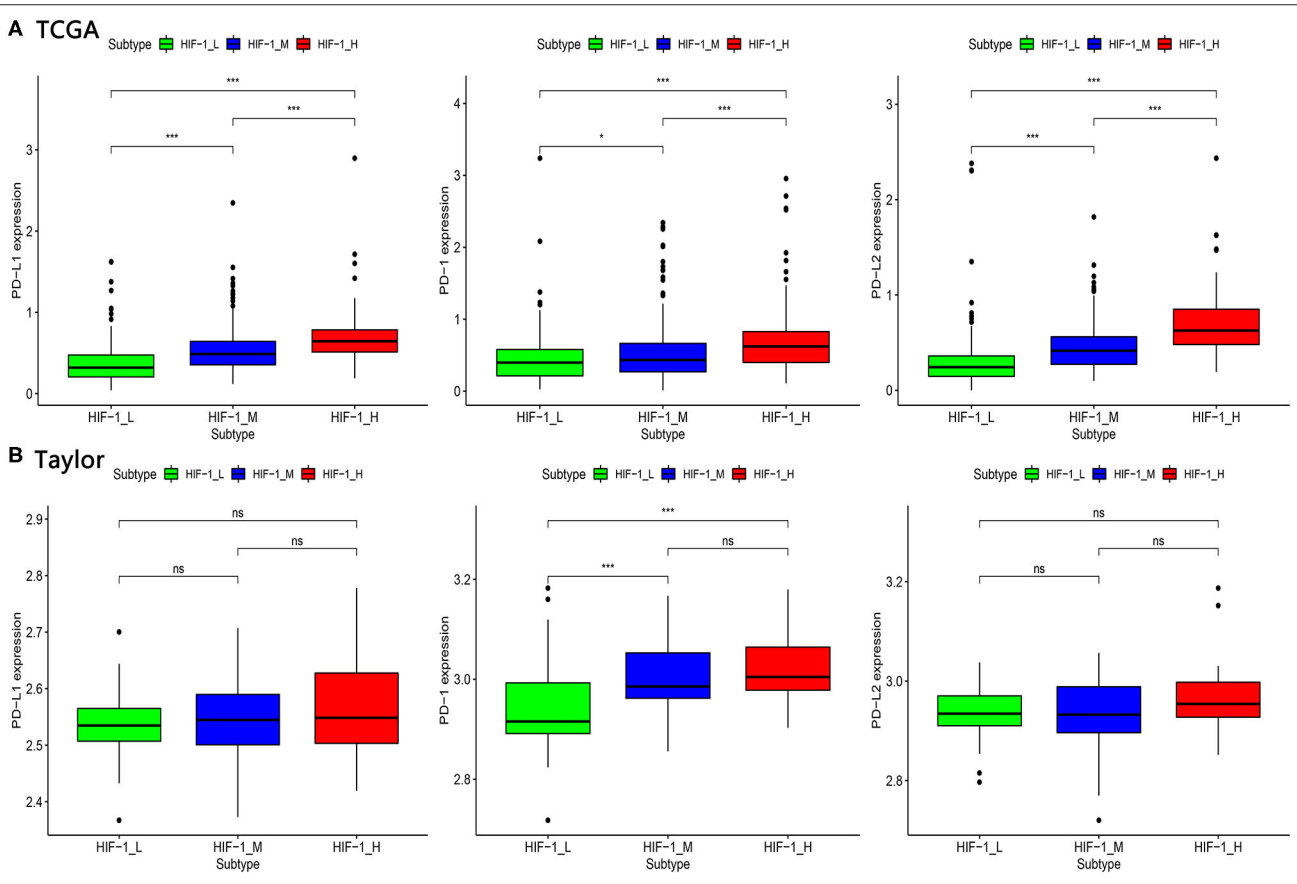

FIGURE 4 | Comparison of the expression of PD-1, PD-L1, and PD-L2 among three PCa subtypes in TCGA **(A)** and Taylor **(B)** dataset. (*$P < 0.05$, **$P < 0.01$; ***$P < 0.001$; ns, $P = 1$).

TCGA dataset. The Kruskal–Wallis test was employed to test the difference between PCa subtypes.

Comparison of the Proportions of Immune Cell Subsets Among PCa Subtypes

CIBERSORT algorithm (25) was used to infer the proportions of LM22 human immune cell subclasses. The 1,000 permutations and $P < 0.05$ was set as the criteria for inclusion of tumor samples. Total T cells were calculated as a sum of CD8+ T cells, CD4+ naïve T cells, CD4+ memory resting T cells, CD4+ memory activated T cells, follicular helper T cells, regulatory T cells (Tregs) and T cells gamma delta fractions between HIF-1_H and HIF-1_L subtypes. Total macrophage fraction was input as a sum of M0, M1, and M2 macrophage fractions. Total B cells were estimated as a sum of B cells memory and B cells naïve.

Survival Analyses

We compared the disease-free survival (DFS) of PCa patients considering tumor subtypes. The Kaplan-Meier survival analysis was used to compare the differences among three PCa subclasses in Taylor and TCGA datasets, which have available survival data. The log-rank test was used to calculate the significance of survival time differences with a threshold of $P < 0.05$.

Gene Set Enrichment Analysis (GSEA) and Gene Set Variation Analysis (GSVA)

Gene Set Enrichment Analysis (GSEA) and Gene Set Variation Analysis (GSVA) were conducted to determine the overall pathway of gene-set activity score for each sample in the Taylor and TCGA datasets (20). The Gene sets based on the c2/c5 curated signatures were downloaded from the Molecular Signature Database (MSigDB) of Broad Institute. KEGG pathways that were upregulated in HIF-1_H and HIF-1_L were then identified. The pathways that were significantly enriched were identified based on FDR < 0.05. The common pathways in both datasets were selected.

Identification of PCa Subtype-Specific Networks

The WGCNA (26) method was used to identify gene modules that are significantly related to genes that are highly associated with immune cell infiltration, based on gene co-expression analysis using the TCGA dataset. The gene-gene interaction network was built using Cytoscape 3.3.2.

Mutation Analysis

Mutation data in the MAF of PCa patients were used in the TCGA dataset for genetic and epigenetic analysis. The R package "maftools" was used to display the mutation profile of each subtype (27). The maftools was also used to impute the mutation rate of each gene and to identify significant mutant genes in the different subtypes ($P < 0.05$).

Prediction for Chemo/Immunotherapeutic Response

Tumor immune dysfunction and exclusion (TIDE) algorithms (28) and subclass mapping (29) are used to predict clinical response to immune checkpoints between the HIF-1_H and HIF-1_L in the TCGA dataset. The chemotherapeutic response of each sample was predicted based on the largest publicly available pharmacogenomics database [Pharmaceutical Sensitivity Genomics in Cancer (GDSC), https://www.cancerrxgene.org/] (24). The prediction procedure was performed by the R software package "pRRophetic," where the half-maximal inhibitory

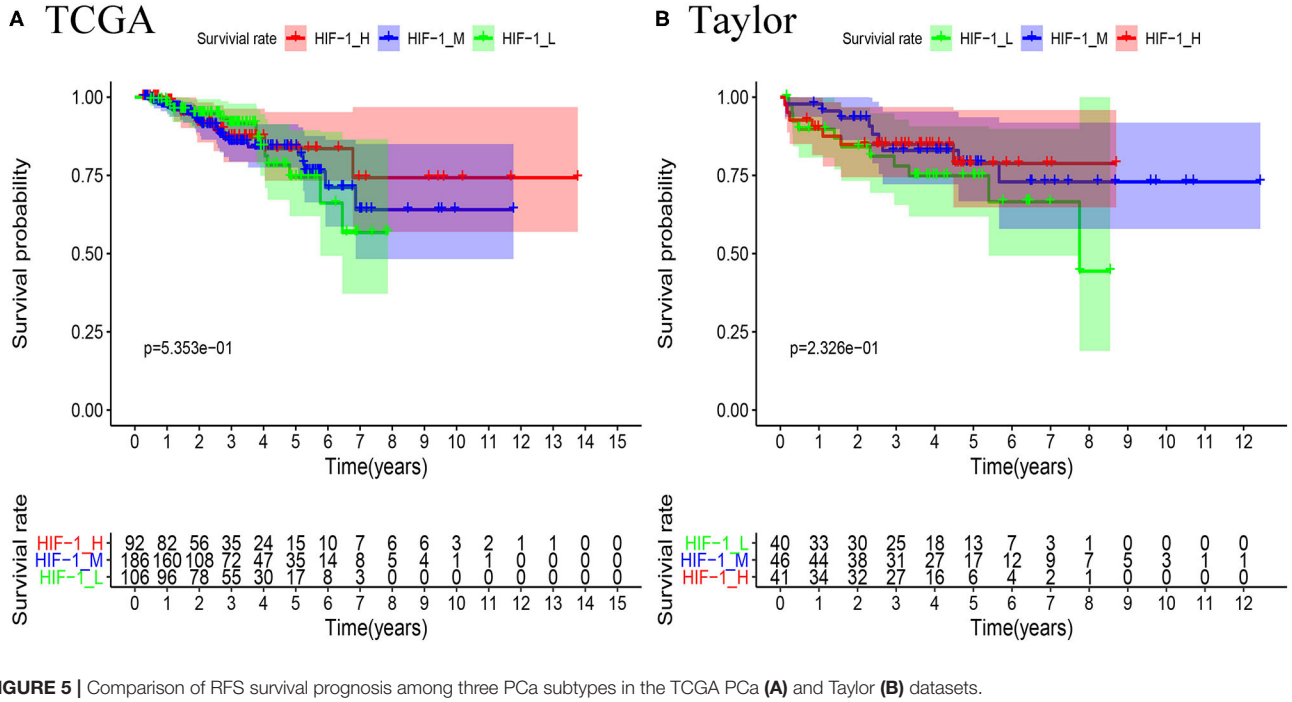

FIGURE 5 | Comparison of RFS survival prognosis among three PCa subtypes in the TCGA PCa **(A)** and Taylor **(B)** datasets.

concentration (IC_{50}) of the samples was demonstrated using ridge regression and the prediction accuracy was assessed using 10-fold cross-validation based on the GDSC training set (30).

Identification of HIF-1a in HPA Dataset

HIF-1a is a core factor in the HIF signaling pathway. Here, immunohistochemistry (IHC) data from the Human Protein Atlas database (HPA, https://www.proteinatlas.org/) was used to determine the protein expression of HIF-1a between PCa and normal tissues (31).

Statistical Analysis

All statistical tests were analyzed using R (3.5.2) utilizing a $\chi 2$ or Fisher's exact test for categorical data. A Wilcoxon test (Mann-Whitney test) and the Kruskal-Wallis test were used for two or more continuous data groups (32). Kaplan-Meier curve (33) was conducted to screen prognostic immune cell subclasses for survival data. Survival analysis was performed using the R package "survival." Fisher's independence exact test is used to statistically classify the relationship between clinical information and defined subtypes. For all statistical analyses, $P < 0.05$ was considered statistically significant.

RESULTS

Identification of Immunogenomic PCa Subtypes

The flowchart was exhibited in **Supplementary Figure 1**. The gene set of the HIF-1 signaling pathway was downloaded from KEGG; a total of 109 genes were included in the KEGG pathway. Then, GSVA was performed to infer the enrichment scores across the PCa samples using the gene set. Unsupervised clustering analysis was conducted across the tumor samples in three PCa databases [Taylor (16), TCGA (17), and [GSE70768 (18) and GSE68555 (19)]]; all the four datasets showed similar clustering results, with three clusters separated. The three clusters: HIF-1 High (HIF-1_H), HIF-1 Medium (HIF-1_M), and HIF-1 Low (HIF-1_L) were defined (**Figures 1A–D**). The results demonstrate that immune cell infiltration increased with an increased enrichment score of the HIF-1 pathway in the TCGA dataset. A similar trend was observed in the GSE70768 and GSE68555 datasets, but the trend was not as distinct in the Taylor dataset.

The immune score was significantly higher in the HIF-1_H subset in all four data sets, whereas stromal score and tumor purity were significantly higher in the HIF-1_L subset

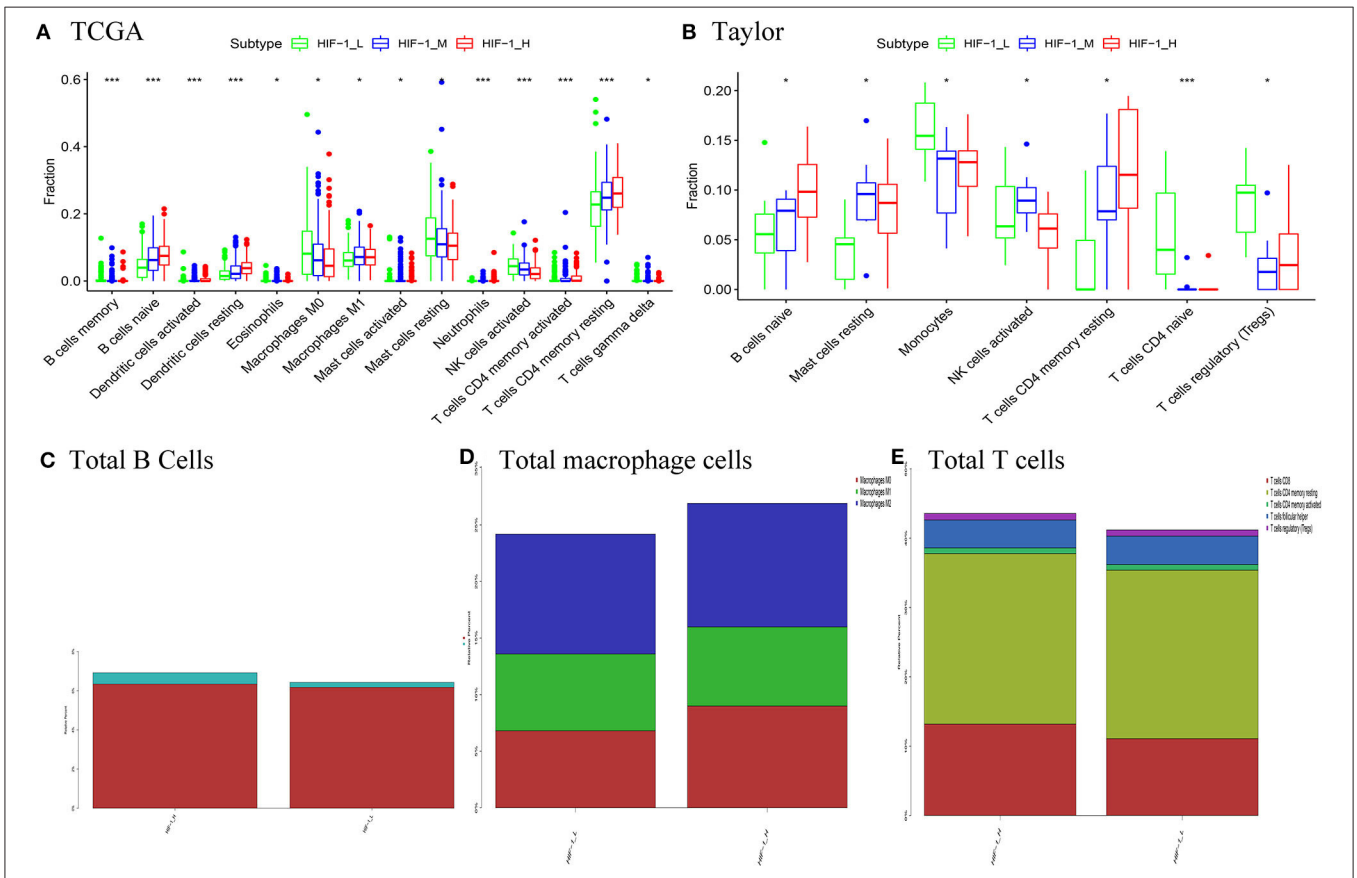

FIGURE 6 | Comparison of the proportions of immune cell subsets among PCa subtypes in TCGA **(A)** and Taylor **(B)** dataset. Comparison of total B cells **(C)**, total Total macrophage cells **(D)**, and total T cells **(E)** among PCa subclasses in the TCGA PCa cohort. (*$P < 0.05$, **$P < 0.01$; ***$P < 0.001$; ns, P = 1).

(Kruskal–Wallis test, $P < 0.05$) (**Figures 2A–D**, **Table 1**). The ABSOLUTE algorithm showed that the purity score was lower in the HIF-1_H subset, for the TCGA dataset (**Supplementary Figure 2**). These results indicate that HIF-1_H contains the highest number of immune cells and stromal cells, while HIF-1_L contains the highest number of tumor cells.

The human leukocyte antigen (HLA) complex is an important component of the immune system. It stimulates immune cells to provide protection and defense against cancer because tumor antigens must be presented in an HLA-restricted manner to be recognized by T cell receptors. In this study, HLA genes exhibited significantly higher expression in HIF-1_H and significantly lower expression in HIF-1_L (Kruskal-Wallis test, $P < 0.05$, **Figures 3A,C**). The expression levels of various immune cell marker genes such as CD8A (cytotoxic T cell), CXCR5 (Tfh cell), FOXP3 (Treg), IL-17 (Th17 cell), CD1A (iDC), and IL3RA (pDC) (34) were highest in HIF-1_H and the lowest in HIF-1_L (**Figures 3B,D**). This finding is consistent with the previous

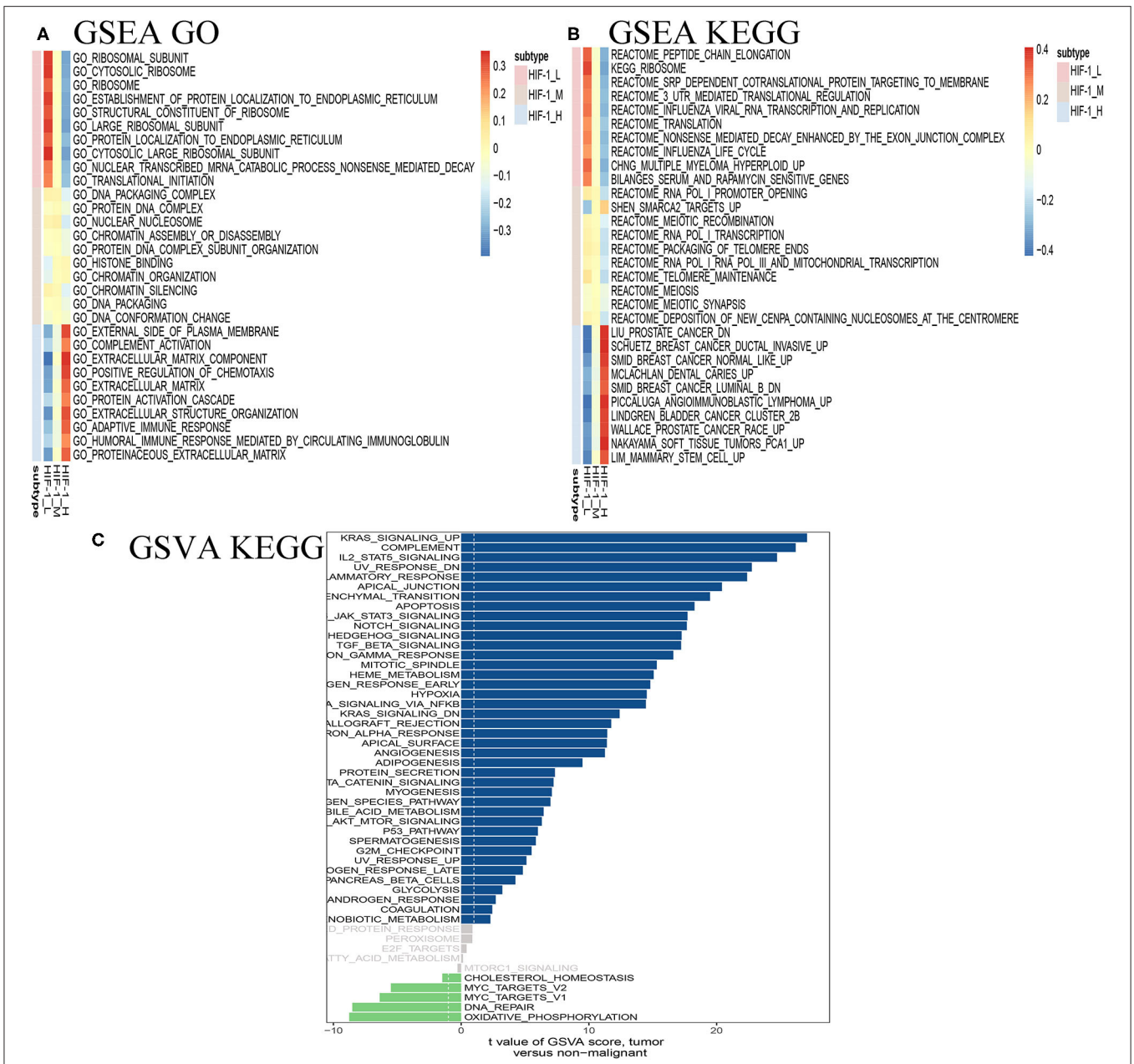

FIGURE 7 | Identification of PCa subtype-specific up-regulated GO **(A)** and KEGG **(B)** among three PCa subtypes using the GSEA method in the TCGA dataset. **(C)** GSVA reveals the disparity in the KEGG pathway between the HIF-1_L and HIF-1_H subset in the TCGA dataset.

observation that the subtype HIF-1_H is enriched in immune cell type.

The expression of PD-L1 (programmed death-ligand 1), PD1 (prephenate dehydratase 1), and PD-L2 (programmed death-ligand 2) for the three PCa subtypes were explored, in the four datasets. The results indicate that HIF-1_H exhibited the highest expression of PD-L1, PD1, and PD-L2, while HIF-1_L had the lowest expression of PD-L1, PD1, and PD-L2 (Kruskal–Wallis test, $P < 0.05$) (**Figures 4A,B**). This suggests that PCa subtype HIF-1_H may have a better response to anti-PD-L1 immunotherapy than other PCa subtypes because PD-1/PD-L1 expression is often positively correlated with immunotherapy response (35).

Survival analyses suggested that these PCa subsets have distinct clinical outcomes. The HIF-1_H subtype likely has a better survival prognosis than the HIF-1_M and HIF-1_L subtypes, but there was no significant survival difference between the HIF-1_M and the HIF-1_L subtypes (**Figures 5A,B**).

Comparisons of the Proportions of Immune Cells and Clonal Heterogeneity Between PCa Subtypes

CIBERSOFT algorithm was conducted to infer the landscape of tumor microenvironment (TME) cell infiltration between PCa subtypes in the TCGA dataset. The findings showed that 14/22 immune cells had significant difference among the PCa subtypes; B cells naïve, dendritic cells resting, T cells CD4 memory activated and T cells CD4 memory resting were significantly higher in the HIF-1_H subset, while Macrophages M1 and NK cells activated were significantly lower in the HIF-1_L subset in the TCGA dataset. In the Taylor dataset, Only 9/22 immune cells had significant difference among the PCa

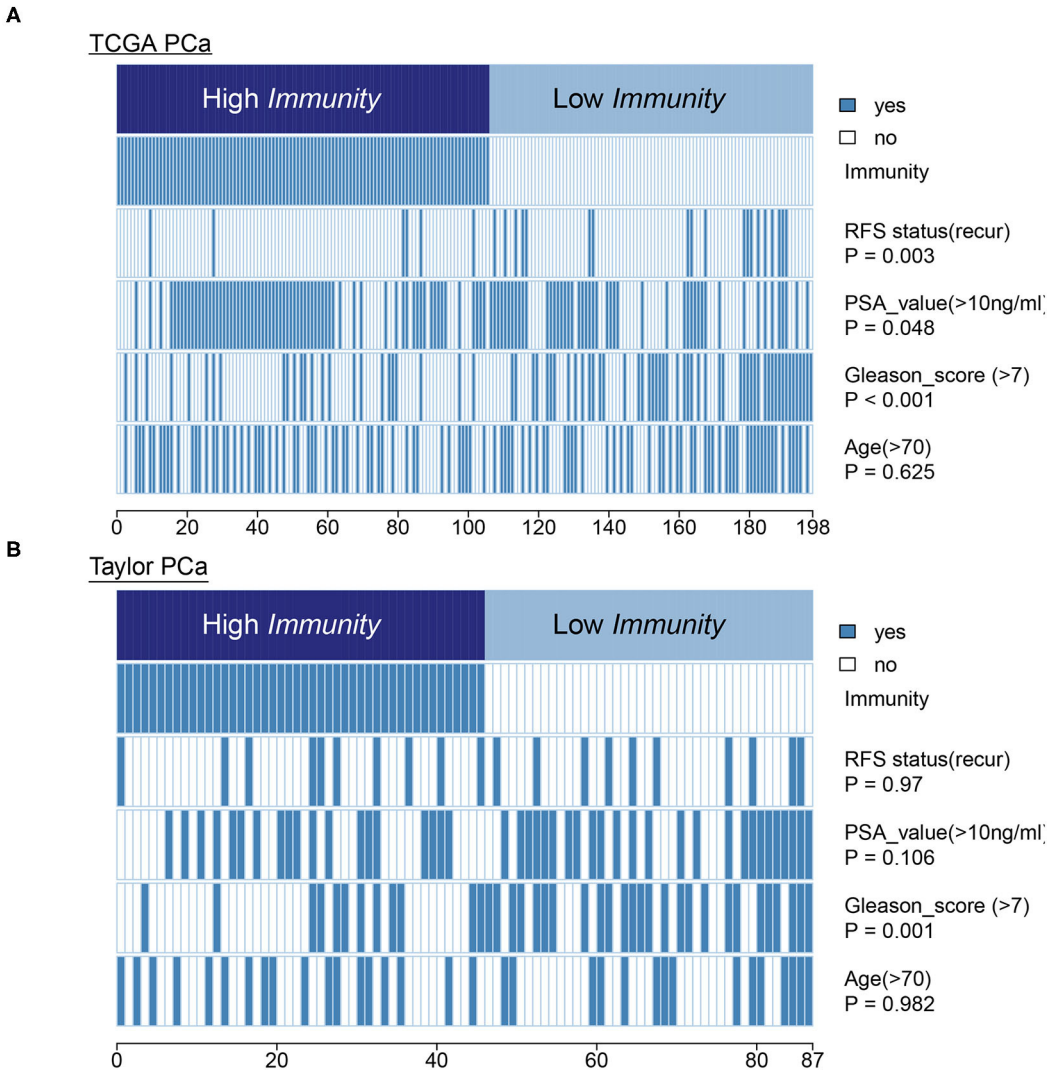

FIGURE 8 | Comparing PSA value, Gleason score, and age between the immune-H and immune-L PCa subsets. Statistical significance was performed using the Chi-square test. The heatmap illustrates the association of different clinical characters with PCa subsets. **(A,B)** TCGA PCa and Taylor, respectively.

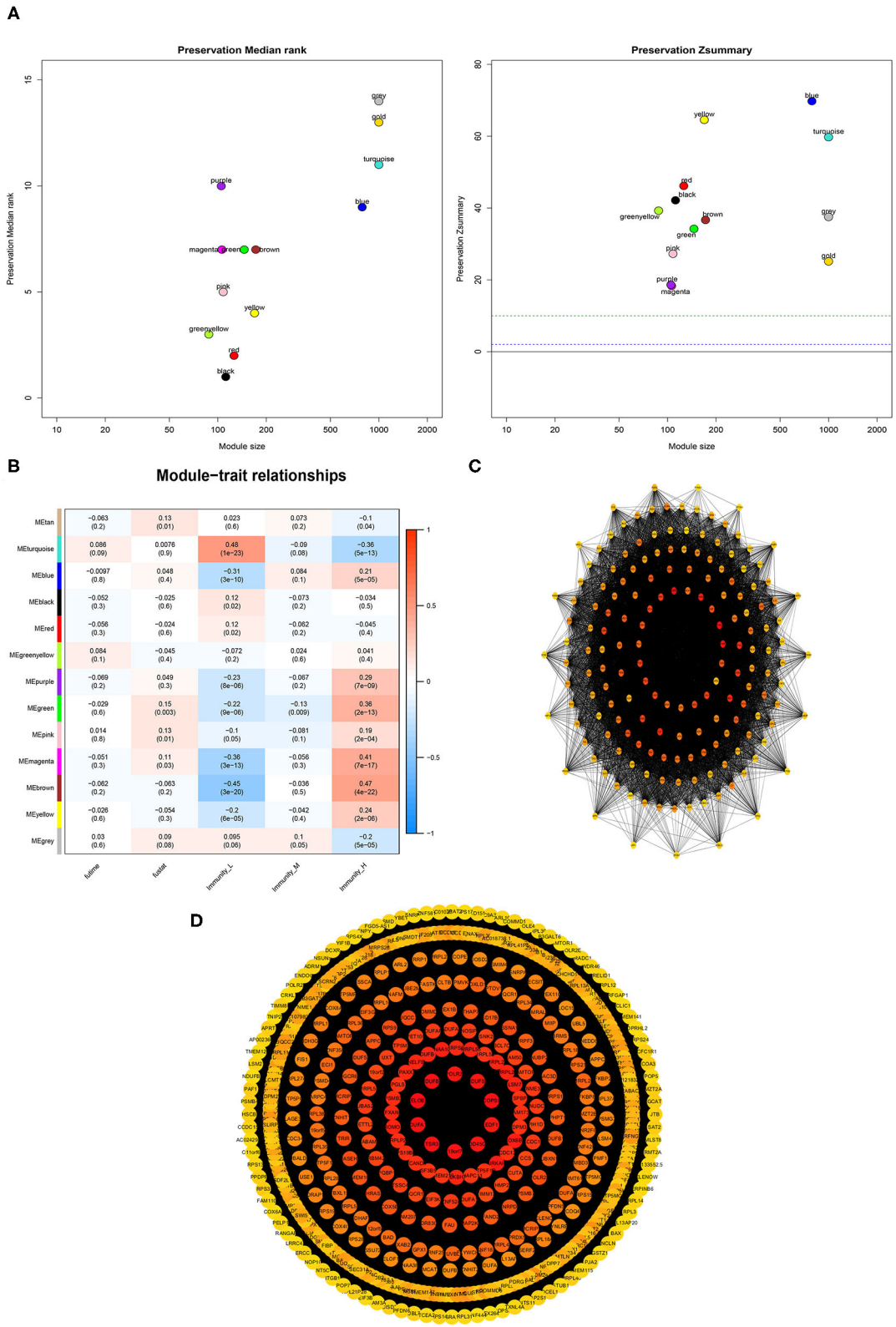

FIGURE 9 | Association between clinical features and PCa subtypes using WGCNA analysis. **(A)** The median Rank and Zsummary statistics of the module preservation. **(B)** The module-feature associations among three PCa subsets. **(C,D)** The protein-protein interaction (PPI) network as constructed in the Brown and Turquoise modules, respectively.

subtypes; B cells naïve and T cells CD4 memory resting were relatively higher in the HIF-1_H subset, monocytes and T cells regulatory (Tregs) were relatively higher in the HIF-1_L subset (**Figures 6A,B**). The fractions of total T cells, total B cells, and total Macrophages were higher in the HIF-1_H subset in the TCGA dataset (**Figures 6C–E**). This finding aligns with the previous observation that the subtype HIF-1_H is enriched with immune cells.

Identification of PCa Subtype-Specific Pathways, Gene Ontology

GSEA revealed distinct enriched up-regulated gene sets between the HIF-1_H and HIF-1_L (**Figures 7A,B**). Typically, the immune-related pathways were highly active in the HIF-1_H subclass. Several immune-related GO terms were identified in the HIF-1_H subtypes, including B cell receptor signaling pathway, T cell differentiation, and B cell-mediated immunity. The HIF-1_H subtypes were enriched in the cell cycle, cell repair, cell adhesion, adherens junction function, including ribosome, RNA binding, and cellular protein complex disassembly. Compared with the HIF-1_L subtype, adaptive immune response, and humoral immune response mediated by circulating immunoglobulin, the extracellular matrix were highly activated. In contrast, cytosolic ribosome and translational initiation were activated in the HIF-1_L subtype. In terms of the KEGG pathway, the immune-related pathways were highly activated in the HIF-1_H subtype

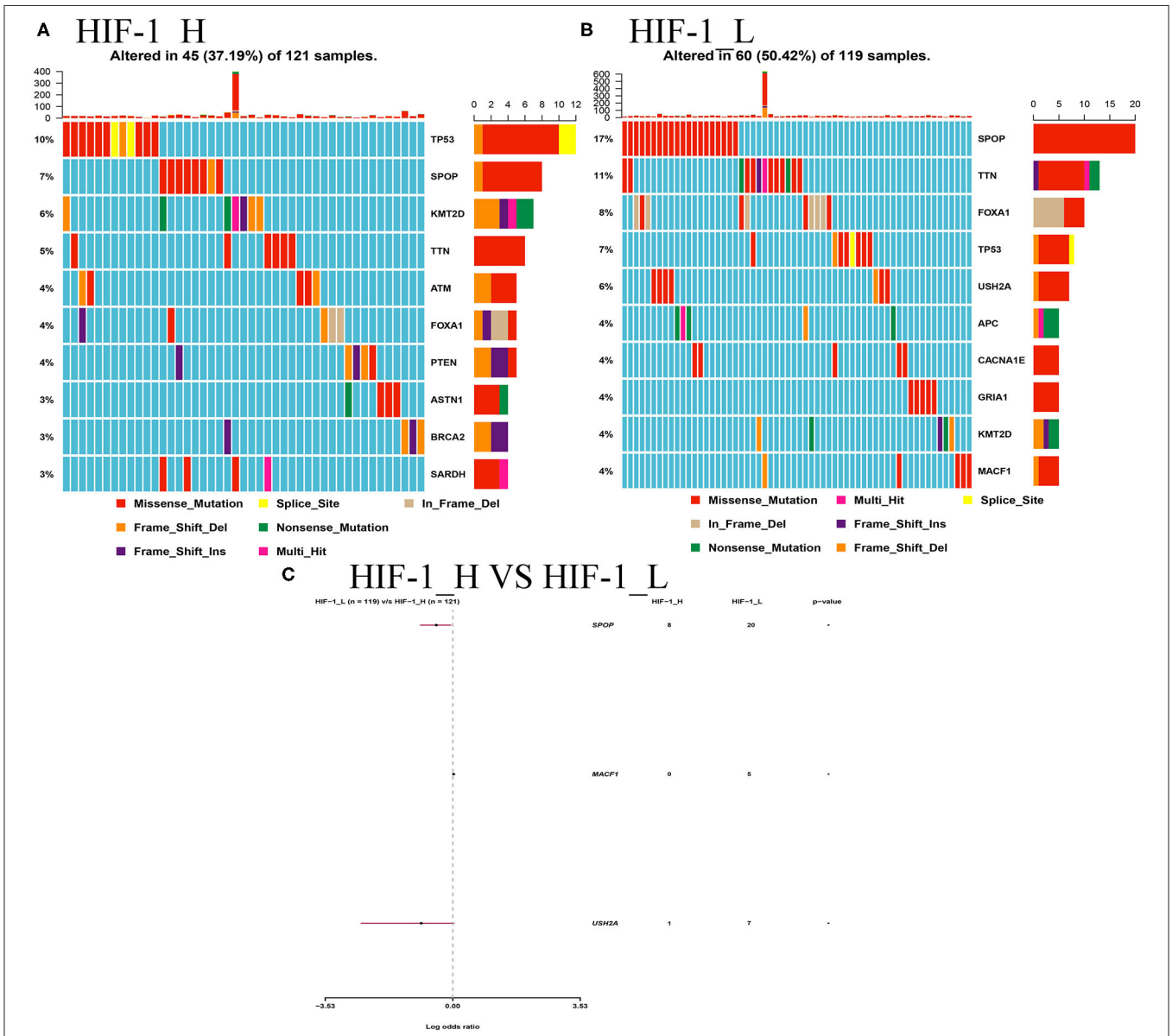

FIGURE 10 | (A) Mutation analysis between the HIF-1_L and HIF-1_H subsets in the TCGA dataset. **(B)** Gene mutation profiles of highly mutated genes among the two subtypes. **(C)** The forest plots show the comparison results of gene mutations (*$P < 0.05$, **$P < 0.01$; ns, $P = 1$).

and included Th1 and Th2 cell differentiation, leukocyte trans-endothelial migration, and B cell and T cell receptor signaling pathways. The findings validated that elevated immune activity is in the HIF-1_H subtype. Besides, multiple cancer-related pathways identified were hyperactivated in HIF-1_H, TNF signaling pathway, PI3K-Akt signaling pathway, prostate cancer, and Wallace prostate cancer race. In contrast, HIF-1_L was mainly enriched in pathways related to peptide chain elongation, ribosome, and influenza life cycle.

The GSVA analysis revealed similar results. KRAS signaling, IL2 stat5 signaling, and epithelial-mesenchymal transition were highly activated in the HIF-1_H, while DNA repair and oxidative phosphorylation were hyperactivated in HIF-1_L (**Figure 7C**).

Clinical Feature of PCa Subtypes

In terms of clinical features, HIF-1_H had a lower Gleason score and PSA level compared to HIF-1_L in the TCGA PCa cohort. The heatmap illustrates the association of the different clinical characters between the two subgroups. However, there was no difference in RFS status and age between the two subtypes (**Figure 8A**). In the Taylor dataset, HIF-1_H had a lower Gleason score (**Figure 8B**). There was no difference in the RFS status, age, and PSA values between the two subtypes. Statistical significance was determined using the Fish's exact test.

Identification of PCa Subtype-Specific Network and Hub Genes

A weighted gene co-expression network analysis of the TCGA dataset was conducted using the WGCNA method. Module preservation analysis demonstrated that 13 modules were the most stable with Zsummary statistics >10. Several gene modules that were significantly different based on PCa subtype, survival time, or survival status were identified (**Figure 9A**). The turquoise and magenta modules were negatively associated with the HIF-1_H subtype, while brown and yellow modules were positively correlated with HIF-1_H, especially the brown module. The opposite trend was observed in the HIF-1_L subtype (**Figure 9B**). A weighted co-expression network from the brown and turquoise modules was constructed (**Figures 9C,D**).

Comparisons of Gene Mutation Between PCa Subtypes

This study examined the association between the HIF-1_H/L subtypes and somatic mutation count. Highly mutated gene profiles are shown in **Figures 10A,B**. The most mutations in the HIF-1_H subtype were found in the TP53, PTEN, and BRCA2 genes, whereas the HIF-1_L subtype had the most mutations in the SPOP, FOXA1, and TP53 genes. SPOP and USH2A genes exhibited a higher mutation rate in the HIF-1_H subtype, and MACF1 exhibited a higher mutation rate in the HIF-1_L subtype with the cut-off point < 0.05 (**Figure 10C**).

Prediction for Response to Immunotherapy or Anti-cancer Drug in PCa Subtypes

The submap algorithm was used to predict the likelihood of responding to immunotherapy in the TCGA PCa cohort, although immunological checkpoint drugs have

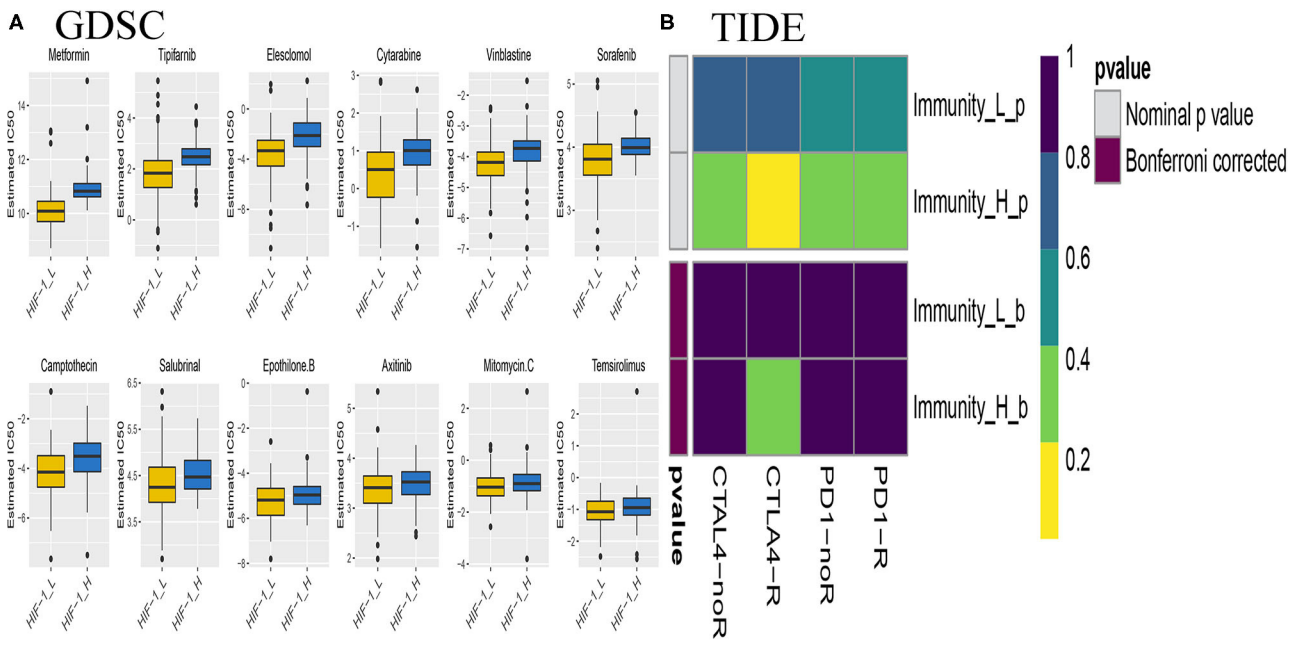

FIGURE 11 | Differential putative chemotherapeutic and immunotherapeutic response. The box plots of the estimated IC_{50} for chemotherapeutic drugs are shown: **(A)** for Immune-H and Immune-L PCa subsets, **(B)** Submap analysis manifested that Immune-H could be more sensitive to the immunotherapy (Bonferroni-corrected $P < 0.05$).

not been approved for conventional use in PCa. The analysis showed that HIF-1_H was likely to respond better to immunotherapy than HIF-1_L ($P = 0.04$). For the TIDE prediction, a subclass mapping method was used to compare the expression profiles of the three PCa subtypes with another published data set containing 47 melanoma patients who responded to immunotherapy. The results showed that HIF-1_H was the most promising subtype for CTLA4 treatment (Bonferroni correction $P < 0.05$) (**Figure 11A**).

Chemotherapy is a common treatment for PCa. The response of the three subtypes to commonly used drugs was evaluated. The prediction model on the GDSC cell line dataset was trained by ridge regression. Satisfactory prediction accuracy was evaluated by 10-fold cross-validation for the TCGA PCa cohort. The IC_{50} for each sample in the TCGA dataset was estimated based on the predictive model of chemo drugs; there were significant differences in the estimated IC_{50} against HIF-1_H, for several drugs. HIF-1_H may be more sensitive to commonly used chemotherapy (ABT 888, Temsirolimus, and EHT 1864, $P < 0.05$) (**Figure 11B**).

Immunohistochemistry Verification of HIF-1a in HPA Database

The protein levels of the HIF-1a were significantly higher in tumor tissues compared with normal tissues based on the HPA database (**Figures 12A,B**).

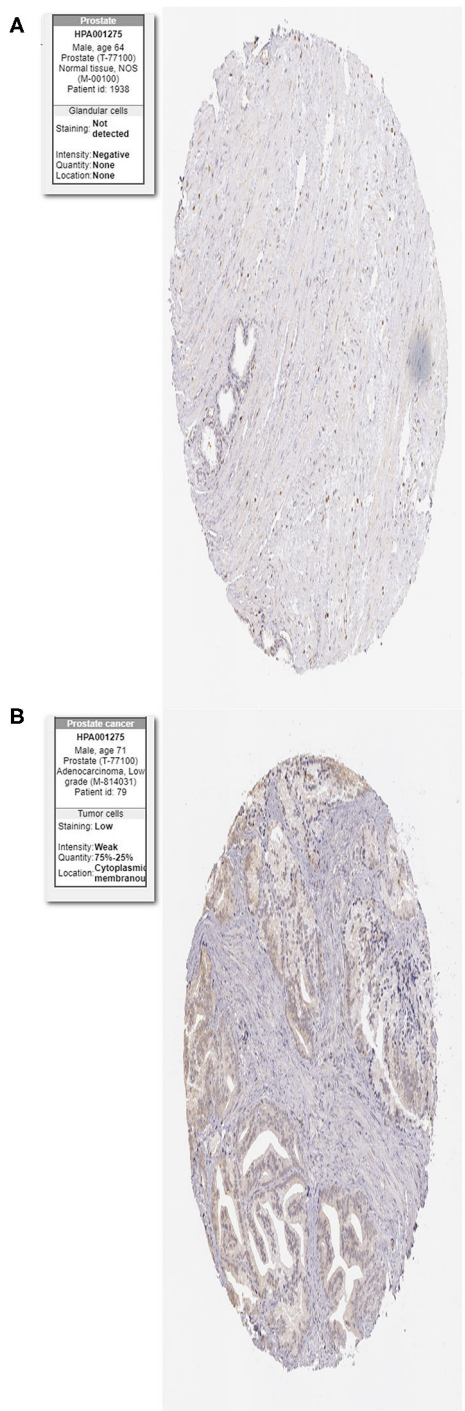

FIGURE 12 | Immunohistochemistry of the HIF-1a in PCa and normal tissues from the human protein atlas (HPA) database. **(A)** Protein levels of HIF-1a in normal prostate tissue, **(B)** Protein levels of HIF-1a in PCa tissues.

DISCUSSION

Prostate cancer remains one of the major tumors threatening male human health all worldwide (36). Prostate cancer therapy includes surgery, radiotherapy, chemotherapy, immunotherapy, and targeted approaches using antiangiogenic monoclonal antibodies and tyrosine kinase inhibitors, if tumors harbor a specific mutation. These modalities have provided therapeutic options, but the prognosis of advanced PCa is still not optimistic; the 5-year overall survival remains low. Prostate cancer causes a hypoxic environment due to the rapidly proliferating cells, structural and functional abnormalities of the tumor vasculature. Increased synthesis and decreased degradation of HIF-1a protein have been observed in PCa (37–39); HIF-1a is expected to be a feasible target considering the disease's insensitivity to immunotherapy.

In this study, the immunogenomic PCa subsets were classified based on enrichment scores and the HIF-1 signaling pathway using the publicly available four PCa datasets. Our results showed that PCa could be classified into three subtypes: HIF-1-H, HIF-1_M, and HIF-1_L. These results were validated in three other datasets; this classification was reproducible and predictable. Details of the subpopulation of the three subtypes in PCa were also revealed. HIF-1_H was enriched where there were greater immune cell infiltration and higher HIF enrichment score, and exhibited a better survival prognosis, whereas HIF-1-_L had higher tumor purity and stromal score. In the functional enrichment analysis, HIF-1_H had many subtype-specific pathways, including apoptosis, TNF signaling pathway, PI3K-Akt signaling pathway, prostate cancer Th1 and Th2 cell differentiation, Leukocyte trans-endothelial migration,

B cell receptor signaling pathway, and T cell receptor signaling pathway. In contrast, the HIF-1_L subtype was enriched in the ribosome, cell cycle and cell repair, cell adhesion, and adherens junction function. The HIF pathway may trigger a hyperactivated immune-related pathway, which may be involved in the pathogenesis of cancer. For example, HIF-1α exerts important functional roles in both innate and adaptive immune cells, including macrophages (40), neutrophils (41), dendritic cells (42), and lymphocytes (43). It is also is an essential regulator of effector T cells responses in the tumor microenvironment (44).

HIF-1_H has a better prognosis, higher HIF-1 pathway enrichment scores, and lower Gleason score and PSA level than HIF-1_L. The submap and TIDE analysis suggested that HIF-1_H was more promising for CTLA4 treatment. Using the GDSC database, we deduced that HIF-1_H could be more sensitive to commonly used chemotherapies than HIF-1_L. The above implies that Cluster I may benefit from the combination of chemotherapy and immunotherapy (ABT 888, Temsirolimus, and EHT 1864, $P < 0.05$). Barreto-Andrade et al. (45) found that veliparib (ABT-888) can enhance the response of prostate cancer cells and tumors to ionizing radiation (IR). In a single-arm, open-label, pilot study, oral PARP inhibitor veliparib and the combination [veliparib and temozolomide (TMZ)] were observed to have antitumor activity in patients with metastatic castration-resistant prostate cancer (mCRPC) (46). Several studies demonstrate that Temsirolimus maintenance therapy is a potential treatment option for castration-resistant PCa (47–49). Comstock et al. (50) using human PCa models and primary tumors, showed that PD-0332991 (a potent and selective CDK4/6 inhibitor) exerts antitumor properties. These findings indicate that HIF-1a is a major regulator of cellular responses to the hypoxic microenvironment, is elevated in prostate cancer, and is considered a viable target in the treatment of prostate cancer.

CONCLUSIONS

The identification of immunogenomic PCa subtypes based on the HIF-1 signaling pathway has potential clinical implications for PCa treatment. Immunopositive PCa subtypes may help to solve the poor response of PCa to immunotherapy; it is expected that immunotherapy will be used in the personalized treatment of PCa patients.

DATA AVAILABILITY STATEMENT

The datasets presented in this study can be found in online repositories. The names of the repository/repositories and accession number(s) can be found in the article/**Supplementary Material**.

ETHICS STATEMENT

The studies involving human participants were reviewed and approved by Guizhou Provincial People's Hospital. The patients/participants provided their written informed consent to participate in this study. Written informed consent was obtained from the individual(s) for the publication of any potentially identifiable images or data included in this article.

AUTHOR CONTRIBUTIONS

JS, JZ, WC, and GZ wrote the main manuscript text. JS prepared **Figures 1–12**. JS and JZ contributed to data analysis. All authors reviewed the manuscript.

FUNDING

The works was supported by Science and Technology Fund of Guizhou Provincial Health Commission, NO: gzwjkj2019-1-130.

ACKNOWLEDGMENTS

This manuscript has been released as a pre-print at Research Square (51).

SUPPLEMENTARY MATERIAL

The Supplementary Material for this article can be found online at: https://www.frontiersin.org/articles/10.3389/fonc.2020.01374/full#supplementary-material

Supplementary Figure 1 | The flowchart of data procession.

Supplementary Figure 2 | Comparison of the expression levels of Immune cell subpopulation marker genes between three PCa subtypes.

Supplementary Table 1 | The gene set of HIF-1 signaling pathway from KEGG dataset.

REFERENCES

1. Bray F, Ferlay J, Soerjomataram I, Siegel RL, Torre LA, Jemal A. Global cancer statistics 2018: GLOBOCAN estimates of incidence and mortality worldwide for 36 cancers in 185 countries. *CA Cancer J Clin.* (2018) 68:394–424. doi: 10.3322/caac.21492
2. Siegel RL, Miller KD, Jemal A. Cancer statistics, 2019. *CA Cancer J Clin.* (2019) 69:7–34. doi: 10.3322/caac.21551
3. Ferlay J, Colombet M, Soerjomataram I, Mathers C, Parkin DM, Pineros M, et al. Estimating the global cancer incidence and mortality in 2018: GLOBOCAN sources and methods. *Int J Cancer.* (2019) 144:1941–53. doi: 10.1002/ijc.31937
4. Liu X, Yu C, Bi Y, Zhang ZJ. Trends and age-period-cohort effect on incidence and mortality of prostate cancer from 1990 to 2017 in China. *Public Health.* (2019) 172:70–80. doi: 10.1016/j.puhe.2019.04.016
5. Carm KT, Hoff AM, Bakken AC, Axcrona U, Axcrona K, Lothe RA, et al. Interfocal heterogeneity challenges the clinical usefulness of molecular classification of primary prostate cancer. *Sci Rep.* (2019) 9:13579. doi: 10.1038/s41598-019-49964-7
6. Kgatle MM, Kalla AA, Islam MM, Sathekge M, Moorad R. Prostate cancer: epigenetic alterations, risk factors, and therapy. *Prostate Cancer.* (2016) 2016:5653862. doi: 10.1155/2016/5653862
7. Kaelin WG Jr, Ratcliffe PJ. Oxygen sensing by metazoans: the central role of the HIF hydroxylase pathway. *Mol Cell.* (2008) 30:393–402. doi: 10.1016/j.molcel.2008.04.009
8. Ruan K, Song G, Ouyang G. Role of hypoxia in the hallmarks of human cancer. *J Cell Biochem.* (2009) 107:1053–62. doi: 10.1002/jcb.22214

9. Sato M, Hirose K, Kashiwakura I, Aoki M, Kawaguchi H, Hatayama Y, et al. LW6, a hypoxia-inducible factor 1 inhibitor, selectively induces apoptosis in hypoxic cells through depolarization of mitochondria in A549 human lung cancer cells. *Mol Med Rep.* (2015) 12:3462–8. doi: 10.3892/mmr.2015.3862
10. Mun J, Jabbar AA, Devi NS, Liu Y, Van Meir EG, Goodman MM. Structure-activity relationship of 2,2-dimethyl-2H-chromene based arylsulfonamide analogs of 3,4-dimethoxy-N-[(2,2-dimethyl-2H-chromen-6-yl)methyl]-N-phenylbenzenesulfonamide, a novel small molecule hypoxia inducible factor-1 (HIF-1) pathway inhibitor and anti-cancer agent. *Bioorg Med Chem.* (2012) 20:4590–7. doi: 10.1016/j.bmc.2012.04.064
11. Doddapaneni BS, Al-Fatease AM, Rao DA, A.Alani WG. Dual-drug loaded micelle for combinatorial therapy targeting HIF and mTOR signaling pathways for ovarian cancer treatment. *J Control Release.* (2019) 307:272–81. doi: 10.1016/j.jconrel.2019.06.036
12. Fallah J, Rini BI. HIF inhibitors: status of current clinical development. *Curr Oncol Rep.* (2019) 21:6. doi: 10.1007/s11912-019-0752-z
13. Kuang Y, Han X, Xu M, Yang Q. Oxaloacetate induces apoptosis in HepG2 cells via inhibition of glycolysis. *Cancer Med.* (2018) 7:1416–29. doi: 10.1002/cam4.1410
14. Kwiatkowska D, Kluska P, Reich A. Beyond PD-1 immunotherapy in malignant melanoma. *Dermatol Ther.* (2019) 9:243–57. doi: 10.1007/s13555-019-0292-3
15. Koller KM, Wang W, Schell TD, Cozza EM, Kokolus KM, Neves RI, et al. Malignant melanoma-The cradle of anti-neoplastic immunotherapy. *Crit Rev Oncol Hematol.* (2016) 106:25–54. doi: 10.1016/j.critrevonc.2016.04.010
16. Taylor BS, Schultz N, Hieronymus H, Gopalan A, Xiao Y, Carver BS, et al. Integrative genomic profiling of human prostate cancer. *Cancer Cell.* (2010) 18:11–22. doi: 10.1016/j.ccr.2010.05.026
17. Cancer Genome Atlas Research Network. The molecular taxonomy of primary prostate cancer. *Cell.* (2015) 163:1011–25. doi: 10.1016/j.cell.2015.10.025
18. Ross-Adams H, Lamb AD, Dunning MJ, Halim S, Lindberg J, Massie CM, et al. Integration of copy number and transcriptomics provides risk stratification in prostate cancer: a discovery and validation cohort study. *EBioMedicine.* (2015) 2:1133–44. doi: 10.1016/j.ebiom.2015.07.017
19. Yu YP, Landsittel D, Jing L, Nelson J, Ren B, Liu L, et al. Gene expression alterations in prostate cancer predicting tumor aggression and preceding development of malignancy. *J Clin Oncol.* (2004) 22:2790–9. doi: 10.1200/JCO.2004.05.158
20. Hanzelmann S, Castelo R, Guinney J. GSVA: gene set variation analysis for microarray and RNA-seq data. *BMC Bioinformatics.* (2013) 14:7. doi: 10.1186/1471-2105-14-7
21. Barbie DA, Tamayo P, Boehm JS, Kim SY, Moody SE, Dunn IF, et al. Systematic RNA interference reveals that oncogenic KRAS-driven cancers require TBK1. *Nature.* (2009) 462:108–12. doi: 10.1038/nature08460
22. Lambrechts D, Wauters E, Boeckx B, Aibar S, Nittner D, Burton O, et al. Phenotype molding of stromal cells in the lung tumor microenvironment. *Nat Med.* (2018) 24:1277–89. doi: 10.1038/s41591-018-0096-5
23. Yoshihara K, Shahmoradgoli M, Martinez E, Vegesna R, Kim H, Torres-Garcia W, et al. Inferring tumour purity and stromal and immune cell admixture from expression data. *Nat Commun.* (2013) 4:2612. doi: 10.1038/ncomms3612
24. Yang W, Soares J, Greninger P, Edelman EJ, Lightfoot H, Forbes S, et al. Genomics of drug sensitivity in cancer (GDSC): a resource for therapeutic biomarker discovery in cancer cells. *Nucleic Acids Res.* (2013) 41:D955–61. doi: 10.1093/nar/gks1111
25. Newman AM, Liu CL, Green MR, Gentles AJ, Feng W, Xu Y, et al. Robust enumeration of cell subsets from tissue expression profiles. *Nat Methods.* (2015) 12:453–7. doi: 10.1038/nmeth.3337
26. Langfelder P, Horvath S. WGCNA: an R package for weighted correlation network analysis. *BMC Bioinformatics.* (2008) 9:559. doi: 10.1186/1471-2105-9-559
27. Mayakonda A, Lin DC, Assenov Y, Plass C, Koeffler HP. Maftools: efficient and comprehensive analysis of somatic variants in cancer. *Genome Res.* (2018) 28:1747–56. doi: 10.1101/gr.239244.118
28. Jiang P, Gu S, Pan D, Fu J, Sahu A, Hu X, et al. Signatures of T cell dysfunction and exclusion predict cancer immunotherapy response. *Nat Med.* (2018) 24:1550–8. doi: 10.1038/s41591-018-0136-1
29. Hoshida Y, Brunet JP, Tamayo P, Golub TR, Mesirov JP. Subclass mapping: identifying common subtypes in independent disease data sets. *PLoS ONE.* (2007) 2:e1195. doi: 10.1371/journal.pone.0001195
30. Geeleher P, Cox NJ, Huang RS. Clinical drug response can be predicted using baseline gene expression levels and *in vitro* drug sensitivity in cell lines. *Genome Biol.* (2014) 15:R47. doi: 10.1186/gb-2014-15-3-r47
31. Thul PJ, Lindskog C. The human protein atlas: a spatial map of the human proteome. *Protein Sci.* (2018) 27:233–44. doi: 10.1002/pro.3307
32. Hazra A, Gogtay N. Biostatistics Series Module 3: comparing groups: numerical variables. *Indian J Dermatol.* (2016) 61:251–60. doi: 10.4103/0019-5154.182416
33. Bland JM, Altman DG. Survival probabilities (the Kaplan-Meier method). *BMJ.* (1998) 317:1572. doi: 10.1136/bmj.317.7172.1572
34. Bindea G, Mlecnik B, Tosolini M, Kirilovsky A, Waldner M, Obenauf AC, et al. Spatiotemporal dynamics of intratumoral immune cells reveal the immune landscape in human cancer. *Immunity.* (2013) 39:782–95. doi: 10.1016/j.immuni.2013.10.003
35. Patel SP, Kurzrock R. PD-L1 expression as a predictive biomarker in cancer immunotherapy. *Mol Cancer Ther.* (2015) 14:847–56. doi: 10.1158/1535-7163.MCT-14-0983
36. Ferlay J, Colombet M, Soerjomataram I, Dyba T, Randi G, Bettio M, et al. Cancer incidence and mortality patterns in Europe: Estimates for 40 countries and 25 major cancers in 2018. *Eur J Cancer.* (2018) 103:356–87. doi: 10.1016/j.ejca.2018.07.005
37. Zhong H, De Marzo AM, Laughner E, Lim M, Hilton DA, Zagzag D, et al. Overexpression of hypoxia-inducible factor 1alpha in common human cancers and their metastases. *Cancer Res.* (1999) 59:5830–5.
38. Zhong H, Hanrahan C, van der Poel H, Simons JW. Hypoxia-inducible factor 1alpha and 1beta proteins share common signaling pathways in human prostate cancer cells. *Biochem Biophys Res Commun.* (2001) 284:352–6. doi: 10.1006/bbrc.2001.4981
39. Talks KL, Turley H, Gatter KC, Maxwell PH, Pugh CW, Ratcliffe PJ, et al. The expression and distribution of the hypoxia-inducible factors HIF-1alpha and HIF-2alpha in normal human tissues, cancers, tumor-associated macrophages. *Am J Pathol.* (2000) 157:411–21. doi: 10.1016/S0002-9440(10)64554-3
40. Cramer T, Yamanishi Y, Clausen BE, Forster I, Pawlinski R, Mackman N, et al. HIF-1α is essential for myeloid cell-mediated inflammation. *Cell.* (2003) 112:645–57. doi: 10.1016/S0092-8674(03)00154-5
41. Walmsley SR, Print C, Farahi N, Peyssonnaux C, Johnson RS, Cramer T, et al. Hypoxia-induced neutrophil survival is mediated by HIF-1α-dependent NF-κB activity. *J Exp Med.* (2005) 201:105–15. doi: 10.1084/jem.20040624
42. Jantsch J, Chakravortty D, Turza N, Prechtel AT, Buchholz B, Gerlach RG, et al. Hypoxia and hypoxia-inducible factor-1α modulate lipopolysaccharide-induced dendritic cell activation and function. *J Immunol.* (2008) 180:4697–705. doi: 10.4049/jimmunol.180.7.4697
43. McNamee EN, Korns Johnson D, Homann D, Clambey ET. Hypoxia and hypoxia-inducible factors as regulators of T cell development, differentiation, and function. *Immunol Res.* (2013) 55:58–70. doi: 10.1007/s12026-012-8349-8
44. Palazon A, Tyrakis PA, Macias D, Velica P, Rundqvist H, Fitzpatrick S, et al. An HIF-1α/VEGF-A axis in cytotoxic t cells regulates tumor progression. *Cancer Cell.* (2017) 32:669–83.e5. doi: 10.1016/j.ccell.2017.10.003
45. Barreto-Andrade JC, Efimova EV, Mauceri HJ, Beckett MA, Sutton HG, Darga TE, et al. Response of human prostate cancer cells and tumors to combining PARP inhibition with ionizing radiation. *Mol Cancer Ther.* (2011) 10:1185–93. doi: 10.1158/1535-7163.MCT-11-0061
46. Hussain M, Carducci MA, Slovin S, Cetnar J, Qian J, McKeegan EM, et al. Targeting DNA repair with combination veliparib (ABT-888) and temozolomide in patients with metastatic castration-resistant prostate cancer. *Invest New Drugs.* (2014) 32:904–12. doi: 10.1007/s10637-014-0099-0
47. Emmenegger U, Booth CM, Berry S, Sridhar SS, Winquist E, Bandali N, et al. Temsirolimus maintenance therapy after docetaxel

induction in castration-resistant prostate cancer. *Oncologist*. (2015) 20:1351–2. doi: 10.1634/theoncologist.2015-0220

48. McHugh DJ, Chudow J, DeNunzio M, Slovin SF, Danila DC, Morris MJ, et al. A Phase I trial of IGF-1R inhibitor cixutumumab and mTOR inhibitor temsirolimus in metastatic castration-resistant prostate cancer. *Clin Genitourin Cancer*. (2020) 18:171–8.e2. doi: 10.1016/j.clgc.2019.10.013
49. Inamura SO, Ito H, Taga M, Tsuchiyama K, Hoshino H, Kobayashi M, et al. Low-dose docetaxel enhanced the anticancer effect of temsirolimus by overcoming autophagy in prostate cancer cells. *Anticancer Res*. (2019) 39:5417–25. doi: 10.21873/anticanres.13735
50. Comstock CE, Augello MA, Goodwin JF, de Leeuw R, Schiewer MJ, Ostrander WF, et al. Targeting cell cycle and hormone receptor pathways in cancer. *Oncogene*. (2013) 32:5481–91. doi: 10.1038/onc.2013.83
51. Song J, He S, Wang W, Su J, Yuan D, Chen W, et al. Identification of immune-based prostate cancer subtypes using mRNA expression. *Trans Med. [Preprint]*. (2020). doi: 10.21203/rs.2.23038/v1

Conflict of Interest: The authors declare that the research was conducted in the absence of any commercial or financial relationships that could be construed as a potential conflict of interest.

Copyright © 2020 Song, Chen, Zhu, Wang, Sun and Zhu. This is an open-access article distributed under the terms of the Creative Commons Attribution License (CC BY). The use, distribution or reproduction in other forums is permitted, provided the original author(s) and the copyright owner(s) are credited and that the original publication in this journal is cited, in accordance with accepted academic practice. No use, distribution or reproduction is permitted which does not comply with these terms.

frontiers in Immunology

ORIGINAL RESEARCH
published: 29 September 2020
doi: 10.3389/fimmu.2020.584458

Tumor-Secreted GRP78 Promotes the Establishment of a Pre-metastatic Niche in the Liver Microenvironment

Lu Chen[1], Hao Zheng[2,3], Xiang Yu[2,3], Lei Liu[2,3], Heli Li[1], Huifen Zhu[1], Zhihong Zhang[2,3], Ping Lei[1] and Guanxin Shen[1]*

[1] Department of Immunology, School of Basic Medicine, Tongji Medical College, Huazhong University of Science and Technology, Wuhan, China, [2] Britton Chance Center for Biomedical Photonics, Wuhan National Laboratory for Optoelectronics, Huazhong University of Science and Technology, Wuhan, China, [3] MoE Key Laboratory for Biomedical Photonics, School of Engineering Sciences, Huazhong University of Science and Technology, Wuhan, China

OPEN ACCESS

Edited by:
Peng Qu,
National Institutes of Health (NIH), United States

Reviewed by:
George S. Karagiannis, Albert Einstein College of Medicine, United States
Gabriela Schneider, University of Louisville, United States
Peter Siegel, McGill University, Canada

***Correspondence:**
Ping Lei
adaleip@hust.edu.cn

Specialty section:
This article was submitted to Cancer Immunity and Immunotherapy, a section of the journal Frontiers in Immunology

Received: *17 July 2020*
Accepted: *11 September 2020*
Published: *29 September 2020*

Citation:
Chen L, Zheng H, Yu X, Liu L, Li H, Zhu H, Zhang Z, Lei P and Shen G (2020) Tumor-Secreted GRP78 Promotes the Establishment of a Pre-metastatic Niche in the Liver Microenvironment. Front. Immunol. 11:584458. doi: 10.3389/fimmu.2020.584458

The liver is an immunologically tolerant organ and a common site of distant metastasis for various cancers. The expression levels of glucose-regulated protein 78 (GRP78) have been associated with tumor malignancy. Secretory GRP78 (sGRP78) released from tumor cells contributes to the establishment of an immunosuppressive tumor microenvironment by regulating cytokine production in macrophages and dendritic cells (DCs). However, the role of sGRP78 on tumor cell colonization and metastasis in the liver remains unclear. Herein, we found that GRP78 was expressed at higher levels in the liver compared to other tissues and organs. We performed intravital imaging using a sGRP78-overexpressing breast cancer cell line (E0771) and found that sGRP78 interacted with dendritic cells (DCs) and F4/80$^+$ macrophages in the liver. Importantly, sGRP78 overexpression inhibited DC activation and induced M2-like polarization in F4/80$^+$ macrophages. Moreover, sGRP78 overexpression enhanced TGF-β production in the liver. In conclusion, sGRP78 promotes tumor cell colonization in the liver by remodeling the tumor microenvironment and promoting immune tolerance. The ability of sGRP78-targeting strategies to prevent or treat liver metastasis should be further examined.

Keywords: tumor-secreted GRP78, liver pro-metastatic niche, dendritic cells, macrophages, natural killers, immunomodulation

INTRODUCTION

Tumor metastasis remains the major cause of cancer-related deaths. The liver represents a common site of distant metastasis for various cancers, including melanoma, breast cancer, and colorectal cancer. The successful colonization of distant organs by circulating tumor cells (CTCs) is key for cancer metastasis (1), and the local microenvironment of these organs plays decisive roles in this process. Prior to cancer cell dissemination, the primary tumor secretes cytokines and vesicles, which create a pre-metastatic niche in secondary organs and metastatic sites. Myeloid-derived suppressor cells (MDSCs) and other immune-suppressive cells and secreted factors are essential for the establishment of the pre-metastatic niche. Upon establishment of a pre-metastatic niche,

CTCs migrate to and colonize secondary organs. Some of the CTCs survive or become dormant until the microenvironment is suitable for the development of micrometastases and eventually macrometastases (1, 2).

Glucose-regulated protein 78 (GRP78) belongs to a group of highly conserved heat shock proteins (HSP) with important stress response functions (3–5). GRP78 is involved in the unfolded protein response (UPR) and endoplasmic reticulum (ER) stress response (5, 6), as well as in cell metabolism, hypoglycemia, hypoxia, acidosis, viral infections, and DNA damage repair (7). GRP78 is upregulated during ER stress; GRP78 translocates from the ER to the cell membrane (mGRP78) or is secreted as soluble GRP78 (sGRP78) (8). sGRP78 has long been recognized as a resolution-associated molecular pattern, facilitating inflammation resolution (9–11). GRP78 is expressed at higher levels in cancer tissues than in adjacent healthy tissues, and its expression levels have been associated with tumor malignancy (12, 13). Furthermore, GRP78 expression has been associated with cancer cell invasion and drug resistance, hindering the efficacy of anti-tumor treatments (14, 15). However, the role of GRP78 in the tumor microenvironment remains unclear. Rodvold et al. (16) reported a potential role of GRP78 in the activation of antigen-presenting cells (APCs) and subsequent innate and adaptive immune responses. Notably, GRP78-deficient macrophages demonstrated adapted UPR with upregulation of activating transcription factor (ATF)-4 and M2-polarization markers (17). We previously demonstrated that sGRP78 promoted B cell differentiation into IL-10-secreting $CD19^{hi}$ regulatory B cells (18) and dendritic cell (DC) differentiation into regulatory DCs (DCreg) (9–11). Moreover, GRP78-treated DCs facilitated the differentiation of regulatory T cells (Tregs) (11). Hence, targeting GRP78 has emerged as a promising approach to enhance the effects of anti-tumor therapies (19–21). For instance, betulinic acid has been shown to induce apoptosis in breast cancer by binding to the ATPase domain of GRP78 (22). Furthermore, antibodies targeting GRP78 enhanced the efficacy of radiotherapy in human glioblastoma and non-small cell lung cancer cells (20). The anticancer effects of the apoptotic cyclic peptide BC71 have been attributed to its ability to inhibit mGRP78 (23). Besides, GRP78 has been shown to affect tumor progression and therapeutic response by modulating the functions of immune cells found in the tumor microenvironment (24).

The liver contains high numbers of natural killer (NK) cells (25), which play important roles in the immune responses against hepatocellular carcinoma and various other cancer types (26). Andre et al. (27) showed that blockade of the NK inhibitory receptor NKG2A enhanced anti-tumor immunity in mice and humans by enhancing the effector functions of NK and $CD8^+$ T cells. The crosstalk between DC and NK is mediated by the phosphorylation of the signal transducer and activator of transcription 3 (STAT3) (28). Zhou et al. (29) demonstrated that TLR7/8 agonists enhanced the anti-tumor effects of NK cells in hepatocellular carcinoma by augmenting NK-DC crosstalk. Furthermore, DCs and MDSCs inhibited NK cell activation in a TGF-β-dependent manner (30, 31). TGF-β directly inhibited NK cell effector functions and reduced the levels of NKG2D on their cell surface (32, 33). Nevertheless, the role of tumor-secreted GRP78 on the ability of hepatic APCs to regulate the pro-metastatic activities of NK cells is understudied.

Herein, we show that GRP78 is highly expressed in the liver of tumor-free mice. To elucidate the relevance of sGRP78 in the hepatic metastatic niche, we established a sGRP78-overexpressing cell line, which was used to establish an experimental liver metastasis mouse model. Using this mouse model, we found that sGRP78 mediates the formation of a pro-metastatic niche, supporting the rationale of sGRP78-targeting as a liver metastasis prevention strategy.

MATERIALS AND METHODS

Mice

Female C57BL/6 mice were purchased from Hunan SJA Laboratory Animal Co., Ltd (Changsha, Hunan, China). CX3CR1-GFP mice in a C57BL/6 background were purchased from the Jackson Laboratory; in these mice, EGFP is expressed in monocytes, DCs, NK cells, and brain microglia, under the control of the endogenous *Cx3cr1* locus. All experiments were performed with mice aged 6–8 weeks. Mice were bred and maintained in specific pathogen-free (SPF) conditions at the Animal Center of Wuhan National Laboratory for Optoelectronics. All procedures involving animals were conducted in compliance with protocols approved by the Hubei Provincial Animal Care and Use Committee of Huazhong University of Science and Technology.

Cell Cultures

The E0771 cell line was kindly provided by Professor Rong Xiang (Nankai University, Tianjin, China) and was authenticated in Beijing Microread Genetics Co., Ltd. by STR analysis. The B16F10 cell line was purchased from the BO STER Company (Wuhan, China). E0771 cells were stably transfected with the PB transposon system (a gift from Dr. Xiaohui Wu, Fudan University, Shanghai, China) (34), which contained a *CMV* promoter-driven mCherry or mCherry-sGRP78 (GRP78 GeneBank No: NM_001163434.1) coding sequence, and named as E0771-mCherry/E0771-mCherry-sGRP78 cells. B16F10 cells were stably transfected with the PB transposon system, which contained the mCherry-sgGRP78, mCherry or mCherry-sGRP78 coding sequence (B16-mCherry-sgGRP78, B16-mCherry and B16-mCherry-sGRP78 cells). All cell lines were regularly tested for mycoplasma using the MycoProbe Mycoplasma Detection Kit (R&D Systems, Minneapolis, MN, United States). E0771 cells were cultured in DMEM containing 10% fetal bovine serum (FBS), 100 U/mL Sodium Pyruvate, 100 U/mL non-essential amino acids, and 100 U/mL penicillin-streptomycin. B16F10 cells were cultured in ROMI-1640 containing 10% FBS and 100 U/mL penicillin-streptomycin. Cells were maintained at 37°C in a 5% CO_2 incubator (Thermo Fisher Scientific, United States).

Protein Quantitation

Tissues and organs of C57BL/6 mice at 8 weeks were harvested and their mass was measured. Tissue samples with the same wet

weight were lysed in NP-40 lysis buffer (5 μL/mg) containing a protease inhibitor cocktail (Sigma-Aldrich). Lysates were separated and stored at −80°C until further use. 1×10^6 cells were seeded in the plates and cultured in serum-free culture media for 24 h. Then supernatants and tissue samples were assayed by ELISA using the BiP (C50B12) Rabbit mAb (CST). The purified GRP78 protein was used as the standard sample. Data were analyzed by Welch's ANOVA.

Cell Proliferation Assay

The 6-well plates were seeded with 10^4 E0771 tumor cells on day 0, and then the cells were counted for 7 consecutive days. Data were analyzed by Welch's ANOVA (versus E0771 group).

Wound Healing Assay

The 6-well plates were seeded with 4×10^5 E0771 tumor cells. After the cells adhere to the wall, the wound was scratched as the 0 h. And CCD photographs record the wound healing at 0 and 24 h.

Liver Metastasis Model

The mice were anesthetized by intraperitoneal (i.p.) injection of a mixture of 10 mg/kg xylazine and 100 mg/kg ketamine hydrochloride (Sigma, St. Louis, MO, United States). During anesthesia, body temperature was maintained at 37°C using a warm plate (Thermo Plate, TOKAI HIT, Shizuoka-ken, Japan). Mouse spleens were exposed by a small upper abdomen incision, followed by injection of 1×10^6 E0771 or 5×10^5 B16F10 cells. Seven minutes later, half of the spleen containing the tumor cell injection site was resected. The hepatic metastatic burden was assessed on day 21 for E0771 and day 15 for B16F10 after tumor cell inoculation. Hematoxylin and eosin (H&E) stain was purchased from Servicebio Biotechnology (Wuhan, China) and slides were scanned using a Nikon Ni-E (Nikon, Minato, Tokyo, Japan). Images were acquired using the NIS-Elements software and analyzed using ImageJ. The metastatic burden was calculated by dividing the area occupied by metastatic foci (mm^2) by the total surface liver area (mm^2).

Isolation of Intrahepatic Leukocytes

Female C57BL/6 mice (7–8 weeks old) were sacrificed by cervical dislocation. The liver was dissected into 1 mm pieces and digested using collagenase IV (Worthington) and DNAase II (Sigma) for 30 min at 37°C. The digested liver extracts were filtered through a 70 μm cell strainer and centrifuged at $500 \times g$ for 5 min. The resulting cell pellet was resuspended in 10 mL 35% Percoll containing 100 U/mL heparin and centrifuged at $700 \times g$ for 15 min at room temperature. The cell pellet containing leukocytes was collected and resuspended in 3 mL red blood cell lysis solution (155 mmol/L NH_4CL, 10 mmol/L $KHCO_3$, 1 mmol/L EDTA, 170 mmol/L Tris; pH 7.3). After incubation for 3 min at room temperature, cells were washed twice with RPMI 1640 containing 5% FBS.

Flow Cytometry

Antibodies against CD45 (104), CD3 (17A2), NK1.1 (PK136), CD19 (6D5), CD69 (H1.2F3), CD4 (RM4-4), CD8 (53-6.7), Ki-67 (11F6), CD146 (ME-9F1), Ly6G (1A8), CD11b (M1/70), F4/80 (BM8), CD11c (N418), MHC-II (M5/114.15.2), CD86 (GL-1), CD80 (16-10A1), PD-1 (RMP1-14), and FoxP3 (MF-14) were purchased from BioLegend. The fixable viability dye eFluor506 was purchased from eBioscience. Liver cell suspensions were subjected to surface staining with fluorescently labeled antibodies according to the manufacturer's instructions. Cell viability was assessed using the fixable viability dye eFluor506 (eBioscience). Subsequently, cells were permeabilized using the Transcription Factor Buffer Set (Biolegend) and stained for Ki-67, FoxP3. Cells were analyzed on a CytoFLEX flow cytometer (Beckman Coulter, United States). Flow cytometry data were analyzed using FlowJo software (FlowJo, Ashland, OR, United States).

Immunofluorescence Analysis

For the immunofluorescence analysis, liver tissues were fixed in 4% paraformaldehyde for 12 h at 4°C and then dehydrated in 30% sucrose solution. The tissues were then frozen in OCT (Sakura, Torrance, CA, United States) compound and sectioned into 20 μm slices using a freezing microtome (Leica, Germany). OCT was removed by washing three times in PBS, and the sections were immunostained with Alexa Fluor 647 anti-mouse F4/80 (BioLegend, Clone: BM8, Catalog: 123122), Alexa Fluor 647 anti-mouse CD11c (BioLegend, Clone: N418, Catalog: 117312) or Alexa Fluor 647 anti-mouse NK1.1 (BioLegend, Clone: PK136, Catalog: 108720) at 1:200 dilution. All the sections were imaged with Olympus IX83 confocal microscope outfitted with an UltraVIEW VoX 3D live cell imaging system (PerkinElmer). Images were analyzed with Image J software (National Institutes of Health).

Cytokine Quantitation

Livers were harvested and their mass was measured at days 4 and 7 after injection. Tissue samples were lysed in NP-40 lysis buffer (5 μL/mg) containing a protease inhibitor cocktail (Sigma-Aldrich). Lysates were separated and stored at −80°C until further use. Samples were assayed using the LEGENDplexTM Mouse Cytokine Panel array (BioLegend) according to the manufacturer's instructions. Data were analyzed with Legendplex software (BioLegend). Mouse TGF-beta ELISA kit (DAKEWE) was used to detect TGF-β levels in the samples.

Intravital Imaging

CX3CR1-GFP C57BL/6 mice (6–10 weeks old) were inoculated with 1×10^6 E0771-mCherry or E0771-mCherry-sGRP78 cells (day 0). On days 4 and 7, mice were anesthetized by i.p. injection of a mixture of 10 mg/kg xylazine and 100 mg/kg ketamine hydrochloride (Sigma, St. Louis, MO, United States). Mice were maintained anesthesia with isoflurane inhalation [1.5–2% (v/v) isoflurane in O_2] and placed within a custom-designed imaging box. Throughout the imaging process, mice were placed on a heating pad to maintain a body temperature of 37°C (Thermo Plate, TOKAI HIT, Shizuoka-ken, Japan). Intravital imaging was performed using an Olympus IX83 confocal microscope outfitted with an UltraVIEW VoX 3D live cell imaging system (PerkinElmer). Images were acquired using a 20 × /0.75 NA

objective and Volocity 6.3 (PerkinElmer) software. Images were analyzed with Image J software (National Institutes of Health).

Data Analysis

Intravital cell movement was assessed using Image-Pro Plus (Media Cybernetics, Inc., Rockville, MD; RRID:SCR-007369) or Imaris 7.6 (Bitplane AG, Switzerland; RRID:SCR-007370) software. The mean velocity, mean displacement, arrest coefficient, and confinement ratio were determined. The mean velocity was used to determine the migratory speed in μm/min. Cells with a mean velocity of less than 2 μm/min were defined as immotile. The mean displacement was used to determine the initial displacement of the cells. The arrest coefficient was calculated as the percentage of time that the instantaneous velocity of each cell was less than 2 μm/min, as previously described (35, 36). The confinement ratio was calculated as the ratio of the maximum displacement of a given cell to its path length within a given time. Linear fitting was performed on the plotted curves to determine whether the cells underwent random movement.

Statistical Analysis

Statistical analysis was performed using GraphPad Prism 6 (GraphPad Software, CA, United States). A one-way ANOVA followed by a *post hoc* test was used for multiple group comparisons, and Student's t-test (two-tailed) was used for comparisons of two groups. Survival data were analyzed using log-rank (Mantel-Cox) test. Values were expressed as mean ± standard error of the mean (SEM). Two-sided $P < 0.05$ was considered statistically significant ($^{*}P \leq 0.05$, $^{**}P \leq 0.01$, $^{***}P < 0.001$). The numbers of animals used in each experiment were indicated in the figure legends.

RESULTS

Tumor-Secreted GRP78 Enhances Tumor Invasion and Liver Metastasis

In this study, we established a sGRP78-overexpressing breast cancer cell line (E0771-mCherry-sGRP78). Confocal microscopy showed that, although mCherry primarily localized in the cytoplasm in E0771-mCherry-sGRP78 cells, it was evenly distributed in E0771-mCherry cells (**Figure 1A**). ELISA assay indicated that the level of sGRP78 in the supernatant of E0771-mCherry-sGRP78 cells was four times higher than that in E0771-mCherry or E0771 control cells (**Figure 1B**). Cell proliferation assay revealed that overexpression of sGRP78 did not affect the proliferation of E0771 cells *in vitro* (**Figure 1C**). To investigate the effect of sGRP78 overexpression on cancer cell migration, we performed a scratch wound healing assay. E0771-mCherry-sGRP78 cells were more migrative than E0771-mCherry control cells (**Figure 1D**).

We also found that the level of GRP78 in the supernatant (SN) of liver homogenate was two times higher than in the NS from spleen and lung (**Supplementary Figure 1**). Flow cytometry 4 days after cell inoculation indicated that the percentage of mCherry-positive cells that metastasized to the liver was 0.158% ± 0.020 in E0771-mCherry-sGRP78-bearing mice and 0.121% ± 0.015 in E0771-mCherry-bearing mice; this difference was no statistically significant (**Figure 1E**). Seven days after cell inoculation, activation of adaptive immune responses was observed in the liver, while the function of innate immune cells was less profound. In E0771-mCherry-sGRP78-injected mice, 0.595% of the living cells expressed mCherry, while the livers of E0771-mCherry-bearing mice contained approximately half as much (**Figure 1E**). Twenty days after splenic injection of tumor cells, we evaluated the effect of sGRP78 overexpression on liver metastasis by measuring the weight of the liver and histology (**Figure 1F** and **Supplementary Figures 2A,B**). Liver weight was higher nearly by a two-fold in E0771-mCherry-sGRP78-bearing mice compared with E0771-mCherry-bearing mice. Histology confirmed the higher metastatic burden in E0771-mCherry-sGRP78-bearing mice (**Figure 1G**). Additionally, widefield fluorescence imaging of different organs indicated that mCherry-expressing metastatic tumor cells were primarily found in the liver. Interestingly, weak mCherry signal was detected in the kidneys of E0771-mCherry-sGRP78-injected mice but not in E0771-mCherry-injected mice, suggesting that sGRP78 was excreted through the kidneys (**Figure 1H**). Notably, all E0771-mCherry-sGRP78-bearing mice died within 40 days after cell inoculation, while 75% of E0771-mCherry-bearing mice were still alive after 50 days (**Figure 1I**). The B16 cell lines had similar results, showing that GRP78 upregulation promoted more tumor cells (B16-mCherry-sGRP78) metastasizing to liver, while down-regulation of GRP78 (B16-mCherry-sgGRP78) significantly improved the survival ability of mice (**Supplementary Figures 2C,D**). These findings suggest that tumor-derived sGRP78 promotes tumor cell dissemination and colonization *in vivo*, accelerating liver metastasis.

Tumor-Secreted GRP78 Induces Tolerogenic Phenotypes in Hepatic Dendritic Cells and Macrophages

Next, we investigated the effects of sGRP78 overexpression on the function of hepatic APCs. Hepatic APCs mainly consist of DCs, Kupffer cells (KCs), macrophages, and liver sinusoidal endothelial cells (LSECs) (37, 38). We performed flow cytometry evaluating the frequencies of different hepatic APCs, as well as quantifying the expression levels of CD86 and MHC-II (**Figure 2A**). We found that 4 days after cell inoculation, the percentages of $F4/80^{+}$ macrophages and DCs in the liver differ significantly between the two groups ($F4/80^{+}$ macrophages were 11.48% in E0771-mCherry-sGRP78-bearing mice vs. 7.98% in E0771-mCherry-bearing mice; $P < 0.05$; DCs were 0.732% in E0771-mCherry-sGRP78-bearing mice vs. 1.136% in E0771-mCherry-bearing mice; $P < 0.01$; **Figure 2B**). This was also the case 7 days after cell inoculation; however, the level of macrophage recruitment was higher compared to 4 days after cell inoculation (**Figure 2C**). Additionally, 7 days after cell inoculation, the expression levels of the M2-type marker CD206 was profoundly higher in mice with

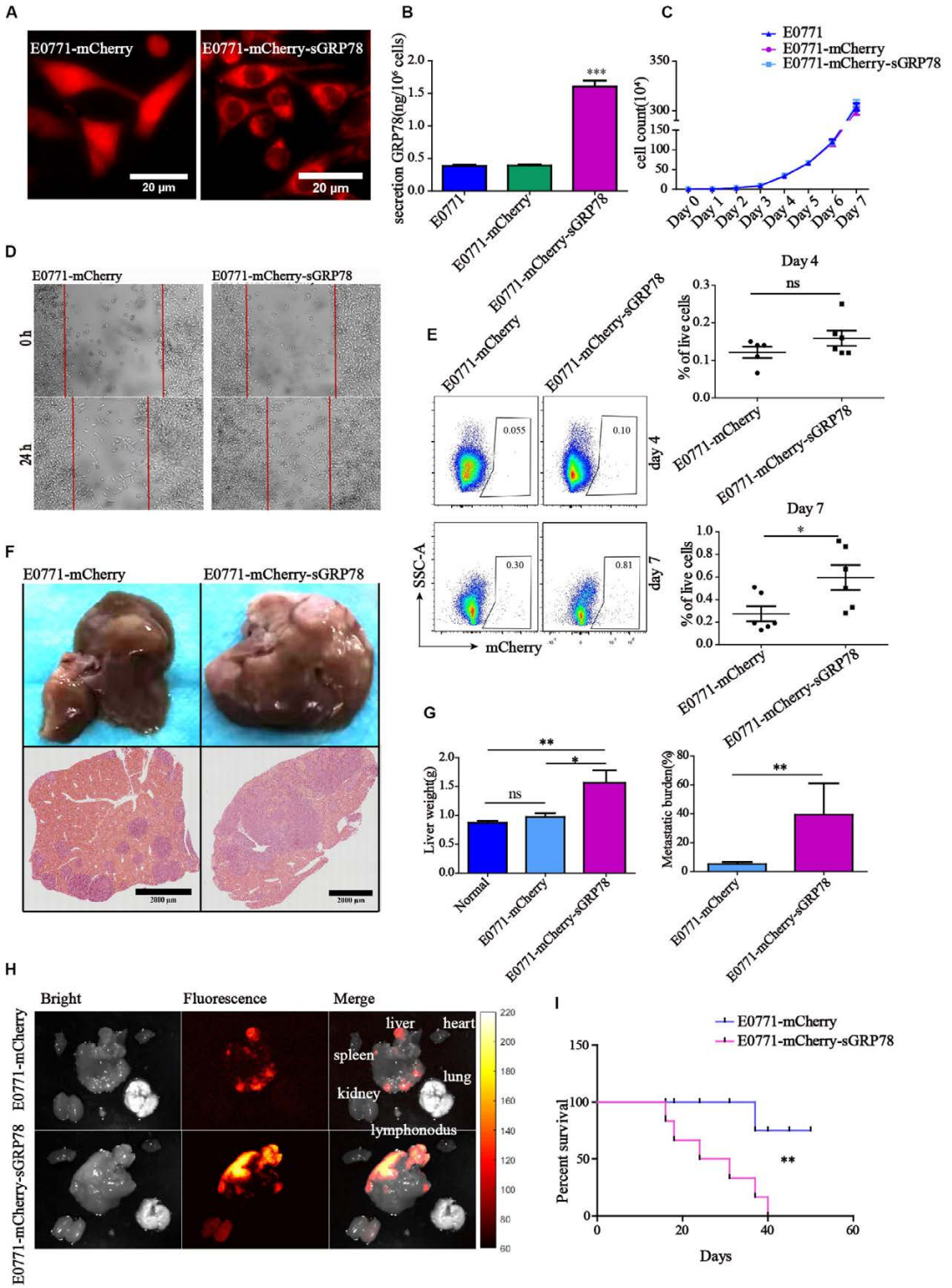

FIGURE 1 | Tumor-secreted GRP78 promotes tumor invasion and liver metastasis. **(A)** sGRP78-overexpressing E0771-sGRP78-mCherry cells were identified by confocal microscopy. Scale bar, 20 μm. **(B)** The levels of sGRP78 in the cell culture supernatant were determined by ELISA. **(C)** Tumor growth curves. **(D)** The migration ability of tumor cells was assessed by wound healing assay. **(E)** Frequencies of mCherry-positive cells in the liver 4 and 7 days after cell inoculation. Representative flow cytometry dot plots (left) and percentage of positive cells (right) are shown. **(F)** Representative images of H&E-stained liver sections from mice sacrificed 20 days after tumor cell intrasplenic injection. Scale bar, 2,000 μm. **(G)** Quantification of liver weight (left panel) and metastatic burden (right panel) in livers (n = 5 mice per group). **(H)** Representative images of organ tumor burden 20 days after tumor cell intrasplenic injection. **(I)** Survival curves (n = 6). Error bars represent SEM. Ns, not significant; $^{*}P < 0.05$; $^{**}P < 0.01$; $^{***}P < 0.001$. Statistical significance was determined by Student's t-test (**E,G** right), by Welch's ANOVA (**B,C,G** left) or by log-rank Mantel-Cox test **(I)**.

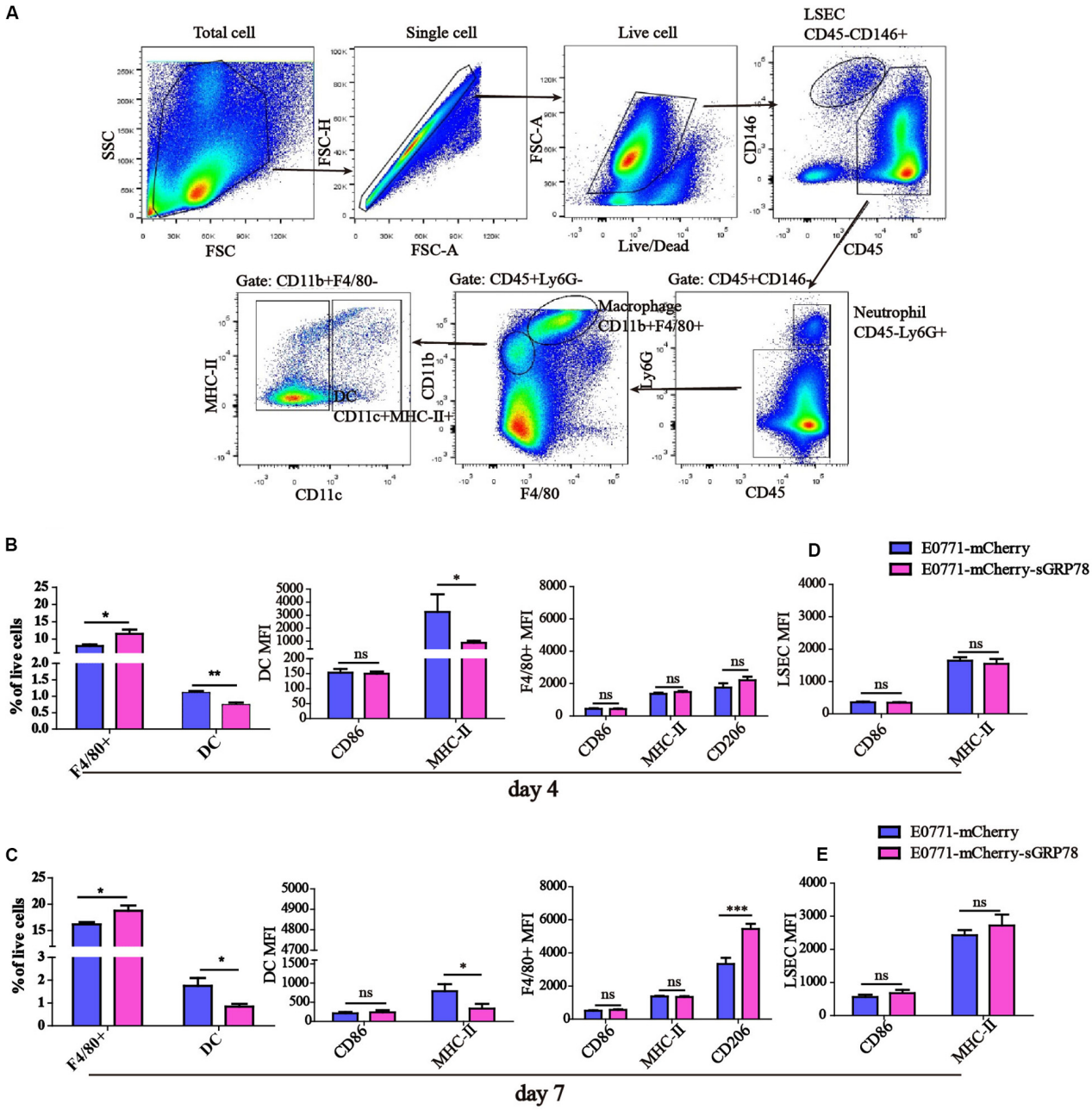

FIGURE 2 | Tumor-secreted GRP78 induces tolerogenic phenotypes in hepatic monocytes/macrophages. **(A)** Gating strategy followed to distinguish the hepatic myeloid cells. Frequencies of hepatic F4/80$^+$ macrophages and DC cells, as well as their expressions of CD86 and MHC-II four **(B)** and seven **(C)** days after tumor cell intrasplenic injection. Expression of CD86 and MHC-II on LSEC cells four **(D)** and seven **(E)** days after tumor cell intrasplenic injection. Graphs represent the mean ± SEM. Ns, not significant; *$P < 0.05$; **$P < 0.01$; ***$P < 0.001$. Statistical significance was determined by Student's *t*-test.

tumor-secreted GRP78 compared with control mice ($P < 0.001$; **Figure 2C**). Although we found no difference in the levels of DC recruitment, the expression levels of MHC-II on DCs was significantly lower in the E0771-mCherry-sGRP78 group compared with control mice ($P < 0.05$; **Figures 2B,C**). sGRP78 did not affect the expression of CD86 or MHC-II on LSECs (**Figures 2D,E**). These results suggest that tumor-secreted GRP78 affects the hepatic immune microenvironment by inducing tolerogenic phenotypes in DC and F4/80$^+$ macrophages, but not in LSEC.

Tumor-Secreted GRP78 Binds to Hepatic DCs and F4/80$^+$ Macrophages

Immunofluorescence staining on liver sections from our experimental liver metastasis mouse model was performed

to evaluate the ability of sGRP78 to bind to $CD11c^+$ DCs (**Figure 3A**) and $F4/80^+$ macrophages (**Figure 3B**). Tumor cells displayed strong mCherry signal, and in E0771-mCherry-sGRP78-bearing mice, sGRP78 was diffusely distributed and partially taken up by $CD11c^+$ DC and $F4/80^+$ macrophages. Although the density of $F4/80^+$ macrophages in metastatic lesions was higher by a 1.3-fold in E0771-mCherry-sGRP78-bearing mice compared with control mice, the numbers of mCherry-positive $CD11c^+$ DCs and $F4/80^+$ macrophages were considerably higher in E0771-mCherry-sGRP78-bearing mice (5.4-fold for $CD11c^+$ cells and 3-fold for $F4/80^+$ cells; **Figure 3C**). These findings suggest that DCs and macrophages directly bind sGRP78.

CX3CR1 is expressed in various cells, including DCs and macrophages (39, 40). In our CX3CR1-GFP liver metastasis mouse model, tumor-secreted GRP78 was taken up by both $F4/80^+CX3CR1^+$ and $F4/80^-CX3CR1^+$ cells (**Figure 3D**). In theory, sGRP78 could also bind on KCs ($F4/80^+CX3CR1^-$). Compared to $CX3CR1^-F4/80^+$ cells, the numbers of mCherry-positive $CX3CR1^+F4/80^-$ and $CX3CR1^+F4/80^+$ cells were 5 times and 3.5 times higher, respectively (**Figure 3E**). These results confirm that CX3CR1 transgenic mice are a promising model for analyzing the behavior of DCs and macrophages during the establishment of the pre-metastatic niche in the liver.

Intravital Imaging of Myeloid $CX3CR1^+$ Cell Migration in Metastatic Lesions

To understand the effects of sGRP78 on the motility of hepatic myeloid DCs and macrophages within the tumor microenvironment, we performed intravital imaging using C57BL/6 CX3CR1-GFP mice. Intravital imaging was performed using confocal laser scanning microscopy (CLSM) (**Figures 4A,B**), followed by $CX3CR1^+$ cell motility quantification (**Figure 4C**). Four days after tumor cell inoculation, the motility of $CX3CR1^+$ cells in the E0771-mCherry-sGRP78-bearing mice was significantly increased. The 25-min mean displacement of $CX3CR1^+$ cells was higher in the E0771-mCherry-sGRP78 group compared with the E0771-mCherry group (13.85 ± 1.177 μm vs. 8.759 ± 0.8735 μm; $P < 0.001$; **Figure 4D**). In the E0771-mCherry-sGRP78 group, $CX3CR1^+$ cells migrated to the tumor periphery with a mean velocity of 7.350 ± 0.5245 μm/min ($n = 175$ cells). However, in E0771-mCherry-bearing mice, $CX3CR1^+$ cells migrated with a mean velocity of 2.899 ± 0.2512 μm/min ($n = 95$ cells). Moreover, in E0771-mCherry-sGRP78-bearing mice, the migration trajectories were more confined (confinement ratio: 0.5610 ± 0.02504; $P < 0.01$) and the arrest coefficient (percentage of cell resting time) was lower compared with the E0771-mCherry group ($36.14\% \pm 2.446$ vs. $79.93\% \pm 1.858$; **Figure 4D**).

Seven days after tumor cell inoculation, the $CX3CR1^+$ cell motility changed significantly. Although the number of moving $CX3CR1^+$ cells was significantly lower in both groups compared with 4 days after cell inoculation, the velocity of movement was significantly increased in E0771-mCherry-sGRP78-bearing mice (102.9 ± 18.28 μm/min). In contrast, in E0771-mCherry-bearing mice, the velocity of movement did not differ significantly between 4 and 7 days after cell inoculation (6.346 ± 0.7385; $n = 46$ cells from 4 to 5 mice; **Figure 4E**). We found no significant differences in the migration trajectories, and arrest coefficient between 4 and 7 days after cell inoculation, suggesting that the effect of sGRP78 was reduced and that $CX3CR1^+$ cells were saturated in sGRP78. These data suggest an association between the level of tumor-secreted GRP78 and the level of $CX3CR1^+$ cell migration in metastatic lesions, particularly during the early stages of cancer cell colonization. The effect of sGRP78 on $CX3CR1^+$ cell motility was less profound 7 days after cell inoculation, suggesting that sGRP78 promotes immune tolerance early during pre-metastatic niche establishment by recruiting $CX3CR1^+$ cells.

Tumor-Secreted GRP78 Inhibits Hepatic NK Cell Activation

NK cells play essential roles in anti-tumor immunity by exerting cytotoxic effects on cancer cells. Hence, we tested the effects of sGRP78 overexpression on NK cells and other effector lymphocytes, including natural killer T (NKT) cells, B cells, $CD4^+$, and $CD8^+$ T cells, as well as on macrophages and neutrophils, during liver metastasis (**Figure 5A**). The frequencies of infiltrated NK ($P < 0.05$) and $CD19^+$ B cells ($P < 0.01$) in E0771-mCherry-sGRP78-bearing mice 4 and 7 days after cell inoculation were lower than those in control mice, respectively (**Figure 5B**). Four days after cell inoculation, the expression of CD69, which is an important marker for activated effector cells (41, 42), was lower on NK cells in sGRP78-expressing mice than control mice ($P < 0.001$; **Figures 5C,D**). However, no differences in CD69 expression were observed 7 days after cell inoculation (**Figure 5E**). T cells, B cells, and other lymphocytes were not influenced by sGRP78. The effects of sGRP78 on the recruitment and activation of immune cells was reflected on cytokines secretion. Compared with control mice, sGRP78-expressing mice exhibited higher levels of IL-10 at both time points. Nevertheless, no differences were observed on the levels of IFN-γ, TNF-α, IL-2, or IL-6 (**Figure 5F**). Notably, compared with control mice, TGF-β levels were increased by 1.12-fold in sGRP78-expressing mice; however, TGF-β upregulation was not observed before day 7 (**Figure 5G**). These results suggest that tumor-secreted GRP78 facilitates tumor metastasis by inhibiting NK activity and inducing the secretion of immune-suppressive cytokines.

DISCUSSION

In this study, we demonstrated that high expression of sGRP78 in the liver promotes immune tolerance. To elucidate the role of sGRP78 in the hepatic pre-metastatic niche, we established an experimental liver metastasis model using sGRP78-overexpressing murine breast cancer cells. We found that tumor-secreted GRP78 reshaping the hepatic microenvironment by recruiting $CX3CR1^+$ myeloid cells. sGRP78 inhibited DC activation by downregulating MHC-II, as well as induced $F4/80^+$ M2-type polarization. Furthermore, sGRP78 affected NK cell infiltration and activation in hepatic metastatic lesions by regulating cytokine production (**Figure 6**).

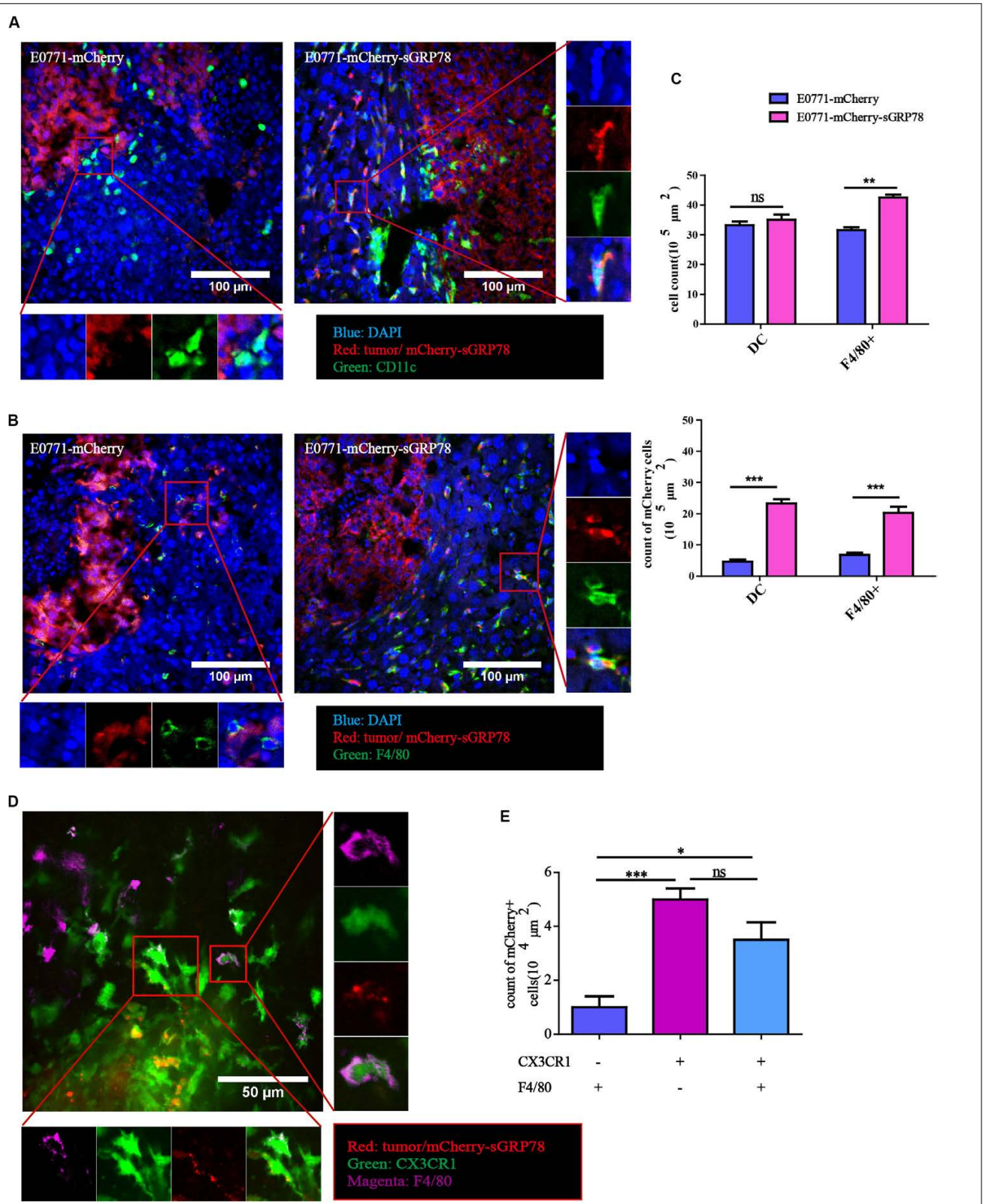

FIGURE 3 | Tumor-secreted GRP78 interacts with hepatic DC and F4/80$^+$ macrophages. Mice liver sections showing sGRP78 interacting with CD11c$^+$ cells **(A)** and F4/80$^+$ cells **(B)**. Scale bar, 100 μm. **(C)** Numbers of infiltrated DC cells and F4/80$^+$ cells (upper), as well as of mCherry$^+$ DC and F4/80$^+$ cells (lower). sGRP78 was detected to interact with CX3CR1$^+$ cells **(D)**. Scale bar, 50 μm. **(E)** Numbers of mCherry$^+$ CX3CR1$^+$ cells. Error bars represent SEM. Ns, not significant; $^*P < 0.05$; $^{**}P < 0.01$; $^{***}P < 0.001$. Statistical significance was determined by Student's *t*-test **(C)** or by Welch's ANOVA **(E)**.

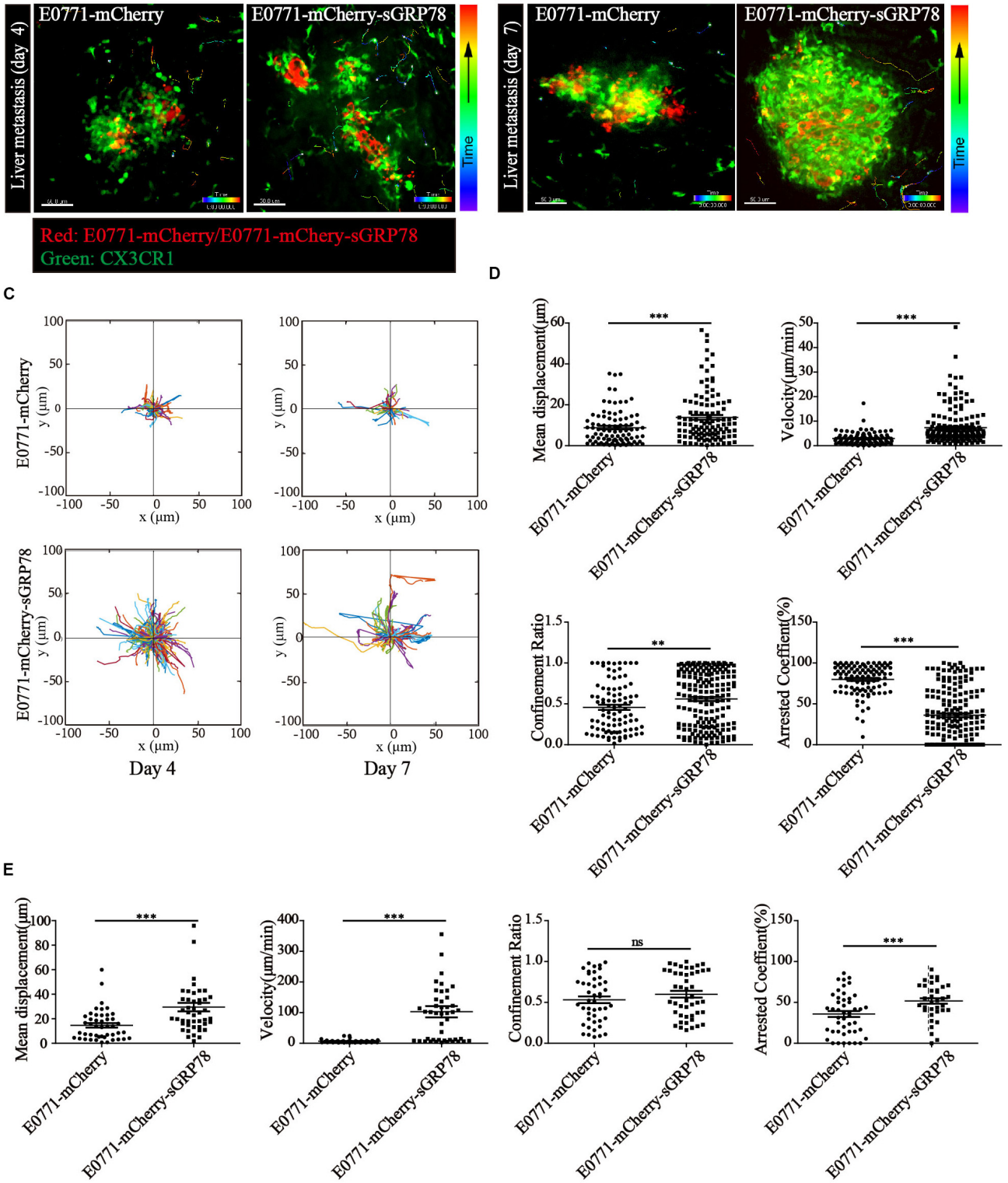

FIGURE 4 | Tumor-secreted GRP78 promotes myeloid CX3CR1^{+} cell recruitment in metastatic lesions. *In vivo* imaging of the livers four **(A)** and seven **(B)** days after E0771-mCherry (left) and E0771-sGRP78-mCherry (right) injection, using confocal microscopy. Trajectories **(C)** and motion parameters of CX3CR1^{+} cells four **(D)** and seven **(E)** days after tumor cell intrasplenic injection. Each data point represents a single cell, and the red bars indicate mean values. $^{**}P < 0.01$; $^{***}P < 0.001$; ns: not significant. The data from 3–5 mice in two independent experiments were pooled. Statistical significance was determined by Student's *t*-test.

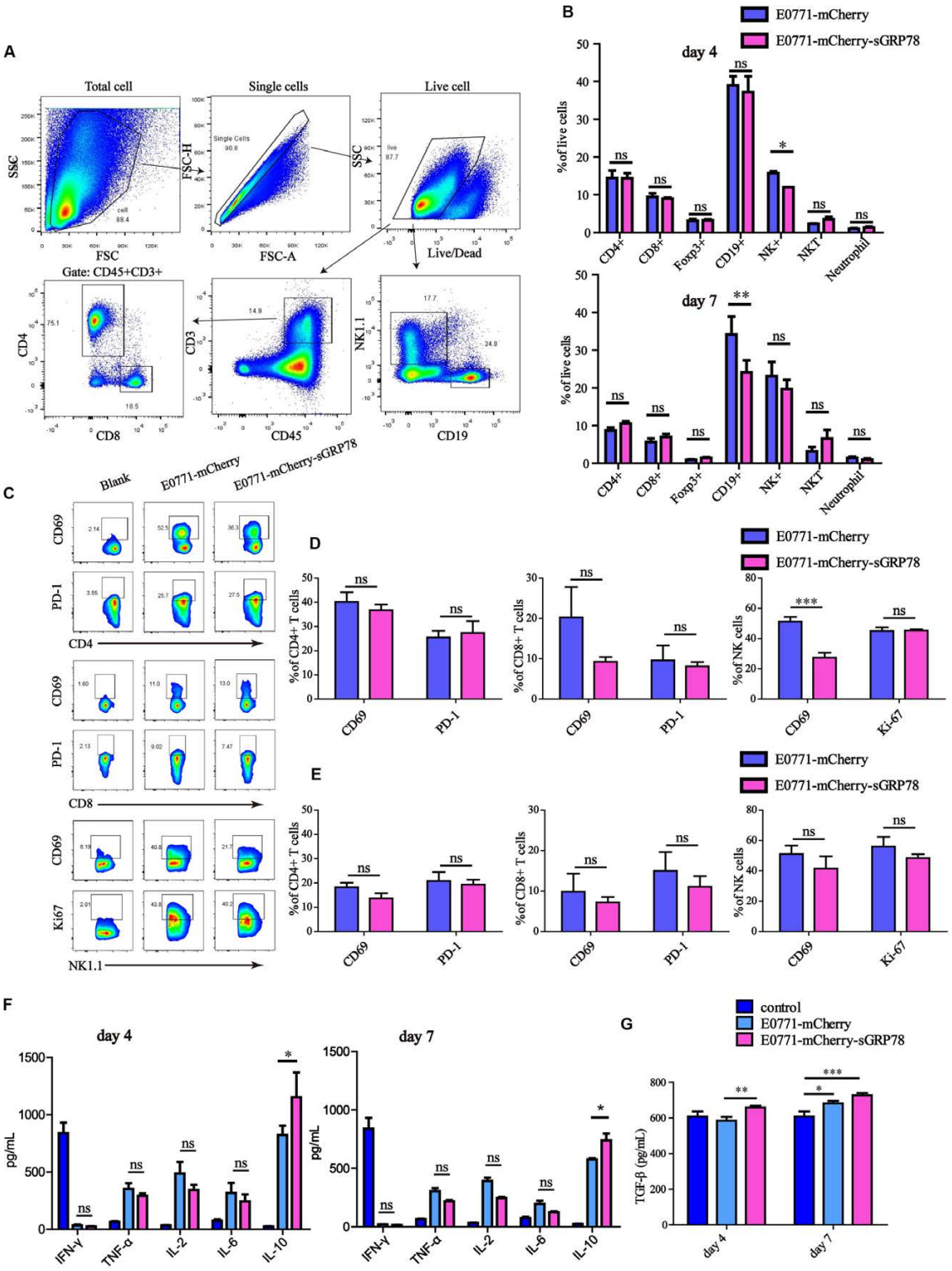

FIGURE 5 | Tumor-secreted GRP78 inhibits hepatic NK cell activation. Liver tissues were excised and their mass was measured at days 4 and 7 after injection. The liver was digested and then filtered. The cell pellet containing leukocytes was collected by Percoll centrifugation. Then cells were stained with antibodies for FCM analysis. **(A)** Gating strategy followed to distinguish the hepatic immune cells. **(B)** Frequencies of immune cell subsets in the liver four (upper panel) and seven (lower panel) days after tumor cell intrasplenic injection. **(C–E)** Frequencies of $CD69^+$ and $PD\text{-}L1^+$ cells among CD4, CD8 subsets, as well as of $CD69^+$ and $Ki\text{-}67^+$ cells in NK1.1 cells. Representative flow cytometry dot plots **(C)** and percentage of positive cells **(D,E)** are shown. **(F,G)** Detection of cytokines. Graphs represent the mean ± SEM. Ns, not significant; $^*P < 0.05$; $^{**}P < 0.01$; $^{***}P < 0.001$. Statistical significance was determined by Student's *t*-test **(B,D,E)** or by Welch's ANOVA **(F,G)**.

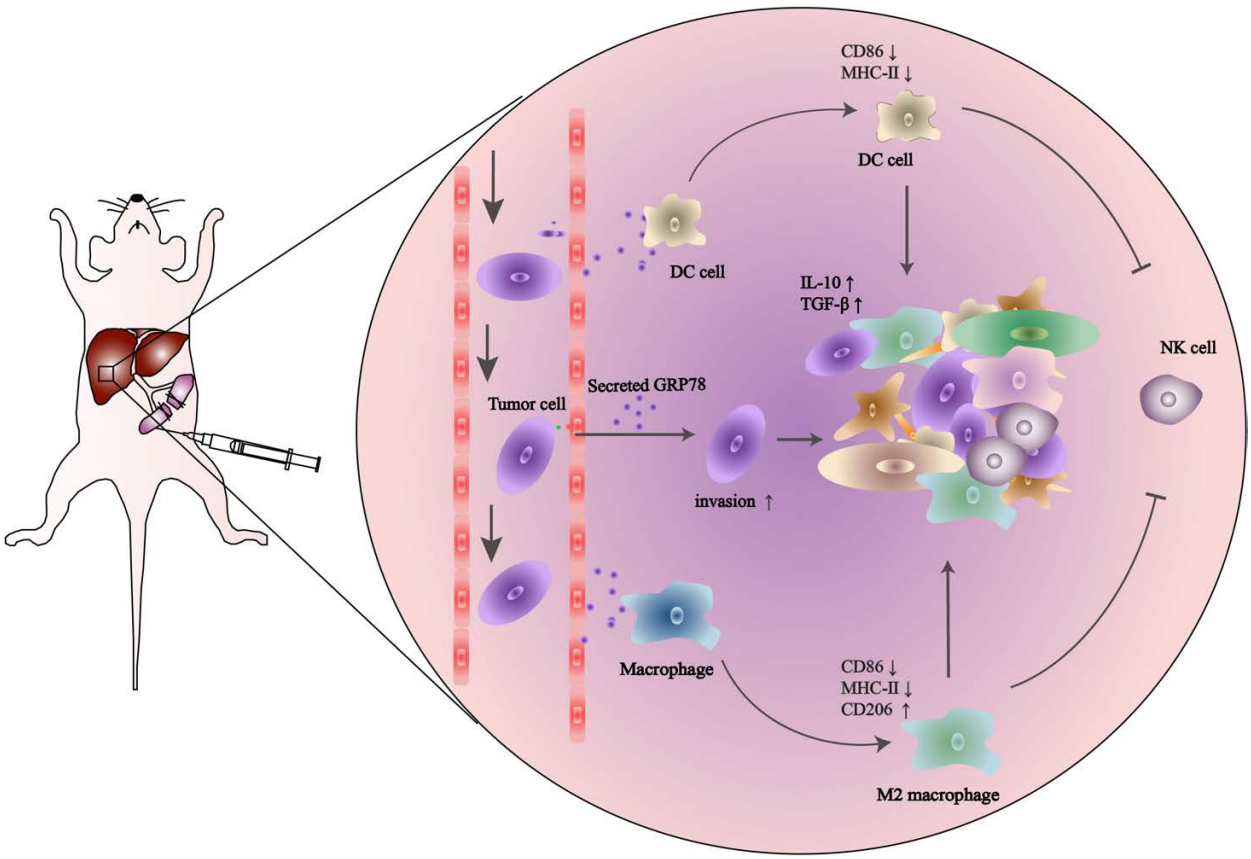

FIGURE 6 | Schematic description of the role of tumor-secreted GRP78 in the pre-metastatic niche. Tumor-secreted GRP78 interacts with hepatic DCs and macrophages in the metastatic niche to induce tolerogenic phenotypes. These impair NK cell recruitment and activation, thereby promoting the establishment of a pre-metastatic niche, which fosters tumor cell colonization, invasion, and metastasis.

GRP78 is expressed at higher levels in tumor tissues compared to adjacent healthy tissues, indicating that GRP78 has potential pro-tumorigenic functions (43–45). In order to investigate the effects of sGRP78 on the establishment of the hepatic pre-metastatic niche, we assessed the concentrations of GRP78 in different tissues. GRP78 was highly expressed in the liver, suggesting a potential role in reshaping the hepatic microenvironment to facilitate liver metastasis. sGRP78 has been implicated in immunomodulation by biding to pattern recognition receptors (9, 18). Moreover, intracellular GRP78 levels have been associated with drug resistance and apoptosis in cancers (11, 46). To assess the ability of sGRP78 to reshape the hepatic microenvironment, we established a sGRP78-overexpressing breast cancer cell line (E0771-mCherry-sGRP78) and found that sGRP78 overexpression promoted tumor cell invasion *in vitro*. In addition, sGRP78 overexpression enhanced the colonization and proliferation of metastatic cells in the liver, suggesting that sGRP78 expression in cancer cells promotes invasion and liver metastasis by modulating the hepatic microenvironment.

The establishment of a pre-metastatic niche is a prerequisite for tumor cell colonization and growth in secondary organs (1). In this study, we found increased numbers of tumor cells in the liver 4 days after cell inoculation when sGRP78 was overexpressed, suggesting that the high levels of GRP78 contributed to the establishment of immune tolerance and pre-metastatic niche in the liver. The mechanisms underlying the sGRP78-mediated immune cell recruitment into the liver during the establishment of the pre-metastatic niche merits further investigation. Zhuoyu Li et al. (47) proposed that tumor-secreted GRP78 facilitates macrophage infiltration into the tumor by binding to intracellular Ca^{2+}, leading to cytoskeleton remodeling. Our results supported the role of sGRP78 on the motility of $CX3CR1^{+}$ cells in the liver, including DCs and macrophages, fostering liver metastasis. We believe that the increased infiltration of DCs and macrophages accompanied by the decreased recruitment and activation of NK cells contributed to the establishment of a microenvironment allowing for tumor cell survival and growth. Nevertheless, future studies are required to determine the mechanisms involved in the sGRP78-mediated NK cell inhibition.

In conclusion, we have demonstrated that sGRP78 promotes tumor cell colonization in the liver. We also identified several mechanisms involved in this phenomenon, including the modulation of DCs and $F4/80^{+}$ macrophages, induction of TGF-β, and suppression of hepatic NK cells. Thus, sGRP78

promotes tumor growth and metastasis by remodeling the tumor microenvironment and promoting immune tolerance. The ability of GRP78-targeting agents to prevent liver metastasis should be further investigated.

DATA AVAILABILITY STATEMENT

The raw data supporting the conclusions of this article will be made available by the authors, without undue reservation.

ETHICS STATEMENT

The animal study was reviewed and approved by the Animal Experimentation Ethics Committee of Huazhong University of Science and Technology.

AUTHOR CONTRIBUTIONS

LC under the direction of ZZ and GS designed and performed the experiments, analyzed the data, and wrote the first version of the manuscript. XY and LL provided technical guidance. HZhe discussed the manuscript and provided feedback and suggestions. ZZ, PL, and GS designed the experiments, wrote the manuscript, and supervised the study. All authors contributed to the critical revision of the manuscript and approved the final version.

FUNDING

This work was supported by the major research plan of the National Natural Science Foundation of China (Grant No. 91842305) and the general program of NSFC (Grant No. 81871307), Program for HUST Basic Medical Immunology Team (PL) and Academic Frontier Youth Team (ZZ).

ACKNOWLEDGMENTS

The authors thank Dr. Xiaohui Wu at Fudan University (China) for providing PB transposon system. They also thank the Optical Bioimaging Core Facility of WNLO-HUST and the Research Core Facilities of Life Science (HUST) for the support in data acquisition, and the Analytical and Testing Center of HUST for the facility support.

SUPPLEMENTARY MATERIAL

The Supplementary Material for this article can be found online at: https://www.frontiersin.org/articles/10.3389/fimmu.2020.584458/full#supplementary-material

Supplementary Figure 1 | GRP78 expression in different mouse organs. GRP78 expression in different tissue homogenates was detected by ELISA. Error bars represent SEM. $^{**}P < 0.01$; $^{***}P < 0.001$. Statistical significance was determined by Welch's ANOVA.

Supplementary Figure 2 | Tumor-secreted GRP78 promotes liver metastasis. **(A)** The photo image of livers ($n = 5$ animals/group) were mice sacrificed on day 20 and day 14 after injected with 1×10^6 E0771 or 5×10^5 B16F10 cells, respectively. **(B)** Representative images of H&E-stained liver sections from mice sacrificed 14 days after tumor cell intrasplenic injection. Scale bar, 2,000 μm. **(C)** Quantification of liver weight (left panel) and metastatic burden (right panel) in livers ($n = 5$ mice per group). **(D)** Survival curves ($n = 6$). Error bars represent SEM. Ns, not significant; $^{*}P < 0.05$; $^{**}P < 0.01$; $^{***}P < 0.001$. Statistical significance was determined by Welch's ANOVA **(C)** or by log-rank Mantel-Cox test **(D)**.

REFERENCES

1. Liu Y, Cao XT. Characteristics and significance of the pre-metastatic Niche. *Cancer Cell.* (2016) 30:668–81. doi: 10.1016/j.ccell.2016.09.011
2. Lee JW, Stone ML, Porrett PM, Thomas SK, Komar CA, Li JH, et al. Hepatocytes direct the formation of a pro-metastatic niche in the liver. *Nature.* (2019) 567:249–52. doi: 10.1038/s41586-019-1004-y
3. Liu H, Bowes RC, vandeWater B, Sillence C, Nagelkerke JF, Stevens JL. Endoplasmic reticulum chaperones GRP78 and calreticulin prevent oxidative stress, Ca2+ disturbances, and cell death in renal epithelial cells. *J Biol Chem.* (1997) 272:21751–9. doi: 10.1074/jbc.272.35.21751
4. Rao RV, Peel A, Logvinova A, del Rio G, Hermel E, Yokota T, et al. Coupling endoplasmic reticulum stress to the cell death program: role of the ER chaperone GRP78. *FEBS Lett.* (2002) 514:122–8. doi: 10.1016/s0014-5793(02)02289-5
5. Zhu GY, Lee AS. Role of the unfolded protein response, GRP78 and GRP94 in organ homeostasis. *J Cell Physiol.* (2015) 230:1413–20. doi: 10.1002/jcp.24923
6. Shen JS, Chen X, Hendershot L, Prywes R. ER stress regulation of ATF6 localization by dissociation of BiP/GRP78 binding and unmasking of golgi localization signals. *Dev Cell.* (2002) 3:99–111. doi: 10.1016/s1534-5807(02)00203-4
7. Dicks N, Gutierrez K, Michalak M, Bordignon V, Agellon LB. Endoplasmic reticulum stress, genome damage, and cancer. *Front Oncol.* (2015) 5:11. doi: 10.3389/fonc.2015.00011
8. Li ZW, Zhuang M, Zhang LC, Zheng XN, Yang P, Li ZY. Acetylation modification regulates GRP78 secretion in colon cancer cells. *Sci Rep.* (2016) 6:30406.
9. Qin K, Ma SM, Li HL, Wu M, Sun YL, Fu MP, et al. GRP78 impairs production of Lipopolysaccharide-induced Cytokines by interaction with CD14. *Front Immunol.* (2017) 8:579. doi: 10.3389/fimmu.2017.00579
10. Fong JJ, Sreedhara K, Deng LW, Varki NM, Angata T, Liu QL, et al. Immunomodulatory activity of extracellular Hsp70 mediated via paired receptors Siglec-5 and Siglec-14. *EMBO J.* (2015) 34:2775–88. doi: 10.15252/embj.201591407
11. Yang MY, Zhang F, Qin K, Wu M, Li HL, Zhu HF, et al. Glucose-regulated protein 78-induced myeloid antigen-presenting cells maintained tolerogenic signature upon LPS stimulation. *Front Immunol.* (2016) 7:552. doi: 10.3389/fimmu.2016.00552
12. Tameire F, Verginadis II, Koumenis C. Cell intrinsic and extrinsic activators of the unfolded protein response in cancer: mechanisms and targets for therapy. *Semin Cancer Biol.* (2015) 33:3–15. doi: 10.1016/j.semcancer.2015.04.002
13. Li ZW, Li ZY. Glucose regulated protein 78: a critical link between tumor microenvironment and cancer hallmarks. *Bba Rev Cancer.* (2012) 1826:13–22. doi: 10.1016/j.bbcan.2012.02.001
14. Dong DZ, Ko BC, Baumeister P, Swenson S, Costa F, Markland F, et al. Vascular targeting and antiangiogenesis agents induce drug resistance effector GRP78 within the tumor microenvironment. *Cancer Res.* (2005) 65:5785–91. doi: 10.1158/0008-5472.can-05-0754
15. Rui L, Gu YJ, He WB, Wang Y, Huang JH, Zheng HC, et al. Secreted GRP78 activates EGFR-SRC-STAT3 signaling and confers the resistance to sorafeinib in HCC cells. *Oncotarget.* (2017) 8:19354–64. doi: 10.18632/oncotarget.15223
16. Rodvold JJ, Mahadevan NR, Zanetti M. Immune modulation by ER stress and inflammation in the tumor microenvironment. *Cancer Lett.* (2016) 380:227–36. doi: 10.1016/j.canlet.2015.09.009

17. Kim JH, Lee E, Friedline RH, Suk S, Jung DY, Dagdeviren S, et al. Endoplasmic reticulum chaperone GRP78 regulates macrophage function and insulin resistance in diet-induced obesity. *FASEB J.* (2018) 32:2292–304. doi: 10.1096/fj.201701017r
18. Tang YF, Jiang Q, Ou YH, Zhang F, Qing K, Sun YL, et al. BIP induces mice CD19(hi) regulatory B cells producing IL-10 and highly expressing PD-L1, FasL. *Mol Immunol.* (2016) 69:44–51. doi: 10.1016/j.molimm.2015.10.017
19. Ge R, Kao C. Cell surface GRP78 as a death receptor and an anticancer drug target. *Cancers (Basel).* (2019) 11:1787. doi: 10.3390/cancers11111787
20. Dadey DYA, Kapoor V, Hoye K, Khudanyan A, Collins A, Thotala D, et al. Antibody targeting GRP78 enhances the efficacy of radiation therapy in human glioblastoma and non-small cell lung cancer cell lines and tumor models. *Clin Cancer Res.* (2017) 23:2556–64. doi: 10.1158/1078-0432.ccr-16-1935
21. Jiang B, Zhang R, Zhang J, Hou Y, Chen X, Zhou M, et al. GRP78-targeted ferritin nanocaged ultra-high dose of doxorubicin for hepatocellular carcinoma therapy. *Theranostics.* (2019) 9:2167–82. doi: 10.7150/thno.30867
22. Cai YL, Zheng YF, Gu JY, Wang SQ, Wang N, Yang BW, et al. Betulinic acid chemosensitizes breast cancer by triggering ER stress-ediated apoptosis by directly targeting GRP78. *Cell Death Dis.* (2018) 9:636.
23. Kao C, Chandna R, Ghode A, Dsouza C, Chen M, Larsson A, et al. Proapoptotic cyclic peptide BC71 targets cell-surface GRP78 and functions as an anticancer therapeutic in mice. *Ebiomedicine.* (2018) 33:22–32. doi: 10.1016/j.ebiom.2018.06.004
24. Ramirez MU, Hernandez SR, Soto-Pantoja DR, Cook KL. Endoplasmic reticulum stress pathway, the unfolded protein response, modulates immune function in the tumor microenvironment to impact tumor progression and therapeutic response. *Int J Mol Sci.* (2019) 21:169. doi: 10.3390/ijms21010169
25. Peng H, Tian ZG. Re-examining the origin and function of liver-resident NK cells. *Trends Immunol.* (2015) 36:293–9. doi: 10.1016/j.it.2015.03.006
26. Liu PY, Chen LL, Zhang HY. Natural killer cells in liver disease and hepatocellular carcinoma and the NK cell-based immunotherapy. *J Immunol Res.* (2018) 2018:1206737.
27. Andre P, Denis C, Soulas C, Bourbon-Caillet C, Lopez J, Arnoux T, et al. Anti-NKG2A mAb is a checkpoint inhibitor that promotes anti-tumor immunity by unleashing both T and NK cells. *Cell.* (2018) 175:1731–43.e13.
28. Sarhan D, Palma M, Mao YM, Adamson L, Kiessling R, Mellstedt H, et al. Dendritic cell regulation of NK-cell responses involves lymphotoxin-, IL-12, and TGF-. *Eur J Immunol.* (2015) 45:1783–93. doi: 10.1002/eji.201444885
29. Zhou ZX, Yu X, Zhang J, Tian ZG, Zhang C. TLR7/8 agonists promote NK-DC cross-talk to enhance NK cell anti-tumor effects in hepatocellular carcinoma. *Cancer Lett.* (2015) 369:298–306. doi: 10.1016/j.canlet.2015.09.017
30. Hernandez-Jimenez E, Cubillos-Zapata C, Toledano V, Perez de Diego R, Fernandez-Navarro I, Casitas R, et al. Monocytes inhibit NK activity via TGF-beta in patients with obstructive sleep apnoea. *Eur Respir J.* (2017) 49:1602456. doi: 10.1183/13993003.02456-2016
31. Peng LS, Zhang JY, Teng YS, Zhao YL, Wang TT, Mao FY, et al. Tumor-associated monocytes/macrophages impair NK-cell function via TGFbeta1 in human gastric cancer. *Cancer Immunol Res.* (2017) 5:248–56. doi: 10.1158/2326-6066.cir-16-0152
32. Ghiringhelli F, Menard C, Terme M, Flament C, Taieb J, Chaput N, et al. CD4(+) CD25(+) regulatory T cells inhibit natural killer cell functions in a transforming growth factor-beta-dependent manner. *J Exp Med.* (2005) 202:1075–85. doi: 10.1084/jem.20051511
33. Lazarova M, Steinle A. Impairment of NKG2D-Mediated Tumor Immunity by TGF-beta. *Front Immunol.* (2019) 10:2689. doi: 10.3389/fimmu.2019.02689
34. Ding S, Wu XH, Li G, Han M, Zhuang Y, Xu T. Efficient transposition of the piggyBac resource (PB) transposon in mammalian cells and mice. *Cell.* (2005) 122:473–83. doi: 10.1016/j.cell.2005.07.013
35. Qi S, Li H, Lu L, Qi Z, Liu L, Chen L, et al. Long-term intravital imaging of the multicolor-coded tumor microenvironment during combination immunotherapy. *eLife.* (2016) 5:e14756. doi: 10.7554/eLife.14756
36. Yang F, Liu S, Liu X, Liu L, Luo M, Qi S, et al. In vivo visualization of tumor antigen-containing microparticles generated in fluorescent-protein-elicited immunity. *Theranostics.* (2016) 6:1453–66. doi: 10.7150/thno.14145
37. Thomson AW, Knolle PA. Antigen-presenting cell function in the tolerogenic liver environment. *Nat Rev Immunol.* (2010) 10:753–66. doi: 10.1038/nri2858
38. Racanelli V, Rehermann B. The liver as an immunological organ. *Hepatology.* (2006) 43:S54–62.
39. David BA, Rezende RM, Antunes MM, Santos MM, Freitas Lopes MA, Diniz AB, et al. Combination of mass cytometry and imaging analysis reveals origin, location, and functional repopulation of liver myeloid cells in mice. *Gastroenterology.* (2016) 151:1176–91. doi: 10.1053/j.gastro.2016.08.024
40. Sutti S, Bruzzi S, Heymann F, Liepelt A, Krenkel O, Toscani A, et al. CX3CR1 mediates the development of monocyte-derived dendritic cells during hepatic inflammation. *Cells.* (2019) 8:1099. doi: 10.3390/cells8091099
41. Marden CM, North J, Anderson R, Bakhsh IA, Addison E, Pittman H, et al. CD69 is required for activated NK cell-mediated killing of resistant targets. *Blood.* (2005) 106:928a–9a.
42. Prado-Drayer A, Teppa J, Sanchez P, Camejo MI. Immunophenotype of peripheral T lymphocytes, NK cells and expression of CD69 activation marker in patients with recurrent spontaneous abortions, during the mid-luteal phase. *Am J Reprod Immunol.* (2008) 60:66–74. doi: 10.1111/j.1600-0897.2008.00591.x
43. Cali G, Insabato L, Conza D, Bifulco G, Parrillo L, Mirra P, et al. GRP78 mediates cell growth and invasiveness in endometrial cancer. *J Cell Physiol.* (2014) 229:1417–26. doi: 10.1002/jcp.24578
44. Ding X, Duan X. Expression of GRP78 protein is increased in rectal adenocarcinoma. *Virchows Arch.* (2017) 471:S189–S.
45. Dong DZ, Ni M, Li JZ, Xiong SG, Ye W, Virrey JJ, et al. Critical role of the stress chaperone GRP78/BiP in tumor proliferation, survival, and tumor anglogenesis in transgene-induced mammary tumor development. *Cancer Res.* (2008) 68:498–505. doi: 10.1158/0008-5472.can-07-2950
46. Wang Q, Shu R, He HJ, Wang L, Ma Y, Zhu HF, et al. Co-silencing of Birc5 (survivin) and Hspa5 (Grp78) induces apoptosis in hepatoma cells more efficiently than single gene interference. *Int J Oncol.* (2012) 41:652–60. doi: 10.3892/ijo.2012.1471
47. La X, Zhang L, Yang Y, Li H, Song G, Li Z. Tumor-secreted GRP78 facilitates the migration of macrophages into tumors by promoting cytoskeleton remodeling. *Cell Signal.* (2019) 60:1–16. doi: 10.1016/j.cellsig.2019.04.004

Conflict of Interest: The authors declare that the research was conducted in the absence of any commercial or financial relationships that could be construed as a potential conflict of interest.

Copyright © 2020 Chen, Zheng, Yu, Liu, Li, Zhu, Zhang, Lei and Shen. This is an open-access article distributed under the terms of the Creative Commons Attribution License (CC BY). The use, distribution or reproduction in other forums is permitted, provided the original author(s) and the copyright owner(s) are credited and that the original publication in this journal is cited, in accordance with accepted academic practice. No use, distribution or reproduction is permitted which does not comply with these terms.

frontiers in Immunology

ORIGINAL RESEARCH
published: 06 October 2020
doi: 10.3389/fimmu.2020.590794

Obesity-Associated Myeloid-Derived Suppressor Cells Promote Apoptosis of Tumor-Infiltrating CD8 T Cells and Immunotherapy Resistance in Breast Cancer

*Justin T. Gibson[1], Rachael M. Orlandella[1], William J. Turbitt[2], Michael Behring[3], Upender Manne[3,4], Robert E. Sorge[5,6] and Lyse A. Norian[2,4,6]**

[1] Graduate Biomedical Sciences, University of Alabama at Birmingham, Birmingham, AL, United States, [2] Department of Nutrition Sciences, University of Alabama at Birmingham, Birmingham, AL, United States, [3] Department of Pathology, University of Alabama at Birmingham, Birmingham, AL, United States, [4] O'Neal Comprehensive Cancer Center, University of Alabama at Birmingham, Birmingham, AL, United States, [5] Department of Psychology, University of Alabama at Birmingham, Birmingham, AL, United States, [6] Nutrition Obesity Research Center, University of Alabama at Birmingham, Birmingham, AL, United States

OPEN ACCESS

Edited by:
Peng Qu,
National Institutes of Health (NIH), United States

Reviewed by:
Richard Eric Davis,
University of Texas MD Anderson Cancer Center, United States
Panayotis Verginis,
Biomedical Research Foundation of the Academy of Athens (BRFAA), Greece
Jiaxin Liang,
Dana–Farber Cancer Institute, United States

***Correspondence:**
Lyse A. Norian
lnorian@uab.edu

Specialty section:
This article was submitted to Cancer Immunity and Immunotherapy, a section of the journal Frontiers in Immunology

Received: 03 August 2020
Accepted: 15 September 2020
Published: 06 October 2020

Citation:
Gibson JT, Orlandella RM, Turbitt WJ, Behring M, Manne U, Sorge RE and Norian LA (2020) Obesity-Associated Myeloid-Derived Suppressor Cells Promote Apoptosis of Tumor-Infiltrating CD8 T Cells and Immunotherapy Resistance in Breast Cancer. Front. Immunol. 11:590794. doi: 10.3389/fimmu.2020.590794

Nearly 70% of adults in the US are currently overweight or obese. Despite such high prevalence, the impact of obesity on antitumor immunity and immunotherapy outcomes remains incompletely understood, particularly in patients with breast cancer. Here, we addressed these gaps in knowledge using two murine models of breast cancer combined with diet-induced obesity. We report that obesity increases CXCL1 concentrations in the mammary tumor microenvironment, driving CXCR2-mediated chemotaxis and accumulation of granulocytic myeloid-derived suppressor cells (G-MDSCs) expressing Fas ligand (FasL). Obesity simultaneously promotes hyperactivation of CD8 tumor-infiltrating lymphocytes (TILs), as evidenced by increased expression of CD44, PD-1, Ki-67, IFNγ, and the death receptor Fas. Accordingly, G-MDSCs induce Fas/FasL-mediated apoptosis of CD8 T cells *ex vivo* and *in vivo*. These changes promote immunotherapy resistance in obese mice. Disruption of CXCR2-mediated G-MDSC chemotaxis in obese mice is sufficient to limit intratumoral G-MDSC accumulation and improve immunotherapy outcomes. The translational relevance of our findings is demonstrated by transcriptomic analyses of human breast tumor tissues, which reveal positive associations between *CXCL1* expression and body mass index, poor survival, and a MDSC gene signature. Further, this MDSC gene signature is positively associated with *FASLG* expression. Thus, we have identified a pathway wherein obesity leads to increased intratumoral CXCL1 concentrations, which promotes CXCR2-mediated accumulation of $FasL^+$ G-MDSCs, resulting in heightened CD8 TIL apoptosis and immunotherapy resistance. Disruption of this pathway may improve immunotherapy outcomes in patients with breast cancer and obesity.

Keywords: myeloid-derived suppressor cells (MDSCs), obesity, immunotherapy resistance, breast cancer, tumor-infiltrating lymphocyte apoptosis, Fas ligand (FasL)

INTRODUCTION

Obesity is a major health epidemic in the US, affecting nearly 40% of adults (1). Excess body weight increases the incidence of 13 types of cancer (2), promotes disease progression (3, 4), impairs antitumor immunity (5, 6), promotes resistance to targeted and chemotherapies (7, 8), and worsens survival for cancer patients (9, 10), especially those with breast cancer. However, the impact of obesity on immunotherapy outcomes in patients with breast cancer is unknown.

In 2019, the FDA granted accelerated approval for the treatment of select triple negative breast cancer patients with an immunotherapy/chemotherapy combination based on results reported from the phase III IMpassion130 clinical trial (11). However, despite immunotherapeutics dramatically improving outcomes for a subset of patients with cancer, many still do not respond. As such, research efforts are concentrated on identifying and targeting factors underlying immunotherapeutic resistance. Obesity may be one such factor. Recent findings from a phase I clinical trial of patients with breast cancer treated with atezolizumab (anti-PD-L1) indicate that elevated baseline plasma levels of interleukin 6 (IL-6) and C-reactive protein (CRP) are associated with reduced progression free and overall survival (12). As both IL-6 and CRP are biomarkers of obesity-associated inflammation, this raises the possibility that obesity may impair immunotherapeutic efficacy in patients with breast cancer. In support of this idea, obesity was previously shown to be associated with impaired responses to targeted and chemotherapies in patients with breast cancer (7, 8). However, given the short duration of its clinical use, the impact of obesity on immunotherapy outcomes in patients with breast cancer has not yet been investigated.

Molecular markers of obesity (e.g. IL-6, CRP, leptin, interleukin 1 beta [IL-1β]) increase the generation of myeloid-derived suppressor cells (MDSCs) (13–16). MDSCs are a heterogeneous immunosuppressive population of cells that function to inhibit protective antitumor immunity to promote tumor growth and progression. To date, only one study has investigated the impact of obesity-associated MDSCs in mediating mammary tumor growth (14). However, this study did not assess the impact of MDSCs on response to immunotherapy. Given that intratumoral accumulation of MDSCs has been identified as a mechanism of immunotherapy resistance (17, 18), we asked if obesity would enhance MDSC-mediated immunotherapy resistance in a preclinical model of breast cancer.

MATERIALS AND METHODS

Research Resource Identifiers

Research Resource Identifiers (RRIDs) and other detailed identifier information (vendor, clone, catalog number etc.) for antibodies and key reagents used in this study can be found in this text and **Supplementary Table 1**.

Murine Models of Obesity

Wildtype C57BL/6 female mice were purchased from Charles River at 7–8 weeks of age. Following one week of acclimation, animals were randomized to a NIH31 formulated low-fat diet (LFD; 14% kcal from fat, LabDiet), standard American diet (SAD; 36% kcal from fat, Envigo), or high-fat diet (HFD; 60% kcal from fat, Research Diets) for 16 weeks, thereby generating lean (LFD) or diet-induced obese (SAD and HFD) mice. All animal experiments were conducted as approved by the Animal Resources Program and Institutional Animal Care and Use Committee at the University of Alabama at Birmingham (UAB).

In Vivo Tumor Modeling

The E0771 murine mammary tumor cell line was purchased from CH3 BioSystems (RRID: CVCL_GR23) and engineered to express firefly luciferase (E0771-fluc) *via* transduction with lentiviral particles (Kerafast) according to the manufacturer's protocol. Cells were maintained in RPMI1640 complete media supplemented with 10% FBS, 10mM HEPES, 100 units/ml Penicillin, and 100 μg/ml Streptomycin. The Py8119 murine mammary tumor cell line was purchased from ATCC (RRID : CVCL_AQ09) and cells were maintained in F-12K complete media supplemented with 5% FBS. Neither cell line was authenticated after purchase and both were determined to be free of mycoplasma contamination.

Mice were injected with 2.5e5 E0771-fluc or 1e6 Py8119 cells subcutaneously into mammary fat pad number four. Tumor outgrowth was monitored using a dial caliper and bioluminescence imaging. To measure E0771-fluc tumor bioluminescence, tumor-bearing mice were injected intraperitoneally with 1mg of luciferin, anesthetized, and imaged using an IVIS Lumina III imaging system and the Living Image Software Version 4.7.2 (Perkin Elmer).

NanoString and Gene Ontology Analysis of Tumor Immune Microenvironment

At day 28 experimental endpoint, E0771-fluc tumors were excised and a portion was preserved in RNAlater. RNA was batch isolated and submitted to the UAB nanoString facility for interrogation using the nCounter PanCancer Immune Profiling Panel (XT-CSO-MIP1-12) according to the manufacturer's instructions. Data analysis was performed using nCounter Analysis Software (Version 4.0) with the Advanced Analysis (Version 2.0) plugin. Differentially expressed genes were identified as those with a p value < 0.05 and fold change $> \pm 1.5$. Due to the exploratory nature of our study and intent for validation, we used raw p values and did not adjust p values for multiple comparisons.

The nanoString tumor immunogenetic profiling dataset expression matrix from n=72 subjects with triple negative breast cancer (TNBC) was obtained from a previously published manuscript (17). Body mass index (BMI) information for this cohort of subjects was kindly provided by Dr. Xiang "Shawn" Zhang, Baylor College of Medicine. Of the 72 patient tissues evaluated, 4 were excluded from analysis due to lack of BMI data, being underweight, or issues with sample quality control. The final cohort for analysis consisted of n=68 samples. Linear regression analyses were performed for BMI versus log2 expression of each of the 730 genes. Due to the exploratory nature of the study, those with a $p<0.1$ were investigated further. Of the 730 genes, 73 were associated with BMI; 8 positively and 65 negatively.

From our murine study, differentially expressed genes were separated into groups of upregulated or downregulated genes and subjected to Gene Ontology enrichment analysis using the PANTHER classification system to identify associated biological processes (http://geneontology.org/) (19). This was also done for the clinical analyses using genes positively associated with BMI, identified as described above.

Flow Cytometry

Spleen and tumor tissues were excised and mechanically homogenized using the Miltenyi gentleMACS Dissociator, followed by enzymatic digestion in 5 μg/ml Liberase TM and 37.5 μg/ml DNase I at 37°C with gentle agitation for 15 or 30 min, respectively. Resulting homogenates were filtered (70um) to obtain single cell suspensions. Cells were stained with fixable Zombie Aqua viability dye, Fc blocked, and incubated with fluorophore-conjugated antibodies to surface markers. Evaluation of intracellular markers was conducted using BD's Cytofix/Cytoperm kit according to manufacturer's protocol. For evaluation of T cell cytokine production, single cell tumor homogenates were stimulated with anti-CD3 (8 μg/ml) and anti-CD28 (10 μg/ml) for 4 h with the addition of GolgiPlug during the last 2 h. Cells were then harvested and stained as indicated above for surface and intracellular markers. Apoptosis was evaluated using the BD Annexin V Apoptosis Detection Kit according to manufacturer's protocol.

Samples were analyzed on an Attune NxT cytometer after compensation using BD Comp Beads. Analyses were conducted using FlowJo (Version 10) and all gates were objectively drawn based on fluorescence minus one (FMO) controls for the tissue of interest. Detailed information for the antibodies used in this study is provided in **Supplementary Table 1**.

Quantification of Soluble Proteins

Tumors were excised and placed in Dulbecco's Phosphate Buffered Saline (DPBS; 0.2g tissue per 1 ml DPBS) followed by mechanical homogenization using a Miltenyi gentleMACS Dissociator. Tumor homogenates were centrifuged and supernatants were collected and stored for batch analysis of soluble proteins using the Bio-Plex Multiplex Immunoassay (Bio-Rad) according to the manufacturer's protocols.

In Vivo Anti-CD8β Antibody-Mediated CD8 T Cell Depletion

On days 1, 3, 5, 7, 14, 21, and 27 post tumor challenge, lean and DIO animals received an intraperitoneal injection containing 100 μg of anti-CD8β or isotype control antibody (Bio X Cell). Animals were euthanized on day 28 post tumor challenge, at which time tumor tissues were excised and CD8 TILs were evaluated by flow cytometry.

In Vivo Anti-Gr-1 Antibody-Mediated MDSC Depletion

On day 19 post tumor challenge, DIO animals received an intratumoral injection containing 200 μg of anti-Gr-1 or isotype control antibody (Bio X Cell). On days 20, 21, and 22 post tumor challenge, animals received a follow-up injection containing 100 μg of their respective antibody. Animals were euthanized on day 23 post tumor challenge, at which time tumor tissues were excised and infiltrating leukocytes were evaluated by flow cytometry.

G-MDSC Induction of Apoptosis

$CD8^+$ T cells were positively selected from spleens of naive 8- to 12-week-old C57BL/6 female mice using Miltenyi MACS Enrichment according to the manufacturer's protocol. Enriched $CD8^+$ T cells were activated *in vitro* for 72 h using 1 μg/ml anti-CD3 and 1 μg/ml anti-CD28 to induce Fas expression. Tumor-infiltrating G-MDSCs from DIO mice were sort-purified on a BD FACSMelody after being pre-enriched using anti-CD11b MACS beads from Miltenyi, as per the manufacturer's protocol. Prior to co-culture, purified G-MDSCs were incubated in the presence or absence of 50 μg/ml anti-FasL neutralizing antibody for 1 h. *In vitro* activated $CD8^+$ T cells were then co-cultured with G-MDSCs in the continued presence or absence of anti-FasL for 24 h. Cells were harvested and stained for flow cytometry to evaluate CD8 T cell apoptosis as indicated above.

Immunotherapy

Mice with established tumors within a 25–100 mm^2 range (~50 mm^2 on average) were randomized to receive saline or immunotherapy. Immunotherapy consisted of $1x10^9$ PFU of adenovirus (Ad) encoding murine TNF-related apoptosis inducing ligand (TRAIL; AdT) and 50 μg of the TLR9 agonist CpG 1826 oligodeoxynucleotide (AdT+CpG) (20). Saline or AdT+CpG were administered in 50uL volumes *via* intratumoral injection.

Disruption of CXCR2 signaling was accomplished using the CXCR2 antagonist SB 225002 (Tocris Bioscience). Beginning 2 days prior to tumor challenge and every 2 days after until day 26, 5 mg/kg of CXCR2a was administered intraperitoneally to lean and DIO animals.

Clinical Outcomes

Kaplan-Meier Plotter (KM Plotter; https://kmplot.com/) was used to evaluate the association of *CXCL1* expression and overall survival in systemically untreated patients with basal breast cancer (21). The following parameters were used for analysis with regard to *CXCL1*: auto select best cutoff, overall survival, intrinsic subtype: basal, and systemically untreated patients. Log rank p value and hazard ratio (HR) were calculated as part of the analysis.

Clinical Transcriptomic Analyses

Transcriptomic data were downloaded from The Cancer Genome Atlas (TCGA) using the curatedTCGAData package (https://bioconductor.org/packages/release/data/experiment/html/curatedTCGAData.html). The most recent version of TCGA RNASeq data (title "BRCA_RNASeq2GeneNorm-20160128") was used for analysis. To approximate expression values, RNASeq2 count data were log2 transformed and the mean expression of a previously published multi-gene MDSC signature (22) was calculated. The MDSC expression score was then separated into tertiles and compared to log2 expression values for genes of interest in tumor tissues from n=88 patients with basal breast cancer.

Statistical Analysis

Statistical analyses were performed using GraphPad Prism Version 7.0. Gaussian distribution was assessed using the Shapiro-Wilk normality test. Comparisons of two groups was accomplished using non-parametric Mann-Whitney U tests or parametric two-tailed unpaired t-tests as appropriate. Comparisons of three groups was accomplished using non-parametric Kruskal-Wallis tests with Dunn's multiple comparisons tests or parametric one-way ANOVAs with Tukey's or Dunnet's multiple comparisons tests as appropriate. Analysis of four groups was carried out using non-parametric Kruskal-Wallis tests or parametric one-way ANOVAs with post-hoc pairwise comparisons of group means of interest using non-parametric Mann-Whitney U tests, parametric two-tailed unpaired t-tests, or Tukey's multiple comparisons test, as appropriate. Differences in tumor growth over time were assessed using repeated measures two-way ANOVAs with Tukey's multiple comparisons test. Associations between clinical gene expression and BMI were evaluated using linear regression analyses. Statistical differences are denoted throughout as $^{*}p < 0.05$, $^{**}p < 0.01$, $^{***}p < 0.001$, $^{****}p < 0.0001$. Non-significant (ns) p values ≤ 0.15 are indicated throughout.

RESULTS

Obesity Promotes Mammary Tumor Growth and Remodeling of the Tumor Immune Microenvironment

To evaluate the impact of obesity on mammary tumor growth, we utilized two models of diet-induced obesity (DIO) wherein animals were randomized to either a standard American diet (SAD; 36% kcal from fat) or high-fat diet (HFD; 60% kcal from fat) for 16 weeks. Low-fat diet-fed (LFD; 14% kcal from fat) animals served as age-matched lean controls. SAD- and HFD-feeding led to significantly increased body weights relative to LFD-fed lean controls, with HFD-fed animals having further increases in body weights relative to SAD-fed animals (**Figure 1A**). Lean and DIO mice were then challenged with E0771 mammary tumor cells expressing firefly luciferase (E0771-fluc) and tumor growth was monitored *via* caliper measurements, bioluminescent imaging, and excised tumor weights. All methods indicated that both SAD- and HFD-induced obesity promote accelerated mammary tumor growth (**Figures 1B–D**).

We next asked how DIO impacted the composition of the tumor immune microenvironment. To this end, we evaluated the immunogenetic profile of tumors from LFD- and HFD-fed animals using nanoString to screen for genes of interest. Doing so revealed differential expression (DE) of 86 of the 730 genes surveyed (**Figure 1E** and **Supplementary Table 2**). Gene Ontology (GO) assessment of biological processes involved with downregulated genes largely identified T cell alterations, whereas upregulated genes were associated with neutrophil/granulocyte trafficking and apoptotic signaling (**Figure 1F**). Flow cytometric analysis confirmed obesity-associated reductions in CD8 tumor-infiltrating lymphocytes (TILs) and increases in myeloid-derived suppressor cells (MDSCs), a subset of which are phenotypically synonymous with tumor-associated neutrophils (**Figure 1G**). Prior studies have shown that these immunologic alterations are associated with negative clinical outcomes in patients with breast cancer, independent of obesity status (23, 24). Most notably, as body weights increased (LFD<SAD<HFD), there were corresponding increases in tumor burden and MDSC abundance, whereas CD8 TIL abundance decreased. Similar obesity-associated alterations to tumor growth and leukocyte composition were also seen in the Py8119 mammary tumor model, indicating that these results were not specific to a single tumor model (**Supplementary Figure 1**).

We next wanted to explore whether a causal relationship existed between the abundance of CD8 TILs and mammary tumor growth in LFD-fed lean and HFD-fed DIO mice. Following depletion of CD8 T cells, lean mice experienced accelerated tumor growth as expected, demonstrating the critical role of CD8 TILs in mediating antitumor immunity in the E0771-fluc tumor model (**Supplementary Figures 2A, B**). Unsurprisingly, depletion of CD8 T cells in DIO mice did not impact mammary tumor growth (**Supplementary Figure 2A**). Quantification of CD8 TILs suggested that this was likely due to the already extremely low levels of CD8 TILs present in the obese tumor microenvironment (**Supplementary Figure 2B**). Thus these data suggested that obesity-associated reductions in CD8 TIL abundance impair antitumor immunity.

Obesity Promotes CD8 TIL Hyperactivation and Apoptosis in the Mammary Tumor Microenvironment

Given that obesity was associated with reductions in total CD8 TILs, we further sought to identify potential alterations in their phenotype and mechanisms underlying their reduction. Surprisingly, the frequency of CD8 TILs with an effector phenotype increased with obesity while naive CD8 TILs decreased (**Figure 2A**). Accordingly, increases were seen in the percentages of PD-1^{+}, Ki-67^{+}, and IFNγ^{+} CD8 TILs, consistent with increased antigen engagement, proliferation, and cytokine production with obesity (**Figures 2B–D**). Notably, regardless of phenotype, total effector and naive CD8 TIL subsets and intratumoral IFNγ concentration were decreased with obesity (**Supplementary Figure 3**). Our immunogenetic profiling results indicated that obesity was associated with increased apoptotic signaling (**Figure 1F**). Thus, we next asked if obesity-associated TIL hyperactivation promoted apoptosis, causing decreased CD8 TIL abundance (**Figure 1G**). Annexin V staining revealed that obesity was indeed associated with increased percentages of apoptotic CD8 TILs (**Figure 2E**). Further, DIO animals had reduced percentages of CD8 TILs expressing antiapoptotic Bcl-2 (**Figure 2F**) and increased percentages of CD8 TILs expressing the death receptor Fas (**Figure 2G**). These results corroborated our immunogenetic profiling results (**Figures 1E, F**) and indicated that CD8 TILs were hyperactivated and poised for apoptosis with obesity.

Having established that a higher percentage of CD8 TILs from DIO animals were expressing Fas and undergoing apoptosis, we

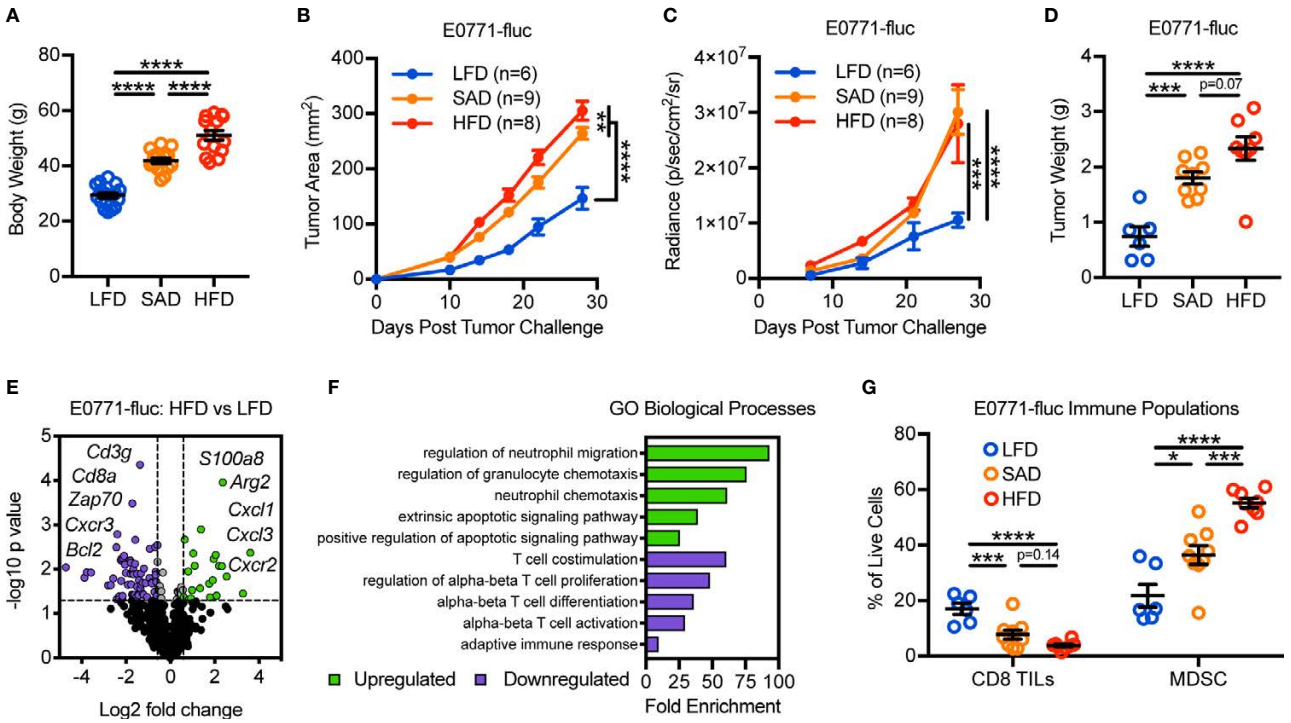

FIGURE 1 | Diet-induced obesity promotes mammary tumor growth and remodeling of the tumor immune microenvironment. **(A)** Body weight of animals 16 weeks after randomization to low-fat diet (LFD; 14% kcal from fat), standard American diet (SAD; 36% kcal from fat), or high-fat diet (HFD; 60% kcal from fat). Following diet randomization, animals were challenged with E0771-fluc mammary tumor cells and tumor growth monitored *via* **(B)** caliper measurements, **(C)** bioluminescent imaging of firefly luciferase expressing E0771 tumor cells (E0771-fluc), and **(D)** excised tumor weights. **(E)** Volcano plot showing differentially expressed (DE) genes from tumors of HFD-fed animals vs LFD-fed animals. Dotted lines indicate p = 0.05 and fold change = ±1.5. **(F)** Gene Ontology (GO) enrichment analysis for biological processes associated with downregulated (purple) and upregulated (green) DE genes from **(E)**. **(G)** Flow cytometric analysis of day 28 excised mammary tumors for $CD3^+CD8^+$ tumor-infiltrating lymphocytes and $CD11b^+Gr\text{-}1^+$ MDSCs. Data are pooled from multiple independent experiments and presented as means ± SEM. Statistical differences were calculated using parametric one-way ANOVAs or repeated measures two-way ANOVAs, both with Tukey's multiple comparisons tests (*p < 0.05, **p < 0.01, ***p < 0.001, ****p < 0.0001).

next asked what sources of FasL existed within the tumor microenvironment that could potentially promote Fas/FasL-mediated apoptosis of CD8 TILs. In both lean and DIO animals, $CD11b^+Gr\text{-}1^+$ MDSCs were the largest contributors of FasL expression (**Figure 2H**). Notably, obesity did not impact the apoptotic phenotype of splenic CD8 T cells where $FasL^+$ MDSCs were minimally abundant (**Figures 2I, J**). These results suggested that the abundance of $FasL^+$ MDSCs was associated with CD8 TIL apoptosis.

Obesity Promotes the Recruitment and Accumulation of $FasL^+$ G-MDSCs Which Induce Fas/FasL-Mediated Apoptosis of Hyperactivated CD8 TILs

We next sought to identify the mechanism(s) by which obesity promoted MDSC accumulation in murine mammary tumors. Murine MDSCs exist as two main sub-types: monocytic MDSCs (M-MDSCs) and granulocytic MDSCs (G-MDSCs). With obesity, only the G-MDSC subset was increased within tumors (**Figure 3A**). Our tumor immunogenetic profiling results revealed that obesity significantly increased the expression of *Il1b*, *Cxcl1*, *Cxcl3*, *S100a8*, and *Csf3*. These genes encode cytokines and chemokines responsible for the generation and trafficking of G-MDSCs, providing evidence for enhanced MDSC generation and chemotaxis with obesity (**Figure 3B**). Intratumoral protein concentrations of CXCL1 were further found to be elevated in the obese tumor microenvironment (**Figure 3C**). CXCL1 and CXCL3 are chemokines that promote G-MDSC chemotaxis *via* their cognate receptor CXCR2 (25). CXCR2 was highly and equivalently expressed on tumor-infiltrating G-MDSCs from both lean and obese animals (**Figure 3D**). Thus, these results suggest that obesity enhances generation and CXCL1/CXCR2-mediated G-MDSC chemotaxis.

We next asked how obesity impacted FasL expression by G-MDSCs and whether MDSCs were, in fact, responsible for CD8 TIL apoptosis. Approximately 90% of G-MDSCs from lean and DIO animals expressed FasL (**Figure 3E**). Interestingly, although the frequency of G-MDSCs expressing FasL was unchanged, the per cell expression of FasL was elevated with obesity (**Figure 3F**). We next sought to confirm that $FasL^+$ G-MDSCs could directly induce Fas/FasL-mediated apoptosis of CD8 T cells. Splenic CD8

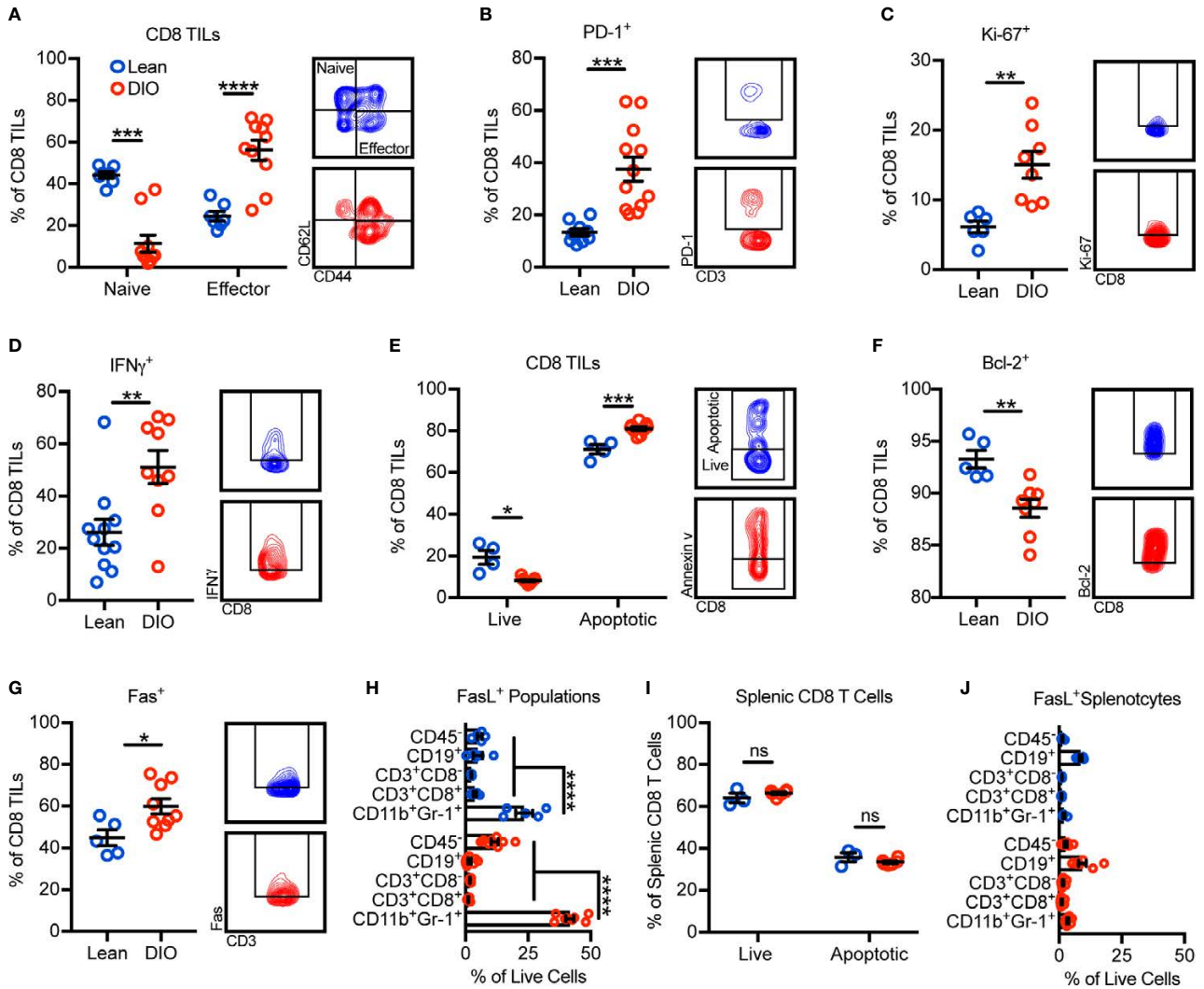

FIGURE 2 | Obesity promotes CD8 TIL hyperactivation and apoptosis in the mammary tumor microenvironment. Flow cytometric analysis of day 28 excised E0771-fluc mammary tumors for **(A)** naive ($CD44^-CD62L^+$) and effector ($CD44^+CD62L^-$) CD8 TILs. Expression of **(B)** PD-1, **(C)** Ki-67, and **(D)** IFNγ by CD8 TILs. **(E)** Quantification of live (annexin V^-) and apoptotic (annexin V^+) CD8 TILs. Expression of **(F)** Bcl-2 and **(G)** Fas by CD8 TILs. **(H)** Quantification of $FasL^+$ tumor infiltrating populations. **(I)** Quantification of live (annexin V^-) and apoptotic (annexin V^+) splenic CD8 T cells and **(J)** $FasL^+$ splenic populations. **(A–D, F)** Data are pooled from multiple independent experiments or **(E, G–J)** are from a single representative experiment and presented as means ± SEM. Statistical differences were calculated using parametric t-tests or non-parametric Mann-Whitney U tests as appropriate and parametric one-way ANOVAs with Dunnet's multiple comparisons tests (*$p < 0.05$, **$p < 0.01$, ***$p < 0.001$, ****$p < 0.0001$, ns = non-significant).

T cells were activated *in vitro* to induce expression of Fas then co-cultured with G-MDSCs sort-purified from the tumors of obese mice in the presence or absence of FasL neutralization. FasL neutralization demonstrated that G-MDSCs were not only capable of inducing CD8 T cell apoptosis, but that they did so in a largely FasL-dependent manner (**Figure 3G**). We also asked whether G-MDSC-induced CD8 TIL apoptosis occurred *in vivo*. Short-term anti-Gr-1-mediated MDSC depletion in DIO animals resulted in decreased percentages of apoptotic CD8 TILs relative to isotype-treated controls (**Figures 3H, I**). Thus, these data demonstrate that obesity promotes the recruitment and intratumoral accumulation of $FasL^+$ G-MDSCs that functionally suppress hyperactivated Fas^+ CD8 TILs *via* the induction of apoptosis.

Obesity Promotes Immunotherapy Resistance and Is Associated With G-MDSC Accumulation

Our findings that obesity negatively impacted antitumor immunity *via* enhanced G-MDSC accumulation and CD8 TIL apoptosis prompted us to ask if these changes impaired immunotherapy outcomes. Because obesity accelerates tumor growth (**Figure 1**), we first normalized tumor areas at treatment initiation so that tumor burdens were equivalent across groups

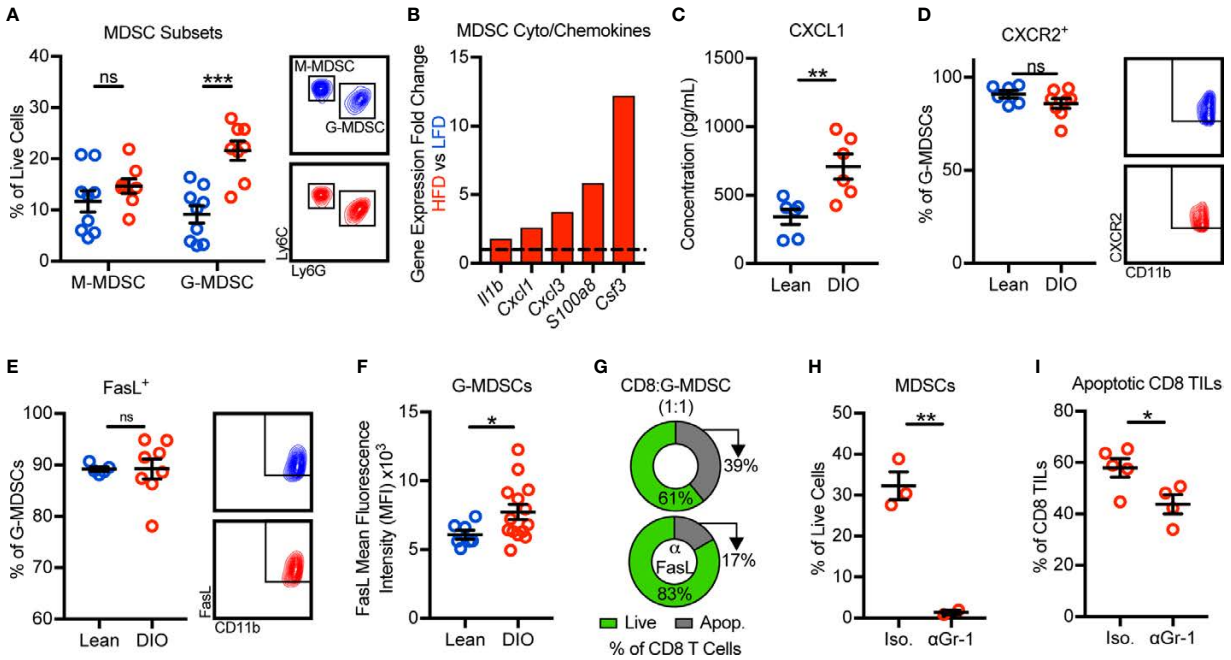

FIGURE 3 | Obesity promotes the recruitment and accumulation of FasL$^+$ granulocytic myeloid-derived suppressor cells (G-MDSCs) which induce Fas/FasL-mediated apoptosis of CD8 TILs. Flow cytometric analysis of day 28 excised E0771-fluc mammary tumors for **(A)** monocytic MDSC (M-MDSCs) (CD45$^+$CD11b$^+$CD11c$^-$I-Ab$^-$Ly6C$^+$Ly6G$^-$) and G-MDSCs (CD45$^+$CD11b$^+$CD11c$^-$I-Ab$^-$Ly6C^{low}Ly6G$^+$). **(B)** Immunogenetic gene expression fold changes of MDSC-related cyto/chemokines in the tumors of HFD- vs LFD-fed animals. **(C)** Concentration of CXCL1 in the tumor microenvironment. Percentage of G-MDSCs expressing **(D)** CXCR2 and **(E)** FasL. **(F)** FasL mean fluorescence intensity of G-MDSCs. **(G)** Percentage of live (annexin V$^-$) and apoptotic (annexin V$^+$) *in vitro* activated splenic CD8 T cells after 24 h of co-culture with sort-purified tumor-infiltrating G-MDSCs from obese mice in the (top) absence or (bottom) presence of FasL neutralizing antibody. DIO animals were treated with intratumoral anti-Gr-1 or isotype control antibody. Quantification of intratumoral **(H)** MDSCs and **(I)** apoptotic (annexin V$^+$) CD8 TILs. Data are pooled from **(A–F, I)** multiple independent experiments or are from **(G, H)** a single representative experiment and presented as means ± SEM. Statistical differences were calculated using parametric t-tests or non-parametric Mann-Whitney U tests as appropriate (*$p < 0.05$, **$p < 0.01$, ***$p < 0.001$, ns = non-significant).

and thus would not be a confounding variable in comparing outcomes in lean and DIO animals (**Figure 4A**). When tumors were 25–100 mm^2 in area, lean and DIO animals were randomized in parallel to receive an intratumoral injection of saline or immunotherapy consisting of non-replicative adenovirus (Ad) encoding murine TNF-related apoptosis inducing ligand (TRAIL; AdT) co-administered with CpG oligodeoxynucleotide 1826 (AdT+CpG) (20). AdT induces tumor cell death, increasing tumor antigen availability, while CpG induces antigen-presenting cell activation and maturation (20). Collectively this therapy promotes the priming of endogenous CD8 T cells that subsequently mediate tumor control (20). Additionally, CpG administration induces MDSCs to mature into macrophages and dendritic cells, relieving immunosuppression (26). E0771-fluc cells express both the coxsackievirus and adenovirus receptor (CAR) that permits viral binding and the TRAIL receptor (TRAIL-R2) that induces tumor cell death (**Supplementary Figure 4**). Notably, normalization of tumor burden at immunotherapy administration resulted in equivalent outgrowth of tumors in lean and DIO animals treated with saline (**Figure 4B** direct comparison not shown, p=0.30). In lean mice, AdT+CpG immunotherapy significantly delayed tumor outgrowth, whereas in DIO animals, tumor growth progressed unchecked, demonstrating immunotherapy resistance (**Figure 4B**).

To discern underlying causes of AdT+CpG immunotherapy resistance in obese mice, we examined immune responses after therapy administration. In this setting, both lean and DIO animals had statistically equivalent increases in total effector and IFNγ^+ CD8 TILs (**Figures 4C, D**). However, following therapy administration, lean mice displayed reductions in CD8 TIL apoptosis and G-MDSC accumulation, whereas neither parameter changed in DIO animals (**Figures 4E, F**). Tumor expression levels of *Cxcl1* followed a similar trend (**Figure 4G**), suggesting that G-MDSC recruitment persisted even after therapy administration in DIO mice. Therefore, although DIO mice mounted CD8 TIL responses equivalent to those of lean animals in response to immunotherapy, high levels of CD8 TIL apoptosis, G-MDSC accumulation, and *Cxcl1* expression remained, corresponding with immunotherapy resistance.

Disruption of G-MDSC Accumulation Sensitizes Obese Animals to Immunotherapy

To determine if disruption of G-MDSC accumulation would improve immunotherapy response in lean animals and overcome

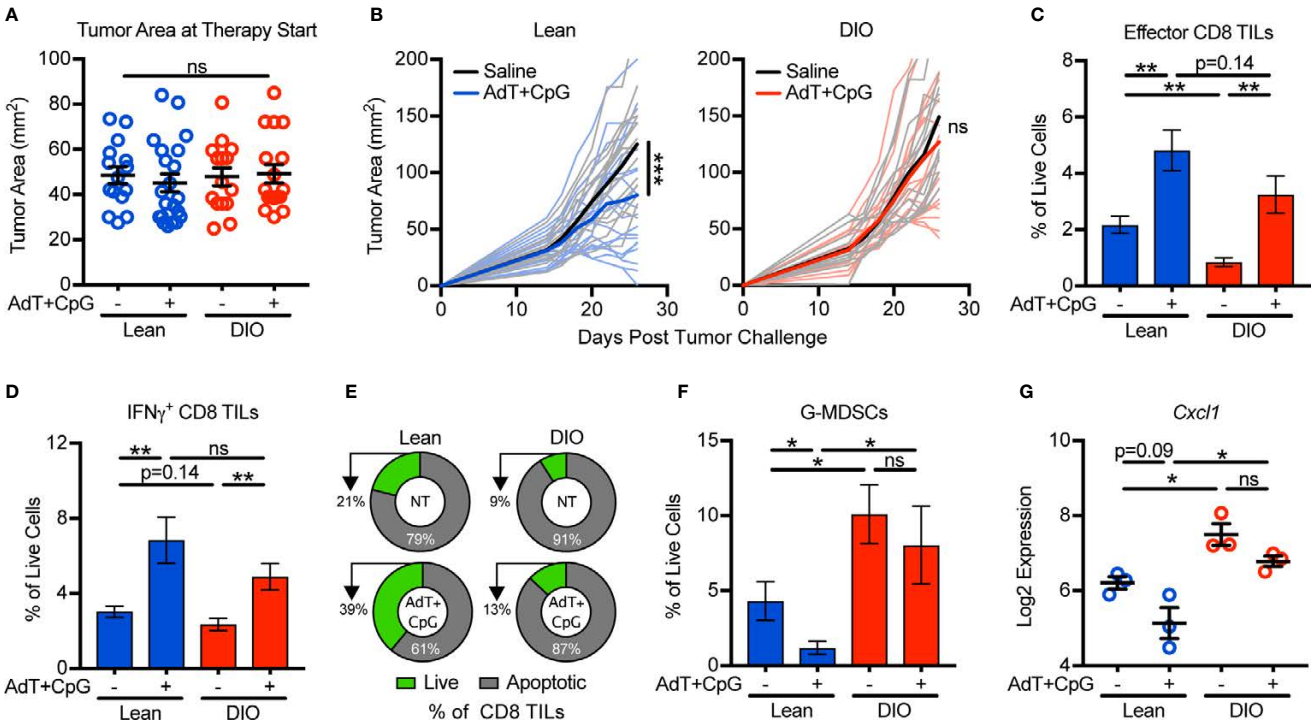

FIGURE 4 | Obesity promotes immunotherapy resistance and is associated with granulocytic myeloid-derived suppressor cell (G-MDSC) accumulation. Lean and DIO mice with established E0771-fluc tumors within a 25–100 mm^2 range were randomized to receive saline control or AdT+CpG immunotherapy. **(A)** Tumor areas at therapy initiation. **(B)** Resulting tumor growth for lean and DIO animals. Flow cytometric analysis of day 28 excised mammary tumors for **(C)** effector ($CD44^+CD62L^-$) and **(D)** $IFN\gamma^+$ CD8 TILs. **(E)** Percentage of live (annexin V^-) and apoptotic (annexin V^+) CD8 TILs. Quantification of **(F)** tumor-infiltrating G-MDSCs ($CD45^+CD11b^+CD11c^-I\text{-}Ab^-Ly6C^{low}Ly6G^+$). **(G)** Log2 expression of *Cxcl1* in the tumor microenvironment. **(A–D,F)** Data are pooled from multiple independent experiments (n=6–21 per group) or **(E)** are from single a representative experiment (n=4-9 per group) and presented as means ± SEM or **(B)** individual outgrowth is shown, with the bold line indicating mean tumor growth. Statistical differences were calculated using repeated measures two-way ANOVAs with Tukey's multiple comparison or non-parametric Kruskal-Wallis tests or parametric one-way ANOVAs with *post hoc* pairwise comparison of group means of interest using non-parametric Mann-Whitney U tests, parametric two-tailed unpaired t-tests, or Tukey's multiple comparisons tests as appropriate (*$p < 0.05$, **$p < 0.01$, ***$p < 0.001$, ns = non-significant).

immunotherapy resistance in obese animals, we targeted CXCR2, which is highly and predominantly expressed on G-MDSCs (**Figures 3D**, **5A**). Treatment of lean animals with combinatorial AdT+CpG+CXCR2 antagonist (CXCR2a) provided no benefit over that of AdT+CpG alone with regard to tumor burden or MDSC accumulation (**Figures 5B–D**). In fact, the combinatorial therapy reduced the proportion of lean animals responding to therapy (7/8 versus 4/9), indicating potential negative effects. Interestingly, no change was seen in G-MDSC accumulation with the addition of the CXCR2a, likely due to the substantial reduction caused by AdT+CpG alone.

Following therapy administration, few beneficial responses were evident in obese animals treated with the CXCR2a (1/5) or AdT+CpG (3/9) alone (**Figure 5E**). However, the combination of the CXCR2a and AdT+CpG led to substantially improved responses in the majority of animals treated (8/13) (**Figure 5E**), corresponding with significant reductions in tumor burdens (**Figure 5F**) and G-MDSC accumulation (**Figure 5G**). Thus, the combinatorial AdT+CpG+CXCR2a immunotherapy was able to reduce G-MDSC accumulation and improve immunotherapy responses, specifically in obese animals.

CXCL1 Expression in Breast Tumors Is Positively Associated With BMI, Poor Overall Survival, and a MDSC Expression Score

Last, we evaluated the clinical relevance of our findings by utilizing previously published immunogenetic and transcriptomic data from tumor tissues of patients with breast cancer. We first used linear regression analyses to evaluate the association of body mass index (BMI), a metric used to define obesity, with the expression of 730 immune-related genes. In a cohort of 68 patients with triple negative breast cancer (17) 73 of 730 total genes were found to be associated with BMI ($p<0.1$) (**Figure 6A**). Of these 73 genes, 65 were negatively associated with BMI and 8 were positively associated with BMI. These 8 genes included *CXCL1*, *S100A8*, *RELA*, *CCL20*, *CDK1*, *NOD2*, *SH2B2*, and *TANK* (**Figure 6A**). GO assessment of biological processes associated with these 8 genes revealed neutrophil/granulocyte chemotaxis/migration, corroborating immunogenetic, protein, and cellular results from our murine study (**Figure 6B**). Importantly, *CXCL1*, *S100A8*, and *NOD2* were also found to be positively associated with obesity in our murine study. Increased expression of *CXCL1* was not only

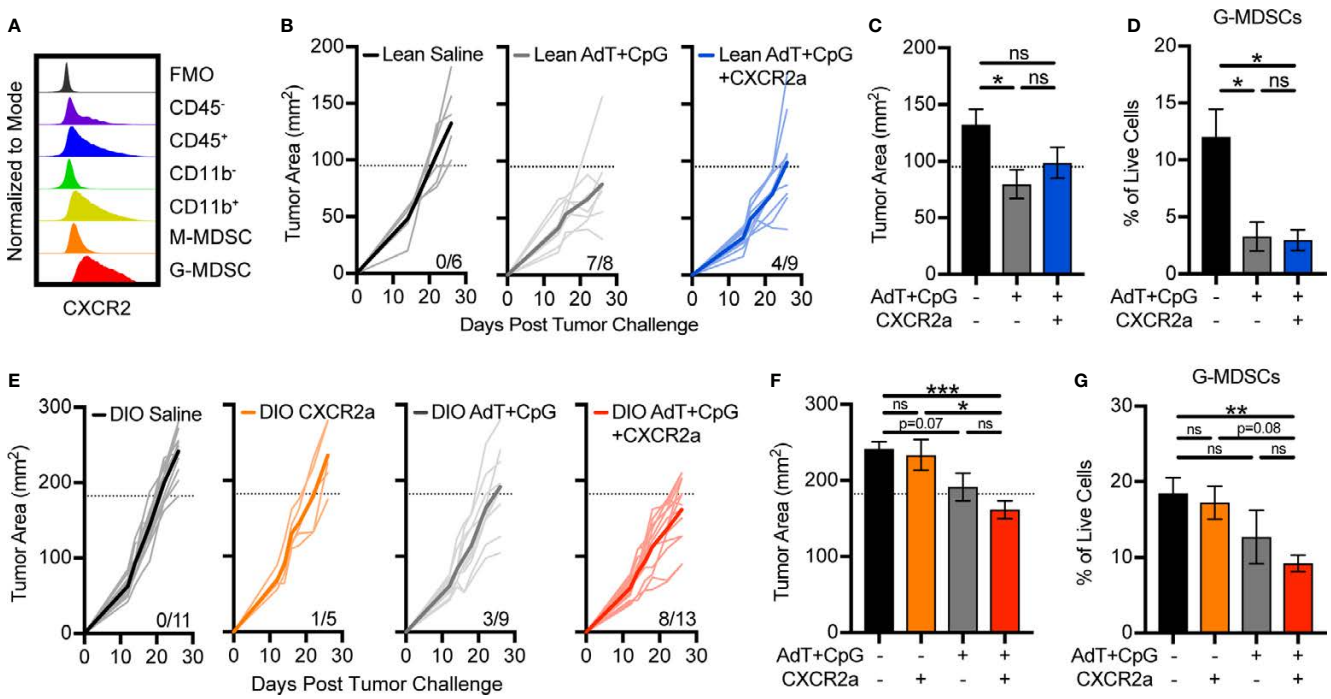

FIGURE 5 | Disruption of granulocytic myeloid-derived suppressor cells (G-MDSC) accumulation sensitizes obese animals to immunotherapy. **(A)** Representative histogram depicting intracellular expression of CXCR2 in different populations in the E0771-fluc tumor microenvironment. Lean and DIO animals bearing E0771-fluc tumors were treated with saline, CXCR2 antagonist (CXCR2a), AdT+CpG, or AdT+CpG+CXCR2a. Resulting tumor growth in **(B)** lean and **(E)** DIO animals is shown. Response thresholds are depicted by the dotted lines which indicate the lower limit of tumor growth in respective saline treated animals. Quantification of **(C, F)** endpoint tumor areas and **(D, G)** tumor-infiltrating G-MDSCs ($CD45^+$ $CD11b^+CD11c^-I\text{-}Ab^-Ly6C^{low}Ly6G^+$). Data are pooled from multiple independent experiments and presented as means ± SEM or individual outgrowth is shown, with the bold line indicating mean tumor growth. Statistical differences were calculated using parametric one-way ANOVAs with Tukey's multiple comparisons tests (*$p < 0.05$, **$p < 0.01$, ***$p < 0.001$, ns = non-significant).

found to be associated with increasing BMI (**Figure 6C**), but also decreased overall survival in a cohort of n=54 systemically untreated patients with basal breast cancer (**Figure 6D**). Analysis of transcriptomic data available from The Cancer Genome Atlas (TCGA) allowed us to quantify the relative abundance of MDSCs using a previously published multi-gene MDSC expression score (22). In breast tumor tissues from n=88 patients with basal breast cancer, *CXCL1* and *FASLG* expression were found to increase significantly as the MDSC expression score increased (**Figure 6E**). These data support the clinical relevance of our murine findings by providing evidence that the expression levels of multiple MDSC chemokines (i.e., *CXCL1* and *S100A8*) were positively associated with BMI in patients with breast cancer. High *CXCL1* expression was further associated with poor overall survival and expression-based MDSC abundance. Additionally, this MDSC score was positively associated with expression of *FASLG*.

DISCUSSION

The prevalence of obesity among adults in the US is currently approaching 40% (1) and is expected to reach 50% by 2030 (27). As many cancer patients are now being treated with immunotherapies, understanding the impact of obesity on antitumor immunity and immunotherapeutic outcomes is critical. Here, we report that, in a preclinical model of breast cancer, obesity impairs antitumor immunity and promotes immunotherapy resistance. Specifically, we have identified a novel pathway wherein obesity drives hyperactivation of and subsequent Fas expression on CD8 TILs, priming them for apoptosis. Concurrently, obesity increases intratumoral CXCL1 concentrations, promoting CXCR2-mediated accumulation of $FasL^+$ G-MDSCs, resulting in heightened Fas/FasL-mediated CD8 TIL apoptosis and immunotherapy resistance (**Figure 7**). We find evidence of this pathway in lean animals, albeit to a lesser extent (i.e. low levels of both $FasL^+$ G-MDSCs and CD8 TIL apoptosis). Thus we posit that the above mechanism is primarily operative in animals with obesity. The clinical relevance of this pathway is illustrated by our transcriptomic data showing high concordant expression of *CXCL1* with increasing BMI, poor survival, and a MDSC expression score in human breast tumors.

Our data add to a growing number of reports detailing the complex role of obesity in modulating antitumor immunity and responses to immunotherapy. Recent reports indicate that obesity not only promotes CD8 T cell dysfunction in a preclinical model of melanoma (28), but also leads to reductions in CD8 TILs in murine and human breast tumors (6). In the latter study, TIL reductions occurred in parallel with increased apoptosis of $CD45^+$ leukocytes,

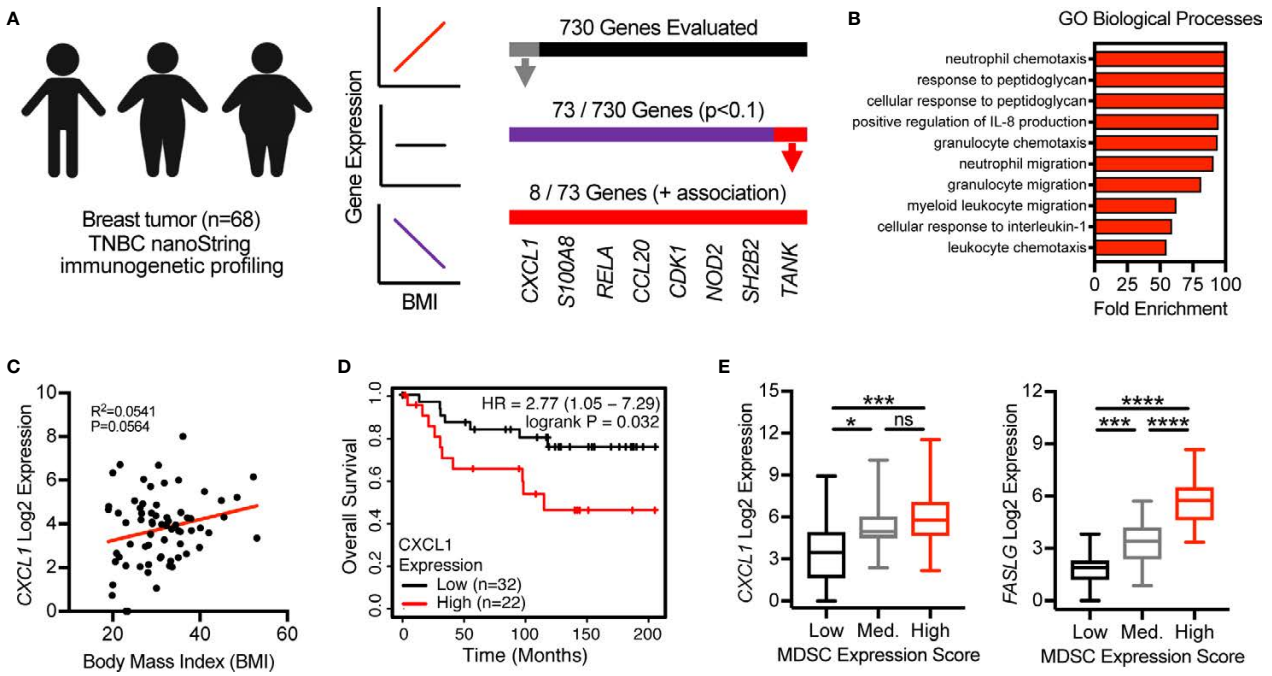

FIGURE 6 | CXCL1 expression in breast tumors is positively associated with BMI, poor overall survival, and a myeloid-derived suppressor cell (MDSC) expression score. **(A)** NanoString immunogenetic profiling of n=68 triple negative breast tumors. Of 730 genes surveyed, 73 were found to be associated (p<0.1) with body mass index (BMI). Of the 73 genes identified, 8/73 were positively associated with BMI and 65/73 were negatively associated with BMI. **(B)** Gene Ontology (GO)-identified biological processes associated with the 8 indicated genes. **(C)** Correlation between BMI and *CXCL1* expression from samples used in **(A, B)**. **(D)** Expression of *CXCL1* and overall survival in systemically untreated patients with basal breast cancer. Data were generated using KM Plotter (kmplot.com). **(E)** The Cancer Genome Atlas (TCGA)-derived transcriptomics data from breast tumor tissue of n=88 patients with basal breast cancer. Multi-gene MDSC expression score was calculated and samples were separated into low (n=20), medium (n=20), and high (n=48) tertiles. Analysis of myeloid-derived suppressor cells (MDSC) expression scores versus expression of (left) *CXCL1* and (right) *FASLG*. Data are presented as linear regression, Kaplan-Meier plots, or boxes defining 25th to 75th percentiles with line at median and whiskers extending to minimum and maximum points. Statistical differences were calculated using linear regression, log rank test, or parametric one-way ANOVAs with Tukey's multiple comparisons tests (*p < 0.05, ***p < 0.001, ****p < 0.0001).

although CD8 TIL apoptosis was not specifically examined. We add to this literature by demonstrating that obesity not only drives hyperactivation of CD8 TILs, but also predisposes them to G-MDSC-mediated apoptosis, thereby impeding antitumor immunity and immunotherapeutic efficacy (29).

Obesity and inflammation expand and mobilize MDSCs and their precursors *via* molecules such as IL-6, CRP, IL-1β, and leptin (13–16, 30), increasing their susceptibility to tumor-derived signals that further drive their recruitment and suppressive capacity. Here, we found that the expression levels of multiple mediators of MDSC development and chemotaxis, including *Cxcl1*, *Cxcl3*, *S100a8*, *Csf3* (G-CSF), and *Il1β* (31), were elevated in the tumors of DIO animals (**Figures 1E**, **3B** and **Supplementary Table 1**). These results were further supported by our clinical analyses which demonstrated positive associations between BMI and the expression of *CXCL1* and *S100A8* in human breast tumors (**Figure 6**). These data provide evidence for redundant mechanisms of MDSC recruitment to the tumor microenvironment in mice and humans with obesity, highlighting the need for further investigation of obesity-associated alterations in the soluble protein milieu of the tumor microenvironment. Here, we targeted CXCR2 for intervention in mice with mammary tumors, disrupting signals from its cognate ligands, CXCL1 and CXCL3. Although a significant therapeutic benefit was observed, chemotactic redundancy (i.e., S100A8) was likely responsible for achieving only a modest reduction in tumor burden. This redundancy may serve as a barrier for the clinical targeting of MDSCs, particularly in the context of obesity. Thus, interventions targeting MDSC generation or function, rather than chemotaxis, may be more efficacious in the clinical setting.

A recent study utilized single cell transcriptomics and the MMTV-PyMT transgenic murine model of breast cancer to identify expression signatures found in G-MDSCs versus their non-suppressive neutrophil counterparts (32). The authors identified genes, including *Arg2*, *Cxcr2*, *Il1b*, *Ifitm1*, *Socs3*, *Osm*, and *Cd14* among others, whose expression was elevated in G-MDSCs. These genes identify particular mechanisms of suppression (i.e., *Arg2*, which encodes arginase 2) and chemotaxis (i.e., *Cxcr2*) utilized by G-MDSCs (25, 33). In our study, all of the aforementioned genes were increased in expression in the tumors of obese mice (**Supplementary Table 2**). These data further support the classification of G-MDSCs in our murine model and emphasize the accumulation of G-MDSCs rather than non-suppressive neutrophils.

Recently, tumor-infiltrating MDSCs have been shown to promote immunotherapy resistance in preclinical models of

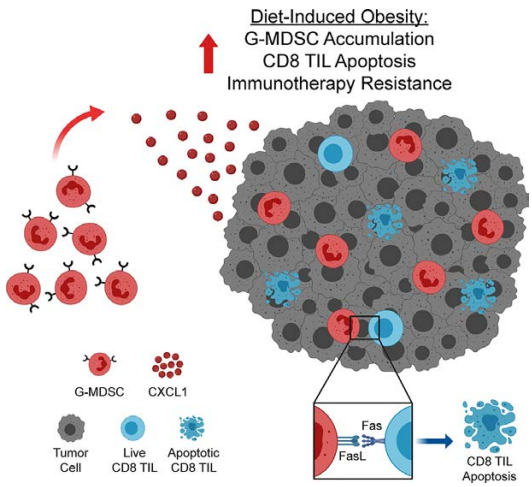

FIGURE 7 | Obesity enhances accumulation of FasL$^+$ granulocytic myeloid-derived suppressor cells (G-MDSCs), driving CD8 TIL apoptosis and immunotherapy resistance. Increased concentration of CXCL1 in the obese mammary tumor microenvironment drives CXCL1/CXCR2-mediated accumulation of FasL$^+$ G-MDSCs. FasL$^+$ G-MDSCs interact with hyperactivated Fas$^+$ CD8 TILs, driving CD8 TIL apoptosis and immunotherapy resistance. Graphic created with BioRender.com.

breast cancer and melanoma (17, 18). In studies of inducible and transplantable melanoma, MDSC-mediated immunotherapy resistance was found to occur in part through expression of FasL and subsequent Fas/FasL-mediated apoptosis of CD8 TILs (18). Here, we substantiated those findings and extended them to breast cancer, where we implicate FasL-expressing MDSCs as part of a broader pathway that links host obesity to heightened CD8 TIL apoptosis and immunotherapy resistance. We find that targeting of MDSCs is sufficient to improve immunotherapy response, although the subsequent impact on CD8 TIL dynamics was not evaluated. Obesity is an incredibly complex and multifactorial disease that elicits numerous changes to the breast tumor microenvironment (34). As such, we recognize the potential for additional known, or currently unknown, factors to contribute to our observed outcomes.

Reports indicate that elevated levels of plasma IL-6 and CRP are associated with reduced progression free and overall survival in patients with breast cancer who were treated with anti-PD-L1 immunotherapy (12). Notably, both IL-6 and CRP are elevated with obesity and modulate MDSC dynamics (15, 16). Although the impact of obesity on immunotherapy outcomes in patients with breast cancer has not yet been evaluated, the aforementioned data suggest that obesity may be associated with worse clinical outcomes in breast cancer, which may be linked to MDSC accumulation. This notion is backed by our transcriptomic analyses, which shows a positive correlation between *CXCL1* expression and BMI, poor survival, and a MDSC expression score in human breast tumor tissues (**Figure 4E**). Additional evidence for this hypothesis comes from earlier work implicating obesity in resistance to targeted and chemotherapies in patients with breast cancer (7, 8). Our preclinical findings concur with these outcomes. Conversely, a retrospective analysis of women with melanoma found that obesity did not impact outcomes to anti-PD-1/PD-L1 immunotherapy (35). As this study was retrospective, there was no evaluation of IL-6, CRP, or MDSCs, indicating areas for future prospective analyses. Thus, these data suggest obesity may be associated with worse immunotherapy outcomes in patients with breast cancer, but also that obesity may differentially impact treatment outcomes based on tumor or immunotherapy type, emphasizing the need for continued study of this critical issue.

With nearly 40% of the adult US population presenting with obesity and an additional 30% presenting with overweight (1), it is critical now more than ever that we consider co-morbidities, such as obesity and diabetes, as the new normal. This is especially needed in preclinical modeling where the use of young lean mice starkly departs from our aging and weighty cancer patient population. Forethought will allow us to more considerately and effectively develop therapeutics to treat what continues to be the increasing majority of our population.

DATA AVAILABILITY STATEMENT

The differentially expressed genes identified from the murine mammary tumor immunogenetic profiling results in this study can be found in **Supplementary Table 2**. Immunogenetic and transcriptomic profiling data from human breast tumors were obtained from a previously published manuscript (17) or TCGA and are publicly available.

ETHICS STATEMENT

All animal experiments were conducted as approved by the Animal Resources Program and Institutional Animal Care and Use Committee at the University of Alabama at Birmingham (UAB).

AUTHOR CONTRIBUTIONS

JG and LN conceptualized the study, designed experiments, and wrote the manuscript. JG managed and led the study under the supervision of LN. JG, RO, WT, and MB performed experiments and analyzed data. All authors contributed to the article and approved the submitted version.

FUNDING

Research reported in this publication was supported by the University of Alabama at Birmingham Department of Nutrition Sciences startup package to LN, Breast Cancer Research Foundation of Alabama Impact Grant to LN, NIH award #T32GM008111 to JG, NCI award #T32CA047888 to RO and MB, NCI award #T32CA183926 to WT, the Rita Allen Foundation grant

#2014701 to RS, and NIH awards #P30CA013148 and #1S10OD021697 to the UAB O'Neal Comprehensive Cancer Center Preclinical Imaging Shared Facility.

ACKNOWLEDGMENTS

The authors would like to thank the following UAB cores and facilities: nanoString laboratory, particularly Debbie Della Manna, flow cytometry core, particularly Vidya Sagar Hanumanthu and Berencia M Fore, and the O'Neal Comprehensive Cancer Center Preclinical Imaging Shared Facility. We would also like to thank Brett P. Gross for generation of the firefly luciferase expressing variant of the E0771 cell line, Dr. Francis E. Lund for use of her ab's MAGPIX Luminex plate reader, Dr. Davide Botta for running the multiplex immunoassays, and Dr. Alexander Szalai and Dr. Douglas Hurst for reading and providing feedback on the manuscript.

SUPPLEMENTARY MATERIAL

The Supplementary Material for this article can be found online at: https://www.frontiersin.org/articles/10.3389/fimmu.2020.590794/full#supplementary-material

REFERENCES

1. Hales CM, Fryar CD, Carroll MD, Freedman DS, Ogden CL. Trends in Obesity and Severe Obesity Prevalence in US Youth and Adults by Sex and Age, 2007-2008 to 2015-2016. *JAMA* (2018) 319(16):1723–5. doi: 10.1001/jama.2018.3060
2. Lauby-Secretan B, Scoccianti C, Loomis D, Grosse Y, Bianchini F, Straif K, et al. Body Fatness and Cancer–Viewpoint of the IARC Working Group. *N Engl J Med* (2016) 375(8):794–8. doi: 10.1056/NEJMsr1606602
3. Kolb R, Phan L, Borcherding N, Liu Y, Yuan F, Janowski AM, et al. Obesity-associated NLRC4 inflammasome activation drives breast cancer progression. *Nat Commun* (2016) 7:13007. doi: 10.1038/ncomms13007
4. Quail DF, Olson OC, Bhardwaj P, Walsh LA, Akkari L, Quick ML, et al. Obesity alters the lung myeloid cell landscape to enhance breast cancer metastasis through IL5 and GM-CSF. *Nat Cell Biol* (2017) 19(8):974–87. doi: 10.1038/ncb3578
5. Michelet X, Dyck L, Hogan A, Loftus RM, Duquette D, Wei K, et al. Metabolic reprogramming of natural killer cells in obesity limits antitumor responses. *Nat Immunol* (2018) 19(12):1330–40. doi: 10.1038/s41590-018-0251-7
6. Zhang C, Yue C, Herrmann A, Song J, Egelston C, Wang T, et al. STAT3 Activation-Induced Fatty Acid Oxidation in CD8(+) T Effector Cells Is Critical for Obesity-Promoted Breast Tumor Growth. *Cell Metab* (2020) 31 (1):148–61.e5. doi: 10.1016/j.cmet.2019.10.013
7. Greenlee H, Unger JM, LeBlanc M, Ramsey S, Hershman DL. Association between Body Mass Index and Cancer Survival in a Pooled Analysis of 22 Clinical Trials. *Cancer Epidemiol Biomarkers Prev* (2017) 26(1):21–9. doi: 10.1158/1055-9965.EPI-15-1336
8. Incio J, Ligibel JA, McManus DT, Suboj P, Jung K, Kawaguchi K, et al. Obesity promotes resistance to anti-VEGF therapy in breast cancer by up-regulating IL-6 and potentially FGF-2. *Sci Transl Med* (2018) 10(432):eaag0945. doi: 10.1126/scitranslmed.aag0945
9. Chan DS, Vieira AR, Aune D, Bandera EV, Greenwood DC, McTiernan A, et al. Body mass index and survival in women with breast cancer-systematic literature review and meta-analysis of 82 follow-up studies. *Ann Oncol* (2014) 25(10):1901–14. doi: 10.1093/annonc/mdu042
10. Caan BJ, Cespedes Feliciano EM, Prado CM, Alexeeff S, Kroenke CH, Bradshaw P, et al. Association of Muscle and Adiposity Measured by Computed Tomography With Survival in Patients With Nonmetastatic Breast Cancer. *JAMA Oncol* (2018) 4(6):798–804. doi: 10.1001/jamaoncol.2018.0137
11. Schmid P, Adams S, Rugo HS, Schneeweiss A, Barrios CH, Iwata H, et al. Atezolizumab and Nab-Paclitaxel in Advanced Triple-Negative Breast Cancer. *N Engl J Med* (2018) 379(22):2108–21. doi: 10.1056/NEJMoa1809615
12. Li Y, Fassò M, Emens LA, Molinero L. Abstract CT001: Biomarkers of systemic inflammation associated to reduced clinical activity of atezolizumab monotherapy in patients with metastatic triple negative breast cancer. *Cancer Res* (2019) 79(13 Supplement):CT001–CT. doi: 10.1158/1538-7445.AM2019-CT001
13. Bunt SK, Sinha P, Clements VK, Leips J, Ostrand-Rosenberg S. Inflammation induces myeloid-derived suppressor cells that facilitate tumor progression. *J Immunol* (2006) 176(1):284–90. doi: 10.4049/jimmunol.176.1.284
14. Clements VK, Long T, Long R, Figley C, Smith DMC, Ostrand-Rosenberg S. Frontline Science: High fat diet and leptin promote tumor progression by inducing myeloid-derived suppressor cells. *J Leukoc Biol* (2018) 103(3):395–407. doi: 10.1002/JLB.4HI0517-210R
15. Jimenez RV, Kuznetsova V, Connelly AN, Hel Z, Szalai AJ. C-Reactive Protein Promotes the Expansion of Myeloid Derived Cells With Suppressor Functions. *Front Immunol* (2019) 10:2183. doi: 10.3389/fimmu.2019.02183
16. Marigo I, Bosio E, Solito S, Mesa C, Fernandez A, Dolcetti L, et al. Tumor-induced tolerance and immune suppression depend on the C/EBPbeta transcription factor. *Immunity* (2010) 32(6):790–802. doi: 10.1016/j.immuni.2010.05.010
17. Kim IS, Gao Y, Welte T, Wang H, Liu J, Janghorban M, et al. Immuno-subtyping of breast cancer reveals distinct myeloid cell profiles and immunotherapy resistance mechanisms. *Nat Cell Biol* (2019) 21(9):1113–26. doi: 10.1038/s41556-019-0373-7
18. Zhu J, Powis de Tenbossche CG, Cane S, Colau D, van Baren N, Lurquin C, et al. Resistance to cancer immunotherapy mediated by apoptosis of tumor-infiltrating lymphocytes. *Nat Commun* (2017) 8(1):1404. doi: 10.1038/s41467-017-00784-1
19. Mi H, Muruganujan A, Ebert D, Huang X, Thomas PD. PANTHER version 14: more genomes, a new PANTHER GO-slim and improvements in enrichment analysis tools. *Nucleic Acids Res* (2019) 47(D1):D419–D26. doi: 10.1093/nar/gky1038
20. Norian LA, Kresowik TP, Rosevear HM, James BR, Rosean TR, Lightfoot AJ, et al. Eradication of metastatic renal cell carcinoma after adenovirus-encoded TNF-related apoptosis-inducing ligand (TRAIL)/CpG immunotherapy. *PLoS One* (2012) 7(2):e31085. doi: 10.1371/journal.pone.0031085
21. Gyorffy B, Lanczky A, Eklund AC, Denkert C, Budczies J, Li Q, et al. An online survival analysis tool to rapidly assess the effect of 22,277 genes on breast cancer prognosis using microarray data of 1,809 patients. *Breast Cancer Res Treat* (2010) 123(3):725–31. doi: 10.1007/s10549-009-0674-9
22. Wang G, Lu X, Dey P, Deng P, Wu CC, Jiang S, et al. Targeting YAP-Dependent MDSC Infiltration Impairs Tumor Progression. *Cancer Discov* (2016) 6(1):80–95. doi: 10.1158/2159-8290.CD-15-0224
23. Ali HR, Provenzano E, Dawson SJ, Blows FM, Liu B, Shah M, et al. Association between CD8+ T-cell infiltration and breast cancer survival in 12,439 patients. *Ann Oncol* (2014) 25(8):1536–43. doi: 10.1093/annonc/mdu191
24. Dominguez GA, Condamine T, Mony S, Hashimoto A, Wang F, Liu Q, et al. Selective Targeting of Myeloid-Derived Suppressor Cells in Cancer Patients Using DS-8273a, an Agonistic TRAIL-R2 Antibody. *Clin Cancer Res* (2017) 23 (12):2942–50. doi: 10.1158/1078-0432.CCR-16-1784
25. Griffith JW, Sokol CL, Luster AD. Chemokines and chemokine receptors: positioning cells for host defense and immunity. *Annu Rev Immunol* (2014) 32:659–702. doi: 10.1146/annurev-immunol-032713-120145
26. Zoglmeier C, Bauer H, Noerenberg D, Wedekind G, Bittner P, Sandholzer N, et al. CpG blocks immunosuppression by myeloid-derived suppressor cells in tumor-bearing mice. *Clin Cancer Res* (2011) 17(7):1765–75. doi: 10.1158/1078-0432.CCR-10-2672
27. Ward ZJ, Bleich SN, Cradock AL, Barrett JL, Giles CM, Flax C, et al. Projected U.S. State-Level Prevalence of Adult Obesity and Severe Obesity. *N Engl J Med* (2019) 381(25):2440–50. doi: 10.1056/NEJMsa1909301
28. Wang Z, Aguilar EG, Luna JI, Dunai C, Khuat LT, Le CT, et al. Paradoxical effects of obesity on T cell function during tumor progression and PD-1

checkpoint blockade. *Nat Med* (2019) 25(1):141–51. doi: 10.1038/s41591-018-0221-5
29. Horton BL, Williams JB, Cabanov A, Spranger S, Gajewski TF. Intratumoral CD8(+) T-cell Apoptosis Is a Major Component of T-cell Dysfunction and Impedes Antitumor Immunity. *Cancer Immunol Res* (2018) 6(1):14–24. doi: 10.1158/2326-6066.CIR-17-0249
30. Nagareddy PR, Kraakman M, Masters SL, Stirzaker RA, Gorman DJ, Grant RW, et al. Adipose tissue macrophages promote myelopoiesis and monocytosis in obesity. *Cell Metab* (2014) 19(5):821–35. doi: 10.1016/j.cmet.2014.03.029
31. Umansky V, Blattner C, Gebhardt C, Utikal J. The Role of Myeloid-Derived Suppressor Cells (MDSC) in Cancer Progression. *Vaccines (Basel)* (2016) 4 (4):36. doi: 10.3390/vaccines4040036
32. Alshetaiwi H, Pervolarakis N, McIntyre LL, Ma D, Nguyen Q, Rath JA, et al. Defining the emergence of myeloid-derived suppressor cells in breast cancer using single-cell transcriptomics. *Sci Immunol* (2020) 5(44):eaay6017. doi: 10.1126/sciimmunol.aay6017
33. Grzywa TM, Sosnowska A, Matryba P, Rydzynska Z, Jasinski M, Nowis D, et al. Myeloid Cell-Derived Arginase in Cancer Immune Response. *Front Immunol* (2020) 11:938. doi: 10.3389/fimmu.2020.00938
34. Gilbert CA, Slingerland JM. Cytokines, obesity, and cancer: new insights on mechanisms linking obesity to cancer risk and progression. *Annu Rev Med* (2013) 64:45–57. doi: 10.1146/annurev-med-121211-091527
35. McQuade JL, Daniel CR, Hess KR, Mak C, Wang DY, Rai RR, et al. Association of body-mass index and outcomes in patients with metastatic melanoma treated with targeted therapy, immunotherapy, or chemotherapy: a retrospective, multicohort analysis. *Lancet Oncol* (2018) 19(3):310–22. doi: 10.1016/S1470-2045(18)30078-0

Conflict of Interest: The authors declare that the research was conducted in the absence of any commercial or financial relationships that could be construed as a potential conflict of interest.

Copyright © 2020 Gibson, Orlandella, Turbitt, Behring, Manne, Sorge and Norian. This is an open-access article distributed under the terms of the Creative Commons Attribution License (CC BY). The use, distribution or reproduction in other forums is permitted, provided the original author(s) and the copyright owner(s) are credited and that the original publication in this journal is cited, in accordance with accepted academic practice. No use, distribution or reproduction is permitted which does not comply with these terms.

frontiers in Immunology

REVIEW
published: 16 October 2020
doi: 10.3389/fimmu.2020.603157

Emerging Blood-Based Biomarkers for Predicting Response to Checkpoint Immunotherapy in Non-Small-Cell Lung Cancer

*Shumin Li, Chengyan Zhang, Guanchao Pang and Pingli Wang**

Department of Respiratory and Critical Care Medicine, The Second Affiliated Hospital of Zhejiang University School of Medicine, Hangzhou, China

Immune checkpoint inhibitors (ICIs) have brought impressive clinical benefits in a variety of malignancies over the past years, which dramatically revolutionized the cancer treatment paradigm. Monotherapy or in combination with chemotherapy of ICIs targeting programmed death 1/programmed death ligand 1 (PD-L1) has emerged as an alternative treatment for patients with advanced non-small-cell lung cancer (NSCLC). However, constrained by primary or acquired resistance, most patients obtain limited benefits from ICIs and occasionally suffer from severe immune-related adverse events. Moreover, owing to the complexity of the tumor microenvironment and the technical limitations, clinical application of PD-L1 and tumor mutation burden as biomarkers shows many deficiencies. Thus, additional predictive biomarkers are required to further advance the precision of proper patient selection, avoiding the exposure of potential non-responders to unnecessary immunotoxicity. Nowadays, an increasing number of investigations are focusing on peripheral blood as a noninvasive alternative to tissue biopsy in predicting and monitoring treatment outcomes. Herein, we summarize the emerging blood-based biomarkers that could predict the clinical response to checkpoint immunotherapy, specifically in patients with NSCLC.

Keywords: immunotherapy, biomarker, programmed death ligand 1, liquid biopsy, non-small-cell lung cancer

OPEN ACCESS

Edited by:
Huanfa Yi,
Jilin University, China

Reviewed by:
Simon Heeke,
University of Texas MD Anderson Cancer Center, United States
Rodabe N. Amaria,
University of Texas MD Anderson Cancer Center, United States

***Correspondence:**
Pingli Wang
pingliwang@zju.edu.cn

Specialty section:
This article was submitted to Cancer Immunity and Immunotherapy, a section of the journal Frontiers in Immunology

Received: *05 September 2020*
Accepted: *30 September 2020*
Published: *16 October 2020*

Citation:
Li S, Zhang C, Pang G and Wang P (2020) Emerging Blood-Based Biomarkers for Predicting Response to Checkpoint Immunotherapy in Non-Small-Cell Lung Cancer. Front. Immunol. 11:603157. doi: 10.3389/fimmu.2020.603157

INTRODUCTION

Immunotherapy has revolutionized the strategy for the treatment of cancer and it aims to activate the immune system to identify and destroy cancer cells. Patients with multiple malignancies, such as melanoma, renal carcinoma, and lung cancer, significantly benefit from immune checkpoint inhibitors (ICIs) (1). Regardless of their use as first- or second-line treatment, ample evidence from several clinical trials demonstrated that ICIs are superior to platinum-based chemotherapy in the treatment of advanced non-small-cell lung cancer (NSCLC) (2–5). Unfortunately, only approximately 20%–40% of patients with advanced NSCLC obtained durable clinical benefits from anti-programmed death (ligand) 1 [anti-PD-(L)1] therapies (2–5). In other words, in most cases, patients have primary or acquired resistance to checkpoint immunotherapy (6, 7). Additionally, non-responders not only suffer from risk of severe immune-related adverse events,

but also meaninglessly afford the high cost of anti-PD-(L)1 drug. Therefore, early identification of potential responders versus non-responders is of great clinical significance. In recent years, research studies aim to identify appropriate biomarkers that could stratify patients into potential responders and non-responders prior to the initiation of immunotherapy, as well as monitor clinical response in real time during treatment.

In clinical practice, PD-L1 expression assessed by immunohistochemistry on tumor samples obtained through biopsy is the most extensively used predictive biomarker. It is approved by the Food and Drug Administration as a companion or complementary diagnostic assay for the administration of ICIs in patients with NSCLC (8). Across multiple clinical trials performed in advanced NSCLC patients treated with anti-PD-(L)1 antibody, high pretreatment PD-L1 expression corresponded to superior clinical outcomes. However, the application of tumor PD-L1 expression as a predictive biomarker remains defective and controversial, as numerous patients with PD-L1-negative tumors may also respond to anti-PD-(L)1 therapy. Furthermore, immunohistochemistry analysis of PD-L1 expression remains technically and biologically limited, namely due to the existence of intra-tumoral heterogeneity, different expression levels between primary and metastatic lesions, and a lack of standardization in the detection antibodies and scoring systems (9, 10). Moreover, archival tissue specimens collected in the past may not reflect current PD-L1 expression levels (11), particularly in patients receiving chemotherapy, radiotherapy, or anti-angiogenic therapy after biopsy (12, 13).

Beyond PD-L1 expression, tumor mutation burden (TMB) was also included into the National Comprehensive Cancer Network guidelines recently as an emerging predictor of response to ICIs. TMB is the total number of non-synonymous somatic mutations per megabase in the coding region of the cancer genome (14). In previous clinical studies conducted in patients with NSCLC, TMB showed value in identifying responders to ICIs, with data supporting that higher TMB values correlated with improved progression-free survival (PFS), superior overall response rate (ORR), and better durable clinical benefits. For example, the Checkmate-227 and Checkmate-568 studies demonstrated that TMB ≥ 10 muts/Mb could predict clinical benefits of nivolumab plus ipilimumab in patients with NSCLC, regardless of PD-L1 expression (15, 16). However, the latest data from the Keynote-021 and Keynote-189 studies yielded inconsistent evidence, indicating that the predictive value of TMB in combined immunotherapy is uncertain (17–19). Similar with PD-L1 expression, TMB is also characterized by a few limitations, such as the high cost of whole-exome sequencing, long result turnaround time, and complicated analytical process. Moreover, techniques used to evaluate TMB level are not standardized, and the predictive threshold differ widely across next-generation sequencing platforms. In addition, multiple preanalytical and analytical factors, such as sample collection, fixation methodology, and sequencing depth, may influence the TMB value (20).

Tissue samples are required to detect the aforementioned biomarkers, while tumor biopsy is invasive, occasionally infeasible, and cannot be repeatedly performed to monitor early disease response in most patients. Furthermore, biopsy specimens are difficult to accurately reflect the overall condition of the tumor due to the existence of intra-tumoral heterogeneity (21). Hence, currently approved tissue biomarkers are characterized by these practical limitations. In contrast, peripheral blood is a non-invasive, low-risk, and convenient source for repetitive sampling. Therefore, researchers show increasing interest in developing blood-based biomarkers for patient selection and treatment monitoring. Furthermore, peripheral blood could provide a holistic insight into the host immune status, which is one of the decisive factors for the efficacy of cancer immunotherapy (22). Numerous studies have explored the potential blood-based predictors of response to anti-PD-(L)1 therapy, such as circulating immune cells, circulating tumor cells (CTCs), and cytokines. In this systematic review, we summarize the findings of recent studies utilizing various components of peripheral blood to predict the efficacy of anti-PD-(L)1 therapy in patients with NSCLC.

ROUTINE PERIPHERAL BLOOD BIOMARKERS

Owing to the easy accessibility and low cost, numerous studies have investigated the predictive value of blood routine parameters in tumor immunotherapy. In multivariable analysis of NSCLC patients treated with nivolumab, the baseline absolute lymphocyte count ≥ 1,000/μl and absolute neutrophil count (ANC) ≤ 7,500/μl were significantly and independently correlated with both prolonged PFS [hazard ratio (HR) = 0.55, p = 0.04 and HR = 3.97, p = 0.001, respectively] and better overall survival (OS) (HR = 0.36, p = 0.03 and HR = 3.46, p = 0.03, respectively) (23). However, another study observed that a high absolute lymphocyte count did not correspond to favorable OS after anti-PD-1 treatment; meanwhile, an increased ANC only correlated with shorter OS (HR = 1.86, p = 0.02) (24). These data suggested that the absolute lymphocyte count or ANC alone cannot adequately predict clinical outcomes and efficacy of response to checkpoint immunotherapy in patients with NSCLC.

An elevated neutrophil-to-lymphocyte ratio (NLR) indicates the chronic inflammation status, which could be used to reflect the immune status of patients with different malignancies (25). In this regard, several studies investigated the negative prognostic value of high NLR in NSCLC patients receiving immunotherapy. Bagley et al. reported that NLR ≥ 5 at baseline was significantly correlated with worse OS (HR = 2.07, p = 0.002) and PFS (HR = 1.43, p = 0.04) (26). Subsequently, data from Suh et al. also supported that NLR ≥ 5 at 6 weeks post anti-PD-1 treatment was associated with poor PFS (HR = 15.09, p < 0.001) and OS (HR = 3.82, p = 0.003) (27). Furthermore, Cao et al. carried out a meta-analysis including 14 retrospective studies with 1,225 NSCLC patients treated with nivolumab, further confirming that a baseline NLR ≥ 5 was associated with inferior PFS (HR = 1.73, p < 0.05) and OS (HR = 1.76, p < 0.05) (28).

Researchers proposed that the derived NLR [dNLR, ANC/(white blood cell−ANC)] may be more relevant to clinical outcomes than the NLR, as the former also takes monocytes and other granulocyte subpopulations into account. In advanced NSCLC patients treated with anti-PD-(L)1 therapy, an association between baseline dNLR > 3 and shorter OS was revealed (HR = 1.70, p < 0.001). In addition, baseline dNLR together with lactate dehydrogenase (LDH) constituted a lung immune prognostic index, which effectively distinguished three groups of patients with different survival outcomes (median OS: 16.5 vs. 10 vs. 4.8 months; p < 0.01) (29). In another study, the advanced lung cancer inflammation index (ALI) was calculated as body mass index × albumin/NLR, and high systemic inflammation was suspected in patients with a low ALI score. Multivariate analyses indicated that pretreatment ALI < 18 was independently related to poor PFS and higher risk of early progression [odds ratio (OR) = 2.76, p = 0.002] in NSCLC patients receiving nivolumab (30).

Investigation of the absolute eosinophil count, absolute monocytic count, platelet-to-lymphocyte ratio, and lymphocyte-to-monocyte ratio as predictors of response to ICIs also attracted considerable interest over the past years. Clinical studies showed that pretreatment absolute eosinophil count ≥ 150/μl and absolute monocytic count ≥ 630/μl negatively impact PFS (HR = 0.53, p = 0.02 and HR = 1.50, p = 0.02, respectively) in NSCLC patients treated with anti-PD-1 agent (23, 24). In addition, platelet-to-lymphocyte ratio ≥ 169 at 6 weeks correlated with longer OS (HR = 1.56, p = 0.002) (27). Except for the aforementioned parameters, Sekine and colleagues proposed and validated that an increased lymphocyte-to-monocyte ratio was significantly associated with higher ORR (50.0% vs. 20.0%; p = 0.015) and prolonged PFS (not reached vs. 3.1 months; p = 0.0092) (31). Early changes in lymphocyte-to-monocyte ratio could be further explored as an effective marker to evaluate whether anti-PD-1 therapy should be continued.

Finally, several exploratory studies provided a clue that baseline level of serum LDH may contribute to the identification of patients with NSCLC gaining better survival benefits from immunotherapy. Researchers evaluated the LDH level in 94 NSCLC patients treated with ICIs, and discovered that baseline LDH < 400 was related to improved OS (HR = 0.45, p = 0.01) (32). Further studies involving large-scale prospective cohorts may facilitate the progress in confirming the function of elevated LDH in NSCLC and its potential value in predicting efficacy.

CIRCULATING IMMUNE CELL SUBSETS

Dynamic Changes in T Lymphocytes

Continuous advancements in the application of high-throughput technologies in multi-parametric flow cytometry, single-cell sequencing, and mass cytometry (CyTOF) make it possible to monitor the dynamic changes in different circulating immune cell subtypes from peripheral blood collected during cancer immunotherapy. Previous studies have provided evidence that utilizing the positive surface expression of PD-1 enables the identification of tumor-specific T cells in multiple malignancies, and PD-1^+ $CD8^+$ T cells could also be detected in peripheral blood (33–35). The proliferation response of circulating PD-1^+ $CD8^+$ T cells is more likely to be tumor-specific, as non-tumor-specific $CD8^+$ T cells do not present an increase in the frequency of Ki-67^+ cells after immunotherapy (36, 37). In this regard, researchers speculated that the anti-tumor cytotoxicity of T cells infiltrated in the tumor microenvironment could be reflected by the reinvigoration status of circulating PD-1^+ $CD8^+$ T cells during anti-PD-(L)1 immunotherapy. Moreover, circulating PD-1^+ $CD8^+$ T cells may be an important determinant of response to ICIs.

Several research studies have paid more attention to the predictive value of the proliferation response of circulating PD-1^+ $CD8^+$ T cells. Huang et al. analyzed the clonal overlap between tumor-infiltrating $CD8^+$ T cells and circulating $CD8^+$ T cells in melanoma patients receiving PD-1-targeted immunotherapy with pembrolizumab. The results showed that top-ranked $CD8^+$ T-cell clones in peripheral blood are also present in tumor tissues, all of which were $CD38^+$ HLA-DR^+ and mostly Ki-67^+ PD-1^+ (38). The frequency of Ki-67^+ cells among PD-1^+ $CD8^+$ T cells 3 weeks post treatment/baseline tumor burden (Ki-67/TB) ratio was applied to predict the clinical efficacy. They found that Ki-67/TB ratio > 1.94 was correlated with increased ORR (p = 0.03), prolonged PFS (p = 0.03), and OS (p = 0.004) in the discovery cohort. However, data from the validation cohort did not show strong association between the Ki-67/TB ratio and survival outcomes (38). Subsequently, Kamphorst et al. observed that the proliferation of peripheral PD-1^+ $CD8^+$ T cells within 4 weeks of anti-PD-(L)1 therapy in patients with NSCLC was associated with good clinical response (37). These proliferating $CD8^+$ T cells presented an effector-like phenotype (HLA-DR^+ $CD38^+$ BCL-2^{low}) and exhibited increased expression of positive costimulatory molecule CD28, suggesting a vital role in response to anti-PD-(L)1 therapy (37). Similarly, results from Kim et al. supported the idea that early proliferation of peripheral PD-1^+ $CD8^+$ T cells could predict response to anti-PD-1 therapy. Fold changes in the frequency of Ki-67^+ cells among PD-1^+ $CD8^+$ T cells 7 days after treatment (Ki-$67_{D7/D0}$) were used to evaluate the rate of early proliferation in three independent cohorts. In the validation NSCLC cohort, a Ki-$67_{D7/D0}$ ≥ 2.8 was closely associated with superior durable clinical benefits (p = 0.001), as well as prolonged PFS (p = 0.002) and OS (p = 0.037) (36). Moreover, this study also indicated that Ki-$67_{D7/D0}$ was more reliable in predicting non-responders, as its negative predictive value ranged 85%–94%. Taken together, the above independent studies highlighted the predictive value of circulating Ki-67^+ PD-1^+ $CD8^+$ T cells. Hence, monitoring this T-cell subpopulation during treatment may provide informative data on outcomes. However, further studies are warranted to confirm their practicality as predictors of efficacy.

Conversely, Simoni et al. demonstrated that PD-1 was also expressed on the surface of non-tumor-specific bystander tumor-infiltrating $CD8^+$ T cells, and CD39 could be a more straightforward marker for distinguishing tumor-specific

T cells (39). The expansion of the circulating $CD39^+$ T-cell subpopulation might be an early sign of cytotoxic anti-tumor-specific responses and could be exploited for the development of promising biomarkers. In addition to $CD8^+$ T cells, $CD4^+$ T cells also play an important role in determining the efficacy of anti-PD-(L)1 therapy. A recent study, which included NSCLC and renal cell carcinoma patients receiving nivolumab and pembrolizumab, indicated that the differential peripheral change between responders and non-responders was observed in the TIM-3^+ T-cell subset. The increase in the frequency of TIM-3^+ cells either among $CD4^+$ T cells or $CD8^+$ T cells was independently correlated with lower PFS (12-month PFS: 0% vs. 81.5%; $p < 0.001$ and 20.8% vs. 85.7%; $p = 0.002$, respectively) (40). Noteworthy, this study was limited by its small sample size, and its main methodological weakness was that blood was collected only 12 weeks after treatment. Further studies are necessary to evaluate these blood parameters at earlier sampling time points.

Baseline Level of T Lymphocytes

Compared with dynamic biomarkers, the advantage of baseline biomarkers is that they can help predict the response to immunotherapy before the initiation of treatment. Whereas the therapeutic response displays features of a critical state transition involving complex immunological processes; therefore, it is notoriously difficult to predict the response far in advance (41–43). Despite these limitations of static biomarkers, researchers have consistently explored the potential value of baseline immune cells as predictive biomarkers in patients treated with anti-PD-(L)1 agent.

Manjarrez-Orduno et al. discovered that melanoma and non-squamous NSCLC patients with increased transcription of inflammatory genes in tumor tissues always presented a high central memory T cell to effector T cell ratio in peripheral blood. In NSCLC patients treated with nivolumab, a high central memory/effector T cell ratio showed a strong correlation with higher tumor PD-L1 expression and prolonged PFS (91 vs. 215 days) (44). The existence of terminally differentiated T cells might explain this un-expected inverse correlation between the number of effector T cells and response to ICIs. These results are concordant with another contemporaneous research study performed in patients with melanoma, which demonstrated that peripheral blood mononuclear cells (PBMCs) obtained from responders exhibited lower frequencies of effector memory $CD4^+$ T cells and naïve $CD8^+$ T cells, and higher frequencies of central memory $CD8^+$ T cells (45). Additionally, Kim and colleagues found that lower frequency of effector memory ($CCR7^-$ $CD45RA^-$) $CD8^+$ T cells and a higher frequency of severely exhausted population ($TIGIT^+$ cells among PD-1^+ $CD8^+$ T cells) at baseline were associated with inferior clinical outcomes and increased risk of hyperprogression disease (HPD) (46). The advantage of this study was the analysis of HPD data from a large population of patients with NSCLC. Prospective validation of these biomarkers in the future will properly guide the selection of patients who will obtain clinical benefits from anti-PD-(L)1 therapy.

Several studies claimed that clinical response to anti-PD-(L)1 therapy requires the existence of functional systemic CD4 immunity. Zuazo et al. reported that NSCLC patients with a higher proportion of highly differentiated ($CD27^-$ $CD28^-$) $CD4^+$ T cells are more prone to superior clinical outcomes (47). Further analysis revealed that these highly differentiated $CD4^+$ T cells were mainly composed of non-exhausted memory ($CD45RA^-$ $CD62L^{+/-}$) CD4 cells, which significantly affect T cell proliferation response during immunotherapy (47). Subsequently, this research team conducted a prospective study in 70 NSCLC patients treated with ICIs, indicating that HPD was closely associated with dysfunctional CD4 immunity and an increased number of peripheral $CD28^-$ $CD4^+$ T cells (48). Julia et al. also highlighted the importance of functional CD4 T cell immunity for anti-tumor response, and they observed higher baseline proportion of central memory $CD4^+$ T cells in responders (40). Closely consistent with these studies, Kagamu et al. reported that patients showing response to nivolumab generally presented a higher frequency of $CD62L^{low}$ $CD4^+$ T cells ($p < 0.0001$) at baseline. In contrast, $CCR7^-$ $CD4^+$ T cells did not show a significant difference between responders and non-responders (49). Furthermore, CyTOF analysis revealed that the majority of $CD62L^{low}$ $CD4^+$ T cells corresponded to double-negative $CD27^-$ $CD28^-$ T cells, and was significantly correlated with the classical Th1 ($CXCR3^+$ $CCR4^-$ $CCR6^-$) subpopulation ($p < 0.0001$) (49). Regretfully, the sample size of these studies was relatively small, and the concluded potential biomarkers remain to be further investigated.

Regulatory T (Treg) cells constitute a special immunosuppressive subset, which could promote immunosuppression and tolerance in patients with tumor. It has been speculated that a low percentage of Treg cells might contribute to the efficacy of ICI therapy. However, researchers found that the frequency of $CD127^-$ $CD25^+$ Treg cells did not show a significant difference between responders and non-responders, either at baseline or post-treatment (45). These results agree well with the observation of Huang et al. that there was no significant correlation between Ki-67^+ proliferating Treg cells and clinical outcomes (38). Consistent with the initial hypothesis, Kagamu et al. reported that the baseline proportion of $CD25^+$ $FOXP3^+$ cells among total $CD4^+$ T cells was significantly higher in non-responders ($p = 0.034$) (49). Based on the ratio of $CD62L^{low}$ T cells to $CD25^+$ $FOXP3^+$ $CD4^+$ T cells, they further developed a formula for the prediction of non-responders with 85.7% sensitivity and 100% specificity (49). In contrast, several studies found that higher Treg cell counts at baseline was associated with better prognosis in patients receiving anti-PD-(L)1 therapy (50, 51). Researchers evaluated the frequency of lectin-type oxidized LDL receptor 1 (LOX-1^+) polymorphonuclear myeloid-derived suppressor cells (PMN-MDSCs) in NSCLC patients treated with nivolumab. They demonstrated that the ratio of Treg cells to PMN-MDSCs could predict clinical outcomes in both discovery and validation cohorts (51). These findings warrant further validation in large cohort studies, and novel strategies should be devised to detect the varying immunosuppressive activity of Treg cells in individual patients. Future exploration of Treg cells as a predictive biomarker should consider the differences in the

immunosuppressive function of Treg cells, rather than focusing merely on the Treg cell count.

T Cell Receptor Repertoire

Activation of the host immune system against cancer cells requires the recognition of neoantigen peptides by clonally proliferating T cell receptors (TCRs) (52). The clonality and diversity of TCRs can be assessed by deep sequencing of the complementary-determinant region 3, which depends on the random variable-(diversity)-joining recombination (53). Studies in various tumors have investigated whether peripheral TCR repertoire analysis could serve as a predictive biomarker of response to immunotherapy (54–58). However, the predictive value of the peripheral TCR repertoire remains controversial, likely because the existence of non-tumor-specific TCRs in PBMCs diluted tumor neoantigen-specific TCRs (59).

Several studies confirmed the observation that exhausted neoantigen-specific T cells can be reinvigorated by ICIs, and their subsequent clonal expansion was associated with the anti-tumor immune response (60, 61). In addition, numerous studies have indicated that the PD-1^+ $CD8^+$ phenotype represents an exhausted T cell subset, and it could be exploited to monitor dynamic changes in neoantigen-specific cytotoxic T cells in multiple malignancies (33–35). Recently, Han et al. collected PBMCs from NSCLC patients treated with ICIs, and specifically investigated the TCR repertoire in PD-1^+ $CD8^+$ exhausted T cells. Patients with higher pretreatment TCR diversity and increased post-treatment TCR clonality in sorted peripheral PD-1^+ $CD8^+$ T cells, were more likely to obtain superior survival outcomes (62). This study is of great significance as it marks the first attempt to evaluate the TCR repertoire specifically in PD-1^+ $CD8^+$ exhausted T cells instead of total T cells. In addition, the independent validation study also enhances the credibility of these conclusions. Overall, more evidence is needed before utilizing the TCR repertoire as a predictive biomarker for immunotherapy in clinical practice.

MDSCs

MDSCs are groups of highly heterogeneous cells derived from immature myeloid progenitors with potent immunosuppressive properties (63). According to morphological characteristics and phenotypic analysis, human MDSCs are usually divided into PMN-MDSCs and monocytic MDSCs (M-MDSCs). In human peripheral blood, $CD11b^+$ $CD14^-$ $CD15^+$ or $CD66b^+$ are generally used to characterize PMN-MDSCs, while $CD11b^+$ HLA-$DR^{-/low}$ $CD14^+$ $CD15^-$ cells are equivalent to M-MDSCs (64). It is generally believed that PMN-MDSCs can be separated from peripheral blood by standard Ficoll density gradient centrifugation. However, a recent study suggested that PMN-MDSCs and activated $CD15^+$ neutrophils without suppressive activity can simultaneously appear in PBMC layer after Ficoll gradient separation (65). Fortunately, a study reported that LOX-1 was specifically expressed on immunosuppressive PMN-MDSCs, but not on neutrophils in peripheral blood (66). Thus, the combination of gradient centrifugation with LOX-1 expression helps distinguish circulating PMN-MDSCs from neutrophils in patients with cancer.

MDSCs participate in the regulation of anti-tumor immunity through various immunosuppressive mechanisms, such as inducing nitric oxide synthase and arginase (67), producing reactive oxygen species (68), increasing Treg cells (69) and directly inhibiting the proliferation of T lymphocytes (70). Based on the immunosuppressive functions of MDSCs, several studies explored the specific role of MDSCs in predicting clinical efficacy of PD-1-targeting antibody in patients with NSCLC. A study performed in such patients reported that, after the first dose of nivolumab, the proportion of LOX-1^+ PMN-MDSCs was significantly higher in non-responders than responders (51). Patients with a higher post-treatment Treg cells to LOX-1^+ PMN-MDSCs ratio showed superior PFS in both discovery and validation cohorts (51). Another study analyzed blood immune parameters in patients with metastatic NSCLC before and during treatment of nivolumab. They noted that high expression of TIM-3 on lymphoid cells and early accumulation of (Lin^- $CD33^+$ $CD14^+$ $CD15^-$ HLA-DR^-) M-MDSC associate with resistance to PD-1 blockade. Moreover, TIM-3^+ lymphoid cells and galectin-9 positive M-MDSC impeded the secretion ability of $CD8^+$ T cells and reduced the efficacy of PD-1-targeting antibody (71). Passaro et al. reported that NSCLC patients with high baseline level of PMN-MDSCs and a low CD8 to PMN-MDSC ratio had significantly improved response to immunotherapy ($p = 0.02$) (72).

These findings suggest that MDSCs have potential in predicting response to anti-PD-(L)1 therapy in patients with NSCLC. However, the underlying mechanisms and interactions involved in this process still require further investigation. Besides, unlike other immunosuppressive cells, various MDSC subsets lack uniform definitions, and the results are inconsistent in different studies. Therefore, more prospective studies yielding solid and definitive evidence are required prior to applying these findings for the guidance of clinical decision.

Monocytes and Natural Killer Cells

Besides T cells and MDSCs, researchers using high-dimensional CyTOF and bioinformatics analysis deeply characterized the peripheral immune cell subsets of melanoma patients treated with immunotherapy. Krieg et al. described that baseline classical monocytes ($CD14^+$ $CD16^-$ HLA-DR^{hi}) was a promising immune predictor of response. The results from the independent validation cohort using conventional flow cytometry also confirmed that classical monocytes may aid in guiding treatment decisions (45). However, to date, there are no study investigating whether circulating monocytes could serve as a predictor of response in NSCLC patients treated with anti-PD-(L)1 therapy.

Regarding natural killer (NK) cells, several studies explored the potential relationship between circulating NK cells and response to ICIs. In NSCLC patients treated with ICIs, Cho et al. discovered that the overall activity of NK cells and their count were significantly higher in responders compared with non-responders (73). However, this preliminary study included only nine patients; thus, a large-scale study will be needed in the future to confirm these results. In patients with NSCLC, Mazzaschi et al. observed that the absolute number of circulating $CD56^+$ NK cells at baseline resulted in a two-fold higher change in responders compared with non-responders ($p < 0.01$). During the

administration of nivolumab, the circulating NK cell count progressively increased in responders, while remained stable or slightly decreased in non-responders (74). Conversely, Ottonello et al. recently reported that a relatively high frequency of baseline NK cells was closely related to poor OS and PFS in NSCLC patients treated with nivolumab (75). These results indicate that the specific function of NK cells in immunotherapy and their potential as biomarkers for predicting response to ICIs require further investigation.

These findings emphasized to the importance of the peripheral immune status in predicting response to anti-PD-(L)1 therapy. Nevertheless, all these divergent investigational biomarkers require further confirmation by prospectively designed studies with large cohorts. We summarized the studies exploring peripheral immune cells as predictive biomarkers of response to ICIs in patients with NSCLC (**Table 1**).

CTCs

CTCs derived from the primary tumor and/or metastatic lesion are dispersed into the bloodstream *via* intravasation, reflecting the genetic and epigenetic variations in tumor tissue. Expression of PD-L1 on CTCs has been extensively demonstrated, and CTCs have emerged as a readily obtainable source for the evaluation of tumor evolution (76–79). According to the available data, PD-L1 expression on NSCLC-derived CTCs and the concordance rate of PD-L1 expression between CTCs and tumor tissue vary markedly in different studies (78, 80, 81). Nonetheless, multiple studies have demonstrated the prognostic value of CTCs in patients with NSCLC, and these studies indicated that dynamic changes in the number of PD-L1$^+$ CTCs may help monitor response to treatment (82–85).

Several studies evaluated the expression of PD-L1 on NSCLC-derived CTCs to investigate its predictive value of selecting patients for immunotherapy. Firstly, Nicolazzo et al. longitudinally evaluated the presence of PD-L1$^+$ CTCs in metastatic NSCLC patients treated with nivolumab. They found that, after 6 months of treatment, all patients with PD-L1$^+$ CTCs experienced disease progression (76). Subsequently, Guibert and colleagues evaluated the expression of PD-L1 on CTCs among 96 patients with NSCLC at the initiation of treatment and time of progression. CTCs were detected in baseline blood samples in 93% of patients, and 83% of those expressed PD-L1 on ≥ 1% of CTCs. In terms of clinical outcomes, responders had lower baseline CTC counts ($p < 0.0001$) compared with non-responders. A high number of CTCs at baseline (> 30/7.5 ml) was significantly associated with worse clinical outcomes

TABLE 1 | Investigational peripheral immune cell biomarkers of response to ICIs in NSCLC.

Biomarker	Cancer type	No. of patients	Peripheral findings associated with clinical response	Reference
Ki-67$^+$ PD-1$^+$ CD8$^+$ T cells	NSCLC	29	Increased proliferative response in PD-1$^+$ CD8$^+$ T cells within 4 weeks of treatment associated with PR or SD	Kamphorst et al. (37)
Ki-67$_{D7/D0}$	NSCLC TET	79 31	Higher fold change of proliferative response in PD-1$^+$ CD8$^+$ T cells at first-week of treatment associated with DCB and prolonged PFS	Kim et al. (36)
TIM-3$^+$ CD4/CD8$^+$ T cells	NSCLC RCC	18 7	Increased frequency of TIM-3$^+$ cells among CD4$^+$ or CD8$^+$ T cells correlated with poor PFS	Julia et al. (40)
CM/Eff T cell ratio	NSCLC Melanoma	62 43	Higher CM/Eff T cell ratio associated with increased tumor inflammatory profile and prolonged PFS	Manjarrez-Orduno et al. (44)
Effector memory CD8$^+$ T cells TIGIT$^+$ PD-1$^+$ CD8$^+$ T cells	NSCLC	263	Lower frequency of effector memory cells among CD8$^+$ T cells associated with HPD, poor PFS and OS Higher frequency of TIGIT$^+$ cells among PD-1$^+$ CD8$^+$ T cells associated with HPD, poor PFS and OS	Kim et al. (46)
CD27$^-$ CD28$^-$ CD4$^+$ T cells	NSCLC	51	Higher baseline frequency of highly differentiated CD4$^+$ T cells associated with prolonged PFS	Zuazo et al. (47)
(%CD62L^{low} CD4$^+$ T cells)^2/(%CD25$^+$ FOXP3$^+$ CD4$^+$ T cells) ratio	NSCLC	126	Higher baseline prediction formula value associated with prolonged PFS and OS	Kagamu et al. (49)
(%Treg cells)/(%LOX-1$^+$ PMN-MDSCs) ratio	NSCLC	63	Higher (%Treg cells)/(%LOX-1$^+$ PMN-MDSCs) ratio associated with prolonged PFS	Kim et al. (51)
TCR diversity in PD-1$^+$ CD8$^+$ T cells	NSCLC	40	Higher baseline TCR diversity in PD-1$^+$ CD8$^+$ T cells and increased TCR clonality after treatment associated with prolonged PFS	Han et al. (62)
Lin$^-$ CD33$^+$ CD14$^+$ CD15$^-$ HLA-DR$^-$ M-MDSC	NSCLC	61	Higher frequency of M-MDSC associated with poor OS	Limagne et al. (71)
Good Immunological asset (PMN-MDSC ≥ 6 cell/μl, ANC < 5,840/μl, AEC > 90/μl, NLR < 3)	NSCLC	53	Good Immunological asset associated with prolonged PFS and OS	Passaro et al. (72)
NK cells	NSCLC	9	Higher frequency and overall activity of NK cells associated with PR or SD	Cho et al. (73)
CD56$^+$ NK cells	NSCLC	31	Increased number of NK cells associated with prolonged survival outcomes	Mazzaschi et al. (74)
NK cells	NSCLC	74	Higher frequency of NK cells at baseline associated with shorter OS and PFS	Ottonello et al. (75)

ICI, immune checkpoint inhibitor; NSCLC, non-small-cell lung cancer; PD-1, programmed death 1; PR, partial response; SD, stable disease; TET, thymic epithelial tumor; DCB, durable clinical benefit; PFS, progression-free survival; RCC, renal cell carcinoma; TIM-3, T-cell immunoglobulin mucin 3; CM, central memory; Eff, Effector; TIGIT, T cell immunoreceptor with Ig and ITIM domains; HPD, hyperprogression disease; OS, overall survival; Treg, regulatory T; LOX-1, lectin-type oxidized LDL receptor 1; PMN-MDSC, polymorphonuclear myeloid-derived suppressor cell; TCR, T cell receptor; M-MDSC, monocytic MDSC; ANC, absolute neutrophil count; AEC, absolute eosinophil count; NLR, neutrophil-to-lymphocyte ratio. NK, natural killer.

(OS: HR = 2.37, p = 0.0088; PFS: HR = 2.44, p = 0.0004). The presence of pre-treatment PD-L1$^+$ CTCs was not significantly correlated with survival outcomes. Nevertheless, patients with higher frequency of baseline PD-L1$^+$ CTCs (≥ 1%) were more likely to be non-responders (p = 0.04) (78). Similarly, another research investigated the correlation between PD-L1$^+$ CTCs and PFS in 17 patients treated with anti-PD-1 therapy. The results indicated that ≥ 2 PD-L1$^+$ CTCs per ml of blood at baseline was not a predictor of response to immunotherapy (86). Overall, to date, the possibility of utilizing PD-L1$^+$ CTCs as a predictive biomarker has not been solidly demonstrated in patients with NSCLC.

Besides the analysis of PD-L1$^+$ CTCs, a prospective exploratory cohort study (including 104 NSCLC patients receiving ICIs) investigated the predictive value of CTCs and tumor-derived extracellular vesicles. Data showed that the presence of CTCs prior to or during treatment was an independent predictor for the lack of durable response, and it was associated with shorter PFS and OS. Elevated level of tumor-derived extracellular vesicles were correlated with shorter survival, but not with the response rate (87).

Limitations of the aforementioned studies include small research cohorts, non-uniform methodology for the capture of CTCs, use of different antibodies for the staining of PD-L1, and lack of clear cut-off criteria for the definition of positive PD-L1 expression. Multicentral studies are needed to ascertain whether CTCs could serve as a predictive biomarker.

SOLUBLE SERUM-BASED BIOMARKERS AND CYTOKINES

Soluble PD-L1

Multiple research studies have demonstrated that both PD-1 and PD-L1 have soluble forms (sPD-1 and sPD-L1) in peripheral blood, and their increasing levels measured by enzyme-linked immunosorbent assay may correlate with the response to immunotherapy (88, 89). Current studies have suggested that lower levels of sPD-L1 may correlate with longer survival in several malignancies (90, 91). Zhou et al. reported that high pretreatment level of sPD-L1 in melanoma patients treated with ICIs was associated with an increased risk of progressive disease (92). However, increased post-treatment level of sPD-1 was associated with favorable clinical responses (92). Consistent with these results, a prospective study involving 39 NSCLC patients treated with PD-1-targeting antibodies also found that higher sPD-L1 level at baseline was related to a shorter OS (93). Furthermore, among patients treated with nivolumab, the ORR was higher in the low sPD-L1 group versus the high sPD-L1 group (59% vs. 25%, p = 0.0069). In addition, another single-center study including 43 NSCLC patients treated with nivolumab yielded similar results (94). Thus, baseline sPD-L1 may represent an immunosuppressive status and indicate poor response to ICIs. However, the underling mechanisms are not fully elucidated.

Recently, a case-control study proposed composite criteria (sCombo) corresponding to sPD-1 and sPD-L1 positivity for the prediction of immune response in individual patients. In the nivolumab group, baseline sCombo positivity was negatively related to PFS (HR = 2.66, p = 0.02) but not OS. Notably, increased or stable sPD-1 levels after two cycles of treatment with nivolumab was correlated with prolonged PFS (HR = 0.49, p = 0.004) and OS (HR = 0.39, p = 0.002) (95). In conclusion, sPD-L1 may represent a novel biomarker for guiding patient selection and predicting clinical outcomes. However, the lack of standardization of measurement and a consistent threshold is the major limitation for the application of sPD-L1 to clinical practice.

Granzyme B

Granzyme B is a serine protease secreted by NK cells and cytotoxic CD8$^+$ T cells, which is involved in mediating target cell apoptosis (96). Preclinical models showed that granzyme B activity can be evaluated through dedicated positron emission tomography imaging, and that tumors with a high signal for granzyme B uptake showed good response to ICIs (97, 98). Furthermore, a clinical study evaluated the concentration of soluble granzyme B in the peripheral blood of NSCLC patients treated with nivolumab. They reported that responders had significantly higher concentration of soluble granzyme B than non-responders at initiation of treatment with nivolumab (p = 0.039) (94). This may reflect an activated and efficient CD8$^+$ cytotoxic immune response, known to be associated with better response to ICIs. During treatment, patients with a stable or decreased concentration of soluble granzyme B had advantages in ORR, OS, and PFS (94). A possible explanation is that the increase in the concentration of granzyme B reflects an expanding, but ineffective T-cell response leading to T-cell exhaustion.

Indoleamine 2,3-Dioxygenase

Indoleamine 2,3-dioxygenase (IDO) is a key enzyme responsible for catalyzing the conversion of essential amino acid l-tryptophan to the main metabolite kynurenine. Moreover, it promotes cancer cell survival through enhanced suppression of immunity (99). Growing preclinical evidence indicates that an increase in IDO activity is involved in resistance to ICIs, and IDO activity may serve as a predictor of immunotherapeutic efficacy (100). The serum kynurenine/tryptophan ratio was measured by high-performance liquid chromatography-tandem mass spectrometry to assess baseline IDO activity. The IDO activity was negatively associated with PFS and OS in advanced NSCLC patients treated with second-line nivolumab (101). These preliminary results suggested that the serum kynurenine/tryptophan ratio may guide the identification of NSCLC patients with intrinsic resistance to anti-PD-1 agents.

Interleukin-6 and Interleukin-8

Various studies have reported that soluble cytokines influence the efficacy of ICIs. For example, Sanmamed et al. demonstrated that early changes in serum interleukin-8 (IL-8) level reflect and predict response to anti-PD-1 therapy in patients with metastatic melanoma and NSCLC. They designed a validation cohort of 19 NSCLC patients receiving anti-PD-1 agents, and they found that responders had significantly decreased levels of serum IL-8 at the best response moment, whereas non-responders presented opposite changes. in patients with NSCLC, an early decrease in

serum IL-8 level was associated with longer OS (p = 0.015) (102). In addition, this study showed that serum IL-8 level could discern the appearance of pseudoprogression. Moreover, Kang et al. reported that serum interleukin-6 level at baseline could be used to predict the clinical efficacy of anti-PD-(L)1 therapy in patients with NSCLC. Patients with low interleukin-6 level (< 13.1 pg/ml) at baseline presented significantly superior PFS (6.3 vs. 1.9 months; p < 0.001) and OS (not reached vs. 7.4 months; p < 0.001) than those with high interleukin-6 level (103). Studies with larger cohorts are warranted to validate these results.

Exosomes

Exosomes are extracellular vesicles secreted by various cells (including cancer cells), and contain DNA, RNA, and proteins (104). A study evaluated the PD-L1 mRNA expression in circulating exosomes to monitor the response to PD-1-targeting antibodies in patients with melanoma or NSCLC. The data showed that, after treatment, PD-L1 mRNA expression in exosomes significantly decreased in responders, remained unchanged in those with stable disease, and significantly increased in patieints with progressive disease (105). This study demonstrated that dynamic measurement of PD-L1 expression in circulating exosomes is feasible and might provide useful information regarding response to treatment with ICIs. Future exploration in larger cohorts of patients are required, as well as a comparison of PD-L1 expression in paired tissue and circulating exosomes.

The levels of soluble proteins and cytokines can be easily determined, providing an automated, highly sensitive, accurate, and straightforward approach to simultaneously analyzing multiple samples. Most of the aforementioned studies were exploratory, and further studies are required to verify the efficacy of these biomarkers in patients with NSCLC.

CONCLUSION AND FUTURE PERSPECTIVES

The clinical exploration of peripheral blood biomarkers for immunotherapy is important and rapidly developing due to its safety and less invasive nature. In this review, we covered various potential blood-based biomarkers, such as peripheral T lymphocytes, TCR repertoire, MDSCs, CTCs, and soluble proteins. Different assays and platforms were used to monitor peripheral immune status in multiple clinical studies, therefore, demonstrating the potential of these biomarkers in predicting the efficacy of ICIs. Nevertheless, most of the available results are preliminary, so the potential biomarkers in these studies cannot be implemented into routine clinical practice until they are validated in further large-scale prospective clinical trials. Furthermore, more clinical trials should be designed to explore differences in the application of the potential biomarkers alone or in combination, and to standardize thresholds for the guidance of clinical decision making. Despite the inherent challenges, peripheral blood-based biomarkers remain attractive tools for personalized clinical management of immunotherapy for patients with NSCLC.

AUTHOR CONTRIBUTIONS

SL wrote the manuscript. CZ and GP provided expertise and advice. PW designed and supervised the project. All authors contributed to the article and approved the submitted version.

FUNDING

This study was supported by the General Project (U1609220 and 81470212) from the National Natural Science Foundation of China and the Key Research and Development Project (2020C03027) from the Department of Science and Technology of Zhejiang Province.

ACKNOWLEDGMENTS

We gratefully thank Yuan Wu and Yongfang Wang for critical reading of the article.

REFERENCES

1. Ribas A, Wolchok JD. Cancer immunotherapy using checkpoint blockade. *Science* (2018) 359(6382):1350–5. doi: 10.1126/science.aar4060
2. Borghaei H, Paz-Ares L, Horn L, Spigel DR, Steins M, Ready NE, et al. Nivolumab versus Docetaxel in Advanced Nonsquamous Non-Small-Cell Lung Cancer. *N Engl J Med* (2015) 373(17):1627–39. doi: 10.1056/NEJMoa1507643
3. Brahmer J, Reckamp KL, Baas P, Crino L, Eberhardt WE, Poddubskaya E, et al. Nivolumab versus Docetaxel in Advanced Squamous-Cell Non-Small-Cell Lung Cancer. *N Engl J Med* (2015) 373(2):123–35. doi: 10.1056/NEJMoa1504627
4. Herbst RS, Baas P, Kim DW, Felip E, Perez-Gracia JL, Han JY, et al. Pembrolizumab versus docetaxel for previously treated, PD-L1-positive, advanced non-small-cell lung cancer (KEYNOTE-010): a randomised controlled trial. *Lancet* (2016) 387(10027):1540–50. doi: 10.1016/S0140-6736(15)01281-7
5. Reck M, Rodriguez-Abreu D, Robinson AG, Hui R, Csoszi T, Fulop A, et al. Pembrolizumab versus Chemotherapy for PD-L1-Positive Non-Small-Cell Lung Cancer. *N Engl J Med* (2016) 375(19):1823–33. doi: 10.1056/NEJMoa1606774
6. Jenkins RW, Barbie DA, Flaherty KT. Mechanisms of resistance to immune checkpoint inhibitors. *Br J Cancer* (2018) 118(1):9–16. doi: 10.1038/bjc.2017.434
7. Seto T, Sam D, Pan M. Mechanisms of Primary and Secondary Resistance to Immune Checkpoint Inhibitors in Cancer. *Med Sci (Basel)* (2019) 7(2):14. doi: 10.3390/medsci7020014
8. Hersom M, Jorgensen JT. Companion and Complementary Diagnostics-Focus on PD-L1 Expression Assays for PD-1/PD-L1 Checkpoint Inhibitors in Non-Small Cell Lung Cancer. *Ther Drug Monit* (2018) 40(1):9–16. doi: 10.1097/FTD.0000000000000460
9. Hirsch FR, McElhinny A, Stanforth D, Ranger-Moore J, Jansson M, Kulangara K, et al. PD-L1 Immunohistochemistry Assays for Lung Cancer: Results from Phase 1 of the Blueprint PD-L1 IHC Assay Comparison Project. *J Thorac Oncol* (2017) 12(2):208–22. doi: 10.1016/j.jtho.2016.11.2228
10. Tsao MS, Kerr KM, Kockx M, Beasley MB, Borczuk AC, Botling J, et al. PD-L1 Immunohistochemistry Comparability Study in Real-Life Clinical

Samples: Results of Blueprint Phase 2 Project. *J Thorac Oncol* (2018) 13 (9):1302–11. doi: 10.1016/j.jtho.2018.05.013
11. Herbst RS, Baas P, Perez-Gracia JL, Felip E, Kim DW, Han JY, et al. Use of archival versus newly collected tumor samples for assessing PD-L1 expression and overall survival: an updated analysis of KEYNOTE-010 trial. *Ann Oncol* (2019) 30(2):281–9. doi: 10.1093/annonc/mdy545
12. Adams DL, Adams DK, He JZ, Kalhor N, Zhang M, Xu T, et al. Sequential Tracking of PD-L1 Expression and RAD50 Induction in Circulating Tumor and Stromal Cells of Lung Cancer Patients Undergoing Radiotherapy. *Clin Cancer Res* (2017) 23(19):5948–58. doi: 10.1158/1078-0432.Ccr-17-0802
13. Shaverdian N, Lisberg AE, Bornazyan K, Veruttipong D, Goldman JW, Formenti SC, et al. Previous radiotherapy and the clinical activity and toxicity of pembrolizumab in the treatment of non-small-cell lung cancer: a secondary analysis of the KEYNOTE-001 phase 1 trial. *Lancet Oncol* (2017) 18(7):895–903. doi: 10.1016/S1470-2045(17)30380-7
14. Yarchoan M, Hopkins A, Jaffee EM. Tumor Mutational Burden and Response Rate to PD-1 Inhibition. *New Engl J Med* (2017) 377(25):2500–1. doi: 10.1056/NEJMc1713444
15. Ready N, Hellmann MD, Awad MM, Otterson GA, Gutierrez M, Gainor JF, et al. First-Line Nivolumab Plus Ipilimumab in Advanced Non-Small-Cell Lung Cancer (CheckMate 568): Outcomes by Programmed Death Ligand 1 and Tumor Mutational Burden as Biomarkers. *J Clin Oncol* (2019) 37 (12):992–+. doi: 10.1200/Jco.18.01042
16. Hellmann MD, Ciuleanu TE, Pluzanski A, Lee JS, Otterson GA, Audigier-Valette C, et al. Nivolumab plus Ipilimumab in Lung Cancer with a High Tumor Mutational Burden. *New Engl J Med* (2018) 378(22):2093–104. doi: 10.1056/NEJMoa1801946
17. Garassino M, Rodriguez-Abreu D, Gadgeel S, Esteban E, Felip E, Speranza G, et al. Evaluation of TMB in KEYNOTE-189: Pembrolizumab Plus Chemotherapy vs Placebo Plus Chemotherapy for Nonsquamous NSCLC. *J Thoracic Oncol* (2019) 14(10):S216–S7. doi: 10.1016/j.jtho.2019.08.427
18. Langer C, Gadgeel S, Borghaei H, Patnaik A, Powell S, Gentzler R, et al. KEYNOTE-021: TMB and Outcomes for Carboplatin and Pemetrexed With or Without Pembrolizumab for Nonsquamous NSCLC. *J Thoracic Oncol* (2019) 14(10):S216–S. doi: 10.1016/j.jtho.2019.08.426
19. Paz-Ares L, Langer CJ, Novello S, Halmos B, Cheng Y, Gadgeel SM, et al. Pembrolizumab (pembro) plus platinum-based chemotherapy (chemo) for metastatic NSCLC: Tissue TMB (tTMB) and outcomes in KEYNOTE-021, 189, and 407. *Ann Oncol* (2019) 30:917–+. doi: 10.1093/annonc/mdz394.078
20. Chan TA, Yarchoan M, Jaffee E, Swanton C, Quezada SA, Stenzinger A, et al. Development of tumor mutation burden as an immunotherapy biomarker: utility for the oncology clinic. *Ann Oncol* (2019) 30(1):44–56. doi: 10.1093/annonc/mdy495
21. Gerlinger M, Rowan AJ, Horswell S, Larkin J, Endesfelder D, Gronroos E, et al. Intratumor Heterogeneity and Branched Evolution Revealed by Multiregion Sequencing. *New Engl J Med* (2012) 366(10):883–92. doi: 10.1056/NEJMoa1113205
22. Spitzer MH, Carmi Y, Reticker-Flynn NE, Kwek SS, Madhireddy D, Martins MM, et al. Systemic Immunity Is Required for Effective Cancer Immunotherapy. *Cell* (2017) 168(3):487–+. doi: 10.1016/j.cell.2016.12.022
23. Tanizaki J, Haratani K, Hayashi H, Chiba Y, Nakamura Y, Yonesaka K, et al. Peripheral Blood Biomarkers Associated with Clinical Outcome in Non-Small Cell Lung Cancer Patients Treated with Nivolumab. *J Thorac Oncol* (2018) 13(1):97–105. doi: 10.1016/j.jtho.2017.10.030
24. Soyano AE, Dholaria B, Marin-Acevedo JA, Diehl N, Hodge D, Luo Y, et al. Peripheral blood biomarkers correlate with outcomes in advanced non-small cell lung Cancer patients treated with anti-PD-1 antibodies. *J Immunother Cancer* (2018) 6(1):129. doi: 10.1186/s40425-018-0447-2
25. Ameratunga M, Chenard-Poirier M, Moreno Candilejo I, Pedregal M, Lui A, Dolling D, et al. Neutrophil-lymphocyte ratio kinetics in patients with advanced solid tumours on phase I trials of PD-1/PD-L1 inhibitors. *Eur J Cancer* (2018) 89:56–63. doi: 10.1016/j.ejca.2017.11.012
26. Bagley SJ, Kothari S, Aggarwal C, Bauml JM, Alley EW, Evans TL, et al. Pretreatment neutrophil-to-lymphocyte ratio as a marker of outcomes in nivolumab-treated patients with advanced non-small-cell lung cancer. *Lung Cancer* (2017) 106:1–7. doi: 10.1016/j.lungcan.2017.01.013
27. Suh KJ, Kim SH, Kim YJ, Kim M, Keam B, Kim TM, et al. Post-treatment neutrophil-to-lymphocyte ratio at week 6 is prognostic in patients with advanced non-small cell lung cancers treated with anti-PD-1 antibody. *Cancer Immunol Immun* (2018) 67(3):459–70. doi: 10.1007/s00262-017-2092-x
28. Cao DD, Xu HL, Xu XM, Guo T, Ge W. A reliable and feasible way to predict the benefits of Nivolumab in patients with non-small cell lung cancer: a pooled analysis of 14 retrospective studies. *Oncoimmunology* (2018) 7(11): e1507262. doi: 10.1080/2162402x.2018.1507262
29. Mezquita L, Auclin E, Ferrara R, Charrier M, Remon J, Planchard D, et al. Association of the Lung Immune Prognostic Index With Immune Checkpoint Inhibitor Outcomes in Patients With Advanced Non-Small Cell Lung Cancer. *JAMA Oncol* (2018) 4(3):351–7. doi: 10.1001/jamaoncol.2017.4771
30. Shiroyama T, Suzuki H, Tamiya M, Tamiya A, Tanaka A, Okamoto N, et al. Pretreatment advanced lung cancer inflammation index (ALI) for predicting early progression in nivolumab-treated patients with advanced non-small cell lung cancer. *Cancer Med* (2018) 7(1):13–20. doi: 10.1002/cam4.1234
31. Sekine K, Kanda S, Goto Y, Horinouchi H, Fujiwara Y, Yamamoto N, et al. Change in the lymphocyte-to-monocyte ratio is an early surrogate marker of the efficacy of nivolumab monotherapy in advanced non-small-cell lung cancer. *Lung Cancer* (2018) 124:179–88. doi: 10.1016/j.lungcan.2018.08.012
32. De Castro AM, Navarro A, Perez SC, Martinez A, Pardo N, Hernando A, et al. Lactate Dehydrogenase (LDH) as a Surrogate Biomarker to Checkpoint-Inhibitors for Patient with Advanced Non-Small-Cell Lung Cancer (NSCLC). *J Thoracic Oncol* (2017) 12(1):S1313–S4. doi: 10.1016/j.jtho.2016.11.1858
33. Gros A, Parkhurst MR, Tran E, Pasetto A, Robbins PF, Ilyas S, et al. Prospective identification of neoantigen-specific lymphocytes in the peripheral blood of melanoma patients. *Nat Med* (2016) 22(4):433–8. doi: 10.1038/nm.4051
34. Gros A, Tran E, Parkhurst MR, Ilyas S, Pasetto A, Groh EM, et al. Recognition of human gastrointestinal cancer neoantigens by circulating PD-1+ lymphocytes. *J Clin Invest* (2019) 129(11):4992–5004. doi: 10.1172/JCI127967
35. Thommen DS, Koelzer VH, Herzig P, Roller A, Trefny M, Dimeloe S, et al. A transcriptionally and functionally distinct PD-1(+) CD8(+) T cell pool with predictive potential in non-small-cell lung cancer treated with PD-1 blockade. *Nat Med* (2018) 24(7):994–1004. doi: 10.1038/s41591-018-0057-z
36. Kim KH, Cho J, Ku BM, Koh J, Sun JM, Lee SH, et al. The First-week Proliferative Response of Peripheral Blood PD-1(+)CD8(+) T Cells Predicts the Response to Anti-PD-1 Therapy in Solid Tumors. *Clin Cancer Res* (2019) 25(7):2144–54. doi: 10.1158/1078-0432.CCR-18-1449
37. Kamphorst AO, Pillai RN, Yang S, Nasti TH, Akondy RS, Wieland A, et al. Proliferation of PD-1+ CD8 T cells in peripheral blood after PD-1-targeted therapy in lung cancer patients. *Proc Natl Acad Sci U S A* (2017) 114 (19):4993–8. doi: 10.1073/pnas.1705327114
38. Huang AC, Postow MA, Orlowski RJ, Mick R, Bengsch B, Manne S, et al. T-cell invigoration to tumour burden ratio associated with anti-PD-1 response. *Nature* (2017) 545(7652):60–5. doi: 10.1038/nature22079
39. Simoni Y, Becht E, Fehlings M, Loh CY, Koo SL, Teng KWW, et al. Bystander CD8(+) T cells are abundant and phenotypically distinct in human tumour infiltrates. *Nature* (2018) 557(7706):575–9. doi: 10.1038/s41586-018-0130-2
40. Julia EP, Mando P, Rizzo MM, Cueto GR, Tsou F, Luca R, et al. Peripheral changes in immune cell populations and soluble mediators after anti-PD-1 therapy in non-small cell lung cancer and renal cell carcinoma patients. *Cancer Immunol Immunother* (2019) 68(10):1585–96. doi: 10.1007/s00262-019-02391-z
41. Blank CU, Haanen JB, Ribas A, Schumacher TN. Cancer Immunology. The "cancer immunogram". *Science* (2016) 352(6286):658–60. doi: 10.1126/science.aaf2834
42. Chen DS, Mellman I. Oncology meets immunology: the cancer-immunity cycle. *Immunity* (2013) 39(1):1–10. doi: 10.1016/j.immuni.2013.07.012
43. Lesterhuis WJ, Bosco A, Millward MJ, Small M, Nowak AK, Lake RA. Dynamic versus static biomarkers in cancer immune checkpoint blockade: unravelling complexity. *Nat Rev Drug Discovery* (2017) 16(4):264–72. doi: 10.1038/nrd.2016.233
44. Manjarrez-Orduno N, Menard LC, Kansal S, Fischer P, Kakrecha B, Jiang C, et al. Circulating T Cell Subpopulations Correlate With Immune Responses

at the Tumor Site and Clinical Response to PD1 Inhibition in Non-Small Cell Lung Cancer. *Front Immunol* (2018) 9:1613. doi: 10.3389/fimmu.2018.01613
45. Krieg C, Nowicka M, Guglietta S, Schindler S, Hartmann FJ, Weber LM, et al. High-dimensional single-cell analysis predicts response to anti-PD-1 immunotherapy. *Nat Med* (2018) 24(2):144–53. doi: 10.1038/nm.4466
46. Kim CG, Kim KH, Pyo KH, Xin CF, Hong MH, Ahn BC, et al. Hyperprogressive disease during PD-1/PD-L1 blockade in patients with non-small-cell lung cancer. *Ann Oncol* (2019) 30(7):1104–13. doi: 10.1093/annonc/mdz123
47. Zuazo M, Arasanz H, Fernandez-Hinojal G, Garcia-Granda MJ, Gato M, Bocanegra A, et al. Functional systemic CD4 immunity is required for clinical responses to PD-L1/PD-1 blockade therapy. *EMBO Mol Med* (2019) 11(7):e10293. doi: 10.15252/emmm.201910293
48. Arasanz H, Zuazo M, Bocanegra A, Gato M, Martinez-Aguillo M, Morilla I, et al. Early Detection of Hyperprogressive Disease in Non-Small Cell Lung Cancer by Monitoring of Systemic T Cell Dynamics. *Cancers* (2020) 12 (2):344. doi: 10.3390/cancers12020344
49. Kagamu H, Kitano S, Yamaguchi O, Yoshimura K, Horimoto K, Kitazawa M, et al. CD4(+) T-cell Immunity in the Peripheral Blood Correlates with Response to Anti-PD-1 Therapy. *Cancer Immunol Res* (2020) 8(3):334–44. doi: 10.1158/2326-6066.CIR-19-0574
50. Martens A, Wistuba-Hamprecht K, Geukes Foppen M, Yuan J, Postow MA, Wong P, et al. Baseline Peripheral Blood Biomarkers Associated with Clinical Outcome of Advanced Melanoma Patients Treated with Ipilimumab. *Clin Cancer Res* (2016) 22(12):2908–18. doi: 10.1158/1078-0432.CCR-15-2412
51. Kim HR, Park SM, Seo SU, Jung I, Yoon HI, Gabrilovich DI, et al. The Ratio of Peripheral Regulatory T Cells to Lox-1(+) Polymorphonuclear Myeloid-derived Suppressor Cells Predicts the Early Response to Anti-PD-1 Therapy in Patients with Non-Small Cell Lung Cancer. *Am J Respir Crit Care Med* (2019) 199(2):243–6. doi: 10.1164/rccm.201808-1502LE
52. Riaz N, Havel JJ, Makarov V, Desrichard A, Urba WJ, Sims JS, et al. Tumor and Microenvironment Evolution during Immunotherapy with Nivolumab. *Cell* (2017) 171(4):934–49 e16. doi: 10.1016/j.cell.2017.09.028
53. van der Merwe PA, Dushek O. Mechanisms for T cell receptor triggering. *Nat Rev Immunol* (2011) 11(1):47–55. doi: 10.1038/nri2887
54. Postow MA, Manuel M, Wong P, Yuan J, Dong ZW, Liu C, et al. Peripheral T cell receptor diversity is associated with clinical outcomes following ipilimumab treatment in metastatic melanoma. *J Immunother Cancer* (2015) 3. doi: 10.1186/s40425-015-0070-4
55. Hopkins AC, Yarchoan M, Durham JN, Yusko EC, Rytlewski JA, Robins HS, et al. T cell receptor repertoire features associated with survival in immunotherapy-treated pancreatic ductal adenocarcinoma. *Jci Insight* (2018) 3(13):e122092. doi: 10.1172/jci.insight.122092
56. Hogan SA, Courtier A, Cheng PF, Jaberg-Bentele NF, Goldinger SM, Manuel M, et al. Peripheral Blood TCR Repertoire Profiling May Facilitate Patient Stratification for Immunotherapy against Melanoma. *Cancer Immunol Res* (2019) 7(1):77–85. doi: 10.1158/2326-6066.Cir-18-0136
57. Looney TJ, Topacio-Hall D, Lowman G, Conroy J, Morrison C, Oh D, et al. TCR Convergence in Individuals Treated With Immune Checkpoint Inhibition for Cancer. *Front Immunol* (2020) 10:2985. doi: 10.3389/fimmu.2019.02985
58. Snyder A, Nathanson T, Funt SA, Ahuja A, Buros Novik J, Hellmann MD, et al. Contribution of systemic and somatic factors to clinical response and resistance to PD-L1 blockade in urothelial cancer: An exploratory multi-omic analysis. *PloS Med* (2017) 14(5):e1002309. doi: 10.1371/journal.pmed.1002309
59. Aversa I, Malanga D, Fiume G, Palmieri C. Molecular T-Cell Repertoire Analysis as Source of Prognostic and Predictive Biomarkers for Checkpoint Blockade Immunotherapy. *Int J Mol Sci* (2020) 21(7):2378. doi: 10.3390/ijms21072378
60. Anagnostou V, Smith KN, Forde PM, Niknafs N, Bhattacharya R, White J, et al. Evolution of neoantigen landscape during immune checkpoint blockade in non-small cell lung cancer. *Cancer Discov* (2017) 7(3):264–76. doi: 10.1158/2159-8290.CD-16-0828
61. Olugbile S, Kiyotani K, Inoue H, Park JH, Hoffman P, Szeto L, et al. In-Depth Molecular Characterization of T Cell Clonal Expansion Induced by Anti-PD1 Therapy in NSCLC. *J Thoracic Oncol* (2017) 12(1):S1310–S1. doi: 10.1016/j.jtho.2016.11.1853
62. Han J, Duan J, Bai H, Wang Y, Wan R, Wang X, et al. TCR Repertoire Diversity of Peripheral PD-1(+)CD8(+) T Cells Predicts Clinical Outcomes after Immunotherapy in Patients with Non-Small Cell Lung Cancer. *Cancer Immunol Res* (2020) 8(1):146–54. doi: 10.1158/2326-6066.CIR-19-0398
63. Gabrilovich DI. Myeloid-Derived Suppressor Cells. *Cancer Immunol Res* (2017) 5(1):3–8. doi: 10.1158/2326-6066.CIR-16-0297
64. Bronte V, Brandau S, Chen SH, Colombo MP, Frey AB, Greten TF, et al. Recommendations for myeloid-derived suppressor cell nomenclature and characterization standards. *Nat Commun* (2016) 7:12150. doi: 10.1038/ncomms12150
65. Negorev D, Beier UH, Zhang T, Quatromoni JG, Bhojnagarwala P, Albelda SM, et al. Human neutrophils can mimic myeloid-derived suppressor cells (PMN-MDSC) and suppress microbead or lectin-induced T cell proliferation through artefactual mechanisms. *Sci Rep* (2018) 8(1):3135. doi: 10.1038/s41598-018-21450-6
66. Condamine T, Dominguez GA, Youn JI, Kossenkov AV, Mony S, Alicea-Torres K, et al. Lectin-type oxidized LDL receptor-1 distinguishes population of human polymorphonuclear myeloid-derived suppressor cells in cancer patients. *Sci Immunol* (2016) 1(2):aaf8943. doi: 10.1126/sciimmunol.aaf8943
67. Liu CY, Wang YM, Wang CL, Feng PH, Ko HW, Liu YH, et al. Population alterations of L-arginase- and inducible nitric oxide synthase-expressed CD11b+/CD14(-)/CD15+/CD33+ myeloid-derived suppressor cells and CD8+ T lymphocytes in patients with advanced-stage non-small cell lung cancer. *J Cancer Res Clin Oncol* (2010) 136(1):35–45. doi: 10.1007/s00432-009-0634-0
68. Ohl K, Tenbrock K. Reactive Oxygen Species as Regulators of MDSC-Mediated Immune Suppression. *Front Immunol* (2018) 9:2499. doi: 10.3389/fimmu.2018.02499
69. Zhang G, Huang H, Zhu Y, Yu G, Gao X, Xu Y, et al. A novel subset of B7-H3(+)CD14(+)HLA-DR(-/low) myeloid-derived suppressor cells are associated with progression of human NSCLC. *Oncoimmunology* (2015) 4 (2):e977164. doi: 10.4161/2162402X.2014.977164
70. Huang A, Zhang B, Wang B, Zhang F, Fan KX, Guo YJ. Increased CD14(+) HLA-DR (-/low) myeloid-derived suppressor cells correlate with extrathoracic metastasis and poor response to chemotherapy in non-small cell lung cancer patients. *Cancer Immunol Immunother* (2013) 62(9):1439–51. doi: 10.1007/s00262-013-1450-6
71. Limagne E, Richard C, Thibaudin M, Fumet JD, Truntzer C, Lagrange A, et al. Tim-3/galectin-9 pathway and mMDSC control primary and secondary resistances to PD-1 blockade in lung cancer patients. *Oncoimmunology* (2019) 8(4):e1564505. doi: 10.1080/2162402X.2018.1564505
72. Passaro A, Mancuso P, Gandini S, Spitaleri G, Labanca V, Guerini-Rocco E, et al. Gr-MDSC-linked asset as a potential immune biomarker in pretreated NSCLC receiving nivolumab as second-line therapy. *Clin Transl Oncol* (2020) 22(4):603–11. doi: 10.1007/s12094-019-02166-z
73. Cho YH, Choi MG, Kim DH, Choi YJ, Kim SY, Sung KJ, et al. Natural Killer Cells as a Potential Biomarker for Predicting Immunotherapy Efficacy in Patients with Non-Small Cell Lung Cancer. *Target Oncol* (2020) 15(2):241–7. doi: 10.1007/s11523-020-00712-2
74. Mazzaschi G, Facchinetti F, Missale G, Canetti D, Madeddu D, Zecca A, et al. The circulating pool of functionally competent NK and CD8+cells predicts the outcome of anti-PD1 treatment in advanced NSCLC. *Lung Cancer* (2019) 127:153–63. doi: 10.1016/j.lungcan.2018.11.038
75. Ottonello S, Genova C, Cossu I, Fontana V, Rijavec E, Rossi G, et al. Association Between Response to Nivolumab Treatment and Peripheral Blood Lymphocyte Subsets in Patients With Non-small Cell Lung Cancer. *Front Immunol* (2020) 11:125. doi: 10.3389/fimmu.2020.00125
76. Nicolazzo C, Raimondi C, Mancini M, Caponnetto S, Gradilone A, Gandini O, et al. Monitoring PD-L1 positive circulating tumor cells in non-small cell lung cancer patients treated with the PD-1 inhibitor Nivolumab. *Sci Rep* (2016) 6:31726. doi: 10.1038/srep31726
77. Boffa DJ, Graf RP, Salazar MC, Hoag J, Lu D, Krupa R, et al. Cellular Expression of PD-L1 in the Peripheral Blood of Lung Cancer Patients is Associated with Worse Survival. *Cancer Epidem Biomar* (2017) 26(7):1139–45. doi: 10.1158/1055-9965.Epi-17-0120

78. Guibert N, Delaunay M, Lusque A, Boubekeur N, Rouquette I, Clermont E, et al. PD-L1 expression in circulating tumor cells of advanced non-small cell lung cancer patients treated with nivolumab. *Lung Cancer* (2018) 120:108–12. doi: 10.1016/j.lungcan.2018.04.001
79. Kallergi G, Vetsika EK, Aggouraki D, Lagoudaki E, Koutsopoulos A, Koinis F, et al. Evaluation of PD-L1/PD-1 on circulating tumor cells in patients with advanced non-small cell lung cancer. *Ther Adv Med Oncol* (2018) 10. doi: 10.1177/1758834017750121
80. Ilie M, Szafer-Glusman E, Hofman V, Chamorey E, Lalvee S, Selva E, et al. Detection of PD-L1 in circulating tumor cells and white blood cells from patients with advanced non-small-cell lung cancer. *Ann Oncol* (2018) 29 (1):193–9. doi: 10.1093/annonc/mdx636
81. Cheng Y, Wang T, Lv X, Li R, Yuan L, Shen J, et al. Detection of PD-L1 Expression and Its Clinical Significance in Circulating Tumor Cells from Patients with Non-Small-Cell Lung Cancer. *Cancer Manag Res* (2020) 12:2069–78. doi: 10.2147/CMAR.S245425
82. Wang Y, Kim TH, Fouladdel S, Zhang Z, Soni P, Qin A, et al. PD-L1 Expression in Circulating Tumor Cells Increases during Radio(chemo) therapy and Indicates Poor Prognosis in Non-small Cell Lung Cancer. *Sci Rep* (2019) 9(1):566. doi: 10.1038/s41598-018-36096-7
83. Shishido SN, Carlsson A, Nieva J, Bethel K, Hicks JB, Bazhenova L, et al. Circulating tumor cells as a response monitor in stage IV non-small cell lung cancer. *J Transl Med* (2019) 17(1):294. doi: 10.1186/s12967-019-2035-8
84. Alama A, Coco S, Genova C, Rossi G, Fontana V, Tagliamento M, et al. Prognostic Relevance of Circulating Tumor Cells and Circulating Cell-Free DNA Association in Metastatic Non-Small Cell Lung Cancer Treated with Nivolumab. *J Clin Med* (2019) 8(7):1011. doi: 10.3390/jcm8071011
85. Kapeleris J, Kulasinghe A, Warkiani ME, Vela I, Kenny L, O' Byrne K, et al. The Prognostic Role of Circulating Tumor Cells (CTCs) in Lung Cancer. *Front Oncol* (2018) 8:311. doi: 10.3389/fonc.2018.00311
86. Dhar M, Wong J, Che J, Matsumoto M, Grogan T, Elashoff D, et al. Evaluation of PD-L1 expression on vortex-isolated circulating tumor cells in metastatic lung cancer. *Sci Rep* (2018) 8(1):2592. doi: 10.1038/s41598-018-19245-w
87. Tamminga M, de Wit S, Hiltermann TJN, Timens W, Schuuring E, Terstappen LWMM, et al. Circulating tumor cells in advanced non-small cell lung cancer patients are associated with worse tumor response to checkpoint inhibitors. *J Immunother Cancer* (2019) 7(1):173. doi: 10.1186/s40425-019-0649-2
88. Nagato T, Ohkuri T, Ohara K, Hirata Y, Kishibe K, Komabayashi Y, et al. Programmed death-ligand 1 and its soluble form are highly expressed in nasal natural killer/T-cell lymphoma: a potential rationale for immunotherapy. *Cancer Immunol Immunother* (2017) 66(7):877–90. doi: 10.1007/s00262-017-1987-x
89. Shi MH, Xing YF, Zhang ZL, Huang JA, Chen YJ. [Effect of soluble PD-L1 released by lung cancer cells in regulating the function of T lymphocytes]. *Zhonghua Zhong Liu Za Zhi* (2013) 35(2):85–8. doi: 10.3760/cma.j.issn.0253-3766.2013.02.002
90. Zhu X, Lang J. Soluble PD-1 and PD-L1: predictive and prognostic significance in cancer. *Oncotarget* (2017) 8(57):97671–82. doi: 10.18632/oncotarget.18311
91. Zhang J, Gao J, Li YY, Nie J, Dai L, Hu WH, et al. Circulating PD-L1 in NSCLC patients and the correlation between the level of PD-L1 expression and the clinical characteristics. *Thoracic Cancer* (2015) 6(4):534–8. doi: 10.1111/1759-7714.12247
92. Zhou J, Mahoney KM, Giobbie-Hurder A, Zhao F, Lee S, Liao X, et al. Soluble PD-L1 as a Biomarker in Malignant Melanoma Treated with Checkpoint Blockade. *Cancer Immunol Res* (2017) 5(6):480–92. doi: 10.1158/2326-6066.CIR-16-0329
93. Okuma Y, Wakui H, Utsumi H, Sagawa Y, Hosomi Y, Kuwano K, et al. Soluble Programmed Cell Death Ligand 1 as a Novel Biomarker for Nivolumab Therapy for Non-Small-cell Lung Cancer. *Clin Lung Cancer* (2018) 19(5):410–+. doi: 10.1016/j.cllc.2018.04.014
94. Costantini A, Julie C, Dumenil C, Helias-Rodzewicz Z, Tisserand J, Dumoulin J, et al. Predictive role of plasmatic biomarkers in advanced non-small cell lung cancer treated by nivolumab. *Oncoimmunology* (2018) 7 (8):e1452581. doi: 10.1080/2162402X.2018.1452581
95. Tiako Meyo M, Jouinot A, Giroux-Leprieur E, Fabre E, Wislez M, Alifano M, et al. Predictive Value of Soluble PD-1, PD-L1, VEGFA, CD40 Ligand and CD44 for Nivolumab Therapy in Advanced Non-Small Cell Lung Cancer: A Case-Control Study. *Cancers (Basel)* (2020) 12(2):473. doi: 10.3390/cancers12020473
96. Martinez-Lostao L, Anel A, Pardo J. How Do Cytotoxic Lymphocytes Kill Cancer Cells? *Clin Cancer Res* (2015) 21(22):5047–56. doi: 10.1158/1078-0432.Ccr-15-0685
97. Larimer BM, Bloch E, Nesti S, Austin EE, Wehrenberg-Klee E, Boland G, et al. The Effectiveness of Checkpoint Inhibitor Combinations and Administration Timing Can Be Measured by Granzyme B PET Imaging. *Clin Cancer Res* (2019) 25(4):1196–205. doi: 10.1158/1078-0432.Ccr-18-2407
98. Larimer BM, Wehrenberg-Klee E, Dubois F, Mehta A, Kalomeris T, Flaherty K, et al. Granzyme B PET Imaging as a Predictive Biomarker of Immunotherapy Response. *Cancer Res* (2017) 77(9):2318–27. doi: 10.1158/0008-5472.Can-16-3346
99. Mbongue JC, Nicholas DA, Torrez TW, Kim NS, Firek AF, Langridge WH. The Role of Indoleamine 2, 3-Dioxygenase in Immune Suppression and Autoimmunity. *Vaccines (Basel)* (2015) 3(3):703–29. doi: 10.3390/vaccines3030703
100. Holmgaard RB, Zamarin D, Munn DH, Wolchok JD, Allison JP. Indoleamine 2,3-dioxygenase is a critical resistance mechanism in antitumor T cell immunotherapy targeting CTLA-4. *J Exp Med* (2013) 210 (7):1389–402. doi: 10.1084/jem.20130066
101. Botticelli A, Cerbelli B, Lionetto L, Zizzari I, Salati M, Pisano A, et al. Can IDO activity predict primary resistance to anti-PD-1 treatment in NSCLC? *J Transl Med* (2018) 16(1):219. doi: 10.1186/s12967-018-1595-3
102. Sanmamed MF, Perez-Gracia JL, Schalper KA, Fusco JP, Gonzalez A, Rodriguez-Ruiz ME, et al. Changes in serum interleukin-8 (IL-8) levels reflect and predict response to anti-PD-1 treatment in melanoma and non-small-cell lung cancer patients. *Ann Oncol* (2017) 28(8):1988–95. doi: 10.1093/annonc/mdx190
103. Kang DH, Park CK, Chung C, Oh IJ, Kim YC, Park D, et al. Baseline Serum Interleukin-6 Levels Predict the Response of Patients with Advanced Non-small Cell Lung Cancer to PD-1/PD-L1 Inhibitors. *Immune Netw* (2020) 20 (3):e27. doi: 10.4110/in.2020.20.e27
104. Chen R, Xu X, Qian Z, Zhang C, Niu Y, Wang Z, et al. The biological functions and clinical applications of exosomes in lung cancer. *Cell Mol Life Sci* (2019) 76(23):4613–33. doi: 10.1007/s00018-019-03233-y
105. Del Re M, Marconcini R, Pasquini G, Rofi E, Vivaldi C, Bloise F, et al. PD-L1 mRNA expression in plasma-derived exosomes is associated with response to anti-PD-1 antibodies in melanoma and NSCLC. *Brit J Cancer* (2018) 118 (6):820–4. doi: 10.1038/bjc.2018.9

Conflict of Interest: The authors declare that the research was conducted in the absence of any commercial or financial relationships that could be construed as a potential conflict of interest.

Copyright © 2020 Li, Zhang, Pang and Wang. This is an open-access article distributed under the terms of the Creative Commons Attribution License (CC BY). The use, distribution or reproduction in other forums is permitted, provided the original author(s) and the copyright owner(s) are credited and that the original publication in this journal is cited, in accordance with accepted academic practice. No use, distribution or reproduction is permitted which does not comply with these terms.

frontiers in Oncology

REVIEW
published: 03 November 2020
doi: 10.3389/fonc.2020.590941

The Crosstalk Between Tumor-Associated Macrophages (TAMs) and Tumor Cells and the Corresponding Targeted Therapy

Zhe Ge[1,2] *and Shuzhe Ding*[1,2]*

[1] School of Physical Education & Health Care, East China Normal University, Shanghai, China, [2] Key Laboratory of Adolescent Health Assessment and Exercise Intervention of Ministry of Education, East China Normal University, Shanghai, China

Tumor microenvironment (TME) is composed of tumor cells and surrounding non-tumor stromal cells, mainly including tumor associated macrophages (TAMs), endothelial cells, and carcinoma-associated fibroblasts (CAFs). The TAMs are the major components of non-tumor stromal cells, and play an important role in promoting the occurrence and development of tumors. Macrophages originate from bone marrow hematopoietic stem cells and embryonic yolk sacs. There is close crosstalk between TAMs and tumor cells. With the occurrence of tumors, tumor cells secrete various chemokines to recruit monocytes to infiltrate tumor tissues and further promote their M2-type polarization. Importantly, M2-like TAMs can in turn accelerate tumor growth, promote tumor cell invasion and metastasis, and inhibit immune killing to promote tumor progression. Therefore, targeting TAMs in tumor tissues has become one of the principal strategies in current tumor immunotherapy. Current treatment strategies focus on reducing macrophage infiltration in tumor tissues and reprogramming TAMs to M1-like to kill tumors. Although these treatments have had some success, their effects are still limited. This paper mainly summarized the recruitment and polarization of macrophages by tumors, the support of TAMs for the growth of tumors, and the research progress of TAMs targeting tumors, to provide new treatment strategies for tumor immunotherapy.

Keywords: tumor, tumor-associated macrophages (TAMs), tumor microenvironment, immune suppression, therapeutic target

OPEN ACCESS

Edited by:
Huanfa Yi,
Jilin University, China

Reviewed by:
Zheng Liu,
Virginia Commonwealth University, United States
Daniel Olive,
Aix Marseille Université, France

***Correspondence:**
Shuzhe Ding
szding@tyxx.ecnu.edu.cn

Specialty section:
This article was submitted to Cancer Immunity and Immunotherapy, a section of the journal Frontiers in Oncology

Received: *03 August 2020*
Accepted: *12 October 2020*
Published: *03 November 2020*

Citation:
Ge Z and Ding S (2020) The Crosstalk Between Tumor-Associated Macrophages (TAMs) and Tumor Cells and the Corresponding Targeted Therapy. Front. Oncol. 10:590941. doi: 10.3389/fonc.2020.590941

INTRODUCTION

Macrophages, the dominant cell type in the tumor milieu, account for ~30–50% of the tumor tissue mass, been referred to as TAMs. Degree of TAMs tumor infiltration is intimately related to the poor prognosis of a series of tumors (1). Macrophages are classified into nonpolarized M0 macrophage, classically activated M1 macrophages, and alternatively activated M2 macrophages, which are further sub-categorized into M2a, M2b, M2c, and M2d based on the stimulation of different cytokines (2, 3). There is close crosstalk between TAMs and tumor cells. For example, TAMs are abundant in many cancers. Due to the influence of various signal factors secreted by tumor cells, they are characterized by an immunosuppressive M2-like phenotype that affects the tumor microenvironment and promotes tumor growth and metastasis by secreting a variety of substances (4).

ORIGIN AND RECRUITMENT OF TAMS

Origin of TAMs

It is traditionally believed that macrophages are released from the bone marrow as immature monocytes and migrate to the tissues after circulation, eventually differentiating into resident macrophages, including Kupffer cells in the liver, alveolar macrophages in the lung, and osteoclasts in the bone (5). However, the main tissue-resident macrophage population, including liver Kupffer cells, alveolar, spleen, and peritoneal macrophages, is derived from the yolk sac precursors and is not dependent on monocytes in the blood (6). TAMs are derived from Ly6C+CCR2+ monocytes in the circulation, which are derived from bone marrow hematopoietic stem cells. Then Ly6C+CCR2+ monocytes are engaged into tumor tissue and differentiated into TAMs (7). In addition, tissue-resident macrophages may also promote tumor growth by switching to TAMs (8). These results suggest that TAMs can be temporarily recruited from the blood circulation or directly transformed from the resident macrophages in tissue where the tumor is located.

Recruitment of TAMs

Tumors Recruit Macrophages by Secreting Cytokines

Tumor cells can secrete some signal molecules and interleukins to recruit macrophages (**Figure 1**). First, it has been found that the expression of colony stimulus factor 1 (CSF-1) and interleukin-6 (IL-6) in non-small cell lung cancer (NSCLC) is closely associated with the infiltration of TAMs in tumor stroma and the progression of lung cancer (9). Indeed, tumor cells can recruit macrophages into tumor tissues through CSF1, the main chemokine, and function regulator of macrophages. It is found that CSF1 overexpression in colon cancer cells is associated with macrophage infiltration, and colon cell-derived CSF1 promotes macrophage recruitment and increases IL-8 production bynbsp;macrophages. Furthermore, IL-8 secreted by macrophages, in turn, activates the protein kinase C (PKC) signaling pathway of colon cancer cells, which enhances the production of CSF1 in colon cancer cells (10), indicating that the interaction between tumor cells and TAMs forms a vicious cycle, thus promoting the recruitment of macrophages in tumor tissues. It is worth noting that hypoxia inducible factor-1 (HIF-1)-dependent production of CSF-1 in tumor cells recruits TAMs with hypoxia (11), which also means that improving the TME with hypoxia is beneficial to prevent the recruitment of TAMs. Secondly, the expression of hippo pathway effector protein (YAP) in hepatocellular carcinoma cells results in the recruitment of TAMs by secreting IL-6 (12). Adipose tissue can also recruit macrophage by secreting IL-6 (13). The expression of IL-6 in THP-1 cells enhances its own migration and infiltration into tissues (14). It is worth noting that the recruited TAMs can also secrete high levels of IL-6 (15), further recruiting macrophages to infiltrate the tumor tissue and form a vicious circle. Therefore, it is

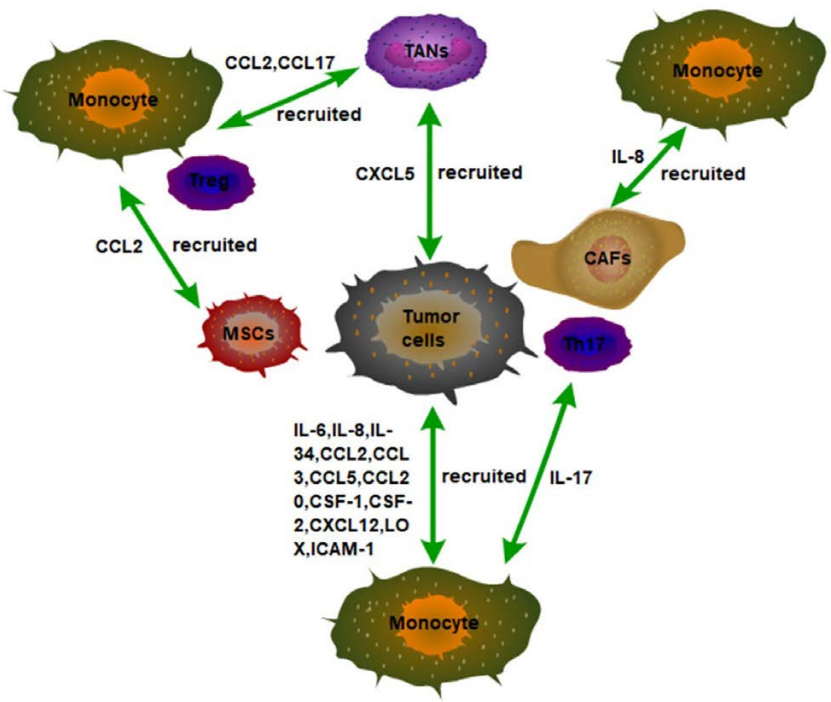

FIGURE 1 | The recruitment of monocytes in the TME in tumor tissues. Tumor cells secrete a variety of inflammatory factors and chemokines to recruit monocytes to infiltrate tumor tissues, such as IL-6, IL-8, and IL34. In addition, non-tumor stromal cells in tumor tissues can also recruit monocytes to infiltrate tumors by secreting inflammatory factors and chemokines. For example, IL-8 secreted by CAFs, IL-17 secreted by Th17, and CCL2 secreted by MSCs recruit monocytes to infiltrate tumor tissues.

speculated that increased IL-6 levels in tumor tissues may lead to the infiltration of macrophages in tumor tissues. Also, lung tumor tissue recruits RAW264.7 macrophages and primary peritoneal macrophages to migrate through the high expression of IL-17, the process mediated by IL-17RA and IL-17RC expressed on TAMs (16). IL-34, the newly discovered cytokine in recent years, shares common features with CSF-1. It can be considered with CSF-1 as twin cytokines that are functionally related. In fact, IL-34 expressed by osteosarcoma cells, is regulated by IL-1β and TNF-α, can also recruit macrophages into tumor tissues (17). Finally, the high expression of CSF2 in breast cancer is associated with more CC chemokine ligand 18 (CCL18)+ macrophage infiltration, epithelial-mesenchymal transition (EMT), enhanced metastasis, and reduced patient survival (18). These results indicate inflammatory TME may be the key for the recruitment of macrophages.

Tumor cells can also secrete chemokines to recruit macrophages to infiltrate the tumors. Tumor cells can also recruit chemokine (C-C motif) receptor 2 (CCR2)-expressing monocytes into tumor tissues by secreting CCL2 (19). This indicates that the CCL2/CCR2 axis participates in the recruitment of TAMs into tumor tissues. Besides, it has been observed that PBMCs in NSCLC patients released higher levels of CCL2 after LPS stimulation compared with non-smokers, supporting the involvement of CCL2 in NSCLC biological processes (20). As we all know, CCL20 is deemed to be produced by intestinal epithelial cells, especially in response to stress. It has been found that colon cancer cells recruit monocytes to infiltrate tumor tissues by secreting CCL20 to bind with the monocyte receptor CCR6 in mouse model of colon cancer (15). Phyllodes tumors of the breast promote malignant progression by secreting CCL5 to recruit macrophages associated with repolarized tumors (21). However, the transfer inhibitor raf kinase inhibitor (RKIP) can regulate TAM recruitment by blocking high mobility group AT-hook 2 (HMGA2), leading to decreased expression of various macrophages chemokines, including CCL5. It is worth noting that the expression of RKIP in tumor cells is decreased in TNBC, which leads to the increase of CCL5 secretion to promote the recruitment of macrophages, thus enhancing the invasion of tumors (22). This also shows that targeted recovery of RKIP expression in TNBC to reduce the secretion of CCL5 in tumor cells is an important strategy to reduce macrophage infiltration. Indeed, in the mouse PDX (patient-derived xenografts) model of human malignant phyllodes tumor, intraperitoneal injection of maraviroc, CCR5 inhibitor, or CCL5 neutralizing antibody prevents the recruitment of monocytes to tumors and dramatically suppress tumor growth (21).

Activation of chemokine receptor CXCR4/CXCL12 signaling is also involved in TAMs recruitment of melanoma (23). Moreover, the invasion of TAMs in tumor tissues and the high expression of CXCL4 in NSCLC cells is intimately related to the development of NSCLC and the higher rate of lymph node metastasis (24). It has been found that glioma cells with PTEN gene deletion can activate transcription factor YAP1, which can lead to a large amount of LOX excretion. Then, LOX recruits macrophages to infiltrate into glioma cells by binding to β1 integrin on macrophages, which secretes SPP1 to support the growth of gliomas (25).

High expression of transcriptional factor Sox2 in breast cancer cells activates nuclear factor of activated T cells (NFAT), signal transducer and activator of transcription 3, (STAT3), and NF-κB signalings to secrete chemokines CCL3 and intercellular adhesion molecule-1 (ICAM-1), which recruit TAMs into the tumor microenvironment and promote tumor metastasis (26). Also, it has been found that the high expression of galectin-3 in tumor cells recruits M2 macrophages to infiltrate tumors and generate blood vessels in mouse melanoma and Lewis lung cancer models (27), but the specific mechanism remains unclear.

Recruitment of Macrophages by Stromal Cellular Compartment in TME

Other cells in the tumor microenvironment can also recruit macrophages into the tumor (**Figure 1**). For example, tumor cells can also recruit macrophages through tumor-associated neutrophils (TANs). Mechanically, CXCL5 derived from hepatocellular carcinoma (HCC) cells is the strongest effector of neutrophil migration under hypoxic conditions. Then, the TANs that are distributed in the HCC stroma, but not in tumor cells or adjacent non-tumor hepatocytes recruit macrophages and Treg cells into HCC by secreting CCL2 and CCL17 to promote the HCC progression (28). Furthermore, the interaction of macrophages, fat cells, and tumor cells in the microenvironment of breast cancer promotes the recruitment of macrophages in tumors and further promotes the development of breast cancer. Specifically, leptin and lauric acid secreted by adipocytes and CCL2 secreted by breast cancer cells together enhance the chemotaxis of macrophages. In addition, leptin also decreases the proportion of M1 TAMs (29). These results also mean that targeting adipocytes in TME may become a new idea for tumor immunotherapy.

Mesenchymal stromal cells (MSCs) are a non-hematopoietic pluripotent progenitor cell derived from bone marrow, capable of differentiating into a variety of cell types, including chondrocytes, adipocytes, and osteocytes. MSCs are an important component of the tumor microenvironment. MSCs can also be recruited into tumors in a CCR2-dependent manner. Moreover, TNFα-pretreated BM-MSCs mimic MSCs from tumors in their chemokine production profile and ability to promote tumorigenesis of lymphoma, melanoma, and breast carcinoma (30). In addition, CAFs recruit macrophages into tumors *via* IL-8/CXCR2 pathway (31). These results indicate that the inflammatory tumor environment is conducive to macrophage recruitment and tumor growth promotion. In addition, liver tumor-initiating cells (TICs) can recruit macrophages to sustain their growth. It has been found that TICs can recruit M2-type macrophages at the early stage of tumorigenesis. Mechanistically, TICs recruit M2-type macrophages for infiltration through activation of YAP, which induces the expression of CCL2 and CSF-1 (32). Therefore, targeting YAP in tumors may be able to slow tumor growth by reducing the recruitment of TAMs.

POLARIZATION OF TAMS IN TUMOR MICROENVIRONMENT

Macrophages can be divided into M1-type macrophages and M2-type macrophages according to their functions. M1 macrophages produce inflammatory cytokines such as IL-1, 6, 12, and 23, TNF-α, ROS, and NO. However, M2 macrophages produce IL-10, TGF-β, VEGF, and matrix metalloproteinase 9 (MMP9), and express argininase-1 (ARG-1), scavenger receptors (CD163 and CD204), and C-type lectin (CD301) (33). In fact, TAMs are characterized by an immunosuppressive M2-like phenotype (4). In the presence of interferon-γ (IFN-γ) and lipopolysaccharide (LPS), monocytes differentiate into M1 macrophages. However, monocytes differentiate into M2 macrophages in the presence of CSF-1, interleukin-4, IL-13, glucocorticoid, IL-10, and in the presence of immune complexes induced jointly with IL-1R or TLR ligands (34). After tumor cells recruit macrophages into tumor tissues, in order to avoid being swallowed by macrophages, they can induce M2-type polarization of macrophages in the following ways.

Interleukins and Chemokines

It has been observed that monocytes are recruited into tumors and then differentiated into TAMs through IL-4 and IL-13 induction (35). IL-4 and IL-13, mainly derived from Th2 cells, promote M2-type polarization of macrophages through activation of STAT6 signaling (36). Importantly, tumor cells also secrete IL-4, IL-10 (37, 38), and IL-10 can also induce M2-type polarization of macrophages (39). Thus, tumor cells can induce M2-type differentiation of macrophages by secreting IL-4 and IL-10. In addition, IFN-γ knockout mice show accelerated tumor growth and M2-type TAMs during urethane-induced lung cancer. However, lung tumor growth is inhibited in IL-4R knockout mice and TAMs phenotype presents M1-type (40). These results also indicate that IFN-γ and IL-4 play an antagonistic role in the differentiation of TAMs and that targeting IL-4 in the TME may contribute to lung cancer treatment. Indeed, it has been found that targeting the elevated IL-4 in the TME also alters inflammation in the tumor microenvironment, reducing the generation of immunosuppressive M2 macrophages and myeloid-derived suppressor cells (MDSCs), which enhances anti-tumor immunity and delays tumor progression (41). Moreover, tumor-derived CSF-1 and IL-4 synergistically induce M2-type polarization of macrophages (42). Except for of the above, myeloma cells can also stimulate macrophage proliferation and TAMs polarization by overexpressing chemokines CCL2, CCL3, and CCL14 (43). Snail expressed tumor cells not only recruited macrophages by secreting cytokines such as CCL2, CCL5, and IL-6, but also secretes tumor-derived exosomes (TEXs) which contains miR-21 to induce M2-type polarization of macrophages (44).

TGF-β

Transforming growth factor β (TGF-β) secreted by tumor cells can also induce M2-type polarization of macrophages. Mechanistically, interleukin-1 receptor associated kinase-M (IRAK-M), an inactive serine/threonine kinase, is mainly expressed in macrophages and a robust negative regulator of TLR signaling. TGF-β secreted by tumor cells induces the expression of IRAK-M in macrophages and promotes the polarization of macrophages toward M2-type, thereby promoting the tumor (45). TGF-β can also induce M2-macrophage polarization by up-regulating Snail expression through smad2/3 and PI3K/AKT signaling pathways (46).

Other Signal Molecules

Tumor cells can also induce M2-type polarization of TAMs through a variety of other signal molecules (**Figure 2**). For example, tumor cells can release vesicles into the extracellular space to be absorbed by macrophages. These special subcellular vesicles are called MPs, which are between 100 and 1,000 nanometers in diameter and contain nuclear histones, caspases, microRNAs, and DNA. With the absorption of MPs, TAMs polarize into M2-type to accelerate tumor progression (47). In addition, the expression of human leucine leucine 37 (LL-37) and its mouse homologous antimicrobial peptide-related AMP (CRAMP) in both human and mouse prostate cancer is positively correlated with tumor progression. Mechanistically, the CRAMP derived from prostate cancer also mediates M2-type polarization of macrophages (48). Furthermore, lung adenocarcinoma cells secrete phosphoprotein 1 (SPP1) to induce the expression of PD-L1 in M2 macrophages and enhance the M2-polarized effect of macrophages, thus promoting tumor progression (49).

It has been found that the expression of angiogenin-like protein 2 (Angptl2) is significantly elevated in NSCLC cells, which is positively correlated with TAM infiltration, tumor size, and poor patient survival. NSCLC cells promote the polarization of M2 in TAMs by secreting Angptl2 and promote the progression of non-small cell lung cancer (50). Tumor cells also utilize Tyro3, Axl, and Mer receptor tyrosine kinases to reduce inflammation and innate immune responses. It has been found that tumor cells can secrete protein S (Pros1), a Mer/Tyro3 ligand, to suppress M1 polarization and lower anti-tumor immune response (51). PGE2, highly expressed in lung cancer tissues, induces M2-type polarization of macrophages by secretion (16). Furthermore, B7-H3, a member of the B7 family, is expressed in some types of human cancer and plays a significant role in the development of tumors. Elevated expression of B7-H3 in lung cancer tissues of NSCLC patients is found to be significantly associated with shorter overall survival (52). In addition, the elevated expression of B7-H3 in hepatocellular carcinoma is also positively correlated with the number of TAMs. Mechanically, HCC cells can induce M2-type differentiation of monocytes by secreting B7-H3 and inducing the expression of B7-H3 in monocytes, thereby stimulating the STAT3 signaling pathway (53). Importantly, cancer cells can utilize protease-mediated shedding strategies to produce soluble MIC (sMIC) to escape host immune recognition. Furthermore, sMIC also promotes MDSCs amplification by activating STAT3 and causes macrophages to be more inclined to a more immunosuppressive phenotype (54), suggesting that sMIC targeting is a target for cancer immunotherapy. It has also

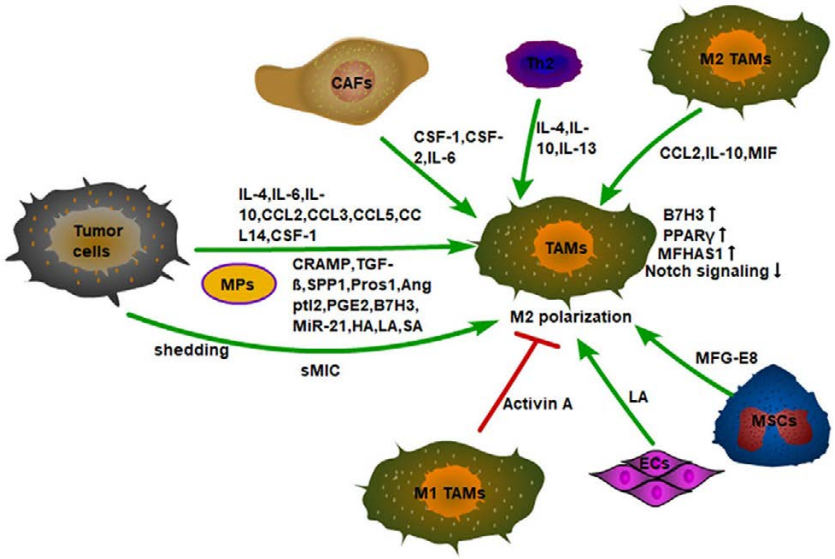

FIGURE 2 | Monocytes recruited into tumor tissue are polarized into M2 macrophages by a variety of cytokines in the TME. First, tumor cells secrete inflammatory factors, chemokines, and signal molecules to promote the M2 polarization of TAMs, such as IL-4, CCL2, TGF-β, etc. Secondly, tumor cells also promote the M2 polarization of TAMs by shedding sMIC. Finally, the non-tumor stromal cells in the TME also induce M2-type polarization of macrophages. For example, CSF-1, CSF-2, and IL-6 secreted by CAFs; IL-4, IL-10, IL-13 secreted by Th2 cells, and MFG-E8 secreted by MSCs. In addition, Activin A secreted by M1 TAMs can also inhibit the M2 polarization of macrophages. ECs also promote the M2-type polarization of macrophages by secreting LA.

found that tumor tissue hypoxia leads to a large upregulation of sialic acid (SA), which is transported to bind with CD45 of MDSCs to upregulate the activity of CD45 protein tyrosine phosphatase (CD45PTP) and suppress the phosphorylation of STAT3, thus promoting the differentiation of MDSCs to TAMs (55). Thus, it is worth noting that whether the activity of STAT3 is beneficial to the differentiation of M2 macrophages still needs to be elucidated. Furthermore, the extracellular matrix (ECM) component hyaluronic acid (HA) can be produced by tumor cells, which is associated with increased tumor progression. HA released by ovarian cancer cells induces the M2 phenotype of TAMs by promoting macrophage cell-cholesterol effervescent (56).

Intermittent hypoxia significantly promotes the metastasis of Lewis lung cancer (LLC) and increased CD209+ macrophage infiltration in the primary tumor tissues. Mechanistically, hypoxia and IL-6 can promote the m2-like phenotype deflection of the tumor from M1-to enhance the metastasis of LLC. Further studies have shown that the M2 polarization of the macrophage caused by hypoxia depends heavily on the activation of its ERK signaling (57). Malignant fibrous histiocytoma amplified sequence 1 (MFHAS1) is a predictive oncoprotein that shows tumorigenic activity *in vivo*. It has been found that with the progress of CRC, the expression of MFHAS1 in TAMs increases gradually. Further studies show that CRC cells could induce MFHAS1 expression in macrophages, and subsequently promote TAMs M2 polarization by activating STAT6 and KLF4 to accelerate CRC progression. In addition, they found that the activation drive of PPAR polarizes macrophage M2 through MFHAS1-mediated activation of STAT6 and KLF4 signaling (58). Indeed, ovarian tumor stem cells (OCSCs) promote M2 polarization of macrophages by increasing PPARγ expression and inhibiting NF-κB expression (59). This also suggests that inhibit PPARγ signaling in macrophages may reverse M2-type polarization.

The Polarization of Macrophages by Stromal Cellular Compartment in TME

M2-type macrophages can convert M1-type macrophages to M2-type macrophages by secreting CCL2 in TME. It is found that after TLR stimulation, CSF-2 polarized macrophages (M1-type macrophages) release large amounts of TNF-α and IL-6, and CSF-1 polarized macrophages (M2-type macrophages) produce low levels of pro-inflammatory cytokines and high levels of IL-10. CCL2 is highly expressed by macrophages under the action of CSF-1, while CCR2 is only expressed by CSF-2 polarized macrophages. CCL2 enhances LPS-induced IL-10 production, while CCL2 blockade leads to increased expression of M1-polarization-related genes, and decreased expression of M2-related gene in macrophages. In fact, CCR2-deficient macrophages show an M1-skewed polarization profile at the transcriptomic level and exhibit a high expression of pro-inflammatory cytokines (TNF-α, IL-6) under the stimulation of LPS (60). Furthermore, a large amount of IL-10 produced by TAMs can inhibit the production of self-IL-12, which facilitates the maintenance of TME (61). Macrophage migration inhibitor (MIF) released by macrophages also promotes M2-type polarization in melanoma (62). Moreover, it has been found that malignant tumor cells, such as glioblastomas and melanomas, can recruit mesenchymal stem cells from surrounding tissue or from the circulation into tumor tissue to sustain their growth. Then, the

MFG-E8, a powerful angiogenic factor secreted by mesenchymal stromal cells can promote M2-type polarization of macrophages and promote tumor angiogenesis (63). In addition, circulating tumor cell CTC can regulate M2-type polarization of TAMs to increase tumor invasiveness, angiogenesis, and immunosuppression (64). It is to be noted that M1-type macrophages can in turn affect the polarization of M2-type macrophages. It has been observed that activin-A secreted by M1-type macrophages can promote the pro-inflammatory phenotype of macrophages and inhibit the acquisition of the M2-type through smad2/3 phosphorylation (65).

CSF-1 and CSF-2 have different polarization effects on macrophage polarization. CSF-1 co-acts with NF-κB and upregulates c-Jun expression to induce M2-type polarization in macrophages (66). Interestingly, CSF-2 can induce M1-type polarization in macrophages, while CSF-2 and IL-6 derived from tumor-associated fibroblasts (CAFs) can synergistically induce the M2-type phenotype of TAMs (67). The specific mechanism remains unclear. Furthermore, the concentration of lactic acid in the TME can also regulate the polarization of macrophages. In tumor cells, glycolysis is strongly enhanced to meet the high ATP demand of these tumor cells (68). It has been found that the energy metabolism of endothelial cells ECs is mainly dependent on glycolysis, and ECs-derived lactic acid can cause macrophages to be polarized into M2-type. However, the loss of phosphofructokinase-2/fructose-2,6-bisphosphatase isoform 3 (PFKFB3), the glycolytic regulator, reduces lactate secretion by ECs and inhibits M2-type macrophage. In addition, MCT1 knockout inhibits M2-type macrophage differentiation (69). This suggests that the production of lactic acid in the tumor microenvironment can promote M2-type differentiation of macrophages. In addition, the presence of a large number of tumor blood vessels in tumor tissues can provide nutrients for tumor cells. Not only can tumor cells produce lactic acid through glycolysis, but also their vascular endothelial cells can produce lactic acid to polarize TAMs into M2-type. The M2-type macrophages can further promote the formation of blood vessels in tumor tissues and these form a vicious circle. In addition, CAFs can increase ROS content in monocytes by secreting CSF-1, to induce M2-type differentiation of macrophages (70).

Notch Signaling

TAMs terminal differentiation is dependent on RBP-J, a DNA-binding protein, which serves as the central transcriptional regulator of the Notch signaling pathway (71). In addition to the regulation of macrophage polarization by the above methods, the tumor also promotes M2-type polarization by inhibiting the Notch signaling of macrophages. For example, M2-like TAMs have a low level of activation of the Notch pathway in mouse tumor models, while activation of the Notch signaling in macrophages promotes M1-type polarization and enhances the anti-tumor ability of macrophages. Further studies found that RBP-J-deficient macrophages show TAM phenotype, and RBP-J-mediated Notch signaling promotes M1 polarization of macrophages through SOCS3 (72). It is worth noting that although the Notch signaling promotes the differentiation of monocyte into TAMs, the Notch signaling can promote the pro-inflammatory polarization of differentiated TAMs toward M1, which suggests that targeting to enhance the expression of RBP-J of TAMs and enhancing Notch signaling to promote the M1 polarization of TAMs may have potential for tumor treatment.

However, other studies have shown that RBP-J is the key to the M2 polarization of macrophages (73). The specific mechanism of these paradoxes is still unclear. In addition, IL-37 can also inhibit the Notch signaling pathway. In fact, IL-37 inhibits M1 macrophage polarization by suppressing the Notch1 and NK-κB pathways (74). However, it has been found that IL-37 is almost not expressed in non-small cell lung cancer tissues, but is highly expressed in adjacent normal tissues (75). In addition, the expression of IL-37 in liver cancer tissues is also decreased, and its expression level is negatively correlated with tumor size (76). These results suggest that tumor cells may not rely on IL-37 to induce M2-type polarization of macrophages.

The Tumor Inhibits Its Phagocytosis by Binding to the TAMs Receptor

Macrophages can engulf and destroy tumor cells to prevent tumor growth. With the exception for inducing the M2 polarization of macrophages, subtle tumor cells can also inhibit their phagocytic activity by binding directly to the macrophages' receptors. CD47 is recognized as a key protein expressed on the surface of many cancer cells, allowing them to evade innate immune surveillance and its overexpression is a common feature of leukemia cells and solid tumors. CD47 on tumor cells binds to and activates the signal regulatory protein-α (SIRPα), an inhibitory protein expressed on the surface of macrophages, to initiate a signal cascade and inhibit the phagocytic activity of macrophages (77). Additionally, recent studies have also discovered new targets for tumor cells to express "don't eat me" signals. In addition to CD47, tumor cells also highly express CD24 molecules to achieve immune escape. CD24 can bind to the inhibitory receptor sialic-acid-binding Ig-like lectin 10 (Siglec-10) highly expressed on TAMs, thereby inhibiting the phagocytic activity of TAM (78). Besides, MHC class I on tumor cells directly protects them from macrophage attack through binding to the inhibitory receptor LILRB1 on the surface macrophages, which is up-regulated by tumor cells (79). Also, tumors also utilize the PD-L1/PD-1 axis to suppress the phagocytosis of TAMs. It has been found that PD-1 is expressed in TAMs in both mice and humans. PD-1 expression in TAM increases with tumor progression in mouse cancer models and primary human cancers. Importantly, this correlates negatively with phagocytic potency against tumor cells (80).

MECHANISM OF TAMS PROMOTING TUMOR PROGRESSION

TAMs can promote tumor progression through a variety of pathways. For example, TAMs secrete TGF-β, vascular endothelial growth factor (VEGF), fibroblast growth factor 2 (FGF2), FGF10, fibroblast growth factor receptor 2 (FGFR2), and several MMPs to support tumor growth and immune

protection (81). Furthermore, it is found that patients with cancers which include pancreas, lung, undifferentiated thyroid, and gallbladder with high TAM density have a lower survival rate (82). In fact, depletion of TAMs slows the growth of urethane-induced lung cancer in mice (83). In addition, the maintenance of TAMs polarization is dependent on the presence of tumor (84), which suggests that tumor cells can maintain the M2-type polarization of TAMs. Tumor tissues are composed of varying numbers of cancer cells and stromal cells, in which the number of macrophages expressing CD204 is associated with lung adenocarcinoma invasion (85). Indeed, the specific location of TAMs in tumor tissues is closely related to tumor progression. An increase in CD204 positive TAMs in the tumor stroma is found to be associated with a poor prognosis of lung adenocarcinoma, rather than the number of TAMs in the tumor islets or alveolar cavity (86). In addition, increased expression of CD163+ TAMs and CXCL12 in tumor stroma (TS) and invasive tumor margin (TM) is intimately associated with tumor progression in GC (87). These studies indicate that the number of TAMs in tumor stroma plays a vital role in promoting tumor progression.

TAMs Promote the Development of Tumors

TAMs in lung tumor tissue also promote lung tumor formation by the activation of NLRP3 inflammasomes that produce IL-1α and IL-1β (88). TAMs also stimulate the expression of IL-1, IL-6, and IL-8 in lung cancer cells through TLR signaling, serving to maintain the inflammatory microenvironment of the tumor and promote the development and progression of lung cancer (89). Indeed, it has been found that infiltrating macrophages secrete inflammatory mediators CCL2, IL-1α, IL-6, and tumor necrosis factor-α (TNF-α) to promote the proliferation of colon cancer cells (15). Furthermore, tumor-derived HSPs activate TLR4 signaling in TAMs to produce cytokines that are beneficial to tumor growth, such as TNF-α and VEGF. Furthermore, TNF-α secreted by TAM leads to the activation of NF-kB in tumor cells. Activation of NF-kB pathway in tumor cells prevents tumor cell death and enhances tumor cell invasion (90).

In fact, there is a large number of inflammatory cell infiltrations in tumors, among which IL-17 produced by Th17 cells and IL-23 produced by TAMs can promote tumor progression. This process may be activated by microbial products in tumors (91). Indeed, recent studies have found a large number of bacteria in tumor tissues (92), which means that inflammation caused by microorganisms in tumors is intimately related to the progression of cancer. How to target and regulate these tumor microorganisms may be the key to the future treatment of tumors.

IL-6 secreted by TAMs encourages the development of HCC through phosphorylation of STAT3 in HCC cells (93). Moreover, with the progression of lung cancer, the high expression of IL-10 in TAMs in NSCLC is associated with poor overall survival, and the expression of IL-10 in lung cancer cells is not changed (94), indicating that IL-10 secreted by TAMs during cancer progression is the key to promote cancer progression. Importantly, IL-10 elevation in TME is intimately associated with TAMs ERK1/2 signaling activation. It is found that the MyD88-dependent pathway in TAMs is selectively blocked. However, LPS and Poly (I:C) can activate downstream ERK-1/2 MAPK activation by TLRs receptors on TAMs independent of MyD88 signal, resulting in phosphorylation of the IL-10 histone promoter region, thereby increasing the expression of IL-10 of TAMs, a process independent of p38MAPK activation. Considering that LPS can induce the activation of p38MAPK and ERK-1/2 activation in normal macrophages, this phenomenon may be specific to TAMs. Additionally, abrogation of ERK1/2 activation significantly reduces IL-10 production in TAM. Moreover, activation of ERK-1/2MAPK leads to enhanced induction of IRAK M in TAM, which negatively regulates the MyD88 signaling pathway, further promoting the immunosuppression function of TAMs. Furthermore, there are also endogenous TLR ligands in tumor sites (95). This also means that these endogenous tumor TLR ligands may maintain the pro-tumor function of TAMs by activating ERK1/2 signaling downstream of the TLR signaling.

IL-6 has long been considered a mediator of tumor cell proliferation by binding to IL-6 receptors (IL-6R) (96). Indeed, IL-6 secreted by TAM acts on glioma cells and promotes 3-phosphoinositide dependent protein kinase 1 (PDPK1) mediated phosphoglycerate kinase 1 (PGK1) phosphorylation (T243), which changed the affinity between PGK1 and the substrate, promoting the activity of the glycolysis direction of PGK1, and the aerobic glycolysis, cell proliferation and tumor growth of glioma cells (97). In mouse and human neuroblastoma cells, TAMs are found to increase STAT3 activation in neuroblastoma cells, and up-regulates MYC oncogenes, a process associated with IL-6 independent expression. However, inhibition of STAT3 activation significantly retards TAMs mediated tumor growth in subcutaneous neuroblastoma in mice (96), which suggests that IL-6 is not the key to the growth of neuroblastoma and may be related to the type of tumor.

Tumor-derived extracellular vesicles (TEVs) include RNA and a variety of cytokines such as TGF-β, activated Src, Wnt3, HIF1α, in which the process also associates with tumor progression. Indeed, studies have shown that TAM can also transfer tumor-derived extracellular vesicles (TEVs) to surrounding stromal cells to make stromal cells become CAF-like cells and forming a pro-tumor microenvironment to promote tumor progression (98).

Tumors Utilize TAMs to Promote Metastasis

TLR4, the receptor mainly expressed on macrophages, its signaling plays an active role in the process of chronic inflammation. Activation of TLR4 on M2-polarized TAMs stimulates an increase in the IL-10, which promotes the EMT of pancreatic cancer cells, specifically in increased the morphology of fibroblasts, up-regulated the expression of mesenchymal markers Vimentin and Snail, and increased the proliferation, migration, and proteolytic activities of MMP 2 and MMP9 in pancreatic cancer cells. M2-polarized TAMs co-culture

with pancreatic cancer cells reduce the expression of E-cadherin, an epithelial marker. In turn, pancreatic cancer cells increased TLR4 expression in M2-polarized TAMs (99). Furthermore, M2-polarized macrophages promote HCC migration and EMT through the TLR4/STAT3 signaling pathway (100). These results suggest that TLR4 is an important target for tumor immunotherapy. Also, IL-4 produced by tumor cells not only promotes M2-type polarization of macrophage, but also promotes tumor growth and invasion by enhancing the cathepsin protease activity in TAMs (38).

COX-2 is overexpressed in all metastatic cancers. It has been found that the high expression of COX-2 in breast cancer TAMs enhances the migration and invasion of breast cancer cells. Mechanistically, the overexpression of COX-2 in TAMs activates the AKT pathway in breast cancer cells by releasing IL-6 and PGE2, thereby inducing the expression of MMP-9 and promoting EMT in breast cancer cells (101). In addition, IL-6 secreted by macrophages can up-regulate COX-2 expression and PGE2 secretion in lung cancer cells, and then COX-2 and PGE2 further promote lung cancer cell metastasis by inducing EMT through β-catenin transposition from the cytoplasm to nucleus (102), which indicates that the high expression of COX-2 in TAMs can also up-regulate the COX-2 in tumor cells through the secretion of IL-6 to promote the process of tumor metastasis. Indeed, TAMs have been proven to promote tumor cell migration and invasion by up-regulating COX-2 and MMP9 expression in osteosarcoma (OS) cells, promoting phosphorylation of STAT3 and inducing epithelial-mesenchymal transformation (EMT) (103). Trigger receptor (TREM)-1, a member of the hyperimmunoglobulin family, is primarily expressed in monocytes/macrophages and is highly expressed in colon, liver, and lung cancer tissues. Moreover, it is found that the expression of TREM-1 in tumors is closely related to tumor invasiveness of liver cancer and lung cancer. Mechanistically, lung cancer cells could induce increased expression of TREM-1 in macrophages through COX-2 signaling (104). These findings also mean that targeted inhibition of COX-2 signaling in tumor tissues may be the key to inhibit tumor metastasis.

TGF-β also causes EMT in tumor cells (105). The mechanism is that TGF-β1/Smad signaling directly activates the expression of EMT transcription factors, such as ZEB1, ZEB2, Snail, Slug, and Twist (106). TGF-β secreted by TAMs can stimulate the expression of SOX9 in lung cancer cells by stimulating the c-Jun/smad3 signaling, promote its EMT, and thus promote the proliferation, migration, and invasion of tumors. Therefore, TGF-β/SOX9 axis may represent an effective therapeutic target for lung cancer (107). Besides, fucosyltransferase IV (FUT4) and its synthetic tumor sugar antigen Lewis Y (LeY) are severely elevated in various solid tumors and play an important role in tumor invasion and metastasis. Importantly, FUT4/LeY is essential in cytoskeletal remodeling and EMT and the density of TAMs is intimately correlated with E-cadherin and LeY levels in lung adenocarcinoma. Moreover, M2 macrophages can promote the expression of FUT4/LeY through TGF-β1/Smad2/3 signaling, which mediates the development of EMT in lung adenocarcinoma by Ezrin phosphorylation (108). Tumor cells also promote TAMs secretion of TGF-β, for example, colon cancer cells with high expression of RBP-J secrete CXCL11 to promote TAMs secretion of TGF-β. Further studies show a negative correlation between RBP-J expression and E-cadherin expression, which are beneficial to the metastasis of colon cancer cells (109). ZEB1 in TAMs, a TGF-β downstream transcription factor, induces the expression of CCR2, MMP9, and CCL2 in cancer cells to accelerate tumor growth (110). Moreover, E2F3, a downstream signaling molecule of CSF-1, has been found to increase expression of E2F3 in prostate cancer, ovarian cancer, and lung cancer, and the expression of E2F3 in TAMs can promote lung metastasis of tumors (111). Overexpression of FOXQ1 has been reported in a variety of cancers, including lung cancer cells, pancreatic ductal adenocarcinoma, and the transition of intestinal epithelial cells from normal to adenoma and adenocarcinoma in APC mice. TGF-β has been proven to promote FOXQ1 expression to induce EMT. In addition, FOXQ1 directly binds to the promoter region of E-cadherin to inhibit E-cadherin expression (112). Indeed, studies have found that TAMs can induce the expression of FOXO1 protein in gastric cancer cells, thus promoting EMT, invasion, and metastasis of tumor cells (113), which indicates that FOXQ1 repression in tumor cells may be the key to inhibiting tumor metastasis.

CCL18 is mainly secreted by M2-TAMs and promotes cancer progression in a variety of human cancers. High expression of CCL18 in TAMs has been found to be associated with lymph node metastasis, distant metastasis, and poor prognosis in NSCLC patients. Mechanistically, CCL18 increases the invasion of NSCLC by binding to the Nir1 in NSCLC, which induces ELMO1-dependent cytoskeletal recombination through RAC1 activation (114). Moreover, mesenchymal breast cancer cells induce macrophages to present the TAM phenotype by GM-CSF. Similarly, CCL18 derived from TAMs induces cancer cell EMT to form a positive feedback loop (18). Furthermore, the TAMs in breast cancer produce large amounts of CCL18, which promotes breast cancer metastasis through the PITPNM3 receptor (115). In addition, the expression of CCL18 in tumor cells is also associated with enhanced invasion and migration. For example, it has been found that the high expression of CCL18 in tumor cells promotes invasion and migration of ovarian cancer cells by activating their own mTOR signaling (116). Notably, lung cancer cells can induce vimentin expression and EMT in non-cancerous receptor cells by secreting exosomes, leading to their migration, invasion, and proliferation (117), which suggests that tumor cells can also induce peripheral cell EMT to promote tumor metastasis and invasion.

TAMs Promote the Cancer Stemness

M2-type macrophages promote cancer stem cell (CSC)-like properties by stimulating the JAK1/STAT1/NF-κB/Notch1 pathway in NSCLCs by secreting IL-10 (118). Furthermore, MUC1 in various types of cancer is a poor prognostic indicator. However, TAMs also secrete MUC1 to enhance the

expression of CSC-related and inflammatory genes in lung cancer cells, such as CD133, SOX2, and NF-κB, thus promoting the generation of lung cancer stem cells (LCSCs) (119). Indeed, studies have found that the number of TAMs is positively correlated with the density of CSCs in the peripheral areas of human HCC. Moreover, TGF-β secreted by M2-type TAMs can promote the cancer stem cell-like properties via inducing EMT (120). Also, IL6 produced by TAMs promotes CSCs expansion in hepatocellular carcinoma (121). In addition, PGE2 levels are associated with colon CSC markers (CD133, CD44, LRG5, and SOX2) in human colorectal cancer samples. Further studies show that PGE2 activates NF-κB by signaling EP4-PI3K and EP4-mitogen-activated protein kinase, which induces proliferation and metastasis of colorectal cancer stem cells (122). In addition, the stemness of glioma cells can in turn recruit microglia cells. Glioma stem cells (GSCs) are the key to tumor drug resistance and heterogeneity. In the GBM study of glioblastoma, it is found that the high expression of CLOCK in GSCs could maintain the stemness of GSCs, which promotes the expression of chemokine OLFML3 as a transcription factor, thus accelerating the infiltration of microglia into GBM, but it did not affect the recruitment of macrophages, and the mechanism remains unclear (123).

TAMs Promote Tumors Escape Immune Surveillance

TAMs can also promote tumor cells to escape immune surveillance through the following multiple ways. First, TAMs induce the expression of B7-H4 on the surface of lung cancer cells, so that lung cancer cells can escape T cell immune recognition and destruction (124). Secondly, IFN-γ is not always effective as an anti-tumor agent. Studies have concluded that it can also promote tumor cells to evade immune surveillance. IFN-γ secreted by TAMs can induce the expression of PD-L1 in lung cancer cells through JAK/STAT3 and PI3K/AKT signaling pathways, thereby promoting tumor progression (125). Furthermore, TGF-β secreted by TAMs in Malignant pleural effusion (MPE) can increase the expression of Tim-3, PD-1, and CTLA-4 on the surface of T cells and reduce the production of IFN-γ and granzyme B to inhibit T cell cytotoxic activity in MPE (126). Moreover, TAM-derived TGF-β in MPE can induce CCL22 expression through c-Fos, which promotes the recruitment of regulatory T cells (Treg). Then, the Treg secretes high levels of IL-8 to further induce TGF-β production from TAMs, thus which forms a vicious circle, and leads to the formation of an immunosuppressive microenvironment in MPE (127). Finally, in addition to the IFN-γ mentioned above, TAMs promote the expression of PD-L1 in tumor cells by secreting IL-10 (128). Intriguingly, tumor cells can induce the expression of PD-L1 on the surface of TAMs. Indeed, tumor cells can secrete phosphoprotein 1 (SPP1) to induce the expression of PD-L1 in TAMs (49). Additionally, peripheral blood monocytes with low initial levels of PD-L1 up-regulates the expression of PD-L1, after incubation with primary tumor cells from OSCC patients, which correlates with the increased IL-10 levels in the TME (129). The increase of IL-6 in the TME also enhances the expression of TAMs PD-L1. These studies indicate that improving the inflammatory TME may be the key to reducing PD-L1 expression and reversing the immunosuppressive TME.

TAMs Promote the Formation of Blood and Lymphatic Vessels in Tumor Tissues

TAMs also promote the production of blood and lymphatic vessels in tumor tissue. It has been found that matrix metalloproteinase 9 (MMP9) secreted by TAMs promotes the migration of tumor cells by promoting the migration of endothelial cells, which promotes angiogenesis (130). In addition, there is a cross-talk between TAM and lung cancer cells, in which the CCR2-CCL2 and CX3CR1-CXCL1 signals are the basis for lung cancer growth and metastasis. Specifically, knockout of CCR2 and CX3CR1 in mice can shift TAMs toward M1 polarization, inhibit local neovascularization signals, and the growth and metastasis of Lewis lung cancer (131). In addition, GBM promotes macrophage infiltration by up-regulating LOX, which secretes SPP1 to stimulate angiogenesis in the PTEN-knockout GBM xenograft mouse model to sustain the growth of glioma cells. However, inhibition of LOX reduces macrophage infiltration and tumor growth (25). Finally, it is found that tumor stromal infiltrating inflammatory cells, TAMs, and (MCs) mast cells synergistic promote tumor angiogenesis and promote the occurrence, invasion, and metastasis of NSCLC (132).

Infiltration of tumor tissue TAMs in patients with lung adenocarcinoma is related to tumor lymphangiogenesis, which in turn leads to a lower survival rate in patients with lung adenocarcinoma (133). Furthermore, CCL2 is produced in all types of cancers and plays a particularly important role in cancer metastasis. Lymph node metastasis-associated transcript 1 (LNMAT1), a long-chain non-coding RNA, is significantly up-regulated in bladder cancer cells to enhance the transcription of CCL2, thereby recruiting TAMs to produce VEGF-C which promotes bladder cancer-associated lymphatic metastasis of tumors. Moreover, LNMAT1 is significantly overexpressed in various types of human cancer, such as bladder, prostate, kidney, colon, lung, and liver cancer (19), which also means that LNMAT1 may be a potential therapeutic target for clinical intervention in metastatic cancer.

THE RELATIONSHIP BETWEEN TUMOR CELLS AND TAMS AND TARGETED THERAPY

Tumor cells recruit TAMs through a variety of ways, which not only inhibit their phagocytosis, but also utilize them to maintain their growth. How to prevent tumors from manipulating macrophages is also the key to current tumor immunotherapy. Nowadays, the research of tumor macrophage targeted therapy is primarily carried out from two aspects. One is to reduce the number of TAMs in tumor tissues, and the other is to reprogram TAMs into anti-tumor macrophages. Current studies have found that targeting multiple targets in the TME can reverse the M2 phenotype of macrophages (**Table 1**).

TABLE 1 | Tumor treatment by targeting TAMs.

Tumor type/Cell line	Treatment of TAMs or tumor-bearing mice	Effect	References
NSCLC	Hydroxychloroquine (HCQ)	CD8+ T cell infiltration↑ Anti-tumor CD8+ T cell↑ The ratio of M1/M2 (TAMs) macrophage ↑	(134)
NSCLC cell	Ginsenoside Rh2	The expression levels of VEGF MMP2 and MMP9 ↓ The ratio of M1/M2 (TAMs) macrophage ↑	(135)
A549	Ginsenoside Rh2	Phosphorylation of α–catenin at S641↑ Wnt and hedgehog signaling↓ E - cadherin↑ vimentin↓ Cell proliferation ↓	(136)
NSCLC	miR-125b	The ratio of M1/M2 (TAMs) macrophage ↑	(137)
Lewis lung cancer cells	β-Elemene	Proliferation migration and invasion↓ EMT↓ The ratio of M1/M2 (TAMs) macrophage ↑	(138)
Cisplatin-resistant A549 and H460	dasatinib	Src CD155, and MIF↓ The ratio of M1/M2 (TAMs) macrophage ↑	(139)
A549	Water extract of ginseng	Proliferation and migration↓	(140)
Lewis lung cancer cells	HangAmDan-B	Growth of LLCs↓ The ratio of M1/M2 (TAMs) macrophage ↑	(141)
Human and mouse lung tumors	ß-catenin knockdown in TAMs	Tumor size↓ The ratio of M1/M2 (TAMs) macrophage ↑	(142)
Lewis lung cancer	Fuzheng Sanjie recipe	IL-4, IL-13, TGF-α in serum ↓ IFN-γ in serum↑	(143)
Malignant pediatric brain tumors	Humanized anti-CD47 antibody	TAMs phagocytosis↑ Tumor growth ↓	(77)
PDAC	CpG	Tumor size↓ TAMs phagocytosis↑ TAMs numbers↑ The ratio of M1/M2 (TAMs) macrophage ↑	(2)
Ovarian cancer and breast cancer	Blockade of the CD24–Siglec-10 interaction	Macrophages phagocytosis↑	(78)
$MHCI^{hi}$ Tumor cells	Disruption of either MHC class I or LILRB1	Macrophages phagocytosis↑	(79)
An *ex vivo* tumor system	PSGL-1 antibodies	Pro-inflammatory cytokine↑ The ratio of M1/M2 (TAMs) macrophage ↑	(144)
MC38-tumor-bearing mice	TLR7/8-agonist-loaded nanoparticles	Tumor size↓ The ratio of M1/M2 (TAMs) macrophage ↑	(4)
Mice bearing TSA, MCA38, 4T1 tumors	CCL16, CpG plus anti-IL-10 receptor antibody	Tumor size↓ Metastases↓ CTL activity↑ TNF IL-12 and NO in macrophage↑ The ratio of M1/M2 (TAMs) macrophage↑	(145)
LLCs MOPC315	IFN-γ + TLR agonists	TNF-α, IL-12p40, IL-12p70 and NO in macrophage↑ IL-10 in macrophage↓ Macrophage tumoricidal activity↑	(146)
Early mammary cancers	Ferumoxytol	Tumor growth↓ caspase-3 of cancer cells↑ Liver and lung metastases↓ The ratio of M1/M2 (TAMs) macrophage↑	(147)
B16F10 tumor-bearing mice	Ferumoxytol (FMT)+TLR3 agonist poly (I:C),	Tumor proliferation↓ TNF-α and iNOS in macrophage↑ Lung metastasis↓ The ratio of M1/M2 (TAMs) macrophage↑	(148)
Mouse fibrosarcoma tumor model	TLR7 ligation/TGF-β receptor I inhibition	iNOS, CD80 and MHC class II↑ TGF-β↓VEGF↓ CD4+ CD8+, CD19+ cells as well as neutrophils infiltrating the tumor↑ The ratio of M1/M2 (TAMs) macrophage↑	(149)
K1735-M2 tumor-bearing mice	Knockout TLR4 in TAMs	TNF-α↓、VEGF↓ NF-kB activity in tumor cells↓ Tumor growth↓	(90)
MC-38 tumor-bearing mice	CB2 antagonists	Tumor progression↓	(150)
C6 and GL261 glioma intracranial and subcutaneous model	Flavonoid CH625 (CYP4X1 inhibitors)	Survival↑ Tumor burden↓ Microvessel density↓ 14 15-EET-EA, VEGF and TGF-β in the TAMs↓ The ratio of M1/M2 (TAMs) macrophage↑	(151)

(Continued)

TABLE 1 | Continued

Tumor type/Cell line	Treatment of TAMs or tumor-bearing mice	Effect	References
NSCLC	Blockade of CCL2	Growth of primary tumors↓ Spontaneous lung metastases↓ Activated intratumoral CD8+T Cells↑ The ratio of M1/M2 (TAMs) macrophage↑	(152)
Lewis lung cancer cells	Luteolin	Phosphorylation of STAT6↓ Secretion of CCL2↓ Recruitment of monocytes↓ Migration of LLCs↓	(153)
4T1	PTEN and NHERF-1	Secretion of CCL2↓VEGF-A↓ Migration of 4T1↓ The ratio of M1/M2 (TAMs) macrophage↑	(154)
Human breast cancer cells	Zoledronic acid	Tumor growth↓ Secretion of CCL2 in MSC↓ Recruitment of macrophages↓	(155)
LLC and B16F10 tumors model	CSF1R inhibitors+ CXCR2 antagonist	MDSC recruitment↓ Tumor growth↓	(156)
Breast cancer	Class IIa HDAC inhibitor (TMP95)	Tumor burden↓ pulmonary metastasis↓ Activated intratumoral CD8+T Cells↑ Vascular density↓ The ratio of M1/M2 (TAMs) macrophage↑	(157)
Colon cancer	Antibody blockade of GM-CSF and IL-6	Metastasis↓ Tumorigenesis↓ The ratio of M1/M2 (TAMs) macrophage↑	(67)
NSCLC	Bu Fei Decoction	Tumor growth↓ IL-10 and CD206 in TAMs↓ PD-L1 in NSCLC cells↓	(128)
NSCLC	IL-33 blockade	Tumor growth↓ Tregs in TME↓ The ratio of M1/M2 (TAMs) macrophage↑	(158)
Glioma	Stat3 inhibition	Tumor growth↓ The ratio of M1/M2 (TAMs) macrophage↑	(159)
	Corosolic acid (CA)-containing liposomes	IL-10↓ TNFα↑ The activation of STAT3↓ The ratio of M1/M2 (TAMs) macrophage↑	(160)
4434 melanoma LL/2 carcinoma	Knockout ERK5 in TAMs	Tumor growth↓ The activation of STAT3↓ The ratio of M1/M2 (TAMs) macrophage↑	(161)
U373 human glioblastoma	Oleanolic acid	IL-10↓ The activation of STAT3↓ The ratio of M1/M2 (TAMs) macrophage↑	(162)
Lewis lung cancer	Resveratrol	Tumor growth↓ The activation of STAT3↓ The ratio of M1/M2 (TAMs) macrophage↑	(163)
B16F10	SOCS3 Knockout	Survival time↑ The activation of STAT3↑ TNFα↓ IL-6↓ CCL8↑ Anti-tumor metastatic effect↑	(164)
Lewis lung cancer	Gefitinib	The activation of STAT6↓ Invasion and migration of LLC cells↓ The ratio of M1/M2 (TAMs) macrophage↑	(165)
4T1	Knockdown STAT6	Tumor growth and metastasis↓ The ratio of M1/M2 (TAMs) macrophage↑	(166)
Lewis lung cancer	Imatinib	The activation of STAT6↓ The migration of LLCs↓ Pulmonary metastasis↓ The ratio of M1/M2 (TAMs) macrophage↑	(167)
Colon cancer	MK2 Knockout	Tumor growth↓ Tumor Angiogenesis↓ The ratio of M1/M2 (TAMs) macrophage↑	(168)
Ovarian cancer	Deletion of ABC transporters	Tumor progression↓ Cholesterol efflux↓	(56)
NSCLC	AXL targeting in tumor cells	ICAM1 and ULBP1 in tumor cells↑ NK and CTL-mediated killing↑ Patient survival↑	(169)
Breast cancer, colon carcinoma, Melanoma,	Antibody targeting of MARCO	Tumor growth and metastasis↓ Immune checkpoint therapy↑ The ratio of M1/M2 (TAMs) macrophage↑	(170)

(Continued)

TABLE 1 | Continued

Tumor type/Cell line	Treatment of TAMs or tumor-bearing mice	Effect	References
PC14PE6 A549	Overexpression of surfactant protein A in tumor cells	NK cells activity↑ The ratio of M1/M2 (TAMs) macrophage↑ Lung cancer progression↓	(171)
Colorectal cancer	MFHAS1 knockdown	Tumor progression↓ Migration↓ E-cadherin↑ F-Cyclin D1 and N-cadherin↓ The activation of STAT6↓ The ratio of M1/M2 (TAMs) macrophage↑	(58)
Lewis lung cancer	Metformin	The AMPKα1 activation↑ Metastases↓ Tumor angiogenesis↓ The ratio of M1/M2 (TAMs) macrophage↑	(172)
Lewis lung cancer	Astragaloside IV	Tumor growth and metastases↓ Survival time↑ The AMPKα activation↓ The ratio of M1/M2 (TAMs) macrophage↑	(173)
Lewis lung cancer	Endostatin	Tumor growth and angiogenesis↓ VEGF↓ IL-6↓ IL-17 ↓ IFN-γ↑ HIF-1α↑ Infiltration of CD8+T cells↑ The ratio of M1/M2 (TAMs) macrophage↑	(174)
Lewis lung cancer	Qing-Re-Huo-Xue (QRHX) formulae	Tumor growth↓ Infiltration of TAMs↓ IL-6↓TNF-α↓Arg-1↓iNOS↑ VEGF↓CD31↓ CXCL12/CXCR4↓ JAK2/STAT3 phosphorylation↓	(175)
Lewis lung cancer	IFNγ and/or celecoxib	Tumor growth↓ MMP-2↓MMP-9↓VEGF↓ The density of microvessels↓ The ratio of M1/M2 (TAMs) macrophage↑	(176)
Lewis lung cancer CMT167	Knockout cPLA2	Infiltration of TAMs↓ Tumor growth and metastases↓ Survival time↑ IL-6↓	(177)
Lewis lung cancer	Melittin	Tumor growth↓ VEGF↓ The ratio of M1/M2 (TAMs) macrophage↑	(178)
Lewis lung cancer	MEL-dKLA (hybrid peptide)	Tumor growth and angiogenesis↓ The ratio of M1/M2 (TAMs) macrophage↑	(179)
CT-26 B16F10	RP-182 (synthetic peptide)	Tumor growth↓ Survival time↑ Antitumor activity of CD8+T cells↑ Conversion of from M2 (TAMs) macrophage into M1	(180)
B16F10	LTF-IC	Tumor growth↓ Survival time↑ Granzyme B↑ VEGF↓ MDSC↓ Treg↓ The ratio of M1/M2 (TAMs) macrophage↑	(181)
B16F10 4T1	High-salt diets	Tumor growth↓ IL-12p40↑ ICAM-1↑ IFN-γ↑ TNF-α↑ IL-6↓ IL-10↓ CSF-2↓ T-cell-mediated antitumor responses↑ M-MDSCs differentiate to M1 macrophage	(182)
Malignant phyllodes tumor	Maraviroc (a FDA-proved CCR5 inhibitor)	Tumor growth↓ Recruitment of monocytes↓	(21)
Lewis lung cancer	glycocalyx-mimicking nanoparticles (GNPs)	IL-12↑IL-10↓Arginase 1↓ CCL22↓ The ratio of M1/M2 (TAMs) macrophage↑ Tumor growth↓	(183)
Metastatic castration-resistant prostate cancer	Carlumab (CNTO 888)	Tumor growth=	(184)
Advanced pancreatic cancer	CCR2 inhibitor PF-04136309 +FOLFIRINOX chemotherapy	Infiltration of TAMs↓ IL-4↓IL-10↓ IL-13↓ TGF-β↓ CD4+T cell infiltration↑ CD8+T cell infiltration↑ Treg infiltration↓ Tumor growth↓	(185)

(Continued)

TABLE 1 | Continued

Tumor type/Cell line	Treatment of TAMs or tumor-bearing mice	Effect	References
PDAC	CCR2 inhibitor, CXCR2 inhibitor +FOLFIRINOX chemotherapy	CD4+ T cell infiltration↑ CD8+ T cell infiltration↑ Tumor-infiltrating myeloid cells↓ Tumor growth↓	(186)
Colorectal cancer	CCR5 inhibitor	Anti-tumor repolarization of macrophages↑ IL-8↓VEGF↓ Tumor growth↓	(187)

Reducing the Accumulation of TAMs in Tumor Tissues

The utilization of liposome-encapsulated clodronate treatment effectively depletes the infiltrating macrophages in the tumor thereby achieving significant inhibition of tumor growth (188). The CCL2/CCR2 axis plays a vital role in the recruitment of TAMs to tumor tissues. After knocking out CCR2 in mice, the macrophages accumulation in tumors is decreased, slowing down the tumor growth (30). In addition, IL-4 activates STAT6 to polarize macrophages to M2 and enhance their CCL2 secretion. However, luteolin inhibits the phosphorylation of STAT6, the main downstream of IL-4, reduces the expression of M2 related genes in macrophages and the secretion of CCL2, and affects the tumor tissue infiltration of M2 macrophages, thereby reducing CCL2-dependent metastasis of Lewis lung cancer cells (153). Furthermore, the expression of PTEN can reduce the secretion of CCL2 and the expression of VEGF-A in macrophages, and inhibit the migration of breast cancer cells. However, NHERF-1 can promote the expression of PTEN on the cell membrane where PTEN performs its function, and NHERF-1 and PTEN cooperate to inhibit the M2-type polarization of macrophages, in which the process is related to the reduction of macrophage CCL2 secretion, which indicates that that targeted enhancement of the expression of NHERF-1 and PTEN of TAMs may be an important strategy to reduce the secretion of CCL2. In addition, treatment with zoledronic acid (ZA) can reduce the expression of CCL2 in MSC cells, thereby reducing the recruitment of TAMs to the tumor site, thereby inhibiting tumor growth (155). However, it has also been found that CCL2 blockade does not inhibit the recruitment of TAMs, but tilts the polarization of TAMs toward M1, showing a stronger anti-tumor phenotype, and activating CD8+ T cells in the tumor to destroy the tumor cell (152). The differences in these studies may be related to the types of different tumors. In addition, these studies also verify the effectiveness of blockade CCL2 in animal models. However, carlumab (CNTO 888) is well-tolerated in phase 2 trial (NCT00992186) but does not block the CCL2/CCR2 axis or show anti-tumor activity as a single agent in metastatic castration-resistant prostate cancer (CRPC) (184). The combination with CCR2 inhibitor PF-04136309 and FOLFIRINOX chemotherapy to treat tumors in a phase Ib trial (NCT01413022) to achieve an objective tumor response, with local tumor control achieved in most patients (185), which suggest that inhibition of CCR2 can improve the effect of tumor chemotherapy. Indeed, it was found that although targeting CCR2+ TAMs or CXCR2+ TANs alone can enhance anti-tumor immunity, unfortunately, this leads to a compensatory influx of alternative myeloid subset, which result persistent immunosuppressive TME. It is worth noting that combined treatment with CCR2 inhibitors and CXCR2 inhibitors can overcome this compensatory effect, and augment anti-tumor immunity and improve response to FOLFIRINOX chemotherapy, prolonging the survival of PDAC mice (187). Therefore, targeting CCR2 and CXCR2 combined with FOLFIRINOX chemotherapy may be a very promising treatment for PDAC. Moreover, given that TANs secrete high levels of CCL2 and CCL17 to recruit macrophages. Therefore, in mouse HCC models, intratumoral injection of antibodies targeting CCL2 and CCL17 reduces the migration activity of macrophages and Treg cells, and delays tumor growth (28). Sorafenib is a drug that inhibits tumor angiogenesis. However, although sorafenib treatment reduces the tumor volume in mice, it increases the number of TANs infiltrating the tumor. More importantly, the combination therapy of sorafenib and anti-Ly6G antibody can reduce the number of TANs and neovascularization, which can further inhibit the tumor growth (28).

CSF1 participates in the recruitment of TAMs to tumor tissues and the M2 polarization process of TAMs, and the survival, proliferation, and function of TAMs depend to a large extent on the CSF1R signaling. The signaling of CSF1R depends on two ligands, CSF-1 and IL-34. Indeed, the high expression of IL-34 and CSF-1 in lung cancer tissues is intimately related to the progression of lung cancer (189), which suggests that IL-34 and CSF-1 secreted by tumor cells may activate and maintain the pro-tumor function of TAMs by interacting with the CSF1R receptor on TAMs. Importantly, further studies have found that IL-34 is highly expressed in ovarian cancer cells and tissues, which is associated with poor progression-free survival (PFS) and overall survival, while the expression of CSF-1 has not changed. Moreover, it's worth noting that compared with CSF-1, IL-34 has a stronger affinity for CSF1R (190). It can be seen that tumor cells may secrete high levels of IL-34 to stimulate the CSF1R signaling of TAMs to promote tumor progression. Therefore, targeting IL-34 may be more effective than CSF-1 for the treatment of cancer. However, studies have shown that the utilization of CSF1R inhibitors to interfere the communication between TAM and tumor cells has not had any delay effect on tumor growth. Surprisingly, it is found that a large number of PMN-MDSC are recruited in tumor tissues after the treatment of CSF1R inhibitors with mice. Mechanistically, CSF1 secreted by tumor cells binds to the CSF1R receptor on CAFs and inhibits the secretion of CXCL1 and other chemokines by CAFs to recruit PMN-MDSCs. CXCR2 is the primary receptor for CXCL1 to function. It is worth noting

that CSF1R inhibitor combined with CXCR2 antagonist intervention can block PMN-MDSC infiltration of tumor tissues, and has a strong tumor treatment effect (156). This study provides a novel strategy for tumor immunotherapy. In addition, class IIa histone deacetylase (Class IIa HDAC) inhibitor TMP95 can also induce macrophages to fight tumors. Additionally, ADM3100, a specific antagonist of the CXCR4/CXCL12 pathway, decreases the accumulation of TAMs and prevents B16 melanoma progression in mice (23).

Reprogramming TAMs Into Anti-tumor Macrophages

Blocking Cytokine

The inflammatory TME is the primary cause of immunosuppression of TAMs. Thus, improving the inflammatory TME is an important strategy to restore phagocytic activity of TAMs. CSF-2 and IL6 antibody blockade can inhibit the occurrence and metastasis of colon cancer in vivo, increase the proportion of M1 macrophages in tumor tissues, and reduce the proportion of M2 phenotypic TAMs in tumor tissues (67). It has been observed that TMP95 can affect the response of human monocytes to CSF-1 and CSF-2 *in vitro*. Further studies have found that TMP95 can induce the M1 polarization of TAMs to phagocytose tumors, normalize tumor vasculature, and prevent tumor cell proliferation and lung metastasis (157). Besides, studies have found that MAPKAP Kinase 2 (MK2), which mediates the synthesis of proinflammatory cytokines, promotes TAMs to the M2 macrophage phenotype and promotes angiogenesis into tumor development, while chemical inhibitors of MK2 in macrophages inhibit M2 polarization and M2 macrophage-induced angiogenesis (168). In addition, in a phase I clinical trial (NCT01736813), CCR5 antagonists leads to TAMs anti-tumor repolarization and mitigates the tumor-promoting inflammation in CRC (186). These studies also show that improving the inflammatory TME is also the key to restoring the anti-tumor polarization of TAMs.

IL-10 secreted by TAMs promotes the expression of PD-L1 in NSCLC cells, while Bufei Decoction can reduce the expression of IL-10 and CD206 in TAMs and PD-L1 in NSCLC cells, delaying the progression of tumors in NSCLC (128), which also means Bufei Decoction reduces the proportion of M2 macrophages in TAMs in tumor tissues to delay tumor progression. In addition, IL-33 is an important carcinogen. It has been found that IL-33 can promote the growth and metastasis of colorectal cancer, breast cancer, gastric cancer, and ovarian cancer. The expression of IL-33 in patients with NSCLC is positively correlated with Ki-67 and the expression of M2 TAMs and Teg related genes. In fact, IL-33 blockade can reduce the polarization of M2 TAMs and the accumulation of Tregs in the tumor microenvironment, thereby inhibiting the growth of NSCLCs (158).

Sialic acid can promote the differentiation of MDSC into TAMs. Theoretically, inhibition of sialic acid can inhibit the differentiation of TAMs. However, intratumoral injection of sialidase in mice alone activates STAT3 in tumor myeloid cells and increased the infiltration of myeloid cells, accelerating the tumor growth. Intratumoral injection of STAT3 inhibitors also does not impede tumor growth, but it is surprising that the combination of sialiadase and STAT3 inhibitor JSI-124 can produce significant anti-tumor effects, which is related to the consumption of MDSCs at the tumor site (55). It suggests that sialidase can sensitize tumor myeloid cells to STAT3 inhibition, and dramatically enhance the anti-tumor effect of STAT3 targeted therapy.

TLR Receptors

Studies have shown that TLR7/8 agonists can be packaged in β-cyclodextrin nanoparticles to be transported to TAM, which can promote the conversion of macrophages from M2 to M1, promoting the antitumor of macrophages (4). In addition, treatment with CpG plus anti-interleukin-10 receptor antibody rapidly transfers TAMs from type M2 to type M1 (145). Moreover, studies have found that the activation of TLR3 alone or IFN-γ in macrophage cannot trigger the anti-tumor activity of macrophages, but the combined intervention of the two can enhance the M1 polarization of macrophages to activate the tumor-killing activity of macrophages (146), which also means that the combined use of IFN-γ and TLR3 agonists may be useful for macrophage-based cancers immunotherapy. Furthermore, nano-iron oxide particles promote the M1 polarization of macrophages (147). Meanwhile, nano-iron oxide particles combined with TLR3 agonists can also induce M1-type polarization of macrophages against tumors (148). The combination with activating TLR7 and inhibiting TGF-β signaling can reprogram TAMs to the M1 phenotype, which can enhance the tumoricidal activity of TAMs and reduce tumor progression (149). Altogether, these results indicate that the activation of TLR7, TLR8, and TLR9 of TAMs can change macrophages from a tumor-promoting effect to an anti-tumor effect.

The TLR4 signaling in TAMs can promote tumor growth. Indeed, blockade of TLR4 in TAMs with antibody reduces the production of cytokines and weakens their pro-tumor activity (90). However, it has been found that the expression of macrophage monoacylglycerol lipase (MGLL) in tumor tissues is reduced, and the lack of monoacylglycerol lipase (MGLL) in TAM can lead to triglyceride lipid overload. Mechanistically, the cannabinoid receptor CB2 can interact with TLR4 and inhibit the pro-inflammatory signaling of TLR4, while lack of MGLL promotes CB2/TLR4-dependent the M2 phenotype in TAMs, thereby inhibiting the function of tumor-related CD8+ T cells and promoting tumor progression. MGLL can inhibit CB2 cannabinoid receptor-dependent tumor progression, and CB2 antagonist treatment can delay tumor progression in mice (150), which indicates that TLR4 activation can also inhibit tumor growth. The specific mechanism still remains to be explored. In addition, MGLL is the switch of CB2/TLR4 dependent macrophage activation. Restoring the expression of MGLL in tumor tissues and targeting CB2 are new strategies for tumor immunotherapy. However, the flavonoid CH625 inhibits CYP4X1 through the CB2 and EGFR-STAT3 axis to reprogram TAMs away from M2 type, and normalizes the blood vessels of gliomas (151). This also indicates that CB2 can inhibit tumor progression, which may be different from tumor types and the specific mechanism deserves further exploration.

STAT3 and STAT6

Tumor cells induce and maintain the M2 phenotype of TAMs in many ways. Nowadays, there are also studies to reprogram TAMs by targeting to block the internal signal molecules of TAMs and restore their anti-tumor activity (**Table 1**). It is found that inhibiting the expression of STAT3 reprograms TAMs into M1 macrophages to inhibit tumor growth (159). Indeed, liposomes are used to carry corosolic acid (CA), a natural compound that inhibits stat3, to target CD163+ macrophages, thereby reprogramming TAMs to the M1 phenotype and promoting the expression of pro-inflammatory factors (160). The activation of the STAT3 signal is related to ERK5. ERK5 belongs to the family of mitogen-activated protein kinases (MAPKs) and plays an important role in the process of extracellular transduction. It has been found that high expression of ERK5 in human TAMs promotes tumor growth. Mechanistically, ERK5 phosphorylates Tyr705 of STAT3, thereby promoting the M2 phenotype of TAMs. However, knockout ERK5 in TAMs reduces the phosphorylation of STAT3 and inhibits its M2 phenotype, which promotes the anti-tumor activity of TAMs, thereby inhibiting the melanoma growth (161), which suggests that targeting ERK5 is an attractive cancer treatment strategy. It is worth noting that the activation of STAT3 is essential for the M2 differentiation of macrophages. Studies have found that oleanolic acid, a triterpene compound, can inhibit the activation of STAT3 in macrophages and glioblastoma cells to suppress the M2 phenotype differentiation of macrophages and the proliferation of glioblastoma cells (162). In addition, resveratrol inhibits the growth of lung cancer by inhibiting the M2-like polarization of TAMs and inhibiting the activation of STAT3 in tumor cells (163). Indeed, STAT3 is also frequently activated in a variety of human cancer cells, STAT3 signaling transduction promotes the growth and survival of tumor cells. However, studies have found that mice whose macrophages specifically knock out the SOCS3 that has been shown to be a negative regulator of STAT3 survive longer than wild-type mice. Mechanistically, tumor lysates stimulated SOCS3 knockout macrophages in vitro, their STAT3 phosphorylation is enhanced and TNF-α and IL-6 are reduced, and higher levels of MCP2/CCL8 via STAT3 are produced to combat tumor metastasis in contrast to normal macrophages. Therefore, inhibition of SOCS3 activity in macrophages may have a therapeutic effect on inhibiting tumor metastasis (164). These results also indicate that whether the activation of STAT3 in macrophages promotes tumor development remains to be clarified.

STAT6 phosphorylation is important signaling for M2-like polarization of macrophages. It has been found that gefitinib can inhibit IL-13-induced phosphorylation of STAT6 in macrophages to inhibit M2-like polarization in the Lewis lung cancer model (165). Indeed, targeting the STAT6 in TAMs can reduce the growth and metastasis of breast cancer tumors (166). Furthermore, imatinib inhibits STAT6 phosphorylation and nuclear translocation, leading to the arrest of M2-like polarization of macrophages and inhibiting the metastasis of Lewis lung cancer (167). Furthermore, glycocalyx-mimicking nanoparticles (GNPs) can be specifically internalized by TAMs via lectin receptors, resulting in to up-regulation IL-12 and down-regulation of IL-10, arginase 1, and CCL22 expression, reversing TAMs to an anti-tumor phenotype, in which the process is associated with suppressing STAT6 and activating NF-κB phosphorylation. Importantly, the combined treatment of GNPs and PD-L1 antibody can significantly improve the immunosuppressive TME and the efficacy of anti-tumor therapy (183). These studies have shown that targeting STAT6 can suppress the M2 polarization of TAMs and delay tumor growth.

Polypeptide

Melittin, a major polypeptide of bee venom, has been extensively studied due to its cytotoxicity to malignant cells. The melittin selectively reduces the number of CD206+ M2-like TAMs in the lewis lung cancer mouse model, which is manifested in the decreased expression of VEGF and CD206 in M2-like TAMs (178). However, the effect of melittin in the treatment of lung cancer is limited. Therefore, studies have utilized melittin's affinity for M2 type macrophages and mixed melittin with pro-apoptotic peptide d (KLAKLAK)2 (dKLA) to target TAMs in the lung cancer tissue. Indeed, MEL-dKLA is more able to inhibit tumor growth rate, tumor weight, and angiogenesis compared with melittin (179). In addition, RP-182, the host defense peptide, can also reprogram M2-like TAMs to an antitumor M1-like phenotype, and selectively induce a conformational switch of CD206 on M2-like TAMs, thereby increasing the cancer cell phagocytosis by TAMs (180). Furthermore, previous studies have found that the immune complex of lactoferrin has a very strong pro-inflammatory effect on human monocytes and macrophages (191). Indeed, the immune complex of lactoferrin drives the transformation of human macrophages from M2- to M1-like phenotype (192), and also mediates anti-tumor effects by resetting TAMs to the M1-like phenotype (181). In addition, iron-loaded tumor-associated macrophages (iTAMs) exhibit a pro-inflammatory phenotype, which has anti-tumor activity and the ability to reduce tumor growth in patients with lung adenocarcinoma, and prolong the survival time of patients. However, the iron in TME does not affect the survival of the patients in patients with lung squamous cell carcinoma, indicating that iron has a unique effect on different histological subtypes of NSCLC (193). The specific mechanism needs to be explored.

High Salt Diets

High-salt diets can also encourage macrophages to swallow tumors to slow the growth of tumors. Recent studies have found that high-salt diets inhibit tumor growth in mice by regulating the differentiation of bone marrow-derived cells. The local sodium chloride concentration in tumor tissues results in high osmolality, which reduces the production of cytokines required for the expansion of MDSCs and the accumulation of MDSCs in the blood, spleen, and tumors. Therefore, two types of MDSCs change their phenotypes: monocytes-MDSCs differentiate into anti-tumor macrophages, and granulocytes-MDSCs adopt pro-inflammatory

functions, thereby reactivating the anti-tumor actions of T cells (182). Although high-salt diets have pro-inflammatory and anti-tumor effects, it has been found that high-salt diets can induce increased production of pro-inflammatory cytokines, and activate p38 MAPK and STAT1 signaling pathways to promote immune activation of DC cells and accelerate the progression of SLE in mice (194). These results also suggest that a high-salt diet is also a double-edged sword. It can cause excessive inflammation while treating tumors, which may induce autoimmune diseases.

Target Other Signaling Molecules

Tumor cell-derived HA drives cholesterol efflux from macrophages to induce their TAMs phenotype, so knocking out the ABC transporter which mediates cholesterol efflux can reverse the tumor-promoting function of TAMs and reduce tumor progression (56). Scavenger receptor MARCO is expressed in tissue-resident macrophages in the lung, lymph nodes, spleen, and peritoneum. In addition, it has been found that targeting MARCO expression in M2 TAMs in mouse breast cancer, melanoma, and colon cancer can increase the infiltration of M1 type macrophages in tumor tissues, reduce M2 type macrophages, and block tumor growth and metastasis (170). Moreover, metformin also inhibits the M2-like polarization of TAMs, which is associated with the enhanced level of AMPKα1 phosphorylation in macrophages. Similarly, another AMPK activator, AIRCA, can prevent IL-13-stimulated M2-like polarization. However, knocking out AMPKα1 has no effect. In addition, metformin can inhibit the pro-angiogenesis of M2-like macrophages to prevent tumor metastasis (172). However, astragaloside IV blocks the M2 polarization of macrophages by inhibiting the AMPK signaling pathway of macrophages and reduces the growth, invasion, migration, and angiogenesis of lung cancer cells. Astragaloside IV inhibits AMPKα activation in M2 macrophages, but silencing AMPKα partially abolishes the inhibitory effect of AS-IV (173). Therefore, the effect of AMPK activation on macrophage polarization remains unclear.

Malignant fibrous histiocytoma amplified sequence 1 (MFHAS1) is a predicted oncogenic protein that shows tumorigenic activity *in vivo*. It is worth noting that CRC cells can induce the expression of MFFAS1 in mouse macrophages. However, knocking down the expression of MFHAS1 in macrophages reduces the number of M2 TAMs and delays the progression of CRC (58), which also means that MFFAS1 in macrophages is also one of the most potential targets for tumor immunotherapy. The expression of TREM-1 on TAMs decreases significantly with tumor growth, which is a feature of lung cancer TAMs. In addition, TREM-1 activation can promote TAM to secrete IL-1β in the intervention of LPS (195). This also indicates that the low expression level of TREM-1 in TAMs may affect the pro-inflammatory effect of TAMs, which is beneficial to tumor growth. Complement component 9 (C9) plays a critical role in killing tumors *in vitro*. C9 is specifically expressed in most alveolar macrophages (AMs) in adjacent lung tissues, but only a few tumor TAMs in NSCLC tissues. More importantly, the percentage of C9 positive cells in AMs or TAMs is related to the increase in tumoricidal activity. In fact, the hypoxic tumor microenvironment can shift the phenotype of macrophages from M1 to M2 and down-regulate the expression of C9 in TAMs (196), which means that improving the hypoxic environment of tumors is an important strategy for tumor treatment. Surfactant protein A (SP-A) is a large multimeric protein that exists in the airways and alveoli of the lung. In addition to performing immunomodulatory functions in infectious respiratory diseases, SP-A can also be used as a marker for lung adenocarcinoma. The deletion of SFTPA1 (alias, SPA) gene in NSCLCs is associated with tumor progression. However, overexpression of SP-A in lung adenocarcinoma cells can inhibit the progression of lung cancer by promoting the M1 polarization of TAMs to recruit and activate NK cells (171). These studies also provide new potential targets for tumor immunotherapy.

Target Interaction Receptors on TAMs and Tumor Cells

After intervention therapy with anti-CD47 antibody, macrophages can be induced to phagocytose tumor cells (77). However, CD47-blocking as a monotherapy shows limited anti-tumor effects in the pancreatic ductal adenocarcinoma (PDAC) model, which may be related to the limited phagocytosis of macrophages after CD47 blockade. Fortunately, it has been found that CpG oligodeoxynucleotide, a toll-like receptor agonist, can directly activate TLR9 to trigger an innate immune response. In addition, its stimulation can cause changes in the central carbon metabolism of macrophages to enhance the anti-tumor activity of macrophages (2). It is worth noting that mitochondrial DNA (mtDNA) contains a large number of unmethylated CpG sequences (197). It is speculated that treatment with mtDNA to target macrophages in tumors may enhance their anti-tumor activity. In addition, therapeutic blockade of the CD24 and SIGLEC10 interaction and the MHC class I molecules and LILRB1 interaction accompanied with enhanced TAM phagocytosis towards tumor cells (78, 79). The expression of PD-1 in TAMs is negatively correlated with the phagocytic ability against tumor cells. Blockade of PD-1/PD-L1 axis *in vivo* can increase macrophage phagocytosis, reduce tumor growth, and prolong the survival time of mice tumor model (80). These results mean that interfering with the interaction of these targets between tumor cells and macrophages can provide new therapeutic strategies for tumor immunotherapy. Furthermore, the latest research found that PSGL-1 is a new macrophage checkpoint. Importantly, targeting PSGL-1 with an antagonist antibody can repolarize M2 macrophages to M1 type (144).

Inhibition of Tumor Angiogenesis

Endostatin has been proven to effectively inhibit the angiogenesis and growth of endothelial cells. Endostatin can reduce the number of M2 macrophages and increase the number of M1 macrophages in tumor tissues, and promote the infiltration of CD8+ T cells into tumors. In addition, endostatin can reduce the expression levels of VEGF, TGF-β, IL-6, and IL-17 in tumor tissues, increase the expression levels of IFN-γ and HIF-1α, suppressing growth and angiogenesis of tumors (174). Besides, QRHX intervention can reduce the infiltration of TAMs in tumor tissues of lung cancer mice, reduce the expression of IL-6, TNF-α, ARG-1, CD31, and

VEGF, and increase the expression of inducible NO synthase (iNOS). It is worth noting that CXCL12/CXCR4 and JAK2/STAT3 are important molecules involved in M2 polarization. QRHX also reduces the expression of CXCL12/CXCR4 and the phosphorylation of JAK2/STAT3 in tumor tissues (175). These results also indicate that QRHX may induce the conversion of M2 type macrophages to M1 type macrophages, reducing tumor tissue angiogenesis. Besides, IFNγ and/or celecoxib, the cyclooxygenase-2 inhibitor, treatment constantly suppress tumor growth in mouse lung cancer models. Mechanistically, IFNγ or celecoxib increases the percentage of M1 macrophages and decreases the percentage of M2 macrophages in tumors. In addition, they also reduce the density of MMP-2, MMP-9, VEGF, and microvessels in tumors (176). Furthermore, the IL-6 secreted by tumor cells and stromal cells contributes to tumor progression and angiogenesis, but the expression of cPLA2 in macrophages is critical to the release of IL-6 from tumor cells. The loss of cytoplasmic phospholipase A2 (cPLA2) in macrophages can reduce the secretion of IL-6 by tumor cells and prevent the progression and metastasis of lung cancer (177), which indicates that cPLA2 plays a key role in tumor progression, and targeting the expression of cPLA2 in TAMs can provide new therapeutic strategies for the clinical treatment of tumors.

SUMMARY

There is a complex crosstalk between tumor cells and TAMs in tumors. Macrophages have the function of engulfing and killing tumor cells. However, a large number of TAMs infiltrated in the tumor microenvironment not only kill tumor cells, but also support tumor growth and metastasis. Specifically, first, tumor cells secrete a large number of chemokines to recruit macrophages into tumor tissues, such as CCL2, CCL3, CCL5, and so on. Then, after the macrophages recruited to the tumor tissue, the tumor cells secrete a variety of cytokines to regulate the signaling pathway of the macrophages, and then promote their differentiation into M2 macrophages. Finally, TAMs differentiated into M2 type maintain tumor growth by promoting tumor cell growth, invasion, and metastasis, inhibiting the killing of tumor cells by immune cells, and angiogenesis in tumor tissues. Importantly, these processes are intimately related to the inflammatory TME. How to regulate the inflammatory TME is the key to improving the immunosuppressive TME. Moreover, the large number of bacteria present in tumor tissues may be an important cause of the inflammatory TME. Therefore, targeting microbes in tumors may be the key to restore tumor phagocytosis of TAMs. There are also numerous corresponding strategies to limit the supporting effect of TAMs on tumor growth. The main strategy is to limit the recruitment of monocytes, which reduces the accumulation of TAMs in tumor tissues, and target TAMs receptors or block key cytokines secreted by tumor cells to reprogram TAMs into M1 macrophages with anti-tumor activity. Because a single antibody targeting TAMs therapy may cause other immune cells to compensately infiltrate the tumor tissue, and then continue to maintain the inflammatory TME, there are certain limitations. In the future, multiple methods should be considered to target TAMs. For example, multi-site targeted combined drug therapy or a suitable high-salt diet may have a better therapeutic effect. In addition, the current clinical trials on TAMs-targeted treatments in animals is still in a lagging stage, and further improvement is urgently needed. It is worth noting that recent studies have found that RXRβ is a new marker on the surface of TAMs. Targeting RXRβ can distinguish TAMs from macrophages in other tissues (116). Similarly, it is found that a new type of bivalent glycosylated targeting ligand packaging nanoparticles can utilize CD206 to selectively target anti-inflammatory M2 macrophages (198). These studies provide new drug carrier tools and targeted markers for targeting M2 macrophages. Nowadays, the drug resistance and heterogeneity of cancer stem cells are the fundamental reasons for the failure of radiotherapy, chemotherapy, and immunotherapy. How to eliminate cancer stem cells in tumor tissues is of great importance. In addition, recent studies have concluded that the growth of cancer stem cells is extremely dependent on methionine (199). These research results provide crucial treatment ideas and strategies for cancer treatment.

AUTHOR CONTRIBUTIONS

ZG is responsible for the retrieval of relevant documents and the writing of article content, and SD is responsible for the design of the overall framework of the article. All authors contributed to the article and approved the submitted version.

FUNDING AND ACKNOWLEDGMENTS

This work was supported by grants from the National Natural Science Foundation of China (No. 31671241).

REFERENCES

1. Morrison C. Immuno-oncologists eye up macrophage targets. *Nat Rev Drug Discovery* (2016) 15:373–4. doi: 10.1038/nrd.2016.111
2. Liu M, O'Connor RS, Trefely S, Graham K, Snyder NW, Beatty GL. Metabolic rewiring of macrophages by CpG potentiates clearance of cancer cells and overcomes tumor-expressed CD47-mediated 'don't-eat-me' signal. *Nat Immunol* (2019) 20:265–75. doi: 10.1038/s41590-018-0292-y
3. Arora S, Dev K, Agarwal B, Das P, Syed MA. Macrophages: Their role, activation and polarization in pulmonary diseases. *Immunobiology* (2018) 223:383–96. doi: 10.1016/j.imbio.2017.11.001
4. Rodell CB, Arlauckas SP, Cuccarese MF, Garris CS, Li R, Ahmed MS, et al. TLR7/8-agonist-loaded nanoparticles promote the polarization of tumour-associated macrophages to enhance cancer immunotherapy. *Nat BioMed Eng* (2018) 2:578–88. doi: 10.1038/s41551-018-0236-8
5. Bingle L, Brown NJ, Lewis CE. The role of tumour-associated macrophages in tumour progression: implications for new anticancer therapies. *J Pathol* (2002) 196:254–65. doi: 10.1002/path.1027
6. Yona S, Kim KW, Wolf Y, Mildner A, Varol D, Breker M, et al. Fate mapping reveals origins and dynamics of monocytes and tissue macrophages underhomeostasis. *Immunity* (2013) 38:79–91. doi: 10.1016/j.immuni.2012.12.001

7. Liu Y, Cao X. The origin and function of tumor-associated macrophages. *Immunol Today* (1992) 265:265–70. doi: 10.1016/0167-5699(92)90008-U
8. Palaga T, Wongchana W, Kueanjinda P. Notch Signaling in Macrophages in the Context of Cancer Immunity. *Front Immunol* (2018) 9:652. doi: 10.3389/fimmu.2018.00652
9. Pei BX, Sun BS, Zhang ZF, Wang AL, Ren P. Interstitial tumor-associated macrophages combined with tumor-derived colony-stimulating factor-1 and interleukin-6, a novel prognostic biomarker in non-small cell lung cancer. *J Thorac Cardiovasc Surg* (2014) 148:1208–1216.e2. doi: 10.1016/j.jtcvs.2014.05.003
10. Wang H, Shao Q, Sun J, Ma C, Gao W, Wang Q, et al. Interactions between colon cancer cells and tumor-infiltrated macrophages depending on cancer cell-derived colony stimulating factor 1. *Oncoimmunology* (2016) 5: e1122157. doi: 10.1080/2162402X.2015.1122157
11. Balamurugan K. HIF-1 at the crossroads of hypoxia, inflammation, and cancer. *Int J Cancer* (2016) 138:1058–66. doi: 10.1002/ijc.29519
12. Zhou TY, Zhou YL, Qian MJ, Fang YZ, Ye S, Xin WX, et al. Interleukin-6 induced by YAP in hepatocellular carcinoma cells recruits tumor-associated macrophages. *J Pharmacol Sci* (2018) 138:89–95. doi: 10.1016/j.jphs.2018.07.013
13. Kraakman MJ, Kammoun HL, Allen TL, Deswaerte V, Henstridge DC, Estevez E, et al. Blocking IL-6 trans-signaling prevents high-fat diet-induced adipose tissue macrophage recruitment but does not improve insulin resistance. *Cell Metab* (2015) 21:403–16. doi: 10.1016/j.cmet.2015.02.006
14. Liao CW, Chou CH, Wu XM, Chen ZW, Chen YH, Chang YY, et al. Interleukin-6 plays a critical role in aldosterone-induced macrophage recruitment and infiltration in the myocardium. *Biochim Biophys Acta Mol Basis Dis* (2020) 1866:165627. doi: 10.1016/j.bbadis.2019.165627
15. Nandi B, Shapiro M, Samur MK, Pai C, Frank NY, Yoon C, et al. Stromal CCR6 drives tumor growth in a murine transplantable colon cancer through recruitment of tumor-promoting macrophages. *Oncoimmunology* (2016) 5: e1189052. doi: 10.1080/2162402X.2016.1189052
16. Liu L, Ge D, Ma L, Mei J, Liu S, Zhang Q, et al. Interleukin-17 and prostaglandin E2 are involved in formation of an M2 macrophage-dominant microenvironment in lung cancer. *J Thorac Oncol* (2012) 7:1091–100. doi: 10.1097/JTO.0b013e3182542752
17. Segaliny AI, Mohamadi A, Dizier B, Lokajczyk A, Brion R, Lanel R, et al. Interleukin-34 promotes tumor progression and metastatic process in osteosarcoma through induction of angiogenesis and macrophage recruitment. *Int J Cancer* (2015) 137:73–85. doi: 10.1002/ijc.29376
18. Su S, Liu Q, Chen J, Chen J, Chen F, He C, et al. A positive feedback loop between mesenchymal-like cancer cells and macrophages is essential to breast cancer metastasis. *Cancer Cell* (2014) 25:605–20. doi: 10.1016/j.ccr.2014.03.021
19. Chen C, He W, Huang J, Wang B, Li H, Cai Q, et al. LNMAT1 promotes lymphatic metastasis of bladder cancer via CCL2 dependent macrophage recruitment. *Nat Commun* (2018) 9:3826. doi: 10.1038/s41467-018-06152-x
20. Miotto D, Boschetto P, Bononi I, Milani G, Legorini C, Cavallesco G, et al. CC ligand 2 levels are increased in LPS-stimulated peripheral monocytes of patients with non-small cell lung cancer. *Respir Med* (2007) 101:1738–43. doi: 10.1016/j.rmed.2007.02.021
21. Nie Y, Huang H, Guo M, Chen J, Wu W, Li W, et al. Breast Phyllodes Tumors Recruit and Repolarize Tumor-Associated Macrophages via Secreting CCL5 to Promote Malignant Progression, Which Can Be Inhibited by CCR5 Inhibition Therapy. *Clin Cancer Res* (2019) 25:3873–86. doi: 10.1158/1078-0432.CCR-18-3421
22. Frankenberger C, Rabe D, Bainer R, Sankarasharma D, Chada K, Krausz T, et al. Metastasis Suppressors Regulate the Tumor Microenvironment by Blocking Recruitment of Prometastatic Tumor-Associated Macrophages. *Cancer Res* (2015) 75:4063–73. doi: 10.1158/0008-5472.CAN-14-3394
23. Mota JM, Leite CA, Souza LE, Melo PH, Nascimento DC, De-Deus-Wagatsuma VM, et al. Post-Sepsis State Induces Tumor-Associated Macrophage Accumulation through CXCR4/CXCL12 and Favors Tumor Progression in Mice. *Cancer Immunol Res* (2016) 4:312–22. doi: 10.1158/2326-6066.CIR-15-0170
24. Yusen W, Xia W, Shengjun Y, Shaohui Z, Hongzhen Z. The expression and significance of tumor associated macrophages and CXCR4 in non-small cell lung cancer. *J BUON* (2018) 23:398–402.
25. Chen P, Zhao D, Li J, Liang X, Li J, Chang A, et al. Symbiotic Macrophage-Glioma Cell Interactions Reveal Synthetic Lethality in PTEN-Null Glioma. *Cancer Cell* (2019) 35:868–884.e6. doi: 10.1016/j.ccell.2019.05.003
26. Mou W, Xu Y, Ye Y, Chen S, Li X, Gong K, et al. Expression of Sox2 in breast cancer cells promotes the recruitment of M2 macrophages to tumor microenvironment. *Cancer Lett* (2015) 358:115–23. doi: 10.1016/j.canlet.2014.11.004
27. Jia W, Kidoya H, Yamakawa D, Naito H, Takakura N. Galectin-3 accelerates M2 macrophage infiltration and angiogenesis in tumors. *Am J Pathol* (2013) 182:1821–31. doi: 10.1016/j.ajpath.2013.01.017
28. Zhou SL, Zhou ZJ, Hu ZQ, Huang XW, Wang Z, Chen EB, et al. Tumor-Associated Neutrophils Recruit Macrophages and T-Regulatory Cells to Promote Progression of Hepatocellular Carcinoma and Resistance to Sorafenib. *Gastroenterology* (2016) 150:1646–1658.e17. doi: 10.1053/j.gastro.2016.02.040
29. Santander AM, Lopez-Ocejo O, Casas O, Agostini T, Sanchez L, Lamas-Basulto E, et al. Paracrine Interactions between Adipocytes and Tumor Cells Recruit and Modify Macrophages to the Mammary Tumor Microenvironment: The Role of Obesity and Inflammation in Breast Adipose Tissue. *Cancers (Basel)* (2015) 7:143–78. doi: 10.3390/cancers7010143
30. Ren G, Zhao X, Wang Y, Zhang X, Chen X, Xu C, et al. CCR2-dependent recruitment of macrophages by tumor-educated mesenchymal stromal cells promotes tumor development and is mimicked by TNFalpha. *Cell Stem Cell* (2012) 11:812–24. doi: 10.1016/j.stem.2012.08.013
31. Zhang R, Qi F, Zhao F, Li G, Shao S, Zhang X, et al. Cancer-associated fibroblasts enhance tumor-associated macrophages enrichment and suppress NK cells function in colorectal cancer. *Cell Death Dis* (2019) 10:273. doi: 10.1038/s41419-019-1435-2
32. Guo X, Zhao Y, Yan H, Yang Y, Shen S, Dai X, et al. Single tumor-initiating cells evade immune clearance by recruiting type II macrophages. *Genes Dev* (2017) 31:247–59. doi: 10.1101/gad.294348.116
33. Tamura R, Tanaka T, Yamamoto Y, Akasaki Y, Sasaki H. Dual role of macrophage in tumor immunity. *Immunotherapy-UK* (2018) 10:899–909. doi: 10.2217/imt-2018-0006
34. Sica A, Larghi P, Mancino A, Rubino L, Porta C, Totaro MG, et al. Macrophage polarization in tumour progression. *Semin Cancer Biol* (2008) 18:349–55. doi: 10.1016/j.semcancer.2008.03.004
35. Van Dyken SJ, Locksley RM. Interleukin-4- and interleukin-13-mediated alternatively activated macrophages: roles in homeostasis and disease. *Annu Rev Immunol* (2013) 31:317–43. doi: 10.1146/annurev-immunol-032712-095906
36. Zhou D, Chen L, Yang K, Jiang H, Xu W, Luan J. SOCS molecules: the growing players in macrophage polarization and function. *Oncotarget* (2017) 8:60710–22. doi: 10.18632/oncotarget.19940
37. Morvan MG, Lanier LL. NK cells and cancer: you can teach innate cells new tricks. *Nat Rev Cancer* (2016) 16:7–19. doi: 10.1038/nrc.2015.5
38. Gocheva V, Wang HW, Gadea BB, Shree T, Hunter KE, Garfall AL, et al. IL-4 induces cathepsin protease activity in tumor-associated macrophages to promote cancer growth and invasion. *Genes Dev* (2010) 24:241–55. doi: 10.1101/gad.1874010
39. Ambade A, Satishchandran A, Saha B, Gyongyosi B, Lowe P, Kodys K, et al. Hepatocellular carcinoma is accelerated by NASH involving M2 macrophage polarization mediated by hif-1alphainduced IL-10. *Oncoimmunology* (2016) 5:e1221557. doi: 10.1080/2162402X.2016.1221557
40. Redente EF, Dwyer-Nield LD, Barrett BS, Riches DW, Malkinson AM. Lung tumor growth is stimulated in IFN-gamma-/- mice and inhibited in IL-4Ralpha-/- mice. *Anticancer Res* (2009) 29:5095–101. doi: 10.1590/S0100-40422008000300028
41. Ito SE, Shirota H, Kasahara Y, Saijo K, Ishioka C. IL-4 blockade alters the tumor microenvironment and augments the response to cancer immunotherapy in a mouse model. *Cancer Immunol Immunother* (2017) 66:1485–96. doi: 10.1007/s00262-017-2043-6
42. Zhao P, Gao D, Wang Q, Song B, Shao Q, Sun J, et al. Response gene to complement 32 (RGC-32) expression on M2-polarized and tumor-associated macrophages is M-CSF-dependent and enhanced by tumor-derived IL-4. *Cell Mol Immunol* (2015) 12:692–9. doi: 10.1038/cmi.2014.108
43. Li Y, Zheng Y, Li T, Wang Q, Qian J, Lu Y, et al. Chemokines CCL2, 3, 14 stimulate macrophage bone marrow homing, proliferation, and polarization

in multiple myeloma. *Oncotarget* (2015) 6:24218–29. doi: 10.18632/oncotarget.4523
44. Hsieh CH, Tai SK, Yang MH. Snail-overexpressing Cancer Cells Promote M2-Like Polarization of Tumor-Associated Macrophages by Delivering MiR-21-Abundant Exosomes. *Neoplasia* (2018) 20:775–88. doi: 10.1016/j.neo.2018.06.004
45. Standiford TJ, Kuick R, Bhan U, Chen J, Newstead M, Keshamouni VG. TGF-beta-induced IRAK-M expression in tumor-associated macrophages regulates lung tumor growth. *Oncogene* (2011) 30:2475–84. doi: 10.1038/onc.2010.619
46. Zhang F, Wang H, Wang X, Jiang G, Liu H, Zhang G, et al. TGF-beta induces M2-like macrophage polarization via SNAIL-mediated suppression of a pro-inflammatory phenotype. *Oncotarget* (2016) 7:52294–306. doi: 10.18632/oncotarget.10561
47. Ma R, Ji T, Chen D, Dong W, Zhang H, Yin X, et al. Tumor cell-derived microparticles polarize M2 tumor-associated macrophages for tumor progression. *Oncoimmunology* (2016) 5:e1118599. doi: 10.1080/2162402X.2015.1118599
48. Cha HR, Lee JH, Hensel JA, Sawant AB, Davis BH, Lee CM, et al. Prostate cancer-derived cathelicidin-related antimicrobial peptide facilitates macrophage differentiation and polarization of immature myeloid progenitors to protumorigenic macrophages. *Prostate* (2016) 76:624–36. doi: 10.1002/pros.23155
49. Zhang Y, Du W, Chen Z, Xiang C. Upregulation of PD-L1 by SPP1 mediates macrophage polarization and facilitates immune escape in lung adenocarcinoma. *Exp Cell Res* (2017) 359:449–57. doi: 10.1016/j.yexcr.2017.08.028
50. Wei X, Nie S, Liu H, Sun J, Liu J, Li J, et al. Angiopoietin-like protein 2 facilitates non-small cell lung cancer progression by promoting the polarization of M2 tumor-associated macrophages. *Am J Cancer Res* (2017) 7:2220–33.
51. Ubil E, Caskey L, Holtzhausen A, Hunter D, Story C, Earp HS. Tumor-secreted Pros1 inhibits macrophage M1 polarization to reduce antitumor immune response. *J Clin Invest* (2018) 128:2356–69. doi: 10.1172/JCI97354
52. Sun J, Mao Y, Zhang YQ, Guo YD, Mu CY, Fu FQ, et al. Clinical significance of the induction of macrophage differentiation by the costimulatory molecule B7-H3 in human non-small cell lung cancer. *Oncol Lett* (2013) 6:1253–60. doi: 10.3892/ol.2013.1586
53. Kang FB, Wang L, Li D, Zhang YG, Sun DX. Hepatocellular carcinomas promote tumor-associated macrophage M2-polarization via increased B7-H3 expression. *Oncol Rep* (2015) 33:274–82. doi: 10.3892/or.2014.3587
54. Xiao G, Wang X, Sheng J, Lu S, Yu X, Wu JD. Soluble NKG2D ligand promotes MDSC expansion and skews macrophage to the alternatively activated phenotype. *J Hematol Oncol* (2015) 8:13. doi: 10.1186/s13045-015-0110-z
55. Kumar V, Cheng P, Condamine T, Mony S, Languino LR, McCaffrey JC, et al. CD45 Phosphatase Inhibits STAT3 Transcription Factor Activity in Myeloid Cells and Promotes Tumor-Associated Macrophage Differentiation. *Immunity* (2016) 44:303–15. doi: 10.1016/j.immuni.2016.01.014
56. Goossens P, Rodriguez-Vita J, Etzerodt A, Masse M, Rastoin O, Gouirand V, et al. Membrane Cholesterol Efflux Drives Tumor-Associated Macrophage Reprogramming and Tumor Progression. *Cell Metab* (2019) 29:1376–1389.e4. doi: 10.1016/j.cmet.2019.02.016
57. Zhang J, Cao J, Ma S, Dong R, Meng W, Ying M, et al. Tumor hypoxia enhances Non-Small Cell Lung Cancer metastasis by selectively promoting macrophage M2 polarization through the activation of ERK signaling. *Oncotarget* (2014) 5:9664–77. doi: 10.18632/oncotarget.1856
58. Chen W, Xu Y, Zhong J, Wang H, Weng M, Cheng Q, et al. MFHAS1 promotes colorectal cancer progress by regulating polarization of tumor-associated macrophages via STAT6 signaling pathway. *Oncotarget* (2016) 7:78726–35. doi: 10.18632/oncotarget.12807
59. Deng X, Zhang P, Liang T, Deng S, Chen X, Zhu L. Ovarian cancer stem cells induce the M2 polarization of macrophages through the PPARgamma and NF-kappaB pathways. *Int J Mol Med* (2015) 36:449–54. doi: 10.3892/ijmm.2015.2230
60. Sierra-Filardi E, Nieto C, Dominguez-Soto A, Barroso R, Sanchez-Mateos P, Puig-Kroger A, et al. CCL2 shapes macrophage polarization by GM-CSF and M-CSF: identification of CCL2/CCR2-dependent gene expression profile. *J Immunol* (2014) 192:3858–67. doi: 10.4049/jimmunol.1302821
61. Sica A, Saccani A, Bottazzi B, Polentarutti N, Vecchi A, van Damme J, et al. Autocrine production of IL-10 mediates defective IL-12 production and NF-kappa B activation in tumor-associated macrophages. *J Immunol* (2000) 164:762–7. doi: 10.4049/jimmunol.164.2.762
62. Yaddanapudi K, Putty K, Rendon BE, Lamont GJ, Faughn JD, Satoskar A, et al. Control of tumor-associated macrophage alternative activation by macrophage migration inhibitory factor. *J Immunol* (2013) 190:2984–93. doi: 10.4049/jimmunol.1201650
63. Yamada K, Uchiyama A, Uehara A, Perera B, Ogino S, Yokoyama Y, et al. MFG-E8 Drives Melanoma Growth by Stimulating Mesenchymal Stromal Cell-Induced Angiogenesis and M2 Polarization of Tumor-Associated Macrophages. *Cancer Res* (2016) 76:4283–92. doi: 10.1158/0008-5472.CAN-15-2812
64. Hamilton G, Rath B, Klameth L, Hochmair MJ. Small cell lung cancer: Recruitment of macrophages by circulating tumor cells. *Oncoimmunology* (2016) 5:e1093277. doi: 10.1080/2162402X.2015.1093277
65. Sierra-Filardi E, Puig-Kroger A, Blanco FJ, Nieto C, Bragado R, Palomero MI, et al. Activin A skews macrophage polarization by promoting a proinflammatory phenotype and inhibiting the acquisition of anti-inflammatory macrophage markers. *Blood* (2011) 117:5092–101. doi: 10.1182/blood-2010-09-306993
66. Yang Y, Qin J, Lan L, Li N, Wang C, He P, et al. M-CSF cooperating with NFkappaB induces macrophage transformation from M1 to M2 by upregulating c-Jun. *Cancer Biol Ther* (2014) 15:99–107. doi: 10.4161/cbt.26718
67. Cho H, Seo Y, Loke KM, Kim SW, Oh SM, Kim JH, et al. Cancer-Stimulated CAFs Enhance Monocyte Differentiation and Protumoral TAM Activation via IL6 and GM-CSF Secretion. *Clin Cancer Res* (2018) 24:5407–21. doi: 10.1158/1078-0432.CCR-18-0125
68. Romero-Garcia S, Lopez-Gonzalez JS B, Ez-Viveros JL, Aguilar-Cazares D, Prado-Garcia H. Tumor cell metabolism. *Cancer Biol Ther* (2011) 12:939–48. doi: 10.4161/cbt.12.11.18140
69. Zhang J, Muri J, Fitzgerald G, Gorski T, Gianni-Barrera R, Masschelein E, et al. Endothelial Lactate Controls Muscle Regeneration from Ischemia by Inducing M2-like Macrophage Polarization. *Cell Metab* (2020) 31:1136–1153.e7. doi: 10.1016/j.cmet.2020.05.004
70. Zhang A, Qian Y, Ye Z, Chen H, Xie H, Zhou L, et al. Cancer-associated fibroblasts promote M2 polarization of macrophages in pancreatic ductal adenocarcinoma. *Cancer Med* (2017) 6:463–70. doi: 10.1002/cam4.993
71. Franklin RA, Liao W, Sarkar A, Kim MV, Bivona MR, Liu K, et al. The cellular and molecular origin of tumor-associated macrophages. *Science* (2014) 344:921–5. doi: 10.1126/science.1252510
72. Wang YC, He F, Feng F, Liu XW, Dong GY, Qin HY, et al. Notch signaling determines the M1 versus M2 polarization of macrophages in antitumor immune responses. *Cancer Res* (2010) 70:4840–9. doi: 10.1158/0008-5472.CAN-10-0269
73. Foldi J, Shang Y, Zhao B, Ivashkiv LB, Hu X. RBP-J is required for M2 macrophage polarization in response to chitin and mediates expression of a subset of M2 genes. *Protein Cell* (2016) 7:201–9. doi: 10.1007/s13238-016-0248-7
74. Zhou P, Li Q, Su S, Dong W, Zong S, Ma Q, et al. Interleukin 37 Suppresses M1 Macrophage Polarization Through Inhibition of the Notch1 and Nuclear Factor Kappa B Pathways. *Front Cell Dev Biol* (2020) 8:56:56. doi: 10.3389/fcell.2020.00056
75. Deng YM, Zhang H, Liang JM, Xian HB, Chen ZC, Tang YC, et al. IL-37 mediates the anti-tumor activity in non-small cell lung cancer through IL-6/STAT3 pathway. *J Appl Biomed* (2017) 16:15–21. doi: 10.1016/j.jab.2017.04.001
76. Zhao JJ, Pan QZ, Pan K, Weng DS, Wang QJ, Li JJ, et al. Interleukin-37 mediates the antitumor activity in hepatocellular carcinoma: role for CD57+ NK cells. *Sci Rep* (2014) 4:5177. doi: 10.1038/srep05177
77. Gholamin S, Mitra SS, Feroze AH, Liu J, Kahn SA, Zhang M, et al. Disrupting the CD47-SIRPalpha anti-phagocytic axis by a humanized anti-CD47 antibody is an efficacious treatment for malignant pediatric brain tumors. *Sci Transl Med* (2017) 9:eaaf2968. doi: 10.1126/scitranslmed.aaf2968
78. Barkal AA, Brewer RE, Markovic M, Kowarsky M, Barkal SA, Zaro BW, et al. CD24 signalling through macrophage Siglec-10 is a target for cancer immunotherapy. *Nature* (2019) 572:392–6. doi: 10.1038/s41586-019-1456-0

79. Barkal AA, Weiskopf K, Kao KS, Gordon SR, Rosental B, Yiu YY, et al. Engagement of MHC class I by the inhibitory receptor LILRB1 suppresses macrophages and is a target of cancer immunotherapy. *Nat Immunol* (2018) 19:76–84. doi: 10.1038/s41590-017-0004-z
80. Gordon SR, Maute RL, Dulken BW, Hutter G, George BM, McCracken MN, et al. PD-1 expression by tumour-associated macrophages inhibits phagocytosis and tumour immunity. *Nature* (2017) 545:495–9. doi: 10.1038/nature22396
81. Hegab AE, Ozaki M, Kagawa S, Hamamoto J, Yasuda H, Naoki K, et al. Tumor associated macrophages support the growth of FGF9-induced lung adenocarcinoma by multiple mechanisms. *Lung Cancer* (2018) 119:25–35. doi: 10.1016/j.lungcan.2018.02.015
82. Jung KY, Cho SW, Kim YA, Kim D, Oh BC, Park DJ, et al. Cancers with Higher Density of Tumor-Associated Macrophages Were Associated with Poor Survival Rates. *J Pathol Transl Med* (2015) 49:318–24. doi: 10.4132/jptm.2015.06.01
83. Fritz JM, Tennis MA, Orlicky DJ, Lin H, Ju C, Redente EF, et al. Depletion of tumor-associated macrophages slows the growth of chemically induced mouse lung adenocarcinomas. *Front Immunol* (2014) 5:587. doi: 10.3389/fimmu.2014.00587
84. Redente EF, Dwyer-Nield LD, Merrick DT, Raina K, Agarwal R, Pao W, et al. Tumor progression stage and anatomical site regulate tumor-associated macrophage and bone marrow-derived monocyte polarization. *Am J Pathol* (2010) 176:2972–85. doi: 10.2353/ajpath.2010.090879
85. Ohtaki Y, Ishii G, Nagai K, Ashimine S, Kuwata T, Hishida T, et al. Stromal macrophage expressing CD204 is associated with tumor aggressiveness in lung adenocarcinoma. *J Thorac Oncol* (2010) 5:1507–15. doi: 10.1097/JTO.0b013e3181eba692
86. Li Z, Maeda D, Yoshida M, Umakoshi M, Nanjo H, Shiraishi K, et al. The intratumoral distribution influences the prognostic impact of CD68- and CD204-positive macrophages in non-small cell lung cancer. *Lung Cancer* (2018) 123:127–35. doi: 10.1016/j.lungcan.2018.07.015
87. Park JY, Sung JY, Lee J, Park YK, Kim YW, Kim GY, et al. Polarized CD163+ tumor-associated macrophages are associated with increased angiogenesis and CXCL12 expression in gastric cancer. *Clin Res Hepatol Gastroenterol* (2016) 40:357–65. doi: 10.1016/j.clinre.2015.09.005
88. Terlizzi M, Colarusso C, Popolo A, Pinto A, Sorrentino R. IL-1alpha and IL-1beta-producing macrophages populate lung tumor lesions in mice. *Oncotarget* (2016) 7:58181–92. doi: 10.18632/oncotarget.11276
89. Ke X, Wu M, Lou J, Zhang S, Huang P, Sun R, et al. Activation of Toll-like receptors signaling in non-small cell lung cancer cell line induced by tumor-associated macrophages. *Chin J Cancer Res* (2015) 27:181–9. doi: 10.3978/j.issn.1000-9604.2015.03.07
90. Lee CH, Wu CL, Shiau AL. Toll-like receptor 4 signaling promotes tumor growth. *J Immunother* (2010) 33:73–82. doi: 10.1097/CJI.0b013e3181b7a0a4
91. Grivennikov SI, Wang K, Mucida D, Stewart CA, Schnabl B, Jauch D, et al. Adenoma-linked barrier defects and microbial products drive IL-23/IL-17-mediated tumour growth. *Nature* (2012) 491:254–8. doi: 10.1038/nature11465
92. Nejman D, Livyatan I, Fuks G, Gavert N, Zwang Y, Geller LT, et al. The human tumor microbiome is composed of tumor type-specific intracellular bacteria. *Science* (2020) 368:973–80. doi: 10.1126/science.aay9189
93. Kong L, Zhou Y, Bu H, Lv T, Shi Y, Yang J. Deletion of interleukin-6 in monocytes/macrophages suppresses the initiation of hepatocellular carcinoma in mice. *J Exp Clin Cancer Res* (2016) 35:131. doi: 10.1186/s13046-016-0412-1
94. Zeni E, Mazzetti L, Miotto D, Lo CN, Maestrelli P, Querzoli P, et al. Macrophage expression of interleukin-10 is a prognostic factor in nonsmall cell lung cancer. *Eur Respir J* (2007) 30:627–32. doi: 10.1183/09031936.00129306
95. Banerjee S, Halder K, Bose A, Bhattacharya P, Gupta G, Karmahapatra S, et al. TLR signaling-mediated differential histone modification at IL-10 and IL-12 promoter region leads to functional impairments in tumor-associated macrophages. *Carcinogenesis* (2011) 32:1789–97. doi: 10.1093/carcin/bgr208
96. Hadjidaniel MD, Muthugounder S, Hung LT, Sheard MA, Shirinbak S, Chan RY, et al. Tumor-associated macrophages promote neuroblastoma via STAT3 phosphorylation and up-regulation of c-MYC. *Oncotarget* (2017) 8:91516–29. doi: 10.18632/oncotarget.21066
97. Zhang Y, Yu G, Chu H, Wang X, Xiong L, Cai G, et al. Macrophage-Associated PGK1 Phosphorylation Promotes Aerobic Glycolysis and Tumorigenesis. *Mol Cell* (2018) 71:201–215.e7. doi: 10.1016/j.molcel.2018.06.023
98. Umakoshi M, Takahashi S, Itoh G, Kuriyama S, Sasaki Y, Yanagihara K, et al. Macrophage-mediated transfer of cancer-derived components to stromal cells contributes to establishment of a pro-tumor microenvironment. *Oncogene* (2019) 38:2162–76. doi: 10.1038/s41388-018-0564-x
99. Liu CY, Xu JY, Shi XY, Huang W, Ruan TY, Xie P, et al. M2-polarized tumor-associated macrophages promoted epithelial-mesenchymal transition in pancreatic cancer cells, partially through TLR4/IL-10 signaling pathway. *Lab Invest* (2013) 93:844–54. doi: 10.1038/labinvest.2013.69
100. Yao RR, Li JH, Zhang R, Chen RX, Wang YH. M2-polarized tumor-associated macrophages facilitated migration and epithelial-mesenchymal transition of HCC cells via the TLR4/STAT3 signaling pathway. *World J Surg Oncol* (2018) 16:9. doi: 10.1186/s12957-018-1312-y
101. Gan L, Qiu Z, Huang J, Li Y, Huang H, Xiang T, et al. Cyclooxygenase-2 in tumor-associated macrophages promotes metastatic potential of breast cancer cells through Akt pathway. *Int J Biol Sci* (2016) 12:1533–43. doi: 10.7150/ijbs.15943
102. Che D, Zhang S, Jing Z, Shang L, Jin S, Liu F, et al. Macrophages induce EMT to promote invasion of lung cancer cells through the IL-6-mediated COX-2/PGE2/β-catenin signalling pathway. *Mol Immunol* (2017) 90:197–210. doi: 10.1016/j.molimm.2017.06.018
103. Han Y, Guo W, Ren T, Huang Y, Wang S, Liu K, et al. Tumor-associated macrophages promote lung metastasis and induce epithelial-mesenchymal transition in osteosarcoma by activating the COX-2/STAT3 axis. *Cancer Lett* (2019) 440-441:116–25. doi: 10.1016/j.canlet.2018.10.011
104. Yuan Z, Mehta HJ, Mohammed K, Nasreen N, Roman R, Brantly M, et al. TREM-1 is induced in tumor associated macrophages by cyclo-oxygenase pathway in human non-small cell lung cancer. *PloS One* (2014) 9:e94241. doi: 10.1371/journal.pone.0094241
105. Katsuno Y, Lamouille S, Derynck R. TGF-beta signaling and epithelial-mesenchymal transition in cancer progression. *Curr Opin Oncol* (2013) 25:76–84. doi: 10.1097/CCO.0b013e32835b6371
106. Zhang J, Yao H, Song G, Liao X, Xian Y, Li W. Regulation of epithelial-mesenchymal transition by tumor-associated macrophages in cancer. *Am J Transl Res* (2015) 7:1699–711.
107. Zhang S, Che D, Yang F, Chi C, Meng H, Shen J, et al. Tumor-associated macrophages promote tumor metastasis via the TGF-beta/SOX9 axis in non-small cell lung cancer. *Oncotarget* (2017) 8:99801–15. doi: 10.18632/oncotarget.21068
108. Wang A, Lu C, Ning Z, Gao W, Xie Y, Zhang N, et al. Tumor-associated macrophages promote Ezrin phosphorylation-mediated epithelial-mesenchymal transition in lung adenocarcinoma through FUT4/LeY up-regulation. *Oncotarget* (2017) 8:28247–59. doi: 10.18632/oncotarget.16001
109. Liu MJ, Fu X, Wang S, Jiang L, Wang W. RBP-Jκ in colon cancer cells facilitates tumour associated macrophages (TAMs)-induced cell metastasis by secreting CXCL11. *Ann Oncol* (2019) 30:v240. doi: 10.1093/annonc/mdz246.114
110. Cortes M, Sanchez-Moral L, de Barrios O, Fernandez-Acenero MJ, Martinez-Campanario MC, Esteve-Codina A, et al. Tumor-associated macrophages (TAMs) depend on ZEB1 for their cancer-promoting roles. *EMBO J* (2017) 36:3336–55. doi: 10.15252/embj.201797345
111. Trikha P, Sharma N, Pena C, Reyes A, Pecot T, Khurshid S, et al. E2f3 in tumor macrophages promotes lung metastasis. *Oncogene* (2016) 35:3636–46. doi: 10.1038/onc.2015.429
112. Fan DM, Feng XS, Qi PW, Chen YW. Forkhead factor FOXQ1 promotes TGF-beta1 expression and induces epithelial-mesenchymal transition. *Mol Cell Biochem* (2014) 397:179–86. doi: 10.1007/s11010-014-2185-1
113. Guo J, Yan Y, Yan Y, Guo Q, Zhang M, Zhang J, et al. Tumor-associated macrophages induce the expression of FOXQ1 to promote epithelial-mesenchymal transition and metastasis in gastric cancer cells. *Oncol Rep* (2017) 38:2003–10. doi: 10.3892/or.2017.5877
114. Shi L, Zhang B, Sun X, Zhang X, Lv S, Li H, et al. CC chemokine ligand 18 (CCL18) promotes migration and invasion of lung cancer cells by binding to

Nir1 through Nir1-ELMO1/DOC180 signaling pathway. *Mol Carcinog* (2016) 55:2051–62. doi: 10.1002/mc.22450
115. Chen J, Yao Y, Gong C, Yu F, Su S, Chen J, et al. CCL18 from tumor-associated macrophages promotes breast cancer metastasis via PITPNM3. *Cancer Cell* (2011) 19:541–55. doi: 10.1016/j.ccr.2011.02.006
116. Tang T, Wei Y, Kang J, She ZG, Kim D, Sailor MJ, et al. Tumor-specific macrophage targeting through recognition of retinoid X receptor beta. *J Control Release* (2019) 301:42–53. doi: 10.1016/j.jconrel.2019.03.009
117. Rahman MA, Barger JF, Lovat F, Gao M, Otterson GA, Nana-Sinkam P. Lung cancer exosomes as drivers of epithelial mesenchymal transition. *Oncotarget* (2016) 7:54852–66. doi: 10.18632/oncotarget.10243
118. Yang L, Dong Y, Li Y, Wang D, Liu S, Wang D, et al. IL-10 derived from M2 macrophage promotes cancer stemness via JAK1/STAT1/NF-kappaB/Notch1 pathway in non-small cell lung cancer. *Int J Cancer* (2019) 145:1099–110. doi: 10.1002/ijc.32151
119. Huang WC, Chan ML, Chen MJ, Tsai TH, Chen YJ. Modulation of macrophage polarization and lung cancer cell stemness by MUC1 and development of a related small-molecule inhibitor pterostilbene. *Oncotarget* (2016) 7:39363–75. doi: 10.18632/oncotarget.8101
120. Fan QM, Jing YY, Yu GF, Kou XR, Ye F, Gao L, et al. Tumor-associated macrophages promote cancer stem cell-like properties via transforming growth factor-beta1-induced epithelial-mesenchymal transition in hepatocellular carcinoma. *Cancer Lett* (2014) 352:160–8. doi: 10.1016/j.canlet.2014.05.008
121. Wan S, Zhao E, Kryczek I, Vatan L, Sadovskaya A, Ludema G, et al. Tumor-associated macrophages produce interleukin 6 and signal via STAT3 to promote expansion of human hepatocellular carcinoma stem cells. *Gastroenterology* (2014) 147:1393–404. doi: 10.1053/j.gastro.2014.08.039
122. Wang D, Fu L, Sun H, Guo L, DuBois RN. Prostaglandin E2 Promotes Colorectal Cancer Stem Cell Expansion and Metastasis in Mice. *Gastroenterology* (2015) 149:1884–1895.e4. doi: 10.1053/j.gastro.2015.07.064
123. Chen P, Hsu WH, Chang A, Tan Z, Lan Z, Zhou A, et al. Circadian Regulator CLOCK Recruits Immune-Suppressive Microglia into the GBM Tumor Microenvironment. *Cancer Discovery* (2020) 10:371–81. doi: 10.1158/2159-8290.CD-19-0400
124. Chen C, Qu QX, Shen Y, Mu CY, Zhu YB, Zhang XG, et al. Induced expression of B7-H4 on the surface of lung cancer cell by the tumor-associated macrophages: a potential mechanism of immune escape. *Cancer Lett* (2012) 317:99–105. doi: 10.1016/j.canlet.2011.11.017
125. Zhang X, Zeng Y, Qu Q, Zhu J, Liu Z, Ning W, et al. PD-L1 induced by IFN-gamma from tumor-associated macrophages via the JAK/STAT3 and PI3K/AKT signaling pathways promoted progression of lung cancer. *Int J Clin Oncol* (2017) 22:1026–33. doi: 10.1007/s10147-017-1161-7
126. Li L, Yang L, Wang L, Wang F, Zhang Z, Li J, et al. Impaired T cell function in malignant pleural effusion is caused by TGF-beta derived predominantly from macrophages. *Int J Cancer* (2016) 139:2261–9. doi: 10.1002/ijc.30289
127. Wang D, Yang L, Yue D, Cao L, Li L, Wang D, et al. Macrophage-derived CCL22 promotes an immunosuppressive tumor microenvironment via IL-8 in malignant pleural effusion. *Cancer Lett* (2019) 452:244–53. doi: 10.1016/j.canlet.2019.03.040
128. Pang L, Han S, Jiao Y, Jiang S, He X, Li P. Bu Fei Decoction attenuates the tumor associated macrophage stimulated proliferation, migration, invasion and immunosuppression of non-small cell lung cancer, partially via IL-10 and PD-L1 regulation. *Int J Oncol* (2017) 51:25–38. doi: 10.3892/ijo.2017.4014
129. Jiang C, Yuan F, Wang J, Wu L. Oral squamous cell carcinoma suppressed antitumor immunity through induction of PD-L1 expression on tumor-associated macrophages. *Immunobiology* (2017) 222:651–7. doi: 10.1016/j.imbio.2016.12.002
130. Morishita A, Gow CH, D'Armiento J. Macrophages-Specific Matrix Metalloproteinase-9 (MMP9) Induces Lung Cancer Metastasis In An Animal Model. *Am Thoracic Soc Int Conf* (2011). doi: 10.1164/ajrccm-conference.2011.183.1_MeetingAbstracts.A2440
131. Schmall A, Al-Tamari HM, Herold S, Kampschulte M, Weigert A, Wietelmann A, et al. Macrophage and cancer cell cross-talk via CCR2 and CX3CR1 is a fundamental mechanism driving lung cancer. *Am J Respir Crit Care Med* (2015) 191:437–47. doi: 10.1164/rccm.201406-1137OC
132. Zou W, Hu TH. [Relation of tumor associated macrophages and mast cells of tumor interstitial and angiogenesis in non-small cell lung cancer]. *Zhong Nan Da Xue Xue Bao Yi Xue Ban* (2007) 32:1037–41.
133. Zhang BC, Gao J, Wang J, Rao ZG, Wang BC, Gao JF. Tumor-associated macrophages infiltration is associated with peritumoral lymphangiogenesis and poor prognosis in lung adenocarcinoma. *Med Oncol* (2011) 28:1447–52. doi: 10.1007/s12032-010-9638-5
134. Li Y, Cao F, Li M, Li P, Yu Y, Xiang L, et al. Hydroxychloroquine induced lung cancer suppression by enhancing chemo-sensitization and promoting the transition of M2-TAMs to M1-like macrophages. *J Exp Clin Cancer Res* (2018) 37:259. doi: 10.1186/s13046-018-0938-5
135. Li H, Huang N, Zhu W, Wu J, Yang X, Teng W, et al. Modulation the crosstalk between tumor-associated macrophages and non-small cell lung cancer to inhibit tumor migration and invasion by ginsenoside Rh2. *BMC Cancer* (2018) 18:579. doi: 10.1186/s12885-018-4299-4
136. Zhang G, He L, Chen J, Xu B, Mao Z. Ginsenoside Rh2 activates alpha-catenin phosphorylation to inhibit lung cancer cell proliferation and invasion. *Exp Ther Med* (2020) 19:2913–22. doi: 10.3892/etm.2020.8543
137. Parayath NN, Parikh A, Amiji MM. Repolarization of Tumor-Associated Macrophages in a Genetically Engineered Nonsmall Cell Lung Cancer Model by Intraperitoneal Administration of Hyaluronic Acid-Based Nanoparticles Encapsulating MicroRNA-125b. *Nano Lett* (2018) 18:3571–9. doi: 10.1021/acs.nanolett.8b00689
138. Yu X, Xu M, Li N, Li Z, Li H, Shao S, et al. beta-elemene inhibits tumor-promoting effect of M2 macrophages in lung cancer. *Biochem Biophys Res Commun* (2017) 490:514–20. doi: 10.1016/j.bbrc.2017.06.071
139. Huang WC, Kuo KT, Wang CH, Yeh CT, Wang Y. Cisplatin resistant lung cancer cells promoted M2 polarization of tumor-associated macrophages via the Src/CD155/MIF functional pathway. *J Exp Clin Cancer Res* (2019) 38:180. doi: 10.1186/s13046-019-1166-3
140. Gao J, Bi L, Jiang YC, Yang Y, Li BY, Chen WP. [Effect of Water Extract of Ginseng on Biological Bechaviors of Lung Cancer A549 Cells and the Expression of F-actin in Co-culture System of TAMs and A549 Cells]. *Zhongguo Zhong Xi Yi Jie He Za Zhi* (2017) 37:345–50.
141. Park HR, Lee EJ, Moon SC, Chung TW, Kim KJ, Yoo HS, et al. Inhibition of lung cancer growth by HangAmDan-B is mediated by macrophage activation to M1 subtype. *Oncol Lett* (2017) 13:2330–6. doi: 10.3892/ol.2017.5730
142. Sarode P, Zheng X, Weigert A, Tretyn A, Guenther S, Pullamsetti SS, et al. Reprogramming of Tumor Associated Macrophages by Modulating Wnt β-Catenin Signalling in Lung Cancer. *In: American Thoracic Soc* (2018). doi: 10.1164/ajrccm-conference.2018.197.1_MeetingAbstracts.A5938
143. Li JH, Tian F, Qiu CS, Chen WJ, Xu DX, Yang LQ, et al. [Relevant studies on effect of Fuzheng Sanjie recipe in regulating immune microenvironment remodeling of TAMs in Lewis lung cancer mice]. *Zhongguo Zhong Yao Za Zhi* (2015) 40:1161–5.
144. Nowakowska D, Phennicie R, Kauffman K, Zafari M, Rooney K, O Nuallain B, et al. PSGL-1 is a novel macrophage checkpoint in immuno-oncology. *J Clin Oncol* (2020) 38:e15090–0. doi: 10.1200/JCO.2020.38.15_suppl.e15090
145. Guiducci C, Vicari AP, Sangaletti S, Trinchieri G, Colombo MP. Redirecting in vivo elicited tumor infiltrating macrophages and dendritic cells towards tumor rejection. *Cancer Res* (2005) 65:3437–46. doi: 10.1158/0008-5472.CAN-04-4262
146. Muller E, Christopoulos PF, Halder S, Lunde A, Beraki K, Speth M, et al. Toll-Like Receptor Ligands and Interferon-gamma Synergize for Induction of Antitumor M1 Macrophages. *Front Immunol* (2017) 8:1383. doi: 10.3389/fimmu.2017.01383
147. Zanganeh S, Hutter G, Spitler R, Lenkov O, Mahmoudi M, Shaw A, et al. Iron oxide nanoparticles inhibit tumour growth by inducing pro-inflammatory macrophage polarization in tumour tissues. *Nat Nanotechnol* (2016) 11:986–94. doi: 10.1038/nnano.2016.168
148. Zhao J, Zhang Z, Xue Y, Wang G, Cheng Y, Pan Y, et al. Anti-tumor macrophages activated by ferumoxytol combined or surface-functionalized with the TLR3 agonist poly (I : C) promote melanoma regression. *Theranostics* (2018) 8:6307–21. doi: 10.7150/thno.29746
149. Peng J, Tsang JY, Li D, Niu N, Ho DH, Lau KF, et al. Inhibition of TGF-beta signaling in combination with TLR7 ligation re-programs a tumoricidal phenotype in tumor-associated macrophages. *Cancer Lett* (2013) 331:239–49. doi: 10.1016/j.canlet.2013.01.001
150. Xiang W, Shi R, Kang X, Zhang X, Chen P, Zhang L, et al. Monoacylglycerol lipase regulates cannabinoid receptor 2-dependent macrophage activation

and cancer progression. *Nat Commun* (2018) 9:2574. doi: 10.1038/s41467-018-04999-8
151. Wang C, Li Y, Chen H, Huang K, Liu X, Qiu M, et al. CYP4X1 Inhibition by Flavonoid CH625 Normalizes Glioma Vasculature through Reprogramming TAMs via CB2 and EGFR-STAT3 Axis. *J Pharmacol Exp Ther* (2018) 365:72–83. doi: 10.1124/jpet.117.247130
152. Fridlender ZG, Kapoor V, Buchlis G, Cheng G, Sun J, Wang LC, et al. Monocyte chemoattractant protein-1 blockade inhibits lung cancer tumor growth by altering macrophage phenotype and activating CD8+ cells. *Am J Respir Cell Mol Biol* (2011) 44:230–7. doi: 10.1165/rcmb.2010-0080OC
153. Choi HJ, Choi HJ, Chung TW, Ha KT. Luteolin inhibits recruitment of monocytes and migration of Lewis lung carcinoma cells by suppressing chemokine (C-C motif) ligand 2 expression in tumor-associated macrophage. *Biochem Biophys Res Commun* (2016) 470:101–6. doi: 10.1016/j.bbrc.2016.01.002
154. Li N, Qin J, Lan L, Zhang H, Liu F, Wu Z, et al. PTEN inhibits macrophage polarization from M1 to M2 through CCL2 and VEGF-A reduction and NHERF-1 synergism. *Cancer Biol Ther* (2015) 16:297–306. doi: 10.1080/15384047.2014.1002353
155. Jia XH, Du Y, Mao D, Wang ZL, He ZQ, Qiu JD, et al. Zoledronic acid prevents the tumor-promoting effects of mesenchymal stem cells via MCP-1 dependent recruitment of macrophages. *Oncotarget* (2015) 6:26018–28. doi: 10.18632/oncotarget.4658
156. Kumar V, Donthireddy L, Marvel D, Condamine T, Wang F, Lavilla-Alonso S, et al. Cancer-Associated Fibroblasts Neutralize the Anti-tumor Effect of CSF1 Receptor Blockade by Inducing PMN-MDSC Infiltration of Tumors. *Cancer Cell* (2017) 32:654–668.e5. doi: 10.1016/j.ccell.2017.10.005
157. Guerriero JL, Sotayo A, Ponichtera HE, Castrillon JA, Pourzia AL, Schad S, et al. Class IIa HDAC inhibition reduces breast tumours and metastases through anti-tumour macrophages. *Nature* (2017) 543:428–32. doi: 10.1038/nature21409
158. Wang K, Shan S, Yang Z, Gu X, Wang Y, Wang C, et al. IL-33 blockade suppresses tumor growth of human lung cancer through direct and indirect pathways in a preclinical model. *Oncotarget* (2017) 8:68571–82. doi: 10.18632/oncotarget.19786
159. Zhang L, Alizadeh D, Van Handel M, Kortylewski M, Yu H, Badie B. Stat3 inhibition activates tumor macrophages and abrogates glioma growth in mice. *Glia* (2009) 57:1458–67. doi: 10.1002/glia.20863
160. Andersen MN, Etzerodt A, Graversen JH, Holthof LC, Moestrup SK, Hokland M, et al. STAT3 inhibition specifically in human monocytes and macrophages by CD163-targeted corosolic acid-containing liposomes. *Cancer Immunol Immunother* (2019) 68:489–502. doi: 10.1007/s00262-019-02301-3
161. Giurisato E, Xu Q, Lonardi S, Telfer B, Russo I, Pearson A, et al. Myeloid ERK5 deficiency suppresses tumor growth by blocking protumor macrophage polarization via STAT3 inhibition. *Proc Natl Acad Sci U S A* (2018) 115:E2801–10. doi: 10.1073/pnas.1707929115
162. Fujiwara Y, Komohara Y, Kudo R, Tsurushima K, Ohnishi K, Ikeda T, et al. Oleanolic acid inhibits macrophage differentiation into the M2 phenotype and glioblastoma cell proliferation by suppressing the activation of STAT3. *Oncol Rep* (2011) 26:1533–7. doi: 10.3892/or.2011.1454
163. Sun L, Chen B, Jiang R, Li J, Wang B. Resveratrol inhibits lung cancer growth by suppressing M2-like polarization of tumor associated macrophages. *Cell Immunol* (2017) 311:86–93. doi: 10.1016/j.cellimm.2016.11.002
164. Hiwatashi K, Tamiya T, Hasegawa E, Fukaya T, Hashimoto M, Kakoi K, et al. Suppression of SOCS3 in macrophages prevents cancer metastasis by modifying macrophage phase and MCP2/CCL8 induction. *Cancer Lett* (2011) 308:172–80. doi: 10.1016/j.canlet.2011.04.024
165. Tariq M, Zhang JQ, Liang GK, He QJ, Ding L, Yang B. Gefitinib inhibits M2-like polarization of tumor-associated macrophages in Lewis lung cancer by targeting the STAT6 signaling pathway. *Acta Pharmacol Sin* (2017) 38:1501–11. doi: 10.1038/aps.2017.124
166. Binnemars-Postma K, Bansal R, Storm G, Prakash J. Targeting the Stat6 pathway in tumor-associated macrophages reduces tumor growth and metastatic niche formation in breast cancer. *FASEB J* (2018) 32:969–78. doi: 10.1096/fj.201700629R
167. Yao Z, Zhang J, Zhang B, Liang G, Chen X, Yao F, et al. Imatinib prevents lung cancer metastasis by inhibiting M2-like polarization of macrophages. *Pharmacol Res* (2018) 133:121–31. doi: 10.1016/j.phrs.2018.05.002
168. Suarez-Lopez L, Sriram G, Kong YW, Morandell S, Merrick KA, Hernandez Y, et al. MK2 contributes to tumor progression by promoting M2 macrophage polarization and tumor angiogenesis. *Proc Natl Acad Sci U S A* (2018) 115:E4236–44. doi: 10.1073/pnas.1722020115
169. Terry S, Buart S, Engelsen A, Baud V, Gausdal G, Lorens J, Baud V, et al. AXL targeting enhances lymphocyte-mediated cytotoxicity of lung cancer cells. In: 第十七届国际免疫学大会. Abstracts of IUIS 2019 Beijing—17th International Congress of Immunology (IV) (2019).
170. Georgoudaki AM, Prokopec KE, Boura VF, Hellqvist E, Sohn S, Ostling J, et al. Reprogramming Tumor-Associated Macrophages by Antibody Targeting Inhibits Cancer Progression and Metastasis. *Cell Rep* (2016) 15:2000–11. doi: 10.1016/j.celrep.2016.04.084
171. Mitsuhashi A, Goto H, Kuramoto T, Tabata S, Yukishige S, Abe S, et al. Surfactant protein A suppresses lung cancer progression by regulating the polarization of tumor-associated macrophages. *Am J Pathol* (2013) 182:1843–53. doi: 10.1016/j.ajpath.2013.01.030
172. Ding L, Liang G, Yao Z, Zhang J, Liu R, Chen H, et al. Metformin prevents cancer metastasis by inhibiting M2-like polarization of tumor associated macrophages. *Oncotarget* (2015) 6:36441–55. doi: 10.18632/oncotarget.5541
173. Xu F, Cui WQ, Wei Y, Cui J, Qiu J, Hu LL, et al. Astragaloside IV inhibits lung cancer progression and metastasis by modulating macrophage polarization through AMPK signaling. *J Exp Clin Cancer Res* (2018) 37:207. doi: 10.1186/s13046-018-0878-0
174. Liu X, Nie W, Xie Q, Chen G, Li X, Jia Y, et al. Endostatin reverses immunosuppression of the tumor microenvironment in lung carcinoma. *Oncol Lett* (2018) 15:1874–80. doi: 10.3892/ol.2017.7455
175. Xu F, Cui W, Zhao Z, Gong W, Wei Y, Liu J, et al. Targeting Tumor Microenvironment: Effects of Chinese Herbal Formulae on Macrophage-Mediated Lung Cancer in Mice. *Evid Based Complement Alternat Med* (2017) 2017:7187168. doi: 10.1155/2017/7187168
176. Ren F, Fan M, Mei J, Wu Y, Liu C, Pu Q, et al. Interferon-gamma and celecoxib inhibit lung-tumor growth through modulating M2/M1 macrophage ratio in the tumor microenvironment. *Drug Des Devel Ther* (2014) 8:1527–38. doi: 10.2147/DDDT.S66302
177. Weiser-Evans MC, Wang XQ, Amin J, Van Putten V, Choudhary R, Winn RA, et al. Depletion of cytosolic phospholipase A2 in bone marrow-derived macrophages protects against lung cancer progression and metastasis. *Cancer Res* (2009) 69:1733–8. doi: 10.1158/0008-5472.CAN-08-3766
178. Lee C, Bae SS, Joo H, Bae H. Melittin suppresses tumor progression by regulating tumor-associated macrophages in a Lewis lung carcinoma mouse model. *Oncotarget* (2017) 8:54951–65. doi: 10.18632/oncotarget.18627
179. Lee C, Jeong H, Bae Y, Shin K, Kang S, Kim H, et al. Targeting of M2-like tumor-associated macrophages with a melittin-based pro-apoptotic peptide. *J Immunother Cancer* (2019) 7:147. doi: 10.1186/s40425-019-0610-4
180. Jaynes JM, Sable R, Ronzetti M, Bautista W, Rudloff U. Mannose receptor (CD206) activation in tumor-associated macrophages enhances adaptive and innate antitumor immune responses. *ence Trans Med* (2020) 12:6337. doi: 10.1126/scitranslmed.aax6337
181. Dong H, Yang Y, Gao C, Sun H, Wang H, Hong C, et al. Lactoferrin-containing immunocomplex mediates antitumor effects by resetting tumor-associated macrophages to M1 phenotype. *J Immunother Cancer* (2020) 8: e000339. doi: 10.1136/jitc-2019-000339
182. He W, Xu J, Mu R, Li Q, Lv DL, Huang Z, et al. High-salt diet inhibits tumour growth in mice via regulating myeloid-derived suppressor cell differentiation. *Nat Commun* (2020) 11:1732. doi: 10.1038/s41467-020-15524-1
183. Zhang Y, Wu L, Li Z, Zhang W, Luo F, Chu Y, et al. Glycocalyx-Mimicking Nanoparticles Improve Anti-PD-L1 Cancer Immunotherapy through Reversion of Tumor-Associated Macrophages. *Biomacromolecules* (2018) 19:2098–108. doi: 10.1021/acs.biomac.8b00305
184. Pienta KJ, Machiels JP, Schrijvers D, Alekseev B, Shkolnik M, Crabb SJ, et al. Phase 2 study of carlumab (CNTO 888), a human monoclonal antibody against CC-chemokine ligand 2 (CCL2), in metastatic castration-resistant prostate cancer. *Invest New Drug* (2013) 31:760–8. doi: 10.1007/s10637-012-9869-8
185. Nywening TM, Wang-Gillam A, Sanford DE, Belt BA, Panni RZ, Cusworth BM, et al. Targeting tumour-associated macrophages with CCR2 inhibition in combination with FOLFIRINOX in patients with borderline resectable and locally advanced pancreatic cancer: a single-centre, open-label, dose-

finding, non-randomised, phase 1b trial. *Lancet Oncol* (2016) 17:651–62. doi: 10.1016/S1470-2045(16)00078-4
186. Halama N, Zoernig I, Berthel A, Kahlert C, Klupp F, Suarez-Carmona M, et al. Tumoral Immune Cell Exploitation in Colorectal Cancer Metastases Can Be Targeted Effectively by Anti-CCR5 Therapy in Cancer Patients. *Cancer Cell* (2016) 29:587–601. doi: 10.1016/j.ccell.2016.03.005
187. Nywening TM, Belt BA, Cullinan DR, Panni RZ, Han BJ, Sanford DE, et al. Targeting both tumour-associated CXCR2(+) neutrophils and CCR2(+) macrophages disrupts myeloid recruitment and improves chemotherapeutic responses in pancreatic ductal adenocarcinoma. *Gut* (2018) 67:1112–23. doi: 10.1136/gutjnl-2017-313738
188. Zeisberger SM, Odermatt B, Marty C, Zehnder-Fjallman AH, Ballmer-Hofer K, Schwendener RA. Clodronate-liposome-mediated depletion of tumour-associated macrophages: a new and highly effective antiangiogenic therapy approach. *Br J Cancer* (2006) 95:272–81. doi: 10.1038/sj.bjc.6603240
189. Baghdadi M, Endo H, Takano A, Ishikawa K, Kameda Y, Wada H, et al. High co-expression of IL-34 and M-CSF correlates with tumor progression and poor survival in lung cancers. *Sci Rep* (2018) 8:418. doi: 10.1038/s41598-017-18796-8
190. Endo H, Hama N, Baghdadi M, Ishikawa K, Otsuka R, Wada H, et al. Interleukin-34 expression in ovarian cancer: a possible correlation with disease progression. *Int Immunol* (2020) 32:175–86. doi: 10.1093/intimm/dxz074
191. Hu L, Hu X, Long K, Gao C, Dong HL, Zhong Q, et al. Extraordinarily potent proinflammatory properties of lactoferrin-containing immunocomplexes against human monocytes and macrophages. *Sci Rep* (2017) 7:4230. doi: 10.1038/s41598-017-04275-7
192. Gao CH, Dong HL, Tai L, Gao XM. Lactoferrin-Containing Immunocomplexes Drive the Conversion of Human Macrophages from M2- into M1-like Phenotype. *Front Immunol* (2018) 9:37. doi: 10.3389/fimmu.2018.00037
193. Thielmann CM, Costa DSM, Muley T, Meister M, Herpel E, Muckenthaler MU. Iron accumulation in tumor-associated macrophages marks an improved overall survival in patients with lung adenocarcinoma. *Sci Rep* (2019) 9:11326. doi: 10.1038/s41598-019-47833-x
194. Xiao ZX, Hu X, Zhang X, Chen Z, Wang J, Jin K, et al. High salt diet accelerates the progression of murine lupus through dendritic cells via the p38 MAPK and STAT1 signaling pathways. *Signal Transduct Target Ther* (2020) 5:34. doi: 10.1038/s41392-020-0139-5
195. Zhang G, Liu H, Huang J, Chen S, Pan X, Huang H, et al. TREM-1low is a novel characteristic for tumor-associated macrophages in lung cancer. *Oncotarget* (2016) 7:40508–17. doi: 10.18632/oncotarget.9639
196. Li L, Yang H, Li Y, Li XD, Zeng TT, Lin SX, et al. Hypoxia restrains the expression of complement component 9 in tumor-associated macrophages promoting non-small cell lung cancer progression. *Cell Death Discovery* (2018) 4:63. doi: 10.1038/s41420-018-0064-3
197. West AP, Shadel GS. Mitochondrial DNA in innate immune responses and inflammatory pathology. *Nat Rev Immunol* (2017) 17:363–75. doi: 10.1038/nri.2017.21
198. Chen P, Zhang X, Venosa A, Lee IH, Myers D, Holloway JA, et al. A Novel Bivalent Mannosylated Targeting Ligand Displayed on Nanoparticles Selectively Targets Anti-Inflammatory M2 Macrophages. *Pharmaceutics* (2020) 12:243. doi: 10.3390/pharmaceutics12030243
199. Wang Z, Yip LY, Lee J, Wu Z, Chew HY, Chong P, et al. Methionine is a metabolic dependency of tumor-initiating cells. *Nat Med* (2019) 25:825–37. doi: 10.1038/s41591-019-0423-5

Conflict of Interest: The authors declare that the research was conducted in the absence of any commercial or financial relationships that could be construed as a potential conflict of interest.

Copyright © 2020 Ge and Ding. This is an open-access article distributed under the terms of the Creative Commons Attribution License (CC BY). The use, distribution or reproduction in other forums is permitted, provided the original author(s) and the copyright owner(s) are credited and that the original publication in this journal is cited, in accordance with accepted academic practice. No use, distribution or reproduction is permitted which does not comply with these terms.

frontiers in Immunology

REVIEW
published: 09 November 2020
doi: 10.3389/fimmu.2020.595207

Hyperthermia Targeting the Tumor Microenvironment Facilitates Immune Checkpoint Inhibitors

Zihui Li, Jie Deng, Jianhai Sun and Yanling Ma *

Oncology Department, The Third People's Hospital of Hubei Province, Affiliated Hospital of Jianghan University, Wuhan, China

Immune checkpoint inhibitors (ICIs) have ushered in a new era of cancer therapy; however, ICIs are only effective in selective patients. The efficacy of ICIs is closely related to the tumor microenvironment. Fever for a long time was thought to directly regulate the immune response, and artificial "fever" from hyperthermia modulates the tumor immune microenvironment by providing danger signals with heat shock proteins (HSPs) as well as subsequent activation of immune systems. Encouraging results have been achieved in preclinical studies focused on potential synergetic effects by combining hyperthermia with ICIs. In this review, we summarized a cluster of immune-related factors that not only make hyperthermia a treatment capable of defending against cancer but also make hyperthermia a reliable treatment that creates a type I-like tumor microenvironment (overexpression of PD-L1 and enrichment of tumor infiltrating lymphocytes) in complementary for the enhancement of the ICIs. Then we reviewed recent preclinical data of the combination regimens involving hyperthermia and ICIs that demonstrated the combined efficacy and illustrated possible approaches to further boost the effectiveness of this combination.

Keywords: hyperthermia, tumor microenvironment, immune checkpoint inhibitors, combined therapy, synergetic effect

OPEN ACCESS

Edited by:
Huanfa Yi,
Jilin University, China

Reviewed by:
Aung Naing,
University of Texas MD Anderson Cancer Center, United States
Chenming Sun,
Xian Jiaotong University, China

***Correspondence:**
Yanling Ma
yanlingma2020@163.com

Specialty section:
This article was submitted to Cancer Immunity and Immunotherapy, a section of the journal Frontiers in Immunology

Received: *15 August 2020*
Accepted: *09 October 2020*
Published: *09 November 2020*

Citation:
Li Z, Deng J, Sun J and Ma Y (2020) Hyperthermia Targeting the Tumor Microenvironment Facilitates Immune Checkpoint Inhibitors. Front. Immunol. 11:595207. doi: 10.3389/fimmu.2020.595207

INTRODUCTION

Immune checkpoint inhibitors (ICIs) aim to reverse the immunosuppressive tumor microenvironment (TME) have ushered in a new era of cancer treatment. Efficacy of ICIS-based cancer immunotherapy relies on the immune status in TME. TME is composed of tumor cells, immune/inflammatory cells, stromal cells, blood/lymph vessels, cytokines, secreted proteins, RNAs, and small organelles (1). Through signal transduction and intercellular interactions, TME constitutes and modulates the cancer-immunity cycle (2). Based on the immune status of TME, tumors can be classified as "cold" and "hot" in which "cold" tumors often have a low response rate to anti-PD-1/PD-L1 mAb due to reduced tumor mutation, less T-cell infiltration, less PD-L1 expression and enrichment in immunosuppressive cells (3). Anti-angiogenesis treatment, radiotherapy, or chemotherapy increases the treatment efficacy of ICIs by transforming the immune status of TME through exposure of tumor-specific antigens, normalization of the endothelium, attraction of immune cells, *etc.* (4–6) Hyperthermia can also modulate the immune status of TME and influence the immune system through cytotoxic effects of high temperatures (7).

Hyperthermia is a method of killing cancer cells or impeding their growth by increasing tissue temperature with an external heat source for a certain period of time. Hippocrates, the father of modern medicine said, "Those who cannot be cured by surgery can be cured by heat. Those who cannot be cured by heat, they are indeed incurable." Early studies found that fever was correlated with spontaneous tumor regression. Since the last century, hyperthermia has been widely used for patients with both locoregional and advanced cancers in prostate cancer, melanoma, bladder cancer, esophageal cancer, and cervical cancer. The combination of hyperthermia and radio-/chemotherapy has also shown effectiveness for tumor control in numerous clinical studies. Hyperthermia can be classified as local (microwaves, radio waves, or ultrasound), regional (hyperthermic intraperitoneal chemotherapy), and whole body hyperthermia depending on the organ to be targeted. While based on temperature ranges, hyperthermia can be classified as fever-range temperature hyperthermia (39–40°C), mild temperature hyperthermia (heat shock temperature, 41–43°C), and thermal ablation (cytotoxic temperature, >43°C). Magnetic nanoparticle hyperthermia, cryo-thermal therapy, and photothermal therapy are newly developed treatments that also belong to the category of hyperthermia.

Hyperthermia modulates the immune status of tumor microenvironment by providing danger signals with HSPs as well as subsequent activation of immune systems. The immunomodulatory effects not only make hyperthermia a treatment capable of defending against cancer but also make hyperthermia a reliable treatment that creates a type I-like tumor microenvironment (overexpression of PD-L1 and enrichment of tumor infiltrating lymphocytes) in complementary for the enhancement of the ICIs. Below, we summarize a cluster of immune-related factors that are inducible by hyperthermia, highlighting the complementary effect of hyperthermia on immunogenicity and immunoreactivity in the tumor microenvironment for the enhancement of ICIs. Then we reviewed recent preclinical data of the combination regimens involving hyperthermia and ICIs that demonstrated the combined efficacy and illustrated possible approaches to further boost the effectiveness of this combination.

HYPERTHERMIA INCREASES TUMOR DNA DAMAGE

The T cell-based immune system frequently responds to neoantigens that arise as a consequence of accumulated DNA damage, known as the tumor mutation burden (8, 9). High tumor mutation achieves a higher response rate to PD-1/PD-L1 mAb and gets a higher objective tumor remission rate. Hyperthermia directly and indirectly induces DNA damage in addition to interacting and interfering with various DNA repair cascades, all of which contribute to mutations in the tumor genome and the production of neoantigens (8, 10). Briefly, hyperthermia can directly induce the DNA damage response by promoting single stranded break (SBS), double stranded break (DBS), histone H2AX with phosphorylated C-terminal serines (γ-H2AX) foci formation and ataxia-telangiectasia mutated protein(ATM) phosphorylation and decelerating DNA replication and repair (downregulate DNA polymerases and topoisomerases activity), and indirectly activate DNA damage response and induce tumor suppressor alternative reading frame (ARF) by promoting ROS production, cell cycle arrest, cell cycle checkpoint arrest, cell death, decelerate DNA replication. Moreover, hyperthermia can significantly promote DNA damage in tumor stem cells that are resistant to most classical treatment regimens, which would be more effective for the formation of tumor neoantigens (11). In addition, exosomes extracted from heat-stressed tumor cells (HS-TEX) induce a bystander effect that can transform DNA damage from heat-stressed tumor cells to the non-heated ones (12). The enhanced irreversible cellular DNA damage accumulation was further proven by that hyperthermia is applied as a complement in treatment combining chemotherapy or irradiation to induce irreversible cellular DNA damage (13). Nevertheless, the identification of neoantigens requires the mapping of tumor-specific genetic aberrations using whole-exosome sequencing, *in silico* predictions, mass spectrometry, and T cell assays (9).

HYPERTHERMIA IS A STRONG ICD INDUCER

Despite mutations and neoantigens for the potential initiation of immunity, only immunogenic characteristic defined by immunogenic cell death (ICD) triggers an immune response. ICD is a novel concept that has emerged during the last decade. ICD depends on the concomitant generation of reactive oxygen species (ROS, Type I) and activation of endoplasmic reticulum stress (ER stress, Type II) (14, 15) to function as "enabler" and "eat me" signals to recruited immune cells (16–18). ICD has emerged as an important sign of a favorable immunogenic TME that provides the various functional immunological cell infiltration and cytokines (15, 19). Clinical studies have suggested that pre-treatment with ICD inducers sensitizes cells to immune checkpoint blockade treatment (20). Though discussed frequently, hyperthermia is a kind of ICD inducer. Below, we will discuss hyperthermia-induced ICD from two aspects including ICD-related biological events (ER stress, ROS, and apoptosis) and the accompanying generated damage-associated molecular patterns (DAMPs) with an emphasis on HSP.

Hyperthermia-Induced ICD Depends on ER Stress and ROS

"Fever"-induced apoptotic, necrotic, or even live cancer cells constitute a relevant natural mode of tumor-associated antigen (TAA) (21, 22). Hyperthermia generates different modes of TAA depending on the temperature change. Generally, temperature at the fever range (37–41°C) leads to a protective function for cancer cells with presentation of their constituents, while temperatures of 41–43°C promote cell death predominantly by

apoptosis with a balance between pro-apoptosis and anti-apoptosis. As temperature rises even higher, the pro-apoptosis becomes dominant. While temperatures rise above 43°C (thermal ablation range), tumor cells experience the destruction mainly by necrosis (23).

Thermal ablation induced necrosis is a pathologic cell death that can produce immunogenic inflammatory response (24). Unlike thermal ablation, fever range hyperthermia can only influence cell membrane fluidity and stability, change cell morphology, and influence intracellular sodium–calcium levels (25). At this temperature, the heat shock response and ER stress can occur simultaneously. Heat shock response-induced HSPs can either diminish the activation or relieve ER stress by activating a negative feedback system of the unfolded protein response (UPR) to avoid excessive activation (26) and can protect tumor cells against both caspase-dependent and caspase-independent apoptosis triggered by oxidative stress (27). Additionally, eIF2α phosphorylation, the hallmark of ICD (28, 29), was rarely induced at this temperature (30). While temperature rises between the "fever range" and "thermal ablation range" at 41–43°C, tumor cells died predominantly by apoptosis with a balance between pro-apoptosis and anti-apoptosis. This process involves the induction of CHOP, the alterations in calcium levels and the activation of ER proteases, calpain–calpastatin proteolytic system and caspase mediated apoptosis (30, 31). This process also accompanies with the upregulation of eIF2α phosphorylation. While both low (43°C) and high (45°C) hyperthermic exposures were capable of inducing cell death by activating apoptotic pathways, mild hyperthermia (43°C) triggers the apoptotic response in a more regulated manner in order to sustain apoptotic cell death (31).

Traditional view holds that apoptosis is non-immunogenic and does not induce an inflammatory response. However, recent studies have suggested that certain kinds of treatment that induce tumor cell apoptosis can also release DAMPs and induce ICD. Calreticulin (CRT) exposure, high mobility group box 1 (HMGB1) release, and adenosine triphosphate (ATP) secretion are essential factors for cell death to be considered ICD (32). In fact, heat-shock conditioning of cancer cells increased their CRT plasma membrane translocation and induced the release of HMGB1 protein. Moreover, both CRT and HMGB1 mobilization were associated with enhanced antigen cross-presentation and antigen present cell maturation after hyperthermia at mild temperature range of 41–43°C (33, 34). It remains to be elucidated that hyperthermia related apoptosis can induce ICD, but apoptosis induced by hyperthermia is involved in the ICD generation (35–37). Nevertheless, considering the ICD-related biological events of ER stress, ROS, and apoptosis and the accompanying generated DAMPs, hyperthermia can be regarded as an ICD inducer as well as other treatments (32, 38). Whereas, it should be noted that hyperthermia-induced ER stress or apoptosis is fostered by focused ROS rather than by secondary or collateral ER stress effects, which were thought to be more effective for ICD-associated immunogenicity (15). Moreover, this referred ICD is different from pathologic necrosis cell death caused by tumor ablation (39).

HSPs Are Among the Most Important DAMPs Induced by Hyperthermia

Hyperthermia induces various kinds of DAMPs, including HMGB1, CRT, and ATP. In addition, study by proteomic profiling found quantitative proteins regulated by heat shock treatment that can be described as potential DAMPs or candidates for further immunological analysis (40). However, the current paradigm of the immunogenicity of hyperthermia mainly relies on HSPs and activated Toll-like receptor-4 (TLR-4) signaling pathways for the initiation of tumor-specific immune responses (38, 41). Here, we discuss various forms of HSPs and the suitable temperature for maximized immunity.

HSPs are a group of highly conserved chaperone proteins synthesized under pressure in a wide range of tumor cells containing HSP70, HSP60, HSP90, and small HSPs. Elevated HSPs are usually associated with poor prognosis in most cancer types. However, these overexpressed HSPs after hyperthermia are also associated with enhanced immune response. There are three forms of HSP: intracellular, membrane, and extracellular HSPs. Intracellular HSPs promote the maintenance of the innate structures and functions of their client proteins by facilitating protein folding when the cells are under homeostatic challenges (42). Unlike intracellular HSPs, studies found that small fractions of several heat-stress cognates are located at or near the cytoplasm inside the membrane along with cytoskeletal proteins, and that additional submembranous localization of HSPs may be a part of cellular responses to heat that associated with membrane damage (43). Whereas, later research found that this membrane HSP70 might also serve as a tumor-specific target for the cytolytic attack of $CD56^{bright}$/$CD94^{+}$ natural killer (NK) cells (25, 44). While, extracellular HSPs released from tumor cells are regarded as potent adjuvants to facilitate the presentation of tumor antigens and the induction of anti-tumor immunity (45, 46).

In accordance with relationship between biological events and temperature, HSPs start to release at 41°C and reach a maximum at 43°C but begin to diminish at 45°C (47). To achieve the optimal extracellular HSP synthesis for anti-tumor immune activation, Lin et al. developed a model to predict the optimal temperature and exposure time by involving factors such as different cell lines, cell incubation times, and heat administration methods into the model. They found that the maximum extracellular HSP synthesis was at 43°C, so was the maximum modulatory effect for tumor regression and decreased metastasis. When the temperature was further increased, HSP synthesis decreased, and the immune modulatory effect of hyperthermia was also downregulated (48). Whereas, through bioinformatic approach, Duzgun et al. identified a series of molecules that determine the thermoresistance and immunogenic cell death in thermotherapy through estimating the percentage of the two kinds of denatured proteins. They found that thermoresistance along with ICD both existed in a broad temperature windows, and that average T_m (50% of the protein is unfolded) of DAMPs

(63.42°C) is remarkably higher compared to the thermal ablation temperature due to the function to interact with their pattern recognition receptors (PRRs) even under thermal stress (49). Although the suitable temperature for maximized immunity remains unclear, these models offer ways to rationally explore suitable conditions to exploit hyperthermia.

HYPERTHERMIA ENHANCED THE IMMUNE RESPONSE IN MULTIPLE STEPS

With increased tumor mutation burden and ICD, immunity is either activated or enhanced by hyperthermia for the subsequent immune response in multiple steps of the cancer-immunity cycle. Hyperthermia-activated immunity appears to be specific, persistent, and memorable. This activated immunity not only makes hyperthermia a capable treatment to defend against cancer but also orient it as a reliable treatment that can facilitate the efficacy of ICIs.

Hyperthermia Promotes APCs' Activation

It has been established for years that mild thermal stress regulates DCs' activities to control infections and tumor growth (50, 51). Although APCs' activation is not directly associated with the prognosis of PD-1/PD-L1 mAb treatment, APCs' activation directly influences tumor-specific T cell responses. APCs' activation includes antigen presentation and APC maturation. During the process of antigen presentation, hyperthermia mainly regulates "phagocytosis checkpoints" by enhancing the immunogenic "eat me" signals and repressing tolerogenic "eat me" signals as well as "do not eat me" signals (52). Specifically, phagocytosis of APCs is mainly enhanced by immunogenic "eat me" signals of DAMPs through receptor-mediated endocytosis *via* PRR. Moreover, hyperthermia represses the "do not eat me" signal through decreasing the expression of CD47 in the cell surface (53). In addition, hyperthermia can also inhibit tolerogenic "eat me" signals by transforming immature APCs and/or APCs exhibiting immunosuppressive phenotypes (M2 macrophages, N2 neutrophils, myeloid-derived suppressor cells) to a relatively mature one (54, 55). This transformations include infiltrating activated monocytes into the tumor microenvironment (56), inducing immature DCs to differentiate into DCs (45), promoting macrophage polarization to the M1 type that exerts pro-inflammatory effects, and promoting the release of inflammatory factors (57, 58). In fact, significantly increased phagocytosis rates of macrophages and DCs have been seen; moreover, this process seems to be temperature sensitive (>43°C).

Along with antigen presentation, APCs initiate a process of maturation by increasing the expression of MHC I, MHC II molecules and costimulatory molecules, and migrating to the draining lymph node. This process can be mediated by antigen presentation, TLR agonists, the standard maturation cocktail of pro-inflammatory cytokines (59), and physiological temperature stress of 40–41°C (50, 51). Traditional views hold that hyperthermia-induced ICD is among the strategies to improve the efficacy of dendritic cell-based immunotherapy for specific cancer types (60). However, studies have suggested that merely heating tumor cells cannot activate immature DCs. Only when tumor cells and immature DCs are both under sequential hyperthermia treatment, can the immature DCs be effectively activated. This result suggests that DCs' maturation not only depends on danger signals with HSPs but also on hyperthermia itself independently (61). Further studies proposed that fever-range hyperthermia promote DCs from a quiescent status to an activated status by promoting the metabolic reprogramming in them (62, 63). The authors proposed that hyperthermia increased the expression of insulin-like growth factor binding protein 6 (IGFBP-6) and HSP70, whose autocrine mechanism increases the glycolysis, decreases the activity of the mitochondrial respiratory chain and consequent oxidative phosphorylation (OxPhos), enhances the production of NO and ROS, and promotes the mitochondrial Ca^{2+} overload. It should also be noted that this metabolic reprogramming of DCs functions more like a kind of checkpoint in DCs' activation or maturation, and this process is an early event for the accomplishment of cell-specific immunologic adaptation.

Hyperthermia Corrects Dysfunctional CD4 T Cell Immune Response

CD4 T cells display a large degree of plasticity to differentiate into Th1, Th2, Th17, and regulatory T cells (Tregs) in response to different tumor environments (64, 65). Th1 cells along with its generated chemokines exert prominent anti-tumor activity by blocking the formation of new blood vessels as well as promoting recruitment of tumor-killing immune cells. Intra-tumoral FoxP3 + Tregs impede effective immune response against cancer and impaired the efficacy of PD-1/PD-L1 mAb. In contrast to function of Tregs, Th17 cells may be prominent candidates for adoptive T-cell therapy (66–68). Functional systemic CD4 T cell immunity is essential for effector cytotoxic T lymphocyte (CTL) priming, memory CTL development, and effective PD-1/PD-L1 blockade (69, 70). Hyperthermia showed the potential of correcting dysfunctional CD4 T cell immune response by drifting CD4 T cells to Th1 and transforming Treg cells into Th17 cells to rebuild a favorable TME that can effectively respond to anti-PD-1/PD-L1 mAb.

DC maturation induced by thermal therapy is a prerequisite for CD4 T cell differentiation (57, 71). Besides fever-range hyperthermia (39–40°C) inhibits Th2 and Treg growth, induces spleen Th1 and Tc1 proliferation, and promotes Th1 cell-associated secretion of IL-2, IFN-γ and TNF-α in spleen (72). While cryothermal therapy not only reduced the percentage of Tregs and myeloid-derived suppressor cells (MDSCs) in spleen, lung and blood but also promoted $CD4^+$ T cell's differentiation into predominant $CD4^+$ CTL, Th1, Th2, and Tfh subsets (73). Moreover, compared with radiotherapy alone, combined radiotherapy with hyperthermia regulated the tumor microenvironment and upregulated the Th1/Th2 ratio (74). In addition, HS-TEX can elicit Th1-polarized immune responses by increasing the production of IgG2a and IFN-γin sensitized tumors (75). Besides, preclinical studies have shown the potential of hyperthermia to promote Th1-related immunity and repress the

function of Treg cells. Last, the correcting of dysfunctional CD4 T cell by hyperthermia has also been proven by that patients with tumor treated with hyperthermia showed increases in Th17 cells and decreases in Tregs in the peripheral blood (76).

Hyperthermia Creates a Favorable Inflammatory Tumor Microenvironment

It is highly dependent on cytokines and chemokines for "cold" tumors with low response rate to PD-1/PD-L1 mAb to transform to a "hot" one that is infiltrated with immune cells in tumor sites. Serum cytokine analysis revealed that hyperthermia at 41°C for 30 min induces an intratumoral inflammatory cytokines and chemokines to increase in enhanced T-cell trafficking (77). Specifically, mild hyperthermia increases the expression of L-selectin, P-selectin, and intercellular cell adhesion molecule-1 (ICAM-1) in the vessel wall (78–80) and drives the production of a number of pro-inflammatory cytokines and chemokines (*i.e.* interleukin−1β, IL-6, IL-8, IL-10, and CCL22) (77, 81). This inflammatory cytokines and chemokines act at multiple discrete steps that favor lymphocyte infiltrate to the tumor microenvironment and attack solid tumors in the immune cascade.

Among cytokines and chemokines induced by thermal stress, IL-6 plays a pivotal role in the tumor immune microenvironment. Specifically, cryo-thermal therapy-induced IL-6-rich acute pro-inflammatory response promotes DC phenotypic maturation, CD4(+) T cell differentiation, and Th1 anti-tumor immunity (71, 82). In addition, hyperthermia induces M1 macrophages to secrete CXCL10 and IL-6 to induce CD4 T cell differentiation into Th1 and CD4 CTL cells, and reduce MDSC aggregation (57). Moreover, IL-6 stimulated by HS-TEX promotes Treg transformation to Th17 cells and induces CD4 T and CD8 T cell-dependent immune responses (76). Though IL-6 also drives tumor growth and promotes survival of neoplastic cells, these tumor-promoting activities are completely counteracted by the effect of T lymphocyte infiltration into the tumor site with a result of tumor cell killing and tumor regression (81, 83). However, most of the research was conducted under physiological temperature stress of 40–41°C. Moreover, hyperthermia alone seems insufficient for tumor cell regression for the result that combination of an artificial cytokine storm and hyperthermia rather than hyperthermia itself can effectively promote the anti-tumor response (84).

HS-TEX Extracted After Hyperthermia Acts as Tumor Vaccine

Exosomes are small membrane vesicles of endocytic origin that have a typical bilayer-membrane structure shuttling from donor cells to recipient cells to communicate and transport information between different cells. In response to a variety of stress conditions, cells employ extracellular vesicle to transmit a pro-survival message in the tumor microenvironment for evasion of cell death and transmitting resistance to therapy (85). Heat stress not only promotes the release of TEX (quantity) (86) but also promotes TEX to pack with more positive immunomodulators (HSP70, adhesion molecules, chemokines) rather than negative regulators (fasL, TGF-β) (87).

HS-TEX is a reliable tumor vaccine for tumor-specific immune response. A study suggested that HS-TEX extracted from ascites of gastric cancer can induce DCs' differentiation and promote tumor-specific immune response (88). Whereas, intra-tumoral injection of HS-TEX derived from colon cancer cells and B lymphoma with hyperthermia efficiently induced tumor-specific anti-tumor immunity in mouse models (89, 90). Besides, HS-TEX can activate DCs to release IL-6 to trigger subsequent transformation of the immune microenvironment to reduce Tregs and promote the chemotaxis of T cells to tumors (76). Contents in the HS-TEX plays an important role for its function in TME. HSP-70 abundant exosomes recruit more NK cells and promote the killing of NK cells better than that of apoptotic fragments and HSP-70 knockout exosomes (91). Chemokines in HS-TEX recruit and activate DCs and tumor-specific T cells through a lipid raft-dependent pathway to promote tumor immune response. Despite the promising role of HS-TEX in TME, a study also suggested a bystander effect induced by HS-TEX from tumor cells that promotes the survival of unstressed ones (12). Moreover, PD-L1 can also express in TEX for immune evasion, but this expression cannot be neutralized by anti-PD-L1 mAb treatment (92). The sophisticated role of HS-TEX in the TME remains to be elucidated *in vivo* rather than as a vaccine. (Thus, this part is presented in **Figure 1** marked with dotted lines.)

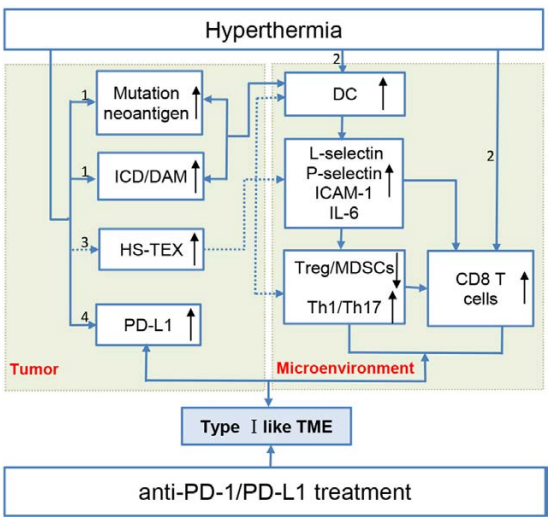

FIGURE 1 | Hyperthermia creates a type I-like tumor microenvironment, and the multifaceted mechanisms make hyperthermia a potent immune checkpoint inhibitor sensitizer. (1) Hyperthermia increases the tumor mutation burden/neoantigen and promotes immunogenic cell death. These two aspects promote DC activation maturation and thus transform the immunosuppressive microenvironment by inhibiting Treg cells and promoting tumor-infiltrating lymphocyte recruitment. (2) Hyperthermia can directly promote DC and T cell maturation. (3) Exosomes extracted from heat-stressed tumor cells (HS-TEX) act as a cancer vaccine to activate DCs and promote cells to secrete IL-6 to transform the immunosuppressive TME (marked with dotted lines) (4) Hyperthermia can upregulate PD-L1 expression in an elevated temperature.

Hyperthermia Promotes CD8 T Cell's Quantity and Quality

Despite the presence and activation of several immunologic components in the TME, tumor cells are not easily eradicated (93). Mechanisms involved in this impaired response are attributed to the immune suppressive agents in the TME, including the depletion of naïve anti-tumor T cells during thymic lymphocyte development, unresponsiveness of CTLs due to impaired of costimulatory or enhanced coinhibitory molecules, prolonged presence of immunosuppressive cells and along with secreted inhibitory molecules from those cells (94). Consequently, although immune cells are found in the TME, they are not fully effective (95, 96). Hyperthermia can break this barrier by promoting antigen-specific naive CD8 T cell differentiation, enhancing the cytotoxic potential of T cells and promoting memory stem T cell generation.

CD8 T cells' differentiation and function of cytotoxicity are both temperature-sensitive events. Study researched the number of Melan-A/Mart-1-specific CD8 T cells in patients after isolated limb perfusion with hyperthermia and found a small increase in tumor-specific T-cells in a subpopulation of patients with melanoma, demonstrating the potential of thermal therapy in the activation and differentiation of immune effector cells in the tumor microenvironment (97). Another study showed that heat-shocked pre-treated melanoma cell lysates promote the proportion of a prototypic effector T cells (PD-1^{lo}CD8 T cell) in the TME to prevent dysfunctional T-cell accumulation and inhibit tumor growth (98). The result that hyperthermia promotes naive CD8 T cells' differentiation are also proved by a study that CD8+ T cells under heat stress (39.5°C) can differentiate into effector cells by reversible clustering of GM1(+) CD-microdomains in the plasma membrane, clustering of TCRβ and the CD8 coreceptor, and enhancing the rate of CD8+ T cell-APC conjugate formation in all spleen, lymph nodes, and peripheral blood T cells. While during the phase of cytotoxicity, the ability IFN-gamma production and cytotoxicity effect of effector CD8+ T cell are also enhanced after hyperthermia (99, 100). The enhanced cytotoxicity effect is associated with the expression of HSF1 that upregulates fas ligand expression by translocation of the transcription factors AP-1 and NF-κB (101). Some researchers believe that exhaustion of CTLs is due to impaired formation of memory T cells (102). Studies have shown that hyperthermia induces differentiation of $CD8^+$ T cells into memory stem T cells (T_{SCM}) (103) and could possibly redistribute the memory T cells of patients with tumor (104). Thus based on the results of enhanced T-cell trafficking and promoted CD8 T cell immunity, hyperthermia can effectively target at the TME to edit the immunity for cancer treatment.

HYPERTHERMIA PROMOTES THE EXPRESSION OF COINHIBITORY MOLECULES

Despite the reliable effects of hyperthermia on the immunogenicity and immunoreactivity of tumors, hyperthermia can also upregulate the expression of coinhibitory molecules. Studies have shown that heating in the range of 37–49°C successively upregulated the expression of PD-L1 and IDO on the surface of tumor cells. They found that with time, the expression of IDO increased at 48 h after the heat treatment and then decreased at 72h. Whereas, the expression of PD-L1 have the highest expression at 72 h. Moreover, the upregulated PD-L1 expression not only showed in tumor margins but also in distant tumors after hyperthermia (ablation temperature) (105–107). It remains to be elucidated that the upregulated coinhibitory molecules of PD-L1, PD-1, and Tim-3 are a cellular protective responses to avoid excessive immune activation or a byproducts from heat shock response when cells under damage. It should be noted that the upregulated coinhibitory molecules on tumor cells can also lead to impaired function of CD8 T cell. However, this upregulated immune checkpoint molecule can be neutralized by ICIs, and synergetic effect has been achieved for the combined hyperthermia and ICIs for tumor remission (see the following section). Thus, based on the foregoing reference that hyperthermia can either activate or enhance the immune response and upregulate PD-L1 in several kinds of tumors, we propose that treatment with hyperthermia creates a type I like tumor immune microenvironment with tumor infiltrating lymphocytes (TILs) and upregulates PD-L1 to work in complement with ICIs for cancer treatment (**Figure 1**).

PRECLINICAL DATA COMBINING HYPERTHERMIA AND ICIs

Discussed and researched for centuries, hyperthermia is seldom applied as a mainstream therapy or an adjuvant approach for cancer therapy. Clinical studies have researched the combination treatment of hyperthermia with cytokines and DCs; however, the results are conflicting. The reasons are mainly attributed to tumor tissue selection, antigen load *in vitro* and *in vivo*, and whether DCs could be recruited effectively. Despite the conflicting results of hyperthermia with traditional immune treatment and the constraint of antigen masking or shielding, thermoresistance, the bystander effect of HS-TEX and possible high expression of PD-L1 in HS-TEX, preclinical research of the combination regimens involving hyperthermia and ICIs has achieved optimistic results. However, hyperthermia is mainly restricted to nanoparticle-mediated hyperthermia and radiofrequency ablation.

Nanoparticle-mediated hyperthermia is a localized non-invasive treatment with controllable irradiation that has emerged as a new paradigm towards precise cancer therapy. Nanoparticle-mediated hyperthermia includes photothermal therapy and magnetic hyperthermia. Studies have found that the combination of ICIs (CTLA-4, PD-L1, IDO) and nanoparticle-mediated hyperthermia can promote antigen capture, enhance ICD effect, inhibit Treg cells' function, promote M1 macrophages' differentiation, recruit several folds of tumor-infiltrating lymphocytes, and achieve lasting memory for the inhibition of tumor growth in primary and distant sites

(106–114). The synergetic role of heat and ICIs is further confirmed by results that enhanced tumor antigen-specific T cell responses and an increased Teff to Treg ratio in distant tumors with a combination of RFA and anti-PD-1 mAb administration (105). Despite the favorable results, several studies have shown limited results for complete tumor remission for ICIs with hyperthermia. Thus, triple combination strategies including ICIs with radio-/chemotherapy or TLR agonists have been studied, and they have also achieved favorable results with decreased tumor volume, increased metastatic dissemination, prevention of tumor rechallenge, and improved overall survival (115–126). A case report also found that hyperthermia and ipilimumab combined with IL-2 achieved complete clinical remission of stage IV triple-negative breast cancer with lung metastasis (127). Despite the favorable results, a preclinical study combining magnetic iron oxide nanoparticle hyperthermia and anti-PD-1 and anti-CTLA-4 with a 4T1-luc cell mouse model also showed decreased tumor volume but increased metastatic dissemination and no improvement in overall survival (128). In fact, a study has shown that tumors quickly overcame immune responses by inhibiting the function of CD8 and CD4 T cells, driving a shift to a higher Treg/Teff ratio and upregulating PD-L1/PD-1 expression, which result suggested that tumor microenvironment after hyperthermia is variable and is favorable

TABLE 1 | Preclinical studies involving hyperthermia and immune checkpoint inhibitors.

Hyperthermia	Immune checkpoint inhibitors	Temperature	Tumor (mouse model)	Reference
CuS NPs-PEG-Mal-mediated PTT	Anti-PD-L1 mAb	55°C	4T1 breast tumor	(108)
Mild photothermal	Anti-PD-L1 mAb	45°C	4T1 breast tumor and B16-F10 melanoma tumor	(107)
CoFe2O4@MnFe2O4 nanoparticle-mediated magnetic hyperthermia	Anti-PD-L1 mAb	50°C	4T1 breast tumor	(109)
FVIOs-mediated magnetic hyperthermia	Anti-PD-L1 mAb	43–44°C	Orthotopic 4T1 breast cancer	(110)
Au nanoparticle-loaded membrane nanosheet photothermal therapy	Anti-PD-L1 mAb	64.4 ± 1.4°C	B16–F10 melanoma-tumor	(111)
GNPs-hPD-L1 siRNA-mediated photothermal therapy	Nanoprism-assisted PD-L1 siRNA	41.2°C	HCC827 lung cancer cell bearing tumor	(112)
APP- and HAuNS-loaded PLGA nanoparticle photothermal ablation	Sustained release anti-PD-1 peptide	50–55°C	4T1 breast tumor and CT26 tumor	(113)
Au@Pt-LMDP conjugated photothermal-immunotherapy	Release of a D-peptide antagonist of PD-L1	+ 20°C	4T1 breast tumor	(114)
NLG919/IR780 micelle-mediated PTT	IDO inhibitor	54°C	MCF-7 breast cancer	(106)
Triple combination				
mPEG-Pep-IDOi/ICG NPs-mediated phototherapy	Anti-PD-L1 mAb and nanoplatform of IDO inhibitor (IDOi)	Maximum 60°C	B16–F10 melanoma tumor	(115)
Magnetic iron oxide nanoparticle hyperthermia	Anti-PD-1 mAb and anti-CTLA-4 mAb	43°C	4T1-luc breast cancer model	(128)
PEG–rGO–FA–IDOi-mediated PTT	Anti-PD-L1 mAb and IDOi	53°C	CT26 colorectal cancer	(116)
PDMN-JQ1 nanoplatform-mediated photothermal therapy	bromodomain and extra-terminal inhibitor JQ1 downregulated the expression of PD-L1 and inhibited the BRD4-c-MYC axis	+21.7–20.3°C	4T1 breast tumor	(117)
PDA-PEG-R848-CD nanoparticle PTT	Anti-PD-L1 mAb + PDA loaded with TLR7 agonist	52.4°C	4T1 breast tumor	(118)
Fe3O4-R837 SP-involved PTT	Anti-PD-L1 mAb and nanoparticles loaded with Toll-like receptor 7 agonist	Ablation temperature	4T1 breast tumor	(119)
Iron nanoparticle-mediated magnetic hyperthermia	Anti-CTLA-4 mAb and TLR7 agonist	55°C	CT26 mouse colon cancer and murine B16 skin melanoma	(120)
WO2.9-WSe2 nanoparticles I RT/PTT	Anti-PD-L1 mAb-based CBT + low radiation dose	48°C	4T1 breast tumor	(121)
COF@ICG@OVA PTT/PDT therapy	Anti-PD-L1 mAb + PDT + PTT	>63.5°C	H22 murine hepatoma	(122)
Hyaluronic acid-shelled PPy/CPT nanoparticles	Anti-PD-L1 mAb and camptothecin	45–50°C	4T1 Breast cancer	(123)
FA-CD@PP-CpG phototherapy	Anti-PD-L1 mAb+low dosage of loaded docetaxel	44°C	4T1 breast tumor	(126)
Pd-Dox@TGMs NPs chemical-photothermal therapy	Anti-PD-L1 mAb and doxorubicin	51.2°C	CT26 colorectal cancer	(124)
Cu-PPT + 650 + 808 nm laser photo/chemodynamic therapy	Glutathione peroxidase-mimicking and PD-L1 mAb	–	CT26 colorectal cancer	(125)
Regional hyperthermia followed by systemic fever-range hyperthermia induced by interleukin-2	Ipilimumab (case report)	<42°C	Stage IV triple-negative breast cancer with lung metastasis	(127)
Radiofrequency ablation				
Radiofrequency ablation	Anti-PD-1 mAbs	>45°C	CT26 mouse colon cancer	(105)
	Atezolizumab (case report)	>45°C	Stage IV non-small cell lung cancer	(129)

for anti-PD-1/PD-L1mAb treatment for only a narrow time window (105). Thus, compared to similar studies mentioned above, the reasons may partially be attributed to the unsynchronized treatment of hyperthermia and ICIs, for which other reasons should be explored to avoid further clinical failure. Detailed information on the combination therapies is shown in **Table 1**.

CONCLUSIONS AND FUTURE CHALLENGES

Providing danger signals and reforming immune cells in the TME, hyperthermia is involved in multiple steps of regulating pathways in the cancer-immunity cycle; the immunomodulatory effect not only makes hyperthermia a treatment capable of defending against cancer but also makes the regimens of hyperthermia and ICIs a promising treatment for clinical use. Two of the major concerns are whether this combination is sufficient for the initiation and clearance of the tumor and that the combination would not drag the result in the opposite direction, *i.e.*, the super-progression of the tumor due to immunotolerance. For the first concern, selective combination with the known treatment would be a way for solution. In fact, both radiotherapy and chemotherapy can directly kill tumor cells, whose cell debris can be recognized as a tumor *in situ* vaccine that can promote the effect of ant-PD-1/PD-L1 mAb. Moreover, hyperthermia is a potent radio-/chemo-sensitizer *via* a series of supplementary cytotoxic effect (130). Thus, it is expected for efficacy of the triple combination of anti-PD-1/PD-L1 mAb, hyperthermia and radio/chemotherapy in clinics. Moreover, it also seems promising for PARPi, anti-angiogenesis treatments and other treatments to substitute radio/chemotherapy to combine with PD-1/PD-L1 mAb and hyperthermia for the treatment of tumors with low mutation, fewer neoantigens or disorganized tumor vessels. Thus, rational different combination therapies are promising for the eradication of tumors (131). For the second question, the authors believe that the patients should also be explored and selected for the combination, which point is also important for the first concern. Studies have found that certain gene mutations, such as *KRAS*, are more sensitive to hyperthermia as they exhibit sustained ERK signaling hyperactivation and increased Wingless/Integrated (WNT)/beta-catenin signalling (132). Moreover, using a bioinformatic approach, a series of molecules have been identified as determinants of resistance/sensitivity to thermotherapy (49). The results of the two studies offer ways for accurate selection when treated with hyperthermia. Last but not least, thermoequipment and procedures should be normalized with schedules based on the model system, the magnitude, the duration of the thermal stress, and the time of recovery after heat exposure (133). However, radiofrequency and local hyperthermia are the most commonly used hyperthermia regimens in clinical practice; they exploit ablation and mild temperature for treatment directly instead of the help of particle media. How they can be properly used with ICIs and whether they can achieve equally promising results remain to be elucidated.

AUTHOR CONTRIBUTIONS

ZL performed the manuscript preparation and drafted the manuscript. JD helped draft the manuscript. JS revised the manuscript and approved the final version. YM contributed to the conception and design of the current study, revised the manuscript, and approved the final version. All authors contributed to the article and approved the submitted version.

REFERENCES

1. Wu T, Dai Y. Tumor microenvironment and therapeutic response. *Cancer Lett* (2017) 387:61–8. doi: 10.1016/j.canlet.2016.01.043
2. Chen DS, Mellman I. Oncology meets immunology: the cancer-immunity cycle. *Immunity* (2013) 39(1):1–10. doi: 10.1016/j.immuni.2013.07.012
3. Teng MW, Ngiow SF, Ribas A, Smyth MJ. Classifying Cancers Based on T-cell Infiltration and PD-L1. *Cancer Res* (2015) 75(11):2139–45. doi: 10.1158/0008-5472.CAN-15-0255
4. Osipov A, Saung MT, Zheng L, Murphy AG. Small molecule immunomodulation: the tumor microenvironment and overcoming immune escape. *J Immunother Cancer* (2019) 7(1):224. doi: 10.1186/s40425-019-0667-0
5. Wang Y, Deng W, Li N, Neri S, Sharma A, Jiang W, et al. Combining Immunotherapy and Radiotherapy for Cancer Treatment: Current Challenges and Future Directions. *Front Pharmacol* (2018) 9:185. doi: 10.3389/fphar.2018.00185
6. Fukumura D, Kloepper J, Amoozgar Z, Duda DG, Jain RK. Enhancing cancer immunotherapy using antiangiogenics: opportunities and challenges. *Nat Rev Clin Oncol* (2018) 15(5):325–40. doi: 10.1038/nrclinonc.2018.29
7. Repasky EA, Evans SS, Dewhirst MW. Temperature matters! And why it should matter to tumor immunologists. *Cancer Immunol Res* (2013) 1 (4):210–6. doi: 10.1158/2326-6066.cir-13-0118
8. Germano G, Lamba S, Rospo G, Barault L, Magri A, Maione F, et al. Inactivation of DNA repair triggers neoantigen generation and impairs tumour growth. *Nature* (2017) 552(7683):116–20. doi: 10.1038/nature24673
9. Schumacher TN, Scheper W, Kvistborg P. Cancer Neoantigens. *Annu Rev Immunol* (2019) 37:173–200. doi: 10.1146/annurev-immunol-042617-053402
10. Mantso T, Goussetis G, Franco R, Botaitis S, Pappa A, Panayiotidis M. Effects of hyperthermia as a mitigation strategy in DNA damage-based cancer therapies. *Semin Cancer Biol* (2016) 37-38:96–105. doi: 10.1016/j.semcancer.2016.03.004
11. Oei AL, Vriend LEM, Krawczyk PM, Horsman MR, Franken NAP, Crezee J. Targeting therapy-resistant cancer stem cells by hyperthermia. *Int J Hyperthermia* (2017) 33(4):419–27. doi: 10.1080/02656736.2017.1279757
12. Bewicke-Copley F, Mulcahy LA, Jacobs LA, Samuel P, Akbar N, Pink RC, et al. Extracellular vesicles released following heat stress induce bystander effect in unstressed populations. *J Extracell Vesicles* (2017) 6(1):1340746. doi: 10.1080/20013078.2017.1340746
13. Hurwitz M, Stauffer P. Hyperthermia, radiation and chemotherapy: the role of heat in multidisciplinary cancer care. *Semin Oncol* (2014) 41(6):714–29. doi: 10.1053/j.seminoncol.2014.09.014
14. Radogna F, Diederich M. Stress-induced cellular responses in immunogenic cell death: Implications for cancer immunotherapy. *Biochem Pharmacol* (2018) 153:12–23. doi: 10.1016/j.bcp.2018.02.006
15. Krysko DV, Garg AD, Kaczmarek A, Krysko O, Agostinis P, Vandenabeele P. Immunogenic cell death and DAMPs in cancer therapy. *Nat Rev Cancer* (2012) 12(12):860–75. doi: 10.1038/nrc3380
16. Garg AD, Krysko DV, Verfaillie T, Kaczmarek A, Ferreira GB, Marysael T, et al. A novel pathway combining calreticulin exposure and ATP secretion in

immunogenic cancer cell death. *EMBO J* (2012) 31(5):1062–79. doi: 10.1038/emboj.2011.497
17. Panaretakis T, Kepp O, Brockmeier U, Tesniere A, Bjorklund AC, Chapman DC, et al. Mechanisms of pre-apoptotic calreticulin exposure in immunogenic cell death. *EMBO J* (2009) 28(5):578–90. doi: 10.1038/emboj.2009.1
18. Nagata S, Tanaka M. Programmed cell death and the immune system. *Nat Rev Immunol* (2017) 17(5):333–40. doi: 10.1038/nri.2016.153
19. Inoue H, Tani K. Multimodal immunogenic cancer cell death as a consequence of anticancer cytotoxic treatments. *Cell Death Differ* (2014) 21(1):39–49. doi: 10.1038/cdd.2013.84
20. Kepp O, Zitvogel L, Kroemer G. Clinical evidence that immunogenic cell death sensitizes to PD-1/PD-L1 blockade. *Oncoimmunology* (2019) 8(10): e1637188. doi: 10.1080/2162402x.2019.1637188
21. González FE, Gleisner A, Falcón-Beas F, Osorio F, López MN, Salazar-Onfray F. Tumor cell lysates as immunogenic sources for cancer vaccine design. *Hum Vaccin Immunother* (2014) 10(11):3261–9. doi: 10.4161/21645515.2014.982996
22. Melief CJ. Mini-review: Regulation of cytotoxic T lymphocyte responses by dendritic cells: peaceful coexistence of cross-priming and direct priming? *Eur J Immunol* (2003) 33(10):2645–54. doi: 10.1002/eji.200324341
23. Diederich CJ. Thermal ablation and high-temperature thermal therapy: overview of technology and clinical implementation. *Int J Hyperthermia* (2005) 21(8):745–53. doi: 10.1080/02656730500271692
24. Kono H, Rock KL. How dying cells alert the immune system to danger. *Nat Rev Immunol* (2008) 8(4):279–89. doi: 10.1038/nri2215
25. de Andrade Mello P, Bian S, Savio LEB, Zhang H, Zhang J, Junger W, et al. Hyperthermia and associated changes in membrane fluidity potentiate P2X7 activation to promote tumor cell death. *Oncotarget* (2017) 8(40):67254–68. doi: 10.18632/oncotarget.18595
26. Homma T, Fujii J. Heat stress promotes the down-regulation of IRE1α in cells: An atypical modulation of the UPR pathway. *Exp Cell Res* (2016) 349 (1):128–38. doi: 10.1016/j.yexcr.2016.10.006
27. Pallepati P, Averill-Bates D. Mild thermotolerance induced at 40 degrees C increases antioxidants and protects HeLa cells against mitochondrial apoptosis induced by hydrogen peroxide: Role of p53. *Arch Biochem Biophys* (2010) 495(2):97–111. doi: 10.1016/j.abb.2009.12.014
28. Bezu L, Sauvat A, Humeau J, Gomes-da-Silva LC, Iribarren K, Forveille S, et al. eIF2α phosphorylation is pathognomonic for immunogenic cell death. *Cell Death Differ* (2018) 25(8):1375–93. doi: 10.1038/s41418-017-0044-9
29. Kepp O, Semeraro M, Bravo-San Pedro JM, Bloy N, Buqué A, Huang X, et al. eIF2α phosphorylation as a biomarker of immunogenic cell death. *Semin Cancer Biol* (2015) 33:86–92. doi: 10.1016/j.semcancer.2015.02.004
30. Bettaieb A, Averill-Bates DA. Thermotolerance induced at a mild temperature of 40°C alleviates heat shock-induced ER stress and apoptosis in HeLa cells. *Biochim Biophys Acta* (2015) 1853(1):52–62. doi: 10.1016/j.bbamcr.2014.09.016
31. Mantso T, Vasileiadis S, Anestopoulos I, Voulgaridou GP, Lampri E, Botaitis S, et al. Hyperthermia induces therapeutic effectiveness and potentiates adjuvant therapy with non-targeted and targeted drugs in an in vitro model of human malignant melanoma. *Sci Rep* (2018) 8(1):10724. doi: 10.1038/s41598-018-29018-0
32. Wang Q, Ju X, Wang J, Fan Y, Ren M, Zhang H. Immunogenic cell death in anticancer chemotherapy and its impact on clinical studies. *Cancer Lett* (2018) 438:17–23. doi: 10.1016/j.canlet.2018.08.028
33. Aguilera R, Saffie C, Tittarelli A, González FE, Ramírez M, Reyes D, et al. Heat-shock induction of tumor-derived danger signals mediates rapid monocyte differentiation into clinically effective dendritic cells. *Clin Cancer Res* (2011) 17(8):2474–83. doi: 10.1158/1078-0432.ccr-10-2384
34. Shi H, Cao T, Connolly JE, Monnet L, Bennett L, Chapel S, et al. Hyperthermia enhances CTL cross-priming. *J Immunol* (2006) 176 (4):2134–41. doi: 10.4049/jimmunol.176.4.2134
35. Meggyeshazi N, Andocs G, Balogh L, Balla P, Kiszner G, Teleki I, et al. DNA fragmentation and caspase-independent programmed cell death by modulated electrohyperthermia. *Strahlenther Onkol* (2014) 190(9):815–22. doi: 10.1007/s00066-014-0617-1
36. Vancsik T, Kovago C, Kiss E, Papp E, Forika G, Benyo Z, et al. Modulated electro-hyperthermia induced loco-regional and systemic tumor destruction in colorectal cancer allografts. *J Cancer* (2018) 9(1):41–53. doi: 10.7150/jca.21520
37. Hou CH, Lin FL, Hou SM, Liu JF. Hyperthermia induces apoptosis through endoplasmic reticulum and reactive oxygen species in human osteosarcoma cells. *Int J Mol Sci* (2014) 15(10):17380–95. doi: 10.3390/ijms151017380
38. Adkins I, Fucikova J, Garg AD, Agostinis P, Spisek R. Physical modalities inducing immunogenic tumor cell death for cancer immunotherapy. *Oncoimmunology* (2014) 3(12):e968434. doi: 10.4161/21624011.2014.968434
39. O'Brien MA, Power DG, Clover AJ, Bird B, Soden DM, Forde PF. Local tumour ablative therapies: opportunities for maximising immune engagement and activation. *Biochim Biophys Acta* (2014) 1846(2):510–23. doi: 10.1016/j.bbcan.2014.09.005
40. González FE, Chernobrovkin A, Pereda C, García-Salum T, Tittarelli A, López MN, et al. Proteomic Identification of Heat Shock-Induced Danger Signals in a Melanoma Cell Lysate Used in Dendritic Cell-Based Cancer Immunotherapy. *J Immunol Res* (2018) 2018:3982942. doi: 10.1155/2018/3982942
41. Chen T, Guo J, Han C, Yang M, Cao X. Heat shock protein 70, released from heat-stressed tumor cells, initiates antitumor immunity by inducing tumor cell chemokine production and activating dendritic cells via TLR4 pathway. *J Immunol* (2009) 182(3):1449–59. doi: 10.4049/jimmunol.182.3.1449
42. Calderwood SK. Heat shock proteins and cancer: intracellular chaperones or extracellular signalling ligands? *Philos Trans R Soc Lond B Biol Sci* (2018) 373 (1738). doi: 10.1098/rstb.2016.0524
43. Tomasovic SP, Simonette RA, Wolf DA, Kelley KL, Updyke TV. Co-isolation of heat stress and cytoskeletal proteins with plasma membrane proteins. *Int J Hyperthermia* (1989) 5(2):173–90. doi: 10.3109/02656738909140446
44. Shevtsov M, Huile G, Multhoff G. Membrane heat shock protein 70: a theranostic target for cancer therapy. *Philos Trans R Soc Lond B Biol Sci* (2018) 373(1738). doi: 10.1098/rstb.2016.0526
45. Zhu J, Zhang Y, Zhang A, He K, Liu P, Xu LX. Cryo-thermal therapy elicits potent anti-tumor immunity by inducing extracellular Hsp70-dependent MDSC differentiation. *Sci Rep* (2016) 6:27136. doi: 10.1038/srep27136
46. Schildkopf P, Frey B, Ott OJ, Rubner Y, Multhoff G, Sauer R, et al. Radiation combined with hyperthermia induces HSP70-dependent maturation of dendritic cells and release of pro-inflammatory cytokines by dendritic cells and macrophages. *Radiother Oncol* (2011) 101(1):109–15. doi: 10.1016/j.radonc.2011.05.056
47. Ito A, Fujioka M, Tanaka K, Kobayashi T, Honda H. Screening of cytokines to enhance vaccine effects of heat shock protein 70-rich tumor cell lysate. *J Biosci Bioeng* (2005) 100(1):36–42. doi: 10.1263/jbb.100.36
48. Lin FC, Hsu CH, Lin YY. Nano-therapeutic cancer immunotherapy using hyperthermia-induced heat shock proteins: insights from mathematical modeling. *Int J Nanomedicine* (2018) 13:3529–39. doi: 10.2147/ijn.s166000
49. Duzgun MB, Theofilatos K, Georgakilas AG, Pavlopoulou A. A Bioinformatic Approach for the Identification of Molecular Determinants of Resistance/Sensitivity to Cancer Thermotherapy. *Oxid Med Cell Longev* (2019) 2019:4606219. doi: 10.1155/2019/4606219
50. Ostberg JR, Repasky EA. Emerging evidence indicates that physiologically relevant thermal stress regulates dendritic cell function. *Cancer Immunol Immunother* (2006) 55(3):292–8. doi: 10.1007/s00262-005-0689-y
51. Knippertz I, Stein MF, Dorrie J, Schaft N, Muller I, Deinzer A, et al. Mild hyperthermia enhances human monocyte-derived dendritic cell functions and offers potential for applications in vaccination strategies. *Int J Hyperthermia* (2011) 27(6):591–603. doi: 10.3109/02656736.2011.589234
52. Feng M, Jiang W, Kim BYS, Zhang CC, Fu YX, Weissman IL. Phagocytosis checkpoints as new targets for cancer immunotherapy. *Nat Rev Cancer* (2019) 19(10):568–86. doi: 10.1038/s41568-019-0183-z
53. Adkins I, Sadilkova L, Hradilova N, Tomala J, Kovar M, Spisek R. Severe, but not mild heat-shock treatment induces immunogenic cell death in cancer cells. *Oncoimmunology* (2017) 6(5):e1311433. doi: 10.1080/2162402x.2017.1311433
54. Garg AD, Romano E, Rufo N, Agostinis P. Immunogenic versus tolerogenic phagocytosis during anticancer therapy: mechanisms and clinical translation. *Cell Death Differ* (2016) 23(6):938–51. doi: 10.1038/cdd.2016.5
55. Dudek AM, Martin S, Garg AD, Agostinis P. Immature, Semi-Mature, and Fully Mature Dendritic Cells: Toward a DC-Cancer Cells Interface That Augments Anticancer Immunity. *Front Immunol* (2013) 4:438. doi: 10.3389/fimmu.2013.00438
56. Kubes J, Svoboda J, Rosina J, Starec M, Fiserova A. Immunological response in the mouse melanoma model after local hyperthermia. *Physiol Res* (2008) 57(3):459–65.

57. Liu P, Jia S, Lou Y, He K, Xu LX. Cryo-thermal therapy inducing MI macrophage polarization created CXCL10 and IL-6-rich pro-inflammatory environment for CD4(+) T cell-mediated anti-tumor immunity. *Int J Hyperthermia* (2019) 36(1):408–20. doi: 10.1080/02656736.2019.1579373
58. He K, Jia S, Lou Y, Liu P, Xu LX. Cryo-thermal therapy induces macrophage polarization for durable anti-tumor immunity. *Cell Death Dis* (2019) 10 (3):216. doi: 10.1038/s41419-019-1459-7
59. Sabado RL, Balan S, Bhardwaj N. Dendritic cell-based immunotherapy. *Cell Res* (2017) 27(1):74–95. doi: 10.1038/cr.2016.157
60. Hargadon KM. Strategies to Improve the Efficacy of Dendritic Cell-Based Immunotherapy for Melanoma. *Front Immunol* (2017) 8:1594. doi: 10.3389/fimmu.2017.01594
61. Matsumoto K, Yamamoto N, Hagiwara S, Saito M, Furue H, Shigetomi T, et al. Optimization of hyperthermia and dendritic cell immunotherapy for squamous cell carcinoma. *Oncol Rep* (2011) 25(6):1525–32. doi: 10.3892/or.2011.1232
62. Menga M, Trotta R, Scrima R, Pacelli C, Silvestri V, Piccoli C, et al. Febrile temperature reprograms by redox-mediated signaling the mitochondrial metabolic phenotype in monocyte-derived dendritic cells. *Biochim Biophys Acta Mol Basis Dis* (2018) 1864(3):685–99. doi: 10.1016/j.bbadis.2017.12.010
63. Liso A, Capitanio N, Gerli R, Conese M. From fever to immunity: A new role for IGFBP-6? *J Cell Mol Med* (2018) 22(10):4588–96. doi: 10.1111/jcmm.13738
64. Zhou L, Chong MM, Littman DR. Plasticity of CD4+ T cell lineage differentiation. *Immunity* (2009) 30(5):646–55. doi: 10.1016/j.immuni.2009.05.001
65. Wan YY. Multi-tasking of helper T cells. *Immunology* (2010) 130(2):166–71. doi: 10.1111/j.1365-2567.2010.03289.x
66. Kim HJ, Cantor H. CD4 T-cell subsets and tumor immunity: the helpful and the not-so-helpful. *Cancer Immunol Res* (2014) 2(2):91–8. doi: 10.1158/2326-6066.CIR-13-0216
67. Fridman WH, Pages F, Sautes-Fridman C, Galon J. The immune contexture in human tumours: impact on clinical outcome. *Nat Rev Cancer* (2012) 12 (4):298–306. doi: 10.1038/nrc3245
68. Najafi S, Mirshafiey A. The role of T helper 17 and regulatory T cells in tumor microenvironment. *Immunopharmacol Immunotoxicol* (2019) 41 (1):16–24. doi: 10.1080/08923973.2019.1566925
69. Zuazo M, Arasanz H, Bocanegra A, Chocarro L, Vera R, Escors D, et al. Systemic CD4 immunity: A powerful clinical biomarker for PD-L1/PD-1 immunotherapy. *EMBO Mol Med* (2020) 12(9):e12706. doi: 10.15252/emmm.202012706
70. Zuazo M, Arasanz H, Fernández-Hinojal G, García-Granda MJ, Gato M, Bocanegra A, et al. Functional systemic CD4 immunity is required for clinical responses to PD-L1/PD-1 blockade therapy. *EMBO Mol Med* (2019) 11(7):e10293. doi: 10.15252/emmm.201910293
71. Liu K, He K, Xue T, Liu P, Xu LX. The cryo-thermal therapy-induced IL-6-rich acute pro-inflammatory response promoted DCs phenotypic maturation as the prerequisite to CD4(+) T cell differentiation. *Int J Hyperthermia* (2018) 34(3):261–72. doi: 10.1080/02656736.2017.1332394
72. Du G, Liu Y, Li J, Liu W, Wang Y, Li H. Hypothermic microenvironment plays a key role in tumor immune subversion. *Int Immunopharmacol* (2013) 17(2):245–53. doi: 10.1016/j.intimp.2013.06.018
73. Duan XH, Li H, Han XW, Ren JZ, Li FY, Ju SG, et al. Upregulation of IL-6 is involved in moderate hyperthermia induced proliferation and invasion of hepatocellular carcinoma cells. *Eur J Pharmacol* (2018) 833:230–6. doi: 10.1016/j.ejphar.2018.06.014
74. Hong M, Jiang Z, Zhou YF. Effects of thermotherapy on Th1/Th2 cells in esophageal cancer patients treated with radiotherapy. *Asian Pac J Cancer Prev* (2014) 15(5):2359–62. doi: 10.7314/apjcp.2014.15.5.2359
75. Cho JA, Lee YS, Kim SH, Ko JK, Kim CW. MHC independent anti-tumor immune responses induced by Hsp70-enriched exosomes generate tumor regression in murine models. *Cancer Lett* (2009) 275(2):256–65. doi: 10.1016/j.canlet.2008.10.021
76. Guo D, Chen Y, Wang S, Yu L, Shen Y, Zhong H, et al. Exosomes from heat-stressed tumour cells inhibit tumour growth by converting regulatory T cells to Th17 cells via IL-6. *Immunology* (2018) 154(1):132–43. doi: 10.1111/imm.12874
77. Newton JM, Flores-Arredondo JH, Suki S, Ware MJ, Krzykawska-Serda M, Agha M, et al. Non-Invasive Radiofrequency Field Treatment of 4T1 Breast Tumors Induces T-cell Dependent Inflammatory Response. *Sci Rep* (2018) 8 (1):3474. doi: 10.1038/s41598-018-21719-w
78. Chen Q, Fisher DT, Kucinska SA, Wang WC, Evans SS. Dynamic control of lymphocyte trafficking by fever-range thermal stress. *Cancer Immunol Immunother* (2006) 55(3):299–311. doi: 10.1007/s00262-005-0022-9
79. Chen Q, Appenheimer MM, Muhitch JB, Fisher DT, Clancy KA, Miecznikowski JC, et al. Thermal facilitation of lymphocyte trafficking involves temporal induction of intravascular ICAM-1. *Microcirculation* (2009) 16(2):143–58. doi: 10.1080/10739680802353850
81. Evans SS, Wang WC, Bain MD, Burd R, Ostberg JR, Repasky EA. Fever-range hyperthermia dynamically regulates lymphocyte delivery to high endothelial venules. *Blood* (2001) 97(9):2727–33. doi: 10.1182/blood.v97.9.2727
80. Chen Q, Fisher DT, Clancy KA, Gauguet JM, Wang WC, Unger E, et al. Fever-range thermal stress promotes lymphocyte trafficking across high endothelial venules via an interleukin 6 trans-signaling mechanism. *Nat Immunol* (2006) 7(12):1299–308. doi: 10.1038/ni1406
82. Xue T, Liu P, Zhou Y, Liu K, Yang L, Moritz RL, et al. Interleukin-6 Induced "Acute" Phenotypic Microenvironment Promotes Th1 Anti-Tumor Immunity in Cryo-Thermal Therapy Revealed By Shotgun and Parallel Reaction Monitoring Proteomics. *Theranostics* (2016) 6(6):773–94. doi: 10.7150/thno.14394
83. Fisher DT, Chen Q, Skitzki JJ, Muhitch JB, Zhou L, Appenheimer MM, et al. IL-6 trans-signaling licenses mouse and human tumor microvascular gateways for trafficking of cytotoxic T cells. *J Clin Invest* (2011) 121 (10):3846–59. doi: 10.1172/JCI44952
84. Kushida S, Ohmae H, Kamma H, Totsuka R, Matsumura M, Takeuchi A, et al. Artificial cytokine storm combined with hyperthermia induces significant anti-tumor effect in mice inoculated with lewis lung carcinoma and B16 melanoma cells. *Int J Hyperthermia* (2006) 22(8):699–712. doi: 10.1080/02656730601088508
85. O'Neill CP, Gilligan KE, Dwyer RM. Role of Extracellular Vesicles (EVs) in Cell Stress Response and Resistance to Cancer Therapy. *Cancers (Basel)* (2019) 11(2). doi: 10.3390/cancers11020136
86. Yang Y, Chen Y, Zhang F, Zhao Q, Zhong H. Increased anti-tumour activity by exosomes derived from doxorubicin-treated tumour cells via heat stress. *Int J Hyperthermia* (2015) 31(5):498–506. doi: 10.3109/02656736.2015.1036384
87. Chen T, Guo J, Yang M, Zhu X, Cao X. Chemokine-containing exosomes are released from heat-stressed tumor cells via lipid raft-dependent pathway and act as efficient tumor vaccine. *J Immunol* (2011) 186(4):2219–28. doi: 10.4049/jimmunol.1002991
88. Zhong H, Yang Y, Ma S, Xiu F, Cai Z, Zhao H, et al. Induction of a tumour-specific CTL response by exosomes isolated from heat-treated malignant ascites of gastric cancer patients. *Int J Hyperthermia* (2011) 27(6):604–11. doi: 10.3109/02656736.2011.564598
89. Dai S, Wan T, Wang B, Zhou X, Xiu F, Chen T, et al. More efficient induction of HLA-A*0201-restricted and carcinoembryonic antigen (CEA)-specific CTL response by immunization with exosomes prepared from heat-stressed CEA-positive tumor cells. *Clin Cancer Res* (2005) 11(20):7554–63. doi: 10.1158/1078-0432.CCR-05-0810
90. Chen W, Wang J, Shao C, Liu S, Yu Y, Wang Q, et al. Efficient induction of antitumor T cell immunity by exosomes derived from heat-shocked lymphoma cells. *Eur J Immunol* (2006) 36(6):1598–607. doi: 10.1002/eji.200535501
91. Gastpar R, Gehrmann M, Bausero MA, Asea A, Gross C, Schroeder JA, et al. Heat shock protein 70 surface-positive tumor exosomes stimulate migratory and cytolytic activity of natural killer cells. *Cancer Res* (2005) 65(12):5238–47. doi: 10.1158/0008-5472.CAN-04-3804
92. Poggio M, Hu T, Pai CC, Chu B, Belair CD, Chang A, et al. Suppression of Exosomal PD-L1 Induces Systemic Anti-tumor Immunity and Memory. *Cell* (2019) 177(2):414–427 e413. doi: 10.1016/j.cell.2019.02.016
93. Verdeil G, Fuertes Marraco SA, Murray T, Speiser DE. From T cell "exhaustion" to anti-cancer immunity. *Biochim Biophys Acta* (2016) 1865 (1):49–57. doi: 10.1016/j.bbcan.2015.06.007
94. Frey AB. Suppression of T cell responses in the tumor microenvironment. *Vaccine* (2015) 33(51):7393–400. doi: 10.1016/j.vaccine.2015.08.096
95. Baitsch L, Fuertes-Marraco SA, Legat A, Meyer C, Speiser DE. The three main stumbling blocks for anticancer T cells. *Trends Immunol* (2012) 33 (7):364–72. doi: 10.1016/j.it.2012.02.006
96. Davoodzadeh Gholami M, Kardar GA, Saeedi Y, Heydari S, Garssen J, Falak R. Exhaustion of T lymphocytes in the tumor microenvironment:

Significance and effective mechanisms. *Cell Immunol* (2017) 322:1–14. doi: 10.1016/j.cellimm.2017.10.002
97. Olofsson R, Lindberg E, Karlsson-Parra A, Lindnér P, Mattsson J, Andersson B. Melan-A specific CD8+ T lymphocytes after hyperthermic isolated limb perfusion: a pilot study in patients with in-transit metastases of malignant melanoma. *Int J Hyperthermia* (2013) 29(3):234–8. doi: 10.3109/02656736.2013.782428
98. Gleisner MA, Pereda C, Tittarelli A, Navarrete M, Fuentes C, Avalos I, et al. A heat-shocked melanoma cell lysate vaccine enhances tumor infiltration by prototypic effector T cells inhibiting tumor growth. *J Immunother Cancer* (2020) 8(2). doi: 10.1136/jitc-2020-000999
99. Mace TA, Zhong L, Kilpatrick C, Zynda E, Lee CT, Capitano M, et al. Differentiation of CD8+ T cells into effector cells is enhanced by physiological range hyperthermia. *J Leukoc Biol* (2011) 90(5):951–62. doi: 10.1189/jlb.0511229
100. Mace TA, Zhong L, Kokolus KM, Repasky EA. Effector CD8+ T cell IFN-gamma production and cytotoxicity are enhanced by mild hyperthermia. *Int J Hyperthermia* (2012) 28(1):9–18. doi: 10.3109/02656736.2011.616182
101. Cippitelli M, Fionda C, Di Bona D, Piccoli M, Frati L, Santoni A. Hyperthermia enhances CD95-ligand gene expression in T lymphocytes. *J Immunol* (2005) 174(1):223–32. doi: 10.4049/jimmunol.174.1.223
102. Jiang Y, Li Y, Zhu B. T-cell exhaustion in the tumor microenvironment. *Cell Death Dis* (2015) 6:e1792. doi: 10.1038/cddis.2015.162
103. He K, Liu P, Xu LX. The cryo-thermal therapy eradicated melanoma in mice by eliciting CD4(+) T-cell-mediated antitumor memory immune response. *Cell Death Dis* (2017) 8(3):e2703. doi: 10.1038/cddis.2017.125
104. Atanackovic D, Pollok K, Faltz C, Boeters I, Jung R, Nierhaus A, et al. Patients with solid tumors treated with high-temperature whole body hyperthermia show a redistribution of naive/memory T-cell subtypes. *Am J Physiol Regul Integr Comp Physiol* (2006) 290(3):R585–594. doi: 10.1152/ajpregu.00014.2005
105. Shi L, Chen L, Wu C, Zhu Y, Xu B, Zheng X, et al. PD-1 Blockade Boosts Radiofrequency Ablation-Elicited Adaptive Immune Responses against Tumor. *Clin Cancer Res* (2016) 22(5):1173–84. doi: 10.1158/1078-0432.ccr-15-1352
106. Peng J, Xiao Y, Li W, Yang Q, Tan L, Jia Y, et al. Photosensitizer Micelles Together with IDO Inhibitor Enhance Cancer Photothermal Therapy and Immunotherapy. *Adv Sci (Weinh)* (2018) 5(5):1700891. doi: 10.1002/advs.201700891
107. Huang L, Li Y, Du Y, Zhang Y, Wang X, Ding Y, et al. Mild photothermal therapy potentiates anti-PD-L1 treatment for immunologically cold tumors via an all-in-one and all-in-control strategy. *Nat Commun* (2019) 10(1):4871. doi: 10.1038/s41467-019-12771-9
108. Wang R, He Z, Cai P, Zhao Y, Gao L, Yang W, et al. Surface-Functionalized Modified Copper Sulfide Nanoparticles Enhance Checkpoint Blockade Tumor Immunotherapy by Photothermal Therapy and Antigen Capturing. *ACS Appl Mater Interfaces* (2019) 11(15):13964–72. doi: 10.1021/acsami.9b01107
109. Pan J, Hu P, Guo Y, Hao J, Ni D, Xu Y, et al. Combined Magnetic Hyperthermia and Immune Therapy for Primary and Metastatic Tumor Treatments. *ACS Nano* (2020) 14(1):1033–44. doi: 10.1021/acsnano.9b08550
110. Liu X, Zheng J, Sun W, Zhao X, Li Y, Gong N, et al. Ferrimagnetic Vortex Nanoring-Mediated Mild Magnetic Hyperthermia Imparts Potent Immunological Effect for Treating Cancer Metastasis. *ACS Nano* (2019) 13 (8):8811–25. doi: 10.1021/acsnano.9b01979
111. Li X, Liu J, Zhang W, Wu Y, Li J, Foda MF, et al. Biogenic Hybrid Nanosheets Activated Photothermal Therapy and Promoted Anti-PD-L1 Efficacy for Synergetic Antitumor Strategy. *ACS Appl Mater Interfaces* (2020) 12 (26):29122–32. doi: 10.1021/acsami.0c09111
112. Liu B, Cao W, Qiao G, Yao S, Pan S, Wang L, et al. Effects of gold nanoprism-assisted human PD-L1 siRNA on both gene down-regulation and photothermal therapy on lung cancer. *Acta Biomater* (2019) 99:307–19. doi: 10.1016/j.actbio.2019.08.046
113. Luo L, Yang J, Zhu C, Jiang M, Guo X, Li W, et al. Sustained release of anti-PD-1 peptide for perdurable immunotherapy together with photothermal ablation against primary and distant tumors. *J Control Release* (2018) 278:87–99. doi: 10.1016/j.jconrel.2018.04.002
114. Yang Q, Peng J, Shi K, Xiao Y, Liu Q, Han R, et al. Rationally designed peptide-conjugated gold/platinum nanosystem with active tumor-targeting for enhancing tumor photothermal-immunotherapy. *J Control Release* (2019) 308:29–43. doi: 10.1016/j.jconrel.2019.06.031
115. Liu Y, Lu Y, Zhu X, Li C, Yan M, Pan J, et al. Tumor microenvironment-responsive prodrug nanoplatform via co-self-assembly of photothermal agent and IDO inhibitor for enhanced tumor penetration and cancer immunotherapy. *Biomaterials* (2020) 242:119933. doi: 10.1016/j.biomaterials.2020.119933
116. Yan M, Liu Y, Zhu X, Wang X, Liu L, Sun H, et al. Nanoscale Reduced Graphene Oxide-Mediated Photothermal Therapy Together with IDO Inhibition and PD-L1 Blockade Synergistically Promote Antitumor Immunity. *ACS Appl Mater Interfaces* (2019) 11(2):1876–85. doi: 10.1021/acsami.8b18751
117. Tian Y, Wang X, Zhao S, Liao X, Younis MR, Wang S, et al. JQ1-Loaded Polydopamine Nanoplatform Inhibits c-MYC/Programmed Cell Death Ligand 1 to Enhance Photothermal Therapy for Triple-Negative Breast Cancer. *ACS Appl Mater Interfaces* (2019) 11(50):46626–36. doi: 10.1021/acsami.9b18730
118. Lu Q, Qi S, Li P, Yang L, Yang S, Wang Y, et al. Photothermally activatable PDA immune nanomedicine combined with PD-L1 checkpoint blockade for antimetastatic cancer photoimmunotherapy. *J Mater Chem B* (2019) 7 (15):2499–511. doi: 10.1039/c9tb00089e
119. Ge R, Liu C, Zhang X, Wang W, Li B, Liu J, et al. Photothermal-Activatable Fe3O4 Superparticle Nanodrug Carriers with PD-L1 Immune Checkpoint Blockade for Anti-metastatic Cancer Immunotherapy. *ACS Appl Mater Interfaces* (2018) 10(24):20342–55. doi: 10.1021/acsami.8b05876
120. Chao Y, Chen G, Liang C, Xu J, Dong Z, Han X, et al. Iron Nanoparticles for Low-Power Local Magnetic Hyperthermia in Combination with Immune Checkpoint Blockade for Systemic Antitumor Therapy. *Nano Lett* (2019) 19 (7):4287–96. doi: 10.1021/acs.nanolett.9b00579
121. Dong X, Cheng R, Zhu S, Liu H, Zhou R, Zhang C, et al. A Heterojunction Structured WO(2.9)-WSe(2) Nanoradiosensitizer Increases Local Tumor Ablation and Checkpoint Blockade Immunotherapy upon Low Radiation Dose. *ACS Nano* (2020) 14(5):5400–16. doi: 10.1021/acsnano.9b08962
122. Zhou Y, Liu S, Hu C, Cai L, Pang M. A covalent organic framework as a nanocarrier for synergistic photothermary and immunotherapy. *J Mater Chem B* (2020) 8(25):5451–9. doi: 10.1039/d0tb00679c
123. Sun W, Du Y, Liang X, Yu C, Fang J, Lu W, et al. Synergistic triple-combination therapy with hyaluronic acid-shelled PPy/CPT nanoparticles results in tumor regression and prevents tumor recurrence and metastasis in 4T1 breast cancer. *Biomaterials* (2019) 217:119264. doi: 10.1016/j.biomaterials.2019.119264
124. Wen Y, Chen X, Zhu X, Gong Y, Yuan G, Qin X, et al. Photothermal-Chemotherapy Integrated Nanoparticles with Tumor Microenvironment Response Enhanced the Induction of Immunogenic Cell Death for Colorectal Cancer Efficient Treatment. *ACS Appl Mater Interfaces* (2019) 11(46):43393–408. doi: 10.1021/acsami.9b17137
125. Hu C, Cai L, Liu S, Liu Y, Zhou Y, Pang M. Copper-Doped Nanoscale Covalent Organic Polymer for Augmented Photo/Chemodynamic Synergistic Therapy and Immunotherapy. *Bioconjug Chem* (2020) 31 (6):1661–70. doi: 10.1021/acs.bioconjchem.0c00209
126. Chen L, Zhou L, Wang C, Han Y, Lu Y, Liu J, et al. Tumor-Targeted Drug and CpG Delivery System for Phototherapy and Docetaxel-Enhanced Immunotherapy with Polarization toward M1-Type Macrophages on Triple Negative Breast Cancers. *Adv Mater* (2019) 31(52):e1904997. doi: 10.1002/adma.201904997
127. Kleef R, Moss R, Szasz AM, Bohdjalian A, Bojar H, Bakacs T. Complete Clinical Remission of Stage IV Triple-Negative Breast Cancer Lung Metastasis Administering Low-Dose Immune Checkpoint Blockade in Combination With Hyperthermia and Interleukin-2. *Integr Cancer Ther* (2018) 17(4):1297–303. doi: 10.1177/1534735418794867
128. Oei AL, Korangath P, Mulka K, Helenius M, Coulter JB, Stewart J, et al. Enhancing the abscopal effect of radiation and immune checkpoint inhibitor therapies with magnetic nanoparticle hyperthermia in a model of metastatic breast cancer. *Int J Hyperthermia* (2019) 36(sup1):47–63. doi: 10.1080/02656736.2019.1685686
129. Yin J, Dong J, Gao W, Wang Y. A case report of remarkable response to association of radiofrequency ablation with subsequent Atezolizumab in stage IV nonsmall cell lung cancer. *Med (Baltimore)* (2018) 97(44):e13112. doi: 10.1097/MD.0000000000013112
130. Datta NR, Ordonez SG, Gaipl US, Paulides MM, Crezee H, Gellermann J, et al. Local hyperthermia combined with radiotherapy and-/or

chemotherapy: recent advances and promises for the future. *Cancer Treat Rev* (2015) 41(9):742–53. doi: 10.1016/j.ctrv.2015.05.009
131. Datta NR, Kok HP, Crezee H, Gaipl US, Bodis S. Integrating Loco-Regional Hyperthermia Into the Current Oncology Practice: SWOT and TOWS Analyses. *Front Oncol* (2020) 10:819. doi: 10.3389/fonc.2020.00819
132. Bordonaro M, Shirasawa S, Lazarova DL. In Hyperthermia Increased ERK and WNT Signaling Suppress Colorectal Cancer Cell Growth. *Cancers (Basel)* (2016) 8(5). doi: 10.3390/cancers8050049
133. Milani V, Noessner E. Effects of thermal stress on tumor antigenicity and recognition by immune effector cells. *Cancer Immunol Immunother* (2006) 55(3):312–9. doi: 10.1007/s00262-005-0052-3

Conflict of Interest: The authors declare that the research was conducted in the absence of any commercial or financial relationships that could be construed as a potential conflict of interest.

Copyright © 2020 Li, Deng, Sun and Ma. This is an open-access article distributed under the terms of the Creative Commons Attribution License (CC BY). The use, distribution or reproduction in other forums is permitted, provided the original author(s) and the copyright owner(s) are credited and that the original publication in this journal is cited, in accordance with accepted academic practice. No use, distribution or reproduction is permitted which does not comply with these terms.

frontiers in Oncology

ORIGINAL RESEARCH
published: 09 November 2020
doi: 10.3389/fonc.2020.586820

Tumor Derived SIGLEC Family Genes May Play Roles in Tumor Genesis, Progression, and Immune Microenvironment Regulation

Zheng Chen, Mincheng Yu, Lei Guo, Bo Zhang, Shuang Liu, Wentao Zhang, Binghai Zhou, Jiuliang Yan, Qianni Ma, Zhangfu Yang, Yongsheng Xiao, Yongfeng Xu*, Hui Li* and Qinghai Ye**

Liver Cancer Institute, Zhongshan Hospital, Fudan University and Key Laboratory of Carcinogenesis and Cancer Invasion, Ministry of Education, Shanghai, China

OPEN ACCESS

Edited by:
Peng Qu,
National Institutes of Health (NIH), United States

Reviewed by:
Laila C. Roisman,
Ben-Gurion University of the Negev, Israel
Ye Zhang,
Koch Institute for Integrative Cancer Research at MIT, United States

***Correspondence:**
Qinghai Ye
ye.qinghai@zs-hospital.sh.cn
Hui Li
li.hui1@zs-hospital.sh.cn
Yongfeng Xu
xu.yongfeng@zs-hospital.sh.cn
Yongsheng Xiao
xiao.yongsheng@zs-hospital.sh.cn

Specialty section:
This article was submitted to Cancer Immunity and Immunotherapy, a section of the journal Frontiers in Oncology

Received: *24 July 2020*
Accepted: *06 October 2020*
Published: *09 November 2020*

Citation:
Chen Z, Yu M, Guo L, Zhang B, Liu S, Zhang W, Zhou B, Yan J, Ma Q, Yang Z, Xiao Y, Xu Y, Li H and Ye Q (2020) Tumor Derived SIGLEC Family Genes May Play Roles in Tumor Genesis, Progression, and Immune Microenvironment Regulation. Front. Oncol. 10:586820. doi: 10.3389/fonc.2020.586820

Background: SIGLEC family genes can also be expressed on tumor cells in different cancer types, and though it has been found that SIGLEC genes expressed by immune cells can be exploited by tumors to escape immune surveillance, functions of tumor derived SIGLEC expression in tumor microenvironment (TME) were barely investigated, which could play roles in cancer patients' survival.

Methods: Using bioinformatic analysis, mutation status of SIGLEC family genes was explored through the cBioPortal database, and expression of them in different tumors was explored through the UALCAN database. The GEPIA database was used to compare SIGLEC family genes' mRNA between cancers and to generate a highly correlated gene list in tumors. A KM-plotter database was used to find the association between SIGLEC genes and survival of patients. The associations between SIGLEC family genes' expression, immune infiltration, and immune regulators' expression in TME were generated and examined by the TIMER 2.0 database; the differential fold changes of SIGLEC family genes in specific oncogenic mutation groups of different cancer types were also yielded by TIMER 2.0. The networks of SIGLEC family genes and highly correlated genes were constructed by the STRING database, and gene ontology and pathway annotation of SIGLEC family highly correlated genes were performed through the DAVID database.

Results: SIGLEC family genes were highly mutated and amplified in melanoma, endometrial carcinoma, non-small cell lung cancer, bladder urothelial carcinoma, and esophagogastric adenocarcinoma, while deep deletion of SIGLEC family genes was common in diffuse glioma. Alteration of SIGLEC family genes demonstrated different levels in specific tumors, and oncogenic mutation in different cancer types could influence SIGLEC family genes' expression. Most SIGLEC family genes were related to patients' overall survival and progression free survival. Also, tumor derived SIGLEC family genes

were related to tumor immune cell infiltration and may regulate TME by influencing chemokine axis.

Conclusion: Our computational analysis showed SIGLEC family genes expressed by tumor cells were associated with tumor behaviors, and they may also influence TME through chemokine axis, playing vital roles in patients' survival. Further experiments targeting tumor derived SIGLEC family genes are needed to confirm their influences on tumor growth, metastasis, and immune environment regulation.

Keywords: pan-cancer, tumor immune microenvironment, tumor genesis, tumor progression, bioinformatic analysis

INTRODUCTION

SIGLEC family genes translate a group of proteins belonging to the immunoglobulin superfamily in mammal animals, and they can be divided into conservative (SIGLEC1, SIGLEC2, SIGLEC4, and SIGLEC15) and highly evolved (SIGLEC3, SIGLEC5, SIGLEC6, SIGLEC7, SIGLEC8, SIGLEC9, SIGLEC10, SIGLEC11, SIGLEC14, and SIGLEC16) teams, which are widely expressed on immune cell populations' membrane, mainly involving endocytosis and immune regulation in various diseases (1–5). SIGLEC family genes' protein on immune cells could bind to sialylated oligosaccharides, a type of glycoprotein, expressed by self or non-self cells, which in turn activate or inhibit immune cell function themselves or by binding to other functional kinase protein, providing targets for immune therapy (6).

It has been found that tumor cells can express sialylated ligands for SIGLEC receptors on immune cells, depressing immune cell function to escape immune surveillance, such as SIGLEC7 and SIGLEC9 on natural killer cell (7–12). However, SIGLEC family genes can also be expressed by tumor cells across cancer types, and recently, studies have found SIGLEC15 expressed by tumor cells or macrophages in mouse melanoma model could directly depress CD8+ T cell infiltration and function in tumor microenvironment through binding to presumptive target on CD8+ T cells (13–15). The explicit roles of tumor intrinsic SIGLEC family genes' expression on patients' survival, disease progression, and immune regulation in tumor microenvironment were still unknown, and we used bioinformatic analysis to find whether tumor derived expression of SIGLEC family genes played roles in those aspects, which could provide new thoughts for cancer immune therapy.

MATERIALS AND METHODS

Mutation and Alteration Frequency of SIGLEC Family Genes

cBioPortal database (https://www.cbioportal.org) was used to explore the mutation frequency of SIGLEC family genes in 33 types of tumors (melanoma, endometrial carcinoma, esophagogastric adenocarcinoma, non-small cell lung cancer, colorectal adenocarcinoma, ovarian epithelial tumor, cervical squamous cell carcinoma, bladder urothelial carcinoma, esophageal squamous cell carcinoma, sarcoma, head and neck squamous cell carcinoma, pancreatic adenocarcinoma, hepatocellular carcinoma, leukemia, prostate adenocarcinoma, invasive breast carcinoma, ocular melanoma, diffuse glioma, non-seminomatous germ cell tumor, renal non-clear cell carcinoma, pleural mesothelioma, adrenocortical carcinoma, glioblastoma, renal clear cell carcinoma, cervical adenocarcinoma, cholangiocarcinoma, mature B-cell neoplasm, pheochromocytoma, miscellaneous neuroepithelial tumor, undifferentiated stomach adenocarcinoma, seminoma, well-differentiated thyroid cancer, thymic epithelial tumor), which is an integrative database for analysis of mutation in various cancer types, containing somatic mutation and copy number variation data from the cancer genome atlas (TCGA) database (https://www.cancer.gov/about-nci/organization/ccg/research/structural-genomics/tcga) and other published articles (16, 17). The data of each tumor in TCGA Pan-Cancer projects were selected for analysis and demonstration. The data of alteration frequency (amplification, deletion, mutation, fusion, log2 transformed expression>=2 or log2 transformed expression<=-2) of each SIGLEC family gene were also generated and downloaded from the official website for further analysis (**Figure 1**).

mRNA Expression Levels of SIGLEC Family Genes and Comparison Between Normal and Tumor Tissues

mRNA expression levels of SIGLEC family genes were compared between normal and tumor tissues of each cancer type, using the UALCAN database (http://ualcan.path.uab.edu), which is an official website for comprehensive analysis of cancer data from the TCGA database (18). The corresponding significance of examination in each comparison test was generated by website, and the results were marked with asterisks for illustration.

Influence of SIELCE Family Gene mRNA Expression on Patients' Overall Survival and Progression Free Survival

The KM-plotter database (http://www.kmplot.com/analysis/index.php?p=service) was used to analyze the association between SIGLEC family genes' mRNA expression and patients' overall survival (OS) and progression free survival (PFS). KM-plotter database is an portal website for analysis of association between gene expression and patients survival, using data from

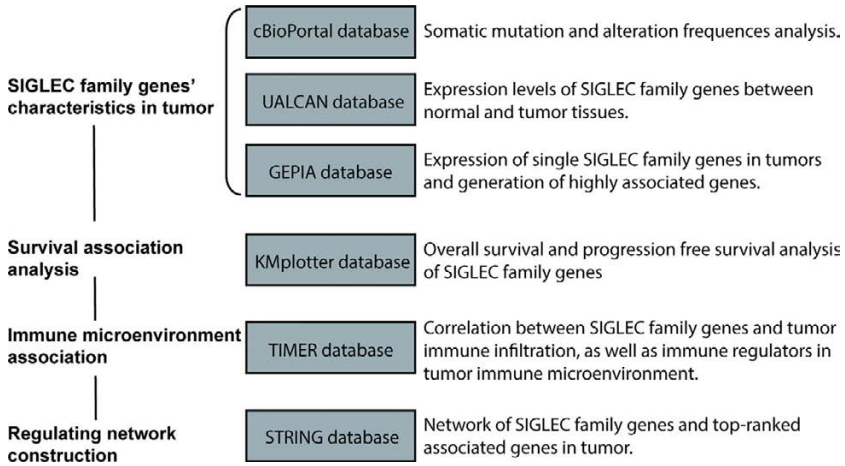

FIGURE 1 | Workflow of this study.

previous performed analysis, such as data from TCGA Pan-cancer projects and GEO database, covering micro RNA, long non-coding RNA, mRNA, and epigenetic information (19). The hazard ratio, 95% confidence interval, and *p* value of each analysis were generated by website, and in this analysis, best cutoff *p* values were deployed to subgroup patients into high- and low-expression groups.

mRNA Expression of SIGLEC Family Genes in Single Tumor and the List of SIGLEC Family Highly Correlated Genes

The Gene Expression Profiling Interactive Analysis (GEPIA) database (http://gepia.cancer-pku.cn) is a comprehensive database for tumor gene expression analysis, providing a portal for analyzing specific genes in 32 types of cancer, using data from TCGA Pan-Cancer project and GTEx database (https://www.gtexportal.org) (20, 21). In this analysis, median expression of SIGLEC family genes (transcript per million base, TPM) in each tumor type were downloaded from the website for demonstration, and the first 50 highly correlated genes of each SIGLEC family gene in tumor were generated through the website and were combined as SIGLEC family highly correlated genes for further analysis.

Correlation Between SIGLEC Family Genes, Immune Infiltration, and Immune Regulators

TIMER 2.0 (http://cistrome.shinyapps.io/timer) is a web-derived tool for analysis of tumor immune infiltration, which provides scores of 6 types of infiltrating immune cells (B cell, CD4+ T cell, CD8+ T cell, myeloid-derived dendritic cell, macrophages, and neutrophils) in tumors (22, 23). The correlation between SIGLEC family genes and six types of infiltrating immune cell were examined in each of 32 cancers, the data of which were from the TCGA database, and the results of examination were downloaded for demonstration. The correlation between SIGLEC family genes and well-known immune regulators were also analyzed through TIMER 2.0 for demonstration. TIMER 2.0 can also analyze differentially expressed genes between specific oncogene mutation groups, and SIGLEC family genes were input for analysis of well-known oncogenic mutation in specific tumors.

Network of SIGLEC Family Genes and Highly Correlated Genes in Tumors

The networks of SIGLEC family genes and highly correlated genes were yielded by STRING database (https://string-db.org), which can construct network of selective genes given results of formerly examined correlation in articles (24). The results were downloaded from the website, and Cytoscape (version: 3.7.1) was used to illustrate the correlation (25). The cytoHubba tool in Cytoscape was used to procure the core network and the top-10 leading node genes (26).

Gene Ontology of SIGLEC Family Highly Correlated Genes

The DAVID database (https://david.ncifcrf.gov) was used for gene ontology annotation of SIGLEC family highly correlated genes, which is a useful web tool for functional annotation (biological process, cellular compartment, and molecular function) of gene lists, and is also a tool for gene symbol transformation (27). It can link to the KEGG database (https://www.kegg.jp) for pathway annotation (28).

Statistics

All statistical examinations were performed by database derived tools, and *p* value under 0.05 was considered significant. All heat maps in this analysis were constructed in R environment (version: 3.6.1), using R studio (version: 1.2.1335) and pheatmap (29–31). R package of graphics was used to construct a forrest graph of hazard ratio in survival analysis,

and ggplot2, topGO, and clusterProfiler were used to generate the gene ontology graph (32–34).

RESULTS

Alteration Frequency of SIGLEC Family Genes Across Different Cancer Types

SIGLEC family genes (SIGLEC1 or CD169, SIGLEC2 or CD22, SIGLEC3 or CD33, SIGLEC4 or MAG, SIGLEC5, SIGLEC6, SIGLEC7, SIGLEC8, SIGLEC9, SIGLEC10, SIGLEC11, SIGLEC14, SIGLEC15, SIGLEC16) were also expressed in tumor cells, and we used the cBioPortal database to find mutation status of SIGLEC family genes in different cancer types. Results showed mutation frequencies of SIGLEC1, SIGLEC2, and SIGLEC10 were relatively high among all SIGLEC family genes, and SIGLEC family genes were highly mutated in melanoma (except SIGLEC15 and SIGLEC16). However, in ocular melanoma, miscellaneous neuroepithelial tumor, seminoma, cholangiocarcinoma, undifferentiated stomach adenocarcinoma, pheochromocytoma, well-differentiated thyroid cancer, non-seminomatous germ cell tumor, cervical adenocarcinoma, and pheochromocytoma mutation of SIGLEC family genes were rare. Of notice, while most SIGLEC family genes rarely mutated in cholangiocarcinoma and undifferentiated stomach adenocarcinoma, SIGLEC10 and SIGLEC7 were respectively highly mutated in each of them. Alteration frequencies (mutation, amplification, deep deletion, and multiple mutation) of SIGLEC family genes were also high in endometrial carcinoma, non-small cell lung cancer, bladder urothelial carcinoma, and esophagogastric adenocarcinoma. For endometrial carcinoma, non-small cell lung cancer and bladder urothelial carcinoma, mutation, and amplification of SIGLEC family genes were both high; for esophagogastric adenocarcinoma, mutation, amplification, and deep deletion of SIGLEC family genes were all common. Also, in diffuse glioma, deep deletion of SIGLEC family genes was common in comparison to 32 other types of tumor, and SIGLEC15 seemed to be deeply deleted in various tumors, while SIGLEC16 was amplified in mutating cancer types (**Figure 2**).

Expression Levels of SIGLEC Family Genes Between Normal and Tumor Tissues Across Cancer Types

We wondered whether SIGLEC family genes were differentially expressed between normal and tumor tissues in various cancer types, and we used the UALCAN database to examine their expression levels. We found mRNA expression levels of SIGLEC family genes were different between normal and tumors tissues, and extremely in breast invasive carcinoma (BRCA), colon adenocarcinoma (COAD), head and neck squamous cell carcinoma (HNSC), kidney renal clear cell carcinoma (KIRC), kidney renal papillary cell carcinoma (KIRP), liver hepatocellular carcinoma (LIHC), lung adenocarcinoma (LUAD), lung squamous cell carcinoma (LUSC), thyroid carcinoma (THCA), stomach adenocarcinoma (STAD), and uterine Corpus Endometrial Carcinoma (UCEC), almost all expressional difference of SIGLEC family genes achieved significance. In glioblastoma multiform (GBM), HNSC, KIRC, KIRP, THCA, and STAD, most SIGLEC family genes were highly expressed in tumor samples, while in COAD, LIHC, LUAD, and LUSC, most SIGLEC family genes were down-regulated in tumors. Also, SIGLEC11 mRNA expression was down-regulated in 19 out of 24 cancer types (except GBM, HNSC, THCA, and sarcoma [SARC], prostate adenocarcinoma [PRAD]), and SIGLEC15 was up-regulated in 18 out of 24 cancer types (except BRCA, KIRC, LUSC, PRAD, thymoma [THYM], and skin cutaneous melanoma [SKCM]) (**Figure 3**).

mRNA Expression of SIGLEC Family Genes Differed in Different Tumors, and Oncogenic Mutation Changes of Different Tumors Were Related to SIGLEC Family Genes

We compared the median TPM expression of SIGLEC family genes between cancer types (from GEPIA database), and results showed some SIGLEC family genes were highly expressed in specific tumors (**Figure 4**). Using TIMER 2.0 database, we found tumor specific oncogenic mutation could influence expression levels of SIGLEC family genes. In APC mutation groups of COAD and rectum adenocarcinoma (READ), most SIGLEC family genes were significantly down-regulated; in the CTNNB1 mutation group of LIHC, all SIGLEC family genes were down-regulated (10 out of 14 achieved significance). In other common mutations of tumors, such as PTEN, TP53, KRAS, and PIK3CA, SIGLEC family genes also demonstrated significant expressional changes in mutation groups of different cancer types (**Figure 5**).

Tumor Derived mRNA Expression of SIGLEC Family Genes Were Highly Correlated to Patients' Overall Survival and Progression Survival Across Cancer Types

We associated mRNA expression of SIGELC family genes with patients' survival, using the KM-plotter database, and found SIGLEC family genes were related to patients' overall survival (OS) and progression free survival (PFS) in most cancer types (**Figures 6A, B**). Concerning OS of patients with various tumors, most SIGLEC family genes in LUAD, THYM, KIRC, and HNSC showed significant correlation, and in HNSC and LUAD, most SIGLEC family genes showed protective roles, while in THYM and KIRC, most SIGLEC family genes were risk factors (**Figures 6C–F**). In LIHC and pancreatic adenocarcinoma (PAAD), only one (SIGLEC6) and three (SIGLEC2, SIGLEC15, and SIGLEC16) SIGLEC family genes were related to patients' OS, respectively; however, when it comes to PFS, most SIGELC family genes changed to protective and risk factors in LIHC and PAAD, correspondingly. Also, in bladder urothelial carcinoma (BLCA) and UCEC, most SIGLEC family genes were significant protecting factors for PFS, and only MAG (SIGLEC4) was a risk factor for PFS in UCEC (**Figures 6G–K**).

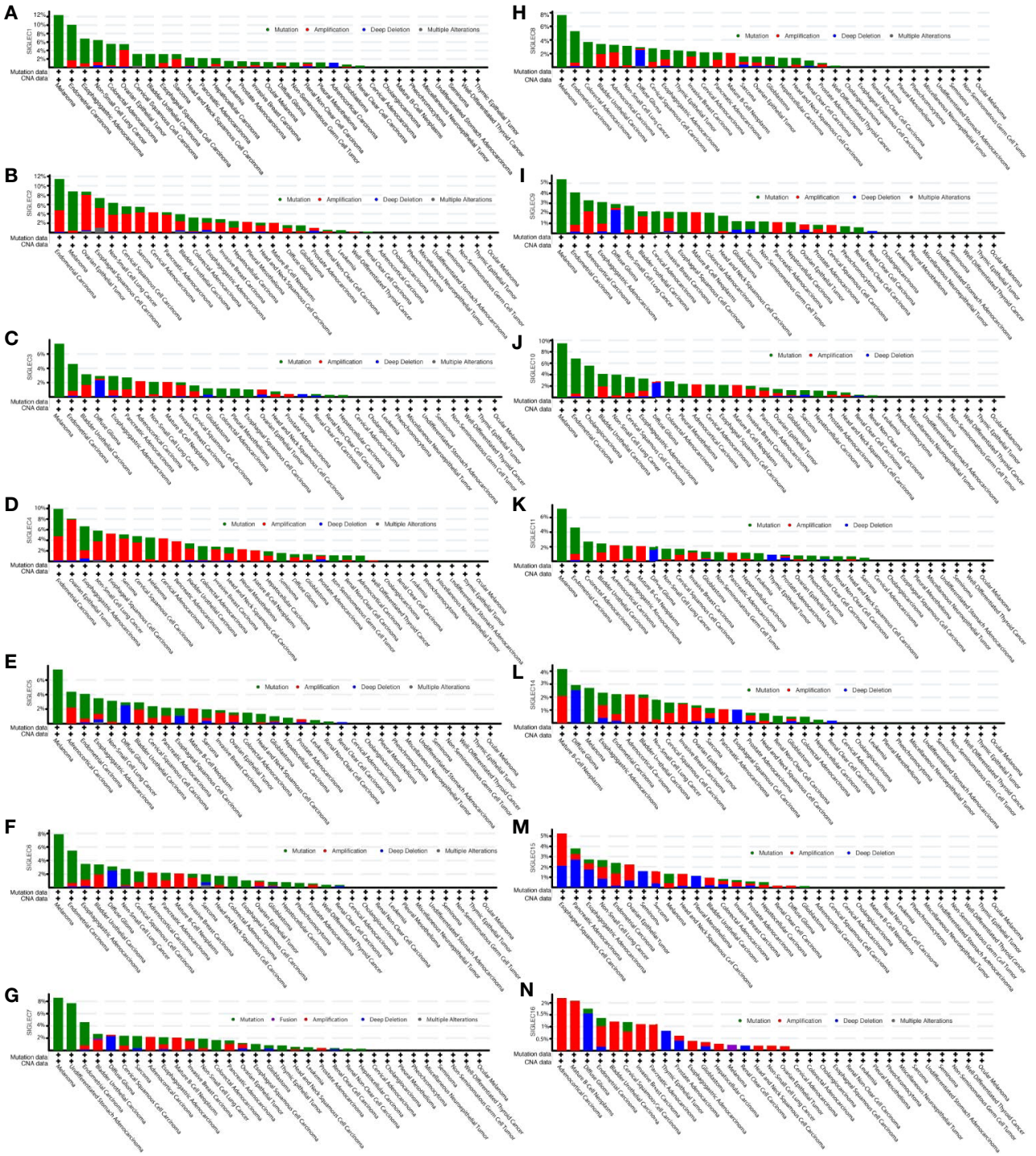

FIGURE 2 | Mutation frequency of SIGLEC family genes across different cancer types in cBioPortal database. **(A)**. Mutation frequency of SIGLEC1 across cancers. **(B)**. Mutation frequency of SIGLEC2 across cancers. **(C)**. Mutation frequency of SIGLEC3 across cancers. **(D)**. Mutation frequency of SIGLEC4 across cancers. **(E)**. Mutation frequency of SIGLEC5 across cancers. **(F)**. Mutation frequency of SIGLEC6 across cancers. **(G)**. Mutation frequency of SIGLEC7 across cancers. **(H)**. Mutation frequency of SIGLEC8 across cancers. **(I)**. Mutation frequency of SIGLEC9 across cancers. **(J)**. Mutation frequency of SIGLEC10 across cancers. **(K)**. Mutation frequency of SIGLEC11 across cancers. **(L)**. Mutation frequency of SIGLEC14 across cancers. **(M)**. Mutation frequency of SIGLEC15 across cancers. **(N)**. Mutation frequency of SIGLEC16 across cancers.

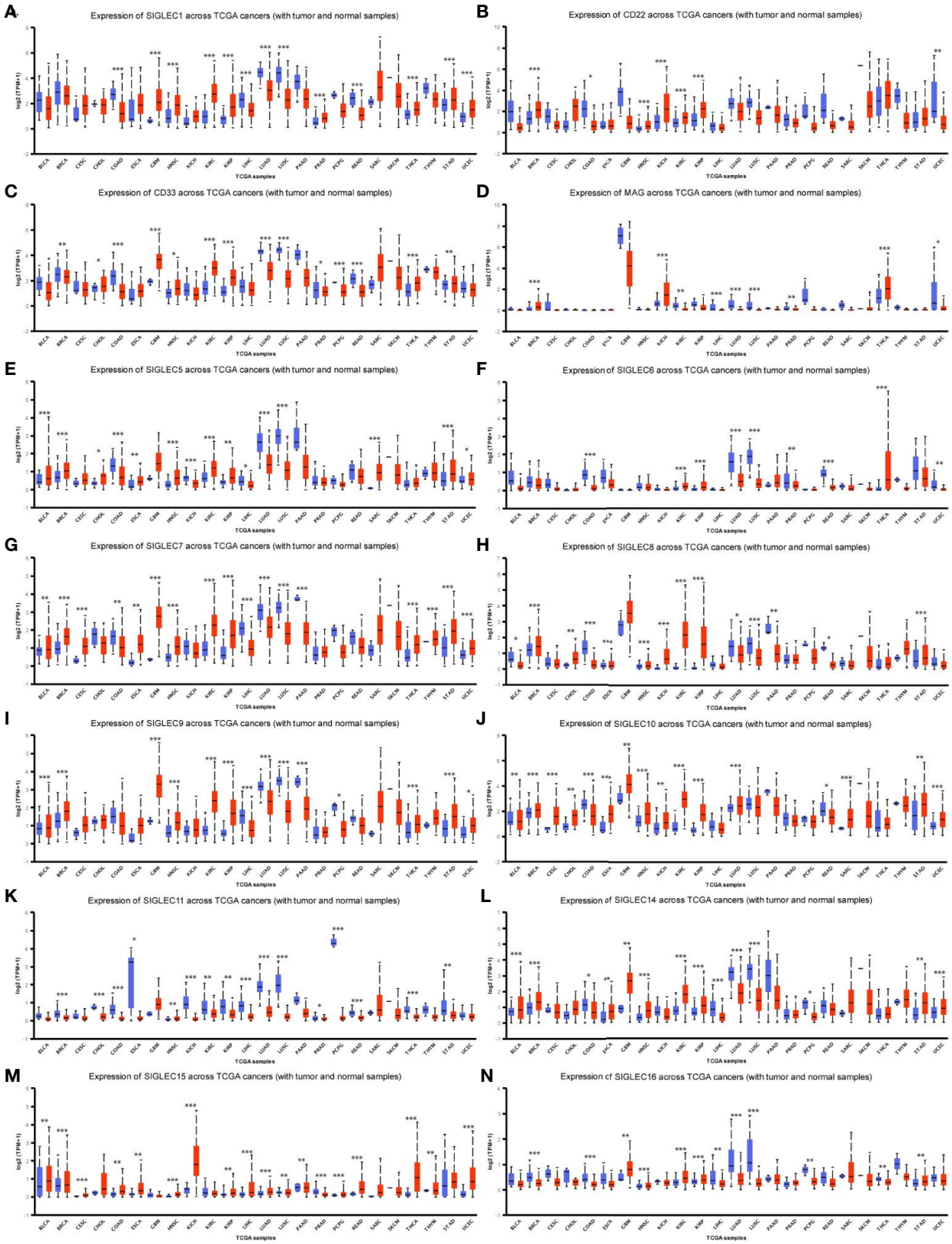

FIGURE 3 | Continued

FIGURE 3 | SIGLEC family genes were differentially expressed between different tumor and corresponding normal tissues. **(A)**. Expression of SIGLEC1 in normal and cancer tissues of TCGA database. **(B)**. Expression of CD22 (SIGLEC2) in normal and cancer tissues of TCGA database. **(C)**. Expression of CD33 (SIGLEC3) in normal and cancer tissues of TCGA database. **(D)**. Expression of MAG (SIGLEC4) in normal and cancer tissues of TCGA database. **(E)**. Expression of SIGLEC5 in normal and cancer tissues of TCGA database. **(F)**. Expression of SIGLEC6 in normal and cancer tissues of TCGA database. **(G)**. Expression of SIGLEC7 in normal and cancer tissues of TCGA database. **(H)**. Expression of SIGLEC8 in normal and cancer tissues of TCGA database. **(I)**. Expression of SIGLEC9 in normal and cancer tissues of TCGA database. **(J)**. Expression of SIGLEC10 in normal and cancer tissues of TCGA database. **(K)**. Expression of SIGLEC11 in normal and cancer tissues of TCGA database. **(L)** Expression of SIGLEC14 in normal and cancer tissues of TCGA database. **(M)**. Expression of SIGLEC15 in normal and cancer tissues of TCGA database. **(N)**. Expression of SIGLEC16 in normal and cancer tissues of TCGA database. (*$p < 0.05$, **$p < 0.01$, ***$p < 0.001$; Bladder Urothelial Carcinoma, BLCA, normal=19, tumor=408; Breast invasive carcinoma, BRCA, normal=114, tumor=1097; Cervical squamous cell carcinoma and endocervical adenocarcinoma, CESC, normal=3, tumor=305; Cholangiocarcinoma, CHOL, normal=9, tumor=36; Colon adenocarcinoma, COAD, normal=41, tumor=286; Esophageal carcinoma, ESCA, normal=11, tumor=184; Glioblastoma multiforme, GBM, normal=5, tumor=156; Head and Neck squamous cell carcinoma, HNSC, normal=44, tumor=520; Kidney Chromophobe, KICH, normal=25, tumor=67; Kidney renal clear cell carcinoma, KIRC, normal=72, tumor=533; Kidney renal papillary cell carcinoma, KIRP, normal=32, tumor=290; Liver hepatocellular carcinoma, LIHC, normal=50, tumor=371; Lung adenocarcinoma, LUAD, normal=59, tumor=515; Lung squamous cell carcinoma, LUSC, normal=52, tumor=503; Pancreatic adenocarcinoma, PAAD, normal=4, tumor=178; Prostate adenocarcinoma, PRAD, normal=52, tumor=497; Pheochromocytoma and Paraganglioma, PCPG, normal=3, tumor=179; Rectum adenocarcinoma, READ, normal=10, tumor=166; Sarcoma, SARC, normal=2, tumor=260; Skin Cutaneous Melanoma, SKCM, normal=1, tumor=472; Thyroid carcinoma, THCA, normal=59, tumor=505; Thymoma, THYM, normal=2, tumor=120; Stomach adenocarcinoma, STAD, normal=34, tumor=415; Uterine Corpus Endometrial Carcinoma, UCEC, normal=35, tumor=546. Blue boxplot: normal expression; red boxplot: tumor expression.)

Tumor Intrinsic mRNA Levels of SIGLEC Family Genes Were Closely Related to Tumor Immune Cell Infiltration

Former studies showed SIGLEC family genes were expressed on immune cells and were involved in immune cell activation and adaptation; also, recently, SIGLEC15 was found to be able to dampen CD8+ T cell infiltration and function in mouse melanoma model. We wondered whether tumor intrinsic expression of SIGLEC family genes could influence immune infiltration in a tumor microenvironment. Using TIMER 2.0 to examine the correlation between SIGLEC family genes and six types of infiltrating immune cells (B cell, CD4+ T cell, CD8+ T cell, myeloid dendritic cell, macrophage, and neutrophil), we found in specific tumors, such as HNSC, THCA, and THYM, SIGLEC family genes were negatively correlated with B cell and CD8+ T cell infiltration, while in cervical squamous cell

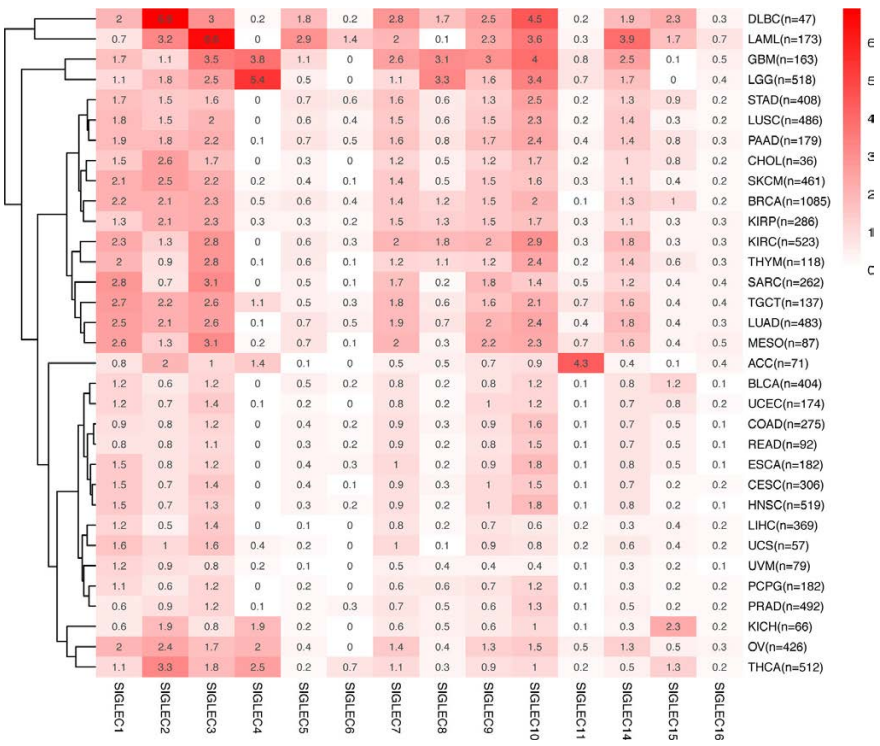

FIGURE 4 | mRNA Expression of SIGLEC family genes differed in various tumors. Average mRNA expression (TPM) of SIGLEC family genes in different tumors from GEPIA database.

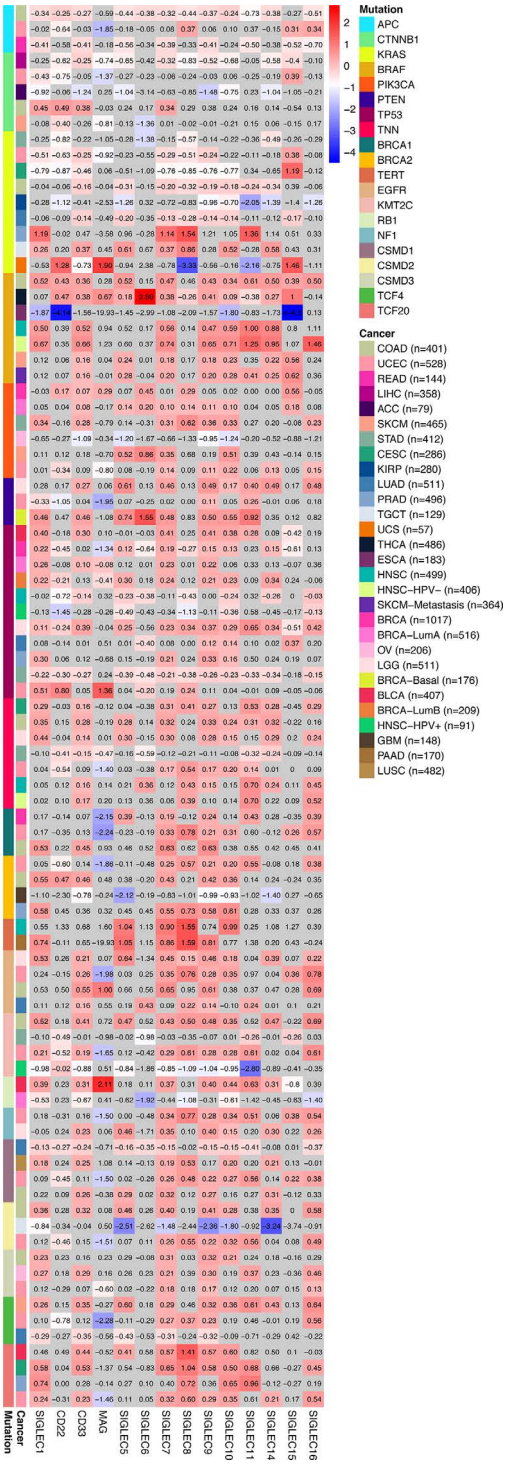

FIGURE 5 | Tumor specific oncogenic gene mutation was related to SIGLEC mRNA expression in tumors of different origin. Fold changes of log2-transformed differential expression of SIGLEC family genes in specific oncogene mutation groups of different tumors (calculated by TIMER 2.0 database). Fold changes with significance were marked with bright colors, and non-significant fold changes were marked with grey background. ($p<0.05$ was considered significant.)

carcinoma and endocervical adenocarcinoma (CESC), esophageal carcinoma (ESCA), and KIRP, most SIGLEC family genes were positively correlated with B cell and CD8+ T cell (**Figures 7A–C**). Also, it turned out that SIGLEC family genes were highly correlated with dendritic cell, macrophage, and neutrophil in various cancer types (**Figures 7D–F**). Of notice, in brain lower grade glioma (LGG), most SIGLEC family genes were highly correlated with CD4+ T cell and negatively correlated with CD8+ T cell infiltration; in LIHC, LUAD, LUSC, PAAD, READ, SARC, SKCM, and stomach adenocarcinoma (STAD), most SIGLEC family genes were positively correlated with CD8+ T cells. Besides, in comparison to READ, COAD tissues additionally showed negative correlation between SIGLEC family genes and B cell infiltration.

SIGLEC Family Genes Expressed in Tumor Cells Could Influence Immune Regulators in Tumor Microenvironment, Such as Chemokine Axis, Immune Stimulator, Immune Inhibitor, and MHC Molecular

After finding SIGLEC family genes expressed by tumor cells of various cancer types were closely related to tumor immune infiltration, we further examined the correlation between SIGLEC family genes and immune regulators in tumor. Since former studies have found SIGLEC1 (CD169), SIGLEC2 (CD22), SIGLEC3 (CD33), SIGLEC7, SIGLEC9, and SIGLEC15 expressed by immune cell populations could be manipulated by tumor cells to escape immune surveillance, we focused on the five SIGLEC family members. We found SIGLEC family genes were significantly correlated to a wide spectrum of immune regulators, including chemokine axis, immune stimulators, inhibitors, and MHC molecular, such as CD28, CD40, CD40LG, ICOS, LAG3, PDCD1, CD274, and CTLA4. Though some SIGLEC genes showed non-significant correlation with immune regulators, most coefficients were significant with absolute value over 0.5, indicating their active roles of immune regulation in tumor microenvironment (**Figure 8**).

Additionally, we generated a list of SIGLEC family highly correlated genes in tumor through GEPIA database, and we constructed a network of them through the STRING database (**Figures 9A–B**). The top ranked 10 node genes were TYROBP, ITGAM, ITGB2, FPR2, C3AR1, LILRB2, FCER1G, FCGR2A, GNGT2, and FPR1. Further gene ontology and pathway enrichment of SIGLEC family highly correlated genes, through DAVID database, showed those genes were most immune function related and enriched in cytokine-cytokine receptor interaction, chemokine signaling pathway, and leukocyte transendothelial migration (**Figure 9C**).

DISCUSSION

In our analysis, the alteration status of SIGLEC family genes differed in different cancer types. In melanoma, endometrial carcinoma, non-small cell lung cancer, bladder urothelial

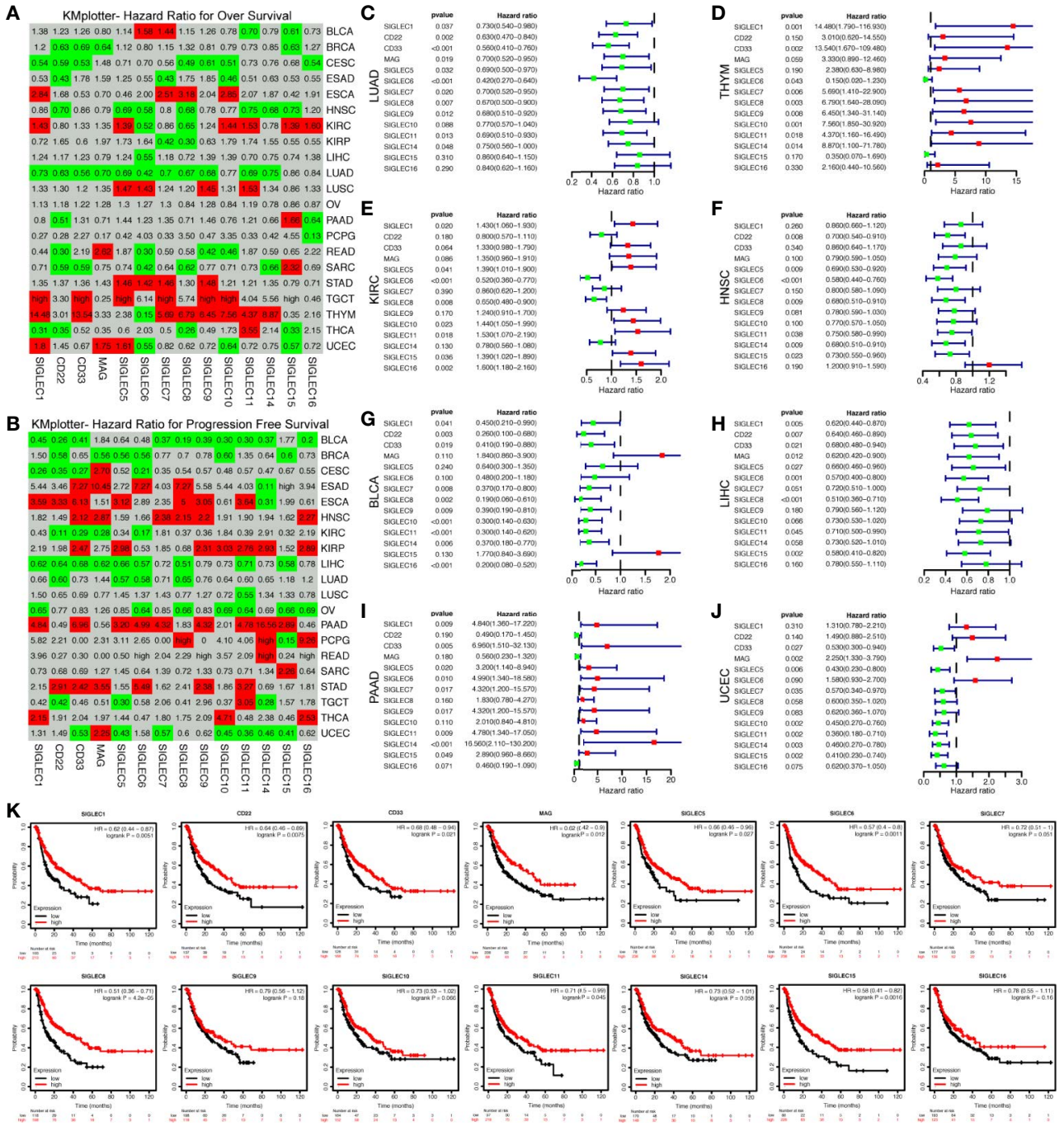

FIGURE 6 | mRNA expression levels of SIGLEC family genes in different tumors were related to patients' overall survival and progression free survival. **(A)**. Hazard ratio (HR) for patients' overall survival (OS) of different tumors (calculated by KMplotter database). **(B)**. Hazard ratio (HR) for patients' progression free survival (PFS) of different tumors (calculated by KMplotter database). (HRs less than 1 with significance were marked with green background as protective factors, and HRs over 1 were marked with red background as risk factors. Non-significant HRs were marked with grey background. HRs over 50 were replaced with "high.") **(C–F)**. HRs, 95% confidence interval and *p* value for SIGLEC family genes in association with patients' OS in LUAD, THYM, KIRC, and HNSC. **(G–J)**. HRs, 95% confidence interval and *p* value for SIGLEC family genes in association with patients' PFS in BLCA, LIHC, PAAD, and UCEC. (Green dots represented protective factors, while red dots represented risk factors.) **(K)**. Survival curves for SIGLEC family genes in association with patients' PFS in LIHC.

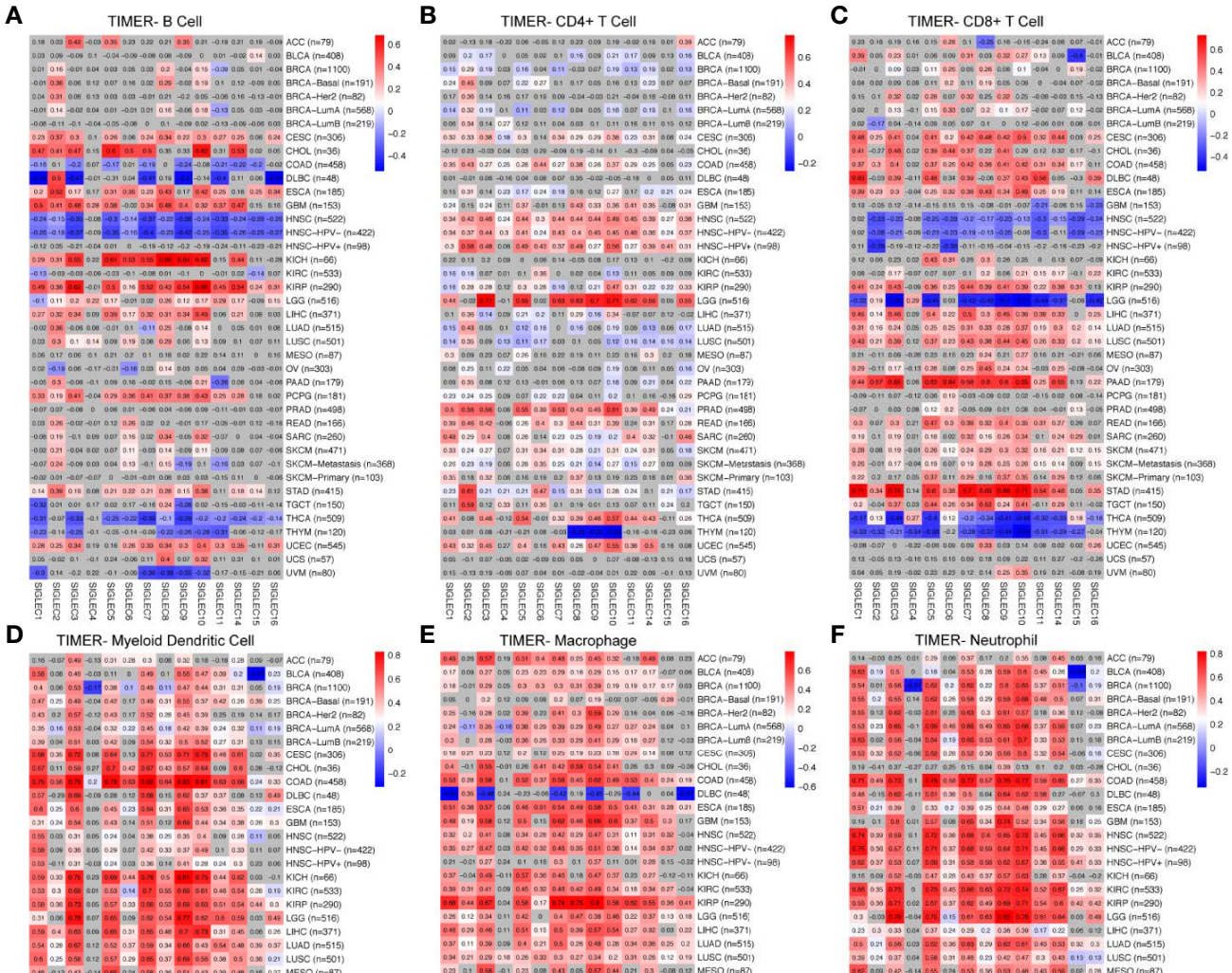

FIGURE 7 | Coefficients for correlation between SIGLEC family genes and immune cell infiltration of different tumors in TIMER database. **(A)**. Coefficients for correlation between B cell infiltration score and SIGLEC family genes in different tumors. **(B)**. Coefficients for correlation between CD4+ T cell infiltration score and SIGLEC family genes in different tumors. **(C)**. Coefficients for correlation between CD8+ T cell infiltration score and SIGLEC family genes in different tumors. **(D)**. Coefficients for correlation between myeloid dendritic cell infiltration score and SIGLEC family genes in different tumors. **(E)**. Coefficients for correlation between macrophage infiltration score and SIGLEC family genes in different tumors. **(F)**. Coefficients for correlation between neutrophil infiltration score and SIGLEC family genes in different tumors. (Coefficients with significance were marked with bright colors, while non-significant coefficients were marked with grey background. *P* value under 0.05 was considered significant. The association was generated with tumor purification adjusted.)

carcinoma, and esophagogastric adenocarcinoma, mutation and amplification of SIGLEC family genes were little, while deep deletion was commonly seen in diffuse glioma. We believed that in epithelium derived tumors, high proliferation status of tumor tissue may cause high frequencies of mutation and amplification of SIGLEC family genes in tumor cells; however, in diffuse glioma, the tumor microenvironment was different from other cancer types, which may redirect the adaptation of tumor cells. SIGLEC

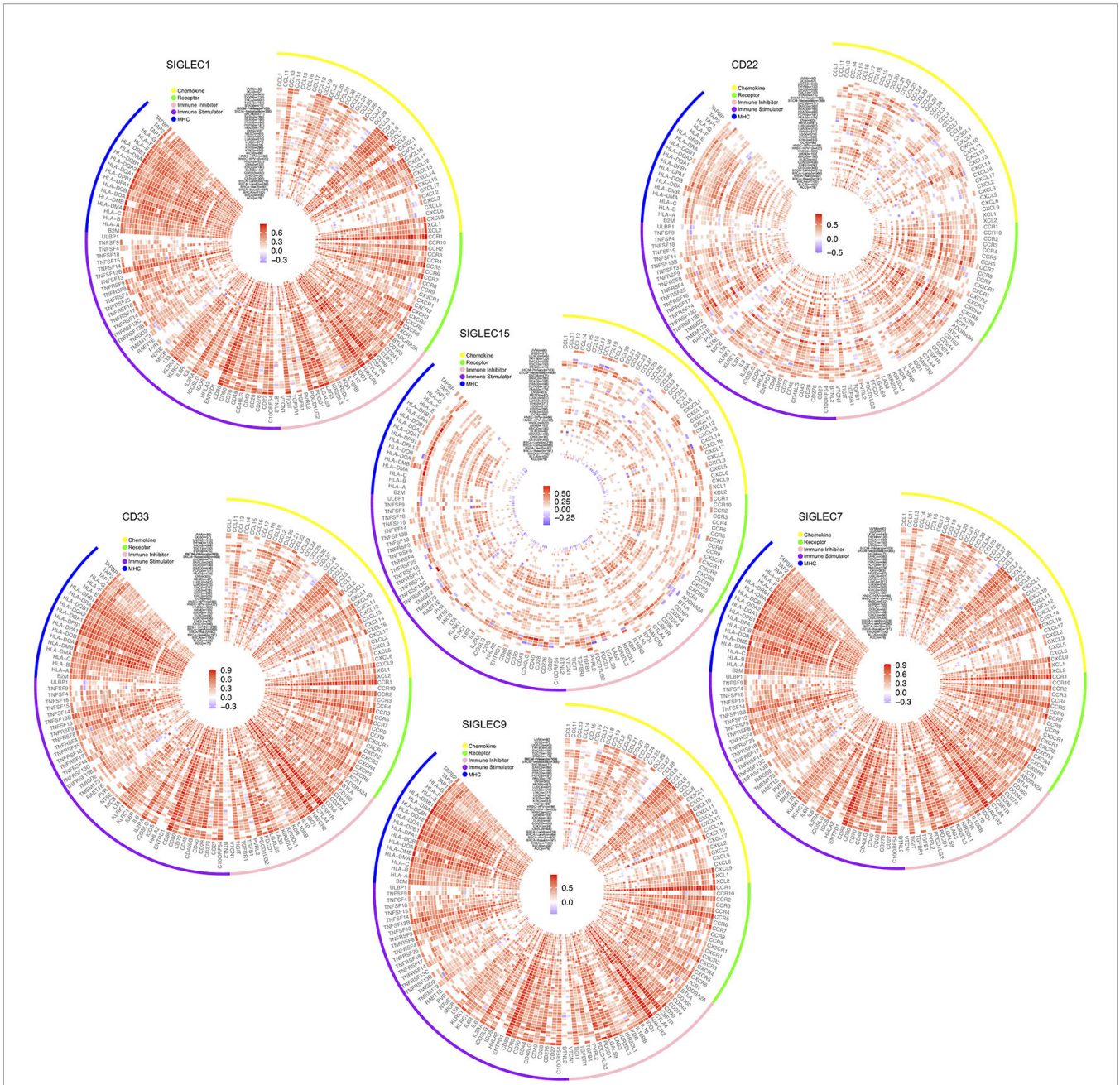

FIGURE 8 | Correlation between mRNA expression of SIGLEC family genes (SIGLEC1, CD22 & SIGLEC2, CD33 & SIGLEC3, SIGLEC7, SIGLEC9, SIGLEC15) and immune regulators. (Coefficients with significance, calculated by TIMER 2.0 database, were shown with gradient color changes, and non-significant coefficients were replaced by blank space. *P* value under 0.05 was considered significant. The association was generated with tumor purification adjusted.)

family genes were further associated with specific oncogene mutation in different cancer types and were differentially expressed between patients of mutation and non-mutation groups, such as APC in COAD and READ, or CTNNB1 in LIHC. Those mutations were formerly found to be related to degrees of tumor malignant behaviors or carcinogenesis, and we thought evolution of tumor cells may somehow drive expression changes of SIGLEC family genes.

SIGLEC family genes were highly correlated with patients' OS and PFS across cancer types. Especially in LUAD, THYM, KIRC, and HNSC, most SIGLEC family genes were related to OS with significance, while in LIHC and PAAD, most of them were involved in PFS of patients. The hazard ratio for SIGLEC family genes differed in different cancer types: most SIGLEC family genes showed protective roles in some cancer types, while they demonstrated risking roles in the other. Also, though the hazard

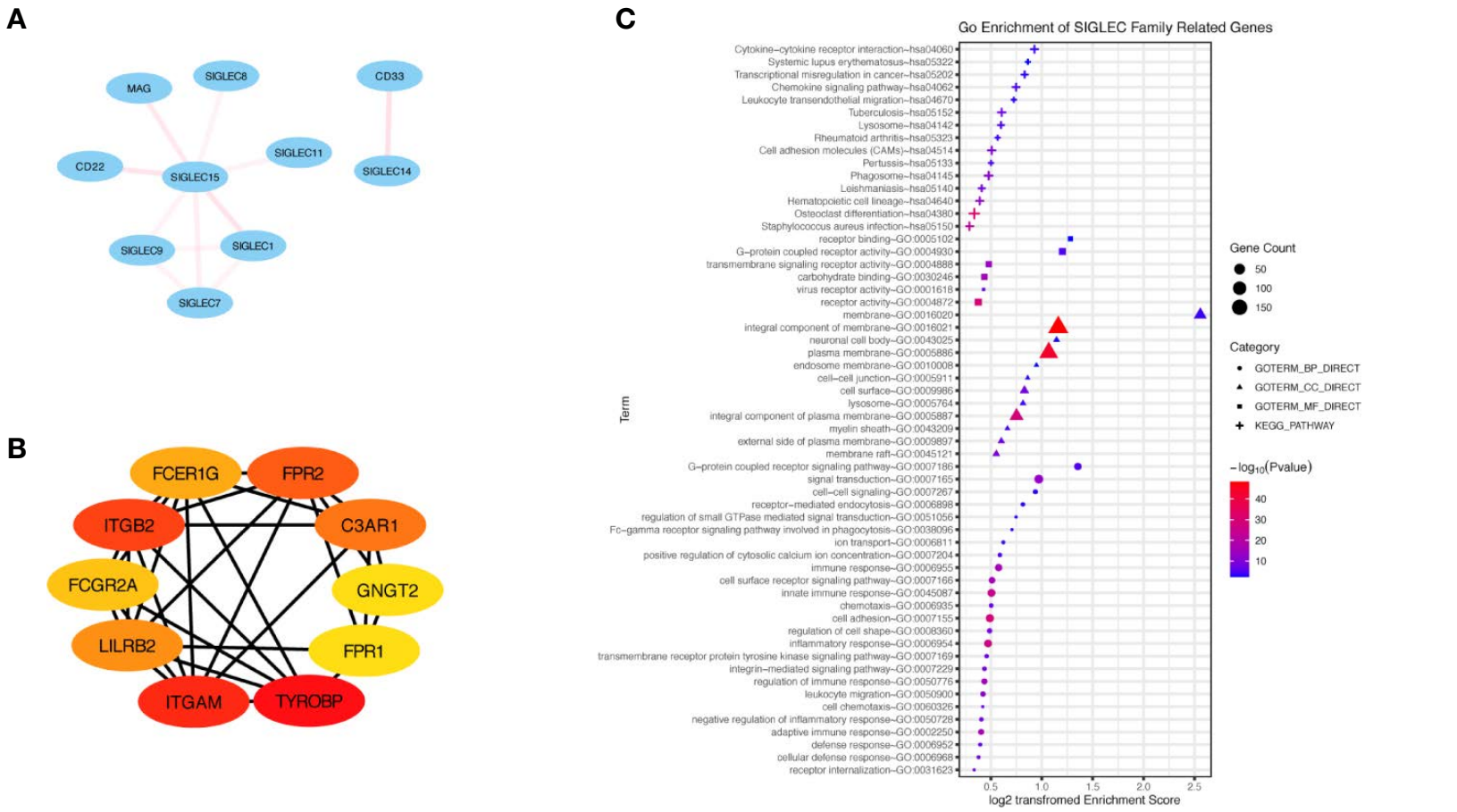

FIGURE 9 | Genes highly correlated with SIGLEC family in tumors were enriched in immune regulation of tumor microenvironment. **(A)** Correlation between SIGLEC family genes. The correlation was calculated by STRING database, and transparency of edges between different genes reflected combined score between two-linked genes. **(B)** Highly SIGLEC family correlated genes (provided by GEPIA database) were calculated by STRING database, and top 10 connecting genes were selected by CytoHuba software. (The rank of genes was demonstrated by color changes, and the first ranked gene was marked with red bubble.) **(C)**. Gene ontology of highly SIGLEC family correlated genes. (Terms with gene count over 6 were shown, and *p* value under 0.05 was considered significant.)

ratios for OS and PFS were consistent for most SIGLEC genes, in a few tumors, some SIGLEC family members were both risk factors and protective factors for OS and PFS. We thought expression levels of SIGLEC family genes in different cancer types may influence tumor malignant traits through different mechanisms, and their involvement in a special tumor microenvironment of different cancer types may also cause the survival difference across cancer types.

Former studies of SIGLEC family genes in tumors were mainly about their functional roles on immune cell populations, facilitating tumor growth, and immune escape in different cancer types, such as inhibitory SIGLEC9 and SIGLEC7 expressed on natural killer cells, or SIGLEC6 expressed on mast cells in colorectal cancer, which could be exploited by tumor cells through increased sialylation and glycosylation (7, 35–41). A recent study concerning SIGLEC15 also showed expression of SIGLEC15 by macrophages or tumor cells could directly depress function of CD8+ T cells in a melanoma model (15). Though some studies mentioned the expression difference of SIGLEC family members between normal and tumor tissue, functions of tumor derived SIGLEC gene expression on tumor growth and progression were rarely investigated. Our results showed all SIGLEC family genes expressed by tumors were survival (OS and PFS) related in various cancer types, and mutation frequencies or expression levels of them differed according to origin or tissue types of tumor, which needs further experiments to undermine the detailed mechanisms in different cancer types. Since SIGLEC genes expressed on immune cells can stimulate or inhibit immune cell function, we examined the correlation between tumor expressed SIGLEC genes and immune infiltration score, as well as immune regulators in tumor microenvironment. Enrichment of SIGLEC family highly correlated genes was also performed. It seemed tumor-expressed SIGLEC genes also were highly correlated with immune microenvironment of tumor, and they may regulate immune infiltration by influencing chemokine axis. SIGLEC family genes were correlated with macrophage, neutrophil, and dendritic cell infiltration in broad cancer types, and in specific tumors, correlation with B cell, CD4+ T cell, and CD8+ T cell infiltration levels were high. Former studies showed expression of SIGLEC genes on immune cells were positively correlated with immune checkpoints, such as PD1, and in our study, tumor expressed SIGLEC genes were also positively correlated with various immune stimulators and inhibitors (8, 36, 38, 42). Also, the recent study about SIGLEC15 additionally demonstrated the similar structure of SIGLEC15 and PDL1, which makes us wonder whether SIGLEC family genes expressed on tumor cells may directly influence immune cell infiltration and function in tumor microenvironment by binding to potential targets on immune cells, since SIGLEC15 has a relatively conservative structure among them (15, 43–45). Those results shed new light on immune blockade therapy to improve patients' prognosis by neutralizing SIGLEC receptors on tumor cells or immune cells (12, 15, 46, 47).

There are several limitations of our study. First, the analysis was performed by using data from online databases, which needs further experiments for validation. Second, the immune infiltration status of different cancer types was calculated by computational methods. Though calculation was performed by multiple algorithms and correlation analysis was performed with tumor purification adjusted, the sequencing data may contain information from other cell sources, which requires tissue sample confirmation.

CONCLUSION

Our computational analysis showed SIGLEC family genes expressed by tumor cells in different cancer types were related to tumor formation and patients' survival, and they could regulate tumor immune microenvironment by influencing chemokine axis. Targeting tumor derived SIGLEC genes may benefit patients' survival by both interfering with tumor malignant behaviors and improving tumor immune microenvironment.

DATA AVAILABILITY STATEMENT

Publicly available datasets were analyzed in this study. This data can be found here: https://www.cancer.gov/about-nci/organization/ccg/research/structural-genomics/tcga https://www.cbioportal.org http://timer.cistrome.org http://gepia.cancer-pku.cn http://kmplot.com/private/http://ualcan.path.uab.edu https://string-db.org https://david.ncifcrf.gov.

ETHICS STATEMENT

Ethical review and approval was not required for the study on human participants in accordance with the local legislation and institutional requirements. Written informed consent for participation was not required for this study in accordance with the national legislation and the institutional requirements.

AUTHOR CONTRIBUTIONS

ZC, HL, and QY designed the investigation, and ZC, MY, QM, and ZY helped to collect data in databases. ZC, MY, LG, BIZ and SL wrote the draft of the paper, and WZ, BOZ, JY, YSX, and YFX helped to revise and make adaptations. All authors contributed to the article and approved the submitted version.

FUNDING

This study was funded by National Nature Science Foundation of China (81871924 to QY, 81572844 to YFX).

SUPPLEMENTARY MATERIAL

The Supplementary Material for this article can be found online at: https://www.frontiersin.org/articles/10.3389/fonc.2020.586820//full#supplementary-material

REFERENCES

1. Varki A, Angata T. Siglecs–the major subfamily of I-type lectins. *Glycobiology* (2006) 16:1r–27r. doi: 10.1093/glycob/cwj008
2. Crocker PR, Redelinghuys P. Siglecs as positive and negative regulators of the immune system. *Biochem Soc Trans* (2008) 36:1467–71. doi: 10.1042/BST0361467
3. Macauley MS, Crocker PR, Paulson JC. Siglec-mediated regulation of immune cell function in disease. *Nat Rev Immunol* (2014) 14:653–66. doi: 10.1038/nri3737
4. Bordon Y. Inflammation: Live long and prosper with Siglecs. *Nat Rev Immunol* (2015) 15:266–7. doi: 10.1038/nri3851
5. Fraschilla I, Pillai S. Viewing Siglecs through the lens of tumor immunology. *Immunol Rev* (2017) 276:178–91. doi: 10.1111/imr.12526
6. Lübbers J, Rodríguez E, van Kooyk Y. Modulation of Immune Tolerance via Siglec-Sialic Acid Interactions. *Front Immunol* (2018) 9:2807. doi: 10.3389/fimmu.2018.02807
7. Jandus C, Boligan KF, Chijioke O, Liu H, Dahlhaus M, Démoulins T, et al. Interactions between Siglec-7/9 receptors and ligands influence NK cell-dependent tumor immunosurveillance. *J Clin Invest* (2014) 124:1810–20. doi: 10.1172/JCI65899
8. Matsumoto T, Takahashi N, Kojima T, Yoshioka Y, Ishikawa J, Furukawa K, et al. Soluble Siglec-9 suppresses arthritis in a collagen-induced arthritis mouse model and inhibits M1 activation of RAW264.7 macrophages. *Arthritis Res Ther* (2016) 18:133. doi: 10.1186/s13075-016-1035-9
9. Pearce OM, Läubli H. Sialic acids in cancer biology and immunity. *Glycobiology* (2016) 26:111–28. doi: 10.1093/glycob/cwv097
10. Bärenwaldt A, Läubli H. The sialoglycan-Siglec glyco-immune checkpoint - a target for improving innate and adaptive anti-cancer immunity. *Expert Opin Ther Targets* (2019) 23:839–53. doi: 10.1080/14728222.2019.1667977
11. Reily C, Stewart TJ, Renfrow MB, Novak J. Glycosylation in health and disease. *Nat Rev Nephrol* (2019) 15:346–66. doi: 10.1038/s41581-019-0129-4
12. van de Wall S, Santegoets KCM, van Houtum EJH, Büll C, Adema GJ. Sialoglycans and Siglecs Can Shape the Tumor Immune Microenvironment. *Trends Immunol* (2020) 41:274–85. doi: 10.1016/j.it.2020.02.001
13. Cao G, Xiao Z, Yin Z. Normalization cancer immunotherapy: blocking Siglec-15! *Signal Transduct Target Ther* (2019) 4:10–0. doi: 10.1038/s41392-019-0045-x
14. Ren X. Immunosuppressive checkpoint Siglec-15: a vital new piece of the cancer immunotherapy jigsaw puzzle. *Cancer Biol Med* (2019) 16:205–10. doi: 10.20892/j.issn.2095-3941.2018.0141
15. Wang J, Sun J, Liu LN, Flies DB, Nie X, Toki M, et al. Siglec-15 as an immune suppressor and potential target for normalization cancer immunotherapy. *Nat Med* (2019) 25:656–66. doi: 10.1038/s41591-019-0374-x
16. Gao J, Aksoy BA, Dogrusoz U, Dresdner G, Gross B, Sumer SO. et al: Integrative analysis of complex cancer genomics and clinical profiles using the cBioPortal. *Sci Signaling* (2013) 6:pl1. doi: 10.1126/scisignal.2004088
17. Tomczak K, Czerwinska P, Wiznerowicz M. The Cancer Genome Atlas (TCGA): an immeasurable source of knowledge. *Contemp Oncol (Poznan Poland)* (2015) 19:A68–77. doi: 10.5114/wo.2014.47136
18. Chandrashekar DS, Bashel B, Balasubramanya SAH, Creighton CJ, Ponce-Rodriguez I, Chakravarthi B, et al. UALCAN: A Portal for Facilitating Tumor Subgroup Gene Expression and Survival Analyses. *Neoplasia (New York NY)* (2017) 19:649–58. doi: 10.1016/j.neo.2017.05.002
19. Nagy Á, Lánczky A, Menyhárt O, Győrffy B. Validation of miRNA prognostic power in hepatocellular carcinoma using expression data of independent datasets. *Sci Rep* (2018) 8:9227. doi: 10.1038/s41598-018-27521-y
20. Human genomics. The Genotype-Tissue Expression (GTEx) pilot analysis: multitissue gene regulation in humans. *Sci (New York NY)* (2015) 348:648–60. doi: 10.1126/science.1262110
21. Tang Z, Li C, Kang B, Gao G, Li C, Zhang Z. GEPIA: a web server for cancer and normal gene expression profiling and interactive analyses. *Nucleic Acids Res* (2017) 45:W98–w102. doi: 10.1093/nar/gkx247
22. Li B, Severson E, Pignon JC, Zhao H, Li T, Novak J, et al. Comprehensive analyses of tumor immunity: implications for cancer immunotherapy. *Genome Biol* (2016) 17:174. doi: 10.1186/s13059-016-1028-7
23. Li T, Fan J, Wang B, Traugh N, Chen Q, Liu JS, et al. TIMER: A Web Server for Comprehensive Analysis of Tumor-Infiltrating Immune Cells. *Cancer Res* (2017) 77:e108–10. doi: 10.1158/0008-5472.Can-17-0307
24. Szklarczyk D, Franceschini A, Wyder S, Forslund K, Heller D, Huerta-Cepas J, et al. STRING v10: protein-protein interaction networks, integrated over the tree of life. *Nucleic Acids Res* (2015) 43:D447–452. doi: 10.1093/nar/gku1003
25. Shannon P, Markiel A, Ozier O, Baliga NS, Wang JT, Ramage D, et al. Cytoscape: a software environment for integrated models of biomolecular interaction networks. *Genome Res* (2003) 13:2498–504. doi: 10.1101/gr.1239303
26. Chin CH, Chen SH, Wu HH, Ho CW, Ko MT, Lin CY. cytoHubba: identifying hub objects and sub-networks from complex interactome. *BMC Syst Biol* (2014) 8 Suppl 4:S11. doi: 10.1186/1752-0509-8-S4-S11
27. Huang da W, Sherman BT, Lempicki RA. Systematic and integrative analysis of large gene lists using DAVID bioinformatics resources. *Nat Protoc* (2009) 4:44–57. doi: 10.1038/nprot.2008.211
28. Kanehisa M, Sato Y, Furumichi M, Morishima K, Tanabe M. New approach for understanding genome variations in KEGG. *Nucleic Acids Res* (2019) 47:D590–5. doi: 10.1093/nar/gky962
29. R Core Team. *R: A language and environment for statistical computing*. Vienna, Austria: R Foundation for Statistical Computing (2019). Available at: https://www.R-project.org/.
30. RStudio Team. *RStudio: Integrated Development for R*. Boston, MA: RStudio, Inc. (2015). Available at: http://www.rstudio.com/.
31. Kolde R. *pheatmap: Pretty Heatmaps. R package version 1.0.12*. (2019). Available at: https://CRAN.R-project.org/package=pheatmap.
32. Wickham H. *ggplot2: Elegant Graphics for Data Analysis*. Springer-Verlag New York (2016). ISBN 978-3-319-24277-4.
33. Alexa A, Rahnenfuhrer J. *topGO: Enrichment Analysis for Gene Ontology. R package version 2.36.0*. (2019).
34. Yu G, Wang LG, Han Y, He QY. clusterProfiler: an R package for comparing biological themes among gene clusters. *Omics J Integr Biol* (2012) 16:284–7. doi: 10.1089/omi.2011.0118
35. Boligan KF, Mesa C, Fernandez LE. and von Gunten S: Cancer intelligence acquired (CIA): tumor glycosylation and sialylation codes dismantling antitumor defense. *Cell Mol Life Sci CMLS* (2015) 72:1231–48. doi: 10.1007/s00018-014-1799-5
36. Beatson R, Tajadura-Ortega V, Achkova D, Picco G, Tsourouktsoglou TD, Klausing S, et al. The mucin MUC1 modulates the tumor immunological microenvironment through engagement of the lectin Siglec-9. *Nat Immunol* (2016) 17:1273–81. doi: 10.1038/ni.3552
37. Huang PJ, Low PY, Wang I, Hsu SD, Angata T. Soluble Siglec-14 glycan-recognition protein is generated by alternative splicing and suppresses myeloid inflammatory responses. *J Biol Chem* (2018) 293:19645–58. doi: 10.1074/jbc.RA118.005676
38. Stanczak MA, Siddiqui SS, Trefny MP, Thommen DS, Boligan KF, von Gunten S, et al. Self-associated molecular patterns mediate cancer immune evasion by engaging Siglecs on T cells. *J Clin Invest* (2018) 128:4912–23. doi: 10.1172/jci120612
39. Yu Y, Blokhuis BRJ, Diks MAP, Keshavarzian A, Garssen J, Redegeld FA. Functional Inhibitory Siglec-6 Is Upregulated in Human Colorectal Cancer-Associated Mast Cells. *Front Immunol* (2018) 9:2138. doi: 10.3389/fimmu.2018.02138
40. Barkal AA, Brewer RE, Markovic M, Kowarsky M, Barkal SA, Zaro BW, et al. CD24 signalling through macrophage Siglec-10 is a target for cancer immunotherapy. *Nature* (2019) 572:392–6. doi: 10.1038/s41586-019-1456-0
41. Santegoets KCM, Gielen PR, Büll C, Schulte BM, Kers-Rebel ED, Küsters B, et al. Expression profiling of immune inhibitory Siglecs and their ligands in patients with glioma. *Cancer Immunol Immunother: CII* (2019) 68:937–49. doi: 10.1007/s00262-019-02332-w
42. Takamiya R, Ohtsubo K, Takamatsu S, Taniguchi N, Angata T. The interaction between Siglec-15 and tumor-associated sialyl-Tn antigen enhances TGF-beta secretion from monocytes/macrophages through the DAP12-Syk pathway. *Glycobiology* (2013) 23:178–87. doi: 10.1093/glycob/cws139
43. Magesh S, Ando H, Tsubata T, Ishida H, Kiso M. High-affinity ligands of Siglec receptors and their therapeutic potentials. *Curr Med Chem* (2011) 18:3537–50. doi: 10.2174/092986711796642580
44. Chang L, Chen YJ, Fan CY, Tang CJ, Chen YH, Low PY, et al. Identification of Siglec Ligands Using a Proximity Labeling Method. *J Proteome Res* (2017) 16:3929–41. doi: 10.1021/acs.jproteome.7b00625

45. Bornhofft KF, Goldammer T, Rebl A, Galuska SP. Siglecs: A journey through the evolution of sialic acid-binding immunoglobulin-type lectins. *Dev Comp Immunol* (2018) 86:219–31. doi: 10.1016/j.dci.2018.05.008
46. Pfeifer M, Zheng B, Erdmann T, Koeppen H, McCord R, Grau M, et al. Anti-CD22 and anti-CD79B antibody drug conjugates are active in different molecular diffuse large B-cell lymphoma subtypes. *Leukemia* (2015) 29:1578–86. doi: 10.1038/leu.2015.48
47. Adams OJ, Stanczak MA, von Gunten S, Läubli H. Targeting sialic acid-Siglec interactions to reverse immune suppression in cancer. *Glycobiology* (2018) 28:640–7. doi: 10.1093/glycob/cwx108

Conflict of Interest: The authors declare that the research was conducted in the absence of any commercial or financial relationships that could be construed as a potential conflict of interest.

Copyright © 2020 Chen, Yu, Guo, Zhang, Liu, Zhang, Zhou, Yan, Ma, Yang, Xiao, Xu, Li and Ye. This is an open-access article distributed under the terms of the Creative Commons Attribution License (CC BY). The use, distribution or reproduction in other forums is permitted, provided the original author(s) and the copyright owner(s) are credited and that the original publication in this journal is cited, in accordance with accepted academic practice. No use, distribution or reproduction is permitted which does not comply with these terms.

frontiers in Immunology

ORIGINAL RESEARCH
published: 19 November 2020
doi: 10.3389/fimmu.2020.544248

Identification of Interleukin-9 Producing Immune Cells in Endometrial Carcinoma and Establishment of a Prognostic Nomogram

Huan Tong[1], Hao Feng[2,3], Xiang Hu[1], Meng-fei Wang[1], Yun-feng Song[1], Xiao-li Wen[1], Yi-ran Li[4] and Xiao-ping Wan[1,4]**

[1] Clinical and Translational Research Center, Shanghai First Maternity and Infant Hospital, Tongji University School of Medicine, Shanghai, China, [2] Department of Liver Surgery, Renji Hospital, School of Medicine, Shanghai Jiao Tong University, Shanghai, China, [3] University Hospital of Munich, Ludwig-Maximilians-University of Munich, Munich, Germany, [4] Department of Gynecology, Shanghai First Maternity and Infant Hospital, Tongji University School of Medicine, Shanghai, China

OPEN ACCESS

Edited by:
Peng Qu,
National Institutes of Health (NIH), United States

Reviewed by:
Hua Jiang,
Indiana University, Purdue University Indianapolis, United States
Xingping Qin,
Renmin Hospital of Wuhan University, China
Hongru Zhang,
University of Pennsylvania, United States

***Correspondence:**
Xiao-ping Wan
wanxiaoping@tongji.edu.cn
Hao Feng
surgeonfeng@live.com

Specialty section:
This article was submitted to Cancer Immunity and Immunotherapy, a section of the journal Frontiers in Immunology

Received: 04 May 2020
Accepted: 13 October 2020
Published: 19 November 2020

Citation:
Tong H, Feng H, Hu X, Wang M-f, Song Y-f, Wen X-l, Li Y-r and Wan X-p (2020) Identification of Interleukin-9 Producing Immune Cells in Endometrial Carcinoma and Establishment of a Prognostic Nomogram. Front. Immunol. 11:544248. doi: 10.3389/fimmu.2020.544248

Background: Interleukin-9 (IL9) plays a critical role in immunity and the pathogenesis of endometrial cancer (EC), especially endometrioid EC (EEC). This study aimed to identify the IL9+ immune cell subsets and their pleiotropic functions and establish an optimized prognostic nomogram towards the promotion of personalized treatment of EEC.

Methods: 1,417 EC patients were involved in the present study. 143 patients from the tertiary gynecology centers in Shanghai between 2013 and 2019 were recruited, and the study protocol was approved by the Institutional Review Board (IRB) of Shanghai First Maternity and Infant Hospital. The genomic data of the other 1,274 patients were extracted from the TCGA and the MSKCC datasets, respectively. Immune and stromal scores were calculated using the ESTIMATE R tool, and the tumor infiltration of immune cells was analyzed using the TIMER platform. Metascape and GEPIA datasets were used for bioinformatic analysis. $P < 0.05$ was considered statistically significant. All statistical analyses were performed with GraphPad Prism and R studio.

Results: 552 genes that were correlated with leukocyte infiltration, lymphocyte activation, and regulation of innate immune response were up-regulated in the high immune score group. More IL9+ cell infiltration was detected in the highly and moderately differentiated EC ($p = 0.04$). High IL9+ lymphocyte infiltration was related to a better overall survival ($p = 0.0027$). IL9 positive cell clusters included ILC2s, Vδ2 $\gamma\delta$T cells, mast cells, macrophages, and Th9 cells. Parameters such as FIGO stage, IL9 score, Vδ2 + $\gamma\delta$T cell infiltration, classification of differentiation, and diabetes mellitus were assigned a weighted number of points in the nomogram for a specific predicted 3-, 5- and 10-year overall survival (OS). IL9–IL9R axis played a vital role in EEC, IL9R positive cell subgroups were also identified, and the related function was analyzed in the present study. Additionally, PR (Progesterone Receptor, or PGR) expression was relevant to a higher density of IL9+ lymphocyte

infiltration. However, PGRMC1 (Progesterone Receptor Membrane Component 1) was negatively relevant to IL9R (p = 4.26e-8).

Conclusion: We observed a significant infiltration of IL9+ cells and the overrepresentation of IL-9R in tissue specimens of patients in EC cases. The nomogram incorporating the IL9 could accurately predict individualized survival probability in EEC. Additionally, this study not only established a prognostic nomogram but also assist in the firmer understanding of the relevance of the IL9-IL9R axis and IL9-producing cells in EC immunity.

Keywords: endometrial carcinoma, γδT cells, interleukin-9, nomogram, survival analysis

INTRODUCTION

Endometrial carcinomas (ECs) are the most common gynecologic malignancies and the majority of uterine corpus cancers globally (1). Moreover, endometrioid endometrial carcinoma (EEC) is the most common subtype of endometrial cancer (EC), representing approximately 87% of all diagnosed ECs (2). EECs are usually diagnosed at early stages and are associated with a favorable prognosis (3). However, for those patients with advanced stages or tumor recurrence, the prognosis is relatively poor, with 5-year overall survival rate of approximately 20% for stage IV EEC (4, 5). The routine treatments of the EC include surgery, hormonal therapy, chemotherapy, and immunotherapy. Recently, biomathematical modeling and recurrence risk estimation basing on patient-related characters have opened a new era of care oriented towards the promotion of personalized medicine.

Additionally, it is more and more apparent that the prognosis of cancer patients is not solely determined by tumor characters, but also the circumstance, particularly the immune microenvironment, which plays an essential role in cancer biology. Interleukin-9 (IL-9) was initially defined as a T_H2-type cytokine but was reported to have pleiotropic functions, inducing the proliferation, differentiation, and effector functions of numerous immune cell subsets and plays a critical role in immunity and the pathogenesis of cancers (6, 7). Most recently, much attention has been focused on a major population of T_H cells that produce IL-9, namely T_H9 cells, which have been reported to have potent abilities in eradicating advanced tumors. The majority of IL-9-producing cells in cancer are T_H9 cells; however, IL-9 can also be secreted by Vδ2+ γδ T cells (the dominant γδT-cell subset), group 2 innate lymphoid cells (ILC2s), and some cytotoxic T cells. ILC2 is a subset of innate lymphoid cells (ILCs), its role in cancer immune response is dependent on cytokine context. ILC2s could produce IL-5, leading to eosinophil activation and an increased anti-tumor immune response in solid cancers (8). In the endometrium, Interleukin-9 (IL-9) plays a unique position in the human endometrial function and embryo implantation (9). However, the presence and role of IL9 within EEC were not thoroughly investigated. Herein, we investigated the expression of IL9, IL9R, and IL9 producing immune cells and proposed a nomogram to predict the prognosis of EEC.

Abbreviations: EC, endometrial carcinoma; EEC, Endometrioid endometrial carcinomas; ESTIMATE, Estimation of STromal and Immune cells in MAlignant Tumor tissues using Expression data; TMA, tissue microarray; TIMER, Tumor Immune Estimation Resource; T_H2, T helper type 2 cells; PGRMC1, Progesterone Receptor Membrane Component 1; CyTOF, cytometry by time-of-flight; OS, overall survival; ER, Estrogen Receptor; PR/PGR, Progesterone Receptor; GO, Gene Ontology; KEGG, Kyoto Encyclopedia of Genes and Genomes; KM, Kaplan–Meier; DEGs, differentially expressed genes; TCGA, The Cancer Genome Atlas; FPKM, Fragments Per Kilobase of transcript per Million mapped reads.

METHODS

Study Population, Data Collection, and Follow-Up

In total, data from 1,417 EC patients were analyzed in the present study (**Supplementary Figure 1**). 143 patients with EC from two tertiary gynecology centers in Shanghai were recruited in the present study. Inclusion criteria included: (1) patients who underwent an operation for EC from 2013 to 2019, (2) patients with final histopathological diagnosis of EC. Exclusion criteria included patients with histologically proven uterine sarcoma or other types of tumors. Tumor tissues and adjacent healthy tissues retrospectively collected from 127 consecutive patients were used for the tissue microarray (TMA, Superbiotek, Shanghai). Tissues of the other 16 patients were prospectively collected for CyTOF (cytometry by time-of-flight) analysis and immunofluorescence staining. Pathological parameters such as the quality, grading, tumor stages of the specimens were evaluated according to FIGO 2009 edition. This study was approved by the Institutional Review Board (IRB) of Shanghai First Maternity and Infant Hospital.

The cohort containing the genomic data (*e.g.*, mRNA, mutation frequency) of 1,274 patients were extracted from the TCGA database (Firehose, Legacy, 548 patients; PanCancer atlas, 529 patients) and the MSKCC dataset (197 patients), respectively. cBioPortal platform (www.cbioportal.org) was used for bioinformatics analysis (10). In the present study, disease-free survival (DFS) was defined as the time for any recurrence. Overall survival (OS) was defined as the time for death from any cause. If the postoperative margin was negative, the operation was considered as R_0 resection. Follow-up consisted of serum tumor marker measurements every one to three months and computed tomography (CT) every six months. Complete follow-up was conducted for the entire cohort of patients.

Characteristic of Immunohistochemistry and Immunofluorescence

Slides of TMA and other samples were fixed with 4% paraformaldehyde for 15 min, permeabilized with 0.1% Triton X-100 for 5 min, blocked with 5% BSA, incubated with indicated primary antibodies: Anti-TCR Vδ2(Catalog-Nr:130-099-664, Miltenyi Biotech, Auburn,CA, USA) and Anti-IL-9 antibody-C-terminal (Catalog-Nr: ab181397, Abcam, Cambridge, UK), human anti-IL5 (Catalog-Nr: 562048) and anti-CD3 (BD Pharmingen, Munich, Germany), at 4°C overnight and followed by anti-rabbit Alexa fluor 488 secondary antibody(CST,4412S) and anti-mouse Alexa Fluor 594-conjugated secondary antibody(CST,8890S). The slides were then stained with anti-fade DAPI (Catalog-Nr: ab104139, Abcam, Cambridge, UK) for nuclear staining. The images were acquired with Fluorescence images and were obtained using confocal microscopy (TCS SP8; Leica, Wetzlar, Germany). Immunohistochemistry staining profiles of EEC tissues were collected from Shanghai First Maternity and Infant Hospital and Human Protein Atlas database [www.proteinatlas.org, (11)]. ULI RNA-seq data of IL9 and IL9R were also extracted from the Human Protein Atlas database.

Calculation of Immune/Stromal Scores and Identification of Differentially Expressed Genes

ESTIMATE (Estimation of STromal and Immune cells in MAlignant Tumor tissues using Expression data) algorithms calculated the immune and stromal scores (12) using Pearson's correlation coefficient. Then, these data were divided into high and low immune/stromal score groups. The selection of differentially expressed genes (DEGs) was performed by using the "limma" R package with p-value <0.05 and log fold change >1 as a filter (13).

CyTOF Staining and Barcoding

Single cells isolated from endometrial tumor tissues were washed with complete RPMI (Sigma) followed by three washes in Barium-free PBS (Sigma) by spinning at 1,800 rpm for 3 min. Cells from each sample were stained with intercalator-103Rh to label dead cells. After one wash in the MaxPar staining buffer, living cells were fixed in Fix I Buffer followed by permeabilization. Each sample was labeled with barcodes from Cell-ID™ 20-plex Pd barcoding kit. Barcoded samples were washed twice in the MaxPar staining buffer and pooled into one sample. Human TruStain FcX Fc receptor blocker (BioLegend) was used to block Fc receptors of cells, which were then incubated with cell-surface antibodies as listed in **Supplemental Table 1** at 4°C for 30 min. After incubation, cells were washed twice in the MaxPar staining buffer and fixed as described above, followed by two washes in Perm-S buffer. Antibodies against intracellular targets were incubated with permeabilized cells in Perm-S buffer for 30 min at 4°C. At the end of the staining, cells were washed twice in MaxPar staining buffer and stored in 1 ml of MaxPar Fix and Perm Buffer containing 125 nM MaxPar Intercalator-Ir (191Ir and 193Ir) at 4°C. After 12 h, cells were washed twice in MaxPar staining buffer and stored as a pellet in MaxPar staining buffer at 4°C until analysis. To minimize the batch effect, samples were stained all in one batch then analyzed by CyTOF in two consecutive days (the day after cell staining). On the day of analysis, cells were washed twice in MaxPar water and re-suspended in MaxPar water containing 10% EQ™ four-element calibration beads followed by acquisition on CyTOF.

Immune Cell Infiltration Analysis

The infiltration of six types of immune cells (CD4+ T cells, CD8+ T cells, B cells, neutrophils, macrophages, and dendritic cells) based on RNA-Seq expression profile data was calculated by using the TIMER (Tumor IMmune Estimation Resource) algorithm (14). The correlation between IL9, IL9R, and immune cells was calculated by Spearman's correlation analysis by TIMER. The correlation coefficient >0.3 indicates a positive/negative correlation.

Enrichment Analysis

Metascape (http://metascape.org/gp/index.html) is an effective and efficient tool for experimental biologists to comprehensively analyze and interpret OMICs-based studies in the big data era. The database was used to perform the Gene Ontology (GO) and Kyoto Encyclopedia of Genes and Genomes (KEGG) pathway enrichment analysis, which is used to predict the potential biological functions of the overlapping genes of the DEGs and target genes. Then, verification was performed by the GEPIA database (http://gepia.cancer-pku.cn) to identify hub genes (15–23).

Statistical Analysis

Pearson's Chi-square test for categorical variables and the Wilcoxon rank-sum test for continuous variables were used to compare various parameters in different groups divided by IL9/IL9R expression. The Kaplan–Meier method was used to estimate OS, DFS, or PFS. Differences in survival outcomes were assessed by the log-rank test. Results were presented as hazard ratios (HRs) and 95% confidence intervals (CIs). $p < 0.05$ was considered statistically significant except in logistic regression ($p < 0.1$) for the coefficient analysis. All statistical analyses were performed with GraphPad Prism (version 8.0; GraphPad Software, La Jolla, California) and R studio (version 3.6.1; R studio, Boston, Massachusetts).

RESULTS

Immune/Stromal Scores, DEGs, and Enrichment Analysis of DEGs in EC

By using ESTIMATE algorithm, immune and stromal scores were calculated for 529 EC patients whose clinical data were extracted from the TCGA Pan-Cancer dataset. And immune-related and stromal related genes were further identified (**Supplemental Table 2**); 552 genes were up-regulated in high immune score group and were selected for enrichment analysis. The correlation includes IFNγ production, B cell activation, lymphocyte activation, and regulation of innate immune response (**Figure 1A**). Both CD4 and CD8 T cells are the primary sources of IFNγ. Next, the tumor infiltration with six types of immune cells was analyzed by TIMER to investigate the consistency of the enrichment analysis. These analyses above

showed that EC patients with high immune scores might experience multiple immune cell infiltration and activation. In contrast, only B cells and CD8+ T cell infiltration, instead of macrophages, dendritic cells (DCs), CD4+ T cells, or neutrophil, were found relevant to the OS of EC patients (**Figure 1B**).

The Component of IL-9 Producing Immune Cells in EC

Based on the Pan-cancer clinical data extracted from the TCGA dataset and TIMER platform, we found that IL9 was up-regulated in various cancer types, including EC (**Supplementary Figure 2A**). However, the expression of IL9 did not correlate with the infiltrating levels of any of the six types of immune cells (**Supplementary Figure 2B**). Through immunofluorescence staining of 143 tumor tissues of EC patients, we found that nearly all the Vδ2 + γδT cells were IL9 positive. However, although most of the IL5+ cells (mostly ILC2 or T_H2) secreted IL9, they only presented as a small subgroup of IL9 positive cells in EC (**Figure 2A**). **Figure 2B** showed the gene skyline presenting the expression profiles of IL9 and its receptor IL9R in the majority of immune cell types through microarray and ULI RNA-seq data. Consistently, IL9 was enriched in ILC2, Vδ2 + γδT cells, memory B cells, CD4+/CD8+ T cells, macrophages, and mast cells. Similarly, the IL9R gene was also up-regulated in B cells. Moreover, IL9R was also found up-regulated in mast cells, dendritic cells, Vδ2 + γδT cells, and ILC2s, with ILC2 expressing a significantly higher level of IL9R compared to other immune cells. To further investigate the

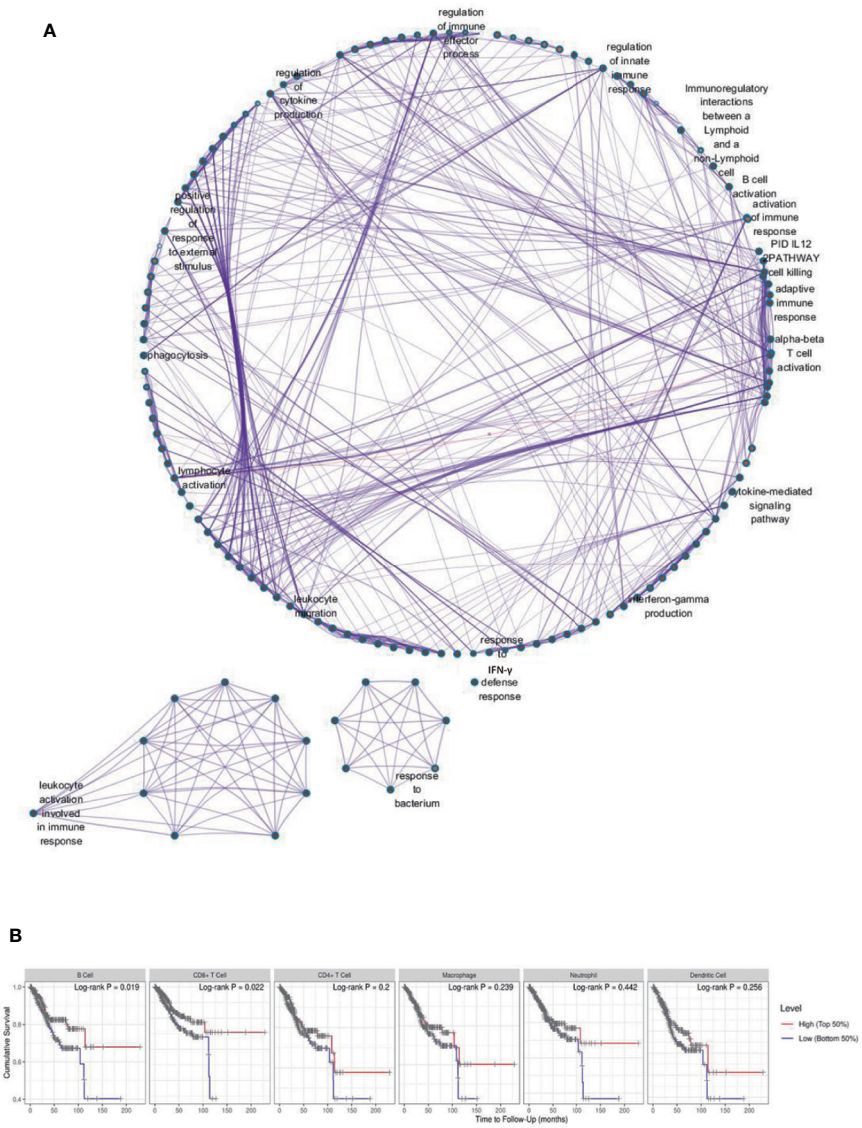

FIGURE 1 | Immune Scores and Enrichment Analysis of DEGs in EC. **(A)** The correlation between high immune score related differentially expressed genes (DEGs) and biological processes GO terms; **(B)** The tumor infiltration with six types of immune cells and cumulative survival rates.

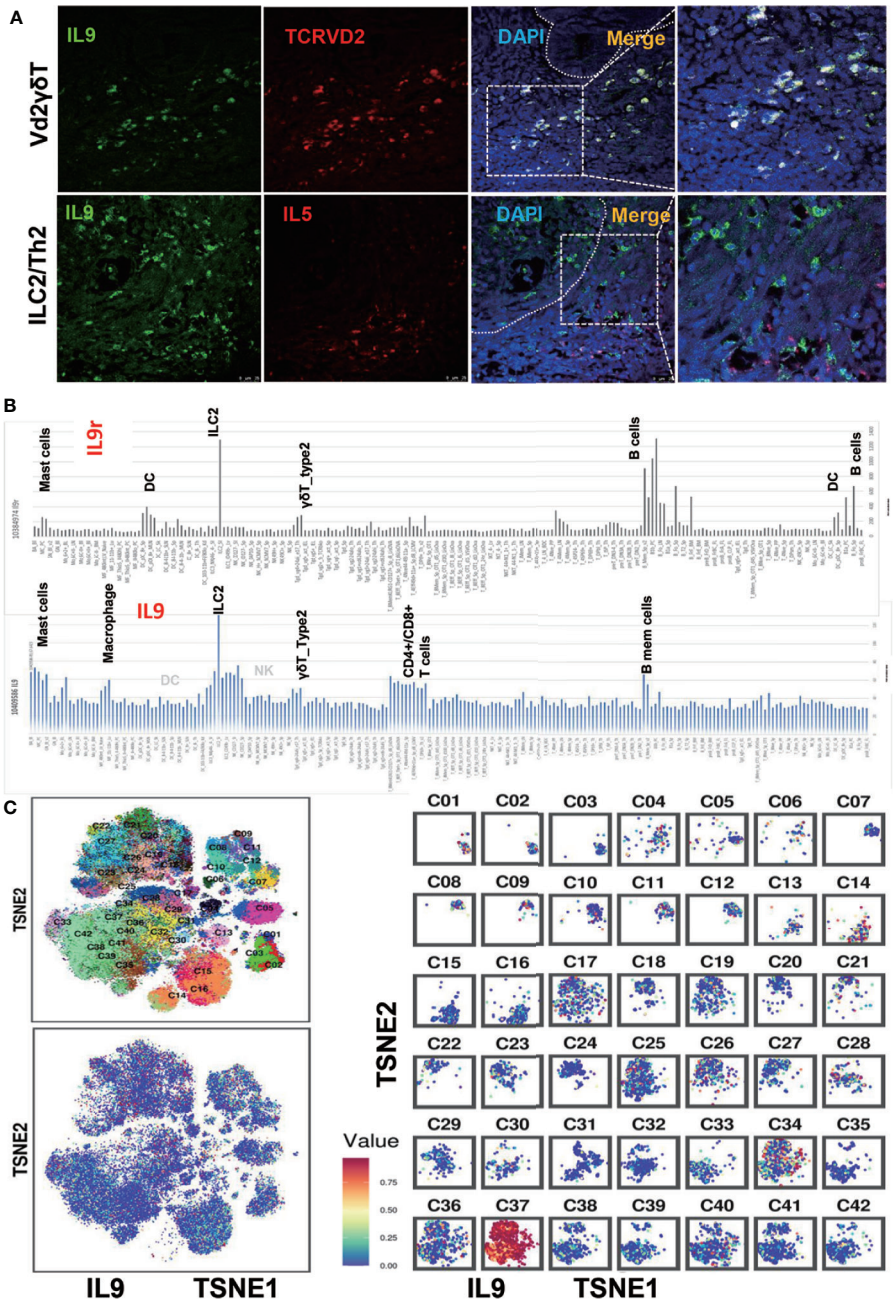

FIGURE 2 | The Component of IL-9 Producing Immune Cells in EC. **(A)** Immunofluorescence staining of IL9 + Vδ2 γδT cells and IL9 + ILC2 cells in EECs. **(B)** This panel showed the gene skyline presenting the expression profiles of IL9 and IL9R in the majority of immune cell types through microarray and ULI RNA-seq data. IL9R was found up-regulated in B cells, mast cells, dendritic cells, Vδ2 + γδT cells, and ILC2, with ILC2 expressing a significantly higher level of IL9R compared to other immune cells. Similarly, it's ligand IL9 was also enriched in ILC2, Vδ2 + γδT cells, memory B cells, and CD4+/CD8+ T cells. **(C)** The tSNE map generated by CyTOF, the IL9 was enriched in cluster 37 (T_H9 cells) , cluster 9 (Vδ2 + γδT cells), cluster 14 (NK cells), cluster 8 (macrophage), cluster 1 (MDSC), and ILC2s. C1–42 means Cluster1–42.

component of IL9+ immune cells in EEC, CyTOF was performed for the specimens from eight patients with EEC. The t-SNE map showed that in EEC, IL9 positive cells were T_H9 (cluster 37), Vδ2 +γδT cells (cluster 9), macrophages (cluster 8), myeloid-derived suppressor cells (MDSCs, cluster1), and innate immune cells (cluster 14, 34) (**Figure 2C**).

Clinicopathologic Features and IL9 Expression in Patients With EC

RNA-seq data were reported as median FPKM (number Fragments Per Kilobase of exon per Million reads) extracted from 541 patients out of 548 patients (lack of data for the other seven patients) from the TCGA database (Firehose, Legacy, 548

patients). DEGs were generated from IL9 ^{high} and IL9 ^{low} subgroups (cutoff: FPKM 0.1, **Supplementary Figure 2C**). The top 10 of biological processes, cellular component, and molecular function GO terms of IL9-low (**Supplementary Figure 2D**) or IL9-high (**Supplementary Figure 2E**) related DEGs. 127 patients with ECs were then included in the current analysis. The mean age of patients at the time of diagnosis was 54 ± 8.7 years. The mean size of the tumor was 7.95 cm^2(1–175 cm^2). 59% (75 patients) of the patients presented with Figo stage Ia ECC, 17.3% (22 patients) presented with stage Ib; patients presented with stages II, III, and IV were 9.4% (12 patients), 9.4% (12 patients), and 0.8% (one patient), respectively. Five patients were without staging data. The IL9+ lymphocyte count was 83.17 ± 122.1 cells/spot(d = 1.5 mm), the Vδ2 + γδT cell count was 9.85 ± 12.15 cells/spot(d = 1.5 mm).

Prognostic Estimation in EEC Patients

Next, the correlation of the number of IL9+ cells with the expression of the biomarkers was evaluated, respectively (**Figure 3A**). And we elucidated that up-regulated Progesterone Receptor (PR) expression(p = 0.04) and high/moderate EC differentiation(p = 0.04) were relevant to more IL9+ lymphocyte infiltration. To detect the connection of IL9+ lymphocyte infiltration and survival, we performed a univariate survival analysis of the IL9+ lymphocytes and Vδ2 + γδT cells for 127 patients after a median follow-up of 81.8 months (range, 25–124 months, specimens from 27 patients were not sufficient for staining or met the exclusion criteria). Specifically, high IL9+ lymphocyte infiltration ($IL9^{hi}$, IL9+ cells ≥100 cells/spot, 0.6 cells/mm^2) was positively correlated with a better overall survival (p = 0.0027) (**Figure 3B**). Vδ2 + γδT cells were reported to be the main resource of IL9 in plenty of solid tumors and also one of the resources of IL9 in EC; however, the present study revealed the opposite that less than high Vδ2 + γδT cell infiltration ($Vδ2^{lo}$, Vδ2 + γδT cell<18 cells/spot, 0.1 cells/mm^2) was related to a better OS (p = 0.0221, HR 7.61) (**Figure 3C**). It might be because that in EC, Vδ2+γδT cell presented 0.15–0.86% of immune cells, T_H9 cells are 3.6–14 times as many as Vδ2 + γδT cells in the present study. Next, all of these covariates were included in the multivariable logistic regression model. Briefly, on multivariable analysis, FIGO stage (Estimate Std. −7.582, Pr(>|t|) = 0.000006), IL9 score (Estimate Std. 8.917, Pr(>|t|) = 0.026), classification of differentiation (Estimate Std. 2.865, Pr(>|t|) = 0.067), and diabetes mellitus (Estimate Std. 9.561, Pr(>|t|) = 0.07) emerged as predictors for the outcome of interest. To predict the overall survival of patients with EC, a prognostic nomogram was established through the Cox regression model analysis. Though the infiltrating Vδ2 + γδT cells did not present as a predictor, it was still considered for the development of the nomogram given its clinical importance in the univariate survival analysis. Each factor in the nomogram was assigned a weighted number of points, and the sum of points for each patient was in accordance with a specific predicted 3-, 5- and 10-year OS (**Figure 3D**). We also validated the nomograms by using the concordance index (C-index) to assess the predictive accuracy of the nomograms. For the internal validation of the nomogram, the concordance index for our survival model was 0.754(SD = 0.148, p = 0.0006, **Figure 3E**), which showed a good agreement between the nomogram-predicted survival and actual survival.

IL9R Expression Enriched in Endometrium and EECs

The expression of IL9R positively correlated with the infiltrating levels of B cells, DC cells, CD8+ T cells, and CD4+T cells (**Figure 4A**). Concerning IL9R RNA expression, it is enriched in normal female tissues, especially in the endometrium (**Figure 4B**). Concerning protein expression in cancer, IL9R significantly enriched in endometrial cancer compared to renal cancer, breast cancer, and other malignancies (**Figure 4C**). Specifically, although in a few cases, IL9R is only expressed in the tumor cells (**Figures 4N, O**). However, mostly, IL9R was not only detected in tumor cells but also infiltrated lymphocytes (**Figures 4D–M**). Thus, we focused on the IL9R RNA expression in immune cells by analyzing Monaco and HPA datasets and found that IL9R up-regulated in Naïve-B cells, T_H2 cells, Treg cells, eosinophils, and neutrophils (**Figures 4P–R**). Firstly, IL9R RNA was found not relevant to the DFS or OS of endometrial cancer based on a small sample size of data(n = 168) from the TCGA dataset (**Figures 5A, B**). However, in a larger cohort of 541 patients, patients with high IL9R expression showed significantly better OS (p < 0.05, **Figure 5C**). Similar to IL9, IL9R RNA was also up-regulated in endometrial cancer tissues (UCEC) compared to adjacent normal tissues (n = 265, p < 0.05, **Figure 5D**). Specifically, the expression level of IL9R RNA was significantly downregulated in Stage IV tumors compared to the early stages (p = 0.0129, **Figure 5E**).

Pathway and Process Enrichment Analysis of IL9R

As IL9R was enriched in B cells, T cells, mast cells, eosinophil, and neutrophils, pathway and process enrichment analysis had been carried out in different cell types with the following ontology sources: KEGG Pathway, GO Biological Processes, Reactome Gene Sets, Canonical Pathways and CORUM. The top 20 clusters with their enriched representative terms were shown in **Figure 5F**. Specifically, the IL9R related genes were associated with several pathways such as oxidative phosphorylation and cell cycle of B cells, RUNX1 pathways, lymphocyte differentiation and activation, Jak-STAT signaling pathway of T cells, and CD28 costimulation of eosinophils, and leukocyte activation of mast cells and so on. To further capture the relationships between the terms, a subset of enriched terms of T cells and mast cells had been selected and rendered as a network plot, where terms with a similarity >0.3 were connected by edges. The network was visualized using Cytoscape, where each node represented an enriched term.

Intriguingly, similar to IL9, which was relevant to the PR/PGR expression level, IL9R was negatively relevant to PGRMC1 (Progesterone Receptor Membrane Component 1) (p = 4.26e-8, **Figure 6A**). Progesterone, acting through the progesterone receptors (PR/PGRs), is one of the most critical regulators of endometrial differentiation. Additionally, PR is the most validated prognostic biomarkers for endometrial cancer. In the present study, PR+ cells were DC (cluster 6), macrophages

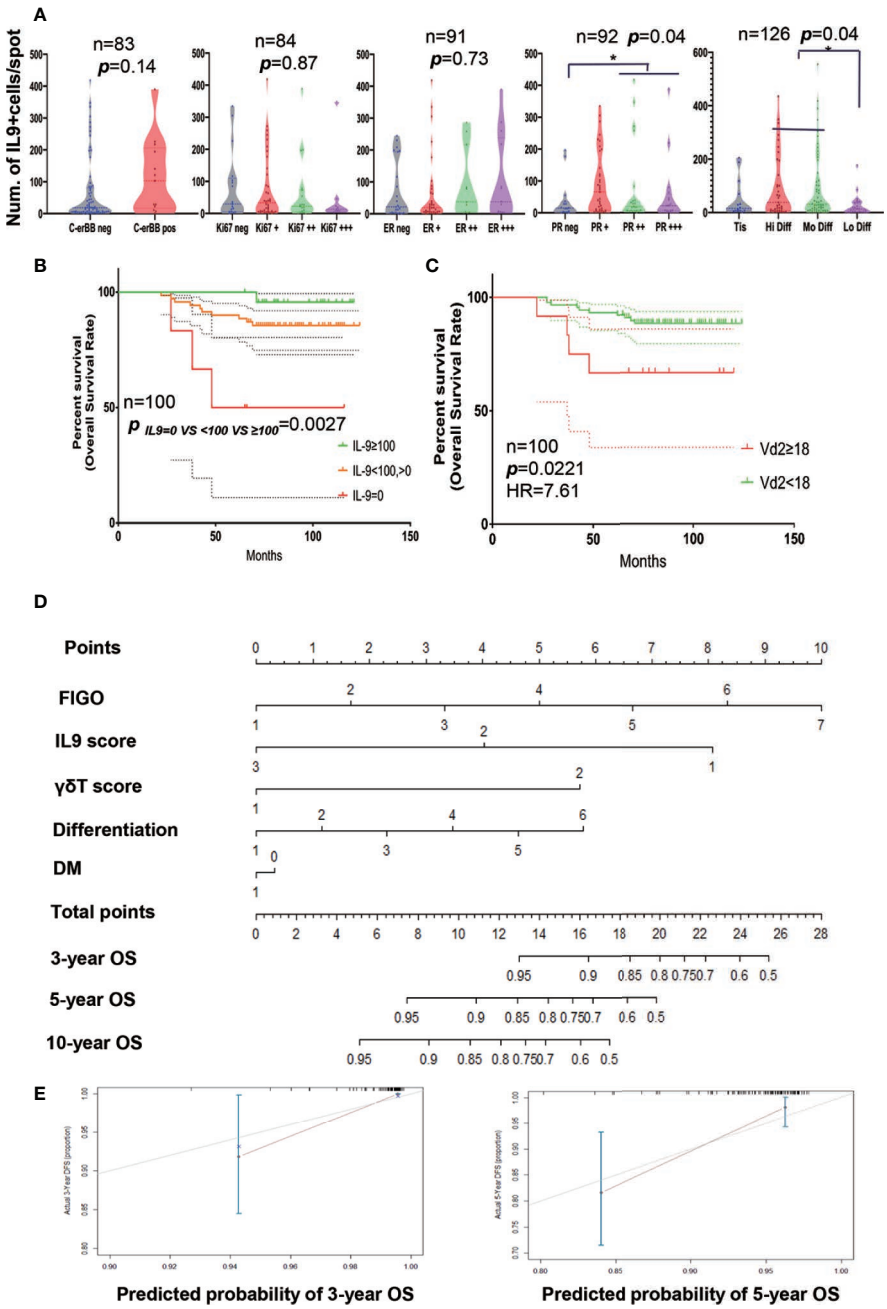

FIGURE 3 | Prognostic Estimation in EC Patients. **(A)** The association between expression of the biomarkers C-erBB, Ki67, Estrogen Receptor (ER), Progesterone Receptor (PR/PGR)), differentiation, and the number of IL9+ cells/spot. **(B)** The overall survival rate of EC patients with different IL9 expression. **(C)** The overall survival rate of EC patients with different density of Vδ2 $\gamma\delta$T cells. **(D)** The nomogram of EC patients. Each factor in the nomogram was assigned a weighted number of points, and the sum of points for each patient was in accordance with a specific predicted 3-, 5- and 10-year OS. IL9 score 1: ~0 cells/mm^2, IL9 score 2: <0.6 cells/mm^2, IL9 score 3: ≥0.6 cells/mm^2; $\gamma\delta$T cell score 1: Vδ2 + $\gamma\delta$T cell <0.1 cells/mm^2; $\gamma\delta$T cell score 2: Vδ2 + $\gamma\delta$T cell ≥0.1 cells/mm^2**.** **(E)** Verification plots of 3-year (up) and 5-year (low) overall survival nomogram verification curves. * means $p < 0.05$.

(cluster 8), Vδ2 + $\gamma\delta$T cells (cluster 9), and innate immune cells (cluster 34); the majority of PR+ immune cells were CD68 + CD206 + CD14 + tumor-associated macrophages (1.7% of immune cells in EC), which were negatively related to patients' survival. Then, for these IL9R and PGR associated genes, protein–protein interaction enrichment analysis had also been carried out. Densely connected network components, including YWHAZ, PGRMC1, CD46, PPT1, RCN2, ATXN10, RAB4A, *etc.*

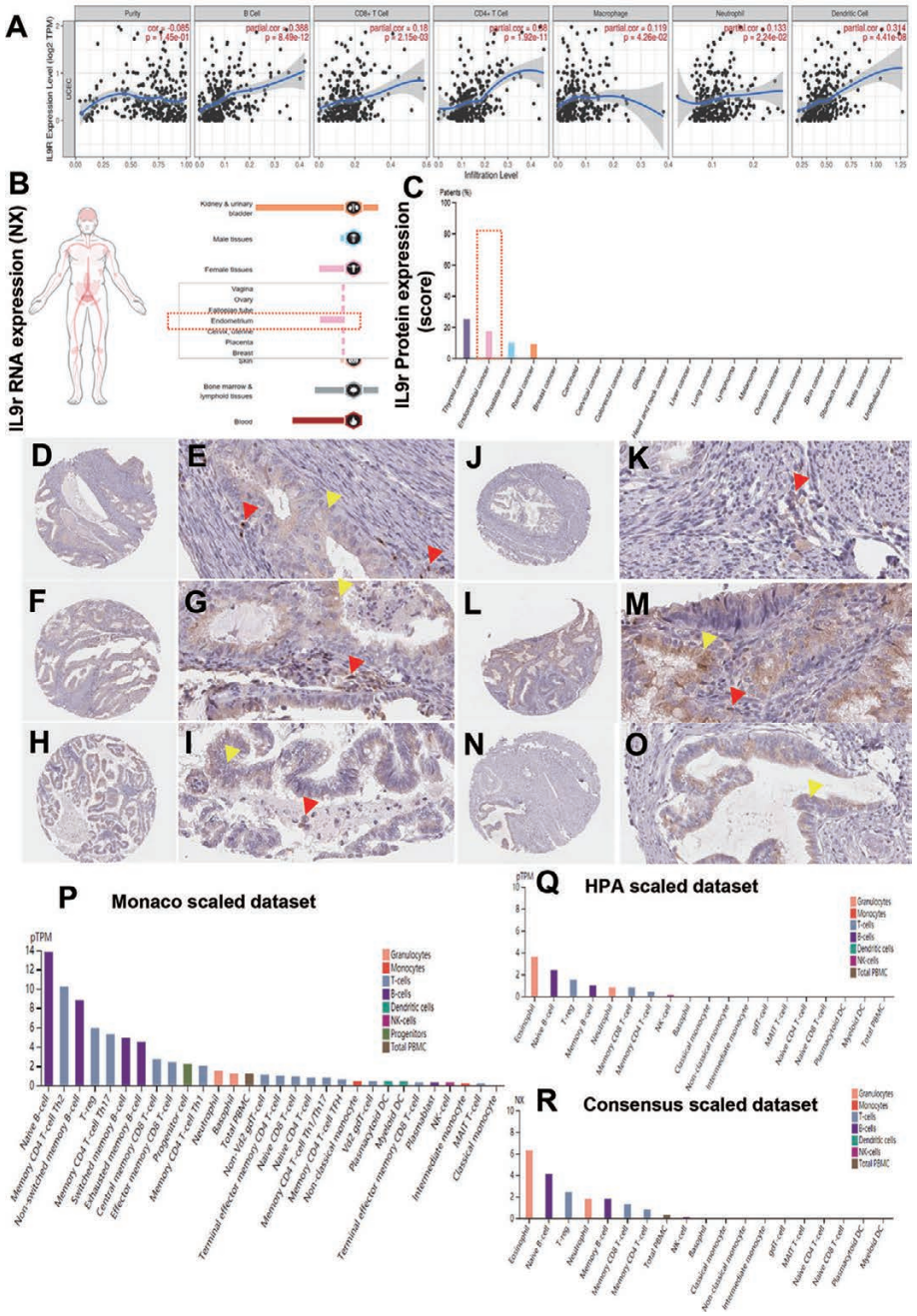

FIGURE 4 | IL-9R Expression in Endometrium and EECs. **(A)** Correlation of IL9R expression level with immune infiltration level. **(B)** IL9R RNA expression was enriched in normal female tissues, especially in the endometrium; **(C)** IL9R protein was increased in endometrial cancer compared to renal cancer, breast cancer, and other malignancies. **(D–M)** In most of the endometrial cancers, IL9R was detected in tumor cells and infiltrated lymphocytes. **(N, O)** In a few cases, IL9R was only expressed in tumor cells. **(P–R)** IL9R RNA expression in immune cells was analyzed in Monaco and HPA datasets and found that IL9R was up-regulated in Naïve-B cells, T_H2 cells, Tregs, eosinophils, and neutrophils.

were identified in **Figure 6B**; the involved network included T cell and B cell activation, T_H17 differentiation, leukocyte migration, IL12 pathway, and IFNγ production (**Figure 6E**). The expression of PGR and PGRMC1 positively correlated with the infiltrating levels of CD8+T cells (**Figures 6C, D**).

DISCUSSIONS

Endometrioid endometrial carcinomas are frequently estrogen-dependent tumors with heterogeneous prognosis (24, 25). Though biomathematical tools have provided an excellent

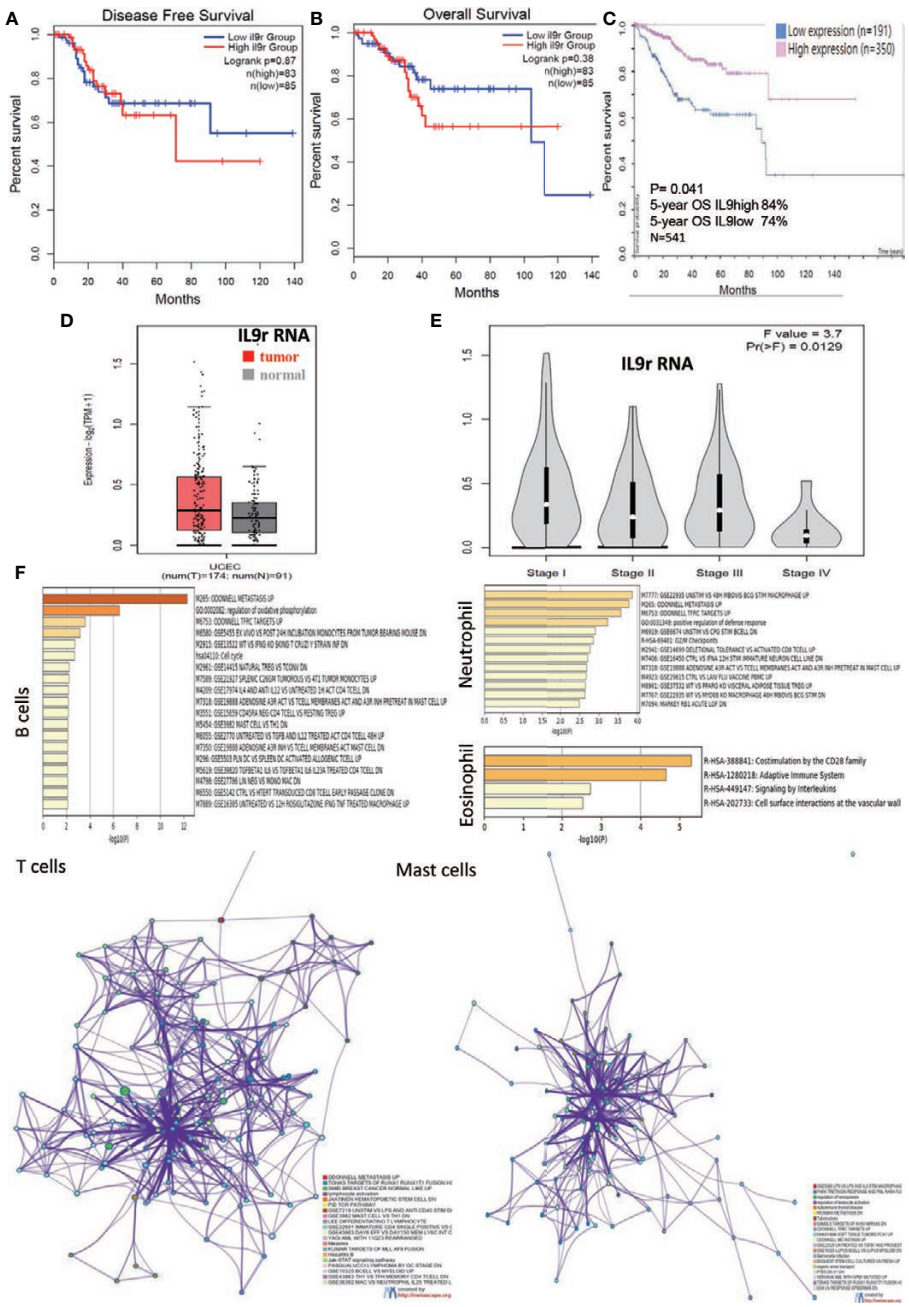

FIGURE 5 | Pathway and Process Enrichment Analysis of IL9R. **(A, B)** Disease-free survival and overall survival analysis based on the expression status of IL9R RNA and a Kaplan–Meier curve was plotted. (n = 168) **(C)** Overall survival analysis based on the expression status of IL9R RNA and a Kaplan–Meier curve was plotted (n = 541). **(D)** The expression of IL9R RNA in tumor and adjacent normal tissue UCEC by analyzing TCGA dataset. UCEC, Uterine Corpus Endometrial Carcinoma (n = 265, $p < 0.05$). **(E)** The expression of IL9R RNA in stages I–IV UCEC by analyzing TCGA dataset. UCEC, Uterine Corpus Endometrial Carcinoma. **(F)** Pathway and process enrichment analysis of IL9R related genes had been carried out in different cell types with the following ontology sources: KEGG Pathway, GO Biological Processes, Reactome Gene Sets, Canonical Pathways, and CORUM. Top 20 clusters with their enriched representative terms were shown here. A subset of enriched terms of T cells and mast cells had been selected and rendered as a network plot of IL9R, where terms with a similarity >0.3 were connected by edges. The network was visualized using Cytoscape, where each node represented an enriched term.

chance for the promotion of targeted therapies and personalized treatments, a tiny fraction of them is sufficient to yield excellent prognostic results for EECs. This might be owing to the heterogeneity of EEC and the comprehensive characterization of the tumor microenvironment. This inspired us that endometrial immune profile and cytokines might be new parameters for prognostic prediction (26, 27). Investigators have shown that the immune score could predict survival in

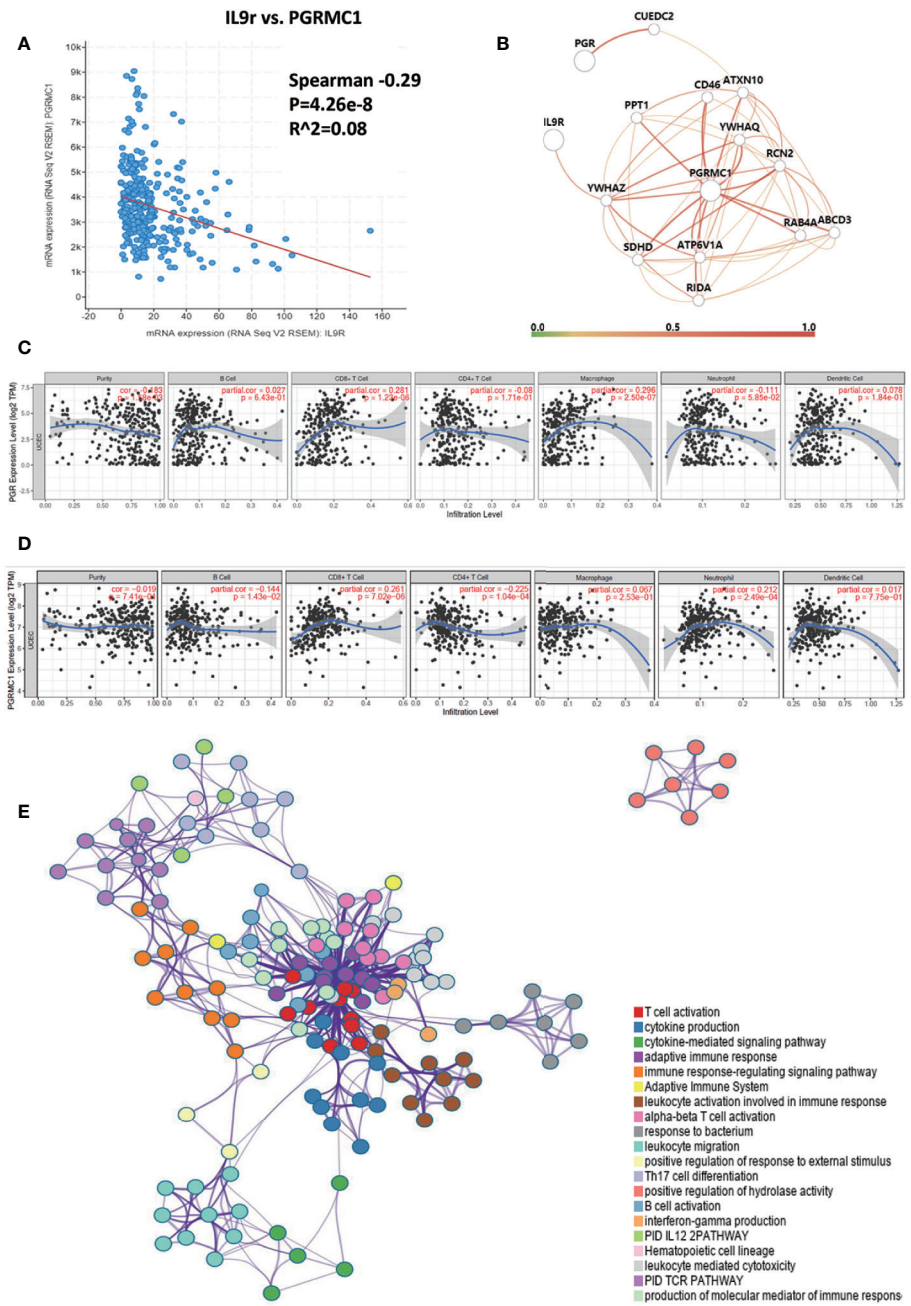

FIGURE 6 | Protein Interaction of IL9/IL9R. **(A)** The correlation analysis of IL9R mRNA and PGR/PR, or PGRMC1 (Progesterone Receptor Membrane Component 1) mRNA. PGRMC1 was negatively relevant to IL9R (p = 4.26e-8); **(B)** protein–protein interaction enrichment analysis of IL9R and PR/PGR associated genes. Densely connected network components, including YWHAZ, PGRMC1, CD46, PPT1, RCN2, ATXN10, RAB4A, *etc*. **(C, D)** Correlation of PGR and PGRMC1 gene's expression with immune infiltration levels. **(E)** A subset of enriched genes of IL9R and terms had been selected and rendered as a network plot, where terms with a similarity >0.3 were connected by edges. The network was visualized using Cytoscape, where each node represented an enriched term; the involved network included T cell and B cell activation, T_H17 differentiation, leukocyte migration, IL12 pathway, and IFNγ production.

cancer patients (28, 29). Specifically, cytokines and chemokines have been highlighted owing to their capability of active or suppress immune cascades in the immune microenvironment (30, 31). The common cytokine receptor γ chain (γc) family of cytokines includes interleukin-2 (IL-2), IL-4, IL-7, IL-9, IL-15, and IL-21. This set of cytokines exhibits broad pleiotropic actions on the immune system, bridging both the innate and adaptive immune systems. IL-9 was first discovered around the 1990s as a late T cell growth factor as well as a mast cell growth factor. IL-9 is produced predominantly by helper T cells such as T_H2 and

T_H9 cells; it could also be provided by ILC2 cells, mast cells, and NK T cells. It usually functions on T and B cells, γδT cells, eosinophils, neutrophils, and mast cells (32) through the activation of a JAK/STAT pathway and plays a critical role in immunity and the pathogenesis of cancer.

IL9 yields different responses depending on the cancer type. This cytokine not only has been shown to exhibit anti-tumor activity but also has been presented as a tolerogenic cytokine in most solid cancers to promote T regulatory cell function (33, 34). However, it has not been extensively studied in endometrial carcinoma. In the present study, we found that the high density of tissue-resident IL9+ cells was associated with a better prognosis. Because Vδ2 T cells were considered as a major source of IL-9 (35), we also evaluated the infiltration of Vδ2 T cells in endometrial cancer. We found that elevated Vδ2 T cell infiltration was relevant to worse overall survival, and multivariable analysis showed an attenuated diagnostic value of this cell type. CyTOF and immunofluorescence were performed to explain the discrepancy. The results revealed that IL-9 was also produced by Vδ2 T cell, ILC2, mast cells, eosinophils, M2 macrophages, T_H9, and NK/NKT cells in the endometrial cancer tissues. Intriguingly, IL9 positive immune cells were also ESR positive according to CyTOF analysis. Besides, IL9R, the receptor of IL9, was up-regulated in the endometrium tissue and endometrial cancer tissues as well. In the present study, IL-9Ra is not only detected on T cells and B cells but also on other hematopoietic cells such as eosinophils, neutrophils, mast cells, and ILC2s. Recent studies have shown that sex hormone levels regulate tissue-resident populations of some tissue-resident immune cells such as ILC2s in homeostasis (36). Ovariectomy of ERα−/− females and orchidectomy of ERα−/− males restored ILC2 numbers and function to WT levels. For advanced stages and recurrence of endometrial cancer, hormone treatment using progesterone could slower the growth of endometrial cancer cells and govern the immune microenvironment. However, the association between endometrioid resident immune cells and estrogen or progesterone remains unclear (37). The present study provided an initial idea of the association between IL9R and PGRMC1.

CONCLUSIONS

In conclusion, we observed a significant infiltration of IL9+ cells and the overrepresentation of IL-9R in tissue specimens of patients in EC cases. Our proposed nomogram, based on FIGO classification, IL9 score, and γδT score, can classify patients into subgroups with different prognosis and will help facilitate personalized strategies for EC patients. We also elucidated that IL9 was relevant to the PR/PGR expression level, IL9R was negatively relevant to PGRMC1. Additionally, this study not only established a prognostic nomogram but also assisted in the firmer understanding of the relevance of the IL9-IL9R axis and IL9-producing cells in EC immunity.

DATA AVAILABILITY STATEMENT

The original contributions presented in the study are included in the article/supplementary material, further inquiries can be directed to the corresponding author/s.

ETHICS STATEMENT

The studies involving human participants were reviewed and approved by the Institutional Review Board (IRB) of Shanghai First Maternity and Infant Hospital. The patients/participants provided their written informed consent to participate in this study.

AUTHOR CONTRIBUTIONS

HT and HF conceived the project, designed the study, and drafted the manuscript. HT, X-PW, and HF designed the study, wrote and revised the manuscript, and approved the final submission. HT, HF, and X-PW revised the manuscript and approved the final submission. XH, M-FW, Y-FS, X-LW, and Y-RL were involved in the design of the study. All authors contributed to the article and approved the submitted version. All authors qualify as per ICJME criteria for authorship.

FUNDING

This study was supported by the Funding Program from Shanghai Jiao Tong University (SJTU) Cross-disciplinary project (HF, YG2017QN54), National Natural Science Foundation, China (HT, 81702545), Shanghai Natural Science Foundation (HF, 18ZR1424200), National Natural Science Foundation, China (X-PW, 81672574), National Natural Science Foundation, China (HF, 81902388).

SUPPLEMENTARY MATERIAL

The Supplementary Material for this article can be found online at: https://www.frontiersin.org/articles/10.3389/fimmu.2020.544248/full#supplementary-material

SUPPLEMENTARY FIGURE 1 | The workflow of the present study.

SUPPLEMENTARY FIGURE 2 | (A) IL9 expression in 31 types of tumors. **(B)** Correlation of IL9 expression with immune infiltration level. **(C)** DEGs in IL9 high and IL9 low subgroups. **(D)** The top 10 of biological processes, cellular component, and molecular function GO terms of IL9-low related DEGs. **(E)** The top eight of biological processes, cellular component, and molecular function GO terms of IL9-high related DEGs.

SUPPLEMENTARY TABLE 1 | Antibody involved in the present study.

SUPPLEMENTARY TABLE 2 | 1. The immune scores and stromal scores of EC. 2. DEG in EC with IL9 high and IL9 low.

REFERENCES

1. Gallo ML, Bell DW. The Emerging Genomic Landscape of Endometrial Cancer. *Clin Chem* (2014) 60(1):98–110. doi: 10.1373/clinchem.2013.205740
2. Dedes KJ, Wetterskog D, Ashworth A, Kaye SB, Reis-Filho JS. Emerging therapeutic targets in endometrial cancer. *Nat Rev Clin Oncol* (2011) 8 (5):261–71. doi: 10.1038/nrclinonc.2010.216
3. Lewin SN, Wright JD. Comparative Performance of the 2009 International Federation of Gynecology and Obstetrics' Staging System for Uterine Corpus Cancer. *Obstet Gynecol* (2010) 116(5):1141–9. doi: 10.1097/AOG.0b013e3181f39849
4. Siegel RL, Miller KD, Jemal A. Cancer statistics, 2019. *CA Cancer J Clin* (2019) 69(1):7–34. doi: 10.3322/caac.21551
5. Wui-Jin KM, Abu-Rustum NM, Bradley KM. *National Comprehensive Cancer Network. Uterine Neoplasms (Version 1.2019)* (Accessed November 22, 2018).
6. Leonard WJ, Lin JX, O'Shea JJ. The γc Family of Cytokines: Basic Biology to Therapeutic Ramifications. *Immunity* (2019) 50(4):832–50. doi: 10.1016/j.immuni.2019.03.028
7. You FP, Zhang J, Cui T, Zhu R, Lv CQ, Tang HT, et al. Th9 cells promote antitumor immunity via IL-9 and IL-21 and demonstrate atypical cytokine expression in breast cancer. *Int Immunopharmacol* (2017) 52:163–7. doi: 10.1016/j.intimp.2017.08.031
8. Bruchard M, Ghiringhelli F. Deciphering the Roles of Innate Lymphoid Cells in Cancer. *Front Immunol* (2019) 10:656. doi: 10.3389/fimmu.2019.00656
9. Gomez-Lopez N, Olson DM, Robertson SA. Interleukin-6 controls uterine Th9 cells and CD8 + T regulatory cells to accelerate parturition in mice. *Immunol Cell Biol* (2016) 94(1):79–89. doi: 10.1038/icb.2015.63
10. Cerami E, Gao J, Dogrusoz U, Gross BE, Sumer SO, Aksoy BA, et al. The cBio cancer genomics portal: an open platform for exploring multidimensional cancer genomics data. *Cancer Discov* (2012) 2(5):401–4. doi: 10.1158/2159-8290.CD-12-0095. Erratum in: Cancer Discov. 2012 Oct;2(10):960.
11. Uhlén M, Fagerberg L, Hallström BM, Lindskog C, Oksvold P, Mardinoglu A, et al. Tissue-based map of the human proteome. *Science* (2015) 347 (6220):1260419. doi: 10.1126/science.1260419
12. Yoshihara K, Shahmoradgoli M, Martínez E, Vegesna R, Kim H, Torres-Garcia W, et al. Inferring tumour purity and stromal and immune cell admixture from expression data. *Nat Commun* (2013) 4:2612. doi: 10.1038/ncomms3612
13. Ritchie ME, Phipson B, Wu D, Hu Y, Law CW, Shi W, et al. limma powers differential expression analyses for RNA-sequencing and microarray studies. *Nucleic Acids Res* (2015) 43:e47. doi: 10.1093/nar/gkv007
14. Li T, Fan J, Wang B, Traugh N, Chen Q, Liu JS, et al. TIMER: A Web Server for Comprehensive Analysis of Tumor-Infiltrating Immune Cells. *Cancer Res* (2017) 77:e108–10. doi: 10.1158/0008-5472.CAN-17-0307
15. Zhou Y, Zhou B, Pache L, Chang M, Khodabakhshi AH, Tanaseichuk O, et al. Metascape provides a biologist-oriented resource for the analysis of systems-level datasets. *Nat Commun* (2019) 10(1):1523. doi: 10.1038/s41467-019-09234-6
16. Zar JH. *Biostatistical Analysis. 4th edn*. Upper Saddle River: NJ Prentice Hall (1999). p. 523.
17. Hochberg Y, Benjamini Y. More powerful procedures for multiple significance testing. *Stat Med* (1990) 9:811–8. doi: 10.1002/sim.4780090710
18. Cohen J. A coefficient of agreement for nominal scales. Educ. Psychol. *Meas* (1960) 20:27–46. doi: 10.1177/001316446002000104
19. Shannon P, Markiel A, Ozier O, Baliga NS, Wang JT, Ramage D, et al. Cytoscape: a software environment for integrated models of biomolecular interaction networks. *Genome Res* (2003) 3(11):2498–504. doi: 10.1101/gr.1239303
20. Stark C, Breitkreutz BJ, Reguly T, Boucher L, Breitkreutz A, Tyers M, et al. BioGRID: a general repository for interaction datasets. *Nucleic Acids Res* (2006) 34:D535–539. doi: 10.1093/nar/gkj109
21. Li T, Wernersson R, Hansen RB, Horn H, Mercer J, Slodkowicz G, et al. A scored human protein-protein interaction network to catalyze genomic interpretation. *Nat Methods* (2017) 14:61–4. doi: 10.1038/nmeth.4083
22. Turei D, Korcsmáros T, Saez-Rodriguez J. OmniPath: guidelines and gateway for literature-curated signaling pathway resources. *Nat Methods* (2016) 13 (12):966–7. doi: 10.1038/nmeth.4077
23. Bader GD, Hogue CW. An automated method for finding molecular complexes in large protein interaction networks. *BMC Bioinf* (2003) 4:2. doi: 10.1186/1471-2105-4-2
24. Mariani A, Dowdy SC, Cliby WA, Gostout BS, Jones MB, Wilson TO, et al. Prospective assessment of lymphatic dissemination in endometrial cancer: A paradigm shift in surgical staging. *Gynecol Oncol* (2008) 109(1):11–8. doi: 10.1016/j.ygyno.2008.01.023
25. Keys HM, Roberts JA, Brunetto VL, Zaino SR, Spirtos NM, Bloss JD, et al. A phase III trial of surgery with or without adjunctive external pelvic radiation therapy in intermediate risk endometrial adenocarcinoma: A Gynecologic Oncology Group study. *Gynecol Oncol* (2004) 92(3):744–51. doi: 10.1016/j.ygyno.2003.11.048. Erratum in: Gynecol Oncol. 2004 Jul;94(1):241-2..
26. Longoria TC, Eskander RN. Immunotherapy in endometrial cancer - an evolving therapeutic paradigm. *Gynecol Oncol Res Pract* (2015) 2:11. doi: 10.1186/s40661-015-0020-3
27. Pardoll DM. The blockade of immune checkpoints in cancer immunotherapy. *Nat Rev Cancer* (2012) 12(4):252–64. doi: 10.1038/nrc3239
28. Wang H, Wu X, Chen Y. Stromal-Immune Score-Based Gene Signature: A Prognosis Stratification Tool in Gastric Cancer. *Front Oncol* (2019) 12(9):1212. doi: 10.3389/fonc.2019.01212
29. Geng Y, Shao Y, Zhu D, Zheng X, Zhou Q, Zhou W, et al. Systemic Immune-Inflammation Index Predicts Prognosis of Patients with Esophageal Squamous Cell Carcinoma: A Propensity Score-matched Analysis. *Sci Rep* (2016) 6(1):39482. doi: 10.1038/srep39482
30. Gogos C, Drosou E, Bassaris HP, Skoutelis A. Pro- versus Anti-inflammatory Cytokine Profile in Patients with Severe Sepsis: A Marker for Prognosis and Future Therapeutic Options. *J Infect Dis* (2000) 181(1):176–80. doi: 10.1086/315214
31. Lippitz B, Harris RA. Cytokine patterns in cancer patients: A review of the correlation between interleukin 6 and prognosis. *OncoImmunology* (2016) 5 (5):e1093722. doi: 10.1080/2162402X.2015.1093722
32. Qayum AA, Koh B, Martin RK, Kenworthy BK, Kharwadkar R, Fu Y, et al. The Il9 CNS-25 Regulatory Element Controls Mast Cell and Basophil IL-9 Production. *J Immunol* (2019) 203(5):1111–21. doi: 10.4049/jimmunol.1900272
33. Lu Y, Hong S, Li H, Park J, Hong B, Wang L, et al. Th9 cells promote antitumor immune responses in vivo. *J Clin Invest* (2012) 122(11):4160–71. doi: 10.1172/JCI65459
34. Purwar R, Schlapbach C, Xiao S, Kang S, Elyaman W, Jiang X, et al. Robust tumor immunity to melanoma mediated by interleukin-9–producing T cells. *Nat Med* (2012) 18(8):1248–53. doi: 10.1038/nm.2856
35. Peters C, Häsler R, Wesch D, Kabelitz D. Human Vδ2 T cells are a major source of interleukin-9. *Proc Natl Acad Sci U S A* (2016) 113(44):12520–5. doi: 10.1073/pnas.1607136113
36. Kadel S, Ainsua-Enrich E, Hatipoglu I, Turner S, Singh S, Khan S, et al. A Major Population of Functional KLRG1- ILC2s in Female Lungs Contributes to a Sex Bias in ILC2 Numbers. *Immunohorizons* (2018) 2 (2):74–86. doi: 10.4049/immunohorizons.1800008
37. Park J, Nam J. Progestins in the Fertility-Sparing Treatment and Retreatment of Patients With Primary and Recurrent Endometrial Cancer. *Oncologist* (2015) 20(3):270–8. doi: 10.1634/theoncologist.2013-0445

Conflict of Interest: The authors declare that the research was conducted in the absence of any commercial or financial relationships that could be construed as a potential conflict of interest.

Copyright © 2020 Tong, Feng, Hu, Wang, Song, Wen, Li and Wan. This is an open-access article distributed under the terms of the Creative Commons Attribution License (CC BY). The use, distribution or reproduction in other forums is permitted, provided the original author(s) and the copyright owner(s) are credited and that the original publication in this journal is cited, in accordance with accepted academic practice. No use, distribution or reproduction is permitted which does not comply with these terms.

frontiers in Oncology

ORIGINAL RESEARCH
published: 09 December 2020
doi: 10.3389/fonc.2020.595082

Reconstruction of Immune Microenvironment and Signaling Pathways in Endometrioid Endometrial Adenocarcinoma During Formation of Lymphovascular Space Involvement and Lymph Node Metastasis

Yuan Cheng[1], *Xiaobo Zhang*[2], *Zhiqi Wang*[1] *and Jianliu Wang*[1]*

[1] Department of Obstetrics and Gynecology, Peking University People's Hospital, Beijing, China, [2] Department of Pathology, Peking University People's Hospital, Beijing, China

OPEN ACCESS

Edited by:
Peng Qu,
National Institutes of Health (NIH),
United States

Reviewed by:
Jing Hao,
Shandong University, China
Guohao Wang,
National Institutes of Health (NIH),
United States

***Correspondence:**
Jianliu Wang
wangjianliu@pkuph.edu.cn

Specialty section:
This article was submitted to Cancer Immunity and Immunotherapy, a section of the journal Frontiers in Oncology

Received: 15 August 2020
Accepted: 16 October 2020
Published: 09 December 2020

Citation:
Cheng Y, Zhang X, Wang Z and Wang J (2020) Reconstruction of Immune Microenvironment and Signaling Pathways in Endometrioid Endometrial Adenocarcinoma During Formation of Lymphovascular Space Involvement and Lymph Node Metastasis. Front. Oncol. 10:595082. doi: 10.3389/fonc.2020.595082

Background: The amplification or mutation of oncogenes and escape from immune surveillance systems promote tumor metastasis. However, subtle changes in the immune microenvironment and signaling pathways are poorly understood during the formation of lymphovascular space involvement (LVSI) and lymph node (LN) metastasis of endometrioid endometrial adenocarcinoma (EEA).

Patients and methods: We detected tumor immunology-related signaling pathways and immunocyte subtypes according to the mRNA levels of 750 oncogenes and genes relating to the tumor microenvironment and immune response using the Nanostring PanCancer IO 360 Panel in 24 paraffin-embedded tissues of EEAs and benign gynecological diseases. Internal reference genes were used for data normalization.

Results: Angiogenesis and immune cell adhesion signaling pathways were activated during LVSI formation of EEA progression. However, during the development of LVSI to LN metastasis, immune system signaling pathways were significantly inhibited, including antigen presentation, cytotoxicity, lymphoid compartment, interferon signaling, and costimulatory signaling pathways. Immune-related genes (CD69, HLA-DOA, ATF3, GBP1, AP2, DTX3L, EGR1, GBP4, TAP1, EIF2AK2, MX1, ISG15, STAT1, and HLA-DRA) were significantly downregulated in EEA with LN metastasis compared to those in EEA with LVSI. Instead, hypoxia, metabolic stress, epigenetic regulation, matrix remodeling, and metastasis signaling pathways were continuously activated in LN metastasis. We also found that neutrophils, macrophages, and mast cells might be involved in LVSI formation and LN metastasis in EEA.

Conclusions: EEA with metastatic LNs showed significant immunosuppressive effects. Some oncogenes, matrix remodeling- and hypoxia-related genes, and neutrophil signatures showed higher expression, suggesting their potential as therapeutic targets and offering new immunotherapy strategies in EEA during LN metastasis.

Keywords: lymphovascular space involvement, lymph node metastasis, immune surveillance, neutrophils, macrophages, mast cells, endometrioid endometrial adenocarcinoma

INTRODUCTION

Endometrial cancer (EC) is ranked 4th and 6th in morbidity and mortality, respectively, among cancers affecting women in the United States in 2019 (1). Statistically, the mortality rate of EC slowly increased from 2012 to 2016 in China (2). The 5-year survival rates of patients with endometrial carcinoma at FIGO stages III and IV were only 57–66% and 20–26%, respectively (3, 4). Endometrial carcinoma with lymphovascular space involvement (LVSI), myometrial invasion, lymph node (LN) metastasis, and high-grade cancer were associated with significantly higher recurrence rates (5). Accumulated studies have shown that LN metastasis is a strong independent prognostic factor for endometrial carcinoma recurrence (6, 7). Recent studies revealed that LVSI is an independent prognostic factor for lymph node metastasis and non-locoregional recurrence in early-stage endometrial carcinoma (8, 9). However, little is known about the regulation of molecular mechanisms and the tumor microenvironment for LVSI and LN metastasis in endometrial carcinoma.

The immune surveillance system and cancer cells fight a seesaw-like battle from occurrence to the early and advanced stages. In the early stage, the immune system produces an anti-inflammatory microenvironment to fight against cancer cells, whereas in the late stage, tumor cells escape immune surveillance, resulting in distant metastasis and recurrence (10). Antomarchi etal. (11) found that grade 1 ECs showed a strong anti-tumor immune microenvironment; however, the high-grade ECs presented immunotolerance and immunosuppression. Pakish etal. (12) showed increased infiltration of immune cells, including granzyme B+ cells, activated cytotoxic T lymphocytes, and PD-L1 + cells, in endometrial carcinomas with high microsatellite instability (MSI-H) compared to those with microsatellite stability (MSS). These studies suggested that low-grade tumors and MSI-positive endometrial carcinoma might be more sensitive to immunotherapy. However, the regulation of the immune microenvironment and signaling pathways remain poorly understood in relation to LVSI formation and LN metastasis of endometrial carcinoma.

Immune system surveillance has been shown to play a role in type I endometrioid endometrial adenocarcinoma (EEA), while it is inert in type II serous carcinoma (13, 14). This study focused on the construction of the spectrum of tumor immune microenvironments of EEA during LVSI formation and LN metastasis. It was determined that immune system activation was present in EEAs with LVSI formation. However, severe immunosuppression and tolerance were observed in ECs with LN metastasis. Hypoxia, metabolic stress, epigenetic regulation, matrix remodeling, and metastasis signaling pathway-related oncogenes and neutrophil signatures showed higher expression, suggesting their potential as therapeutic targets and offering new immunotherapy strategies for LN metastasis in EEA.

METHODS

Patients and Specimens

Paraffin sections from 24 patients with EEA and benign gynecological disease were obtained from the pathology department of Peking University People's Hospital. LVSI and LN metastasis were important pathological progress indicators of EEA. Cases were separated into 4 groups of 6 cases: Normal control, LVSI-LN-, LVSI+LN-, and LVSI+LN+. The clinicopathological data of 18 EEAs are listed in **Table 1**. LVSI and LN metastasis of endometrial carcinoma were re-identified by a senior pathologist. The study was approved by the ethics committee of Peking University People's Hospital (2019PHB031-01).

Analysis of mRNA Expression

There or four formalin-fixed, paraffin-embedded curls (10 μm; effective tissue sample area > 1.5 × 1.5 cm) were prepared for RNA extraction using the High Pure RNA Paraffin Kit (Roche Applied

TABLE 1 | The clinicopathological characteristics of 18 endometrial cancer patients.

Variables	n=18 (No. of patients) %
Age (median)	54 years (49–63 years)
FIGO stage	
I	12 (66.7)
III	6 (33.3)
Histological grade	
Grade 1	4 (22.2)
Grade 2	9 (50.0)
Grade 3	5 (27.8)
Tumor diameter	
<2	4 (22.2)
≥2	14 (77.8)
LVSI	
No	6 (33.3)
Yes	12 (66.7)
LN metastasis	
No	12 (66.7)
Yes	6 (33.3)

Data are expressed as n (%). Abbreviations: FIGO, International Federation of Gynecology and Obstetrics; LVSI, lymphovascular space involvement; LN, lymph node.

Science, Penzberg, Germany). RNAs were at least 300 nt in length, and ≥50% RNA content was obtained. At least 300 ng total RNA was obtained per sample. RNA quality was detected by Nanodrop (A260/A280: 1.7–2.3; A260/A230: 1.8–2.3). The tumor-related signaling pathways and tumor-infiltrating lymphocyte (TIL) counts were examined according to the mRNA levels of 750 genes relating to the tumor microenvironment and immune response as well as internal reference genes for data normalization using the Nanostring PanCancer IO 360 Panel (Agilent 2100 Bioanalyzer and an Agilent RNA 6000 Nano Kit, Nanostring Technologies, Inc., Seattle, WA, USA); (https://www.nanostring.com/products/gene-expression-panels/gene-expression-panels-overview/360-series-panel-collection/pancancer-io360-gene-expression-panel). These 770 genes were classified into13 annotations and selected reference genes as follows: release of cancer cell antigens (74), cancer antigen presentation (101), T-cell priming and activation (150), immune cell localization to tumors (292), stromal factors (102), recognition of cancer cells by T-cells (105), killing of cancer cells (179), myeloid cell activity (260), natural killer (NK) cell activity (28), cell cycle and proliferation (54), tumor-intrinsic factors (155), immunometabolism (101), common signaling pathways (162), and internal reference genes (20).

Genes were classified as 14 immune cell type metagenes (B-cells, CD45, CD8 T cells, cytotoxic cells, dendritic cells [DCs], exhausted CD8, macrophages, mast cells, neutrophils, NK CD56dim cells, NK cells, T cells, Th1 cells, and Tregs). Besides, 39 signaling pathways were analyzed in 13 annotations as follows: release of cancer cell antigens (microsatellite instability/MSI, double strand break repair, chromatin modification/epigenetics, DNA damage repair), cancer antigen presentation (MHC class-I/II genes, non-MHC antigen presentation, antigen processing machinery, proteasome and immunoproteosome, cross-presenting DC genes), T-cell priming and activation (costimulatory molecules), immune cell localization to tumors (chemokines, integrins, selectins, immune cell populations in tumors), stromal factors (extracellular matrix remodeling, collagens, angiogenesis, metastasis), recognition of cancer cells by T-cells (immune checkpoints), killing of cancer cells (interferon signaling, JAK-STAT1/2 pathway, cytolytic activity, phagocytosis), myeloid cell activity (inflammation, Fc-gamma receptor signaling), NK cell activity, cell cycle and proliferation, tumor-intrinsic factors (apoptosis, autophagy, nutrient depletion, metastasis), immunometabolism (oxygen sensing, nutrient regulation), and common signaling pathways (Wnt, Hedgehog, TGF-β, NF-κB, Notch, PI3K-Akt, RAS, MAPK).

Bioinformatics and Statistical Analysis

The raw gene expression values were normalized to those of housekeeping genes using the NanoString nSolver 4.0 software (nanoString, Seattle, WA) and log2 transformation. Differentially expressed genes, along with false discovery rate (FDR) corrected p-values was screened out for signaling pathway analysis according to Kyoto Encyclopedia of Genes and Genomes (KEGG) pathways. Signaling pathway scores were clustered by unsupervised hierarchical clustering, and the 1-euclidean distance was used as the similarity measure. The P-values were adjusted using the Benjamini-Yekutieli (BY) false discovery rate and the Bonferroni correction. The false discovery rate was limited to ≤5% using P-values. Furthermore, the absolute and relative abundance of an immune cell subtype was estimated by simply taking the average log2 expression of the characteristic genes. Along with nanoString n-Solver software, one-way ANONA were used for statistical analysis. P-value for significance was set at $p<0.05$. Scatter plots charts were obtained using Graphpad Prism 8.

Immunohistochemical Staining

Three-μm-thick slices stained with H&E or immunohistochemical (IHC) were obtained from formalin-fixed paraffin-embedded (FFPE) EEAs tissues, which were the same wax blocks as the previous nanostring analysis. IHC staining of FFPE slides was performed using monoclonal mAbs against BIRC5(ab76424), CD68(ab213363) and CD163(ab213612) (Abcam, Cambridge, UK), with 1:500 working dilution. Paraffin sections are first dewaxed in steps from xylene to different concentrations of alcohol, and finally placed in tap water for washing. The slices were treated with heated citric acid repair fluid for antigen repair. After incubation with 3% H2O2 for 10 min, endogenous peroxidase was removed. Goat serum was used for blocking for 30 min. The first antibody was incubated overnight at 4 degrees. The next day, the second antibody labeled with horseradish peroxidase was incubated for 30 min. In the middle of each step, 1 x PBS should be used for cleaning at 5 min * 3 times. DAB was used for IHC staining observed under the microscope.

Scoring for BIRC5, CD68, and CD163 was evaluated by percentage of cells stained in tumor and stromal tissue compartments by a pathologist.

RESULTS

Heatmap of Signaling Pathway and Differentially Expressed Genes (DEGs) Between EEAs and Benign Gynecological Lesions

HE staining from 24 patients with EEA and benign gynecological disease was showed in **Figure 1**. Cases were separated into 4 groups of 6 cases: Normal control (Non-cancer), LVSI-LN-, LVSI+LN-, and LVSI+LN+. The clinicopathological data of 18 EEAs are listed in **Table 1**. First of all, we analyzed the signal pathways and differentially expressed genes between 6 cases of normal control group and 18 cases of EEAs. The data showed that MAPK, Hedgehog signaling, Wnt signaling were significantly suppressed in EEAs. The other 22 signaling pathways, including cell proliferation, DNA damage repair and so on, are greatly activated in EEAs (**Figure 2A**). Differentially expressed genes (DEGs) between EEAs and normal control were showed in **Figure 2B**. Top 20 DEGs including MELK, EXO1, SLC7A5, CCNB1, CXCL8, IL2RA, TYMS, CXCL10, CEP55, ANLN, MMP9, IL7R, CXCL9, RRM2, HMGA1, FCGR3A/B, MKI67, CXCL1, CXCL11, CENPF were showed in **Table 2**.

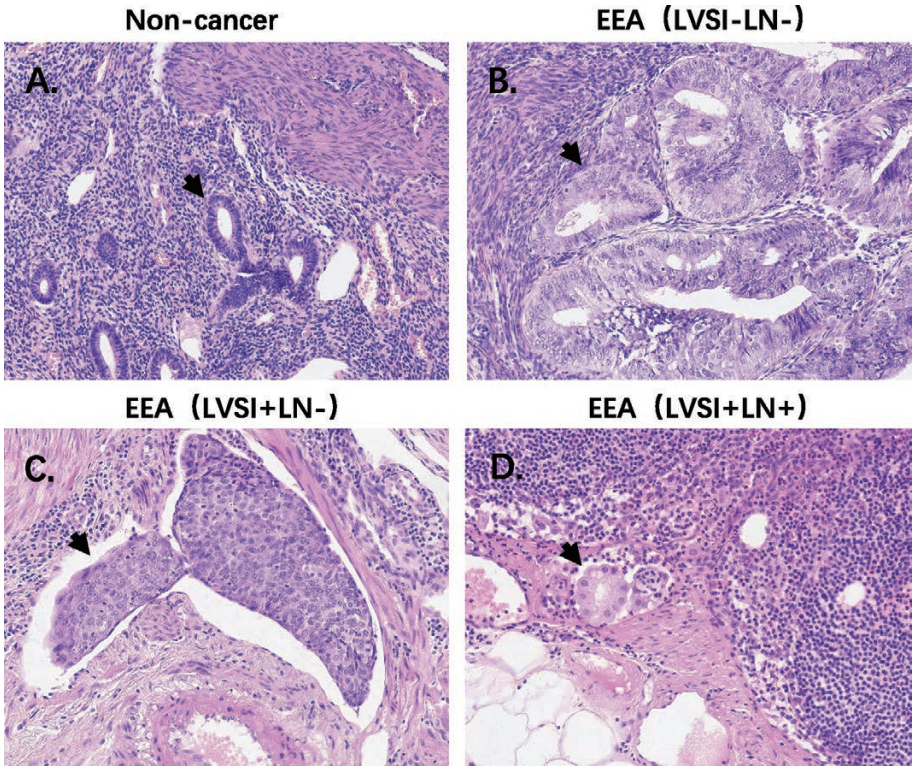

FIGURE 1 | HE staining of endometrioid endometrial adenocarcinomas (EEAs) and benign gynecological lesions in 4 groups of 6 cases. LVSI, lymphovascular space involvement; LN, lymph node. **(A)** Non-cancer group. The black arrow refers to the normal gland; **(B)** LVSI-LN-group, the black arrow refers to the gland of EEA; **(C)** LVSI+LN-group, the black arrow refers to the LVSI. **(D)** LVSI+LN+ group, the black arrow refers to EEAs in LN.

Signaling Pathway Characteristics of EEA During LVSI Formation and LN Metastasis

Signaling pathways involved in LVSI formation and LN metastasis compared to LVSI-LN- group were shown in **Figure 3**. We found significantly different distributions of signaling pathways among the three groups (LVSI-LN-, LVSI +LN-, and LVSI+LN+) in EEA progression. Persistent activation of cell proliferation and PI3K-AKT signaling pathways was observed in the LVSI+LN- group LVSI+LN+ group compared to the LVSI-LN- group without metastasis in EEA progression (**Figures 3A, B**). Hedgehog signaling pathways were downregulated whereas the angiogenesis, immune cell adhesion, apoptosis, DNA damage repair, and JAK-STAT signaling pathways were upregulated in EEA with LVSI compared to those in the LVSI-LN- group without metastasis (**Figures 3C–H**). Hypoxia, metabolic stress, epigenetic regulation, matrix remodeling, and metastasis signaling pathways were upregulated in EEA with LN metastasis compared to the LVSI-LN- group without metastasis (**Figures 3I–M**). However, antigen presentation, cytotoxicity, lymphoid compartment, interferon, and costimulatory signaling pathways were all downregulated in EEA with LN metastasis compared to EEA with LVSI (**Figures 3N–Q**). Cytokine and chemokine, myeloid compartment, autophagy, TGF-β, MAPK, NF-κB, Notch, and Wnt signaling pathways showed no significant changes in the absence of LVSI, LVSI formation, and LN metastasis during EEA progression (**Supplementary Figure 1**).

Regulation of Critical mRNA Expression in EEA During LVSI Formation and LN Metastasis

Compared to the LVSI-LN- group without metastasis, the top 20 genes showing differential mRNA expression in EEA with LVSI were as follows: BIRC5, COMP, CENPF, AXIN1, CCL3/L1, GMIP, CDC20, CCNE1, CCNB1, EZH2, IL21R, MELK, BLM, FANCA, H2AFX, CCL18, BRCA2, VEGFB, BRCA1, and RRM2 (**Table 3**). For EEA with LN metastasis compared to the LVSI-LN- group, the top 20 differentially expressed mRNAs were: COMP, AXIN1, APH1B, PSMB5, EIF2AK2, ATF3, SLC11A1, MELK, EZH2, BIRC5, CCNE1, ANLN, CENPF, IL1RN, TGFB2, PRLR, AQP9, CCL18, TRIM21, and FGF13 (**Table 4**).

Finally, the top 20 differentially expressed mRNAs in the EEAs with LN group compared with EEAs with LVSI were as follows: ATF3, ARNT2, WNT4, HLA-DOA, DUSP1, CD69, TAP1, IL6, STAT1, TGFB2, GBP4, GBP1, MX1, HERC6, PSMB9, NLRC5, EGR1, TAP2, SAMSN1, and DTX3L (**Table 5**).

Compared with the LVSI-LN- group without metastasis, various regulated signaling pathway-related genes were

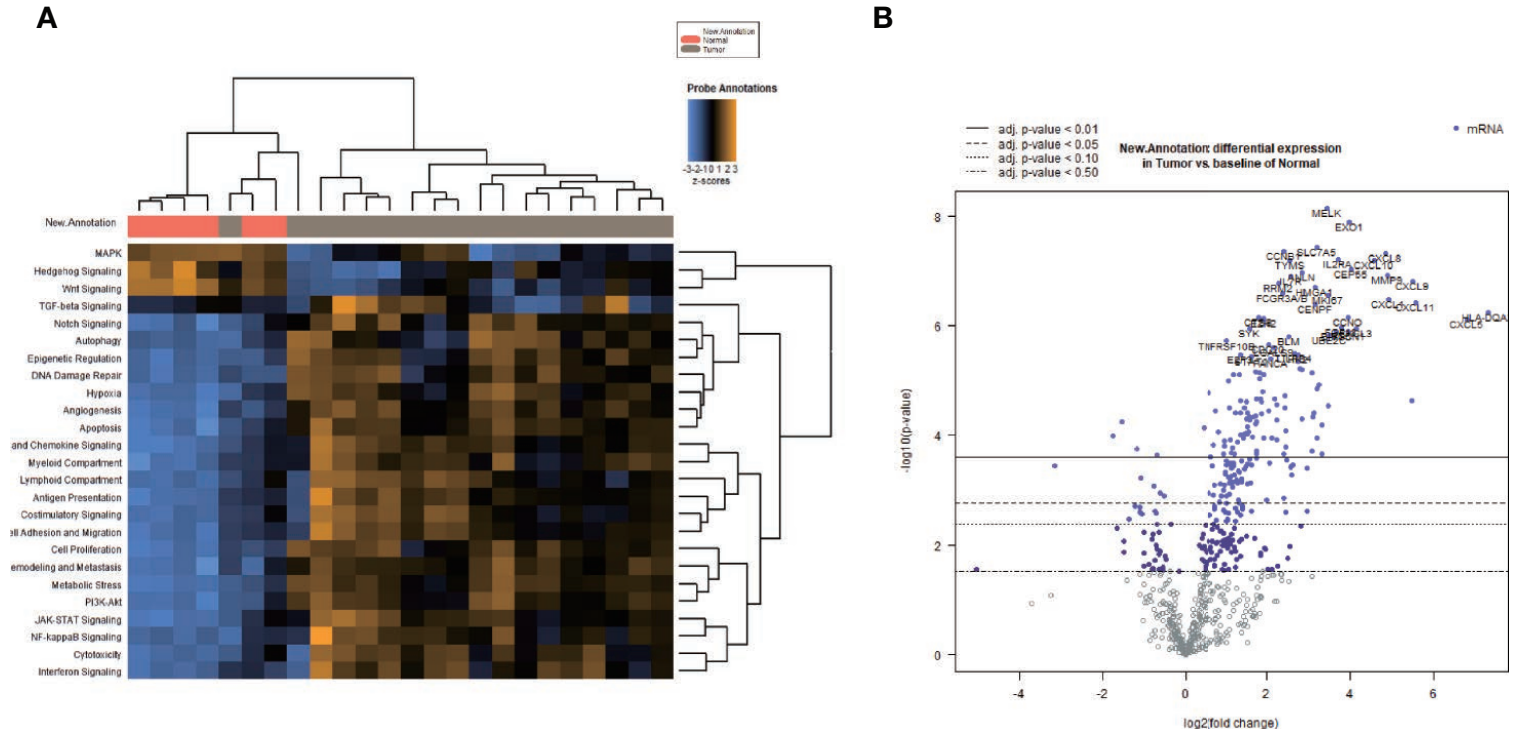

FIGURE 2 | Heatmap of signaling pathway and differentially expressed genes (DEGs) between endometrioid endometrial adenocarcinomas (EEAs) and benign gynecological lesions. **(A)** The heatmap of all signaling pathways in EEAs compared to those of the benign gynecological lesions Red, gray bars represent normal and tumor, respectively. The transition between blue, black, and yellow represents the level scores of signaling pathways ranging from –3 to 3. Vertical lines or horizontally focused lines represent unsupervised clustering. In total, 25 signaling pathways are marked on the left side of the heat map. **(B)** DEGs between EEAs and benign gynecological lesions. Blue and purple dots represent DEGs, and a dot represents a gene. The left side of 0 represents the down regulated mRNA, and the right side of 0 represents the up-regulated mRNA on the X-axis. The log2 expression value of the gene corresponds to the Y-axis. Four different virtual and real lines represent different stages of P value, from $P < 0.5$ to $P < 0.01$.

TABLE 2 | Top 20 differentially expressed mRNA in endometrioid endometrial adenocarcinomas (EEAs) compared to benign gynecological lesions.

Gene name	Log2 fold change	P-value	Gene.sets
MELK	3.45	7.27E-09	Cell Proliferation
EXO1	3.97	1.27E-08	Cell Proliferation, DNA Damage Repair
SLC7A5	3.2	3.73E-08	Metabolic Stress
CCNB1	2.4	4.46E-08	Cell Proliferation
CXCL8	4.85	4.77E-08	Cytokine and Chemokine Signaling, Metabolic Stress
IL2RA	3.72	6.18E-08	Costimulatory Signaling, Cytokine and Chemokine Signaling, JAK-STAT Signaling, PI3K-Akt
TYMS	2.54	6.36E-08	Cell Proliferation
CXCL10	4.57	6.37E-08	Cytokine and Chemokine Signaling, Lymphoid Compartment
CEP55	4.03	9.46E-08	Cell Proliferation
ANLN	2.85	1.05E-07	Cell Proliferation
MMP9	4.9	1.19E-07	Angiogenesis, Immune Cell Adhesion and Migration, Matrix Remodeling and Metastasis
IL7R	2.57	1.26E-07	Cytokine and Chemokine Signaling, JAK-STAT Signaling, PI3K-Akt
CXCL9	5.5	1.53E-07	Cytokine and Chemokine Signaling, Lymphoid Compartment
RRM2	2.29	1.7E-07	Cell Proliferation
HMGA1	3.16	1.99E-07	Epigenetic Regulation, Metabolic Stress
FCGR3A/B	2.39	2.62E-07	
MKI67	3.47	2.81E-07	Cell Proliferation
CXCL1	4.91	3.35E-07	Antigen Presentation, Cytokine and Chemokine Signaling, Myeloid Compartment
CXCL11	5.56	3.77E-07	Cytokine and Chemokine Signaling, Lymphoid Compartment
CENPF	3.15	4.11E-07	Cell Proliferation

observed in EEA with LVSI, including those related to the Hedgehog signaling pathways (PSMB5), angiogenesis (CCNE1, EZH2, VEGFB, and MMP9), immune cell adhesion (ICOSLG, ITGA6, and MMP9), cell proliferation and apoptosis (BIRC5, BLM, PSMB5), DNA damage repair (BLM, FANCA, H2AFX, BRCA2, BRCA1, EXO1, POLD1), and JAK-STAT signaling pathways (IL21R, PRLR) (P<0.01) (**Figure 4A**).

Signaling pathway-related genes identified in EEA with LN metastasis compared to the results of the LVSI-LN- group without metastasis were as follows: genes relating to hypoxia (ERBB2, HK1, PIK3CA), metabolic stress (EZH2, CCNE1, AQP9, ERBB2, HK1, HRAS, H2AFX, HMGA1, ATM, PIK3CA, UBE2C), epigenetic regulation (EZH2, H2AFX, HMGA1), and matrix remodeling and metastasis (COMP, TGFB2, ITGA6, RELN, and NCAM1) (P<0.01) (**Figure 4B**).

Immune-related genes in EEA with LN metastasis compared to those in EEA with LVSI were as follows: genes relating to antigen presentation (ATF3, HLA-DOA, TAP1, DTX3L, CXCL1, HLA-DRA), cytotoxicity (STAT1, MX1, ISG15), lymphoid compartment (STAT1, MX1, EGR1, ISG15), interferon signaling (STAT1, GBP4, GBP1, MX1, EGR1, ISG15, EIF2AK2, HLA-DRA), and costimulatory signaling (CD69, EGR1, HLA-DRA) (P<0.01) (**Figure 4C**).

Distribution Characteristics of Immunocyte Subsets in EEA During LVSI Formation and LN Metastasis

The results revealed that immunocyte subtypes and genes relating to immune surveillance and immune escape, such as NK cells, CD8 T cells, Treg cells, DCs, exhausted CD8, TIL count, PD-L1, and CTLA4, showed no significant differences in expression in the absence of LVSI or with LVSI and LN metastasis in EEA progression (**Supplementary Figures 2** and **3**). However, total neutrophils were upregulated in the LVSI+LN+ group compared to the LVSI-LN- group (P<0.05) (**Figure 5B**). Total macrophages also showed an upward trend, though not statistically significant. Whereas mast cells showed a downward trend, although there was no statistical significance (P=0.093) (**Figures 5A, C**). The ratio of neutrophils in TIL was up-regulated in LVSI+LN+ group, compared to LVSI+LN- and LVSI-LN- group (**Figures 5E, F**). The ratio of macrophages in TIL showed an upward trend in LVSI+LN+ group, compared to LVSI+LN- group and LVSI-LN- group (**Figure 5D**).

We further analyzed gene expression relating to macrophages, neutrophils, and mast cells. Macrophage-related gene CD68 was upregulated in the LVSI+LN group compared to the LVSI-LN- group. However, CSFIR and CCL2 were downregulated in the LVSI+LN+ group compared to the LVSI+LN- group (**Figure 6A**). Neutrophil-related gene FCAR was upregulated in the LVSI+LN- group and LVSI+LN+ group compared to the LVSI-LN- group. Neutrophil-related gene CXCL1 were upregulated in the LVSI +LN+ group compared to those in the LVSI+LN- group (**Figure 6B**). Among mast cell-related genes, tumor necrosis factor (TNF) was upregulated in the LVSI+LN- group compared to the LVSI-LN- group. Moreover, the mast cell-related genes CAP3, HDC, and MS4A2 were downregulated in the LVSI+LN+ group compared to those in the LVSI-LN- group (**Figure 6C**).

HE Staining and Immunohistochemical Staining Confirmed the Expression of Hub Genes and Immunocytes

Compared to the LVSI-LN- group without metastasis, BIRC5 related to cell proliferation was in top 20 gene in LVSI+LN- group and LVSI+LN+ group. So, we further verified the BIRC5 *in situ* protein expression in EEAs tissues. We observed that the brown black positive granules were expressed in the LVSI+LN- group and LVSI+LN+ group, but were absent in the LVSI-LN- group tissues without LVSI and LN metastasis (**Figure 7**). The total number of neutrophils was significantly increased in the LVSI+ LN+ group

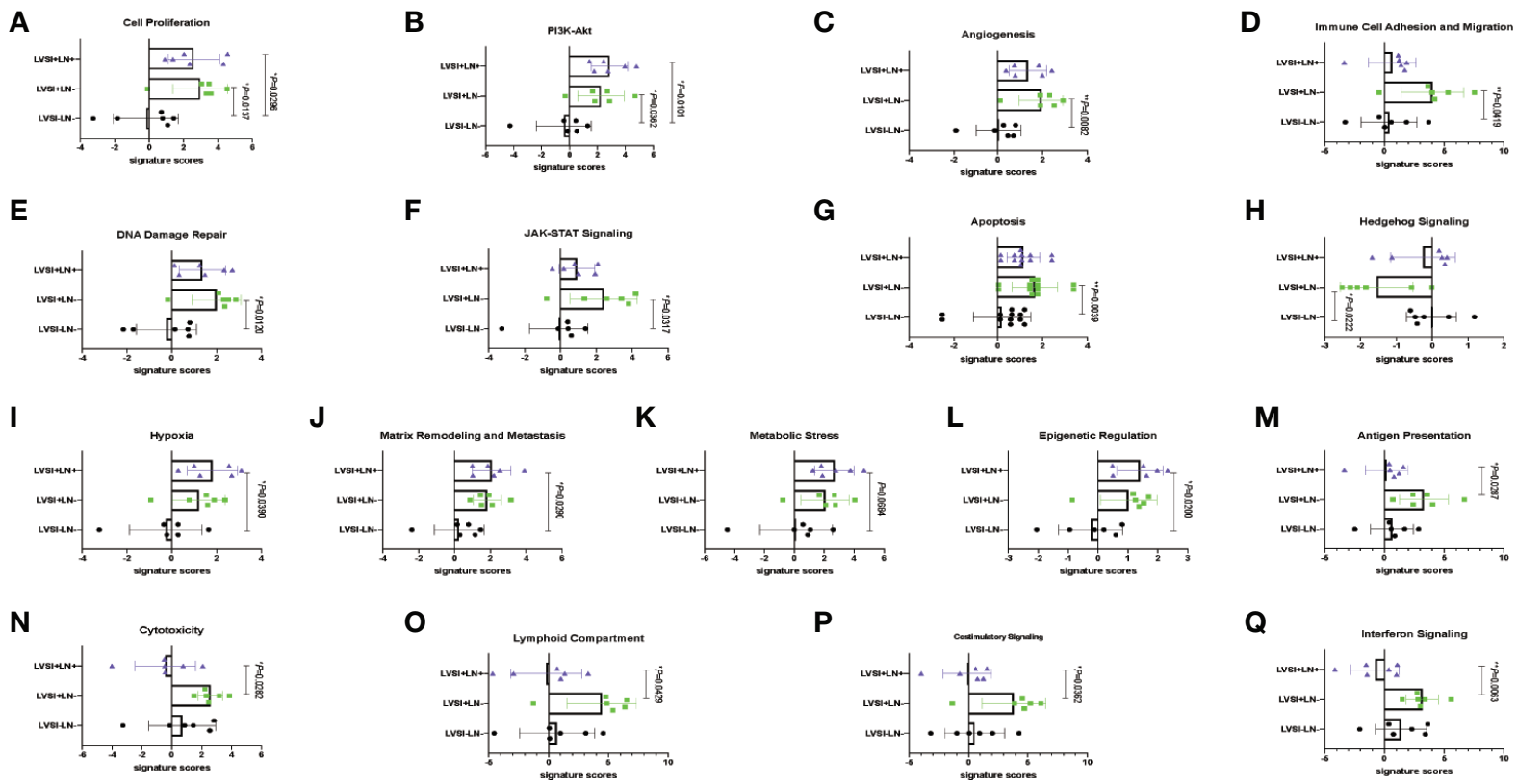

FIGURE 3 | Changes of signaling pathways in lymphovascular space involvement (LVSI) formation and lymph node (LN) metastasis in endometrioid endometrial adenocarcinomas (EEAs) progression. Points represent the number of cases. Each group has 6 cases. Black, green, and purple represent LVSI-LN-, LVSI+LN-, and LVSI+LN+, respectively. **(A)** Cell proliferation **(B)** PI3K-Akt. **(C)** Angiogenesis. **(D)** Immune cell adhesion and migration. **(E)** DNA damage repair. **(F)** JAK-STAT signaling. **(G)** Apoptosis. **(H)** Hedgehog signaling. **(I)** Hypoxia. **(J)** Matrix remodeling and metastasis. **(K)** Metabolic stress. **(L)** Epigenetic regulation. **(M)** Antigen presentation. **(N)** Cytotoxicity. **(O)** Costimulatory signaling. **(P)** Interferon signaling. $^{*}P < 0.05$, $^{**}P < 0.01$.

TABLE 3 | Top 20 differentially expressed mRNAs in endometrial adenocarcinoma with lymphovascular space involvement (LVSI) compared to expression in the LVSI-LN- group without metastasis.

Gene name	Log2 fold change	P-value	Gene sets
BIRC5	1.95	0.000298	Apoptosis, Cell Proliferation
COMP	3.86	0.000402	Matrix Remodeling and Metastasis, PI3K-Akt
CENPF	1.97	0.000546	Cell Proliferation
AXIN1	0.687	0.000639	Wnt Signaling
CCL3/L1	1.31	0.00137	Cytokine and Chemokine Signaling
GMIP	0.65	0.00143	–
CDC20	1.33	0.00145	Antigen Presentation, Cell Proliferation
CCNE1	1.67	0.00153	Angiogenesis, Cell Proliferation, Metabolic Stress, PI3K-Akt
CCNB1	1.21	0.00158	Cell Proliferation
EZH2	1.05	0.00165	Angiogenesis, Epigenetic Regulation, Metabolic Stress
IL21R	2	0.00205	Cytokine and Chemokine Signaling, JAK-STAT Signaling
MELK	1.25	0.00207	Cell Proliferation
BLM	1.14	0.00222	Apoptosis, Cell Proliferation, DNA Damage Repair
FANCA	1.49	0.00268	DNA Damage Repair
H2AFX	1.14	0.00292	Cell Proliferation, DNA Damage Repair, Epigenetic Regulation, Metabolic Stress
CCL18	1.83	0.00295	Cytokine and Chemokine Signaling
BRCA2	1.23	0.00323	Cell Proliferation, DNA Damage Repair
VEGFB	0.492	0.00352	Angiogenesis, MAPK, PI3K-Akt
BRCA1	0.833	0.00356	Cell Proliferation, DNA Damage Repair, PI3K-Akt
RRM2	0.957	0.00376	Cell Proliferation

LVSI, lymphovascular space involvement; LN, lymph node.

TABLE 4 | Top 20 differentially expressed mRNAs in endometrial adenocarcinoma with lymph node (LN) metastasis compared to expression in the lymphovascular space involvement (LVSI-LN-) group without metastasis.

Gene name	Log2 fold change	P-value	Gene sets
COMP	4.46	1.4E-05	Matrix Remodeling and Metastasis, PI3K-Akt
AXIN1	0.849	1.62E-05	Wnt Signaling
APH1B	-1.23	4.54E-05	Notch Signaling
PSMB5	0.718	0.000213	Antigen Presentation, Apoptosis, Cell Proliferation, Costimulatory Signaling, Hedgehog Signaling, NF-κB Signaling
EIF2AK2	-0.659	0.000496	Interferon Signaling
ATF3	-2.6	0.000498	Antigen Presentation
SLC11A1	1.95	0.000669	Myeloid Compartment
MELK	1.31	0.000681	Cell Proliferation
EZH2	1.13	0.000728	Angiogenesis, Epigenetic Regulation, Metabolic Stress
BIRC5	1.77	0.00073	Apoptosis, Cell Proliferation
CCNE1	2.38	0.000805	Angiogenesis, Cell Proliferation, Metabolic Stress, PI3K-Akt
ANLN	1.19	0.000912	Cell Proliferation
CENPF	1.69	0.000913	Cell Proliferation
IL1RN	2.14	0.00102	Cytokine and Chemokine Signaling, Myeloid Compartment
TGFB2	-1.42	0.00103	MAPK, Matrix Remodeling and Metastasis, TGF-β Signaling
PRLR	-1.96	0.00107	Cytotoxicity, JAK-STAT Signaling, PI3K-Akt
AQP9	1.83	0.00109	Metabolic Stress
CCL18	2.06	0.00119	Cytokine and Chemokine Signaling
TRIM21	-0.564	0.00121	Antigen Presentation, Interferon Signaling
FGF13	-1.36	0.00129	MAPK, PI3K-Akt

LVSI, lymphovascular space involvement; LN, lymph node.

compared with the LVSI-LN- group observed in the HE staining EEAs sections (**Figure 8**). The expression of macrophage-associated genes CD68 and CD163 was stronger and more positive in LVSI +LN- group, compared to LVSI-LN- group (**Figure 9**). The expression trends of BIRC5, CD68, CD163, and neutrophiles in tissues detected by immunohistochemistry and HE staining were consistent with the result of nanostring mRNA analysis.

DISCUSSION

T cell-mediated adaptive immunity plays an active role in the anti-tumor process. DCs, macrophages, and B cells present tumor antigens to CD4+ helper T cells. In turn, they cooperate to induce CD8+ T cells and B cells as well as activate NK cells and macrophages. These pathways ultimately eliminate tumor cells through the CD8+ cytotoxic T cell-dependent apoptosis pathway. Moreover, an imbalance in T cell-mediated responses plays a negative role in cancer progression, leading to an immunosuppressive environment and tumor escape (15–17). High TIL levels occur in anti-tumor immune response and indicate a good prognosis in gastric cancer and breast cancer (18, 19). Moreover, regulation of lymph node function by NK cells is associated with prognosis in patients with stage II colon cancer (20). Study have shown that the average fluorescence intensity of CD8 staining in peripheral blood of patients with grade 3 EEC is lower than that of healthy donors. Cytotoxic T cells with decreased CD8 expression were positively correlated with EEAs (21). Endometrial tumor microenvironment reduces the recruitment of NK cells and changes the phenotype and function of NK cells (22). The profiles of immune infiltration NK cells, DCs and CD8+T cells showed associated with patients survival in TCGA uterine cancer cohort (23). This study showed that immunocytes (CD8, NK cells and DC) tended to recede in the advanced stage of LN metastasis compared to those in the LVSI+LN- group, leading to immunotolerance or immunosuppression. However, due to the limited sample size, these immune cells did not show significant difference. The obtained expression profile of immune microenvironment regulation during LN metastasis in endometrial carcinoma was consistent with the results of previous studies.

In this study, the ratio of macrophages in TILs showed an upward trend in the LVSI+LN+ group compared to that in the LVSI+LN- and LVSI-LN- groups. Various studies have shown that tumor-associated macrophages (TAMs) in endometrial carcinoma are associated with increases in LVSI and LN metastasis and a poor survival outcome (24). TAMs are polarized M2 macrophages, which secrete cytokines, chemokines, and growth factors to promote EC development and inhibit the anti-tumor immune system. CTHRC1 increases the recruitment of M2-like macrophages, prompting myometrial invasion in endometrial carcinoma by regulating the integrin-Akt signaling pathway (25). TAM reduced the ERα expression in

TABLE 5 | Top 20 differentially expressed mRNAs in endometrial adenocarcinoma with lymph node (LN) metastasis compared to those in endometrial adenocarcinoma with lymphovascular space involvement (LVSI).

Gene name	Log2 fold change	P-value	Gene sets
ATF3	-3.02	0.000553	Antigen Presentation
ARNT2	-0.597	0.00147	_
WNT4	1.56	0.0019	Hedgehog Signaling, Wnt Signaling
HLA-DOA	-1.15	0.00208	Antigen Presentation, Immune Cell Adhesion and Migration
DUSP1	-2.1	0.00244	MAPK
CD69	-1.52	0.00285	Costimulatory Signaling
TAP1	-1.4	0.0034	Antigen Presentation
IL6	-2.43	0.00377	Cytokine and Chemokine Signaling, Hypoxia, JAK-STAT Signaling, Metabolic Stress, PI3K-Akt
STAT1	-0.954	0.00407	Cytokine and Chemokine Signaling, Cytotoxicity, Interferon Signaling, JAK-STAT Signaling, Lymphoid Compartment
TGFB2	-0.99	0.00432	MAPK, Matrix Remodeling and Metastasis, TGF-β Signaling
GBP4	-1.59	0.00436	Interferon Signaling
GBP1	-1.51	0.00455	Interferon Signaling
MX1	-1.23	0.00506	Cytotoxicity, Interferon Signaling, Lymphoid Compartment
HERC6	-0.99	0.00573	_
PSMB9	-1.21	0.0059	Antigen Presentation, Apoptosis, Cell Proliferation, Costimulatory Signaling, Hedgehog Signaling, NF-κB Signaling
NLRC5	-0.848	0.00619	_
EGR1	-1.79	0.00678	Costimulatory Signaling, Interferon Signaling, Lymphoid Compartment
TAP2	-0.737	0.00745	Antigen Presentation
SAMSN1	-0.965	0.00866	_
DTX3L	-0.406	0.0087	Antigen Presentation, Notch Signaling

LVSI, lymphovascular space involvement; LN, lymph node.

EC cells *via* HOXB13 by increasing CXCL8 secretion, thus promoting EC invasion and metastasis (26). Invasive macrophages induce ERα expression through epigenetic mechanism mediated by IL17A, which makes endometrial cancer cells sensitive to estrogen (27).

For a long time, the function of neutrophils in the tumor microenvironment has been ignored. Recently, accumulating studies have shown that neutrophils are involved in promoting tumor progression and metastasis (28, 29). Wculek & Malanchi (30) showed that neutrophils are involved in lung metastasis in mouse breast cancer models, whereas drug- or gene-mediated suppression of the leukotriene-generating enzyme arachidonate 5-lipoxygenase abolished neutrophil-associated pro-metastatic functions. During the formation of the tumor metastasis microenvironment, increased secretion of CXCL1 and CXCL2 by endothelial cells and megakaryocytes promotes the release of neutrophils into circulation *via* the regulation of CXCR2 signaling. Neutrophil-derived MMP9 is more likely to activate and participate in pre-tumor functions (31). Neutrophils produce rEEAtive oxygen species, which cause DNA damage, genomic instability, and gene mutations in precancerous epithelial cells, thus promoting the carcinogenic transformation (32). For the first time, this study found that neutrophils showed a rising trend when LN metastasis develop in EC. Compared to the LVSI-LN- group, VEGFB and MMP9 showed higher expression in the LVSI+LN- group. VEGFB, MMP9, and neutrophils may cooperatively regulate angiogenesis in the primary metastasis of endometrial carcinoma. Moreover, CXCL1 mRNA expression was upregulated in the LVSI+LN+ group compared to that in the LVSI+LN- group, suggesting that the high expression of chemokine CXCL1 may be involved in the recruitment of neutrophils to lymph vessels during the progression of lymph node metastasis in EEA.

Studies have also found that mast cells play a dual role in regulating cancer progression (33, 34). First, mast cells participate in the internal and acquired immune process, promote DC migration and maturation, and interact with T and B cells. Additionally, they can promote the release of inflammatory factors such as TNF-α, MIP, and MCP and participate in the formation of an anti-tumor inflammatory

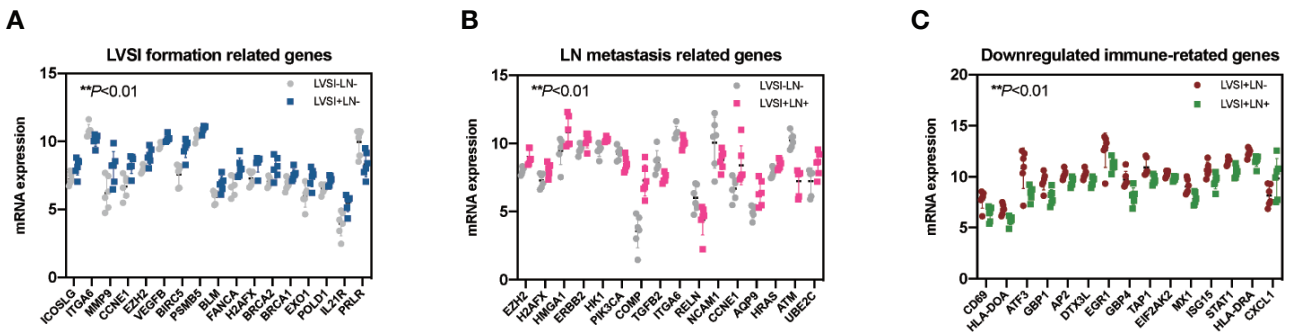

FIGURE 4 | Regulated genes in endometrioid endometrial adenocarcinomas (EEAs) with LVSI and LN metastasis. LVSI, lymphovascular space involvement; LN, lymph node. Points represent the number of cases. Each group has 6 cases. **(A)** Seventeen genes with differential expression in LVSI formation (**$P < 0.01$). EEAh point represents a case number. Gray dots represent the LVSI-LN- group; dark blue dots represent the LVSI+LN- group. **(B)** Sixteen genes with differential expression in LN metastasis compared to the LVSI-LN- group (**$P < 0.01$). EEAh point represents a case number. Gray dots represent the LVSI-LN- group; pink dots represent the LVSI+LN+ group. **(C)** Fifteen genes with differential expression in LN metastasis compared to the LVSI+LN- group (**$P < 0.01$). EEAh point represents a case number. Green dots represent the LVSI-LN- group; red dots represent the LVSI+LN+ group.

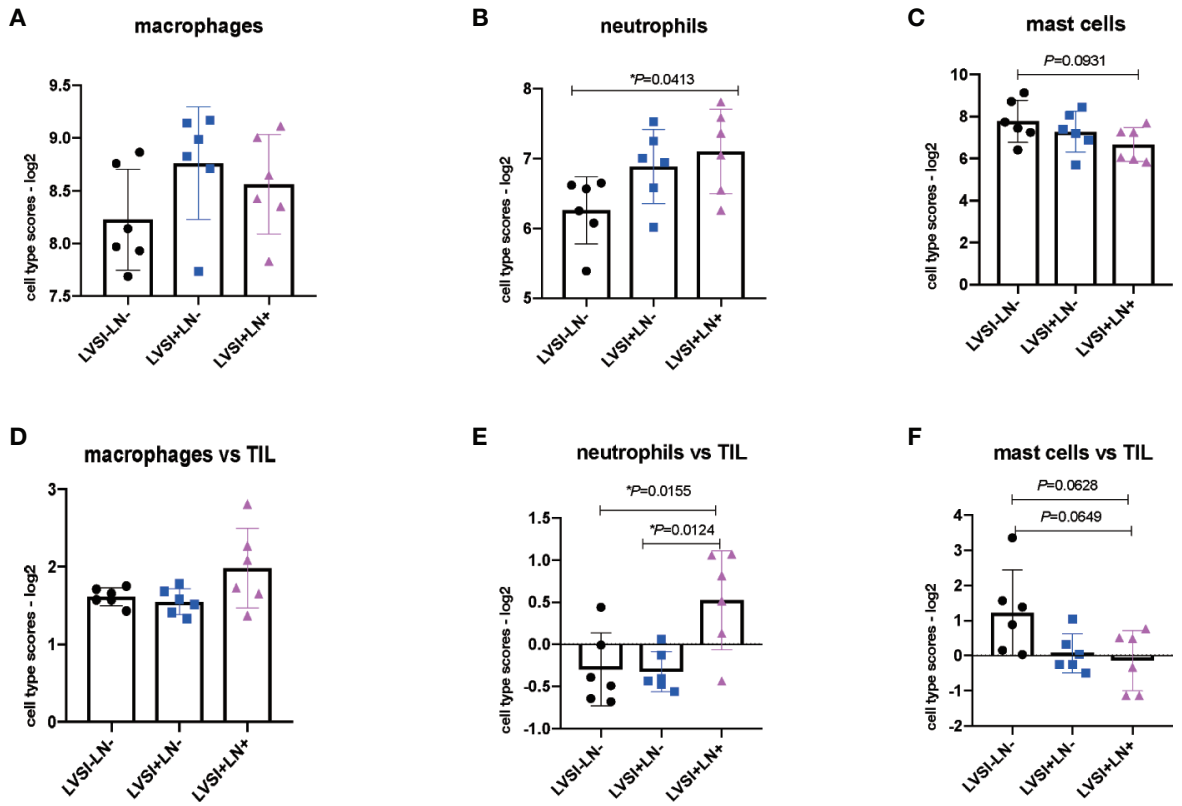

FIGURE 5 | Changes in the distribution of immunocyte subtypes during LVSI formation and LN metastasis of endometrial adenocarcinoma. LVSI, lymphovascular space involvement; LN, lymph node. Points represent the number of cases. Each group has 6 cases. Black, blue, and pink represent LVSI-LN-, LVSI+LN-, and LVSI +LN+, respectively. TIL: tumor infiltrating lymphocyte. Different scores of **(A)** total macrophages, **(B)** total neutrophils, and **(C)** total mast cells are shown for the three groups (LVSI-LN-, LVSI+LN-, LVSI+LN+). The ratios of **(D)** macrophages, **(E)** neutrophils, and **(F)** mast cells in TILs are shown for the three groups (LVSI-LN-, LVSI +LN-, LVSI+LN+). *$P < 0.05$.

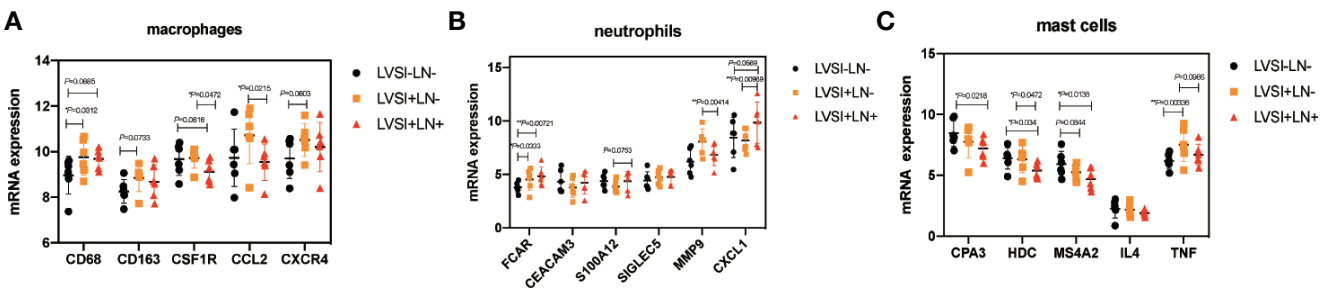

FIGURE 6 | Changes in the distribution of immunocyte subtype-related genes during LVSI formation and LN metastasis of endometrial adenocarcinoma. LVSI, lymphovascular space involvement; LN, lymph node. Points represent the number of cases. Each group has 6 cases. Black, orange, and red represent LVSI-LN-, LVSI+LN-, and LVSI+LN+, respectively. The mRNA expression of **(A)** 5 macrophage-related genes, **(B)** 6 neutrophil-related genes, and **(C)** 5 mast cell-related genes is shown in the three groups (LVSI-LN-, LVSI+LN-, LVSI+LN+). *$P < 0.05$, ** $P < 0.01$.

microenvironment. However, tryptases secreted by mast cells can promote angiogenesis and lymphangiogenesis, providing a platform and channel for tumor metastasis (33). Accumulating studies have shown controversial and variable results regarding the role of mast cells in different types of tumors and in different stages of cancer progression. Mast cells derived from adipose tissue promote apoptosis of breast cancer cells by secreting TNF-α and granulocyte-macrophage colony-stimulating factor (35). A previous study revealed that activated mast cells were downregulated in breast cancer tissues of the LN-positive

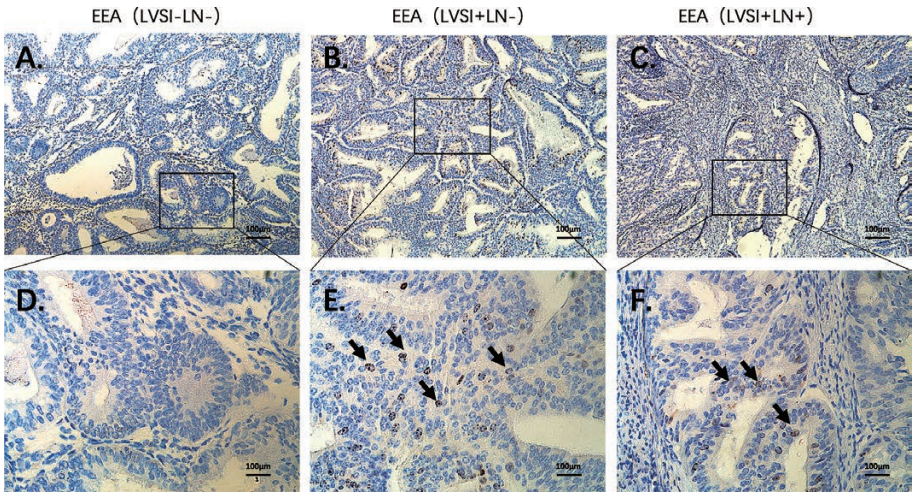

FIGURE 7 | Immunohistochemical staining of BIRC5 during LVSI formation and LN metastasis of endometrioid endometrial adenocarcinomas (EEAs). **(A)** LVSI-LN- group. 100X magnification **(B)** LVSI+LN- group. 100X magnification. **(C)** LVSI+LN+ group. 100X magnification. **(D)** LVSI-LN- group. 400X magnification. **(E)** LVSI +LN- group. 400X magnification. **(F)** LVSI+LN+ group. 400X magnification. The black arrow indicates brown black positive expression particles.

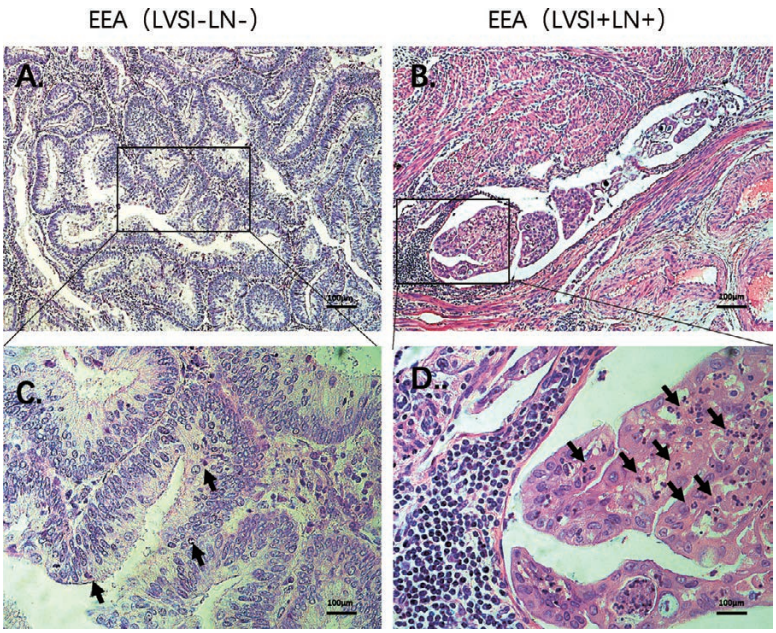

FIGURE 8 | HE staining of neutrophils during metastasis of endometrioid endometrial adenocarcinomas (EEAs). **(A)** LVSI-LN- group. 100X magnification **(B)** LVSI +LN+ group. 100X magnification. **(C)** LVSI-LN-group. 400X magnification. **(D)** LVSI+LN-+group. 400X magnification. The black arrow represents neutrophils.

group compared to those of the LN-negative group (36). Conversely, another study found that mast cell density was increased in metastatic LNs in breast cancer (37). In this study, we found downregulated expression of mast cell-related genes in both LVSI formation and LN metastasis, suggesting that mast cells play a negative role in regulating immune response tolerance and LN metastasis in EEA.

The important upregulated genes involved in LVSI were BIRC5, CDC20, CCNE1, EZH2, MMP9, et al. It is clear that cell proliferation, angiogenesis, immune cell adhesion, DNA damage, and JAK-STAT signaling pathways were involved in EC with LVSI formation. Furthermore, the antigen presentation-related genes ATF3, HLA-DOA, TAP1, DTX3L, and HLA-DRA were significantly decreased in the LVSI+LN+ group compared

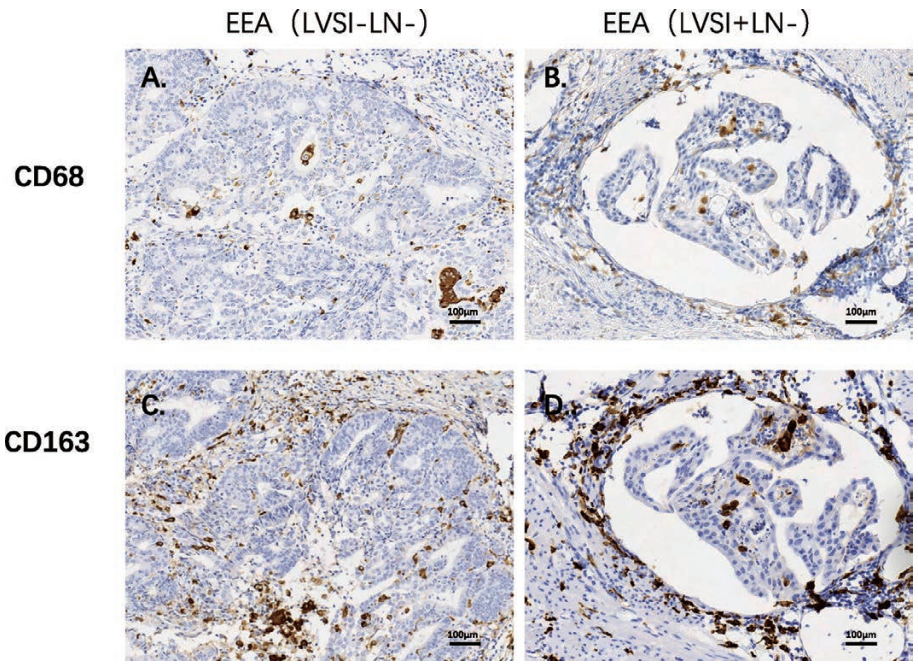

FIGURE 9 | Immunohistochemical staining of macrophages-related genes during LVSI formation of endometrioid endometrial adenocarcinomas (EEAs). **(A)** CD68 protein expression in LVSI-LN- group. 200X magnification **(B)** CD68 protein expression in LVSI+LN- group. 200X magnification **(C)** CD163 protein expression in LVSI-LN- group. 200X magnification. **(D)** CD163 protein expression in LVSI+LN- group. 200X magnification.

to the LVSI+LN- group. Moreover, genes relating to costimulatory signaling (CD69, EGR1, and HLA-DRA), interferon signaling (STAT1, GBP4, GBP1, MX1, EGR1, ISG15, EIF2AK2, and HLA-DR), and the lymphoid compartment (STAT1, MX1, EGR1, and ISG15) were significantly downregulated in the LVSI+LN+ group compared to the LVSI+LN- group. Overall, the immune surveillance system was devastated during the development of LN metastasis in endometrial carcinoma. However, metabolic stress, matrix remodeling and metastasis, PI3K-AKT, and hypoxia signaling pathways were always activated during LN metastasis.

In conclusion, this study found that ECs with metastatic LNs showed significant immunosuppressive effects. Some oncogenes as well as genes relating to matrix remodeling, hypoxia, macrophages, and neutrophil signatures showed higher expression, suggesting their potential for use as therapeutic targets and offering new immunotherapy strategies in EEA during LN metastasis.

DATA AVAILABILITY STATEMENT

According to national legislation/guidelines, specifically the Administrative Regulations of the People's Republic of China on Human Genetic Resources (http://www.gov.cn/zhengce/content/2019-06/10/content_5398829.htm, http://english.www.gov.cn/policies/latest_releases/2019/06/10/content_281476708945462.htm), no additional raw data is available at this time. Data of this project can be accessed after an approval application to the China National Genebank (CNGB, https://db.cngb.org/cnsa/). Please refer to https://db.cngb.org/, or email: CNGBdb@cngb.org for detailed application guidance. The accession code CRA003336 (http://bigd.big.ac.cn/gsa/s/L5wcNuAp) should be included in the application.

ETHICS STATEMENT

The studies involving human participants were reviewed and approved by the ethics committee of Peking University People's hospital. The patients/participants provided their written informed consent to participate in this study. Written informed consent was obtained from the individual(s) for the publication of any potentially identifiable images or data included in this article.

AUTHOR CONTRIBUTIONS

YC chiefly wrote this manuscript and collected clinical data and samples. XZ was primarily responsible for pathological diagnosis. ZW gave advice on the selection of clinical samples. JW was mainly responsible for project design. All authors contributed to the article and approved the submitted version.

FUNDING

The National Natural Science Foundation of China (Grant no. 81802607, 81874108, and 81672571), the Beijing Municipal Natural Science Foundation (Grant no.7202213), the Fund for Fostering Young Scholars of Peking University Health Science Center (Grant no. BMU2017PY011), the Research and Development Fund of Peking University People's Hospital (Grant no. RDY2017-12), and National Key Technology R&D Program of China (Grant No. 2019YFC1005200 and 2019YFC1005201).

SUPPLEMENTARY MATERIAL

The Supplementary Material for this article can be found online at: https://www.frontiersin.org/articles/10.3389/fonc.2020.595082/full#supplementary-material

SUPPLEMENTARY FIGURE 1 | Some signaling pathways showed no significant changes in the groups without LVSI or with LVSI formation or LN metastasis in endometrial adenocarcinoma progression. LVSI: lymphovascular space involvement; LN: lymph node. Points represent the number of cases. Black, green, and purple represent LVSI-LN-, LVSI+LN-, and LVSI+LN+, respectively. Scores of **(A)** cytokine and chemokine signaling, **(B)** myeloid compartment, **(C)** autophagy, **(D)** TGF-β signaling, **(E)** MAPK, **(F)** NF-κB signaling, **(G)** Notch signaling, and **(H)** Wnt signaling are shown in the three groups (LVSI-LN-, LVSI+LN-, LVSI+LN+).

SUPPLEMENTARY FIGURE 2 | Some immunocyte subtypes showed no significant changes in the groups without LVSI or with LVSI formation or LN metastasis in endometrial adenocarcinoma progression. LVSI: lymphovascular space involvement; LN: lymph node; TIL: tumor-infiltrating lymphocyte. Points represent the number of cases. Black, blue, and pink represent LVSI-LN-, LVSI +LN-, and LVSI+LN+, respectively. Scores for **(A)** CD8, **(B)** natural killer cells, **(C)** dendritic cells, **(D)** Tregs, and **(E)** exhausted CD8 cells are shown in the three groups (LVSI-LN-, LVSI+LN-, LVSI+LN+). Ratios of **(F)** CD8, **(G)** natural killer cells, **(H)** dendritic cells, **(I)** Tregs, and **(J)** exhausted CD8 cells are shown in the three groups (LVSI-LN-, LVSI+LN-, LVSI+LN+).

SUPPLEMENTARY FIGURE 3 | TIL counts and PD-L1 expression showed no significant changes in the groups without LVSI or with LVSI formation or LN metastasis in endometrial adenocarcinoma progression. LVSI: lymphovascular space involvement; LN: lymph node; TIL: tumor-infiltrating lymphocyte. Points represent the number of cases. Black, blue, and pink represent LVSI-LN-, LVSI +LN-, and LVSI+LN+, respectively. **(A)** TIL count scores, **(B)** PD-L1 mRNA expression, and **(C)** CTLA4 mRNA expression are shown in the three groups (LVSI-LN-, LVSI+LN-, LVSI+LN+).

REFERENCES

1. Bray F, Ferlay J, Soerjomataram I, Siegel RL, Torre LA, Jemal A. Global cancer statistics 2018: GLOBOCAN estimates of incidence and mortality worldwide for 36 cancers in 185 countries. *CA Cancer J Clin* (2018) 68(6):394–424. doi: 10.3322/caac.21492
2. Siegel RL, Miller KD, Jemal A. Cancer statistic. *CA Cancer J Clin* (2017) 67:7–30. doi: 10.3322/caac.21387
3. Siegel RL, Miller KD, Jemal A. Cancer statistic. *CA Cancer J Clin* (2015) 65:5–29. doi: 10.3322/caac.21254
4. Creasman WT, Odicino F, Maisonneuve P, Quinn MA, Beller U, Benedet JL, et al. Carcinoma of the corpus uteri. FIGO 26th annual report on the results of treatment in gynecological cancer. *Int J Gynaecol Obstet* (2006) 95(suppl 1): S105–43. doi: 10.1016/S0020-7292(06)60031-3
5. Loizzi V, Cormio G, Lorusso M, Latorre D, Falagario M, Demitri P, et al. The impact of lymph vascular space invasion on recurrence and survival in patients with early stage endometrial cancer. *Eur J Cancer Care (Engl)* (2014) 23(3):380–4. doi: 10.1111/ecc.12115
6. Zanfagnin V, Huang Y, Mc Gree ME, Weaver AL, Casarin J, Multinu F, et al. Predictors of extensive lymphatic dissemination and recurrences in node-positive endometrial cancer. *Gynecol Oncol* (2019) 154(3):480–6. doi: 10.1016/j.ygyno.2019.07.006
7. Owen C, Bendifallah S, Jayot A, Ilenko A, Arfi A, Boudy AS, et al. Lymph node management in endometrial cancer. *Bull Cancer* (2020) 107(6):686–95. doi: 10.1016/j.bulcan.2019.06.015
8. Ørtoft G, Lausten-Thomsen L, Høgdall C, Hansen ES, Dueholm M. Lymph-vascular space invasion (LVSI) as a strong and independent predictor for non-locoregional recurrences in endometrial cancer: a Danish Gynecological Cancer Group Study. *J Gynecol Oncol* (2019) 30(5):e84. doi: 10.3802/jgo.2019.30.e84
9. Cusano E, Myers V, Samant R, Sudai T, Keller A, Le T, et al. Prognostic Significance of Lymphovascular Space Invasion in the Absence of Lymph Node Metastases in Early-Stage Endometrial Cancer. *Int J Gynecol Cancer* (2018) 28(5):890–4. doi: 10.1097/IGC.0000000000001229
10. López-Soto A, Gonzalez S, Smyth MJ, Galluzzi L. Control of Metastasis by NK Cells. *Cancer Cell* (2017) 32(2):135–54. doi: 10.1016/j.ccell.2017.06.009
11. Antomarchi J, Ambrosetti D, Cohen C, Delotte J, Chevallier A, Karimdjee-Soilihi B, et al. Immunosuppressive Tumor Microenvironment Status and Histological Grading of Endometrial Carcinoma. *Cancer Microenviron* (2019) 12(2-3):169–79. doi: 10.1007/s12307-019-00225-1
12. Pakish JB, Zhang Q, Chen Z, Liang H, Chisholm GB, Yuan Y, et al. Immune Microenvironment in Microsatellite-Instable Endometrial Cancers: Hereditary or Sporadic Origin Matters. *Clin Cancer Res* (2017) 23 (15):4473–81. doi: 10.1158/1078-0432.CCR-16-2655
13. Kucukgoz Gulec U, Kilic Bagir E, Paydas S, Baris Guzel A, Gumurdulu D, Ali Vardar M, et al. Programmed death-1 (PD-1) and programmed death-ligand 1 (PD-L1) expressions in type 2 endometrial cancer. *Arch Gynecol Obstet* (2019) 300(2):377–82. doi: 10.1007/s00404-019-05180-2
14. Talhouk A, Derocher H, Schmidt P, Leung S, Milne K, Gilks CB, et al. Molecular Subtype Not Immune Response Drives Outcomes in Endometrial Carcinoma. *Clin Cancer Res* (2019) 25(8):2537–48. doi: 10.1158/1078-0432.CCR-18-3241
15. Farhood B, Najafi M, Mortezaee K. CD8 + cytotoxic T lymphocytes in cancer immunotherapy: A review. *J Cell Physiol* (2019) 234(6):8509–21. doi: 10.1002/jcp.27782
16. Borst J, Ahrends T, Bąbała N, Melief CJM, Kastenmüller W. CD4 + T cell help in cancer immunology and immunotherapy. *Nat Rev Immunol* (2018) 18 (10):635–47. doi: 10.1038/s41577-018-0044-0
17. Gardner A, Ruffell B. Dendritic Cells and Cancer Immunity. *Trends Immunol* (2016) 37(12):855–65. doi: 10.1016/j.it.2016.09.006
18. Zhang D, He W, Wu C, Tan Y, He Y, Xu B, et al. Scoring System for Tumor-Infiltrating Lymphocytes and Its Prognostic Value for Gastric Cancer. *Front Immunol* (2019) 10:71. doi: 10.3389/fimmu.2019.00071
19. Krishnamurti U, Wetherilt CS, Yang J, Peng L, Li X. Tumor-infiltrating lymphocytes are significantly associated with better overall survival and disease-free survival in triple-negative but not estrogen receptor-positive breast cancers. *Hum Pathol* (2017) 64:7–12. doi: 10.1016/j.humpath.2017.01.004
20. Okada K, Sadahiro S, Chan LF, Ogimi T, Miyakita H, Saito G, et al. The Number of Natural Killer Cells in the Largest Diameter Lymph Nodes Is Associated with the Number of Retrieved Lymph Nodes and Lymph Node Size, and Is an Independent Prognostic Factor in Patients with Stage II Colon Cancer. *Oncology* (2018) 95(5):288–96. doi: 10.1159/000491019
21. Pascual-García M, Bértolo C, Nieto JC, Serrat N, Espinosa Í, D'Angelo E, et al. CD8 down-regulation on cytotoxic T lymphocytes of patients with endometrioid endometrial carcinomas. *Hum Pathol* (2016) 56:180–8. doi: 10.1016/j.humpath.2016.05.025
22. Degos C, Heinemann M, Barrou J, Boucherit N, Lambaudie E, Savina A, et al. Endometrial Tumor Microenvironment Alters Human NK Cell Recruitment, and Resident NK Cell Phenotype and Function. *Front Immunol* (2019) 10:877. doi: 10.3389/fimmu.2019.00877

23. Li BL, Wan XP. Prognostic significance of immune landscape in tumour microenvironment of endometrial cancer. *J Cell Mol Med* (2020) 24(14):7767–77. doi: 10.1111/jcmm.15408
24. De Nola R, Menga A, Castegna A, Loizzi V, Ranieri G, Cicinelli E, et al. The Crowded Crosstalk between Cancer Cells and Stromal Microenvironment in Gynecological Malignancies: Biological Pathways and Therapeutic Implication. *Int J Mol Sci* (2019) 20(10):2401. doi: 10.3390/ijms20102401
25. Li LY, Yin KM, Bai YH, Zhang ZG, Di W, Zhang S. CTHRC1 promotes M2-like macrophage recruitment and myometrial invasion in endometrial carcinoma by integrin-Akt signaling pathway. *Clin Exp Metastasis* (2019) 36(4):351–63. doi: 10.1007/s10585-019-09971-4
26. Tong H, Ke JQ, Jiang FZ, Wang XJ, Wang FY, Li YR, et al. Tumor-associated macrophage-derived CXCL8 could induce ERα suppression via HOXB13 in endometrial cancer. *Cancer Lett* (2016) 376(1):127–36. doi: 10.1016/j.canlet.2016.03.036
27. Ning C, Xie B, Zhang L, Li C, Shan W, Yang B, et al. Infiltrating Macrophages Induce ERα Expression through an IL17A-mediated Epigenetic Mechanism to Sensitize Endometrial Cancer Cells to Estrogen. *Cancer Res* (2016) 76 (6):1354–66. doi: 10.1158/0008-5472.CAN-15-1260
28. Mollinedo F. Neutrophil Degranulation, Plasticity, and Cancer Metastasis. *Trends Immunol* (2019) 40(3):228–42. doi: 10.1016/j.it.2019.01.006
29. Coffelt SB, Wellenstein MD, de Visser KE. Neutrophils in cancer: neutral no more. *Nat Rev Cancer* (2016) 16(7):431–46. doi: 10.1038/nrc.2016.52
30. Wculek SK, Malanchi I. Neutrophils support lung colonization of metastasis-initiating breast cancer cells. *Nature* (2015) 528(7582):413–7. doi: 10.1038/nature16140
31. Mizuno R, Kawada K, Itatani Y, Ogawa R, Kiyasu Y, Sakai Y. The Role of Tumor-Associated Neutrophils in Colorectal Cancer. *Int J Mol Sci* (2019) 20 (3):529. doi: 10.3390/ijms20030529
32. Mensurado S, Rei M, Lança T, Ioannou M, Gonçalves-Sousa N, Kubo H, et al. Tumor-associated neutrophils suppress pro-tumoral IL-17+ γδ T cells through induction of oxidative stress. *PloS Biol* (2018) 16(5):e2004990. doi: 10.1371/journal.pbio.2004990
33. Aponte-López A, Fuentes-Pananá EM, Cortes-Muñoz D, Muñoz-Cruz S. Mast Cell, the Neglected Member of the Tumor Microenvironment: Role in Breast Cancer. *J Immunol Res* (2018) 2018:2584243. doi: 10.1155/2018/2584243
34. Ribatti D, Tamma R, Crivellato E. The dual role of mast cells in tumor fate. *Cancer Lett* (2018) 433:252–8. doi: 10.1016/j.canlet.2018.07.005
35. Plotkin JD, Elias MG, Fereydouni M, Daniels-Wells TR, Dellinger AL, Penichet ML, et al. Human Mast Cells From Adipose Tissue Target and Induce Apoptosis of Breast Cancer Cells. *Front Immunol* (2019) 10:138. doi: 10.3389/fimmu.2019.00138
36. Rajput AB, Turbin DA, Cheang MC, Voduc DK, Leung S, Gelmon KA, et al. Stromal mast cells in invasive breast cancer are a marker of favourable prognosis: a study of 4,444 cases. *Breast Cancer Res Treat* (2008) 107 (2):249–57. doi: 10.1007/s10549-007-9546-3
37. Keser SH, Kandemir NO, Ece D, Gecmen GG, Gul AE, Barisik NO, et al. Relationship of mast cell density with lymphangiogenesis and prognostic parameters in breast carcinoma. *Kaohsiung J Med Sci* (2017) 33(4):171–80. doi: 10.1016/j.kjms.2017.01.005

Conflict of Interest: The authors declare that the research was conducted in the absence of any commercial or financial relationships that could be construed as a potential conflict of interest.

Copyright © 2020 Cheng, Zhang, Wang and Wang. This is an open-access article distributed under the terms of the Creative Commons Attribution License (CC BY). The use, distribution or reproduction in other forums is permitted, provided the original author(s) and the copyright owner(s) are credited and that the original publication in this journal is cited, in accordance with accepted academic practice. No use, distribution or reproduction is permitted which does not comply with these terms.

frontiers in Oncology

ORIGINAL RESEARCH
published: 15 December 2020
doi: 10.3389/fonc.2020.607622

Identification and Verification of Immune-Related Gene Prognostic Signature Based on ssGSEA for Osteosarcoma

Bo Xiao[1,2], *Liyan Liu*[1,2], *Aoyu Li*[1,2], *Cheng Xiang*[1,2], *Pingxiao Wang*[1,2], *Hui Li*[1,2*] *and Tao Xiao*[1,2*]

[1] Department of Orthopedics, Second Xiangya Hospital, Central South University, Changsha, China, [2] Orthopedic Biomedical Materials Engineering Laboratory of Hunan Province, Changsha, China

OPEN ACCESS

Edited by:
Peng Qu,
National Institutes of Health (NIH), United States

Reviewed by:
Meng Xu,
National Institutes of Health (NIH), United States
Ming Yi,
Frederick National Laboratory for Cancer Research (NIH), United States

***Correspondence:**
Hui Li
lihuix@csu.edu.cn
Tao Xiao
xiaotaoxyl@csu.edu.cn

Specialty section:
This article was submitted to Cancer Immunity and Immunotherapy, a section of the journal Frontiers in Oncology

Received: 17 September 2020
Accepted: 17 November 2020
Published: 15 December 2020

Citation:
Xiao B, Liu L, Li A, Xiang C, Wang P, Li H and Xiao T (2020) Identification and Verification of Immune-Related Gene Prognostic Signature Based on ssGSEA for Osteosarcoma. Front. Oncol. 10:607622. doi: 10.3389/fonc.2020.607622

Osteosarcoma is the most common malignant bone tumor in children and adolescence. Multiple immune-related genes have been reported in different cancers. The aim is to identify an immune-related gene signature for the prospective evaluation of prognosis for osteosarcoma patients. In this study, we evaluated the infiltration of immune cells in 101 osteosarcoma patients downloaded from TARGET using the ssGSEA to the RNA-sequencing of these patients, thus, high immune cell infiltration cluster, middle immune cell infiltration cluster and low immune cell infiltration cluster were generated. On the foundation of high immune cell infiltration cluster vs. low immune cell infiltration cluster and normal vs. osteosarcoma, we found 108 common differentially expressed genes which were sequentially submitted to univariate Cox and LASSO regression analysis. Furthermore, GSEA indicated some pathways with notable enrichment in the high- and low-immune cell infiltration cluster that may be helpful in understanding the potential mechanisms. Finally, we identified seven immune-related genes as prognostic signature for osteosarcoma. Kaplan-Meier analysis, ROC curve, univariate and multivariate Cox regression further confirmed that the seven immune-related genes signature was an innovative and significant prognostic factor independent of clinical features. These results of this study offer a means to predict the prognosis and survival of osteosarcoma patients with uncovered seven-gene signature as potential biomarkers.

Keywords: immune, gene, prognostic, osteosarcoma, ssGSEA, TARGET

INTRODUCTION

Osteosarcoma is one of the most common primary malignant bone tumor and the second chief cause of cancer-related deaths in children and adolescence, accounting about 5% of childhood cancers (1, 2). Currently, the chief treatment for osteosarcoma is surgery combined with chemotherapy. Five-year survival rate of osteosarcoma patients has increase to ~70% over the last 30 years (3). However, because of drugs resistance, metastasis or recurrence, prognosis of osteosarcoma patients remains poor

(2). Thus, to identify prognostic biomarkers that associate with biological heterogeneity of osteosarcoma is urgently needed to improve prognosis.

Nowadays, immune oncology has attracted much attention for its particular clinical benefits of many cancers. Immuotherapy, a novel treatment, has achieved favorable results for some cancers, such as breast cancer, hepatocellular carcinoma (4, 5). As a cellular environment, tumor microenvironment was composed of mesenchymal cells, endothelial cells, immune cells, inflammatory mediators, and extracellular matrix molecules. The bone microenvironment of osteosarcoma contains osteoblasts, osteoclasts and hematopoietic cells. Macrophages/monocytes were derived from these cells (6, 7). Multiple cytokines and growth factors were released from these cells. Immune-related genes and immune cells infiltration act as an indispensable role in tumor development and progression (8). Therefore, the comprehensive analysis of the relationship between immune-related genes and overall survival maybe provide a new reference for the treatment and prognosis of osteosarcoma.

In this study, we used ssGSEA to assign osteosarcoma patients into high-, middle- and low-immune cell infiltration clusters, and validated by ESTIMATE, CIBERSORT and K-M analysis. Then, we identified a seven immune-related genes signature correlated with the prognosis in differentially expressed genes in both osteosarcoma group and high immune cell infiltration cluster using univariate Cox and LASSO regression analysis. Finally, we assessed the accuracy of immune-related gene prognosis signature. The immune-related gene signature not only can enhance the ability to predict prognosis in osteosarcoma patients but also maybe explain the underlying mechanisms.

MATERIALS AND METHODS

Collect and Cluster of Osteosarcoma Data

The RNA-sequencing data of osteosarcoma (n = 101) were downloaded from TARGET (Therapeutically Applicable Research to Generate Effective Treatments) (https://ocg.cancer.gov/programs/target). 95 samples of them with corresponding clinical information. The gene expression of GSE42352 were obtained from Gene Expression Omnibus (GEO) database. GSE42352 is a microarray dataset that contains 15 normal cells/tissues (12 mesenchymal stem cells, 3 osteoblast), 103 osteosarcoma tissues/cells (84 biopsies of osteosarcoma tissue, 19 cell lines). The platform of the dataset is GPL10295. We obtained 29 immune-related cells and types (9). The ssGSEA was applied to explore the different infiltration degrees of immune cell types, immune-related functions, and immune-related pathways in osteosarcoma expression profile of TARGET and GSE42352 database using the R package "GSVA". By applying unsupervised hierarchical clustering algorithm (cutoff = 1.0), osteosarcoma samples were assigned into three clusters based on immune infiltration. Samples of osteosarcoma in the TARGET and GSE42352 were classified as high immune cell infiltration cluster, middle immune cell infiltration cluster and low immune cell infiltration cluster based on the result of ssGSEA using the R package "sparcl". Besides, the GSE42352 was applied to analyze the differentially expressed genes between normal tissue/cells and osteosarcoma tissue/cells using the R package "limma".

Validation of the Effectuality of Immune Clustering

ESTIMATE was designed to count scores for reflecting the infiltration levels of immune cells and stromal cells within the tumor microenvironment on the foundation of the specific genes expression level of immune and stromal cells using the R package "ESTIMATE" (10). First, we used ESTIMATE algorithm based on the expression level of RNA-seq to count the Tumor Purity, ESTIMATE Score, Immune Score, and Stromal Score of 101 osteosarcoma samples in three clusters of TARGET database using the R package "estimate" to validate the effectuality of ssGSEA grouping and to picture clustering heatmap. The vioplots of Tumor Purity, ESTIMATE Score, Immune Score, and Stromal Score in three clusters were presented employing the R package "ggpubr". Next, to investigate the difference of immune cell subtypes, the R package "CIBERSORT" was applied to count the proportion of 22 immune cells of all osteosarcoma samples on the foundation of expression file (11), and the difference of three clusters was validated again. Besides, we also used K-M analysis and the expression of HLA family and PD-L1 to validate the difference between three clusters applying the R package "survival" and "ggpubr" respectively.

Distinction of Immune-Related Genes in Osteosarcoma

Based on the above-mentioned clusters, mRNA-seq expression data of TARGET and expression profiling of GSE42352 were divided into high immune cell infiltration, middle immune cell infiltration and low immune cell infiltration cluster with the same cutoff. We obtained the differentially expressed genes ($|lgFC| > 1$ and adj.P.Val/FDR < 0.05) between high immune cell infiltration and low immune cell infiltration cluster in two databases using the R package "edgeR". The same criterion was applied to obtain the differentially expressed genes associated with tumorigenesis between normal tissue/cells and osteosarcoma tissue/cells using the R package "limma". Finally, we used Venn analysis to investigate the immune-related genes from the above-mentioned results.

GSEA Enrichment Analysis

Gene set enrichment analysis was conducted between high immune cell infiltration and low immune cell infiltration clusters of TARGET database using the R "clusterprofiler" package. The R "enrichplot" package was used to generate visual gene set enrichment maps with annotations. $p < 0.05$ was considered statistically significant.

Distinction and Confirmation of Immune-Related Gene Prognostic Signature for Osteosarcoma

First, we used univariate Cox regression analysis to distinct immune-related gene in osteosarcoma samples (n = 95) with

complete clinical information in TARGET dataset with significant correlation to overall survival using the R "survival" package. We then used LASSO regression analysis to screen survival related genes for significant results of univariate Cox regression analysis using the R "glmnet" package. 1000-round cross-validation for tuning parameter selection was used to prevent overfitting and the partial likelihood deviance met the minimum criteria. Finally, we constructed the prognostic signature of osteosarcoma according to the expression of immune-related genes and their relevant coefficients result from LASSO regression analysis. The formula as follows: risk score = $\sum \sum i$coefficient (gene$i$) × expression(gene$i$). The median value of risk score was defined using the "Survminer" package, in which the osteosarcoma patients were divided into high-risk and low-risk groups. The time-dependent receiver-operating characteristic (ROC) and Kaplan-Meier (K-M) curves were used to assess the clinical prognostic capacity of the risk score using the R "timeROC", "survival", and "survminer" packages. Further, to assess whether risk score can be regarded as an independent predictor of overall survival of osteosarcoma patients, univariate Cox and multivariate Cox regression analysis were performed with risk score, gender, age and metastasis status as variables using the R "survival" package.

Construction and Verification of Nomogram

The nomogram was designed to predict survival of osteosarcoma patients. Risk score, age, gender, primary tumor site and metastasis status were used to build the nomogram using R "rms" and "survival" packages. The calibration curve was used to evaluate the accuracy of the nomogram in differentiating between patient groups.

Statistical Analysis

All statistical analyses were conducted using the R software version 4.0.1. Kaplan-Meier analysis and log-rank test were applied to assess survival and compare difference in survival between clusters as well as risk groups. $p < 0.05$ was regarded statistically significant.

RESULTS

Construction and Validation of Osteosarcoma Clustering

We obtained 101 osteosarcoma samples data from the TARGET. The ssGSEA method was applied to the RNA-sequencing data of osteosarcoma samples to assess the immune cells infiltration. Then, the richness levels of 29 immune-related cells and types in osteosarcoma samples was obtained. By applying unsupervised hierarchical clustering algorithm (cutoff = 1.0), osteosarcoma samples were assigned into three clusters based on immune infiltration, which include the high immune cell infiltration cluster (n = 9), middle immune cell infiltration cluster (n = 65), and low immune cell infiltration cluster (n = 27) (**Figure 1A** and **Supplementary Figure 1A**). To validate the practicability of the above clustering result, Stromal Score, Immune Score, ESTIMATE Score and Tumor Purity were calculated according to the expression level of osteosarcoma using the ESTIMATE algorithm. The result has shown that Stromal Score, Immune Score, and ESTIMATE Score of high immune cell infiltration cluster were higher than that of other two clusters, but Tumor Purity was opposite (**Figure 1A**). The violin plot also has shown that Stromal Score, Immune Score and ESTIMATE Score in low-, middle-, high- immune cell infiltration cluster become higher and higher, while Tumor Purity become lower and lower ($p < 0.05$) (**Figure 1B**). Besides, boxplot has also shown that the expression of most of HLAs and PD-L1 in low-, middle-, high-immune cell infiltration cluster become higher and higher ($p < 0.01$) (**Figures 1C, D**). In addition, we discovered that most of immune cells were displayed in higher proportions in high immune cell infiltration cluster using CIBERSORT algorithm (**Figure 1E**). Finally, the Kaplan-Meier (K-M) curve has shown that the osteosarcoma patients in low immune cell infiltration cluster have worse survival rate and the survival rate of three clusters have significant difference ($p = 0.009$) (**Figure 1F**). Obviously, all of these results demonstrate that the osteosarcoma clustering can be used for further analysis. Similarly, osteosarcoma samples in GSE42352 were also assigned into three clusters based on the richness levels of 29 immune-related cells and types, which include the high immune cell infiltration cluster (n = 44), middle immune cell infiltration cluster (n = 40), and low immune cell infiltration cluster (n = 19) *via* applying unsupervised hierarchical clustering algorithm with the same cutoff value (**Supplementary Figure 1B**).

Identification of Differentially Expressed Genes Between Osteosarcoma and Normal Groups and Between High and Low Immune Cell Infiltration Clusters

PCA 3D plot showed the mesenchymal stem cells and osteoblast are relatively closed compared to osteosarcoma (**Supplementary Figure 2**). Using a threshold of $|lgFC| > 1$ and adj.P.Val/FDR < 0.05, we explored the differentially expressed genes between normal group (15 cases) and osteosarcoma group (103 cases) in the GSE42352. Then, 945 differentially expressed genes including 524 up-regulated and 421 down-regulated were obtained (**Figure 2A**). Basing on the same criterion, we obtained 1075 differentially expressed genes between high immune cell infiltration cluster and low immune cell infiltration cluster in TARGET database, with 245 up-regulated and 597 down-regulated (**Figure 2B**). Besides, 842 differentially expressed genes were obtained between high immune cell infiltration cluster and low immune cell infiltration cluster in GSE42352, with 808 up-regulated and 267 down-regulated (**Figure 2C**). Finally, through using Venn analysis of three sets of differentially expressed genes, 108 differentially expressed genes were identified in both high immune cell infiltration cluster and osteosarcoma group (**Figure 2D**).

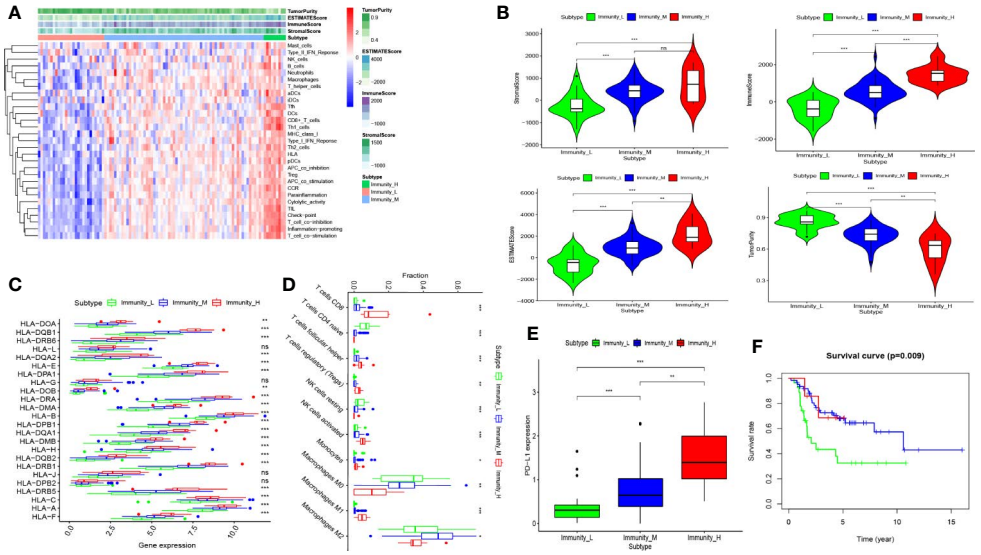

FIGURE 1 | Construction and validation of osteosarcoma clustering. **(A)** The enrichment levels of 29 immune-related cells and types in the high immune cell infiltration group (Immunity_H), middle immune cell infiltration group (Immunity_M), and the low immune cell infiltration group (Immunity_L). The Tumor Purity, ESTIMATE Score, Immune Score and Stromal Score of every patient gene were showed combine with the clustering information. **(B)** The violin plot showed the difference in ESTIMATE Score, Immune Score, Stromal Score, and Tumor Purity between three clusters. **(C, D)** The expression of most HLAs and PD-L1 was a significant difference in high- (red), middle- (blue), and low- (green) immune cell infiltration cluster. **(E)** the boxplot showed the proportion of immune cells among the high- (red), middle- (blue), and low-immune cell infiltration cluster(green) using CIBERSORT algorithm. **(F)** Patients in low immune cell infiltration cluster (green) showed worse overall survival than those in (middle- (blue), and low- (green) immune cell infiltration) cluster. nap > 0.05, *p < 0.05, **p < 0.01, ***p < 0.001. ns, no statistically significant.

GSEA Enrichment Analysis

The GO analysis of genes in the high immune cell infiltration cluster and low immune cell infiltration cluster in TARGET database has shown that these associated with MHC class II protein complex, immunoglobulin receptor binding, regulation of apoptotic cell clearance and so on (**Figure 3A**). The KEGG analysis indicated that the genes correlated with primary immunodeficiency, Intestinal immune network for IgA production, Th1 and Th2 cell differentiation, PD−L1 expression and PD−1 checkpoint pathway in cancer, B cell receptor signaling pathway and so on (**Figure 3B**).

Distinction and Evaluation of Seven Immune-Related Genes Prognostic Signature for Osteosarcoma

We selected 95 osteosarcoma patients with complete clinical data for the further analysis. Univariate Cox regression analysis was applied to the expression profiles of 108 genes in osteosarcoma patients. From this analysis, 44 differentially expressed genes were found to have significant association with overall survival ($p < 0.05$) (**Figure 4A**). Then, by the LASSO regression analysis, seven genes, including IFITM3, VAMP8, ACTA2, GZMA, CDCA7, EVI2B, and SLC7A7, were identified (**Figures 4B, C**). The risk score was counted based on the expression level and its coefficient of these seven genes. Risk score = (−0.0297667 *expression of VAMP8) + (−0.0842312 * expression of GZMA) + (−0.3625101*expression of ACTA2) + (−0.3627611 * expression of IFITM3) + (0.15067589*expression of CDCA7) + (−0.0458604 * expression of EVI2B) +(−0.2311853*expression of SLC7A7).

We divided patients into high-risk and low-risk groups based on the median risk score. Kaplan-Meier (K-M) curves demonstrated low-risk group had a noticeably better survival than patients in high-risk group ($p = 4.952e{-}03$), showing the risk score has an effective value of prognosis (**Figure 5A**). Risk score and survival status of all osteosarcoma patients were exhibited in the risk curve and scatterplot. The mortality and risk coefficient of patients in the low-risk group were lower than that of high-risk group (**Figures 5B, C**). The heatmap of these seven immune-related genes expression level in GSE42352 indicated that five of these genes (CDCA7, GZMA, SLC7A7, VAMP8, and EVI2B) were highly expressed in the osteosarcoma group, but two of these genes (IFITM3 and ACTA2) were highly expressed in the normal group (**Figure 5D**). Besides, Time-dependent ROC curves was used to assess the precision of the seven immune-related genes signature in predicting overall survival of osteosarcoma patients at 3-, 5-, and 10- year. The area under the ROC (AUC) values of 3-, 5-, and 10- year were 0.750, 0.808, and 0.704, respectively (**Figure 5E**), showing a good capacity of our seven immune-related genes signature in predicting overall survival. As a whole, all of these analyses identify seven immune-related genes as prognostic signature for osteosarcoma.

Assessment of Seven Immune-Related Genes Signature as Independent Prognostic Factor in Osteosarcoma Patients

We applied univariate and multivariate Cox regression analysis to test whether the seven immune-related genes signature was an

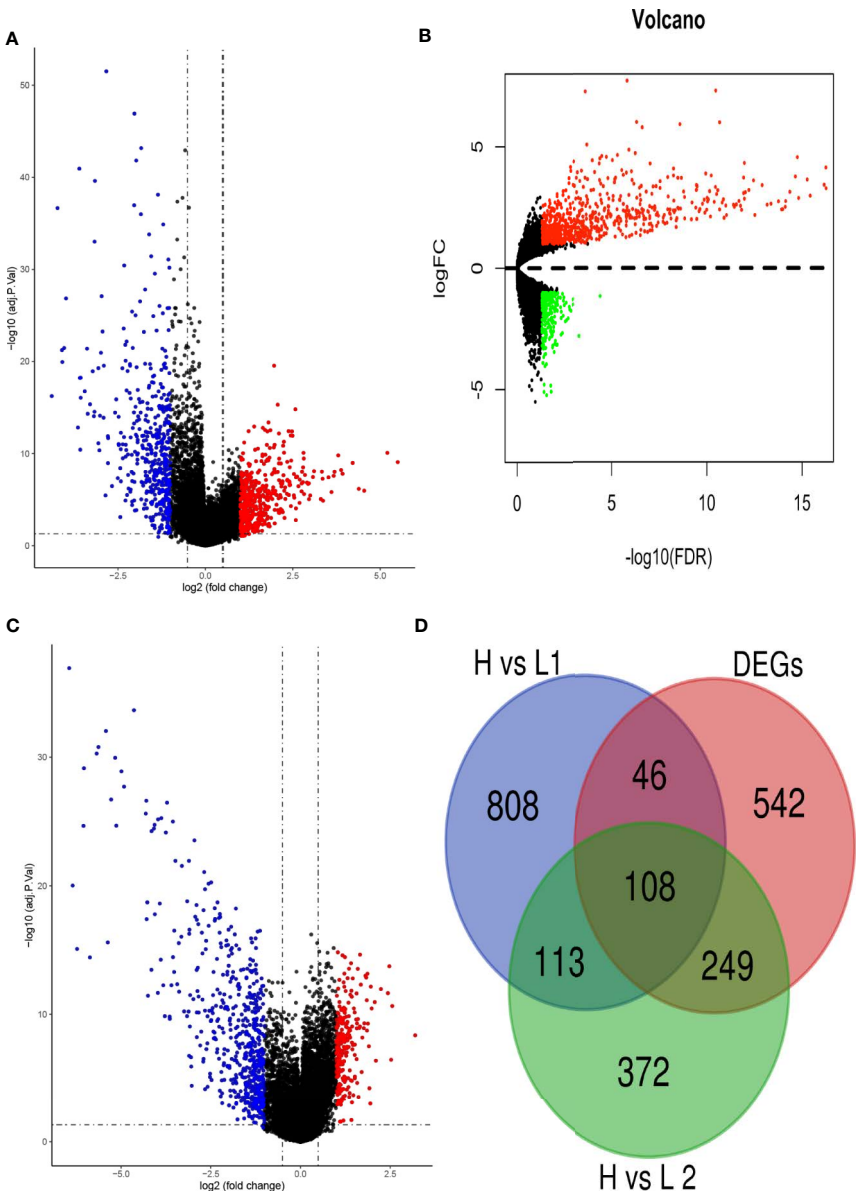

FIGURE 2 | Identification of differentially expressed genes. **(A)** The volcano plot showed that 524 up-regulated genes (red) and 421 down-regulated genes (green) between osteosarcoma (T) and normal (N) tissues/cells. **(B)** the volcano plot showed that 808 up-regulated genes (red) and 267 down-regulated genes (green) between high and low immune cell infiltration cluster in TARGET dataset. **(C)** The volcano plot showed that 245 up-regulated genes (red) and 597 down-regulated genes (green) between high and low immune cell infiltration cluster in GSE42354. **(D)** Using Draw Venn Diagram to pick up the intersection, 108 differentially expressed genes were obtained.

independent prognostic factor for other features, such as gender, age, and metastasis status. Both univariate and multivariate Cox regression analysis illustrated risk score and metastasis status were the independent prognostic factors ($P < 0.001$) (**Figures 6A, B**). Time-dependent ROC curves were used to evaluate the precision of metastasis status in predicting overall survival of osteosarcoma patients at 3-, 5-, and 10- year. The area under the ROC (AUC) values of 3-, 5-, and 10- year were 0.669, 0.667, and 0.64, respectively (**Figure 6C**) were lower than that of risk score. Both of results indicated that the seven immune-related genes signature was an independent prognostic factor in osteosarcoma patients.

Construction and Validation of Nomogram

In order to predict the 3-year, 5-year, and 10-year overall survival of each patient, a nomogram was designed based on the TARGET. The expression signature for the seven immune-related genes, age, gender, and metastasis status were used as variables (**Figure 7A**). The calibration curve obtained compared well with the ideal model (**Figures 7B, C**).

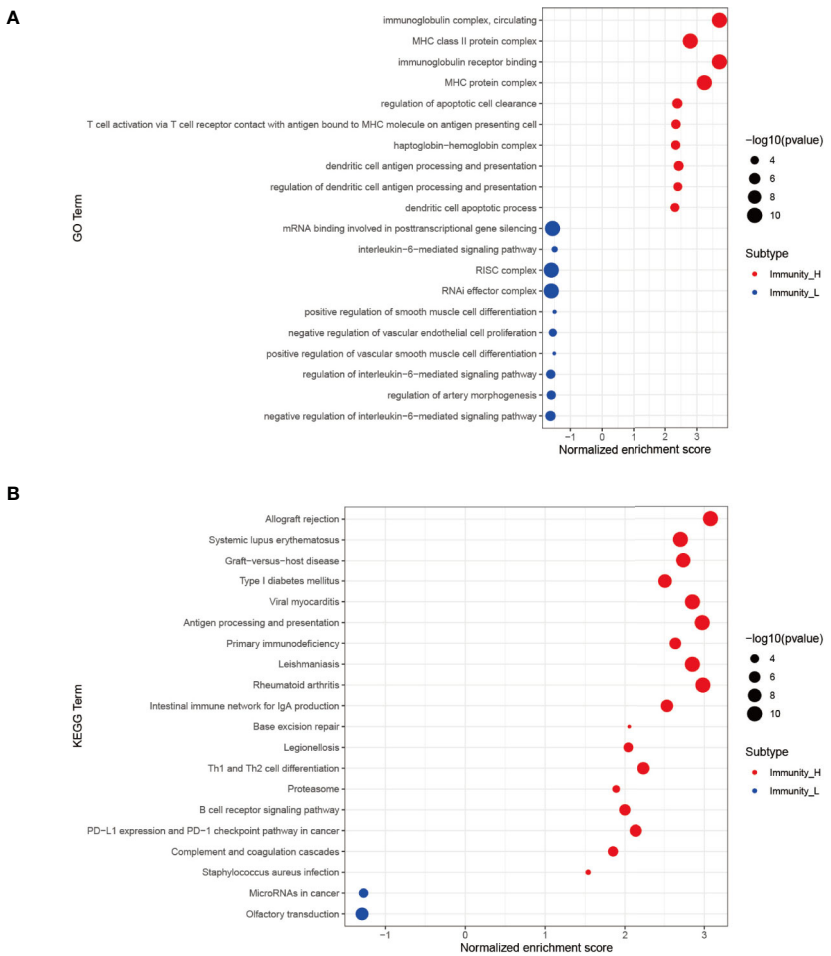

FIGURE 3 | GSEA enrichment analysis. **(A)** The top 10 results of GO analysis in Immunity_H (red) and Immunity_L (green). **(B)** The results of KEGG analysis in Immunity_H (red) and Immunity_L (green).

DISCUSSION

Osteosarcoma derives from mesenchymal stem cells, is the most common malignant bone tumor in children and adolescence, with the highest level of heterogeneity in humans (12, 13). This heterogeneity occurs not only in the macroscopic and microscopic aspects, with heterogeneous tumor microenvironment, but in genotypes and phenotypes aspects (13). Osteosarcoma tissue is not only composed of osteoblastic, chondroblastic and/or fibroblastic but also blended with immune cells and stromal cell (14, 15). That is to say, each sample has different types of cells composition. Thus, we concentrate on the heterogeneity of osteosarcoma and correlation between tumor immune cells infiltration and tumor cells, which was of remarkable meanings to study the mechanism of tumor development and progression, and to discover new approaches of diagnosis and therapy. By using the mRNA sequencing data and clinical data of osteosarcoma obtained from TARGET, we identified and validated the seven gene prognostic signature associated with immune cell infiltration.

In this study, we divided the samples into three clusters based on the enrichment of 29 immune cell types by applying unsupervised hierarchical clustering algorithm. There were significant differences in Immune Score, Stromal Score, ESTIMATE Score and Tumor Purity between the high-, middle- and low- immune cell infiltration cluster. Then, the heterogeneity of immune microenvironment in osteosarcoma was validated by the expression level of HLAs and PD-L1 (16–18). Besides, there were also obviously difference in the proportion of most of 22 immune cells of three clusters using CIBERSORT algorithm. Finally, K-M curve indicated that the osteosarcoma patients in low immune cell infiltration cluster have lower survival rate and the survival rate of three clusters have significant difference. The seven immune-related genes signature for overall survival was constructed on the differentially expressed genes among high immune cell infiltration cluster and osteosarcoma to predict the prognosis of osteosarcoma patients. The samples were assigned into low-risk group and high-risk group based on the median risk score.

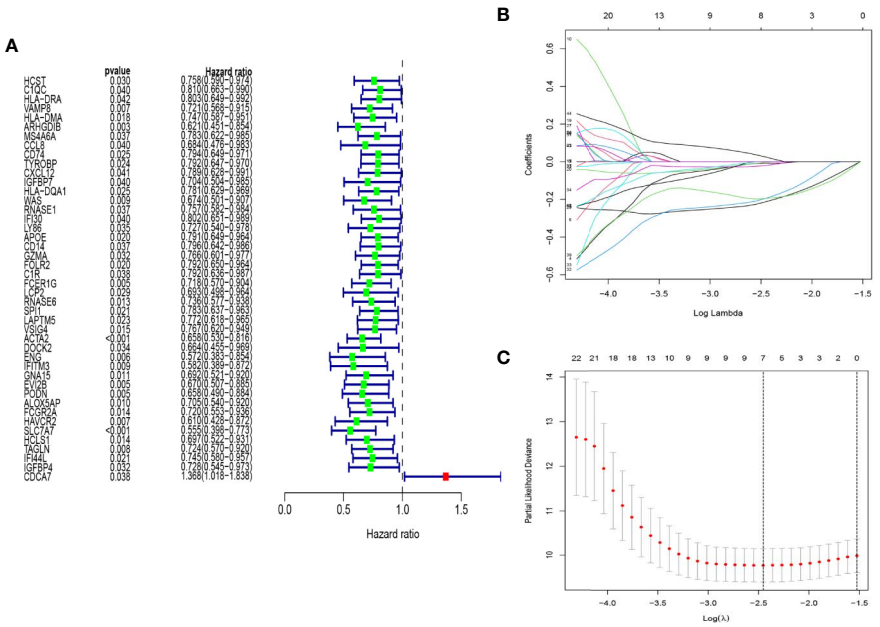

FIGURE 4 | Construction of immune-related gene prognostic signature. **(A)** The p-value and HR of selected genes in univariable Cox regression analysis ($p < 0.05$). **(B)** The LASSO Cox analysis identified seven genes associated with prognosis. **(C)** The optimal values of the penalty parameter were defined by 1,000-round cross-validation.

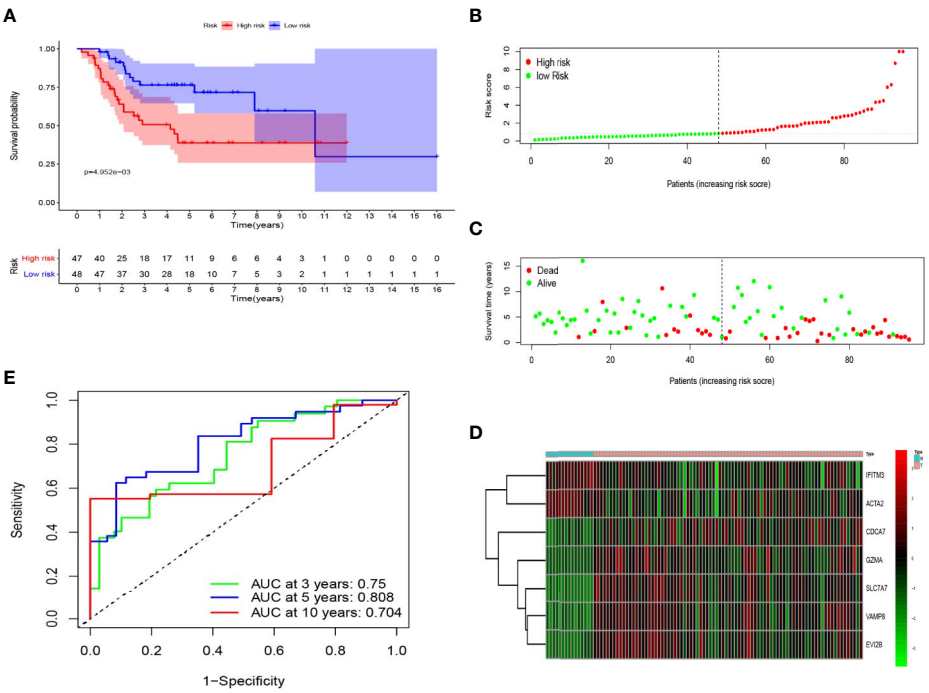

FIGURE 5 | The prognostic value of seven immune-related genes. **(A)** Patients in the low-risk group (blue) showed better overall survival than those in the high-risk group (red). **(B)** The risk curve of every sample arranged by risk score. **(C)** The scatter plot of osteosarcoma samples survival overview. The red and green dots stand for death and survival, respectively. **(D)** Heatmap showed the expression level of seven genes in the normal group (blue) and osteosarcoma group (red). **(E)** The ROC curve for 3-, 5-, and 10-year overall survival of osteosarcoma patients.

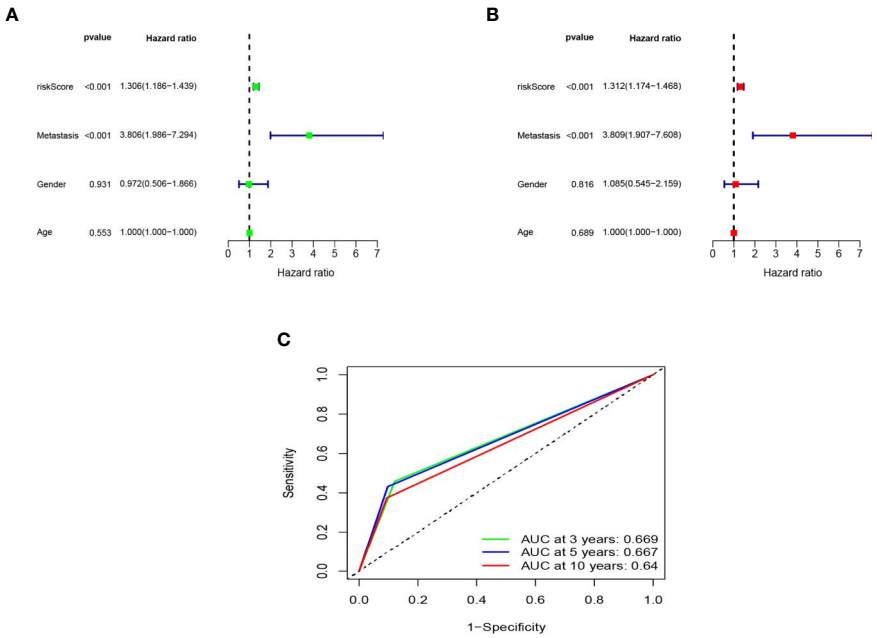

FIGURE 6 | Assessment of the independent prognostic value. The univariate **(A)** and multivariate **(B)** Cox regression analysis of risk score, age, gender and metastasis. **(C)** The AUC of metastasis model based on ROC curve.

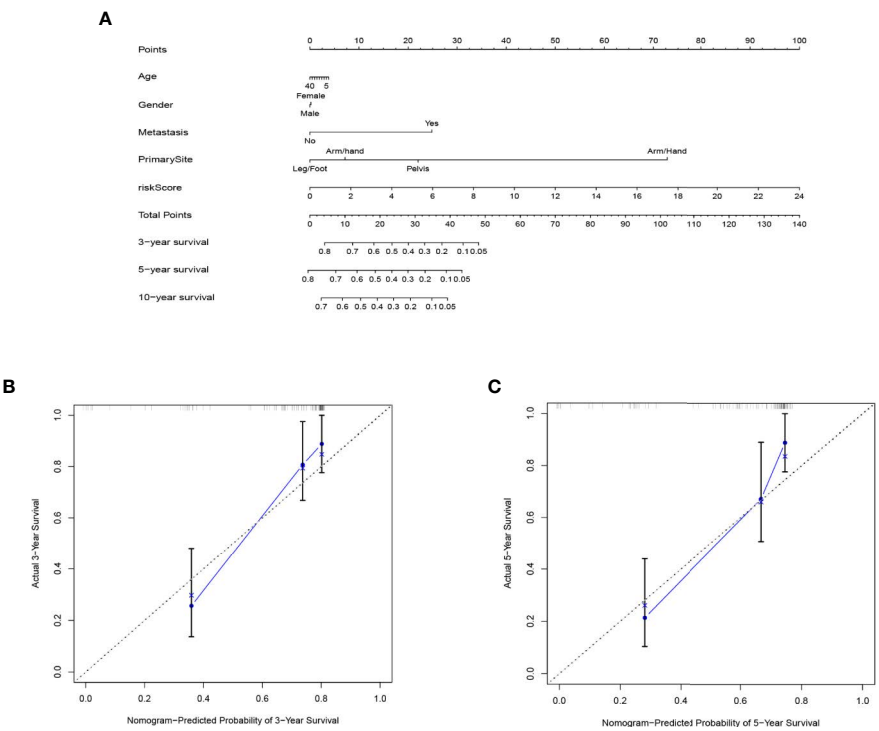

FIGURE 7 | The nomogram to predict the survival rate of osteosarcoma patients. **(A)** nomogram of TARGET cohort used to predict the survival time. **(B, C)** calibration maps used to predict the 3-year **(B)** and 5-year survival **(C)**.

K-M curve, ROC curve, and score plot and plot of survival status shown that the seven immune-related gene had a favorable predictive ability.

Five of the seven immune-related genes (CDCA7, GZMA, SLC7A7, VAMP8, and EVI2B) were highly expressed in the osteosarcoma group, while two of these immune-related genes (IFITM3 and ACTA2) were lowly expressed. Most of the seven immune-related genes have been found associate with prognosis of different types of cancers. IFITM3 enhanced the invasion and metastasis of hepatocellular carcinoma through regulating expression of MMP9 *via* the p38/MAPK pathway and promoted proliferation of hepatocellular carcinoma *via* regulating expression of c-myc through the ERK1/2 signaling pathway (19, 20). Overexpression of IFITM3 was correlated with poor prognosis and associated with some molecules of immune checkpoint and biomarkers of tumor-associated macrophage in head and neck squamous cell carcinoma (21). Previous study identified that high expression of VAMP8 was associated with oncogenesis and metastasis of osteosarcoma (22). High expression of VAMP8 enhanced the cell proliferation of glioma and glioma growth by regulating cell cycle in the G0/G1 phase (23). ACTA2 was associated with maintenance of cell shape and mechanical tension and played an important role in tumor cell migration and invasion (24). Overexpression of ACTA2 had an increased risk of distant metastasis and worse survival for lung adenocarcinoma patients (25). It has been found that immune-related gene (GZMA) is high expressed in endometrial cancer at early stage and associated with prognosis, but the mechanism of tumor progression is unclear (26). As a family member of the cell division cycle proteins, CDCA7 was markedly overexpressed in colorectal cancer and lung adenocarcinoma. CDCA7 enhance cell proliferation in lung adenocarcinoma by mediating G1 phase and regulating apoptosis. besides, colorectal cancer patients with low expression of CDCA7 had better overall survival (27, 28). It has been found that low expression of EVI2B could enhance cell proliferation, invasion and migration in colorectal cancer cells and remarkably promote tumor growth. besides, EVI2B participated in PPIs (protein-protein interactions) of T-cell-mediated system-wide modulation (29). Similarly, EVI2B was a potential prognostic biomarker for colorectal cancer (CRC) (30). SLC7A7 was a significant and independent biomarker for predicting poor prognosis and was a potential prognosis predicter of glioblastoma (31). Mounting evidence showed dysregulation of SLC7A7 was associated with resistance of chemotherapy and radiation in ovarian cancers and non-small cell lung cancer, respectively (32, 33). Studies about the tumor progression part of SLC7A7 are too limited. APOE regulates lipid homeostasis in the systemic circulation and induces inflammatory immune responses in the tumor microenvironment (34).

Then, we investigated the correlation between risk score, gender, age and metastasis status in patients with osteosarcoma by univariate Cox and multivariate Cox regression analysis. Both of results showed that risk score and metastasis status maybe the independent prognostic factors in osteosarcoma patients ($p < 0.001$). To find out which of the two independent prognostic factors can better predict overall survival in osteosarcoma patients, we constructed a metastasis status model. The AUC values of ROC curve were applied to assess the accuracy of the model. The AUC values of 3-, 5-, and 10- year are obviously lower than those of the immune-related gene signature, suggesting that risk score is an independent prognostic factor and the predictive ability is significantly better than that of metastasis status.

Finally, we designed a nomogram to predict prognosis of osteosarcoma patients based on the risk score of seven immune-related gene signature, age, gender, metastasis status and primary tumor site. From this nomogram we were able to predict the 3-, 5-, and 10-year survival of osteosarcoma. Consistently, the plots of calibration demonstrated that the signature could accurately evaluate the survival of osteosarcoma patients. Although, our prognostic signature had a favorable predictive capability, the prognostic model can be optimized by consolidating with other independent datasets or even improved by optimizing the LASSO results in the future.

Some limitations of our study should be admitted. First, lack of sufficient samples and some other clinical pathological features. Second, the performance of our prognostic signature should be validated in more osteosarcoma datasets. Finally, all the results were based on public datasets and should be further confirmed by actual experiments.

In conclusion, the seven immune-related genes signature identified as the independent prognostic significance for osteosarcoma. These results of this study offer a means to predict the prognosis and survival of osteosarcoma patients and maybe provide promising targets for immunotherapy.

DATA AVAILABILITY STATEMENT

The original contributions presented in the study are included in the article/**Supplementary Material**. Further inquiries can be directed to the corresponding authors.

AUTHOR CONTRIBUTIONS

BX had the idea, collected data and wrote the first draft, HL, LL and AL did statistical analysis, BX, CX, and PW created the figures, HL and TX drafted the final manuscript. All authors contributed to the article and approved the submitted version.

FUNDING

This work was supported by Key Research and Development Program of Hunan Province 2017GK2120 (to TX).

SUPPLEMENTARY MATERIAL

The Supplementary Material for this article can be found online at: https://www.frontiersin.org/articles/10.3389/fonc.2020.607622/full#supplementary-material

REFERENCES

1. Hameed M, Mandelker D. Tumor Syndromes Predisposing to Osteosarcoma. *Adv Anat Pathol* (2018) 25(4):217–22. doi: 10.1097/PAP.0000000000000190
2. Yan GN, Lv YF, Guo QN. Advances in osteosarcoma stem cell research and opportunities for novel therapeutic targets. *Cancer Lett* (2016) 370(2):268–74. doi: 10.1016/j.canlet.2015.11.003
3. Chen J, Liu G, Wu Y, Ma J, Wu H, Xie Z, et al. CircMYO10 promotes osteosarcoma progression by regulating miR-370-3p/RUVBL1 axis to enhance the transcriptional activity of beta-catenin/LEF1 complex via effects on chromatin remodeling. *Mol Cancer* (2019) 18(1):150. doi: 10.1186/s12943-019-1076-1
4. Liu Y, Qiao L, Zhang S, Wan G, Chen B, Zhou P, et al. Dual pH-responsive multifunctional nanoparticles for targeted treatment of breast cancer by combining immunotherapy and chemotherapy. *Acta Biomater* (2018) 66:310–24. doi: 10.1016/j.actbio.2017.11.010
5. Guerra AD, Yeung OWH, Qi X, Kao WJ, Man K. The Anti-Tumor Effects of M1 Macrophage-Loaded Poly (ethylene glycol) and Gelatin-Based Hydrogels on Hepatocellular Carcinoma. *Theranostics* (2017) 7(15):3732–44. doi: 10.7150/thno.20251
6. Winslow S, Lindquist KE, Edsjo A, Larsson C. The expression pattern of matrix-producing tumor stroma is of prognostic importance in breast cancer. *BMC Cancer* (2016) 16(1):841. doi: 10.1186/s12885-016-2864-2
7. Senbabaoglu Y, Gejman RS, Winer AG, Liu M, Van Allen EM, de Velasco G, et al. Tumor immune microenvironment characterization in clear cell renal cell carcinoma identifies prognostic and immunotherapeutically relevant messenger RNA signatures. *Genome Biol* (2016) 17(1):231. doi: 10.1186/s13059-016-1092-z
8. Gonzalez H, Hagerling C, Werb Z. Roles of the immune system in cancer: from tumor initiation to metastatic progression. *Genes Dev* (2018) 32(19-20):1267–84. doi: 10.1101/gad.314617.118
9. Shen Y, Peng X, Shen C. Identification and validation of immune-related lncRNA prognostic signature for breast cancer. *Genomics* (2020) 112 (3):2640–6. doi: 10.1016/j.ygeno.2020.02.015
10. Yoshihara K, Shahmoradgoli M, Martinez E, Vegesna R, Kim H, Torres-Garcia W, et al. Inferring tumour purity and stromal and immune cell admixture from expression data. *Nat Commun* (2013) 4:2612. doi: 10.1038/ncomms3612
11. Newman AM, Liu CL, Green MR, Gentles AJ, Feng W, Xu Y, et al. Robust enumeration of cell subsets from tissue expression profiles. *Nat Methods* (2015) 12(5):453–7. doi: 10.1038/nmeth.3337
12. Geller DS, Gorlick R. Osteosarcoma: a review of diagnosis, management, and treatment strategies. *Clin Adv Hematol Oncol* (2010) 8(10):705–18.
13. Schiavone K, Garnier D, Heymann MF, Heymann D. The Heterogeneity of Osteosarcoma: The Role Played by Cancer Stem Cells. *Adv Exp Med Biol* (2019) 1139:187–200. doi: 10.1007/978-3-030-14366-4_11
14. Hong W, Yuan H, Gu Y, Liu M, Ji Y, Huang Z, et al. Immune-related prognosis biomarkers associated with osteosarcoma microenvironment. *Cancer Cell Int* (2020) 20:83. doi: 10.1186/s12935-020-1165-7
15. Heymann MF, Lezot F, Heymann D. The contribution of immune infiltrates and the local microenvironment in the pathogenesis of osteosarcoma. *Cell Immunol* (2019) 343:103711. doi: 10.1016/j.cellimm.2017.10.011
16. Koirala P, Roth ME, Gill J, Piperdi S, Chinai JM, Geller DS, et al. Immune infiltration and PD-L1 expression in the tumor microenvironment are prognostic in osteosarcoma. *Sci Rep* (2016) 6:30093. doi: 10.1038/srep30093
17. Pan Y, Lu L, Chen J, Zhong Y, Dai Z. Identification of potential crucial genes and construction of microRNA-mRNA negative regulatory networks in osteosarcoma. *Hereditas* (2018) 155:21. doi: 10.1186/s41065-018-0061-9
18. Guan X, Guan Z, Song C. Expression profile analysis identifies key genes as prognostic markers for metastasis of osteosarcoma. *Cancer Cell Int* (2020) 20:104. doi: 10.1186/s12935-020-01179-x
19. Min J, Feng Q, Liao W, Liang Y, Gong C, Li E, et al. IFITM3 promotes hepatocellular carcinoma invasion and metastasis by regulating MMP9 through p38/MAPK signaling. *FEBS Open Bio* (2018) 8(8):1299–311. doi: 10.1002/2211-5463.12479
20. Min J, Hu J, Luo C, Zhu J, Zhao J, Zhu Z, et al. IFITM3 upregulates c-myc expression to promote hepatocellular carcinoma proliferation via the ERK1/2 signalling pathway. *Biosci Trends* (2020) 13(6):523–9. doi: 10.5582/bst.2019.01289
21. Li H, Yang LL, Wu CC, Xiao Y, Mao L, Chen L, et al. Expression and Prognostic Value of IFIT1 and IFITM3 in Head and Neck Squamous Cell Carcinoma. *Am J Clin Pathol* (2020) 153(5):618–29. doi: 10.1093/ajcp/aqz205
22. Liu J, Wu S, Xie X, Wang Z, Lei Q. Identification of potential crucial genes and key pathways in osteosarcoma. *Hereditas* (2020) 157(1):29. doi: 10.1186/s41065-020-00142-0
23. Chen Y, Meng D, Wang H, Sun R, Wang D, Wang S, et al. VAMP8 facilitates cellular proliferation and temozolomide resistance in human glioma cells. *Neuro Oncol* (2015) 17(3):407–18. doi: 10.1093/neuonc/nou219
24. Gao X, Chen Y, Chen M, Wang S, Wen X, Zhang S. Identification of key candidate genes and biological pathways in bladder cancer. *PeerJ* (2018) 6: e6036. doi: 10.7717/peerj.6036
25. Lee HW, Park YM, Lee SJ, Cho HJ, Kim DH, Lee JII, et al. Alpha-smooth muscle actin (ACTA2) is required for metastatic potential of human lung adenocarcinoma. *Clin Cancer Res* (2013) 19(21):5879–89. doi: 10.1158/1078-0432.CCR-13-1181
26. Ikeda Y, Kiyotani K, Yew PY, Sato S, Imai Y, Yamaguchi R, et al. Clinical significance of T cell clonality and expression levels of immune-related genes in endometrial cancer. *Oncol Rep* (2017) 37(5):2603–10. doi: 10.3892/or.2017.5536
27. Li S, Huang J, Qin M, Zhang J, Liao C. High expression of CDCA7 predicts tumor progression and poor prognosis in human colorectal cancer. *Mol Med Rep* (2020) 22(1):57–66. doi: 10.3892/mmr.2020.11089
28. Wang H, Ye L, Xing Z, Li H, Lv T, Liu H, et al. CDCA7 promotes lung adenocarcinoma proliferation via regulating the cell cycle. *Pathol Res Pract* (2019) 215(11):152559. doi: 10.1016/j.prp.2019.152559
29. Yuan Y, Chen J, Wang J, Xu M, Zhang Y, Sun P, et al. Identification Hub Genes in Colorectal Cancer by Integrating Weighted Gene Co-Expression Network Analysis and Clinical Validation in vivo and vitro. *Front Oncol* (2020) 10:638:638. doi: 10.3389/fonc.2020.00638
30. Huang MY, Wang HM, Tok TS, Chang HJ, Chang MS, Cheng TL, et al. EVI2B, ATP2A2, S100B, TM4SF3, and OLFM4 as potential prognostic markers for postoperative Taiwanese colorectal cancer patients. *DNA Cell Biol* (2012) 31(4):625–35. doi: 10.1089/dna.2011.1365
31. Fan S, Meng D, Xu T, Chen Y, Wang J, Li X, et al. Overexpression of SLC7A7 predicts poor progression-free and overall survival in patients with glioblastoma. *Med Oncol* (2013) 30(1):384. doi: 10.1007/s12032-012-0384-8
32. Cheng L, Lu W, Kulkarni B, Pejovic T, Yan X, Chiang JH, et al. Analysis of chemotherapy response programs in ovarian cancers by the next-generation sequencing technologies. *Gynecol Oncol* (2010) 117(2):159–69. doi: 10.1016/j.ygyno.2010.01.041
33. Xie L, Song X, Yu J, Guo W, Wei L, Liu Y, et al. Solute carrier protein family may involve in radiation-induced radioresistance of non-small cell lung cancer. *J Cancer Res Clin Oncol* (2011) 137(12):1739–47. doi: 10.1007/s00432-011-1050-9
34. An HJ, Koh HM, Song DH. Apolipoprotein E is a predictive marker for assessing non-small cell lung cancer patients with lymph node metastasis. *Pathol Res Pract* (2019) 215(10):152607. doi: 10.1016/j.prp.2019.152607

Conflict of Interest: The authors declare that the research was conducted in the absence of any commercial or financial relationships that could be construed as a potential conflict of interest.

Copyright © 2020 Xiao, Liu, Li, Xiang, Wang, Li and Xiao. This is an open-access article distributed under the terms of the Creative Commons Attribution License (CC BY). The use, distribution or reproduction in other forums is permitted, provided the original author(s) and the copyright owner(s) are credited and that the original publication in this journal is cited, in accordance with accepted academic practice. No use, distribution or reproduction is permitted which does not comply with these terms.

frontiers in Oncology

REVIEW
published: 15 December 2020
doi: 10.3389/fonc.2020.610104

Myeloid-Derived Suppressor Cells: A New and Pivotal Player in Colorectal Cancer Progression

Kai Yin[1], Xueli Xia[2], Ke Rui[3], Tingting Wang[4]* and Shengjun Wang[2]**

[1] Department of General Surgery, Affiliated Hospital of Jiangsu University, Zhenjiang, China, [2] Department of Immunology, Jiangsu Key Laboratory of Laboratory Medicine, School of Medicine, Jiangsu University, Zhenjiang, China, [3] Department of Laboratory Medicine, Affiliated Hospital of Jiangsu University, Zhenjiang, China, [4] Department of Laboratory Medicine, Affiliated Wuxi People's Hospital of Nanjing Medical University, Wuxi Children's Hospital, Wuxi, China

OPEN ACCESS

Edited by:
Peng Qu,
National Institutes of Health (NIH),
United States

Reviewed by:
Anurag Singh,
Tübingen University Hospital,
Germany
Hua Jiang,
Medical University of South Carolina,
United States

***Correspondence:**
Kai Yin
jsyinkai@163.com
Tingting Wang
3288689388@qq.com
Shengjun Wang
sjwjs@ujs.edu.cn

Specialty section:
This article was submitted to Cancer Immunity and Immunotherapy, a section of the journal Frontiers in Oncology

Received: *25 September 2020*
Accepted: *10 November 2020*
Published: *15 December 2020*

Citation:
Yin K, Xia X, Rui K, Wang T and Wang S (2020) Myeloid-Derived Suppressor Cells: A New and Pivotal Player in Colorectal Cancer Progression. Front. Oncol. 10:610104. doi: 10.3389/fonc.2020.610104

Colorectal cancer (CRC) remains a devastating human malignancy with poor prognosis. Of the various factors, immune evasion mechanisms play pivotal roles in CRC progression and impede the effects of cancer therapy. Myeloid-derived suppressor cells (MDSCs) constitute an immature population of myeloid cells that are typical during tumor progression. These cells have the ability to induce strong immunosuppressive effects within the tumor microenvironment (TME) and promote CRC development. Indeed, MDSCs have been shown to accumulate in both tumor-bearing mice and CRC patients, and may therefore become an obstacle for cancer immunotherapy. Consequently, numerous studies have focused on the characterization of MDSCs and their immunosuppressive capacity, as well as developing novel approaches to suppress MDSCs function with different approaches. Current therapeutic strategies that target MDSCs in CRC include inhibition of their recruitment and alteration of their function, alone or in combination with other therapies including chemotherapy, radiotherapy and immunotherapy. Herein, we summarize the recent roles and mechanisms of MDSCs in CRC progression. In addition, a brief review of MDSC-targeting approaches for potential CRC therapy is presented.

Keywords: myeloid-derived suppressor cells, colorectal cancer, cancer immunology, colorectal cancer immunotherapy, tumor microenvironment

INTRODUCTION

Colorectal cancer (CRC) remains the third most common cancer and the third leading cause of cancer-related deaths in males and females (1). Despite improvements in systemic treatments for advanced CRC in recent years, only 12–14% of patients with metastatic CRC survive for five years (2). Moreover, patients with advanced CRC develop resistance to chemotherapy, radiotherapy, immunotherapy and targeted drug therapy, which results in increasing challenges in treating CRC. Recently, different types of immune cells such as myeloid-derived suppressor cells (MDSCs), dendritic cells (DCs), tumor-associated macrophages (TAMs), natural killer (NK) cells, and regulatory T cells (Tregs) were shown to impact CRC progression (3, 4).

CRC patients' responses to chemotherapy, radiation therapy, targeted drugs therapy and immunotherapy are affected by the tumor immune microenvironment (5, 6). Growing evidence has demonstrated that MDSCs accumulate and expand in the peripheral blood and tumor tissues, where they regulate host anti-tumor immune responses (7, 8). Once the MDSC population is expanded and activated in the immune system, it executes its numerous functions in tumor progression. MDSCs not only suppress anti-tumor immunity but also impede the efficacy of therapeutic agents for cancer treatment (9).

Immunosuppression is an important hallmark of most cancer growth and progression (10). In recent years, accumulating data have indicated that MDSCs, as one of the main immunosuppressive cell populations, are pivotal for cancer development (11). MDSCs represent a heterogeneous population of immature myeloid cells (IMCs) that fail to complete their differentiation into macrophages, DCs, or granulocytes (12). MDSCs consist of two large groups of cells: granulocytic or polymorphonuclear MDSCs (PMN-MDSCs) and monocytic MDSCs (M-MDSCs) (13). In general, the immunosuppressive function of MDSCs is regulated by multiple signaling pathways as well as interactions with several immune cell populations and mediators, which directly or indirectly suppress anti-tumor immunity and support cancer progression (7, 9). An increasing number of studies have focused on MDSCs, which are involved in regulation of the immune response in many types of cancer, but are poorly understood in CRC. It has been shown that different populations of MDSCs are observed in the peripheral blood and tumor tissue of CRC patients (14). A positive relationship between MDSCs and CRC progression including growth, metastasis, invasion, and angiogenesis has also been reported (15). Therapeutic agents targeting MDSCs have been proven to promote anti-tumor immunity and enhance the effects of immunotherapy against CRC. In this review, we discuss developments on the role of MDSCs in CRC: (1) MDSCs and their functional correlation with cancer, (2) MDSCs-mediated signaling pathways in CRC progression, and (3) MDSCs-targeting approaches for potential CRC treatment.

Abbreviations: DCs, Dendritic cells; TAMs, tumor-associated macrophages; NK, natural killer; Tregs, regulatory T cells; UCB, umbilical cord blood; MDSCs, myeloid-derived suppressor cells; IMCs, immature myeloid cells; PMN-MDSCs, polymorphonuclear MDSCs; M-MDSCs, monocytic MDSCs; e-MDSCs, early-stage MDSCs; PBMCs, peripheral blood mononuclear cells; F-MDSCs, fibrocytic MDSCs; PGE2, prostaglandin E2; TGF-β, transforming growth factor beta; HIF-1α, hypoxia-inducible factor-1α; CRC, colorectal cancer; CCR2, C-C chemokine receptor type 2; iNOS, inducible nitric oxide synthase; CCL2, chemokine ligand 2; CXCR, C-X-C motif chemokine receptor; ENTPD2, ectonucleoside triphosphate diphosphohydrolase 2; RONS, reactive oxygen and nitrogen species; RNS, reactive nitrogen species; G-CSF, granulocyte colony-stimulating factor, GM-CSF, granulocytes macrophage colony-stimulating factor; M-CSF, macrophage colony-stimulating factor; STAT3, signal transducer and activator of transcription 3; NADPH, nicotinamide adenine dinucleotide phosphate; TME, tumor microenvironment; NF-κB, nuclear factor-κB; NO, nitric oxide; ROS, reactive oxygen species; VEGF, vascular endothelial growth factor; JAK3, Janus kinase 3; MHC, major histocompatibility complex; IDO, indoleamine 2,3dioxygenase; Bcl-2, B-cell lymphoma 2; TIM3, T-cell immunoglobulin domain and mucin domain 3; ADAM17, disintegrin and metalloproteinase domain17; IFN-γ, interferon gamma; HCC, hepatocellular carcinoma; IRF2, interferon regulatory factor 2; RIPK3, receptor-interacting protein kinase 3; COX-2, cyclooxygenase-2; IBD, inflammatory bowel disease; VISTA, V-domain Ig suppressor of T-cell activation; GNAI1, G protein subunit alpha i1; PAR2, protease-activated receptor 2; S1PR1, sphingosine-1-phosphate receptor 1; ATRA, all-trans-retinoic acid; HDC, histamine dihydrochloride; XIAP, X-linked inhibitor of apoptosis protein; PI3K, phosphatidylinositol 3-kinase; CTLA-4, cytotoxic T lymphocyte-associated antigen-4.

MOLECULAR FEATURES AND SUPPRESSIVE FUNCTION OF MDSCs

Phenotypic Features

Under normal circumstances, IMCs do not have immunosuppressive functions and are believed to be constitutively present in healthy individuals. The generation of IMCs occurs in the bone marrow and is regulated by growth factors including granulocyte colony-stimulating factor (G-CSF), granulocyte macrophage colony-stimulating factor (GM-CSF), and macrophage colony-stimulating factor (M-CSF) (16, 17). During this process, IMCs migrate to the blood and various peripheral organs, where they differentiate into myeloid cells such as macrophages, neutrophils, and DCs. However, in pathological conditions including cancers, chronic infections and autoimmune diseases, IMC differentiation is impaired leading to an accumulation of MDSCs (18–20).

MDSCs are IMCs that expand during the growth and metastasis of malignant tumors and in inflammatory conditions. Their heterogeneity is tumor-dependent, and their phenotype and functions change with cancer progression (21). Recently, neutrophils were distinguished from MDSCs by the expression of the lectin-type oxidized LDL receptor 1 (LOX-1). LOX-1$^+$ neutrophils have been shown to suppress T cells proliferation (22). These cells, also called tumor-associated neutrophils (TANs), were found in the tumor microenvironment (TME) and promote cancer cell migration and invasion (23). However, the main difference between MDSCs, neutrophils, and monocytes is their functions, with MDSCs having the potential to suppress immune activity.

There are two types of macrophages, namely, M1-like macrophage and M2-like macrophage. The macrophages found in the TME are known as TAMs and are predominantly M2 macrophages (24). TAMs are abundant in the microenvironment of CRC and are strong promoters of angiogenesis and lymphogenesis, thus contributing to tumor progression (25). Interferon gamma (IFN-γ), LPS, and GM-CSF induce polarization of M1 TAMs from monocytes, which are involved in antitumor immunity (26). In contrast, CSF-1, interleukin (IL)-4, IL-10, transforming growth factor beta (TGF)-β, and IL-13 contribute to M2 TAM polarization (27). M2 macrophages suppress cytotoxic T cell activities and attract Tregs, which promote tumor growth and immune escape (28). Furthermore, while M1 macrophages express CD64, suppressor of cytokine signaling 1 (SOCS1), indoleamine 2,3-dioxygenase (IDO) and chemokine (C-X-C motif) ligand 1 (CXCL1), M2 macrophages express mannose receptor C-type 1 (MRC1), CD23, and chemokine ligand 22 (CCL22) (29). Macrophages are highly plastic, and under certain physiological and pathological conditions, M1 macrophages can repolarize into M2 macrophages, and vice versa (30). However, the molecular mechanisms that regulate the macrophage polarization remain poorly understood.

Although TAMs and MDSCs are distinct cell types, they are not clearly distinguishable and have several characteristics in common. In the TME, cytokines and chemokines from tumor cells can influence normal myelopoiesis and increase the differentiation of M-MDSCs into PMN-MDSCs (31). M-MDSCs and inflammatory monocytes migrate to the tumor site *via* the CCL2/CCR2 pathways and differentiated into TAMs in response to various factors secreted by tumor cells (32). In addition, infiltrating MDSCs can also differentiate into TAMs through a combination of Toll-like receptor (TLR) and cytokine signaling (33, 34). MDSCs are phenotypically distinct from neutrophils, macrophages and monocytes. They can be divided into two major types based on their cell surface markers. In mice, PMN-MDSCs are defined as $CD11b^{+}Gr\text{-}1^{+}Ly6G^{high}Ly6C^{low}$ cells, whereas M-MDSCs are defined as $CD11b^{+}Gr\text{-}1^{+}Ly6G^{low}Ly6C^{high}$ cells. The frequencies of PMN-MDSCs and M-MDSC subsets differ between tumors and organs in tumor-bearing mice with PMN-MDSCs accounting for 70–80% of MDSCs and M-MDSCs representing 20–30% (35). In humans, PMN-MDSCs are HLA-DR-$CD11b^{+}CD14^{-}CD33^{+}$ ($CD15^{+}$ or $CD66^{+}$) cells and M-MDSCs are HLA-$DR^{low/-}CD11b^{+}CD14^{+}CD15^{-}$ cells (36). Other cell surface molecules can also be used to identify other subsets of MDSCs, such as CD115, CD80, and CD124 (37, 38). Moreover, M-MDSCs express inducible nitric oxide synthase (iNOS) and generate nitric oxide (NO), while PMN-MDSCs produce reactive oxygen species (ROS) and arginase-1 (39).

In human peripheral blood, early-stage MDSCs (e-MDSCs), which are comprised of more immature progenitors than conventional MDSCs, are defined by Lin^{-} (including CD3, CD14, CD15, CD19, CD56) HLA-DR-$CD33^{+}$. While e-MDSCs markers for murine cells have yet to be determined (36, 40–42), a subset of e-MDSCs with the phenotype of $CD11b^{+}Gr\text{-}1^{-}F4/80^{-}MHC\text{-}II^{-}$ has been described in IL-6 high-expressing 4T1 mice mammary carcinoma models (43). Human fibrocytic MDSCs (F-MDSCs), which can be differentiated from umbilical cord blood (UCB) precursors, have been identified as a new MDSCs subset with fibrocytic phenotypes and immunosuppressive functions. They are defined as $CD11b^{low}CD11c^{low}CD33^{+}IL\text{-}4Ra^{+}$ (44, 45). In addition, PMN-MDSCs and M-MDSCs are also phenotypically different from neutrophils. Compared to neutrophils, PMN-MDSCs have fewer granules and low expression of CD16 and CD62L (36, 41, 42, 46). The phenotypes and markers of MDSCs are shown in **Table 1**.

Recruitment and Expansion of MDSCs

Cytokines can facilitate the recruitment and expansion of MDSCs in the TME. Tumor-induced factors, including prostaglandin E2 (PGE2), IL-6, IL-10, IL-1β, and transforming growth factor beta (TGF)-β have been shown to result in the recruitment and activation of MDSCs in the TME in malignant tumors (47). For example, IL-1β and IL-6 can induce the accumulation and activation of MDSCs at tumor sites (48–50). IL-1β not only promotes the accumulation of MDSCs but also induces expression of other molecules that are necessary for the expansion of MDSCs such as vascular endothelial growth factor (VEGF), IL-6 and GM-CSF (51). Other cytokines, such as IL-10 and TGF-β have the ability to generate MDSCs populations, as well as mediate their suppressive functions (52, 53). Thus, MDSCs are able to produce TGF-β and create a feedback loop that sustains their antitumor immunity. Furthermore, IL-17, which is secreted by Th17 cells, is overexpressed in cancer cells and promote MDSCs translocation from the periphery to the tumor sites (54).

Chemokines also influence MDSCs expansion and activation. Some of them, such as chemokine ligand 2 (CCL2) can interact with its corresponding receptor C-C chemokine receptor type 2 (CCR2) to promote chemotaxis to areas of inflammation (55, 56). IL-8 is released by cancer cells and binds to G protein-coupled receptors C-X-C motif chemokine receptor 1 and 2 (CXCR1 and CXCR2) on MDSCs (57). Moreover, the CCL3/CCR5 axis has been reported to induce the maintenance of immunosuppressive myeloid cells in tumor areas (55).

Hypoxia is commonly found in the TME and is recognized as an important factor that mediates MDSCs expansion. It has been shown that hypoxia inducible factor 1 alpha (HIF-1α) can induce the expression of ectonucleoside triphosphate diphosphohydrolase 2 (ENTPD2), an ectoenzyme on MDSCs, resulting in MDSCs expansion in the TME (40). In addition, hypoxia can upregulate VEGF and functional molecule expression and lead to MDSCs accumulation in both mice and patients with lung cancer (58, 59). This process is mediated by the VEGF receptor, which is expressed on MDSCs (58).

MDSCs Immunosuppressive Mechanism

Notably, one of the features of MDSCs in TME is the immune suppressive function. MDSCs suppress the activity of immune cells through multiple mechanisms, including the generation of reactive oxygen and nitrogen species (RONS), the degradation of L-arginine, the production of immunosuppressive cytokines such as IL-10 and TGF-β, the inhibition of T cells, and the induction of other immunosuppressive cells (41, 60). Firstly, MDSCs can regulate anti-tumor immune responses through the production of RONS including NO and ROS (61, 62). MDSCs require activation of signal transducer and activator of transcription 3 (STAT3) and increase nicotinamide adenine

TABLE 1 | Summary of commonly expressed markers in mice and human MDSCs.

MDSCs	PMN-MDSCs Markers	M-MDSCs Markers	e-MDSCs	F-MDSCs
Mice	$CD11b^{+}Gr\text{-}1^{+}Ly6G^{high}$ $Ly6C^{low}$	$CD11b^{+}Gr\text{-}1^{+}Ly6G^{low}Ly6C^{high}$	–	–
Human	HLA-DR-$CD11b^{+}$ $CD14^{-}CD33^{+}(CD15^{+}/CD66^{+})$	HLA-$DR^{low/-}CD11b^{+}$ $CD14^{+}$ $CD15^{-}$	Lin^{-}(CD3/CD14/CD15/CD19/ CD56)HLA-DR-$CD33^{+}$	$CD11b^{low}CD11c^{low}CD33^{+}IL\text{-}4Ra^{+}$

dinucleotide phosphate (NADPH) oxidase activity to produce ROS (13, 41). However, NADPH oxidase may also synthesize reactive nitrogen species (RNS) like NO by metabolizing L-arginine (63). ROS are also activated *via* the STAT3 transcription factor and are associated with the metabolism of L-arginine (52, 64). Taken together, these data suggest that production of ROS, NO, and RNS are dependent on L-arginine metabolism. Furthermore, these factors can suppress T cell populations, thus rendering them incapable of facilitating an anti-cancer response (65). In the TME, S100A8/A9 has been shown to activate the production of ROS in a STAT3-dependent manner. This leads to nitration of the T cell receptor-alpha-beta (TCR$\alpha\beta$) chain, resulting in T cells that lack the ability to interact with the peptide antigen bound to the major histocompatibility complex class II (MHC-II) and are therefore unable to initiate an anti-cancer response (51). Similarly, iNOS released by MDSCs is an additional mechanism responsible for inducing oxidative stress in the TME. NO produced by iNOS can suppress the T cells' response and induce T cell apoptosis *via* various mechanisms, including the inhibition of Janus kinase 3 (JAK3), STAT5, and MHC-II expression (11, 13). Synergistically, S100A8/A9 also increases the production of iNOS through activation of STAT1 (66).

Secondly, MDSCs can suppress T cell activation and proliferation by depleting essential amino acids. MDSCs increase arginase-1 activity and induce T cell suppression *via* the depletion of L-arginine (11, 13, 67). The lack of L-arginine suppresses proliferation of activated T cells and decreases the expression of the T cell receptor-zeta (TCR-ζ) chain (68). As a result, arginase-1 leading to depletion of L-arginine in the TME suppresses the ability of the T cells to exert their anti-tumor functions (69). Indeed, MDSCs have the ability to inhibit T cell proliferation by regulating the G0/G1 phase of their cell cycle (70). Expression of IDO by MDSCs can also suppress T cell proliferation by decreasing tryptophan levels and producing cytotoxic metabolites (71). Furthermore, it was reported that chronic psychological stress can also lead to MDSCs accumulation in the bone marrow of Balb/c mice where they inhibit T cells proliferation (72).

Other mechanisms that result in MDSCs-induced T cell apoptosis have been described. For example, MDSCs can decrease expression level of B-cell lymphoma 2 (Bcl-2) expression and increase FAS (CD95 ligand) expression in T cells. Furthermore, MDSCs express galectin-9, which binds to T-cell immunoglobulin domain and mucin domain 3 (TIM3), an inhibitory surface molecule on lymphocytes, leading to decreased T cell viability (73, 74). Interestingly, different subtypes of MDSCs utilize different mechanisms to mediate immunosuppressive functions in the TME. M-MDSCs produce high levels of NO and immunosuppressive cytokines such as IL-10, which suppress both antigen-specific and non-specific T-cell responses (55). In contrast, PMN-MDSCs suppress T-cell responses by generating ROS based on an antigen-specific approach (75, 76).

Thirdly, MDSCs-mediated lymphocyte trafficking and viability are restricted. MDSCs can suppress T cell movement to the lymph nodes *via* down-regulation of L-selectin (CD62L) on the surface of T cells by increasing expression of disintegrin and metalloproteinase domain17 (ADAM17). MDSCs can also interrupt the migration of CD8+ T cells to tumor sites by peroxynitrite modification of CCL2 (77, 78). Finally, MDSCs can promote the induction of other immunosuppressive cells. MDSCs have been shown to induce the generation of FoxP3$^+$ Treg cells *in vivo* through the production of IFN-γ, TGF-β and IL-10. This effect is independent of NO production (38). Furthermore, the CCR5 ligands CCL3, CCL4, and CCL5 were shown to promote CCR5$^+$ Treg cell recruitment in mouse models of melanoma (74). It has been reported that CD14$^+$HLA-DR$^{-/low}$ M-MDSCs could induce CD4$^+$CD25$^+$Foxp^{3+}Treg cells when co-cultured with autologous T cells in hepatocellular carcinoma (HCC) patients (79). Moreover, F-MDSCs can inhibit T cell proliferation by releasing IDO and promoting the expansion of Tregs (80). With the exception of Tregs stimulation, MDSCs can also reverse macrophages to an M2-like phenotype with low IL-12 production, thereby promoting tumor growth (81). In addition, MDSCs impair NK cell function and cytotoxicity by suppressing the production of IFN-γ from NK cells and decreasing the expression of natural killer group 2 member D (NKG2D) (82). Induction of MDSCs in a tumor-bearing mouse model of lung cancer can lead to impairment of B cell differentiation and function though an IL-7 and STAT5-dependent manner (83). The MDSCs immunosuppressive mechanisms described above are outlined in **Figure 1**.

ROLES OF MDSCs IN COLORECTAL CANCER

Prognostic Values of MDSCs in CRC

MDSCs play an important role in the immunosuppressive mechanism associated with CRC progression. Several studies have demonstrated that MDSCs in the peripheral blood and tumor tissues are associated with tumor stage, histological grade of cancer and lymph node metastases in CRC (84, 85). It has been reported that the peripheral blood of CRC patients contains a significantly increased percentage and absolute number of CD33$^+$CD11b$^+$HLA-DR$^{-/low}$ MDSCs compared with healthy donors. This increasement was closely correlated with clinical cancer stage and tumor metastasis but not primary tumor size. Interestingly, radical operation can significantly decrease the level of circulating MDSCs in CRC patients (76, 85). Moreover, the proportion of PMN-MDSCs and immature MDSCs (I-MDSCs) was found to be higher in the tumor tissues of CRC patients compared to tumor-adjacent tissues (86).

In a recent study, CD33$^+$ MDSCs and Yes-associated protein 1 (YAP1) were identified as predictors for the prognosis of CRC patients. This study demonstrated that CD33$^+$MDSCs numbers and YAP1 expression levels were increased in tumor tissues compared with those of tumor-adjacent tissues from the same CRC patients (87). Furthermore, CD33$^+$CD11b$^+$HLA-DR$^{-/low}$ myeloid cells were shown to be expanded in the peripheral blood of CRC patients, with the number of circulating MDSCs positively correlating with

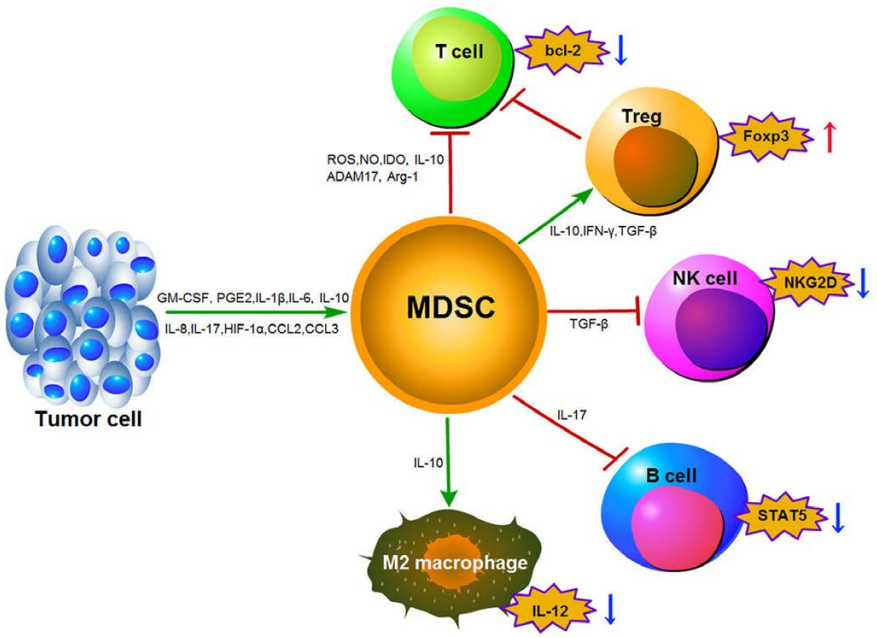

FIGURE 1 | Main mechanisms of immunosuppression function mediated by MDSCs in the tumor microenvironment.

poor prognosis and low survival rates (88). In addition, a lower lymphocyte-to-monocyte ratio (LMR) was associated with poor prognosis in CRC patients, who were found to have higher levels of circulating MDSCs (89). Unresectable metastatic CRC patients with high M-MDSCs levels in their peripheral blood were also shown to have a significantly shorter progression-free survival (90). Interestingly, it was proven that although Tregs, Th17, and PMN-MDSCs were significantly increased in metastatic CRC, only high levels of PMN-MDSCs were associated with a poor prognosis for CRC patients (91).

Signaling Pathways for MDSCs-Mediated Functions in CRC

The immunosuppressive function of MDSCs relies on the activation of different intracellular signaling pathways. Many studies indicate that MDSCs-associated signaling pathways are involved in CRC development. KRAS mutations, for example, are frequently observed in human CRC and correlate positively with tumor aggressiveness and metastasis (92–94). KRAS-mediated repression of interferon regulatory factor 2 (IRF2) was associated with high expression of CXCL3, which led to MDSCs migration to the TME through binding to CXCR2 on the MDSCs (95). Receptor-interacting protein kinase 3 (RIPK3) is essential for mucosal repair in CRC. It has been reported that reduction of RIPK3 in CRC cells induces expansion of MDSCs and increases cyclooxygenase-2 (COX-2) expression, which then catalyze PGE2 and enhance MDSCs function (96). Similarly, RIPK3 signaling in an I-MDSCs subset promoted intestinal tumor development in MC38 cell tumors by expanding IL17-producing T cells (97).

It has been suggested that down-regulation of mucin 1 (MUC1) in hematopoietic cells increases MDSCs expansion in inflammatory bowel disease (IBD) leading to the development of CRC (98). Moreover, MUC13 promotes colitis-associated colorectal tumors development through the β-catenin signaling pathway and increases MDSCs expansion in the TME (99). In addition, MDSCs can increase the expression levels of ROS and NO, which may result in DNA damage and promote tumor progression in CRC (100). Previous studies have also demonstrated that CRC cells secrete VEGF-A, which leads to TAMs induction and subsequent production of chemokine (C-X-C motif) ligand 1 (CXCL1) in the primary tumor. Increased CXCL1 in liver tissue was shown to recruit CXCR2-positive MDSCs to form a premetastatic niche in CRC (101). In addition, overexpression of CXCR4 has been found to play a crucial role in the invasion of CRC, as well as promoting the epithelial–mesenchymal transition (EMT) and infiltration of MDSCs in colonic tissue, accelerating colitis-associated and Apc mutation-driven colorectal tumorigenesis (102). Recently, Varun Sasidharan Nair et al. reported some genes associated with histone deacetylases (HDAC) activation, DNA methylation, Wnt and IL-6 signaling pathways are upregulated in CRC tumor infiltrating I-MDSCs, and propose that they could be exploited as potential targets for CRC therapy (86).

The JAK/STAT pathway is considered to be a major player in mediating immunosuppression (103, 104). MDSCs isolated from the spleen of CT26 cell-bearing mice exhibited inhibition of phosphorylation of STAT1 (p-STAT1) in response to IFN-α or IFN-γ (105). However, another study demonstrated that IFN-γ is not a key regulator of MDSCs and that targeting it would be

unlikely to alter MDSCs accumulation or function in tumor-bearing mice (106). It has been reported that IL-6 activates expansion of MDSCs *via* the JAK2/STAT3/NF-κB signaling pathway, resulting in AOM/DSS-induced colon tumor development in G protein subunit alpha i1 (GNAI1) and GNAI3 (GNAI1;3) double-knockout (DKO) mice (107). It has also been shown that protease-activated receptor 2 (PAR2) deficiency significantly promotes tumor development in the AOM/DSS-induced colitis-associated colon cancer model through accumulation of MDSCs and enhancement of their immunosuppressive activity *via* STAT3-mediated ROS production (108). Previous studies have demonstrated that G-CSF could promote MDSCs' survival and activation through the STAT3 signaling pathway in a mouse colitis-associated cancer model (109). Additionally, CCL2 was initially characterized as a cytokine that was found to be increased in CRC tissues and reported to enhance PMN-MDSCs' function in a STAT3-mediated manner (110). Xu et al. demonstrated that sphingosine-1-phosphate receptor 1 (S1PR1) and STAT3 are elevated in human CRC tissues and propose that they recruit MDSCs through the S1PR1–STAT3–IL-6 axis to promote tumor growth and liver metastasis niche (111). In addition, STAT6 appears to promote expansion of MDSCs and contributes to intestinal tumor progression in ApcMin/+ mice (112). Finally, S100A8/A9 is another pro-inflammatory molecular that activates the STAT3 signaling pathway, which is responsible for maintaining the MDSCs suppressive function (113).

Of significance, a highly hypoxic environment leads to the accumulation and activation of MDSCs in CRC development. Hypoxia within the TME is associated with increased V-domain Ig suppressor of T-cell activation (VISTA) expression, which promotes MDSCs function. VISTA is highly expressed in the CRC microenvironment, while both VISTA and HIF-1α activity were found to be increased in a cohort of CRC patients (114). Notably, malignant tumors can potentially recruit MDSCs from the bone marrow by releasing exosomes. Previous studies have shown that hypoxia can induce MDSCs to secrete more exosomes in a HIF-1α dependent manner (115). The exosomal contents can reprogram the target cell and increase mobility of MDSCs to the tumor sites. Inhibition of S100A9 was found to suppress the susceptibility of mice to AOM/DSS-induced colitis-associated colon cancer (116).

Targeting MDSCs in CRC Therapy

The safety and efficacy of using MDSCs inhibition as a CRC therapy have been evaluated in an increasing number of studies (**Table 2**). Here we summarize novel preclinical approaches targeting MDSCs in CRC (**Figure 2**). Current treatments aim to deplete MDSCs, inhibit their immunosuppressive function, and block their expansion to the tumor site (128). Several studies have proved that depletion of the number of MDSCs and inhibition of their function in tumor tissue are an important strategy for CRC therapy. For example, targeting MDSCs with all-trans-retinoic acid (ATRA) has been shown to decrease their number and suppress their function in tumor bearing mice (117). Consequently, ATRA may consider being a novel immunotherapeutic protocols to target CRC in the future. Similarly, histamine dihydrochloride (HDC), a NADPH oxidase 2 (NOX2) inhibitor, has also been shown to inhibit tumor progression by reducing the accumulation of tumor MDSCs in MC-38 cell-bearing mice (118). Embelin (2,5-dihydroxy-3-undecyl-1,4-benzoquinone) is a non-peptidic small molecule inhibitor of X-linked inhibitor of apoptosis protein (XIAP). Wu et al. found that embelin can significantly reduce the accumulation number of MDSCs in the peripheral lymphoid organ and tumor tissue, and impair the immunosuppressive function of MDSCs by reducing the production of ROS and arginase-1 level in colitis-associated tumorgenesis (119). Naringin (4′,5,7-trihydroxyavanone-7-rhamnoglucoside), a major flavanone glycoside that occurs naturally in citrus fruits, inhibits the severity of colitis and CRC development through regulation of the MDSCs' immunosuppressive function *via* the NF-κB/IL-6/STAT3 axis in colorectal tissues (120).

Recruitment of tumor MDSCs is dependent on the receptor tyrosine kinase CSF-1R. Thus, inhibition of CSF-1R signaling can significantly block the number of tumor-infiltrating MDSCs number and enhance anti-tumor T cells responses in tumor bearing mice (121). In addition, blocking the immunosuppressive function of MDSCs can be achieved by targeting anti-G-CSF monoclonal antibody. Treatment with an anti-G-CSF

TABLE 2 | Summary of preclinical studies analyzing the role of MDSCs in CRC and therapeutic agents.

Mouse models	Cells lines	Therapeutic agents	Targets	Ref.
C57/BL6 mice	MC38 cells	all-trans-retinoic acid (ATRA)	–	(117)
C57/BL6 mice and Nox2-KO mice	MC38 cells	Histamine dihydrochloride (HDC)	NOX2	(118)
C57BL/6 mice	–	Embelin	XIAP	(119)
C57BL/6 mice	–	Naringin	–	(120)
Balb/c mice	CT26 cells	CSF-1R kinase inhibitors (PLX647 and PLX5622)	CSF-1R	(121)
C57/BL6 mice and SCID mice	–	anti-G-CSF mAb	G-CSF	(109)
C57BL/6 mice	MC38 cells	anti-DC-HIL mAb	DC-HIL	(122)
Balb/c mice	CT26 cells	Curcumin	–	(123)
Balb/c mice	CT26 cells	TLR7/8 agonist, R848	TLR7/8	(124)
C57BL/6 mice,CCR2$^{-/-}$ and CCL2$^{-/-}$ mice	MC38 cells	anti-CCR2 mAb	CCR2	(125)
Balb/c mice and C57BL/6 mice	CT26 cells and MC38 cells	anti-IL-6 mAb	IL-6	(126)
Balb/c mice	CT26 cells	(-)-4-O- (4-O-β-D-glucopyranosylcaffeoyl) quinic acid (QA)	PI3Kδ/γ	(127)

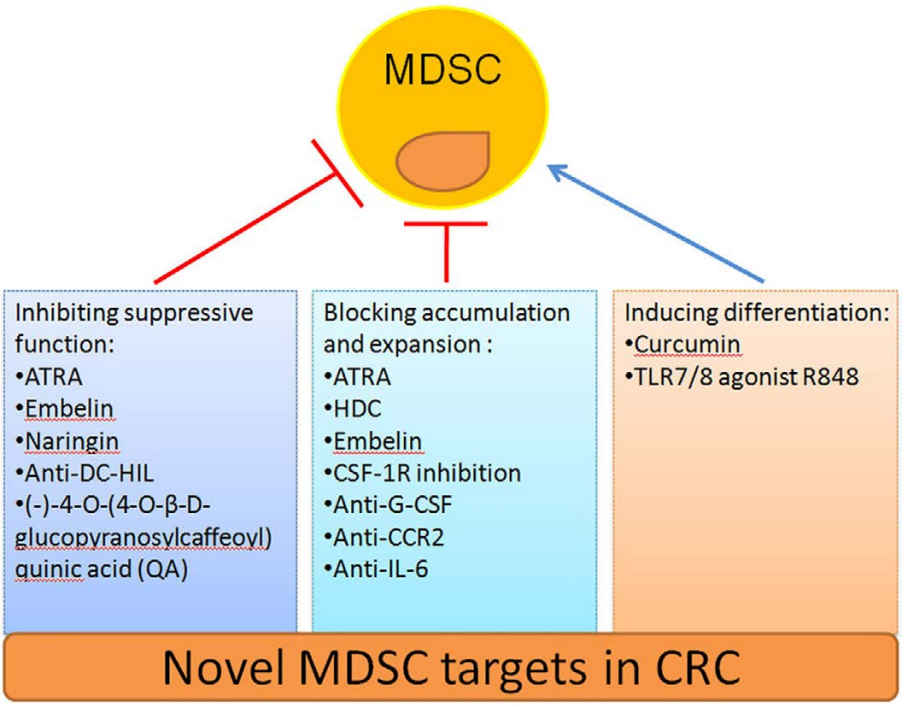

FIGURE 2 | Novel strategies to target MDSCs in CRC.

monoclonal antibody reduces MDSCs accumulation and decreases the migration, proliferation, and functional maintenance of MDSCs and could therefore become a potential therapeutic agent for colitis-associated cancer (109). Previous results have indicated that DC-HIL^{+}MDSCs are expanded in the blood of metastatic CRC patients. Since, anti-DC-HIL mAb treatment can suppress the function of MDSCs isolated from treated mice, functionally blocking DC-HIL on MDSCs could also be potentially beneficial in the treatment of metastatic CRC (122).

Other treatments include the induction of MDSCs differentiation alone or in combination with radiotherapy, chemotherapy, surgery or other kinds of immunotherapy to target CRC (129). Curcumin has been shown to inhibit the expansion of MDSCs, activate STAT3 and NF-κB in MDSCs, and polarize MDSCs toward a M1-like phenotype in CT26 cell-bearing mice (123). Recently, the TLR7/8 agonist R848, as a new immunologic adjuvant, was found to reverse the functional orientation of MDSCs towards M1 macrophages, suggesting that R848 may be a potential immunologic adjuvant in chemotherapy for oxaliplatin-resistant CRC (124). It has been reported that treatment with anti-CCR2 antibody can alleviate radiation-induced MDSCs infiltration in CRC tumor tissues by activation of the STING pathway (125). Hence, anti-CCR2 antibody treatment may improve radiotherapy for advanced CRC patients. A previous study indicated that IL-6 induces strong immunosuppression in the CRC microenvironment by recruiting MDSCs and impairing T cells infiltration. Interestingly, an anti-IL-6 and anti-PD-L1 combination treatment prolonged tumor-bearing mouse survival, providing a novel strategy to overcome anti-PD-L1 resistance in CRC (126). In addition, blocking the immunosuppressive function of MDSCs can also be achieved by targeting phosphatidylinositol 3-kinase (PI3K)δ/γ. Hence, (-)-4-O-(4-O-β-D-glucopyranosylcaffeoyl) quinic acid (QA), a selective small molecule inhibitor of PI3Kδ/γ, has the ability to reshape the tumor immune microenvironment and promote responses to anti-PD-1 treatment in a colon tumor model (127).

While there is an abundance of preclinical data supporting the theory that suppression of MDSCs could be a beneficial therapeutic tool. Several clinical studies have also indicated that inhibition of MDSCs is beneficial to CRC patients. Metastatic CRC patients treated with a first-line combination regimen of 5-FU, oxaliplatin, and bevacizumab (FOLFOX-bevacizumab) were associated with a better survival outcome. Furthermore, the FOLFOX-bevacizumab treatment was found to decrease the PMN-MDSC population in metastatic CRC patients (91). While docosahexaenoic acid (DHA) has been shown to inhibit caspase-1 activity in 5-fluorouracil (5-FU) treated MDSCs, a negative relationship between the DHA content in plasma and the induction of caspase-1 activity in MDSCs of CRC patients treated with 5-FU-based chemotherapy has been reported (130). Thus, these data provide new insights into the regulation of DHA and its potential benefit in 5-FU-based chemotherapy for CRC patients. Previous studies demonstrated that CD38 is a

transmembrane receptor–ectoenzyme expressed by MDSCs in esophageal cancer and multiple myeloma (131, 132). Interestingly, a significant expansion of $CD38^+$M-MDSCs were observed in PBMCs of CRC patients when compared with healthy donors, and $CD38^+$M-MDSCs frequencies were significantly higher in CRC patients who had previously received any form of cancer treatment (surgery, chemotherapy or radiotherapy, targeted therapy, or a combination of these methods) when compared with treatment-naive patients (133). This study supported a method to target M-MDSCs with an anti-CD38 monoclonal antibody could be a valuable therapeutic tool for the treatment of metastatic CRC patients.

Immune Checkpoints

Growing evidence suggests that the immunosuppressive microenvironments in tumors result from the activation of MDSCs, PD-1/PD-L1 and cytotoxic T lymphocyte-associated antigen-4(CTLA-4) pathways (134). PD-1 has been found to bind to its ligand PD-L1 and then induce T cell anergy and apoptosis (135). CTLA-4 is another receptor expressed on the surface of T cells, which inhibits T cells activities by competing with CD28 to bind to the two T cell activation antigens, CD80 and CD86 (136). PD-1 and CTLA-4 are immune checkpoint proteins expressed on activated T cells (**Figure 3**). Blocking PD-L1 or CTLA-4 signaling has been shown to be beneficial for cancer patient survival. MDSCs express high levels of PD-L1, and this upregulation of PD-L1 has been associated with expression of S100A9 and HIF-1α (69, 137). It has been indicated that PD-L1 expression on MDSCs is increased in CRC patients and colon tumor bearing mice, suggesting that it may be a potent mediator of immunosuppression function (138, 139). Furthermore, PD-$L1^+$MDSCs were significantly decreased after neutralization of IFN-γ in the TME (139). Interestingly, PD-$L1^+$MDSCs are significantly increased in HCC patients, while M-CSF and VEGFA have been shown to induce PD-$L1^+$MDSCs *in vitro* (140). Compared to responding patients, PMN-MDSCs also expressed high levels of PD-L1 in non-responding melanoma patients treated by ipilimumab (141).

Several studies found that MDSCs and other molecules such as PD-L1 and CTLA-4 in tumor tissues are sensitive predictive markers for patients' response to chemoradiotherapy for rectal cancer patients (142). In the latest study, it was demonstrated that blockade of CXCR2 on MDSCs can overcome resistance to anti-PD-1 therapy in CRC-expressing oncogenic KRAS (95). Similarly, MDSCs elimination can reverse resistance to anti-PD-L1 or combination of normo-fractionated radiotherapy plus immunotherapy in CRC (143). Moreover, HDC can reduce the accumulation of intratumoral MDSCs in colon tumor-bearing mice and improve the anti-tumor efficacy of the PD-1/PD-L1 checkpoint blockade (118). Interestingly, IL-6 blockade was also reported to reverse the anti-PD-L1 resistance and inhibit CRC growth by reducing the number of MDSCs (126). MUC13-deficient mice have fewer MDSCs and are sensitive to anti-PD-L1 therapy, suggesting that MUC13 may be useful for in the treatment of colitis-associated cancer (99). Additionally, it has been revealed that treatment using an anti-KIT monoclonal antibody in a mouse colon cancer model enhanced the anti-tumor activity of anti-CTLA-4 and anti-PD-1 therapy by selectively reducing the MDSCs population (144).

Several studies have shown that the increasing number of TAMs in tumor correlates with favorable 5-year overall survival (OS) for CRC patients (145, 146). Increased M2 macrophage numbers in the TME promote the initiation and growth of tumor. However, few strategies are currently available to modulate TAMs by repolarizing the M2 macrophages to become M1 macrophages. A recent study demonstrated that PD-$L1^+$ T cells can engage PD-1^+ macrophages, inducing an alternative M2-like program, which have effects on adaptive

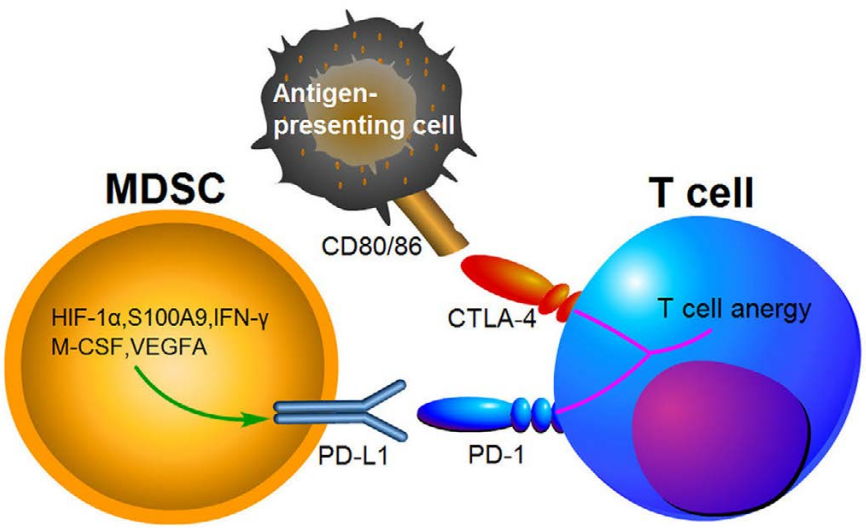

FIGURE 3 | The expression of PD-L1 in MDSCs causing T cell anergy *via* binding to its respective receptor.

antitumor immunity (147). In addition, Wang et al. showed that CD30L deficiency promote the accumulation of MDSCs, increase the expression of PD-L1 on MDSCs and TAMs, and enhance immunosuppressive function in an AOM/DSS-induced CAC model, suggesting that CD30L/CD30 signaling could be a potential candidate target for immunotherapy in CAC (148).

CONCLUSIONS

In conclusion, numerous studies have documented the important role of immunosuppressive MDSCs in CRC development in mice and cancer patients. During CRC progression, MDSCs-mediated immunosuppressive activity is regulated by many different signaling pathways. MDSCs promote CRC progression by increasing cell proliferation, cancer stemness, enhancing tumor invasiveness and metastasis. Given that the mechanisms controlling expansion and activation of MDSCs in tumor tissues or in the peripheral blood are distinct, it is difficult to devise a therapeutic approach to reduce their numbers or arrest their function. Furthermore, monotherapies targeting MDSCs have shown promising but limited efficacy. Thus, it is important to elucidate novel mechanisms involving different stromal components and myeloid cells such as cancer associated fibroblasts (CAFs), TAMs and neutrophils. Further studies are required to strengthen the knowledge about MDSCs and to better understand the effects in combination with other therapies involving different immunotherapeutic approaches for CRC therapy.

AUTHOR CONTRIBUTIONS

KY drafted the manuscript. XX and KR discussed and revised the manuscript. TW and SW designed the study and provided critical suggestions. All authors contributed to the article and approved the submitted version.

FUNDING

This study was conducted with support from the Natural Science Foundation of Jiangsu (Grant No. BK20190242 and BK20170563), Jiangsu Province's Key Medical Talents Program (Grant No.ZDRCB2016018), Research Project of Jiangsu Commission of Health (Grant No. K2019019).

REFERENCES

1. Siegel RL, Miller KD, Jemal A. Cancer statistics, 2019. *CA Cancer J Clin* (2019) 69:7–34. doi: 10.3322/caac.21551
2. Siegel RL, Miller KD, Fedewa SA, Ahnen DJ, Meester RGS, Barzi A, et al. Colorectal cancer statistics, 2017. *CA Cancer J Clin* (2017) 67:177–93. doi: 10.3322/caac.21395
3. Le DT, Hubbard-Lucey VM, Morse MA, Heery CR, Dwyer A, Marsilje TH, et al. A Blueprint to Advance Colorectal Cancer Immunotherapies. *Cancer Immunol Res* (2017) 5:942–9. doi: 10.1158/2326-6066.CIR-17-0375
4. Fletcher R, Wang YJ, Schoen RE, Finn OJ, Yu J, Zhang L. Colorectal cancer prevention: Immune modulation taking the stage. *Biochim Biophys Acta Rev Cancer* (2018) 1869:138–48. doi: 10.1016/j.bbcan.2017.12.002
5. Gotwals P, Cameron S, Cipolletta D, Cremasco V, Crystal A, Hewes B, et al. Prospects for combining targeted and conventional cancer therapy with immunotherapy. *Nat Rev Cancer* (2017) 17:286–301. doi: 10.1038/nrc.2017.17
6. Roelands J, Kuppen PJK, Vermeulen L, Maccalli C, Decock J, Wang E, et al. Immunogenomic Classification of Colorectal Cancer and Therapeutic Implications. *Int J Mol Sci* (2017) 18:2229. doi: 10.3390/ijms18102229
7. Tian X, Zheng Y, Yin K, Ma J, Tian J, Zhang Y, et al. LncRNA AK036396 inhibits maturation and accelerates immunosuppression of polymorphonuclear myeloid-derived suppressor cells by enhancing the stability of ficolin B. *Cancer Immunol Res* (2020) 8:565–77. doi: 10.1158/2326-6066.CIR-19-0595
8. Zhang Y, Velez-Delgado A, Mathew E, Li D, Mendez FM, Flannagan K, et al. Myeloid cells are required for PD-1/PD-L1 checkpoint activation and the establishment of an immunosuppressive environment in pancreatic cancer. *Gut* (2017) 66:124–36. doi: 10.1136/gutjnl-2016-312078
9. Markowitz J, Brooks TR, Duggan MC, Paul BK, Pan X, Wei L, et al. Patients with pancreatic adenocarcinoma exhibit elevated levels of myeloid-derived suppressor cells upon progression of disease. *Cancer Immunol Immunother* (2015) 64:149–59. doi: 10.1007/s00262-014-1618-8
10. Cavallo F, De Giovanni C, Nanni P, Forni G, Lollini PL. 2011: the immune hallmarks of cancer. *Cancer Immunol Immunother* (2011) 60:319–26. doi: 10.1007/s00262-010-0968-0
11. Consonni FM, Porta C, Marino A, Pandolfo C, Mola S, Bleve A, et al. Myeloid-Derived Suppressor Cells: Ductile Targets in Disease. *Front Immunol* (2019) 10:949. doi: 10.3389/fimmu.2019.00949
12. Veglia F, Perego M, Gabrilovich D. Myeloid-derived suppressor cells coming of age. *Nat Immunol* (2018) 19:108–19. doi: 10.1038/s41590-017-0022-x
13. Gabrilovich DI, Nagaraj S. Myeloid-derived suppressor cells as regulators of the immune system. *Nat Rev Immunol* (2009) 9:162–74. doi: 10.1038/nri2506
14. Fedorova L, Pilatova K, Selingerova I, Bencsikova B, Budinska E, Zwinsova B, et al. Circulating Myeloid-Derived Suppressor Cell Subsets in Patients with Colorectal Cancer - Exploratory Analysis of Their Biomarker Potential. *Klin Onkol* (2018) 31:88–92. doi: 10.14735/amko20182S88
15. Zhang Y, Xu J, Zhang N, Chen M, Wang H, Zhu D. Targeting the tumour immune microenvironment for cancer therapy in human gastrointestinal malignancies. *Cancer Lett* (2019) 458:123–35. doi: 10.1016/j.canlet.2019.05.017
16. Gabrilovich DI. Myeloid-Derived Suppressor Cells. *Cancer Immunol Res* (2017) 5:3–8. doi: 10.1158/2326-6066.CIR-16-0297
17. Solito S, Marigo I, Pinton L, Damuzzo V, Mandruzzato S, Bronte V. Myeloid-derived suppressor cell heterogeneity in human cancers. *Ann N Y Acad Sci* (2014) 1319:47–65. doi: 10.1111/nyas.12469
18. Tian J, Rui K, Hong Y, Wang X, Xiao F, Lin X, et al. Increased GITRL impairs the function of myeloid-derived suppressor cells and exacerbates primary Sjögren's syndrome. *J Immunol* (2019) 202:1693–703. doi: 10.4049/jimmunol.1801051
19. Dorhoi A, Du Plessis N. Monocytic Myeloid-Derived Suppressor Cells in Chronic Infections. *Front Immunol* (2017) 8:1895. doi: 10.3389/fimmu.2017.01895
20. Meyer C, Sevko A, Ramacher M, Bazhin AV, Falk CS, Osen W, et al. Chronic inflammation promotes myeloid-derived suppressor cell activation blocking antitumor immunity in transgenic mouse melanoma model. *Proc Natl Acad Sci USA* (2011) 108:17111–6. doi: 10.1073/pnas.1108121108
21. Katoh H, Watanabe M. Myeloid-Derived Suppressor Cells and Therapeutic Strategies in Cancer. *Mediators Inflammation* (2015) 2015:159269. doi: 10.1155/2015/159269
22. Kumar V, Cheng P, Condamine T, Mony S, Languino LR, McCaffrey JC, et al. CD45 Phosphatase Inhibits STAT3 Transcription Factor Activity in Myeloid

Cells and Promotes Tumor-Associated Macrophage Differentiation. *Immunity* (2016) 44:303–15. doi: 10.1016/j.immuni.2016.01.014
23. Sagiv JY, Michaeli J, Assi S, Mishalian I, Kisos H, Levy L, et al. Phenotypic diversity and plasticity in circulating neutrophil subpopulations in cancer. *Cell Rep* (2015) 10:562–73. doi: 10.1016/j.celrep.2014.12.039
24. Biswas SK, Gangi L, Paul S, Schioppa T, Saccani A, Sironi M, et al. A distinct and unique transcriptional program expressed by tumor-associated macrophages (defective NF-kappaB and enhanced IRF-3/STAT1 activation). *Blood* (2006) 107:2112–22. doi: 10.1182/blood-2005-01-0428
25. Barbera-Guillem E, Nyhus JK, Wolford CC, Friece CR, Sampsel JW. Vascular endothelial growth factor secretion by tumor-infiltrating macrophages essentially supports tumor angiogenesis, and IgG immune complexes potentiate the process. *Cancer Res* (2002) 62:7042–9.
26. Mantovani A, Marchesi F, Malesci A, Laghi L, Allavena P. Tumour-associated macrophages as treatment targets in oncology. *Nat Rev Clin Oncol* (2017) 14:399–416. doi: 10.1038/nrclinonc.2016.217
27. Biswas SK, Mantovani A. Macrophage plasticity and interaction with lymphocyte subsets: cancer as a paradigm. *Nat Immunol* (2010) 11:889–96. doi: 10.1038/ni.1937
28. Calabretta E, d'Amore F, Carlo-Stella C. Immune and Inflammatory Cells of the Tumor Microenvironment Represent Novel Therapeutic Targets in Classical Hodgkin Lymphoma. *Int J Mol Sci* (2019) 20:5503. doi: 10.3390/ijms20215503
29. Martinez FO, Gordon S. The M1 and M2 paradigm of macrophage activation: time for reassessment. *F1000Prime Rep* (2014) 6:13. doi: 10.12703/P6-13
30. Yahaya MAF, Lila MAM, Ismail S, Zainol M, Afizan N. Tumour-Associated Macrophages (TAMs) in Colon Cancer and How to Reeducate Them. *J Immunol Res* (2019) 2019:2368249. doi: 10.1155/2019/2368249
31. Schreiber RD, Old LJ, Smyth MJ. Cancer immunoediting: integrating immunity's roles in cancer suppression and promotion. *Science* (2011) 331:1565–70. doi: 10.1126/science.1203486
32. Korbecki J, Kojder K, Barczak K, Siminska D, Gutowska I, Chlubek D, et al. Hypoxia Alters the Expression of CC Chemokines and CC Chemokine Receptors in a Tumor-A Literature Review. *Int J Mol Sci* (2020) 21:5647. doi: 10.3390/ijms21165647
33. Trellakis S, Bruderek K, Hutte J, Elian M, Hoffmann TK, Lang S, et al. Granulocytic myeloid-derived suppressor cells are cryosensitive and their frequency does not correlate with serum concentrations of colony-stimulating factors in head and neck cancer. *Innate Immun* (2013) 19:328–36. doi: 10.1177/1753425912463618
34. Mishalian I, Bayuh R, Levy L, Zolotarov L, Michaeli J, Fridlender ZG. Tumor-associated neutrophils (TAN) develop pro-tumorigenic properties during tumor progression. *Cancer Immunol Immunother* (2013) 62:1745–56. doi: 10.1007/s00262-013-1476-9
35. Jiang J, Guo W, Liang X. Phenotypes, accumulation, and functions of myeloid-derived suppressor cells and associated treatment strategies in cancer patients. *Hum Immunol* (2014) 75:1128–37. doi: 10.1016/j.humimm.2014.09.025
36. Youn JI, Collazo M, Shalova IN, Biswas SK, Gabrilovich DI. Characterization of the nature of granulocytic myeloid-derived suppressor cells in tumor-bearing mice. *J Leukoc Biol* (2012) 91:167–81. doi: 10.1189/jlb.0311177
37. Gallina G, Dolcetti L, Serafini P, De Santo C, Marigo I, Colombo MP, et al. Tumors induce a subset of inflammatory monocytes with immunosuppressive activity on CD8+ T cells. *J Clin Invest* (2006) 116:2777–90. doi: 10.1172/JCI28828
38. Huang B, Pan PY, Li Q, Sato AI, Levy DE, Bromberg J, et al. Gr-1+CD115+ immature myeloid suppressor cells mediate the development of tumor-induced T regulatory cells and T-cell anergy in tumor-bearing host. *Cancer Res* (2006) 66:1123–31. doi: 10.1158/0008-5472.CAN-05-1299
39. Cha YJ, Koo JS. Role of Tumor-Associated Myeloid Cells in Breast Cancer. *Cells* (2020) 9:1785. doi: 10.3390/cells9081785
40. Groth C, Hu X, Weber R, Fleming V, Altevogt P, Utikal J, et al. Immunosuppression mediated by myeloid-derived suppressor cells (MDSCs) during tumour progression. *Br J Cancer* (2019) 120:16–25. doi: 10.1038/s41416-018-0333-1
41. Bronte V, Brandau S, Chen SH, Colombo MP, Frey AB, Greten TF, et al. Recommendations for myeloid-derived suppressor cell nomenclature and characterization standards. *Nat Commun* (2016) 7:12150. doi: 10.1038/ncomms12150
42. Rodriguez PC, Ernstoff MS, Hernandez C, Atkins M, Zabaleta J, Sierra R, et al. Arginase I-producing myeloid-derived suppressor cells in renal cell carcinoma are a subpopulation of activated granulocytes. *Cancer Res* (2009) 69:1553–60. doi: 10.1158/0008-5472.CAN-08-1921
43. Zhang W, Jiang M, Chen J, Zhang R, Ye Y, Liu P, et al. SOCS3 Suppression Promoted the Recruitment of CD11b(+)Gr-1(-)F4/80(-)MHCII(-) Early-Stage Myeloid-Derived Suppressor Cells and Accelerated Interleukin-6-Related Tumor Invasion via Affecting Myeloid Differentiation in Breast Cancer. *Front Immunol* (2018) 9:1699. doi: 10.3389/fimmu.2018.01699
44. Gunaydin G, Kesikli SA, Guc D. Cancer associated fibroblasts have phenotypic and functional characteristics similar to the fibrocytes that represent a novel MDSC subset. *Oncoimmunology* (2015) 4:e1034918. doi: 10.1080/2162402X.2015.1034918
45. Mazza EM, Zoso A, Mandruzzato S, Bronte V, Serafini P, Inverardi L, et al. Gene expression profiling of human fibrocytic myeloid-derived suppressor cells (f-MDSCs). *Genom Data* (2014) 2:389–92. doi: 10.1016/j.gdata.2014.10.018
46. Condamine T, Ramachandran I, Youn JI, Gabrilovich DI. Regulation of tumor metastasis by myeloid-derived suppressor cells. *Annu Rev Med* (2015) 66:97–110. doi: 10.1146/annurev-med-051013-052304
47. Lechner MG, Liebertz DJ, Epstein AL. Characterization of cytokine-induced myeloid-derived suppressor cells from normal human peripheral blood mononuclear cells. *J Immunol* (2010) 185:2273–84. doi: 10.4049/jimmunol.1000901
48. Song X, Krelin Y, Dvorkin T, Bjorkdahl O, Segal S, Dinarello CA, et al. CD11b+/Gr-1+ immature myeloid cells mediate suppression of T cells in mice bearing tumors of IL-1beta-secreting cells. *J Immunol* (2005) 175:8200–8. doi: 10.4049/jimmunol.175.12.8200
49. Bunt SK, Yang L, Sinha P, Clements VK, Leips J, Ostrand-Rosenberg S. Reduced inflammation in the tumor microenvironment delays the accumulation of myeloid-derived suppressor cells and limits tumor progression. *Cancer Res* (2007) 67:10019–26. doi: 10.1158/0008-5472.CAN-07-2354
50. Wu CT, Hsieh CC, Lin CC, Chen WC, Hong JH, Chen MF. Significance of IL-6 in the transition of hormone-resistant prostate cancer and the induction of myeloid-derived suppressor cells. *J Mol Med (Berl)* (2012) 90:1343–55. doi: 10.1007/s00109-012-0916-x
51. Parker KH, Beury DW, Ostrand-Rosenberg S. Myeloid-Derived Suppressor Cells: Critical Cells Driving Immune Suppression in the Tumor Microenvironment. *Adv Cancer Res* (2015) 128:95–139. doi: 10.1016/bs.acr.2015.04.002
52. Umansky V, Blattner C, Gebhardt C, Utikal J. The Role of Myeloid-Derived Suppressor Cells (MDSC) in Cancer Progression. *Vaccines (Basel)* (2016) 4:36. doi: 10.3390/vaccines4040036
53. Lee CR, Lee W, Cho SK, Park SG. Characterization of Multiple Cytokine Combinations and TGF-beta on Differentiation and Functions of Myeloid-Derived Suppressor Cells. *Int J Mol Sci* (2018) 19:869. doi: 10.3390/ijms19030869
54. Guan X, Liu Z, Zhang J, Jin X. Myeloid-derived suppressor cell accumulation in renal cell carcinoma is correlated with CCL2, IL-17 and IL-18 expression in blood and tumors. *Adv Clin Exp Med* (2018) 27:947–53. doi: 10.17219/acem/70065
55. Kumar V, Patel S, Tcyganov E, Gabrilovich DI. The Nature of Myeloid-Derived Suppressor Cells in the Tumor Microenvironment. *Trends Immunol* (2016) 37:208–20. doi: 10.1016/j.it.2016.01.004
56. Ding AS, Routkevitch D, Jackson C, Lim M. Targeting Myeloid Cells in Combination Treatments for Glioma and Other Tumors. *Front Immunol* (2019) 10:1715. doi: 10.3389/fimmu.2019.01715
57. Alfaro C, Sanmamed MF, Rodriguez-Ruiz ME, Teijeira A, Onate C, Gonzalez A, et al. Interleukin-8 in cancer pathogenesis, treatment and follow-up. *Cancer Treat Rev* (2017) 60:24–31. doi: 10.1016/j.ctrv.2017.08.004
58. Ostrand-Rosenberg S, Fenselau C. Myeloid-Derived Suppressor Cells: Immune-Suppressive Cells That Impair Antitumor Immunity and Are Sculpted by Their Environment. *J Immunol* (2018) 200:422–31. doi: 10.4049/jimmunol.1701019

59. Zheng Y, Tian X, Wang T, Xia X, Cao F, Tian J, et al. Long noncoding RNA Pvt1 regulates the immunosuppression activity of granulocytic myeloid-derived suppressor cells in tumor-bearing mice. *Mol Cancer* (2019) 18:61. doi: 10.1186/s12943-019-0978-2
60. Cassetta L, Baekkevold ES, Brandau S, Bujko A, Cassatella MA, Dorhoi A, et al. Deciphering myeloid-derived suppressor cells: isolation and markers in humans, mice and non-human primates. *Cancer Immunol Immunother* (2019) 68:687–97. doi: 10.1007/s00262-019-02302-2
61. Brandau S, Moses K, Lang S. The kinship of neutrophils and granulocytic myeloid-derived suppressor cells in cancer: cousins, siblings or twins? *Semin Cancer Biol* (2013) 23:171–82. doi: 10.1016/j.semcancer.2013.02.007
62. Dumitru CA, Lang S, Brandau S. Modulation of neutrophil granulocytes in the tumor microenvironment: mechanisms and consequences for tumor progression. *Semin Cancer Biol* (2013) 23:141–8. doi: 10.1016/j.semcancer.2013.02.005
63. de Haas N, de Koning C, Spilgies L, de Vries IJ, Hato SV. Improving cancer immunotherapy by targeting the STATe of MDSCs. *Oncoimmunology* (2016) 5:e1196312. doi: 10.1080/2162402X.2016.1196312
64. Pinton L, Solito S, Damuzzo V, Francescato S, Pozzuoli A, Berizzi A, et al. Activated T cells sustain myeloid-derived suppressor cell-mediated immune suppression. *Oncotarget* (2016) 7:1168–84. doi: 10.18632/oncotarget.6662
65. Cimen Bozkus C, Elzey BD, Crist SA, Ellies LG, Ratliff TL. Expression of Cationic Amino Acid Transporter 2 Is Required for Myeloid-Derived Suppressor Cell-Mediated Control of T Cell Immunity. *J Immunol* (2015) 195:5237–50. doi: 10.4049/jimmunol.1500959
66. Sinha P, Okoro C, Foell D, Freeze HH, Ostrand-Rosenberg S, Srikrishna G. Proinflammatory S100 proteins regulate the accumulation of myeloid-derived suppressor cells. *J Immunol* (2008) 181:4666–75. doi: 10.4049/jimmunol.181.7.4666
67. Pawelec G, Verschoor CP, Ostrand-Rosenberg S. Myeloid-Derived Suppressor Cells: Not Only in Tumor Immunity. *Front Immunol* (2019) 10:1099. doi: 10.3389/fimmu.2019.01099
68. Rodriguez PC, Quiceno DG, Zabaleta J, Ortiz B, Zea AH, Piazuelo MB, et al. Arginase I production in the tumor microenvironment by mature myeloid cells inhibits T-cell receptor expression and antigen-specific T-cell responses. *Cancer Res* (2004) 64:5839–49. doi: 10.1158/0008-5472.CAN-04-0465
69. Noman MZ, Desantis G, Janji B, Hasmim M, Karray S, Dessen P, et al. PD-L1 is a novel direct target of HIF-1alpha, and its blockade under hypoxia enhanced MDSC-mediated T cell activation. *J Exp Med* (2014) 211:781–90. doi: 10.1084/jem.20131916
70. Fujimura T, Mahnke K, Enk AH. Myeloid derived suppressor cells and their role in tolerance induction in cancer. *J Dermatol Sci* (2010) 59:1–6. doi: 10.1016/j.jdermsci.2010.05.001
71. Yu J, Du W, Yan F, Wang Y, Li H, Cao S, et al. Myeloid-derived suppressor cells suppress antitumor immune responses through IDO expression and correlate with lymph node metastasis in patients with breast cancer. *J Immunol* (2013) 190:3783–97. doi: 10.4049/jimmunol.1201449
72. Jin J, Wang X, Wang Q, Guo X, Cao J, Zhang X, et al. Chronic psychological stress induces the accumulation of myeloid-derived suppressor cells in mice. *PloS One* (2013) 8:e74497. doi: 10.1371/journal.pone.0074497
73. Bronte V, Zanovello P. Regulation of immune responses by L-arginine metabolism. *Nat Rev Immunol* (2005) 5:641–54. doi: 10.1038/nri1668
74. Schlecker E, Stojanovic A, Eisen C, Quack C, Falk CS, Umansky V, et al. Tumor-infiltrating monocytic myeloid-derived suppressor cells mediate CCR5-dependent recruitment of regulatory T cells favoring tumor growth. *J Immunol* (2012) 189:5602–11. doi: 10.4049/jimmunol.1201018
75. Marvel D, Gabrilovich DI. Myeloid-derived suppressor cells in the tumor microenvironment: expect the unexpected. *J Clin Invest* (2015) 125:3356–64. doi: 10.1172/JCI80005
76. OuYang LY, Wu XJ, Ye SB, Zhang RX, Li ZL, Liao W, et al. Tumor-induced myeloid-derived suppressor cells promote tumor progression through oxidative metabolism in human colorectal cancer. *J Transl Med* (2015) 13:47. doi: 10.1186/s12967-015-0410-7
77. Molon B, Ugel S, Del Pozzo F, Soldani C, Zilio S, Avella D, et al. Chemokine nitration prevents intratumoral infiltration of antigen-specific T cells. *J Exp Med* (2011) 208:1949–62. doi: 10.1084/jem.20101956
78. Ostrand-Rosenberg S, Sinha P, Beury DW, Clements VK. Cross-talk between myeloid-derived suppressor cells (MDSC), macrophages, and dendritic cells enhances tumor-induced immune suppression. *Semin Cancer Biol* (2012) 22:275–81. doi: 10.1016/j.semcancer.2012.01.011
79. Zhao F, Korangy F, Greten TF. Cellular immune suppressor mechanisms in patients with hepatocellular carcinoma. *Dig Dis* (2012) 30:477–82. doi: 10.1159/000341695
80. Zoso A, Mazza EM, Bicciato S, Mandruzzato S, Bronte V, Serafini P, et al. Human fibrocytic myeloid-derived suppressor cells express IDO and promote tolerance via Treg-cell expansion. *Eur J Immunol* (2014) 44:3307–19. doi: 10.1002/eji.201444522
81. Beury DW, Parker KH, Nyandjo M, Sinha P, Carter KA, Ostrand-Rosenberg S. Cross-talk among myeloid-derived suppressor cells, macrophages, and tumor cells impacts the inflammatory milieu of solid tumors. *J Leukoc Biol* (2014) 96:1109–18. doi: 10.1189/jlb.3A0414-210R
82. Liu C, Yu S, Kappes J, Wang J, Grizzle WE, Zinn KR, et al. Expansion of spleen myeloid suppressor cells represses NK cell cytotoxicity in tumor-bearing host. *Blood* (2007) 109:4336–42. doi: 10.1182/blood-2006-09-046201
83. Wang Y, Schafer CC, Hough KP, Tousif S, Duncan SR, Kearney JF, et al. Myeloid-Derived Suppressor Cells Impair B Cell Responses in Lung Cancer through IL-7 and STAT5. *J Immunol* (2018) 201:278–95. doi: 10.4049/jimmunol.1701069
84. Sun HL, Zhou X, Xue YF, Wang K, Shen YF, Mao JJ, et al. Increased frequency and clinical significance of myeloid-derived suppressor cells in human colorectal carcinoma. *World J Gastroenterol* (2012) 18:3303–9. doi: 10.3748/wjg.v18.i25.3303
85. Zhang B, Wang Z, Wu L, Zhang M, Li W, Ding J, et al. Circulating and tumor-infiltrating myeloid-derived suppressor cells in patients with colorectal carcinoma. *PloS One* (2013) 8:e57114. doi: 10.1371/journal.pone.0057114
86. Sasidharan Nair V, Saleh R, Toor SM, Taha RZ, Ahmed AA, Kurer MA, et al. Transcriptomic profiling disclosed the role of DNA methylation and histone modifications in tumor-infiltrating myeloid-derived suppressor cell subsets in colorectal cancer. *Clin Epigenet* (2020) 12:13. doi: 10.1186/s13148-020-0808-9
87. Yang R, Cai TT, Wu XJ, Liu YN, He J, Zhang XS, et al. Tumour YAP1 and PTEN expression correlates with tumour-associated myeloid suppressor cell expansion and reduced survival in colorectal cancer. *Immunology* (2018) 155:263–72. doi: 10.1111/imm.12949
88. Toor SM, Syed Khaja AS, El Salhat H, Bekdache O, Kanbar J, Jaloudi M, et al. Increased Levels of Circulating and Tumor-Infiltrating Granulocytic Myeloid Cells in Colorectal Cancer Patients. *Front Immunol* (2016) 7:560. doi: 10.3389/fimmu.2016.00560
89. Shimura T, Shibata M, Gonda K, Hayase S, Sakamoto W, Okayama H, et al. Prognostic impact of preoperative lymphocyte-to-monocyte ratio in patients with colorectal cancer with special reference to myeloid-derived suppressor cells. *Fukushima J Med Sci* (2018) 64:64–72. doi: 10.5387/fms.2018-10
90. Tada K, Kitano S, Shoji H, Nishimura T, Shimada Y, Nagashima K, et al. Pretreatment Immune Status Correlates with Progression-Free Survival in Chemotherapy-Treated Metastatic Colorectal Cancer Patients. *Cancer Immunol Res* (2016) 4:592–9. doi: 10.1158/2326-6066.CIR-15-0298
91. Limagne E, Euvrard R, Thibaudin M, Rebe C, Derangere V, Chevriaux A, et al. Accumulation of MDSC and Th17 Cells in Patients with Metastatic Colorectal Cancer Predicts the Efficacy of a FOLFOX-Bevacizumab Drug Treatment Regimen. *Cancer Res* (2016) 76:5241–52. doi: 10.1158/0008-5472.CAN-15-3164
92. Wood LD, Parsons DW, Jones S, Lin J, Sjoblom T, Leary RJ, et al. The genomic landscapes of human breast and colorectal cancers. *Science* (2007) 318:1108–13. doi: 10.1126/science.1145720
93. Pereira AA, Rego JF, Morris V, Overman MJ, Eng C, Garrett CR, et al. Association between KRAS mutation and lung metastasis in advanced colorectal cancer. *Br J Cancer* (2015) 112:424–8. doi: 10.1038/bjc.2014.619
94. Vakiani E, Janakiraman M, Shen R, Sinha R, Zeng Z, Shia J, et al. Comparative genomic analysis of primary versus metastatic colorectal carcinomas. *J Clin Oncol* (2012) 30:2956–62. doi: 10.1200/JCO.2011.38.2994
95. Liao W, Overman MJ, Boutin AT, Shang X, Zhao D, Dey P, et al. KRAS-IRF2 Axis Drives Immune Suppression and Immune Therapy Resistance in

Colorectal Cancer. *Cancer Cell* (2019) 35:559–72.e557. doi: 10.1016/j.ccell.2019.02.008
96. Yan G, Zhao H, Zhang Q, Zhou Y, Wu L, Lei J, et al. A RIPK3-PGE2 Circuit Mediates Myeloid-Derived Suppressor Cell-Potentiated Colorectal Carcinogenesis. *Cancer Res* (2018) 78:5586–99. doi: 10.1158/0008-5472.CAN-17-3962
97. Jayakumar A, Bothwell ALM. RIPK3-Induced Inflammation by I-MDSCs Promotes Intestinal Tumors. *Cancer Res* (2019) 79:1587–99. doi: 10.1158/0008-5472.CAN-18-2153
98. Poh TW, Madsen CS, Gorman JE, Marler RJ, Leighton JA, Cohen PA, et al. Downregulation of hematopoietic MUC1 during experimental colitis increases tumor-promoting myeloid-derived suppressor cells. *Clin Cancer Res* (2013) 19:5039–52. doi: 10.1158/1078-0432.CCR-13-0278
99. Sheng YH, Wong KY, Seim I, Wang R, He Y, Wu A, et al. MUC13 promotes the development of colitis-associated colorectal tumors via beta-catenin activity. *Oncogene* (2019) 38:7294–310. doi: 10.1038/s41388-019-0951-y
100. Grivennikov SI, Greten FR, Karin M. Immunity, inflammation, and cancer. *Cell* (2010) 140:883–99. doi: 10.1016/j.cell.2010.01.025
101. Wang D, Sun H, Wei J, Cen B, DuBois RN. CXCL1 Is Critical for Premetastatic Niche Formation and Metastasis in Colorectal Cancer. *Cancer Res* (2017) 77:3655–65. doi: 10.1158/0008-5472.CAN-16-3199
102. Yu X, Wang D, Wang X, Sun S, Zhang Y, Wang S, et al. CXCL12/CXCR4 promotes inflammation-driven colorectal cancer progression through activation of RhoA signaling by sponging miR-133a-3p. *J Exp Clin Cancer Res* (2019) 38:32. doi: 10.1186/s13046-018-1014-x
103. Villarino AV, Kanno Y, O'Shea JJ. Mechanisms and consequences of Jak-STAT signaling in the immune system. *Nat Immunol* (2017) 18:374–84. doi: 10.1038/ni.3691
104. Trikha P, Carson WE,3. Signaling pathways involved in MDSC regulation. *Biochim Biophys Acta* (2014) 1846:55–65. doi: 10.1016/j.bbcan.2014.04.003
105. Mundy-Bosse BL, Lesinski GB, Jaime-Ramirez AC, Benninger K, Khan M, Kuppusamy P, et al. Myeloid-derived suppressor cell inhibition of the IFN response in tumor-bearing mice. *Cancer Res* (2011) 71:5101–10. doi: 10.1158/0008-5472.CAN-10-2670
106. Sinha P, Parker KH, Horn L, Ostrand-Rosenberg S. Tumor-induced myeloid-derived suppressor cell function is independent of IFN-gamma and IL-4Ralpha. *Eur J Immunol* (2012) 42:2052–9. doi: 10.1002/eji.201142230
107. Li ZW, Sun B, Gong T, Guo S, Zhang J, Wang J, et al. GNAI1 and GNAI3 Reduce Colitis-Associated Tumorigenesis in Mice by Blocking IL6 Signaling and Down-regulating Expression of GNAI2. *Gastroenterology* (2019) 156:2297–312. doi: 10.1053/j.gastro.2019.02.040
108. Ke Z, Wang C, Wu T, Wang W, Yang Y, Dai Y. PAR2 deficiency enhances myeloid cell-mediated immunosuppression and promotes colitis-associated tumorigenesis. *Cancer Lett* (2020) 469:437–46. doi: 10.1016/j.canlet.2019.11.015
109. Li W, Zhang X, Chen Y, Xie Y, Liu J, Feng Q, et al. G-CSF is a key modulator of MDSC and could be a potential therapeutic target in colitis-associated colorectal cancers. *Protein Cell* (2016) 7:130–40. doi: 10.1007/s13238-015-0237-2
110. Chun E, Lavoie S, Michaud M, Gallini CA, Kim J, Soucy G, et al. CCL2 Promotes Colorectal Carcinogenesis by Enhancing Polymorphonuclear Myeloid-Derived Suppressor Cell Population and Function. *Cell Rep* (2015) 12:244–57. doi: 10.1016/j.celrep.2015.06.024
111. Lin Q, Ren L, Jian M, Xu P, Li J, Zheng P, et al. The mechanism of the premetastatic niche facilitating colorectal cancer liver metastasis generated from myeloid-derived suppressor cells induced by the S1PR1-STAT3 signaling pathway. *Cell Death Dis* (2019) 10:693. doi: 10.1038/s41419-019-1922-5
112. Jayakumar A, Bothwell ALM. Stat6 Promotes Intestinal Tumorigenesis in a Mouse Model of Adenomatous Polyposis by Expansion of MDSCs and Inhibition of Cytotoxic CD8 Response. *Neoplasia* (2017) 19:595–605. doi: 10.1016/j.neo.2017.04.006
113. Zoller M. Janus-Faced Myeloid-Derived Suppressor Cell Exosomes for the Good and the Bad in Cancer and Autoimmune Disease. *Front Immunol* (2018) 9:137. doi: 10.3389/fimmu.2018.00137
114. Deng J, Li J, Sarde A, Lines JL, Lee YC, Qian DC, et al. Hypoxia-Induced VISTA Promotes the Suppressive Function of Myeloid-Derived Suppressor Cells in the Tumor Microenvironment. *Cancer Immunol Res* (2019) 7:1079–90. doi: 10.1158/2326-6066.CIR-18-0507
115. Tian X, Shen H, Li Z, Wang T, Wang S. Tumor-derived exosomes, myeloid-derived suppressor cells, and tumor microenvironment. *J Hematol Oncol* (2019) 12:84. doi: 10.1186/s13045-019-0772-z
116. Wang Y, Yin K, Tian J, Xia X, Ma J, Tang X, et al. Granulocytic Myeloid-Derived Suppressor Cells Promote the Stemness of Colorectal Cancer Cells through Exosomal S100A9. *Adv Sci (Weinh)* (2019) 6:1901278. doi: 10.1002/advs.201901278
117. Heine A, Flores C, Gevensleben H, Diehl L, Heikenwalder M, Ringelhan M, et al. Targeting myeloid derived suppressor cells with all-trans retinoic acid is highly time-dependent in therapeutic tumor vaccination. *Oncoimmunology* (2017) 6:e1338995. doi: 10.1080/2162402X.2017.1338995
118. Grauers Wiktorin H, Nilsson MS, Kiffin R, Sander FE, Lenox B, Rydstrom A, et al. Histamine targets myeloid-derived suppressor cells and improves the anti-tumor efficacy of PD-1/PD-L1 checkpoint blockade. *Cancer Immunol Immunother* (2019) 68:163–74. doi: 10.1007/s00262-018-2253-6
119. Wu T, Wang C, Wang W, Hui Y, Zhang R, Qiao L, et al. Embelin impairs the accumulation and activation of MDSCs in colitis-associated tumorigenesis. *Oncoimmunology* (2018) 7:e1498437. doi: 10.1080/2162402X.2018.1498437
120. Zhang YS, Wang F, Cui SX, Qu XJ. Natural dietary compound naringin prevents azoxymethane/dextran sodium sulfate-induced chronic colorectal inflammation and carcinogenesis in mice. *Cancer Biol Ther* (2018) 19:735–44. doi: 10.1080/15384047.2018.1453971
121. Holmgaard RB, Zamarin D, Lesokhin A, Merghoub T, Wolchok JD. Targeting myeloid-derived suppressor cells with colony stimulating factor-1 receptor blockade can reverse immune resistance to immunotherapy in indoleamine 2,3-dioxygenase-expressing tumors. *EBioMedicine* (2016) 6:50–8. doi: 10.1016/j.ebiom.2016.02.024
122. Kobayashi M, Chung JS, Beg M, Arriaga Y, Verma U, Courtney K, et al. Blocking Monocytic Myeloid-Derived Suppressor Cell Function via Anti-DC-HIL/GPNMB Antibody Restores the In Vitro Integrity of T Cells from Cancer Patients. *Clin Cancer Res* (2019) 25:828–38. doi: 10.1158/1078-0432.CCR-18-0330
123. Tu SP, Jin H, Shi JD, Zhu LM, Suo Y, Lu G, et al. Curcumin induces the differentiation of myeloid-derived suppressor cells and inhibits their interaction with cancer cells and related tumor growth. *Cancer Prev Res (Phila)* (2012) 5:205–15. doi: 10.1158/1940-6207.CAPR-11-0247
124. Liu Z, Xie Y, Xiong Y, Liu S, Qiu C, Zhu Z, et al. TLR 7/8 agonist reverses oxaliplatin resistance in colorectal cancer via directing the myeloid-derived suppressor cells to tumoricidal M1-macrophages. *Cancer Lett* (2020) 469:173–85. doi: 10.1016/j.canlet.2019.10.020
125. Liang H, Deng L, Hou Y, Meng X, Huang X, Rao E, et al. Host STING-dependent MDSC mobilization drives extrinsic radiation resistance. *Nat Commun* (2017) 8:1736. doi: 10.1038/s41467-017-01566-5
126. Li J, Xu J, Yan X, Jin K, Li W, Zhang R. Targeting Interleukin-6 (IL-6) Sensitizes Anti-PD-L1 Treatment in a Colorectal Cancer Preclinical Model. *Med Sci Monit* (2018) 24:5501–8. doi: 10.12659/MSM.907439
127. Lin H, Wu Y, Chen J, Huang S, Wang Y. (-)-4-O-(4-O-beta-D-glucopyranosylcaffeoyl) Quinic Acid Inhibits the Function of Myeloid-Derived Suppressor Cells to Enhance the Efficacy of Anti-PD1 against Colon Cancer. *Pharm Res* (2018) 35:183. doi: 10.1007/s11095-018-2459-5
128. Fleming V, Hu X, Weber R, Nagibin V, Groth C, Altevogt P, et al. Targeting Myeloid-Derived Suppressor Cells to Bypass Tumor-Induced Immunosuppression. *Front Immunol* (2018) 9:398. doi: 10.3389/fimmu.2018.00398
129. Seliger B. Combinatorial Approaches With Checkpoint Inhibitors to Enhance Anti-tumor Immunity. *Front Immunol* (2019) 10:999. doi: 10.3389/fimmu.2019.00999
130. Dumont A, de Rosny C, Kieu TL, Perrey S, Berger H, Fluckiger A, et al. Docosahexaenoic acid inhibits both NLRP3 inflammasome assembly and JNK-mediated mature IL-1beta secretion in 5-fluorouracil-treated MDSC: implication in cancer treatment. *Cell Death Dis* (2019) 10:485. doi: 10.1038/s41419-019-1723-x
131. Karakasheva TA, Waldron TJ, Eruslanov E, Kim SB, Lee JS, O'Brien S, et al. CD38-Expressing Myeloid-Derived Suppressor Cells Promote Tumor Growth in a Murine Model of Esophageal Cancer. *Cancer Res* (2015) 75:4074–85. doi: 10.1158/0008-5472.CAN-14-3639

132. Krejcik J, Casneuf T, Nijhof IS, Verbist B, Bald J, Plesner T, et al. Daratumumab depletes CD38+ immune regulatory cells, promotes T-cell expansion, and skews T-cell repertoire in multiple myeloma. *Blood* (2016) 128:384–94. doi: 10.1182/blood-2015-12-687749
133. Karakasheva TA, Dominguez GA, Hashimoto A, Lin EW, Chiu C, Sasser K, et al. CD38+ M-MDSC expansion characterizes a subset of advanced colorectal cancer patients. *JCI Insight* (2018) 3:e97022. doi: 10.1172/jci.insight.97022
134. Zumwalt TJ, Goel A. Immunotherapy of Metastatic Colorectal Cancer: Prevailing Challenges and New Perspectives. *Curr Colorectal Cancer Rep* (2015) 11:125–40. doi: 10.1007/s11888-015-0269-2
135. Sambi M, Bagheri L, Szewczuk MR. Current Challenges in Cancer Immunotherapy: Multimodal Approaches to Improve Efficacy and Patient Response Rates. *J Oncol* (2019) 2019:4508794. doi: 10.1155/2019/4508794
136. Sansom DM. CD28, CTLA-4 and their ligands: who does what and to whom? *Immunology* (2000) 101:169–77. doi: 10.1046/j.1365-2567.2000.00121.x
137. Cheng P, Eksioglu EA, Chen X, Kandell W, Le Trinh T, Cen L, et al. S100A9-induced overexpression of PD-1/PD-L1 contributes to ineffective hematopoiesis in myelodysplastic syndromes. *Leukemia* (2019) 33:2034–46. doi: 10.1038/s41375-019-0397-9
138. Yamauchi Y, Safi S, Blattner C, Rathinasamy A, Umansky L, Juenger S, et al. Circulating and Tumor Myeloid-derived Suppressor Cells in Resectable Non-Small Cell Lung Cancer. *Am J Respir Crit Care Med* (2018) 198:777–87. doi: 10.1164/rccm.201708-1707OC
139. Lu C, Redd PS, Lee JR, Savage N, Liu K. The expression profiles and regulation of PD-L1 in tumor-induced myeloid-derived suppressor cells. *Oncoimmunology* (2016) 5:e1247135. doi: 10.1080/2162402X.2016.1247135
140. Iwata T, Kondo Y, Kimura O, Morosawa T, Fujisaka Y, Umetsu T, et al. PD-L1 (+)MDSCs are increased in HCC patients and induced by soluble factor in the tumor microenvironment. *Sci Rep* (2016) 6:39296. doi: 10.1038/srep39296
141. Gebhardt C, Sevko A, Jiang H, Lichtenberger R, Reith M, Tarnanidis K, et al. Myeloid Cells and Related Chronic Inflammatory Factors as Novel Predictive Markers in Melanoma Treatment with Ipilimumab. *Clin Cancer Res* (2015) 21:5453–9. doi: 10.1158/1078-0432.CCR-15-0676
142. Teng F, Meng X, Kong L, Mu D, Zhu H, Liu S, et al. Tumor-infiltrating lymphocytes, forkhead box P3, programmed death ligand-1, and cytotoxic T lymphocyte-associated antigen-4 expressions before and after neoadjuvant chemoradiation in rectal cancer. *Transl Res* (2015) 166:721–732 e721. doi: 10.1016/j.trsl.2015.06.019
143. Grapin M, Richard C, Limagne E, Boidot R, Morgand V, Bertaut A, et al. Optimized fractionated radiotherapy with anti-PD-L1 and anti-TIGIT: a promising new combination. *J Immunother Cancer* (2019) 7:160. doi: 10.1186/s40425-019-0634-9
144. Garton AJ, Seibel S, Lopresti-Morrow L, Crew L, Janson N, Mandiyan S, et al. Anti-KIT Monoclonal Antibody Treatment Enhances the Antitumor Activity of Immune Checkpoint Inhibitors by Reversing Tumor-Induced Immunosuppression. *Mol Cancer Ther* (2017) 16:671–80. doi: 10.1158/1535-7163.MCT-16-0676
145. Edin S, Wikberg ML, Dahlin AM, Rutegard J, Oberg A, Oldenborg PA, et al. The distribution of macrophages with a M1 or M2 phenotype in relation to prognosis and the molecular characteristics of colorectal cancer. *PloS One* (2012) 7:e47045. doi: 10.1371/journal.pone.0047045
146. Li J, Li L, Li Y, Long Y, Zhao Q, Ouyang Y, et al. Tumor-associated macrophage infiltration and prognosis in colorectal cancer: systematic review and meta-analysis. *Int J Colorectal Dis* (2020) 35:1203–10. doi: 10.1007/s00384-020-03593-z
147. Diskin B, Adam S, Cassini MF, Sanchez G, Liria M, Aykut B, et al. PD-L1 engagement on T cells promotes self-tolerance and suppression of neighboring macrophages and effector T cells in cancer. *Nat Immunol* (2020) 21:442–54. doi: 10.1038/s41590-020-0620-x
148. Wang X, Gao Y, Zhang X, Wang X, Wang B, Meng X, et al. CD30L/CD30 signaling regulates the formation of the tumor immune microenvironment and inhibits intestinal tumor development of colitis-associated colon cancer in mice. *Int Immunopharmacol* (2020) 84:106531. doi: 10.1016/j.intimp.2020.106531

Conflict of Interest: The authors declare that the research was conducted in the absence of any commercial or financial relationships that could be construed as a potential conflict of interest.

Copyright © 2020 Yin, Xia, Rui, Wang and Wang. This is an open-access article distributed under the terms of the Creative Commons Attribution License (CC BY). The use, distribution or reproduction in other forums is permitted, provided the original author(s) and the copyright owner(s) are credited and that the original publication in this journal is cited, in accordance with accepted academic practice. No use, distribution or reproduction is permitted which does not comply with these terms.

frontiers in Immunology

REVIEW
published: 16 December 2020
doi: 10.3389/fimmu.2020.606859

Tumor-Derived Extracellular Vesicles and the Immune System—Lessons From Immune-Competent Mouse-Tumor Models

Marvin Droste[1,2], *Basant K. Thakur*[3] *and Brian P. Eliceiri*[1*]

[1] Department of Surgery, Division of Trauma, Surgical Critical Care and Burns, UC San Diego School of Medicine, San Diego, CA, United States, [2] Department of Pediatrics II (Pediatric Nephrology), University Hospital Essen, Essen, Germany, [3] Cancer Exosomes Laboratory, Department of Pediatrics III, University Hospital Essen, Essen, Germany

OPEN ACCESS

Edited by:
Peng Qu,
National Institutes of Health (NIH), United States

Reviewed by:
Qiubai Li,
Huazhong University of Science and Technology, China
Reza Rahbarghazi,
Tabriz University of Medical Sciences, Iran
Rui-Cheng Ji,
Oita University, Japan

***Correspondence:**
Brian P. Eliceiri
beliceiri@health.ucsd.edu

Specialty section:
This article was submitted to Cancer Immunity and Immunotherapy, a section of the journal Frontiers in Immunology

Received: 15 September 2020
Accepted: 13 November 2020
Published: 16 December 2020

Citation:
Droste M, Thakur BK and Eliceiri BP (2020) Tumor-Derived Extracellular Vesicles and the Immune System—Lessons From Immune-Competent Mouse-Tumor Models. Front. Immunol. 11:606859. doi: 10.3389/fimmu.2020.606859

Tumor-derived extracellular vesicles (TEVs) are important regulators of the immune response in cancer; however, most research so far has been carried out using cell culture systems. Immune-competent murine tumor models currently provide the best platform to assess proposed roles of TEVs using *in vivo* animal models and therefore are important for examining interactions between TEVs and the immune system. In this review, we present the current knowledge on TEVs using *in vivo* tumor-bearing animal models, with a focus on the role of TEVs in mediating crosstalk between tumor cells and both adaptive and innate immune cells. In particular, we address the question how animal models can clarify the reported heterogeneity of TEV effects in both anti-tumor responses and evasion of immune surveillance. The potential of TEVs in mediating direct antigen-presenting functions supports their potential as cancer vaccine therapeutics, therefore, we provide an overview of key findings of TEV trials that have the potential as novel immunotherapies, and shed light on challenges in the path toward the first in-human trials. We also highlight the important updates on the methods that continue to enhance the rigor and reproducibility of EV studies, particularly in functional animal models.

Keywords: extracellular vesicles, tumor exosomes, adaptive immunity, extracellular vesicle heterogeneity, cancer, immunotherapy, mouse tumor models, immune system

INTRODUCTION

Metastatic cancers are among the deadliest diseases worldwide, yet, therapy options remain limited. Escaping the host's immune response is one of the characteristic properties of tumors that are essential for malignancy, tumor growth and metastasis (1). During the past few decades, immuno-oncology research has focused on deciphering the molecular mechanisms that tumors develop to influence their microenvironment as well as the global immune response. More recently, extracellular vesicles (EVs) released by tumor cells have been studied extensively for their potential as antigen-presenting particles and regulators of immune cells (2). EVs are nanoparticles that are formed intracellularly, and are composed of a proteo-lipid bilayer, and luminal proteins and nucleic acids, which together determine their functionality. The complex

mechanism of EVs biogenesis has been recently outlined elsewhere (3). Of note, the packaging of EVs may be altered upon changes of the cellular microenvironment or after therapeutic interventions (4). EVs are categorized by size and the organelle from which they are derived. The three predominant classes of EVs are endosomal-derived exosomes that are 50–150 nm in diameter, microvesicles, or "ectosomes" that are 200–1,000 nm in diameter and are derived from plasma membrane shedding, and apoptotic bodies that have a wide size range of 100–5,000 nm in diameter. Recent work has pointed toward the existence of a plethora of additional EV classes not described above, a prominent example being so-called exomeres. Exomeres were described to be smaller than exosomes (<50 nm) and enriched in metabolism-associated enzymes and antigens, which has led to the assumption that they might influence the metabolic state of recipient cells and take part in tumor-related mechanisms such as metastasis (5, 6).

The heterogeneity of extracellular vesicles is further underscored by studies that continue to refine our understanding of their cargo (7), and challenges with standardized isolation and characterization techniques to define the function of specific subpopulations of EVs. It remains a common approach in the field to focus studies on pellets acquired following ultracentrifugation. These fractions are referred to as "exosomes", even though the International Society for Extracellular Vesicles (ISEV) is encouraging researchers to use the term "small EVs" to better capture the spectrum of vesicle types (8). To meet the requirements of more precise terminology and biological accuracy, we will use the term "tumor-derived extracellular vesicles" (TEVs), which includes vesicles released by an endosomal pathway ("classical" exosomes), membrane-derived vesicles and apoptotic-derived vesicles since all three are frequently observed in malignancy.

Many investigators have identified and classified TEVs using various cancer cell lines to obtain an insight into their pathophysiological relevance in tumor progression and immune responses, however, the potential of TEVs as immune regulators in immune-competent animal tumor models remains understudied. The importance of an immune-competent model is highlighted by the need to understand tumor-immune cell-crosstalk mediated by TEVs in the complexity of an animal model, which we argue have the greatest potential to provide insight into the TEV-dependent mechanisms relevant to metastasis and translation to humans. We point out where findings from animal studies and cell culture experiments may appear to be contradictory and identify areas for future research on the role of TEVs and the regulation of tumor-associated immune cells.

An understanding of the basis of the most utilized methods, such as direct injection of TEVs and immune cell pulsing by TEVs before injection, is important to consider with respect to their potential influences on experimental outcomes. Work by Andre and colleagues (9) first showed that TEVs carry antigens derived from their cells of origin that are presented by dendritic cells (DCs) to induce the proliferation of specific T cell subsets. The observation that bodily fluids contain TEVs that are reservoirs for tumor antigens demonstrated the relevance of TEVs in tumor immunotherapy research that has been followed by cancer vaccine trials (10) and TEV bioengineering approaches (11, 12). While specific aspects of TEV immunology remain poorly understood, TEVs remain promising targets for future research, with the regulation of their release being a prominent example (13–16). Moreover, the rapid evolution of EV methodologies in general will benefit *in vivo* studies of TEVs. Progress in these areas will likely lead to new therapy options in cancer, autoimmune disease and many other chronic conditions where EVs can mediate immune activity to distal end organs.

TEV EFFECTS ON THE ADAPTIVE IMMUNITY: DENDRITIC CELLS AND T CELLS

Our current understanding of anti-tumor immunity emphasizes the role of $CD8^+$ cytotoxic T-lymphocytes (CTLs) as key protective agents. The presentation of tumor antigens by dendritic cells induces the activation and clonal proliferation of anti-tumor CTLs, however, tumors regularly develop mechanisms and factors to evade this response. It has been recognized that TEVs might carry such factors as a payload or express tumor antigens on their surface. Therefore, both immunosuppressive and immune-stimulatory roles have been proposed and described for TEVs (2).

In terms of the immunosuppressive effects of TEVs, direct as well as indirect effects on cellular immunity have been proposed (17). Ning and colleagues demonstrated in a murine model that TEVs owe the potential to block the differentiation and function of dendritic cells and Th1 $CD4^+$ lymphocytes, whereas the activity of regulatory T cells (Tregs) is increased by TEVs (18). However, functional conclusions should be drawn with caution as certain Treg subtypes may also suppress cancer progression especially in tumors with extended tumor-induced inflammation (19).

Although not much is known about the pathways by which TEVs can directly suppress effector cell function, there is some recent evidence that apoptosis induction, at least in $CD4^+$ T cells, is mediated by miRNA that is associated with TEVs (20), a mode of EV signaling that has been well established since the recognition of various RNA types as a common EV cargo (21). The immunosuppressive effects of TEVs were partially reversible by blockage of PD-L1, allowing the interpretations that either TEVs carry PD-L1 on their surface to interact with PD-1 receptors on activated CTL, or that TEVs induced the expression of PD-L1 on dendritic cells. It was recently demonstrated that tumor cells actively secrete TEVs carrying PD-L1 that are released in a mechanism that is dependent on the EV release regulators such as Rab27a and nSMase2 (22, 23). In mice, the TEV-associated PD-L1 enhanced tumor progression, suppressed T cell activity, and was resistant to antibody therapy. Interestingly, when TEV-associated PD-L1 secretion was blocked, distant secondary tumor growth was inhibited (23). This effect was synergistic with anti-PD-L1 antibody treatments

and led the authors to the conclusion that blocking of PD-L1 secretion associated with TEVs could provide an additive treatment to current antibody therapies, which would have a high clinical relevance (24). Interestingly, PD-L1 has been shown to be present in TEVs from various cancer cell lines in different concentrations, which could explain the heterogeneous results obtained from therapeutic PD-L1 antibody treatment (23). Further studies are warranted to clarify whether other tumor-derived ligands are also differentially packaged into TEVs dependent on the cancer cell line.

Another example for a mechanism of $CD4^+$ and $CD8^+$ T cell suppression is arginase-1 carried by TEVs. Such TEVs were isolated from patients with ovarian cancer and inhibited effector cell function after previous uptake into dendritic cells in an ovarian cancer mouse model (25). The resulting tumor progression could be reversed by applying arginase inhibitors, thus underlining the potential for therapeutic manipulation.

Despite suppression of T cell function, it has also been reported that TEVs carry out tumor antigen-presenting functions, similar to antigen-presenting cells. When $CD8^+$ CTL are stimulated *in vitro* with TEVs, a strong specific anti-tumor effect of these CTL was reported (26). This finding might open up a new strategy for potential tumor vaccines. Additionally, this observation raises the question whether TEVs alone have the capacity to induce T cell responses independently of the contribution by dendritic cells. Indeed, another group has also described a direct antigen-presenting effect of TEVs on $CD8^+$ CTL *via* transfer of so-called pioneer translation peptides that originate from pre-mRNAs (27). In contrast, others have shown that TEVs alone do not exert T cell-activating functions in the absence of DCs even though they carry MHC cargo (28). This finding has been attributed to the fact that TEVs, due to their small size, might not carry enough MHC molecules to activate the T cell receptor (29). It remains controversial whether TEVs may act as "mini-DCs" to directly promote T cell activation, which can be addressed in the future by comparison of multiple tumor models. The potential role of vesicle size can be addressed by the use of different TEV isolation protocols.

During the last decade, multiple groups have investigated the processes by which TEVs interact with T cells to promote the effects discussed above. Most evidence which is available to date points toward a receptor-ligand interaction between T cells and TEVs which controls cellular homeostasis. For instance, it has been demonstrated that binding of TEVs to target receptors on T cells alters the amount of Ca^{2+} influx and comes along with transcriptional reprogramming of the targeted cell (30, 31). In this context, the signaling ligands of TEVs may function in the same way as cells carrying the surface molecule (32). However, the proposed transfer of RNA to T cells would require internalization of TEVs and subsequent intracellular cargo release. Indeed, recent work has suggested the existence of a relatively small subpopulation of T cells that is able to internalize TEVs by micropinocytosis, at least in a growth factor-enriched microenvironment such as the tumor bed (33). Given the fact that the variety of TEV uptake mechanisms is thought to be large, other processes, such as receptor-mediated endocytosis, may also play a role, as comprehensively outlined elsewhere (34, 35).

Antigen-presenting cells, such as DCs, are another important target of TEVs, as they largely facilitate the connection between tumor-derived, antigen-containing material, and immune effector cells. TEVs have been described to either induce or decrease the intensity by which dendritic cells are activated, comparable to what is known regarding the TEV effects on T cells. It was reported by several groups that TEVs severely interfere with differentiation of DCs from bone marrow myeloid precursor cells and $CD14^+$ monocytes, resulting in impaired migratory behavior and apoptosis of the precursor cells (18, 36). Moreover, when incubated with TEVs, these cells produce increased amounts of interleukin-6 (IL-6) (36). Interestingly, IL-6 induction was also shown in TEV-activated differentiated DCs and one study reported that this is related to metastasis and tumor invasion in a STAT3-dependent manner (37). However, this trial did not provide evidence that this can be attributed to TEVs *in vivo*, as IL-6 induction by TEVs was solely demonstrated *in vitro*. In addition, the effect has been linked to HSP72 on the TEVs, which conversely has been shown by another group to induce IL-12 production and thus increase tumor surveillance (38). It is therefore controversial whether differentiated DCs are also capable of producing immunosuppressive cytokines. Recent work, which applied lymphatic-derived TEVs from melanoma patients, has further supported the theory that DC maturation is targeted by TEV contents. Proteomic profiling of vesicles revealed that this effect might be linked to S100A9, which had been previously described to suppress DC differentiation (39).

The above described findings support the conclusion that the differentiation phase of DCs is particularly susceptible to interference by TEVs. However, when differentiated DCs are incubated *in vitro* with TEVs, some groups were able to use these DCs as a potent DC vaccine against the tumor after expansion in cell culture, underlining the role of TEVs in antigen presentation and induction of the adaptive immune response (40). This provides some evidence that at least a certain subset of TEVs might be part of a tightly regulated cellular anti-tumor signal, but also allows the hypothesis that fully differentiated DCs are less prone to dysregulation by TEVs than their precursors (41). In a pioneering trial applying human material, it was shown that differentiated DCs pulsed with autologous TEVs isolated from patient ascites can be used for inducing tumor-specific CTL, in some cases even expanding restricted T cell repertoires (9). This was the foundation for further TEV/DC-based vaccine trials. Subsequently, antigen transfer from TEVs to DCs has been well characterized. DCs have the capacity to readily internalize TEVs and process their associated antigens in an MHC-dependent manner (28, 42, 43). The uptake of TEVs into DCs has been shown to be mediated by LFA-1/CD54 and C-type lectin/C-type lectin receptor interactions and is dependent on the actin cytoskeleton (40). After internalization, TEV contents are predominantly recruited to MHCII loading compartments (41). Interestingly, TEVs with luminally loaded antigens induce stronger class I MHC responses than TEVs with antigens located

at the outside of the vesicle membrane (44). Moreover, TEVs seem to be the most efficient route of presentation for some tumor antigens. Using MUC1, a well-known tumor antigen, Rughetti et al. were able to demonstrate that TEV-associated MUC1 is translocated from endolysosomes to MHCII loading compartments in DCs. This was however not the case when soluble MUC1 was used (45). TEVs also have the capacity to reprogram the uptaking DC by inducing reactive oxygen species (ROS) and alkalinization in the phagosomal compartment, which enhances antigen processing (46). Apart from this, TEV internalization by DCs was also described to result in an increase in expression of the costimulatory receptors CD40, CD80, and CD54 on the DCs (40).

However, it is probable that not all types of TEVs interact with DCs efficiently. For example, a recent study examined glycocalyxes on TEVs, especially ligands of sialic acid binding Ig-like lectin (Siglec) receptors, to determine the extent to which they mediate internalization (47). Indeed, the authors found evidence that these glycocalyx components directly affect TEV-DC interaction and can be experimentally modified to alter the uptake of TEVs by DCs. This finding could explain differences in DC pulsing efficacy, while also allowing for positive selection or artificial generation of TEV subtypes that are well-suited for immunotherapy.

There is also evidence that certain therapeutic interventions shift the payload of TEVs toward a phenotype that favors anti-tumor immune responses. For example, double-stranded DNA (dsDNA) is shed in TEVs (48, 49), but is markedly increased after radiotherapy (RT). This RT-induced dsDNA can be delivered to DCs by TEVs, increasing the production of type 1 interferon to promote the survival of tumor-bearing mice (50). Another study reported that treatment of tumor cells with IFN-γ results in the release of TEVs which have the capacity to induce IL-12 secretion in cultured DCs, thus promoting tumor surveillance (38). This is particularly interesting as this effect was attributed to TEV-associated HSP72, which has been described by other groups as an inducer of pro-tumoral phenotypes in DCs (37). Moreover, others have argued that IFN-γ upregulates the expression of TEV-associated PD-L1, thus inhibiting CTL (22). Further studies to assess how cancer therapy potentially alters the TEV profile toward immune stimulation or suppression are clearly needed as such approaches owe a potential for biomarkers for therapy response.

Taking all these considerations together, the existing evidence points toward several pivotal effects of TEVs on T cells and dendritic cells. First, TEVs are capable of interfering with DC differentiation. Thereby, they inhibit the recognition of tumor-derived antigens and reduce T cell responses in the tumor microenvironment. This is further augmented by activation of regulatory T cells and targeting of $CD4^+$/$CD8^+$ T cells, in which apoptosis is induced. The potency of TEVs is probably influenced by three factors. First, TEVs circulate within the bloodstream and can therefore reach distant sites of metastasis, where local immunosuppression can contribute to pre-metastatic niche formation (51). Second, a single tumor cell can release thousands of extracellular vesicles during its lifespan and upon undergoing apoptosis. Thereby, the magnitude by which tumor-promoting ligands such as PD-L1 interact with a recipient immune cell is markedly increased compared to single tumor cells (23). Thus, TEVs function like an amplifier of the communication between a tumor and the immune cells in its microenvironment. Third, due to their heterogeneity in biophysical properties and cargo, TEVs can target a large variety of different immune cells, which increases the efficacy by exploiting redundant systems to promote aligned effects. Thus, TEVs largely take part in the cellular reprogramming which is induced by malignant tumors during disease progression (52).

However, as outlined above, it has been also recognized that DCs can process TEV-associated antigens to promote T cell responses. This apparently contradictory finding has prompted irritation in the field whether TEVs are "friends or foes" (53). We aim to answer this question by addressing important experimental differences in the underlying studies in *Explanations for the Reported Heterogeneity of TEV Effects* section.

TEV EFFECTS ON THE INNATE IMMUNITY: MACROPHAGES AND NEUTROPHILS

Few groups have focused on deciphering the interaction of TEVs and the innate immune system. Some evidence exists that macrophages are able to capture TEVs derived from apoptosis from circulation in a CD169 dependent process (54). Knockout of CD169 led to an enhanced immune response after immunization with ovalbumin, suggesting that macrophages eliminate TEVs, thus promoting tolerance. On the other hand, the same group demonstrated that in non-tumor bearing mice, injected TEVs suppress the immune response toward the ovalbumin antigen independent of macrophages (54). In an *in vitro* approach, Bardi et al. found that TEVs polarize macrophages toward a mixed phenotype of both M1 and M2 macrophages, thus promoting both inflammation and tissue regeneration (55). This could be explained by previous studies on macrophages in cancer that described both tumor-suppressing and tumor-promoting roles (56, 57). However, the authors interpreted the mixed macrophage polarization induced by TEVs as evidence of a certain flexibility a tumor would need to induce a vast subset of tumorigenic processes.

In concert with macrophages, neutrophils perform important tasks in immune response, based on recent studies defining interactions of neutrophils with TEVs. Leal and colleagues reported that TEVs induce the formation of neutrophil extracellular traps (NET) that promote cancer-related thrombosis (58). TEVs from tumor stem-like cells, as well differentiated tumor cells were described to induce a pro-tumoral phenotype in neutrophils. This occurs, for example, by polarization toward the N2 subpopulation, which induces production of several factors that promote angiogenesis, invasion and metastasis (59–62). This effect might be due to the uptake of vesicular RNA that exerts signaling functions or the uptake of circulating oncogenic DNA (63). These

findings underline the potential of deciphering TEV-based mechanisms by which neutrophils are altered toward a phenotype that promotes tumor survival and progression.

A PERSPECTIVE ON TEVS IN IMMUNOTHERAPY AND BIOENGINEERING

Three leading hypotheses have made TEVs attractive for immunotherapeutic research. First, their potential roles in antigen presentation, possibly owing the potential of an anti-tumor vaccination-like approach, second, their immunosuppressive abilities and, third, their internalization in living cells, making them potential biological vehicles of artificially engineered therapeutic components. Interestingly, as outlined above, immunotherapeutic effects have been described when isolated TEVs are not injected separately into an animal, but are used to educate dendritic cells which are then administered (41). This DC vaccine might be more desirable in terms of therapeutic application compared to the injection of directly tumor-derived material. This approach has been used by several groups to treat cancer in animal models and evaluated in clinical trials that are currently registered using tumor-sensitized autologous dendritic cells or DC-derived EVs (64, 65). However, it remains unknown which tumor antigen source would be most effective for the pulsing of dendritic cells, since it has been reported that certain isolated tumor proteins would be more beneficial than whole tumor cell lysates (66). Gu and colleagues compared tumor lysates and TEVs in a murine model of DC vaccine, finding that the pre-incubation with TEVs is more efficient in terms of tumor growth restriction and survival (41). Furthermore, TEVs could be engineered to have increased MHC expression on the surface of TEVs, and thus enhance the efficacy of DC sensitization (67).

As the field is still at the beginning of exploiting the benefits of EVs for therapeutic purposes, research effort is needed to understand how therapeutic EVs, including TEVs, influence the tumor progression *in vivo*. We have learned from clinical trials that immunomodulatory EVs derived from mesenchymal stromal cells (MSCs) are sufficient to treat steroid-refractory human Graft-versus-Host-Disease (68). However, the experiences with MSC-EVs also demonstrate that various subsets of EVs differ in their immunomodulatory capacities (69). Taking into account the contradictory functional results from studies on TEVs, translation to the clinics could potentially be aggravated by the lack of techniques which are suitable to reliably predict therapeutic efficiency. Therefore, standardized assays, such as those recently proposed by Kordelas et al. (69), are needed in the field to determine the immunomodulatory properties of EV preparations prior to administration. Likewise, the same group has reported that recipients vary in MSC-EV responsiveness which complicates EV therapy (69). Regarding TEVs, this heterogeneity has not been widely addressed in animal models and requires further study. It was recently reported that an *in vitro* assay based on a co-culture of TEVs with splenocytes from an experimental model of murine encephalomyelitis detects TEV-mediated activity that distinguishes MSC-EVs from TEVs based on the expression pattern on targeted splenocytes (70). Further development and validation of similar approaches will likely lead to a platform that has the potential for pre-clinical testing and enhance patient safety, which would be a major step toward the first in-human trials based on TEVs.

Engineered EVs are often investigated with a focus on targeting specific tissues or tumors, respectively. Biodistribution analyses have revealed that EVs are rapidly recruited to tumors after intravenous injection, possibly due to the increased vascularization (71). However, the transport of EVs within the bloodstream to tumor sites would still be unspecific. As integrins have been demonstrated to play a pivotal role in organotropic delivery of EVs (72), this observation could support the loading of specific integrins onto EVs to target the tumor bed. Moreover, exosome-mimetic nanoplatforms (EMN) are potentially useful for the generation of vesicles from cultured tumor cells that are customized to contain specific integrins with a therapeutic payload (73). Such tumor cell-derived EMN share relevant biological properties with "natural" TEVs, but are easier to obtain in therapeutically applicable concentrations. Moreover, the patient safety concerns regarding tumor cell-derived EMN could be addressed by using non-tumor cell lines that retain targeting specificity *in vivo*. For example, Jang et al. reported that monocytes and macrophages can be used for EMN production and that these EMN can be recruited to tumor sites (74), a promising approach avoiding the use of tumor cells.

EXPLANATIONS FOR THE REPORTED HETEROGENEITY OF TEV EFFECTS

One of the most enigmatic questions in the study of TEVs remains why TEVs have immunosuppressive as well as immune-stimulatory roles (**Figures 1**, **2**, **Tables 1**, **2**). As outlined above, *in vivo*, TEVs may suppress functionality of dendritic cells and $CD4^+$ T cells, and increase activation of Tregs and myeloid-derived suppressor cells (81). However, one could hypothesize that the antigen-presenting component of some TEVs might predominate under certain *in vitro* conditions when the suppressive effect by impaired antigen-presenting cells and supporter cells is lacking. Still, this would not explain why *in vivo* DC vaccines are quite effective when TEVs are used for antigen delivery (9, 41). As a consequence, neither isolated TEVs + effector cells alone nor isolated TEV-pulsed DCs shift the phenotype toward immunosuppression. Of note, the major difference between studies using pulsed DCs vs. direct injection of TEVs in a living animal, is that there is an *in vitro* incubation step of TEVs directly with differentiated DCs, suggesting the following two hypotheses:

a. In living organisms, TEVs might strongly influence the differentiation phases of immune cells. This effect has been well described for DCs (36). Rather than interfering with fully

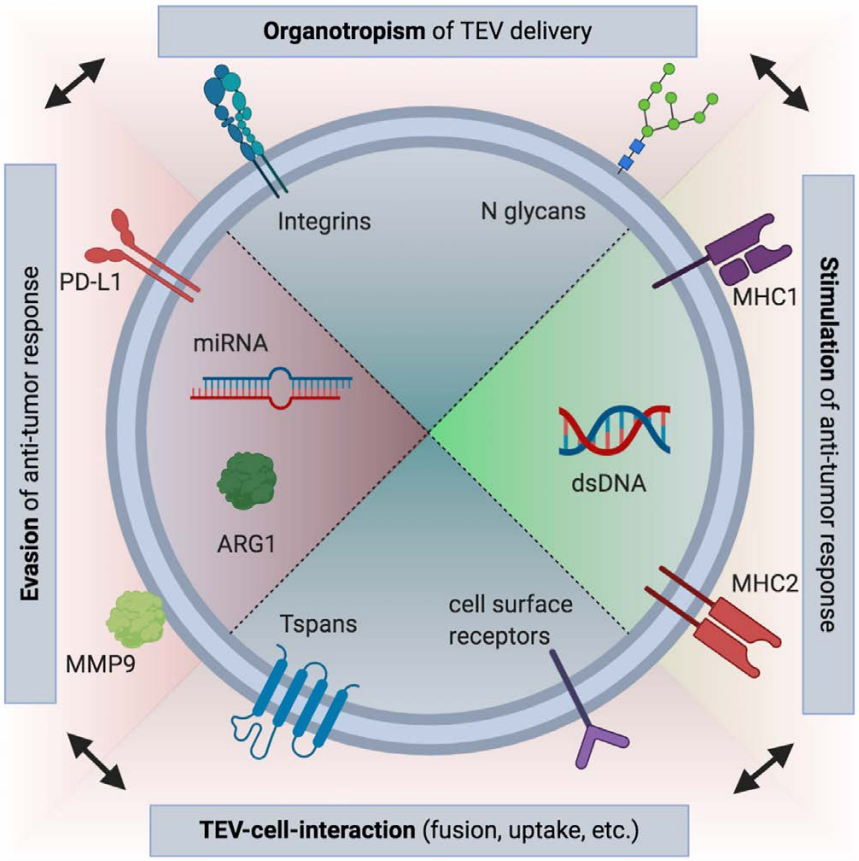

FIGURE 1 | Overview of selected immune-modulatory tumor-derived extracellular vesicle (TEV) cargo. Both immunosuppressive and immune-stimulating roles have been proposed for TEVs. These effects can be mediated by receptors bound to the surface of TEVs, such as PD-L1, or by nucleic acid or protein contents (e.g., arginin-1, ARG1) encapsulated in the interior of the vesicles (21, 22, 25). However, if uptake occurs, interaction of vesicular and cellular receptors is probably needed (75). Tetraspanins (Tspans) such as CD9, CD63, and CD81 are frequently used for characterization of EVs and are likely involved in fusion of TEVs and recipient cells, similar to what has been described for some viruses (76, 77). While also promoting TEV uptake, integrins and other adhesion molecules are responsible for tissue-specific binding of TEVs (78). Thus, immune responses can be modified by TEVs not only globally, but also influence local local responses. This may promote pre-metastatic niche formation (51). Recently, a role in immune cell targeting has been also revealed for N glycans (47). (Figure created using BioRender.com).

differentiated immune cells, TEVs might potently suppress the differentiation of precursor cells.

b. In immune-competent animal models as well as in human cancer, TEVs may interact directly with Tregs (activation) (18, 30), $CD4^+$ T cells (apoptosis induction) (20), and myeloid-derived suppressor cells (activation) (81). The direct interaction is underlined by the finding that TEV-pulsed dendritic cells do not induce these processes when injected into an animal.

Taking *(a)* and *(b)* together, one can conclude that at least some subtypes of TEVs have the capacity to present tumor antigens to $CD8^+$ T cells and DCs. However, in a living organism, interactions are much more complex. Direct effects of TEVs on T-suppressor cells have to be considered where TEVs themselves are involved in a system of linking regulatory immune pathways. Moreover, naïve immune cells might react substantially differently to TEVs than exhausted T cells or DCs in the tumor microenvironment. Therefore, one explanation for the efficacy of DC vaccines could be that the injected DCs are not excessively reprogrammed toward a pro-tumoral phenotype, unlike the endogenous DCs. Once more, this implicates distinct functions of TEVs under various conditions.

Moreover, the role of TEVs has to be integrated into the complex network of the tumor secretome. This includes soluble factors that are not released in vesicles, but might – due to their biochemical properties – adhere to the surface of vesicles or might as well remain completely unassociated with TEVs (87). Therefore, it might be even harder than expected to match the biological origin of TEVs with their function, and to establish the effect of TEVs that could be over- or underestimated. For example, Madera and colleagues demonstrated that the macrophage-related effects of breast cancer cell conditioned media are partly, but not exclusively, due to TEVs (79). These observations underscore the importance of detailed attention to controls in functional studies, such as the methodology for the collection of conditioned media depleted of TEVs.

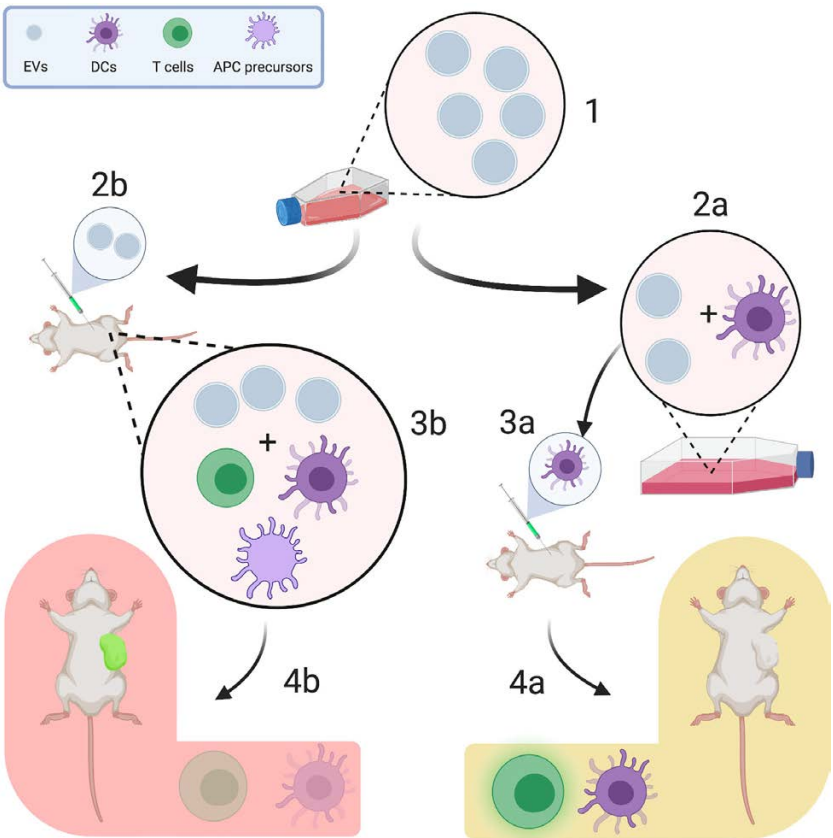

FIGURE 2 | Experimental design influences the heterogeneity of reported tumor-derived extracellular vesicle (TEV) effects. TEVs are regularly harvested from the supernatants of tumor cell lines (*1*). They can be either used for *in vitro* pulsing of immune cells (e.g., differentiated dendritic cells, *2a*) or for direct injection *(2b)*. In pulsing experiments, TEV-associated antigens are presented to dendritic cells, which are then injected into an animal and induce strong T cell responses *(3a)* (41). This promotes tumor growth restriction and increases survival of tumor-bearing mice *(4a)*. On the other hand, when TEVs are injected separately, they interact with a plenitude of other immune cells, such as regulatory T cells, $CD34^+$ dendritic cell precursors and myeloid derived suppressor cells *(3b)*, which are commonly activated by TEVs to enable immune evasion (18, 36). This, in turn, reduces the tumor-specific T cell response and enhances tumor progression *(4b)*. (Figure created using BioRender.com).

Apart from these considerations, another explanation could be the heterogeneity of EVs themselves. However, the question of which subtype of TEVs is most likely involved in the various processes of immunomodulation has not been widely assessed, as there are hardly any well-established markers that could easily distinguish exosomes from microvesicles or apoptotic bodies, respectively. Nevertheless, some groups have targeted this question, including further characterization of the immune-modulatory TEVs. Muhsin-Sharafaldine and colleagues observed that the antigen-presenting role of TEVs is mostly mediated by apoptotic vesicles, as tumor antigens were only detected in the "apoptotic vesicle-enriched fraction" (86). Subsequently, when mice were first immunized by B16-F1 cell line-derived EVs and then subject to B16 melanoma implantation, the group of animals which had been "vaccinated" with apoptotic vesicles were protected for longer from the tumor than animals that were administered exosomes and microvesicles. However, apoptotic bodies were identified as vesicles larger than 200 nm, although it is also accepted that some apoptotic bodies are actually as small as 100 nm (88). Of note, exosomes were – among other markers – characterized by the presence of histones. It is currently extremely controversial whether histone proteins are presents in EVs at all, and the characterization of exosomes by histone payload is therefore not recommended at the moment (7). Regardless, the hypothesis that apoptotic-derived vesicles carry at least a larger amount of tumor antigens than exosomes is consistent with the understanding of exosome biogenesis as a tightly controlled process versus apoptotic vesicle formation as a part of "cell waste" disposal. Moreover, the immunogenicity of apoptotic tumor cells has been well described (89, 90). Indeed, apoptotic vesicles could induce comparably strong anti-tumor immune responses, as the variety of genetic material and tumor-derived protein content is probably the largest among the vesicle types.

Recently, new light was shed on the functional differences between the several types of TEVs. In a study published by Temoche-Diaz et al., two subtypes of small TEVs from a breast cancer cell line were successfully separated by high-resolution

TABLE 1 | Tumor-derived extracellular vesicle (TEV)-associated effects on immune cells promoting immune evasion and tumor progression.

Cancer type	Material/cells	Identified cargo	Model	Proposed mode of action	Reference
Mammary carcinoma	4T1	PD-L1	*In vitro; in vivo*	Inhibition of DC/Th1 function and differentiation, enhancement of tolerance (Treg induction), partly due to PD-L1	(18)
		MMP9	*In vitro*	Elicitation of pro-inflammatory phenotypes in macrophages ➔ tumor progression	(79)
			In vitro	Rab27a-dependent MMP9 secretion independently of TEVs, but may associate with TEV surface	(80)
	TSA	–	*In vitro; in vivo*	Inhibition of bone marrow-derived precursor cell differentiation; induction of IL-6	(36)
	MDA-MB-231	–	*In vitro*	Inhibition of monocyte differentiation into DC	(36)
Melanoma	B16-F10	HSP72/105	*In vitro; in vivo*	HSP72/105 induces IL-6 secretion in DCs, dependent on TLR2/4 and STAT3	(37)
		miRNA	*In vitro; in vivo*	miRNA induces apoptosis of CD4+ T cells	(20)
	+ patient material	PD-L1	*In vitro; in vivo*	PD-1-dependent inhibition of CTL proliferation	(22)
	Human melanoma	18 immuno-suppressive proteins	*In vitro*	Direct delivery of inhibitory proteins	(39)
Prostate carcinoma	TRAMP-C2	PD-L1	*In vitro; in vivo*	Promotion of tumor growth/progression; suppression of T cell activity	(23)
Renal cell carcinoma	RenCa	PD-L1	*In vitro; in vivo*	DC pulsing with TEV enables potent DC vaccine	(41)
		HSP70	*In vitro*	Induction of myeloid-derived suppressor cells, dependent on TLR2/STAT3	(81)
Lymphoma	EL4	–	*In vitro; in vivo*	Macrophages eliminate antigen-carrying TEVs to promote tumor tolerance	(54)
Ovarian cancer	OvCa + patient material	ARG-1	*In vitro; in vivo*	Delivery of metabolic checkpoint modulators that decrease proliferation of T cells	(25)
	Patient material	FasL	*In vitro*	T cell apoptosis and loss of CD3 zeta chain expression	(82)
Head and neck cancer	PCI-13 + patient material	FasL	*In vitro*	Apoptosis induction in activated T cells	(83)
Acute myeloid leukemia	Patient material	TGF-β	*In vitro*	Suppression of natural killer cell function	(84)
Colon carcinoma	CT26	HSP72	*In vitro; in vivo*	STAT3-mediated activation of myeloid-derived suppressor cells	(85)

density gradient fractionation and then further characterized (91). These authors demonstrated that these two subtypes of small TEVs exploit distinct mechanisms of RNA loading and recruit miRNA in a selective way. As gene ontology analysis revealed different subcellular origins of these vesicles, corresponding to endosomes and the plasma membrane, it can be hypothesized that the rough EV pellet typically obtained by ultracentrifugation contains at least two biologically different populations of TEVs with possibly distinct functions. Given the fact that these subtypes were shown to differ in terms of their density, even minimal differences in ultracentrifugation parameters such as k-factor, speed, time, and rotor (swing-out vs. fixed angle) or tube type used might predominantly enrich one of these subtypes. As a remarkable number of publications do not contain any characterization of the proposed EVs or only provide evidence that significantly falls below the experimental guidelines of the ISEV (8), findings should also be interpreted with a view to the utilized TEV isolation and characterization techniques.

Finally, it is notable that tumor cell lines differ substantially in terms of their invasiveness, apoptosis rate and metastatic potential. All of these factors are probably reflected in the formation of TEVs and therefore contribute to the heterogeneity of reported TEV effects, as well *in vitro* as *in vivo*. Of note, it was demonstrated that cancer cell lines differ in the expression of Rab27a, one of the known regulators of EV release (80). Another example is Rab7, which regulates MVB transport toward the plasma membrane and is differentially expressed in ovarian/peritoneal serous carcinoma and malignant peritoneal mesothelioma (92). Differences in the abundance of SNARE proteins, which mediate the fusion of MVBs and the plasma membrane, have been described for various types of hematopoietic and lymphoid neoplasia (93). Apart from

TABLE 2 | Tumor-derived extracellular vesicle (TEV)-associated effects on immune cells promoting tumor surveillance and immune response.

Cancer type	Material/cells	Identified cargo	Model	Proposed mode of action	Reference
Mammary carcinoma	4T1	HSP72	*In vitro*	HSP72 induces IL-12 release by DCs	(38)
	TSA	dsDNA	*In vitro; in vivo*	Delivery of dsDNA to DCs after radiotherapy	(50)
Melanoma	B16-F10	–	*In vitro*	Macrophage polarization toward mixed, pro-tumoral phenotypes	(55)
	B16-F1	–	*In vivo*	Protection against tumor growth after TEV injection	(86)
	Human melanoma	Matr1 antigen	*In vitro*	Induction of DCs and antigen-specific CTL	(9)
Renal cell carcinoma	RCC	–	*In vitro; in vivo*	Stimulation of CTL through FasL/Fas signaling	(26)

release-associated proteins and enzymes, molecules that exert direct signaling functions are differentially expressed in various tumors. For example, PD-L1 is a prominent example that has been linked to TEV-induced immunosuppression and is a promising clinical outcomes marker following immunotherapy (23, 94).

Taking all these considerations together, several lessons have to be learned from functional animal experiments studying the effect of TEVs on the immune response. Obviously, findings from *in vivo* and *in vitro* experiments differ notably (**Figure 2**). Although comparative studies are largely lacking, preliminary evidence suggests that experimental differences in *in vitro* vs. *in vivo* trials account for a proportion of the reported heterogeneity of TEV effects (95). Cell culture experiments are especially useful if interactions between well-defined components are studied. These components should be arbitrarily manipulatable by the researcher. However, this is not the case for functional TEV-immunity experiments, as two complex systems – the vesicle population and the immune system – are studied, which are necessarily oversimplified in this experimental setting. Therefore, cell culture trials of immune cell interactions with TEVs resemble a burning lens – they apply a strong focus on specific details but leave the rest blurred out. This is underlined by two major observations that have been outlined above:

First, mouse models have shown that many different immune cells and precursors are influenced by TEVs. The immune cells, in turn, influence each other's functionality but also the tumor microenvironment. It is therefore conceivable that the TEV composition changes after targeting of the tumor by immune cells. Moreover, tumor progression leads to a substantial reprogramming of cellular functions, thus, in later tumor stages, e.g., the antigen-presenting role of TEVs could be heavily impaired. Certain TEV types themselves could contribute to this process (96). These complex biological crosslinks are impossible to mimic in a cell culture experiment which cannot simulate reciprocal interactions.

Second, any experimental TEV population is highly heterogeneous. Researchers are confronted with two sides of the same coin: on one hand, technical purification of TEVs is necessary for pulsing immune cells *in vitro*. On the other hand, extreme purification can also mean a significant loss of EV subpopulations. Moreover, the purity of EV preparations is an issue that has led to misinterpretations in terms of cargo (7). Thus, an impact on experimental outcomes cannot be excluded.

From a technical perspective, animal models owe the unique potential to address currently understudied questions more rigorously. For instance, *in vivo* TEV tracking could provide insight into details on the kinetics of TEV-immune cell interactions. Lipid dyes, including, e.g., CFSE, PKH26/67 and DiR, have been applied in functional mouse models of tumor progression (97), although there are remaining concerns regarding their lack of staining specificity. A main issue is the labelling of non-EV-lipid particles, such as lipoproteins, which surpass EVs in terms of abundancy. Thus, results may not be exclusively attributed to EVs. A comprehensive review of fluorescent dyes for EV staining has been recently published elsewhere (98). The problem of TEV pre-staining has been addressed by multiple groups, who applied transfection of tumor cells with a fluorescent reporter such as green fluorescent protein (GFP) under the regulation of known EV associated proteins like the tetraspanins CD9, CD63, and CD81 (99, 100). Combined with recent advances in high resolution imaging and nanoscale flow cytometry, TEV release and trafficking can be further addressed (101, 102). Another important aspect is the mode of administration of TEVs in laboratory animals. If non-tumor bearing animals are used, immunological effects might differ notably from the effects observed in tumor-bearing animals, in which TEVs are constitutively released. Additionally, the optimal amount of TEVs injected into animals as well as the administration route will likely have an impact on functional results (103). To overcome the problems of TEV pre-isolation, staining, and administration, the above described expression of fluorescent or bioluminescent TEV fusion protein reporters could be further investigated in murine tumors. Bridging techniques, such as a recently reported spheroid co-culture model of PBMCs and tumor cells stably releasing GFP-tagged TEVs (33), offer a valuable chance to assess functional hypotheses before planning such animal trials.

CONCLUDING REMARKS

During the past decade, our understanding of tumor-derived EVs has grown tremendously. However, translation into clinical research has been delayed by contradictory findings and the technical complexity of EV studies. As substantial progress has been recently made especially in the field of nanotechnology, further advances in nanoscale bioimaging might ultimately enable rigorous animal trials, which could elucidate the enigmatic dichotomy of TEV functions in cancer immunity. This, in turn, will lead to a more detailed understanding of the mechanisms by which TEVs alter immune responses toward a pro-tumoral phenotype, owing the potential for therapeutic manipulation. We have argued that animal models can much better account for the heterogeneity of both the TEV populations and immune cell functions. They also accurately display physiological phenomena such as immune cell exhaustion, tumor apoptosis and invasion. Moreover, they owe the potential to study alterations of the TEV profile in different phases of tumor development and progression. Given these premises, future research efforts should focus on pathophysiological models in the tumor-bearing living animal rather than characterization of TEV-single-cell-interactions. Multiparametric readouts, using techniques that combine high-resolution imaging and biochemical characterization, e.g., *via* nanoscale flow cytometry, are valuable to cover a broad spectrum of immune cell interactions.

Moreover, the antigen-carrying functions of TEVs and their role in dendritic cell vaccines will likely cause further research enthusiasm in clinical oncology. However, to fully exploit the undoubted potential of TEVs as immunotherapeutic agents, standardized assays will be necessary to evaluate the biological activity of TEV preparations. Ultimately, ongoing efforts might

open the door for TEVs as a novel component of personalized tumor therapy, either as a novel treatment or a therapeutic target.

AUTHOR CONTRIBUTIONS

MD wrote the review with editorial advice from BT and BE. All authors contributed to the article and approved the submitted version.

FUNDING

MD received funding support by the Else Kroener Fresenius-Stiftung foundation and the German Academic Scholarship Foundation ("Studienstiftung des deutschen Volkes"). BT is supported by Stiftung Universitätsmedizin Essen. Additional support (BE) was provided by the National Institutes of Health (R01 GM140137) and the Academic Senate of UC San Diego and the Department of Surgery.

REFERENCES

1. Gajewski TF, Schreiber H, Fu YX. Innate and adaptive immune cells in the tumor microenvironment. *Nat Immunol* (2013) 14(10):1014–22. doi: 10.1038/ni.2703
2. Robbins PD, Morelli AE. Regulation of immune responses by extracellular vesicles. *Nat Rev Immunol* (2014) 14(3):195–208. doi: 10.1038/nri3622
3. Mir B, Goettsch C. Extracellular Vesicles as Delivery Vehicles of Specific Cellular Cargo. *Cells* (2020) 9(7):1601. doi: 10.3390/cells9071601
4. Jabbari N, Karimipour M, Khaksar M, Akbariazar E, Heidarzadeh M, Mojarad B, et al. Tumor-derived extracellular vesicles: insights into bystander effects of exosomes after irradiation. *Lasers Med Sci* (2020) 35 (3):531–45. doi: 10.1007/s10103-019-02880-8
5. Zhang H, Freitas D, Kim HS, Fabijanic K, Li Z, Chen H, et al. Identification of distinct nanoparticles and subsets of extracellular vesicles by asymmetric flow field-flow fractionation. *Nat Cell Biol* (2018) 20(3):332–43. doi: 10.1038/s41556-018-0040-4
6. Zhang Q, Higginbotham JN, Jeppesen DK, Yang YP, Li W, McKinley ET, et al. Transfer of Functional Cargo in Exomeres. *Cell Rep* (2019) 27(3):940–54.e6. doi: 10.1016/j.celrep.2019.01.009
7. Jeppesen DK, Fenix AM, Franklin JL, Higginbotham JN, Zhang Q, Zimmerman LJ, et al. Reassessment of Exosome Composition. *Cell* (2019) 177(2):428–45.e18. doi: 10.1016/j.cell.2019.02.029
8. Thery C, Witwer KW, Aikawa E, Alcaraz MJ, Anderson JD, Andriantsitohaina R, et al. Minimal information for studies of extracellular vesicles 2018 (MISEV2018): a position statement of the International Society for Extracellular Vesicles and update of the MISEV2014 guidelines. *J Extracell Vesicles* (2018) 7(1):1535750. doi: 10.1080/20013078.2018.1461450
9. Andre F, Schartz NE, Movassagh M, Flament C, Pautier P, Morice P, et al. Malignant effusions and immunogenic tumour-derived exosomes. *Lancet* (2002) 360(9329):295–305. doi: 10.1016/S0140-6736(02)09552-1
10. Markov O, Oshchepkova A, Mironova N. Immunotherapy Based on Dendritic Cell-Targeted/-Derived Extracellular Vesicles-A Novel Strategy for Enhancement of the Anti-tumor Immune Response. *Front Pharmacol* (2019) 10:1152. doi: 10.3389/fphar.2019.01152
11. Zuo B, Qi H, Lu Z, Chen L, Sun B, Yang R, et al. Alarmin-painted exosomes elicit persistent antitumor immunity in large established tumors in mice. *Nat Commun* (2020) 11(1):1790. doi: 10.1038/s41467-020-15569-2
12. Taghikhani A, Farzaneh F, Sharifzad F, Mardpour S, Ebrahimi M, Hassan ZM. Engineered Tumor-Derived Extracellular Vesicles: Potentials in Cancer Immunotherapy. *Front Immunol* (2020) 11:221. doi: 10.3389/fimmu.2020.00221
13. Peng X, Yang L, Ma Y, Li Y, Li H. Focus on the morphogenesis, fate and the role in tumor progression of multivesicular bodies. *Cell Commun Signal* (2020) 18(1):122. doi: 10.1186/s12964-020-00619-5
14. Armacki M, Polaschek S, Waldenmaier M, Morawe M, Ruhland C, Schmid R, et al. Protein Kinase D1, Reduced in Human Pancreatic Tumors, Increases Secretion of Small Extracellular Vesicles From Cancer Cells That Promote Metastasis to Lung in Mice. *Gastroenterology* (2020) 159(3):1019–35.e22. doi: 10.1053/j.gastro.2020.05.052
15. Huang C, Hays FA, Tomasek JJ, Benyajati S, Zhang XA. Tetraspanin CD82 interaction with cholesterol promotes extracellular vesicle-mediated release of ezrin to inhibit tumour cell movement. *J Extracell Vesicles* (2020) 9 (1):1692417. doi: 10.1080/20013078.2019.1692417
16. Hyenne V, Apaydin A, Rodriguez D, Spiegelhalter C, Hoff-Yoessle S, Diem M, et al. RAL-1 controls multivesicular body biogenesis and exosome secretion. *J Cell Biol* (2015) 211(1):27–37. doi: 10.1083/jcb.201504136
17. Whiteside TL. Exosomes and tumor-mediated immune suppression. *J Clin Invest* (2016) 126(4):1216–23. doi: 10.1172/JCI81136
18. Ning Y, Shen K, Wu Q, Sun X, Bai Y, Xie Y, et al. Tumor exosomes block dendritic cells maturation to decrease the T cell immune response. *Immunol Lett* (2018) 199:36–43. doi: 10.1016/j.imlet.2018.05.002
19. Whiteside TL. Regulatory T cell subsets in human cancer: are they regulating for or against tumor progression? *Cancer Immunol Immunother* (2014) 63 (1):67–72. doi: 10.1007/s00262-013-1490-y
20. Zhou J, Yang Y, Wang W, Zhang Y, Chen Z, Hao C, et al. Melanoma-released exosomes directly activate the mitochondrial apoptotic pathway of CD4(+) T cells through their microRNA cargo. *Exp Cell Res* (2018) 371 (2):364–71. doi: 10.1016/j.yexcr.2018.08.030
21. Valadi H, Ekstrom K, Bossios A, Sjostrand M, Lee JJ, Lotvall JO. Exosome-mediated transfer of mRNAs and microRNAs is a novel mechanism of genetic exchange between cells. *Nat Cell Biol* (2007) 9(6):654–9. doi: 10.1038/ncb1596
22. Chen G, Huang AC, Zhang W, Zhang G, Wu M, Xu W, et al. Exosomal PD-L1 contributes to immunosuppression and is associated with anti-PD-1 response. *Nature* (2018) 560(7718):382–6. doi: 10.1038/s41586-018-0392-8
23. Poggio M, Hu T, Pai CC, Chu B, Belair CD, Chang A, et al. Suppression of Exosomal PD-L1 Induces Systemic Anti-tumor Immunity and Memory. *Cell* (2019) 177(2):414–27.e13. doi: 10.1016/j.cell.2019.02.016
24. Czystowska-Kuzmicz M, Whiteside TL. The potential role of tumor-derived exosomes in diagnosis, prognosis and response to therapy in cancer. *Expert Opin Biol Ther* (2020) 1–18. doi: 10.1080/14712598.2020.1813276
25. Czystowska-Kuzmicz M, Sosnowska A, Nowis D, Ramji K, Szajnik M, Chlebowska-Tuz J, et al. Small extracellular vesicles containing arginase-1 suppress T-cell responses and promote tumor growth in ovarian carcinoma. *Nat Commun* (2019) 10(1):3000. doi: 10.1038/s41467-019-10979-3
26. Xu HY, Li N, Yao N, Xu XF, Wang HX, Liu XY, et al. CD8+ T cells stimulated by exosomes derived from RenCa cells mediate specific immune responses through the FasL/Fas signaling pathway and, combined with GMCSF and IL12, enhance the antirenal cortical adenocarcinoma effect. *Oncol Rep* (2019) 42(2):866–79. doi: 10.3892/or.2019.7208
27. Duvallet E, Boulpicante M, Yamazaki T, Daskalogianni C, Prado Martins R, Baconnais S, et al. Exosome-driven transfer of tumor-associated Pioneer Translation Products (TA-PTPs) for the MHC class I cross-presentation pathway. *Oncoimmunology* (2016) 5(9):e1198865. doi: 10.1080/2162402X.2016.1198865
28. Wolfers J, Lozier A, Raposo G, Regnault A, Théry C, Masurier C, et al. Tumor-derived exosomes are a source of shared tumor rejection antigens for CTL cross-priming. *Nat Med* (2001) 7(3):297–303. doi: 10.1038/85438
29. Vincent-Schneider H, Stumptner-Cuvelette P, Lankar D, Pain S, Raposo G, Benaroch P, et al. Exosomes bearing HLA-DR1 molecules need dendritic cells to efficiently stimulate specific T cells. *Int Immunol* (2002) 14(7):713–22. doi: 10.1093/intimm/dxf048
30. Muller L, Simms P, Hong CS, Nishimura MI, Jackson EK, Watkins SC, et al. Human tumor-derived exosomes (TEX) regulate Treg functions via cell surface signaling rather than uptake mechanisms. *Oncoimmunology* (2017) 6 (8):e1261243. doi: 10.1080/2162402X.2016.1261243
31. Muller L, Mitsuhashi M, Simms P, Gooding WE, Whiteside TL. Tumor-derived exosomes regulate expression of immune function-related genes in human T cell subsets. *Sci Rep* (2016) 6:20254. doi: 10.1038/srep20254

32. Schuler PJ, Saze Z, Hong CS, Muller L, Gillespie DG, Cheng D, et al. Human CD4+ CD39+ regulatory T cells produce adenosine upon co-expression of surface CD73 or contact with CD73+ exosomes or CD73+ cells. *Clin Exp Immunol* (2014) 177(2):531–43. doi: 10.1111/cei.12354
33. Sadovska L, Zandberga E, Sagini K, Jekabsons K, Riekstina U, Kalnina Z, et al. A novel 3D heterotypic spheroid model for studying extracellular vesicle-mediated tumour and immune cell communication. *Biochem Biophys Res Commun* (2018) 495(2):1930–5. doi: 10.1016/j.bbrc.2017.12.072
34. Mulcahy LA, Pink RC, Carter DR. Routes and mechanisms of extracellular vesicle uptake. *J Extracell Vesicles* (2014) 3(1):24641. doi: 10.3402/jev.v3.24641
35. Abels ER, Breakefield XO. Introduction to Extracellular Vesicles: Biogenesis, RNA Cargo Selection, Content, Release, and Uptake. *Cell Mol Neurobiol* (2016) 36(3):301–12. doi: 10.1007/s10571-016-0366-z
36. Yu S, Liu C, Su K, Wang J, Liu Y, Zhang L, et al. Tumor exosomes inhibit differentiation of bone marrow dendritic cells. *J Immunol* (2007) 178 (11):6867–75. doi: 10.4049/jimmunol.178.11.6867
37. Shen Y, Guo D, Weng L, Wang S, Ma Z, Yang Y, et al. Tumor-derived exosomes educate dendritic cells to promote tumor metastasis via HSP72/HSP105-TLR2/TLR4 pathway. *Oncoimmunology* (2017) 6(12):e1362527. doi: 10.1080/2162402X.2017.1362527
38. Bausero MA, Gastpar R, Multhoff G, Asea A. Alternative mechanism by which IFN-gamma enhances tumor recognition: active release of heat shock protein 72. *J Immunol* (2005) 175(5):2900–12. doi: 10.4049/jimmunol.175.5.2900
39. Maus RLG, Jakub JW, Hieken TJ, Nevala WK, Christensen TA, Sutor SL, et al. Identification of novel, immune-mediating extracellular vesicles in human lymphatic effluent draining primary cutaneous melanoma. *Oncoimmunology* (2019) 8(12):e1667742. doi: 10.1080/2162402X.2019.1667742
40. Hao S, Bai O, Li F, Yuan J, Laferte S, Xiang J. Mature dendritic cells pulsed with exosomes stimulate efficient cytotoxic T-lymphocyte responses and antitumour immunity. *Immunology* (2007) 120(1):90–102. doi: 10.1111/j.1365-2567.2006.02483.x
41. Gu X, Erb U, Buchler MW, Zoller M. Improved vaccine efficacy of tumor exosome compared to tumor lysate loaded dendritic cells in mice. *Int J Cancer* (2015) 136(4):E74–84. doi: 10.1002/ijc.29100
42. Yao Y, Chen L, Wei W, Deng X, Ma L, Hao S. Tumor cell-derived exosome-targeted dendritic cells stimulate stronger CD8+ CTL responses and antitumor immunities. *Biochem Biophys Res Commun* (2013) 436(1):60–5. doi: 10.1016/j.bbrc.2013.05.058
43. Piao YJ, Kim HS, Moon WK. Noninvasive Photoacoustic Imaging of Dendritic Cell Stimulated with Tumor Cell-Derived Exosome. *Mol Imaging Biol* (2020) 22(3):612–22. doi: 10.1007/s11307-019-01410-w
44. Arima Y, Liu W, Takahashi Y, Nishikawa M, Takakura Y. Effects of Localization of Antigen Proteins in Antigen-Loaded Exosomes on Efficiency of Antigen Presentation. *Mol Pharm* (2019) 16(6):2309–14. doi: 10.1021/acs.molpharmaceut.8b01093
45. Rughetti A, Rahimi H, Belleudi F, Napoletano C, Battisti F, Zizzari IG, et al. Microvesicle cargo of tumor-associated MUC1 to dendritic cells allows cross-presentation and specific carbohydrate processing. *Cancer Immunol Res* (2014) 2(2):177–86. doi: 10.1158/2326-6066.CIR-13-0112-T
46. Battisti F, Napoletano C, Rahimi Koshkaki H, Belleudi F, Zizzari IG, Ruscito I, et al. Tumor-Derived Microvesicles Modulate Antigen Cross-Processing via Reactive Oxygen Species-Mediated Alkalinization of Phagosomal Compartment in Dendritic Cells. *Front Immunol* (2017) 8:1179. doi: 10.3389/fimmu.2017.01179
47. Dusoswa SA, Horrevorts SK, Ambrosini M, Kalay H, Paauw NJ, Nieuwland R, et al. Glycan modification of glioblastoma-derived extracellular vesicles enhances receptor-mediated targeting of dendritic cells. *J Extracell Vesicles* (2019) 8(1):1648995. doi: 10.1080/20013078.2019.1648995
48. Thakur BK, Zhang H, Becker A, Matei I, Huang Y, Costa-Silva B, et al. Double-stranded DNA in exosomes: a novel biomarker in cancer detection. *Cell Res* (2014) 24(6):766–9. doi: 10.1038/cr.2014.44
49. Kahlert C, Melo SA, Protopopov A, Tang J, Seth S, Koch M, et al. Identification of double-stranded genomic DNA spanning all chromosomes with mutated KRAS and p53 DNA in the serum exosomes of patients with pancreatic cancer. *J Biol Chem* (2014) 289(7):3869–75. doi: 10.1074/jbc.C113.532267
50. Diamond JM, Vanpouille-Box C, Spada S, Rudqvist NP, Chapman JR, Ueberheide BM, et al. Exosomes Shuttle TREX1-Sensitive IFN-Stimulatory dsDNA from Irradiated Cancer Cells to DCs. *Cancer Immunol Res* (2018) 6 (8):910–20. doi: 10.1158/2326-6066.CIR-17-0581
51. Becker A, Thakur BK, Weiss JM, Kim HS, Peinado H, Lyden D. Extracellular Vesicles in Cancer: Cell-to-Cell Mediators of Metastasis. *Cancer Cell* (2016) 30(6):836–48. doi: 10.1016/j.ccell.2016.10.009
52. Palucka AK, Coussens LM. The Basis of Oncoimmunology. *Cell* (2016) 164 (6):1233–47. doi: 10.1016/j.cell.2016.01.049
53. Barros FM, Carneiro F, Machado JC, Melo SA. Exosomes and Immune Response in Cancer: Friends or Foes? *Front Immunol* (2018) 9:730. doi: 10.3389/fimmu.2018.00730
54. Black LV, Saunderson SC, Coutinho FP, Muhsin-Sharafaldine MR, Damani TT, Dunn AC, et al. The CD169 sialoadhesin molecule mediates cytotoxic T-cell responses to tumour apoptotic vesicles. *Immunol Cell Biol* (2016) 94 (5):430–8. doi: 10.1038/icb.2015.111
55. Bardi GT, Smith MA, Hood JL. Melanoma exosomes promote mixed M1 and M2 macrophage polarization. *Cytokine* (2018) 105:63–72. doi: 10.1016/j.cyto.2018.02.002
56. Qian BZ, Pollard JW. Macrophage diversity enhances tumor progression and metastasis. *Cell* (2010) 141(1):39–51. doi: 10.1016/j.cell.2010.03.014
57. Sica A, Mantovani A. Macrophage plasticity and polarization: in vivo veritas. *J Clin Invest* (2012) 122(3):787–95. doi: 10.1172/JCI59643
58. Leal AC, Mizurini DM, Gomes T, Rochael NC, Saraiva EM, Dias MS, et al. Tumor-Derived Exosomes Induce the Formation of Neutrophil Extracellular Traps: Implications For The Establishment of Cancer-Associated Thrombosis. *Sci Rep* (2017) 7(1):6438. doi: 10.1038/s41598-017-06893-7
59. Zhang X, Shi H, Yuan X, Jiang P, Qian H, Xu W. Tumor-derived exosomes induce N2 polarization of neutrophils to promote gastric cancer cell migration. *Mol Cancer* (2018) 17(1):146. doi: 10.1186/s12943-018-0898-6
60. Hwang WL, Lan HY, Cheng WC, Huang SC, Yang MH. Tumor stem-like cell-derived exosomal RNAs prime neutrophils for facilitating tumorigenesis of colon cancer. *J Hematol Oncol* (2019) 12(1):10. doi: 10.1186/s13045-019-0699-4
61. Cheng WC, Liao TT, Lin CC, Yuan LE, Lan HY, Lin HH, et al. RAB27B-activated secretion of stem-like tumor exosomes delivers the biomarker microRNA-146a-5p, which promotes tumorigenesis and associates with an immunosuppressive tumor microenvironment in colorectal cancer. *Int J Cancer* (2019) 145(8):2209–24. doi: 10.1002/ijc.32338
62. Wang X, Qiu L, Li Z, Wang XY, Yi H. Understanding the Multifaceted Role of Neutrophils in Cancer and Autoimmune Diseases. *Front Immunol* (2018) 9:2456. doi: 10.3389/fimmu.2018.02456
63. Chennakrishnaiah S, Meehan B, D'Asti E, Montermini L, Lee TH, Karatzas N, et al. Leukocytes as a reservoir of circulating oncogenic DNA and regulatory targets of tumor-derived extracellular vesicles. *J Thromb Haemost* (2018) 16(9):1800–13. doi: 10.1111/jth.14222
64. Zitvogel L, Regnault A, Lozier A, Wolfers J, Flament C, Tenza D, et al. Eradication of established murine tumors using a novel cell-free vaccine: dendritic cell-derived exosomes. *Nat Med* (1998) 4(5):594–600. doi: 10.1038/nm0598-594
65. Salem ML. The use of dendritic cells for peptide-based vaccination in cancer immunotherapy. *Methods Mol Biol* (2014) 1139:479–503. doi: 10.1007/978-1-4939-0345-0_37
66. Groh V, Li YQ, Cioca D, Hunder NN, Wang W, Riddell SR, et al. Efficient cross-priming of tumor antigen-specific T cells by dendritic cells sensitized with diverse anti-MICA opsonized tumor cells. *Proc Natl Acad Sci U.S.A.* (2005) 102(18):6461–6. doi: 10.1073/pnas.0501953102
67. Lee YS, Kim SH, Cho JA, Kim CW. Introduction of the CIITA gene into tumor cells produces exosomes with enhanced anti-tumor effects. *Exp Mol Med* (2011) 43(5):281–90. doi: 10.3858/emm.2011.43.5.029
68. Kordelas L, Rebmann V, Ludwig AK, Radtke S, Ruesing J, Doeppner TR, et al. MSC-derived exosomes: a novel tool to treat therapy-refractory graft-versus-host disease. *Leukemia* (2014) 28(4):970–3. doi: 10.1038/leu.2014.41
69. Kordelas L, Schwich E, Dittrich R, Horn PA, Beelen DW, Borger V, et al. Individual Immune-Modulatory Capabilities of MSC-Derived Extracellular Vesicle (EV) Preparations and Recipient-Dependent Responsiveness. *Int J Mol Sci* (2019) 20(7):1642. doi: 10.3390/ijms20071642
70. Fathollahi A, Hashemi SM, Haji Molla Hoseini M, Yeganeh F. In vitro analysis of immunomodulatory effects of mesenchymal stem cell- and tumor

cell -derived exosomes on recall antigen-specific responses. *Int Immunopharmacol* (2019) 67:302–10. doi: 10.1016/j.intimp.2018.12.009
71. Lai CP, Mardini O, Ericsson M, Prabhakar S, Maguire C, Chen JW, et al. Dynamic biodistribution of extracellular vesicles in vivo using a multimodal imaging reporter. *ACS Nano* (2014) 8(1):483–94. doi: 10.1021/nn404945r
72. Hoshino A, Costa-Silva B, Shen TL, Rodrigues G, Hashimoto A, Tesic Mark M, et al. Tumour exosome integrins determine organotropic metastasis. *Nature* (2015) 527(7578):329–35. doi: 10.1038/nature15756
73. Vazquez-Rios AJ, Molina-Crespo A, Bouzo BL, Lopez-Lopez R, Moreno-Bueno G, de la Fuente M. Exosome-mimetic nanoplatforms for targeted cancer drug delivery. *J Nanobiotechnol* (2019) 17(1):85. doi: 10.1186/s12951-019-0517-8
74. Jang SC, Kim OY, Yoon CM, Choi DS, Roh TY, Park J, et al. Bioinspired exosome-mimetic nanovesicles for targeted delivery of chemotherapeutics to malignant tumors. *ACS Nano* (2013) 7(9):7698–710. doi: 10.1021/nn402232g
75. Bobrie A, Colombo M, Raposo G, Théry C. Exosome secretion: molecular mechanisms and roles in immune responses. *Traffic* (2011) 12(12):1659–68. doi: 10.1111/j.1600-0854.2011.01225.x
76. Andreu Z, Yáñez-Mó M. Tetraspanins in extracellular vesicle formation and function. *Front Immunol* (2014) 5:442. doi: 10.3389/fimmu.2014.00442
77. Cormier EG, Tsamis F, Kajumo F, Durso RJ, Gardner JP, Dragic T. CD81 is an entry coreceptor for hepatitis C virus. *Proc Natl Acad Sci U S A* (2004) 101 (19):7270–4. doi: 10.1073/pnas.0402253101
78. Wortzel I, Dror S, Kenific CM, Lyden D. Exosome-Mediated Metastasis: Communication from a Distance. *Dev Cell* (2019) 49(3):347–60. doi: 10.1016/j.devcel.2019.04.011
79. Madera L, Greenshields A, Coombs MR, Hoskin DW. 4T1 Murine Mammary Carcinoma Cells Enhance Macrophage-Mediated Innate Inflammatory Responses. *PloS One* (2015) 10(7):e0133385. doi: 10.1371/journal.pone.0133385
80. Bobrie A, Krumeich S, Reyal F, Recchi C, Moita LF, Seabra MC, et al. Rab27a supports exosome-dependent and -independent mechanisms that modify the tumor microenvironment and can promote tumor progression. *Cancer Res* (2012) 72(19):4920–30. doi: 10.1158/0008-5472.CAN-12-0925
81. Diao J, Yang X, Song X, Chen S, He Y, Wang Q, et al. Exosomal Hsp70 mediates immunosuppressive activity of the myeloid-derived suppressor cells via phosphorylation of Stat3. *Med Oncol* (2015) 32(2):453. doi: 10.1007/s12032-014-0453-2
82. Taylor DD, Gerçel-Taylor C, Lyons KS, Stanson J, Whiteside TL. T-cell apoptosis and suppression of T-cell receptor/CD3-zeta by Fas ligand-containing membrane vesicles shed from ovarian tumors. *Clin Cancer Res* (2003) 9(14):5113–9.
83. Kim JW, Wieckowski E, Taylor DD, Reichert TE, Watkins S, Whiteside TL. Fas ligand-positive membranous vesicles isolated from sera of patients with oral cancer induce apoptosis of activated T lymphocytes. *Clin Cancer Res* (2005) 11(3):1010–20.
84. Szczepanski MJ, Szajnik M, Welsh A, Whiteside TL, Boyiadzis M. Blast-derived microvesicles in sera from patients with acute myeloid leukemia suppress natural killer cell function via membrane-associated transforming growth factor-beta1. *Haematologica* (2011) 96(9):1302–9. doi: 10.3324/haematol.2010.039743
85. Chalmin F, Ladoire S, Mignot G, Vincent J, Bruchard M, Remy-Martin JP, et al. Membrane-associated Hsp72 from tumor-derived exosomes mediates STAT3-dependent immunosuppressive function of mouse and human myeloid-derived suppressor cells. *J Clin Invest* (2010) 120(2):457–71. doi: 10.1172/JCI40483
86. Muhsin-Sharafaldine MR, Saunderson SC, Dunn AC, Faed JM, Kleffmann T, McLellan AD. Procoagulant and immunogenic properties of melanoma exosomes, microvesicles and apoptotic vesicles. *Oncotarget* (2016) 7 (35):56279–94. doi: 10.18632/oncotarget.10783
87. Buzas EI, Toth EA, Sodar BW, Szabo-Taylor KE. Molecular interactions at the surface of extracellular vesicles. *Semin Immunopathol* (2018) 40(5):453–64. doi: 10.1007/s00281-018-0682-0
88. Poon IKH, Parkes MAF, Jiang L, Atkin-Smith GK, Tixeira R, Gregory CD, et al. Moving beyond size and phosphatidylserine exposure: evidence for a diversity of apoptotic cell-derived extracellular vesicles in vitro. *J Extracell Vesicles* (2019) 8(1):1608786. doi: 10.1080/20013078.2019.1608786
89. Chen Z, Moyana T, Saxena A, Warrington R, Jia Z, Xiang J. Efficient antitumor immunity derived from maturation of dendritic cells that had phagocytosed apoptotic/necrotic tumor cells. *Int J Cancer* (2001) 93(4):539–48. doi: 10.1002/ijc.1365
90. Goldszmid RS, Idoyaga J, Bravo AI, Steinman R, Mordoh J, Wainstok R. Dendritic cells charged with apoptotic tumor cells induce long-lived protective CD4+ and CD8+ T cell immunity against B16 melanoma. *J Immunol* (2003) 171(11):5940–7. doi: 10.4049/jimmunol.171.11.5940
91. Temoche-Diaz MM, Shurtleff MJ, Nottingham RM, Yao J, Fadadu RP, Lambowitz AM, et al. Distinct mechanisms of microRNA sorting into cancer cell-derived extracellular vesicle subtypes. *Elife* (2019) 8:e47544. doi: 10.7554/eLife.47544
92. Davidson B, Zhang Z, Kleinberg L, Li M, Florenes VA, Wang TL, et al. Gene expression signatures differentiate ovarian/peritoneal serous carcinoma from diffuse malignant peritoneal mesothelioma. *Clin Cancer Res* (2006) 12(20 Pt 1):5944–50. doi: 10.1158/1078-0432.CCR-06-1059
93. Bhat R, Bhattacharyya PK, Ratech H. An Immunohistochemical Survey of SNARE Proteins Shows Distinct Patterns of Expression in Hematolymphoid Neoplasia. *Am J Clin Pathol* (2016) 145(5):604–16. doi: 10.1093/ajcp/aqw022
94. Patel SP, Kurzrock R. PD-L1 Expression as a Predictive Biomarker in Cancer Immunotherapy. *Mol Cancer Ther* (2015) 14(4):847–56. doi: 10.1158/1535-7163.MCT-14-0983
95. Chen Z, You L, Wang L, Huang X, Liu H, Wei JY, et al. Dual effect of DLBCL-derived EXOs in lymphoma to improve DC vaccine efficacy in vitro while favor tumorgenesis in vivo. *J Exp Clin Cancer Res* (2018) 37(1):190. doi: 10.1186/s13046-018-0863-7
96. Whiteside TL. Tumor-Derived Exosomes and Their Role in Cancer Progression. *Adv Clin Chem* (2016) 74:103–41. doi: 10.1016/bs.acc.2015.12.005
97. Guo M, Wu F, Hu G, Chen L, Xu J, Xu P, et al. Autologous tumor cell-derived microparticle-based targeted chemotherapy in lung cancer patients with malignant pleural effusion. *Sci Transl Med* (2019) 11(474):eaat5690. doi: 10.1126/scitranslmed.aat5690
98. Simonsen JB. Pitfalls associated with lipophilic fluorophore staining of extracellular vesicles for uptake studies. *J Extracell Vesicles* (2019) 8 (1):1582237. doi: 10.1080/20013078.2019.1582237
99. Ludwig AK, De Miroschedji K, Doeppner TR, Borger V, Ruesing J, Rebmann V, et al. Precipitation with polyethylene glycol followed by washing and pelleting by ultracentrifugation enriches extracellular vesicles from tissue culture supernatants in small and large scales. *J Extracell Vesicles* (2018) 7 (1):1528109. doi: 10.1080/20013078.2018.1528109
100. Lai CP, Kim EY, Badr CE, Weissleder R, Mempel TR, Tannous BA, et al. Visualization and tracking of tumour extracellular vesicle delivery and RNA translation using multiplexed reporters. *Nat Commun* (2015) 6:7029. doi: 10.1038/ncomms8029
101. van der Vos KE, Abels ER, Zhang X, Lai C, Carrizosa E, Oakley D, et al. Directly visualized glioblastoma-derived extracellular vesicles transfer RNA to microglia/macrophages in the brain. *Neuro Oncol* (2016) 18(1):58–69. doi: 10.1093/neuonc/nov244
102. Ricklefs FL, Maire CL, Reimer R, Duhrsen L, Kolbe K, Holz M, et al. Imaging flow cytometry facilitates multiparametric characterization of extracellular vesicles in malignant brain tumours. *J Extracell Vesicles* (2019) 8(1):1588555. doi: 10.1080/20013078.2019.1588555
103. Wiklander OP, Nordin JZ, O'Loughlin A, Gustafsson Y, Corso G, Mäger I, et al. Extracellular vesicle in vivo biodistribution is determined by cell source, route of administration and targeting. *J Extracell Vesicles* (2015) 4:26316. doi: 10.3402/jev.v4.26316

Conflict of Interest: The authors declare that the research was conducted in the absence of any commercial or financial relationships that could be construed as a potential conflict of interest.

Copyright © 2020 Droste, Thakur and Eliceiri. This is an open-access article distributed under the terms of the Creative Commons Attribution License (CC BY). The use, distribution or reproduction in other forums is permitted, provided the original author(s) and the copyright owner(s) are credited and that the original publication in this journal is cited, in accordance with accepted academic practice. No use, distribution or reproduction is permitted which does not comply with these terms.

frontiers in Immunology

REVIEW
published: 21 December 2020
doi: 10.3389/fimmu.2020.601497

Anti-Cancer Nanomedicines: A Revolution of Tumor Immunotherapy

Wei Li[1†], Anghui Peng[2†], Huajun Wu[1], Yingyao Quan[2,3], Yong Li[2], Ligong Lu[2] and Min Cui[1*]*

[1] Department of General Surgery, Zhuhai People's Hospital, Zhuhai Hospital Affiliated with Jinan University, Jinan University, Zhuhai, China, [2] Zhuhai Interventional Medical Center, Zhuhai Precision Medical Center, Zhuhai People's Hospital, Zhuhai Hospital Affiliated with Jinan University, Jinan University, Zhuhai, China, [3] Faculty of Health Sciences, University of Macau, Macau, China

Immunotherapies have been accelerating the development of anti-cancer clinical treatment, but its low objective responses and severe off-target immune-related adverse events (irAEs) limit the range of application. Strategies to remove these obstacles primarily focus on the combination of different therapies and the exploitation of new immunotherapeutic agents. Nanomedicine potentiates the effects of activating immune cells selectively and reversing tumor induced immune deficiency microenvironment through multiple mechanisms. In the last decade, a variety of nano-enabled tumor immunotherapies was under clinical investigation. As time goes by, the advantages of nanomedicine are increasingly prominent. With the continuous development of nanotechnology, nanomedicine will offer more distinctive perspectives in imaging diagnosis and treatment of tumors. In this Review, we wish to provide an overview of tumor immunotherapy and the mechanisms of nanomaterials that aim to enhance the efficacy of tumor immunotherapy under development or in clinic treatment.

Keywords: tumor, immunotherapy, nanomedicine, nanotherapy, review

OPEN ACCESS

Edited by:
Huanfa Yi,
Jilin University, China

Reviewed by:
Zong Sheng Guo,
University of Pittsburgh, United States
Yuan Cheng,
Peking University People's Hospital, China

***Correspondence:**
Min Cui
cuimw@hotmail.com
Ligong Lu
luligong1969@126.com

†These authors have contributed equally to this work

Specialty section:
This article was submitted to Cancer Immunity and Immunotherapy, a section of the journal Frontiers in Immunology

Received: *01 September 2020*
Accepted: *20 November 2020*
Published: *21 December 2020*

Citation:
Li W, Peng A, Wu H, Quan Y, Li Y, Lu L and Cui M (2020) Anti-Cancer Nanomedicines: A Revolution of Tumor Immunotherapy. Front. Immunol. 11:601497. doi: 10.3389/fimmu.2020.601497

INTRODUCTION

Nanoparticles have become a promising strategy for anti-cancer treatment due to their inherent properties. To date, the clinical approvals for tumor therapy are organic materials, including liposomes (pegylated or non-pegylated) and albumin, while inorganic materials are used for tracking and molecular imaging functions, and only superparamagnetic iron oxide (SPIO) nanoparticles are approved in clinical (1). Nanoparticles for tumor therapy are mainly used for drug delivery, photothermal therapy, modification and preparation of engineered cells, imaging diagnosis, and lymph node (LN) tracing. Normally, nanoparticles are used as a drug-loading platform to improve the efficacy of existed anti-tumor agents. Nanoparticles loaded chemotherapeutic agents and targeting delivery into tumor sites have been applied to clinical treatment (2). However, the tumor immunotherapy based on nanoplatforms still stay at the stage of pre-clinical research. However, it is noteworthy that nanoparticles themselves trigger immunogenic tumor cell death and elicit both innate and adaptive immune responses for tumor control and metastasis prevention (3), which showed a broad-spectrum anti-cancer mechanism.

LIMITATIONS OF CONVENTIONAL TUMOR IMMUNOTHERAPIES

Immunotherapy aims to activate immune system to discover and eradicate tumor cells and to inhibit tumor development durable by producing immunological memory (4, 5), while non-specific stimulate immune system directly enhances the reactivity to tumor antigens (6). Until recent years cancer immunotherapies have achieved higher objective response rates (ORR) in patients because of the promotion of T cell function by immune checkpoint blocking (ICB) with monoclonal antibodies (mAbs). Currently, ICB is often chosen as first-line therapy due to the long duration of response in some patients, even after cessation of therapy (**Supplementary Table S1 and S2**) (7, 8). However, there are two major obstacles in tumor immunotherapies, namely the low response rate and the severe immune-related adverse immunotherapy events (irAEs), which are still insurmountable issues in conventional tumor immunotherapy.

Low Response Rate

Although immunotherapy has shown substantial benefit in treatment of a variety of tumors and exhibit durable response, the majority of patients failed to respond to PD-1/PD-L1 blockers (9–12). 50% patients with PD-L1 positive show tolerance after the initial response to PD-1/PD-L1 blockers, most patients will develop acquired resistance (13). Similarly, Anti-CTLA-4 has low level of ORR (14, 15). Moreover, the ORR of HDIL-2 monotherapy is 10%–19% with complete ORR of 6%–8% (16). Therefore, how to improve the ORR of immunotherapy and how to select appropriate indicators to predict the effectiveness of immunotherapy are the two hotspots of current research. At present, combined therapy is the major way to improve clinical response rate, such as the combination of different ICBs (17–20), the combination of various immunotherapies including tumor vaccines, CAR-T, and IL-2, immunotherapy combined with anti-angiogenic therapies (21) and immunotherapy combined with chemotherapy (12, 22–24). Diverse chemotherapeutics can induce the expression of PD-L1 through distinct mechanisms (25, 26), so the chemotherapy combined PD-L1 inhibitors may produce a synergistic effect. Combining nivolumab with radiotherapy could induce immunosensitization to improve the efficacy of PD-1 blocker (27, 28), while immunotherapy combined with small molecule inhibitors therapies reflects immunomodulatory effects, such as the increase of tumor antigenicity and the promotion of T cell infiltration in tumors (29–31). Overall, given the current clinical projects, except the optimization of the current drug combinative strategies, new platform should be founded to improve the treatment status, reduce side effects and recognize the tumor-specific antigens by engineered lymphocyte.

Immune-Related Adverse Events

Immunotherapy often results in irAEs (14, 32), whose pathogenesis can be comprehended by the immune-pathophysiology that excessive and systemic immune system activation can occur at any point during treatment course (33–35). Generally, irAEs include skin toxicity, diarrhea, colitis, pneumonia, liver toxicity, and endocrine system toxicity, and the severity of irAEs is divided into 1–4 grades (36). Approximately 30% patients with melanoma who had accepted the CTLA-4 blocking strategy developed to toxicity grades 3–4, suggesting that the inhibitor activated the systemic immune response rather than tumor-specific T cells (14). In most cases, the combined therapy increases the incidence of irAEs (17, 31, 37, 38). Patients with asymptomatic can be carefully observed and followed up. If it cannot reach a higher level stage and relieve the patients' suffering, withdrawal temporarily or permanently and medical interventions including steroids and immunosuppressive agents are required. Notably, the potential risk of toxicity should not outweigh the overall survival (OS) benefit.

APPLICABLE SYSTEMS OF NANOMODIFIED IMMUNOTHERAPY

As a versatile platform, nanoparticles can not only be loaded with agents to improve their efficacy but also play a role of therapeutic media themselves (**Table 1**). In recent years, nanomedicine has continued to solve existing problems and has achieved the desired therapeutic effects in cancer immunotherapy.

Drug Delivery Systems

In terms of ICB and cytokine therapies' low affinities with the targeted proteins and the obstacle of precise delivery, it is necessary to improve the targeting and the controlled releasing

TABLE 1 | The types and functions of nanoparticles commonly used in clinical trials.

Particle type	Application in clinical trials	Functions
Organic NPs		
Cyclodextrin NPs	CRLX101	improve drug solubility deliver drug to tumor
Liposome NPs	Tecemotide, Lipo-MERIT, DPX-0907, DPX-Survivac, OncoQuest-L, Lipovaxin MM, ISCOMATRIX, AS15, JVRS-100,	improve drug-loading efficiency provide efficient cell affinity increase cellular uptake
Polymeric NPs	CHP-NY-ESO-1, IMF-001, ZYC300	deliver antigen
Solid Lipid NPs	ONT-10 Vaccine	adjuvant
Exosomes NPs	Dex2	extracellular vesicles target and dock to recipient cells stimulate CD8+ and CD4+ T cells
Autophagosome NPs	DRibbles	induce B-cell proliferation and activation induce antibody production induce cytokine secretion antigen cross- presentation
Virus-Like NPs	Melan-A VLPs	restore immune response Induce CTL response antigen cross- presentation
Tumor lysate NPs	WDVAX	activate the immune system
Inorganic NPs		
Gold NPs	Colloidal gold	deliver protein biologics

capabilities of anti-cancer drugs to make them work in specific sites and minimize off-target effects (39). Surprisingly, as a drug carrier, nanoparticles increase the biocompatibility and solubility of reagents, prolong their blood circulation time to provide unique advantages in the precise delivery of drugs to target sites (**Figure 1**). Briefly, the nanomodified immunotherapies reduce peripheral toxicity and side effects, making clinical treatment more compliant and precise.

AlbiVax is a novel nanovaccine complex that the antigen is conjugated to Evans blue and can be self-assembled in combination with albumin *in vivo*. Compared with incomplete Freund's adjuvant, AlbiVax had an almost 100-fold higher efficacy in delivering antigen to LNs, and its ability to elicit immunological memory of peripheral antigen-specific $CD8^+$ T cells was approximately 10 times higher than that of incomplete Freund's adjuvant. AlbiVax restrains the growth of various tumors, and the combination of AlbiVax with anti-PD-1 agents Abraxane enhances immunotherapy and eradicates most tumors (40). Encapsulation of anti-PD-1 antibodies with PLGA nanoparticles improves the anti-tumor effect but exhibits higher mortality due to the overactivation of T cells, which can be reversed by reducing dose (41). A multifunctional immunoliposomes named CAT@aPDL1-SSLs promoted the delivery and accumulation of anti-PDL1 antibodies in tumor tissues to activate the infiltration of $CD8^+$ T cells at the tumor site with low systemic toxicity (42). In addition to direct drug delivery, nanoparticles package small interfering RNAs (siRNAs) targeting PD-1 and T-cell immunoglobulin mucin 3 (TIM-3) to restore T cell immunity and sensitize the response of cancer cells to T cell killing (43, 44). Loading the PD-L1 trap plasmid into a lipid-protamine-DNA nanoparticle enhanced the local level of PD-L1 trap in tumor microenvironment (TME) but did not induce the appearance of Th17 cells in spleens, indicating that this formulation was better tolerated and had a lower tendency to induce irAEs than the unmodified plasmid (45). Collectively, targeted delivery of agents is based on the enhanced permeability and retention (EPR) effect of nanomaterials and abnormal tumor blood vessels, but the characteristics of nanomaterials have a profound and lasting effect due to their surface modifiability.

Regulation of the Hypoxic Microenvironment

Hypoxia is a hallmark of TME that induces the tumor resistance to immunotherapy (42, 46, 47). Preclinical and clinical data indicate that hypoxia can significantly reduce the efficacy of anti-tumor immunity (48–51). This mechanism includes the following immunity reactions: a) Hypoxia limits infiltration and proliferation of anti-tumor immune cells; b) Hypoxia acts as an intrinsic immunosuppressive for T cells to inhibit tumor-killing function; c) Hypoxia up-regulates the expression of PD-L1, which promotes the binding of HIF-1α to a transcriptionally active hypoxia-response element (HRE) (50, 52); d) Hypoxia induces high expression of forkhead box P3 (FOXP3), transforming growth factor-β (TGF-β) and CC-chemokine ligand 28 (CCL28) that selectively attracts regulatory T cells (Treg) and increases their functions, which results in antigen tolerance and suppression of the response to effector T cells; e) Hypoxia reduces the production of interferon-γ (IFN-γ) and interleukin-2 (IL-2) by both CD4+ and CD8+ T cells (52). Therefore, reverse the hypoxic TME may potentially increase the immune response.

Nanotechnology has been increasingly used to reverse tumor hypoxic microenvironment (42, 53, 54). Modified nanoparticles could attenuate the unfavorable factors by normalizing oxygen levels through tumor vascular normalization (55, 56), external oxygen delivery, capture and delivery of oxygen from the lungs and generation of oxygen through catalysis of water (47).

Vascular function dictates the efficacy of immunotherapy. Tumor vascular normalization is an important measure to reduce the hypoxic microenvironment (57). Some pure inorganic nanoparticles, including gold or silver nanoparticles, can modulate tumor blood vessels (58, 59). Moreover, many reagents (60) and siRNAs (61) targeting blood vessels can be loaded into nanoparticles to retain vascular normalization (62). In addition, the remodeling of blood vessels increases the enrichment and infiltration of anti-tumor drugs and $GrzB^+$ effector T cells in tumors, which sensitize tumor to immunotherapy (63, 64).

Since intelligent nanoparticles respond to TME, they may induce the generation of oxygen. MnO_2-based nanoplatforms

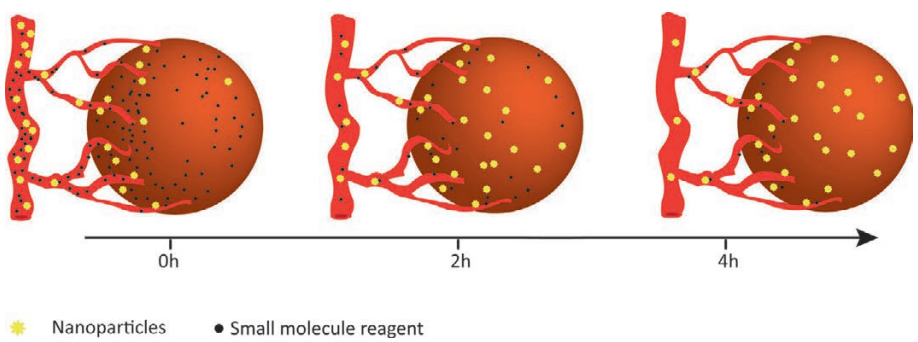

FIGURE 1 | Enhanced retention of nanoparticles. Compared to small-molecule drugs, nanoparticles appear to be gradually enriched in tumors and maintained for a longer period of time.

could react with excessive endogenous H_2O_2 in TME to generate oxygen *in situ* and to overcome hypoxia limitations for cancer therapy (65, 66). A novel TiO-porphyrin nanosystem (FA-TiOPs) was designed by encapsulating TiO-porphyrin into folic acid liposomes. FA-TiOPs can photosplit water to produce oxygen, which overcomes hypoxia in TME, boosts specific anticancer effects while being harmless to normal tissues, especially under acidic conditions (67). FeSiAuO contains Fe_3O_4, mesoporous SiO_2 and magnetic Au_2O_3, which decompose into O_2 in TME under light irradiation (68).

Oxygen-carrying is a direct strategy in which nanocarriers load oxygen in oxygen-rich areas and release oxygen in hypoxic areas depending on the partial oxygen pressure (**Figure 2**) (53). Perfluorocarbon is a safe O_2 carrier that has been already demonstrated in clinic, and the encapsulation of perfluorocarbon with albumin enhanced its accumulation in the tumor site and rapidly released the oxygen that was physically dissolved (69). Fluorocarbon-functionalized nanoparticles enhanced the effects of both photodynamic therapy (PDT) (70) and oxygen-sensitive anti-tumor drugs (71) by increasing tumor oxygenation. Besides, perfluorocarbons have entered clinical trials for ischemia and imaging theranostic strategies to ensure that the simple O_2 transport system can be rapidly and easily transformed into clinical applications. Hemoglobin (Hb) is another appreciating functional material for the development of oxygen-carrying nanoparticles. Hemoglobin nanoparticles (H-NPs) are assembled after re-emulsion. They are Hb-based oxygen nanocarriers that attenuate the hypoxia-induced decrease in decitabine activity and sensitize renal cell carcinoma to combination therapy of decitabine with oxaliplatin (72). Overall, hypoxic TME is a critical variable for immunotherapy. The development of nanomaterials targeting the hypoxic TME is one of the fastest growing branches of nanomedicine.

Nano-Based Photothermal Therapy Induced Tumor Immune Response

By effectively generating lethal doses of heat under near-infrared (NIR) light irradiation, photothermal therapy adopts material with high photothermal conversion efficiency to kill tumor cells (73, 74). The nanomaterials that initially provided photothermal therapy were mainly precious metals, but they have gradually developed into nanocarbons, metal organic compounds and organic dyes. For instance, PLGA nanoparticles loaded with indocyanine green (ICG) stimulate physicochemical and physiological changes in TME under mild heating, leading to increased infiltration of chondroitin sulfate proteoglycan-4 (CSPG4)-specific CAR T cells (73). Silica sealed by gold nanoshells (AuroShell) is the only inorganic material approved by Food and Drug Administration (FDA) for clinical photothermal therapy (75). AuroShell particles can be passively accumulated in solid tumors through the vasculature and were demonstrated safe when they were used systemically in focal ablations in prostate (74).

Intriguingly, tumor immune effect induced by photothermal therapy has been recognized. Photothermal therapy induces deep tissue immunogenic cell death, potentiates cancer immunotherapy and synergistically enhances immune efficacy (**Figure 3**). Gold nanostars (GNS) induced the anti-tumor immune response following the highly immunogenic thermal death of cancer cells, and the combination of GNS-mediated photothermal therapy with ICB reversed tumor-mediated immunosuppression (76). Al_2O_3 nanoparticle coating with polydopamine acts as an adjuvant for photothermal therapy, triggering a series of powerful cell-mediated immune responses to eliminate residual tumor cells and reduce the risk of tumor recurrence (77).

The therapeutic outcome of photothermal therapy is limited by the degree of light transmission (78), while the deep internal

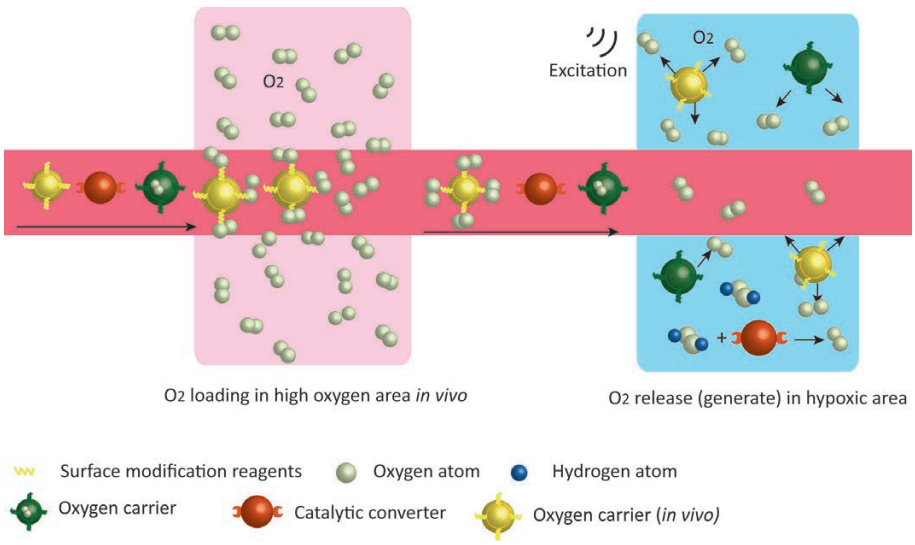

FIGURE 2 | Strategies of nanoparticles to increase tissue oxygen content. Oxygen carriers wrap O2 *in vitro*, or bind O2 in high oxygen areas *in vivo* and release them in low oxygen environment. Nanoparticles with catalytic effects react with excessive endogenous H2O2 in the TME to generate oxygen.

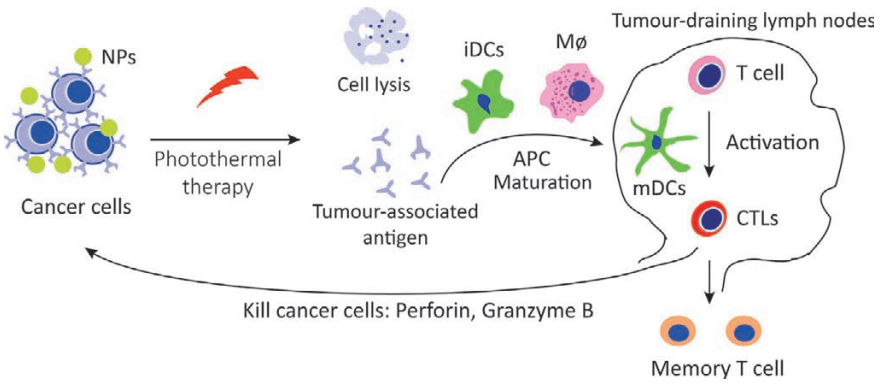

FIGURE 3 | Immunotherapy induced by photothermal therapy. Photothermal therapy increases the tissue immunogenic cell death and release antigens, which are presented to T cells by DCs and macrophages, enhance the recognition and killing to tumor cells.

area of the tumor lacks lymphocytic infiltration and experiences in various immune escape mechanisms (3). However, these issues could be solved by the combined nano-based photothermal therapy with immunotherapy. A multiplex nanoparticle assembled by a NIR photosensitizer named IR780 and an IDO inhibitor named NLG919 enhanced accumulation in the tumor site *via* passive targeting, increased the infiltration and differentiation of T cells into $CD8^+$ T cells, suppressed the tumor margin beyond the border of effective photothermal therapy and strengthened the immune response to inhibit the distal tumor (78).The assembly of gold nanoparticles into fluid liposomes produced photothermal sensors that have NIR-I and NIR-II biological windows and respond to different absorptions of red light. NIR-II light activates both innate and adaptive immune responses, achieves effective tumor control (3) and triggers more homogeneous and deeper immunogenic cancer cell death than NIR-I light. In addition, photothermal therapy facilitates the accumulative and effective function of CAR-T cells within solid tumors by reducing tumor interstitial pressure, increasing blood perfusion and releasing antigens (73). Briefly, these findings demonstrate the great potential of nano-based photothermal therapy in immunotherapy.

Reprogramming the Immune Microenvironment

The efficacy of immunotherapy depends on the infiltration of immune cells and immune factors in TME. Tumor cells reprogram the microenvironment to facilitate immune escape and induce immunotherapy tolerance. Therefore, reversing the immunosuppressive microenvironment is an insightful perspective for the improvement of immunotherapy. The increasing numbers of multifunctional modified nanoparticles are being created, which shows us a diversity of anti-tumor mechanisms. In addition to a role of carrier, nanoparticles also directly activate immune cells to participate in anti-tumor responses.

At present, most of the nanoparticles that activate immune cells are coupled with immune activators, such as ICB molecules (34, 79, 80) and tumor vaccines. Luo and colleagues first discovered that Fe_3O_4 NPs act as immunopotentiators to stimulate dendritic cell (DC)-based immunotherapy and to potentially activate macrophages and T cells. Fe_3O_4-OVA vaccines successfully inhibit the subcutaneous growth and lung metastasis of melanoma (1). Because iron-based nanomaterials have been approved by FDA, they are expected to be used in clinical tumor treatment in future. Nanospheres, as a new vaccine adjuvant, elicited prominent antigen cross-presentation effects on DCs and bone marrow dendritic cells (BMDCs), enhanced humoral and cellular immune responses *in vivo* (81, 82). Although the application of ICB is impeded by TME, the modified nanoparticles co-loaded with CRISPR/Cas9 and paclitaxel (PTX) to reduce Tregs and repolarize tumor associated macrophages (TAMs), which can reverse the TME and enhance anti-tumor immunity (83). Collectively, we can continuously obtain the optimal efficacy of immunotherapy thanks to the nanomaterials' function of crosstalk reprogramming and immune cells activation in various ways.

Interestingly, some nondrug-loaded nanoparticles have been shown to directly modulate the immune microenvironment. Zhang et al. assembled ursonic acid with liposomes into nanoparticles to increase the solubility, which modulated TME by reducing $CD4^+CD25^+Foxp3^+$ Tregs, and this reduction was correlated with the inhibition of STAT5 phosphorylation and the reduction of IL-10 expression (81). Systemic exposure to nanoparticles enabled transient immune recognition of tumor, increased the number of immune cells, such as NK cells, monocytes, $CD4^+$ T cells, and $CD8^+$ T cells, reconfigured TME immune system and delayed tumor growth; Of note, all of these changes were independent of antibody therapeutic activity and therapeutic payload (84). Natural nanoparticles can be easily obtained with their application prospects. Nanoparticles extracted from cuttlefish ink (CINPs) increase $CD8^+$ T cells and repolarize M2 macrophages to the M1 phenotype through activation of the MAPK pathway. CINPs almost completely restrained tumor growth when synergizing with the photothermal effect, which induces tumor-specific antigen release (85). In general, the immunosuppressive microenvironment of solid tumors represents a severe obstacle for immunotherapy. However, nanomedicine

potentiates the effects of TME modulation by activating immunosupportive cells and inhibiting immunosuppressive cells.

In addition to tumor tissues, LN is another important target for nanoparticles to produce anti-tumor effects. For instance, compared with its parent compound, the structure-optimized CpG-DNA/peptide vaccine increases the efficiency of T cell initialization and improves anti-tumor function and reduces systemic toxicity due to its advantages of a significant increase in LN accumulation and a decrease in systemic diffusion (86). Nanoparticle-bound tumor-associated antigens can transform immunosuppressive environment of the LNs draining the tumor into the more immunogenic environment. Compared with non-targeted vaccines, vaccines that target tumor draining lymph nodes (tdLN) can regress tumors and retain a higher host survival rate, because they induce intense cytotoxic $CD8^+$ T cells reactions (87).

Nanomaterials increase anti-tumor effects in the progress of both cell-mediated immunity and humoral immune regulation. For one thing, multiple nanoparticles effectively stimulate the proliferation of $CD4^+$ and $CD8^+$ T cells, thereby further promote the production of antibodies, which together trigger more dramatic humoral and cellular immune responses than free antigen alone (88). For another, some nanoparticles can directly increase the binding robustness of antibodies. As a result, manipulating the chemistry of polyanhydride nanoparticles promotes the differential kinetics of antibody titer, affinity and epitope specificity development, and eventually, induces continuous and mature antibody responses (89).

Nano-Engineered Cells

Currently, viral delivery vector is a major medium of chimeric antigen receptor (CAR)-engineered T cells, which induce permanent expression of CAR but may cause serve adverse reactions (90). Nanotechnology promotes the adoptive T cell therapy, effectively delivers CAR cargo to T cells or other effector cells, and then quickly programs T cells to recognize tumor cell antigens (91). Nanocarriers present TCR stimulation signals or pro-survival cytokines, accelerate T cell transduction *in vivo* and improve their survival rate (91). Biodegradable nanomaterials take advantages of structural flexibility, the ability to deliver soluble paracrine to T cells and surface-bound molecules will be lost over time, which prevents excessive activation of T cells (92). In a word, nanotechnology-based CAR T cell modification is a promising approach to improve the efficacy of adoptive cell therapy (**Figure 4**).

Nanotechnology efficiently delivers pEGFRvIII-CARs to Jurkat T cells transiently and expresses EGFRvIII-CAR on the transfected cell membrane, enabling Jurkat T cells specifically to recognize and bind to EGFRvIII-positive tumor cells (93). Nanoparticles which encapsulated with an A2aR-specific small molecule antagonist attached to the surface of CAR-T cells *in vitro* had no effect on the recognition of target cells, IFN-γ secretion, cell cytotoxicity or migration but increased the active targeting of the tissue of interest and ameliorated intratumoral T cell hypofunction (94).

Therapeutic nanoparticles click into the surface of CAR-T cells modified with IL-13 targeting quadruple mutant (TQM-13), which increases the affinity with glioblastoma (95). Nanoparticles encoding FOXO1 gene promote the transformation of effector T cells into memory cells (96). Compared with traditional methods, ionizable lipid nanoparticles deliver mRNA to T cells to induce CAR expression in an equal level, but decrease cytotoxicity and enhance the potential of mRNA-based CAR-T cell engineering methods (90). Conjugating IL-2 to liposomes is inclined to target adoptive cell therapy (ACT) cells and induce ACT-T cell proliferation in tumor-tolerant mice, proving the feasibility of repetitive functional targeting of T cells *in vivo* (97). Dextran-coated superparamagnetic iron oxide nanoparticles have been designed for the expansion of T cells, while MHC-Ig antibodies and anti-CD28 antibodies are conjugated to them to provide antigen-specific and co-stimulatory signals. This Nano-aAPC provoked the activation of tumor-specific T cells through "enrichment plus amplification" (98).

In addition, nanoparticles can self-assemble into CAR-like complex which activate T cells while targeting tumors. Bai et al.

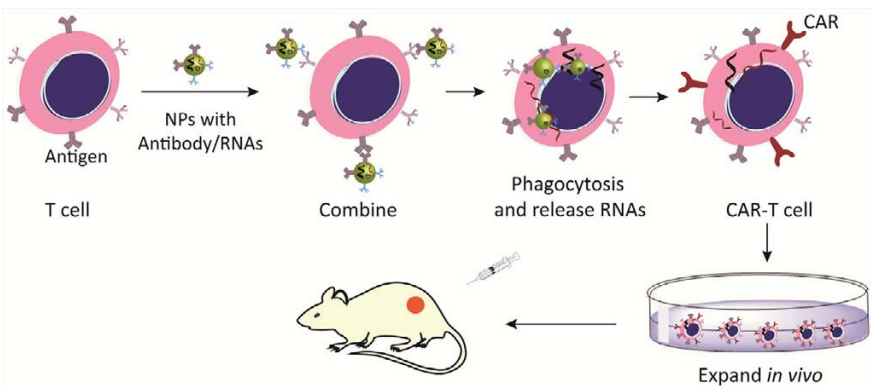

FIGURE 4 | Nanomaterials activate and expand adoptive T cells. Nano-modified CAR-T cells increase the expression of CAR antigens and improve the recognition of tumor cells.

developed CAR-like multivalent aptamer nanoparticles which were assembled with CD28 RNA aptamer and the tetramer of CTLA-4 RNA aptamer, as well as a folic acid labeled single stranded DNA fragment in a stable nucleic acid three-way junction scaffold. These nanoparticles increase T cell proliferation, reverse the inhibitory effect of IL-2 secreting caused by exogenous B7.1 molecules on T cells *in vitro* and promise a novel approach to develop a multi-functional design of aptamer drugs with potential CAR-like characteristics to enhance the safety of CAR-T cell immunotherapy (99).

Nanoparticles also harbor both the function of NK cells modification (100) and the potential of CAR-NK therapy achievement. For one thing, nanoparticles promote the transfection of siRNA to NK92 cells which have been used for NK-based cancer immune therapy in clinical trials (101); For another, nanoparticles are used to enhance the expansion of adoptively transferred NK cells. For instance, particles prepared from the plasma membrane of K562-mb21-41BBL cells that express 562BBL and membrane-bound IL-21 (PM21 particles) induce PBMCs from healthy donors and patients with AML to produce specific NK cell expansion (102).

Combination of Nanotechnology With Monoclonal Antibodies Therapy

The combination of Abs with nanomedicine includes nanobiosensors, Ab-based nanomachines and active targeted drug delivery systems (103). Some tumor-specific markers have been discovered, and the usage of corresponding Abs modified nanoparticles can transform the passive targeting into active condition and functionalize them as "guided missiles" to increase the specificity of enrichment in tumor sites and to minimize damage to healthy tissues. For example, anti-CD133 Ab-conjugated SN-38-loaded nanoparticles recognize CD133 on the surface of colorectal cancer cells, thereby increasing the targeting of nanometers (104). CD-340-conjugated DOX-loaded PLGA nanoparticles preferentially deliver drug to breast cancer tissue, and reduce DOX-mediated cardiotoxicity due to its tumor-specific distribution (105). In addition, antibodies for more markers were conjugated to a variety of nanoparticles which have been extensively verified in preclinical studies. Most of them have shown good targeting and anti-tumor activity. For example, daunorubicin-loaded CdTe QDs conjugated to anti-CD123 mAbs (DNR-CdTe-CD123) treatment was designed for high-risk myelodysplastic syndromes (MDS) (106), the nanocomposite displayed higher inhibition rate and apoptosis rate in MDS cells than monotherapy, enhanced the therapeutic efficacy and reduced the side effects of daunorubicin. Genetically engineering cell-derived exosomes with anti-CD3 and anti-HER2 antibodies (aCD3-aHER2 SMART-Exos) dually target T cells and $HER2^+$ breast cancer, selectively inducing HER2-expressing tumor-specific immunity and activating cytotoxic T cells toward attacking breast cancer cells (107).

At present, some clinically approved drugs are gradually being nano-sized to improve their therapeutic effects. Herceptin-conjugated paclitaxel loaded PCL-PEG worm-like nanocrystal micelles (PTX@PCL-PEG-Herceptin) remained relatively stable in the circulation and in TME. PTX@PCL-PEG-Herceptin greatly enhanced the binding robustness of the nanoparticle to the $HER2^+$ breast cancer cells, enriched target cells rapidly and protected normal tissues from the toxic effects (108). The conjugation of HER2 protein 1-146 with cholesteryl pullulan (CHP) nanoparticles (also named CHP-HER2 vaccine) was safer than HER2 protein 1-146 used only, the complex induced HER2-specific $CD8^+$ and $CD4^+$ T cell immune responses in patients who received four to eight vaccinations (109).

Anti-EGFR Abs are mainly used to bind gold nanoparticles based on active targeting function (110, 111), and phase I clinical trials have been launched on the basis of a large number of preclinical studies. For example, anti-EGFR-immunoliposomes loaded with doxorubicin (C225-ILs-dox) were used for patients with relapsed or refractory high-grade gliomas (NCT03603379). Anti-EGFR ILs-dox nanoparticles were designed by pegylated liposomes which encapsulated doxorubicin into antigen-binding fragments (Fab') of cetuximab, this nanoplatform was well tolerated, and showed more effective than non-targeted liposomes at destroying EGFR-overexpressing target cells because of its active and specific internalization (NCT01702129) (112).

POSSIBILITIES OF NANOMATERIALS IN CLINICAL TUMOR IMMUNOTHERAPY

A large number of nanomaterials have been synthesized for tumor treatment in clinical trials (**Supplementary Table S3**). However, there are few approved in clinical applications. Only liposomes and albumin carriers were formed into stable dosage types. The clinical nanomaterials applied for tumor therapy are listed in **Supplementary Table S4**.

Liposome is an outstanding drug delivery platform due to its biocompatibility and drug encapsulating efficiency (100), which can be loaded with hydrophobic and hydrophilic molecules. Immunoliposomes directly target tumors to provide a bystander killing effect through diffusion of loading agents to neighboring tumor cells (42, 112). Liposomes have been extensively applied in clinical management of cancers. The first nanomedicine for tumor clinical treatment is doxorubicin (Doxil™), a PEGylated long-circulating liposome loaded with doxorubicin approved in 1995, whose main indications are advanced ovarian cancer, multiple myeloma and HIV-combined Kaposi's sarcoma (113). Nano-platform based vincristine sulfate liposome (Marqibo™) was proved for treatment of adult patients with Philadelphia chromosome–negative (Ph^-) acute lymphoblastic leukemia (ALL) (114, 115) while Irinotecan liposome (Onivyde™) for metastatic pancreatic cancer (116). Other liposome-based nano-drug in tumor treatment includes daunorubicin liposome (DaunoXome®), doxorubicin liposomes, cisplatin liposomes and so on. Furthermore, modification of nano-liposomes increases the functional characteristics of the nano-drug platform with greater targeting effect. Temperature-sensitive liposomes could passively load with gemcitabine and copper complex to release drugs with tumor vasculature in response of ultrasound hyperthermia (117). Oleuropein loaded folate-targeted-PEG liposomes was prepared

by the method of film hydration-cum-extrusion technique which enhanced the anti-cancer effect of oleuropein (118).

Albumin is a well-tolerated material with the advantages of highly solution and stability, no toxicity, no immunogenicity and easily chemical function (119). Albumin could protect circulating nanoparticles from the recognition and elimination of mononuclear phagocytic systems with half-life of 19 days, and they can avoid renal clearance because of the reabsorption by receptor-mediated endocytosis in the renal proximal tubule (120), thus albumin-based nanoparticles can be enriched in solid tumor tissues based on their increased consumption by cancer cells and the interaction with TME (121). All of these processes make nanoparticles become helpful carriers for anti-cancer agents. Onafuye and colleagues designed doxorubicin-loaded albumin nanoparticles by desolvation and crosslink using glutaraldehyde which could reverse transporter mediated drug resistance, whereas other nano-carrier systems have not found the similar effect (122). Choi and colleagues prepared inhalable self-assembling doxorubicin albumin nano-system which was treated with tumor necrosis factor (TNF)-related apoptosis-inducing ligand (TRAIL) and was based on albumin, demonstrating synergistic anti-tumor efficacy, and providing a new inhalation-based combination therapies to treat drug-resistant lung cancer with the obvious reduction of the dose of doxorubicin (119). Currently, the most extensively used albumin nanoparticles is nab-paclitaxel (Abraxane^{TM}), which approved for the treatment of breast cancer, metastatic non-small cell lung cancer (NSCLC) and pancreatic cancer. Besides, there are still many clinical trials based on the combination of nab-paclitaxel and other drugs (such as cisplatin, oxaliplatin, toripalimab, and S1) to obtain better therapeutic effect through combination therapy.

Polyethylene glycol (PEG) is the chief ingredient used to synthesize nanoparticles and modify the surface of nanomaterials. PEG-b-PLA micelles are the first-generation platform with a hydrodynamic diameter of 33 nm in the usage of systemic multiple administration of poorly water-soluble anti-cancer agents (123). The combination of PEG-b-PLA micelles with paclitaxel (Genexol-PM®) has been used in clinical cancer treatment with a high response rate in clinical trials in patients with NSCLC, gastric cancer, breast cancer and fewer acute hypersensitivity reactions (123).

Cyclodextrins (CDs) and other polymers were often combined with water-insoluble pharmaceutical drugs to increase their solubility and availability (124). Cyclodextrins- camptothecin (CRLX101) complex optimized the plasma pharmacokinetics and then facilitated drug delivery to tumors (125). The preferential uptake of cyclodextrins and camptothecin conjugation may promote the selective release of tumor antigens into TME and enhance the effect of tumor immune drugs (126). Preclinical studies have proven that CRLX101 could reduce adverse reactions and increase NK cell and T cell populations, which may potentially improve the anti-PD1/PDL1 therapy (127).

Cholesteryl pullulan (CHP) nanogel is a novel antigen delivery system based on CHP nanogel that has been accomplished phase I clinical trials. CHP is conjugated to HER2 and NY-ESO-1 antigen-related cancer vaccine. Additionally, HP-NY-ESO-1 is a safe and promising cancer vaccine. In previous studies, CHP-NY-ESO-1 vaccination showed $CD4^+$ and $CD8^+$ T cell response activities (128). The addition of anti-PD-1 activates NY-ESO-1 specific T cells as well as other tumor antigen-reactive T cells. Afterwards, clinical trials of combined therapies including cancer vaccines, adjuvants and ICBs, are ready to proceed (129). Comparatively, the CHP-HER2 vaccine is well tolerated, and HER2-specific $CD8^+$ and $CD4^+$ T cell immune responses have been detected in patients who had received the vaccine (109).

Autophagy in tumor cells also plays a key role in the cross-presentation of tumor antigens (130). Tumor-derived autophagasomes vaccine named DRibbles is defined as a novel type of multivalent vaccine which was produced by disrupting the ubiquitin proteasome system to degrade intracellular proteins. DRibbles vaccine consists of autophagic vesicles which are rich in defective ribosomal products and short-lived proteins, known tumor-associated antigens, mediators of innate immunity and surface markers that promote phagocytosis and cross-presentation of antigen-presenting cells (131). Human antigen-specific memory T cells can be activated by specific viral antigens during immune monitoring and adoptive immunotherapy. As a result, Dribbles vaccine will be a vaccine for cancer patients in the future (132). In the phase I of clinical trials, DRibbles had been derived from autologous tumor cells and applied to vaccinate patients with NSCLC, following a randomized multi-center phase II clinical trial was initiated to use allogeneic DRibbles vaccine (132). The available evidence supported that DRibbles vaccine is a human treatment strategy in the latest clinical development and it promises to be a delivery mechanism for other vaccines in the future.

Virus-like particles (VLPs) are nanoparticles that self-assembled by one or more viral proteins, with the diameter of about 10-200nm (133). VLPs do not contain nuclei acids which exhibit non-infectious function for the vaccinated individuals. By contrast, the structure of VLPs are similar to the conformation of wild type viruses which can activate adaptive immunity (134). VLPs can be modified by chemical or genetic fusion technologies to express chimeras or targeted delivery of small molecule drugs and nucleic acids as a result of the improvement of bioavailability of the delivered substance (135). Thus, VLPs can restore immune response, cross-present and induce CTL responses. Furthermore, VLPs identify and combine specific pattern recognition receptors on the surface of DCs followed by internalizing into activate DCs, and then present peptides which was loaded into MHC-I/II. Eventually, they in turn initiate $CD8^+$ or $CD4^+$ T cell immunity (134). Collectively, the ability to engineer VLPs with exquisite detail makes them popular candidates for the design of a platform to produce vaccines against various diseases.

APPLICATION PROSPECTS OF NANOMEDICINE IN IMMUNOTHERAPY

Immunotherapy has become a vital tool of cancer treatment. The effectiveness of immunotherapy is various in tumor subtypes. The development mechanism of primary tumors and immune regulation mechanisms have been the key to clarify the difference in efficacy of

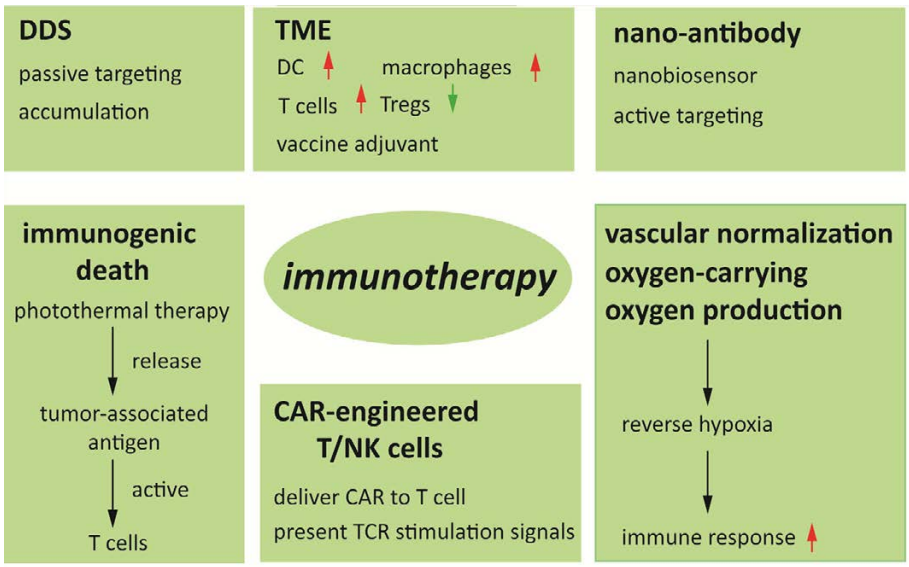

FIGURE 5 | Mechanism of nanoparticles in immunotherapy.

immunotherapy. Even so, the hurdles existed in conventional tumor immunotherapy hindered the progress of tumor immunotherapy. With the advancement of nanotechnology, the use of nanomaterials should not be ignored in tumor therapy due to their intrinsic immune modulation activities. The auxiliary applications of nanomaterials will provide a predictable guarantee for the effectiveness and safety of immune interventions (**Figure 5**). Nanomedicines take advantages of immunotherapies in four aspects. 1) Immunomodulators, such as immunopharmaceuticals, vaccines, siRNAs, etc. carried by nanomaterials can be slowly released on specific targets to prolong the effect of immunotherapy and reduce systemic side effects. 2) The photothermal effect mediated by nanomaterials triggers immunogenic cell death. 3) The modified nanomaterials can activate cytotoxic T cells and antigen-presenting cells, reverse the polarization of macrophages and inhibit Treg cells, thereby enhancing the tumor killing effect. 4) Regulating tumor blood vessels and tumor hypoxic microenvironment not only enhances the sensitivity of immunotherapy, but also strengthens the therapeutic effect of radiotherapy and chemotherapy. In summary, nanomedicine has extremely high variability in material and particle size selection, surface modification, packaged drug selection, and drug delivery schemes. Therefore, there is extensive optimization space for nanomedicine to improve. In the past decades, the practicality of biomaterials has been verified in the field of tumor therapy. Afterwards, more than ten kinds of nano-based drugs have been approved for tumor or other diseases clinical treatment. And now, the clinical transformation of material-based cancer immunotherapy is accelerating. In the future, the principles we have learned from the existing experience of using nanomaterials will guide us to design more effective cancer immunotherapies, allowing for extend the frontiers of more successful cancer treatment.

AUTHOR CONTRIBUTIONS

WL wrote the majority of the manuscript. AP cowrote the manuscript. HW and YQ drew images and summarized tables. YL supervised the research. LL and MC designed and cowrote the manuscript, and supervised the research. All authors contributed to the article and approved the submitted version.

FUNDING

This work is partially supported by National Key Research and Development Program of China (No. 2017YFA0205200) and the National Natural Science Foundation of China (No. 81571785, 81771957, 81801811).

SUPPLEMENTARY MATERIAL

The Supplementary Material for this article can be found online at: https://www.frontiersin.org/articles/10.3389/fimmu.2020.601497/full#supplementary-material

REFERENCES

1. Luo L, Iqbal MZ, Liu C, Xing J, Akakuru OU, Fang Q, et al. Engineered nano-immunopotentiators efficiently promote cancer immunotherapy for inhibiting and preventing lung metastasis of melanoma. *Biomaterials* (2019) 223:119464. doi: 10.1016/j.biomaterials.2019.119464
2. Schmid P, Adams S, Rugo HS, Schneeweiss A, Barrios CH, Iwata H, et al. Atezolizumab and Nab-Paclitaxel in Advanced Triple-Negative Breast

Cancer. *N Engl J Medicine* (2018) 379(22):2108–21. doi: 10.1056/NEJMoa1809615
3. Ma Y, Zhang Y, Li X, Zhao Y, Li M, Jiang W, et al. Near-Infrared II Phototherapy Induces Deep Tissue Immunogenic Cell Death and Potentiates Cancer Immunotherapy. *ACS Nano* (2019) 13(10):11967–80. doi: 10.1021/acsnano.9b06040
4. Zhang R, Zhu Z, Lv H, Li F, Sun S, Li J, et al. Immune Checkpoint Blockade Mediated by a Small-Molecule Nanoinhibitor Targeting the PD-1/PD-L1 Pathway Synergizes with Photodynamic Therapy to Elicit Antitumor Immunity and Antimetastatic Effects on Breast Cancer. *Small* (2019) 15 (49):e1903881. doi: 10.1002/smll.201903881
5. Friedman J, Moore EC, Zolkind P, Robbins Y, Clavijo PE, Sun L, et al. Neoadjuvant PD-1 Immune Checkpoint Blockade Reverses Functional Immunodominance among Tumor Antigen-Specific T Cells. *Clin Cancer Res* (2020) 26(3):679–89. doi: 10.1158/1078-0432.CCR-19-2209
6. Sussman JJ, Shu S, Sondak VK, Chang AE. Activation of T lymphocytes for the adoptive immunotherapy of cancer. *Ann Surg Oncol* (1994) 1(4):296–306. doi: 10.1007/bf02303568
7. Hodi FS, Chiarion-Sileni V, Gonzalez R, Grob JJ, Rutkowski P, Cowey CL, et al. Nivolumab plus ipilimumab or nivolumab alone versus ipilimumab alone in advanced melanoma (CheckMate 067): 4-year outcomes of a multicentre, randomised, phase 3 trial. *Lancet Oncol* (2018) 19(11):1480–92. doi: 10.1016/S1470-2045(18)30700-9
8. Hargadon KM, Johnson CE, Williams CJ. Immune checkpoint blockade therapy for cancer: An overview of FDA-approved immune checkpoint inhibitors. *Int Immunopharmacol* (2018) 62:29–39. doi: 10.1016/j.intimp.2018.06.001
9. Skoulidis F, Goldberg ME, Greenawalt DM, Hellmann MD, Awad MM, Gainor JF, et al. STK11/LKB1 Mutations and PD-1 Inhibitor Resistance in KRAS-Mutant Lung Adenocarcinoma. *Cancer Discov* (2018) 8(7):822–35. doi: 10.1158/2159-8290.CD-18-0099
10. O'Donnell JS, Teng MWL, Smyth MJ. Cancer immunoediting and resistance to T cell-based immunotherapy. *Nat Rev Clin Oncol* (2019) 16(3):151–67. doi: 10.1038/s41571-018-0142-8
11. Yau T, Hsu C, Kim TY, Choo SP, Kang YK, Hou MM, et al. Nivolumab in advanced hepatocellular carcinoma: Sorafenib-experienced Asian cohort analysis. *J Hepatol* (2019) 71(3):543–52. doi: 10.1016/j.jhep.2019.05.014
12. Horn L, Mansfield AS, Szczesna A, Havel L, Krzakowski M, Hochmair MJ, et al. First-Line Atezolizumab plus Chemotherapy in Extensive-Stage Small-Cell Lung Cancer. *N Engl J Med* (2018) 379(23):2220–9. doi: 10.1056/NEJMoa1809064
13. Finn RS, Ryoo BY, Merle P, Kudo M, Bouattour M, Lim HY, et al. Pembrolizumab As Second-Line Therapy in Patients With Advanced Hepatocellular Carcinoma in KEYNOTE-240: A Randomized, Double-Blind, Phase III Trial. *J Clin Oncol* (2020) 38(3):193–202. doi: 10.1200/JCO.19.01307
14. Sanmamed MF, Chen L. A Paradigm Shift in Cancer Immunotherapy: From Enhancement to Normalization. *Cell* (2019) 176(3):677. doi: 10.1016/j.cell.2019.01.008
15. Schachter J, Ribas A, Long GV, Arance A, Grob JJ, Mortier L, et al. Pembrolizumab versus ipilimumab for advanced melanoma: final overall survival results of a multicentre, randomised, open-label phase 3 study (KEYNOTE-006). *Lancet* (2017) 390(10105):1853–62. doi: 10.1016/S0140-6736(17)31601-X
16. McQuade JL, Homsi J, Torres-Cabala CA, Bassett R, Popuri RM, James ML, et al. A phase II trial of recombinant MAGE-A3 protein with immunostimulant AS15 in combination with high-dose Interleukin-2 (HDIL2) induction therapy in metastatic melanoma. *BMC Cancer* (2018) 18(1):1274. doi: 10.1186/s12885-018-5193-9
17. Larkin J, Chiarion-Sileni V, Gonzalez R, Grob JJ, Cowey CL, Lao CD, et al. Combined Nivolumab and Ipilimumab or Monotherapy in Untreated Melanoma. *N Engl J Med* (2015) 373(1):23–34. doi: 10.1056/NEJMoa1504030
18. Larkin J, Chiarion-Sileni V, Gonzalez R, Grob JJ, Rutkowski P, Lao CD, et al. Five-Year Survival with Combined Nivolumab and Ipilimumab in Advanced Melanoma. *N Engl J Med* (2019) 381(16):1535–46. doi: 10.1056/NEJMoa1910836
19. Hellmann MD, Paz-Ares L, Bernabe Caro R, Zurawski B, Kim SW, Carcereny Costa E, et al. Nivolumab plus Ipilimumab in Advanced Non-Small-Cell Lung Cancer. *N Engl J Med* (2019) 381(21):2020–31. doi: 10.1056/NEJMoa1910231
20. Motzer RJ, Tannir NM, McDermott DF, Aren Frontera O, Melichar B, Choueiri TK, et al. Nivolumab plus Ipilimumab versus Sunitinib in Advanced Renal-Cell Carcinoma. *N Engl J Med* (2018) 378(14):1277–90. doi: 10.1056/NEJMoa1712126
21. Hodi FS, Lawrence D, Lezcano C, Wu X, Zhou J, Sasada T, et al. Bevacizumab plus ipilimumab in patients with metastatic melanoma. *Cancer Immunol Res* (2014) 2(7):632–42. doi: 10.1158/2326-6066.CIR-14-0053
22. Apetoh L, Ladoire S, Coukos G, Ghiringhelli F. Combining immunotherapy and anticancer agents: the right path to achieve cancer cure? *Ann Oncol* (2015) 26(9):1813–23. doi: 10.1093/annonc/mdv209
23. Voorwerk L, Slagter M, Horlings HM, Sikorska K, van de Vijver KK, de Maaker M, et al. Immune induction strategies in metastatic triple-negative breast cancer to enhance the sensitivity to PD-1 blockade: the TONIC trial. *Nat Med* (2019) 25(6):920–8. doi: 10.1038/s41591-019-0432-4
24. Langer CJ, Gadgeel SM, Borghaei H, Papadimitrakopoulou VA, Patnaik A, Powell SF, et al. Carboplatin and pemetrexed with or without pembrolizumab for advanced, non-squamous non-small-cell lung cancer: a randomised, phase 2 cohort of the open-label KEYNOTE-021 study. *Lancet Oncol* (2016) 17(11):1497–508. doi: 10.1016/S1470-2045(16)30498-3
25. Zhang P, Ma Y, Lv C, Huang M, Li M, Dong B, et al. Upregulation of programmed cell death ligand 1 promotes resistance response in non-small-cell lung cancer patients treated with neo-adjuvant chemotherapy. *Cancer Sci* (2016) 107(11):1563–71. doi: 10.1111/cas.13072
26. Gilad Y, Eliaz Y, Yu Y, Han SJ, O'Malley BW, Lonard DM. Drug-induced PD-L1 expression and cell stress response in breast cancer cells can be balanced by drug combination. *Sci Rep* (2019) 9(1):15099. doi: 10.1038/s41598-019-51537-7
27. Bozorgmehr F, Hommertgen A, Krisam J, Lasitschka F, Kuon J, Maenz M, et al. Fostering efficacy of anti-PD-1-treatment: Nivolumab plus radiotherapy in advanced non-small cell lung cancer - study protocol of the FORCE trial. *BMC Cancer* (2019) 19(1):1074. doi: 10.1186/s12885-019-6205-0
28. Qin Q, Nan X, Miller T, Fisher R, Teh B, Pandita S, et al. Complete Local and Abscopal Responses from a Combination of Radiation and Nivolumab in Refractory Hodgkin's Lymphoma. *Radiat Res* (2018) 190(3):322–9. doi: 10.1667/RR15048.1
29. Hughes PE, Caenepeel S, Wu LC. Targeted Therapy and Checkpoint Immunotherapy Combinations for the Treatment of Cancer. *Trends Immunol* (2016) 37(7):462–76. doi: 10.1016/j.it.2016.04.010
30. Ascierto PA, Ferrucci PF, Fisher R, Del Vecchio M, Atkinson V, Schmidt H, et al. Dabrafenib, trametinib and pembrolizumab or placebo in BRAF-mutant melanoma. *Nat Med* (2019) 25(6):941–6. doi: 10.1038/s41591-019-0448-9
31. Ribas A, Lawrence D, Atkinson V, Agarwal S, Miller WHJr., Carlino MS, et al. and MEK inhibition with PD-1 blockade immunotherapy in BRAF-mutant melanoma. *Nat Med* (2019) 25(6):936–40. doi: 10.1038/s41591-019-0476-5
32. Pauken KE, Dougan M, Rose NR, Lichtman AH, Sharpe AH. Adverse Events Following Cancer Immunotherapy: Obstacles and Opportunities. *Trends Immunol* (2019) 40(6):511–23. doi: 10.1016/j.it.2019.04.002
33. Rapoport BL, van Eeden R, Sibaud V, Epstein JB, Klastersky J, Aapro M, et al. Supportive care for patients undergoing immunotherapy. *Support Care Cancer Off J Multinational Assoc Support Care Cancer* (2017) 25(10):3017–30. doi: 10.1007/s00520-017-3802-9
34. Ishihara J, Ishihara A, Sasaki K, Lee SS, Williford JM, Yasui M, et al. Targeted antibody and cytokine cancer immunotherapies through collagen affinity. *Sci Trans Med* (2019) 11(487):eaau3259. doi: 10.1126/scitranslmed.aau3259
35. Winer A, Bodor JN, Borghaei H. Identifying and managing the adverse effects of immune checkpoint blockade. *J Thoracic Dis* (2018) 10(Suppl 3): S480–9. doi: 10.21037/jtd.2018.01.111
36. Spain L, Diem S, Larkin J. Management of toxicities of immune checkpoint inhibitors. *Cancer Treat Rev* (2016) 44:51–60. doi: 10.1016/j.ctrv.2016.02.001

37. Postow MA, Chesney J, Pavlick AC, Robert C, Grossmann K, McDermott D, et al. Nivolumab and ipilimumab versus ipilimumab in untreated melanoma. *N Engl J Med* (2015) 372(21):2006–17. doi: 10.1056/NEJMoa1414428
38. Zhang B, Wu Q, Zhou YL, Guo X, Ge J, Fu J. Immune-related adverse events from combination immunotherapy in cancer patients: A comprehensive meta-analysis of randomized controlled trials. *Int Immunopharmacol* (2018) 63:292–8. doi: 10.1016/j.intimp.2018.08.014
39. Riley RS, June CH, Langer R, Mitchell MJ. Delivery technologies for cancer immunotherapy. *Nat Rev Drug Discov* (2019) 18(3):175–96. doi: 10.1038/s41573-018-0006-z
40. Zhu G, Lynn GM, Jacobson O, Chen K, Liu Y, Zhang H, et al. Albumin/vaccine nanocomplexes that assemble *in vivo* for combination cancer immunotherapy. *Nat Commun* (2017) 8(1):1954. doi: 10.1038/s41467-017-02191-y
41. Ordikhani F, Uehara M, Kasinath V, Dai L, Eskandari SK, Bahmani B, et al. Targeting antigen-presenting cells by anti-PD-1 nanoparticles augments antitumor immunity. *JCI Insight* (2018) 3(20):e122700. doi: 10.1172/jci.insight.122700
42. Hei Y, Teng B, Zeng Z, Zhang S, Li Q, Pan J, et al. Multifunctional Immunoliposomes Combining Catalase and PD-L1 Antibodies Overcome Tumor Hypoxia and Enhance Immunotherapeutic Effects Against Melanoma. *Int J Nanomed* (2020) 15:1677–91. doi: 10.2147/IJN.S225807
43. Qian Y, Qiao S, Dai Y, Xu G, Dai B, Lu L, et al. Molecular-Targeted Immunotherapeutic Strategy for Melanoma via Dual-Targeting Nanoparticles Delivering Small Interfering RNA to Tumor-Associated Macrophages. *ACS Nano* (2017) 11(9):9536–49. doi: 10.1021/acsnano.7b05465
44. Teo PY, Yang C, Whilding LM, Parente-Pereira AC, Maher J, George AJ, et al. Ovarian cancer immunotherapy using PD-L1 siRNA targeted delivery from folic acid-functionalized polyethylenimine: strategies to enhance T cell killing. *Adv Healthcare Mater* (2015) 4(8):1180–9. doi: 10.1002/adhm.201500089
45. Song W, Shen L, Wang Y, Liu Q, Goodwin TJ, Li J, et al. Synergistic and low adverse effect cancer immunotherapy by immunogenic chemotherapy and locally expressed PD-L1 trap. *Nat Commun* (2018) 9(1):2237. doi: 10.1038/s41467-018-04605-x
46. Graham K, Unger E. Overcoming tumor hypoxia as a barrier to radiotherapy, chemotherapy and immunotherapy in cancer treatment. *Int J Nanomed* (2018) 13:6049–58. doi: 10.2147/IJN.S140462
47. Jahanban-Esfahlan R, de la Guardia M, Ahmadi D, Yousefi B. Modulating tumor hypoxia by nanomedicine for effective cancer therapy. *J Cell Physiol* (2018) 233(3):2019–31. doi: 10.1002/jcp.25859
48. Jayaprakash P, Ai M, Liu A, Budhani P, Bartkowiak T, Sheng J, et al. Targeted hypoxia reduction restores T cell infiltration and sensitizes prostate cancer to immunotherapy. *J Clin Invest* (2018) 128(11):5137–49. doi: 10.1172/JCI96268
49. Daniel SK, Sullivan KM, Labadie KP, Pillarisetty VG. Hypoxia as a barrier to immunotherapy in pancreatic adenocarcinoma. *Clin Trans Med* (2019) 8(1):10. doi: 10.1186/s40169-019-0226-9
50. Noman MZ, Hasmim M, Lequeux A, Xiao M, Duhem C, Chouaib S, et al. Improving Cancer Immunotherapy by Targeting the Hypoxic Tumor Microenvironment: New Opportunities and Challenges. *Cells* (2019) 8(9):1083. doi: 10.3390/cells8091083
51. Chouaib S, Messai Y, Couve S, Escudier B, Hasmim M, Noman MZ. Hypoxia promotes tumor growth in linking angiogenesis to immune escape. *Front Immunol* (2012) 3:21. doi: 10.3389/fimmu.2012.00021
52. Palazon A, Aragones J, Morales-Kastresana A, de Landazuri MO, Melero I. Molecular pathways: hypoxia response in immune cells fighting or promoting cancer. *Clin Cancer Res* (2012) 18(5):1207–13. doi: 10.1158/1078-0432.CCR-11-1591
53. Wang H, Li J, Wang Y, Gong X, Xu X, Wang J, et al. Nanoparticles-mediated reoxygenation strategy relieves tumor hypoxia for enhanced cancer therapy. *J Controlled Release* (2020) 319:25–45. doi: 10.1016/j.jconrel.2019.12.028
54. Chung CH, Lu KY, Lee WC, Hsu WJ, Lee WF, Dai JZ, et al. Fucoidan-based, tumor-activated nanoplatform for overcoming hypoxia and enhancing photodynamic therapy and antitumor immunity. *Biomaterials* (2020) 257:120227. doi: 10.1016/j.biomaterials.2020.120227
55. Chen Q, Xu L, Chen J, Yang Z, Liang C, Yang Y, et al. Tumor vasculature normalization by orally fed erlotinib to modulate the tumor microenvironment for enhanced cancer nanomedicine and immunotherapy. *Biomaterials* (2017) 148:69–80. doi: 10.1016/j.biomaterials.2017.09.021
56. Sung YC, Jin PR, Chu LA, Hsu FF, Wang MR, Chang CC, et al. Delivery of nitric oxide with a nanocarrier promotes tumour vessel normalization and potentiates anti-cancer therapies. *Nat Nanotechnol* (2019) 14(12):1160–9. doi: 10.1038/s41565-019-0570-3
57. Mpekris F, Voutouri C, Baish JW, Duda DG, Munn LL, Stylianopoulos T, et al. Combining microenvironment normalization strategies to improve cancer immunotherapy. *Proc Natl Acad Sci U S A* (2020) 117(7):3728–37. doi: 10.1073/pnas.1919764117
58. Li W, Li X, Liu S, Yang W, Pan F, Yang XY, et al. Gold nanoparticles attenuate metastasis by tumor vasculature normalization and epithelial-mesenchymal transition inhibition. *Int J Nanomed* (2017) 12:3509–20. doi: 10.2147/IJN.S128802
59. Gurunathan S, Lee KJ, Kalishwaralal K, Sheikpranbabu S, Vaidyanathan R, Eom SH. Antiangiogenic properties of silver nanoparticles. *Biomaterials* (2009) 30(31):6341–50. doi: 10.1016/j.biomaterials.2009.08.008
60. Taleb M, Ding Y, Wang B, Yang N, Han X, Du C, et al. Dopamine Delivery via pH-Sensitive Nanoparticles for Tumor Blood Vessel Normalization and an Improved Effect of Cancer Chemotherapeutic Drugs. *Adv Healthcare Mater* (2019) 8(18):e1900283. doi: 10.1002/adhm.201900283
61. Wang B, Ding Y, Zhao X, Han X, Yang N, Zhang Y, et al. Delivery of small interfering RNA against Nogo-B receptor via tumor-acidity responsive nanoparticles for tumor vessel normalization and metastasis suppression. *Biomaterials* (2018) 175:110–22. doi: 10.1016/j.biomaterials.2018.05.034
62. Zheng D, Li B, Xu L, Zhang QL, Fan JX, Li CX, et al. Normalizing Tumor Microenvironment Based on Photosynthetic Abiotic/Biotic Nanoparticles. *ACS Nano* (2018) 12(6):6218–27. doi: 10.1021/acsnano.8b02977
63. Ruscetti M, Morris J, Mezzadra R, Russell J, Leibold J, Romesser PB, et al. Senescence-Induced Vascular Remodeling Creates Therapeutic Vulnerabilities in Pancreas Cancer. *Cell* (2020) 181(2):424–41.e21. doi: 10.1016/j.cell.2020.03.008
64. He B, Johansson-Percival A, Backhouse J, Li J, Lee GYF, Hamzah J, et al. Remodeling of Metastatic Vasculature Reduces Lung Colonization and Sensitizes Overt Metastases to Immunotherapy. *Cell Rep* (2020) 30(3):714–24.e5. doi: 10.1016/j.celrep.2019.12.013
65. Hu D, Chen L, Qu Y, Peng J, Chu B, Shi K, et al. Oxygen-generating Hybrid Polymeric Nanoparticles with Encapsulated Doxorubicin and Chlorin e6 for Trimodal Imaging-Guided Combined Chemo-Photodynamic Therapy. *Theranostics* (2018) 8(6):1558–74. doi: 10.7150/thno.22989
66. Meng L, Cheng Y, Tong X, Gan S, Ding Y, Zhang Y, et al. Tumor Oxygenation and Hypoxia Inducible Factor-1 Functional Inhibition via a Reactive Oxygen Species Responsive Nanoplatform for Enhancing Radiation Therapy and Abscopal Effects. *ACS Nano* (2018) 12(8):8308–22. doi: 10.1021/acsnano.8b03590
67. Chen H, Ma A, Yin T, Chen Z, Liang R, Pan H, et al. In Situ Photocatalysis of TiO-Porphyrin-Encapsulated Nanosystem for Highly Efficient Oxidative Damage against Hypoxic Tumors. *ACS Appl Mater Interf* (2020) 12(11):12573–83. doi: 10.1021/acsami.0c00921
68. Zhang Z, Niu N, Gao X, Han F, Chen Z, Li S, et al. A new drug carrier with oxygen generation function for modulating tumor hypoxia microenvironment in cancer chemotherapy. *Colloids Surfaces B Biointerf* (2019) 173:335–45. doi: 10.1016/j.colsurfb.2018.10.008
69. Zhou Z, Zhang B, Wang H, Yuan A, Hu Y, Wu J. Two-stage oxygen delivery for enhanced radiotherapy by perfluorocarbon nanoparticles. *Theranostics* (2018) 8(18):4898–911. doi: 10.7150/thno.27598
70. Ma S, Zhou J, Zhang Y, Yang B, He Y, Tian C, et al. An Oxygen Self-sufficient Fluorinated Nanoplatform for Relieved Tumor Hypoxia and Enhanced Photodynamic Therapy of Cancers. *ACS Appl Mater Interf* (2019) 11(8):7731–42. doi: 10.1021/acsami.8b19840
71. Zhou Z, Zhang B, Wang S, Zai W, Yuan A, Hu Y, et al. Perfluorocarbon Nanoparticles Mediated Platelet Blocking Disrupt Vascular Barriers to Improve the Efficacy of Oxygen-Sensitive Antitumor Drugs. *Small* (2018) 14(45):e1801694. doi: 10.1002/smll.201801694

72. Chen L, Wang Z, Xu Q, Liu Y, Chen L, Guo S, et al. The failure of DAC to induce OCT2 expression and its remission by hemoglobin-based nanocarriers under hypoxia in renal cell carcinoma. *Theranostics* (2020) 10(8):3562–78. doi: 10.7150/thno.39944
73. Chen Q, Hu Q, Dukhovlinova E, Chen G, Ahn S, Wang C, et al. Photothermal Therapy Promotes Tumor Infiltration and Antitumor Activity of CAR T Cells. *Adv Mater* (2019) 31(23):e1900192. doi: 10.1002/adma.201900192
74. Stern JM, Kibanov Solomonov VV, Sazykina E, Schwartz JA, Gad SC, Goodrich GP. Initial Evaluation of the Safety of Nanoshell-Directed Photothermal Therapy in the Treatment of Prostate Disease. *Int J Toxicol* (2016) 35(1):38–46. doi: 10.1177/1091581815600170
75. Liu C, Luo L, Zeng L, Xing J, Xia Y, Sun S, et al. Porous Gold Nanoshells on Functional NH2 -MOFs: Facile Synthesis and Designable Platforms for Cancer Multiple Therapy. *Small* (2018) 14(35):e1801851. doi: 10.1002/smll.201801851
76. Liu Y, Crawford BM, Vo-Dinh T. Gold nanoparticles-mediated photothermal therapy and immunotherapy. *Immunotherapy* (2018) 10 (13):1175–88. doi: 10.2217/imt-2018-0029
77. Chen W, Qin M, Chen X, Wang Q, Zhang Z, Sun X. Combining photothermal therapy and immunotherapy against melanoma by polydopamine-coated Al2O3 nanoparticles. *Theranostics* (2018) 8 (8):2229–41. doi: 10.7150/thno.24073
78. Peng J, Xiao Y, Li W, Yang Q, Tan L, Jia Y, et al. Photosensitizer Micelles Together with IDO Inhibitor Enhance Cancer Photothermal Therapy and Immunotherapy. *Adv Sci* (2018) 5(5):1700891. doi: 10.1002/advs.201700891
79. Chiang CS, Lin YJ, Lee R, Lai YH, Cheng HW, Hsieh CH, et al. Combination of fucoidan-based magnetic nanoparticles and immunomodulators enhances tumour-localized immunotherapy. *Nat Nanotechnol* (2018) 13(8):746–54. doi: 10.1038/s41565-018-0146-7
80. Mi Y, Smith CC, Yang F, Qi Y, Roche KC, Serody JS, et al. Dual Immunotherapy Nanoparticle Improves T-Cell Activation and Cancer Immunotherapy. *Adv Mater* (2018) 30(25):e1706098. doi: 10.1002/adma.201706098
81. Zheng S, Qin T, Lu Y, Huang Y, Luo L, Liu Z, et al. Maturation of dendritic cells *in vitro* and immunological enhancement of mice *in vivo* by pachyman- and/or OVA-encapsulated poly(d,l-lactic acid) nanospheres. *Int J Nanomed* (2018) 13:569–83. doi: 10.2147/IJN.S153567
82. Dong H, Wen ZF, Chen L, Zhou N, Liu H, Dong S, et al. Polyethyleneimine modification of aluminum hydroxide nanoparticle enhances antigen transportation and cross-presentation of dendritic cells. *Int J Nanomed* (2018) 13:3353–65. doi: 10.2147/IJN.S164097
83. Tu K, Deng H, Kong L, Wang Y, Yang T, Hu Q, et al. Reshaping Tumor Immune Microenvironment through Acidity-Responsive Nanoparticles Featured with CRISPR/Cas9-Mediated Programmed Death-Ligand 1 Attenuation and Chemotherapeutics-Induced Immunogenic Cell Death. *ACS Appl Mater Interf* (2020) 12(14):16018–30. doi: 10.1021/acsami.9b23084
84. Korangath P, Barnett JD, Sharma A, Henderson ET, Stewart J, Yu SH, et al. Nanoparticle interactions with immune cells dominate tumor retention and induce T cell-mediated tumor suppression in models of breast cancer. *Sci Adv* (2020) 6(13):eaay1601. doi: 10.1126/sciadv.aay1601
85. Deng RH, Zou MZ, Zheng D, Peng SY, Liu W, Bai XF, et al. Nanoparticles from Cuttlefish Ink Inhibit Tumor Growth by Synergizing Immunotherapy and Photothermal Therapy. *ACS Nano* (2019) 13(8):8618–29. doi: 10.1021/acsnano.9b02993
86. Liu H, Moynihan KD, Zheng Y, Szeto GL, Li AV, Huang B, et al. Structure-based programming of lymph-node targeting in molecular vaccines. *Nature* (2014) 507(7493):519–22. doi: 10.1038/nature12978
87. Jeanbart L, Ballester M, de Titta A, Corthesy P, Romero P, Hubbell JA, et al. Enhancing efficacy of anticancer vaccines by targeted delivery to tumor-draining lymph nodes. *Cancer Immunol Res* (2014) 2(5):436–47. doi: 10.1158/2326-6066.CIR-14-0019-T
88. Bo R, Sun Y, Zhou S, Ou N, Gu P, Liu Z, et al. Simple nanoliposomes encapsulating Lycium barbarum polysaccharides as adjuvants improve humoral and cellular immunity in mice. *Int J Nanomed* (2017) 12:6289–301. doi: 10.2147/IJN.S136820
89. Haughney SL, Ross KA, Boggiatto PM, Wannemuehler MJ, Narasimhan B. Effect of nanovaccine chemistry on humoral immune response kinetics and maturation. *Nanoscale* (2014) 6(22):13770–8. doi: 10.1039/c4nr03724c
90. Billingsley MM, Singh N, Ravikumar P, Zhang R, June CH, Mitchell MJ. Ionizable Lipid Nanoparticle-Mediated mRNA Delivery for Human CAR T Cell Engineering. *Nano Lett* (2020) 20(3):1578–89. doi: 10.1021/acs.nanolett.9b04246
91. Nawaz W, Xu S, Li Y, Huang B, Wu X, Wu Z. Nanotechnology and immunoengineering: How nanotechnology can boost CAR-T therapy. *Acta Biomater* (2020) 109:21–36. doi: 10.1016/j.actbio.2020.04.015
92. Dunn ZS, Mac J, Wang P. T cell immunotherapy enhanced by designer biomaterials. *Biomaterials* (2019) 217:119265. doi: 10.1016/j.biomaterials.2019.119265
93. Yu Q, Zhang M, Chen Y, Chen X, Shi S, Sun K, et al. Self-Assembled Nanoparticles Prepared from Low-Molecular-Weight PEI and Low-Generation PAMAM for EGFRvIII-Chimeric Antigen Receptor Gene Loading and T-Cell Transient Modification. *Int J Nanomed* (2020) 15:483–95. doi: 10.2147/IJN.S229858
94. Siriwon N, Kim YJ, Siegler E, Chen X, Rohrs JA, Liu Y, et al. CAR-T Cells Surface-Engineered with Drug-Encapsulated Nanoparticles Can Ameliorate Intratumoral T-cell Hypofunction. *Cancer Immunol Res* (2018) 6(7):812–24. doi: 10.1158/2326-6066.CIR-17-0502
95. Kim GB, Aragon-Sanabria V, Randolph L, Jiang H, Reynolds JA, Webb BS, et al. High-affinity mutant Interleukin-13 targeted CAR T cells enhance delivery of clickable biodegradable fluorescent nanoparticles to glioblastoma. *Bioactive Mater* (2020) 5(3):624–35. doi: 10.1016/j.bioactmat.2020.04.011
96. Moffett HF, Coon ME, Radtke S, Stephan SB, McKnight L, Lambert A, et al. Hit-and-run programming of therapeutic cytoreagents using mRNA nanocarriers. *Nat Commun* (2017) 8(1):389. doi: 10.1038/s41467-017-00505-8
97. Zheng Y, Stephan MT, Gai SA, Abraham W, Shearer A, Irvine DJ. In vivo targeting of adoptively transferred T-cells with antibody- and cytokine-conjugated liposomes. *J Controlled Release* (2013) 172(2):426–35. doi: 10.1016/j.jconrel.2013.05.037
98. Perica K, Bieler JG, Schutz C, Varela JC, Douglass J, Skora A, et al. Enrichment and Expansion with Nanoscale Artificial Antigen Presenting Cells for Adoptive Immunotherapy. *ACS Nano* (2015) 9(7):6861–71. doi: 10.1021/acsnano.5b02829
99. Bai C, Gao S, Hu S, Liu X, Li H, Dong J, et al. Self-Assembled Multivalent Aptamer Nanoparticles with Potential CAR-like Characteristics Could Activate T Cells and Inhibit Melanoma Growth. *Mol Ther Oncolytics* (2020) 17:9–20. doi: 10.1016/j.omto.2020.03.002
100. Matosevic S. Viral and Nonviral Engineering of Natural Killer Cells as Emerging Adoptive Cancer Immunotherapies. *J Immunol Res* (2018) 2018:4054815. doi: 10.1155/2018/4054815
101. Nakamura T, Kuroi M, Fujiwara Y, Warashina S, Sato Y, Harashima H. Small-sized, stable lipid nanoparticle for the efficient delivery of siRNA to human immune cell lines. *Sci Rep* (2016) 6:37849. doi: 10.1038/srep37849
102. Oyer JL, Pandey V, Igarashi RY, Somanchi SS, Zakari A, Solh M, et al. Natural killer cells stimulated with PM21 particles expand and biodistribute in vivo: Clinical implications for cancer treatment. *Cytotherapy* (2016) 18 (5):653–63. doi: 10.1016/j.jcyt.2016.02.006
103. Hillman Y, Lustiger D, Wine Y. Antibody-based nanotechnology. *Nanotechnology* (2019) 30(28):282001. doi: 10.1088/1361-6528/ab12f4
104. Ning ST, Lee SY, Wei MF, Peng CL, Lin SY, Tsai MH, et al. Targeting Colorectal Cancer Stem-Like Cells with Anti-CD133 Antibody-Conjugated SN-38 Nanoparticles. *ACS Appl Mater Interf* (2016) 8(28):17793–804. doi: 10.1021/acsami.6b04403
105. Mondal L, Mukherjee B, Das K, Bhattacharya S, Dutta D, Chakraborty S, et al. CD-340 functionalized doxorubicin-loaded nanoparticle induces apoptosis and reduces tumor volume along with drug-related cardiotoxicity in mice. *Int J Nanomedicine* (2019) 14:8073–94. doi: 10.2147/IJN.S220740
106. Guo D, Xu P, Chen D, Wang L, Zhu Y, Zuo Y, et al. Daunorubicin-Loaded CdTe QDs Conjugated with Anti-CD123 mAbs: A Novel Delivery System for Myelodysplastic Syndromes Treatment. *Int J Nanomed* (2020) 15:521–36. doi: 10.2147/IJN.S233395
107. Shi X, Cheng Q, Hou T, Han M, Smbatyan G, Lang JE, et al. Genetically Engineered Cell-Derived Nanoparticles for Targeted Breast Cancer

Immunotherapy. *Mol Therapy: J Am Soc Gene Ther* (2020) 28(2):536–47. doi: 10.1016/j.ymthe.2019.11.020
108. Peng J, Chen J, Xie F, Bao W, Xu H, Wang H, et al. Herceptin-conjugated paclitaxel loaded PCL-PEG worm-like nanocrystal micelles for the combinatorial treatment of HER2-positive breast cancer. *Biomaterials* (2019) 222:119420. doi: 10.1016/j.biomaterials.2019.119420
109. Kitano S, Kageyama S, Nagata Y, Miyahara Y, Hiasa A, Naota H, et al. HER2-specific T-cell immune responses in patients vaccinated with truncated HER2 protein complexed with nanogels of cholesteryl pullulan. *Clin Cancer Res* (2006) 12(24):7397–405. doi: 10.1158/1078-0432.CCR-06-1546
110. Chen CH, Wu YJ, Chen JJ. Photo-thermal therapy of bladder cancer with Anti-EGFR antibody conjugated gold nanoparticles. *Front Biosci* (2016) 21:1211–21. doi: 10.2741/4451
111. Liszbinski RB, Romagnoli GG, Gorgulho CM, Basso CR, Pedrosa VA, Kaneno R. Anti-EGFR-Coated Gold Nanoparticles *In vitro* Carry 5-Fluorouracil to Colorectal Cancer Cells. *Materials* (2020) 13(2):375. doi: 10.3390/ma13020375
112. Mamot C, Ritschard R, Wicki A, Stehle G, Dieterle T, Bubendorf L, et al. Tolerability, safety, pharmacokinetics, and efficacy of doxorubicin-loaded anti-EGFR immunoliposomes in advanced solid tumours: a phase 1 dose-escalation study. *Lancet Oncol* (2012) 13(12):1234–41. doi: 10.1016/S1470-2045(12)70476-X
113. Russell LM, Hultz M, Searson PC. Leakage kinetics of the liposomal chemotherapeutic agent Doxil: The role of dissolution, protonation, and passive transport, and implications for mechanism of action. *J Controlled Release* (2018) 269:171–6. doi: 10.1016/j.jconrel.2017.11.007
114. Schiller GJ, Damon LE, Coutre SE, Hsu P, Bhat G, Douer D. High-Dose Vincristine Sulfate Liposome Injection, for Advanced, Relapsed, or Refractory Philadelphia Chromosome-Negative Acute Lymphoblastic Leukemia in an Adolescent and Young Adult Subgroup of a Phase 2 Clinical Trial. *J Adolesc Young Adult Oncol* (2018) 7(5):546–52. doi: 10.1089/jayao.2018.0041
115. Sasaki K, Kantarjian H, Wierda W, Ravandi-Kashani F, Jorgensen J, Wang SA, et al. Phase 2 study of hyper-CMAD with liposomal vincristine for patients with newly diagnosed acute lymphoblastic leukemia. *Am J Hematol* (2020) 95(7):734–9. doi: 10.1002/ajh.25784
116. Passero FCJr., Grapsa D, Syrigos KN, Saif MW. The safety and efficacy of Onivyde (irinotecan liposome injection) for the treatment of metastatic pancreatic cancer following gemcitabine-based therapy. *Expert Rev Anticancer Ther* (2016) 16(7):697–703. doi: 10.1080/14737140.2016.1192471
117. Tucci ST, Kheirolomoom A, Ingham ES, Mahakian LM, Tam SM, Foiret J, et al. Tumor-specific delivery of gemcitabine with activatable liposomes. *J Controlled Release* (2019) 309:277–88. doi: 10.1016/j.jconrel.2019.07.014
118. Nassir AM, Ibrahim IAA, Md S, Waris M, Tanuja, Ain MR, et al. Surface functionalized folate targeted oleuropein nano-liposomes for prostate tumor targeting: Invitro and invivo activity. *Life Sci* (2019) 220:136–46. doi: 10.1016/j.lfs.2019.01.053
119. Choi SH, Byeon HJ, Choi JS, Thao L, Kim I, Lee ES, et al. Inhalable self-assembled albumin nanoparticles for treating drug-resistant lung cancer. *J Controlled Release* (2015) 197:199–207. doi: 10.1016/j.jconrel.2014.11.008
120. Hoogenboezem EN, Duvall CL. Harnessing albumin as a carrier for cancer therapies. *Adv Drug Deliv Rev* (2018) 130:73–89. doi: 10.1016/j.addr.2018.07.011
121. Hyun H, Park J, Willis K, Park JE, Lyle LT, Lee W, et al. Surface modification of polymer nanoparticles with native albumin for enhancing drug delivery to solid tumors. *Biomaterials* (2018) 180:206–24. doi: 10.1016/j.biomaterials.2018.07.024
122. Onafuye H, Pieper S, Mulac D, Cinatl JJr., Wass MN, Langer K, et al. Doxorubicin-loaded human serum albumin nanoparticles overcome transporter-mediated drug resistance in drug-adapted cancer cells. *Beilstein J Nanotechnol* (2019) 10:1707–15. doi: 10.3762/bjnano.10.166
123. Cho H, Gao J, Kwon GS. PEG-b-PLA micelles and PLGA-b-PEG-b-PLGA sol-gels for drug delivery. *J Controlled Release* (2016) 240:191–201. doi: 10.1016/j.jconrel.2015.12.015
124. Pacheco PA, Rodrigues LNC, Ferreira JFS, Gomes ACP, Verissimo CJ, Louvandini H, et al. Inclusion complex and nanoclusters of cyclodextrin to increase the solubility and efficacy of albendazole. *Parasitol Res* (2018) 117 (3):705–12. doi: 10.1007/s00436-017-5740-3
125. Schmidt KT, Peer CJ, Huitema ADR, Williams MD, Wroblewski S, Schellens JHM, et al. Measurement of NLG207 (formerly CRLX101) nanoparticle-bound and released camptothecin in human plasma. *J Pharm Biomed Anal* (2020) 181:113073. doi: 10.1016/j.jpba.2019.113073
126. Chao J, Lin J, Frankel P, Clark AJ, Wiley DT, Garmey E, et al. Pilot trial of CRLX101 in patients with advanced, chemotherapy-refractory gastroesophageal cancer. *J Gastrointest Oncol* (2017) 8(6):962–9. doi: 10.21037/jgo.2017.08.10
127. Chen YF, Wang YH, Lei CS, Changou CA, Davis ME, Yen Y. Host immune response to anti-cancer camptothecin conjugated cyclodextrin-based polymers. *J Biomed Sci* (2019) 26(1):85. doi: 10.1186/s12929-019-0583-0
128. Uenaka A, Wada H, Isobe M, Saika T, Tsuji K, Sato E, et al. T cell immunomonitoring and tumor responses in patients immunized with a complex of cholesterol-bearing hydrophobized pullulan (CHP) and NY-ESO-1 protein. *Cancer Immunity* (2007) 7:9.
129. Ishihara M, Tono Y, Miyahara Y, Muraoka D, Harada N, Kageyama S, et al. First-in-human phase I clinical trial of the NY-ESO-1 protein cancer vaccine with NOD2 and TLR9 stimulants in patients with NY-ESO-1-expressing refractory solid tumors. *Cancer Immunol Immunother: CII* (2020) 69 (4):663–75. doi: 10.1007/s00262-020-02483-1
130. Yi Y, Zhou Z, Shu S, Fang Y, Twitty C, Hilton TL, et al. Autophagy-assisted antigen cross-presentation: Autophagosome as the argo of shared tumor-specific antigens and DAMPs. *Oncoimmunology* (2012) 1(6):976–8. doi: 10.4161/onci.20059
131. Page DB, Hulett TW, Hilton TL, Hu HM, Urba WJ, Fox BA. Glimpse into the future: harnessing autophagy to promote anti-tumor immunity with the DRibbles vaccine. *J Immunother cancer* (2016) 4:25. doi: 10.1186/s40425-016-0130-4
132. Ye W, Xing Y, Paustian C, van de Ven R, Moudgil T, Hilton TL, et al. Cross-presentation of viral antigens in dribbles leads to efficient activation of virus-specific human memory T cells. *J Trans Med* (2014) 12:100. doi: 10.1186/1479-5876-12-100
133. Anzaghe M, Schulke S, Scheurer S. Virus-Like Particles as Carrier Systems to Enhance Immunomodulation in Allergen Immunotherapy. *Curr Allergy Asthma Rep* (2018) 18(12):71. doi: 10.1007/s11882-018-0827-1
134. Zepeda-Cervantes J, Ramirez-Jarquin JO, Vaca L. Interaction Between Virus-Like Particles (VLPs) and Pattern Recognition Receptors (PRRs) From Dendritic Cells (DCs): Toward Better Engineering of VLPs. *Front Immunol* (2020) 11:1100. doi: 10.3389/fimmu.2020.01100
135. Qian C, Liu X, Xu Q, Wang Z, Chen J, Li T, et al. Recent Progress on the Versatility of Virus-Like Particles. *Vaccines* (2020) 8(1):139. doi: 10.3390/vaccines8010139

Conflict of Interest: The authors declare that the research was conducted in the absence of any commercial or financial relationships that could be construed as a potential conflict of interest.

Copyright © 2020 Li, Peng, Wu, Quan, Li, Lu and Cui. This is an open-access article distributed under the terms of the Creative Commons Attribution License (CC BY). The use, distribution or reproduction in other forums is permitted, provided the original author(s) and the copyright owner(s) are credited and that the original publication in this journal is cited, in accordance with accepted academic practice. No use, distribution or reproduction is permitted which does not comply with these terms.

frontiers in Immunology

REVIEW
published: 07 January 2021
doi: 10.3389/fimmu.2020.612202

Exploring the Emerging Role of the Gut Microbiota and Tumor Microenvironment in Cancer Immunotherapy

Qin Qiu[1†], Yuqi Lin[2†], Yucui Ma[3†], Xiaoling Li[4], Juan Liang[1], Zhiyan Chen[5], Kaifeng Liu[5], Yuge Huang[6], Hui Luo[3], Riming Huang[2] and Lianxiang Luo[3,7,8*]*

[1] Graduate School, Guangdong Medical University, Zhanjiang, China, [2] Guangdong Provincial Key Laboratory of Food Quality and Safety, College of Food Science, South China Agricultural University, Guangzhou, China, [3] The Marine Biomedical Research Institute, Guangdong Medical University, Zhanjiang, China, [4] Animal Experiment Center, Guangdong Medical University, Zhanjiang, China, [5] The First Clinical College, Guangdong Medical University, Zhanjiang, China, [6] Department of Pediatrics, The Affiliated Hospital of Guangdong Medical University, Zhanjiang, China, [7] The Marine Biomedical Research Institute of Guangdong Zhanjiang, Zhanjiang, China, [8] Southern Marine Science and Engineering Guangdong Laboratory (Zhanjiang), Zhanjiang, China

OPEN ACCESS

Edited by:
Peng Qu,
National Institutes of Health (NIH), United States

Reviewed by:
Francesca Romana Ponziani, Fondazione Policlinico Universitario Agostino Gemelli IRCCS, Italy
Mingxiao Feng, Johns Hopkins University, United States

***Correspondence:**
Riming Huang
huangriming@scau.edu.cn
Lianxiang Luo
luolianxiang321@gdmu.edu.cn

[†]These authors have contributed equally to this work

Specialty section:
This article was submitted to Cancer Immunity and Immunotherapy, a section of the journal Frontiers in Immunology

Received: *30 September 2020*
Accepted: *23 November 2020*
Published: *07 January 2021*

Citation:
Qiu Q, Lin Y, Ma Y, Li X, Liang J, Chen Z, Liu K, Huang Y, Luo H, Huang R and Luo L (2021) Exploring the Emerging Role of the Gut Microbiota and Tumor Microenvironment in Cancer Immunotherapy. Front. Immunol. 11:612202. doi: 10.3389/fimmu.2020.612202

The tumor microenvironment (TME) is a complex ecosystem, which includes many different types of cells, abnormal vascular systems, and immunosuppressive cytokines. TME serves an important function in tumor tolerance and escapes from immune surveillance leading to tumor progression. Indeed, there is increasing evidence that gut microbiome is associated with cancer in a variety of ways, as specific microbial signatures are known to promote cancer development and influence safety, tolerability, and efficacy of therapies. Studies over the past five years have shown that the composition of the intestinal microbiota has a significant impact on the efficacy of anticancer immunosurveillance, which contribute to the therapeutic activity of cancer immunotherapies based on targeting cytotoxic T lymphocyte protein 4 (CTLA-4) or programmed cell death protein 1 (PD-1)–programmed cell death 1 ligand 1 (PD-L1) axis. In this review, we mainly discuss the impact of TME on cancer and immunotherapy through immune-related mechanisms. We subsequently discuss the influence of gut microbiota and its metabolites on the host immune system and the formation of TME. In addition, this review also summarizes the latest research on the role of gut microbiota in cancer immunotherapy.

Keywords: tumor microenvironment, gut microbiota, immunotherapy, host immunity, programmed cell death protein 1/programmed cell death 1 ligand 1

INTRODUCTION

Cancer is a major public health problem with high rates of incidence and mortality (1). Over the past few decades, significant progress has been achieved in the field of cancer treatment, the main treatment methods included surgery, chemotherapy, radiotherapy, target therapy, and immunotherapy, among them, immunotherapy has become a research hotspot in recent years

among these (2, 3). However, the effect of tumor immunotherapy is largely affected by tumor microenvironment (TME) (4, 5). The TME consisted of a variety of different cell types, which plays an important role in tumor tolerance and the evasion of immune surveillance (6). Studies have shown that multiple cells in TME play a significant role in tumor immunotherapy, including T cell, fibroblasts, natural killer (NK) cell, dendritic cells (DCs), and so on (7–9), NK cells stimulate cDC1 to enter into the TME and promote tumor immune control (10). More than 1,000 microorganisms are living in the human gut, called the gut microbiota, which is closely related to a variety of diseases, for example, chronic inflammation, autoimmunity, cancer, and so on (7, 11). Gut microbiota can shape TME by regulating the immune and hormonal factors of the whole host (7), in other words, host gut microbiota is emerging as a critical modulator of the TME. It is also reported that regulating gut microbiota can enhance the effect of cancer immunotherapy (12). It is worth mentioning that the metabolites of gut microbiota [such as short-chain fatty acids (SCFAs), lipopolysaccharide, and Gallic acid] also have effects on TME and tumor immunosuppressive therapy (13–15). Besides, gut microbiota acts tumor immunotherapy directly or indirectly through immune-related mechanisms. The gut microbiota has been found to inhibit the cancer-suppressing effect of p53 mutations, while antibiotic treatment (elimination of gut microbiota) can restore it (16). Exploring roles of gut microbiota and TME in cancer immunotherapy as well as their interaction based on literature survey, which obtains answer of problems existed in cancer immunotherapy, and clarifies the future research direction of tumor immunotherapy. Meanwhile, it provides a theoretical basis for immunotherapy based on TME and gut microbiota.

THE ROLE OF TME IN CANCER IMMUNOTHERAPY

TME is composed of immune cells, such as T cells, B cells, and NK cells, a variety of myeloid cell populations including granulocytes, monocytes, macrophages, and DCs, abnormal vasculature and immunosuppressive cytokines, which play different roles in TME (17, 18). The progress of cancer growth, invasion, metastasis, drug resistance, and immune escape are affected by TME (19, 20). For example, TME promotes the occurrence of hepatocellular carcinoma (HCC) in many ways, mainly in that NK cells and DCs participate in immune escape mechanisms, macrophages are involved in promotion of angiogenesis and tissue remodeling, and the production of cytokines and chemokines lead to persistent inflammation-related damage (21–23). On the other hand, well expression of co-inhibitory molecules, especially CTLA-4, PD-1 and PD-L1 are associated with immune-system exhaustion and immune tolerance (24, 25). The regulation of the TME could be used as an effective strategy to prevent as well as treat cancer (2). The purpose of tumor immunotherapy is to stimulate tumor-specific cytotoxic T lymphocytes (CTLs) and subsequent transports, to enable them to reach and persist in TME in order to identify and eliminate malignant target cells (26). TME show different important effects and mechanisms in the tumor and its immunotherapy with different channels (**Figure 1**).

Dendritic Cells and T Cells

T cells play an irreplaceable role in tumor immunotherapy. T cells through the T cell receptor (TCR) to identify major histocompatibility complex class I/II (MHC- I/MHC-II) molecules that existed on the surface of the specific antigen peptide of malignant cells, which plays an important role in defense against cancer. Tumor targets are mainly achieved by releasing the content of cytolytic granules containing perforin and granzyme. To destroy their targets, CTLs must first migrate to tumor sites, infiltrate tumor tissue, interact with cancer cells, and eventually eliminate transformed cells due to trigger effector functions (27). It is indicated that a better prognosis of lung, melanoma, brain, breast, colorectal cancer is associated with that infiltration of T cells, particularly CD8+ T cells infiltrate into the TME (28, 29). CD8+ T cell mediated anti-tumor immunity of promising cancer immunotherapy, including DC cancer vaccines, adaptability of reactive T cell tumor cell metastasis (ACT) and free of disease checkpoint blockade, such as resistance to PD-1, PD-L1, and resisting CTLA-4 (26), PD-1 therapy is associated with the abundance of CD8+ T cells that support tumor invasion, tumor mutation load, and interferon signaling (30).

Although tumor cells have directly present tumor antigens to MHC-I playing a strong part in the effector function of $CD8^+$ T cells, it is necessary that primary $CD8^+$ T cells need to be cross-presented by specialized antigen-presenting cells (especially DCs) to maintain the cytotoxic immune response. TME plays a key role not only in initiating the primary immune response, but also in initiating the acquired immune response (31, 32). In fact, DCs in tumors mainly act on T cells and can be divided into two subgroups: conventional DC type 1 (cDC1) and conventional DC type 2 (cDC2) (33). On the one hand, cDC1 can attract T cells in the tumor, to stimulate and magnified the role of tumor specific CD8+ T cells, meanwhile, which can induce the death of tumor cells and the drainage of tumor antigens to lymph nodes (34, 35), where the formation is responsible for the staggered start anti-tumor key DC subtype of CD8+ T cells, so as to achieve the effect of the removal of the tumor (36). On the other hand, conventional type 1 DCs in TME can be induced to support T cell effector function by secreting interleukin-12 (37) and recruiting chemokines such as CCL5 and XCL1 (38, 39).

The response will be activated by cDC2 when $CD4^+$ T cells migrate to lymph nodes. Interestingly, regulatory T cells (Tregs) inhibit tumor-responsive activated $CD4^+$ T cells by inhibiting cDC2, and Tregs also inhibit mature DCs and prevent their migration to draining lymph nodes (40, 41). The DCs, the main companions of T cells, not only are crucial for initiating a primary immune response, but also play a vital role in initiating acquired immune response in TME (31, 32). Many researches provide new evidence for the wider role of DCs in tumors, including maintaining and supporting effect function in T-cell responses (30). DCs and T cells complement each other in the role of cancer immunotherapy and play an anti-tumor role

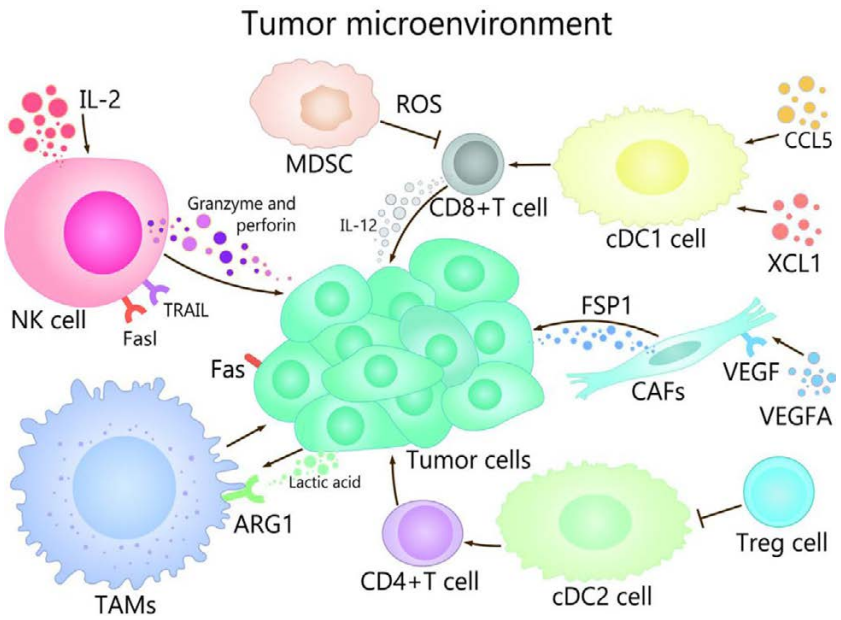

FIGURE 1 | The role of TME in cancer and its immunotherapy. The main cells of the TME in cancer immunity are NK cells, DC cells, CD8 + T cells, Treg cells, fibroblasts, TAMs, and MDSCs. Among them, NK cells induce the death of tumor cells by the ways of releasing perforin and granzyme, secreting tumor necrosis factor-a, and mediating cytotoxicity by TRAIL and FasI receptors. CDC1 cells are able to promote the differentiation and maturation of $CD8^+$ T cells, and cDC1 cells can recruit CCL5 and XCL1, which induce the accumulation of cDC1 cells in the TME, thereby improving the immune control of tumors. IL-2 contributes to enhancing the antitumor activity of NK cells. When CD4 + T cells migrate to lymph nodes, cDC2 can activate $CD4^+$ T cell responses. cDC2 resistant $CD4^+$ T cells can be inhibited by Treg cells. VEGFA activates fibroblasts, which secrete FSP1. TAMs can promote the growth and metastasis of tumor cells through multiple pathways, lactate produced by cancer and acidification of the microenvironment increase ARG1 expression in TAMs. MDSCs affect the ability to respond to non-specific stimulation by producing ROS, etc., which leads to the inability of $CD8^+$ T cells combined with pMHC.

together. But many unknown mechanisms remain to be further studied in order to better grasp prospects in cancer therapy.

NK Cell

Although current tumor immunotherapy mainly focuses on T cells, NK cells also are gradually being considered as the key target of tumor immunotherapy. NK cell-based therapy is becoming a safe and effective treatment for some cancers (42). The enhanced anti-tumor response mediated by $CD8^+$ T cells was associated with altered the acquired immune response, which related to the interaction between NK cells and immune cells (43, 44). In addition, NK cells recognize and mediate direct cytotoxic activity against tumor cells in early cancer (45). NK cells distinguish tumor cells and viral infections of cancer cells by encoding a series of receptor activation and inhibition of receptors (10). The activated receptor and inhibitory receptor signal are balanced to positively promote the activation of NK cells, which induce the target cell death through releasing granzyme and perforin by exocytosis, the cytotoxicity mediated receptor of by TNF-related apoptosis inducing ligand (TRAIL) and Fas ligand (FasL) (46).

PD-1 is mainly expressed on activated T cells, but also on NK cells, called "$PD\text{-}1^+$NK cells" accounting for 25% of NK cells, whose expression is increased in a variety of cancers indicating a poor prognosis (47, 48). Blocking the PD-1/PD-L1 interaction with anti–PD-L1 or PD-L1 antibody restores, could reverse the dysfunctional status of $PD\text{-}1^+$ NK cells and restore the anti-tumor response of NK cells (49, 50). At the same time, the increase in the frequency and activation of NK cells can enhance the response to anti-PD-1 therapy, and the rescue of NK cell activity can enhance the anti-tumor activity of adaptive T cells, thus increasing the overall survival rate of patients with multiple types of cancer (44). The anti-tumor activity of NK cells can be enhanced by cytokines, especially IL-2, but with toxic (51). IL-12 has a huge potential for increasing ADCC-mediated NK cell killing activity in solid tumors (52). It has been found that immunomodulatory drugs like lenalidomide can enhance the cytotoxicity mediated by NK cell and ADCC (16). However, in most studies, a small number and impaired function of NK cells isolated from primary tumors were observed, which was mainly due to the accumulation of suppressors in the TME, which inhibited the anti-tumor activity of NK cells and reduced the recruitment and persistence of NK cells in tumor nests (53). The complex interaction of cancer cells and the immune system has great limitations to the immunogenicity of cancer and promotes immunosuppression, which is the key factor affecting the drug resistance and validity of NK cell therapy. Therefore, a deeper understanding of the complex interactions between NK cells and TME in solid tumors will open up new prospects for cancer treatment (54).

Tumor-Associated Fibroblasts

Fibroblasts are repeatedly activated by a diverse set of factors secreted from cancer or immune cells, resulting in phenotypic transformation and becoming tumor-associated fibroblasts (CAFs), which are not only the source of immunosuppressive molecules, but also a physical barrier (55). CAFs are indispensable in the immunosuppression within TME and has the role of promoting cancer, thus it has become a target to enhance cancer immunotherapy (56). The occurrence and development of tumors could be inhibited by antifibrotic drugs (57).

CAFs inhibit the activity of CTLs and recruit lymphocytes that produce inflammatory signals to promote cancer progression (58). CAFs can direct or coordinate the infiltration of immune cells directly or through secreted cytokines and surface proteins, or indirectly and coordinate the infiltration of immune cells by depositing various ECM substrates and remodeling matrices, thereby promote cancer (59, 60). For example, the protein-1 (FSP1) secreted by fibroblasts, which cause metastasis of colon and breast cancer, and the factor A (VEGFA) induce the development of cancer cell (61). In addition, CAFs promotes resistance to anticancer drugs or therapies and provides protective or proliferative factors in cancer cells (62). Genetic variation has been found in cancer-associated fibroblasts, which is more genetically stable than tumor cells, making it an alternative target for immunotherapy (63). CAFs have several potential therapeutic targets, such as VEGF, which is the most important signal mediating vascular growth, and several VEGF inhibitors are currently being tested in phase I or II trials for colon and lung cancer (60). Pirfenidone, an orally active synthetic anti-fibrotic, which not only reduces the risk of lung cancer in patients with idiopathic pulmonary fibrosis, but also inhibits tumor growth and distant metastasis of refractory breast and pancreatic cancer (64–66). Anti-fibrosis therapy holds great promise.

Tumor-Associated Macrophages and Myeloid-Derived Suppressor Cells

Tumor-associated macrophages (TAMs), one of the most dominant immune cells in TME, can promote the growth and metastasis of tumor cells in many ways (67). In addition, TAMs in some settings stimulate anti-tumor immunity or kill tumor cells directly (68). Macrophages differentiate into typically activated macrophages (M1), induced by IFN-γ and/or lipopolysaccharide (LPS), which is important to host defense and anti-tumor immunity and activated macrophages (M2), induced by IL-4/IL-13, which play a critical role in fibrosis, promote wound healing, dampen inflammation and tumorigenesis (46, 69). TAMs play an M2 role to produce high levels of reactive oxygen free radicals, promote DNA damage and genomic instability, tumor infiltration and metastasis, participate in the digestion and reconstruction of extracellular matrix (ECM), inhibit anti-tumor immunity and so on (70). IFN-γ and celecoxib inhibits M2 differentiation, thus inhibiting tumor growth (71). Tumor cells release too much tumor-promoting and angiogenic cytokines/chemokines with TAMs and tumor-associated neutrophils (TANs), targeting these mediators and blocking immunosuppressive molecules expressed by tumor cells or tumor-infiltrating immune cells (9).

Myeloid-derived suppressor cells (MDSCs) are also one of the important components of TME (72). MDSCs are an effective inhibitor of innate and adaptive immunity, especially on T cells (73, 74). MDSCs can induce $CD8^+$ T cell tolerance, this $CD8^+$ T cell tolerance is one of the major mechanisms of tumor escape. The specific manifestation is that MDSCs induce the nitration of TCR/CD8 complex through the excessive production of reactive oxygen species (ROS) and peroxynitrite in the process of cell-cell direct contact, which leads to the inability of $CD8^+$ T cells to bind to peptide-MHC (pMHC) and affect the ability to respond to non-specific stimulation (75). In addition, MDSCs increase the metabolism of L-arginine (L-Arg) by producing arginase I, which inhibits T cell-lymphocyte reaction and block T-cell activation by consuming cysteine (76, 77).

The stimulating factor 1 receptor (CSF1R) is significantly expressed in MDSCs and TAMs, which cause functionally reprogram the response of macrophage and enhance antigen presentation and anti-tumor T cell response. Meanwhile, T cell checkpoint molecules, including PDL1 and CTLA4, are upregulated by CSF1R blockade, thus inhibiting beneficial therapeutic effects, but the combination of PD1 and CTLA4 antagonists could enhance the efficacy of checkpoint-based immunotherapics (78). Other tumor-infiltrating cells of myeloid lineage such as TANs, releasing excessive amounts of pro-tumor and pro-angiogenic cytokines/chemokines. Targeting these mediators, blocking immunosuppressive molecules expressed by tumor cells or tumor-infiltrating immune cells, and promoting anti-tumor immune responses, which can effectively treat a variety of tumors (9). Thus, TAMs and MDSCs affect the growth and metastasis of tumor cells and the efficacy of tumor immunotherapy through a variety of channels.

Cell Metabolism and Other Tumor-Infiltrating Cells

Cellular metabolism also has a critical important effect on the viability and function of both cancer cells and immune cells (79). Cancer cells up-regulate the absorption of nutrients and the production of waste metabolites, thus creating an immunosuppressive TME that allows it to escape and grow, and determines the fate of immune cells (80). Cell metabolism can be regulated using a combination of metabolic disruptors and immune checkpoint blockade (81). In addition to consuming key nutrients, tumors also produce large amounts of waste products such as lactic acid, arginine and tryptophan byproducts, and phosphoenolpyruvate, which can impair T-cell metabolism and function, then lead to a worse prognosis for patients (82). So cell metabolism becomes an attractive target for restoring anti-tumor immunity and developing anticancer therapies (81). Lactic acid is the primary cause of acidic PH and the inhibition of pH-dependent T cell function in the tumor micro-environment. Lactic acid generated by tumors and acidification of the microenvironment improves the expression of ARG1 in TAMs, which is characteristic of the M2-assisted phenotype (83). The inhibition of the production of lactic acid in cancer cells helps to

recover active oxygen homeostasis of physiological mitochondrial and restore normal function of cells (84). Therefore, the recovery of the anticancer immune response can be achieved by targeting inhibition of the lactic acid production pathway (85).

To sum up, it is strongly demonstrated that TME plays a critical role in tumor immunotherapy. But solutions to these two problems is that overcome the inherent immunosuppressive tumor environment and stimulate a strong adaptive response (8).

THE EFFECT OF GUT MICROBIOTA AND ITS METABOLITES ON THE HOST IMMUNE SYSTEM AFFECTS TME SHAPING

Gut microbiota plays fundamental roles in the development in the function, maintenance and development of the host immune system (86, 87). In the early stage of life, gut microbiota shapes the immune system, and the changes of gut microbiota will affect many aspects of the immune system in the later stage of life (88). Otherwise, the diversity of gut microbiota is crucial for the establishment of immune regulation networks (89). Generally, multiple gut microbiota establishes a symbiotic relationship with the host immune system and promotes the host homeostasis, the perturbation of this relationship will result in chronic inflammatory and autoimmune immunopathology, thereby may causing or aggravating the formation and development of cancer (90). TME is the environment in which tumors grow, it can regulate tumor growth, promote tumor invasion and metastasis, mediate tumor immune escape, and promote or weaken the carcinogenic process (86, 91). The crosstalk between gut microbiomes and microbiome metabolites in TME is continuous and beneficial, that affects the TME by affecting host immunity and intestinal epithelium, and promotes or inhibits the development of tumor (**Figure 2**) (53, 92). For example, the efficacy of conventional chemotherapy and immunotherapy for pancreatic cancer are affected by the involvement of gut microbiota in the metabolism of TME (93). Based on the close interaction between host microbiota and immune response in TME, it is suggested that manipulating gut microbiota is a feasible strategy for anticancer therapy (94).

Interaction Between Gut Microbiota and Microbiome Metabolites With Host Immunity Affects TME

Normal or pathological immune response will occur in the tumor treatment (95). Gut microbiota modulates the whole host immune, which impacts the distant preneoplastic lesions toward malignancy or regression. The interaction between gut microbiota and host immune enhances the possibility that the TME interacts with broader systemic microbial-immune networks, that reminds that the gut microbiota is emerging as an essential modulator of TME (96–100).

It is known that among immune cells, neutrophils and Treg as key cells in cancer development and growth (98, 101–103). Neutrophils can activate the interaction between cancer cells and endothelial cells in the primary TME, thus promoting tumor metastasis. In melanoma, neutrophils recruited by Toll-like receptor 4 (TLR4) signal can induce cancer cells to migrate to

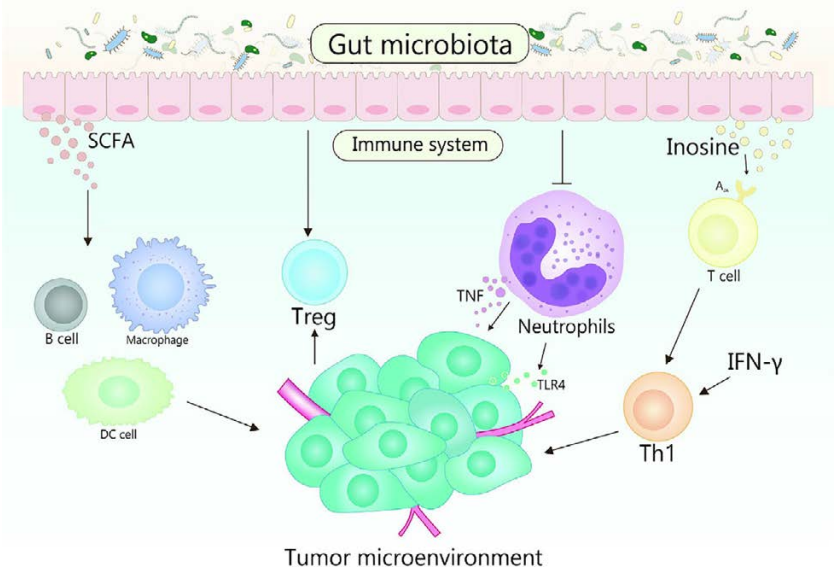

FIGURE 2 | Gut microbiota and its metabolites act on the host immune system to influence the shaping of the TME. TLR4 signaling in tumor cells is able to recruit neutrophils, while TNF released by neutrophils is able to induce metastasis of tumor cells. Gut microbiota is beneficial to reduce the number of neutrophils, which plays a promoting role in the treatment of tumors. Gut microbiota metabolite inosine significantly promotes the differentiation of Th1 cells in the presence of exogenous interferon-γ by acting on the A2A receptor on T cells, while SCFA can regulate the production of cytokines, affect the class conversion of B cells, activate DC cells and macrophages, and affect the differentiation of memory T cells, which also plays an important role in cancer therapy.

endothelial cells through tumor necrosis factor (TNF), resulting in enhancing cancer metastasis (104). Meanwhile, the adhesion of cancer cells is mediated by neutrophil Mac-1/ICAM-1, thus affecting its metastasis (1). Moreover, cytokines, chemokines, growth factors, and serine proteases of neutrophils shape microenvironment that contribute to the tumor growth (102). Cytokines released by tumor and TME send out an emergency signal to stimulate a large number of neutrophils to enter the blood circulation and accelerate the metastasis of cancer cells (105). However, the number of neutrophils in circulation is reduced by abundant gut microbiota. One research found the mice applying with *L.reuteri* showed a better capacity of wound healing, which is achieved by reducing the number of neutrophils in circulation through the increase of Foxp3 and Tregs (106). Another research pointed out the same result that the cachexia mice treated with *L.reuteri* showed decreased systemic inflammation and better tumor inhibition, which also associated with the reduction of neutrophils in the blood (107). And, the neutrophil homeostasis will be affected by microbiota through enterocyte CXCL5-mediated signaling and IL-17 (108).

Treg is essential for maintaining the homeostasis of the immune system and the balance of beneficial inflammatory response during infection (109). Treg regulates the host immune response which gathers near TME, suppresses the anti-tumor inflammatory response and counteracts antigen-specific effector T-cell responses, consequently (109–111). The differentiation and proliferation of Treg, and the secretion and recruitment of immunosuppressive factors will be activated by TME, then contribute to the immunosuppression of tumor tissue (112). Based on the data of animal models, it has been found that the Treg induced by some specific gut microbiota could change the TME, which is beneficial to relieve the induction of cancer. For example, $CD4^+$ $CD25^+$ Treg cells inhibit the occurrence of colon cancer by inhibiting the development of *H. hepaticus*-induced inflammation and dysplasia (113), the effectiveness of Treg cells will be enhanced by the infection from gut pathogens, thereby inhibiting the occurrence of breast cancer (114). Gut microbiota response mediated by $IL22^+$ innate lymphoid cells, Th17 cells and Treg cells occurred in mice lacking adaptive immunity, indicating that gut microbiota can promote the innate immunity (115). The mechanism of tumor reduction driven by microbiota may induce the anticancer immune response (102, 116).

Otherwise, the intestinal epithelial barrier, a physical barrier, that are extremely essential in maintaining the balance of the intestinal environment (117). On the one hand, the common gut microbiota can enhance immunoglobulin A production in the intestinal tract by regulating the response of B cells to maintain an intact epithelial barrier (118, 119), which also is a key figure in the development of the immune system (92, 120). Once this barrier is broken, the main inflammation-activating transcription factor NF-κB will be activated (121). The activation of NF-κB in ovarian cancer cells responds to inflammatory chemokines and cytokines in the TME, which helps to create an immune escape environment and attract infiltrating immune cells with tumor-promoting phenotypes (122). The origin of tumor-promoting inflammation is quite clear in gastrointestinal cancer, most of which can be attributed to the destruction of epithelial barrier integrity (123). On the other hand, intestinal epithelial cells can activate the NOTCH1 signal and lead to a high penetrating transfer of colorectal cancer (124).

Thus, the interaction between neutrophils and TME accelerates the progression of tumors, and the dynamic balance of neutrophils is affected by gut microbiota. Treg gathers near TME with an immunosuppressive effect, which is induced by specific gut microbiota to changes TME, thereby alleviate cancer. Maintaining the integrity of the intestinal epithelium can be maintained by gut microbiota, which is conducive to reduce e the incidence of cancer.

Interaction Between Gut Microbiota Metabolites and Host Immunity Affects TME

Gut microbiota metabolites enter host cells and mutually interact thereby affecting the immune response and disease risk, promote a variety of tumor inhibitory and immunomodulatory effects, and inhibit inflammation by maintaining the integrity of epithelial barrier and intestinal tract (9, 125). Accumulating evidence suggests that gut microbiota metabolites and products of their metabolic activities influence important metabolic pathways of the host related to food intake, adiposity, lipid and energy homeostasis (114, 126–131).

Some fatty acids and cholic acids are related to inflammation. SCFAs contribute to maintaining intestinal homeostasis and regulating intestines' barrier function (132, 133). It acts on G protein-coupled receptors (GPCRs) to inhibit the metastasis of breast cancer (134). Butyrate, an SCFAs, produced by *Faecalibacterium prausnitzii*, which has the ability to suppress angiogenesis and reduce the expression of pro-angiogenic factors, so increasing the concentration of butyrate can play a role in protecting and preventing cancer (135–137). In addition, Deoxycholic acid (DCA) and petrocholic acid (LCA) potentially cause DNA damage by enhancing the production of ROS (138). DNA damage causes cell senescence, chronic inflammation, and tumorigenesis (139). Recent studies have suggested that the metabolite inosine was produced by intestinal bacteria *B. pseudolongum*, which significantly promoted Th1 cell differentiation in the presence of exogenous IFN-γ and enhanced the therapeutic response of ICB therapy including anti–CTLA-4 and anti–PD-L1, by acting on adenosine A_{2A} receptor on T cells (12). Understanding how the metabolites and sub-metabolites of gut microbiota affect immune cell subsets and their actions to reshape TME may be the direction of future research.

Specific gut microbiota interacts with immune cells to promote tumor clearance, slow metastasis of cancer cells and inhibit chronic inflammation, thus mitigating against cancer. The gut microbiota metabolites, such as SCFAs and inosine, directly or indirectly interact with TME to reshape TME, and

affect the cancer process. However, a study has found that some gut microbiota (such as *Bacteroides* and *Ruminococcaceae*) can participate in the occurrence of HCC by aggravating hepatocyte inflammation, accumulating toxic compounds and leading to liver steatosis (23). Therefore, a comprehensive understanding of the interaction mechanism between gut microbiota and its metabolites with the host immune system in reshaping and regulating TME through gut microbiota is profound for cancer immunotherapy.

THE EFFECT OF GUT MICROBIOTA IN CANCER IMMUNOTHERAPY

Immunotherapy realizes the result of eliminating tumors by suppressing negative immune regulatory factors, activating the immune system and enhancing the recognition, thereby killing of immune cells to tumors (140). With further research, it has been verified that the gut microbiota could regulate the immune response, thus affect the effectiveness of cancer immunotherapy (120, 141). Various mechanisms mediated by gut microbiota affect the therapeutic response and toxicity of immune checkpoint inhibitors (ICIs), chemotherapy, and stem cell transplant (**Figure 3**) (142). In fact, some studies indicate that there is a strong correlation between gut microbiota and immune checkpoint response (143–145). Gut microorganisms play a crucial role in cancer treatment by eliminating anticancer effects and mediating toxicity.

Anti-CD47 Therapy

Tumor immunotherapy identified and kills tumor cells through the host immune system, and more and more attention has been paid to the research in this field (146–148). CD47, as a signal molecule to help tumor cells escape, conveys the "don't eat me" signal to immune cells and produces a good effect of tumor immunotherapy by blocking the CD47 (149, 150). CD47 is a kind of transmembrane protein that has interactions with signal regulatory protein (SIRP) expressed on macrophages and DCs (151). It is a hint of a poor prognosis when CD47 can highly express in malignant tumors, for example, leukemia, myeloma, ovarian tumor, and so on (152, 153).

Anti-CD47 antibody therapy makes not only cancer cells swallowed by macrophages but also anti-tumor cytotoxic T cell immune response initiated (154). Researches have shown that $CD8^+$ T cells are essential for anti-CD47-mediated tumor regression, and tumor-resident DCs can enhance anti-CD47 by cross-stimulation of antigen-specific T cells (150). In addition, DC-specific type I IFN plays a critical role in enhancing the adaptive immune response to anti-CD47 antibody therapy (149, 150). A research pointed out that the main anti-tumor effect of anti-CD47 monoclonal antibodies is attributed to the activation of host cGAS-STING pathway mediated by mitochondrial DNA in DC (150).

Anaerobes play a dominant role in the gastrointestinal tract, among common anaerobes, *Bifidobacterium* is a functional gut microbiota, which is widely used in the treatment of inflammatory gastrointestinal diseases such as ulcerative colitis (155, 156). TME in a low oxygen state creates a good growth

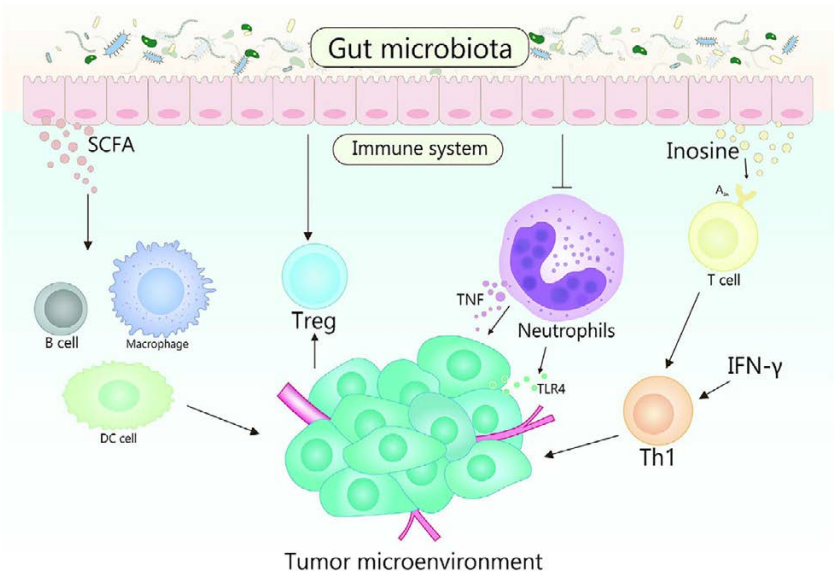

FIGURE 3 | Role of gut microbiota in cancer immunotherapy. Gut microbes can stimulate the body to produce CD47 antibodies by activating STING signaling, thereby promoting immunotherapy. It is reported that the cross-priming of antigen-specific T cells of tumor-resident DCs can be enhanced by anti-CD47 therapy. In addition, type I IFN plays an important role in enhancing the adaptive immune response to anti-CD47 antibody therapy in tumor-resident DCs. Accumulation of *Bifidobacteria* in the TME can significantly improve the antitumor efficacy of anti-CD47 immunotherapy, which is dependent on STING signaling and type I IFN within DCs. *Bifidobacteria* may affect activating DC cells, thereby improving the activity of tumor-specific $CD8^+$ T cells. The key role of B. fragilis is to restore the anti–CTLA-4 treatment response associated with Th1 immune responses in tumor-draining lymph nodes.

environment for anaerobic bacteria (157). A study indicated that the accumulation of *Bifidobacterium* in TME can significantly improve the anti-tumor effect of anti-CD47 immunotherapy, which depends on the STING signal and the type I IFN within DC (158). CD47 is widely expressed in a variety of solid human tumors. At present, the related mechanism of CD47 has been extensive and in-depth research. However, there are few studies on the influence of gut microbiota on anti-CD47 immunotherapy, which has a great prospect.

Interaction Between Gut Microbiota and ICIs

Immune checkpoints are a type of membrane-bound molecules, which can impede uncontrolled T-cell response after initial stimulation. This mechanism can be used for cancer cells to escape immune surveillance. ICIs, however, can reactivate the inefficient T cells and recover the response to tumor antigens (159). Based on the current research background, CTLA-4, PD-1, and PD-L1 are the most in-depth target of immune checkpoint therapy. CTLA-4, PD-1, or PD-L1 have shown strong antitumor activity in the experimental animal models and the long-lasting clinical efficacy in cancer patients, such as melanoma, renal cell cancer, and lung cancer (159). Clinical studies and preclinical trials have shown that the efficacy of ICIs is affected by gut microbiota, which explains the large individual differences in patients' responses to ICIs (160, 161). At present, a variety of inhibitions about them have been invented and used or used or tested in the clinic (**Table 1**). Obviously, the response of ICIs is closely decided by the diversity and composition of gut microbiota (160, 162).

PD-1 and PD-L1 are members of the immune checkpoint proteins relating to the suppression of the immune system and delivering inhibitory signals to T cells (163). Cancer immunotherapy targeting PD-L1 and PD-1 has been widely carried out, and gut microbiota has been proposed to affect its efficacy and toxicity. Maston et al. analysis of 38 fecal samples from patients with metastatic melanoma who received anti-PD1 therapy, it is found that *Bifidobacterium longum*, *Enterococcus faecalis*, and *Collinsella aerofaciens* contribute to a better prognosis (145). Researchers transferred the fecal material from Jackson Laboratory (JAX) or Taconic Farms (TAC) from one mouse to another by oral gavage before tumor implantation and pointed out that the DCs may be activated by the increasing abundance of *Bifidobacterium longum*, thus improve tumor-specific $CD8^+$ T cells activity (160). With researches obtain more attention to identifying the specific bacteria genres that play a critical role in human immunity by clinical experiments. Gopalakrishnan et al. found the melanoma patient respond to anti-PD1 treatment has higher microbial diversity, including the abundance of *Ruminococcaceae*, *Clostridiales*, and *Faecalibacterium*, patients with more *Faecalibacterium* has a significantly prolonged progression-free survival with a higher level of effector T cells and a stabilized cytokine response to PD-1 blockade, simultaneously, systemic and anti-tumor immunity are also enhanced (144). Another research also achieved the same opinions, they found the *Alistipes putredinis*, *Bifidobacterium longum*, and *Prevotella copri* were enriched in responsive patients with advanced non-small-cell lung carcinoma who were being treated with PD-1 blockade therapies, expectedly, a greater frequency of memory $CD8^+$ T cell and NK cell subgroups was observed in the periphery blood of responding patients (164). The abundance of the gut microbial flora acting as immune adjuvants in the immunotherapy of PD-1 and the T cell response may deeply connect with the PD-1/PD-L1 immunotherapy, and relevant researches have shown that the patients with endogenous T cell response in TME are more effective in immunotherapy (165, 166). The hot tumor with a large number of T cell infiltration, which has the highest response rate to tumor immunotherapy (167). Targeted inhibition of Vps34, can transform "cold tumor" into "hot tumor", thus enhancing the efficacy of PD-L1/PD-1 blocking therapy (168).

TABLE 1 | Modulatory function of gut microbiome in ICIs therapy.

Bacteria	Model	Modulatory function of gut microbiome in ICIs therapy	References
Bifidobacterium adolescentis	Mouse	(1) Stimulating DCs directly, inducing DCs maturation and cytokine secretion (2) Anti-tumor function and synergistic effect with PD-1 blockade	(160)
Bacteroides fragilis	Mouse	(1) Immunostimulation induced by CTLA-4 blockade (2) Promoting the maturation of DCs in tumor cells and inducing Th1 cell activation	(161)
Bacteroides thetaiotaomicron	Mouse	(1) Anti-tumor effect of CTLA-4 blockade (2) Promoting Th1 immune response	(161)
Blautia obeum	Human	Related to impaired efficacy of PD-1 blockers	(103)
Collinsella aerofaciens	Human	(1) Results in decreased peripheral blood Treg (2) Associated with enhanced efficacy of PD-1 blockade	(103)
Enterococcus faecium	Human	(1) Results in decreased peripheral blood Treg (2) Associated with enhanced efficacy of PD-1 blockade	(103)
Klebsiella pneumonia	Human	(1) Associated with enhanced efficacy of PD-1 blockade	(103)
Parabacteroides merdae	Human	(1) Results in decreased peripheral blood Treg (2) Associated with enhanced efficacy of PD-1 blockade	(103)
Roseburia intestinalis	Human	Related to impaired efficacy of PD-1 blockers	(103)
Veillonella parvula	Human	Associated with enhanced efficacy of PD-1 blockade	(103)
Ruminococcaceae	Human/mouse	(1) Associated with enhanced efficacy of PD-1 blockade (2) Increasing effector T cell levels in peripheral blood and TILs	(11)
Enterococcus hirae	Human/mouse	(1) Synergistic effect with PD-1 blockers in combination with Ackerman mucilaginosa (2) Improving traditional Chinese medicine combined with Ackerella Sinensis	(12)
Alistipes indistinctus	Human/mouse	Restoring the anti-tumor efficacy of PD-1 blockers	(12)

CTLA-4, also known as CD152, is constitutively expressed in Tregs and acts as an immune checkpoint that decreases immune responses (169). Vetizou et al. found that a key role of *Bacteroides thetaiotaomicron* or *Bacteroides fragilis* restores response to the anti–CTLA-4 therapy associated with T-helper 1 immune responses in tumor-draining lymph nodes and maturation of intratumoral DCs, activation of effector CD4+ T cells and TILs elicited by CTLA-4 blockade was considerably dampened in germ-free or antibiotics mice, otherwise, the intestinal reconstitution of antibiotic-treated mice with *Bacteroides* and *Burkholderia* genres could restore the CTLA-4 blockade-mediated anticancer responses (161). The abundance of *Bacteroides* in patients with new immune-mediated colitis treated with anti–CTLA-4 was significantly lower than that in patients without colitis treated with ipilimumab. Meanwhile, the response of mice to anti-CTLA4 antibody could be restored and the degree of immune-mediated colitis could be significantly reduced by taken orally administration of *Bacillus fragilis* and *Bacillus cepacia* (170). However, a single dose of *Bacillus fragilis* or *B.thaiotaomicron* could not receive the same effect (161, 171). Vancomycin enhances the blocking effect of CTLA-4 by increasing the proportion of Gram-negative *Burkholderia* and *Bacteroides* in the intestines (161). It may prove that *Bacillus* can be used to regulate the efficacy of anti–CTLA-4 therapy.

Another research suggested that the special gut microbiota contributes to both CTLA4 and anti–PD-L1 immunotherapy. Three bacteria from the intestinal tract, *Bifidobacterium pseudolongum*, *Lactobacillus johnsonii*, and *Olsenella* from the intestinal tract significantly enhanced the efficacy of anti-CTLA4 and anti–PD-L1 immunotherapy in four different cancer mice when they were introduced into aseptic mice with ICIs, and the *Bifidobacterium pseudolongum* in the intestine contributes to regulating and enhancing the immunotherapeutic response by producing inosine (12). Based on these reports suggest that the commensal microbiome may have a mechanistic impact on antitumor immunity in cancer patients, and a growing number of studies have also emphasized that the gut microbiota could modulate response to cancer immunotherapy. Consequently, the further research about the effect and the potential mechanism of gut microbiota in ICIs is profound for cancer treatment. Innovative treatments were used to study and not widely applicate in patients, so it is necessary that further works must unlock the mystery of microbial modulation in various anticancer immunotherapies.

Gut Microbiota Affect the Efficacy of Cancer Immunotherapy

Abundant gut microbiota plays a regulatory role in tumor therapy, which has a critical role in regulating the efficacy and toxicity of cancer immunotherapy (172). The effect of gut microbiota on the efficacy and interaction of ICIS has been verified in melanoma, non-small cell lung cancer, urethral epithelial carcinoma, and renal cell carcinoma (144, 145, 173). Lukas F Mager et al. found that *Bifidobacterium pseudolongum*, *Lactobacillus johnsonii*, and *Olsenella* enhanced efficacy quadrupled of ICIs in four mouse models of cancer (12). It is suggested that selective regulation of gut microbial population may help to overcome the resistance to ICIs (159, 167).

Among radiotherapy, ionizing radiation therapy (RTX) is an effective method for tumors treatment, but severe oral mucositis and bowel disease caused by RTX may limit the completion of treatment, fortunately, the probiotics such as Lactobacillus casei, Rhamnose and Bifidobacterium have been shown to reduce radiotherapy-associated diarrhoea in mouse models by inhibiting the expression of TNF, IL1b, and IL6mRNA (174–176). It is reported that complete response of tumor cells with local temperature causing by infrared radiation of a specific wavelength, and the formation of the tumor specific thrombus can achieve effective photothermal immunotherapy of cancer through the action of attenuated Salmonella in an innovative photothermal therapy (177). On the other hand, gut microbiota may reduce the side effects of a variety of chemotherapy. In chemotherapy, cyclophosphamide (CTX), one of the most commonly used chemotherapeutic drugs in treating lymphomas and solid tumors, inducing immunogenic cancer cell death and immunomodulatory effects (178). Orally administrated with Enterococcus hirae cause a restoration of CTX anti-tumor efficacy by inducing differentiation of TH17 and pathogenic TH17 cells, promoting tumor-specific Th1 and CTL activity (179). Abiraterone acetate is both an inhibitor of androgen biosynthesis and a highly effective drug of prostate cancer, which reduces the harmful microorganisms and promotes the growth of anticancer microorganisms through metabolizing the gut microbiota (180). Otherwise, Pushalkar et al. suggested that bacterial ablation can reshape TME in the orthotopic mouse model of pancreatic cancer (PDAC), induce activation of T cell and increase the sensitivity of immunotherapy (181).

Excepting the related advantages, the correlation between the composition of intestinal microbial community and the degree of TNF shows that some *Lactobacillus strains*, such as fermented *Lactobacillus*, are considered as weakening the response to immunotherapy (182). The composition of gut microbiota is related to the different development of graft-versus-host disease (GVHD). It has high morbidity and mortality, when the cross reaction occurs between the donor cells (usually T cells) the graft and the patient's major histocompatibility. On the contrary, it was found that increased bacterial diversity and increased amounts of *Blautia* to be related to reduce GVHD mortality and improve survival (183).

At present, research has moved away from the approach based on association toward mechanism as the advances in sequencing technology and the development of powerful computing tools. Elucidating the relationship between the gut microbiome and cancer as well as the potential mechanism has become the priorities of further research, which also the main method for cancer immunotherapy.

CONCLUSION AND FUTURE PERSPECTIVE

The gut microbiota activates the host immune system further and has an anti-cancer effect, and more superiority than the traditional way of treating cancer. In addition, the interaction between gut microbiota and cancer ICIs play an antitumor immune therapy, this way of targeted therapy in cancer immunotherapy is getting more and more recognition. Targeting and manipulating cells and factors in TME during cancer therapy, which contribute to control malignancies and obtain positive health outcomes (132). An in-depth understanding of TME, its role and related molecules will provide important insights into the biological behavior of different tumor types. Molecules and tumorigenic processes in TME are considered as the key targets of the new therapy strategy of cancer (86, 184). The refining of molecular cells and immune regulation of therapeutic targets is increasing in the TME, and the clinical application also is growing more and more widely, for example, that resistance to PD-1/PD-L1 plays multiple roles in tumor immunotherapy, however, the test of limited activity PD-1 of resisting tumor types may have a good therapeutic effect in the strategy of reshaping the tumor inert environment in the future. Namely the possibility of immunotoxicity and immunotherapy to enhance antitumor immunity, in other words, use reasonable and selective combined immunotherapy in a limited TME to reactivate the anti-tumor immune response (185).

In the previous introduction, we have known that gut microbiota is essential in maintaining the host balance, promoting physiological responses including the protection of pathogen, host metabolism, host immunity response, and so on. More and more scientific evidence showed that broken the delicate balance of gut microbiota can lead to the occurrence of cancer and other diseases, which indicates that modulating strategy is very important. In fact, gut microbiota has great inter-individual heterogeneity due to the impact of host, including the age, living environment, genetic factor, and diet habit. Among them, diet habit and host age are the main determinants of gut microbiota according to the biological relationship between gut microbiota and host in nutrient digestion (186). It is reported that the diversity of gut microbiota and its metabolites were changed by diet habit (187). The overall richness of gut microbiota decreases with age, and some microbial taxa related to unhealthy aging appear, which leads to the malnutrition of gut microbiota, then finally affect the host's innate immune response (188). Fecal microbiota transplant (FMT), live biotherapeutics, diet habits, and prebiotics are the main strategies to regulate gut microbiota, making it more healthy (189). For example, patients with colon cancer have obvious characteristics and diversity of gut microbiota in tumor tissue and nearby mucosa. After taking probiotics, the abundance of *butyrate-producing bacteria* in tumors, non-tumor mucosa, and fecal flora increased in these patients, that helps maintain the intact intestinal barrier to avoid the activation of inflammation-related factors in TME (190, 191). The report pointed out that non-responders lack beneficial bacteria which are critical to the anti-tumor effect of immunotherapy, however, the effect of them on ICIS can be restored by transplanting these bacteria from responders to non-responders by some means, such as FMT, probiotic therapy, and so on (192).

In addition, determining the composition of individual gut microbiota is also a way to solve the huge heterogeneity among individuals in the gut microbiota. Searching for microbial signals to determine the degree of response to cancer treatment may help determine gut microbiota composition associated with specific treatment categories or overlapping signals, which is suitable for a wide range of immune therapy. But the microbe signal is a continuous work, the differences of sequencing technology and patient cohort were all factors that affect microbial expression (193). The composition of gut microbiota havs undergone a similar change during cancer progression and treatment, and this change causes more additional challenges. Cancer cells grow and evolve under the therapy of selective pressure. Molecular evolution of tumors may still occur when gut microbiota is manipulated to maximize immunotherapeutic efficacy. Therefore, future research may be able to use DNA sequencing, metabolomics technologies and high-dimensional data, as well as to give them intervention, the interdependence of individual host-intestinal microflora can provide more effective treatment and greatly promote the development of microbial alliance to treat specific disease (194). More challenges need to be overcome by combination with basic experimental and clinical research. Therefore, we look forward to getting more precise therapies targeted cancer coming from gut microbiota and the TME in the future. It is also suggested that further studies should focus on the precise targets and mechanisms of action in this field.

AUTHOR CONTRIBUTIONS

LL and RH conceived and designed the review. QQ, YM, YL, ZC, JL, XL, and LL wrote the manuscript. LL, YH, and HL reviewed the paper and provided comments. All authors contributed to the article and approved the submitted version.

FUNDING

This project was supported by the Ph.D. Start-up Fund of Guangdong Medical University (B2019016); Administration of Traditional Chinese Medicine of Guangdong Province (20201180); Science and Technology Special Project of Zhanjiang (2019A01009); Natural Science Foundation of Guangdong Province (2016B030309002); Basic and Applied Basic Research Program of Guangdong Province (2019A1515110201); GDNRC[2020]038; Educational Commission of Guangdong Province (4SG20138G); and Fund of Southern Marine Science and Engineering Guangdong Laboratory (Zhanjiang) (ZJW-2019-007).

REFERENCES

1. Arneth B. Tumor Microenvironment. *Medicina (Kaunas Lithuania)* (2019) 56(1):15. doi: 10.3390/medicina56010015
2. Casey SC, Amedei A, Aquilano K, Azmi AS, Benencia F, Bhakta D, et al. Cancer prevention and therapy through the modulation of the tumor microenvironment. *Semin Cancer Biol* (2015) 35Suppl(Suppl):S199–s223. doi: 10.1016/j.semcancer.2015.02.007
3. Janji B, Berchem G, Chouaib S. Targeting Autophagy in the Tumor Microenvironment: New Challenges and Opportunities for Regulating Tumor Immunity. *Front Immunol* (2018) 9:887. doi: 10.3389/fimmu.2018.00887
4. Binnewies M, Roberts EW, Kersten K, Chan V, Fearon DF, Merad M, et al. Understanding the tumor immune microenvironment (TIME) for effective therapy. *Nat Med* (2018) 24(5):541–50. doi: 10.1038/s41591-018-0014-x
5. Jiao S, Subudhi SK, Aparicio A, Ge Z, Guan B, Miura Y, et al. Differences in tumor microenvironment dictate T helper lineage polarization and response to immune checkpoint therapy. *Cell* (2019) 179(5):1177–90.e13. doi: 10.1016/j.cell.2019.10.029
6. Vinay DS, Ryan EP, Pawelec G, Talib WH, Stagg J, Elkord E, et al. Immune evasion in cancer: Mechanistic basis and therapeutic strategies. *Semin Cancer Biol* (2015) 35(Suppl):S185–s98. doi: 10.1016/j.semcancer.2015.03.004
7. Poutahidis T, Erdman SE. Commensal bacteria modulate the tumor microenvironment. *Cancer Lett* (2016) 380(1):356–8. doi: 10.1016/j.canlet.2015.12.028
8. Zhang Y, Yu G, Chu H, Wang X, Xiong L, Cai G, et al. Macrophage-associated PGK1 phosphorylation promotes aerobic glycolysis and tumorigenesis. *Mol Cell* (2018) 71(2):201–15.e7. doi: 10.1016/j.molcel.2018.06.023
9. Zhou Y, Fei M, Zhang G, Liang WC, Lin W, Wu Y, et al. Blockade of the Phagocytic Receptor MerTK on Tumor-Associated Macrophages Enhances P2X7R-Dependent STING Activation by Tumor-Derived cGAMP. *Immunity* (2020) 52(2):357–73.e9. doi: 10.1016/j.immuni.2020.01.014
10. Böttcher JP, Bonavita E, Chakravarty P, Blees H, Cabeza-Cabrerizo M, Sammicheli S, et al. NK cells stimulate recruitment of cDC1 into the tumor microenvironment promoting cancer immune control. *Cell* (2018) 172(5):1022–37. e14. doi: 10.1016/j.cell.2018.01.004
11. Erdman SE, Poutahidis T. The microbiome modulates the tumor macroenvironment. *Oncoimmunology* (2014) 3:e28271. doi: 10.4161/onci.28271
12. Mager LF, Burkhard R, Pett N, Cooke NC, Brown K, Ramay H, et al. Microbiome-derived inosine modulates response to checkpoint inhibitor immunotherapy. *Science* (2020) 369(6510):1481–9. doi: 10.1126/science.abc3421
13. Yang W, Yu T, Huang X, Bilotta AJ, Xu L, Lu Y, et al. Intestinal microbiota-derived short-chain fatty acids regulation of immune cell IL-22 production and gut immunity. *Nat Commun* (2020) 11(1):4457. doi: 10.1038/s41467-020-18262-6
14. Ohtani N. Microbiome and cancer. *Semin Immunopathol* (2015) 37(1):65–72. doi: 10.1007/s00281-014-0457-1
15. Dibra D, Xia X, Mitra A, Cutrera JJ, Lozano G, Li S. Mutant p53 in concert with an interleukin-27 receptor alpha deficiency causes spontaneous liver inflammation, fibrosis, and steatosis in mice. *Hepatology (Baltimore Md)* (2016) 63(3):1000–12. doi: 10.1002/hep.28379
16. Ben-Shmuel A, Biber G, Barda-Saad M. Unleashing Natural Killer Cells in the Tumor Microenvironment-The Next Generation of Immunotherapy? *Front Immunol* (2020) 11:275. doi: 10.3389/fimmu.2020.00275
17. Wu J, Chen J, Feng Y, Tian H, Chen X. Tumor microenvironment as the "regulator" and "target" for gene therapy. *J Gene Med* (2019) 21(7):e3088. doi: 10.1002/jgm.3088
18. Vito A, El-Sayes N, Mossman K. Hypoxia-Driven Immune Escape in the Tumor Microenvironment. *Cells* (2020) 9(4):992. doi: 10.3390/cells9040992
19. Wang T, Green R, Howell M, Martinez T, Dutta R, Mohapatra S, et al. The design and characterization of a gravitational microfluidic platform for drug sensitivity assay in colorectal perfused tumoroid cultures. *Nanomedicine* (2020) 30:102294. doi: 10.1016/j.nano.2020.102294
20. Quail DF, Joyce JA. Microenvironmental regulation of tumor progression and metastasis. *Nat Med* (2013) 19(11):1423–37. doi: 10.1038/nm.3394
21. Wan S, Kuo N, Kryczek I, Zou W, Welling TH. Myeloid cells in hepatocellular carcinoma. *Hepatology* (2015) 62(4):1304–12. doi: 10.1002/hep.27867
22. Yang L, Zhang Y. Tumor-associated macrophages: from basic research to clinical application. *J Hematol Oncol* (2017) 10(1):58. doi: 10.1186/s13045-017-0430-2
23. Ponziani FR, Nicoletti A, Gasbarrini A, Pompili M. Diagnostic and therapeutic potential of the gut microbiota in patients with early hepatocellular carcinoma. *Ther Adv Med Oncol* (2019) 11:1758835919848184. doi: 10.1177/1758835919848184
24. Li Z, Li N, Li F, Zhou Z, Sang J, Chen Y, et al. Immune checkpoint proteins PD-1 and TIM-3 are both highly expressed in liver tissues and correlate with their gene polymorphisms in patients with HBV-related hepatocellular carcinoma. *Medicine (Baltimore)* (2016) 95(52):e5749. doi: 10.1097/md.0000000000005749
25. Cho H, Kang H, Lee HH, Kim CW. Programmed Cell Death 1 (PD-1) and Cytotoxic T Lymphocyte-Associated Antigen 4 (CTLA-4) in Viral Hepatitis. *Int J Mol Sci* (2017) 18(7):1517. doi: 10.3390/ijms18071517
26. Wang T, Shen Y, Luyten S, Yang Y, Jiang X. Tissue-resident memory CD8 (+) T cells in cancer immunology and immunotherapy. *Pharmacol Res* (2020) 159:104876. doi: 10.1016/j.phrs.2020.104876
27. Corgnac S, Boutet M, Kfoury M, Naltet C, Mami-Chouaib F. The Emerging Role of CD8(+) Tissue Resident Memory T (T(RM)) Cells in Antitumor Immunity: A Unique Functional Contribution of the CD103 Integrin. *Front Immunol* (2018) 9:1904. doi: 10.3389/fimmu.2018.01904
28. Mami-Chouaib F, Blanc C, Corgnac S, Hans S, Malenica I, Granier C, et al. Resident memory T cells, critical components in tumor immunology. *J Immunother Cancer* (2018) 6(1):87. doi: 10.1186/s40425-018-0399-6
29. Blanc C, Hans S, Tran T, Granier C, Saldman A, Anson M, et al. Targeting Resident Memory T Cells for Cancer Immunotherapy. *Front Immunol* (2018) 9:1722. doi: 10.3389/fimmu.2018.01722
30. Fu C, Jiang A. Dendritic Cells and CD8 T Cell Immunity in Tumor Microenvironment. *Front Immunol* (2018) 9:3059. doi: 10.3389/fimmu.2018.03059
31. Banchereau J, Steinman RM. Dendritic cells and the control of immunity. *Nature* (1998) 392(6673):245–52. doi: 10.1038/32588
32. Ma Y, Shurin GV, Peiyuan Z, Shurin MR. Dendritic cells in the cancer microenvironment. *J Cancer* (2013) 4(1):36–44. doi: 10.7150/jca.5046
33. Guilliams M, Ginhoux F, Jakubzick C, Naik SH, Onai N, Schraml BU, et al. Dendritic cells, monocytes and macrophages: a unified nomenclature based on ontogeny. *Nat Rev Immunol* (2014) 14(8):571–8. doi: 10.1038/nri3712
34. Spranger S, Dai D, Horton B, Gajewski TF. Tumor-Residing Batf3 Dendritic Cells Are Required for Effector T Cell Trafficking and Adoptive T Cell Therapy. *Cancer Cell* (2017) 31(5):711–23.e4. doi: 10.1016/j.ccell.2017.04.003
35. Broz ML, Binnewies M, Boldajipour B, Nelson AE, Pollack JL, Erle DJ, et al. Dissecting the tumor myeloid compartment reveals rare activating antigen-presenting cells critical for T cell immunity. *Cancer Cell* (2014) 26(5):638–52. doi: 10.1016/j.ccell.2014.09.007
36. Salmon H, Idoyaga J, Rahman A, Leboeuf M, Remark R, Jordan S, et al. Expansion and Activation of CD103(+) Dendritic Cell Progenitors at the Tumor Site Enhances Tumor Responses to Therapeutic PD-L1 and BRAF Inhibition. *Immunity* (2016) 44(4):924–38. doi: 10.1016/j.immuni.2016.03.012
37. Ruffell B, Chang-Strachan D, Chan V, Rosenbusch A, Ho CM, Pryer N, et al. Macrophage IL-10 blocks CD8+ T cell-dependent responses to chemotherapy by suppressing IL-12 expression in intratumoral dendritic cells. *Cancer Cell* (2014) 26(5):623–37. doi: 10.1016/j.ccell.2014.09.006
38. Dorner BG, Dorner MB, Zhou X, Opitz C, Mora A, Güttler S, et al. Selective expression of the chemokine receptor XCR1 on cross-presenting dendritic cells determines cooperation with CD8+ T cells. *Immunity* (2009) 31(5):823–33. doi: 10.1016/j.immuni.2009.08.027
39. McColl SR. Chemokines and dendritic cells: a crucial alliance. *Immunol Cell Biol* (2002) 80(5):489–96. doi: 10.1046/j.1440-1711.2002.01113.x
40. Kennedy R, Celis E. Multiple roles for CD4+ T cells in anti-tumor immune responses. *Immunol Rev* (2008) 222:129–44. doi: 10.1111/j.1600-065X.2008.00616.x

41. Kitano M, Yamazaki C, Takumi A, Ikeno T, Hemmi H, Takahashi N, et al. Imaging of the cross-presenting dendritic cell subsets in the skin-draining lymph node. *Proc Natl Acad Sci U S A* (2016) 113(4):1044–9. doi: 10.1073/pnas.1513607113
42. Myers JA, Miller JS. Exploring the NK cell platform for cancer immunotherapy. *Nat Rev Clin Oncol* (2020) 1–16. doi: 10.1038/s41571-020-0426-7
43. Zhang Q, Bi J, Zheng X, Chen Y, Wang H, Wu W, et al. Blockade of the checkpoint receptor TIGIT prevents NK cell exhaustion and elicits potent anti-tumor immunity. *Nat Immunol* (2018) 19(7):723–32. doi: 10.1038/s41590-018-0132-0
44. Zhang C, Liu Y. Targeting NK Cell Checkpoint Receptors or Molecules for Cancer Immunotherapy. *Front Immunol* (2020) 11:1295. doi: 10.3389/fimmu.2020.01295
45. Fang L, Gong J, Wang Y, Liu R, Li Z, Wang Z, et al. MICA/B expression is inhibited by unfolded protein response and associated with poor prognosis in human hepatocellular carcinoma. *J Exp Clin Cancer Res* (2014) 33(1):76. doi: 10.1186/s13046-014-0076-7
46. Zamai L, Ahmad M, Bennett IM, Azzoni L, Alnemri ES, Perussia B. Natural killer (NK) cell-mediated cytotoxicity: differential use of TRAIL and Fas ligand by immature and mature primary human NK cells. *J Exp Med* (1998) 188(12):2375–80. doi: 10.1084/jem.188.12.2375
47. Pesce S, Greppi M, Tabellini G, Rampinelli F, Parolini S, Olive D, et al. Identification of a subset of human natural killer cells expressing high levels of programmed death 1: A phenotypic and functional characterization. *J Allergy Clin Immunol* (2017) 139(1):335–46.e3. doi: 10.1016/j.jaci.2016.04.025
48. Liu Y, Cheng Y, Xu Y, Wang Z, Du X, Li C, et al. Increased expression of programmed cell death protein 1 on NK cells inhibits NK-cell-mediated anti-tumor function and indicates poor prognosis in digestive cancers. *Oncogene* (2017) 36(44):6143–53. doi: 10.1038/onc.2017.209
49. Hsu J, Hodgins JJ, Marathe M, Nicolai CJ, Bourgeois-Daigneault MC, Trevino TN, et al. Contribution of NK cells to immunotherapy mediated by PD-1/PD-L1 blockade. *J Clin Invest* (2018) 128(10):4654–68. doi: 10.1172/jci99317
50. Oyer JL, Gitto SB, Altomare DA, Copik AJ. PD-L1 blockade enhances anti-tumor efficacy of NK cells. *Oncoimmunology* (2018) 7(11):e1509819. doi: 10.1080/2162402x.2018.1509819
51. Jiang T, Zhou C, Ren S. Role of IL-2 in cancer immunotherapy. *Oncoimmunology* (2016) 5(6):e1163462. doi: 10.1080/2162402x.2016.1163462
52. Parihar R, Dierksheide J, Hu Y, Carson WE. IL-12 enhances the natural killer cell cytokine response to Ab-coated tumor cells. *J Clin Invest* (2002) 110(7):983–92. doi: 10.1172/jci15950
53. Barry KC, Hsu J, Broz ML, Cueto FJ, Binnewies M, Combes AJ, et al. A natural killer-dendritic cell axis defines checkpoint therapy-responsive tumor microenvironments. *Nat Med* (2018) 24(8):1178–91. doi: 10.1038/s41591-018-0085-8
54. Muntasell A, Ochoa MC, Cordeiro L, Berraondo P, López-Díaz de Cerio A, Cabo M, et al. Targeting NK-cell checkpoints for cancer immunotherapy. *Curr Opin Immunol* (2017) 45:73–81. doi: 10.1016/j.coi.2017.01.003
55. Kuzet SE, Gaggioli C. Fibroblast activation in cancer: when seed fertilizes soil. *Cell Tissue Res* (2016) 365(3):607–19. doi: 10.1007/s00441-016-2467-x
56. De Jaeghere EA, Denys HG, De Wever O. Fibroblasts Fuel Immune Escape in the Tumor Microenvironment. *Trends Cancer* (2019) 5(11):704–23. doi: 10.1016/j.trecan.2019.09.009
57. Yoshida GJ, Azuma A, Miura Y, Orimo A. Activated Fibroblast Program Orchestrates Tumor Initiation and Progression; Molecular Mechanisms and the Associated Therapeutic Strategies. *Int J Mol Sci* (2019) 20(9):2256. doi: 10.3390/ijms20092256
58. Murata T, Mekada E, Hoffman RM. Reconstitution of a metastatic-resistant tumor microenvironment with cancer-associated fibroblasts enables metastasis. *Cell Cycle (Georgetown Tex)* (2017) 16(6):533–5. doi: 10.1080/15384101.2017.1281486
59. Avery D, Govindaraju P, Jacob M, Todd L, Monslow J, Puré E. Extracellular matrix directs phenotypic heterogeneity of activated fibroblasts. *Matrix Biol* (2018) 67:90–106. doi: 10.1016/j.matbio.2017.12.003
60. Zhu Y, Herndon JM, Sojka DK, Kim KW, Knolhoff BL, Zuo C, et al. Tissue-Resident Macrophages in Pancreatic Ductal Adenocarcinoma Originate from Embryonic Hematopoiesis and Promote Tumor Progression. *Immunity* (2017) 47(2):323–38.e6. doi: 10.1016/j.immuni.2017.07.014
61. Guo S, Deng CX. Effect of Stromal Cells in Tumor Microenvironment on Metastasis Initiation. *Int J Biol Sci* (2018) 14(14):2083–93. doi: 10.7150/ijbs.25720
62. Zhu Y, Zhang L, Zha H, Yang F, Hu C, Chen L, et al. Stroma-derived Fibrinogen-like Protein 2 Activates Cancer-associated Fibroblasts to Promote Tumor Growth in Lung Cancer. *Int J Biol Sci* (2017) 13(6):804–14. doi: 10.7150/ijbs.19398
63. Liu T, Han C, Wang S, Fang P, Ma Z, Xu L, et al. Cancer-associated fibroblasts: an emerging target of anti-cancer immunotherapy. *J Hematol Oncol* (2019) 12(1):86. doi: 10.1186/s13045-019-0770-1
64. Takai K, Le A, Weaver VM, Werb Z. Targeting the cancer-associated fibroblasts as a treatment in triple-negative breast cancer. *Oncotarget* (2016) 7(50):82889–901. doi: 10.18632/oncotarget.12658
65. Kozono S, Ohuchida K, Eguchi D, Ikenaga N, Fujiwara K, Cui L, et al. Pirfenidone inhibits pancreatic cancer desmoplasia by regulating stellate cells. *Cancer Res* (2013) 73(7):2345–56. doi: 10.1158/0008-5472.Can-12-3180
66. Azuma A. Pirfenidone treatment of idiopathic pulmonary fibrosis. *Ther Adv Respir Dis* (2012) 6(2):107–14. doi: 10.1177/1753465812436663
67. Komohara Y, Jinushi M, Takeya M. Clinical significance of macrophage heterogeneity in human malignant tumors. *Cancer Sci* (2014) 105(1):1–8. doi: 10.1111/cas.12314
68. Chen X, Wang Y, Nelson D, Tian S, Mulvey E, Patel B, et al. CCL2/CCR2 Regulates the Tumor Microenvironment in HER-2/neu-Driven Mammary Carcinomas in Mice. *PloS One* (2016) 11(11):e0165595. doi: 10.1371/journal.pone.0165595
69. Goerdt S, Orfanos CE. Other functions, other genes: alternative activation of antigen-presenting cells. *Immunity* (1999) 10(2):137–42. doi: 10.1016/s1074-7613(00)80014-x
70. Nejman D, Livyatan I, Fuks G, Gavert N, Zwang Y, Geller LT, et al. The human tumor microbiome is composed of tumor type-specific intracellular bacteria. *Science (New York NY)* (2020) 368(6494):973–80. doi: 10.1126/science.aay9189
71. Ren F, Fan M, Mei J, Wu Y, Liu C, Pu Q, et al. Interferon-γ and celecoxib inhibit lung-tumor growth through modulating M2/M1 macrophage ratio in the tumor microenvironment. *Drug Des Devel Ther* (2014) 8:1527–38. doi: 10.2147/dddt.S66302
72. Gordon S. Alternative activation of macrophages. *Nat Rev Immunol* (2003) 3(1):23–35. doi: 10.1038/nri978
73. Raber PL, Thevenot P, Sierra R, Wyczechowska D, Halle D, Ramirez ME, et al. Subpopulations of myeloid-derived suppressor cells impair T cell responses through independent nitric oxide-related pathways. *Int J Cancer* (2014) 134(12):2853–64. doi: 10.1002/ijc.28622
74. Gabrilovich DI, Ostrand-Rosenberg S, Bronte V. Coordinated regulation of myeloid cells by tumours. *Nat Rev Immunol* (2012) 12(4):253–68. doi: 10.1038/nri3175
75. Nagaraj S, Gupta K, Pisarev V, Kinarsky L, Sherman S, Kang L, et al. Altered recognition of antigen is a mechanism of CD8+ T cell tolerance in cancer. *Nat Med* (2007) 13(7):828–35. doi: 10.1038/nm1609
76. Srivastava MK, Sinha P, Clements VK, Rodriguez P, Ostrand-Rosenberg S. Myeloid-derived suppressor cells inhibit T-cell activation by depleting cystine and cysteine. *Cancer Res* (2010) 70(1):68–77. doi: 10.1158/0008-5472.Can-09-2587
77. Raber P, Ochoa AC, Rodríguez PC. Metabolism of L-arginine by myeloid-derived suppressor cells in cancer: mechanisms of T cell suppression and therapeutic perspectives. *Immunol Invest* (2012) 41(6-7):614–34. doi: 10.3109/08820139.2012.680634
78. Zhu Y, Knolhoff BL, Meyer MA, Nywening TM, West BL, Luo J, et al. CSF1/CSF1R blockade reprograms tumor-infiltrating macrophages and improves response to T-cell checkpoint immunotherapy in pancreatic cancer models. *Cancer Res* (2014) 74(18):5057–69. doi: 10.1158/0008-5472.Can-13-3723
79. Leone RD, Powell JD. Metabolism of immune cells in cancer. *Nat Rev Cancer* (2020) 20(9):516–31. doi: 10.1038/s41568-020-0273-y
80. Kouidhi S, Ben Ayed F, Benammar Elgaaied A. Targeting Tumor Metabolism: A New Challenge to Improve Immunotherapy. *Front Immunol* (2018) 9:353. doi: 10.3389/fimmu.2018.00353

81. Wei F, Wang D, Wei J, Tang N, Tang L, Xiong F, et al. Metabolic crosstalk in the tumor microenvironment regulates antitumor immunosuppression and immunotherapy resisitance. *Cell Mol Life Sci CMLS* (2020). doi: 10.1007/s00018-020-03581-0
82. Ohta A, Gorelik E, Prasad SJ, Ronchese F, Lukashev D, Wong MK, et al. A2A adenosine receptor protects tumors from antitumor T cells. *Proc Natl Acad Sci U S A* (2006) 103(35):13132–7. doi: 10.1073/pnas.0605251103
83. Domblides C, Lartigue L, Faustin B. Control of the Antitumor Immune Response by Cancer Metabolism. *Cells* (2019) 8(2):104. doi: 10.3390/cells8020104
84. Fischer K, Hoffmann P, Voelkl S, Meidenbauer N, Ammer J, Edinger M, et al. Inhibitory effect of tumor cell-derived lactic acid on human T cells. *Blood* (2007) 109(9):3812–9. doi: 10.1182/blood-2006-07-035972
85. Choi SY, Collins CC, Gout PW, Wang Y. Cancer-generated lactic acid: a regulatory, immunosuppressive metabolite? *J Pathol* (2013) 230(4):350–5. doi: 10.1002/path.4218
86. Khan MAW, Ologun G, Arora R, McQuade JL, Wargo JA. Gut Microbiome Modulates Response to Cancer Immunotherapy. *Dig Dis Sci* (2020) 65(3):885–96. doi: 10.1007/s10620-020-06111-x
87. Shi N, Li N, Duan X, Niu H. Interaction between the gut microbiome and mucosal immune system. *Mil Med Res* (2017) 4:14. doi: 10.1186/s40779-017-0122-9
88. Maynard CL, Elson CO, Hatton RD, Weaver CT. Reciprocal interactions of the intestinal microbiota and immune system. *Nature* (2012) 489(7415):231–41. doi: 10.1038/nature11551
89. Wesemann DR, Portuguese AJ, Meyers RM, Gallagher MP, Cluff-Jones K, Magee JM, et al. Microbial colonization influences early B-lineage development in the gut lamina propria. *Nature* (2013) 501(7465):112–5. doi: 10.1038/nature12496
90. Kau AL, Ahern PP, Griffin NW, Goodman AL, Gordon JI. Human nutrition, the gut microbiome and the immune system. *Nature* (2011) 474(7351):327–36. doi: 10.1038/nature10213
91. Zeng MY, Cisalpino D, Varadarajan S, Hellman J, Warren HS, Cascalho M, et al. Gut Microbiota-Induced Immunoglobulin G Controls Systemic Infection by Symbiotic Bacteria and Pathogens. *Immunity* (2016) 44(3):647–58. doi: 10.1016/j.immuni.2016.02.006
92. Sethi V, Kurtom S, Tarique M, Lavania S, Malchiodi Z, Hellmund L, et al. Gut Microbiota Promotes Tumor Growth in Mice by Modulating Immune Response. *Gastroenterology* (2018) 155(1):33–7.e6. doi: 10.1053/j.gastro.2018.04.001
93. Zhang X, Liu Q, Liao Q, Zhao Y. Pancreatic Cancer, Gut Microbiota, and Therapeutic Efficacy. *J Cancer* (2020) 11(10):2749–58. doi: 10.7150/jca.37445
94. Ling Z, Shao L, Liu X, Cheng Y, Yan C, Mei Y, et al. Regulatory T Cells and Plasmacytoid Dendritic Cells Within the Tumor Microenvironment in Gastric Cancer Are Correlated With Gastric Microbiota Dysbiosis: A Preliminary Study. *Front Immunol* (2019) 10:533. doi: 10.3389/fimmu.2019.00533
95. Ma W, Mao Q, Xia W, Dong G, Yu C, Jiang F. Gut Microbiota Shapes the Efficiency of Cancer Therapy. *Front Microbiol* (2019) 10:1050. doi: 10.3389/fmicb.2019.01050
96. Erdman SE, Poutahidis T. Cancer inflammation and regulatory T cells. *Int J Cancer* (2010) 127(4):768–79. doi: 10.1002/ijc.25430
97. Erdman SE, Poutahidis T. Gut bacteria and cancer. *Biochim Biophys Acta* (2015) 1856(1):86–90. doi: 10.1016/j.bbcan.2015.05.007
98. Erdman SE, Rao VP, Olipitz W, Taylor CL, Jackson EA, Levkovich T, et al. Unifying roles for regulatory T cells and inflammation in cancer. *Int J Cancer* (2010) 126(7):1651–65. doi: 10.1002/ijc.24923
99. Lakritz JR, Poutahidis T, Levkovich T, Varian BJ, Ibrahim YM, Chatzigiagkos A, et al. Beneficial bacteria stimulate host immune cells to counteract dietary and genetic predisposition to mammary cancer in mice. *Int J Cancer* (2014) 135(3):529–40. doi: 10.1002/ijc.28702
100. Rao VP, Poutahidis T, Fox JG, Erdman SE. Breast cancer: should gastrointestinal bacteria be on our radar screen? *Cancer Res* (2007) 67(3):847–50. doi: 10.1158/0008-5472.Can-06-3468
101. Poutahidis T, Haigis KM, Rao VP, Nambiar PR, Taylor CL, Ge Z, et al. Rapid reversal of interleukin-6-dependent epithelial invasion in a mouse model of microbially induced colon carcinoma. *Carcinogenesis* (2007) 28(12):2614–23. doi: 10.1093/carcin/bgm180
102. Coffelt SB, Wellenstein MD, de Visser KE. Neutrophils in cancer: neutral no more. *Nat Rev Cancer* (2016) 16(7):431–46. doi: 10.1038/nrc.2016.52
103. Erdman SE, Rao VP, Poutahidis T, Rogers AB, Taylor CL, Jackson EA, et al. Nitric oxide and TNF-alpha trigger colonic inflammation and carcinogenesis in Helicobacter hepaticus-infected, Rag2-deficient mice. *Proc Natl Acad Sci U S A* (2009) 106(4):1027–32. doi: 10.1073/pnas.0812347106
104. Bald T, Quast T, Landsberg J, Rogava M, Glodde N, Lopez-Ramos D, et al. Ultraviolet-radiation-induced inflammation promotes angiotropism and metastasis in melanoma. *Nature* (2014) 507(7490):109–13. doi: 10.1038/nature13111
105. Dumitru CA, Lang S, Brandau S. Modulation of neutrophil granulocytes in the tumor microenvironment: mechanisms and consequences for tumor progression. *Semin Cancer Biol* (2013) 23(3):141–8. doi: 10.1016/j.semcancer.2013.02.005
106. Poutahidis T, Kearney SM, Levkovich T, Qi P, Varian BJ, Lakritz JR, et al. Microbial symbionts accelerate wound healing via the neuropeptide hormone oxytocin. *PloS One* (2013) 8(10):e78898. doi: 10.1371/journal.pone.0078898
107. Varian BJ, Gourishetti S, Poutahidis T, Lakritz JR, Levkovich T, Kwok C, et al. Beneficial bacteria inhibit cachexia. *Oncotarget* (2016) 7(11):11803–16. doi: 10.18632/oncotarget.7730
108. Varian BJ, Poutahidis T, DiBenedictis BT, Levkovich T, Ibrahim Y, Didyk E, et al. Microbial lysate upregulates host oxytocin. *Brain Behav Immun* (2017) 61:36–49. doi: 10.1016/j.bbi.2016.11.002
109. Poutahidis T, Kleinewietfeld M, Erdman SE. Gut microbiota and the paradox of cancer immunotherapy. *Front Immunol* (2014) 5:157. doi: 10.3389/fimmu.2014.00157
110. Mougiakakos D, Choudhury A, Lladser A, Kiessling R, Johansson CC. Regulatory T cells in cancer. *Adv Cancer Res* (2010) 107:57–117. doi: 10.1016/s0065-230x(10)07003-x
111. Nishikawa H, Sakaguchi S. Regulatory T cells in cancer immunotherapy. *Curr Opin Immunol* (2014) 27:1–7. doi: 10.1016/j.coi.2013.12.005
112. Wang YA, Li XL, Mo YZ, Fan CM, Tang L, Xiong F, et al. Effects of tumor metabolic microenvironment on regulatory T cells. *Mol Cancer* (2018) 17(1):168. doi: 10.1186/s12943-018-0913-y
113. Erdman SE, Poutahidis T, Tomczak M, Rogers AB, Cormier K, Plank B, et al. CD4+ CD25+ regulatory T lymphocytes inhibit microbially induced colon cancer in Rag2-deficient mice. *Am J Pathol* (2003) 162(2):691–702. doi: 10.1016/s0002-9440(10)63863-1
114. Rao VP, Poutahidis T, Ge Z, Nambiar PR, Boussahmain C, Wang YY, et al. Innate immune inflammatory response against enteric bacteria Helicobacter hepaticus induces mammary adenocarcinoma in mice. *Cancer Res* (2006) 66(15):7395–400. doi: 10.1158/0008-5472.Can-06-0558
115. Mao K, Baptista AP, Tamoutounour S, Zhuang L, Bouladoux N, Martins AJ, et al. Innate and adaptive lymphocytes sequentially shape the gut microbiota and lipid metabolism. *Nature* (2018) 554(7691):255–9. doi: 10.1038/nature25437
116. Leschner S, Westphal K, Dietrich N, Viegas N, Jablonska J, Lyszkiewicz M, et al. Tumor invasion of Salmonella enterica serovar Typhimurium is accompanied by strong hemorrhage promoted by TNF-alpha. *PloS One* (2009) 4(8):e6692. doi: 10.1371/journal.pone.0006692
117. Pott J, Hornef M. Innate immune signalling at the intestinal epithelium in homeostasis and disease. *EMBO Rep* (2012) 13(8):684–98. doi: 10.1038/embor.2012.96
118. Macpherson AJ, Yilmaz B, Limenitakis JP, Ganal-Vonarburg SC. IgA Function in Relation to the Intestinal Microbiota. *Annu Rev Immunol* (2018) 36:359–81. doi: 10.1146/annurev-immunol-042617-053238
119. Donaldson GP, Ladinsky MS, Yu KB, Sanders JG, Yoo BB, Chou WC, et al. Gut microbiota utilize immunoglobulin A for mucosal colonization. *Science (New York NY)* (2018) 360(6390):795–800. doi: 10.1126/science.aaq0926
120. Roy S, Trinchieri G. Microbiota: a key orchestrator of cancer therapy. *Nat Rev Cancer* (2017) 17(5):271–85. doi: 10.1038/nrc.2017.13
121. Xia Y, Shen S, Verma IM. NF-κB, an active player in human cancers. *Cancer Immunol Res* (2014) 2(9):823–30. doi: 10.1158/2326-6066.Cir-14-0112
122. Harrington BS, Annunziata CM. NF-κB Signaling in Ovarian Cancer. *Cancers* (2019) 11(8):1182. doi: 10.3390/cancers11081182
123. Shalapour S, Karin M. Cruel to Be Kind: Epithelial, Microbial, and Immune Cell Interactions in Gastrointestinal Cancers. *Annu Rev Immunol* (2020) 38:649–71. doi: 10.1146/annurev-immunol-082019-081656

124. Jackstadt R, van Hooff SR, Leach JD, Cortes-Lavaud X, Lohuis JO, Ridgway RA, et al. Epithelial NOTCH Signaling Rewires the Tumor Microenvironment of Colorectal Cancer to Drive Poor-Prognosis Subtypes and Metastasis. *Cancer Cell* (2019) 36(3):319–36.e7. doi: 10.1016/j.ccell.2019.08.003
125. Rooks MG, Garrett WS. Gut microbiota, metabolites and host immunity. *Nat Rev Immunol* (2016) 16(6):341–52. doi: 10.1038/nri.2016.42
126. Poutahidis T, Kleinewietfeld M, Smillie C, Levkovich T, Perrotta A, Bhela S, et al. Microbial reprogramming inhibits Western diet-associated obesity. *PloS One* (2013) 8(7):e68596. doi: 10.1371/journal.pone.0068596
127. Poutahidis T, Varian BJ, Levkovich T, Lakritz JR, Mirabal S, Kwok C, et al. Dietary microbes modulate transgenerational cancer risk. *Cancer Res* (2015) 75(7):1197–204. doi: 10.1158/0008-5472.Can-14-2732
128. Flint HJ, Scott KP, Louis P, Duncan SH. The role of the gut microbiota in nutrition and health. *Nat Rev Gastroenterol Hepatol* (2012) 9(10):577–89. doi: 10.1038/nrgastro.2012.156
129. Nicholson JK, Holmes E, Kinross J, Burcelin R, Gibson G, Jia W, et al. Host-gut microbiota metabolic interactions. *Science (New York NY)* (2012) 336 (6086):1262–7. doi: 10.1126/science.1223813
130. Clemente JC, Ursell LK, Parfrey LW, Knight R. The impact of the gut microbiota on human health: an integrative view. *Cell* (2012) 148(6):1258–70. doi: 10.1016/j.cell.2012.01.035
131. Yoshimoto S, Loo TM, Atarashi K, Kanda H, Sato S, Oyadomari S, et al. Obesity-induced gut microbial metabolite promotes liver cancer through senescence secretome. *Nature* (2013) 499(7456):97–101. doi: 10.1038/nature12347
132. Soysal SD, Tzankov A, Muenst SE. Role of the Tumor Microenvironment in Breast Cancer. *Pathobiology* (2015) 82(3-4):142–52. doi: 10.1159/000430499
133. Wang Y, Mumm JB, Herbst R, Kolbeck R, Wang Y. IL-22 Increases Permeability of Intestinal Epithelial Tight Junctions by Enhancing Claudin-2 Expression. *J Immunol (Baltimore Md 1950)* (2017) 199 (9):3316–25. doi: 10.4049/jimmunol.1700152
134. Thirunavukkarasan M, Wang C, Rao A, Hind T, Teo YR, Siddiquee AA, et al. Short-chain fatty acid receptors inhibit invasive phenotypes in breast cancer cells. *PloS One* (2017) 12(10):e0186334. doi: 10.1371/journal.pone.0186334
135. Davie JR. Inhibition of histone deacetylase activity by butyrate. *J Nutr* (2003) 133(7 Suppl):2485s–93s. doi: 10.1093/jn/133.7.2485S
136. Louis P, Flint HJ. Diversity, metabolism and microbial ecology of butyrate-producing bacteria from the human large intestine. *FEMS Microbiol Lett* (2009) 294(1):1–8. doi: 10.1111/j.1574-6968.2009.01514.x
137. Zgouras D, Wächtershäuser A, Frings D, Stein J. Butyrate impairs intestinal tumor cell-induced angiogenesis by inhibiting HIF-1alpha nuclear translocation. *Biochem Biophys Res Commun* (2003) 300(4):832–8. doi: 10.1016/s0006-291x(02)02916-9
138. Payne CM, Weber C, Crowley-Skillicorn C, Dvorak K, Bernstein H, Bernstein C, et al. Deoxycholate induces mitochondrial oxidative stress and activates NF-kappaB through multiple mechanisms in HCT-116 colon epithelial cells. *Carcinogenesis* (2007) 28(1):215–22. doi: 10.1093/carcin/bgl139
139. Rodier F, Coppé JP, Patil CK, Hoeijmakers WA, Muñoz DP, Raza SR, et al. Persistent DNA damage signalling triggers senescence-associated inflammatory cytokine secretion. *Nat Cell Biol* (2009) 11(8):973–9. doi: 10.1038/ncb1909
140. Beatty GL, Gladney WL. Immune escape mechanisms as a guide for cancer immunotherapy. *Clin Cancer Res* (2015) 21(4):687–92. doi: 10.1158/1078-0432.Ccr-14-1860
141. Hooper LV, Macpherson AJ. Immune adaptations that maintain homeostasis with the intestinal microbiota. *Nat Rev Immunol* (2010) 10 (3):159–69. doi: 10.1038/nri2710
142. Helmink BA, Khan MAW, Hermann A, Gopalakrishnan V, Wargo JA. The microbiome, cancer, and cancer therapy. *Nat Med* (2019) 25(3):377–88. doi: 10.1038/s41591-019-0377-7
143. McQuade JL, Daniel CR, Helmink BA, Wargo JA. Modulating the microbiome to improve therapeutic response in cancer. *Lancet Oncol* (2019) 20(2):e77–91. doi: 10.1016/s1470-2045(18)30952-5
144. Gopalakrishnan V, Spencer CN, Nezi L, Reuben A, Andrews MC, Karpinets TV, et al. Gut microbiome modulates response to anti-PD-1 immunotherapy in melanoma patients. *Science (New York NY)* (2018) 359(6371):97–103. doi: 10.1126/science.aan4236
145. Matson V, Fessler J, Bao R, Chongsuwat T, Zha Y, Alegre ML, et al. The commensal microbiome is associated with anti-PD-1 efficacy in metastatic melanoma patients. *Science (New York NY)* (2018) 359(6371):104–8. doi: 10.1126/science.aao3290
146. Ngambenjawong C, Gustafson HH, Pun SH. Progress in tumor-associated macrophage (TAM)-targeted therapeutics. *Adv Drug Deliv Rev* (2017) 114:206–21. doi: 10.1016/j.addr.2017.04.010
147. Wculek SK, Cueto FJ, Mujal AM, Melero I, Krummel MF, Sancho D. Dendritic cells in cancer immunology and immunotherapy. *Nat Rev Immunol* (2020) 20(1):7–24. doi: 10.1038/s41577-019-0210-z
148. Wang Y, Luan Z, Zhao C, Bai C, Yang K. Target delivery selective CSF-1R inhibitor to tumor-associated macrophages via erythrocyte-cancer cell hybrid membrane camouflaged pH-responsive copolymer micelle for cancer immunotherapy. *Eur J Pharm Sci* (2020) 142:105136. doi: 10.1016/j.ejps.2019.105136
149. Liu X, Pu Y, Cron K, Deng L, Kline J, Frazier WA, et al. CD47 blockade triggers T cell-mediated destruction of immunogenic tumors. *Nat Med* (2015) 21(10):1209–15. doi: 10.1038/nm.3931
150. Xu MM, Pu Y, Han D, Shi Y, Cao X, Liang H, et al. Dendritic cells but not macrophages sense tumor mitochondrial DNA for cross-priming through signal regulatory protein α signaling. *Immunity* (2017) 47(2):363–73.e5. doi: 10.1016/j.immuni.2017.07.016
151. Barclay AN, Van den Berg TK. The interaction between signal regulatory protein alpha (SIRPα) and CD47: structure, function, and therapeutic target. *Annu Rev Immunol* (2014) 32:25–50. doi: 10.1146/annurev-immunol-032713-120142
152. Majeti R, Chao MP, Alizadeh AA, Pang WW, Jaiswal S, Gibbs KDJr., et al. CD47 is an adverse prognostic factor and therapeutic antibody target on human acute myeloid leukemia stem cells. *Cell* (2009) 138(2):286–99. doi: 10.1016/j.cell.2009.05.045
153. Jaiswal S, Jamieson CH, Pang WW, Park CY, Chao MP, Majeti R, et al. CD47 is upregulated on circulating hematopoietic stem cells and leukemia cells to avoid phagocytosis. *Cell* (2009) 138(2):271–85. doi: 10.1016/j.cell.2009.05.046
154. Tseng D, Volkmer JP, Willingham SB, Contreras-Trujillo H, Fathman JW, Fernhoff NB, et al. Anti-CD47 antibody-mediated phagocytosis of cancer by macrophages primes an effective antitumor T-cell response. *Proc Natl Acad Sci U S A* (2013) 110(27):11103–8. doi: 10.1073/pnas.1305569110
155. Furrie E, Macfarlane S, Kennedy A, Cummings JH, Walsh SV, O'Neil DA, et al. Synbiotic therapy (Bifidobacterium longum/Synergy 1) initiates resolution of inflammation in patients with active ulcerative colitis: a randomised controlled pilot trial. *Gut* (2005) 54(2):242–9. doi: 10.1136/gut.2004.044834
156. Zhou S, Gravekamp C, Bermudes D, Liu K. Tumour-targeting bacteria engineered to fight cancer. *Nat Rev Cancer* (2018) 18(12):727–43. doi: 10.1038/s41568-018-0070-z
157. Deng X, Tian H, Yang R, Han Y, Wei K, Zheng C, et al. Oral Probiotics Alleviate Intestinal Dysbacteriosis for People Receiving Bowel Preparation. *Front Med* (2020) 7:73. doi: 10.3389/fmed.2020.00073
158. Shi Y, Zheng W, Yang K, Harris KG, Ni K, Xue L, et al. Intratumoral accumulation of gut microbiota facilitates CD47-based immunotherapy via STING signaling. *J Exp Med* (2020) 217(5):e20192282. doi: 10.1084/jem.20192282
159. Sharma P, Allison JP. The future of immune checkpoint therapy. *Science (New York NY)* (2015) 348(6230):56–61. doi: 10.1126/science.aaa8172
160. Sivan A, Corrales L, Hubert N, Williams JB, Aquino-Michaels K, Earley ZM, et al. Commensal Bifidobacterium promotes antitumor immunity and facilitates anti-PD-L1 efficacy. *Science (New York NY)* (2015) 350 (6264):1084–9. doi: 10.1126/science.aac4255
161. Vétizou M, Pitt JM, Daillère R, Lepage P, Waldschmitt N, Flament C, et al. Anticancer immunotherapy by CTLA-4 blockade relies on the gut microbiota. *Science (New York NY)* (2015) 350(6264):1079–84. doi: 10.1126/science.aad1329
162. Huang J, Jiang Z, Wang Y, Fan X, Cai J, Yao X, et al. Modulation of gut microbiota to overcome resistance to immune checkpoint blockade in cancer

immunotherapy. *Curr Opin Pharmacol* (2020) 54:1–10. doi: 10.1016/j.coph.2020.06.004
163. Chemnitz JM, Parry RV, Nichols KE, June CH, Riley JL. SHP-1 and SHP-2 associate with immunoreceptor tyrosine-based switch motif of programmed death 1 upon primary human T cell stimulation, but only receptor ligation prevents T cell activation. *J Immunol (Baltimore Md 1950)* (2004) 173 (2):945–54. doi: 10.4049/jimmunol.173.2.945
164. Jin Y, Dong H, Xia L, Yang Y, Zhu Y, Shen Y, et al. The Diversity of Gut Microbiome is Associated With Favorable Responses to Anti-Programmed Death 1 Immunotherapy in Chinese Patients With NSCLC. *J Thorac Oncol* (2019) 14(8):1378–89. doi: 10.1016/j.jtho.2019.04.007
165. Ji RR, Chasalow SD, Wang L, Hamid O, Schmidt H, Cogswell J, et al. An immune-active tumor microenvironment favors clinical response to ipilimumab. *Cancer Immunol Immunother* (2012) 61(7):1019–31. doi: 10.1007/s00262-011-1172-6
166. Spranger S, Spaapen RM, Zha Y, Williams J, Meng Y, Ha TT, et al. Up-regulation of PD-L1, IDO, and T(regs) in the melanoma tumor microenvironment is driven by CD8(+) T cells. *Sci Trans Med* (2013) 5 (200):200ra116. doi: 10.1126/scitranslmed.3006504
167. Galon J, Bruni D. Approaches to treat immune hot, altered and cold tumours with combination immunotherapies. *Nat Rev Drug Discov* (2019) 18(3):197–218. doi: 10.1038/s41573-018-0007-y
168. Noman MZ, Parpal S, Van Moer K, Xiao M, Yu Y, Viklund J, et al. Inhibition of Vps34 reprograms cold into hot inflamed tumors and improves anti-PD-1/PD-L1 immunotherapy. *Sci Adv* (2020) 6(18):eaax7881. doi: 10.1126/sciadv.aax7881
169. Parry RV, Chemnitz JM, Frauwirth KA, Lanfranco AR, Braunstein I, Kobayashi SV, et al. CTLA-4 and PD-1 receptors inhibit T-cell activation by distinct mechanisms. *Mol Cell Biol* (2005) 25(21):9543–53. doi: 10.1128/mcb.25.21.9543-9553.2005
170. Dubin K, Callahan MK, Ren B, Khanin R, Viale A, Ling L, et al. Intestinal microbiome analyses identify melanoma patients at risk for checkpoint-blockade-induced colitis. *Nat Commun* (2016) 7:10391. doi: 10.1038/ncomms10391
171. Dasgupta S, Erturk-Hasdemir D, Ochoa-Reparaz J, Reinecker HC, Kasper DL. Plasmacytoid dendritic cells mediate anti-inflammatory responses to a gut commensal molecule via both innate and adaptive mechanisms. *Cell Host Microbe* (2014) 15(4):413–23. doi: 10.1016/j.chom.2014.03.006
172. Kroemer G, Zitvogel L. Cancer immunotherapy in 2017: The breakthrough of the microbiota. *Nat Rev Immunol* (2018) 18(2):87–8. doi: 10.1038/nri.2018.4
173. Routy B, Le Chatelier E, Derosa L, Duong CPM, Alou MT, Daillère R, et al. Gut microbiome influences efficacy of PD-1-based immunotherapy against epithelial tumors. *Science (New York NY)* (2018) 359(6371):91–7. doi: 10.1126/science.aan3706
174. Urbancsek H, Kazar T, Mezes I, Neumann K. Results of a double-blind, randomized study to evaluate the efficacy and safety of Antibiophilus in patients with radiation-induced diarrhoea. *Eur J Gastroenterol Hepatol* (2001) 13(4):391–6. doi: 10.1097/00042737-200104000-00015
175. Salminen E, Elomaa I, Minkkinen J, Vapaatalo H, Salminen S. Preservation of intestinal integrity during radiotherapy using live Lactobacillus acidophilus cultures. *Clin Radiol* (1988) 39(4):435–7. doi: 10.1016/s0009-9260(88)80296-4
176. Delia P, Sansotta G, Donato V, Messina G, Frosina P, Pergolizzi S, et al. Prevention of radiation-induced diarrhea with the use of VSL#3, a new high-potency probiotic preparation. *Am J Gastroenterol* (2002) 97(8):2150–2. doi: 10.1111/j.1572-0241.2002.05946.x
177. Yi X, Zhou H, Chao Y, Xiong S, Zhong J, Chai Z, et al. Bacteria-triggered tumor-specific thrombosis to enable potent photothermal immunotherapy of cancer. *Sci Adv* (2020) 6(33):eaba3546. doi: 10.1126/sciadv.aba3546
178. Kroemer G, Galluzzi L, Kepp O, Zitvogel L. Immunogenic cell death in cancer therapy. *Annu Rev Immunol* (2013) 31:51–72. doi: 10.1146/annurev-immunol-032712-100008
179. Viaud S, Saccheri F, Mignot G, Yamazaki T, Daillère R, Hannani D, et al. The intestinal microbiota modulates the anticancer immune effects of cyclophosphamide. *Science (New York NY)* (2013) 342(6161):971–6. doi: 10.1126/science.1240537
180. Daisley BA, Chanyi RM, Abdur-Rashid K, Al KF, Gibbons S, Chmiel JA, et al. Abiraterone acetate preferentially enriches for the gut commensal Akkermansia muciniphila in castrate-resistant prostate cancer patients. *Nat Commun* (2020) 11(1):4822. doi: 10.1038/s41467-020-18649-5
181. Pushalkar S, Hundeyin M, Daley D, Zambirinis CP, Kurz E, Mishra A, et al. The Pancreatic Cancer Microbiome Promotes Oncogenesis by Induction of Innate and Adaptive Immune Suppression. *Cancer Discovery* (2018) 8 (4):403–16. doi: 10.1158/2159-8290.Cd-17-1134
182. Iida N, Dzutsev A, Stewart CA, Smith L, Bouladoux N, Weingarten RA, et al. Commensal bacteria control cancer response to therapy by modulating the tumor microenvironment. *Science (New York NY)* (2013) 342(6161):967–70. doi: 10.1126/science.1240527
183. Jenq RR, Taur Y, Devlin SM, Ponce DM, Goldberg JD, Ahr KF, et al. Intestinal Blautia Is Associated with Reduced Death from Graft-versus-Host Disease. *Biol Blood Marrow Transplant* (2015) 21(8):1373–83. doi: 10.1016/j.bbmt.2015.04.016
184. DeBerardinis RJ. Tumor Microenvironment, Metabolism, and Immunotherapy. *New Engl J Med* (2020) 382(9):869–71. doi: 10.1056/NEJMcibr1914890
185. Ngiow SF, Young A. Re-education of the Tumor Microenvironment With Targeted Therapies and Immunotherapies. *Front Immunol* (2020) 11:1633. doi: 10.3389/fimmu.2020.01633
186. Yadav M, Verma MK, Chauhan NS. A review of metabolic potential of human gut microbiome in human nutrition. *Arch Microbiol* (2018) 200 (2):203–17. doi: 10.1007/s00203-017-1459-x
187. De Angelis M, Garruti G, Minervini F, Bonfrate L, Portincasa P, Gobbetti M. The Food-gut Human Axis: The Effects of Diet on Gut Microbiota and Metabolome. *Curr Med Chem* (2019) 26(19):3567–83. doi: 10.2174/0929867324666170428103848
188. Kim S, Jazwinski SM. The Gut Microbiota and Healthy Aging: A Mini-Review. *Gerontology* (2018) 64(6):513–20. doi: 10.1159/000490615
189. Wargo JA. Modulating gut microbes. *Science* (2020) 369(6509):1302–3. doi: 10.1126/science.abc3965
190. Geirnaert A, Calatayud M, Grootaert C, Laukens D, Devriese S, Smagghe G, et al. Butyrate-producing bacteria supplemented in vitro to Crohn's disease patient microbiota increased butyrate production and enhanced intestinal epithelial barrier integrity. *Sci Rep* (2017) 7(1):11450. doi: 10.1038/s41598-017-11734-8
191. Hibberd AA, Lyra A, Ouwehand AC, Rolny P, Lindegren H, Cedgård L, et al. Intestinal microbiota is altered in patients with colon cancer and modified by probiotic intervention. *BMJ Open Gastroenterol* (2017) 4(1):e000145. doi: 10.1136/bmjgast-2017-000145
192. Cheng WY, Wu CY, Yu J. The role of gut microbiota in cancer treatment: friend or foe? *Gut* (2020) 69(10):1867–76. doi: 10.1136/gutjnl-2020-321153
193. Gharaibeh RZ, Jobin C. Microbiota and cancer immunotherapy: in search of microbial signals. *Gut* (2019) 68(3):385–8. doi: 10.1136/gutjnl-2018-317220
194. Kelly CR, Kahn S, Kashyap P, Laine L, Rubin D, Atreja A, et al. Update on Fecal Microbiota Transplantation 2015: Indications, Methodologies, Mechanisms, and Outlook. *Gastroenterology* (2015) 149(1):223–37. doi: 10.1053/j.gastro.2015.05.008

Conflict of Interest: The authors declare that the research was conducted in the absence of any commercial or financial relationships that could be construed as a potential conflict of interest.

Copyright © 2021 Qiu, Lin, Ma, Li, Liang, Chen, Liu, Huang, Luo, Huang and Luo. This is an open-access article distributed under the terms of the Creative Commons Attribution License (CC BY). The use, distribution or reproduction in other forums is permitted, provided the original author(s) and the copyright owner(s) are credited and that the original publication in this journal is cited, in accordance with accepted academic practice. No use, distribution or reproduction is permitted which does not comply with these terms.

frontiers in Immunology

ORIGINAL RESEARCH
published: 20 January 2021
doi: 10.3389/fimmu.2020.622467

GBP1 Facilitates Indoleamine 2,3-Dioxygenase Extracellular Secretion to Promote the Malignant Progression of Lung Cancer

*Yinnan Meng[1], Wei Wang[1], Meng Chen[2], Kuifei Chen[2], Xinhang Xia[1], Suna Zhou[1] and Haihua Yang[1,2]**

[1] Laboratory of Cellular and Molecular Radiation Oncology, Radiation Oncology Institute of Enze Medical Health Academy, Department of Radiation Oncology, Affiliated Taizhou Hospital of Wenzhou Medical University, Taizhou, China, [2] School of Medicine, Shaoxing University, Shaoxing, China

IDO1-mediated immune escape can lead to the malignant progression of tumors. However, the precise mechanism of IDO1 remains unclear. This study showed that IDO1 can bind to GBP1 and increase the extracellular secretion of IDO1 with the assistance of GBP1, thereby promoting the malignant proliferation and metastasis of lung cancer. In vitro study showed that the high expression levels of IDO1 and GBP1 in lung cancer cells promoted cell invasion and migration. In vivo study revealed that knockdown of IDO1 and GBP1 inhibited tumor growth and metastasis. In addition, Astragaloside IV reduces the extracellular secretion of IDO1 by blocking the interaction of IDO1 and GBP1, thereby reducing T cell exhaustion and inhibiting tumor progression. These results suggest that blocking the extracellular secretion of IDO1 may prevent T cell exhaustion and thereby enhance the effect of PD-1 inhibitors on cancer treatment.

Keywords: lung cancer, indoleamine 2,3-dioxygenase 1 (IDO1), GBP1, PD-1, astragaloside IV

OPEN ACCESS

Edited by:
Peng Qu,
National Institutes of Health (NIH), United States

Reviewed by:
Erik Richard Ladomersky, Northwestern University, United States
Paolo Puccetti, University of Perugia, Italy

***Correspondence:**
Haihua Yang
yhh93181@163.com

Specialty section:
This article was submitted to Cancer Immunity and Immunotherapy, a section of the journal Frontiers in Immunology

Received: *28 October 2020*
Accepted: *04 December 2020*
Published: *20 January 2021*

Citation:
Meng Y, Wang W, Chen M, Chen K, Xia X, Zhou S and Yang H (2021) GBP1 Facilitates Indoleamine 2,3-Dioxygenase Extracellular Secretion to Promote the Malignant Progression of Lung Cancer. Front. Immunol. 11:622467. doi: 10.3389/fimmu.2020.622467

INTRODUCTION

Lung cancer is the leading cause of cancer deaths in the world. Non-small cell lung cancer accounts for 80% of all lung cancers. It is usually diagnosed in the advanced stage, and the 5-year survival rate is very low (1, 2). Non-small cell lung cancer includes squamous cell carcinoma, adenocarcinoma and large cell carcinoma. Compared with that of other subtypes of lung cancer, the incidence of lung adenocarcinoma is relatively low, but the prevalence has increased, and blood metastases often occur early (3, 4). Surgery remains the standard method to treat lung cancer. Chemotherapy drugs and targeted drugs for EGFR mutation, BRAF mutation and ALK translocation are also used in the treatment of lung cancer. In addition, the development of programmed cell death 1 (PD-1)/PD-1 ligand 1 (PD-L1) checkpoint inhibitors has changed the pattern of non-small cell lung cancer treatment and achieved certain therapeutic effects (5).

Indoleamine 2,3-dioxygenase (IDO) is a home-containing enzyme that is highly expressed in myeloid cells and catalyzes the initial step of tryptophan degradation. Tryptophan starvation caused by IDO inhibits T cell function through several mechanisms (6, 7). An increasing number of studies linked the overexpression of IDO with cancer progression. High levels of IDO have been found in

patients with ovarian cancer, hepatocellular carcinoma, invasive cervical cancer, non-small cell lung cancer, and are associated with poor prognosis (8–12). Although some studies support that blocking IDO exerts a positive anti-tumor effect, the mechanism of how to regulate IDO in tumor cells remains unclear.

This study showed that IDO1 can bind to GBP1. With the assistance of GBP1, the extracellular secretion of IDO1 increased. In vivo and *in vitro* experiments showed that the simultaneous overexpression of IDO1 and GBP1 can promote the migration and invasion of lung cancer cells. In addition, astragaloside IV can block the combination of IDO1 and GBP1 to inhibit the progression of lung cancer. These results provide a certain theoretical basis for the combined targeted therapy of IDO1 and PD-1 and may provide a new idea for the clinical treatment of lung cancer.

MATERIALS AND METHODS

Cell Culture

Lung cancer cell lines NCI-H460, A549 were purchased from cell resource center of Chinese academy of medical sciences, and NCI-H345, NCI-H1299, NCI-H146, NCI-H1341 cells were purchased from ATCC. Mouse Lewis Lung Cancer cell LLT was obtained from cell resource center of Chinese academy of medical sciences. NCI-H345, NCI-H1299, NCI-H146, NCI-H1341 cells were purchased from ATCC. Cells were maintained in RPMI-1640 (Gibco, USA) or DMEM (Gibco, USA) medium supplement with 10% FBS (Gibco, USA). All cells were cultured at 37°C under a humidified atmosphere of 5% CO2.

Silver Staining

At 48 h after cell transfection, cell extracts were obtained using lysis buffer (0.2 mM EDTA, 50 mM Tris-HCl, 150 mM NaCl and 0.3% NP-40). The anti-Flag tag affinity beads (Sigma, USA) were incubated with cell extracts at 4°C overnight. After washing the beads with a cold lysis buffer containing 0.1% NP-40, Flag peptide was applied to the beads to elute the Flag protein complex. The obtained protein was separated *via* 10% SDS-PAGE and then identified using a silver staining kit (Beyotime, China). After the electrophoresis, the gel was placed in the fixative for about 1 h, washed with 30% ethanol for 10 min and then washed with 200 ml of pure water for 10 min. Then, silver solution was added for 10 min and then rinsed with ice and water until color developed. Finally, a stop solution was added to stop the reaction and obtain different bands.

Colony Formation Assay

After reaching the logarithmic growth phase, the transfected cells were digested with 0.25% trypsin and gently pipetted to make them single cells. After the cell count, the cells were seeded into a six-well plate at a density of 1000 cells per dish and placed in a 37°C 5% CO2 incubator for 15 days. When macroscopically visible clones were present, the supernatant was discarded, and the cells were washed twice with PBS. The cells were fixed with 4% paraformaldehyde for 15 min and then stained with GIMSA staining solution for 20 min. After washing with running water and drying, the number of colonies that formed was counted.

Transwell

Cells with a 1:6 dilution of 50 mg/L Matrigel (BD, USA) were inoculated with a final concentration of 1×10^5 cells per well and then cultured in top chamber (Corning, USA) with serum-free medium (Gibco, USA). The complete medium containing 10% FBS was added to bottom and then cultured for 16 h. Then, the cells were removed, and those cells that have not passed were wiped off with a cotton swab. After fixing with formaldehyde for 30 min at room temperature, the cells were stained with 0.1% crystal violet for 20 min. After washing three times with clean water, the cells were observed under a microscope (Nikon, Japan) and then counted.

WOUND HEALING

The cells were seeded into six-well plates. When the cell confluence reached 90% after transfection, a straight scratch was made with a 100-μl pipette tip. The cells were washed with PBS three times to remove the suspended cells, added with medium and then placed in a 37°C, 5% CO2 incubator. After 24 h, photographs of the cells were taken, and then the cell migration rate was calculated.

Plasmid and Lentivirus

Wild-type GBP1 and IDO1 overexpression plasmids were purchased from Sinobiogical (Beijing, China). The mutant IDO1 plasmid was synthesized by Genwiz (Suzhou, China) and inserted into the pCMV3-N-FLAG vector and was verified by DNA sequencing. The synthesized NRP1 and IDO1 shRNA sequences were annealed and inserted into the pLKD-CMV-Puro-U6-shRNA vector, and finally packaged into lentivirus in 293FT cells. shRNA sequences were as follows: GBP1-top: 5′-CACCGCCTCATTGAGAACACTAATGCGAACATTAGTGTTCTCAATGAGGC-3′, GBP1-bot: 5′-AAAAGCCTCATTGAGAACACTAATGTTCGCATTAGTGTTCTCAATGAGGC-3′, IDO1-top: 5′-CACCGCCAAGAAATATTGCTGTTCCCGAAGGAACAGCAATATTTCTTGGC-3′, IDO1-bot: 5′-AAAAGCCAAGAAATATTGCTGTTCCTTCGGGAACAGCAATATTTCTTGGC-3′. All plasmid transfections were performed using Lipofectamine 3000 in accordance with the instructions. A lentivirus was constructed and used in the *in vivo* experiments.

Molecular Docking

The GBP1 and IDO1 protein crystal structures were downloaded from the PDB database (http://www.rcsb.org). HEX software was used for molecular docking, and the binding force was analyzed based on protein surface potential and surface structure. On the basis of the docking results, the protein interaction interface was used as the active pocket for the high-throughput screening of inhibitors.

Western Blot

After discarding the medium and washing with 1× PBS, the cells were treated with PMSF-containing lysis solution (50 mM Tris, 150 mM NaCl, 1% Triton X-100, 1%sodium deoxycholate, 0.1% SDS) and incubated for 30 min. For the detection of the IDO1 protein level in the medium, we collected 60 ml of the medium and centrifuged at 3,000*g* for 20 min using a 30-kDa protein concentrator (Millipore, USA) to obtain a protein mixture. The total protein obtained was harvested, quantified by BCA method, separated through SDS-PAGE and then transferred onto the PVDF membrane (Millipore, USA). After blocking with 5% BSA for 2 h, the membrane was incubated with primary antibodies for 4 h at room temperature and then with HRP-labeled secondary antibodies for 2 h at room temperature. Finally, the band was visualized using an enhanced chemiluminescence system (Millipore, USA) in accordance with the manufacturer's instructions. Primary antibodies were as followed: IDO1 (Abcam, USA, ab134197, 1:1000), GBP1 (Proteintech, China, 67161-1-Ig, 1:500). GAPDH (Abcam, USA, ab8245, 1:3000). Each experiment was repeated three times.

Immunofluorescence

The treated cells were seeded on a glass slide in a 24-well plate and cultured at 37 ℃ and 5% CO2 for 48 h. After immersion in 1× PBS for three times, the cells were fixed with 4% paraformaldehyde (Beyotime, China) for 15 min. Then, the cells were treated with 0.5% Triton X-100 at room temperature for 20 min, washed with 1× PBS, added with normal goat serum (Solarbio, Beijing, China) and blocked for 30 min at room temperature to remove non-specific binding. The slides were incubated with the following primary antibodies at 4°C overnight. GBP1 (Proteintech, China, 67161-1-Ig, 1:500), IDO1 (Abcam, USA, ab134197, 1:1000). After washing with PBST for three times, the cells were added with the diluted fluorescent-labeled secondary antibody (Santa Cruz, USA), incubated at 37° C for 1 h and finally incubated with DAPI for 5 min in the dark. The collected images were observed under a fluorescence microscope (Nikon, Japan).

Xenograft Model

Thirty-two 6-week-old Balb/c nude mice were randomly divided into four groups. NCI-H1299 cells were inoculated subcutaneously at a concentration of 5×10^6 cells per mouse. When the diameter of the tumor reaches 5 mm, GBP1 and IDO1 knock-down lentivirus were used for intertumoral injection. For the metastasis model, luciferase-labeled NCI-H1299 cells were injected into the tail vein to establish a tumor metastasis model. Ten days later, GBP1 and IDO1 knock-down lentivirus were used for intertumoral injection. In order to test the synergistic effect of astragaloside IV and PD-1 inhibitors, C57 mice inoculated with Lewis lung cancer cells. 9 days after inoculation, the tumor diameter reaches 5 to 7 mm, mice were injected with either astragaloside IV (5 mg/kg), anti-PD-1 antibody (BioXCell, 200 μg/mouse, intraperitoneally administered) or the combination of both agents. The tumor volume and animal survival status were monitored every 3 days. Thirty days after cell inoculation, the animals were euthanized by intravenous injection of pentobarbital sodium at the final concentration of 100 mg/kg. The solid tumors were harvested and fixed with formalin for immunohistochemical detection. The tumor volume was calculated as follows: V(volume)=(length × $width^2$)/2. All animal experiments were conducted in accordance with the ethical standards of the Institutional Animal Care and Use Committee of the Affiliated Taizhou hospital of Wenzhou Medical University.

Flow Cytometry

Solid tumors were digested in collagenase and DNase I and dissociated according to the instructions of tumor dissociation kit (Miltenyi Biotec, Auburn, CA). Tumor-infiltrating lymphocyte were enriched and harvested separately by Percoll gradient (Sigma, USA). The lymphocytes were then washed and subsequently blocked with Fc antibody (BD Pharmingen) for 10 min on ice followed by incubation or staining with cell surface antibodies: CD3-APC (Biolegend, USA), CD8-PE (Biolegend, USA) for a 30-min incubation on ice. Cells were washed with Fix/Perm buffer and assayed on a guava easyCyte flow cytometer (MILLIPORE, USA).

Immunohistochemistry

After deparaffinization of 4-μm paraffin sections, 0.3% H_2O_2 was added to inhibit endogenous peroxidase activity. The slices were placed in 0.01 M sodium citrate buffer solution (pH 6.0) and then heated in a microwave oven for antigen retrieval. Subsequently, the slices were added with 5% negative serum to block non-specific proteins and with the corresponding primary antibodies and then incubated overnight at 4°C. After discarding the primary antibodies and washing with 1× PBS, the slices were added with the diluted secondary antibody and incubated at 37°C for 30 min. Finally, DAB was added for color visualization, and the staining intensity was recorded under a microscope.

Statistical Analysis

All statistical analyses were performed using SPSS 19.0 (SPSS, Chicago, USA). The results are expressed as mean ± standard deviation (SD). Student's t test was used to compare the significant differences between the two groups. Comparisons between three or more groups were performed using ANOVA and Dunnett's post-test. Statistical significance was considered at $P < 0.05$ and marked with *.

RESULTS

Indoleamine 2,3-dioxygenase 1 Interacts With GBP1 in Lung Cancer Cells

Flag-tagged IDO1 overexpression plasmid was transfected into A549 cells. Anti-flag magnetic beads were used to obtain the IDO1 binding protein complex and separated by PAGE gel. After silver staining, it was found that there was an obvious band near 65 kDa, which was identified as GBP1 by mass spectrometry (**Figure 1A**). In order to confirm the interaction between IDO1

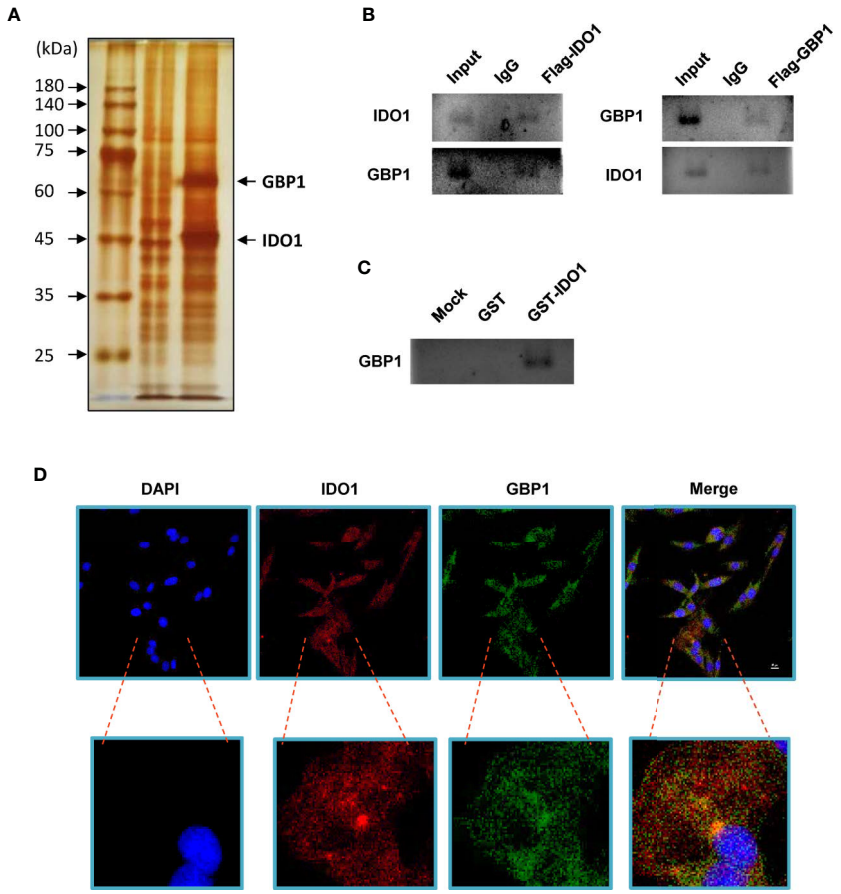

FIGURE 1 | IDO1 binds GBP1 in A549 cells. **(A)** Identification of IDO1 binding protein by silver staining. **(B)** Use Co-IP to detect the interaction between IDO1 and GBP1. **(C)** GST pull-down was performed to analyze the interaction between IDO1 and GBP1 in vitro. **(D)**. Immunofluorescence confirms the co-localization of IDO1 and GBP1 in A549 cells.

and GBP1 *in vivo*, Co-immunoprecipitation was performed. Results showed that GBP1 signal could be detected in the protein complex obtained with anti-flag magnetic beads after transfection of Flag-IDO1. Similarly, GBP1 could also capture IDO1 in cell lysates (**Figure 1B**). GST pull-down experiment was used to detect the interaction between IDO1 and GBP1 *in vitro*. It was found that GST fused IDO1 and transcribed GBP1 *in vitro* can indeed bind to each other (**Figure 1C**). In addition, we used immunofluorescence to determine the co-localization of IDO1 and GBP1 in A549 cell species. The results showed that IDO1 and GBP1 had colocalization signals (**Figure 1D**).

Indoleamine 2,3-dioxygenase 1 and GBP1 Promotes Lung Cancer Cell Migration and Invasion

In order to verify the role of IDO1 and GBP1 in lung cancer species, western blot was performed to detect the expression levels of IDO1 and GBP1 in 6 lung cancer cell lines. The results showed that the protein levels of IDO1 and GBP1 were the highest in NCI-H1299 cells and the lowest in A549 cells (**Figure 2A**). Therefore, we selectively overexpressed IDO1 and GBP1 in A549 cells (**Figure 2B**) and knock down IDO1 and GBP1 in NCI-H1299 cells (**Figure 2C**). We found that GBP1 contributed to the extracellular secretion of IDO1. Then the effects of IDO1 and GBP1 on the invasion, migration and colony formation ability of lung cancer cells were tested by transwell (**Figure 2D**), wound healing (**Figure 2E**) and colony formation (**Figure 2F**) assay. Results showed that overexpression of IDO1 or GBP1 promoted the invasion, migration and colony formation ability of A549 cells compared that of control vector group. Compared with the overexpression of IDO1 or GBP1 respectively, co-overexpression of IDO1 or GBP1 promoted the cells more obviously. In NCI-H1299 cells, knocking down IDO1 or GBP1 could inhibit cell invasion, migration. These experiments indicated that IDO1 and GBP1 contributed to the malignant progression of lung cancer, which may due to the interaction between IDO1 and GBP1.

GBP1 Contributes to the Extracellular Secretion of Indoleamine 2,3-dioxygenase 1

In order to verify the precise mechanism of GBP1 and IDO1 interaction and its role in lung cancer cells, we simulated the

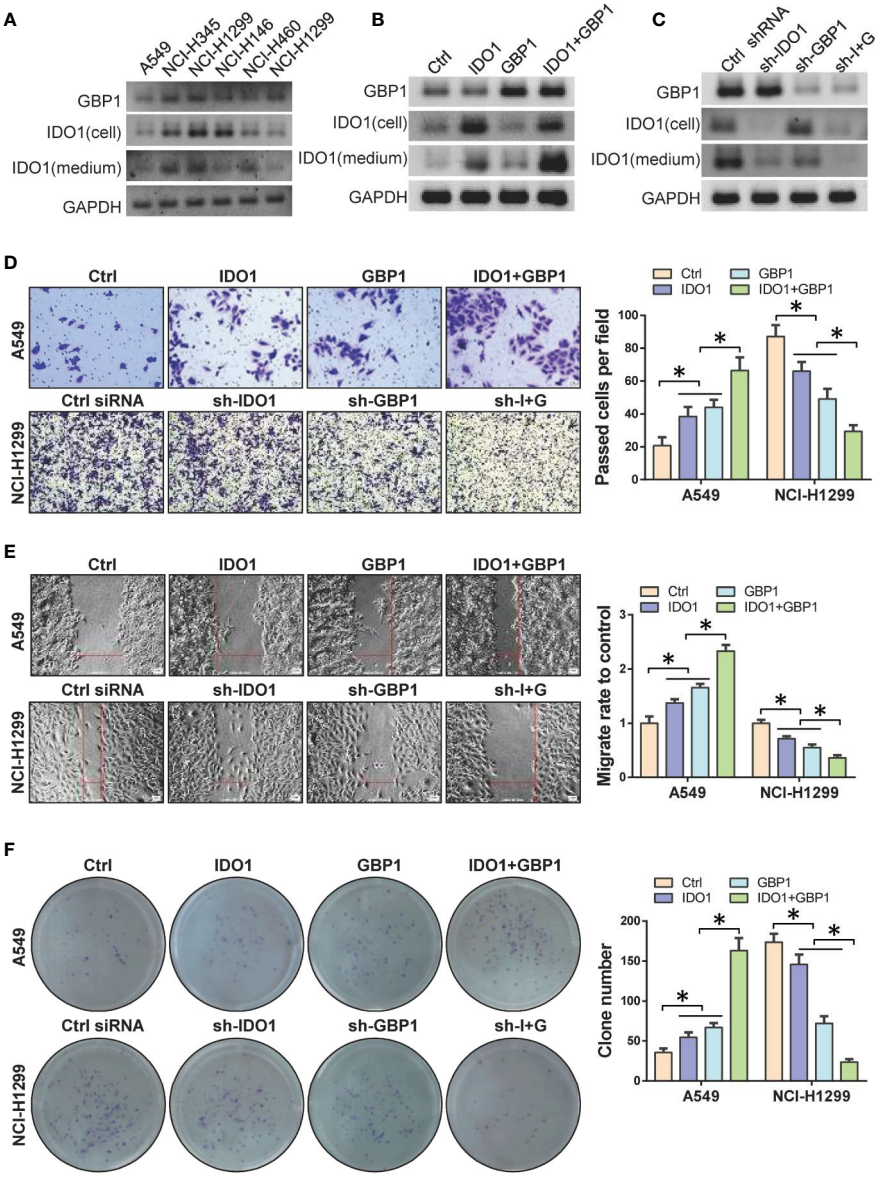

FIGURE 2 | DO1 and GBP1 promotes lung cancer cell invasion, migration and colony formation ability. **(A)** Western blot to detect the protein of IDO1 and GBP1 in 6 lung cancer cell lines. **(B)** Protein levels of GBP1 and IDO1 in cell and culture medium after ectopic expression of IDO1 and GBP1. **(C)** Protein levels of GBP1 and IDO1 in cell and culture medium after knocking down of IDO1 and GBP1. **(D)** Transwell to analyze cell invasion ability after GBP1 and IDO1 overexpression. **(E)** Wound healing to analyze cell migration ability after GBP1 and IDO1 ectopic expression. **(F)** Detection of cell colony formation ability. Statistical significance was considered at $P < 0.05$ and marked with *.

interaction between GBP1 and IDO1 using molecular docking. The results showed that IDO1 protein have strong binding capacity to GBP1 (**Figure 3A**). Next, we performed in GST pull-down between truncated GST-fused IDO1 proteins and *in vitro* transcribed GBP1 proteins. The results showed that after removing the 45 amino acids at the N-terminus, the binding ability of the truncated IDO1 and GBP1 was weakened (**Figure 3B**). In addition, we co-express wild-type or mutant IDO1 with GBP1 in A549 cells. The results showed that GBP1 could assist the secretion of wild-type IDO1 out of the cell. However, after IDO1 mutation, GBP1's carrying effect is weakened (**Figure 3C**). These results suggest that the interaction with GBP1 may contribute to extracellular localization of IDO1 is closely related to GBP1.

Indoleamine 2,3-dioxygenase 1 and GBP1 Promotes Tumor Genesis and Metastasis *In Vivo*

The above results suggested that GBP1 can promote the extracellular secretion of IDO1, which may be involved in the

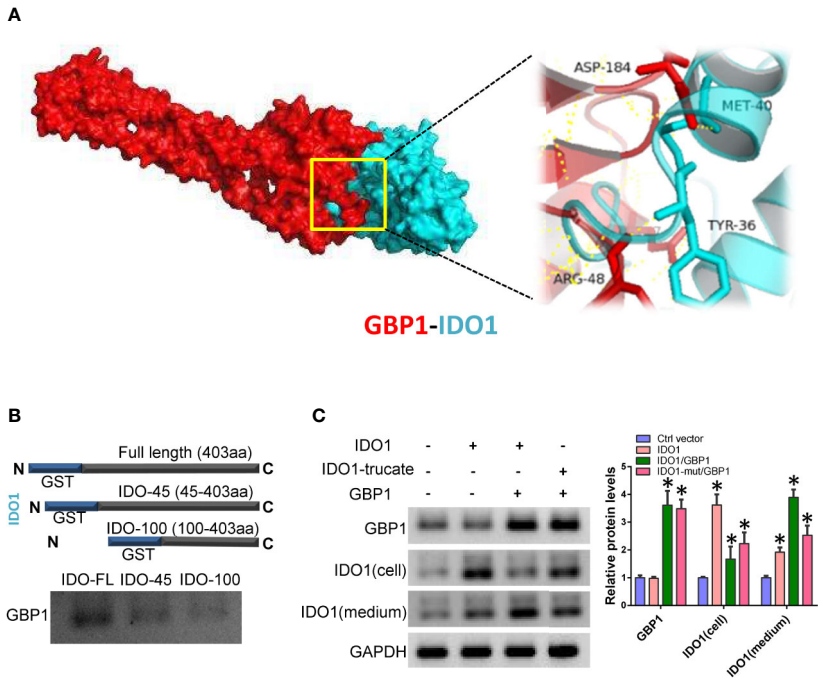

FIGURE 3 | GBP1 contributes to IDO1 extracellular secretion. **(A)** Molecular docking simulates the binding between IDO1 and GBP1. **(B)** Interaction of truncated IDO1 and GBP1 *in vitro*. **(C)** Expression of GBP1 and IDO1 in cells and culture media. Statistical significance was considered at $P < 0.05$ and marked with *.

malignant progression of lung cancer *in vitro*. Here we inoculated NCI-H1299 cells into Balb/c nude mice by subcutaneous inoculation and tail vein injection at a concentration of 10^6 cells per mice. Seven days after inoculation, sh-IDO1 and sh-GBP1 lentiviruses were injected into tumors individually or jointly every 5 days. For tail vein inoculated animals, after 7 days of inoculation, sh-IDO1 and sh-GBP1 lentiviruses were injected through the tail vein alone or jointly transfected with two retroviruses every 5 days. After 35 days, all the mice were euthanized by carbon dioxide asphyxiation. Then tumor volume was measured, and the tumor tissue was formalin fixed and used for immunohistochemical staining to detect the protein expression of IDO1 and GBP1. The results showed that after IDO1 and GBP1 were knocked down, tumor volumes were decreased, and the tumor volume was the smallest in the IDO1 and GBP1 group (**Figure 4A**). The results of immunohistochemistry showed that knocking down IDO1 and GBP1 can reduce the extracellular secretion of IDO1, while knocking down IDO1 and GBP1 simultaneously prevented the extracellular secretion of IDO1 to a greater extent (**Figure 4B**). In tail vein mice, knocking down IDO1 and GBP1 can inhibit the metastasis of lung cancer cells (**Figure 4C**).

Astragaloside IV Blocks Indoleamine 2,3-dioxygenase 1 and GBP1 Interaction and Inhibits Lung Cancer Cell Progression

Based on the above results, we speculate that GBP1-mediated extracellular secretion of IDO1 enhances the malignancy of tumor cells. According to the results of molecular docking, the interaction region of GBP1 and IDO1 was used as the active pocket for screening of interface inhibitors. The results showed that astragaloside IV has a stronger binding force in the interaction area and may block the combination of IDO1 and GBP1 (**Figure 5A**). Considering that the existing studies have proved the anti-tumor effect of astragaloside IV, we selected astragaloside IV as a candidate interface inhibitor for IDO1 and GBP1. After treating NCI-H1299 cells with 5 and 10 μM astragaloside IV, the binding ability of the truncated IDO1 and GBP1 was weakened (**Figure 5B**). To detect the protein expression of GBP1 and IDO1, we found that astragaloside IV can prevent the extracellular localization of IDO1 (**Figure 5C**). Next, we use transwell, wound healing and colony formation assays to analyze the effects of astragaloside IV on the invasion, migration of lung cancer cells. The results show that compared with control group, Astragaloside IV (5 and 10 μM) can inhibit cell invasion (**Figure 5D**), migration (**Figure 5E**) and colony formation ability (**Figure 5F**). This indicated that inhibiting the extracellular secretion of IDO1 by blocking the interaction of IDO1 and GBP1 can also inhibit the malignant progression of lung cancer cells.

Astragaloside IV Inhibits Tumor Genesis and Metastasis *In Vivo*

Because IDO1 can inhibit the anti-tumor effect of T cells by degrading tryptophan. Therefore, blocking the extracellular secretion of IDO1 may enhance the anti-tumor effect of PD-1 inhibitors. Here we inoculate Lewis lung cancer cells into C57 mice by subcutaneous injection. After combined treatment with astragaloside IV and PD-1 antibody, the effect on tumor growth

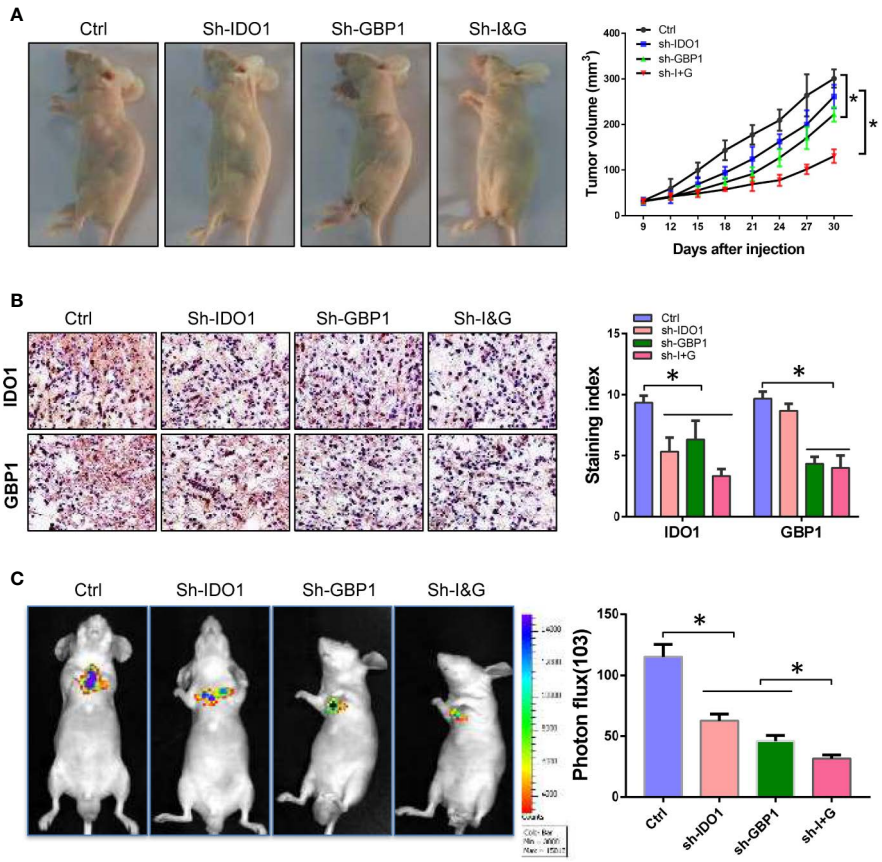

FIGURE 4 | Knock-down of IDO1 and GBP1 inhibits lung cancer tumorigenesis and metastasis. **(A)** Pictures of tumor-bearing mice and tumor volume. **(B)** The expression and subcellular location of IDO1 and GBP1 detected by immunohistochemistry. **(C)** Images of lung metastases and relative fluorescence intensity of metastatic tumor. Statistical significance was considered at $P < 0.05$ and marked with *.

was evaluated. The results showed that astragaloside IV can enhance the inhibitory effect of PD-1 inhibitors on tumor growth (**Figure 6A**). By using IHC, it was found that astragaloside IV had no effect on the expression of GBP1, but the amount of extracellular secretion of IDO1 was reduced (**Figure 6B**). This can further confirm that astragaloside IV blocks the extracellular localization of IDO1 to enhance the anti-tumor effect of PD-1 inhibitors. In addition, the use of flow cytometry analysis found that the proportion of CD3+CD8+ T cells increased after treatment with astragaloside IV (**Figure 6C**). This showed that astragaloside IV can promote the activation of T cells and enhance the effect of anti-tumor immunotherapy. All the above experiments showed that GBP1 combined with IDO1 to increase the secretion of IDO1 and promotes the malignant progression of lung cancer. And astragaloside IV can assist the anti-tumor effect of PD-1 by blocking the binding of GBP1 and IDO1 (**Figure 6D**). These results indicate that astragaloside IV can block the combination of IDO1 and GBP1 and reduce the secretion of IDO1, and further enhance the anti-tumor effect of PD-1 inhibitors by reducing T cell exhaustion.

DISCUSSION

The combination of surgical resection and chemotherapy improves the prognosis of patients with lung cancer. However, additional chemotherapy and targeted therapies remain ineffective in improving the prognosis of patients with metastasis (5, 13). Although the application of immune checkpoint inhibitors has brought hope for cancer immunotherapy, many patients still do not respond to the therapy (14, 15). This phenomenon may be related to the expression of PD-L1 in tumor cells and the tumor microenvironment. Previous study found that inhibiting IDO1 can restore the activity of T cells and improve the ability to kill tumor cells (16–18). Hence, a variety of drug candidates have been developed and are in clinical trials. Most laboratories researching IDO1 agree that it is a cytoplasmic protein. Only Rita Romani's research has shown that human amniotic fluid stem cells exert immunoregulatory functions through secreted IDO1 (19). However, the role of extracellular secretion of IDO1 in cancer progression has not yet been described. The present study showed that IDO1 can bind to GBP1 and then be secreted

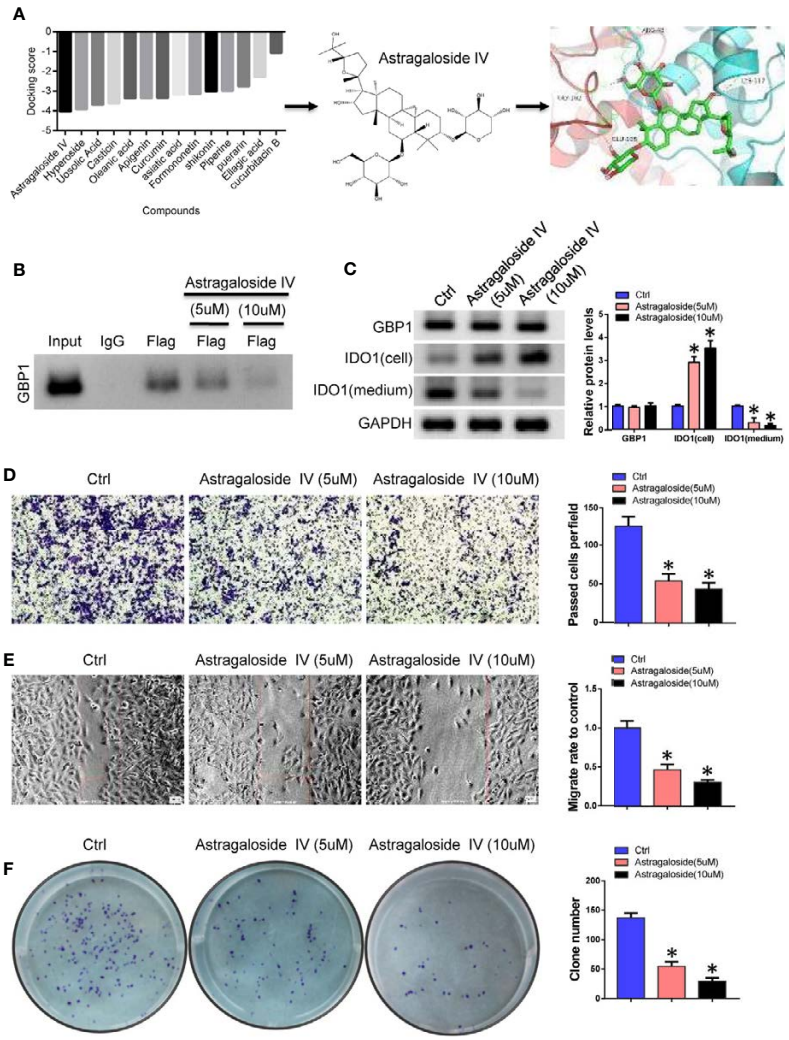

FIGURE 5 | Astragaloside IV blocks the interaction of IDO1 and GBP1. **(A)**. Screening of interface inhibitors and the binding of astragaloside IV to IDO1 and GBP1 interaction regions. **(B)** Co-IP was performed to detect the effect of astragaloside IV between IDO1 and GBP1 binding. **(C)** Western blot detects the expression of GBP1 and IDO1. **(D)** Transwell to evaluate the role of astragaloside IV on cell invasion. **(E)** Cell migration was detected by wound healing assay. **(F)** The role of astragaloside IV on cell colony formation ability. Statistical significance was considered at $P < 0.05$ and marked with *.

outside the cell with the assistance of GBP1. This phenomenon may explain why the high expression of IDO1 alone is not significantly related to the prognosis of patients with lung adenocarcinoma.

GBP1, as a member of the GTPase superfamily, participates in membrane, cytoskeleton and cell verification reactions (20–22). However, in tumors, GBP1 is a double-edged sword. High GBP1 expression has been previously related to better or worse prognosis in different human tumors. In colorectal cancer, GBP1 can inhibit tumor cell proliferation (23). However, in oral squamous cell carcinoma and ovarian cancer, GBP1 confers tumor cells with stronger drug resistance, and its expression level is related to the poor prognosis of patients (24–26). The expression and activity of GBP1 are closely related to the tumor microenvironment (27). Stimulation of inflammatory factors can induce the expression of GBP1, 2 and 5, but only GBP1 is secreted outside the cell (25, 28). In the present study, GBP1 can bind IDO1, thereby transporting IDO1 to the extracellular matrix during the secretion of GBP1. This result suggests that IDO1 only responds to IDO1 inhibitors after it is secreted into the cell matrix through a similar pathway. However, how GBP1 is secreted out of cells in the body and its relationship with tumor microenvironment and inflammation warrant further verification.

The recognition of tumor cells by T cells must be enhanced and T cells must have strong killing ability to promote the clinical application of immune checkpoint inhibitors. If IDO1 is secreted into the extracellular matrix with the assistance of GBP1, it is bound to have a certain inhibitory effect on the activity of T cells (29, 30). In animal models of glioma, the combination of IDO1 and PD-1 inhibitors prolongs the survival time of animals (31, 32). These seem to indicate that inhibiting the activity of IDO1 can enhance the anti-tumor effect of PD-1 inhibitors. In the present study, we used interface inhibitors to break the combination of GBP1 and IDO1,

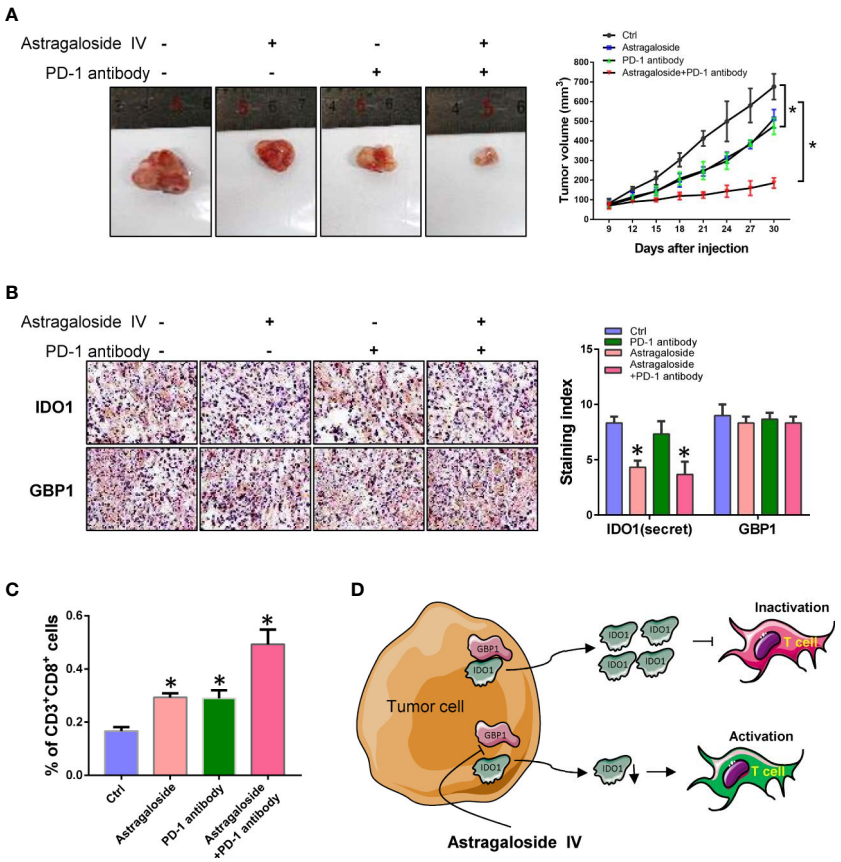

FIGURE 6 | Astragaloside IV combined with PD-1 inhibitor represses tumor growth of lung cancer. **(A)**. The effect of astragaloside IV combined with PD-1 inhibitors on tumor growth. **(B)**. Detection of IDO1 and GBP1 expression by immunohistochemistry. **(C)**. Percentage of tumor infiltrating $CD3^+CD8^+$ T cells. **(D)**. Schematic diagram of this study. Statistical significance was considered at $P < 0.05$ and marked with *.

avoid the extracellular localization of IDO1 and solve the root cause of IDO1's inhibitory effect on T cell activity. Astragaloside IV can block the combination of IDO1 and GBP1 to prevent the exhaustion of T cells caused by the extracellular secretion of IDO1, and further enhance the inhibitory effect of PD-1 inhibitors in lung cancer. Studies have shown that Astragaloside IV has anti-inflammatory and chemotherapy sensitization effects (33–35). Here we found the synergistic anti-tumor effect of astragaloside IV combined with PD-1. Of course, other effects of astragaloside IV may play a certain role in tumor growth in this experiment. However, we did detect that astragaloside IV can block the combination of IDO1 and GBP1. In addition, studies have suggested that astragaloside IV can inhibit the expression of IDO1, which may be inconsistent with our conclusions (36). Our results prove that blocking the extracellular secretion of IDO1 can enhance the therapeutic effect of PD-1.

The interaction of GBP1 and IDO1 induced the extracellular secretion of IDO1 promote lung cancer cell progression. In addition, astragaloside IV can block the interaction between GBP1 and IDO1 and enhance the inhibitory effect of PD-1 inhibitors of lung cancer cell *in vivo* and *in vitro*. These results explain the mechanism of IDO1 in regulating T cell infiltration in lung cancer and provide a certain possibility for its clinical combination therapy with PD-1 inhibitors.

DATA AVAILABILITY STATEMENT

The original contributions presented in the study are included in the article/**Supplementary Material**; further inquiries can be directed to the corresponding author.

ETHICS STATEMENT

The animal study was reviewed and approved by Affiliated Taizhou hospital of Wenzhou Medical University.

AUTHOR CONTRIBUTIONS

HY conceived and designed the study. YM performed the cell and animal experiments and wrote the paper. WW and KC

performed cell and molecular experiments. XX performed the pathological analysis. SZ analyzed data. All authors contributed to the article and approved the submitted version.

FUNDING

This work was funded by the National Natural Science Foundation of China (81874221) and the Taizhou Science and Technology Bureau (20ywa09).

REFERENCES

1. Brody H. Lung cancer. *Nature* (2014) 513:S1. doi: 10.1038/513S1a
2. Hamann HA, Ver Hoeve ES, Carter-Harris L, Studts JL, Ostroff JS. Multilevel Opportunities to Address Lung Cancer Stigma across the Cancer Control Continuum. *J Thorac Oncol* (2018) 13:1062–75. doi: 10.1016/j.jtho.2018.05.014
3. Duruisseaux M, Esteller M. Lung cancer epigenetics: From knowledge to applications. *Semin Cancer Biol* (2018) 51:116–28. doi: 10.1016/j.semcancer.2017.09.005
4. Calvayrac O, Pradines A, Pons E, Mazieres J, Guibert N. Molecular biomarkers for lung adenocarcinoma. *Eur Respir J* (2017) 49. doi: 10.1183/13993003.01734-2016
5. Hirsch FR, Scagliotti GV, Mulshine JL, Kwon R, Curran WJ Jr., Wu YL, et al. Lung cancer: current therapies and new targeted treatments. *Lancet* (2017) 389:299–311. doi: 10.1016/S0140-6736(16)30958-8
6. Munn DH, Mellor AL. Indoleamine 2,3 dioxygenase and metabolic control of immune responses. *Trends Immunol* (2013) 34:137–43. doi: 10.1016/j.it.2012.10.001
7. Munn DH, Mellor AL. Indoleamine 2,3-dioxygenase and tumor-induced tolerance. *J Clin Invest* (2007) 117:1147–54. doi: 10.1172/JCI31178
8. Goyne HE, Cannon MJ. Dendritic cell vaccination, immune regulation, and clinical outcomes in ovarian cancer. *Front Immunol* (2013) 4:382. doi: 10.3389/fimmu.2013.00382
9. Asghar K, Farooq A, Zulfiqar B, Rashid MU. Indoleamine 2,3-dioxygenase: As a potential prognostic marker and immunotherapeutic target for hepatocellular carcinoma. *World J Gastroenterol* (2017) 23:2286–93. doi: 10.3748/wjg.v23.i13.2286
10. Ferns DM, Kema IP, Buist MR, Nijman HW, Kenter GG, Jordanova ES. Indoleamine-2,3-dioxygenase (IDO) metabolic activity is detrimental for cervical cancer patient survival. *Oncoimmunology* (2015) 4:e981457. doi: 10.4161/2162402X.2014.981457
11. Schalper KA, Carvajal-Hausdorf D, McLaughlin J, Altan M, Velcheti V, Gaule P, et al. Differential Expression and Significance of PD-L1, IDO-1, and B7-H4 in Human Lung Cancer. *Clin Cancer Res* (2017) 23:370–8. doi: 10.1158/1078-0432.CCR-16-0150
12. Astigiano S, Morandi B, Costa R, Mastracci L, D'Agostino A, Ratto GB, et al. Eosinophil granulocytes account for indoleamine 2,3-dioxygenase-mediated immune escape in human non-small cell lung cancer. *Neoplasia* (2005) 7:390–6. doi: 10.1593/neo.04658
13. Osmani L, Askin F, Gabrielson E, Li QK. Current WHO guidelines and the critical role of immunohistochemical markers in the subclassification of non-small cell lung carcinoma (NSCLC): Moving from targeted therapy to immunotherapy. *Semin Cancer Biol* (2018) 52:103–9. doi: 10.1016/j.semcancer.2017.11.019
14. Yang Y. Cancer immunotherapy: harnessing the immune system to battle cancer. *J Clin Invest* (2015) 125:3335–7. doi: 10.1172/JCI83871
15. O'Donnell JS, Teng MWL, Smyth MJ. Cancer immunoediting and resistance to T cell-based immunotherapy. *Nat Rev Clin Oncol* (2019) 16:151–67. doi: 10.1038/s41571-018-0142-8
16. Labadie BW, Bao R, Luke JJ. Reimagining IDO Pathway Inhibition in Cancer Immunotherapy via Downstream Focus on the Tryptophan-Kynurenine-Aryl Hydrocarbon Axis. *Clin Cancer Res* (2019) 25:1462–71. doi: 10.1158/1078-0432.CCR-18-2882
17. Munn DH, Mellor AL. IDO in the Tumor Microenvironment: Inflammation, Counter-Regulation, and Tolerance. *Trends Immunol* (2016) 37:193–207. doi: 10.1016/j.it.2016.01.002
18. Li A, Barsoumian HB, Schoenhals JE, Caetano MS, Wang X, Menon H, et al. IDO1 Inhibition Overcomes Radiation-Induced "Rebound Immune Suppression" by Reducing Numbers of IDO1-Expressing Myeloid-Derived Suppressor Cells in the Tumor Microenvironment. *Int J Radiat Oncol Biol Phys* (2019) 104:903–12. doi: 10.1016/j.ijrobp.2019.03.022
19. Romani R, Pirisinu I, Calvitti M, Pallotta MT, Gargaro M, Bistoni G, et al. Stem cells from human amniotic fluid exert immunoregulatory function via secreted indoleamine 2,3-dioxygenase1. *J Cell Mol Med* (2015) 19:1593–605. doi: 10.1111/jcmm.12534
20. Piro AS, Hernandez D, Luoma S, Feeley EM, Finethy R, Yirga A, et al. Detection of Cytosolic Shigella flexneri via a C-Terminal Triple-Arginine Motif of GBP1 Inhibits Actin-Based Motility. *mBio* (2017) 8. doi: 10.1128/mBio.01979-17
21. Scheffzek K, Shivalingaiah G. Ras-Specific GTPase-Activating Proteins-Structures, Mechanisms, and Interactions. *Cold Spring Harb Perspect Med* (2019) 9. doi: 10.1101/cshperspect.a031500
22. Mizuno-Yamasaki E, Rivera-Molina F, Novick P. GTPase networks in membrane traffic. *Annu Rev Biochem* (2012) 81:637–59. doi: 10.1146/annurev-biochem-052810-093700
23. Britzen-Laurent N, Lipnik K, Ocker M, Naschberger E, Schellerer VS, Croner RS, et al. GBP-1 acts as a tumor suppressor in colorectal cancer cells. *Carcinogenesis* (2013) 34:153–62. doi: 10.1093/carcin/bgs310
24. Andreoli M, Persico M, Kumar A, Orteca N, Kumar V, Pepe A, et al. Identification of the first inhibitor of the GBP1:PIM1 interaction. Implications for the development of a new class of anticancer agents against paclitaxel resistant cancer cells. *J Med Chem* (2014) 57:7916–32. doi: 10.1021/jm5009902
25. Honkala AT, Tailor D, Malhotra SV. Guanylate-Binding Protein 1: An Emerging Target in Inflammation and Cancer. *Front Immunol* (2019) 10:3139. doi: 10.3389/fimmu.2019.03139
26. De Donato M, Mariani M, Petrella L, Martinelli E, Zannoni GF, Vellone V, et al. Class III beta-tubulin and the cytoskeletal gateway for drug resistance in ovarian cancer. *J Cell Physiol* (2012) 227:1034–41. doi: 10.1002/jcp.22813
27. Sahu M, Mallick B. An integrative approach predicted co-expression sub-networks regulating properties of stem cells and differentiation. *Comput Biol Chem* (2016) 64:250–62. doi: 10.1016/j.compbiolchem.2016.07.006
28. Tretina K, Park ES, Maminska A, MacMicking JD. Interferon-induced guanylate-binding proteins: Guardians of host defense in health and disease. *J Exp Med* (2019) 216:482–500. doi: 10.1084/jem.20182031
29. Zhai L, Ladomersky E, Lenzen A, Nguyen B, Patel R, Lauing KL, et al. IDO1 in cancer: a Gemini of immune checkpoints. *Cell Mol Immunol* (2018) 15:447–57. doi: 10.1038/cmi.2017.143
30. Blair AB, Kleponis J, Thomas DL, Muth ST, Murphy AG, Kim V, et al. IDO1 inhibition potentiates vaccine-induced immunity against pancreatic adenocarcinoma. *J Clin Invest* (2019) 129:1742–55. doi: 10.1172/JCI124077
31. Ladomersky E, Zhai L, Lenzen A, Lauing KL, Qian J, Scholtens DM, et al. IDO1 Inhibition Synergizes with Radiation and PD-1 Blockade to Durably Increase Survival Against Advanced Glioblastoma. *Clin Cancer Res* (2018) 24:2559–73. doi: 10.1158/1078-0432.CCR-17-3573
32. Liu S, Wang Z, Wang Y, Fan X, Zhang C, Ma W, et al. PD-1 related transcriptome profile and clinical outcome in diffuse gliomas. *Oncoimmunology* (2018) 7:e1382792. doi: 10.1080/2162402X.2017.1382792

SUPPLEMENTARY MATERIAL

The Supplementary Material for this article can be found online at: https://www.frontiersin.org/articles/10.3389/fimmu.2020.622467/full#supplementary-material

SUPPLEMENTARY FIGURE 1 | IDO1 binds GBP1 in A549 cells. **(A)** Identification of IDO1 binding protein by silver staining. **(B)** Use Co-IP to detect the interaction between IDO1 and GBP1. **(C)** GST pull-down was performed to analyze the interaction between IDO1 and GBP1 *in vitro*. D. Immunofluorescence confirms the co-localization of IDO1 and GBP1 in A549 cells.

33. Zheng Y, Dai Y, Liu W, Wang N, Cai Y, Wang S, et al. Astragaloside IV enhances taxol chemosensitivity of breast cancer via caveolin-1-targeting oxidant damage. *J Cell Physiol* (2019) 234:4277–90. doi: 10.1002/jcp.27196
34. Ye Q, Su L, Chen D, Zheng W, Liu Y. Astragaloside IV Induced miR-134 Expression Reduces EMT and Increases Chemotherapeutic Sensitivity by Suppressing CREB1 Signaling in Colorectal Cancer Cell Line SW-480. *Cell Physiol Biochem* (2017) 43:1617–26. doi: 10.1159/000482025
35. Jiang P, Ma D, Wang X, Wang Y, Bi Y, Yang J, et al. Astragaloside IV Prevents Obesity-Associated Hypertension by Improving Pro-Inflammatory Reaction and Leptin Resistance. *Mol Cells* (2018) 41:244–55. doi: 10.14348/molcells.2018.2156
36. Zhang A, Zheng Y, Que Z, Zhang L, Lin S, Le V, et al. Astragaloside IV inhibits progression of lung cancer by mediating immune function of Tregs and CTLs by interfering with IDO. *J Cancer Res Clin Oncol* (2014) 140:1883–90. doi: 10.1007/s00432-014-1744-x

Conflict of Interest: The authors declare that the research was conducted in the absence of any commercial or financial relationships that could be construed as a potential conflict of interest.

Copyright © 2021 Meng, Wang, Chen, Chen, Xia, Zhou and Yang. This is an open-access article distributed under the terms of the Creative Commons Attribution License (CC BY). The use, distribution or reproduction in other forums is permitted, provided the original author(s) and the copyright owner(s) are credited and that the original publication in this journal is cited, in accordance with accepted academic practice. No use, distribution or reproduction is permitted which does not comply with these terms.

frontiers in Immunology

ORIGINAL RESEARCH
published: 20 January 2021
doi: 10.3389/fimmu.2020.612547

Nocardia Rubra Cell Wall Skeleton Up-Regulates T Cell Subsets and Inhibits PD-1/PD-L1 Pathway to Promote Local Immune Status of Patients With High-Risk Human Papillomavirus Infection and Cervical Intraepithelial Neoplasia

Wei Chen[1], Yi Zhang[2], Chunfang Zhao[1], Suxia Shao[1], Yanan Zhang[1], Xuehui Li[3], Xue Bai[4], Qianyu Guo[1], Qianwen Liu[1], Junmin Tang[5] and Lei Zhang[1]**

[1] Department of Histology and Embryology, Hebei Medical University, Shijiazhuang, China, [2] Department of Medicine, Weihai Greatest Pharmaceutical Research Institute Co., Ltd., Weihai, China, [3] Department of Gynaecology, The First Hospital of Hebei Medical University, Shijiazhuang, China, [4] Department of Gynaecology, The Fourth Hospital of Hebei Medical University, Shijiazhuang, China, [5] Department of Histology and Embryology, Peking University Health Science Centre, Beijing, China

The Nocardia rubra cell wall skeleton (Nr-CWS) for external use is an immune enhancer, which has been widely used in human cervix diseases such as cervical erosion, but the mechanism of Nr-CWS enhancing immunity is still unclear. The purpose of this study was to explore the effect and mechanism of Nr-CWS on the local immune status of cervical tissue in patients with high-risk human papillomavirus (HR-HPV) infection and cervical precancerous lesion, cervical intraepithelial neoplasia (CIN). The recruited patients with HR-HPV infection and CIN were treated with Nr-CWS. The specimens were taken from these patients before and after local application of Nr-CWS respectively. The normal control specimens were tested simultaneously. Serial section analysis of immunohistochemistry and co-expression analysis were performed to characterize populations of T cells and the expressions of programmed cell death-1 (PD-1) and programmed cell death-ligand 1 (PD-L1). The levels of cytokines in local cervical tissue were also detected. Nr-CWS significantly increased T cells including $CD4^+$, $CD8^+$ T cells, and reduced the expression of PD-L1 in the patients' local cervical tissues. Co-expression analyses showed that the proportions of $PD\text{-}1^+CD4^+$ cells in $CD4^+$ T cells and $PD\text{-}1^+CD8^+$ cells in $CD8^+$ T cells decreased after Nr-CWS application. Furthermore, the increase in the number of immune cells was accompanied by increased pro-inflammatory cytokines interleukin-12 (IL-12), interferon-γ (IFN-γ), tumor necrosis factor-α (TNF-α), and decreased

OPEN ACCESS

Edited by:
Peng Qu,
National Institutes of Health (NIH), United States

Reviewed by:
Zhenying Nie,
Oregon Health and Science University, United States
Huiwen Liu,
Harbin Medical University, China

***Correspondence:**
Lei Zhang
zhang13903210199@163.com
Junmin Tang
jmtang242@163.com

Specialty section:
This article was submitted to Cancer Immunity and Immunotherapy, a section of the journal Frontiers in Immunology

Received: *30 September 2020*
Accepted: *02 December 2020*
Published: *20 January 2021*

Citation:
Chen W, Zhang Y, Zhao C, Shao S, Zhang Y, Li X, Bai X, Guo Q, Liu Q, Tang J and Zhang L (2021) Nocardia Rubra Cell Wall Skeleton Up-Regulates T Cell Subsets and Inhibits PD-1/PD-L1 Pathway to Promote Local Immune Status of Patients With High-Risk Human Papillomavirus Infection and Cervical Intraepithelial Neoplasia. Front. Immunol. 11:612547. doi: 10.3389/fimmu.2020.612547

suppressive cytokine IL-10. The results indicate that Nr-CWS, as an immunotherapeutic agent for HR-HPV infection and CIN, plays an immune promoting role related to the upregulation of T cell subsets and the inhibition of PD-1/PD-L1 pathway.

Keywords: Nocardia rubra cell wall skeleton, high-risk human papillomavirus, cervical intraepithelial neoplasia, CD4+ T cell, CD8+ T cell, programmed cell death-1, programmed cell death-ligand 1

INTRODUCTION

Cervical cancer is the fourth most common cancer in females worldwide. China together with India, contributed more than one-third of the global cervical burden in 2018, with 106,000 cases and 48,000 deaths in China (1). Cervical cancer is still an important cause of mortality among females in developing countries (2). It has been well known that human papillomavirus (HPVs) are the etiological agents of cervical cancer and its premalignant precursor cervical intraepithelial neoplasia (CIN) (3). However, not all women who harbor HPV infection will develop cervical cancer. With normal immune function, most HPV infections can be cleared by an incompletely understood immune response within 6–18 months (4). Nevertheless, the risk of CIN increases with the type of HPV, duration of infection, immunosuppression, and environmental factors like cigarette smoking in the patient. The presence of persistent infection with high-risk HPV (HR-HPV) (5) and those who have associated cofactors like immunodeficiency or smoking are at higher risk for the progression of lesions to the development of invasive cancer. In China, the reported HR-HPV persistent infection rate among women (ages 16–69) was 13.30%–22.94% (6). It was reported that 21% of patients progressed to CIN 2 or higher, if HR-HPV infection persisted for more than 1 year (7).

The host immune response serves a pivotal role in eliminating HR-HPV and determining the regression of a cervical abnormality or persistence and progression to a malignancy (8). Improving body's immunity to HR-HPV and avoiding immune escape should be important methods for the treatment of CIN and even cervical cancer.

The Nocardia rubra cell wall skeleton (Nr-CWS) is the cell wall skeleton obtained from N. rubra, a gram-positive bacterium, and mainly contains arabinogalactan, muramic acid and mucopeptide. Nr-CWS was first reported by Azuma et al. in 1976 (9) and was subsequently shown to exert antitumor effects and affect the complex immune network formed by interactions of immunocompetent cells (10). Recently, it has been proved *in vitro* that Nr-CWS could stimulate macrophages (11), dendritic cells, natural killer cells (12), $CD4^+$ T cells (13), and $CD8^+$ T cells (14), which imply its potential application in immunotherapy.

As an approved National Category II New Drug in China, the Nr-CWS for external use has been used for human cervix diseases, but the mechanism of Nr-CWS enhancing immunity in cervix is still unclear. The purpose of this study was to explore the effect and mechanism of Nr-CWS on the local immune status of cervical tissue in patients with HR-HPV infection and CIN, revealing its potential broad application prospects in the immunotherapy of cervical precancerous lesions and even cancer.

MATERIALS AND METHODS

Reagents

The Nr-CWS for external use (Drug approval number: S20030009) was provided by Weihai Greatest Pharmaceutical Research Institute Co., Ltd. (China).

Samples and Patients

After obtaining ethical approval from the First Hospital and the Fourth Hospital of Hebei Medical University, People's Republic of China, the study participants were recruited from these two hospitals in 2019 and 2020. All participants gave written informed consent. Available clinical information included the Pap smear report, histology diagnosis, HPV DNA genotyping, prior cervical pathology, and HPV history.

Twenty-three patients suffered with CIN and HR-HPV infection in female lower genital tract were recruited and treated with Nr-CWS. HPV DNA genotyping and biopsy report were the gold standards for defining final disease status. Participants with the following conditions were excluded from the study: pregnancy, women with any signs and symptoms of sexually transmitted infections, severe heart, lung, liver and kidney disease, any other neoplastic diseases, immunocompromised state, and those under any anti-inflammatory or immunosuppressive treatment. The cervical specimens were taken from these patients at the times before and 1 and 3 months after local application of Nr-CWS respectively. During the re-examination 3 months after Nr-CWS treatment, HPV DNA genotyping and biopsy were detected.

Five normal control cervical specimens were taken from the patients without HPV infection who underwent hysteroscopic endometrial electrotomy or hysteroscopic transcervical resection of myoma because of their endometrium polyp or submucosal myoma of uterus.

Nr-CWS Administration Method

The patients were given Nr-CWS on the 3^{rd} day after menstruation. The drug was administered once every other day at a dose of 120 μg for 10 times. The cervix was exposed and cleaned with a cotton ball soaked with normal saline, and wiped repeatedly with a dry gauze to form minor wounds. The Nr-CWS solution (60 μg Nr-CWS dissolved in 0.5 ml normal saline) was injected into the cervical canal with a Pasteur pipette. The Nr-CWS solution (60 μg Nr-CWS dissolved in 2 ml normal saline) was soaked with a cotton ball with tail thread and then pressed on the cervical surface with forceps for 1 min. After Nr-CWS application, the patient can move freely after lying down for 10 min. The cotton ball with tail thread was kept in the body for 24 h and then taken out.

Immunohistochemical Method

Immunohistochemical method was performed to detect the infiltration of T cells and the expressions of programmed cell death-1 (PD-1) and programmed cell death-ligand 1 (PD-L1) in the local cervix. Cervical tissue samples were fixed in 10% formalin. Immunohistochemistry was performed using our previously published protocol (15). In brief, tissue sections were incubated with one of the following primary antibodies: anti-CD3 (1 : 500; ZsBio, Beijing, China), anti-CD4 (1 : 500; Abways Technology, Shanghai, China), anti-CD8 (1 : 500; Abways Technology), anti-PD-1 (1 : 1000; Abcam, Cambridge, Massachusetts, USA) and anti-PD-L1 (1 : 1000; Abcam). Immunodetection was performed using an appropriate biotinylated immunoglobulin and a horseradish peroxidase-labeled avidin kit (ZsBio) with diaminobenzidine (DAB) as the substrate. Finally, the sections were lightly counterstained with hematoxylin for 30 s.

Scoring System and Analysis of Immunohistochemical Method

The modified McCarty's "H" scoring system was used to evaluate the immunohistochemistry method (16).

$$\textit{Modified H - score}\ (0-300) = \textit{intensity}\ (0-3) \times \textit{percentage of immunohistochemical positive cells}$$

One hundred cells were counted sequentially and percentage of immunohistochemical positive cells was calculated. In order to make intensity assessments more objective, the intensity of immunohistochemical positive was not assessed visually, but measured as mean grey value (MGV). The MGV was analysed using Image-J software (NIH, Bethesda, MA, USA). The following MGV ranges were used to grade the intensity of staining (191.5–255, 0 = negative; 127.5–191.5, 1 = weak positive; 63.5–127.5, 2 = moderate intensity; < 63.5, 3 = strong positive). With values obtained, the total modified H-scores were calculated. Ten fields were chosen randomly in each specimen.

Co-Expression Analysis

In order to detect the co-expression characteristics of PD-1 and T cell subsets, serial section immunohistochemistry and analysis of the percentage of CD4, CD8, and PD-1 positive cells were carried out. Patient specimens before and 1 month and 3 months after administration of Nr-CWS were immersed into 10% formalin for 24 h at room temperature and then embedded with paraffin. Consecutive 4-μm sections were cut from each paraffin-embedded block. Adjacent consecutive sections were used to detect the expressions of CD4, CD8 and PD-1 using immunohistochemical method. Ten fields of the same position in each specimen of the three indexes were randomly selected and the percentages of CD4, CD8, and PD-1 positive cells were calculated respectively.

Then we used double label immunofluorescence histochemical method and laser scanning confocal microscopy (LSCM) to analyze the co-expression of PD-1 and CD4 or CD8 in patient specimens before and 1 month and 3 months after administration of Nr-CWS. The 4-μm paraffin-embedded sections were subjected to the following treatments: Gradual alcohol dewaxing, PBS rinsing, incubation in 3% H_2O_2, PBS rinsing, antigen repair in 0.01 Mol/L citrate buffer and PBS rinsing. Sections were incubated with two primary antibodies of anti-PD-1 (1 : 200; Abcam) and anti-CD4 (1 : 200; Abways Technology) or anti-CD8 (1 : 200; Abways Technology). Subsequently, sections were incubated with secondary antibodies of goat anti-mouse IgG Alexa Fluor 594 (1 : 200; Abways Technology) and goat anti-rabbit IgG Alexa Fluor 488 (1 : 200; Abways Technology) and mounted. LSCM was performed on an Olympus FV1200MPE LSCM. For the results of double label staining, the $PD\text{-}1^+CD4^+$ cells/$CD4^+$ cells ratio and $PD\text{-}1^+CD8^+$ cells/$CD8^+$ cells ratio in the cervical epithelium and stroma were calculated.

Total RNA Isolation and qRT-PCR

To analyze the mRNA levels of cytokines including interleukin-10 (IL-10), interleukin-12 (IL-12), interferon-γ (IFN-γ) and tumor necrosis factor-α (TNF-α), total RNAs were extracted from cervical tissue samples using TRIzol and reverse transcribed with a PrimeScript® RT reagent Kit (TaKaRa Biotechnology, Dalian, China) for qRT-PCR using SYBR® Premix Ex Taq™ (TaKaRa Biotechnology) following the manufacturer's instructions. The purity and amount of RNA were determined by measuring the OD260/280 nm ratio. The mRNA levels were normalized using β-actin as the housekeeping gene and analyzed by the $2^{-}\delta\delta^{Ct}$ method. The primers were provided by Invitrogen (Carlsbad, CA, USA) (**Table 1**).

Statistical Analysis

Data are presented as means ± SDs. Statistical analysis was performed with SPSS version 19.0 (SPSS, Inc., Chicago, IL, USA). Statistical significance was determined by independent samples T-test or one-way Analysis of Variance (ANOVA). A P value less than 0.05 was considered to be significant.

RESULTS

Subject Characteristics of the Study Groups

The subject characteristics of the study groups are summarized in **Table 2**. The 23 recruited patients for Nr-CWS treatment were

TABLE 1 | Forward and reverse primers of cytokines and their oligo sequences.

Primer name	Oligo sequence (5′ to 3′)
IL-12 forward	AGAACTTGCAGCTGAAGCC
IL-12 reverse	CCTGGACCTGAACGCAGAAT
IFN-γ forward	CTTGAATGTCCAACGCAAAGC
IFN-γ reverse	TCTTCGACCTCGAAACAGCAT
TNF-α forward	GCTGCACTTTGGAGTGATCG
TNF-α reverse	TCACTCGGGGTTCGAGAAGA
IL-10 forward	AGGCAACCTGCCTAACATGC
IL-10 reverse	GTTCTCAGCTTGGGGCATCA
β-actin forward	CGCCACCAGTTCGCCATGGA
β-actin reverse	TACAGCCCGGGGAGCATCGT

TABLE 2 | Subject characteristics of the study groups.

	Nr-CWS group (n=23)			normal control group (n=5)
	Before Nr-CWS	1-Month After Nr-CWS	3-Month After Nr-CWS	
Age range (years)		22–56		32–39
Mean age (years)[1]		37.39 ± 9.15		35.6 ± 2.61
Subjects infected with HR-HPV type				
Single infection	47.83% (11/23)	–	26.09% (6/23)	0
Multiple infection	52.17% (12/23)	–	13.04% (3/23)	0
HR-HPV overcast rate	–	–	60.87% (14/23)	–
Pathological features				
CIN I	20	–	2	–
CIN II	3	–	0	–
Effective rate in pathological changes	–	–	91.3% (21/23)	–

CIN, cervical intraepithelial neoplasia; HR-HPV, high-risk human papillomavirus.
[1]mean ± SD.

aged between 22 and 56 years old (mean 37.39 ± 9.15 years old). In these 23 patients, a single HR-HPV type was detected in 11 (47.83%, 11/23), and two or more HR-HPV types were found in the same sample from 12 (52.17%, 12/23) women. The 5 patients in the normal control group were aged between 32 and 39 years old (mean 35.6 ± 2.61 years old), and no significant differences were found compared with the Nr-CWS treatment group. No HR-HPV infection was detected in these normal control patients.

At 3 months after Nr-CWS treatment, the results of HR-HPV detection in 14 out of the 23 cases became negative, and HR-HPV overcast rate was 60.87% (14/23). Besides, HR-HPV types were reduced in 3 other patients with multiple HR-HPV infections. Pathological efficient changes were observed in 21 out of the 23 cases, and the effective rate was 91.3% (21/23) at 3 months after Nr-CWS treatment.

Expressions of $CD3^+$ T, $CD4^+$ T and $CD8^+$ T Cell Detected by Immunohistochemistry

The $CD3^+$ T, $CD4^+$ T, or $CD8^+$ T cells were found both in human cervical squamous epithelium and in the underlying stroma in each group (**Figures 1A–L**). The brownish-yellowish deposits were distributed in the cytoplasm and on the cell membrane of the positive cells. The positive cells in human cervical epithelium were mainly located in the basal or intermediate layers and rarely appeared in the superficial layers.

Figures 1M–O showed that in the human cervical epithelial tissues of these recruited patients at 1 month after Nr-CWS administration, the modified H-scores of $CD3^+$ T, $CD4^+$ T, and $CD8^+$ T cells were significantly higher than those before Nr-CWS treatment ($P < 0.05$). At 3 months after Nr-CWS treatment, the $CD3^+$ T and $CD8^+$ T cells expression scores continued to increase and reached the highest level ($P < 0.05$). The $CD4^+$ T cells scores peaked at 1 month and dropped at 3 months. In the stroma underlying human cervical epithelium, the scores of $CD3^+$ T, $CD4^+$ T, and $CD8^+$ T cells were significantly higher at 1 month than those before Nr-CWS ($P < 0.05$) and reached the highest level. At 3 months, $CD3^+$ T, $CD4^+$ T, and $CD8^+$ T cells expression scores dropped, but were still significantly higher than those before treatment ($P < 0.05$).

Expressions of PD-1 and PD-L1 Detected by Immunohistochemistry

Figures 2A–D, I showed the PD-1 expression in normal control and recruited patients. The $PD\text{-}1^+$ cells with brownish-yellowish deposits in cytoplasm and cell membrane were distributed in human cervical epithelium and stroma. In the normal control group, PD-1 expression was almost absent. Before these patients were treated with Nr-CWS, the expression scores of PD-1 in human cervical epithelium and stroma were significantly higher than those of normal controls ($P < 0.05$). After Nr-CWS treatment, the PD-1 expression in the human cervical epithelial tissue decreased gradually with the extension of repair time, which was statistically significant compared with that before Nr-CWS treatment ($P < 0.05$). However, in human cervical stroma, the expression of PD-1 increased after Nr-CWS treatment ($P < 0.05$), which might be due to increased lymphocyte infiltration.

Figures 2E–H, J showed the PD-L1 expression in normal control and recruited patients. No PD-L1 expression was detected in human cervical tissue of the normal control group. Before the Nr-CWS treatment of these patients, PD-L1 expression was detected in human cervical epithelial cells, mainly in the basal layer of epithelium. The brownish-yellowish deposits were located in the cytoplasm and membrane of the PD-L1 positive cells. After administration of Nr-CWS, the expression level of PD-L1 strikingly reduced ($P < 0.05$) as the repair time prolonged.

Co-Expression Analysis of PD-1 and CD4 or CD8

The immunohistochemical results of co-expression analysis revealed the expressions of CD4, CD8 and PD-1 at the same position in the serial sections of human cervical tissue (**Figures 3A–I**). **Figure 3J** showed that in the human cervical epithelial

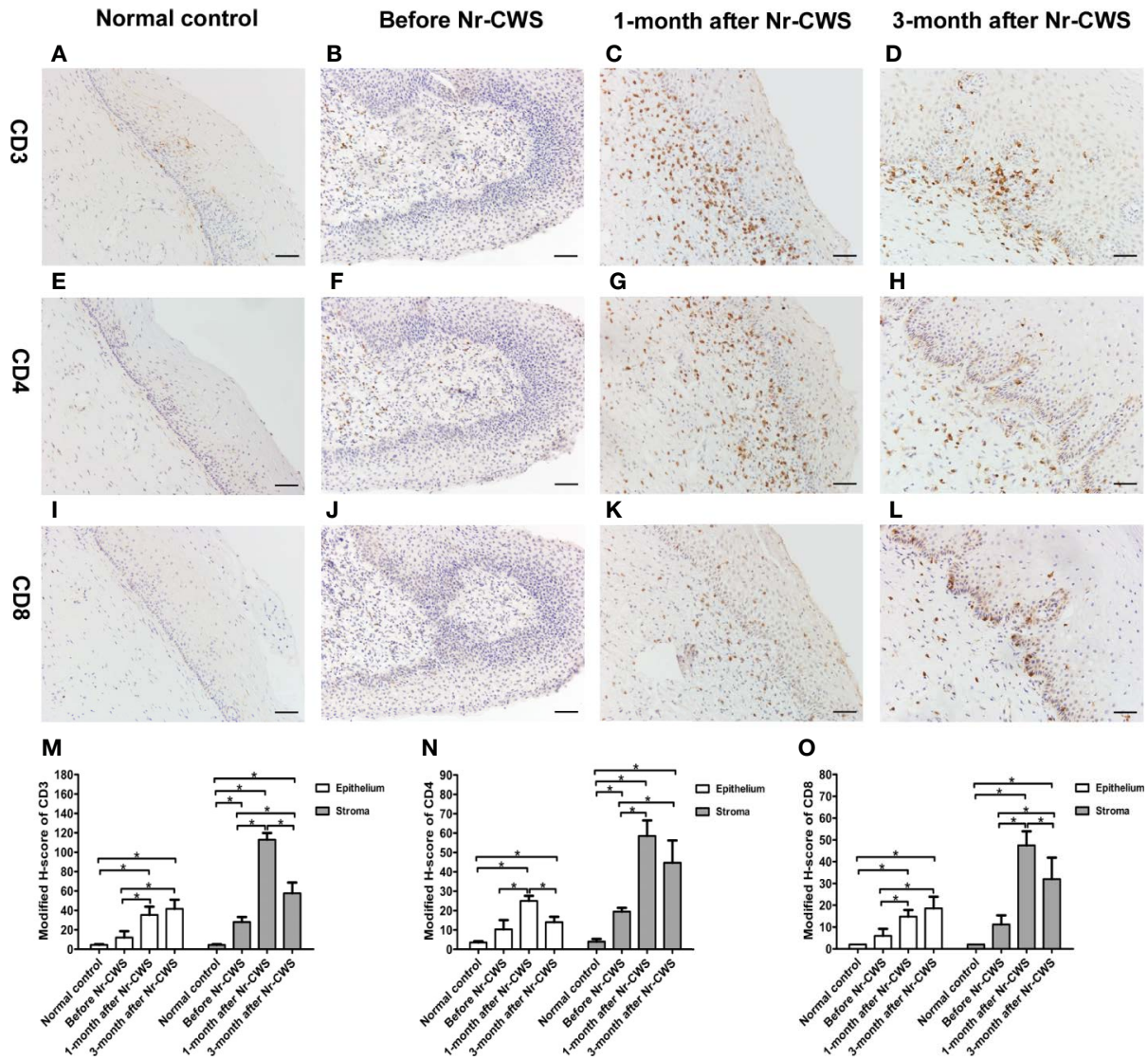

FIGURE 1 | Expressions of CD3, CD4, and CD8 detected by immunohistochemistry. The expressions of CD3 were detected in cervical tissues of the normal control group **(A)**, recruited patients before Nr-CWS treatment **(B)**, 1 month after Nr-CWS **(C)**, and 3 months after Nr-CWS **(D)**. Statistical data of CD3 **(M**: $^*P < 0.05$). The expressions of CD4 were detected in the normal control group **(E)**, recruited patients before Nr-CWS treatment **(F)**, 1 month after Nr-CWS **(G)**, and 3 months after Nr-CWS **(H)**. Statistical data of CD4 **(N**: $^*P < 0.05$). The expressions of CD8 were detected in the normal control group **(I)**, recruited patients before Nr-CWS treatment **(J)**, 1 month after Nr-CWS **(K)** and 3 months after Nr-CWS **(L)**. Statistical data of CD8 (**O**: $^*P < 0.05$). (**A–L**, scale bars = 50 μm).

tissue, the percentage of CD4 positive cells increased significantly after Nr-CWS treatment from 5.14% to 12.5% at 1 month ($P < 0.05$) and 7% at 3 months ($P < 0.05$), and reached a peak at 1 month. The percentage of CD8 positive cells kept increasing significantly after Nr-CWS treatment from 3% to 7.4% (at 1 month) ($P < 0.05$) and 9.29% (at 3 months) ($P < 0.05$), and peaked at 3 months. However, after Nr-CWS treatment, the percentage of PD-1^+ cells showed a continuous downward trend, from 6.2% before Nr-CWS treatment to 4.2% at 1 month and 1.71% at 3 months, and was significantly lower at 3 months than before Nr-CWS treatment ($P < 0.05$). In human cervical stroma (**Figure 3K**), the percentages of $CD4^+$ T and $CD8^+$ T cells increased significantly from 9.75% and 5.6% respectively after Nr-CWS treatment, reaching their respective peaks of 29.25% ($P < 0.05$) and 23.75% ($P < 0.05$) at 1 month. The percentages of $CD4^+$ T and $CD8^+$ T cells at 3 months were 22.33% and 16% respectively, both of which were significantly higher than those before Nr-CWS treatment ($P < 0.05$). The percentage of PD-1 positive cells was 5.33% before treatment, and significantly increased to 13.25% (at 1 month) ($P < 0.05$) and 13% (at 3 months) ($P < 0.05$) after Nr-CWS treatment.

Figures 4 and **5** showed the results of PD-1 and CD4 (or CD8) double label immunofluorescence histochemical method. Besides PD-$1^+$$CD4^+$ (or PD-$1^+$$CD8^+$) cells, much more PD-$1^-$

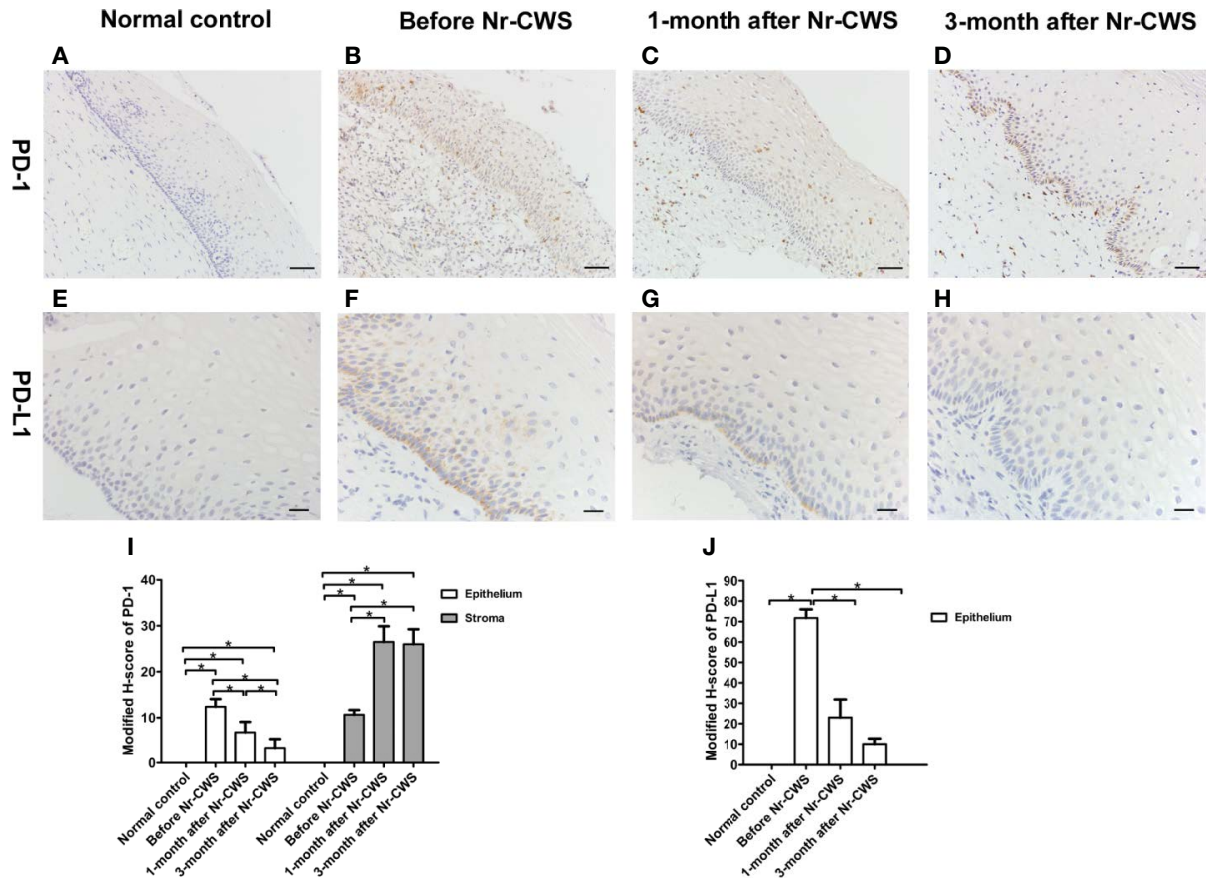

FIGURE 2 | Expressions of PD-1 and PD-L1 detected by immunohistochemistry. The expressions of PD-1 were detected in cervical tissues of the normal control group **(A)**, recruited patients before Nr-CWS treatment **(B)**, 1 month after Nr-CWS **(C)** and 3 months after Nr-CWS **(D)**. Statistical data of PD-1 (**I**: *$P < 0.05$). The expressions of PD-L1 were detected in the normal control group **(E)**, recruited patients before Nr-CWS treatment **(F)**, 1 month after Nr-CWS **(G)** and 3 months after Nr-CWS **(H)**. Statistical data of PD-L1 (**J**: *$P < 0.05$). (**A–D**, scale bars = 50 μm; **E–H**, scale bars = 20 μm).

$CD4^+$ (or $PD\text{-}1^-CD8^+$) cells appeared in human cervical epithelium and stroma after Nr-CWS treatment. In addition, some $PD\text{-}1^+CD4^-$ (or $PD\text{-}1^+CD8^-$) cells were observed in human epithelium and stroma before treatment. The $PD\text{-}1^+CD4^+$ cells/$CD4^+$ cells ratio and $PD\text{-}1^+CD8^+$ cells/$CD8^+$ cells ratio in human cervical epithelium and stroma were calculated separately. After Nr-CWS treatment, the $PD\text{-}1^+CD4^+$ cells/$CD4^+$ cells ratio significantly fell from 89.26% to 35% at 1 month ($P < 0.05$) and 5% at 3 month ($P < 0.05$) in the cervical epithelium, from 73.15% to 7% at 1 month ($P < 0.05$) and 14.7% at 3 month ($P < 0.05$) in the cervical stroma. The $PD\text{-}1^+CD8^+$ cells/$CD8^+$ cells ratio significantly fell from 85.16% to 30.14% at 1 month ($P < 0.05$) and 8.74% at 3 month ($P < 0.05$) in the cervical epithelium, from 89.83% to 32.03% at 1 month ($P < 0.05$) and 6.69% at 3 month ($P < 0.05$) in the cervical stroma.

Detection of Cytokine Levels in Human Cervical Tissue by qRT-PCR

The effect of Nr-CWS on cytokines in human cervical tissues was analyzed by qRT-PCR (**Figure 6**). Results showed that compared with those in the normal control, the mRNA levels of local pro-inflammatory cytokines (IL-12, IFN-γ, and TNF-α) were higher and the mRNA level of suppressive cytokine IL-10 was lower in the cervical tissues of these patients before Nr-CWS treatment. At 3 months after Nr-CWS, the mRNA levels of IL-12, IFN-γ, and TNF-α elevated significantly ($P < 0.05$) while the level of IL-10 decreased significantly ($P < 0.05$).

DISCUSSION

Over 100 subtypes of HPV exist with 15 being identified as high risk. Persistence of HR-HPV infection in tissues is critical factor in the development of CIN and ultimately, carcinoma. Therefore, in this study, patients with HR-HPV infection and CIN were selected as research objects to detect the therapeutic effect of Nr-CWS on cervical cancer-related precancerous lesions, so as to prevent the occurrence of human cervical cancer. Nevertheless, the standard-of-care management of CIN 2 and CIN 3 is mainly surgical therapy which ablates or excises in human cervical

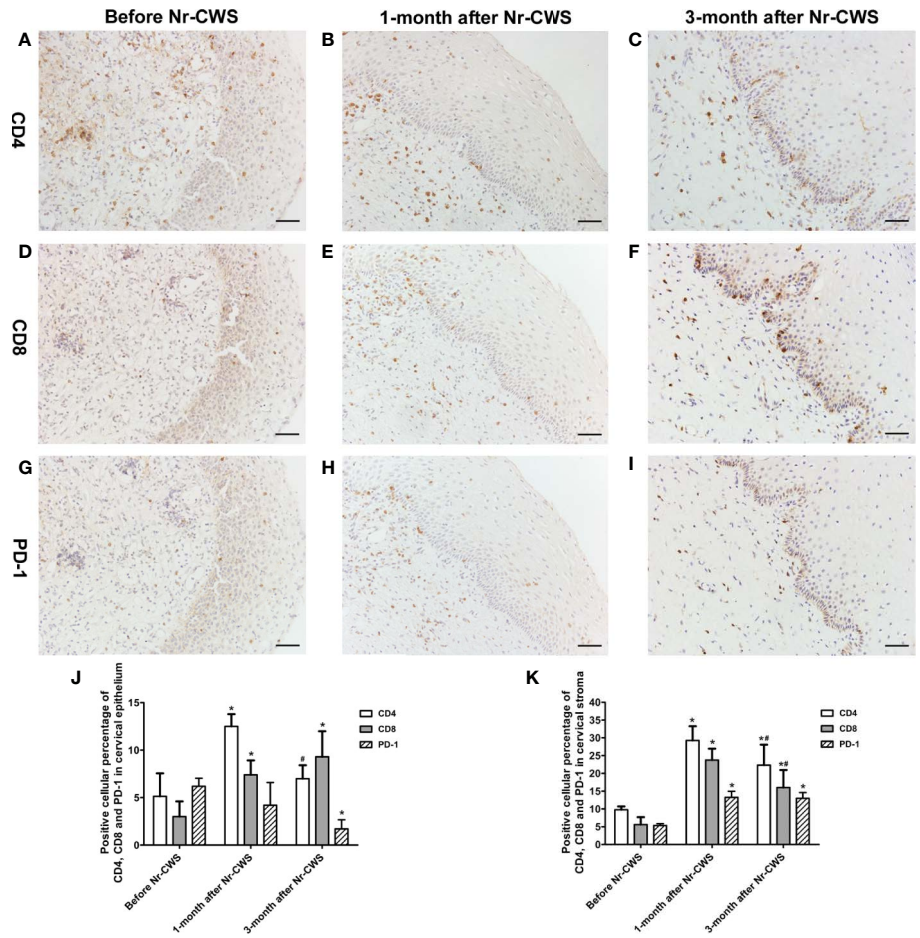

FIGURE 3 | Co-expression analysis of PD-1 and CD4 or CD8 by serial section immunohistochemistry. The immunohistochemistry results of co-expression analysis revealed the expressions of CD4, CD8, and PD-1 at the same position in the serial sections. CD4 expression in recruited patients before Nr-CWS **(A)**, 1 month after Nr-CWS **(B)** and 3 months after Nr-CWS **(C)**; CD8 expression in recruited patients before Nr-CWS **(D)**, 1 month after Nr-CWS **(E)** and 3 months after Nr-CWS **(F)**; PD-1 expression in recruited patients before Nr-CWS **(G)**, 1 month after Nr-CWS **(H)** and 3 months after Nr-CWS **(I)**. Statistical data of CD4, CD8, and PD-1 in the cervical epithelial tissue (**J**: $^{*}P < 0.05$ vs Before Nr-CWS, $^{\#}P < 0.05$ vs 1-month after Nr-CWS). Statistical data of CD4, CD8 and PD-1 in the cervical stroma (**K**: $^{*}P < 0.05$ vs Before Nr-CWS, $^{\#}P < 0.05$ vs 1-month after Nr-CWS). (**A–I**, scale bars = 50 μm).

transformation zone (17). So in this study, the subjects recruited in the actual clinical practice were mainly CIN 1 and few CIN 2 or higher patients.

The surgical therapy carries potential risks such as preterm birth (17). For patients with fertility requirements, there has been a long-standing and continued interest in the development of a safe, effective topical therapy. In the present study, Nr-CWS was applied locally in cervical tissues of patients with HR-HPV infection and CIN. Tissue samples from recruited patients were collected at 1 month after the application of Nr-CWS to detect short-term changes in cervical local immunity, and cervical tissue samples were collected at 3 months after Nr-CWS to detect local immune changes after repair for a period of time. For some reasons of clinical application, the placebo group was not set in this study, but the cervical local immune status of the patients before Nr-CWS treatment was compared with that of the normal control group. The former reflected the immune status in the absence of drug treatment for HR-HPV infection. The results showed that the HR-HPV overcast rate was about 60.87% after 3 months of repair, which was higher than the natural HPV negative conversion rate (26.9%) within 3 months (18). Meanwhile, the effective rate of pathological changes by removing dysplastic cells was 91.3% at 3 months after Nr-CWS treatment. The results showed that clinical application of Nr-CWS had a good clinical effect and may eliminate the HR-HPV infection and dysplastic cells in cervix of a considerable proportion of patients.

Cell-mediated immunity of an individual is considered to be a vital mechanism in protection against the virus and elimination of virus-infected cells. The activation of $CD4^+$ T cells and consequently synthesis of cytokines are essential in the immune response because these mediators could activate or inhibit other cells types including cytotoxic $CD8^+$ T cells (19). Cytotoxic $CD8^+$ T cell infiltrates appear to be principal effectors

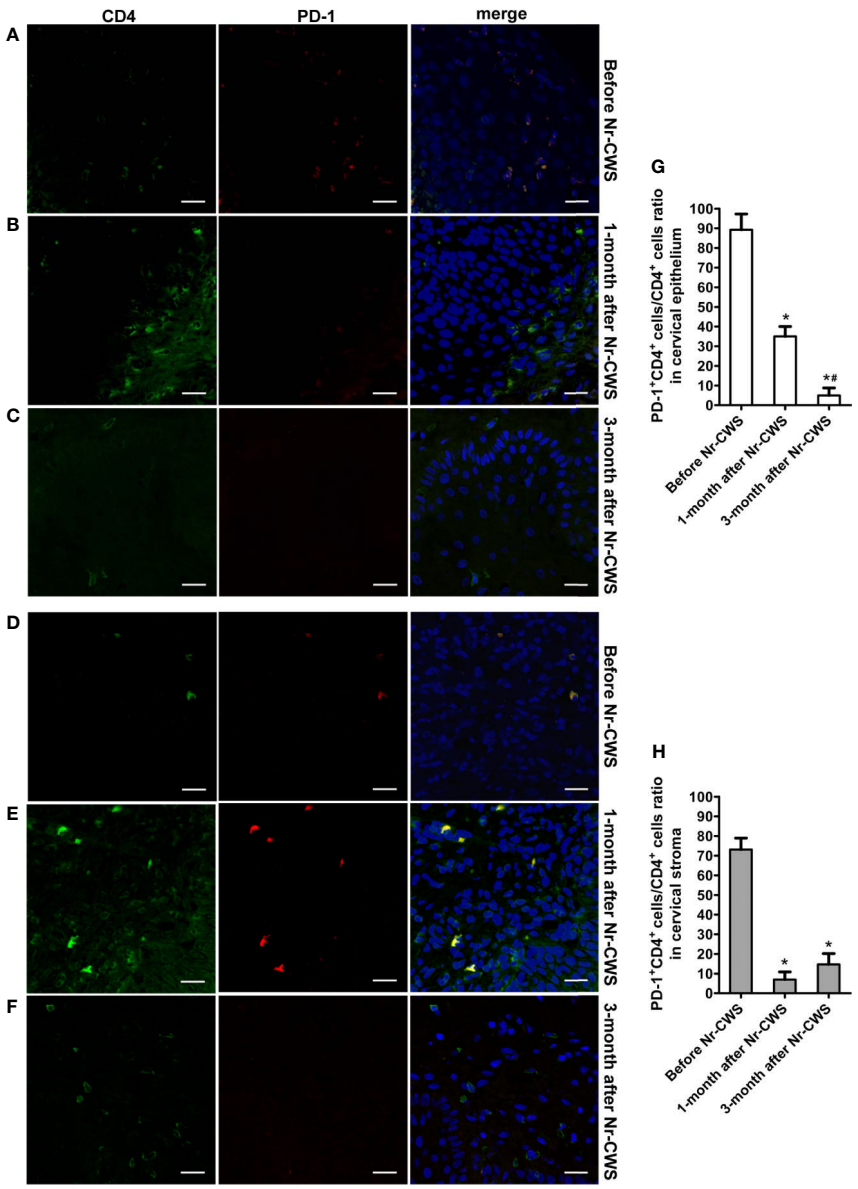

FIGURE 4 | Co-expression analysis of PD-1 and CD4 by double label immunofluorescence histochemical method. The co-expression of PD-1 and CD4 was detected by double label immunofluorescence histochemical method: the co-expression of PD-1 and CD4 in human cervical epithelium of the recruited patients before Nr-CWS treatment **(A)**, 1 month after Nr-CWS **(B)** and 3 months after Nr-CWS **(C)**; the co-expression of PD-1 and CD4 in human cervical stroma of the patients before Nr-CWS treatment **(D)**, 1 month after Nr-CWS **(E)** and 3 months after Nr-CWS **(F)**; statistical data of co-expression of PD-1 and CD4 (**G, H**: $^{*}P < 0.05$ vs Before Nr-CWS, $^{\#}P < 0.05$ vs 1-month after Nr-CWS) (**A–F**, scale bars = 20 μm).

in eliminating HPV infected pre-neoplastic human cervical epithelial cells and severe dysplastic cells (20). An increasing number of documents have described the relationship between CIN and T cell subsets. The women presenting CIN had a higher $CD4^+$ T and $CD8^+$ T cell infiltrates than the healthy ones (21), which was consistent with our results. The presence of $CD4^+$ T cells in the stroma of women with CIN 2/3 was predictor for the regression of lesions (22). The patients with regressed CIN 2/3 had higher $CD8^+$ T cells than patients that presented persistent lesions (23). Low $CD3^+$ T and $CD8^+$ T cells infiltrates were reported as being predictive markers of progressive cervical disease (24). In this study, after administration of Nr-CWS treatment, the infiltrates of $CD3^+$ T, $CD4^+$ T, and $CD8^+$ T cells improved significantly both in human cervical epithelium and stroma, suggesting an improvement in local cell immunity by Nr-CWS. Additionally, T cells infiltrate from human cervical stroma to the epithelium, which is matched by our results. We found the positive cells in epithelium were mainly located in the basal or intermediate layers and rarely appeared in the superficial layers. Under the stimulation of Nr-CWS, T cells in human

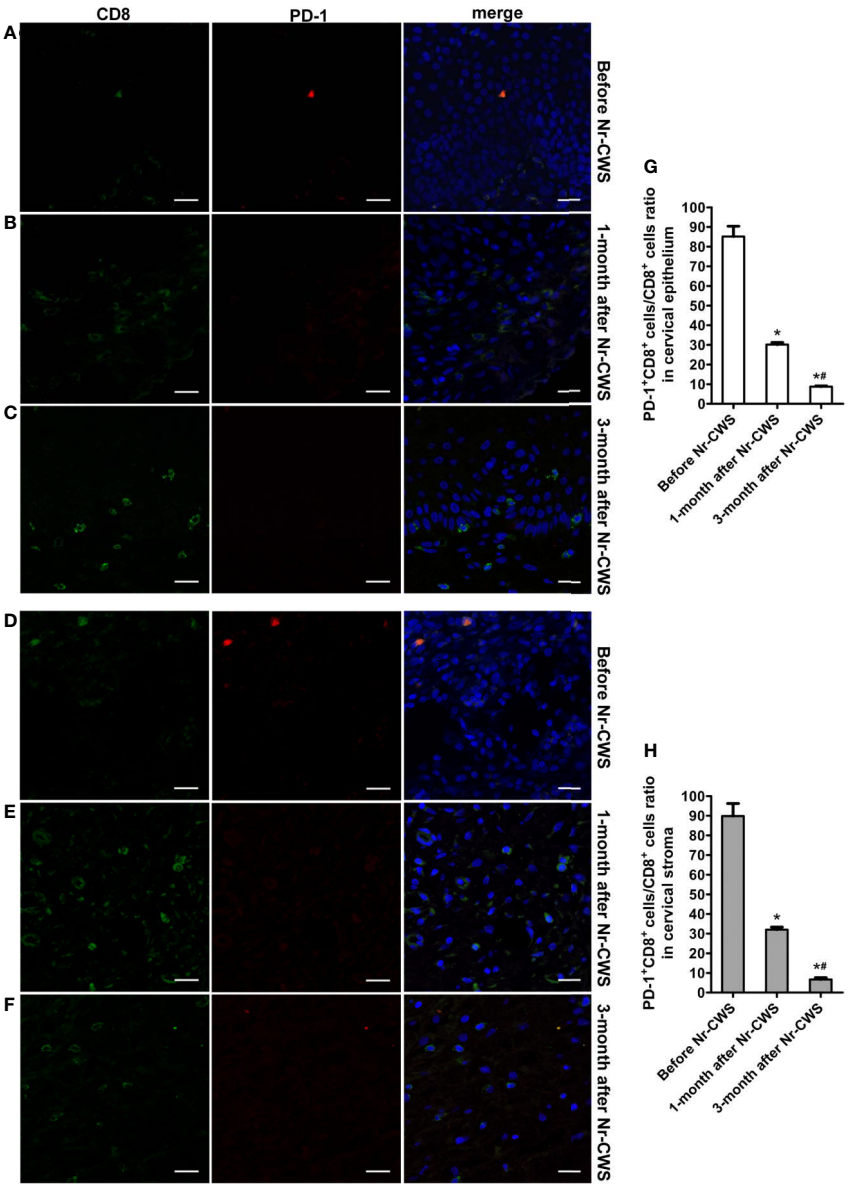

FIGURE 5 | Co-expression analysis of PD-1 and CD8 by double label immunofluorescence histochemical method. The co-expression of PD-1 and CD8 was detected by double label immunofluorescence histochemical method: the co-expression of PD-1 and CD8 in human cervical epithelium of the recruited patients before Nr-CWS treatment **(A)**, 1 month after Nr-CWS **(B)** and 3 months after Nr-CWS **(C)**; the co-expression of PD-1 and CD8 in human cervical stroma of the patients before Nr-CWS treatment **(D)**, 1 month after Nr-CWS **(E)** and 3 months after Nr-CWS **(F)**; statistical data of co-expression of PD-1 and CD8 (**G, H**: $^{*}P < 0.05$ vs Before Nr-CWS, $^{\#}P < 0.05$ vs 1-month after Nr-CWS) (**A–F**, scale bars = 20 μm).

cervical stroma changed more rapidly than those in human cervical epithelium, and the increase was higher than that in human cervical epithelium. Furthermore, cytotoxic $CD8^+$ T cells are orchestrated by $CD4^+$ T cell responses. The activation of $CD4^+$ T cells occurs earlier, with the production of cytokines that are essential to the recruitment and activation of $CD8^+$ T cells. In line with this, we found that the $CD4^+$ T cells in the epithelium reached the highest level at 1 month after Nr-CWS, while the $CD8^+$ T cells gradually increased and peaked at 3 months after Nr-CWS. In addition, the results showed that the scores of $CD3^+$ T, $CD4^+$ T and $CD8^+$ T cells in the stroma increased significantly at 1 month, indicating a strong local immune response, while the decrease in the scores of immune cells at 3 months indicated a decrease in the intensity of the immune response. This may be related to the reduction of HPV, the improvement of the condition, and therefore the corresponding weakening of the immune response. The changes of T cells in the cervical epithelium were slower than those in the stroma, and only

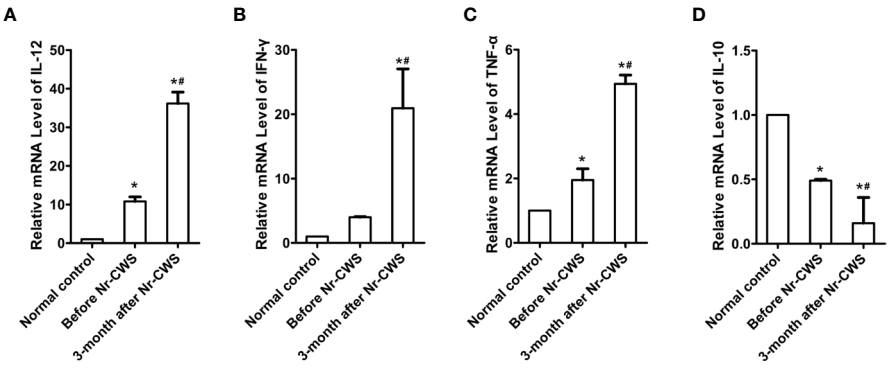

FIGURE 6 | Detection of cytokine mRNA levels in cervical tissue by qRT-PCR. Statistical data of the mRNA levels of local pro-inflammatory cytokines: IL-12 **(A)**, IFN-γ **(B)**, TNF-α **(C)**; Statistical data of the mRNA level of suppressive cytokine IL-10 **(D)** (*$P < 0.05$ vs Normal control, $^{\#}P < 0.05$ vs Before Nr-CWS).

$CD4^+$ T cells showed a similar trend, while the $CD8^+$ T cells showed a later change than $CD4^+$ T cells, reaching a peak at 3 months.

Inhibitory receptors are crucial negative regulatory pathways, controlling autoreactivity and immunopathology. Although inhibitory receptors are transiently expressed in functional effector T cells during activation, their sustained high expression are hallmarks of exhausted T cells (25). PD-1 is illustrated as an important negative costimulatory molecule. The binding of PD-1 and PD-L1 can block TCR and its co-stimulus signal transduction, inhibit the activation and proliferation of T cells, deplete the function of effector T cells. The PD-1/PD-L1 pathway has been revealed to inhibit a wide range of immune responses against pathogens, tumors and self-antigens (26).

PD-L1 is widely expressed in activated T and B cells, antigen presenting cells and thymic cortical epithelial cells (27). Relevant studies have found abnormal PD-L1 expression in various cancers including cervical squamous cell carcinoma (CSCC). Mezache et al. reported that PD-L1 was a solid biomarker of productive HPV infection in cervix and was significantly upregulated in both cancer cells and surrounding inflammatory cells in human cervical cancer (28). As for CIN, Yang et al. proved that increase in PD-L1 and PD-1 expression negatively regulated cervical cell immunity to HPV, and contributed to the progression of HR-HPV related CIN (29). The expressions of PD-1 and PD-L1 in CIN and CSCC were of prognostic value and associated with HPV status (30). In the study of Mezache et al (28), the percentage of cases with high PD-L1 expression in the abnormal squamous cells of CIN 1-2 lesions was 95%. PD-L1 positive mononuclear cells, which were abundant in the invasive squamous cell nests of CSCC, were rarely evident in the epithelial layer of CIN 1-2. Consistent with that, because the participants were mainly CIN 1 or CIN 2 patients, our results showed that PD-L1 was expressed in the cervical epithelial cells. However, PD-L1 expression was not detected in other cells such as mononuclear cells, which may be related to the relatively mild lesion level of the recruited patients. In addition, similar to previous findings, the PD-L1 expression was located mainly toward the basal layer of epithelium, where E6 and E7 RNAs might be relatively abundant (28). After treatment with Nr-CWS, the expression of PD-L1 decreased significantly, demonstrating that Nr-CWS had a certain inhibitory effect on the PD-1/PD-L1 pathway.

PD-1 is expressed on activated T cells, B cells and some myeloid cells, though its functions are best characterized for T cells. PD-1 interacts with its ligands, PD-L1 and PD-L2. There is accumulating evidence indicating the relationship between PD-1 expression and impaired cellular immunity. The sustained upregulation of PD-1 in $CD4^+$ T cells and $CD8^+$ T cells was one of the characteristic features of T cell exhaustion during chronic infection or cancer (25, 31). As for HPV infection and CIN, PD-1 expression on cervical T cells was associated with HR-HPV positivity and increased in parallel with increasing CIN grade (29). The PD-1 expression levels on peripheral $CD4^+$ T and $CD8^+$ T cells were significantly elevated in samples from patients with cancer and CIN (26). As for the function of exhausted T cells, the exhausted $CD8^+$ T cells lose effector functions including production of IL-2, IFN-γ, TNF-α and β-chemokines, high proliferative capacity, ex-vivo cytolytic activity and degranulation (32). The exhaustion of $CD4^+$ T cells shares many characteristics with $CD8^+$ T cell exhaustion, including impaired production of effector cytokines (e.g. IFN-γ, TNF-α) (33). On the other hand, soluble molecules are also important signals in regulating T cell exhaustion, including suppressive cytokines such as IL-10 and transforming growth factor-β (TGF-β) and pro-inflammatory cytokines such as type I IFN and IL-6 (25).

The present study first demonstrated that Nr-CWS treatment remarkably raised the percentages of $CD4^+$ T and $CD8^+$ T cells in both the cervical epithelium and the stroma of the patients, and the percentage of $PD\text{-}1^+$ cells decreased in human cervical epithelium. However, the percentage of $PD\text{-}1^+$ cells in human cervical stroma increased after Nr-CWS treatment. In order to find out the exact effect of Nr-CWS on PD-1 and T cells, we designed a co-expression analysis experiment. The results showed that $PD\text{-}1^+CD4^+$ cells/$CD4^+$ T cells ratio and $PD\text{-}1^+CD8^+$ cells/$CD8^+$ T cells ratio decreased both in cervical epithelium and stroma, suggesting that Nr-CWS treatment reduced local exhausted $CD4^+$ T and $CD8^+$ T cells and more uninhibited $CD4^+$ T and $CD8^+$ T cells were present in human cervix. The increase in the percentage of $PD\text{-}1^+$ cells in the stroma after Nr-CWS treatment may be caused by the significant

increase in the percentages of $CD4^+$ T and $CD8^+$ T cells. Additionally, PD-1 is also expressed on other immune cells besides $CD4^+$ T and $CD8^+$ T cells. We found some $PD\text{-}1^+CD4^-$ (or $PD\text{-}1^+CD8^-$) cells in the image of double label staining, which may be other cells expressing PD-1 except $CD4^+$ T or $CD8^+$ T cells. On the other hand, the mRNA levels of local pro-inflammatory cytokines (IL-12, IFN-γ, and TNF-α) were elevated while the mRNA level of suppressive cytokine IL-10 decreased after Nr-CWS treatment, which also verified the efficient role of Nr-CWS in reversal T cell exhaustion. The role of Nr-CWS in regulating cytokines may also be caused by affecting other immune cells. In short, the mechanisms of Nr-CWS in subverting T cell exhaustion and revitalizing host immunity are complex. Much more researches are needed to clarify the immune enhancing effect of Nr-CWS.

CONCLUSION

In light of these results, we propose that Nr-CWS, as an immunotherapeutic agent for HR-HPV infection and CIN, plays an efficient part in immune enhancement and treatment, through upregulating T cell subsets and inhibiting PD-1/PD-L1 signal pathway.

DATA AVAILABILITY STATEMENT

The original contributions presented in the study are included in the article/supplementary materials. Further inquiries can be directed to the corresponding authors.

ETHICS STATEMENT

The studies involving human participants were reviewed and approved by the ethics committee of the First Hospital of Hebei Medical University and the ethics committee of the Fourth Hospital of Hebei Medical University. The patients/participants provided their written informed consent to participate in this study.

AUTHOR CONTRIBUTIONS

LZ and JT contributed to the conception and design of the study. WC designed experiments, analyzed the samples, and contributed to the manuscript preparation. YiZ contributed to the design of the experiments and study supervision. CZ performed experiments. SS contributed to the project administration. XL and XB were responsible for clinical patient recruitment and treatment. YaZ, QG and QL collected samples from the patients and performed experiments. All authors contributed to the article and approved the submitted version.

FUNDING

This work was supported by Technology Development Agreement of Hebei Medical University and Weihai Greatest Pharmaceutical Research Institute Co., Ltd., RP China, and Nature Science Foundation of Hebei Province [Grant No. H2017206078]. The funder bodies were not involved in the study design, collection, analysis, interpretation of data, the writing of this article or the decision to submit it for publication.

REFERENCES

1. Arbyn M, Weiderpass E, Bruni L, de Sanjose S, Saraiya M, Ferlay J, et al. Estimates of incidence and mortality of cervical cancer in 2018: a worldwide analysis. *Lancet Glob Health* (2020) 8(2):e191–203. doi: 10.1016/S2214-109X(19)30482-6
2. Correnti M, Medina F, Cavazza ME, Rennola A, Avila M, Fernandes A. Human papillomavirus (HPV) type distribution in cervical carcinoma, low-grade, and high-grade squamous intraepithelial lesions in Venezuelan women. *Gynecol Oncol* (2011) 121(3):527–31. doi: 10.1016/j.ygyno.2011.02.003
3. Hochmann J, Parietti F, Martinez J, Lopez AC, Carreno M, Quijano C, et al. Human papillomavirus type 18 E5 oncoprotein cooperates with E6 and E7 in promoting cell viability and invasion and in modulating the cellular redox state. *Mem Inst Oswaldo Cruz* (2020) 115:e190405. doi: 10.1590/0074-02760190405
4. Plummer M, Schiffman M, Castle PE, Maucort-Boulch D, Wheeler CM, Group A. A 2-year prospective study of human papillomavirus persistence among women with a cytological diagnosis of atypical squamous cells of undetermined significance or low-grade squamous intraepithelial lesion. *J Infect Dis* (2007) 195(11):1582–9. doi: 10.1086/516784
5. Venuti A, Paolini F, Nasir L, Corteggio A, Roperto S, Campo MS, et al. Papillomavirus E5: the smallest oncoprotein with many functions. *Mol Cancer* (2011) 10:140. doi: 10.1186/1476-4598-10-140
6. Luo M, Yu J, Zhu S, Huang L, Chen Y, Wei S. Detoxification therapy of traditional Chinese medicine for genital tract high-risk human papillomavirus infection: A systematic review and meta-analysis. *PloS One* (2019) 14(3):e0213062. doi: 10.1371/journal.pone.0213062
7. Massad LS, Einstein MH, Huh WK, Katki HA, Kinney WK, Schiffman M, et al. updated consensus guidelines for the management of abnormal cervical cancer screening tests and cancer precursors. *Obstet Gynecol* (2012) 2013) 121(4):829–46. doi: 10.1097/AOG.0b013e3182883a34
8. Woo YL, Sterling J, Damay I, Coleman N, Crawford R, van der Burg SH, et al. Characterising the local immune responses in cervical intraepithelial neoplasia: a cross-sectional and longitudinal analysis. *BJOG* (2008) 115(13):1616–21. doi: 10.1111/j.1471-0528.2008.01936.x. discussion 21-2.
9. Azuma I, Taniyama T, Yamawaki M, Sugimura K, Yamamura Y. Adjuvant and antitumor activities of Nocardia cell-wall skeletons. *Gan* (1976) 67(5):733–6.
10. Hozawa S, Ishioka S, Yanagida J, Takaishi M, Matsuzaka S, Ohsaki M, et al. Effects of periodic administration of Nocardia rubra cell-wall skeleton on immunoglobulin production and B-cell-stimulatory factor activity in vitro in workers at a poison gas factory. *Cancer Immunol Immunother* (1989) 30(3):190–4. doi: 10.1007/BF01669429
11. Wang Y, Hu Y, Ma B, Wang F, Liu S, Xu J, et al. Nocardia rubra cell wall skeleton accelerates cutaneous wound healing by enhancing macrophage activation and angiogenesis. *J Int Med Res* (2018) 46(6):2398–409. doi: 10.1177/0300060518764210
12. Meng Y, Sun J, Wang X, Ma Y, Kong C, Zhang G, et al. The biological macromolecule Nocardia rubra cell-wall skeleton as an avenue for cell-based immunotherapy. *J Cell Physiol* (2019). doi: 10.1002/jcp.28182
13. Wang G, Wu J, Miao M, Dou H, Nan N, Shi M, et al. Nocardia rubra cell-wall skeleton promotes CD4(+) T cell activation and drives Th1 immune

response. *Int J Biol Macromol* (2017) 101:398–407. doi: 10.1016/j.ijbiomac.2017.03.060
14. Tao Y, Wang G, Zhai J, Zhang N. Functional modulation of CD8+ T cell by approved novel immune enhancer: Nocardia rubra Cell-Wall Skeletons (Nr-CWS). *Int Immunopharmacol* (2020) 78:106023. doi: 10.1016/j.intimp.2019.106023
15. Chen W, Zhang L, Shao SX, Wang HP, Cui SJ, Zhang YN, et al. Transcription factors GATA4 and TBX5 promote cardiomyogenic differentiation of rat bone marrow mesenchymal stromal cells. *Histol Histopathol* (2015) 30(12):1487–98. doi: 10.14670/HH-11-644
16. Vijayashree R, Aruthra P, Rao KR. A comparison of manual and automated methods of quantitation of oestrogen/progesterone receptor expression in breast carcinoma. *J Clin Diagn Res* (2015) 9(3):EC01–5. doi: 10.7860/JCDR/2015/12432.5628
17. Desravines N, Miele K, Carlson R, Chibwesha C, Rahangdale L. Topical therapies for the treatment of cervical intraepithelial neoplasia (CIN) 2-3: A narrative review. *Gynecol Oncol Rep* (2020) 33:100608. doi: 10.1016/j.gore.2020.100608
18. He Y, Wu YM, Yin CH, Geng YN, Yang SL, Kang LD. [Natural changes of high-risk HPV in women with negative for intraepithelial lesion or malignancy: a prospective 1 year study]. *Zhonghua Fu Chan Ke Za Zhi* (2017) 52(11):740–4. doi: 10.3760/cma.j.issn.0529-567X.2017.11.005
19. Lucena AA, Guimaraes MV, Michelin MA, Lodi CT, Lima MI, Murta EF, et al. Evaluation of T, B and natural killer lymphocyte in the cervical stroma of HIV-positive and negative patients with cervical intraepithelial neoplasia. *Immunol Lett* (2016) 169:98–103. doi: 10.1016/j.imlet.2015.10.016
20. Maskey N, Thapa N, Maharjan M, Shrestha G, Maharjan N, Cai H, et al. Infiltrating CD4 and CD8 lymphocytes in HPV infected uterine cervical milieu. *Cancer Manag Res* (2019) 11:7647–55. doi: 10.2147/CMAR.S217264
21. Jacobs N, Renard I, Al-Saleh W, Hubert P, Doyen J, Kedzia W, et al. Distinct T cell subsets and cytokine production in cultures derived from transformation zone and squamous intraepithelial lesion biopsies of the uterine cervix. *Am J Reprod Immunol* (2003) 49(1):6–13. doi: 10.1034/j.1600-0897.2003.01109.x
22. Munk AC, Gudlaugsson E, Ovestad IT, Lovslett K, Fiane B, Hidle B, et al. Interaction of epithelial biomarkers, local immune response and condom use in cervical intraepithelial neoplasia 2-3 regression. *Gynecol Oncol* (2012) 127(3):489–94. doi: 10.1016/j.ygyno.2012.09.010
23. Ovestad IT, Gudlaugsson E, Skaland I, Malpica A, Kruse AJ, Janssen EA, et al. Local immune response in the microenvironment of CIN2-3 with and without spontaneous regression. *Mod Pathol* (2010) 23(9):1231–40. doi: 10.1038/modpathol.2010.109
24. Piersma SJ, Jordanova ES, van Poelgeest MI, Kwappenberg KM, van der Hulst JM, Drijfhout JW, et al. High number of intraepithelial CD8+ tumor-infiltrating lymphocytes is associated with the absence of lymph node metastases in patients with large early-stage cervical cancer. *Cancer Res* (2007) 67(1):354–61. doi: 10.1158/0008-5472.CAN-06-3388
25. Wherry EJ, Kurachi M. Molecular and cellular insights into T cell exhaustion. *Nat Rev Immunol* (2015) 15(8):486–99. doi: 10.1038/nri3862
26. Zhang Y, Zhu W, Zhang X, Qu Q, Zhang L. Expression and clinical significance of programmed death-1 on lymphocytes and programmed death ligand-1 on monocytes in the peripheral blood of patients with cervical cancer. *Oncol Lett* (2017) 14(6):7225–31. doi: 10.3892/ol.2017.7105
27. Folkl A, Bienzle D. Structure and function of programmed death (PD) molecules. *Vet Immunol Immunopathol* (2010) 134(1-2):33–8. doi: 10.1016/j.vetimm.2009.10.006
28. Mezache L, Paniccia B, Nyinawabera A, Nuovo GJ. Enhanced expression of PD L1 in cervical intraepithelial neoplasia and cervical cancers. *Mod Pathol* (2015) 28(12):1594–602. doi: 10.1038/modpathol.2015.108
29. Yang W, Song Y, Lu YL, Sun JZ, Wang HW. Increased expression of programmed death (PD)-1 and its ligand PD-L1 correlates with impaired cell-mediated immunity in high-risk human papillomavirus-related cervical intraepithelial neoplasia. *Immunology* (2013) 139(4):513–22. doi: 10.1111/imm.12101
30. Yang W, Lu YP, Yang YZ, Kang JR, Jin YD, Wang HW. Expressions of programmed death (PD)-1 and PD-1 ligand (PD-L1) in cervical intraepithelial neoplasia and cervical squamous cell carcinomas are of prognostic value and associated with human papillomavirus status. *J Obstet Gynaecol Res* (2017) 43(10):1602–12. doi: 10.1111/jog.13411
31. Pauken KE, Wherry EJ. Overcoming T cell exhaustion in infection and cancer. *Trends Immunol* (2015) 36(4):265–76. doi: 10.1016/j.it.2015.02.008
32. McLane LM, Abdel-Hakeem MS, Wherry EJ. CD8 T Cell Exhaustion During Chronic Viral Infection and Cancer. *Annu Rev Immunol* (2019) 37:457–95. doi: 10.1146/annurev-immunol-041015-055318
33. Crawford A, Angelosanto JM, Kao C, Doering TA, Odorizzi PM, Barnett BE, et al. Molecular and transcriptional basis of CD4(+) T cell dysfunction during chronic infection. *Immunity* (2014) 40(2):289–302. doi: 10.1016/j.immuni.2014.01.005

Conflict of Interest: YiZ was employed by the company Weihai Greatest Pharmaceutical Research Institute Co., Ltd.

The remaining authors declare that the research was conducted in the absence of any commercial or financial relationships that could be construed as a potential conflict of interest.

Copyright © 2021 Chen, Zhang, Zhao, Shao, Zhang, Li, Bai, Guo, Liu, Tang and Zhang. This is an open-access article distributed under the terms of the Creative Commons Attribution License (CC BY). The use, distribution or reproduction in other forums is permitted, provided the original author(s) and the copyright owner(s) are credited and that the original publication in this journal is cited, in accordance with accepted academic practice. No use, distribution or reproduction is permitted which does not comply with these terms.

frontiers in Immunology

REVIEW
published: 21 January 2021
doi: 10.3389/fimmu.2020.609705

Research Status and Molecular Mechanism of the Traditional Chinese Medicine and Antitumor Therapy Combined Strategy Based on Tumor Microenvironment

Yang Zhang[1†], *Yanni Lou*[2†], *Jingbin Wang*[3], *Cunguo Yu*[4] *and Wenjuan Shen*[5*†]

[1] Department of Internal Medicine, First Affiliated Hospital, Heilongjiang University of Chinese Medicine, Harbin, China, [2] Oncology Department of Integrated Traditional Chinese and Western Medicine, China-Japan Friendship Hospital, Beijing, China, [3] Department of Spleen and Stomach Disease, Chinese Medicine Shenzhen Hospital, Guangzhou University, Shenzhen, China, [4] Department of Chinese Medicine, Qinhuangdao Haigang Hospital, Qinhuangdao, China, [5] Department of Obstetrics and Gynecology, First Affiliated Hospital, Heilongjiang University of Chinese Medicine, Harbin, China

OPEN ACCESS

Edited by:
Peng Qu,
National Institutes of Health (NIH), United States

Reviewed by:
Haoming Luo,
Changchun University of Chinese Medicine, China
Bangwei Cao,
Capital Medical University, China

***Correspondence:**
Wenjuan Shen
shenwenjuankx@163.com

[†]*These authors have contributed equally to this work*

Specialty section:
This article was submitted to Cancer Immunity and Immunotherapy, a section of the journal Frontiers in Immunology

Received: *24 September 2020*
Accepted: *03 December 2020*
Published: *21 January 2021*

Citation:
Zhang Y, Lou Y, Wang J, Yu C and Shen W (2021) Research Status and Molecular Mechanism of the Traditional Chinese Medicine and Antitumor Therapy Combined Strategy Based on Tumor Microenvironment. Front. Immunol. 11:609705. doi: 10.3389/fimmu.2020.609705

Treatment of malignant tumors encompasses multidisciplinary comprehensive diagnosis and treatment and reasonable combination and arrangement of multidisciplinary treatment, which is not a simple superimposition of multiple treatment methods, but a comprehensive consideration of the characteristics and specific conditions of the patients and the tumor. The mechanism of tumor elimination by restoring the body's immune ability is consistent with the concept of "nourishing positive accumulation and eliminating cancer by itself" in traditional Chinese medicine (TCM). The formation and dynamic changes in the tumor microenvironment (TME) involve many different types of cells and multiple signaling pathways. Those changes are similar to the multitarget and bidirectional regulation of immunity by TCM. Discussing the relationship and mutual influence of TCM and antitumor therapy on the TME is a current research hotspot. TCM has been applied in the treatment of more than 70% of cancer patients in China. Data have shown that TCM can significantly enhance the sensitivity to chemotherapeutic drugs, enhance tumor-suppressing effects, and significantly improve cancer-related fatigue, bone marrow suppression, and other adverse reactions. TCM treatments include the application of Chinese medicine monomers, extracts, classic traditional compound prescriptions, listed compound drugs, self-made compound prescriptions, as well as acupuncture and moxibustion. Studies have shown that the TCM functional mechanism related to the positive regulation of cytotoxic T cells, natural killer cells, dendritic cells, and interleukin-12, while negatively regulating of regulatory T cells, tumor-associated macrophages, myeloid-derived suppressive cells, PD-1/PD-L1, and other immune regulatory factors. However, the application of TCM in cancer therapy needs further study and confirmation. This article summarizes the existing research on the molecular mechanism of TCM regulation of the TME and provides a theoretical basis for further screening of the predominant population.

Moreover, it predicts the effects of the combination of TCM and antitumor therapy and proposes further developments in clinical practice to optimize the combined strategy.

Keywords: traditional Chinese medicine, cancer, immune ability, anti-tumor therapy, tumor microenvironment

INTRODUCTION

Cancer is one of the major noncommunicable chronic diseases that seriously affect human health (1–3). Although treatment methods and drug research and development continue to improve, many problems such as drug resistance and recurrence still hinder progress (4–9). The treatment of malignant tumors encompasses multidisciplinary comprehensive diagnosis and treatment (10–12) and reasonable combination and arrangement of multiple treatment methods including surgery, radiotherapy, chemotherapy, targeted therapy, immunotherapy, endocrine therapy, interventional therapy (13–19). Multidisciplinary treatment is not a simple superimposition of multiple treatment methods, but a comprehensive consideration of the characteristics and specific conditions of the patients and the tumor, leading to a planned and reasonable choice (20). While pursuing prolonged survival (21), attention should also be given to improving the quality of life of the patients (22).

Due to its huge population, China accounts for about a quarter of the world's new tumors and deaths, leading to a serious disease burden (23–25). Traditional Chinese medicine (TCM) is a unique diagnosis and treatment method with thousands of years of history (26, 27). It is reported that most Chinese cancer patients have used TCM during the diagnosis and treatment process (28, 29). TCM is mostly used in the form of compound prescriptions in clinical oncology, including oral herbal medicines, granules or capsules, and injections (30). There are many pieces of research on Chinese medicine monomers and their active ingredients (31). Many researches have shown that TCM combined with antitumor therapy can achieve significant tumor suppression effects, reduce drug resistance, and improve adverse reactions and patient quality of life (32–36). In recent years, targeting the immune checkpoints CTLA-4, PD-1, and PD-L1 has led to breakthroughs in a variety of cancer types (37–39). The mechanism of tumor eradication by restoring the body's immune ability is consistent with the concept of "nourishing positive accumulation and eliminating cancer by itself" or "strengthening vital Qi to treat cancer" in TCM (40, 41).

The tumor microenvironment (TME) (42, 43) is formed by the structural components such as tumor cells, endothelial cells, fibroblasts, immune cells, extracellular matrix, and secreted cytokines. It has three main roles: inhibiting the immune response, promoting angiogenesis, and growing cancer stem cells. Chronic inflammation (44, 45) and immunosuppression (46, 47) are the core features of the TME. Chronic inflammation leads to low oxygen levels, low pH, high pressure in the microenvironment, and the prolonged existence of inflammatory factors such as tumor necrosis factor (TNF) that maintain and continuously aggravate the inflammatory features of the TME. The hypoxic microenvironment increases hypoxia inducible factor (HIF) levels, induces the formation of new blood vessels, modifies the vascular endothelial growth factor (VEGF), and recruits bone marrow-derived endothelial progenitor cells to form new blood vessels. The TME enables a large number of regulatory T cells (Tregs) that penetrate and accumulate in tumor tissues, inhibit the differentiation and maturation of effector cells such as lymphocytes, macrophages, dendritic cells (DC), and isolate them from tumor tissues to inhibit immune responses. The immunosuppressive microenvironment is closely related to the "deficiency of vital Qi" in Chinese medicine (48). The "syndrome" of TCM involves multiple systems and levels of Western medicine. TCM treatment of cancer pays attention to overall regulation whether it is to strengthen the body (Fu Zheng) or eliminate evil (Qu Xie). Its advantage lies in regulating the tumor-host microenvironment, allowing normal immune cells to perform their duties, so that there is no environment for tumor cells to survive, and causing apoptosis or autophagy (49–51).

In this review, we mainly discuss, from the perspective of TME regulation, the studies on the combined application of TCM and anticancer treatments. Further screening of dominant populations and predictors will help optimize the joint strategy and provide a theoretical basis for clinical practice.

TCM COMBINED WITH CHEMOTHERAPY

Chemotherapy is still the cornerstone of anticancer therapy. As one of the most important treatments for advanced stage cancer, chemotherapy compatibility ensures the correct combination of chemotherapeutic drugs and the combination of chemotherapy and other types of treatment. There are many clinical and preclinical studies on the combination of TCM treatment and chemotherapy.

The clinical studies on TCM combined with chemotherapy for anticancer treatment research have been mainly published in Chinese journals (**Table 1**). The studied cancer types include lung cancer (52–58), digestive system cancer (gastric/liver/esophageal cancer) (59–63), gynecological cancer (ovarian

Abbreviations: Non-small cell lung cancer, NSCLC; Chemotherapy, CT; Traditional Chinese medicine, TCM; Disease control rate, DCR; Interleukin 2, IL-2; Interleukin 10, IL-10; Interferon-γ, IFN-γ; Gemcitabine, G; Matrix metalloprotein-2, MMP-2; Matrix metalloprotein-9, MMP-9; Natural killer cells, NK; Tumor necrosis factor α, TNF-α; High sensitivity C-reactive protein, hs-CRP; Vascular endothelial growth factor, VEGF; Gemcitabine & cisplatin, GP; Paclitaxel & cisplatin, TP; Transforming growth factor β 1, TGF-β_1; Fluorouracil & Oxaliplatin & calcium folinate, FOLFOX; Doxorubin, DOX; Hypoxia inducible factor-1 α, HIF-1α; Monocyte chemoattractant protein-1, MCP-1,; Myeloid suppressor cells, MDSCs; Insulin-like growth factor-2, IGF-2; Fluorouracil & adriamycin & chloramphenicol, FAP; Cisplatin, DDP; Paclitaxel & cyclophosphamide, TC; Methotrexate & actinomycete D & calcium folinate & vincristine sulfate & cyclophosphamide, EMA-CO; Paclitaxel & gemcitabine, GT; Cisplatin & docetaxel, DC; Gemcitabine & Cisplatin, GP.

TABLE 1 | Influence of traditional Chinese medicine (TCM) Combined Chemotherapy (CT) on tumor microenvironment (TME)-Clinical Study.

Cancers	Formulation	Herbal medicine	Group and Number of cases	Effect of Combination	Upregulate	Downregulate	Refs.
Lung Cancer							
NSCLC	Compound (Classic, oral)	Baihe Gujin Decoction (Rehmannia, Rehmannia, Carlo, album AGLAOPHOTIS, lilium, Fritillaria, Ophiopogon, Bellflower, Scrophulariaceae, rudis Licoricia)	TCM + DC vs DC = 48 vs 48	DCR 89.6% vs 72.9% ($p<0.05$)	$CD3^+$, $CD4^+$, $CD4^+/CD8^+$, IL-2, and INF-γ	$CD8^+$, IL-4, IL-10	He and Huang (52)
NSCLC	Compound (Self-made, oral)	Bushen Yifei Jiedu Decoction (Xianling lienis contegentem membranam, Ligustrum lucidum, Ganoderma lucidum, Cruda Astragalus, Radix Angelicae Ginseng, Pinellia, Atractylodes, Germen Stone, aesculus aesculus, Shansi Fungorum aurea Buckwheat, etc)	TCM + CT vs CT = 30 vs 30	/	/	Foxp3, B7-H3	Wang et al. (53)
NSCLC	Compound (Listed drug, Oral Liquid)	Jinfukang Oral Liquid (Astragalus, Ophiopogon japonicus, Adenophora glabra, Ligustrum lucidum, Cornus alba, etc)	TCM + G vs G = 60 vs 60	DCR 91.67% vs 75% ($p<0.05$)	/	MMP-9	Zhang et al. (54)
NSCLC	Compound (Listed drug, oral)	Yifei Qinghua Granule (American Ginseng, Adenophora, Astragalus, Ophiopogon japonicus, Patrinia vulgaris, Oldenlandia diffusa, Panax notoginseng, etc)	TCM + CT vs CT = 101 vs 101	DCR 81.19% vs 64.36% ($p<0.05$)	$CD3^+$, $CD4^+$, $CD4^+/CD8^+$, NK	$CD8^+$, IL-6, TNF-α, hs-CPR	Wang et al. (55)
NSCLC	Compound (Self-made, oral)	Yifei Xiaoai Decoction (Houttuynia, Cattus BRACHIUM, Mountain Conch, Codonopsis, Asparagus, Fritillaria, Populus tremula Reed Stein, Loquat Folium, Panax notoginseng, Citrus aurantium, STILIO, etc)	TCM + TP vs TP = 32 vs 32	DCR 84.4% vs 68.9% ($p<0.05$)	/	VEGF, MMP-2, MMP-9	Liu and Yang (56)
NSCLC	Compound (Listed drug, injection)	Shenqi Fuzheng Injection (Codonopsis, Astragalus)	TCM + TP vs TP = 41 vs 38	DCR 90.2% vs 76.3%, PFS 19m vs 13m, OS 43m vs 29m ($p<0.05$)	Th17	Treg	Chen et al. (57)
NSCLC	Compound (Listed drug, injection)	Kanglaite Injection (Coix Oil)	TCM + GP vs GP = 36 vs 36	DCR 91.67% vs 69.34% ($p<0.05$)	/	VEGF, P53, anti-Survivin antibody	Wang et al. (58)
Digestive system cancer							
Gastric Cancer	Compound (Listed drug, injection)	Compound Kushen Injection (Sophora flavescens, Berberis vulgaris uniseriale) Aidi Injection (Astragalus, Acanthopanax senticosus, Ginseng, Cantharidin)	TCM + FOLFOX vs FOLFOX = 39 vs 39	DCR 97.44% vs 87.18% ($p<0.05$)	hydrogen sulfide, $CD3^+$, $CD4^+$, $CD8^+$, $CD4^+/CD8^+$	IL-6, TGF-β1	Meng et al. (59)
Gastric Cancer	Compound (Self-made, oral)	Buzhong Guben Yiwei Decoction (Atractylodes movent-frixum, Ginseng, Astragalus, Poria, tangerine cortices, Chuanxiong, Carlo, Fritillaria, Cyperus rotundus, album AGLAOPHOTIS, Bupleurum falcatum, amomi, Platycodon, lignei, Licoricia, gingiberi, Jujube)	TCM + FOLFOX vs FOLFOX = 50 vs 50	DCR 66% vs 38% ($p<0.05$)	$CD3^+$, $CD4^+$, $CD4^+/CD8^+$	/	Wang and Zhang (60)
Gastric Cancer	Compound (Classic, oral)	Yanghe Decoction (Muta Rehmannia, cornibus gum, eruca alba semina, ephedra, cinnamo, gingiberi, Licoricia)	TCM + DOX vs DOX = 60 vs 60	DCR 85% vs 68.3% ($p<0.05$)	IFN-γ	HIF-1α, IL-10, TGF-β1, TNF-α, MCP-1, MDSCs, Tregs	Tian et al. (61)
Hepatocelllar Carcinoma	Compound (Self-made, oral)	Chaihu Zaoxiu Decoction (Bupleurum falcatum, Fusarium oxysporum, Poria, rubrum AGLAOPHOTIS, album AGLAOPHOTIS, Rubia, Angelica, Turmeric, Cyperus rotundus: Scutellaria, Curcuma, totum cucumis, Cruda turtur, Polygonum cuspidatum, Licorice)	TCM + FAP vs FAP = 40 vs 40	ORR 35% vs 22.5% ($p<0.05$)	IL-2	MMP-2, MMP-9, VEGF, IGF-2	Wang and Jiao (62)
Esophageal Cancer	Compound (Self-made, oral)	Buyi Zhiai Decoction (Ginseng, Poria, Astragalus, Carlo, album AGLAOPHOTIS, Rehmannia, Atractylodes, Licoricia, Shouwu, CISSANTHEMOS, dandelion, Taraxacum)	TCM + DDP vs DDP = 53 vs 53	/	$CD4^+$, $CD4^+/CD8^+$, IgA, IgG, IgM	$CD8^+$	Feng et al. (63)
Gynecological cancer							

(Continued)

TABLE 1 | Continued

Cancers	Formulation	Herbal medicine	Group and Number of cases	Effect of Combination	Upregulate	Downregulate	Refs.
Ovarian Cancer	Compound (Listed drug, injection)	Shenqi Fuzheng Injection (Codonopsis, Astragalus)	TCM + TC vs TC = 55 vs 50	DCR 70.9% vs 50% (p<0.05)	$CD3^+$, $CD4^+$, $CD4^+/CD8^+$	/	Wei and Li (64)
Choriocarcinoma	Compound (Self-made, oral)	Fuzheng Yiliu Formula (Astragalus, Ligustrum lucidum, Oldenlandia diffusa, Scutellaria barbata, Fritillaria, Salvia, muta Rehmannia, Codonopsis, rubrum AGLAOPHOTIS, futurist awards, Poria, Atractylodes, Carlo, Polygonatum, Zihe, Gynostemma, Pinellia, Licoricia, aurantiaco cortices, three-lens)	TCM + EMA-CO vs EMA-CO = 46 vs 46	DCR 73.91% vs 47.83% (p<0.05)	$CD3^+$, $CD4^+$, $CD4^+/CD8^+$	$CD8^+$	Zhang et al. (65)
Triple-negative Breast Cancer	Compound (Self-made, oral)	Huangqi Jiedu Decoction (Astragalus, Scutellaria barbata, Coix semen Oldenlandia diffusa, Radix Angelicae Scrophulariaceae, Gentianaceae, Ligustrum lucidum, solanum, Atractylodes, Poria Cocos, Ophiopogon japonicus: Fungorum Shanzi, Fritillaria, Licorice)	TCM + GT vs GT = 51 vs 51	DCR 78.4% vs 58.8% (p<0.05)	IL-2, IFN-γ, IL-2/IL-6, IFN-γ/IL-6	IL-6	Yang et al. (66)
Breast Cancer	Compound (Listed drug, injection)	Shenqi Fuzheng Injection (Codonopsis, Astragalus)	TCM + D vs DEC = 50 vs 50	DCR 84% vs 64% (p<0.05)	$CD3^+$, $CD4^+$, $CD4^+/CD8^+$, CD80, CD83, CD86	$CD8^+$	Lu et al. (67)
Cervical Cancer	Monomer (Listed drug, injection)	Matrine Injection	TCM + DC vs DC = 35 vs 35	DCR 94.29% vs 71.43% (p<0.05)	IL-18, IFN-γ, $CD3^+$, $CD4^+$, $CD4^+/CD8^+$	IL-6	Du et al. (68)
Others							
Bladder Cancer	Monomer (Listed drug, injection)	Matrine Injection	TCM + GP vs GP = 39 vs 42	DCR 97.43% vs 87.5% (p = 0.034), PFS 12.64m vs 10.37m, OS 18.63m vs 15.09m (p<0.001)	CTL, NK	Treg	Han et al. (69)

cancer, choriocarcinoma, breast cancer) (64–68), and bladder cancer (69). The observed drugs are mainly compound herbal medicines, including classic prescriptions [Baihe Gujin decoction (52), Yanghe decoction (61)], listed drugs [Shenqi Fuzheng injection (57, 64, 67), Kanglaite injection (58), compound Kushen injection (59), Aidi injection (59), Jinfukang oral liquid (54), Yifei Qinghua granules (55)], a variety of self-made empirical formulas (53, 56, 60, 62, 63, 65, 66), and monomeric Chinese medicines or their components (matrine) (68, 69). The results consistently show that TCM can help improve the sensitivity to chemotherapeutic drugs, enhance tumor-suppressing effects, and significantly improve cancer-related fatigue, bone marrow suppression, and other adverse reactions. The quality of life self-report scores also show significant improvement. Regarding the regulation of tumor immune function, clinical studies mainly detected immune-related factors in peripheral blood. The results concluded that TCM combined with chemotherapy can upregulate $CD3^+$, $CD4^+$, and $CD4^+/CD8^+$ (52, 55, 59, 60, 64, 65, 67, 68), interleukin-2 (IL-2) (52, 62, 66), interferon-gamma (INF-γ) (52, 61, 66, 68), natural killer cells (NK) (55, 69), and cytotoxic T lymphocytes (CTL) (69), while downregulating IL-6 (55, 59, 66, 68), IL-10 (52, 61), transforming growth factor-β1 (TGF-β1) (59, 61), vascular endothelial growth factor(VEGF) (58, 62), matrix metalloproteinase-2 (MMP-2), MMP-9 (54, 56, 62), Forkhead box protein 3 (Foxp3), and B7-H3 (53), and Tregs (57, 61, 69). However, there are also inconsistencies between different research results for some indicators.

Experimental studies were conducted through in vivo and in vitro research (**Table 2**). Cell and animal experiments present more in-depth research on the mechanism of TCM improvement of chemotherapeutic efficacy. The observed drugs include Chinese medicine monomers [curcumin (70–73), ginsenoside Rg3 (74)], extracts [Ginseng and Astragalus (75)], classic traditional compound prescriptions [Huangqin decoction PHY906 (76, 77), Shiquan Dabu decoction (78)], listed compound drugs [Shexiang Baoxin pill (79)], and self-made compound prescriptions (80, 81). The most representative ones are curcumin, PHY906, and tonic Chinese medicines. The combination of curcumin and chemotherapy has been proven to overcome multidrug resistance [FOLFOX (70), oxaliplatin (71, 73), 5-Fu (72)] through a number of in vivo and in vitro studies. The effect of this combined therapy may upregulate Bax, caspase-3, and PARP and downregulate EGFRs (such as IGF-1R), Bcl-2, survivin, HSP70, Nrf2, Bcl-2/Bax, NF-κB, p-p65, and TGF-β/Smad2/3. PHY906 is derived from the classic formula prescription Huangqin decoction; however, instead of the separation and purification of the possible active compounds, it is taken as a whole. In-depth research via animal experiments, clinical trials, and quality control of PHY906 have been conducted. Results showed that PHY906 could significantly increase the antitumor activity of CPT-11, decreasing toxicity in normal tissues while promoting cell death within the TME, and that its effect may be upregulated by IRF-1, IRF-5, CCL-2/MCP-1, and CCL-5/RANTES. Tonic Chinese medicines include monomers, water extracts, the classic compound Shiquan Dabu decoction, or self-made prescriptions, and their mechanism of action may be related to the regulation of macrophage polarization, the reduction of epithelial cell-mesenchymal transition, and cell stemness.

TCM COMBINED WITH TARGETED THERAPY OR IMMUNOTHERAPY

Unlike the destructive antitumor effects of traditional chemotherapy, new molecular targeted therapies target specific molecular changes in cancer (16). They have achieved significant effects in clinical practice in recent years and have also triggered a change in the concept of anticancer treatment. The immunotherapeutic approach involves the restart and maintenance of the tumor immune cycle, the restoration of the body's normal antitumor immune response, and the control and elimination of cancer, by means such as monoclonal antibody immune checkpoint inhibitors, therapeutic antibodies, tumor vaccines, cell therapy, and small molecule inhibitors. Among them, PD-1 inhibitors lead the treatment of malignant tumors into a new era of immunotherapy (17, 38, 39). There are currently many studies on the combined application of TCM and targeted drugs or immunotherapy, focusing on improving efficacy, reversing drug resistance, and reducing adverse reactions. Some research results describing the impact of TCM combined with targeted drugs (**Table 3**) and immunotherapy (**Table 4**) on the TME have been released; however, there are still more treatment aspects that need further clarification.

In addition to evaluating the immune function of peripheral blood, some studies involved the detection of tumor-specific markers and tumor tissue-related factors to evaluate the invasion ability of tumors. Clinical studies on non-small-cell lung carcinoma (NSCLC) (82), hepatocellular carcinoma (83), and ovarian cancer (84) use compound preparations, including classic traditional formula Xuefu Zhuyu decoction (82) and listed compound herbal medicine Shenqi Fuzheng injection (83). During *in vitro* and *in vivo* studies, apart from observing the effects on tumor cell proliferation, the related signaling pathways were explored, including the NF-κB and p38 MAPK signaling cascades mediated by TNFR1 in hepatocellular carcinoma cells (compound Kushen injection) (85) and the AKT pathway in gastric cancer and pancreatic cancer cells (Astragalus polysaccharide) (86, 87). YIV-906, which is based on PHY906 (88), is a clinical observation drug that ensures >90% consistency in product quality (89). It is also the first Chinese medicinal project to be awarded a grant from the PO1 program of the National Cancer Center of the United States. Animal experiments show that PHY906 may potentiate sorafenib action and that its mechanism of action involves an increase in hMCP1 expression, enhanced infiltration of macrophages into tumors with a higher M1/M2 expression pattern, and upregulation of AMPKα-P and ULK1-S555-P. Computer simulation methods have also been used in the analysis of its mechanism of action and key components (90).

TABLE 2 | Influence of traditional Chinese medicine (TCM) Combined Chemotherapy (CT) on tumor microenvironment (TME) - Experimental Study.

Cells	Type	Formulation	Herbal medicine	Chemo	Effect of Combination	Upregulate	Downregulate	Refs.
HCT-116 and HT-29; LoVo-xenograft; HCT –8/5–Fu cells	In vitro and in vivo	Monomer	Curcumin	FOLFOX/ Oxa/5 –Fu	Confirmed the reversal effect on multidrug resistance	Bax, caspase-3, and PARP	EGFRs and IGF-1R; Bcl-2, survivin, HSP70; Nrf2, Bcl-2/Bax; NF-κB; p-p65, TGF-β/Smad2/3	Patel et al. (70) Guo et al. (71) Zhang et al. (72) Yin et al. (73)
SPC-A1, H1299, A549 cell lines	In vitro and in vivo	Monomer	Ginsenoside Rg3	DDP	Increase the sensitivity to DDP	/	NF-κB, EMT and stemness	Wang et al. (74)
A549 cells and Lewis lung carcinoma (LLC1)	In vitro in and vivo	Compound extract	WEGA (Water extract of ginseng and astragalus)	DDP	Effectively inhibited the transplanted tumor growth and improved weight loss and immunosuppressive	inhibited A549 cell proliferation, M1 macrophage markers	M2 TAMs markers	Chen et al. (75)
Colon 38 tumors	In vivo	Compound (Classic)	PHY906 (Glycyrrhiza uralensis Fisch, Paeonia lactiflora Pall, Scutelleriabaicalensis Georgi, and Ziziphus jujuba Mill)	CPT-11	Increased the antitumor activity of CPT-11 while decreasing animal weight loss caused by CPT-11; decrease toxicity in normal tissues while promoting cell death within the tumor microenvironment	IRF-1, IRF-5, CCL-2/MCP-1 and CCL-5/ RANTES	/	Lam et al. (76) Wang et al. (77)
B6F10 Melanoma cells	In vitro and in vivo	Compound (Classic)	Shiquan Dabu Decoction (Ginseng, calami similiter ducentos quinquaginta, Chuanxiong, Rehmannia, Poria, Atractylodes, Licoricia, Astragalus, Carlo, etc)	DDP	Inhibit the proliferation of melanoma, promote apoptosis and the proliferation of mouse spleen lymphocytes, enhance the anti-tumor effect	IL-4	IL-1β	Zhang et al. (78)
Murine LLC cells	In vitro and in vivo	Compound (Listed drug)	Shexiang Baoxin Pill (Artificial Moschus, Cortex cinnamomic, Borneolum, Radix ginseng, Calculus bovis, Styrax, Venenum Bufonis)	GEM	Enhance the effective treatment performancewhile minimizing the toxic side effects	tumor angiogenesis, blood perfusion, vascular permeability, and vessel dilation	a-SMA, collagen	Yang et al. (79)
Lewis lung carcinoma (LLC1)	In vitro and vivo	Compound (Self-made)	**JC-001** (Bupleurum chinense DC, Gentiana scabra Bge., Rheum palmatum L., Clematis montana Buch.-Ham., Carthamus tinctorius L., Prunus persica (L.) Batsch , Angelicadahurica (Fisch. ex Hoffm.) Benth. et Hook. f., Siegesbeckia orientalis L., Glycyrrhiza uralensis Fisch. and Solanum incanum L.)	DDP	JC-001 suppressed foci formation and reduced the viability of LLC1 cells in vitro, increased the chemosensitivity to CDDP in vivo	IL-2, IL-10, TNF-α and INF-γ, enhanced the Th1 response	IL-17A, TGF-β	Chuang et al. (80)
CNE2 cells nasopharyngeal carcinoma	In vivo	Compound Granules	**Qi-Boosting Toxin-Resolving Granules** (Rudis Astragalus, Coptis, Oldenlandia diffusa, etc)	DDP	Apoptotic rate was significantly higher	INF-γ, Foxp3	IL-17, TGF-β, ROR-γt mRNA	Hu et al. (81)

TABLE 3 | Influence of TCM Combined Targeted therapy.

Cancers	Type	Formulation	Herbal medicine	Targeted therapy	Effect of Combination	Upregulate	Downregulate	Refs.
NSCLC	Clinical	Compound (Classic, oral)	Xuefu Zhuyu Decoction (Angelica, peach kernel, chuanxiong, safflower, red peony root, achyranthes, bupleurum, citrus aurantium, platycodon, habitat, mountain mushroom, oldenlandia diffusa, shuyangquan, gecko, licorice)	TCM + gefitinib/ erlotinib vs gefitinib/ erlotinib = 39 vs 39	DCR 56.4% vs 48.7% ($p<0.05$)	T cell, Th, Tc	Protease activated receptor (PAR)-1 expression in tumor tissue	Li et al. (82)
Hepatocellular Carcinoma	Clinical	Compound (Listed drug, injection)	Shenqi Fuzheng Injection (Codonopsis, Astragalus)	TCM + sorafenib vs sorafenib = 44 vs 44	DCR 97.7% vs 86.4% ($p<0.05$)	$CD4^+$	$CD8^+$, CXCR3, miR-103	Lu et al. (83)
Ovarian cancer	Clinical	Compound (Self-made, oral)	Yiqi Yangyin Decoction (Seres yam, Astragalus, Habitat, Polygonatum, Scrophulariaceae, Ligustrum lucidum, Zingiber turmeric, Shanzi fungus Prunella vulgaris, Platycodon grandiflorum, Jujube)	TCM + bevacizumab vs bevacizumab = 43 vs 37	/	$CD3^+$, $CD4^+$, $CD4^+/CD8^+$, NK IL-2, INF-γ	$CD4^+CD25^+$, IL-6, IL-10, VEGF, CD133, DDX4	Guli et al. (84)
HCC cells	in vitro and in vivo	Compound (Listed drug, injection)	Compound Kushen Injection (Sophora flavescens, Berberis vulgaris uniseriale)	sorafenib	Enhanced the anticancer activity of sorafenib at a subclinical dose with no obvious side effects.	triggering TNFR1, mediated NF-κB and p38 MAPK signaling cascades	/	Yang et al. (85)
Gastric AGS cells	in vitro	Monomer component	Astragalus polysaccharide (APS)	apatinib	Remarkable increase in apoptosis	/	p-AKT, MMP-9	Wu et al. (86)
Pancreatic cancer cell lines	in vitro	Monomer component	Astragalus polysaccharide (APS)	apatinib	Enhanced inhibitory effects on cell migration and invasion, and increased cell apoptosis percentage	/	p-AKT, p-ERK, MMP-9	Wu et al. (87)
HepG2 xenografts	in vivo	Compound (Classic, oral)	PHY906 (KD018)	sorafenib	potentiate the anti-hepatoma activity	hMCP1, M1/M2, AMPKα-P and ULK1-S555-P, ERK1/2-P	/	Lam et al. (88)

TABLE 4 | Influence of traditional Chinese medicine (TCM) Combined Immunotherapy.

Cancers	Type	Formulation	Herbal medicine	Immunotherapy	Effect of Combination	Upregulate	Downregulate	Refs.
WEHI-3 leukemia or EL4 lymphoblast cells	in vitro	Monomer component	PG2 (A polysaccharide isolated from the radix of Astragalus membranaceus)	/	*via* the protein kinase B (Akt)/mammalian target of rapamycin (mTOR)/ribosomal protein S6 kinase beta-1 (p70S6K) pathway	/	PD-L1 on the cell surface	Chang et al. (91)
Diffuse large B cell lymphoma	in vitro	Monomer component	Ginsenoside Rg3	PD-1 inhibitor	enhances the anti-tumor effect and proliferation of T cells, inhibiting apoptosis, increasing the secretion of cytokine	IL-2, IFN-γ	/	Guo et al. (92)
TC-1	in vivo	Monomer	Glycyrrhiza uralensis water extract	HPV dendritic cell-based vaccine	dose-dependently promoted DC maturation and cytokine secretion through TLR4 signaling pathway	CD4+ and CD8+ T cells	iTregs: CD4 +CD25- Fopx3+	Aipire et al. (93)
MB79 bladder cancer	in vivo	Monomer component	Bisdemethoxycurcumin	α-PD-L1	significantly prolonged survival of intraperitoneal metastasized bladder cancer bearing mice	intratumoral $CD8^+$ T-cell infiltration, IFN-γ in the blood	intratumoral MDSCs	Shao et al. (94)
CT26 colon cancer	in vivo	Compound (Classic)	Gegen Qinlian Decoction	anti-mouse PD-1	Gut microbiota analysis revealed that combination significantly enriched for s: Bacteroides_acidifaciens and s:uncultured_organism_g:norank_f: Bacteroidales_S24-7_group.	CD8+ T cells in peripheral blood, IFN-γ, IL-2,	PD-1	Lv et al. (95)
CT26 colon cancer	in vivo	Compound (Classic)	ninjin'yoeito (NYT, Renshen Yangrong Decoction)	tumor vaccine	synergistically enhances the effects of the prophylactic tumor vaccine	CD8+ T cells	Tregs: CD4 +CD25-Fopx3 +	Takaku et al. (96)
B16 melanoma cancer	in vivo	Compound (Classic)	Juzentaihoto (JTT, Shiquan Dabu Decoction)	anti-PD-1 antibody	significantly suppressed B16 cell metastasis	IL-12, IFN-γ, NK	/	Ishikawa et al. (97)
Advanced stage cancer	Clinical	Compound (Classic, oral)	Guipi Decoction	NK cell	TCM symptoms improved (shortness of breath, over fatigued, tiredness)	$CD3^+$, $CD4^+$, $CD8^+$, NK	/	Lu and Peng (98)
Castration-resistant prostate cancer	Clinical	Compound (Classic, oral)	Hochu-ekki-to (Buzhong Yiqi Decoction) and Keishi-bukuryo-gan (Guizhi Fuling Pills)	Personalized Peptide Vaccine (PPV)	well tolerated without severe adverse events.		Mo-MDSC, IL-6	Koga et al. (99)

Whether tonic herbal medicine be used in combination with immunotherapy is one of the issues that Chinese cancer patients are extremely concerned about; moreover, it is a very controversial issue for cancer clinicians. Research on the combination of TCM and immunotherapy mainly includes ***in vivo*** and ***in vitro*** studies, while clinical studies are rarely conducted. The TCM studied mostly include tonic drugs or their components: Astragalus (91), ginsenoside Rg3 (92), Glycyrrhiza uralensis water extract (93), and bisdemethoxycurcumin (94). Most of the compound prescriptions are classic medicines, including Gegen Qinlian decoction (95), Renshen Yangrong decoction (96), Shiquan Dabu decoction (97), Guipi decoction (98), and Buzhong Yiqi decoction (99). The components of Astragalus can downregulate PD-L1 on the tumor cell surface, which may be related to the AKT/mTOR/p70S6K pathway (91). *In vivo* studies have shown that TCM combinations have a positive effect on therapeutic curative potential and tumor inhibition. Some studies also explored the intestinal flora; however, in clinical observation, the main observed effect remains the improvement of symptoms. Both TCM treatment and immunotherapy have systematic and complex characteristics. Determining whether TCM affects the efficacy or the adverse effects of immunotherapy by regulating the TME and related factors necessitates further research.

TCM COMBINED WITH LOCAL TREATMENT

Malignant tumors require different treatment strategies according to the different stages of the disease. Additionally, local treatment plays an important role in the treatment of cancer. Early radical surgery is the most effective way to obtain a curative effect and long-term survival. Radiotherapy and interventional therapy can obtain survival benefits and symptom improvement through the control of local lesions. The combined citation of TCM and local treatment have been clinically observed to reduce perioperative complications, promote the recovery of immune function, reduce recurrence and metastasis, and improve long-term prognosis. The TCM involved are mostly listed drugs (**Table 5**), and research on their mechanism of action is relatively lacking and limited to peripheral blood immune function detection.

DISCUSSION

The clinical application of TCM has a long history, and its treatment principles and philosophy have a unique system. With the continuous improvement of research methods, our understanding of TCM is deepening. The study of herbal medicine monomers and their components is relatively easy to explain; however, compound prescription and compatibility are more characteristic of TCM holistic thinking. TCM has its advantages and specifics in the treatment of cancer. In addition to reducing the side effects of antitumor treatment and improving the symptoms and patient quality of life, it also

TABLE 5 | Influence of traditional Chinese medicine (TCM) Combined Local treatment (Peri-operation, γ-knife, interventional therapy).

Cancer	Type	Formulation	Herbal medicine	Local treatment	Effect of Combination	Upregulate	Downregulate	Refs.
NSCLC	Clinical	Compound (Listed drug, injection)	Aidi Injection	Neoadjuvant Chemo: TCM + Neo-Chemo vs Neo-Chemo = 35 vs 20	Decreased blood loss in operation: 530. 15 ± 104. 55 ml vs 615. 49 ± 114. 08 ml ($P<0.05$); Increased curative effect: 45. 71% vs 30. 00% ($P<0.05$); Decreased leucopenia: 37. 14% vs 60. 00% ($P<0.05$)	/	$CD4^+$, $CD25^+$	Teng et al. (100)
Lung cancer	Clinical	Compound (Listed drug, oral)	Zilongjin Tablets	Post operation: TCM vs control = 30 vs 30	promote the recovery of immune function	IgA, IgG, $CD4^+$, $CD4^+$/$CD8^+$, NK	/	Huang et al. (101)
Triple-negative Breast Cancer	Clinical	Compound (Self-made, oral)	Shenghe Powder	Post operation Chemo-Radio Therapy(CRT): TCM + CRT vs CRT = 84 vs 84	5-year survival rate: 76. 2% vs 64. 3% ($P<0.05$); Recurrence and metastasis rate: 25.0% vs 39.3% ($P<0.01$)	$CD3^+$, $CD4^+$, $CD4^+$/$CD8^+$, NK; miR-34a,	LDHA	Wang et al. (102)
Primary liver cancer	Clinical	Compound (Listed drug, injection)	Compound Danshen Injection	TCM + γ-knife vs γ-knife = 20 vs 20	/	IgA, IgG, IgM, $CD3^+$, $CD4^+$, $CD4^+$/$CD8^+$,	/	Zhu and Yi (103)
Primary liver cancer	Clinical	Compound (Listed drug, oral)	Jinlong Capsule	TCM + intervention vs intervention = 30 vs 30	facilitates the cellular immunity recovery	keep stable: $CD3^+$, $CD4^+$, $CD4^+$/$CD8^+$, NK; SIL-2R, TSGF	/	Yuan et al. (104)

"supports the healthy Qi" and restores the body's own immune system. It can improve efficacy and prolong survival in the comprehensive treatment of cancer.

Many studies on the monomers or components of herbal medicine have confirmed that they affect related factors in the TME; however, their effects in a more complex system are relatively unexplored. This review summarizes and analyzes the influence and effect of TCM in combination with antitumor therapy, including chemotherapy, targeted therapy, immunotherapy, the perioperative period, radiotherapy, and interventional therapy. Relevant Chinese medicines include marketed drugs (injections, oral liquids, and tablets), traditional prescriptions, and self-developed experiential prescriptions, as well as many Chinese medicinal monomers or ingredients. Tonic drugs are the main active agents, including multiple treatments such as replenishing Qi, invigorating the spleen, promoting blood circulation, eliminating phlegm, clearing heat, and dispelling stagnation. It is well known that the immune system of body, plays defensive, protective and eliminative roles on tumor cells. For example, NK cells can directly recognize and eradicate tumor cells; Dendritic cells (DCs) can activate adaptive immunity; macrophages (M) can kill tumor cells by generating cytotoxicity, which related to the production of effector molecules and accompanying phagocytosis. Clinical studies have shown that adding TCM to the treatment strategy can significantly improve patient symptoms without increasing adverse reactions, with a tendency to prolong survival. The detection of peripheral blood-related immune factors suggests that TCM has a regulatory effect on immune function and that it can promote a healthy Th1/Th2 balance and regulate the polarization of macrophages. Peripheral blood is the most commonly used medium for disease diagnosis and has been widely accepted by patients for noninvasive molecular diagnosis. In addition, compared with the tumor tissue sample, the dynamic change of microenvironment is ignored, and the peripheral blood can be sampled for many times regularly, which is convenient for monitoring. In relevant *in vivo* and *in vitro* studies, possible mechanisms of action have been discussed, including the classical NF-κB, AKT, and TLR4 signaling pathways and the intestinal flora. However, TCM treatment still needs to go through top-level design, good quality control, reverse verification, and in-depth research that can reproduce results to demonstrate the role of TCM in the comprehensive treatment of tumors and clarify its therapeutic mechanism.

CONCLUSIONS

Cancer treatment has multiple stages and high complexity, and the optimal approach includes multidisciplinary comprehensive diagnosis and treatment. TCM has its unique advantages and characteristics that are different from other types of antineoplastic treatment, and these should not be ignored. However, current research results cannot clearly explain the dominant population and mechanism of effect of TCM combined with antitumor therapy; however, the impact on the TME may be the core principle of this approach. More evidence-based experimental research is still needed to provide a basis for formulating better combined strategies for cancer treatment.

AUTHOR CONTRIBUTIONS

YZ, YL, and WS concepted and designed the review. YZ and YL wrote the manuscript. JW, CY, and WS revised the manuscript. All authors contributed to the article and approved the submitted version.

FUNDING

This work is supported by the National Natural Science Foundation of China (No. 81973601 and No. 81904003), and the Beijing Municipal Natural Science Foundation (No. 7202184).

ACKNOWLEDGMENTS

We would like to thank Editage (www.editage.cn) for English language editing.

REFERENCES

1. Freddie BBMP, JF ME. Isabelle Soerjomataram MD MP, MPH RLS, MSPH LAT, Ahmedin Jemal PhD D. Global cancer statistics 2018: GLOBOCAN estimates of incidence and mortality worldwide for 36 cancers in 185 countries. *CA: A Cancer J Clin* (2018) 68:394–424. doi: 10.3322/caac.21492
2. Fidler MM, Bray F, Soerjomataram I. The global cancer burden and human development: A review. *Scand J Public HEALT* (2018) 46:27–36. doi: 10.1177/1403494817715400
3. Camilla M, Giuseppe L. Cancer statistics: a comparison between World Health Organization (WHO) and Global Burden of Disease (GBD). *Eur J Public Health* (2019) 30:1026–27. doi: 10.1093/eurpub/ckz216
4. Neil V, José B, M HD. A view on drug resistance in cancer. *Nature* (2019) 575:299–309. doi: 10.1038/s41586-019-1730-1
5. Nikolaou M, Pavlopoulou A, Georgakilas AG, Kyrodimos E. The challenge of drug resistance in cancer treatment: a current overview. *Clin Exp Metastas* (2018) 35:309–18. doi: 10.1007/s10585-018-9903-0
6. Ankur G, Kumardeep C, Rahul K, Sudheer G, Harinder S, RGP S. Managing Drug Resistance in Cancer: Role of Cancer Informatics. *Methods Mol Biol (Clifton NJ)* (2016) 1395:299–312. doi: 10.1007/978-1-4939-3347-1_17
7. Assaraf YG, Brozovic A, Gonçalves AC, Jurkovicova D, Linē A, Machuqueiro M, et al. The multi-factorial nature of clinical multidrug resistance in cancer. *Drug Resist Update* (2019) 46:100645. doi: 10.1016/j.drup.2019.100645
8. M GM, Orit L, D HM, Jean-Pierre G. Toward a Better Understanding of the Complexity of Cancer Drug Resistance. *Annu Rev Pharmacol* (2016) 56:85–102. doi: 10.1146/annurev-pharmtox-010715-103111
9. N AS, Robert E, R SE, D SCM. Fear of cancer recurrence: A qualitative systematic review and meta-synthesis of patients' experiences. *Clin Psychol Rev* (2019) 68:13–24. doi: 10.1016/j.cpr.2018.12.001
10. Pillay B, Wootten AC, Crowe H, Corcoran N, Tran B, Bowden P, et al. The impact of multidisciplinary team meetings on patient assessment, management and outcomes in oncology settings: A systematic review of the literature. *Cancer Treat Rev* (2016) 42:56–72. doi: 10.1016/j.ctrv.2015.11.007

11. Rogers MJ, Matheson L, Garrard B, Maher B, Cowdery S, Luo W, et al. Comparison of outcomes for cancer patients discussed and not discussed at a multidisciplinary meeting. *Public Health* (2017) 149:74–80. doi: 10.1016/j.puhe.2017.04.022
12. PhD IPD, MB MPH, CA MPH, Kathleen M, Castro RN MA, Brandys B, et al. multidisciplinary treatment planning in US cancer care settings. *Outcomes Cancer-Am Cancer Soc* (2018) 124:3656–67. doi: 10.1002/cncr.31394
13. Wyld L, Audisio RA, Poston GJ. The evolution of cancer surgery and future perspectives. *Nat Rev Clin Oncol* (2015) 12:115–24. doi: 10.1038/nrclinonc.2014.191
14. Schaue D, McBride WH. Opportunities and challenges of radiotherapy for treating cancer. *Nat Rev Clin Oncol* (2015) 12:527–40. doi: 10.1038/nrclinonc.2015.120
15. Stefan B. Molecular precision chemotherapy: overcoming resistance to targeted therapies? *Clin Cancer Res* (2014) 20:1064–6. doi: 10.1158/1078-0432.CCR-13-3194
16. Lee YT, Tan YJ, Oon CE. Molecular targeted therapy: Treating cancer with specificity. *Eur J Pharmacol* (2018) 834:28–32. doi: 10.1016/j.ejphar.2018.07.034
17. Guo Q, Huang F, Goncalves C, Rincón SVD, Miller WH. Translation of cancer immunotherapy from the bench to the bedside. *Adv Cancer Res* (2019) 143:1–62. doi: 10.1016/bs.acr.2019.03.001
18. Fabian CJ, Visvanathan K, Somerfield MR. Use of Endocrine Therapy for Breast Cancer Risk Reduction: ASCO Clinical Practice Guideline Update Summary. *J Oncol Pract* (2019) 15:607–10. doi: 10.1200/JOP.19.00379
19. AS S, CM R, TP T, KP G, BG M, Helen B, et al. Clinical Development of Novel Drug-Radiotherapy Combinations. *Clin Cancer Res An Off J Am Assoc Cancer Res* (2019) 25:1455–61. doi: 10.1158/1078-0432.CCR-18-2466
20. Linda H, Cath T, Magda Z, Ross W, Emma P, James G. Improving the effectiveness of cancer multidisciplinary team meetings: analysis of a national survey of MDT members' opinions about streamlining patient discussions. *BMJ Open Qual* (2019) 8:e000631. doi: 10.1136/bmjoq-2019-000631
21. Stone E, Rankin N, Kerr S, Fong K, Currow DC, Phillips J, et al. Does presentation at multidisciplinary team meetings improve lung cancer survival? Findings from a consecutive cohort study. *Lung Cancer* (2018) 124:199–204. doi: 10.1016/j.lungcan.2018.07.032
22. Elena CM, Romano D, Corrado G, Pietro I, Alessandra E, Massimo U. Management of toxicities associated with targeted therapies for HR-positive metastatic breast cancer: a multidisciplinary approach is the key to success. *Breast Cancer Res TR* (2019) 176:483–94. doi: 10.1007/s10549-019-05261-5
23. Wu C, Li M, Meng H, Liu Y, Niu W, Zhou Y, et al. Analysis of status and countermeasures of cancer incidence and mortality in China. *Sci China(Life Sci)* (2019) 62:640–7. doi: 10.1007/s11427-018-9461-5
24. Feng RM, Zong YN, Cao SM, Xu RH. Current cancer situation in China: good or bad news from the 2018 Global Cancer Statistics? *Cancer Commun* (2019) 39:22. doi: 10.1186/s40880-019-0368-6
25. Wanqing Chen PhD MD, RZ MPH, PDB P, BMedSc SZ, Hongmei Zeng PhD MD, PhD FB, et al. Cancer statistics in China, 2015. *CA: A Cancer J Clin* (2016) 66:115–32. doi: 10.3322/caac.21338
26. Ma Y, Zhou K, Fan J, Sun S. Traditional Chinese medicine: potential approaches from modern dynamical complexity theories. *Front Med-PRC* (2016) 10:28–32. doi: 10.1007/s11684-016-0434-2
27. Xu Q, Bauer R, Hendry BM, Fan TP, Zhao Z, Duez P, et al. The quest for modernisation of traditional Chinese medicine. *BMC Complem Altern M* (2013) 13:132. doi: 10.1186/1472-6882-13-132
28. So T, Chan S, Lee V, Chen B, Kong F, Lao L. Chinese Medicine in Cancer Treatment - How is it Practiced in the East and the West? *Clin ONCOL-UK* (2019) 31:578–88. doi: 10.1016/j.clon.2019.05.016
29. Nie J, Zhao C, Deng L, Chen J, Yu B, Wu X, et al. Efficacy of traditional Chinese medicine in treating cancer (Review). *Biomed Rep* (2016) 4:3–14. doi: 10.3892/br.2015.537
30. Liu J, Mao JJ, Wang XS, Lin H. Evaluation of Traditional Chinese Medicine Herbs in Oncology Clinical Trials. *Cancer J* (2019) 25:367–71. doi: 10.1097/PPO.0000000000000404
31. Xiang Y, Guo Z, Zhu P, Chen J, Huang Y. Traditional Chinese medicine as a cancer treatment: Modern perspectives of ancient but advanced science. *Cancer Med* (2019) 8:1958–75. doi: 10.1002/cam4.2108
32. Liu X, Li M, Wang X, Dang Z, Yu L, Wang X, et al. Effects of adjuvant traditional Chinese medicine therapy on long-term survival in patients with hepatocellular carcinoma. *Phytomedicine* (2019) 62:152930. doi: 10.1016/j.phymed.2019.152930
33. Tang M, Wang S, Zhao B, Wang W, Zhu Y, Hu L, et al. Traditional Chinese Medicine Proton vs Progression-Free Survival and Enhances Therapeutic Effects in Epidermal Growth Factor Receptor Tyrosine Kinase Inhibitor (EGFR-TKI) Treated Non-Small-Cell Lung Cancer (NSCLC) Patients Harboring EGFR Mutations. *Med Sci Monitor* (2019) 25:8430–7. doi: 10.12659/MSM.917251
34. Huang S, Peng W, Mao D, Zhang S, Xu P, Yi P, et al. Kangai Injection, a Traditional Chinese Medicine, Improves Efficacy and Reduces Toxicity of Chemotherapy in Advanced Colorectal Cancer Patients: A Systematic Review and Meta-Analysis. *Evid-Based Compl Alt* (2019) 2019:8423037. doi: 10.1155/2019/8423037
35. Wong W, Chen BZ, Lee AKY, Chan AHC, Wu JCY, Lin Z. Chinese Herbal Medicine Effectively Prolongs the Overall Survival of Pancreatic Cancer Patients: A Case Series. *Integr Cancer Ther* (2019) 18:1534735419828836. doi: 10.1177/1534735419828836
36. FuuJen T, Xiang L, ChaoJung C, TeMao L, JianShiun C, PoHeng C, et al. Chinese herbal medicine therapy and the risk of overall mortality for patients with liver cancer who underwent surgical resection in Taiwan. *Complement Ther Med* (2019) 47:102213. doi: 10.1016/j.ctim.2019.102213
37. Muenst S, Läubli H, Soysal SD, Zippelius A, Tzankov A, Hoeller S. The immune system and cancer evasion strategies: therapeutic concepts. *J Intern Med* (2016) 279:541–62. doi: 10.1111/joim.12470
38. Hongxing S, Shih-Hsin YE, Marty C, John F, Carlo C, BJ A, et al. Predictive biomarkers for immune checkpoint blockade and opportunities for combination therapies. *Genes Dis* (2019) 6:232–46. doi: 10.1016/j.gendis.2019.06.006
39. Andrews LP, Yano H, Vignali DAA. Inhibitory receptors and ligands beyond PD-1, PD-L1 and CTLA-4: breakthroughs or backups. *Nat Immunol* (2019) 20:1425–34. doi: 10.1038/s41590-019-0512-0
40. Jinjing W, Fanghua Q, Zhixue W, Zhikun Z, Ni P, Lei H, et al. A review of traditional Chinese medicine for treatment of glioblastoma. *Biosci Trends* (2020) 13:476–87. doi: 10.5582/bst.2019.01323
41. Tian JH, Xi ZC, Luo B, Que ZJ, Xu HX, Liu JX. Scientific Connotation of the Theory of "Strengthening Vital Qi to Treat Cancer". *Modernization Tradit Chin Med Mater Med-World Sci Technol* (2019) 21:943–8. doi: 10.11842/wst.2019.05.017
42. HD C, SL A. The Tumor Microenvironment Innately Modulates Cancer Progression. *Cancer Res* (2019) 79:4557–66. doi: 10.1158/0008-5472.CAN-18-3962
43. Pitt JM, Marabelle A, Eggermont A, Soria JC, Kroemer G, Zitvogel L. Targeting the tumor microenvironment: removing obstruction to anticancer immune responses and immunotherapy. *Ann Oncol* (2016) 27:1482–92. doi: 10.1093/annonc/mdw168
44. IN M, Ayca G, DAJ, HC A. Obesity and Cancer Mechanisms: Tumor Microenvironment and Inflammation. *J Clin Oncol* (2016) 34:4270–6. doi: 10.1200/JCO.2016.67.4283
45. Glauben L, De la Fuente, Peti T, Chanitra T, HM A. Chronic inflammation and cytokines in the tumor microenvironment. *J Immunol Res* (2014) 2014:149–85. doi: 10.1155/2014/149185
46. Dingzhi W, DR N. Immunosuppression associated with chronic inflammation in the tumor microenvironment. *Carcinogenesis* (2015) 36:1085–93. doi: 10.1093/carcin/bgv123
47. Nakamura K, Yaguchi T, Ohmura G, Kobayashi A, Kawamura N, Iwata T, et al. Involvement of local renin-angiotensin system in immunosuppression of tumor microenvironment. *Cancer Sci* (2018) 109:54–64. doi: 10.1111/cas.13423
48. Du J, Cheng BCY, Fu XQ, Su T, Li T, Guo H, et al. In vitro assays suggest Shenqi Fuzheng Injection has the potential to alter melanoma immune microenvironment. *J Ethnopharmacol* (2016) 194:15–9. doi: 10.1016/j.jep.2016.08.038
49. Zhaokun Y, Zijun L, Jiumao L. Anticancer Properties of Traditional Chinese Medicine. *COMB Chem High T SCR* (2017) 20:423–9. doi: 10.2174/1386207320666170116141818
50. Lin W, Lu J, Cheng B, Ling C. Progress in research on the effects of traditional Chinese medicine on the tumor microenvironment. *J Integr Med* (2017) 15:282–7. doi: 10.1016/S2095-4964(17)60345-5
51. Qiujun G, Jie L, Hongsheng L. Effect and Molecular Mechanisms of Traditional Chinese Medicine on Regulating Tumor Immunosuppressive Microenvironment. *BioMed Res Int* (2015) 2015:261620. doi: 10.1155/2015/261620

52. He SM, Huang QQ. Effect of Baihe Gujin Decoction with TP chemotherapy on advanced non-small cell lung carcinoma differentiated by lung-kidney yin deficiency and on the immune function. *World J Integrated Tradit Western Med* (2020) 15:682–686+690. doi: 10.13935/j.cnki.sjzx.200425
53. Wang JY, Lin Y, Li HG, Zhou L, Zhu LH, Zhao LH, et al. Effect of Bushen Yifei Jiedu decoction combined with chemotherapy on expression of serum Foxp3 and B7-H3 in advanced non-small cell lung cancer of type of lung and kidney deficiency. *Modern J Integrated Tradit Chin Western Med* (2020) 29:1608–11. doi: 10.3969/j.issn.1008-8849.2020.15.003
54. Zhang JH, Wang J, Cui QR. Effect of Jinfukang Oral Liquid Combined with Gemcitabine on Serum Level of MMP-9 in the Treatment of Non-Small Cell Lung Cancer with Deficiency of Both Qi and Yin. *Inf Tradit Chin Med* (2019) 36:65–8. doi: 10.19656/j.cnki.1002-2406.190048
55. Wang ZF, Geng L, Wang S, Liu XB, Zhang RX, Liu SL, et al. Effect of Feiliuping ointment combined with chemotherapy on cellular immune function and related inflammatory factors in patients with lung cancer. *Chin Tradit Herbal Drugs* (2018) 49:5368–72. doi: 10.7501/j.issn.0253-2670.2018.22.022
56. Liu JX, Yang LL. Yifei Xiaoai Decoction in Treatment of Advanced Non-small Cell Lung Cancer. *Acta Chin Med* (2018) 33:2064–8. doi: 10.16368/j.issn.1674-8999.2018.11.489
57. Chen R, Li M, Ji BY, Qi SJ. Clinical Observation of Shenqi Fuzheng Injection Combined with Chemotherapy in Treatment of Non Small Cell Lung Cancer and The Regulation of Th17/Treg Cells in Patients. *Chin Arch Tradit Chin Med* (2018) 36:1994–7. doi: 10.13193/j.issn.1673-7717.2018.08.054
58. Wang Y, Hui S, Li M, Zhang CH. Clinical trial of Kanglaite injection in gemcitabine combined cisplatin regimen chemotherapy for advanced non-small cell lung cancer. *Chin J Clin Pharmacol* (2017) 33:2354–2356+2360. doi: 10.13699/j.cnki.1001-6821.2017.23.008
59. Meng XY, Meng WY, Ye Q, Dai L, Hu J, Wang XH, et al. Effect of Modified FOLFOX7 Regimen Combined With Compound Kushen Injection and Aidi Injection on Levels of CA125,CEA,IL-6,TGFβ1 and Hydrogen Sulfide in Advanced Gastric Cancer and Analysis of Drug Safety. *Chin Arch Tradit Chin Med* (2020) 38:208–11. doi: 10.13193/j.issn.1673-7717.2020.07.048
60. Wang DD, Zhang K. Clinical study of Buzhong Guben Yiwei decoction combined with chemotherapy in the treatment of patients with advanced gastric cancer after operation. *Hebei J Tradit Chin Med* (2020) 42:240–244 +248. doi: 10.3969/j.issn.1002-2619.2020.02.018
61. Tian TD, Yang F, Yue LY, Wang XX, Shi B. Effect of Yanghetang in Chemotherapeutic Enhancement Response Among Patients of Advanced Gastric Cancer with Syndrome of Yang Deficiency and Cancer Inflammatory Factors Treg and MDSCs. *Chin J Exp Tradit Med Formulae* (2016) 22:160–4. doi: 10.13422/j.cnki.syfjx.2016220160
62. Wang KR, Jiao HJ. Clinical Efficacy of Chaihu Zaoxiu Decoction Combined with Chemotherapy in Treatment of Primary Hepatocellular Carcinoma and Its Influence on Related Serum Indicators. *Chin Arch Tradit Chin Med* (2020) 38:173–6. doi: 10.13193/j.issn.1673-7717
63. Feng XF. Effect of Buyi Zhiai Decoction on Quality of Life and Immune Function in Patients with Middle and Late Stage Esophageal Cancer Chemotherapy. *Chin Arch Tradit Chin Med* (2019) 37:1006–8. doi: 10.13193/j.issn.1673-7717.2019.04.057
64. Wei HL, Li LN. The Influence of the Life Quality of Shengqi Fuzheng Injection on the Immune Function of Ovarian Cancer after Chemotherapy. *Pract J Cancer* (2019) 34:1032–4. doi: 10.3969/j.issn.1001-5930.2019.06.046
65. Zhang BP, Meng M, Lv SY. Therapeutic effects on choriocarcinoma treated with fuzheng yiliu formula and EMA-CO chemotherapy and the impacts on immune function in the patients. *World J Integrated Tradit Western Med* (2019) 14:86–89+93. doi: 10.13935/j.cnki.sjzx.190122
66. Yang SY, Gao ZQ, Liu LL, Lai Q, Xie D. Curative Effects of Huangqi Jiedu Decoction Combined with GT Chemotherapy on Metastatic Triple-negative Breast Cancer and its Influence on Th1/Th2 Cytokine Balance. *Anti-tumor Pharm* (2019) 9:312–316+324. doi: 10.3969/j.issn.2095-1264.2019.02.29
67. Lu R, Shen ZW, Cao LY. Effect of Shenqi Fuzheng Injection combined with Docetaxel on Cellular Immune Function in Patients with Terminal Breast Cancer. *Chin J Surg Integrated Tradit Western Med* (2018) 24:149–55. doi: 10.3969/j.issn.1007-6948.2018.02.005
68. Du R, Zhang YY, Hu QF. Effect of Matrine Injection on Chemosensitivity, Quality of Life and Immune Function in Patients with Cervical Cancer. *Chin Arch Tradit Chin Med* (2018) 36:3051–5. doi: 10.13193/j.issn.1673-7717.2018.12.059
69. Han ZX, Zhao YQ, Liu QJ, Ji SQ, Cheng WL, Zhang HJ, et al. Short-term Effects of Matrine Injection Combined with Gemcitabine + Cisplatin Chemotherapy on Advanced Bladder Cancer Patients and on the Survival Time. *Anti-tumor Pharm* (2019) 9:112–6. doi: 10.3969/j.issn.2095-1264.2019.01.24
70. PB B, Radha S, Sadia Q, HEtal V, Yingjie Y, RA K, et al. Curcumin enhances the effects of 5-fluorouracil and oxaliplatin in mediating growth inhibition of colon cancer cells by modulating EGFR and IGF-1R. *Int J Cancer* (2008) 122:267–73. doi: 10.1002/ijc.23097
71. Li-da G, Yong-qing S, Xiao-han Z, Li-jian G, Zhi-jun Y, Duo W, et al. Curcumin combined with oxaliplatin effectively suppress colorectal carcinoma in vivo through inducing apoptosis. *Phytother Res PTR* (2015) 29:357–65. doi: 10.1002/ptr.5257
72. Chao Z, Lian-Jun H, Hai-Zhu Y, Ding-Feng L, Yi-Bao Z, Dong-Dong M, et al. Nrf2 is a key factor in the reversal effect of curcumin on multidrug resistance in the HCT–8/5–Fu human colorectal cancer cell line. *Mol Med Rep* (2018) 18:5409–16. doi: 10.3892/mmr.2018.9589
73. Jiahuan Y, Li W, Yong W, Hailong S, Xiaojie W, Lei W. Curcumin reverses oxaliplatin resistance in human colorectal cancer via regulation of TGF-β/Smad2/3 signaling pathway. *Oncotarg Ther* (2019) 12:3893–903. doi: 10.2147/OTT.S199601
74. Wang J, Tian L, Khan MN, Zhang L, Liu J. Ginsenoside Rg3 sensitizes hypoxic lung cancer cells to cisplatin via blocking of NF-κB mediated epithelial–mesenchymal transition and stemness. *Cancer Lett* (2018) 415:73–85. doi: 10.1016/j.canlet.2017.11.037
75. Yingna C, Lei B, Huijuan L, Yucui J, Feiyan C, Yunshan W, et al. Water extract of ginseng and astragalus regulates macrophage polarization and synergistically enhances DDP's anticancer effect. *J Ethnopharmacol* (2018) 232:11–20. doi: 10.1016/j.jep.2018.12.003
76. Lam W, Bussom S, Guan F, Jiang Z, Zhang W, Gullen EA, et al. The Four-Herb Chinese Medicine PHY906 Reduces Chemotherapy-Induced Gastrointestinal Toxicity. *Sci Transl Med* (2010) 2:45ra59. doi: 10.1126/scitranslmed.3001270
77. Wang E, Bussom S, Chen J, Quinn C, Bedognetti D, Lam W, et al. Interaction of a traditional Chinese Medicine (PHY906) and CPT-11 on the inflammatory process in the tumor microenvironment. *BMC Med Genomics* (2011) 4:38. doi: 10.1186/1755-8794-4-38
78. Zhang TT, Zou W, Yang CM, Qian C, Wu YY, Li XM, et al. Study on the Anti-Melanoma Effect of Shiquan Dabu Decoction and its Combination Therapy with Cisplatin. *J Nanjing Univ Tradit Chin Med* (2019) 35:160–5. doi: 10.14148/j.issn.1672-0482.2019.0160
79. Yang LQ, Li RY, Yang XY, Cui QF, Zhang JG. Co-administration of Shexiang Baoxin Pill and Chemotherapy Drugs Potentiated Cancer Therapy by Vascular-Promoting Strategy. *Front Pharmacol* (2019) 10:565. doi: 10.3389/fphar.2019.00565
80. Chuang M, Jan M, Chang JT, Lu F. The Chinese medicine JC-001 enhances the chemosensitivity of Lewis lung tumors to cisplatin by modulating the immune response. *BMC Complem Altern M* (2017) 17:210. doi: 10.1186/s12906-017-1728-x
81. Hu M, Zhou FL, Song L, Li L, He YC. Effect of Qi-Boosting Toxin-Resolving Granules and cisplatin on transplanted tumor of nasopharyngeal carcinoma and balance of Foxp3/ROR-γt. *Chin Tradit Herbal Drugs* (2019) 50:2121–6. doi: 10.7501/j.issn.0253-2670.2019.09.016
82. Li Y, Jiang LF, Ma DY, Cui QL, Hu YH, Fu BF. Effect and Mechanism of Resolving Stasis and Detoxication Method Combined with EGFR-TKI on NSCLC Based on Modulating PAR1 to Remodel Immune Surveillance. *Liaoning J Tradit Chin Med* (2020) 47:145–7+222. doi: 10.13192/j.issn.1000-1719.2020.06.044
83. Lu XY, Hua GD, Bai J, Tian XL, Liu C, Li YH. Effect of Shenqi Fuzheng injection combined with sorafenib on miR-103,CXCR3 and AFP in postoperative patients with liver cancer. *Chin J Integrated Tradit Western Med Liver Dis* (2020) 30:218–20+230+ 290. doi: 10.3969/j.issn.1005-0264.2020.03.009
84. Gulimire· BRJ, Reziya· KEB, Ailikemu· ABDWK, Li XW, Gulina· KEB. Effects of Yiqi Yangyin decoction combined with bevacizumab on immune function, inflammatory factors and tumor markers in patients with ovarian

cancer. *Oncol Prog* (2019) 17:827–30. doi: 10.11877/j.issn.1672-1535.2019.17.07.23
85. Yang Y, Mayu S, Wenbo Y, Feng W, Xiaoguang L, Wei W, et al. Compound kushen injection relieves tumor-associated macrophage-mediated immunosuppression through TNFR1 and sensitizes hepatocellular carcinoma to sorafenib. *J Immunother Cancer* (2020) 8:e000317. doi: 10.1136/jitc-2019-000317
86. Jun W, Junxian Y, Jing W, Chenguang Z, Kun S, Xiaojun Y, et al. Astragalus polysaccharide enhanced antitumor effects of Apatinib in gastric cancer AGS cells by inhibiting AKT signalling pathway. *Biomed Pharmacother Biomed Pharmacother* (2018) 100:176–83. doi: 10.1016/j.biopha.2018.01.140
87. Jun W, Jing W, Qiang S, Wei D, Teng L, Junxian Y, et al. Traditional Chinese medicine Astragalus polysaccharide enhanced antitumor effects of the angiogenesis inhibitor apatinib in pancreatic cancer cells on proliferation, invasiveness, and apoptosis. *Oncotarg Ther* (2018) 11:2685–98. doi: 10.2147/OTT.S157129
88. Wing L, Zaoli J, Fulan G, Xiu H, Rong H, Jing W, et al. PHY906(KD018), an adjuvant based on a 1800-year-old Chinese medicine, enhanced the anti-tumor activity of Sorafenib by changing the tumor microenvironment. *Sci REP-UK* (2015) 5:9384. doi: 10.1038/srep09384
89. Chang H, Kuo Y, Wu L, Chang C, Cheng K, Tyan Y, et al. The extracts of Astragalus membranaceus overcome tumor immune tolerance by inhibition of tumor programmed cell death protein ligand-1 expression. *Int J Med Sci* (2020) 17:939–45. doi: 10.7150/ijms.42978
90. Guo YW, Guo XC, Zhang JB, Liu AC, Quan LN. Effect of Ginsenoside Rg3 Enhancing the Immunity of PD-1 Inhibitor in Treatment of DLBCL: A Study in Vitro. *Acta Chin Med Pharmacol* (2018) 46:24–9. doi: 10.19664/j.cnki.1002-2392.180140
91. Aipire A, Li J, Yuan P, He J, Hu Y, Liu L, et al. Glycyrrhiza uralensis water extract enhances dendritic cell maturation and antitumor efficacy of HPV dendritic cell- based vaccine. *Sci Rep-UK* (2017) 7. doi: 10.1038/srep43796
92. Shao Y, Zhu W, Da J, Xu M, Wang Y, Zhou J, et al. Bisdemethoxycurcumin in combination with alpha-PD-L1 antibody boosts immune response against bladder cancer. *Oncotarg Ther* (2017) 10:2675–83. doi: 10.2147/OTT.S130653
93. Lv J, Jia Y, Li J, Kuai W, Li Y, Guo F, et al. Gegen Qinlian decoction enhances the effect of PD-1 blockade in colorectal cancer with microsatellite stability by remodelling the gut microbiota and the tumour microenvironment. *Cell Death Dis* (2019) 10415:43796. doi: 10.1038/s41419-019-1638-6
94. Takaku S, Shimizu M, Takahashi H. Japanese Kampo medicine ninjin'yoeito synergistically enhances tumor vaccine effects mediated by CD8(+) T cells. *Oncol Lett* (2017) 13:3471–8. doi: 10.3892/ol.2017.5937
95. Lu SB, Peng XF. Effect of guipi decoction combined with NK cell on the quality of life and immune function in patients with advanced malignant neoplasm. *Chin J Cancer Prev Treat* (2018) 025:1733–6. doi: 10.16073/j.cnki.cjcpt.2018.24.011
96. Koga N, Moriya F, Waki K, Yamada A, Itoh K, Noguchi M. Immunological efficacy of herbal medicines in prostate cancer patients treated by personalized peptide vaccine. *Cancer Sci* (2017) 108:2326–32. doi: 10.1111/cas.13397
97. Ishikawa S, Ishikawa T, Tezuka C, Asano K, Sunagawa M, Hisamitsu T. Efficacy of Juzentaihoto for Tumor Immunotherapy in B16 Melanoma Metastasis Model. *Evid-Based Compl Alt Med* (2017) 2017:6054706. doi: 10.1155/2017/6054706
98. Lam W, Ren Y, Guan F, Jiang Z, Cheng W, Xu CH, et al. Mechanism Based Quality Control (MBQC) of Herbal Products: A Case Study YIV-906 (PHY906). *Front Pharmacol* (2018) 9:1324. doi: 10.3389/fphar.2018.01324
99. Liu S, He X, Man VH, Ji B, Wang J. New application of in silico methods in identifying mechanisms of action and key components of anti-cancer herbal formulation YIV-906 (PHY906). *Phys Chem Chem Phys* (2019) 21:23501–13. doi: 10.1039/C9CP03803E
100. Teng Y, Xiao JR, Lin P, Zhang J. Effects of Combination of Aidi Injection and Neoadjuvant Chemotherapy on Patients with Non-Small-Cell Lung Cancer and Number of CD4~+CD25~+T Regulatory Cells. *Chin J Exp Tradit Med Formulae* (2012) 18:291–4. doi: 10.13422/j.cnki.syfjx.2012.18.095
101. Huang ZR, Chen YM, Lin H, Lin JP, Chen NJ. Effect of Zilongjin Tablets on immune function of patients with lung cancer after operation. *Chin Tradit Herbal Drugs* (2019) 50:2941–4. doi: 10.7501/j.issn.0253-2670.2019.12.029
102. Wang H, Li XJ, Cai ZH, Wang JH, Xia YS. Effect of Shenghe Powder on Recurrence and Metastasis Rate of Post-operative Triple-negative Breast Cancer. *Chin Arch Tradit Chin Med* (2018) 36:2983–6. doi: 10.13193/j.issn.1673-7717.2018.12.043
103. Zhu YL, Yi FT. The effect of γ knife the combined application of danshen injections on immune function in patients with primary liver cancer. *Chin J Integrated Tradit Western Med Liver Dis* (2020) 30:111–3. doi: 10.3969/j.issn.1005-0264.2020.02.005
104. Yuan TW, Wen SW, Dang ZJ, Zhang XQ, Chang JP, Xue YQ. Regulation of immune functions by combined Jinlong capsule and interventional therapy in patients with primary liver cancer. *Chin J Clin Oncol* (2013) 40:1116–8. doi: 10.3969/j.issn.1000-8179.20130206

Conflict of Interest: The authors declare that the research was conducted in the absence of any commercial or financial relationships that could be construed as a potential conflict of interest.

Copyright © 2021 Zhang, Lou, Wang, Yu and Shen. This is an open-access article distributed under the terms of the Creative Commons Attribution License (CC BY). The use, distribution or reproduction in other forums is permitted, provided the original author(s) and the copyright owner(s) are credited and that the original publication in this journal is cited, in accordance with accepted academic practice. No use, distribution or reproduction is permitted which does not comply with these terms.

frontiers in Immunology

ORIGINAL RESEARCH
published: 22 January 2021
doi: 10.3389/fimmu.2020.594212

Stereotactic Body Radiotherapy Is Effective in Modifying the Tumor Genome and Tumor Immune Microenvironment in Non-Small Cell Lung Cancer or Lung Metastatic Carcinoma

Pu Zhou[1†], Diangang Chen[1†], Bo Zhu[1†], Wei Chen[2†], Qichao Xie[3], Yali Wang[4], Qiulin Tan[4], Bibo Yuan[1], Xuejiao Zuo[1], Changlin Huang[1], Hongfan Zhu[5] and Guanghui Li[1]*

[1] Institute of Cancer, Xinqiao Hospital, Army Medical University, Chongqing, China, [2] Zhongyuan Union Clinical Laboratory Co. Ltd, Beijing, China, [3] Department of Oncology, Third Affiliated Hospital, Chongqing Medical University, Chongqing, China, [4] Department of Pathology, Xinqiao Hospital, Army Medical University, Chongqing, China, [5] Department of Internal Medicine, Army 956 Hospital, Linzhi, China

Background and Purpose: To directly reveal the change in genome mutation, RNA transcript of tumor cells, and tumor microenvironment (TME) after stereotactic body radiotherapy (SBRT) in paired human lung tumor specimens.

Materials and Methods: Paired tumor samples were collected from 10 patients with non-small cell lung cancer (NSCLC) or lung metastatic carcinoma within a week before and after SBRT. DNA and RNA of tumor tissues was extracted from the paired samples. Whole-exome and RNA sequencing assays were performed by next-generation sequencing. Gene mutation, genomic expression, T-cell receptor (TCR) repertoire, and profiling of tumor-infiltrating immune cells were analyzed through bioinformatics analysis in paired tumor samples. CD8+ T-cell infiltration and PD-L1 expressions were detected by immunostaining in tumor tissues.

Results: The diversity of TCR repertoire and PD-L1 expression increased significantly in the TME, and the most enriched term of the gene ontology analysis was the immune response gene after receiving SBRT. SBRT induced neo-mutation of genes in tumor cells but did not increase tumor mutation burden in tumor tissues. TME displayed complex immune cell changes and infiltration and expression of immune-regulating factors such as C-X-C motif chemokine (CXCL) 10, CXCL16, interferons (IFNs), and IFN receptors. CD8+ T-cells in tumor tissues did not improve significantly after SBRT while the infiltrating TH1 and TH2 cells decreased remarkably.

OPEN ACCESS

Edited by:
Peng Qu,
National Institutes of Health (NIH), United States

Reviewed by:
John-William Sidhom, Johns Hopkins Medicine, United States
Hua Jiang, Medical University of South Carolina, United States

***Correspondence:**
Guanghui Li
liguanghui_2000@aliyun.com

†These authors have contributed equally to this work

Specialty section:
This article was submitted to Cancer Immunity and Immunotherapy, a section of the journal Frontiers in Immunology

Received: *12 August 2020*
Accepted: *04 December 2020*
Published: *22 January 2021*

Citation:
Zhou P, Chen D, Zhu B, Chen W, Xie Q, Wang Y, Tan Q, Yuan B, Zuo X, Huang C, Zhu H and Li G (2021) Stereotactic Body Radiotherapy Is Effective in Modifying the Tumor Genome and Tumor Immune Microenvironment in Non-Small Cell Lung Cancer or Lung Metastatic Carcinoma. Front. Immunol. 11:594212. doi: 10.3389/fimmu.2020.594212

Conclusion: SBRT improved the TCR repertoire diversity and PD-L1 expression in the TME and induced neo-mutation of genes in tumor cells but did not increase CD8+ T-cell infiltration and IFN expression in the tumor tissue within a week.

Keywords: stereotactic body radiotherapy, tumor microenvironment, tumor-infiltrating immune cells, T-cell receptor, whole-exome sequencing, RNA sequencing

INTRODUCTION

Significant synergy between radiotherapy and treatment with immune checkpoint inhibitors (ICIs) would potentiate the effect of irradiation on antitumor immune response. Immunotherapy combined with radiotherapy is more effective than monotherapy alone for various types of tumors (1–3). Radiotherapy could even rescue a nivolumab-refractory immune response in patients with metastatic lung carcinoma (4). Radiation-induced antitumor immune response in patients varied widely depending on the doses delivered, fraction, and irradiation site of radiotherapy (5). Several reports confirmed that stereotactic body radiotherapy (SBRT) is more potent in terms of improving ICI anti-tumor response compared with conventional fraction radiation in patients with non-small cell lung cancer (NSCLC) (6, 7).

Although numerous reports demonstrated that radiotherapy enhanced the therapeutic effect of immunotherapy (8), the direct impact of SBRT on the tumor cell genome and the tumor microenvironment (TME) remains unclear in patients with cancer. Here, we examined the genomic variance of cancer cells, immune cell infiltration, and immune-regulating factor expression of the TME in 10 patients with lung tumors who received SBRT.

MATERIALS AND METHODS

Study Patients

Thirteen patients aged 43–68 years were included. They had histologically documented malignant tumor, recurrent or metastatic; World Health Organization (WHO) performance status score of 0 to 2; life expectancy of at least 3 months at day 1; and indication for local radiotherapy. Four patients had metastatic lung tumor from colorectal carcinoma (CRC), seven had NSCLC, one had metastatic esophageal carcinoma in the lungs, and one had metastatic cervical cancer in the lungs. The medical ethics committee of Xinqiao Hospital of Army Medical University approved the study (Ethical No: 2019-Res 032-1). All patients provided informed consent.

Biopsy and Radiotherapy

Computed tomography-guided puncture biopsy of the lung deposit was performed a week before SBRT. Peripheral blood samples were collected in ethylenediaminetetraacetic acid vacutainer tubes at the same time. Mononuclear cells separated by centrifugation at 1,600 *g* were transferred to a new microcentrifuge tube and were fixed with a preserving buffer (Geneplus Biotech, China) for 24 h at 4°C and were then placed in the refrigerator (−80°C) to preserve sample integrity. Lung targeted tumors received 60 Gy irradiation in 10 fractions using Varian Triology Linear Accelerator (Varian Medical System Inc, USA). The second samples of irradiated tumors and peripheral white blood cells were collected within a week after radiotherapy in the same manner as the first collection. Three pieces of tissue were taken from each tumor biopsy. One piece was fixed with formalin for pathological examination and was set for quality control (QC) to ensure samples have adequate tumor cells. Two pieces were fixed with a preserving buffer (Geneplus Biotech, China) for 24 h at 4°C and were then placed in a refrigerator (−80°C) for RNA extraction and DNA extraction, respectively.

Nucleic Acid Extraction, Library Construction, and Sequencing

Paired tumor samples and lymphocytes were submitted for next-generation sequencing (NGS) in Zhongyuan-Vcan Genetic Technology Co., Ltd (Tianjing, China). Genomic DNA was extracted from tumor tissues and blood cells using the TIANamp Genomic DNA Kit (Tiangen) for whole-exome sequencing (WES). Paired analysis of tumor and matched-lymphocyte samples was performed for definitive identification of somatic variations. DNA integrity was assessed by agarose gel electrophoresis. DNA concentrations were measured using a Qubit fluorometer (Thermo Fisher Scientific). WES libraries were constructed using the KAPA HyperPrep Kits (KAPA) and enriched using Agilent SureSelect^{XT} target enrichment kit ILM (Agilent). Genomic DNA from tumor paired samples and matched-lymphocyte samples were sequenced using the NextSeq 500 platform. Exome capture was performed using SureSelect^{XT} Human All Exon 60 MB (Agilent). Tumor exomes were sequenced at 200× coverage, while blood cell exomes were sequenced at 100×. Burrows-Wheeler Aligner (BWA) (version 0.7.15-r1140) was used to align sequences over the human reference genome HG19.

Total RNA was extracted from tumor tissues using TRIzol™ Reagent (Life Technologies) for transcriptome analyses. RNA integrity, purity, and concentration were evaluated using an Agilent 2100 Bioanalyzer (Agilent Technologies). Nanodrop and Qubit 3.0. RNA-seq libraries were constructed using KAPA mRNA HyperPrep Kit. WES and RNA-seq were performed in the Illumina Novaseq System. All libraries were sequenced on the Novaseq using 2×150 bp paired-end sequencing. Adaptor sequences were trimmed, and reads were processed into clean reads. Each RNA-seq data required approxiimately 10 G.

Analysis of Gene Expression, Fusion Gene, Tumor-Infiltrating Immune Cells, and TCR Repertoire

The paired-end clean reads were mapped to the human reference genome GRCh37.75 using STAR (version 020201) with default parameters (9). A novel network flow algorithm used in StringTie (version 2.2.1) (10) was applied to perform transcript assembly and quantify gene expression in fragments per kilobase of transcript per million fragment mapped units for RNA-seq. Then, DESeq (version 1.24.0) (11) was used to identify differentially expressed genes (DEGs). Results were considered significant if the Benjamini–Hochberg adjusted p-value, represented by false discovery rate, was <0.01 and fold change was >2. DEGs were used in the enrichment analysis and significance was detected using Fisher's exact test. The cases were grouped by cancer type, and the differential gene expression characteristics were analyzed before and after SBRT. Then, we further analyzed the differential expression of each case before and after SBRT. Based on paired-end RNA-seq data, we aligned the fastq files that passed QC to the reference genome using the STAR software program and prepared a count matrix, which tallies the number of RNA-seq reads/fragments within each gene for each sample using StringTie and DESeq.

Fusion gene analysis was performed based on the RNA-seq data. The fusion point of each gene and the 5′- and 3′-chromosomal ends were examined. The count of read pairs supported the fusion including the multi-mapping reads and count of unique mapped reads on the fusion junction. Then, all reads were counted as maps on the fusion junction minus the polymerase chain reaction duplicated reads. In this study, fusion genes were detected using FusionCatcher. It is a tool used for finding novel and known somatic fusion genes in paired-end RNA-seq data in diseased samples collected from vertebrates that had available annotation data in the Ensembl database (12).

The T-cell receptor (TCR) comprises a heterodimer of two chains (αβ or γδ), both of which are products of variable (V), diversity (D), and joining (J) (V(D)J) recombination. This somatic rearrangement occurs only in the T-cell genome and produces an extremely diverse repertoire of TCRs. The most variable region in TCR is CDR3, which has a critical role in antigen recognition. In this study, we utilized a method to assemble *de novo* the CDR3 sequences generated from TCR locus transcripts in paired-end RNA-seq data by deep sequencing. This method first maps the reads to the human genome and searches for read pairs, with one mate properly mapped to a TCR gene and the other mate unmappable to the genome, potentially owing to the V(D)J recombination. It then initiates pairwise comparisons between the unmapped reads and constructs a read-overlap matrix, represented by an undirected graph, with each node corresponding to a read and edges indicating partial sequence overlap between the two connected reads. This graph is further divided into disjoint cliques to represent potentially different CDR3 sequences. Finally, all reads in each clique were assembled to obtain the contigs of DNA sequence and annotate them with information, including amino acid sequence and the associated V and J genes. TCR repertoire analysis was performed using iXCR (version 3.0.5) that processes large immune data from raw sequences into quantitated clonotypes (13).

Tumor-infiltrating immune cell analysis was performed using xCell (14), which is a gene signature-based method learned from thousands of pure cell types from various sources and applies a novel technique to reduce the associations between closely related cell types. Based on transcriptome sequencing data, a cell-type enrichment analysis of gene expression data for 64 immune cell types was performed using xCell.

Exome Sequencing

WES assays of tumor biopsy samples and peripheral white blood cells were performed to analyze genomic mutations, copy-number alterations, and select fusions involving cancer-associated genes. The paired-end reads were mapped to the human reference genome GRCh37.75 using BWA (version 0.7.15-r1140) with default parameters. Variant calling was executed using GATK MuTect2 (v3.7-0-gcfedb67), Verdict (v1.4.8-0), and VarScan (v2.4.2). Variants were annotated with ANNOVAR (2016-02-01), according to the genomic coordinates GRCh37.75, and complex variants were further annotated with SnpEff (v4.3). Then, we examined whether the variants were present in the dbSNP (v147) common database. Variants not found in the dbSNP database were further filtered using the ClinVar (20181028) database, Cosmic (70), 1000g_EAS, ExAC_ALL, and ExAC_EAS. Pathogenic variants were annotated as "likely pathogenic," "pathogenic," or "drug response" in the ClinVar database. Raw exome sequencing data were also used to analyze the copy-number variation (CNV), which was performed using the CNVkit (v0.9.6).

Tumor mutational burden (TMB) assay was performed to examine the number of base substitutions, deletions, and insertion mutations in the protein coding region. The variations determined on NGS analysis include three parts: germline variation, somatic variation, and sequencing error. The original somatic variation set must be filtered before performing subsequent analysis. The filtration criteria are as follows:

1. The ratio is greater than 3% for mutations present in the Cosmic database and greater than 5% for mutations absent in the Cosmic database.
2. 1000g2015aug_all, ESP6500si, 1000g_EAS, ExAC_ALL, and ExAC_EAS mutation rate in the five normal human mutation databases is less than 1%.
3. Synonymous mutations must be removed from the dataset, and the mutation site is controlled only in the exonic and splicing regions.

When the above filtration criteria are met, it can be ensured that the mutations for subsequent analysis are rare in the normal population. The TMB value was obtained in accordance with the TMB algorithm from FMI[①]. The FMI method (FoundationOne CDx™) was approved by the Food and Drug Administration in 2017 for clinical drug selection decision making. Furthermore, raw exome sequencing data were also used to search for CNVs and single-nucleotide variants (SNVs)/Indel analysis.

Immunohistochemical Analyses

The biopsy specimens were embedded in paraffin, and immunohistochemical (IHC) staining was performed on 5-μm-thick tissue sections using affinity mouse monoclonal antibodies against CD8 (clone C8-144B, dilution 1:1; Maixin Biotech, Fuzhou, China) and PD-L1 (clone 22c3, dilution 1:40, Agilent Tech, Inc., USA). Tissue sections were deparaffinized and stained using the Ventana BenchMark ULTRA in automatic mode (Roche Diagnostics GmbH, Germany) for analyzing CD8+ T-cell infiltration and PD-L1 expression in tumor cells.

Statistical Analysis

The difference between the two groups was analyzed using Student's t-test, and the comparisons were two-sided, with a significance level of 0.05. Pearson's correlation coefficients between TMB and neoantigen, TCRseqs, and T cell were calculated as follows: $\gamma<0.30$=low, $0.3<\gamma<0.60$ =moderate, and $\gamma>0.60$=high.

RESULTS

Two paired samples did not meet the QC for pathological examination because of not enough tumor cells. One paired sample for lung metastasis from rectal cancer could not be analyzed using WES and RNA-seq due to the bad quality or quantity of DNA/RNA. Ten paired samples were analyzed with WES, and RNA-seq was detected in nine paired samples except in case 2 (**Supplementary 1**). Clinical and pathologic characteristics of ten patients whose samples underwent WES and RNA-seq analysis are shown in **Table 1**.

SBRT Causing New Genomic Mutations but Not Increasing TMB

Radiation can trigger new mutations. Whether SBRT could improve TMB remains unclear. WES as a standard method for TMB analysis can detect somatic mutations present within the entire exome. We analyzed a series of genomic variations including CNVs, SNVs, and fusion genes using WES in tumor tissue before and after SBRT. Surprisingly, the TMB value of the tumor tissue did not increase coincidentally in 10 samples treated with SBRT (**Figure 1A**, *P*=0.612). However, all 10 tumor samples showed new mutations after radiation (**Figures 1B, C**). Then, we analyzed the mutations or aberrations of the genome in detail. The results (**Figure 1D**) showed that SNV in tumor deposits had no significant difference before and after irradiation (*P*=0.518); the CNV of tumor specimens that received SBRT decreased significantly (*P*=0.031). In contrast, the fusion genes increased significantly in tumor samples after receiving radiation (*P*=0.017). The absence of significant changes in TMB may be due to inconsistent changes in CNVs and fusion genes. The changes in neoantigen number was similar to TMB in paired samples (**Figure 1E**, r=0.63, *P*=0.003). Moreover, the neoantigen number in paired samples had no obvious changes (**Figure 1F**, *P*=0.522). These results implied that SBRT can trigger only new mutations and induce neoantigen rather than increasing the TMB in the TME.

Increased PD-L1 Expression With No Significant Change in CXCL10, CXCL16, MHC-I, IFNs, and IFNs Receptors in the TME After SBRT

In addition to WES analysis, whole transcriptomes in TME were detected with RNA-seq. We analyzed the differential expression characteristics of the tumor tissue before and after radiation treatment, and DEGs were analyzed using paired-sample t-test. The top 50 DEGs are listed in the heat map (**Figure 2A**). Then, we performed gene ontology (GO) enrichment analysis of these altered genes by biological process classification. The most enriched term was the immune response gene (six genes, *P*=4.67E-05), followed by gene of DNA repair (five genes, *P*=2.55E-06) and regulating gene of signal transduction by p53 class mediator (five genes, *P*=7.71E-05) (**Figure 2B**). The differential genes of immune responses included many TCRs and immunoglobulin superfamily as listed in **Figure 2C**. Moreover, PD-L1 (CD274) expression in the TME significantly increased after SBRT than before radiation (**Figure 2D**, *P*=0.012). To confirm this result, we performed an IHC assay

TABLE 1 | Clinical and pathologic characteristics of patients.

No.	Diagnosis	Clinical stage[a]	Histology	Lesion of irradiation	Fraction of radiotherapy	WES	RNA-seq
Case 1	EC	Metastasis	ASC	metastastic lesion	60 Gy/10F	Yes	No
Case 2	CC	Metastasis	SCC	Metastatic lesion	60 Gy/10F	Yes	Yes
Case 3	NSCLC	T4N3M1	AC	Primary lesion	60 Gy/10F	Yes	Yes
Case 4	CRC	Metastasis	AC	Metastatic lesion	60 Gy/10F	Yes	Yes
Case 5	NSCLC	T2N2M1c	AC	Primary lesion	60 Gy/10F	Yes	Yes
Case 6	CRC	TxNxM1b	AC	Metastatic lesion	60 Gy/10F	Yes	Yes
Case 7	NSCLC	T2N3M1c	AC	Primary lesion	60 Gy/10F	Yes	Yes
Case 8	CRC	Metastasis	AC	Metastatic lesion	60 Gy/10F	No	No
Case 9	NSCLC	T2N3M1b	AC	Primary lesion	60 Gy/10F	Yes	Yes
Case10	CRC	Metastasis	AC	Metastatic lesion	60 Gy/10F	Yes	Yes
Case11	NSCLC	T2N3M1c	AC	Primary lesion	60 Gy/10F	Yes	Yes

EC, Esophageal cancer; CC, Cervical cancer; NSCLC, non-small-cell lung cancer; CRC, colorectal cancer; ASC, Adenosquamous cancer; SCC, Squamous cell carcinoma; AC, Adenocarcinoma.
[a]Cancer stage were assigned in accordance with American Joint Committee on Cancer (AJCC) TNM Staging Classification for NSCLC, cervical cancer, colorectal cancer, and esophageal cancer (8th ed, 2017).

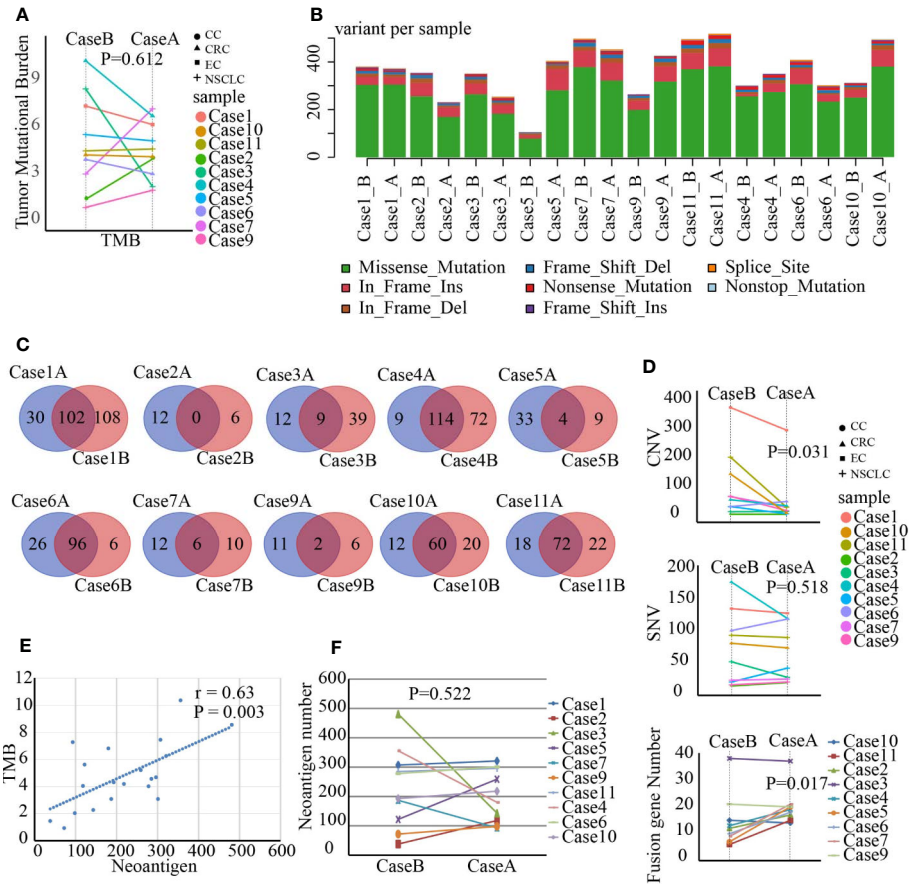

FIGURE 1 | Gene mutations, fusion genes, and neoantigen prediction were analyzed by whole-exome sequencing and RNA-seq in paired tumor samples before and after stereotactic body radiotherapy (SBRT). *_B indicates the values before SBRT, *_A indicates the values after SBRT. **(A)** Changes in the tumor mutation burden (TMB) value after SBRT (*P*=0.612). **(B)** The number of variants in each sample is shown in a stacked bar plot and the variant types in a boxplot and summarized based on variant classification. **(C)** Number of unique mutations owned in paired tumor samples compared to the somatic mutations of peripheral white blood cells and number of unique mutations in Venn plots for each patient. The left number indicates unique mutations in tumor tissue after SBRT compared to those in the paired sample before radiation treatment, while the right number shows unique mutations in the tumor tissue before SBRT compared to the paired sample after receiving SBRT. The middle number specifies co-owned mutations in paired samples before and after SBRT. **(D)** Differences in copy-number variation (CNV; *P* = 0.031), single-nucleotide variant (SNV; *P* = 0.518), and fusion gene (*P* = 0.017) in the tumor microenvironment (TME) before and after SBRT. **(E)** Linear relationship between TMB and neoantigen and the value of neoantigen prediction (r = 0.63, *P* = 0.003). **(F)** Comparison of neoantigen number before and after radiotherapy (*P* = 0.522).

and found that PD-L1expression in tumor tissue increased significantly after SBRT (**Figure 2E**).

Furthermore, several studies have revealed that chemokines and pro-inflammatory factors such as CXCL10, CXCL16, IFNs, and its receptors could be induced by radiation in mice models and were essential for recruiting and activating CD8+ T cells (15, 16). However, in this study, expression of IFN-I, IFN-II, CXCL10, CXCL16, IFN-I receptor, and IFN-II receptor did not show significant differences in paired samples before and after SBRT (**Figure 2F**). MHC-I expression in tumor tissues that received SBRT also showed no significant differences when compared to that before radiation (**Figure 2F**), although it can be enhanced by radiation, thus inducing antitumor immunotherapy in murine tumor transplant models (17). Furthermore, there was no significant difference in PD1 expression in the TME before and after SBRT (**Figure 2F**).

Effect of SBRT on the Diversity of TCR Repertoire and Frequency of TCR in the TME

The landscape of neoantigens is thought to determine the immunogenicity of cancers, and in particular, the antitumor responses mediated by T-cells. Therefore, we characterized the TCR repertoire in the TME. The diversity and frequency of TCRs, including TRA, TRB, TRD, and TRG, reflect the diversity and activity of cellular immunity. We amplified and sequenced the TCR repertoire including approximately 260 distinct TCR genes in paired samples. The results showed that TCR gene expression in the TME was modified by SBRT (**Figures 3A, B**). However, no significant difference was observed in the frequency of TCRs in tumor tissues after receiving SBRT when compared with that before irradiation (**Figures 3C, D**, *P*=0.877), although

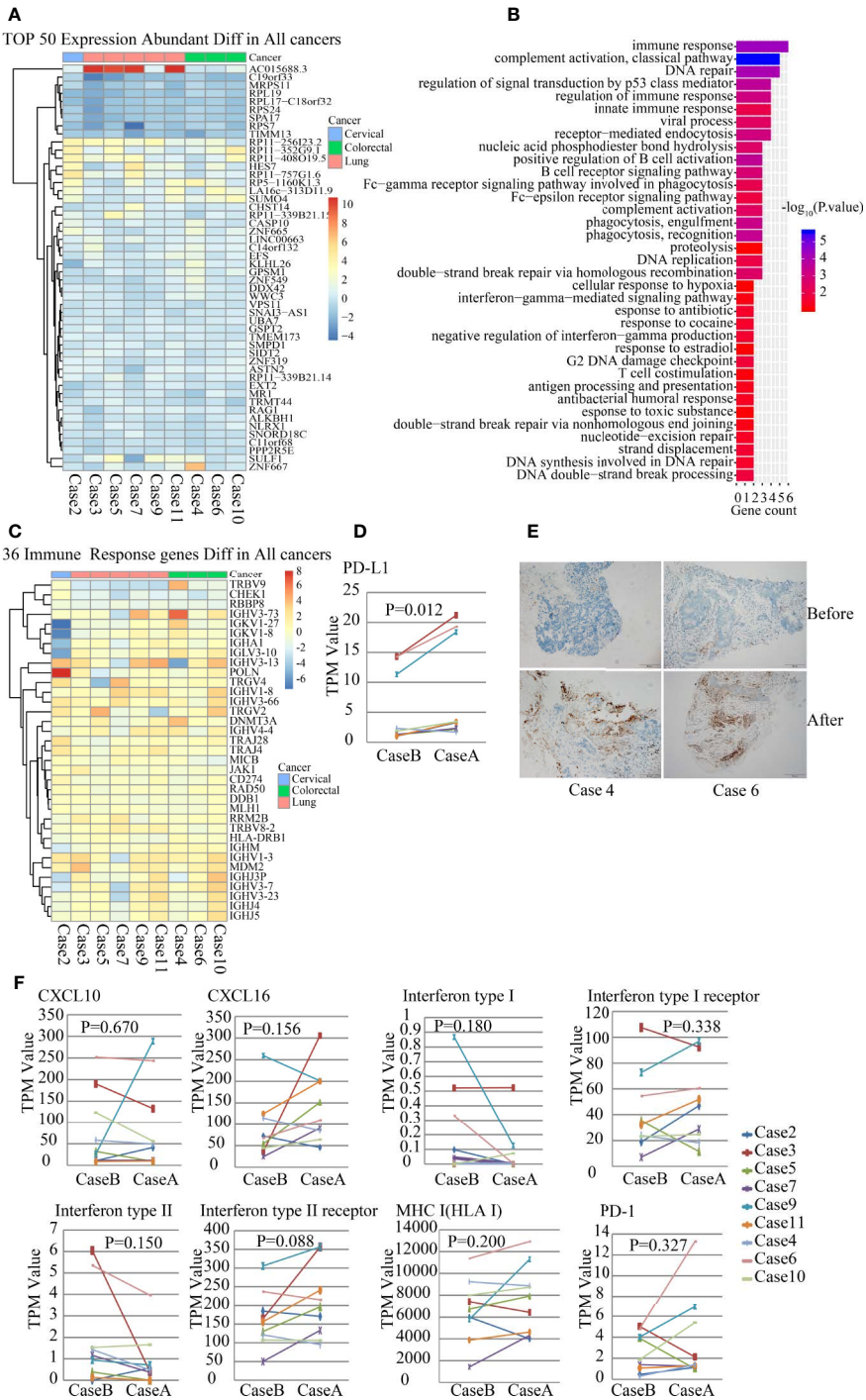

FIGURE 2 | Gene expression analysis of the paired samples before and after stereotactic body radiotherapy (SBRT) by RNA-seq. *_B indicates the values before SBRT; *_A indicates the values after SBRT. **(A)** Heatmap of 50 differentially expressed genes abundant in nine paired tumor samples. **(B)** Gene ontology (GO) enrichment pathway analysis of nine paired tumor samples. **(C)** Heatmap of the expression of 36 immune responsive genes abundant in nine tumor samples before and after SBRT. **(D)** Differences in PD-L1 expression in the tumor microenvironment (TME) before and after SBRT (P = 0.012). **(E)** PD-L1 expression was detected in tumor tissue using IHC and it increased significantly in tumor cells after SBRT compared to before SBRT. **(F)** Comparison of the expression of CXCL10, CXCL16, IFN I receptor, IFN II receptor, IFN I, IFN II, MHC-1, and PD-1 in the TME before and after SBRT.

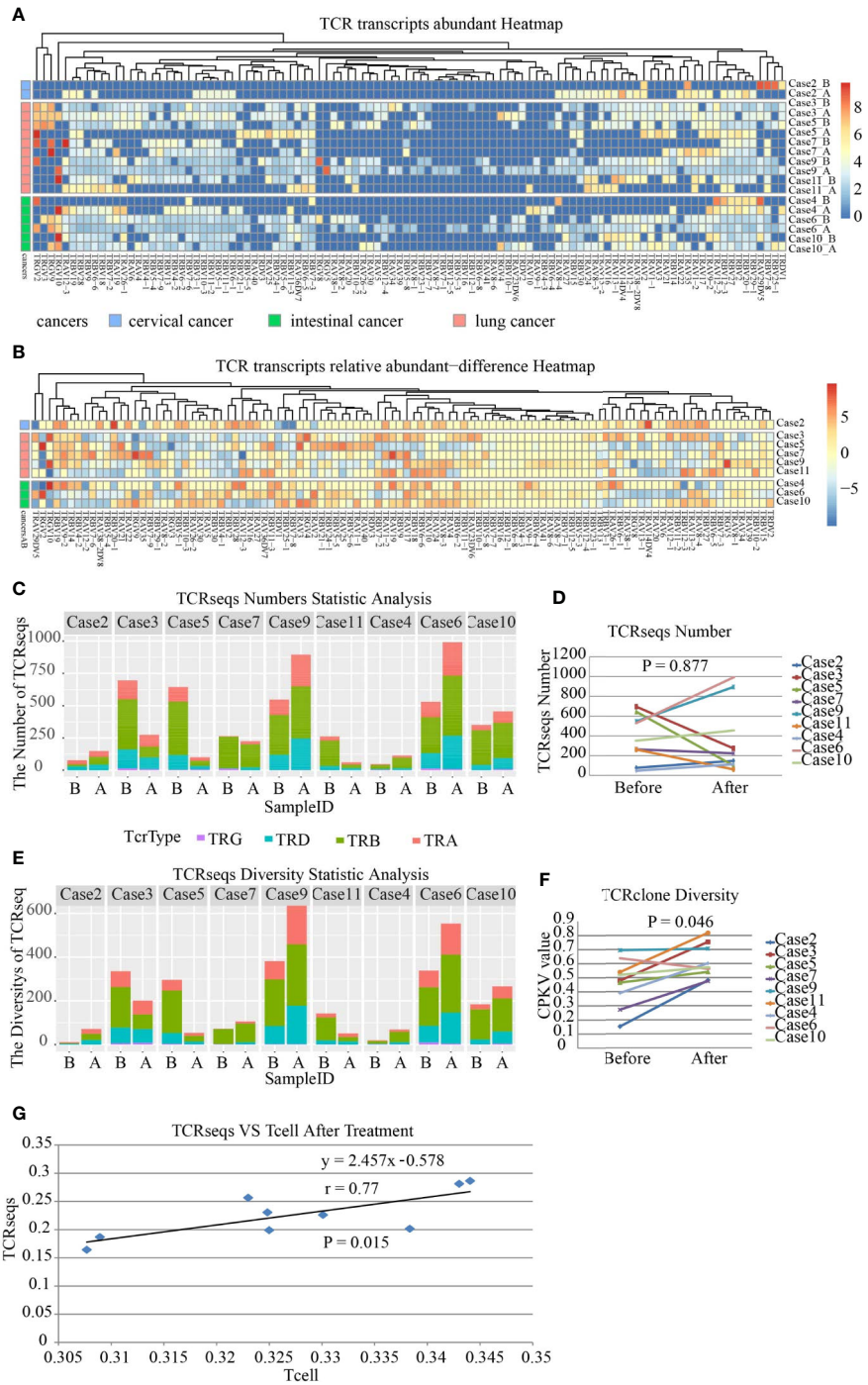

FIGURE 3 | Transcript abundance and repertoire diversity of T-cell receptor (TCR) in nine patients before and after stereotactic body radiotherapy (SBRT). TRA, TRB, TRD, and TRG mean Vα, Vβ, Vγ, and Vδ segment usage of TCR, respectively. *A represents samples after SBRT, while *B represents samples before SBRT. **(A)** Frequency and distribution of TRA, TRB, TRD, and TRG gene usage and productive sequences in all samples. **(B)** The heatmap shows the difference in abundance in TRA, TRB, TRD, and TRG transcripts in each case after SBRT compared to that before radiation. **(C)** Transcript abundance of TCRs comprising TRA, TRB, TRD, and TRG in each sample on the x axis; the value on the y axis represents the number of TCRseqs. **(D)** Comparison of TCR transcript abundance in the tumor microenvironment (TME) before and after SBRT ($P = 0.877$). **(E)** Diversity of TCR repertoire in each sample. **(F)** Diversity of TCR repertoire assessed by CPKV value after SBRT increased significantly ($P = 0.046$). The values on the y axis represent the diversity of TCRseqs. **(G)** Relationship between the amount of TCRseqs and the relative amount of T cell ($R^2 = 0.594$). Each point represents one sample. The value on the x axis represents the amount of TCR clones, while the value on the y axis represents the amount of TCRseqs.

the frequency of TCRs in the tumor samples increased in five cases that underwent SBRT.

The diversity of TCR repertoire was analyzed using the ratio of the number of unique TCRseqs to the number of total TCRseqs as an indicator. The indicator was defined as the CPKV value and was more accurate than the CPK value (18). The results demonstrated that the diversity of TCR repertoire in samples treated with SBRT was significantly higher than that before irradiation (**Figures 3E, F**, P=0.046). This finding indicated that SBRT might promote T-cell-mediated immune responses against tumors by increasing the diversity of TCR repertoire in the TME. Lastly, we analyzed the consistency between TCRseqs and T cell and found a high consistency between them (**Figure 3G**, r=0.77, P=0.015).

Profiling Tumor-Infiltrating Immune Cells in the TME Before and After SBRT

Tumor-infiltrating immune cells are associated with promoting or inhibiting antitumor immune response, which corresponds to good or poor outcomes in different cancers (19). We analyzed tumor-infiltrating immune cells including 34 subsets in paired tumor samples. The results revealed striking differences in the immune cells in the TME in different patients after SBRT (**Figures 4A, B**). There were no significant changes in the number of tumor-infiltrating NK and Treg cells in most paired samples before and after irradiation. The number of tumor-infiltrating CD8+ T cells in the TME did not increase remarkably a week after SBRT (P=0.753). On the contrary, it reduced in five samples after radiotherapy (**Figure 4C**, P=0.753). The result was confirmed by the IHC detection of CD8+ T cells in TME (**Figure 4D**). In addition, only a significant reduction in TH1 and TH2 cells was observed in tumor deposits receiving SBRT (**Figure 4E**). The changes in tumor-infiltrating immune cell number implied that the responses of immune cell subsets vary in different patients after SBRT.

DISCUSSION

The success of ICIs combined with radiotherapy in several types of cancers ignited the interest of oncologists to explore the effects of immunotherapy fueled by radiotherapy. This phenomenon has also been verified indirectly in mouse tumor models (20, 21). Thus, understanding the immunologic effects induced by radiation is important to design rational combination strategies of radiotherapy and immunotherapy.

Irradiation may increase nonsynonymous mutation burden and trigger neoantigen production in cancer cells, possibly favoring *in situ* vaccine development and TME reprogramming (22). Rizvi et al. found that a higher TMB in tumors was associated with an improved pembrolizumab effect in NSCLC patients (23). Therefore, we detected the genomic variance of tumor tissues a week after SBRT. Beyond our conjecture, SBRT did not promote TMB increase in the TME, although the CNV decreased significantly and the fusion genes increased markedly after radiation. The changes in TMB, CNV, and fusion genes could be due to double-strand breaks (DSBs) of DNA induced by SBRT in cancer cells, leading to the repair of DNA DSBs. While the radiation-induced production of DNA damage is linear, the radiobiological effects are generally non-linear. Cancer cells repair DNA damage and survive by inducing DNA repair and cell cycle arrest or start cellular death without DNA repairing after irradiation treatment (24). New nonsynonymous gene mutations were observed in each patient. Thus, SBRT may not improve the quantity of TMB and neoantigen in the TME but trigger new nonsynonymous mutations, possibly inducing tumor-specific neoantigen development.

Biological responses of cancer cells to radiation involved damage, repair, apoptosis, or necrosis, leading to the activation or inhibition of signal transductions of DNA repair, metabolism, and cell cycle arrest (25). In this study, RNA-seq results demonstrated that several genes regulating cancer proliferation, invasion, and immune response might be under-expressed or over-expressed in tumor tissues after SBRT. Expression of a large number of immune-related genes has changed. Tumor immune microenvironment comprises inflammatory factors, infiltrating immune cells, and stroma cells and can be reprogrammed by radiotherapy (26). Expression of CXCL10, CXCL16, IFNs, and IFN receptors could be induced by irradiation in an experimental animal model (15, 16, 27, 28). However, expression of CXCL10, CXCL16, IFNs, and IFN receptor showed various changes, including an increase and decrease in the TME after SBRT. There was no significant difference in the expression of CXCL10, CXCL16, IFNs, and IFN receptors before and after SBRT. This result was contrary to that of other experimental animal studies but was similar in relation to that of tumor-infiltrating immune cells in this study.

Tumor-infiltrating lymphocytes (TILs) are integral components of the TME and correlate with response to immune therapy (29, 30). Neoadjuvant chemoradiation therapy increased the density of TILs in post-treatment resected rectal cancer specimens (31). However, our results showed that SBRT did not promote CD8+ T-cell and NK-cell infiltration in the TME. With regard to infiltrating immune cells in the TME in this study, which were different from that reported in other studies, the discrepancy might be due to the differences in the fractionated dosage of radiotherapy or time point of sample collection.

The antitumor responses of effector T-cells comprised recognizing tumor antigen and attacking cancer cells, which are associated with MHC-I, PD-1/PD-L1 axis, and TCR. The increase in MHC-I expression in tumor tissues after SBRT promoted recognition of *in situ* tumor-specific antigen to CD8+ T cells. It was supported by the improvement in the diversity of TCR repertoire in the TME after SBRT. The high diversity of TCR repertoire reflected a better immune status, which indicated clinical benefit in cancer patients (32). Based on the result of MHC-I and TCR repertoire diversity, this study supported that SBRT promoted the antitumor immune response. An important study finding was the upregulation of PD-L1/PD-1 expression in the TME, which was supported by the results of Sato's research that revealed that DNA DSBs upregulated PD-L1 expression in an ATM/ATR/Chk1-dependent manner (33).

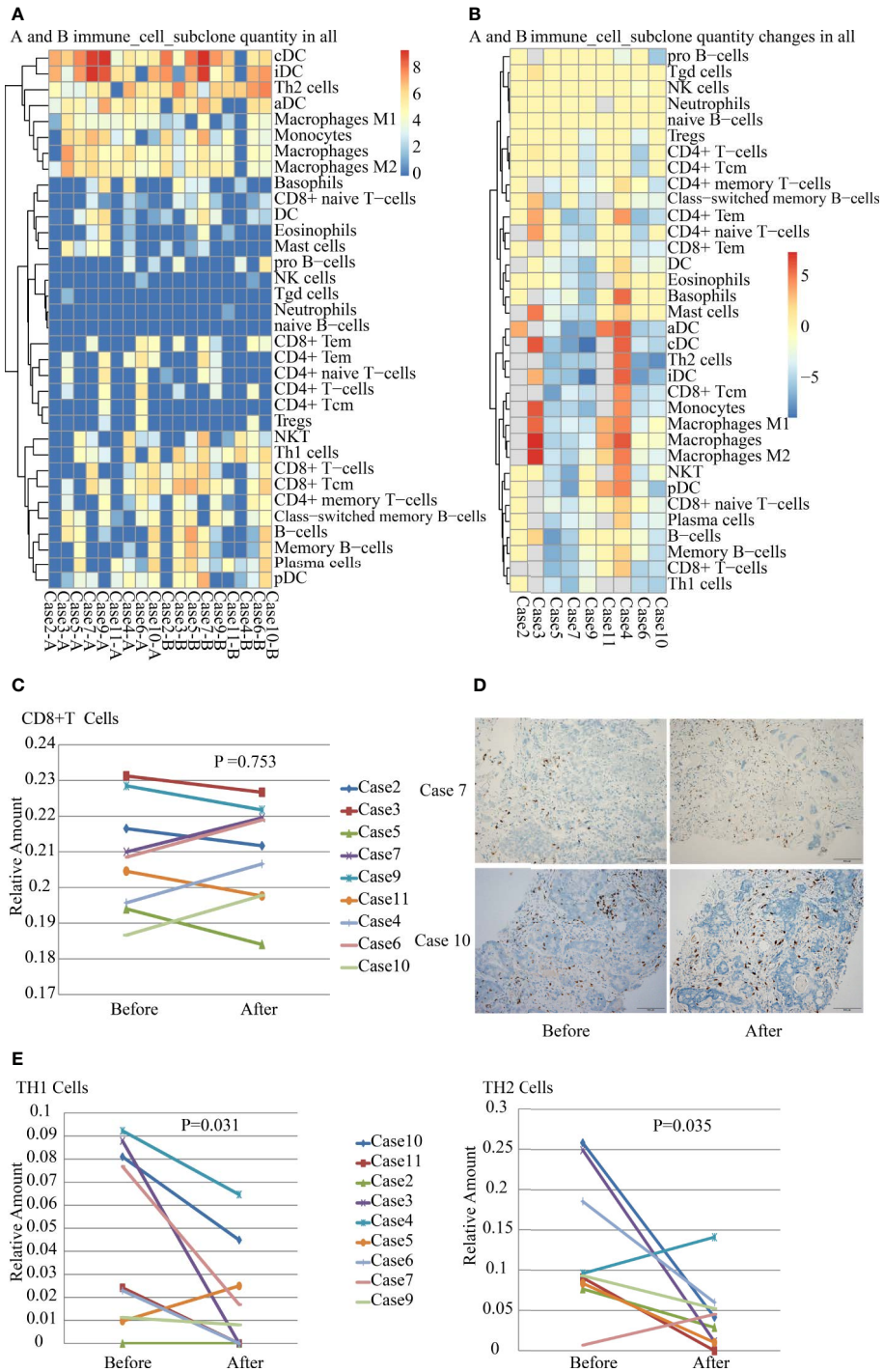

FIGURE 4 | Analysis of tumor-infiltrating immune cells in nine paired samples before and after stereotactic body radiotherapy (SBRT). **(A)** Inferred composition of 34 immune cell subsets in samples of each patient before and after SBRT. The results were generated from gene expression data for 64 immune cell types using xCell. **(B)** Differences in the number of tumor-infiltrating immune cell subsets before and after SBRT in nine patients. **(C)** Differences in CD8+ T-cell infiltration in the tumor microenvironment (TME) before and after SBRT ($P = 0.753$). **(D)** CD8+ T cells infiltration were detected by IHC in tumor tissues before and after SBRT. **(E)** Differences in TH1 cell (P = 0.031) and TH2 cell (P = 0.035) infiltration in the TME before and after SBRT.

This is the first study to report the direct effect of SBRT on genomic mutation, differences in gene expression, and tumor immune microenvironment. Notably, the diversity of TCR repertoire increased and PD-L1 expression upregulated in the TME after SBRT. SBRT induced neo-mutation and new fusion gene in cancer cells, which induced the generation of tumor-specific neoantigen but did not increase TMB in tumor tissues. It displayed complex changes in tumor-infiltrating immune cells and expression of immune-regulating factor in the TME after receiving SBRT. However, SBRT did not increase CD8+ T-cell infiltration and IFN-I/II expression in tumor tissues a week after radiation. Certainly, this study had some limitations. The study used a small sample size and did not perform a dynamic observation of the TME after SBRT. A few metastatic tumors to lung was grouped in analysis of this study. The changes of genome and tumor immune microenvironment induced by SBRT could not be considered as a specific results of SBRT because it lacked of a control group for conventional radiotherapy. Hence, further studies are warranted to address these concerns.

DATA AVAILABILITY STATEMENT

The data presented in the study are deposited in the NCBI GEO database repository, accession number: GSE162946. (https://www.ncbi.nlm.nih.gov/geo/query/acc.cgi?acc=GSE162946).

ETHICS STATEMENT

The studies involving human participants were reviewed and approved by the Ethics Committee of Xinqiao Hospital (Ethical No: 2019-Res 032-1), Chongqing 40037, China. Written informed consent for participation was not required for this study in accordance with the national legislation and the institutional requirements.

AUTHOR CONTRIBUTIONS

PZ and DC performed the collection and preservation of samples including analysis of some parts of the results. BZ took part in the analysis and interpretation of the TCR results. WC wrote the methods of RNA-seq and WES. QX analyzed and interpreted the tumor-infiltrating immune cell results. YW and QT performed the pathological diagnosis for the patients. BY, XZ, CH, and HZ provided treatment to patients. GL conceived and designed the experiments, summarized the results, guided SBRT for the patients in this study. He also wrote and revised this manuscript. All authors contributed to the article and approved the submitted version.

FUNDING

This work was supported by the Medical Research Foundation Project of CQ Health Commission (No. 2019ZDXM043) and Science and Technology Innovation Ability Promotion Project of AMU (No. 2019XLC2011).

ACKNOWLEDGMENTS

We extend our thanks to Prof. Ying Wan, Biomedical Analysis Center, Army Medical University, Chongqing, China, for the insightful discussion. We would like to thank Editage (www.editage.cn) for English language editing.

SUPPLEMENTARY MATERIAL

The Supplementary Material for this article can be found online at: https://www.frontiersin.org/articles/10.3389/fimmu.2020.594212/full#supplementary-material

REFERENCES

1. Haymaker CL, Kim D, Uemura M, Vence LM, Phillip A, McQuail N, et al. Metastatic melanoma patient had a complete response with clonal expansion after whole brain radiation and PD-1 blockade. *Cancer Immunol Res* (2017) 5:100–5. doi: 10.1158/2326-6066.CIR-16-0223
2. Antonia SJ, Villegas A, Daniel D, Vicente D, Murakami S, Hui R, et al. Overall survival with durvalumab after chemoradiotherapy in stage III NSCLC. *N Engl J Med* (2018) 379:2342–50. doi: 10.1056/NEJMoa1809697
3. Shaverdian N, Lisberg AE, Bornazyan K, Veruttipong D, Goldman JW, Formenti SC, et al. Previous radiotherapy and the clinical activity and toxicity of pembrolizumab in the treatment of non-small-cell lung cancer: a secondary analysis of the KEYNOTE-001 phase 1 trial. *Lancet Oncol* (2017) 18:895–903. doi: 10.1016/S1470-2045(17)30380-7
4. Yuan Z, Fromm A, Ahmed KA, Grass GD, Yang GQ, Oliver DE, et al. Radiotherapy rescue of a nivolumab-refractory immune response in a patient with PD-L1-negative metastatic squamous cell carcinoma of the lung. *J Thorac Oncol* (2017) 12:e135–6. doi: 10.1016/j.jtho.2017.04.029
5. Siva S, MacManus MP, Martin RF, Martin OA. Abscopal effects of radiation therapy: a clinical review for the radiobiologist. *Cancer Lett* (2015) 356:82–90. doi: 10.1016/j.canlet.2013.09.018
6. Theelen WSME, Peulen HMU, Lalezari F, van der Noort V, de Vries JF, Aerts J, et al. Effect of pembrolizumab after stereotactic body radiotherapy vs pembrolizumab alone on tumor response in patients with advanced non-small cell lung cancer: results of the PEMBRO-RT phase 2 randomized clinical trial. *JAMA Oncol* (2019). doi: 10.1001/jamaoncol2019.1478
7. Wersäll PJ, Blomgren H, Pisa P, Lax I, Kalkner KM, Svedman C. Regression of non-irradiated metastases after extracranial stereotactic radiotherapy in metastatic renal cell carcinoma. *Acta Oncol* (2006) 45:493–7. doi: 10.1080/02841860600604611
8. Twyman-Saint Victor C, Rech AJ, Maity A, Rengan R, Pauken KE, Stelekati E, et al. Radiation and dual checkpoint blockade activates non-redundant immune mechanisms in cancer. *Nature* (2015) 520:373–7. doi: 10.1038/nature14292
9. Dobin A, Davis CA, Schlesinger F, Drenkow J, Zaleski C, Jha S, et al. STAR: ultrafast universal RNA-seq aligner. *Bioinformatics* (2013) 29:15–21. doi: 10.1093/bioinformatics/bts635
10. Pertea M, Pertea GM, Antonescu CM, Chang TC, Mendell JT, Salzberg SL. StringTie enables improved reconstruction of a transcriptome from RNA-seq reads. *Nat Biotechnol* (2015) 33:290–5. doi: 10.1038/nbt.3122
11. Wang L, Feng Z, Wang X, Wang X, Zhang X. DEGseq: an R package for identifying differentially expressed genes from RNA-seq data. *Bioinformatics* (2010) 26:136–8. doi: 10.1093/bioinformatics/btp612

12. Nicorici D, Satalan M, Edgren H, Kangaspeska S, Murumagi A, Kalioniemi O, et al. FusionCatcher – a tool for finding somatic fusion genes in paired-end RNA-sequencing data. *Genome Biol* (2014) 11:R104. doi: 10.1101/011650
13. Bolotin D, Poslavsky S, Mitrophanov I, Shugay M, Mamedov IZ, Putintseva EV, et al. MiXCR: software for comprehensive adaptive immunity profiling. *Nat Methods* (2015) 12:380–1. doi: 10.1038/nmeth.3364
14. Aran D, Hu Z, Butte AJ. xCell: digitally portraying the tissue cellular heterogeneity landscape. *Genome Biol* (2017) 18:220. doi: 10.1186/s13059-017-1349-1
15. Matsumura S, Wang B, Kawashima N, Braunstein S, Badura M, Cameron TO, et al. Radiation-induced CXCL16 release by breast cancer cells attracts effector T cells. *J Immunol* (2008) 181:3099–107. doi: 10.4049/jimmunol.181.5.3099
16. Deng L, Liang H, Xu M, Yang X, Burnette B, Arina A, et al. STING-dependent cytosolic DNA sensing promotes radiation-induced type I interferon-dependent antitumor immunity in immunogenic tumors. *Immunity* (2014) 41:843–52. doi: 10.1016/j.immuni.2014.10.019
17. Reits EA, Hodge JW, Herberts CA, Groothuis TA, Chakraborty M, Wansley EK, et al. Radiation modulates the peptide repertoire, enhances MHC class I expression, and induces successful antitumor immunotherapy. *J Experi Med* (2006) 203:1259–71. doi: 10.1084/jem.20052494
18. Jin Y, Luo W, Zhang G, Lin KR, Cui JH, Chen XP, et al. TCR repertoire profiling of tumors, adjacent normal tissues, and peripheral blood predicts survival in nasopharyngeal carcinoma. *Cancer Immunol Immunother* (2018) 67:1719–30. doi: 10.1007/s00262-018-2237-6
19. Fridman WH, Pagès F, Sautès-Fridman C, Galon J. The immune contexture in human tumours: impact on clinical outcome. *Nat Rev Cancer* (2012) 12:298–306. doi: 10.1038/nrc3245
20. Camphausen K, Moses MA, Menard C, Sproull M, Beecken WD, Folkman J, et al. Radiation abscopal antitumor effect is mediated through p53. *Cancer Res* (2003) 63:1990–3.
21. Demaria S, Ng B, Devitt ML, Babb JS, Kawashima N, Liebes L, et al. Ionizing radiation inhibition of distant untreated tumors (abscopal effect) is immune mediated. *Int J Radiat Oncol Biol Phys* (2004) 58:862–70. doi: 10.1016/j.ijrobp.2003.09.012
22. Herrera FG, Bourhis J, Coukos G. Radiotherapy combination opportunities leveraging immunity for the next oncology practice. *CA Cancer J Clin* (2017) 67:65–85. doi: 10.3322/caac.21358
23. Rizvi NA, Hellmann MD, Snyder A, Kvistborg P, Makarov V, Havel JJ, et al. Cancer immunology. Mutational landscape determines sensitivity to PD-1 blockade in non-small cell lung cancer. *Science* (2015) 348:124–8.
24. Lavelle C, Foray N. Chromatin structure and radiation-induced DNA damage: from structural biology to radiobiology. *Int J Biochem Cell Biol* (2014) 49:84–97.
25. Broustas CG, Xu Y, Harken AD, Garty G, Amundson SA. Comparison of gene expression response to neutron and x-ray irradiation using mouse blood. *BMC Genomics* (2017) 18:2.
26. Barker HE, Paget JT, Khan AA, Harrington KJ. The tumour microenvironment after radiotherapy: mechanisms of resistance and recurrence. *Nat Rev Cancer* (2015) 15:409–25.
27. Rentoft M, Coates PJ, Loljung L, Wilms T, Laurell G, Nylander K. Expression of CXCL10 is associated with response to radiotherapy and overall survival in squamous cell carcinoma of the tongue. *Tumour Biol* (2014) 35:4191–8.
28. Wang X, Schoenhals JE, Li A, Valdecanas DR, Ye H, Zang F, et al. Suppression of Type I IFN Signaling in Tumors Mediates Resistance to Anti-PD-1 Treatment That Can Be Overcome by Radiotherapy. *Cancer Res* (2017) 77:839–50.
29. Gentles AJ, Newman AM, Liu CL, Bratman SV, Feng W, Kim D, et al. The prognostic landscape of genes and infiltrating immune cells across human cancers. *Nat Med* (2015) 21:938–45.
30. Chen B, Khodadoust MS, Liu CL, Newman AM, Alizadeh AA. Profiling Tumor Infiltrating Immune Cells with CIBERSORT. *Methods Mol Biol* (2018) 1711:243–59.
31. Matsutani S, Shibutani M, Maeda K, Nagahara H, Fukuoka T, Nakao S, et al. Significance of tumor-infiltrating lymphocytes before and after neoadjuvant therapy for rectal cancer. *Cancer Sci* (2018) 109:966–79.
32. Liu YY, Yang QF, Yang JS, Cao RB, Liang JY, Liu YT, et al. Characteristics and prognostic significance of profiling the peripheral blood T-cell receptor repertoire in patients with advanced lung cancer. *Int J Cancer* (2019) 145:1423–31.
33. Sato H, Niimi A, Yasuhara T, Permata TBM, Hagiwara Y, Isono M, et al. DNA double-strand break repair pathway regulates PD-L1 expression in cancer cells. *Nat Commun* (2017) 8:1751.

Conflict of Interest: Author WC was employed in Zhongyuan Union Clinical Laboratory Co. Ltd.

The remaining authors declare that the research was conducted in the absence of any commercial or financial relationships that could be construed as a potential conflict of interest.

Copyright © 2021 Zhou, Chen, Zhu, Chen, Xie, Wang, Tan, Yuan, Zuo, Huang, Zhu and Li. This is an open-access article distributed under the terms of the Creative Commons Attribution License (CC BY). The use, distribution or reproduction in other forums is permitted, provided the original author(s) and the copyright owner(s) are credited and that the original publication in this journal is cited, in accordance with accepted academic practice. No use, distribution or reproduction is permitted which does not comply with these terms.

frontiers in Immunology

REVIEW
published: 25 January 2021
doi: 10.3389/fimmu.2020.612072

Advances in Hypofractionated Irradiation-Induced Immunosuppression of Tumor Microenvironment

*Yuxia Wang**

Department of Radiation Oncology, Peking University Third Hospital, Beijing, China

Hypofractionated radiotherapy is external beam irradiation delivered at higher doses in fewer fractions than conventional standard radiotherapy, which can stimulate innate and adaptive immunity to enhance the body's immune response against cancer. The enhancement effect of hypofractionated irradiation to immune response has been widely investigated, which is considered an approach to expand the benefit of immunotherapy. Meanwhile, increasing evidence suggests that hypofractionated irradiation may induce or enhance the suppression of immune microenvironments. However, the suppressive effects of hypofractionated irradiation on immunomicroenvironment and the molecular mechanisms involved in these conditions are largely unknown. In this context, we summarized the immune mechanisms associated with hypofractionated irradiation, highlighted the advances in its immunosuppressive effect, and further discussed the potential mechanism behind this effect. In our opinion, besides its immunogenic activity, hypofractionated irradiation also triggers homeostatic immunosuppressive mechanisms that may counterbalance antitumor effects. And this may suggest that a combination with immunotherapy could possibly improve the curative potential of hypofractionated radiotherapy.

Keywords: hypofractionated irradiation, immunosuppression, tumor, immune microenvironment, radiotherapy

OPEN ACCESS

Edited by:
Huanfa Yi,
Jilin University, China

Reviewed by:
Kawaljit Kaur,
University of California, Los Angeles, United States
Yuzhu Hou,
University of Chicago, United States

***Correspondence:**
Yuxia Wang
lily31415926@126.com

Specialty section:
This article was submitted to Cancer Immunity and Immunotherapy, a section of the journal Frontiers in Immunology

Received: *30 September 2020*
Accepted: *06 November 2020*
Published: *25 January 2021*

Citation:
Wang Y (2021) Advances in Hypofractionated Irradiation-Induced Immunosuppression of Tumor Microenvironment. Front. Immunol. 11:612072. doi: 10.3389/fimmu.2020.612072

INTRODUCTION

Radiation therapy (RT) is the mainstay of treatment in cancers, and up to 50% of cancer patients receive radiotherapy to improve local control, survival, or quality of life (1). Conventional fractionated radiotherapy usually delivers in small fractions (1.8–2.0Gy per fraction) over a number of weeks, while hypofractionated radiotherapy delivers higher dose (3–20Gy) in fewer fractions (2, 3). Emerging evidence suggests that hypofractionated radiotherapy—clinically called stereotactic body radiotherapy (SBRT) or radiosurgery (SRS)—may elicit a pronounced anti-tumor effect (4, 5). In addition to directly killing tumor cells, hypofractionated irradiation can induce tumor cells death *via* antitumor immunity (6) and vascular damage (7). There are two types of RT-induced nontargeted effects: (1) the bystander effect, which describes the additional regression of nonirradiated surrounding tumor sites after local radiation therapy (8, 9), and (2) the abscopal effect, which describes the tumor regression of distant unirradiated tumor site (10, 11). Preliminary

studies suggest that radiation-induced immune responses are probably dose-dependent (12, 13). Substantial work has demonstrated that the nontargeted effects are attributed to the interaction between tumor irradiation and the host immune system (14, 15).

The tumor microenvironment (TME) is the stroma surrounding cancer cells that modulates the progression of cancer (16, 17). The TME consists of immune cells, tumor blood vessels, fibroblasts, and epithelial cells (18–21). Immune cells—such as tumor-associated macrophages (TAMs), tumor-associated neutrophils (TANs), myeloid-derived suppressor cells (MDSCs), mast cells, and natural killer (NK) cells—can produce a variety of factors (chemokines, cytokines, and enzymes) that directly or indirectly act as initiator or coordinator of the cellular immune responses to irradiation. Among all the stromal cells present in the TME, cancer-associated fibroblasts (CAFs) are one of the most abundant components of the tumor mesenchyme, which play a key role in promoting or retarding tumorigenesis in a context-dependent manner (22). In addition, radiotherapy may induce vascular damages or stimulate angiogenesis according to different regimens (23).

A large number of studies have shown that hypofractionated radiotherapy exerts a stimulating effect on the anti-tumor immune responses by inducing tumor cell death, normalizing aberrant tumor vasculature, releasing tumor associated antigens (TAAs) and inflammatory cytokines (24, 25). However, pre-clinical studies in some tumor models have suggested that radiotherapy-induced changes in the TME may induce an immunosuppressive TME, which may promote tumor invasion and spread in some situations (26, 27).

In this review, we summarized the immune mechanisms associated with hypofractionated radiotherapy, highlighted the advances in its immunosuppressive effect, and further discussed the potential mechanism behind this effect.

HYPOFRACTIONATED IRRADIATION INFLUENCES IMMUNOLOGICAL RESPONSES

Higher physical or biologic dose is associated with better local control and with better survival in some cases (28–30). In clinical practice, a typical example of hypofractionated radiotherapy is stereotactic body radiation, which delivers one to five fractions of doses above 6Gy per fraction to small target volumes (31). SBRT achieved high local control in the treatment of many cancers, such as early lung cancer, brain metastases, spinal metastases, and so on. The excellent efficacy of SBRT mainly attributed to the precisely delivered high dose to tumor site and the minimized dose to adjacent normal tissue. Besides this, SBRT can induce tumor cell death and tumor size reduction in non-radiotherapy sites, named bystander effect and abscopal effect (8–11).

The radiobiological mechanisms of hypofractionated radiotherapy are largely different from that of conventional radiotherapy. The reoxygenation, repopulation, repair, and redistribution (4Rs) are important components in the response of tumor to conventional fractionated radiotherapy (32, 33), and tumor cells are killed directly through irreparable DNA double-strand breaks in the forms of mitotic catastrophe and cellular apoptosis (34). Low-dose irradiation induces DNA damage and initiate apoptosis by activation of p53-dependent mechanisms, upregulating plasma membrane death receptor, and activation of the pro-apoptotic SAPK/JNK pathway (35, 36). However, in the setting of high dose irradiation, tumor cells may be eliminated in the form of necrosis (32). Necrosis is considered an immunogenic pathway and often accompanied by the release of pro-inflammatory cytokines and damage-associated molecular patterns, which promote tumor cell killing by anti-tumor T cell response (37).

Hypofractionated radiotherapy may change the tumor cell phenotype and the tumor microenvironment. After hypofractionated irradiation, tumor cells demonstrate increased cell-surface expression of immunogenic molecules, such as adhesion molecules, death receptors, stress-induced ligands, heat shock proteins, and stimulatory molecules (such as MHC-I and CD80) (38, 39). These immunophenotype changes make human tumors more amenable to be recognized by immune system and more sensitive to T cell-mediated cytotoxicity (40). Additionally, pro-inflammatory molecules and danger signals increase in the tumor microenvironment (41–43). Immune cells, such as CD8+ T cells and dendritic cells, are activated and recruited into the tumor and play an important role in anti-cancer immunity (44).

TME PLAYS A CENTRAL ROLE IN RESPONSE TO RADIOTHERAPY

The tumor microenvironment is the internal environment which tumors depend on survival and development. TME is associated with tumor growth, progression, and metastasis (16, 17). Cancer is an extremely complex and heterogeneous disease. Cancer cells present distinct features and various mutations, which is an important clinical determinant of patient outcomes. Dynamic changes occurring in the TME cause tumor cell variants selection, which may promote the complexity of cancer heterogeneity and impact the response to different treatment strategies (45, 46).

The TME consists of tumor stroma cells, immune cells, and a variety of factors produced by these cells (chemokines, cytokines, and enzymes) (47–49). Tumor stroma cells include cancer-associated fibroblasts, epithelial cells (ECs), and mesenchymal stromal cells (MSCs). CAFs are the most abundant cells in TME and play an important role in angiogenesis and tumor growth after irradiation (22). The damage of ECs has been shown to be a major factor in the biological mechanism in response to SBRT (50, 51). Cells of the immune system include tumor-associated macrophages, tumor-associated neutrophils, myeloid-derived suppressor cells, natural killer cells (NKs), T cells, B cells, dendritic cells (DCs), and mast cells. These cells significantly differ in radiosensitivity. In general, NKs and B lymphocytes are the most radiosensitive immune cells, while DCs, CAFs, and ECs are more radioresistant cells (27). Among the immune cells, regulatory T cells (Tregs) are more radioresistant than any other kinds of T cells (such as CD8+ T

cells) and B cells (27). As a result, the response of TME after irradiation varies according to the dose and fractionation schedule, which causes different outcomes in different cell types in TME.

Radiotherapy is a double-edged sword that can activate or suppress the immune response of TME under different conditions. The "hot" TME refers to a "inflamed" phenotype with highly infiltration of T cell lymphocytes (52, 53). Typical features for a hot TME include high number of effector cells (NK cells, CD8+ T cells, and Th1 cells) and functional antigen-presenting cells (APCs), and TAMs with the M1 phenotype. On the contrary, the "cold" TME refers to a "noninflamed" phenotype lack of T cell lymphocytes infiltration (52, 53). Characteristics of a cold TME include high numbers of Treg cells and MDSCs, lack of effector cells, and enrichment of immunosuppressive cytokines (47, 54). Activated NK cells and CD8+ T cells can eliminate tumor cells, while immunosuppressive TME is associated with enhanced metastasis and poor prognosis in patients (55, 56). Currently, it is not fully understood what dose and fractional radiotherapy induces the immune activated TME, and what dose and fractional radiotherapy causes the immunosuppressive TME.

HYPOFRACTIONATED IRRADIATION INDUCES ANTI-TUMOR IMMUNE RESPONSES

Emerging evidence demonstrates that hypofractionated radiotherapy can induce a pronounced anti-tumor effect ((57–62), **Figure 1**). The immunoreactive effect of radiation therapy is dose-dependent, and preclinical studies revealed that more than 8–10Gy per fraction are more effective in enhancing the anti-tumor immune response (63). In addition to the direct killing effects, hypofractionated radiotherapy can induce immunogenic death of tumor cells and orchestrate a spectrum of cellular and molecular alterations in the anti-tumor immune response (64).

After high-dose irradiation, cellular and DNA damage facilitate the generation and release of tumor-associated antigens, while necrosis or apoptosis cancer cells can generate pro-inflammatory "danger" signals and damage associated molecular patterns (DAMPs) (24, 62, 65). DAMPs and "danger" molecules stimulate dendritic cells *via* toll-like receptors (TLRs), and facilitate the uptake of TAAs and their presentation on major histocompatibility complex class 1 (MHC-1) to activate the tumor-specific cytotoxic T lymphocytes (24, 66). Dendritic cells are the major antigen-presenting cell that can process antigenic materials and present TAAs to CD8+ T cells (57, 65–67). Many preclinical studies have demonstrated that hypofractionated irradiation can increase presentation of TAAs to CD8+ T cells and enhance the antitumor T-cell-mediated immune response (68).

Irradiation also increases MHC-I expression by tumor cells, which presents TAAs to specific cytotoxic T cells, leading to the lysis of tumor cells (69). Garnett et al. (70) reported that, when irradiated by a single dose of 10–20Gy, colon and lung cell lines up-regulated the expression of MHC-I, while all of 4 prostate cancer cell lines did not. These results may suggest that the antitumor immunity response induced by hypofractionated radiotherapy differs among different cancer types.

In addition, radiation therapy exerts an immunostimulating activity by increasing NK cell cytotoxicity, facilitating the infiltration and accumulation of CD8+ T cells and tumor-associated M1 macrophages (inhibiting tumor growth), reducing the infiltration of Tregs (71), enhancing the

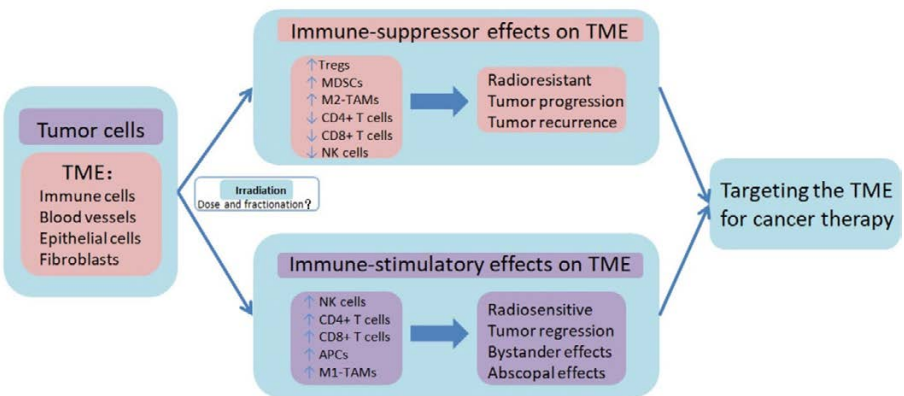

FIGURE 1 | Immune-suppressor effects and immune-stimulatory effects of radiotherapy on tumor microenvironment. Radiotherapy, especially hypofractionated irradiation, contributes to the induction of anti-tumor immune responses, which promote tumor control. Besides the immune-suppressor effects, radiotherapy also induces immunosuppression of TME, resulting in tumor progression and recurrence. The high infiltration of T cell lymphocytes in TME, known as immune hot or inflamed phenotype, is characterized by high number of effector cells (NK cells, CD8+ T cells, and Th1 cells) and functional antigen-presenting cells (APCs), and TAMs with the M1 phenotype. On the contrary, the lack of T cell lymphocytes infiltration in TME, known as immune cold or noninflamed phenotype, is characterized by high numbers of Treg cells and MDSCs, lack of effector cells, and enrichment of immunosuppressive cytokines. However, it is not fully understood what dose and fractional radiotherapy induces the immune activated TME, and what dose and fractional radiotherapy causes the immunosuppressive TME. Combination therapy targeting TME may help to improve the therapeutic benefit of radiotherapy. TME tumor microenvironment, Tregs regulatory T lymphocytes, MDSCs myeloid-derived suppressor cells, M2-TAMs tumor-associated M2 macrophages, NK cells natural killer cells, APCs antigen-presenting cells, M1-TAMs tumor-associated M1 macrophages.

expression of Fas and IFN-γ, and inhibiting the PD-1/PD-L1 pathway (24, 27).

Clinical evidences of the effect of radiation on TME include bystander effect and abscopal effect, in which local irradiation can induce regression in non-irradiated tumor or metastasis. Clinical reports of bystander or abscopal effects induced by radiation alone are relatively rare, and these phenomena are mainly observed in relatively high-dose radiotherapy (10). Tubin et al. (8, 9, 72, 73) conducted a series studies to explore the by stander and abscopal effects in unresectable stage IIIB/IV bulky non-small cell lung cancer (NSCLC), which were inoperable or unsuitable for radical radio-chemotherapy. They delivered 1–3 fractions each of 10–12Gy to 30% of the bulky tumor. As a result, they observed that the bystander and abscopal effects induced by partial irradiation were 95% and 45% (8), respectively. Furthermore, partial irradiation improved survival and tumor control compared to the standard of care. The researchers speculate that the induction of the bystander and abscopal effect are attribute to the irradiation to the hypoxic clonogenic cells and the sparing of peritumoral immune microenvironment and regional circulating lymphocytes. These results imply that irradiating a partial tumor may be enough to initiate immune modulation.

HYPOFRACTIONATED IRRADIATION INDUCES IMMUNOSUPPRESSIVE TME

Preclinical studies have suggested that irradiation-induced changes in tumor microenvironment may favor tumor growth, promoting tumor invasion and metastasis ((74, 75), **Figure 1**). This issue must be taken seriously, because suppression of the immune microenvironment not only leads to worse prognosis, but it may also be a legitimate therapeutic target.

Radiotherapy could eliminate radiosensitive immune cells, while radioresistant immune cells survive from it, thereby changing the proportion of immune cells in TME and causing suppression of the immune microenvironment. In the immune system, NK cells are the most radiosensitive immune cells (25, 76). On the contrary, immunosuppressive Tregs and MDSCs are more radioresistant than other population of T cells (27, 77). Kachikwu et al. (78) evaluated the impact of 0, 10, or 20Gy irradiation on Treg cells in murine model of prostate cancer. They found that Treg cells are more resistant to radiation than other lymphocytes, resulting in their preferential increase. In addition, Shi et al. (79) demonstrated that local irradiation with 10, 20, or 30Gy in cervical cancer patients significantly decreases CD8+ T cells, while having no effects on Tregs. Similarly, the MDSCs have been shown to accumulate in TME and suppress the activation of CD4+ and CD8+ T-cells (80, 81). Therefore, after certain doses and fractionated irradiation, NK cells and CD8+ T cells with anti-tumor effects are eliminated, while Treg cells and MDSCs with immunosuppressive effects are left. Changes in the types and numbers of immune cells result in the TME transformation from sensitive to resistant for response to radiotherapy (27).

High dose irradiation induces tumor vascular damage, which limits the infiltration of cytotoxic T lymphocytes into the tumor and increases the area of hypoxia (82, 83), leading to the resistance to radiotherapy (84, 85). Tumor blood vessels are more permeable and morphologically immature, and they are more sensitive to radiation (86). Vascular destruction is mainly observed at dose greater than 5 to 10Gy (27, 87), which drastically reduces the blood flow and induces hypoxia. Sonveaux et al. (88) reported that irradiation by a 6Gy dose up-regulates the expression and activity of endothelial nitric oxide synthase (eNOS). This activates the nitric oxide (NO) pathway in ECs and generates tumor angiogenesis. The process of vasculogenesis leads to the recruitment of radioresistant suppressor cells, including MDSCs, Tregs, and TAMs with the M2 phenotype (87, 89).

CAFs are the most abundant cells in the tumor stroma and play an important role in tumor angiogenesis, growth, and metastasis (90–94). CAFS are radioresistant, being able to survive at doses of up to 50Gy (95–97). CAFs can stimulate the recruitment of cells, which promotes tumor blood vessel formation and facilitates tumor recurrence (98, 99). The CAFs also secrete enzymes such as matrix metalloproteinases, which degrade the extracellular matrix, promote the migration of CAFS, and facilitate the invasion of tumor cells (90, 100). Furthermore, in vitro studies have demonstrated that a dose >10Gy to fibroblasts induces an irreversible senescent phenotype. Metabolically activated CAFs release growth factors, proteolytic enzymes, and cytokines, inducing an environment that promotes tumor growth and spread (82, 96, 101–103). However, the cancer promoting effects of senescent fibroblasts may depend on the dose and fraction of radiotherapy and vary in different tumor types (104).

Understanding the immunosuppressive effects of hypofractionated radiotherapy on the TME may help to explore new treatment strategies to block the immunosuppressive responses of radiotherapy and augment the antitumor effects (105). Previous studies suggested that both enhancing the function of tumor suppressor cells and inhibiting the function of tumor promoting cells could improve the therapeutic efficiency of radiotherapy (106–109). For example, the combination of radiotherapy and immunotherapy may prevent early exhaustion of anti-tumor immunity by boosting the activation of NK cells and cytotoxic T lymphocytes (106, 107). Moreover, inhibiting the immunosuppressive cells like Tregs, MDSCs, and TAMs can induce durable anti-tumor immunity and prevent tumor progression. A previous study by Xu et al. (108) showed that inhibition of macrophage colony-stimulating factor CSF-1 could reduce the recruitment of both TAMs and MDSCs, thereby suppressing tumor growth more effectively than irradiation alone. Furthermore, vascular-targeted agents are demonstrated to alter the tumor microenvironment to increase the radiosensitivity of tumor (110). Targeting the tumor immune microenvironment is an interesting strategy to enhance the efficacy of radiotherapy, and much remains to be investigated before realizing its potential therapeutic effects clinically.

DISCUSSION

Recent technological advances in external beam radiotherapy have allowed larger doses per fraction delivered to tumor, while minimizing doses to normal tissues adjacent. However, despite the increasing effectiveness of hypofractionated radiotherapy, we still can't completely avoid tumor recurrence and progression. A large number of studies have shown that hypofractionated radiotherapy can induce immune-activated TME and improve treatment efficacy. However, increasing studies have suggested that hypofractionated radiotherapy can promote immune-suppressive TME and play a significant role in radioresistance and tumor recurrence. There is a delicate balance between TME suppression and activation triggered by hypofractionated irradiation. We still don't know which doses and fractionation schedule activate the anti-tumor immune response and which induce the immune suppression. Moreover, different sites and types of tumors may respond differently to the same dose and fractionated irradiation. More knowledge is needed to optimize the radiotherapy strategy. Understanding the immune effects of hypofractionated radiotherapy on the TME may help to improve therapeutic benefit and explore new combination therapy strategies.

AUTHOR CONTRIBUTIONS

YW designed this work and wrote and revised the manuscript.

REFERENCES

1. Sato H, Okonogi N, Nakano T. Rationale of combination of anti-PD-1/PD-L1 antibody therapy and radiotherapy for cancer treatment. *Int J Clin Oncol* (2020) 25:801–9. doi: 10.1007/s10147-020-01666-132246277
2. Frey B, Ruckert M, Weber J, Mayr X, Derer A, Lotter M, et al. Hypofractionated Irradiation Has Immune Stimulatory Potential and Induces a Timely Restricted Infiltration of Immune Cells in Colon Cancer Tumors. *Front Immunol* (2017) 8:231. doi: 10.3389/fimmu.2017.00231
3. Prasanna A, Ahmed MM, Mohiuddin M, Coleman CN. Exploiting sensitization windows of opportunity in hyper and hypo-fractionated radiation therapy. *J Thorac Dis* (2014) 6:287–302. doi: 10.3978/j.issn.2072-1439.2014.01.14
4. Chen Y, Gao M, Huang Z, Yu J, Meng X. SBRT combined with PD-1/PD-L1 inhibitors in NSCLC treatment: a focus on the mechanisms, advances, and future challenges. *J Hematol Oncol* (2020) 13:105. doi: 10.1186/s13045-020-00940-z
5. Ijsseldijk MA, Shoni M, Siegert C, Wiering B, van Engelenburg A, Tsai TC, et al. Oncologic Outcomes of Surgery Versus SBRT for Non-Small-Cell Lung Carcinoma: A Systematic Review and Meta-analysis. *Clin Lung Cancer* (2020) S1512–7304(20):30140–6. doi: 10.1016/j.cllc.2020.04.017
6. Chajon E, Castelli J, Marsiglia H, De Crevoisier R. The synergistic effect of radiotherapy and immunotherapy: A promising but not simple partnership. *Crit Rev Oncol Hematol* (2017) 111:124–32. doi: 10.1016/j.critrevonc 2017.01.017
7. Zhuang H, Zhuang H, Lang N, Liu J. Precision Stereotactic Radiotherapy for Spinal Tumors: Mechanism, Efficacy, and Issues. *Front Oncol* (2020) 10:826. doi: 10.3389/fonc.2020.00826
8. Tubin S, Khan MK, Salerno G, Mourad WF, Yan W, Jeremic B. Mono-institutional phase 2 study of innovative Stereotactic Body RadioTherapy targeting PArtial Tumor HYpoxic (SBRT-PATHY) clonogenic cells in unresectable bulky non-small cell lung cancer: profound non-targeted effects by sparing peri-tumoral immune microenvironment. *Radiat Oncol* (2019) 14:212. doi: 10.1186/s13014-019-1410-1
9. Tubin S, Ashdown M, Jeremic B. Time-synchronized immune-guided SBRT partial bulky tumor irradiation targeting hypoxic segment while sparing the peritumoral immune microenvironment. *Radiat Oncol* (2019) 14:220. doi: 10.1186/s13014-019-1423-9
10. Ashrafizadeh M, Farhood B, Eleojo MA, Taeb S, Rezaeyan A, Najafi M. Abscopal effect in radioimmunotherapy. *Int Immunopharmacol* (2020) 85:106663. doi: 10.1016/j.intimp.2020.106663
11. Chicas-Sett R, Morales-Orue I, Castilla-Martinez J, Zafra-Martin J, Kannemann A, Blanco J, et al. Stereotactic Ablative Radiotherapy Combined with Immune Checkpoint Inhibitors Reboots the Immune Response Assisted by Immunotherapy in Metastatic Lung Cancer: A Systematic Review. *Int J Mol Sci* (2019) 20(9):2173. doi: 10.3390/ijms20092173
12. Bernstein MB, Garnett CT, Zhang H, Velcich A, Wattenberg MM, Gameiro SR, et al. Radiation-induced modulation of costimulatory and coinhibitory T-cell signaling molecules on human prostate carcinoma cells promotes productive antitumor immune interactions. *Cancer Biother Radiopharm* (2014) 29:153–61. doi: 10.1089/cbr.2013.1578
13. Schaue D, Ratikan JA, Iwamoto KS, McBride WH. Maximizing tumor immunity with fractionated radiation. *Int J Radiat Oncol Biol Phys* (2012) 83:1306–10. doi: 10.1016/j.ijrobp.2011.09.049
14. de Olza MO, Bourhis J, Irving M, Coukos G, Herrera FG. High versus low dose irradiation for tumor immune reprogramming. *Curr Opin Biotechnol* (2020) 65:268–83. doi: 10.1016/j.copbio.2020.08.001
15. Demaria S, Ng B, Devitt ML, Babb JS, Kawashima N, Liebes L, et al. Ionizing radiation inhibition of distant untreated tumors (abscopal effect) is immune mediated. *Int J Radiat Oncol Biol Phys* (2004) 58:862–70. doi: 10.1016/j.ijrobp.2003.09.012
16. Hanahan D, Weinberg RA. Hallmarks of cancer: the next generation. *Cell* (2011) 144:646–74. doi: 10.1016/j.cell.2011.02.013
17. Mantovani A, Ponzetta A, Inforzato A, Jaillon S. Innate immunity, inflammation and tumour progression: double-edged swords. *J Intern Med* (2019) 285:524–32. doi: 10.1111/joim.12886
18. Cui Y, Guo G. Immunomodulatory Function of the Tumor Suppressor p53 in Host Immune Response and the Tumor Microenvironment. *Int J Mol Sci* (2016) 17(11):1942. doi: 10.3390/ijms17111942
19. Chen DS, Mellman I. Elements of cancer immunity and the cancer-immune set point. *Nature* (2017) 541:321–30. doi: 10.1038/nature21349
20. Albini A, Bruno A, Noonan DM, Mortara L. Contribution to Tumor Angiogenesis From Innate Immune Cells Within the Tumor Microenvironment: Implications for Immunotherapy. *Front Immunol* (2018) 9:527. doi: 10.3389/fimmu.2018.00527
21. Tugues S, Ducimetiere L, Friebel E, Becher B. Innate lymphoid cells as regulators of the tumor microenvironment. *Semin Immunol* (2019) 41:101270. doi: 10.1016/j.smim.2019.03.002
22. Ansems M, Span PN. The tumor microenvironment and radiotherapy response; a central role for cancer-associated fibroblasts. *Clin Transl Radiat Oncol* (2020) 22:90–7. doi: 10.1016/j.ctro.2020.04.001
23. Martinez-Zubiaurre I, Chalmers AJ, Hellevik T. Radiation-Induced Transformation of Immunoregulatory Networks in the Tumor Stroma. *Front Immunol* (2018) 9:1679. doi: 10.3389/fimmu.2018.01679
24. Tharmalingam H, Hoskin PJ. The optimism surrounding stereotactic body radiation therapy and immunomodulation. *Chin Clin Oncol* (2017) 6:S9. doi: 10.21037/cco.2017.05.01
25. Kotera Y, Shimizu K, Mule JJ. Comparative analysis of necrotic and apoptotic tumor cells as a source of antigen(s) in dendritic cell-based immunization. *Cancer Res* (2001) 61:8105–9.
26. Barker HE, Paget JT, Khan AA, Harrington KJ. The tumour microenvironment after radiotherapy: mechanisms of resistance and recurrence. *Nat Rev Cancer* (2015) 15:409–25. doi: 10.1038/nrc3958
27. Jarosz-Biej M, Smolarczyk R, Cichon T, Kulach N. Tumor Microenvironment as A "Game Changer" in Cancer Radiotherapy. *Int J Mol Sci* (2019) 20(13):3212. doi: 10.3390/ijms20133212

28. Offersen BV, Alsner J, Nielsen HM, Jakobsen EH, Nielsen MH, Krause M, et al. Hypofractionated Versus Standard Fractionated Radiotherapy in Patients With Early Breast Cancer or Ductal Carcinoma In Situ in a Randomized Phase III Trial: The DBCG HYPO Trial. *J Clin Oncol* (2020) 38(31):3615–25. doi: 10.1200/JCO.20.01363
29. Oliinyk D, Augustin T, Koehler VF, Rauch J, Belka C, Spitzweg C, et al. Hypofractionated Radiotherapy for Anaplastic Thyroid Cancer: Systematic Review and Pooled Analysis. *Cancers (Basel)* (2020) 12(9):2506. doi: 10.3390/cancers12092506
30. Tamihardja J, Schortmann M, Lawrenz I, Weick S, Bratengeier K, Flentje M, et al. Moderately hypofractionated radiotherapy for localized prostate cancer: updated long-term outcome and toxicity analysis. *Strahlenther Onkol* (2020). doi: 10.1007/s00066-020-01678-w
31. Xing D, Siva S, Hanna GG. The Abscopal Effect of Stereotactic Radiotherapy and Immunotherapy: Fool's Gold or El Dorado? *Clin Oncol (R Coll Radiol)* (2019) 31:432–43. doi: 10.1016/j.clon.2019.04.006
32. Kim MS, Kim W, Park IH, Kim HJ, Lee E, Jung JH, et al. Radiobiological mechanisms of stereotactic body radiation therapy and stereotactic radiation surgery. *Radiat Oncol J* (2015) 33:265–75. doi: 10.3857/roj.2015.33.4.265
33. Brown JM, Carlson DJ, Brenner DJ. The tumor radiobiology of SRS and SBRT: are more than the 5 Rs involved? *Int J Radiat Oncol Biol Phys* (2014) 88:254–62. doi: 10.1016/j.ijrobp.2013.07.022
34. Eriksson D, Stigbrand T. Radiation-induced cell death mechanisms. *Tumour Biol* (2010) 31:363–72. doi: 10.1016/j.ijrobp.2013.07.022
35. Verheij M, Bartelink H. Radiation-induced apoptosis. *Cell Tissue Res* (2000) 301(1):133–42. doi: 10.1007/s004410000188
36. Sia J, Szmyd R, Hau E, Gee HE. Molecular Mechanisms of Radiation-Induced Cancer Cell Death: A Primer. *Front Cell Dev Biol* (2020) 8:41. doi: 10.3389/fcell.2020.00041
37. Tesniere A, Panaretakis T, Kepp O, Apetoh L, Ghiringhelli F, Zitvogel L, et al. Molecular characteristics of immunogenic cancer cell death. *Cell Death Differ* (2008) 15(1):3–12. doi: 10.1038/sj.cdd.4402269
38. Moding EJ, Mowery YM, Kirsch DG. Opportunities for Radiosensitization in the Stereotactic Body Radiation Therapy (SBRT) Era. *Cancer J* (2016) 22:267–73. doi: 10.1097/PPO.0000000000000203
39. Schaue D, McBride WH. Opportunities and challenges of radiotherapy for treating cancer. *Nat Rev Clin Oncol* (2015) 12:527–40. doi: 10.1038/nrclinonc.2015.120
40. Diegeler S, Hellweg CE. Intercellular Communication of Tumor Cells and Immune Cells after Exposure to Different Ionizing Radiation Qualities. *Front Immunol* (2017) 8:664. doi: 10.3389/fimmu.2017.00664
41. Wattenberg MM, Fahim A, Ahmed MM, Hodge JW. Unlocking the combination: potentiation of radiation-induced antitumor responses with immunotherapy. *Radiat Res* (2014) 182:126–38. doi: 10.1667/RR13374.1
42. Frey B, Rubner Y, Kulzer L, Werthmoller N, Weiss EM, Fietkau R, et al. Antitumor immune responses induced by ionizing irradiation and further immune stimulation. *Cancer Immunol Immunother* (2014) 63:29–36. doi: 10.1007/s00262-013-1474-y
43. Gameiro SR, Jammeh ML, Wattenberg MM, Tsang KY, Ferrone S, Hodge JW. Radiation-induced immunogenic modulation of tumor enhances antigen processing and calreticulin exposure, resulting in enhanced T-cell killing. *Oncotarget* (2014) 5:403–16. doi: 10.18632/oncotarget.1719
44. Deng L, Liang H, Burnette B, Weicheslbaum RR, Fu YX. Radiation and anti-PD-L1 antibody combinatorial therapy induces T cell-mediated depletion of myeloid-derived suppressor cells and tumor regression. *Oncoimmunology* (2014) 3:e28499. doi: 10.4161/onci.28499
45. Noman MZ, Hasmim M, Lequeux A, Xiao M, Duhem C, Chouaib S, et al. Improving Cancer Immunotherapy by Targeting the Hypoxic Tumor Microenvironment: New Opportunities and Challenges. *Cells-Basel* (2019) 8(9):1083. doi: 10.3390/cells8091083
46. Wu J, Chen J, Feng Y, Tian H, Chen X. Tumor microenvironment as the "regulator" and "target" for gene therapy. *J Gene Med* (2019) 21:e3088. doi: 10.1002/jgm.3088
47. Portella L, Scala S. Ionizing radiation effects on the tumor microenvironment. *Semin Oncol* (2019) 46:254–60. doi: 10.1053/j.seminoncol.2019.07.003
48. Junttila MR, de Sauvage FJ. Influence of tumour micro-environment heterogeneity on therapeutic response. *Nature* (2013) 501:346–54. doi: 10.1038/nature12626
49. Wu T, Dai Y. Tumor microenvironment and therapeutic response. *Cancer Lett* (2017) 387:61–8. doi: 10.1016/j.canlet.2016.01.043
50. Song CW, Lee YJ, Griffin RJ, Park I, Koonce NA, Hui S, et al. Indirect Tumor Cell Death After High-Dose Hypofractionated Irradiation: Implications for Stereotactic Body Radiation Therapy and Stereotactic Radiation Surgery. *Int J Radiat Oncol Biol Phys* (2015) 93:166–72. doi: 10.1016/j.ijrobp.2015.05.016
51. Maeda A, Chen Y, Bu J, Mujcic H, Wouters BG, DaCosta RS. In Vivo Imaging Reveals Significant Tumor Vascular Dysfunction and Increased Tumor Hypoxia-Inducible Factor-1alpha Expression Induced by High Single-Dose Irradiation in a Pancreatic Tumor Model. *Int J Radiat Oncol Biol Phys* (2017) 97:184–94. doi: 10.1016/j.ijrobp.2016.09.005
52. Duan Q, Zhang H, Zheng J, Zhang L. Turning Cold into Hot: Firing up the Tumor Microenvironment. *Trends Cancer* (2020) 6:605–18. doi: 10.1016/j.trecan.2020.02.022
53. Fan Z, Liu H, Xue Y, Lin J, Fu Y, Xia Z, et al. Reversing cold tumors to hot: An immunoadjuvant-functionalized metal-organic framework for multimodal imaging-guided synergistic photo-immunotherapy. *Bioact Mater* (2021) 6:312–25. doi: 10.1016/j.bioactmat.2020.08.005
54. Shimizu K, Iyoda T, Okada M, Yamasaki S, Fujii SI. Immune suppression and reversal of the suppressive tumor microenvironment. *Int Immunol* (2018) 30:445–54. doi: 10.1093/intimm/dxy042
55. Qian BZ, Pollard JW. Macrophage diversity enhances tumor progression and metastasis. *Cell* (2010) 141:39–51. doi: 10.1016/j.cell.2010.03.014
56. Chen J, Yao Y, Gong C, Yu F, Su S, Chen J, et al. CCL18 from tumor-associated macrophages promotes breast cancer metastasis via PITPNM3. *Cancer Cell* (2011) 19:541–55. doi: 10.1016/j.ccr.2011.02.006
57. Lee Y, Auh SL, Wang Y, Burnette B, Wang Y, Meng Y, et al. Therapeutic effects of ablative radiation on local tumor require CD8+ T cells: changing strategies for cancer treatment. *Blood* (2009) 114:589–95. doi: 10.1182/blood-2009-02-206870
58. Lugade AA, Sorensen EW, Gerber SA, Moran JP, Frelinger JG, Lord EM. Radiation-induced IFN-gamma production within the tumor microenvironment influences antitumor immunity. *J Immunol* (2008) 180:3132–9. doi: 10.4049/jimmunol.180.5.3132
59. Hennel R, Brix N, Seidl K, Ernst A, Scheithauer H, Belka C, et al. Release of monocyte migration signals by breast cancer cell lines after ablative and fractionated gamma-irradiation. *Radiat Oncol* (2014) 9:85. doi: 10.1186/1748-717X-9-85
60. Golden EB, Demaria S, Schiff PB, Chachoua A, Formenti SC. An abscopal response to radiation and ipilimumab in a patient with metastatic non-small cell lung cancer. *Cancer Immunol Res* (2013) 1:365–72. doi: 10.1158/2326-6066.CIR-13-0115
61. Gulley JL, Arlen PM, Bastian A, Morin S, Marte J, Beetham P, et al. Combining a recombinant cancer vaccine with standard definitive radiotherapy in patients with localized prostate cancer. *Clin Cancer Res* (2005) 11:3353–62. doi: 10.1158/1078-0432.CCR-04-2062
62. Garg AD, Nowis D, Golab J, Vandenabeele P, Krysko DV, Agostinis P. Immunogenic cell death, DAMPs and anticancer therapeutics: an emerging amalgamation. *Biochim Biophys Acta* (2010) 1805:53–71. doi: 10.1016/j.bbcan.2009.08.003
63. Popp I, Grosu AL, Niedermann G, Duda DG. Immune modulation by hypofractionated stereotactic radiation therapy: Therapeutic implications. *Radiother Oncol* (2016) 120:185–94. doi: 10.1016/j.radonc.2016.07.013
64. Menon H, Ramapriyan R, Cushman TR, Verma V, Kim HH, Schoenhals JE, et al. Role of Radiation Therapy in Modulation of the Tumor Stroma and Microenvironment. *Front Immunol* (2019) 10:193. doi: 10.3389/fimmu.2019.00193
65. Apetoh L, Ghiringhelli F, Tesniere A, Obeid M, Ortiz C, Criollo A, et al. Toll-like receptor 4-dependent contribution of the immune system to anticancer chemotherapy and radiotherapy. *Nat Med* (2007) 13:1050–9. doi: 10.1038/nm1622
66. Yang Y, Liu B, Dai J, Srivastava PK, Zammit DJ, Lefrancois L, et al. Heat shock protein gp96 is a master chaperone for toll-like receptors and is important in the innate function of macrophages. *Immunity* (2007) 26:215–26. doi: 10.1016/j.immuni.2006.12.005
67. Gupta A, Probst HC, Vuong V, Landshammer A, Muth S, Yagita H, et al. Radiotherapy promotes tumor-specific effector CD8+ T cells via dendritic

cell activation. *J Immunol* (2012) 189:558–66. doi: 10.4049/jimmunol.1200563
68. Arnold KM, Flynn NJ, Raben A, Romak L, Yu Y, Dicker AP, et al. The Impact of Radiation on the Tumor Microenvironment: Effect of Dose and Fractionation Schedules. *Cancer Growth Metastasis* (2018) 11:1406729127. doi: 10.1177/1179064418761639
69. Peters HL, Yan Y, Solheim JC. APLP2 regulates the expression of MHC class I molecules on irradiated Ewing's sarcoma cells. *Oncoimmunology* (2013) 2: e26293. doi: 10.4161/onci.26293
70. Garnett CT, Palena C, Chakraborty M, Tsang KY, Schlom J, Hodge JW. Sublethal irradiation of human tumor cells modulates phenotype resulting in enhanced killing by cytotoxic T lymphocytes. *Cancer Res* (2004) 64:7985–94. doi: 10.1158/0008-5472.CAN-04-1525
71. Wennerberg E, Lhuillier C, Vanpouille-Box C, Pilones KA, Garcia-Martinez E, Rudqvist NP, et al. Barriers to Radiation-Induced In Situ Tumor Vaccination. *Front Immunol* (2017) 8:229. doi: 10.3389/fimmu.2017.00229
72. Tubin S, Popper HH, Brcic L. Novel stereotactic body radiation therapy (SBRT)-based partial tumor irradiation targeting hypoxic segment of bulky tumors (SBRT-PATHY): improvement of the radiotherapy outcome by exploiting the bystander and abscopal effects. *Radiat Oncol* (2019) 14:21. doi: 10.1186/s13014-019-1227-y
73. Tubin S, Yan W, Mourad WF, Fossati P, Khan MK. The future of radiation-induced abscopal response: beyond conventional radiotherapy approaches. *Future Oncol* (2020) 16:1137–51. doi: 10.2217/fon-2020-0063
74. Basler L, Andratschke N, Ehrbar S, Guckenberger M, Tanadini-Lang S. Modelling the immunosuppressive effect of liver SBRT by simulating the dose to circulating lymphocytes: an in-silico planning study. *Radiat Oncol* (2018) 13:10. doi: 10.1186/s13014-018-0952-y
75. Muroyama Y, Nirschl TR, Kochel CM, Lopez-Bujanda Z, Theodros D, Mao W, et al. Stereotactic Radiotherapy Increases Functionally Suppressive Regulatory T Cells in the Tumor Microenvironment. *Cancer Immunol Res* (2017) 5:992–1004. doi: 10.1158/2326-6066.CIR-17-0040
76. Philippou Y, Sjoberg HT, Murphy E, Alyacoubi S, Jones KI, Gordon-Weeks AN, et al. Impacts of combining anti-PD-L1 immunotherapy and radiotherapy on the tumour immune microenvironment in a murine prostate cancer model. *Br J Cancer* (2020) 123(7):1089–100. doi: 10.1038/s41416-020-0956-x
77. Oweida AJ, Darragh L, Phan A, Binder D, Bhatia S, Mueller A, et al. STAT3 Modulation of Regulatory T Cells in Response to Radiation Therapy in Head and Neck Cancer. *J Natl Cancer Inst* (2019) 111:1339–49. doi: 10.1093/jnci/djz036
78. Kachikwu EL, Iwamoto KS, Liao YP, DeMarco JJ, Agazaryan N, Economou JS, et al. Radiation enhances regulatory T cell representation. *Int J Radiat Oncol Biol Phys* (2011) 81:1128–35. doi: 10.1016/j.ijrobp.2010.09.034
79. Qinfeng S, Depu W, Xiaofeng Y, Shah W, Hongwei C, Yili W. In situ observation of the effects of local irradiation on cytotoxic and regulatory T lymphocytes in cervical cancer tissue. *Radiat Res* (2013) 179:584–9. doi: 10.1667/RR3155.1
80. Yang X, Lu Y, Hang J, Zhang J, Zhang T, Huo Y, et al. Lactate-modulated immunosuppression of myeloid-derived suppressor cells contributes to the radioresistance of pancreatic cancer. *Cancer Immunol Res* (2020) 8 (11):1440–51. doi: 10.1158/2326-6066.CIR-20-0111
81. Chen HY, Xu L, Li LF, Liu XX, Gao JX, Bai YR. Inhibiting the CD8(+) T cell infiltration in the tumor microenvironment after radiotherapy is an important mechanism of radioresistance. *Sci Rep* (2018) 8:11934. doi: 10.1038/s41598-018-30417-6
82. Hellevik T, Martinez-Zubiaurre I. Radiotherapy and the tumor stroma: the importance of dose and fractionation. *Front Oncol* (2014) 4:1. doi: 10.3389/fonc.2014.00001
83. Begg K, Tavassoli M. Inside the hypoxic tumour: reprogramming of the DDR and radioresistance. *Cell Death Discovery* (2020) 6:77. doi: 10.1038/s41420-020-00311-0
84. Wang Y, Liu ZG, Yuan H, Deng W, Li J, Huang Y, et al. The Reciprocity between Radiotherapy and Cancer Immunotherapy. *Clin Cancer Res* (2019) 25:1709–17. doi: 10.1158/1078-0432.CCR-18-2581
85. Sun X, Lv X, Yan Y, Zhao Y, Ma R, He M, et al. Hypoxia-mediated cancer stem cell resistance and targeted therapy. *BioMed Pharmacother* (2020) 130:110623. doi: 10.1016/j.biopha.2020.110623
86. Grabham P, Hu B, Sharma P, Geard C. Effects of ionizing radiation on three-dimensional human vessel models: differential effects according to radiation quality and cellular development. *Radiat Res* (2011) 175:21–8. doi: 10.1667/RR2289.1
87. Park HJ, Griffin RJ, Hui S, Levitt SH, Song CW. Radiation-induced vascular damage in tumors: implications of vascular damage in ablative hypofractionated radiotherapy (SBRT and SRS). *Radiat Res* (2012) 177:311–27. doi: 10.1667/rr2773.1
88. Sonveaux P, Brouet A, Havaux X, Gregoire V, Dessy C, Balligand JL, et al. Irradiation-induced angiogenesis through the up-regulation of the nitric oxide pathway: implications for tumor radiotherapy. *Cancer Res* (2003) 63:1012–9.
89. Sun X, Deng L, Lu Y. Challenges and opportunities of using stereotactic body radiotherapy with anti-angiogenesis agents in tumor therapy. *Chin J Cancer Res* (2018) 30:147–56. doi: 10.21147/j.issn.1000-9604.2018.01.15
90. Bhowmick NA, Neilson EG, Moses HL. Stromal fibroblasts in cancer initiation and progression. *Nature* (2004) 432:332–7. doi: 10.1038/nature03096
91. Kalluri R, Zeisberg M. Fibroblasts in cancer. *Nat Rev Cancer* (2006) 6:392–401. doi: 10.1038/nrc1877
92. Orimo A, Weinberg RA. Stromal fibroblasts in cancer: a novel tumor-promoting cell type. *Cell Cycle* (2006) 5:1597–601. doi: 10.4161/cc.5.15.3112
93. Shimoda M, Mellody KT, Orimo A. Carcinoma-associated fibroblasts are a rate-limiting determinant for tumour progression. *Semin Cell Dev Biol* (2010) 21:19–25. doi: 10.1016/j.semcdb.2009.10.002
94. Liu L, Zhang Z, Zhou L, Hu L, Yin C, Qing D, et al. Cancer associated fibroblasts-derived exosomes contribute to radioresistance through promoting colorectal cancer stem cells phenotype. *Exp Cell Res* (2020) 391:111956. doi: 10.1016/j.yexcr.2020.111956
95. Hawsawi NM, Ghebeh H, Hendrayani SF, Tulbah A, Al-Eid M, Al-Tweigeri T, et al. Breast carcinoma-associated fibroblasts and their counterparts display neoplastic-specific changes. *Cancer Res* (2008) 68:2717–25. doi: 10.1158/0008-5472.CAN-08-0192
96. Papadopoulou A, Kletsas D. Human lung fibroblasts prematurely senescent after exposure to ionizing radiation enhance the growth of malignant lung epithelial cells in vitro and in vivo. *Int J Oncol* (2011) 39:989–99. doi: 10.3892/ijo.2011.1132
97. Tachiiri S, Katagiri T, Tsunoda T, Oya N, Hiraoka M, Nakamura Y. Analysis of gene-expression profiles after gamma irradiation of normal human fibroblasts. *Int J Radiat Oncol Biol Phys* (2006) 64:272–9. doi: 10.1016/j.ijrobp.2005.08.030
98. Orimo A, Gupta PB, Sgroi DC, Arenzana-Seisdedos F, Delaunay T, Naeem R, et al. Stromal fibroblasts present in invasive human breast carcinomas promote tumor growth and angiogenesis through elevated SDF-1/CXCL12 secretion. *Cell* (2005) 121:335–48. doi: 10.1016/j.cell.2005.02.034
99. Tseng D, Vasquez-Medrano DA, Brown JM. Targeting SDF-1/CXCR4 to inhibit tumour vasculature for treatment of glioblastomas. *Br J Cancer* (2011) 104:1805–9. doi: 10.1038/bjc.2011.169
100. Gaggioli C, Hooper S, Hidalgo-Carcedo C, Grosse R, Marshall JF, Harrington K, et al. Fibroblast-led collective invasion of carcinoma cells with differing roles for RhoGTPases in leading and following cells. *Nat Cell Biol* (2007) 9:1392–400. doi: 10.1038/ncb1658
101. Nguyen HQ, To NH, Zadigue P, Kerbrat S, De La Taille A, Le Gouvello S, et al. Ionizing radiation-induced cellular senescence promotes tissue fibrosis after radiotherapy. A review. *Crit Rev Oncol Hematol* (2018) 129:13–26. doi: 10.1016/j.critrevonc.2018.06.012
102. Rodier F, Coppe JP, Patil CK, Hoeijmakers WA, Munoz DP, Raza SR, et al. Persistent DNA damage signalling triggers senescence-associated inflammatory cytokine secretion. *Nat Cell Biol* (2009) 11:973–9. doi: 10.1038/ncb1909
103. Piper M, Mueller AC, Karam SD. The interplay between cancer associated fibroblasts and immune cells in the context of radiation therapy. *Mol Carcinog* (2020) 59:754–65. doi: 10.1002/mc.23205
104. Hellevik T, Pettersen I, Berg V, Winberg JO, Moe BT, Bartnes K, et al. Cancer-associated fibroblasts from human NSCLC survive ablative doses of radiation but their invasive capacity is reduced. *Radiat Oncol* (2012) 7:59. doi: 10.1186/1748-717X-7-59
105. Ashrafizadeh M, Farhood B, Eleojo MA, Taeb S, Najafi M. The interactions and communications in tumor resistance to radiotherapy: Therapy

perspectives. *Int Immunopharmacol* (2020) 87:106807. doi: 10.1016/j.intimp.2020.106807
106. Bolli E, D'Huyvetter M, Murgaski A, Berus D, Stange G, Clappaert EJ, et al. Stromal-targeting radioimmunotherapy mitigates the progression of therapy-resistant tumors. *J Control Release* (2019) 314:1–11. doi: 10.1016/j.jconrel.2019.10.024
107. Gaipl US, Multhoff G, Pockley AG, Rodel F. Editorial: Radioimmunotherapy-Translational Opportunities and Challenges. *Front Oncol* (2020) 10:190. doi: 10.3389/fonc.2020.00190
108. Xu J, Escamilla J, Mok S, David J, Priceman S, West B, et al. CSF1R signaling blockade stanches tumor-infiltrating myeloid cells and improves the efficacy of radiotherapy in prostate cancer. *Cancer Res* (2013) 73:2782–94. doi: 10.1158/0008-5472.CAN-12-3981
109. Najafi M, Mortezaee K, Majidpoor J. Stromal reprogramming: A target for tumor therapy. *Life Sci* (2019) 239:117049. doi: 10.1016/j.lfs.2019.117049
110. Ciric E, Sersa G. Radiotherapy in combination with vascular-targeted therapies. *Radiol Oncol* (2010) 44:67–78. doi: 10.2478/v10019-010-0025-92293389

Conflict of Interest: The author declares that the research was conducted in the absence of any commercial or financial relationships that could be construed as a potential conflict of interest.

Copyright © 2021 Wang. This is an open-access article distributed under the terms of the Creative Commons Attribution License (CC BY). The use, distribution or reproduction in other forums is permitted, provided the original author(s) and the copyright owner(s) are credited and that the original publication in this journal is cited, in accordance with accepted academic practice. No use, distribution or reproduction is permitted which does not comply with these terms.

frontiers in Immunology

ORIGINAL RESEARCH
published: 26 January 2021
doi: 10.3389/fimmu.2020.620166

CU06-1004-Induced Vascular Normalization Improves Immunotherapy by Modulating Tumor Microenvironment *via* Cytotoxic T Cells

Songyi Park[1], Ji Hoon Oh[1], Dong Jin Park[1], Haiying Zhang[2], Minyoung Noh[1], Yeomyung Kim[1], Ye-Seul Kim[1], Hyejeong Kim[1], Young-Myeong Kim[3], Sang-Jun Ha[1] and Young-Guen Kwon[1]**

[1] Department of Biochemistry, College of Life Science and Biotechnology, Yonsei University, Seoul, South Korea, [2] R&D Department, Curacle Co. Ltd, Seongnam-si, South Korea, [3] Vascular System Research Center, Kangwon National University, Chuncheon, South Korea

Blocking the immune evasion mechanism of tumor cells has become an attractive means for treating cancers. However, the usage of a drug such as nivolumab (αPD-1), which blocks programmed cell death protein 1 (PD-1), turned out to be only effective against certain types of cancer. Especially, vascular abnormal structures of which deter delivery route by leakage and cause the poor perfusion were considered to be environment unfavorable to T cells and immune checkpoint blockade (ICB) delivery within the tumor microenvironment (TME). Herein, we report stabilization of tumor blood vessels by endothelial dysfunctional blocker CU06-1004, which modified the TME and showed synergistic effects with immunotherapy anti-PD-1 antibody. CU06-1004 combination therapy consistently prolonged the survival of tumor-bearing mice by decreasing tumor growth. T-cell infiltration increased in the tumors of the combination group, with cytotoxic $CD8^+$ T cell activity within the tumor parenchyma upregulated compared with anti-PD-1 monotherapy. Tumor inhibition was associated with reduced hypoxia and reduced vessel density in the central region of the tumor. These effects correlated significantly with enhanced expression of IFN gamma and PD-L1 in tumors. Taken together, our findings suggest that CU06-1004 is a potential candidate drug capable of improving therapeutic efficacy of anti-PD-1 through beneficial changes in the TME.

Keywords: CU06-1004, anti-PD-1, combination therapy, drug delivery, tumor microenvironment (TME), immune checkpoint blockade (ICB), vascular leakage blocker, cytotoxic T lymphocytes

OPEN ACCESS

Edited by:
Peng Qu,
National Institutes of Health (NIH), United States

Reviewed by:
Nuray Bayar Muluk,
Kırıkkale University, Turkey
Guohao Wang,
National Institutes of Health (NIH), United States

***Correspondence:**
Sang-Jun Ha
sjha@yonsei.ac.kr
Young-Guen Kwon
ygkwon@yonsei.ac.kr

Specialty section:
This article was submitted to Cancer Immunity and Immunotherapy, a section of the journal Frontiers in Immunology

Received: *22 October 2020*
Accepted: *10 December 2020*
Published: *26 January 2021*

Citation:
Park S, Oh JH, Park DJ, Zhang H, Noh M, Kim Y, Kim Y-S, Kim H, Kim Y-M, Ha S-J and Kwon Y-G (2021) CU06-1004-Induced Vascular Normalization Improves Immunotherapy by Modulating Tumor Microenvironment via Cytotoxic T Cells. Front. Immunol. 11:620166. doi: 10.3389/fimmu.2020.620166

INTRODUCTION

Immunotherapy is an innovative way of treating cancers. However, response rates and effects vary among tumors expressing specific biomarkers (1, 2). Therefore, immunosuppression may be a critical factor contributing to tumor growth (3). Tumors can also evade T cells by expressing immunosuppressive molecules or receptors, such as programmed death-ligand 1 (PD-L1) (4). Programmed cell death 1 (PD-1) binds PD-L1 and is expressed on the surface of immune cells, including activated T cells, B cells, monocytes, natural killer (NK) cells, and dendritic cells (5). PD-1/PD-L1 interactions trigger intracellular signaling, preventing immune cell activation and cytokine secretion (6). Immune checkpoint blockade (ICB) targeting PD-L1/PD-1, galectin-9/TIM-3, IDO1, LAG-3, and CTLA4 seeks to increase the number and activity of CTLs in tumors (7). These therapies share some properties but commonly face drug delivery challenges (8, 9). Enhanced delivery technologies, increased interactions of drugs with target proteins, and reduced extratumoral drug release, may improve efficacy (10).

The solid tumor microenvironment (TME) is a major cause of tumor progression and treatment resistance (11). Oncotic pressure, acidosis, and hypoxia interfere with normal functions and promote immunological and metabolic changes (12, 13). TME changes are strongly associated with abnormalities in tumor vessels, including reduced vascular density and structurally disordered expansion (14). These changes may result in hyper-permeable vasculature (15). Endothelial cells support tumor cell apoptosis by accommodating the movement of CTLs and oxygen to the TME (16). Immunosuppression created by the abnormal TME vasculature cannot be modified by anti-PD-1 therapy (17), which may restore TME structure but does not abolish blood vessels (18). Thus, vascular stabilization by cancer treatment may increase the efficacy of immunotherapy by normalizing blood vessel perfusion (19).

CU06-1004 is a small molecule that sustains vascular stabilization and prevents endothelial loss (20–22). CU06-1004 forms cortical actin rings through cAMP/Rac/Cortactin and strengthens the endothelial barrier, inhibiting vascular leakage (20). In addition, CU06-1004 regulates various factors such as vascular endothelial growth factor (VEGF), histamine, and thrombin and decreases IL-1β cytokine level. CU06-1004 also reduces vascular hyper-permeability and tumor hypoxia (21). In an *in vivo* model of ischemic stroke, injection of CU06-1004 inhibited IL-1β-induced endothelial permeability and NF-κB activation, significantly reducing neurological deficits, cerebral infarction, and glial activation (22). Additionally, in a model of tumor angiogenesis, CU06-1004 normalized the tumor vasculature and improved delivery and efficacy of the anti-angiogenesis drug sunitinib (20). This drug combination, which directly regulates expression of vascular junction proteins, pericytes, and smooth muscle actin to induce vascular normalization, may overcome tumor progression and treatment resistance (20). Surprisingly, CU06-1004 injection improved direct drug delivery to tissue by blocking disruption of vascular structure and maximizing binding to target proteins (20–22).

Here, we examine the impact of CU06-1004, an endothelial dysfunctional blocker, on the TME in MC38 tumor models in combination with an anti-PD-1 antibody. We demonstrate that direct drug delivery of CU06-1004 results in tumor-infiltrating immune cell populations containing NK and T cells and tumor apoptosis induced by increased $CD8^+$ T cell activity. Analysis of tumor cytokines showed that IFNγ expression was highly regulated within the TME. Conversely, NK and T cell depletion experiments showed that the $CD8^+$ T cell population in the tumor was important for the combination of CU06-1004 and ICB therapy. Our findings indicate that CU06-1004, which blocks endothelial dysfunction, improves efficacy of ICB in the TME compared with anti-PD-1 therapy alone.

Abbreviations: 1004, CU06-1004; αPD-1, anti-PD-1; TME, tumor microenvironment; IFNγ, interferon gamma; TNFα, tumor necrosis factor-alpha; IL-1β, interleukin-1 beta; IFNα& β, interferon alpha & beta; IL-10, interleukin-10; GAPDH, glyceraldehyde 3-phosphate dehydrogenase; VE-cad, vascular endothelial cadherin; α-SMA, alpha-smooth muscle actin; NG2, neuron-glial antigen 2; Coll IV, collagen IV; HIF1α, hypoxia-inducible factor 1-alpha; PMA, phorbol myristate acetate; STAT1, signal transducer and activator of transcription1; TUNEL, terminal deoxynucleotidyl transferase dUTP nick end labeling.

MATERIALS AND METHODS

Mice

Male C57BL/6 mice, aged 7–8 weeks, were purchased from DBL Korea under semi-SPF conditions. All experiments were approved by the committee (IACUC-A-20201015-117).

Drugs

Anti-PD-1 immunotherapy (*InVivo*MAb anti-mouse PD-1 (CD279); RMP1-14; BE0146) and IgG2a control antibody (*InVivo*MAb rat IgG2a isotype control; 2A3; BE0089) were purchased from BioXcell Korea. A stock solution of anti-PD-1 and isotype control (2 mg/ml) in PBS was used for dilutions. CU06-1004 was previously reported (20–22). To synthesize CU06-1004, a tetrahydropyran analog was prepared by reacting dihydropyran and pregnenolone in p-toluenesulfonic acid. After Wittig olefination using 4- (carboxybutyl) triphenylphosphonium bromide, acid-moiety methylation was performed by trimethylsilyl diazomethane. CU06-1004 was synthesized *via* tetrahydropyran deprotection with subsequent glycosidation with 4, 6-di-O-acetyl-2, 3-didieoxyhex-2-enopyran in the presence of acid (23).

Cell Culture

MC38 colon adenocarcinoma cells (kind gift from Prof. Sang-Jun Ha; Yonsei University, Seoul, Korea) were cultured in complete Dulbecco's modified Eagle's media (DMEM; Hyclone; SH30022.01) supplemented with 10% fetal bovine serum (FBS; GE Healthcare UK Ltd) and 1% penicillin/streptomycin (Gibco Laboratories) at 37°C in a 5% CO_2 incubator in a humidified atmosphere.

In Vivo Models

Tumors were subcutaneously implanted into the right flanks of 7- to 8-week-old C57BL/6 mice. Tumor volumes were measured every 2 or 3 days according to the formula (0.523 x (length x

width^2)). The drug was injected approximately 1 week after the tumor was implanted.

Anti-PD-1 and CU06-1004 Treatment

*InVivo*Mab rat IgG2a isotype control antibody 200 μg/dose was injected intraperitoneally (i.p.) in vehicle and CU06-1004-alone groups on days 0, 3, and 6 after all tumors were visible. Similarly, *InVivo*Mab anti-mouse PD-1 antibody 200 μg/dose was injected i.p. in the anti-PD-1-alone and combination anti-PD-1 plus CU06-1004 groups on days 0, 3, and 6 after all tumors were visible. CU06-1004 1mpk (1 mg/kg) was injected intravenously (i.v.) in the CU06-1004-alone and combination group during daily a week at the same time point as the anti-PD-1 drug.

Immunofluorescence Staining

Mice were anesthetized with i.p. 2.5% avertin and then perfused with 50 ml PBS or saline *via* the left ventricle of the heart. Whole tumors were collected, fixed with 4% paraformaldehyde (PFA) for 16 hours (h), dehydrated in 15% sucrose solution, and followed by a 30% sucrose solution until tumors sank to the bottom of the container. Mouse tumor tissues were sectioned 20–30 μm thick using a cryostat (Leica, Wetzlar, Germany). One of every 7 to 10 slices was collected. Sections were stored at -80°C. To examine vascular leakage, tumor tissue slices were permeabilized in 0.5% PBS Triton X-100 (PBST) for 5 minutes (min), incubated in blocking solution at room temperature (RT) for 1 h, and incubated with primary antibodies for double staining of CD31/PECAM1 (R&D systems; AF3628; 1:200, Santa Cruz, SC-1506; 1:200) with VE-cadherin (Santa Cruz; SC-9989; 1:200), α-SMA (Abcam; ab7817; 1:200), NG2 (Millipore; 92950; 1:200), or collagen IV (Millipore; 1982483; 1:200) at 4°C for 16 h and then at RT for 1 h. To examine increased T cells in the tumor, double staining of CD31/PECAM1 with CD8 (Abcam; ab22378; 1:200) or CD3 (Abcam; ab16669; 1:200) was performed at 4°C for 16 h and then at RT for 1 h. After washing, slides were incubated with the appropriate Alexa-Flour 488-, 594-conjugated secondary antibodies (1:500) at RT for 1 h. For nuclear staining, slides were treated with DAPI (1:1000) for 20 min before mounting. Immunofluorescence was imaged using confocal microscopy (Carl Zeiss 700, Germany). Quantification of fluorescence intensity and cell counting were performed using Image J (NIH) or Photoshop version CS6 (Adobe Systems, San Jose, CA). Data represent twice independent experiments.

Phycoerythrin-Anti-PD-1 Staining

CU06-1004 was injected daily i.v. for a week in the CU06-1004-treated group, and PE anti-mouse CD279 (PD-1) (BioLegend; RMP1-14; 114118) 100 μg/dose was injected i.v. in vehicle and CU06-1004-alone groups. Mice were harvested and perfused on day 7. All tumors were fixed in 4% PFA and dehydrated in 15% sucrose solution, 30% sucrose solution, and followed by sectioning (20–30 μm thick). Nuclei in tumor tissue slices were stained with DAPI (1:1000) for 20 min and mounted. Immunofluorescence was imaged using confocal microscopy (Carl Zeiss 700, Germany). Quantification of fluorescence intensity and cell counting were performed using Image J (NIH).

In Situ Apoptosis Detection

Fresh tumor tissue was immediately frozen in optimal cutting temperature (OCT) compound and sectioned onto a *silanized slide*. Tumor tissue slices were washed with PBS for 20 to 30 min. Labeling reaction mixture plus 100 μl permeabilization buffer was maintained on ice for 2 to 5 min. The labeling reaction mixture (50 μl) consisting of 5 μl TdT enzyme and 45 μl labeling-safe buffer was incubated on the slide at 37°C for 60 to 90 min. To prevent drying, the glass slide was covered with a plastic coverslip. The reaction was terminated, and the slide was washed 3 times in PBS for 5 min each time. The tumor tissue slide was analyzed by confocal microscopy (Carl Zeiss 700, Germany).

Cell Preparation

Cells from spleen and peripheral blood were isolated as described (24). Spleens were passed through a 70-μm cell strainer (BD Falcon), and red blood cells were lysed using ACK lysing buffer (Gibco Laboratories). Peripheral blood from the retro-orbital sinus was underlaid with Histopaque-1077 (Sigma-Aldrich). The gradient was centrifuged at 2000 rpm without braking for 20 min at 20°C, and mononuclear cells were recovered from the interface. To isolate tumor-infiltrating lymphocytes, tumors were removed, weighed, and chopped into small pieces. Following incubation in 1 mg/ml collagenase IV (Worthington Biochemical Corp.) and 0.01 mg/ml DNase (Sigma-Aldrich) in RPMI containing 10% FBS and 1% penicillin/streptomycin at 37°C for 30 min, digested cells were passed through a 70-μm cell strainer (BD Falcon), and red blood cells were lysed using ACK lysing buffer (Gibco Laboratories). After washing with RPMI containing 2% FBS and 1% penicillin/streptomycin, cells were counted using a hemocytometer.

Flow Cytometry and Antibodies

For flow cytometry analysis, cells in single-cell suspension were plated in each well of 96-well plate(round-bottom) which also contains PBS consisting of 2% FBS. The cells were stained with fluorochrome-conjugated antibodies for 20 min in 4°C. Antibodies used for cell labelling were BV605 anti-CD45.2 (BioLegend Cat. No. 109841, clone: 104), BV421 anti-CD4 (BioLegend Cat. No. 100544, clone: RM4-5), BV421 anti-CD11c (BioLegend Cat. No. 117329, clone: N418), APC anti-PD-L1 (BioLegend Cat. No. 124312, clone: 10F.9G2), PerCP-Cy5.5 anti-CD107a (BioLegend Cat. No. 121626, clone: 1D4B), PE-Cy7 anti-CD25 (eBioscience Cat. No. 25-0251-82, clone: PC61.5), PE-Cy7 anti-CD8a (eBioscience Cat. No. 25-0081-82, clone: 53-6.7), PerCP-Cy5.5 anti-CD8a (eBioscience Cat. No. 45-0081-82, clone: 53-6.7), FITC anti-F4/80 (eBioscience Cat. No. 11-4801-82, clone: BM8), PE anti-Foxp3 (eBioscience Cat. No. 12-4771-80, clone: NRRF-30), PE-Cy7 anti-CD11b (BD Biosciences Cat. No. 552850, clone: M1/70), APC anti-NK1.1 (BD Biosciences Cat. No. 554420, clone: PK136), PerCP-Cy5.5 anti-Ly6G (BD Biosciences Cat. No. 565797, clone: 1A8), Alexa Fluor 488 anti-Ki-67 (BD Biosciences Cat. No. 561165, clone: B56), PE anti-NK1.1 (BD Biosciences Cat. No. 553165, clone: PK136) FITC anti-IFNγ (BD Biosciences Cat. No. 554411, clone: XMG1.2), and APC anti-

TNF (BD Biosciences Cat. No. 554420, clone: MP6-XT22). The LIVE/DEAD fixable dead cell stain kit (Invitrogen) was used to remove the dead cell population in all staining procedures. Additionally, for intracellular staining process, cells were first stained with surface antigens followed by permeabilization and fixation with either Foxp3 Fixation/Permeabilization Kit and Protocol (eBioscience) or Cytofix/Cytoperm Kit (BD Biosciences) according to the manufacturer's instructions before the appropriate antibodies were added. All the stained samples were analyzed using FACSCantoII instrument (BD Biosciences) and FlowJo software (Tree Star).

Cytokine Analysis

To detect cytokines, spleen and tumor cells were either stimulated with MC38 epitope peptide (p15E, KSPWFTTL) or with 25 ng/ml phorbol myristate acetate (PMA) and 1 μM ionomycin (Sigma-Aldrich) in the presence of Golgi plug/Golgi stop (BD Biosciences) and CD107a (BioLegend; clone: 1D4B) antibody at 37°C for 5 h. Subsequently, surface staining was performed, and cells were permeabilized with Cytofix/Cytoperm Kit (BD Biosciences) solution to stain intracellular cytokines.

Reverse Transcriptase-Polymerase Chain Reaction and Quantitative PCR

Tumor tissue was harvested in 1 ml Trizol and stored at −80°C until processing. Total RNA was isolated from tumor tissues, and cDNA was synthesized using Moloney murine leukemia virus reverse transcriptase. RT-PCR was performed with a cDNA template, primer, dNTP, 10χ buffer, and Taq polymerase. And qRT-PCR was performed with SYBR Green (Invitrogen) in a Bio-Rad real-time PCR detection system. Data represent three independent experiments. Primers were: *Ifnγ*, 5'-GCTTTGCAG CTCTTCCTCAT-3', 5'-GTCACCATCCTTTTGCCAGT-3; *Tnfα*, 5'-CCAGACCCTCACACTCACAA-3', 5'-GTGGGTG AGGACACGTAGT-3; *Il-1β*, 5'-GGGCCTCAAAGGAAA GAATC-3', 5'-TACCAGTTGGGGAACTCTGC-3'; *Ifnα&β*, 5'-ATGGGCAGTGTGACCTTTTC-3', 5'-CCCTTCCTCTGCT CTGACAC-3'; *Tgfβ*, 5'-TGCGCTTGCAGAGATTAAAA-3', 5'-CTGCCGTACAACTCCAGTGA-3'; *Gapdh*, 5'-ACCCAGAAG ACTGTG GATGG-3', 5'-CACATTGGGGGTAGGAACAC-3'.

Western Blotting

Tumor tissues were washed with cold PBS, harvested in cytosolic buffer (10 mM Tris [pH 7.5], 0.05% NP-40, 3 mM MgCl2, 100 mM NaCl, 1 mM EGTA, 1 mM Na3VO4), and centrifuged at 15,000 rpm for 15 min. After centrifugation, nuclei were pelleted and suspended in nuclear buffer (1 mM EDTA, 3.5% SDS, 10% glycerol, and 70 mM Tris-Cl) as previously described. Proteins were separated by SDS polyacrylamide gel electrophoresis. Immunoblotting was performed with antibodies to VE-cadherin, α-SMA, pSTAT1, STAT1, PD-L1, and β-actin (Santa Cruz Biotechnology, Santa Cruz, CA). Data represent three independent experiments.

In Vivo Depletion of Immune Cells

To deplete NK, CD4+, or CD8+ T cells, 200 μg *InVivo*MAb anti-mouse NK1.1 (BioXCell; PK136; BE0036), 200 μg *InVivo*MAb anti-mouse CD4 (BioXCell; GK1.5; BE0003-1) or 200 μg *InVivo*MAb anti-mouse CD8a (BioXCell; 2.43; BE0061) was injected i.v. twice for 2 weeks before tumor injection and before drug injection. Depletion was evaluated by flow cytometry 7 days after drug treatment. Data represent twice independent experiments.

Live Imaging of Lewis Lung Cancer -Green Fluorescent Protein Tumor-Bearing Mice

A dorsal skinfold chamber model was constructed by injecting $1 \chi 10^6$ LLC-GFP mouse lung carcinoma cells into BALB/c-nu/nu mice. Diameter and density were measured daily in groups injected with drugs and vehicle 7 days after tumor injection, and permeability was measured daily 10 days after tumor injection. Anti-CD31 antibody conjugated to a fluorescent dye was injected i.v. Vessel diameter and density were measured before drug and vehicle treatment and after 4, 24 h, 3, and 7 days. Permeability was measured 4 days after drug or vehicle injection.

In Vitro Cell Cytotoxicity

Cell viability and proliferation were compared by 3- (4,5-dimethylthiazol-2-yl) -2,5-diphenyl tetrazolium-bromide (MTT) assay. MC38 cells were seeded in 24-well plates ($2 \chi 10^4$ cells/well). After treatment with CU06-1004 and anti-PD-1 or isotype control, cells were maintained for 48 h in media containing 0.2% FBS. MTT (0.5 mg/ml) was added to each well, and cells were incubated at 37°C for 3 h. The supernatant was removed, and 200 μl DMSO + isopropyl alcohol was added to dissolve the formazan product. Absorbance, which is proportional to the number of living cells and proliferation rate, was measured at 540 nm on a microplate reader (FLUOstar Omega, BMG LABTECH). Data represent four independent experiments.

Enzyme-Linked Immunosorbent Assay

To analyze cytokine levels between drug-treated groups, protein was collected from each tumor tissue. Quantification was performed with BCA protein reagent (SMART™ BCA Protein Assay Kit Solution A and B; iNtRON BIOTECHNOLOGY; 21071) and RIPA buffer assay (cOmplete ULTRA Tablets; Roche). IFNγ (Mouse IFN-gamma DuoSet ELISA; R&D Systems; DY485) and TNFα (Mouse TNF-alpha DuoSet ELISA; R&D Systems; DY410) were measured by ELISA kit. Data represent three independent experiments.

Survival Analysis

Standard Kaplan–Meier survival analysis was used to determine associations with survival, with 1 indicating alive and 0 dead. Data represent three independent experiments.

Statistical Analysis

Data are presented as mean ± standard error of the mean (SEM). All statistical analyses were performed using GraphPad Prism (version 8; GraphPad Software, La Jolla, CA). The mean difference between groups was analyzed by two-way ANOVA to reveal differences in tumor growth rates. The mean difference between groups was also analyzed by one-way ANOVA. $^*p < 0.05$; $^{**}p < 0.01$; $^{***}p < 0.001$; $^{****}p < 0.0001$. ns, not significant.

RESULTS

CU06-1004 Aids Anti-PD-1-Mediated Tumor Growth Inhibition and Overall Survival

To observe the synergistic effect of using immune checkpoint blockade drug and CU06-1004, which is a drug known for its high ability to normalize blood vessel, we conducted monotherapy or combinatory therapy to MC38 tumor-bearing mice with anti-PD-1 and CU06-1004. Four different treatment groups were decided depending on types of drug administered (**Figure 1A**). As treatment began, tumor volumes were measured, and some mice were sacrificed seven days after the day of initial treatment to further measure the tumor weight difference. The growth of tumor volume between these groups of mice showed that the combination therapy effectively controlled the tumor progression compared to the other three groups (**Figures 1B–D**). Since the tumor volume of mice in combination group were maintained in small volume, the size and the weight were the lowest as well (**Figures 1E, F**). As it can be expected from the increment of tumor volume and weight, the mouse that were treated with both CU06-1004 and anti-PD-1 showed higher survival rate than any other mouse groups (**Figure 1G**). The suppression of tumor growth using combination therapy was also observed when the drugs were administered for longer period of time (**Figure S1A**). In the case of anti-PD-1 monotherapy, the rate of tumor growth increased significantly after 12 days, which indicated loss of drug efficiency. However, in combination group it inhibited the tumor progression considerably (**Figure S1B**). Also looking at the survival outcome, while anti-PD-1 monotherapy did not show any differences between short- and long-term treatment, group that received combination therapy showed noticeable survival benefit even in long-term treatment period (**Figure S1C**). In addition to MC38 tumor model, CT26 tumor model was also used to demonstrate the effect of CU06-1004 in other tumor model that do not respond to anti-PD-1(**Figure S2**). This became the basis for showing the importance of blocking blood vessel leakage and vascular normalization in the early stages in changing the tumor microenvironment.

CU06-1004 Obstructs Vascular Collapse by Maintaining Blood Vessel Structure and Prevents Uncontrolled Angiogenesis Within Central Tumor Region in MC38 Tumors

Tumor regression observed in combination group showed that CU06-1004 can complement the effect of anti-PD-1 treatment significantly. Thus, these results prompted us to see if blood vessel normalization effect of CU06-1004 can also be observed in MC38 tumor model which may be the reason for improved immunotherapy response. We previously reported that CU06-1004 inhibits vascular leakage in endothelial cells and maintains stabilization of human umbilical vein endothelial cells (20). The effect of CU06-1004 was measured using immunofluorescence staining and first, the markers for vessel and adherent junctions were selected which included CD31/PECAM1, and VE-Cadherin, respectively. CD31 and VE-Cadherin were clearly detected and seem to form a normal vessel structure only when CU06-1004 is given (**Figure 2A**). Additionally, other markers that are related to vessel structures such as α-SMA, NG2, and collagen IV were measured. The fluorescent figures indicate that intact vessel structures are present only in groups that are treated with CU06-1004 (**Figures 2B–D**). To further confirm these fluorescent data, western blot was conducted and showed significant increase in VE-Cadherin and a-SMA (**Figure 2E**). Lastly, by injecting Evans blue into the tumor tissue of CU06-1004 untreated and treated group, 20-s time-lapse movie was made. The perfusion of Evans blue into the vessels showed that in CU06-1004 treated group, the chemical is dispersed following the blood vessel without any leakage (**Figure S3** and **Figure SV1**). These results showed that vascular leakage was prevented by inhibiting structural deformation. Treating CU06-1004 not only kept the vessels intact but also seem to have prevented abnormal and uncontrolled angiogenesis. Vessel density within the tumor central region was significantly decreased when CU06-1004 was treated. In contrast, the blood vessel density in peripheral region did not show any difference (**Figures 2F, G**). Since the abrupt angiogenesis and vessel breakage were prevented, we postulated that transportation of substances such as oxygen would be more effective. In fact, assessment of HIF1α protein marker which indicates hypoxia level showed that the level of hypoxia decreased in CU06-1004 treated group (**Figure 2H**).

Effective Trafficking of Anti-PD-1 Drug Through Normalized Blood Vessels Expands Tumor Infiltrated Lymphocytes

Next, in order to see whether tumor vessel normalization induced by CU06-1004 enhanced the infiltration of lymphocyte from periphery into tumor central region, we conducted flow cytometry analysis of tumor infiltrating lymphocyte (TIL) retrieved from mice sacrificed at 7 days after the treatment. Compared to the control group, the percentage of CD4, CD8 and NK cells was significantly increased in the anti-PD-1 monotherapy group and combination treatment group, but not in the CU06-1004 monotherapy group. Additionally, the comparison between anti-PD-1 monotherapy group and combination therapy group showed increased frequency of CD8 T cell in combination treatment group, excluding CD4 and NK cells (**Figure 3A**). Immunofluorescence staining data also supported the flow cytometry data by showing accumulation of $CD3^+$ and $CD8^+$ T cell in tumor site in anti-PD-1 monotherapy group and combination treatment group, but not in the monotherapy group. (**Figures 3B, C**). The frequency of T cell in the tumor center region with many abnormal blood vessels showed a significant difference by combination treatment, but the frequency of T cell in the relatively stable structure of the tumor periphery region did not show a significant difference between groups (**Figure 3B** and **Figure S4**). In contrast to the effective transportation of oxygen to the tumor site through normalized blood vessels (**Figure 2**), the accumulation of T cells

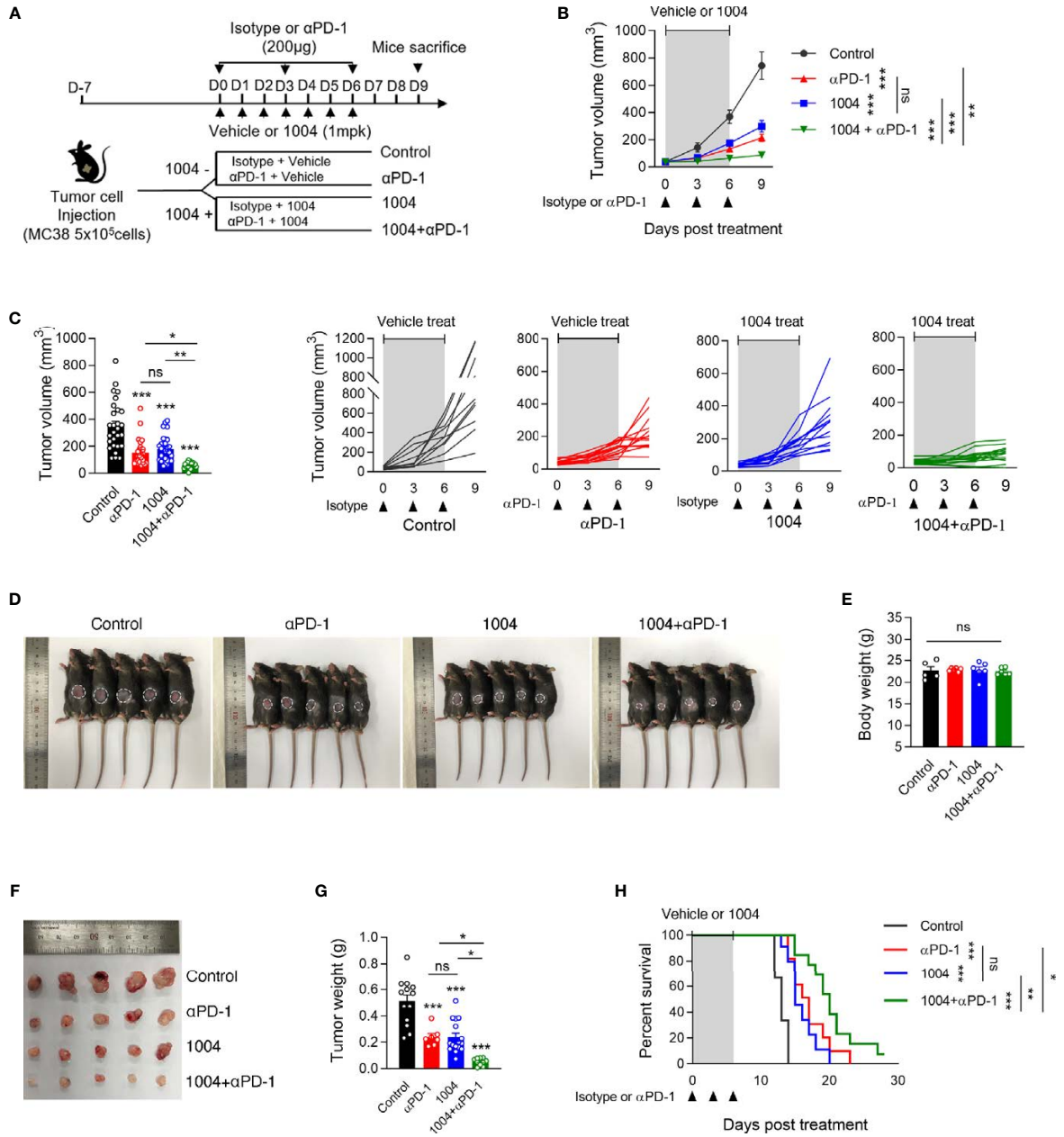

FIGURE 1 | Combined Vascular leakage blocker, CU06-1004 and anti-PD-1 delayed MC38 tumor growth and extended mice survival. MC38 tumor cells (5×10^5 cells/mouse) were injected subcutaneously into the right flank of C57BL/6 mice. At 7 days post tumor inoculation (tumor size <100 mm^3), tumor-bearing mice were treated with control IgG, anti-PD-1, CU06-1004, or anti-PD-1 + CU06-1004. The control IgG or anti-PD-1 was treated 200ug intraperitoneally once every 3 days (total 3 times), and CU06-1004 was treated intravenously at 1 mg/kg daily. **(A)** Schematic diagram depicting treated schedule for the MC38 tumor-bearing mice model. **(B, C)** Tumor size was measured every 3 days from the start of the treatment. Growth curve graphs show mean (top) and individual (bottom) tumor growth and bar graphs show tumor volume on 6-days post treatment. B, n = 10–14 per group and C, n = 23–28 per group (Data are pooled from three B, or six C, independent experiments). Statistical analysis by two-way B, or one-way C, ANOVA with Tukey's multiple comparisons. **(D, E)** At 7 days post treatment, Body weight were measured from each group of mice. Scale bars indicate 1 cm. n = 5-6 per group (Data are representative of at least four independent experiments). Statistical analysis by one-way ANOVA with Tukey's multiple comparisons. **(F, G)** At 7 days post treatment, tumor weight were measured from each group of mice. Scale bars indicate 1 cm. n = 7–16 per group. Statistical analysis by one-way ANOVA with Tukey's multiple comparisons. **(H)** Kaplan-Meier survival curves of MC38 tumor-bearing mice treated as indicated. Mice were euthanized when the mean tumor size reached 2000mm^3. n = 9-13 per group. *$p < 0.05$; **$p < 0.01$; ***$p < 0.001$. ns, not significant. Data represent ± SEM.

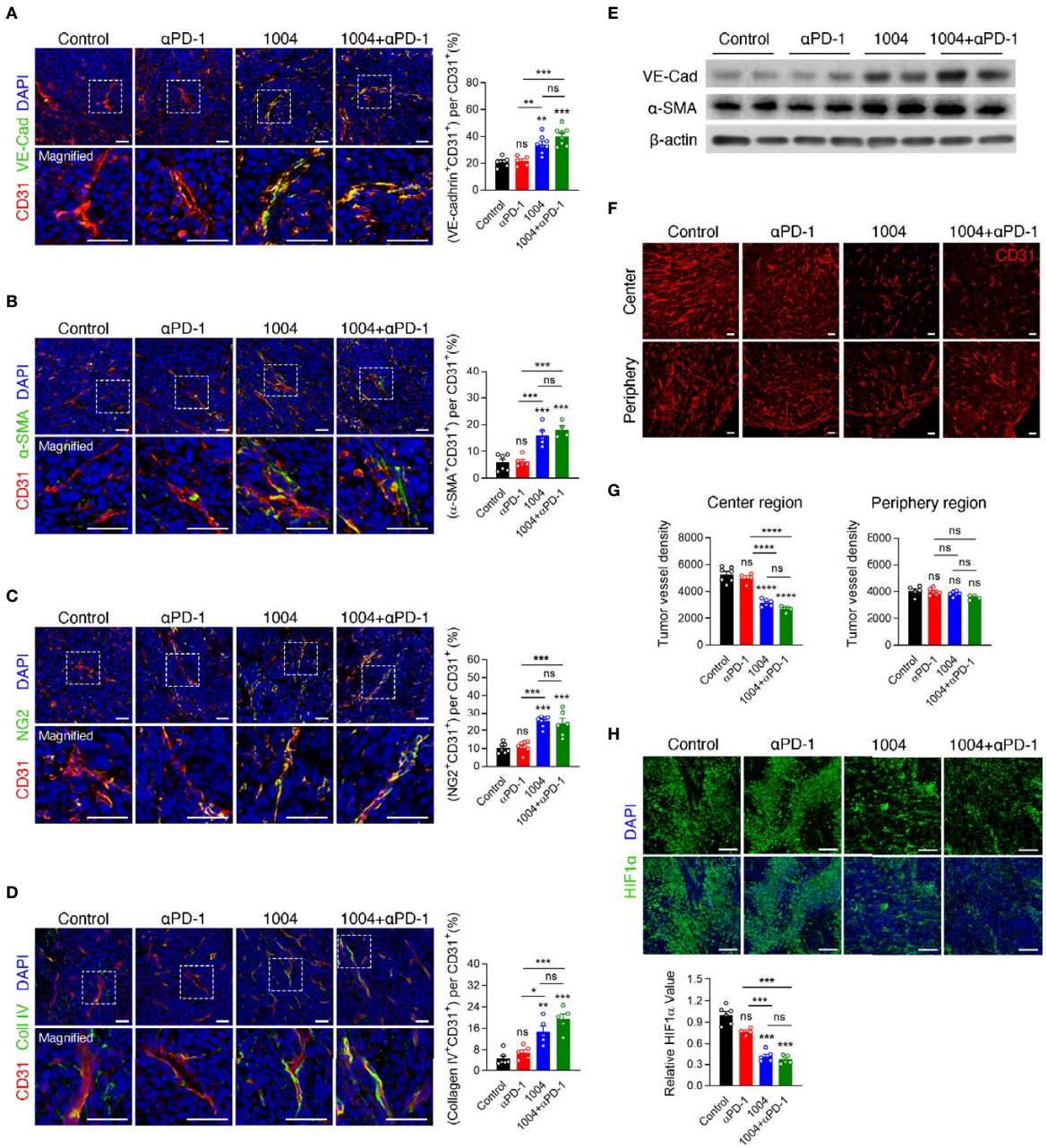

FIGURE 2 | CU06-1004 improved tumor vascular normalization and decreased hypoxia and abnormal vessel density. **(A)** Representative immunofluorescence staining for adherent junction coverage (the ratio VE-cadherin$^+$CD31$^+$/CD31$^+$ area) on day 7. Red, CD31 staining; green, VE-cadherin staining; blue, DAPI staining, Scale bars; 20 μm. *n* = 5-8 per group. Statistical analysis by one-way ANOVA with Tukey's multiple comparisons. **(B)** Representative immunofluorescence staining for α-smooth muscle actin coverage (the ratio αSMA$^+$CD31$^+$/CD31$^+$ area) on day 7. Red, CD31 staining; green, αSMA staining; blue, DAPI staining, Scale bars; 20 μm. *n* = 4-6 per group. Statistical analysis by one-way ANOVA with Tukey's multiple comparisons. **(C)** Representative immunofluorescence staining for pericyte coverage (the ratio NG2$^+$CD31$^+$/CD31$^+$ area) on day 7. Red, CD31 staining; green, NG2 staining; blue, DAPI staining, Scale bars; 20 μm. *n* = 6-8 per group. Statistical analysis by one-way ANOVA with Tukey's multiple comparisons. **(D)** Representative immunofluorescence staining for collagen IV (the ratio Collagen IV$^+$ CD31 $^+$/CD31$^+$ area) on day 7. Red, CD31 staining; green, Collagen IV staining; blue, DAPI staining, Scale bars; 20 μm. *n* = 5-6 per group. Statistical analysis by one-way ANOVA with Tukey's multiple comparisons. **(E)** Western blotting for adherent junction protein of VE-cadherin and αSMA protein in tumor tissue on day 7. **(F)** The entire blood vessel density was stained in the tumor center region and periphery region. Red, CD31 staining, Scale bars; 100 μm. **(G)** Quantification of the vessel density in the MC38 tumor center region and periphery region. *n* = 4–7 per group. Statistical analysis by one-way ANOVA with Tukey's multiple comparisons. **(H)** Representative images of HIF1α$^+$ area in core tumor region on day 7. Green, HIF1α staining; blue, DAPI staining, Scale bars; 100 μm. Quantification of the hypoxic area on day 7. *n* = 4-6 per group. Statistical analysis by one-way ANOVA with Tukey's multiple comparisons. **p* < 0.05; ***p* < 0.01; ****p* < 0.001; *****p* < 0.0001. ns, not significant. Data represent ± SEM.

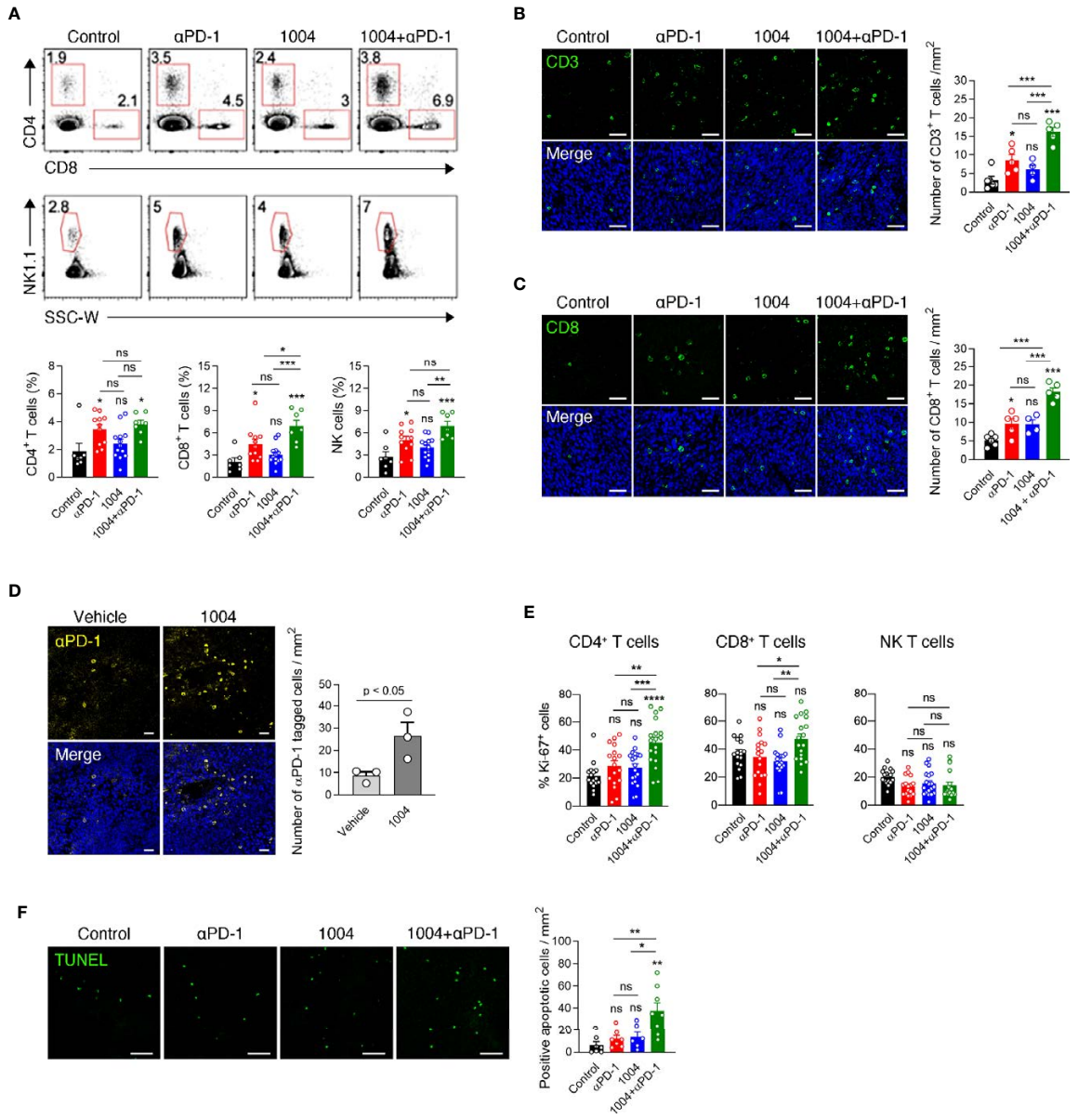

FIGURE 3 | Combined CU06-1004 and anti-PD-1 treatment promotes the accumulation of specific $CD8^+$ T cells and apoptosis in tumors. **(A)** Flow cytometry analysis of the $CD4^+$($CD45.2^+CD3^+NK1.1$-$CD8$-$CD4^+$), CD8+ ($CD45.2^+CD3^+NK1.1$-$CD8^+CD4$-), T and NK cells ($CD45.2^+CD3$-$NK1.1^+$), in subcutaneous MC38 tumors from each group of mice on 7 days post treatment. Numbers in the representative flow cytometric plots indicate the percentages of each cell type among CD45.2+ cells. Data are pooled from two independent experiments (Control, $n = 7$; αPD-1, $n = 11$; CU06-1004, $n = 13$; Combination, $n = 7$). Statistical analysis by one-way ANOVA with Tukey's multiple comparisons. **(B)** Representative immunofluorescence staining for $CD3^+$T cells infiltration in the center region on day 7. Green, CD3 staining; blue, DAPI staining, Scale bars; 50 μm. Quantification of infiltrated T cells on day 7. $n = 4$–6 per group. Statistical analysis by one-way ANOVA with Tukey's multiple comparisons. **(C)** Representative immunofluorescence staining for $CD8^+$ T cells infiltrating MC38 tumor on day 7. Red, CD31 staining; green, CD8 staining; blue, DAPI staining, Scale bars; 50 μm. Quantification of infiltrated $CD8^+$ T cell numbers in MC38 tumor on day 7. $n = 4$–6 per group. Statistical analysis by one-way ANOVA with Tukey's multiple comparisons. **(D)** Representative immunofluorescence staining for PE-conjugated anti-PD-1 in the tumor on day 7. Yellow, PE-anti-PD-1; blue, DAPI staining, Scale bars; 20 μm. PE-conjugated anti-PD-1 intravenously treated one day before harvesting a tumor. $n = 3$ per group. Statistical analysis by one-way ANOVA with Tukey's multiple comparisons. **(E)** Representative graph showing the percentages of Ki-67^+ cells among $CD4^+$, $CD8^+$ T and NK cells. Data are pooled from five independent experiments (Control, $n = 16$; αPD-1, $n = 17$; CU06-1004, $n = 19$; Combination, $n = 18$). Statistical analysis by one-way ANOVA with Tukey's multiple comparisons. **(F)** Representative immunofluorescence staining for apoptotic areas in the tumor on day 7. Green, TUNEL staining, Scale bars; 50 μm. $n = 6$–8 per group. Statistical analysis by one-way ANOVA with Tukey's multiple comparisons. $^*p < 0.05$; $^{**}p < 0.01$; $^{***}p < 0.001$. ns, not significant. Data represent ± SEM.

in tumor site between the CU06-1004 monotherapy group and the control group was slight difference, indicating that CU06-1004 treatment alone does not lead to significant infiltration of immune cells into tumor site. Thus, we hypothesized that treatment of CU06-1004 allows the trafficking of anti-PD-1 into tumor central region *via* normalized vessels which leads to the expansion of tumor infiltrated lymphocytes instead of increasing the ability of effective infiltration of immune cells. To assess the trafficking efficacy of anti-PD-1 drug *via* normalized blood vessel, immunofluorescence staining was conducted with tumor tissue that was injected with PE-tagged anti-PD-1 antibody at the 6 days instead of anti-PD-1 treatment. Based on the data, more anti-PD-1 drug was detected in CU06-1004 treated group than that of control group and anti-PD-1 antibody implied that vessel normalization by CU06-1004 treatment induces increased trafficking of drug to the lymphocyte within the tumor site. (**Figure 3D**). Since anti-PD-1 drug has been known to rejuvenate and induce expansion of lymphocyte within tumor, the proliferation of T cells was assessed by analyzing Ki67 expression level. As expected, the increased Ki67 expression level of T cells in combination treatment group was observed which indicated proliferation of T cells by anti-PD-1 drug (**Figure 3E**). Additionally, TUNEL assay was conducted and the results indicated that the number of apoptotic cells were increased in combination therapy group which suggests that increment of cytolytic immune cells could lead to induction of apoptosis in cancer cells (**Figure 3F**). Additionally, neither CU06-1004 nor anti-PD-1 alone affected tumor cell viability (**Figure S5**).

Combination Therapy Enhances the Function of Tumor Infiltration CD8$^+$ T Cells

Increased frequency of CD8$^+$ T cells within the tumor of combination therapy group led us to analyze the functionality of TIL by measuring intracellular cytokines and cytotoxic marker CD107a. Lymphocytes from spleen and tumor were re-stimulated with either p15E peptide, which is a known CD8$^+$ T cell-specific antigen of MC38 tumor, or with PMA and Ionomycin. Although the expression level was not significant between anti-PD-1 and combination group, stimulating these two groups of spleen cells with p15E showed statistically significant IFNγ expression compared to control group. In contrast to the splenocytes, when tumor infiltrated lymphocytes (TIL) are stimulated with p15E, much higher percentage of IFNγ and CD107a expressing cells were observed. Also, TILs retrieved from combination therapy group showed the highest frequency of IFNγ$^+$ and IFNγ$^+$CD107a$^+$CD8$^+$ T cells compared to other treatment groups (**Figure 4A**). These results indicate that combination therapy allows tumor antigen-specific T cells to be maintained in the tumor site while keeping their cytolytic activity and restrains from entering exhausted state. Stimulating the same immune cells with PMA and Ionomycin showed similar trend compared to p15E peptide stimulation. In splenic T cells, although every group expressed quite amount of IFNγ as PMA/Ionomycin was treated, the combination treatment group showed evidently higher percentage of expression. IFNγ, TNFα and CD107a expression levels in TILs were dramatically increased compared to expression levels in splenic T cells. In addition, CD8$^+$ T cells in combination treatment group not only higher expression level of IFNγ but also showed higher frequency of CD8$^+$ T cells expressing TNFα or CD107a with higher frequency than CD8$^+$ T cells retrieved from other treatment groups. (**Figure 4B**). In sharp contrast to the effect of combination therapy, monotherapy of either drug had not shown such expression level of cytokines from CD8$^+$ T cells. In addition, expression of IFNγ was also measured in CD4$^+$ T cells and in NK cells in the spleen and tumor. CD4$^+$ T cells in the spleen and tumor did not show a significant difference in IFNγ expression between each group. Similarly, there was no difference in the expression level of IFNγ in NK cells from the spleen, but NK cells retrieved from tumors treated with combination therapy showed some different expression level (**Figure S7A**). These results indicates that many functional CD8$^+$ T cells are present in tumor due to combination therapy of CU06-1004 and anti-PD-1. We also observed high expression level of IFNγ in tumor from combination therapy group by performing RT-PCR, QPCR and ELISA (**Figures 4C, D** and **Figure S6**). Looking at IFNγ down signaling markers by western blot showed that p-STAT1, STAT1 and PD-L1 were prominently higher in combination group where expression level of IFNγ were very high (**Figure 4E** and **Figure S8**). These results indicate that the secretion of IFNγ by T cells in the tumor from combination group is physiologically increased.

CD8$^+$ T Cells Are Directly Involved in Controlling Progression Tumor Growth

Since we have seen that combination therapy led to the expansion of functional CD8$^+$ T cells in the tumor, we sought to determine if tumor suppression is indeed dependent on CD8$^+$ T cells by depleting each immune cell type including CD4$^+$ T, CD8$^+$ T cells, and NK cells. The experiment was conducted using same scheme as previous experiments except depletion antibody was injected twice, once a day before tumor injection and the other on the day before drug injection (**Figure 5A**). After seven days of first depletion antibody injection, we confirmed depletion efficacy of corresponding cell types in PBMC (**Figure 5B**). In combination treatment group, the depletion of any immune cell subtypes led to more rapid tumor growth compared to the non-depleted group, of which the most accelerated tumor growth rate was observed when the CD8+ T cells were depleted (**Figures 5C, D**). Such increment of tumor volume inevitably induced very poor survival rate for the group that was depleted of CD8$^+$ T cells (**Figure 5E**). Additionally, we performed QPCR to determine how changed expression of IFNγ in the combined group was changed after depleting CD4+ T cells, CD8+ T cells, and NK cells. Interestingly, the results showed that the expression of IFNγ, which was increased in the combination group, was significantly reduced in the group depleted of CD8+ T cells, there was no difference in the group depleted of CD4+ T cells, and slightly different in the group depleted of NK cells (**Figure S7B**). Comprehensively, these data illustrate that tumor regression observed when treating both CU06-1004 and anti-PD-1 are caused by CD8$^+$ T cells which were actively participating in controlling the tumor growth.

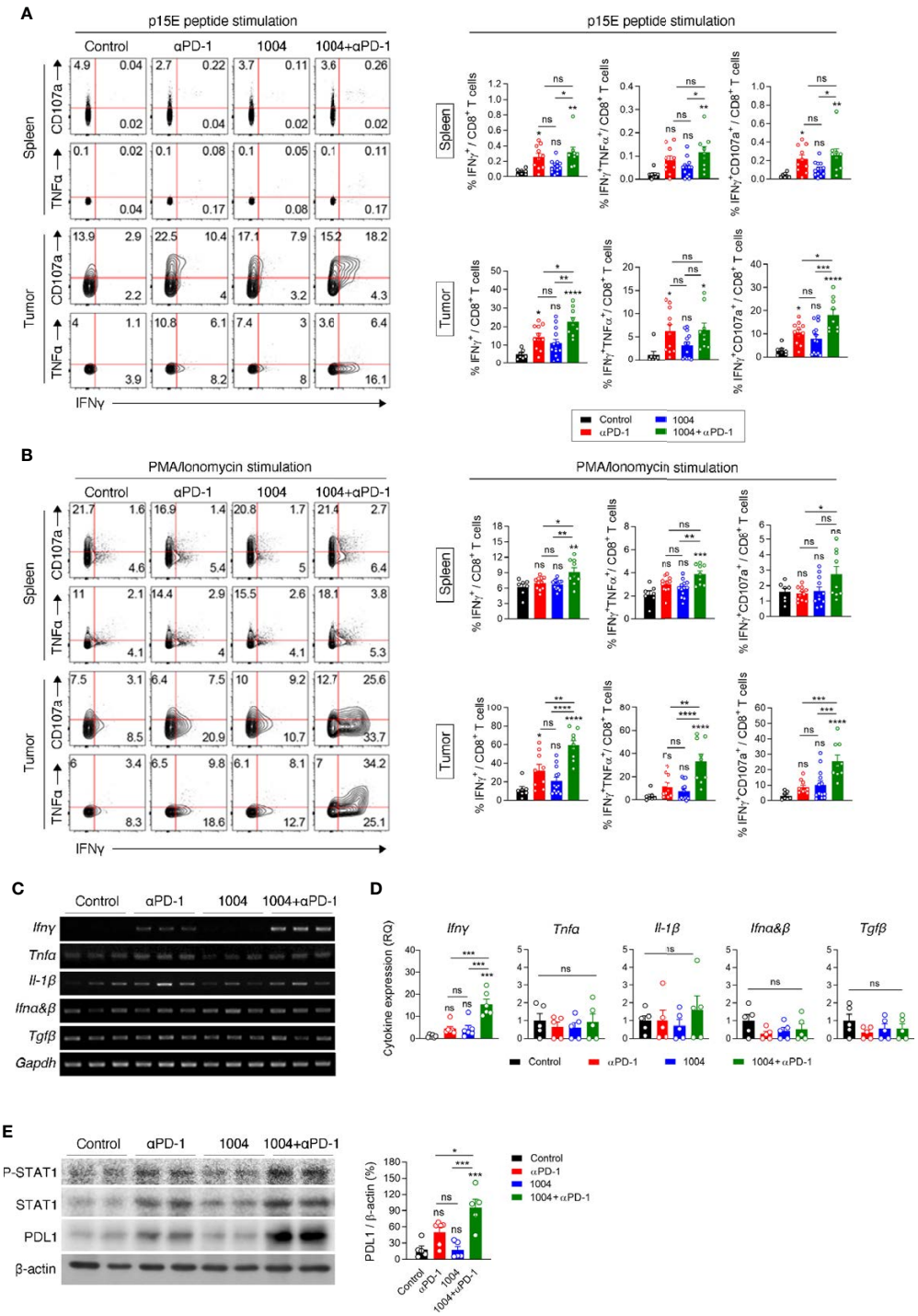

FIGURE 4 | Combination therapy improves tumor specific CD8$^+$ T cell response in spleen and tumor tissue. **(A, B)** Lymphocytes isolated from the spleen and tumor of each group of mice at 7 days post treatment were re-stimulated *in vitro* with MC38 epitope peptide **(A)** or PMA/Ionomycin **(B)**. Representative plots (left) are shown for co-expression of IFNγ and CD107a or IFNγ and TNFα on CD8$^+$ T cells; summarized graph (right) for the frequency of IFNγ$^+$, IFNγ$^+$TNFα$^+$ and IFNγ$^+$CD107a$^+$ cells among CD8$^+$ T cells. Data are pooled from three independent experiments (Control, n = 7; αPD-1, n = 9; CU06-1004, n = 13; Combination, n = 9). Statistical analysis by one-way ANOVA with Tukey's multiple comparisons. **(C)** RT-PCR analysis for cytokine and chemokine expression in tissue after drug-treated tumor harvest. **(D)** qRT-PCR analysis of inflammatory cytokines *Ifnγ, Tnfα, Il-1β, Ifnα&β*, and *Tgfβ* in tumor tissue. n = 5–6 per group. Statistical analysis by one-way ANOVA with Tukey's multiple comparisons. **(E)** Western blotting analysis of p-STAT1, STAT1, and PD-L1 expression in tumor tissue. n = 5-6 per group. Statistical analysis by one-way ANOVA with Tukey's multiple comparisons. *p < 0.05; **p < 0.01; ***p < 0.001; ****p < 0.0001. ns, not significant. Data represent ± SEM.

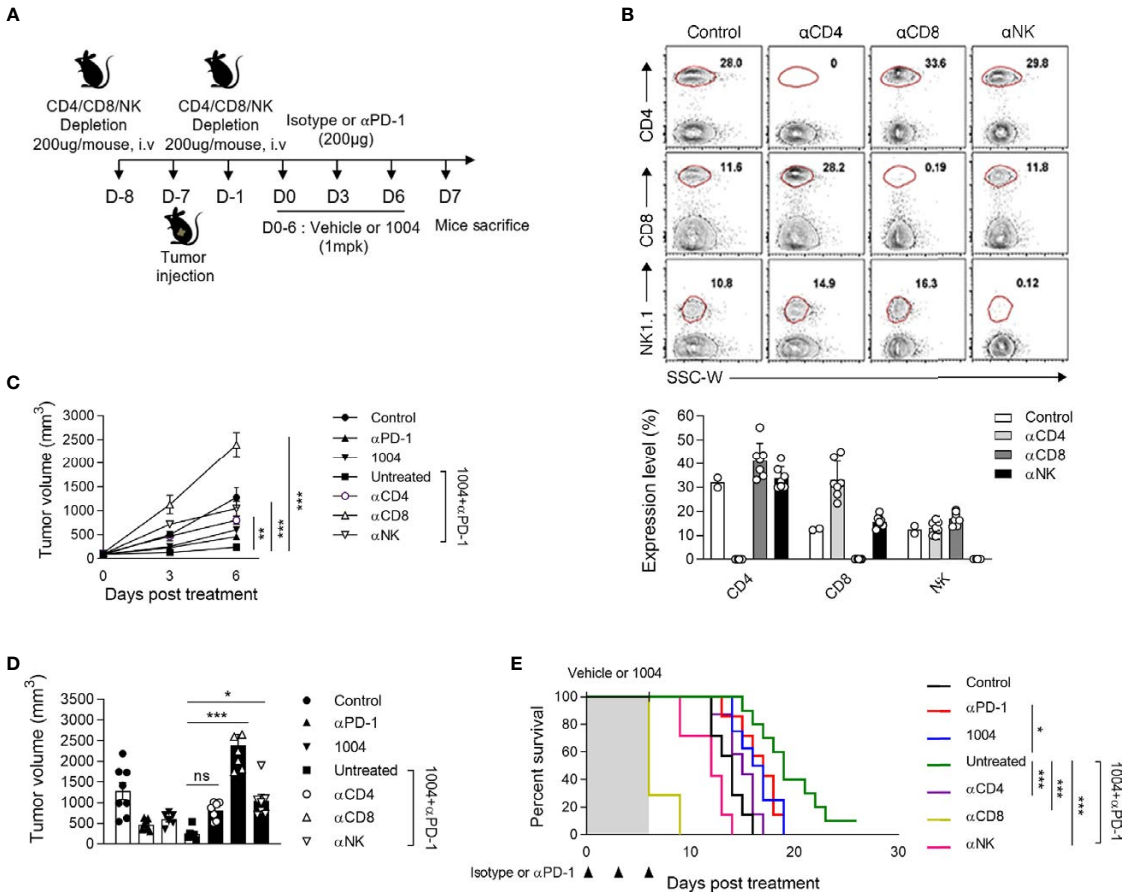

FIGURE 5 | Specific CD8$^+$ T cells are indispensable for suppressing tumor growth by combination therapy. **(A)** αCD4, αCD8 or αNK1.1-depleting mAb was administrated intravenously into each group of mice prior to tumor injection (0.2 mg) and prior to treatment (0.2 mg). **(B)** At day 7 after first depletion, CD4$^+$, CD8$^+$ T cells, and NK cells were analyzed in the PBMC from each group of mice. Representative flow cytometric plots and graphs show the frequencies of CD4$^+$, CD8$^+$ T cells, and NK cells in PBMC. **(C, D)** Tumor size was measured every 3 days from the start of the treatment. Growth curve graphs show mean tumor growth and bar graphs show tumor volume on 6-days post treatment. n = 5–6 per group. Statistical analysis by two-way **(C)** or one-way **(D)** ANOVA with Tukey's multiple comparisons. **(E)** Kaplan-Meier survival curves of MC38 tumor-bearing mice treated as indicated. Mice were euthanized when the mean tumor size reached 2000mm^3. n = 7–10 per group. *p < 0.05; **p < 0.01; ***p < 0.001. ns, not significant. Data represent ± SEM.

DISCUSSION

Cancer immunotherapies that enhance T cells using blocking antibodies are more effective than chemo- or radiotherapy due to low toxicity and higher response rates (2, 25, 26). However, tumor heterogeneity, including PD-L1 expression, anti-PD-1 resistance, and TME, causes variability in treatment response (27). Leaky and hyper-permeable tumor vessels are inefficient in anti-PD-1 antibody delivery, resulting in low infiltration and activation of T cells at the tumor site (28). Despite attempts to overcome immuno-suppression by the TME, the problems remain unresolved (3, 29). In this study, CU06-1004, which normalizes the TME vasculature, was combined with ant-PD-1 immune checkpoint blockade therapy. The modified TME induced T-cell recruitment and activation, which increased the anti-tumor response. This effect was mediated by IFNγ signaling directly induced by cytotoxic CD8$^+$ T cells. These effects may improve current drawbacks of PD-1/PD-L1 treatment by enhancing drug delivery and T-cell infiltration and function. Thus, combination therapy consisting of anti-PD-1 plus CU06-1004 has potential value compared with existing combination therapy (**Figure 6B**).

TME contributes to the abnormal proliferation, angiogenesis, and secretion of chemicals that promote drug resistance and induce vascular leakage and inhibition of drug delivery (15, 30, 31). Tumor vessels are irregular and highly permeable, resulting in intratumoral protein loss and fluid increase (19). Uncontrolled angiogenesis due to vessel breakage creates a favorable environment for tumor progression, including increased hypoxia (13, 32–34). However, when vascular leakage was blocked with CU06-1004 in the B16F10 melanoma mouse model, vessels were normalized, reducing hypoxia (20). Combination treatment with other anti-tumor drugs, such as doxorubicin and sunitinib, reduced tumor progression (20). Based on this observation, we used the MC38 tumor model, which is respond to anti-PD-1 therapy, and the CT26 tumor

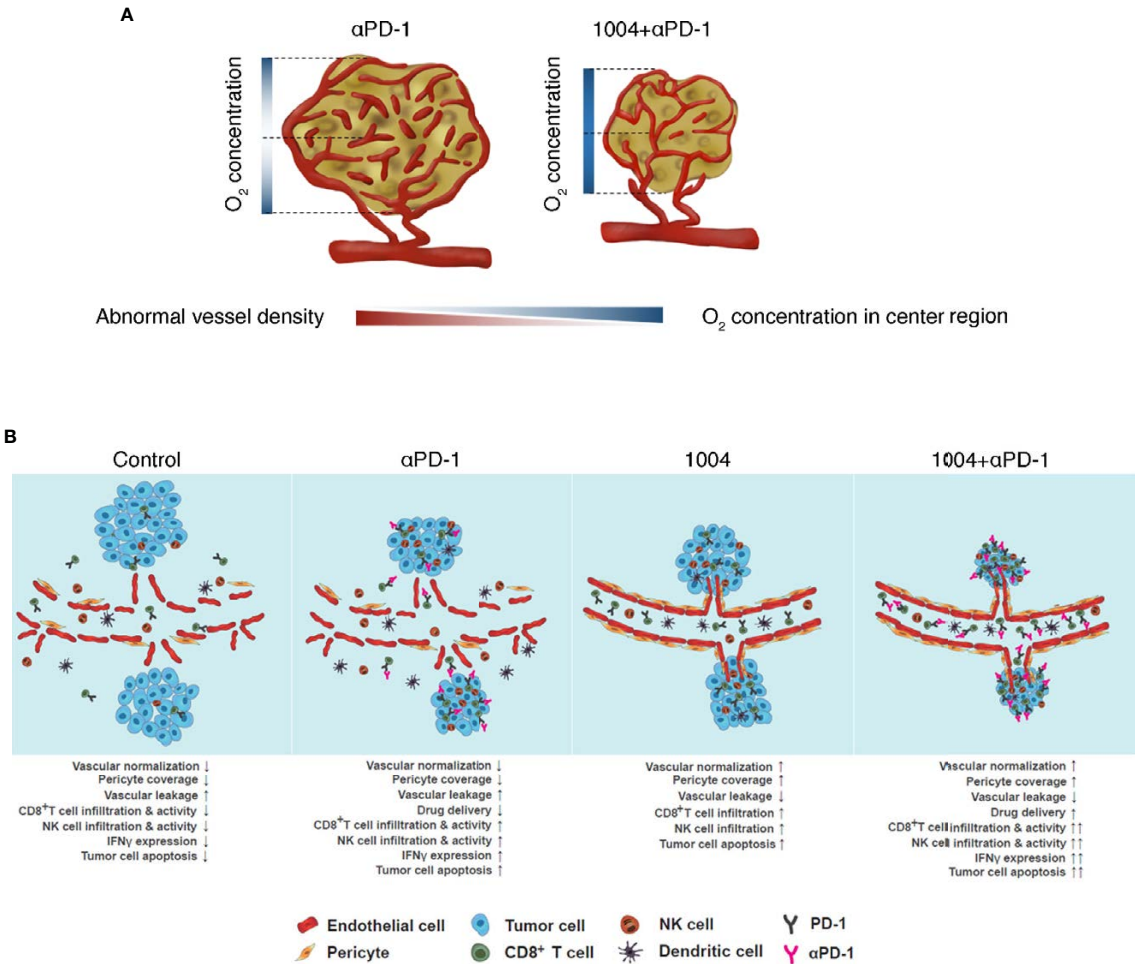

FIGURE 6 | CU06-1004 enhanced the therapeutic efficacy of anti-PD-1 antibody in MC38 tumors. **(A)** In the absence of CU06-1004, the center region in the tumor had a lower O_2 concentration and induced abnormal vascular density than the periphery region. However, when CU06-1004 was injected into the tumor, it maintained the proper O_2 concentration in the center region as well as the periphery region, and changed it into a stable center region by reducing the relatively abnormal vascular density. **(B)** In the TME without CU06-1004 treatment, migration of immune cells was suppressed by blood vascular leakage in the tumor. When CU06-1004 was injected into the tumor, the blood vessel was normalized in tumors, decreasing vascular leakage. Penetration of immune cells was successfully achieved by the CU06-1004 injection. Production of pro-inflammatory cytokine *Ifnγ* was enhanced by $CD8^+$ T cell populations after CU06-1004 injection. In conclusion, the combination of CU06-1004 and anti-PD-1 increased therapeutic efficacy in MC38 tumors.

model, which is not respond to anti-PD-1 therapy and examined combination therapy using anti-PD-1 and CU06-1004. In groups treated with CU06-1004, the number of aggressive blood vessels located in the central region of the tumor mass was greatly reduced. Structural differences between the central and peripheral regions of solid tumors were significant. Vessels in the central region of solid tumors are generally unstable compared with peripheral vessels (35), reducing oxygen levels and drug transport in the central region. However, CU06-1004 reduced non-functional vessels and reduced hypoxia within the central region of the tumor mass (**Figure 6A**). These effects were observed in the MC38 cancer model and in BALB/c-nu/nu mice injected with LLC-GFP. CU06-1004 induced an anti-tumor effect similar to anti-PD-1 monotherapy. CU06-1004 did not directly affect MC38 tumor growth but caused changes in the TME that increased the number of activated cytotoxic T cells. Immune activity in tumor tissue was related to the TME changes, with hypoxia playing an important role (36). TME has a wide variety of structures depending on the type of tumor, and these TMEs are closely related to tumor vessel normalization (23). Perhaps, in ICB treatment, the difference in anti-cancer efficacy according to the type of tumor is related to differences in vascular structure (37).

Changes in T-cell function are related to increased intratumoral delivery of anti-PD-1 therapy (34). Here, we have shown that the number of cells bound to anti-PD-1 drug was lower in groups that were not treated with CU06-1004. By contrast, CU06-1004 treated groups increased the number of anti-PD-1-bound cells. CU06-1004 normalizes the vessels within the tumor mass and allows seamless movement for both the drug

and immune cells. We examined changes in the T-cell population within the tumor of groups treated with both anti-PD-1 and CU06-1004. Anti-PD-1 alone can prevent PD-1/PD-L1 signaling, but only allows a portion of activated T cells to infiltrate (36). When CU06-1004 is added with anti-PD-1, the number of T cells within the tumor significantly increased due to changes in the TME. Although changing TME can influence the amount of infiltrated T cells within the tumor, it is important to assess that increased T cell population is indeed activated $CD8^+$ T cells. In particular, among many T cells, $CD8^+$ Tcells have been reported to directly kill tumor cells by inducing perforin/granzyme, FasL/Fas binding, or secreting cytokine/chemokine (23). Our results predict that activated $CD8^+$ T cells are responsible for significant tumor suppressive effects. In order to prove that infiltrated T cells are cytotoxic $CD8^+$ T cells, we analyzed FACS and fluorescence data. CU06-1004 plus anti-PD-1 increased activated T cells more than any other treatment method while unaffecting the number of regulatory T cells. Thus, combination treatment with CU06-1004 and anti-PD-1 increased the number of activated $CD8^+$ T cells and improved the efficacy of immune therapy.

Generally, activated $CD8^+$ T cells inhibit tumor progression by increasing the secretion of cytokines and chemokines. Cytokines secreted from $CD8^+$ T cells include IFNγ, TNFα, and IL-2 (38, 39). We examined if combination treatment induced activated CD8+ T cells to express pro-inflammatory cytokines, such as IFNγ, TNFα, and IL-1β. We also checked other cytokines, such as anti-inflammatory markers IFNα, IFNβ, and TGFβ, using RT-PCR, qPCR, and ELISA. As already documented, treatment using anti-PD-1 alone can reactivate CD8+Tcells and induce cytokine secretion of tumor-antigen specific T cells. In contrast, experiments using only CU06-1004 caused lower levels of cytokine secretion compared to the anti-PD-1 treated group. Lower secretion of cytokines in the CU06-1004-treated group may be due to less activation of $CD8^+$ T cells, in contrast to anti-PD-1, with only movement and infiltration enhanced. Indeed, expression of cytokines was higher in the combination group compared with the anti-PD-1 mono-treatment group, thus enhancing the anti-tumor activity of $CD8^+$ T cells by combination treatment.

Defining mechanisms that affect immune response in cancer patients is important (40). Anti-PD-1 therapy strengthens T cell-derived immune responses by binding IFNγ receptors (IFNGR) in tumors, increasing PD-L1 expression through JAK1 and JAK2 activation and mobilizing surrounding STAT1 (41–43). Combination therapy compared with anti-PD-1 monotherapy showed higher expression levels of PD-L1 on cancer cells due to increased secretion of IFNγ, which increased recruitment of STAT1. Although the increase in PD-L1 on cancer cells can increase immune evasion, anti-PD-1 treatment prevented immune evasion by cancer cells and allowed T cells to mediate anti-tumor responses in our studies. A modified TME allows drugs and activated T cells to move efficiently into the central tumor region. Anti-tumor activity by these cells was supported by IFNγ expression and signaling.

Combination therapy with an immune checkpoint blocker and anti-VEGF drug inhibits angiogenesis (44, 45). Although the effect of anti-VEGF treatment may seem similar compared with CU06-1004 in that it stabilized the tumor vessels in early stage, anti-VEGF can induce hypoxia by eliminating vessels inside the tumor. By contrast, CU06-1004 normalizes vessels to yield long-lasting effects by raising oxygen and T-cell infiltration. Anti-VEGF treatment may occasionally normalize vessels, but the steady increase in hypoxia promotes tumor progression (46–48). Therefore, anti-VEGF may be effective only during early stages when a tumor is small. Combination treatment with CU06-1004 showed favorable responses at early time points of tumor development and maintained effects for a longer period. Thus, the novel combination therapy examined in this study may be effective for cancer patients, including those who require long-term treatment.

We showed that combination treatment including CU06-1004 can normalize vessels and directly change the TME, enhancing drug transfer and T-cell activity. Further, changes in IFNγ and PD-L1 expression indicate that the combination therapy is highly effective in generating an anti-tumor response. Finally, these data suggest that the combination of CU06-1004 and anti-PD-1 is highly synergistic and long-lasting with potential benefits for early and late stages of cancer.

CONCLUSIONS

We demonstrate that the antitumor effects of CU06-1004 combined ICB through enhanced specific $CD8^+$T cell activity and increased antitumor cytokine, Ifnγ. CU06-1004 used for the treatment of cancer by changing the TME and had a new promising candidate drug efficacy.

DATA AVAILABILITY STATEMENT

The original contributions presented in the study are included in the article/**Supplementary Material**; further inquiries can be directed to the corresponding authors.

ETHICS STATEMENT

The animal study was reviewed and approved by IACUC-A-201901-843-02.

AUTHOR CONTRIBUTIONS

Y-GK and S-JH provided expertise and research financing, and contributed to the writing of the manuscript. SP performed all the experiments and quantifications and wrote the manuscript. JHO and DJP contributed to the experiment, quantification, and revised the manuscript. HZ, MN, YK, Y-SK, and HK helped with the experiments, and Y-MK commented. All authors contributed to the article and approved the submitted version.

FUNDING

This work was supported by the Basic Science Research Program through the National Research Foundation of Korea funded by the Ministry of Education, Science and Technology (grant number 2019R1A2C3007142) and (grant number 2018R1A2A1A05076997), and the Bio & Medical Technology Development Program of the National Research Foundation of Korea (NRF-2015M3A9B6066835). The work was supported in part by Brain Korea 21(BK21) FOUR program / SP are fellowship awardee by BK21 FOUR program.

SUPPLEMENTARY MATERIAL

The Supplementary Material for this article can be found online at: https://www.frontiersin.org/articles/10.3389/fimmu.2020.620166/full#supplementary-material

REFERENCES

1. Ventola CL. Cancer Immunotherapy, Part 3: Challenges and Future Trends. *P T* (2017) 42p(8):514–21. doi: 10.1155/2019/4508794
2. Chiriva-Internati M, Bot A. A new era in cancer immunotherapy: discovering novel targets and reprogramming the immune system. *Int Rev Immunol* (2015) 34(2):101–3. doi: 10.3109/08830185.2015.1015888
3. Rabinovich GA, Gabrilovich D, Sotomayor EM. Immunosuppressive strategies that are mediated by tumor cells. *Annu Rev Immunol* (2007) 25:267–96. doi: 10.1146/annurev.immunol.25.022106.141609
4. Escors D, Gato-Canas M, Zuazo M, Arasanz H, Garcia-Granda MJ, Vera R, et al. The intracellular signalosome of PD-L1 in cancer cells. *Signal Transd Target Ther* (2018) 3:26. doi: 10.1038/s41392-018-0022-9
5. Santarpia M, Gonzalez-Cao M, Viteri S, Karachaliou N, Altavilla G, Rosell R. Programmed cell death protein-1/programmed cell death ligand-1 pathway inhibition and predictive biomarkers: understanding transforming growth factor-beta role. *Transl Lung Cancer Res* (2015) 4(6):728–42. doi: 10.3978/j.issn.2218-6751.2015.12.04
6. Arasanz H, Gato-Canas M, Zuazo M, Ibanez-Vea M, Breckpot K, Kochan G, et al. PD1 signal transduction pathways in T cells. *Oncotarget* (2017) 8 (31):51936–45. doi: 10.18632/oncotarget.17232
7. Shi T, Ma Y, Yu L, Jiang J, Shen S, Hou Y, et al. Cancer Immunotherapy: A Focus on the Regulation of Immune Checkpoints. *Int J Mol Sci* (2018) 19(5). doi: 10.3390/ijms19051389
8. Wang H, Mao L, Zhang T, Zhang L, Wu Y, Guo W, et al. Altered expression of TIM-3, LAG-3, IDO, PD-L1, and CTLA-4 during nimotuzumab therapy correlates with responses and prognosis of oral squamous cell carcinoma patients. *J Oral Pathol Med* (2019) 48(8):669–76. doi: 10.1111/jop.12883
9. Wang X, Guo G, Guan H, Yu Y, Lu J, Yu J. Challenges and potential of PD-1/PD-L1 checkpoint blockade immunotherapy for glioblastoma. *J Exp Clin Cancer Res* (2019) 38(1):87. doi: 10.1186/s13046-019-1085-3
10. Sambi M, Bagheri L, Szewczuk MR. Current Challenges in Cancer Immunotherapy: Multimodal Approaches to Improve Efficacy and Patient Response Rates. *J Oncol* (2019) 2019:4508794. doi: 10.1155/2019/4508794
11. Quail DF, Joyce JA. Microenvironmental regulation of tumor progression and metastasis. *Nat Med* (2013) 19(11):1423–37. doi: 10.1038/nm.3394
12. Jain RK. Normalizing tumor microenvironment to treat cancer: bench to bedside to biomarkers. *J Clin Oncol* (2013) 31(17):2205–18. doi: 10.1200/JCO.2012.46.3653
13. Jing X, Yang F, Shao C, Wei K, Xie M, Shen H, et al. Role of hypoxia in cancer therapy by regulating the tumor microenvironment. *Mol Cancer* (2019) 18 (1):157. doi: 10.1186/s12943-019-1089-9
14. Zhao Y, Ting KK, Li J, Cogger VC, Chen J, Johansson-Percival A, et al. Targeting Vascular Endothelial-Cadherin in Tumor-Associated Blood Vessels Promotes T-cell-Mediated Immunotherapy. *Cancer Res* (2017) 77(16):4434–47. doi: 10.1158/0008-5472.CAN-16-3129
15. Azzi S, Hebda JK, Gavard J. Vascular permeability and drug delivery in cancers. *Front Oncol* (2013) 3:211. doi: 10.3389/fonc.2013.00211
16. Klein D. The Tumor Vascular Endothelium as Decision Maker in Cancer Therapy. *Front Oncol* (2018) 8:367. doi: 10.3389/fonc.2018.00367
17. Datta M, Coussens LM, Nishikawa H, Hodi FS, Jain RK. Reprogramming the Tumor Microenvironment to Improve Immunotherapy: Emerging Strategies and Combination Therapies. *Am Soc Clin Oncol Educ Book* (2019) 39:165–74. doi: 10.1200/EDBK_237987
18. Goel S, Wong AH, Jain RK. Vascular normalization as a therapeutic strategy for malignant and nonmalignant disease. *Cold Spring Harb Perspect Med* (2012) 2(3):a006486. doi: 10.1101/cshperspect.a006486
19. Zheng X, Fang Z, Liu X, Deng S, Zhou P, Wang X, et al. Increased vessel perfusion predicts the efficacy of immune checkpoint blockade. *J Clin Invest* (2018) 128(5):2104–15. doi: 10.1172/JCI96582
20. Lee K, Agrawal V, Kim K, Kim J, Park H, Lee S, et al. Combined effect of vascular-leakage-blocker Sac-1004 and antiangiogenic drug sunitinib on tumor angiogenesis. *Biochem Biophys Res Commun* (2014) 450(4):1320–6. doi: 10.1016/j.bbrc.2014.06.139
21. Maharjan S, Kim K, Agrawal V, Choi HJ, Kim NJ, Kim YM, et al. Sac-1004, a novel vascular leakage blocker, enhances endothelial barrier through the cAMP/Rac/cortactin pathway. *Biochem Biophys Res Commun* (2013) 435 (3):420–7. doi: 10.1016/j.bbrc.2013.04.104
22. Zhang H, Park JH, Maharjan S, Park JA, Choi KS, Park H, et al. Sac-1004, a vascular leakage blocker, reduces cerebral ischemia-reperfusion injury by suppressing blood-brain barrier disruption and inflammation. *J Neuroinflam* (2017) 14(1):122. doi: 10.1186/s12974-017-0897-3
23. Oh JH, Kim MJ, Choi SJ, Ban YH, Lee HK, Shin EC, et al. Sustained Type I Interferon Reinforces NK Cell-Mediated Cancer Immunosurveillance during Chronic Virus Infection. *Cancer Immunol Res* (2019) 7p(4):584–99. doi: 10.1158/2326-6066.CIR-18-0403
24. Koury J, Lucero M, Cato C, Chang L, Geiger J, Henry D, et al. Immunotherapies: Exploiting the Immune System for Cancer Treatment. *J Immunol Res* (2018) 2018:9585614. doi: 10.1155/2018/9585614
25. Ventola CL. Cancer Immunotherapy, Part 2: Efficacy, Safety, and Other Clinical Considerations. *P T* (2017) 42(7):452–63.
26. Kim JM, Chen DS. Immune escape to PD-L1/PD-1 blockade: seven steps to success (or failure). *Ann Oncol* (2016) 27(8):1492–504. doi: 10.1093/annonc/mdw217
27. Ishihara J, Ishihara A, Sasaki K, Lee SS, Williford JM, Yasui M, et al. Targeted antibody and cytokine cancer immunotherapies through collagen affinity. *Sci Transl Med* (2019) 11(487). doi: 10.1126/scitranslmed.aau3259
28. Hegde PS, Chen DS. Top 10 Challenges in Cancer Immunotherapy. *Immunity* (2020) 52(1):17–35. doi: 10.1016/j.immuni.2019.12.011
29. Stylianopoulos T, Munn LL, Jain RK. Reengineering the Physical Microenvironment of Tumors to Improve Drug Delivery and Efficacy: From Mathematical Modeling to Bench to Bedside. *Trends Cancer* (2018) 4 (4):292–319. doi: 10.1016/j.trecan.2018.02.005
30. Roma-Rodrigues C, Mendes R, Baptista PV, Fernandes AR. Targeting Tumor Microenvironment for Cancer Therapy. *Int J Mol Sci* (2019) 20(4). doi: 10.3390/ijms20040840
31. Martin JD, Seano G, Jain RK. Normalizing Function of Tumor Vessels: Progress, Opportunities, and Challenges. *Annu Rev Physiol* (2019) 81:505–34. doi: 10.1146/annurev-physiol-020518-114700
32. Jain RK, Martin JD, Stylianopoulos T. The role of mechanical forces in tumor growth and therapy. *Annu Rev BioMed Eng* (2014) 16:321–46. doi: 10.1146/annurev-bioeng-071813-105259
33. Martin JD, Fukumura D, Duda DG, Boucher Y, Jain RK. Reengineering the Tumor Microenvironment to Alleviate Hypoxia and Overcome Cancer Heterogeneity. *Cold Spring Harb Perspect Med* (2016) 6(12). doi: 10.1101/cshperspect.a031195
34. Nguyen L, Fifis T, Malcontenti-Wilson C, Chan LS, Costa PN, Nikfarjam M, et al. Spatial morphological and molecular differences within solid tumors

may contribute to the failure of vascular disruptive agent treatments. *BMC Cancer* (2012) 12:522. doi: 10.1186/1471-2407-12-522
35. Jin MZ, Jin WL. The updated landscape of tumor microenvironment and drug repurposing. *Signal Transd Target Ther* (2020) 5(1):166. doi: 10.1038/s41392-020-00280-x
36. Huang Y, Goel S, Duda DG, Fukumura D, Jain RK. Vascular normalization as an emerging strategy to enhance cancer immunotherapy. *Cancer Res* (2013) 73(10):2943–8. doi: 10.1158/0008-5472.CAN-12-4354
37. Mpekris F, Voutouri C, Baish JW, Duda DG, Munn LL, Stylianopoulos T, et al. Combining microenvironment normalization strategies to improvecancer immunotherapy. *Proc Natl Acad Sci U S A* (2020) 117 (7):3728–37. doi: 10.1073/pnas.1919764117
38. Gallego A, Vargas JA, Castejon R, Citores MJ, Romero Y, Millan I, et al. Production of intracellular IL-2, TNF-alpha, and IFN-gamma by T cells in B-CLL. *Cytometry B Clin Cytom* (2003) 56(1):23–9. doi: 10.1002/cyto.b.10052
39. Freeman BE, Hammarlund E, Raue HP, Slifka MK. Regulation of innate CD8+ T-cell activation mediated bycytokines. *Proc Natl Acad Sci U S A* (2012) 109 (25):9971–6. doi: 10.1073/pnas.1203543109
40. Gonzalez H, Hagerling C, Werb Z. Roles of the immune system in cancer: from tumor initiation to metastatic progression. *Genes Dev* (2018) 32(19-20):1267–84. doi: 10.1101/gad.314617.118
41. Bellucci R, Martin A, Bommarito D, Wang K, Hansen SH, Freeman GJ, et al. Interferon-gamma-induced activation of JAK1 and JAK2 suppresses tumor cell susceptibility to NK cells through upregulation of PD-L1 expression. *Oncoimmunology* (2015) 4(6):e1008824. doi: 10.1080/2162402X.2015.1008824
42. Nowicki TS, Hu-Lieskovan S, Ribas A. Mechanisms of Resistance to PD-1 and PD-L1 Blockade. *Cancer J* (2018) 24(1):47–53. doi: 10.1097/PPO.0000000000000303
43. Castro F, Cardoso AP, Goncalves RM, Serre K, Oliveira MJ. Interferon-Gamma at the Crossroads of Tumor Immune Surveillance or Evasion. *Front Immunol* (2018) 9:847. doi: 10.3389/fimmu.2018.00847
44. Niu G, Chen X. Vascular endothelial growth factor as an anti-angiogenic target for cancer therapy. *Curr Drug Targets* (2010) 11(8):1000–17. doi: 10.2174/138945010791591395
45. Browder T, Butterfield CE, Kraling BM, Shi B, Marshall B, O'Reilly MS, et al. Antiangiogenic scheduling of chemotherapy improves efficacy against experimental drug-resistant cancer. *Cancer Res* (2000) 60 (7):1878–86.
46. Maimela NR, Liu S, Zhang Y. Fates of CD8+ T cells in Tumor Microenvironment. *Comput Struct Biotechnol J* (2019) 17:1–13. doi: 10.1016/j.csbj.2018.11.004
47. Lee CT, Mace T, Repasky EA. Hypoxia-driven immunosuppression: a new reason to use thermal therapy in the treatment of cancer? *Int J Hyperthermia* (2010) 26(3):232–46. doi: 10.3109/02656731003601745
48. Liu Z, Wang Y, Huang Y, Kim BYS, Shan H, Wu D, et al. Tumor Vasculatures: A New Target for Cancer Immunotherapy. *Trends Pharmacol Sci* (2019) 40 (9):613–23. doi: 10.1016/j.tips.2019.07.001

Conflict of Interest: HZ was employed by the company Curacle Co. Ltd.

The remaining authors declare that the research was conducted in the absence of any commercial or financial relationships that could be construed as a potential conflict of interest.

Copyright © 2021 Park, Oh, Park, Zhang, Noh, Kim, Kim, Kim, Kim, Ha and Kwon. This is an open-access article distributed under the terms of the Creative Commons Attribution License (CC BY). The use, distribution or reproduction in other forums is permitted, provided the original author(s) and the copyright owner(s) are credited and that the original publication in this journal is cited, in accordance with accepted academic practice. No use, distribution or reproduction is permitted which does not comply with these terms.

frontiers in Oncology

ORIGINAL RESEARCH
published: 28 January 2021
doi: 10.3389/fonc.2020.618374

Pan-Cancer Molecular Characterization of m^{6}A Regulators and Immunogenomic Perspective on the Tumor Microenvironment

Jie Zhu[1], *Jiani Xiao*[2], *Min Wang*[3] *and Daixing Hu*[4]*

[1] Department of Intensive Care Unit, The People's Hospital of Tongliang District, Chongqing, China, [2] Department of Pediatric Dentistry, West China Hospital of Stomatology, Sichuan University, Chengdu, China, [3] Department of Respiratory and Geriatrics, Chongqing Public Health Medical Center, Chongqing, China, [4] Department of Urology, First Affiliated Hospital of Chongqing Medical University, Chongqing, China

Purpose: N6-methyladenosine (m^{6}A) methylation plays a critical role in diverse biological processes. However, knowledge regarding the constitution of m^{6}A on tumor microenvironment (TME) and tumor-infiltrating lymphocytes (TILs) across cancer types is still lacking. We performed comprehensive immuno-genomic analyses to reveal molecular characterization of the m^{6}A regulators and immune-related genes (IRGs) across TME and TIL heterogeneity.

Methods: We comprehensively analyzed the properties of m^{6}A regulators in genomic profiles from The Cancer Genome Atlas (TCGA) according to expression perturbations of crucial IRGs, CD274, CD8A, GZMA, and PRF1. The four IRGs were proved to be reliable biomarkers of TILs and TME *via* CIBERSORT and ESTIMATE analyses, and their co-expression relationship was certified by TIMER analysis. Based on their median values, the samples from the pan-cancer tissues (N = 11,057) were classified into eight TME types. The RNA expression levels of 13 m^{6}A regulators were compared across TME subtypes. Single-sample Gene Set Enrichment Analysis (ssGSEA) was also used to classify TME clusters, expression variants of IRGs and m^{6}A regulators were verified among TME clusters. Meanwhile, the correlation between m^{6}A regulators and tumor mutational burden (TMB) were tested. Finally, the impacts of IRGs and TME clusters in clinical characteristics and outcomes were revealed.

Results: CD274, CD8A, GZMA, and PRF1 showed similar TILs' characteristics, of which the level of T cells CD8 and T cells CD4 memory activated are consistent with the expression levels of the four IRGs and higher immune infiltration. Besides, CD274, CD8A, GZMA, and PRF1 were positively correlated with the stromal score or immune score in almost all 33 tumor types. All of four IRGs showed impact between tumor pathological stages or clinical outcomes. Among TME type I to type IV, m^{6}A regulators' expression drift changed from high-level to low-level in ESCA, BLCA, HNSC, CESC, BRCA, and GBM. However among TME type V to type VIII, m^{6}A regulators drew a shift from low-level to high-level expression in CESC, BLCA, ESCA, KIRP, HNSC, BRCA, KIRC, COAD, LAML,

OPEN ACCESS

Edited by:
Huanfa Yi,
Jilin University, China

Reviewed by:
Meng Xu,
Carnegie Mellon University, United States
Feng Geng,
The Ohio State University, United States

***Correspondence:**
Daixing Hu
hudaixing523@163.com

Specialty section:
This article was submitted to Cancer Immunity and Immunotherapy, a section of the journal Frontiers in Oncology

Received: *16 October 2020*
Accepted: *04 December 2020*
Published: *28 January 2021*

Citation:
Zhu J, Xiao J, Wang M and Hu D (2021) Pan-Cancer Molecular Characterization of m^{6}A Regulators and Immunogenomic Perspective on the Tumor Microenvironment. Front. Oncol. 10:618374. doi: 10.3389/fonc.2020.618374

GBM, and KICH. In ssGSEA analyses, IRGs' expression levels were elevated with the immune infiltration degree and m^{6}A regulators' expression level varied among three TIL subgroups. With different TMB levels, expression differences of m^{6}A regulators were observed in BLCA, BRCA, COAD, LGG, LUAD, LUSC, STAD, THCA, and UCEC.

Conclusion: We identified four crucial IRGs affecting TILs, TME characteristics and clinical parameters. Expression variants of m^{6}A regulators among the subgroups of TME types and ssGSEA clusters suggested that m^{6}A regulators may be essential factors for phenotypic modifications of IRGs and thus affecting TME characteristics across multiple tumor types.

Keywords: N6-methyladenosine methylation, tumor microenvironment, tumor-infiltrating lymphocytes, The Cancer Genome Atlas (TCGA), pancancer analysis

INTRODUCTION

Immunotherapy, as a viable treatment for multiple cancers, has recently received extensive attention. T cell-based immunotherapy has been called as immune checkpoint inhibitors (ICIs), such as anti-cytotoxic T-lymphocyte-associated protein 4 (CTLA4), anti-programmed death protein-1 (PD-1), or anti-programmed death-ligand 1 (PD-L1) antibodies (1–3). Immune-related treatments targeting T cell exhaustion markers can improve cancer outcomes by enhancing antitumor immunity (1), which have shown significant clinical efficacy in immunogenic tumors such as melanoma, renal cell carcinoma, bladder cancer, non-small cell lung cancer, and hodgkin's lymphoma (2, 4–6). However, not all patients respond well to ICIs therapy. The variable response is also associated with patients' genomic characteristics such as tumor microenvironment (TME) and tumor mutation burden (TMB) (7–9). Accumulating researches have shown that tumor cells could change the TME to serve as contributors that ensure rapid cell proliferation (10). The dynamic alteration of molecular and cellular processes in TME relying on the interactions between tumor cells and immune cells (11), which highlights the role of tumor-infiltrating lymphocytes (TILs) in the context of protumorigenic inflammation and anticancer immunosurveillance (12). Hence, researchers have attempted to analyze the detailed composition, density, and function of TILs in TME context, which turn out to be challenging.

Several studies have shown that the mRNA-seq value of some crucial immune-related genes (IRGs) could constitute appropriate models for assessing TME. Rooney et al. reported a quantitative measure of immune cytolytic activity (CYT) based on the expression levels of granzyme A (GZMA) and perforin 1 (PRF1), which was also a model to assess TME (13). A study used the median PD-L1 (assessed by CD274 expression) and CD8A expression levels as the cut-off values to define subgroups in TME, of which the response to ICIs treatment was proved to differ among subgroups (14). Another published research proposed to classify TME depending on PD-L1 status and presence or absence of TILs, which also indicated specific TILs with PD-L1 positive would benefit more from anti-PD-L1/PD-1 therapies (15).

In most eukaryotes, m^{6}A methylation is the most abundant internal chemical modification around the 3′ untranslated region (3′ UTR) of mRNA (16). Protein complexes and related coding genes have been classified as methyltransferases ("writers"), binding proteins ("readers"), and demethylases ("erasers"). Based on current research, the writers mainly include WT1-associated protein (WTAP), methyltransferase like 3 (METTL3), methyltransferase like 14 (METTL14), RNA binding motif protein 15 (RBM15), zinc finger CCCH-type containing 13 (ZC3H13), and the readers include YTH domain-containing 1 (YTHDC1), YTH domain-containing 1 (YTHDC2), YTH N6-methyl-adenosine RNA binding protein 1 (YTHDF1), YTH N6-methyladenosine RNA binding protein 2 (YTHDF2), YTH N6-methyladenosine RNA binding protein 3 (YTHDF3) and heterogeneous nuclear ribonucleoprotein C (HNRNPC). The erasers contain fat mass- and obesity-associated protein (FTO) and α-ketoglutarate-dependent dioxygenase alkB homolog 5 (ALKBH5) (17–19). M^{6}A methylation controls many mRNA features, such as structure formation, maturation, stability, splicing, export, translation, and decay (20). It also regulates cell fate, cell cycle arrest, cell differentiation, eventually leading to the occurrence of cancer (21, 22). Recently, it has been recognized as a crucial factor in T cell homeostasis (23). Selectively altered m^{6}A regulator levels may be effective adjuvant therapy strategies in a variety of immunological diseases (24–26). But knowledge regarding the fluctuation of m^{6}A regulators in TILs, TME, and immunotherapies has not been clearly elucidated. Research based on the heterogeneity of m^{6}A regulators to identify distinct subtypes of sepsis (27), of which the GSEA and CIBERSORT analyses found different immunocompetent status (such as Th1 cells, T cells CD4 activated, NK cells activated and B cells activated) among subtypes and indicated the potential relation among m^{6}A regulators and leukocyte infiltration. Studies also have shown that m^{6}A regulators contribute to TME formation (28) and affect the abundance of TILs (29) as well as response to ICIs treatment (30).

In our study, we performed comprehensive immuno-genomic analyses to provide a thorough understanding of the m^{6}A regulator alterations and IRGs expression perturbations across

TME and TILs heterogeneity. We extracted the data of patients with 33 tumor types from The Cancer Genome Atlas (TCGA) database and systematically characterized them into subgroups depending on TME or TILs characteristics. We found specific and widespread genetic alteration patterns in m^6A regulators and IRGs in this context. We also assessed the relationship between TMB and m^6A regulators and explored the prognostic value of IRGs or TME clusters. Our analysis emphasizes the vital effect of m6A regulators on the crucial IRGs, which lays a foundation for further research to improve ICIs treatment strategies.

MATERIALS AND METHODS

Data Availabilities

The original contributions presented in the study are publicly available in the TCGA database (https://portal.gdc.cancer.gov/). This data can be found in the UCSC Xena browser (https://xenabrowser.net);. Tumor gene expression data, TMB data, and corresponding clinical data, including survival time (overall survival, OS; disease-specific survival, DSS; progression-free interval, PFI), survival status, age, and tumor stages, as well as the somatic mutation (SNPs and small INDELs) data, were obtained across 33 tumor types. Data of TMB in this study were directly generated from the somatic mutation data. A total of 11,057 tumor samples in the TCGA cohort were included, and gene expression levels were presented as the log 2-transformed (FPKM+1) values.

Cancer Types Investigated in this Study

Adrenocortical carcinoma (ACC), Bladder Urothelial Carcinoma (BLCA), Breast invasive carcinoma (BRCA), Cervical squamous cell carcinoma and endocervical adenocarcinoma (CESC), cholangiocarcinoma (CHOL), Colorectal adenocarcinoma (COAD), Diffuse large B-cell lymphoma (DLBC), Esophageal Carcinoma (ESCA), Glioblastoma multiforme (GBM), Head and Neck squamous cell carcinoma (HNSC), kidney chromophobe (KICH), Kidney renal clear cell carcinoma (KIRC), Kidney Renal Papillary Cell Carcinoma (KIRP), Acute myeloid leukemia (LAML), Brain Lower Grade Glioma (LGG), Liver hepatocellular carcinoma (LIHC), Lung adenocarcinoma (LUAD), Lung squamous cell carcinoma (LUSC), mesothelioma (MESO), Ovarian serous cystadenocarcinoma (OV), pancreatic adenocarcinoma (PAAD), Pheochromocytoma and Paraganglioma (PCPG), Prostate Adenocarcinoma (PRAD), rectum adenocarcinoma (READ), Sarcoma (SARC), Skin Cutaneous Melanoma (SKCM), Stomach adenocarcinoma (STAD), Testicular germ cell tumors (TGCT), Papillary Thyroid Carcinoma (THCA), Thymoma (THYM), Uterine Corpus Endometrial Carcinoma (UCEC), Uterine carcinosarcoma (UCS), Uveal Melanoma (UVM).

Tumor Immune Estimation Resource

TIMER is a comprehensive resource (http://timer.cistrome.org/) that consists of six major analytic modules that allow users to explore the association of TILs abundance with gene expression, overall survival, somatic mutations, and DNA somatic copy number alterations (SCNAs), as well as analysis of differential gene expression (DiffExp) and gene–gene correlations (31, 32).

CIBERSORT

The proportions of the 22 tumor-infiltrating immune cells from each sample were determined by using the "CIBERSORT" (R package) (33), and gene expression profiles were transformed into the proportion of 22 TILs, namely: B cells naive, B cells memory, Plasma cells, T cells CD8, T cells CD4 naive, T cells CD4 memory resting, T cells CD4 memory activated, T cells follicular helper, T cells regulatory (Tregs), T cells gamma delta, NK. cells resting, NK. cells activated, Monocytes, Macrophages M0, Macrophages M1, Macrophages M2, Dendritic cells resting, Dendritic cells activated, Mast cells resting, Mast cells activated, Eosinophils, and Neutrophils. The relative expression of 22 tumor-infiltrating immune cells in each sample was determined. Significant results ($P < 0.05$) were selected for subsequent analysis.

Estimation of Stromal and Immune Cells in Malignant Tumor Tissues Using Expression Data Scores and Immune Subtype Analyses

ESTIMATE (Estimation of Stromal and Immune cells in Malignant Tumor tissues using Expression data) is a newly developed algorithm that takes advantage of the unique properties of the transcriptional profiles of cancer tissues to infer tumor cellularity as well as the different infiltrating normal cells (34). The algorithm imputes stromal and immune scores to predict the level of infiltrating stromal and immune cells based on specific gene expression signatures of stromal and immune cells. Stromal and immune scores were calculated by using the "estimate" package with default parameters.

The immune-related prognostic signature was generated by a previously conducted TILs study (9). The aforementioned previous study comprehensively described the immune landscape of >10,000 samples, comprising 33 different cancer types, and integrated 160 immune-related signatures containing 2,995 immune genes. Six immune subtypes were defined as Wound Healing (Immune C1), IFN-gamma Dominant (Immune C2), Inflammatory (Immune C3), Lymphocyte Depleted (Immune C4), Immunologically Quiet (Immune C5), TGF-beta Dominant (Immune C6), measuring immune infiltrates in TME.

Gene Enrichment Analysis

Single-sample Gene Set Enrichment Analysis (ssGSEA) is used to analyze TME features. It is an extension of Gene Set Enrichment Analysis (GSEA), which calculates separate enrichment scores for each pairing of a sample and gene set (35). Pearson's correlation coefficient was used to calculate the correlation of the ssGSEA scores across the gene sets. The ssGSEA scores for most immune cell populations obtained using the gene sets from Angelova et al. (36). Those with ssGSEA scores consistent with known immune cell markers were retained for the gene sets included in no less than two published studies. Finally, a total of

29 gene sets representing distinct immune cell populations were selected, and the ssGSEA scores of each were calculated across 11,057 samples in the pan-cancer cohort. The following 29 types of immune-related gene sets were obtained: aDCs, APC co-inhibition, APC co-stimulation, CCR, CD8+ T cells, Checkpoint, Cytolytic activity, DCs, HLA, iDCs, Inflammation-promoting, Macrophages, Mast cells, MHC class I, Neutrophils, NK cells, Parainflammation, pDCs, T cell co-inhibition, T cell co-stimulation, T helper cells, Tfh, Th1 cells, Th2 cells, TIL, Treg, Type I IFN Reponse, Type II IFN Reponse. In this manner, ssGSEA transforms a single sample's gene expression profile to a gene set enrichment profile. The enrichment scores calculated by ssGSEA analysis were utilized to represent the relative abundance of TME infiltrating cells in each sample.

Statistical Analyses

Statistical analyses and data plotting were performed using R program (3.6.2). Unless noted otherwise, Fisher's exact and equal-variance t-tests were, respectively, used in group comparisons for categorical and continuous variables. Spearman's correlation analysis test was used to analyzed the correlation relationship in different cancer types. A threshold of 0.05 was used to deem significance from p values of statistical tests.

RESULTS

The Tumor-Infiltrating Lymphocytes' Distribution Related to Immune-Related Genes

According to previous studies we mentioned above, CD274, CD8A, GZMA, and PRF1 were chosen as the crucial IRGs to represent TILs' characteristics in TME. To evaluate whether the four IRGs could tell the TILs' characteristics, we further focused on TILs' distribution in patients with differential expression of CD274, CD8A, GZMA, and PRF1. By taking the median value as threshold and using CIBERSORT as TILs component analysis, T cells CD4 memory activated (in 26 tumor types) expressed the most extensive infiltration differences in pan-cancer tissues and followed by Macrophages M1 (in 24 tumor types), T cells CD8 (in 20 tumor types), Macrophages M0 (in 15 tumor types) between the high- and low-expression groups of CD274 (**Supplement Figure 1**). A comparable result could be observed in high- and low-expression groups of CD8A, T cells CD8 (in 31 tumor types), T cells CD4 memory activated (in 26 tumor types), Macrophages M1 (in 26 tumor types), Macrophages M0 (in 24 tumor types) were also identified as differential infiltrated TIL types (**Supplement Figure 2**). Further analyses suggested that the TILs' features did not change much in high- and low-expression groups of GZMA and PRF1. T cells CD8 (31 tumor types *versus* 32 tumor types), T cells CD4 memory activated (26 tumor types *versus* 26 tumor types), Macrophages M1 (26 tumor types *versus* 23 tumor types), Macrophages M0 (23 tumor types *versus* 20 tumor types) turned to be the consistent TILs pattern of inter-group differences (**Supplement Figures 3** and **4**). Additionally, T cells CD8 and T cells CD4 memory activated were always co-expressed with gene expression level. The high-expression groups of CD274, CD8A, GZMA, and PRF1 always tended to show higher infiltration of T cells CD8 and T cells CD4 memory activated. On the contrary, Macrophages M0 always showed higher infiltration in low-expression groups of CD274, CD8A, GZMA, and PRF1. There were no consistencies observed in Macrophages M2, Macrophages M1, NK cells resting, and Mast cells activated in groups of various tumor types.

Relationship Between Estimation of Stromal and Immune Cells in Malignant Tumor Tissues Using Expression Data Scores and Immune-Related Genes

The ESTIMATE immune score and stromal score were used to analyze the infiltration levels of immune cells and stromal cells in different tumors. The correlation between the four IRGs and immune or stromal score was analyzed by Spearman's correlation analysis. The results suggested a surprising degree of consistency, CD274 (in 32 tumor types, except THYM, **Supplement Figure 5**), CD8A (in 32 tumor types, except UCS, **Supplement Figure 6**), GZMA (in 33 tumor types, **Supplement Figure 7**), and PRF1 (in 33 tumor types, **Supplement Figure 8**) were all positively correlated with the stromal score or immune score in almost all 33 tumor types, which gave us the basis for continued classification of samples according to the IRG characteristics.

M^6A Regulators Distribution Across Immune Subtype of Tumor Microenvironment and Relationship With Immune-Related Genes Across Cancer Types

The differential expressions of m^6A regulators were tested across the six immune subtypes (C1 to C6) reported by Thorsson, V. et al. METTL3, METTL14, WTAP, RBM15, ZC3H13, HNRNPC, FTO, ALKBH5, YTHDC1, YTHDC2, YTHDF1, YHDF2, and YTHDF3 were all significantly differentially expressed among six immune subtypes ($p < 0.001$) (**Figure 1**). Across 33 tumor types, CD274 and CD8A had broader positive correlations with m^6A regulators (**Figures 1B, C**). By contrast, GZMA and PRF1 presented broader negative correlations (**Figures 1D, E**). By taking the median of the log 2-transformed (FPKM+1) values, we compared the expressions of m^6A regulators between high- and low-expression groups of CD274 (**Supplement Figure 9**), CD8A (**Supplement Figure 10**), GZMA (**Supplement Figure 11**), and PRF1 (**Supplement Figure 12**) respectively. The results showed that m6A regulators' levels had vast differences among these groups across various tumor types, of which KIRC, PAAD, and UVM are the top three tumor types showed the widest differences.

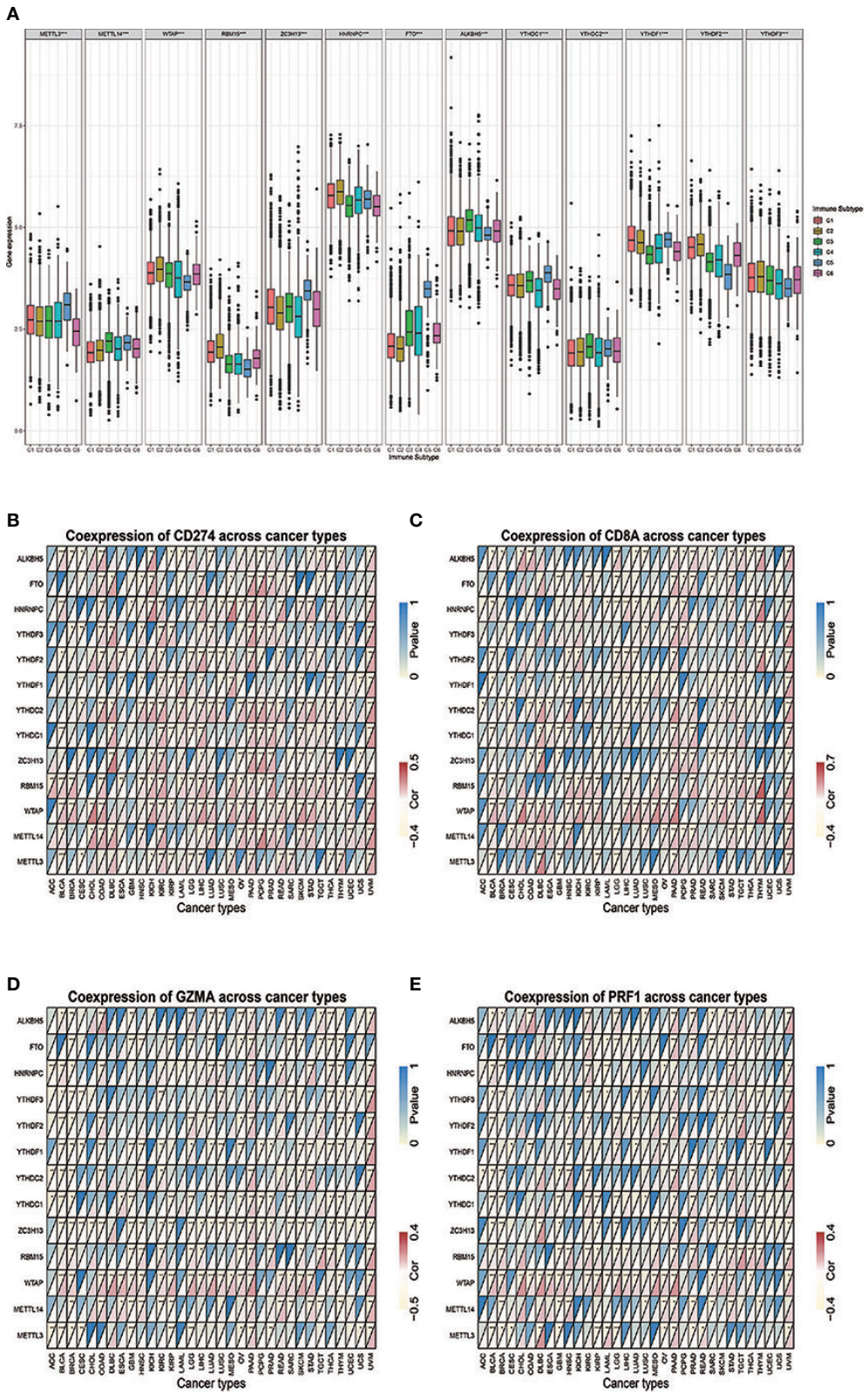

FIGURE 1 | **(A)** The differential expression of m^{6}A regulators was tested across the six immune subtypes (C1 to C6). **(B–E)** The correlations between IRGs and m^{6}A regulators. * represents P < 0.05, ** represents P < 0.01, *** represents P < 0.001.

M^{6}A Regulator Distribution Across Immune-Related Gene Immune Types in Pan-Cancer Types

Through TIMER analysis, we observed positive correlations between CD274 and CD8A across 29 tumor types (more specifically, ACC, BLCA, BRCA, CESC, CHOL, COAD, DLBC, ESCA, HNSC, KIRC, KIRP, LGG, LIHC, LUAD, LUSC, MESO, OV, PAAD, PCPG, PRAD, READ, SARC, SKCM, STAD, TGCT, THCA, UCEC, UCS, UVM) (**Supplement Figure 13**). Moreover, GZMA and PRF1 also showed a tightly co-expressed correlation in 32 of the 33 tumor types (except for LAML) (**Supplement Figure 14**), which is consistent with the previous study (13). Based on the co-expression relationship of the four IRGs, it is suggested that by dividing four IRGs into two groups (CD274 and CD8A, GZMA, and PRF1, respectively), we may reveal a certain TME commonality and TILs similarity. After merging log 2-transformed values of the (FPKM+1) of CD274, CD8A, GZMA, and PRF1, we divided all of the TCGA samples into four groups as follows: type I, CD274 expression higher than the median and CD8A expression higher than the median; type II, CD274 expression higher than the median and CD8A expression lower than the median; type III, CD274 expression lower than the median and CD8A expression higher than the median; and type IV, CD274 expression lower than the median and CD8A expression lower than the median. Between type I and type II, tumor tissues showed higher m^{6}A regulators expressions compared with normal tissues across multiple tumor types (**Figure 2A**). A similar analysis in type III and type IV revealed that m^{6}A regulators turned to expressed in lower level (**Figure 2B**).

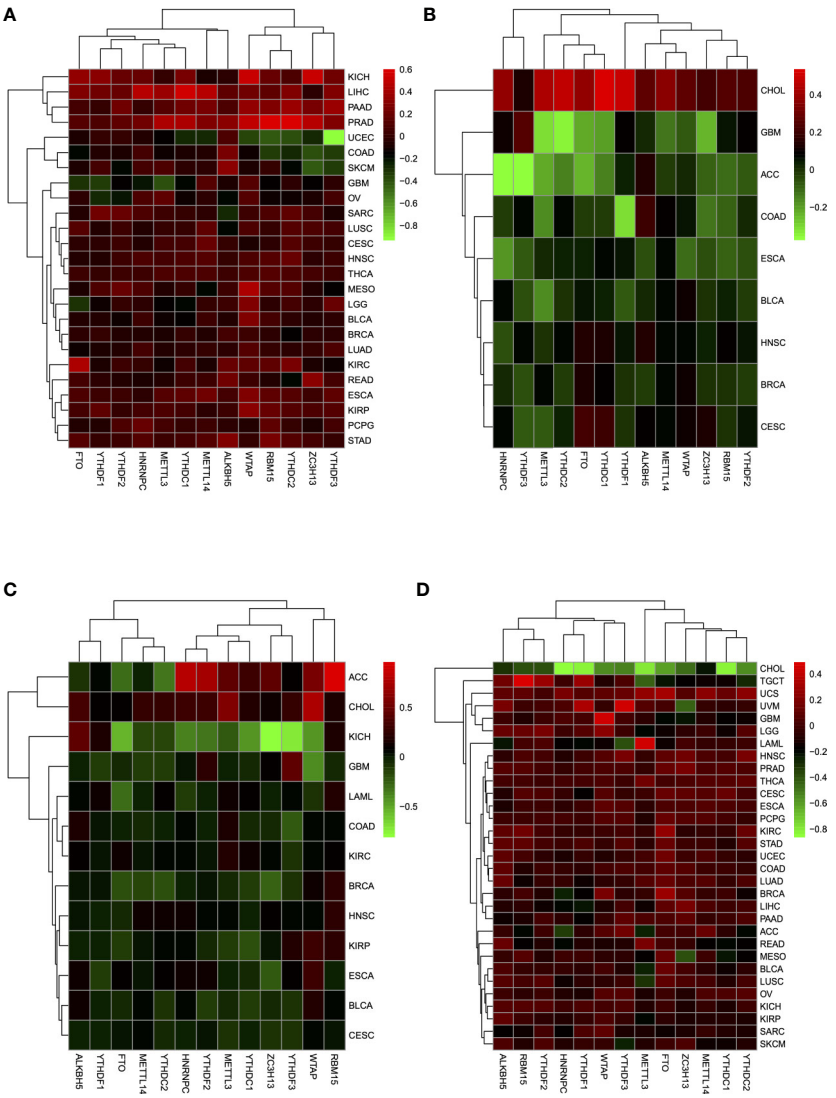

FIGURE 2 | **(A)** Expression of m^{6}A regulators between tumor tissues and normal tissues in type I and type II groups, which showed a higher expression tendency in tumor tissues. **(B)** In type III and type IV, m^{6}A regulators tended to show a lower expression tendency in tumor tissues. **(C)** M^{6}A regulators in tumor tissues showed a lower expression level between type V and type VI. **(D)** Between type VII and type VIII, m^{6}A regulators showed a higher expression level in tumor tissues.

More specifically, m^{6}A regulators' expression drift changed from high-level to low-level in ESCA, BLCA, HNSC, CESC, BRCA, and GBM.

In the same way, we divided all of the TCGA samples into four groups as follows: type V, GZMA expression higher than the median and PRF1 expression higher than the median; type VI, GZMA expression higher than the median and PRF1 expression lower than the median; type VII, GZMA expression lower than the median and PRF1 expression higher than the median; and type VIII, GZMA expression lower than the median and PRF1 expression lower than the median. Compared with type V and type VI, m^{6}A regulators drew a shift from lower expression level to higher level in type VII and type VIII between tumor tissues and normal tissues in CESC, BLCA, ESCA, KIRP, HNSC, BRCA, KIRC, COAD, LAML, GBM, and KICH (**Figures 2C, D**). Only in CHOL, m^{6}A regulators changed from higher to lower expression tendency. Overall, when we grouped the patients depending on the expression levels of IRGs, m^{6}A regulators reflected dramatic

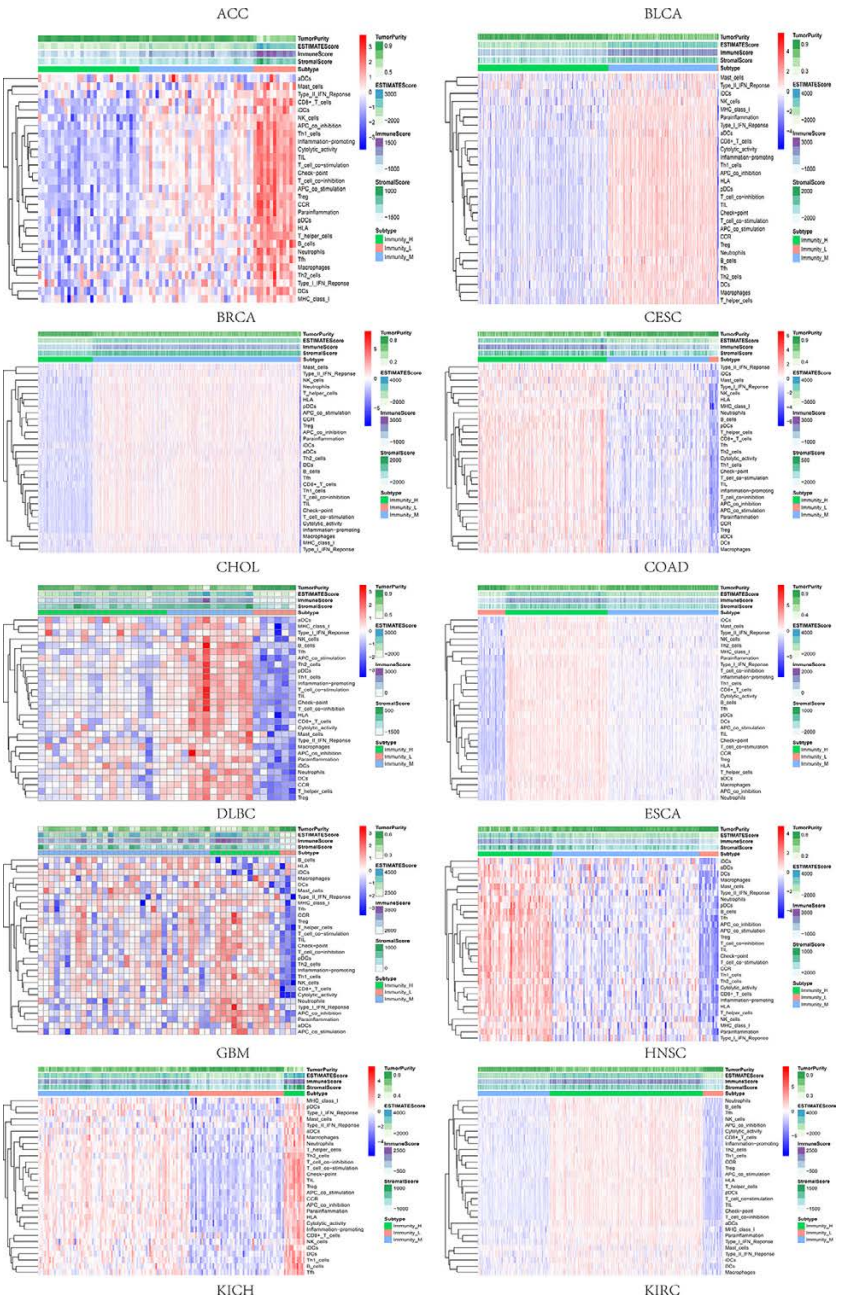

FIGURE 3 | Three subgroups were defined as immunity-high, immunity-medium, and immunity-low by ssGSEA scores across 33 tumor types.

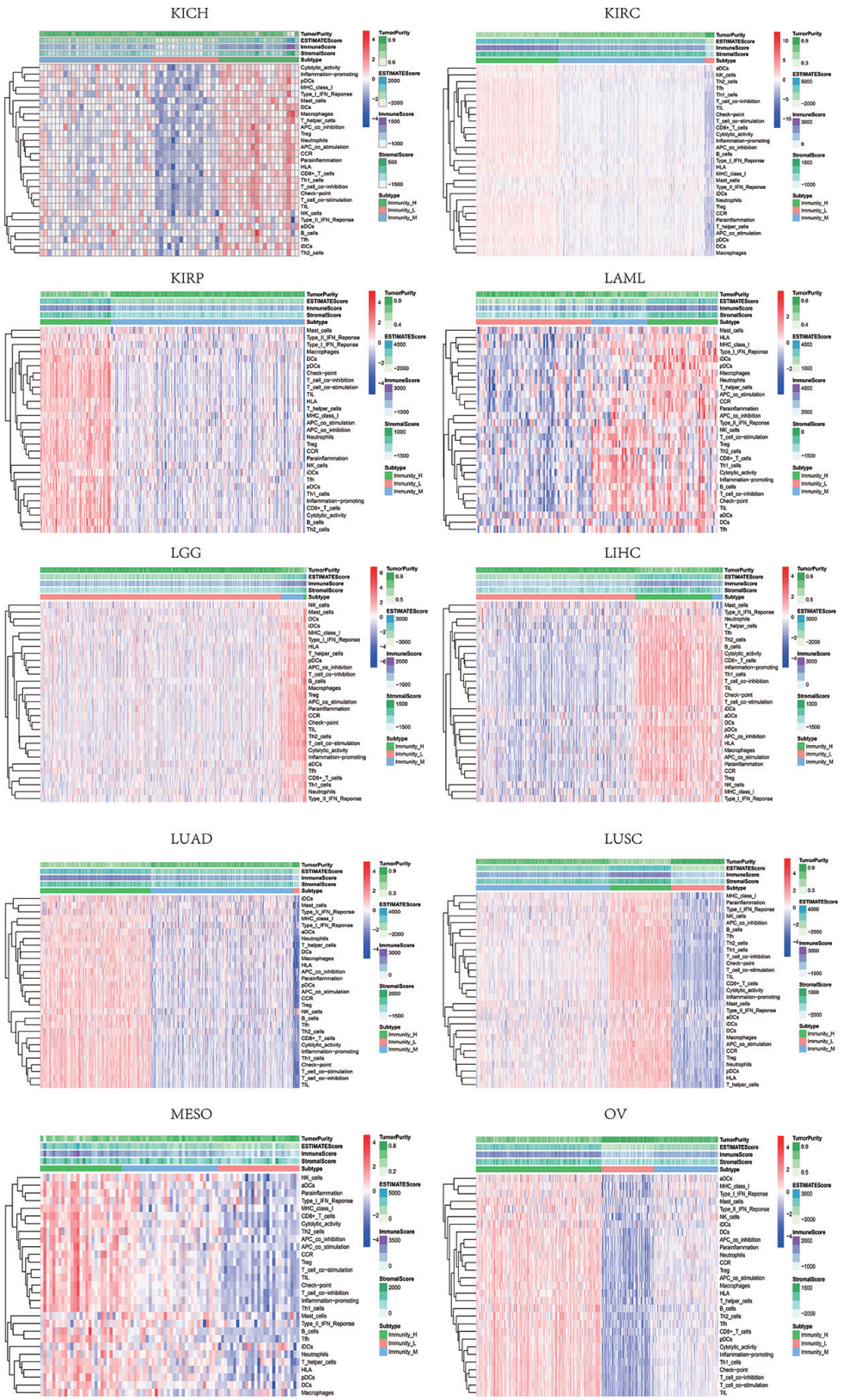

FIGURE 4 | Three subgroups were defined as immunity-high, immunity-medium, and immunity-low by ssGSEA scores across 33 tumor types.

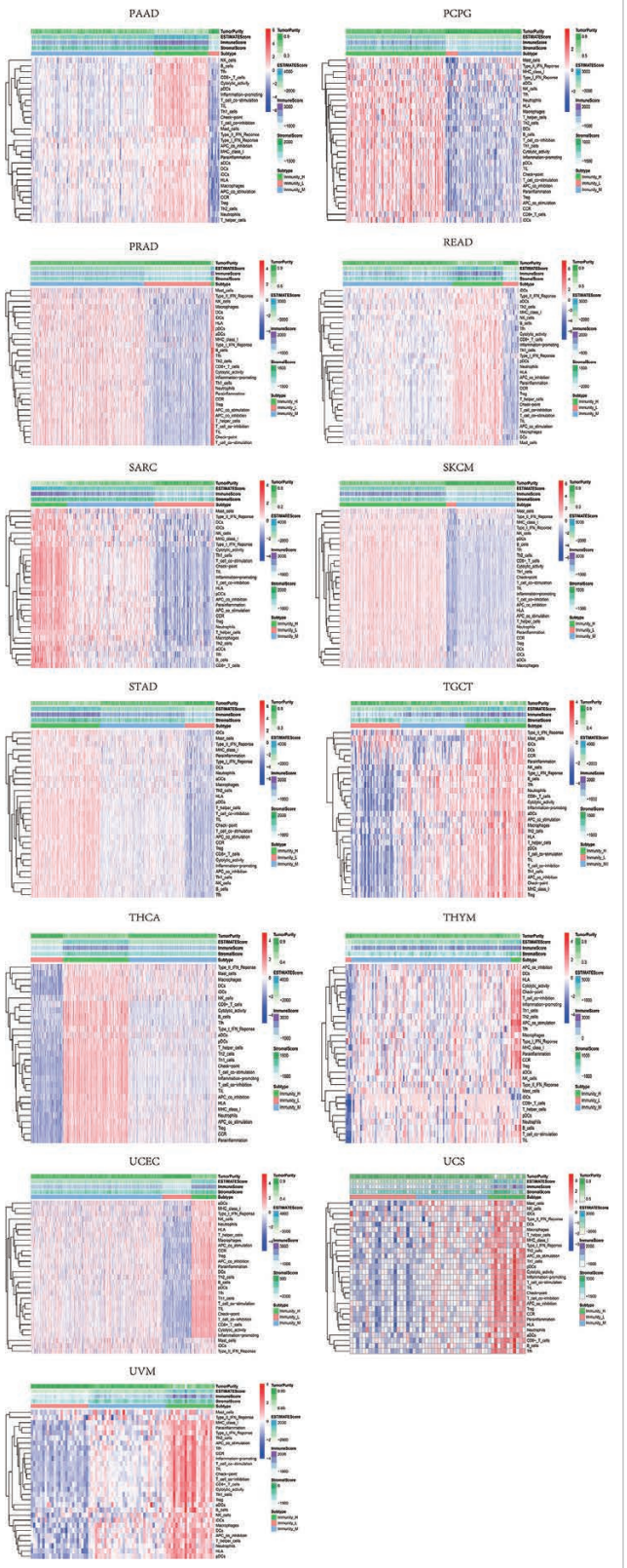

FIGURE 5 | Three subgroups were defined as immunity-high, immunity-medium, and immunity-low by ssGSEA scores across 33 tumor types.

contrast changes among groups. The considerable expression fluctuation among groups revealed that m^{6}A regulators might be the crucial factors affecting IRGs expression and thus affecting TME immune infiltration.

The Relevance of Immune-Related Genes and m^{6}A Regulators With Tumor Microenvironment Features

Based on the ssGSEA scores of infiltrated immune cells, the hierarchical clustering method divided the samples across 33 tumor types into three subgroups as immunity-high, immunity-medium, and immunity-low, representing the density of TILs (**Figures 3**–**5**). Meanwhile, by combining ESTIMATE analysis, we revealed the distribution of immune score, stromal score, ESTIMATE score, and tumor purity between the three immune subgroups. We found that the subgroup's immune infiltration degree was remarkably consistent with its immune score, stromal score, and ESTIMATE score. Conversely, high immune infiltration, observed in the immunity-high group, was related to low tumor purity, which indicated that we successfully divided all samples into subgroups depending on their TILs and TME characteristics. The next, we found some commonalities between the four IRGs and TILs once again. High immune infiltration was strongly related to high expressions of CD274 (**Figure 6**), CD8A (**Figure 7**), GZMA (**Figure 8**), and PRF1 (**Figure 9**). Almost all the four IRGs showed the rising expression trend with the degree of immune infiltration in 18 tumor types (ACC, BLCA, CESC, CHOL, COAD, DLBC, ESCA, GBM, HNSC, KICH, KIRP, LGG, LIHC, LUAD, LUSC, MESO, OV, PAAD, PRAD, READ, SARC, SKCM, STAD, TGCT, THCA, UCEC, UCS, and UVM). Additionally, we measured the diversity of m^{6}A regulators among three subtypes (**Figures 10**–**12**). METTL3 showed vast expression differences in 22 tumor types (ACC, BLCA, BRCA, CESC, CHOL, COAD, GBM, HNSC, KIRC, KIRP, LAML, LGG, LUAD, LUSC, OV, PRAD, SARC, SKCM, STAD, THCA, UCEC, and UVM), although no uniform expression trend was observed among the three subgroups. YTHDF1 and YTHDC1 followed it, showing subgroup-to-group expression varieties in 21 and 19 tumor types. Similarly, no significant expression tendency was observed among subgroups. Besides, high immune infiltration indicated better prognosis in CESC, LGG, OV, SARC, SKCM, THYM, UCEC, and UVM (**Figure 13**). These results showed that m^{6}A regulators may affect TILs and result in heterogeneous prognostic outcomes by affecting the expression of IRGs.

Correlation Between Tumor Mutational Burden and m^{6}A Regulators in Pan-Cancer Tissues

TMB has been reported to closely influence immunotherapy's effectiveness across tumor types (8, 37, 38). Tumors with highly mutated burdens are more susceptible to immune cells because of the neoantigens making them respond to ICIs better (8, 39). Considering the close ties between TMB and immune infiltration, TMB could be a predictor of multiple tumors with either anti-CTLA-4 or anti-PD-L1 treatment. Besides, CYT has

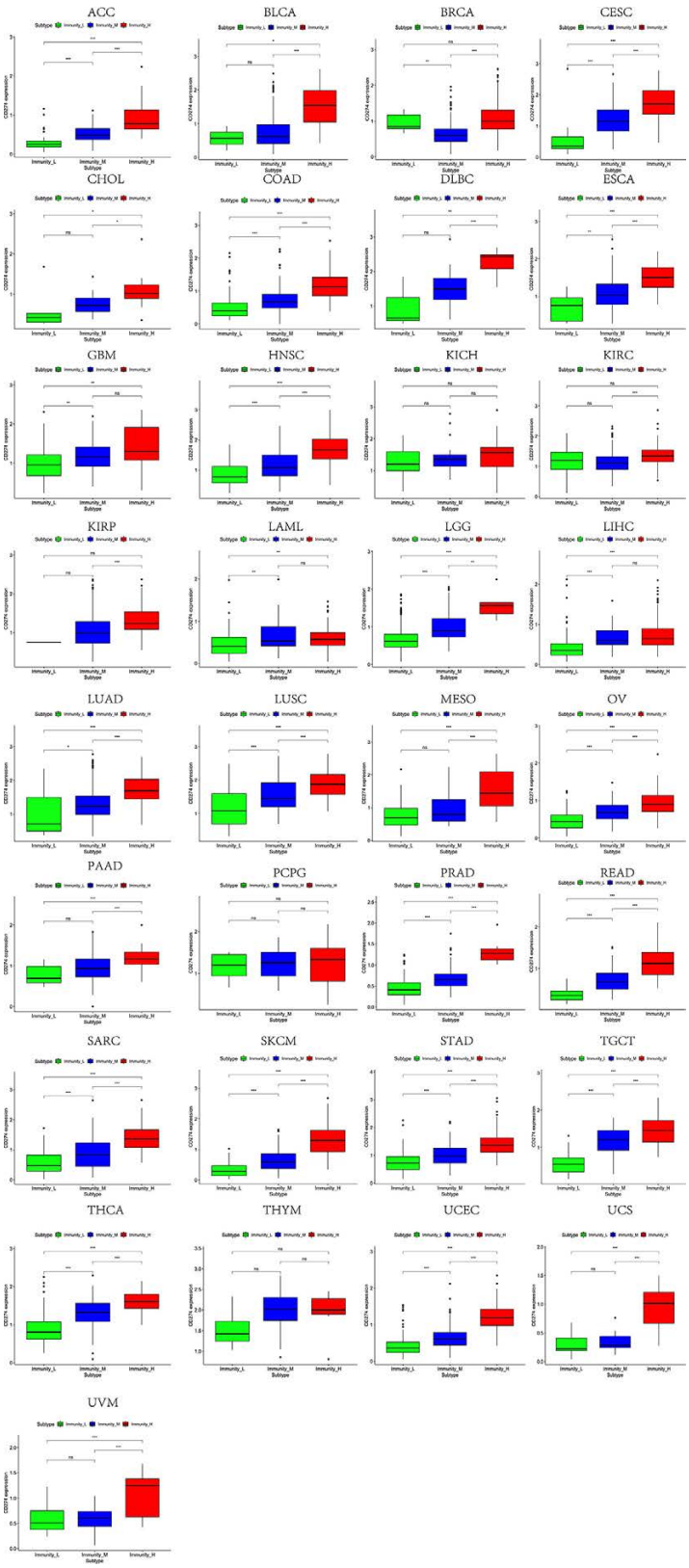

FIGURE 6 | High expression level of CD274 was presented in high immune infiltration across 33 tumor types.

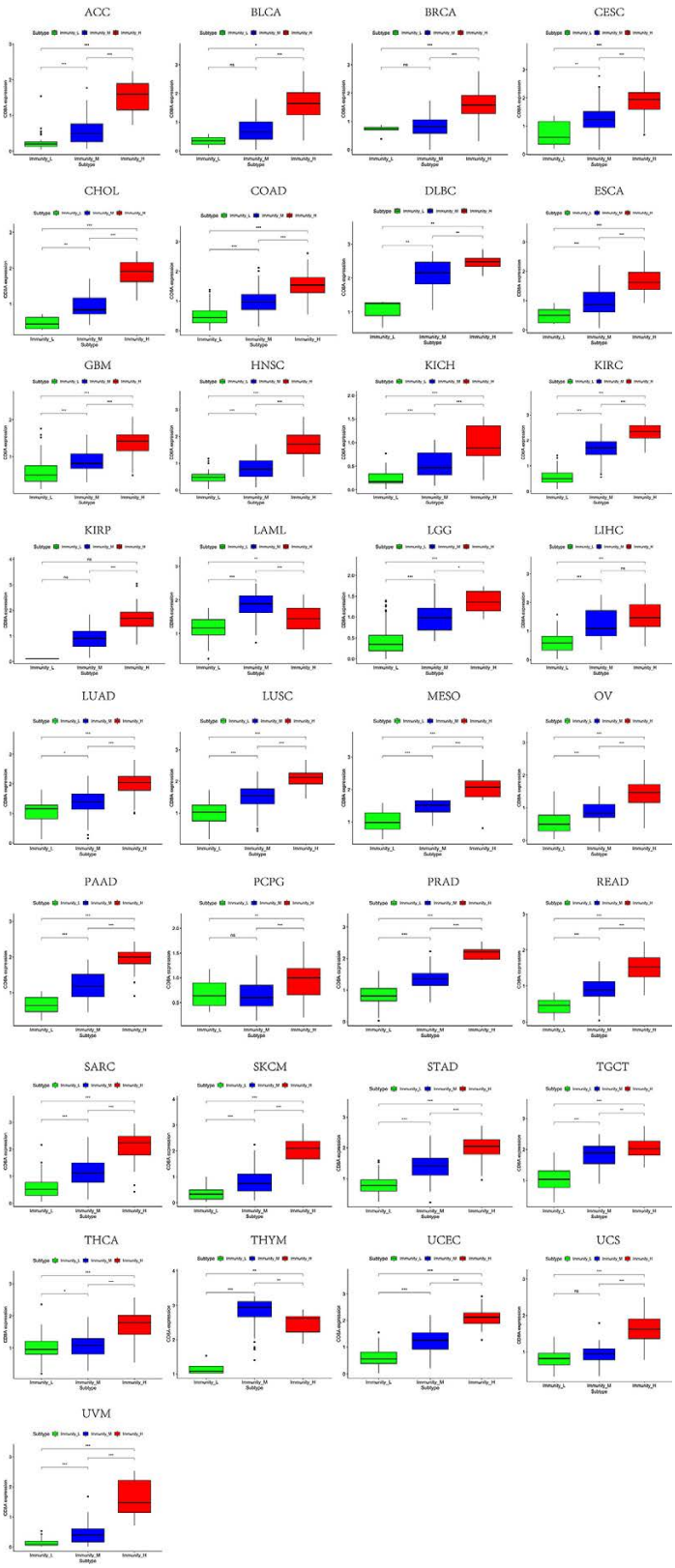

FIGURE 7 | High expression level of CD8A was presented in high immune infiltration across 33 tumor types.

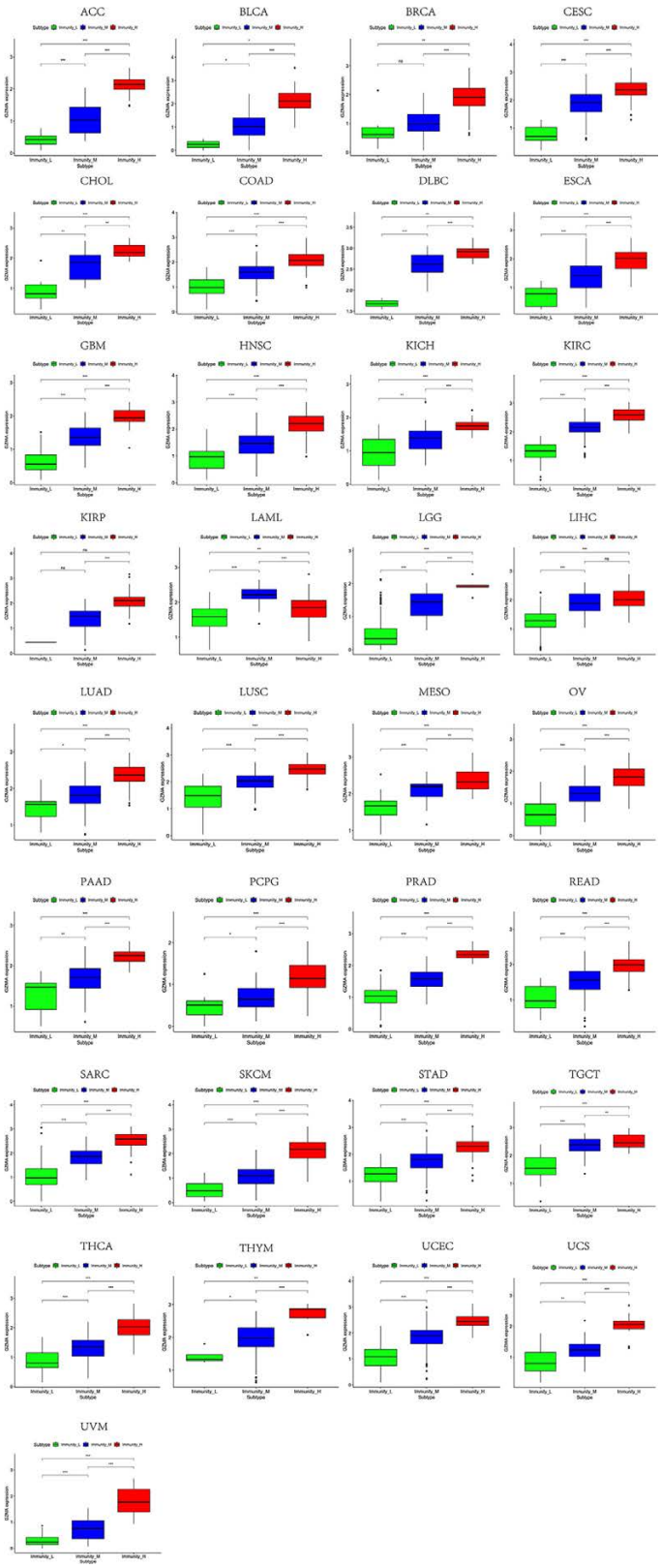

FIGURE 8 | High expression level of GZMA was presented in high immune infiltration across 33 tumor types.

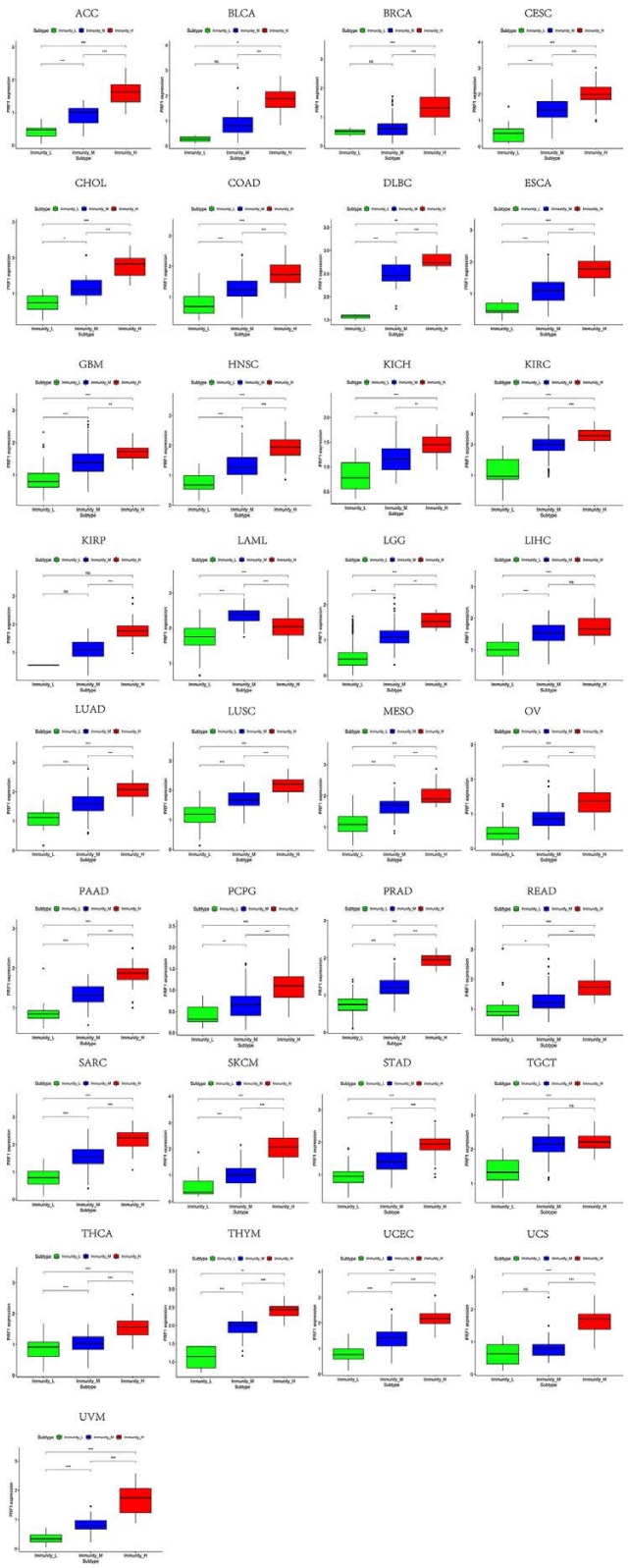

FIGURE 9 | High expression level of PRF1 was presented in high immune infiltration across 33 tumor types.

also been reported to positively correlate with somatic mutations of IRGs (13). Furthermore, high-level co-expression of CD274 and CD8A is usually associated with higher tumor mutation and oncogenic viral infection (14, 40). Nevertheless, we do not know much about the impact of TMB on m^{6}A regulators. Since we have demonstrated in the foregoing process that m6A regulators' impacts on IRGs may extend to the whole TILs and TME, we analyzed the correlation between TMB and m6A regulators in pan-cancer tissues. By taking the median value of TMB, patients' profiles were divided into high and low TMB groups in each tumor type. It could be seen that large inter-group differences of m^{6}A regulators were observed in BLCA, BRCA, COAD, LGG, LUAD, LUSC, STAD, THCA, and UCEC (**Figure 14**). Especially, FTO (in all of nine tumor types), RBM15 (in seven of nine tumor types), and YTHDF1 (in six of nine tumor types) showed a wide range of inter-group expression differences.

Relationship Between Immune-Related Genes and Clinical Parameters

Chi-square test and Wilcoxon test analyses were performed to explore the associations between clinical parameters and expression levels' values. The results showed that the level of CD274 varies at tumor stages in COAD, ESCA, READ, SKCM, and THCA, mostly between early (stage I and II) and late-stage (stage III and IV) patients (**Figure 15**). Meanwhile, CD8A and GZMA also had similar expression variants in several tumor types such as COAD, SKCM, STAD, KIRC, and THCA (**Figure 15**). As for PRF1, we only observed this expression differences between stages in ACC and SKCM (**Figure 15**). Overall, the differences of IRGs' expression levels between early and late-stage patients are more evident in COAD, SKCM, KIRC, THCA, and SKCM. We still used the mean expression value of IRGs as the threshold to compare whether there are differences in OS, DSS, and PFI in various tumor types. The high-expression group of CD274 performed better at OS, DSS, and PFI in ACC and SKCM (**Supplement Figure 15**). The high-expression group of CD8A showed better OS, DSS, and PFI performance in CESC, SKCM, and UCEC (**Supplement Figure 15**). The high-expression group of GZMA had longer survival time, DSS, and PFI in BRCA, SKCM, and UCEC (**Supplement Figure 15**). The high-expression group of PRF1 showed better survival performance or longer PFI in ACC, SKCM, and UCEC (**Supplement Figure 15**).

DISCUSSION

Immunotherapy has recently received extensive attention and shows efficacy in many cancers (1). However, the variable clinical response has been associated with patients' immune genomic characteristics as much as other features such as TME and TILs (7, 9, 41, 42). Due to the regulation of the m^{6}A, modifications are associated with almost any step of mRNA metabolism. There is convincing evidence that m6A modification is particularly critical in a variety of pathological and physiological immune responses, including T cell homeostasis and differentiation, dendritic cell activation (43–45).

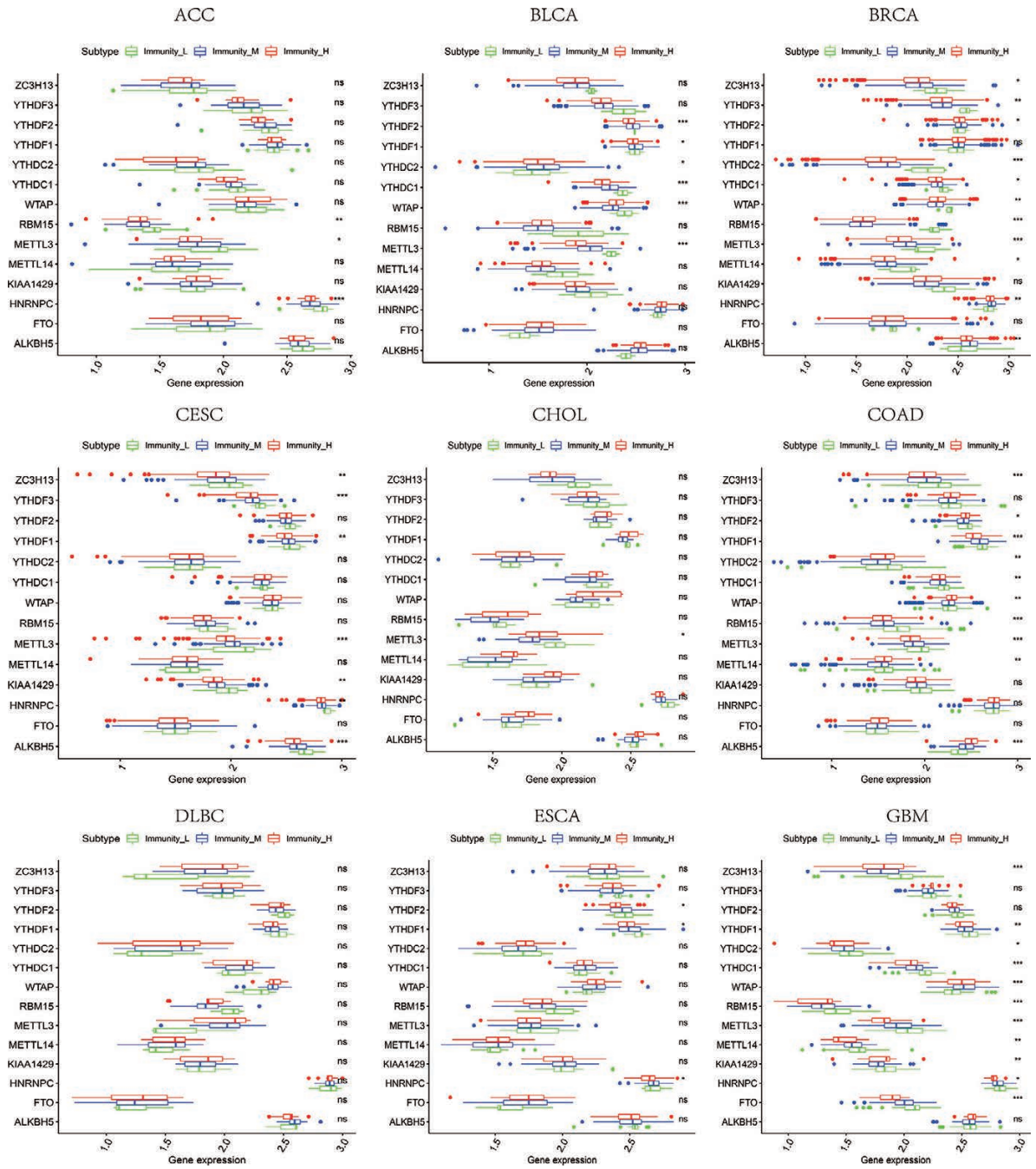

FIGURE 10 | The expression diversity of m^{6}A regulators among high, medium, and low immune infiltration levels. * represents P < 0.05, ** represents P < 0.01, *** represents P < 0.001, ns represents P ≥ 0.05.

Our study intends to prove that m^{6}A regulators could alter TME properties by influencing key IRGs and TILs. Based on the previous researches, CD274, CD8A, GZMA, and PRF1 were selected for further analysis as being iconic targets of ICIs and key genes affecting TILs. CD274, also known as PD-L1, was found to have high expression on the surface of various tumor cells (46, 47), involving the development of tumors and affecting response to ICIs' treatment and clinical outcomes (48). CD8A encodes part of cell surface glycoprotein on most cytotoxic T lymphocyte, which includes adaptive immune response-induced CD8+ cytolytic T cells (49, 50), plays a crucial role in the antitumor activity of anti-PD-L1 (51). GZMA and PRF1 serve as two key cytolytic effectors, which are proved to bond with CD8+ T cell activation and affect clinical responses to ICIs (13).

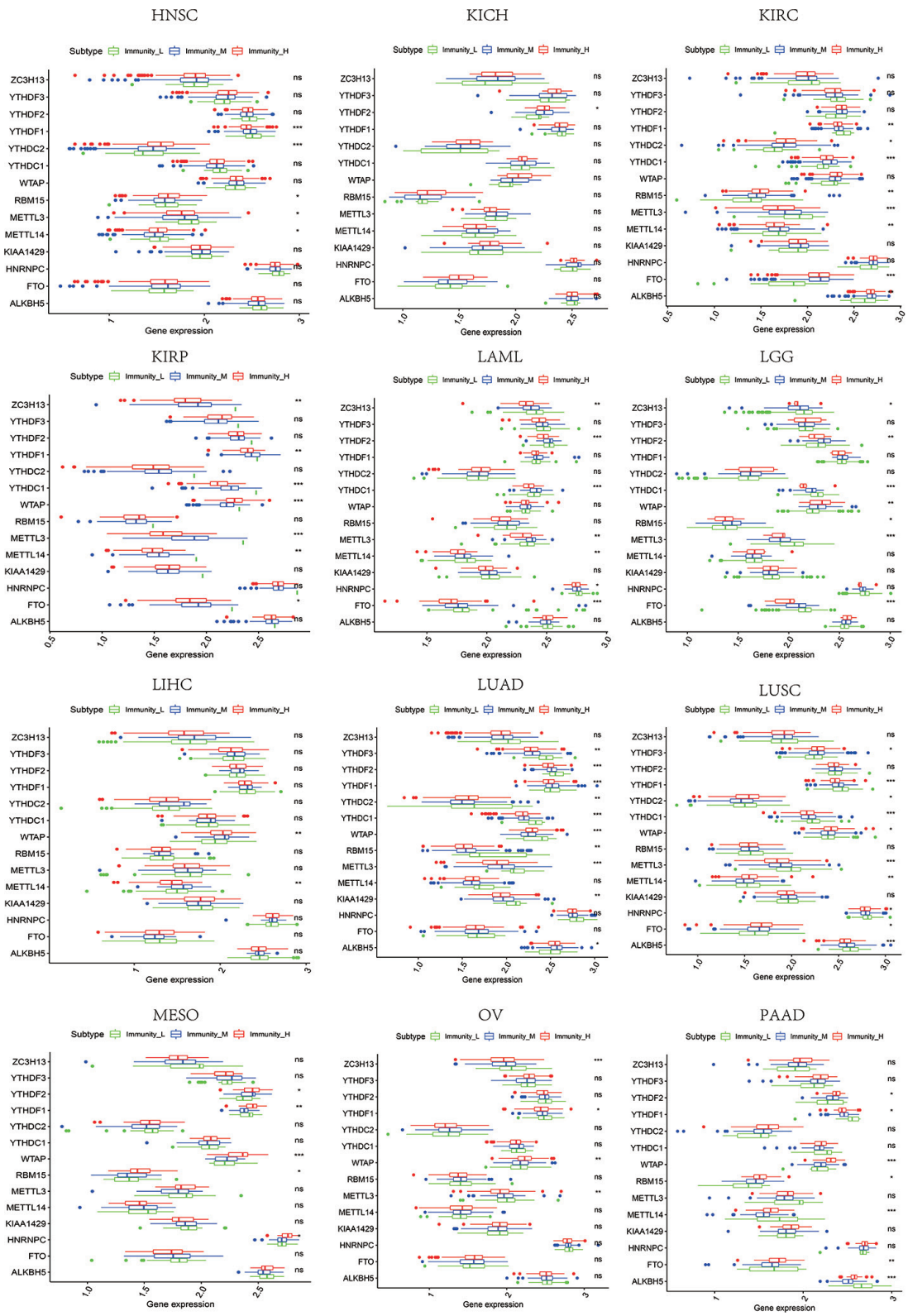

FIGURE 11 | The expression diversity of m^{6}A regulators among high, medium, and low immune infiltration levels. * represents $P < 0.05$, ** represents $P < 0.01$, *** represents $P < 0.001$, ns represents $P \geq 0.05$.

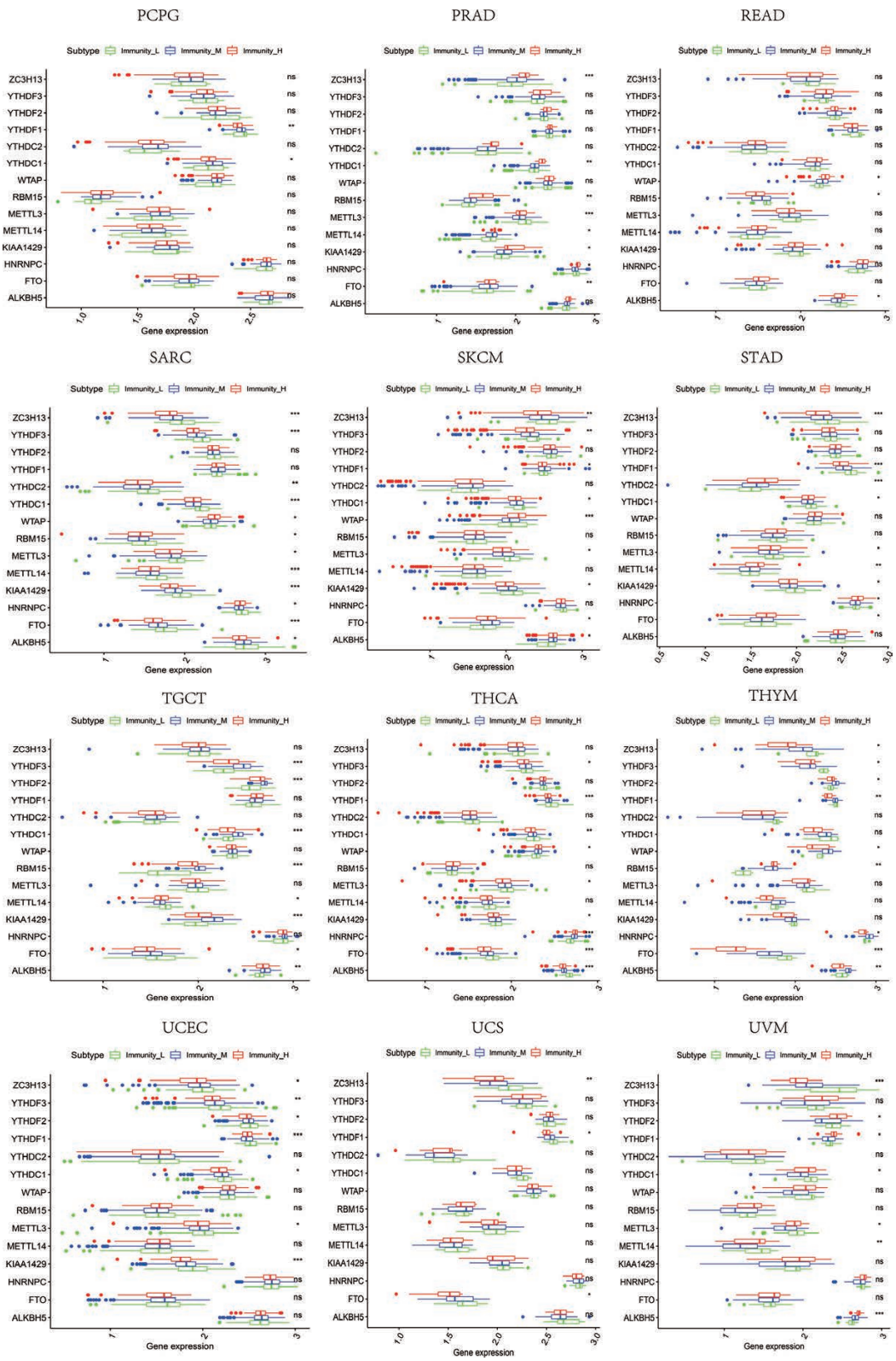

FIGURE 12 | The expression diversity of m^{6}A regulators among high, medium, and low immune infiltration levels. * represents $P < 0.05$, ** represents $P < 0.01$, *** represents $P < 0.001$, ns represents $P \geq 0.05$.

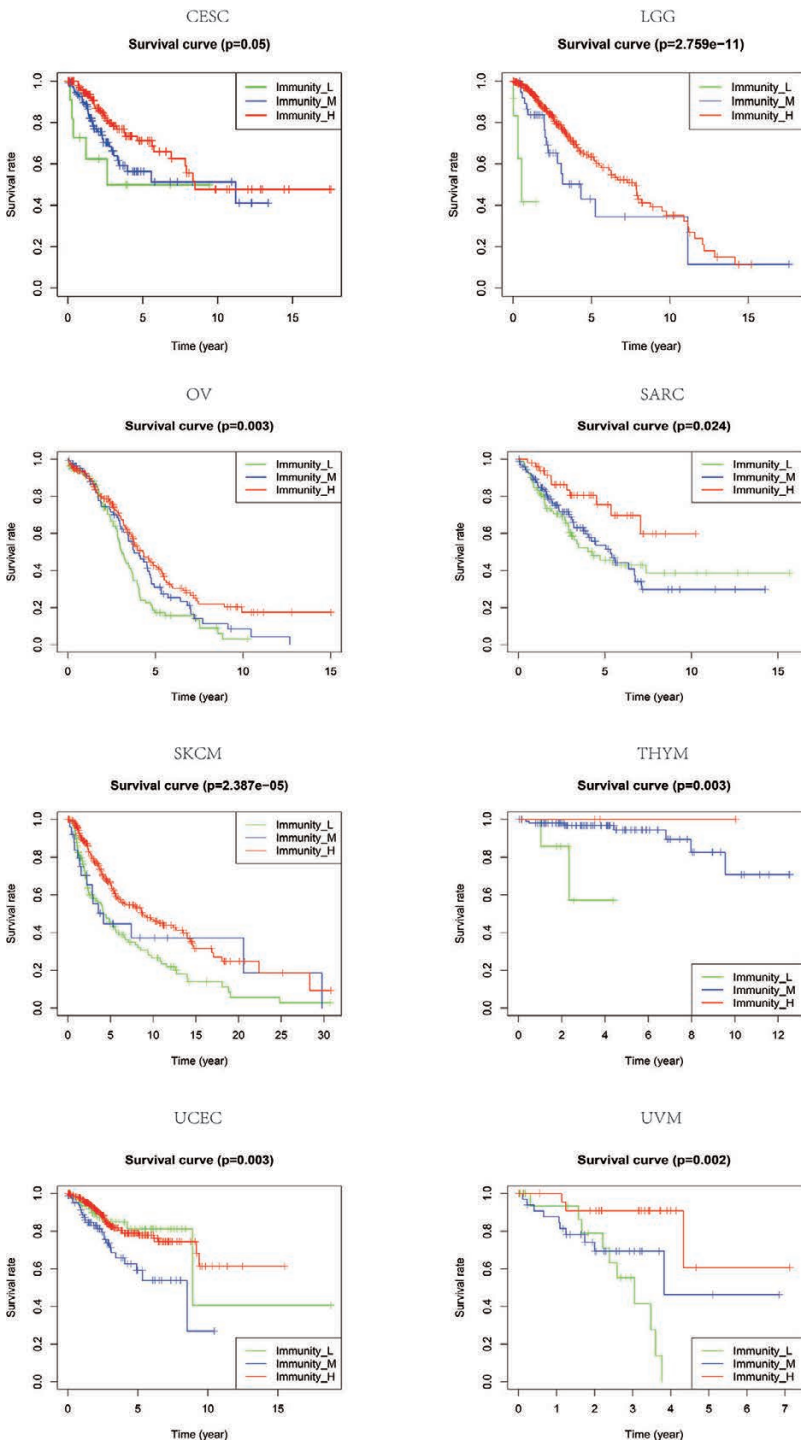

FIGURE 13 | The patients that grouped into high immune infiltration showed better prognosis in CESC, LGG, OV, SARC, SKCM, THYM, UCEC, and UVM.

All four IRGs were proved to have impacts on pathological stages and clinical outcomes. Furthermore, they showed similar TILs characteristics, of which it is worth noting that the expression tendency of T cells CD8, T cells CD4 memory activated is consistent with the expression levels of all four immune-related genes. Not surprisingly, ICIs had been proved to rely heavily on functional T cells CD8 (CD8+ T cells) (52). Moreover, activated memory CD4 T cells also play a crucial role in effective antitumor

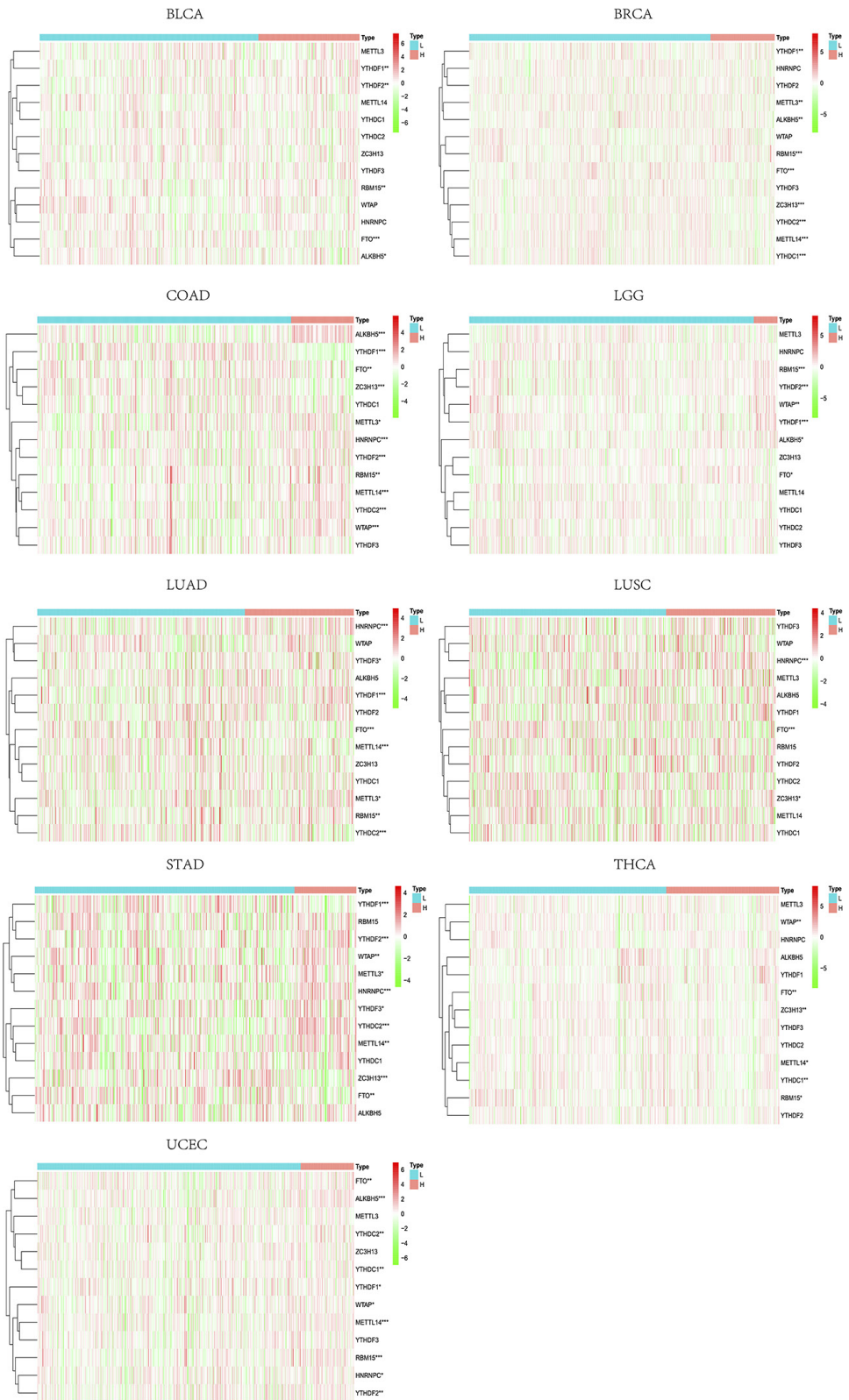

FIGURE 14 | Inter-group differences of m^{6}A regulators between high- and low-TMB levels. * represents P < 0.05, ** represents P < 0.01, *** represents P < 0.001.

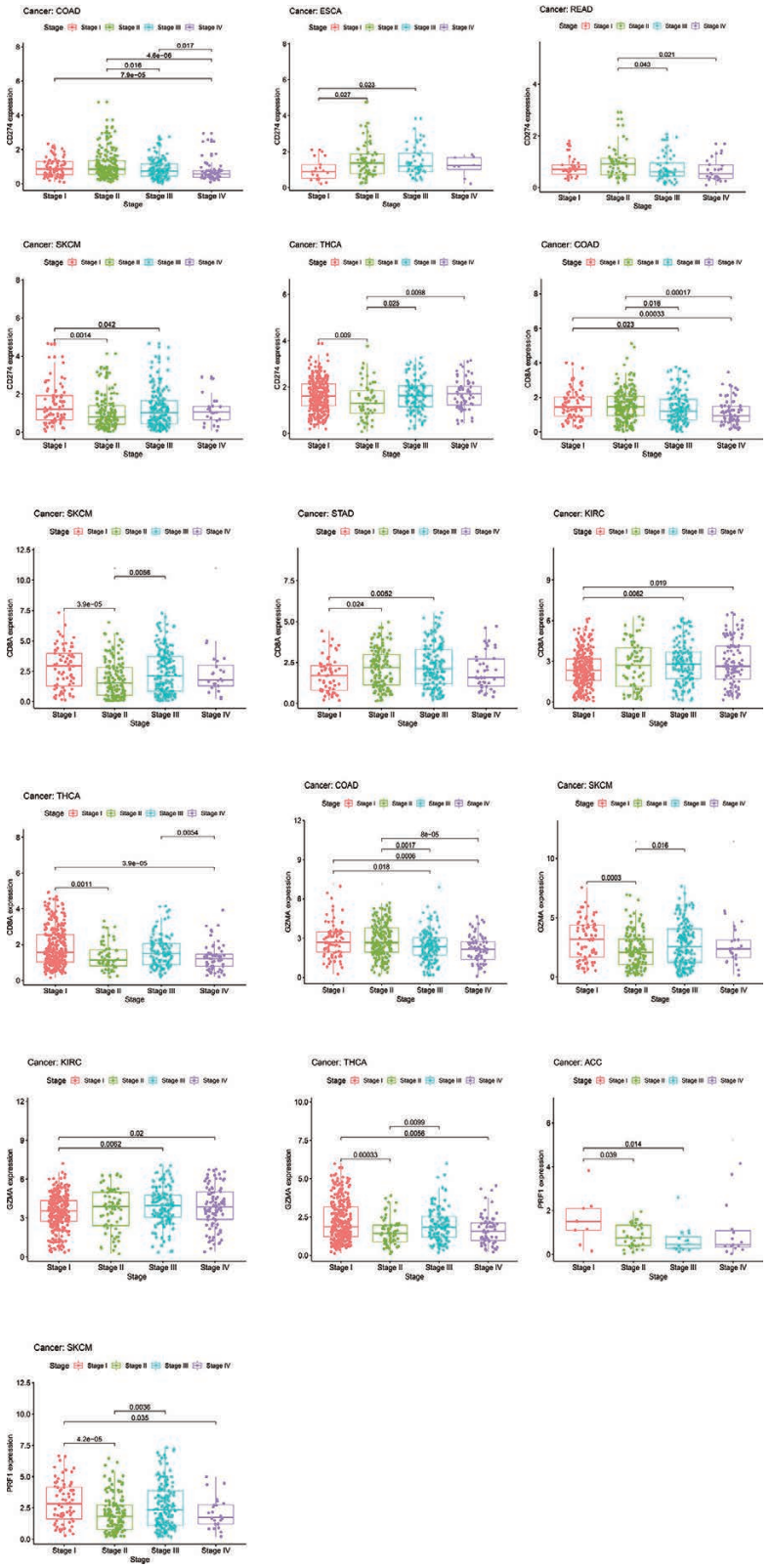

FIGURE 15 | The levels of CD274, CD8A, GZMA, and PRF1 varied between early (stage I and II) and late-stage (stage III and IV) patients.

immunity (53). And ssGSEA analyses revealed expression levels of CD274, CD8A, GZMA, and PRF1 were positively correlated with high immune infiltration in 18 tumor types, which was consistent with the result of ESTIMATE analyses that all the four IRGs were positively expressed with the immune score or stromal score in almost all of 33 tumor types. High immune infiltration and high-level of the four IRGs were found to predict better prognosis in multiple tumor types like CESC, SKCM, THYM, and UCEC. So far, we believed that the four IRGs could represent the TILs characteristics of tumor tissues and to be used to classify TME. Based on the co-expression correlation between CD274 and CD8A in 29 tumor types, and between GZMA and PRF1 in 32 tumors, we further classified TME into eight groups according to IRGs' expression level. The exact opposite expression tendency of m6A regulators was found among the subgroups of type I to type VIII, suggesting that m6A regulators may be essential for phenotypic modifications of IRGs. To further confirm this correlation, the ssGSEA method was used to classify immuno-subtypes and genomic expression diversities. IRGs and m^6A regulators were proved to vary with immuno-subtypes in different TME characteristics.

Neoantigens are carried by highly mutated tumors, which are susceptible to immune cells and own a better response to ICIs (38). Previous studies have shown that TMB could predict patients' survival in diverse tumor types with either anti-CTLA-4 or anti-PD-1 treatment (8, 39). We further evaluated the correlation between TMB and m^6A regulators. In nine tumor types (BLCA, BRCA, COAD, LGG, LUAD, LUSC, STAD, THCA, and UCEC), m^6A regulators' expressions also differ along with TMB levels. In conclusion, we have demonstrated the prevalent genetic expression alterations of the crucial IRGs are related to m^6A regulators across tumor types. Both of IRGs and m^6A regulators are tightly correlated with TME characteristics and TILs features. Our systematic and comprehensive analyses in the landscape of molecular alterations and clinical relevance provide a foundation for understanding the internal mechanisms of TME and its overall prognosis and the development of potential therapeutic targets.

DATA AVAILABILITY STATEMENT

Publicly available datasets were analyzed in this study. These data can be found here: The original contributions presented in the study are publicly available in TCGA database (https://portal.gdc.cancer.gov/). This data can be found in the UCSC Xena browser (https://xenabrowser.net).

AUTHOR CONTRIBUTIONS

JZ, JX, MW, and DH handled the conceptualization and methodology. JZ, MW, and JX handled the software. JX and DH handled the validation. JZ and MW were in charge of the original draft preparation. JX and DH were responsible for the review and editing. The first authors of this manuscript are JZ and JX. These authors contributed equally to this work. All authors contributed to the article and approved the submitted version.

FUNDING

This work was supported by the Science and Technology Project in Tongliang District (No.TL2019-25).

SUPPLEMENTARY MATERIAL

The Supplementary Material for this article can be found online at: https://www.frontiersin.org/articles/10.3389/fonc.2020.618374/full#supplementary-material

SUPPLEMENTARY FIGURE 1 | Pancancer TILs component analyses of CD274 *via* CIBERSORT.

SUPPLEMENTARY FIGURE 2 | Pancancer TILs component analyses of CD8A *via* CIBERSORT.

SUPPLEMENTARY FIGURE 3 | Pancancer TILs component analyses of GZMA *via* CIBERSORT.

SUPPLEMENTARY FIGURE 4 | Pancancer TILs component analyses of PRF1 *via* CIBERSORT.

SUPPLEMENTARY FIGURE 5 | Correlation analysis between CD274 and ESTIMATE immune score or stromal score across pancancer tissues.

SUPPLEMENTARY FIGURE 6 | Correlation analysis between CD8A and ESTIMATE immune score or stromal score across pancancer tissues.

SUPPLEMENTARY FIGURE 7 | Correlation analysis between GZMA and ESTIMATE immune score or stromal score across pancancer tissues.

SUPPLEMENTARY FIGURE 8 | Correlation analysis between PRF1 and ESTIMATE immune score or stromal score across pancancer tissues.

SUPPLEMENTARY FIGURE 9 | Expression analysis of m^6A regulators between high- and low-expression levels of CD274.

SUPPLEMENTARY FIGURE 10 | Expression analysis of m^6A regulators between high- and low-expression levels of CD8A.

SUPPLEMENTARY FIGURE 11 | Expression analysis of m^6A regulators between high- and low-expression levels of GZMA.

SUPPLEMENTARY FIGURE 12 | Expression analysis of m^6A regulators between high- and low-expression levels of PRF1.

SUPPLEMENTARY FIGURE 13 | Co-expression relationship between CD274 and CD8A across pancancer tissues.

SUPPLEMENTARY FIGURE 14 | Co-expression relationship between GZMA and PRF1 across pancancer tissues.

SUPPLEMENTARY FIGURE 15 | The high-expression level of CD274 performed better at OS, DSS, and PFI in ACC and SKCM; The high-expression level of CD8A showed better OS, DSS, and PFI performance in CESC, SKCM, and UCEC; The high-expression level of GZMA had longer survival time, DSS, and PFI in BRCA, SKCM, and UCEC; The high-expression level of PRF1 showed better survival performance or longer PFI in ACC, SKCM, and UCEC.

REFERENCES

1. Topalian SL, Hodi FS, Brahmtpb 2er JR, Gettinger SN, Smith DC, McDermott DF, et al. Safety, activity, and immune correlates of anti-PD-1 antibody in cancer. *N Engl J Med* (2012) 366(26):2443–54. doi: 10.1056/NEJMoa1200690
2. Xu W, Atkins MB, McDermott DF. Checkpoint inhibitor immunotherapy in kidney cancer. *Nat Rev Urol* (2020) 17(3):137–50. doi: 10.1038/s41585-020-0282-3
3. Lee CK, Man J, Lord S, Links M, Gebski V, Mok T, et al. Checkpoint Inhibitors in Metastatic EGFR-Mutated Non-Small Cell Lung Cancer-A Meta-Analysis. *J Thorac Oncol* (2017) 12(2):403–7. doi: 10.1016/j.jtho.2016.10.007
4. Hamid O, Robert C, Daud A, Hodi FS, Hwu WJ, Kefford R, et al. Safety and tumor responses with lambrolizumab (anti-PD-1) in melanoma. *N Engl J Med* (2013) 369(2):134–44. doi: 10.1056/NEJMoa1305133
5. Garon EB, Rizvi NA, Hui R, Leighl N, Balmanoukian AS, Eder JP, et al. Pembrolizumab for the treatment of non-small-cell lung cancer. *N Engl J Med* (2015) 372(21):2018–28. doi: 10.1056/NEJMoa1501824
6. Ansell SM, Lesokhin AM, Borrello I, Halwani A, Scott EC, Gutierrez M, et al. PD-1 blockade with nivolumab in relapsed or refractory Hodgkin's lymphoma. *N Engl J Med* (2015) 372(4):311–9. doi: 10.1056/NEJMoa1411087
7. Keenan TE, Burke KP, Van Allen EM. Genomic correlates of response to immune checkpoint blockade. *Nat Med* (2019) 25(3):389–402. doi: 10.1038/s41591-019-0382-x
8. Samstein RM, Lee CH, Shoushtari AN, Hellmann MD, Shen R, Janjigian YY, et al. Tumor mutational load predicts survival after immunotherapy across multiple cancer types. *Nat Genet* (2019) 51(2):202–6. doi: 10.1038/s41588-018-0312-8
9. Thorsson V, Gibbs DL, Brown SD, Wolf D, Bortone DS, Ou Yang TH, et al. The Immune Landscape of Cancer. *Immunity* (2019) 51(2):411–2. doi: 10.1016/j.immuni.2019.08.004
10. Casey SC, Amedei A, Aquilano K, Azmi AS, Benencia F, Bhakta D, et al. Cancer prevention and therapy through the modulation of the tumor microenvironment. *Semin Cancer Biol* (2015) 35 Suppl:S199–223. doi: 10.1016/j.semcancer.2015.02.007
11. Chen DS, Mellman I. Elements of cancer immunity and the cancer-immune set point. *Nature* (2017) 541(7637):321–30. doi: 10.1038/nature21349
12. El-Khoueiry AB, Sangro B, Yau T, Crocenzi TS, Kudo M, Hsu C, et al. Nivolumab in patients with advanced hepatocellular carcinoma (CheckMate 040): an open-label, non-comparative, phase 1/2 dose escalation and expansion trial. *Lancet* (2017) 389(10088):2492–502. doi: 10.1016/S0140-6736(17)31046-2
13. Rooney MS, Shukla SA, Wu CJ, Getz G, Hacohen N. Molecular and genetic properties of tumors associated with local immune cytolytic activity. *Cell* (2015) 160(1-2):48–61. doi: 10.1016/j.cell.2014.12.033
14. Ock CY, Keam B, Kim S, Lee JS, Kim M, Kim TM, et al. Pan-Cancer Immunogenomic Perspective on the Tumor Microenvironment Based on PD-L1 and CD8 T-Cell Infiltration. *Clin Cancer Res* (2016) 22(9):2261–70. doi: 10.1158/1078-0432.CCR-15-2834
15. Teng MW, Ngiow SF, Ribas A, Smyth MJ. Classifying Cancers Based on T-cell Infiltration and PD-L1. *Cancer Res* (2015) 75(11):2139–45. doi: 10.1158/0008-5472.CAN-15-0255
16. Yue Y, Liu J, Cui X, Cao J, Luo G, Zhang Z, et al. VIRMA mediates preferential m(6)A mRNA methylation in 3'UTR and near stop codon and associates with alternative polyadenylation. *Cell Discov* (2018) 4:10. doi: 10.1038/s41421-018-0019-0
17. Yang Y, Hsu PJ, Chen YS, Yang YG. Dynamic transcriptomic m(6)A decoration: writers, erasers, readers and functions in RNA metabolism. *Cell Res* (2018) 28(6):616–24. doi: 10.1038/s41422-018-0040-8
18. Li A, Chen YS, Ping XL, Yang X, Xiao W, Yang Y, et al. Cytoplasmic m(6)A reader YTHDF3 promotes mRNA translation. *Cell Res* (2017) 27(3):444–7. doi: 10.1038/cr.2017.10
19. Yue Y, Liu J, He C. RNA N6-methyladenosine methylation in post-transcriptional gene expression regulation. *Genes Dev* (2015) 29(13):1343–55. doi: 10.1101/gad.262766.115
20. Lan Q, Liu PY, Haase J, Bell JL, Huttelmaier S, Liu T. The Critical Role of RNA m(6)A Methylation in Cancer. *Cancer Res* (2019) 79(7):1285–92. doi: 10.1158/0008-5472.CAN-18-2965
21. Liu ZX, Li LM, Sun HL, Liu SM. Link Between m6A Modification and Cancers. *Front Bioeng Biotechnol* (2018) 6:89. doi: 10.3389/fbioe.2018.00089
22. Dai D, Wang H, Zhu L, Jin H, Wang X. N6-methyladenosine links RNA metabolism to cancer progression. *Cell Death Dis* (2018) 9(2):124. doi: 10.1038/s41419-017-0129-x
23. Zhang C, Fu J, Zhou Y. A Review in Research Progress Concerning m6A Methylation and Immunoregulation. *Front Immunol* (2019) 10:922. doi: 10.3389/fimmu.2019.00922
24. Luo S, Wang Y, Zhao M, Lu Q. The important roles of type I interferon and interferon-inducible genes in systemic lupus erythematosus. *Int Immunopharmacol* (2016) 40:542–9. doi: 10.1016/j.intimp.2016.10.012
25. Shah K, Lee WW, Lee SH, Kim SH, Kang SW, Craft J, et al. Dysregulated balance of Th17 and Th1 cells in systemic lupus erythematosus. *Arthritis Res Ther* (2010) 12(2):R53. doi: 10.1186/ar2964
26. Li LJ, Fan YG, Leng RX, Pan HF, Ye DQ. Potential link between m(6)A modification and systemic lupus erythematosus. *Mol Immunol* (2018) 93:55–63. doi: 10.1016/j.molimm.2017.11.009
27. Zhang S, Liu F, Wu Z, Xie J, Yang Y, Qiu H. Contribution of m6A subtype classification on heterogeneity of sepsis. *Ann Transl Med* (2020) 8(6):306. doi: 10.21037/atm.2020.03.07
28. Li Y, Gu J, Xu F, Zhu Q, Chen Y, Ge D, et al. Molecular characterization, biological function, tumor microenvironment association and clinical significance of m6A regulators in lung adenocarcinoma. *Brief Bioinform* (2020) 00(00):1–17. doi: 10.1093/bib/bbaa225
29. Yi L, Wu G, Guo L, Zou X, Huang P. Comprehensive Analysis of the PD-L1 and Immune Infiltrates of m(6)A RNA Methylation Regulators in Head and Neck Squamous Cell Carcinoma. *Mol Ther Nucleic Acids* (2020) 21:299–314. doi: 10.1016/j.omtn.2020.06.001
30. Mo P, Xie S, Cai W, Ruan J, Du Q, Ye J, et al. N(6)-methyladenosine (m(6)A) RNA methylation signature as a predictor of stomach adenocarcinoma outcomes and its association with immune checkpoint molecules. *J Int Med Res* (2020) 48(9):300060520951405. doi: 10.1177/0300060520951405
31. Li T, Fan J, Wang B, Traugh N, Chen Q, Liu JS, et al. TIMER: A Web Server for Comprehensive Analysis of Tumor-Infiltrating Immune Cells. *Cancer Res* (2017) 77(21):e108–e10. doi: 10.1158/0008-5472.CAN-17-0307
32. Li B, Li T, Liu JS, Liu XS. Computational Deconvolution of Tumor-Infiltrating Immune Components with Bulk Tumor Gene Expression Data. *Methods Mol Biol* (2020) 2120:249–62. doi: 10.1007/978-1-0716-0327-7_18
33. Newman AM, Liu CL, Green MR, Gentles AJ, Feng W, Xu Y, et al. Robust enumeration of cell subsets from tissue expression profiles. *Nat Methods* (2015) 12(5):453–7. doi: 10.1038/nmeth.3337
34. Yoshihara K, Shahmoradgoli M, Martinez E, Vegesna R, Kim H, Torres-Garcia W, et al. Inferring tumour purity and stromal and immune cell admixture from expression data. *Nat Commun* (2013) 4:2612. doi: 10.1038/ncomms3612
35. Barbie DA, Tamayo P, Boehm JS, Kim SY, Moody SE, Dunn IF, et al. Systematic RNA interference reveals that oncogenic KRAS-driven cancers require TBK1. *Nature* (2009) 462(7269):108–12. doi: 10.1038/nature08460
36. Angelova M, Charoentong P, Hackl H, Fischer ML, Snajder R, Krogsdam AM, et al. Characterization of the immunophenotypes and antigenomes of colorectal cancers reveals distinct tumor escape mechanisms and novel targets for immunotherapy. *Genome Biol* (2015) 16:64. doi: 10.1186/s13059-015-0620-6
37. Chan TA, Yarchoan M, Jaffee E, Swanton C, Quezada SA, Stenzinger A, et al. Development of tumor mutation burden as an immunotherapy biomarker: utility for the oncology clinic. *Ann Oncol* (2019) 30(1):44–56. doi: 10.1093/annonc/mdy495
38. Chalmers ZR, Connelly CF, Fabrizio D, Gay L, Ali SM, Ennis R, et al. Analysis of 100,000 human cancer genomes reveals the landscape of tumor mutational burden. *Genome Med* (2017) 9(1):34. doi: 10.1186/s13073-017-0424-2
39. van Rooij N, van Buuren MM, Philips D, Velds A, Toebes M, Heemskerk B, et al. Tumor exome analysis reveals neoantigen-specific T-cell reactivity in an ipilimumab-responsive melanoma. *J Clin Oncol* (2013) 31(32):e439–42. doi: 10.1200/JCO.2012.47.7521
40. Zhang L, Li B, Peng Y, Wu F, Li Q, Lin Z, et al. The prognostic value of TMB and the relationship between TMB and immune infiltration in head and neck squamous cell carcinoma: A gene expression-based study. *Oral Oncol* (2020) 110:104943. doi: 10.1016/j.oraloncology.2020.104943

41. Mlecnik B, Tosolini M, Kirilovsky A, Berger A, Bindea G, Meatchi T, et al. Histopathologic-based prognostic factors of colorectal cancers are associated with the state of the local immune reaction. *J Clin Oncol* (2011) 29(6):610–8. doi: 10.1200/JCO.2010.30.5425
42. Das S, Camphausen K, Shankavaram U. Cancer-Specific Immune Prognostic Signature in Solid Tumors and Its Relation to Immune Checkpoint Therapies. *Cancers (Basel)* (2020) 12(9):2476–90. doi: 10.3390/cancers12092476
43. Furlan M, Galeota E, de Pretis S, Caselle M, Pelizzola M. m6A-Dependent RNA Dynamics in T Cell Differentiation. *Genes (Basel)* (2019) 10(1):28–35. doi: 10.3390/genes10010028
44. Li HB, Tong J, Zhu S, Batista PJ, Duffy EE, Zhao J, et al. m(6)A mRNA methylation controls T cell homeostasis by targeting the IL-7/STAT5/SOCS pathways. *Nature* (2017) 548(7667):338–42. doi: 10.1038/nature23450
45. Wang H, Hu X, Huang M, Liu J, Gu Y, Ma L, et al. Mettl3-mediated mRNA m(6)A methylation promotes dendritic cell activation. *Nat Commun* (2019) 10(1):1898. doi: 10.1038/s41467-019-09903-6
46. Wu Z, Yang L, Shi L, Song H, Shi P, Yang T, et al. Prognostic Impact of Adenosine Receptor 2 (A2aR) and Programmed Cell Death Ligand 1 (PD-L1) Expression in Colorectal Cancer. *BioMed Res Int* (2019) 2019:8014627. doi: 10.1155/2019/8014627
47. Li M, Li A, Zhou S, Xu Y, Xiao Y, Bi R, et al. Heterogeneity of PD-L1 expression in primary tumors and paired lymph node metastases of triple negative breast cancer. *BMC Cancer* (2018) 18(1):4. doi: 10.1186/s12885-017-3916-y
48. Zhang W, Xu GX, Li JJ, Liu X, Chen YJ, Zhang F. [Expression of PD-1/PD-L1 in triple-negative breast carcinoma and its significance]. *Zhonghua Bing Li Xue Za Zhi* (2017) 46(1):20–4. doi: 10.3760/cma.j.issn.0529-5807.2017.01.005
49. Xu Q, Chen Y, Zhao WM, Huang ZY, Zhang Y, Li X, et al. DNA methylation and regulation of the CD8A after duck hepatitis virus type 1 infection. *PloS One* (2014) 9(2):e88023. doi: 10.1371/journal.pone.0088023
50. Fumet JD, Richard C, Ledys F, Klopfenstein Q, Joubert P, Routy B, et al. Prognostic and predictive role of CD8 and PD-L1 determination in lung tumor tissue of patients under anti-PD-1 therapy. *Br J Cancer* (2018) 119(8):950–60. doi: 10.1038/s41416-018-0220-9
51. Tumeh PC, Harview CL, Yearley JH, Shintaku IP, Taylor EJ, Robert L, et al. PD-1 blockade induces responses by inhibiting adaptive immune resistance. *Nature* (2014) 515(7528):568–71. doi: 10.1038/nature13954
52. Park J, Kwon M, Kim KH, Kim TS, Hong SH, Kim CG, et al. Immune Checkpoint Inhibitor-induced Reinvigoration of Tumor-infiltrating CD8(+) T Cells is Determined by Their Differentiation Status in Glioblastoma. *Clin Cancer Res* (2019) 25(8):2549–59. doi: 10.1158/1078-0432.CCR-18-2564
53. Spitzer MH, Carmi Y, Reticker-Flynn NE, Kwek SS, Madhireddy D, Martins MM, et al. Systemic Immunity Is Required for Effective Cancer Immunotherapy. *Cell* (2017) 168(3):487–502.e15. doi: 10.1016/j.cell.2016.12.022

Conflict of Interest: The authors declare that the research was conducted in the absence of any commercial or financial relationships that could be construed as a potential conflict of interest.

Copyright © 2021 Zhu, Xiao, Wang and Hu. This is an open-access article distributed under the terms of the Creative Commons Attribution License (CC BY). The use, distribution or reproduction in other forums is permitted, provided the original author(s) and the copyright owner(s) are credited and that the original publication in this journal is cited, in accordance with accepted academic practice. No use, distribution or reproduction is permitted which does not comply with these terms.

frontiers in Immunology

REVIEW
published: 01 February 2021
doi: 10.3389/fimmu.2020.629722

Tumor Burden and Immunotherapy: Impact on Immune Infiltration and Therapeutic Outcomes

Samuel I. Kim[1], *Christopher R. Cassella*[2] *and Katelyn T. Byrne*[2,3]*

[1] Program in Biochemistry, College of Arts and Sciences, University of Pennsylvania, Philadelphia, PA, United States,
[2] Department of Medicine, Perelman School of Medicine, University of Pennsylvania, Philadelphia, PA, United States,
[3] Parker Institute for Cancer Immunotherapy, University of Pennsylvania, Philadelphia, PA, United States

Cancer immunotherapy has revolutionized the treatment landscape in medical oncology, but its efficacy has been variable across patients. Biomarkers to predict such differential response to immunotherapy include cytotoxic T lymphocyte infiltration, tumor mutational burden, and microsatellite instability. A growing number of studies also suggest that baseline tumor burden, or tumor size, predicts response to immunotherapy. In this review, we discuss the changes in immune profile and therapeutic responses that occur with increasing tumor size. We also overview therapeutic approaches to reduce tumor burden and favorably modulate the immune microenvironment of larger tumors.

Keywords: tumor burden, immunotherapy, immune infiltrate, tumor microenvionment, immunosuppression

OPEN ACCESS

Edited by:
Peng Qu,
National Institutes of Health (NIH), United States

Reviewed by:
Limin Zheng,
Sun Yat-Sen University, China
Zong Sheng Guo,
University of Pittsburgh, United States

***Correspondence:**
Katelyn T. Byrne
byrnek@upenn.edu

Specialty section:
This article was submitted to Cancer Immunity and Immunotherapy, a section of the journal Frontiers in Immunology

Received: *15 November 2020*
Accepted: *18 December 2020*
Published: *01 February 2021*

Citation:
Kim SI, Cassella CR and Byrne KT (2021) Tumor Burden and Immunotherapy: Impact on Immune Infiltration and Therapeutic Outcomes. Front. Immunol. 11:629722. doi: 10.3389/fimmu.2020.629722

INTRODUCTION

Nearly 50 years ago, Whitney and colleagues reported that mice bearing large carcinogen-induced sarcomas displayed defective spontaneous immune responses (1). These immunological defects were reversible with tumor resection, providing a link between tumor burden and dysfunctional immune responses. In the intervening decades, further interrogation into the immunobiology of the tumor microenvironment (TME) reveals significant local and systemic impacts on immune responses (2, 3). With the advent and success of immune checkpoint blockade (ICB) in patients with advanced disease (4), there is a need to understand biomarkers of response to improve outcomes in patients that remain resistant to immunotherapy. Despite the identification of several correlates of response to ICB, including CD8 T cell infiltration of the tumor site, tumor mutational burden, and cytolytic T cell gene expression profiles (5–7), these metrics are not universal predictors of response across all tumor types and patient subsets. Here, we review the literature with regard to total tumor burden as an important negative correlate of response and explore potential mechanisms to mitigate the local and systemic impact of high tumor burden on immune interventions.

TUMOR BURDEN IMPACTS BASELINE IMMUNITY

The complex immunobiology of the TME is regulated by a number of factors, including tumor cell-intrinsic determinants of immune cell infiltration (8), the tissue in which the tumor is located (9),

and the stromal and vasculature content of the tumor [reviewed elsewhere (10, 11)]. Immune cell intrinsic defects also contribute to tumor progression, including T cell exhaustion or tolerization to high avidity tumor antigens (12). This multitude of factors contribute to tumor progression, but preclude mechanistic insight in heterogeneous clinical samples, even across tumors harvested from a single patient (13). Mouse models provide crucial insight into the impact of tumor burden on immune features in the TME by allowing for isolation of the impact of tumor size as a variable regulating immune infiltration and immunotherapy sensitivity. Preclinical data support the clinical findings that large tumors are more immunosuppressive compared to small tumors on both the local and systemic level, directly impacting the ability of the host immune system to effectively mount natural or immunotherapy-induced immune responses.

The immunosuppressive nature of the tumor site is locally enforced *via* immune cell subsets recruited or induced within the TME. Pro-tumorigenic myeloid derived suppressor cells (MDSCs) mediate T cell suppression through a variety of mechanisms including depletion of arginine, oxidative stress of target cells, and release of the dicarbonyl radical methylglyoxal (14–16). MDSCs have been found to increasingly infiltrate the TME in a murine model of renal adenocarcinoma (RENCA) even as the populations of other immune cells (including T cells and dendritic cells; DCs) decreased (17, 18). Similarly, in a murine model of pancreatic ductal adenocarcinoma (PDAC), MDSCs and tumor-associated macrophages have been shown to increasingly infiltrate the TME as tumors progress (19). The same trends are observed in regulatory T cells (Tregs) in multiple tumor types, concurrent with a decrease or even absence of CD8 T cells, NK cells, and DCs during tumor progression (17, 19–22). These data suggest that targeting suppressive immune cell populations may help convert the TME of large tumors to more closely resemble the immune infiltrate of small tumors, augmenting the impact of immunotherapeutic interventions.

In addition to increased proportions of immunosuppressive cells in the TMEs, the cytokine production in large tumors is also skewed to a more suppressive profile as compared to small tumors. Transforming growth factor-β (TGF-β), a pleiotropic cytokine shown to exert anti-tumor effects in early-stage cancer but tumor-promoting effects in late-stage cancer (23), is amplified in large murine T cell leukemia and RENCA tumors (17, 24). IL-10 and nitric oxide synthase 2 (NOS2) similarly increase as tumors progress (17, 24). This likely reflects progressive increases of MDSCs and Tregs in growing tumors (19–22), as both cell populations are major producers of these suppressive cytokines.

However, not all TMEs follow the same positive correlation between suppressor cell infiltration and increased tumor size. In patients with colorectal cancer, CXCL9 – an IFN-γ inducible chemokine that recruits CD8 T cells – is not differentially expressed according to high or low tumor burden (25). In a mouse model of melanoma, B16 tumors show very little perturbation in the relative frequencies of effector or regulatory T cell subsets as tumors increase in size (17). Similarly, CD8 T cells are actually increased (while Tregs are decreased) in large vs. small tumors in a mouse model of colon carcinoma (17). However, chronic antigen exposure has the potential for tumor-specific T cell deletion, resulting in functional "holes" in the immune cell repertoire, a mechanism first reported in the context of chronic viral infections (26). High avidity T cell interactions also have the potential for deletion, as observed in a mouse model of lymphoma where tumor-specific T cells were rapidly lost in the context of a highly immunogenic tumor antigen when the number of target tumor cells was above a certain threshold (27). The failure of these effector cells in large tumors highlights the contribution of other suppressive mechanisms – beyond those mediated by sheer numbers of suppressive MDSC or Treg populations – in established and progressing tumors.

One such mechanism by which tumors escape T cell-mediated destruction is *via* negative immune checkpoints including programmed death-1 (PD-1) or cytotoxic T lymphocyte-associated protein 4 (CTLA-4). Ligation of immune checkpoints on T cells drives exhaustion and dysfunction, preventing autoimmunity and immunopathology in the context of extenuating immune activation, but usurped by the tumor to disable anti-tumor immunity. Immune checkpoint ligands such as programmed death ligand 1 (PD-L1) are abundant in the TME of many tumor types, independently of tumor mutation burden (28). Multiple tumor types exhibit increased PD-L1 expression as a direct correlate with tumor size including gastroenteropancreatic neuroendocrine tumors (29), advanced gastric cancer (30), and meningiomas (31). Furthermore, in primary and metastatic melanoma samples, PD-L1 levels are higher in primary and local metastases and lower in distant metastases (32) with similar findings in cutaneous squamous cell carcinoma (33) suggesting that expression of checkpoint ligands may be linked to tumor progression.

The immunosuppressive impacts of bearing a large tumor are often not limited to the local TME. Recently, Allen and colleagues revealed that the presence of a tumor negatively impacts the systemic immune landscape, including a global suppression of T cell responses to tumor-unrelated antigen challenges as a result of increased IL-1 and G-CSF (3). Similarly, conventional dendritic cells responsible for priming CD8+ T cells were found to be systematically and progressively dysregulated in mice bearing PDAC, leading to deficient T cell priming even in the presence of strong tumor neoantigens (34, 35). In murine PDAC, tumor cell-derived G-CSF impaired differentiation of type 1 conventional dendritic cells in the bone marrow and blood (36), and elevated serum levels of the cytokine IL-6 in tumor-bearing mice induced apoptosis of conventional dendritic cells (34). Thus the findings of failed systemic immunity in mice bearing large tumors have come full circle (1), revealing that both local and global suppression of the immune response is heightened in the context of increased tumor burden. Targeting both deficits may provide the signal necessary to drive immune responses in currently treatment-resistant tumor types.

IMPACT OF TUMOR BURDEN ON THERAPY-INDUCED IMMUNE RESPONSES

Spontaneous or natural cancer-immunity cycles have failed by the time a tumor is detected in the clinical setting, requiring therapeutic interventions to drive immune-mediated rejection of tumors. ICB has thus far garnered the most success and has shown remarkable clinical benefit in patients with aggressive disease (4), but gene therapy approaches such as chimeric antigen receptor (CAR) T cells have become standard-of-care for some patients with previously incurable malignancies (37), and oncolytic viruses have shown great promise in treatment-refractory brain tumors (38). Integrating knowledge about the impact of tumor burden on the efficacy of these therapies may enhance clinical outcomes.

Immune Checkpoint Blockade

Immune checkpoints such as PD-1/PD-L1 or CTLA-4 are negative regulators of activated T cells. Using monoclonal antibodies (mAbs) to disrupt the ligand/receptor pairing of these immune checkpoint molecules enables tumor-associated T cells to overcome immunosuppression and effectively perform anti-tumor functions (39). ICB has drastically improved clinical outcomes for patients with advanced disease including metastatic melanoma (40–42) and non-small cell lung cancer (NSCLC) (43–45).

Despite the immense positive impact of ICB in the clinical setting, many patients do not respond, and tumor burden is one metric that negatively correlates with ICB efficacy. Preclinical data reveals that PD-1 blockade is more effective in mice bearing smaller lung squamous cell tumors (22). Similarly, mice with advanced ovarian tumors are more resistant to PD-L1 blockade than mice with earlier stage tumors (21, 46). This negative correlation of tumor size and ICB sensitivity is borne out in patients where total tumor volume is predictive of response to αPD-1 with local or metastatic melanoma (47, 48). In patients with NSCLC, metabolic tumor volume was also a prognostic factor for sensitivity to PD-1 blockade in both retrospective and prospective studies (22, 49). Furthermore, dual ICB, which targets both PD-1 and CTLA-4 at the same time, has shown greater efficacy than single ICB in patients with metastatic NSCLC and melanoma (40, 43), and is more effective in melanoma patients with smaller baseline tumor diameters (50). Despite the plethora of studies correlating tumor size and ICB outcomes, the threshold of tumor burden at which ICB efficacy is reduced has not been defined. Given this, a dynamic metric, such as the ratio of proliferating T cells specifically reinvigorated by anti-PD-1 compared to the total tumor burden (51) may be the best approach for identifying patients that are resistant to ICB and would benefit from additional therapeutic interventions.

T Cell Costimulation

In contrast to alleviating suppressive signals *via* ICB, direct co-stimulation of T cells using mAbs targeting molecules such as OX40 and 4-1BB has also been explored. OX40 is a member of the TNF receptor superfamily expressed by activated T cells, and agonistic OX40 mAbs have direct stimulatory activities on effector T cells with the benefit of inhibiting Treg function in the tumor site, showing early promise in clinical trials (52). Preclinical studies reveal that small MCA205 fibrosarcoma tumors and CT26 colon carcinomas are sensitive to OX40 agonism as a single agent, but larger tumors (50–120 mm^2) require the addition of transforming growth factor-β (TGF-β) receptor antagonists to further reduce immune suppression (53). Similar to OX40, 4-1BB is a co-stimulatory receptor expressed on T cells and antigen-presenting cells, and 4-1BB agonists enhance the anti-tumor effector functions of cytotoxic T cells (54). In preclinical studies using an MC38 colon carcinoma model, 4-1BB agonist therapy had little impact on tumor progression when administered early (less than 48 h after tumor implantation), while the combination of 4-1BB and anti-CTLA-4 together was effective even in established tumors (14 days after implantation) (55). However, this approach failed in B16 melanoma tumors (55), suggesting that the unique tumor microenvironment, in addition to tumor size, dictates therapeutic efficacy.

Cancer Vaccines and Oncolytic Viruses

In contrast to ICB, where T cells are indiscriminately "rescued" from exhaustion regardless of antigen specificity, cancer vaccines aim to induce a tumor-specific adaptive immune response through delivery of whole tumor cells or tumor-derived antigens (56). Preclinical mouse models reveal cancer vaccine platforms are efficacious in small, but not large, tumors (21, 57). Coupling a bacteria Type II secretion protein with the model antigen ovalbumin (OVA), Binder and colleagues show that tumor rejection cannot be fully rescued in late stage B16 melanoma tumors, even with a strong OVA-specific CD8 T cell response (57). Similarly, two reports using killed tumor cells to vaccinate tumor-bearing mice find that late stage ovarian cancer or mammary tumors cannot be controlled, even with the addition of costimulatory or ICB mAbs (21, 58). These reports highlight the existence of a threshold of tumor burden below which the tumors are sensitive to immunotherapy, but above which the tumors are highly resistant.

Oncolytic vaccines offer the ability to prime T cell responses against tumor antigens *via* robust stimulation of the innate immune system. However, an adenovirus vaccine encoding tumor-specific somatic mutations (Gad-CT26-31) that works prophylactically or as a very early therapeutic intervention for small CT26 colon carcinomas was insufficient to eradicate large (>70mm^3) established tumors (59). Similarly, a HPV vaccine resulted in the cures of small herpes poliovirus (HPV)-expressing TC-1 tumors whereas large tumors were more resistant, failing to achieve complete clearance (60). The inverse relationship between the success of viral vaccines or oncolytic viruses and high tumor burden holds true for patients with melanoma: treatment with the oncolytic virus talimogene laherparepvec, or T-VEC (which drives tumor cell killing and *in situ* priming against tumor antigens *via* cytokine release), results in better outcomes if tumor burden is low at the start of therapy (61). However, rational pairing of oncolytic viruses with ICB may hold

promise: PD-1 blockade rescued anti-tumor immunity in mice bearing large tumors in both colon cancer and HPV models (59, 60). The potential beneficial impact of oncolytic viruses for diseases such as glioblastoma highlight the need to better understand the TME, to optimally pair treatment modalities for improved outcomes.

Direct Antigen-Presenting Cell Activation

Cancer vaccines are often utilizing *ex vivo* DC activation, or *in vivo* innate immune sensors for activation of antigen presenting cells (APCs) to improve T cell priming, with the underlying hypothesis that insufficient T cell priming is one reason for the failure of ICB or co-stimulation mAbs to "rescue" T cell responses in the TME (62). However, direct activation of APCs such as by using an agonist CD40 mAb is another option for driving newly primed T cell responses against tumors. Ligation of CD40, expressed on APCs, promotes the rapid licensing and maturation of dendritic cells and other APC subsets independently of CD4 T cell help (the natural source of CD40 ligand) (63–65) normally provided upstream of immune checkpoint expression. We have shown that CD40 stimulation drives T cell immunity in a genetically engineered mouse model of PDAC when used in combination with chemotherapy (66), ICB (67), or combinations of chemotherapy and radiotherapy with ICB (68, 69), and there are promising data from a clinical trial in patients with metastatic PDA receiving agonistic CD40 in combination with chemotherapy (70). To assess the impact of tumor size in response to agonistic CD40 mAb therapy, we segregated tumor-bearing mice from previous studies according to therapeutic response and assessed the baseline tumor size in each group (66, 67). As shown in **Figure 1**, mice that responded to anti-CD40 in combination with chemotherapy (gemcitabine, Gem; and nab-paclitaxel, nP) or dual ICB had smaller baseline tumors than mice that were resistant to treatment. Mice with smaller tumors also survived longer in both treatment cohorts, although treatment with CD40/ICB resulted in slightly larger tumors responding to therapy as compared to mice treated with chemotherapy and CD40, supporting findings in cancer vaccine studies where a multi-pronged approach is more effective. Thus, non-redundant methods of stimulation T cell priming—directly *via* costimulatory mAbs, or *via* activation of APCs *via* CD40 mAb—still reveal the baseline tumor size as a major determinant of response.

Adoptive and CAR T Cell Therapies

Given the systemic inhibition of immune responses in the presence of large tumors, adoptive cell therapy (ACT) is an

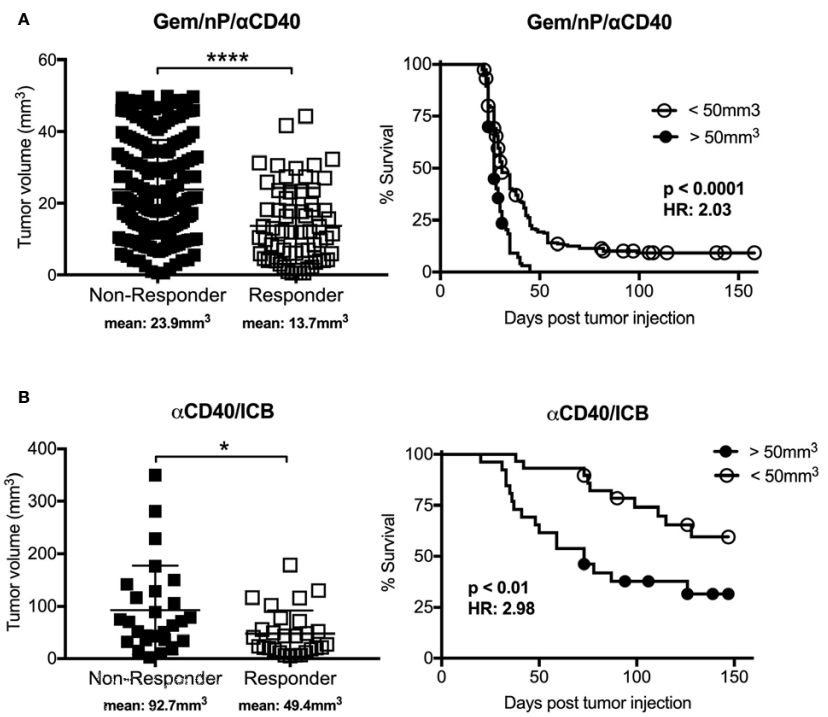

FIGURE 1 | Efficacy of tumor rejection after combination treatment with agonistic CD40 antibody correlates with tumor size. Graphs from studies reported in (66) **(A)** and (67) **(B)**, reported here stratified by tumor response (defined as cured of primary tumor; scatter plots) or baseline tumor size (survival curves). Briefly, C57Bl/6 mice were implanted subcutaneously with $2.5x10^5$ 4,662 pancreatic ductal adenocarcinoma (PDAC) cell lines and treated with **(A)** agonistic CD40 (αCD40) in combination with chemotherapy (gemcitabine, Gem; and nab-paclitaxel, nP) as described in (66), or treated with **(B)** αCD40 in combination with αPD-1 and αCTLA-4 (ICB) as reported in (67). Each symbol represents a single mouse, horizontal lines indicate mean (also denoted below graph), and error bars indicate standard deviation. **** indicates p value < 0.0001 and * p < 0.05 as determined by an unpaired t test. For survival curves analysis was performed using log-rank test with indicated p values, HR indicates Hazard Ratio according to the size cutoff of $50mm^3$, calculated using log-rank. Analyses were performed using Graphpad Prism.

appealing therapeutic option that bypasses the requirement for *in vivo* T cell priming or reactivation. Tumor-specific T cells are enriched *via ex vivo* expansion and activation before reinjection into the patient, and ACT of tumor infiltrating lymphocytes (TILs) has shown promise in metastatic melanoma (71, 72). However, tumor burden presents an issue even with antigen specific T cell therapies, as shown in a mouse model of lymphoma where ACT is effective only against small tumors (27). In large tumors, the authors found functional impairment and rapid deletion of the transferred CD8+ T cells, which was reversed *via* pretreatment with chemotherapy to reduce tumor size (27). Similar observations were made in a mouse model of sarcoma, where small tumors regressed after ACT, but large tumors on the contralateral flank did not (73). Recent studies show that the impairment and deletion of ACTs observed in large (but not small) tumors is reflective of suppressive local TME, as T cell affinity and expression of the tumor specific antigen was similar in both tumor sizes (74).

In addition to TILs, genetically modified T cells can also be used for ACT, including CAR T cells, where success has been made in many hematological malignancies, but solid tumors remain a more difficult problem (37). Hematological cancers such as acute lymphoblastic leukemia have a direct correlation between total tumor burden and response to CD19 CAR T cell treatment (75). In a mouse model of hepatocellular carcinomas, CAR T cells targeting glypican 3 were sufficient to drive regressions of small tumors but had no effect on large tumors, which was reversed upon the addition of sorafenib as a result of increased IL-12 production from intratumoral macrophages (76). In contrast, CAR T cells targeting glypican 1 were sufficient to drive tumor regressions in both large and small murine colorectal tumors (77). Thus the local TME can impact treatment efficacy (and can be targeted with rational therapeutic combinations) but the systemic impact on the immune response as a result of bearing large tumors is a significant barrier to treatment outcomes.

STRATEGIES TO REDUCE TUMOR-BURDEN ASSOCIATED IMPACTS ON IMMUNITY

Given that large tumors are more resistant to immunotherapy and harbor greater populations of suppressive cells, targeting tumor burden-associated alterations in the tumor microenvironment may exert therapeutic effects. Here, we briefly cover two major categories of approaches that may improve immune responses against tumors: directly reducing tumor size and modulating the tumor immune microenvironment.

Traditional Interventions

Surgery

Tumor resection is the oldest method of treating cancer, and one of the original methods of restoring defective tumor surveillance in mouse models (1). The use of tumor resection prior to administration of immunotherapy improves control of tumor growth in multiple mouse models (3, 22, 78). This "resetting" of the immune response has been linked to the alleviation of immune suppression by tumor-derived IL-1 and granulocyte colony-stimulating factor (G-CSF) and could be phenocopied by mAb blockade of either cytokine (3). However, the trauma of surgical resection and the ensuing wound-healing process can lead to the outgrowth of otherwise immune-controlled metastases (79–81), which can be reversed by neoadjuvant administration of immunotherapies in some settings (81, 82). For example, patients with metastatic renal cell cancer benefited when surgery was combined with IFNα-2b treatment, resulting in a three-month increase in median survival with combination treatment compared to IFN treatment alone (83). In addition to immunotherapies, anti-inflammatory medication also prevents surgery-induced outgrowth of metastases by reducing the proportion of suppressive tumor-associated macrophages (82). Thus, surgical resection with careful management of the immunosuppressive wound-healing process could be considered prior to adjuvant immunotherapy.

Chemotherapy

Cytotoxic chemotherapy is another viable strategy to reduce tumor size that has been employed in the clinic for decades. Moreover, some chemotherapy regimens drive immunogenic cell death of tumor cells, leading to release of tumor antigens that can be presented by APCs to prime cytotoxic T cells (84). In this way, chemotherapy can exert both a local anti-tumor effect as well as systemic positive pressure on the immune system; these two outcomes are not mutually exclusive but highly interdependent. For example, a pre-clinical study showed that administering a low dose of the chemotherapy cyclophosphamide (CTX) one day before ACT of tumor-specific CD8 T cells is effective in reducing tumor burden and thereby prevents deletion of the transferred CD8 T cells in a murine lymphoma model (27). In the clinic, combination chemo-immunotherapy regimens have shown increased efficacy over chemotherapy alone in patients with advanced NSCLC (44) and metastatic melanoma (85).

However, given the cytotoxic nature of chemotherapy on any proliferating cell including T cells (86, 87), the impact of combination chemo-immunotherapy has variable results. The use of CTX followed by αCTLA-4 resulted in significant tumor regressions in a mouse model of colon cancer, while reversing the order resulted in apoptosis of tumor-reactive T cells (88), and we and others have observed similar detrimental impacts on sequencing gemcitabine with αCD40 in a mouse model of PDAC (89, 90). Furthermore, we have reported that the addition of the chemotherapy to agonistic CD40 and dual ICB significantly reduced the long-term survival of tumor bearing mice compared to immunotherapy alone (67). These findings suggest that chemotherapy, while important to restrain tumor growth, may not synergize with some types of immunotherapy. Additional investigations are necessary to determine optimal sequencing strategies such that chemotherapy can be employed to shrink large tumors without negatively impacting a developing immune response.

Radiation Therapy

Radiotherapy delivers high-energy rays directly to tumor sites as a form of curative control locally at the tumor, and the resultant abscopal effect can be beneficial for immune responses. The administration of radiation treatment completely ablates the tumor and surrounding stroma, effectively debulking the tumors. The immune impact is therefore complex—immune suppression may be alleviated by the eradication of the local tumor, while increased tumor cell death enhances systemic anti-tumor T cell response by generating novel tumor antigens presented on major histocompatibility complex (MHC)-I (91). In preclinical and clinical studies, the addition of radiotherapy to immunotherapy treatments such as ICB (92–94) and/or αCD40 (68) significantly improved immune response and survival. Mechanistically, radiation can upregulate expression of neoantigens (94), diversify the T cell repertoire (92), and enhance antigen presentation and co-stimulation on dendritic cells (68). Thus, in contrast to the detrimental immune impact of chemotherapy, radiation may promote immune cell activation while reducing tumor burden as a rational therapy partner for many immunotherapies.

SIMULATING A "SMALL" IMMUNE MICROENVIRONMENT

Physical Barriers to Immune Infiltration

Some of the highest hurdles for immune cell infiltration of the TME are the physical barriers of entry to the tumor site. Large tumors have reduced vascularization which creates regions of hypoxia that are particularly prominent in large tumors (95, 96), but reduced vascularization also compromises the delivery of a number of different types of therapies into the TME itself (97). This is further compromised when the TME is highly fibrotic, as is the case with PDAC and reviewed elsewhere in greater detail (98). While several mechanisms to target the stroma, such as inhibition of fibroblast activation protein (99), inhibition of Hedgehog signaling (100), or the use of chemotherapeutic agents such as nab-paclitaxel (101–103) have been devised, immune therapies can also be modified to overcome this barrier. For example, Maute et al. engineered a PD-1 ectodomain capable of blocking PD-1:PD-L1 interactions that is an order of magnitude smaller than anti-PDL1, and able to more effectively penetrate the TME (104). As a result, the PD-1 ectodomain was more effective against both large (150 mm^3) and small (50 mm^3) mouse CT26 colon carcinomas as compared to anti-PD-L1, which was only effective against small tumors (104). Thus, designing drugs with a higher degree of tumor penetration is a feasible approach for improved delivery of some immunotherapies.

Overcoming Tumor-Associated Suppressive Cells

As discussed in Part I, the proportions of suppressive cell populations such as MDSCs are increased in large and progressing tumors. Blocking MDSC recruitment to or activity in the TME renders the tumor sensitive to immunotherapy [reviewed in depth elsewhere (105)]. We and others have shown that MDSCs are rapidly recruited to the PDAC TME *via* multiple chemokine and cytokine axes including CXCR2 (8, 106, 107), GM-CSF (108, 109), and G-CSF (8). Perturbation of these pathways reduces MDSC recruitment to the tumor site (8, 107, 108), increases CD8 T cells in the TME (8, 107, 108), and converts the tumor to immunotherapy-sensitive (8). MDSC reduction can be achieved *via* depletion, using CD33-specific immunotoxin Gemtuzumab ozogamicin (110) or ADH-503, a small-molecule agonist for CD11b (111), while the immunosuppressive activity of MDSCs can be blunted using anti-TIGIT (112) or CD73 blockade (113).

Tumor-associated macrophages (TAMs) play a similarly suppressive role in the TME and can also be targeted using depletion strategies. Colony-stimulating factor-1 (CSF-1), a key regulator of macrophage differentiation, can be blocked *via* CSF-1R mAb or antagonists, resulting in a sensitization of the TME to immune cell killing (114). Skewing TAMs to an anti-tumor functional profile also reduces the immunosuppression in hosts bearing large tumors. For example, pharmacological inhibition of PI3K-γ, which is highly expressed on myeloid cells, shifted TAMs from a M2-like immunosuppressive phenotype to an inflammatory M1-like phenotype in the murine 4T1 mammary carcinoma and B16 melanoma models (115). Paradoxically, reducing TAMs can result in a compensatory increase of MDSCs (116, 117). However, this effect can be overcome by blocking both TAMs and gMDSCs, which augments the efficacy of PD-1 blockade in a mouse model of cholangiocarcinoma (116) and bolsters chemotherapy in a mouse model of PDAC (117). The suppressive myeloid and macrophages subsets in the TME are thus a major immune cell barrier that must be overcome to generate effective anti-tumor responses.

Suppression in the TME is also closely regulated by Tregs, including both natural Tregs and tumor-induced Tregs. Selective depletion of Tregs by αCD25 shows promise in preclinical tumor-bearing animal models [reviewed in (118)], but can have unintended consequences of deleting effector $CD25^+$ CD4 T cells. While effector CD4 T cell depletion does not negatively impact all immunotherapies (119), there is a growing appreciation of the contributions of CD4 T cells in mediating anti-tumor responses (67, 120–122). Some data suggest that αCTLA-4 specifically depletes CTLA-4^+ Tregs in mouse models (123), but not in patients (124). Similarly, targeting glucocorticoid-induced TNFR family related protein (GITR) *via* agonistic antibody has also been shown to deplete Tregs in mouse models (125), while agonistic CD40 administration results in a drastic reduction in Tregs in the murine PDAC TME (66). These findings support targeting Tregs as well as other suppressive cell populations in the large TME to render the ratio of effector cell to suppressive cell more in alignment with ratios found in small tumor sites.

Stimulating Immune Responses

In contrast to removing suppression, many immunotherapies specifically aim to promote immune activation and, to a certain extent, inflammation. The stimulation of innate immune signaling pathways is the original immunotherapy approach,

used by William Coley in the early 1900s. "Coley's Toxins" included a mix of bacterial products that he applied to the tumor lesions of patients, and he observed striking tumor regressions (126). Over the next century, immunologists deconstructed the immune response, resulting in the identification of cell types, receptors, and ligands that can be utilized to mount immune reactions.

Toll-like receptors (TLRs) are canonical pattern recognition receptors, and ligation by toll-like agonists stimulate the innate immune sensing pathways. In the context of the cancer-immunity cycle, providing TLR agonists licenses APCs to enhance antigen presentation and production of inflammatory cytokines (127). TLR agonists have significant anti-tumor roles by driving polarization of TAMs toward an anti-tumor, pro-inflammatory M1 phenotype (128). This conversion of TAMs to an M1 phenotype renders the TME more permissive to downstream activation of CD8+ T cells and infiltration to the tumor site naturally or *via* orthogonal combinations (129). Furthermore, TLR2 agonists alleviate the immunosuppression mediated by Tregs by reprogramming the Tregs to effector Th17 cells (130).

Despite these positive changes in the TME after TLR agonist administration, there are some tumor cells that express—and are activated—by TLR ligation (127, 131), which promotes tumor growth and chemoresistance in TLR7/TLR8 overexpressing human pancreatic cancer cells (132) and production of immunosuppressive cytokines (TGF-β, vascular endothelial growth factor (VEGF), IL-8) and resistance to apoptosis in human lung cancer cells (133). Implementation of TLR agonists may therefore have a number of benefits to reducing tumor suppression, but the type of TLR stimulated and the downstream impact may be regulated by the immunobiology of a specific TME.

A second class of innate immune sensor stimulation bypasses the binding of TLRs and instead directly stimulates the cyclic GMP-AMP synthase (cGAS) - stimulator of IFN genes (STING) pathway, which is triggered in the presence of cytosolic DNA (134). Activation of the cGAS-STING pathway in cancer cells leads to secretion of pro-inflammatory molecules that attract immune cells and restrict tumorigenesis (135, 136). Furthermore, tumor-cell derived DNA is transferred to APCs, activating the cGAS-STING pathway and production of type I interferons, leading to improved CD8 T cell priming (137, 138). STING activation has also been shown to act on tumor endothelial cells, leading to potent production of type I IFNs (139), further enhancing the anti-tumor response. STING agonists therefore offer an effective method of increasing CD8 T cell infiltration in the TME of large tumors, and have the potential to synergize in combination with a number of treatment modalities including ICB (140), VEGF receptor 2 blockade (141), and chemotherapy (142).

The TLR and STING agonist pathways are dependent downstream on signaling *via* type I IFNs. In contrast, CD40 stimulation bypasses the use of innate immune sensors and Type I IFN signaling, thus presenting an alternate bridge between innate and adaptive immunity (66, 67). Agonistic CD40 can drive the priming of a robust anti-tumor T cell response dependent on IFN-γ and Batf3 expression (8, 66, 67), while CD40 ligation on TAMs drives a tumoricidal response that depletes the stroma in the TME (143). As such CD40 activation is an important mechanism of increasing effector T cell trafficking to immunologically cold tumors, a finding that can be extended to treatment of large tumors that harbor more immunosuppressive cells and fewer effector immune cells.

Oncolytic Viruses

Oncolytic viruses (OVs), originally designed to specifically kill tumor cells, have more recently been utilized as potent activators of local and systemic immune responses. OVs drive tumor cell death, resulting in the release of inflammatory signals (cell stress danger-associated molecular patterns or DAMPS) and the liberation of tumor-associated antigens to promote anti-tumor immunity. Most recently, clinical trials in patients with brain tumors have shown promising results using OVs (144), such as PVSRIPO (a modified poliovirus OV) in patients with glioblastoma, where some patients have shown complete and durable remissions (145). Future investigations into combinatorial approaches may further enhance the outcomes of OVs in tumors and help delineate which patients with brain tumors may require additional resections vs. orthogonal treatment combinations.

The immunostimulatory impacts of OVs can also be modulated by "cytokine-arming," whereby the virus also contains a cytokine payload that re-educates, recruits, or stimulates immune cells locally in the TME [reviewed in (146)]. One highly successful example of a cytokine-armed OV is T-VEC, which selectively targets tumor cells while also producing GM-CSF (147). Mechanistically, T-VEC modulates the TME by activating and attracting tumor-specific CD8 T cells (148) *via* tumor cell lysis (resulting in the liberation of tumor antigens and DAMPs) and the recruitment of DCs [reviewed in (149)]. T-VEC has shown remarkable efficacy in clinical trials for patients with advanced melanoma both as monotherapy (150) and in combination with anti-CTLA-4 (151, 152). OVs thus have the potential to specifically target tumor cells for destruction while delivering a payload that promotes immune activation, a multi-pronged approach that may be ideal for large tumors that are otherwise not amenable to traditional tumor debulking approaches.

Tumor Cell Intrinsic Mechanisms of Immune Regulation

In addition to contributing to aberrant tumor cell growth, oncogenic signaling pathways have the potential to regulate immune responses within the TME, suggesting that precision medicine in combination with immunotherapy should be explored for improved outcomes. For example, the Wnt/β-catenin signaling in a mouse model of melanoma hindered T-cell infiltration and established an immune "cold" TME by downregulating the expression of the chemokine CCL4 (153). Targeting the gene encoding β-catenin *via* RNA interference synergizes with dual ICB in a mouse model of breast cancer mice

and results in complete tumor regressions (154), and small molecule inhibitors of Wnt signaling are being explored for potential application in tumor-bearing hosts (155). Similarly, we found increased expression of MYC in immune "cold" tumors, resulting in increased CXCL1 production and MDSC recruitment concomitant with a lack of T cells in the TME (8). JQ1 is a small molecule that binds competitively to bromodomains and inhibits MYC gene transcription by displacing bromodomain 4 (BRD4) (156), and has the added benefit of reducing PD-L1 expression by tumor cells and APCs (157) while also directly promoting T cell persistence and effector functions in the TME (157, 158). Although JQ1 shows promise in driving tumor responses when used in combination with ACT and ICB (158, 159), it has also been shown to activate and promote tumor invasion and metastasis pathways in mouse models of prostate cancer (160), suggesting further investigation is necessary for optimal application in the clinical setting.

There has been significant effort to develop effective inhibitors against the mitogen-activated protein kinase (MAPK) signaling pathway, given that it is one of the most commonly mutated pathways across all types of cancer (161). RAS proteins are activated upstream of MAPK and direct the establishment of the immunosuppressive TME *via* GM-CSF production (108) and upregulation of PD-L1 (162), but have proved difficult to target [reviewed elsewhere in detail (163)]. Interestingly, using ACT of T cells specific for an MHC I epitope derived from mutated Kras controlled tumor growth in a patient with metastatic colorectal cancer (164) and is being further investigated preclinically (165) and *via* Kras-directed cancer vaccine trials (163). Recently, the clinical development of Sotorasib, an inhibitor to mutant G12C KRAS, has yielding promising results in a phase I clinical study performed on patients with advanced solid tumors harboring the KRAS p.G12C mutation (166). It has also been shown to increase T cell, dendritic cell, and macrophage infiltration into the tumor site of CT26 KRAS G12C colon carcinoma-bearing mice, either alone or in combination with anti-PD-1 therapy (167). However, it is likely that tumor burden will continue to be a major barrier to these approaches as discussed above, and thus targeting RAS *via* immune-mediated mechanisms may require combinatorial approaches for optimal outcomes.

Targeting proteins downstream of RAS in the MAPK pathway has been more successful. BRAFV600E is one of the most common mutations, and a class of RAF monomer inhibitors specifically target this mutation to block mutant BRAF signaling (161). Vemurafenib is one such small molecule and administration significantly enhanced the survival of patients with metastatic melanoma harboring the BRAFV600E mutation (168). Critically, vemurafenib directly alters immune-associated features of malignant cells, such that blocking mutant BRAF signaling results in the reduction of suppressive cytokine production and increased MHC expression by tumor cells (169). This alters the local TME, resulting in decreased recruitment and survival of suppressive MDSCs (170) and Tregs (20), with a concomitant increase in MHC expression of melanocyte differentiation antigens [known targets of the endogenous T cell response against melanoma (171)] and with some BRAFi, T cell infiltration in to the TME (172). Thus BRAF inhibition controls tumor progression while also altering the tumor site toward a "small" TME, suggesting combination with other immune interventions may be highly effective.

Similar to BRAFi, mitogen/extracellular signal regulated kinase (MEK) inhibition controls tumor progression, but has been shown to negatively impact T cell priming and proliferation *in vitro* and in lymph nodes (173). However, MEKi appears to have a negligible negative impact on the local immune response against the tumor when administered *in vivo* (173). Indeed, MEKi increases infiltration of antigen-specific CD8 T cells into CT26 colon carcinoma tumors and protects intratumoral T cells from TCR-driven exhaustive apoptosis (174). These findings support the rational combination of MEKi with ICB, and accordingly, MEKi augments PD-1 or PD-LI blockade in mouse models of colon carcinoma and melanoma (174–176).

Despite the positive immune impacts of inhibiting mutant BRAF or MEK, many patients still progress after a period of tumor control, leading to the combination of BRAF/MAPKi in the clinical setting (177). This combination rendered tumors more sensitive to ICB, and adding PD-1 blockade further potentiated BRAF/MEKi in a mouse model of melanoma (178), and has been translated to the clinic for patients with mutant BRAF (179). Given the potential negative impact of MEKi on T cell priming in tumor-draining lymph nodes, rational immunotherapy combinations are crucial – e.g., pairing with CD40 stimulation may not be ideal while ICB or certain types of ACT may work very well with MEKi and these early combination trials are very promising.

Epigenomic Modifiers

Abnormal gene expression is a hallmark of cancer progression, and histone deacetylases (HDAC), which regulate chromatin remodeling, are aberrantly expressed in many cancer types. HDACi results in cytostatic or cytotoxic effects on tumor cells, but this approach has been more effective in hematological malignancies than in solid tumors when used as a monotherapy or combined with other drugs including chemotherapy, reviewed by Suraweera and colleagues (180). Despite this, HDACi does reverse some of the gene repression found in tumor cells, thereby increasing expression of MHC and costimulatory molecules for both T and NK cells on tumor cells in the TME (181). In addition to tumor cell intrinsic effects, HDACi can also have direct effects on lymphocytes in the TME, similar to MEKi. Here the data are somewhat contradictory, as HDACi has differential impacts on T cell subsets, alternatively promoting IFN-γ production (182) and survival (183), while also restraining proliferation and cytotoxic functions *in vitro* (184). Importantly, tumor-associated Tregs are sensitive to Class I HDACi, with reductions in frequencies and suppressive function in a dose-dependent manner in a mouse model of renal cell carcinoma or prostate cancer (185). The impact of HDACi on APC subsets in the TME remains less clear, with some TAM subsets becoming less suppressive, other subsets acquiring an alternatively activated phenotype and DCs losing licensing and activation markers (181). These studies support the

use of HDACi to help remodel the TME and associated immune response, but preclinical modeling will be crucial to elucidate the impact of HDACi on the initiation and maintenance of tumor immunity.

Autophagy Inhibition

Autophagy is a mechanism by which cancer cells (and other cell types) degrade intracellular organelles as a source of nutrients under both basal and stress-induced conditions (186). Two FDA-approved drugs developed to treat malaria – chloroquine (CQ) and hydroxychloroquine (HCQ) – have been used extensively in the clinical setting but are also potent autophagy inhibitors. Initial *in vitro* studies revealed a cytotoxic impact after blocking autophagy in cancer cells and the first clinical trial was run in glioblastoma where patient survival was significantly extended when CQ was combined with radiation and chemotherapy (187), and CQ or HCQ have now been studied in the context of a number of different tumor types with somewhat variable results (186). In a mouse model of pancreatic cancer, a recent study highlighted the autophagy-mediated downregulation of MHC expression by tumor cells, which was reversible upon autophagy inhibition (188). Combining CQ with dual ICB drove potent tumor regressions and responses (188), revealing autophagy as a determinant of tumor cell immunogenicity. While this alone helps skew the TME toward a "small" TME phenotype with increased T cell infiltration (188), the benefits of systemic autophagy inhibition are much broader (186). CD8 T cells display enhanced anti-tumor effector function (189), while DCs upregulate MHC I expression after autophagy inhibition. However, tumor-intrinsic autophagy may be required for chemotherapy-induced tumor cell death, which can be a potent immune stimulator (190), highlighting the need for preclinical investigations to identify rational therapeutic partners for autophagy inhibition and successful immune responses against cancer.

CONCLUDING REMARKS

Clinical and pre-clinical data indicate that tumor burden negatively correlates with response to a range of immunotherapies that include ICB, adoptive T cell therapy, and activation of antigen-presenting cells. Mechanistically, large tumors exert greater local and systemic changes to the immune system, and harbor more immunosuppressive cells and molecules that dampen antitumor activity. Many of the alterations locally and systemically reflect a more immunosuppressive tumor microenvironment; however, integrating this within the context of tumor burden may help stratify patients for optimally designed combination therapy approaches. Targeting features of the "large" TME can skew the immune microenvironment more toward phenotype of a "small" TME, rendering the tumor more sensitive to immunotherapeutic interventions as highlighted in **Figure 2**. A patient presenting with a large tumor burden that is amenable to debulking or size reduction to help alleviate system immunosuppression may require one approach, while a patient presenting with a relatively small but highly immunosuppressive tumor may require an entirely different therapeutic intervention. Small tumors that display an immunosupportive phenotype and are, at baseline, more amenable to immune interventions may require less invasive treatments than large tumors of the same type. Further studies interrogating the impact of bearing a large vs. small tumor are

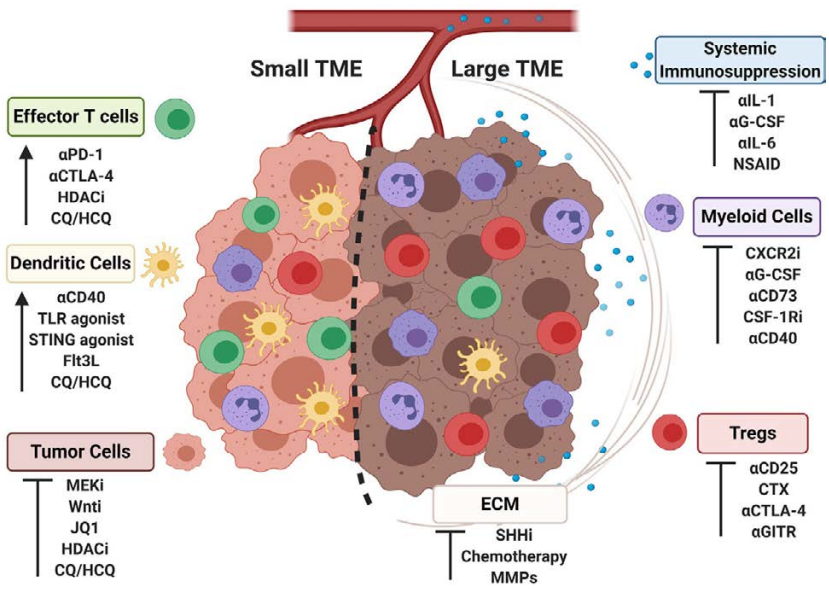

FIGURE 2 | Strategies for skewing immune aspects of the large tumor microenvironment to a small tumor microenvironment. Representative cell populations frequencies found in large or small tumor microenvironments (TMEs) are shown (cell identities labeled on figure according to colors as shown). Strategies to target the TME are listed under cell populations known to response to specific interventions, with the outcomes indicated by an arrow or an inhibitory symbol.

warranted, including investigations into the systemic impact on the immune response, the spatio-temporal localization of immune cell subsets within the TME as tumors progress, and opportunities to harness precision medicine with personalized immunotherapies. These investigations may reveal novel combinations of interventions that have the greatest impact on therapeutic outcome for patients with the greatest unmet clinical need.

AUTHOR CONTRIBUTIONS

SK and KB wrote the manuscript; all authors edited the manuscript. All authors contributed to the article and approved the submitted version.

FUNDING

This work was supported by the Roy and Diana Vagelos Scholars Program in the Molecular Life Sciences at the University of Pennsylvania (SK) and Parker Institute for Cancer Immunotherapy (KB).

ACKNOWLEDGMENTS

We thank Robert Vonderheide, Alexander Morrison, and members of the Byrne and Vonderheide laboratories for helpful discussions pertaining to this review. **Figure 2** was generated using Biorender.com.

REFERENCES

1. Whitney RB, Levy JG, Smith AG. Influence of tumor size and surgical resection on cell-mediated immunity in mice. *J Natl Cancer Inst* (1974) 53 (1):111–6. doi: 10.1093/jnci/53.1.111
2. Hinshaw DC, Shevde LA. The Tumor Microenvironment Innately Modulates Cancer Progression. *Cancer Res* (2019) 79(18):4557–66. doi: 10.1158/0008-5472.CAN-18-3962
3. Allen BM, Hiam KJ, Burnett CE, Venida A, DeBarge R, Tenvooren I, et al. Systemic dysfunction and plasticity of the immune macroenvironment in cancer models. *Nat Med* (2020) 26(7):1125–34. doi: 10.1038/s41591-020-0892-6
4. Ribas A, Wolchok JD. Cancer immunotherapy using checkpoint blockade. *Science* (2018) 359(6382):1350–5. doi: 10.1126/science.aar4060
5. Tumeh PC, Harview CL, Yearley JH, Shintaku IP, Taylor EJM, Robert L, et al. PD-1 blockade induces responses by inhibiting adaptive immune resistance. *Nature* (2014) 515(7528):568–71. doi: 10.1038/nature13954
6. Yarchoan M, Hopkins A, Jaffee EM. Tumor Mutational Burden and Response Rate to PD-1 Inhibition. *N Engl J Med* (2017) 377(25):2500–1. doi: 10.1056/NEJMc1713444
7. Cristescu R, Mogg R, Ayers M, Albright A, Murphy E, Yearley J, et al. Pan-tumor genomic biomarkers for PD-1 checkpoint blockade-based immunotherapy. *Science* (2018) 362(6411):eaar3593. doi: 10.1126/science.aar3593
8. Li J, Byrne KT, Yan F, Yamazoe T, Chen Z, Baslan T, et al. Tumor Cell-Intrinsic Factors Underlie Heterogeneity of Immune Cell Infiltration and Response to Immunotherapy. *Immunity* (2018) 49(1):178–93.e7. doi: 10.1016/j.immuni.2018.06.006
9. Horton BL, Fessenden TB, Spranger S. Tissue Site and the Cancer Immunity Cycle. *Trends Cancer* (2019) 5(10):593–603. doi: 10.1016/j.trecan.2019.07.006
10. Yamauchi M, Barker TH, Gibbons DL, Kurie JM. The fibrotic tumor stroma. *J Clin Invest* (2018) 128(1):16–25. doi: 10.1172/JCI93554
11. Schaaf MB, Garg AD, Agostinis P. Defining the role of the tumor vasculature in antitumor immunity and immunotherapy article. *Cell Death Dis* (2018) 9 (115):1–14. doi: 10.1038/s41419-017-0061-0
12. Janicki CN, Jenkinson SR, Williams NA, Morgan DJ. Loss of CTL function among high-avidity tumor-specific CD8+ T cells following tumor infiltration. *Cancer Res* (2008) 68(8):2993–3000. doi: 10.1158/0008-5472.CAN-07-5008
13. Stanta G, Bonin S. Overview on Clinical Relevance of Intra-Tumor Heterogeneity. *Front Med* (2018) 5:85:85. doi: 10.3389/fmed.2018.00085
14. Kumar V, Patel S, Tcyganov E, Gabrilovich DI. The Nature of Myeloid-Derived Suppressor Cells in the Tumor Microenvironment. *Trends Immunol* (2016) 37(3):208–20. doi: 10.1016/j.it.2016.01.004
15. Ostrand-Rosenberg S, Fenselau C. Myeloid-Derived Suppressor Cells: Immune-Suppressive Cells That Impair Antitumor Immunity and Are Sculpted by Their Environment. *J Immunol* (2018) 200(2):422–31. doi: 10.4049/jimmunol.1701019
16. Baumann T, Dunkel A, Schmid C, Schmitt S, Hiltensperger M, Lohr K, et al. Regulatory myeloid cells paralyze T cells through cell-cell transfer of the metabolite methylglyoxal. *Nat Immunol* (2020) 21(5):555–66. doi: 10.1038/s41590-020-0666-9
17. Yu JW, Bhattacharya S, Yanamandra N, Kilian D, Shi H, Yadavilli S, et al. Tumor-immune profiling of murine syngeneic tumor models as a framework to guide mechanistic studies and predict therapy response in distinct tumor microenvironments. *PloS One* (2018) 13(11):e0206223. doi: 10.1371/journal.pone.0206223
18. Najjar YG, Rayman P, Jia X, Pavicic PGJr., Rini BI, Tannenbaum C, et al. Myeloid-Derived Suppressor Cell Subset Accumulation in Renal Cell Carcinoma Parenchyma Is Associated with Intratumoral Expression of IL1β, IL8, CXCL5, and Mip-1α. *Clin Cancer Res* (2017) 23(9):2346–55. doi: 10.1158/1078-0432.CCR-15-1823
19. Clark CE, Hingorani SR, Mick R, Combs C, Tuveson DA, Vonderheide RH. Dynamics of the immune reaction to pancreatic cancer from inception to invasion. *Cancer Res* (2007) 67(19):9518–27. doi: 10.1158/0008-5472.CAN-07-0175
20. Shabaneh TB, Molodtsov AK, Steinberg SM, Zhang P, Torres GM, Mohamed GA, et al. Tumor Biology and Immunology Oncogenic BRAF V600E Governs Regulatory T-cell Recruitment during Melanoma Tumorigenesis. *Cancer Res* (2018) 78(17):5038–49. doi: 10.1158/0008-5472.CAN-18-0365
21. Duraiswamy J, Freeman GJ, Coukos G. Dual blockade of PD-1 and CTLA-4 combined with tumor vaccine effectively restores T-cell rejection function in tumors-response. *Cancer Res* (2014) 74)2:633–4. doi: 10.1158/0008-5472.CAN-13-2752
22. Guisier F, Cousse S, Jeanvoine M, Thiberville L, Salaun M. A rationale for surgical debulking to improve anti-PD1 therapy outcome in non small cell lung cancer. *Sci Rep* (2019) 9(1):16902. doi: 10.1038/s41598-019-52913-z
23. Colak S, Ten Dijke P. Targeting TGF-beta Signaling in Cancer. *Trends Cancer* (2017) 3(1):56–71. doi: 10.1016/j.trecan.2016.11.008
24. Hsieh CL, Chen DS, Hwang LH. Tumor-induced immunosuppression: A barrier to immunotherapy of large tumors by cytokine-secreting tumor vaccine. *Hum Gene Ther* (2000) 11(5):681–92. doi: 10.1089/10430340050015581
25. Wu Z, Huang X, Han X, Li Z, Zhu Q, Yan J, et al. The chemokine CXCL9 expression is associated with better prognosis for colorectal carcinoma patients. *BioMed Pharmacother* (2016) 78:8–13. doi: 10.1016/j.biopha.2015.12.021
26. Mueller SN, Ahmed R. High antigen levels are the cause of T cell exhaustion during chronic viral infection. *Proc Natl Acad Sci* (2009) 106(21):8623–8. doi: 10.1073/pnas.0809818106
27. Prato S, Zhan Y, Mintern JD, Villadangos JA. Rapid Deletion and Inactivation of CTLs upon Recognition of a Number of Target Cells over a Critical Threshold. *J Immunol* (2013) 191(7):3534–44. doi: 10.4049/jimmunol.1300803
28. Yarchoan M, Albacker LA, Hopkins AC, Montesion M, Murugesan K, Vithayathil TT, et al. PD-L1 expression and tumor mutational burden are

independent biomarkers in most cancers. *JCI Insight* (2019) 4(6):e126908. doi: 10.1172/jci.insight.126908
29. Sampedro-Nunez M, Serrano-Somavilla A, Adrados M, Cameselle-Teijeiro JM, Blanco-Carrera C, Cabezas-Agricola JM, et al. Analysis of expression of the PD-1/PD-L1 immune checkpoint system and its prognostic impact in gastroenteropancreatic neuroendocrine tumors. *Sci Rep* (2018) 8(1):17812. doi: 10.1038/s41598-018-36129-1
30. Wang Y, Zhu C, Song W, Li J, Zhao G, Cao H. PD-L1 Expression and CD8 (+) T Cell Infiltration Predict a Favorable Prognosis in Advanced Gastric Cancer. *J Immunol Res* (2018) 2018:4180517. doi: 10.1155/2018/4180517
31. Karimi S, Mansouri S, Mamatjan Y, Liu J, Nassiri F, Suppiah S, et al. Programmed death ligand-1 (PD-L1) expression in meningioma; prognostic significance and its association with hypoxia and NFKB2 expression. *Sci Rep* (2020) 10(1):14115. doi: 10.1038/s41598-020-70514-z
32. Chapon M, Randriamampita C, Maubec E, Badoual C, Fouquet S, Wang SF, et al. Progressive upregulation of PD-1 in primary and metastatic melanomas associated with blunted TCR signaling in infiltrating T lymphocytes. *J Invest Dermatol* (2011) 131(6):1300–7. doi: 10.1038/jid.2011.30
33. Slater NA, Googe PB. PD-L1 expression in cutaneous squamous cell carcinoma correlates with risk of metastasis. *J Cutan Pathol* (2016) 43 (8):663–70. doi: 10.1111/cup.12728
34. Lin JH, Huffman AP, Wattenberg MM, Walter DM, Carpenter EL, Feldser DM, et al. Type 1 conventional dendritic cells are systemically dysregulated early in pancreatic carcinogenesis. *J Exp Med* (2020) 217(8):e20190673. doi: 10.1084/jem.20190673
35. Hegde S, Krisnawan VE, Herzog BH, Zuo C, Breden MA, Knolhoff BL, et al. Dendritic Cell Paucity Leads to Dysfunctional Immune Surveillance in Pancreatic Cancer. *Cancer Cell* (2020) 37(3):289–307.e9. doi: 10.1016/j.ccell.2020.02.008
36. Meyer MA, Baer JM, Knolhoff BL, Nywening TM, Panni RZ, Su X, et al. Breast and pancreatic cancer interrupt IRF8-dependent dendritic cell development to overcome immune surveillance. *Nat Commun* (2018) 9 (1):1250. doi: 10.1038/s41467-018-03600-6
37. June CH, Sadelain M. Chimeric Antigen Receptor Therapy. *N Engl J Med* (2018) 379(1):64–73. doi: 10.1056/NEJMra1706169
38. Martikainen M, Essand M. Virus-Based Immunotherapy of Glioblastoma. *Cancers* (2019) 11(2):186. doi: 10.3390/cancers11020186
39. Wei SC, Duffy CR, Allison JP. Fundamental mechanisms of immune checkpoint blockade therapy. *Cancer Discov* (2018) 8(9):1069–86. doi: 10.1158/2159-8290.CD-18-0367
40. Larkin J, Chiarion-Sileni V, Gonzalez R, Grob JJ, Rutkowski P, Lao CD, et al. Five-Year Survival with Combined Nivolumab and Ipilimumab in Advanced Melanoma. *N Engl J Med* (2019) 381(16):1535–46. doi: 10.1056/NEJMoa1910836
41. Hodi FS, O'Day SJ, McDermott DF, Weber RW, Sosman JA, Haanen JB, et al. Improved survival with ipilimumab in patients with metastatic melanoma. *N Engl J Med* (2010) 363(8):711–23. doi: 10.1056/NEJMoa1003466
42. Hamid O, Robert C, Daud A, Hodi FS, Hwu WJ, Kefford R, et al. Safety and tumor responses with lambrolizumab (anti-PD-1) in melanoma. *N Engl J Med* (2013) 369(2):134–44. doi: 10.1056/NEJMoa1305133
43. Hellmann MD, Paz-Ares L, Bernabe Caro R, Zurawski B, Kim SW, Carcereny Costa E, et al. Nivolumab plus Ipilimumab in Advanced Non-Small-Cell Lung Cancer. *N Engl J Med* (2019) 381(21):2020–31. doi: 10.1056/NEJMoa1910231
44. Gandhi L, Rodriguez-Abreu D, Gadgeel S, Esteban E, Felip E, De Angelis F, et al. Pembrolizumab plus Chemotherapy in Metastatic Non-Small-Cell Lung Cancer. *N Engl J Med* (2018) 378(22):2078–92. doi: 10.1056/NEJMoa1801005
45. Parikh PM, Vaid A, Advani SH, Digumarti R, Madhavan J, Nag S, et al. Randomized, double-blind, placebo-controlled phase II study of single-agent oral talactoferrin in patients with locally advanced or metastatic non-small-cell lung cancer that progressed after chemotherapy. *J Clin Oncol* (2011) 29 (31):4129–36. doi: 10.1200/JCO.2010.34.4127
46. Duraiswamy J, Freeman GJ, Coukos G. Therapeutic PD-1 pathway blockade augments with other modalities of immunotherapy T-cell function to prevent immune decline in ovarian cancer. *Cancer Res* (2013) 73 (23):6900–12. doi: 10.1158/0008-5472.CAN-13-1550
47. Joseph RW, Elassaiss-Schaap J, Kefford R, Hwu WJ, Wolchok JD, Joshua AM, et al. Baseline tumor size is an independent prognostic factor for overall survival in patients with melanoma treated with pembrolizumab. *Clin Cancer Res* (2018) 24(20):4960–7. doi: 10.1158/1078-0432.CCR-17-2386
48. Lee JHJ, Lyle M, Menzies AM, Chan MMK, Lo S, Clements A, et al. Metastasis-specific patterns of response and progression with anti-PD-1 treatment in metastatic melanoma. *Pigment Cell Melanoma Res* (2018) 31 (3):404–10. doi: 10.1111/pcmr.12675
49. Chardin D, Paquet M, Schiappa R, Darcourt J, Bailleux C, Poudenx M, et al. Baseline metabolic tumor volume as a strong predictive and prognostic biomarker in patients with non-small cell lung cancer treated with PD1 inhibitors: a prospective study. *J Immunother Cancer* (2020) 8(2):e000645. doi: 10.1136/jitc-2020-000645
50. Nishino M, Giobbie-Hurder A, Ramaiya NH, Hodi FS. Response assessment in metastatic melanoma treated with ipilimumab and bevacizumab: CT tumor size and density as markers for response and outcome. *J Immunother Cancer* (2014) 2(1):40. doi: 10.1186/s40425-014-0040-2
51. Huang AC, Postow MA, Orlowski RJ, Mick R, Bengsch B, Manne S, et al. T-cell invigoration to tumour burden ratio associated with anti-PD-1 response. *Nature* (2017) 545:60–5. doi: 10.1038/nature22079
52. Marin-Acevedo JA, Dholaria B, Soyano AE, Knutson KL, Chumsri S, Lou Y. Next generation of immune checkpoint therapy in cancer: New developments and challenges. *J Hematol Oncol* (2018) 11(1):39. doi: 10.1186/s13045-018-0582-8
53. Triplett TA, Tucker CG, Triplett KC, Alderman Z, Sun L, Ling LE, et al. STAT3 signaling is required for optimal regression of large established tumors in mice treated with anti-OX40 and TGFβ Receptor Blockade. *Cancer Immunol Res* (2015) 3(5):526–35. doi: 10.1158/2326-6066.CIR-14-0187
54. Bartkowiak T, Curran MA. 4-1BB agonists: Multi-potent potentiators of tumor immunity. *Front Oncol* (2015) 5:117:117. doi: 10.3389/fonc.2015.00117
55. Kocak E, Lute K, Chang X, May KFJr., Exten KR, Zhang H, et al. Combination therapy with anti-CTL antigen-4 and anti-4-1BB antibodies enhances cancer immunity and reduces autoimmunity. *Cancer Res* (2006) 66 (14):7276–84. doi: 10.1158/0008-5472.CAN-05-2128
56. Vermaelen K. Vaccine strategies to improve anticancer cellular immune responses. *Front Immunol* (2019) 10:8:8. doi: 10.3389/fimmu.2019.00008
57. Binder DC, Engels B, Arina A, Yu P, Slauch JM, Fu YX, et al. Antigen-specific bacterial vaccine combined with anti-PD-L1 rescues dysfunctional endogenous T cells to reject long-established cancer. *Cancer Immunol Res* (2013) 1(2):123–33. doi: 10.1158/2326-6066.CIR-13-0058
58. Cuadros C, Dominguez AL, Lollini P-L, Croft M, Mittler RS, Borgström P, et al. Vaccination with dendritic cells pulsed with apoptotic tumors in combination with anti-OX40 and anti-4-1BB monoclonal antibodies induces T cell-mediated protective immunity in Her-2/neu transgenic mice. *Int J Cancer* (2005) 116(6):934–43. doi: 10.1002/ijc.21098
59. D'Alise AM, Leoni G, Cotugno G, Troise F, Langone F, Fichera I, et al. Adenoviral vaccine targeting multiple neoantigens as strategy to eradicate large tumors combined with checkpoint blockade. *Nat Commun* (2019) 10 (1):2688. doi: 10.1038/s41467-019-10594-2
60. Rice AE, Latchman YE, Balint JP, Lee JH, Gabitzsch ES, Jones FR. An HPV-E6/E7 immunotherapy plus PD-1 checkpoint inhibition results in tumor regression and reduction in PD-L1 expression. *Cancer Gene Ther* (2015) 22 (9):454–62. doi: 10.1038/cgt.2015.40
61. Kaufman H, Amatruda T, Nemunaitis JJ, Chesney JA, Delman KA, Spitler LE, et al. Tumor size and clinical outcomes in melanoma patients treated with talimogene laherparepvec (T-VEC). *J Clin Oncol* (2015) 33 (15_suppl):9074. doi: 10.1200/jco.2015.33.15_suppl.9074
62. Vonderheide RH. The Immune Revolution: A Case for Priming, Not Checkpoint. *Cancer Cell* (2018) 33(4):563–9. doi: 10.1016/j.ccell.2018.03.008
63. French RR, Chan HT, Tutt AL, Glennie MJ. CD40 antibody evokes a cytotoxic T-cell response that eradicates lymphoma and bypasses T-cell help. *Nat Med* (1999) 5(5):548–53. doi: 10.1038/8426
64. Diehl L, den Boer AT, Schoenberger SP, van der Voort EI, Schumacher TN, Melief CJ, et al. CD40 activation in vivo overcomes peptide-induced

peripheral cytotoxic T-lymphocyte tolerance and augments anti-tumor vaccine efficacy. *Nat Med* (1999) 5(7):774–9. doi: 10.1038/10495
65. Schoenberger SP, Toes REM, van der Voort EIH, Offringa R, Melief CJM. T-cell help for cytotoxic T lymphocytes is mediated by CD40-CD40L interactions. *Nature* (1998) 393(6684):480–3. doi: 10.1038/31002
66. Byrne KT, Vonderheide RH. CD40 Stimulation Obviates Innate Sensors and Drives T Cell Immunity in Cancer. *Cell Rep* (2016) 15(12):2719–32. doi: 10.1016/j.celrep.2016.05.058
67. Morrison AH, Diamond MS, Hay CA, Byrne KT, Vonderheide RH. Sufficiency of CD40 activation and immune checkpoint blockade for T cell priming and tumor immunity. *Proc Nat Acad Sci* (2020) 117(14):8022–31. doi: 10.1073/pnas.1918971117
68. Rech AJ, Dada H, Kotzin JJ, Henao-Mejia J, Minn AJ, Twyman-Saint Victor C, et al. Radiotherapy and CD40 Activation Separately Augment Immunity to Checkpoint Blockade in Cancer. *Cancer Res* (2018) 78(15):4282–91. doi: 10.1158/0008-5472.CAN-17-3821
69. Winograd R, Byrne KT, Evans RA, Odorizzi PM, Meyer ARL, Bajor DL, et al. Induction of T-cell immunity overcomes complete resistance to PD-1 and CTLA-4 blockade and improves survival in pancreatic carcinoma. *Cancer Immunol Res* (2015) 3(4):399–411. doi: 10.1158/2326-6066.CIR-14-0215
70. O'Hara MH, O'Reilly EM, Mick R, Varadhachary G, Wainberg ZA, Ko A, et al. A Phase Ib study of CD40 agonistic monoclonal antibody APX005M together with gemcitabine and nab-paclitaxel with or without nivolumab in untreated metastatic ductal pancreatic adenocarcinoma patients. *Cancer Res* (2019) 79(13):CT004. doi: 10.1158/1538-7445.SABCS18-CT004
71. Rosenberg SA, Yang JC, Sherry RM, Kammula US, Hughes MS, Phan GQ, et al. Durable complete responses in heavily pretreated patients with metastatic melanoma using T-cell transfer immunotherapy. *Clin Cancer Res* (2011) 17(13):4550–7. doi: 10.1158/1078-0432.CCR-11-0116
72. Andersen R, Donia M, Ellebaek E, Borch TH, Kongsted P, Iversen TZ, et al. Long-Lasting Complete Responses in Patients with Metastatic Melanoma after Adoptive Cell Therapy with Tumor-Infiltrating Lymphocytes and an Attenuated IL2 Regimen. *Clin Cancer Res* (2016) 22(15):3734–45. doi: 10.1158/1078-0432.CCR-15-1879
73. Hanson HL, Donermeyer DL, Ikeda H, White JM, Shankaran V, Old LJ, et al. Eradication of established tumors by CD8+ T cell adoptive immunotherapy. *Immunity* (2000) 13(2):265–76. doi: 10.1016/S1074-7613(00)00026-1
74. Segal G, Prato S, Zehn D, Mintern JD, Villadangos JA. Target Density, Not Affinity or Avidity of Antigen Recognition, Determines Adoptive T Cell Therapy Outcomes in a Mouse Lymphoma Model. *J Immunol* (2016) 196 (9):3935–42. doi: 10.4049/jimmunol.1502187
75. Park JH, Riviere I, Gonen M, Wang X, Senechal B, Curran KJ, et al. Long-Term Follow-up of CD19 CAR Therapy in Acute Lymphoblastic Leukemia. *N Engl J Med* (2018) 378(5):449–59. doi: 10.1056/NEJMoa1709919
76. Wu X, Luo H, Shi B, Di S, Sun R, Su J, et al. Combined Antitumor Effects of Sorafenib and GPC3-CAR T Cells in Mouse Models of Hepatocellular Carcinoma. *Mol Ther* (2019) 27(8):1483–94. doi: 10.1016/j.ymthe.2019.04.020
77. Kato D, Yaguchi T, Iwata T, Katoh Y, Morii K, Tsubota K, et al. GPC1 specific CAR-T cells eradicate established solid tumor without adverse effects and synergize with anti-PD-1 Ab. *Elife* (2020) 9:e49392. doi: 10.7554/eLife.49392
78. Shimizu T, Fuchimoto Y, Okita H, Fukuda K, Kitagawa Y, Ueno S, et al. A curative treatment strategy using tumor debulking surgery combined with immune checkpoint inhibitors for advanced pediatric solid tumors: An in vivo study using a murine model of osteosarcoma. *J Pediatr Surg* (2018) 53 (12):2460–4. doi: 10.1016/j.jpedsurg.2018.08.023
79. Demicheli R, Retsky MW, Hrushesky WJ, Baum M. Tumor dormancy and surgery-driven interruption of dormancy in breast cancer: learning from failures. *Nat Clin Pract Oncol* (2007) 4(12):699–710. doi: 10.1038/ncponc0999
80. Giancotti FG. Mechanisms governing metastatic dormancy and reactivation. *Cell* (2013) 155(4):750–64. doi: 10.1016/j.cell.2013.10.029
81. Bakos O, Lawson C, Rouleau S, Tai LH. Combining surgery and immunotherapy: turning an immunosuppressive effect into a therapeutic opportunity. *J Immunother Cancer* (2018) 6(1):86. doi: 10.1186/s40425-018-0398-7
82. Krall JA, Reinhardt F, Mercury OA, Pattabiraman DR, Brooks MW, Dougan M, et al. The systemic response to surgery triggers the outgrowth of distant immune-controlled tumors in mouse models of dormancy. *Sci Transl Med* (2018) 10(436):eaan3464. doi: 10.1126/scitranslmed.aan3464
83. Flanigan RC, Salmon SE, Blumenstein BA, Bearman SI, Roy V, McGrath PC, et al. Nephrectomy Followed by Interferon Alfa-2b Compared with Interferon Alfa-2b Alone for Metastatic Renal-Cell Cancer. *N Engl J Med* (2001) 345(23):1655–9. doi: 10.1056/NEJMoa003013
84. Galluzzi L, Buque A, Kepp O, Zitvogel L, Kroemer G. Immunogenic cell death in cancer and infectious disease. *Nat Rev Immunol* (2017) 17(2):97–111. doi: 10.1038/nri.2016.107
85. Robert C, Thomas L, Bondarenko I, O'Day S, Weber J, Garbe C, et al. Ipilimumab plus dacarbazine for previously untreated metastatic melanoma. *N Engl J Med* (2011) 364(26):2517–26. doi: 10.1056/NEJMoa1104621
86. Mackall CL. T-cell immunodeficiency following cytotoxic antineoplastic therapy: a review. *Oncologist* (1999) 4(5):370–8. doi: 10.1634/theoncologist.4-5-370
87. McCoy MJ, Lake RA, van der Most RG, Dick IM, Nowak AK. Post-chemotherapy T-cell recovery is a marker of improved survival in patients with advanced thoracic malignancies. *Br J Cancer* (2012) 107(7):1107–15. doi: 10.1038/bjc.2012.362
88. Iida Y, Harashima N, Motoshima T, Komohara Y, Eto M, Harada M. Contrasting effects of cyclophosphamide on anti-CTL-associated protein 4 blockade therapy in two mouse tumor models. *Cancer Sci* (2017) 108 (10):1974–84. doi: 10.1111/cas.13337
89. Byrne KT, Leisenring NH, Bajor DL, Vonderheide RH. CSF-1R-Dependent Lethal Hepatotoxicity When Agonistic CD40 Antibody Is Given before but Not after Chemotherapy. *J Immunol* (2016) 197(1):179–87. doi: 10.4049/jimmunol.1600146
90. Long KB, Gladney WL, Tooker GM, Graham K, Fraietta JA, Beatty GL. IFN and CCL2 Cooperate to Redirect Tumor-Infiltrating Monocytes to Degrade Fibrosis and Enhance Chemotherapy Efficacy in Pancreatic Carcinoma. *Cancer Discov* (2016) 6(4):400–13. doi: 10.1158/2159-8290.CD-15-1032
91. Reits EA, Hodge JW, Herberts CA, Groothuis TA, Chakraborty M, Wansley EK, et al. Radiation modulates the peptide repertoire, enhances MHC class I expression, and induces successful antitumor immunotherapy. *J Exp Med* (2006) 203(5):1259–71. doi: 10.1084/jem.20052494
92. Twyman-Saint Victor C, Rech AJ, Maity A, Rengan R, Pauken KE, Stelekati E, et al. Radiation and dual checkpoint blockade activate non-redundant immune mechanisms in cancer. *Nature* (2015) 520(7547):373–7. doi: 10.1038/nature14292
93. Maity A, Mick R, Huang AC, George SM, Farwell MD, Lukens JN, et al. A phase I trial of pembrolizumab with hypofractionated radiotherapy in patients with metastatic solid tumours. *Br J Cancer* (2018) 119(10):1200–7. doi: 10.1038/s41416-018-0281-9
94. Formenti SC, Rudqvist NP, Golden E, Cooper B, Wennerberg E, Lhuillier C, et al. Radiotherapy induces responses of lung cancer to CTLA-4 blockade. *Nat Med* (2018) 24(12):1845–51. doi: 10.1038/s41591-018-0232-2
95. Muz B, de la Puente P, Azab F, Azab AK. The role of hypoxia in cancer progression, angiogenesis, metastasis, and resistance to therapy. *Hypoxia* (2015) 3:83–92. doi: 10.2147/HP.S93413
96. Petrova V, Annicchiarico-Petruzzelli M, Melino G, Amelio I. The hypoxic tumour microenvironment. *Oncogenesis* (2018) 7(1):10. doi: 10.1038/s41389-017-0011-9
97. Lee CM, Tannock IF. The distribution of the therapeutic monoclonal antibodies cetuximab and trastuzumab within solid tumors. *BMC Cancer* (2010) 10:255. doi: 10.1186/1471-2407-10-255
98. Oberstein PE, Olive KP. Pancreatic cancer: why is it so hard to treat? *Therap Adv Gastroenterol* (2013) 6(4):321–37. doi: 10.1177/1756283X13478680
99. Lo A, Li CP, Buza EL, Blomberg R, Govindaraju P, Avery D, et al. Fibroblast activation protein augments progression and metastasis of pancreatic ductal adenocarcinoma. *JCI Insight* (2017) 2(19):e92232. doi: 10.1172/jci.insight.92232
100. Olive KP, Jacobetz MA, Davidson CJ, Gopinathan A, McIntyre D, Honess D, et al. Inhibition of Hedgehog signaling enhances delivery of chemotherapy in a mouse model of pancreatic cancer. *Science* (2009) 324(5933):1457–61. doi: 10.1126/science.1171362

101. Alvarez R, Musteanu M, Garcia-Garcia E, Lopez-Casas PP, Megias D, Guerra C, et al. Stromal disrupting effects of nab-paclitaxel in pancreatic cancer. *Br J Cancer* (2013) 109(4):926–33. doi: 10.1038/bjc.2013.415
102. Von Hoff DD, Ramanathan RK, Borad MJ, Laheru DA, Smith LS, Wood TE, et al. Gemcitabine plus nab-paclitaxel is an active regimen in patients with advanced pancreatic cancer: a phase I/II trial. *J Clin Oncol* (2011) 29 (34):4548–54. doi: 10.1200/JCO.2011.36.5742
103. Neesse A, Frese KK, Chan DS, Bapiro TE, Howat WJ, Richards FM, et al. SPARC independent drug delivery and antitumour effects of nab-paclitaxel in genetically engineered mice. *Gut* (2014) 63(6):974–83. doi: 10.1136/gutjnl-2013-305559
104. Maute RL, Gordon SR, Mayer AT, McCracken MN, Natarajan A, Ring NG, et al. Engineering high-affinity PD-1 variants for optimized immunotherapy and immuno-PET imaging. *Proc Nat Acad Sci* (2015) 112(47):e6506–e14. doi: 10.1073/pnas.1519623112
105. Kramer ED, Abrams SI. Granulocytic Myeloid-Derived Suppressor Cells as Negative Regulators of Anticancer Immunity. *Front Immunol* (2020) 11:1963:1963. doi: 10.3389/fimmu.2020.01963
106. Steele CW, Karim SA, Leach JDG, Bailey P, Upstill-Goddard R, Rishi L, et al. CXCR2 Inhibition Profoundly Suppresses Metastases and Augments Immunotherapy in Pancreatic Ductal Adenocarcinoma. *Cancer Cell* (2016) 29(6):832–45. doi: 10.1016/j.ccell.2016.04.014
107. Chao T, Furth EE, Vonderheide RH. CXCR2-dependent accumulation of tumor-associated neutrophils regulates T-cell immunity in pancreatic ductal adenocarcinoma. *Cancer Immunol Res* (2016) 4(11):968–82. doi: 10.1158/2326-6066.CIR-16-0188
108. Bayne LJ, Beatty GL, Jhala N, Clark CE, Rhim AD, Stanger BZ, et al. Tumor-Derived Granulocyte-Macrophage Colony-Stimulating Factor Regulates Myeloid Inflammation and T Cell Immunity in Pancreatic Cancer. *Cancer Cell* (2012) 21(6):822–35. doi: 10.1016/j.ccr.2012.04.025
109. Pylayeva-Gupta Y, Lee KE, Hajdu CH, Miller G, Bar-Sagi D. Oncogenic Kras-induced GM-CSF production promotes the development of pancreatic neoplasia. *Cancer Cell* (2012) 21(6):836–47. doi: 10.1016/j.ccr.2012.04.024
110. Fultang L, Panetti S, Ng M, Collins P, Graef S, Rizkalla N, et al. MDSC targeting with Gemtuzumab ozogamicin restores T cell immunity and immunotherapy against cancers. *EBioMedicine* (2019) 47:235–46. doi: 10.1016/j.ebiom.2019.08.025
111. Panni RZ, Herndon JM, Zuo C, Hegde S, Hogg GD, Knolhoff BL, et al. Agonism of CD11b reprograms innate immunity to sensitize pancreatic cancer to immunotherapies. *Sci Trans Med* (2019) 11(499):eaau9240. doi: 10.1126/scitranslmed.aau9240
112. Wu L, Mao L, Liu JF, Chen L, Yu GT, Yang LL, et al. Blockade of TIGIT/CD155 signaling reverses t-cell exhaustion and enhances antitumor capability in head and neck squamous cell carcinoma. *Cancer Immunol Res* (2019) 7(10):1700–13. doi: 10.1158/2326-6066.CIR-18-0725
113. Roh M, Wainwright DA, Wu JD, Wan Y, Zhang B. Targeting CD73 to augment cancer immunotherapy. *Curr Opin Pharmacol* (2020) 53:66–76. doi: 10.1016/j.coph.2020.07.001
114. Neubert NJ, Schmittnaegel M, Bordry N, Nassiri S, Wald N, Martignier C, et al. T cell-induced CSF1 promotes melanoma resistance to PD1 blockade. *Sci Transl Med* (2018) 10(436):eaan3311. doi: 10.1126/scitranslmed.aan3311
115. De Henau O, Rausch M, Winkler D, Campesato LF, Liu C, Cymerman DH, et al. Overcoming resistance to checkpoint blockade therapy by targeting PI3Kgamma in myeloid cells. *Nature* (2016) 539(7629):443–7. doi: 10.1038/nature20554
116. Loeuillard E, Yang J, Buckarma E, Wang J, Liu Y, Conboy CB, et al. Targeting tumor-associated macrophages and granulocytic-myeloid-derived suppressor cells augments pd-1 blockade in cholangiocarcinoma. *J Clin Invest* (2020) 130(10):5380–96. doi: 10.1172/JCI137110
117. Nywening TM, Belt BA, Cullinan DR, Panni RZ, Han BJ, Sanford DE, et al. Targeting both tumour-associated CXCR2(+) neutrophils and CCR2(+) macrophages disrupts myeloid recruitment and improves chemotherapeutic responses in pancreatic ductal adenocarcinoma. *Gut* (2018) 67(6):1112–23. doi: 10.1136/gutjnl-2017-313738
118. Tanaka A, Sakaguchi S. Targeting Treg cells in cancer immunotherapy. *Eur J Immunol* (2019) 49(8):1140–6. doi: 10.1002/eji.201847659
119. Cote AL, Byrne KT, Steinberg SM, Zhang P, Turk MJ. Protective CD8 memory T cell responses to mouse melanoma are generated in the absence of CD4 T cell help. *PloS One* (2011) 6(10):e26491. doi: 10.1371/journal.pone.0026491
120. Alspach E, Lussier DM, Miceli AP, Kizhvatov I, DuPage M, Luoma AM, et al. MHC-II neoantigens shape tumour immunity and response to immunotherapy. *Nature* (2019) 574(7780):696–701. doi: 10.1038/s41586-019-1671-8
121. Ferris ST, Durai V, Wu R, Theisen DJ, Ward JP, Bern MD, et al. cDC1 prime and are licensed by CD4(+) T cells to induce anti-tumour immunity. *Nature* (2020) 584(7822):624–9. doi: 10.1038/s41586-020-2611-3
122. Sledzinska A, Vila de Mucha M, Bergerhoff K, Hotblack A, Demane DF, Ghorani E, et al. Regulatory T Cells Restrain Interleukin-2- and Blimp-1-Dependent Acquisition of Cytotoxic Function by CD4(+) T Cells. *Immunity* (2020) 52(1):151–66 e6. doi: 10.1016/j.immuni.2019.12.007
123. Simpson TR, Li F, Montalvo-Ortiz W, Sepulveda MA, Bergerhoff K, Arce F, et al. Fc-dependent depletion of tumor-infiltrating regulatory T cells co-defines the efficacy of anti–CTLA-4 therapy against melanoma. *J Exp Med* (2013) 210(9):1695–710. doi: 10.1084/jem.20130579
124. Sharma A, Subudhi SK, Blando J, Scutti J, Vence L, Wargo J, et al. Anti-CTLA-4 Immunotherapy Does Not Deplete FOXP3(+) Regulatory T Cells (Tregs) in Human Cancers. *Clin Cancer Res* (2019) 25(4):1233–8. doi: 10.1158/1078-0432.CCR-18-0762
125. Mahne AE, Mauze S, Joyce-Shaikh B, Xia J, Bowman EP, Beebe AM, et al. Dual Roles for Regulatory T-cell Depletion and Costimulatory Signaling in Agonistic GITR Targeting for Tumor Immunotherapy. *Cancer Res* (2017) 77 (5):1108–18. doi: 10.1158/0008-5472.CAN-16-0797
126. Starnes CO. Coley's toxins in perspective. *Nature* (1992) 357(6373):11–2. doi: 10.1038/357011a0
127. Urban-Wojciuk Z, Khan MM, Oyler BL, Fåhraeus R, Marek-Trzonkowska N, Nita-Lazar A, et al. The role of tlrs in anti-cancer immunity and tumor rejection. *Front Immunol* (2019) 10:2388:2388. doi: 10.3389/fimmu.2019.02388
128. Rodell CB, Arlauckas SP, Cuccarese MF, Garris CS, Li R, Ahmed MS, et al. TLR7/8-agonist-loaded nanoparticles promote the polarization of tumour-associated macrophages to enhance cancer immunotherapy. *Nat BioMed Engl* (2018) 2(8):578–88. doi: 10.1038/s41551-018-0236-8
129. Mullins SR, Vasilakos JP, Deschler K, Grigsby I, Gillis P, John J, et al. Intratumoral immunotherapy with TLR7/8 agonist MEDI9197 modulates the tumor microenvironment leading to enhanced activity when combined with other immunotherapies. *J Immunother Cancer* (2019) 7(1):244. doi: 10.1186/s40425-019-0724-8
130. Nyirenda MH, Sanvito L, Darlington PJ, O'Brien K, Zhang G-X, Constantinescu CS, et al. TLR2 Stimulation Drives Human Naive and Effector Regulatory T Cells into a Th17-Like Phenotype with Reduced Suppressive Function. *J Immunol* (2011) 187(5):2278–90. doi: 10.4049/jimmunol.1003715
131. Kaczanowska S, Joseph AM, Davila E. TLR agonists: our best frenemy in cancer immunotherapy. *J Leukoc Biol* (2013) 93(6):847–63. doi: 10.1189/jlb.1012501
132. Grimmig T, Matthes N, Hoeland K, Tripathi S, Chandraker A, Grimm M, et al. TLR7 and TLR8 expression increases tumor cell proliferation and promotes chemoresistance in human pancreatic cancer. *Int J Oncol* (2015) 47 (3):857–66. doi: 10.3892/ijo.2015.3069
133. He W, Liu Q, Wang L, Chen W, Li N, Cao X. TLR4 signaling promotes immune escape of human lung cancer cells by inducing immunosuppressive cytokines and apoptosis resistance. *Mol Immunol* (2007) 44(11):2850–9. doi: 10.1016/j.molimm.2007.01.022
134. Sun L, Wu J, Du F, Chen X, Chen ZJ. Cyclic GMP-AMP synthase is a cytosolic DNA sensor that activates the type I interferon pathway. *Science* (2013) 339(6121):786–91. doi: 10.1126/science.1232458
135. Kwon J, Bakhoum SF. The Cytosolic DNA-Sensing cGAS-STING Pathway in Cancer. *Cancer Discov* (2020) 10(1):26–39. doi: 10.1158/2159-8290.CD-19-0761
136. Yum S, Li M, Frankel AE, Chen ZJ. Roles of the cGAS-STING pathway in cancer immunosurveillance and immunotherapy. *Ann Rev Cancer Biol* (2019) 3(1):323–44. doi: 10.1146/annurev-cancerbio-030518-055636
137. Woo SR, Fuertes MB, Corrales L, Spranger S, Furdyna MJ, Leung MY, et al. STING-dependent cytosolic DNA sensing mediates innate immune recognition of immunogenic tumors. *Immunity* (2014) 41(5):830–42. doi: 10.1016/j.immuni.2014.10.017

138. Diamond MS, Kinder M, Matsushita H, Mashayekhi M, Dunn GP, Archambault JM, et al. Type I interferon is selectively required by dendritic cells for immune rejection of tumors. *J Exp Med* (2011) 208 (10):1989–2003. doi: 10.1084/jem.20101158
139. Demaria O, De Gassart A, Coso S, Gestermann N, Di Domizio J, Flatz L, et al. STING activation of tumor endothelial cells initiates spontaneous and therapeutic antitumor immunity. *Proc Nat Acad Sci* (2015) 112(50):15408–13. doi: 10.1073/pnas.1512832112
140. Wang H, Hu S, Chen X, Shi H, Chen C, Sun L, et al. cGAS is essential for the antitumor effect of immune checkpoint blockade. *Proc Nat Acad Sci* (2017) 114(7):1637–42. doi: 10.1073/pnas.1621363114
141. Yang H, Lee WS, Kong SJ, Kim CG, Kim JH, Chang SK, et al. STING activation reprograms tumor vasculatures and synergizes with VEGFR2 blockade. *J Clin Invest* (2019) 129(10):4350–64. doi: 10.1172/JCI125413
142. Li T, Cheng H, Yuan H, Xu Q, Shu C, Zhang Y, et al. Antitumor Activity of cGAMP via Stimulation of cGAS-cGAMP-STING-IRF3 Mediated Innate Immune Response. *Sci Rep* (2016) 6:19049. doi: 10.1038/srep19049
143. Beatty GL, Chiorean EG, Fishman MP, Saboury B, Teitelbaum UR, Sun W, et al. CD40 Agonists Alter Tumor Stroma and Show Efficacy Against Pancreatic Carcinoma in Mice and Humans. *Science* (2011) 331 (6024):1612–6. doi: 10.1126/science.1198443
144. Zhang Q, Liu F. Advances and potential pitfalls of oncolytic viruses expressing immunomodulatory transgene therapy for malignant gliomas. *Cell Death Dis* (2020) 11(6):485. doi: 10.1038/s41419-020-2696-5
145. Desjardins A, Gromeier M, Herndon JE, Beaubier N, Bolognesi DP, Friedman AH, et al. Recurrent Glioblastoma Treated with Recombinant Poliovirus. *N Engl J Med* (2018) 379(2):150–61. doi: 10.1056/NEJMoa1716435
146. de Graaf JF, de Vor L, Fouchier RAM, van den Hoogen BG. Armed oncolytic viruses: A kick-start for anti-tumor immunity. *Cytokine Growth Factor Rev* (2018) 41:28–39. doi: 10.1016/j.cytogfr.2018.03.006
147. Liu BL, Robinson M, Han ZQ, Branston RH, English C, Reay P, et al. ICP34.5 deleted herpes simplex virus with enhanced oncolytic, immune stimulating, and anti-tumour properties. *Gene Ther* (2003) 10(4):292–303. doi: 10.1038/sj.gt.3301885
148. Ribas A, Dummer R, Puzanov I, VanderWalde A, Andtbacka RHI, Michielin O, et al. Oncolytic Virotherapy Promotes Intratumoral T Cell Infiltration and Improves Anti-PD-1 Immunotherapy. *Cell* (2017) 170(6):1109–19 e10. doi: 10.1016/j.cell.2017.08.027
149. Kohlhapp FJ, Kaufman HL. Molecular Pathways: Mechanism of Action for Talimogene Laherparepvec, a New Oncolytic Virus Immunotherapy. *Clin Cancer Res* (2016) 22(5):1048–54. doi: 10.1158/1078-0432.CCR-15-2667
150. Andtbacka RH, Kaufman HL, Collichio F, Amatruda T, Senzer N, Chesney J, et al. Talimogene Laherparepvec Improves Durable Response Rate in Patients With Advanced Melanoma. *J Clin Oncol* (2015) 33(25):2780–8. doi: 10.1200/JCO.2014.58.3377
151. Puzanov I, Milhem MM, Minor D, Hamid O, Li A, Chen L, et al. Talimogene Laherparepvec in Combination With Ipilimumab in Previously Untreated, Unresectable Stage IIIB-IV Melanoma. *J Clin Oncol* (2016) 34(22):2619–26. doi: 10.1200/JCO.2016.67.1529
152. Chesney J, Puzanov I, Collichio F, Singh P, Milhem MM, Glaspy J, et al. Randomized, Open-Label Phase II Study Evaluating the Efficacy and Safety of Talimogene Laherparepvec in Combination With Ipilimumab Versus Ipilimumab Alone in Patients With Advanced, Unresectable Melanoma. *J Clin Oncol* (2018) 36(17):1658–67. doi: 10.1200/JCO.2017.73.7379
153. Spranger S, Bao R, Gajewski TF. Melanoma-intrinsic beta-catenin signalling prevents anti-tumour immunity. *Nature* (2015) 523(7559):231–5. doi: 10.1038/nature14404
154. Ganesh S, Shui X, Craig KP, Park J, Wang W, Brown BD, et al. RNAi-Mediated beta-Catenin Inhibition Promotes T Cell Infiltration and Antitumor Activity in Combination with Immune Checkpoint Blockade. *Mol Ther* (2018) 26(11):2567–79. doi: 10.1016/j.ymthe.2018.09.005
155. Qu Y, Olsen JR, Yuan X, Cheng PF, Levesque MP, Brokstad KA, et al. Small molecule promotes beta-catenin citrullination and inhibits Wnt signaling in cancer. *Nat Chem Biol* (2018) 14(1):94–101. doi: 10.1038/nchembio.2510
156. Filippakopoulos P, Qi J, Picaud S, Shen Y, Smith WB, Fedorov O, et al. Selective inhibition of BET bromodomains. *Nature* (2010) 468(7327):1067–73. doi: 10.1038/nature09504
157. Zhu H, Bengsch F, Svoronos N, Rutkowski MR, Bitler BG, Allegrezza MJ, et al. BET Bromodomain Inhibition Promotes Anti-tumor Immunity by Suppressing PD-L1 Expression. *Cell Rep* (2016) 16(11):2829–37. doi: 10.1016/j.celrep.2016.08.032
158. Kagoya Y, Nakatsugawa M, Yamashita Y, Ochi T, Guo T, Anczurowski M, et al. BET bromodomain inhibition enhances T cell persistence and function in adoptive immunotherapy models. *J Clin Invest* (2016) 126(9):3479–94. doi: 10.1172/JCI86437
159. Adeegbe DO, Liu S, Hattersley MM, Bowden M, Zhou CW, Li S, et al. BET Bromodomain Inhibition Cooperates with PD-1 Blockade to Facilitate Antitumor Response in Kras-Mutant Non-Small Cell Lung Cancer. *Cancer Immunol Res* (2018) 6(10):1234–45. doi: 10.1158/2326-6066.CIR-18-0077
160. Wang L, Xu M, Kao CY, Tsai SY, Tsai MJ. Small molecule JQ1 promotes prostate cancer invasion via BET-independent inactivation of FOXA1. *J Clin Invest* (2020) 130(4):1782–92. doi: 10.1172/JCI126327
161. Yaeger R, Corcoran RB. Targeting Alterations in the RAF-MEK Pathway. *Cancer Discov* (2019) 9(3):329–41. doi: 10.1158/2159-8290.CD-18-1321
162. Coelho MA, de Carne Trecesson S, Rana S, Zecchin D, Moore C, Molina-Arcas M, et al. Oncogenic RAS Signaling Promotes Tumor Immunoresistance by Stabilizing PD-L1 mRNA. *Immunity* (2017) 47 (6):1083–99. doi: 10.1016/j.immuni.2017.11.016
163. Ryan MB, Corcoran RB. Therapeutic strategies to target RAS-mutant cancers. *Nat Rev Clin Oncol* (2018) 15(11):709–20. doi: 10.1038/s41571-018-0105-0
164. Tran E, Robbins PF, Lu YC, Prickett TD, Gartner JJ, Jia L, et al. T-Cell Transfer Therapy Targeting Mutant KRAS in Cancer. *N Engl J Med* (2016) 375(23):2255–62. doi: 10.1056/NEJMoa1609279
165. Wang QJ, Yu Z, Griffith K, Hanada K, Restifo NP, Yang JC. Identification of T-cell Receptors Targeting KRAS-Mutated Human Tumors. *Cancer Immunol Res* (2016) 4(3):204–14. doi: 10.1158/2326-6066.CIR-15-0188
166. Hong DS, Fakih MG, Strickler JH, Desai J, Durm GA, Shapiro GI, et al. KRAS(G12C) Inhibition with Sotorasib in Advanced Solid Tumors. *N Engl J Med* (2020) 383(13):1207–17. doi: 10.1056/NEJMoa1917239
167. Canon J, Rex K, Saiki AY, Mohr C, Cooke K, Bagal D, et al. The clinical KRAS(G12C) inhibitor AMG 510 drives anti-tumour immunity. *Nature* (2019) 575(7781):217–23. doi: 10.1038/s41586-019-1694-1
168. Chapman PB, Hauschild A, Robert C, Haanen JB, Ascierto P, Larkin J, et al. Improved survival with vemurafenib in melanoma with BRAF V600E mutation. *N Engl J Med* (2011) 364(26):2507–16. doi: 10.1056/NEJMoa1103782
169. Reddy SM, Reuben A, Wargo JA. Influences of BRAF Inhibitors on the Immune Microenvironment and the Rationale for Combined Molecular and Immune Targeted Therapy. *Curr Oncol Rep* (2016) 18(7):42. doi: 10.1007/s11912-016-0531-z
170. Steinberg SM, Zhang P, Malik BT, Boni A, Shabaneh TB, Byrne KT, et al. BRAF inhibition alleviates immune suppression in murine autochthonous melanoma. *Cancer Immunol Res* (2014) 2(11):1044–50. doi: 10.1158/2326-6066.CIR-14-0074
171. Boni A, Cogdill AP, Dang P, Udayakumar D, Njauw CN, Sloss CM, et al. Selective BRAFV600E inhibition enhances T-cell recognition of melanoma without affecting lymphocyte function. *Cancer Res* (2010) 70(13):5213–9. doi: 10.1158/0008-5472.CAN-10-0118
172. Wilmott JS, Long GV, Howle JR, Haydu LE, Sharma RN, Thompson JF, et al. Selective BRAF inhibitors induce marked T-cell infiltration into human metastatic melanoma. *Clin Cancer Res* (2012) 18(5):1386–94. doi: 10.1158/1078-0432.CCR-11-2479
173. Kuske M, Westphal D, Wehner R, Schmitz M, Beissert S, Praetorius C, et al. Immunomodulatory effects of BRAF and MEK inhibitors: Implications for Melanoma therapy. *Pharmacol Res* (2018) 136:151–9. doi: 10.1016/j.phrs.2018.08.019
174. Ebert PJR, Cheung J, Yang Y, McNamara E, Hong R, Moskalenko M, et al. MAP Kinase Inhibition Promotes T Cell and Anti-tumor Activity in Combination with PD-L1 Checkpoint Blockade. *Immunity* (2016) 44 (3):609–21. doi: 10.1016/j.immuni.2016.01.024
175. Yarchoan M, Mohan AA, Dennison L, Vithayathil T, Ruggieri A, Lesinski GB, et al. MEK inhibition suppresses B regulatory cells and augments anti-tumor immunity. *PloS One* (2019) 14(10):e0224600. doi: 10.1371/journal.pone.0224600

176. Deken MA, Gadiot J, Jordanova ES, Lacroix R, van Gool M, Kroon P, et al. Targeting the MAPK and PI3K pathways in combination with PD1 blockade in melanoma. *Oncoimmunology* (2016) 5(12):e1238557. doi: 10.1080/2162402X.2016.1238557
177. Eroglu Z, Ribas A. Combination therapy with BRAF and MEK inhibitors for melanoma: latest evidence and place in therapy. *Ther Adv Med Oncol* (2016) 8(1):48–56. doi: 10.1177/1758834015616934
178. Hu-Lieskovan S, Mok S, Homet Moreno B, Tsoi J, Robert L, Goedert L, et al. Improved antitumor activity of immunotherapy with BRAF and MEK inhibitors in BRAF(V600E) melanoma. *Sci Transl Med* (2015) 7 (279):279ra41. doi: 10.1126/scitranslmed.aaa4691
179. Ribas A, Lawrence D, Atkinson V, Agarwal S, Miller WHJr., Carlino MS, et al. Combined BRAF and MEK inhibition with PD-1 blockade immunotherapy in BRAF-mutant melanoma. *Nat Med* (2019) 25(6):936–40. doi: 10.1038/s41591-019-0476-5
180. Suraweera A, O'Byrne KJ, Richard DJ. Combination Therapy With Histone Deacetylase Inhibitors (HDACi) for the Treatment of Cancer: Achieving the Full Therapeutic Potential of HDACi. *Front Oncol* (2018) 8:92:92. doi: 10.3389/fonc.2018.00092
181. Shen L, Orillion A, Pili R. Histone deacetylase inhibitors as immunomodulators in cancer therapeutics. *Epigenomics* (2016) 8(3):415–28. doi: 10.2217/epi.15.118
182. Chang S, Collins PL, Aune TM. T-bet dependent removal of Sin3A-histone deacetylase complexes at the Ifng locus drives Th1 differentiation. *J Immunol* (2008) 181(12):8372–81. doi: 10.4049/jimmunol.181.12.8372
183. Lisiero DN, Soto H, Everson RG, Liau LM, Prins RM. The histone deacetylase inhibitor, LBH589, promotes the systemic cytokine and effector responses of adoptively transferred CD8+ T cells. *J Immunother Cancer* (2014) 2:8. doi: 10.1186/2051-1426-2-8
184. Moreira JM, Scheipers P, Sorensen P. The histone deacetylase inhibitor Trichostatin A modulates CD4+ T cell responses. *BMC Cancer* (2003) 3:30. doi: 10.1186/1471-2407-3-30
185. Shen L, Ciesielski M, Ramakrishnan S, Miles KM, Ellis L, Sotomayor P, et al. Class I histone deacetylase inhibitor entinostat suppresses regulatory T cells and enhances immunotherapies in renal and prostate cancer models. *PloS One* (2012) 7(1):e30815. doi: 10.1371/journal.pone.003081
186. Mulcahy Levy JM, Thorburn A. Autophagy in cancer: moving from understanding mechanism to improving therapy responses in patients. *Cell Death Differ* (2020) 27(3):843–57. doi: 10.1038/s41418-019-0474-7
187. Briceno E, Reyes S, Sotelo J. Therapy of glioblastoma multiforme improved by the antimutagenic chloroquine. *Neurosurg Focus* (2003) 14(2):e3. doi: 10.3171/foc.2003.14.2.4
188. Yamamoto K, Venida A, Yano J, Biancur DE, Kakiuchi M, Gupta S, et al. Autophagy promotes immune evasion of pancreatic cancer by degrading MHC-I. *Nature* (2020) 581(7806):100–5. doi: 10.1038/s41586-020-2229-5
189. DeVorkin L, Pavey N, Carleton G, Comber A, Ho C, Lim J, et al. Autophagy Regulation of Metabolism Is Required for CD8(+) T Cell Anti-tumor Immunity. *Cell Rep* (2019) 27(2):502–13 e5. doi: 10.1016/j.celrep.2019.03.037
190. Michaud M, Martins I, Sukkurwala AQ, Adjemian S, Ma Y, Pellegatti P, et al. Autophagy-dependent anticancer immune responses induced by chemotherapeutic agents in mice. *Science* (2011) 334(6062):1573–7. doi: 10.1126/science.1208347

Conflict of Interest: The authors declare that the research was conducted in the absence of any commercial or financial relationships that could be construed as a potential conflict of interest.

Copyright © 2021 Kim, Cassella and Byrne. This is an open-access article distributed under the terms of the Creative Commons Attribution License (CC BY). The use, distribution or reproduction in other forums is permitted, provided the original author (s) and the copyright owner(s) are credited and that the original publication in this journal is cited, in accordance with accepted academic practice. No use, distribution or reproduction is permitted which does not comply with these terms.

frontiers in Immunology

ORIGINAL RESEARCH
published: 04 February 2021
doi: 10.3389/fimmu.2020.621623

An Immune Cell Signature Is Associated With Disease-Free Survival and Adjuvant Chemosensitivity of Patients With Resectable Gastric Cancer

Hongfei Yan[1,2,3,4], *Yang Chen*[2,5], *Zichang Yang*[1,2,3,4], *Zhi Li*[1,2,3,4], *Xiaofang Che*[1,2,3,4], *Jiawen Xiao*[6], *Yunpeng Liu*[1,2,3,4*] *and Xiujuan Qu*[1,2,3,4*]

[1] Department of Medical Oncology, The First Hospital of China Medical University, Shenyang, China, [2] Key Laboratory of Anticancer Drugs and Biotherapy of Liaoning Province, The First Hospital of China Medical University, Shenyang, China, [3] Liaoning Province Clinical Research Center for Cancer, The First Hospital of China Medical University, Shenyang, China, [4] Key Laboratory of Precision Diagnosis and Treatment of Gastrointestinal Tumors, Ministry of Education, The First Hospital of China Medical University, Shenyang, China, [5] Department of Respiratory and Infectious Disease of Geriatrics, The First Hospital of China Medical University, Shenyang, China, [6] Department of Medical Oncology, Shenyang Fifth People Hospital, Shenyang, China

OPEN ACCESS

Edited by:
Peng Qu,
National Institutes of Health (NIH), United States

Reviewed by:
Meng Xu,
Carnegie Mellon University, United States
Jie Chen,
University of Pennsylvania, United States

***Correspondence:**
Xiujuan Qu
xiujuanqu@yahoo.com
Yunpeng Liu
ypliu@cmu.edu.cn

Specialty section:
This article was submitted to Cancer Immunity and Immunotherapy, a section of the journal Frontiers in Immunology

Received: 26 October 2020
Accepted: 21 December 2020
Published: 04 February 2021

Citation:
Yan H, Chen Y, Yang Z, Li Z, Che X, Xiao J, Liu Y and Qu X (2021) An Immune Cell Signature Is Associated With Disease-Free Survival and Adjuvant Chemosensitivity of Patients With Resectable Gastric Cancer. Front. Immunol. 11:621623. doi: 10.3389/fimmu.2020.621623

Increasing evidence has indicated that current tumor-node-metastasis (TNM) stage alone cannot predict prognosis and adjuvant chemotherapy benefits accurately for stages II and III gastric cancer (GC) patients after surgery. In order to improve the predictive ability of survival and adjuvant chemotherapy benefits of GC patients after surgery, this study aimed to establish an immune signature based on the composition of infiltrating immune cells. Twenty-eight types of immune cell fractions were evaluated based on the expression profiles of GC patients from the Gene Expression Omnibus (GEO) database using single-sample gene set enrichment analysis (ssGSEA). The immunoscore (IS) was constructed using a least absolute shrinkage and selection operator (LASSO) Cox regression model. Through the LASSO model, an IS classifier consisting of eight immune cells was constructed. Significant difference was found between high-IS and low-IS groups in the training cohort in disease-free survival (DFS, $P < 0.0001$) and overall survival (OS, $P < 0.0001$). Multivariate analysis showed that the IS classifier was an independent prognostic indicator. Moreover, a combination of IS and TNM stage exhibited better prognostic value than TNM stage alone. Further analysis demonstrated that low-IS patients who had more tumor-infiltrating lymphocytes had better response to adjuvant chemotherapy. More importantly, we found that patients with high-IS were more likely to benefit from a Xeloda plus cisplatin regimen after surgery. Finally, we established two nomograms to screen the stage II and III GC patients who benefitted from adjuvant chemotherapy after surgery. The combination of IS classifier and TNM stage could predict DFS and OS of GC patients. The IS model has been proven as a promising tool that can be used to identify the patients with stages II and III GC who may benefit from adjuvant chemotherapy.

Keywords: immunoscore, gastric cancer, adjuvant chemotherapy, DFS, XP

INTRODUCTION

Gastric cancer (GC) is the fifth most common malignant cancer and the third leading cause of cancer-related deaths around the world (1). Although treatments for GC have improved rapidly, for patients with resectable GC, as stage I, II, and partial III GC, surgical resection is the preferred treatment. As the rates of recurrence for GC patients following surgery range from 25% to 40% (2–5), adjuvant chemotherapy is important; however, much research has revealed variations in clinical outcomes in patients with similar treatments at the same TNM stage (5, 6), indicating the insufficient clinical information provided by TNM stage which is the most useful staging system for cancers in clinical practice (7–9). Although several studies have developed models to reinforce the prognostic ability of TNM stage (10, 11), most of which are established with the expression of proteins in cancer cells detected by immunohistochemistry based on the OS of patients (11, 12), ignoring the effects of tumor microenvironment (TME) and DFS.

The concept, immunoscore (IS), was proposed for use in analysis of colon cancer at the first time, consisting of two markers of cytotoxic and memory T cells (13). Consequently, studies have reported that the scores assessed by immune cell markers could predict recurrence, DFS and OS of patients with stage I-IV colon cancer (14, 15). Moreover, a recent investigation demonstrated the predictive value of IS in oxaliplatin-based adjuvant chemotherapy. The International Duration Evaluation of Adjuvant Therapy (IDEA) France cohort study showed that 3-year DFS rates of patients who received mFOLFOX6 for 6 months were not dramatically superior to those treated for 3 months (72% *vs.* 76%; HR, 1.44; 95% CI, 1.14–1.82) (16), however, a follow-up study on IS, consisting of CD3 and CD8, revealed that patients whose tumor had been infiltrated by more lymphocytes (IS-Intermediate+ High) benefited more from 6 months of oxaliplatin-based adjuvant chemotherapy compared with those treated with 3 months of adjuvant chemotherapy (HR, 0.528; 95% CI, 0.372-0.750; $P = 0.0004$), indicating that tumor-infiltrating immune cells (TIICs) have critical effects on DFS and adjuvant chemosensitivity in cancers (17).

Like colon cancer, adjuvant chemotherapy has been verified to improve DFS and OS compared with surgery alone in GC in many studies (5, 18–20). Results of CLASSIC trial showed that the 5-year DFS in adjuvant chemotherapy group was 68% *versus* 53% in the observation group though the median OS was only a moderate benefit of 9% (5), indicating that adjuvant chemotherapy could significantly improve DFS of GC patients; however, subgroup analysis of the Adjuvant Chemotherapy Trial of TS-1 Gastric Cancer (ACTS-GC) revealed that adjuvant chemotherapy did not improve OS in stage III patients compared with observation alone, but conversely increased adverse effects (21). Therefore, it is necessary to improve patient selection for adjuvant chemotherapy and outcome prediction for individual treatment. Recent studies have developed models with protein markers in GC cells detected by immunohistochemistry (10, 22). However, in these studies, tumor microenvironment (TME) was ignored, which plays a critical role during tumorigenesis, progression, and therapeutic efficacy (23–25).

In this study, we described the landscape of 28 immune cells in GC applying ssGSEA and established a novel immune cells-based model using LASSO Cox regression, IS, to predict DFS and OS in patients after surgery. Moreover, the model could select the patients who might benefit from adjuvant chemotherapy. To apply the IS classifier to clinical practice, we constructed two nomograms to screen benefit population for adjuvant chemotherapy with accurate clinicopathological risk factors.

MATERIALS AND METHODS

Patients Selection and Data Collection

Microarray dataset GSE62254, used as a training cohort for its complete clinicopathological and survival information, was downloaded from GEO database (https://www.ncbi.nlm.nih.gov/geo/). GSE26253 dataset, which included 432 GC patients with complete survival information, was used as a testing cohort. The inclusion and exclusion criteria were exhibited in **Figure 1**.

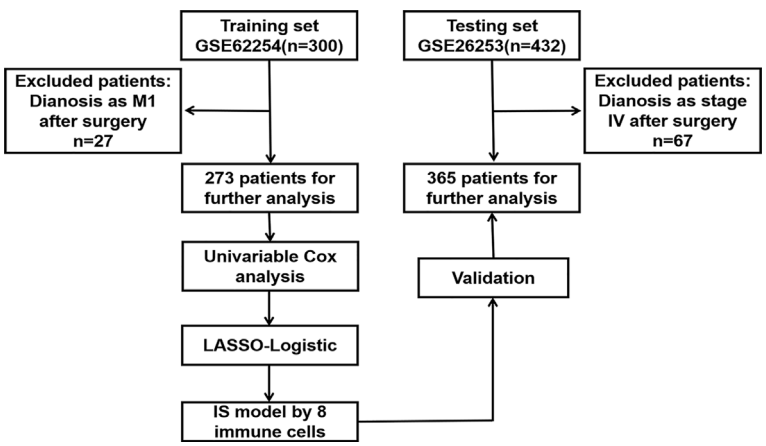

FIGURE 1 | The flowchart through the identification procedure and analyses. *LASSO* least absolute shrinkage and selection operator.

The patients diagnosed as IV stage after surgery were filtered by the criteria since DFS was the main endpoint in this study.

Estimation of Immune Cell Type Fractions

Gene expression profiles of GSE62254 and GSE26253 datasets downloaded from GEO database were analyzed by ssGSEA, which classifies gene sets with common physiological regulation, chromosomal localization and biological functions (26). Gene markers of 28 immune cells [activated $CD4^+$ T cells ($CD4^+$ Ta), activated $CD8^+$ T cells ($CD8^+$ Ta), activated dendritic cells (aDC), $CD56^{bright}$ natural killer cells ($CD56^+$ NK), $CD56^{dim}$ natural killer cells ($CD56^-$ NK), activated B cells (Ba), central memory $CD4^+$ T cells ($CD4^+$ Tcm), central memory $CD8^+$ T cells ($CD8^+$ Tcm), effector memory $CD4^+$ T cells ($CD4^+$ Tem), effector memory $CD8^+$ T cells ($CD8^+$ Tem), eosinophils, gamma delta T cells (γδT), immature B cells (Bi), immature dendritic cells (DCi), mast cells, myeloid-derived suppressor cells (MDSC), memory B cells (Bm), monocytes, natural killer cells (NK), natural killer T cells (NK T), neutrophils, plasmacytoid dendritic cells (pDC), macrophages, regulatory T cells (Tregs), follicular helper T cells (Tfh), type-1 T helper cells (Th1), type-17 T helper cells (Th17), and type-2 T helper cells (Th2)] were obtained from a previous study (27). On the basis of the expression of these markers, the infiltration levels of immune cell types were quantified by ssGSEA in the R package GSVA (28).

The Construction of Immunoscore Using LASSO Algorithm

To select the most useful prognostic immune cells, the "glmnet" package in R was utilized to perform the COX regression analysis with LASSO algorithm (29). Eight immune cells were selected from candidate cells by LASSO algorithm, where the data were subsampled and the tuning parameters were determined according to the expected generalization error estimated from 10-fold cross-validation. The optimal cut-off values were evaluated based on the association between DFS and cell fraction in the training cohort using the "survminer" package, dividing the patients into low-IS and high-IS groups.

Construction of Nomograms

Following the multivariate Cox regression analysis for the selection of independent prognostic factors, IS and other clinical pathological characteristics were used to generate the nomograms and calibration plots by "rms" package in R. In this model, each factor was assigned a weight score based on the results of the multivariate Cox regression analysis. Calibration was used to assess the performance of the nomograms. Receiver operating characteristic (ROC) analysis was also performed to estimate the accuracy of the nomograms for survival prediction using the "survival ROC" package of R. In addition, C-index was calculated with "survival" package.

Statistical Analysis

Group comparisons were performed for continuous and categorical variables using one-way ANOVA and the χ^2 test. Survival curves were constructed by the Kaplan–Meier method and compared by means of the log rank test. Hazard ratios for univariable analyses were calculated using a univariable Cox proportional hazards regression model. A multivariable Cox regression model with the enter method was used to determine independent prognostic factors. Correlations between the immunoscore and mRNA expression of genes were analyzed by means of Pearson's correlation test. The sensitivity and specificity of the survival prediction based on the immunoscore were depicted by a time-dependent receiver operating characteristic (ROC) curve, with quantification of the area under the ROC curve using the "timeROC" package. All statistical tests were two-sided and $P < 0.050$ was considered statistically significant. Statistical analyses were conducted using R software and SPSS® version 19.0 (IBM, Armonk, New York, USA).

RESULTS

Patient Characteristics

As shown by the flowchart (**Figure 1**), 273 patients from the GSE62254 dataset and 365 patients from the GSE26253 dataset with DFS and OS information were included after applying the exclusion criteria. The patients' clinicopathological characteristics are detailed in **Table 1**. Of the 273 patients in the training cohort, 186 (68.1%) were men and the median age was 64 (28–84) years. In addition, the median DFS was 35.7 months and OS was 53.3 months. Of the 365 patients in the testing cohort, 239 (65.5%) were men and the median age was 53 (23–74) years. The median DFS and OS were 60.4 and 69.6 months, respectively, in the testing cohort. **Figure S1** shows the distribution of the immune cells in patients in the training cohort (**Figure S1A**) and the relationship between 28 TIICs (**Figure S1B**).

Construction of IS Model

Based on the relationship between 28 TIICs and DFS, we then constructed an immune-cell model. The forest plot in **Figure 2A** calculated by univariate Cox analysis shows the association between each immune cell subset and DFS. In general, $CD4^+$ Ta (HR = 0.21, $P < 0.001$), aDC (HR = 0.44, $P = 0.047$), Th17 (HR = 0.35, $P = 0.013$), and $CD56^-$ NK (HR = 0.21, $P < 0.001$) are protective factors for DFS. On the contrary, mast cell (HR = 2.6, $P = 0.019$) and pDC (HR = 2.3, $P = 0.038$) are risk factors. Then through LASSO Cox regression model eight immune cells were selected to build the IS and the formula was as follows: IS = 0.20810997 × DC + 0.79762920 × Mast cell - 0.8729771 × $CD4^+$ Ta - 0.37309914 × $CD8^+$ Tem - 0.04459008×Th17 - 0.88370283 × $CD56^+$ NK - 0.12005145 × Ba-0.39656416×Bm (**Figures 2B, C**). We calculated an IS for each patient based on their personalized levels of the eight cells. The predictive accuracy of the model in the training cohort was assessed by time-dependent ROC analysis at 1, 2, and 3 years where AUC values were 0.733, 0.779, and 0.784, respectively (**Figure 2D**).

IS and Prognosis

Using the optimum cut-off value (IS = -0.65) obtained by the "survminer" package, patients in the training cohort were divided into high-IS and low-IS groups. **Figure 3A** shows the distribution of clinicopathological characteristics between high-

TABLE 1 | Characteristics of patients in the training (GSE62254) and testing (GSE26253) cohorts.

Characteristics	GSE62254		GSE26253	
	Number of patients	Percentage (%)	Number of patients	Percentage (%)
Number of patients	273		365	
Gender				
Male	186	68.1	239	65.5
Female	87	31.9	126	34.5
Age				
≤60	104	38.1	276	75.6
>60	169	61.9	89	24.4
Depth of invasion				
T2	176	64.5		
T3+T4	97	35.5		
Lymph node metastasis				
N0	37	13.6		
N1+N2+N3	236	86.4		
TNM stage				
I	32	11.7	68	18.6
II	163	59.7	167	45.8
III	78	28.6	130	35.6
Lauren classification				
Intestinal	142	52	122	33.4
Diffuse	115	42.1	232	63.6
Mixed	16	5.9	11	3
Status of microsatellite				
MSS	206	75.5		
MSI	67	24.5		
Adjuvant Chemotherapy				
No	131	48		
Yes	142	52		

MSS, microsatellite stability; MSI, microsatellite instability.

IS and low-IS groups. The Kaplan-Meier curve in the training cohort revealed that patients in the low-IS group had longer DFS ($P < 0.001$) as well as OS ($P < 0.001$) compared with the high-IS group (**Figures 3B, C**). The 5-year DFS and OS for low-IS group were 28.2% and 60%, respectively and 14.1% and 22.5% respectively, for high-IS group. Similar results were observed in the testing cohort ($P < 0.001$ for both DFS and OS, **Figures 3D, E** and **Figure S2**). The ROC analysis of the testing cohort indicated that the model could predict the prognosis of GC patients accurately (**Figure 3F**). The multivariate Cox regression analysis showed that high-IS and TNM stage were independent prognostic indicators for both poor DFS and OS in either training cohort (**Table 2**, **Table S1**) or testing cohort (**Tables S2** and **S3**). Additionally, different distributions of immune cells between high-IS and low-IS groups are illustrated in **Figure 3G**. The infiltration of $CD4^+$ Ta, $CD8^+$ Ta, aDC, Th17, and $CD56^-$ NK cells in the TME of low-IS patients was significantly greater than that in high-IS patients. These data demonstrated that the eight-immune cells model, IS, could precisely predict the DFS and OS of GC patients with surgery.

We also assessed the relationships between IS, the status of relapse and survival, and the distribution of the eight cells in the training and testing cohorts. **Figure S3** shows that patients in the high-IS group had more recurrence and death events than among those in the low-IS group, which further verified the accuracy of the model.

IS and TNM Stage

So far, the TNM stage has been regarded as a powerful indicator to predict the outcomes of patients with cancers, however, variable prognosis of patients was observed in clinical practice due to the heterogeneity. Here, to examine the value of the model, we respectively performed stratified analysis of the patients in stages I, II, and III in both the training and testing cohorts. Consistently, DFS and OS were all much longer in low-IS patients with stages I, II, and III GC than high-IS patients in either the training or testing cohort (**Figures 4A–C**, **Figures S4A–C**). Cox regression and forest plots were used to demonstrate that high-IS was a risk factor for both DFS and OS in stages I, II, and III (**Figure 4D**). Moreover, **Figure S5A** demonstrates that IS showed a better prognostic accuracy for DFS in GC patients with surgery than the TNM stage in the training cohort. Meanwhile, compared with the TNM stage alone, combining the data with IS showed a better prognostic value for DFS and OS in two cohorts (**Figure S5**). In conclusion, the prognostic value of IS is independent of TNM stage. For GC patients with surgery, the combination of IS and TNM stage for prediction of DFS and OS is superior to that of TNM alone.

IS and the Subtype of GC

For GC patients, Lauren subtype and the status of microsatellite are the two recognized indicators to predict the outcomes and the efficacy of treatments. Therefore, we identified the value of IS based on Lauren classification and the status of microsatellite by using stratified analysis. **Figures S6A, B** show that low-IS patients had longer DFS (all $P < 0.001$ for intestinal and diffuse subtypes) and OS ($P = 0.00046$ for intestinal subtype, $P < 0.001$ for diffuse subtype, respectively) than high-IS patients. However, this phenomenon was not observed in mixed subtype patients (**Figure S6C**). Forest plots revealed that high-IS was the risk factor for DFS and OS simultaneously in both intestinal and diffuse subtypes (**Figure S6D**). Similarly, for patients with MSI, DFS and OS of high-IS patients were significantly shorter than those of low-IS patients (all $P < 0.001$, **Figure S7A**). Similar results were obtained in patients with microsatellite stability (MSS) on DFS ($P < 0.001$) and OS ($P < 0.001$) (**Figure S7B**). Meanwhile, high-IS was also a risk factor for DFS and OS regardless of the status of microsatellite stability (**Figure S7C**). Taken together, IS remains a statistically and clinically significant prognostic model when stratified by GC subtypes.

IS and Adjuvant Chemotherapy

For patients with surgery, especially stages II and III, adjuvant chemotherapy is indispensable. In the current study, the patients' clinicopathological characteristics distributing in the group accepting adjuvant chemotherapy were similar to that in the group without chemotherapy after surgery (**Figure S8**). As shown in **Figure 5A**, adjuvant chemotherapy could improve DFS and OS simultaneously in the total cohort (P = 0.00047 for DFS). For

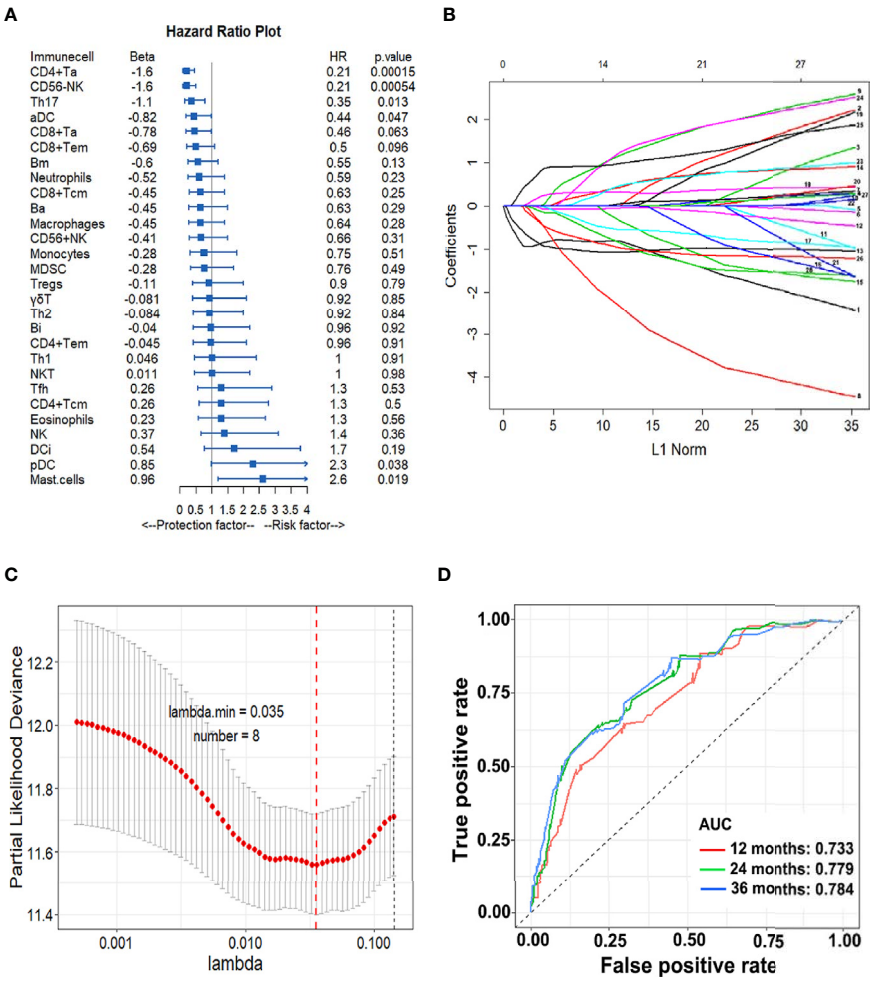

FIGURE 2 | Construction of the IS model. **(A)** Forest plots of HRs for tumor infiltrating cells by univariate Cox analysis; **(B)** LASSO coefficient profiles of the 28 immune cell fractions; Immune cell types: 1.CD4$^+$Ta; 2.CD8$^+$Ta; 3.aDC; 4.CD56$^+$ NK; 5.CD4$^+$ Tcm; 6.CD8$^+$ Tem; 7. CD4$^+$ Tem; 8.CD8$^+$Tcm; 9.NK; 10.NKT; 11.Th1; 12.Th17; 13.CD56$^-$NK; 14.DCi; 15. Macrophages; 16.MDSC; 17.Neutrophils; 18.pDC; 19.Tregs; 20.Th2; 21.Ba; 22.Eosinophils; 23.γδT; 24.Bi; 25.Mast cells; 26.Bm; 27.Monocytes; 28.Tfh; **(C)** Ten-fold cross-validation for tuning parameter selection in the LASSO model. Error bars represent confidence intervals for partial likelihood deviance as Λ was changed. The dotted line indicates the optimal values; **(D)** The IS measured by time-dependent ROC curves in the training cohort. The area under the ROC curve is defined as AUC. *HR*, hazard ratio; *LASSO*, least absolute shrinkage and selection operator; *ROC*, receiver-operating characteristic.

TABLE 2 | Univariable and multivariable association of IS classifier, clinicopathological characteristics with DFS in the training cohort.

	Univariate analysis		Multivariate analysis	
	HR(95% CI)	**P value**	**HR(95% CI)**	**P value**
Gender	0.962(0.637–1.453)	0.855		
Age	1.005(0.987–1.023)	0.614		
T stage(T2+T3 vs. T1+T2)	2.602(1.772–3.822)	<0.01		
N stage(N1+N2+N3 vs. N0)	3.052(1.338–6.955)	0.008		
TNM stage(III vs. I+II)	3.744(2.386–5.875)	<0.01	2.279(1.278–4.055)	0.005
Lauren type	1.394(1.018–1.908)	0.038		
Status of microsatellite (MSI vs. MSS)	1.356(1.039–1.770)	0.025		
IS	1.794(1.492–2.158)	<0.01	1.581(1.279–1.954)	<0.01

MSS, microsatellite stability; MSI, microsatellite instability; HR, hazard ratio; IS, immunoscore.

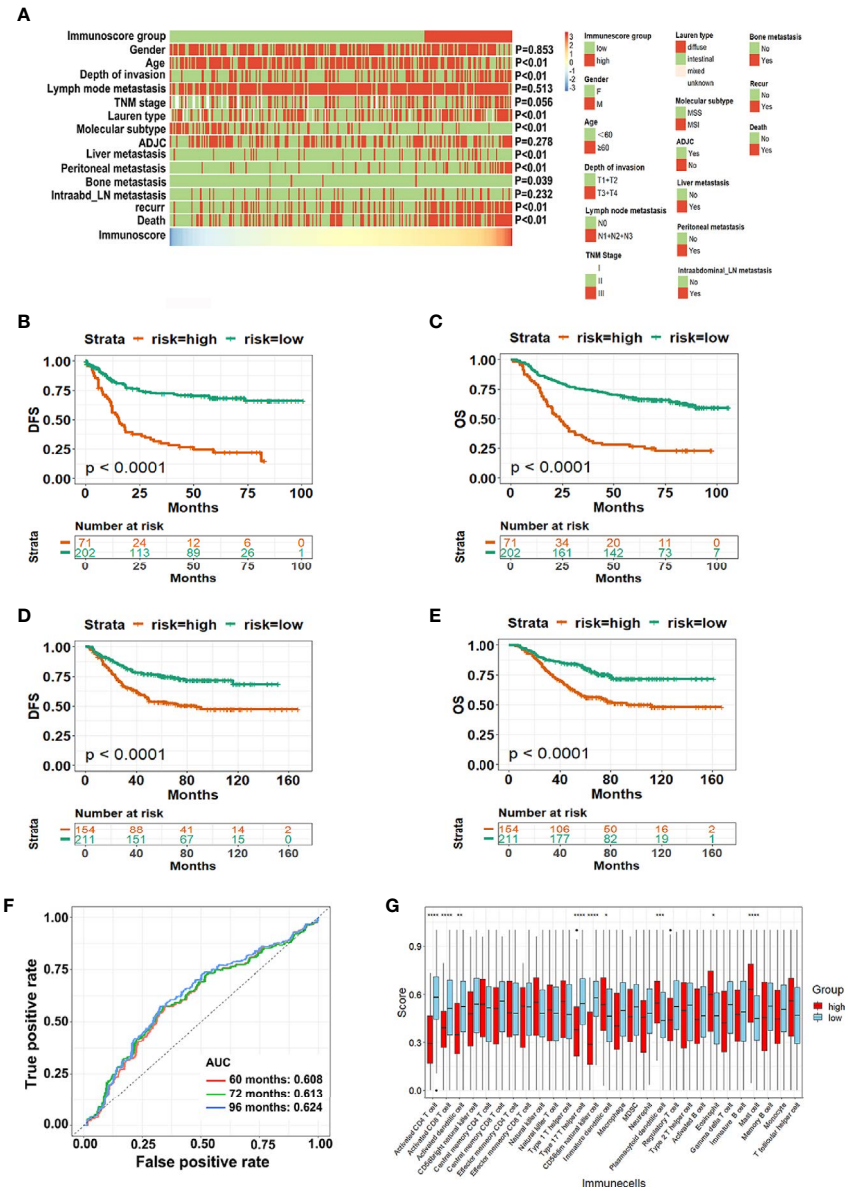

FIGURE 3 | The predictive value of IS for GC patients with surgery. **(A)** Heatmaps summarizing the distribution of IS and clinical pathological characteristics in the training cohort; **(B, C)** Kaplan-Meier analysis for the DFS and OS of GC patients in the GSE62254 dataset; **(D, E)** Kaplan-Meier analysis for the DFS and OS of GC patients in the GSE26253 dataset; **(F)** The IS measured by time-dependent ROC curves in the testing cohort. The area under the ROC curve was defined as AUC; **(G)** Distribution of 28 immune cells transformed using ssGSEA in high-IS and low-IS groups. *ADJC*, adjuvant chemotherapy; *Intraabd_LN* intraabdominal lymph nodes; *DFS*, disease free survival; *OS*, overall survival; *GC*, gastric cancer; *ssGSEA* single-sample gene set enrichment analysis; *IS*, immunoscore; *ROC*, receiver-operating characteristic. *$P < 0.05$; **$P < 0.01$; ***$P < 0.001$; ****$P < 0.0001$.

patients in the low-IS group, adjuvant chemotherapy improved DFS ($P = 0.0061$), which was not observed in the high-IS group ($P = 0.19$; **Figure 5A**). The results from subset analysis in stage I showed no difference in DFS between patients receiving adjuvant chemotherapy and not receiving adjuvant chemotherapy (**Figure 5B**). However, the subset analysis in stages II and III patients demonstrated that adjuvant chemotherapy significantly improved DFS in the low-IS group ($P = 0.0041$), but no significant effect was found in the high-IS group ($P = 0.071$; **Figure 5C**). Stages II and III GC patients with low-IS would obtain longer DFS by receiving chemotherapy after surgery. To explain this phenomenon, we performed the relationship between IS value and the expression of immune checkpoint regulators and inflammatory mediators. Notably, IS value was shown to be negatively correlated with PD-L1 ($P < 0.001$, $r = -0.19$), CD40 ($P < 0.001$, $r = -0.23$), CD47 ($P < 0.001$, $r = -0.42$), CTLA4 ($P < 0.001$, $r = -0.37$), GZMB

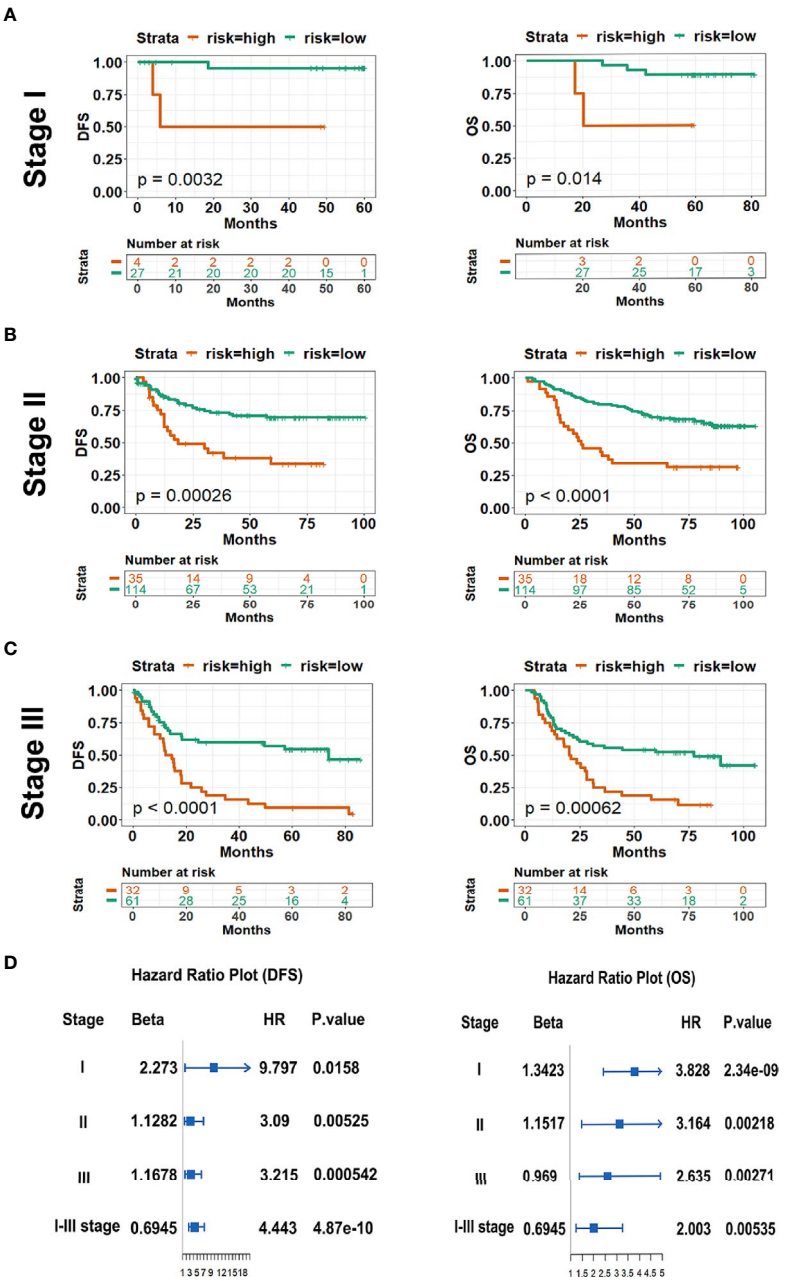

FIGURE 4 | Kaplan-Meier survival analysis of DFS (left pane) and OS (right pane) according to IS in subgroups of patients with GC in the training cohort. **(A)** Stage I (*n* = 30); **(B)** Stage II (*n* = 97); **(C)** Stage III (*n* = 146); **(D)** The survival impact of IS in TNM stage subgroup. *HR*, hazard ratio; *IS*, immunoscore; *DFS*, disease free survival; *OS*, overall survival.

($P < 0.001$, $r = -0.52$), Tim-3 ($P < 0.001$, $r = -0.29$), ICOS ($P < 0.001$, $r = -0.30$), IDO1 ($P < 0.001$, $r = -0.53$), LAG3 ($P < 0.001$, $r = -0.55$), and IFNG ($P < 0.001$, $r = -0.56$), whereas the interleukin family and TGF showed no statistical correlation (**Figure 5D**). Further, we compared the expression of these immune checkpoint regulators and inflammatory mediator between low-IS and high-IS groups. As **Figure S9** shown, the expression of PD-L1 (P<0.001), CD40 (P=0.001), CD47 (P<0.001), CTLA-4 (P<0.0001), GZMB (P<0.0001), Tim-3 (P<0.0001), ICOS (P<0.0001), IDO1 (P<0.0001), LAG3 (P<0.0001), and IFNG (P<0.0001) in low-IS group were all higher than that in high-IS group. In summary, these results indicated that IS could identify candidate stages II and III patients with surgery who would benefit from adjuvant chemotherapy.

It is generally known that patients with stage II-III should receive adjuvant chemotherapy after surgery according to NCCN

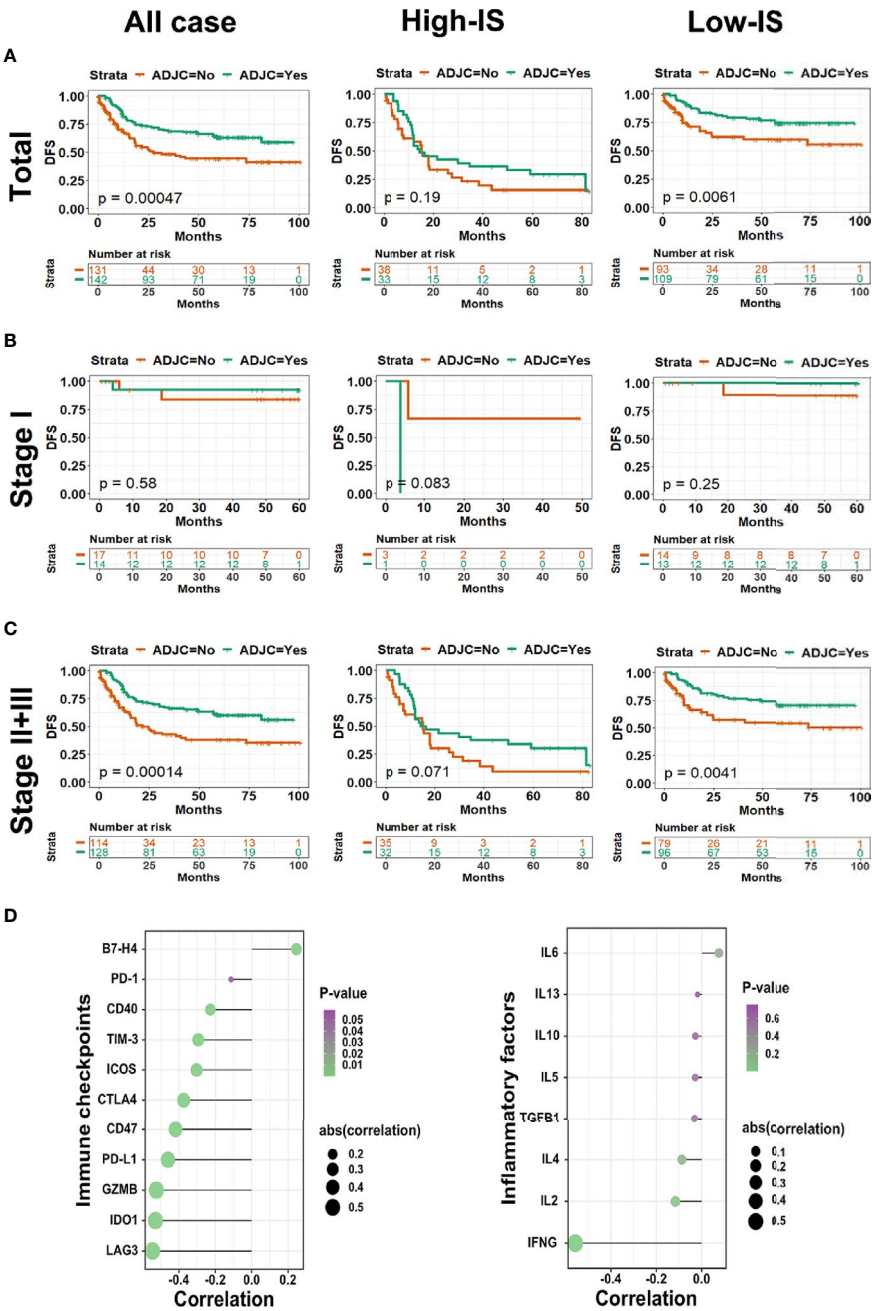

FIGURE 5 | Comparing adjuvant chemotherapy benefit by DFS in total and TNM stage subgroups. Kaplan-Meier curves of **(A)** total cohort, **(B)** stage I and **(C)** stages II and III patients with GC stratified by the receipt of adjuvant chemotherapy; **(D)** Bubble diagrams describing the association between IS value and immune checkpoint regulators (left pane) and inflammatory cytokines (right pane). Bubble size represents the degree of correlation, bubble color denotes P-value. *DFS*, disease free survival; *GC*, gastric cancer.

guidelines. Next, we investigated the effects of chemoregimen in the training dataset. Patients with stage II-III GC were divided into two groups, patients with Xeloda plus cisplatin (XP, 83 patients) and patients with chemoregimen based on fluorouracil (5-Fu, 44 patients), according to the adjuvant chemoregimen. As shown in **Figure 6A**, patients with low-IS had significantly longer DFS regardless of the adjuvant chemoregimen (P = 0.0021 and P = 0.00011 for the XP group and 5-Fu group, respectively). However, as patients were divided into low-IS and high-IS groups based on the IS classifier, we found that in high-IS group patients who received XP regimen after surgery had longer DFS compared with patients who received regimen 5-Fu

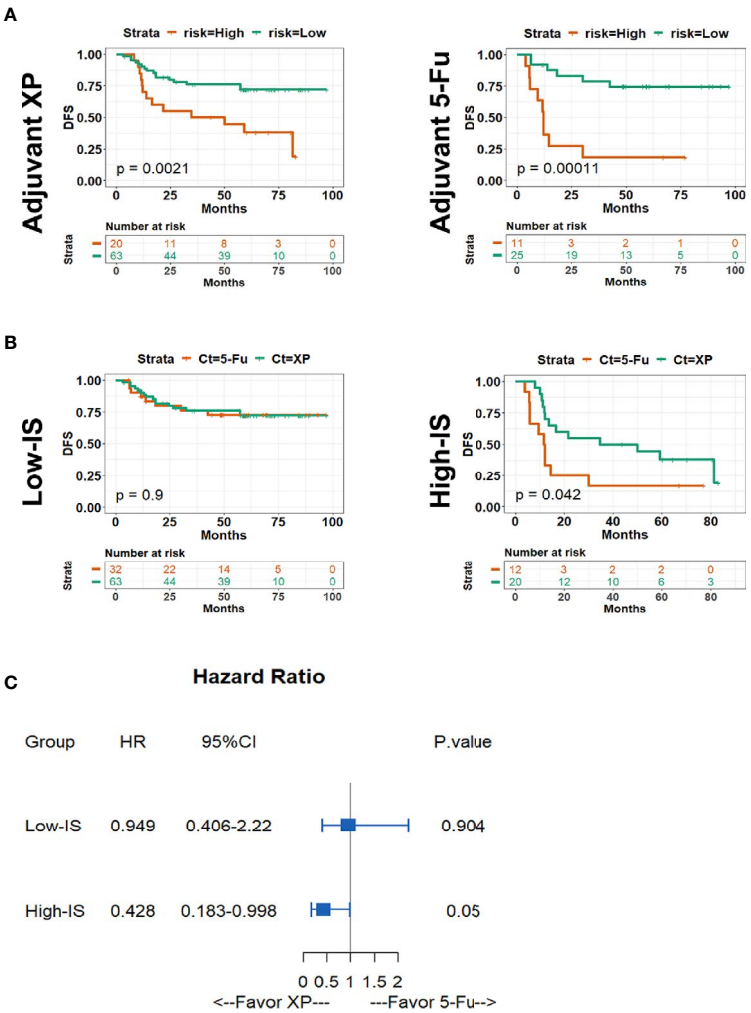

FIGURE 6 | Kaplan-Meier survival analysis of DFS stratified by types of adjuvant chemotherapy among stages II and III patients. **(A)** Kaplan-Meier curves of patients in XP group (left panel) and 5-Fu group (right panel) stratified by IS; **(B)** Kaplan-Meier curves of patients in Low-IS group (left panel) and high-IS group (right panel) stratified by chemotherapy regimen; **(C)** Forest plot describing the benefit of chemotherapy regimen in different IS groups. *IS*, immunoscore; *XP*, Xeloda plus cisplatin; *5-Fu* 5-fluorouracil.

(**Figure 6B**, $P = 0.042$), while in low-IS group patients there was no difference between two chemoregimen (**Figure 6B**, $P = 0.9$). Cox regression analysis notably demonstrated that patients with high-IS might benefit from XP rather than 5-Fu after surgery (**Figure 6C**).

To provide a quantitative method in clinical practice to predict the probability of 1-, 2-, and 3-year DFS in patients with stages II and III GC after surgery, we established two nomograms integrating clinicopathological factors and IS on the basis of multivariate Cox regression analysis (**Figure 7**). The *c*-index values were 0.7 and 0.677 for the nomograms with adjuvant chemotherapy and without adjuvant chemotherapy after surgery respectively, indicating a satisfactory overlap with actual observations. The two nomograms based on IS could be used to predict the prognosis of patients with or without adjuvant chemotherapy in clinical practice.

DISCUSSION

In the present study, we analyzed the pattern of TIICs by using ssGSEA and constructed an eight-immune cells model through LASSO Cox regression based on DFS. In recent years, many immune score models have been generated to predict the prognosis and the therapeutic efficacy by immunohistochemical method (10, 22, 30); however, the results of immunohistochemistry would be limited by the small quantity of cell types and sample size. In our study, immune cells were assessed by high-throughput gene expression generated through ssGSEA which supplied an expanded view of immune contexts, allowing us to investigate more tumor subtypes with greater precision within a larger patient cohort. Moreover, other than previous studies which generated models mostly based on OS (11, 31, 32), our study mainly focused on the DFS of GC patients. Though OS is a recognized and widely used

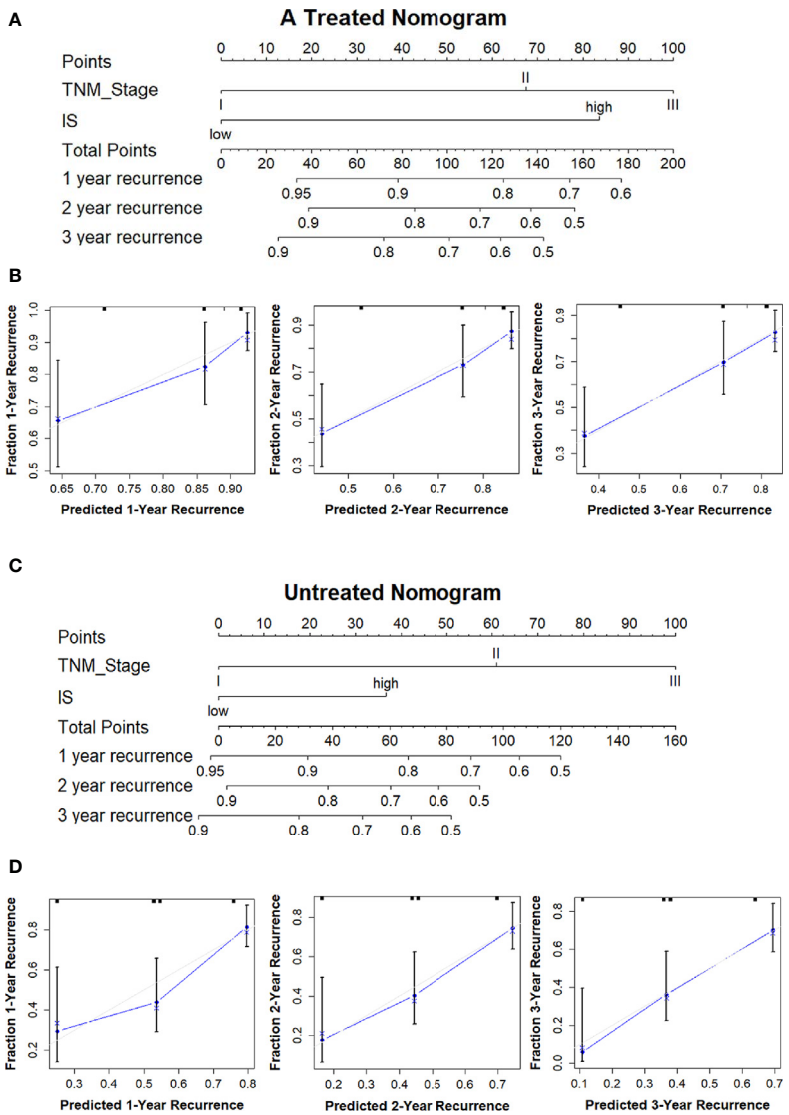

FIGURE 7 | Treated and untreated nomograms to predict the probability of 1, 2, and 3-year recurrence with or without adjuvant chemotherapy in GC. **(A)** Treated nomogram predicting 1-, 2-, and 3-year DFS for GC patients after surgery with adjuvant chemotherapy; **(B)** Calibration curves to validate treated nomogram for 1-, 2-, and 3-year DFS; **(C)** Untreated nomogram predicting 1-, 2-, and 3-year DFS for GC patients after surgery without adjuvant chemotherapy; **(D)** Calibration curves to validate untreated nomogram for 1-, 2-, and 3-year DFS. *DFS*, disease free survival; *OS*, overall survival; *GC*, gastric cancer.

outcome measure for patients with tumors, its use as a marker of therapeutic benefit remains controversial (33, 34). Recurrence and metastasis are the two important factors shortening the OS of patients, indicating that it is essential to assess the relapse risk accurately to improve prognosis. In this study, our data demonstrated that patients in the low-IS group whose tumors are infiltrated more lymphocytes have longer DFS than those in the high-IS group and the same results were obtained in stages I, II, and III, respectively, by way of stratification analysis. Furthermore, ROC analysis showed that the predictive accuracy for DFS of this IS classifier was superior to TNM stage. In contrast with TNM staging system which is described based on anatomical characteristics, the IS model could provide the immunological information in the microenvironment of GC. According to our analysis, the combination of TNM stage and IS classifier had better predictive ability than TNM alone. In general, GC patients at the same TNM stage could be divided into different risk groups based on IS for receiving appropriate treatments to improve the outcome.

According to National Comprehensive Cancer Network (NCCN) guidelines and previous studies, adjuvant chemotherapy is regarded as a standard treatment for stage II and III patients (35). However, results of the ACTS-GC trial implied that adjuvant chemotherapy did not improve OS in stage III patients compared with observation alone, conversely it

increased adverse effects (21). Therefore, many studies have been committed to identify low-risk patients with stage II and III GC who might not need adjuvant chemotherapy. In present study, the results demonstrated that DFS and OS of patients with low-IS were significantly longer than patients with high-IS, indicating that low-IS patients are more likely benefit from adjuvant chemotherapy. Previous research has found that TIICs are essential for chemotherapy response in various cancers (36), indicating that patients with more immune-cell infiltration are chemotherapy-sensitive (37). Consistently, our results stated that low-IS patients who are more likely to benefit from adjuvant chemotherapy had more activated $CD4^+$ T cell, activated $CD8^+$ T cell, aDC, Th17, and $CD56^-$ NK cells infiltrating in their tumors. The underlying mechanisms might be that chemotherapy exerts an anti-tumor effect by triggering immunogenic cell death (ICD) beyond cytotoxicity *via* TIICs (37–39). The immune cells activated by chemotherapeutic agents secrete cytokines, such as interferon and interleukin, leading to the death of cancers. Coincidently, the results revealed that the expression of IFNG in the low-IS group was dramatically higher, indicating that IFNG might participate in the process of chemotherapy sensitization in low-IS GC patients whose tumors have more TIICs. Further studies were needed to investigate the underlying mechanisms of action between IS and chemosensitivity in GC.

Additionally, to further explore why there was no difference between patients receiving adjuvant chemotherapy or not in high-IS group, we analyzed subsets according to chemotherapy regimens. Interestingly, the results demonstrated that patients with high-IS are more likely to benefit from the XP regimen after surgery. Recent decade, studies have verified the advantage of postoperative chemotherapy in GC compared with surgery alone (4, 40). ACTS-GC and CLASSIC, two randomized phase III trials, showed that postoperative chemotherapy with S-1 or capecitabine plus oxaliplatin could decrease the risk of recurrence (5, 21). Similarly, the Intergroup 0116 (INT-0116) trial (4) and the Adjuvant Chemoradiation Therapy in Stomach Cancer (ARTIST) trial (2) demonstrated the efficacy of 5-Fu plus leucovorin (LV) and XP regimens in patients after surgery, however, little evidence has been supplied to compare these regimens to screen the patients who can benefit from each regimen. Similar to colon cancer that the MSI status is a biomarker to predict the lack of efficacy of adjuvant 5-Fu chemotherapy and recommend an adjuvant chemotherapy combining fluoropyrimidine and oxaliplatin for stage III patients (41), our IS classifier offers a method with which to select patients who benefit from XP and 5-Fu regimens respectively. Generally speaking, in our opinion patients with low-IS are always sensitive to adjuvant chemotherapy no matter the regimens after surgery. For patients with high-IS, we suggested XP regimen as their adjuvant chemotherapy after surgery.

In recent years, immune checkpoint inhibitors (ICIs) have opened a new era of immunotherapy in vary cancers, represented by anti-CTLA-4 and anti-PD (42–44). The concept of "immune checkpoints" was regarded as the important immune switch regulating the "activity" and "inhibitory" state of immune cells (45, 46). Increasing evidence has demonstrated that the expression of immune checkpoints genes could be used as predictive biomarkers for therapeutic response of ICIs (47, 48). In this study, we found a significantly negative correlation between IS value and several important immune checkpoint biomarkers. PD-L1 has been regarded as the most useful biomarker to predict the immunotherapeutic efficacy in clinical practice. Several studies have reported that PD-L1 expression could be induced by IFNγ as an exogenous regulation which is consistent with our result that low-IS patients with high expression of PD-L1 secreted more IFNγ (49). Therefore, we speculate that patients with low-IS might also benefit from immunotherapy, which warrants further investigation.

Our study has some limitations. Firstly, it was a retrospective study based on publicly available datasets, the potential bias inferring to unbalanced clinicopathological characteristics cannot be ignored. Secondly, due to the incompleteness of the information we obtained, it is possible that patients with immune system disorders or acute infection were included in our study, which ideally should have been excluded. Thus, further prospective studies are needed to validate our findings.

CONCLUSIONS

In summary, the IS classifier is a novel prognostic tool based on the presence of eight immune cells that could significantly improve the prediction of recurrence and survival in GC patients with surgery. Moreover, the IS classifier is a useful model to identify patients who would be more likely to benefit from adjuvant chemotherapy. Stages II and III GC patients with low-IS could benefit from either 5-Fu or XP regimens as adjuvant chemotherapy, however, patients with high-IS are more sensitive to XP regimen. In conclusion, the IS might help make decisions that improve individual treatment regimes in clinical practice.

DATA AVAILABILITY STATEMENT

The datasets presented in this study can be found in online repositories. The names of the repository/repositories and accession number(s) can be found below: https://www.ncbi.nlm.nih.gov/geo/, 62254 https://www.ncbi.nlm.nih.gov/geo/, 26253.

AUTHOR CONTRIBUTIONS

HY conceived and designed the study. HY, YC and ZY collected and analyzed the data. ZL and JX reviewed the methods. HY wrote the manuscript. XC, YL, and XQ reviewed the manuscript. All authors contributed to the article and approved the submitted version.

FUNDING

This work was supported by the National Key Research and Development Program of China (2017YFC1308900), Technological Special Project of Liaoning Province of China (2019020176-JH1/103), Science and Technology Plan Project of Liaoning Province (NO.2013225585), The Key Research and Development Program of Liaoning Province (2018225060), The General Projects of Liaoning Province Colleges and Universities (LFWK201706), Science and Technology Plan Project of Shenyang city (19-112-4-099).

ACKNOWLEDGMENTS

The authors would like to acknowledge the Key Laboratory of Precision Diagnosis and Treatment of Gastrointestinal Tumors, Ministry of Education (China Medical University, Shenyang, China) for providing the space and equipment for conducting the experiments.

SUPPLEMENTARY MATERIAL

The Supplementary Material for this article can be found online at: https://www.frontiersin.org/articles/10.3389/fimmu.2020.621623/full#supplementary-material

Supplementary Figure 1 | The distribution of tumor-infiltrating cells in GC patients in the training cohort. **(A)** The tumor-infiltrating cell composition profile for each GC sample. **(B)** The correlation between different infiltrating immune cells. *GC*, gastric cancer.

Supplementary Figure 2 | Heatmap summarizing the correlation between IS and clinicalpathological characteristics in the testing cohort.

Supplementary Figure 3 | IS analysis of GC patients. **(A)** IS distribution, status of recurrence and survival, distribution of eight immune cells of 273 training cohort patients. **(B)** IS distribution, status of recurrence and survival, distribution of eight immune cells of 365 testing cohort patients. *DFS*, disease free survival; *OS*, overall survival; *GC*, gastric cancer.

Supplementary Figure 4 | Kaplan-Meier survival analysis of DFS (left pane) and OS (right pane) according to IS in TNM subgroups of patients with GC in the testing cohort. **(A)** Stage I (n = 68); **(B)** Stage II (n = 167); **(C)** Stage III (n = 130). *DFS*, disease free survival; *OS*, overall survival; *GC*, gastric cancer.

Supplementary Figure 5 | ROC curves compare the prognostic accuracy of the IS with TNM in the training and testing cohorts. **(A)** Comparison of the accuracy of DFS by IS and TNM in the training and testing cohorts. **(B)** Comparison of the accuracy of OS by IS and TNM in the training and testing cohorts. *ROC*, receiver operator characteristic; *AUC*, area under curve.

Supplementary Figure 6 | Kaplan-Meier survival analysis of DFS (left pane) and OS (right pane) according to IS in Lauren subtype of the training cohort. **(A)** Intestinal subtype (n = 142); **(B)** Diffuse subtype (n = 115); **(C)** Mixed subtype (n = 16); **(D)** The survival impact of IS in Lauren subtype. *HR*, hazard ratio; *DFS*, disease free survival; *OS*, overall survival.

Supplementary Figure 7 | Kaplan-Meier survival analysis of DFS (left pane) and OS (right pane) according to IS in MSS/MSI subtypes of the training cohort. **(A)** MSI subtype (n = 67); **(B)** MSS subtype (n = 206); **(C)** The survival impact of IS in MSI/MSS subtypes. *HR*, hazard ratio; *MSS*, microsatellite stability; *MSI*, microsatellite instability; *DFS*, disease free survival; *OS* overall survival.

Supplementary Figure 8 | Effects of adjuvant chemotherapy on DFS in different subgroups.

Supplementary Figure 9 | PD-L1, CD40, CD47, CTLA4, GZMB, Tim-3, ICOS, IDO1, LAG3, and IFNG mRNA expression between the low- and high-IS groups. * $P < 0.05$

REFERENCES

1. Ferlay J, Soerjomataram I, Dikshit R, Eser S, Mathers C, Rebelo M, et al. Cancer incidence and mortality worldwide: sources, methods and major patterns in GLOBOCAN 2012. *Int J Cancer* (2015) 136(5):E359–386. doi: 10.1002/ijc.29210
2. Lee J, Lim DH, Kim S, Park SH, Park JO, Park YS, et al. Phase III trial comparing capecitabine plus cisplatin versus capecitabine plus cisplatin with concurrent capecitabine radiotherapy in completely resected gastric cancer with D2 lymph node dissection: the ARTIST trial. *J Clin Oncol Off J Am Soc Clin Oncol* (2012) 30(3):268–73. doi: 10.1200/JCO.2011.39.1953
3. Kim S, Lim DH, Lee J, Kang WK, MacDonald JS, Park CH, et al. An observational study suggesting clinical benefit for adjuvant postoperative chemoradiation in a population of over 500 cases after gastric resection with D2 nodal dissection for adenocarcinoma of the stomach. *Int J Radiat Oncol Biol Physics* (2005) 63(5):1279–85. doi: 10.1016/j.ijrobp.2005.05.005
4. Macdonald JS, Smalley SR, Benedetti J, Hundahl SA, Estes NC, Stemmermann GN, et al. Chemoradiotherapy after surgery compared with surgery alone for adenocarcinoma of the stomach or gastroesophageal junction. *New Engl J Med* (2001) 345(10):725–30. doi: 10.1056/NEJMoa010187
5. Noh SH, Park SR, Yang HK, Chung HC, Chung IJ, Kim SW, et al. Adjuvant capecitabine plus oxaliplatin for gastric cancer after D2 gastrectomy (CLASSIC): 5-year follow-up of an open-label, randomised phase 3 trial. *Lancet Oncol* (2014) 15(12):1389–96. doi: 10.1016/S1470-2045(14)70473-5
6. Sasako M, Inoue M, Lin JT, Khor C, Yang HK, Ohtsu A. Gastric Cancer Working Group report. *Japan J Clin Oncol* (2010) 40 Suppl 1:i28–37. doi: 10.1093/jjco/hyq124
7. Cristescu R, Lee J, Nebozhyn M, Kim KM, Ting JC, Wong SS, et al. Molecular analysis of gastric cancer identifies subtypes associated with distinct clinical outcomes. *Nat Med* (2015) 21(5):449–56. doi: 10.1038/nm.3850
8. Shah MA, Khanin R, Tang L, Janjigian YY, Klimstra DS, Gerdes H, et al. Molecular classification of gastric cancer: a new paradigm. *Clin Cancer Res An Off J Am Assoc Cancer Res* (2011) 17(9):2693–701. doi: 10.1158/1078-0432.CCR-10-2203
9. Cancer Genome Atlas Research N. Comprehensive molecular characterization of gastric adenocarcinoma. *Nature* (2014) 513(7517):202–9. doi: 10.1038/nature13480
10. Jiang Y, Zhang Q, Hu Y, Li T, Yu J, Zhao L, et al. ImmunoScore Signature: A Prognostic and Predictive Tool in Gastric Cancer. *Ann Surg* (2018) 267 (3):504–13. doi: 10.1097/SLA.0000000000002116
11. Zeng D, Zhou R, Yu Y, Luo Y, Zhang J, Sun H, et al. Gene expression profiles for a prognostic immunoscore in gastric cancer. *Br J Surg* (2018) 105 (10):1338–48. doi: 10.1002/bjs.10871
12. Peng D, Wang L, Li H, Cai C, Tan Y, Xu B, et al. An immune infiltration signature to predict the overall survival of patients with colon cancer. *IUBMB Life* (2019) 71(11):1760–70. doi: 10.1002/iub.2124
13. Pages F, Kirilovsky A, Mlecnik B, Asslaber M, Tosolini M, Bindea G, et al. In situ cytotoxic and memory T cells predict outcome in patients with early-stage colorectal cancer. *J Clin Oncol Off J Am Soc Clin Oncol* (2009) 27(35):5944–51. doi: 10.1200/JCO.2008.19.6147
14. Galon J, Mlecnik B, Bindea G, Angell HK, Berger A, Lagorce C, et al. Towards the introduction of the 'Immunoscore' in the classification of malignant tumours. *J Pathol* (2014) 232(2):199–209. doi: 10.1002/path.4287
15. Pagès F, Mlecnik B, Marliot F, Bindea G, Ou F-S, Bifulco C, et al. International validation of the consensus Immunoscore for the classification of colon cancer: a prognostic and accuracy study. *Lancet* (2018) 391(10135):2128–39. doi: 10.1016/s0140-6736(18)30789-x
16. Andre T, Vernerey D, Mineur L, Bennouna J, Desrame J, Faroux R, et al. Three Versus 6 Months of Oxaliplatin-Based Adjuvant Chemotherapy for

Patients With Stage III Colon Cancer: Disease-Free Survival Results From a Randomized, Open-Label, International Duration Evaluation of Adjuvant (IDEA) France, Phase III Trial. *J Clin Oncol Off J Am Soc Clin Oncol* (2018) 36 (15):1469–77. doi: 10.1200/JCO.2017.76.0355

17. Pages F, Andre T, Taieb J, Vernerey D, Henriques J, Borg C, et al. Prognostic and predictive value of the Immunoscore in stage III colon cancer patients treated with oxaliplatin in the prospective IDEA France PRODIGE-GERCOR cohort study. *Ann Oncol Off J Eur Soc Med Oncol* (2020) 31(7):921–9. doi: 10.1200/JCO.2019.37.15_suppl.3513
18. Ychou M, Boige V, Pignon JP, Conroy T, Bouche O, Lebreton G, et al. Perioperative chemotherapy compared with surgery alone for resectable gastroesophageal adenocarcinoma: an FNCLCC and FFCD multicenter phase III trial. *J Clin Oncol Off J Am Soc Clin Oncol* (2011) 29(13):1715–21. doi: 10.1200/JCO.2010.33.0597
19. Sasako M, Sakuramoto S, Katai H, Kinoshita T, Furukawa H, Yamaguchi T, et al. Five-year outcomes of a randomized phase III trial comparing adjuvant chemotherapy with S-1 versus surgery alone in stage II or III gastric cancer. *J Clin Oncol Off J Am Soc Clin Oncol* (2011) 29(33):4387–93. doi: 10.1200/JCO.2011.36.5908
20. Smalley SR, Benedetti JK, Haller DG, Hundahl SA, Estes NC, Ajani JA, et al. Updated analysis of SWOG-directed intergroup study 0116: a phase III trial of adjuvant radiochemotherapy versus observation after curative gastric cancer resection. *J Clin Oncol Off J Am Soc Clin Oncol* (2012) 30(19):2327–33. doi: 10.1200/JCO.2011.36.7136
21. Sakuramoto S, Sasako M, Yamaguchi T, Kinoshita T, Fujii M, Nashimoto A, et al. Adjuvant chemotherapy for gastric cancer with S-1, an oral fluoropyrimidine. *New Engl J Med* (2007) 357(18):1810–20. doi: 10.1056/NEJMoa072252
22. Jiang Y, Xie J, Huang W, Chen H, Xi S, Han Z, et al. Tumor Immune Microenvironment and Chemosensitivity Signature for Predicting Response to Chemotherapy in Gastric Cancer. *Cancer Immunol Res* (2019) 7(12):2065–73. doi: 10.1158/2326-6066.CIR-19-0311
23. Wu T, Dai Y. Tumor microenvironment and therapeutic response. *Cancer Lett* (2017) 387:61–8. doi: 10.1016/j.canlet.2016.01.043
24. Qu JL, Qu XJ, Li Z, Zhang JD, Liu J, Teng YE, et al. Prognostic Model Based on Systemic Inflammatory Response and Clinicopathological Factors to Predict Outcome of Patients with Node-Negative Gastric Cancer. *PloS One* (2015) 10 (6):e0128540. doi: 10.1371/journal.pone.0128540
25. Wang J, Qu J, Li Z, Che X, Liu J, Teng Y, et al. Pretreatment platelet-to-lymphocyte ratio is associated with the response to first-line chemotherapy and survival in patients with metastatic gastric cancer. *J Clin Lab Analysis* (2018) 32(1):e22185. doi: 10.1002/jcla.22185
26. Subramanian A, Tamayo P, Mootha VK, Mukherjee S, Ebert BL, Gillette MA, et al. Gene set enrichment analysis: a knowledge-based approach for interpreting genome-wide expression profiles. *Proc Natl Acad Sci United States America* (2005) 102(43):15545–50. doi: 10.1073/pnas.0506580102
27. Bindea G, Mlecnik B, Tosolini M, Kirilovsky A, Waldner M, Obenauf Anna C, et al. Spatiotemporal Dynamics of Intratumoral Immune Cells Reveal the Immune Landscape in Human Cancer. *Immunity* (2013) 39(4):782–95. doi: 10.1016/j.immuni.2013.10.003
28. Hanzelmann S, Castelo R, Guinney J. GSVA: gene set variation analysis for microarray and RNA-seq data. *BMC Bioinf* (2013) 14:7. doi: 10.1186/1471-2105-14-7
29. Friedman J, Hastie T, Tibshirani R. Regularization Paths for Generalized Linear Models via Coordinate Descent. *J Stat Software* (2010) 33(1):1–22. doi: 10.18637/jss.v033.i01
30. Jiang Y, Xie J, Han Z, Liu W, Xi S, Huang L, et al. Immunomarker Support Vector Machine Classifier for Prediction of Gastric Cancer Survival and Adjuvant Chemotherapeutic Benefit. *Clin Cancer Res An Off J Am Assoc Cancer Res* (2018) 24(22):5574–84. doi: 10.1158/1078-0432.CCR-18-0848
31. Qu Y, Cheng B, Shao N, Jia Y, Song Q, Tan B, et al. Prognostic value of immune-related genes in the tumor microenvironment of lung adenocarcinoma and lung squamous cell carcinoma. *Aging* (2020) 12 (6):4757–77. doi: 10.18632/aging.102871
32. Song Y, Sun Y, Sun T, Tang R. Comprehensive bioinformatics analysis identifies tumor microenvironment and immune-related genes in small cell lung cancer. *Combinatorial Chem High Throughput Screen* (2020) 23(5):381–91. doi: 10.2174/1386207323666200407075004
33. Wilson MK, Karakasis K, Oza AM. Outcomes and endpoints in trials of cancer treatment: the past, present, and future. *Lancet Oncol* (2015) 16(1): e32–42. doi: 10.1016/S1470-2045(14)70375-4
34. Tanaka K, Kawano M, Iwasaki T, Itonaga I, Tsumura H. A meta-analytic evaluation of the correlation between event-free survival and overall survival in randomized controlled trials of newly diagnosed Ewing sarcoma. *BMC Cancer* (2020) 20(1):379. doi: 10.1186/s12885-020-06871-9
35. Bang YJ, Kim YW, Yang HK, Chung HC, Park YK, Lee KH, et al. Adjuvant capecitabine and oxaliplatin for gastric cancer after D2 gastrectomy (CLASSIC): a phase 3 open-label, randomised controlled trial. *Lancet* (2012) 379(9813):315–21. doi: 10.1016/S0140-6736(11)61873-4
36. Casares N, Pequignot MO, Tesniere A, Ghiringhelli F, Roux S, Chaput N, et al. Caspase-dependent immunogenicity of doxorubicin-induced tumor cell death. *J Exp Med* (2005) 202(12):1691–701. doi: 10.1084/jem.20050915
37. Galluzzi L, Buque A, Kepp O, Zitvogel L, Kroemer G. Immunological Effects of Conventional Chemotherapy and Targeted Anticancer Agents. *Cancer Cell* (2015) 28(6):690–714. doi: 10.1016/j.ccell.2015.10.012
38. Schiavoni G, Sistigu A, Valentini M, Mattei F, Sestili P, Spadaro F, et al. Cyclophosphamide synergizes with type I interferons through systemic dendritic cell reactivation and induction of immunogenic tumor apoptosis. *Cancer Res* (2011) 71(3):768–78. doi: 10.1158/0008-5472.CAN-10-2788
39. Shalapour S, Font-Burgada J, Di Caro G, Zhong Z, Sanchez-Lopez E, Dhar D, et al. Immunosuppressive plasma cells impede T-cell-dependent immunogenic chemotherapy. *Nature* (2015) 521(7550):94–8. doi: 10.1038/nature14395
40. Cunningham D, Allum WH, Stenning SP, Thompson JN, Van de Velde CJH, Nicolson M, et al. Perioperative Chemotherapy versus Surgery Alone for Resectable Gastroesophageal Cancer. *New Engl J Med* (2006) 355(1):11–20. doi: 10.1056/NEJMoa055531
41. Zaanan A, Taieb J. Predictive and prognostic value of MSI phenotype in adjuvant colon cancer: Who and how to treat? *Bull Du Cancer* (2019) 106 (2):129–36. doi: 10.1016/j.bulcan.2018.10.011
42. Leach DR, Krummel MF, Allison JP. Enhancement of antitumor immunity by CTLA-4 blockade. *Science* (1996) 271(5256):1734–6. doi: 10.1126/science.271.5256.1734
43. Harding FA, McArthur JG, Gross JA, Raulet DH, Allison JP. CD28-mediated signalling co-stimulates murine T cells and prevents induction of anergy in T-cell clones. *Nature* (1992) 356(6370):607–9. doi: 10.1038/356607a0
44. Freeman GJ, Long AJ, Iwai Y, Bourque K, Chernova T, Nishimura H, et al. Engagement of the PD-1 immunoinhibitory receptor by a novel B7 family member leads to negative regulation of lymphocyte activation. *J Exp Med* (2000) 192(7):1027–34. doi: 10.1084/jem.192.7.1027
45. Sadreddini S, Baradaran B, Aghebati-Maleki A, Sadreddini S, Shanehbandi D, Fotouhi A, et al. Immune checkpoint blockade opens a new way to cancer immunotherapy. *J Cell Physiol* (2019) 234(6):8541–9. doi: 10.1002/jcp.27816
46. Fan L, Li Y, Chen JY, Zheng YF, Xu XM. Immune checkpoint modulators in cancer immunotherapy: Recent advances and combination rationales. *Cancer Lett* (2019) 456:23–8. doi: 10.1016/j.canlet.2019.03.050
47. Duffy MJ, Crown J. Biomarkers for Predicting Response to Immunotherapy with Immune Checkpoint Inhibitors in Cancer Patients. *Clin Chem* (2019) 65 (10):1228–38. doi: 10.1373/clinchem.2019.303644
48. Havel JJ, Chowell D, Chan TA. The evolving landscape of biomarkers for checkpoint inhibitor immunotherapy. *Nat Rev Cancer* (2019) 19(3):133–50. doi: 10.1038/s41568-019-0116-x
49. Zhang J, Dang F, Ren J, Wei W. Biochemical Aspects of PD-L1 Regulation in Cancer Immunotherapy. *Trends Biochem Sci* (2018) 43(12):1014–32. doi: 10.1016/j.tibs.2018.09.004

Conflict of Interest: The authors declare that the research was conducted in the absence of any commercial or financial relationships that could be construed as a potential conflict of interest.

Copyright © 2021 Yan, Chen, Yang, Li, Che, Xiao, Liu and Qu. This is an open-access article distributed under the terms of the Creative Commons Attribution License (CC BY). The use, distribution or reproduction in other forums is permitted, provided the original author(s) and the copyright owner(s) are credited and that the original publication in this journal is cited, in accordance with accepted academic practice. No use, distribution or reproduction is permitted which does not comply with these terms.

frontiers in Oncology

ORIGINAL RESEARCH
published: 08 February 2021
doi: 10.3389/fonc.2020.622251

Screening and Identification of Four Prognostic Genes Related to Immune Infiltration and G-Protein Coupled Receptors Pathway in Lung Adenocarcinoma

Yan Wang[1,2†], Liwei Qiu[3†], Yu Chen[2], Xia Zhang[2], Peng Yang[1] and Feng Xu[1*]*

[1] Department of Emergency Medicine, The First Affiliated Hospital of Soochow University, Suzhou, China, [2] Department of Emergency Medicine, Affiliated Hospital of Nantong University, Nantong, China, [3] Research Center of Clinical Medicine, Affiliated Hospital of Nantong University, Nantong, China

OPEN ACCESS

Edited by:
Keqiang Chen,
National Cancer Institute at Frederick, United States

Reviewed by:
Ruoxi Yuan,
Hospital for Special Surgery, United States
Haiwei Mou,
Cold Spring Harbor Laboratory, United States

***Correspondence:**
Peng Yang
yangpeng@suda.edu.cn
Feng Xu
sz_xf@suda.edu.cn

†These authors have contributed equally to this work

Specialty section:
This article was submitted to Cancer Immunity and Immunotherapy, a section of the journal Frontiers in Oncology

Received: *28 October 2020*
Accepted: *21 December 2020*
Published: *08 February 2021*

Citation:
Wang Y, Qiu L, Chen Y, Zhang X, Yang P and Xu F (2021) Screening and Identification of Four Prognostic Genes Related to Immune Infiltration and G-Protein Coupled Receptors Pathway in Lung Adenocarcinoma. Front. Oncol. 10:622251. doi: 10.3389/fonc.2020.622251

Background: Lung adenocarcinoma (LUAD) is a common malignant tumor with the highest morbidity and mortality worldwide. The degree of tumor immune infiltration and clinical prognosis depend on immune-related genes, but their interaction with the tumor immune microenvironment, the specific mechanism driving immune infiltration and their prognostic value are still not very clear. Therefore, the aim of this work was focused on the elucidation of these unclear aspects.

Methods: TCGA LUAD samples were divided into three immune infiltration subtypes according to the single sample gene set enrichment analysis (ssGSEA), in which the associated gene modules and hub genes were screened by weighted correlation network analysis (WGCNA). Four key genes related to immune infiltration were found and screened by differential expression analysis, univariate prognostic analysis, and Lasso-COX regression, and their PPI network was constructed. Finally, a Nomogram model based on the four genes and tumor stages was constructed and confirmed in two GEO data sets.

Results: Among the three subtypes—high, medium, and low immune infiltration subtype—the survival rate of the patients in the high one was higher than the rate in the other two subtypes. The four key genes related to LUAD immune infiltration subtypes were CD69, KLRB1, PLCB2, and P2RY13. The PPI network revealed that the downstream genes of the G-protein coupled receptors (GPCRs) pathway were activated by these four genes through the S1PR1. The risk score signature based on these four genes could distinguish high and low-risk LUAD patients with different prognosis. The Nomogram constructed by risk score and clinical tumor stage showed a good ability to predict the survival rate of LUAD patients. The universality and robustness of the Nomogram was confirmed by two GEO datasets.

Conclusions: The prognosis of LUAD patients could be predicted by the constructed risk score signature based on the four genes, making this score a potential independent

biomarker. The screening, identification, and analysis of these four genes could contribute to the understanding of GPCRs and LUAD immune infiltration, thus guiding the formulation of more effective immunotherapeutic strategies.

Keywords: lung adenocarcinoma, tumor immune infiltration, single sample gene set enrichment analysis, weighted correlation network analysis, prognosis

INTRODUCTION

Lung cancer is a common malignant tumor worldwide. More than 2 million new lung cancer cases and nearly 1.8 million deaths occurred in 2018 (1). The incidence and mortality of lung cancer rank first among all malignant tumors (2). Lung cancer is mainly divided into two pathological forms: small cell lung cancer (SCLC) and non-small cell lung cancer (NSCLC), the latter being the prevalent one, accounting for 85~90% of lung cancers. NSCLC is mainly divided into lung squamous cell carcinoma and lung adenocarcinoma (LUAD), which is the most common lung cancer subtype. About half of patients with LUAD are at an advanced stage at the time of diagnosis, with an average 5-year survival rate of only 4% (3).

In recent years, immunotherapy based on blocking strategies of immune checkpoints (PD-1/PD-L1/CTLA-4) revealed considerable survival benefits in a variety of solid tumors, including LUAD (4–6), although only a small number of tumor patients showed a sustained response to immunotherapy (7). More and more evidence is available on the importance of tumor microenvironment (TME) in tumor proliferation, metastasis, and resistance to immunotherapy (8–10). The interaction between tumor cells and immune modulatory factors in TME is the key factor influencing the positive response of tumor patients to immunotherapy (11, 12).

TME represents the environment around tumor cells, composed of extracellular matrix, blood vessels and immune cells, all playing an important role in tumor immunity and closely related to tumor progression and treatment results (13, 14). Many studies confirmed the involvement of TME in the response of immunotherapy and resistance to different drugs in different types of cancer, including LUAD, thus compromising the prognosis of patients (15–17).

However, at present, most of the studies on prognostic models of LUAD only have focused on the changes of gene expression, while the relationship between differentially expressed genes and different levels of immune infiltration is not yet well understood because of the limitation of the existing literature. In addition, the articles available did not study the specific mechanism involved in the aforementioned relationship, and there are too many screening genes involved in the models that maybe lead to overfitting, thus preventing satisfactory results from being achieved (18–20). In this study, our aim was to identify genes that are highly associated with different immune infiltration conditions in LUAD using the RNA-seq data downloaded from The Cancer Genome Atlas (TCGA) database, and to analyze the potential pathways in which these genes are involved when regulating the immune infiltration by the use of bioinformatics. Furthermore, a prognostic model was constructed based on these genes, the applicability, and the value of the model in LUAD were evaluated, and the universality of the model was investigated by the external validation of multiple data sets from the Gene Expression Omnibus (GEO) database. The results of this study might highlight a potentially useful systematic and comprehensive screening process of immune infiltration-related genes resulting in the discovery of potential targets for immunotherapy, and a model for predicting the prognosis of LUAD.

MATERIAL AND METHODS

LUAD Data Download

The RNA-seq data and clinical information of 487 LUAD patients were downloaded from the TCGA database through the GDC website (https://portal.gdc.cancer.gov/). The RNA-seq data include HTSeq-FPKM data and counts data (the latter used only for the identification of differentially expressed genes). After data cleaning consisting of the removal of the repeated samples, paraffin section samples and samples with missing prognostic data, a total of 426 LUAD samples with complete clinical data were included in this study (Training cohort, **Table 1**). Five microarray datasets were downloaded from the GEO database to confirm the results, and two of them were used as validation cohorts by incorporating them into the external validation of the prognostic model (**Tables 1** and **2**).

Identification of the Immune Infiltration Subtypes in LUAD

A total of 29 gene sets associated to tumor immune cells and immune functions were obtained from several articles (21–25).

Abbreviations: AUC, Area Under the Curve; BP, Biological Process; CC, Cellular Component; CCR, Cell Surface Chemokine Receptor; CD, Cluster of Differentiation; CTLA-4, Cytotoxic T Lymphocyte associated Antigen 4; DCs, Dendritic Cells; DEGs, Differential Expressed Genes; FPKM, Fragments Per Kilobase Million; GEO, Gene Expression Omnibus; GPCRs, G-Protein Coupled Receptors; GS, Gene Significance; HLA, Human Leukocyte Antigen; HR, Hazard Ratio; IFN, Interferon; KEGG, Kyoto Encyclopedia of Genes and Genomes; KLRB1, Killer Cell Lectin Like Receptor B1; LASSO, Least Absolute Shrinkage and Selection Operator; LUAD, Lung Adenocarcinoma; MEs, Module Eigengenes; MF, Molecular Function; MHC, Major Histocompatibility Complex; MM, Module Membership; NK, Natural Killer; NSCLC, Non-Small Cell Lung Cancer; OS, Overall Survival; PCA, Principal Component Analysis; PD-1, Programmed cell Death 1; PD-L1, Programmed cell Death Ligand 1; PLCB2, Phospholipase C Beta 2; PPI, Protein-Protein Interaction; P2RY13, Purinergic Receptor P2Y13; ROC, Receiver Operating Characteristic curve; SCLC, Small Cell Lung Cancer; ssGSEA, single sample Gene Set Enrichment Analysis; S1PR1, Sphingosine-1-Phosphate Receptor 1; TCGA, The Cancer Genome Atlas; TIL, Tumor Infiltrating Lymphocyte; TME, Tumor Microenvironment; WGCNA, Weighted Correlation Network Analysis.

TABLE 1 | Clinical data of LUAD patients.

	Training Cohort (TCGA)	Validation Cohort 1 (GSE 41271)	Validation Cohort 2 (GSE 72094)
Number of LUAD	426	182	398
Age (years old)			
Medium	66	64	69
Average	65	64	69
Min	33	30	38
Max	88	86	89
Gender			
Male	190	92	176
Female	236	90	222
Tumor Stage			
Stage I	224	101	254
Stage II	107	28	67
Stage III and IV	95	53	77
T Stage		not provided	not provided
T1 and T2	368		
T3 and T4	55		
TX	3		
M Stage		not provided	not provided
M0	283		
M1	22		
MX	121		
N Stage		not provided	not provided
N0	270		
N1	82		
N2 & N3	63		
NX	11		

The "GSVA" R package was used to perform the single sample gene set enrichment analysis (ssGSEA) on these 29 immune-related gene data sets to obtain the immune infiltration score in each sample to allow the clustering of all samples into three immune infiltration subtypes (26). Next, the "ESTIMATE" R package was used to calculate the tumor purity (representing the proportion of cancer cells in the tumor), the immune score (representing the infiltration of immune cells in the tumor), the stromal score (capturing the presence of stroma in the tumor), and the ESTIMAT score (sum of immune and stromal score) of each sample, which were included in the heat map of ssGSEA to verify the relationship between these subtypes and tumor purity (27). Finally, the relative fractions of 22 kinds of tumor immune cells were calculated in the subgroups by a deconvolution algorithm using the "CIBERSORT" R package (28).

Screen of Coordinated Expression Genes Related With Immune Infiltration

The coordinated expression genes related with clinical traits and immune infiltration subtypes of LUAD were screened out using weighted correlation network analysis (WGCNA) of the "WGCNA" R package (29). A scale-free topological network model was built using 18,748 genes obtained after data filtering (removing the duplicate genes and genes with average FPKM <5 in total samples), by calculating the correlation of the expression of these genes among each other. TOM-based differences through dynamic tree cutting were used to form modules related to traits (patients' clinical phenotype and immune infiltration). The minimum module size in this WGCNA network was set at 30 and the height was set at 0.25. The coordinated expression gene network was plotted based on the evaluation of the module eigengenes (MEs), gene significance (GS), and module membership (MM).

Construction of the Protein-Protein Interaction (PPI) Network and GO/KEGG Enrichment Analysis

Top 300 gene pairs in the two modules screened by WGCNA with the highest GS in each module were selected to construct the PPI network using the "Cytoscape" software (Version 3.8.0). The immune infiltration key genes finally screened were analyzed by inputting the names into the "STRING" website (https://STRING-db.org/) (30). The minimum required interaction score was set as 0.4 during the STRING PPI analysis, while the max number of interactions was set as no more than 10, the line color was set to indicate the type of interaction and the node color was set to indicate the gene ontology (GO) terms to which the gene belongs. The "ClusterProfiler" R package was used to perform GO and the Kyoto Encyclopedia of Genes and Genomes (KEGG) enrichment analysis (31). Three aspects were mainly investigated by the GO analysis: biological process, molecular function, and cellular component.

Construction and Validation of the Risk Score Signature and Nomogram Model

The "Least Absolute Shrinkage and Selection Operator" (Lasso)-Cox algorithm in "glmnet" R package was used to screen the independent prognostic genes (32) and the selected ones were subsequently used to construct a risk score signature according to a coefficient calculated by Lasso regression. Univariate/multivariate COX regression analysis was performed, a Nomogram prediction model was established, and an external validation in GEO datasets was carried out, all of them using the

TABLE 2 | Validation cohorts from GEO database.

Data Set	Pathology	Type	Platform	Samples	LUAD
GSE 41271	NSCLC	Microarray	GPL6884	275	182
GSE 72094	LUAD	Microarray	GPL15048	442	398
GSE 50081	NSCLC	Microarray	GPL570	181	127
GSE 68465	LUAD	Microarray	GPL96	462	442
GSE 42127	NSCLC	Microarray	GPL6884	176	133

"Survival" R package. The Time-dependent receiver operating characteristic (ROC) curve was plotted by the "survivalROC" R package.

Statistical Analysis

The differentially expressed genes (based on counts data) between high immune infiltration subtype and medium-low immune infiltration subtype were found using the "DEseq2" R package. Genes with a false discovery rate (FDR) less than 0.05 were defined as differentially expressed genes (DEGs). The "networkD3" R package was used to perform the principal component analysis (PCA) and to plot the Sankey diagram. The Kaplan-Meier survival curves were tested by the log-rank method, the data in two groups were compared by Mann–Whitney test, the data in multiple groups were compared by Wilcox test, and the Pearson correlation coefficient test was performed to the linear relationship between two quantitative measures. The *P* values (or adjusted *P*-values, *P*adj) of all statistical analysis were calculated using R software (Vision 4.0.2), and a value less than 0.05 was considered statistically significant.

RESULTS

Immune Infiltration Subtypes in LUAD

Immune cells and immune-related pathways cause a different immune infiltration and anti-tumor effect in the immune TME. The immune infiltration status of the transcriptome LUAD data was evaluated using the ssGSEA algorithm. A total of 575 immune-related genes included in 29 immune-related gene sets were used to evaluate the immune infiltration in LUAD. The samples in the training cohort were clustered into three immune infiltration subtypes using the hierarchical and K-means clustering method as follows: 44 cases with low immune infiltration, 265 cases with medium immune infiltration, and 118 cases with high immune infiltration (**Figures 1A** and **S1A**). The relationship between the immune infiltration status and tumor purity was evaluated using the ESTIMATE algorithm, and the tumor purity, ESTIMATE score, stromal score, and immune score of the TCGA cohort were calculated. The heatmap and violin plots revealed that the LUAD cases with high immune infiltration were often with lower tumor purity and higher ESTIMATE, stromal and immune scores compared with the cases with low and medium immune infiltration (**Figures 1A, B** and **S1B–D**). The CIBERSORT algorithm was used to quantify the relative fractions of immune cells in the LUAD samples to evaluate more accurately the infiltration status of immune cells in the different immune infiltration subtypes (**Figure S1E**). Fourteen types among the 22 types of immune cells defined by the algorithm were present in different counts in the immune infiltration subtypes ($P < 0.05$). Six types of immune cells, such as immature B cells, CD8 T cells, activated memory CD4 T cells, M1 macrophage cells, and dendritic cells, have the highest significances of infiltration degree in different immune infiltration subtypes ($P < 0.001$), and showed a progressive increasing or decreasing trend (**Figure 1C**). The Kaplan-Meyer survival curve of the three immune infiltration subtypes in the TCGA cohort showed that the 5-year overall survival rate of the high immune infiltration subtype was significantly higher than that in the medium and low immune infiltration subtypes (P = 4.394000e-4, **Figure 1D**).

Screen of the Coordinated Expression Genes Related With Immune Infiltration by WGCNA

The WGCNA algorithm was used to construct a weighted correlation gene network to screen the coordinated expression genes associated with immune infiltration. A total of 18,748 genes were included in the WGCNA analysis after the removal of the duplicate genes and genes with low expression. WGCNA clustered all these genes into 14 gene modules by selecting the appropriate soft threshold (**Figures S2A, B**) according to the coordinated pattern (**Figure 2A**). These gene modules were associated with both the clinical traits and the immune infiltration subtypes of LUAD patients. The results revealed that the red module (containing 1,028 genes) and the light yellow module (containing 643 genes) showed a high correlation with the immune infiltration subtypes (r = 0.62, P = 9e-47; r = 0.69, P = 2e-60, respectively; **Figure 2B**). A high correlation between red modules and bright yellow modules was also revealed by the correlation cluster heatmap (**Figure 2C**). In addition, the high reliability of the WGCNA result was confirmed by the high correlation between GS and MM inside the modules (**Figures S2C, D**). The gene pairs with the Top 300 GS weighted coefficients in the two modules aforementioned were extracted, and the gene-related PPI map was constructed and plotted using the "Cytoscape" software. The PPI showed that the genes with the largest number of associated nodes in the weighted network of the two gene modules, such as NCKAP1L, CD53, SASH3, and CD3E, were present in the ssGSEA gene set (**Figures 2D, E**), and it revealed a strong correlation between the screened genes by WGCNA and the immune infiltration subtypes. The total 1,671 genes in the two modules were then analyzed by GO and KEGG pathway. The GO terms T cell activation, regulation of lymphocyte activation, external side of plasma membrane, and cytokine receptor binding were the enriched GO terms (**Figures 2F**, **S2E** and **S2G**). The cytokine −cytokine receptor interaction and chemokine signaling pathways were also enriched in the two modules as revealed by the KEGG pathway analysis (**Figures 2G**, **S2F** and **S2H**). These results confirmed that the genes in the two modules were immune related genes.

Further Screening and Identification of Immune Infiltration Related Genes

DESeq2 standard procedure was used to screen DEGS in LUAD patients with high immune infiltration in comparison with patients with low or medium immune infiltration to further define the genes related to immune infiltration and their prognostic survival in LUAD patients (**Figures S3A, B**). In addition, a total of 2,601 genes related to the prognosis of

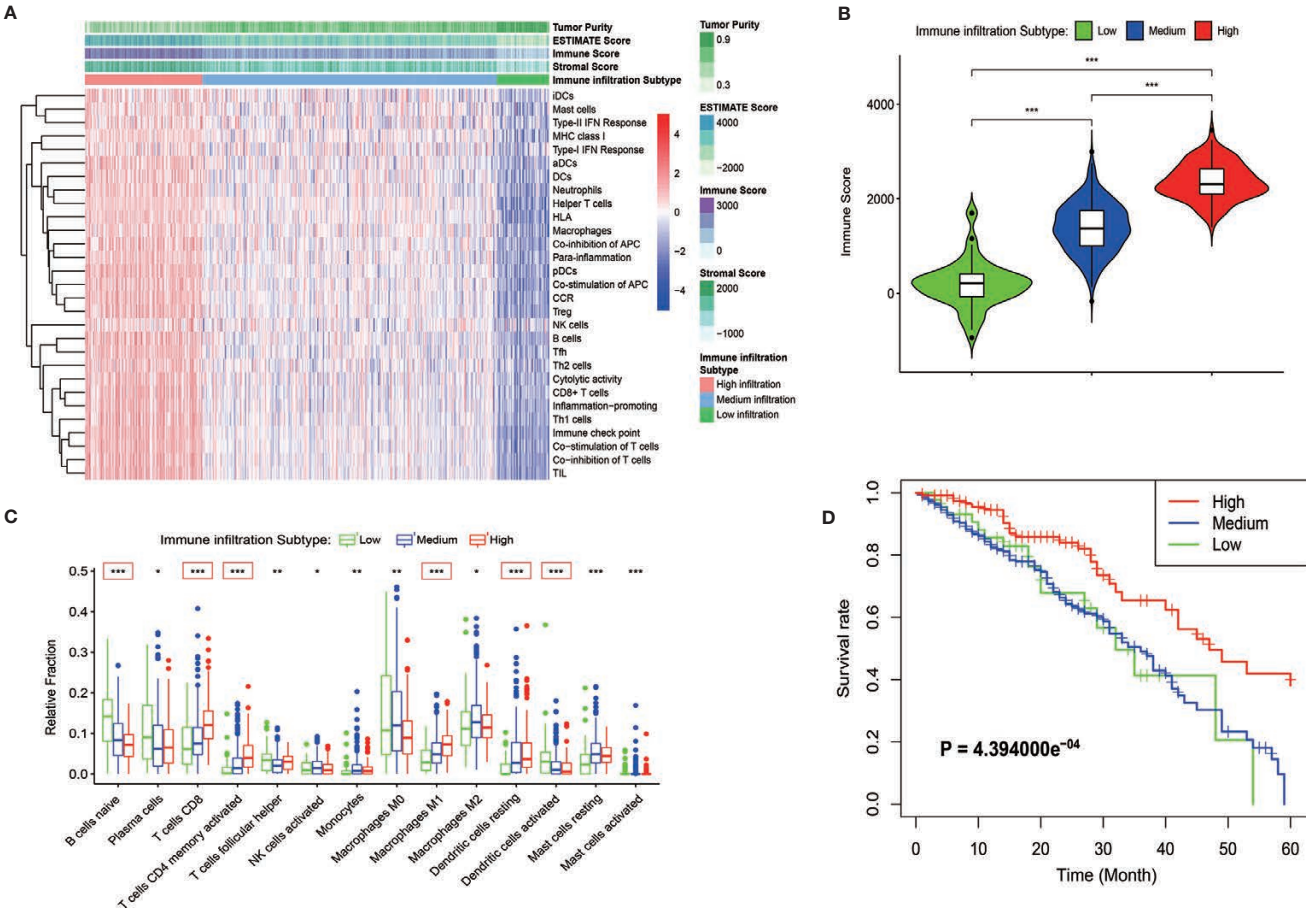

FIGURE 1 | Identification of the immune infiltration subtypes in LUAD in the TCGA cohort. **(A)** According to 29 immune-related gene sets, three immune infiltration subtypes were identified in LUAD samples by ssGSEA. The results of the ESTIMATE algorithm are also shown in the heatmap. **(B)** The immune score calculated by the ESTIMATE algorithm in different immune infiltration subtypes. **(C)** Relative fractions of 14 immune cells in different immune infiltration subtypes. The red box indicated that the relative expression of immune cells increased or decreased in the three immune infiltration subtypes. **(D)** Kaplan-Meyer survival curve of the three immune infiltration subtypes in the TCGA cohort. $^{*}P < 0.05$; $^{**}P < 0.01$; $^{***}P < 0.001$.

LUAD were screened by univariate log-rank test. The coordinate expression genes associated to immune infiltration screened by WGCNA were intersected with DEGs and prognosis-related genes, and 325 genes were found as common genes (**Figure 3A**). The genes already included in ssGSEA analysis, non-coding genes (lincRNA and miRNA), pseudogenes, and antisense chains of coding genes were removed and a total of 178 genes remained that were used to construct a PPI network by the "STRING" website (which does not show single-node genes). In this network, some members of the G-protein coupled receptor pathway, such as GNG2, GNB2, and P2RY13, as the central nodes, had more associated genes, and the evidence of gene association is also more sufficient (thicker the lines, more sufficient the evidences) (**Figure 3B**). The GO analysis of the 178 genes revealed three molecular functional GO terms with the highest enrichment degree, such as non–membrane spanning protein tyrosine kinase activity, carbohydrate binding, and G protein–coupled purinergic nucleotide receptor activity (**Figure 3C**). The biological process and cellular component of the GO analysis revealed that immune response–activating related signaling pathways and cell membrane component were the mainly enriched GO terms (**Figures S3C, D**). The KEGG pathway analysis revealed that chemokine signaling pathway and B cell receptor pathway were the mainly enriched pathways (**Figure 3D**). Finally, the lasso-cox algorithm applied to these 178 genes revealed that CD69, KLRB1, PLCB2, and P2RY13 were independent prognostic genes (**Figure 3E**). These four genes showed specific interactions with various immune-related genes or immune-related signaling pathways as revealed by the PPI network (**Figures S3E–H**). The LUAD patients were divided into high expression group and low expression group according to the median expression value of these four key genes used as the cutoff value. The results showed that the 5-year survival rate in LUAD patients with high expression of these four genes was significantly higher than that in patients with low expression of these genes (**Figure 3F**).

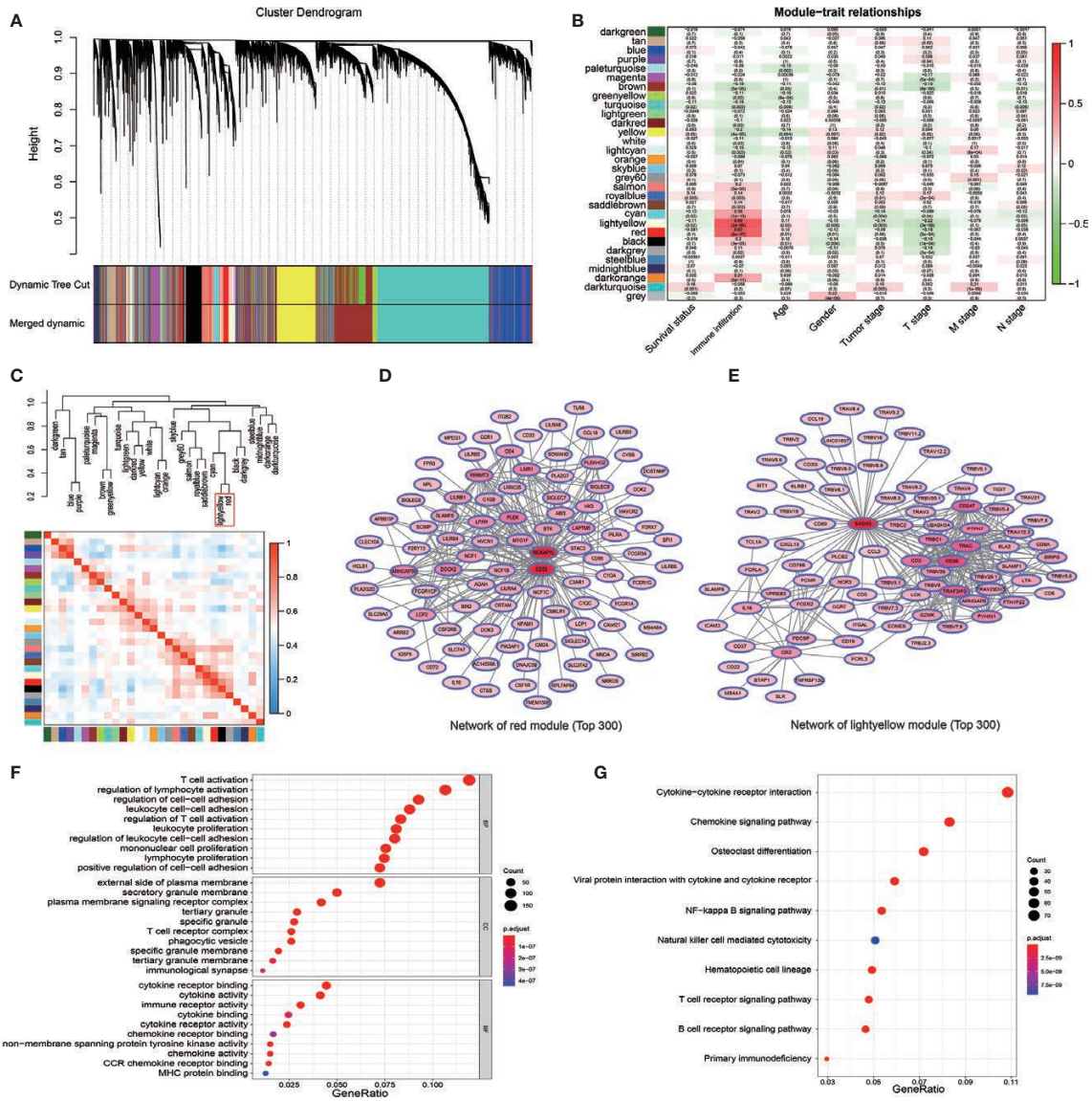

FIGURE 2 | Detection of the immune infiltration related modules and genes by WGCNA. **(A)** The gene dendrogram obtained by the different clusters based on scale-free topological network corresponding to the module represented by the colors in the row. Each colored module contains a group of highly coordinated expression genes. **(B)** Relationship between the gene modules and the different clinical traits of LUAD in the TCGA cohort. **(C)** Dendrogram and heatmap of the correlation of modules. The red box shows the high correlation between the red module and light-yellow module. **(D, E)** The PPI network of the top 300 gene pairs with the highest GS in the red module **(D)** and in the light-yellow module **(E)**. The intensity of the red color of the nodes represents the number of coordinated expression genes in this node gene. **(F)** GO enriched analysis of the coordinated expression genes in red and light-yellow modules. **(G)** KEGG pathway analysis of the coordinated expression genes in red and light-yellow modules.

Relationship Between the Four Key Genes and LUAD Immune Microenvironment

The expression of these four genes in different immune infiltration subgroups were analyzed to further explore the relationship between the four key genes and LUAD immune microenvironment and the potential mechanism regulating this relationship. A significant difference in the expression of these genes among the three immune infiltration subgroups was found (**Figure 4A**), all showing a progressive increase in their expression from the low immune infiltration subgroup to the high one. The PCA suggested that different immune infiltration states could be distinguished to some extent just only using the expression of these four key genes (**Figure 4B**). A correlation between the expression of these key genes and the infiltration of various immune cells was indeed found (**Figures 4C** and **S4A**). CD69 is a marker of macrophage activation and, as such, is negatively correlated with the relative number of M0 cell. KLRB1 expression was positively correlated with the activation of CD8

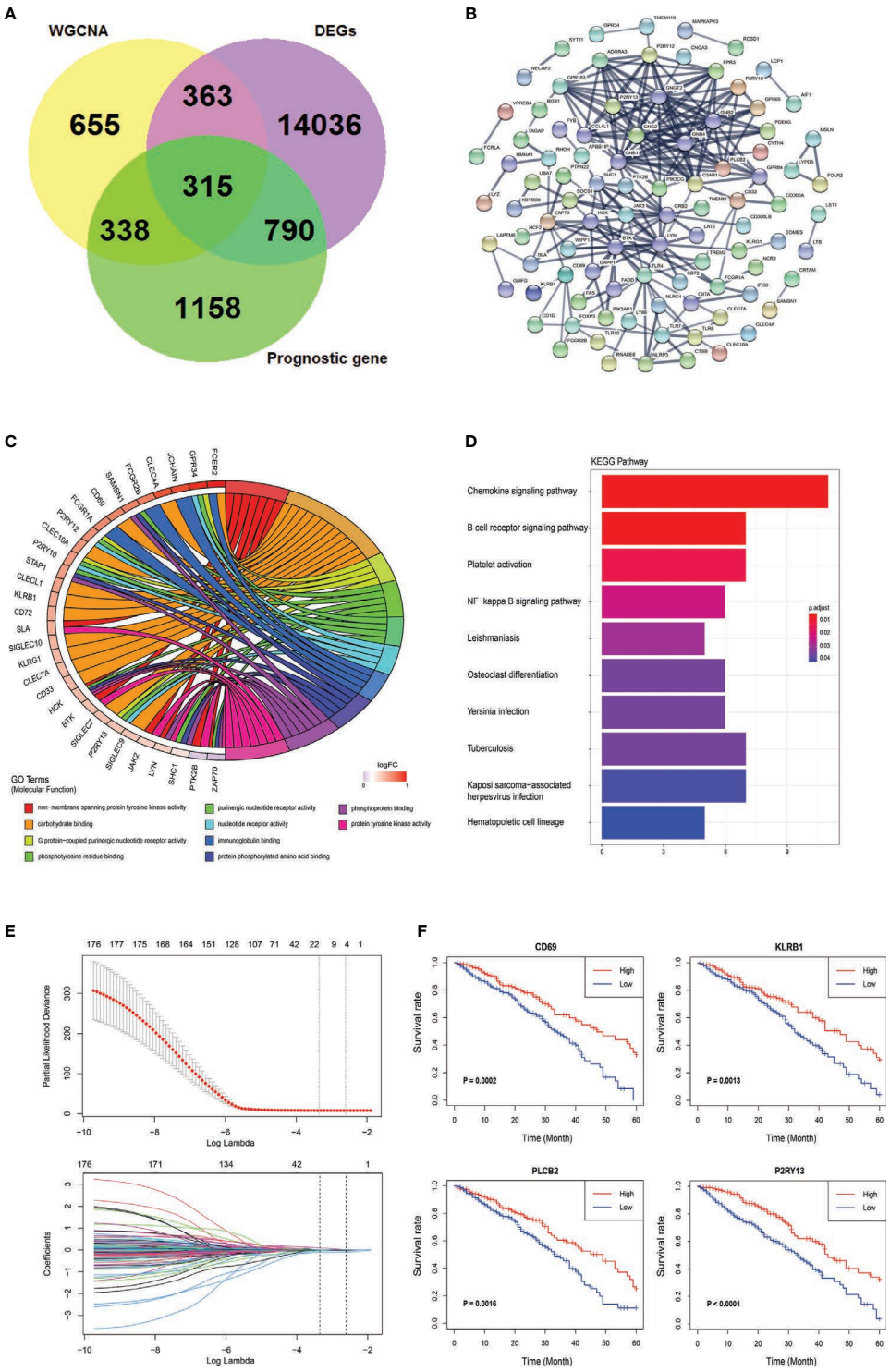

FIGURE 3 | Further screening and identification of immune infiltration related genes. **(A)** Venn diagram showing the intersection (315 genes) of the genes related with immune infiltration screened by WGCNA and DEGs in different immune infiltration subtypes and the prognostic genes screened by log-rank test. **(B)** PPI network of the 178 genes. The line thickness indicates the strength of the data supporting the interaction. **(C)** A Chord graph showing the genes in the top 10 enriched GO terms in the molecular function level. **(D)** KEGG pathway analysis of the 178 genes. **(E)** Lasso-Cox regression showing the independent prognostic genes. The top graph shows the coefficient shrinkage, the bottom graph shows the 10-fold cross-validation. **(F)** The Kaplan-Meyer survival curves of the four genes (CD69, KLRB1, PLCB2, and P2RY13) screened by the Lasso-Cox regression.

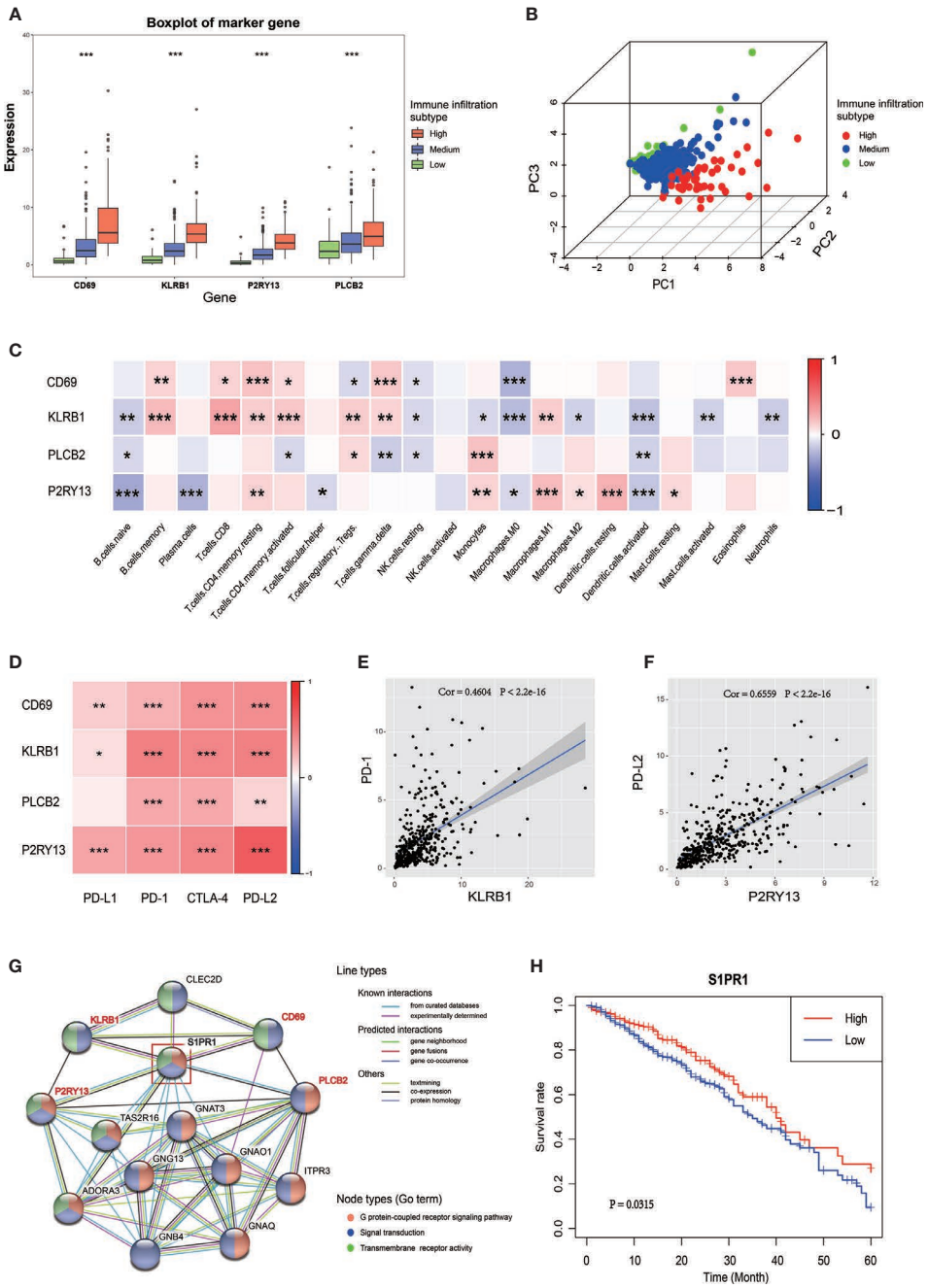

FIGURE 4 | Relationship between the four key genes and LUAD immune microenvironment. **(A)** The boxplot shows the expression trends of the four key genes in different immune infiltration subtypes. **(B)** 3D PCA of the four key genes shows the spatial distribution of different immune infiltrations. **(C)** Correlation between the four key genes and 22 immune cell types. The blue box indicates a negative correlation, the red box indicates a positive correlation, and the increase of the color indicates the increase of the correlation coefficient. **(D)** Correlation between the four key genes and the four immune checkpoints. The increase of the color indicates the increase of the correlation coefficient. **(E)** Correlation between KLRB1 and PD-1. **(F)** Correlation between P2RY13 and PD-L2. **(G)** PPI network of the four key genes. The colors of the lines indicate the types of interaction, the colors of the node indicate which GO term the gene belong to. The node in the red box (S1PR1 gene) was the common interaction of the four key genes. **(H)** The Kaplan-Meyer survival curve of S1PR1 in LUAD. $^{*}P < 0.05$; $^{**}P < 0.01$; $^{***}P < 0.001$.

positive T cells, PLCB2 expression was positively correlated with monocyte infiltration, and P2RY13 expression was negatively correlated with the number of naive B cell, but positively correlated with the number of resting dendritic cells. A correlation between the expression of the four key genes and immune checkpoint genes was also found, as shown in **Figures 4D** and **S4B–J**, in which the correlation between KLRB1 and PD-1, as well as P2RY13 and PD-L2 was significant (**Figures 4E, F**).

The potential interaction between these four key genes was also evaluated. The use of the STRING website revealed that both P2RY13 and PLCB2 belong to the G-protein coupled receptor pathway, while CD69 and KLRB1 belong to the signal transduction pathway, but these four genes had a common interaction gene, such as S1PR1, which is a member of both the G-protein coupled receptor pathway and the signal transduction pathway (**Figure 4G**). The subsequent investigation of S1PR1 revealed that it might also be a prognostic gene in LUAD (in TCGA cohort and GSE72094), with interactions with some well-known tumor genes such as AKT1, STAT3 and CXCR4 (**Figures 4H**, **S4K–4N**).

Establishment of a Prognostic Model Based on Four Immune-Related Genes

A risk score signature was constructed to integrate the roles of these four key genes by the coefficients of LASSO-Cox regression in view of their role in the prognosis and immune infiltration in LUAD (**Figure 5A**). The coefficients are shown in **Table S1**. The LUAD patients were divided into high-risk group and low-risk group according to the median value of the risk score. The survival rate of the patients in the low-risk group was significantly higher than that of the patients in the high-risk group, with a 5-year survival rate of 46.0 and 29.0%, respectively (**Figure 5B**). The combination of the risk score with the clinical baseline index of LUAD by univariate COX analysis revealed that tumor stage, TNM stage, and risk score were prognosis predictors, but after the correction by multivariate COX, only the tumor stage and risk score resulted as independent predictors of LUAD prognosis (**Figures 5C, D**). The result of the multivariate COX model was then quantified and visualized through the construction of a Nomogram to predict the 3-year and 5-year survival rates of LUAD patients (**Figure 5E**). A high coincidence rate between the predicted probability and the actual probability in the 3-year and 5-year survival prediction of LUAD was found through the internal calibration curves (**Figure 5F**). The time-dependent ROC curve showed that the area under the curve (AUC) of the Nomogram to predict the 3-year survival rate was 0.715, which was higher than that of the TNM stage (0.618), while the AUC to predict the 5-year survival rate was 0.829, also higher than 0.699 of the TNM (**Figures 5G, H**). The Sankey diagram visualized the relationship between the risk score and the final outcome of patients with different immune infiltration subtypes (**Figure 5I**).

Validation of the Prognostic Value of the Four Immune-Related Genes in GEO Datasets

Universality is an important index to evaluate a prognostic model, thus, it is necessary to use data from different sources to externally verify the Nomogram (33). Five GEO datasets using different chip platforms were selected to confirm the prognostic prediction ability of the immune-related genes and the Nomogram. All the four key genes had a prognostic significance in both GSE41271 and GSE72094 (**Figures S5A, B**). As regard the other GEO datasets, CD69 and KLRB1 in GSE50081, KLRB1 and PLCB2 in GSE68465, and PLCB2 and P2RY13 in GSE42127 also had a prognostic significance. The risk score constructed by the four key genes in GSE41271 and GSE72094 had a significant prognostic value (**Figures 6A, B** and **S5C, D**). The external calibration curves of the Nomogram to predict the two GEO datasets showed that the prediction of the 3-year and 5-year survival rate was in good agreement with the actual survival rates (**Figures 6C, D**). The ROC curves also revealed that the predicted AUCs of other survival periods were higher than 0.7, except for the AUC of the 5-year survival in GSE41271 (**Figures 6E, F**).

DISCUSSION

The continuous development of high-throughput sequencing technology allowed a deeper understanding of the genetic and epigenetic pathological characteristics of tumors, including LUAD. A variety of clustering and deconvolution algorithms are used to determine the state of TME (especially the immune TME) through the high-throughput RNA sequencing data, resulting in a great improvement of tumor treatment and prognosis (34). Moreover and more importantly, the potential association of the changes in tumor immune microenvironment with the gene expression changes may be helpful in finding the key genes leading to tumor immune infiltration. These key genes may represent novel biomarkers to predict the clinical outcome of patients or potential immunotherapeutic targets to develop effective anti-tumor drugs. However, most of the studies available based on bioinformatics only focus on algorithms to screen DEGs, lacking the in-depth investigation of the interaction network among these key genes, or single-source data creating an overfitting model with a weak universal survival prediction.

In this work the tumor immune status of LUAD patients in the TCGA database at the genetic level was considered. Based on ssGSEA algorithm, LUAD patients were divided into high, medium, and low immune infiltration subtype, and the Kaplan-Meyer analysis revealed a better prognosis of the patients with high immune infiltration subtype. These results suggested that a high immune infiltration specifically localized in the tumor might be considered as an anti-tumor factor. The expression of genes implicated in immunotherapy and specific genes of immune cells, along with the abundance of immune cell infiltrates in a tumor, is substantially inversely correlated with tumor purity (35). This aspect underlines the need to consider tumor purity when evaluating the gene expression of markers obtained from tumor transcriptome data. The ESTIMATE algorithm was used to calculate the tumor purity and the immune and stromal score in LUAD, thus, the negative regulation relationship between the immune infiltration state and tumor burden in LUAD was confirmed. Unlike the ssGSEA, CIBERSORT deconvolution algorithm, only focus on the proportion of immune cells in tumors. The CIBERSORT results showed that mainly CD8+ cells, activated CD4 memory cells and M1 macrophages are the ones highly infiltrated in a

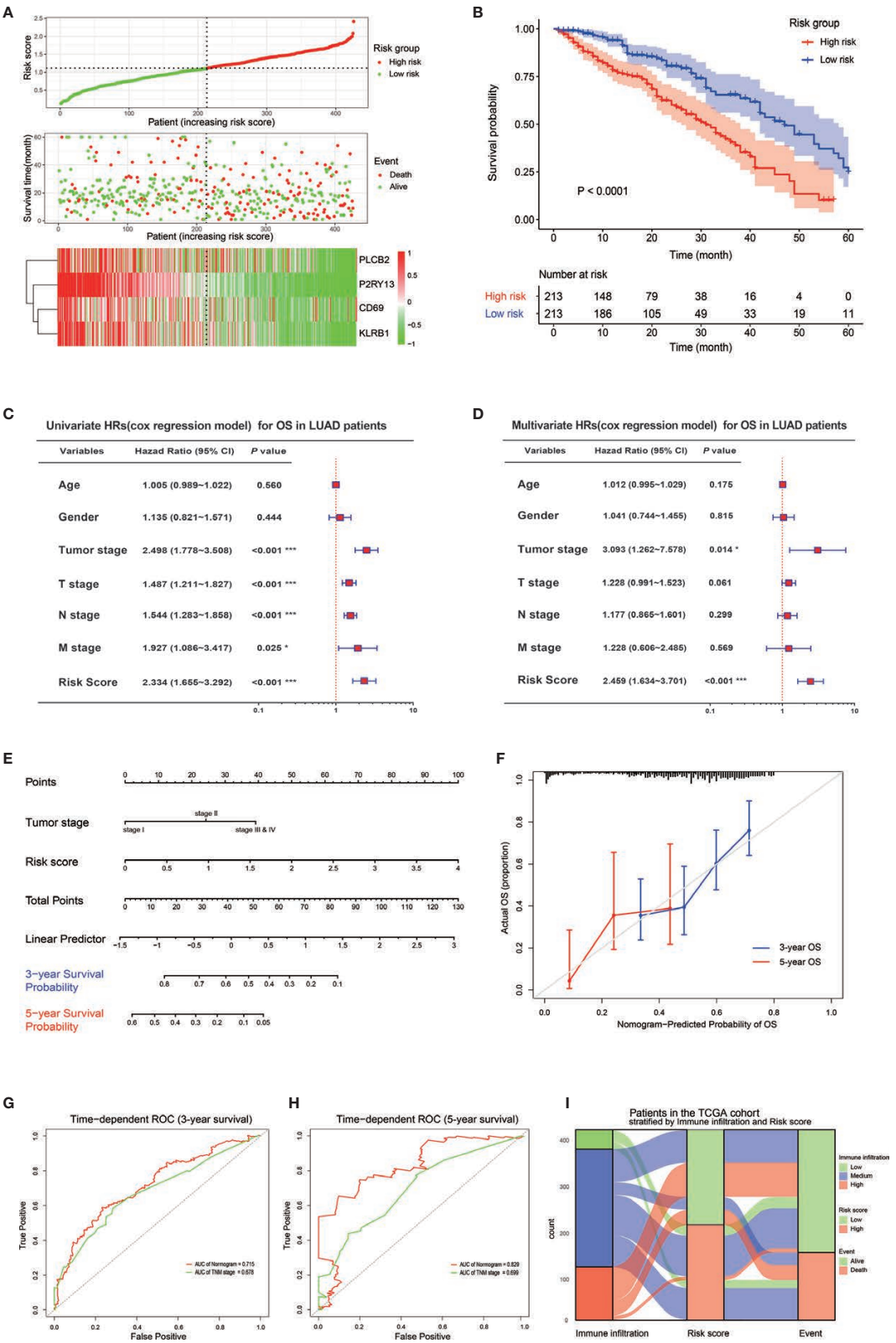

FIGURE 5 | Continued

FIGURE 5 | Prognostic value of the four key genes. **(A)** Risk score signature based on the four key genes. The top graph shows the calculation formula and the value of the risk score; the middle graph shows the distribution of the survival status based on the risk score; the bottom graph shows the cluster heatmap of the four key genes. **(B)** The Kaplan-Meyer survival curve shows the different survival rate between LUAD patients with high-risk score and low-risk score. **(C)** The forest plot shows the result of the univariate cox regression for the overall survival in TCGA cohort. **(D)** The forest plot shows the result of the multivariate cox regression for the overall survival in the TCGA cohort. **(E)** Nomogram based on the multivariate cox regression for the prediction of the 3-year and 5-year survival rates in the TCGA cohort. **(F)** An internal calibration curve shows the fitness between the actual overall survival probability and the nomogram-predicted overall survival probability. **(G, H)** The time-dependent ROCs show the accuracy of the Nomogram and TNM for the 3-year overall survival prediction **(G)** and 5-year overall survival prediction **(H)**. **(I)** The Sankey diagram shows the final survival status of LUAD patients with different immune infiltrations and with different risk scores. *$P < 0.05$; **$P < 0.01$; ***$P < 0.001$.

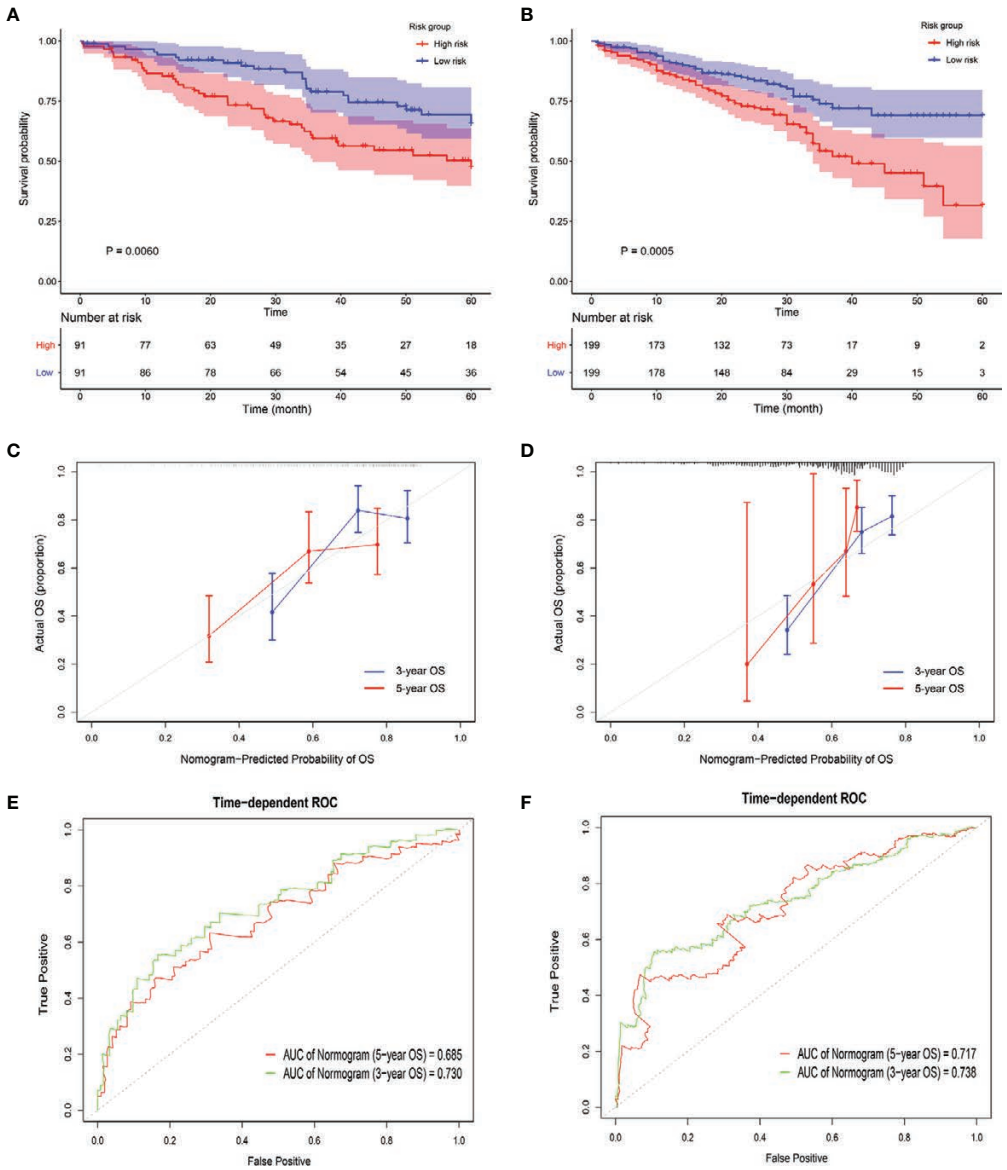

FIGURE 6 | Validation of the prognostic value of the four key genes in the GEO datasets. **(A, B)** The Kaplan-Meyer survival curves show the different survival rate between high-risk group and low-risk group in GSE 41271 **(A)** and GSE 72094 **(B)**. **(C, D)** The external calibration curves show the fitness of the overall survival probability in GSE 41271 **(C)** and in GSE 72094 **(D)**. **(E, F)** The time-dependent ROCs show the accuracy of the 3-year overall survival prediction and 5-year overall survival prediction in GSE 41271 **(E)** and in GSE 72094 **(F)**.

tumor in a condition of high immune infiltration, and these cells are important anti-tumor immune cells (36).

Whether it is tumor immune cells or tumor immune-related genes, there is often a network-based synergistic relationship between them often exists (37–39). If the immune infiltration state of LUAD is classified and confirmed, it is important to evaluate which are the coordinate expression genes, and the correlation between them and the immune infiltration in LUAD. For this reason, the immune infiltration of LUAD in this work was considered as a clinical trait, and the WGCNA algorithm was used to screen the coordinate expressed genes in the form of gene modules that were associated with the immune infiltration of LUAD. A total of 1,671 genes included in two gene modules were screened and the PPI network analysis showed that the hub gene in the two modules were included in the gene set of ssGSEA algorithm. GO and KEGG analysis also confirmed that these genes were mainly enriched in immune-related pathways. These results suggested that the WGCNA method used in our study to screen immune-related genes was effective and reliable.

A further cleaning of the aforementioned 1,671 genes resulted in the selection of 178 genes and their PPI network was constructed by "STRING" website. In this network, some hub genes such as GNB2, GNB4, GNG2, GNGT2, and P2RY13 had more interactional genes and more sufficient evidences of the interactions. These hub genes are all members of the G protein-coupled receptor pathway. The GO enriched analysis revealed that the G protein-coupled purinergic nucleotide receptor activity pathway also ranked third in the molecular function Go terms. The G protein-coupled receptor pathway is nowadays a hot spot in cancer immune research, and some members of GPCRs are actually demonstrated as having a role as prognostic factors in a variety of cancers (40–42).

The LASSO algorithm was used to find independent prognostic molecules and avoid co-linearity between genes since the genes screened by WGCNA are often coordinate expression genes, and four key genes such as CD69, KLRB1, PLCB2, and P2RY13 were finally found. The relationship between CD69 and tumor immunity is known, although it was initially considered as a marker of early activation of T cells and macrophages, but the latest research revealed that it is a surface marker of tissue resident memory T cells, and high infiltration of these cells often indicates a better tumor outcome (43, 44). KLRB1 (also called CD161) is a gene encoding for a surface marker of many subtypes of T cells and NK cells, and its widespread expression is associated with a better prognosis of NSCLC (45, 46). PLCB2 and P2RY13 are members of the phosphatidyl C family and purine subunit family, respectively (47, 48). These two genes are classified as belonging to the GPCRs pathways that are closely related to tumor immunity and despite reports on the relationship between these two genes and tumor immunity are still rare, new progress has been made revealing their relationship with macrophages and NK cells (49, 50). In this study, the expression of these four genes was increased with the increase of LUAD immune infiltration level. The important aspect was that these four genes were correlated with the amount of immune cell infiltration (such as CD69 and M0 macrophage), but also with the expression of immune checkpoint genes (such as KLRB1 and PD-1, P2RY13, and PD-L2) suggesting that these four genes might predict the immunotherapy response and could be potentially considered as new immunotherapeutic targets. These four genes interact with a gene common to all of them, such as S1PR1, which is a core gene of the G protein coupled pathway (51). S1PR1 is usually considered as an oncogene, since it promotes the proliferation, invasion, and metastasis of tumor cells through the STAT3, PI3K/AKT, and CCR signaling pathway in many types of malignant tumors (52–54). However, some recent studies revealed that S1PR1 is also able to promote tumor cell apoptosis, thus, its high expression is an indicator of a good prognosis (55–57). In the present study, our hypothesis was that an interacting gene network was formed among CD69, KLRB1 and GPRCs family members PLCB2, P2RY13, and S1PR1. This gene network further activated the downstream genes in GPRCs signaling pathway, promoting the immune infiltration in LUAD tissues and the consequent anti-tumor effect of immune cells. This finding provided a new basis clarifying the mechanism of immune infiltration in LUAD, and providing a potential therapeutic target for the immunotherapy against LUAD.

Finally, these four genes were used to construct a risk score signature in training cohort to explore the role of these four genes in the clinical prognosis of LUAD. This risk score signature allowed the identification of high-risk LUAD patients with poor prognosis. This score signature was also used as an independent prognostic index to construct an effective Nomogram prediction model combined with the tumor stage in LUAD TCGA cohort. This model could predict the 3-year and 5-year survival rates of TCGA LUAD with a high accuracy. The ROC curves revealed that the AUC of the Nomogram were better than AUC of the TNM stage. Tumor heterogeneity is an unavoidable problem, thus, it should be considered in all tumor studies, being also a problem in the prognostic prediction of LUAD patients (58, 59). The model was externally validated in two GEO datasets using different microarray platforms to further improve the universality and robustness of the Nomogram in LUAD samples. The validation further confirmed the prognostic value of these four genes and the ability of the Nomogram to predict the survival rates in LUAD patients. These results indicated that these four LUAD genes had a universal prognostic value, thus, they might be potentially considered for further clinical applications.

Our study had several limitations that should be acknowledged while indicating necessary future studies in the relevant areas. As shown in the results, the prognostic significance of the four genes and S1PR1 were found in some of the examined GEO datasets, not all. It may be due to the limitations of the data obtained from open datasets. The data were shared by studies using inconsistent experimental study design, such as different detected objects, various detected platforms, and diverse sample sizes. For example, the GSE50081 only focused on early-stage NSCLC, and the GSE41271 and the GSE42127 did not contain S1PR1 detection probes. The heterogeneity of tumors, which was also hard to control using open data, may have impacted and resulted in these

inconsistent findings among datasets as well. Specifically, the individual differences, difference of tumor development stages, and difference of tumor sites could all affect the analysis results of immune cell infiltration and gene expression levels. All these factors can be impactful to the data analysis, lower the validation of the prognostic value of these genes, and thus affect the universality of the prognostic prediction model. For future studies, the clinical application value of this gene signature needs to be further verified in more independent LUAD cohorts. Our research team has just launched a new validation study at the protein level based on an independent cohort of which the samples are being collected from our own hospital. Meanwhile, a larger sample size should be considered in future studies to help reduce the interference caused by tumor heterogeneity and ensure statistic power.

CONCLUSIONS

Our study identified four key genes significantly correlated with tumor immune infiltration and in LUAD and its prognosis. These four genes formed a network with S1PR1, which is a mutual interaction gene, activating the downstream genes in GPRCs to promote the immune infiltration in LUAD. The constructed risk score signature based on the key genes could be used as an independent biomarker to predict the prognosis of LUAD. Therefore, the screening, identification, and analysis of these four genes made a contribution in the understanding of GPCRs and the immune infiltration in LUAD, opening up new perspectives for more effective immunotherapeutic strategies.

DATA AVAILABILITY STATEMENT

The datasets presented in this study can be found in online repositories. The names of the repository/repositories and accession number(s) can be found in the article/ **Supplementary Material**.

AUTHOR CONTRIBUTIONS

YW and FX conceived, designed, and wrote the manuscript. LQ and PY analyzed the data. YC and XZ helped with manuscript and data review. All authors contributed to the article and approved the submitted version.

FUNDING

This study was funded by the National Natural Science Foundation of China (Grant No. 81701213), the Natural Science Foundation of Jiangsu Province of China (Grant No. BK20170369) and Science and Technology Project of Nantong (Grant No. JCZ20209).

SUPPLEMENTARY MATERIAL

The Supplementary Material for this article can be found online at: https://www.frontiersin.org/articles/10.3389/fonc.2020.622251/full#supplementary-material

REFERENCES

1. Bray F, Ferlay J, Soerjomataram I, Siegel RL, Torre LA, Jemal A. Global cancer statistics 2018: GLOBOCAN estimates of incidence and mortality worldwide for 36 cancers in 185 countries. *CA Cancer J Clin* (2018) 68(6):394–424. doi: 10.3322/caac.21492
2. Siegel RL, Miller KD, Jemal A. Cancer statistics, 2016. *CA Cancer J Clin* (2016) 66(1):7–30. doi: 10.3322/caac.21332
3. Miller KD, Siegel RL, Lin CC, Mariotto AB, Kramer JL, Rowland JH, et al. Cancer treatment and survivorship statistics, 2016. *CA Cancer J Clin* (2016) Jul66(4):271–89. doi: 10.3322/caac.21349
4. Topalian SL, Taube JM, Anders RA, Pardoll DM. Mechanism-driven biomarkers to guide immune checkpoint blockade in cancer therapy. *Nat Rev Cancer* (2016) 16(5):275–87. doi: 10.1038/nrc.2016.36
5. Li B, Chan HL, Chen P. Immune Checkpoint Inhibitors: Basics and Challenges. *Curr Med Chem* (2019) 26(17):3009–25. doi: 10.2174/0929867324666170804143706
6. Sasidharan Nair V, Elkord E. Immune checkpoint inhibitors in cancer therapy: a focus on T-regulatory cells. *Immunol Cell Biol* (2018) 96(1):21–33. doi: 10.1111/imcb.1003
7. Sharma P, Hu-Lieskovan S, Wargo JA, Ribas A. Primary, Adaptive, and Acquired Resistance to Cancer Immunotherapy. *Cell* (2017) 168(4):707–23. doi: 10.1016/j.cell.2017.01.017
8. Quail DF, Joyce JA. Microenvironmental regulation of tumor progression and metastasis. *Nat Med* (2013) Nov19(11):1423–37. doi: 10.1038/nm.3394
9. Osipov A, Saung MT, Zheng L, Murphy AG. Small molecule immunomodulation: the tumor microenvironment and overcoming immune escape. *J Immunother Cancer* (2019) 7(1):224. doi: 10.1186/s40425-019-0667-0
10. Saleh R, Elkord E. Acquired resistance to cancer immunotherapy: Role of tumor-mediated immunosuppression. *Semin Cancer Biol* (2020) 65:13–27. doi: 10.1016/j.semcancer.2019.07.017
11. Giraldo NA, Sanchez-Salas R, Peske JD, Vano Y, Becht E, Petitprez F, et al. The clinical role of the TME in solid cancer. *Br J Cancer* (2019) 120(1):45–53. doi: 10.1038/s41416-018-0327-z
12. Schulz M, Salamero-Boix A, Niesel K, Alekseeva T, Sevenich L. Microenvironmental Regulation of Tumor Progression and Therapeutic Response in Brain Metastasis. *Front Immunol* (2019) 10:1713. doi: 10.3389/fimmu.2019.01713
13. Belli C, Trapani D, Viale G, D'Amico P, Duso BA, Della Vigna P, et al. Targeting the microenvironment in solid tumors. *Cancer Treat Rev* (2018) 65:22–32. doi: 10.1016/j.ctrv.2018.02.004
14. Hinshaw DC, Shevde LA. The Tumor Microenvironment Innately Modulates Cancer Progression. *Cancer Res* (2019) 79(18):4557–66. doi: 10.1158/0008-5472.CAN-18-3962
15. Bacolod MD, Barany F, Fisher PB. Can CpG methylation serve as surrogate markers for immune infiltration in cancer? *Adv Cancer Res* (2019) 143:351–84. doi: 10.1016/bs.acr.2019.03.007
16. Pinto R, Petriella D, Lacalamita R, Montrone M, Catino A, Pizzutilo P, et al. KRAS-Driven Lung Adenocarcinoma and B Cell Infiltration: Novel Insights for Immunotherapy. *Cancers (Basel)* (2019) 11(8):1145. doi: 10.3390/cancers11081145
17. Seo JS, Kim A, Shin JY, Kim YT. Comprehensive analysis of the tumor immune micro-environment in non-small cell lung cancer for efficacy of

checkpoint inhibitor. *Sci Rep* (2018) 8(1):14576. doi: 10.1038/s41598-018-32855-8
18. Ni KW, Sun GZ. The identification of key biomarkers in patients with lung adenocarcinoma based on bioinformatics. *Math Biosci Eng* (2019) 16 (6):7671–87. doi: 10.3934/mbe.2019384
19. Yu Y, Tian X. Analysis of genes associated with prognosis of lung adenocarcinoma based on GEO and TCGA databases. *Medicine (Baltimore)* (2020) 99(19):e20183. doi: 10.1097/MD.0000000000020183
20. Wang Z, Xu H, Zhu L, He T, Lv W, Wu Z. Establishment and Evaluation of a 6-Gene Survival Risk Assessment Model Related to Lung Adenocarcinoma Microenvironment. *BioMed Res Int* (2020) 2020:6472153. doi: 10.1155/2020/6472153
21. Rooney MS, Shukla SA, Wu CJ, Getz G, Hacohen N. Molecular and genetic properties of tumors associated with local immune cytolytic activity. *Cell* (2015) 160(1-2):48–61. doi: 10.1016/j.cell.2014.12.033
22. Aran D, Lasry A, Zinger A, Biton M, Pikarsky E, Hellman A, et al. Widespread parainflammation in human cancer. *Genome Biol* (2016) 17(1):145. doi: 10.1186/s13059-016-0995-z
23. Wong HS, Chang CM, Liu X, Huang WC, Chang WC. Characterization of cytokinome landscape for clinical responses in human cancers. *Oncoimmunology* (2016) 5(11):e1214789. doi: 10.1080/2162402X.2016.1214789
24. Charoentong P, Finotello F, Angelova M, Mayer C, Efremova M, Rieder D, et al. Pan-cancer Immunogenomic Analyses Reveal Genotype-Immunophenotype Relationships and Predictors of Response to Checkpoint Blockade. *Cell Rep* (2017) 18(1):248–62. doi: 10.1016/j.celrep.2016.12.019
25. De Simone M, Arrigoni A, Rossetti G, Gruarin P, Ranzani V, Politano C, et al. Transcriptional Landscape of Human Tissue Lymphocytes Unveils Uniqueness of Tumor-Infiltrating T Regulatory Cells. *Immunity* (2016) 45 (5):1135–47. doi: 10.1016/j.immuni.2016.10.021
26. Subramanian A, Tamayo P, Mootha VK, Mukherjee S, Ebert BL, Gillette MA, et al. Gene set enrichment analysis: a knowledge-based approach for interpreting genome-wide expression profiles. *Proc Natl Acad Sci U S A* (2005) 102(43):15545–50. doi: 10.1073/pnas.0506580102
27. Yoshihara K, Shahmoradgoli M, Martínez E, Vegesna R, Kim H, Torres-Garcia W, et al. Inferring tumour purity and stromal and immune cell admixture from expression data. *Nat Commun* (2013) 4:2612. doi: 10.1038/ncomms3612
28. Newman AM, Liu CL, Green MR, Gentles AJ, Feng W, Xu Y, et al. Robust enumeration of cell subsets from tissue expression profiles. *Nat Methods* (2015) 12(5):453–7. doi: 10.1038/nmeth.3337
29. Langfelder P, Horvath S. WGCNA: an R package for weighted correlation network analysis. *BMC Bioinf* (2008) 9:559. doi: 10.1186/1471-2105-9-559
30. von Mering C, Jensen LJ, Snel B, Hooper SD, Krupp M, Foglierini M, et al. STRING: known and predicted protein-protein associations, integrated and transferred across organisms. *Nucleic Acids Res* (2005) 33(Database issue): D433–7. doi: 10.1093/nar/gki005
31. Ritchie ME, Phipson B, Wu D, Hu Y, Law CW, Shi W, et al. limma powers differential expression analyses for RNA-sequencing and microarray studies. *Nucleic Acids Res* (2015) 43(7):e47. doi: 10.1093/nar/gkv007
32. Gao J, Kwan PW, Shi D. Sparse kernel learning with LASSO and Bayesian inference algorithm. *Neural Netw* (2010) 23(2):257–64. doi: 10.1016/j.neunet.2009.07.001
33. Iasonos A, Schrag D, Raj GV, Panageas KS. How to build and interpret a nomogram for cancer prognosis. *J Clin Oncol* (2008) 26(8):1364–70. doi: 10.1200/JCO.2007.12.9791
34. Isaeva OI, Sharonov GV, Serebrovskaya EO, Turchaninova MA, Zaretsky AR, Shugay M, et al. Intratumoral immunoglobulin isotypes predict survival in lung adenocarcinoma subtypes. *J Immunother Cancer* (2019) 7(1):279. doi: 10.1186/s40425-019-0747-1
35. Rhee JK, Jung YC, Kim KR, Yoo J, Kim J, Lee YJ, et al. Impact of Tumor Purity on Immune Gene Expression and Clustering Analyses across Multiple Cancer Types. *Cancer Immunol Res* (2018) 6(1):87–97. doi: 10.1158/2326-6066.CIR-17-0201
36. Gajewski TF, Schreiber H, Fu YX. Innate and adaptive immune cells in the tumor microenvironment. *Nat Immunol* (2013) 14(10):1014–22. doi: 10.1038/ni.2703
37. Zhong Z, Hong M, Chen X, Xi Y, Xu Y, Kong D, et al. Transcriptome analysis reveals the link between lncRNA-mRNA co-expression network and tumor immune microenvironment and overall survival in head and neck squamous cell carcinoma. *BMC Med Genomics* (2020) 13(1):57. doi: 10.1186/s12920-020-0707-0
38. Schelker M, Feau S, Du J, Ranu N, Klipp E, MacBeath G, et al. Estimation of immune cell content in tumour tissue using single-cell RNA-seq data. *Nat Commun* (2017) 8(1):2032. doi: 10.1038/s41467-017-02289-3
39. Hubel P, Urban C, Bergant V, Schneider WM, Knauer B, Stukalov A, et al. A protein-interaction network of interferon-stimulated genes extends the innate immune system landscape. *Nat Immunol* (2019) 20(4):493–502. doi: 10.1038/s41590-019-0323-3
40. Sriram K, Moyung K, Corriden R, Carter H, Insel PA. GPCRs show widespread differential mRNA expression and frequent mutation and copy number variation in solid tumors. *PloS Biol* (2019) 17(11):e3000434. doi: 10.1371/journal.pbio.3000434
41. Wu V, Yeerna H, Nohata N, Chiou J, Harismendy O, Raimondi F, et al. Illuminating the Onco-GPCRome: Novel G protein-coupled receptor-driven oncocrine networks and targets for cancer immunotherapy. *J Biol Chem* (2019) 294(29):11062–86. doi: 10.1074/jbc.REV119.005601
42. Xiong Z, Xiong Y, Liu H, Li C, Li X. Identification of purity and prognosis-related gene signature by network analysis and survival analysis in brain lower grade glioma. *J Cell Mol Med* (2020) 24(19):11607–12. doi: 10.1111/jcmm.15805.PMID:32869484
43. Marzio R, Jirillo E, Ransijn A, Mauël J, Corradin SB. Expression and function of the early activation antigen CD69 in murine macrophages. *J Leukoc Biol* (1997) 62(3):349–55. doi: 10.1002/jlb.62.3.349
44. Mami-Chouaib F, Blanc C, Corgnac S, Hans S, Malenica I, Granier C, et al. Resident memory T cells, critical components in tumor immunology. *J Immunother Cancer* (2018) 6(1):87. doi: 10.1186/s40425-018-0399-6
45. Gentles AJ, Newman AM, Liu CL, Bratman SV, Feng W, Kim D, et al. The prognostic landscape of genes and infiltrating immune cells across human cancers. *Nat Med* (2015) 21(8):938–45. doi: 10.1038/nm.3909
46. Braud VM, Biton J, Becht E, Knockaert S, Mansuet-Lupo A, Cosson E, et al. Expression of LLT1 and its receptor CD161 in lung cancer is associated with better clinical outcome. *Oncoimmunology* (2018) 7(5):e1423184. doi: 10.1080/2162402X.2017.1423184
47. Zhang T, Song X, Liao X, Wang X, Zhu G, Yang C, et al. Distinct Prognostic Values of Phospholipase C Beta Family Members for Non-Small Cell Lung Carcinoma. *BioMed Res Int* (2019) 2019:4256524. doi: 10.1155/2019/4256524
48. Maiga A, Lemieux S, Pabst C, Lavallée VP, Bouvier M, Sauvageau G, et al. Transcriptome analysis of G protein-coupled receptors in distinct genetic subgroups of acute myeloid leukemia: identification of potential disease-specific targets. *Blood Cancer J* (2016) 6(6):e431. doi: 10.1038/bcj.2016.36
49. Xiao W, Kawakami Y, Kawakami T. Immune regulation by phospholipase C-β isoforms. *Immunol Res* (2013) 56(1):9–19. doi: 10.1007/s12026-012-8341-3
50. Akhtari M, Zargar SJ, Vojdanian M, Ashraf-Ganjouei A, Javinani A, Hamzeh E, et al. P2 receptors mRNA expression profiles in macrophages from ankylosing spondylitis patients and healthy individuals. *Int J Rheum Dis* (2020) 23(3):350–7. doi: 10.1111/1756-185X.13783
51. Spiegel S, Milstien S. The outs and the ins of sphingosine-1-phosphate in immunity. *Nat Rev Immunol* (2011) 11(6):403–15. doi: 10.1038/nri2974
52. Liu Y, Zhi Y, Song H, Zong M, Yi J, Mao G, et al. S1PR1 promotes proliferation and inhibits apoptosis of esophageal squamous cell carcinoma through activating STAT3 pathway. *J Exp Clin Cancer Res* (2019) 38(1):369. doi: 10.1186/s13046-019-1369-7
53. Rostami N, Nikkhoo A, Ajjoolabady A, Azizi G, Hojjat-Farsangi M, Ghalamfarsa G, et al. S1PR1 as a Novel Promising Therapeutic Target in Cancer Therapy. *Mol Diagn Ther* (2019) 23(4):467–87. doi: 10.1007/s40291-019-00401-5
54. Balaji Ragunathrao VA, Anwar M, Akhter MZ, Chavez A, Mao Y, Natarajan V, et al. Sphingosine-1-Phosphate Receptor 1 Activity Promotes Tumor Growth by Amplifying VEGF-VEGFR2 Angiogenic Signaling. *Cell Rep* (2019) 29(11):3472–3487.e4. doi: 10.1016/j.celrep.2019.11.036
55. Lei FJ, Cheng BH, Liao PY, Wang HC, Chang WC, Lai HC, et al. Survival benefit of sphingosin-1-phosphate and receptors expressions in breast cancer patients. *Cancer Med* (2018) 7(8):3743–54. doi: 10.1002/cam4.1609
56. Gao C, Zhuang J, Li H, Liu C, Zhou C, Liu L, et al. Exploration of methylation-driven genes for monitoring and prognosis of patients with lung

adenocarcinoma. *Cancer Cell Int* (2018) 18:194. doi: 10.1186/s12935-018-0691-z

57. Patrussi L, Capitani N, Martini V, Pizzi M, Trimarco V, Frezzato F, et al. Enhanced Chemokine Receptor Recycling and Impaired S1P1 Expression Promote Leukemic Cell Infiltration of Lymph Nodes in Chronic Lymphocytic Leukemia. *Cancer Res* (2015) 75(19):4153–63. doi: 10.1158/0008-5472.CAN-15-0986
58. Sun J, Zhao T, Zhao D, Qi X, Bao X, Shi R, et al. Development and validation of a hypoxia-related gene signature to predict overall survival in early-stage lung adenocarcinoma patients. *Ther Adv Med Oncol* (2020) 12:1758835920937904. doi: 10.1177/1758835920937904
59. Song C, Guo Z, Yu D, Wang Y, Wang Q, Dong Z, et al. A Prognostic Nomogram Combining Immune-Related Gene Signature and Clinical Factors Predicts Survival in Patients With Lung Adenocarcinoma. *Front Oncol* (2020) 10:1300. doi: 10.3389/fonc.2020.01300

Conflict of Interest: The authors declare that the research was conducted in the absence of any commercial or financial relationships that could be construed as a potential conflict of interest.

Copyright © 2021 Wang, Qiu, Chen, Zhang, Yang and Xu. This is an open-access article distributed under the terms of the Creative Commons Attribution License (CC BY). The use, distribution or reproduction in other forums is permitted, provided the original author(s) and the copyright owner(s) are credited and that the original publication in this journal is cited, in accordance with accepted academic practice. No use, distribution or reproduction is permitted which does not comply with these terms.

frontiers in Oncology

ORIGINAL RESEARCH
published: 22 February 2021
doi: 10.3389/fonc.2021.618187

CCR4, *CCR8*, and *P2RY14* as Prognostic Factors in Head and Neck Squamous Cell Carcinoma Are Involved in the Remodeling of the Tumor Microenvironment

Liangliang Meng[1,2,3†], Xiaoxi He[4†], Quan Hong[5], Bo Qiao[6], Xiao Zhang[2], Bin Wu[2,3], Xiaobo Zhang[2], Yingtian Wei[2], Jing Li[2], Zhaoxiang Ye[4] and Yueyong Xiao[2*]*

[1] Medical School of Chinese PLA, Beijing, China, [2] Department of Radiology, The First Medical Centre, Chinese PLA General Hospital, Beijing, China, [3] Department of Radiology, Chinese PAP Beijing Corps Hospital, Beijing, China, [4] Department of Radiology, Tianjin Medical University Cancer Institute and Hospital, National Clinical Research Center for Cancer, Tianjin's Clinical Research Center for Cancer, Key Laboratory of Cancer Prevention and Therapy, Tianjin, China, [5] Department of Nephrology, The First Medical Center, Chinese PLA General Hospital, Chinese PLA Institute of Nephrology, State Key Laboratory of Kidney Diseases, National Clinical Research Center of Kidney Diseases, Beijing, China, [6] Department of Stomatology, The First Medical Center, Chinese PLA General Hospital, Beijing, China

The tumor microenvironment (TME) plays a critical role in the initiation and progression of cancer. However, the specific mechanism of its regulation in head and neck squamous cell carcinoma (HNSCC) remains unclear. In this study, we first applied the ESTIMATE method to calculate the immune and stromal scores in patients' tumor tissues from The Cancer Genome Atlas (TCGA) database. GSE41613, GSE30784, and GSE37991 data sets from the Gene Expression Omnibus (GEO) database were recruited for further validation. Differentially expressed genes (DEGs) were identified and then analyzed by Cox regression analysis and protein-protein interaction (PPI) network construction. DEGs significantly associated with prognosis and TME will be identified as hub genes. These genes were also validated at the protein level by immunohistochemical analysis of 10 pairs of primary tumor tissues and the adjacent normal tissues from our institution. The relationship between hub genes expression and immune cell fraction estimated by CIBERSORT software was also examined. 275 DEGs were significantly associated with TME. *CCR4, CCR8*, and *P2RY14* have then identified as hub genes by intersection Cox and PPI analysis. Further investigation revealed that the expression of *CCR4, CCR8*, and *P2RY14* was negatively correlated with clinicopathological characteristics (clinical stage, T stage) and positively associated with survival in HNSCC patients, especially in male patients. The expression of *CCR8* and *P2RY14* was lower in males than in females. *CCR8* and *P2RY14* were differentially expressed in tumor tissues than normal tissues, and the results were validated at the protein level by immunohistochemistry experiments. Gene set enrichment analysis (GSEA) showed that the high expression groups' hub genes were mainly enriched for immune-related activities. In the low-expression groups, genes were primarily enriched in metabolic pathways. CIBERSORT results showed that the

OPEN ACCESS

Edited by:
Keqiang Chen,
National Cancer Institute at Frederick, United States

Reviewed by:
Ruoxi Yuan,
Hospital for Special Surgery, United States
Xiang Yi,
Ruijin Hospital, China
Hanli Xu,
Beijing Jiaotong University, China

***Correspondence:**
Zhaoxiang Ye
yezhaox@hotmail.com
Yueyong Xiao
yueyongxiao@yahoo.com

[†]These authors share first authorship

Specialty section:
This article was submitted to Cancer Immunity and Immunotherapy, a section of the journal Frontiers in Oncology

Received: *27 November 2020*
Accepted: *06 January 2021*
Published: *22 February 2021*

Citation:
Meng L, He X, Hong Q, Qiao B, Zhang X, Wu B, Zhang X, Wei Y, Li J, Ye Z and Xiao Y (2021) CCR4, CCR8, and P2RY14 as Prognostic Factors in Head and Neck Squamous Cell Carcinoma Are Involved in the Remodeling of the Tumor Microenvironment. Front. Oncol. 11:618187. doi: 10.3389/fonc.2021.618187

expression of these genes was all negatively correlated with the fraction of memory B cells and positively correlated with the fraction of the other four cells, including naive B cells, resting T cells CD4 memory, T cells follicular helper, and T cells regulatory (Tregs). The results suggest that *CCR4, CCR8*, and *P2RY14* may be responsible for maintaining the immune dominance of TME, thus leading to a better prognosis.

Keywords: tumor microenvironment, squamous cell carcinoma, survival, immune, gene

INTRODUCTION

The most common pathologic type of tumor occurring in the head and neck region is mucosal squamous cell carcinoma, which mainly affects the oral mucosa, palate, tongue, oropharynx, hypopharynx, larynx, and other parts (1). The global incidence of head and neck squamous cell carcinoma (HNSCC) has risen significantly and is estimated to increase by 30% until 2030 (1.08 million new cases annually) (https://gco.iarc.fr/) (2, 3). The 5-year survival rate for patients with HNSCC is less than 50% before 2014 (4), primarily because approximately 80% to 90% of patients with advanced HNSCC develop local recurrence or distant metastasis (5, 6). Besides, patients with HNSCC have the second-highest suicide rate, less than patients with pancreatic cancer, which may be attributed to excessive stress and low life quality (7). Treatment strategies for HNSCC vary depending on the site of disease, disease stage, etc., and mainly include surgery (8), local radiotherapy (9), and systemic chemotherapy (10). Immunotherapy, especially immune checkpoint inhibitors, have also shown encouraging results in the advanced tumor (11, 12). However, for advanced squamous cell carcinoma, the currently existing therapies were of limited benefit.

Tumor microenvironment (TME) is the internal environment for the production and growth of tumor cells, which provides conditions for the initiation, proliferation, invasion, and metastasis of the tumor. It is closely related to the survival of tumor cells (13, 14). These immune cells and related stromal components, recruited and activated by tumor cells, form a tumor-suppressive inflammatory microenvironment in the early stages of tumor colonization or growth, thereby impeding tumor progression. However, after continuous tumor antigen stimulation and immune activation, the relevant effector cells in the microenvironment are in a state of depletion or remodeling. They cannot perform their normal functions or even promote tumors' malignant manifestation, resulting in an immunosuppressive microenvironment (15). According to most previous studies, multiple immune cells and cytokines in the tumor microenvironment are closely associated with tumor prognosis (16). Currently, immunotherapy has achieved great success and long-term clinical benefits in treating various types of cancer. However, a significant proportion of patients still have limited or no response to immunotherapy. Strong immunosuppressive TME will cause tumor-reactive CD8+ T cells exhausted and lose their ability to eliminate cancer cells, thus reducing the effect of immunotherapy (15).

To investigate the TME status in patients with HNSCC and the underlying mechanism of prognostic influence, a series of analyses have been conducted around the relationship between TME and prognosis. In the present study, we used ESTIMATE software to analyze immune and stromal components' scores in tumor tissues. The relationships between microenvironment and tumor prognosis in HNSCC were further explored through prognostic-related Cox regression analysis and TME-associated protein interaction networks (PPI) to search for predictive hub genes significantly associated with TME. CIBERSORT software was used to analyze the relative fraction of 22 immune cells in tumor tissues. The relationships between the expression of hub genes and the fraction of these tumor-infiltrating immune cells were also further analyzed.

MATERIALS AND METHODS

Data Sources

The level 3 HTSeq-FPKM RNA-seq expression data and corresponding clinical data of HNSCC patients were retrieved from a data set of the Cancer Genome Atlas database (TCGA-HNSC) (https://portal.gdc.cancer.gov). A total of 546 RNA-seq expression data, including 502 tumor tissues and 44 normal tissues, were included in TCGA-HNSC data set, and were applied in the following analyses. A total of 499 patients had both clinical data containing survival information and gene expression data included for survival analysis (**Table S1**). GSE41613 data set retrieved from the Gene Expression Omnibus (GEO) database (http://www.ncbi.nlm.nih.gov/geo) with both expression data and the corresponding survival information of 97 patients were recruited for external survival validation. However, GSE41613 data set does not include gene expression data from normal tissues. Therefore, GSE30784 and GSE37991 data sets from the GEO database with the expression data of both tumor and normal tissues were then used for external RNA-seq expression validation. The GSE30784 data set includes gene expression data from 167 tumor tissues and 45 normal controls. A total of 80 tumor and non-tumor pair-wise samples obtained from 40 male oral squamous cell cancer (OSCC) patients were recruited in the GSE37991.

Clinical Samples for Immunohistochemical Staining

To validate the target genes' protein levels, we obtained a total of 10 pairs of primary tumor tissues and the corresponding adjacent normal tissues from OSCC patients who underwent surgical resection at the Department of Stomatology, Chinese PLA General Hospital, between March 2020 and July 2020. The location of tumor occurrence in 10 patients included six cases of the mouth's fundus, 4 cases of the gingiva. There were seven cases in

males and three cases in females. All patients had postoperative pathology confirmed as oral squamous cell carcinoma. All patients underwent surgery prior to chemotherapy or radiotherapy. All samples were used for immunohistochemical staining. Our study was conducted following the Declaration of Helsinki and approved by the Chinese PLA General Hospital's Ethics Committee. All patients signed an informed consent form.

Scores for TME Using ESTIMATE Package

The ratio of immune and stromal cells in the TME of each sample was calculated using the ESTIMATE package (Version 1.0.13) based on the R software version 3.6.1. The data used were HTSeq-FPKM RNA-seq expression data. Results are presented in the form of three scores, including ImmuneScore, StromalScore, and ESTIMATEScore.The higher the respective score, the greater the ratios of the corresponding components in the TME. If the overall score is higher, the proportion of tumor cells in the tumor tissue is lower with lower tumor purity.

DEGs Between High- and Low-Score Groups Regarding ImmuneScore and StromalScore

The 502 tumor samples were labeled as high scores or low scores based on the median value of ImmuneScore or StromalScore, respectively. DEGs were obtained by performing differential analysis of gene expression between groups using the "limma" package based on R software. DEGs with a log2(folder change) >1 and a false discovery rate (FDR) adjusted *P*-value < 0.05 were considered statistically significant. Genes that were differentially expressed in both immune and stromal components were included in the next step of the analysis. A total of 275 DEGs associated with changes in the TME were included in the next stage of analysis after matching.

Survival Analysis

Survival analysis was performed by applying the R software package "survminer" (Version 0.4.7) and "survival" (Version 2.44.1.1). Patients included in the survival analysis must have both gene expression data and corresponding survival clinical data. A total of 499 individuals were eventually included in the survival analysis. Tumors were categorized into high and low scoring groups based on the above microenvironmental scores, and the survival differences between the groups were compared. Also, patients were grouped according to their gender, followed by survival analysis. Survival curves were plotted using the Kaplan-Meier method. A *P* value < 0.05 of the log-rank test was considered statistically significant.

Gene Ontology (GO) and The Kyoto Encyclopedia of Genes and Genomes (KEGG) Pathway Functional Enrichment Analysis

GO and KEGG enrichment analysis was performed utilizing DEGs. We completed the GO and KEGG pathway analysis using R packages ("enrichplot," "clusterProfiler," and "ggplot2") (17). We used both *P*-value < 0.05 and FDR adjusted *P*-value < 0.05 as the threshold for GO and KEGG enrichment analysis.

Protein-Protein Interaction (PPI) Network of DEGs and Hub Genes

DEGs that are significantly associated with TME were used to construct the PPI network to analyze the model's intrinsic function. The PPI network construction was based on the STRING database (https://string-db.org/), and we subsequently applied Cytoscape software (version:3.8.0) for the reconstruction and visualization of the network. Nodes with the confidence of an interactive relationship > 0.7 were used for building the network.

After constructing the PPI, the core genes of the network need to be identified. We counted the number of neighboring nodes for each gene and selected the top 30 genes with the most neighboring nodes as the PPI network's core genes.

Prognosis-Related Genes in DEGs

First, Univariate Cox regression analysis was used to identify the genes associated with prognosis. A forest plot was constructed based on the Cox analysis. *P* <0.05 indicated a significant association with prognosis. Hazard Ratio (HR) >1 indicated a high-risk gene. Kaplan–Meier test was also used. Patients were divided into two groups with high and low expression according to the median value of gene expression to compare whether there was a difference in survival between them. The genes that were significant by both methods were used as the final prognosis-related genes.

Gene Set Enrichment Analysis (GSEA)

GSEA is used to assess genes' distribution trends in a predefined set of genes in a gene set sequenced for phenotypic relevance and determine their contribution to the phenotype (18). We applied the GSEA software (Version 4.0.3, http://software.broadinstitute.org/gsea/) with 1,000 phenotype permutations for GSEA enrichment analysis. The statistically significant gene sets threshold was set to Nominal *P*-value < 0.05 with an FDR adjusted *P*-value < 0.25. We classified the patients into two groups according to the median value of a target gene. We then performed a GESA analysis to compare the pathways of differential enrichment between the two groups. MSigDB oncogenic signatures gene sets (version 7.1, https://www.gsea-msigdb.org/gsea/downloads.jsp) was applied in the GSEA analysis.

Estimation of Immune Cell Abundance in Tumor Tissue

To analyze whether there were differences in the immune cell abundance of tumor tissue between High and low expression groups of hub genes, we used CIBERSORT (https://cibersort.stanford.edu/) to evaluate the relative abundance of predefined cell types in mixed solid tissues. The data used were normalized FPKM gene expression data of tumor tissue. We used the default LM22 leukocyte gene signature matrix from the CIBERSORT website. LM22 contains 547 genes distinguishing 22 types of immune-related cells. Disabling quantile normalization was checked. We set the number of permutations to 1000 for robust analyses. CIBERSORT enumerated the relative

proportions of the 22 infiltrating immune cells, including B cells, dendritic cells, T cells, natural killer cells, macrophages, and others.

Differential Expression Analysis of Target Genes

The Wilcox rank-sum test was used to compare the differences in the expression of target genes between tumor and normal tissues. The R package "beeswarm" was used to generate the corresponding expression figures. Besides, we then performed paired differentiation analyses of target gene expression in tumor and normal samples from the same patient using the Wilcoxon rank-sum test. Statistical thresholds were set at $P<0.05$. The figures were generated using the "ggpaired" command of the R package "ggpubr."

Data Sets Validations of the Hub Genes

The relationships between hub genes and prognosis were analyzed in TCGA-HNSC and were validated using the GSE41613 external data set (n = 97) and two randomly generated subsets of TCGA-HNSC (n = 250 and n = 249). Another two external data sets (GSE30784 (n = 212) and GSE37991 (n = 80)) were used to validate the expression of hub genes (CCR4, CCR8, and P2RY14) between normal and tumor tissues. To validate the gender differences, we then divided TCGA-HNSC data set into two sub-data sets by gender (male = 366, female = 133).

Correlation of Target Gene Expression With Clinicopathological Characteristics

The Kruskal-Wallis rank-sum test was used to compare statistical differences between multiple groups. Wilcoxon rank-sum test was used to perform statistical analysis for comparison between two groups. P <0.05 was considered statistically significant. Subsequently, both univariate and multivariate Cox proportional hazards regression analyses of the hub genes and other clinical factors for the overall survival (OS) time were performed in the TCGA cohort.

Immunohistochemical Staining

Tumor tissues and control tissues were fixed with formalin, dehydrated, paraffin-embedded, and cut into 5-μm-thick continuous sections. After dewaxing and hydration, the sections were infiltrated with closed permeabilization solution for 30 min, washed three times with 0.01 mol/L PBS for 3 min each time, blocked with 5% BSA for 1 h, and treated with anti-*CCR8* antibody (ZENBIO, No. 860154) or anti-*P2RY14* antibody (Bioss, Bs-15356R) (diluted to 1:250) in 4°C overnight incubation. After a brief wash with PBS, the antibody was incubated with a horseradish peroxidase-conjugated anti-rabbit IgG antibody (1:500) for 2 h, and the staining was then developed with 0.003% H_2O_2 and 0.03% 3,3′-diaminobenzidine in 0.05 mol/L Tris-HCl. The staining was observed, the dye was poured off, and the color development time was controlled for about 3 to 10 min. The neutral resin was used to seal the slices and then observed and photographed under the microscope. For the quantification, 10 non-overlapping cortical section at a magnification of 400× (high power field, HPF) were counted using Image-pro plus software. Multiple t-test was used to evaluate the difference between tumor and normal samples. The statistical threshold was set at $P<0.05$.

RESULTS

The flowchart for the entire analysis is shown in **Figure 1**.

Clinical Relevance of TME Scores

According to the median value of the TME scores, respectively, 502 patients in TCGA-HNSC data set were stratified into the high- or low-score group. All TME scores analyses did not find a significant correlation with survival ($P > 0.05$) (**Figures 2A–C**). However, we can observe a tendency that patients with higher immune scores have a better prognosis (**Figure 2A**). In addition, we found that female patients had a significantly worse prognosis than male patients ($P < 0.05$) (**Figure 2D**). There was a significant correlation between immune score and T stage ($P < 0.05$) (**Figure 2E**). Immune scores of tumor tissues were significantly lower in male patients than in female patients ($P < 0.05$) (**Figure 2F**). No correlation between tumor immune score and lymph node metastasis in patients was found (**Figure S1A**). No significant correlation between tumor StromalScore and any clinical features was found in TCGA-HNSC data set ($P > 0.05$) (**Figures S1B–D**).

DEGs Between High- and Low-Score Groups Regarding ImmuneScore and StromalScore

The 502 tumor samples were labeled as a high-score or low-score based on the median value of ImmuneScore or StromalScore, respectively. Regarding ImmuneScore, 776 genes were up-regulated, and 161 genes were down-regulated in the high-score group compared to the low-score group. For the stromal component scores, 985 genes were up-regulated, and 63 genes were down-regulated in the high-score group compared to the low-score group. There were 275 genes whose expression was simultaneously and significantly correlated with either the immune component or the stromal component (**Figures 3A, B**).

GO and KEGG Pathway Analyses of the DEGs

Since these 275 DEGs were significantly associated with TME status, we sought to explore these genes' function through GO and KEGG enrichment analysis. Results of GO enrichment analysis revealed that DEGs were enriched significantly in neutrophil activation, neutrophil degranulation, neutrophil-mediated immunity, leukocyte chemotaxis, regulation of inflammatory response, lymphocyte proliferation ($P<0.05$ and FDR adjusted $P<0.05$) (**Figures 3C, D**, **Figure S2A**). Results of KEGG functional enrichment analysis revealed that DEGs were significantly enriched in Cytokine–cytokine receptor interaction, Chemokine signaling pathway, Staphylococcus aureus infection,

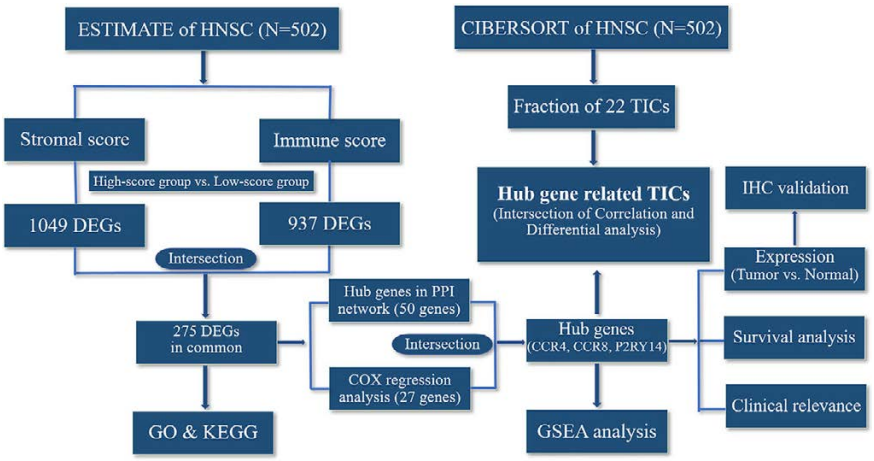

FIGURE 1 | Flowchart of the entire analysis.

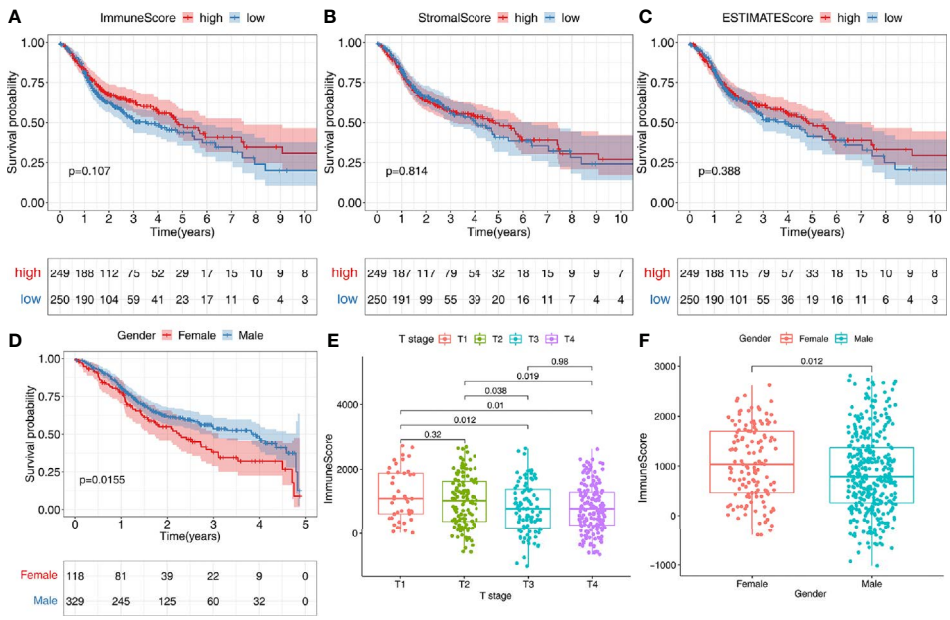

FIGURE 2 | Correlation of tumor microenvironment (TME) with survival and clinical characteristics. **(A–C)** According to the median value of the immune score, stromal score, or estimate score, 502 patients were stratified into the high- or low-score group. Kaplan-Meier curves were used for survival analyses between different score groups in the TCGA-HNSC data set. **(D)** Females have a worse prognosis than male patients with an OS<5 years (P<0.05). **(E)** There was a significant correlation between immune score and T stage (P<0.05). **(F)** Immune scores of tumor tissues were significantly lower in male patients than in female patients (P<0.05).

and others (P < 0.05 and FDR adjusted P<0.05) (**Figures 3E, F**, **Figure S2B**).

Prognosis-Related Genes in DEGs

Univariate Cox regression analysis and the Kaplan–Meier method were both used to identify the genes associated with prognosis. A total of 27 genes were found to be significantly associated with prognosis (P<0.05 in both Cox regression analysis and Kaplan–Meier analysis) (**Figure 4A**).

PPI Network and Hub Genes

With the 275 DEGs, the PPI network construction was based on the STRING database, and we subsequently applied Cytoscape software for the reconstruction and visualization of the network. A total of

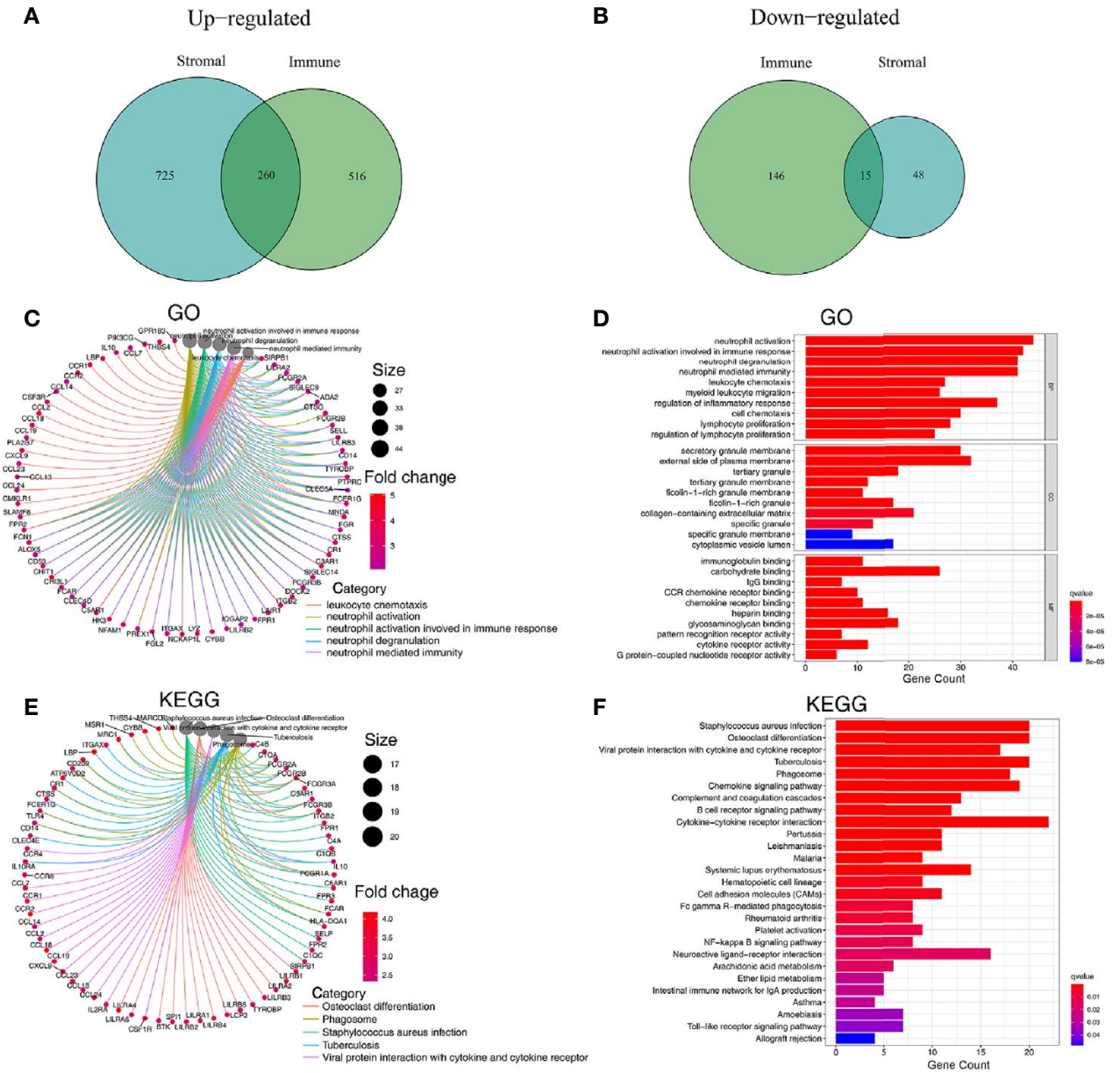

FIGURE 3 | Analysis of genes affecting the TME and their associated GO and KEGG enrichment. **(A, B)** Venn plots showing 260 up-regulated DEGs and 15 down-regulated DEGs shared by ImmuneScore and StromalScore (thresholds for differential gene expression set at an FDR adjusted *P*-value <0.05 and log2FC>1). **(C, D)** GO enrichment analysis for 275 microenvironmentally relevant DEGs, the statistical threshold set at *P*-value < 0.05 with an FDR adjusted *P*-value < 0.05. **(E, F)** KEGG enrichment analysis for 275 microenvironmentally relevant DEGs, the statistical threshold set at *P* value < 0.05 with an FDR adjusted *P*-value < 0.05.

182 network nodes with the confidence of an interactive relationship larger than 0.7 existed in the PPI network. We counted the number of neighboring nodes for each gene and selected the top 30 genes with the most neighboring nodes as the hub genes of the PPI network (**Figure 4B**).

Hub Genes Related to TME and Prognosis

To further explore the relationship between TME and prognosis, the intersection analysis between the critical nodes in the PPI network and the prognosis related DEGs was carried out, and only three genes, *CCR4*, *CCR8*, and *P2RY14*, were overlapping from the above analyses (**Figure 4C**).

Differential Expression of Key Genes Between Tumor and Normal Tissues

A total of 502 tumor tissues and 44 normal tissues were included in TCGA-HNSC data set. We used the "limma" package to analyze the expression of these three key genes and found that *CCR8* and *P2RY14* were differentially expressed in tumor tissues compared with normal tissues ($P<0.01$), while *CCR4* exhibited

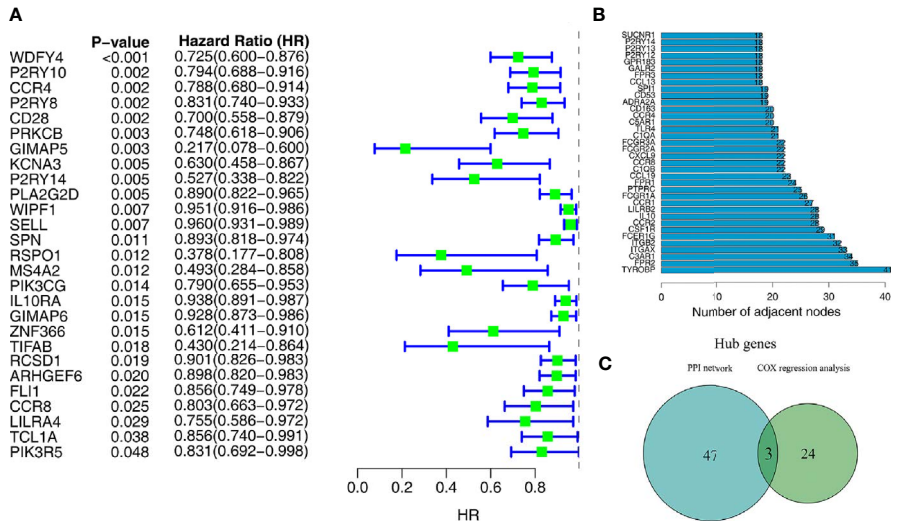

FIGURE 4 | Screening of target genes by PPI network and survival analysis. **(A)** Univariate Cox regression analysis of 275 microenvironment-associated DEGs. **(B)** Core genes with the highest number of neighboring nodes in the PPI network. **(C)** The Wayne plot shows three hub genes that belong to both the PPI network and prognosis-related genes.

no significant difference in expression between tumor and normal tissues (**Figures 5A–C**). Paired differentiation analyses using the Wilcoxon rank-sum test exhibited similar results. A total of 43 pairs of tumors and normal tissues from 43 patients were included in this analysis. *CCR8* and *P2RY14* were significantly differentially expressed in tumor tissues compared with normal tissues, while *CCR4* was not significantly different (**Figures 5D–F**).

GSE30784 and GSE37991 were used to validate the above-mentioned expression results of hub genes. According to the results from TCGA-HNSC data set, compared to normal tissues, *CCR4* exhibited a similar expression level in the tumor tissues ($P>0.05$) (**Figures 6A, D**). The expression of *CCR8* was significantly increased in tumor tissues ($P<0.001$) (**Figures 6B, E**), while the expression of *P2RY14* was significantly decreased ($P<0.001$) (**Figures 6C, F**).

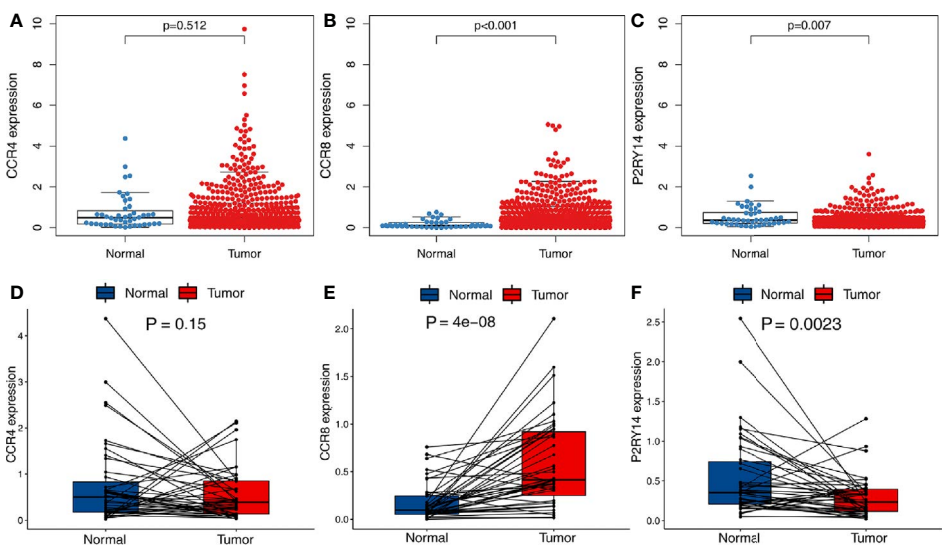

FIGURE 5 | Differential expression analysis of hub genes in tumor and normal tissues in TCGA-HNSC data set. **(A)** There was no significant difference in the expression of *CCR4* in tumor and normal tissues. **(B, C)** Significant differences were observed in the expression of *CCR8* and *P2RY14* in tumor and normal tissues ($P<0.01$). **(D–F)** A paired analysis of tumor and normal tissues from the same patients confirmed the previous analysis results.

To validate the gender differences, we then divided TCGA-HNSC data set into two groups by gender. We found no significant correlation between higher or lower immune scores and tumor prognosis in either the male or female groups (P>0.05) (**Figures S3A, B**). However, in the male group, there was a trend for better prognosis in the higher immune score group (**Figure S3A**). Within these two groups, respectively, we performed survival analysis based on the high and low expression of the hub genes. Interestingly, in the male group, the expression of all genes was significantly correlated with survival (P<0.005), while in the female group, the expression of all hub genes was not correlated with survival (P>0.05) (**Figures S3C–H**).

Immunohistochemical analysis of HNSCC specimens and adjacent normal tissues for *CCR8* and *P2RY14* proteins revealed that *CCR8* was significantly over-expressed in HNSCC specimens, whereas *P2RY14* was significantly lower expressed than in normal tissues (P<0.05) (**Figures 7A, B**).

The Correlation of Gene Expression With the Survival and Clinical Characteristics

CCR4 showed a significant correlation with survival in TCGA-HNSC data set (P<0.001), and the higher the gene expression, the better the patient's prognosis (**Figure 8A**). To eliminate the non-proportional hazard, according to the survival period of the patients, we classified those with less than 5 years as a group and those with more than 5 years were included in another group for separate analysis of *CCR8* and *P2RY14*. We found the vast majority (447/499) of patients with a survival of less than 5 years. The results of the survival analysis showed that the expression of *CCR8*, *P2RY14* were significantly associated with survival in patients with OS less than 5 years (**Figures 8B, C**). However, the results were not significant in patients with OS more than 5 years (n=52) (**Figures S4A, B**).

In the two randomly generated sub-data sets of TCGA-HNSC, we obtained results from the survival analysis that were highly consistent with previous results, with higher expression of the hub genes predicting a better prognosis (P<0.05) (**Figures 8D–I**).

We also validated the results on the external GSE41613 data set and found that no significant differences were found for any of the three genes, but CCR8 and P2RY14 showed highly identical trends to those in TCGA-HNSC (**Figures 8J–L**).

CCR4 gene expression was significantly correlated with pathological tumor stage and T-stage (P<0.05) (**Figure 8**). Both *CCR8* and *P2RY14* gene expression was significantly correlated with pathological tumor stage, T-stage, and gender (P<0.05) (**Figure 9**).

CCR4 demonstrated its independent predictive value of OS in the univariate Cox regression analysis in TCGA-HNSC data set (P<0.05). In the multivariate regression analysis of CCR4, although not significant, it showed a predictive value that was not weaker than that of the T-stage (P = 0.057) (**Figure 10A**). CCR8 expression did not reveal its independent prognostic value over other factors in the regression analyses (**Figure 10B**). Notably, compared to gender and stage, we found the expression of P2RY14 exhibits an independent prognostic value in both the univariate and multivariate Cox regression analyses (P <0.05) (see in **Figure 10C**).

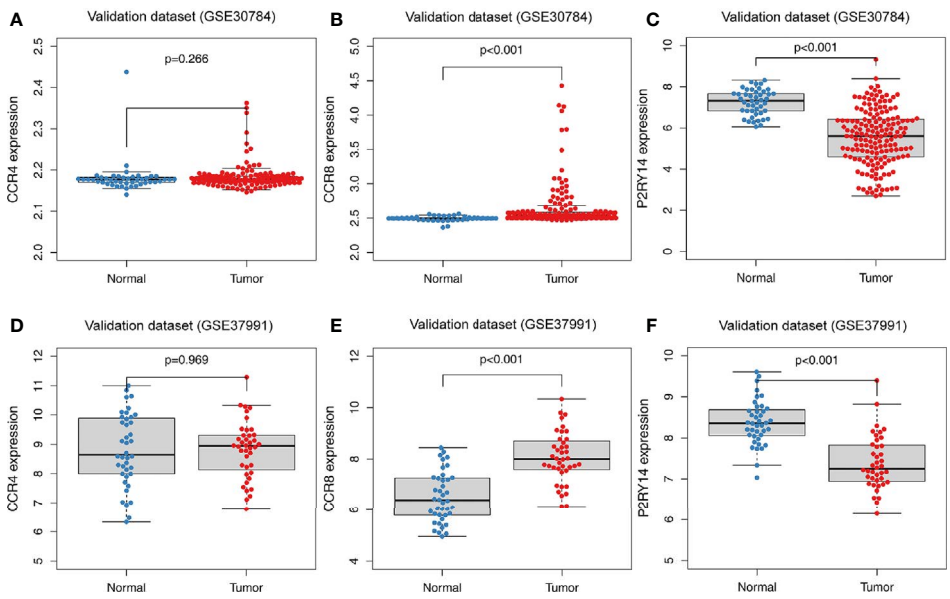

FIGURE 6 | Differential expression analysis of hub genes in tumor and normal tissues in GEO data sets. **(A)** There was no significant difference in the expression of *CCR4* in the GSE30784 data set. **(B, C)** Significant differences were observed in the expression of *CCR8* and *P2RY14* between tumor and normal tissues in the GSE30784 data set (P<0.001). **(D)** No significant difference in *CCR4* was observed in the GSE37991 data set. **(E, F)** In the GSE37991 data set, *CCR8* expression was increased in tumor tissues compared to normal tissues, while *P2RY14* expression was significantly decreased.

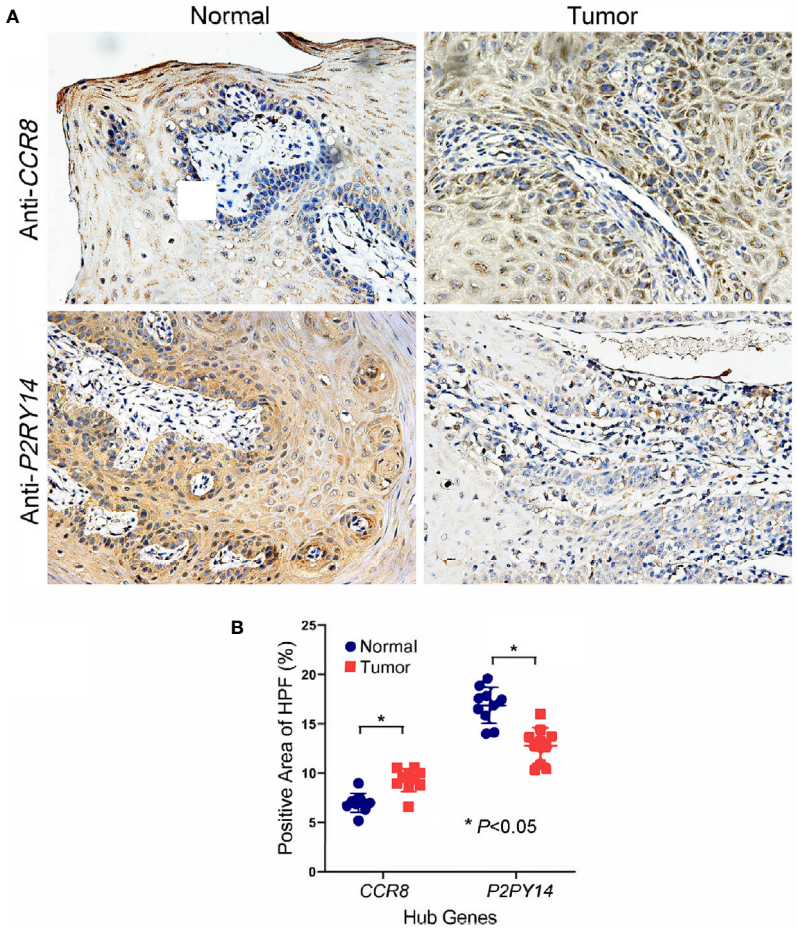

FIGURE 7 | Immunohistochemical analysis of oral squamous cell carcinoma specimens and adjacent normal tissues for *CCR8* and *P2RY14* protein. **(A)** *CCR8* was highly expressed in tumor specimens of HNSCC patients compared to normal tissues. *P2RY14* was highly expressed in normal tissues compared to tumor specimens. **(B)** The quantification of IHC results (FDR adjusted P-value < 0.05).

Pathways Enriched for These Hub Genes as Revealed by GSEA Analysis

Given that the expression levels of all three key genes mentioned above were significantly correlated with the survival and T stage of patients in TCGA-HNSC data set, we categorized the patients into high and low expression groups according to their median expression levels and then performed GSEA analysis. The results showed that in the high-expression group, all three hub genes were significantly enriched in immune-related pathways such as "CYTOKINE_CYTOKINE_RECEPTOR_INTERACTION," "JAK_STAT_SIGNALING_PATHWAY," "CHEMOKINE_SIGNALING_PATHWAY," "NATURAL_KILLER_CELL_MEDIATED_CYTOTOXICITY" (**Figures 11A–C**). In the low-expression group, all three genes are significantly enriched in metabolism-related pathways, including "OXIDATIVE_PHOSPHORYLATION," "RNA_POLYMERASE," "RIBOSOME," and so on (**Figures 11D–F**).

Correlation Between Gene Expression and Immune Cell Infiltration

CIBERSORT was used to estimate the fractions of 22 infiltrated immune cells using the RNA-sequence data. The relative abundance of parts of the 22 infiltrated immune cells exhibited significant differences between the high- and low-expression groups. Combining the results of differential analysis (**Figure 12A**, **Figure S5A**, **Figure S6A**) and correlation analysis (**Figure 12B**, **Figure S5B**, **Figure S6B**), we found that the content of a total of 14 immune cells was significantly correlated with the expression of *CCR4*, 11 with the expression of *CCR8*, and 13 with the expression of *P2RY14* (**Figure 12C**). For example, six immune cells were positively correlated with the expression of *CCR8*, including naive B cells, T cells regulatory (Tregs), T cells CD4 memory resting, T cells follicular helper, resting Mast cells, and activated T cells CD4 memory. Five cells were negatively correlated with *CCR8* expression, including memory B cells, Macrophages M0, activated

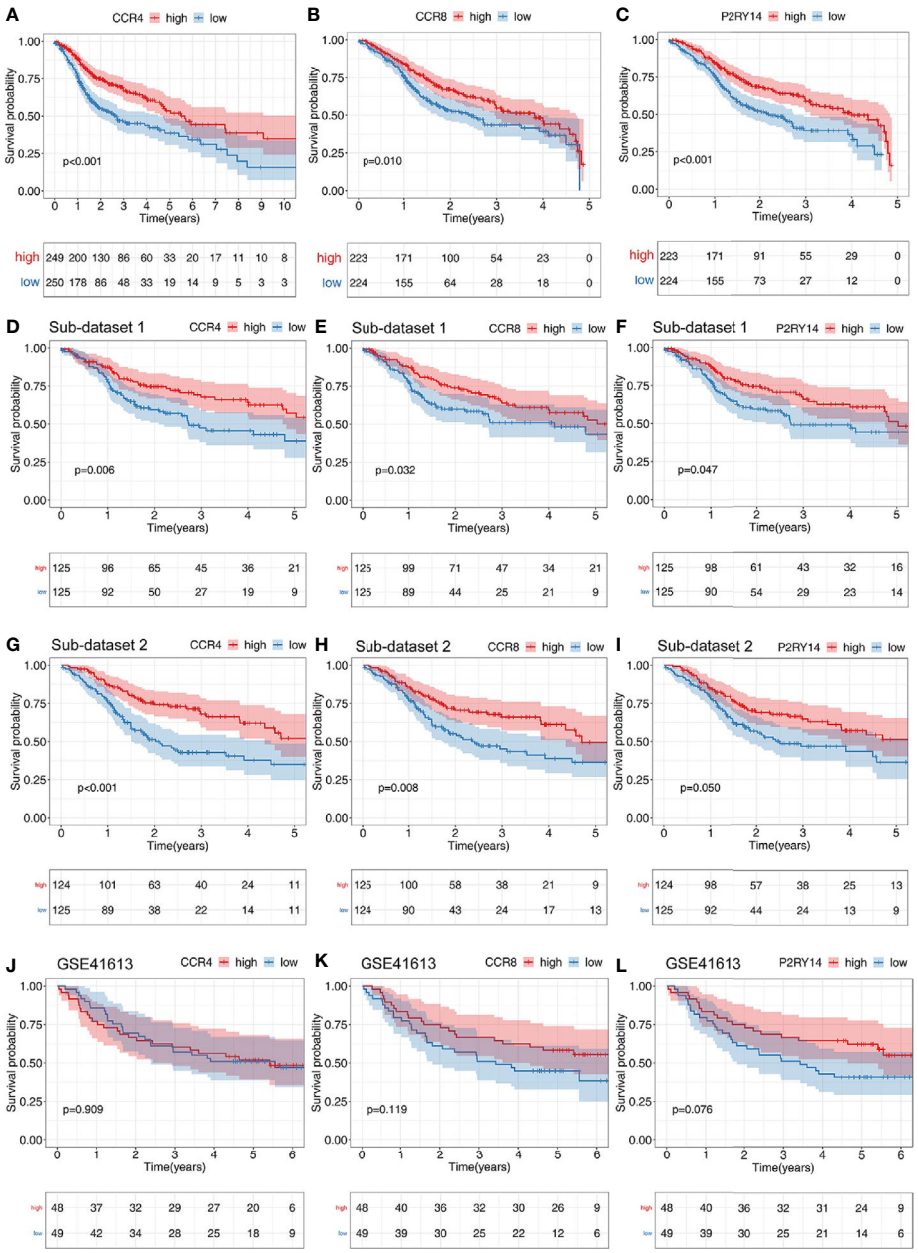

FIGURE 8 | Results of survival analyses of hub genes. The expression of *CCR4* **(A)**, *CCR8* **(B)**, and *P2RY14* **(C)** were all significantly correlated with patient prognosis in the TCGA data set, and the higher the level of gene expression, the better the patient's prognosis. **(D–I)** Survival analysis of two randomly distributed subsets showed results consistent with the original data set, with the expression of all of the three hub genes significantly correlated with survival. **(J–L)** Survival analysis was performed on another validation data set GSE41613.

Mast cells, Eosinophils, and activated NK cells. Notably, five of the infiltrating cells had similar correlations with all three hub genes. The expression of these genes was negatively correlated with the fraction of memory B cells and positively correlated with the fraction of the other four cells, including naive B cells, resting T cells CD4 memory, T cells follicular helper, and Tregs. These results further support that the expression of *CCR4*, *CCR8*, and *P2RY14* affect the immunoreactivity of TME.

DISCUSSION

In this study, we identified three hub genes (*CCR4*, *CCR8*, and *P2RY14*) that were significantly associated with both TME and prognosis through a combination of correlation analysis and survival analysis for the TME related DEGs. Among them, there were significant differences in the expression of *CCR8* and *P2RY14* in tumor tissues and normal tissues. Enrichment

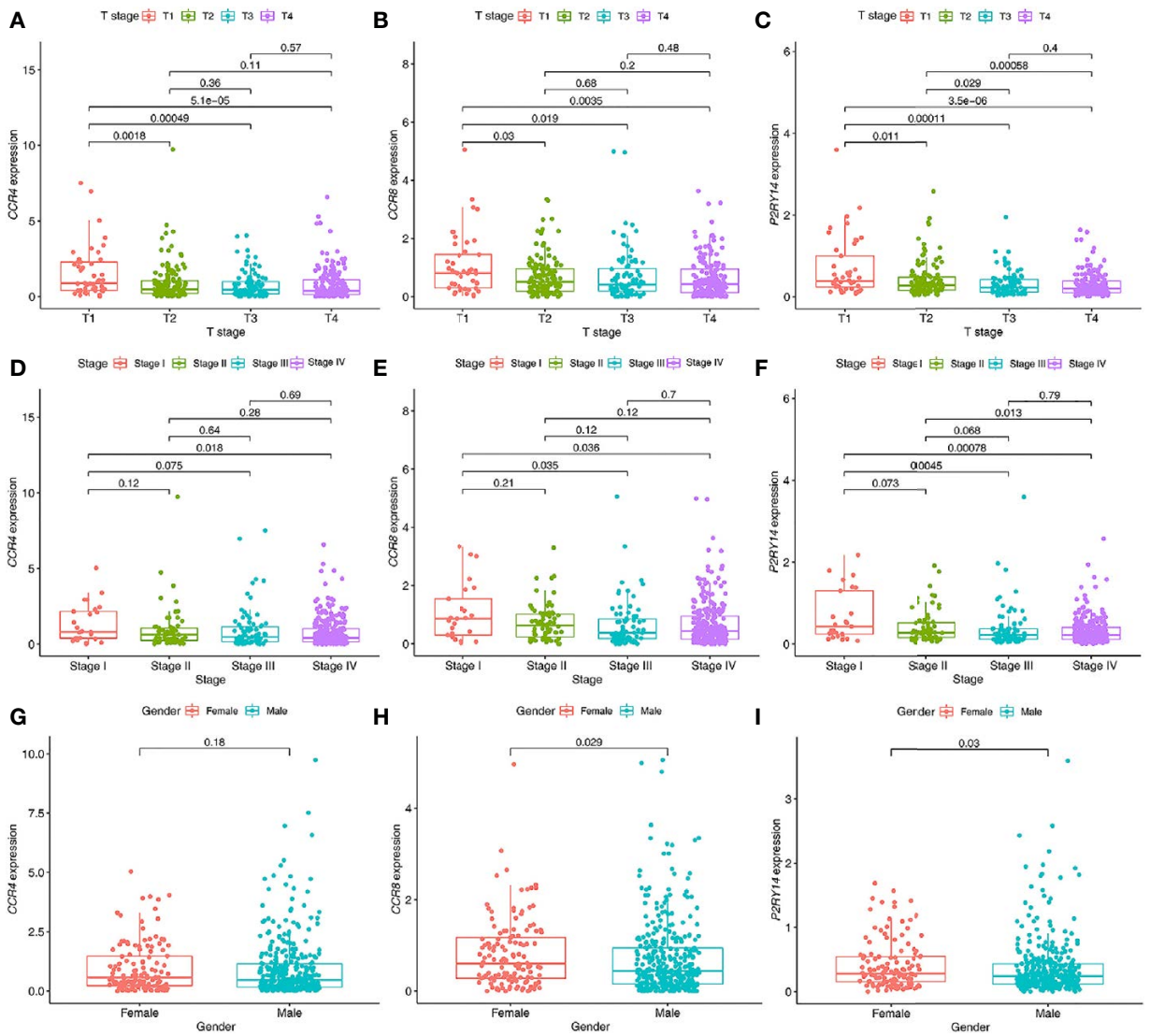

FIGURE 9 | Relationship between the expression levels of hub genes in tumor tissues and clinical characteristics of patients. **(A–C)** The expression of *CCR4* **(A)**, *CCR8* **(B)**, and *P2RY14* **(C)** were all significantly correlated with the T staging. The expression levels of these genes all decreased gradually with the progression of the T stage. **(D–F)** Similar results were seen with the pathological staging in all three hub genes, but not as significant as for T staging. **(G–I)** All of these genes were less expressed in males than in females, with no significant difference was shown in CCR4 (P>0.05), and significant differences were demonstrated in both *CCR8* and *P2RY14* (P<0.05).

analysis revealed that the functions of these genes are primarily associated with the immune system. In a subsequent analysis of tumor-infiltrating cells, we found that the expression of these genes was all significantly correlated with the fraction of multiple immune cells in the tumor tissue. This is further evidence that these genes influence the immune system and the tumor microenvironment by influencing the immune system and, thus, tumorigenesis, progression, and prognosis. They can also be used as reliable predictors of the tumor microenvironment and prognosis.

A great number of studies have confirmed that TME plays an essential role in tumor initiation and development (19–21). An aggressive TME may support continued tumor growth, invasion, and metastasis. The interactions between numerous components of TME may result in different tumor growth patterns and prognosis, but the precise mechanisms remain to be elucidated and thoroughly investigated. Li et al. recently found that three immune-related genes (*COL1A1*, *COMP*, and *SERPINE2*) are significantly correlated in both TME and tumor prognosis, thus revealing the possible effects and pathways of microenvironment on tumor prognosis (22). Huo et al. analyzed the scores of 22 immune cells in tumor tissues using gene expression data from 816 HNSCC patients and developed a TME score-based prognostic risk model accordingly. The model was significantly

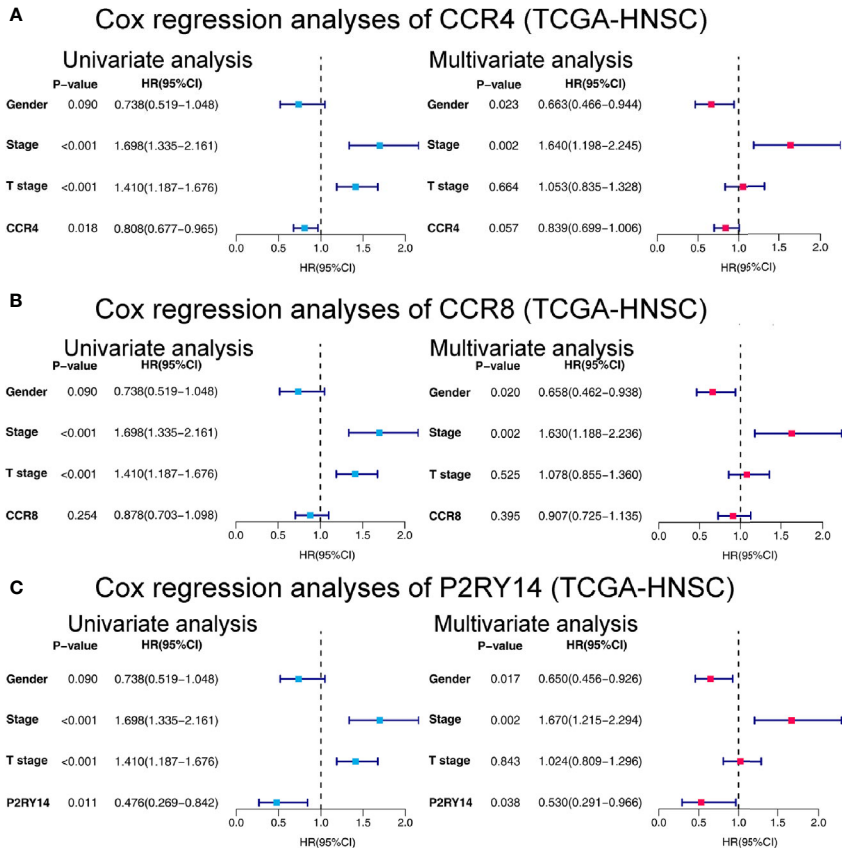

FIGURE 10 | Forest plots of univariate and multivariate Cox regression analyses in TCGA-HNSC. **(A)** Cox regression analyses on the relationship between CCR4 expression and prognosis. **(B)** Cox regression analyses of CCR8. **(C)** Cox regression analyses of P2RY14. HR, hazard ratio.

correlated with tumor stage, grade, HPV infection, and prognosis (23).

Both *CCR4* and *CCR8* belong to chemokine receptors, and the proteins encoded by these genes belong to the family of G-protein-coupled receptors (24). Chemokines consist of a set of small polypeptides that regulate cellular transport in various types of leukocytes. Chemokines also have essential roles in the development, homeostasis, and function of the immune system, and they have effects on endothelial cells involved in angiogenesis or vasorelaxation (25). Besides, these genes are also strongly associated with tumor development. Xu et al. found that *CCR4* and CCR6 are independent prognostic indicators for patients with lung adenocarcinoma (26). One animal study in canines confirmed that the expression of *CCR4* was significantly higher in tumor tissues than in normal tissues and was significantly correlated with the content of Treg cells. They suggest that the *CCL17*/*CCR4* axis may drive Treg recruitment in a variety of canine cancers. *CCR4* blockade may be a potential therapeutic option to eradicate tumors through Treg depletion (27). Based on the mechanism of *CCR4*, Mogamulizumab is a new humanized anti-*CCR4* antibody that is currently being used in the clinical treatment of advanced cutaneous T-cell lymphoma (CTCL) (28).

P2RY14 is a purinergic receptor for UDP-glucose and other UDP-glycans coupled to G-proteins. It plays a role in the immune system by participating in the regulation of the stem cell compartment (29). *P2RY14* is now thought to be closely associated with tumorigenesis and development. For instance, Wang et al. found that *P2RY14* is significantly down-regulated in lung cancer tissues based on analysis of different data sets, and the higher the expression level of this gene, the better the patient's prognosis (30). Similar to the results we obtained in TCGA-HNSC data set, the higher the expression of *P2RY14* in the tumor tissue, the better the prognosis of the patient (**Figure 8C**). And in tumor tissues, the levels of the gene are significantly down-regulated compared to normal tissues (**Figures 5C, F**). Immunohistochemical analysis also validated the results of these genetic analyses.

In addition, we analyzed the correlation between these hub genes and clinical features, and several meaningful results were obtained. The first was that the expression of these genes was significantly correlated with the T-stage, with differences in the expression of the genes in the different stages. In all three genes, this significance was observed, and the difference in their expression between T1 and all other stages became increasingly significant with increasing staging. We also observed such differences in

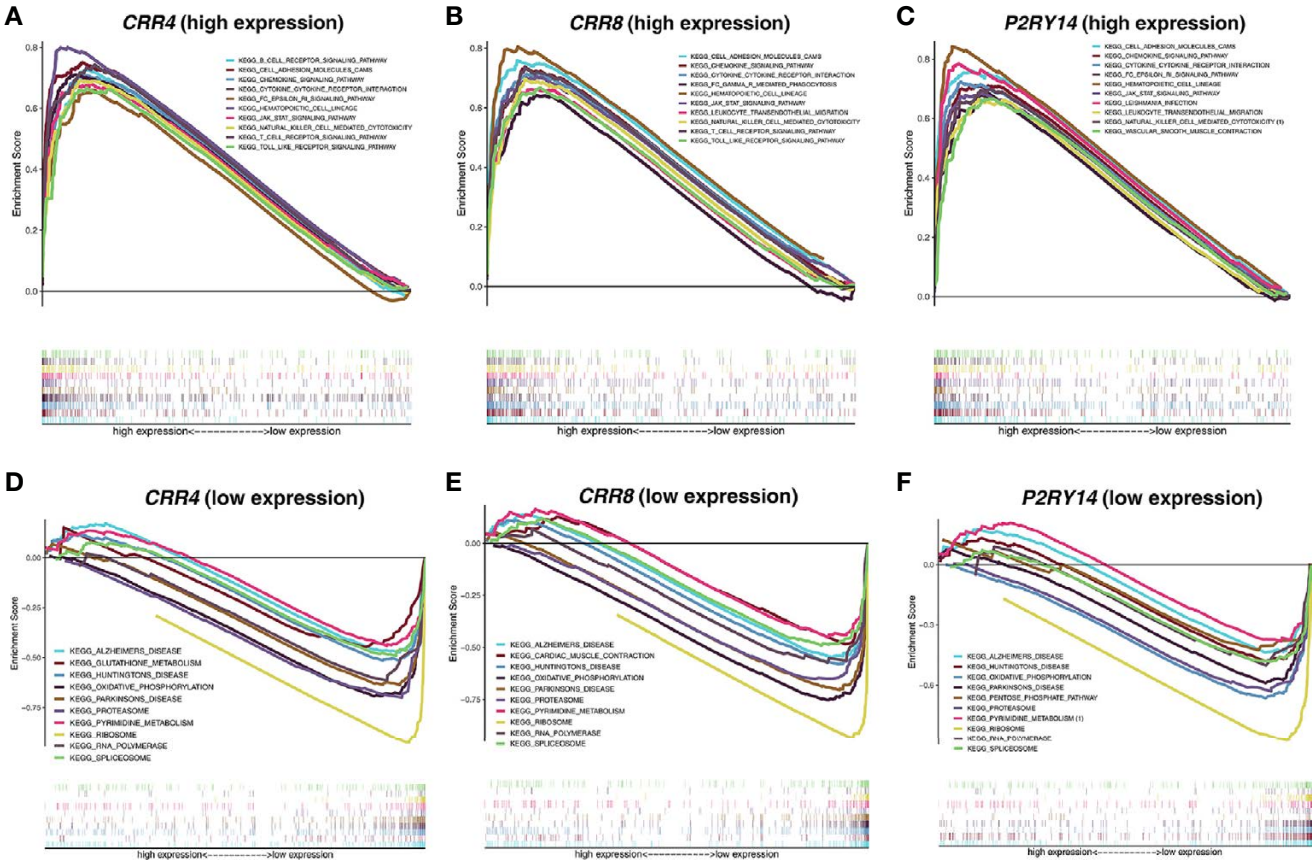

FIGURE 11 | Functional enrichment analyses regarding the expression of the hub genes. **(A–C)** Results of enrichment analysis with higher expression of the hub genes. **(D–F)** Results of enrichment analysis with lower expression of the hub genes. The threshold was set to Nominal *P*-value < 0.05 with an FDR adjusted *P*-value < 0.25.

pathological staging. This supports that the expression of these genes was significantly correlated with tumor progression. Interestingly, the expression levels of *CCR8* and *P2RY14* in tumor tissues were significantly correlated with gender, with women showing significantly higher levels of gene expression than men. The expression of *CCR4*, although non-significant, showed a similar tendency. However, these findings have not been reported in previous studies. Notably, a similar result was seen in a previous analysis of TME scores, with male patients having significantly lower immune scores than females. Related studies have found significant differences in incidence, outcome, and response to immunotherapy across tumors (31, 32). For example, in urothelial bladder carcinoma, although the incidence was lower in women than in men, the disease's aggressiveness and mortality were higher in women than in men (33). Similar to these studies, we grouped the data by gender in this study and found that female patients had a poorer prognosis than male patients ($P < 0.05$, HR= 1.328 (0.981 to 1.799)) (**Figure 2D**). Although we found that immune scores were higher in women than in men, the results showed that the prognosis of female patients was not better than men as expected from the immune scores. Therefore, it is reasonable to assume that although females have more immune infiltrates and highly expressed hub genes than males, this is not sufficient to have a decisive impact on the survival prognosis. The reasons for this may be related firstly to the smaller sample size of women and more likely, to the fact that female HNSCC patients differ significantly from men at the molecular level (34). These results suggest that there may be differences in TME between male and female patients. No significant gender-related pathways were also found in the results of the KEGG enrichment analysis. We may need to do more gender-related studies to reveal the possible underlying mechanisms.

The relative fraction of tumor infiltrated immune cells are estimated by Cibersort software using the FPKM RNA-seq expression data. By correlation and differential analyses, we found that the content of these immune-related cells in tumor tissues was closely associated with the three hub genes' expression. We found that both in *CCR4*, *CCR8*, and *P2RY14*, the abundance of CD8 T-lymphocytes was significantly higher in the group with high expression of these genes than in the lower expression group. T cells expressing CD8 usually differentiate into cytotoxic T-lymphocytes after being activated and are able

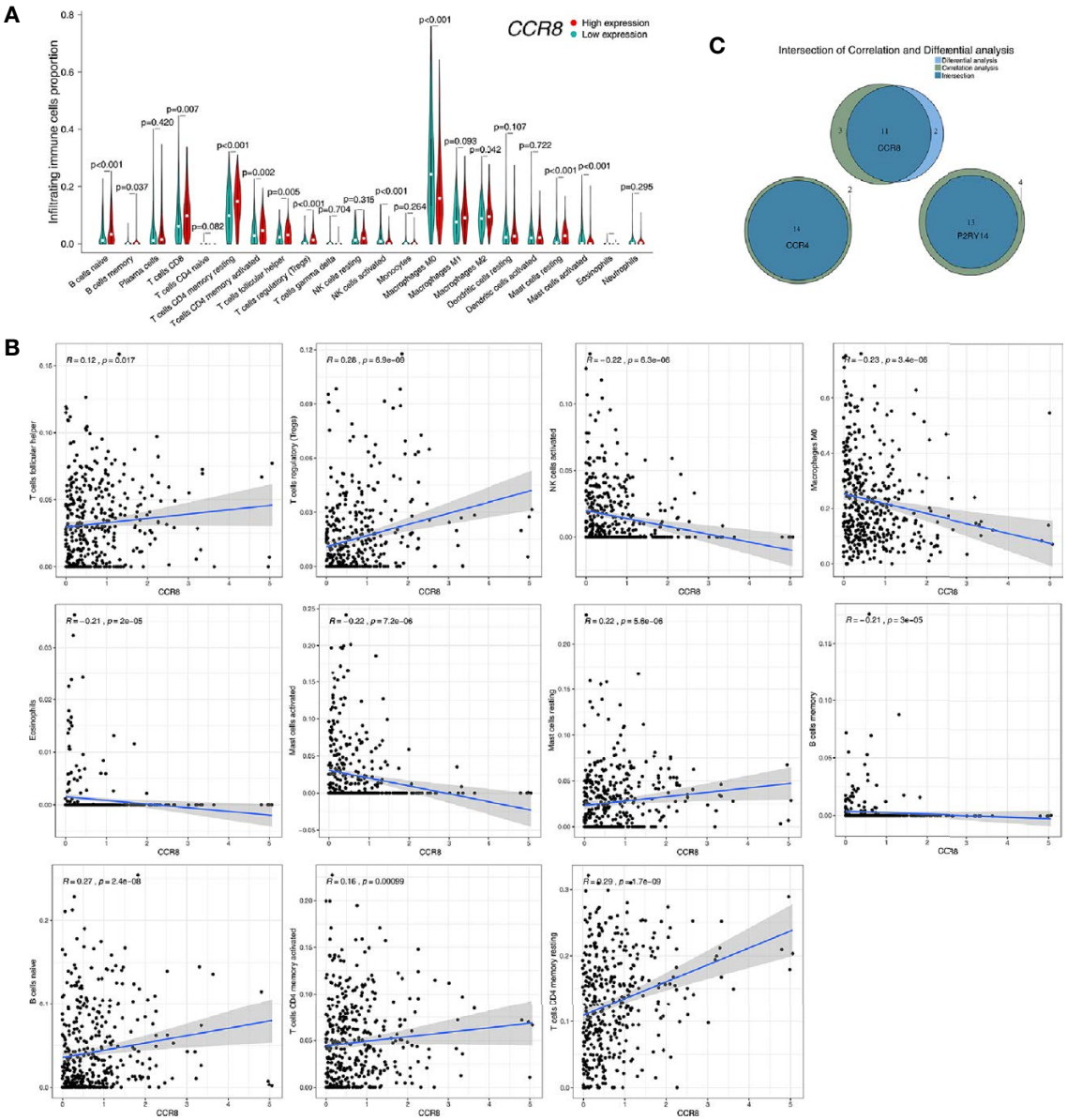

FIGURE 12 | Correlation of *CCR8* expression with immune cell fraction in tumor tissues in TCGA-HNSC. **(A)** Patients were divided into high- and low-expression groups based on the median value of *CCR8* gene expression. There were significant differences in the fraction of some immune cells in the tumor tissue ($P<0.05$). **(B)** Correlation analysis of *CCR8* and immune cell content was used to validate the above differential analysis results. **(C)** Wayne plots showed that the expression of *CCR4*, *CCR8*, and *P2RY14* was associated with the fraction of several immune cells, respectively.

to kill tumor cells specifically. Therefore, studies have confirmed that the higher the level of CD8+ T cells, the stronger the body's anti-tumor immune response and the better the prognosis of patients (35, 36). In all of the three hub genes, we also found that the content of M0 macrophages was significantly lower in the high-expression group of the gene. The primary function of macrophages is phagocytosis and digestion of cellular debris and pathogens, and activation of other immune cells. M0 macrophages are non-activated macrophages without any inflammatory or tumor-associated function and can be transformed into classically activated M1 macrophages and alternatively activated M2 macrophages (37, 38). M1 macrophages have a primary anti-tumor role, distinguishing tumor cells from healthy cells, recognizing and then killing tumor cells by mediating cytotoxic effects. In contrast, the role of M2 macrophages is to promote the growth and metastasis of tumors. In this study, we found that the content of M0 macrophages was significantly reduced in the high expression

group while M1 macrophages were increased although there was no significant difference, while there was no significant change in M2 macrophages, which suggested an enhanced anti-tumor immune response in the high expression group. These results are also consistent with the changes in immune status caused by altered CD8 T cells. Furthermore, in the present study, we found that, like the other two key genes, high expression of the *CCR8* gene was significantly associated with an enrichment of Tregs in tumor tissue, which in turn predicted a better prognosis. This is consistent with previous findings in colorectal cancer, which suggested that enrichment of Tregs in tumors favors a better prognosis (39, 40). Salama et al. found that improved survival associated with a high density of tumor-infiltrating FOXP3(+) Tregs in colorectal cancer (40). These results confirm the influence of hub genes on different types of tumor immune cells and also preliminarily reveal possible mechanisms that may influence the microenvironment and prognosis.

There are several limitations to this study. Firstly, this study calculated the TME score of tumor tissues based on mRNA expression data using the ESTIMATE algorithm and the fraction of the immune cells using the CIBERSORT algorithm. These algorithms are still in the exploratory stage. More optimization of the algorithms is needed in the future to be closer to the real world. Second, we found three hub genes, but it is unclear through what functions and pathways these genes affect TME and prognosis, and further studies are needed in the future. In addition, we included a limited number of patients for IHC validation. The sample size should be enlarged in future studies.

CONCLUSION

In the present study, we identified three hub genes (*CCR4*, *CCR8*, and *P2RY14*) that are significantly associated with TME and prognosis. We found that these genes are essential in building a microenvironment that stimulates anti-tumor immune responses and thus inhibits tumor growth and migration. These findings may shed new light on future anti-tumor therapies that target TME status.

DATA AVAILABILITY STATEMENT

The data sets presented in this study can be found in online repositories. The names of the repository/repositories and accession number(s) can be found in the article/**Supplementary Material**.

ETHICS STATEMENT

The studies involving human participants were reviewed and approved by the Ethics Committee of Chinese PLA General Hosptial. The patients/participants provided their written informed consent to participate in this study.

AUTHOR CONTRIBUTIONS

LM and YX conceived and designed the study. BQ was responsible for patients' samples collection. QH and JL helped to conduct some experiments including IHC staining. LM and XH performed the data analyses. XBZ and BW validated the results. LM drafted the manuscript with YW. YX, ZY and XZ reviewed and revised the manuscript. ZY guided the article revision and the selection of statistical methods. All authors contributed to the article and approved the submitted version.

ACKNOWLEDGMENTS

Some of the results published here are based on data downloaded from the TCGA (http://cancergenome.nih.gov) and GEO databases (http://www.ncbi.nlm.nih.gov/geo/). We are grateful to TCGA and GEO for the convenient sources of data.

SUPPLEMENTARY MATERIAL

The Supplementary Material for this article can be found online at: https://www.frontiersin.org/articles/10.3389/fonc.2021.618187/full#supplementary-material

Supplementary Figure 1 | Correlation of TME scores with clinical characteristics. **(A)** No correlation between tumor immune score and lymph node metastasis in patients was found. There was no significant correlation between stromal score and T stage **(B)**, lymph node metastasis **(C)**, or gender **(D)**, respectively.

Supplementary Figure 2 | Dot plots of GO and KEGG enrichment analysis for the 275 DEGs. **(A)** GO enrichment analysis for 275 TME-related DEGs, statistical threshold set at *P*-value < 0.05 with an FDR adjusted *P*-value < 0.05. (**B**) KEGG enrichment analysis for the 275 DEGs, statistical threshold set at p-value < 0.05 with an FDR adjusted *P*-value < 0.05.

Supplementary Figure 3 | Results of survival analyses in male and female sub-cohorts of TCGA-HNSC. **(A, B)** No significant correlation between immune score and survival was observed in males or females (P>0.05). **(C–E)** The expression of all hub genes was significantly correlated with survival in the male group (P<0.005). **(F–H)** In the females, all hub genes' expression was not associated with survival (P>0.05).

Supplementary Figure 4 | Results of survival analyses of hub genes and gender in TCGA-HNSC patients with an OS >5 years. **(A, B)** Neither CCR8 nor P2RY14 gene expression levels in patients with survival beyond 5 years were significantly associated with prognosis (P>0.05). **(C)** The patients did not exhibit survival-related gender differences (P>0.05).

Supplementary Figure 5 | Correlation of *CCR4* expression with immune cell fraction in tumor tissues. **(A)** There were significant differences in the fraction of some immune cells in the tumor tissue *(P*<0.05). **(B)** Correlation analysis of *CCR4* and immune cell content was used to validate the above differential analysis results.

Supplementary Figure 6 | Correlation of *P2RY14* expression with immune cell fraction in tumor tissues. **(A)** There were significant differences in the fraction of some immune cells in the tumor tissue (*P*<0.05). **(B)** Correlation analysis of *P2RY14* and immune cell content was used to validate the above differential analysis results.

REFERENCES

1. Marur S, Forastiere AA. Head and Neck Squamous Cell Carcinoma: Update on Epidemiology, Diagnosis, and Treatment. *Mayo Clin Proc* (2016) 91 (3):386–96. doi: 10.1016/j.mayocp.2015.12.017
2. Johnson DE, Burtness B, Leemans CR, Lui VWY, Bauman JE, Grandis JR. Head and neck squamous cell carcinoma. *Nat Rev Dis Primers* (2020) 6(1):92. doi: 10.1038/s41572-020-00224-3
3. Bray F, Ferlay J, Soerjomataram I, Siegel RL, Torre LA, Jemal A. Global cancer statistics 2018: GLOBOCAN estimates of incidence and mortality worldwide for 36 cancers in 185 countries. *CA Cancer J Clin* (2018) 68(6):394–424. doi: 10.3322/caac.21492
4. Shen S, Bai J, Wei Y, Wang G, Li Q, Zhang R, et al. A seven-gene prognostic signature for rapid determination of head and neck squamous cell carcinoma survival. *Oncol Rep* (2017) 38(6):3403–11. doi: 10.3892/or.2017.6057
5. Zhang Y, Sun X. Role of Focal Adhesion Kinase in Head and Neck Squamous Cell Carcinoma and Its Therapeutic Prospect. *Onco Targets Ther* (2020) 13:10207–20. doi: 10.2147/OTT.S270342
6. Siegel RL, Miller KD, Jemal A. Cancer statistics, 2018. *CA: Cancer J Clin* (2018) 68(1):7–30. doi: 10.3322/caac.21442
7. Osazuwa-Peters N, Simpson MC, Zhao L, Boakye EA, Olomukoro SI, Deshields T, et al. Suicide risk among cancer survivors: Head and neck versus other cancers. *Cancer* (2018) 124(20):4072–9. doi: 10.1002/cncr.31675
8. Nguyen AT, Luu M, Mallen-St Clair J, Mita AC, Scher KS, Lu DJ, et al. Comparison of Survival After Transoral Robotic Surgery vs Nonrobotic Surgery in Patients With Early-Stage Oropharyngeal Squamous Cell Carcinoma. *JAMA Oncol* (2020) 6(10):1555–62. doi: 10.1001/jamaoncol.2020.3172
9. Chen X, Fu E, Lou H, Mao X, Yan B, Tong F, et al. IL-6 induced M1 type macrophage polarization increases radiosensitivity in HPV positive head and neck cancer. *Cancer Lett* (2019) 456:69–79. doi: 10.1016/j.canlet.2019.04.032
10. Rosenberg AJ, Vokes EE. Optimizing Treatment De-Escalation in Head and Neck Cancer: Current and Future Perspectives. *Oncol* (2020) 26(1):40–8. doi: 10.1634/theoncologist.2020-0303
11. Elbehi AM, Anu RI, Ekine-Afolabi B, Cash E. Emerging role of immune checkpoint inhibitors and predictive biomarkers in head and neck cancers. *Oral Oncol* (2020) 109:104977. doi: 10.1016/j.oraloncology.2020.104977
12. Carlisle JW, Steuer CE, Owonikoko TK, Saba NF. An update on the immune landscape in lung and head and neck cancers. *CA: Cancer J Clin* (2020) 70 (6):505–17. doi: 10.3322/caac.21630
13. Wondergem NE, Nauta IH, Muijlwijk T, Leemans CR, van de Ven R. The Immune Microenvironment in Head and Neck Squamous Cell Carcinoma: on Subsets and Subsites. *Curr Oncol Rep* (2020) 22(8):81. doi: 10.1007/s11912-020-00938-3
14. Yang Y, Yang Y, Yang J, Zhao X, Wei X. Tumor Microenvironment in Ovarian Cancer: Function and Therapeutic Strategy. *Front Cell Dev Biol* (2020) 8:758. doi: 10.3389/fcell.2020.00758
15. Hossain MA, Liu G, Dai B, Si Y, Yang Q, Wazir J, et al. Reinvigorating exhausted CD8 cytotoxic T lymphocytes in the tumor microenvironment and current strategies in cancer immunotherapy. *Med Res Rev* (2020) 41(1):156–201. doi: 10.1002/med.21727
16. Jin M-Z, Jin W-L. The updated landscape of tumor microenvironment and drug repurposing. *Signal Transduct Targ Ther* (2020) 5(1):166. doi: 10.1038/s41392-020-00280-x
17. Kanehisa M, Furumichi M, Tanabe M, Sato Y, Morishima K. KEGG: new perspectives on genomes, pathways, diseases and drugs. *Nucleic Acids Res* (2017) 45(D1):D353–D61. doi: 10.1093/nar/gkw1092
18. Reimand J, Isserlin R, Voisin V, Kucera M, Tannus-Lopes C, Rostamianfar A, et al. Pathway enrichment analysis and visualization of omics data using g: Profiler, GSEA, Cytoscape and EnrichmentMap. *Nat Protoc* (2019) 14(2):482–517. doi: 10.1038/s41596-018-0103-9
19. Jena BC, Das CK, Bharadwaj D, Manda M. Cancer associated fibroblast mediated chemoresistance: A paradigm shift in understanding the mechanism of tumor progression. *Biochim Biophys Acta Rev Cancer* (2020) 1874 (2):188416. doi: 10.1016/j.bbcan.2020.188416
20. Hu C, Liu C, Tian S, Wang Y, Shen R, Rao H, et al. Comprehensive analysis of prognostic tumor microenvironment-related genes in osteosarcoma patients. *BMC Cancer* (2020) 20(1):814. doi: 10.1186/s12885-020-07216-2
21. De Cicco P, Ercolano G, Ianaro A. The New Era of Cancer Immunotherapy: Targeting Myeloid-Derived Suppressor Cells to Overcome Immune Evasion. *Front Immunol* (2020) 11:1680. doi: 10.3389/fimmu.2020.01680
22. Li F, Teng H, Liu M, Liu B, Zhang D, Xu Z, et al. Prognostic Value of Immune-Related Genes in the Tumor Microenvironment of Bladder Cancer. *Front Oncol* (2020) 10:1302. doi: 10.3389/fonc.2020.01302
23. Huo M, Zhang Y, Chen Z, Zhang S, Bao Y, Li T. Tumor microenvironment characterization in head and neck cancer identifies prognostic and immunotherapeutically relevant gene signatures. *Sci Rep* (2020) 10 (1):11163. doi: 10.1038/s41598-020-68074-3
24. Ohue Y, Nishikawa H, Regulatory T. (Treg) cells in cancer: Can Treg cells be a new therapeutic target? *Cancer Sci* (2019) 110(7):2080–9. doi: 10.1111/cas.14069
25. Bünemann E, Hoff N-P, Buhren BA, Wiesner U, Meller S, Bölke E, et al. Chemokine ligand-receptor interactions critically regulate cutaneous wound healing. *Eur J Med Res* (2018) 23(1):4. doi: 10.1186/s40001-017-0299-0
26. Xu Z-Y, Zhao M, Chen W, Li K, Qin F, Xiang W-W, et al. Analysis of prognostic genes in the tumor microenvironment of lung adenocarcinoma. *PeerJ* (2020) 8:e9530. doi: 10.7717/peerj.9530
27. Maeda S, Nakazawa M, Uchida M, Yoshitake R, Nakagawa T, Nishimura R, et al. Foxp3 Regulatory T Cells Associated With CCL17/CCR4 Expression in Carcinomas of Dogs. *Vet Pathol* (2020) 57(4):497–506. doi: 10.1177/0300985820921535
28. Ohuchi K, Fujimura T, Lyu C, Amagai R, Muto Y, Aiba S. Serum CCL22 levels decreased in parallel with disease activity in CCR4-positive mycosis fungoides treated with mogamulizumab. *Dermatol Ther* (2020) 33(6):e14099. doi: 10.1111/dth.14099
29. Shah K, Moharram SA, Kazi JU. Acute leukemia cells resistant to PI3K/mTOR inhibition display upregulation of P2RY14 expression. *Clin Epigenet* (2018) 10:83. doi: 10.1186/s13148-018-0516-x
30. Wang H, Wang X, Xu L, Zhang J, Cao H. High expression levels of pyrimidine metabolic rate-limiting enzymes are adverse prognostic factors in lung adenocarcinoma: a study based on The Cancer Genome Atlas and Gene Expression Omnibus datasets. *Purinergic Signal* (2020) 16(3):347–66. doi: 10.1007/s11302-020-09711-4
31. Koti M, Ingersoll MA, Gupta S, Lam CM, Li X, Kamat AM, et al. Sex Differences in Bladder Cancer Immunobiology and Outcomes: A Collaborative Review with Implications for Treatment. *Eur Urol Oncol* (2020) 3(5):622–30. doi: 10.1016/j.euo.2020.08.013
32. Fernandez-Gomez J, Solsona E, Unda M, Martinez-Piñeiro L, Gonzalez M, Hernandez R, et al. Prognostic factors in patients with non-muscle-invasive bladder cancer treated with bacillus Calmette-Guérin: multivariate analysis of data from four randomized CUETO trials. *Eur Urol* (2008) 53(5):992–1001. doi: 10.1016/j.eururo.2007.10.006
33. Radkiewicz C, Edgren G, Johansson ALV, Jahnson S, Häggström C, Akre O, et al. Sex Differences in Urothelial Bladder Cancer Survival. *Clin Genitourin Cancer* (2020) 18(1):26–34. doi: 10.1016/j.clgc.2019.10.020
34. Yuan Y, Liu L, Chen H, Wang Y, Xu Y, Mao H, et al. Comprehensive Characterization of Molecular Differences in Cancer between Male and Female Patients. *Cancer Cell* (2016) 29(5):711–22. doi: 10.1016/j.ccell.2016.04.001
35. Mardanpour K, Rahbar M, Mardanpour S, Mardanpour N, Rezaei M. CD8+ T-cell lymphocytes infiltration predict clinical outcomes in Wilms' tumor. *Tumour Biol: J Int Soc Oncodevelopmental Biol Med* (2020) 42 (12):1010428320975976. doi: 10.1177/1010428320975976
36. van der Leun AM, Thommen DS, Schumacher TN. CD8 T cell states in human cancer: insights from single-cell analysis. *Nat Rev Cancer* (2020) 20 (4):218–32. doi: 10.1038/s41568-019-0235-4
37. Meng L, He X, Zhang X, Zhang X, Wei Y, Wu B, et al. Predicting the clinical outcome of melanoma using an immune-related gene pairs signature. *PLoS One* (2020) 15(10):e0240331. doi: 10.1371/journal.pone.0240331
38. Genin M, Clement F, Fattaccioli A, Raes M, Michiels C. M1 and M2 macrophages derived from THP-1 cells differentially modulate the response of cancer cells to etoposide. *BMC Cancer* (2015) 15:577. doi: 10.1186/s12885-015-1546-9
39. Lee W-S, Park S, Lee WY, Yun SH, Chun H-K. Clinical impact of tumor-infiltrating lymphocytes for survival in stage II colon cancer. *Cancer* (2010) 116(22):5188–99. doi: 10.1002/cncr.25293

40. Salama P, Phillips M, Grieu F, Morris M, Zeps N, Joseph D, et al. Tumor-infiltrating FOXP3+ T regulatory cells show strong prognostic significance in colorectal cancer. *J Clin Oncol* (2009) 27(2):186–92. doi: 10.1200/JCO.2008.18.7229

Conflict of Interest: The authors declare that the research was conducted in the absence of any commercial or financial relationships that could be construed as a potential conflict of interest.

Copyright © 2021 Meng, He, Hong, Qiao, Zhang, Wu, Zhang, Wei, Li, Ye and Xiao. This is an open-access article distributed under the terms of the Creative Commons Attribution License (CC BY). The use, distribution or reproduction in other forums is permitted, provided the original author(s) and the copyright owner(s) are credited and that the original publication in this journal is cited, in accordance with accepted academic practice. No use, distribution or reproduction is permitted which does not comply with these terms.

frontiers in Immunology

PERSPECTIVE
published: 23 February 2021
doi: 10.3389/fimmu.2021.636081

Tryptophan: A Rheostat of Cancer Immune Escape Mediated by Immunosuppressive Enzymes IDO1 and TDO

*Minah Kim and Petr Tomek**

Auckland Cancer Society Research Centre, Faculty of Medical and Health Sciences, University of Auckland, Auckland, New Zealand

Blockade of the immunosuppressive tryptophan catabolism mediated by indoleamine 2,3-dioxygenase 1 (IDO1) and tryptophan 2,3-dioxygenase (TDO) holds enormous promise for sensitising cancer patients to immune checkpoint blockade. Yet, only IDO1 inhibitors had entered clinical trials so far, and those agents have generated disappointing clinical results. Improved understanding of molecular mechanisms involved in the immune-regulatory function of the tryptophan catabolism is likely to optimise therapeutic strategies to block this pathway. The immunosuppressive role of tryptophan metabolite kynurenine is becoming increasingly clear, but it remains a mystery if tryptophan exerts functions beyond serving as a precursor for kynurenine. Here we hypothesise that tryptophan acts as a rheostat of kynurenine-mediated immunosuppression by competing with kynurenine for entry into immune T-cells through the amino acid transporter called System L. This hypothesis stems from the observations that elevated tryptophan levels in TDO-knockout mice relieve immunosuppression instigated by IDO1, and that the vacancy of System L transporter modulates kynurenine entry into CD4+ T-cells. This hypothesis has two potential therapeutic implications. Firstly, potent TDO inhibitors are expected to indirectly inhibit IDO1 hence development of TDO-selective inhibitors appears advantageous compared to IDO1-selective and dual IDO1/TDO inhibitors. Secondly, oral supplementation with System L substrates such as leucine represents a novel potential therapeutic modality to restrain the immunosuppressive kynurenine and restore anti-tumour immunity.

Keywords: IDO1, TDO, inhibitors, immunotherapy, tryptophan, kynurenine, AhR, System L

OPEN ACCESS

Edited by:
Keqiang Chen,
National Cancer Institute at Frederick, United States

Reviewed by:
Haiwei Mou,
Cold Spring Harbor Laboratory, United States
Shuo Geng,
Virginia Tech, United States

***Correspondence:**
Petr Tomek
p.tomek@auckland.ac.nz

Specialty section:
This article was submitted to Cancer Immunity and Immunotherapy, a section of the journal Frontiers in Immunology

Received: *30 November 2020*
Accepted: *04 January 2021*
Published: *23 February 2021*

Citation:
Kim M and Tomek P (2021) Tryptophan: A Rheostat of Cancer Immune Escape Mediated by Immunosuppressive Enzymes IDO1 and TDO. Front. Immunol. 12:636081. doi: 10.3389/fimmu.2021.636081

INTRODUCTION

The human immune system can recognise and eradicate tumour cells. Thus, the immunity plays a key role in reducing cancer incidence (1). However, the immunity is a double-edged sword. Elimination of immune-sensitive tumour cells drives evolution of tumours towards the immune-resistant phenotype in a process called cancer immune-editing (2). This, in turn, leads to malignant

Abbreviations: AhR, Aryl hydrocarbon Receptor; GCN2, General control non-derepressible 2; IDO1, Indoleamine 2,3-dioxygenase 1; KP, Kynurenine Pathway; mTOR, Mammalian target of rapamycin; PD-1, Programmed cell death protein 1; TDO, Tryptophan 2,3-dioxygenase.

and clinically apparent cancer. It is of utmost importance to identify and silence tumoural immune escape mechanisms to restore the patient's anti-tumour immunity. Inhibiting the T-cell regulatory checkpoints, such as the programmed cell death protein 1 (PD-1) axis, by monoclonal antibodies have shown remarkable clinical responses (3). Some patients on the anti-PD-1 inhibitors experience durable tumour regressions but a sizeable fraction of patients do not benefit from these agents (4). This has triggered a search for mechanisms that could be modulated to optimise cancer patients' responses to immune checkpoint inhibitors (5, 6). One of the key candidates are enzymes IDO1 and TDO that accelerate immunosuppressive tryptophan catabolism along the kynurenine pathway (7).

Initially thought of as a "holy grail" for potentiating cancer immunotherapy, the disappointing outcomes of IDO1 inhibitors in clinical trials (8–10) have generated scepticism (11–13). However, the evidence indicates that the concept of blocking the kynurenine pathway for potentiating immunotherapy is sound and holds true in preclinical models. It is likely that the most optimal therapeutic approaches to silence the kynurenine pathway have not yet been identified. We envision that improved understanding of the immunosuppression induced by the kynurenine pathway will yield insights into optimised therapeutic strategies.

In this perspective, we summarise the current knowledge about the mechanisms mediating immunosuppression by IDO1/TDO, propose a novel immune-regulatory function for the IDO1/TDO's substrate tryptophan, and discuss the potential impact of this novel function on therapeutic strategies to block the immunosuppressive tryptophan catabolism.

IMMUNOSUPPRESSIVE TRYPTOPHAN CATABOLISM

Mammals metabolise more than 90% of tryptophan *via* the kynurenine pathway (KP) (14). The resulting tryptophan metabolites are involved in essential biological processes such as immune regulation, energy metabolism and production of an important enzyme co-factor NAD (15–17). The first and rate limiting step of the KP, tryptophan oxidation, is catalysed by intracellular enzymes IDO1 and TDO (18). There is also a third enzyme called IDO2, but its low catalytic activity suggests that its principal role is unlikely to oxidise tryptophan (19, 20).

Although both IDO1 and TDO catalyse the identical biochemical reaction, their physiological roles differ. IDO1 regulates peripheral immunity (21) and is induced by pro-inflammatory molecules including type I and II interferons, TNF-α, lipopolysaccharide, and prostaglandin E (22–25) in a wide range of cells including myeloid cells, fibroblasts, and cancer cells (26). Due to its inducible nature, IDO1 is absent in most tissues except for the sites where the body is exposed to non-self antigens such as lung, intestine, pregnant placenta, and lymphoid organs (27). In contrast, the evolutionarily older TDO is primarily expressed in the liver where it degrades excess dietary tryptophan (28–30). TDO can be induced by corticosteroids and activated by excess tryptophan (31–33).

The immunosuppressive role of the KP came to the fore in 1998 as a mechanism that confers an allogeneic foetus the ability to evade destruction by the mother's T-cells (34). Researchers soon realised that the powerful immunosuppressive effect of KP could be co-opted by cancers to escape immune destruction (35, 36). It is now well established that a wide range of different cancer types thrive on accelerated tryptophan catabolism (27, 37–39). However, the mechanisms whereby KP regulates immunity are not completely understood.

Mechanisms Involved in Immunosuppression Mediated by Accelerated Tryptophan Catabolism

As KP is a metabolic pathway, its immune regulatory role has been attributed mainly to tryptophan deprivation and the accumulation of the kynurenine pathway metabolites (**Figure 1**) (40). However, IDO1 also has a non-enzymatic function in which the enzyme acts as a signalling protein in a non-canonical NF-κB pathway driven by immunosuppressive cytokine TGF-β (41–43). The contribution of each of these mechanisms to the immune regulation is actively discussed in the research community but accumulating evidence suggests that kynurenine is likely the main culprit (44). Increased kynurenine levels have been associated with reduced function of Natural Killer cells (45) and T-cells (46, 47). Mechanistically, kynurenine's immune regulatory function is primarily linked to a transcription factor called aryl hydrocarbon receptor (AhR). Binding of kynurenine to AhR induces differentiation and activation of immunosuppressive T-regulatory cells (48–53), contributes to the recruitment of tolerogenic myeloid cells such as macrophages (54), and increases expression of the immune checkpoint molecule PD-1 on tumour-specific $CD8^+$ T-cells (**Figure 1**) (55).

In contrast, the role of tryptophan deprivation in immune regulation is somewhat controversial. An earlier study has demonstrated that tryptophan deprivation inhibits proliferation and induces apoptosis in T-cells (56). But these experiments have been mostly carried out in the dish where tryptophan can get depleted. As tumours accelerating tryptophan catabolism still contain sufficient levels of tryptophan (57–59), it is likely that tumoural tryptophan levels cannot reach levels sufficiently low to activate the stress response pathways to low amino acid levels such as the general control non-derepressible-2 (GCN2) and the mammalian target of rapamycin (mTOR) (**Figure 1**). The key protagonist involved in regulation of T-cell responses to tryptophan deprivation was initially suspected to be the GCN2 kinase (60). GCN2 mediates conserved stress response pathway to amino acid deprivation in eukaryotes and was shown to be activated in T-cells in response to tryptophan deprivation (60, 61). However, this finding was recently challenged by two studies. Sonner and colleagues demonstrated no difference in the level of immune responses between the GCN2-proficient and GCN2-deficient T-cells against B16 melanomas (59). Similarly, tryptophan deprived T-cells ceased proliferation even in the absence of the *GCN2* gene (62). The unlikely role of GCN2 as a low tryptophan sensor in

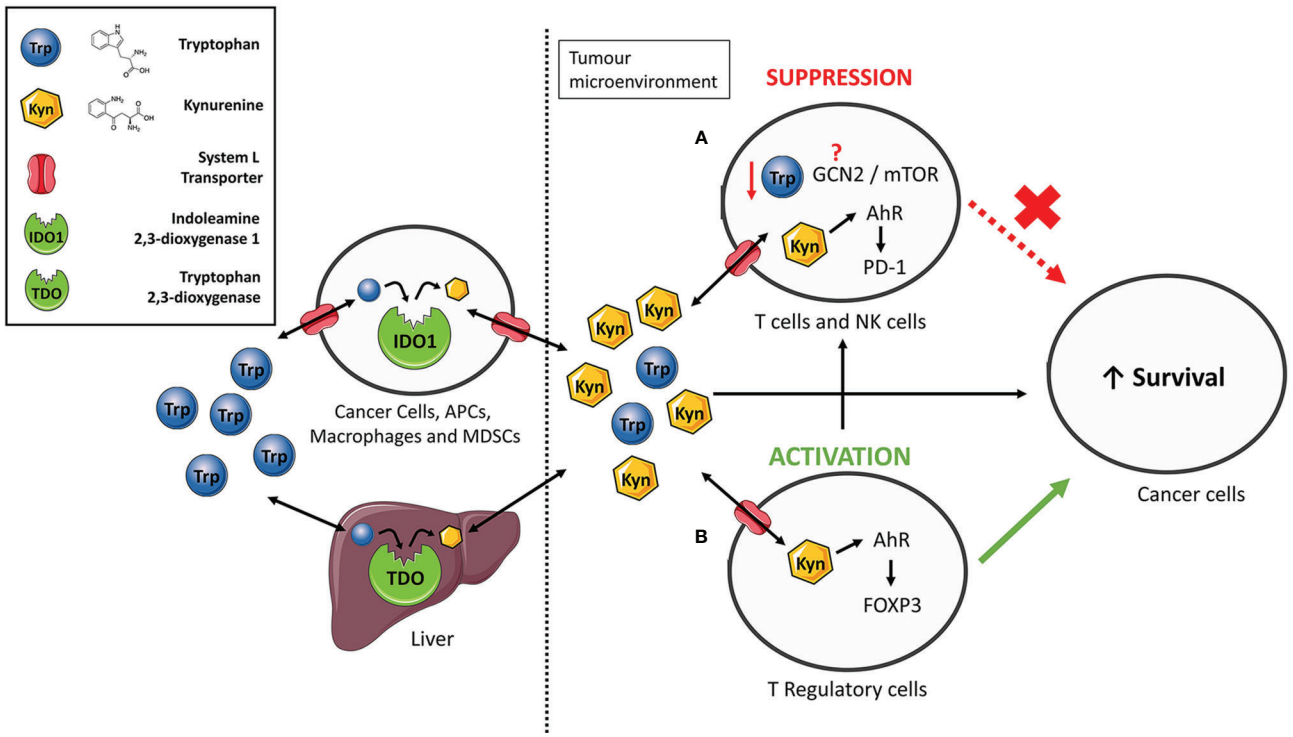

FIGURE 1 | The immunosuppressive functions of IDO1/TDO-mediated tryptophan catabolism. Extrahepatic and hepatic cells express indoleamine 2,3-dioxygenase 1 (IDO1) and tryptophan 2,3-dioxygenase (TDO) to consume tryptophan and give rise to numerous bioactive metabolites such as kynurenine. Elevated expression of IDO1 or TDO, such as in cancer, increases the relative kynurenine levels while reducing tryptophan content. Kynurenine enters cells *via* System L transporters. **(A)** Increased kynurenine levels inhibit proliferation of T-cells and natural killer (NK) cells by interacting with aryl hydrocarbon receptor (AhR) to express programmed cell death protein 1 (PD-1). Previous studies have suggested the involvement of the general control non-deprepressible-2 (GCN2) kinase and mammalian target of rapamycin (mTOR) in proliferation inhibition but the exact mechanism through which this occurs still remains unresolved. **(B)** Kynurenine induces differentiation of naïve $CD4^+$ T-cells to immunosuppressive T-regulatory cells by activation of AhR and induction of the FoxP3 transcription factor. Taken together, an immune suppressed tumour microenvironment is created that promotes survival of cancer cells.

immune cells is further corroborated by studies questioning the canonical role of GCN2 as a sensor of amino acid deficiency in mammals. GCN2 stress response pathway has been widely accepted as a mechanism for maintenance of amino acid homeostasis by controlling the feeding behaviour of omnivores (63). However, more recent studies challenged this paradigm as no significant difference in feeding behaviour was observed between the GCN2-deficient and GCN2-proficient mice that were amino acid-deprived (64). Complementary to GCN2, the mTOR senses amino acid sufficiency (65) and was proposed as a mediator of cellular stress response to low tryptophan levels. Metz and colleagues reported the repression of mTOR kinase activity in tryptophan-deprived HeLa cells, which eventually led to cell cycle arrest and apoptosis (66). It is not yet understood if mTOR could sense low tryptophan levels in immune cells.

The collective evidence accumulated to date tends to favour the conclusion that tryptophan serves primarily as a kynurenine precursor rather than inducing stress by its deprivation in vivo (67). However, a recent study by Schramme and colleagues provides a clue to a new immune regulatory function of tryptophan (57). In this study, elevated (5 to 10-fold) systemic tryptophan levels reaching 500 μM in TDO2- knockout mice overturned tumoural immune suppression induced by IDO1. Consequently, anti-PD1 immune checkpoint therapy alone was sufficient to impede the growth of IDO1-proficient MC38 colon tumours in these TDO2-knockout mice (57). That is a striking observation but how can it be explained mechanistically? How can elevation in circulating tryptophan levels overcome IDO1-mediated immunosuppression in the tumour? We posit that elevated tryptophan levels reverse the immunosuppression by outcompeting kynurenine for entry into T-cells through a shared amino acid transporter.

Tryptophan and Kynurenine: Transporter Competitors

IDO1 and TDO are intracellular enzymes; hence they require the cells to import tryptophan from the extracellular space. Import of large amino acids such as tryptophan typically occurs through the transporter called System L (68, 69). System L transporters are heterodimeric transmembrane proteins comprising a glycoprotein heavy chain (CD98) and a catalytic light chain (LAT1 or LAT2). Kynurenine can also be transported into cells through the System L transporters (70). It has been suggested that the transporters are bidirectional and can exchange

tryptophan for kynurenine in cancer cells (71). This would explain the ability of cancer cells to siphon tryptophan from the microenvironment and enrich it with kynurenine to create an immunosuppressive milieu. As System L transports a broad range of amino acids, the transporter substrates compete with each other, and the probability of interacting with the transporter depends on the relative levels of the specific amino acid and their respective affinity for the transporter (72).

This observation indicates that the relative ratio of tryptophan to kynurenine will influence the amount of kynurenine entering T-cells. Therefore, tryptophan concentration can be viewed as a rheostat that modulates kynurenine entry into T-cells and the resulting immunosuppression (**Figure 2**). This concept is supported by literature evidence. The vacancy of System L transporter influences the ability of kynurenine to enter the CD4+ T-cells and activate AhR (73). Further, both low tryptophan levels and kynurenine accumulation appear to be pivotal for immunosuppression mediated by tryptophan catabolism (47), and tryptophan supplementation reverses the proliferation arrest of IDO1-mediated tryptophan deprivation in T-cells (60, 74). Tryptophan acting as a rheostat of kynurenine-mediated immunosuppression has two important therapeutic implications. Firstly, it can aid to resolve the conundrum whether the IDO1-selective, TDO-selective or dual IDO1/TDO inhibitors would be the most optimal therapeutic agents to block KP. Secondly, it can serve as a basis for a new approach to silence kynurenine-mediated immunosuppression by oral supplementation with System L transporter substrates. We will discuss these two areas in the following section.

DISCUSSION

Efficient Silencing of Kynurenine Pathway May Require Only TDO-Selective Inhibitors

Many cancer types co-opt IDO1, TDO or both enzymes (27, 39, 75) to accelerate tryptophan catabolism and escape immune destruction. Upregulation of IDO1 or elevated kynurenine levels associate with poor patient outcomes (37, 76–79) and resistance to immune checkpoint therapy such as anti-PD-1 inhibitors (80, 81). Moreover, anti-PD-L1 therapy promotes tryptophan catabolism as a consequence of IDO1 upregulation by IFN-γ secreted by re-invigorated tumour-infiltrating lymphocytes (82). These observations provide a strong mechanistic rationale for combining the tryptophan catabolism blockade with immune checkpoint inhibitors and potentially other cancer immunotherapies. Targeting the KP also offers certain advantages over targeting cell surface immune-regulatory molecules such as PD-1. Proteins on the KP including IDO1 and TDO are intracellular enzymes (40, 83) that harbour active sites easily

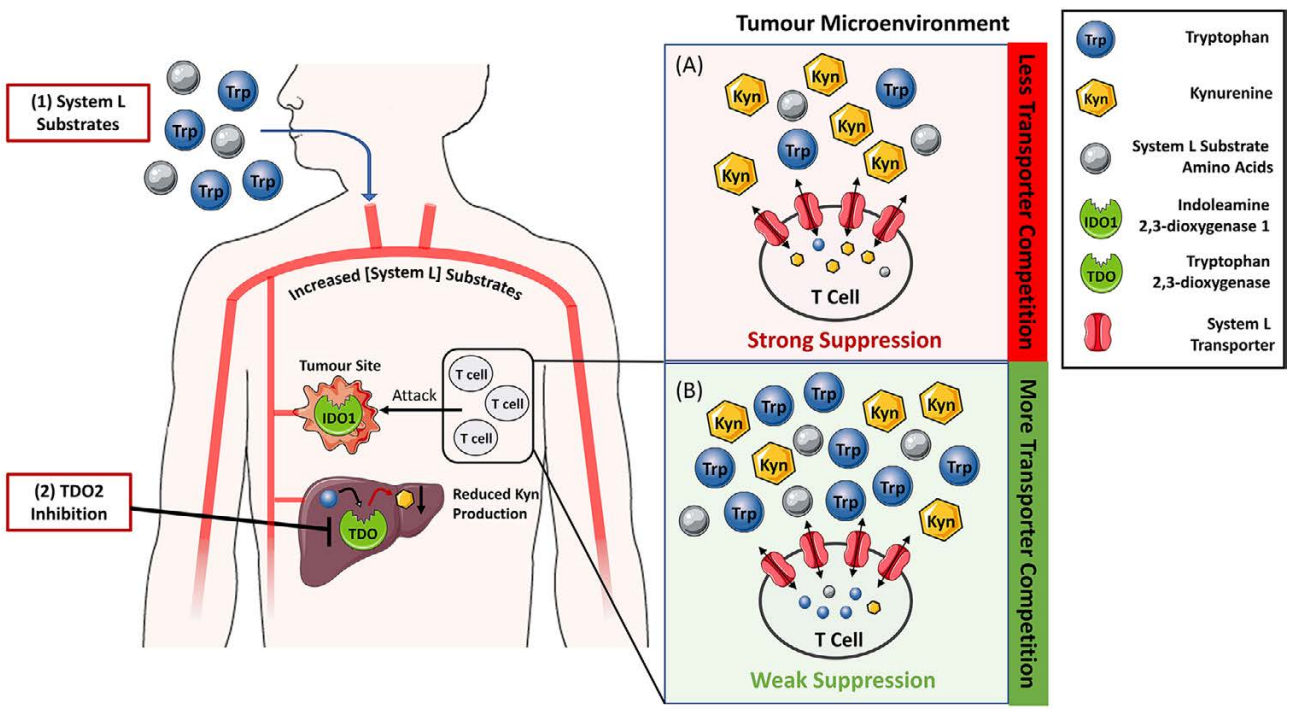

FIGURE 2 | Reversing IDO1/TDO-mediated immunosuppression by increasing the levels of System L transporter substrates to limit kynurenine entry into T-cells. **(A)** In tumour microenvironment rich in indoleamine 2,3-dioxygenase 1 (IDO1) and tryptophan 2,3-dioxygenase 2 (TDO), the tryptophan to kynurenine ratio is typically low leading to the suppression of T-cell activity and tumour killing. Blockade of TDO enzymatic activity by small molecule inhibitors (2) and/or supplementation with System L substrates such as leucine (1) is expected to increase their blood levels. Hence, the ratio of System L substrates to kynurenine in the tumour microenvironment **(B)** will also be increased. Elevated System L substrate levels competitively inhibit kynurenine entry into T cells so that T cell suppression is reduced.

targetable with inexpensive and non-immunogenic small molecules. Such molecules are stable on storage, can be administered orally, and penetrate into the brain. This is in contrast to immune checkpoint molecules such as PD-1 that do not catalyse a biochemical reaction hence lack an active site, and typically require costly antibodies for therapeutic modulation. Due to their size and instability, antibodies need to be administered by injection and cannot pass the blood brain barrier. Of note, small molecules that disrupt PD-1/PD-L1 interaction are currently in development (84, 85).

Major effort has been devoted to disable tryptophan catabolism using IDO1 inhibitors (7, 86, 87). Whilst IDO1 inhibitors can boost immunotherapy in mouse cancer models (88–91), the most advanced IDO1 inhibitor Epacadostat (INCB024360) could not potentiate anti-PD1 inhibitor pembrolizumab in a recent Phase III trial involving about 700 advanced melanoma patients (9, 92). Reasons for this negative outcome are unclear and discussed extensively elsewhere (11–13, 93, 94) but poor target engagement, compensatory expression of TDO or IDO2, dose-limiting toxicities or the lack of selection for IDO1-positive patients are likely one of the contributing factors.

Unlike IDO1 inhibitors, no TDO-specific inhibitor has yet reached clinical trials. This is not surprising given the paucity of potent TDO-selective inhibitors. High affinity TDO inhibitors seems to be much more difficult to develop than IDO1 inhibitors. That is likely because the TDO's active site is less flexible than that of IDO1 and thus cannot accommodate bulky ligands (7, 95). As a consequence, the majority of TDO-specific inhibitors [reviewed in (7, 96)] mimic tryptophan (28, 36, 97–100). Currently, the most promising TDO inhibitors appear to be the derivatives of IDO1-specific clinical candidate Navoximod (100) reported by Genentech, and PF06845102 (57) developed by iTeos Therapeutics. These inhibitors display submicromolar potencies, up to 100-fold TDO selectivity over IDO1, good metabolic stability and ability to raise systemic tryptophan levels in mice (57, 100). PF06845102 has also been shown to potentiate anti-tumour activity of the anti-CTLA4 immune checkpoint inhibitor in a mouse model of colorectal cancer (57). These promising data support further development of next-generation TDO inhibitors.

The hypothesis presented in this perspective suggests that TDO inhibition can be advantageous to IDO1 inhibition. Firstly, TDO inhibition is expected to indirectly inhibit the immunosuppressive action of IDO1 by raising the systemic levels of tryptophan and limiting entry of IDO1-generated kynurenine into T-cells (**Figure 2**). This concept assumes relatively low contribution of non-enzymatic signalling function of IDO1 to the overall immunosuppression. Secondly, unlike IDO1 inhibitors, TDO inhibitors do not require tumoural TDO expression because TDO is constitutively expressed in the liver. This is clearly demonstrated in studies where TDO2-knockout mice but not IDO1-knockout mice have markedly increased plasma tryptophan levels compared to their respective wild-type counterparts (29, 57). Therefore, TDO inhibition is anticipated to silence kynurenine-mediated immunosuppression in a greater subset of patients. The potential toxicity of hepatic TDO blockade in humans still remains unresolved. However, the absence of serious clinical pathologies of a woman diagnosed with hypertryptophanaemia due to TDO deficiency (101) suggests that TDO inhibition will be well tolerated in humans.

As cancers can express both IDO1 and TDO, the industry has been pursuing the development of dual IDO1/TDO inhibitors. This concept has not yet been supported by strong evidence but some dual inhibitors are in preclinical development or Phase I trials (40, 102, 103) including Navoximod (89) which was originally thought to be an IDO1-selective inhibitor. Similarly to IDO1 inhibitors, we contend that development of dual inhibitors may be unnecessary. However, it cannot be excluded that IDO1 inhibition will be needed to complement TDO blockade. Inhibition of hepatic TDO may not increase tryptophan levels significantly in humans. Further, it is possible that kynurenine enters cells through a transporter other than System L or triggers the immunosuppressive effect in the absence of secretion from the IDO1/TDO-expressing cells.

Can High-Dose Amino Acid Supplementation Reverse Kynurenine Mediated Immunosuppression and Potentiate Immunotherapy?

We propose that any strategy that safely increases the levels of circulating System L substrates to out-compete kynurenine has potential to reverse the IDO1/TDO mediated immunosuppression. One additional possibility to TDO inhibition is oral supplementation with amino acids that are System L substrates (**Figure 2**) such as leucine, isoleucine, valine, phenylalanine, tyrosine, tryptophan, methionine, or histidine. Whilst tryptophan supplementation emerges as a possibility, it is unlikely to increase systemic tryptophan levels because hepatic TDO efficiently breaks down excess tryptophan. This is consistent with the study of Schramme et al. showing that three-fold increase of tryptophan in the diet from 0.06 to 0.18% did not increase circulating tryptophan levels of the mice (57). Further, tryptophan supplementation (30 mg per mouse) did not significantly impede growth of mouse CT26 colon tumours (104). On the other hand, there are preclinical data showing that leucine, a high affinity substrate of System L, limits System L-mediated entry of kynurenine into brain (105). There are no data available to show if high-dose dietary supplementation with leucine or any other amino acid would translate into improved tumour control or blockade of kynurenine-mediated immunosuppression. However, the above-mentioned study strongly supports the feasibility of limiting kynurenine transport *in vivo* at leucine doses that are well tolerated by an organism.

The safety of high dose amino acid supplementation raises a potential concern. It is generally assumed that amino acids do not pose serious health hazards as they are natural substances produced endogenously and part of human diet and supplements (106). Perhaps not surprisingly, toxicities associated with high dose amino acid supplementation to mammals differ significantly (107) but leucine appears to be the least toxic amino acid. Oral or intravenous supplementation of leucine (5 g–6 g) increased systemic leucine levels in humans

in the absence of overt toxicities (108, 109). Similarly, as stated in the preceding paragraph, elevated leucine levels sufficient to prevent kynurenine transport are well tolerated by mice. This is in contrast to methionine and histidine which, at high doses, appear to be one of the most toxic amino acids to humans (110–112). However, the toxicity of a substance depends on its dose. It is therefore likely that even the seemingly most toxic amino acids may prevent kynurenine entry into T-cells at levels which are well tolerated by an organism. Experimental studies will be necessary to rigorously investigate this concept and determine which amino acids and at what doses will provide therapeutic benefit, if any.

Overall, the therapeutic supplementation with a high dose of amino acids with the intent to inhibit kynurenine-mediated immunosuppression appears like a highly feasible and exciting research prospect. It offers a simple and economical alternative to synthetic drugs inhibiting tryptophan catabolising enzymes or downstream kynurenine targets such as AhR.

SUMMARY

The disappointing outcome of the Phase III trial of Epacadostat (9) has stimulated search for alternative approaches to silence the KP. Such approaches include kynurenine depletion by kynureninase (44), small molecule inhibitors to the kynurenine's downstream target AhR (81, 94), and perhaps we will see small molecule inhibitors to a recently discovered tryptophan metabolising enzyme IL4I1 that produces AhR agonists (113). This perspective proposes a novel function for the IDO1's substrate tryptophan that could lead to an additional therapeutic strategy to block KP. We posit that tryptophan acts as a rheostat of kynurenine-mediated immunosuppression, *i.e.*, high tryptophan to kynurenine ratio limits kynurenine's entry into immune T-cells through the shared System L amino acid transporter.

Therefore, increasing circulating levels of System L substrates can relieve kynurenine-induced immunosuppression. One way to achieve this is *via* inhibition of hepatic kynurenine pathway by TDO inhibitors. This supports the development of TDO-selective inhibitors that, unlike IDO1 inhibitors, are not contingent on tumoural TDO expression. Alternatively, kynurenine can be out-competed by therapeutic supplementation of amino acids such as leucine which is a high-affinity System L substrate. Leucine supplementation appears highly feasible. Leucine has low toxicity to mammals and was shown to block kynurenine entry into the mouse brain. If confirmed, we envision the amino acid supplementation strategy will enrich the armamentarium of therapeutic approaches modulating KP, and increase the likelihood of realising the prospect of silencing the KP for cancer immunotherapy.

DATA AVAILABILITY STATEMENT

The original contributions presented in the study are included in the article/supplementary material. Further inquiries can be directed to the corresponding author.

AUTHOR CONTRIBUTIONS

PT conceived, designed and supervised the study. MK drafted the manuscript and figures. All authors contributed to the article and approved the submitted version.

FUNDING

PT and MK acknowledge support from Health Research Council New Zealand through the Emerging Researcher First Grants 17/586 awarded to PT. PT acknowledges additional support from Auckland Medical Research Foundation Project grant 1120009 awarded to PT, School of Medical Sciences at the University of Auckland in New Zealand and Auckland Cancer Society Research Centre. The funding bodies had no role in design of this study, decision to publish and preparation of the manuscript.

REFERENCES

1. Shankaran V, Ikeda H, Bruce AT, White JM, Swanson PE, Old LJ, et al. IFN [gamma] and lymphocytes prevent primary tumour development and shape tumour immunogenicity. *Nature* (2001) 410:1107–11. doi: 10.1038/35074122
2. Dunn GP, Bruce AT, Ikeda H, Old LJ, Schreiber RD. Cancer immunoediting: from immunosurveillance to tumor escape. *Nat Immunol* (2002) 3:991–8. doi: 10.1038/ni1102-991
3. Hoos A. Development of immuno-oncology drugs [mdash] from CTLA4 to PD1 to the next generations, Nature reviews. *Drug Discov* (2016) 15:235–47. doi: 10.1038/nrd.2015.35
4. Havel JJ, Chowell D, Chan TA. The evolving landscape of biomarkers for checkpoint inhibitor immunotherapy. *Nat Rev Cancer* (2019) 19:133–50. doi: 10.1038/s41568-019-0116-x
5. Bader JE, Voss K, Rathmell JC. Targeting metabolism to improve the tumor microenvironment for cancer immunotherapy. *Mol Cell* (2020) 78:1019–33. doi: 10.1016/j.molcel.2020.05.034
6. Egen JG, Ouyang W, Wu LC. Human anti-tumor immunity: insights from immunotherapy clinical trials. *Immunity* (2020) 52:36–54. doi: 10.1016/j.immuni.2019.12.010
7. Dolšak A, Gobec S, Sova M. Indoleamine and tryptophan 2,3-dioxygenases as important future therapeutic targets. *Pharmacol Ther* (2020), 107746. doi: 10.1016/j.pharmthera.2020.107746
8. Jung KH, LoRusso P, Burris H, Gordon M, Bang Y-J, Hellmann MD, et al. Phase I study of the indoleamine 2,3-Dioxygenase 1 (IDO1) inhibitor Navoximod (GDC-0919) administered with PD-L1 inhibitor (Atezolizumab) in advanced solid tumors. *Clin Cancer Res* (2019) 25:3220–8. doi: 10.1158/1078-0432.CCR-18-2740
9. Long GV, Dummer R, Hamid O, Gajewski TF, Caglevic C, Dalle S, et al. Epacadostat plus pembrolizumab versus placebo plus pembrolizumab in patients with unresectable or metastatic melanoma (ECHO-301/KEYNOTE-252): a phase 3, randomised, double-blind study. *Lancet Oncol* (2019) 20:1083–97. doi: 10.1016/S1470-2045(19)30274-8

10. Reardon DA, Desjardins A, Rixe O, Cloughesy T, Alekar S, Williams JH, et al. A phase 1 study of PF-06840003, an oral indoleamine 2,3-dioxygenase 1 (IDO1) inhibitor in patients with recurrent malignant glioma. *Invest New Drugs* (2020) 10:1784–95. doi: 10.1007/s10637-020-00950-1
11. Günther J, Däbritz J, Wirthgen E. Limitations and off-target effects of tryptophan-related ido inhibitors in cancer treatment. *Front Immunol* (2019) 10:1–8. doi: 10.3389/fimmu.2019.01801
12. Eynde BJV, Baren N, Baurain J-F. Is There a clinical future for ido1 inhibitors after the failure of epacadostat in melanoma? *Annu Rev Cancer Biol* (2020) 4:241–56. doi: 10.1146/annurev-cancerbio-030419-033635
13. Muller AJ, Manfredi MG, Zakharia Y, Prendergast GC. Inhibiting IDO pathways to treat cancer: lessons from the ECHO-301 trial and beyond. *Semin Immunopathol* (2018) 41:41–8. doi: 10.1007/s00281-018-0702-0
14. Leklem JE. Quantitative aspects of tryptophan metabolism in humans and other species: a review. *Am J Clin Nutr* (1971) 24:659–72. doi: 10.1093/ajcn/24.6.659
15. Hopper AT, Campbell BM, Kao H, Pintchovski SA, Staal RGW. Recent developments in targeting neuroinflammation in disease. In: . *Annual Reports in Medicinal Chemistry Volume*, vol. 47. Elsevier (2012). p. 37–53.
16. Badawy AA. Hypothesis kynurenic and quinolinic acids: The main players of the kynurenine pathway and opponents in inflammatory disease. *Med Hypotheses* (2018) 118:129–38. doi: 10.1016/j.mehy.2018.06.021
17. Kolodziej LR, Paleolog EM, Williams RO. Kynurenine metabolism in health and disease. *Amino Acids* (2011) 41:1173–83. doi: 10.1007/s00726-010-0787-9
18. Ball HJ, Jusof FF, Bakmiwewa SM, Hunt NH, Yuasa H. Tryptophan catabolizing enzymes – party of three. *Front Immunol* (2014) 5:1–10. doi: 10.3389/fimmu.2014.00485
19. Ball HJ, Sanchez-Perez A, Weiser S, Austin CJD, Astelbauer F, Miu J, et al. Characterization of an indoleamine 2,3-dioxygenase-like protein found in humans and mice. *Gene* (2007) 396:203–13. doi: 10.1016/j.gene.2007.04.010
20. Metz R, DuHadaway JB, Kamasani U, Laury-Kleintop L, Muller AJ, Prendergast GC. Novel Tryptophan Catabolic Enzyme IDO2 Is the Preferred Biochemical Target of the Antitumor Indoleamine 2,3-Dioxygenase Inhibitory Compound d-1-Methyl-Tryptophan. *Cancer Res* (2007) 67:7082–7. doi: 10.1158/0008-5472.CAN-07-1872
21. Mellor AL, Munn DH. IDO expression by dendritic cells: tolerance and tryptophan catabolism. *Nat Rev Immunol* (2004) 4:762–74. doi: 10.1038/nri1457
22. Fujigaki S, Saito K, Sekikawa K, Tone S, Takikawa O, Fujii H, et al. Lipopolysaccharide induction of indoleamine 2,3-dioxygenase is mediated dominantly by an IFN-γ-independent mechanism. *Eur J Immunol* (2001) 31:2313–8. doi: 10.1002/1521-4141(200108)31:8<2313::AID-IMMU2313>3.0.CO;2-S
23. Grant RS. Indoleamine 2,3-Dioxygenase Activity Increases NAD+ Production in IFN-gamma-Stimulated human primary mononuclear cells. *Int J Tryptophan Res* (2018) 11:1–8. doi: 10.1177/1178646917751636
24. Taylor MW, Feng GS. Relationship between interferon-gamma, indoleamine 2,3-dioxygenase, and tryptophan catabolism. *FASEB J* (1991) 5:2516–22. doi: 10.1096/fasebj.5.11.1907934
25. Trabanelli S, Očadlíková D, Ciciarello M, Salvestrini V, Lecciso M, Jandus C, et al. The SOCS3-independent expression of ido2 supports the homeostatic generation of t regulatory cells by human dendritic cells. *J Immunol* (2014) 192:1231–40. doi: 10.4049/jimmunol.1300720
26. Meireson A, Devos M, Brochez L. IDO expression in cancer: different compartment, different functionality? *Front Immunol* (2020) 11:1–17. doi: 10.3389/fimmu.2020.531491
27. Théate I, van Baren N, Pilotte L, Moulin P, Larrieu P, Renauld J-C, et al. Extensive profiling of the expression of the indoleamine 2,3-dioxygenase 1 protein in normal and tumoral human tissues. *Cancer Immunol Res* (2015) 3:161–72. doi: 10.1158/2326-6066.CIR-14-0137
28. Salter M, Hazelwood R, Pogson CI, Iyer R, Madge DJ. The effects of a novel and selective inhibitor of tryptophan 2,3-dioxygenase on tryptophan and serotonin metabolism in the rat. *Biochem Pharmacol* (1995) 49:1435–42. doi: 10.1016/0006-2952(95)00006-L
29. Kanai M, Funakoshi H, Takahashi H, Hayakawa T, Mizuno S, Matsumoto K, et al. Tryptophan 2,3-dioxygenase is a key modulator of physiological neurogenesis and anxiety-related behavior in mice. *Mol Brain* (2009) 2:1–16. doi: 10.1186/1756-6606-2-8
30. Mehler AH, Knox WE. The conversion of tryptophan to kynurenine in liver: II. The enzymatic hydrolysis of formylkynurenine. *J Biol Chem* (1950) 187:431–8. doi: 10.1016/S0021-9258(19)50968-1
31. Li JS, Han Q, Fang J, Rizzi M, James AA, Li J. Biochemical mechanisms leading to tryptophan 2,3-dioxygenase activation. *Arch Insect Biochem Physiol* (2007) 64:74–87. doi: 10.1002/arch.20159
32. Green AR, Joseph MH, Woods HF. Proceedings: tryptophan metabolism by the isolated perfused rat liver. *Br J Pharmacol* (1975) 55:253–4. doi: 10.1111/j.1476-5381.1976.tb07660.x
33. Danesch U, Gloss B, Schmid W, Schütz G, Schüle R, Renkawitz R. Glucocorticoid induction of the rat tryptophan oxygenase gene is mediated by two widely separated glucocorticoid-responsive elements. *EMBO J* (1987) 6:625–30. doi: 10.1002/j.1460-2075.1987.tb04800.x
34. Munn DH, Zhou M, Attwood JT, Bondarev I. Prevention of allogeneic fetal rejection by tryptophan catabolism. *Science* (1998) 281:1191–3. doi: 10.1126/science.281.5380.1191
35. Uyttenhove C, Pilotte L, Théate I, Stroobant V, Colau D, Parmentier N, et al. Evidence for a tumoral immune resistance mechanism based on tryptophan degradation by indoleamine 2,3-dioxygenase. *Nat Med* (2003) 9:1269–74. doi: 10.1038/nm934
36. Pilotte L, Larrieu P, Stroobant V, Colau D, Dolušić E, Frédérick R, et al. Reversal of tumoral immune resistance by inhibition of tryptophan 2,3-dioxygenase. *Proc Natl Acad Sci* (2012) 109:2497–502. doi: 10.1073/pnas.1113873109
37. Sucher R, Kurz K, Weiss G, Margreiter R, Fuchs D, Brandacher G. IDO-mediated tryptophan degradation in the pathogenesis of malignant tumor disease. *Int J Tryptophan Res* (2010) 3:113–20. doi: 10.4137/IJTR.S4157
38. van Baren N, Van den Eynde BJ. Tryptophan-degrading enzymes in tumoral immune resistance. *Front Immunol* (2015) 6:1–9. doi: 10.3389/fimmu.2015.00034
39. Hoffmann D, Dvorakova T, Stroobant V, Bouzin C, Daumerie A, Solvay M, et al. Tryptophan 2,3-dioxygenase expression identified in human hepatocellular carcinoma cells and in intratumoral pericytes of most cancers. *Cancer Immunol Res* (2019) 8:19–31. doi: 10.1158/2326-6066.CIR-19-0040
40. Platten M, Nollen EAA, Röhrig UF, Fallarino F, Opitz CA. Tryptophan metabolism as a common therapeutic target in cancer, neurodegeneration and beyond. *Nat Rev Drug Discov* (2019) 18:379–401. doi: 10.1038/s41573-019-0016-5
41. Pallotta MT, Orabona C, Volpi C, Vacca C, Belladonna ML, Bianchi R, et al. Indoleamine 2,3-dioxygenase is a signaling protein in long-term tolerance by dendritic cells. *Nat Immunol* (2011) 12:870–8. doi: 10.1038/ni.2077
42. Bessede A, Gargaro M, Pallotta MT, Matino D, Servillo G, Brunacci C, et al. Aryl hydrocarbon receptor control of a disease tolerance defence pathway. *Nature* (2014) 511:184–90. doi: 10.1038/nature13323
43. Pallotta MT, Fallarino F, Matino D, Macchiarulo A, Orabona C. AhR-mediated, non-genomic modulation of IDO1 function. *Front Immunol* (2014) 5:1–6. doi: 10.3389/fimmu.2014.00497
44. Triplett TA, Garrison KC, Marshall N, Donkor M, Blazeck J, Lamb C, et al. Reversal of indoleamine 2,3-dioxygenase–mediated cancer immune suppression by systemic kynurenine depletion with a therapeutic enzyme. *Nat Biotechnol* (2018) 36:758–64. doi: 10.1038/nbt.4180
45. Chiesa MD, Carlomagno S, Frumento G, Balsamo M, Cantoni C, Conte R, et al. The tryptophan catabolite L-kynurenine inhibits the surface expression of NKp46- and NKG2D-activating receptors and regulates NK-cell function. *Blood* (2006) 108:4118–25. doi: 10.1182/blood-2006-03-006700
46. Rad Pour S, Morikawa H, Kiani NA, Yang M, Azimi A, Shafi G, et al. Exhaustion of CD4+ T-cells mediated by the Kynurenine Pathway in Melanoma. *Sci Rep* (2019) 9:12150. doi: 10.1038/s41598-019-48635-x
47. Fallarino F, Grohmann U, You S, McGrath BC, Cavener DR, Vacca C, et al. The Combined Effects of Tryptophan Starvation and Tryptophan Catabolites Down-Regulate T Cell Receptor ζ-Chain and Induce a Regulatory Phenotype in Naive T Cells. *J Immunol* (2006) 176:6752–61. doi: 10.4049/jimmunol.176.11.6752
48. Opitz CA, Litzenburger UM, Sahm F, Ott M, Tritschler I, Trump S, et al. An endogenous tumour-promoting ligand of the human aryl hydrocarbon receptor. *Nature* (2011) 478:197–203. doi: 10.1038/nature10491
49. Mezrich JD, Fechner JH, Zhang X, Johnson BP, Burlingham WJ, Bradfield CA. An interaction between kynurenine and the aryl hydrocarbon receptor can

generate regulatory T cells. *J Immunol* (2010) 185:3190–8. doi: 10.4049/jimmunol.0903670
50. Gutierrez-Vazquez C, Quintana FJ. Regulation of the Immune Response by the Aryl Hydrocarbon Receptor. *Immunity* (2018) 48:19–33. doi: 10.1016/j.immuni.2017.12.012
51. Brenk M, Scheler M, Koch S, Neumann J, Takikawa O, Hacker G, et al. Tryptophan deprivation induces inhibitory receptors ILT3 and ILT4 on dendritic cells favoring the induction of human CD4+CD25+ Foxp3+ T regulatory cells. *J Immunol* (2009) 183:145–54. doi: 10.4049/jimmunol.0803277
52. Vignali DAA, Collison LW, Workman CJ. How regulatory T cells work. *Nat Rev Immunol* (2008) 8:523–32. doi: 10.1038/nri2343
53. Nguyen NT, Kimura A, Nakahama T, Chinen I, Masuda K, Nohara K, et al. Aryl hydrocarbon receptor negatively regulates dendritic cell immunogenicity via a kynurenine-dependent mechanism. *Proc Natl Acad Sci* (2010) 107:19961–6. doi: 10.1073/pnas.1014465107
54. Takenaka MC, Gabriely G, Rothhammer V, Mascanfroni ID, Wheeler MA, Chao C-C, et al. Control of tumor-associated macrophages and T cells in glioblastoma via AHR and CD39. *Nat Neurosci* (2019) 22:729–40. doi: 10.1038/s41593-019-0370-y
55. Liu Y, Liang X, Dong W, Fang Y, Lv J, Zhang T, et al. Tumor-Repopulating Cells Induce PD-1 Expression in CD8+ T Cells by Transferring Kynurenine and AhR Activation. *Cancer Cell* (2018) 33:480–94.e487. doi: 10.1016/j.ccell.2018.02.005
56. Lee GK, Park HJ, Macleod M, Chandler P, Munn DH, Mellor AL. Tryptophan deprivation sensitizes activated T cells to apoptosis prior to cell division. *Immunology* (2002) 107:452–60. doi: 10.1046/j.1365-2567.2002.01526.x
57. Schramme F, Crosignani S, Frederix K, Hoffmann D, Pilotte L, Stroobant V, et al. Inhibition of tryptophan-dioxygenase activity increases the antitumor efficacy of immune checkpoint inhibitors. *Cancer Immunol Res* (2019) 8:32–45. doi: 10.1158/2326-6066.CIR-19-0041
58. Koblish HK, Hansbury MJ, Bowman KJ, Yang G, Neilan CL, Haley PJ, et al. Hydroxyamidine Inhibitors of Indoleamine-2,3-dioxygenase Potently Suppress Systemic Tryptophan Catabolism and the Growth of IDO-Expressing Tumors. *Mol Cancer Ther* (2010) 9:489–98. doi: 10.1158/1535-7163.MCT-09-0628
59. Sonner JK, Deumelandt K, Ott M, Thomé CM, Rauschenbach KJ, Schulz S, et al. The stress kinase GCN2 does not mediate suppression of antitumor T cell responses by tryptophan catabolism in experimental melanomas. *Oncoimmunology* (2016) 5:e1240858. doi: 10.1080/2162402X.2016.1240858
60. Munn DH, Sharma MD, Baban B, Harding HP, Zhang Y, Ron D, et al. GCN2 kinase in T cells mediates proliferative arrest and anergy induction in response to indoleamine 2,3-dioxygenase. *Immunity* (2005) 22:633–42. doi: 10.1016/j.immuni.2005.03.013
61. Castilho BA, Shanmugam R, Silva RC, Ramesh R, Himme BM, Sattlegger E. Keeping the eIF2 alpha kinase Gcn2 in check. *Biochim Biophys Acta (BBA) - Mol Cell Res* (2014) 1843:1948–68. doi: 10.1016/j.bbamcr.2014.04.006
62. Van de Velde LA, Guo XJ, Barbaric L, Smith AM, Oguin TH3, Thomas PG, et al. Stress Kinase GCN2 Controls the Proliferative Fitness and Trafficking of Cytotoxic T Cells Independent of Environmental Amino Acid Sensing. *Cell Rep* (2016) 17:2247–58. doi: 10.1016/j.celrep.2016.10.079
63. Maurin A-C, Jousse C, Averous J, Parry L, Bruhat A, Cherasse Y, et al. The GCN2 kinase biases feeding behavior to maintain amino acid homeostasis in omnivores. *Cell Metab* (2005) 1:273–7. doi: 10.1016/j.cmet.2005.03.004
64. Leib DE, Knight ZA. Re-examination of Dietary Amino Acid Sensing Reveals a GCN2-Independent Mechanism. *Cell Rep* (2015) 13:1081–9. doi: 10.1016/j.celrep.2015.09.055
65. Guertin DA, Sabatini DM. Defining the Role of mTOR in Cancer. *Cancer Cell* (2007) 12:9–22. doi: 10.1016/j.ccr.2007.05.008
66. Metz R, Rust S, Duhadaway JB, Mautino MR, Munn DH, Vahanian NN, et al. IDO inhibits a tryptophan sufficiency signal that stimulates mTOR: A novel IDO effector pathway targeted by D-1-methyl-tryptophan. *Oncoimmunology* (2012) 1:1460–8. doi: 10.4161/onci.21716
67. Badawy AAB, Namboodiri AMA, Moffett JR. The end of the road for the tryptophan depletion concept in pregnancy and infection. *Clin Sci* (2016) 130:1327–33. doi: 10.1042/CS20160153
68. Segawa H, Fukasawa Y, Miyamoto K, Takeda E, Endou H, Kanai Y. Identification and Functional Characterization of a Na+ independent Neutral Amino Acid Transporter with Broad Substrate Selectivity. *J Biol Chem* (1999) 274:19745–51. doi: 10.1074/jbc.274.28.19745
69. Kudo Y, Boyd CAR. The role of L-tryptophan transport in L-tryptophan degradation by indoleamine 2,3-dioxygenase in human placental explants. *J Physiol* (2001) 531:417–23. doi: 10.1111/j.1469-7793.2001.0417i.x
70. Sekine A, Okamoto M, Kanatani Y, Sano M, Shibata K, Fukuwatari T. Amino acids inhibit kynurenic acid formation via suppression of kynurenine uptake or kynurenic acid synthesis in rat brain in vitro. *Springerplus* (2015) 4:48. doi: 10.1186/s40064-015-0826-9
71. Verrey F. System L: heteromeric exchangers of large, neutral amino acids involved in directional transport. *Pflugers Arch* (2003) 445:529–33. doi: 10.1007/s00424-002-0973-z
72. Hoglund E, Overli O, Winberg S. Tryptophan Metabolic Pathways and Brain Serotonergic Activity: A Comparative Review. *Front Endocrinol (Lausanne)* (2019) 10:158. doi: 10.3389/fendo.2019.00158
73. Sinclair LV, Neyens D, Ramsay G, Taylor PM, Cantrell DA. Single cell analysis of kynurenine and System L amino acid transport in T cells. *Nat Commun* (2018) 9:1981. doi: 10.1038/s41467-018-04366-7
74. Silk JD, Lakhal S, Laynes R, Vallius L, Karydis I, Marcea C, et al. IDO induces expression of a novel tryptophan transporter in mouse and human tumor cells. *J Immunol* (2011) 187:1617–25. doi: 10.4049/jimmunol.1000815
75. Li H, Ning S, Ghandi M, Kryukov GV, Gopal S, Deik A, et al. The landscape of cancer cell line metabolism. *Nat Med* (2019) 25:850–60. doi: 10.1038/s41591-019-0404-8
76. Ferns DM, Kema IP, Buist MR, Nijman HW, Kenter GG, Jordanova ES. Indoleamine-2,3-dioxygenase (IDO) metabolic activity is detrimental for cervical cancer patient survival. *OncoImmunology* (2015) 4:e981457. doi: 10.4161/2162402X.2014.981457
77. Weinlich G, Murr C, Richardsen L, Winkler C, Fuchs D. Decreased serum tryptophan concentration predicts poor prognosis in malignant melanoma patients. *Dermatology* (2007) 214:8–14. doi: 10.1159/000096906
78. Tanizaki Y, Kobayashi A, Toujima S, Shiro M, Mizoguchi M, Mabuchi Y, et al. Indoleamine 2,3-dioxygenase promotes peritoneal metastasis of ovarian cancer by inducing an immunosuppressive environment. *Cancer Sci* (2014) 105:966–73. doi: 10.1111/cas.12445
79. Masaki A, Ishida T, Maeda Y, Suzuki S, Ito A, Takino H, et al. Prognostic significance of tryptophan catabolism in adult T-cell leukemia/lymphoma. *Clin Cancer Res* (2015) 21:2830–9. doi: 10.1158/1078-0432.CCR-14-2275
80. Li H, Bullock K, Gurjao C, Braun D, Shukla SA, Bosse D, et al. Metabolomic adaptations and correlates of survival to immune checkpoint blockade. *Nat Commun* (2019) 10:4346. doi: 10.1038/s41467-019-12361-9
81. Campesato LF, Budhu S, Tchaicha J, Weng C-H, Gigoux M, Cohen IJ, et al. Blockade of the AHR restricts a Treg-macrophage suppressive axis induced by L-Kynurenine. *Nat Commun* (2020) 11:4011. doi: 10.1038/s41467-020-17750-z
82. Gomes B, Driessens G, Bartlett D, Cai D, Cauwenberghs S, Crosignani S, et al. Characterization of the Selective Indoleamine 2,3-Dioxygenase-1 (IDO1) Catalytic Inhibitor EOS200271/PF-06840003 Supports IDO1 as a Critical Resistance Mechanism to PD-(L)1 Blockade Therapy. *Mol Cancer Ther* (2018) 17:2530–42. doi: 10.1158/1535-7163.MCT-17-1104
83. Dounay AB, Tuttle JB, Verhoest PR. Challenges and Opportunities in the Discovery of New Therapeutics Targeting the Kynurenine Pathway. *J Med Chem* (2015) 58:8762–82. doi: 10.1021/acs.jmedchem.5b00461
84. Guzik K, Tomala M, Muszak D, Konieczny M, Hec A, Błaszkiewicz U, et al. Development of the Inhibitors That Target the PD-1/PD-L1 Interaction—A Brief Look at Progress on Small Molecules, Peptides and Macrocycles. *Molecules* (2019) 24:2071. doi: 10.3390/molecules24112071
85. Konieczny M, Musielak B, Kocik J, Skalniak L, Sala D, Czub M, et al. Di-bromo-Based Small-Molecule Inhibitors of the PD-1/PD-L1 Immune Checkpoint. *J Med Chem* (2020) 63:11271–85. doi: 10.1021/acs.jmedchem.0c01260
86. Cheong JE, Ekkati A, Sun L. A patent review of IDO1 inhibitors for cancer. *Expert Opin Ther Pat* (2018) 28:317–30. doi: 10.1080/13543776.2018.1441290
87. Sun L. Advances in the discovery and development of selective heme-displacing IDO1 inhibitors. *Expert Opin Drug Discov* (2020) 15(10): 1–10. doi: 10.1080/17460441.2020.1781811

88. Spranger S, Koblish H, Horton B, Scherle P, Newton R, Gajewski T. Mechanism of tumor rejection with doublets of CTLA-4, PD-1/PD-L1, or IDO blockade involves restored IL-2 production and proliferation of CD8+ T cells directly within the tumor microenvironment. *J Immunother Cancer* (2014) 2:3. doi: 10.1186/2051-1426-2-3
89. Tu W, Yang F, Xu G, Chi J, Liu Z, Peng W, et al. Discovery of Imidazoisoindole Derivatives as Highly Potent and Orally Active Indoleamine-2,3-dioxygenase Inhibitors. *ACS Med Chem Lett* (2019) 10:949–53. doi: 10.1021/acsmedchemlett.9b00114
90. Zhang H, Liu K, Pu Q, Achab A, Ardolino MJ, Cheng M, et al. Discovery of Amino-cyclobutarene-derived Indoleamine-2,3-dioxygenase 1 (IDO1) Inhibitors for Cancer Immunotherapy. *ACS Med Chem Lett* (2019) 10:1530–6. doi: 10.1021/acsmedchemlett.9b00344
91. Watanabe T, Gaedicke S, Guffart E, Firat E, Niedermann G. Adding Indoximod to Hypofractionated Radiotherapy with Anti-PD-1 Checkpoint Blockade Enhances Early NK and CD8+ T-Cell–Dependent Tumor Activity. *Clin Cancer Res* (2020) 26:945–56. doi: 10.1158/1078-0432.CCR-19-0476
92. Jochems C, Fantini M, Fernando RI, Kwilas AR, Donahue RN, Lepone LM. The IDO1 selective inhibitor epacadostat enhances dendritic cell immunogenicity and lytic ability of tumor antigen-specific T cells. *Oncotarget* (2016) 7:37762–72. doi: 10.18632/oncotarget.9326
93. Sondak VK, Khushalani NI. Echoes of a failure: what lessons can we learn? *Lancet Oncol* (2019) 20(8):1037–9. doi: 10.1016/S1470-2045(19)30312-2
94. Opitz CA, Somarribas Patterson LF, Mohapatra SR, Dewi DL, Sadik A, Platten M, et al. The therapeutic potential of targeting tryptophan catabolism in cancer. *Br J Cancer* (2019) 122:30–44. doi: 10.1038/s41416-019-0664-6
95. Pham KN, Lewis-Ballester A, Yeh S-R. Structural Basis of Inhibitor Selectivity in Human Indoleamine 2,3-Dioxygenase 1 and Tryptophan Dioxygenase. *J Am Chem Soc* (2019) 141(47):18771–9. doi: 10.1021/jacs.9b08871
96. Kozlova A, Frédérick R. Current state on tryptophan 2,3-dioxygenase inhibitors: a patent review. *Expert Opin Ther Pat* (2019) 29:11–23. doi: 10.1080/13543776.2019.1556638
97. Dolušić E, Larrieu P, Moineaux L, Stroobant V, Pilotte L, Colau D, et al. Tryptophan 2,3-Dioxygenase (TDO) Inhibitors. 3-(2-(Pyridyl)ethenyl) indoles as Potential Anticancer Immunomodulators. *J Med Chem* (2011) 54:5320–34. doi: 10.1021/jm2006782
98. Pantouris G, Loudon-Griffiths J, Mowat CG. Insights into the mechanism of inhibition of tryptophan 2,3-dioxygenase by isatin derivatives. *J Enzyme Inhib Med Chem* (2016) 1–9:70–8. doi: 10.3109/14756366.2016.1170013
99. Pei Z, Mendonca R, Gazzard L, Pastor R, Goon L, Gustafson A, et al. Aminoisoxazoles as Potent Inhibitors of Tryptophan 2,3-Dioxygenase 2 (TDO2). *ACS Med Chem Lett* (2018) 9:417–21. doi: 10.1021/acsmedchemlett.7b00427
100. Parr BT, Pastor R, Sellers BD, Pei Z, Jaipuri FA, Castanedo GM, et al. Implementation of the CYP Index for the Design of Selective Tryptophan-2,3-dioxygenase Inhibitors. *ACS Med Chem Lett* (2020) 11:541–9. doi: 10.1021/acsmedchemlett.0c00004
101. Ferreira P, Shin I, Sosova I, Dornevil K, Jain S, Dewey D, et al. Hypertryptophanemia due to tryptophan 2,3-dioxygenase deficiency. *Mol Genet Metab* (2017) 120:317–24. doi: 10.1016/j.ymgme.2017.02.009
102. Gyulveszi G, Fischer C, Mirolo M, Stern M, Green L, Ceppi M, et al. Abstract LB-085: RG70099: A novel, highly potent dual IDO1/TDO inhibitor to reverse metabolic suppression of immune cells in the tumor microenvironment. *AACR* (2016) 76(14 Supplement). doi: 10.1158/1538-7445.AM2016-LB-085
103. Gullapalli S, Roychowdhury A, Khaladkar T, Sawargave S, Janrao R, Kalhapure V, et al. EPL-1410, a novel fused heterocycle based orally active dual inhibitor of IDO1/TDO2, as a potential immune-oncology therapeutic. *Cancer Res* (2018) 78:1701. doi: 10.1158/1538-7445.AM2018-1701
104. Satoh Y, Kotani H, Iida Y, Taniura T, Notsu Y, Harada M. Supplementation of l-arginine boosts the therapeutic efficacy of anticancer chemoimmunotherapy. *Cancer Sci* (2020) 111:2248–58. doi: 10.1111/cas.14490
105. Walker AK, Wing EE, Banks WA, Dantzer R. Leucine competes with kynurenine for blood-to-brain transport and prevents lipopolysaccharide-induced depression-like behavior in mice. *Mol Psychiatry* (2019) 24:1523–32. doi: 10.1038/s41380-018-0076-7
106. Roberts A. The Safety and Regulatory Process for Amino Acids in Europe and the United States. *J Nutr* (2016) 146:2635S–42S. doi: 10.3945/jn.116.234591
107. Garlick PJ. The Nature of Human Hazards Associated with Excessive Intake of Amino Acids. *J Nutr* (2004) 134:1633S–9S. doi: 10.1093/jn/134.6.1633S
108. Anderson SA, Raiten DJ. *Safety of amino acids used as dietary supplements*. Bethesda, Md. (9650 Rockville Pike, Bethesda 20814-3998): Life Sciences Research Office, Federation of American Societies for Experimental Biology (1992).
109. Lupton JR, Brooks J, Butte N, Caballero B, Flatt J, Fried S. *Dietary reference intakes for energy, carbohydrate, fiber, fat, fatty acids, cholesterol, protein, and amino acids*. vol. 5. Washington, DC, USA: National Academy Press (2002). p. 589–768.
110. Benevenga N, Steele R. Adverse effects of excessive consumption of amino acids. *Annu Rev Nutr* (1984) 4:157–81. doi: 10.1146/annurev.nu.04.070184.001105
111. Matsueda S, Niiyama Y. The effects of excess amino acids on maintenance of pregnancy and fetal growth in rats. *J Nutr Sci Vitaminol* (1982) 28:557–73. doi: 10.3177/jnsv.28.557
112. Benevenga N, Yeh M-H, Lalich J. Growth depression and tissue reaction to the consumption of excess dietary methionine and S-methyl-L-cysteine. *J Nutr* (1976) 106:1715–20. doi: 10.1093/jn/106.12.1715
113. Sadik A, Somarribas Patterson LF, Öztürk S, Mohapatra SR, Panitz V, Secker PF, et al. IL4I1 Is a Metabolic Immune Checkpoint that Activates the AHR and Promotes Tumor Progression. *Cell* (2020) 182:1252–70.e34. doi: 10.1016/j.cell.2020.07.038

Conflict of Interest: The authors declare that the research was conducted in the absence of any commercial or financial relationships that could be construed as a potential conflict of interest.

Copyright © 2021 Kim and Tomek. This is an open-access article distributed under the terms of the Creative Commons Attribution License (CC BY). The use, distribution or reproduction in other forums is permitted, provided the original author(s) and the copyright owner(s) are credited and that the original publication in this journal is cited, in accordance with accepted academic practice. No use, distribution or reproduction is permitted which does not comply with these terms.

frontiers in Immunology

ORIGINAL RESEARCH
published: 24 February 2021
doi: 10.3389/fimmu.2021.624789

Changes in the Peripheral Blood Treg Cell Proportion in Hepatocellular Carcinoma Patients After Transarterial Chemoembolization With Microparticles

Zhizhong Ren[1†], Yuanxun Yue[2†], Yuewei Zhang[1], Jiahong Dong[1*], Ying Liu[1], Xiaowei Yang[1], Xin Lin[3], Xueqiang Zhao[3], Zhanqi Wei[3], Yu Zheng[3] and Tianxiao Wang[1]*

[1] Hepatobiliary Pancreatic Center Department, Beijing Tsinghua Changgung Hospital Affiliated to Tsinghua University, Beijing, China, [2] Department of Interventional and Pain, Beijing Luhe Hospital, Capital Medical University, Beijing, China, [3] School for Medicine, Institute for Immunology, Tsinghua University, Beijing, China

OPEN ACCESS

Edited by:
Peng Qu,
National Institutes of Health (NIH), United States

Reviewed by:
Joseph Barbi, University at Buffalo, United States
Ajithkumar Vasanthakumar, Peter Doherty Institute for Infection and Immunity, Australia

***Correspondence:**
Yuewei Zhang
zhangyuewei1121@sina.com
Jiahong Dong
djha00988@btch.edu.cn

[†]These authors share first authorship

Specialty section:
This article was submitted to Cancer Immunity and Immunotherapy, a section of the journal Frontiers in Immunology

Received: *01 November 2020*
Accepted: *04 January 2021*
Published: *24 February 2021*

Citation:
Ren Z, Yue Y, Zhang Y, Dong J, Liu Y, Yang X, Lin X, Zhao X, Wei Z, Zheng Y and Wang T (2021) Changes in the Peripheral Blood Treg Cell Proportion in Hepatocellular Carcinoma Patients After Transarterial Chemoembolization With Microparticles. Front. Immunol. 12:624789. doi: 10.3389/fimmu.2021.624789

Objective: Transarterial chemoembolization (TACE) stands for an ideal therapy for patients with intermediate stage HCC. This study was carried out to observe the effect of microparticles-transarterial chemoembolization (microparticles-TACE, m-TACE) on the immune function of hepatocellular carcinoma (HCC) patients by detecting the proportion of regulatory (Treg) cells in the peripheral blood of HCC patients before and after m-TACE, and to determine whether m-TACE has a positive regulatory effect on the immune function of HCC patients.

Methods: 33 HCC patients treated with Gelatn Sponge Microparticles (GSMs-TACE) were enrolled. Flow cytometry was used to determine the proportion of Treg cells and CD4+/CD8+ T cells in peripheral blood of HCC patients 1 day before GSMs-TACE, 1 to 2 weeks and 3 to 5 weeks after GSMs-TACE, respectively.

Results: The Tregs cell proportion of HCC patients was significantly higher than that of the healthy and cirrhosis controls and was associated with various clinical indicators of HCC patients. The Treg cell proportion in HCC patients with BCLC stage C was higher than that of stage B patients; The Treg cell proportion at 1 to 2 weeks postoperatively was 8.54 ± 1.27%, which was significantly lower than that before the GSMs-TACE. The Treg cell proportion at 3 to 5 weeks postoperatively was 7.59 ± 1.27%, which continued to decline. The ratio of CD4+/CD8+ T cells was 1.31 ± 0.56, 1.86 ± 0.73, 1.76 ± 0.58% ($P<0.01$) respectively.

Conclusion: These results indicated that m-TACE could exert a positive regulatory effect on the anticancer immune function of HCC patients, which may be used in combination with immune adjuvant therapies to enhance the efficacy of HCC.

Keywords: hepatocellular carcinoma, Treg cells, m-TACE, tumor immunity, flow cytometry

INTRODUCTION

Hepatocellular carcinoma (HCC) is the most common malignancy worldwide. Currently, liver transplantation and surgical resection remain the primary choice for HCC, but the overall survival of HCC patients is still depressing mainly due to local recurrence, distant metastasis, treatment resistance, and the lack of early diagnosis (1–3). TACE is one of the first-line treatment choices for HCC patients with specific clinical characteristics, such as stage B according to Barcelona Clinic Liver Cancer (BCLC) (4). The transcatheter delivery of both chemotherapeutic agents and embolizing agents contributes to a dual effect of cytotoxicity and ischemia in tumor tissues (4). Currently, there are many TACE modalities in clinical practice, such as conventional TACE (c-TACE), m-TACE and Doxorubicin Eluting Beads TACE (DEB-TACE) (4).

As the representative of absorbable particles, Gelatn Sponge Microparticles(GSMs) are characterized by chemical cross-linking and physical adsorption since they can be absorbed 7–15 days after arterial embolization. Since 2009, satisfactory efficacy and safety of GSMs-TACE in the treatment of HCC patients at stage B and C (BCLC classification) with a diameter of 150–350 μm/350–560 μm GSMs have been achieved in our team (5, 6). During GSMs-TACE procedures, under the premise of good liver function, the standard of terminating embolization is that the tumor blood supply artery is completely embolized. Compared with c-TACE, the application of TACE combined with different diameters microparticles in the treatment of HCC can lead to more significant tumor necrosis, especially the huge HCC.

Since the identification of tumor antigens, various approaches manipulating the immune system have been developed for cancer therapies (7). However, not all patients respond to immunotherapies, and one of the major obstacles is the formation of immunosuppressive tumor microenvironment which is filled with immunosuppressive cells such as Treg cells (8). Treg cells are a T-lymphocyte subset and help maintain immune homeostasis by controlling abnormal/excessive immune responses. Studies have found that Treg cells are also involved in development and progression of tumors *via* acting as s suppressor of effective antitumor immunity (7, 9). High infiltration by Treg cells into TME was observed in various types of tumors including HCC and was found to be correlated with poor prognosis (8–10). Therefore, strategies to reduce Treg cells and control the functions of Treg cells would be potentially effective anticancer therapies.

Many studies have confirmed the efficacy and safety of TACE procedures in treating HCC, and it was considered that the effects were mainly attributed to the blood supply blockade and the cytotoxic effects (11, 12). Except for the tumor necrosis, it was also observed that extrahepatic metastasis were reduced or even disappeared after GSMs-TACE in our clinical practice. Considering the close relationship between tumor metastasis and the immunosuppressive TME, these findings prompted us wonder if the effect of m-TACE was also partly lead to tumor necrosis, which promoted the positive regulatory effects on the anticancer immunity. However, there have been no related studies to testify this hypothesis. Thus, this study aimed to determine the changes in immune function indicated by the peripheral blood Treg cell proportion in HCC patients after m-TACE. The results of this study provided a piece of preliminary evidence that m-TACE may be used in combination with immune adjuvant therapies to increase the efficacy of HCC treatment.

PATIENTS AND METHODS

Patients

Seventy-nine patients with HCC diagnosed in our hospital from July 2017 to June 2020 were enrolled (**Figure 1**, **Table 1**). All patients were confirmed as HCC by two or more imaging examinations or liver tumor biopsy, according to the Expert Consensus on Regulation of Standardized Diagnosis and Treatment of Primary Liver Cancer. Thirty-three patients were followed up regularly after GSMs -TACE treatment for 3 to 5 weeks and the Treg cells proportion in peripheral blood was examined. Twenty healthy volunteers and 20 cirrhosis were selected as control group.

The Standardized GSMs-TACE

The enrolled patients were treated with GSMs-TACE, all the blood supply arteries of the tumors were identified according to the location, size and staining integrity of the tumors. Microparticles of different sizes (150μm, 350–560 μm, and 560–710 μm) were selected during the procedure according to the tumor size and degree of staining. The appropriate dose of epirubicin (30–50 mg) was decided according to the tumor volume, and the dose of GSMs embolic agent (50–200 mg) was selected according to the tumor volume and degree of staining. Epirubicin was diluted with 50–100 mL of saline and then mixed with embolic agents of GSMs evenly. When the GSMs achieved a uniform and sparse suspension in epirubicin dilution, the mixture was used to slowly embolize the feeding artery of the tumor until the tumor staining disappeared completely, and the embolization usually lasted for 20–30 min.

Collection and Process of Blood Sample

All patients signed the informed consent. Functions of liver and kidney, blood test and tumor marker (AFP and PIVKA-II) were routinely examined 1 day before GSMs-TACE and 4, 10, and 30 days after TACE. Upper abdominal CT plain scan was performed 4 days after operation, and enhanced CT or MRI was performed 30 days after TACE. Two milliliter forearm venous blood was collected from all patients with HCC 1 day before GSMs-TACE, 1 to 2 weeks and 3 to 5 weeks after TACE using blood collection tube treated with heparin sodium anticoagulant. Flow cytometry was used to determine Treg, CD4+T, CD8+T and NK cell proportions in peripheral blood. Two milliliter of forearm venous blood was also collected from the healthy and cirrhosis control group, and the data were collected for statistical analysis.

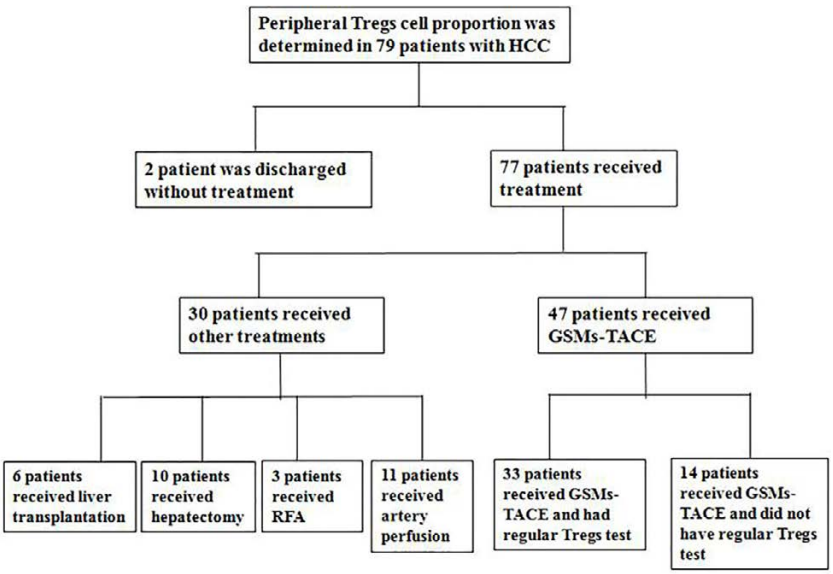

FIGURE 1 | Flow chart of the enrollment of 33 HCC patients treated with GSMs-TACE. (RFA, radiofrequency ablation; HCC, hepatocellular carcinoma; GSMs-TACE, transarterial chemoembolization with gelatin sponge microparticles).

Blood Preparation and Determination of Treg Cell Proportion by Flow Cytometry

1. Venipuncture blood was collected using anticoagulant tube;
2. One hundred milliliter whole blood was added to the bottom of the dry powder reagent tube which has antibodies of CD25/CD4/CD127/CD3 in the bottom;
3. the tube was vortexed for 0.5-1 s to mix well and incubated for 15 min at room temperature with light avoided;
4. Five hundred microliter of erythrocyte lysate was added to the tube. The tube was then incubated for 15 min at room temperature with light avoided;
5. Two milliliter PBS solution was added to each tube, and then oscillate the tube. Then the mixture was centrifuged at room temperature for 5 min with a centrifugal force of 300 g;
6. the supernatant was removed, and then step 5 was repeated for one more time.
7. the supernatant was removed, and then 500 mL PBS solution was added to each tube. The sample was then used for flow cytometry within 1 h;
8. the gating strategy of flow cytometry was set as follows: Treg: cell population of ①$CD4^+$ and $CD3^+$; ②$CD25^+$ and $CD127^+$ low.

Flow Cytometry for CD4+T CD8+T in Peripheral Blood

The cell surface expression levels of CD4, CD8 were evaluated using flow cytometry, followed by incubation with PE-CY5-conjugated anti-CD4 antibody and FITC-conjugated anti-CD8 antibody at room temperature. After 10 min, red cells were removed using lysis buffer, and were washed twice with PBS. The cells were resuspended in 0.5 ml PBS. Analysis was performed on the results obtained from at least 10,000 cells, which were acquired on a CytoFLEX (Beckman Coulter).

Statistical Analysis

The statistical analysis was conducted by SPSS software (provided by IBM, version 20.0). Results were expressed as mean ± SD. The *t* test was used to compare the data of different groups. The test level was α=0.05, and $P < 0.05$ was considered statistically significant.

RESULTS

The Increased Proportion of Treg Cells in Peripheral Blood of Cirrhosis and HCC Patients

The proportion of Treg cells ($CD25^+$, CD127+ Low) in Th cells (CD3+, CD4+) was 11.74 ± 1.67% in HCC patients, 5.51 ± 1.22% in healthy group and 7.69 ± 1.07 in Cirrhosis. The proportion of Treg cells in peripheral blood of Cirrhosis and HCC patients was significantly higher than that of healthy group ($P < 0.01$). See **Figure 2A**.

The Association Between the Treg Cells Proportion and Clinical Characteristics of HCC Patients

The peripheral blood Treg cell proportion in HCC patients was associated with tumor stage, AFP, PIVKA-II, tumor size, tumor encapsulation, vascular invasion. The proportion of Treg cells in peripheral blood of HCC patients at stage C was higher than that

TABLE 1 | Characteristics of 79 patients with HCC and 33 patients treated by GSMs-TACE who had regular Tregs test.

Variables	79 patient	33 patient
Average age (years, mean ± SD)	55 ± 12	54 ± 12
Gender		
Male	65	26
Female	14	7
Child-Pugh grade		
A	67	29
B	12	4
BCLC stage		
B	31	13
C	48	20
AFP (ng/mL)		
<400	32	17
≥400	47	16
PIVKA-II(mAU/ml)		
<1000	35	12
≥1000	44	21
Tumor size (cm)		
<10	41	12
≥10	38	21
Tumor number		
<4	43	14
≥4	36	19
Extrahepatic metastasis (cases)		
Yes	33	12
no	46	21
Portal or hepatic vein invasion (cases)		
Yes	42	19
no	37	14
Tumor encapsulation		
Yes	37	15
no	42	18
Type of hepatitis		
Hepatitis B	67	28
No hepatitis	12	5
HBeAg		
Positive	18	9
Negative	49	24

AFP, alpha-fetoprotein; PIVKA-II, Protein Induced by Vitamin K Absence or Antagonist-II; BCLC, Barcelona Clinic Liver Cancer (BCLC) staging system.

of patients at stage B. The Treg cells proportion in AFP and PIVKA-II positive (≥400 ng/mL; ≥1,000 mAU/ml) HCC patients was higher than that in AFP and PIVKA-II negative patients. In addition, the larger the tumor size (>10cm), the higher the Treg cell proportion in peripheral blood ($P < 0.05$). According to the enhanced CT examination and Digital Subtraction Angiography (DSA) tumor staining, the Treg proportion in HCC patients without tumor encapsulation or with vascular invasion was higher than that with tumor encapsulation or without vascular invasion ($P < 0.01$) (**Table 2**). Analysis showed the number of tumor, extrahepatic metastasis, hepatitis B virus-related was not positively correlated with the Treg cell proportion ($P>0.05$).

The Treg Cell Proportion in Peripheral Blood of 33 HCC Patients Before and After GSMs-TACE

In this study, the Treg cell proportion in HCC patients before and at 1 to 2 weeks, 3 to 5 weeks after GSMs-TACE showed a decreasing trend, 11.74 ± 1.67% before GSMs-TACE to 8.54 ± 1.27% at 1 to 2 weeks and 7.59 ± 1.27% at 3 to 5 weeks after GSMs-TACE, which was statistically significantly lower after GSMs-TACE ($P < 0.01$) (**Table 3**, **Figure 2B**). Representative profiles of high CD25 and low CD127 expressions in the peripheral blood of a HCC patient are shown in **Figure 3A**.

Moreover, the analysis of the BCLC subgroup showed that the Treg proportion of both stage B and stage C patients decreased significantly at 1 to 2 weeks and 3 to 5 weeks after GSMs-TACE ($P < 0.01$) (**Table 4**).

The CD4+ CD8+ and NK Cell Proportions in Peripheral Blood of 33 Patients With HCC Before and After GSMs-TACE

The comparison between prior to and after GSMs-TACE is demonstrated in **Table 5**, **Figure 4**. The proportion of CD4+T cells of HCC patients was 31.45 ± 6.82, 39.87 ± 8.96, 39.64 ± 8.83% respectively prior to and 1–2 weeks and 3–5weeks after

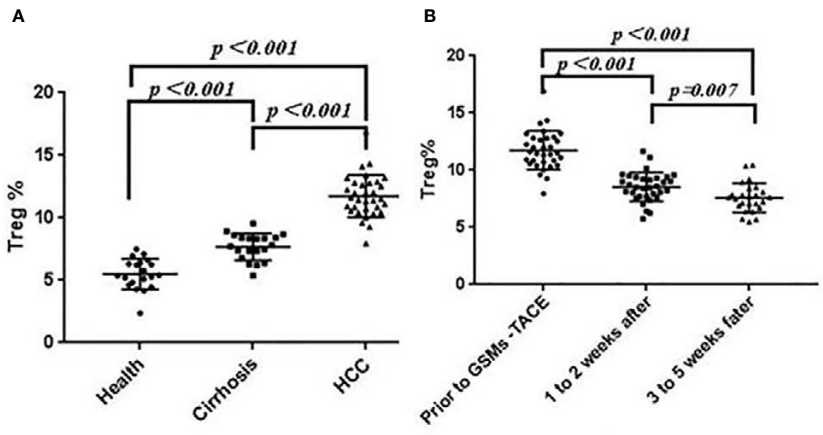

FIGURE 2 | **(A)** Comparison of Treg Cell proportions in Health, Cirrhosis and HCC patients. **(B)** Changes of Treg cell proportions in peripheral blood of HCC patients before and after GSMs-TACE.

TABLE 2 | The association between the Treg cell proportion with clinical characteristics of HCC patients.

Characteristics		Number	Treg cells proportion	*t* value	*p*
Tumor stage	stage B	31	9.88 ± 1.89		
(BCLC)	stage C	48	11.49 ± 2.20	3.438	0.001
AFP (ng/mL)	<400	32	10.10 ± 1.77		
	≥400	47	11.37 ± 2.40	2.735	0.008
PIVKA-II(mAU/ml)	<1,000	35	10.08 ± 1.66		
	≥1,000	44	11.47 ± 2.42	2.899	0.005
Tumor size (cm)	<10	41	10.35 ± 1.87		
	≥10	38	11.40 ± 2.45	2.138	0.036
Number of Tumor	<4	43	10.73 ± 1.98		
	≥4	36	11.00 ± 2.50	0.513	0.609
Tumor encapsulation	yes	37	10.12 ± 1.94		
	no	42	11.50 ± 2.27	2.909	0.005
Extrahepatic	yes	33	10.88 ± 2.46		
Metastasis	no	46	10.84 ± 2.05	0.070	0.945
Portal or hepatic	yes	42	11.58 ± 2.28		
Vein invasion	no	37	10.04 ± 1.87	3.294	0.001
Type of hepatitis B	Positive	67	10.87 ± 2.09		
	Negative	12	10.80 ± 2.97	0.075	0.942
HBeAg	Positive	18	10.67 ± 2.04		
	Negative	49	10.94 ± 2.12	0.474	0.638

GSMs-TACE (P<0.01), CD8+T cells was 28.01 ± 7.56, 22.64 ± 5.59, 25.47 ± 7.70% respectively. The ratio of CD4+/CD8+T cells was 1.31 ± 0.56, 1.86 ± 0.73, 1.76 ± 0.58% (P<0.01) respectively. These results suggested that the partial T lymphocytes immune function was restored in HCC patients following GSMs-TACE.

Imaging Changes of HCC Patients Before and After GSMs-TACE

DSA imaging during GSMs-TACE procedures showed intrahepatic tumor staining, and the feeding artery came from the right hepatic artery. After GSMs-TACE, the blood supply artery of the tumor was blocked, and the tumor staining disappeared according to the angiography. On the 4th day after interventional therapy, CT scan of the upper abdomen of 33 patients with HCC showed honeycomb necrosis to different degrees (**Figure 5**).

DISCUSSION

Currently, HCC is still one of the primary causes of cancer deaths, although the survival rates and prognosis of HCC have been greatly improved by liver transplantation and surgical resection (2). TACE procedures are currently widely used for various cases of HCC, mostly patients at BCLC stage B. Gelatin sponge microparticle (GSM) is an effective embolization agent, and a study reported that when compared with the ethiodized oil which is a permanent embolization agent, GSMs had many advantages, such as a higher tumor response rate at 1 month after treatment, especially in large tumors (13). Our previous clinical practices have confirmed the safety and efficacy of GSMs-TACE (5, 14, 15). It was found that 350–560 μm GSMs combined with single chemotherapy drug TACE procedures was effective and safe in treating elderly HCC without surgical resection, and more elderly patients may have better prognosis (5). GSMs combined with trans-arterial p53-gene-embolization also achieved satisfactory efficacy in treating BCLC stage B HCC as evidenced by favorable survival rates (100% for both 6 and 12 months) and no significant complications (14). Therefore, GSMs were adopted in this study, and imaging scan confirmed the efficacy of GSMs-TACE. DSA angiography during the procedure revealed that after GSMs embolization, the blood flow velocity of tumor feeding arteries, slowed down, and the tumor staining basically disappeared. Moreover, 4 days after GSMs-TACE, CT plain scan showed some honeycomb-like low-density changes in tumors compared with before the procedure. In addition, in a previous study, after analyzing the data of 37 patients who received GSMs-TACE for liver metastases after gastrointestinal tumor surgery, it was observed that the treatment produced various degrees of necrosis and shrinkage of lesions, and even 2 patients achieved a complete response (16). Considering the close relationship between tumor metastasis and the immunosuppressive TME, these findings prompted us to wonder whether tumor necrosis after GSMs-TACE improved the therapeutic efficacy *via* regulating the immune-mediated elimination of tumor cells.

Regulatory T (Treg) cells are a subset of $CD4^+$ T cells in immune system known to function as "immune-suppressor". It is well recognized that Treg cells play an important role in protecting against excessive inflammation and immune response in physiological or some pathological conditions. Furthermore, it has been noticed that Treg cells are involved in liver diseases including HCC (17). The infiltration of Treg cells into tumor sites can exert a suppressive effect on host anticancer immunity and thereby become an obstacle to curative anticancer therapy (10, 18, 19). In the current study, we first compared the Treg cell proportion in peripheral blood in HCC patients, healthy volunteers and Cirrhosis (11.74 ± 1.67%, vs. 5.51 ± 1.22%, vs. 7.69 ± 1.07%, p<0.01), which was in accordance with the previous study (19). Besides, we analyzed the association between the Treg cell proportion and various clinical indicators of HCC, and it was found that the Treg cell proportion was closely related to tumor stage, tumor markers:

TABLE 3 | Comparison of Treg cell proportions in 33 HCC patients before and at 1 to 2 weeks, 3 to 5 weeks after GSMs-TACE.

Time point	No.	Tregs proportion	*t*	*P*
Prior to GSMs -TACE		33	11.74 ± 1.67	
1 to 2 weeks after GSMs -TACE	33	8.54 ± 1.27[#]	8.737	<0.001
3 to 5 weeks after GSMs -TACE	25	7.59 ± 1.27[#]	10.707	<0.001

[#]*Treg proportions at 1 to 2 weeks, 3 to 5 weeks after GSMs -TACE were compared with those before GSMs -TACE, P < 0.05.*

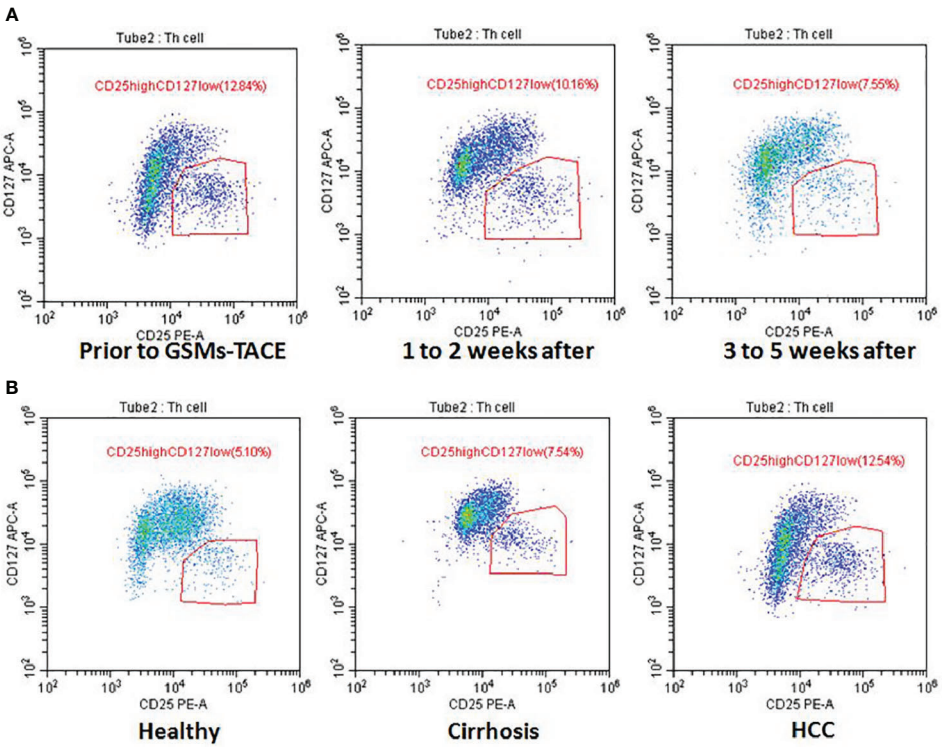

FIGURE 3 | **(A)** Flow Cytometry Chart: The Treg cell proportion of a HCC patient before GSMs-TACE and at 1 to 2 weeks and 3 to 5 weeks after GSMs-TACE was 12.84, 10.16, 7.55%, respectively. **(B)** Flow Cytometry Chart: The Treg cell proportion of healthy people, cirrhosis and HCC patient was 5.10, 7.54, 12.54%, respectively.

AFP and PIVKA-II, tumor diameter, tumor encapsulation and vascular invasion, which further confirmed the association between the Treg cell proportion and HCC. However, the mechanism of the association between circulating Treg cells and HCC pathophysiological characteristics has not been fully elucidated. Shi et al. proposed that Tregs could modify HCC in the way that potentiates the metastasis since it was found that Treg cell proportions in HCC patients were significantly correlated with biomarkers of tumor cell metastasis such as E-cadherin, vimentin and SNAIL, although these findings were based on the analysis of limited cases (20). In addition, tumor encapsulation was an important clinicopathological invasive marker of HCC, and it was observed that the high Treg cell proportion in HCC patients was significantly correlated with the presence of tumor encapsulation, which was inconsistent with the published literature, where Gao et al. reported that a high Tregs proportion was associated with the absence of tumor encapsulation (21). Nevertheless, these await further studies.

The 33 patients enrolled in this study received GSMs-TACE, and the imaging techniques confirmed the success of the procedure. To testify our hypothesis that TACE procedures may also have an impact on anti-cancer immunity, the Treg cell proportion in peripheral blood was determined before and at 1 to 2 weeks and 3 to 5 weeks after GSMs-TACE. It was found

TABLE 4 | Comparison of Treg Cell proportions in HCC patients with BCLC staging B and staging C HCC before and after GSMs-TACE.

Stage	Time	No.	Treg(%)	*t*	*P*
B	Prior to GSMs -TACE	13	11.16 ± 1.43		
	1 to 2 weeks after	13	8.09 ± 1.10[#]	6.126	<0.001
	3 to 5 weeks after	8	7.07 ± 1.23[#]	16.691	<0.001
C	Prior to GSMs -TACE	20	12.12 ± 1.76		
	1 to 2 weeks after	20	8.83 ± 1.31[#]	6.714	<0.001
	3 to 5 weeks after	17	7.83 ± 1.48[#]	8.630	<0.001

[#]*Treg proportions at 1 to 2 weeks and 3 to 5 weeks after GSMs-TACE were both compared with those before GSMs-TACE, P < 0.01.*

TABLE 5 | Comparison of CD4+T, CD8+T, CD4+/CD8+T and NK cell proportions in the peripheral blood of HCC patients before GSMs-TACE and at 1 to 2 weeks, 3 to 5 weeks after GSMs-TACE.

Group	Time	HCC patients (n=33)	*t*	*P*
CD4+T (%)	Prior to GSMs -TACE	31.45 ± 6.82		
	1 to 2 weeks after	39.87 ± 8.96	4.294	<0.001
	3 to 5 weeks after	39.64 ± 8.83	3.847	<0.001
CD8+T (%)	Prior to GSMs -TACE	28.01 ± 7.56		
	1 to 2 weeks after	22.64 ± 5.59	3.283	0.002
	3 to 5 weeks after	25.47 ± 7.70	1.256	0.215
CD4+T/CD8+T	Prior to GSMs -TACE	1.31 ± 0.56		
	1 to 2 weeks after	1.86 ± 0.73	3.382	0.001
	3 to 5 weeks after	1.76 ± 0.58	2.939	0.005
NK (%)	Prior to GSMs -TACE	15.38 ± 7.94		
	1 to 2 weeks after	14.85 ± 7.45	0.285	0.777
	3 to 5 weeks after	18.14 ± 9.67	1.161	0.252

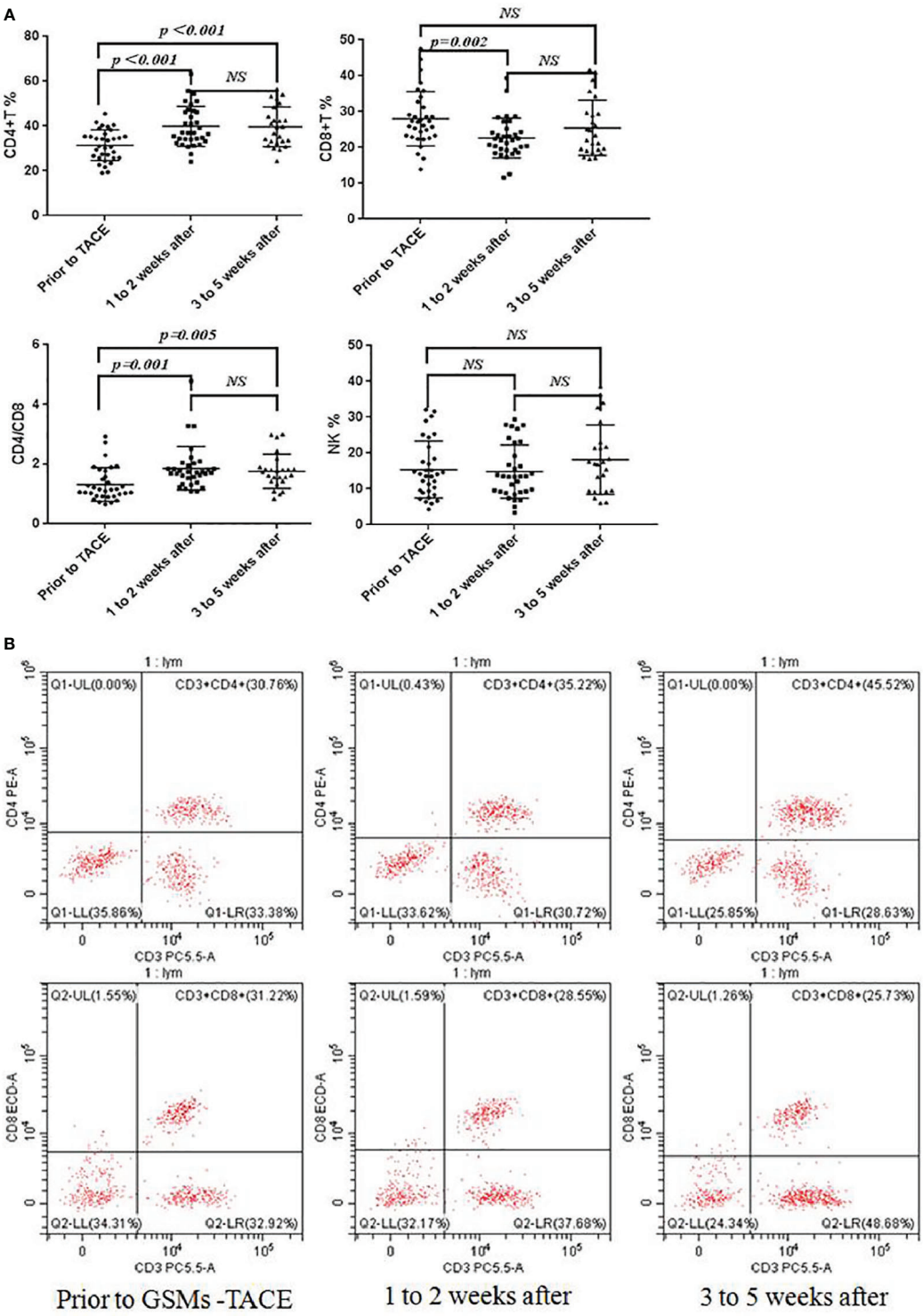

FIGURE 4 | **(A)** Flow Cytometry Chart: Changes of CD4+T, CD8+T, CD4+/CD8+T and NK cell proportions in peripheral blood of HCC patients before and after GSMs-TACE. **(B)** Changes of CD4+T, CD8+T cell proportions in peripheral blood of a representative HCC patient before and after GSMs-TACE detected by flow cytometry.

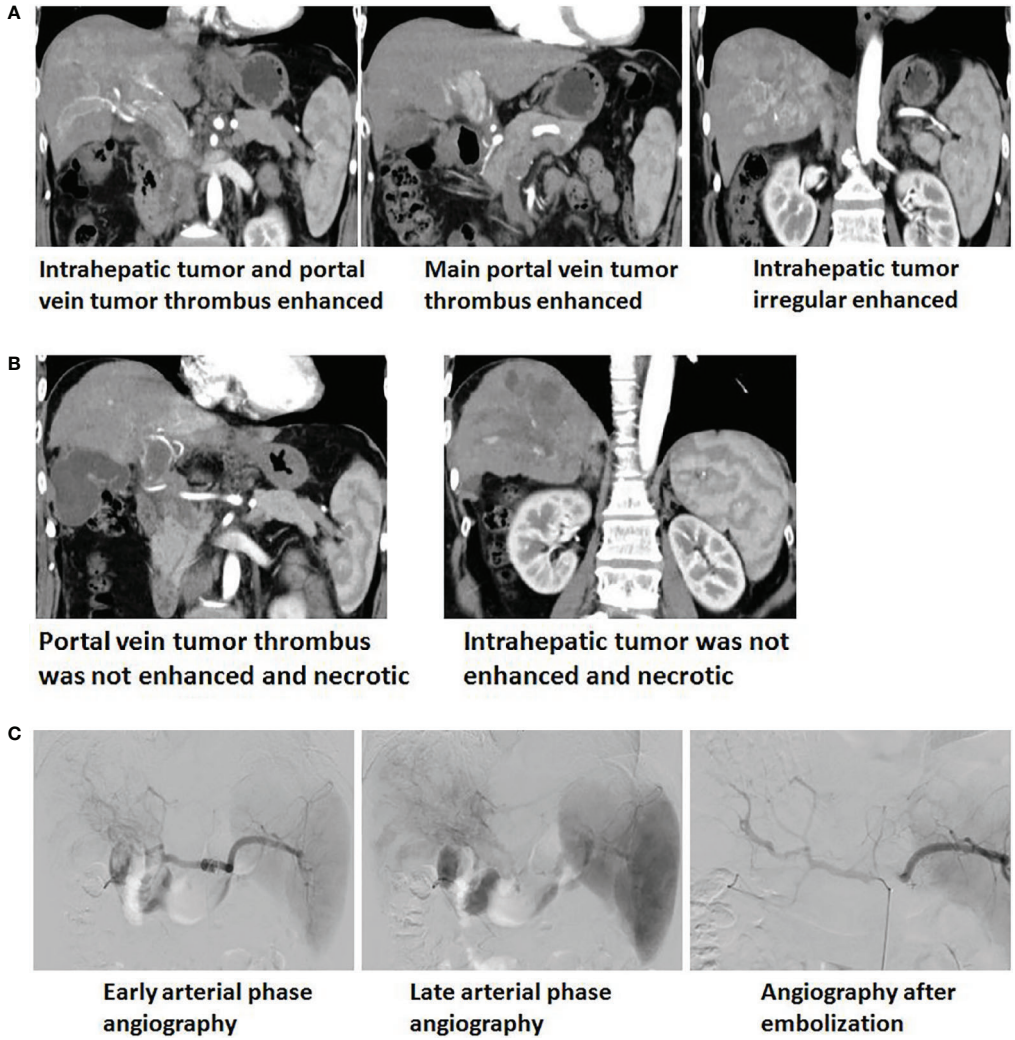

FIGURE 5 | **(A)** Enhanced upper abdominal CT(Arterial phase) showed that the obviously enhanced of irregular tumor and tumor thrombi in the left and right branches of portal vein, which extending to the main portal vein and the opening of splenic vein. **(B)** One month after GSMs-TACE, enhanced CT of the upper abdomen showed that reduction and necrosis of intrahepatic tumor and portal vein tumor thrombus. **(C)** Early and late arterial phase angiography showed arterial staining of intrahepatic tumor and tumor thrombi of portal vein and no distinct boundary with normal liver tissue. Angiography after embolization showed staining of intrahepatic tumor and thrombi disappeared and local arterial blood stasis.

that circulating Treg cell after TACE was significantly lower than that of before the TACE. These results indicated that GSMs-TACE may have a positive regulatory effect on immune function. The possible reason is that after the effective embolization of tumor feeding artery, the tumor cell necrosis is induced significantly in a short time, and the tumor load is also significantly reduced, which is related to the significant reduction of the immunosuppressive effect on the body. It is well recognized that many tumors bear tumor antigens and can induce T-cell cytotoxic responses (22). The release of tumor antigens then led to local microenvironment immune response and a subsequent reduction of Treg cells. We considered that the "reduction of Tregs" seen in these studies was a relative reduction in frequency reflecting the heightened generation and effectors potentially stimulated by immune-stimulating damage to the tumor itself. The comparison between prior to and after GSMs-TACE, the ratio of CD4+/CD8+T cells increased in HCC patients. These results suggested that the partial T lymphocytes cellular immune function was restored in HCC patients following GSMs-TACE. Our results showed that the improvement of immune function can be maintained within at least one month, which indicated that it may be the optimal time for immunoadjuvant therapy. Therefore, the follow-up treatment including TACE, targeted therapy and immunotherapy can further reduce the burden of tumors in order to better restore and enhance the body's anti-tumor immunity.

In recent years, tumor immunotherapies have gained promising results. Programmed cell death protein 1 (PD-1), expressed by various activated immune cells, is an immune

checkpoint and can protect against autoimmune responses. It has been revealed that in cancer immunity, tumor cells express PD-L1, the ligand of PD-1, and combine with PD-1 in T cells, thereby suppressing T cell activities and promoting the differentiation of Treg cells (23). As a result, the anticancer immune responses are inhibited in tumor microenvironment. The immunotherapies targeting PD-1/PD-L1 have successfully improved the outcomes of various types of cancer worldwide, including HCC (24). A pioneering study analyzed the PD-L1 expression in 240 HCC patients who received surgical resection, and it was found that patients who were positive for PD-L1 showed significant shorter disease-free survival or overall survival than those PD-L1 negative patients (25). Antibodies of PD-1 or PD-L1 in HCC immunology have shown promising efficacies (26). However, there are still unmet clinical needs considering that many patients show no response. Since one of the important mechanisms of PD-1/PD-L1 pathway is the promotion of Treg cells differentiation, an interesting and promising suggestion was drawn from this study that GSMs-TACE has the potential to be used in combination with immune adjuvant therapies such as PD-1/PD-L1 pathway targeting therapies to increase the efficacy of HCC treatment.

In conclusion, the Treg cell proportion of HCC patients was higher than that of healthy and cirrhosis controls and was closely related to the clinical characteristics of HCC. The GSMs-TACE procedure significantly reduced the peripheral blood Treg cell proportions at 1 to 2 weeks and 3 to 5 weeks days after TACE. These results indicated that GSMs-TACE could exert a positive regulatory effect on the Treg, CD4+, CD8+T cell immune function of HCC patients. This study provides a piece of preliminary evidence that GSMs-TACE has the potential to be used in combination with immune adjuvant therapies such as therapies targeting PD-1 or PDL-1 to increase the efficacy of HCC treatment.

However, there are also some limitations of this study, the subgroups of nTreg, iTreg, and tTreg were not detected in detail. Next we're going to expand our research to supplement data on the activation status of Tregs and the expression of its markers (such as tumor invasion potential, inhibitory medium level). The expression of other molecules or biomarkers involved in tumor immunity should be assessed along with the Treg cell proportion to better explain the mechanism of GSMs-TACE procedures affecting tumor immunity, so as to provide references for the treatment design of HCC patients.

DATA AVAILABILITY STATEMENT

The original contributions presented in the study are included in the article/supplementary material. Further inquiries can be directed to the corresponding authors.

ETHICS STATEMENT

The studies involving human participants were reviewed and approved by Tsinghua University Affiliated Beijing Tsinghua Changgung Hospital ethics committee. The patients/participants provided their written informed consent to participate in this study. Written informed consent was obtained from the individual(s) for the publication of any potentially identifiable images or data included in this article.

AUTHOR CONTRIBUTIONS

First author: ZR. Co-first author: YY. Corresponding author: YWZ. Co-corresponding author: JD. All authors, contributed to the article and approved the submitted version.

FUNDING

This work was supported by National Natural Science Foundation of China (81930119), Grant from the Tsinghua Precision Medicine Foundation (12020B7028).

REFERENCES

1. Kulik L, El-Serag HB. Epidemiology and management of hepatocellular carcinoma. *Gastroenterology* (2019) 156(2):477–91.e1. doi: 10.1053/j.gastro.2018.08.065
2. Schlachterman A, Craft WW Jr, Hilgenfeldt E, Mitra A, Cabrera R. Current and future treatments for hepatocellular carcinoma. *World J Gastroenterol* (2015) 21(28):8478–91. doi: 10.3748/wjg.v21.i28.8478
3. Bruix J, Gores GJ, Mazzaferro V. Hepatocellular carcinoma: clinical frontiers and perspectives. *Gut* (2014) 63(5):844–55. doi: 10.1136/gutjnl-2013-306627
4. Raoul JL, Forner A, Bolondi L, Cheung TT, Kloeckner R, Baere T. Updated use of TACE for hepatocellular carcinoma treatment: How and when to use it based on clinical evidence. *Cancer Treat Rev* (2019) 72:28–36. doi: 10.1016/j.ctrv.2018.11.002
5. Zhao GS, Li C, Liu Y, Ren ZZ, Yuan XL, Zhang YW, et al. 350-560 mum gelatin sponge particles combined with transcatheter arterial chemoembolization for the treatment of elderly hepatocellular carcinoma: The safety and efficacy. *Med (Baltimore)* (2017) 96(16):e6629. doi: 10.1097/MD.0000000000006629
6. Liu S, Zhang YW, Zhao GS, Liu Y. Complete remission of diffuse hepatocellular carcinoma in a young adult after GSP-TACE: a case report. *World J Surg Oncol* (2014) 12:300. doi: 10.1186/1477-7819-12-300
7. Ohue Y, Nishikawa H. Regulatory T (Treg) cells in cancer: Can Treg cells be a new therapeutic target? *Cancer Sci* (2019) 110(7):2080–9. doi: 10.1111/cas.14069
8. Pacella I, Piconese S. Immunometabolic checkpoints of Treg dynamics: adaptation to microenvironmental opportunities and challenges. *Front Immunol* (2019) 8(10):1–17. doi: 10.3389/fimmu.2019.01889
9. Tanaka A, Sakaguchi S. Targeting Treg cells in cancer immunotherapy. *Eur J Immunol* (2019) 49(8):1140–6. doi: 10.1002/eji.201847659
10. Hu Z-Q, Xin HY, Luo CB, Li J, Zhou ZJ, Zou JX, et al. Associations among the mutational landscape, immune microenvironment, and prognosis in Chinese patients with hepatocellular carcinoma. *Cancer Immunol Immunother* (2020) 8(6):942–9. doi: 10.1007/s00262-020-02685-7
11. Burrel M, Reig M, Forner A, Barrufet M, Tremosini S, Ayuso C, et al. Survival of patients with hepatocellular carcinoma treated by transarterial chemoembolisation (TACE) using Drug Eluting Beads. Implications for clinical practice and trial design. *J Hepatol* (2012) 56(6):1330–5. doi: 10.1016/j.jhep.2012.01.008

12. Meyer T, Fox R, Ma YT, Ross PJ, James MW, Sturgess R, et al. Sorafenib in combination with transarterial chemoembolisation in patients with unresectable hepatocellular carcinoma (TACE 2): a randomised placebo-controlled, double-blind, phase 3 trial. *Lancet Gastroenterol Hepatol* (2017) 2(8):565–75. doi: 10.1016/S2468-1253(17)30156-5
13. Ma X-L, Qu XD, Yang WJ, Wang BL, Shen MN, Yan Zhou Y, et al. Elevated soluble programmed death-ligand 1 levels indicate immunosuppression and poor prognosis in hepatocellular carcinoma patients undergoing transcatheter arterial chemoembolization. *Clin Chim Acta* (2020) 24(511):67–74. doi: 10.1016/j.cca.2020.09.026
14. Liu Y, Zhang YW, Bautista D, Tang SX, Zhou J, Chuang L, et al. Trans-arterial p53-gene-embolization with gelatin sponge microparticles for hepatocellular carcinoma with BCLC stage B: single-center experience. *Cell Biochem Biophys* (2015) 71(1):99–104. doi: 10.1007/s12013-014-0167-2
15. Zhou J, Liu Y, Ren ZZ, Zhang YW, Zhang ZM. Transarterial chemoembolization with gelatin sponge microparticles for barcelona clinic liver cancer Stage C and large hepatocellular carcinoma: Initial clinical experience. *J Cancer Res Ther* (2017) 13(5):767–72. doi: 10.4103/jcrt.JCRT_297_17
16. Li C, Liu Y, Zhou J, Zhang YW. A retrospective analysis of the efficacy of microparticle-mediated chemoembolization in liver metastases arising from gastrointestinal tumors. *J Cancer Res Ther* (2017) 13(4):642–6. doi: 10.4103/jcrt.JCRT_213_17
17. Zhang HR, Jiang ZZ, Zhang LY. Dual effect of T helper cell 17 (Th17) and regulatory T cell (Treg) in liver pathological process: From occurrence to end stage of disease. *Int Immunopharmacol* (2019) 69:50–9. doi: 10.1016/j.intimp.2019.01.005
18. Liua F, Liu W, Sanin DE, Jia G, Tian M, Wang H, et al. Heterogeneity of exhausted T cells in the tumor microenvironment is linked to patient survival following resection in hepatocellular carcinoma. *Oncoimmunology* (2020) 9(1):e1746573. doi: 10.1080/2162402X.2020.1746573
19. Li F, Guo Z, Lizée G, Yu H, Wang H, Si T. Clinical prognostic value of CD4+ CD25+FOXP3+regulatory T cells in peripheral blood of Barcelona Clinic Liver Cancer (BCLC) stage B hepatocellular carcinoma patients. *Clin Chem Lab Med* (2014) 52(9):1357–65. doi: 10.1515/cclm-2013-0878
20. Shi C, Chen Y, Chen Y, Yang Y, Bing W, Qi J. CD4(+) CD25(+) regulatory T cells promote hepatocellular carcinoma invasion via TGF-beta1-induced epithelial-mesenchymal transition. *Onco Targets Ther* (2019) 12:279–89. doi: 10.2147/OTT.S172417
21. Gao Q, Qiu S, Fan J, Zhou J, Wang X, Xiao Y, et al. Intratumoral balance of regulatory and cytotoxic T cells is associated with prognosis of hepatocellular carcinoma after resection. *J Clin Oncol* (2007) 25(18):2586–93. doi: 10.1200/JCO.2006.09.4565
22. Lee JC, Mehdizadeh S, Smith J, Young A, Mufazalov IA, Mowery CT, et al. Regulatory T cell control of systemic immunity and immunotherapy response in liver metastasis. *Sci Immunol* (2020) 5(52):eaba0759. doi: 10.1126/sciimmunol.aba0759
23. Salmaninejad A, Valilou SF, Shabgah AG, Aslani S, Alimardani M, Pasdar A, et al. PD-1/PD-L1 pathway: Basic biology and role in cancer immunotherapy. *J Cell Physiol* (2019) 234(10):16824–37. doi: 10.1002/jcp.28358
24. Seidel JA, Otsuka A, Kabashima K. Anti-PD-1 and Anti-CTLA-4 therapies in cancer: mechanisms of action, efficacy, and limitations. *Front Oncol* (2018) 8:86. doi: 10.3389/fonc.2018.00086
25. Gao Q, Wang XY, Qiu SJ, Yamato I, Sho M, Nakajima Y, et al. Overexpression of PD-L1 significantly associates with tumor aggressiveness and postoperative recurrence in human hepatocellular carcinoma. *Clin Cancer Res* (2009) 15 (3):971–9. doi: 10.1158/1078-0432.CCR-08-1608
26. Ng HHM, Lee RY, Goh S, Tay ISY, Lim X, Lee B, et al. Immunohistochemical scoring of CD38 in the tumor microenvironment predicts responsiveness to anti-PD-1/PD-L1 immunotherapy in hepatocellular carcinoma. *J Immunother Cancer* (2020) 8(2):e000987. doi: 10.1136/jitc-2020-000987

Conflict of Interest: The authors declare that the research was conducted in the absence of any commercial or financial relationships that could be construed as a potential conflict of interest.

Copyright © 2021 Ren, Yue, Zhang, Dong, Liu, Yang, Lin, Zhao, Wei, Zheng and Wang. This is an open-access article distributed under the terms of the Creative Commons Attribution License (CC BY). The use, distribution or reproduction in other forums is permitted, provided the original author(s) and the copyright owner(s) are credited and that the original publication in this journal is cited, in accordance with accepted academic practice. No use, distribution or reproduction is permitted which does not comply with these terms.

frontiers in Immunology

ORIGINAL RESEARCH
published: 25 February 2021
doi: 10.3389/fimmu.2021.649020

TRAF6 Regulates the Immunosuppressive Effects of Myeloid-Derived Suppressor Cells in Tumor-Bearing Host

Ge Song[1,2†], Yue Zhang[1], Jie Tian[2], Jie Ma[2], Kai Yin[3*], Huaxi Xu[2] and Shengjun Wang[1,2*]*

[1] Department of Laboratory Medicine, Affiliated People's Hospital, Jiangsu University, Zhenjiang, China, [2] Institute of Laboratory Medicine, Jiangsu Key Laboratory for Laboratory Medicine, Jiangsu University School of Medicine, Zhenjiang, China, [3] Department of General Surgery, Affiliated Hospital of Jiangsu University, Zhenjiang, China

OPEN ACCESS

Edited by:
Peng Qu,
National Institutes of Health (NIH), United States

Reviewed by:
Yafeng He,
National Heart, Lung, and Blood Institute (NHLBI), United States
Hongru Zhang,
University of Pennsylvania, United States

***Correspondence:**
Shengjun Wang
sjwjs@ujs.edu.cn
Kai Yin
jsyinkai@163.com
Yue Zhang
13952815636@163.com

†Present address:
Ge Song,
Department of Clinical Laboratory, Haian People's Hospital, Haian, China

Specialty section:
This article was submitted to Cancer Immunity and Immunotherapy, a section of the journal Frontiers in Immunology

Received: *03 January 2021*
Accepted: *04 February 2021*
Published: *25 February 2021*

Citation:
Song G, Zhang Y, Tian J, Ma J, Yin K, Xu H and Wang S (2021) TRAF6 Regulates the Immunosuppressive Effects of Myeloid-Derived Suppressor Cells in Tumor-Bearing Host. Front. Immunol. 12:649020. doi: 10.3389/fimmu.2021.649020

Myeloid-derived suppressor cells (MDSCs) are immature heterogeneous cells derived from the bone marrow and they are the major component of the tumor-induced immunosuppressive environment. Tumor necrosis factor receptor-associated factor 6 (TRAF6), an E3 ubiquitin ligase, catalyzes the polyubiquitination of target proteins. TRAF6 plays a critical role in modulating the immune system. However, whether TRAF6 is involved in the regulation of MDSCs has not been thoroughly elucidated to date. In this study, we found that the expression of TRAF6 in MDSCs derived from tumor tissue was significantly upregulated compared with that of MDSCs from spleen of tumor-bearing mice. Knockdown of TRAF6 remarkably attenuated the immunosuppressive effects of MDSCs. Mechanistically, TRAF6 might improve the immunosuppression of MDSCs by mediating K63-linked polyubiquitination and phosphorylation of signal transducer and activator of transcription 3 (STAT3). Additionally, it was discovered that the accumulation of MDSCs was abnormal in peripheral blood of lung cancer patients. TRAF6 and arginase 1 were highly expressed in MDSCs of patients with lung cancer. Taken together, our study demonstrated that TRAF6 participates in promoting the immunosuppressive function of MDSCs and provided a potential target for antitumor immunotherapy.

Keywords: myeloid-derived suppressor cells, TRAF6, STAT3, tumor immunology, tumor microenvironment

INTRODUCTION

The tumor microenvironment provides a suitable environment for the survival and development of tumor cells. There are a large number of cytokines and chemokines in the tumor microenvironment that recruit immunosuppressive cells to accumulate in local tumors and promote tumor immune escape (1–3). Myeloid-derived suppressor cells (MDSCs) are crucial immunosuppressive cells in the tumor microenvironment, which have powerful suppressive effects (4–6). In mice, MDSCs are immature myeloid cells that co-express CD11b and Gr1, which are further divided into 2 subsets: $CD11b^{+}Ly6G^{+}Ly6C^{low}$ polymorphonuclear MDSCs (PMN-MDSCs) and $CD11b^{+}Ly6G^{-}Ly6C^{hi}$ mononuclear MDSCs (M-MDSCs) according to the expression of LY6G and LY6C (7–10). However, human MDSCs have a more complex phenotype and are usually characterized by $CD11b^{+}CD33^{+}HLA\text{-}DR^{low/-}$ expression (9, 11). In tumor-bearing mice, the proportion of MDSCs is significantly increased compared with that in wild type mice. MDSCs reach 20 to 40%

in the spleen in tumor-bearing mice, and the massive aggregation of MDSCs in tumor tissue is particularly obvious (12). Studies have shown that the immunosuppressive function of MDSCs derived from tumor tissue was stronger than that of spleen-derived MDSCs from tumor-bearing mice (13–15).

Accumulating evidence has indicated that the suppressive function of MDSCs is correlated with the high production of arginase 1 (Arg1), inducible nitric oxide synthase (iNOS) and reactive oxygen species (ROS), which can inhibit T cell proliferation and antitumor responses (16–18). The two subsets of MDSCs exert immunosuppressive effects in different ways. Although both PMN-MDSCs and M-MDSCs highly express Arg1, the expression of iNOS and ROS are notably different (19, 20). Signal transducer and activator of transcription 3 (STAT3) is one of the key transcription factors regulating the expansion, activation and function of MDSCs (21–24). Abnormal activation of STAT3 signaling hinders the normal differentiation of myeloid cells, leading to the expansion and activation of MDSCs (25–27). STAT3 activation is mainly affected by posttranslational modifications. In addition to phosphorylation modification, ubiquitination also plays a critical role in modulating the activity of STAT3 (28, 29).

Tumor necrosis factor receptor-associated factor 6 (TRAF6) is an important member of the TRAF family (30). Unlike other TRAF members, TRAF6 is both an adaptor protein and E3 ubiquitin ligase (31–33). As a non-conventional E3 ubiquitin ligase, TRAF6 catalyzes the K63-linked polyubiquitination of target proteins further affecting functions. Studies have shown that the E3 ubiquitin ligase TRAF6 binds to STAT3 (28, 34). Moreover, TRAF6 promotes STAT3 phosphorylation by mediating the K63-linked polyubiquitination of STAT3 (29). However, whether TRAF6 affects the function of MDSCs by mediating STAT3 activity is unclear.

In this study, we explored the role of TRAF6 in modulating the immunosuppressive function of MDSCs and elaborated the potential molecular mechanism. Our research pointed out that the expression of TRAF6 is significantly increased in MDSCs derived from the tumor tissue of tumor-bearing mice. TRAF6 promoted the immunosuppressive function of MDSCs by mediating the activation of STAT3. These data elucidate a novel mechanism of the regulation of MDSCs in the tumor microenvironment and propose new ideas for therapeutic strategies targeting TRAF6.

METHODS

Cell Line, Mice, and Tumor Models

Male C57BL/6 mice, aged 6–8 weeks, were purchased from the Laboratory Animal Center of Jiangsu University (Zhenjiang, China). Murine Lewis lung carcinoma (LLC) cells were obtained from the Cell Bank of Shanghai Institutes for Biological Sciences (Shanghai, China). The cells were cultured in DMEM (Gibco, Carlsbad, CA) with 10% fetal calf serum (Gibco, Carlsbad, CA) at 37°C in a humidified 5% CO_2 atmosphere. 1×10^6 LLC cells were injected subcutaneously into the mice to establish tumor-bearing mouse model. All animal experiments were approved by the Committee on the Use of Live Animals in Research and Teaching of Jiangsu University.

Preparation of Single-Cell Suspensions

The murine spleen was ground and treated with ACK buffer. After centrifugation, PBE buffer was added to obtain a spleen cell suspension. In addition, the tumor tissue was stripped and cut into pieces, and then collagenase, hyaluronidase and DNase I (Sigma-Aldrich, St. Louis, MO) were used to digest the tissue in a water bath at 37°C for 2 h. The filtrate was collected through a 70 μm cell strainer. After centrifugation, PBE buffer was added to obtain single-cell suspensions.

Isolation of MDSCs and CD4$^+$ T Cells

Murine Gr1$^+$ CD11b$^+$ MDSCs were isolated using a mouse MDSC kit (Miltenyi Biotec, Auburn, CA) according to the manufacturer's instructions. To improve the purity of MDSCs isolated from tumor tissues, enriched MDSCs were subsequently isolated using flow cytometry (FCM).

Simultaneously, murine CD4$^+$ T cells were isolated from the spleens of wild-type C57BL/6 mice via using a mouse CD4$^+$ T cell isolation kit (Miltenyi Biotec, Auburn, CA). The purity of MDSCs and CD4$^+$ T cells were determined by FCM.

Flow Cytometry

Single-cell suspensions were stained with relevant fluorochrome-conjugated anti-mouse/human CD11b, anti-mouse Gr-1, Ly6G, and Ly6C antibodies (Biolegend, San Diego, CA) and anti-human-CD33 and HLA-DR antibodies (eBioscience, San Diego, CA). To examine cytotoxic T lymphocytes (CTLs) and T helper 1 (Th1) cells, single-cell suspensions derived from tumor tissues of tumor-bearing mice were treated with 1 μg/mL ionomycin, 2 ng/mL monensin (eBioscience, San Diego, CA), and 50 ng/mL PMA (Sigma-Aldrich, St. Louis, MO) for 5 h. After resuspending in PBS, the cells were stained with anti-mouse CD3e, anti-mouse CD8a or anti-mouse CD4 mAb (eBioscience, San Diego, CA). The cells were incubated at 4°C for 30 min, fixed, permeabilized, and stained with anti-mouse IFN-γ mAbs (BD Pharmingen™) according to the instructions in the intracellular cytokine staining kit (eBioscience, San Diego, CA). Flow cytometry (BD FACSCalibur) was used to determine the proportion of cells.

Quantitative Real-Time PCR (qRT-PCR)

Total RNA was extracted by using TRIzol reagent (Invitrogen, Carlsbad, CA) and reverse-transcribed to cDNA with a PrimeScript RT reagent kit (Takara, Osaka, Japan) according to the manufacturer's instructions. Quantitative PCR was performed by using SYBR Premix Ex Taq (Tli RNaseH Plus) (Takara, Osaka, Japan). The primer sequences are listed in **Table 1**.

Abbreviations: Arg1, Arginase 1; CTL, cytotoxic T lymphocyte; FCM, flow cytometry; iNOS, inducible nitric oxide synthase; IP, immunoprecipitation; MDSCs, myeloid-derived suppressor cells; M-MDSCs, monocytic myeloid-derived suppressor cells; NO, nitric oxide; PMN-MDSCs, polymorphonuclear myeloid-derived suppressor cells; ROS, reactive oxygen species; STAT3, signal transducer and activator of transcription 3; TRAF6, tumor necrosis factor receptor-associated factor 6; Ub, ubiquitin.

TABLE 1 | The gene primer sequences.

Gene	Primer sequence
Arg1	Forward: 5′-GCTGGTCTGCTGGAAAAACTT-3′
	Reverse: 5′-AGGGGAGTGTTGATGTCAGTGT-3′
iNOS	Forward: 5′-GAGCCCTCAGCAGCATCCAT-3′
	Reverse: 5′-GGTGAGGGCTTGGCTGAGTG-3′
18S	Forward: 5′-TCCGGAGAGGGAGCCTGAGA-3′
	Reverse: 5′-GCACCAGACTTGCCCTCCAA-3′
TRAF6	Forward: 5′-TGCTTTGCGTCCGTGCGATG-3′
	Reverse: 5′-GGGTCCGAATGGTCCGTTTG-3′
β-actin	Forward: 5′-AGCCATGTACGTAGCCATCC-3′
	Reverse: 5′-GCTGTGGTGGTGAAGCTGTA-3′

Immunoprecipitation and Western Blotting

MDSCs were lysed by immunoprecipitation cell lysis buffer. After centrifugation, the supernatant was collected and incubated with anti-STAT3 Abs (Santa Cruz Biotechnology, Santa Cruz, CA) or IgG Abs (Cell Signaling Technology, Beverly, MA) for 30 min at 4°C. Then, Protein A/G plus-agarose beads (Santa Cruz Biotechnology, Santa Cruz, CA) were added and blended on a shaker overnight at 4°C. After being washed 3 times, the lysates were boiled in SDS-PAGE protein loading buffer. TRAF6 and STAT3 protein were detected by Western blotting.

Proteins extracted from cells were denatured and subsequently separated by SDS-PAGE. Then, the proteins were transferred to PVDF membranes (Bio-Rad, Hercules, CA), and the membranes were incubated in primary antibodies overnight at 4°C, followed by incubation with HRP-conjugated secondary antibodies. Detection was performed by using LAS4000 chemiluminescence gel imaging and analysis system (Champion Chemical, Whittier, CA). Rabbit anti-TRAF6 mAb, rabbit anti-ubiquitin (linkage-specific K63) mAb, and HRP-conjugated goat anti-rat IgG Ab were purchased from Abcam (Cambridge, UK). Rabbit anti–p-STAT3 (Y705) mAb and rat anti-β-actin mAb were obtained from Cell Signaling Technology (Beverly, MA).

Transfection

Tumor tissue-derived MDSCs were cultured in 24-well plates with RPMI 1640 medium containing 10% FBS. MDSCs were transfected with TRAF6 siRNA or negative control siRNA using Lipofectamine ™ 2,000 transfection reagent (Invitrogen, Carlsbad, CA) according to the manufacturer's instructions. The siRNA transfection efficiency was determined by qRT-PCR and Western blotting. TRAF6 siRNA and negative control siRNA were purchased from RiboBio (Guangzhou, China).

Assessment of MDSCs Suppressive Activity

In order to determine the immunosuppressive function of MDSCs, the sorted MDSCs were co-cultured with CFSE-labeled splenic $CD4^+$ T cells in the study. Splenic $CD4^+$ T cells were stained with fluorescent dye CFSE (5 μM, Invitrogen) for 10 min at 37°C protected from light. RPMI 1640 medium (Gibco, Carlsbad, CA) containing 10% fetal calf serum (Gibco, Carlsbad, CA) was added to wash the cell pellets for 3 times. Sorted MDSCs were co-cultured with CFSE-stained $CD4^+$ T cells at a ratio of 1:1 in 96-well round-bottomed plates (Costar, Corning, NY) in the presence of anti-CD3 mAbs and anti-CD28 mAbs (Biolegend, San Diego, CA). The cells were incubated in RPMI 1640 medium supplemented with 10% fetal calf serum at 37°C in a humidified 5% CO2 atmosphere for 72 h protected from light. The proliferation of $CD4^+$ T cells was detected by flow cytometry at 488 nm excitation light to determinate the suppressive activity of MDSCs.

Measurement of Arginase 1 Activity and NO Content

MDSCs were lysed with an appropriate amount of RIPA buffer for 30 min, and the lysate supernatant was collected after centrifugation. A QuantiChrom arginase assay kit (BioAssay systems, Hayward, CA) was used to determine the Arg1 activity in the lysate supernatant.

The content of NO was measured by the Griess reagent system kit (Promega, Madison, WI) according to the manufacturer's instructions.

In vivo Experiments

To study the effect of TRAF6 on the immunosuppressive function of MDSCs *in vivo*, C57BL/6 mice were divided into siRNA control group and siTRAF6-MDSC group. The mice in the siRNA control group were subcutaneously injected with 1×10^6 MDSCs transfected with siNC mixed with 1×10^6 LLC cells, and the mice in the siTRAF6-MDSC group were subcutaneously injected with 1×10^6 MDSCs transfected with siTRAF6 mixed with 1×10^6 LLC cells. We constantly monitored the length and width of the tumor, and the tumor volume was calculated using the formula $V = 1/2 \times a^2 \times b$ ("a" represents the width and "b" represents the length). The mice were sacrificed on the 28th day after inoculation with LLC cells and MDSCs. The proportions of Th1 cells and CTLs from tumor tissue were analyzed by FCM.

Patients and Sampling

Fresh peripheral blood samples from 33 patients with lung cancer and healthy controls were collected at the Affiliated People's Hospital, Jiangsu University. The peripheral blood mononuclear cells (PBMCs) were isolated by density-gradient centrifugation via using Ficoll-Hypaque solution (Haoyang Biological Technology Co.) and subsequently analyzed by flow cytometry. The protocol was approved by the Ethics Committee of the Affiliated People's Hospital of Jiangsu University (Zhenjiang, China). Written informed consent was obtained from all patients before study enrollment.

Statistical Analysis

The experimental data are expressed as the mean ± SD. Student's *t*-test and ANOVA were used to determine significant differences. Correlations were determined by the Spearman correlation coefficient. Differences were considered significant at a $p < 0.05$.

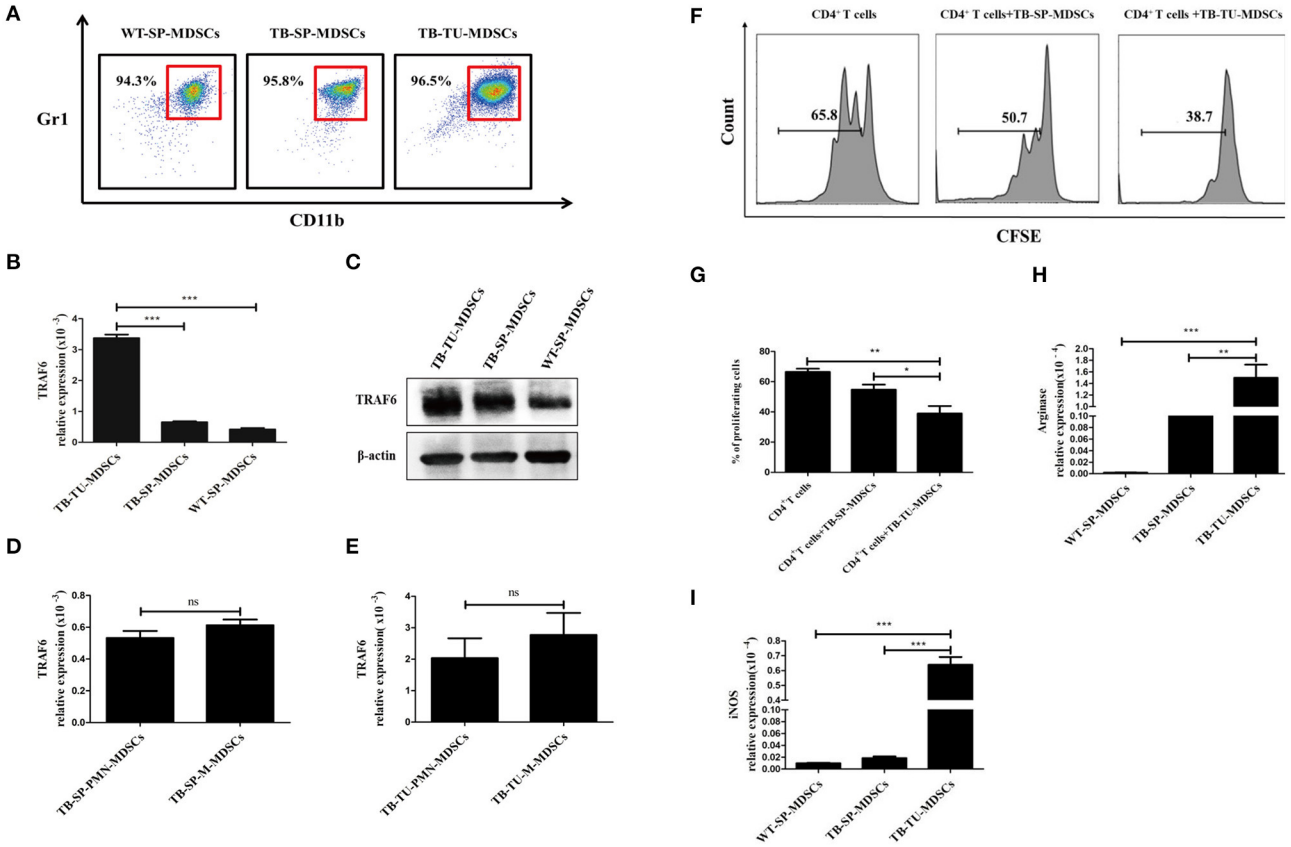

FIGURE 1 | TRAF6 is highly expressed in MDSCs derived from the tumor tissue of tumor-bearing mice. Approximately 1 × 10^6 LLC cells were s.c. injected in the backs of C57BL/6 mice for 28 d to establish a tumor-bearing (TB) mouse model. MDSCs were isolated by immunomagnetic beads from the spleens of TB mice, the tumor tissue of TB mice or the spleens of wild-type (WT) mice. **(A)** The purity of the isolated MDSCs was determined using flow cytometry via the detection of the $CD11b^+Gr1^+$ phenotype. The expression of TRAF6 in MDSCs derived from different sources was determined by qRT-PCR **(B)** or Western blotting **(C)**. The mRNA expression of TRAF6 in PMN-MDSCs and M-MDSCs derived from the spleen **(D)** or tumor tissue **(E)**. **(F)** CFSE-labeled $CD4^+$ T cells were co-cultured with MDSCs derived from the spleen or tumor tissue in the presence of CD3 and CD28 stimulation. After 72 h, the proliferation of $CD4^+$ T cells was tested via flow cytometry. **(G)** Statistical analyses of the percentage of proliferating $CD4^+$ T cells co-cultured with MDSCs derived from the spleen or tumor tissue of TB mice. The mRNA expression levels of Arg1 **(H)** and iNOS **(I)** in MDSCs were measured by qRT-PCR. ***$p < 0.001$, **$p < 0.01$, *$p < 0.05$; ns, no significance; TB-TU-MDSCs, MDSCs derived from the tumor tissue of tumor-bearing mice; TB-SP-MDSCs, MDSCs derived from the spleens of tumor-bearing mice; WT-SP-MDSCs, MDSCs derived from the spleens of wild-type mice.

RESULTS

TRAF6 Is Highly Expressed in MDSCs Derived From Tumor Tissue of Tumor-Bearing Mice

To investigate whether TRAF6 is involved in regulating MDSCs, we evaluated the expression of TRAF6 in MDSCs. The purity of MDSCs isolated from the spleen or tumor tissue of mice was >90% (**Figure 1A**). Compared with that of MDSCs from the spleens of wild-type (WT) mice or tumor-bearing (TB) mice, the expression of TRAF6 in MDSCs from tumor tissue was significantly increased (**Figures 1B,C**). The expression of TRAF6 in PMN-MDSCs and M-MDSCs were determined by qRT-PCR, and the results showed that there was no difference in the mRNA expression of TRAF6 in the two subgroups of MDSCs (**Figures 1D,E**).

In addition, we analyzed the suppressive function of tumor tissue-derived MDSCs. Compared with MDSCs from spleen of TB mice, tumor tissue-derived MDSCs had stronger suppressive effects on the proliferation of $CD4^+$ T cells (**Figures 1F,G**). Moreover, the expressions of Arg1 and iNOS in tumor tissue-derived MDSCs were higher than that in splenic MDSCs (**Figures 1H,I**). These results indicated that the immunosuppressive function of MDSCs derived from tumor tissue was stronger than those of splenic MDSCs from TB mice, which was consistent with previous reports (1).

TRAF6 Knockdown Impairs the Immunosuppressive Activity of MDSCs *in vitro*

To evaluate whether TRAF6 is involved in the suppressive effects of MDSCs, specific siRNA was used to knock down

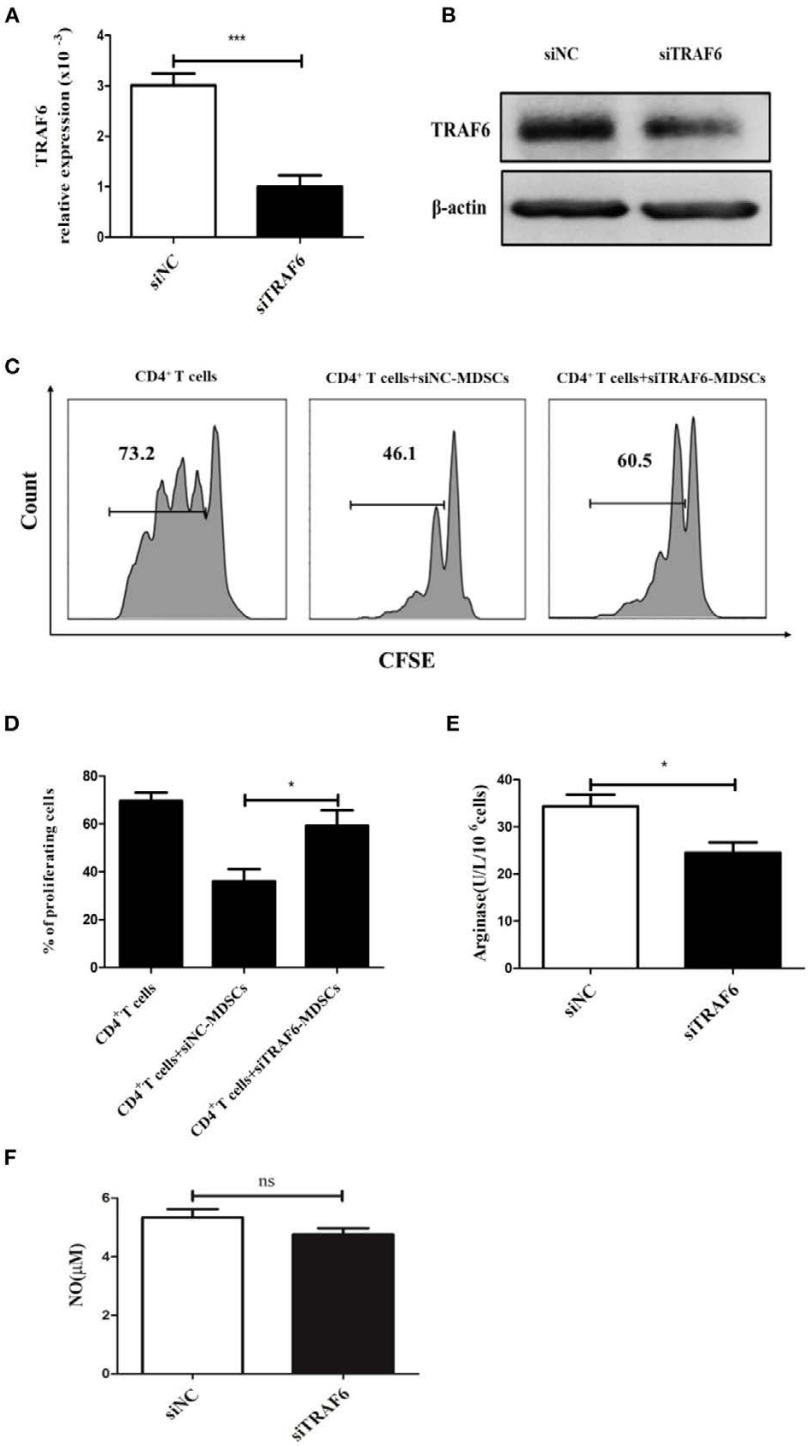

FIGURE 2 | TRAF6 knockdown impairs the immunosuppressive effects of MDSCs *in vitro*. Specific siRNA (siTRAF6) was used to knockdown the expression of TRAF6 in MDSCs, and the efficiency of siTRAF6 knockdown was validated by qRT-PCR **(A)** and Western blotting **(B)**. **(C)** Tumor-derived MDSCs were transfected with siTRAF6 and cocultured with CFSE-labeled $CD4^+$ T cells, and proliferation was measured by flow cytometry after 72 h. **(D)** Statistical analyses of the percentage of proliferating $CD4^+$ T cells co-cultured with MDSCs transfected with siTRAF6. After TRAF6 knockdown, the activity of Arg1 was measured by a QuantiChrom arginase assay kit **(E)**, and the concentration of NO was determined via a Griess reagent system kit **(F)**. $^{***}p < 0.001$, $^{*}p < 0.05$; ns, no significance.

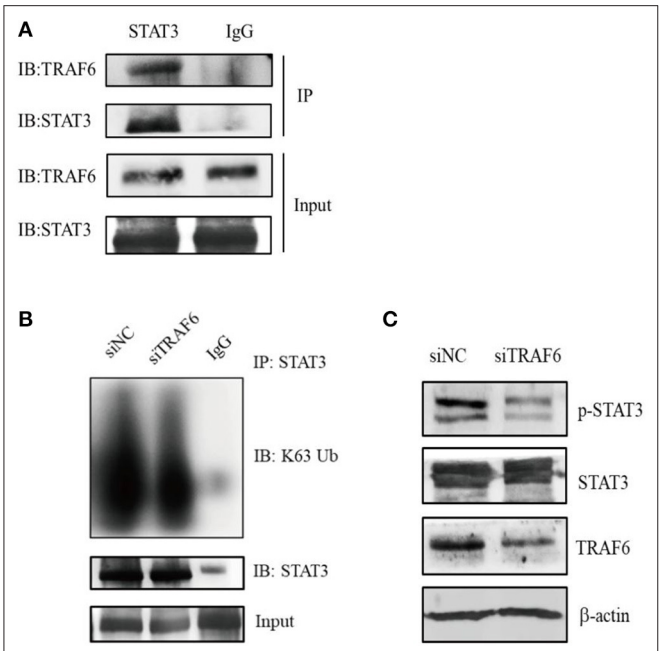

FIGURE 3 | TRAF6 alters the activity of STAT3 by mediating the K63-linked polyubiquitination of STAT3 in MDSCs. **(A)** The interaction between TRAF6 and STAT3 in tumor-derived MDSCs was determined by co-immunoprecipitation (Co-IP) assays. **(B)** After knockdown of TRAF6 in MDSCs, the level of STAT3 K63-linked polyubiquitination was measured by Co-IP assays. **(C)** After knockdown of TRAF6 in MDSCs, the level of STAT3 phosphorylation was assessed by Western blotting.

TRAF6 in MDSCs. After treatment with TRAF6-specific siRNA, the expression of TRAF6 in MDSCs from tumor tissue was effectively decreased (**Figures 2A,B**). Remarkably, the inhibitory effect of MDSCs transfected with siTRAF6 on $CD4^+$ T cell proliferation was significantly attenuated (**Figures 2C,D**). Consistently, knockdown of TRAF6 distinctly decreased the activity of Arg1 in MDSCs (**Figure 2E**), although the content of NO did not noticeably altered (**Figure 2F**). These data indicate that knockdown of TRAF6 impairs the immunosuppressive effects of MDSCs *in vitro*.

TRAF6 Alters the Activity of STAT3

Next, we explored the potential molecular mechanism by which TRAF6 regulates MDSC function. It is widely known that the transcription factor STAT3 plays a dominant role in MDSC expansion, activation and function. Recent studies have revealed that the E3 ubiquitin ligase TRAF6 mediates the K63-linked polyubiquitination of STAT3 but has no effect on STAT3 degradation (34). To determine whether TRAF6 impacts the function of MDSCs by STAT3, we conducted the interaction between TRAF6 and STAT3 in MDSCs by co-immunoprecipitation (Co-IP) assays. The results of Co-IP showed that TRAF6 was co-immunoprecipitated with STAT3, suggesting that endogenous TRAF6 binds to endogenous STAT3 in MDSCs (**Figure 3A**). Furthermore, we examined the regulation of TRAF6 on the posttranslational modification of STAT3. After knockdown of TRAF6 in MDSCs, the K63-linked polyubiquitination of STAT3 was significantly downregulated (**Figure 3B**). Moreover, silencing of TRAF6 remarkably decreased the levels of phosphorylated STAT3 in MDSCs from tumor tissue of TB mice (**Figure 3C**).

TRAF6 Knockdown Attenuates the Ability of MDSCs to Accelerate Tumor Progression in Tumor-Bearing Mice

As shown in the *in vitro* experiments, knockdown of TRAF6 impaired the immunosuppressive activity of MDSCs. Thus, we further investigated the effects of TRAF6 on the suppressive effects of MDSCs *in vivo*. 1×10^6 Lewis lung carcinoma cells and 1×10^6 MDSCs transfected with TRAF6 siRNA or negative control siRNA were subcutaneously injected into C57BL/6 mice. As shown in **Figure 4A**, the tumor growth of mice injected with siTRAF6-transfected MDSCs (siTRAF6) group was evidently delayed. Furthermore, the tumor volume and weight were significantly less than those of the control (siNC) group (**Figures 4B,C**). Given that MDSCs mainly suppress the function of T cells in the tumor microenvironment, we measured the proportion of $CD4^+$ Th1 cells and $CD8^+$ CTLs from tumor tissue of TB mice. Compared with that of the control group, the proportion of Th1 cells was no significant difference in the siTRAF6 group (**Figure 4D**), while the proportion of CTLs in the siTRAF6 group was significantly increased (**Figure 4E**). Our data showed that knockdown of TRAF6 attenuated the ability of MDSCs to accelerate tumor progression and partly suppressed the antitumor T cell response.

TRAF6 Expression Was Augmented in MDSCs From the PBMCs of Lung Cancer Patients

Considering that TRAF6 improves the function of MDSCs in mice, we examined whether TRAF6 had similar characteristics in MDSCs from lung cancer patients. We performed flow cytometry to analyze the proportion of $CD11b^+CD33^+HLA\text{-}DR^-$ MDSCs in PBMCs from lung cancer patients. The percentage of MDSCs in PBMCs from lung cancer patients was higher than that from healthy controls, which indicated that the abnormal accumulation of MDSCs in peripheral blood was correlated with lung cancer (**Figure 5A**). We further examined the expression of TRAF6 in human MDSCs. Compared with that of healthy control, the expression of TRAF6 was markedly augmented in MDSCs from PBMCs of lung cancer patients (**Figure 5B**). In addition, Arg1 is the important immunosuppressive molecule in MDSCs, which was also upregulated in MDSCs from PBMCs of patients (**Figure 5C**). Furthermore, there was a positive correlation between the expression levels of TRAF6 and Arg1 (**Figure 5D**), indicating that TRAF6 may be participate in the regulation of Arg1 expression in MDSCs.

DISCUSSION

As an adaptor protein and E3 ubiquitin ligase, TRAF6 is involved in mediating various cellular signaling pathways and

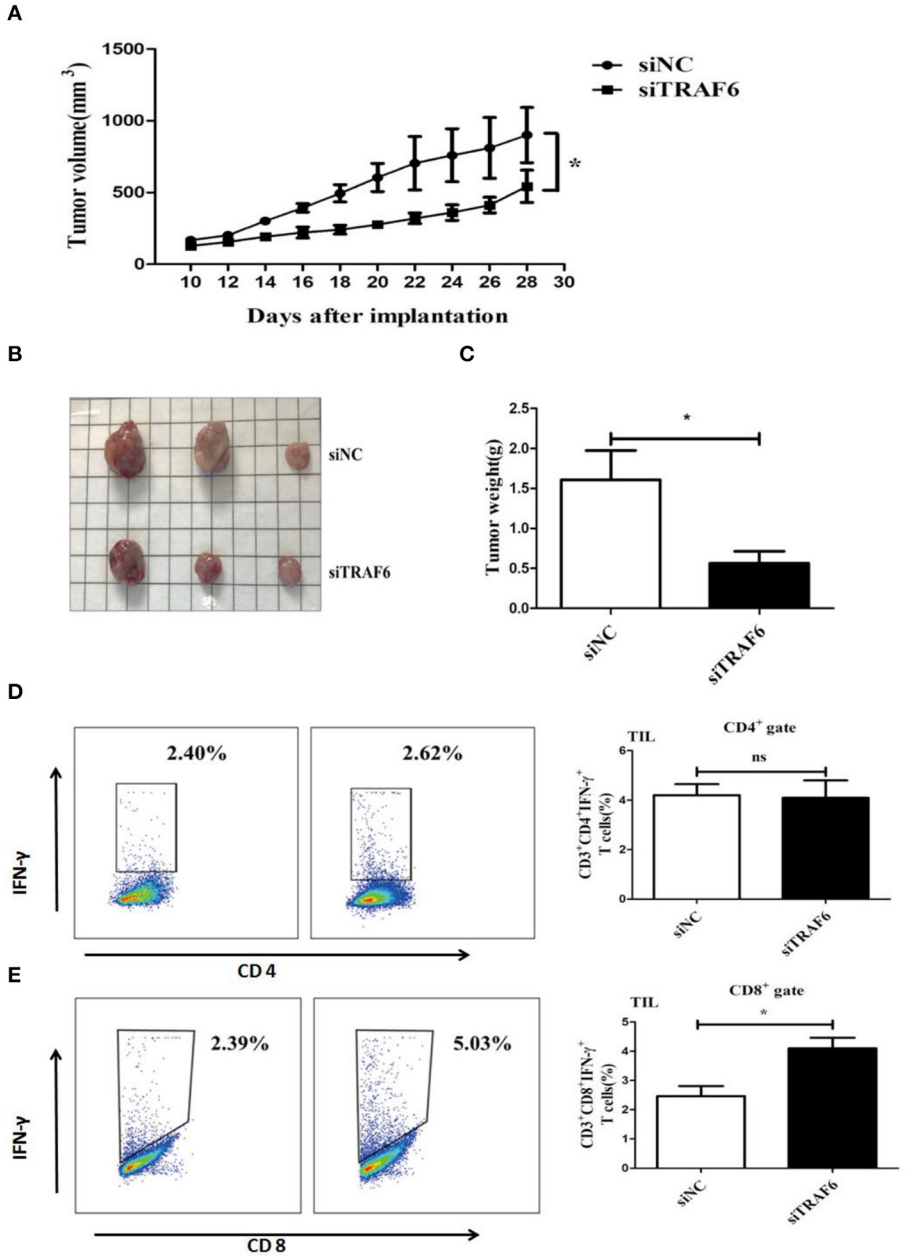

FIGURE 4 | TRAF6 knockdown attenuates the ability of MDSCs to accelerate tumor progression in tumor-bearing mice. To investigate the effects of TRAF6 on the suppressive activity of MDSCs *in vivo*, 2 groups of wild-type C57BL/6 mice were s.c. injected with 1×10^6 LLC cells and 1×10^6 MDSCs transfected with siTRAF6 (siTRAF6 group) or MDSCs transfected with siNC (control group). **(A)** Tumor growth was constantly monitored. The width "a" and length "b" were measured, and tumor volume was calculated. **(B,C)** On the 28th day after the inoculation of LLC cells, the mice were sacrificed, and the tumor image and weights were showed in both groups. **(D)** The proportion of $CD4^+IFN\text{-}\gamma^+$ Th1 cells in the tumor tissue of both groups was analyzed by FCM. **(E)** The proportion of $CD8^+IFN\text{-}\gamma^+$ CTLs in the tumor tissue of both groups was analyzed by FCM. *$p < 0.05$; ns, no significance.

regulating a series of physiological process (35–40). In addition, the oncogenic role of TRAF6 in tumors has been widely reported. TRAF6 is abnormally highly expressed in multiple tumor tissues and modulates the malignant behavior of tumor cells (41–46). Furthermore, mounting evidence has revealed that TRAF6 plays a critical role in the development and activation of lymphocytes and myeloid cells (42, 47, 48). However, whether TRAF6 regulates MDSCs which are pivotal immunosuppressive cells has not been reported to date.

To shed light on the potential effect of TRAF6 on MDSC functions, we constructed murine Lewis lung carcinoma models. Our research suggested that the expression of TRAF6 was higher

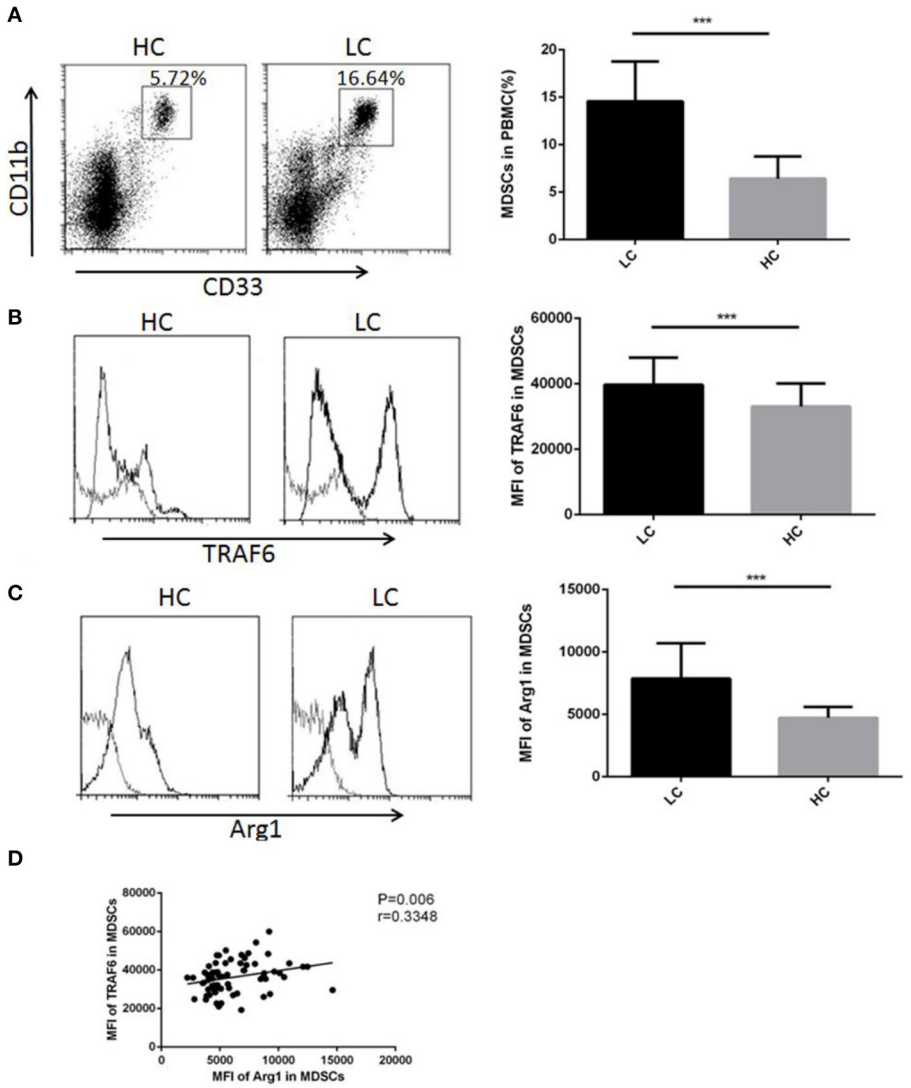

FIGURE 5 | TRAF6 expression was augmented in MDSCs from lung cancer patients. To examine the modulation of TRAF6 in MDSCs from lung cancer patients, the level of TRAF6 in MDSCs was measured in the lung cancer patient group (LC) and healthy control group (HC). **(A)** The proportions of MDSCs in the PBMCs of lung cancer patients and healthy persons were analyzed by flow cytometry. Representative dot plots of $CD11b^{+}CD33^{+}HLA\text{-}DR^{-}$ MDSCs in the blood of patients with LC and healthy controls are shown. **(B)** The mean fluorescence intensity (MFI) of TRAF6 in MDSCs was determined by flow cytometry. **(C)** The MFI of arginase-1 in MDSCs was determined by flow cytometry. **(D)** The correlation between TRAF6 and arginase-1 in MDSCs was analyzed. ***$p < 0.001$.

in MDSCs from tumor tissue than that in MDSCs from spleen. Consistent with previous research, we noted that the suppressive function of MDSCs derived from tumor tissue was stronger than that of spleen-derived MDSCs. Thus, we hypothesized that the strong suppressive activity of MDSCs from tumor tissues may be attributed to the high expression of TRAF6. After TRAF6 knockdown, the inhibitory effect of MDSCs on $CD4^{+}$ T cell proliferation was significantly decreased, with reduced Arg1 activity. Moreover, knockdown of TRAF6 attenuated the ability of MDSCs to accelerate tumor progression in tumor-bearing mice. Many clinical studies have demonstrated that increased levels of both circulating and tumor-infiltrating MDSCs were associated with poor prognosis in cancer patients. We further confirmed that the percentage of MDSCs was markedly increased in lung cancer patients. In addition, the expression of TRAF6 was increased in MDSCs from lung cancer patients, which was positively correlated with the level of Arg1 in MDSCs. These results highlighted the key role of TRAF6 in enhancing the function of MDSCs *in vitro* and *in vivo*.

STAT3 is one of the most important transcription factors regulating the expansion, activation and function of MDSCs. STAT3 is abnormally activated in MDSCs in the tumor microenvironment (23, 24, 49, 50). In addition to phosphorylation, ubiquitination is also involved in STAT3

activation. In our study, we demonstrated that TRAF6 binds to STAT3 in MDSCs. TRAF6 knockdown markedly reduced the K63-linked polyubiquitination and phosphorylation of STAT3 in MDSCs, indicating that TRAF6 elevated the suppressive function of MDSCs by interacting with STAT3. Indeed, it has been reported that TRAF6 mediates K63 ubiquitination via the SH2 domain of STAT3, which is an essential step for STAT3 phosphorylation in response to bacterial infections (29). Thus we assumed that TRAF6 fosters the suppressive effect of MDSCs by inducing STAT3 K63 ubiquitination and subsequent STAT3 phosphorylation. However, further studies are required to reveal the detailed molecular mechanism by which TRAF6 affects the function of MDSCs via STAT3.

CONCLUSIONS

In summary, we demonstrate that TRAF6 regulates the immunosuppressive activity of MDSCs by modulating the K63-linked polyubiquitination and phosphorylation of STAT3. Targeting of TRAF6 might be a potential clinical therapeutic strategy for enhancing antitumor immune response.

DATA AVAILABILITY STATEMENT

The original contributions presented in the study are included in the article/supplementary material, further inquiries can be directed to the corresponding author/s.

ETHICS STATEMENT

The studies involving human participants were reviewed and approved by the Ethics Committee of the Affiliated People's Hospital of Jiangsu University. The patients/participants provided their written informed consent to participate in this study. The animal study was reviewed and approved by the Committee on the Use of Live Animals in Research and Teaching of Jiangsu University. Written informed consent was obtained from the individual(s) for the publication of any potentially identifiable images or data included in this article.

AUTHOR CONTRIBUTIONS

GS performed the experiments, analyzed the data, and wrote the paper. YZ analyzed the data, and wrote the paper. JT and JM analyzed the data. KY and HX revised the paper. SW designed the study and wrote the paper. All authors read and approved the final manuscript.

FUNDING

This work was supported by the Jiangsu Province's Key Medical Talents Program (Grant No. ZDRCB2016018), Research Project of the Jiangsu Commission of Health (Grant No. K2019019), Natural Science Foundation of Jiangsu (Grant No. BK20190242), and Science and Technology Support Program (Social Development) of Zhenjiang (Grant No. SH 2020041).

REFERENCES

1. Kumar V, Patel S, Tcyganov E, Gabrilovich DI. The nature of myeloid-derived suppressor cells in the tumor microenvironment. *Trends Immunol.* (2016) 37:208–20. doi: 10.1016/j.it.2016.01.004
2. Li M, Zha X, Wang S. The role of N6-methyladenosine mRNA in the tumor microenvironment. *Biochim Biophys Acta Rev Cancer.* (2021). doi: 10.1016/j.bbcan.2021.188522. [Epub ahead of print].
3. Xie F, Xu M, Lu J, Mao L, Wang S. The role of exosomal PD-L1 in tumor progression and immunotherapy. *Mol Cancer.* (2019) 18:146. doi: 10.1186/s12943-019-1074-3
4. Ostrand-Rosenberg S, Fenselau C. Myeloid-Derived suppressor cells: immune-suppressive cells that impair antitumor immunity and are sculpted by their environment. *J Immunol.* (2018) 200:422–31. doi: 10.4049/jimmunol.1701019
5. Zheng Y, Tian X, Wang T, Xia X, Cao F, Tian J, et al. Long noncoding RNA Pvt1 regulates the immunosuppression activity of granulocytic myeloid-derived suppressor cells in tumor-bearing mice. *Mol Cancer.* (2019) 18:61. doi: 10.1186/s12943-019-0978-2
6. Tian X, Zheng Y, Yin K, Ma J, Tian J, Zhang Y, et al. LncRNA AK036396 inhibits maturation and accelerates immunosuppression of polymorphonuclear myeloid-derived suppressor cells by enhancing the stability of ficolin B. *Cancer Immunol Res.* (2020) 8:565–77. doi: 10.1158/2326-6066.CIR-19-0595
7. Bosiljcic M, Cederberg RA, Hamilton MJ, LePard NE, Harbourne BT, Collier JL, et al. Targeting myeloid-derived suppressor cells in combination with primary mammary tumor resection reduces metastatic growth in the lungs. *Breast Cancer Res.* (2019) 21:103. doi: 10.1186/s13058-019-1189-x
8. Tian J, Rui K, Hong Y, Wang X, Xiao F, Lin X, et al. Increased GITRL impairs the function of myeloid-derived suppressor cells and exacerbates primary sjögren's syndrome. *J Immunol.* (2019) 202:1693–703. doi: 10.4049/jimmunol.1801051
9. Zhou J, Liu M, Sun H, Feng Y, Xu L, Chan AWH, et al. Hepatoma-intrinsic CCRK inhibition diminishes myeloid-derived suppressor cell immunosuppression and enhances immune-checkpoint blockade efficacy. *Gut.* (2018) 67:931–44. doi: 10.1136/gutjnl-2017-314032
10. Tam JW, Kullas AL, Mena P, Bliska JB, van der Velden AW. CD11b+ Ly6Chi Ly6G- immature myeloid cells recruited in response to *Salmonella enterica Serovar typhimurium* infection exhibit protective and immunosuppressive properties. *Infect Immun.* (2014) 82:2606–14. doi: 10.1128/IAI.01590-13
11. Tian X, Ma J, Wang T, Tian J, Zhang Y, Mao L, et al. Long non-coding RNA HOXA transcript antisense RNA myeloid-specific 1-HOXA1 axis downregulates the immunosuppressive activity of myeloid-derived suppressor cells in lung cancer. *Front Immunol.* (2018) 9:473. doi: 10.3389/fimmu.2018.00473
12. Movahedi K, Guilliams M, Van den Bossche J, Van den Bergh R, Gysemans C, Beschin A, et al. Identification of discrete tumor-induced myeloid-derived suppressor cell subpopulations with distinct T cell-suppressive activity. *Blood.* (2008) 111:4233–44. doi: 10.1182/blood-2007-07-099226
13. Sumida K, Wakita D, Narita Y, Masuko K, Terada S, Watanabe K, et al. Anti-IL-6 receptor mAb eliminates myeloid-derived suppressor cells and inhibits tumor growth by enhancing T-cell responses. *Eur J Immunol.* (2012) 42:2060–72. doi: 10.1002/eji.201142335
14. Nefedova Y, Nagaraj S, Rosenbauer A, Muro-Cacho C, Sebti SM, Gabrilovich DI. Regulation of dendritic cell differentiation and antitumor immune response in cancer by pharmacologic-selective inhibition of the janus-activated kinase 2/signal transducers and activators of transcription 3 pathway. *Cancer Res.* (2005) 65:9525–35. doi: 10.1158/0008-5472.CAN-05-0529

15. Noman MZ, Desantis G, Janji B, Hasmim M, Karray S, Dessen P, et al. PD-L1 is a novel direct target of HIF-1α, and its blockade under hypoxia enhanced MDSC-mediated T cell activation. *J Exp Med.* (2014) 211:781–90. doi: 10.1084/jem.20131916
16. Fleet JC, Burcham GN, Calvert RD, Elzey BD, Ratliff TL. 1α, 25 Dihydroxyvitamin D (1,25(OH)(2)D) inhibits the T cell suppressive function of myeloid derived suppressor cells (MDSC). *J Steroid Biochem Mol Biol.* (2020) 198:105557. doi: 10.1016/j.jsbmb.2019.105557
17. Zhu D, Tian J, Wu X, Li M, Tang X, Rui K, et al. G-MDSC-derived exosomes attenuate collagen-induced arthritis by impairing Th1 and Th17 cell responses. *Biochim Biophys Acta Mol Basis Dis.* (2019) 1865:165540. doi: 10.1016/j.bbadis.2019.165540
18. Si Y, Merz SF, Jansen P, Wang B, Bruderek K, Altenhoff P, et al. Multidimensional imaging provides evidence for down-regulation of T cell effector function by MDSC in human cancer tissue. *Sci Immunol.* (2019) 4:eaaw9159. doi: 10.1126/sciimmunol.aaw9159
19. Koehn BH, Apostolova P, Haverkamp JM, Miller JS, McCullar V, Tolar J, et al. GVHD-associated, inflammasome-mediated loss of function in adoptively transferred myeloid-derived suppressor cells. *Blood.* (2015) 126:1621–28. doi: 10.1182/blood-2015-03-634691
20. Gabrilovich D I, Ostrand-Rosenberg S, Bronte V. Coordinated regulation of myeloid cells by tumours. *Nat Rev Immunol.* (2012) 12:253–68. doi: 10.1038/nri3175
21. Liu YF, Zhuang KH, Chen B, Li PW, Zhou X, Jiang H, et al. Expansion and activation of monocytic-myeloid-derived suppressor cell via STAT3/arginase-I signaling in patients with ankylosing spondylitis. *Arthritis Res Ther.* (2018) 20:168. doi: 10.1186/s13075-018-1654-4
22. Namkoong H, Ishii M, Fujii H, Yagi K, Asami T, Asakura T, et al. Clarithromycin expands CD11b+Gr-1+ cells via the STAT3/Bv8 axis to ameliorate lethal endotoxic shock and post-influenza bacterial pneumonia. *PLoS Pathog.* (2018) 14:e1006955. doi: 10.1371/journal.ppat.1006955
23. Hellsten R, Lilljebjörn L, Johansson M, Leandersson K, Bjartell A. The STAT3 inhibitor galiellalactone inhibits the generation of MDSC-like monocytes by prostate cancer cells and decreases immunosuppressive and tumorigenic factors. *Prostate.* (2019) 79:1611–21. doi: 10.1002/pros.23885
24. Trovato R, Fiore A, Sartori S, Canè S, Giugno R, Cascione L, et al. Immunosuppression by monocytic myeloid-derived suppressor cells in patients with pancreatic ductal carcinoma is orchestrated by STAT3. *J Immunother Cancer.* (2019) 7:255. doi: 10.1186/s40425-019-0734-6
25. Jiang M, Chen J, Zhang W, Zhang R, Ye Y, Liu P, et al. Interleukin-6 trans-signaling pathway promotes immunosuppressive myeloid-derived suppressor cells suppression of suppressor of cytokine signaling 3 in breast cancer. *Front Immunol.* (2017) 8:1840. doi: 10.3389/fimmu.2017.01840
26. Mao F, Zhao Y, Lv Y, Teng Y, Kong H, Liu Y, et al. CD45CD33CD11b myeloid-derived suppressor cells suppress CD8 T cell activity via the IL-6/IL-8-arginase I axis in human gastric cancer. *Cell Death Dis.* (2018) 9:763. doi: 10.1038/s41419-018-0803-7
27. Guha P, Gardell J, Darpolor J, Cunetta M, Lima M, Miller G, et al. STAT3 inhibition induces Bax-dependent apoptosis in liver tumor myeloid-derived suppressor cells. *Oncogene.* (2019) 38:533–48. doi: 10.1038/s41388-018-0449-z
28. Xin J, Zhang Z, Su X, Wang L, Zhang Y, Yang R. Epigenetic component p66a modulates myeloid-derived suppressor cells by modifying STAT3. *J Immunol.* (2017) 198:2712–20. doi: 10.4049/jimmunol.1601712
29. Ruan H, Zhang Z, Wang S, Nickels LM, Tian L, Qiao J, et al. Tumor necrosis factor receptor-associated factor 6 (TRAF6) mediates ubiquitination-dependent STAT3 activation upon *Salmonella enterica Serovar typhimurium* infection. *Infect Immun.* (2017) 85(8). doi: 10.1128/IAI.00081-17
30. Dou Y, Tian X, Zhang J, Wang Z, Chen G. Roles of TRAF6 in central nervous system. *Curr Neuropharmacol.* (2018) 16:1306–13. doi: 10.2174/1570159X16666180412094655
31. Chung J, Lu M, Yin Q, Lin S, Wu H. Molecular basis for the unique specificity of TRAF6. *Adv Exp Med Biol.* (2007) 597:122–30. doi: 10.1007/978-0-387-70630-6_10
32. Inoue J, Gohda J, Akiyama T. Characteristics and biological functions of TRAF6. *Adv Exp Med Biol.* (2007) 597:72–9. doi: 10.1007/978-0-387-70630-6_6
33. Mukhopadhyay D, Sangaré LO, Braun L, Hakimi MA, Saeij JP. Toxoplasma GRA15 limits parasite growth in IFNγ-activated fibroblasts through TRAF ubiquitin ligases. *EMBO J.* (2020) 39:e103758. doi: 10.15252/embj.2019103758
34. Wei J, Yuan Y, Jin C, Chen H, Leng L, He F, et al. The ubiquitin ligase TRAF6 negatively regulates the JAK-STAT signaling pathway by binding to STAT3 and mediating its ubiquitination. *PLoS ONE.* (2012) 7:e49567. doi: 10.1371/journal.pone.0049567
35. Biswas R, Bagchi A. Structural Characterization of the trimerization of TRAF6 protein through molecular dynamics simulations. *Interdiscip Sci.* (2019) 11:428–36. doi: 10.1007/s12539-017-0259-y
36. Xie C, Zhang LZ, Chen ZL, Zhong WJ, Fang JH, Zhu Y, et al. A hMTR4-PDIA3P1-miR-125/124-TRAF6 regulatory axis and its function in NF kappa B signaling and chemoresistance. *Hepatology.* (2020) 71:1660–77. doi: 10.1002/hep.30931
37. Wu H, Lu XX, Wang JR, Yang TY, Li XM, He XS, et al. TRAF6 inhibits colorectal cancer metastasis through regulating selective autophagic CTNNB1/β-catenin degradation and is targeted for GSK3B/GSK3β-mediated phosphorylation and degradation. *Autophagy.* (2019) 15:1506–22. doi: 10.1080/15548627.2019.1586250
38. Khusbu FY, Zhou X, Roy M, Chen FZ, Cao Q, Chen HC. Resveratrol induces depletion of TRAF6 and suppresses prostate cancer cell proliferation and migration. *Int J Biochem Cell Biol.* (2020) 118:105644. doi: 10.1016/j.biocel.2019.105644
39. Peng SJ, Yao RR, Yu SS, Chen HY, Pang X, Zhang Y, et al. UBL4A augments innate immunity by promoting the K63-linked ubiquitination of TRAF6. *J Immunol.* (2019) 203:1943–1951. doi: 10.4049/jimmunol.1800750
40. Cao C, An R, Yu Y, Dai H, Qu Z, Gao M, et al. BICP0 negatively regulates TRAF6-mediated NF-κB and interferon activation by promoting K48-linked polyubiquitination of TRAF6. *Front Microbiol.* (2019) 10:3040. doi: 10.3389/fmicb.2019.03040
41. Wu H, Yang TY, Li Y, Ye WL, Liu F, He XS, et al. Tumor necrosis factor receptor-associated factor 6 promotes hepatocarcinogenesis by interacting with histone deacetylase 3 to enhance c-Myc gene expression and protein stability. *Hepatology.* (2020) 71:148–63. doi: 10.1002/hep.30801
42. Wu X, Xue R, Peng H, Gan X, Lu X, Yan W, et al. Traf6 inhibitor boosts antitumor immunity by impeding regulatory T cell migration in Hepa1-6 tumor model. *Int Immunopharmacol.* (2019) 77:105965. doi: 10.1016/j.intimp.2019.105965
43. Zhu G, Cheng Z, Huang Y, Zheng W, Yang S, Lin C, et al. TRAF6 promotes the progression and growth of colorectal cancer through nuclear shuttle regulation NF-kB/c-jun signaling pathway. *Life Sci.* (2019) 235:116831. doi: 10.1016/j.lfs.2019.116831
44. Park Y, Pang K, Park J, Hong E, Lee J, Ooshima A, et al. Destablilization of TRAF6 by DRAK1 suppresses tumor growth and metastasis in cervical cancer cells. *Cancer Res.* (2020) 80:2537–49. doi: 10.1158/0008-5472.CAN-19-3428
45. Zhang T, Wang H, Han L. Expression and clinical significance of tumor necrosis factor receptor-associated factor 6 in patients with colon cancer. *Iran Red Crescent Med J.* (2016) 18:e23931. doi: 10.5812/ircmj.23931
46. Luo Z, Zhang X, Zeng W, Su J, Yang K, Lu L, et al. TRAF6 regulates melanoma invasion and metastasis through ubiquitination of basigin. *Oncotarget.* (2016) 7:7179–92. doi: 10.18632/oncotarget.6886
47. Zeng XZ, Zhang YY, Yang Q, Wang S, Zou BH, Tan YH, et al. Artesunate attenuates LPS-induced osteoclastogenesis by suppressing TLR4/TRAF6 and PLCγ1-Ca(2+)-NFATc1 signaling pathway. *Acta Pharmacol Sin.* (2020) 41:229–36. doi: 10.1038/s41401-019-0289-6
48. Ni X, Kou W, Gu J, Wei P, Wu X, Peng H, et al. TRAF6 directs FOXP3 localization and facilitates regulatory T-cell function through K63-linked ubiquitination. *EMBO J.* (2019) 38:99766. doi: 10.15252/embj.201899766
49. Dysthe M, Parihar R. Myeloid-derived suppressor cells in the tumor microenvironment. *Adv Exp Med Biol.* (2020) 1224:117–40. doi: 10.1007/978-3-030-35723-8_8

50. Jing B, Wang T, Sun B, Xu J, Xu D, Liao Y, et al. IL6/STAT3 signaling orchestrates premetastatic niche formation and immunosuppressive traits in lung. *Cancer Res.* (2020) 80:784–97. doi: 10.1158/0008-5472.CAN-19-2013

Conflict of Interest: The authors declare that the research was conducted in the absence of any commercial or financial relationships that could be construed as a potential conflict of interest.

Copyright © 2021 Song, Zhang, Tian, Ma, Yin, Xu and Wang. This is an open-access article distributed under the terms of the Creative Commons Attribution License (CC BY). The use, distribution or reproduction in other forums is permitted, provided the original author(s) and the copyright owner(s) are credited and that the original publication in this journal is cited, in accordance with accepted academic practice. No use, distribution or reproduction is permitted which does not comply with these terms.

frontiers in Oncology

MINI REVIEW
published: 26 February 2021
doi: 10.3389/fonc.2021.637504

Cyclooxygenase-2 Inhibitor: A Potential Combination Strategy With Immunotherapy in Cancer

*Dan Pu[1], Liyuan Yin[1], Lin Huang[1], Changlong Qin[1], Yuwen Zhou[2], Qiang Wu[1], Yan Li[1], Qinghua Zhou[1] and Lu Li[1]**

[1] Department of Lung Cancer Center, Lung Cancer Center, West China Hospital, Sichuan University, Chengdu, China, [2] Oncology Department, West China Hospital, Sichuan University, Chengdu, China

The clinical application of immunotherapy is the milestone of cancer treatment. However, some patients have bad reaction. Cyclooxygenase-2 (COX-2) is frequently expressed in multiple cancer cells and is associated with poor prognosis. It is the key enzyme of prostaglandin E_2 (PGE2) that has been proved to promote the development, proliferation and metastasis of tumor cells. Recent studies further find the PGE2 in tumor microenvironment (TME) actively triggers tumor immune evasion *via* many ways, leading to poor response of immunotherapy. COX-2 inhibitor is suggested to restrain the immunosuppression of PGE2 and may enhance or reverse the response of immune checkpoint inhibitors (ICIs). This review provides insight into the mechanism of COX-2/PGE2 signal in immunosuppressive TME and summarizes the clinical application and trials in cancer treatment.

Keywords: cyclooxygenase-2, immunotherapy, cancer, combination therapy, celecoxib

OPEN ACCESS

Edited by:
Peng Qu,
National Institutes of Health (NIH), United States

Reviewed by:
Mingxiao Feng,
Johns Hopkins University, United States
Guolin Zhang,
mprobe INC, United States

****Correspondence:***
Lu Li
windflower1991@vip.163.com

Specialty section:
This article was submitted to Cancer Immunity and Immunotherapy, a section of the journal Frontiers in Oncology

Received: *03 December 2020*
Accepted: *20 January 2021*
Published: *26 February 2021*

Citation:
Pu D, Yin L, Huang L, Qin C, Zhou Y, Wu Q, Li Y, Zhou Q and Li L (2021) Cyclooxygenase-2 Inhibitor: A Potential Combination Strategy With Immunotherapy in Cancer. Front. Oncol. 11:637504. doi: 10.3389/fonc.2021.637504

INTRODUCTION

Cancer is a global health problem. In recent years, immunotherapy has become a hot spot. ICIs, the most popular kind of immunotherapy, for variety of cancers have shown better efficacy than conventional chemotherapy. However, there are remaining questions needed to be resolved. The main two important questions were: Why the response to ICIs are different in different patients? How to increase the population benefiting from immunotherapy? Programmed death receptor-1 (PD-L1) expression, tumor infiltration lymph cells (TILs) and tumor mutation burden (TMB) are considered to be associated with ICIs efficacy (1). But even though the expression of PD-L1, the rate of TILs and the TMB are high in some patients, the efficacy of ICIs is still limited, which points out a non-PD-1/PD-L1 axis mediated immunosuppression (2). The leading theory explaining this phenomenon includes two aspects. One is the intrinsic factors, such as cancer-driven signaling pathways, MHC downregulation, microsatellite stability, etc. (3, 4). The another is extrinsic factors, known as TME. Cancer cells are closely related to extracellular matrix, stromal cells, and immune cells, which together constitute TME (5) and these components in TME impact the efficacy of ICIs, for example, the number of regulatory T cells (Tregs), myeloid suppressor cells (MDSCs), dendritic cells (DCs) and the activity of indoleamine 2,3-dioxygenase (IDO). TME is closely associated with inflammatory response and the inflammatory mediators in TME can be produced by stroma, TILs or cancer cells themselves. Prostaglandin E2 (PGE2) is one of the most important inflammatory factors in TME, which is related to the survival, growth, migration, invasion,

angiogenesis and immune evasion of cancer cells (6). Cyclooxygenase (COX) is the rate-limiting step enzyme that produces PGE2. There are three isoforms: COX-1, COX-2, COX-3 (7). COX-1, constitutively expressed in a wide range of normal tissues, works as a housekeeping enzyme responsible for maintaining tissue homeostasis. COX-3 is a splice variant of COX-1, which is also called COX-1b or COX-1v. COX-2 barely presents in most normal cells, but can be highly induced by inflammation and cancer (8). Previous studies have shown that COX-2 is overexpressed in most cancers and is associated with poor prognosis (9, 10). With the rise of immunotherapy, more and more studies have shown that COX-2 mediates immunosuppression *via* multiple ways. This review summarizes the roles of COX-2 in the resistance of ICIs and proposes a position and opportunity for COX-2 inhibitors in combination with immunotherapy in cancers.

THE ACTIVATION OF COX-2/PGE2 PATHWAY IN CANCER

Gene encoding COX-2 is located on the chromosome 1q25.2-q25.3 in human, known as *PTGS2*. COX-2 is a membrane-bound enzyme that plays a key role in synthesis of important biological hormones-prostaglandins (PGs), such as PGE2, PGF2α and thromboxane (11). COX-2 is usually negligible in normal cells except basal expressed in a few organs, such as stomach, kidney, central nervous and female reproduction. While it is frequently expressed in most types of cancers, including lung cancer (12), gastrointestinal cancer (13), breast cancer (14), head and neck carcinoma (15), hepatocellular carcinoma, and etc (16). COX-2 overexpression is linked to many properties of malignant cells including promoting carcinogenesis, increasing the rate of cancer recurrence, reducing survival and mediating resistance of tumor cells to treatment, through overproduction of PGs (17).

Oncogenic viruses, inflammatory cytokines can elevate the expression of COX-2. Tumor intrinsic factors also upregulate COX-2/PGE2 axis. Markosyan and his colleagues identified *PTGS2* was upregulated by EPHA2, a candidate tumor intrinsic driver of immunosuppression, through TGF-β pathway in pancreatic cancer (18). The reduction of RIPK3 in colorectal cancer cells and MDSCs elicited NF-κβ-transcribed COX-2, thus to exacerbate the immunosuppressive activity of MDSCs (19). In breast cancer, HDAC6 was frequently upregulated in the cancer-associated fibroblasts(CAFs) and increased the expression of COX-2/PGE2 by regulating STAT3 activation (20), leading to poor survival outcomes. In addition, the aberrant activation of EGF (21), KRAS (22), p38MAPK (23, 24) signals, which frequently present in cancers, also induce COX-2 expression, thus to mediate immunosuppression.

THE MECHANISM OF IMMUNOSUPPRESSION MEDIATED BY COX-2

Malignant cells can escape immune-surveillance by exhaustion of CD8+ T cells expressing programmed cell death protein 1 (PD-1) and cytotoxic T-lymphocyte-associated protein (CTLA-4). ICIs are a class of inhibitors that targeted immune checkpoint proteins marked on the surface of cancer cells, like CTLA-4 receptor and programmed cell death protein ligand 1 (PD-L1), so that to remove the inhibition of T cells by cancer cells. Previous evidences suggested that the impact of COX-2/PGE2 signal pathway in TME plays an important role in immunosuppression and further induces ICIs resistance. Long before the advent of immunotherapy in clinic, the role of COX-2/PGE2 in immunosuppression was deeply studied in laboratory.

COX-2/PGE2 Signal Inhibits T Cell Infiltration

T cells infiltrated to tumors recognize and fight against antigen-targeted tumor cells. The non-T cell inflamed tumors are usually difficult to treat with ICIs (25). Markosyan showed that compared with wild-type, the onset of breast tumors in ErbB2 transgenic mice with mammary epithelial cell COX-2 deficiency (COX-2^{MEK}KO) was delayed. COX-2^{MEK}KO TME contained more $CD4^+$ T helper cells and $CD8^+$ cytotoxic T lymphocytes (CTL). The Th1 marker Tbet and Th2 marker GATA3 were overexpressed, while Retnla, the marker of M2 macrophage cell was lower expressed in COX-2^{MEK}KO tumor than the wild-type, suggesting an enhanced immune-surveillance (26).

Analysis of samples from human and mouse cancer cells with low or high TIL density again confirmed the association between COX-2 expression and T cell exclusion. In pancreatic cancer (18), the intrinsic TGF-β signaling of tumor cells drives the upregulation of EPHA2 on cell surface, which promotes the overexpression of *PTGS2*. In vivo study, researchers inoculated control and *Ptgs2*-knockdown (*Ptgs2*-KD) cells into immunocompetent mice, with or without $CD4^+$ and $CD8^+$ T cell depletion, resulting in a higher rate of tumor formation in control cells. T cell depletion abolished the tumor growth suppression afforded by *Ptgs2* KD or celecoxib, which indicates that the tumor suppression of *PTGS*2 is T cell dependent. In *PTGS2* overexpression tumors, the proportion of $CD4^+$ and $CD8^+$ T cells and the percentage of activated $CD8^+$ T cells were significantly reduced. In addition, *PTGS2* overexpression increased the proportion of infiltrated myeloid cells, especially myeloid-derived suppressor cells (MDSCs), with a decrease in the dendritic cells (DCs) population.

A series of human cancer cells constitutively express indoleamine 2,3-dioxygenase 1 (IDO1) that degrades tryptophan and produces equimolar amounts of kynurenine, also mediates immunosuppression. Marc Hennequart's study indicated that COX-2 expression drives the constitutive expression of IDO1. In human tumor cell lines, constitutive IDO1 expression depends on COX-2 and PGE2 *via* EP receptor through PKC and PI3K pathways. Celecoxib treatment decreased IDO1 expression and increased $CD3^+$ and $CD8^+$ cells infiltration in ovarian SKOV3 tumors (27).

COX-2/PGE2 Signal in NK-DC Crosstalk

Nature kill (NK) cell as a part of innate immunity plays an important role in tumor immune surveillance. NK cells not only directly recognize and kill tumor cells, but also release cytokines that

promote CTL activation and proliferation. Park. A and his colleagues showed thyroid cancer-derived PGE2 represses NK maturation and the expression of NK receptors, such as NK44, NK30, TRAIL and NKG2D (28). Inhibition of COX-2/PGE2 signal pathway can recover the activation of NK cells in tumor-bearing mice (29). Besides, Böttcher revealed the intercommunication between NK cell and dendritic cells (DCs) (30). NK cells recruit conventional type 1 DCs (cDC1) by release of CCL5 and XCL1. Tumor-derived PGE2 impairs NK cell viability and chemokine production, then decreases the recruitment of cDC1s to TME. DCs, especially Batf3$^+$ CD103$^+$ cDC1, are essential in presenting tumor antigen and secreting cytokines, such as CXCL9, CXCL10, that regulate T cell function (31). CD103$^+$ DCs were selectively absent in tumor expressing COX-2. In an obesity-associated hepatocellular carcinoma mice model, the daily systemic therapy of PGE2 receptor inhibitor for 3 weeks showed significant induction of cDC1 (CD103$^+$ DC) frequency (32).

COX-2/PGE2 Signal Induces MDSCs

MDSCs can inhibit CTL activation by overexpression of argininase 1 (ARG-1), inducing nitric oxide synthase (iNOS or NOS2) and reactivating oxygen species (ROS), thus inducing immune escape. COX-2/PGE2 signal pathway is associated with the accumulation of MDSCs. In colorectal cancer, the reduction of PIRK3 elicited NF-κβ transcribed COX-2 expression and boosted the synthesis of PGE2. Inhibition of COX-2 or PGE2 receptors reversed the immunosuppressive activity of MDSCs and dampened tumorigenesis (19). Porta et al. (33) also demonstrated tumor-derived PGE2 mediated induction of nuclear p50 NF-κB epigenetically reprograms the response of monocytic cells to IFN-γ toward an immunosuppressive phenotype, thus retrieving the anticancer properties of IFN-γ. Inhibition of the PGE2 axis can prevents MDSC suppressive functions and restores the efficacy of anticancer immunotherapy.

Multiple tumor cell lines, like Braf V600E melanoma, 4T1 breast cancer, CT26 colorectal cancer, *Nras* G12D-drive mouse melanoma, methylcholine-induced fibrosarcoma (34, 35) aberrant expressed COX-2/PGE2. The conditional medium of Braf V600E melanoma cells regulated the function of myeloid cells by expressing COX-2 and PGE2. COX-2 deficiency resulted in low expression of immunosuppression factors like IL-6, IL-10, and CXCL1, while the mRNA of anti-tumor immune mediators are significantly increased, such as IFN-γ, T-bet, CXCL10, and IL-12 (36).

MDSCs can also negatively regulate NK function. MDSCs from patients with advanced melanoma inhibited the activity of co-cultured NK cells. PGE2 binding to EP2 and EP4 receptors on MDSC activates p38MAPK/ERK pathway, leading to TGF secretion and thereby inhibiting NK cells (37).

COX-2/PGE2 Signal Induced M2

Macrophages are the most plastic cells in the hematopoietic system, which are found in all tissues, and they also have strong functional diversity. There are at least two subtypes of macrophages, namely M1 and M2. M1 macrophages are involved in the pro-inflammatory response and play a central role in the host's defense against bacterial and viral infections. M2 macrophages are associated with resolution of inflammatory response, parasite infection, tissue remodeling, fibrosis, and tumor disease development. Previous studies had pointed out an important role of PGE2 in the polarization of macrophage to M2, leading to an immunosuppression TME. In vitro experiments, a human peripheral blood mononuclear cell primary culture in the presence of GM-CSF plus IL-4 promoted differentiation to DCs. An addition of PGE_2 in this culture suppressed the formation of DCs and skewed the differentiation into the M2-like macrophage (38, 39). PGE2 also induces the differentiation from MDSC to M2 macrophage. The cross-talk between miR-21 and PGE_2 may be a determining factor in macrophage polarization. PGE2 and its downstream effectors PKA and Epac inhibited mRNA-21 and enhance the expression of M2 gene (40).

Based on previous studies, COX-2 derived PGE2 helps TME transformed from an anti-tumor response to an immunosuppressive response in a variety of ways, becoming an accomplice of cancer cell immune escape (**Figure 1**).

CLINICAL APPLICATION OF COX-2 INHIBITORS IN CANCER TREATMENT

The current focus of immunotherapy is to improve the therapeutic response of ICIs by simultaneously stimulating immune function and targeting immunoregulatory factors in TME. A variety of combinations are in clinical trials, such as ICIs combined with GM-CSF, targeted drugs, oncolytic virus, chemotherapy, radiotherapy, IDO inhibitor, etc. (41, 42).

Researchers have long noticed the important role of COX-2 in the occurrence and development of cancer. Once upon a time, the clinical trials of COX-2 inhibitor combination therapy in cancers were popular. However, no satisfactory results were obtained in such combinations. A phase II clinical trial of COX-2 inhibitor combined with erlotinib, one of the epidermal growth factor receptor tyrosine kinase inhibitor (EGFR TKI), seemed to have an increase trend in time to progression (TTP) and overall survival (OS) in non-small cell lung cancer (NSCLC) (43). While compared with conventional chemotherapy regiments, combined with COX-2 inhibitor did not achieve survival improvement (44, 45). The conclusion was controversial. Csiki et al. (46) performed a stratified analysis of the decreased levels of urine PGE-M (the main urinary metabolite of PGE2) after using celecoxib, and showed that patients with a large decline rate obtained a longer survival (14.8 months, 6.3 months, 5.0 months, respectively). Are COX-2 inhibitors really useful in cancer treatment? COX-2 expression level, metabolites or COX-2-dependent inflammatory mediators may be useful biomarkers for predicting prognosis and outcomes of combination therapy. Based on the mechanism of COX-2 and PGE2 in TME described above, the combination of COX-2 inhibitor and ICI is a potential choice. This idea has been further verified in animal experiments (36). The combination of COX inhibitors (including aspirin and celecoxib) with anti-PD-1 antibodies can promote tumor regression more than the single use of anti-PD-1 antibodies. What's more, it has been known that ICI combined with chemotherapy would increase disease

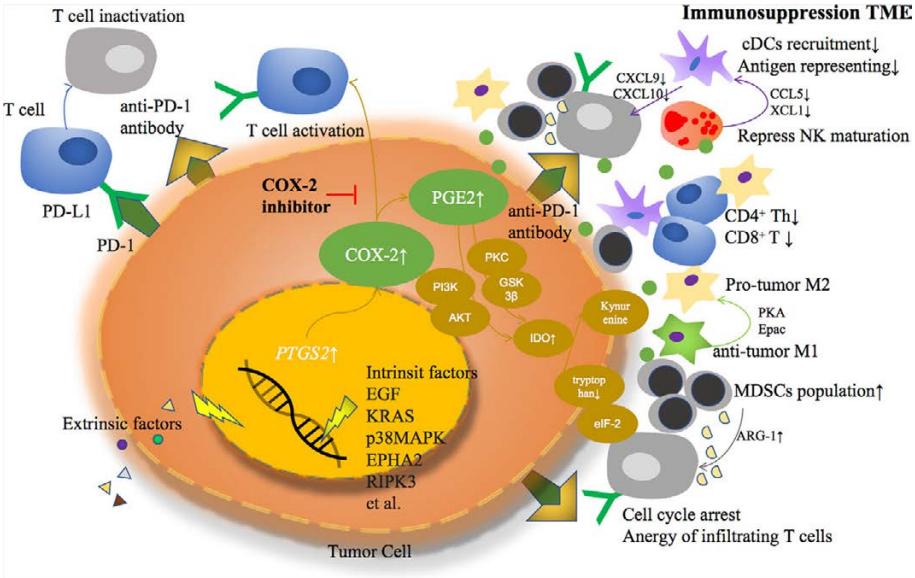

FIGURE 1 | Extrinsic or intrinsic factors lead to COX-2 overexpression and PGE2 over production in tumor cells, formatting an immunosuppressive tumor microenvironment through multiple ways.

control, because of the antigen release induced by chemotherapy. So the benefit of COX-2 inhibitor might be based on the immune activation combined with ICI and chemotherapy plays a supporting role in it, which need to be further study in clinical practice.

In order to further find patients who may benefit from this combination, the relationship between COX-2 and cancers in previous studies were also reviewed. An analysis of 170 cases of surgically resected lung adenocarcinoma showed that high COX-2 expression accounted for 46%, and the number of $CD8^+$ T lymphocytes in tumors with high COX-2 expression was significantly less than that in the low expression group, while the Treg count was in the opposite (47). Shimizu et al. reported correlations between COX-2 and immune checkpoint proteins. Double fluorescence staining showed co-localization of PD-L1 and COX-2 expression in resected lung cancer specimens (48). Besides, Kim's study analyzed the relationship between PD-L1 RNA and COX-2 expression in 60 human melanoma cell lines in CCLE database and also showed a significant correlation (r=0.312, P=0.014). But *in vitro*, COX-2 inhibitor, celecoxib did not affect the expression of PD-L1 induced by IFN-γ in melanoma cell lines, A375, SB2 and LOX-IMVI (49). So, COX-2 might be an intrinsic characteristic of certain cancer cells, and mediates immunosuppression *via* not only PD-1/PD-L1 axis.

In terms of the safety of ICI combined with COX-2 inhibitor, several aspects should be taken into consideration. First of all, ICIs are a kind of monoclonal antibody. Their metabolic pathways are similar to that of endogenous IgG, not go through the cytochrome P450 enzyme metabolic pathway. While celecoxib is mainly metabolized by CYP2C9 (50), so there might be no drug interaction between them theoretically. Secondly, we take Celecoxib, the most representative selective COX-2 inhibitor, as an example, to illustrate the side-effects of COX-2 inhibitor. The most common side-effects of Celecoxib at a dose of 400–800 mg/day for 3 years are diarrhea (10.5% in Celecoxib group vs. 7.0% in placebo), Gastroesophageal reflux (4.7% in Celecoxib group vs. 3.1% in placebo), nausea (6.8% in Celecoxib group vs. 5.3% in placebo), vomit (3.2% in Celecoxib group vs. 2.1% in placebo), dyspnea (2.8% in Celecoxib group vs. 1.6% in placebo), hypertension (12.5% in Celecoxib group vs. 9.8% in placebo). The occurrence of heart abnormalities and thrombotic event were between 0.1% and 1%. The previous trials of celecoxib combined chemotherapy regimens were well tolerated and did not show an increase in serious adverse events (45, 51). Especially when compared with the placebo group, there was no increase in cardiovascular events in celecoxib group (45). Finally, it is very likely that the main risks of the combination therapy of COX-2 inhibitor and ICI come from their own separately. According to the dose of celecoxib used in CLASS study, the incidence of complicated and symptomatic ulcers was only 0.78% and the incidence of severe cardiovascular thromboembolic events was only 1.2% continuously taking 400 mg twice daily for 9 months (52). And Csiki et al. (46) have also shown that at this dose intensity, urine PGE-M is significantly reduced, indicating that COX-2 and its derived PGE2 are significantly restrained.

Some clinical trials about COX-2 inhibitor combination therapies are ongoing (**Table 1**). In colorectal cancer, trials to evaluate PD-1 inhibitors with celecoxib as neoadjuvant therapy are recruiting (NCT03026140, NCT03926338). In breast cancer, NCT04188119 and NCT04348747 are registered. There are also some other combined treatments in progress. For example,

TABLE 1 | The clinical trials that study the COX inhibitor and immunotherapy registered in clinicaltrial.gov.

Clinical Trial	Cancer	Therapy	Phase	Status
NCT03026140	Colon carcinoma	Ipilimumab, Nivolumab; Ipilimumab, Nivolumab, Celecoxib	II	Recruiting
NCT04188119	Breast cancer	Avelumab, PPI; Avelumab, Aspirin, PPI	II	Not yet recruiting
NCT03926338	Colorectal cancer	PD-1 inhibitor, Celecoxib; PD-1 inhibitor	I, II	Recruiting
NCT04348747	Breast cancer	DC vaccine, pembrolizumab, celecoxib, IFNα-2b,rintatolimod	II	Not yet recruiting
NCT03728179	TIL-negative solid tumors	Low dose irradiation+Nivolumab+Ipilimumab or Cyclophosphamide + Aspirin/ Celecoxib	I	Recruiting
NCT03245489	Squamous Cell Carcinoma of the Head and Neck	Pembrolizumab, Clopidogrel, Aspirin; Pembrolizumab	I	Recruiting

TIL, Tumor Infiltrating Lymphocytes; PPI, Proton Pump Inhibitor.

RACIN (NCT03728179) is designed to explore the combination of PD-1 inhibitor with or without CTLA-4 inhibitor, aspirin (non-selective COX inhibitor) or celecoxib (selective COX-2 inhibitor) and low-dose radiotherapy in TIL negative solid tumors, which might answer the immunomodulation effect of aspirin or celecoxib. Selective COX-2 inhibitor induces less gastrointestinal reaction, one of the most common side-effects of COX inhibitors, like gastric ulcer. What's more, a large clinical study in 2017 showed that compared with the COX-2 selective inhibitor Celecoxib, the non-selective COX inhibitors ibuprofen and naproxen significantly increased the systolic blood pressure, and the occurrence of new hypertension was higher (53). In fact, taking Celecoxib or non-selective ones (such as ibuprofen) for up to three years have shown that the risk of cardiovascular events increases. So, theoretically, selective or non-selective COX inhibitor, as long as drugs targeting COX2/PGE2 signal pathway, could be further studied in clinical practices, but selective one at least reduces gastrointestinal reaction. Thus the side effect of COX-2 inhibitor should be taken into consideration carefully and exclude patients that have contraindications. The appropriate dose of these drugs is uncertain by now. Some scientists considered that whether PGE2 receptor inhibitor, instead of COX-2 inhibitor, could also combined with immunotherapy. The COX-2 product PGE2 binds to four G-protein-coupled EP receptors designated EP1-EP4. Recent drugs7nbsp;only designed to block EP4. EP4 is commonly upregulated in cancers, while MDSCs are induced by PGE2 acting on myeloid-expressed EP2 and EP4 (54). So, the effect of EP4 inhibitor combined with ICI remains to be seen. Anyway, the COX-2/PGE2 signal is a promising target in combination with immunotherapy.

CONCLUSION

Given that COX-2/PGE2 axis promotes immunosuppression, it is conceivable that COX inhibitors have a role in anti-tumor therapy. Unfortunately, former clinical attempt of combination COX inhibitor with chemotherapy or targeted therapy failed. But COX inhibitor might enhance or expand the response of immunotherapy in consideration of its mechanism. Several clinical trials are ongoing. They will provide us a new thought of therapeutic approach in cancer immunotherapy.

AUTHOR CONTRIBUTIONS

DP wrote the manuscript. LY, LH, and CQ searched the references. YZ, QW, and YL contributed to the scientific discussion. QZ modified the manuscript. LL supported the research. All authors contributed to the article and approved the submitted version.

FUNDING

2020HXFH046, 1·3·5 Project for Disciplines of Excellence-Clinical Research Incubation Project, West China Hospital, Sichuan University.

ACKNOWLEDGMENTS

We would like to thank QZ and LL for reviewing the manuscript.

REFERENCES

1. Yi M, Jiao D, Xu H, Liu Q, Zhao W, Han X, et al. Biomarkers for predicting efficacy of PD-1/PD-L1 inhibitors. *Mol Cancer* (2018) 17(1):129. doi: 10.1186/s12943-018-0864-3
2. Pitt Jonathan M, Vétizou M, Daillère R, Roberti María P, Yamazaki T, Routy B, et al. Resistance Mechanisms to Immune-Checkpoint Blockade in Cancer: Tumor-Intrinsic and -Extrinsic Factors. *Immunity* (2016) 44(6):1255–69. doi: 10.1016/j.immuni.2016.06.001
3. Pardoll DM. The blockade of immune checkpoints in cancer immunotherapy. *Nat Rev Cancer* (2012) 12(4):252–64. doi: 10.1038/nrc3239
4. Topalian SL, Wolchok JD, Chan TA, Mellman I, Palucka K, Banchereau J, et al. Immunotherapy: The path to win the war on cancer? *Cell* (2015) 161 (2):185–6. doi: 10.1016/j.cell.2015.03.045
5. Hanahan D, Coussens Lisa M. Accessories to the Crime: Functions of Cells Recruited to the Tumor Microenvironment. *Cancer Cell* (2012) 21(3):309–22. doi: 10.1016/j.ccr.2012.02.022

6. Wang D, DuBois RN. Eicosanoids and cancer. *Nat Rev Cancer* (2010) 10 (3):181–93. doi: 10.1038/nrc2809
7. Hashemi Goradel N, Najafi M, Salehi E, Farhood B, Mortezaee K. Cyclooxygenase-2 in cancer: A review. *J Cell Physiol* (2019) 234(5):5683–99. doi: 10.1002/jcp.27411
8. Ferrer MD, Busquets-Cortés C, Capó X, Tejada S, Tur JA, Pons A, et al. Cyclooxygenase-2 Inhibitors as a Therapeutic Target in Inflammatory Diseases. *Curr Med Chem* (2019) 26(18):3225–41. doi: 10.2174/0929867325666180514112124
9. Hu Z, Yang Y, Zhao Y, Huang Y. The prognostic value of cyclooxygenase-2 expression in patients with esophageal cancer: evidence from a meta-analysis. *Onco Targets Ther* (2017) 10:2893–901. doi: 10.2147/ott.S134599
10. Kunzmann AT, Murray LJ, Cardwell CR, McShane CM, McMenamin UC, Cantwell MM. PTGS2 (Cyclooxygenase-2) expression and survival among colorectal cancer patients: a systematic review. *Cancer Epidemiol Biomarkers Prev* (2013) 22(9):1490–7. doi: 10.1158/1055-9965.Epi-13-0263
11. Wang D, DuBois RN. Prostaglandins and cancer. *Gut* (2006) 55(1):115–22. doi: 10.1136/gut.2004.047100
12. Jiang H, Wang J, Zhao W. Cox-2 in non-small cell lung cancer: a meta-analysis. *Clin Chim Acta* (2013) 419:26–32. doi: 10.1016/j.cca.2013.01.012
13. Nagaraju GP, El-Rayes BF. Cyclooxygenase-2 in gastrointestinal malignancies. *Cancer* (2019) 125(8):1221–7. doi: 10.1002/cncr.32010
14. Chen EP, Smyth EM. COX-2 and PGE2-dependent immunomodulation in breast cancer. *Prostaglandins Other Lipid Mediat* (2011) 96(1-4):14–20. doi: 10.1016/j.prostaglandins.2011.08.005
15. Zhu Y, Shi C, Zeng L, Liu G, Jiang W, Zhang X, et al. High COX-2 expression in cancer-associated fibiroblasts contributes to poor survival and promotes migration and invasiveness in nasopharyngeal carcinoma. *Mol Carcinog* (2020) 59(3):265–80. doi: 10.1002/mc.23150
16. Yang Y, Zhu J, Gou H, Cao D, Jiang M, Hou M. Clinical significance of Cox-2, Survivin and Bcl-2 expression in hepatocellular carcinoma (HCC). *Med Oncol (Northwood London England)* (2011) 28(3):796–803. doi: 10.1007/s12032-010-9519-y
17. Williams CS, Mann M, DuBois RN. The role of cyclooxygenases in inflammation, cancer, and development. *Oncogene* (1999) 18(55):7908–16. doi: 10.1038/sj.onc.1203286
18. Conejo-Garcia JR. Breaking barriers for T cells by targeting the EPHA2/TGF-β/COX-2 axis in pancreatic cancer. *J Clin Invest* (2019) 129(9):3521–3. doi: 10.1172/jci130316
19. Yan G, Zhao H, Zhang Q, Zhou Y, Wu L, Lei J, et al. A RIPK3-PGE2 Circuit Mediates Myeloid-Derived Suppressor Cell-Potentiated Colorectal Carcinogenesis. *Cancer Res* (2018) 78(19):5586–99. doi: 10.1158/0008-5472.Can-17-3962
20. Li A, Chen P, Leng Y, Kang J. Histone deacetylase 6 regulates the immunosuppressive properties of cancer-associated fibroblasts in breast cancer through the STAT3-COX2-dependent pathway. *Oncogene* (2018) 37 (45):5952–66. doi: 10.1038/s41388-018-0379-9
21. Chiang KH, Shieh JM, Shen CJ, Chang TW, Wu PT, Hsu JY, et al. Epidermal growth factor-induced COX-2 regulates metastasis of head and neck squamous cell carcinoma through upregulation of angiopoietin-like 4. *Cancer Sci* (2020) 111(6):2004–15. doi: 10.1111/cas.14400
22. Smakman N, Kranenburg O, Vogten JM, Bloemendaal AL, van Diest P, Borel Rinkes IH. Cyclooxygenase-2 is a target of KRASD12, which facilitates the outgrowth of murine C26 colorectal liver metastases. *Clin Cancer Res An Off J Am Assoc Cancer Res* (2005) 11(1):41–8.
23. Uchida K. HNE as an inducer of COX-2. *Free Radic Biol Med* (2017) 111:169–72. doi: 10.1016/j.freeradbiomed.2017.02.004
24. Lim HJ, Park JH, Jo C, Yoon K, Koh YH. Cigarette smoke extracts and cadmium induce COX-2 expression through γ-secretase-mediated p38 MAPK activation in C6 astroglia cells. *PloS One* (2019) 14(2):e0212749. doi: 10.1371/journal.pone.0212749
25. Chen DS, Mellman I. Elements of cancer immunity and the cancer–immune set point. *Nature* (7637) 2017) 541:321–30. doi: 10.1038/nature21349
26. Markosyan N, Chen EP, Evans RA, Ndong V, Vonderheide RH, Smyth EM. Mammary Carcinoma Cell Derived Cyclooxygenase 2 Suppresses Tumor Immune Surveillanceby Enhancing Intratumoral Immune Checkpoint Activity. *Breast Cancer Res* (2013) 15(5):R75. doi: 10.1186/bcr3469
27. Hennequart M, Pilotte L, Cane S, Hoffmann D, Stroobant V, Plaen ED, et al. Constitutive IDO1 Expression in Human Tumors Is Driven by Cyclooxygenase-2 and Mediates Intrinsic Immune Resistance. *Cancer Immunol Res* (2017) 5(8):695. doi: 10.1158/2326-6066.CIR-16-0400
28. Park A, Lee Y, Kim MS, Kang YJ, Park Y-J, Jung H, et al. Prostaglandin E2 Secreted by Thyroid Cancer Cells Contributes to Immune Escape Through the Suppression of Natural Killer (NK) Cell Cytotoxicity and NK Cell Differentiation. *Front Immunol* (2018) 9:1859. doi: 10.3389/fimmu.2018.01859
29. Ma X, Holt D, Kundu N, Reader J, Goloubeva O, Take Y, et al. (PGE) receptor EP4 antagonist protects natural killer cells from PGE2-mediated immunosuppression and inhibits breast cancer metastasis. *OncoImmunology* (2013) 2(1):e22647. doi: 10.4161/onci.22647
30. Böttcher JP, Bonavita E, Chakravarty P, Blees H, Cabeza-Cabrerizo M, Sammicheli S, et al. NK Cells Stimulate Recruitment of cDC1 into the Tumor Microenvironment Promoting Cancer Immune Control. *Cell* (2018) 172(5):1022–1037.e1014. doi: 10.1016/j.cell.2018.01.004
31. Spranger S, Dai D, Horton B, Gajewski TF. Tumor-Residing Batf3 Dendritic Cells Are Required for Effector T Cell Trafficking and Adoptive T Cell Therapy. *Cancer Cell* (2017) 31(5):711–723.e714. doi: 10.1016/j.ccell.2017.04.003
32. Loo TM, Kamachi F, Watanabe Y, Yoshimoto S, Kanda H, Arai Y, et al. Gut Microbiota Promotes Obesity-Associated Liver Cancer through PGE(2)-Mediated Suppression of Antitumor Immunity. *Cancer Discovery* (2017) 7 (5):522–38. doi: 10.1158/2159-8290.Cd-16-0932
33. Porta C, Consonni FM, Morlacchi S, Sangaletti S, Bleve A, Totaro MG, et al. Tumor-Derived Prostaglandin E2 Promotes p50 NF-κB-Dependent Differentiation of Monocytic MDSCs. *Cancer Res* (2020) 80(13):2874–88. doi: 10.1158/0008-5472.Can-19-2843
34. Matsushita H, Vesely MD, Koboldt DC, Rickert CG, Uppaluri R, Magrini VJ, et al. Cancer exome analysis reveals a T-cell-dependent mechanism of cancer immunoediting. *Nature* (2012) 482(7385):400–4. doi: 10.1038/nature10755
35. Pedersen M, Küsters-Vandevelde HVN, Viros A, Groenen PJTA, Sanchez-Laorden B, Gilhuis JH, et al. Primary Melanoma of the CNS in Children Is Driven by Congenital Expression of Oncogenic <em<NRAS</em< in Melanocytes. *Cancer Discovery* (2013) 3(4):458. doi: 10.1158/2159-8290.CD-12-0464
36. Zelenay S, van der Veen Annemarthe G, Böttcher Jan P, Snelgrove Kathryn J, Rogers N, Acton Sophie E, et al. Cyclooxygenase-Dependent Tumor Growth through Evasion of Immunity. *Cell* (2015) 162(6):1257–70. doi: 10.1016/j.cell.2015.08.015
37. Mao Y, Sarhan D, Steven A, Seliger B, Kiessling R, Lundqvist A. Inhibition of Tumor-Derived Prostaglandin-E2 Blocks the Induction of Myeloid-Derived Suppressor Cells and Recovers Natural Killer Cell Activity. *Clin Cancer Res* (2014) 20(15):4096. doi: 10.1158/1078-0432.CCR-14-0635
38. Take Y, Koizumi S, Nagahisa A. Prostaglandin E Receptor 4 Antagonist in Cancer Immunotherapy: Mechanisms of Action. *Front Immunol* (2020) 11:324. doi: 10.3389/fimmu.2020.00324
39. Albu DI, Wang Z, Huang K-C, Wu J, Twine N, Leacu S, et al. EP4 Antagonism by E7046 diminishes Myeloid immunosuppression and synergizes with Treg-reducing IL-2-Diphtheria toxin fusion protein in restoring anti-tumor immunity. *OncoImmunology* (2017) 6(8):e1338239. doi: 10.1080/2162402X.2017.1338239
40. Wang Z, Brandt S, Medeiros A, Wang S, Wu H, Dent A, et al. MicroRNA 21 is a homeostatic regulator of macrophage polarization and prevents prostaglandin E2-mediated M2 generation. *PloS One* (2015) 10(2):e0115855. doi: 10.1371/journal.pone.0115855
41. Tang J, Yu JX, Hubbard-Lucey VM, Neftelinov ST, Hodge JP, Lin Y. The clinical trial landscape for PD1/PDL1 immune checkpoint inhibitors. *Nat Rev Drug Discovery* (2018) 17(12):854–5. doi: 10.1038/nrd.2018.210
42. LaRocca CJ, Warner SG. Oncolytic viruses and checkpoint inhibitors: combination therapy in clinical trials. *Clin Trans Med* (2018) 7(1):35. doi: 10.1186/s40169-018-0214-5
43. Gitlitz BJ, Bernstein E, Santos ES, Otterson GA, Milne G, Syto M, et al. A randomized, placebo-controlled, multicenter, biomarker-selected, phase 2 study of apricoxib in combination with erlotinib in patients with advanced non-small-cell lung cancer. *J Thoracic Oncol Off Publ Int Assoc Study Lung Cancer* (2014) 9(4):577–82. doi: 10.1097/jto.0000000000000082
44. Edelman MJ, Wang X, Hodgson L, Cheney RT, Baggstrom MQ, Thomas SP, et al. Phase III Randomized, Placebo-Controlled, Double-Blind Trial of Celecoxib in

Addition to Standard Chemotherapy for Advanced Non–Small-Cell Lung Cancer With Cyclooxygenase-2 Overexpression: CALGB 30801 (Alliance). *J Clin Oncol* (2017) 35(19):2184–92. doi: 10.1200/JCO.2016.71.3743

45. Groen HJM, Sietsma H, Vincent A, Hochstenbag MMH, van Putten JWG, van den Berg A, et al. Randomized, Placebo-Controlled Phase III Study of Docetaxel Plus Carboplatin With Celecoxib and Cyclooxygenase-2 Expression As a Biomarker for Patients With Advanced Non–Small-Cell Lung Cancer: The NVALT-4 Study. *J Clin Oncol* (2011) 29(32):4320–6. doi: 10.1200/JCO.2011.35.5214
46. Csiki I, Morrow JD, Sandler A, Shyr Y, Oates J, Williams MK, et al. Targeting cyclooxygenase-2 in recurrent non-small cell lung cancer: a phase II trial of celecoxib and docetaxel. *Clin Cancer Res An Off J Am Assoc Cancer Res* (2005) 11(18):6634–40. doi: 10.1158/1078-0432.Ccr-05-0436
47. Shimizu K, Okita R, Saisho S, Maeda A, Nojima Y, Nakata M. Prognostic value of Cox-2 and PD-L1 expression and its relationship with tumor-infiltrating lymphocytes in resected lung adenocarcinoma. *Cancer Manag Res* (2017) 9:741–50. doi: 10.2147/cmar.S146897
48. Shimizu K, Okita R, Saisho S, Maeda AI, Nojima Y, Nakata M. Impact of COX2 Inhibitor for Regulation of PD-L1 Expression in Non-small Cell Lung Cancer. *Anticancer Res* (2018) 38(8):4637–44. doi: 10.21873/anticanres.12768
49. Kim SH, Roszik J, Cho SN, Ogata D, Milton DR, Peng W, et al. The COX2 Effector Microsomal PGE2 Synthase 1 is a Regulator of Immunosuppression in Cutaneous Melanoma. *Clin Cancer Res An Off J Am Assoc Cancer Res* (2019) 25(5):1650–63. doi: 10.1158/1078-0432.Ccr-18-1163
50. Kim S-H, Kim D-H, Byeon J-Y, Kim Y-H, Kim D-H, Lim H-J, et al. Effects of CYP2C9 genetic polymorphisms on the pharmacokinetics of celecoxib and its carboxylic acid metabolite. *Arch Pharmacal Res* (2017) 40(3):382–90. doi: 10.1007/s12272-016-0861-2
51. Lilenbaum R, Socinski MA, Altorki NK, Hart LL, Keresztes RS, Hariharan S, et al. Randomized Phase II Trial of Docetaxel/Irinotecan and Gemcitabine/Irinotecan With or Without Celecoxib in the Second-Line Treatment of Non–Small-Cell Lung Cancer. *J Clin Oncol* (2006) 24(30):4825–32. doi: 10.1200/JCO.2006.07.4773
52. Panadol. *MIMS Annual Report on China Drug Manual 2011 to 2012 (15th edition) (Chinese Edition)[M]* HongKong: MIMS Limited Press (2012).
53. Ruschitzka F, Borer JS, Krum H, Flammer AJ, Yeomans ND, Libby P, et al. Differential blood pressure effects of ibuprofen, naproxen, and celecoxib in patients with arthritis: the PRECISION-ABPM (Prospective Randomized Evaluation of Celecoxib Integrated Safety Versus Ibuprofen or Naproxen Ambulatory Blood Pressure Measurement) Trial. *Eur Heart J* (2017) 38(44):3282–92. doi: 10.1093/eurheartj/ehx508
54. Ching MM, Reader J, Fulton AM. Eicosanoids in Cancer: Prostaglandin E(2) Receptor 4 in Cancer Therapeutics and Immunotherapy. *Front Pharmacol* (2020) 11:819. doi: 10.3389/fphar.2020.00819

Conflict of Interest: The authors declare that the research was conducted in the absence of any commercial or financial relationships that could be construed as a potential conflict of interest.

Copyright © 2021 Pu, Yin, Huang, Qin, Zhou, Wu, Li, Zhou and Li. This is an open-access article distributed under the terms of the Creative Commons Attribution License (CC BY). The use, distribution or reproduction in other forums is permitted, provided the original author(s) and the copyright owner(s) are credited and that the original publication in this journal is cited, in accordance with accepted academic practice. No use, distribution or reproduction is permitted which does not comply with these terms.

frontiers in Immunology

ORIGINAL RESEARCH
published: 02 March 2021
doi: 10.3389/fimmu.2021.645320

Effects of Hypoxia in Intestinal Tumors on Immune Cell Behavior in the Tumor Microenvironment

Luping Zhang[1†], Shaokun Wang[2†], Yachen Wang[1], Weidan Zhao[1], Yingli Zhang[1], Nan Zhang[1] and Hong Xu[1*]*

[1] Department of Gastroenterology, The First Hospital of Jilin University, Changchun, China, [2] Department of Emergency, The First Hospital of Jilin University, Changchun, China

OPEN ACCESS

Edited by:
Peng Qu,
National Institutes of Health (NIH), United States

Reviewed by:
Hou Yuzhu,
University of Chicago, United States
Feng Geng,
The Ohio State University, United States

***Correspondence:**
Nan Zhang
zhangnan@jlu.edu.cn
Hong Xu
x_hong@jlu.edu.cn

[†]These authors have contributed equally to this work

Specialty section:
This article was submitted to Cancer Immunity and Immunotherapy, a section of the journal Frontiers in Immunology

Received: 22 December 2020
Accepted: 20 January 2021
Published: 02 March 2021

Citation:
Zhang L, Wang S, Wang Y, Zhao W, Zhang Y, Zhang N and Xu H (2021) Effects of Hypoxia in Intestinal Tumors on Immune Cell Behavior in the Tumor Microenvironment. Front. Immunol. 12:645320. doi: 10.3389/fimmu.2021.645320

Background: Imbalanced nutritional supply and demand in the tumor microenvironment often leads to hypoxia. The subtle interaction between hypoxia and immune cell behavior plays an important role in tumor occurrence and development. However, the functional relationship between hypoxia and the tumor microenvironment remains unclear. Therefore, we aimed to investigate the effect of hypoxia on the intestinal tumor microenvironment.

Method: We extracted the names of hypoxia-related genes from the Gene Set Enrichment Analysis (GSEA) database and screened them for those associated with colorectal cancer prognosis, with the final list including *ALDOB*, *GPC1*, *ALDOC*, and *SLC2A3*. Using the sum of the expression levels of these four genes, provided by The Cancer Genome Atlas (TCGA) and Gene Expression Omnibus (GEO) databases, and the expression coefficients, we developed a hypoxia risk score model. Using the median risk score value, we divided the patients in the two databases into high- and low-risk groups. GSEA was used to compare the enrichment differences between the two groups. We used the CIBERSORT computational method to analyze immune cell infiltration. Finally, the correlation between these five genes and hypoxia was analyzed.

Result: The prognosis of the two groups differed significantly, with a higher survival rate in the low-risk group than in the high-risk group. We found that the different risk groups were enriched by immune-related and inflammatory pathways. We identified activated M0 macrophages in TCGA and GEO databases and found that *CCL2/4/5*, and *CSF1* contributed toward the increased infiltration rate of this immune cell type. Finally, we observed a positive correlation between the five candidate genes' expression and the risk of hypoxia, with significant differences in the level of expression of each of these genes between patient risk groups.

Conclusion: Overall, our data suggest that hypoxia is associated with the prognosis and rate of immune cell infiltration in patients with colorectal cancer. This finding may improve immunotherapy for colorectal cancer.

Keywords: colorectal cancer, hypoxia, immune cell infiltration, tumor microenvironment, risk score

INTRODUCTION

Since Stephen Paget proposed the "seed and soil" theory of cancer development and tumor metastasis (1), the understanding of the tumor microenvironment has gradually deepened. Several components of the tumor microenvironment contribute toward tumor occurrence and development (2, 3). An imbalance between nutrient supply and demand within the tumor often leads to hypoxia, glucose deficiency, and consequently an acidic tumor microenvironment (4). Specifically, tumor cells can use immune escape mechanisms to drive metastasis and invasion in anoxic environments (5). This has increased research interest into the relationship between hypoxia and the tumor immune microenvironment.

Hypoxia can reduce the activity of various immune cells in the tumor microenvironment and the production of corresponding immune stimulators to increase the release of suppressors and the expression of immune checkpoint inhibitors (5, 6), suggesting a close relationship between hypoxia and immune cells.

This study aimed to investigate the relationship between hypoxia-related genes and the immune microenvironment of colorectal cancer by (1) quantifying the influence of these genes on the tumor immune microenvironment, (2) screening hypoxia-related genes associated with intestinal tumor prognosis, (3) developing a hypoxia risk score model, (4) validating the model's ability to predict patient prognosis and risk using data from The Cancer Genome Atlas (TCGA) and Gene Expression Omnibus (GEO) databases, (5) identifying the enrichment of model-related pathways, (6) using the hypoxia risk score as the entry point to explore differences in the infiltration rate of immune cells, and (7) identifying genes that affect immune cell infiltration to evaluate the relationship between hypoxia risk score and the tumor immune microenvironment.

MATERIALS AND METHODS

Raw Data

The intestinal cancer-related RNA-sequencing and clinical data used in this study were obtained from TCGA (https://portal.gdc.cancer.gov/) and GEO (gse39582) databases.

Construction and Grouping of the Hypoxia Model

The screening of hypoxia-related genes identified the genes independently related to the prognosis of intestinal cancer. We then multiplied the expression levels of each gene in TCGA and GEO databases by their respective expression coefficients, with the resulting sum defined as the risk score for each patient. Based on the median risk score value, the patients in the two databases were divided into high- and low-risk groups for the follow-up evaluations.

Survival Analysis

The survival and survminer R packages (The R Foundation for Statistical Computing, Vienna, Austria) were used to analyze the prognosis of 445 and 579 patients in TCGA and GEO databases, respectively. Patients in TCGA database were followed up for 12 years, while those in the GEO database were followed up for 16 years. The Kaplan–Meier method was used to plot the survival curves, and the log-rank test was used to evaluate the statistical significance between them, with p-values <0.05 considered statistically significant.

ROC Curve Analysis

ROC curve analysis was conducted using the survival, survminer, and timeROC packages in R. The 1-, 3-, and 5-year survival rates of patients in TCGA and GEO databases were evaluated. The area under the ROC curve for the 1-, 3-, and 5-year survival rates increased gradually and exceeded 0.5, which was defined as the threshold for the accurate prediction of survival by the model. Survival for each group is shown as risk columns and risk curves in **Figures 2A, B**.

Heat Maps

In this study, heat maps of gene expression were drawn using the pheatmap package in R.

PPI Network Analysis

A network of anoxic genes was constructed using the STRING database. R software was used to select the 50 genes with the largest numbers of adjacent nodes for subsequent analysis.

Cox Regression Analysis

We applied the "survival" package in R and performed univariate Cox regression analysis to identify hypoxia-related genes that were closely related to prognosis. Univariate and multivariate prognostic analyses included factors such as age, sex, TNM stage, and the proposed risk score.

Correlations Between Gene Expression and Hypoxia Risk

After screening for genes that play a key role in immune cell regulation, the ggplot2, GGPUBR, and ggExtra packages in R were used to analyze the correlations between gene expression and the risk of hypoxia, and the differences in expression levels between patients at high- and low-risk of hypoxia.

Gene Set Enrichment Analysis

We downloaded the HALLMARK gene set and gene symbols from the GSEA website (https://www.gsea-msigdb.org/gsea/index.jsp) to extract hypoxia-related genes. The entire transcriptome of all tumor samples was used for GSEA, and only gene sets with nominal p-values <0.05 and FDR q values <0.06 were considered significant.

RESULTS

Extraction and Screening of Hypoxia-Related Genes

We first downloaded the HALLMARK gene sets. The gene symbol set was obtained from the Gene Set Enrichment Analysis (GSEA) website (https://www.gsea-msigdb.org/gsea/index.jsp), which

provides the names of all hypoxia-related genes. We then used the Search Tool for the Retrieval of Interacting Genes/Proteins (STRING) (http://string-db.org/cgi/input.pl), a protein-protein interaction (PPI) network database, to construct a model of PPIs between hypoxia-related genes (**Figure 1A**). By counting the number of adjacent nodes for each protein, we identified the core genes. The top 50 core genes with adjacent nodes are presented in **Figure 1B**. We then downloaded the intestinal tumor gene expression data and associated clinical information available from TCGA database. We extracted the data on hypoxia-related gene expression and screened genes associated with prognosis using univariate Cox regression analysis (**Figure 1C**). Among the identified genes, *ALDOB* was associated with a low risk, while five genes (*GPC1, ALDOC, ENO2, SERPINE1*, and *SLC2A3*) were associated with a high risk of developing tumor malignancy. The multivariate Cox regression analysis of genes associated with patient prognosis revealed four genes (**Figure 1D**) that were then used to construct prognostic models. These four genes (*ALDOB*, *GPC1, ALDOC*, and *SLC2A3*) had model coefficients of −0.1574, 0.2994, 0.2647, and 0.2074, respectively.

Effects of Hypoxia-Related Genes on Prognosis

Multivariate Cox regression analysis identified four hypoxia-related genes associated with intestinal tumor prognosis, which were used for modeling. We multiplied the expression levels of these genes (as reported in TCGA and GEO databases) by the corresponding coefficients to obtain the risk score for each patient. The median risk score value was then used to divide the patients in TCGA database into high- and low-risk groups. The subsequent survival analysis revealed significant differences between the high- and low-risk groups ($p < 0.05$; **Figures 2A, B**). Receiver operating characteristic (ROC) curve analysis was used to verify the accuracy of the survival estimates derived from the present model, showing a gradually increasing accuracy of predicting the 1-, 3-, and 5-year survival rates of patients

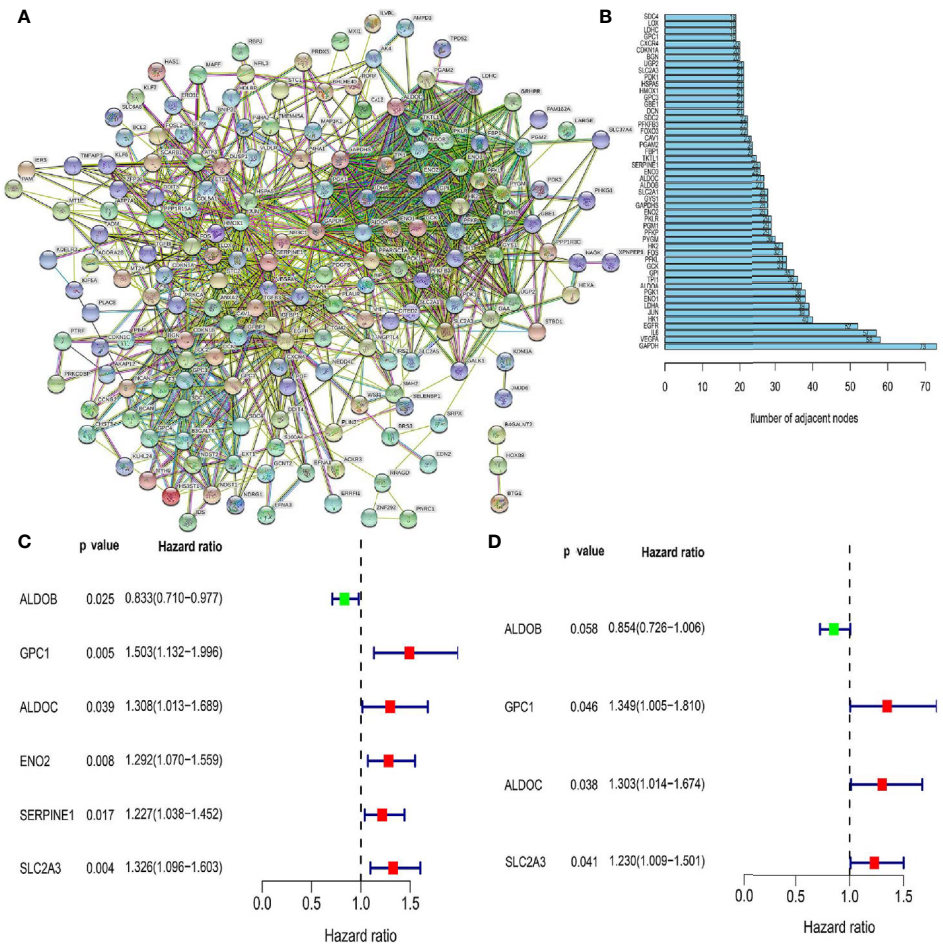

FIGURE 1 | Screening for hypoxia-related genes and their relationship with patient prognosis. **(A)** Protein-protein interaction network containing members with interaction confidence values >0.4. **(B)** The top 50 genes selected based on the number of nodes and their sub-nodes. **(C)** Univariate Cox regression analysis identified candidate genes with p-values <0.05. **(D)** Among the genes related to colorectal cancer prognosis, the genes shown are those independently related to patient prognosis in a multifactor prognostic model of hypoxia.

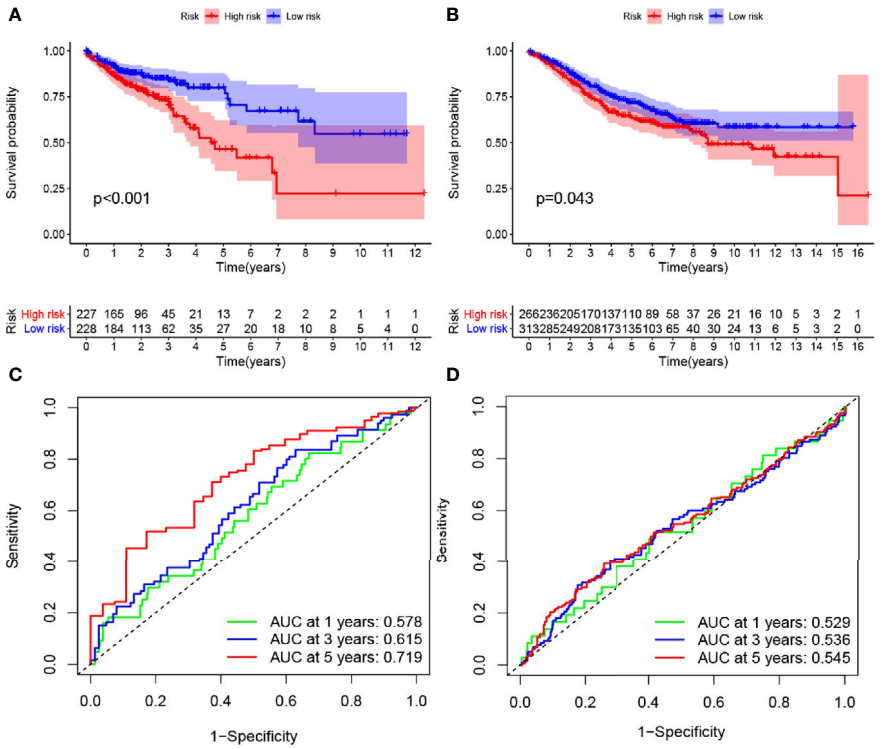

FIGURE 2 | Effects of the hypoxia model on patient prognosis. **(A, B)** Kaplan–Meier survival curves for patients with colon cancer in The Cancer Genome Atlas and Gene Expression Omnibus databases, stratified according to risk scores (high vs. low); comparisons of the median survival time in both groups with log-rank tests ($p<0.01$ and $p = 0.043$, respectively). **(C, D)** Receiver operating characteristic curve analysis of the prognostic accuracy of the model.

included in TCGA database (**Figure 2C**). The area under the ROC curve for the GEO database was > 0.05 (**Figure 2D**), indicating that the model accurately predicted the survival rate. To value the survival rate of patients more intuitively in the high- and low-risk groups, we used risk histograms to show the differences in survival status between the two databases (**Figures 3A, B**). We observed a higher proportion of surviving patients in the low-risk group than in the high-risk group. These results further demonstrated that our model effectively distinguished between high- and low-risk patients. We also analyzed the interactions between the hypoxia-related genes that were identified as affecting patient prognosis in the model (**Figures 3C, D**). We further demonstrated the relationship between patient risk and survival using risk curves, in which the risk scores for both groups of patients were plotted (**Figures 3E, F**). We observed a longer survival time in the low-risk group than in the high-risk group. Moreover, the number of deaths in the low-risk group decreased over time (**Figures 3G, H**). Finally, we compared the expression level of each gene included in the model between the high- and low-risk groups using thermography (**Figures 3I, J**).

Effects of Different Clinical Characteristics on Intestinal Tumor Prognosis

Clinical characteristics differ in the impact they have on patient prognosis. Thus, we analyzed the impact of clinical characteristics on the prognosis of patients included in TCGA and GEO databases. We first used univariate Cox regression analysis to evaluate the impact of clinical characteristics on the survival time and prognosis of patients included in the two databases (**Figures 4A, B**). We found that patient sex affected neither survival nor prognosis, while other factors affected survival and prognosis and were associated with increased risk. However, the p-value of the risk score in our model was <0.05 for patients in TCGA database, indicating that the risk score also affected patient prognosis and survival. In contrast, the p-value was >0.05 for patients in the GEO database. Multivariate analysis of these factors showed that the p-values for age and tumor–node–metastasis (TNM) stage were both <0.05, indicating that these variables were independent prognostic factors (**Figures 4C, D**). We also observed differences in the expression levels of hypoxia-related genes between patients with different T stages included in the two databases (**Figures 4E–H**). The expression level of *SLC2A3* in different T stages (T1, T2, T3, and T4) differed significantly between patients in TCGA and GEO databases ($p < 0.05$).

Enrichment of Pathways in Hypoxia-Related Risk Groups

We observed differences in the enrichment level of hypoxia-related genes and associated pathways between the high- and low-risk groups. To understand the level of pathway enrichment, we used GSEA software (UC San Diego, San Diego, CA, USA; Broad Institute, Cambridge, MA, USA) to compare the pathways

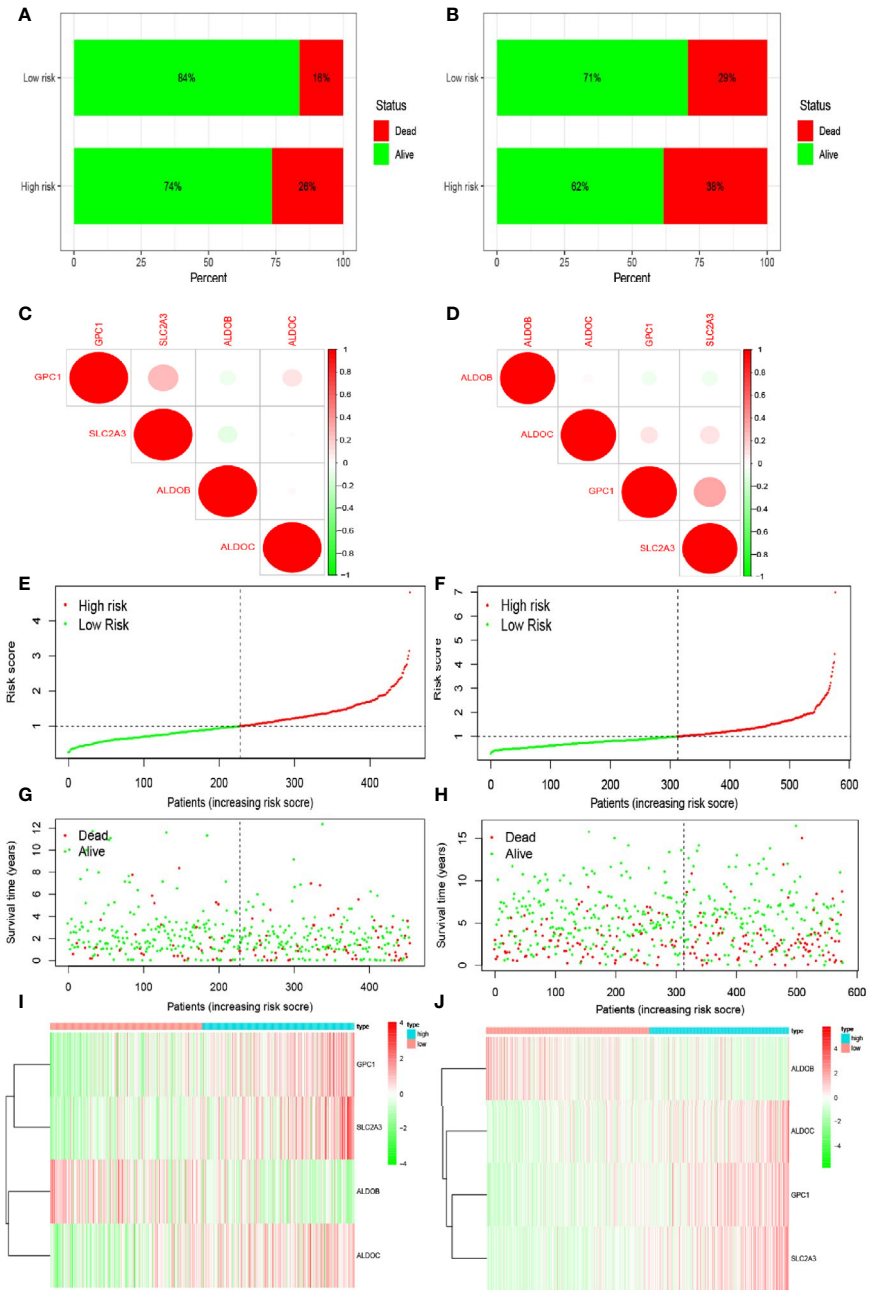

FIGURE 3 | Prediction of patient risk in the hypoxia model and the expression levels of the genes included in the model. **(A, B)** Patient survival in The Cancer Genome Atlas (TCGA) and Gene Expression Omnibus (GEO) databases. **(C, D)** Correlations between the genes included in the risk model based on TCGA and GEO databases. Positive and negative correlations are indicated in red and green, respectively. **(E, F)** Patient risk scores in TCGA and GEO databases. **(G, H)** Survival rates in the high- and low-risk patient groups in TCGA and GEO databases. **(I, J)** Heat maps of gene expression levels in the risk model for the high- and low-risk groups in TCGA and GEO databases.

between different risk groups. The high-risk group in TCGA database showed many enriched pathways related to apoptotic and immune functions (**Figure 5A**) compared with the low-risk group. Among these were apoptosis, hypoxia, interleukin (IL) 2/ signal transducer and activator of transcription (STAT) 5 signaling, IL6-STAT3 signaling, and the inflammatory response pathways. The other related pathways are shown in **Table 1**. In contrast, the pathways enriched in the low-risk group mainly included those associated with oxidative phosphorylation and lipid metabolism, among others. The pathways with false discovery rate (FDR) q values >0.05 are shown in **Table 2**. The low-risk group of patients in the GEO database also showed the

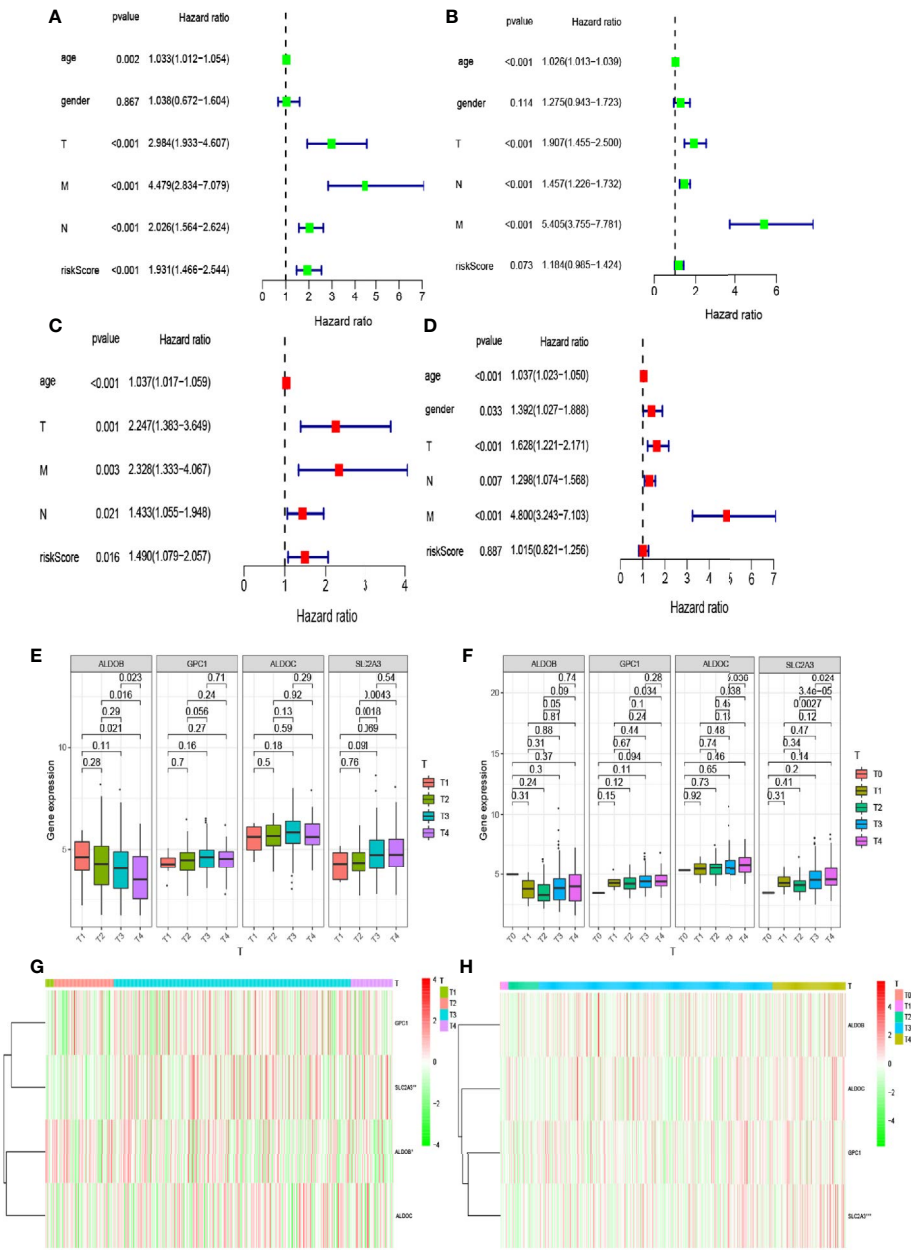

FIGURE 4 | Relationship between the risk model and clinical factors. **(A, B)** Single-factor prognostic analysis included age, sex, tumor–node–metastasis (TNM) stage, and the risk scores of patients with colorectal cancer in The Cancer Genome Atlas (TCGA) and Gene Expression Omnibus (GEO) databases. **(C, D)** Multifactor prognostic analysis included age, sex, TNM stage, and the risk scores of patients with colorectal cancer in TCGA and GEO databases. **(E, F)** Comparisons of the expression levels of various genes in the hypoxia model in TCGA and GEO databases for different T stages. **(G, H)** Heat maps showing the expression levels of genes in the risk model in TCGA and GEO databases for different T stages.

enrichment of apoptosis and IL2-STAT5 signaling pathways, in addition to, the p53 and peroxisome and phosphatidylinositol 3-kinase-mammalian target of rapamycin serine/threonine protein kinase B signaling pathways (**Figure 5B**). The enrichment of other pathways is shown in **Table 3**. The high-risk group also showed the enrichment of the Hedgehog and Wnt/beta-catenin signaling pathways. Pathways with FDR values >0.05 are shown in **Table 4**.

Immune Cell Infiltration

The results of the pathway enrichment analysis of hypoxia-related genes for both risk groups in TCGA and GEO databases showed the

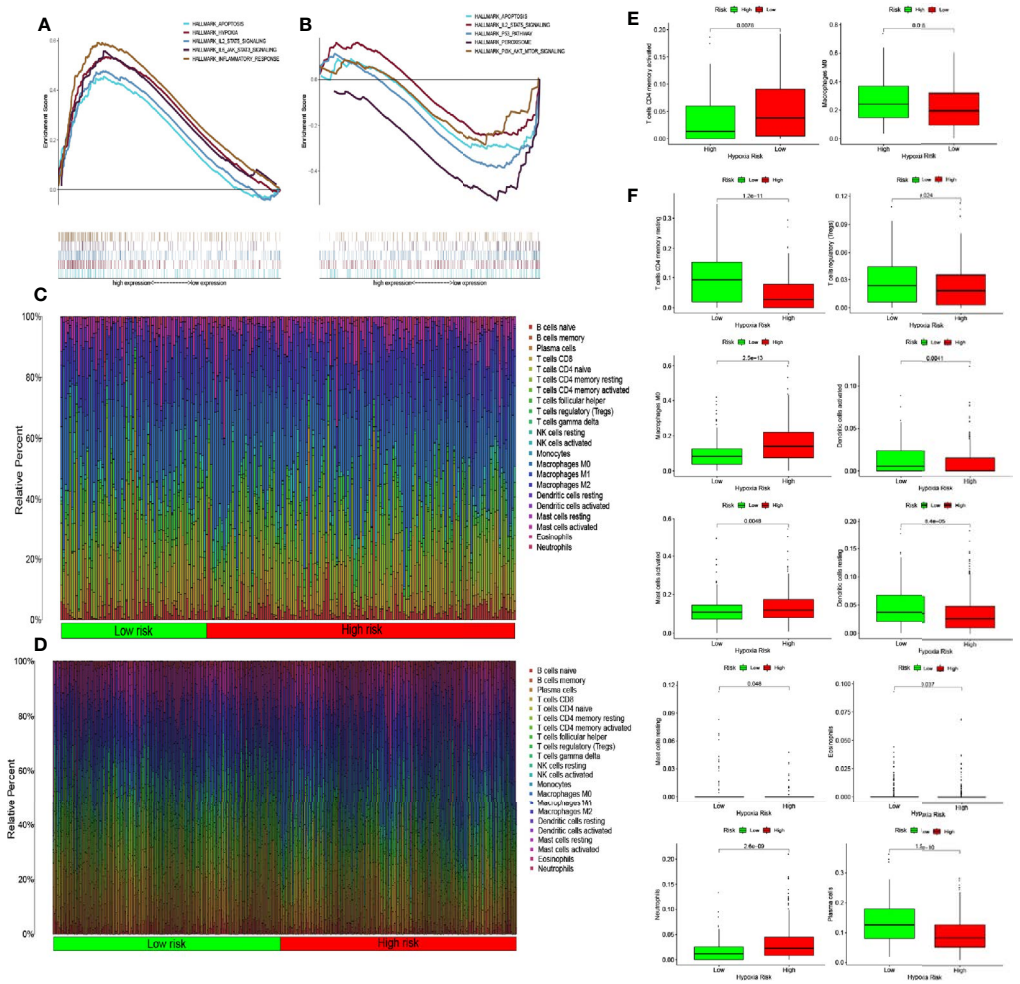

FIGURE 5 | Enrichment of hypoxia pathways and infiltration of hypoxia-related immune cells. **(A)** Enriched gene sets in the HALLMARK collection according to high-risk scores in The Cancer Genome Atlas (TCGA) database. Each line represents one particular gene set with a unique color, with upregulated genes appearing on the left side approaching the origin of the coordinates and downregulated genes appearing on the right side of the x-axis. Only gene sets with nominal (NOM) p-values <0.05 and false discovery rate (FDR) q values <0.06 were considered statistically significant. A selection of leading gene sets is shown in the plot. **(B)** The enriched gene sets in the HALLMARK collection by low-risk scores in the Gene Expression Omnibus (GEO) database. Only gene sets with NOM p-values <0.05 and FDR q values of <0.06 were considered statistically significant. A selection of leading gene sets is shown in the plot. **(C, D)** Heat map of hypoxia risk and immune cell infiltration in TCGA and GEO databases. **(E)** Immune cells whose infiltration is significantly associated with the risk of hypoxia in TCGA database ($p < 0.05$). **(F)** Immune cells whose infiltration is significantly associated with the risk of hypoxia in the GEO database ($p < 0.05$).

enrichment of pathways related to inflammation, immunity, and other factors. Based on these findings, we assessed the rate of immune cell infiltration in each risk group according to the constructed hypoxia-related gene model. **Figures 5C, D** shows the infiltration rate of immune cells in the high- and low-risk groups in TCGA and GEO databases, respectively. TCGA database showed differences in the infiltration rate of two types of immune cells in the high- and low-risk groups (**Figure 5E**; $p < 0.05$). In contrast, the rate of infiltration of 10 types of immune cells differed between the high- and low-risk groups in the GEO database (**Figure 5F**; $p < 0.05$). Among them, the infiltration rate of activated M0 macrophages differed between the high- and low-risk groups in both databases. Using the Tracking Tumor Immunophenotype online platform (http://biocc.hrbmu.edu.cn/TIP/index.jsp), we screened the immune-related genes for those that played important roles in the regulation of this immune cell type. Heat maps were then drawn to visualize the expression of these genes relative to that of hypoxia-related genes in the high- and low-risk groups of patients in TCGA and GEO databases (**Figures 6A, B**). The expression levels of *CCL2/4/5, CSF1*, and *CX3CL1* were significantly different between the high- and low-risk groups in both databases ($p < 0.05$). Next, we plotted the correlation curves between the expression levels of these four genes and the risk scores, which showed that the expression levels of these four genes were positively correlated with the patients' risk score. We also observed differences in the expression levels of these four genes between the high- and low-risk groups (**Figures 6C–L**).

TABLE 1 | Pathway enrichment in the group of patients at high risk of hypoxia in The Cancer Genome Atlas database.

NAME	SIZE	ES	NES	NOM p-val	FDR q-val	FWER p-val
MYOGENESIS	199	0.64095765	2.2988102	0	0	0
EPITHELIAL_MESENCHYMAL_TRANSITION	198	0.7808052	2.2663856	0	9.73E-04	0.001
COAGULATION	138	0.5881612	2.2491221	0	6.49E-04	0.001
APICAL_JUNCTION	200	0.5725273	2.210138	0	7.86E-04	0.002
HYPOXIA	197	0.5341002	2.1750667	0	0.001029189	0.003
ANGIOGENESIS	36	0.7042173	2.1259532	0	0.002047737	0.007
KRAS_SIGNALING_UP	199	0.53099084	2.0836837	0	0.003663993	0.015
UV_RESPONSE_DN	142	0.5923043	2.0315046	0.001988072	0.00553734	0.022
HEDGEHOG_SIGNALING	36	0.6280092	2.0067165	0.003913894	0.005807516	0.026
RESPONSE	200	0.5912703	2.0001185	0.003738318	0.005448199	0.027
COMPLEMENT	200	0.5222255	1.9398772	0.001926782	0.008785588	0.045
IL2_STAT5_SIGNALING	199	0.47638285	1.9347376	0.001923077	0.008227405	0.047
NOTCH_SIGNALING	32	0.53026545	1.8844135	0.005928854	0.011401303	0.078
APICAL_SURFACE	44	0.52808076	1.8692672	0	0.012468602	0.085
APOPTOSIS	159	0.45459515	1.8656777	0.003846154	0.012308807	0.089
TNFA_SIGNALING_VIA_NFKB	199	0.5475131	1.8406801	0.009380863	0.014613844	0.114
IL6_JAK_STAT3_SIGNALING	87	0.5565036	1.7961316	0.0056926	0.020605113	0.158
TGF_BETA_SIGNALING	54	0.47515002	1.6418401	0.034951456	0.059671924	0.381
ALLOGRAFT_REJECTION	196	0.5172241	1.5929213	0.06	0.07578372	0.456
WNT_BETA_CATENIN_SIGNALING	42	0.47698218	1.5757742	0.045454547	0.079787806	0.484
ESTROGEN_RESPONSE_EARLY	198	0.32408136	1.4306225	0.055984557	0.15474646	0.701
CHOLESTEROL_HOMEOSTASIS	73	0.38557705	1.4078543	0.10685484	0.16225821	0.734
KRAS_SIGNALING_DN	199	0.34252158	1.3754886	0.07129095	0.17926803	0.779
UV_RESPONSE_UP	156	0.28952506	1.2597458	0.12741312	0.27369708	0.891
INTERFERON_GAMMA_RESPONSE	198	0.4217492	1.2542942	0.2848723	0.2676427	0.894
MITOTIC_SPINDLE	198	0.31854162	1.188202	0.31697342	0.3293753	0.935
P53_PATHWAY	195	0.27196786	1.1832048	0.21314742	0.3224601	0.937
ADIPOGENESIS	198	0.27874216	1.1698754	0.27734375	0.32397935	0.943
GLYCOLYSIS	199	0.26324964	1.1427033	0.26070037	0.34104726	0.956
ANDROGEN_RESPONSE	99	0.30673286	1.1124011	0.33870968	0.36284208	0.966
ESTROGEN_RESPONSE_LATE	198	0.2458808	1.1081452	0.2615694	0.35552585	0.967
HEME_METABOLISM	193	0.23562211	1.0899739	0.30113637	0.36277255	0.972
MTORC1_SIGNALING	197	0.24964637	0.90750676	0.5214724	0.5825153	0.997
PI3K_AKT_MTOR_SIGNALING	105	0.209095	0.88849974	0.634	0.59227496	0.997
PANCREAS_BETA_CELLS	40	0.23578233	0.70691955	0.8606061	0.83144087	1
INTERFERON_ALPHA_RESPONSE	96	0.19630556	0.54184294	0.8392157	0.95013	1

DISCUSSION

Hypoxia is a feature of tumor physiology specifically that of mechanisms associated with the acquisition of some malignant attributes, such as metastasis, invasion (7–9), and drug resistance (10). In these processes, hypoxia-related genes act on the corresponding pathways or on the regulating immune cells. Hypoxia-inducible factor (HIF) is activated during hypoxia. Some immunosuppressive factors, such as vascular endothelial growth factor, are HIF target genes, which affect both angiogenesis and immunosuppression (11). Hypoxia also results in upregulated *EGFR* expression, which promotes ligand-independent epidermal growth factor receptor signaling (12, 13). This process increases the rate of tumor glycolysis, resulting in metabolic competition (14). In our study, we screened for hypoxia-related genes in the gut and found that the core genes (*ALDOB*, *GPC1*, *ALDOC*, and *SLC2A3*) were closely related to patient prognosis. The rate of aldolase-B and fructose-bisphosphate B-driven fructose metabolism is significantly increased in patients with colon cancer and liver metastasis, and in those with colorectal villous polyps (15, 16). *GPC1* has also been shown to be overexpressed in various malignancies (17, 18). A recent study has reported *GPC1* enrichment in tumor-derived exosomes (17). In melanoma, *NME1* has been shown to inhibit metastasis by activating *ALDOC* transcription (19). Solute carrier family 2, member 3 can increase glucose uptake in anoxic cells and, thus, increase the rate of glycolysis. These findings suggest that hypoxia-related gene expression levels are closely related to tumor development and metabolism (20); therefore, they were included in our hypoxia-related gene model.

With a deepening understanding of the mechanisms of hypoxia, its influence on tumor prognosis is also increasingly being understood (21, 22). To further investigate the relationship between the expression of hypoxia-related genes and patient prognosis, we evaluated patient prognosis by taking the product sum of the expression levels and the coefficients of *ALDOB*, *GPC1*, *ALDOC*, and *SLC2A3* in TCGA and GEO databases as the risk score. The prognosis of patients in the high- and low-risk groups differed significantly; the survival rate of patients in the

TABLE 2 | Pathway enrichment in the group of patients at low risk of hypoxia in The Cancer Genome Atlas database.

NAME	SIZE	ES	NES	NOM p-val	FDR q-val	FWER p-val
OXIDATIVE_PHOSPHORYLATION	200	-0.6354224	-1.8517317	0.02	0.09670171	0.108
MYC_TARGETS_V1	196	-0.55293024	-1.5802475	0.091976516	0.29567894	0.452
E2F_TARGETS	198	-0.5320485	-1.5347565	0.115830116	0.25026736	0.533
FATTY_ACID_METABOLISM	156	-0.37549332	-1.483107	0.078125	0.24727894	0.605
PEROXISOME	104	-0.34722096	-1.4177548	0.08267716	0.26794004	0.708
BILE_ACID_METABOLISM	112	-0.33064038	-1.4166067	0.052529182	0.22491534	0.711
XENOBIOTIC_METABOLISM	197	-0.23699556	-1.0814732	0.31225297	0.6670434	0.973
MYC_TARGETS_V2	58	-0.4065364	-1.0632117	0.4333996	0.6178284	0.977
G2M_CHECKPOINT	195	-0.33763614	-1.0606128	0.425	0.55348146	0.978
DNA_REPAIR	150	-0.28392524	-1.0543846	0.39078155	0.50790316	0.981
PROTEIN_SECRETION	96	-0.30276886	-1.0146313	0.45114344	0.5174334	0.986
REACTIVE_OXYGEN_SPECIES_PATHWAY	49	-0.27658382	-0.960691	0.49802372	0.5441408	0.99
SPERMATOGENESIS	133	-0.2188226	-0.8435639	0.7213439	0.67120385	0.999
UNFOLDED_PROTEIN_RESPONSE	110	-0.18729709	-0.7100693	0.8192771	0.8042398	1

TABLE 3 | Pathway enrichment in the group of patients at high risk of hypoxia in the Gene Expression Omnibus database.

NAME	SIZE	ES	NES	NOM p-val	FDR q-val	FWER p-val
HEDGEHOG_SIGNALING	35	0.47144	1.277345	0.14038461	1	0.749
WNT_BETA_CATENIN_SIGNALING	41	0.430082	1.2600657	0.15187377	0.96750426	0.763
EPITHELIAL_MESENCHYMAL_TRANSITION	195	0.5649699	1.176124	0.33539096	0.9005055	0.86
ANGIOGENESIS	35	0.46240142	1.0144869	0.45738044	1	0.956
MYOGENESIS	196	0.3335677	0.9412718	0.5278351	1	0.983
UV_RESPONSE_DN	135	0.3387805	0.9249301	0.5495868	0.99989307	0.985
TGF_BETA_SIGNALING	52	0.33623004	0.9151217	0.5373737	0.88053614	0.985
KRAS_SIGNALING_DN	190	0.263007	0.8919948	0.642562	0.81584287	0.987
APICAL_SURFACE	43	0.27583465	0.7981121	0.813278	0.91715556	0.996
KRAS_SIGNALING_UP	192	0.30013293	0.7668628	0.806	0.8810992	0.997
ANDROGEN_RESPONSE	93	0.22268894	0.7156268	0.86470586	0.8806738	0.998
COAGULATION	136	0.2703017	0.67810416	0.9207317	0.8534861	0.998

low-risk group was significantly higher than that of their counterparts. However, the ROC curve analysis, which aimed to evaluate the accuracy of the survival estimates, showed that the curves obtained from the GEO database corresponded poorly to the observed prognosis. Thus, we also analyzed the influence of other factors, including age, sex, TNM staging, and our proposed risk score, on patient prognosis. We concluded that our proposed risk score showed a good correspondence with patient prognosis. However, the results of the multivariate analysis in the GEO database were not statistically significant. This finding suggests that the risk score alone cannot be used as an independent prognostic factor. The samples in the GEO database were all colorectal adenocarcinoma samples that had been obtained in France. Because the tumor type and region are very specific, these samples may not accurately reflect the relationship between hypoxia and colon cancer prognosis. Moreover, the prognosis of colon cancer is related to disease stage and clinical, histological, genetic, and molecular factors, among others. These factors should be considered in future studies.

We next applied GSEA to identify pathways enriched in the high- and low-risk groups in the two databases. We found that most of the enriched pathways were related to inflammation, immune response, and apoptosis. Hypoxia and cell death in tumor tissue produce large amounts of cell debris and trigger the release of inflammatory factors, which can attract macrophages and monocytes, and can induce macrophage polarization. After polarization, macrophages secrete inflammatory factors (23). These findings suggest a close relationship between hypoxia, inflammation, and the immune response. In addition, some apoptosis-related genes, such as p53, which is a tumor suppressor gene, are closely related to tumor apoptosis. Nilay et al. (24) found that mutations in p53 in gastric and esophageal cancer cells can induce hypoxia signaling. This finding was confirmed in a study involving nude mice.

The results of many previous studies and those of the present study have shown that hypoxia can recruit immune cells into the tumor microenvironment. Hypoxia-induced tumor-derived cytokines, such as IL-10 and transforming growth factor-beta, can induce tumor-associated macrophages to differentiate into M2 macrophages with immunosuppressive effects (25). When monocytes are stimulated by inflammatory factors, such as interferon-gamma and lipopolysaccharide, they activate M1 macrophages, which can secrete inflammatory factors, such as IL-6 and tumor necrosis factor-alpha, and can phagocytize invasive pathogens and tumor cells (23, 26). Hypoxia can also

TABLE 4 | Pathway enrichment in the group of patients at low risk of hypoxia in the Gene Expression Omnibus database.

NAME	SIZE	ES	NES	NOM p-val	FDR q-val	FWER p-val
OXIDATIVE_PHOSPHORYLATION	180	-0.5181038	-1.8664485	0.017612524	0.052985493	0.035
FATTY_ACID_METABOLISM	153	-0.5680401	-1.8461372	0.00203666	0.03559099	0.046
PEROXISOME	101	-0.53683174	-1.8330911	0	0.029562779	0.051
CHOLESTEROL_HOMEOSTASIS	71	-0.54806143	-1.6309602	0.021276595	0.15649396	0.239
ADIPOGENESIS	189	-0.41682148	-1.5094645	0.035433073	0.32561186	0.449
XENOBIOTIC_METABOLISM	193	-0.52328324	-1.5083747	0.028985508	0.2722546	0.449
REACTIVE_OXYGEN_SPECIES_PATHWAY	47	-0.4019267	-1.376308	0.11977186	0.51835406	0.644
GLYCOLYSIS	194	-0.39022183	-1.3331028	0.12045889	0.56736577	0.716
P53_PATHWAY	188	-0.3891394	-1.2930824	0.124756336	0.61373806	0.757
BILE_ACID_METABOLISM	109	-0.45229995	-1.2606792	0.17364016	0.63521326	0.791
ESTROGEN_RESPONSE_LATE	197	-0.3940817	-1.2011873	0.156	0.73189086	0.858
UV_RESPONSE_UP	153	-0.34357396	-1.175342	0.19662921	0.73222524	0.88
MYC_TARGETS_V2	56	-0.4696598	-1.1727189	0.37304688	0.6814103	0.88
MTORC1_SIGNALING	189	-0.38030684	-1.1696959	0.29032257	0.6386857	0.882
PI3K_AKT_MTOR_SIGNALING	103	-0.29268706	-1.132223	0.27868852	0.6835487	0.904
ESTROGEN_RESPONSE_EARLY	193	-0.32482004	-1.0662084	0.33464566	0.79412293	0.936
PANCREAS_BETA_CELLS	40	-0.42545584	-1.057426	0.38690478	0.767329	0.94
HEME_METABOLISM	189	-0.2667636	-1.0508605	0.36575875	0.7411266	0.942
DNA_REPAIR	144	-0.298164	-1.0362988	0.42330098	0.73253185	0.943
APOPTOSIS	159	-0.3165646	-0.9227984	0.57114625	0.955858	0.981
SPERMATOGENESIS	132	-0.24104334	-0.86871046	0.6871287	1	0.988
COMPLEMENT	194	-0.32908297	-0.8492691	0.6442308	1	0.991
APICAL_JUNCTION	188	-0.27416155	-0.83836824	0.64705884	1	0.992
MYC_TARGETS_V1	185	-0.271399	-0.80545324	0.628	1	0.995
INTERFERON_GAMMA_RESPONSE	194	-0.3529506	-0.7729238	0.6927593	1	0.996
INTERFERON_ALPHA_RESPONSE	92	-0.36440378	-0.7677859	0.6827853	1	0.996
ALLOGRAFT_REJECTION	193	-0.32352465	-0.7621619	0.69921875	1	0.996
IL2_STAT5_SIGNALING	193	-0.24943894	-0.74676377	0.8172888	1	0.997
UNFOLDED_PROTEIN_RESPONSE	103	-0.20758167	-0.70057595	0.7745665	1	0.998
TNFA_SIGNALING_VIA_NFKB	194	-0.30261576	-0.6995795	0.80670613	1	0.998
HYPOXIA	190	-0.24055389	-0.6963746	0.8644401	1	0.998
MITOTIC_SPINDLE	198	-0.19739081	-0.6422138	0.87279844	1	0.999
NOTCH_SIGNALING	31	-0.2139055	-0.6397593	0.9166667	1	0.999
E2F_TARGETS	190	-0.2648517	-0.622124	0.78019804	1	0.999
INFLAMMATORY_RESPONSE	198	-0.25689715	-0.6020838	0.9265873	0.99692255	0.999
IL6_JAK_STAT3_SIGNALING	87	-0.23669887	-0.56183934	0.9643564	0.99789304	1
PROTEIN_SECRETION	95	-0.16205812	-0.5151241	0.97137016	0.9930653	1
G2M_CHECKPOINT	185	-0.19927993	-0.5018363	0.89065605	0.9723166	1

lead to immune escape through the role of immune cells (5); for example, hypoxia can reduce T-cell activity (27). Hypoxia is closely related to immune cell function. In our study, we observed significant differences in the level of activated M0 macrophages between the high- and low-risk groups in TCGA database. In the GEO database, the level of infiltration of activated CD4 memory T cells and M0 macrophages, activated and resting mast cells, and neutrophils differed significantly between the high- and low-risk groups. Both databases showed significant differences in the infiltration rate of activated M0 macrophages between the high- and low-risk groups. When we screened the genes that regulated this immune cell type, we found different levels of *CCL2/4/5* and *CSF1*expression between the high- and low-risk groups. Further analyses confirmed the significant correlation between the expression level of each of these genes and the risk of hypoxia.

Three of these four genes encode chemokines, which play a chemotactic role in immune cells, such as natural killer cells and monocytes, which are closely related to tumor development. *CCL2* and *CCL5* play important roles in prostate cancer metastasis and drug resistance (28, 29), while *CCL4* is associated with the clinical characteristics of breast cancer (30). *CSF1* is expressed in almost all tumors (31, 32). It recruits macrophages other than alveolar macrophages through *CSF1* receptors and regulates their differentiation (31, 33). Macrophages, a major component of the tumor microenvironment, contribute to tumorigenesis by promoting angiogenesis, immunosuppression, invasion, and metastasis (34, 35).

In conclusion, hypoxia plays an important role in the tumor microenvironment. Screening for genes that can affect the rate of immune cell infiltration revealed a correlation between these genes and the hypoxia risk score. Our findings show that hypoxia-related genes can affect the prognosis of intestinal cancer and may play a role in immune infiltration in intestinal cancer. Analysis of the relationship between hypoxia and immune cells may improve immunotherapy and tumor treatment.

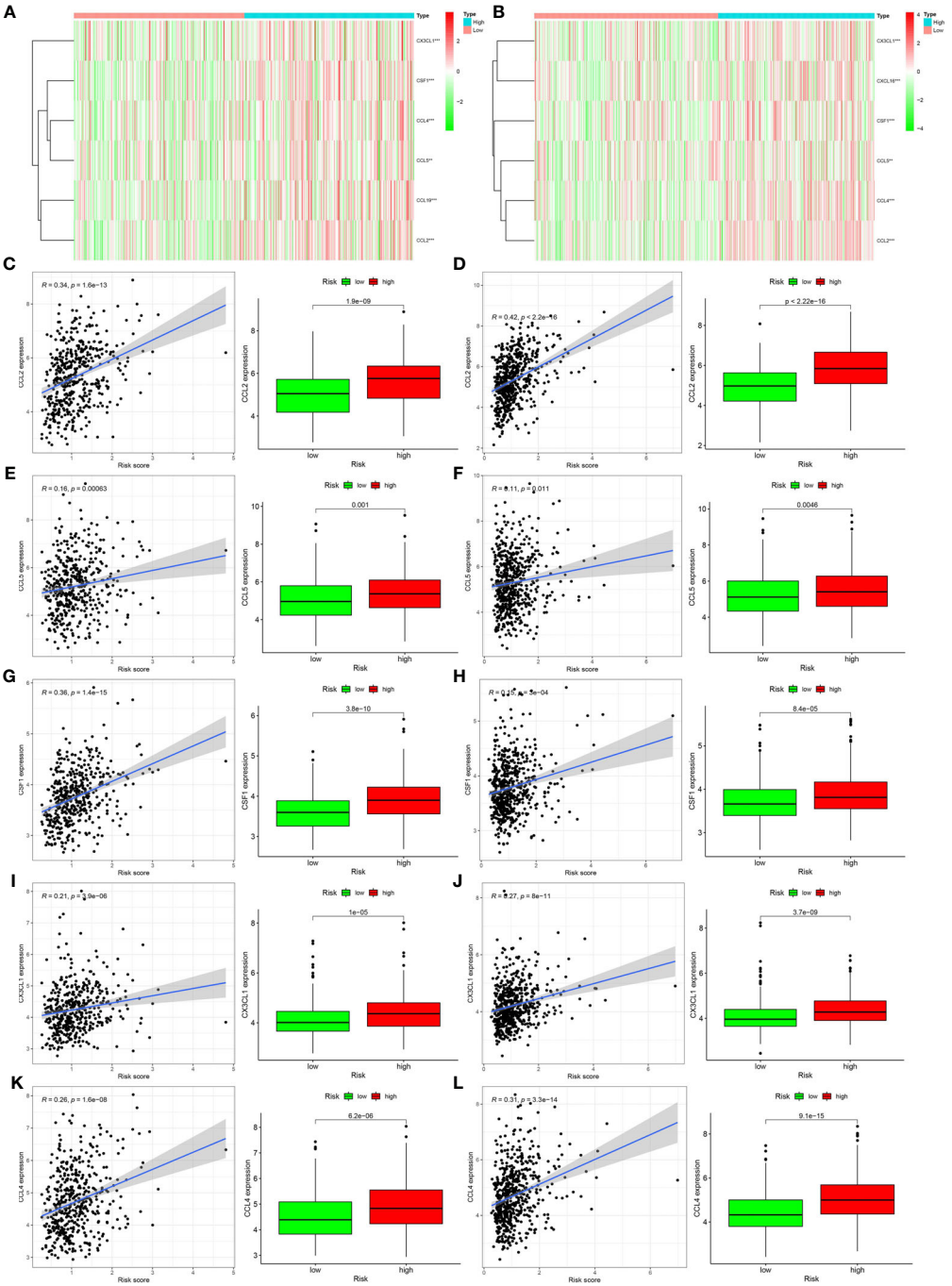

FIGURE 6 | Relationships between genes regulating immune cell behavior and hypoxia risk. **(A, B)** Heat maps showing the expression levels of genes regulating activated CD4 memory T cells and M0 macrophages in different hypoxia risk groups (**p < 0.01; ***p < 0.001). **(C–L)** Scatter plots showing the correlations of the expression of four genes from The Cancer Genome Atlas and Gene Expression Omnibus databases with immune cell regulation, showing differences in the expression levels between the different hypoxia risk groups (p < 0.05). The blue line in each plot is a fitted linear model indicating the relationship between gene expression and the risk of hypoxia. Pearson coefficients were used to assess the correlation between the two factors. The box plots show the differences in the levels of gene expression between groups at risk of hypoxia (p < 0.05).

DATA AVAILABILITY STATEMENT

The original contributions presented in the study are included in the article/supplementary material. Further inquiries can be directed to the corresponding authors.

ETHICS STATEMENT

All participants provided a signed informed consent.

AUTHOR CONTRIBUTIONS

The data analysis and original writing of the draft were conducted by LZ and SW. HX and NZ came up with the design and critical revision of the manuscript. The original writing of the draft and its editing were by YW, WZ, and YZ. All authors contributed to the article and approved the submitted version.

FUNDING

Finance Department of Jilin (2018SCZWSZX-039); Finance Department of Jilin (JLSWSRCZX2020-083); Science and Technology of Jilin (20170623092TC-119).

ACKNOWLEDGMENTS

We would like to acknowledge the reviewers for their helpful comments on this study.

REFERENCES

1. Stephen P. The distribution of secondary growths in cancer of the breast. *Lancet* (1889) 133(3421):571–3. doi: 10.1016/S0140-6736(00)49915-0
2. Hanahan D, Coussens Lisa M. Accessories to the Crime: Functions of Cells Recruited to the Tumor Microenvironment. *Cancer Cell* (2012) 21(3):309–22. doi: 10.1016/j.ccr.2012.02.022
3. Lebleu VS. Imaging the tumor microenvironment. *Cancer J* (2015) 21:174–8. doi: 10.1007/978-3-319-67577-0_15
4. Klemm F, Joyce JA. Microenvironmental regulation of therapeutic response in cancer. *Trends Cell Biol* (2015) 25(4):198–213. doi: 10.1016/j.tcb.2014.11.006
5. Barsoum IB, Koti M, Siemens DR, Graham CH. Mechanisms of hypoxia-mediated immune escape in cancer. *Cancer Res* (2014) 74(24):7185–90. doi: 10.1158/0008-5472.CAN-14-2598
6. Multhoff G, Vaupel P. Hypoxia Compromises Anti-Cancer Immune Responses. *Adv Exp Med Biol* (2020) 1232:131–43. doi: 10.1007/978-3-030-34461-0_18
7. Chaturvedi P, Gilkes DM, Wong CCL, Shitiz K, Luo W, Zhang H, et al. Hypoxia-inducible factor–dependent breast cancer–mesenchymal stem cell bidirectional signaling promotes metastasis. *J Clin Invest* (2013) 123(1):189–205. doi: 10.1172/JCI64993
8. Cheng JC, Klausen C, Leung PCK. Hypoxia-inducible factor 1 alpha mediates epidermal growth factor-induced down-regulation of E-cadherin expression and cell invasion in human ovarian cancer cells. *Cancer Lett* (2013) 329 (2):197–206. doi: 10.1016/j.canlet.2012.10.029
9. Rankin EB, Giaccia AJ. Hypoxic control of metastasis. *Science* (2016) (6282):175–80. doi: 10.1126/science.aaf4405
10. Facciabene A, Peng X, Hagemann IS, Balint K, Barchetti A, Wang LP, et al. Tumour hypoxia promotes tolerance and angiogenesis via CCL28 and T(reg) cells. *Nature* (2011) 475(7355):226–30. doi: 10.1038/nature10169
11. Gavalas NG, Tsiatas M, Tsitsilonis O, Politi E, Ioannou K, Ziogas AC, et al. VEGF directly suppresses activation of T cells from ascites secondary to ovarian cancer via VEGF receptor type 2. *Br J Cancer* (2012) 107(11):1869–75. doi: 10.1038/bjc.2012.468
12. Franovic A, Gunaratnam L, Smith K, Robert I, Patten D, Lee S. Translational up-regulation of the EGFR by tumor hypoxia provides a nonmutational explanation for its overexpression in human cancer. *Proc Natl Acad Sci* (2007) 104(32):13092–7. doi: 10.1073/pnas.0702387104
13. Misra A, Pandey C, Sze SK, Thanabalu T. Hypoxia activated egfr signaling induces epithelial to mesenchymal transition (EMT). *PloS One* (2012) 7(11): e49766. doi: 10.1371/journal.pone.0049766
14. Wang Y, Roche O, Xu C, Moriyama EH, Heir P, Chung J, et al. Hypoxia promotes ligand-independent EGF receptor signaling via hypoxia-inducible factor–mediated upregulation of caveolin-1. *Proc Natl Acad Sci* (2012) 109 (13):4892–7. doi: 10.1073/pnas.1112129109
15. Lin WR, Chiang JM, Lim SN, Su MY, Yeh CT. Dynamic bioenergetic alterations in colorectal adenomatous polyps and adenocarcinomas. *EBioMedicine* (2019) 44:334–45. doi: 10.1016/j.ebiom.2019.05.031
16. Bu P, Chen KY, Xiang K, Johnson C, Crown SB, Rakhilin N, et al. Aldolase B-Mediated Fructose Metabolism Drives Metabolic Reprogramming of Colon Cancer Liver Metastasis. *Cell Metab* (2018) 27:1249. doi: 10.1016/j.cmet.2018.04.03
17. Melo SA, Luecke LB, Kahlert C, Fernandez AF, Gammon ST, Kaye J, et al. Glypican-1 identifies cancer exosomes and detects early pancreatic cancer. *Nature* (2015) 523(7559):177–82. doi: 10.1038/nature14581
18. Chamorro-Jorganes A, Araldi E, Rotllan N, Cirera-Salinas D, Suarez Y. Autoregulation of glypican-1 by intronic microRNA-149 fine tunes the angiogenic response to FGF2 in human endothelial cells. *J Cell Ence* (2014) 127(6):1169. doi: 10.1242/jcs.130518
19. Pamidimukkala NV, Leonard MK, Snyder D, McCorkle JR, Kaetzel DM. Metastasis Suppressor NME1 Directly Activates Transcription of the ALDOC Gene in Melanoma Cells. *Anticancer Res* (2018) 38(11):6059–68. doi: 10.21873/anticanres.12956
20. Debangshu S, Semenza GL. Metabolic adaptation of cancer and immune cells mediated by hypoxia-inducible factors. *Biochim Biophys Acta (BBA) Rev Cancer* (2018) 1870:15–22. doi: 10.1016/j.bbcan.2018.07.002
21. Brooks JM, Menezes AN, Ibrahim M, Archer L, Lal N, Bagnall CJ, et al. Development and validation of a combined hypoxia and immune prognostic classifier for head and neck cancer. *Clin Cancer Res* (2019) 17):5315–28. doi: 10.1158/1078-0432.CCR-18-3314
22. Yang L, Roberts D, Takhar M, Erho N, Bibby BAS, Thiruthaneeswaran N, et al. Development and Validation of a 28-gene Hypoxia-related Prognostic Signature for Localized Prostate Cancer. *EBioMedicine* (2018) 31:182–9. doi: 10.1016/j.ebiom.2018.04.019
23. Zhou D, Huang C, Lin Z. Macrophage polarization and function with emphasis on the evolving roles of coordinated regulation of cellular signaling pathways. *Cell SIGNALLING* (2014) (2):192–7. doi: 10.1016/j.cellsig.2013.11.004
24. Sethi N, Kikuchi O, Mcfarland J, Zhang Y, Bass AJ. Mutant p53 induces a hypoxia transcriptional program in gastric and esophageal adenocarcinoma. *JCI Insight* (2019) 4(15):e128439. doi: 10.1172/jci.insight.128439
25. Hao N-B, Lü M-H, Fan Y-H, Cao Y-L, Zhang Z-R, Yang S-M, et al. Macrophages in tumor microenvironments and the progression of tumors. *Clin Dev Immunol* (2012) 2012:948098. doi: 10.1155/2012/948098
26. Murray PJ. Macrophage Polarization. *Annu Rev Physiol* (2016) 79(1):541. doi: 10.1146/annurev-physiol-022516-034339
27. Sun J, Zhang Y, Yang M, Yang M, Zhang Y, Xie Q, et al. Hypoxia induces T-cell apoptosis by inhibiting chemokine C receptor 7 expression: the role of adenosine receptor A2. *Cell Mol Immunol* (2010) 7(1):77–82. doi: 10.1038/cmi.2009.105
28. Urata S, Izumi K, Hiratsuka K, Maolake A, Natsagdorj A, Shigehara K, et al. C-C motif ligand 5 promotes migration of prostate cancer cells in the prostate

cancer bone metastasis microenvironment. *Cancer Ence* (2018) 109(3):724–31. doi: 10.1111/cas.13494
29. Izumi K, Fang L, Mizokami A, Namiki M, Li L, Lin W, et al. Targeting the androgen receptor with siRNA promotes prostate cancer metastasis through enhanced macrophage recruitment via CCL2/CCR2-induced STAT3 activation. *EMBO Mol Med* (2013) 5(9):1383–401. doi: 10.1002/emmm.201202367
30. Hu G, Tzeng H, Chen P, Wang C, Zhao Y, Wang Y, et al. Correlation between CCL4 gene polymorphisms and clinical aspects of breast cancer. *Int J Of Med Sci* (2018) 11):1179–86. doi: 10.7150/ijms.26771
31. Lin W, Xu D, Austin CD, Caplazi P, Senger K, Sun Y, et al. Function of CSF1 and IL34 in Macrophage Homeostasis, Inflammation, and Cancer. *Front Immunol* (2019) 10:2019. doi: 10.3389/fimmu.2019.02019
32. Baghdadi M, Endo H, Takano A, Ishikawa K, Kameda Y, Miyagi Y, et al. High co-expression of IL-34 and M-CSF correlates with tumor progression and poor survival in lung cancers. *Sci Rep* (2018) 8. doi: 10.1038/s41598-017-18796-8
33. Barreda DR, Hanington PC, Belosevic M. Regulation of myeloid development and function by colony stimulating factors. *Dev Comp Immunol* (2004) 28:509–54. doi: 10.1016/j.dci.2003.09.010
34. Olingy CE, Dinh HQ, Hedrick CC. Monocyte Heterogeneity and Functions in Cancer. *J Leukocyte Biol* (2019) 106(2):309–22. doi: 10.1002/JLB.4RI0818-311R
35. Poh AR, Matthias E. Targeting Macrophages in Cancer: From Bench to Bedside. *Front Oncol* (2018) 8:49. doi: 10.3389/fonc.2018.00049

Conflict of Interest: The authors declare that the research was conducted in the absence of any commercial or financial relationships that could be construed as a potential conflict of interest.

Copyright © 2021 Zhang, Wang, Wang, Zhao, Zhang, Zhang and Xu. This is an open-access article distributed under the terms of the Creative Commons Attribution License (CC BY). The use, distribution or reproduction in other forums is permitted, provided the original author(s) and the copyright owner(s) are credited and that the original publication in this journal is cited, in accordance with accepted academic practice. No use, distribution or reproduction is permitted which does not comply with these terms.

frontiers in Immunology

ORIGINAL RESEARCH
published: 03 March 2021
doi: 10.3389/fimmu.2021.637933

Analysis of m6A-Related Signatures in the Tumor Immune Microenvironment and Identification of Clinical Prognostic Regulators in Adrenocortical Carcinoma

Yi Jin[1,2,3†], Zhanwang Wang[1†], Dong He[4], Yuxing Zhu[1], Xueying Hu[1], Lian Gong[1], Mengqing Xiao[1], Xingyu Chen[1], Yaxin Cheng[1] and Ke Cao[1]*

[1] Department of Oncology, Third Xiangya Hospital, Central South University, Changsha, China, [2] Department of Radiation Oncology, Hunan Cancer Hospital, The Affiliated Cancer Hospital of Xiangya School of Medicine, Central South University, Changsha, China, [3] Key Laboratory of Translational Radiation Oncology, Department of Radiation Oncology, Hunan Cancer Hospital and The Affiliated Cancer Hospital of Xiangya School of Medicine, Central South University, Changsha, China, [4] Department of Respiratory, The Second People's Hospital of Hunan Province, Changsha, China

OPEN ACCESS

Edited by:
Peng Qu,
National Institutes of Health (NIH), United States

Reviewed by:
Xingping Qin,
Renmin Hospital of Wuhan University, China
Hua Jiang,
Medical University of South Carolina, United States

***Correspondence:**
Ke Cao
csucaoke@163.com

[†] These authors have contributed equally to this work

Specialty section:
This article was submitted to Cancer Immunity and Immunotherapy, a section of the journal Frontiers in Immunology

Received: 04 December 2020
Accepted: 29 January 2021
Published: 03 March 2021

Citation:
Jin Y, Wang Z, He D, Zhu Y, Hu X, Gong L, Xiao M, Chen X, Cheng Y and Cao K (2021) Analysis of m6A-Related Signatures in the Tumor Immune Microenvironment and Identification of Clinical Prognostic Regulators in Adrenocortical Carcinoma. Front. Immunol. 12:637933. doi: 10.3389/fimmu.2021.637933

Adrenocortical carcinoma (ACC) is a rare endocrine malignancy with a high rate of mortality and recurrence. N6-methyladenosine methylation (m6A) is the most common modification to affect cancer development, but to date, the potential role of m6A regulators in ACC prognosis is not well understood. In this study, we systematically analyzed 21 m6A regulators in ACC samples from The Cancer Genome Atlas (TCGA) and the Gene Expression Omnibus (GEO) database. We identified three m6A modification patterns with different clinical outcomes and discovered a significant relationship between diverse m6A clusters and the tumor immune microenvironment (immune cell types and ESTIMATE algorithm). Additionally, Gene Ontology (GO), Kyoto Encyclopedia of Genes and Genomes (KEGG), and Gene Set Enrichment Analysis (GSEA) revealed that the m6A clusters were strongly associated with immune infiltration in the ACC. Next, to further explore the m6A prognostic signatures in ACC, we implemented Lasso (Least Absolute Shrinkage and Selection Operator) Cox regression to establish an eight-m6A-regulator prognostic model in the TCGA dataset, and the results showed that the model-based high-risk group was closely correlated with poor overall survival (OS) compared with the low-risk group. Subsequently, we validated the key modifications in the GEO datasets and found that high HNRNPA2B1 expression resulted in poor OS and event-free survival (EFS) in ACC. Moreover, to further decipher the molecular mechanisms, we constructed a competing endogenous RNA (ceRNA) network based on HNRNPA2B1, which consists of 12 long noncoding RNAs (lncRNAs) and 1 microRNA (miRNA). In conclusion, our findings indicate the potential role of m6A modification in ACC, providing novel insights into ACC prognosis and guiding effective immunotherapy.

Keywords: adrenocortical carcinoma, M6A, tumor immune microenvironment, prognostic signatures, HNRNPA2B1

INTRODUCTION

Adrenocortical carcinoma (ACC) is an uncommon endocrine malignancy with an annual incidence of 0.7–2.0 cases per million (1). Despite its rarity, the 5-year survival rate in most series is <35% (2). Currently, the only curative therapy for localized ACC is surgery. Even with complete excision, rates of local recurrence typically range from 19–34% (3, 4). Adjuvant treatments which aim to decrease recurrence, including chemotherapy and radiotherapy, show limited therapeutic effectiveness (5). Nevertheless, the most widely used tumor, lymph node, and metastasis (TNM) classification system remains unacceptable for heterogeneous outcomes and poor survival (6, 7). Therefore, unraveling the genomic properties underlying ACC is crucial for developing effective treatments and predicting individual survival and recurrence risk.

N6-methyladenosine (m6A), which was first discovered in the 1970s, is recognized as the most prominent and abundant form of internal modification that occurs in messenger RNAs (mRNAs) and long non-coding RNAs (lncRNAs) in many eukaryotic species (8, 9). m6A methylation is thought to affect every aspect of RNA metabolism, including RNA splicing, translocation, stability, and translation into protein (10). The m6A modification is dynamically deposited by three types of homologous factors: methyltransferases ("writers"), demethylases ("erasers"), and m6A binding proteins ("readers") (11). Methyltransferases, with core members, METTL3, METTL14, WTAP, ZC3H13, RBM15, and RBM15B, catalyze the methyl group directly attached to the nitrogen on the sixth carbon of the aromatic ring of an adenosine residue (12). Demethylases, which mediate the m6A removal process, with core members FTO and ALKBH5, selectively remove the methyl code from specific mRNAs (11). m6A binding proteins, including the YTHDF family (YTHDF1/2/3), nuclear heterogeneous riboprotein family (HNRNPA2B1 and HNRNPC), and eukaryotic initiation factor (eIF or EIF1A), aim to decode RNA methylation and recognize the m6A motif (11).

To date, N6-methyladenosine, a potential biomarker, has been reported to actively participate in various important physiological processes such as stem cell differentiation, circadian periods, and DNA damage response *in vivo* (13–15). Aberrant expression and mutation of m6A were confirmed to result in the abnormal processes, including dysregulation of cell death and proliferation, developmental defects, and impaired self-renewal capacity (16, 17). Recent studies have demonstrated that abnormal m6A methylation modification is closely associated with a variety of human diseases, especially cancer, including bladder cancer, head and neck squamous cell carcinoma, gastric cancer, breast cancer, hepatocellular carcinoma, and colorectal cancer (18). For instance, in breast cancer, high FTO levels are significantly associated with poor survival rates. Furthermore, in a series of *in vitro* and *in vivo* assays, FTO dramatically alleviated and degraded BNIP3 (a tumor suppressor) *via* a YTHDF2-independent mechanism to induce cancer cell proliferation, colony formation, and metastasis (19). Additionally, Zewei Tu reportedly built a ceRNA network and established a 9 m6A-related lncRNA prognostic model in lower-grade glioma patients (20). Accumulating evidence has shown that m6A-related mRNAs and lncRNAs can serve as novel potential targets for predicting prognosis and developing personalized treatments for many types of cancer. However, little is known about the relationship between the effect of m6A methylation modification and ACC.

The tumor microenvironment (TME), which includes cancer cells, stromal cells, and distant recruited cells, such as infiltrating immune cells (myeloid cells and lymphocytes), bone marrow-derived cells (BMDCs), and secreted factors such as cytokines and chemokines, play a crucial role in tumor progression and affect the clinical benefit from novel strategies of immunological checkpoint blockade (ICB, PD-1/L1, and CTLA-4) (21, 22). In advanced ACC, no investigated therapy has offered long-term disease control, except for immune checkpoint blockade. A phase II study indicated that pembrolizumab (an anti-PD-1 monoclonal antibody) can provide meaningful and durable antitumor activity (23). Emerging studies have focused on research interests that enhance the in-depth understanding of the heterogeneity and complexity of the TME to improve immunotherapy strategies by comprehensive analysis of particular m6A regulators (24, 25). For instance, inhibiting ALKBH5 may enhance the efficacy of anti-PD-1 therapy in melanoma patients by mediating the level of Mct4/Slc16a3, which is involved in regulating suppressive lymphocyte Treg and myeloid-derived suppressor cell accumulations in the TME (24). Currently, none of these studies have extended their research into the frontiers of knowledge in ACC.

In this study, we performed a retrospective analysis based on The Cancer Genome Atlas (TCGA) and the Gene Expression Omnibus (GEO) databases to estimate the effect of m6A-related genes on the prognostic value. We identified multiple m6A regulators and related lncRNAs or microRNAs (miRNAs) as potential biomarkers by shaping individual TME characterizations.

MATERIALS AND METHODS

Data Processing of the ACC Dataset

The public RNA sequencing, mutation expression, and full clinical information of ACC were downloaded from TCGA and GEO. Patients without survival information were excluded from further evaluation. The RNA sequencing data (FPKM value) and somatic mutation data from TCGA-ACC (The Cancer Genome Atlas - Adrenocortical carcinoma) were downloaded from the Genomic Data Commons (GDC; https://portal.gdc.cancer.gov/) and gathered as a training set for further analysis. In total, six eligible data from GEO (GSE10927, GSE19750, GSE33371,

Abbreviations: ACC, adrenocortical carcinoma; TNM, tumor, lymph node, and metastasis; m6A, N6-methyladenosine; TME, the tumor microenvironment; BMDCs, bone marrow-derived cells; TCGA, the cancer genome atlas; GEO, the gene expression omnibus database; GDC, genomic data commons; OS, the overall survival; DEG differentially expressed gene; GSEA, gene set enrichment analysis; LASSO, the least absolute shrinkage and selection operator; HR, the hazard ratio; ROC, the receiver operating characteristic; SNP, single nucleotide polymorphism; AUC, the area under the curve; EFS, the event-free survival; TMB, the tumor burden; SNV, single nucleotide variants; DDS, the disease-specific survival; DFI, the disease-free interval; PFI, the progression-free interval; TILs, tumor infiltrating lymphocytes; HOTAIR, HOX transcript antisense intergenic RNA.

GSE76019, GSE76021, and GSE49280) were downloaded and an averaging method with the affy and simpleaffy packages was used to perform background adjustment and quantile normalization.

Consensus Clustering of m6A Regulators

We first selected 21 m6A RNA methylation regulators from previously published articles (26, 27). These 21 m6A regulators included 8 writers (METTL3, METTL14, RBM15, RBM15B, WTAP, KIAA1429, CBLL1, and ZC3H13), 2 erasers (ALKBH5, FTO), and 11 readers (YTHDC1, YTHDC2, YTHDF1, YTHDF2, YTHDF3, IGF2BP1, HNRNPA2B1, HNRNPC, FMR1, LRPPRC, and ELAVL1). Based on the expression of the 21 m6A modulators, the patients were classified into three groups using the optimal k-means clustering ("kmeans" function in R). Cluster analysis was performed using the ConsensusClusterPlus R package with cycle computation 1,000 times to ensure stability and reliability (28). The overall survival (OS) between different clusters was calculated using the Kaplan-Meier method.

Identification of Differentially Expressed Genes (DEGs) Between m6A Patterns

To identify the DEGs between three clusters in the TCGA-ACC cohort, the empirical Bayesian approach of the limma R package was applied in the standard comparison mode. The significance criteria for determining DEGs was set to $|\log FC| > 1$ and P-value < 0.05. To investigate the pathways enriched in the different subgroups, we performed Kyoto Encyclopedia of Genes and Genomes (KEGG) pathway analysis and Gene Ontology (GO) biological processes by applying a threshold P-value < 0.05, minimum count of 5, and enrichment factor > 0.15. Gene set enrichment analysis (GSEA) was used to evaluate all genes based on their log2 fold change and assess the functions associated with subtypes by implementing the clusterProfiler R package.

Comparison of Immune Cell Infiltration Among m6A Patterns

To explore the degree of immune cell infiltration among the three subgroups, we applied the ESTIMATE algorithm, in which R script was downloaded from the website (https://sourceforge.net/projects/estimateproject/) to calculate the estimate scores, immune scores, and stromal scores for further predicting tumor purity and analyzing the TME (29). To explore the differences in immune cell subtypes among multiple clusters, we utilized the CIBERSORT package to assess the proportions of 22 immune cell subtypes based on TCGA-ACC samples. The results with $P < 0.05$ in CIBERSORT analysis were used for further analysis. The Mann-Whitney U test was used to compare the differences among the three subgroups.

Least Absolute Shrinkage and Selection Operator Cox Regression and Validation of the Prognostic m6A Signatures

To enhance the prediction accuracy and interpretability of the statistical model, Lasso Cox regression analysis was carried out to examine the relationship between m6A prognosis signatures and ACC risk. Using the "glmnet" software package of R, 8 m6A-related genes were screened to construct the best prognostic model. The risk score was generated using the following formula: risk score $= \text{Expression}_{\text{mRNA1}} \times \text{Coefficient}_{\text{mRNA1}} + \text{Expression}_{\text{mRNA2}} \times \text{Coefficient}_{\text{mRNA2}} + \ldots \text{Expression}_{\text{mRNAn}} \times \text{Coefficient}_{\text{mRNAn}}$. According to the predictive model, the patients were divided into high-risk and low-risk groups using the median cutoff of risk score. The Cox proportional hazard regression model includes age and TNM stage. The hazard ratio (HR) from Cox regression analysis was used to distinguish the prognostic factors positively or negatively. A gene with HR > 1 was considered a risk gene, and a gene with HR < 1 was considered a protective gene. Subsequently, the Kaplan-Meier survival method was used to evaluate the availability of the prognostic model, and the sensitivity and specificity of the receiver operating characteristic (ROC) curve were used to evaluate the prognostic accuracy of the signature building. Similarly, the five validated GEO cohorts were further calculated to validate the prognostic value of selected m6A-related genes by OS and PFS (progression-free survival) analyses.

Gene Mutation Screening and Analysis

The SNP dataset was based on VarScan2 variant aggregation and masking data in TCGA. Here, we analyzed the SNP mutation and carried out visualization using the R maftools package (30). The SNP2APA database was designed to explore the effects of single nucleotide polymorphisms (SNPs) and provided OS across different cancer types (31). Based on this database, we searched for specific SNPs that have prognostic value in ACC, and assessed the relationship between these SNPs and key m6A-related genes.

Construction of the ceRNA Network

Using the TCGA cohort, differentially expressed genes between m6A patterns were identified with the standards of $|\log2(\text{Fold change})| > 1$ and $P < 0.05$ using the R package "limma." Perl programming language was applied to target miRNAs-lncRNAs and miRNAs-mRNAs in the prediction analysis. Furthermore, miRcode was used to collect and target experimentally validated lncRNAs (32). StarBase v3.0 was used to predict miRNA-mRNA interactions (http://starbase.sysu.edu.cn/) (33). The ceRNA network was visualized using the "Cytoscape" software (34).

Statistical Analysis

Most analyses were performed using R software (version 3.6.1, http://www.R-project.org). Kaplan-Meier curves and the log-rank test were used to compare the OS between various subgroups based on the expression of m6A-related genes. Univariate and multivariate Cox proportional hazard regression analyses were used to evaluate the independent prognostic value of the clinical characteristics of OS. The prognostic ability of the predictive models for 1/3/5-year OS was evaluated by ROC curves (R package "timeROC") and the area under the curve (AUC) values. In all analyses, all statistical P-values were bilateral, and $P < 0.05$ was considered statistically significant.

Clinical Specimens

Adrenocortical carcinoma tissues and normal adrenocortical tissues were obtained from five patients who received operation at the Third Xiangya Hospital (Changsha, Hunan, China) from January 2016 to December 2020. The patients were diagnosed by pathological analysis and were not subjected to chemotherapy or radiotherapy. The Institutional Review Board of the Ethics Committee of Third Xiangya Hospital approved the consent procedure, and written informed consent was provided by all patients in this research.

Immunohistochemistry

Paraffin-embedded ACC tissues and normal tissues were sliced, dewaxed, hydrated, and antigen-repaired, then endogenous peroxidase was blocked; anti-HNRNPA2B1 (1:100, 14813-1-AP, Proteintech Group, Wuhan, China), anti-LRPPRC (1:100, 21175-1-AP, Proteintech Group), and anti-ELAVL1 (1:100, 11910-1-AP, Proteintech Group) were added and incubated them together at 4°C overnight, respectively. Polymer enhancers were incubated for 30 min at room temperature, then biotinlabeled secondary antibodies were added and incubated for 30 min at room temperature. Next, the sections were stained by using diaminobenzidine staining solution, followed by counterstaining with hematoxylin, and then the sections were mounted in glycerol-vinyl-alcohol. Two independent professional pathologists were blinded to analysis the data and histopathological features of the patients, and also evaluated the IHC scores according to the scoring standards.

RESULTS

Consensus Clustering of m6A Genes in Three Clusters With Different Clinical Outcomes of ACC

Here, the clinical data and corresponding gene expression profiles of ACC patients were downloaded from the TCGA and GEO databases. The workflow is shown in **Figure 1**. We first analyzed 21 m6A regulators and mapped the correlation between m6A patterns and ACC survival. As a result, the expression levels of m6A regulators and clinical characteristics were obtained from TCGA and GEO. Pearson correlation analysis was performed to determine the relationship between m6A regulators (**Figure 2A**). Some highly correlated ($|\text{correlation coefficient}| \geq 0.5$, $P < 0.05$) m6A regulators were identified, such as YTHDF1, YTHDF2, HNRNPC, KIAA1429, ELAVL1, HNRNPA2B1, CBLL1, and YTHDF3. Based on the ConsensusClusterPlus R package, the TCGA-ACC cohort was clustered into different groups by consensus expression of m6A regulators. When the consensus matrix k value was equal to 3, there was the least crossover between the ACC samples (**Figures 2B,C** and **Supplementary Figure 1**). The OS difference between different clusters was calculated using the Kaplan-Meier method. Significantly better OS was found in patients specifically in cluster1 compared with other clusters **(Figure 2D)**. Further, we plotted a boxplot **(Figure 2E)** and heatmap **(Figure 4A)** for visualizing the expression of the 21 m6A regulatory factors in clusters and found that the expression of CBLL1, ELAVL1, HNRNPA2B1, HNRNPC, KIAA1429, LRPPRC, RBM15, RBM15B, WTAP, YTHDF2, and YTHDF3 in cluster3 was higher than that in other clusters ($P < 0.01$), while the expression of ALKBH5, IGF2BP1, METTL3, and YTHDF1, was higher in cluster2 than in other clusters.

The Interaction and Correlation Among the m6A Regulators in Three Patterns

To explore the potential biological differences among the three different m6A modification patterns, we identified DEGs by comparing clusters with the threshold of $|\text{logFC (fold change)}| \geq 1$ and adj. $P < 0.05$. When comparing cluster1 and cluster2, there were 371 up-regulated and 292 down-regulated genes. GO analysis of biological processes showed that the DEGs were enriched in extracellular structure organization, matrix organization, and humoral immune response. Cellular component analysis indicated that DEGs were abundant in the extracellular matrix and collagen-containing extracellular matrix. Molecular function analysis indicated that DEGs were mainly located in receptor regulator and ligand activities. Furthermore, KEGG analysis showed that the DEGs were enriched in tyrosine metabolism, viral protein interaction with cytokine and cytokine receptor, and IL-17 signaling pathways **(Figures 3A–C)**. Additionally, GSEA was performed for further signaling pathway enrichment analysis, and in a comparison between clusters1 and cluster2, the IL-17 signaling pathway, TNF, and NF-kappa B signaling pathway were enriched relative to cluster2 **(Figure 3D)**. These signaling pathways are related to core biological carcinogenic processes, most of which are involved in the regulation of immune checkpoint expression, and have potential for further exploration of the effect of m6A modifications on immunotherapy (25, 35, 36).

Immune Landscape in ACC Patients

The ESTIMATE algorithm provided stromal and immune scores, and tumor purity for all ACC samples. The heatmap of m6A-related gene expression and the stromal, immune, and ESTIMATE scores, and tumor purity are shown and clustered in **Figure 4A**. From the clustering, we found that such m6A genes showed a similar expression trend with tumor purity, and an opposite trend with stromal, immune, and ESTIMATE scores, indicating that the m6A pathway plays an important role in the tumor immune microenvironment and determines tumor progression and metastatic dissemination. Moreover, the density and location of immune cells can be quantified as a tangible indicator by an immune score. Here, there was a significant difference in the immune scores between the m6A clusters, and cluster1 showed the highest immune score. Furthermore, the ESTIMATE and stromal scores were also calculated, and the expression of cluster1 was higher than that of cluster2. Conversely, the distribution of tumor purity was different from the stromal, immune, and ESTIMATE scores, and cluster1 showed a lower tumor purity score than the others **(Figure 4B)**.

The 22 different immune cell types among different clusters were analyzed using the CIBERSORT algorithm. The results revealed that the macrophages M0, MI, M2 macrophages,

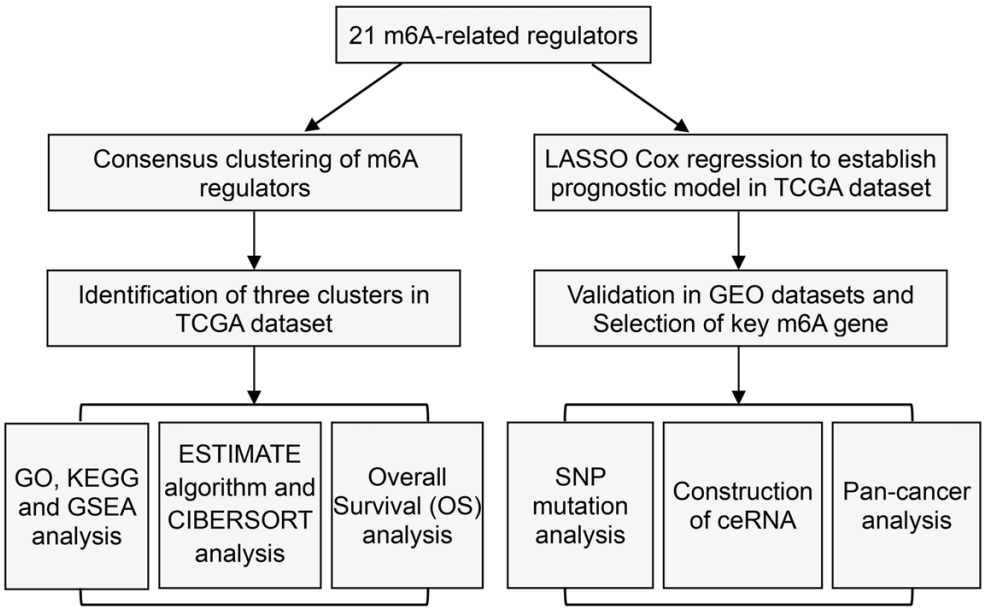

FIGURE 1 | Study flow chart.

dendritic cells activated, dendritic, cells resting, eosinophils mast cells resting, natural killer (NK) cells activated, and NK cells resting accounted for a large proportion of immune cell infiltration. Furthermore, cluster1, which had better survival, displayed a greater number of M1, M2 macrophages, and NK cells activated compared with other clusters with worse prognosis **(Figure 4C)**. In addition, we found that the levels of dendritic cells, macrophages M0, and NK cells activated in cluster1 were significantly lower than those in cluster2 and cluster3. The outcome revealed that m6A-related patterns may remarkably suppress or strengthen the expression of specific immune cell types, thus potentially influencing the response to immunotherapy.

Prognostic Analysis of Risk Model and m6A Genes

To develop a signature for prognosis prediction of ACC, we performed Lasso Cox regression analysis on 21 m6A-related genes based on the TCGA database. Next, we obtained eight genes (METTL14, ZC3H13, FTO, YTHDF1, YTHDF3, HNRNPA2B1, LRPPRC, and ELAVL1) to build the risk model, and the coefficients of these genes were used to calculate the risk score **(Figure 5A)**. The risk score = METTL14 × (−0.1750) + ZC3H13 × (−0.0212) + FTO × (−0.0984) + YTHDF1 × 0.0159 + YTHDF3 × (−0.0073) + HNRNPA2B1 × 0.0405 + LRPPRC × 0.0437 + ELAVL1 × 0.0376. Patients with ACC were separated into low-risk or high-risk groups with the median cutoff of risk score. As shown in **Figures 5B,C**, we found that as the risk score increased, high-risk patients had significantly worse OS than low-risk patients ($P = 1.617e^{-08}$). Univariate and multivariate analyses were used to evaluate the prognostic value of age, sex, M, N, T, and clinical stage (**Supplementary Figure 2**); however, only T stage was significantly correlated with OS. The ROC curve showed that the risk score had strong predictive ability, with an AUC of 0.844, 0.945, and 0.893 in 1, 3, and 5 years compared with other factors (**Figure 5D**). These results indicate that the risk model may serve as an important indicator for evaluating the prognosis of ACC.

Validation of the m6A-Genes in the GEO Dataset

To verify and identify the key genes of m6A patterns, we evaluated the prognostic values of the eight genes and the risk model in the GEO datasets. Three datasets (GSE10927, GSE19750, and GSE33371) containing OS statistics and two datasets (GSE76019 and GSE76021) containing event-free survival (EFS) statistics were selected for further validation. Fortunately, the results indicated that the risk model have potential value of prediction in all GEO datasets (**Supplementary Figure 3**). Considering the similarities of identified genes in the TCGA and GEO data, it is believed that the overlapping m6A regulators might be significant, including HNRNPA2B1, LRPPRC, FTO, YTHDC1, and ELAVL1 (**Supplementary Table 1**). HNRNPA2B1 was validated as a significant indicator of poor OS and EFS based on all GEO datasets (**Figure 6A**). LRPPRC might be regarded as a crucial biomarker of poor survival, which was successfully validated on four GEO datasets (GSE10927, GSE33371, GSE76019, and GSE76021) (**Figure 6B**). Furthermore, ELAVL1 was re-verified as a potential biomarker based on two GEO containing EFS data (**Figure 6C**). However, other m6A-related genes received a failed verification on most GEO datasets (**Supplementary Figures 3**, **4**). Subsequently, compared with the normal tissue, the

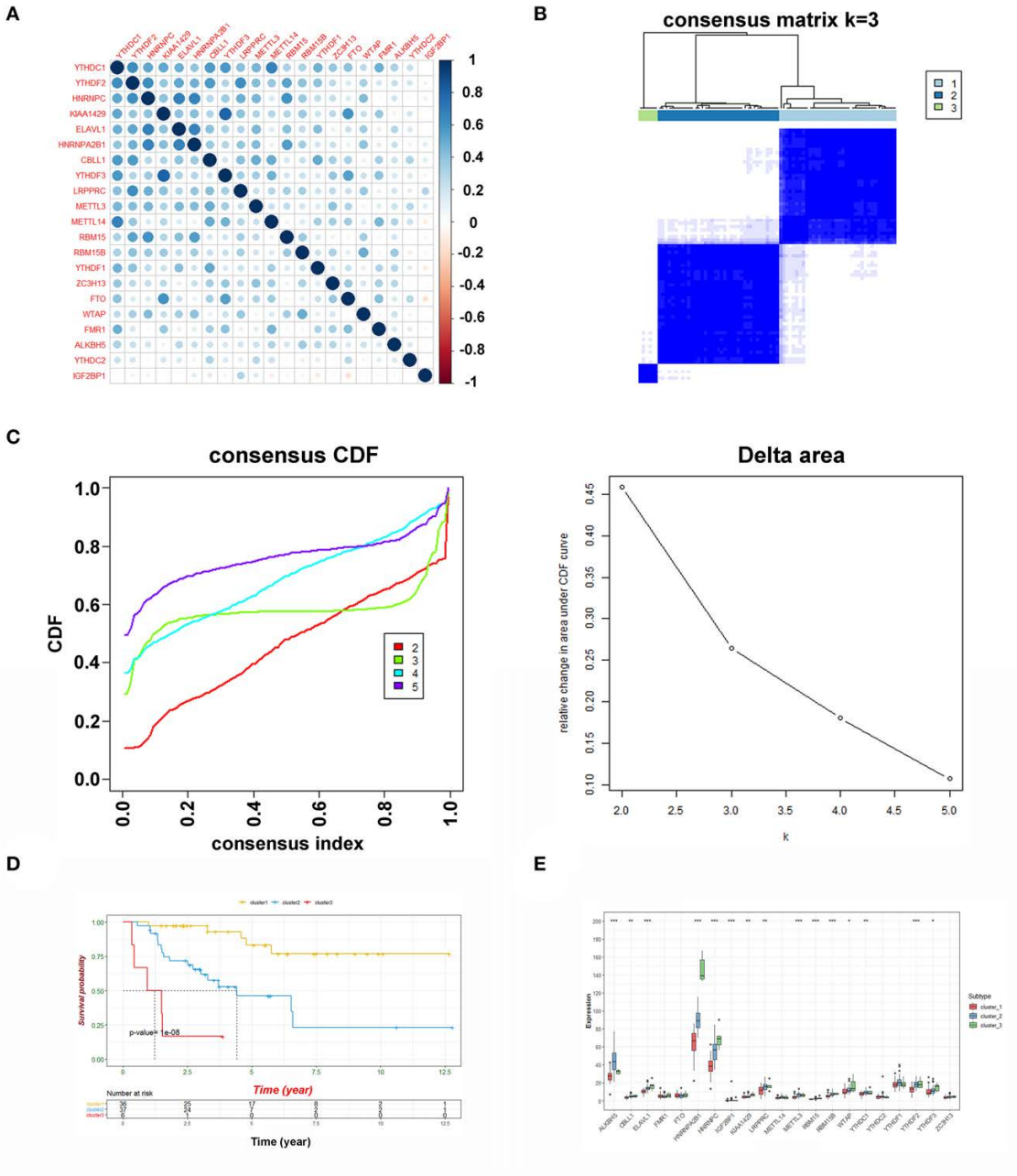

FIGURE 2 | Consensus clustering of m6A genes. **(A)** The Pearson correlation analysis was used to search the relationship among m6A regulators. **(B)** Consensus clustering matrix for k = 3. **(C)** Consensus clustering cumulative distribution function (CDF) and relative change in area under CDF curve for k = 2 to 5. **(D)** Kaplan-Meier curves of OS for three clusters in ACC. **(E)** The expression of the 21 m6A regulatory factors in clusters (***$P < 0.001$; **$P < 0.01$; *$P < 0.05$).

expression of these three m6A regulators was upregulated in ACC by performing IHC (**Supplementary Figure 5**).

SNP Analysis of m6A Genes Among Three Patterns

Tumor mutational burden (TMB) was considered a promising indicator and exhibited predictive utility in identifying responders and non-responders to immune checkpoint inhibitors (37, 38). Here, the most frequent variants were missense mutations, followed by nonsense mutations and splice sites. SNP was responsible for most variants, and single nucleotide variants (SNVs) mostly occurred as C > T and C > A. The top ten mutated genes in ACC samples were TTN, MUC16, PKHD1, TP53, CTNNB1, CNTNAP5, SVEP1, LRP1, HMCN1, and ASXL3 (**Figure 7A**). However, we failed to observe significant differences in these genes among the three clusters and other clinical characteristics (**Figure 7B**).

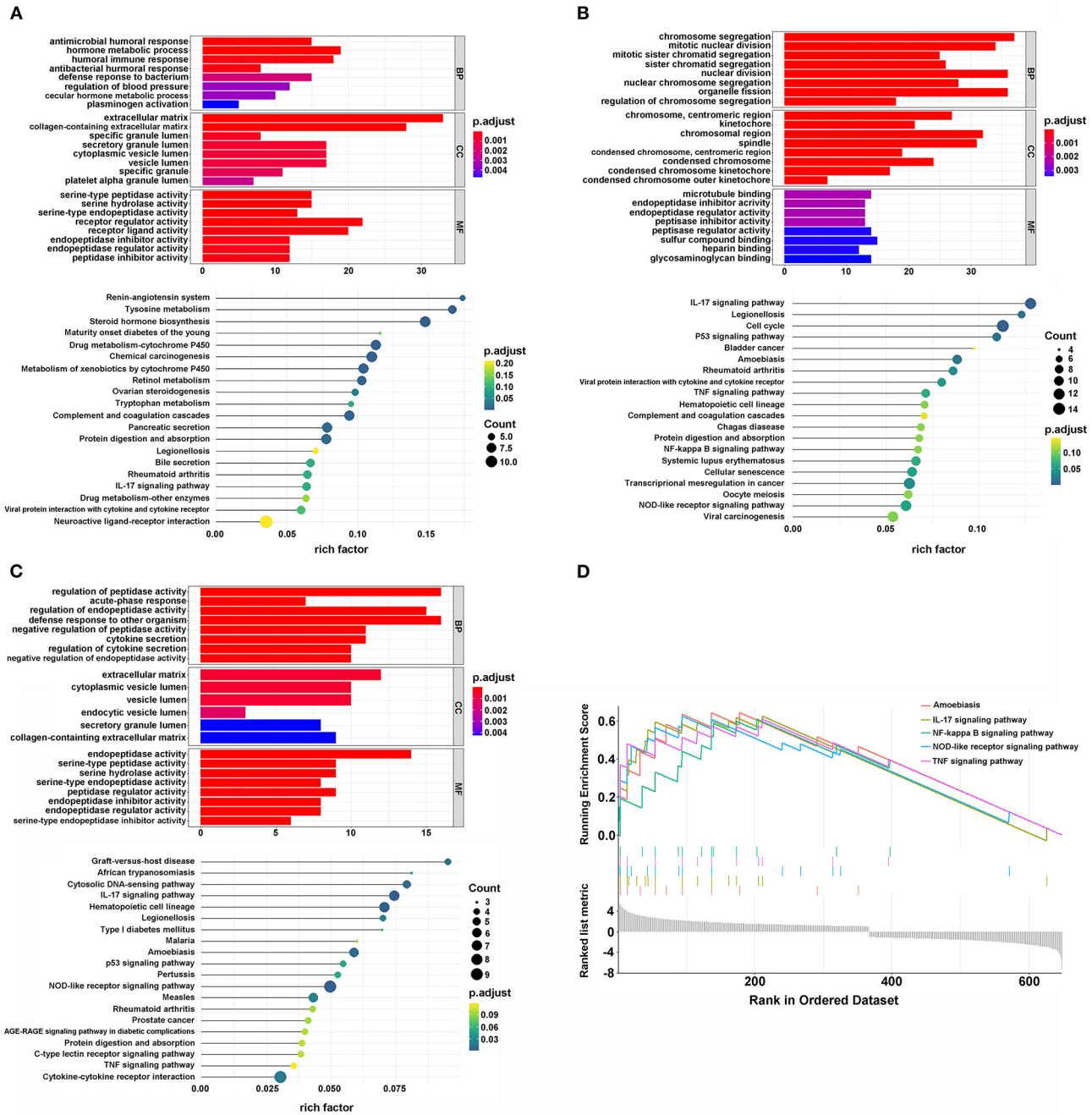

FIGURE 3 | The interaction and correlation among clusters. **(A)** The GO and KEGG analysis of DEGs between cluster1 and cluster2. **(B)** The GO and KEGG analysis of DEGs between cluster1 and cluster3. **(C)** The GO and KEGG analysis of DEGs between cluster2 and cluster3. **(D)** The GSEA analysis of DEGs between cluster1 and cluster2.

To further analyze the relationship between m6A key genes and SNPs, we sorted out all the positive polymorphisms based on the SNP2APA database. Eight polymorphisms from four mRNAs (MID1IP1, CEBPZ, CNPY2, and TIPRL) were considered positive by the Kaplan-Meier survival method (**Supplementary Table 2**). The results of Pearson's correlation analysis indicated that these mRNAs were significantly correlated with the expression level of key m6A-related mRNAs, especially HNRNPA2B1, LRPPRC, and ELAVL1 (**Supplementary Figure 6**).

ceRNA Network Construction Based on the Key Gene

To reveal the function regulated by the m6A regulator pathway, we obtained 318 lncRNAs and 138 miRNAs in cluster2 compared with cluster1 (**Supplementary Tables 3**, **4**).

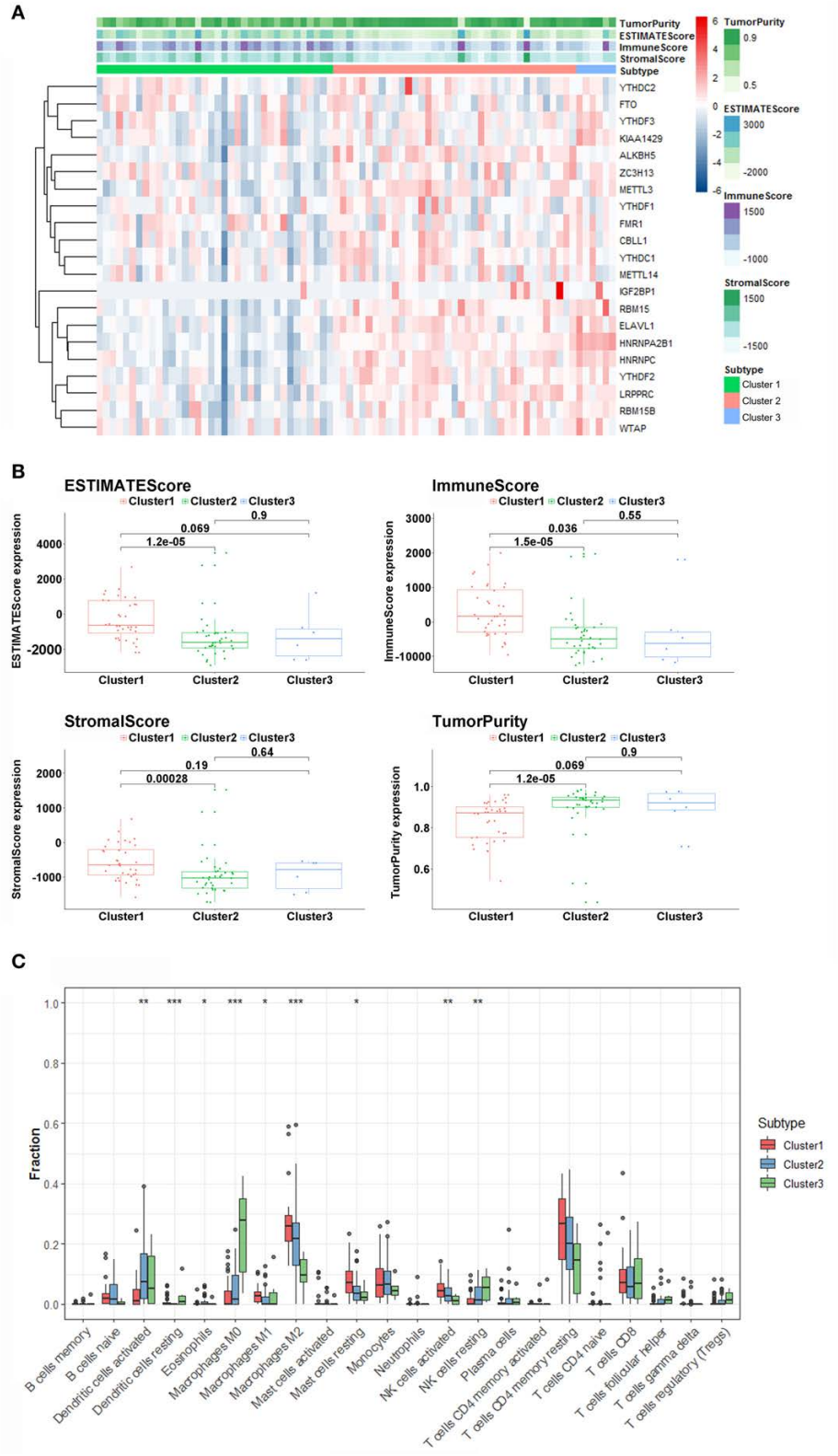

FIGURE 4 | Immune characteristics among three m6A patterns. **(A)** The heatmap of m6A regulators from 3 clusters and ESTIMATE algorithm. **(B)** Different expression of ESTIMATE score, immune score, stromal score, and tumor purity in three m6A Patterns. **(C)** Differences in the levels of infiltration of the 22 immune cells in three m6A patterns (***$P < 0.001$; **$P < 0.01$; *$P < 0.05$).

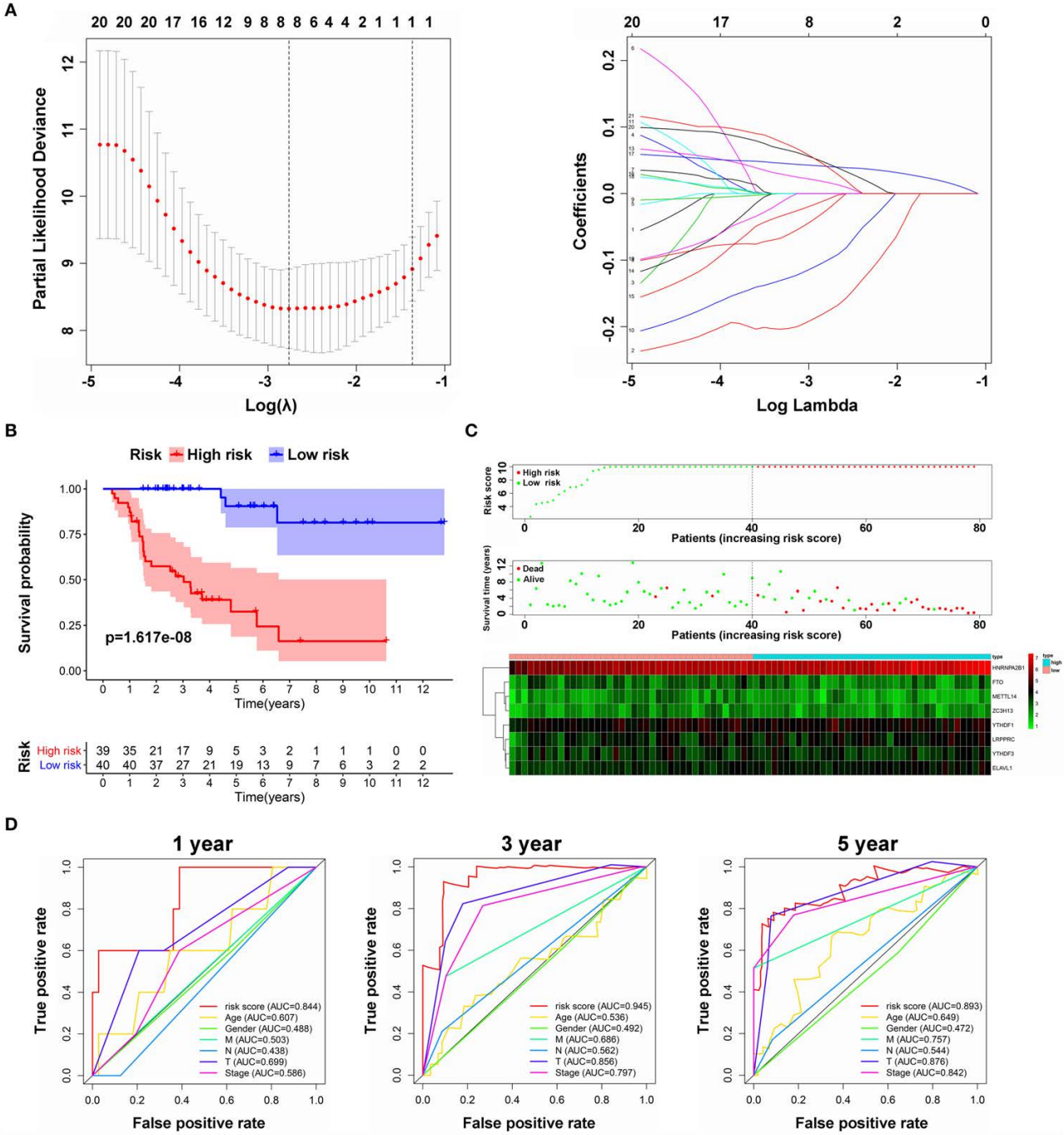

FIGURE 5 | Risk model from m6A-related genes. **(A)** Lasso Cox regression analysis of 21 m6A-related genes. **(B)** Overall survival analysis for patients in high/low risk. **(C)** The distributions of risk scores, alive/dead status, and expression of three m6A-related genes. **(D)** The ROC curve of risk score and clinical characteristics.

The heatmap of DEGs with |logFC (fold change)| ≥ 2 and FDR < 0.05 is shown in **Figures 8A,B**. To further understand how m6A-related lncRNAs mediate mRNA expression by sponging miRNAs, we constructed a ceRNA network based on m6A-related lncRNAs. Twenty-nine lncRNAs were selected from the miRcode database, which targeted 85 miRNAs and 19 miRNAs, were further identified after taking the intersection of DEGs of miRNAs. We then used StarBase to search for mRNAs, and a total of 455 mRNAs were selected based on three databases (miRTarBase, miRDB, and TargetScan) (**Supplementary Table 5**). Furthermore, taking the intersection of these mRNAs and 21 m6A-related genes as potential functional

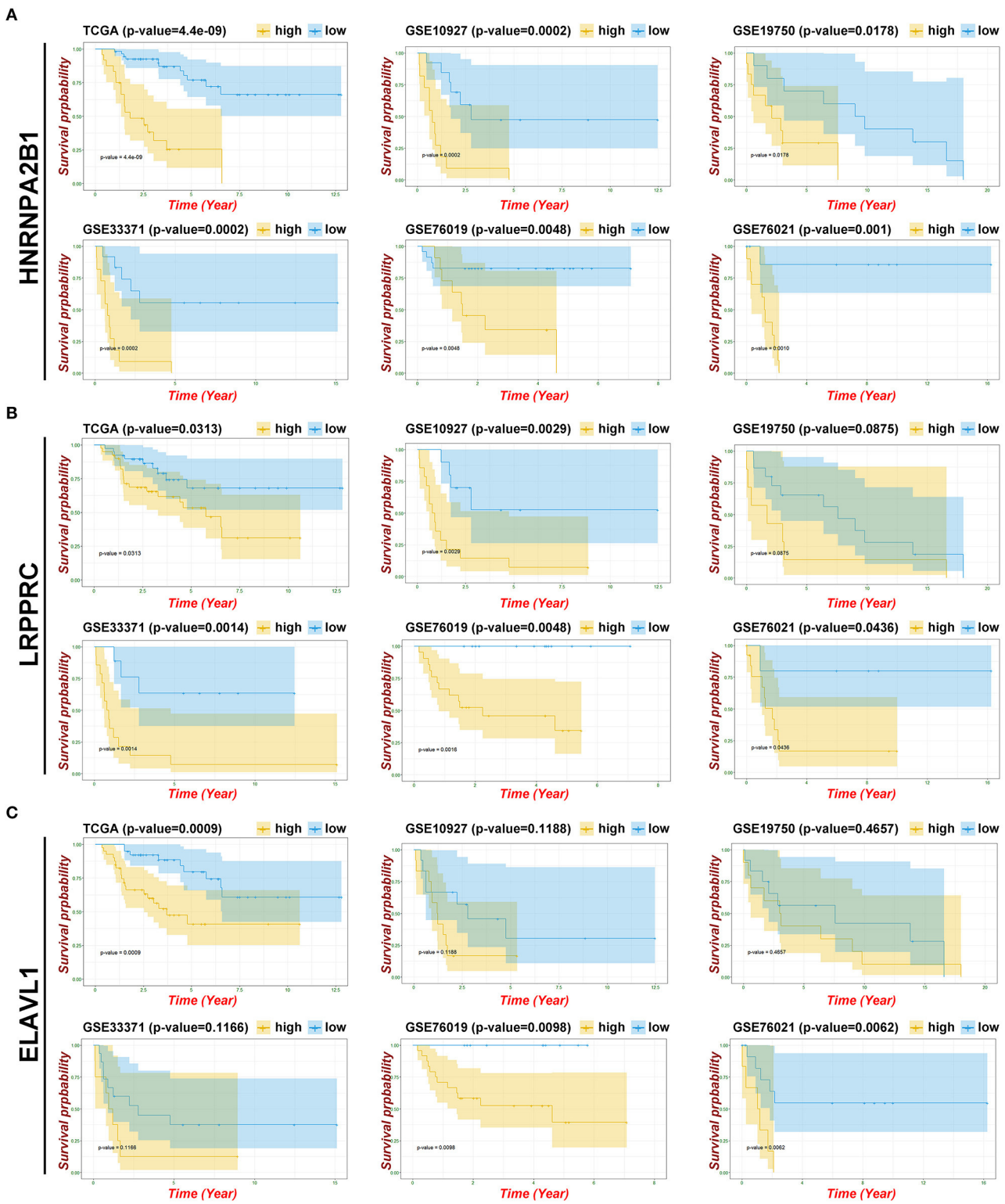

FIGURE 6 | Identifying the key gene of m6A patterns. **(A)** Kaplan-Meier OS curves and EFS curves for patients in HNRNPA2B1. **(B)** Kaplan-Meier OS curves and EFS curves for patients in LRPPRC. **(C)** Kaplan-Meier OS curves and EFS curves for patients in ELAVL1.

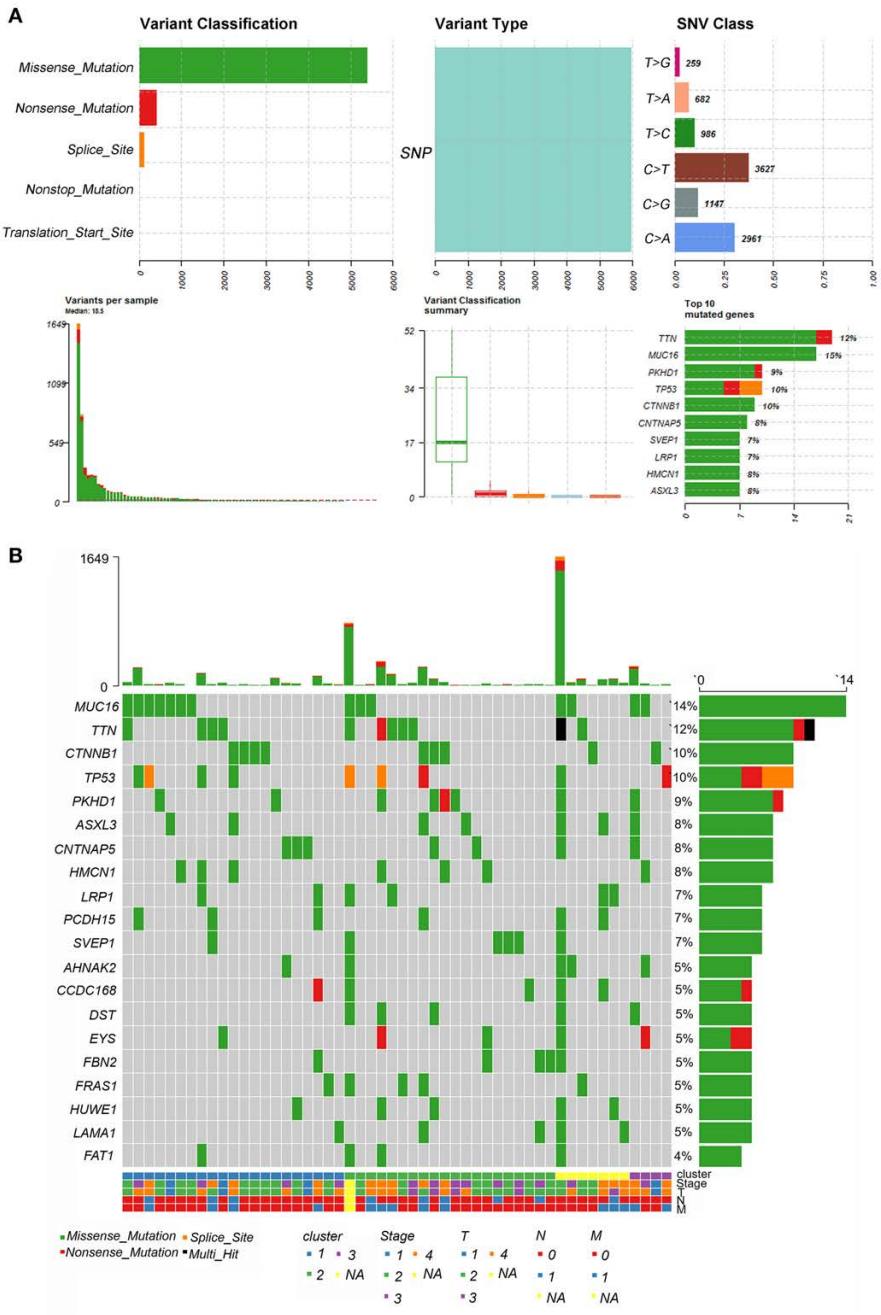

FIGURE 7 | Landscape of TMB in ACC. **(A)** The summary plot of genetic alteration in ACC. **(B)** The oncoplot of genetic alteration in ACC.

molecules, these data indicated that 12 lncRNAs (C17orf100, C8orf31, SNHG14, PLCL2-AS1, HCG11, HOTAIR, LINC00332, IDI2-AS1, ZFY-AS1, TTTY15, LINC00461, and DIO3OS) may dysregulate the behavior of hsa-mir-211 so that it promotes the expression of key m6A gene HNRNPA2B1 (**Figures 8C,D**).

Pan-Cancer Analysis of the Key Gene

To further confirm the key role of HNRNPA2B1 in the m6A modification process, we adopted a pan-cancer analysis and downloaded all the data from the UCSC Cancer Genomics Browser (https://genome-cancer.ucsc.edu), which offers interactive visualization and exploration of TCGA genomic and clinical data. HNRNPA2B1 expression was re-evaluated and was notably found to significantly impact prognosis in ACC. High HNRNPA2B1 expression was associated with decreased disease-specific survival (DSS) ($P < 0.001$), disease-free interval (DFI) ($P = 0.034$), and progression-free interval (PFI) ($P < 0.001$) **(Figures 9A–C)**. In addition, as shown in **Figure 9D**, the

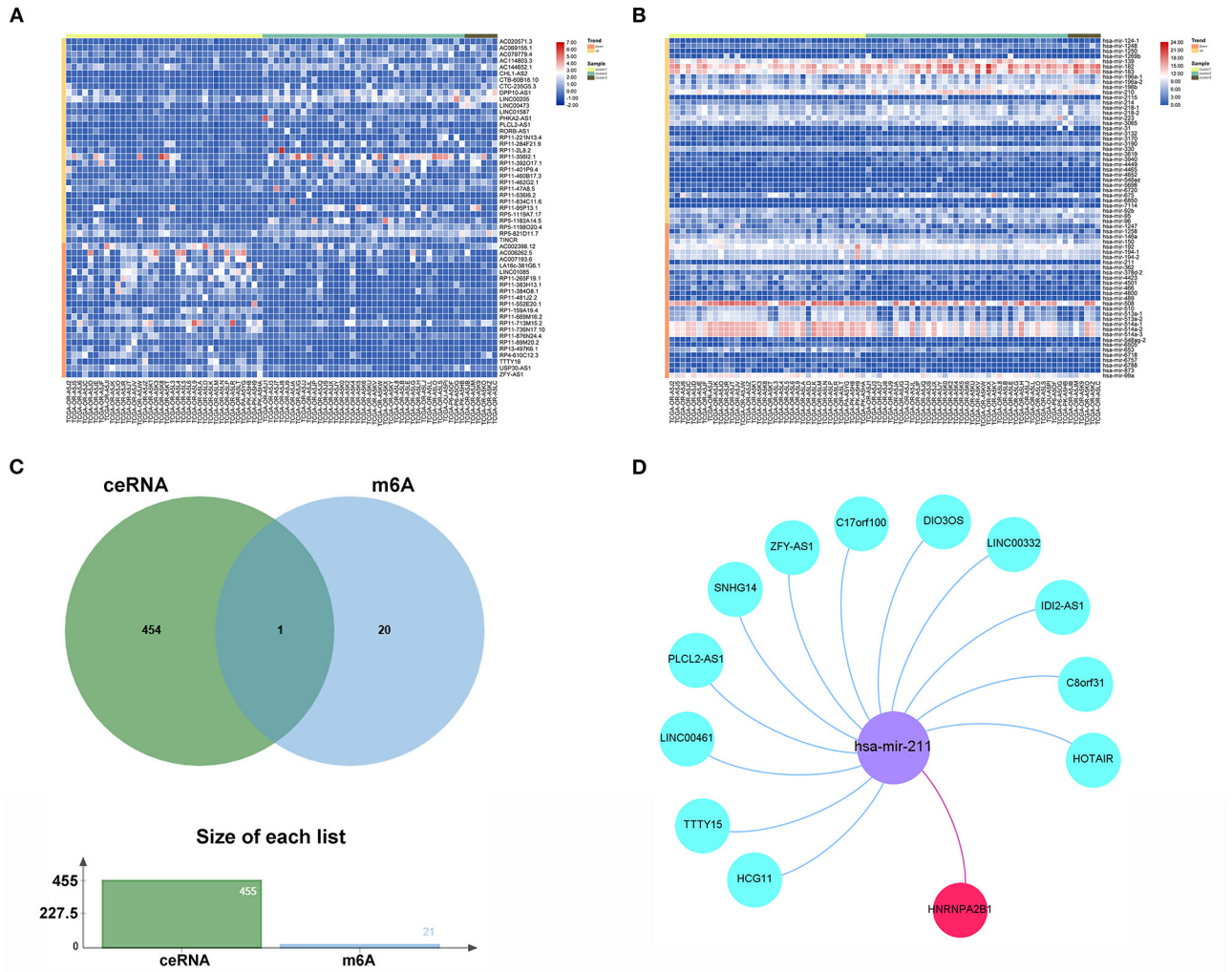

FIGURE 8 | ceRNA network construction of key m6A-related gene. **(A)** The heatmap of significant differential expression lncRNAs. **(B)** The heatmap of significant differential expression miRNAs. **(C)** The Venn plot of 455mRNAs and 21 m6A regulators. **(D)** The ceRNA network of the 12 m6A-related lncRNAs (blue) and target miRNAs (purple) and mRNAs (red).

expression of HNRNPA2B1 was significantly correlated with TNM stage. Furthermore, we analyzed the correlation among HNRNPA2B1 expression, ESTIMATE score, and infiltrating immune cells. The results showed that HNRNPA2B1 levels were significantly negatively correlated with immune score ($r = -0.43$, $P = 0.00011$), stromal score ($r = -0.40$, $P = 0.00033$), and resting mast cells ($r = -0.56$, $P = 0.00012$) **(Figure 9E)**. Additionally, increased TMB has been linked to PD1/PD-L1 therapeutic response, and we found that HNRNPA2B1 mRNA levels were correlated to multiple types of cancers, including ACC, stomach adenocarcinoma (STAD), thymoma (THYM) etc. Microsatellite instability (MSI) is a pattern of hypermutation caused by defects in the mismatch repair system and has been known to be both predictive and prognostic to better profile responses to anti-PD-1 immunotherapy (39). Next, we found that HNRNPA2B1 was associated with diffuse large B-cell lymphoma (DBLC) and lung squamous cell carcinoma (LUSC), but not ACC, as shown in the radar plot **(Figure 9F)**. Moreover, Spearman's correlation was used to show the relationship between HNRNPA2B1 and immune-related mRNAs in 33 cancer types **(Figure 9G)**.

DISCUSSION

With a heterogeneous clinical characteristic and poor OS, treating this complex malignant tumor, adrenocortical carcinoma, is a substantial clinical challenge (40). Further, the current TNM classification system remains inapplicable to predict prognosis. Here, we used univariate and multivariate analyses to evaluate the clinical prognostic value, and the results indicated that most clinical characteristics, including M stage and N stage, failed to guide treatment options. Previous studies have shown that the invasion and proliferation of ACC is regulated by genomic molecular characteristics (41).

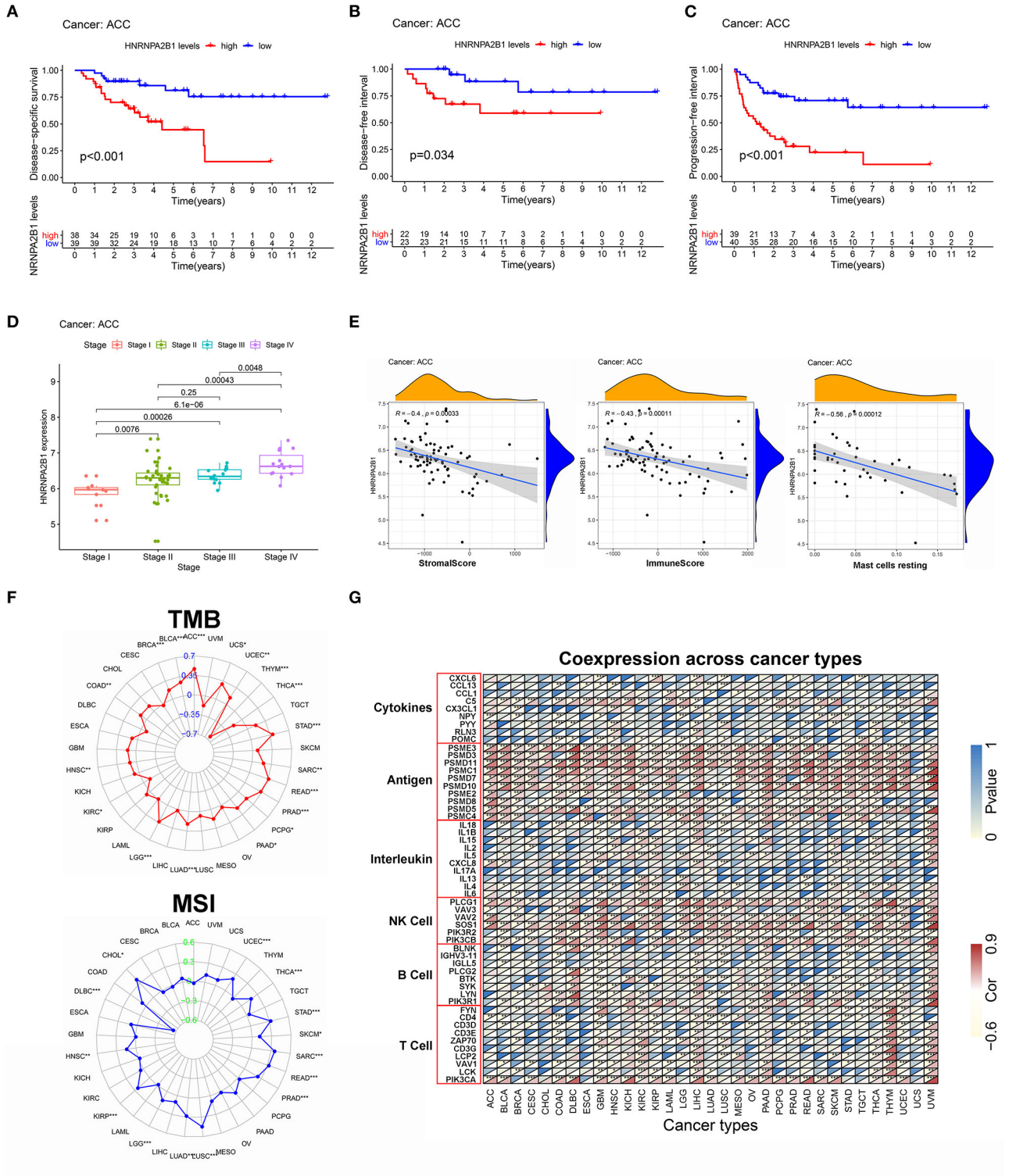

FIGURE 9 | The pan-cancer analysis of HNRNPA2B1. **(A)** The relationship between HNRNPA2B1 expression and DSS. **(B)** The relationship between HNRNPA2B1 expression and DFI. **(C)** The relationship between HNRNPA2B1 expression and PFI. **(D)** The HNRNPA2B1 expression was significantly correlated with TNM stage. **(E)** The correlation among HNRNPA2B1 expression and immune landscape. **(F)** Pan-cancer analysis of the relationship between HNRNPA2B1 expression and TMB (above) or MSI (below). **(G)** The correlation among HNRNPA2B1 expression and immune-related mRNAs.

m6A is the most common and plentiful modification to affect cancer development through the regulation of m6A methyltransferases, demethylases, and binding proteins, but to date, the potential role of m6A regulators in ACC prognosis is not well-understood. Based on the TCGA dataset, we identified three clusters according to the optimal k-means clustering, and we observed a significant difference in OS among the three clusters, suggesting that the expression of m6A-related regulators is intimately related to the prognosis and malignancy of ACC.

Accumulating studies have focused on the tumor immune microenvironment and ACC is characterized as a highly immunogenic tumor, with 86.3% of ACC specimens showing high rates of tumor infiltrating lymphocytes (TILs) (42). Here, GO, KEGG, and GSEA analyses revealed that the DEGs among clusters were enriched in immune-related signaling pathways, such as IL-17 signaling pathway. Furthermore, the ESTIMATE score, especially the immune score, was significantly correlated with the expression of m6A patterns. Similarly, the infiltration of immune cells (M1, M2 macrophages, and NK cells activated) was significantly increased and the infiltration of immune cells (dendritic cells, macrophages M0, and NK cells activated) was significantly decreased in the low-risk score group (cluster1) compared with the high-risk score groups (cluster2 or cluster3). These results indicate a comprehensive evaluation of the m6A modification patterns that will facilitate understanding the characteristics of TME cell infiltration and promote individualized novel therapies by determining the response to immunotherapy.

Here, we systematically explored the effects of multiple m6A regulators on OS in ACC and attempted to construct a risk model for prediction. Next, we distinguished a prognostic risk signature with eight identified m6A regulators (METTL14, ZC3H13, FTO, YTHDF1, YTHDF3, HNRNPA2B1, LRPPRC, and ELAVL1), which divided the OS in ACC into high-risk subgroups with high mortality and low-risk subgroup with remarkably better survival. Notably, compared with the previous prognostic markers (T, N, M clinical stage), our prognostic risk signature can achieve higher accuracy, with AUC values >0.8. In summary, the risk signature we constructed might be viewed as a new potential and promising biomarker that can provide more precise clinical applications and an efficient guide for treatment. However, owing to the limited number of samples in most GEO databases, this model needs to be re-confirmed in other databases with large populations. Meanwhile, we applied survival analysis to further detect the eight identified genes in the TCGA and GEO datasets, and we served overlapping m6A regulators as significant biomarkers, particularly HNRNPA2B1, which was proven to have a positive association with poor OS, EFS, DSS, DFI, and PFI in TCGA and all GEO datasets.

The role of HNRNPA2B1 in cancer has recently garnered increasing attention. On the one hand, HNRNPA2B1 acted as a nuclear m6A reader that recruited the miRNA microprocessor complex protein DGCR8 to a subset of precursor miRNAs and mediated the mature miRNA processing (43). On the other hand, HNRNPA2B1 functioned as an adaptor and modulated the molecular changes to alternative splicing combined with METTL3 (44). Here, the results showed that lower immune scores, stromal scores, and ESTIMATE scores were significantly associated with higher HNRNPA2B1 expression, which demonstrated that this m6A gene signature played a non-negligible role in shaping diverse stromal and immune TME landscapes, implying that HNRNPA2B1 may affect the therapeutic efficacy of immune checkpoint blockade. Moreover, using the CIBERSORT algorithm, we found that HNRNPA2B1 mediated the TME infiltration patterns to accelerate ACC progression partly by regulating macrophages M0. Tumor mutational burden, defined as the total number of somatic coding mutations per million bases, has emerged as a notable biomarker of response to immunotherapy (45). Recent studies showed that HNRNPA2B1 with high frequency of mutation may have an influence on promoting tumorigenesis in melanoma (46). Similarly, by analyzing the mutation annotation files of the TCGA cohort, the results showed that HNRNPA2B1 has a close correlation with TMB in multiple types of cancer, particularly ACC. Based on the SNP2APA database, we identified four highly variant mutated genes, most of which were highly correlated with the HNRNPA2B1 expression level. These findings indicated that high HNRNPA2B1 expression is related to dysregulation of the TME landscape and a sharp accumulation of gene mutations, thus becoming a promising therapeutic target for ACC.

Furthermore, several selected lncRNAs were reported to be associated with cancer progression (47), but there have been few reports on lncRNAs regarding ACC progression, and how m6A-related genes act in an lncRNA-miRNA-dependent manner during ACC progression is still unknown. In our research, we constructed a ceRNA network to target m6A-related miRNA and lncRNAs, which consist of twelve lncRNAs and one miRNA. Therefore, we should pay more attention to filter key lncRNAs that could predict OS and EFS and have a close relationship with HNRNPA2B1. Finally, we identified two lncRNAs, HOTAIR and IDI2-AS1, according to the above-mentioned conditions. Located on chromosome.12q13.13, lncRNA HOTAIR (HOX Transcript Antisense Intergenic RNA) was regarded as a regulator of chromatin states (48). In immune cells, HOTAIR has the ability to interfere with the TME landscape by inducing IκBα degradation, with the consequent activation of NF-κB pathways and secretion of pro-inflammatory cytokines (49, 50). Moreover, HOTAIR also led to the downregulation of the tumor suppressor gene SETD2, promoting MSI and high TMB (50, 51). In ACC, HOTAIR is overexpressed in tumor tissues compared with normal tissues. For *in vitro* experiments, HOTAIR can prompt the progression of ACC by shortening the cell cycle and promoting the proliferation of ACC cells (52). Hence, we planned to take the next step to deeply explore the interaction of HOTAIR and HNRNPA2B1 *in vitro*. In our study, IDI2-AS1 was also found to play a

significant role in ACC. However, there are few reports on how IDI2-AS1 acts as an oncogene. Thus, we carried out a pan-cancer analysis of IDI2-AS1 and hoped our results help to identify the prognostic value. We found that high IDI2-AS1 expression was obviously associated with poor DSS, DFI, PFI, and high TMB rate. Furthermore, the findings revealed that IDI2-AS1 had a stable association with the expression of PD1 (PDCD1) and PD-L1 (CD274) to serve as a potential prognostic marker or therapeutic targets of cancers integrated with m6A-related regulators (**Supplementary Figure 7**). Moreover, previous studies have reported the different functions of miR-211, which can facilitate platinum chemosensitivity by blocking the DNA damage response (53) or by stimulating the emergence of BRAF inhibitor resistance (54). Most speculations that miR-211 may regulate the m6A modification pathway need to be confirmed by further validation or experiments.

In conclusion, this study is the first to comprehensively identify and systematically profile the gene signatures of m6A-related regulators in ACC. The different m6A modification patterns played an important role in the heterogeneity and complexity of the TME. We also developed an eight-gene-signature prognostic model, in particular HNRNPA2B1, which might determine the clinical progression of ACC. Moreover, we constructed a ceRNA network to further decipher the molecular mechanisms based on HNRNPA2B1. Our results indicate that m6A genes are promising predictive indicators that may provide novel insights into ACC therapeutic strategies and guide effective immunotherapy.

DATA AVAILABILITY STATEMENT

The datasets presented in this study can be found in online repositories. The names of the repository/repositories and accession number(s) can be found in the article/**Supplementary Material**.

ETHICS STATEMENT

Written informed consent was obtained from the individual(s), and minor(s)' legal guardian/next of kin, for the publication of any potentially identifiable images or data included in this article.

AUTHOR CONTRIBUTIONS

KC: designed the study. YJ: analyzed, interpreted the data, and wrote original draft. ZW, DH, YZ, and XH: wrote this manuscript. LG, MX, XC, and YC: edited and revised the manuscript. All authors have seen and approved the final version of the manuscript.

FUNDING

This work was supported by the National Natural Science Foundation of China (81874137), the Outstanding Youth Foundation of Hunan Province (2018JJ1047), the Hunan Province Science and Technology Talent Promotion Project (2019TJ-Q10), Hunan Cancer Hospital Climb Plan (No. QH201905), and the Special Foundation for Cancer Research from the National Cancer Center (NCC2017L01, and NCC2017A17), China.

SUPPLEMENTARY MATERIAL

The Supplementary Material for this article can be found online at: https://www.frontiersin.org/articles/10.3389/fimmu.2021.637933/full#supplementary-material

Supplementary Figure 1 | Consensus clustering matrix for k = 2 to 5.

Supplementary Figure 2 | (A) The univariate analysis of age, sex, M, N, T, and clinic stage. **(B)** The multivariate analysis of age, sex, M, N, T, and clinic stage.

Supplementary Figure 3 | Prognostic value of risk model, YTHDF1 and YTHDF3. **(A)** Kaplan-Meier OS curves and EFS curves for patients in risk model. **(B)** Kaplan-Meier OS curves and EFS curves for patients in YTHDF1. **(C)** Kaplan-Meier OS curves and EFS curves for patients in YTHDF3.

Supplementary Figure 4 | Prognostic value of FTO, METTL14 and ZC3H13. **(A)** Kaplan-Meier OS curves and EFS curves for patients in FTO. **(B)** Kaplan-Meier OS curves and EFS curves for patients in METTL14. **(C)** Kaplan-Meier OS curves and EFS curves for patients in ZC3H13.

Supplementary Figure 5 | Verification of key m6A regulators expression in immunohistochemistry. **(A)** The expression of HNRNPA2B1 in tumor and normal tissue. **(B)** The expression of LRPPRC in tumor and normal tissue. **(C)** The expression of ELAVL1 in tumor and normal tissue. (＊＊＊P<0.001; ＊＊P<0.01).

Supplementary Figure 6 | Pearson's correlation analysis of positive polymorphisms and key m6A regulators.

Supplementary Figure 7 | The pan-cancer analysis of IDI2-AS1. **(A)** The relationship between IDI2-AS1 expression and OS. **(B)** The relationship between IDI2-AS1 expression and DSS. **(C)** The relationship between IDI2-AS1 expression and DFI. **(D)** The relationship between IDI2-AS1 expression and PFI. **(E)** The correlation among IDI2-AS1 expression and immune landscape. **(F)** Pan-cancer analysis of the relationship between IDI2-AS1 expression and TMB. **(G)** The correlation among IDI2-AS1 expression and PD1/PD-L1 from starBase V3.0 project.

Supplementary Table 1 | Cox analysis of 21 m6A genes in ACC patients.

Supplementary Table 2 | Positive polymorphisms based on SNP2APA database.

Supplementary Table 3 | All differential expression lncRNAs in cluster2 compared with cluster1.

Supplementary Table 4 | All differential expression miRNAs in cluster2 compared with cluster1.

Supplementary Table 5 | Targeted mRNAs base on miRTarBase, miRDB, and TargetScan databases.

REFERENCES

1. Kebebew E, Reiff E, Duh QY, Clark OH, McMillan A. Extent of disease at presentation and outcome for adrenocortical carcinoma: have we made progress. *World J Surg.* (2006) 30:872–8. doi: 10.1007/s00268-005-0329-x
2. Allolio B, Fassnacht M. Clinical review: adrenocortical carcinoma: clinical update. *J Clin Endocrinol Metab.* (2006) 91:2027–37. doi: 10.1210/jc.2005-2639
3. Gonzalez RJ, Tamm EP, Ng C, Phan AT, Vassilopoulou-Sellin R, Perrier ND, et al. Response to mitotane predicts outcome in patients with

recurrent adrenal cortical carcinoma. *Surgery.* (2007) 142:867–75. doi: 10.1016/j.surg.2007.09.006
4. Icard P, Chapuis Y, Andreassian B, Bernard A, Proye C. Adrenocortical carcinoma in surgically treated patients: a retrospective study on 156 cases by the French Association of Endocrine Surgery. *Surgery.* (1992) 112:972–9.
5. Else T, Kim AC, Sabolch A, Raymond VM, Kandathil A, Caoili EM, et al. Adrenocortical carcinoma. *Endocr Rev.* (2014) 35:282–326. doi: 10.1210/er.2013-1029
6. Assié G, Jouinot A, Fassnacht M, Libé R, Garinet S, Jacob L, et al. Value of molecular classification for prognostic assessment of adrenocortical carcinoma. *JAMA Oncol.* (2019) 5. doi: 10.1001/jamaoncol.2019.1558
7. Fassnacht M, Johanssen S, Quinkler M, Bucsky P, Willenberg HS, Beuschlein F, et al. European Network for the Study of Adrenal, Limited prognostic value of the 2004 International Union Against Cancer staging classification for adrenocortical carcinoma: proposal for a Revised TNM Classification. *Cancer.* (2009) 115:243–50. doi: 10.1002 /cncr.24030
8. Alarcón CR, Lee H, Goodarzi H, Halberg N, Tavazoie SF, Alarcón CR, et al. N6-methyladenosine marks primary microRNAs for processing. *Nature.* (2015) 519:482–5. doi: 10.1038/ nature14281
9. Zhao BS, Roundtree IA, He C. Post-transcriptional gene regulation by mRNA modifications. *Nat Rev Mol Cell Biol.* (2017) 18:31–42. doi: 10.1038/nrm.2016.132
10. Lan Q, Liu PY, Haase J, Bell JL, Hüttelmaier S, Liu T. The critical role of RNA m6A methylation in cancer. *Cancer Res.* (2019) 79:1285–92. doi: 10.1158/00 08-5472.CAN-18-2965
11. Chen XY, Zhang J, Zhu JS. The role of m6A RNA methylation in human cancer. *Mol Cancer.* (2019) 18:103. doi: 10.1186/s12943-019-1033-z
12. Meyer KD, Jaffrey SR. Rethinking m6A readers, writers, and erasers. *Annu Rev Cell Dev Biol.* (2017) 33:319–42. doi: 10.1146/annurev-cellbio-100616-060758
13. Geula S, Moshitch-Moshkovitz S, Dominissini D, Mansour AA, Kol N, Salmon-Divon M. m6A mRNA methylation facilitates resolution of naive pluripotency toward differentiation. *Science.* (2015) 347:1002–6. doi: 10.1126/science.1261417
14. Fustin JM, Doi M, Yamaguchi Y, Hida H, Nishimura S, Yoshida M. RNA-methylation-dependent RNA processing controls the speed of the circadian clock. *Cell.* (2013) 55:793–806. doi: 10.1016/j.cell.2013. 10.026
15. Xiang Y, Laurent B, Hsu CH, Nachtergaele S, Lu Z, Sheng W, et al. RNA m(6)A methylation regulates the ultraviolet-induced DNA damage response. *Nature.* (2017) 543:573–6. doi: 10.1038/nature21671
16. Tong J, Cao G, Zhang T, Sefik E, Amezcua Vesely MC, Broughton JP, et al. m(6)A mRNA methylation sustains Treg suppressive functions. *Cell Res.* (2018) 28:253–6. doi: 10.1038/cr.2018.7
17. Pinello N, Sun S, Wong JJ. Aberrant expression of enzymes regulating m6A mRNA methylation: implication in cancer. *Cancer Biol Med.* (2018) 15:323–34. doi: 10.20892/j.issn.2095-3941.2018.0365
18. Hong K. Emerging function of N6-methyladenosine in cancer. *Oncol Lett.* (2018) 16:5519–24. doi: 10.3892/ol.2018.9395
19. Niu Y, Lin Z, Wan A, Chen H, Liang H, Sun L, et al. RNA N6-methyladenosine demethylase FTO promotes breast tumor progression through inhibiting BNIP3. *Mol Cancer.* (2019) 18:46. doi: 10.1186/s12943-019-1004-4
20. Tu Z, Wu L, Wang P, Hu Q, Tao C, Li K, et al. N6-Methylandenosine-related lncRNAs are potential biomarkers for predicting the overall survival of lower-grade glioma patients. *Front Cell Dev Biol.* (2020) 8:642. doi: 10.33 89/fcell.2020.00642
21. Wang Q, Hu B, Hu X, Kim H, Squatrito M, Scarpace L, et al. Tumor evolution of glioma-intrinsic gene expression subtypes associates with immunological changes in the microenvironment. *Cancer Cell.* (2017) 32:42–56.e6. doi: 10.1016/j.ccell.2017. 06.003
22. Topalian SL, Hodi FS, Brahmer JR, Gettinger SN, Smith DC, McDermott DF, et al. Safety, activity, and immune correlates of anti-PD-1 antibody in cancer. *N Engl J Med.* (2012) 366:2443–54. doi: 10.1056/NEJMoa1200690
23. Raj N, Zheng Y, Kelly V, Katz SS, Chou J, Do RKG, et al. PD-1 blockade in advanced adrenocortical carcinoma. *J Clin Oncol.* (2020) 38:71–80. doi: 10.1200/ JCO.19.01586
24. Li N, Kang Y, Wang L, Huff S, Tang R, Hui H, et al. ALKBH5 regulates anti-PD-1 therapy response by modulating lactate and suppressive immune cell accumulation in tumor microenvironment. *Proc Natl Acad Sci USA.* (2020) 117:20159–70. doi: 10.1073/pnas.1918986117
25. Yang S, Wei J, Cui YH, Park G, Shah P, Deng Y, et al. m(6)A mRNA demethylase FTO regulates melanoma tumorigenicity and response to anti-PD-1 blockade. *Nat Commun.* (2019) 10:2782. doi: 10.1038/s41467-019-10669-0
26. Shi H, Wei J, He C. Where, when, and how: context-dependent functions of RNA methylation writers, readers, and erasers. *Mol Cell.* (2019) 74:640–50. doi: 10.1016/j.molcel.2019.04.025
27. Yang Y, Hsu PJ, Chen YS, Yang YG. Dynamic transcriptomic m(6)A decoration: writers, erasers, readers and functions in RNA metabolism. *Cell Res.* (2018) 28:616–24. doi: 10.1038/s41422-018-0040-8
28. Wilkerson MD, Hayes DN. ConsensusClusterPlus: a class discovery tool with confidence assessments and item tracking. *Bioinformatics.* (2010) 26:1572–3. doi: 10.1093/bioinformatics/btq170
29. Newman AM, Liu CL, Green MR, Gentles AJ, Feng W, Xu Y, et al. Robust enumeration of cell subsets from tissue expression profiles. *Nat Method.* (2015) 12:453–7. doi: 10.1038/nmeth.3337
30. Mayakonda A, Lin DC, Assenov Y, Plass C, Koeffler HP. Maftools: efficient and comprehensive analysis of somatic variants in cancer. *Genome Res.* (2018) 28:1747–56. doi: 10.1101/gr.239244.118
31. Yang Y, Zhang Q, Miao YR, Yang J, Yang W, Yu F, et al. SNP2APA: a database for evaluating effects of genetic variants on alternative polyadenylation in human cancers. *Nucleic Acids Res.* (2020) 48:D226–32. doi: 10.1093/nar/gkz793
32. Jeggari A, Marks DS, Larsson E. miRcode: a map of putative microRNA target sites in the long non-coding transcriptome. *Bioinformatics.* (2012) 28:2062–3. doi: 10.1 093/bioinformatics/bts344
33. Li JH, Liu S, Zhou H, Qu LH, Yang JH. starBase v2.0: decoding miRNA-ceRNA, miRNA-ncRNA and protein-RNA interaction networks from large-scale CLIP-Seq data. *Nucleic acids Res.* (2014) 42:D92–7. doi: 10.1093/nar/gkt1248
34. Shannon P, Markiel A, Ozier O, Baliga NS, Wang JT, Ramage D, et al. Cytoscape: a software environment for integrated models of biomolecular interaction networks. *Genome Res.* (2003) 13:2498–504. doi: 10.1101/gr.1239303
35. Kim HD, Song GW, Park S, Jung MK, Kim MH, Kang HJ, et al. Association between expression level of PD1 by tumor-infiltrating CD8(+) T cells and features of hepatocellular carcinoma. *Gastroenterology.* (2018) 155:1936–50.e17. doi: 10.1 053/j.gastro.2018.08.030
36. Wang X, Yang L, Huang F, Zhang Q, Liu S, Ma L, et al. Inflammatory cytokines IL-17 and TNF-alpha up-regulate PD-L1 expression in human prostate and colon cancer cells. *Immunol Lett.* (2017) 184:7–14. doi: 10.1016/j.imlet.2017.02.006
37. Cristescu R, Mogg R, Ayers M, Albright A, Murphy E, Yearley J, et al. Pan-tumor genomic biomarkers for PD-1 checkpoint blockade-based immunotherapy. *Science.* (2018) 362:eaar3593. doi: 10.1126/science.aar3593
38. Chalmers ZR, Connelly CF, Fabrizio D, Gay L, Ali SM, Ennis R, et al. Analysis of 100,000 human cancer genomes reveals the landscape of tumor mutational burden. *Genome Med.* (2017) 9:34. doi: 10.1186/s13073-017-0 424-2
39. Mandal R, Samstein RM, Lee KW, Havel JJ, Wang H, Krishna C, et al. Genetic diversity of tumors with mismatch repair deficiency influences anti-PD-1 immunotherapy response. *Science.* (2019) 364:485–91. doi: 10.1126/science.aau 0447
40. Assié G, Letouzé E, Fassnacht M, Jouinot A, Luscap W, Barreau O, et al. Integrated genomic characterization of adrenocortical carcinoma. *Nat Genet.* (2014) 46:607–12. doi: 10.1038/ng.2953
41. Wasserman JD, Novokmet A, Eichler-Jonsson C, Ribeiro RC, Rodriguez-Galindo C, Zambetti GP, et al. Prevalence and functional consequence of TP53 mutations in pediatric adrenocortical carcinoma: a children's oncology group study. *J Clin Oncol.* (2015) 33:602–9. doi: 10.1200/JCO.2013. 52.6863
42. Landwehr LS, Altieri B, Schreiner J, Sbiera I, Weigand I, Kroiss M, et al. Interplay between glucocorticoids and tumor-infiltrating lymphocytes on the prognosis of adrenocortical carcinoma. *J Immunother Cancer.* (2020) 8:e000469. doi: 10.1136/jitc -2019-000469

43. Alarcón CR, Goodarzi H, Lee H, Liu X, Tavazoie S, Tavazoie SF. HNRNPA2B1 is a mediator of m(6)a-dependent nuclear RNA processing events. *Cell.* (2015) 162:1299–308. doi: 10.1016/j.cell.2015.08.011
44. Spitale RC, Flynn RA, Zhang QC, Crisalli P, Lee B, Jung JW, et al. Structural imprints *in vivo* decode RNA regulatory mechanisms. *Nature.* (2015) 519:486–90. doi: 10.1038/nature14263
45. Allgäuer M, Budczies J, Christopoulos P, Endris V, Lier A, Rempel E, et al. Implementing tumor mutational burden (TMB) analysis in routine diagnostics-a primer for molecular pathologists and clinicians. *Transl Lung Cancer Res.* (2018) 7:703–15. doi: 10.21037/tlcr.2018.08.14
46. Li T, Gu M, Deng A, Qian C. Increased expression of YTHDF1 and HNRNPA2B1 as potent biomarkers for melanoma: a systematic analysis. *Cancer Cell Int.* (2020) 20:239. doi: 10.1186/s12935-020-01309-5
47. Loewen G, Jayawickramarajah J, Zhuo Y, Shan B. Functions of lncRNA HOTAIR in lung cancer. *J Hematol Oncol.* (2014) 7:90. doi: 10.1186/s13045-014-0090-4
48. Rinn JL, Kertesz M, Wang JK, Squazzo SL, Xu X, Brugmann SA, et al. Functional demarcation of active and silent chromatin domains in human HOX loci by noncoding RNAs. *Cell.* (2007) 29:1311–23. doi: 10.1016/j.cell.2007.05.022
49. Xia Y, Shen S, Verma IM. NF-kappaB, an active player in human cancers. *Cancer Immunol Res.* (2014) 2:823–30. doi: 10.1158/2326-6066.CIR-14-0112
50. Botti G, Scognamiglio G, Aquino G, Liguori G, Cantile M. LncRNA HOTAIR in tumor microenvironment: what role? *Int J Mol Sci.* (2019) 20:2279. doi: 10.3390/ijms20092279
51. Li F, Mao G, Tong D, Huang J, Gu L, Yang W, et al. The histone mark H3K36me3 regulates human DNA mismatch repair through its interaction with MutSalpha. *Cell.* (2013) 153:590–600. doi: 10.1016/j.cell.2013.03.025
52. Yan ZC, He L, Qiu JH, Deng WT, Lu JR, Yuan Z, et al. LncRNA HOTAIR participates in the development and progression of adrenocortical carcinoma via regulating cell cycle. *Eur Rev Med Pharmacol Sci.* (2018) 22:6640–49. doi: 10.26355/eurrev_201810_16139
53. Wang T, Hao D, Yang S, Ma J, Yang W, Zhu Y, et al. miR-211 facilitates platinum chemosensitivity by blocking the DNA damage response (DDR) in ovarian cancer. *Cell Death Dis.* (2019) 10:495. doi: 10.1038/s41419-019-1715-x
54. Díaz-Martínez M, Benito-Jardón L, Alonso L, Koetz-Ploch L, Hernando E, Teixidó J. miR-204-5p and miR-211-5p contribute to BRAF inhibitor resistance in melanoma. *Cancer Res.* (2018) 78:1017–30. doi: 10.1158/0008-5472.CAN-17-1318

Conflict of Interest: The authors declare that the research was conducted in the absence of any commercial or financial relationships that could be construed as a potential conflict of interest.

Copyright © 2021 Jin, Wang, He, Zhu, Hu, Gong, Xiao, Chen, Cheng and Cao. This is an open-access article distributed under the terms of the Creative Commons Attribution License (CC BY). The use, distribution or reproduction in other forums is permitted, provided the original author(s) and the copyright owner(s) are credited and that the original publication in this journal is cited, in accordance with accepted academic practice. No use, distribution or reproduction is permitted which does not comply with these terms.

frontiers in Immunology

REVIEW
published: 04 March 2021
doi: 10.3389/fimmu.2021.653358

Roles of the Dynamic Tumor Immune Microenvironment in the Individualized Treatment of Advanced Clear Cell Renal Cell Carcinoma

Enyu Lin[1,2], *Xuechao Liu*[3], *Yanjun Liu*[4], *Zedan Zhang*[1,2], *Lu Xie*[1], *Kaiwen Tian*[1], *Jiumin Liu*[1] *and Yuming Yu*[1]*

[1] Department of Urology, Guangdong Provincial People's Hospital, Guangdong Academy of Medical Sciences, Guangzhou, China, [2] Shantou University Medical College, Shantou, China, [3] Department of Gastrointestinal Surgery, Affiliated Hospital of Qingdao University, Qingdao, China, [4] Department of Immunology, School of Basic Medical Science, Southern Medical University, Guangzhou, China

Immune checkpoint inhibitors (ICIs) are currently a first-line treatment option for clear cell renal cell carcinoma (ccRCC). However, recent clinical studies have shown that a large number of patients do not respond to ICIs. Moreover, only a few patients achieve a stable and durable response even with combination therapy based on ICIs. Available studies have concluded that the response to immunotherapy and targeted therapy in patients with ccRCC is affected by the tumor immune microenvironment (TIME), which can be manipulated by targeted therapy and tumor genomic characteristics. Therefore, an in-depth understanding of the dynamic nature of the TIME is important for improving the efficacy of immunotherapy or combination therapy in patients with advanced ccRCC. Here, we explore the possible mechanisms by which the TIME affects the efficacy of immunotherapy and targeted therapy, as well as the factors that drive dynamic changes in the TIME in ccRCC, including the immunomodulatory effect of targeted therapy and genomic changes. We also describe the progress on novel therapeutic modalities for advanced ccRCC based on the TIME. Overall, this review provides valuable information on the optimization of combination therapy and development of individualized therapy for advanced ccRCC.

Keywords: clear cell renal cell carcinoma, tumor immune microenvironment, immunotherapy, targeted therapy, genomic characteristics

OPEN ACCESS

Edited by:
Peng Qu,
National Institutes of Health (NIH), United States

Reviewed by:
Mingxiao Feng,
Johns Hopkins University, United States
Nirmish Singla,
Johns Hopkins University, United States

***Correspondence:**
Yuming Yu
yuym72@163.com

Specialty section:
This article was submitted to Cancer Immunity and Immunotherapy, a section of the journal Frontiers in Immunology

Received: *14 January 2021*
Accepted: *12 February 2021*
Published: *04 March 2021*

Citation:
Lin E, Liu X, Liu Y, Zhang Z, Xie L, Tian K, Liu J and Yu Y (2021) Roles of the Dynamic Tumor Immune Microenvironment in the Individualized Treatment of Advanced Clear Cell Renal Cell Carcinoma. Front. Immunol. 12:653358. doi: 10.3389/fimmu.2021.653358

INTRODUCTION

As one of the most common malignancies of the genitourinary system, renal cell carcinoma (RCC) affects ~400,000 people worldwide each year, resulting in ~175,000 deaths (1). The most common histological type of RCC is clear cell RCC (ccRCC), accounting for about 80% of all cases (2, 3). Unlike other urinary tumors, ccRCC is insensitive to chemotherapy. In 2005, sorafenib, the first anti-angiogenic drug, was approved by the US Food & Drug Administration (FDA) to treat patients with advanced RCC. Although anti-angiogenic agents have been continuously optimized over the last decade to improve response rates and safety, many patients will still develop primary or acquired resistance. Therefore, the use of immunotherapy has been explored for metastatic renal cell carcinoma (mRCC) patients who have developed resistance to anti-angiogenic drugs, including immune checkpoint inhibitors (ICIs).

ICIs can achieve excellent therapeutic outcomes in several cancer types, including ccRCC (4–6). However, only a small proportion of patients responded to ICI monotherapy, and the improvement in overall survival (OS) as a result of ICIs is largely attributed to the long-term survival in a minority of patients (7). Additionally, several studies have shown that vascular endothelial growth factor (VEGF) inhibitors promoted T cell infiltration and reversed the inhibitory effect on antigen-presenting cells (APCs) (8–10). These findings provided the theoretical foundations for combination therapy involving anti-angiogenic drugs and ICIs. However, not all patients benefit from the current combination regimens. Therefore, as more therapeutic options for mRCC become available, individualized treatment (i.e., using different combinations and sequences of treatments for different patients) will be critical for optimizing clinical outcomes.

Of note, the therapeutic effects of anti-angiogenic drugs and ICIs are influenced by the tumor immune microenvironment (TIME). Several studies suggest that high levels of tumor-associated macrophages (TAMs), interleukin-8 (IL-8), and IL-6 in the TIME are related to the poor therapeutic effect of anti-angiogenic drugs (11–18). Moreover, high levels of myeloid-derived suppressor cells (MDSCs) and overexpression of immune checkpoints (e.g., LAG-3 and Tim-3) can lead to resistance to ICIs (14–18). Furthermore, a dynamic change in the TIME was observed during treatment with VEGF/VEGFR inhibitors and mammalian target of rapamycin (mTOR) inhibitors (19, 20). Indeed, relatively unique genomic alterations in ccRCC (e.g., VHL mutations and PBRM1 mutations) may also impact the TIME (21, 22). Therefore, ccRCC with different genomic signatures may respond differently to various treatments. The abovementioned results may partially explain the inconsistent efficacy of ICIs or combination therapy for ccRCC.

Herein, we briefly describe the characteristics of the TIME in ccRCC and present detailed analysis of the mechanism by which the TIME influences immunotherapy response. In particular, we discuss the bidirectional relationship between targeted therapy and TIME, and the tumor genomic signature that manipulates the TIME. Finally, we present the progress in the treatment of advanced ccRCC based on the TIME. Overall, this review provides some insights into the optimization of combination therapy and development of individual treatment options for patients with advanced ccRCC.

The Relatively Unique TIME in ccRCC

In contrast to other tumor types, the TIME in ccRCC is characterized by a high level of immune cell infiltration and a high degree of angiogenesis. Several pan-cancer analyses have shown that ccRCC have prominent inflammatory profiles, which is one of the tumor types with the highest degree of T-cell infiltration (23–25). Chevrier and colleagues showed the major immune cell subsets in ccRCC were T cells (22 different phenotypes) and TAMs (with 17 phenotypes), accounting for ∼51 and 31% of immune cells, respectively (26).

High numbers of $CD8^+$ tumor-infiltrating T lymphocytes (TILs) typically correlate with a favorable prognosis in most tumors (including prostatic adenocarcinoma, bladder cancer and breast cancer, etc.), except ccRCC (27). Indeed, $CD8^+$ TILs in ccRCC are characterized by exhaustion and functional deficiency rather than defective recruitment, and express high levels of immune checkpoint molecules and low levels of Ki-67, which fail to efficiently activate anti-tumor immune responses (26, 28–31). TAMs, MDSCs, and regulatory T cells (Tregs) are the main immunosuppressive cells in the TIME. In ccRCC, the TAMs are mostly similar to $CD163^+$ and $CD206^+$ M2 macrophages, which have immunosuppressive actions (32). Meanwhile, MDSCs are generated in the bone marrow under pathological conditions such as tumorigenesis (33), and migrate to tumor tissues or peripheral lymphoid organs mainly under the influence of various chemokines secreted by the tumor cells (34). MDSCs are primarily divided into mononuclear MDSCs (M-MDSCs) and polymorphonuclear MDSCs (PMN-MDSCs), with PMN-MDSCs the predominant type in ccRCC (34). Many studies have shown that M2-like TAMs, MDSCs, and Tregs are associated with poor prognosis in ccRCC (35–37).

Tertiary lymphoid structures (TLS) in the TIME are sites of adaptive immune activation, where dendritic cells (DCs) present local cancer antigens to T cells and induce B cell-mediated humoral immunity and differentiation of effector T (Teff) cells (38, 39). Increasingly, researchers have found that a high density of TLS is related to good prognosis in several cancers, including ccRCC (40–42). However, the density of TLS in ccRCC is lower than in other tumors including non-small cell lung cancer (NSCLC), melanoma, and prostate cancer, in both primary and metastatic cases, suggesting that ccRCC cells may impede the formation of TLS (40, 42, 43).

The reduced TLS formation in ccRCC may be due to the influence of the tumor on DCs. DCs have a great degree of functional plasticity, and different microenvironmental signals can determine the functional phenotypes of DCs by affecting their differentiation, maturation, activation, and polarization (44). DCs can be roughly divided into two categories in ccRCC: TLS-DCs, which are characterized as $HLA\text{-}DR^{hi}$ $CD83^+$ $DC\text{-}LAMP^+$, and non-TLS-DCs (NTLS-DCs) in the tumor core, characterized as $CD209^+$ $CD83^-$ (45). Further studies have shown that these two DC subsets have opposite effects on the clinical outcomes of patients with ccRCC, namely, a high density of TLS-DCs and NTLS-DCs correspond to favorable and poor clinical outcomes, respectively (40, 45). Similarly, Figel et al. found that DCs were dominated by $CD209^+$ NTLS-DCs in RCC, while $CD83^+$ $DC\text{-}LAMP^+$ TLS-DCs were rare, which indirectly confirms the low density of TLS in ccRCC (46).

In summary, the majority of ccRCC are inflammatory neoplasia showing a high degree of infiltration of exhausted $CD8^+$ TILs, which is a prerequisite for the response to ICIs (47). However, immunosuppression from M2-like TAMs, Tregs, MDSCs, and NTLS-DCs in the TIME may also lead to an insensitivity of ccRCC toward immunotherapy, which makes the tumor microenvironment in a proportion of ccRCC patients have immunosuppressive properties. Additionally, the permeability of abnormal neovascularization in ccRCC limits the Teff cell infiltration, which promotes the formation of an immune-silenced microenvironment (8, 48, 49). Indeed, a multi-omics analysis by Clark et al. found that the TIME of ccRCC can be classified into different subtypes, namely the

immunoinflammatory subtype with infiltration of $CD8^+$ T cells that have high expression of immune checkpoint molecules, the immunosuppressive subtype with predominant infiltration of suppressor cells such as TAMs, and the immune-silenced subtype with active angiogenesis and the lack of immune cell infiltration (50). Different TIME subtypes of ccRCC have different prognoses and may also have different degrees of sensitivity to systemic therapy (50). Several studies have found that ccRCC which responded better to anti-VEGF treatment showed lower levels of immune checkpoint molecules, similar to the immune-silenced subtype of ccRCC described above (51, 52). Thus, the high level of immune infiltration and angiogenic features together build a relatively unique and dynamic TIME in ccRCC, making it an ideal target for precision-targeted immunotherapy or combination therapy.

Potential Mechanisms Affecting the Efficacy of Immunotherapy in the TIME in ccRCC

Immunotherapy that have been approved and recommended for advanced ccRCC currently includes cytokines and ICIs. In the 1990s, cytokines such as interferon-α (IFN-α) and interleukin-2 (IL-2) that non-specifically activate the anti-tumor immune response began to be used to treat metastatic ccRCC (53). However, high doses of IL-2 can result in capillary leak syndrome and cause multiple organ damage (53). As immune checkpoints are important components in maintaining the immunosuppressive tumor microenvironment, they are an ideal target for immunotherapy. Nowadays, the PD-1/PD-L1 and CTLA-4/CD28 pathways have been extensively studied, and multiple ICIs targeting these pathways have been approved for systemic therapy of advanced ccRCC. Nevertheless, there are still a large proportion of patients have tumor progression after receiving ICIs (5, 54). As opposed to targeted therapies that directly affect tumor cell survival, the anti-tumor effects of immunotherapy are based on the TIME. Reversing the immunosuppressive nature of the TIME and stimulating tumor-infiltrating NK cells and cytotoxic T lymphocytes (CTLs) are key steps in immunotherapy. Thus, the TIME may be a critical factor affecting immunotherapeutic response, particularly the resistance to immunotherapy. This section discusses the mechanism of resistance to cytokines and ICIs in ccRCC from the perspective of the TIME.

Cytokines

IL-2 exerts its anti-tumor effect mainly by driving the proliferation and activation of NK cells and $CD8^+$ TILs (**Figure 1A**) (55). However, low-dose IL-2 can induce the preferential amplification of $CD4^+$ $Foxp3^+$ Tregs, which mainly manifested as a reduction in autoimmune response (**Figure 1B**) (56, 57). Although high-dose IL-2 has certain ability to activate the anti-tumor immune response, the consequent severe adverse effect and high levels of Tregs significantly limit its clinical benefit. Additional studies have demonstrated that low levels of $CD57^+$ NK cells were found to be an independent immune risk factor affecting the prognosis of mRCC patients treated with IL-2, indicating that activated NK cells may be critical for IL-2 to exert its anti-tumor activity (58). Immunosuppressive factors in the tumor microenvironment, including IL-6, TGF-β, PGE2, and indoleamine 2,3-dioxygenase (IDO), can block NK cell activation (59, 60). Moreover, under hypoxic conditions, metabolites in the tumor microenvironment, such as lactate and adenosine, can attenuate the cytotoxic effects of NK cells (**Figure 1B**) (61, 62). Studies on immunometabolism also revealed that the excessive consumption of glucose and amino acids caused by tumor cell proliferation impairs NK cell proliferation and IFN-γ secretion (60, 63, 64). Prinz et al. verified that tumor-infiltrating NK cells show phenotypic alterations and dysfunction in RCC (primarily poor degranulation activity) compared with those in normal and para-cancerous tissues (65). Based on the above findings, we speculate that the dual immunomodulatory effects of IL-2 and dysfunctional NK cells influenced by the immunosuppressive tumor microenvironment contribute to the insensitivity of ccRCC to IL-2 treatment. Therefore, improving the therapeutic targeting of IL-2 and the activity of NK cells may be effective ways to optimize cytokine therapies.

Immune Checkpoint Inhibitors

Reversing the exhaustion of $CD8^+$ TILs is a key step in the anti-tumor effects of ICIs (**Figure 1C**) (66). O'Donnell et al. found that exhausted $CD8^+$ TILs that only mildly express PD-1 could be reactivated by PD-1/PD-L1 blockade, while over-exhausted $CD8^+$ TILs were unresponsive to PD-1/PD-L1 inhibitors (67). The reasons for this phenomenon can be summarized as follows: first, severely exhausted $CD8^+$ TILs overexpress PD-1, and thus PD-1/PD-L1 inhibitors cannot completely block the PD-1/PD-L1 signaling pathway to reactivate the T cells. Second, severely exhausted $CD8^+$ TILs overexpress other immune checkpoints such as CTLA-4, LAG-3, and Tim-3 (**Figure 1D**) (67). LAG-3 on $CD4^+$ T cells can bind to major histocompatibility complex class II (MHC-II) molecules with a higher affinity than CD4, and directly block T cell receptor signaling, resulting in T cell dysfunction (16). Additionally, LAG-3 on $CD8^+$ TILs inhibits the secretion of IFN-γ by binding to two other ligands, galectin-3 and liver sinusoidal endothelial cell lectin (68). Moreover, the binding of Tim-3, a type I transmembrane protein, with a galectin-9 molecule from MDSCs induces dysregulation and apoptosis of $CD8^+$ TILs (18). Therefore, in the presence of other upregulated immune checkpoints, only blocking the PD-1/PD-L1 pathway would not reverse T-cell exhaustion.

The current evidence also indicates that severely exhausted Teff cells cannot fully restore effector function even under the influence of ICIs, but can promote resistance to ICIs. An animal model study confirmed that ICIs could rejuvenate T cells that express relatively low levels of PD-1, while relatively high levels of PD-1 were associated with severe T-cell exhaustion and a poor response to ICIs (69). In the phase III JAVELIN renal 101 trial, increased numbers of $CD8^+$ TILs in mRCC were associated with improved PFS in the avelumab plus axitinib arm and worse PFS in sunitinib arm (70). Likewise, the phase II IMmotion150 and phase III IMmotion151 trials showed that atezolizumab plus bevacizumab improved PFS compared with sunitinib in mRCC

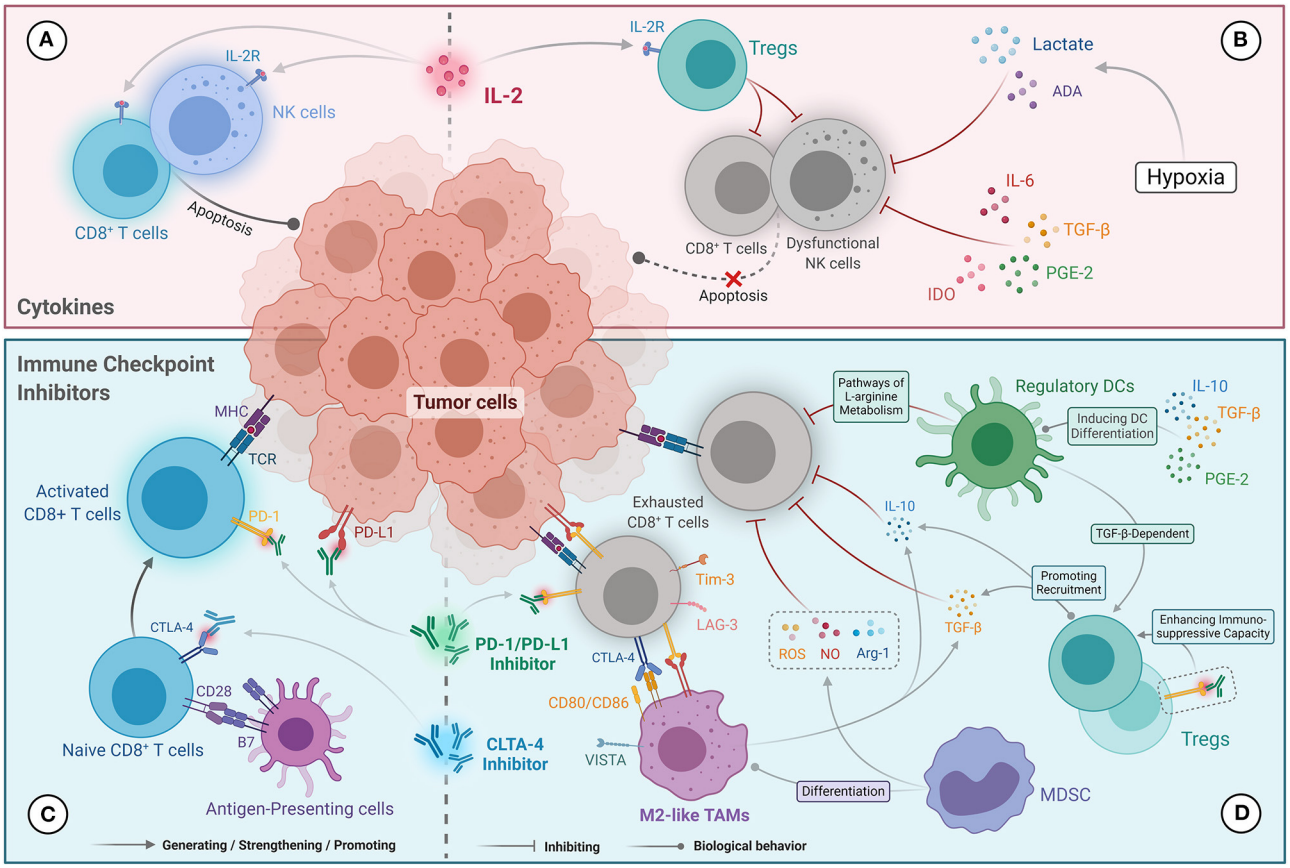

FIGURE 1 | Potential mechanisms influencing immunotherapy response in the TIME in ccRCC. **(A)** The anti-tumor activity of cytokine (IL-2) therapies was primarily mediated by driving the proliferation and activation of NK cells and $CD8^+$ TILs. **(B)** Resistance to cytokine (IL-2) therapies was correlated with the amplification of Tregs level mediated by IL-2 and NK cell dysfunction. IL-6, TGF-β, PGE2, and IDO, as well as lactate and adenosine generated under hypoxic conditions, inhibit the cytotoxic effects of NK cells. **(C)** The anti-tumor mechanisms of immune checkpoint inhibitors that contribute to the reactivation of $CD8^+$ T cells were mediated by blocking the PD-1/PD-L1 and CTLA-4/CD28 pathways. **(D)** Resistance to immune checkpoint inhibitors is mainly mediated by $CD8^+$ TILs anergy, which abundantly express immunosuppressive molecules (e.g., PD-1, CTLA-4, Tim-3, and LAG-3). Tregs and M2-like TAMs secrete IL-10 and TGF-β, which inhibit the cytotoxicity of $CD8^+$ TILs and recruit Tregs. Tregs present a stronger immunosuppressive capacity under the action of PD-1 inhibitors. Ligands expressed on M2-like TAMs (including PD-L1/L2, CD80/86, and VISTA) can also promote exhaustion of $CD8^+$ TILs. NO, ROS, and Arg-1 produced by MDSCs inhibit the anti-tumor immune function of $CD8^+$ TILs, and promote differentiation into M2-like TAMs. Regulatory DCs can also inhibit $CD8^+$ T-cell function via the L-arginine metabolic pathway and promote Tregs proliferation.

with a high level of Teff cells (14, 71). The findings of these three clinical trials confirm the view that Teff cells play an important role in the therapeutic response to ICIs in mRCC.

In contrast, other studies found no significant correlation between PD-1 levels in mRCC and the benefit of ICIs alone or as a combination therapy, which was not observed in NSCLC and melanoma (14, 54, 70–76). We speculate that severely exhausted $CD8^+$ TILs that overexpress PD-1 exist in mRCC, which is in line with the observation that a high infiltration of $CD8^+$ TILs is related to poor prognosis in ccRCC. This severe exhaustion of $CD8^+$ TILs is likely responsible for resistance to ICIs in mRCC, and also explains why PD-1 status cannot be used alone as a predictor of response to ICI therapy.

Tregs can block the function of T cells and APCs by producing IL-10 and TGF-β to mediate immunosuppression (**Figure 1D**) (77, 78). Surprisingly, Tregs are activated and proliferate in the presence of PD-1 inhibitors, which confers a poor prognosis (79). In addition, an animal model study found that exhaustion of Tregs could improve the therapeutic response of ICIs (80). Thus, the immunosuppressive properties of Tregs may also contribute to drug resistance or progression in patients treated with PD-1/PD-L1 inhibitors.

IL-10 and TGF-β secreted by M2-like TAMs can also recruit Tregs and directly inhibit the function of $CD8^+$ TILs (**Figure 1D**) (81). M2-like TAMs can also induce T-cell exhaustion by expressing PD-1 ligands (PD-L1 and PD-L2), CTLA-4 ligands (CD80 and CD86), and VISTA (a potent negative regulator of T cell function) (**Figure 1D**) (81). A recent retrospective study confirmed that high infiltration of M2-like TAMs was associated with poor OS in mRCC patients treated with ICIs (82). Moreover, several animal model studies have found that targeting M2-like TAMs can improve the response to ICIs

in various tumors, including pancreatic cancer, colon cancer, breast cancer, and glioblastoma (83). Collectively, M2-like TAMs counteract the anti-tumor effects of ICIs by expressing and secreting immunosuppressive molecules, and participating in immune escape.

MDSCs in ccRCC can significantly inhibit the T cell-specific immune response by producing large amounts of nitric oxide (NO), reactive oxygen species (ROS), and arginase-1 (Arg-1) (**Figure 1D**) (84). Additionally, MDSCs can also differentiate into M2-like TAMs to mediate immunosuppression (**Figure 1D**) (85). A significant correlation has been found between high levels of MDSCs and poor treatment response to ICIs in melanoma and prostate cancer (86). Furthermore, the IMmotion150 trial showed that in mRCC patients with a high level of myeloid cells, the combination of atezolizumab and bevacizumab or bevacizumab monotherapy was superior to atezolizumab monotherapy (14). These findings indicate that myeloid cells could lead to the development of resistance to ICIs in mRCC.

Finally, DCs with complex immune function phenotypes may also influence the efficacy of ICIs. HLA-DR^{hi} CD83^{+} DC-LAMP^{+} TLS-DC subpopulations, which belong to the immune-activated phenotype, activate CD4^{+} T cells and CD8^{+} TILs by processing and presenting antigens, as well as inducing their clonal proliferation and immune response (38). However, as mentioned above, TLS-DCs were less abundant in ccRCC. In contrast, the CD209^{+} CD83^{-} NTLS-DC subpopulation has an immunosuppressive phenotype and develops under the stimulation of various tumor-derived factors, including IL-10, TGF-β, prostaglandin E2 (PGE2), and chemokines (44). NTLS-DCs, the major DC subpopulation in ccRCC, secrete high levels of MMP-9 and tumor necrosis factor-α, which promote tumor cell growth and invasion (46, 87). NTLS-DCs can selectively promote the proliferation of Tregs in a TGF-β-dependent way, but also inhibit the function of effector CD8^{+} TILs through the L-arginine metabolic pathway (**Figure 1D**) (88–90). Therefore, we speculate the large ratio of NTLS-DCs to TLS-DCs in ccRCC enhances the robustness of the immunosuppressive microenvironment, which interferes with the activity of ICIs. Finally, it should be noted that the density of a single DC subpopulation may not fully represent the immune status of the tumor microenvironment, as different DC subpopulations may have different immunophenotypes and function in ccRCC.

The Bidirectional Relationship Between Targeted Therapies and TIME in ccRCC

The effectiveness of targeted therapies is largely dependent on mutations of the drug target and the corresponding signaling pathway. However, the TIME can also influence angiogenesis in ccRCC and eventually lead to resistance to anti-angiogenic agents. In contrast to the cell-autonomous resistance of tumors caused by genomic or epigenetic changes, the non-cell-autonomous resistance caused by the TIME may be more dynamic and complex. Furthermore, besides immunotherapy, targeted therapies (including VEGF/VEGFR inhibitors and mTOR inhibitors) may have immunomodulatory effects on ccRCC and may remodel the TIME. Therefore, understanding the mutual influences between targeted therapies and the TIME is instructive for optimizing the first-line combination therapy or second-line regimens for patients with advanced ccRCC.

Resistance to VEGF/VEGFR Inhibitors in TIME

Growing evidence suggests that MDSCs enhance resistance to anti-angiogenesis via a range of non-immune related pathways in multiple tumors, including ccRCC (91). Specifically, MDSCs activate alternative pro-angiogenic pathways by producing multiple pro-angiogenic factors, including VEGF and fibroblast growth factor 2 (FGF2) (**Figure 2A**) (91, 92). VEGF and FGF2 stimulate the migration and proliferation of tumor-associated endothelial cells, leading to tumor angiogenesis and stability in RCC (93, 94). In addition, granulocyte-macrophage colony-stimulating factor (GM-CSF) secreted by tumor cells mediates the proliferation of MDSCs through the pSTAT5 pathway, and induces them to secrete pro-angiogenic proteins including IL-8 and matrix metalloproteinase-9 (MMP-9), resulting in reduced sensitivity to VEGF/VEGFR inhibitors in RCC (**Figure 2A**) (95). Besides dynamically remodeling the extracellular matrix, MMP-9 can enhance the pro-angiogenic effect of VEGF (96). Therefore, the presence of MDSCs in the TIME causes RCC to become unresponsive to anti-angiogenic drugs.

M2-like TAMs have also been shown to promote tumor vascularization by producing multiple angiogenic factors. In a hypoxic tumor microenvironment, M2-like TAMs can produce high levels of VEGF-A and hypoxia-inducible factor (HIF)-1α. VEGF-A activates tumor angiogenesis by binding to VEGFR, and HIF-1α enhances this process by upregulating VEGF expression (**Figure 2A**) (97). In breast and colon cancers, high levels of TAM infiltration were associated with increased expression of proteins related to the Wnt pathway (i.e., Wnt5a and Wnt7b), which is involved in the regulation of angiogenesis (98–100). M2-like TAMs can also secrete MMP-9 to mobilize VEGF (**Figure 2A**) (101). Indeed, the phase 3 COMPARZ study showed that high infiltration of TAMs was associated with poor prognosis in mRCC patients treated with VEGFR-TKIs, suggesting that TAMs may contribute to the resistance of RCC to anti-angiogenic agents (102).

Cytokines in the tumor microenvironment, which are mainly secreted by MDSCs and tumor cells, are also thought to assist tumor angiogenesis. For example, the pro-inflammatory cytokines IL-1α and IL-1β can induce VEGF and VEGFR2 expression via the Notch pathway, and upregulate MMP-9, IL-6, and IL-8 levels, to form a pro-angiogenic factor network (**Figure 2A**) (103). Significantly increased levels of IL-1α and IL-1β were observed by Carbone et al. in pancreatic cancers that were resistant to VEGF inhibitors (104). Alternatively, IL-6 can promote the expression of downstream genes, including VEGF and MMP-9, by activating the JAK/STAT3 cascade (**Figure 2A**) (105, 106). IL-8 interacts with its receptor (CXCR2) to activate NF-κB and promote VEGF expression and VEGFR2 autocrine activation (**Figure 2A**) (11). Ishibashi et al. confirmed that RCC

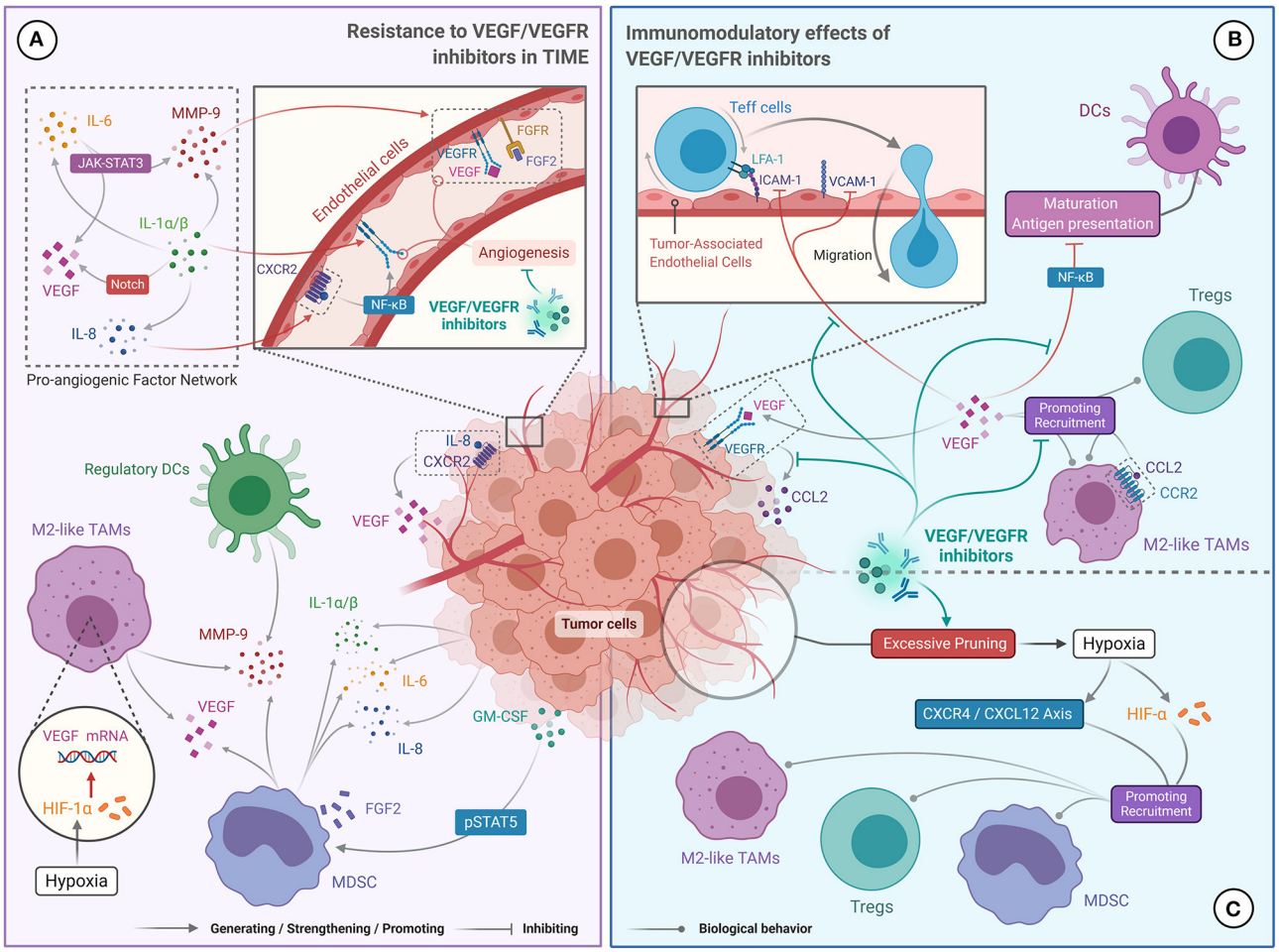

FIGURE 2 | The Bidirectional Relationship between targeted therapies (VEGF/VEGFR inhibitors) and TIME in ccRCC. **(A)** Resistance to VEGF/VEGFR inhibitors is due to a complex network of pro-angiogenic factors (IL-1, IL-6, IL-8, MMP-9, VEGF, and FGF2), which promote excessive tumor angiogenesis. IL-1 promotes the production of IL-6, IL-8, and MMP-9, and enhances the expression of VEGF and VEGFR via the Notch pathway. IL-6 upregulates MMP-9 and VEGF levels via the JAK-STAT3 pathway. IL-8 promotes the secretion of VEGF and the self-activation of the VEGFR. MMP-9 enhances the angiogenic effect of VEDF. Tumor produced GM-CSF can also promote MMP-9 and IL-8 production. Finally, HIF-α promotes VEGF secretion. **(B)** The role of VEGF/VEGFR inhibitors in stimulating the immune response was achieved by blocking the immunosuppressive effect of VEGF. VEGF/VEGFR inhibitors can prevent VEGF-mediated recruitment of TAMs and Tregs, restore DC maturation and antigen presentation, and promote Teff cell migration to tumor microenvironment. **(C)** Immunosuppression mediated by VEGF/VEGFR inhibitors may have resulted from hypoxia. High doses of VEGF/VEGFR inhibitors can excessively prune tumor vessels, leading to hypoxia in the tumor microenvironment, which facilitates recruitment of Tregs, TAMs and MDSCs.

overexpressed IL-6 and showed drug resistance under VEGFR-TKI treatment, and significant tumor regression was observed after blocking the IL-6 receptor (12). Likewise, Huang et al. demonstrated that IL-8 is an important factor for the resistance of ccRCC to VEGFR-TKI (107). Therefore, the presence of IL-1, IL-6, and IL-8 in the TIME may promote the resistance of ccRCC to VEGF/VEGFR inhibitors by multiple non-redundant pathways.

Immunomodulatory Effects of VEGF/VEGFR Inhibitors

Numerous preclinical studies have found that VEGF serves a dual function in angiogenesis and immunosuppression. VEGF recruits $CD4^+$ $Foxp3^+$ Tregs to the tumor microenvironment by interacting with neuropilin 1 on their cell surface (108). Similarly, VEGF promotes the migration of $CD11b^+$ MDSCs and TAMs into the tumor microenvironment by binding to the VEGFR on the surface of these cells (**Figure 2B**) (109, 110). In a ccRCC xenograft model, the binding of VEGF to VEGFR-1 prompted tumor cells to secrete CCL2, which mediated the infiltration of TAMs (111). Besides, binding of VEGF to its receptor inhibits the maturation of DCs and antigen presentation, primarily by blocking the activation of NF-κB (**Figure 2B**) (110). VEGF also restricts the migration of Teff cells into the tumor microenvironment by downregulating the expression of adhesion molecules including ICAM-1 and VCAM-1 on tumor-associated endothelial cells (**Figure 2B**) (112).

Overall, the evidence suggests that VEGF recruits immunosuppressive cells to the tumor microenvironment,

thereby reducing the anti-tumor immune response. Therefore, VEGF/VEGFR inhibitors may reverse the immunosuppressive nature of the TIME. Indeed, in a clinical trial of bevacizumab combined with atezolizumab for the treatment of mRCC, Wallin et al. found that bevacizumab promoted tumor-specific T-cell infiltration and enhanced the tumor-specific immune response (9). Interestingly, sunitinib has also been shown to improve the anti-tumor response of Teff cells and reduce the recruitment of Tregs and MDSCs (113, 114). Zizzari et al. also found that pazopanib promotes DC activation in mRCC by inhibiting the p-Erk and Wnt-β-catenin pathways (19). Therefore, VEGF/VEGFR inhibitors can inhibit the recruitment of immunosuppressive cells to the tumor microenvironment, restore the function and phenotype of APCs, and promote infiltration of Teff cells, which supports the synergistic effect of immunotherapy and anti-angiogenic therapy. Several phase III clinical trials showed that PD-1/PD-L1 inhibitors combined with anti-angiogenic agents significantly improved survival and therapeutic response in untreated patients with advanced ccRCC compared with anti-angiogenic monotherapy (70, 71, 76). Currently, the latest National Comprehensive Cancer Network (NCCN) and European Society for Medical Oncology (ESMO) guidelines recommend pembrolizumab combined with axitinib as the first-line treatment for mRCC patients from all International Metastatic RCC Database Consortium (IMDC) risk categories (115, 116). Likewise, the combination of VEGF/VEGFR inhibitors with IFN-α had also yielded favorable results. A multicenter phase III trial (AVOREN) of mRCC showed that, when compared with single-agent IFN-α, IFN-α combined with bevacizumab significantly increased PFS (10.2 vs. 5.4 months; hazard ratio [HR] = 0.63, 95% confidence interval [95% CI] 0.52–0.75; $p = 0.0001$) and objective response rates (ORR) (31 vs. 13%; $p = 0.0001$), and did not lead to significantly increasing or new adverse reactions (117). Therefore, the combination of IFN-α and bevacizumab is currently recommended by the European Society for Medical Oncology (ESMO) guidelines as a first-line option for mRCC patients with favorable risk (category 3B) or intermediate risk (category 2C) (116).

Despite this, VEGF/VEGFR inhibitors may also have immunosuppressive effects in some cases. For example, increased infiltration of $CD4^+$ $Foxp3^+$ Tregs and upregulation of PD-L1 expression were observed in primary RCC patients treated with sunitinib (118). Several studies have also shown that high doses of anti-angiogenic agents could lead to hypoxia of the tumor microenvironment and upregulation of the CXCR4/CXCL12 axis and HIF-α levels due to excessive pruning of tumor vessels, which facilitates the recruitment of TAMs, MDSCs, and Tregs (**Figure 2C**) (119, 120).

Based on these observations, we propose the following conjecture: moderate doses of VEGF/VEGFR inhibitors are beneficial for enhancing anti-tumor immune responses, while excessive doses can cause hypoxia-induced immunosuppression, which could partially explain the development of acquired resistance and progression in some mRCC patients treated with anti-angiogenic agents alone. Therefore, the dual modulatory effects of anti-angiogenic drugs on the TIME should be considered when choosing the individualized treatment in patients with advanced ccRCC. It is also worth exploring how to determine the optimal dose of anti-angiogenic drugs and how to reduce their immunosuppressive effects.

Immunomodulatory Effects of mTOR Inhibitors

As a downstream effector of the PI3K/Akt pathway, mTOR regulates various modulators of cell growth (e.g., eIF4E, S6K1, and cyclin-D) and pro-angiogenic factors (e.g., HIF, bFGF, and VEGF) (121, 122). Several studies have shown that the levels of mTOR pathway-related proteins (including p70S6K, p-mTOR, PI3K, and pAkt) in RCC were significantly higher than those in normal kidney tissues, and positively correlated with tumor progression (122). mTOR inhibitors can effectively inhibit tumor proliferation and angiogenesis in RCC and are recommended as second-line therapies for patients with mRCC (115). In fact, mTOR inhibitors were first approved for the prevention of immune rejection in solid organ transplant recipients because of their immunosuppressive properties (123). Thus, it is hypothesized that mTOR inhibitors may also have immunomodulatory functions in the tumor microenvironment.

An increased percentage of Tregs and MDSCs, as well as a decreased frequency of $CD56^{bright}$ NK cells and DCs, were found in mRCC patients treated with the mTOR inhibitor everolimus (124). These results suggest that mTOR inhibitors can promote immunosuppression of the tumor microenvironment in RCC, which limits their anti-cancer efficacy. As cyclophosphamide (CTX) was previously shown to selectively suppress Tregs and restore effector function of Teff cells and NK cells (125), a phase I clinical study attempted to assess whether CTX can counteract the immunosuppression of everolimus (126). CTX combined with everolimus significantly reduced the percentage of Tregs and MDSCs and increased the frequency of $CD8^+$ T cells and DC subsets in mRCC patients (126). Currently, the efficacy and safety of this combination therapy are being evaluated in a phase II trial. Thus, using treatments that modulate immunosuppressive cells or enhance the immune response may improve the therapeutic effect of mTOR inhibitors in mRCC.

Genomic Changes in ccRCC That Influence the TIME

ccRCC has relatively unique genomic features compared to other RCC types, namely chromosomal 3p deletion (>90%), chromosomal 5q gain (>67%), and somatic mutations closely related to 3p deletion events, including mutations in *VHL*, *PBRM1*, *SETD2*, and *BAP1* (127). Other common genomic alterations in ccRCC include chromosome 14q deletions, *MTOR* mutations, and *PTEN* mutations (31). Analyses of tumor evolutionary trajectories have shown significant intra-tumor heterogeneity in ccRCC (128); that is, the majority of mutations in ccRCC are subclonal, indicating the existence of significant variations in most trunk mutations from different individuals.

In recent years, the correlation between tumor genomic features and the TIME has received increasing attention. A growing number of studies have found that the TIME of ccRCC presents inherent complexity and individual differences under

the manipulation of a heterogeneous genomic landscape, which can partly explain the different responses of advanced ccRCC to immunotherapy or combination therapy.

VHL Mutations

The *VHL* deletion mutation is located at the short arm of chromosome 3 (3p25.3) and is the most common mutation in ccRCC (found in approximately 80% of cases) (129). The protein encoded by *VHL* has E3 ubiquitin ligase activity and can degrade HIF-α that modulates glucose metabolism and angiogenesis in a hypoxic environment (130). *VHL* deficiency in ccRCC will lead to the accumulation of HIF-α (including HIF-1α and HIF-2α) (**Figure 3A**), which causes ccRCC to present a unique pathologic manifestation, namely glycogen and lipid accumulation and abundant angiogenesis (127). Besides, under conditions of HIF-1α excess, MDSCs secrete more inducible nitric oxide synthase (iNOS) and Arg-1, and have a greater tendency to differentiate into TAMs with an immunosuppressive phenotype (**Figure 3A**) (85). iNOS participate in immunosuppression by catalyzing NO formation (131). TAMs preferentially inhibit T-cell proliferation and IFN-γ expression under the action of HIF-1α/iNOS (132). HIF-1α, which stably exists in the tumor microenvironment, could also facilitate the recruitment of $Foxp3^+$ Tregs by a TGF-β-independent mechanism (**Figure 3A**) (133). In addition, using a ccRCC model, HIF-1α and HIF-2α were found to upregulate PD-L1 expression on MDSCs, TAMs, and DCs through directly binding to hypoxia response element (HRE) (**Figure 3A**) (134, 135). Therefore, overall, *VHL* deletion mutations in ccRCC lead to a large amount of HIF-α accumulation and indirectly promote the formation of immunosuppressive microenvironment via HIF-α-mediated immunosuppressive cell recruitment and upregulation of immunosuppressive molecules.

PBRM1, *BAP1*, and *SETD2* Mutations

In ccRCC, somatic mutations in *PBRM1* (38.0%), *STED2* (13.2%), and *BAP1* (11.0%) located on the short arm of chromosome 3 are strongly associated with 3p deletion events (31). The bromodomain-containing proteins encoded by the *PBRM1* gene participate in the construction of the PBRM1-Brg1/Brm-associated factors (PBAF) chromatin remodeling complex that is involved in DNA repair processes (136). Meanwhile, histone methyltransferase encoded by the *SETD2* gene is involved in the methylation of histone H3 lysine 36 (H3K36), which plays a role in homologous recombination repair and genome stabilization (137). Indeed, loss of *SETD2* has been shown to cause an increased frequency of deletion-associated mutations (137). The *BAP1* gene encodes the BRCA1 associated protein-1, which influences the cell cycle by regulating the activity of key proteins involved in various cellular processes (138). All three genes are involved in the biological pathways related to tumorigenesis and have frequent mutations, supporting their role as tumor suppressors in ccRCC (139).

The loss of PBAF function caused by *PBRM1* deletion mutations has an impact on the TIME (22). On the one hand, PBAF inactivation enhances the chromatin accessibility of transcription factors on the promoters or enhancers of IFN-γ-inducible genes, leading to increased sensitivity of tumor cells to IFN-γ (**Figure 3B**). On the other hand, PBAF inactivation promotes the secretion of chemokines CXCL9 and CXCL10 by tumor cells, which contributes to the increased recruitment of Teff cells to the tumor microenvironment (**Figure 3B**) (22). Furthermore, follow-up results from the CheckMate 025 trial showed that *PBRM1* mutations were strongly associated with improved PFS and OS in advanced ccRCC patients treated with nivolumab, which was not observed in the everolimus group (140, 141). Similar results were reported by Sarah et al. (142). We thus speculate that the *PBRM1* mutation makes tumor cells more sensitive to T-cell-mediated cytotoxicity, and may help improve the therapeutic response to PD-L1/PD-1 blockade therapies. However, no correlation between PBRM1 mutations and OS was observed in a study including 143 patients with metastatic ccRCC treated with ICIs (143). These seemingly conflicting results suggest that the immunostimulatory effects of PBRM1 mutations may be confounded by their direct effects on the biological behavior of ccRCC. Besides, several studies have shown that PBRM1 loss was associated with enhancement of angiogenesis (144, 145), which may affect the response to ICIs of ccRCC by preventing immune cell infiltration. However, it is noteworthy that the above evidence indicated no adverse effects of PBRM1 mutations in patients with advanced RCC treated with ICIs. Overall, further prospective studies to clarify the predictive value of PBRM1 mutations for the therapeutic effects of immunotherapy are warranted given the discrepancy in the results of different studies.

Beuselinck et al. carried out unsupervised clustering analysis for the molecular characteristics of 53 patients with advanced ccRCC and classified them into four four subtypes (ccRCC1 to ccRCC4) (146). The results showed that *SETD2* mutations were related to the immune desert subtype with the poorest T-cell infiltration and lower expression of immunosuppressive markers (ccRCC1). In contrast, *BAP1* mutations were related to the inflammatory subtype with the highest T-cell infiltration (ccRCC4). Among these subtypes, ccRCC4 tumors had the poorest prognosis, which correlated with a high expression of immunosuppressive markers (including PD-L1, PD-1, LAG-3, and TIM-3) and excessive T-cell exhaustion. Besides, ccRCC4 tumors showed no response to sunitinib, which was related to high levels of expression of markers of Tregs (i.e., FOXP3, IL-10., and TGF-β). Similar results were obtained in a study on the immune characterization of ccRCC tumor grafts (147), in which *BAP1* mutations were associated with a highly inflammatory immune phenotype with abundant T-cell infiltration and poor prognosis. Taken together, we speculate that *SETD2* mutations may mediate immune silencing, while *BAP1* mutations may be involved in regulating T-cell infiltration and exhaustion in the TIME in ccRCC (**Figure 3B**). However, the above conclusions on SETD2 and BAP1 mutations were solely observational in nature, and further investigations were required to determine the immunomodulatory mechanism of them.

PTEN Mutations

The *PTEN* gene is one of the most commonly mutated tumor suppressor genes in human cancer, and negatively regulates the PI3K/AKT pathway by encoding a protein

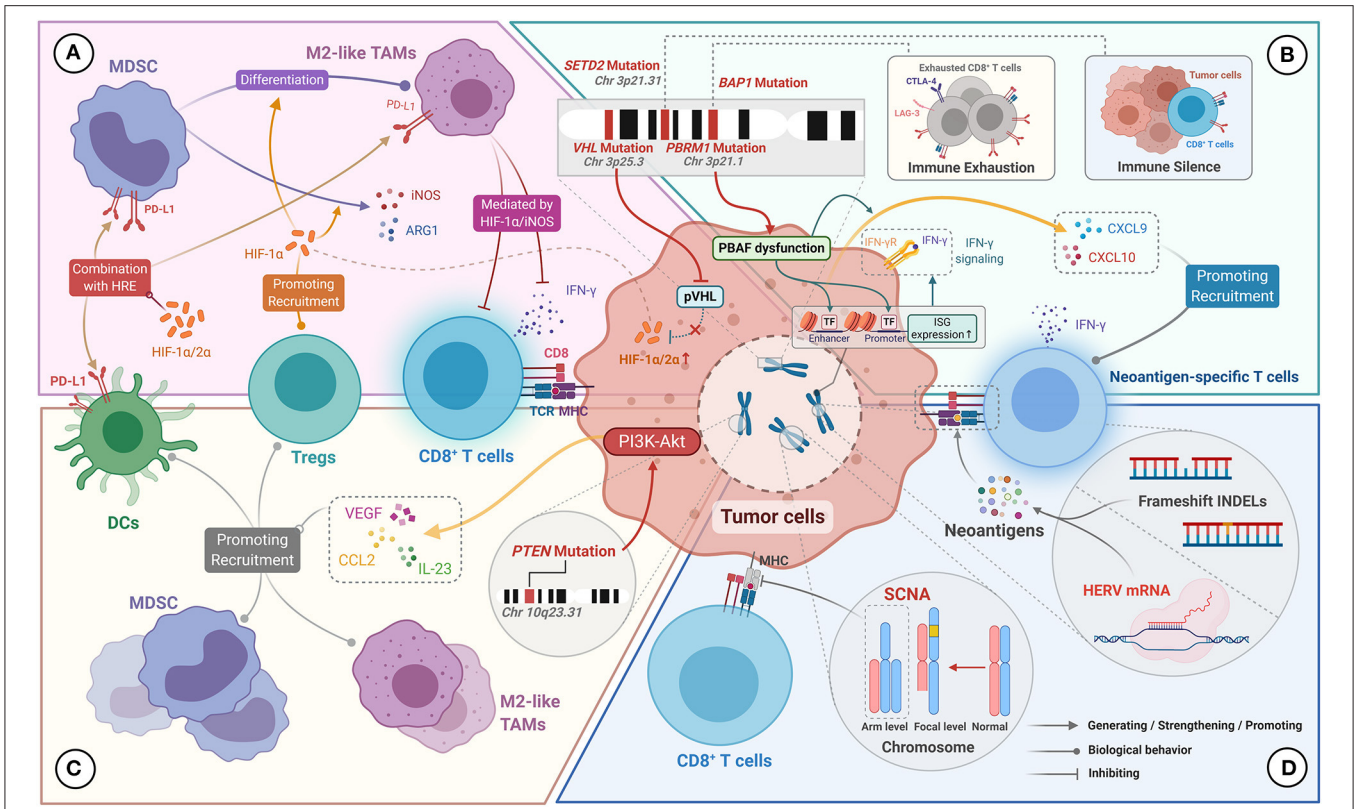

FIGURE 3 | Genomic characteristics of ccRCC for manipulating the TIME. **(A)** *VHL* mutations result in reduced pVHL production and reduced HIF-1α/2α degradation. Excess HIF-1α/2α upregulates the expression of PD-L1 on MDSC, M2-like TAMs, and DCs by binding to the hypoxia response element (HRE). HIF-1α promotes MDSCs to produce iNOS and Arg-1 and to differentiate into M2-like TAMs. HIF-1α promotes the recruitment of Tregs, and mediates the inhibitory effect of M2-like TAMs on the effector function of $CD8^+$ TILs. **(B)** *PBRM1* mutation leads to PBAF complex dysfunction, which upregulates interferon-stimulated gene (ISG) expression, thereby enhancing the tumor killing effect mediated by IFN-γ signaling. PBAF inactivation also promotes the secretion of CXCL9 and CXCL10 by tumor cells. *BAP1* mutations are associated with the immuno-exhausted tumor microenvironment. *SETD2* mutations are associated with the immune-silenced tumor microenvironment. **(C)** *PTEN* mutations activate the P13K-Akt pathway, resulting in upregulation of VEGF, CCL2, and IL-23 expression, which contribute to the recruitment of Tregs, DCs, and MDSCs. **(D)** Frameshift INDELs and HERV expression can generate abundant neoantigens, which stimulate the production of neoantigen-specific T cells. Arm level SCNA can disrupt the antigen-presenting capacity of MHC on tumor cells, resulting in inactivation of tumor-specific immune responses.

with phosphatase activity (148). *PTEN* mutations, which occur in approximately 4.5% of cases of ccRCC, remove the inhibitory effect on the PI3K/AKT pathway, leading to increased proliferation and migration of tumor cells (31, 148). Several studies have found that the sustained activation of the PI3K/AKT pathway caused by *PTEN* mutation upregulates the secretion of several immunosuppressive cytokines, including VEGF, IL-23, and CCL2 via NF-κB-JAK/STAT3 signaling (**Figure 3C**) (149–152). In addition to its role in angiogenesis, VEGF can recruit immature DCs, MDSCs, and Tregs to help sustain the immunosuppressive tumor microenvironment (153, 154). Moreover, *PTEN* loss can increase tumor cell resistance to T-cell killing by significantly upregulating CCL2 and VEGF (155). Besides, *PTEN*-deficient metastatic uterine smooth muscle sarcoma, accompanied by increased expression of VEGF-A and STAT3, were resistant to PD-1/PD-L1 therapy (156). More critically, *PTEN* mutations observed in ccRCC correlated with high infiltration of M2-like TAMs (157). Overall, *PTEN* mutations may upregulate the expression of multiple immunosuppressive factors by eliminating the negative regulation of the downstream PI3K/AKT pathway, thus inducing the immune escape of tumor cells.

Human Endogenous Retroviruses

HERVs form about 8% of the human genome, and are predominantly located in heterochromatin (158). Throughout millions of years of evolution, exogenous retroviruses have repeatedly infected hosts and integrated into their genomes, leading to the formation of HERVs. Under normal physiological conditions, most HERVs are usually inactive because of the presence of epigenetic silencing. However, HERV expression can be induced due to the lack of CpG methylation in tumor tissues (159). In a pan-cancer analysis of HERVs, Smith et al. found that HERV-derived proteins could participate in the regulation of the TIME and correlated with prognosis, particularly in ccRCC (160). Significant upregulation of HERV expression was observed in ccRCC that were responsive to PD-1 blockade, and positively correlated with Teff cell infiltration and the level of cytotoxic markers. Further studies revealed that HERV

expression products could serve as tumor-specific antigenic epitopes to induce HERV-specific T cell production (**Figure 3D**) (160). Taken together, HERVs could be a source of neoantigens and contribute to the cytotoxic effects of Teff cells, thereby shaping the TIME.

Tumor Mutational Burden and Somatic Copy-Number Alterations

The observation that patients with higher TMB are more likely to respond to PD-1/PD-L1 blockade has been reported in a variety of malignant tumors (161). High TMB indicates the presence of more mutation-associated antigens (MANA) in the tumor microenvironment, which facilitates the induction of MANA-specific T cells and activation of the adaptive anti-tumor immune response (162). However, it has been found that ccRCC has a lower TMB than other malignancies that were responsive to immunotherapy, which seems inconsistent with the above point (163).

The TMB mainly depends on the reads of non-synonymous single nucleotide variation (nsSNV) in the tumor cell genome. Frameshift mutations caused by insertional or deletion mutations (INDELs) can similarly produce immunogenic neoantigens (**Figure 3D**) (164). In a pan-cancer analysis, ccRCC had the highest frequency of frameshift INDELs, which seems to explain the phenomenon that PD-1/PD-L1 inhibitors are effective for the treatment of ccRCC with low TMB. However, in the genomic analysis of the IMmotion150 trial, no significant association was found between TMB or frameshift mutation burden (FMB) and the response to atezolizumab alone (anti-PD-L1) or in combination with bevacizumab (anti-VEGF) (14). Similarly, there was no significant correlation between TMB or FMB and the gene signature of Teff cells in the TIME.

In tumor genome aneuploidy studies, Davoli et al. showed that the expression levels of genes associated with adaptive immunity and the ratio of pro-inflammatory cytokines to immunosuppressive molecules were significantly reduced in tumors with high levels of arm-level SCNA (including ccRCC) (165). This finding indicates that tumors with high levels of SCNA may have more significant immunosuppressive properties. The authors hypothesized that arm-level SCNA could impair the antigen-extraction capacity of MHC or affect the balance of proteins associated with cytotoxic immune cell infiltration, resulting in blocking the activation of the tumor-specific immune response (**Figure 3D**) (165). Overall, frameshift INDELs and arm-level SCNA in ccRCC appear to exert diametrically opposed effects on the TIME, and thus, their underlying mechanisms should be further explored.

Novel Therapeutic Strategies for Advanced ccRCC Based on the TIME

As emphasized above, various immune cell subsets and immunomodulatory molecules in the TIME impact on the response to immunotherapy and targeted therapy. Moreover, with the in-depth study of the TIME, multiple immune regulation pathways have been found to affect tumor cell survival. Therefore, by targeting different immune microenvironment components or non-redundant immunomodulatory pathways, we may be able to overcome the therapeutic resistance of advanced ccRCC.

Other Immune Checkpoint Molecules

Besides PD-1 and CTLA-4, other immune checkpoints (e.g., LAG-3 and Tim-3) are involved in the immune escape of tumor cells and resistance to ICIs. Therefore, strategies targeting these other immune checkpoints have great therapeutic potential. Indeed, several early clinical trials of anti-LAG-3 monoclonal antibodies or anti-Tim-3 monoclonal antibodies combined with PD-1 inhibitors are being conducted in several tumor types, including RCC (**Table 1**). Besides, a bispecific antibody (bsAb) that combines two two immune checkpoints is receiving increasing attention, which can reactivate Teff cells more efficiently by blocking different immunosuppressive pathways. Currently, XmAb22841 (a bsAb targeting CTLA-4 and LAG-3) is being evaluated in a phase I trial in mRCC patients (**Table 1**). Stimulatory checkpoint molecules, including OX40 (also known as CD134) and CD27, are also potential therapeutic targets for the treatment of tumors such as RCC. OX40, mainly expressed on activated T cells, stimulates T cell proliferation and enhances effector function when binding to its ligand (OX40L) expressed on antigen-presenting cells (166). CD27, mainly expressed on T cells and NK cells, enhances NK cell-dependent and T cell-dependent anti-tumor immunity when binding to CD70 (166). Thus, activating co-stimulatory molecules can enhance the anti-tumor immune response by a mechanism distinct from inhibitory checkpoint molecules, which is a novel immunotherapeutic strategy for mRCC (167). Indeed, PF-04518600 (an OX40 agonist) combined with axitinib and varlilumab (a CD27 agonist) combined with nivolumab are currently in clinical development for mRCC (**Table 1**).

Modified Cytokine Therapies

NKTR-214 (also called bempegaldesleukin) is a PEGylated IL-2 that drives proliferation and activation of $CD8^+$ TILs and NK cells within the TIME by binding to the dimeric IL2Rβγ (CD122). Compared to traditional IL-2, NKTR-214 does not cause significant amplification of $CD4^+$ $Foxp3^+$ Tregs, and thus, has greater anti-tumor activity and fewer adverse effects (168). This is because NKTR-214 has a limited affinity for IL2Rα subunit, and thus, cannot bind to the IL2Rαβγ heterotrimer on Tregs (169). Currently, NTRK-214 combined with nivolumab is being evaluated in mRCC in the phase III PIVOT-09 trial (**Table 1**). AM0010 (also called pegilodecakin) is a modified PEGylated IL-10 that may enhance the anti-tumor immune response by harnessing the immunostimulatory function of IL-10. The latest results from the ongoing phase I/Ib IVY study confirm that second-line treatment with AM0010 in combination with a PD-1 inhibitor has a good response rate in mRCC (ORR: 33–43%), which is even

TABLE 1 | Novel treatment strategies for advanced ccRCC based on the tumor immune microenvironment.

Drug Type	NCT Number	Intervention	Comparison	Histology	Primary endpoint	Status	Phase	Number of patients	Allocation
Immune checkpoint molecules	NCT01968109	Relatlimab (anti-LAG-3) +/– Nivolumab	–	RCC and others	Safety, efficacy	Recruiting	Phase I/II	1,500	Randomized
	NCT02996110	Relatlimab + Nivolumab	Nivolumab + Ipilimumab	RCC	Safety	Recruiting	Phase II	200	Randomized
	NCT02460224	LAG525 (anti-LAG-3) +/– PDR001 (anti-PD-1)	–	RCC	Safety, ORR	Active, not recruiting	Phase I/II	490	Non-randomized
	NCT02608268	MBG453 (anti-Tim-3) +/– PDR001 (anti-PD-1)	–	RCC	Safety, ORR	Recruiting	Phase I/II	269	Non-randomized
	NCT03849469	XmAb22841 (anti-CTLA-4 & LAG-3) +/–Pembrolizumab	–	RCC	Safety	Recruiting	Phase I	242	Non-randomized
	NCT03092856	PF-04518600 (OX40 agonist) + Axitinib	Axitinib	ccRCC, nccRCC	PFS	Recruiting	Phase II	104	Randomized
	NCT02335918	Varlilumab (CD27 agonist) +Nivolumab	–	RCC and others	ORR	Completed	Phase II	175	N/A
Modified cytokines	NCT03729245	NKTR-214 (CD122 agonist) + Nivolumab	Sunitinib or Cabozantinib	RCC	OS, ORR	Recruiting	Phase III	600	Randomized
	NCT02009449	AM0010 (PEG-IL-10)	–	RCC and others	Safety	Active, not recruiting	Phase I	350	Non-randomized
Small-molecule immunomodulators	NCT02667886	X4P-001 (CXCR4 inhibitor) +/– Axitinib	–	ccRCC	Safety	Active, not recruiting	Phase I/II	74	Randomized
	NCT02923531	X4P−001 + Nivolumab	–	ccRCC	Safety	Completed	Phase I/II	9	N/A
	NCT02675439	MIW815 (STING agonist) +/– Ipilimumab	–	RCC and others	Safety, RD	Active, not recruiting	Phase I	47	Non-randomized
Targeting immunometabolism	NCT02655822	Ciforadenant (A2aR antagonist) +/– Atezolizumab	–	RCC and others	Safety, ORR, DLT, MDL	Recruiting	Phase I	336	Randomized
	NCT02754141	BMS-986179 (anti-CD73) +/– Nivolumab or rHuPH20	–	RCC and others	Safety	Recruiting	Phase I/II	268	Non-randomized

A2aR, adenosine A2a Receptor; ccRCC, clear cell renal cell carcinoma; CTLA-4, cytotoxic T-lymphocyte-associated protein 4; DLT, dose-limiting toxicities; LAG-3, lymphocyte-activation gene 3; MDL, maximum dose level; nccRCC, non-clear cell renal cell carcinoma; ORR, objective response rate; OS, overall survival; PD-1, programmed cell death-1; PEG-IL-10, pegylated interleukin-10; PFS, progression-free survival; RCC, renal cell carcinoma; RD, Recommended dose; rHuPH20, recombinant human hyaluronidase PH20 enzyme; STING, stimulator of interferon genes; Tim-3, T-cell immunoglobulin mucin-3.

better than the currently recommended second-line regimen (**Table 1**) (170).

Small-Molecule Immunomodulators

Activation of the CXCR4/CXCL12 pathway is associated with the formation of an immunosuppressive tumor microenvironment (171), and X4P-001 (a CXCR4 antagonist) can block excessive activation of this pathway to reverse tumor immune escape (172). Preclinical studies have demonstrated that CXCR4 antagonists could reduce the inhibitory effect of immunosuppressive cells on Teff cells and increase T-cell sensitivity to tumor antigens (173, 174). Currently, combination of X4P-001 with other anticancer therapies are in development (**Table 1**). Another potential target is the stimulator of interferon genes (STING), which is activated upon binding to cyclic dinucleotide (CDN), and initiates Teff cell-mediated adaptive immunity by inducing type I IFN production and DC activation (175). The STING agonist MIW815 (also called ADU-S100) was found to activate an anti-tumor immune response in preclinical trials (176), and phase I trials of MIW815 alone or in combination with ipilimumab are currently evaluating the efficacy and safety in multiple cancer types, including RCC (**Table 1**).

Targeting Immunometabolism

Hypoxia, the rapid proliferation of tumor cells, and upregulated expression of CD39 and CD73 can accelerate adenosine production in the tumor microenvironment (177). Several studies have shown that adenosine inhibits the proliferation and effector function of Teff cells, as well as the maturation and antigen-presenting ability of DCs by binding to A2a receptors (A2AR) (177, 178). Adenosine also upregulates the expression of FOXP3 and immune checkpoints, including PD-1, CTLA-4, and LAG-3 (178). CPI-444 (also called ciforadenant) is a selective inhibitor of the A2AR that reverses the immunosuppressive effect by blocking adenosine signaling. Early results from an ongoing phase I/Ib clinical study showed disease control rate of 75% and 100% for CPI-444 alone and in combination with atezolizumab in mRCC, respectively (**Table 1**) (179). Additionally, an anti-CD73 antibody (BMS-986179) that targets the pathway toward adenosine production is currently being evaluated in a phase 1 clinical trial (**Table 1**) (177).

CONCLUSION AND FUTURE PERSPECTIVES

Although ICI-based combination therapies have improved the prognosis of patients with advanced ccRCC, some patients show no response or progress during the treatment process. Increasing evidence suggests that the TIME is an important factor affecting therapeutic response in such cases. Both genomic characteristics and immunomodulatory effects of systemic therapy cause dynamic changes in the TIME in advanced ccRCC, which, in turn, impacts the therapeutic response. Several novel therapeutic strategies optimized according to the components of the TIME are under development to improve outcomes for patients with advanced ccRCC. However, the integration of tumor genomic and immune signatures to more accurately predict therapeutic response is an important task to be refined in the future. Moreover, there are obvious unmet needs in developing the optimal treatment sequencing and combination strategy based on the interaction between the TIME and systemic therapy. We believe that comprehensive correlation analysis combining the TIME, tumor genome, and therapeutic modalities could provide more accurate prediction and decision-making for the individualized treatment of advanced ccRCC patients in the near future.

AUTHOR CONTRIBUTIONS

EL, XL, YL, and YY conceived the idea for the research and designed the review. EL and XL created the figures. All authors participated in the drafting and revision of the manuscript, performed the literature review and approved the submitted version.

FUNDING

This work was supported by the Natural Science Foundation of Guangdong Province (2019A1515010234).

ACKNOWLEDGMENTS

All figures were generated with the help from BioRender.

REFERENCES

1. Bray F, Ferlay J, Soerjomataram I, Siegel RL, Torre LA, Jemal A. Global cancer statistics 2018: GLOBOCAN estimates of incidence and mortality worldwide for 36 cancers in 185 countries. *CA Cancer J Clin.* (2018) 68:394–424. doi: 10.3322/caac.21492
2. Moch H, Cubilla AL, Humphrey PA, Reuter VE, Ulbright TM. The 2016 WHO classification of tumours of the urinary system and male genital organs-part a: renal, penile, and testicular tumours. *Eur Urol.* (2016) 70. doi: 10.1016/j.eururo.2016.02.029
3. Linehan WM. Genetic basis of kidney cancer: role of genomics for the development of disease-based therapeutics. *Genome Res.* (2012) 22:2089–100. doi: 10.1101/gr.131110.111
4. Farolfi A, Schepisi G, Conteduca V, Burgio SL, Lolli C, De Giorgi U. Pharmacokinetics, pharmacodynamics and clinical efficacy of nivolumab in the treatment of metastatic renal cell carcinoma. *Expert Opin Drug Metab Toxicol.* (2016) 12:1089–96. doi: 10.1080/17425255.2016.1214713
5. Motzer RJ, Rini BI, McDermott DF, Redman BG, Kuzel TM, Harrison MR, et al. Nivolumab for metastatic renal cell carcinoma: results of a randomized phase II trial. *J Clin Oncol.* (2015) 33:1430–7. doi: 10.1200/JCO.2014.59.0703
6. Topalian SL, Hodi FS, Brahmer JR, Gettinger SN, Smith DC, McDermott DF, et al. Safety, activity, and immune correlates of anti-PD-1 antibody in cancer. *N Engl J Med.* (2012) 366:2443–54. doi: 10.1056/NEJMoa1200690
7. Xu W, Atkins MB, McDermott DF. Checkpoint inhibitor immunotherapy in kidney cancer. *Nat Rev Urol.* (2020) 17:137–50. doi: 10.1038/s41585-020-0282-3
8. Hegde PS, Wallin JJ, Mancao C. Predictive markers of anti-VEGF and emerging role of angiogenesis inhibitors as immunotherapeutics. *Semin Cancer Biol.* (2018) 52(Pt 2):117–24. doi: 10.1016/j.semcancer.2017.12.002
9. Wallin JJ, Bendell JC, Funke R, Sznol M, Korski K, Jones S, et al. Atezolizumab in combination with bevacizumab enhances antigen-specific

T-cell migration in metastatic renal cell carcinoma. *Nat Commun.* (2016) 7:12624. doi: 10.1038/ncomms12624
10. Kandalaft LE, Motz GT, Busch J, Coukos G. Angiogenesis and the tumor vasculature as antitumor immune modulators: the role of vascular endothelial growth factor and endothelin. *Curr Top Microbiol Immunol.* (2011) 344:129–48. doi: 10.1007/82_2010_95
11. Martin D, Galisteo R, Gutkind JS. CXCL8/IL8 stimulates vascular endothelial growth factor (VEGF) expression and the autocrine activation of VEGFR2 in endothelial cells by activating NFkappaB through the CBM (Carma3/Bcl10/Malt1) complex. *J Biol Chem.* (2009) 284:6038–42. doi: 10.1074/jbc.C800207200
12. Ishibashi K, Haber T, Breuksch I, Gebhard S, Sugino T, Kubo H, et al. Overriding TKI resistance of renal cell carcinoma by combination therapy with IL-6 receptor blockade. *Oncotarget.* (2017) 8:55230–45. doi: 10.18632/oncotarget.19420
13. Dalton HJ, Pradeep S, McGuire M, Hailemichael Y, Ma S, Lyons Y, et al. Macrophages facilitate resistance to anti-VEGF therapy by altered VEGFR expression. *Clin Cancer Res.* (2017) 23:7034–46. doi: 10.1158/1078-0432.CCR-17-0647
14. McDermott DF, Huseni MA, Atkins MB, Motzer RJ, Rini BI, Escudier B, et al. Clinical activity and molecular correlates of response to atezolizumab alone or in combination with bevacizumab versus sunitinib in renal cell carcinoma. *Nat Med.* (2018) 24:749–57. doi: 10.1038/s41591-018-0053-3
15. Nguyen LT, Ohashi PS. Clinical blockade of PD1 and LAG3–potential mechanisms of action. *Nat Rev Immunol.* (2015) 15:45–56. doi: 10.1038/nri3790
16. Andrews LP, Marciscano AE, Drake CG, Vignali DAA. LAG3 (CD223) as a cancer immunotherapy target. *Immunol Rev.* (2017) 276:80–96. doi: 10.1111/imr.12519
17. Das M, Zhu C, Kuchroo VK. Tim-3 and its role in regulating anti-tumor immunity. *Immunol Rev.* (2017) 276. doi: 10.1111/imr.12520
18. Sakuishi K, Apetoh L, Sullivan JM, Blazar BR, Kuchroo VK, Anderson AC. Targeting Tim-3 and PD-1 pathways to reverse T cell exhaustion and restore anti-tumor immunity. *J Exp Med.* (2010) 207:2187–94. doi: 10.1084/jem.20100643
19. Zizzari IG, Napoletano C, Botticelli A, Caponnetto S, Calabrò F, Gelibter A, et al. TK inhibitor pazopanib primes DCs by downregulation of the β-catenin pathway. *Cancer Immunol Res.* (2018) 6:711–22. doi: 10.1158/2326-6066.CIR-17-0594
20. Choueiri TK, Fishman MN, Escudier B, McDermott DF, Drake CG, Kluger H, et al. Immunomodulatory activity of nivolumab in metastatic renal cell carcinoma. *Clin Cancer Res.* (2016) 22:5461–71. doi: 10.1158/1078-0432.CCR-15-2839
21. Trotta AM, Santagata S, Zanotta S, D'Alterio C, Napolitano M, Rea G, et al. Mutated Von Hippel-Lindau-renal cell carcinoma (RCC) promotes patients specific natural killer (NK) cytotoxicity. *J Exp Clin Cancer Res.* (2018) 37:297. doi: 10.1186/s13046-018-0952-7
22. Pan D, Kobayashi A, Jiang P, Ferrari de Andrade L, Tay RE, Luoma AM, et al. A major chromatin regulator determines resistance of tumor cells to T cell-mediated killing. *Science.* (2018) 359:770–5. doi: 10.1126/science.aao1710
23. Yoshihara K, Shahmoradgoli M, Martínez E, Vegesna R, Kim H, Torres-Garcia W, et al. Inferring tumour purity and stromal and immune cell admixture from expression data. *Nat Commun.* (2013) 4:2612. doi: 10.1038/ncomms3612
24. Senbabaoglu Y, Gejman RS, Winer AG, Liu M, Van Allen EM, de Velasco G, et al. Tumor immune microenvironment characterization in clear cell renal cell carcinoma identifies prognostic and immunotherapeutically relevant messenger RNA signatures. *Genome Biol.* (2016) 17:231. doi: 10.1186/s13059-016-1092-z
25. Ock C-Y, Keam B, Kim S, Lee J-S, Kim M, Kim TM, et al. Pan-cancer immunogenomic perspective on the tumor microenvironment based on PD-L1 and CD8 T-cell infiltration. Clin Cancer Res. (2016) 22:2261–70. doi: 10.1158/1078-0432.CCR-15-2834
26. Chevrier S, Levine JH, Zanotelli VRT, Silina K, Schulz D, Bacac M, et al. An immune atlas of clear cell renal cell carcinoma. *Cell.* (2017) 169:736–49.e18. doi: 10.1016/j.cell.2017.04.016
27. Fridman WH, Pagès F, Sautès-Fridman C, Galon J. The immune contexture in human tumours: impact on clinical outcome. *Nat Rev Cancer.* (2012) 12:298–306. doi: 10.1038/nrc3245
28. Giraldo NA, Becht E, Vano Y, Petitprez F, Lacroix L, Validire P, et al. Tumor-infiltrating and peripheral blood t-cell immunophenotypes predict early relapse in localized clear cell renal cell carcinoma. *Clin Cancer Res.* (2017) 23:4416–28. doi: 10.1158/1078-0432.CCR-16-2848
29. Wang QJ, Hanada K-I, Robbins PF, Li YF, Yang JC. Distinctive features of the differentiated phenotype and infiltration of tumor-reactive lymphocytes in clear cell renal cell carcinoma. *Cancer Res.* (2012) 72:6119–29. doi: 10.1158/0008-5472.CAN-12-0588
30. Matsushita H, Sato Y, Karasaki T, Nakagawa T, Kume H, Ogawa S, et al. Neoantigen load, antigen presentation machinery, and immune signatures determine prognosis in clear cell renal cell carcinoma. *Cancer Immunol Res.* (2016) 4:463–71. doi: 10.1158/2326-6066.CIR-15-0225
31. Ricketts CJ, De Cubas AA, Fan H, Smith CC, Lang M, Reznik E, et al. The cancer genome atlas comprehensive molecular characterization of renal cell carcinoma. *Cell Rep.* (2018) 23:313–26.e5. doi: 10.1016/j.celrep.2018.03.075
32. Chávez-Galán L, Olleros ML, Vesin D, Garcia I. Much more than M1 and M2 macrophages, there are also CD169(+) and TCR(+) macrophages. *Front Immunol.* (2015) 6:263. doi: 10.3389/fimmu.2015.00263
33. Fleming V, Hu X, Weber R, Nagibin V, Groth C, Altevogt P, et al. Targeting myeloid-derived suppressor cells to bypass tumor-induced immunosuppression. *Front Immunol.* (2018) 9:398. doi: 10.3389/fimmu.2018.00398
34. Najjar YG, Rayman P, Jia X, Pavicic PG, Rini BI, Tannenbaum C, et al. Myeloid-derived suppressor cell subset accumulation in renal cell carcinoma parenchyma is associated with intratumoral expression of IL1β, IL8, CXCL5, and Mip-1α. *Clin Cancer Res.* (2017) 23:2346–55. doi: 10.1158/1078-0432.CCR-15-1823
35. Siddiqui SA, Frigola X, Bonne-Annee S, Mercader M, Kuntz SM, Krambeck AE, et al. Tumor-infiltrating Foxp3-CD4+CD25+ T cells predict poor survival in renal cell carcinoma. *Clin Cancer Res.* (2007) 13:2075–81. doi: 10.1158/1078-0432.CCR-06-2139
36. Komohara Y, Hasita H, Ohnishi K, Fujiwara Y, Suzu S, Eto M, et al. Macrophage infiltration and its prognostic relevance in clear cell renal cell carcinoma. *Cancer Sci.* (2011) 102:1424–31. doi: 10.1111/j.1349-7006.2011.01945.x
37. Walter S, Weinschenk T, Stenzl A, Zdrojowy R, Pluzanska A, Szczylik C, et al. Multipeptide immune response to cancer vaccine IMA901 after single-dose cyclophosphamide associates with longer patient survival. *Nat Med.* (2012) 18:1254–61. doi: 10.1038/nm.2883
38. Goc J, Germain C, Vo-Bourgais TKD, Lupo A, Klein C, Knockaert S, et al. Dendritic cells in tumor-associated tertiary lymphoid structures signal a Th1 cytotoxic immune contexture and license the positive prognostic value of infiltrating CD8+ T cells. *Cancer Res.* (2014) 74:705–15. doi: 10.1158/0008-5472.CAN-13-1342
39. Kroeger DR, Milne K, Nelson BH. Tumor-infiltrating plasma cells are associated with tertiary lymphoid structures, cytolytic t-cell responses, and superior prognosis in ovarian cancer. *Clin Cancer Res.* (2016) 22:3005–15. doi: 10.1158/1078-0432.CCR-15-2762
40. Giraldo NA, Becht E, Pagès F, Skliris G, Verkarre V, Vano Y, et al. Orchestration and prognostic significance of immune checkpoints in the microenvironment of primary and metastatic renal cell cancer. Clin Cancer Res. (2015) 21:3031–40. doi: 10.1158/1078-0432.CCR-14-2926
41. Colbeck EJ, Ager A, Gallimore A, Jones GW. Tertiary lymphoid structures in cancer: drivers of antitumor immunity, immunosuppression, or bystander sentinels in disease? *Front Immunol.* (2017) 8:1830. doi: 10.3389/fimmu.2017.01830
42. Dieu-Nosjean M-C, Goc J, Giraldo NA, Sautès-Fridman C, Fridman WH. Tertiary lymphoid structures in cancer and beyond. *Trends Immunol.* (2014) 35:571–80. doi: 10.1016/j.it.2014.09.006
43. Remark R, Alifano M, Cremer I, Lupo A, Dieu-Nosjean M-C, Riquet M, et al. Characteristics and clinical impacts of the immune environments in colorectal and renal cell carcinoma lung metastases: influence of tumor origin. *Clin Cancer Res.* (2013) 19:4079–91. doi: 10.1158/1078-0432.CCR-12-3847
44. Ma Y, Shurin GV, Gutkin DW, Shurin MR. Tumor associated regulatory dendritic cells. *Semin Cancer*

Biol. (2012) 22:298–306. doi: 10.1016/j.semcancer.2012.02.010
45. Dieu-Nosjean M-C, Giraldo NA, Kaplon H, Germain C, Fridman WH, Sautès-Fridman C. Tertiary lymphoid structures, drivers of the anti-tumor responses in human cancers. *Immunol Rev.* (2016) 271:260–75. doi: 10.1111/imr.12405
46. Figel A-M, Brech D, Prinz PU, Lettenmeyer UK, Eckl J, Turqueti-Neves A, et al. Human renal cell carcinoma induces a dendritic cell subset that uses T-cell crosstalk for tumor-permissive milieu alterations. *Am J Pathol.* (2011) 179:436–51. doi: 10.1016/j.ajpath.2011.03.011
47. Tang H, Wang Y, Chlewicki LK, Zhang Y, Guo J, Liang W, et al. Facilitating T cell infiltration in tumor microenvironment overcomes resistance to PD-L1 blockade. *Cancer Cell.* (2016) 29:285–96. doi: 10.1016/j.ccell.2016.02.004
48. Fukumura D, Kloepper J, Amoozgar Z, Duda DG, Jain RK. Enhancing cancer immunotherapy using antiangiogenics: opportunities and challenges. *Nat Rev Clin Oncol.* (2018) 15:325–40. doi: 10.1038/nrclinonc.2018.29
49. Georganaki M, van Hooren L, Dimberg A. Vascular targeting to increase the efficiency of immune checkpoint blockade in cancer. *Front Immunol.* (2018) 9:3081. doi: 10.3389/fimmu.2018.03081
50. Clark DJ, Dhanasekaran SM, Petralia F, Pan J, Song X, Hu Y, et al. Integrated proteogenomic characterization of clear cell renal cell carcinoma. *Cell.* (2019) 179:964–83.e31. doi: 10.1158/1538-7445.SABCS18-2458
51. Hara T, Miyake H, Fujisawa M. Expression pattern of immune checkpoint-associated molecules in radical nephrectomy specimens as a prognosticator in patients with metastatic renal cell carcinoma treated with tyrosine kinase inhibitors. *Urol Oncol.* (2017) 35:363–9. doi: 10.1016/j.urolonc.2017.01.002
52. Shin SJ, Jeon YK, Cho YM, Lee JL, Chung DH, Park JY, et al. The association between PD-L1 expression and the clinical outcomes to vascular endothelial growth factor-targeted therapy in patients with metastatic clear cell renal cell carcinoma. *Oncologist.* (2015) 20:1253–60. doi: 10.1634/theoncologist.2015-0151
53. Dhupkar P, Gordon N. Interleukin-2: old and new approaches to enhance immune-therapeutic efficacy. *Adv Exp Med Biol.* (2017) 995:33–51. doi: 10.1007/978-3-319-53156-4_2
54. Motzer RJ, Escudier B, McDermott DF, George S, Hammers HJ, Srinivas S, et al. Nivolumab versus everolimus in advanced renal-cell carcinoma. *N Engl J Med.* (2015) 373:1803–13. doi: 10.1056/NEJMoa1510665
55. Gaffen SL, Liu KD. Overview of interleukin-2 function, production and clinical applications. *Cytokine.* (2004) 28:109–23. doi: 10.1016/j.cyto.2004.06.010
56. Berntsen A, Brimnes MK, thor Straten P, Svane IM. Increase of circulating CD4+CD25highFoxp3+ regulatory T cells in patients with metastatic renal cell carcinoma during treatment with dendritic cell vaccination and low-dose interleukin-2. *J Immunother.* (2010) 33:425–34. doi: 10.1097/CJI.0b013e3181cd870f
57. Zorn E, Nelson EA, Mohseni M, Porcheray F, Kim H, Litsa D, et al. IL-2 regulates FOXP3 expression in human CD4+CD25+ regulatory T cells through a STAT-dependent mechanism and induces the expansion of these cells in vivo. *Blood.* (2006) 108:1571–9. doi: 10.1182/blood-2006-02-004747
58. Donskov F, von der Maase H. Impact of immune parameters on long-term survival in metastatic renal cell carcinoma. *J Clin Oncol.* (2006) 24:1997–2005. doi: 10.1200/JCO.2005.03.9594
59. Konjević GM, Vuletić AM, Mirjačić Martinović KM, Larsen AK, Jurišić VB. The role of cytokines in the regulation of NK cells in the tumor environment. *Cytokine.* (2019) 117:30–40. doi: 10.1016/j.cyto.2019.02.001
60. Terrén I, Orrantia A, Vitallé J, Zenarruzabeitia O, Borrego F. NK Cell metabolism and tumor microenvironment. *Front Immunol.* (2019) 10:2278. doi: 10.3389/fimmu.2019.02278
61. Husain Z, Huang Y, Seth P, Sukhatme VP. Tumor-derived lactate modifies antitumor immune response: effect on myeloid-derived suppressor cells and NK cells. *J Immunol.* (2013) 191:1486–95. doi: 10.4049/jimmunol.1202702
62. Wang J, Matosevic S. Adenosinergic signaling as a target for natural killer cell immunotherapy. *J Mol Med.* (2018) 96:903–13. doi: 10.1007/s00109-018-1679-9
63. Keppel MP, Saucier N, Mah AY, Vogel TP, Cooper MA. Activation-specific metabolic requirements for NK Cell IFN-γ production. *J Immunol.* (2015) 194:1954–62. doi: 10.4049/jimmunol.1402099
64. Lukey MJ, Katt WP, Cerione RA. Targeting amino acid metabolism for cancer therapy. *Drug Discov Today.* (2017) 22:796–804. doi: 10.1016/j.drudis.2016.12.003
65. Prinz PU, Mendler AN, Brech D, Masouris I, Oberneder R, Noessner E. NK-cell dysfunction in human renal carcinoma reveals diacylglycerol kinase as key regulator and target for therapeutic intervention. *Int J Cancer.* (2014) 135:1832–41. doi: 10.1002/ijc.28837
66. Ribas A, Wolchok JD. Cancer immunotherapy using checkpoint blockade. *Science.* (2018) 359:1350–5. doi: 10.1126/science.aar4060
67. O'Donnell JS, Long GV, Scolyer RA, Teng MWL, Smyth MJ. Resistance to PD1/PDL1 checkpoint inhibition. *Cancer Treat Rev.* (2017) 52:71–81. doi: 10.1016/j.ctrv.2016.11.007
68. Long L, Zhang X, Chen F, Pan Q, Phiphatwatchara P, Zeng Y, et al. The promising immune checkpoint LAG-3: from tumor microenvironment to cancer immunotherapy. Genes Cancer. (2018) 9:176–89. doi: 10.18632/genesandcancer.180
69. Ngiow SF, Young A, Jacquelot N, Yamazaki T, Enot D, Zitvogel L, et al. A threshold level of intratumor CD8+ T-cell PD1 expression dictates therapeutic response to anti-PD1. *Cancer Res.* (2015) 75:3800–11. doi: 10.1158/0008-5472.CAN-15-1082
70. Motzer RJ, Penkov K, Haanen J, Rini B, Albiges L, Campbell MT, et al. Avelumab plus axitinib versus sunitinib for advanced renal-cell carcinoma. *N Engl J Med.* (2019) 380:1103–15. doi: 10.1056/NEJMoa1816047
71. Rini BI, Powles T, Atkins MB, Escudier B, McDermott DF, Suarez C, et al. Atezolizumab plus bevacizumab versus sunitinib in patients with previously untreated metastatic renal cell carcinoma (IMmotion151): a multicentre, open-label, phase 3, randomised controlled trial. *Lancet.* (2019) 393:2404–15. doi: 10.1016/S0140-6736(19)30723-8
72. Robert C, Long GV, Brady B, Dutriaux C, Maio M, Mortier L, et al. Nivolumab in previously untreated melanoma without BRAF mutation. *N Engl J Med.* (2015) 372:320–30. doi: 10.1056/NEJMoa1412082
73. Borghaei H, Paz-Ares L, Horn L, Spigel DR, Steins M, Ready NE, et al. Nivolumab versus docetaxel in advanced nonsquamous non-small-cell lung cancer. *N Engl J Med.* (2015) 373:1627–39. doi: 10.1056/NEJMoa1507643
74. Gandhi L, Rodríguez-Abreu D, Gadgeel S, Esteban E, Felip E, De Angelis F, et al. Pembrolizumab plus chemotherapy in metastatic non-small-cell lung cancer. *N Engl J Med.* (2018) 378:2078–92. doi: 10.1056/NEJMoa1801005
75. Motzer RJ, Tannir NM, McDermott DF, Arén Frontera O, Melichar B, Choueiri TK, et al. Nivolumab plus Ipilimumab versus sunitinib in advanced renal-cell carcinoma. *N Engl J Med.* (2018) 378:1277–90. doi: 10.1056/NEJMoa1712126
76. Rini BI, Plimack ER, Stus V, Gafanov R, Hawkins R, Nosov D, et al. Pembrolizumab plus axitinib versus sunitinib for advanced renal-cell carcinoma. *N Engl J Med.* (2019) 380:1116–27. doi: 10.1056/NEJMoa1816714
77. Byrne WL, Mills KHG, Lederer JA, O'Sullivan GC. Targeting regulatory T cells in cancer. *Cancer Res.* (2011) 71:6915–20. doi: 10.1158/0008-5472.CAN-11-1156
78. Beyer M, Schultze JL. Regulatory T cells in cancer. *Blood.* (2006) 108:804–11. doi: 10.1182/blood-2006-02-002774
79. Togashi Y, Shitara K, Nishikawa H. Regulatory T cells in cancer immunosuppression - implications for anticancer therapy. *Nat Rev Clin Oncol.* (2019) 16:356–71. doi: 10.1038/s41571-019-0175-7
80. Simpson TR, Li F, Montalvo-Ortiz W, Sepulveda MA, Bergerhoff K, Arce F, et al. Fc-dependent depletion of tumor-infiltrating regulatory T cells co-defines the efficacy of anti-CTLA-4 therapy against melanoma. *J Exp Med.* (2013) 210:1695–710. doi: 10.1084/jem.20130579
81. Quaranta V, Schmid MC. Macrophage-mediated subversion of anti-tumour immunity. *Cells.* (2019) 8:747. doi: 10.3390/cells8070747
82. Falasiri S, Hajiran A, Kim Y, McCarthy S, Nguyen J, Spiess P, et al. MP18-07 high expression of tumor-associated macrophage (tam) markers within the tumor microenvironment signals poor overall survival in patients with metastatic renal cell carcinoma treated with immunotherapy. *J Urol.* (2020) 203:e237. doi: 10.1097/JU.0000000000000843.07
83. Cassetta L, Kitamura T. Targeting tumor-associated macrophages as a potential strategy to enhance the response to immune checkpoint inhibitors. *Front Cell Dev Biol.* (2018) 6:38. doi: 10.3389/fcell.2018.00038
84. Ostrand-Rosenberg S, Fenselau C. Myeloid-derived suppressor cells: immune-suppressive cells that impair antitumor immunity and

are sculpted by their environment. *J Immunol.* (2018) 200:422–31. doi: 10.4049/jimmunol.1701019
85. Corzo CA, Condamine T, Lu L, Cotter MJ, Youn J-I, Cheng P, et al. HIF-1α regulates function and differentiation of myeloid-derived suppressor cells in the tumor microenvironment. *J Exp Med.* (2010) 207:2439–53. doi: 10.1084/jem.20100587
86. Weber R, Fleming V, Hu X, Nagibin V, Groth C, Altevogt P, et al. Myeloid-derived suppressor cells hinder the anti-cancer activity of immune checkpoint inhibitors. *Front Immunol.* (2018) 9:1310. doi: 10.3389/fimmu.2018.01310
87. Fa B, Luo C, Tang Z, Yan Y, Zhang Y, Yu Z. Pathway-based biomarker identification with crosstalk analysis for robust prognosis prediction in hepatocellular carcinoma. *EBioMedicine*. (2019) 44:250–60. doi: 10.1016/j.ebiom.2019.05.010
88. Ghiringhelli F, Puig PE, Roux S, Parcellier A, Schmitt E, Solary E, et al. Tumor cells convert immature myeloid dendritic cells into TGF-beta-secreting cells inducing CD4+CD25+ regulatory T cell proliferation. *J Exp Med.* (2005) 202:919–29. doi: 10.1084/jem.20050463
89. Norian LA, Rodriguez PC, O'Mara LA, Zabaleta J, Ochoa AC, Cella M, et al. Tumor-infiltrating regulatory dendritic cells inhibit CD8+ T cell function via L-arginine metabolism. *Cancer Res.* (2009) 69:3086–94. doi: 10.1158/0008-5472.CAN-08-2826
90. Liu Q, Zhang C, Sun A, Zheng Y, Wang L, Cao X. Tumor-educated CD11bhighIalow regulatory dendritic cells suppress T cell response through arginase I. *J Immunol.* (2009) 182:6207–16. doi: 10.4049/jimmunol.0803926
91. Bruno A, Mortara L, Baci D, Noonan DM, Albini A. Myeloid derived suppressor cells interactions with natural killer cells and pro-angiogenic activities: roles in tumor progression. *Front Immunol.* (2019) 10:771. doi: 10.3389/fimmu.2019.00771
92. Shojaei F, Wu X, Malik AK, Zhong C, Baldwin ME, Schanz S, et al. Tumor refractoriness to anti-VEGF treatment is mediated by CD11b+Gr1+ myeloid cells. *Nat Biotechnol.* (2007) 25:911–20. doi: 10.1038/nbt1323
93. Ichikawa K, Watanabe Miyano S, Minoshima Y, Matsui J, Funahashi Y. Activated FGF2 signaling pathway in tumor vasculature is essential for acquired resistance to anti-VEGF therapy. *Sci Rep.* (2020) 10:2939. doi: 10.1038/s41598-020-59853-z
94. Laddha AP, Kulkarni YA. VEGF and FGF-2: promising targets for the treatment of respiratory disorders. *Respir Med.* (2019) 156:33–46. doi: 10.1016/j.rmed.2019.08.003
95. Finke J, Ko J, Rini B, Rayman P, Ireland J, Cohen P. MDSC as a mechanism of tumor escape from sunitinib mediated anti-angiogenic therapy. *Int Immunopharmacol.* (2011) 11:856–61. doi: 10.1016/j.intimp.2011.01.030
96. Quintero-Fabián S, Arreola R, Becerril-Villanueva E, Torres-Romero JC, Arana-Argáez V, Lara-Riegos J, et al. Role of matrix metalloproteinases in angiogenesis and cancer. *Front Oncol.* (2019) 9:1370. doi: 10.3389/fonc.2019.01370
97. Riabov V, Gudima A, Wang N, Mickley A, Orekhov A, Kzhyshkowska J. Role of tumor associated macrophages in tumor angiogenesis and lymphangiogenesis. *Front Physiol.* (2014) 5:75. doi: 10.3389/fphys.2014.00075
98. Liu Q, Yang C, Wang S, Shi D, Wei C, Song J, et al. Wnt5a-induced M2 polarization of tumor-associated macrophages via IL-10 promotes colorectal cancer progression. *Cell Commun Signal.* (2020) 18:51. doi: 10.1186/s12964-020-00557-2
99. Pukrop T, Klemm F, Hagemann T, Gradl D, Schulz M, Siemes S, et al. Wnt 5a signaling is critical for macrophage-induced invasion of breast cancer cell lines. *Proc Natl Acad Sci USA.* (2006) 103:5454–9. doi: 10.1073/pnas.0509703103
100. Yeo E-J, Cassetta L, Qian B-Z, Lewkowich I, Li J-f, Stefater JA, et al. Myeloid WNT7b mediates the angiogenic switch and metastasis in breast cancer. *Cancer Res.* (2014) 74:2962–73. doi: 10.1158/0008-5472.CAN-13-2421
101. Liu L, Ye Y, Zhu X. MMP-9 secreted by tumor associated macrophages promoted gastric cancer metastasis through a PI3K/AKT/Snail pathway. *Biomed Pharmacother.* (2019) 117:109096. doi: 10.1016/j.biopha.2019.109096
102. Motzer RJ, Hutson TE, Cella D, Reeves J, Hawkins R, Guo J, et al. Pazopanib versus sunitinib in metastatic renal-cell carcinoma. *N Engl J Med.* (2013) 369:722–31. doi: 10.1056/NEJMoa1303989
103. Voronov E, Carmi Y, Apte RN. The role IL-1 in tumor-mediated angiogenesis. *Front Physiol.* (2014) 5:114. doi: 10.3389/fphys.2014.00114
104. Carbone C, Moccia T, Zhu C, Paradiso G, Budillon A, Chiao PJ, et al. Anti-VEGF treatment-resistant pancreatic cancers secrete proinflammatory factors that contribute to malignant progression by inducing an EMT cell phenotype. *Clin Cancer Res.* (2011) 17:5822–32. doi: 10.1158/1078-0432.CCR-11-1185
105. Ishibashi K, Koguchi T, Matsuoka K, Onagi A, Tanji R, Takinami-Honda R, et al. Interleukin-6 induces drug resistance in renal cell carcinoma. *Fukushima J Med Sci.* (2018) 64:103–10. doi: 10.5387/fms.2018-15
106. Kothari P, Pestana R, Mesraoua R, Elchaki R, Khan KMF, Dannenberg AJ, et al. IL-6-mediated induction of matrix metalloproteinase-9 is modulated by JAK-dependent IL-10 expression in macrophages. *J Immunol.* (2014) 192:349–57. doi: 10.4049/jimmunol.1301906
107. Huang D, Ding Y, Zhou M, Rini BI, Petillo D, Qian C-N, et al. Interleukin-8 mediates resistance to antiangiogenic agent sunitinib in renal cell carcinoma. *Cancer Res.* (2010) 70:1063–71. doi: 10.1158/0008-5472.CAN-09-3965
108. Hansen W. Neuropilin 1 guides regulatory T cells into VEGF-producing melanoma. *Oncoimmunol.* (2013) 2:e23039. doi: 10.4161/onci.23039
109. Vetsika E-K, Koukos A, Kotsakis A. Myeloid-derived suppressor cells: major figures that shape the immunosuppressive and angiogenic network in cancer. *Cells.* (2019) 8:1647. doi: 10.3390/cells8121647
110. Li Y-L, Zhao H, Ren X-B. Relationship of VEGF/VEGFR with immune and cancer cells: staggering or forward? *Cancer Biol Med.* (2016) 13:206–14. doi: 10.20892/j.issn.2095-3941.2015.0070
111. Li C, Liu B, Dai Z, Tao Y. Knockdown of VEGF receptor-1 (VEGFR-1) impairs macrophage infiltration, angiogenesis and growth of clear cell renal cell carcinoma (CRCC). *Cancer Biol Ther.* (2011) 12:872–80. doi: 10.4161/cbt.12.10.17672
112. Dirkx AEM, oude Egbrink MGA, Castermans K, van der Schaft DWJ, Thijssen VLJL, Dings RPM, et al. Anti-angiogenesis therapy can overcome endothelial cell anergy and promote leukocyte-endothelium interactions and infiltration in tumors. *FASEB J.* (2006) 20:621–30. doi: 10.1096/fj.05-4493com
113. Finke JH, Rini B, Ireland J, Rayman P, Richmond A, Golshayan A, et al. Sunitinib reverses type-1 immune suppression and decreases T-regulatory cells in renal cell carcinoma patients. *Clin Cancer Res.* (2008) 14:6674–82. doi: 10.1158/1078-0432.CCR-07-5212
114. Ko JS, Zea AH, Rini BI, Ireland JL, Elson P, Cohen P, et al. Sunitinib mediates reversal of myeloid-derived suppressor cell accumulation in renal cell carcinoma patients. *Clin Cancer Res.* (2009) 15:2148–57. doi: 10.1158/1078-0432.CCR-08-1332
115. RJ, Jonasch E, Michaelson MD, Nandagopal L, Gore JL, George S, et al. NCCN guidelines insights: kidney cancer, version 2.2020. *J Natl Compr Canc Netw.* (2019) 17:1278–85. doi: 10.6004/jnccn.2019.0054
116. Escudier B, Porta C, Schmidinger M, Rioux-Leclercq N, Bex A, Khoo V, et al. Renal cell carcinoma: ESMO clinical practice guidelines for diagnosis, treatment and follow-up†. *Ann Oncol.* (2019) 30:706–20. doi: 10.1093/annonc/mdz056
117. Escudier B, Pluzanska A, Koralewski P, Ravaud A, Bracarda S, Szczylik C, et al. Bevacizumab plus interferon alfa-2a for treatment of metastatic renal cell carcinoma: a randomised, double-blind phase III trial. *Lancet.* (2007) 370:2103–11. doi: 10.1016/S0140-6736(07)61904-7
118. Liu X-D, Hoang A, Zhou L, Kalra S, Yetil A, Sun M, et al. Resistance to antiangiogenic therapy is associated with an immunosuppressive tumor microenvironment in metastatic renal cell carcinoma. *Cancer Immunol Res.* (2015) 3:1017–29. doi: 10.1158/2326-6066.CIR-14-0244
119. Huang Y, Yuan J, Righi E, Kamoun WS, Ancukiewicz M, Nezivar J, et al. Vascular normalizing doses of antiangiogenic treatment reprogram the immunosuppressive tumor microenvironment and enhance immunotherapy. *Proc Natl Acad Sci USA.* (2012) 109:17561–6. doi: 10.1073/pnas.1215397109
120. Albini A, Bruno A, Noonan DM, Mortara L. Contribution to tumor angiogenesis from innate immune cells within the tumor microenvironment: implications for immunotherapy. *Front Immunol.* (2018) 9:527. doi: 10.3389/fimmu.2018.00527
121. Pópulo H, Lopes JM, Soares P. The mTOR signalling pathway in human cancer. *Int J Mol Sci.* (2012) 13:1886–918. doi: 10.3390/ijms13021886

122. Voss MH, Molina AM, Motzer RJ. mTOR inhibitors in advanced renal cell carcinoma. *Hematol Oncol Clin North Am.* (2011) 25:835–52. doi: 10.1016/j.hoc.2011.04.008
123. Macdonald AS. Use of mTOR inhibitors in human organ transplantation. *Expert Rev Clin Immunol.* (2007) 3:423–36. doi: 10.1586/1744666X.3.3.423
124. Huijts CM, Santegoets SJ, de Jong TD, Verheul HM, de Gruijl TD, van der Vliet HJ. Immunological effects of everolimus in patients with metastatic renal cell cancer. *Int J Immunopathol Pharmacol.* (2017) 30:341–52. doi: 10.1177/0394632017734459
125. Ghiringhelli F, Menard C, Puig PE, Ladoire S, Roux S, Martin F, et al. Metronomic cyclophosphamide regimen selectively depletes CD4+CD25+ regulatory T cells and restores T and NK effector functions in end stage cancer patients. *Cancer Immunol Immunother.* (2007) 56:641–8. doi: 10.1007/s00262-006-0225-8
126. CM, Lougheed SM, Bodalal Z, van Herpen CM, Hamberg P, Tascilar M, et al. The effect of everolimus and low-dose cyclophosphamide on immune cell subsets in patients with metastatic renal cell carcinoma: results from a phase I clinical trial. *Cancer Immunol Immunother.* (2019) 68:503–15. doi: 10.1007/s00262-018-2288-8
127. Sanchez DJ, Simon MC. Genetic and metabolic hallmarks of clear cell renal cell carcinoma. *Biochim Biophys Acta Rev Cancer.* (2018) 1870:23–31. doi: 10.1016/j.bbcan.2018.06.003
128. Gerlinger M, Horswell S, Larkin J, Rowan AJ, Salm MP, Varela I, et al. Genomic architecture and evolution of clear cell renal cell carcinomas defined by multiregion sequencing. *Nat Genet.* (2014) 46:225–33. doi: 10.1038/ng.2891
129. Cancer Genome Atlas Research N. Comprehensive molecular characterization of clear cell renal cell carcinoma. *Nature.* (2013) 499:43–9. doi: 10.1038/nature12222
130. Maxwell PH, Wiesener MS, Chang GW, Clifford SC, Vaux EC, Cockman ME, et al. The tumour suppressor protein VHL targets hypoxia-inducible factors for oxygen-dependent proteolysis. *Nature.* (1999) 399:271–5. doi: 10.1038/20459
131. Ekmekcioglu S, Grimm EA, Roszik J. Targeting iNOS to increase efficacy of immunotherapies. *Hum Vaccin Immunother.* (2017) 13:1105–8. doi: 10.1080/21645515.2016.1276682
132. Doedens AL, Stockmann C, Rubinstein MP, Liao D, Zhang N, DeNardo DG, et al. Macrophage expression of hypoxia-inducible factor-1 alpha suppresses T-cell function and promotes tumor progression. *Cancer Res.* (2010) 70:7465–75. doi: 10.1158/0008-5472.CAN-10-1439
133. Clambey ET, McNamee EN, Westrich JA, Glover LE, Campbell EL, Jedlicka P, et al. Hypoxia-inducible factor-1 alpha-dependent induction of FoxP3 drives regulatory T-cell abundance and function during inflammatory hypoxia of the mucosa. *Proc Natl Acad Sci USA.* (2012) 109:E2784-E93. doi: 10.1073/pnas.1202366109
134. Noman MZ, Desantis G, Janji B, Hasmim M, Karray S, Dessen P, et al. PD-L1 is a novel direct target of HIF-1α, and its blockade under hypoxia enhanced MDSC-mediated T cell activation. *J Exp Med.* (2014) 211:781–90. doi: 10.1084/jem.20131916
135. Messai Y, Gad S, Noman MZ, Le Teuff G, Couve S, Janji B, et al. Renal cell carcinoma programmed death-ligand 1, a new direct target of hypoxia-inducible factor-2 alpha, is regulated by von hippel-lindau gene mutation status. *Eur Urol.* (2016) 70:623–32. doi: 10.1016/j.eururo.2015.11.029
136. Carril-Ajuria L, Santos M, Roldán-Romero JM, Rodriguez-Antona C, de Velasco G. Prognostic and predictive value of in clear cell renal cell carcinoma. *Cancers.* (2019) 12. doi: 10.3390/cancers12010016
137. Pfister SX, Ahrabi S, Zalmas L-P, Sarkar S, Aymard F, Bachrati CZ, et al. SETD2-dependent histone H3K36 trimethylation is required for homologous recombination repair and genome stability. *Cell Rep.* (2014) 7:2006–18. doi: 10.1016/j.celrep.2014.05.026
138. Ventii KH, Devi NS, Friedrich KL, Chernova TA, Tighiouart M, Van Meir EG, et al. BRCA1-associated protein-1 is a tumor suppressor that requires deubiquitinating activity and nuclear localization. *Cancer Res.* (2008) 68:6953–62. doi: 10.1158/0008-5472.CAN-08-0365
139. Bihr S, Ohashi R, Moore AL, Rüschoff JH, Beisel C, Hermanns T, et al. Expression and mutation patterns of PBRM1, BAP1 and SETD2 mirror specific evolutionary subtypes in clear cell renal cell carcinoma. *Neoplasia.* (2019) 21:247–56. doi: 10.1016/j.neo.2018.12.006
140. Braun DA, Ishii Y, Walsh AM, Van Allen EM, Wu CJ, Shukla SA, et al. Clinical validation of PBRM1 alterations as a marker of immune checkpoint inhibitor response in renal cell carcinoma. *JAMA Oncol.* (2019) 5:1631–3. doi: 10.1001/jamaoncol.2019.3158
141. Miao D, Margolis CA, Gao W, Voss MH, Li W, Martini DJ, et al. Genomic correlates of response to immune checkpoint therapies in clear cell renal cell carcinoma. *Science.* (2018) 359:801–6. doi: 10.1126/science.aan5951
142. Alaiwi SA, Nassar A, Bakouny ZE, Berchuck JE, Nuzzo P, Flippot R, et al. Association of polybromo-associated BAF (PBAF) complex mutations with overall survival (OS) in cancer patients (pts) treated with checkpoint inhibitors (ICIs). *J Clin Oncol.* (2019) 37(15_suppl):103. doi: 10.1200/JCO.2019.37.15_suppl.103
143. Hakimi AA, Ged Y, Flynn J, Hoen DR, Natale RGD, Blum KA, et al. The impact of PBRM1 mutations on overall survival in greater than 2,100 patients treated with immune checkpoint blockade (ICB). *J Clin Oncol.* (2019) 37(7_Suppl):666. doi: 10.1200/JCO.2019.37.7_suppl.666
144. Hakimi AA, Voss MH, Kuo F, Sanchez A, Liu M, Nixon BG, et al. Transcriptomic profiling of the tumor microenvironment reveals distinct subgroups of clear cell renal cell cancer: data from a randomized phase III trial. *Cancer Discov.* (2019) 9:510–25. doi: 10.1158/2159-8290.CD-18-0957
145. Singla N, Xie Z, Zhang Z, Gao M, Yousuf Q, Onabolu O, et al. Pancreatic tropism of metastatic renal cell carcinoma. *JCI Insight.* (2020) 5:e134564. doi: 10.1172/jci.insight.134564
146. Beuselinck B, Job S, Becht E, Karadimou A, Verkarre V, Couchy G, et al. Molecular subtypes of clear cell renal cell carcinoma are associated with sunitinib response in the metastatic setting. *Clin Cancer Res.* (2015) 21:1329–39. doi: 10.1158/1078-0432.CCR-14-1128
147. Wang T, Lu R, Kapur P, Jaiswal BS, Hannan R, Zhang Z, et al. An empirical approach leveraging tumorgrafts to dissect the tumor microenvironment in renal cell carcinoma identifies missing link to prognostic inflammatory factors. *Cancer Discov.* (2018) 8:1142–55. doi: 10.1158/2159-8290.CD-17-1246
148. Carnero A, Paramio JM. The PTEN/PI3K/AKT pathway in vivo, cancer mouse models. *Front Oncol.* (2014) 4:252. doi: 10.3389/fonc.2014.00252
149. Ying H, Elpek KG, Vinjamoori A, Zimmerman SM, Chu GC, Yan H, et al. PTEN is a major tumor suppressor in pancreatic ductal adenocarcinoma and regulates an NF-κB-cytokine network. *Cancer Discov.* (2011) 1:158–69. doi: 10.1158/2159-8290.CD-11-0031
150. Grivennikov SI, Karin M. Dangerous liaisons: STAT3 and NF-kappaB collaboration and crosstalk in cancer. *Cytokine Growth Factor Rev.* (2010) 21:11–9. doi: 10.1016/j.cytogfr.2009.11.005
151. Romanque P, Piguet A-C, Dufour J-F. Targeting vessels to treat hepatocellular carcinoma. *Clin Sci.* (2008) 114:467–77. doi: 10.1042/CS20070310
152. Cheng F, Eng C. PTEN mutations trigger resistance to immunotherapy. *Trends Mol Med.* (2019) 25:461–3. doi: 10.1016/j.molmed.2019.03.003
153. Kortylewski M, Xin H, Kujawski M, Lee H, Liu Y, Harris T, et al. Regulation of the IL-23 and IL-12 balance by Stat3 signaling in the tumor microenvironment. *Cancer Cell.* (2009) 15:114–23. doi: 10.1016/j.ccr.2008.12.018
154. Bonecchi R, Galliera E, Borroni EM, Corsi MM, Locati M, Mantovani A. Chemokines and chemokine receptors: an overview. *Front Biosci.* (2009) 14:540–51. doi: 10.2741/3261
155. Peng W, Chen JQ, Liu C, Malu S, Creasy C, Tetzlaff MT, et al. Loss of PTEN promotes resistance to t cell-mediated immunotherapy. *Cancer Discov.* (2016) 6:202–16. doi: 10.1158/1538-7445.AM2016-4363
156. George S, Miao D, Demetri GD, Adeegbe D, Rodig SJ, Shukla S, et al. Loss of PTEN Is associated with resistance to anti-PD-1 checkpoint blockade therapy in metastatic uterine leiomyosarcoma. *Immunity.* (2017) 46:197–204. doi: 10.1016/j.immuni.2017.02.001
157. Zhang S, Zhang E, Long J, Hu Z, Peng J, Liu L, et al. Immune infiltration in renal cell carcinoma. *Cancer Sci.* (2019) 110:1564–72. doi: 10.1111/cas.13996
158. Alcazer V, Bonaventura P, Depil S. Human endogenous retroviruses (HERVs): shaping the innate immune response in cancers. *Cancers.* (2020) 12:610. doi: 10.3390/cancers12030610
159. Kassiotis G. Endogenous retroviruses and the development of cancer. *J Immunol.* (2014) 192:1343–9. doi: 10.4049/jimmunol.1302972

160. Smith CC, Beckermann KE, Bortone DS, De Cubas AA, Bixby LM, Lee SJ, et al. Endogenous retroviral signatures predict immunotherapy response in clear cell renal cell carcinoma. *J Clin Invest.* (2018) 128:4804–20. doi: 10.1172/JCI121476
161. Klempner SJ, Fabrizio D, Bane S, Reinhart M, Peoples T, Ali SM, et al. Tumor mutational burden as a predictive biomarker for response to immune checkpoint inhibitors: a review of current evidence. *Oncologist.* (2020) 25:e147–e59. doi: 10.1634/theoncologist.2019-0244
162. Drake CG, Stein MN. The immunobiology of kidney cancer. *J Clin Oncol.* (2018) 36:3547–52. doi: 10.1200/JCO.2018.79.2648
163. Zehir A, Benayed R, Shah RH, Syed A, Middha S, Kim HR, et al. Mutational landscape of metastatic cancer revealed from prospective clinical sequencing of 10,000 patients. *Nat Med.* (2017) 23:703–13. doi: 10.1038/nm.4333
164. Turajlic S, Litchfield K, Xu H, Rosenthal R, McGranahan N, Reading JL, et al. Insertion-and-deletion-derived tumour-specific neoantigens and the immunogenic phenotype: a pan-cancer analysis. *Lancet Oncol.* (2017) 18:1009–21. doi: 10.1016/S1470-2045(17)30516-8
165. Davoli T, Uno H, Wooten EC, Elledge SJ. Tumor aneuploidy correlates with markers of immune evasion and with reduced response to immunotherapy. *Science.* (2017) 355. doi: 10.1126/science.aaf8399
166. Chen L, Flies DB. Molecular mechanisms of T cell co-stimulation and co-inhibition. *Nat Rev Immunol.* (2013) 13:227–42. doi: 10.1038/nri3405
167. Capece D, Verzella D, Fischietti M, Zazzeroni F, Alesse E. Targeting costimulatory molecules to improve antitumor immunity. *J Biomed Biotechnol.* (2012) 2012:926321. doi: 10.1155/2012/926321
168. Bentebibel S-E, Hurwitz ME, Bernatchez C, Haymaker C, Hudgens CW, Kluger HM, et al. A first-in-human study and biomarker analysis of NKTR-214, a novel IL2Rβγ-biased cytokine, in patients with advanced or metastatic solid tumors. *Cancer Discov.* (2019) 9:711–21. doi: 10.1158/2159-8290.CD-18-1495
169. Charych DH, Hoch U, Langowski JL, Lee SR, Addepalli MK, Kirk PB, et al. NKTR-214, an engineered cytokine with biased IL2 receptor binding, increased tumor exposure, and marked efficacy in mouse tumor models. *Clin Cancer Res.* (2016) 22:680–90. doi: 10.1158/1078-0432.CCR-15-1631
170. Naing A, Papadopoulos KP, Wong DJL, Aljumaily R, Hung A, Afable M, et al. Pegilodecakin as monotherapy or in combination with anti-PD-1 or tyrosine kinase inhibitor in heavily pretreated patients with advanced renal cell carcinoma (RCC): updated results from phase I/Ib IVY study. *J Clin Oncol.* (2020) 38(6_suppl):679. doi: 10.1200/JCO.2020.38.6_suppl.679
171. Susek KH, Karvouni M, Alici E, Lundqvist A. The role of CXC chemokine receptors 1–4 on immune cells in the tumor microenvironment. *Front Immunol.* (2018) 9:2159. doi: 10.3389/fimmu.2018.02159
172. Eckert F, Schilbach K, Klumpp L, Bardoscia L, Sezgin EC, Schwab M, et al. Potential role of CXCR4 targeting in the context of radiotherapy and immunotherapy of cancer. *Front Immunol.* (2018) 9:3018. doi: 10.3389/fimmu.2018.03018
173. Panka D, Wang Y, Arbeit R, Mier J. MDSC trafficking and function in RCC by CXCR4 in the presence of a VEGF-R antagonist is dependent on HIF-2α expression. *Eur J Cancer.* (2016) 69:S105. doi: 10.1016/S0959-8049(16)32912-4
174. D'Alterio C, Buoncervello M, Ieranò C, Napolitano M, Portella L, Rea G, et al. Targeting CXCR4 potentiates anti-PD-1 efficacy modifying the tumor microenvironment and inhibiting neoplastic PD-1. *J Exp Clin Cancer Res.* (2019) 38:432. doi: 10.1186/s13046-019-1420-8
175. Wu J-J, Zhao L, Hu H-G, Li W-H, Li Y-M. Agonists and inhibitors of the STING pathway: potential agents for immunotherapy. *Med Res Rev.* (2020) 40:1117–41. doi: 10.1002/med.21649
176. Foote JB, Kok M, Leatherman JM, Armstrong TD, Marcinkowski BC, Ojalvo LS, et al. A STING agonist given with OX40 receptor and PD-L1 modulators primes immunity and reduces tumor growth in tolerized mice. *Cancer Immunol Res.* (2017) 5:468–79. doi: 10.1158/2326-6066.CIR-16-0284
177. Leone RD, Emens LA. Targeting adenosine for cancer immunotherapy. *J Immunother Cancer.* (2018) 6:57. doi: 10.1186/s40425-018-0360-8
178. Leone RD, Sun I-M, Oh M-H, Sun I-H, Wen J, Englert J, et al. Inhibition of the adenosine A2a receptor modulates expression of T cell coinhibitory receptors and improves effector function for enhanced checkpoint blockade and ACT in murine cancer models. *Cancer Immunol Immunother.* (2018) 67:1271–84. doi: 10.1007/s00262-018-2186-0
179. Fong L, Forde PM, Powderly JD, Goldman JW, Nemunaitis JJ, Luke JJ, et al. Safety and clinical activity of adenosine A2a receptor (A2aR) antagonist, CPI-444, in anti-PD1/PDL1 treatment-refractory renal cell (RCC) and non-small cell lung cancer (NSCLC) patients. *J Clin Oncol.* (2017) 35(15_suppl):3004. doi: 10.1200/JCO.2017.35.15_suppl.3004

Conflict of Interest: The authors declare that the research was conducted in the absence of any commercial or financial relationships that could be construed as a potential conflict of interest.

Copyright © 2021 Lin, Liu, Liu, Zhang, Xie, Tian, Liu and Yu. This is an open-access article distributed under the terms of the Creative Commons Attribution License (CC BY). The use, distribution or reproduction in other forums is permitted, provided the original author(s) and the copyright owner(s) are credited and that the original publication in this journal is cited, in accordance with accepted academic practice. No use, distribution or reproduction is permitted which does not comply with these terms.

frontiers in Immunology

ORIGINAL RESEARCH
published: 10 March 2021
doi: 10.3389/fimmu.2021.648917

Deciphering the Prognostic Implications of the Components and Signatures in the Immune Microenvironment of Pancreatic Ductal Adenocarcinoma

Rong Tang[1,2,3,4†], *Xiaomeng Liu*[1,2,3,4†], *Chen Liang*[1,2,3,4†], *Jie Hua*[1,2,3,4], *Jin Xu*[1,2,3,4], *Wei Wang*[1,2,3,4], *Qingcai Meng*[1,2,3,4], *Jiang Liu*[1,2,3,4], *Bo Zhang*[1,2,3,4], *Xianjun Yu*[1,2,3,4*] *and Si Shi*[1,2,3,4*]

[1] Department of Pancreatic Surgery, Fudan University Shanghai Cancer Center, Shanghai, China, [2] Department of Oncology, Shanghai Medical College, Fudan University, Shanghai, China, [3] Shanghai Pancreatic Cancer Institute, Shanghai, China, [4] Pancreatic Cancer Institute, Fudan University, Shanghai, China

OPEN ACCESS

Edited by:
Keqiang Chen,
National Cancer Institute at Frederick,
United States

Reviewed by:
Hanli Xu,
Beijing Jiaotong University, China
Thomas A. Mace,
The Ohio State University,
United States

***Correspondence:**
Si Shi
shisi@fudanpci.org
Xianjun Yu
yuxianjun@fudanpci.org

† These authors have contributed equally to this work

Specialty section:
This article was submitted to Cancer Immunity and Immunotherapy, a section of the journal Frontiers in Immunology

Received: 02 January 2021
Accepted: 12 February 2021
Published: 10 March 2021

Citation:
Tang R, Liu X, Liang C, Hua J, Xu J, Wang W, Meng Q, Liu J, Zhang B, Yu X and Shi S (2021) Deciphering the Prognostic Implications of the Components and Signatures in the Immune Microenvironment of Pancreatic Ductal Adenocarcinoma. Front. Immunol. 12:648917. doi: 10.3389/fimmu.2021.648917

Background: The treatment modalities for pancreatic ductal adenocarcinoma (PDAC) are limited and unsatisfactory. Although many novel drugs targeting the tumor microenvironment, such as immune checkpoint inhibitors, have shown promising efficacy for some tumors, few of them significantly prolong the survival of patients with PDAC due to insufficient knowledge on the tumor microenvironment.

Methods: A single-cell RNA sequencing (scRNA-seq) dataset and seven PDAC cohorts with complete clinical and bulk sequencing data were collected for bioinformatics analysis. The relative proportions of each cell type were estimated using the gene set variation analysis (GSVA) algorithm based on the signatures identified by scRNA-seq or previous literature.

Results: A meta-analysis of 883 PDAC patients showed that neutrophils are associated with worse overall survival (OS) for PDAC, while CD8+ T cells, CD4+ T cells, and B cells are related to prolonged OS for PDAC, with marginal statistical significance. Seventeen cell categories were identified by clustering analysis based on single-cell sequencing. Among them, CD8+ T cells and NKT cells were universally exhausted by expressing exhaustion-associated molecular markers. Interestingly, signatures of CD8+ T cells and NKT cells predicted prolonged OS for PDAC only in the presence of "targets" for pyroptosis and ferroptosis induction. Moreover, a specific state of T cells with overexpression of ribosome-related proteins was associated with a good prognosis. In addition, the hematopoietic stem cell (HSC)-like signature predicted prolonged OS in PDAC. Weighted gene co-expression network analysis identified 5 hub genes whose downregulation may mediate the observed survival benefits of the HSC-like signature. Moreover, trajectory analysis revealed that myeloid cells evolutionarily consisted of 7 states, and antigen-presenting molecules and complement-associated genes were lost along the pseudotime flow. Consensus clustering based on the differentially expressed genes between two states harboring the longest pseudotime span identified two PDAC

groups with prognostic differences, and more infiltrated immune cells and activated immune signatures may account for the survival benefits.

Conclusion: This study systematically investigated the prognostic implications of the components of the PDAC tumor microenvironment by integrating single-cell sequencing and bulk sequencing, and future studies are expected to develop novel targeted agents for PDAC treatment.

Keywords: single cell sequencing, immune microenvironment, pancreatic cancer, prognosis, tumor immune

INTRODUCTION

Pancreatic ductal adenocarcinoma (PDAC) is the most aggressive gastrointestinal tumor, with a 5-year overall survival (OS) rate of ∼9% (1). Unfortunately, the treatment modalities for PDAC remain limited and unsatisfactory (2, 3). Although many novel drugs targeting the tumor microenvironment, such as immune checkpoint inhibitors (ICIs), have shown promising efficacy in the clinic for some tumors (4–6), few significantly prolong the survival of patients with PDAC due to insufficient knowledge on the tumor microenvironment (7).

In fact, the crosstalk between tumor cells and stromal components could inspire many initiatives for novel treatment modalities. For example, a recent study showed that CD8+ T cells could induce ferroptosis, which is a non-apoptotic cell death mechanism, in multiple tumor cells, and this antitumor efficacy could be expanded by combination with ICIs (8). Similarly, CD8+ T cells and NKT cells could induce pyroptosis in tumors, and pyroptotic tumor cells reciprocally trigger more robust anticancer immunity (9–11). In addition, many studies have demonstrated that cancer-associated fibroblasts (CAFs) promote tumor proliferation and metastasis via the secretion of various cytokines (12, 13). These studies suggested that enhanced treatment efficacy could be achieved when targeting the crosstalk between tumor cells and stromal components.

Hence, elucidating the role of the components and signatures of the tumor microenvironment is significant and imperative. The advancement of single-cell sequencing technology has provided researchers with a high-throughput method for interpreting intratumoral heterogeneity by presenting the molecular characteristics of various cell components. However, a stringent limitation of single-cell sequencing is the difficulty of correlating the sequencing findings with patients' clinical information, such as survival expectancy. In this context, appropriate combination with the strength of single-cell and bulk sequencing results would optimize the utilization of sequencing data, given the availability of complete clinical information in bulk sequencing cohorts. Many single-cell sequencing-based studies have realized this limitation and tended to confirm their findings in traditional bulk sequencing cohorts (14, 15).

An increasing number of algorithms have been generated to estimate the percentage of intratumorally infiltrated stromal cells using transcriptome data (16–18). However, the association between infiltrated stromal cells in the tumor microenvironment and patient prognoses has not yet been well-established in PDAC, especially for some immune cells that theoretically exert antitumor functions. A major reason that potentially accounts for this phenomenon might be that each type of stromal cell is subdivisible and that different subtypes of a specific cell cluster may mediate contrary functions (19, 20). A classic example is the opposite roles of M1- and M2-polarizing macrophages—the former suppress tumor development, while the latter promote tumor progression in some kinds of tumors (21, 22).

Here, we annotated the cell clusters in PDAC using single-cell sequencing data and comprehensively analyzed their prognostic implications with bulk sequencing data. Multiple bioinformatic methods and *ex silico* experiments were used to identify the prognosis-related molecular traits and potential treatment targets of PDAC.

METHODS

Sources of Datasets

A single-cell sequencing dataset (GSE155698) including 16 PDAC and 3 adjacent normal samples was obtained from the Gene Expression Omnibus (GEO). The bulk sequencing datasets were derived from The Cancer Genome Atlas (TCGA) (TCGA-PAAD), International Cancer Genome Consortium (ICGC) (ICGC-AU), GEO (GSE21501, GSE57495, GSE71729, and GSE85916), and ArrayExpress (E-MTAB-6134) databases. Both the transcriptome information and clinical information of each dataset were concurrently downloaded from the respective websites. The transcriptome data were transformed to the format of Log_2[transcripts per million (TPM) + 1]. Only PDAC tissues were included in the subsequent analysis, while other histological subtypes, such as neuroendocrine tumors, acinar cell carcinoma, and intraductal papillary mucinous neoplasms, were excluded. T-exhaust and immune checkpoint blockade (ICB) resistance signatures were downloaded from the Tumor Immune Dysfunction and Exclusion (TIDE) database.

Bioinformatics Analysis

Estimation of Intra-Tumoral Infiltrated Immune Cells

The fractions of six infiltrated immune cells, namely, CD8+ T cells, CD4+ T cells, B cells, macrophages, neutrophils, and dendritic cells, were estimated using Tumor IMmune Estimation Resource (TIMER) 2.0 (23). We also estimated the proportions of infiltrated immune cells using other algorithms, such as XCELL, CIBERSORT, and MCP-counter, in TIMER 2.0 (23). Univariate Cox regression was performed using the R package "survival."

Meta-Analysis of the Prognostic Implications of Infiltrated Immune Cells for PDAC

The hazard ratio (HR) for each infiltrated immune cell against the OS of PDAC was computed with the log-rank test. The HRs of each immune cell in different bulk sequencing-based cohorts were pooled in a fixed-effects model if no robust heterogeneity was observed ($I^2 < 50\%$ and $P > 0.05$). The meta-analysis was performed using Stata 15.1, and the forest plot was depicted via GraphPad Prism 7.0.

Processing of Single-Cell RNA Sequencing (scRNA-seq) Data

The "Seurat" package was used to perform the single-cell sequencing analysis. The batch effect of studies was removed through regularized negative binomial regression by the "Seurat" package (24). Genes detected in <3 cells were excluded, and cells with <200 total detected genes were excluded. Afterwards, we calculated the standardized variance of each gene across different cells, and only the top 2,000 variable genes were selected for subsequent analysis. Principal component analysis (PCA) was performed to identify significant dimensions with $P < 0.05$ (25). Then, the t-distributed stochastic neighbor embedding (tSNE) algorithm was applied for dimensionality reduction with the 20 initial PCs and for performing cluster classification analysis across all cells (26). Non-linear dimensional reduction was also performed with the UMAP method. Then, different cell clusters were determined and annotated by the "singleR" package according to the composition patterns of the marker genes and were then manually verified and corrected with the CellMarker database (27, 28). Given that both "singleR" and CellMarker could only classify cell clusters into basic types, we also referred to previously published scRNA-seq analyses to further classify each cell cluster into more precise subtypes (14, 15, 29–31).

Single-Sample Gene Set Enrichment Analysis (ssGSEA)

The enrichment scores of the hallmark genes were evaluated using ssGSEA with the R package "GSVA" (32). Hallmark genes were defined as the top 50 genes with the largest fold change (FC) in each cluster. Using ssGSEA, each sample with complete bulk sequencing data and clinical information was labeled with an enrichment score of the specific hallmark gene signature. The samples were divided into two groups based on the median enrichment score. Then, a Kaplan-Meier curve was plotted to visualize the survival difference between the two groups. The log-rank test and Gehan-Breslow-Wilcoxon test were performed to verify the statistical significance of the survival difference. A $P < 0.05$ was regarded as indicative of a significant difference.

Weighted Gene Co-expression Network (WGCNA)

We utilized the transcriptome profile of the E-MTAB-6134 cohort, which was the largest PDAC cohort with transcriptome and clinical data, to qualify and construct the co-expression network by the "WGCNA" package in R (33). Next, Pearson's correlation matrices were constructed for pairwise genes. We constructed a weighted adjacency matrix using a power function: $a_{mn} = |c_{mn}|^{\beta}$ (c_{mn} = Pearson's correlation between gene m and gene n; a_{mn} = adjacency between gene m and gene n). The β value emphasizes strong correlations between genes and penalizes weak correlations. After choosing the appropriate β value, the adjacency matrix was transformed into a topological overlap matrix (TOM), which measures the network connectivity of a gene defined as the sum of its adjacency with all other genes for network construction. To divide genes with similar expression patterns into gene modules, average linkage hierarchical clustering was performed according to the TOM-based dissimilarity measure with a minimum size of 50 for the gene dendrogram. Then, we further calculated the dissimilarity of module eigengenes (MEs), chose a cut line for the module dendrogram and merged some modules.

MEs were regarded as the major component in PCA for each gene module. We calculated the correlation between MEs and clinical traits or hallmark gene signatures to identify the relevant modules. Gene significance (GS) was defined as the log10 transformation of the *P* value in the linear regression between the gene expression level and clinical data. In addition, module significance (MS) was defined as the average GS for all the genes in a module. When the modules of interest were established, the core genes in a module were identified by GS > 0.2 and MS > 0.8. Specifically, in the present study, we also compared the expression levels of the selected core genes between tumor and normal tissues using GEPIA 2.0 (34), which incorporates the transcriptome data of normal pancreas tissue and thus facilitates the identification of differentially expressed genes.

Trajectory Analysis and Consensus Clustering

The single-cell pseudotime trajectories of the scRNA-seq data were constructed using the Monocle 2 algorithm (35). This algorithm uses a machine learning technique, learning a parsimonious principal graph to reduce the given high-dimensional expression profiles to a low-dimensional space. Single cells were projected to this space and ordered into a trajectory with branch points. For data interpretation, the cells that were located in the same branch were thought to be in the same differentiation state, while cells located in different branches were thought to have different cell differentiation characteristics. Differentially expressed genes between different differentiation states were identified by the R package "limma" (36). Unsupervised consensus clustering based on the differentially expressed genes was conducted using the "ConsensusClusterPlus" package. The clustering procedure included 1,000 iterations, and 80% of the data were sampled in each iteration. The optimal number of clusters was determined by the relative change in the area under the cumulative distribution function (CDF) curves of the consensus score.

Cell Culture and qRT-PCR

CAFs were first separated and purified from human pancreatic cancer tissues in our laboratory based on the study by Walter et al. and then subjected to immortalization treatment (37).

Fresh pancreatic cancer tissue was minced into 1–3 mm^3 fragments and digested with 0.25% trypsin at 37°C for 30 min. The resulting fragments were centrifuged at 600 × g for 5 min and washed once with Dulbecco's modified Eagle's medium (DMEM) containing 10% fetal bovine serum (FBS). The tissue fragments were then plated and allowed to adhere. After incubation at 37°C for several days, fibroblast outgrowth from the tissue fragments occurred. The fibroblasts were sub-cultured by trypsinization for 2–3 passages until free of epithelial cell contamination and maintained in DMEM supplemented with 10% FBS, 2% penicillin, and streptomycin (Invitrogen). The cells were grown at 37°C in a humidified atmosphere containing 5% CO_2. CAFs and the pancreatic cancer cell line SW1990 were cultured in DMEM supplemented with 10% FBS. The non-cell supernatant from SW1990 cultures was extracted through centrifugation at 800 rpm/min. Then, CAFs were treated with SW1990-derived supernatant during medium changing. TGF-beta (3 ng/ml) was added to CAF cultures as a positive control.

RESULTS

A Meta-Analysis Revealed the Correlation Between Infiltrating Immune Cells and the OS of Patients With PDAC

In past decades, many approaches have been developed to estimate or quantify the infiltration level of immune cells in tumor tissues, such as immunohistochemical staining and transcriptome-based estimation (16–18, 38, 39). We applied six algorithms, TIMER, CIBERSORT, XCELL, EPIC, QUANTISEQ, and MCP-counter, to estimate the infiltration percentage of immune cells (**Supplementary Table 1**). Then, we integrated the survival data of patients in seven PDAC cohorts with the infiltration level of each immune cell and performed univariate Cox regression to screen prognosis-related components (**Supplementary Table 1**). Given the difficulty of pooling the Cox regression-derived HR values due to the large confidence interval (CI) in this case, we performed a meta-analysis using the log-rank test-derived HR values. Six basic immune cell types (CD8+ T cells, CD4+ T cells, B cells, macrophages, neutrophils, and dendritic cells) estimated by the TIMER algorithm were selected for meta-analysis. Null or only minor heterogeneity was detected in the fixed effect model; hence, we generated the results of the meta-analysis with low bias. The results showed that neutrophil infiltration was associated with worse OS for PDAC, while CD8+ T cell, CD4+ T cell, and B cell infiltration was related to prolonged OS for PDAC with marginal statistical significance (**Figure 1**).

Single-Cell Sequencing Results Delineated the Heterogeneity of Stromal Cells in the PDAC Microenvironment

Interestingly, many theoretical anticancer cells, such as CD8+ T cells, did not show obvious survival relevance in the meta-analysis. We assumed that at least some of these anticancer immune cells were exhausted or experienced differentiation into protumoral cells, which deprived them of their tumor-killing capability. To investigate the alteration of stromal cells in PDAC, we reanalyzed the scRNA-seq dataset and annotated cell types according to their perturbation in the transcriptome. After carrying out the quality control procedures described in the Methods section (**Supplementary Figures 1A,B**), the top 2,000 variable genes were used in cell clustering (**Figure 2A**; **Supplementary Figures 1C,D**), which identified 26 clusters (**Supplementary Figures 1E,F**) and then classified these clusters into 17 cell types (**Supplementary Figure 1G**). The proportions of each cell type are shown in **Figure 2B**, and their clustering distribution is presented in **Figures 2C–E**; **Supplementary Figure 1H**. For some clusters, we took a conservative approach and annotated them as basic cell categories, such as T cells and myeloid cells. However, when specific cell markers were highly overexpressed in a cluster, we tended to annotate them into more precise clusters, such as NKT and CD8+ T cells. The significant gene markers are presented in **Supplementary Table 2**.

T Cells With a Cytotoxic Signature Predict Prolonged Survival Only in PDAC Patients With the Presence of "Targets" for Pyroptosis and Ferroptosis Induction

NKT and CD8+ T cells are theoretically capable of killing tumor cells through cytotoxic effects; however, most of these cells seem to lose their anticancer ability in the real tumor microenvironment. Through scRNA-seq, we verified that these T cells with a cytotoxic signature universally expressed exhaustion-related or ICB resistance markers (**Figures 3A,B**), which not only produced immune evasion among tumor cells but also caused a low response to immunotherapy, such as ICB. Then, we tested whether such signatures of exhausted cytotoxic T cells were associated with patient prognoses. As expected, no obvious association was observed between the signature of CD8+ T cells and OS in most cohorts except for GSE57495 (**Supplementary Figure 2**; **Figure 3C**). Then, we explored why the signatures of exhausted CD8+ T cells could still predict prolonged OS in some patients. Several recent studies suggested a novel mechanism by which cytotoxic cells trigger tumor cell death, as we reviewed previously (10). These studies demonstrated that cytotoxic T cells, including CD8+ T cells and NKT cells, could kill tumor cells through ferroptosis and pyroptosis induction. Then, we validated this hypothesis in GSE57495, which was the only dataset that showed a correlation between exhausted cytotoxic T cell signatures and patient prognoses. Survival analysis showed that the signature of CD8+ T cells was positively associated with prolonged OS only in samples harboring overexpression of targets for ferroptosis (SLC7A11) and pyroptosis (GSDMB, GSDMC, and GSDME) induction (**Figure 3C**). We continued to investigate the association between the NKT cell signature and patient OS and found that the NKT signature predicted better OS in only two datasets (E-MTAB-6134 and GSE57495). We generated a new index called the target score, which is defined

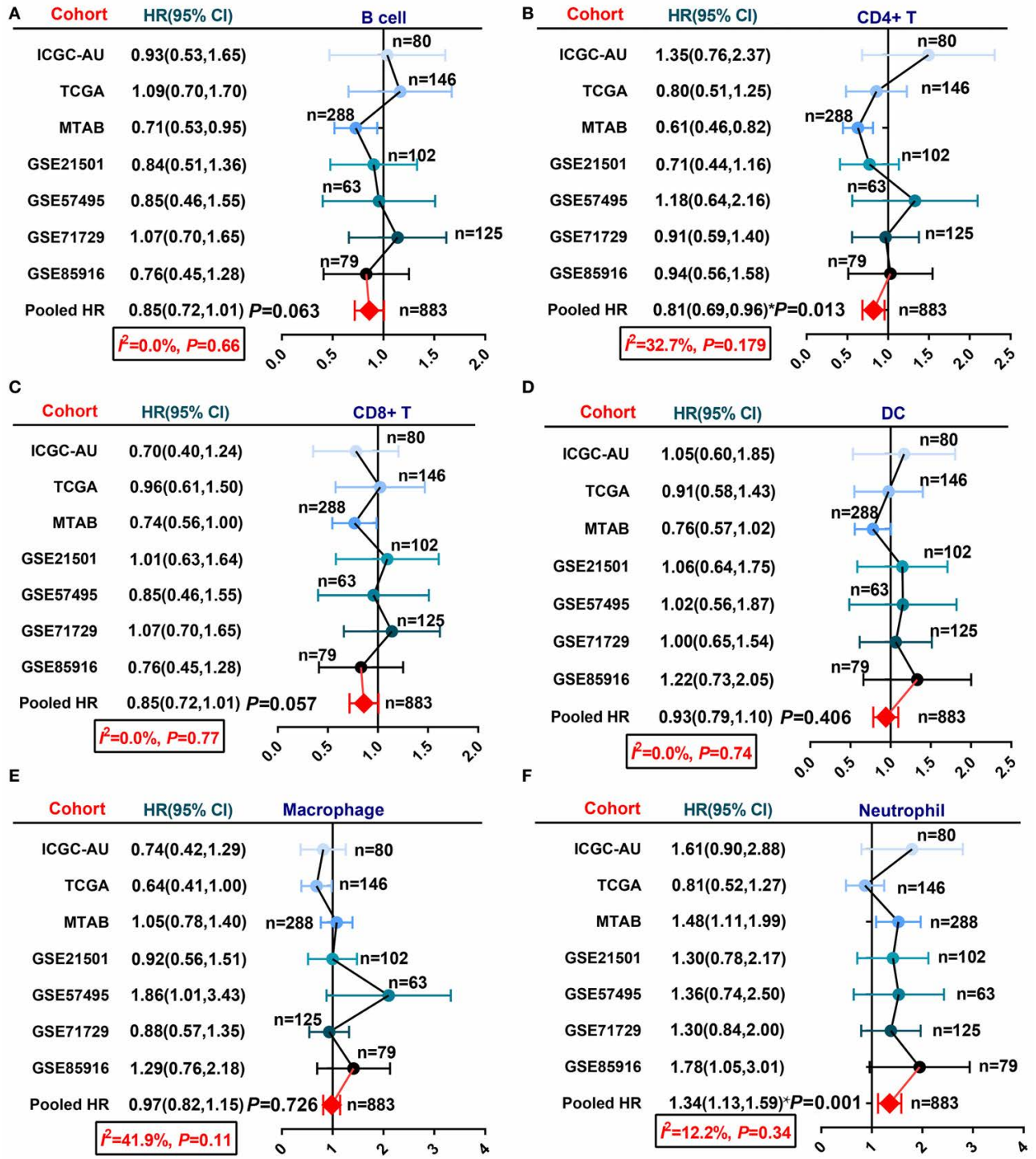

FIGURE 1 | A meta-analysis revealed the association between infiltrated immune cells and PDAC patient OS. **(A)** B cells, **(B)** CD4+ T cells, **(C)** CD8+ T cells, **(D)** dendritic cells, **(E)** macrophages, and **(F)** neutrophils.

as target score $= \frac{\text{HR(targets high expression)}}{\text{HR(targets low expression)}}$. In this equation, HR(targets high expression) reflects the influence of the NKT signature on patients' OS in PDAC samples with overexpression of specific targets for ferroptosis or pyroptosis, while HR (targets low expression) reflects the influence of the NKT signature on patients' OS in PDAC samples with downregulation of specific

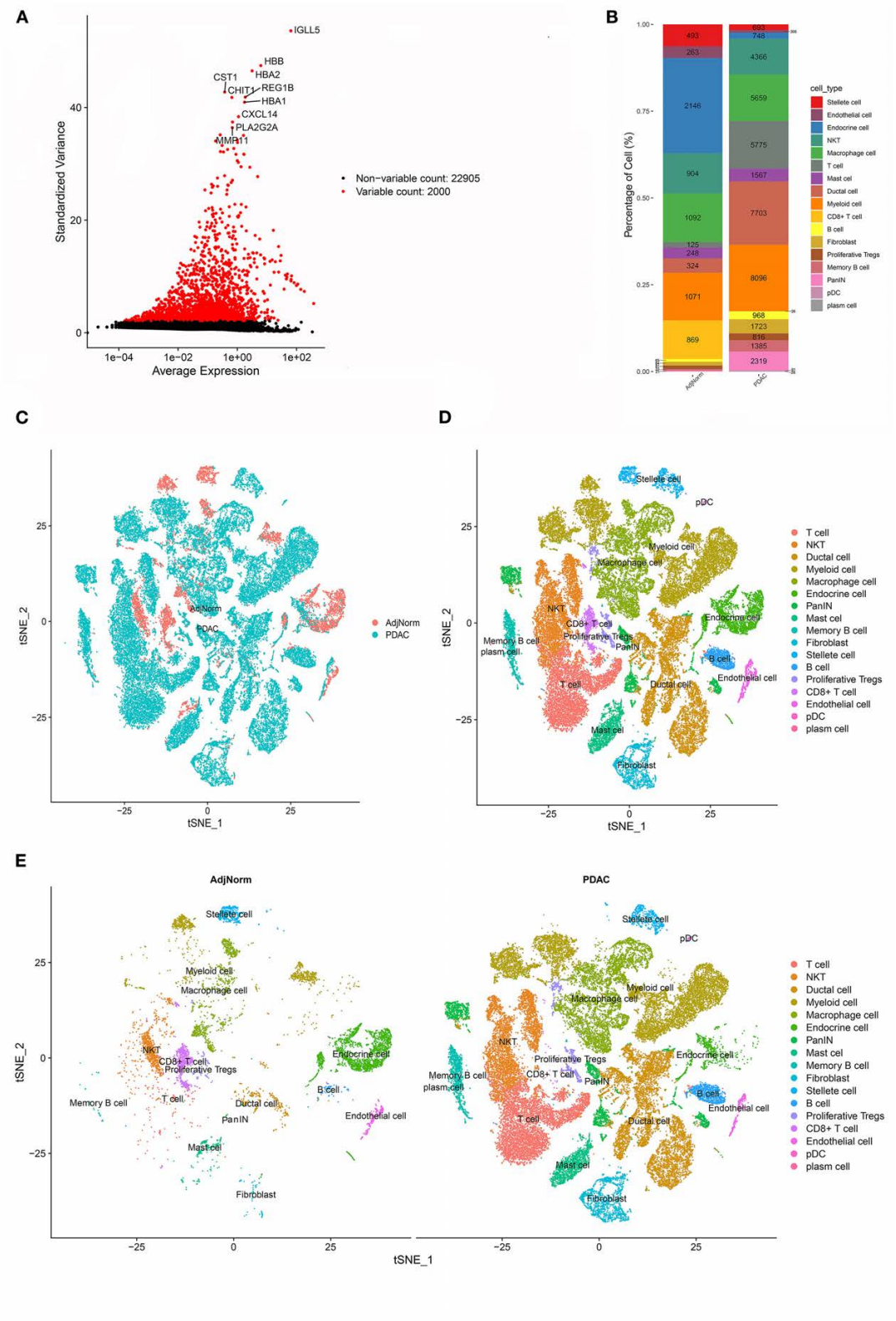

FIGURE 2 | scRNA-seq identified 17 cell types in the PDAC microenvironment. **(A)** The top 2000 variable genes with large, standardized variances were selected for subsequent analysis. **(B)** The percentage of each cell type in PDAC tissues and normal adjacent tissues. **(C–E)** tSNE algorithm classified cell clusters based on transcriptome data.

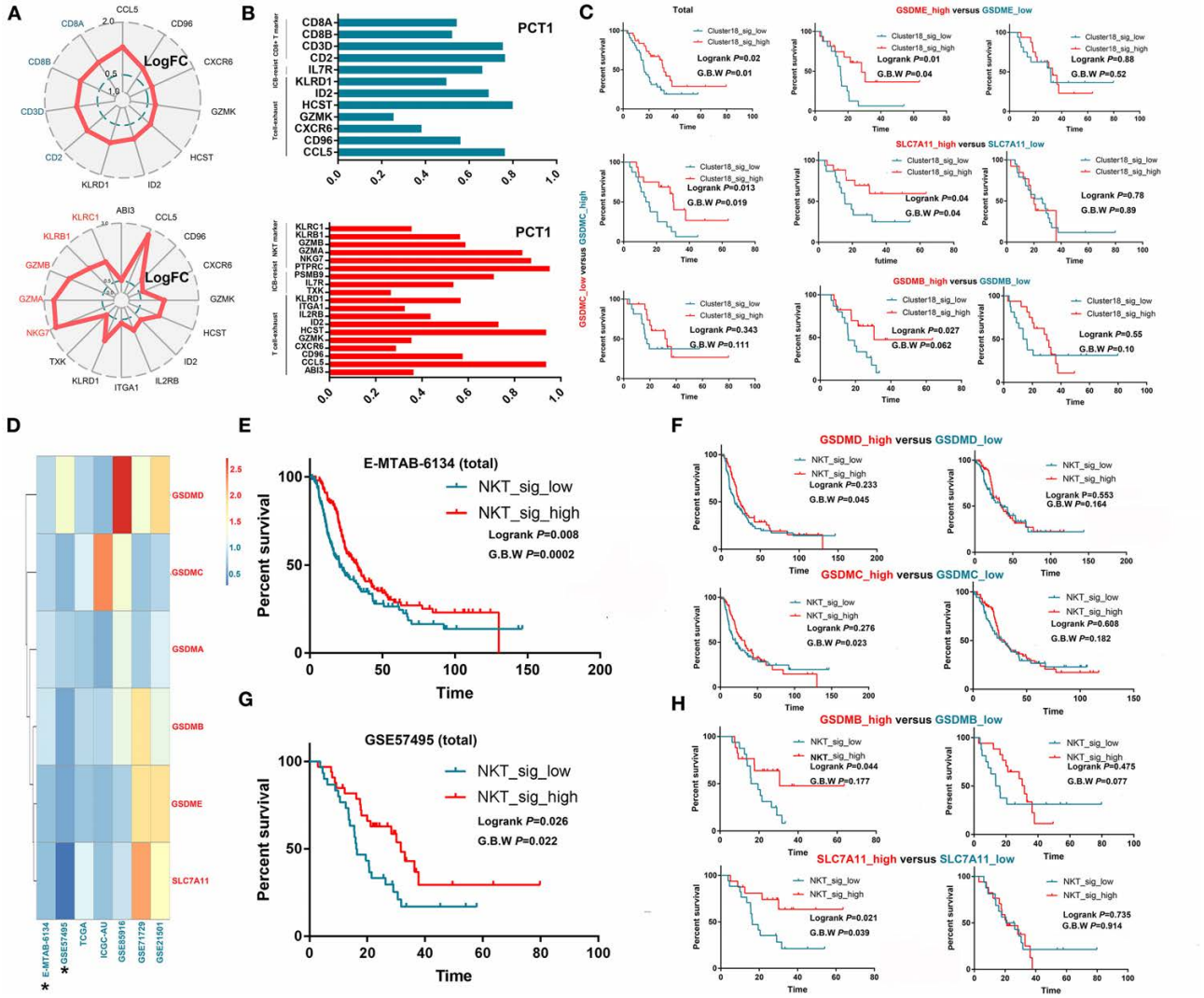

FIGURE 3 | Exhausted cytotoxic T cells predict prolonged survival only in PDACs with the presence of "targets" for pyroptosis and ferroptosis induction. **(A,B)** Intratumorally infiltrated cytotoxic T cells universally expressed exhaustion markers and ICB resistance signatures. LogFC refers to $\log_2$ (fold change); fold change equals the ratio between the mRNA level of a specific gene in one cell cluster and that in the other cell clusters. PCT1 refers to the percentage of cells that express a specific gene. **(C)** CD8+ T cell infiltration predicts prolonged OS only in samples overexpressing GSDMB, GSDMC, GSDME and SLC7A11, which are targets for cytotoxic T cells to induce pyroptosis and ferroptosis. **(D)** Heatmap showing the distribution of target scores among different PDAC cohorts. **(E–H)** NKT cell infiltration predicts prolonged OS only in samples overexpressing GSDMB-D and SLC7A11, which are targets for cytotoxic T cells to induce pyroptosis and ferroptosis.

targets for ferroptosis or pyroptosis. A heatmap was generated to visualize the Target_score of different targets across various datasets (**Figure 3D**), which suggested universal survival benefits caused by high NKT signature expression in samples with high target expression. Survival analysis further demonstrated that the high expression of some ferroptosis and pyroptosis targets was a precondition for the NKT signature predicting a benefit in terms of OS (**Figures 3E–H**). Then, we determined the independency of the prognostic implication of the NKT signature from other infiltrated immune cells. Multivariate Cox regression showed that the cytotoxic T cell signature was associated with prolonged OS, independent of other components in the PDAC microenvironment (**Supplementary Table 3**).

T Cells With Increased Ribosome-Related Protein Signatures Predict a Better Prognosis in PDAC

An LTB(+)IL-7R(+)CD3(+) cell cluster was identified by scRNA-seq (cluster 0). We analyzed the top 100 upregulated genes in this cluster and showed that 51 genes were ribosome-related proteins (**Figure 4A**). Then, we performed survival analysis and found that the cluster 0 signatures could predict prolonged OS in PDAC in multiple datasets (**Figures 4B–E**).

In addition, we investigated the prognostic implications of the three states of B cells in PDAC. Overall, these signatures predict prolonged OS in only some cohorts (**Supplementary Figure 3A**). Notably, plasma cell infiltration

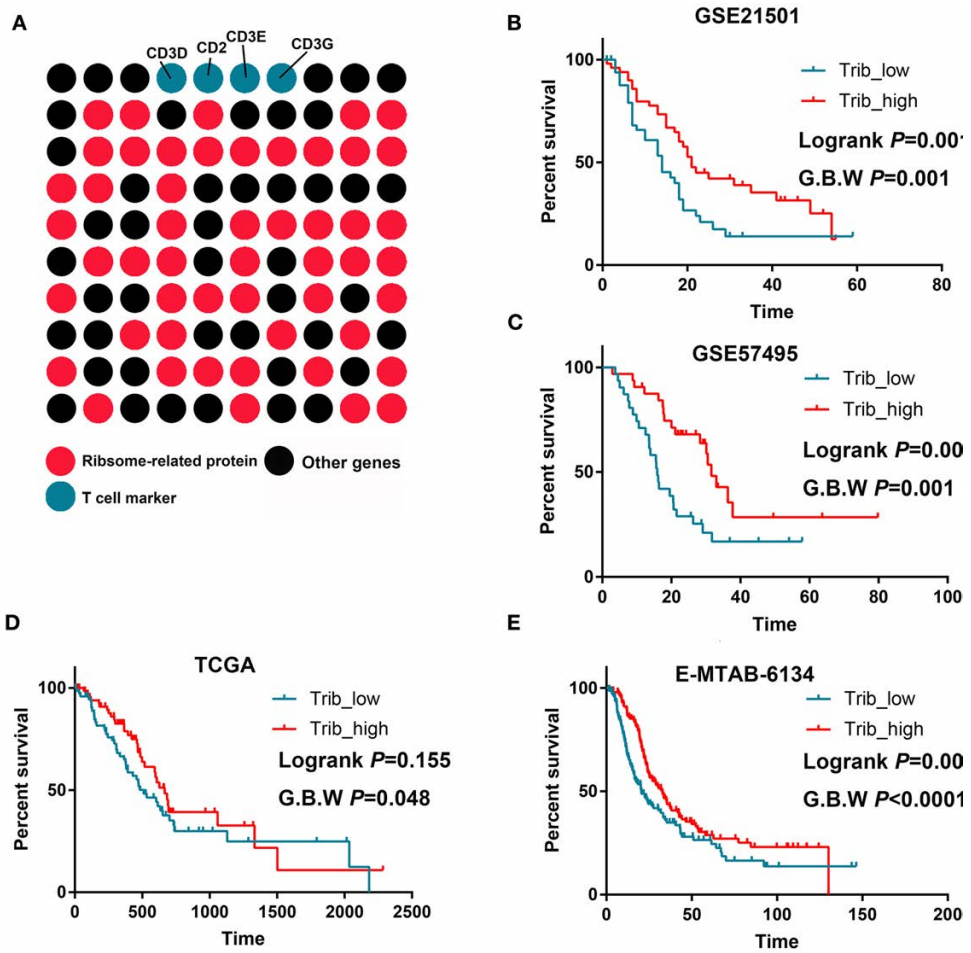

FIGURE 4 | T cells with increased ribosome-related protein signatures predict better prognoses for PDAC. **(A)** Approximately 50% of the markers of this T cell cluster were ribosome-related proteins. **(B–E)** High infiltration of this T cell cluster predicts prolonged OS in GSE21501, GSE57495, TCGA, and MTAB.

predicted better OS in the three cohorts (MTAB, ICGC, and GSE57495) (**Supplementary Figure 3B**).

Increased Hematopoietic Stem Cell (HSC)-Like Signatures Predict Better Prognoses in Patients With PDAC

The XCELL algorithm calculated the infiltration percentage of HSCs in the PDAC microenvironment; however, no direct evidence indicated the existence of intratumoral HSCs in previous studies, and scRNA-seq was performed here. It is biologically plausible that some cell clusters retain parts of the molecular signatures of HSCs. For example, we found that CD34, as a classical marker of HSCs, was significantly upregulated in cluster 19, which we identified through scRNA-seq (logFC = 1.48). Furthermore, we conducted a meta-analysis to investigate whether the HSC signature was associated with the patient prognosis. The results showed that increased HSC signatures significantly predicted prolonged OS in PDAC (HR = 0.72, 95% CI 0.61–0.85) (**Figure 5A**). To further analyze the mechanism by which HSC signatures could predict prolonged OS in PDAC, we performed WGCNA to explore the gene modules associated with HSC signatures in the MTAB cohort, which is the largest PDAC cohort with completed transcriptome and follow-up data (**Figure 5B**). Interestingly, the dark turquoise module was negatively associated with HSC signatures and the OS and DFS of patients ($r = -0.47$, $r = -0.31$, and $r = -0.28$, respectively) (**Figure 5C**). According to the criteria GS > 0.2 and MS > 0.8, we identified 5 core genes associated with HSC signatures (**Figures 5D,E**) and patient prognoses (**Figure 5F**). Given that all five genes were related to unfavorable prognoses, we speculated that these genes may be differentially expressed between tumor and normal tissues. Then, we validated the prognostic implications of these five hub genes in six other cohorts, where each gene was associated with unfavorable OS in at least two validation datasets (**Supplementary Figure 4**). Using the integrated data of the tumor transcriptome from the TCGA database and the normal pancreas transcriptome from the Genotype-Tissue Expression (GTEx) database, we showed that LDHA, SLC2A1, and PGK1 were upregulated in tumor samples (logFC > 2, $P < 0.05$).

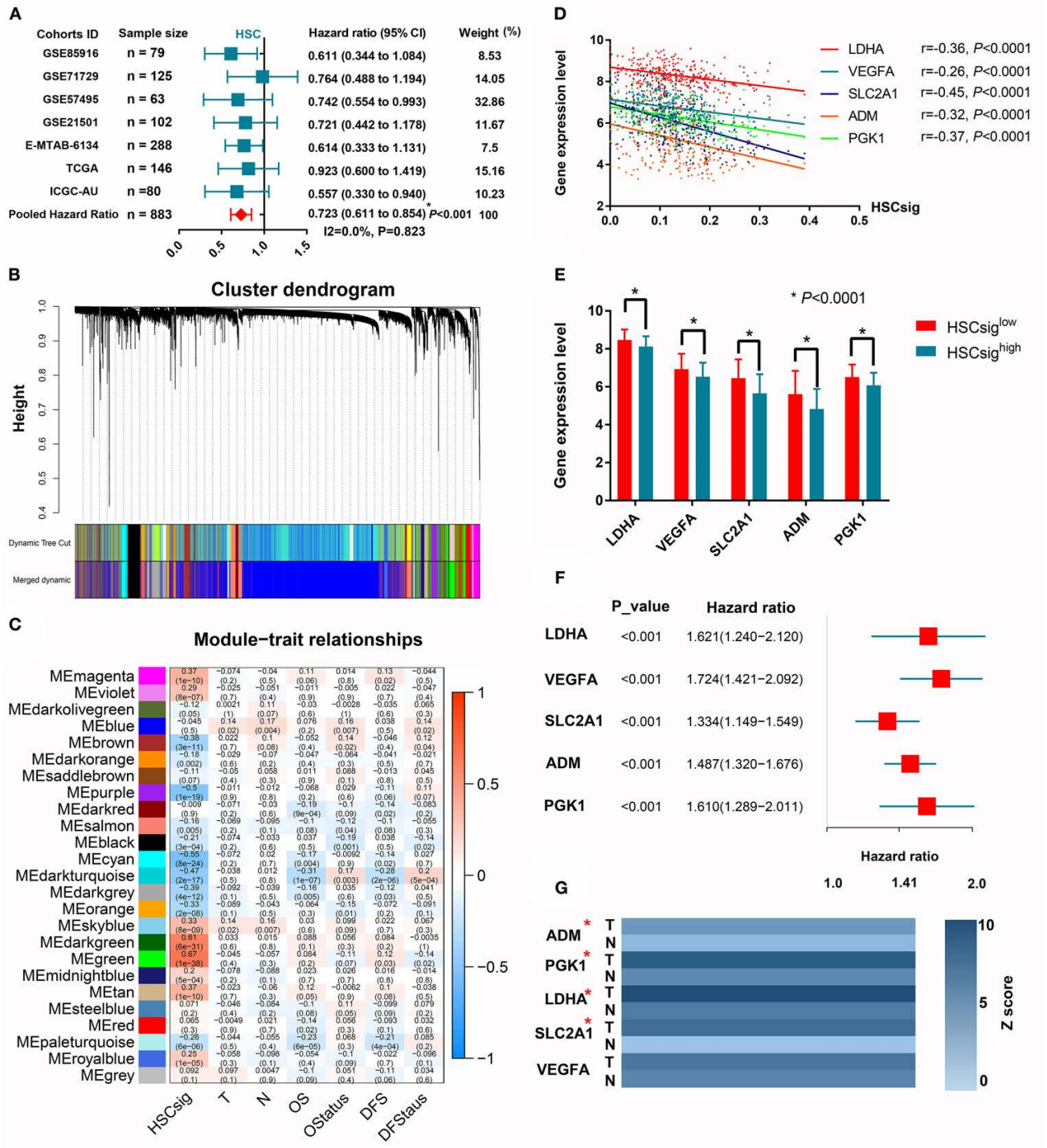

FIGURE 5 | Increased hematopoietic stem cell-like signatures predict better prognoses in patients with PDAC. **(A)** A meta-analysis revealed that HSC-like signatures predict prolonged OS in PDAC patients. **(B)** WGCNA identified gene modules with high coexpression correlation. **(C)** The correlations between 25 coexpressed gene modules and HSC-like signatures and clinical characteristics. **(D)** The linear correlations between the expression of five core genes and HSC-like signatures. **(E)** Comparison of the expression levels between groups with high or low levels of HSC-like signatures. **(F)** The survival implications of five core genes in PDAC. **(G)** The differential expression of core genes between tumor and adjacent normal tissues. *$P < 0.05$.

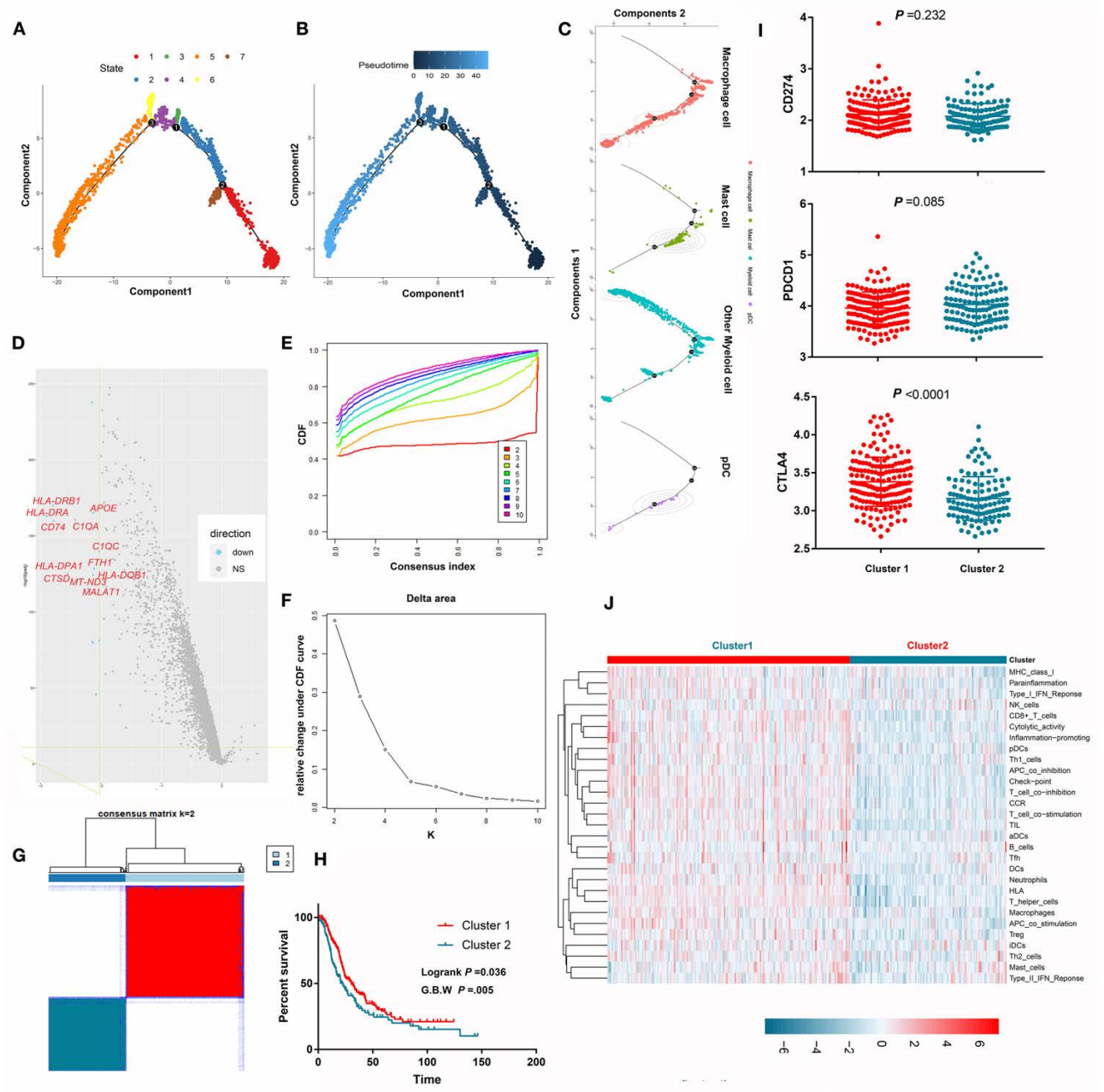

FIGURE 6 | Pseudotime trajectory analysis revealed the evolutionary characteristics of myeloid cells. **(A)** Pseudotime trajectory analysis revealed 7 different states of myeloid cells. **(B)** The gradation of color reflects pseudotime flows. **(C)** The pseudotime trajectory of each cell type in PDAC. **(D)** The volcano plot shows that many antigen-presenting molecules and complement-associated genes were lost along the pseudotime flow. **(E–G)** Unsupervised consensus clustering identified two independent subclusters based on the expression levels of the differentially expressed genes between two cell states spanning the longest pseudotime. **(H)** Survival analysis showed that the prognosis of patients in subcluster 1 was significantly better than that of patients in subcluster 2. **(I)** Comparison the expression of immune-check point between subcluster 1 and subcluster 2. **(J)** Comparison of the activity of 29 immune signatures between subcluster 1 and subcluster 2.

The Evolutionary Trajectory and Prognostic Implications of Myeloid Cells in PDAC

Myeloid cells are important components in the PDAC microenvironment and consist of macrophage cells, myeloid derived suppressive cells, dendritic cells, and granulocytes. Through scRNA-seq, we identified nine myeloid cell clusters (clusters 3–6, 10, 12, 22–23, and 25) and further annotated them as macrophages, mast cells, plasma dendritic cells, and other myeloid cells. Pseudotime trajectory analysis revealed seven different cell states (**Figure 6A**) and showed

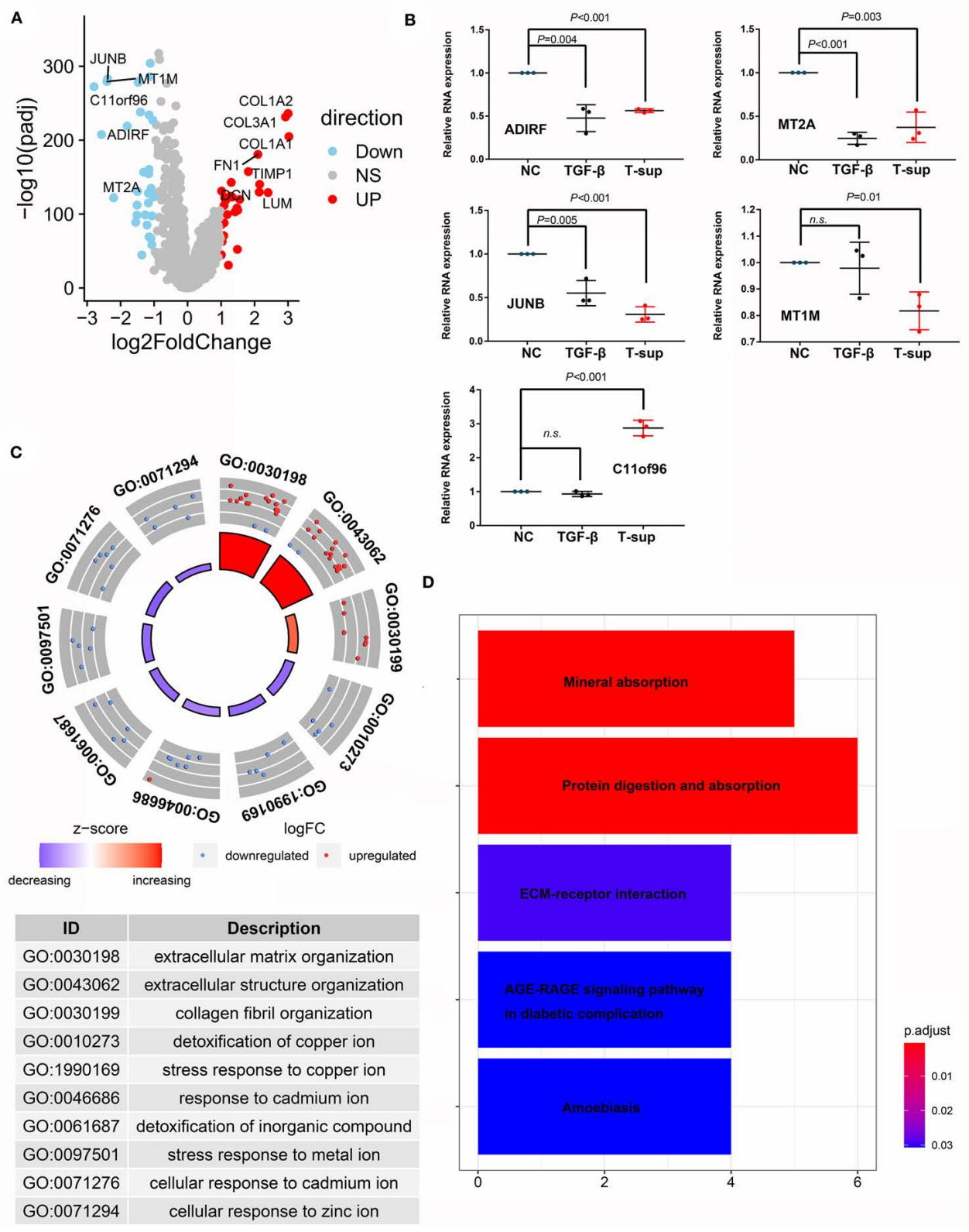

ID	Description
GO:0030198	extracellular matrix organization
GO:0043062	extracellular structure organization
GO:0030199	collagen fibril organization
GO:0010273	detoxification of copper ion
GO:1990169	stress response to copper ion
GO:0046686	response to cadmium ion
GO:0061687	detoxification of inorganic compound
GO:0097501	stress response to metal ion
GO:0071276	cellular response to cadmium ion
GO:0071294	cellular response to zinc ion

FIGURE 7 | Differences in the transcriptome between CAFs and fibroblasts/PSCs. **(A)** Volcano plot showing differentially expressed genes between CAFs and fibroblasts/PSCs in PDAC tissues and adjacent normal tissues. **(B)** Validation of the downregulated genes in CAFs using tumor supernatant or TGF-beta followed by qPCR. **(C,D)** GO and KEGG analyses revealed the functions of the differentially expressed genes.

the distributions of cell states along with pseudotime flows (**Figure 6B**). We also mapped cell classifications to pseudotime trajectories (**Figure 6C**). The difference in the transcriptome between the two cell states with the longest pseudotime span was compared, wherein many antigen-presenting molecules and complement-associated genes were lost along the pseudotime flow (**Figure 6D**). Unsupervised consensus clustering identified two independent clusters based on the pseudotime-related differentially expressed genes in the MTAB cohort (**Figures 6E–G**). Notably, the OS of patients in cluster 1 was significantly better than that of patients in cluster 2 ($P < 0.05$) (**Figure 6H**). This result was marginally confirmed in the ICGC cohort (**Supplementary Figure 5**). Next, we compared the activity of 29 immune signatures between cluster 1 and cluster 2. The results showed that cluster 1 harbored more activated immune signatures, which may account for its survival advantage (**Figures 6I,J**; **Supplementary Figure 4**).

Differentially Expressed Genes Between CAFs in PDAC Tissues and Fibroblasts in Normal Pancreas Tissues

Fibroblasts or pancreatic satellite cells exist in normal pancreatic tissues; however, many studies have suggested that the formation of tumors alters the states and function of these cells. Through scRNA-seq analysis, we compared the mRNA expression landscape of fibroblasts and satellite cells between PDAC and normal pancreas tissues (**Figure 7A**). We found that multiple genes involved in stromal formation, such as COL1A2, COL3A1, COL1A1, FN1, TIMP1, DCN, and LUM, were upregulated in CAFs (logFC > 2, adjusted $P < 0.05$). However, the genes that were downregulated in CAFs have rarely been investigated in CAFs. Hence, we investigated whether PDAC cells could induce alterations in these genes using *in vitro* experiments. Given that TGF-beta is an important mediator regulating the crosstalk between CAFs and PDAC cells, we also established a positive control group using TGF-beta to mimic the activated states of CAFs. Our results showed that the relative mRNA expression of ADIRF, MT2A, MT1M, and JUNB was downregulated after TGF-beta treatment and/or tumor stimulation, while the expression level of C11orf96 was upregulated, even after tumor stimulation (**Figure 7B**). Gene Ontology (GO) analysis indicated that the upregulated genes in CAFs were mainly related to the extracellular matrix and structural organization, while the downregulated genes in CAFs were associated with the response to mental ions (**Figure 7C**). Kyoto Encyclopedia of Genes and Genomes (KEGG) analysis also showed that the differentially expressed genes were enriched in mineral absorption and the extracellular-receptor interaction (**Figure 7D**).

DISCUSSION

The treatment modalities for multiple cancers, except for PDAC, have entered a new era of targeted and immunological therapy (40). A stringent obstacle in optimizing the efficacy of PDAC treatment is its immunosuppressive and desmoplastic microenvironment, which causes difficulties in drug delivery and low responses to targeted therapy, including ICI-based immunotherapy (41). The key to exploring optimized treatment modalities is the comprehension of the intratumoral heterogeneity of PDAC. Next-generation sequencing (NGS) techniques have led to a rush of researchers exploring cancer genomics or transcriptomes (42). Although NGS interprets numerous biological behaviors of PDAC by defining the dysregulation of oncogenic or tumor-suppressive pathways, it is hard for NGS to decipher the role of each cell type in PDAC development, given that bulk sequencing only reflects the average levels of the tissue being detected (43). Even the same cell type sometimes has a different state and manifests distinguished functions. The development of scRNA-seq has provided researchers with an opportunity to explore intratumoral heterogeneity (44). The expression levels of markers could reflect the infiltration of specific cell types in tumor tissues using algorithms such as ssGSEA and TIMER. In addition, the correlation between the relative infiltration level of a specific cell type and patient survival could be established with complete follow-up data in multiple PDAC cohorts.

In the present study, we first observed the paradox that multiple theoretically tumor-suppressive cell types were not associated with patient prognoses. Then, we tried to explore the underlying mechanism by analyzing the intratumoral heterogeneity in PDAC using scRNA-seq data and 7 PDAC cohorts with bulk sequencing. We found that cytotoxic T cells, including CD8+ T cells and NKT cells, predict prolonged OS only in samples with overexpression of targets for pyroptosis and ferroptosis induction, which was the recently reported potential mechanism by which cytotoxic T cells mediate tumor cell killing (8, 11, 45–47). In addition, a specific state of T cells with overexpression of ribosome-related proteins is associated with a better prognosis. Previous studies have shown the importance of function-intact ribosomes in allowing T cells to execute immune effects (48, 49), while ribosome-targeting antibiotics impair T cell effector function and ameliorate autoimmunity by blocking mitochondrial protein synthesis (50). Hence, maintaining normal ribosome function in intratumoral T cells may contribute to their antitumor efficacy and further improve patient prognoses. In addition, an HSC-like signature predicts better OS in PDAC. WGCNA identified 5 hub genes (LDHA, VEGFA, SLC2A1, ADM, and PGK1) whose downregulation may mediate the observed survival benefits of the HSC-like signature. Interestingly, among these core genes, SLC2A1, LDHA, and PGK1 are classical oncogenic glycolytic enzymes in PDAC (51–53), and glycolytic products such as lactate acids could upregulate the level of VEGFA (54), suggesting that the negative correlation between the HSC-like signature and glycolytic activity may account for the survival benefit associated with high HSC-like signature expression. Moreover, pseudotime trajectory analysis uncovered myeloid cells evolutionarily consisting of 7 states, and antigen-presenting molecules and complement-associated genes were lost with the pseudotime flow. Consensus clustering based on the differentially expressed genes between two states harboring the longest pseudotime span identified two PDAC groups with prognostic differences, and more infiltrated immune cells and activated immune signatures may account for the survival benefits.

This study has some strengths that are noteworthy. On one hand, we integrated the scRNA-seq and bulk sequencing data from 7 PDAC cohorts with complete follow-up data to investigate the prognostic implications of cell components, which is a heavy task with a large sample size. Using the cell markers identified in single-cell sequencing for the same cancer type to calculate the cell fractions in tissues through bulk sequencing has distinguished benefits in avoiding the bias derived from cell heterogeneity among different cancer types. In addition, we yielded several findings that might be implicated for future study and clinical translation. For example, we proposed that cytotoxic T cells, including CD8+ T cells and NKT cells, predict prolonged OS only in samples with overexpression of targets for pyroptosis and ferroptosis induction. Given that we have shown that most intratumorally infiltrated T cells were exhausted using scRNA-seq, this novel tumor-killing approach might also help theoretically exhausted T cells defend against tumor cells. Certainly, the present manuscript also has several limitations. On one hand, we analyzed only transcriptome data; however, proteome data would be an appropriate supplement for validating our conclusions. On the other hand, this is a horizontal bioinformatics study lacking longitudinal mechanistic investigation. Notably, certain signatures predict prolonged OS only in some cohorts not in all cohorts. Several reasons could explain it as follows. First, the transcriptome of tissue samples is easily disturbed, especially when preservation measures are inappropriate. Additionally, the inherent systemic error in RNA sequencing also leads to some unexpected bias. Therefore, the expression levels of some genes may not be accurate in all cohorts. Second, the follow-up OS was in fact influenced by many factors, such as chemotherapy modalities, surgical factors, loss of follow-up bias, etc. As a result, even if a gene is associated with the pathophysiological behavior of PDAC, the association of its gene expression level may not tightly reflect OS in some cases. Third, we defined signature_high and signature_low groups based on the median value, which is a common method that has been widely applied in published studies (55–58).

In conclusion, this study systematically investigated the prognostic implications of the components of the PDAC tumor microenvironment by integrating single-cell sequencing and bulk sequencing, and future studies are expected to develop novel targeted agents for PDAC treatment.

DATA AVAILABILITY STATEMENT

The original contributions presented in the study are included in the article/**Supplementary Material**, further inquiries can be directed to the corresponding authors.

ETHICS STATEMENT

This study was approved by the Institutional Research Ethics Committee of Fudan University Shanghai Cancer Center (FUSCC), and written informed consent was obtained from all patients prior to the investigation.

AUTHOR CONTRIBUTIONS

RT and XL performed the bioinformatic analysis. WW and JH were in charge of the statistical analysis. JX, CL, and JL checked the tables and figures. BZ, XY, and SS designed the study.

FUNDING

This work was supported in part by the National Natural Science Foundation of China (No. 81802352), the National Science Foundation for Distinguished Young Scholars of China (No. 81625016), the Scientific Innovation Project of Shanghai Education Committee (2019-01-07-00-07-E00057) and the Clinical and Scientific Innovation Project of Shanghai Hospital Development Center (SHDC12018109).

ACKNOWLEDGMENTS

We would like to acknowledge Dr. Heng Zhu and Dr. Yuan Zhang, who are good instructors in providing laboratory technique support.

SUPPLEMENTARY MATERIAL

The Supplementary Material for this article can be found online at: https://www.frontiersin.org/articles/10.3389/fimmu.2021.648917/full#supplementary-material

Supplementary Figure 1 | scRNA-seq identified 26 independent cell clusters in PDAC. **(A)** The mitochondrial RNA level is not associated with increased read counts, while qualified RNA is positively correlated with increased read counts. **(B)** The distribution of qualified RNA, total read counts and mitochondrial RNA levels in tumor and adjacent tissues. **(C)** The standard deviation and the number of principal components. **(D)** PDAC and adjacent normal tissues could be distinguished by two principal components. **(E,F)** The tSNE and UMAP algorithms classified PDAC samples into 26 independent clusters. **(G)** The 26 clusters were annotated into 17 cell types according to specific cell markers.

Supplementary Figure 2 | Null survival benefits of CD8+ T cells were detected in six PDAC cohorts.

Supplementary Figure 3 | The association between B cell signatures and the OS of PDAC patients. **(A)** The whole landscape. **(B)** The survival curve showed results with statistical significance.

Supplementary Figure 4 | Validation of the prognostic implications of the hub genes identified from WGCNA.

Supplementary Figure 5 | Validation of the consensus clustering results in another dataset (ICGC). **(A–C)** Unsupervised consensus clustering identified two independent subclusters based on the expression levels of the differentially expressed genes between two cell states spanning the longest pseudotime. **(D)** Survival analysis showed that the prognosis of patients in subcluster 1 was marginally better than that of patients in subcluster 2.

Supplementary Table 1 | The raw data and univariate COX analysis for the 119 cell signatures and PDACs' survival in 7 cohorts.

Supplementary Table 2 | The gene markers of different cell clusters.

Supplementary Table 3 | Multivariate cox regression validates the association between OS and cytotoxic T cell signatures in targets_high group is independent of other infiltrated cell components.

REFERENCES

1. Siegel RL, Miller KD, Jemal A. Cancer statistics, 2020. *CA Cancer J Clin*. (2020) 70:7–30. doi: 10.3322/caac.21590
2. Moore A, Donahue T. Pancreatic cancer. *JAMA*. (2019) 322:1426. doi: 10.1001/jama.2019.14699
3. Shi S, Hua J, Liang C, Meng Q, Liang D, Xu J, et al. Proposed modification of the 8th edition of the AJCC staging system for pancreatic ductal adenocarcinoma. *Ann Surg*. (2019) 269:944–50. doi: 10.1097/SLA.0000000000002668
4. Emens LA, Ascierto PA, Darcy PK, Demaria S, Eggermont AMM, Redmond WL, et al. Cancer immunotherapy: opportunities and challenges in the rapidly evolving clinical landscape. *Eur J Cancer*. (2017) 81:116–29. doi: 10.1016/j.ejca.2017.01.035
5. Segal NH, Diaz LAJr, Moskovitz J, Moy J, Ferris RL. Immunotherapy for head and neck squamous cell carcinoma. *Nat Rev Gastroenterol Hepatol*. (2018) 20:22. doi: 10.1007/s11912-018-0654-5
6. Ganesh K, Stadler ZK, Cercek A, Mendelsohn RB, Shia J. Immunotherapy in colorectal cancer: rationale, challenges and potential. *Nat Rev Gastroenterol Hepatol*. (2019) 16:361–75. doi: 10.1038/s41575-019-0126-x
7. Balachandran VP, Beatty GL, Dougan SK. Broadening the impact of immunotherapy to pancreatic cancer: challenges and opportunities. *Gastroenterology*. (2019) 156:2056–72. doi: 10.1053/j.gastro.2018.12.038
8. Wang W, Green M, Choi JE, Gijón M, Kennedy PD, Johnson JK, et al. CD8(+) T cells regulate tumour ferroptosis during cancer immunotherapy. *Nature*. (2019) 569:270–4. doi: 10.1038/s41586-019-1170-y
9. Xi G, Gao J, Wan B, Zhan P, Xu W, Lv T, et al. GSDMD is required for effector CD8(+) T cell responses to lung cancer cells. *Int Immunopharmacol*. (2019) 74:105713. doi: 10.1016/j.intimp.2019.105713
10. Tang R, Xu J, Zhang B, Liu J, Liang C, Hua J, et al. (2020). Ferroptosis, necroptosis, and pyroptosis in anticancer immunity. *J Hematol Oncol*. (2020) 13:110. doi: 10.1186/s13045-020-00946-7
11. Zhang Z, Zhang Y, Xia S, Kong Q, Li S, Liu X, et al. Gasdermin E suppresses tumour growth by activating anti-tumour immunity. *Nature*. (2020) 579:415–20. doi: 10.1038/s41586-020-2071-9
12. Qin X, Yan M, Wang X, Xu Q, Wang X, Zhu X, et al. Cancer-associated fibroblast-derived IL-6 promotes head and neck cancer progression via the osteopontin-NF-kappa b signaling pathway. *Theranostics*. (2018) 8:921–40. doi: 10.7150/thno.22182
13. Wen S, Hou Y, Fu L, Xi L, Yang D, Zhao M, et al. Cancer-associated fibroblast. (CAF)-derived IL32 promotes breast cancer cell invasion and metastasis via integrin β3-p38 MAPK signalling. *Cancer Lett*. (2019) 442:320–32. doi: 10.1016/j.canlet.2018.10.015
14. Ligorio M, Sil S, Malagon-Lopez J, Nieman LT, Misale S, Di Pilato M, et al. Stromal microenvironment shapes the intratumoral architecture of pancreatic cancer. *Nat Biotechnol*. (2019) 178:e127. doi: 10.1016/j.cell.2019.05.012
15. Moncada R, Barkley D. Integrating microarray-based spatial transcriptomics and single-cell RNA-seq reveals tissue architecture in pancreatic ductal adenocarcinomas. *Nat Biotechnol*. (2020). 38:333–42. doi: 10.1038/s41587-019-0392-8
16. Aran D, Hu Z, Butte AJ. xCell: digitally portraying the tissue cellular heterogeneity landscape. *Genome Biol*. (2017) 18:220. doi: 10.1186/s13059-017-1349-1
17. Li T, Fan J, Wang B, Traugh N, Chen Q, Liu JS, et al. TIMER: a web server for comprehensive analysis of tumor-infiltrating immune cells. *Cancer Res*. (2017) 77:e108–10. doi: 10.1158/0008-5472.CAN-17-0307
18. Chen B, Khodadoust MS, Liu CL, Newman AM, Alizadeh AA. Profiling tumor infiltrating immune cells with CIBERSORT. *Methods Mol Biol*. (2018) 1711:243–59. doi: 10.1007/978-1-4939-7493-1_12
19. Philip M, Schietinger A. Heterogeneity and fate choice: T cell exhaustion in cancer and chronic infections. *Curr Opin Immunol*. (2019) 58:98–103. doi: 10.1016/j.coi.2019.04.014
20. van der Leun AM, Thommen DS. CD8(+) T cell states in human cancer: insights from single-cell analysis. *Nat Rev Cancer*. (2020) 20:218–32. doi: 10.1038/s41568-019-0235-4
21. Yuan A, Hsiao YJ, Chen HY, Chen HW, Ho CC, Chen YY, et al. Opposite effects of M1 and M2 macrophage subtypes on lung cancer progression. *Sci Rep*. (2015) 5:14273. doi: 10.1038/srep14273
22. Orecchioni M, Ghosheh Y, Pramod AB, Ley K. Macrophage polarization: different gene signatures in M1(LPS+) vs. classically and M2(LPS-) vs. alternatively activated macrophages. *Front Immunol*. (2019) 10:1084. doi: 10.3389/fimmu.2019.01084
23. Li T, Fu J, Zeng Z, Cohen D, Li J, Chen Q, et al. TIMER2.0 for analysis of tumor-infiltrating immune cells. *Nucleic Acids Res*. (2020) 48:W509–14. doi: 10.1093/nar/gkaa407
24. Stuart T, Butler A, Hoffman P, Hafemeister C, Papalexi E, Mauck WM, et al. Comprehensive integration of single-cell data. *Cell*. (2019) 177:e1821. doi: 10.1016/j.cell.2019.05.031
25. Lall S, Sinha D, Bandyopadhyay S, Sengupta D. Structure-aware principal component analysis for single-cell RNA-seq data. *J Comput Biol*. (2018) 25:1365–73. doi: 10.1089/cmb.2018.0027
26. Satija R, Farrell JA, Gennert D, Schier AF, Regev A. Spatial reconstruction of single-cell gene expression data. *Nat Biotechnol*. (2015) 33:495–502. doi: 10.1038/nbt.3192
27. Aran D, Looney AP, Liu L, Wu E, Fong V, Hsu A, et al. Reference-based analysis of lung single-cell sequencing reveals a transitional profibrotic macrophage. *Nat Immunol*. (2019) 20:163–72. doi: 10.1038/s41590-018-0276-y
28. Zhang X, Lan Y, Xu J, Quan F, Zhao E, Deng C, et al. CellMarker: a manually curated resource of cell markers in human and mouse. *Nucleic Acids Res*. (2019) 47:D721–8. doi: 10.1093/nar/gky900
29. Peng J, Sun BF, Chen CY, Zhou JY, Chen YS. Single-cell RNA-seq highlights intra-tumoral heterogeneity and malignant progression in pancreatic ductal adenocarcinoma. *Cell Res*. (2019) 29:725–38. doi: 10.1038/s41422-019-0195-y
30. Wu W, Elyada E, Bolisetty M, Laise P, Flynn WF. Cross-species single-cell analysis of pancreatic ductal adenocarcinoma reveals antigen-presenting cancer-associated fibroblasts. *Cell Res*. (2019) 9:1102–23. doi: 10.1158/2159-8290.CD-19-0094
31. Schlesinger Y, Yosefov-Levi O, Kolodkin-Gal D, Granit RZ, Peters L, Kalifa R. Single-cell transcriptomes of pancreatic preinvasive lesions and cancer reveal acinar metaplastic cells' heterogeneity. *Nat Biotechnol*. (2020) 11:4516. doi: 10.1038/s41467-020-18207-z
32. Hänzelmann S, Castelo R, Guinney J. GSVA: gene set variation analysis for microarray and RNA-seq data. *BMC Bioinformat*. (2013) 14:7. doi: 10.1186/1471-2105-14-7
33. Langfelder P, Horvath S. WGCNA: an R package for weighted correlation network analysis. *BMC Bioinformat*. (2008) 9:559. doi: 10.1186/1471-2105-9-559
34. Tang Z, Kang B, Li C, Chen T, Zhang Z. GEPIA2: an enhanced web server for large-scale expression profiling and interactive analysis. *Nucleic Acids Res*. (2019) 47:W556–60. doi: 10.1093/nar/gkz430
35. Qiu X, Mao Q, Tang Y, Wang L, Chawla R, Pliner HA, et al. Reversed graph embedding resolves complex single-cell trajectories. *Nat Methods*. (2017). 14:979–82. doi: 10.1038/nmeth.4402
36. Ritchie ME, Phipson B, Wu D, Hu Y, Law CW, Shi W, et al. limma powers differential expression analyses for RNA-sequencing and microarray studies. *Nucleic Acids Res*. (2015) 43:e47. doi: 10.1093/nar/gkv007
37. Walter K, Omura N, Hong SM, Griffith M, Goggins M. Pancreatic cancer associated fibroblasts display normal allelotypes. *Cancer Biol Ther*. (2008) 7:882–8. doi: 10.4161/cbt.7.6.5869
38. Scanziani E. Immunohistochemical staining of fixed tissues. *Methods Mol Biol*. (1998) 104:133–40. doi: 10.1385/0-89603-525-5:133
39. Otali D, Fredenburgh J, Oelschlager DK, Grizzle WE. A standard tissue as a control for histochemical and immunohistochemical staining. *Biotech Histochem*. (2016) 91:309–26. doi: 10.1080/10520295.2016.1179342
40. Gotwals P, Cameron S, Cipolletta D, Cremasco V, Crystal A, Hewes B, et al. Prospects for combining targeted and conventional cancer therapy with immunotherapy. *Nat Rev Cancer*. (2017) 17:286–301. doi: 10.1038/nrc.2017.17
41. Li KY, Yuan JL, Trafton D, Wang JX, Niu N, Yuan CH, et al. Pancreatic ductal adenocarcinoma immune microenvironment and immunotherapy prospects. *Chronic Dis Transl Med*. (2020) 6:6–17. doi: 10.1016/j.cdtm.2020.01.002
42. Kamps R, Brandão RD, Bosch BJ, Paulussen AD, Xanthoulea S, Blok MJ, et al. Next-generation sequencing in oncology: genetic diagnosis, risk prediction and cancer classification. *Int J Mol Sci*. (2017) 18:308. doi: 10.3390/ijms18020308

43. Morganti S, Tarantino P, Ferraro E, D'Amico P, Duso BA, Curigliano G. Next generation sequencing (NGS): a revolutionary technology in pharmacogenomics and personalized medicine in cancer. *Adv Exp Med Biol*. (2019) 1168:9–30. doi: 10.1007/978-3-030-24100-1_2
44. Papalexi E, Satija R. Single-cell RNA sequencing to explore immune cell heterogeneity. *Nat Rev Immunol*. (2018) 18:35–45. doi: 10.1038/nri.2017.76
45. Minton K. Pyroptosis heats tumour immunity. *Nat Rev Immunol*. (2020) 20:274–5. doi: 10.1038/s41577-020-0297-2
46. Nicolai CJ, Raulet DH. Killer cells add fire to fuel immunotherapy. *Science*. (2020) 368:943–4. doi: 10.1126/science.abc2502
47. Zhou Z, He H. Granzyme A from cytotoxic lymphocytes cleaves GSDMB to trigger pyroptosis in target cells. *Science*. (2020) 368:eaaz7548. doi: 10.1126/science.aaz7548
48. Tan TCJ, Knight J, Sbarrato T, Dudek K, Willis AE, Zamoyska R. Suboptimal T-cell receptor signaling compromises protein translation, ribosome biogenesis, and proliferation of mouse CD8 T cells. *Proc Natl Acad Sci USA*. (2017) 114:E6117–26. doi: 10.1073/pnas.1700939114
49. Wolf T, Jin W, Zoppi G, Vogel IA, Akhmedov M, Bleck CKE. Dynamics in protein translation sustaining T cell preparedness. *Nat Immunol*. (2020) 21:927–37. doi: 10.1038/s41590-020-0714-5
50. Almeida L, Dhillon-LaBrooy A, Castro CN, Adossa N, Carriche GM, Guderian M, et al. Ribosome-targeting antibiotics impair T cell effector function and ameliorate autoimmunity by blocking mitochondrial protein synthesis. *Immunity*. (2020) 92:1408–19. doi: 10.1101/832956
51. Nagarajan A, Dogra SK, Sun L, Gandotra N, Ho T, Cai G, et al. Paraoxonase 2 facilitates pancreatic cancer growth and metastasis by stimulating GLUT1-mediated glucose transport. *Mol Cell*. (2017) 67:e686. doi: 10.1016/j.molcel.2017.07.014
52. Fleming JB, Fukuhisa H, Seki N, Idichi T, Kurahara H, Yamada Y, et al. Gene regulation by antitumor miR-130b-5p in pancreatic ductal adenocarcinoma: the clinical significance of oncogenic EPS8. *J Hum Genet*. (2019) 64:521–34. doi: 10.1038/s10038-019-0584-6
53. Liang C, Shi S, Qin Y, Meng Q, Hua J, Hu Q, et al. Localisation of PGK1 determines metabolic phenotype to balance metastasis and proliferation in patients with SMAD4-negative pancreatic cancer. *Gut*. (2020) 69:888–900. doi: 10.1136/gutjnl-2018-317163
54. Song J, Lee K, Park SW, Chung H, Jung D, Na YR, et al. Lactic acid upregulates VEGF expression in macrophages and facilitates choroidal neovascularization. *Invest Ophthalmol Vis Sci*. (2018) 59:3747–54. doi: 10.1167/iovs.18-23892
55. Brooks JM, Menezes AN, Ibrahim M, Archer L, Lal N, Bagnall CJ, et al. Development and validation of a combined hypoxia and immune prognostic classifier for head and neck cancer. *Clin Cancer Res*. (2019) 25:5315–28. doi: 10.1158/1078-0432.CCR-18-3314
56. Karasinska JM, Topham JT, Kalloger SE, Jang GH, Denroche RE, Culibrk L, et al. Altered gene expression along the glycolysis-cholesterol synthesis axis is associated with outcome in pancreatic cancer. *Clin Cancer Res*. (2020) 26:135–46. doi: 10.1158/1078-0432.CCR-19-1543
57. Lv J, Zhu Y, Ji A, Zhang Q, Liao G. Mining TCGA database for tumor mutation burden and their clinical significance in bladder cancer. *Biosci Rep*. (2020) 40:BSR20194337. doi: 10.1042/BSR20194337
58. Zhang M, Wang X, Chen X, Guo F, Hong J. Prognostic value of a stemness index-associated signature in primary lower-grade glioma. *Front Genet*. (2020) 11:441. doi: 10.3389/fgene.2020.00441

Conflict of Interest: The authors declare that the research was conducted in the absence of any commercial or financial relationships that could be construed as a potential conflict of interest.

Copyright © 2021 Tang, Liu, Liang, Hua, Xu, Wang, Meng, Liu, Zhang, Yu and Shi. This is an open-access article distributed under the terms of the Creative Commons Attribution License (CC BY). The use, distribution or reproduction in other forums is permitted, provided the original author(s) and the copyright owner(s) are credited and that the original publication in this journal is cited, in accordance with accepted academic practice. No use, distribution or reproduction is permitted which does not comply with these terms.

frontiers in Immunology

REVIEW
published: 18 March 2021
doi: 10.3389/fimmu.2021.645242

Fundamentals of T Cell Metabolism and Strategies to Enhance Cancer Immunotherapy

Guillermo O. Rangel Rivera[1,2,3]*, *Hannah M. Knochelmann*[1,2,3], *Connor J. Dwyer*[1], *Aubrey S. Smith*[1,2,3], *Megan M. Wyatt*[2,3], *Amalia M. Rivera-Reyes*[2,3], *Jessica E. Thaxton*[1,4] and *Chrystal M. Paulos*[2,3]*

[1] Department of Microbiology and Immunology, Medical University of South Carolina, Charleston, SC, United States, [2] Department of Surgery, Emory University, Atlanta, GA, United States, [3] Department of Microbiology and Immunology, Emory University, Atlanta, GA, United States, [4] Department of Orthopaedics and Physical Medicine, Medical University of South Carolina, Charleston, SC, United States

OPEN ACCESS

Edited by:
Peng Qu,
National Institutes of Health (NIH), United States

Reviewed by:
Yiming Yin,
University of Florida, United States
Xiaobin Huang,
University of Pennsylvania, United States

***Correspondence:**
Guillermo O. Rangel Rivera
rangelar@musc.edu
Chrystal M. Paulos
chrystal.mary.paulos@emory.edu

Specialty section:
This article was submitted to Cancer Immunity and Immunotherapy, a section of the journal Frontiers in Immunology

Received: 22 December 2020
Accepted: 01 March 2021
Published: 18 March 2021

Citation:
Rangel Rivera GO, Knochelmann HM, Dwyer CJ, Smith AS, Wyatt MM, Rivera-Reyes AM, Thaxton JE and Paulos CM (2021) Fundamentals of T Cell Metabolism and Strategies to Enhance Cancer Immunotherapy. Front. Immunol. 12:645242. doi: 10.3389/fimmu.2021.645242

Emerging reports show that metabolic pathways can be targeted to enhance T cell-mediated immunity to tumors. Yet, tumors consume key metabolites in the host to survive, thus robbing T cells of these nutrients to function and thrive. T cells are often deprived of basic building blocks for energy in the tumor, including glucose and amino acids needed to proliferate or produce cytotoxic molecules against tumors. Immunosuppressive molecules in the host further compromise the lytic capacity of T cells. Moreover, checkpoint receptors inhibit T cell responses by impairing their bioenergetic potential within tumors. In this review, we discuss the fundamental metabolic pathways involved in T cell activation, differentiation and response against tumors. We then address ways to target metabolic pathways to improve the next generation of immunotherapies for cancer patients.

Keywords: T cell metabolism, tumor microenvironment, adoptive T cell transfer, immune checkpoint therapy, tumor metabolism, tumor infiltrating lymphocytes

INTRODUCTION

It has long been appreciated that glycolysis and mitochondrial respiration work together to satisfy the long-term energetic demands of T cells in the host (1). As T cell survival is often impaired in patients with cancer and chronic infectious disease (1, 2), it is necessary to have an effective metabolic capacity for a productive immune response (1). For example, in patients, one reason T cells do not thrive amidst tumor cells is that they compete for the same energy sources (1). Herein, we review the fundamental metabolic requirements for T cells to survive, proliferate and mount antigen-specific responses in the context of effector and memory responses. We then outline how the harsh tumor microenvironment manipulates T cell metabolism to impair effector functions. Finally, we contemplate emerging data where metabolic manipulations have been performed and have shown promise for augmenting T cell-based immunotherapies for patients with cancer.

A BRIEF HISTORY OF T CELL METABOLISM

Studies in the mid-20th century first detailed the nutrient requirements for quiescent and activated T cells to survive. It was discovered that energy production and nutrient uptake shifts when a resting T cell is activated *via* signaling cues (3, 4). In the 1960's, work by Hedeskov et al. initially described the metabolism of T lymphocytes at the resting state. Surprisingly, resting T cells largely depended on oxidative phosphorylation (OXPHOS) to survive. Additional investigations, published nearly a decade later, uncovered that resting T cells shift from OXPHOS to avid glycolysis and amino acid consumption upon TCR-mediated recognition of antigen (5). While this finding is obvious now, it was unexpected at the time, especially given that exploiting glycolysis for energy was largely thought less efficient than OXPHOS for T cells to generate ATP (3). For many years, these observations remained as descriptive findings of the highly dynamic ways T cells use bioenergetics to thrive. However, from the 1980's to present day, the significance of bioenergetic requirements for the activation, effector functions and lasting memory of T cell responses against tumors have begun to be elucidated and exploited to improve medicine.

T cells use different metabolic pathways based on their differentiation and memory status (6–8). **Figure 1** visually portrays how T cells exploit distinct metabolic pathways throughout their lifetime and during encounters with foreign antigen, such as viruses or transformed cells (9–11). As mentioned, naïve T cells rely on OXPHOS to survive in their resting state (12, 13). However, upon primary exposure to antigen, naïve T cells differentiate into effector cells and use glycolysis to help them effectively secrete cytokines, such as IFN-gamma and TNF-alpha (14–17). Following activation, naïve T cells shift from mostly oxidizing glutamine to lactate (75% of lactate produced from glutamine oxidation) through OXPHOS towards mostly using anaerobic glycolysis and partial glutamine oxidation (67% of all lactate from glucose metabolism, and 33% from glutamine), surprisingly without significantly changing their ATP production (5). After effector T cells encounter an antigen challenge, many of them die (18). However, a few prevail and survive long-term to battle re-infections or tumor relapse (17, 19, 20). These T cells are termed memory T cells. When memory T cells encounter the same antigen, they can more rapidly induce their effector functions to clear the insult (6, 21). These T cells are termed effector memory cells (EM) (22, 23). Effector T cells derived from memory rather than antigen naïve precursors more efficiently produce cytolytic cytokines by improving the coupling of glycolytic enzymes and mitochondrial machinery to rapidly utilize glucose following a secondary encounter with antigen (11, 24). Most effector memory T cells perish, but the few survivors employ OXPHOS to persist (8, 25). Below, we elaborate on the metabolic requirements of T cells at various stages of differentiation.

METABOLIC REQUIREMENTS DISTINGUISH EFFECTOR AND MEMORY T CELL SUBSETS

Naïve T Cell Metabolism

Naïve T cells can live for the entire duration of the host's life. In fact, naïve T cells can be detected in humans as old as 100 years (26). Only after they encounter their respective antigens, do they

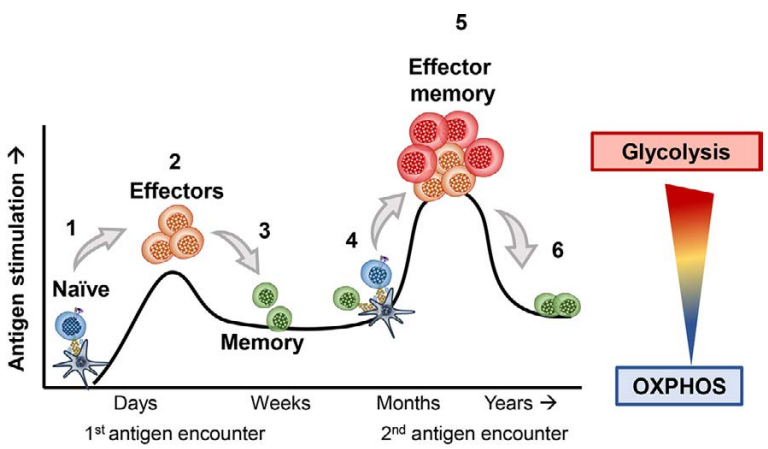

FIGURE 1 | 1) Naive T cells breakdown glucose and efficiently break it down through the tricarboxylic acid (TCA) cycle and oxidative phosphorylation (OXPHOS) to survive, until they encounter their antigen. 2) Upon a primary exposure to antigen, naïve T cells differentiate into effector T cells. As effectors they shift towards the use of amino acids as well as glucose, both required for their proliferation and cytolytic activity. 3) After clearing their inciting antigen, many effector T cells die. However, a fraction of surviving T cells can form memory T cells, which adapt towards improved mitochondrial biogenesis and OXPHOS. 4) These memory T cells can survive for many months to years until they encounter a similar antigen. 5) If these memory T cells re-encounter the same antigen, they rapidly become effectors and more efficiently engage in glycolysis and amino acid usage to robustly proliferate and secrete cytokines. 6) The T cells that survive maintain their usage of OXPHOS to persist long-term within hosts.

either become effector T cells that perish or transition into memory T cells that continue to thrive (19). But how do naïve cells remain viable for so long? As in **Figure 2A**, naïve T cells can only survive when homeostatic cytokines, like interleukin 7 (IL-7) provide signaling cues (27). IL-7 provides the signaling necessary to enable the mechanisms that nurture the survival of naïve T through Akt signaling (28). This pathway, in naïve T cells promotes the translocation of the glucose transporter 1 (Glut1)

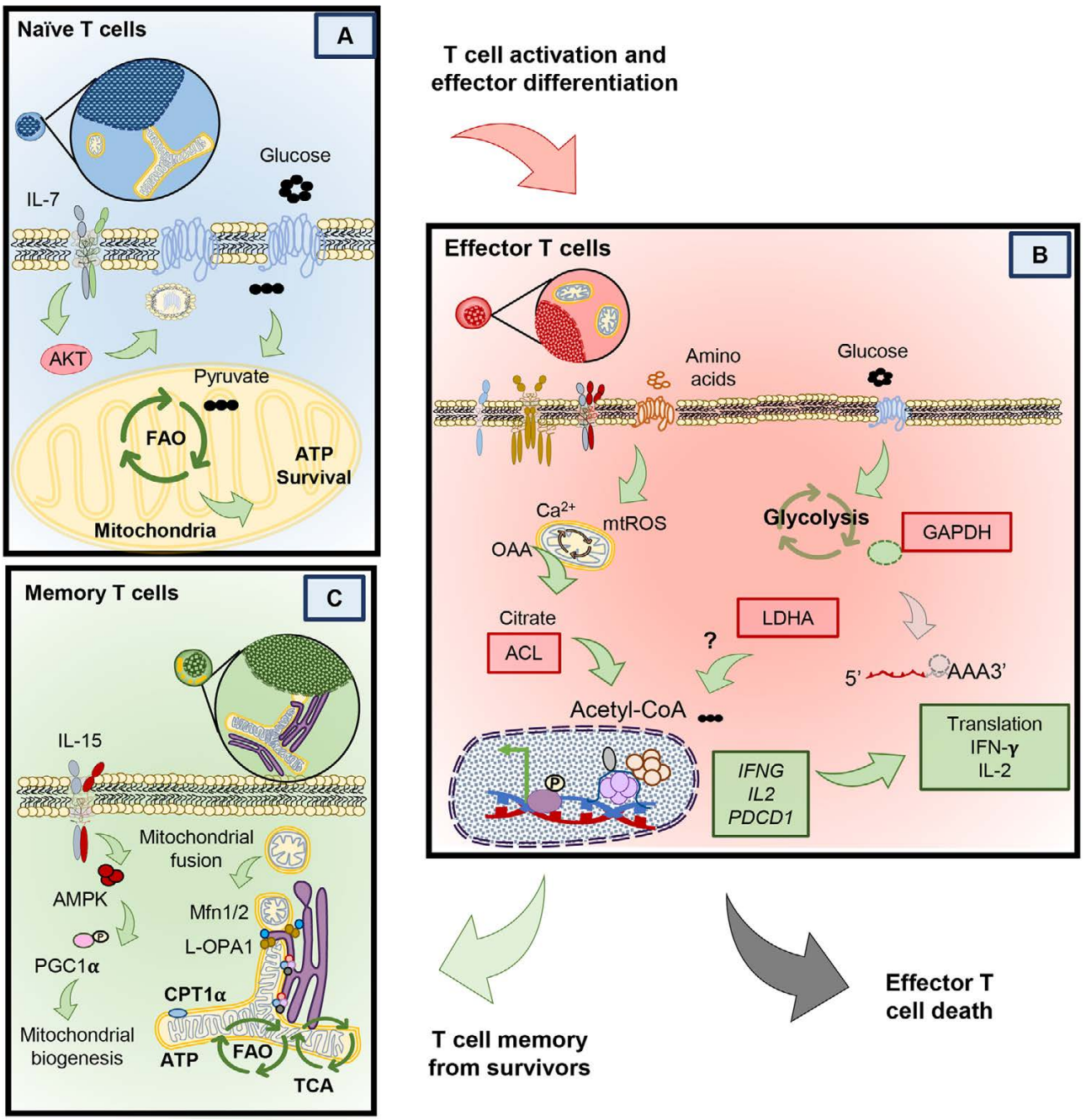

FIGURE 2 | Different metabolic programs between naïve, memory and effector T cells. **(A)** Naïve T cells rely on the full oxidation of glucose through OXPHOS, in the absence of TCR stimulation. **(B)** Upon T cell stimulation T cells undergo protein and transcriptional changes in metabolism that allow the sustained activity of glycolysis and other amino acid uptake and usage. Glycolysis by products in effector T cells mediate changes that help sustain effector cytokine release and cytolytic function. Effector T cells that clear antigen either die or contract to form memory T cells. **(C)** Compared to effectors, memory T cells possess an enhanced metabolic profile dependent on mitochondrial biogenesis, mitochondrial fusion and reliance on fatty acid oxidation.

to take up glucose. Glucose is then broken down into pyruvate, a substrate that enters the mitochondria to activate the synthesis of triacyl glycerol, which serves as a source of lipids that fuels into the fatty acid oxidation (FAO) pathway (28–30). In contrast to this maintenance phase, many nutrients (glucose, glutamine, L-arginine, and other amino acids) are needed to differentiate naïve T cells into the effector phenotype upon antigen encounter (5). We next will detail how activated T cells engage in transcriptional and metabolic changes to license them to proliferate and secrete effector cytokines.

Glycolysis in Effector T Cell Function

Naïve T cells become activated upon TCR engagement with an antigen presented *via* the major histocompatibility complex (MHC) on antigen presenting cells (signal 1). However naïve T cells require a second signal *via* costimulatory molecules (signal 2) to become fully activated and proliferate (31–33). Along with these two signals, cytokines in the host play a key role in fine tuning the fate and metabolic profile of naïve T cells into either an effector or memory phenotype (**Figure 2B**) (12, 34–36). Effector T cells secrete cytotoxic cytokines, such as interferon-γ, TNF-α and granzyme B. These cytokines and cytotoxic molecules destroy cancer cells or clear viruses (37–39). T cells require many metabolic resources to mediate clearance of these foreign antigens. However, instead of engaging in the highly energetically favorable OXPHOS pathway, effector T cells use Warburg metabolism to proliferate and to produce cytokines (24, 40, 41). Warburg metabolism, initially discovered as an important pathway for the survival of malignant cells, is characterized by an extraordinary ability to breakdown glucose by anaerobic glycolysis and amino acids such as glutamine (as in **Figure 2B**) (42, 43). In contrast to naïve T cells, effectors break down glucose to pyruvate and lactate with minimal engagement of mitochondrial respiration (44–46).

Although the metabolic adaptations T cells undergo when activated may appear obvious given the increased energetic demand to proliferate and synthesize proteins, recent findings suggest that these changes are tightly coupled to T cell differentiation and acquisition of effector function. Interestingly, two key enzymes in the anaerobic glycolysis pathway— GAPDH and LDHA—are critical in regulating cytokine production in T cells. Glyceraldehyde 3-phosphate Dehydrogenase (GAPDH), aside from its role in metabolizing glucose, can directly bind the mRNA of key cytokines such as *IL-2*, *IFNG* and *TNFA* in $CD4^+$ effector T cells to prevent their protein translation in the absence of glucose (right side of **Figure 2B**) (41). In contrast to preventing the direct protein translation of cytokines by GAPDH in $CD4^+$ T cells, $CD8^+$ T cells instead utilize lactate dehydrogenase (LDHA), the key enzyme in the conversion of pyruvate into lactate for anaerobic glycolysis, to enforce effector gene expression *via* histone acetylation (46, 47). Genetic loss of *LDHA* prevents acetylation at the promoters of effector genes such as *IFNG* and *PDCD1*, without compromising proliferation (41, 48). Although glucose is a critical metabolite for T cell function, the enzymes involved in anaerobic glycolysis are also tightly coupled to effector function in both $CD4^+$ and $CD8^+$ T cells (49). A potential mechanism explaining the functional effect of using glycolysis to promote effector functions may lie in production of citrate downstream of glucose breakdown. Citrate is shuttled from the mitochondria where it is converted into acetyl-coA by the action of cytosolic ATP Citrate Lyase (ACL) (50). ACL is an enzyme that is upregulated in both $CD4^+$ and $CD8^+$ effector T cells that can translocate from the cytoplasm to the nucleus and has the ability to directly acetylate histones of effector gene promoters (49). Thus, glycolysis regulates effector T cell functionality; while $CD4^+$ T cells moonlight GAPDH to regulate cytokine translation, both $CD4^+$ and $CD8^+$ T cells use acetyl co-A to regulate histone acetylation of effector genes (left side of **Figure 2B**).

In addition to glucose, amino acids are critical for T cell proliferation and function. For example, glutamine breakdown in T cells is required for their proliferation but not for their cytokine production (48, 51). In fact, in the absence of L-Glutamine, T cells are unable to proliferate but can still secrete cytokines (48, 52). These findings suggest synergism from the breakdown of glucose and amino acids (such as glutamine) for T cell proliferation and effector functions. How other amino acids regulate T cell function under nutritional stress remains poorly understood, but is likely to be essential for immunity to tumors as we will discuss in later sections.

Because malignant cells use the same nutrients as effector T cells, they compete form them to thrive. Deprivation of glucose or glutamine in the tumor microenvironment vastly impairs T cell proliferation, function and survival (53–57). Although there may be recent findings that suggest inhibiting glutamine metabolism in the tumor may benefit T cells while impairing tumor metabolism (58). Often this tug of war forces effector T cells to use alternative carbon sources to survive (59–61). It is now clear that T cells use glycolysis to sustain their inflammatory potential, not only as a means to an end, but also as a regulatory component in T cell immunity.

Although metabolic changes permit effector T cells to become highly inflammatory, they come at the price of compromising their mitochondrial quality and capacity to self-renew (36, 62). However, the small T cell fraction that survive the initial antigen encounter acquire a different set of metabolic adaptations to prevail longer-term (63). Next, we discuss how changes to mitochondrial metabolism and morphology impact the development of memory T cells and their recall capacity.

Mitochondrial Properties of Effector and Memory T Cells

Memory T cells develop after a primary antigen challenge, persisting from the pool of lymphocytes with specific metabolic adaptations permitting self-renewal and survival long-term (**Figure 2C**) (64). Given the vast differences in function comparing effector and memory cells, alteration of mitochondrial networking and morphology is critical to fulfill the metabolic needs of these T cells. For example, mitochondria are recruited to the immune synapse after an antigen encounter in effector cells following cleavage from mitochondrial-endoplasmic reticulum (ER) contact sites to enable calcium influx and T cell activation (**Figure 2B**) (65). In contrast, as memory T cells develop

they re-organize their mitochondria to associate tightly with the ER, a feature lacking in terminal effector and naïve T cells (66), which provides a pool of mitochondria primed to sustain aerobic glucose metabolism (67), directly enhancing IFN-gamma production during a secondary response to antigen.

Further, remodeling of mitochondrial morphology is critical for the specialized metabolic needs of effector versus memory T cells. In effector cells, mitochondrial fragmentation, also called fission, produces mitochondria with loose cristae and poorly efficient electron transport but high capacity to buffer calcium (68–71). This morphological and functional change enables the production of reactive oxygen species (ROS) and upregulation of anaerobic glycolysis, needed for the expression of NFAT, a transcription factor required for T cell activation (70, 72–74). In contrast to effectors, memory T cells adapt their mitochondrial morphology for cell-intrinsic usage of lipids and FAO (25). Memory T cells undergo mitochondrial fusion to protect against DNA damage from accumulated ROS to sustain survival under nutritional restriction (71, 75). Cells that acquire the tubular network of fused mitochondria produce less ROS, have tight cristae arrangement and electron transport complexes in close proximity to each other, indicating efficient mitochondrial respiration (70, 76). For example, spare respiratory capacity (SRC) and ATP production is elevated in memory T cells, indicating that they shift towards OXPHOS metabolism with reduced mtROS (36).

Due to these robust differences in metabolic state, manipulation of mitochondrial properties is an active area of research to direct T cells to specific phenotypes. Mitochondrial respiration can be driven by many different types of fuel. For example, IL-7 and IL-15 support the survival of memory T cells, in part, by inducing mitochondrial biogenesis and allowing utilization of alternative substrates to glucose for FAO, such as long chain fatty acids and triacylglycerols (**Figure 2C**) (11, 35). Seminal work by the Pearce group and others demonstrated that spare respiratory capacity and FAO was key for the development of T cell memory (8, 11, 36). Importantly, memory T cell formation could be induced by AMP-dependent-Protein Kinase (AMPK) activity *via* metformin, an FDA approved drug for diabetes (8).

AMPK is a serine threonine kinase responsive to AMP production or energy depletion and has critical function in the development of memory T cells without compromising a primary antigen challenge (77, 78). Mitochondrial respiration and memory formation are compromised in T cells deficient in the catalytic subunit of AMPK (63). In fact, AMPK is a critical regulator of the mitochondrial biogenesis transcription factor, peroxisome proliferator-activated coactivator 1α (PGC1α), which bolsters mitochondrial formation (**Figure 2C**) (79, 80). The importance of mitochondrial biogenesis and function has been recently highlighted by studies showing that either induction of PGC1α through 4-1BB signaling or genetic its overexpression in T cells enhances memory formation against tumors (81, 82). Based on our understanding of how metabolism and mitochondrial homeostasis changes through a T cell's lifetime, under nutrient competent environments, we next discuss how T cell metabolism is altered in the tumor.

NUTRITIONAL TUG OF WAR: T CELLS VS THE TUMOR MICROENVIRONMENT

Nutrient Competition

It has long been appreciated that the cytotoxic potential of $CD8^+$ (CTL) T cells is impaired in the tumor (83). Emerging reports reveal that tumors and activated T cells share common metabolic programs to survive, thus setting the stage for a continuous battle (or tug of war) for nutrients (40, 42, 84). Several lines of evidence support this notion as tumors with gain-of-function mutations in enzymes involved in glycolysis have increased resistance to T cell mediated immunity. This feature presides independent of checkpoint inhibitory receptor expression (84). For example, in renal cell carcinoma, Glut1 expression in tumors is inversely correlated to $CD8^+$ T cell infiltration and cytolytic capacity (43). Moreover, solid tumors are composed of heterogenous populations with differing metabolic adaptations that outcompete T cells in consuming glutamine, glucose and amino acids (**Figure 3A**). Within hypoxic regions, tumors use glucose and glutamine *via* the action of HIF-1α, a hypoxia inducible transcription factor, critical for maintaining glucose and glutamine breakdown under oxygen stress (84, 85). The same mechanism that allows tumors to thrive can further hinder the anti-tumor potential of T cells as hypoxia sensed by prolyl-hydroxylase (PHD) proteins can prevent T cell protection against metastatic lesions in the lungs by downregulating glycolysis genes (86). Because of the heterogenous nature of the tumor mass, areas of hypoxia allow for the development of highly glycolytic tumor regions that contribute to the acidic tumor microenvironment (TME) (87, 88). This contribution can be attributed, in part, to lactate secretion, which relies in proton co-transporters and can be detrimental to T cell activation (89, 90). Lactate must be exported out of the cell along with H^+ ions to maintain homeostasis and to sustain glycolysis (91). When exported by tumor cells, lactate hinders T cell activation by altering the gradient across lactate transporters, thereby preventing recycling of glycolytic byproducts and preventing glycolysis in T and NK cells (87–89, 92). Lactate and proton build up leads to acidification (pH <6.4) of the tumor, in turn blunting T cell effector functions (93, 94). Furthermore, recent evidence suggests that lactate can serve as a substrate to promote immunosuppressive populations of regulatory T cells (T_{regs}) present in the TME (95, 96).

Metabolism of Intratumoral Tregs

Regulatory T cells (T_{regs}) can directly and indirectly blunt cytotoxic $CD8^+$ T cell response against the tumors (97). Similarly to conventional inflammatory CD4 T cells, T_{regs} can induce the glycolytic machinery upon TCR engagement, however T_{regs} complement their metabolism by inducing fatty acid biosynthesis and oxidative phosphorylation which allows them to survive longer than their inflammatory counterparts (98). In fact, T_{regs} rely on the expression and function of the electron transport chain complex III to sustain their suppressive function, as deletion of components of complex III leads to fatal autoimmunity within 25 days in mice and promote tumor

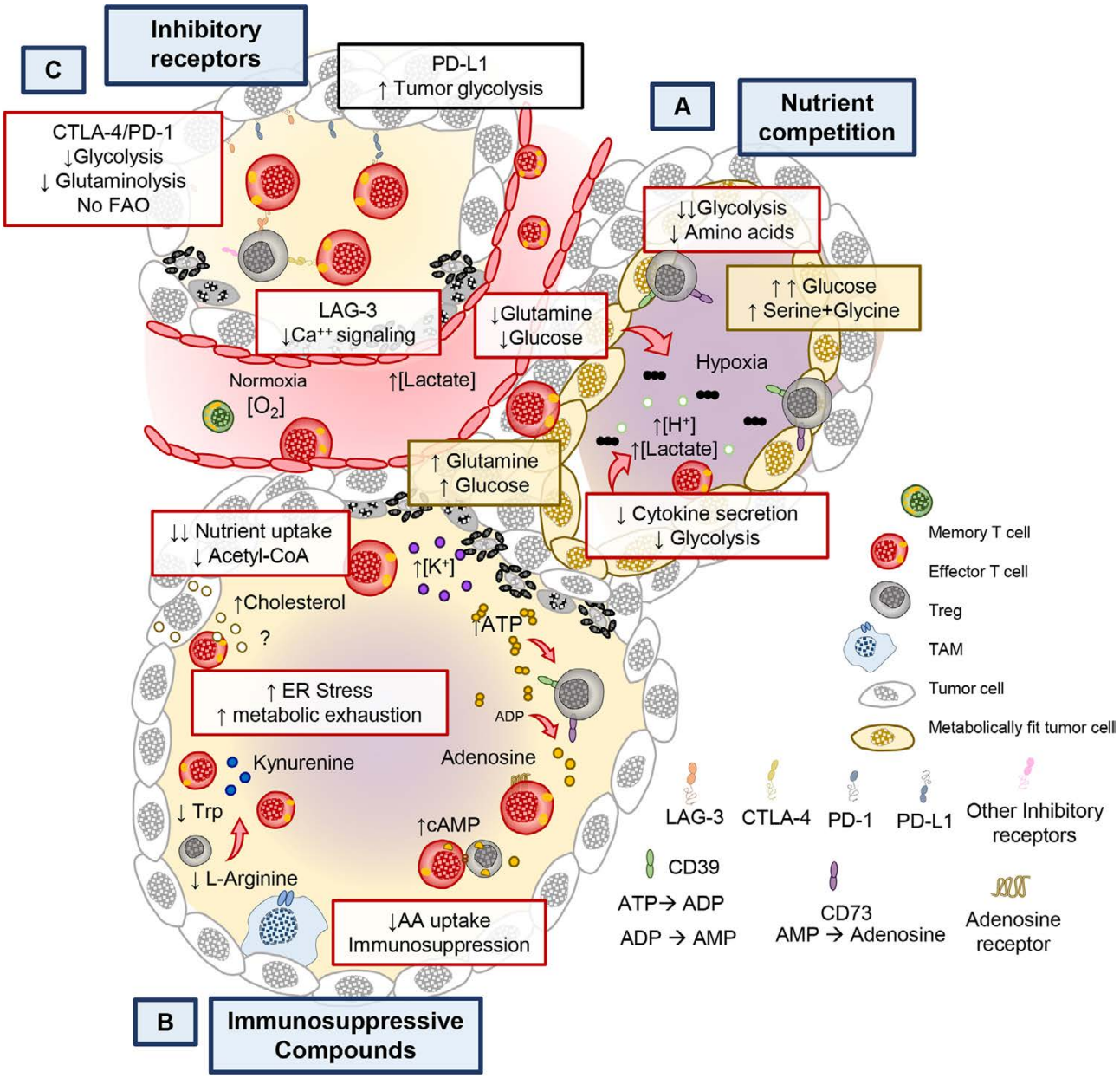

FIGURE 3 | Metabolic and immunological checkpoints that hinder T cell mediated tumor immunity. **(A)** Tumors can adapt their metabolism in response to nutritional stress to better compete and scavenge for glucose and amino acids to suppress T cell bioenergetics. **(B)** Chronic stimulation in the tumor bed leads to the expression of immune checkpoint receptors such as PD-1/PD-L1, CTLA-4, LAG-3, and they exert negative metabolic functions in T cells. **(C)** Furthermore, Ionic imbalances, oxygen availability, and metabolites impact the function of T cells. By products of immunosuppressive immune cells, cell debris and tumor metabolites create the conditions that contribute to the metabolic exhaustion of tumor specific T cells.

immunity in B16 melanoma tumors after inducible deletion (99). The reliance on fatty acid metabolism and the respiratory chain provides T_{regs} with a metabolic advantage to thrive within tumors as they have scarce levels of glucose available and produce high lactate levels, a metabolic state that not only blunts cytotoxic activity but also provides an alternative fuel source to tumor infiltrating T_{regs} (100). As noted with deletion of complex III, a targetable vulnerability of tumor infiltrating T_{regs} exists and can be exploited to destabilize their suppressive function. Indeed, T_{regs} stability can be perturbed when CTA-4 blockade is used in glycolysis impaired tumors, through metabolic reprograming of T_{regs} towards glycolysis and a skewing towards an inflammatory phenotype, a process that is inhibited when tumors have high glycolytic capacity (101). This

finding has tremendous potential for translation into the clinic, as it can be targeted using pharmaceutical agents.

Immunosuppressive Compounds

Tumors indirectly deprive effector $CD8^+$ and helper $CD4^+$ T cells of the metabolic nutrients required for their function and survival. One example of this scarcity of nutrients for immune cells is driven by the accumulation of potassium [K+] in the interstitial fluid of the tumor, which acts to suppress transporters for amino acid and glucose in T cells (**Figure 3B**) (102). Nutrient deprivation depletes the nucleocytosolic pools of acetyl CoA in T cells, preventing the acetylation of the *IFNG* promoter and therefore impairing their production of IFNγ (49, 103). This pathway plays a key role in modulating the epigenetic landscape of effector T cells.

Another mechanism of indirect nutrient deprivation is mediated by the byproducts of suppressive T_{reg} cells, tumor cells, and other suppressive immune cells within the TME. T_{regs} produce adenosine in tumors by CD39/CD73-mediated catalysis (ATP → ADP → Adenosine, as shown in **Figure 3B**. Adenosine is a suppressive molecule that binds to adenosine receptors (A2AR) on cytotoxic T cells and suppresses their function *via* reducing NfkB signaling (104) or by inducing suppressive function on regulatory T cells (105). Furthermore, tumor metabolic byproducts, such as cholesterol, can induce metabolic stress in T cells. Specifically, tumor derived cholesterol induces ER stress which prevents the ability of T cells to secrete cytokines. Furthermore, the ER stress response promotes the factor XBP-1 which can directly increase PD-1, TIM-3, and LAG-3 expression, important immunosuppressive molecules that mediate T cell exhaustion (106). Not only do tumors secrete immunosuppressive molecules, but also other immune cells take up nutrients that are beneficial to T cells and can produce immunosuppressive metabolites. For example, M2 type macrophages in the tumor consume L-arginine in an arginase-1 dependent manner and can deplete tryptophan by breaking it down into immunosuppressive kynurenine derivatives through indoleamine-2,3-oxygenase (IDO) (56). These are just a few of the mechanisms that drive metabolic cross talk between tumors and immune cells. Thus, many byproducts of cellular metabolism synergize in the tumor to suppress T cells from fulfilling their potential to eradicate tumors and are likely to also play an obstacle in the growth of TILs from tumor biopsies (**Figure 3B**). In addition to this metabolic tug of war, the effector functions of T cells are limited by inhibitory receptor on tumors and immunosuppressive host elements, such as myeloid and T_{regs} cells.

IMMUNE CHECKPOINTS IN T CELL METABOLISM

Tumors evade the immune system in order to survive in the host. Tumors do this in many ways, as depicted in **Figure 3C**. One such mechanism is by promoting T cell exhaustion (107). T cells that become exhausted had a reduced capacity to survive, proliferate and secrete cytokines (108). T cell dysfunction is marked by the progressive acquisition of inhibitory receptors (IRs), including programmed cell death protein 1 (PD-1), lymphocyte activation gene-3 (LAG-3), cytotoxic T-lymphocyte association protein 4 (CTLA4), and T cell immunoglobulin and mucin domain-containing protein 3 (TIM3) (109–111). These IRs alter T cell responses against tumors in part by perturbing their metabolism.

T cell function and proliferation are compromised *via* immune checkpoint inhibitory pathways in the tumor (15, 112). PD-1 impairs effector function by downregulating glycolysis and increasing the FAO rate limiting enzyme CPT1α, a feature that supports T cell persistence in the tumor but prevents their cytotoxic potential (112). Although mitochondrial FAO supports T cell persistence but not function, $PD\text{-}1^+$ T cells exhibit markedly decreased mitochondrial respiration (**Figure 3C**) (112, 113). Furthermore, Akt signaling is elevated in tumor infiltrating lymphocytes experience, which potent inhibits PGC1α, a key regulator of mitochondrial biogenesis (81, 113). This data suggests that part of the suppressive mechanism of PD-1 and chronic antigen stimulation is attributed to their negative effect on T cell mitochondrial biogenesis, substrate utilization and glycolytic capacity (**Figure 3C**). Conversely, PD-L1 on tumor cells enhances glucose uptake, further depriving T cells use of this critical energy substrate (84). Collectively this body work suggests that PD-1/PD-L1 blockade can bolster T cell glycolysis to support their antitumor activity (84, 114).

CTLA-4 is a member of the immunoglobulin family on APCs and tumors that antagonizes CD28 on T cells. CTLA-4 activation on T cells suppresses their function and nutrient acquisition (115–118). Moreover, CTLA-4 downregulates the glutamine transporters (SNAT1, SNAT2) and Glut1, ultimately diminishing the bioenergetic potential of T cells in the tumor (112). LAG-3 also impaired T cell activation and proliferation (111, 119). It has been reported that LAG-3 specifically perturbs calcium influx downstream of CD3/TCR signaling, in turn preventing the differentiation of naïve T cells into effectors (120). As checkpoint blockade mediates remarkable responses in patients with a wide variety of malignancies (121, 122), it is critical to understand how IRs regulate T cell biology. Expanding our knowledge on these mechanisms will inform intelligent design of tumor immunotherapies.

T cells face many challenges to sustain effective immunity to tumors. However, it has become evident that modulating the nutritional demands of the tumor is key for sustaining proper anti-tumor T cell potential. Below we highlight the most exciting findings demonstrating how metabolically manipulating T cell *ex vivo* for adoptive immunotherapy can enhance and improve future immunotherapies.

MODULATING METABOLISM TO ENHANCE ADOPTIVE T CELL THERAPY

Introduction to Adoptive T Cell Transfer Therapy

Some patients become resistant to checkpoint inhibition therapy. Consequently, many investigators are trying alternative

therapeutic approaches that can prevent resistance or relapse, including the transfer of tumor specific T cells. Cellular therapies, such as autologous tumor infiltrating lymphocytes (TIL) or engineered chimeric antigen receptor (CAR) T cell approaches have demonstrated great potential in mediating long-lasting responses against tumors (2). Generally, whether TIL or CAR adoptive T cell therapies rely on three basic principles, a) conditioning of host with nonmyeloablative chemotherapy or total body irradiation, b) growth of T cells to large therapeutic doses and 3) treatment post-transfer with high dose IL-2 (123). This therapeutic approach holds the promise of vastly improving cancer treatment, especially for tumors rich in neoantigens, as reported for epithelial cancers such as ovarian and triple negative breast cancer (124–126). However, two major limitations for this approach are the ability to generate enough tumor specific T cells for infusion into patients and the capacity of the infused T cell products to persist long-term.

In situations where naturally arising TILs cannot be generated from a patient, gene therapy has opened the door for synthesizing T cells by directing them against tumors with chimeric antigen receptors (CAR). CD19-specific CAR T cells, designed to recognize B cell malignancies, have mediated long-lasting responses in some patients that have exhausted all other treatment options (127–129). The efficacy of these CAR T cells resulted in FDA approval of three different CD19-CAR T cell preparations thus far: two with CD28 costimulatory domains (axicabtagene ciloleucel and brexacabtagene autoleucel), and one with 4-1BB as a costimulatory domain (tisagenlecleucel). Although both TIL and CAR therapy have shown promise, sustaining prolonged and durable responses in all patients remains a challenge. Yet, the manipulation of T cells in an *ex vivo* setting provides a unique opportunity to specifically empower T cells with antitumor properties, including remodeling their metabolism, without indirect effects on the tumor. Herein we describe new advances in how TIL, CAR and TCR-based cellular therapies have been improved by altering both T cell and tumor bioenergetics.

Metabolic Reprogramming in the Design of CAR T Cells

CAR T cell construct design has evolved to include many flavors of signaling domains, kill switches, switch receptors and regulatory functions. These factors in CAR design have been reported to exquisitely control T cell functionality and selectivity against tumor targets, as reviewed previously (130). Results from early trials of CD28ζ and 4-1BBζ CAR T cells made functional differences between these cells apparent; while the CD28ζ CAR had high incidence of cytokine release syndrome and persistence on the order of months (131), the 41BBζ CAR T was able to persist on the order of years after treatment (132) and exhibited lower rates of T cell exhaustion (133). Early on, understanding of these differences was unclear; however, the June lab discovered a mechanism relating these functional differences to effects of the costimulatory domain on mitochondrial function and bioenergetics (82). 4-1BB signaling enhanced T cell bioenergetics by directly upregulating PGC1α, a transcription factor that promotes increased mitochondrial biogenesis and OXPHOS of T cells (82), supporting their long-term persistence (**Figure 4A**). In contrast, CD28ζ CAR T cells were highly glycolytic and were driven to a terminal effector phenotype (82). Further, reports have also shown that strong and chronic signaling from the CAR domain impaired T cell persistence and function due to impaired mitochondrial metabolism (133). Given these results, it is clear that the costimulatory domains incorporated into CAR T cell designs have functional and metabolic consequences which could be harnessed based on the needs of the patient. 4-1BB is part of the tumor necrosis factor related super family (TNFRSF), which consists of many other members that can be expressed in T cells such as ICOS, OX40, GITR, and CD27. Although their signaling mechanisms are known, whether they affect metabolic fitness or could empower CAR T cell persistence in patients is an active area of study.

Cytokine Priming and Metabolic Re-Programming

The generation of TIL products is possible through the use of high dose IL-2 in tumor digests. Current protocols promote the proliferation of T cells from tumor biopsies and can yield billions of cells after weeks to months of manufacturing. However, TIL products expanded *in vitro* are fully differentiated and show features of senescence, which impairs their persistence and antitumor capacity (2, 108). In contrast, T cells generated with central or stem-cell memory properties *in vitro* have increased potential for antitumor immunity (20, 39, 134). It has long been appreciated that priming T cells with the common γ chain cytokines IL-7, IL-15 or IL-21, can generate and sustain memory T cells and have shown promise in preclinical models of adoptive T cell therapy (135). In fact, expansion of TIL from patient biopsies using a combination of the common γ chain cytokines have yielded less differentiated T cells with improved stemness features, however whether they synergize in combination to improve T cell bioenergetics remains to be fully elucidated (136, 137). Compared to IL-2 conditioning, expanding T cells with IL-15 vastly improves mitochondrial fitness, prevents overt T cell differentiation and improves tumor immunity (12, 36). Furthermore, when compared with IL-15, IL-21 appears to be most effective at preventing T cell differentiation prior to ACT and promotes greater tumor immunity than IL-15 (138); however, whether IL-21 alters T cell metabolism in a similar manner as IL-15 remains to be determined. Recently two independent reports showed that targeting IL-21 directly to T cells rather than systemic delivery in combination with PD-1 therapy improved tumor immunity. They also showed that systemic delivery of soluble IL-21 did not improve the therapeutic efficacy of PD-1 blockade, however when the anti-PD-1 antibody was fused to IL-21 synergetic improvement in tumor immunity was noticed (139, 140). There are currently many efforts to translate the use of single and combinations of these cytokines to expand TIL and CAR products for ACT, as well as novel ways to incorporate cytokine releasing switches in CAR constructs and fusion proteins. However, these studies highlight a need to better understand

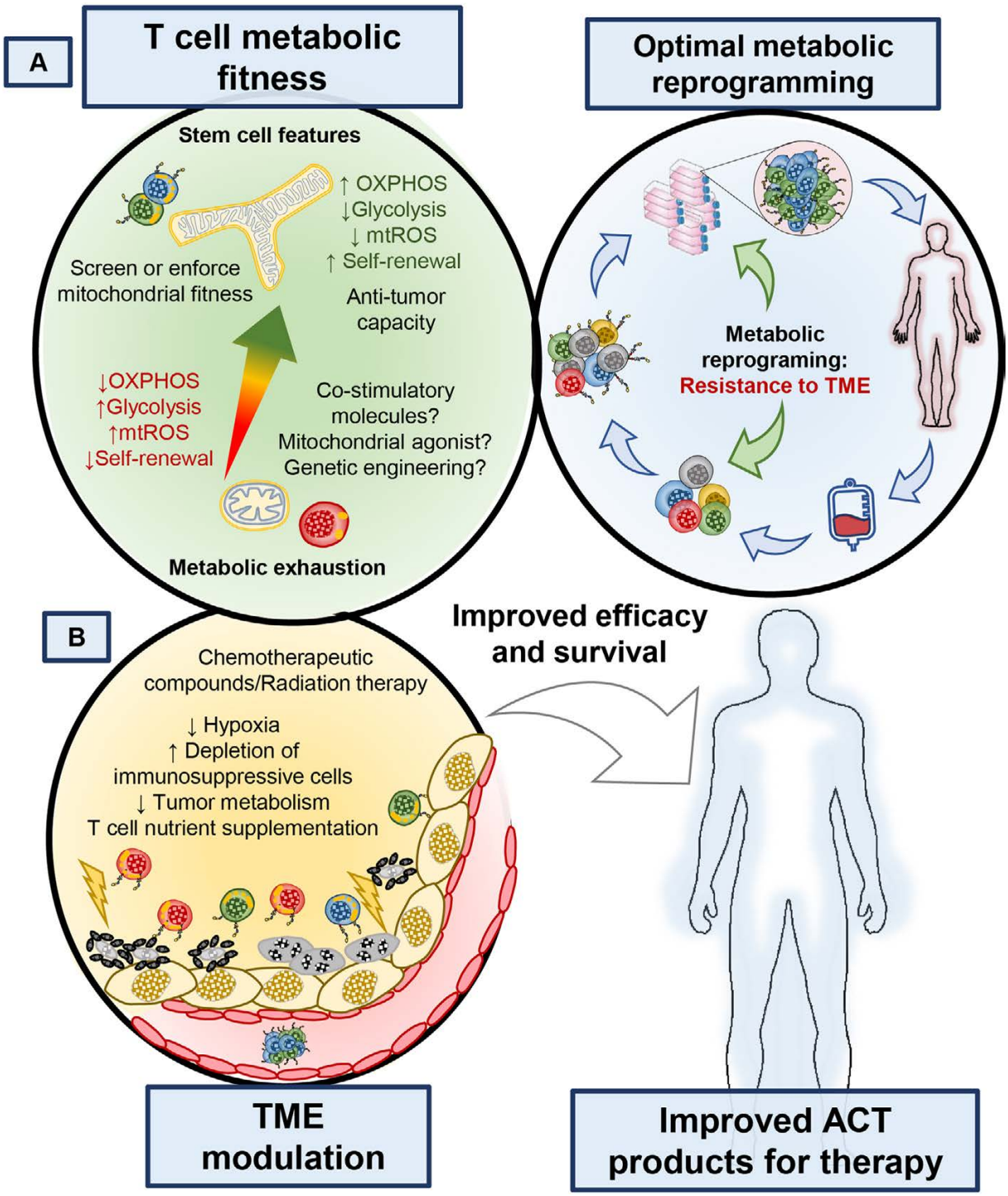

FIGURE 4 | Manipulating the ability of T cells to withstand metabolic stress or altering the metabolism of tumors can enhance the therapeutic potential of T cell-based therapies. **(A)** Identifying markers that identify metabolically competent T cells, as well as understanding how small molecule compounds, biologics or receptor ligands could improve T cell metabolism will bring new targets to improve the efficacy of T cell products. **(B)** Better understanding of how the tumor microenvironment is affected by current therapies could provide new avenues to target both T cell and tumor metabolism to bolster immunotherapies. Enriching metabolically fit T cells during T cell isolation from whole blood or including metabolism modulating agents during TIL and CAR T cell expansion or altering CAR design of T cells could improve the survival of patients treated with cellular therapies.

how and when to use these modulatory cytokines, as they may compromise T cell growth or functionality due to their effect on other immune cells within tumors.

Inhibiting Signaling Pathways to Improve T Cell Therapies

Engagement of TCR, costimulatory molecules and cytokines mediate many internal cascades that contribute to T cell differentiation. These signals promote immunological memory; however, depending on the type and strength, these signals can also drive to T cell differentiation and exhaustion (141). An attractive approach is to use pharmacologic inhibitors against signaling cascades downstream of these signaling cues (**Figure 4A**) to generate antitumor T cells with durable memory traits. Canonical signaling downstream of T cell activation turns on the PI3K/ATK/mTOR signaling pathway and leads to T cell effector differentiation (142). This signaling axis is critical for rewiring metabolism to enable growth, protein translation and function in all proliferating cells, thus using compounds that target components of this pathway is a sensible approach to modulate T cell biology to improve their anti-tumor potential. Our lab and others have shown that targeting the delta subunit of PI3K, which is expressed specifically in lymphocytes, generates T cells with a less differentiated state (143), including murine and human antitumor $CD8^+$ CTLs or $CD4^+$ Th17 cells (144, 145). In fact, Dwyer et al. reported that blocking the PI3Kδ or PI3Kγ subunits were most advantageous for the production of highly effective anti-tumor T cells compared to those treated with drugs that inhibited both PI3Kδ and PI3Kγ subunits (146). Although is predicted that PI3K inhibition should dampen glucose metabolism and reciprocally improve T cell mitochondrial function it is still to be explored if selectively inhibiting the delta or gamma subunit have lasting effects on T cell metabolism reprograming or mitochondrial fitness (146). Downstream of PI3K, Akt blockade was also found to increase T cell stemness as well as FAO metabolism without perturbation of glycolysis upon restimulation (147, 148). Furthermore, inhibition of mTOR with rapamycin generates T cells that resemble a rare stem-memory like T cell population with enhanced survival capacity, mitochondrial respiration and lasting persistence in hosts (149–151). These findings reveal an interesting approach in modulating T cell differentiation and metabolism, which endow T cells with enhanced tumor-killing capacity. However, the question is raised as to which approach is most effective and what mechanisms govern the efficacy of this therapeutic inhibition during ACT expansion. A potential mechanism is that inhibiting the PI3K/Akt/mTOR pathway leads to enhanced autophagy, which is a well described homeostatic process involved promoting T cell memory and mitochondrial fitness (152, 153). This idea is further strengthened by a new report shown an important role for T cell intrinsic mitochondrial regulation by autophagy as an important part sustained immunity against tumors (154).

Another clue as to how blocking signaling cascades may overlap to improve T cell therapies was recently identified by the Restifo group (155). They used a multi-phenotype CRISPR screen to identify more than 25 targets downstream of T cell activation. They identified the stress response p38 MAP kinase as a key driver involved in preventing T cell mediated tumor immunity (155). This finding reinforces previous studies that elegantly demonstrated that ER stress, a target regulated by p38, impairs intratumoral T cell protein translation of cytotoxic molecules and regulates mitochondrial and T cell exhaustion (156–159). Nonetheless, the current efforts exploring inhibition of these key signaling pathways *in vitro* may provide TIL and CAR T cell with enhanced bioenergetics, persistence and anti-tumor capacity during their expansion. A potential benefit of using inhibitors of these key proliferation pathways is their effect on tumor and other suppressive immune cells, such as T_{regs} (160, 161) and myeloid cells (162) as they are sensitive to PI3K inhibition and may enhance the expansion of TIL. Based on current the literature, inhibition of growth and differentiation pathways such as the PI3K/AKT/mTOR signaling axis directly alters the development and metabolic programing of T cells *in vitro*, which improves their bioenergetics and persistence *in vivo* (**Figure 4A**).

Exploiting Nutritional Stress *in Vitro* for Beneficial Metabolic Adaptations

Recent reports show that T cells expanded in the presence of metabolic stress are surprisingly better at delaying tumor growth (103, 163). Although this finding is counterintuitive, this discovery may be explained by the ability of T cells to adapt to scarce environments by upregulating alternative sources of fuel through metabolic adaptations. For example, Sukumar et al. found that depriving T cells of glucose *in vitro* increased the number of less differentiated CTLs and supported their stem and central memory profile. These glucose-starved T cells regained potent effector functions in the tumor when infused into mice (163). Moreover, these cells upregulated AMPK activity, known to enhance mitochondrial respiration and fatty acid usage, and mediated robust regression of melanoma compared to conventionally cultured T cells (163). Most recently this finding has been supported by transient glucose restriction which improves T cell immunity against tumors *via* increased pentose phosphate pathway activity (164). Note that this study is not diminishing the importance of glucose for T cell survival and effector functions. Instead, it highlights the unexpected finding that the biology of T cells can be altered simply by transiently denying them this metabolite *in vitro*, an adaptation likely to be driven by mitochondrial compensation (62). In fact, T cells engineered to overexpress the gluconeogenesis enzyme phosphoenolpyruvate carboxykinase (PCK) can improve antitumor immunity, putatively by increasing the pool of glucose available to enter glycolysis and other ancillary pathways like the pentose phosphate pathway (165).

Glucose availability is a requirement for T cell mediated immunity *in vivo*, so how does depriving T cells of glucose *in vitro* enhance tumor immunity? An explanation could be provided by recent work showing that nutritional deprivation can be a double-edged sword depending on the context. In this work,

priming T cells *in vitro* with high potassium concentrations lead to metabolic reprogramming to increase Acetyl Co-A Synthase (ACCS1) which enhanced mitochondrial respiration, conferred stem memory qualities in T cell and enhanced tumor immunity *in vivo* (49, 153). This data revealed that priming T cells *in vitro* with nutritional deprivation can improve antitumor activity, in part due to improved bioenergetic plasticity in a similar fashion as depriving glucose *in vitro*. Pressuring T cells to undergo metabolic adaptations that allow survival under cellular stress, such as promoting mitochondrial biogenesis, enhancing mitochondrial respiration, or enhancing ancillary pathways such as PPP or gluconeogenesis can benefit tumor control.

Nutritional Support for Anti-tumor T Cells

Collectively, this rich body of work on T cell metabolism highlights the need for T cells to adapt and use alternative fuel sources to thrive in the harsh tumor microenvironment. So, the question is posed, which fuels are most effective at supporting T cell antitumor activity? Recent work suggests that select amino acids and nucleotides may contribute. For example, supplementation of L-arginine *in vitro* and *in vivo* improves T cell tumoricidal activity by enhancing their memory formation and mitochondrial respiration (166). Additionally, supplementing inosine (a nucleoside capable of entering the central carbon pathways of glycolysis and the pentose phosphate pathway) under glucose deprivation enhanced the ability of T cells to clear tumors in mice (59). Identifying unique metabolites to augment cancer immunotherapy is attractive, as they can be delivered directly into T cell cultures or *in vivo* without overt expected side effects. A recent report suggests that highly therapeutic $CD26^{high}$ T cells might have those properties (167), as CD26 docks adenosine deaminase (ADA), which cleaves suppressive adenosine [produced by tumors and T_{regs} (105)] into inosine an important precursor for nucleotide synthesis and feedback into one carbon metabolism (59). This idea is particularly attractive given how potent $CD26^{high}$ T cells are at ablating large tumors, and suggest that ADA-induced inosine might play a role in their potency. Furthermore, methionine is a metabolite that enters the central carbon cycle and is a required amino acid for supporting T cells with effector properties (60, 61). *In vivo*, supplementing T cells with surplus L-arginine, inosine or potentially methionine could be an attractive way to enhance tumor immunity by providing alternative fuels for T cells exogenously (**Figure 4B**).

Direct Mitochondrial Agonists to Enhance Anti-tumor T Cells

Modulating nutrients to directly fuel T cells within tumors may not be the most efficient way to help their support their bioenergetic needs. Instead, directly stimulating the mitochondrial function of T cells using pharmacologic agonists might be more effective (**Figure 4B**). In fact, several reports have shown that small molecule agonists of AMPK, mTOR and PPARα or γ in combination with immune checkpoint blockade (ICB) therapy can promote mitochondrial function in T cells, leading to a positive immune response against tumors (168). For example, PD-L1 blockade in combination with an agonist of peroxisome proliferator–activated receptor γ and co-activator of PGC1α was remarkably effective at mediating curative responses in mice with melanoma (169). This approach is supported by a recent study revealing that T cell mitochondrial function is a marker for responsiveness in patients treated with ICB (168). Thus, it is likely that mitochondrial T cell health and regulation may play an important role in patient responses to immunotherapy (62, 68). Also, survival cues (such as AMPK, PKA and the Sirtuin family of acetylating enzymes) regulate T cell metabolism under energetic stress. This action improves T cell survival *via* bolstering mitochondrial biogenesis (PGC1a), remodeling (fused mitochondria) and recycling (i.e. mitochondrial autophagy) (70, 81, 154). However, direct perturbation of the tumor itself is also likely to modulate metabolites that promote T cell immunity (**Figure 4B**). Many investigators are thus focused on combining radiation or chemotherapy with ICB to help patients, but exactly how these therapies impact the nutrient tug of war between tumor and T cells is still up for debate as well as whether these approaches can be exploited for the expansion of TIL and CAR T cells.

MANIPULATION OF TUMOR CELL METABOLISM

New insights into the metabolic requirements for tumors has sparked interest in manipulating their metabolism to improve immunity (54, 102). Nonetheless, there is limited but promising data regarding the benefit of combining current chemotherapeutic strategies or inhibition of tumor metabolism. Although glucose availability is a key determinant of T cell response, the heterogenous nature of the tumor warrants exploration of multiple targets (55, 57).

Preventing tumors from using the nutrients they need to survive can provide an advantage for T cell effector functions. For example, targeting the lactate dehydrogenase (LDHA), an enzyme that converts pyruvate to lactate and regeneration of NAD+ in tumors, improves T and NK cell function (47, 170, 171). Additionally, altering the hypoxic tumor environment can improve the therapeutic potential of ICB and adoptive transfer therapies, given the critical role of HIF1-α in altering the metabolic requirements of tumors under oxygen stress (172). For example, metformin plus PD-1 therapy enhanced the antitumor capacity of endogenous T cells in mice, in part by reducing the hypoxic nature of the melanoma (173). Another approach to target the tumor to augment immunity has been the neutralization of the highly acidic TME with sodium bicarbonate or other proton pump inhibitors prior to ICB or ACT (174). Combination of tumor metabolism inhibition and chemotherapeutic regiments may relieve the nutritional tug of war between tumors and T cells (93, 175). One promising strategy is to block glutamine metabolism within tumors, as this can also empower T cell immunity, a remarkable feat for single chemotherapy agents (58). Finally, another example of targeting the tumor to augment outcomes is found in pre-conditioning patients with systemic cisplatin to enhance T cell immunity at a secondary tumor site following radiotherapy, also known as the abscopal effect (176, 177). Thus, identifying FDA

approved chemotherapeutics that alter tumor metabolism to augment the therapeutic potential of immunotherapies will be key to improve current therapeutic approaches (**Figure 4**).

SUMMARY AND PERSPECTIVES

It has 70 years since the first studies on T cell metabolism (178). The importance of T cell bioenergetics and its effect on immunity are gaining a new level of appreciation today and are being explored by multiple investigators. Yet, many key questions remain unanswered about how T cell metabolism impacts immunotherapy. For example, how do expression of inhibitory receptors and co-stimulatory molecules [such as LAG-3, TIM3, ICOS and other TNFRSF receptors (i.e. OX40, 4-1BB] impact T cell and tumor metabolism? Moreover, how do "suffering" T cells preconditioned under nutritional deficits gain antitumor activity *in vivo*? Insights into these mechanisms will be critical to design optimal therapies as mono- or combination approaches.

Herein, we have highlighted the myriad of ways metabolism is emerging as a major target for next generation immunotherapies. While the optimal therapeutic approach is unclear, promising strategies include targeting the tumor/immune axis either altogether or as individual branches. Chemotherapy and irradiation as preconditioning agents hinder the tumor directly, permit release of antigens and host immune activation. After effective tumor priming, administration of potent immune activating agents can help overcome immune evasion by the tumor. These immune therapies include checkpoint inhibitors, costimulatory agonists, and adoptively transferred T cells, each have the potential to harness a metabolic advantage for antitumor immune cells. Additionally, direct administration of agents which alter nutrient plasticity or promote metabolic adaptation of T cells over tumors could also synergize. However, as highlighted by the effect of tumor glycolysis and CTLA-4 blockade and the ability of other immunosuppressive cells to benefit from metabolism modulators there is always a possibility that fostering a metabolic advantage for the T cells in the tumor could also benefit the immunosuppressive microenvironment of the tumor, thus defining the timing and sequence of intervention is a challenge that needs to be addressed. One advantage of adoptive T cell therapy as an alternative, is the flexibility to manipulate the T cell directly obviating the challenge of competing immunosuppressive cells and the tumor. However, there are challenges that remain in designing optimal methods to reliably and potently alter the metabolism and function of *ex vivo* expanded T cells. This body of work suggest that by using inhibitors of key differentiation/stress pathways or conditioning with cytokines or co-receptors that improve metabolic function, we could provide the competitive advantage needed to ablate tumors long-term in patients. Regardless of the specific method, metabolic rewiring is likely to play a significant role in eliciting durable and long-lasting immunity in tumors resistant to conventional therapies.

AUTHOR CONTRIBUTIONS

GR and CP designed, wrote and edited the manuscript. HK, CD, AS, MW, AR and JT provided feedback and edited the manuscript. All authors contributed to the article and approved the submitted version.

FUNDING

This work was supported by the NIH Training grant T32 5T32GM008716-19 and MUSC CGS Provost Scholarship to GR. NIH Training grant T32 GM08716 and NCI F30 243307 to HK. NIH training grant T32 AI132164-01 to CD. Hollings Cancer Center Graduate Fellowship to AS. NIH R50 CA233186 to MW. NIH R01 CA175061 and R01 CA208514 grants, KL2 South Carolina Clinical and Translational Research grant UL1 TR000062, ACS-IRG grant 016623-004 and MUSC Start-up funds to CP.

ACKNOWLEDGMENTS

We would like to thank the researchers and clinicians for their dedication and passion to improve cancer immunotherapy, and the patients whose sacrifice and courage inspire us to move research forward. We also greatly appreciate the researchers that have contributed to this body of knowledge.

REFERENCES

1. Allison KE, Coomber BL, Bridle BW. Metabolic reprogramming in the tumour microenvironment: a hallmark shared by cancer cells and T lymphocytes. *Immunology* (2017) 152:175–84. doi: 10.1111/imm.12777
2. Rosenberg SA, Yang JC, Sherry RM, Kammula US, Hughes MS, Phan GQ, et al. Durable complete responses in heavily pretreated patients with metastatic melanoma using T-cell transfer immunotherapy. *Clin Cancer Res* (2011) 17:4550–7. doi: 10.1158/1078-0432.CCR-11-0116
3. Roos D, Loos JA. Changes in the carbohydrate metabolism of mitogenically stimulated human peripheral lymphocytes. II. Relative importance of glycolysis and oxidative phosphorylation on phytohaemagglutinin stimulation. *Exp Cell Res* (1973) 77:127–35. doi: 10.1016/0014-4827(73)90561-2
4. Ardawi MS, Newsholme EA. Glutamine metabolism in lymphocytes of the rat. *Biochem J* (1983) 212:835–42. doi: 10.1042/Bj2120835
5. Bental M, Deutsch C. Metabolic changes in activated T cells: an NMR study of human peripheral blood lymphocytes. *Magn Reson Med* (1993) 29:317–26. doi: 10.1002/mrm.1910290307
6. Kaech SM, Hemby S, Kersh E, Ahmed R. Molecular and functional profiling of memory CD8 T cell differentiation. *Cell* (2002) 111:837–51. doi: 10.1016/S0092-8674(02)01139-X
7. Wherry EJ, Ha SJ, Kaech SM, Haining WN, Sarkar S, Kalia V, et al. Molecular signature of CD8+ T cell exhaustion during chronic viral infection. *Immunity* (2007) 27:670–84. doi: 10.1016/j.immuni.2007.09.006
8. Pearce EL, Walsh MC, Cejas PJ, Harms GM, Shen H, Wang LS, et al. Enhancing CD8 T-cell memory by modulating fatty acid metabolism. *Nature* (2009) 460:103–7. doi: 10.1038/nature08097

9. Gett AV, Hodgkin PD. Cell division regulates the T cell cytokine repertoire, revealing a mechanism underlying immune class regulation. *Proc Natl Acad Sci U S A* (1998) 95:9488–93. doi: 10.1073/pnas.95.16.9488
10. Youngblood B, Hale JS, Ahmed R. T-cell memory differentiation: insights from transcriptional signatures and epigenetics. *Immunology* (2013) 139:277–84. doi: 10.1111/imm.12074
11. van der Windt GJ, O'Sullivan D, Everts B, Huang SC, Buck MD, Curtis JD, et al. CD8 memory T cells have a bioenergetic advantage that underlies their rapid recall ability. *Proc Natl Acad Sci U S A* (2013) 110:14336–41. doi: 10.1073/pnas.1221740110
12. Cieri N, Camisa B, Cocchiarella F, Forcato M, Oliveira G, Provasi E, et al. IL-7 and IL-15 instruct the generation of human memory stem T cells from naive precursors. *Blood* (2013) 121:573–84. doi: 10.1182/blood-2012-05-431718
13. Cho BK, Wang C, Sugawa S, Eisen HN, Chen J. Functional differences between memory and naive CD8 T cells. *Proc Natl Acad Sci U S A* (1999) 96:2976–81. doi: 10.1073/pnas.96.6.2976
14. Gudmundsdottir H, Wells AD, Turka LA. Dynamics and requirements of T cell clonal expansion in vivo at the single-cell level: effector function is linked to proliferative capacity. *J Immunol* (1999) 162:5212–23.
15. Ahn E, Araki K, Hashimoto M, Li W, Riley JL, Cheung J, et al. Role of PD-1 during effector CD8 T cell differentiation. *Proc Natl Acad Sci U S A* (2018) 115:4749–54. doi: 10.1073/pnas.1718217115
16. Wherry EJ, Blattman JN, Ahmed R. Low CD8 T-cell proliferative potential and high viral load limit the effectiveness of therapeutic vaccination. *J Virol* (2005) 79:8960–8. doi: 10.1128/JVI.79.14.8960-8968.2005
17. Badovinac VP, Porter BB, Harty JT. Programmed contraction of CD8(+) T cells after infection. *Nat Immunol* (2002) 3:619–26. doi: 10.1038/ni804
18. Smith CA, Williams GT, Kingston R, Jenkinson EJ, Owen JJ. Antibodies to CD3/T-cell receptor complex induce death by apoptosis in immature T cells in thymic cultures. *Nature* (1989) 337:181–4. doi: 10.1038/337181a0
19. Veiga-Fernandes H, Walter U, Bourgeois C, McLean A, Rocha B. Response of naive and memory CD8+ T cells to antigen stimulation in vivo. *Nat Immunol* (2000) 1:47–53. doi: 10.1038/76907
20. Hinrichs CS, Borman ZA, Cassard L, Gattinoni L, Spolski R, Yu Z, et al. Adoptively transferred effector cells derived from naive rather than central memory CD8+ T cells mediate superior antitumor immunity. *Proc Natl Acad Sci U S A* (2009) 106:17469–74. doi: 10.1073/pnas.0907448106
21. Kaech SM, Ahmed R. Memory CD8+ T cell differentiation: initial antigen encounter triggers a developmental program in naïve cells. *Nat Immunol* (2001) 2:415–22. doi: 10.1038/87720
22. Lanzavecchia A, Sallusto F. Progressive differentiation and selection of the fittest in the immune response. *Nat Rev Immunol* (2002) 2:982–7. doi: 10.1038/nri959
23. Smith NL, Patel RK, Reynaldi A, Grenier JK, Wang J, Watson NB, et al. Developmental Origin Governs CD8(+) T Cell Fate Decisions during Infection. *Cell* (2018) 174:117–30.e114. doi: 10.1016/j.cell.2018.05.029
24. Gubser PM, Bantug GR, Razik L, Fischer M, Dimeloe S, Hoenger G, et al. Rapid effector function of memory CD8+ T cells requires an immediate-early glycolytic switch. *Nat Immunol* (2013) 14:1064–72. doi: 10.1038/ni.2687
25. O'Sullivan D, van der Windt GJ, Huang SC, Curtis JD, Chang CH, Buck MD, et al. Memory CD8(+) T cells use cell-intrinsic lipolysis to support the metabolic programming necessary for development. *Immunity* (2014) 41:75–88. doi: 10.1016/j.immuni.2014.06.005
26. Nasi M, Troiano L, Lugli E, Pinti M, Ferraresi R, Monterastelli E, et al. Thymic output and functionality of the IL-7/IL-7 receptor system in centenarians: implications for the neolymphogenesis at the limit of human life. *Aging Cell* (2006) 5:167–75. doi: 10.1111/j.1474-9726.2006.00204.x
27. Rathmell JC, Vander Heiden MG, Harris MH, Frauwirth KA, Thompson CB. In the absence of extrinsic signals, nutrient utilization by lymphocytes is insufficient to maintain either cell size or viability. *Mol Cell* (2000) 6:683–92. doi: 10.1016/S1097-2765(00)00066-6
28. Wofford JA, Wieman HL, Jacobs SR, Zhao Y, Rathmell JC. IL-7 promotes Glut1 trafficking and glucose uptake via STAT5-mediated activation of Akt to support T-cell survival. *Blood* (2008) 111:2101–11. doi: 10.1182/blood-2007-06-096297
29. Edinger AL, Thompson CB. Akt maintains cell size and survival by increasing mTOR-dependent nutrient uptake. *Mol Biol Cell* (2002) 13:2276–88. doi: 10.1091/mbc.01-12-0584
30. Deberardinis RJ, Lum JJ, Thompson CB. Phosphatidylinositol 3-kinase-dependent modulation of carnitine palmitoyltransferase 1A expression regulates lipid metabolism during hematopoietic cell growth. *J Biol Chem* (2006) 281:37372–80. doi: 10.1074/jbc.M608372200
31. Borowski AB, Boesteanu AC, Mueller YM, Carafides C, Topham DJ, Altman JD, et al. Memory CD8+ T cells require CD28 costimulation. *J Immunol* (2007) 179:6494–503. doi: 10.4049/jimmunol.179.10.6494
32. Vezys V, Penaloza-MacMaster P, Barber DL, Ha SJ, Konieczny B, Freeman GJ, et al. 4-1BB signaling synergizes with programmed death ligand 1 blockade to augment CD8 T cell responses during chronic viral infection. *J Immunol* (2011) 187:1634–42. doi: 10.4049/jimmunol.1100077
33. Kundig TM, Shahinian A, Kawai K, Mittrucker HW, Sebzda E, Bachmann MF, et al. Duration of TCR stimulation determines costimulatory requirement of T cells. *Immunity* (1996) 5:41–52. doi: 10.1016/S1074-7613(00)80308-8
34. Richer MJ, Pewe LL, Hancox LS, Hartwig SM, Varga SM, Harty JT. Inflammatory IL-15 is required for optimal memory T cell responses. *J Clin Invest* (2015) 125:3477–90. doi: 10.1172/JCI81261
35. Cui G, Staron MM, Gray SM, Ho PC, Amezquita RA, Wu J, et al. IL-7-Induced Glycerol Transport and TAG Synthesis Promotes Memory CD8+ T Cell Longevity. *Cell* (2015) 161:750–61. doi: 10.1016/j.cell.2015.03.021
36. van der Windt GJ, Everts B, Chang CH, Curtis JD, Freitas TC, Amiel E, et al. Mitochondrial respiratory capacity is a critical regulator of CD8+ T cell memory development. *Immunity* (2012) 36:68–78. doi: 10.1016/j.immuni.2011.12.007
37. Barber DL, Wherry EJ, Masopust D, Zhu B, Allison JP, Sharpe AH, et al. Restoring function in exhausted CD8 T cells during chronic viral infection. *Nature* (2006) 439:682–7. doi: 10.1038/nature04444
38. Nowacki TM, Kuerten S, Zhang W, Shive CL, Kreher CR, Boehm BO, et al. Granzyme B production distinguishes recently activated CD8(+) memory cells from resting memory cells. *Cell Immunol* (2007) 247:36–48. doi: 10.1016/j.cellimm.2007.07.004
39. Klebanoff CA, Gattinoni L, Palmer DC, Muranski P, Ji Y, Hinrichs CS, et al. Determinants of successful CD8+ T-cell adoptive immunotherapy for large established tumors in mice. *Clin Cancer Res* (2011) 17:5343–52. doi: 10.1158/1078-0432.CCR-11-0503
40. Cham CM, Gajewski TF. Glucose availability regulates IFN-gamma production and p70S6 kinase activation in CD8+ effector T cells. *J Immunol* (2005) 174:4670–7. doi: 10.4049/jimmunol.174.8.4670
41. Chang CH, Curtis JD, Maggi LBJr., Faubert B, Villarino AV, O'Sullivan D, et al. Posttranscriptional control of T cell effector function by aerobic glycolysis. *Cell* (2013) 153:1239–51. doi: 10.1016/j.cell.2013.05.016
42. Warburg O, Wind F, Negelein E. The Metabolism of Tumors in the Body. *J Gen Physiol* (1927) 8:519–30. doi: 10.1085/jgp.8.6.519
43. Singer K, Kastenberger M, Gottfried E, Hammerschmied CG, Buttner M, Aigner M, et al. Warburg phenotype in renal cell carcinoma: high expression of glucose-transporter 1 (GLUT-1) correlates with low CD8(+) T-cell infiltration in the tumor. *Int J Cancer* (2011) 128:2085–95. doi: 10.1002/ijc.25543
44. Jacobs SR, Herman CE, Maciver NJ, Wofford JA, Wieman HL, Hammen JJ, et al. Glucose uptake is limiting in T cell activation and requires CD28-mediated Akt-dependent and independent pathways. *J Immunol* (2008) 180:4476–86. doi: 10.4049/jimmunol.180.7.4476
45. Michalek RD, Gerriets VA, Jacobs SR, Macintyre AN, MacIver NJ, Mason EF, et al. Cutting edge: distinct glycolytic and lipid oxidative metabolic programs are essential for effector and regulatory CD4+ T cell subsets. *J Immunol* (2011) 186:3299–303. doi: 10.4049/jimmunol.1003613
46. Peng M, Yin N, Chhangawala S, Xu K, Leslie CS, Li MO. Aerobic glycolysis promotes T helper 1 cell differentiation through an epigenetic mechanism. *Science* (2016) 354:481–4. doi: 10.1126/science.aaf6284
47. Brand A, Singer K, Koehl GE, Kolitzus M, Schoenhammer G, Thiel A, et al. LDHA-Associated Lactic Acid Production Blunts Tumor Immunosurveillance by T and NK Cells. *Cell Metab* (2016) 24:657–71. doi: 10.1016/j.cmet.2016.08.011
48. Carr EL, Kelman A, Wu GS, Gopaul R, Senkevitch E, Aghvanyan A, et al. Glutamine uptake and metabolism are coordinately regulated by ERK/MAPK during T lymphocyte activation. *J Immunol* (2010) 185:1037–44. doi: 10.4049/jimmunol.0903586

49. Wellen KE, Hatzivassiliou G, Sachdeva UM, Bui TV, Cross JR, Thompson CB. ATP-citrate lyase links cellular metabolism to histone acetylation. *Science* (2009) 324:1076–80. doi: 10.1126/science.1164097
50. Vodnala SK, Eil R, Kishton RJ, Sukumar M, Yamamoto TN, Ha NH, et al. T cell stemness and dysfunction in tumors are triggered by a common mechanism. *Science* (2019) 363. doi: 10.1126/science.aau0135
51. Yaqoob P, Calder PC. Glutamine requirement of proliferating T lymphocytes. *Nutrition* (1997) 13:646–51. doi: 10.1016/S0899-9007(97)83008-0
52. Horig H, Spagnoli GC, Filgueira L, Babst R, Gallati H, Harder F, et al. Exogenous glutamine requirement is confined to late events of T cell activation. *J Cell Biochem* (1993) 53:343–51. doi: 10.1002/jcb.240530412
53. Sukumar M, Kishton RJ, Restifo NP. Metabolic reprograming of anti-tumor immunity. *Curr Opin Immunol* (2017) 46:14–22. doi: 10.1016/j.coi.2017.03.011
54. Luengo A, Gui DY, Vander Heiden MG. Targeting Metabolism for Cancer Therapy. *Cell Chem Biol* (2017) 24:1161–80. doi: 10.1016/j.chembiol.2017.08.028
55. Reina-Campos M, Moscat J, Diaz-Meco M. Metabolism shapes the tumor microenvironment. *Curr Opin Cell Biol* (2017) 48:47–53. doi: 10.1016/j.ceb.2017.05.006
56. Mazzone M, Menga A, Castegna A. Metabolism and TAM functions-it takes two to tango. *FEBS J* (2018) 285:700–16. doi: 10.1111/febs.14295
57. Cascone T, McKenzie JA, Mbofung RM, Punt S, Wang Z, Xu C, et al. Increased Tumor Glycolysis Characterizes Immune Resistance to Adoptive T Cell Therapy. *Cell Metab* (2018) 27:977–87.e974. doi: 10.1016/j.cmet.2018.02.024
58. Leone RD, Zhao L, Englert JM, Sun IM, Oh MH, Sun IH, et al. Glutamine blockade induces divergent metabolic programs to overcome tumor immune evasion. *Science* (2019) 366:1013–21. doi: 10.1126/science.aav2588
59. Wang T, Gnanaprakasam JNR, Chen X, Kang S, Xu X, Sun H, et al. Inosine is an alternative carbon source for CD8(+)-T-cell function under glucose restriction. *Nat Metab* (2020) 2:635–47. doi: 10.1038/s42255-020-0219-4
60. Chisolm DA, Weinmann AS. Connections Between Metabolism and Epigenetics in Programming Cellular Differentiation. *Annu Rev Immunol* (2018) 36:221–46. doi: 10.1146/annurev-immunol-042617-053127
61. Sinclair LV, Howden AJ, Brenes A, Spinelli L, Hukelmann JL, Macintyre AN, et al. Antigen receptor control of methionine metabolism in T cells. *Elife* (2019) 8. doi: 10.7554/eLife.44210
62. Sedlackova L, Korolchuk VI. Mitochondrial quality control as a key determinant of cell survival. *Biochim Biophys Acta Mol Cell Res* (2019) 1866:575–87. doi: 10.1016/j.bbamcr.2018.12.012
63. Blagih J, Coulombe F, Vincent EE, Dupuy F, Galicia-Vazquez G, Yurchenko E, et al. The energy sensor AMPK regulates T cell metabolic adaptation and effector responses in vivo. *Immunity* (2015) 42:41–54. doi: 10.1016/j.immuni.2014.12.030
64. Youngblood B, Davis CW, Ahmed R. Making memories that last a lifetime: heritable functions of self-renewing memory CD8 T cells. *Int Immunol* (2010) 22:797–803. doi: 10.1093/intimm/dxq437
65. Quintana A, Schwindling C, Wenning AS, Becherer U, Rettig J, Schwarz EC, et al. T cell activation requires mitochondrial translocation to the immunological synapse. *Proc Natl Acad Sci U S A* (2007) 104:14418–23. doi: 10.1073/pnas.0703126104
66. Bantug GR, Fischer M, Grahlert J, Balmer ML, Unterstab G, Develioglu L, et al. Mitochondria-Endoplasmic Reticulum Contact Sites Function as Immunometabolic Hubs that Orchestrate the Rapid Recall Response of Memory CD8(+) T Cells. *Immunity* (2018) 48:542–55.e546. doi: 10.1016/j.immuni.2018.02.012
67. Rieusset J. The role of endoplasmic reticulum-mitochondria contact sites in the control of glucose homeostasis: an update. *Cell Death Dis* (2018) 9:388. doi: 10.1038/s41419-018-0416-1
68. Wu S, Zhou F, Zhang Z, Xing D. Mitochondrial oxidative stress causes mitochondrial fragmentation via differential modulation of mitochondrial fission-fusion proteins. *FEBS J* (2011) 278:941–54. doi: 10.1111/j.1742-4658.2011.08010.x
69. Quintana A, Hoth M. Mitochondrial dynamics and their impact on T cell function. *Cell Calcium* (2012) 52:57–63. doi: 10.1016/j.ceca.2012.02.005
70. Buck MD, O'Sullivan D, Klein Geltink RI, Curtis JD, Chang CH, Sanin DE, et al. Mitochondrial Dynamics Controls T Cell Fate through Metabolic Programming. *Cell* (2016) 166:63–76. doi: 10.1016/j.cell.2016.05.035
71. Rambold AS, Pearce EL. Mitochondrial Dynamics at the Interface of Immune Cell Metabolism and Function. *Trends Immunol* (2018) 39:6–18. doi: 10.1016/j.it.2017.08.006
72. Friedman JR, Lackner LL, West M, DiBenedetto JR, Nunnari J, Voeltz GK. ER tubules mark sites of mitochondrial division. *Science* (2011) 334:358–62. doi: 10.1126/science.1207385
73. Cribbs JT, Strack S. Reversible phosphorylation of Drp1 by cyclic AMP-dependent protein kinase and calcineurin regulates mitochondrial fission and cell death. *EMBO Rep* (2007) 8:939–44. doi: 10.1038/sj.embor.7401062
74. Cereghetti GM, Stangherlin A, Martins de Brito O, Chang CR, Blackstone C, Bernardi P, et al. Dephosphorylation by calcineurin regulates translocation of Drp1 to mitochondria. *Proc Natl Acad Sci U S A* (2008) 105:15803–8. doi: 10.1073/pnas.0808249105
75. Rambold AS, Kostelecky B, Elia N, Lippincott-Schwartz J. Tubular network formation protects mitochondria from autophagosomal degradation during nutrient starvation. *Proc Natl Acad Sci U S A* (2011) 108:10190–5. doi: 10.1073/pnas.1107402108
76. Wang D, Wang J, Bonamy GM, Meeusen S, Brusch RG, Turk C, et al. A small molecule promotes mitochondrial fusion in mammalian cells. *Angew Chem Int Ed Engl* (2012) 51:9302–5. doi: 10.1002/anie.201204589
77. Garcia D, Shaw RJ. AMPK: Mechanisms of Cellular Energy Sensing and Restoration of Metabolic Balance. *Mol Cell* (2017) 66:789–800. doi: 10.1016/j.molcel.2017.05.032
78. Mayer A, Denanglaire S, Viollet B, Leo O, Andris F. AMP-activated protein kinase regulates lymphocyte responses to metabolic stress but is largely dispensable for immune cell development and function. *Eur J Immunol* (2008) 38:948–56. doi: 10.1002/eji.200738045
79. Ito K, Ito K. Metabolism and the Control of Cell Fate Decisions and Stem Cell Renewal. *Annu Rev Cell Dev Biol* (2016) 32:399–409. doi: 10.1146/annurev-cellbio-111315-125134
80. Jeninga EH, Schoonjans K, Auwerx J. Reversible acetylation of PGC-1: connecting energy sensors and effectors to guarantee metabolic flexibility. *Oncogene* (2010) 29:4617–24. doi: 10.1038/onc.2010.206
81. Scharping NE, Menk AV, Moreci RS, Whetstone RD, Dadey RE, Watkins SC, et al. The Tumor Microenvironment Represses T Cell Mitochondrial Biogenesis to Drive Intratumoral T Cell Metabolic Insufficiency and Dysfunction. *Immunity* (2016) 45:374–88. doi: 10.1016/j.immuni.2016.07.009
82. Kawalekar OU, O'Connor RS, Fraietta JA, Guo L, McGettigan SE, Posey AD Jr, et al. Distinct Signaling of Coreceptors Regulates Specific Metabolism Pathways and Impacts Memory Development in CAR T Cells. *Immunity* (2016) 44:380–90. doi: 10.1016/j.immuni.2016.01.021
83. Almeida L, Lochner M, Berod L, Sparwasser T. Metabolic pathways in T cell activation and lineage differentiation. *Semin Immunol* (2016) 28:514–24. doi: 10.1016/j.smim.2016.10.009
84. Chang CH, Qiu J, O'Sullivan D, Buck MD, Noguchi T, Curtis JD, et al. Metabolic Competition in the Tumor Microenvironment Is a Driver of Cancer Progression. *Cell* (2015) 162:1229–41. doi: 10.1016/j.cell.2015.08.016
85. Guillaumond F, Leca J, Olivares O, Lavaut MN, Vidal N, Berthezene P, et al. Strengthened glycolysis under hypoxia supports tumor symbiosis and hexosamine biosynthesis in pancreatic adenocarcinoma. *Proc Natl Acad Sci U S A* (2013) 110:3919–24. doi: 10.1073/pnas.1219555110
86. Clever D, Roychoudhuri R, Constantinides MG, Askenase MH, Sukumar M, Klebanoff CA, et al. Oxygen Sensing by T Cells Establishes an Immunologically Tolerant Metastatic Niche. *Cell* (2016) 166:1117–31.e1114. doi: 10.1016/j.cell.2016.07.032
87. Broer S. Lactate transportation is required for lymphocyte activation. *Nat Chem Biol* (2005) 1:356–7. doi: 10.1038/nchembio1205-356
88. Fischer K, Hoffmann P, Voelkl S, Meidenbauer N, Ammer J, Edinger M, et al. Inhibitory effect of tumor cell-derived lactic acid on human T cells. *Blood* (2007) 109:3812–9. doi: 10.1182/blood-2006-07-035972
89. Murray CM, Hutchinson R, Bantick JR, Belfield GP, Benjamin AD, Brazma D, et al. Monocarboxylate transporter MCT1 is a target for immunosuppression. *Nat Chem Biol* (2005) 1:371–6 doi: 10.1038/nchembio744.

90. Doherty JR, Cleveland JL. Targeting lactate metabolism for cancer therapeutics. *J Clin Invest* (2013) 123:3685–92. doi: 10.1172/JCI69741
91. Gatenby RA, Gillies RJ. Why do cancers have high aerobic glycolysis? *Nat Rev Cancer* (2004) 4:891–9. doi: 10.1038/nrc1478
92. Sommer F, Bischof S, Rollinghoff M, Lohoff M. Demonstration of organic anion transport in T lymphocytes. L-lactate and fluo-3 are target molecules. *J Immunol* (1994) 153:3523–32.
93. Calcinotto A, Filipazzi P, Grioni M, Iero M, De Milito A, Ricupito A, et al. Modulation of microenvironment acidity reverses anergy in human and murine tumor-infiltrating T lymphocytes. *Cancer Res* (2012) 72:2746–56. doi: 10.1158/0008-5472.CAN-11-1272
94. van Stipdonk MJ, Hardenberg G, Bijker MS, Lemmens EE, Droin NM, Green DR, et al. Dynamic programming of CD8+ T lymphocyte responses. *Nat Immunol* (2003) 4:361–5. doi: 10.1038/ni912
95. Angelin A, Gil-de-Gomez L, Dahiya S, Jiao J, Guo L, Levine MH, et al. Foxp3 Reprograms T Cell Metabolism to Function in Low-Glucose, High-Lactate Environments. *Cell Metab* (2017) 25:1282–93.e1287. doi: 10.1016/j.cmet.2016.12.018
96. Comito G, Iscaro A, Bacci M, Morandi A, Ippolito L, Parri M, et al. Lactate modulates CD4(+) T-cell polarization and induces an immunosuppressive environment, which sustains prostate carcinoma progression via TLR8/miR21 axis. *Oncogene* (2019) 38:3681–95. doi: 10.1038/s41388-019-0688-7
97. Szymczak-Workman AL, Delgoffe GM, Green DR, Vignali DA. Cutting edge: regulatory T cells do not mediate suppression via programmed cell death pathways. *J Immunol* (2011) 187:4416–20. doi: 10.4049/jimmunol.1100548
98. Pacella I, Procaccini C, Focaccetti C, Miacci S, Timperi E, Faicchia D, et al. Fatty acid metabolism complements glycolysis in the selective regulatory T cell expansion during tumor growth. *Proc Natl Acad Sci U S A* (2018) 115:E6546–55. doi: 10.1073/pnas.1720113115
99. Weinberg SE, Singer BD, Steinert EM, Martinez CA, Mehta MM, Martinez-Reyes I, et al. Mitochondrial complex III is essential for suppressive function of regulatory T cells. *Nature* (2019) 565:495–9. doi: 10.1038/s41586-018-0846-z
100. Watson MJ, Vignali PDA, Mullett SJ, Overacre-Delgoffe AE, Peralta RM, Grebinoski S, et al. Metabolic support of tumour-infiltrating regulatory T cells by lactic acid. *Nature* (2021). doi: 10.1038/s41586-020-03045-2
101. Zappasodi R, Serganova I, Cohen IJ, Maeda M, Shindo M, Senbabaoglu Y, et al. CTLA-4 blockade drives loss of Treg stability in glycolysis-low tumours. *Nature* (2021). doi: 10.1038/s41586-021-03326-4
102. DeVita VT Jr, Chu E. A history of cancer chemotherapy. *Cancer Res* (2008) 68:8643–53. doi: 10.1158/0008-5472.CAN-07-6611
103. Eil R, Vodnala SK, Clever D, Klebanoff CA, Sukumar M, Pan JH, et al. Ionic immune suppression within the tumour microenvironment limits T cell effector function. *Nature* (2016) 537:539–43. doi: 10.1038/nature19364
104. Ohta A, Madasu M, Subramanian M, Kini R, Jones G, Chouker A, et al. Hypoxia-induced and A2A adenosine receptor-independent T-cell suppression is short lived and easily reversible. *Int Immunol* (2014) 26:83–91. doi: 10.1093/intimm/dxt045
105. Ohta A, Sitkovsky M. Extracellular adenosine-mediated modulation of regulatory T cells. *Front Immunol* (2014) 5:304. doi: 10.3389/fimmu.2014.00304
106. Ma X, Bi E, Lu Y, Su P, Huang C, Liu L, et al. Cholesterol Induces CD8(+) T Cell Exhaustion in the Tumor Microenvironment. *Cell Metab* (2019) 30:143–56.e145. doi: 10.1016/j.cmet.2019.04.002
107. Ando M, Ito M, Srirat T, Kondo T, Yoshimura A. Memory T cell, exhaustion, and tumor immunity. *Immunol Med* (2020) 43:1–9. doi: 10.1080/25785826.2019.1698261
108. Ahmadzadeh M, Johnson LA, Heemskerk B, Wunderlich JR, Dudley ME, White DE, et al. Tumor antigen-specific CD8 T cells infiltrating the tumor express high levels of PD-1 and are functionally impaired. *Blood* (2009) 114:1537–44. doi: 10.1182/blood-2008-12-195792
109. Sakuishi K, Apetoh L, Sullivan JM, Blazar BR, Kuchroo VK, Anderson AC. Targeting Tim-3 and PD-1 pathways to reverse T cell exhaustion and restore anti-tumor immunity. *J Exp Med* (2010) 207:2187–94. doi: 10.1084/jem.20100643
110. Parry RV, Chemnitz JM, Frauwirth KA, Lanfranco AR, Braunstein I, Kobayashi SV, et al. CTLA-4 and PD-1 receptors inhibit T-cell activation by distinct mechanisms. *Mol Cell Biol* (2005) 25:9543–53. doi: 10.1128/MCB.25.21.9543-9553.2005
111. Woo SR, Turnis ME, Goldberg MV, Bankoti J, Selby M, Nirschl CJ, et al. Immune inhibitory molecules LAG-3 and PD-1 synergistically regulate T-cell function to promote tumoral immune escape. *Cancer Res* (2012) 72:917–27. doi: 10.1158/0008-5472.CAN-11-1620
112. Patsoukis N, Bardhan K, Chatterjee P, Sari D, Liu B, Bell LN, et al. PD-1 alters T-cell metabolic reprogramming by inhibiting glycolysis and promoting lipolysis and fatty acid oxidation. *Nat Commun* (2015) 6:6692. doi: 10.1038/ncomms7692
113. Bengsch B, Johnson AL, Kurachi M, Odorizzi PM, Pauken KE, Attanasio J, et al. Bioenergetic Insufficiencies Due to Metabolic Alterations Regulated by the Inhibitory Receptor PD-1 Are an Early Driver of CD8(+) T Cell Exhaustion. *Immunity* (2016) 45:358–73. doi: 10.1016/j.immuni.2016.07.008
114. Cham CM, Driessens G, O'Keefe JP, Gajewski TF. Glucose deprivation inhibits multiple key gene expression events and effector functions in CD8+ T cells. *Eur J Immunol* (2008) 38:2438–50. doi: 10.1002/eji.200838289
115. Walunas TL, Lenschow DJ, Bakker CY, Linsley PS, Freeman GJ, Green JM, et al. CTLA-4 can function as a negative regulator of T cell activation. *Immunity* (1994) 1:405–13 doi: 10.1084/jem.183.6.2541.
116. Walunas TL, Bakker CY, Bluestone JA. CTLA-4 ligation blocks CD28-dependent T cell activation. *J Exp Med* (1996) 183:2541–50. doi: 10.1084/jem.183.6.2541
117. Brunet JF, Denizot F, Luciani MF, Roux-Dosseto M, Suzan M, Mattei MG, et al. A new member of the immunoglobulin superfamily–CTLA-4. *Nature* (1987) 328:267–70. doi: 10.1038/328267a0
118. Gribben JG, Freeman GJ, Boussiotis VA, Rennert P, Jellis CL, Greenfield E, et al. CTLA4 mediates antigen-specific apoptosis of human T cells. *Proc Natl Acad Sci U S A* (1995) 92:811–5. doi: 10.1073/pnas.92.3.811
119. Triebel F, Jitsukawa S, Baixeras E, Roman-Roman S, Genevee C, Viegas-Pequignot E, et al. LAG-3, a novel lymphocyte activation gene closely related to CD4. *J Exp Med* (1990) 171:1393–405. doi: 10.1084/jem.171.5.1393
120. Hannier S, Tournier M, Bismuth G, Triebel F. CD3/TCR complex-associated lymphocyte activation gene-3 molecules inhibit CD3/TCR signaling. *J Immunol* (1998) 161:4058–65.
121. Daskivich TJ, Belldegrun A. Words of wisdom. Re: Safety, activity, and immune correlates of anti-PD-1 antibody in cancer. *Eur Urol* (2015) 67:816–7. doi: 10.1016/j.eururo.2014.12.052
122. Brahmer JR, Tykodi SS, Chow LQ, Hwu WJ, Topalian SL, Hwu P, et al. Safety and activity of anti-PD-L1 antibody in patients with advanced cancer. *N Engl J Med* (2012) 366:2455–65. doi: 10.1056/NEJMoa1200694
123. Rosenberg SA, Restifo NP. Adoptive cell transfer as personalized immunotherapy for human cancer. *Science* (2015) 348:62–8. doi: 10.1126/science.aaa4967
124. Tran E, Robbins PF, Rosenberg SA. 'Final common pathway' of human cancer immunotherapy: targeting random somatic mutations. *Nat Immunol* (2017) 18:255–62. doi: 10.1038/ni.3682
125. Lee H, Lee M, Seo JH, Gong G, Lee HJ. Changes in Tumor-infiltrating Lymphocytes After Neoadjuvant Chemotherapy and Clinical Significance in Triple Negative Breast Cancer. *Anticancer Res* (2020) 40:1883–90. doi: 10.21873/anticanres.14142
126. Yossef R, Tran E, Deniger DC, Gros A, Pasetto A, Parkhurst MR, et al. Enhanced detection of neoantigen-reactive T cells targeting unique and shared oncogenes for personalized cancer immunotherapy. *JCI Insight* (2018) 3. doi: 10.1172/jci.insight.122467
127. Kochenderfer JN, Dudley ME, Kassim SH, Somerville RP, Carpenter RO, Stetler-Stevenson M, et al. Chemotherapy-refractory diffuse large B-cell lymphoma and indolent B-cell malignancies can be effectively treated with autologous T cells expressing an anti-CD19 chimeric antigen receptor. *J Clin Oncol* (2015) 33:540–9. doi: 10.1200/JCO.2014.56.2025
128. Maude SL, Frey N, Shaw PA, Aplenc R, Barrett DM, Bunin NJ, et al. Chimeric antigen receptor T cells for sustained remissions in leukemia. *N Engl J Med* (2014) 371:1507–17. doi: 10.1056/NEJMoa1407222
129. Brentjens RJ, Davila ML, Riviere I, Park J, Wang X, Cowell LG, et al. CD19-targeted T cells rapidly induce molecular remissions in adults with chemotherapy-refractory acute lymphoblastic leukemia. *Sci Transl Med* (2013) 5:177ra138. doi: 10.1126/scitranslmed.3005930

130. Knochelmann HM, Smith AS, Dwyer CJ, Wyatt MM, Mehrotra S, Paulos CM. CAR T Cells in Solid Tumors: Blueprints for Building Effective Therapies. *Front Immunol* (2018) 9:1740. doi: 10.3389/fimmu.2018.01740
131. Davila ML, Riviere I, Wang X, Bartido S, Park J, Curran K, et al. Efficacy and Toxicity Management of 19-28z CAR T Cell Therapy in B Cell Acute Lymphoblastic Leukemia. *Sci Trans Med* (2014) 6:224ra225. doi: 10.1126/scitranslmed.3008226
132. Porter DL, Hwang WT, Frey NV, Lacey SF, Shaw PA, Loren AW, et al. Chimeric antigen receptor T cells persist and induce sustained remissions in relapsed refractory chronic lymphocytic leukemia. *Sci Transl Med* (2015) 7:303ra139. doi: 10.1126/scitranslmed.aac5415
133. Long AH, Haso WM, Shern JF, Wanhainen KM, Murgai M, Ingaramo M, et al. 4-1BB costimulation ameliorates T cell exhaustion induced by tonic signaling of chimeric antigen receptors. *Nat Med* (2015) 21:581–90. doi: 10.1038/nm.3838
134. Gattinoni L, Lugli E, Ji Y, Pos Z, Paulos CM, Quigley MF, et al. A human memory T cell subset with stem cell-like properties. *Nat Med* (2011) 17:1290–7. doi: 10.1038/nm.2446
135. Dwyer CJ, Knochelmann HM, Smith AS, Wyatt MM, Rangel Rivera GO, Arhontoulis DC, et al. Fueling Cancer Immunotherapy With Common Gamma Chain Cytokines. *Front Immunol* (2019) 10:263. doi: 10.3389/fimmu.2019.00263
136. Liu S, Riley J, Rosenberg S, Parkhurst M. Comparison of common gamma-chain cytokines, interleukin-2, interleukin-7, and interleukin-15 for the in vitro generation of human tumor-reactive T lymphocytes for adoptive cell transfer therapy. *J Immunother* (2006) 29:284–93. doi: 10.1097/01.cji.0000190168.53793.6b
137. Yang S, Ji Y, Gattinoni L, Zhang L, Yu Z, Restifo NP, et al. Modulating the differentiation status of ex vivo-cultured anti-tumor T cells using cytokine cocktails. *Cancer Immunol Immunother* (2013) 62:727–36. doi: 10.1007/s00262-012-1378-2
138. Hinrichs CS, Spolski R, Paulos CM, Gattinoni L, Kerstann KW, Palmer DC, et al. IL-2 and IL-21 confer opposing differentiation programs to CD8+ T cells for adoptive immunotherapy. *Blood* (2008) 111:5326–33. doi: 10.1182/blood-2007-09-113050
139. Shen S, Sckisel G, Sahoo A, Lalani A, Otter DD, Pearson J, et al. Engineered IL-21 Cytokine Muteins Fused to Anti-PD-1 Antibodies Can Improve CD8+ T Cell Function and Anti-tumor Immunity. *Front Immunol* (2020) 11:832. doi: 10.3389/fimmu.2020.00832
140. Li Y, Cong Y, Jia M, He Q, Zhong H, Zhao Y, et al. Targeting IL-21 to tumor-reactive T cells enhances memory T cell responses and anti-PD-1 antibody therapy. *Nat Commun* (2021) 12:951. doi: 10.1038/s41467-021-21241-0
141. Catakovic K, Klieser E, Neureiter D, Geisberger R. T cell exhaustion: from pathophysiological basics to tumor immunotherapy. *Cell Commun Signal* (2017) 15:1. doi: 10.1186/s12964-016-0160-z
142. Frauwirth KA, Riley JL, Harris MH, Parry RV, Rathmell JC, Plas DR, et al. The CD28 signaling pathway regulates glucose metabolism. *Immunity* (2002) 16:769–77. doi: 10.1016/s1074-7613(02)00323-0
143. Petersen CT, Hassan M, Morris AB, Jeffery J, Lee K, Jagirdar N, et al. Improving T-cell expansion and function for adoptive T-cell therapy using ex vivo treatment with PI3Kdelta inhibitors and VIP antagonists. *Blood Adv* (2018) 2:210–23. doi: 10.1182/bloodadvances.2017011254
144. Bowers JS, Majchrzak K, Nelson MH, Aksoy BA, Wyatt MM, Smith AS, et al. PI3Kdelta Inhibition Enhances the Antitumor Fitness of Adoptively Transferred CD8(+) T Cells. *Front Immunol* (2017) 8:1221. doi: 10.3389/fimmu.2017.01221
145. Majchrzak K, Nelson MH, Bowers JS, Bailey SR, Wyatt MM, Wrangle JM, et al. beta-catenin and PI3Kdelta inhibition expands precursor Th17 cells with heightened stemness and antitumor activity. *JCI Insight* (2017) 2. doi: 10.1172/jci.insight.90547
146. Dwyer CJ, Arhontoulis DC, Rangel Rivera GO, Knochelmann HM, Smith AS, Wyatt MM, et al. Ex vivo blockade of PI3K gamma or delta signaling enhances the antitumor potency of adoptively transferred CD8(+) T cells. *Eur J Immunol* (2020) 50:1386–9. doi: 10.1002/eji.201948455
147. Crompton JG, Sukumar M, Roychoudhuri R, Clever D, Gros A, Eil RL, et al. Akt inhibition enhances expansion of potent tumor-specific lymphocytes with memory cell characteristics. *Cancer Res* (2015) 75:296–305. doi: 10.1158/0008-5472.CAN-14-2277
148. Mousset CM, Hobo W, Ji Y, Fredrix H, De Giorgi V, Allison RD, et al. Ex vivo AKT-inhibition facilitates generation of polyfunctional stem cell memory-like CD8(+) T cells for adoptive immunotherapy. *Oncoimmunology* (2018) 7:e1488565. doi: 10.1080/2162402X.2018.1488565
149. He S, Kato K, Jiang J, Wahl DR, Mineishi S, Fisher EM, et al. Characterization of the metabolic phenotype of rapamycin-treated CD8+ T cells with augmented ability to generate long-lasting memory cells. *PLoS One* (2011) 6:e20107. doi: 10.1371/journal.pone.0020107
150. Scholz G, Jandus C, Zhang L, Grandclement C, Lopez-Mejia IC, Soneson C, et al. Modulation of mTOR Signalling Triggers the Formation of Stem Cell-like Memory T Cells. *EBioMedicine* (2016) 4:50–61. doi: 10.1016/j.ebiom.2016.01.019
151. Klebanoff CA, Crompton JG, Leonardi AJ, Yamamoto TN, Chandran SS, Eil RL, et al. Inhibition of AKT signaling uncouples T cell differentiation from expansion for receptor-engineered adoptive immunotherapy. *JCI Insight* (2017) 2. doi: 10.1172/jci.insight.95103
152. Xu X, Araki K, Li S, Han JH, Ye L, Tan WG, et al. Autophagy is essential for effector CD8(+) T cell survival and memory formation. *Nat Immunol* (2014) 15:1152–61. doi: 10.1038/ni.3025
153. Semenza GL. Mitochondrial autophagy: life and breath of the cell. *Autophagy* (2008) 4:534–6. doi: 10.4161/auto.5956
154. Yu YR, Imrichova H, Wang H, Chao T, Xiao Z, Gao M, et al. Disturbed mitochondrial dynamics in CD8(+) TILs reinforce T cell exhaustion. *Nat Immunol* (2020) 21:1540–51. doi: 10.1038/s41590-020-0793-3
155. Gurusamy D, Henning AN, Yamamoto TN, Yu Z, Zacharakis N, Krishna S, et al. Multi-phenotype CRISPR-Cas9 Screen Identifies p38 Kinase as a Target for Adoptive Immunotherapies. *Cancer Cell* (2020) 37:818–33. doi: 10.1016/j.ccell.2020.05.004
156. Thaxton JE, Wallace C, Riesenberg B, Zhang Y, Paulos CM, Beeson CC, et al. Modulation of Endoplasmic Reticulum Stress Controls CD4(+) T-cell Activation and Antitumor Function. *Cancer Immunol Res* (2017) 5:666–75. doi: 10.1158/2326-6066.CIR-17-0081
157. Hurst KE, Lawrence KA, Reyes Angeles L, Ye Z, Zhang J, Townsend DM, et al. Endoplasmic Reticulum Protein Disulfide Isomerase Shapes T Cell Efficacy for Adoptive Cellular Therapy of Tumors. *Cells* (2019) 8. doi: 10.3390/cells8121514
158. Hurst KE, Lawrence KA, Essman MT, Walton ZJ, Leddy LR, Thaxton JE. Endoplasmic Reticulum Stress Contributes to Mitochondrial Exhaustion of CD8(+) T Cells. *Cancer Immunol Res* (2019) 7:476–86. doi: 10.1158/2326-6066.CIR-18-0182
159. Hurst KE, Lawrence KA, Robino RA, Ball LE, Chung D, Thaxton JE. Remodeling Translation Primes CD8(+) T-cell Antitumor Immunity. *Cancer Immunol Res* (2020) 8:587–95. doi: 10.1158/2326-6066.CIR-19-0516
160. Chellappa S, Kushekhar K, Munthe LA, Tjonnfjord GE, Aandahl EM, Okkenhaug K, et al. The PI3K p110delta Isoform Inhibitor Idelalisib Preferentially Inhibits Human Regulatory T Cell Function. *J Immunol* (2019) 202:1397–405. doi: 10.4049/jimmunol.1701703
161. Ahmad S, Abu-Eid R, Shrimali R, Webb M, Verma V, Doroodchi A, et al. Differential PI3Kdelta Signaling in CD4(+) T-cell Subsets Enables Selective Targeting of T Regulatory Cells to Enhance Cancer Immunotherapy. *Cancer Res* (2017) 77:1892–904. doi: 10.1158/0008-5472.CAN-16-1839
162. Akhiani AA, Hallner A, Kiffin R, Aydin E, Werlenius O, Aurelius J, et al. Idelalisib Rescues Natural Killer Cells from Monocyte-Induced Immunosuppression by Inhibiting NOX2-Derived Reactive Oxygen Species. *Cancer Immunol Res* (2020) 8:1532–41. doi: 10.1158/2326-6066.CIR-20-0055
163. Sukumar M, Liu J, Ji Y, Subramanian M, Crompton JG, Yu Z, et al. Inhibiting glycolytic metabolism enhances CD8+ T cell memory and antitumor function. *J Clin Invest* (2013) 123:4479–88. doi: 10.1172/JCI69589
164. Klein Geltink RI, Edwards-Hicks J, Apostolova P, O'Sullivan D, Sanin DE, Patterson AE, et al. Metabolic conditioning of CD8(+) effector T cells for adoptive cell therapy. *Nat Metab* (2020) 2:703–16. doi: 10.1038/s42255-020-0256-z
165. Ho PC, Bihuniak JD, Macintyre AN, Staron M, Liu X, Amezquita R, et al. Phosphoenolpyruvate Is a Metabolic Checkpoint of Anti-tumor T Cell Responses. *Cell* (2015) 162:1217–28. doi: 10.1016/j.cell.2015.08.012
166. Geiger R, Rieckmann JC, Wolf T, Basso C, Feng Y, Fuhrer T, et al. L-Arginine Modulates T Cell Metabolism and Enhances Survival and Anti-tumor Activity. *Cell* (2016) 167:829–42.e813. doi: 10.1016/j.cell.2016.09.031
167. Bailey SR, Nelson MH, Majchrzak K, Bowers JS, Wyatt MM, Smith AS, et al. Human CD26(high) T cells elicit tumor immunity against multiple

malignancies via enhanced migration and persistence. *Nat Commun* (2017) 8:1961. doi: 10.1038/s41467-017-01867-9

168. Chamoto K, Chowdhury PS, Kumar A, Sonomura K, Matsuda F, Fagarasan S, et al. Mitochondrial activation chemicals synergize with surface receptor PD-1 blockade for T cell-dependent antitumor activity. *Proc Natl Acad Sci U S A* (2017) 114:E761–70. doi: 10.1073/pnas.1620433114
169. Chowdhury PS, Chamoto K, Kumar A, Honjo T. PPAR-Induced Fatty Acid Oxidation in T Cells Increases the Number of Tumor-Reactive CD8(+) T Cells and Facilitates Anti-PD-1 Therapy. *Cancer Immunol Res* (2018) 6:1375–87. doi: 10.1158/2326-6066.CIR-18-0095
170. Doherty JR, Yang C, Scott KE, Cameron MD, Fallahi M, Li W, et al. Blocking lactate export by inhibiting the Myc target MCT1 Disables glycolysis and glutathione synthesis. *Cancer Res* (2014) 74:908–20. doi: 10.1158/0008-5472.CAN-13-2034
171. Xie H, Hanai J, Ren JG, Kats L, Burgess K, Bhargava P, et al. Targeting lactate dehydrogenase–a inhibits tumorigenesis and tumor progression in mouse models of lung cancer and impacts tumor-initiating cells. *Cell Metab* (2014) 19:795–809. doi: 10.1016/j.cmet.2014.03.003
172. Hatfield SM, Kjaergaard J, Lukashev D, Belikoff B, Schreiber TH, Sethumadhavan S, et al. Systemic oxygenation weakens the hypoxia and hypoxia inducible factor 1alpha-dependent and extracellular adenosine-mediated tumor protection. *J Mol Med (Berl)* (2014) 92:1283–92. doi: 10.1007/s00109-014-1189-3
173. Scharping NE, Menk AV, Whetstone RD, Zeng X, Delgoffe GM. Efficacy of PD-1 Blockade Is Potentiated by Metformin-Induced Reduction of Tumor Hypoxia. *Cancer Immunol Res* (2017) 5:9–16. doi: 10.1158/2326-6066.CIR-16-0103
174. Pilon-Thomas S, Kodumudi KN, El-Kenawi AE, Russell S, Weber AM, Luddy K, et al. Neutralization of Tumor Acidity Improves Antitumor Responses to Immunotherapy. *Cancer Res* (2016) 76:1381–90. doi: 10.1158/0008-5472.CAN-15-1743
175. Sborov DW, Haverkos BM, Harris PJ. Investigational cancer drugs targeting cell metabolism in clinical development. *Expert Opin Investig Drugs* (2015) 24:79–94. doi: 10.1517/13543784.2015.960077
176. Kroon P, Frijlink E, Iglesias-Guimarais V, Volkov A, van Buuren MM, Schumacher TN, et al. Radiotherapy and Cisplatin Increase Immunotherapy Efficacy by Enabling Local and Systemic Intratumoral T-cell Activity. *Cancer Immunol Res* (2019) 7:670–82. doi: 10.1158/2326-6066.CIR-18-0654
177. Hong M, Puaux AL, Huang C, Loumagne L, Tow C, Mackay C, et al. Chemotherapy induces intratumoral expression of chemokines in cutaneous melanoma, favoring T-cell infiltration and tumor control. *Cancer Res* (2011) 71:6997–7009. doi: 10.1158/0008-5472.CAN-11-1466
178. Hedeskov CJ, Esmann V. Respiration and glycolysis of normal human lymphocytes. *Blood* (1966) 28:163–74. doi: 10.1182/blood.V28.2.163.163

Conflict of Interest: The authors declare that the research was conducted in the absence of any commercial or financial relationships that could be construed as a potential conflict of interest.

Copyright © 2021 Rangel Rivera, Knochelmann, Dwyer, Smith, Wyatt, Rivera-Reyes, Thaxton and Paulos. This is an open-access article distributed under the terms of the Creative Commons Attribution License (CC BY). The use, distribution or reproduction in other forums is permitted, provided the original author(s) and the copyright owner(s) are credited and that the original publication in this journal is cited, in accordance with accepted academic practice. No use, distribution or reproduction is permitted which does not comply with these terms.

frontiers in Immunology

REVIEW
published: 30 March 2021
doi: 10.3389/fimmu.2021.658753

Engineered TCR-T Cell Immunotherapy in Anticancer Precision Medicine: Pros and Cons

Qijie Zhao[1,2,3†], Yu Jiang[1,2†], Shixin Xiang[1,2], Parham Jabbarzadeh Kaboli[1,2], Jing Shen[1,2], Yueshui Zhao[1,2], Xu Wu[1,2], Fukuan Du[1,2], Mingxing Li[1,2], Chi Hin Cho[1,2], Jing Li[4], Qinglian Wen[5], Tao Liu[6], Tao Yi[7*] and Zhangang Xiao[1,8*]*

[1] Laboratory of Molecular Pharmacology, Department of Pharmacology, School of Pharmacy, Southwest Medical University, Luzhou, China, [2] South Sichuan Institute of Translational Medicine, Luzhou, China, [3] Department of Pathophysiology, College of Basic Medical Science, Southwest Medical University, Luzhou, China, [4] Department of Oncology and Hematology, Hospital (T.C.M.) Affiliated to Southwest Medical University, Luzhou, China, [5] Department of Oncology, The Affiliated Hospital of Southwest Medical University, Luzhou, China, [6] Department of Oncology Rehabilitation, Shenzhen Luohu People's Hospital, Shenzhen, China, [7] School of Chinese Medicine, Hong Kong Baptist University, Hong Kong, Hong Kong, [8] Department of Pharmacy, The Affiliated Hospital of Southwest Medical University, Luzhou, China

OPEN ACCESS

Edited by:
Peng Qu,
National Institutes of Health (NIH), United States

Reviewed by:
Guoyuan Zhu,
Macau University of Science and Technology, Macau
Menghua Wu,
Jinan University, China

***Correspondence:**
Tao Liu
tao2020@sohu.com
Tao Yi
yitao@hkbu.edu.hk
Zhangang Xiao
xzg555898@hotmail.com

[†]These authors have contributed equally to this work

Specialty section:
This article was submitted to Cancer Immunity and Immunotherapy, a section of the journal Frontiers in Immunology

Received: 26 January 2021
Accepted: 02 March 2021
Published: 30 March 2021

Citation:
Zhao Q, Jiang Y, Xiang S, Kaboli PJ, Shen J, Zhao Y, Wu X, Du F, Li M, Cho CH, Li J, Wen Q, Liu T, Yi T and Xiao Z (2021) Engineered TCR-T Cell Immunotherapy in Anticancer Precision Medicine: Pros and Cons. Front. Immunol. 12:658753. doi: 10.3389/fimmu.2021.658753

This review provides insight into the role of engineered T-cell receptors (TCRs) in immunotherapy. Novel approaches have been developed to boost anticancer immune system, including targeting new antigens, manufacturing new engineered or modified TCRs, and creating a safety switch for endo-suicide genes. In order to re-activate T cells against tumors, immune-mobilizing monoclonal TCRs against cancer (ImmTAC) have been developed as a novel class of manufactured molecules which are bispecific and recognize both cancer and T cells. The TCRs target special antigens such as NY-ESO-1, AHNAK^{S2580F} or ERBB2^{H473Y} to boost the efficacy of anticancer immunotherapy. The safety of genetically modified T cells is very important. Therefore, this review discusses pros and cons of different approaches, such as ImmTAC, Herpes simplex virus thymidine kinase (HSV-TK), and inducible caspase-9 in cancer immunotherapy. Clinical trials related to TCR-T cell therapy and monoclonal antibodies designed for overcoming immunosuppression, and recent advances made in understanding how TCRs are additionally examined. New approaches that can better detect antigens and drive an effective T cell response are discussed as well.

Keywords: ImmTAC, immunosuppression, immunotherapy, T-cell receptors, suicide genes

INTRODUCTION

In 2018, GLOBOCAN reported 18.1 million new cancer cases and 9.6 million related deaths worldwide (1). Recent studies have examined the role of neo-antigens in promoting immunotherapy pointing to their promising potential to treat cancer and increase overall survival rates of patients (2). Antibodies which inhibit T-cell inhibitory receptor, programmed death 1 (PD-1), and target its ligand on tumor surface, PD-L1, in order to decrease T cell tolerance in the tumor microenvironment (TME), have recently been approved by US Food and Drug Administration (FDA) (3). Suppression of PD-1 and PD-L1 has achieved promising antitumor

effects in metastatic bladder, pancreatic, ovarian, breast, gastric, and renal-cell cancers (4–9). However, more potent and targeted approaches are crucial to combat certain cancers resistant to conventional therapies (10).

The one of most powerful therapeutic strategy in immunotherapy is adoptive cell transfer (ACT) (**Figure 1**). Chimeric antigen receptors (CAR) and engineered T cell receptors (TCRs) are recent therapeutic manufactured receptors of T cells which are used in adoptive T-cell immunotherapy (11, 12). The TCR-engineered T cells express tumor antigen-specific receptors with α and β chains which are produced from high-quality and high-avidity antigen-specific T-cell clones. They are utilized to develop antigen-specific immunotherapy (13). Recent clinical trials assessing the effectiveness of ACT therapy, TCR modified T (TCR-T) cells, and immune checkpoint inhibitors showed good outcomes. The high affinity and cellular avidity of TCR-T cells determine specific binding of several cellular proteins, which mean TCRs play a key role in activating T cellular avidity. In contrast to low affinity of TCRs which reduce the efficiency of TCR-based therapy, the high-affinity TCRs (Affinity ≥ 2.5nM) are specific and sensitive for targeting cell-surface human leukocyte antigens (HLAs) (14). The TCR molecules belong to a superfamily of immunoglobulin and they consist of two covalently-bound polymorphic subunits, each of which is antigen-specific, and they are related to at least four different types of signal transduction chains.

In order to activate T lymphocyte, there has to be an interaction between TCR and major histocompatibility complex (MHC) (**Figure 2**). The strength of interaction between TCRs and pMHC (peptide-MHC) determines the fate of immature thymocytes, which is very important for the survival of naive T cells. Thus, TCR-T immunotherapy technique activates the host's immune system through efficient interaction with MHC, especially class II molecules; the latter are specifically recognized by TCR-T cells and CAR-T cells (15). The TCR-T cells penetrate tumors but CAR-T cells are mainly distributed on the tumor periphery to access surface antigens. This makes TCR-T cells more efficient in cancer treatment (16).

This review provides insights into TCR-T cells with a special focus on its role in clinical anticancer immunotherapy. It also discusses advantages and disadvantages of different approaches in anticancer immunotherapy, including immune mobilizing monoclonal T-cell receptors against cancer (ImmTAC), inducible caspase-9, and Herpes simplex virus-thymidine kinase (HSV-TK) systems. Clinical trials on TCR-T cell therapy are discussed as well. Further, various strategies in

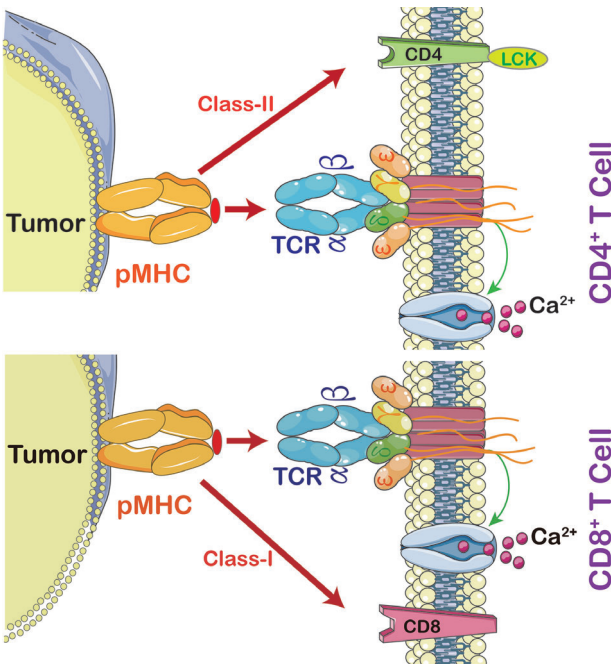

FIGURE 2 | The interaction between peptide MHC and T cells. Cytotoxic T cells ($CD8^+$) recognize MHC-I, CD3 coupled TCRs which activate T cell signaling cascade, including calcium-dependent and protein kinase C signaling pathways (PKC). Calcium is required for activation of nuclear factor of activated T cells (NFAT) leading to expression and secretion of Interleukin (IL)-2 and activation of PKC leading to tuning and regulating the production and secretion of ILs, including IL-2, T cell migration, T cell proliferation, and autoimmunity and graft rejection. $CD4^+$ T cells are able to switch off the immune system by promoting regulatory T cells (Treg). In order to activate T cell proliferation, TCR also triggers p38MAPK and PI3K/Akt pathways. Once CD4 or CD8 activates TCR, it then activates Lymphocyte-Specific Protein-Tyrosine Kinase (Lck) which triggers phosphorylation of CD3 ζ chains.

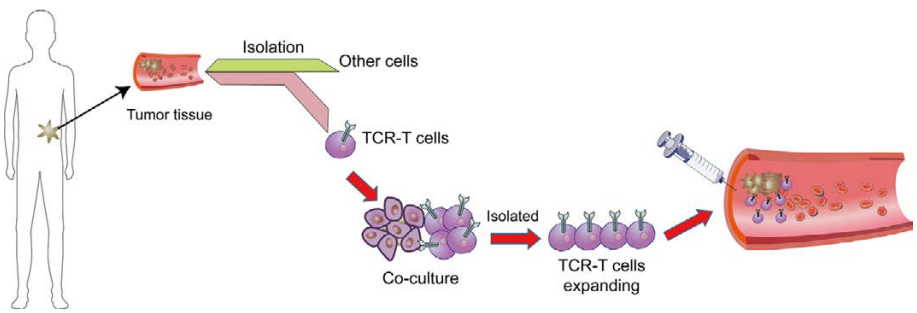

FIGURE 1 | Adoptive T cell therapy. In adoptive cell therapy (ACT), cells are collected from cancer tissues/T cells which are then isolated from other cells, genetically manipulated by engineered TCR or CAR, co-cultured and proliferated, and eventually sent back into circulation.

anticancer immunotherapy with a special focus on TCR-T cell therapy are examined, highlighting efficacy and safety of each method in diagnostic and targeted cancer immunotherapy.

COMPARISON OF CAR AND TCR THERAPIES

In ACT, TCRs and CARs therapies, modified T cells have been successfully used as a paradigm-shifting clinical immunotherapy to treat solid tumors (17) (**Figure 3**). CAR T cells were engineered to transfer arbitrary specificity onto an immune effector cell, like T cell, which specifically eliminates antigen-bearing tumor cells (17). The CAR has scFv derived from antibody, CD3ζ and transmembrane domain (so-called first-generation CARs) (18). In this way, engineered CAR is able to recognize specific tumor associated-antigens (19). Therefore, the CAR has the ability to bind unprocessed tumor surface antigens without MHC processing (20) while TCRs engage with both tumor intracellular and surface antigenic peptides embedded in MHC (**Table 1**) (21). Generally, CAR scFv domain is used to engage with cell surface antigens (22). The scFv fragments could guide the constitutive activation and proliferation of T cells in an antigen-dependent mechanism; however, some scFv may guide T cells into an antigen-independent mechanism which lead to an unsuccessful treatment (23).

Furthermore, first-generation CARs T cells showed limited expansion and relatively short persistence, which failed to evoke robust anti-tumor activity in the clinical studies (24, 25). The

TABLE 1 | Comparative characteristics of TCR and CAR.

Receptor Property	TCR	CAR
MHC involvement	Requires MHC matching	MHC-independent
Disadvantage	Redundant cytokine releasing	Off-tumor toxicities
Subunits	10	1
ITAMs number	10	3
Antigens required on target cells	1	100
Range of affinities for antigen	10^4-10^6/M^{-1}	10^6-10^9/M^{-1}
Recognition enhancing	Higher-order	Surface antigen density

'second-generation' CARs clinical activity can be induced by the CD3ζ domain insertion, namely co-stimulatory receptors CD28 (28ζ), 4-1BB/CD137 (BBζ) and OX40 (OX40ζ) CARs (26–28). The CD28 or CD137/4–1BB was added to CD3ζ endodomain of CAR-T cells which then promotes a more robust and durable T cells response (29, 30). Moreover, these second-generation CARs, which target CD19 antigen (CD19-specific scFv), are highly active against B cell malignancies and have promising clinical benefit (31, 32). In order to overcome the limitations of each individual costimulatory domain, the third generation CARs were proposed to simultaneously combine two co-stimulatory signaling (CD28 and 4-1BB), which presents a superior expansion and longer persistence than second-generation (33).

In contrast, TCRs are α/β heterodimers that bind to the MHC-bound antigens (**Figure 3**). As discussed above, CARs recognize tumor antigen which led to T cell activation with

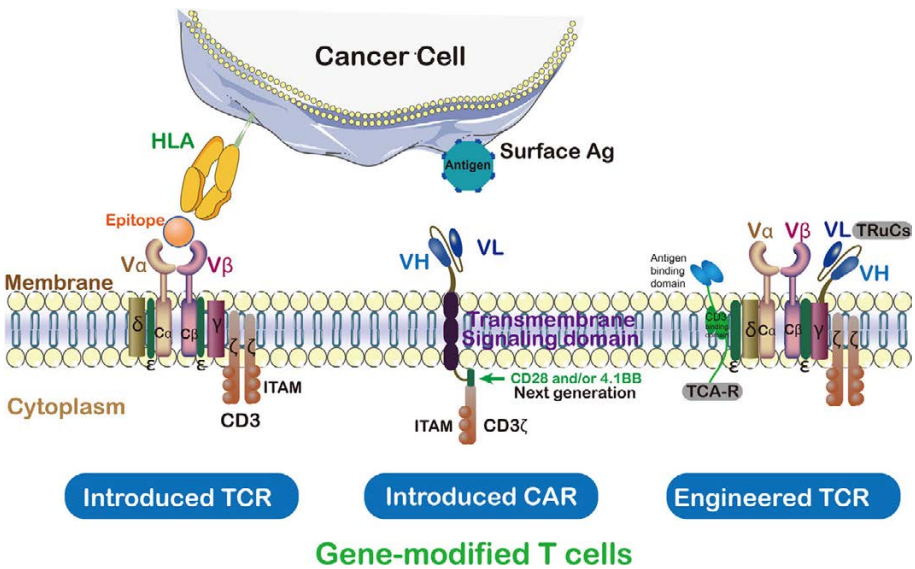

FIGURE 3 | TCRs vs CAR and genetically modified T cells in immunotherapy. Cancer targeting receptors, TCR and CAR, are introduced to the activated T cells to empower them against special type of cancer. ζ subunit of CD3 on the surface of T cell is essential for triggering signaling cascade of T cells. In contrast to TCR which needs to be activated by endogenous CD3, CARs are hybrid receptors manufactured from a single-chain variable fragment (scFv) attached to ζ subunit of CD3. Both introduced and endogenous TCRs recognize HLA peptides on cancer cells. The CARs, instead, do not recognize HLA directly which trigger T cell signaling cascade in a TCR-independent manner.

different functions compared with TCR. CAR-T cell therapy has certain disadvantages like off-tumor toxicities when targeting tumor-specific antigen (34). Compared with CARs, TCRs have several structural advantages in T cell-based therapy because they, such as more subunits in their receptor structure (ten subunits vs one subunit), greater immunoreceptor tyrosine-based activation motif (ITAMs) (ten vs three), less dependence on antigens (one vs 100), and more co-stimulate receptors (CD3, CD4, CD28, *etc.*) (20). The TCRs with low MHC interaction affinity range (10^4-$10^6 M^{-1}$) have been suggested for efficient T-cell stimulation (35). On the contrary, CARs possess a higher affinity range of (10^6-$10^9 M^{-1}$) and off-rates to recognize cell surface antigen (20). In order to maintain high-antigen sensitivity and to recognize pMHCs, exclusively monomeric TCR-CD3 complexes have been suggested (21). In contrast, the CAR-mediated cell sensitivity depends on higher density of cell surface antigen (36). Furthermore, T cell/antigen interaction is initiated in an immune synapse (IS) structure in which the TCR presents a ring region with peripheral LFA-1 adhesion, while CAR shows diffuse LFA-1 distribution without ring region (37). As a result, TCR-IS initiates a slower but longer duration signaling than that of CAR-IS. Meanwhile, the CAR-T cells presents faster killing function and move on to the next tumor target (serial killing), this was in stark contrast to the TCR-T cells protracted signaling and more extended killing.

Clinical trials involving with TCRs and CARs therapies have potential to suppress tumors progression. The CARs have been unable to effectively suppress malignant cells of some solid tumors and this is due to the presence of various types of antigens, their expression level, immunosuppressive environment, and construction of CARs. However, TCR-T cell transfer therapy has effectively treated some solid and hematological tumors (37).

RECOMBINANT TCRS

The TCR is one of the body's most complex receptors, which contain six different receptor subunits to its very broad signaling activities in T cells (38). Tumor-infiltrating lymphocytes (TILs)-TCR changes dramatically influence the tumor-dominant T cells (39). Among which, the changes in TCR will contribute to the expansion/proliferation of T cells. The TCR diversity and increased TILs were associated with anti-tumor effects, and TCR engineering in selective TILs is optimal therapy for the tumor rather than periphery (40). The TCR is composed of α and β chains that together bind to the peptide-MHC ligand, and signaling subunits of CD3 complex (ϵ, γ and δ) as well as the CD3ζ homodimer (41). All subunits except CD3ζ have extracellular immunoglobulin (Ig) domains. Based on these structures, the immune mobilizing monoclonal modified T-cell receptors (ImmTAC) were designed so that can specifically recognize the target HLA-peptide. There are some emerging techniques that utilize signaling subunits of the TCR and improve immunotherapy efficiency in HLA-independent manners, such as ImmTAC, TRuCs and TAC.

Immune Mobilizing Monoclonal T-Cell Receptors (ImmTAC)

The ImmTACs were designed using engineered, soluble, and affinity-enhanced monoclonal TCRs (mTCRs). ImmTACs are basically fusion proteins which combine an engineered TCR-based targeting system with a single chain antibody fragment (scFv) effector function. In the construction of ImmTACs, TCRs was deemed as antibodies which possess antigen recognition within the immune system. However, while antibodies only target cell surface or secreted proteins, TCRs are able to recognize peptides derived from intracellular targets presented by human leukocyte antigen (HLA) (42) (**Figure 4**).

ImmTACs have the potential to suppress tumor growth as they exert their activity through T cell redirection. Generally, ImmTACs comprising tumor-associated antigen-specific monoclonal TCR which strongly boost the affinity to pMHC (43). They effectively redirect these cells to eliminate cancer cells (44). The ImmTAC binds to the cancer cell through specific targeting of HLA-peptide complexes on their cell surface. The picomolar affinity of TCR to pMHC results in the coating of target cells by ImmTACs, and facilitates T-cell mediated effector function *via* interaction between scFv antibody fragments and CD3. Moreover, ImmTAC also activates $CD8^+$ T cells in a dose-dependent manner with a low picomolar range of EC_{50} values (45). It has been shown that an ImmTAC, IMCgp100 effectively redirects and activates effector and memory $CD8^+$ and $CD4^+$ cells (46). The ImmTAC exhibits a polyfunctional response through secretion of several types of cytokines, such as tumor necrosis factor-α (TNF-α), interferon-γ, IL-6 pro-inflammatory cytokines, macrophage inflammatory protein-1α-β (MIP1α-β) and IFN-γ-inducible protein-10. The TNF-α and IFN-γ are highly effective inflammatory agents which promote apoptosis of tumor cell and stimulate inflammation of endothelial cells to enhance immune cell adhesion and extravasation in TME (47). MIP1α-β proteins involved in tumor proliferation or associated inflammation are potent chemo-attractants for monocytes. The MIP1α-β proteins are only secreted by CTLs and are mainly modulated by $CD4^+$ T lymphocytes. An earlier study has shown IMCgp100-redirected T cells have a polyfunctional phenotype, a powerful anti-cancer response (46).

Furthermore, selecting appropriate target antigens is crucial for manufacturing ImmTACs. Certain dysregulated non-mutated proteins are presented as a tumor-associated antigen. Two decades ago, it was necessary to distinguish whether these targets are useful for immunotherapy by comparing their expression levels between tumor and normal tissues. Mass spectrometry has been used to identify low-abundance peptides because it has the sensitivity and ability to identify post-translational modifications for tumor antigens. While, failure to detect a pHLA complex using mass spectrometry does not mean it is absent. A pHLA target has the ability to induce an antigen-specific T cell response. The MHC-multimer technology can be used to profile T cell responses from immuno-stimulated patients. It also facilitates identification of suitable antigens (46). In order to compare ImmTAC targets, antigen

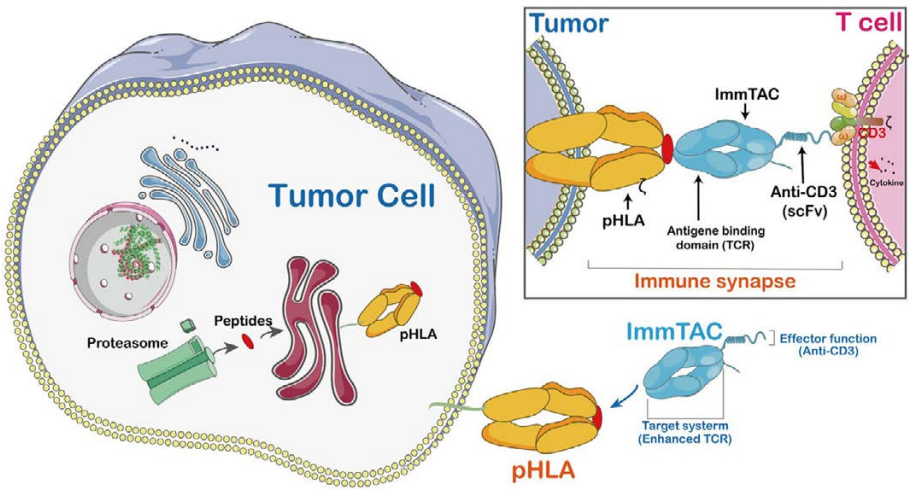

FIGURE 4 | The mechanism of ImmTAC action. ImmTACs are designed to activate T cells against cancer and virus-infected cells. ImmTAC is specific to both MHC-peptides (pHLA) located on the surface of the tumor and CD3s located on T cells. The ImmTAC is able to directly activate CD3 and its corresponding pathways in activated T cells. In fact, the specific role of CD4 and CD8 is to stabilize the immune synapse, an important process of T cells shortened and empowered by ImmTACs.

expression, which is correlated with ImmTAC-mediated response, can be analyzed *in vitro* and *in vivo* studies (48). Of note, unexpected off-target reactivity of TCR-engineered T cells has been led to fatal cardiac toxicity, which was observed to recognize both epitope of MAGE-A3 and unrelated muscle protein titin in cardiac tissue in two series of clinical events (49). Hence, natural presentation of off-target peptide must be first confirmed using mass spectroscopy, and then followed by *in vitro* assessment of ImmTAC recognition. Since the therapeutic window maybe affected by ImmTAC off-target interactions, their affinity should be estimated (44). Overall, ImmTACs have been shown to enhance TCR-T cell anti-tumor response, but its safety needs further scrutiny.

T Cell Receptor Fusion Constructs (TRuCs)

More recently, reprogrammed TCR-T cells with a new target specificity and the potential for HLA-independent cells was developed. T cell receptor fusion constructs (TRuCs), antibody-based binding domain fused to T cell receptor (TCR) subunit, which was designed for effective recognition of tumor surface antigens (29, 50). The TRuCs, consisted of specific ligand antibody fused to the extracellular N-termini of five TCR subunits (TCRα, TCRβ, CD3ϵ, CD3γ and CD3δ), provide the engineered T cell with new target specificity and HLA-independent target cell elimination ability which can be activated by corresponding target cells (51). Upon lentiviral transduction, the TRuCs will be integrated into native TCR complex on the T cells surface. Therefore, activation and effector function of T cells are retained. This method on TCR engineering showed better anti-tumor effect compared to the second-generation CAR-T cells. Moreover, the TRuCs dominate full signaling machinery of the TCR complex, while CARs only utilized limited signaling of isolated CD3ζ cytoplasmic tail (50).

T Cell Antigen Coupler (TAC)

The T cell antigen coupler (TAC) is another platform that co-opts the endogenous TCR with MHC-independent manner to induce more efficient anti-tumor responses and reduces toxicity (52). The TAC chimeric proteins coupled the TCR to recognize antigen *via* CD3 domain binding, resulting in a TCR/CD3 complex formation and achieving more T cell responses (52). In addition, the activity of TAC receptor was critically dependent upon the choice of CD3-binding domain; hence, the appropriate scFvs improve the combination of phenotypic and functional characteristics. For example, the scFv derived from OKT3 (muromonab-CD3), one of the most commonly used agonistic anti-CD3 antibodies has lower cytokine production and cytotoxicity compared to UCHT1 (53). Thus, the delicate difference in integrating with the CD3 complex may contribute to substantially different functional outcomes. Compared to the second-generation CARs, the TAC engineered T cells did not merely favor the greater infiltration of solid tumors after adoptive injected but also reduced T cells expansion in healthy tissues that express antigens and off-tumor toxicities.

Others

Recently, several novel ACT technologies have been proposed. The Natural killer cells (NKs) were emerged as a promising source of CAR-based therapies (CAR-NKs), which is safety and availability (54). The NKs initiate innate immune responses against infections and malignancies with natural cytotoxicity (55). The CAR modified NKs shown specific and potent cytotoxic activity against target cells (56), and the CAR-NKs treatment significantly reduced the tumor growth (57, 58). Some

preclinical data indicated that CAR-NKs may be advantageous over CAR-T cells in T-lymphoid malignancies, as the shared expression of targetable antigens on both malignant and normal T lymphocytes (e.g. CD5 and CD28) (54, 59). Moreover, recent studies have demonstrated that stem cells can differentiate into functional immune cells and/or crosstalk with immune cells to modulate the tumor immune environment (60). The pluripotent stem cells differentiated Cytotoxic T cells and NKs shown several advantages compared to primary immune cells, such as improved anti-tumor activity and produced in essentially unlimited numbers (61). Meanwhile, induced pluripotent stem cells (iPSC) as a novel cancer vaccine achieved a promising preventive and therapeutic effects to various types of cancers (62). Kooreman et, al. indicated that autologous iPSC-based vaccine can elicit anti-tumor responses in breast cancer, mesothelioma, and melanoma models and reduce the local or distant relapse after primary tumor resection (63). Among which, in melanoma, iPSC vaccine is associated with fewer Th17 cells and promoted antigen-specific anti-tumor T cells response. Furthermore, the iPSC plus CpG vaccine can evoked a strong cancer-immunity by upregulating mature APCs, effector T cells and cytotoxic T cells, as well as decreasing the amount of regulatory T cells (Tregs) (62).

TCRS SIDE-EFFECTS

The ACT with genetically engineered T cells has shown high sensitivity but with some severe adverse events in some clinical studies (11). Optimal TCR affinity in engineered T cells is vital and accordingly, receptor avidity is able to determine the safety/efficacy of T cell therapy (64). For example, in melanoma and neuroblastoma, some preclinical studies indicated the advanced intensity and durable antitumor effect of T cells. In a recent multi-target cell-based immunotherapy, patients were treated with CAR-Ts/TCRs against certain tumorigenic antigens, such as interventional studies of 10 and 4 tumor specific CAR-T/TCR in combination with cyclophosphamide or fludarabine (NCT03638206; NCT03941626). Meanwhile, the treatment-related adverse events were monitored based on Common Terminology Criteria for Adverse Events (CTCAE) v4.03 within 30 days after the last infusion. Not surprising, increased TCR expression and high frequency of TCR modified T cells within the graft improved TCR-modified T cells anti-tumor potency. In addition, combing the TCR therapy with irradiation therapy further improves efficiency of TCR therapy (65) (**Table 2**).

With on-target off-tumor toxicities, avidity becomes a main obstacle to the clinical success of ACT. When an antigen-specific receptor is used, in terms of efficacy, the avidity should be high enough for proper T cell activation (66). On the other hand, low avidity TCR interaction is sufficient to activate T cells, but strong avidity is required to sustain T-cell expansion (67). In phase I/II ACT clinical trial, the low-avidity engineered T cells showed safer profile, but they had a weaker anti-tumor response (68). Therefore, optimal avidity is a key factor in safety/efficacy of ACT. Recently, the reversible Ni^{2+}-nitrilotriacetic acid histidine tags (NTAmers) technique was developed to efficiently separate high-avidity cytotoxic T-cells (69). Through recognizing TCR–pMHC interaction of T cells, engineered T cells can be isolated into high and low-intermediate avidity subtypes. Herein, an advance technology for avidity monitoring is necessary to ensure safe treatment.

Herpes Simplex Virus Thymidine Kinase

Immunotherapy using T lymphocytes is an attractive strategy to treat many types of malignancies. However, the side-effects and off-target of T cell immunotherapy necessitates finding a safety switch mechanism which should be based on engineered T cells. Many clinical trials tried to eliminate potentially harmful cells using suicide genes (70). Thymidine kinase gene derived from herpes simplex virus I (HSV-TK) is one of the most common suicide genes. Therefore, transcriptional connection between HSV-TK and cell-division gene (CDK1) has been engineered and quantified based on mathematical models to determine the safety of this therapy (71). Cell batches in the suicide system and a homozygous HSV-TK-CDK1 boost safe-cell level (SCL) while ensuring a clinically validated safety range.

A serious complication related to hematopoietic allografts can happen when the Graft-versus-host disease (GvHD) is occurred. This, as a result of T cell transplantation, can cause tissue and organ damage. Transplantation of T cells recognizes the host's histocompatibility in about 80% of patients (72). In order to prevent GvHD, T cells have been genetically modified with suicide gene HSV-TK using prodrug ganciclovir (GCV) (73) (**Figure 5**). Safety switches (suicide genes) are of particular value in long-term cell-dependent immunotherapies. They also avoid T cell off-target interactions. Herein, the suicide genes were able to control therapeutic process and can be initiated by early clinical interventions. For example, in clinical trial, HSV-TK modified T cells can be monitored by positron emission tomography (PET)/CT when they are migrating to an unexpected location (74).

There are several limitations. First, previous studies observed a small number of patients with HSV-TK engineered T cells had lost sensitivity to GCV. Second, the pro-drug GCV not only activates HSV-TK which precludes its administration, but it also acts as an anti-viral drug for other indications like cytomegalovirus (CMV) infections (75). Finally, HSV-TK engineered T cells have potential immunogenic activity. Autologous immune response to activate the suicide gene may result in transduced T-cell elimination, and therefore, reduces their therapeutic efficiency (76). Non-immunogenic suicide genes with low toxicity, stable expression, and high eliminating strength are urgently required in newly engineered transduced T cells.

Inducible Caspase-9

Although HSV-TK shows safety in cell-based immunotherapy, the phosphorylated nucleoside analogs into DNA synthesis is required to complete elimination of tumor cells (77). Specifically, a quick elimination of the infused cells is required for cancer cellular therapies and regenerative medicine. An original inducible T-cell safety switch is brought to the donor T cell called caspase-9 (78) (**Figure 5**). Inducible caspase-9 is a fusion

TABLE 2 | Clinical trials activated on engineered TCR-T cells.

ID	Study Title	Cancers	Interventions	Participants
NCT03578406	HPV-E6-Specific Anti-PD1 TCR-T Cells in the Treatment of HPV-Positive NHSCC or Cervical Cancer	Cervical Cancer Head and Neck Squamous Cell Carcinoma	**Drug:** HPV E6-specific TCR-T cells	20
NCT03941626	Autologous CAR-T/TCR-T Cell Immunotherapy for Solid Malignancies	Esophagus Cancer Hepatoma Glioma Gastric Cancer	**Biological:** CAR-T/TCR-T cells immunotherapy	50
NCT03891706	Individualized Tumor Specific TCR- T Cells in the Treatment of Advanced Solid Tumors	Lung Cancer Melanoma	**Drug:** tumor-specific TCR-T cells	30
NCT03638206	Autologous CAR-T/TCR-T Cell Immunotherapy for Malignancies	B-cell Acute Lymphoblastic Leukemia Lymphoma Myeloid Leukemia (and 13 more…)	**Biological:** CAR-T cell immunotherapy Multi-target tumor specific CAR-Ts for CD19 and CD22 in B cell leukemia and lymphoma, CD33 in myeloid leukemia, B-cell maturation antigen (BCMA) and CD38 in multiple myeloma, NY-ESO-1 in multiple myeloma, esophagus cancer, lung cancer, and synovial sarcoma, DR5 in hepatoma, C-met in hepatoma, colorectal cancer, ovarian cancer and renal carcinoma, EGFR V III in hepatoma, lung cancer and glioma, and mesothelin in gastric cancer, pancreatic cancer and mesothelioma	73
NCT03139370	Safety and Efficacy of MAGE-A3/A6 T Cell Receptor Engineered T Cells (KITE-718) in HLA-DPB1*04:01 Positive Adults With Advanced Cancers	Solid Tumor	**Drug:** KITE-718 **Drug:** Cyclophosphamide **Drug:** Fludarabine **Device:** MAGE - A3/A6 Screening Test	75
NCT03691376	NY-ESO-1 TCR Engineered T Cell and HSC After Melphalan Conditioning Regimen in Treating Participants With Recurrent or Refractory Ovarian, Fallopian Tube, or Primary Peritoneal Cancer	HLA-A*0201 Positive Cells HLA-DP4 Positive Cells Platinum-Resistant Ovarian Carcinoma (and 6 more…)	**Biological:** Aldesleukin **Biological:** Autologous NY-ESO-1-specific CD8-positive T Lymphocytes **Other:** Cellular Therapy **Drug:** Melphalan	15
NCT02858310	E7 TCR T Cells for Human Papillomavirus-Associated Cancers	Papillomavirus Infections Cervical Intraepithelial Neoplasia Carcinoma *In Situ* (and 2 more…)	**Biological:** E7 TCR cells **Drug:** Aldesleukin **Drug:** Fludarabine **Drug:** Cyclophosphamide	180
NCT03686124	TCR-engineered T Cells in Solid Tumors	Refractory Cancer Recurrent Cancer Solid Tumor, Adult Cancer	**Biological:** IMA203 Product **Device:** IMADetect	16
NCT03029273	NY-ESO-1 TCR (TAEST16001)for Patients With Advanced NSCLC	Lung Cancer, Nonsmall Cell, Recurrent	**Drug:** Cyclophosphamide and Fludarabine **Biological:** Anti-NY-ESO-1 TCR transduced T cells	20
NCT03503968	TCR Modified T Cells MDG1011in High Risk Myeloid and Lymphoid Neoplasms	Safety Tolerability Feasibility Treatment Efficacy	**Drug:** MDG1011 **Other:** Investigator Choice therapy	92
NCT03912831	Safety and Efficacy of KITE-439 in HLA-A*02:01 + Adults With Relapsed/Refractory HPV16^{+} Cancers	Human Papillomavirus 16^{+} Relapsed/Refractory Cancer	**Drug:** KITE-439 **Drug:** Cyclophosphamide **Drug:** Fludarabine	75
NCT03247309	TCR-engineered T Cells in Solid Tumors With Emphasis on NSCLC and HNSCC (ACTengine)	Solid Tumor Cancer Head and Neck Squamous Cell Carcinoma Non-small Cell Lung Cancer	**Biological:** IMA201 Product **Diagnostic Test:** IMA_Detect **Diagnostic Test:** ACT-HLA	16
NCT03441100	TCR-engineered T Cells in Solid Tumors Including NSCLC and HCC Patients	Solid Tumor, Adult Cancer Hepatocellular Carcinoma (and 4 more…)	**Drug:** IMA202 Product **Device:** IMA_Detect	16
NCT02650986	Gene-Modified T Cells in Treating Patients With Locally Advanced or Stage IV Solid Tumors Expressing NY-ES0-1	Adult Solid Neoplasm	**Drug:** Cyclophosphamide **Other:** Laboratory Biomarker Analysis **Biological:** NY-ESO-1 Reactive TCR Retroviral Vector Transduced Autologous PBL **Biological:** TGFbDNRII-transduced Autologous Tumor Infiltrating Lymphocytes	24
NCT03431311	T Cell Receptor Based Therapy of Metastatic Colorectal Cancer	Colorectal Cancer	**Biological:** Adoptive Cell Therapy (ACT)	5

(Continued)

TABLE 2 | Continued

ID	Study Title	Cancers	Interventions	Participants
NCT03326921	HA-1 T TCR T Cell Immunotherapy for the Treating of Patients With Relapsed or Refractory Acute Leukemia After Donor Stem Cell Transplant	HLA-A*0201 HA-1 Positive Cells Present Juvenile Myelomonocytic Leukemia Recurrent Acute Biphenotypic Leukemia (and 24 more…)	**Biological:** $CD8^+$ and $CD4^+$ Donor Memory T-cells-expressing HA1-Specific TCR **Drug:** Fludarabine Phosphate **Other:** Laboratory Biomarker Analysis	24
NCT03462316	NY-ESO-1-specific T Cell Receptor (TCR) T Cell in Sarcoma	Bone Sarcoma Soft Tissue Sarcoma	**Biological:** NY-ESO-1(TCR Affinity Enhancing Specific T cell Therapy)	20
NCT02686372	TCR-Redirected T Cell Infusions to Prevent Hepatocellular Carcinoma Recurrence Post Liver Transplantation	Hepatocellular Carcinoma	**Biological:** HBV antigen specific TCR redirected T cell	10
NCT02719782	A Study of TCR-Redirected T Cell Infusion in Subject With Recurrent HBV-related HCC Post Liver Transplantation	Recurrent Hepatocellular Carcinoma	**Biological:** TCR-T	10

Interventions include Drugs, Medical devices, Biological agents and Other products that are either investigational or already available.

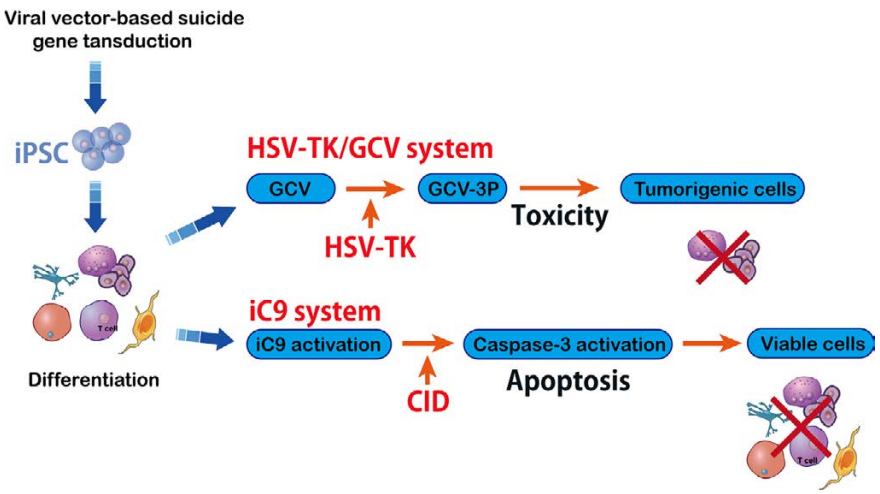

FIGURE 5 | HSV-TK/GCV system vs inducible caspase-9 system. The herpes simplex virus–Thymidine Kinase/ganciclovir (HSV-TK/GCV) system eliminates tumorigenic cells and it is efficient and specific against inducible pluripotent stem cells (iPSC) that can kill the cells whose HSV-TK expression has been silenced. The HSV-TK/GCV system is used as a safety switch and it produces a toxic compound that kills the transduced cells. Another method in suicide gene therapy is introducing inducible caspase-9 (iC9) into iPSC. The iC9 dimerization activates iC9 which then triggers a caspase cascade leading to elimination of tumors originating from iPSC. Specific chemical inducers of dimerization (CID) induce iC9.

of human induced caspase-9 (iC9) which is a modified human FK-binding protein and it can be activated *via* a small-molecule compound AP1903 (79). This process depends on mitochondrial apoptotic pathway. After the pro-drug administration, the iC9-mediated cell clearance ratio was raised to ninety percent in half an hour (79). The iC9 suicide gene is less immunogenic, triggering reduced immune response against transgenic cells. This is to maintain a stable cell level in patients. After AP1903 treatment for one or two weeks in one study, polyclonal iC9-positive T cells were detected in peripheral blood with specific reactivity (79). Thus, the iC9 cell-suicide system is proven to be activated to guard T-cell-based immunotherapies and expand their clinical applications. The iC9-based safety switch has been shown to have better potential than the preexisting suicide genes for cellular therapy. In previous studies, iC9-T cells have been reported which deplete their alloreactive components *ex vivo* (80). A new study showed iC9 allodepletion could be done *in vivo* instead, and iC9-T cells can be eliminated within 30 minutes of AP1903 absorption (81).

The transferred T cells can also secrete pro-inflammatory cytokines leading to life-threatening GvHD-associated cytokine release syndrome (CRS) (82). The CRS is caused by increased levels of cytokines including IL-6 and IFN-γ. Immunosuppressants, for example tocilizumab as an anti-IL-6 receptor, with or without corticosteroids, can reverse this situation (83). The results indicate iC9 activation is sufficiently potent to promote allodepletion and treat GvHD, which leads to rapid resolution of CRS. Despite the iC9 system is engineered to

prevent side-effect of T cell immunotherapy, integration of any transgene is mutagenic and potentially oncogenic. Hence, it is vital to assess its potential risks and benefits.

DISCUSSION AND CONCLUDING REMARKS

Tyrosine kinases belong to a key category of oncogenic proteins including Her2, EGFR, and VEGFR which are targeted by tyrosine kinase inhibitors (TKIs), such as lapatinib, gefitinib and sunitinib (84, 85). However, treatment with TKIs showed acquired resistance to chemotherapy after a few weeks of administration (86). Hence, lower toxicity and higher efficacy in anticancer therapeutic strategy are vital. Recently, gene-modified T cells with least adverse effects have been shown as extremely effective in treating solid and liquid tumors. Therapies which activate the immune system, such as those using antibodies against immune checkpoint PD-1, were shown to have a great potential (87). In addition, antigen-targeted approaches of monoclonal antibodies, CAR-T cell therapy, and TCR-based therapy have shown varied successes against specific tumors (11, 88). Therapies that use modified TCR-T cells for preclinical and clinical investigations have tremendous potential (89, 90). In lung cancer, however, solo use of ImmTAC therapy has failed. In order to recovery ImmTAC potency and tumor regression, the anti-PD-1 monoclonal antibody showed beneficial effects (91). ImmTAC efficiently redirects and activates effector and memory T cells within the $CD8^+$ and $CD4^+$ repertoires. This results in cytotoxic activity against melanoma cells. Apart from its direct therapy effect, ImmTAC can redirect lymphocytes to secrete several key cytokines and chemokines in T cells, such as IFN-γ, ILs (IL-2 and IL-6) and TNF-α, which result in a sustained anti-tumor defense in ACT (46).

The TME is known to suppress TILs (92). Engineered TCRs are able to boost T-cell trafficking and activation in TME (93, 94). Recently, E7 TCR gene therapy showed potential therapeutic value against HPV cancers (89). The ACT from TCR engineered human T cells has shown encouraging results. However, these approaches need further validation (95). In ACT, GVHD maybe observable with different and unpredictable kinetics (96). It has also been shown TCR/CD3 inhibition triggers T cell apoptosis (97).

A quick elimination of infused cells is important for cancer cellular therapies as engineered T cells expressing suicide genes with a specific prodrug are rapidly eliminated by apoptosis. Caspase-9 is a key element in apoptosis and is involved in various chemotherapy stimuli (78). Incorporating NK cells with an iC9 suicide switch enhances safety of anti-leukemia approaches which allows for their safe clinical application (98). However, this method also leads to a rapid inactivation of effector T cells in the event of adverse reactions (99). Anti-cancer and suicide mechanisms can co-exist without effects on cells and hamper tumoricidal activity (100). The iC9 safety switch of transduced T-cells also proved to be reliable in Phase I trial involving patients undergoing haplo-identical stem cell transplantation (90). Furthermore, HSV-TK has been observed to be another safety switch to trigger apoptosis in the cell line of head and neck carcinoma (101). Novel and highly efficient technique called TransfeX delivers HSV-TK into cervical, oral and pharyngeal with tumoricidal effects (102). Hence, TCR-T cell engineered with HSV-TK suicide gene may also enhance oncotherapy. It is evident therefore that TCR-T-cell immunotherapy has the potential to eradicate tumors in addition to lowering risks associated with immunotherapy (103).

In conclusion, TCR-T ACT has a good potential to treat cancers. TCR tuning is vital for T cell re-activity, immune responses, and its clinical effects on foreign antigens. The engineered TCRs targeting special antigens also boost efficiency of immunotherapy. The safety of genetically modified T cells for ACT is also vital. The present article reviewed advances of TCR T cell immunotherapy and proximal new techniques which can detect antigens and drive a T cell response. However, there are some limitations which need to be addressed in future research.

AUTHOR CONTRIBUTIONS

QJZ, YJ, JS, PJK and SXX wrote the paper, YSZ, XW, FKD and MXL edited the manuscript, CHO, JL and QLW prepared and adjusted the figures, TL, TY and ZGX designed the study, provided funding and reviewed the manuscript. All authors contributed to the article and approved the submitted version.

FUNDING

This work was supported by the National Natural Science Foundation of China (Grants: 81503093, 81972643, and 81672444) and the Joint Funds of the Southwest Medical University & Luzhou (Grants: 2016LZXNYD-T01, 2017LZXNYD-Z05 and 2019LXXNYKD-07) and Science & Technology Department of Sichuan Province(Grants: 2018JY0079).

REFERENCES

1. Bray F, Ferlay J, Soerjomataram I, Siegel RL, Torre LA, Jemal A. Global cancer statistics 2018: GLOBOCAN estimates of incidence and mortality worldwide for 36 cancers in 185 countries. *CA: Cancer J Clin* (2018) 68:394–424. doi: 10.3322/caac.21492
2. Yarchoan M, Johnson BA,3, Lutz ER, Laheru DA, Jaffee EM. Targeting neoantigens to augment antitumour immunity. *Nat Rev Cancer* (2017) 17:569. doi: 10.1038/nrc.2017.74
3. Pardoll DM. The blockade of immune checkpoints in cancer immunotherapy. *Nat Rev Cancer* (2012) 12:252–64. doi: 10.1038/nrc3239
4. Fan Z, Liang Y, Yang X, Li B, Cui L, Luo L, et al. A meta-analysis of the efficacy and safety of PD-1/PD-L1 immune checkpoint inhibitors as treatments for metastatic bladder cancer. *OncoTargets Ther* (2019) 12:1791–801. doi: 10.2147/ott.S186271
5. Feng M, Xiong G, Cao Z, Yang G, Zheng S, Song X, et al. PD-1/PD-L1 and immunotherapy for pancreatic cancer. *Cancer Lett* (2017) 407:57–65. doi: 10.1016/j.canlet.2017.08.006

6. Hurkmans DP, Basak EA, van Dijk T, Mercieca D, Schreurs MWJ, Wijkhuijs AJM, et al. A prospective cohort study on the pharmacokinetics of nivolumab in metastatic non-small cell lung cancer, melanoma, and renal cell cancer patients. *J Immunother Cancer* (2019) 7:192. doi: 10.1186/s40425-019-0669-y
7. Pawłowska A, Suszczyk D, Okła K, Barczyński B, Kotarski J, Wertel I. Immunotherapies based on PD-1/PD-L1 pathway inhibitors in ovarian cancer treatment. *Clin Exp Immunol* (2019) 195:334–44. doi: 10.1111/cei.13255
8. Solinas C, Aiello M, De Silva P, Gu-Trantien C, Migliori E, Willard-Gallo K. Targeting PD-1 in cancer: Biological insights with a focus on breast cancer. *Crit Rev Oncol Hematol* (2019) 142:35–43. doi: 10.1016/j.critrevonc.2019.07.011
9. Wang F, Wei XL, Wang FH, Xu N, Shen L, Dai GH, et al. Safety, efficacy and tumor mutational burden as a biomarker of overall survival benefit in chemo-refractory gastric cancer treated with toripalimab, a PD-1 antibody in phase Ib/II clinical trial NCT02915432. *Ann Oncol Off J Eur Soc Med Oncol* (2019) 30:1479–86. doi: 10.1093/annonc/mdz197
10. Kaboli PJ, Zhang L, Xiang S, Shen J, Li M, Zhao Y, et al. Molecular Markers of Regulatory T Cells in Cancer Immunotherapy with Special Focus on Acute Myeloid Leukemia (AML) - A Systematic Review. *Curr Med Chem* (2020) 27:4673–98. doi: 10.2174/0929867326666191004164041
11. Ikeda H. T-cell adoptive immunotherapy using tumor-infiltrating T cells and genetically engineered TCR-T cells. *Int Immunol* (2016) 28:349–53. doi: 10.1093/intimm/dxw022
12. Scherer LD, Brenner MK, Mamonkin M. Chimeric Antigen Receptors for T-Cell Malignancies. *Front Oncol* (2019) 9:126:6. doi: 10.3389/fonc.2019.00126
13. Xu Y, Morales AJ, Cargill MJ, Towlerton AMH, Coffey DG, Warren EH, et al. Preclinical development of T-cell receptor-engineered T-cell therapy targeting the 5T4 tumor antigen on renal cell carcinoma. *Cancer Immunol Immunother CII* (2019) 68:1979–93. doi: 10.1007/s00262-019-02419-4
14. Ohta R, Demachi-Okamura A, Akatsuka Y, Fujiwara H, Kuzushima K. Improving TCR affinity on 293T cells. *J Immunol Methods* (2019) 466:1–8. doi: 10.1016/j.jim.2018.11.010
15. Maus MV, Plotkin J, Jakka G, Stewart-Jones G, Rivière I, Merghoub T, et al. An MHC-restricted antibody-based chimeric antigen receptor requires TCR-like affinity to maintain antigen specificity. *Mol Ther Oncolytics* (2016) 3:1–9. doi: 10.1038/mto.2016.23
16. Segaliny AI, Li G, Kong L, Ren C, Chen X, Wang JK, et al. Functional TCR T cell screening using single-cell droplet microfluidics. *Lab Chip* (2018) 18:3733–49. doi: 10.1039/c8lc00818c
17. June CH, O'Connor RS, Kawalekar OU, Ghassemi S, Milone MC. CAR T cell immunotherapy for human cancer. *Sci (New York NY)* (2018) 359:1361–5. doi: 10.1126/science.aar6711
18. Zhang C, Liu J, Zhong JF, Zhang X. Engineering CAR-T cells. *Biomarker Res* (2017) 5:22. doi: 10.1186/s40364-017-0102-y
19. Liu D, Zhao J, Song Y. Engineering switchable and programmable universal CARs for CAR T therapy. *J Hematol Oncol* (2019) 12:69. doi: 10.1186/s13045-019-0763-0
20. Harris DT, Kranz DM. Adoptive T Cell Therapies: A Comparison of T Cell Receptors and Chimeric Antigen Receptors. *Trends Pharmacol Sci* (2016) 37:220–30. doi: 10.1016/j.tips.2015.11.004
21. Brameshuber M, Kellner F, Rossboth BK, Ta H, Alge K, Sevcsik E, et al. Monomeric TCRs drive T cell antigen recognition. *Nat Immunol* (2018) 19:487–96. doi: 10.1038/s41590-018-0092-4
22. Boyiadzis MM, Dhodapkar MV, Brentjens RJ, Kochenderfer JN, Neelapu SS, Maus MV, et al. Chimeric antigen receptor (CAR) T therapies for the treatment of hematologic malignancies: clinical perspective and significance. *J Immunother Cancer* (2018) 6:137. doi: 10.1186/s40425-018-0460-5
23. Frigault MJ, Lee J, Basil MC, Carpenito C, Motohashi S, Scholler J, et al. Identification of chimeric antigen receptors that mediate constitutive or inducible proliferation of T cells. *Cancer Immunol Res* (2015) 3:356–67. doi: 10.1158/2326-6066.Cir-14-0186
24. Pule MA, Savoldo B, Myers GD, Rossig C, Russell HV, Dotti G, et al. Virus-specific T cells engineered to coexpress tumor-specific receptors: persistence and antitumor activity in individuals with neuroblastoma. *Nat Med* (2008) 14:1264–70. doi: 10.1038/nm.1882
25. Till BG, Jensen MC, Wang J, Chen EY, Wood BL, Greisman HA, et al. Adoptive immunotherapy for indolent non-Hodgkin lymphoma and mantle cell lymphoma using genetically modified autologous CD20-specific T cells. *Blood* (2008) 112:2261–71. doi: 10.1182/blood-2007-12-128843
26. Maude SL, Laetsch TW, Buechner J, Rives S, Boyer M, Bittencourt H, et al. Tisagenlecleucel in Children and Young Adults with B-Cell Lymphoblastic Leukemia. *New Engl J Med* (2018) 378:439–48. doi: 10.1056/NEJMoa1709866
27. Neelapu SS, Locke FL, Bartlett NL, Lekakis LJ, Miklos DB, Jacobson CA, et al. Axicabtagene Ciloleucel CAR T-Cell Therapy in Refractory Large B-Cell Lymphoma. *New Engl J Med* (2017) 377:2531–44. doi: 10.1056/NEJMoa1707447
28. Park JH, Rivière I, Gonen M, Wang X, Sénéchal B, Curran KJ, et al. Long-Term Follow-up of CD19 CAR Therapy in Acute Lymphoblastic Leukemia. *New Engl J Med* (2018) 378:449–59. doi: 10.1056/NEJMoa1709919
29. Getts D, Hofmeister R, Quintás-Cardama A. Synthetic T cell receptor-based lymphocytes for cancer therapy. *Adv Drug Deliv Rev* (2019) 141:47–54. doi: 10.1016/j.addr.2019.04.002
30. Savoldo B, Ramos CA, Liu E, Mims MP, Keating MJ, Carrum G, et al. CD28 costimulation improves expansion and persistence of chimeric antigen receptor-modified T cells in lymphoma patients. *J Clin Invest* (2011) 121:1822–6. doi: 10.1172/jci46110
31. Brentjens RJ, Rivière I, Park JH, Davila ML, Wang X, Stefanski J, et al. Safety and persistence of adoptively transferred autologous CD19-targeted T cells in patients with relapsed or chemotherapy refractory B-cell leukemias. *Blood* (2011) 118:4817–28. doi: 10.1182/blood-2011-04-348540
32. Gardner RA, Finney O, Annesley C, Brakke H, Summers C, Leger K, et al. Intent-to-treat leukemia remission by CD19 CAR T cells of defined formulation and dose in children and young adults. *Blood* (2017) 129:3322–31. doi: 10.1182/blood-2017-02-769208
33. Nonon Saa KB, Maneh N, Vonor K, Amedome K, Togo M, Dzidzinyo K, et al. [Erratum to "Manual small incision cataract surgery: Experience of a regional eye care service in Togo" [J. Fr. Ophtalmol. 41 (3) (2018) 255-61 https://doi.org/10.1016/j.jfo.2017.09.009]]. *J Francais D'ophtalmol* (2018) 41:898. doi: 10.1016/j.jfo.2018.09.002
34. Bedoya F, Frigault MJ, Maus MV. The Flipside of the Power of Engineered T Cells: Observed and Potential Toxicities of Genetically Modified T Cells as Therapy. *Mol Ther J Am Soc Gene Ther* (2017) 25:314–20. doi: 10.1016/j.ymthe.2016.11.011
35. Huang J, Brameshuber M, Zeng X, Xie J, Li QJ, Chien YH, et al. A single peptide-major histocompatibility complex ligand triggers digital cytokine secretion in CD4(+) T cells. *Immunity* (2013) 39:846–57. doi: 10.1016/j.immuni.2013.08.036
36. Stone JD, Aggen DH, Schietinger A, Schreiber H, Kranz DM. A sensitivity scale for targeting T cells with chimeric antigen receptors (CARs) and bispecific T-cell Engagers (BiTEs). *Oncoimmunology* (2012) 1:863–73. doi: 10.4161/onci.20592
37. Davenport AJ, Cross RS, Watson KA, Liao Y, Shi W, Prince HM, et al. Chimeric antigen receptor T cells form nonclassical and potent immune synapses driving rapid cytotoxicity. *Proc Natl Acad Sci USA* (2018) 115:E2068–e76. doi: 10.1073/pnas.1716266115
38. Schamel WW, Alarcon B, Höfer T, Minguet S. The Allostery Model of TCR Regulation. *J Immunol (Baltimore Md 1950)* (2017) 198:47–52. doi: 10.4049/jimmunol.1601661
39. Poschke IC, Hassel JC, Rodriguez-Ehrenfried A, Lindner KAM, Heras-Murillo I, Appel LM, et al. The Outcome of Ex Vivo TIL Expansion Is Highly Influenced by Spatial Heterogeneity of the Tumor T-Cell Repertoire and Differences in Intrinsic In Vitro Growth Capacity between T-Cell Clones. *Clin Cancer Res* (2020) 26:4289–301. doi: 10.1158/1078-0432.CCR-19-3845
40. Hosoi A, Takeda K, Nagaoka K, Iino T, Matsushita H, Ueha S, et al. Increased diversity with reduced "diversity evenness" of tumor infiltrating T-cells for the successful cancer immunotherapy. *Sci Rep* (2018) 8:1058. doi: 10.1038/s41598-018-19548-y
41. Schamel WW, Arechaga I, Risueño RM, van Santen HM, Cabezas P, Risco C, et al. Coexistence of multivalent and monovalent TCRs explains high sensitivity and wide range of response. *J Exp Med* (2005) 202:493–503. doi: 10.1084/jem.20042155

42. Harper J, Adams KJ, Bossi G, Wright DE, Stacey AR, Bedke N, et al. An approved in vitro approach to preclinical safety and efficacy evaluation of engineered T cell receptor anti-CD3 bispecific (ImmTAC) molecules. *PloS One* (2018) 13:e0205491. doi: 10.1371/journal.pone.0205491
43. He Q, Jiang X, Zhou X, Weng J. Targeting cancers through TCR-peptide/MHC interactions. *J Hematol Oncol* (2019) 12:139. doi: 10.1186/s13045-019-0812-8
44. McCormack E, Adams KJ, Hassan NJ, Kotian A, Lissin NM, Sami M, et al. Bi-specific TCR-anti CD3 redirected T-cell targeting of NY-ESO-1- and LAGE-1-positive tumors. *Cancer Immunol Immunother CII* (2013) 62:773–85. doi: 10.1007/s00262-012-1384-4
45. Liddy N, Bossi G, Adams KJ, Lissina A, Mahon TM, Hassan NJ, et al. Monoclonal TCR-redirected tumor cell killing. *Nat Med* (2012) 18:980–7. doi: 10.1038/nm.2764
46. Boudousquie C, Bossi G, Hurst JM, Rygiel KA, Jakobsen BK, Hassan NJ. Polyfunctional response by ImmTAC (IMCgp100) redirected CD8(+) and CD4(+) T cells. *Immunology* (2017) 152:425–38. doi: 10.1111/imm.12779
47. Croft M. The role of TNF superfamily members in T-cell function and diseases. *Nat Rev Immunol* (2009) 9:271–85. doi: 10.1038/nri2526
48. Oates J, Hassan NJ, Jakobsen BK. ImmTACs for targeted cancer therapy: Why, what, how, and which. *Mol Immunol* (2015) 67:67–74. doi: 10.1016/j.molimm.2015.01.024
49. Linette GP, Stadtmauer EA, Maus MV, Rapoport AP, Levine BL, Emery L, et al. Cardiovascular toxicity and titin cross-reactivity of affinity-enhanced T cells in myeloma and melanoma. *Blood* (2013) 122:863–71. doi: 10.1182/blood-2013-03-490565
50. Baeuerle PA, Ding J, Patel E, Thorausch N, Horton H, Gierut J, et al. Synthetic TRuC receptors engaging the complete T cell receptor for potent anti-tumor response. *Nat Commun* (2019) 10:2087. doi: 10.1038/s41467-019-10097-0
51. Alcover A, Alarcón B, Di Bartolo V. Cell Biology of T Cell Receptor Expression and Regulation. *Annu Rev Immunol* (2018) 36:103–25. doi: 10.1146/annurev-immunol-042617-053429
52. Helsen CW, Hammill JA, Lau VWC, Mwawasi KA, Afsahi A, Bezverbnaya K, et al. The chimeric TAC receptor co-opts the T cell receptor yielding robust anti-tumor activity without toxicity. *Nat Commun* (2018) 9:3049. doi: 10.1038/s41467-018-05395-y
53. Arnett KL, Harrison SC, Wiley DC. Crystal structure of a human CD3-epsilon/delta dimer in complex with a UCHT1 single-chain antibody fragment. *Proc Natl Acad Sci USA* (2004) 101:16268–73. doi: 10.1073/pnas.0407359101
54. Rafei H, Daher M, Rezvani K. Chimeric antigen receptor (CAR) natural killer (NK)-cell therapy: leveraging the power of innate immunity. *Br J Haematol* (2020). doi: 10.1111/bjh.17186
55. Hesker PR, Krupnick AS. The role of natural killer cells in pulmonary immunosurveillance. *Front Biosci (Schol Ed)* (2013) 5:575–87. doi: 10.2741/s391
56. Jamali A, Hadjati J, Madjd Z, Mirzaei HR, Thalheimer FB, Agarwal S, et al. Highly Efficient Generation of Transgenically Augmented CAR NK Cells Overexpressing CXCR4. *Front Immunol* (2020) 11:2028. doi: 10.3389/fimmu.2020.02028
57. Xia N, Haopeng P, Gong JU, Lu J, Chen Z, Zheng Y, et al. Robo1-specific CAR-NK Immunotherapy Enhances Efficacy of (125)I Seed Brachytherapy in an Orthotopic Mouse Model of Human Pancreatic Carcinoma. *Anticancer Res* (2019) 39:5919–25. doi: 10.21873/anticanres.13796
58. Han J, Chu J, Keung Chan W, Zhang J, Wang Y, Cohen JB, et al. CAR-Engineered NK Cells Targeting Wild-Type EGFR and EGFRvIII Enhance Killing of Glioblastoma and Patient-Derived Glioblastoma Stem Cells. *Sci Rep* (2015) 5:11483. doi: 10.1038/srep11483
59. Pui CH, Behm FG, Crist WM. Clinical and biologic relevance of immunologic marker studies in childhood acute lymphoblastic leukemia. *Blood* (1993) 82:343–62. doi: 10.1182/blood.V82.2.343.bloodjournal822343
60. Wildes TJ, Flores CT, Mitchell DA. Concise Review: Modulating Cancer Immunity with Hematopoietic Stem and Progenitor Cells. *Stem Cells* (2019) 37:166–75. doi: 10.1002/stem.2933
61. Zhu H, Lai YS, Li Y, Blum RH, Kaufman DS. Concise Review: Human Pluripotent Stem Cells to Produce Cell-Based Cancer Immunotherapy. *Stem Cells* (2018) 36:134–45. doi: 10.1002/stem.2754
62. Wang L, Pegram MD, Wu JC. Induced pluripotent stem cells as a novel cancer vaccine. *Expert Opin Biol Ther* (2019) 19:1191–7. doi: 10.1080/14712598.2019.1650909
63. Kooreman NG, Kim Y, de Almeida PE, Termglinchan V, Diecke S, Shao NY, et al. Autologous iPSC-Based Vaccines Elicit Anti-tumor Responses In Vivo. *Cell Stem Cell* (2018) 22:501–13.e7. doi: 10.1016/j.stem.2018.01.016
64. D'Ippolito E, Schober K, Nauerth M, Busch DH. T cell engineering for adoptive T cell therapy: safety and receptor avidity. *Cancer Immunol Immunother CII* (2019) 68:1701–12. doi: 10.1007/s00262-019-02395-9
65. de Witte MA, Jorritsma A, Kaiser A, van den Boom MD, Dokter M, Bendle GM, et al. Requirements for effective antitumor responses of TCR transduced T cells. *J Immunol (Baltimore Md 1950)* (2008) 181:5128–36. doi: 10.4049/jimmunol.181.7.5128
66. Tan MP, Gerry AB, Brewer JE, Melchiori L, Bridgeman JS, Bennett AD, et al. T cell receptor binding affinity governs the functional profile of cancer-specific CD8+ T cells. *Clin Exp Immunol* (2015) 180:255–70. doi: 10.1111/cei.12570
67. Zehn D, Lee SY, Bevan MJ. Complete but curtailed T-cell response to very low-affinity antigen. *Nature* (2009) 458:211–4. doi: 10.1038/nature07657
68. Ahmed N, Brawley VS, Hegde M, Robertson C, Ghazi A, Gerken C, et al. Human Epidermal Growth Factor Receptor 2 (HER2) -Specific Chimeric Antigen Receptor-Modified T Cells for the Immunotherapy of HER2-Positive Sarcoma. *J Clin Oncol Off J Am Soc Clin Oncol* (2015) 33:1688–96. doi: 10.1200/jco.2014.58.0225
69. Hebeisen M, Schmidt J, Guillaume P, Baumgaertner P, Speiser DE, Luescher I, et al. Identification of Rare High-Avidity, Tumor-Reactive CD8+ T Cells by Monomeric TCR-Ligand Off-Rates Measurements on Living Cells. *Cancer Res* (2015) 75:1983–91. doi: 10.1158/0008-5472.Can-14-3516
70. Li W, Xiang AP. Safeguarding clinical translation of pluripotent stem cells with suicide genes. *Organogenesis* (2013) 9:34–9. doi: 10.4161/org.24317
71. Liang Q, Monetti C, Shutova MV, Neely EJ, Hacibekiroglu S, Yang H, et al. Linking a cell-division gene and a suicide gene to define and improve cell therapy safety. *Nature* (2018) 563:701–4. doi: 10.1038/s41586-018-0733-7
72. Daron C, Soubrier M, Mathieu S. Occurrence of rheumatic symptoms in celiac disease: A meta-analysis: Comment on the article "Osteoarticular manifestations of celiac disease and non-celiac gluten hypersensitivity" by Dos Santos and Lioté. Joint Bone Spine 2016, doi:10.1016/j.jbspin.2016.09.007. *Joint Bone Spine* (2017) 84:645–6. doi: 10.1016/j.jbspin.2017.03.006
73. Zhan H, Gilmour K, Chan L, Farzaneh F, McNicol AM, Xu JH, et al. Production and first-in-man use of T cells engineered to express a HSVTK-CD34 sort-suicide gene. *PloS One* (2013) 8:e77106. doi: 10.1371/journal.pone.0077106
74. Eissenberg LG, Rettig M, Dehdashti F, Piwnica-Worms D, DiPersio JF. Suicide genes: monitoring cells in patients with a safety switch. *Front Pharmacol* (2014) 5:241. doi: 10.3389/fphar.2014.00241
75. Vanpouille C, Bernatchez JA, Lisco A, Arakelyan A, Saba E, Götte M, et al. A common anti-cytomegalovirus drug, ganciclovir, inhibits HIV-1 replication in human tissues ex vivo. *AIDS (London England)* (2017) 31:1519–28. doi: 10.1097/qad.0000000000001532
76. Bonini C, Mondino A. Adoptive T-cell therapy for cancer: The era of engineered T cells. *Eur J Immunol* (2015) 45:2457–69. doi: 10.1002/eji.201545552
77. Ciceri F, Bonini C, Stanghellini MT, Bondanza A, Traversari C, Salomoni M, et al. Infusion of suicide-gene-engineered donor lymphocytes after family haploidentical haemopoietic stem-cell transplantation for leukaemia (the TK007 trial): a non-randomised phase I-II study. *Lancet Oncol* (2009) 10:489–500. doi: 10.1016/s1470-2045(09)70074-9
78. Li P, Zhou L, Zhao T, Liu X, Zhang P, Liu Y, et al. Caspase-9: structure, mechanisms and clinical application. *Oncotarget* (2017) 8:23996–4008. doi: 10.18632/oncotarget.15098
79. Di Stasi A, Tey SK, Dotti G, Fujita Y, Kennedy-Nasser A, Martinez C, et al. Inducible apoptosis as a safety switch for adoptive cell therapy. *New Engl J Med* (2011) 365:1673–83. doi: 10.1056/NEJMoa1106152
80. Zhou X, Di Stasi A, Tey SK, Krance RA, Martinez C, Leung KS, et al. Long-term outcome after haploidentical stem cell transplant and infusion of T cells expressing the inducible caspase 9 safety transgene. *Blood* (2014) 123:3895–905. doi: 10.1182/blood-2014-01-551671

81. Zhou X, Dotti G, Krance RA, Martinez CA, Naik S, Kamble RT, et al. Inducible caspase-9 suicide gene controls adverse effects from alloreplete T cells after haploidentical stem cell transplantation. *Blood* (2015) 125:4103–13. doi: 10.1182/blood-2015-02-628354
82. Morgan RA, Yang JC, Kitano M, Dudley ME, Laurencot CM, Rosenberg SA. Case report of a serious adverse event following the administration of T cells transduced with a chimeric antigen receptor recognizing ERBB2. *Mol Ther J Am Soc Gene Ther* (2010) 18:843–51. doi: 10.1038/mt.2010.24
83. Lee DW, Gardner R, Porter DL, Louis CU, Ahmed N, Jensen M, et al. Current concepts in the diagnosis and management of cytokine release syndrome. *Blood* (2014) 124:188–95. doi: 10.1182/blood-2014-05-552729
84. Jabbarzadeh Kaboli P, Leong MP, Ismail P, Ling KH. Antitumor effects of berberine against EGFR, ERK1/2, P38 and AKT in MDA-MB231 and MCF-7 breast cancer cells using molecular modelling and in vitro study. *Pharmacol Rep PR* (2019) 71:13–23. doi: 10.1016/j.pharep.2018.07.005
85. Zhao Y, Zhao Q, Kaboli PJ, Shen J, Li M, Wu X, et al. m1A Regulated Genes Modulate PI3K/AKT/mTOR and ErbB Pathways in Gastrointestinal Cancer. *Trans Oncol* (2019) 12:1323–33. doi: 10.1016/j.tranon.2019.06.007
86. Jabbarzadeh Kaboli P, Ismail P, Ling KH. Molecular modeling, dynamics simulations, and binding efficiency of berberine derivatives: A new group of RAF inhibitors for cancer treatment. *PloS One* (2018) 13:e0193941. doi: 10.1371/journal.pone.0193941
87. Wu Y, Gu W, Li J, Chen C, Xu ZP. Silencing PD-1 and PD-L1 with nanoparticle-delivered small interfering RNA increases cytotoxicity of tumor-infiltrating lymphocytes. *Nanomed (London England)* (2019) 14:955–67. doi: 10.2217/nnm-2018-0237
88. Rosenberg SA, Restifo NP. Adoptive cell transfer as personalized immunotherapy for human cancer. *Sci (New York NY)* (2015) 348:62–8. doi: 10.1126/science.aaa4967
89. Jin BY, Campbell TE, Draper LM, Stevanović S, Weissbrich B, Yu Z, et al. Engineered T cells targeting E7 mediate regression of human papillomavirus cancers in a murine model. *JCI Insight* (2018) 3:e99488. doi: 10.1172/jci.insight.99488
90. Zhang P, Raju J, Ullah MA, Au R, Varelias A, Gartlan KH, et al. Phase I Trial of Inducible Caspase 9 T Cells in Adult Stem Cell Transplant Demonstrates Massive Clonotypic Proliferative Potential and Long-term Persistence of Transgenic T Cells. *Clin Cancer Res Off J Am Assoc Cancer Res* (2019) 25:1749–55. doi: 10.1158/1078-0432.Ccr-18-3069
91. Zhang H, Li Y, Liu X, Liang Z, Yan M, Liu Q, et al. ImmTAC/Anti-PD-1 antibody combination to enhance killing of cancer cells by reversing regulatory T-cell-mediated immunosuppression. *Immunology* (2018) 155:238–50. doi: 10.1111/imm.12954
92. Zhang J, Wang L. The Emerging World of TCR-T Cell Trials Against Cancer: A Systematic Review. *Technol Cancer Res Treat* (2019) 18:1533033819831068. doi: 10.1177/1533033819831068
93. Liu B, Chen W, Evavold BD, Zhu C. Accumulation of dynamic catch bonds between TCR and agonist peptide-MHC triggers T cell signaling. *Cell* (2014) 157:357–68. doi: 10.1016/j.cell.2014.02.053
94. Lou J, Rossy J, Deng Q, Pageon SV, Gaus K. New Insights into How Trafficking Regulates T Cell Receptor Signaling. *Front Cell Dev Biol* (2016) 4:77. doi: 10.3389/fcell.2016.00077
95. Chhabra A, Mukherji B, Batra D. Activation induced cell death (AICD) of human melanoma antigen-specific TCR engineered CD8 T cells involves JNK, Bim and p53. *Expert Opin Ther Targets* (2017) 21:117–29. doi: 10.1080/14728222.2017.1270941
96. Anwer F, Shaukat AA, Zahid U, Husnain M, McBride A, Persky D, et al. Donor origin CAR T cells: graft versus malignancy effect without GVHD, a systematic review. *Immunotherapy* (2017) 9:123–30. doi: 10.2217/imt-2016-0127
97. Zhu L, Anasetti C. Cell cycle control of apoptosis in human leukemic T cells. *J Immunol (Baltimore Md 1950)* (1995) 154:192–200.
98. Liu E, Tong Y, Dotti G, Shaim H, Savoldo B, Mukherjee M, et al. Cord blood NK cells engineered to express IL-15 and a CD19-targeted CAR show long-term persistence and potent antitumor activity. *Leukemia* (2018) 32:520–31. doi: 10.1038/leu.2017.226
99. Oelsner S, Waldmann A, Billmeier A, Röder J, Lindner A, Ullrich E, et al. Genetically engineered CAR NK cells display selective cytotoxicity against FLT3-positive B-ALL and inhibit in vivo leukemia growth. *Int J Cancer* (2019) 145:1935–45. doi: 10.1002/ijc.32269
100. Rossignoli F, Grisendi G, Spano C, Golinelli G, Recchia A, Rovesti G, et al. Inducible Caspase9-mediated suicide gene for MSC-based cancer gene therapy. *Cancer Gene Ther* (2019) 26:11–6. doi: 10.1038/s41417-018-0034-1
101. Srivastava D, Joshi G, Somasundaram K, Mulherkar R. Mode of cell death associated with adenovirus-mediated suicide gene therapy in HNSCC tumor model. *Anticancer Res* (2011) 31:3851–7.
102. Düzgüneş N, Cheung J, Konopka K. Non-viral suicide gene therapy in cervical, oral and pharyngeal carcinoma cells with CMV- and EEV-plasmids. *J Gene Med* (2018) 20:e3054. doi: 10.1002/jgm.3054
103. Ye B, Stary CM, Gao Q, Wang Q, Zeng Z, Jian Z, et al. Genetically Modified T-Cell-Based Adoptive Immunotherapy in Hematological Malignancies. *J Immunol Res* (2017) 2017:5210459. doi: 10.1155/2017/5210459

Conflict of Interest: The authors declare that the research was conducted in the absence of any commercial or financial relationships that could be construed as a potential conflict of interest.

Copyright © 2021 Zhao, Jiang, Xiang, Kaboli, Shen, Zhao, Wu, Du, Li, Cho, Li, Wen, Liu, Yi and Xiao. This is an open-access article distributed under the terms of the Creative Commons Attribution License (CC BY). The use, distribution or reproduction in other forums is permitted, provided the original author(s) and the copyright owner(s) are credited and that the original publication in this journal is cited, in accordance with accepted academic practice. No use, distribution or reproduction is permitted which does not comply with these terms.

frontiers in Immunology

REVIEW
published: 01 April 2021
doi: 10.3389/fimmu.2021.670324

Interaction Networks Converging on Immunosuppressive Roles of Granzyme B: Special Niches Within the Tumor Microenvironment

Weinan Wang[1], *Rui Zou*[1], *Ye Qiu*[1], *Jishuang Liu*[1], *Yu Xin*[1], *Tianzhu He*[1,2*] *and Zhidong Qiu*[1*]

[1] School of Pharmaceutical Sciences, Changchun University of Chinese Medicine, Changchun, China, [2] School of Basic Medical Sciences, Changchun University of Chinese Medicine, Changchun, China

OPEN ACCESS

Edited by:
Peng Qu,
National Institutes of Health (NIH), United States

Reviewed by:
Ke-Wu Zeng,
Peking University Health Science Centre, China
Guohao Wang,
National Institutes of Health (NIH), United States

***Correspondence:**
Tianzhu He
35677553@qq.com
Zhidong Qiu
qzdcczy@163.com

Specialty section:
This article was submitted to Cancer Immunity and Immunotherapy, a section of the journal Frontiers in Immunology

Received: 21 February 2021
Accepted: 15 March 2021
Published: 01 April 2021

Citation:
Wang W, Zou R, Qiu Y, Liu J, Xin Y, He T and Qiu Z (2021) Interaction Networks Converging on Immunosuppressive Roles of Granzyme B: Special Niches Within the Tumor Microenvironment. Front. Immunol. 12:670324. doi: 10.3389/fimmu.2021.670324

Granzyme B is a renowned effector molecule primarily utilized by CTLs and NK cells against ill-defined and/or transformed cells during immunosurveillance. The overall expression of granzyme B within tumor microenvironment has been well-established as a prognostic marker indicative of priming immunity for a long time. Until recent years, increasing immunosuppressive effects of granzyme B are unveiled in the setting of different immunological context. The accumulative evidence confounded the roles of granzyme B in immune responses, thereby arousing great interests in characterizing detailed feature of granzyme B-positive niche. In this paper, the granzyme B-related regulatory effects of major suppressor cells as well as the tumor microenvironment that defines such functionalities were longitudinally summarized and discussed. Multiplex networks were built upon the interactions among different transcriptional factors, cytokines, and chemokines that regarded to the initiation and regulation of granzyme B-mediated immunosuppression. The conclusions and prospect may facilitate better interpretations of the clinical significance of granzyme B, guiding the rational development of therapeutic regimen and diagnostic probes for anti-tumor purposes.

Keywords: granzyme B, immunosuppression, tumor microenvironment, suppressor cells, regulation networks

INTRODUCTION

Granzyme B (GrB) is a serine protease famous for its activity in proteolysis-mediated apoptosis and works as a critical effector molecule of cytotoxic lymphocytes (CLs) against pathogens during immunosurveillance (1). Upon being properly activated, CLs could recognize the ill-defined cells and secrete cytotoxic granules into an immunological synapse where granzyme B is endocytosed into the cytosol of target cells and triggers the downstream apoptotic pathways (2).

For a long time, granzyme B has been well-accepted as a representative marker for the priming of immunity and efficient killing of tumor cells. In light of the anti-tumor reputation of granzyme B, the development of GrB-based/targeted theranostics has been advanced rapidly in recent years (3, 4). However, the expression of granzyme B is not always positively correlated with anti-tumor

performance. Some researchers even noticed that GrB-deficient mice demonstrated better eradication ability of either allogeneic or syngeneic tumor cells than did wild-type mice (5). Although granzyme B is selective on conserved amino acid sequences of its substrates, its cytotoxicity is non-specific to tumor cells, suggesting that granzyme B in active form, especially the one released to extracellular space, might harm both parties of the immune responses within the tumor microenvironment (TME) (5). These observations and hypothesis bring up a question: is granzyme B always a noteworthy ally against tumors or a waverer that sometimes works in the opposite way.

Increasing evidence has emerged to support the pleiotropic roles of granzyme B within which the immunosuppressive effects being highlighted. Aside from $CD4^+$/$CD8^+$ T cells and NK cells, the expression of active granzyme B is observed in many other types of cells such as B cells, dendritic cells, macrophages, mast cells, basophils, keratinocytes and chondrocytes etc., some are even the bystanders of lymphocytes (6). One part of them constitutively expresses granzyme B, while the other part only expresses it under proper stimulations. The significance of granzyme B expressed by these cells lies in not only their intrinsic feature but also the context that defines their roles. So far, several cell types, exemplified by T regulatory cells (Tregs), B regulatory cells (Bregs), and plasmacytoid dendritic cells (pDCs) are discovered to secrete granzyme B for immunosuppressive purposes as demonstrated in **Figure 1**, though the regulation networks are yet to be established (5, 7–9).

The immunosuppressive role of granzyme B was initially observed in the degradation of T cell receptor (TCR) zeta chain that is essential to the surface expression of TCRs for T cell development (10). The loss of TCR zeta chain seems to be a common phenomenon in tumor-infiltrating lymphocytes, especially the ones suffering from immune exhaustion. Although several mechanisms might involve the loss of TCR zeta chain, the degradation caused by granzyme B practically linked granzyme B with the immunosuppressive components in TME. Nevertheless, the degradation of TCR zeta chain is not the only way in which granzyme B suppresses the priming immunity. More mechanisms and participants have been unearthed in association with immunosuppressive roles of granzyme B, summing up a clearer picture of the GrB-expressing niches in TME, which we are going to discuss detailly in this review.

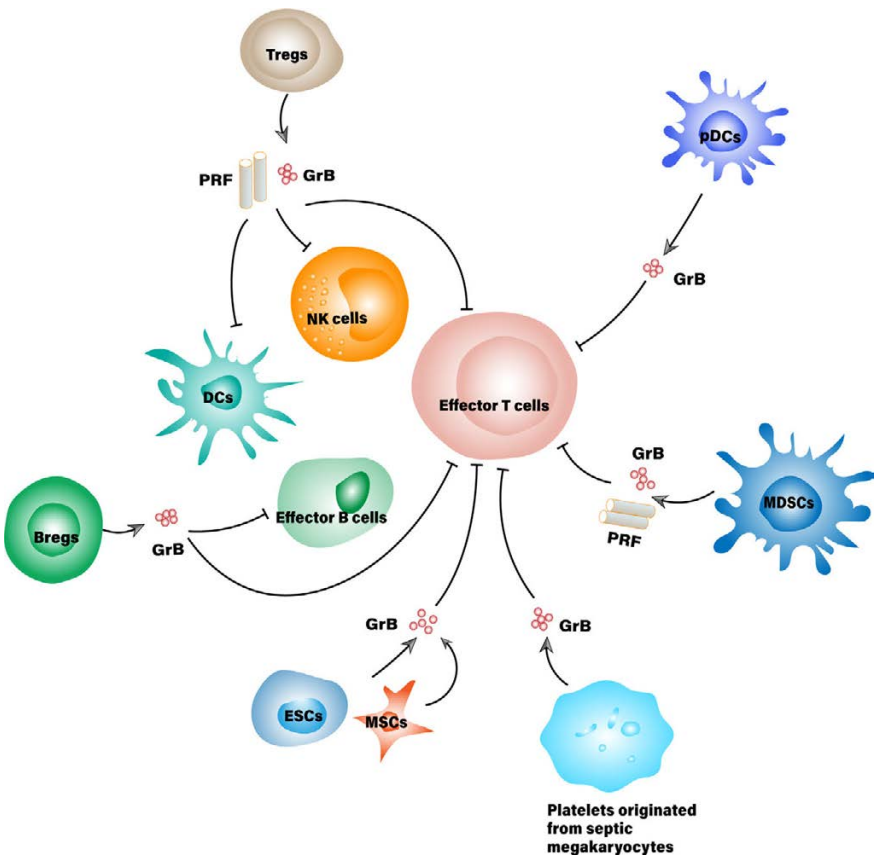

FIGURE 1 | Suppressor cells that secrete granzyme B for immunosuppressive purposes. MDSCs, Myeloid-derived suppressor cell; ESCs, Embryonic stem cell; MSCs, Mesenchymal stem cells; PRF, Perforin.

GRB$^+$ SUPPRESSOR CELLS

T Regulatory Cells

Tregs are a suppressive subset of T cells with the typical hallmarks of CD25 and Foxp3 expression. Although Tregs only occupy a small proportion of CD4$^+$ T cells, they play central roles within the whole immunosuppressive microenvironment either in healthy or ill-defined conditions (11). They are essential to maintaining peripheral tolerance and immune homeostasis in the setting of autoimmune diseases while suppressing beneficial anti-tumor immunity in TME to facilitate tumor evasion and metastasis.

Varied stimulatory molecules induce the differentiation of Tregs into diversified subsets, thereby exerting their immunosuppressive functions against different immune cells *via* multiple pathways (12). For instance, Tregs competitively consume interleukin 2 (IL-2) with weakly activated T effector cells (Teff), causing the suppression of adaptive immune responses (13). Moreover, Tregs secrete IL-10, IL-35, adenosine, and transforming growth factor-β (TGF-β) while express surface molecules, such as cytotoxic T-lymphocyte antigen 4 (CTLA-4), lymphocyte activation gene 3 (LAG-3), and programmed death-1 (PD-1) for general immunosuppressive purposes (14). Other than inhibiting cell function or decreasing cell viability, Tregs can directly induce apoptosis or cytolysis of B cells, antigen-presenting cells (APCs) and Teff, etc., through a GrB-mediated manner (15, 16). This immunosuppression pattern may or may not require cell-to-cell contact, indicating different mechanisms that trigger granzyme B attack.

The association between granzyme B and immunosuppressive effects in Tregs was initially established based on the frequent presence of GrB$^+$ Tregs in malignant tumor lesions (17). Also, high levels of GrB$^+$ Treg was found to negatively correlated with the occurrence of acute graft-versus-host disease after hematopoietic stem cell transplantation, implying a regulatory effect on active participants of adaptive immunity (18). The expression and secretion of granzyme B by Tregs seem to be context-dependent, as evidenced by the disproportionate level of granzyme B in naturally occurring Tregs (nTregs) from thymus comparing to stimuli-inducible Tregs (iTregs) in TME (19).

CD4$^+$CD25$^+$FoxP3$^+$ Treg is a typical phenotype that bears granzyme B for immunosuppressive purposes. In contrast to CD4$^+$CD25$^+$ Tregs, they present an elevated expression of CD275 (ICOSL), CD278 (ICOS), major histocompatibility complex (MHC) II and loss of CD73, which could suppress primed T cells *in vivo via* a GrB-dependent way (5, 20, 21). Unlike tumor-infiltrating Tregs, the circulating Tregs demonstrate very few GrB$^+$ cells with frequencies of lower than 0.3% in all subtypes, further highlights the latent stimuli in specific niches that determine the presence of GrB$^+$ Tregs (15).

Generally, the expression of granzyme B in T cells can be activated by prolonged TCR stimulation through CD3/CD28. However, the generation of GrB$^+$ Tregs needs the participation of IL-2, as either TCR stimulation or IL-2 treatment alone would fail to induce granzyme B in Tregs (22). In addition to CD3/CD28, stimulation of naive CD4$^+$ T cells with anti-CD46 monoclonal antibodies could convert them into granzymes/perforin/IL-10 producing Tregs that kill allogeneic cells as well as autologous immune cells (23, 24).

The induction of other immunosuppressive molecules often accompanies the generation of granzyme B in Tregs. Latency-associated peptide (LAP), the N-terminal pro-peptide of the TGF-β precursor, could facilitate the conversion of naive Tregs to iTregs. Studies have shown that these iTregs expressed more granzyme B and TGF-β than their LAP negative counterpart, exerting their immunosuppressive effects *via* both granzyme B and TGF-β mediated mechanisms (25–28). In another case, the up-regulation of granzyme B was observed in a "self-feeding" process of Tregs caused by an intercellular CC motif ligand (CCL) 1-CC chemokine receptor (CCR) 8 interaction, leading to synchronized up-regulation of FoxP3, CD39 and IL-10, which substantiated the *in vivo* proliferation and immunosuppressive activities of these Tregs (29). Even when encountered with OX40 agonist, potential immunotherapy that enhances anti-tumor immune responses, it did not harm the regulatory ability of Tregs due to the simultaneous increase in granzyme B, IFN-γ, and T-bet expression.

Although the immunosuppressive ability of Tregs would sometimes be reprogrammed or overwhelmed by a subtle environment, the expression and secretion of active granzyme B in Tregs could be a valuable prognostic for immunosuppressive status (30).

B Regulatory Cells

B cells have been classically associated with antibody secretion, antigen presentation, and T cell activation. However, the presence of B cell-mediated immune response does not always positively correlate with a benign prognosis during anti-tumor therapy. Some subsets of B cells, particularly the ones from tumor-derived lymph node (TDLN), exhibit regulatory phenotype and inhibitory activity toward other anti-tumor participants, probably contributing to the immunological tolerance of malignancies (31). These B cells with regulatory effects are termed as Bregs though there are no consensus markers about this classification (32).

The typical phenotype that different Bregs share is the secretion of IL-10 and expression of CD1d and CD5, although subsets of Bregs are known to express not only IL-10 but also other inhibitory molecules, including PD-L1, granzyme B, and TGF-β. Bregs express these cytokines for specific reasons. For instance, TGF-β from Bregs could induce iTregs which would, in turn, facilitate the differentiation of immature B cells into Bregs, hence synergistically controlling the inflammatory responses (33). GrB$^+$ Breg is a special and potent regulatory subtype phenotypically and functionally distinct from IL-10-producing Bregs (B10 cells) in humans. In human GrB$^+$ Bregs, most of the regulatory molecules are expressed primarily on GrB$^+$, but not GrB$^-$ B cells. This suggests that granzyme B might be an important novel marker indicative of immunosuppressive effects of human Bregs (34). IL-21 derived from CD4$^+$ T cells was found to dominantly drive the generation of GrB$^+$ B cells, during which CD40L was identified as an important determinant for the differentiation of B cells into either plasma cells or GrB$^+$ B cells (35). Only when cultured with IL-21$^+$ CD40L$^-$ Th cells

would B cells directly differentiate into GrB^+ Bregs (36). The population of GrB^+ Bregs is also positively correlated with IL-21 production. B cells from tolerant recipients but no other patients could regulate both the number of IL-21^+ T cells and IL-21 production, suggesting a feedback loop that increases excessive B cell activation and endows the regulatory ability (37). Subsequently, GrB^+ Bregs potently suppress the proliferation of co-cultured $CD4^+$ T cells in a GrB-dependent manner. Aside from IL-21 producing cells such as $CD4^+$ T cells, follicular helper T (Tfh) cells, and Natural killer T (NKT) cells, GrB^+ Bregs also target excessive B cells for self-regulatory purposes as well as other bystander immune cells *via* paracrine mechanisms (7).

GrB^+ B cells were unveiled to have pleiotropic roles in immune responses. One is the regulatory role that could maintain allospecific tolerance, and the other is the effector role against infected or ill-defined intruders (38). Within peripheral circulation, B cells from healthy individuals could produce and secrete granzyme B while encountering sufficient IL-21 and the stimulation of B cell receptors. A higher frequency of GrB^+ B cells in peripheral blood often correlated with immune tolerance in the settings of autoimmune diseases, viral infection, and tumor progression (39). On the other hand, some GrB^+ B cells were evidenced to initiate an attack against tumor cells due to its MHC-independent recognition of antigens. Such phenomenon often occurred in the early stage of neoplastic process, and, as the oncogenesis progressed, GrB^+ B cells were gradually polarized into Bregs that might lead to malignancies during late-stage cancer (7, 38). That explains why GrB^+ B cells found within the microenvironment of different tumor types were usually associated with the progress and metastasis of tumors.

The immunosuppressive mechanism exerted by GrB^+ Bregs mainly converged on the GrB-dependent degradation of T cell receptor zeta-chain, which is similar to that by Tregs and pDCs. However, the ways Bregs work on other immunological participants for suppressive goals, especially those independent of T cell receptors for activation, still remain obscure (40, 41). In addition to direct inhibition of effector cells, Bregs with activated STAT3 are found in proximity to tumor vasculature and proved to be proangiogenic and positively correlated with tumor progression. Considering that STAT3 is a critical upstream transcription factor for granzyme B expression, such tumorigenic effects of B cells might partially attribute to either the cytotoxicity of granzyme B toward ambient effector cells or the proteolysis of extracellular matrix (ECM) by granzyme B (42).

Some researchers have tried to decipher the phenotypic signature of Bregs that could signify the expression level of GrB, leading to a few meaningful results as presented in **Table 1** (33, 34). Nevertheless, puzzles delineating the phenotypes of GrB^+ Bregs are yet to be settled. The ambiguity might relate to the origin of B cells which confer different phenotypes to Bregs in TDLNs, peripheral blood, and tonsil (43).

Plasmacytoid Dendritic Cells

Dendritic cells comprise versatile subsets designated to carry out different missions in response to immunologic stimuli. Some of them are determined effector cells against pathogen while others exert pleiotropic effects under different circumstances (44). Plasmacytoid dendritic cells (pDCs) play a crucial role during innate immunity by secreting bulk amounts of type I interferons (IFNs) in response to Toll-like receptor (TLR)–mediated pathogen recognition. Besides, pDCs can contribute to adaptive anti-tumor immunity by activation of antigen-specific T cells (45).

However, the presence of pDCs is not always beneficial to the boost of immunities. It has been evidenced in some cases that the complex interaction of pDCs with tumor cells and their microenvironment might lead to immunologic tolerance (46). For instance, factors such as TNF-α, TGF-β and IL-10 would abrogate the anti-tumor responses from pDCs and facilitate their pro-tumorigenic effects (47). The immunosuppressive roles of pDCs are closely associated with the functionality of Tregs because pDCs are one of the main driving forces for the development of Tregs in T-lymphocyte-rich areas of lymphatic organs (48). Hence an increase in intratumoral pDCs was often observed with simultaneous increase of Foxp3+ regulatory T cells in the same lesion and positively correlated with tumor vascular density (49). In a resting state, pDCs might induce unbiased Th1, Th2, or Treg responses, whereas, upon being activated with CD40 ligand (CD40L) and interleukin-3, pDCs specific of ICOS ligand (ICOSL) expression preferentially enhanced the generation of IL-10-secreting nTregs in periphery blood (47, 50). Such CD40-CD40L-mediated interaction between pDCs and nTregs established a feedback loop critical to pDC maturation and nTreg differentiation in the steady-state human thymus (51). In addition to the indirect immunosuppressive effect relating to Tregs, pDCs could directly participate in the immunomodulatory process *via* autocrine and/or paracrine mechanisms, such as *via* the secretion of IDO, ICOSL and Granzyme B, etc (8, 52, 53). Unlike effector T cells and NK cells which express and secrete perforin and granzyme B synergistically to fight against cancer, pDCs can produce and utilize a bulk amount of granzyme B independent of perforin. pDCs secrete granzyme B to the extracellular area, where it plays dual roles for anti-tumor immunity as it would help process peptide antigen to facilitate cross-presentation while generally suppress T cell activation and expansion through degrading the zeta chain of its TCR (54, 55).

TABLE 1 | General information of GrB^+ Bregs documented.

No.	Phenotype	Origin	Key regulatory molecules	Disease model
1	$CD19^+CD38^+CD1d^+CD14^+IgM^+$	Human	CD25, IDO, IL-10, GrB	Epithelial cancers (breast,cervical, ovarian, colorectal, and prostate carcinoma)
2	$CD19^+CD5^+CD43^+CD86^+CD147^+$	Human	GrB	HIV-1
3	$CD19^+CD5^+CD27^+CD138^+CD38^+$	Human	GrB	Kidney transplant

Some researchers thought only specific subtypes of pDCs highly express and secrete granzyme B, as evidenced in a squamous carcinoma model (56). Another well-accepted notion suggested that the production of granzyme B could be induced and promoted in pDC precursors by certain immunosuppressive cytokines, including IL-3, IL-10, and IL-21. IL-3 was proved to be pivotal to GrB induction in pDCs (8). Literature has reported that IL-3 stimulated pDCs were able to decrease the population of both $CD4^+$ and $CD8^+$ T cells in a GrB-dependent manner. Such immunosuppressive effect of pDCs was further enhanced by IL-10, probably due to its contribution to granzyme B production, but inhibited by TLR stimulation which would downmodulate granzyme B expression in pDCs and polarize them into tumoricidal phenotypes (34, 57). IL-21 is a pleiotropic cytokine with a broad range of actions converging on immunogenicity (58). However, it could also induce the expression and secretion of granzyme B in pDCs, which is partially responsible for the pDC-mediated downregulation of $CD4^+$ T cell proliferation (45). The regulatory side of IL-21 induced pDC can be reversed by the autocrine of type I IFNs which is consistent with the observation that TLR stimulation would convert GrB^{high} pDCs into its GrB^{low} counterpart with immunogenic feature (59).

Other Cell Types

Expression of granzyme B is not specific to cytotoxic lymphocytes as many other cell types have been proved to express and secrete granzyme B under defined circumstances.

Except for conventional participants in immune responses (dendritic cells, macrophages, myeloid-derived suppressor cells, mast cells, basophils and B cells, etc.), these GrB expressing cells also include non-lymphocytes such as keratinocytes, platelets, human articular chondrocytes, and even cancer cells (60). Some cell types express GrB with perforin and other members of the granzyme family, which are often regarded as effector cells against cancer, while others express GrB independent of those cytotoxic components that might lead to pleiotropic effects (6).

Myeloid-derived suppressor cells (MDSCs) are one of the critical immunosuppressive cells against effector T cells, NK cells, dendritic cells and macrophages in the TME (61, 62). Even though their mechanisms of action are yet to be established, the clinical and experimental practice has demonstrated that tumors densely infiltrated with MDSCs are associated with poor prognosis and resistance to immunotherapies (63). Previous studies unearthed the metabolism of L-arginine and the generation of excessive ROS as major strategies that MDSCs invited to suppress immunological responses (64, 65). In recent years, some researchers had noticed a contact-dependent suppression of T lymphocytes by MDSCs and linked such phenomenon to the way cytotoxic T cells kill their targets *via* granzyme B/perforin (66). Then the expression of perforin and Granzyme B was validated in *in vitro* model of MDSC culture, ex vivo experiments of MDSCs isolated from tumor-bearing mice, and MDSCs from human. After deleting perforin/GzmB in MDSCs *in vivo*, an increased amount of CD8+ T cells appeared in the tumor lesion together with better therapeutic performance, suggesting an immunosuppressive role of granzyme B from MDSCs. Nevertheless, the detailed interaction between Granzyme B in MDSCs and the promotion of tumor growth still keep in the dark and warrant further investigation (9).

Sometimes seemingly innocent bystanders in body fluid could be educated into "granzyme B-armed killers" toward active lymphocytes. As in the case of sepsis, platelets were found accumulating in lymphoid microvasculature and suspicious of contributing to sepsis-related lymphoid apoptosis. Granzyme B, independent of perforin, secreted by these platelets, was a prerequisite to the lymphodepletion process, which required cell-to-cell contact with healthy lymphocytes. The immunosuppressive roles of GrB^+ platelets were further substantiated in either the *in vivo* experiment that the absence of granzyme B slows sepsis progression or the ex vivo proof that platelets from septic mice radically decrease the population of healthy splenocytes through GrB-induced apoptosis (67, 68). Such unique platelets originated from septic megakaryocytes with an upregulated *Itga2b* gene which altered the mRNA profiles of the platelets and empowers them with the functions of granzyme B (69).

Embryonic stem cells (ESCs) and mesenchymal stem cells (MSCs) are long known to possess immunosuppressive potential, though the mechanisms are still unclear. ESCs could increase the proportion of $FoxP3^+$ Tregs during alloimmunity as well as direct their regulatory effects toward $CD4^+$ T cells through expression and secretion of granzyme B. The immunosuppressive process mediated by these stem cells requires cell-to-cell contact and is independent of perforin, PDL-1, or Fas ligand, etc. (70). While in the case of MSCs, the situation is more complicated and debatable. MSCs freshly isolated from healthy donor bone marrow were found to express and secrete a bulk amount of enzymatically active granzyme B, which was initially hypothesized to be a major suppressive molecule. Nonetheless unambiguous immunosuppression occurred in a co-culture of MSCs and $CD4^+$ T cells, researchers failed to validate the immunosuppressive roles of granzyme B by one of its inhibitors. Therefore further studies are necessary to elucidate the genuine suppressive mechanisms of MSCs and whether or not they have any relationship with the regulation of granzyme B as presented in ESCs.

IMMUNOSUPPRESSIVE MECHANISMS OF GRANZYME B

Activation Induced Cell Death of T Lymphocytes

Activation-induced cell death (AICD) is a regulatory program co-opted for maintaining the population of activated T lymphocytes induced by repeated stimulation of TCRs (59, 71).

It had been widely accepted that AICD was mediated through the Fas-Fas ligand death pathway until recent literature found granzyme B could promote such process in patients with nonfunctioning Fas (1). Further investigations unveiled a relationship between GrB-induced AICD and the degradation of T cell zeta-chain, a critical component of TCR complex that

works with TCR and CD3 molecules to activate both cytotoxic T cells, T helper cells and NK cells (72). Tregs, pDCs and Bregs are frequently witnessed with such consequences. While these suppressor cells making contact with effector lymphocytes, their granzyme B could enter into the target cells *via* three potential pathways: a) passes through membrane pores formed by perforin; b) being endocytosed by membrane repair response during perforin-mediated Ca^{2+} influx; c) adsorbes onto the surface of target cell by electrostatic force that triggers endocytosis (2). Thereafter granzyme B could either directly degrade T cell zeta-chain at multiple sites or trigger the caspase cascade to indirectly cleave it, because T cell zeta-chain is a direct substrate for both caspase 3 and granzyme B. Either way it can abrogate the surface expression of TCR, resulting in malfunctioning T cell activation. Considering the predominance of effector T cells in the setting of anti-tumor immunity, AICD is supposed to be a primary cause for granzyme B-mediated immunosuppression.

Within cytotoxic lymphocytes, granzyme B was expressed and stored in a lysosomal granule if being properly stimulated. However, lysosomal membrane permeabilization (LMP) happens in proliferating and activated lymphocytes and leaks granzyme B into the cytosol, especially when host cells encounter excessive stimulation by TCR. Thereafter, serpin proteinase inhibitor 9 (SERPINB9) would counteract with active granzyme B, preventing it from damaging its host. The competition between SERPINB9 and granzyme B determines the destiny of host cells. If granzyme B overwhelms SERPINB9, it would consequently trigger a series of adverse effects such as direct Bid to the mitochondrial membrane as well as activate caspase 3 and other death substrates, thereby executing AICD (73, 74). Hence AICD is like a suicide program hardwired into cytotoxic lymphocytes that contribute to auto-regulatory apoptosis. This is an important mechanism of self-tolerance to control the size of the lymphocyte pool during and after immunological responses (75).

GrB-Mediated Cell Death in a Paracrine Manner

In addition to AICD-induced "suicide," granzyme B could be either intentionally secreted to extracellular space or randomly escape from the immunological synapse between cytotoxic lymphocytes and their target cells during immune surveillance. This diffusive granzyme B would adsorb onto the cell membrane of other bystanders and being endocytosed inside the cells by different mechanisms to induce cell death (76, 77). The randomly escaped granzyme B would flow with body fluid and initiate an indiscriminate attack to any cells it makes contact with, leading to the increased inflammatory status, which might facilitate tumor progression (6). In contrast, vectorial granzyme B secretion is programmed under specific stimulation and often conducted in a contact-dependent manner. For instance, granzyme B can be released from Tregs due to prolonged IL-2 stimulation and non-specific TCR signaling and kills target DCs *via* a perforin-dependent way to undermine adaptive immunity. By analyzing the mobility of Tregs and DCs in TDLNs, a positive correlation between the death rate of DCs and their duration of contact with GrB^+ Tregs was established, further highlighting the contact-dependent killing mode of extracellular granzyme B (78). Paracrine signaling of granzyme B is a "double-edged sword" that contributes to either immunogenic or immunosuppressive responses, which depends on the origin of those granzymes. Both cytotoxic lymphocytes and suppressor cells (including cancer cells) could fight against each other *via* paracrine granzyme B. Thus results from the overall detection of granzyme B are hard to be interpreted and need scrutinization on the components of specific niche where granzyme B is presented.

Emperitosis

Secreted granzyme B can be taken back up by its host with potential harm, especially if it were trapped in a confined space (79). During immune surveillance, cytotoxic T lymphocytes (CTLs) could be engulfed into the vacuoles of tumor cells where granzyme B was degranulated. Due to the vacuole restriction, granzyme B cannot be transferred to the cytosol of tumor cells, hence being re-uptaken by its host and initiate a suicide-like death. Such cell-in-cell death is termed Emperitosis (80). It occurred in a variety of tumor types and promoted tumor progression in most cases, which could be leveraged to probe the stages of tumor development (81). Ex vivo and *in vitro* experiments revealed that IL-6 could enhance the adsorption between colon cancer cells and CTLs by upregulating the expression of cell adhesion molecule ICAM1 and polarize CTLs into cancer cells through STAT3, STAT5, ERK, and Rho-ROCK signaling pathways, both of which facilitated the formation of cell-in-cell structure. Furthermore, IL-6 could promote the autophagic activity of target cancer cells after engulfing CTLs, so that protect them from toxic effects and help them survive immune surveillance (82, 83). These results suggested a unique mechanism for immune evasion of cancer cells in TME.

Facilitate Tumor Angiogenesis

As a potent serine protease, granzyme B can modulate the configuration and components of ECM by degrading vital conjunctions and proteins, which releases some proinflammatory cytokines initially inert or sequestered in ECM. These cytokines would then underlie a favorable TME (84). The immunosuppressive effects that granzyme B enforces through ECM degradation and remodeling were suggested in some reports. For example, granzyme B could release VEGF and TGF-β by cleaving a number of glycoproteins, their anchors to ECM, thereby promoting vascular permeability and tumor angiogenesis during chronic inflammation. Such a process is similar to that presented in the case of MMP-2 and MMP-9 induced tumor angiogenesis (85, 86). Besides, extracellular granzyme B could directly degrade IL-1α within ECM into its fragments that favor the chronic inflammatory environment (87). Therefore, targeting granzyme B in ECM could be a promising strategy to attenuate tumor angiogenesis and mitigate the inflammatory response in TME.

Potential Determinants for the Immunosuppressive Roles of GrB in TME

Granzyme B expression within TME always experiences dynamic variation along with the pathophysiological changes (88). Except for the aforementioned cells that could express active granzyme B for immunosuppressive purposes, many factors potentially involved in switching the tumoricidal/tumorigenic roles of granzyme B, predisposing a specific niche within TME.

At the initiation phase of carcinogenesis, first responders in the immune system such as macrophages and NK cells recognize and eliminate the immunogenic cancer cells. Within this stage, these first arrivals not only play a direct tumoricidal role but also secrete chemokines like CCL5 and X-C Motif Chemokine Ligand (XCL) 1, which, combining with dangerous signals generated from necrotic cancer cells, recruit other active participants to enhance anti-tumor immunity (89). Once cytotoxic NK cells and effector T cells all got involved, a cytokine storm of granzyme B would show up and is presented as a tumoricidal molecule accompanied by perforin (90). However, the first wave of attack from the immune system is often inadequate for eradicating the cancer cell variants that are less immunogenic. These escaped cancer cells would utilize every resource they have to instigate their bystander cells to establish immune tolerance in a way termed as cancer immunoediting (91, 92). Subsequently, suppresser cells, including tumor-associated macrophages (TAMs), tumor-associated neutrophils (TANs), Tregs, Bregs, MDSCs, and pDCs, etc. are assembled in context-dependent manners and intervene with the anti-tumor immunity shaped by effector cells, where granzyme B possesses dual opposing roles depending on the cell source and relative abundance of those cells in TME (88, 93).

Mechanisms regarding the recruitment of potential immunosuppressive cells into TME have been explicitly described elsewhere. However, a comprehensive understanding of the induction and regulation of granzyme B in these cells is yet to be clarified (94). Though crosstalk between GrB-secreting cells and other players in TME is rather complicated considering the individual differences of host immunity and tumor heterogeneity, GrB^+ Tregs are generally accepted as central suppressor cells to form the immunosuppressive environment (95, 96). Actually, Tregs share some common routes with effector T cells in the production of granzyme B, such as the JAK/STAT pathway (97). Opposing to the tumor-killing nature of effector T cell-derived GrB, high levels of Treg-derived GrB are confirmed to promote tumor growth (2). Since tumor-specific antigens could both recruit effector T cells and promote the activation and proliferation of autologous Tregs in TME, whatever breaks the balance between Tregs and effector T cells would greatly influence the tumor fate (19).

During immunosurveillance, unconventional TCR stimulation, as well as specific costimulatory molecules and cytokines, could drive the differentiation of $CD4^+$ $Foxp3^-$ conventional T cells into $CD4^+$ $Foxp3^+$ iTregs with elevated granzyme B level comparing to nTregs (25, 98). Such iTregs can induce NK cell death in a GrB- and perforin-dependent fashion and inhibit the priming of T helper and effector T cells by GrB-mediated cleavage of their T cell zeta chain (5). Besides, they can kill DCs within TDLNs and TME in a contact-dependent way where Tregs recognize tumor-specific antigens presented by class 2 MHC ligand on DCs and release granzyme B/perforin granules to eliminate them. Hence GrB^+ Tregs could both impair autoimmunity and prevent the onset of DC-mediated adaptive immunity (77).

IL-2 has an essential impact on the differentiation and proliferation of both regulatory and effector T cells, hence playing important roles in the tradeoff between anti-tumor tolerance and immunity (99). It could also enhance the expression of granzyme B in both cell types and trigger a GrB-mediated reciprocal death between them, as illustrated in **Figure 2** (100). Detailed investigations of different IL-2 concentrations fed to the co-culture of autologous Tregs and responder T cells (RC) revealed a favorable RC killing toward Tregs under low concentration of IL-2 (150 IU/mL) in opposite to a reverse scenario when its concentration reached 1000 IU/mL. Combined with the fact that IL-2 concentration would experience a phased increase during immune responses, the results above could partially explain T cell exhaustion within TME in the case of malignancies and underline the significance of granzyme B in the setting of immunosuppression (101, 102). Some Tregs, such as $Gata3^+IRF4^+IL4^+Foxp3^+$ Th2-like Tregs, are hardwired with enhanced autocrine IL-2-mediated activation so that they could express more granzyme B than other subsets, which helps them survive effector T cells in TME and maintains a tumorigenic environment (103).

IL-3 is another promotive factor for the differentiation of Tregs and often works with IL-2 to facilitate granzyme B expression. After being secreted by activated T cells, monocytes, and/or tumor-associated stromal cells, IL-3 could induce a concomitant increase in the percentage of both $Foxp3^+$ Tregs and IL-2 secreting Th cells in a dose-dependent manner (104, 105). The resulting IL-2 would enhance the differentiation of naive T cells into iTregs with high levels of granzyme B. Intriguingly, Tregs could express IL-3 themselves in response to TGF-β, which would further increase the concentration of IL-2 in TME and forms a self-feeding loop to stall anti-tumor immunity (106).

In addition to cytokines, CCL1, a potent chemokine for Treg recruitment in TME, was recently proved to be closely related to granzyme B expression in Tregs (29, 107, 108). It could be secreted by activated monocytes, macrophages, T lymphocytes, endothelial cells, and tumor cells (109, 110). After being released, it can bind with its specific receptor, namely CCR8, on peripheral Tregs and attract them to tumor sites where it induces a STAT3-dependent elevation of granzyme B level that would confer Tregs with a powerful weapon against their targets (29). Other chemokines that could draw Tregs into tumor lesions, such as the ligands for CCR4 and CCR10, are also largely produced in TME, whereas their contribution to granzyme B expression in Tregs is yet to be established (107).

Except for secreting granzyme B themselves, Tregs could underlay GrB-mediated suppression in several indirect ways

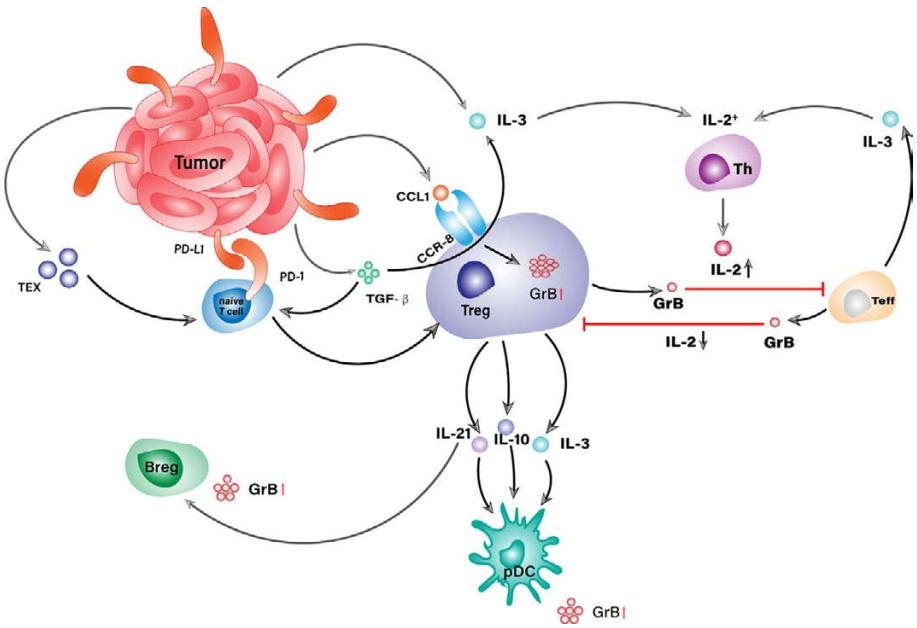

FIGURE 2 | GrB$^+$ Treg is a central orchestrator in the GrB-mediated immunosuppressive niche within TME. Tumor cells conjugate with naive T cells *via* PD-L1/PD-1 ligation and convert them into Tregs with the assist of TEX and TGF-β. No matter derived from TME or periphery, Tregs orchestrate the generation of other GrB$^+$ suppressor cells as well as the attack against Teffs through the secretion of IL-2, IL-3, and IL-21.

(**Figure 3**). Tumor-infiltrating Tregs were often found in aggregates of other suppressor cells exemplified by TAMs, Bregs, pDCs, and MDSCs, etc. (32, 34). Within the aggregates, Tregs could secrete IL-3, IL-10, and IL-21 that empowers their neighbors with elevated levels of granzyme B. These cytokines are vital factors to granzyme B expression in pDCs, among which IL-21 is the dominant driving force for the generation of GrB$^+$ Bregs (8).

However, some immunogenic components could counteract the granzyme B expression in suppressor cells where these cells have been adapted to fight against such adversities. TLR-mediated stimulation is a general response in leukocytes encountering pathogen-associated molecular patterns (PAMPs) derived from cellular components (111). When pDCs recognize PAMPs, the upcoming stimulation will activate their type I IFN signaling pathway and quench the granzyme B expression, thereby converting tolerogenic pDCs into immunogenic pDCs. Interestingly, type I IFNs generated from pDCs could promote IL-10 production in Tregs, which would, in turn, abrogate the type I IFN signaling pathway in pDCs and gradually restore their expression of granzyme B (112, 113). To add fuel to the fire, TLR stimulated pDCs could express the inducible costimulatory molecule (ICOS) ligand, which binds with ICOS on Tregs to promote their expansion and IL-10 secretion (114). Meanwhile, pDC-derived IDO can catabolize surrounding tryptophan into kynurenine derivatives which work on the aryl hydrocarbon receptor (AhR) of Tregs and stabilize their suppressor phenotype with productive granzyme B expression (115–117).

In another respect, IL-21-induced GrB$^+$ Bregs contribute to the granzyme B regulation networks within these suppressor cells in similar ways as described above. Put aside whether or not GrB$^+$ Bregs could express TGF-β, which still remains to be determined, they are definitely capable of IL-10 and IDO secretion, which positively relate to granzyme B production in both Tregs and pDCs (32, 118). Some components in TME, even not directly linked with granzyme B expression, can skew the immune homeostasis in favor of suppressor cells, facilitating the GrB-mediated immunosuppressive responses. CD40 and CD40 ligand (CD40L) are pivotal costimulatory molecules to the licensing of DCs and activation of effect T cells (119–121). Suppressor cells such as pDCs and Bregs also express CD40 and interact with CD40L on effector cells (122, 123). Unfortunately, CD40-CD40L interaction between regulatory and effector cells is most likely detrimental to granzyme B expression in the regulatory types and even transforms them into tumoricidal cells (34, 51). But that does not stop tumor cells from fighting a way out from their demise. Some neoplastic cells constitutively express CD40 and competitively consume CD40L from activated T cells, thus protecting granzyme B-expressing regulatory cells from turning anergy (124, 125).

Tumor-derived exosomes (TEX) are another powerful weapon tumor bears to inhibit the proliferation and viability of multiple immune effector cells. Researches indicated that exosomes from either the *in vitro* culture of tumor cells or the peripheral blood of tumor-bearing patients could educate CD4$^+$CD25$^-$ T cell into iTregs with elevated granzyme B level, which effectively suppressed the immune responses against tumors (126, 127). But the understanding of what in TEX and how these components elicit such effect keeps limited.

In contrast, TGF-β is a common regulatory factor in immune response and could explicitly increase granzyme B level in Tregs (128).

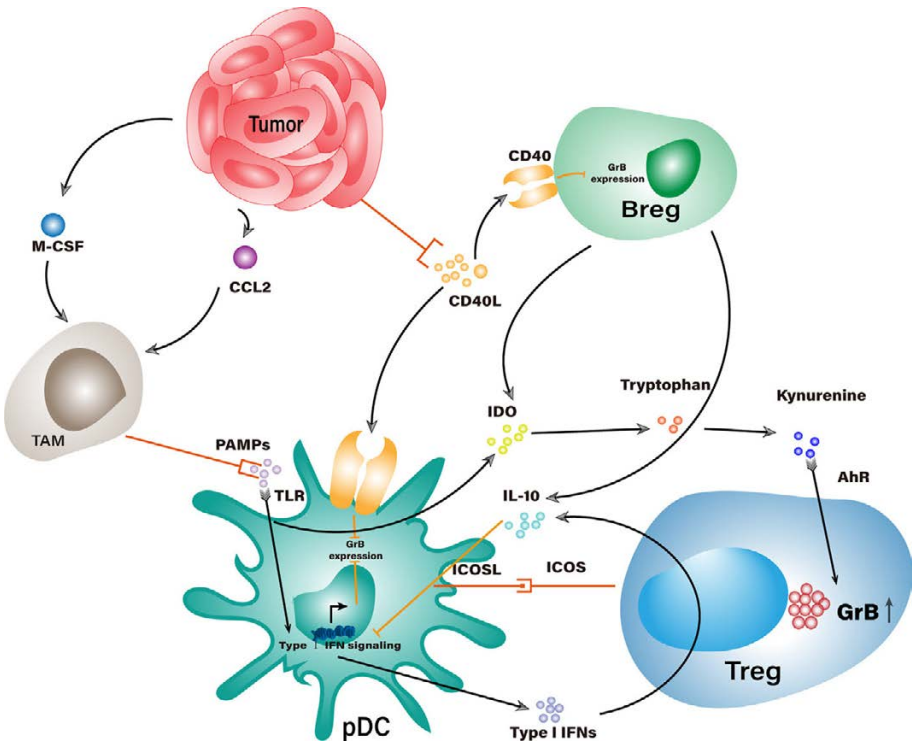

FIGURE 3 | Potential interaction networks that indirectly elevate GrB levels in suppressor cells within TME. Stimulation of TLR would trigger Type I IFN signaling that counteracts with GrB expression in pDCs. Tumor cells recruit TAMs to competitively consume TLR agonists and work with IL-10 from Tregs and Bregs to impair Type I IFN signaling, which indirectly increases the GrB level in pDCs. Tumor cells could consume CD40L and bring down the CD40-CD40L mediated inhibition of GrB expression in Bregs and pDCs. IDO from pDCs and Bregs could enhance GrB expression in Tregs through the catabolite of tryptophan.

Tumor cells, TAMs, tumor-associated neutrophils (TANs), Tregs, and MDSCs generally secrete TGF-β while express surface PD-L1 that binds with PD-1 on T cells, which all together promote the expression of FoxP3, thus differentiating T cells into GrB^{high} iTregs (129).

Tumors in both mice and humans secrete high levels of macrophage colony-stimulating factor (M-CSF) and CCL2, potent chemoattractants that could recruit macrophages to tumor sites where they would be educated into TAMs (130, 131). In malignant tumors, TAMs are the most densely populated cell type among all white blood cells, therefore deemed as the major driving force for TME formation (132). Other than direct suppression on T cell function through the surface presentation of several immunosuppressive ligands, TAMs are an abundant source of IL-10 and TGF-β, both of which crosslink with the regulation network of granzyme B and might boost its levels in Tregs, Bregs, and pDCs (133). Although they act aggressively in ingesting tumor antigens, they have been proved relatively inert to trigger adaptive immunity in contrast to effector DCs (134). Given the high density of TAMs in TME, they are speculated to consume most of the immunogenic cellular segments, including TLR agonists, so that might alleviate TLR-mediated granzyme B reduction in pDCs.

The last concern regarding the immunosuppressive roles of granzyme B might focus on its attack mode against effector cells. Since cell-to-cell contact is not necessary to all GrB-mediated immunosuppressive processes, one may wonder if the secreted granzyme B would escape from its original mission and harm adjacent tumor cells instead. Theoretically, the ubiquitous secretion of granzyme B into extracellular space is somehow harmful to every cell that it gets in contact with. That might explain the contradictory discoveries on some GrB-expressing suppressor cells that also pose threats to tumor cells in a GrB-dependent manner (135–137). Among the strategies that tumor cells employ to survive the adversities caused by effector lymphocytes, the one for overcoming GrB-mediated apoptosis is unique and convergent on SERPINB9, the well-defined granzyme B inhibitor that protects its host from being killed by this cytotoxic molecule (138, 139). While upregulation of SERPINB9 has been observed in several tumor types and linked with their resistance to T cell-mediated killing, a comprehensive understanding of SERPINB9 regulation in tumor cells within TME remains in the dark (140–143).

Some researchers confirmed increasing concentrations of estrogen, as well as elevated expression of estrogen receptor alpha (ERα), significantly elevated SERPINB9 level in breast cancer cells, thus effectively deactivated granzyme B and mitigated NK cell-induced cell death. Such effect might be tissue- and/or cell-line-specific due to the causation between estrogen and breast cancer, which is doubtful if it could apply to the increased expression of SERPINB9 in other cancers (144).

Another meaningful discovery unearthed that type I IFNs could upregulate SERPINB9 in certain cancer cells, thereby blocking GrB-mediated apoptosis and leading to a subsequent insusceptibility to T cell killing after radiotherapy. Since type I IFNs are frequent participants in TME and most cancer cells express their receptors, induction of SERPINB9 should be a more plausible mechanism underlying the evasion of tumor cells from GrB-dependent proteolysis (145).

CONCLUSION

Though granzyme B demonstrates pleiotropic effects in different hosts, excessive expression of granzyme B within the same context has been proved to culminate in anti-tumor propensity due to its innate cytotoxicity (89). In many cases, the GrB-mediated immunosuppression had been treated as collateral events to the interaction between the immune system and pathogens. However, if we zoom in on the battlefield of tumor immune microenvironment (TIME), granzyme B could be evidenced in most fights. The truth is we focused too much on the tumoricidal effects of granzyme B and somehow neglected what it can do to other participants in immunosurveillance. In this review, we introduced several suppressor cells that could secrete active granzyme B for immunosuppressive purposes and discussed possible mechanisms involved in the occurrence of such effects based on what has been documented. Cells with a sporadical expression of granzyme B were not included because little is known about what they utilize granzyme B for. Besides, the gene expression of granzyme B in some suppressor cells is not parallel to the actual level of secreted protein, suggesting the involvement of post-transcriptional regulation (146, 147). All we know now is the signaling pathways of granzyme B in suppressor cells are similar to those seen in effector cells, which converged on the transcription factors of JAK1, STAT3, and STAT5 (8, 148). Recent studies demonstrated that JunB, the AP-1 transcription factor, was essential to the differentiation of effector Tregs and the expression of their effector molecules, including granzyme B (149, 150). But that study did not go deep into detailed investigations of regulation networks around granzyme B. Another noteworthy issue is some tumor cells are observed with endogenous granzyme B and suspect of expressing such proteinase themselves. Nonetheless, the reason why tumor cells evolved to produce granzyme B, which might lead to their suicide, is still unknown (151, 152). Further researches are encouraged to address these issues and should include the GrB^+ suppressor cells developed from all organs of the immune system for a comprehensive understanding of the immunosuppressive roles of granzyme B.

AUTHOR CONTRIBUTIONS

WW wrote the manuscript. TH and ZQ conceived the review and designed the figures. RZ helped with the literature and polish the manuscript. YQ, JL, and YX gleaned the material and scruntinized the manuscript. All authors contributed to the article and approved the submitted version.

FUNDING

This research was funded by National Natural Science Foundation of China (Grant No. 81703643 and No.81973712).

ACKNOWLEDGMENTS

Key laboratory for substance basis of genuine medicinal herbs originated from Changbai Mountain (Jilin Administration of Traditional Chinese Medicine) financially supported this work.

REFERENCES

1. Cullen SP, Brunet M, Martin SJ. Granzymes in cancer and immunity. *Cell Death Differentiation* (2010) 17(4):616–23. doi: 10.1038/cdd.2009.206
2. Arias M, Martínez-Lostao L, Santiago L, Ferrandez A, Granville DJ, Pardo J. The Untold Story of Granzymes in Oncoimmunology: Novel Opportunities with Old Acquaintances. *Trends Cancer* (2017) 3(6):407–22. doi: 10.1016/j.trecan.2017.04.001
3. Voskoboinik I, Whisstock JC, Trapani JA. Perforin and granzymes: function, dysfunction and human pathology. *Nat Rev Immunol* (2015) 15 (6):388–400. doi: 10.1038/nri3839
4. Turner CT, Hiroyasu S, Granville DJ. Granzyme B as a therapeutic target for wound healing. *Expert Opin Ther Targets* (2019) 23(9):745–54. doi: 10.1080/14728222.2019.1661380
5. Cao X, Cai SF, Fehniger TA, Song J, Collins LI, Piwnica-Worms DR, et al. Granzyme B and perforin are important for regulatory T cell-mediated suppression of tumor clearance. *Immunity* (2007) 27(4):635–46. doi: 10.1016/j.immuni.2007.08.014
6. Boivin WA, Cooper DM, Hiebert PR, Granville DJ. Intracellular versus extracellular granzyme b in immunity and disease: challenging the dogma. *Lab Invest* (2009) 89(11):1195–220. doi: 10.1038/labinvest.2009.91
7. Hagn M, Jahrsdörfer B. Why do human B cells secrete granzyme B? Insights into a novel B-cell differentiation pathway. *Oncoimmunology* (2012) 1 (8):1368–75. doi: 10.4161/onci.22354
8. Jahrsdörfer B, Vollmer A, Blackwell SE, Maier J, Sontheimer K, Beyer T, et al. Granzyme B produced by human plasmacytoid dendritic cells suppresses T-cell expansion. *Blood* (2010) 115(6):1156–65. doi: 10.1182/blood-2009-07-235382
9. Dufait I, Pardo J, Escors D, De Vlaeminck Y, Jiang H, Keyaerts M, et al. Perforin and Granzyme B Expressed by Murine Myeloid-Derived Suppressor Cells: A Study on Their Role in Outgrowth Cancer Cells. *Cancers* (2019) 11(6):808. doi: 10.3390/cancers11060808
10. Wieckowski E, Wang GQ, Gastman BR, Goldstein LA, Rabinowich H. Granzyme B-mediated degradation of T-cell receptor zeta chain. *Cancer Res* (2002) 62(17):4884–9.
11. Wing JB, Sakaguchi S. Multiple treg suppressive modules and their adaptability. *Front Immunol* (2012) 3:178. doi: 10.3389/fimmu.2012.00178
12. Whiteside TL. Induced regulatory T cells in inhibitory microenvironments created by cancer. *Expert Opin Biol Ther* (2014) 14(10):1411–25. doi: 10.1517/14712598.2014.927432
13. Höfer T, Krichevsky O, Altan-Bonnet G. Competition for IL-2 between Regulatory and Effector T Cells to Chisel Immune Responses. *Front Immunol* (2012) 3:268. doi: 10.3389/fimmu.2012.00268

14. Taylor A, Verhagen J, Blaser K, Akdis M, Akdis CA. Mechanisms of immune suppression by interleukin-10 and transforming growth factor-beta: the role of T regulatory cells. *Immunology* (2006) 117(4):433–42. doi: 10.1111/j.1365-2567.2006.02321.x
15. Sun B, Liu M, Cui M, Li T. Granzyme B-expressing treg cells are enriched in colorectal cancer and present the potential to eliminate autologous T conventional cells. *Immunol Lett* (2020) 217:7–14. doi: 10.1016/j.imlet.2019.10.007
16. Xu A, Liu Y, Chen W, Wang J, Xue Y, Huang F, et al. TGF-β-Induced Regulatory T Cells Directly Suppress B Cell Responses through a Noncytotoxic Mechanism. *J Immunol (Baltimore Md 1950)* (2016) 196 (9):3631–41. doi: 10.4049/jimmunol.1501740
17. Aggarwal S, Sharma SC, N Das S. Dynamics of regulatory T cells (Tregs) in patients with oral squamous cell carcinoma. *J Surg Oncol* (2017) 116 (8):1103–13. doi: 10.1002/jso.24782
18. Drokov MY, Davydova JO, Kuzmina LA, Galtseva IV, Kapranov NM, Vasilyeva VA, et al. Level of Granzyme B-positive T-regulatory cells is a strong predictor biomarker of acute Graft-versus-host disease after day +30 after allo-HSCT. *Leukemia Res* (2017) 54:25–9. doi: 10.1016/j.leukres.2017.01.014
19. Li C, Jiang P, Wei S, Xu X, Wang J. Regulatory T cells in tumor microenvironment: new mechanisms, potential therapeutic strategies and future prospects. *Mol Cancer* (2020) 19(1):116. doi: 10.1186/s12943-020-01234-1
20. Salti SM, Hammelev EM, Grewal JL, Reddy ST, Zemple SJ, Grossman WJ, et al. Granzyme B regulates antiviral CD8+ T cell responses. *J Immunol (Baltimore Md 1950)* (2011) 187(12):6301–9. doi: 10.4049/jimmunol.1100891
21. Christiansen D, Mouhtouris E, Hodgson R, Sutton VR, Trapani JA, Ierino FL, et al. Antigen-specific CD4+ CD25+ T cells induced by locally expressed ICOS-Ig: the role of Foxp3, Perforin, Granzyme B and IL-10 - an experimental study. *Transplant Int Off J Eur Soc Organ Transplant* (2019) 32(11):1203–15. doi: 10.1111/tri.13474
22. Efimova OV, Kelley TW. Induction of granzyme B expression in T-cell receptor/CD28-stimulated human regulatory T cells is suppressed by inhibitors of the PI3K-mTOR pathway. *BMC Immunol* (2009) 10:59. doi: 10.1186/1471-2172-10-59
23. Grossman WJ, Verbsky JW, Barchet W, Colonna M, Atkinson JP, Ley TJ. Human T regulatory cells can use the perforin pathway to cause autologous target cell death. *Immunity* (2004) 21(4):589–601. doi: 10.1016/j.immuni.2004.09.002
24. Wei X, Zhang J, Gu Q, Huang M, Zhang W, Guo J, et al. Reciprocal Expression of IL-35 and IL-10 Defines Two Distinct Effector Treg Subsets that Are Required for Maintenance of Immune Tolerance. *Cell Rep* (2017) 21 (7):1853–69. doi: 10.1016/j.celrep.2017.10.090
25. Schmitt EG, Williams CB. Generation and function of induced regulatory T cells. *Front Immunol* (2013) 4:152. doi: 10.3389/fimmu.2013.00152
26. Miyazono K, Ichijo H, Heldin CH. Transforming growth factor-beta: latent forms, binding proteins and receptors. *Growth factors (Chur Switzerland)* (1993) 8(1):11–22. doi: 10.3109/08977199309029130
27. Nakamura K, Kitani A, Fuss I, Pedersen A, Harada N, Nawata H, et al. TGF-beta 1 plays an important role in the mechanism of CD4+CD25+ regulatory T cell activity in both humans and mice. *J Immunol (Baltimore Md 1950)* (2004) 172(2):834–42. doi: 10.4049/jimmunol.172.2.834
28. Mahalingam J, Lin CY, Chiang JM, Su PJ, Chu YY, Lai HY, et al. $CD4^+$ T cells expressing latency-associated peptide and Foxp3 are an activated subgroup of regulatory T cells enriched in patients with colorectal cancer. *PloS One* (2014) 9(9):e108554. doi: 10.1371/journal.pone.0108554
29. Barsheshet Y, Wildbaum G, Levy E, Vitenshtein A, Akinseye C, Griggs J, et al. CCR8+FOXp3+ Treg cells as master drivers of immune regulation. *Proc Natl Acad Sci United States America* (2017) 114(23):6086–91. doi: 10.1073/pnas.1621280114
30. Polesso F, Sarker M, Weinberg AD, Murray SE, Moran AE. OX40 Agonist Tumor Immunotherapy Does Not Impact Regulatory T Cell Suppressive Function. *J Immunol (Baltimore Md 1950)* (2019) 203(7):2011–9. doi: 10.4049/jimmunol.1900696
31. Maglioco A, Machuca DG, Camerano G, Costa HA, Ruggiero R, Dran GI. Regulatory B cells present in lymph nodes draining a murine tumor. *Medicina* (2014) 74(3):185–8.
32. Zhang Y, Gallastegui N, Rosenblatt JD. Regulatory B cells in anti-tumor immunity. *Int Immunol* (2015) 27(10):521–30. doi: 10.1093/intimm/dxv034
33. Hasan MM, Thompson-Snipes L, Klintmalm G, Demetris AJ, O'Leary J, Oh S, et al. CD24hiCD38hi and CD24hiCD27+ Human Regulatory B Cells Display Common and Distinct Functional Characteristics. *J Immunol (Baltimore Md 1950)* (2019) 203(8):2110–20. doi: 10.4049/jimmunol.1900488
34. Lindner S, Dahlke K, Sontheimer K, Hagn M, Kaltenmeier C, Barth TF, et al. Interleukin 21-induced granzyme B-expressing B cells infiltrate tumors and regulate T cells. *Cancer Res* (2013) 73(8):2468–79. doi: 10.1158/0008-5472.CAN-12-3450
35. Hagn M, Sontheimer K, Dahlke K, Brueggemann S, Kaltenmeier C, Beyer T, et al. Human B cells differentiate into granzyme B-secreting cytotoxic B lymphocytes upon incomplete T-cell help. *Immunol Cell Biol* (2012) 90 (4):457–67. doi: 10.1038/icb.2011.64
36. Kaltenmeier C, Gawanbacht A, Beyer T, Lindner S, Trzaska T, van der Merwe JA, et al. CD4+ T cell-derived IL-21 and deprivation of CD40 signaling favor the in vivo development of granzyme B-expressing regulatory B cells in HIV patients. *J Immunol (Baltimore Md 1950)* (2015) 194(8):3768–77. doi: 10.4049/jimmunol.1402568
37. Chesneau M, Michel L, Dugast E, Chenouard A, Baron D, Pallier A, et al. Tolerant Kidney Transplant Patients Produce B Cells with Regulatory Properties. *J Am Soc Nephrol JASN* (2015) 26(10):2588–98. doi: 10.1681/ASN.2014040404
38. Zhu J, Zeng Y, Dolff S, Bienholz A, Lindemann M, Brinkhoff A, et al. Granzyme B producing B-cells in renal transplant patients. *Clin Immunol (Orlando Fla)* (2017) 184:48–53. doi: 10.1016/j.clim.2017.04.016
39. Xu L, Liu X, Liu H, Zhu L, Zhu H, Zhang J, et al. Impairment of Granzyme B-Producing Regulatory B Cells Correlates with Exacerbated Rheumatoid Arthritis. *Front Immunol* (2017) 8:768. doi: 10.3389/fimmu.2017.00768
40. He Y, Qian H, Liu Y, Duan L, Li Y, Shi G. The roles of regulatory B cells in cancer. *J Immunol Res* (2014) 2014:215471. doi: 10.1155/2014/215471
41. Ding T, Yan F, Cao S, Ren X. Regulatory B cell: New member of immunosuppressive cell club. *Hum Immunol* (2015) 76(9):615–21. doi: 10.1016/j.humimm.2015.09.006
42. Yang C, Lee H, Pal S, Jove V, Deng J, Zhang W, et al. B cells promote tumor progression via STAT3 regulated-angiogenesis. *PloS One* (2013) 8(5):e64159. doi: 10.1371/journal.pone.0064159
43. Arabpour M, Rasolmali R, Talei AR, Mehdipour F, Ghaderi A. Granzyme B production by activated B cells derived from breast cancer-draining lymph nodes. *Mol Immunol* (2019) 114:172–8. doi: 10.1016/j.molimm.2019.07.019
44. Patente TA, Pinho MP, Oliveira AA, Evangelista G, Bergami-Santos PC, Barbuto J. Human Dendritic Cells: Their Heterogeneity and Clinical Application Potential in Cancer Immunotherapy. *Front Immunol* (2019) 9:3176. doi: 10.3389/fimmu.2018.03176
45. Karrich JJ, Jachimowski LC, Nagasawa M, Kamp A, Balzarolo M, Wolkers MC, et al. IL-21-stimulated human plasmacytoid dendritic cells secrete granzyme B, which impairs their capacity to induce T-cell proliferation. *Blood* (2013) 121(16):3103–11. doi: 10.1182/blood-2012-08-452995
46. Saadeh D, Kurban M, Abbas O. Plasmacytoid dendritic cell role in cutaneous malignancies. *J Dermatol Sci* (2016) 83(1):3–9. doi: 10.1016/j.jdermsci.2016.05.008
47. Li S, Wu J, Zhu S, Liu YJ, Chen J. Disease-Associated Plasmacytoid Dendritic Cells. *Front Immunol* (2017) 8:1268. doi: 10.3389/fimmu.2017.01268
48. Kawamura K, Kadowaki N, Kitawaki T, Uchiyama T. Virus-stimulated plasmacytoid dendritic cells induce CD4+ cytotoxic regulatory T cells. *Blood* (2006) 107(3):1031–8. doi: 10.1182/blood-2005-04-1737
49. Zhou ZJ, Xin HY, Li J, Hu ZQ, Luo CB, Zhou SL. Intratumoral plasmacytoid dendritic cells as a poor prognostic factor for hepatocellular carcinoma following curative resection. *Cancer Immunol Immunother CII* (2019) 68 (8):1223–33. doi: 10.1007/s00262-019-02355-3
50. Tel J, Smits EL, Anguille S, Joshi RN, Figdor CG, de Vries IJ. Human plasmacytoid dendritic cells are equipped with antigen-presenting and tumoricidal capacities. *Blood* (2012) 120(19):3936–44. doi: 10.1182/blood-2012-06-435941
51. Martín-Gayo E, Sierra-Filardi E, Corbí AL, Toribio ML. Plasmacytoid dendritic cells resident in human thymus drive natural Treg cell

development. *Blood* (2010) 115(26):5366–75. doi: 10.1182/blood-2009-10-248260
52. Boasso A, Herbeuval JP, Hardy AW, Anderson SA, Dolan MJ, Fuchs D, et al. HIV inhibits CD4+ T-cell proliferation by inducing indoleamine 2,3-dioxygenase in plasmacytoid dendritic cells. *Blood* (2007) 109(8):3351–9. doi: 10.1182/blood-2006-07-034785
53. Ito T, Yang M, Wang YH, Lande R, Gregorio J, Perng OA, et al. Plasmacytoid dendritic cells prime IL-10-producing T regulatory cells by inducible costimulator ligand. *J Exp Med* (2007) 204(1):105–15. doi: 10.1084/jem.20061660
54. Fabricius D, Trzaska T, Jahrsdörfer B. Granzyme B produced by Plasmacytoid Dendritic Cells Promotes Antigen uptake While Suppressing Premature T cell Activation. *Int J Vaccine Res* (2016) 1 (3):2473–176. doi: 10.15226/2473-2176/1/2/00113
55. Fabricius D, Nußbaum B, Busch D, Panitz V, Mandel B, Vollmer A, et al. Antiviral vaccines license T cell responses by suppressing granzyme B levels in human plasmacytoid dendritic cells. *J Immunol (Baltimore Md 1950)* (2013) 191(3):1144–53. doi: 10.4049/jimmunol.1203479
56. Thiel A, Kesselring R, Pries R, Wittkopf N, Puzik A, Wollenberg B. Plasmacytoid dendritic cell subpopulations in head and neck squamous cell carcinoma. *Oncol Rep* (2011) 26(3):615–20. doi: 10.3892/or.2011.1350
57. Koucký V, Bouček J, Fialová A. Immunology of Plasmacytoid Dendritic Cells in Solid Tumors: A Brief Review. *Cancers* (2019) 11(4):470. doi: 10.3390/cancers11040470
58. Spolski R, Leonard WJ. Interleukin-21: a double-edged sword with therapeutic potential. *Nat Rev Drug Discovery* (2014) 13(5):379–95. doi: 10.1038/nrd4296
59. Salvi V, Vermi W, Cavani A, Lonardi S, Carbone T, Facchetti F, et al. IL-21 May Promote Granzyme B-Dependent NK/Plasmacytoid Dendritic Cell Functional Interaction in Cutaneous Lupus Erythematosus. *J Invest Dermatol* (2017) 137(7):1493–500. doi: 10.1016/j.jid.2017.03.016
60. Afonina IS, Cullen SP, Martin SJ. Cytotoxic and non-cytotoxic roles of the CTL/NK protease granzyme B. *Immunol Rev* (2010) 235(1):105–16. doi: 10.1111/j.0105-2896.2010.00908.x
61. Mantovani A. The growing diversity and spectrum of action of myeloid-derived suppressor cells. *Eur J Immunol* (2010) 40(12):3317–20. doi: 10.1002/eji.201041170
62. Gabrilovich DI, Nagaraj S. Myeloid-derived suppressor cells as regulators of the immune system. *Nat Rev Immunol* (2009) 9(3):162–74. doi: 10.1038/nri2506
63. Veglia F, Perego M, Gabrilovich D. Myeloid-derived suppressor cells coming of age. *Nat Immunol* (2018) 19(2):108–19. doi: 10.1038/s41590-017-0022-x
64. Kusmartsev S, Nefedova Y, Yoder D, Gabrilovich DI. Antigen-specific inhibition of CD8+ T cell response by immature myeloid cells in cancer is mediated by reactive oxygen species. *J Immunol (Baltimore Md 1950)* (2004) 172(2):989–99. doi: 10.4049/jimmunol.172.2.989
65. Ohl K, Tenbrock K. Reactive Oxygen Species as Regulators of MDSC-Mediated Immune Suppression. *Front Immunol* (2018) 9:2499. doi: 10.3389/fimmu.2018.02499
66. Chen X, Eksioglu EA, Zhou J, Zhang L, Djeu J, Fortenbery N, et al. Induction of myelodysplasia by myeloid-derived suppressor cells. *J Clin Invest* (2013) 123(11):4595–611. doi: 10.1172/JCI67580
67. Sharron M, Hoptay CE, Wiles AA, Garvin LM, Geha M, Benton AS, et al. Platelets induce apoptosis during sepsis in a contact-dependent manner that is inhibited by GPIIb/IIIa blockade. *PloS One* (2012) 7(7):e41549. doi: 10.1371/journal.pone.0041549
68. Freishtat RJ, Natale J, Benton AS, Cohen J, Sharron M, Wiles AA, et al. Sepsis alters the megakaryocyte-platelet transcriptional axis resulting in granzyme B-mediated lymphotoxicity. *Am J Respir Crit Care Med* (2009) 179(6):467–73. doi: 10.1164/rccm.200807-1085OC
69. Middleton EA, Rowley JW, Campbell RA, Grissom CK, Brown SM, Beesley SJ, et al. Sepsis alters the transcriptional and translational landscape of human and murine platelets. *Blood* (2019) 134(12):911–23. doi: 10.1182/blood.2019000067
70. Han KH, Ro H, Hong JH, Lee EM, Cho B, Yeom HJ, et al. Immunosuppressive mechanisms of embryonic stem cells and mesenchymal stem cells in alloimmune response. *Transplant Immunol* (2011) 25(1):7–15. doi: 10.1016/j.trim.2011.05.004
71. Zhang J, Xu X, Liu Y. Activation-induced cell death in T cells and autoimmunity. *Cell Mol Immunol* (2004) 1(3):186–92.
72. Ida H, Nakashima T, Kedersha NL, Yamasaki S, Huang M, Izumi Y, et al. Granzyme B leakage-induced cell death: a new type of activation-induced natural killer cell death. *Eur J Immunol* (2003) 33(12):3284–92. doi: 10.1002/eji.200324376
73. Bird CH, Christensen ME, Mangan MS, Prakash MD, Sedelies KA, Smyth MJ, et al. The granzyme B-Serpinb9 axis controls the fate of lymphocytes after lysosomal stress. *Cell Death Differentiation* (2014) 21(6):876–87. doi: 10.1038/cdd.2014.7
74. Ida H, Utz PJ, Anderson P, Eguchi K. Granzyme B and natural killer (NK) cell death. *Modern Rheumatol* (2005) 15(5):315–22. doi: 10.1007/s10165-005-0426-6
75. Gorak-Stolinska P, Truman JP, Kemeny DM, Noble A. Activation-induced cell death of human T-cell subsets is mediated by Fas and granzyme B but is independent of TNF-alpha. *J Leukocyte Biol* (2001) 70(5):756–66. doi: 10.1189/jlb.70.5.756
76. Rousalova I, Krepela E. Granzyme B-induced apoptosis in cancer cells and its regulation (review). *Int J Oncol* (2010) 37(6):1361–78. doi: 10.3892/ijo_00000788
77. Yang J, Pemberton A, Morrison WI, Connelley T. Granzyme B Is an Essential Mediator in CD8+ T Cell Killing of Theileria parva-Infected Cells. *Infection Immun* (2018) 87(1):e00386–18. doi: 10.1128/IAI.00386-18
78. Boissonnas A, Scholer-Dahirel A, Simon-Blancal V, Pace L, Valet F, Kissenpfennig A, et al. Foxp3+ T cells induce perforin-dependent dendritic cell death in tumor-draining lymph nodes. *Immunity* (2010) 32 (2):266–78. doi: 10.1016/j.immuni.2009.11.015
79. Hiebert PR, Granville DJ. Granzyme B in injury, inflammation, and repair. *Trends Mol Med* (2012) 18(12):732–41. doi: 10.1016/j.molmed.2012.09.009
80. Salvesen GS. Dying from within: granzyme B converts entosis to emperitosis. *Cell Death Differentiation* (2014) 21(1):3–4. doi: 10.1038/cdd.2013.157
81. Wang X, Li Y, Li J, Li L, Zhu H, Chen H, et al. Cell-in-Cell Phenomenon and Its Relationship With Tumor Microenvironment and Tumor Progression: A Review. *Front Cell Dev Biol* (2019) 7:311. doi: 10.3389/fcell.2019.00311
82. Wang S, Li L, Zhou Y, He Y, Wei Y, Tao A. Heterotypic cell-in-cell structures in colon cancer can be regulated by IL-6 and lead to tumor immune escape. *Exp Cell Res* (2019) 382(1):111447. doi: 10.1016/j.yexcr.2019.05.028
83. Wang S, He MF, Chen YH, Wang MY, Yu XM, Bai J, et al. Rapid reuptake of granzyme B leads to emperitosis: an apoptotic cell-in-cell death of immune killer cells inside tumor cells. *Cell Death Dis* (2013) 4(10):e856. doi: 10.1038/cddis.2013.352
84. Matsubara JA, Tian Y, Cui JZ, Zeglinski MR, Hiroyasu S, Turner CT, et al. Retinal Distribution and Extracellular Activity of Granzyme B: A Serine Protease That Degrades Retinal Pigment Epithelial Tight Junctions and Extracellular Matrix Proteins. *Front Immunol* (2020) 11:574. doi: 10.3389/fimmu.2020.00574
85. Hendel A, Hsu I, Granville DJ. Granzyme B releases vascular endothelial growth factor from extracellular matrix and induces vascular permeability. *Lab Investigation J Tech Methods Pathol* (2014) 94(7):716–25. doi: 10.1038/labinvest.2014.62
86. Zhao M, Hu Y, Jin J, Yu Y, Zhang S, Cao J, et al. Interleukin 37 promotes angiogenesis through TGF-β signaling. *Sci Rep* (2017) 7(1):6113. doi: 10.1038/s41598-017-06124-z
87. Afonina IS, Tynan GA, Logue SE, Cullen SP, Bots M, Lüthi AU, et al. Granzyme B-dependent proteolysis acts as a switch to enhance the proinflammatory activity of IL-1α. *Mol Cell* (2011) 44(2):265–78. doi: 10.1016/j.molcel.2011.07.037
88. Frankel T, Lanfranca MP, Zou W. The Role of Tumor Microenvironment in Cancer Immunotherapy. *Adv Exp Med Biol* (2017) 1036:51–64. doi: 10.1007/978-3-319-67577-0_4
89. Gonzalez H, Hagerling C, Werb Z. Roles of the immune system in cancer: from tumor initiation to metastatic progression. *Genes Dev* (2018) 32(19-20):1267–84. doi: 10.1101/gad.314617.118
90. Binnewies M, Roberts EW, Kersten K, Chan V, Fearon DF, Merad M, et al. Understanding the tumor immune microenvironment (TIME) for effective therapy. *Nat Med* (2018) 24(5):541–50. doi: 10.1038/s41591-018-0014-x

91. O'Donnell JS, Teng M, Smyth MJ. Cancer immunoediting and resistance to T cell-based immunotherapy. *Nat Rev Clin Oncol* (2019) 16(3):151–67. doi: 10.1038/s41571-018-0142-8
92. Schreiber RD, Old LJ, Smyth MJ. Cancer immunoediting: integrating immunity's roles in cancer suppression and promotion. *Sci (N Y NY)* (2011) 331(6024):1565–70. doi: 10.1126/science.1203486
93. Headley MB, Bins A, Nip A, Roberts EW, Looney MR, Gerard A, et al. Visualization of immediate immune responses to pioneer metastatic cells in the lung. *Nature* (2016) 531(7595):513–7. doi: 10.1038/nature16985
94. Gajewski TF, Schreiber H, Fu YX. Innate and adaptive immune cells in the tumor microenvironment. *Nat Immunol* (2013) 14(10):1014–22. doi: 10.1038/ni.2703
95. Sula Karreci E, Eskandari SK, Dotiwala F, Routray SK, Kurdi AT, Assaker JP, et al. Human regulatory T cells undergo self-inflicted damage via granzyme pathways upon activation. *JCI Insight* (2017) 2(21):e91599. doi: 10.1172/jci.insight.91599
96. Duhen T, Duhen R, Lanzavecchia A, Sallusto F, Campbell DJ. Functionally distinct subsets of human FOXP3+ Treg cells that phenotypically mirror effector Th cells. *Blood* (2012) 119(19):4430–40. doi: 10.1182/blood-2011-11-392324
97. Owen KL, Brockwell NK, Parker BS. JAK-STAT Signaling: A Double-Edged Sword of Immune Regulation and Cancer Progression. *Cancers* (2019) 11 (12):2002. doi: 10.3390/cancers11122002
98. Kanamori M, Nakatsukasa H, Okada M, Lu Q, Yoshimura A. Induced Regulatory T Cells: Their Development, Stability, and Applications. *Trends Immunol* (2016) 37(11):803–11. doi: 10.1016/j.it.2016.08.012
99. Arenas-Ramirez N, Woytschak J, Boyman O. Interleukin-2: Biology, Design and Application. *Trends Immunol* (2015) 36(12):763–77. doi: 10.1016/j.it.2015.10.003
100. Janas ML, Groves P, Kienzle N, Kelso A. IL-2 regulates perforin and granzyme gene expression in CD8+ T cells independently of its effects on survival and proliferation. *J Immunol (Baltimore Md 1950)* (2005) 175 (12):8003–10. doi: 10.4049/jimmunol.175.12.8003
101. Czystowska M, Strauss L, Bergmann C, Szajnik M, Rabinowich H, Whiteside TL. Reciprocal granzyme/perforin-mediated death of human regulatory and responder T cells is regulated by interleukin-2 (IL-2). *J Mol Med (Berlin Germany)* (2010) 88(6):577–88. doi: 10.1007/s00109-010-0602-9
102. Carmenate T, Ortíz Y, Enamorado M, García-Martínez K, Avellanet J, Moreno E, et al. Blocking IL-2 Signal In Vivo with an IL-2 Antagonist Reduces Tumor Growth through the Control of Regulatory T Cells. *J Immunol (Baltimore Md 1950)* (2018) 200(10):3475–84. doi: 10.4049/jimmunol.1700433
103. Halim L, Romano M, McGregor R, Correa I, Pavlidis P, Grageda N, et al. An Atlas of Human Regulatory T Helper-like Cells Reveals Features of Th2-like Tregs that Support a Tumorigenic Environment. *Cell Rep* (2017) 20(3):757–70. doi: 10.1016/j.celrep.2017.06.079
104. Yang YC, Ciarletta AB, Temple PA, Chung MP, Kovacic S, Witek-Giannotti JS, et al. Human IL-3 (multi-CSF): identification by expression cloning of a novel hematopoietic growth factor related to murine IL-3. *Cell* (1986) 47 (1):3–10. doi: 10.1016/0092-8674(86)90360-0
105. Srivastava RK, Tomar GB, Barhanpurkar AP, Gupta N, Pote ST, Mishra GC, et al. IL-3 attenuates collagen-induced arthritis by modulating the development of Foxp3+ regulatory T cells. *J Immunol (Baltimore Md 1950)* (2011) 186(4):2262–72. doi: 10.4049/jimmunol.1002691
106. Kumar A, Rani L, Mhaske ST, Pote ST, Behera S, Mishra GC, et al. IL-3 Receptor Expression on Activated Human Th Cells Is Regulated by IL-4, and IL-3 Synergizes with IL-4 to Enhance Th2 Cell Differentiation. *J Immunol (Baltimore Md 1950)* (2020) 204(4):819–31. doi: 10.4049/jimmunol.1801629
107. Stockis J, Roychoudhuri R, Halim T. Regulation of regulatory T cells in cancer. *Immunology* (2019) 157(3):219–31. doi: 10.1111/imm.13064
108. Karin N. Chemokines and cancer: new immune checkpoints for cancer therapy. *Curr Opin Immunol* (2018) 51:140–5. doi: 10.1016/j.coi.2018.03.004
109. Korbecki J, Grochans S, Gutowska I, Barczak K, Baranowska-Bosiacka I. CC Chemokines in a Tumor: A Review of Pro-Cancer and Anti-Cancer Properties of Receptors CCR5, CCR6, CCR7, CCR8, CCR9, and CCR10 Ligands. *Int J Mol Sci* (2020) 21(20):7619. doi: 10.3390/ijms21207619
110. Kuehnemuth B, Piseddu I, Wiedemann GM, Lauseker M, Kuhn C, Hofmann S, et al. CCL1 is a major regulatory T cell attracting factor in human breast cancer. *BMC Cancer* (2018) 18(1):1278. doi: 10.1186/s12885-018-5117-8
111. Urban-Wojciuk Z, Khan MM, Oyler BL, Fåhraeus R, Marek-Trzonkowska N, Nita-Lazar A, et al. The Role of TLRs in Anti-cancer Immunity and Tumor Rejection. *Front Immunol* (2019) 10:2388. doi: 10.3389/fimmu.2019.02388
112. Stewart CA, Metheny H, Iida N, Smith L, Hanson M, Steinhagen F, et al. Interferon-dependent IL-10 production by Tregs limits tumor Th17 inflammation. *J Clin Invest* (2013) 123(11):4859–74. doi: 10.1172/JCI65180
113. Zhang L, Yuan S, Cheng G, Guo B. Type I IFN promotes IL-10 production from T cells to suppress Th17 cells and Th17-associated autoimmune inflammation. *PloS One* (2011) 6(12):e28432. doi: 10.1371/journal.pone.0028432
114. Faget J, Bendriss-Vermare N, Gobert M, Durand I, Olive D, Biota C, et al. ICOS-ligand expression on plasmacytoid dendritic cells supports breast cancer progression by promoting the accumulation of immunosuppressive CD4+ T cells. *Cancer Res* (2012) 72(23):6130–41. doi: 10.1158/0008-5472.CAN-12-2409
115. Baban B, Chandler PR, Sharma MD, Pihkala J, Koni PA, Munn DH, et al. IDO activates regulatory T cells and blocks their conversion into Th17-like T cells. *J Immunol (Baltimore Md 1950)* (2009) 183(4):2475–83. doi: 10.4049/jimmunol.0900986
116. Wu H, Gong J, Liu Y. Indoleamine 2, 3-dioxygenase regulation of immune response (Review). *Mol Med Rep* (2018) 17(4):4867–73. doi: 10.3892/mmr.2018.8537
117. Goettel JA, Gandhi R, Kenison JE, Yeste A, Murugaiyan G, Sambanthamoorthy S, et al. AHR Activation Is Protective against Colitis Driven by T Cells in Humanized Mice. *Cell Rep* (2016) 17(5):1318–29. doi: 10.1016/j.celrep.2016.09.082
118. Olkhanud PB, Damdinsuren B, Bodogai M, Gress RE, Sen R, Wejksza K, et al. Tumor-evoked regulatory B cells promote breast cancer metastasis by converting resting $CD4^+$ T cells to T-regulatory cells. *Cancer Res* (2011) 71 (10):3505–15. doi: 10.1158/0008-5472.CAN-10-4316
119. Tay NQ, Lee D, Chua YL, Prabhu N, Gascoigne N, Kemeny DM. CD40L Expression Allows CD8+ T Cells to Promote Their Own Expansion and Differentiation through Dendritic Cells. *Front Immunol* (2017) 8:1484. doi: 10.3389/fimmu.2017.01484
120. Elgueta R, Benson MJ, de Vries VC, Wasiuk A, Guo Y, Noelle RJ. Molecular mechanism and function of CD40/CD40L engagement in the immune system. *Immunol Rev* (2009) 229(1):152–72. doi: 10.1111/j.1600-065X.2009.00782.x
121. Karnell JL, Rieder SA, Ettinger R, Kolbeck R. Targeting the CD40-CD40L pathway in autoimmune diseases: Humoral immunity and beyond. *Advanced Drug Deliv Rev* (2019) 141:92–103. doi: 10.1016/j.addr.2018.12.005
122. Mathan TS, Figdor CG, Buschow SI. Human plasmacytoid dendritic cells: from molecules to intercellular communication network. *Front Immunol* (2013) 4:372. doi: 10.3389/fimmu.2013.00372
123. Soares RR, Antinarelli L, Abramo C, Macedo GC, Coimbra ES, Scopel K. What do we know about the role of regulatory B cells (Breg) during the course of infection of two major parasitic diseases, malaria and leishmaniasis? *Pathog Global Health* (2017) 111(3):107–15. doi: 10.1080/20477724.2017.1308902
124. Kim H, Kim Y, Bae S, Kong JM, Choi J, Jang M, et al. Direct Interaction of CD40 on Tumor Cells with CD40L on T Cells Increases the Proliferation of Tumor Cells by Enhancing TGF-β Production and Th17 Differentiation. *PloS One* (2015) 10(5):e0125742. doi: 10.1371/journal.pone.0125742
125. Bereznaya NM, Chekhun VF. Expression of CD40 and CD40L on tumor cells: the role of their interaction and new approach to immunotherapy. *Exp Oncol* (2007) 29(1):2–12.
126. Whiteside TL. Immune modulation of T-cell and NK (natural killer) cell activities by TEXs (tumour-derived exosomes). *Biochem Soc Trans* (2013) 41 (1):245–51. doi: 10.1042/BST20120265
127. Olejarz W, Dominiak A, Żołnierzak A, Kubiak-Tomaszewska G, Lorenc T. Tumor-Derived Exosomes in Immunosuppression and Immunotherapy. *J Immunol Res* (2020) 2020:6272498. doi: 10.1155/2020/6272498
128. Freudenberg K, Lindner N, Dohnke S, Garbe AI, Schallenberg S, Kretschmer K. Critical Role of TGF-β and IL-2 Receptor Signaling in Foxp3 Induction by an

Inhibitor of DNA Methylation. *Front Immunol* (2018) 9:125. doi: 10.3389/fimmu.2018.00125
129. Wang YA, Li XL, Mo YZ, Fan CM, Tang L, Xiong F, et al. Effects of tumor metabolic microenvironment on regulatory T cells. *Mol Cancer* (2018) 17 (1):168. doi: 10.1186/s12943-018-0913-y
130. Lin EY, Nguyen AV, Russell RG, Pollard JW. Colony-stimulating factor 1 promotes progression of mammary tumors to malignancy. *J Exp Med* (2001) 193(6):727–40. doi: 10.1084/jem.193.6.727
131. Cassetta L, Fragkogianni S, Sims AH, Swierczak A, Forrester LM, Zhang H, et al. Human Tumor-Associated Macrophage and Monocyte Transcriptional Landscapes Reveal Cancer-Specific Reprogramming, Biomarkers, and Therapeutic Targets. *Cancer Cell* (2019) 35(4):588–602.e10. doi: 10.1016/j.ccell.2019.02.009
132. Azizi E, Carr AJ, Plitas G, Cornish AE, Konopacki C, Prabhakaran S, et al. Single-Cell Map of Diverse Immune Phenotypes in the Breast Tumor Microenvironment. *Cell* (2018) 174(5):1293–1308.e36. doi: 10.1016/j.cell.2018.05.060
133. Zhou J, Tang Z, Gao S, Li C, Feng Y, Zhou X. Tumor-Associated Macrophages: Recent Insights and Therapies. *Front Oncol* (2020) 10:188. doi: 10.3389/fonc.2020.00188
134. Broz ML, Binnewies M, Boldajipour B, Nelson AE, Pollack JL, Erle DJ, et al. Dissecting the tumor myeloid compartment reveals rare activating antigen-presenting cells critical for T cell immunity. *Cancer Cell* (2014) 26(5):638–52. doi: 10.1016/j.ccell.2014.09.007
135. Lombardi VC, Khaiboullina SF, Rizvanov AA. Plasmacytoid dendritic cells, a role in neoplastic prevention and progression. *Eur J Clin Invest* (2015) 45 (Suppl 1):1–8. doi: 10.1111/eci.12363
136. Drobits B, Holcmann M, Amberg N, Swiecki M, Grundtner R, Hammer M, et al. Imiquimod clears tumors in mice independent of adaptive immunity by converting pDCs into tumor-killing effector cells. *J Clin Invest* (2012) 122 (2):575–85. doi: 10.1172/JCI61034
137. Demoulin S, Herfs M, Delvenne P, Hubert P. Tumor microenvironment converts plasmacytoid dendritic cells into immunosuppressive/tolerogenic cells: insight into the molecular mechanisms. *J Leukocyte Biol* (2013) 93 (3):343–52. doi: 10.1189/jlb.0812397
138. Ashton-Rickardt PG. An emerging role for Serine Protease Inhibitors in T lymphocyte immunity and beyond. *Immunol Lett* (2013) 152(1):65–76. doi: 10.1016/j.imlet.2013.04.004
139. Bladergroen BA, Meijer CJ, ten Berge RL, Hack CE, Muris JJ, Dukers DF, et al. Expression of the granzyme B inhibitor, protease inhibitor 9, by tumor cells in patients with non-Hodgkin and Hodgkin lymphoma: a novel protective mechanism for tumor cells to circumvent the immune system? *Blood* (2002) 99(1):232–7. doi: 10.1182/blood.v99.1.232
140. Medema JP, de Jong J, Peltenburg LT, Verdegaal EM, Gorter A, Bres SA, et al. Blockade of the granzyme B/perforin pathway through overexpression of the serine protease inhibitor PI-9/SPI-6 constitutes a mechanism for immune escape by tumors. *Proc Natl Acad Sci United States America* (2001) 98(20):11515–20. doi: 10.1073/pnas.201398198
141. Uhlen M, Zhang C, Lee S, Sjöstedt E, Fagerberg L, Bidkhori G, et al. A pathology atlas of the human cancer transcriptome. *Sci (N Y NY)* (2017) 357 (6352):eaan2507. doi: 10.1126/science.aan2507
142. Cunningham TD, Jiang X, Shapiro DJ. Expression of high levels of human proteinase inhibitor 9 blocks both perforin/granzyme and Fas/Fas ligand-mediated cytotoxicity. *Cell Immunol* (2007) 245(1):32–41. doi: 10.1016/j.cellimm.2007.03.004
143. Rousalova I, Krepela E, Prochazka J, Cermak J, Benkova K. Expression of proteinase inhibitor-9/serpinB9 in non-small cell lung carcinoma cells and tissues. *Int J Oncol* (2010) 36(1):275–83. doi: 10.3892/ijo_00000498
144. Jiang X, Ellison SJ, Alarid ET, Shapiro DJ. Interplay between the levels of estrogen and estrogen receptor controls the level of the granzyme inhibitor, proteinase inhibitor 9 and susceptibility to immune surveillance by natural killer cells. *Oncogene* (2007) 26(28):4106–14. doi: 10.1038/sj.onc.1210197
145. Chen J, Cao Y, Markelc B, Kaeppler J, Vermeer JA, Muschel RJ. Type I IFN protects cancer cells from CD8+ T cell-mediated cytotoxicity after radiation. *J Clin Invest* (2019) 129(10):4224–38. doi: 10.1172/JCI127458
146. Balkhi MY. Receptor signaling, transcriptional, and metabolic regulation of T cell exhaustion. *Oncoimmunology* (2020) 9(1):1747349. doi: 10.1080/2162402X.2020.1747349
147. Ciucci T, Vacchio MS, Bosselut R. A STAT3-dependent transcriptional circuitry inhibits cytotoxic gene expression in T cells. *Proc Natl Acad Sci United States America* (2017) 114(50):13236–41. doi: 10.1073/pnas.1711160114
148. Villarino AV, Kanno Y, O'Shea JJ. Mechanisms and consequences of Jak-STAT signaling in the immune system. *Nat Immunol* (2017) 18(4):374–84. doi: 10.1038/ni.3691
149. Koizumi SI, Sasaki D, Hsieh TH, Taira N, Arakaki N, Yamasaki S, et al. JunB regulates homeostasis and suppressive functions of effector regulatory T cells. *Nat Commun* (2018) 9(1):5344. doi: 10.1038/s41467-018-07735-4
150. Wheaton JD, Ciofani M. JunB Controls Intestinal Effector Programs in Regulatory T Cells. *Front Immunol* (2020) 11:444. doi: 10.3389/fimmu.2020.00444
151. Pearson JD, Zhang J, Wu Z, Thew KD, Rowe KJ, Bacani JT, et al. Expression of granzyme B sensitizes ALK+ ALCL tumour cells to apoptosis-inducing drugs. *Mol Cancer* (2014) 13:199. doi: 10.1186/1476-4598-13-199
152. Hu SX, Wang S, Wang JP, Mills GB, Zhou Y, Xu HJ. Expression of endogenous granzyme B in a subset of human primary breast carcinomas. *Br J Cancer* (2003) 89(1):135–9. doi: 10.1038/sj.bjc.6601051

Conflict of Interest: The authors declare that the research was conducted in the absence of any commercial or financial relationships that could be construed as a potential conflict of interest.

Copyright © 2021 Wang, Zou, Qiu, Liu, Xin, He and Qiu. This is an open-access article distributed under the terms of the Creative Commons Attribution License (CC BY). The use, distribution or reproduction in other forums is permitted, provided the original author(s) and the copyright owner(s) are credited and that the original publication in this journal is cited, in accordance with accepted academic practice. No use, distribution or reproduction is permitted which does not comply with these terms.

frontiers in Oncology

ORIGINAL RESEARCH
published: 02 April 2021
doi: 10.3389/fonc.2021.639059

Characterization of Immune Infiltration and Construction of a Prediction Model for Overall Survival in Melanoma Patients

Gang Li, Xuran Zhu and Chao Liu*

Plastic Surgery, The Second Affiliated Hospital of Zhengzhou University, Zhengzhou, China

Reports indicate that the use of anti-programmed cell death-1 (PD-1) and death ligand-1 (PD-L1) monoclonal antibodies for the treatment of patients diagnosed with melanoma has demonstrated promising efficacy. Nonetheless, this therapy is limited by the resistance induced by the tumor microenvironment (TME). As such, understanding the complexity of the TME is vital in enhancing the efficiency of immunotherapy. This study used four different methods to estimate the infiltrating level of immune cells. Besides, we analyzed their infiltration pattern in primary and metastatic melanoma obtained from The Cancer Genome Atlas (TCGA) database. As a consequence, we discovered a significantly higher infiltration of immune cells in metastatic melanoma compared to primary tumor. Consensus clustering identified four clusters in melanoma with different immune infiltration and clusters with higher immune infiltration demonstrated a better overall survival. To elucidate the underlying mechanisms of immune cell infiltration, the four clusters were subdivided into two subtypes denoted as hot and cold tumors based on immune infiltration and predicted immune response. Enrichment analysis of differentially expressed genes (DEGs) revealed different transcriptome alterations in two types of tumors. Additionally, we found tyrosinase-related protein1 (TYRP1) was negatively correlated with CD8A expression. *In vitro* experiments showed that knockdown TYRP1 promoted the expression of HLA-A, B, and C. Eventually, we constructed a prediction model which was validated in our external cohort. Notably, this model also performed effectively in predicting the survival of patients under immunotherapy. In summary, this work provides a deeper understanding of the state of immune infiltration in melanoma and a prediction model that might guide the clinical treatment of patients with melanoma.

Keywords: melanoma, immune infiltration, immunotherapy, tumor microenvironment, prediction model

OPEN ACCESS

Edited by:
Peng Qu,
National Institutes of Health (NIH), United States

Reviewed by:
Chao Wang,
Moffitt Cancer Center, United States
Yafeng He,
National Heart, Lung and Blood Institute (NHLBI), United States

****Correspondence:***
Gang Li
gangli_zzu@163.com

Specialty section:
This article was submitted to Cancer Immunity and Immunotherapy, a section of the journal Frontiers in Oncology

Received: *08 December 2020*
Accepted: *10 March 2021*
Published: *02 April 2021*

Citation:
Li G, Zhu X and Liu C (2021) Characterization of Immune Infiltration and Construction of a Prediction Model for Overall Survival in Melanoma Patients. Front. Oncol. 11:639059. doi: 10.3389/fonc.2021.639059

INTRODUCTION

Malignant melanoma is one of the most prevalent cancers accounting for up to 1.5% of all cancer-related deaths (1). Melanoma arises from melanocytes, which are found on the skin and mucosal membranes (2). Based on primary tumor location, melanoma is broadly subdivided into cutaneous and non-cutaneous tumors. The former is a rare subtype with an extremely poor prognosis

attributed to delayed diagnosis and the aggressive nature of these tumors (3–5). The treatment options for melanoma ranges from surgical excision with free margins, to radiotherapy and chemotherapy (6, 7). In recent years, strides made in the genomic, transcriptomic, and immunological structure of melanoma has enabled the development of novel therapies, thereby causing changes in the paradigm of therapeutic interventions (8, 9).

The current approaches for cancer immunotherapies, led by immune checkpoint inhibitors (ICIs), have shown significant efficacy in patients diagnosed with various cancers (10–12). Malignant melanoma is one of the most immunogenic tumors because of high genomic mutational load, which is considered a benefit from immunotherapy (13–15). An increase of high tumor mutation load produces immunogenic neoantigens, which stimulate immune response (16, 17). Notably, the first immune checkpoint inhibitors, anti-T-lymphocyte-associated protein 4 (Ipilimumab), and programmed cell death legend-1 (Nivolumab) were approved by the US Food and Drug Administration (FDA) in 2011 and 2014, respectively, for the treatment of unresectable or metastatic melanoma (18, 19). Data from clinical trials revealed that the use of immune checkpoint inhibitors prolonged the survival of the patient. A 3-year overall survival rate of patients treated with anti-PD-1 alone or in combination with ipilimumab and a 4-year survival rate for nivolumab plus ipilimumab exceeded 50%. Of note, the 5-year survival rate of patients treated with PD-1 alone could reach 35–40% (20–22).

Although the remarkable benefits of immunotherapy are evident, evidence from recent studies demonstrated that ICIs are associated with acquired or innate resistance (23). Immunotherapy focuses on harnessing the immune system to target and eradicate malignant cells. In melanoma, the level of infiltrating T cells correlate with immune response (24, 25). However, in most cases, the intro-tumoral immune response cannot be effectively activated due to the tumor microenvironment (TME) (26, 27). Notably, TME is an integral part of cancer forming an "ecosystem" to support tumor growth. It comprises numerous different cells and non-cellular factors at different stages of tumor development (28). TME is characterized by hypoxia and nutritional deficiency, i.e., conditions that limit the survival and function of effector T cells, but promote the formation of immunosuppressive cells, including myeloid-derived suppressor cell (MDSC), regulatory T cells (Tregs), and tumor-associated macrophages (29–31). Thus, understanding and targeting the TME is a promising approach for enhancing immunotherapy.

Herein, we performed a comprehensive analysis to explore immune infiltration in melanoma using four methods and constructed a prediction model. Consequently, we observed a higher infiltration and correlation of immune cells in metastatic tumors compared to primary tumors. Besides, patients with higher immune infiltration demonstrated a better survival. To uncover the underlying mechanisms of immune infiltration, the tumor was subdivided into hot and cold tumors then we calculated the DEGs between the two types of tumors. We found that TYRP1 was negatively correlated with CD8A expression while knockdown of TYRP1 promoted the expression of HLA-A, B, and C in tumor cells. Additionally, the prediction model performed efficiently in predicting the overall survival of patients with melanoma under immunotherapy.

METHODS AND MATERIALS

Ethics Statement

Treatment naïve melanoma specimens were obtained after surgical treatment in the Second Affiliated Hospital of Zhengzhou University. All specimens were frozen in the biobank, and patients received conventional chemotherapy and were followed up every 6 months. All participants signed an informed consent form approved by the ethics committee of Second Affiliated Hospital of Zhengzhou University (Ethics number: 2020026).

Cell Culture

Human melanoma cell line RPMI 1846 was purchased from the Chinese Academy of Sciences Cell Repertoire (Shanghai, China). Cells were cultured using a complete Roswell Park Memorial Institute (RPMI)-1640 medium containing 10% fetal bovine serum, 100 units/ml of penicillin, and 100 μg/ml of streptomycin (Thermo Fisher Scientific, USA) in a humidified incubator at 37°C with 5% CO_2.

Data Collection

The level 3 RNA-sequencing data and clinical information of skin cutaneous melanoma were downloaded from the online website UCSC Xena (https://xenabrowser.net/) (32), as in log2(x+1) transformed RSEM normalized count. Besides, the count data and survival information of metastatic urothelial cancercancer were downloaded from the platform supplied in the article (http://research-pub.gene.com/IMvigor210CoreBiologies/) (33). The RNA sequencing data and survival information of the melanoma were downloaded from the GEO database (https://www.ncbi.nlm.nih.gov/) with accession numbers: GSE78220, GSE91061 (9, 34).

Immune Estimation

Further, ssGSEA (Single-Sample Gene Set Enrichment Analysis) was performed to derive the enrichment score of each immune-related term using an R package "GSVA" (35). Online web tool CIBERSORT (http://cibersort.stanford.edu/) algorithm was used to estimate the proportion of 22 immune cell types. Samples with CIBERSORT output p-value <0.05 were considered eligible for further analysis (36). The infiltrating level of $CD4^+$ T cells, $CD8^+$ T cells, B cells, macrophages, Dendritic Cells, and Neutrophils was downloaded from an online website, TIMER (https://cistrome.shinyapps.io/timer/) (37). The "MCP-Counter" package in R was used for analysis of microenvironment cell populations (MCPs) and quantification of immune cells (38). The immune score, stromal score, and tumor purity were calculated by R package "ESTIMATE."

Analysis of Differently Expressed Genes (DEGs)

Based on the immune score and immune cell infiltration, the samples were subdivided into two groups, i.e., hot and cold tumors. Subsequently, the differential expression analyses were conducted between the two groups using the R package "Limma," with parameters of logFC >1.5 or <−0.5 and *p* value <0.05. Volcano diagram and heatmap were used to visualize the DEGs using R packages"ggplot2" and "pheatmap."

Enrichment Analysis and Protein-Protein Network Analysis

For the enrichment analysis, this study selected genes with $p < 0.05$ differently expressed in hot and cold tumors. R packages "clusterprofile" were used to analyze gene ontology (GO) terms and Kyoto Encyclopedia of Genes and Genomes (KEGG) enrichment analysis. $P < 0.05$ and $q < 0.05$ showed statistical significance. Genes with $p < 0.05$ and logFC > 2 and logFC < −0.5 were utilized to perform protein-protein interaction (PPI) network *via* online tool STRING (https://string-db.org/) with 0.9 confidence (39). For upregulated genes in PPI network, we used k means method to cluster the network. Nodes with less than two links were excluded for visualization.

Consensus Clustering

The consensus clustering value method provides quantitative and visual stability evidence for estimating the number of unsupervised classes in a dataset (40). ConsensusClusterPlus implements the CC method in R extending it with new functionality and visualizations including item tracking, item-consensus, and cluster-consensus plots. Clustering was performed using the cluster Cons package with 100 iterations using a Manhattan distance metric then the most robust number of clusters was selected. The optimal number of clusters was established by the heat map and dela diagram.

siRNA Transfections

The siRNA sequence was designed by BIODEV (http://biodev.cea.fr/DSIR/) and synthesized by Sangon Biotech (Shanghai, China). The sequence of si 1F: 5′-GGUCUUAACUACUAUGUUAUA-3′, R:5′-UAACAUAGUAGUUAAGACCAG-3′andsi2F:5′-GGUUCUGAUUAUUACGUUAAU-3′, R:5′-UAACGUAAUAAUCAGAACCUG-3′. Sangon Negative Control siRNA was used as control. The cells were seeded in an antibiotic-free complete medium at a density of 5 × 105 cells and cultured for 24 h. Transient transfection of cells with siRNA for 24 h was performed using Lipofectamine 2000 based on the manufacturer's protocol. At 24 h after transfection, the medium was changed and the cells were allowed to recover.

Quantitative Real-Time PCR

The fresh tumor specimens were obtained after the surgery then washed three times using PBS. Thereafter, tumor tissues were cut using scissors and added with Trizol (TaKaRa, Tokyo, Japan). To detect mRNA expression in tumor cell lines, tumor cells were transfected with siTYRP1 for 48 h then cells were obtained. The concentration and purity of total RNA were detected by NanoDrop 2000 (Thermo Fisher Scientific, MA, USA). Exactly 1 ug of total RNA was used to reverse into cDNA using ReverTra Ace qPCR RT Kit (TOYOBO, OSAKA, Japan). The primers used were designed and purchased from Sangon Biotech (Shanghai, China) (**Supplementary Table 1**). Glyceraldehyde-3-phosphate dehydrogenase (GAPDH) was used as control.

Correlation Analysis

The spearman correlation of immune cells was performed by R packages,"ggcor." The spearman correlation of CD8A expression and TYRP1 expression in the TCGA database and clinical samples was performed by GraphPadPrism (version 7.00).

Construction of Prediction Model

The RNA-sequencing data with survival information of melanoma was randomly divided into training and testing cohort by R package "caret." Genes differently expressed in hot and cold tumors were used to perform univariate survival analysis, and genes with $p < 0.05$ were selected. Then, R packages"glmnet" was used to perform LASSO analysis with maix = 20,000. To optimize the model, this work used a step-wise proportional hazards model. The survival analysis was analyzed by R package "survival," while AUC was analyzed by R package" survivalROC." To validate the model, clinical samples with survival information were obtained and the expression of genes in the model was calculated by RT-PCR. The RNA-sequencing data and survival information of patients under immunotherapy treatment were obtained from the GEO database or supplied in the article. The count and FPKM data were transferred into TPM and made a log2(x+1) normalization.

Statistical Analysis

All analyses were performed using R version 3.6.1. WilcoxTest was used to compare the infiltration of immune cells in primary and metastatic melanoma, as well as in hot and cold tumors, whereas ANOVA was used to compare immune score, stromal score, and tumor purity among the four clusters. For the survival analysis, the p-value was calculated with a log-rank test. In all analyses, $P < 0.05$ was considered statistically significant.

RESULTS

Infiltration Patterns Between Primary and Metastatic Melanoma

To dissect the difference of the immune infiltration between primary and metastatic melanoma, the proportion of immune cells was calculated using four different methods, including ssGSEA, CIBERSORT, TIMER, and MCP-Counter. The four methods exhibited various algorithms focusing on different sets of immune cells. ssGSEA, TIMER, and MCP-Counter demonstrated consistent results, while CIBERSORT results differed from others (**Figures 1A–D**). The proportion of the most of immune-related cells in metastatic melanoma was higher than in primary melanoma, specifically B cells, $CD4^+$ T cells,

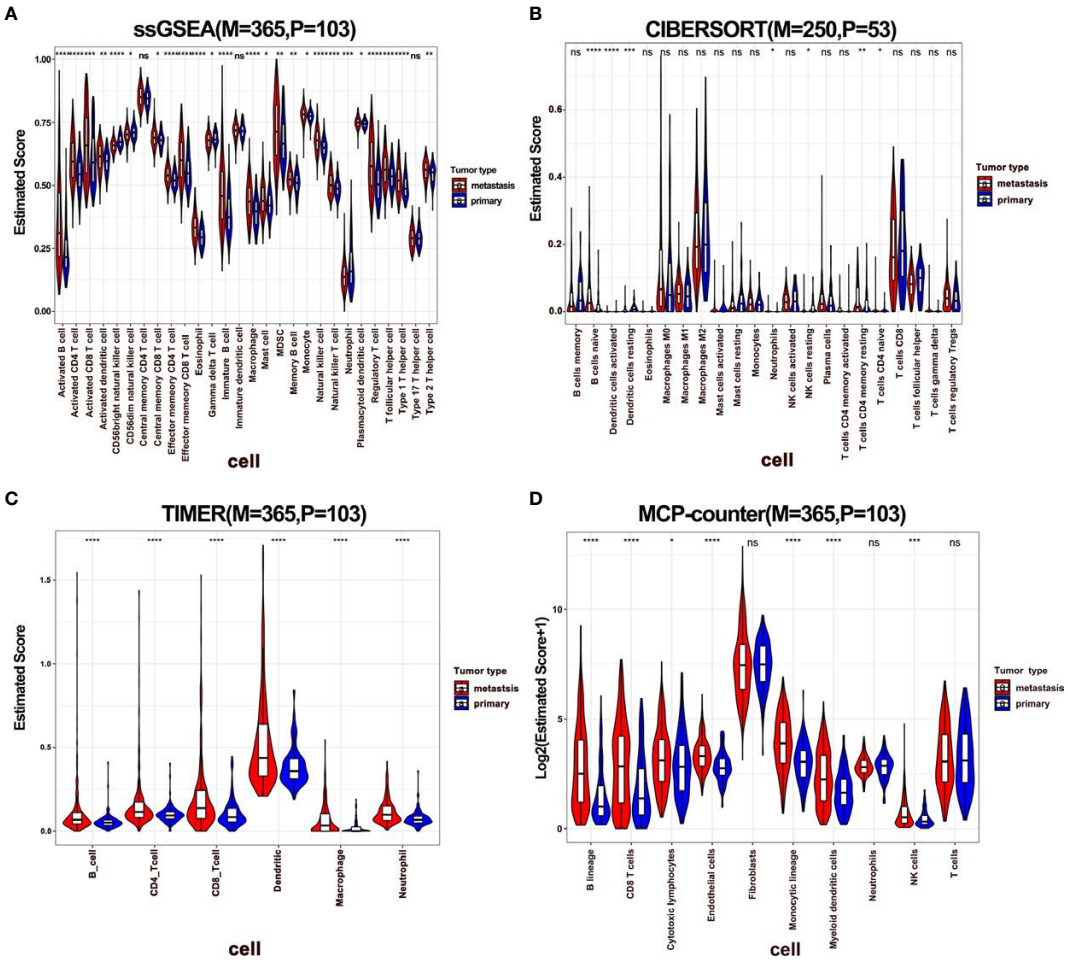

FIGURE 1 | The difference of immune infiltration between primary and metastatic tumors. **(A–D)** Violin plot showed the score of immune cells estimated by ssGSEA, CIBERSORT, TIMER, and MCP-Counter. P represents primary, M represents metastatic.

$CD8^+$ T cells, and DCs. These findings indicate a stronger immune response in metastatic melanoma compared to primary melanoma. Also, a few immune immunosuppressive cells were enriched in metastatic tumors, including myeloid-derived suppressive cells (MDSCs), regulatory T cells (Tregs). Moreover, neutrophils and CD56 bright natural killer (NK) cells were enriched in primary melanoma, indicating the significance of innate immunity in primary tumors. Additionally, a higher infiltration of mast cells was noted in metastatic tumors (**Figures 1A, B**). Notably, mast cells exhibit an important role in connecting innate and adaptive immunity, but also with pro-tumor function in TME (41). Nevertheless, its role in metastatic melanoma remains unclear hence warrants further investigation.

Correlation of Immune Cells in Primary and Metastatic Melanoma

Notably, immune infiltration requires synergic activity of multiple cells in tumor tissues. To this end, we performed a correlation analysis of immune cells in melanoma, where the results of ssGSEA, TIMER, and MCP-Counter revealed that immune cells exhibited a relatively strong correlation (**Figures 2A, C, D**). However, this phenomenon was not observed with the immune cells estimated by the CIBERSORT method (**Figure 2B**). Specifically, $CD8^+$ T cells were positively correlated with follicular helper T cells (Tfhs), activated NK, and DCs, indicating a cooperation across these cells in immune response. Further, it was observed that activated $CD8^+$ and $CD4^+$ T cells were positively correlated with macrophages M1, while negatively associated with M0 and M2 macrophages, demonstrating that M1 exhibits the function of antigen presentation (**Figure 2B**). Besides, neutrophils were negatively correlated with T cells. Furthermore, a correlation analysis was performed in metastatic melanoma and primary melanoma, respectively. Consequently, a higher correlation of immune cells was discovered in metastatic tumors compared to primary tumors (**Supplementary Figures 1A–D**).

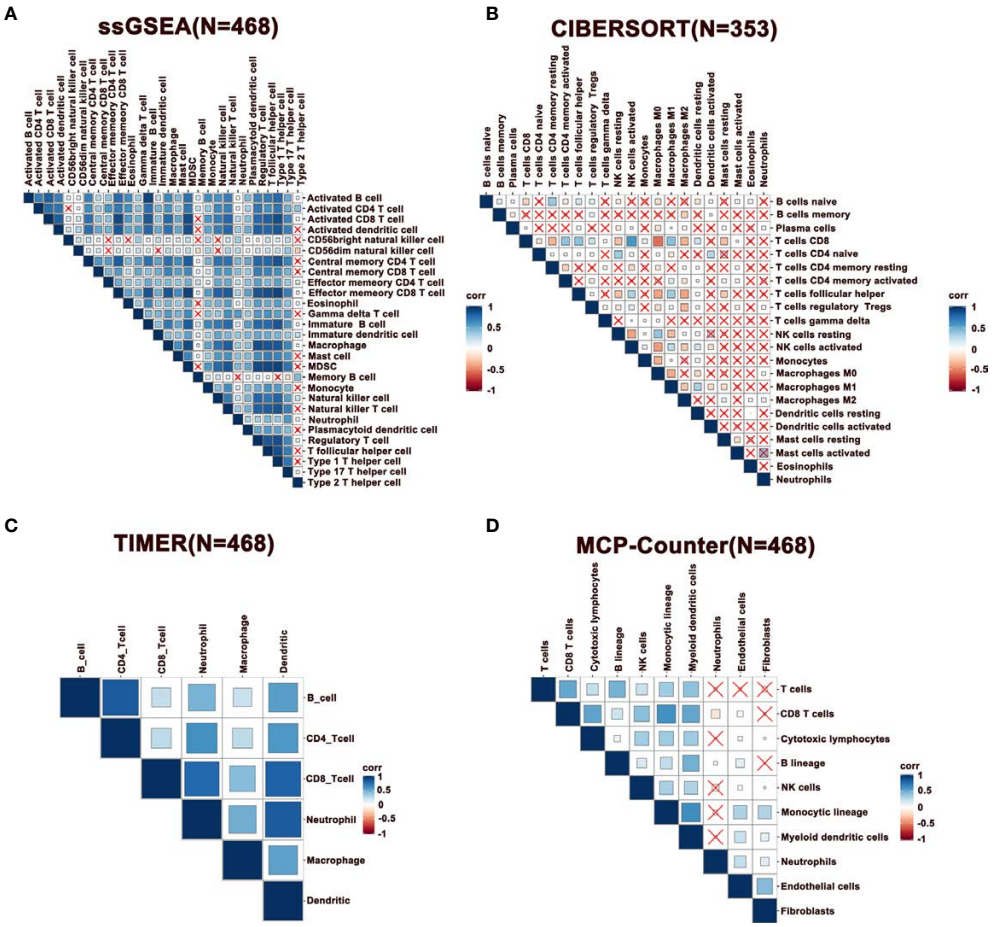

FIGURE 2 | Correlation of immune cells in melanoma. **(A–D)** Spearman correlation analysis of immune cells estimated by ssGSEA, CIBERSORT, TIMER, and MCP-Counter. N represents number of patients.

Immune Subtyping of Melanoma

To further characterize the immune infiltration in melanoma, we performed a consensus clustering analysis of immune cells calculated by ssGSEA. The heatmap revealed that the melanoma could be divided into four clusters (**Figure 3A**). From clusters 1 to 4, there was a gradual increase of immune infiltration in tumor tissue. Cluster1 lacked infiltration of immune cells, clusters 2 and 3 had modest infiltration of immune cells, while cluster 4 showed a phenotype of abundant immune infiltration. This was also reflected by the immune and stromal scores across four clusters (**Figure 3B**). Consistently, activated B cells, $CD4^+$ T cells, $CD8^+$ T cells, and DCs had the highest score in cluster 4 (**Figure 3C**). Notably, a few innate immune cells, including NK cells and neutrophils, showed no changes in four clusters. On other hand, clusters 3 and 4 had high infiltration of Tregs, MDSCs, and immature DCs, which inhibited immune response in tumors. These findings potentially suggest that immune activation is also accompanied with immune suppression mediated by the TME. Survival analysis revealed that clusters 3 and 4 had better survival relative to clusters 1 and 2 (**Figure 3D**). These outcomes indicate that the degree of immune infiltration positively correlates with patient survival.

The Difference of Immune-Related Genes in Four Clusters of Melanoma

To further reveal the mechanisms of cellular immunity among the four clusters, the expression of immune checkpoints, antigen presentation, cytokines, and chemokine-related genes were analyzed in four clusters. Results revealed that these molecules showed a higher expression in clusters 4 and 3 relative to clusters 1 and 2. Nevertheless, the expression of CD276 gradually showed the opposite trend, being highly expressed in clusters 1 and 2, while downregulated in clusters 3 and 4. The mutually exclusive expression pattern of CD276 and other immune checkpoints might provide potential treatment options for patients who do not respond to anti-PD-1, PD-L1, and CTLA-4 treatment (**Figures 4A–D**).

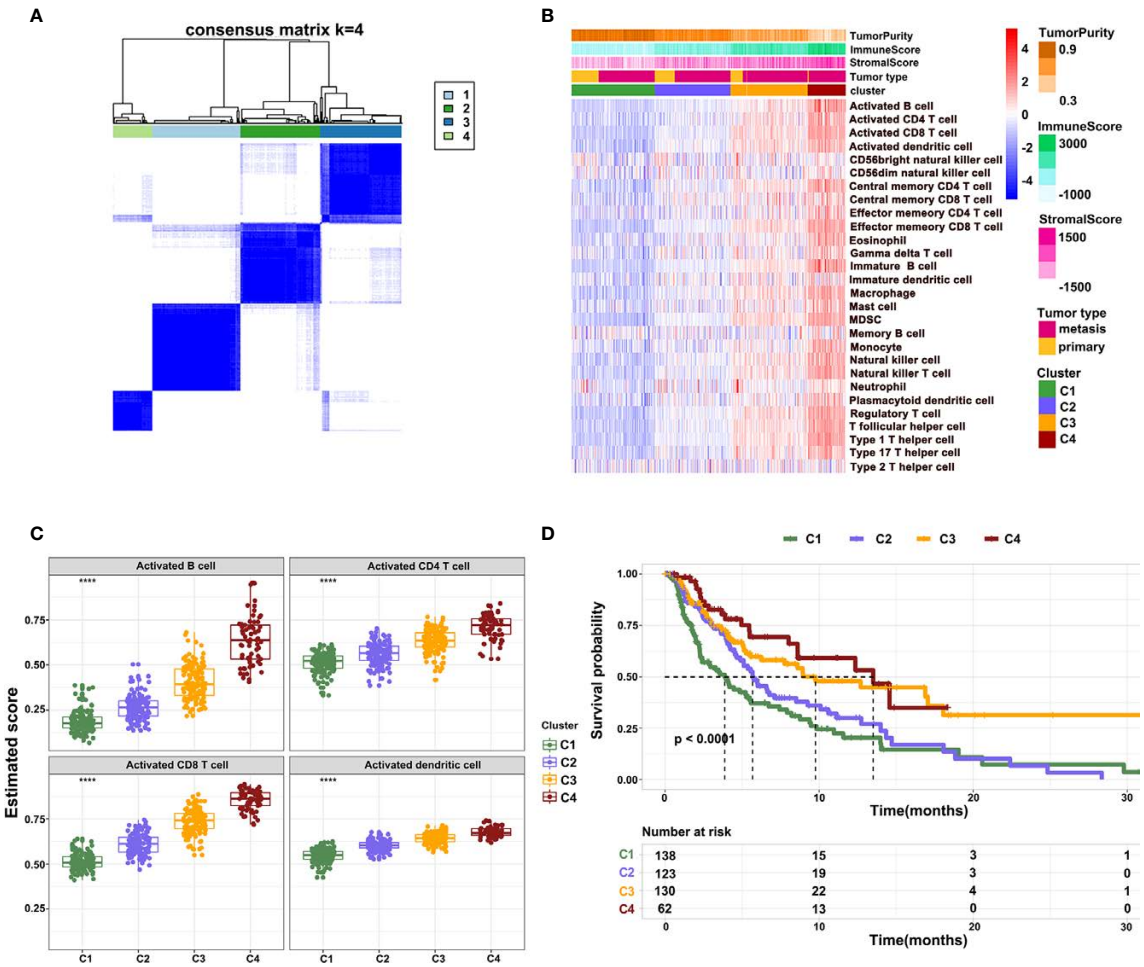

FIGURE 3 | Different patterns of immune cell infiltration in normal and tumor tissue. **(A)** Heatmap showing the consensus clustering of immune cells. **(B)** Heatmap showing the distribution of 28 immune cells across four clusters. **(C)** The infiltration of activated B cells, $CD4^+$ T cells, $CD8^+$ T cells, and DCs across four clusters. **(D)** Kaplan-Meier survival curve showing overall survival of patients across four clusters.

Alterations of Signaling in Hot and Cold Tumor

To predict the response of four clusters to immunotherapy, an online website Tumor Immune Dysfunction and Exclusion(TIDE) was used to calculate the tumor immune dysfunction and exclusion score. As a consequence, clusters 4 and 3 had significantly lower scores compared to clusters 1 and 2 (**Figure 5A**). In line with these findings, clusters 4 and 3 had a higher rate of responders to immunotherapy estimated by TIDE (**Figure 5B**). To further explore the mechanisms of immune infiltration, melanoma was subdivided into two subtypes, i.e., hot and cold tumor, with hot tumor comprising clusters 3 and 4, while cold tumor comprising clusters 1 and 2. Survival analysis revealed that hot tumor was expected to exhibit a better survival (**Figure 5C**). Subsequently, the difference between the two types of tumors was analyzed at the transcription level. Hot and cold tumors demonstrated distinct transcription patterns as illustrated by the volcano map and heatmap (**Figures 5D** and **Supplementary Figure 2**). The top 10 DEGs between hot and cold tumors were marked in the volcano map. Several genes related to immune activation enriched in hot tumors have been reported, including CD3D, PLA2G2D, NKG7, CXCL13, CD79A, and CXCL9. Additionally, tyrosinase-related protein1 (TYRP1) was upregulated in cold tumors and negatively correlated with CD8A expression (**Figure 5E**). *In vitro* experiments revealed that knockdown TYRP1 promoted the expression of HLA-A, B, and C. These findings indicate that inhibition of TYRP1 potentially promote the antigen presentation of MHC class I in tumor cells (**Figures 5F, G**). To investigate the interactions of DEGs, a PPI network of DEGs was performed. As a consequence, the PPI network in hot tumors formed four groups. Group 1 comprised genes in HLA families and B cell lineage, such as FCER1G, FCGR3A, CD79, CD19, which represent antigen presentation. Group 2 were genes implicated in T cell stimulation and recruitment, etc. Group 3 included cytokine and exhausted-related genes, such as GZMB, PRF1, HAVCR2, etc. Group 4 also contained

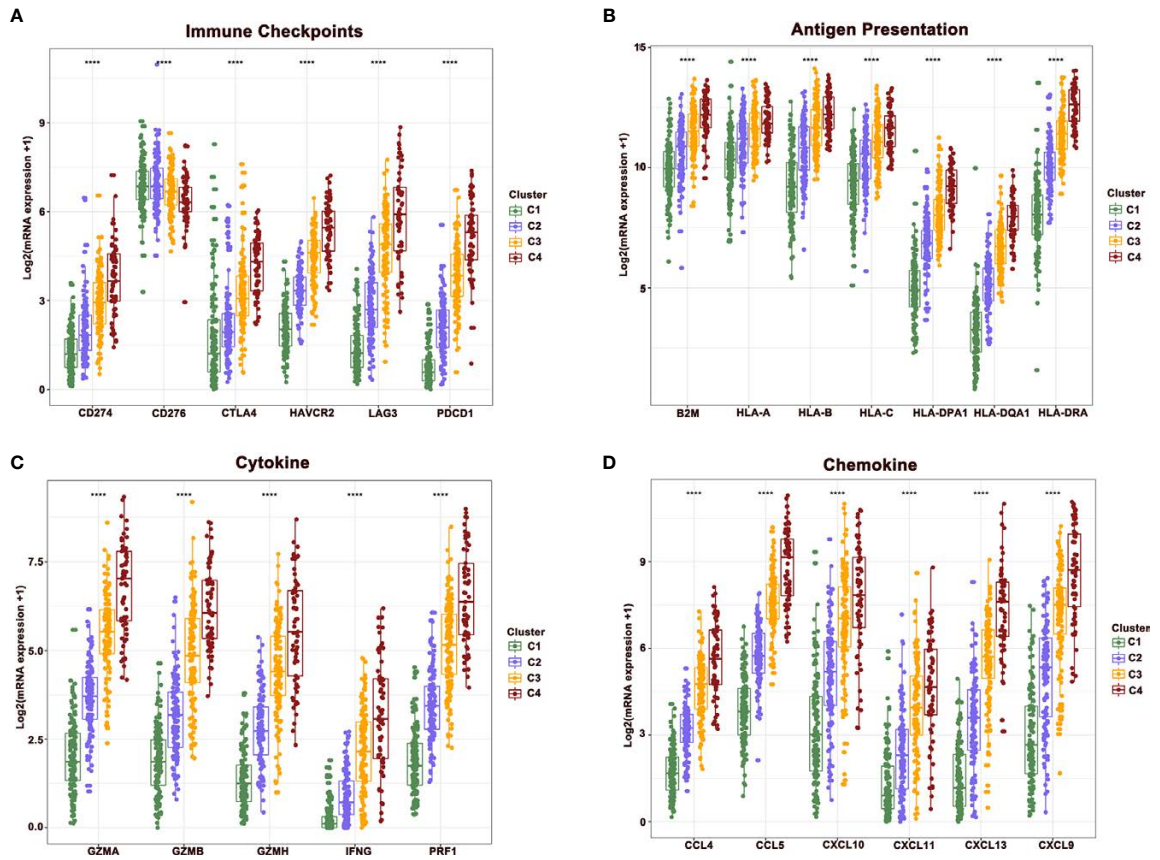

FIGURE 4 | The difference of central immune molecules in melanoma. **(A–D)** The expression of immune checkpoint, antigen presentation, cytokine and chemokine-related genes across four clusters.

several T cells-related chemokines and activated genes, including CCL4, CXCL9, SLAMF1, etc. The PPI network in cold tumor comprises a cluster of small proline-rich proteins (SPRR) family, while its role in melanoma is unclear (**Figures 5H**).

GO and KEGG Pathway Enrichment Analysis of DEGs

To further explore the function of DEGs, GO and KEGG enrichment analyses were performed. In line with the above results, GO analysis revealed that DEGs in hot tumors were primarily enriched in the regulation of leukocyte activation and leukocyte cell-cell adhesion. On the other hand, DEGs in cold tumors were significantly enriched in epidermis development, epidermal cell keratinocyte differentiation, structural constituent of cytoskeleton, structural constituent of epidermis, and ion antiporter activity. These outcomes suggest that the immunity was comprehensively activated in hot tumors, particularly leukocyte-mediated immune responses. In contrast, it was inclined to form a tough structure, including cytoskeleton and cornified envelope in cold tumor, which might prevent the infiltration of immune cells (**Figures 6A, B**). Moreover, the results of KEGG pathways enrichment analysis confirmed that activated immune response was observed in hot tumors (**Figure 6C**). Notably, the KEGG pathway in cold tumor was melanogenesis (**Figure 6D**).

Construction and Validation of Prediction Model for Overall Survival

The above results revealed that immune infiltration was correlated with the survival of patients. Therefore, the value of DEGs in predicting the overall survival of melanoma patients in TCGA and our external validation cohort should be explored. The detailed information of patients in TCGA and our clinical samples is shown in **Table 1**. Based on equal mortality rates, patients from the TCGA dataset were randomly divided into training and testing cohorts. Then, a LASSO regression model was used to identify the best gene sets for predicting OS in the training cohort (**Supplementary Figures 3A, B**). To optimize the model, a stepwise multi-Cox regression model was performed to select the most predictive gene sets (**Supplementary Figure 3C**). Eventually, a gene set containing seven genes was identified; where six of seven (CALHM1, OCSTAMP, HRASLS2, CEBPB,

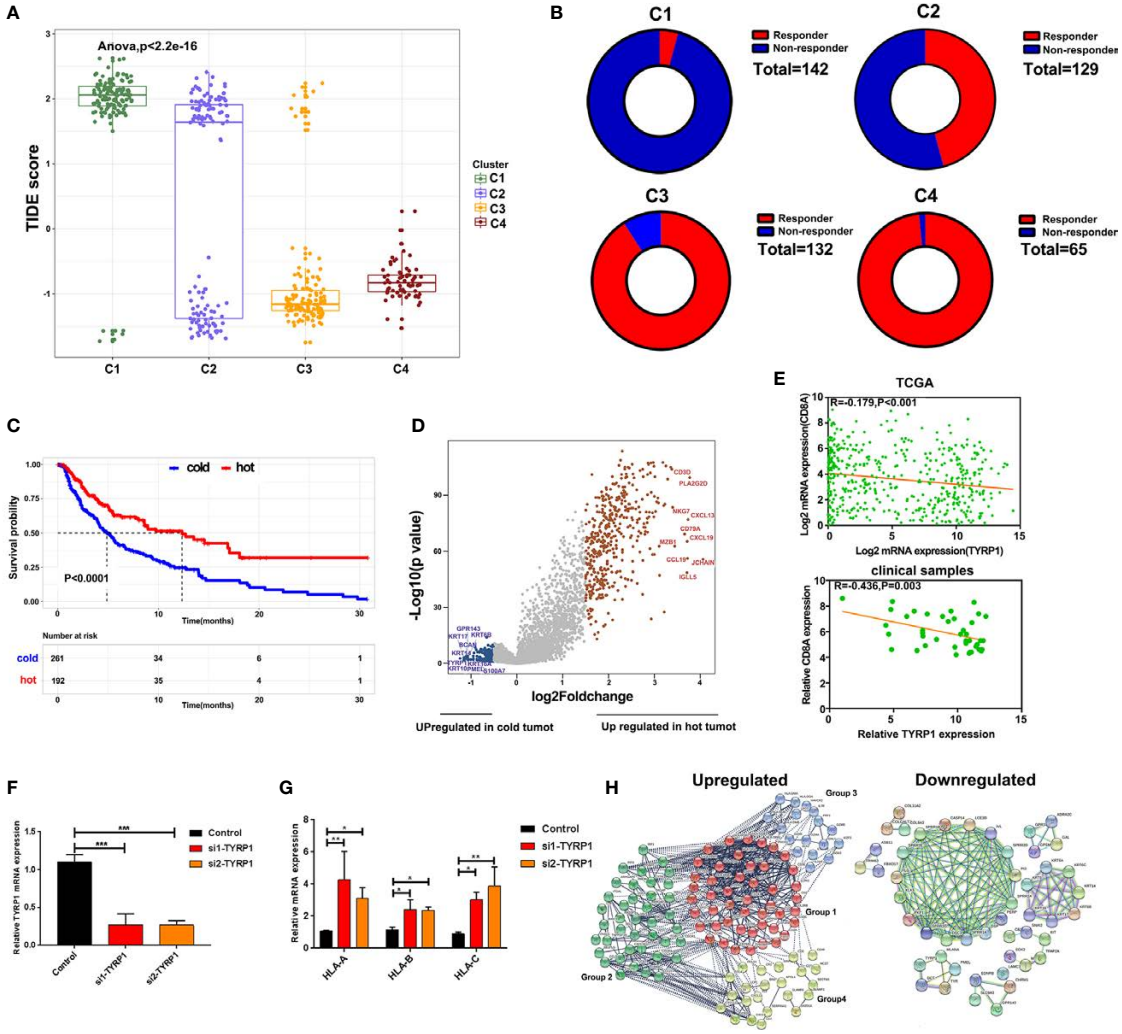

FIGURE 5 | Alterations of signaling in hot and cold tumor. **(A)** Boxplot showed the TIDE score of four clusters. **(B)** Ring plot showed the response rate of immunotherapy across four clusters. **(C)** Kaplan-Meier survival curve showed the survival of patients in hot and cold tumor. **(D)** Volcano showing DEGs between hot and cold tumor. **(E)** Correlation analysis of TYRP1 in TCGA (upper) and clinical samples (lower). **(F)** RT-PCR analyzed the efficiency of knockdown FABP6. **(G)** RT-PCR analyzed the expression of HLA-A, B, and C transfected with si-TYRP1. **(H)** The PPI network of DEGs in hot tumor and cold tumor.

ICAM1, IFITM1) genes were upregulated in the low-risk group, one of seven (TTYH3) was upregulated in the high-risk group (**Supplementary Figures 4A–C**). Then, a risk value was calculated based on the expression levels of selected genes and the corresponding regression coefficients: Risk score = 0.2577 × TTYH3 expression −3.3455 × CALHM1 expression − 1.3156 × OCSTAMP expression − 0.7372 × HRASLS2 expression − 0.2322 × CEBPB expression − 0.1963 × ICAM1 expression − 0.1219 × IFITM1 expression in three cohorts (**Supplementary Figures 4D–F**). Results revealed that the risk score effectively distinguished the survival time of patients in training, testing, and validating cohorts (**Figures 7A–C**). Consistent with these findings, patients with high risk predicted a poor survival (**Figures 7D–F**). The AUC of the predicting model for the training dataset at 1st year, 2nd year, and 3rd year was 0.73, 0.76, 0.75, while 0.64, 0.6, and 0.63 for the testing cohort (**Figures 7G, H**). The AUC in the validating cohort were 0.73, 0.77, and 0.81 at 1st, 2nd, and 3rd year, respectively, indicating a satisfactory value for predicting the overall survival of patients (**Figure 7I**). For further analysis, the seven gene signatures were subsequently evaluated in predicting survival of patients receiving immunotherapy in three independent cohorts, where one was metastatic urothelial cancer cancer and the other two were melanoma. Results revealed that patients with high risk had an unfavorable overall survival in two cohorts, showing no significant difference in a melanoma cohort (**Figures 7J–L**).

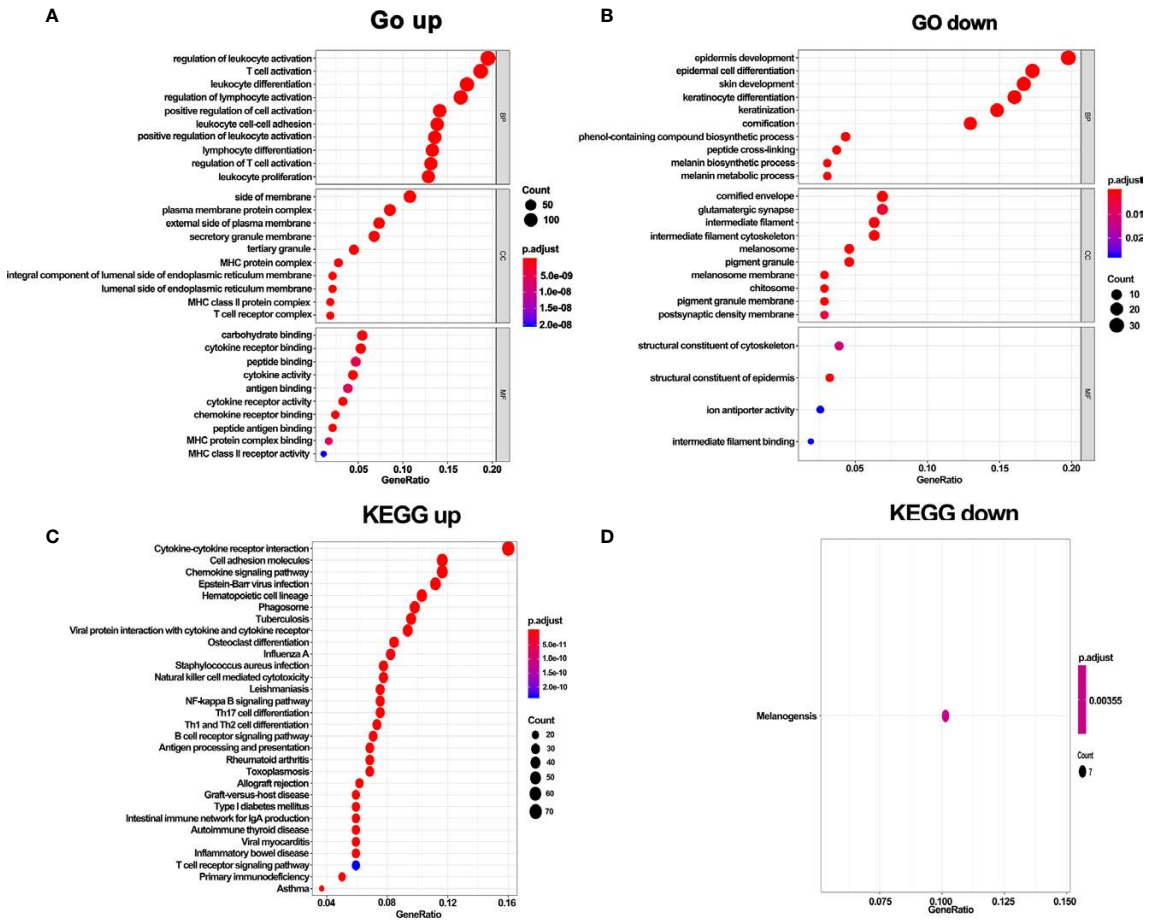

FIGURE 6 | GO terms and KEGG enrichment analysis of DEGs. **(A)** GO enrichment analysis of upregulate DEGs. **(B)** GO enrichment analysis of downregulate DEGs. **(C)** KEGG pathway enrichment analysis of upregulate DEGs. **(D)** KEGG pathway enrichment analysis of downregulate DEGs.

Generally, these findings suggest that the prediction model performed efficiently in predicting overall survival and can guide the clinical treatment of patients with melanoma.

DISCUSSION

Melanoma is evolving as the most threatening form of skin tumor with its global incidence rapidly increasing. In the early stages, surgery is the effective treatment option for melanoma where the survival rates are significantly high, however, they significantly drop after metastasis. Reports indicate that the median overall survival of metastatic melanoma was less than 1 year (42). Early misdiagnosis of melanoma minimizes the survival of melanoma patients, causing metastasis which accounts for the majority of mortalities (43). Considering tumor recurrence and resistance manifesting within a relatively short time for most patients (44, 45) and elevated mutation load of melanoma (46), the treatment with new drug combinations has become a vital strategy in achieving a sustainable effect. Data from clinical trials revealed that advanced melanoma patients treated with ICIs alone or in combination prolonged the survival and demonstrated a higher objective response rate (20). Nonetheless, accumulated data reveals several patients with zero response to treatment, and a few patients initially responding to treatment but eventually develop resistance due to the complex TME (47). As such, an in-depth understanding of immune status in melanoma is essential to guide its clinical treatment.

This study used four methods to investigate the immune infiltration in melanoma. Specifically, we compared the immune infiltration in primary and metastatic melanoma, respectively, as a result, metastatic melanoma showed a higher immune infiltration. Also, previous studies demonstrated that metastatic melanoma is considered a perfect example of an immunogenic tumor since it is characterized by the consistent presence of lymphoid infiltrate (48). While, most of cells estimated by these four methods are different, although same cells are belong to the same cell linage, such as T cell lineage (CD4 and $CD8^+$ T cells), B cell lineage, and macrophage lineage. For a single cell type, it may

TABLE 1 | Clinical and pathologic characteristics of the patients in TCGA and external validation cohort analyzed in this study.

Characteristics	TCGA	Validation cohort
Number of samples	453	60
Age median (range)	58 (15–90)	53 (29–73)
Gender		
Male	282 (62%)	36 (60%)
Female	171 (38%)	24 (40%)
Additional_pharmaceutical_therapy		
Yes	32 (7%)	39 (65%)
NO	32 (7%)	21 (35%)
NA	389 (86%)	
Additional_radiation_therapy		
Yes	46 (10%)	8 (13%)
NO	19 (4%)	52 (87%)
NA	388 (86%)	
Pathologic_M		
M0	403 (89%)	50 (83%)
M1	24 (5%)	10 (17%)
NA	26 (6%)	
Pathologic_N		
N0	221 (49%)	32 (53%)
N1	73 (16%)	18 (30%)
N2	49 (11%)	6 (10%)
N3	56 (12%)	4 (7%)
NX	35 (8%)	
NA	19 (4%)	
Pathologic_T		
T0	23 (5%)	
T1	41 (9%)	14 (23%)
T2	76 (17%)	28 (47%)
T3	89 (20%)	13 (22%)
T4	152 (34%)	5 (8%)
TX	45 (10%)	
NA	27 (6%)	
Pathologic_Stage		
Stage 1	86 (19%)	19 (32%)
Stage 2	138 (30%)	21 (35%)
Stage 3	170 (38%)	14 (23%)
Stage 4	23 (5%)	6 (10%)
NA	36 (8%)	

be difficult to draw a consistent conclusion from these four methods. But different cell types also provide more information for exploring the heterogeneity of the tumor microenvironment. Meanwhile, a strong correlation of immune cells was noted in metastatic melanoma. Besides, mast cells were enriched in metastatic tumors as showed by ssGSEA. Notably, mast cells play critical roles in both innate and adaptive immunity producing large subsets of mediators and reshaping the tumor microenvironment of melanoma. Several case reports and studies have confirmed an enhanced incidence of melanoma among patients with mastocytosis (49–51). Mast cells act as pro-tumor in the TME (52–54). Targeting mast cells infiltrated in TME combined with immune checkpoint inhibitors or turning tumor-promoting mast cells into tumor-inhibiting mast cells might be an effective approach for the treatment of melanoma (55). Here, we calculated the relative expression level of immune cells in each sample using CIBERSORT. Notably, the immune levels estimated by CIBERSORT were not similar to other methods. This method effectively reflects the ratios of cells in each sample but it cannot represent the absolute number of cells. The CIBERSORT algorithm considers a signature matrix built from microarray data, comprising 22 immune cell types, and estimates the cell fractions using nu support vector regression (36). Unlike CIBERSORT, TIMER estimates six immune cell types based on immune-specific markers. However, TIMER cannot used to compare across different cell types (56), and both of the two methods use deconvolution. ssGSEA and MCP-counter calculate score based on marker genes and ranks the genes *via* their absolute expression in a sample and computes enrichment score for each cell type. This method has been widely used since individual gene sets can be defined. MCP-counter is computed as the geometric mean of the expression values of cell-type-specific genes. Different methods have their advantages and disadvantages. CIBERSORT focuses on the ratios of each cell in each sample, thus, cell comparisons between different samples may bring a relatively large deviation. The data analyzed by CIBERSORT can be microarray and RNA-seq, but for RNAseq, the data in Transcripts Per Kilobase of exonmodel per Million mapped reads (TPM) format is more accurate. Although the online webtool TIMER only score six cell types, the markers used in this method contain specific genes in each tumor. Therefore, it may be more accurate to assess the degree of cell infiltration. ssGSEA has fewer restrictions on the format of the data, and the calculated cell score can be used for comparison of different samples. At the same time, it can be more flexible to calculate the cell composition in the microenvironment based on the accurate marker gene (35, 38). Therefore ssGSEA may be a better choice for most sequencing data. Nevertheless, among the above, an effective method remains controversial.

Several distinguishable subtypes of melanoma from clinical and pathology have been reported. Also, studies have reported that these subtypes usually exhibit distinct genetic characteristics in molecular biology (5). Recent empirical studies and reviews have revealed that the efficacy of immune checkpoint inhibitors differ depending on the subtype of melanoma. Moreover, studies have found that tumors with a higher mutation burden usually obtain more benefit from immune checkpoint inhibitors.

This paper clustered melanoma samples based on immune infiltration, and consequently, patients with higher immune response demonstrated better survival, affirming our definition of clusters. Additionally, immune-related genes were upregulated in clusters 4 and 3 relative to clusters 1 and 2, however, this did not include CD276. CD276, known as B7-H3, belongs to the B7 family of immunoregulatory proteins and has been implicated in cancer progression and metastasis. Research has confirmed the expression of CD276 in primary and metastatic melanoma as well as its significant role in the progression of melanoma and events of metastasis (57, 58). Additionally, our findings suggest that CD276 might serve as a potential target for patients with zero response to immunotherapy.

TIDE is a computational method that predicts the outcome of tumor patients treated with anti-PD1 or anti-CTLA4 and calculates the score by evaluating the degree of T cell dysfunction (59). The patients with a high score of TIDE imply a high possibility of tumor immune evasion and lower

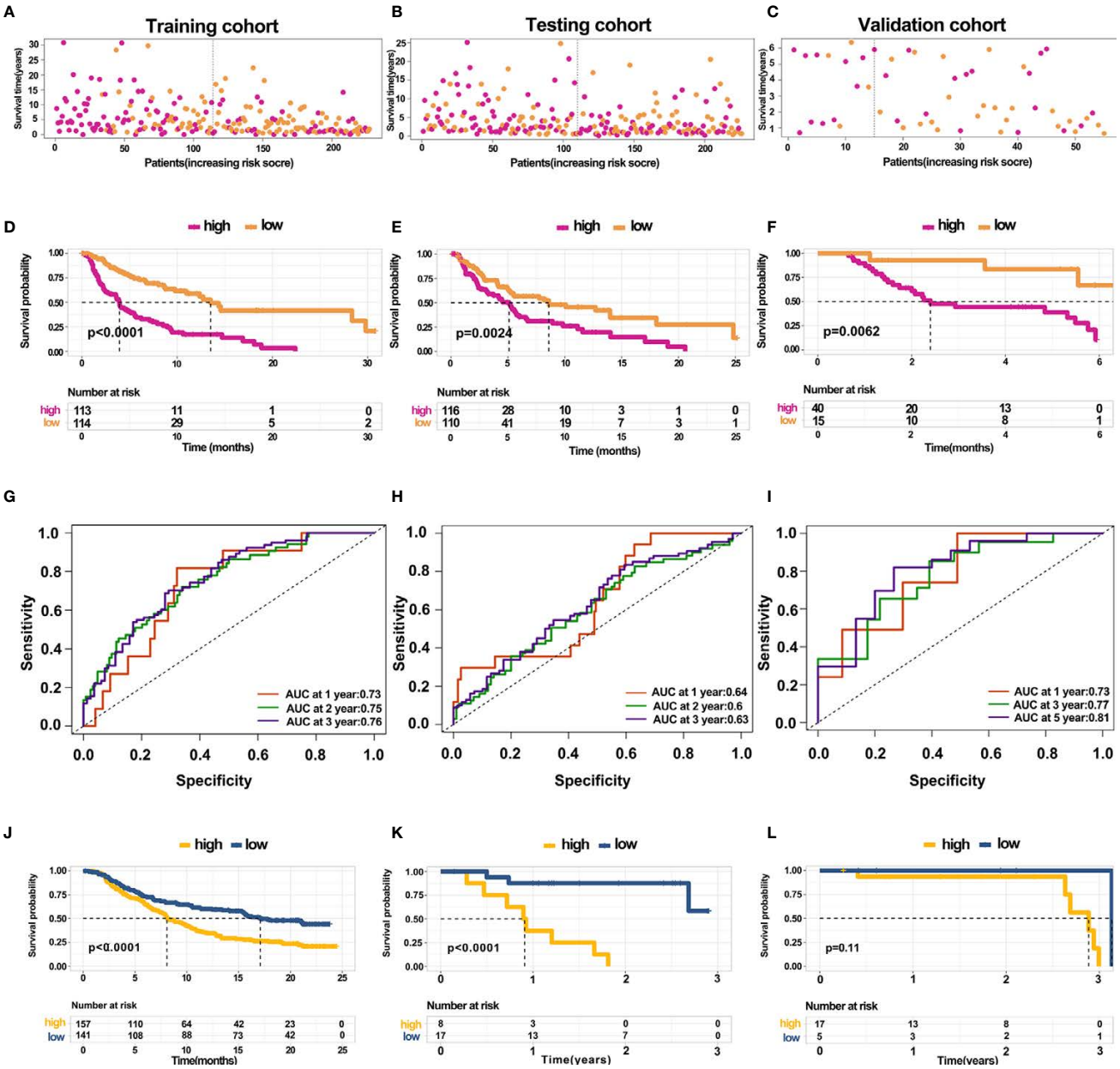

FIGURE 7 | Construction and validation of predicting model for overall survival **(A–C)** Distribution of survival time in the training cohort, testing cohort, and external validation cohort. **(D–F)** Kaplan-Meier survival curve showed the survival of patients with high and low risk in the training cohort, testing cohort, and external validation cohort. **(G–I)** AUC curve of 1, 3, and 5 years for training cohort, testing cohort, and external validation cohort. **(J–L)** Kaplan-Meier survival curve showed the survival of patients under immunotherapy treatment with low and high risk in bladder cancer and melanoma.

benefits from immunotherapy. In line with immune states across all the four clusters, clusters 4 and 3 had lower scores compared to clusters 1 and 2. Notably, the TIDE score of cluster 1, cluster 2, and cluster 3 had two clear subsets, particularly in cluster 2, indicating that these clusters still exits distinct subtypes and need further exploration. To explore the mechanisms of immune infiltration, the four clusters were divided into two major types, i.e., cold and hot tumors. We found that TYRP1 negatively correlated with CD8A expression. *In vitro* experiments revealed that the knockdown of TYRP1 promoted the expression of MHC class I. TYRP1 correlated with the formation of melanogenesis and was a cancer antigen of melanoma (60). Previous studies demonstrated that TYRP1 is linked to a poor clinical outcome for patients diagnosed with metastatic melanoma (61). Besides, it acts as a biomarker candidate for response and survival to checkpoint inhibitors in

melanoma patients (62). Nonetheless, the mechanism of TYRP1 in regulating the immune response warrants further investigation.

Eventually, a prediction model based on the DEGs between hot and cold tumors was constructed, and this model could predict the overall survival of patients with treatment naïve melanoma. The model comprises seven genes which can be easily detected and guide the clinical treatment of melanoma. Notably, we found that this model performed efficiently in predicting the survival of patients under immunotherapy. However, the model has a few limitations; first, we only used one data set as an external validation cohort with a limited number of patients. Secondly, an optimal cut-off of risk score was used to divide the patients into high and low-risk scores, potentially reducing the predictive performance of the model. Thirdly, this model did not apply to melanoma patients under all types of therapies.

CONCLUSION

In this conclusion, we performed a detailed analysis of immune infiltration in melanoma. Our findings revealed that patients with high immune infiltration had a better survival and immune response. Moreover, the knockdown of TYRP1 promoted the expression of MHC class I and serving as a potential target. We constructed a prediction model with seven genes, which performed effectively in predicting survival of treatment naïve melanoma patients or untreated with anti-PD1. This work provides an in-depth insight into immune infiltration and the prediction model can used to guide the treatment of patients with melanoma.

DATA AVAILABILITY STATEMENT

Publicly available datasets were analyzed in this study. This data can be found here: (https://xenabrowser.net/); GSE78220, GSE91061.

AUTHOR CONTRIBUTIONS

GL designed the experiments. GL and XZ performed the experiments and analyzed the data. XZ and CL conceived the work, analyzed the data, and prepared the manuscript. All authors critically revised the manuscript and agreed to be accountable for all aspects of the manuscript. All authors contributed to the article and approved the submitted version.

ACKNOWLEDGMENTS

This study had no grants to support. We thank the TCGA program for providing the RNA-sequencing data and clinical data of patients with melanoma.

SUPPLEMENTARY MATERIAL

The Supplementary Material for this article can be found online at: https://www.frontiersin.org/articles/10.3389/fonc.2021.639059/full#supplementary-material

Supplementary Figure 1 | Correlation of immune cells in primary and metastatic melanoma respectively. **(A–D)** Correlation analysis of immune cells in primary and metastatic tumor estimated by ssGSEA, CIBERSORT, TIMER, and MCP-Counter.

Supplementary Figure 2 | Heatmap showing the DEGs between hot and cold tumor.

Supplementary Figure 3 | Identification of prognostic related genes. **(A, B)** LASSO and partial likelihood deviance coefficient profiles of survival-related genes analyzed by univariate survival analysis. **(C)** Frost plots showed the HRs of selected genes by multivariate Cox analysis.

Supplementary Figure 4 | Construction and validation of predicting model. The expression of selected genes in high and low risk group in training cohort, testing cohort, and external validation cohort.

REFERENCES

1. Siegel RL, Miller KD, Jemal A. Cancer Statistics, 2017. *CA Cancer J Clin* (2017) 67(1):7–30. doi: 10.3322/caac.21387
2. Mackintosh JA. The antimicrobial properties of melanocytes, melanosomes and melanin and the evolution of black skin. *J Theor Biol* (2001) 211(2):101–13. doi: 10.1006/jtbi.2001.2331
3. Tyrrell H, Payne M. Combatting mucosal melanoma: recent advances and future perspectives. *Melanoma Manag* (2018) 5(3):Mmt11. doi: 10.2217/mmt-2018-0003
4. Wilkins DK, Nathan PD. Therapeutic opportunities in noncutaneous melanoma. *Ther Adv Med Oncol* (2009) 1(1):29–36. doi: 10.1177/1758834009337664
5. Curtin JA, Fridlyand J, Kageshita T, Patel HN, Busam KJ, Kutzner H, et al. Distinct sets of genetic alterations in melanoma. *N Engl J Med* (2005) 353 (20):2135–47. doi: 10.1056/NEJMoa050092
6. Xin Y, Huang Q, Zhang P, Yang M, Hou XY, Tang JQ, et al. Meta-Analysis of the Safety and Efficacy of Interferon Combined With Dacarbazine Versus Dacarbazine Alone in Cutaneous Malignant Melanoma. *Med (Baltimore)* (2016) 95(16):e3406. doi: 10.1097/MD.0000000000003406
7. Velho TR. Metastatic melanoma - a review of current and future drugs. *Drugs Context* (2012) 2012:212242. doi: 10.7573/dic.212242
8. Weiss SA, Wolchok JD, Sznol M. Immunotherapy of Melanoma: Facts and Hopes. *Clin Cancer Res* (2019) 25(17):5191–201. doi: 10.1158/1078-0432.CCR-18-1550
9. Riaz N, Havel JJ, Makarov V, Desrichard A, Urba WJ, Sims JS, et al. Tumor and Microenvironment Evolution during Immunotherapy with Nivolumab. *Cell* (2017) 171(4):934–49.e16. doi: 10.1016/j.cell.2017.09.028
10. Mellman I, Coukos G, Dranoff G. Cancer immunotherapy comes of age. *Nature* (2011) 480(7378):480–9. doi: 10.1038/nature10673
11. Brahmer J, Reckamp KL, Baas P, Crinò L, Eberhardt WE, Poddubskaya E, et al. Nivolumab versus Docetaxel in Advanced Squamous-Cell Non-Small-Cell Lung Cancer. *N Engl J Med* (2015) 373(2):123–35. doi: 10.1056/NEJMoa1504627
12. Ferris RL, Blumenschein GJr., Fayette J, Guigay J, Colevas AD, et al. Nivolumab for Recurrent Squamous-Cell Carcinoma of the Head and Neck. *N Engl J Med* (2016) 375(19):1856–67. doi: 10.1056/NEJMoa1602252
13. Marzagalli M, Ebelt ND, Manuel ER. Unraveling the crosstalk between melanoma and immune cells in the tumor microenvironment. *Semin Cancer Biol* (2019) 59:236–50. doi: 10.1016/j.semcancer.2019.08.002
14. Rizvi NA, Hellmann MD, Snyder A, Kvistborg P, Makarov V, Lee W, et al. Cancer immunology. Mutational landscape determines sensitivity to PD-1 blockade in non-small cell lung cancer. *Science* (2015) 348(6230):124–8. doi: 10.1126/science.aaa1348

15. Genomic Classification of Cutaneous Melanoma. *Cell* (2015) 161(7):1681–96. doi: 10.1016/j.cell.2015.05.044
16. Rosenberg JE, Hoffman-Censits J, Powles T, van der Heijden MS, Balar AV, Bellmunt J, et al. Atezolizumab in patients with locally advanced and metastatic urothelial carcinoma who have progressed following treatment with platinum-based chemotherapy: a single-arm, multicentre, phase 2 trial. *Lancet* (2016) 387 (10031):1909–20. doi: 10.1016/S0140-6736(16)32455-2
17. Spranger S, Bao R, Gajewski TF. Melanoma-intrinsic β-catenin signalling prevents anti-tumour immunity. *Nature* (2015) 523(7559):231–5. doi: 10.1038/nature14404
18. Luke JJ, Flaherty KT, Ribas A, Long GV. Targeted agents and immunotherapies: optimizing outcomes in melanoma. *Nat Rev Clin Oncol* (2017) 14(8):463–82. doi: 10.1038/nrclinonc.2017.43
19. Hogan SA, Levesque MP, Cheng PF, Lao CD. Melanoma Immunotherapy: Next-Generation Biomarkers. *Front Oncol* (2018) 8:178. doi: 10.3389/fonc.2018.00178
20. Wolchok JD, Chiarion-Sileni V, Gonzalez R, Rutkowski P, Grob JJ, Lao CD, et al. Overall Survival with Combined Nivolumab and Ipilimumab in Advanced Melanoma. *N Engl J Med* (2017) 377(14):1345–56. doi: 10.1056/NEJMoa1910836
21. Hodi FS, Chiarion-Sileni V, Gonzalez R, Grob JJ, Rutkowski P, et al. Nivolumab plus ipilimumab or nivolumab alone versus ipilimumab alone in advanced melanoma (CheckMate 067): 4-year outcomes of a multicentre, randomised, phase 3 trial. *Lancet Oncol* (2018) 19(11):1480–92. doi: 10.1016/S1470-2045(18)30700-9
22. Hamid O, Robert C, Daud A, Hodi FS, Ribas A. Five-year survival outcomes for patients with advanced melanoma treated with pembrolizumab in KEYNOTE-001. *Ann Oncol* (2019) 30(4):582–8. doi: 10.1093/annonc/mdz011
23. Pérez-Ruiz E, Melero I, Kopecka J, Sarmento-Ribeiro AB, García-Aranda M, De Las Rivas J. Cancer immunotherapy resistance based on immune checkpoints inhibitors: Targets, biomarkers, and remedies. *Drug Resist Update* (2020) 53:100718. doi: 10.1016/j.drup.2020.100718
24. Tumeh PC, Harview CL, Yearley JH, Shintaku IP, Taylor EJ, et al. PD-1 blockade induces responses by inhibiting adaptive immune resistance. *Nature* (2014) 515(7528):568–71. doi: 10.1038/nature13954
25. Hugo W, Zaretsky JM, Sun L, Song C, Moreno BH, Hu-Lieskovan S, et al. Genomic and Transcriptomic Features of Response to Anti-PD-1 Therapy in Metastatic Melanoma. *Cell* (2016) 165(1):35–44. doi: 10.1016/j.cell.2016.02.065
26. Pitt JM, Marabelle A, Eggermont A, Soria JC, Kroemer G, Zitvogel L. Targeting the tumor microenvironment: removing obstruction to anticancer immune responses and immunotherapy. *Ann Oncol* (2016) 27(8):1482–92. doi: 10.1093/annonc/mdw168
27. Roma-Rodrigues C, Mendes R, Baptista PV, Fernandes AR. Targeting Tumor Microenvironment for Cancer Therapy. *Int J Mol Sci* (2019) 20(4). doi: 10.3390/ijms20040840
28. Wu T, Dai Y. Tumor microenvironment and therapeutic response. *Cancer Lett* (2017) 387:61–8. doi: 10.1016/j.canlet.2016.01.043
29. Veglia F, Perego M, Gabrilovich D. Myeloid-derived suppressor cells coming of age. *Nat Immunol* (2018) 19(2):108–19. doi: 10.1038/s41590-017-0022-x
30. De Palma M, Biziato D, Petrova TV. Microenvironmental regulation of tumour angiogenesis. *Nat Rev Cancer* (2017) 17(8):457–74. doi: 10.1038/nrc.2017.51
31. Togashi Y, Shitara K, Nishikawa H. Regulatory T cells in cancer immunosuppression - implications for anticancer therapy. *Nat Rev Clin Oncol* (2019) 16(6):356–71. doi: 10.1038/s41571-019-0175-7
32. Goldman MJ, Craft B, Hastie M, Repečka K, McDade F, Kamath A, et al. Visualizing and interpreting cancer genomics data via the Xena platform. *Nat Biotechnol* (2020) 38(6):675–8. doi: 10.1038/s41587-020-0546-8
33. Mariathasan S, Turley SJ, Nickles D, Castiglioni A, Yuen K, Wang Y, et al. TGFβ attenuates tumour response to PD-L1 blockade by contributing to exclusion of T cells. *Nature* (2018) 554(7693):544–8. doi: 10.1038/nature25501
34. Hugo W, Zaretsky JM, Sun L, Song C, Moreno BH, Hu-Lieskovan S, et al. Genomic and Transcriptomic Features of Response to Anti-PD-1 Therapy in Metastatic Melanoma. *Cell* (2017) 168(3):542. doi: 10.1016/j.cell.2017.01.010
35. Subramanian A, Tamayo P, Mootha VK, Mukherjee S, Ebert BL, Gillette MA, et al. Gene set enrichment analysis: A knowledge-based approach for interpreting genome-wide expression profiles. *Proc Natl Acad Sci* (2005) 102(43):15545–50. doi: 10.1073/pnas.0506580102
36. Newman AM, Liu CL, Green MR, Gentles AJ, Feng W, Xu Y, et al. Robust enumeration of cell subsets from tissue expression profiles. *Nat Methods* (2015) 12(5):453–7. doi: 10.1038/nmeth.3337
37. Li T, Fan J, Wang B, Traugh N, Chen Q, Liu JS, et al. TIMER: A Web Server for Comprehensive Analysis of Tumor-Infiltrating Immune Cells. *Cancer Res* (2017) 77(21):e108–10. doi: 10.1158/0008-5472.CAN-17-0307
38. Becht E, Giraldo NA, Lacroix L, Buttard B, Elarouci N, Petitprez F, et al. Estimating the population abundance of tissue-infiltrating immune and stromal cell populations using gene expression. *Genome Biol* (2016) 17 (1):218. doi: 10.1186/s13059-016-1113-y
39. Bader GD, Hogue CWV. An automated method for finding molecular complexes in large protein interaction networks. *BMC Bioinf* (2003) 4(1):2. doi: 10.1186/1471-2105-4-2
40. Wilkerson MD, Hayes DN. ConsensusClusterPlus: a class discovery tool with confidence assessments and item tracking. (1367-4811 (Electronic)). doi: 10.1093/bioinformatics/btq170
41. Aponte-López A, Muñoz-Cruz S. Mast Cells in the Tumor Microenvironment. *Adv Exp Med Biol* (2020) 1273:159–73. doi: 10.1007/978-3-030-49270-0_9
42. Poklepovic AS, Luke JJ. Considering adjuvant therapy for stage II melanoma. *Cancer* (2020) 126(6):1166–74. doi: 10.1002/cncr.32585
43. Gajos-Michniewicz A, Czyz M. Role of miRNAs in Melanoma Metastasis. *Cancers (Basel)* (2019) 11(3):326. doi: 10.3390/cancers11030326
44. Rebecca VW, Sondak VK, Smalley KS. A brief history of melanoma: from mummies to mutations. *Melanoma Res* (2012) 22(2):114–22. doi: 10.1097/CMR.0b013e328351fa4d
45. Scolyer RA, Long GV, Thompson JF. Evolving concepts in melanoma classification and their relevance to multidisciplinary melanoma patient care. *Mol Oncol* (2011) 5(2):124–36. doi: 10.1016/j.molonc.2011.03.002
46. Persi E, Wolf YI, Leiserson MDM, Koonin EV, Ruppin E. Criticality in tumor evolution and clinical outcome. *Proc Natl Acad Sci USA* (2018) 115(47): E11101–e11110. doi: 10.1073/pnas.1807256115
47. Schoenfeld AJ, Hellmann MD. Acquired Resistance to Immune Checkpoint Inhibitors. *Cancer Cell* (2020) 37(4):443–55. doi: 10.1016/j.ccell.2020.03.017
48. Sanlorenzo M, Vujic I, Posch C, Dajee A, Yen A, Kim S, et al. Melanoma immunotherapy. *Cancer Biol Ther* (2014) 15(6):665–74. doi: 10.4161/cbt.28555
49. Vojvodic A, Vlaskovic-Jovicevic T, Vojvodic P, Vojvodic J, Goldust M, Peric-Hajzler Z, et al. Melanoma and Mastocytosis. *Open Access Maced J Med Sci* (2019) 7(18):3050–2. doi: 10.3889/oamjms.2019.772
50. Capo A, Goteri G, Mozzicafreddo G, Serresi S, Giacchetti A. Melanoma and mastocytosis: is really only a coincidence? *Clin Exp Dermatol* (2019) 44(1):76–7. doi: 10.1111/ced.13717
51. Donati P, Paolino G, Donati M, Panetta C. Cutaneous mastocytosis combined with eruptive melanocytic nevi and melanoma. Coincidence or a linkage in the pathogenesis? *J Dermatol Case Rep* (2014) 8(3):70–4. doi: 10.3315/jdcr.2014.1179
52. Kurihara-Shimomura M, Sasahira T, Shimomura H, Bosserhoff AK, Kirita T. Mast cell chymase promotes angiogenesis and lymphangiogenesis mediated by activation of melanoma inhibitory activity gene family members in oral squamous cell carcinoma. *Int J Oncol* (2020) 56(5):1093–100. doi: 10.3892/ijo.2020.4996
53. Grimbaldeston MA, Pearce AL, Robertson BO, Coventry BJ, Marshman G, Finlay-Jones JJ, et al. Association between melanoma and dermal mast cell prevalence in sun-unexposed skin. *Br J Dermatol* (2004) 150(5):895–903. doi: 10.1111/j.1365-2133.2004.05966.x
54. Jeong HJ, Oh HA, Nam SY, Han NR, Kim YS, et al. The critical role of mast cell-derived hypoxia-inducible factor-1α in human and mice melanoma growth. *Int J Cancer* (2013) 132(11):2492–501. doi: 10.1002/ijc.27937
55. Saakyan SV, Zakharova GP, Myakoshina EB. [Mast cells in the microenvironment of uveal melanoma]. *Arkh Patol* (2019) 81(6):63–70. doi: 10.17116/patol20198106163
56. Li B, Severson E, Pignon JC, Zhao H, Li T, Novak J, et al. Comprehensive analyses of tumor immunity: implications for cancer immunotherapy. *Genome Biol* (2016) 17(1):174. doi: 10.1186/s13059-016-1028-7
57. Wang J, Chong KK, Nakamura Y, Nguyen L, Huang SK, Kuo C, et al. B7-H3 associated with tumor progression and epigenetic regulatory activity in cutaneous melanoma. *J Invest Dermatol* (2013) 133(8):2050–8. doi: 10.1038/jid.2013.114
58. Flem-Karlsen K, Tekle C, Andersson Y, Flatmark K, Fodstad Ø, Nunes-Xavier CE, et al. Immunoregulatory protein B7-H3 promotes growth and decreases

sensitivity to therapy in metastatic melanoma cells. *Pigment Cell Melanoma Res* (2017) 30(5):467–76. doi: 10.1111/pcmr.12599
59. Jiang P, Gu S, Pan D, Fu J, Sahu A, Hu X, et al. Signatures of T cell dysfunction and exclusion predict cancer immunotherapy response. *Nat Med* (2018) 24 (10):1550–8. doi: 10.1038/s41591-018-0136-1
60. Zhu ML, Nagavalli A, Su MA. Aire deficiency promotes TRP-1-specific immune rejection of melanoma. *Cancer Res* (2013) 73(7):2104–16. doi: 10.1158/0008-5472.CAN-12-3781
61. Gautron A, Migault M, Bachelot L, Corre S, Galibert MD, Gilot D, et al. Human TYRP1: two functions for a single gene? *Pigment Cell Melanoma Res* (2020). doi: 10.1111/pcmr.12951
62. Fässler M, Diem S, Mangana J, Hasan Ali O, Berner F, Bomze D, et al. Antibodies as biomarker candidates for response and survival to checkpoint inhibitors in melanoma patients. *J Immunother Cancer* (2019) 7(1):50. doi: 10.1186/s40425-019-0523-2

Conflict of Interest: The authors declare that the research was conducted in the absence of any commercial or financial relationships that could be construed as a potential conflict of interest.

Copyright © 2021 Li, Zhu and Liu. This is an open-access article distributed under the terms of the Creative Commons Attribution License (CC BY). The use, distribution or reproduction in other forums is permitted, provided the original author(s) and the copyright owner(s) are credited and that the original publication in this journal is cited, in accordance with accepted academic practice. No use, distribution or reproduction is permitted which does not comply with these terms.

frontiers in Immunology

ORIGINAL RESEARCH
published: 07 April 2021
doi: 10.3389/fimmu.2021.653836

Identification of Prognostic Genes in the Tumor Microenvironment of Hepatocellular Carcinoma

Shixin Xiang[1,2†], Jing Li[3†], Jing Shen[1,2], Yueshui Zhao[1,2], Xu Wu[1,2], Mingxing Li[1,2], Xiao Yang[1], Parham Jabbarzadeh Kaboli[1,2], Fukuan Du[1,2], Yuan Zheng[4], Qinglian Wen[5], Chi Hin Cho[1,2,6], Tao Yi[7] and Zhangang Xiao[1,8]**

[1] Laboratory of Molecular Pharmacology, Department of Pharmacology, School of Pharmacy, Southwest Medical University, Luzhou, China, [2] South Sichuan Institute of Translational Medicine, Luzhou, China, [3] Department of Oncology and Hematology, Hospital (T.C.M) Affiliated to Southwest Medical University, Luzhou, China, [4] Neijiang Health and Health Vocational College, Neijiang, China, [5] Department of Oncology, Affiliated Hospital of Southwest Medical University, Luzhou, China, [6] Faculty of Medicine, School of Biomedical Sciences, The Chinese University of Hong Kong, Hong Kong, China, [7] School of Chinese Medicine, Hong Kong Baptist University, Hong Kong, China, [8] Department of Pharmacy, The Affiliated Hospital of Southwest Medical University, Luzhou, China

OPEN ACCESS

Edited by:
Huanfa Yi,
Jilin University, China

Reviewed by:
Zheng Liu,
Virginia Commonwealth University, United States
Tao Su,
Guangzhou University of Chinese Medicine, China

***Correspondence:**
Zhangang Xiao
xzg555898@hotmail.com
Tao Yi
yitao@hkbu.edu.hk

[†] These authors have contributed equally to this work

Specialty section:
This article was submitted to Cancer Immunity and Immunotherapy, a section of the journal Frontiers in Immunology

Received: 15 January 2021
Accepted: 10 February 2021
Published: 07 April 2021

Citation:
Xiang S, Li J, Shen J, Zhao Y, Wu X, Li M, Yang X, Kaboli PJ, Du F, Zheng Y, Wen Q, Cho CH, Yi T and Xiao Z (2021) Identification of Prognostic Genes in the Tumor Microenvironment of Hepatocellular Carcinoma. Front. Immunol. 12:653836. doi: 10.3389/fimmu.2021.653836

Background: Hepatocellular carcinoma (HCC) is one of the most common malignant tumors in the world. The efficacy of immunotherapy usually depends on the interaction of immunomodulation in the tumor microenvironment (TME). This study aimed to explore the potential stromal-immune score-based prognostic genes related to immunotherapy in HCC through bioinformatics analysis.

Methods: ESTIMATE algorithm was applied to calculate the immune/stromal/Estimate scores and tumor purity of HCC using the Cancer Genome Atlas (TCGA) transcriptome data. Functional enrichment analysis of differentially expressed genes (DEGs) was analyzed by the Database for Annotation, Visualization, and Integrated Discovery database (DAVID). Univariate and multivariate Cox regression analysis and least absolute shrinkage and selection operator (LASSO) regression analysis were performed for prognostic gene screening. The expression and prognostic value of these genes were further verified by KM-plotter database and the Human Protein Atlas (HPA) database. The correlation of the selected genes and the immune cell infiltration were analyzed by single sample gene set enrichment analysis (ssGSEA) algorithm and Tumor Immune Estimation Resource (TIMER).

Results: Data analysis revealed that higher immune/stromal/Estimate scores were significantly associated with better survival benefits in HCC within 7 years, while the tumor purity showed a reverse trend. DEGs based on both immune and stromal scores primarily affected the cytokine–cytokine receptor interaction signaling pathway. Among the DEGs, three genes (CASKIN1, EMR3, and GBP5) were found most significantly associated with survival. Moreover, the expression levels of CASKIN1, EMR3, and GBP5 genes were significantly correlated with immune/stromal/Estimate scores or tumor purity and multiple immune cell infiltration. Among them, GBP5 genes were highly related to immune infiltration.

Conclusion: This study identified three key genes which were related to the TME and had prognostic significance in HCC, which may be promising markers for predicting immunotherapy outcomes.

Keywords: tumor microenvironment, Hepatocellular carcinoma, TCGA, ESTIMATE algorithm, Prognosis

INTRODUCTION

Hepatocellular carcinoma (HCC), one of the digestive tract cancers, is also the most common primary liver cancer (1). Hepatocarcinogenesis is a multistep and complex biological process in which many signaling cascades are altered, resulting in heterogeneous molecular profiles and ultimately in tumorigenesis, progression, and metastasis (2). Surgical treatment and chemotherapy are the main therapies for HCC (3), but incidence rates of HCC are continuing to grow, and the probability is rising faster than any other cancer in both men and women (4). A systematic analysis for the Global Burden of Disease Study (GBD) has shown that the incidence and mortality of HCC rank among the top 10 cancers, and death in adults with cirrhosis is the leading cause for the mortality of HCC (5). With the improvement of medical standards, the treatment of HCC has indeed made progress. But currently, HCC treatment is still a global research hotspot, and more and more attention has been paid to cancer immunotherapy, one of the most promising methods for cancer treatment (6). Besides, studies have shown that immune tolerance and escape in the immunosuppressive microenvironment of HCC can be promoted by multiple mechanisms (7, 8). Therefore, it is essential to understand the microenvironment of HCC.

The tumor microenvironment (TME), which is comprised of a mixture of immune cells, stromal cells, cancer cells, the intricate cytokine and chemokines environment, and other components (6, 9), is a dynamic system. Immune cells and stromal cells within the TME are the two main types of non-tumor components which are considered to play important role in the diagnosis and prognosis of tumors (10). Evidence from studies indicates that stromal cells within the TME are genetically stable and are attractive therapeutic targets with reduced risk of resistance and tumor recurrence (11). In addition, due to the dysregulation of the metabolic activity of tumor cells, tumor-infiltrating immune cells usually experience metabolic stress, resulting in an impaired anti-tumor immune response (12). A multi-target approach that simultaneously suppresses TME components may provide a more effective method of treating cancer (13). Therefore, understanding the TME is critical for inhibiting tumorigenesis, invasion, and metastasis, and in effectively managing the immune response (14–16).

Bioinformatics resolve the problems of biology through the methods of applied mathematics, informatics, statistics, and computer science (17, 18). At the same time, with the growth of the amount of biological tumor data, bioinformatics is essential for the storage, analysis, and visualization of cancer immunotherapy data (19, 20). Its rapid development has provided a user-friendly and convenient platform for researchers, guiding the implementation of basic experiments (21, 22). In 2013, Yoshihara et al. created a method to infer the ratio of stromal cells and immune cells in malignant tumors through gene expression signatures that can be derived from The Cancer Genome Atlas (TCGA)–ESTIMATE algorithm. In addition, the algorithm can also predict tumor purity, which helps understand the influence of the microenvironment on neoplastic cells (23). Researchers have extensively verified and confirmed the accuracy of the prediction. In recent years, the ESTIMATE algorithm has been applied to glioblastoma (10), gastric cancer (16), clear cell renal cell carcinoma (9), colon cancer (24), and so on. However, the application of HCC remains to be elucidated.

In this study, we obtained transcriptome data of HCC from the TCGA database, and analyzed the immune/stromal/Estimate scores and tumor purity within the microenvironment using the ESTIMATE algorithm. The relationship between immune/stromal/Estimate scores and tumor purity with survival and clinical parameters were explored. Hub genes associated with immune and stromal scores and with prognostic values were chosen.

MATERIALS AND METHODS

Data Processing

RNA sequencing (RNA-Seq) and clinicopathological data of patients with HCC were downloaded from Genomic Data Commons

(GDC) database (https://portal.gdc.cancer.gov/) (25, 26). About 374 tumor samples were used for the analysis. ESTIMATE algorithm was used to calculate the stromal/immune/Estimate scores and tumor purity using "estimate" package through the R project (http://r-forge.r-project.org; repos=rforge, dependencies=TRUE) (23). The Human Protein Atlas (HPA) (https://www.proteinatlas.org/about/download) was used to verify the immunohistochemistry staining of genes. Kaplan–Meier plotter (http://kmplot.com/analysis/) was applied to assess the prognostic value of the biomarkers.

Differential Expression Analysis

The median was set as the cut-off value of the immune and stromal scores. Patient samples were divided into two groups, respectively, namely the high-score group and the low-score group. Differential expression analysis was analyzed on the matrix of the sample using the R package, LIMMA. The filtering conditions for the differential genes were as follows: Fold Change $> |\pm 1|$, with adjusted $p < 0.05$.

Enrichment Analysis

The differentially expressed genes (DEGs) from differential expression analysis that meet the conditions were used for enrichment analysis, including Kyoto Encyclopedia of Genes and Genomes (KEGG) and Gene Ontology (GO) enrichment analysis *via* Database for Annotation, Visualization, and Integrated Discovery database (DAVID) function annotation tool (https://david.ncifcrf.gov) (27). GO contains biological processes (BPs), cell components (CCs), and molecular functions (MFs), and the signaling pathways were identified by considering both *p*-value and count number.

Prognostic Gene Selection by Cox Regression Analysis and Least Absolute Shrinkage and Selection Operator (LASSO)

In order to select the survival-related genes, univariate Cox regression analysis was performed on DEGs. At the same time, in order to prevent overfitting and increase the credibility of selecting core genes, we used the least absolute shrinkage and selection operator (LASSO) Cox regression model for signature construction (28, 29). LASSO regression modeling was conducted using the R package, glmnet (30). Finally, multivariable Cox regression analyses were used for feature selection, and calculating hazard ratios (HRs) with 95% confidence intervals (CIs) (31). Genes with $p < 0.05$ was chosen for further analysis.

Tumor Immune Infiltration Through RNA-Sequencing Expression Profiling Data

Single sample gene set enrichment analysis (ssGSEA) algorithm (https://doi.org/10.1016/j.celrep.2016.12.019, https://doi.org/10.21203/rs.3.rs-33230/v1) is scored based on 29 published immune-related genes (the immune gene set includes immune cell types, functions, and pathways) to quantify the immune infiltration level of 29 immune signatures in each HCC sample using the R package, GSVA (32), and the scores were standardized for each individual immune cell type. Besides, Tumor Immune Estimation Resource (TIMER, https://cistrome.shinyapps.io/timer/) was used to analyze the correlation between six kinds of tumor-infiltrating immune cells and selected hub genes.

Statistical Analysis

Student's *t*-test is analyzed for comparison between two groups and one-way ANOVA is used to compare multiple groups. Survival analysis was performed using Kaplan–Meier curve by using the R packages, such as survival and survminer, and the *p*-value was calculated using the log-rank test. Chi-square test was applied to test the association of the expression of the three hub genes with clinicopathological parameters. The value of $p < 0.05$ was considered statistically significant.

RESULTS

Stromal/Immune/Estimate Scores and Tumor Purity Were Significantly Associated With Prognosis and Tumor Mutation Burden

Transcriptome data and clinical information of HCC were downloaded from the TCGA database and integrated. Totally, 369 cancer samples were used for survival analysis (**Supplementary Table 1**). At the same time, in order to better understand the impact of tumor infiltrating immune and stromal cells on prognosis, we calculated the immune/stromal/Estimate scores and tumor purity based on the ESTIMATE algorithm, which helps to quantify the immune and stromal components in HCC. Sample information of overall survival (OS), disease-specific survival (DSS), disease-free interval (DFI), and progression-free interval (PFI) were collected (**Supplementary Table 2**). The results in **Figure 1A** showed that the four survival periods were significantly correlated with stromal/immune/Estimate scores and tumor purity. Elevated stromal, immune, and Estimate scores were significantly correlated with better prognosis, while higher tumor purity was significantly associated with poor patient survival rate. In addition, we also combined the clinicopathological parameters of HCC to analyze the correlation with immune score, stromal score, Estimate score, and tumor purity (**Supplementary Table 3**). As can be seen from **Supplementary Figure 1**, patients with metastasis tended to have higher immune and Estimate scores and lower tumor purity. For tumor and pathological stage, patients with increased stage tended to have high stromal, immune and Estimate score and lower tumor purity.

Tumor mutation burden (TMB) is the total number of somatic gene coding errors, base substitutions, gene insertion, or deletion errors detected per million bases (33). It is a quantitative biomarker that reflects the total number of mutations carried by tumor cells (34). In order to explore the relationship between TMB and immune/stromal/Estimate scores, tumor purity, and the mutation data of HCC from the TCGA database was downloaded for calculating the TMB. Then we divided the tumor samples into high and low groups according to the median of immune/stromal/Estimate scores and tumor purity, respectively. As can be seen from **Figure 1B**, TMB was significantly higher in the immune/stromal/Estimate scores in the low group, whereas it was higher in tumor purity in the high group.

DEGs Based on Immune and Stromal Scores and Their Associated Pathways Were Identified

To find out novel genes in HCC microenvironment associated with both immune and stromal scores, we performed RNA sequencing (RNA-Seq) differential expression analysis of 374 HCC cases from TCGA cohort. First, we grouped the samples based on the median of the immune score and the stromal score, and then we conducted a difference analysis between the high and low group samples. The DEGs were displayed in the

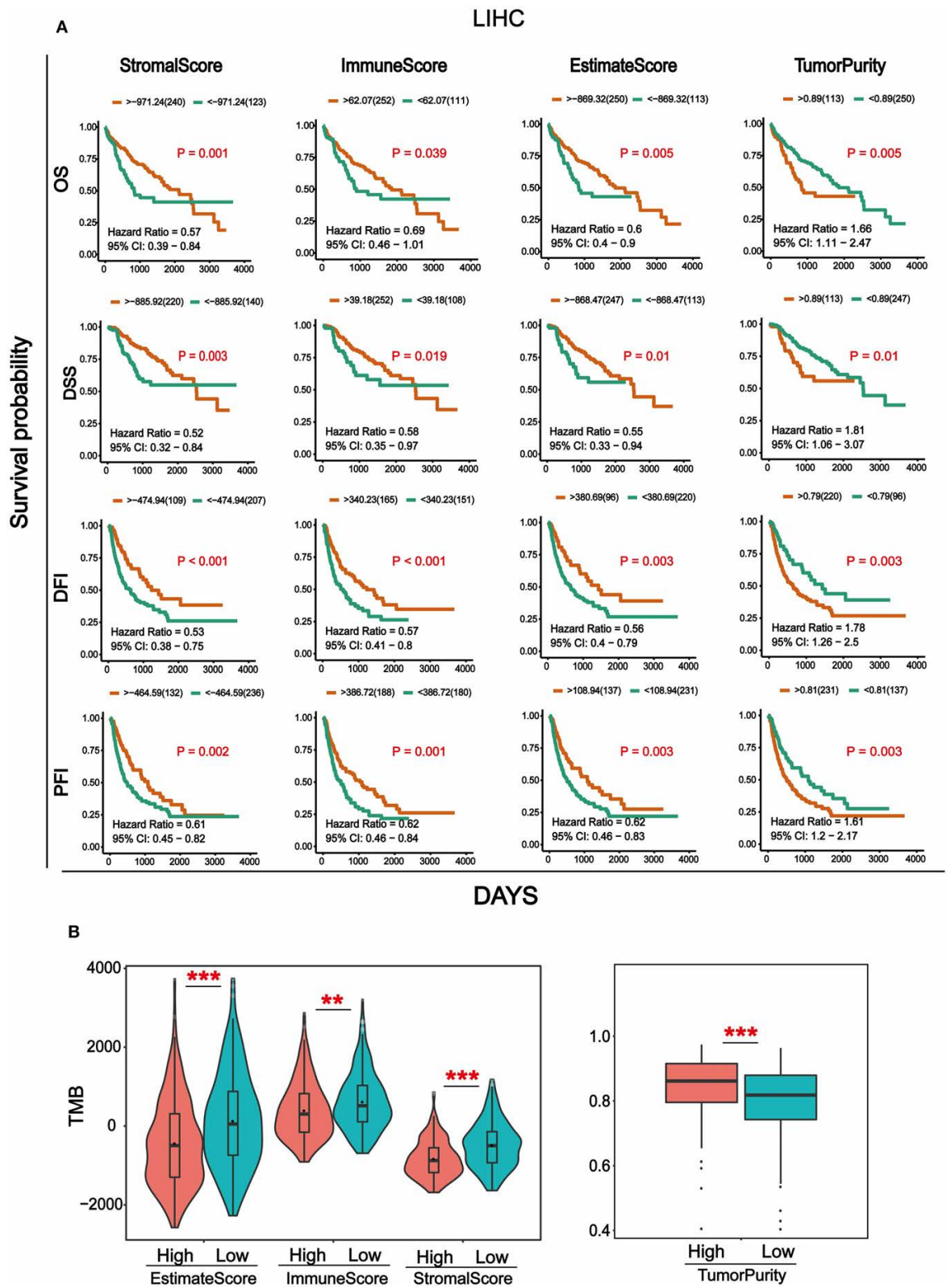

FIGURE 1 | Analysis of survival and Tumor mutation burden (TMB) associated with immune/stromal/Estimate scores and tumor purity. **(A)** Kaplan–Meier survival analysis based on immune/stromal/Estimate/scores and tumor purity. Overall survival (OS), disease-specific survival (DSS), disease-free interval (DFI), progression-free interval (PFI). **(B)** The relationship of immune/stromal/Estimate/scores and tumor purity with tumor mutation burden (TMB). The samples were divided into high and low groups according to the median of score. * $p < 0.05$, ** $p < 0.01$, and *** $p < 0.001$ between the two groups.

heatmap and volcano plot in **Figures 2A,B**. The results showed that there were 1,065 significantly upregulated genes and 105 significantly downregulated genes between high and low immune scores. Based on the difference analysis between the high and low stromal scores, 1,597 significantly upregulated genes and 112 significantly downregulated genes were obtained. By overlapping the DEGs of immune and stromal scores, we obtained a total of 896 genes (850 upregulated genes and 46 downregulated genes) for functional enrichment analysis including GO and KEGG (pathways; **Figure 2C**). The top 10 functional annotations of GO analysis are shown in **Figure 2D**. DEGs were mostly enriched in receptor activity, plasma membrane, and immune response. In addition, the enriched pathways of DEGs are displayed in **Figure 2D**. Considering the number of genes enriched in each pathway and the FDR value, the most important pathway was cytokine–cytokine receptor interaction (FDR = 4.24E-19). The interaction of DEGs enriched in the cytokine–cytokine receptor interaction signaling pathway is shown in **Figure 3**.

Identification and Validation of Optimal Prognostic Biomarkers in HCC

Through a well-known mathematical model, the prognostic DEGs related to the stromal–immune score that can be used as independent prognostic factors in patients with HCC was identified. We performed a univariate Cox regression analysis on the 896 DEGs related to both stromal and immune scores. Eighty-nine genes with a $p < 0.5$ were included for further analysis (**Supplementary Table 4**). To avoid overfitting the variables, 18 genes were screened using LASSO regression analysis (**Figure 4A**). Finally, three genes including guanylate binding protein 5 (GBP5), adhesion G protein-coupled receptor E3 (EMR3) and CASK interacting protein 1 (CASKIN1) were found significantly associated with HCC prognosis by multivariate Cox regression analysis (**Figure 4B**).

We then further verified the prognostic value of the three genes in Kaplan– Meier plotter. Survival analysis of OS, PFS, relapse-free survival (RFS), and DSS according to the expression level of the three genes were performed (**Figure 4C**). Our results showed that all three genes were significantly associated with the four survival parameters. High expression of the three genes predicted prolonged PFS, RFS, and DSS. High expression of EMR3 was also associated with better OS, while high expression of GBP5 was associated with better OS within 80 months and high expression of CASKIN1 was associated with worse OS before 80 months. To further validate the results, we downloaded and sorted out the GSE76427 gene expression and clinical data of a cohort of 115 HCC cases and 52 adjacent non-tumor tissue from the gene expression omnibus (GEO) database. In addition, we also collected the LIRI–JP dataset in the International Cancer Genome Consortium (ICGC) database, including 243 HCC samples and 202 adjacent samples. Similar to TCGA results, the expression of CASKIN1 gene in HCC is significantly higher than that of normal tissues, and the high expression of GBP5 gene is associated with good OS in the GEO and ICGC data analysis (**Supplementary Figure 2**).

The Expression Level of GBP5, EMR3, and CASKIN1 and Their Association With Clinicopathological Parameters in HCC

To further confirm the importance of GBP5, EMR3, and CASKIN1 in HCC, Human Protein Atlas (HPA) database was used to compare their protein expression in normal and HCC tissues. As demonstrated in **Figure 5A**, GBP5 and CASKIN1 were highly expressed in HCC tissue, while EMR3 was downregulated in HCC. At the same time, we also used TCGA database to compare their expression level. CASKIN1 and GBP5 mRNA expression level was significantly increased in HCC tissue compared to adjacent normal tissues, while significantly decreased EMR3 mRNA expression was found in HCC samples compared to normal samples (**Figure 5B**). Moreover, we also analyzed the association of the three genes with clinicopathological parameters of HCC according to the median of their expressions (**Figure 5C**). Low expression of EMR3 was often found in low tumor and pathological grade and there was increased proportion of its high expression in late stage. Similar result was observed for pathological stage and tumor grade for CASKIN1 expression.

The Association of GBP5, EMR3, and CASKIN1 Expression With Immune Cell Infiltration

After identifying the prognostic value and expression level of CASKIN1, EMR3, and GBP5, we performed correlation analysis between CASKIN1, EMR3, and GBP5 expression levels and immune/stromal/Estimate scores, and tumor purity in HCC, respectively. As shown in **Figure 6A**, CASKIN1 expression was negatively correlated with the immune/stromal/Estimate scores and positively correlated with tumor purity. In contrast, the expression of both EMR3 and GBP5 were positively correlated with immune/stromal/Estimate scores, while negatively correlated with tumor purity. Moreover, the association of GBP5 expression with immune/stromal/Estimate scores and tumor purity was stronger than the other two genes.

To study the relationship between the expression of the three genes and immune infiltration level for HCC, scatter plots are shown with partial Spearman's correlation and statistical significance in **Figure 6B**. The expression of GBP5 was significantly associated with purity ($R = -0.461$). In addition, elevated EMR3 and GBP5 were significantly correlated with B cell, CD4+ T cell, macrophage, neutrophil, and dendritic cell infiltration ($p < 0.05$) and a general increase in the immune infiltration level ($R > 0.3$). It is worth noting that there is a significant positive correlation between the infiltration levels of six kinds of immune cells and the GBP5 gene expression level. Then, based on the gene expression data, we enriched the proportion of 29 immune cells in each patient with HCC through the ssGSEA algorithm, and finally obtained the infiltration level of various immune cells. The correlation of the infiltration level of the immune cells with the expression levels of three genes was calculated. As shown in **Figure 6C**, the CASKIN1 gene was mainly negatively correlated with immune cell infiltration and the GBP5 gene showed a positive correlation with 29 immune

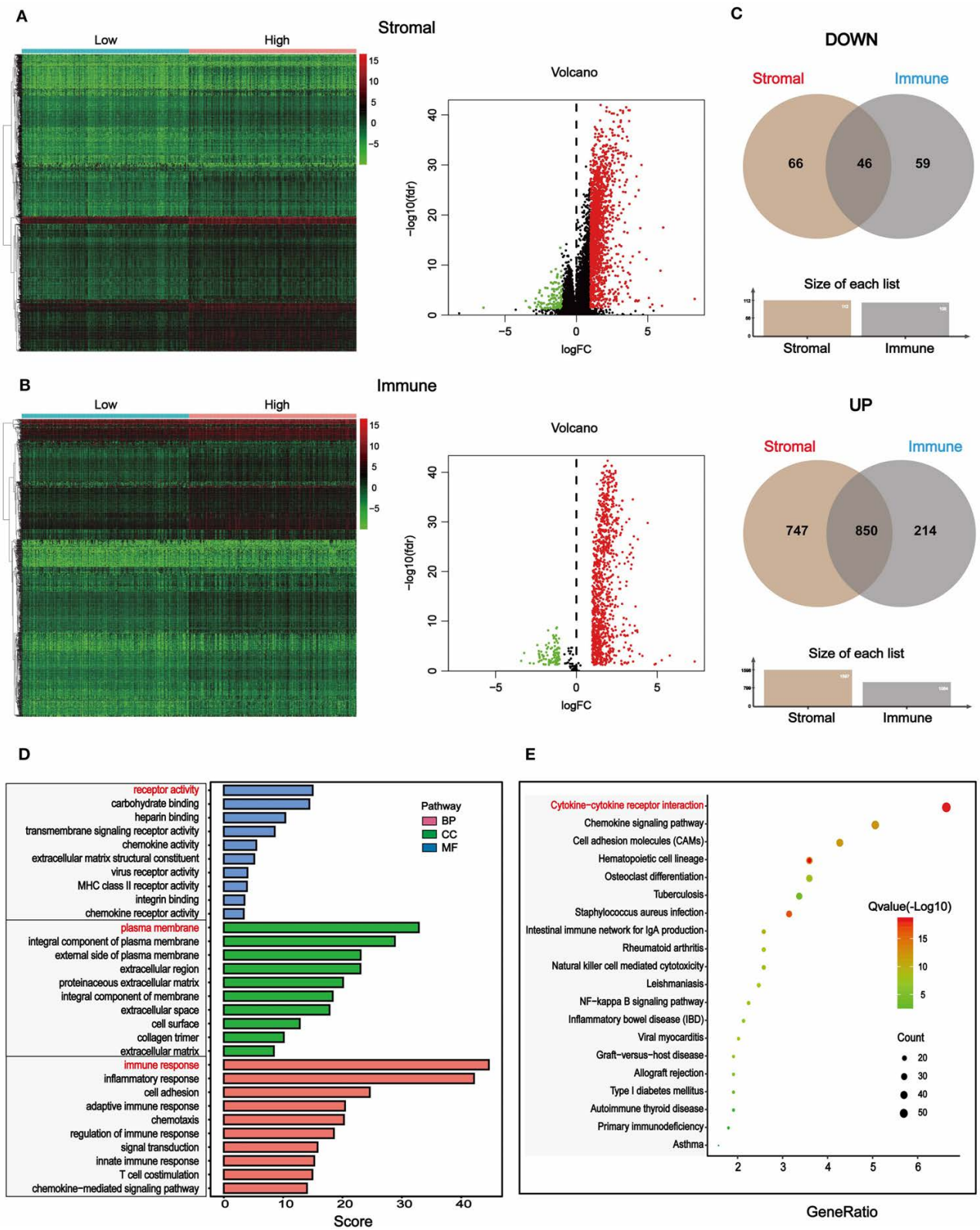

FIGURE 2 | Differentially expressed genes (DEGs) based on immune and stromal scores of tumor microenvironment (TME) and their functional annotations in HCC. **(A)** Heatmaps and volcano plot of the DEGs of stromal scores ($p < 0.05$, fold change > |±1|). **(B)** Heatmaps and volcano plot of the DEGs of immune scores ($p < 0.5$,

(Continued)

FIGURE 2 | fold change > |±1|). **(C)** 46 common downregulated genes and 850 common upregulated genes of both stromal and immune scores were shown by a Venn diagram, and a total of 896 significantly different genes were obtained. **(D)** The selected DEGs were used for Gene Ontology (GO)-enrichment analysis, biological process (BP), cellular component (CC), and molecular function (MF). Top 10 GO terms were displayed, respectively. **(E)** The selected DEGs were used for Kyoto Encyclopedia of Genes and Genomes (KEGG) enrichment analysis *via* Kyoto Encyclopedia of Genes and Genomes (DAVID). Considering both the *p*-value and count number, the optimal pathway was determined.

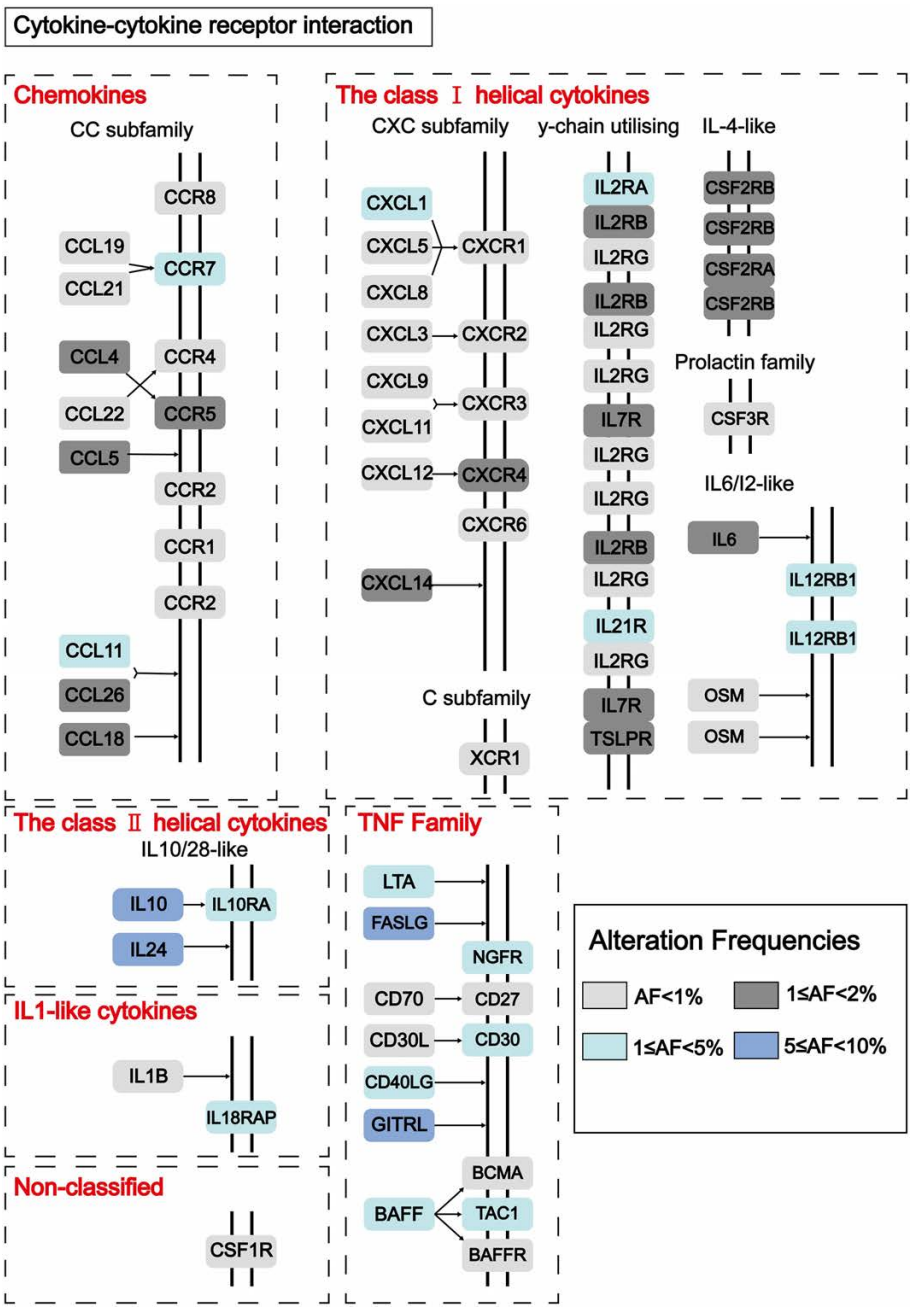

FIGURE 3 | Pathway diagram showing the interaction of DEGs in the cytokine–cytokine receptor interaction pathway. Alteration frequencies of each gene were represented by the color intensity.

cells and was highly correlated with 12 immune cells (R > 0.3), including T-cell co-inhibition, CD8+_T cells, check-point, inflammation-promoting, TIL, Th1 cells, APC co-inhibition, cytolytic activity, HLA, pDCs, Treg, and Th2 cells. EMR3 gene showed both positive and negative correlation with 29 immune cells.

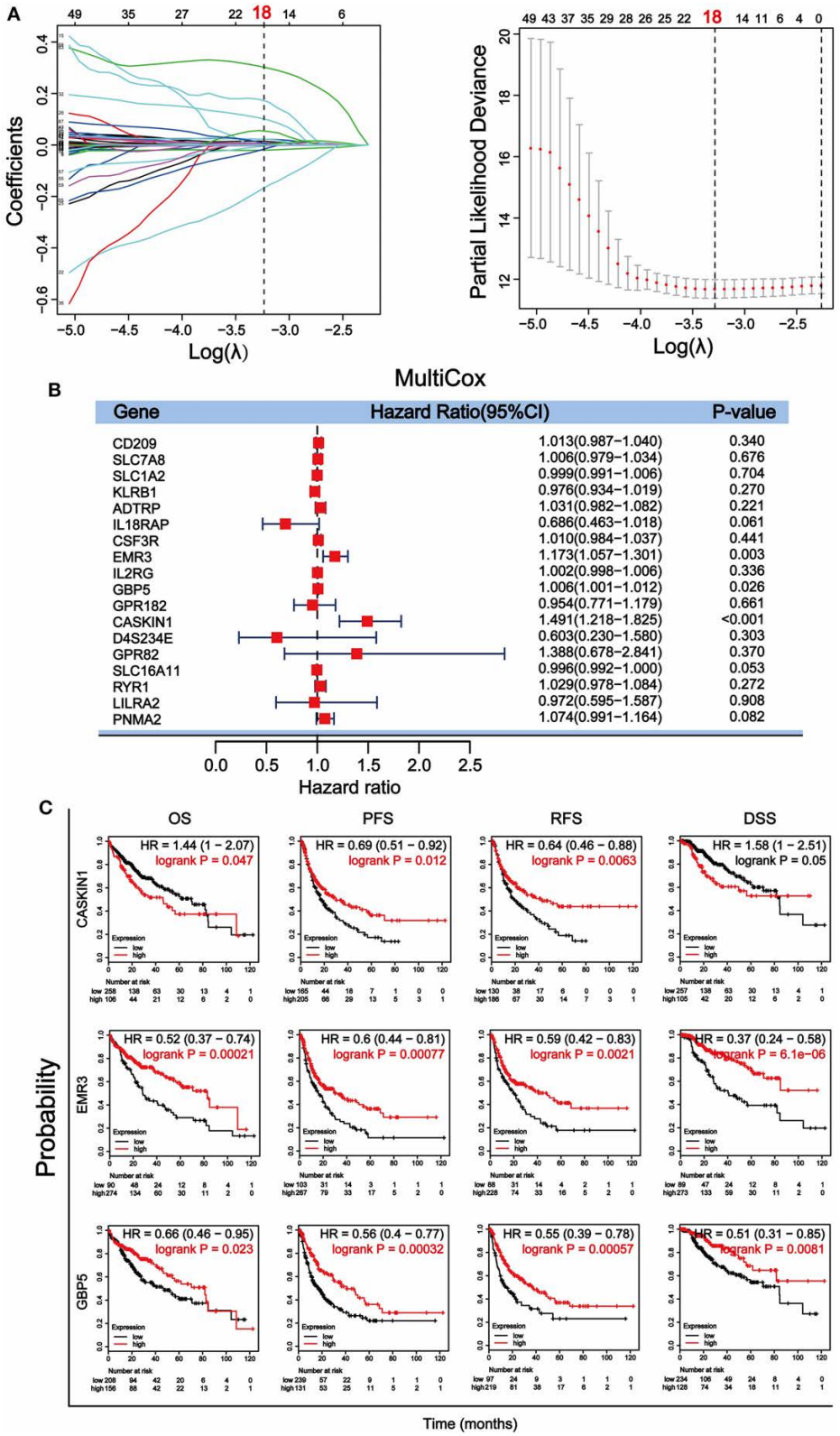

FIGURE 4 | Screening and verification of prognostic genes in HCC. **(A)** Least absolute shrinkage and selection operator (LASSO) regression analysis was used to screen for genetic variables. The dotted line indicates the number of genes after screening. **(B)** Multivariate Cox regression analysis was used to further screen genes that can be used as independent prognostic factors. The value, $p < 0.5$ was considered statistically significant. **(C)** Survival verification of the three selected genes by Kaplan–Meier plotter database in HCC. Prognostic indicators include overall survival (OS), progression-free survival (PFS), relapse-free survival (RFS), disease-specific survival (DSS).

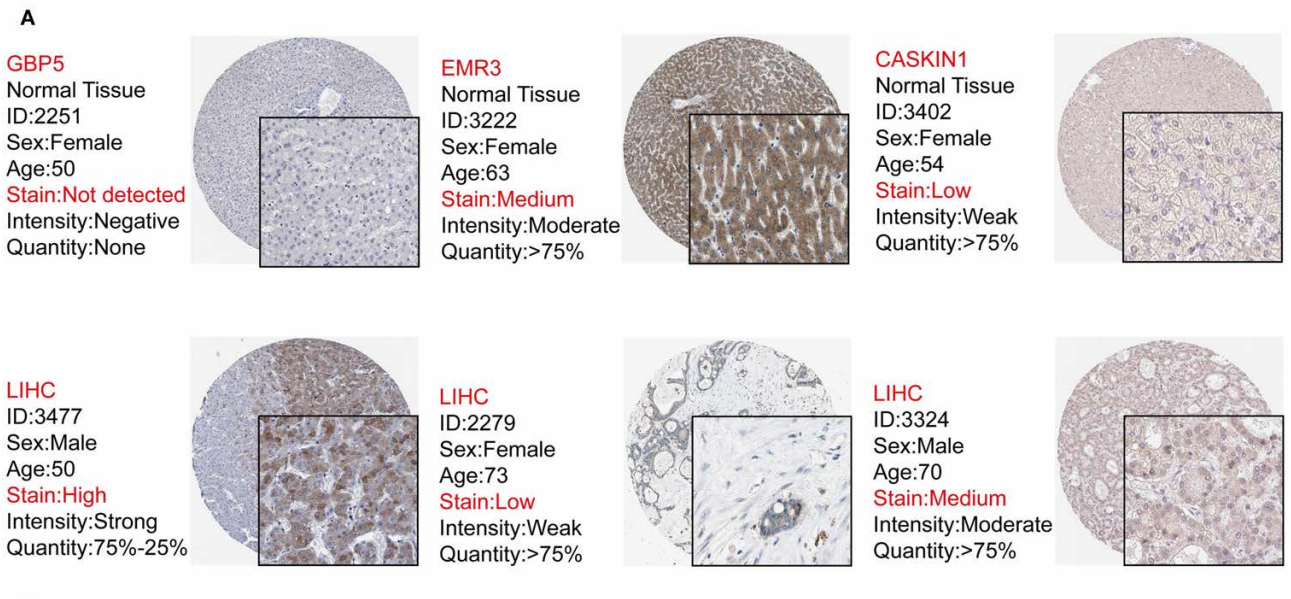

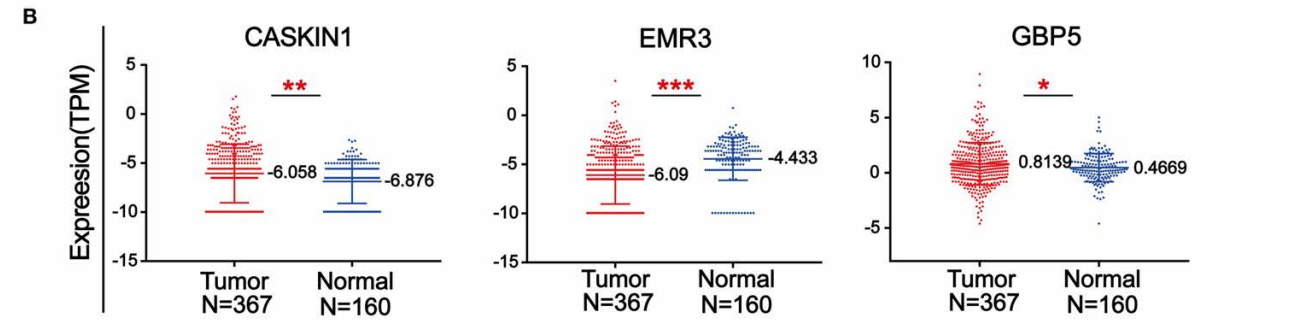

C

Parameter		EMR3 expression			GBP5 expression			CASKIN1 expression		
		Low	High	P value	Low	High	P value	Low	High	P value
OS	Alive	123	116	0.5334	116	123	0.3646	120	119	0.9130
	Dead	62	67		69	60		64	65	
Tumor	T1	103	78		88	93		101	80	
	T2	49	45	0.0030	46	48	0.5886	41	53	0.0711
	T3+T4	32	59		50	41		40	51	
Pathological Stage	Stage Ⅰ	97	74		83	88		97	74	
	Stage Ⅱ	46	40	0.0068	42	44	0.7412	36	50	0.0387
	Stage Ⅲ +Stage Ⅳ	32	56		47	41		39	49	
Grade	G1	35	20		32	23		31	24	
	G2	90	87	0.0613	92	85	0.1995	97	80	0.0148
	G3+G4	59	73		59	73		52	80	
Cancer status	Tumor Free	108	93	0.1697	93	108	0.1697	103	98	0.8665
	With Tumor	69	80		80	69		75	74	

FIGURE 5 | The expression level of three genes in HCC. **(A)** The immunohistochemistry (IHC) results from the Human Protein Atlas (HPA) was used to detect the protein level of three genes in normal and tumor tissues. **(B)** Comparison of the expression levels of CASKIN1, EMR3, and GBP5 genes in HCC tissues and adjacent normal tissues form the Cancer Genome Atlas (TCGA) database. The values of $^{*}p < 0.5$, $^{**}p < 0.01$, and $^{***}p < 0.001$ between the two groups. **(C)** Chi-square test of the clinical parameters according to the median of the expressions of the three genes.

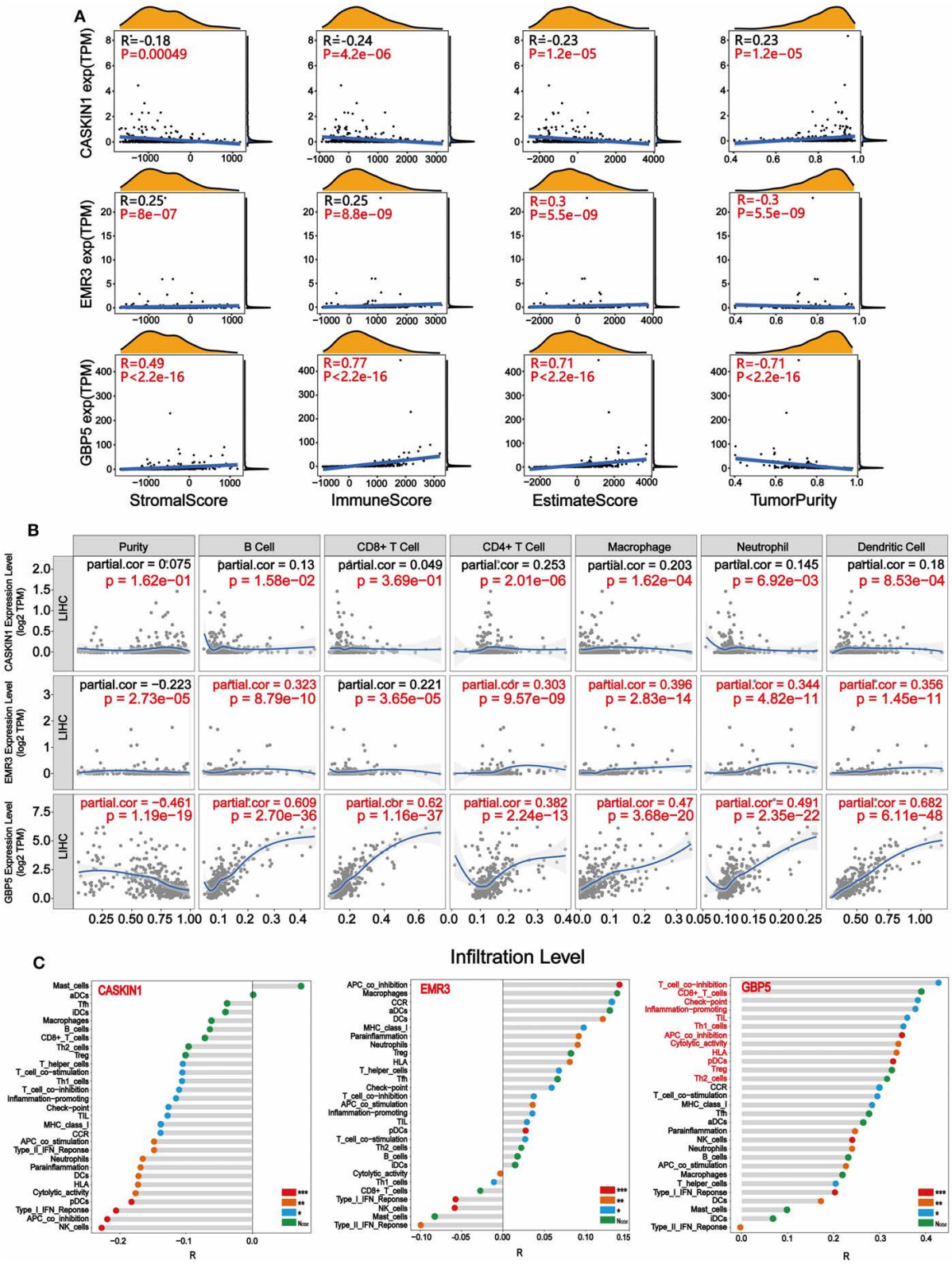

FIGURE 6 | Immune infiltration related to CASKIN1, EMR3, and GBP5. **(A)** Correlation analysis between CASKIN1, EMR3, and GBP5 mRNA expression levels and immune/stromal/Estimate scores and tumor purity in hepatocellular carcinoma (HCC). **(B)** The relationship between the CASKIN1, EMR3, and GBP5 gene expression

(Continued)

FIGURE 6 | and the infiltration level of six types of immune cells in HCC *via* Tumor Immune Estimation Resource (TIMER) database. Partial Spearman's correlation and statistical analysis were performed. **(C)** Single sample gene set enrichment analysis (ssGSEA) algorithm was used to obtain the immune-infiltration levels of 29 immune cells. The correlation between the expression levels of CASKIN1, EMR3, and GBP5 expression levels and the infiltration levels of 29 immune cells was displayed using Lollipop Chart.

DISCUSSION

A large number of studies have shown that the TME plays a significant role in the occurrence, development, and metastasis of tumors (11, 13, 35). With the rapid development of bioinformatics based on tumor immunotherapy and microarray sequencing, researchers are increasingly using statistical algorithms to explore new targets for immunotherapy of HCC (19, 36, 37), including ESTIMATE algorithm, and some progress has been made (38–41).

In this study, the ESTIMATE algorithm was used to obtain the immune/stromal/Estimate scores and tumor purity of TME in (HCC). To explore the impact of the immune/stromal/Estimate scores and tumor purity on survival, we collected four types of survival data: OS, DSS, DPI, and PFI. The results showed that the differential immune/stromal/Estimate scores and tumor purity scores significantly affect survival rates. Remarkably, the high score groups of stromal/immune/Estimate scores were significantly associated with longer OS in patients with HCC among the four survival types within 7 years (**Figure 1A**). These findings are consistent with previous studies showing that the immune/stromal scores were significantly related to OS (40, 42). Findings in multiple cancer types revealed that TMB may play an important role in tumor immunotherapy (43–45), including bladder cancer, colorectal cancer, and non-small cell lung cancer. Therefore, we expect that the immune/stromal/Estimate scores and tumor purity in the microenvironment of HCC are related to TMB. We divided the samples into high and low groups according to the median of the TMB value to compare the correlation between the immune/stromal/Estimate scores, tumor purity, and TMB. The results showed that the higher the immune/stromal scores, the lower is the TMB value. However, the result for tumor purity was the opposite (**Figure 1B**). This means that the more immune/stromal cells in HCC, the harder it is to identify cancer cells (46). Previous studies have revealed that high TMB predicted worse patient outcomes than those with low TMB in patients with HCC. This is consistent with our survival results (47). In addition, we combined the immune/stromal/Estimate scores and tumor purity with the clinical parameters of HCC, such as metastasis, OS, and grade. However, there was no significant difference (**Supplementary Figure 1**).

Next, we grouped the samples according to the median of immune score and stromal score to find DEGs. Based on the stromal score, we got 1,579 significantly upregulated and 112 downregulated genes, and based on immune score, 1,046 significantly upregulated genes and 105 significantly downregulated genes were found (**Figures 2A,B**). We collected 46 DEGs that were jointly downregulated and 850 DEGs that were jointly upregulated in both immune and stromal scores for functional enrichment analysis (**Figure 2C**), including GO functional annotation analysis (**Figure 2D**) and KEGG pathway enrichment analysis (**Figure 2E**). The results indicated that these genes were mainly enriched in receptor activity, plasma membrane, and immune response. It can be seen from the biological process (BP), that the DEGs were closely related to immune response. Consistent with previous studies (48–50), this evidence proved that TME plays a vital role in the immunotherapy of HCC. At the same time, these genes were significantly enriched in the cytokine–cytokine receptor interaction pathway. A simplified pathway diagram in **Figure 3** showed DEGs enriched in the pathway.

To evaluate the prognostic significance of these DEGs in HCC, univariate Cox regression analysis, LASSO regression analysis (**Figure 4A**), multivariate Cox regression analysis (**Figure 4B**), and Kaplan–Meier survival analysis (**Figure 4C**) were performed. The results demonstrated that CASKIN1, EMR3, and GBP5 were the most significant prognostic markers. Previous study has demonstrated that EMR3 is one of the adhesion G protein-coupled receptors (aGPCRs), which can be used as a modulator of immune cell function (51). It has prognostic significance in Dukes'B colon cancer (52) and glioblastoma (53). Besides, the GBP5 gene has been studied in a variety of cancers, including gastric adenocarcinoma (54), skin cutaneous melanoma (55, 56), pancreatic adenocarcinoma (57), and HCC, and GBP5 was one of the key genes in the malignant transformation induced by microcystin-LR (MC-LR) in the cell of HCC (58). In addition, GBP5 promotes immunity in mammals. It also plays an important role in regulating human macrophage pyroptosis and uniquely regulates the induction of apoptosis (59). However, the involvement of CASKIN1 gene in cancer has rarely been studied.

Besides, we tested whether these three genes are abnormally expressed in HCC. The results indicated that the expression of CASKIN1, EMR3, and GBP5 showed significant difference between the tumor and normal samples in both TCGA database and HPA (**Figures 5A,B**). Then, the relationship of the expression of the three genes and their clinical parameters were analyzed *via* the Chi-square test (**Figure 5C**). Among them, the expression of EMR3 showed significant difference in the clinical parameters of tumor and pathological stage. There was also significant difference for CASKIN1 in the pathological stage and grade. These results indicated that CASKIN1 and EMR3 were possibly involved in the progression of HCC. At the same time, we also verified the significance of the three prognostic genes in the GEO and ICGC database (**Supplementary Figure 2**).

Finally, to further analyze the significance of the three genes in tumor immune infiltration, we analyzed the correlation between the three genes and the immune/stromal/Estimate scores and tumor purity, respectively (**Figure 6A**). At the same time, the TIMER database was applied to assess the correlation

between the expression of the three genes and the infiltration scores of six immune cell types. In both the analyses, the GBP5 gene showed a strong correlation with the degree of immune infiltration (**Figure 6B**). Next, the ssGSEA algorithm was used to evaluate RNA-Seq expression profile data to detect the infiltration of immune cells in tumor tissues of HCC. The correlation analysis between the expression of CASKIN1, EMR3, and GBP5 genes and the immune infiltration scores of 29 immune cell types was performed (**Figure 6C**). The results showed that GBP5 gene expression exhibited strong positive correlation with 12 kinds of immune cells ($R > 0.3$, $p < 0.5$), which verified the results in **Figures 6A,B**, suggesting that GBP5 may be an important target for targeted immunotherapy of HCC.

In summary, our study identified three TME-related prognostic markers in HCC. CASKIN1 was overexpressed in tumor and its high expression was associated with poor OS, while high expression of EMR3 and GBP5 were associated with better survival. However, the prognostic value of the three genes warrants further validation by more clinical data. Importantly, the GBP5 gene was highly expressed in HCC and strongly correlated with immune cell infiltration. It holds a great potential as a candidate for targeted immunotherapy of HCC.

DATA AVAILABILITY STATEMENT

RNA sequencing and clinicopathological data of HCC patients were downloaded from GDC database (https://portal.gdc.cancer.gov/) - https://gdc-hub.s3.us-east-1.amazonaws.com/latest/TCGA-LIHC.htseq_fpkm.tsv.gz.

AUTHOR CONTRIBUTIONS

SX, JL, and JS wrote the paper. YZha, XW, XY, and ML edited the manuscript. PK, CC, FD, QW, and YZhe prepared and adjusted the figures. TY and ZX designed the study, provided funding, and reviewed the manuscript.

FUNDING

This work was supported by the National Natural Science Foundation of China (Grants 81503093, 81972643, and 81672444), the Joint Funds of the Southwest Medical University & Luzhou (Grants 2016LZXNYD-T01, 2017LZXNYD-Z05, and 2019LXXNYKD-07), and the Science & Technology Department of Sichuan Province (Grant 2018JY0079).

SUPPLEMENTARY MATERIAL

The Supplementary Material for this article can be found online at: https://www.frontiersin.org/articles/10.3389/fimmu.2021.653836/full#supplementary-material

Supplementary Figure 1 | Analysis of clinicopathological indicators associated with immune/stromal/Estimate scores and tumor purity. Clinical parameters include metastasis (M0, M1), overall survival (OS) (alive, dead), grade (G1, G2, G3, and G4), tumor (T1, T2, T3, and T4) and pathological stage (Stage I; Stage II, Stage III, Stage IV). Student's *t*-test was used for comparison between the two groups of data, and a one-way ANOVA was applied to compare multiple groups.

Supplementary Figure 2 | Validation of prognostic genes in the gene expression omnibus (GEO) and the International Cancer Genome Consortium (ICGC) database. **(A)** The expression levels and verification of CASKIN1, EMR3, and GBP5 genes in HCC tissues and adjacent normal tissues from GSE76427 dataset in the GEO database. $^{*}p < 0.05$, $^{**}p < 0.01$, and $^{***}p < 0.001$ between the two groups. **(B)** Survival verification of the three prognostic genes by gene expression omnibus (GEO) database in hepatocellular carcinoma (HCC) ($p < 0.05$ in Log-rank test). **(C)** The expression levels and verification of CASKIN1, EMR3, and GBP5 genes in HCC samples and adjacent samples from LIRI-JP dataset in the ICGC database. $^{*}p < 0.05$, $^{**}p < 0.01$, and $^{***}p < 0.001$ between the two groups. **(D)** Survival validation of the three prognostic genes using data from ICGC database in HCC ($p < 0.05$ in Log-rank test).

Supplementary Table 1 | The immune/stromal/Estimate scores and tumor purity of HCC were calculated by using ESTIMATE algorithm.

Supplementary Table 2 | The sample information of overall survival (OS), disease-specific survival (DSS), disease-free interval (DFI), and progression-free interval (PFI).

Supplementary Table 3 | The immune/stromal/Estimate scores and tumor purity with the clinical parameters of hepatocellular carcinoma (HCC), including tumor, metastasis, OS, grade, stage, and cancer status.

Supplementary Table 4 | The results of univariate COX regression analysis.

REFERENCES

1. Fu Q, Yang F, Xiang T, Huai G, Yang X, Wei L, et al. Author correction: a novel microRNA signature predicts survival in liver hepatocellular carcinoma after hepatectomy. *Sci Rep.* (2018) 8:9395. doi: 10.1038/s41598-018-27641-5
2. Farazi PA, DePinho RA. Hepatocellular carcinoma pathogenesis: from genes to environment. *Nat Rev Cancer.* (2006) 6:674–87. doi: 10.1038/nrc1934
3. Llovet JM, Montal R, Villanueva A. Randomized trials and endpoints in advanced HCC: role of PFS as a surrogate of survival. *J Hepatol.* (2019) 70:1262–77. doi: 10.1016/j.jhep.2019.01.028
4. DeSantis CE, Ma J, Gaudet MM, Newman LA, Miller KD, Goding Sauer A, et al. Breast cancer statistics, 2019. *CA Cancer J Clin.* (2019) 69:438–51. doi: 10.3322/caac.21583
5. Global Burden of Disease Cancer Collaboration, Fitzmaurice C, Abate D, Abbasi N, Abbastabar H, Abd-Allah F, et al. Global, regional, and national cancer incidence, mortality, years of life lost, years lived with disability, and disability-adjusted life-years for 29 cancer groups, 1990 to 2017: a systematic analysis for the Global Burden of Disease Study. *JAMA Oncol.* (2019) 5:1749–68. doi: 10.1001/jamaoncol.2019.2996
6. Fu Y, Liu S, Zeng S, Shen H. From bench to bed: the tumor immune microenvironment and current immunotherapeutic strategies for hepatocellular carcinoma. *J Exp Clin Cancer Res.* (2019) 38:396. doi: 10.1186/s13046-019-1396-4
7. Hato T, Goyal L, Greten TF, Duda DG, Zhu AX. Immune checkpoint blockade in hepatocellular carcinoma: current progress and future directions. *Hepatology.* (2014) 60:1776–82. doi: 10.1002/hep.27246
8. Zhang HH, Mei MH, Fei R, Liu F, Wang JH, Liao WJ, et al. Regulatory T cells in chronic hepatitis B patients affect the immunopathogenesis of hepatocellular carcinoma by suppressing the anti-tumour immune responses. *J Viral Hepat.* (2010) 17(Suppl. 1):34–43. doi: 10.1111/j.1365-2893.2010.01269.x
9. Xu WH, Xu Y, Wang J, Wan FN, Wang HK, Cao DL, et al. Prognostic value and immune infiltration of novel signatures in clear cell renal cell carcinoma microenvironment. *Aging.* (2019) 11:6999–7020. doi: 10.18632/aging.102233

10. Jia D, Li S, Li D, Xue H, Yang D, Liu Y. Mining TCGA database for genes of prognostic value in glioblastoma microenvironment. *Aging.* (2018) 10:592–605. doi: 10.18632/aging.101415
11. Quail DF, Joyce AJ. Microenvironmental regulation of tumor progression and metastasis. *Nat Med.* (2013) 19:1423–37. doi: 10.1038/nm.3394
12. Li X, Wenes M, Romero P, Huang SC, Fendt SM, Ho PC. Navigating metabolic pathways to enhance antitumour immunity and immunotherapy. *Nat Rev Clin Oncol.* (2019) 16:425–41. doi: 10.1038/s41571-019-0203-7
13. Belli C, Trapani D, Viale G, D'Amico P, Duso BA, Della Vigna P, et al. Targeting the microenvironment in solid tumors. *Cancer Treat Rev.* (2018) 65:22–32. doi: 10.1016/j.ctrv.2018.02.004
14. Eggert T, Greten FT. Tumor regulation of the tissue environment in the liver. *Pharmacol Ther.* (2017) 173:47–57. doi: 10.1016/j.pharmthera.2017.02.005
15. Yang S, Gao H. Nanoparticles for modulating tumor microenvironment to improve drug delivery and tumor therapy. *Pharmacol Res.* (2017) 126:97–108. doi: 10.1016/j.phrs.2017.05.004
16. Zhou L, Huang W, Yu HF, Feng YJ, Teng X. Exploring TCGA database for identification of potential prognostic genes in stomach adenocarcinoma. *Cancer Cell Int.* (2020) 20:264. doi: 10.1186/s12935-020-01351-3
17. Oliver GR, Hart SN, Klee EW. Bioinformatics for clinical next generation sequencing. *Clin Chem.* (2015) 61:124–35. doi: 10.1373/clinchem.2014.224360
18. Yin Z, Lan H, Tan G, Lu M, Vasilakos AV, Liu W. Computing platforms for big biological data analytics: perspectives and challenges. *Comput Struct Biotechnol J.* (2017) 15:403–11. doi: 10.1016/j.csbj.2017.07.004
19. Hohenberger P. Locoregional recurrence of rectal cancer: biological and technical aspects of surgical failure. *Recent Results Cancer Res*. (1998) 146:127–40. doi: 10.1007/978-3-642-71967-7_12
20. Olsen LR, Campos B, Barnkob MS, Winther O, Brusic V, Andersen MH. Bioinformatics for cancer immunotherapy target discovery. *Cancer Immunol Immunother.* (2014) 63:1235–49. doi: 10.1007/s00262-014-1627-7
21. He KY, Ge D, He MM. Big data analytics for genomic medicine. *Int J Mol Sci.* (2017) 18:412. doi: 10.3390/ijms18020412
22. Wu J, Xu WH, Wei Y, Qu YY, Zhang HL, Ye DW. An integrated score and nomogram combining clinical and immunohistochemistry factors to predict high ISUP grade clear cell renal cell carcinoma. *Front Oncol.* (2018) 8:634. doi: 10.3389/fonc.2018.00634
23. Yoshihara K, Shahmoradgoli M, Martinez E, Vegesna R, Kim H, Torres-Garcia W, et al. Inferring tumour purity and stromal and immune cell admixture from expression data. *Nat Commun.* (2013) 4:2612. doi: 10.1038/ncomms3612
24. Alonso MH, Ausso S, Lopez-Doriga A, Cordero D, Guino E, Sole X, et al. Comprehensive analysis of copy number aberrations in microsatellite stable colon cancer in view of stromal component. *Br J Cancer.* (2017) 117:421–31. doi: 10.1038/bjc.2017.208
25. Hutter C, Zenklusen JC. The cancer genome atlas: creating lasting value beyond its data. *Cell.* (2018) 173:283–5. doi: 10.1016/j.cell.2018.03.042
26. Wang Z, Jensen MA, Zenklusen JC. A practical guide to The Cancer Genome Atlas (TCGA). *Methods Mol Biol.* (2016) 1418:111–41. doi: 10.1007/978-1-4939-3578-9_6
27. Huang da W, Sherman BT, Lempicki RA. Systematic and integrative analysis of large gene lists using DAVID bioinformatics resources. *Nat Protoc.* (2009) 4:44–57. doi: 10.1038/nprot.2008.211
28. Lao J, Chen Y, Li ZC, Li Q, Zhang J, Liu J, et al. A deep learning-based radiomics model for prediction of survival in glioblastoma multiforme. *Sci Rep.* (2017) 7:10353. doi: 10.1038/s41598-017-10649-8
29. Li J, Liu C, Chen Y, Gao C, Wang M, Ma X, et al. Tumor characterization in breast cancer identifies immune-relevant gene signatures associated with prognosis. *Front Genet.* (2019) 10:1119. doi: 10.3389/fgene.2019.01119
30. Friedman J, Hastie T, Tibshirani R. Regularization paths for generalized linear models via coordinate descent. *J Stat Softw.* (2010) 33:1–22. doi: 10.18637/jss.v033.i01
31. Bolzetta F, Wetle T, Besdine R, Noale M, Cester A, Crepaldi G, et al. The relationship between different settings of medical service and incident frailty. *Exp Gerontol.* (2018) 108:209–14. doi: 10.1016/j.exger.2018.04.023
32. Hanzelmann S, Castelo R, Guinney J. GSVA: gene set variation analysis for microarray and RNA-seq data. *BMC Bioinformatics.* (2013) 14:7. doi: 10.1186/1471-2105-14-7
33. Chan TA, Yarchoan M, Jaffee E, Swanton C, Quezada SA, Stenzinger A, et al. Development of tumor mutation burden as an immunotherapy biomarker: utility for the oncology clinic. *Ann Oncol.* (2019) 30:44–56. doi: 10.1093/annonc/mdy495
34. Fancello L, Gandini S, Pelicci PG, Mazzarella L. Tumor mutational burden quantification from targeted gene panels: major advancements and challenges. *J Immunother Cancer.* (2019) 7:183. doi: 10.1186/s40425-019-0647-4
35. Laplane L, Duluc D, Bikfalvi A, Larmonier N, Pradeu T. Beyond the tumour microenvironment. *Int J Cancer.* (2019) 145:2611–2618. doi: 10.1002/ijc.32343
36. Deng F, Chen D, Wei X, Lu S, Luo X, He J, et al. Development and validation of a prognostic classifier based on HIF-1 signaling for hepatocellular carcinoma. *Aging.* (2020) 12:3431–50. doi: 10.18632/aging.102820
37. Kiprenskii Iu V, Erofeev GP. [The immunogenicity of different organs and the characteristics of immunosuppressive therapy during their allotransplantation]. *Khirurgiia*. (1992) 3:123–32.
38. Deng Z, Wang J, Xu B, Jin Z, Wu G, Zeng, et al. Mining TCGA database for tumor microenvironment-related genes of prognostic value in hepatocellular carcinoma. *Biomed Res Int.* (2019) 2019:2408348. doi: 10.1155/2019/2408348
39. Hsiao YW, Chiu LT, Chen CH, Shih WL, Lu TP. Tumor-infiltrating leukocyte composition and prognostic power in hepatitis B- and hepatitis C-related hepatocellular carcinomas. *Genes.* (2019) 10:630. doi: 10.3390/genes10080630
40. Pan L, Fang J, Chen MY, Zhai ST, Zhang B, Jiang ZY, et al. Promising key genes associated with tumor microenvironments and prognosis of hepatocellular carcinoma. *World J Gastroenterol.* (2020) 26:789–803. doi: 10.3748/wjg.v26.i8.789
41. Zanjani HS, Mariani J, Herrup K. Cell loss in the inferior olive of the staggerer mutant mouse is an indirect effect of the gene. *J Neurogenet.* (1990) 6:229–41. doi: 10.3109/01677069009107113
42. Tian Z, Wang Z, Chen Y, Qu S, Liu C, Chen F, et al. Bioinformatics analysis of prognostic tumor microenvironment-related genes in the tumor microenvironment of hepatocellular carcinoma. *Med Sci Monit.* (2020) 26:e922159. doi: 10.12659/MSM.922159
43. Rizvi NA, Hellmann MD, Snyder A, Kvistborg P, Makarov V, Havel JJ, et al. Cancer immunology. Mutational landscape determines sensitivity to PD-1 blockade in non-small cell lung cancer. *Science.* (2015) 348:124–8. doi: 10.1126/science.aaa1348
44. Samstein RM, Lee CH, Shoushtari AN, Hellmann MD, Shen R, Janjigian YY, et al. Tumor mutational load predicts survival after immunotherapy across multiple cancer types. *Nat Genet.* (2019) 51:202–06. doi: 10.1038/s41588-018-0312-8
45. Snyder A, Wolchok JD, Chan TA. Genetic basis for clinical response to CTLA-4 blockade. *N Engl J Med.* (2015) 372:783. doi: 10.1056/NEJMc1415938
46. Gandara DR, Paul SM, Kowanetz M, Schleifman E, Zou W, Li Y, et al. Blood-based tumor mutational burden as a predictor of clinical benefit in non-small-cell lung cancer patients treated with atezolizumab. *Nat Med.* (2018) 24:1441–8. doi: 10.1038/s41591-018-0134-3
47. Shrestha R, Prithviraj P, Anaka M, Bridle KR, Crawford DHG, Dhungel B, et al. Monitoring immune checkpoint regulators as predictive biomarkers in hepatocellular carcinoma. *Front Oncol.* (2018) 8:269. doi: 10.3389/fonc.2018.00269
48. Pineiro Fernandez J, Luddy KA, Harmon C, O'Farrelly C. Hepatic tumor microenvironments and effects on NK cell phenotype and function. *Int J Mol Sci.* (2019) 20:4131. doi: 10.3390/ijms20174131
49. Wu Q, Zhou L, Lv D, Zhu X, Tang H. Exosome-mediated communication in the tumor microenvironment contributes to hepatocellular carcinoma development and progression. *J Hematol Oncol.* (2019) 12:53. doi: 10.1186/s13045-019-0739-0
50. Zhang FP, Huang YP, Luo WX, Deng WY, Liu CQ, Xu LB, et al. Construction of a risk score prognosis model based on hepatocellular carcinoma microenvironment. *World J Gastroenterol.* (2020) 26:134–53. doi: 10.3748/wjg.v26.i2.134
51. Hamann J, Hsiao CC, Lee CS, Ravichandran KS, Lin HH. Adhesion GPCRs as modulators of immune cell function. *Handb Exp Pharmacol.* (2016) 234:329–50. doi: 10.1007/978-3-319-41523-9_15
52. Wang Y, Jatkoe T, Zhang Y, Mutch MG, Talantov D, Jiang J, et al. Gene expression profiles and molecular markers to predict recurrence of Dukes' B colon cancer. *J Clin Oncol.* (2004) 22:1564–71. doi: 10.1200/JCO.2004.08.186

53. Kane AJ, Sughrue ME, Rutkowski MJ, Phillips JJ, Parsa AT. EMR-3: a potential mediator of invasive phenotypic variation in glioblastoma and novel therapeutic target. *Neuroreport*. (2010) 21:1018–22. doi: 10.1097/WNR.0b013e32833f19f2
54. Patil PA, Blakely AM, Lombardo KA, Machan JT, Miner TJ, Wang LJ, et al. Expression of PD-L1, indoleamine 2,3-dioxygenase and the immune microenvironment in gastric adenocarcinoma. *Histopathology*. (2018) 73:124–36. doi: 10.1111/his.13504
55. Chen W, Cheng P, Jiang J, Ren Y, Wu D, Xue D. Epigenomic and genomic analysis of transcriptome modulation in skin cutaneous melanoma. *Aging*. (2020) 12:12703–25. doi: 10.18632/aging.103115
56. Wang Q, Wang X, Liang Q, Wang S, Xiwen L, Pan F, et al. Distinct prognostic value of mRNA expression of guanylate-binding protein genes in skin cutaneous melanoma. *Oncol Lett*. (2018) 15:7914–2. doi: 10.3892/ol.2018.8306
57. He QL, Jiang HX, Zhang XL, Qin SY. Relationship between a 7-mRNA signature of the pancreatic adenocarcinoma microenvironment and patient prognosis (a STROBE-compliant article). *Medicine*. (2020) 99:e21287. doi: 10.1097/MD.0000000000021287
58. Chen HQ, Zhao J, Li Y, He LX, Huang YJ, Shu WQ, et al. Gene expression network regulated by DNA methylation and microRNA during microcystin-leucine arginine induced malignant transformation in human hepatocyte L02 cells. *Toxicol Lett*. (2018) 289:42–53. doi: 10.1016/j.toxlet.2018.03.003
59. Fisch D, Bando H, Clough B, Hornung V, Yamamoto M, Shenoy AR, et al. Human GBP1 is a microbe-specific gatekeeper of macrophage apoptosis and pyroptosis. *EMBO J*. (2019) 38:e100926. doi: 10.15252/embj.2018100926

Conflict of Interest: The authors declare that the research was conducted in the absence of any commercial or financial relationships that could be construed as a potential conflict of interest.

Copyright © 2021 Xiang, Li, Shen, Zhao, Wu, Li, Yang, Kaboli, Du, Zheng, Wen, Cho, Yi and Xiao. This is an open-access article distributed under the terms of the Creative Commons Attribution License (CC BY). The use, distribution or reproduction in other forums is permitted, provided the original author(s) and the copyright owner(s) are credited and that the original publication in this journal is cited, in accordance with accepted academic practice. No use, distribution or reproduction is permitted which does not comply with these terms.

frontiers in Immunology

ORIGINAL RESEARCH
published: 14 April 2021
doi: 10.3389/fimmu.2021.657950

ATP2C2 Has Potential to Define Tumor Microenvironment in Breast Cancer

Jiazhou Liu[1,2], Yuxian Wei[1,2], Yushen Wu[1,2], Jie Li[1,2], Jiazheng Sun[1,2], Guosheng Ren[1,2] and Hongzhong Li[2]**

[1] Department of Endocrine and Breast Surgery, The First Affiliated Hospital of Chongqing Medical University, Chongqing, China, [2] Key Laboratory of Molecular Oncology and Epigenetics, The First Affiliated Hospital of Chongqing Medical University, Chongqing, China

OPEN ACCESS

Edited by:
Keqiang Chen,
National Cancer Institute at Frederick, United States

Reviewed by:
Shuo Geng,
Virginia Tech, United States
Haiwei Mou,
Cold Spring Harbor Laboratory, United States
Xiang Yi,
Ruijin Hospital, China

***Correspondence:**
Hongzhong Li
203851@hospital.cqmu.edu.cn
Guosheng Ren
rengs726@126.com

Specialty section:
This article was submitted to Cancer Immunity and Immunotherapy, a section of the journal Frontiers in Immunology

Received: 24 January 2021
Accepted: 24 March 2021
Published: 14 April 2021

Citation:
Liu J, Wei Y, Wu Y, Li J, Sun J, Ren G and Li H (2021) ATP2C2 Has Potential to Define Tumor Microenvironment in Breast Cancer. Front. Immunol. 12:657950. doi: 10.3389/fimmu.2021.657950

Tumor microenvironment (TME) is vital for the occurrence and development of breast cancer (BRCA). However, it remains challenging to understand the dynamic modulation of the stromal and immune components comprehensively in TME. Herein, we used ESTIMATE and CIBERSORT algorithm to estimate the number of stromal and immune components and the abundance of tumor-infiltrating immune cells (TICs) in 582 BRCA cases from gene expression omnibus (GEO) database. We employed three regression models including univariable Cox proportion, LASSO regression model and multivariate Cox regression, and identified 7 immune-specific genes related to BRCA survival. Of 7 genes, ATPase Secretory Pathway Ca^{2+} Transporting 2 (ATP2C2) attracts our attention for significantly predicting prognosis of BRCA patients. Further analysis indicated that ATP2C2 expression was closely related to the clinicopathological features (age, T- and N-staging) and negatively correlated with patients' survival in BRCA. Gene Set Enrichment Analysis (GSEA) was performed to reveal pathway enrichment between $ATP2C2^{high}$ and $ATP2C2^{low}$ groups. The low ATP2C2 expression groups' genes were mainly enriched for immune-related activities, while those in the ATP2C2 high-expression group were largely enriched in metabolic-related pathways. Notably, Pearson's correlation analysis identified that ATP2C2 expression was positively correlated with T follicular helper (Tfh) cells, and negatively correlated with gamma delta (γδ) T cell, suggesting that ATP2C2 might be accountable for the maintenance of immune-dominant status for TME. To sum up, this study comprehensively analyzed the TME and shed light on prognostic immune-related biomarkers for BRCA. In particular, ATP2C2 might be helpful for predicting the prognosis of BRCA patients, which provided an extra insight for BRCA treatment.

Keywords: breast cancer, ATP2C2, tumor microenvironment, tumor-infiltrating immune cells, LASSO, nomogram
ATP2C2 modulates TME in BRCA

INTRODUCTION

Breast cancer (BRCA) with high aggressiveness is one of the most common malignant tumors that seriously endanger women's health (1). However, the mechanism of its occurrence and development is not yet fully understood. Therefore, in-depth study of the molecular mechanisms of BRCA development and finding effective therapeutic targets are of great significance for improving the prognosis of BRCA patients.

The "seed-soil" theory of tumors believes that the growth of tumor cells requires the surrounding normal cells and extracellular matrix to provide a permissive environment, that is, the tumor microenvironment (TME) (2). TME is the local environment for tumor cells to survive. In addition to tumor cells, it also contains resident stromal cells and recruited immune cells. These components are crucial in the occurrence, development, and immune evasion of tumors (3). Although stromal cells can promote tumor angiogenesis, cancer cell proliferation, invasion and metastasis, the detailed molecular mechanism to promote cancer progression has not been fully elucidated. Meanwhile, increasing attention has been paid to the influence of the immune cells in TME on tumor development. It was revealed that high levels of immune cell infiltration into cancer tissues were correlated with favorable outcomes, suggesting that valuing TME heterogeneity and remodeling the immune microenvironment may hold promise for cancer treatment (4). Immune cells in the TME can affect the host immune response by secreting chemokines, cytokines and other factors that directly or indirectly suppress or support tumor progression (5). Therefore, to better understand the immune status of the TME and investigating the distribution pattern and function of immune cells are essential for improving the effectiveness of cancer immunotherapy.

In the present study, we used ESTIMATE and CIBERSORT algorithm to quantify the tumor-infiltrating immune cell (TIC) proportion and the ratio of immune and stromal components of BRCA samples from the gene expression omnibus (GEO) database and identified a novel predictive biomarker, ATPase Secretory Pathway Ca^{2+} Transporting 2 (ATP2C2). Gene dysregulation of ATP2C2 has been linked to breast cancers: ATP2C2 (also known as SPCA2) promotes tumor growth by increasing Ca^{2+} entry through activation of the Orai1 calcium channel (6). Recently, the literature has demonstrated a novel association among ATP2C2, Kv10.1 and Orai1 involved in mediating transduction signals from TME to the BRCA cells, suggesting that ATP2C2 may play an important role in TME (7). Here we set out to compare differentially expressed genes (DEGs) produced by comparison between stromal components and immune components in BRCA cases, revealing that the ATP2C2 may be a potential indicator for the alteration of TME status in BRCA.

MATERIALS AND METHODS

BRCA Datasets and Samples

mRNA expression data for breast cancer (BRCA) were procured from GEO (https://www.ncbi.nlm.nih.gov/geo/). The keywords "Breast cancer" and "Survival" were used for retrieval. Finally, five gene expression microarray datasets were chosen as a training set, including (GSE42568, n=121), (GSE88770, n=117), (GSE16446, n=120), (GSE37751, n=108), and (GSE7390, n=198). 582 samples with the survival status and survival time were downloaded for DEG analysis from the five datasets. In addition, the GSE20711 cohort (n = 88) were used as a validation set.

Harmonized RNA sequencing data and related clinical information for BRCA were downloaded for clinical correlation and GSEA analysis from TCGA (https://portal.gdc.cancer.gov/, up to July 30, 2020), which included 1222 samples, 113 normal tissue samples, and 1109 tumor samples.

ESTIMATE

The stromal, immune and ESTIMATE scores were outputted by the R package "estimate" (8).

DEGs Identification Based on StromalScore and ImmuneScore

Based on the comparison with the median scores of StromalScore and ImmuneScore, 582 BRCA cases were divided into high or low score groups. Limma R package was applied to determine DEGs between high-scoring samples and low-scoring samples. Genes with $p < 0.05$ and $|\log2 \text{ FC (fold-change)}| > 1$ were screened DEGs. A flowchart for constructing DEG signature is displayed in **Figure 1**.

Heatmaps

Heatmaps were plotted with the R package pheatmap (9).

Functional Enrichment and Pathway Analysis

To understand the potential function of the common DEGs that stemmed from the immune scores and stromal scores, Gene Ontology (GO) and the Kyoto Encyclopedia of Genes and Genomes (KEGG) pathway enrichment analysis were performed by "clusterProfiler" package in R. GO and KEGG terms with a p- and q-value of both <0.05 were considered significantly enriched.

Construction and Validation of the Prognostic Prediction Models

A univariate Cox model was conducted to screen potential prognostic immune-related genes (IRGs) and TICs. A LASSO Cox regression model was further applied to narrow the range of prognostic IRGs and TICs. Next, a multivariate Cox regression model was utilized to select IRGs and TICs most closely related to survival, and those IRGs and TICs were used to construct two risk models. Two formulas for the IRGs risk score and TICs risk score was established to predict patient survival: IRGs risk score = (−0.212 × expression level of ADRB2) + (0.208 × expression level of ATP2C2) + (−0.287 × expression level of CELF2) + (−0.129 × expression level of CXCL12) + (0.257 × expression level of LGMN) + (−0.204 × LIPA) + (0.214 × expression level of SLCO2B1), TICs risk score = (3.359 × abundance of naïve B cells) + (4.957 × abundance of T follicular helper (Tfh) cells) + (−4.349 × abundance of gamma delta (γδ) T cells) + (−3.966 × abundance of resting mast cells). The individual IRGs risk score

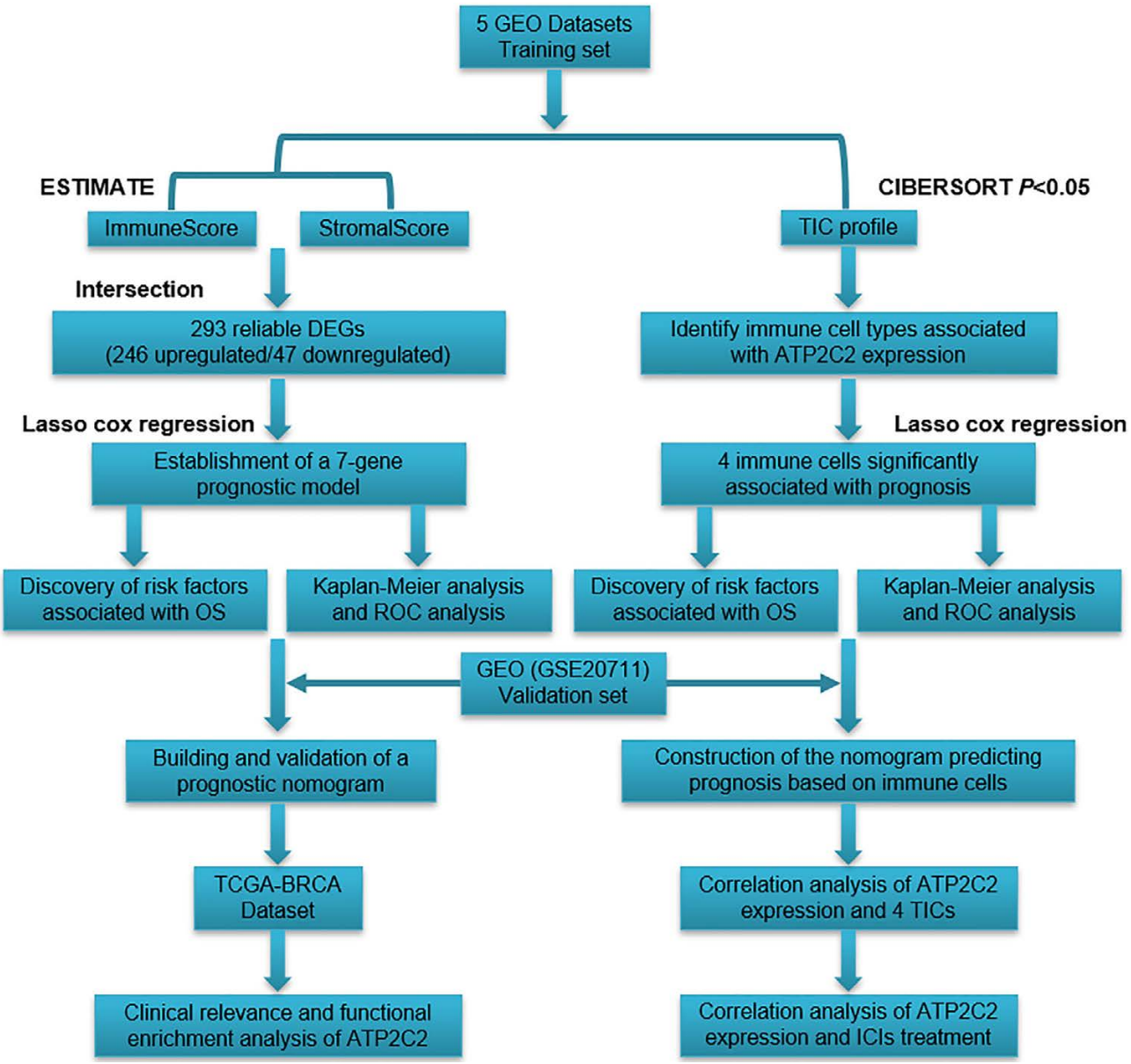

FIGURE 1 | Experimental technical roadmap.

and TICs risk score in both training set and validation set were calculated according to the formulas accordingly.

The Kaplan-Meier method and the ROC curves were used to analyze OS and to assess signature's sensitivity and specificity of the models.

Construction and Validation of Nomograms

Based on seven IRGs and four TICs, we separately plotted the nomograms to predict the probability of 1-, 2-, and 3-OS of BRCA patients. Validation of the nomograms was evaluated by the discrimination and calibration.

Gene Set Enrichment Analysis (GSEA)

GSEA was performed between high- and low-ATP2C2 expression (10). The number of random sample permutations was set at 1000, and NOM p-value < 0.05, FDR q-value < 0.25, and | NES | > 1 were set as the significance threshold.

Estimation of TIC Types

CIBERSORT algorithm was utilized to evaluate the relative abundance of 22 types of TICs. After the quality filtering (p-value < 0.05), 545 BRCA samples were selected for following analysis.

Tumor Immune Dysfunction and Exclusion (TIDE) Analysis

TIDE is a computational framework construct to predict immune checkpoint inhibitors (ICIs) response (11).

RESULTS

DEGs Based on ImmuneScore and StromalScore Were Mainly Presented as the Enrichment of IRGs

To explore the accurate alterations of gene profile in TME regarding immune and stromal components, a comparative analysis of high- and low-scoring samples was performed. A total 1091 DEGs including 692 upregulated and 399 downregulated genes were obtained from ImmuneScore (**Figure 2A**). Similarly, a total of 1261 DEGs including 852 upregulated and 409 downregulated genes were obtained from StromalScore (**Figure 2B**). By intersecting these DEGs from ImmuneScore and StromalScore, a total of 246 up-regulated genes and 47 down-regulated genes (**Figures 2C, D**). These DEGs were probably key factors for the status of TME. GO enrichment analysis showed that the functions of the DEGs were predominantly associated with the immune response, such as leukocyte proliferation and leukocyte migration (**Figure 2E**; **Figure S1A**). The KEGG enrichment analysis also indicated that the DEGs were involved in hematopoietic cell lineage, Th1 and Th2 cell differentiation, and cytokine–cytokine receptor interaction (**Figure 2F**; **Figure S1B**). Therefore, immune-related activities tended to represent the main functions of DEGs, implying that the involvement of immune components was a predominant feature of TME of BRCA.

Screening of Prognosis-Specific IRGs and Construction of Prognosis Prediction Model

293 differentially expressed IRGs were further subjected to the univariate Cox regression model; we identified 67 IRGs significantly related with OS (**Table S1**). Then, these 67 IRGs were used in the LASSO regression for feature selection. A set of seventeen genes (ADD3, ADRB2, ALDH1A1, ATP2C2, CCR2, CELF2, CRTAM, CXCL12, EPN3, HOXC8, IL2RB, ITM2A, KLRG1, LGMN, LIPA, SLCO2B1, and TMEM243) and their coefficients were computed (**Figures 3A, B**). Then, the Akaike information criterion (AIC) was utilized to screen significant prognostic IRGs in multivariate Cox regression models (**Figure 3C**).

The risk score of each BRCA patient was calculated, and the patients were classified into the high-risk (n = 291) or low-risk (n = 291) group by the median cut-off value (**Figure 3D**). Remarkably, the number of deaths was significantly higher in the high-risk group (**Figure 3E**). A heatmap revealed that patients in the high-risk group tended to have increased LGMN, ATP2C2, and SLCO2B1 expression levels, as well as decreased expression levels of CXCL12, LIPA, ADRB2 and CELF2 (**Figure 3F**). The Kaplan–Meier analysis indicated that low-risk patients had a better OS than high-risk patients ($P < 0.001$) (**Figure 3J**). The accuracy of the prognostic model was displayed in the ROC curve. The AUCs under ROC curve for predicting OS in the first, third, and fifth year were 0.831, 0.731, and 0.723, respectively (**Figure 3L**). To demonstrate the robustness of the prognostic signature, the predictive ability was assessed in a GSE20711 cohort. The risk score for each patient was calculated based on the same formula, and the best threshold was chosen as the cut-off for patients stratified as high- and low-risk. The risk score profiles and gene expression are displayed in **Figures 3G–I**. Patients in high-risk group had a shorter OS than patients in the low-risk group in the GSE20711 cohort, which was consistent with the results of the training set (**Figure 3K**). The AUC of the signature for OS was 0.92, 0.668 and 0.693 at 1, 3 and 5 years, respectively (**Figure 3M**).

Based on the multivariate Cox analysis results, seven IRGs were integrated in the nomogram to predict the OS of BRCA patients (**Figures 4A, B**). The calibration curves revealed acceptable accuracy. These results indicated that the IRGs risk model nomogram had very appropriate calibration.

ATP2C2 Is Highly Expressed in BRCA and Correlates With Unfavorable Prognosis

Ion channels have a key role in mediating TME signal (12). Previous studies had shown that ATP2C2 can regulate the localization and the activity of Kv10.1 and Orai1 channels, mediating transduction signals from TME to the BRCA cells (7). However, the clinical role of the ATP2C2 has not yet been determined. Here we divided all BRCA samples into ATP2C2 high and low expression groups based on ATP2C2 median expression. The Kaplan–Meier analysis elucidated that BRCA patients with ATP2C2 low expression had longer survival than those with ATP2C2 high expression (**Figure 5A**). In addition, we further found that ATP2C2 levels are associated with poor prognosis of various cancers, including thyroid carcinoma (THCA), head-neck squamous cell carcinoma (HNSC), kidney renal clear cell carcinoma (KIRC), lung squamous cell carcinoma (LUSC), and esophageal squamous cell carcinoma (ESCC) on a web platform Kaplan–Meier Plotter (http://kmplot.com/analysis/) (**Figures S2A–E**). After that, clinical pathologic features and ATP2C2 expression were downloaded from the TCGA database. The expression of ATP2C2 in the BRCA samples was significantly higher than that in normal breast tissues or paired breast non-tumor by Wilcoxon rank sum test (**Figures 5B, C**). We also observed a similar up-regulation of ATP2C2 expression in BRCA in the HPA dataset (https://www.proteinatlas.org/) (**Figures S3A–F**). Collectively, these outcomes clearly demonstrated that high ATP2C2 expression in TME was correlated with worse prognosis of BRCA patients. Remarkably, the levels of ATP2C2 were increased along with the progression of age, T- and N- staging (**Figures 5D–I**).

ATP2C2 Had Potential to Be an Indicator for TME Modulation

Given the expressions of ATP2C2 were negatively associated with the OS, T- and N- staging of patients with BRCA, GSEA was

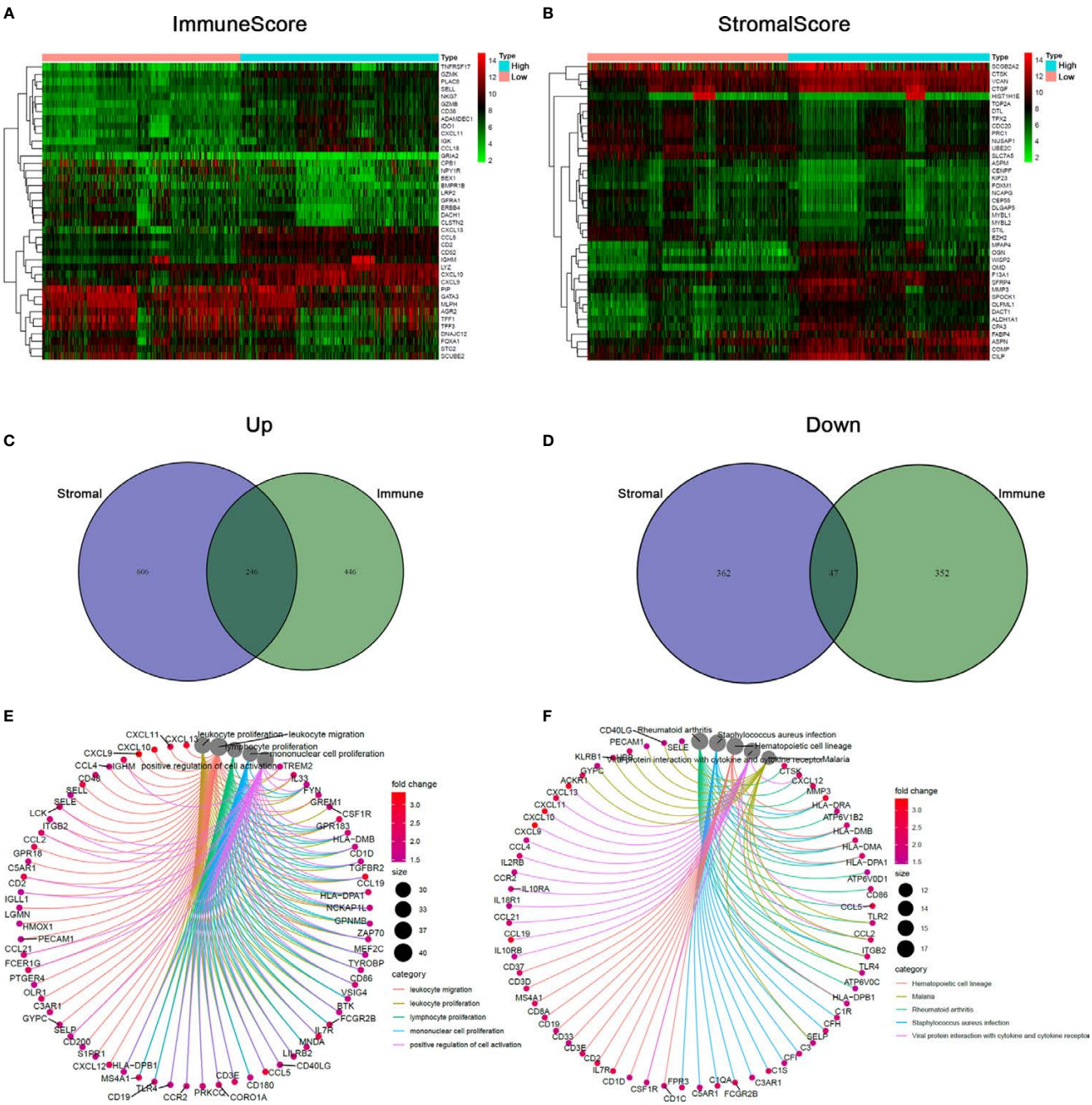

FIGURE 2 | Comparison of gene expression profile with stromal and immune scores of BRCA. **(A, B)** The heatmap presenting the top 20 upregulated and downregulated DEGs in ImmuneScore and StromalScore. DEGs were detected by Wilcoxon rank sum test ($q < 0.05$ & $|\log2FC| > 0.5$). **(C, D)** Venn diagram analysis of aberrantly expressed genes based on stromal and immune scores. **(E, F)** DEGs-related biological functions and pathways in BRCA, terms with p and $q < 0.05$ were considered to be significantly enriched.

performed to explore the gene sets enriched in different ATP2C2 subgroups. As shown in **Figure 6A**, ATP2C2 low-expression group' genes were significantly enriched in immune-related activities, such as cytokine–cytokine receptor interaction, hematopoietic cell lineage and primary immunodeficiency, while those in ATP2C2 high-expression group were mainly enriched in metabolic pathways, including citrate cycle TCA cycle, amino sugar and nucleotide sugar metabolism, and fructose and mannose metabolism (**Figure 6B**). Together, these findings implied that ATP2C2 might be a potential indicator for the status of TME.

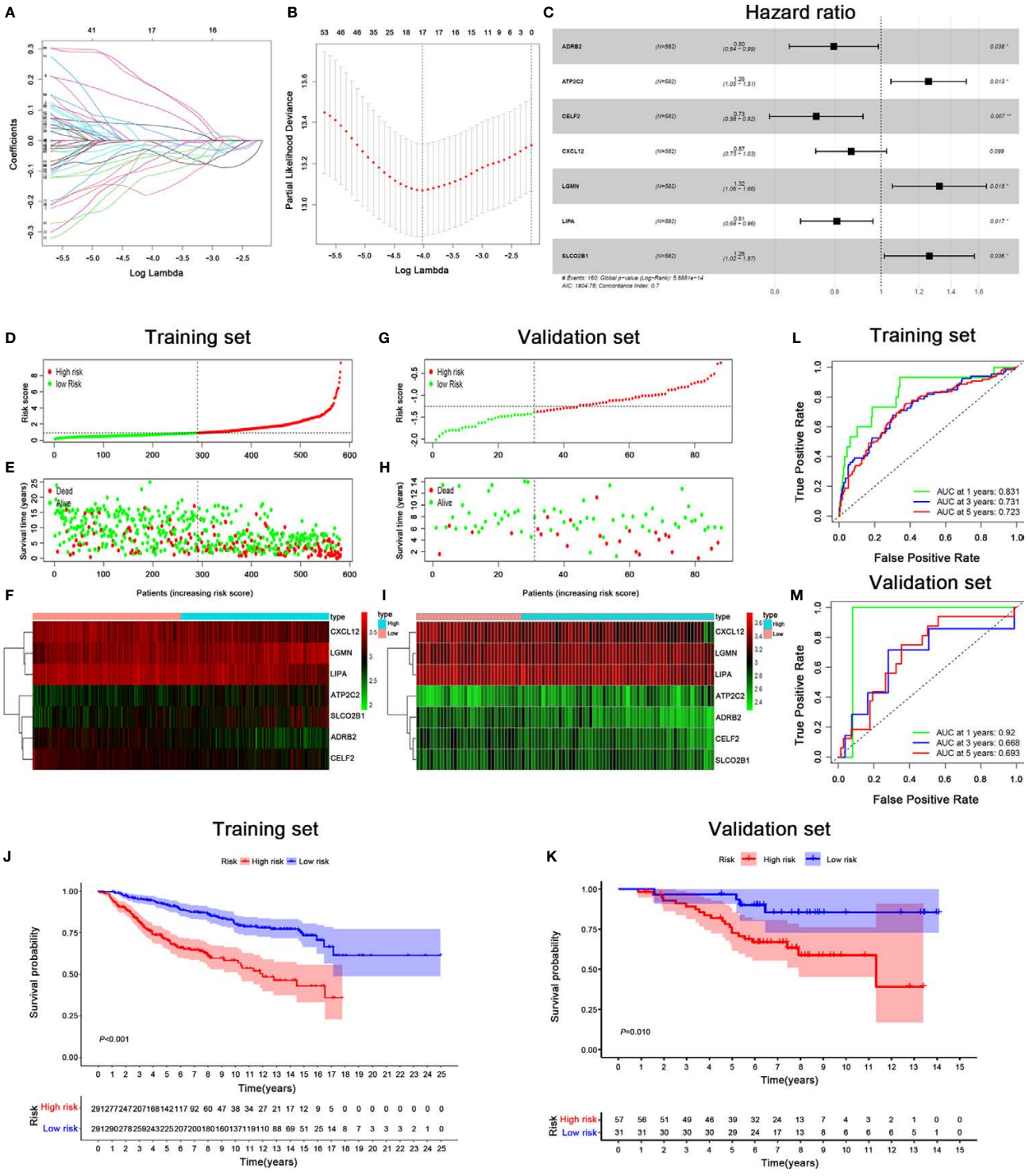

FIGURE 3 | Signature-based risk score is a promising marker of survival in BRCA patients. **(A, B)** LASSO Cox analysis identified seven genes most correlated with OS, and 10-round cross validation was performed to prevent overfitting. **(C)** Multivariate Cox analysis of 7 immune-related hub genes. **(D, G)** Risk score distribution in training set **(D)** and validation set **(G)**. **(E, H)** Survival overview in training set **(E)** and validation set **(H)**. **(F, I)** Expression profile of 7 immune genes in training set **(F)** and validation set **(I)**. **(J, K)** Kaplan–Meier estimates of OS according to the seven-immune-related gene signature in training set **(J)** and validation set **(K)**. The differences between the two curves were evaluated by the two-side log-rank test. **(L, M)** The ROC curve analysis of the seven-immune-related gene signature for predicting OS in training set **(L)** and validation set **(M)**.

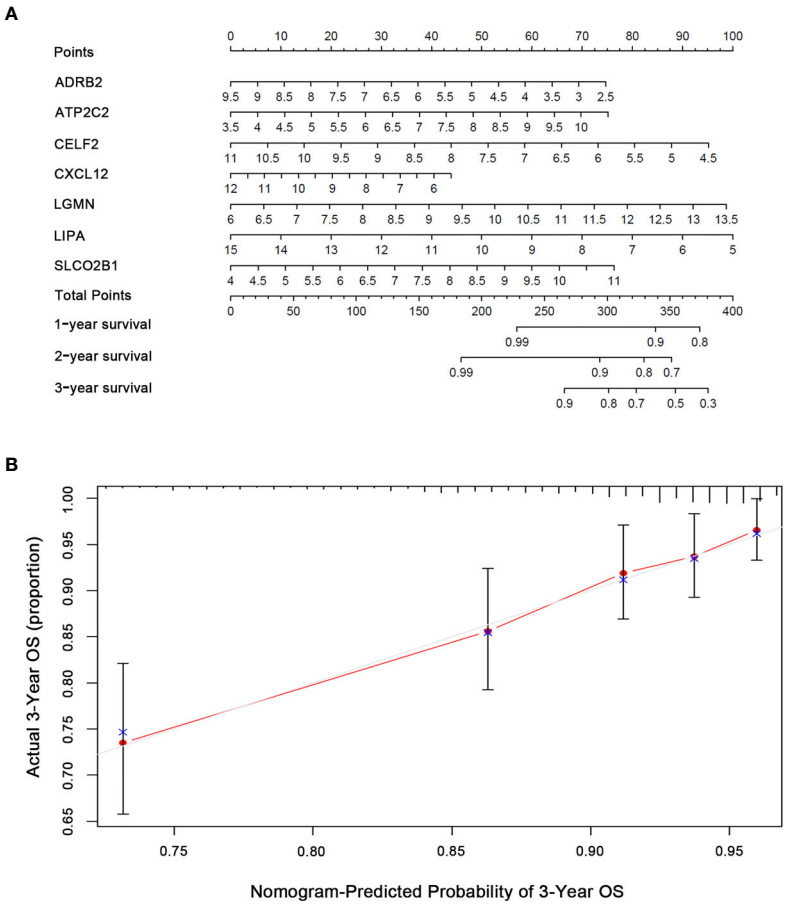

FIGURE 4 | Nomogram predicting OS for BRCA patients based on risk score. **(A)** Nomogram model for predicting the probability of 1-, 2-, and 3-year OS of BRCA. Points are assigned for seven features. The sum of these points is located on the total points axis. The total points on the bottom scales correspond to the predicted 1-, 2-, and 3-year survival. **(B)** Calibration plots of the nomogram for predicting the probability of OS at 1, 2, and 3 years. The X-axis represents nomogram-predicted survival, and the Y-axis represents actual survival.

ATP2C2 Predicts the Infiltration of Immune Cells Into BRCA Microenvironment

To further explore the indicative roles of ATP2C2 on TME, we used the CIBERSORT algorithm to detect the proportions of 22 kinds of immune cells in the BRCA microenvironment (**Figure 7A**). Besides, the results of the Wilcoxon-Mann-Whitney test showed that the fractions of the naïve B cells, γδ T cells, activated memory $CD4^+$ T cells, naïve $CD4^+$ T cells, monocytes, M0 macrophages, M2 macrophages, and activated dendritic cells in ATP2C2 high-expression group was relatively less than that in ATP2C2 low-expression group, and regulatory T cells (Tregs), activated NK cells, and M1 macrophages were relatively greater in ATP2C2 high-expression group (**Figure 7B**).

ATP2C2 Was Correlated With Distribution Pattern of T Cell Subsets

All TICs were integrated into a univariate Cox regression model (**Table 1**). The significative TICs, screened by univariate Cox regression analysis were subjected to LASSO Cox regression analysis. The results of the Lasso regression suggested that the model was not overfitting (**Figure S4A, B**). After that, multivariate Cox regression analysis revealed that the model composed of naïve B cells, Tfh cells, γδ T cells, and resting mast cells had the smallest AIC (**Figure S4C**). According to the median cut-off value of TICs risk score, BRCA patients were classified into high- and low-risk groups. The distribution of risk score, survival status and expression profile of the four TICs of each patient are presented in **Figures S4D–F** (training set) and **Figures S4G–I** (validation set). The Kaplan–Meier survival analysis in the two datasets revealed significantly worse prognosis in the high-risk group (**Figures S4J, K**). Next, the prognostic accuracy of the TICs risk score was examined in the training set and validation set by using time-dependent ROC curves analysis (**Figures S4L, M**).

To further improve the accuracy of the prognostic, the nomogram based on the multivariate analysis was constructed (**Figure S5A**). In addition, the calibration curve and the ROC

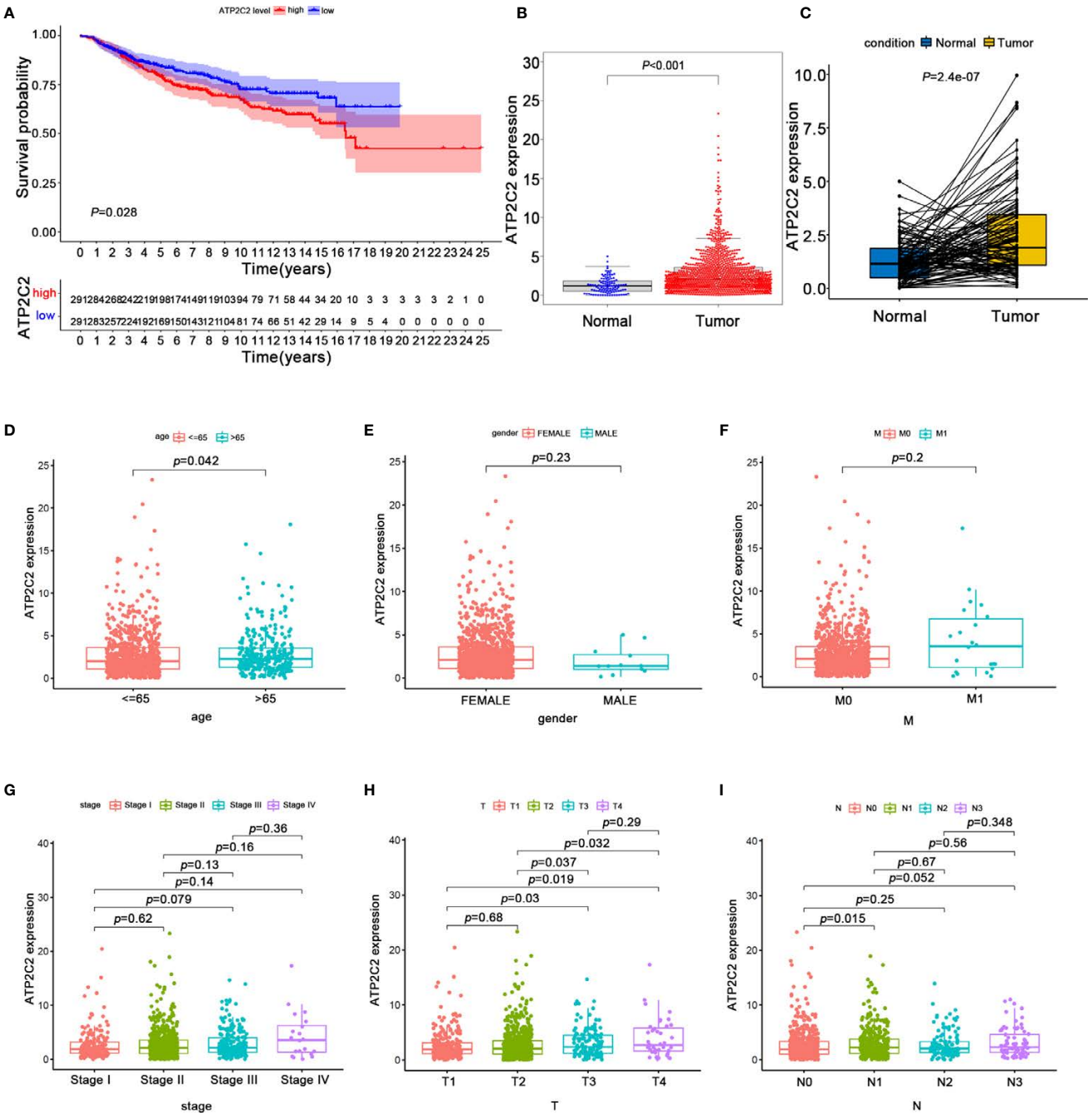

FIGURE 5 | The expression of ATP2C2 and correlation with OS and clinicopathological features of BRCA patients revealed by bioinformatic analysis. **(A)** Survival outcome for BRCA patients with different ATP2C2 expression. The differences between the two curves were detected by the two-side log-rank test. **(B)** ATP2C2 mRNA is highly expressed in BRCA tissues. Statistical significance was evaluated using Wilcoxon-Mann-Whitney test. **(C)** ATP2C2 mRNA levels in the paired BRCA tissues were evaluated. *P*-values are based on the Wilcoxon Test. **(D–I)** The correlation of ATP2C2 expression with clinicopathological features. Statistical significance was evaluated using Wilcoxon rank sum test.

demonstrated good discrimination and concordance (**Figure S5B**).

Pearson analysis was applied to demonstrate the co-expression patterns among diversified immune cells (**Figure 8A**). Likewise, correlation relationship between immune cells and key genes was further analyzed and illustrated (**Figure 8B**). Here we emphatically analyzed the correlation between T cells and ATP2C2. Among them, Tfh cells were positively correlated with ATP2C2 expression

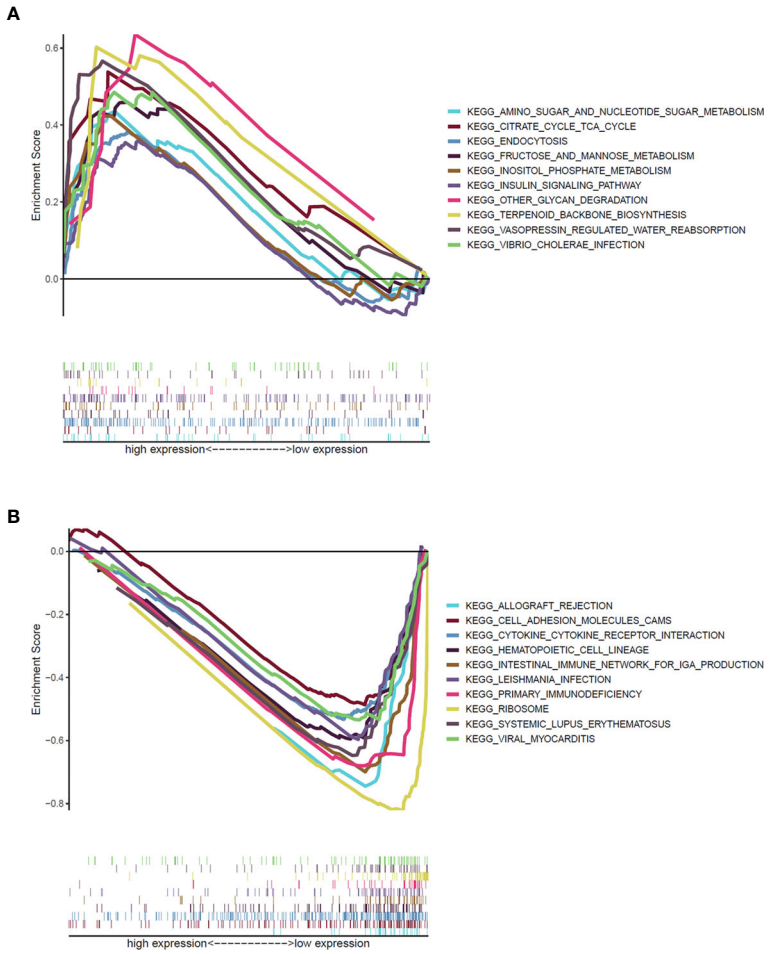

FIGURE 6 | GSEA revealed biological pathways correlated with ATP2C2 in the cohort from TCGA. **(A)** Gene sets enriched in ATP2C2 high-expression group. **(B)** Gene sets enriched in ATP2C2 low-expression group. NOM $p < 0.05$, FDR $q < 0.25$, and |NES| > 1 are set as the significance threshold.

(R = 0.12, P = 0.0059) (**Figure 8C**); γδ T cells was negatively correlated with ATP2C2 expression (R = -0.18, P = 1.9e-05) (**Figure 8D**). These outcomes further verified that the expressions of ATP2C2 influenced the immune activity of TME.

ATP2C2 Promotes Immune Evasion and Resistance to ICIs

Accumulating evidence suggests that the level of cytotoxic T lymphocytes (CTL) is correlated with a better prognosis of patients. Through the analysis of the TIDE algorithm, we found that in BRCA patients with low ATP2C2 expression levels, high CTL levels indicate a better prognosis, while the above phenomenon is not observed in BRCA patients with high ATP2C2 expression levels (http://tide.dfci.harvard.edu/) (**Figure 9**). Similar results are observed in acute myeloid leukemia (AML), lung adenocarcinoma (LUAD), and ovarian serous cystadenocarcinoma (OV) patients (**Figures S6A–C**). In addition, we further used the TIDE algorithm to predict the efficacy of patients with ICIs. We found that the expression level of ATP2C2 is related to the enhanced efficacy of ICIs treatment in melanoma and KIRC (**Figures S6D, E**). These results suggested that ATP2C2 may be appropriate candidates for immunotherapy, especially ICIs.

DISCUSSION

Herein, we sought to mine TME-related genes that contributed to the classification of TNM stages and the OS in BRCA patients from the GEO and TCGA-BRCA datasets. ATP2C2 was determined to be involved in immune activities. Interestingly, we found that ATP2C2 might be an indicator for the status of TME in BRCA patients through bioinformatics analysis.

TME is the key regulator of carcinogenesis and consists of tumor cells, stromal cells, and immune cells (13, 14). TICs are closely associated with tumorigenesis, angiogenesis and the growth and metastatic potential of tumor cells, which could alternately modulate the pattern of immune cells (15–18). Now,

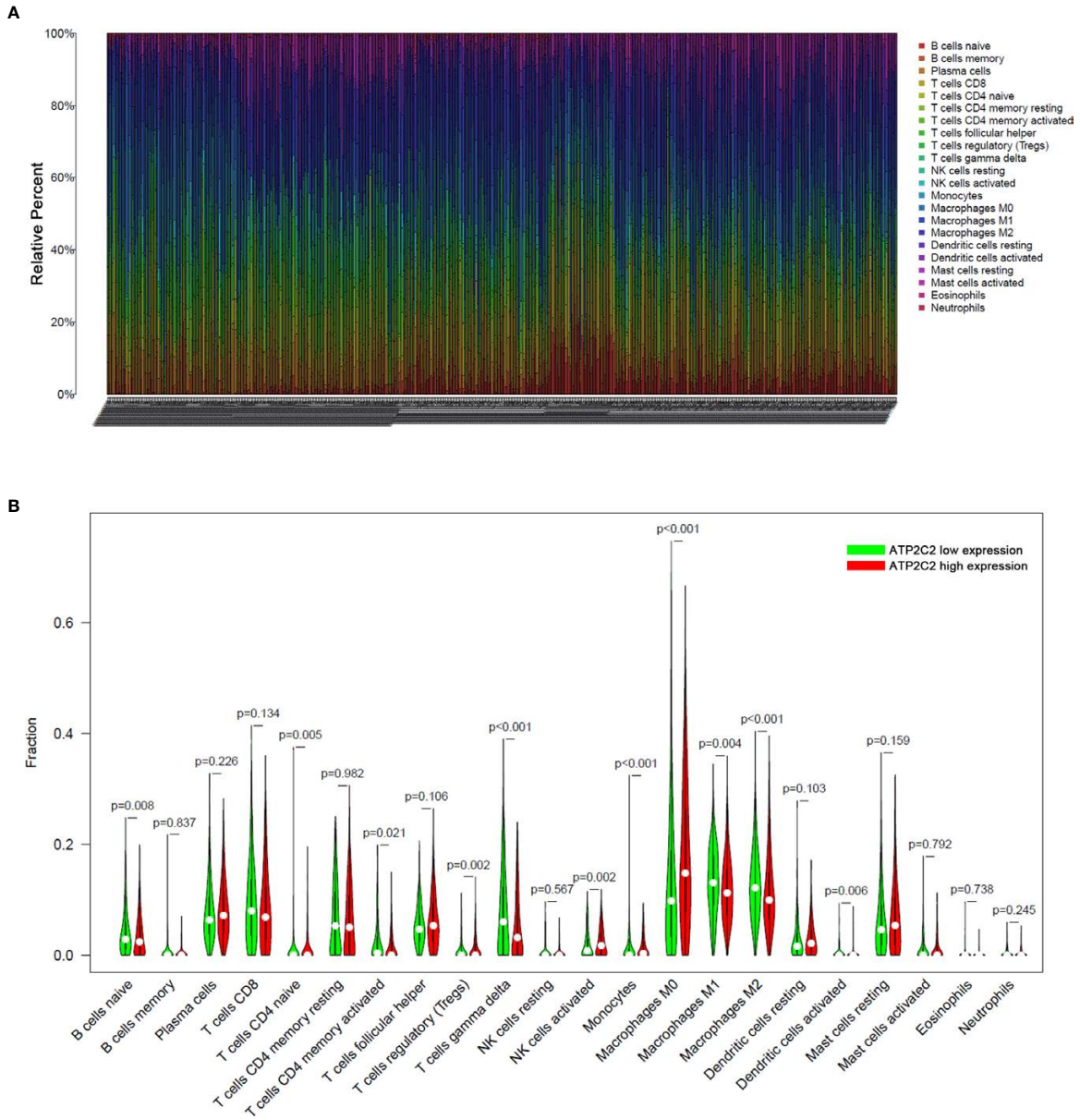

FIGURE 7 | Analysis of immune cell infiltration. **(A)** Fraction data of the 22 types of immune cells. **(B)** Differential immune cell type expression was observed between the high and low-ATP2C2 groups. Significant statistical differences between the two subgroups were assessed using the Wilcoxon test.

immunotherapy has been widely used to treat a broad spectrum of cancers including BRCA (19–22). However, not all patients can benefit from it. Thus, it is of crucial significance to improve treatment efficacy of BRCA and to uncover strong prognostic biomarkers for BRCA. Here, 7 prognosis-specific IRGs were identified by a series of bioinformatics analysis. The risk score calculated using the 7 IRGs was an independent prognostic factor for BRCA. Among all 7 prognosis-specific IRGs, four (e.g., ADRB2, CXCL12, LGMN, LIPA) have been reported to be involved in the immune microenvironment-associated pathogenesis of BRCA, implying that our bioinformatics analysis using GEO cohorts has prognostic value. The remaining three genes including ATP2C2, CELF2, and SLCO2B1 have not been formerly reported to be associated with BRCA patients' prognosis and could serve as novel potential biomarkers for BRCA. Here we gave special attention to ATP2C2 and then embarked from the transcriptomic analysis of BRCA in TCGA database, which revealed that increased ATP2C2 expression was significantly correlated with the advanced clinicopathological characteristics (age, T- and N-staging) and unfavorable prognosis of BRCA patients.

TABLE 1 | Univariate analysis showing associations between different immune cell subsets and OS in BRCA. Unadjusted HRs are shown with 95 percent confidence intervals.

Variables	Univariate analysis			
	HR	**HR.95L**	**HR.95H**	***P*-value**
Naïve B cells	51.91709028	1.393224791	1934.637024	0.032386271
T follicular helper cells	60.68385192	1.593168431	2311.450448	0.027054021
Gamma delta T cells	0.018187256	0.001155435	0.286278542	0.004380174
M0 macrophages,	5.614738081	1.866935106	16.88611651	0.002131852
Resting dendritic cells	0.003802593	1.49E-05	0.970254058	0.048764644
Resting mast cells	0.013876877	0.000785406	0.245182503	0.00350731

HR, hazard ratio.

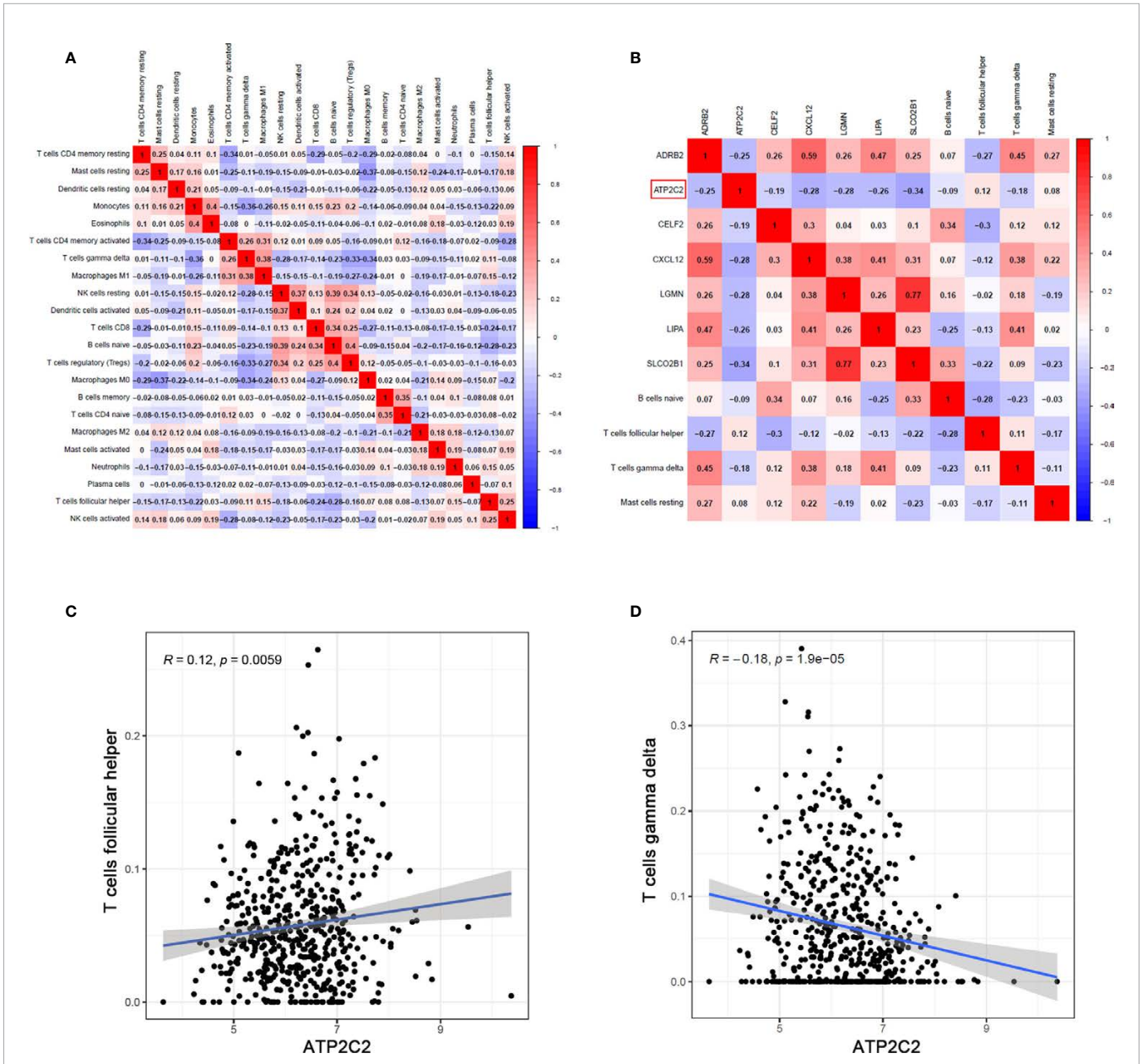

FIGURE 8 | Correlation of TICs proportion with ATP2C2 expression. **(A, B)** Correlation analysis of different TICs and the relationships between different TICs and DEGs in tumor tissues of BRCA. Pearson's correlation coefficient (*r*) was used for the significance test. **(C, D)** Correlation between Tfh cells, γδ T cells and ATP2C2 expression. Correlation test is conducted by the Pearson coefficient. *p*-value < 0.01 is the significance threshold.

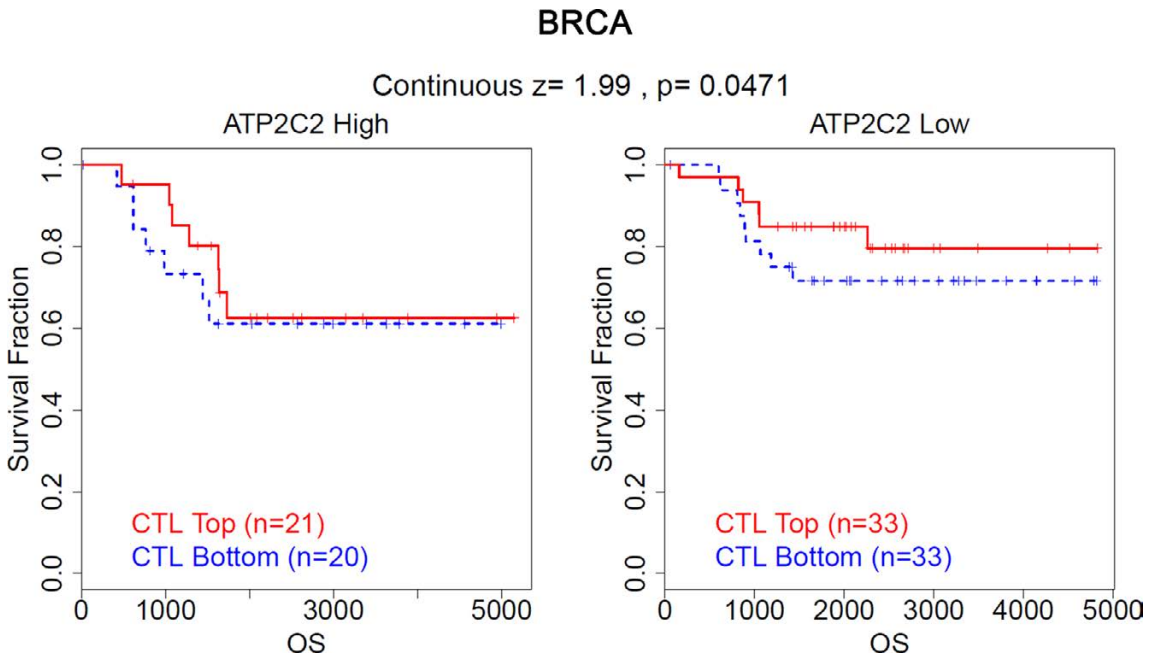

FIGURE 9 | Validation of ATP2C2 as a regulator of tumor immune escape. The association between the CTL level and OS for BRCA with different ATP2C2 levels.

ATP2C2 is mainly expressed in salivary glands, gastrointestinal and respiratory tracts, and mammary gland, and participates in Ca^{2+} transport in secretion (23). ATP2C2 has been shown to be involved in many important biological functions, such as the regulation of calcium homeostasis, and modulation of phonological short-term memory in language impairment (24, 25). In addition, it was shown that ATP2C2 helps colon cancer cells adapt to hypoxia, prevents cancer cells death, increases proliferation capacity and promotes tumor growth (26). ATP2C2 can serve as an independent prognostic factor and has better prediction for the survival of thyroid cancer patients (27). Therefore, ATP2C2 seems to play an antitumor role in BRCA. Here, relationship between ATP2C2 expression and TME were further studied. GSEA results revealed that high ATP2C2 expression was associated with metabolic-related signaling pathways, such as fructose and mannose metabolism, citrate cycle TCA cycle, and amino sugar and nucleotide sugar metabolism. In the ATP2C2 low-expression group, immune pathways including cytokine–cytokine receptor interaction, hematopoietic cell lineage and primary immunodeficiency were significantly enriched. Previous studies have validated that hypoxia-reprogrammed TCA cycle promotes breast tumorigenic cells growth (28). The expression of ATP2C2 is highly related to the TCA cycle, which may affect the prognosis of BRCA patients through the TCA cycle. Changes in cytosolic Ca^{2+} trigger events critical for tumorigenesis, such as cellular motility, proliferation, and apoptosis (6). Suppression of ATP2C2 attenuates basal intracellular Ca^{2+} levels and breast tumorigenicity (6). ATP2C2 can regulate Ca^{2+} metabolism and affect the prognosis of BRCA patients. Consistent with this, our analysis verified that BRCA patients with higher ATP2C2 expression had shorter OS time. In another study, the authors concluded that ATP2C2 antagonizes epithelial mesenchymal transition and suppresses BRCA cell migration and tumor metastasis (29). This study is inconsistent with our present observations and other studies (6, 7, 30). Perhaps it emphasizes that ATP2C2 can regulate epithelial to mesenchymal transition and BRCA metastasis, rather than studying the effect of ATP2C2 on the growth of BRCA. Together, our results suggested that ATP2C2 could participate in the conversion of TME from immune-dominant to metabolic-dominant status.

Considering the importance of immune cell infiltration in tumors (31–33), CIBERSORT was further applied to evaluate the abundance ratios of 22 types of immune cells in each BRCA specimen from GEO. Mounting evidence suggests that the interaction between the tumor and the microenvironment plays an important role in the progression of BRCA and immunotherapeutic efficacy. Therefore, we evaluated the potential of ATP2C2 to reflect the infiltration of immune cells. We found out the different proportions of numerous immune cells in different ATP2C2 subgroups. ATP2C2 low-expression group had significantly higher proportions of the naïve B cells, naïve $CD4^+$ T cells, activated memory $CD4^+$ T cells, monocytes, γδ T cells, M0 macrophages, M2 macrophages, and activated dendritic cells and significantly lower proportions of M1 macrophages, activated NK cells, and Tregs than ATP2C2 high-expression group. Tumor-infiltrating macrophages play a crucial role in tumor behavior and clinical outcome. Classically (M1) and alternatively activated (M2) macrophages exhibit different phenotypes and functions. M1 macrophages secrete

cytokines, including TNF-α, IL-6, and IL-12 (34), killing tumor cells in the TME (35). M2 macrophages can secrete anti-inflammatory factors such as TGF-β and IL-10, and promote tumor growth and metastasis (36). We found that more M1 macrophages infiltrated in ATP2C2 high-expression group compared with ATP2C2 low-expression group, implying that tumor infiltrated macrophages exert immune response functions and exhibit anti-tumor effects.

With further use of LASSO Cox regression models, as a statistical method for screening cell variables to establish the TICs risk model, the predictive accuracy could be improved significantly. Moreover, a nomogram was made based on four immune infiltrating cells to establish a more accurate prognostic prediction model for BRCA. Finally, the correlation analysis revealed that there was a significantly positive correlation between Tfh cells and ATP2C2 expression, and a negative correlation between γδ T cells and ATP2C2 expression. The main function of Tfh cells is to help B cells produce antibodies. As early as 2013, Tfh cells were first found in BRCA (37). However, the role of these Tfh cells in BRCA is not clear. It is discovered that the original Tfh cells in BRCA secrete CXCL13 to promote the accumulation of Tregs in the tumor, inhibit the body's anti-tumor immunity, and ultimately promote the development of BRCA (38). One small component of this microenvironment in humans is γδT lymphocytes, which display both innate and adaptive functions (39). Early studies have shown that γδ T lymphocytes in the BRCA cell lines have anti-tumor activity (40). Previous studies have shown that γδ T lymphocytes inhibit angiogenic signalling pathways associated with AKT and ERK, and increase apoptosis (41, 42). Interestingly, ATP2C2 promotes BRCA cell-cycle progression and cell proliferation *via* RAS-ERK pathway (6). Therefore, ATP2C2 might be responsible for the preservation of immune-active status in TME.

DATA AVAILABILITY STATEMENT

The datasets presented in this study can be found in online repositories. The names of the repository/repositories and accession number(s) can be found in the article/**Supplementary Material**.

AUTHOR CONTRIBUTIONS

HL and GR conceived and designed the study. JZL, YXW, and YSW searched and selected studies, analyzed the data, wrote and revised the paper. JL and JS prepared the figures and tables. All authors contributed to the article and approved the submitted version.

FUNDING

This study was supported by National Natural Science Foundation of China (#31420103915, #81472475).

ACKNOWLEDGMENTS

Thanks to the GEO for providing the original data.

SUPPLEMENTARY MATERIAL

The Supplementary Material for this article can be found online at: https://www.frontiersin.org/articles/10.3389/fimmu.2021.657950/full#supplementary-material

REFERENCES

1. Krug K, Jaehnig EJ, Satpathy S, Blumenberg L, Karpova A, Anurag M, et al. Proteogenomic Landscape of Breast Cancer Tumorigenesis and Targeted Therapy. *Cell* (2020) 183(5):1436–56 e31. doi: 10.1016/j.cell.2020.10.036
2. Kaymak I, Williams KS, Cantor JR, Jones RG. Immunometabolic Interplay in the Tumor Microenvironment. *Cancer Cell* (2020) 39(1):28–37. doi: 10.1016/j.ccell.2020.09.004
3. Toyama T, Iwase H, Yamashita H, Hara Y, Omoto Y, Sugiura H, et al. Reduced expression of the Syk gene is correlated with poor prognosis in human breast cancer. *Cancer Lett* (2003) 189(1):97–102. doi: 10.1016/s0304-3835(02)00463-9
4. Janes PW, Vail ME, Ernst M, Scott AM. Eph receptors in the immune-suppressive tumor microenvironment. *Cancer Res* (2020) 81(4):801–5. doi: 10.1158/0008-5472.CAN-20-3047
5. Akhand SS, Liu Z, Purdy SC, Abdullah A, Lin H, Cresswell GM, et al. Pharmacologic Inhibition of FGFR Modulates the Metastatic Immune Microenvironment and Promotes Response to Immune Checkpoint Blockade. *Cancer Immunol Res* (2020) 8(12):1542–53. doi: 10.1158/2326-6066.CIR-20-0235
6. Feng M, Grice DM, Faddy HM, Nguyen N, Leitch S, Wang Y, et al. Store-independent activation of Orai1 by SPCA2 in mammary tumors. *Cell* (2010) 143(1):84–98. doi: 10.1016/j.cell.2010.08.040
7. Peretti M, Badaoui M, Girault A, Van Gulick L, Mabille MP, Tebbakha R, et al. Original association of ion transporters mediates the ECM-induced breast cancer cell survival: Kv10.1-Orai1-SPCA2 partnership. *Sci Rep* (2019) 9 (1):1175. doi: 10.1038/s41598-018-37602-7
8. Bi KW, Wei XG, Qin XX, Li B. BTK Has Potential to Be a Prognostic Factor for Lung Adenocarcinoma and an Indicator for Tumor Microenvironment Remodeling: A Study Based on TCGA Data Mining. *Front Oncol* (2020) 10:424. doi: 10.3389/fonc.2020.00424
9. Li H, Zhao X, Wang J, Zong M, Yang H. Bioinformatics analysis of gene expression profile data to screen key genes involved in pulmonary sarcoidosis. *Gene* (2017) 596:98–104. doi: 10.1016/j.gene.2016.09.037
10. Kuleshov MV, Jones MR, Rouillard AD, Fernandez NF, Duan Q, Wang Z, et al. Enrichr: a comprehensive gene set enrichment analysis web server 2016 update. *Nucleic Acids Res* (2016) 44(W1):W90–7. doi: 10.1093/nar/gkw377
11. Jiang P, Gu S, Pan D, Fu J, Sahu A, Hu X, et al. Signatures of T cell dysfunction and exclusion predict cancer immunotherapy response. *Nat Med* (2018) 24 (10):1550–8. doi: 10.1038/s41591-018-0136-1
12. Arcangeli A. Ion channels and transporters in cancer. 3. Ion channels in the tumor cell-microenvironment cross talk. *Am J Physiol Cell Physiol* (2011) 301 (4):C762–71. doi: 10.1152/ajpcell.00113.2011
13. Karamitopoulou E. The Tumor Microenvironment of Pancreatic Cancer. *Cancers (Basel)* (2020) 12(10):3076. doi: 10.3390/cancers12103076
14. Anderson NM, Simon MC. The tumor microenvironment. *Curr Biol* (2020) 30(16):R921–R5. doi: 10.1016/j.cub.2020.06.081
15. Liu Y, Li X, Zhang Y, Wang H, Rong X, Peng J, et al. An miR-340-5p-macrophage feedback loop modulates the progression and tumor microenvironment of glioblastoma multiforme. *Oncogene* (2019) 38 (49):7399–415. doi: 10.1038/s41388-019-0952-x
16. Kumagai S, Togashi Y, Sakai C, Kawazoe A, Kawazu M, Ueno T, et al. An Oncogenic Alteration Creates a Microenvironment that Promotes Tumor

Progression by Conferring a Metabolic Advantage to Regulatory T Cells. *Immunity* (2020) 53(1):187–203 e8. doi: 10.1016/j.immuni.2020.06.016
17. Bustos SO, Antunes F, Rangel MC, Chammas R. Emerging Autophagy Functions Shape the Tumor Microenvironment and Play a Role in Cancer Progression - Implications for Cancer Therapy. *Front Oncol* (2020) 10:606436. doi: 10.3389/fonc.2020.606436
18. Fabris L, Sato K, Alpini G, Strazzabosco M. The Tumor Microenvironment in Cholangiocarcinoma Progression. *Hepatology* (2020) 18(S1):75–85. doi: 10.1002/hep.31410
19. Di Cosimo S. Advancing immunotherapy for early-stage triple-negative breast cancer. *Lancet* (2020) 396(10257):1046–8. doi: 10.1016/S0140-6736(20)31962-0
20. Lieben L. Immunotherapy: Keeping breast cancer in check. *Nat Rev Cancer* (2017) 17(8):454–5. doi: 10.1038/nrc.2017.55
21. Nathan MR, Schmid P. The emerging world of breast cancer immunotherapy. *Breast* (2018) 37:200–6. doi: 10.1016/j.breast.2017.05.013
22. Salatino M, Girotti MR, Rabinovich GA. Glycans Pave the Way for Immunotherapy in Triple-Negative Breast Cancer. *Cancer Cell* (2018) 33 (2):155–7. doi: 10.1016/j.ccell.2018.01.015
23. Vanoevelen J, Dode L, Van Baelen K, Fairclough RJ, Missiaen L, Raeymaekers L, et al. The secretory pathway Ca2+/Mn2+-ATPase 2 is a Golgi-localized pump with high affinity for Ca2+ ions. *J Biol Chem* (2005) 280(24):22800–8. doi: 10.1074/jbc.M501026200
24. Fenech MA, Carter MM, Stathopulos PB, Pin CL. The pancreas-specific form of secretory pathway calcium ATPase 2 regulates multiple pathways involved in calcium homeostasis. *Biochim Biophys Acta Mol Cell Res* (2020) 1867 (1):118567. doi: 10.1016/j.bbamcr.2019.118567
25. Newbury DF, Winchester L, Addis L, Paracchini S, Buckingham LL, Clark A, et al. CMIP and ATP2C2 modulate phonological short-term memory in language impairment. *Am J Hum Genet* (2009) 85(2):264–72. doi: 10.1016/j.ajhg.2009.07.004
26. Jenkins J, Papkovsky DB, Dmitriev RI. The Ca2+/Mn2+-transporting SPCA2 pump is regulated by oxygen and cell density in colon cancer cells. *Biochem J* (2016) 473(16):2507–18. doi: 10.1042/BCJ20160477
27. Zhao H, Zhang S, Shao S, Fang H. Identification of a Prognostic 3-Gene Risk Prediction Model for Thyroid Cancer. *Front Endocrinol (Lausanne)* (2020) 11:510. doi: 10.3389/fendo.2020.00510
28. Tang K, Yu Y, Zhu L, Xu P, Chen J, Ma J, et al. Hypoxia-reprogrammed tricarboxylic acid cycle promotes the growth of human breast tumorigenic cells. *Oncogene* (2019) 38(44):6970–84. doi: 10.1038/s41388-019-0932-1
29. Dang DK, Makena MR, Llongueras JP, Prasad H, Ko M, Bandral M, et al. A Ca (2+)-ATPase Regulates E-cadherin Biogenesis and Epithelial-Mesenchymal Transition in Breast Cancer Cells. *Mol Cancer Res* (2019) 17(8):1735–47. doi: 10.1158/1541-7786.MCR-19-0070
30. Dang D, Prasad H, Rao R. Secretory pathway Ca(2+) -ATPases promote in vitro microcalcifications in breast cancer cells. *Mol Carcinog* (2017) 56 (11):2474–85. doi: 10.1002/mc.22695
31. Sui S, An X, Xu C, Li Z, Hua Y, Huang G, et al. An immune cell infiltration-based immune score model predicts prognosis and chemotherapy effects in breast cancer. *Theranostics* (2020) 10(26):11938–49. doi: 10.7150/thno.49451
32. Grabovska Y, Mackay A, O'Hare P, Crosier S, Finetti M, Schwalbe EC, et al. Pediatric pan-central nervous system tumor analysis of immune-cell infiltration identifies correlates of antitumor immunity. *Nat Commun* (2020) 11(1):4324. doi: 10.1038/s41467-020-18070-y
33. Braun DA, Hou Y, Bakouny Z, Ficial M, Sant' Angelo M, Forman J, et al. Interplay of somatic alterations and immune infiltration modulates response to PD-1 blockade in advanced clear cell renal cell carcinoma. *Nat Med* (2020) 26(6):909–18. doi: 10.1038/s41591-020-0839-y
34. Shapouri-Moghaddam A, Mohammadian S, Vazini H, Taghadosi M, Esmaeili SA, Mardani F, et al. Macrophage plasticity, polarization, and function in health and disease. *J Cell Physiol* (2018) 233(9):6425–40. doi: 10.1002/jcp.26429
35. Hedbrant A, Wijkander J, Seidal T, Delbro D, Erlandsson A. Macrophages of M1 phenotype have properties that influence lung cancer cell progression. *Tumour Biol* (2015) 36(11):8715–25. doi: 10.1007/s13277-015-3630-9
36. Valeta-Magara A, Gadi A, Volta V, Walters B, Arju R, Giashuddin S, et al. Inflammatory Breast Cancer Promotes Development of M2 Tumor-Associated Macrophages and Cancer Mesenchymal Cells through a Complex Chemokine Network. *Cancer Res* (2019) 79(13):3360–71. doi: 10.1158/0008-5472.CAN-17-2158
37. Gu-Trantien C, Loi S, Garaud S, Equeter C, Libin M, de Wind A, et al. CD4(+) follicular helper T cell infiltration predicts breast cancer survival. *J Clin Invest* (2013) 123(7):2873–92. doi: 10.1172/JCI67428
38. Gu-Trantien C, Migliori E, Buisseret L, de Wind A, Brohee S, Garaud S, et al. CXCL13-producing TFH cells link immune suppression and adaptive memory in human breast cancer. *JCI Insight* (2017) 2(11):e91487. doi: 10.1172/jci.insight.91487
39. Davey MS, Willcox CR, Baker AT, Hunter S, Willcox BE. Recasting Human Vdelta1 Lymphocytes in an Adaptive Role. *Trends Immunol* (2018) 39 (6):446–59. doi: 10.1016/j.it.2018.03.003
40. Bank I, Book M, Huszar M, Baram Y, Schnirer I, Brenner H. V delta 2+ gamma delta T lymphocytes are cytotoxic to the MCF 7 breast carcinoma cell line and can be detected among the T cells that infiltrate breast tumors. *Clin Immunol Immunopathol* (1993) 67(1):17–24. doi: 10.1006/clin.1993.1040
41. Morrow ES, Roseweir A, Edwards J. The role of gamma delta T lymphocytes in breast cancer: a review. *Transl Res* (2019) 203:88–96. doi: 10.1016/j.trsl.2018.08.005
42. Aggarwal R, Lu J, Kanji S, Das M, Joseph M, Lustberg MB, et al. Human Vgamma2Vdelta2 T cells limit breast cancer growth by modulating cell survival-, apoptosis-related molecules and microenvironment in tumors. *Int J Cancer* (2013) 133(9):2133–44. doi: 10.1002/ijc.28217

Conflict of Interest: The authors declare that the research was conducted in the absence of any commercial or financial relationships that could be construed as a potential conflict of interest.

Copyright © 2021 Liu, Wei, Wu, Li, Sun, Ren and Li. This is an open-access article distributed under the terms of the Creative Commons Attribution License (CC BY). The use, distribution or reproduction in other forums is permitted, provided the original author(s) and the copyright owner(s) are credited and that the original publication in this journal is cited, in accordance with accepted academic practice. No use, distribution or reproduction is permitted which does not comply with these terms.

frontiers in Immunology

ORIGINAL RESEARCH
published: 16 April 2021
doi: 10.3389/fimmu.2021.678999

IDO1 Expression in Ovarian Cancer Induces PD-1 in T Cells *via* Aryl Hydrocarbon Receptor Activation

Adaobi Amobi-McCloud[1†], Ravikumar Muthuswamy[1†], Sebastiano Battaglia[1], Han Yu[2], Tao Liu[2], Jianmin Wang[2], Vasanta Putluri[3], Prashant K. Singh[4], Feng Qian[1], Ruea-Yea Huang[1], Nagireddy Putluri[3,5], Takemasa Tsuji[1,6], Amit A. Lugade[1], Song Liu[2] and Kunle Odunsi[1,6,7]*

[1] Center for Immunotherapy, Roswell Park Comprehensive Cancer Center, Buffalo, NY, United States, [2] Department of Biostatistics & Bioinformatics, Roswell Park Comprehensive Cancer Center, Buffalo, NY, United States, [3] Department of Molecular and Cell Biology, Baylor College of Medicine, Houston, TX, United States, [4] Center for Personalized Medicine, Roswell Park Comprehensive Cancer Center, Buffalo, NY, United States, [5] Molecular and Cellular Biology, Advanced Technology Cores, Baylor College of Medicine, Houston, TX, United States, [6] Obstetrics and Gynecology-Gynecologic Oncology, University of Chicago Medicine Comprehensive Cancer Center, Chicago, IL, United States, [7] Department of Gynecologic Oncology, Roswell Park Comprehensive Cancer Center, Buffalo, NY, United States

OPEN ACCESS

Edited by:
Peng Qu,
National Institutes of Health (NIH), United States

Reviewed by:
Darina Ocadlikova, University of Bologna, Italy
Theodoros Eleftheriadis, University of Thessaly, Greece

***Correspondence:**
Kunle Odunsi
odunsia@bsd.uchicago.edu

[†]These authors have contributed equally to this work

Specialty section:
This article was submitted to Cancer Immunity and Immunotherapy, a section of the journal Frontiers in Immunology

Received: 10 March 2021
Accepted: 30 March 2021
Published: 16 April 2021

Citation:
Amobi-McCloud A, Muthuswamy R, Battaglia S, Yu H, Liu T, Wang J, Putluri V, Singh PK, Qian F, Huang R-Y, Putluri N, Tsuji T, Lugade AA, Liu S and Odunsi K (2021) IDO1 Expression in Ovarian Cancer Induces PD-1 in T Cells via Aryl Hydrocarbon Receptor Activation. Front. Immunol. 12:678999. doi: 10.3389/fimmu.2021.678999

The immunoregulatory enzyme, indoleamine 2,3-dioxygenase (IDO1) and the PD-1/PD-L1 axis are potent mechanisms that impede effective anti-tumor immunity in ovarian cancer. However, whether the IDO pathway regulates PD-1 expression in T cells is currently unknown. Here we show that tumoral IDO1 expression led to profound changes in tryptophan, nicotinate/nicotinamide, and purine metabolic pathways in the ovarian tumor microenvironment, and to an increased frequency of PD-1^{+}CD8^{+} tumor infiltrating T cells. We determined that activation of the aryl hydrocarbon receptor (AHR) by kynurenine induced PD-1 expression, and this effect was significantly abrogated by the AHR antagonist CH223191. Mechanistically, kynurenine alters chromatin accessibility in regulatory regions of T cell inhibitory receptors, allowing AHR to bind to consensus XRE motifs in the promoter region of PD-1. These results enable the design of strategies to target the IDO1 and AHR pathways for enhancing anti-tumor immunity in ovarian cancer.

Keywords: IDO, indoleamine 2, 3-dioxygenase, KYN, kynurenine, AhR (aryl hydrocarbon Receptor), PD-1, immunosuppression

INTRODUCTION

Epithelial ovarian cancer (EOC) is the most lethal gynecologic malignancy in the U.S (1). Despite initial response to frontline treatments (i.e. surgery and platinum-based chemotherapy), the majority of patients relapse and ultimately die from their disease within five years (2, 3). Although several studies have demonstrated a positive correlation between EOC prognosis and magnitude of tumor-infiltrating effector T lymphocytes (TIL) (4–6), the clinical benefit of TIL-promoting immunotherapies – such as immune checkpoint inhibitors (ICI), vaccines, and adoptive cell therapy – is limited by the presence of multiple tolerogenic mechanisms within the ovarian tumor microenvironment (TME).

Among several immunosuppressive mechanisms, indoleamine 2,3-dioxygenase (IDO1) has emerged as a key targetable pathway impacting the anti-tumor function of TIL. IDO1 is a heme enzyme which catabolizes the first and rate-limiting step of tryptophan (Trp) catabolism along the kynurenine pathway (KP) to generate active immunosuppressive metabolites. Depletion of tryptophan leads to arrest of T cell proliferation (7), and inducing a stress response *via* activation of the general control nondepressible-2 (GCN2) kinase (8). In addition, kynurenine (Kyn) promotes the differentiation of CD4+ T cells into immunosuppressive regulatory T (Treg) cells *via* activation of the aryl hydrocarbon receptor (AHR) (9, 10). In EOC patients, elevated IDO1 expression correlated with a lower Trp:Kyn ratio in the ovarian tumor microenvironment (11), reduced $CD8^+$ TIL frequency (12), poor prognosis (13, 14), and suppression of T cell responses (15). The vital role of targeting IDO1 for effective immunotherapeutic control of established tumors was observed in pre-clinical models by the synergistic effect of IDO1 inhibition and immune checkpoint inhibitors to mediate the rejection of poorly immunogenic tumors, indicating that IDO1 may be a major mechanism of immunotherapy resistance (16).

Although these observations support therapeutic targeting of the IDO1 pathway, EOC patients treated with epacadostat, an IDO1 inhibitor, did not exhibit objective responses with a median progression-free survival (PFS) of 3.75 months versus 5.56 months for the control group receiving tamoxifen (17). Moreover, a subsequent randomized phase 3 clinical trial in patients with unresectable metastatic melanoma (18) failed to demonstrate improvement in clinical responses when epacadostat was added to pembrolizumab (19–21). These findings suggest that a gap still exists in understanding the full biological consequences of IDO1 enzyme activity in the TME.

Since high IDO1 enzyme activity (11) occurs concomitantly with elevated PD-1 expression on antigen-specific $CD8^+$ T cells as a marker of exhaustion and dysfunction (22), we reasoned that IDO1 may play a role in regulating the expression of PD-1 and other T cell inhibitory receptors in EOC. As the IDO1 metabolite Kyn is an endogenous ligand of AHR transcription factor (23), we investigated a possible role for AHR as the mechanism by which IDO1 facilitates TIL dysfunction associated with inhibitory checkpoint receptor upregulation. In this study, we observed profound IDO1-mediated metabolic and immunoregulatory changes in the ovarian TME, and importantly, induction of inhibitory receptors on $CD8^+$ TIL *via* Kyn-mediated AHR signaling. These data implicate a novel role for Kyn in regulating the exhausted phenotype of $CD8^+$ T cells.

RESULTS

IDO1 Reduces the Prognostic Benefit of TIL in Human EOC and Impacts Overall Survival

We evaluated the clinical outcome of 265 patients with high-grade serous ovarian cancers available in The Cancer Genome Atlas (TCGA) stratified by TIL expression and 44 genes (**Supplemental Table 1**) related to tryptophan catabolism and AHR signaling. TCGA EOC patient cohorts stratified into four distinct populations (TIL^{High}/IDO^{Low}, TIL^{Low}/IDO^{Low}, TIL^{Low}/IDO^{High}, and TIL^{High}/IDO^{High}) (**Figure 1A**). TIL^{High}/IDO^{Low} patients had a significantly improved disease-free survival (DFS) and overall survival (OS) compared with the other groups (**Figure 1B**). Additionally, elevated IDO1 and AHR pathway expression negated the beneficial impact of increased TIL signature (TIL^{High}/IDO^{High} patients), further highlighting a critical role for this pathway. These data suggest that the relationship between IDO1 expression and TIL infiltration is critical in shaping EOC patient outcomes.

To delineate the mechanisms by which IDO1 mediates immune suppression, we generated a stable IDO1-expressing EOC cell line by retroviral transduction (**Supplemental Figure 1A**) of an aggressive ID8 variant, IE9mp1 (24, 25). IE9mp1-mIDO1 tumor cells expressed the murine IDO1 (mIDO1) gene (**Supplemental Figure 1B**) and the gene product demonstrated functional enzyme activity, as measured by elevated Kyn production compared to empty vector (IE9mp1-EV) controls (**Supplemental Figure 1C**). The addition of the mIDO1 gene did not alter *in vitro* cell viability compared with EV control (**Supplemental Figure 1D**). Consistent with the TCGA EOC data, syngeneic wild-type (WT) C57BL/6 mice challenged with IE9mp1-mIDO1 displayed earlier onset of tumor burden (**Figure 1C**) and a significant decrease in overall survival compared with tumors that lack IDO1 expression (**Figure 1D**).

Expression of IDO1 Profoundly Alters the Metabolic Profile of Ovarian Tumors

Dynamic changes in the metabolic profile of intraperitoneal IDO1-expressing ovarian tumors were evaluated by LC-MS measurement of Kyn and its downstream catabolites (26). IDO1 expression at endpoint (Day 47) had the largest effect on the tryptophan, nicotinate/nicotinamide, and purine metabolism pathways ($p<0.05$; Global-ANCOVA) (**Figure 2** and **Table 1**). As expected, IDO1-expressing tumors demonstrated lower levels of tryptophan compared to EV tumors, alongside elevated expression of downstream Kyn metabolites (**Figure 2A**). The metabolite signature also revealed elevation in nicotinic acid, nicotinamide, and quinolinic acid (**Figure 2B**), consistent with enhanced *de-novo* nicotinamide generation *via* the Kyn pathway (27, 28). Nicotinate and nicotinamide metabolites (which include adenosine and thymine) were increased in the IE9mp1-mIDO1 tumors compared with IE9mp1-EV tumors on day 47 (**Figures 2C, D**). Altogether, the impact of tumoral IDO1 expression in ovarian cancer was not only confined to the kynurenine pathway, but also affected nicotinamide, purine and pyrimidine metabolic pathways, and the magnitude of change was influenced by the tumor burden.

Host- and Tumor-Derived IDO1 Expression Drive an Immunosuppressive Cell Profile in the Ovarian TME

To delineate the relative contribution of host- versus tumor-derived IDO1 on the TME immune cell profile, IDO1-sufficient

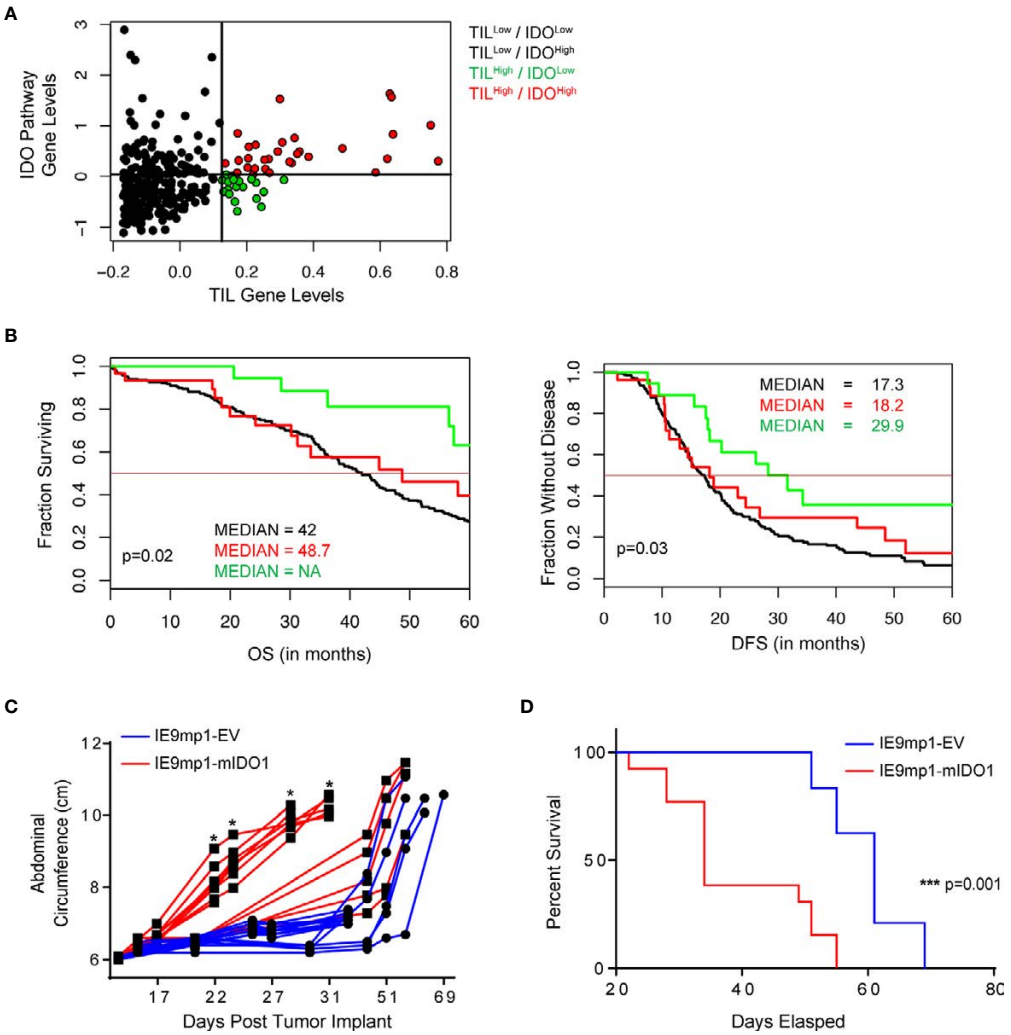

FIGURE 1 | IDO1 reduces the prognostic benefit of tumor infiltrating CD8+ T cells in human ovarian cancer and reduces overall survival in a murine model of ovarian cancer. **(A)** Scatterplot and **(B)** Kaplan-Meier curves of 4 distinct populations comprised of 265 high grade serous ovarian cancer patients from The Cancer Genome Atlas (TCGA) data set. RNA-seq data was analyzed in the context of 44 genes from the tryptophan metabolism and AHR(Aryl Hydrocarbon Receptor) signaling pathways, and CD3E, CD8A, IL2, and Granzyme B. Confidence intervals for the stratified population of patients include OS (Overall Survival): black line median 42.0 [38.0, 46], red line median 48.7[31.2, NA] and green line median NA[57.4, NA] p=0.02; DFS (Disease Free Survival): black line median 17.3[15.1, 19.9], red line median 18.2[13.0, 48.5], and green line median 29.9[18.2, NA] p=0.03). **(C)** 6- to 8- week old WT C57BL/6 mice challenged i.p. with $1x10^7$ IE9mp1-EV (n=10) or IE9mp1-mIDO1 (n=12) tumor cells. Tumor progression was quantified by measuring the abdominal circumference of tumor-bearing mice. **(D)** Kaplan-Meier curves of the survival analysis of IE9mp1-EV (n=14) and IE9mp1-mIDO1 (n=15) tumor-bearing WT C57BL/6 mice. *p < 0.05, ***p < 0.001, by the Log-rank (Mantel-Cox) test **(B, D)**, or Student's t test **(C)**. NA, Not available.

C57BL/6 (WT) mice and IDO1-knockout mice (IDOKO, C57BL/6 background) were challenged intraperitoneally with either IE9mp1-EV or IE9mp1-mIDO1. WT mice bearing IE9mp1-mIDO1 tumors exhibited a non-significant decrease in $CD8^+$ TIL frequency at all time points of tumor growth compared to animals whose tumors lack IDO1 expression (**Figure 3A**, left panel). IDO1 deficient mice also exhibited diminished $CD8^+$ TIL frequency (**Figure 3A**, right panel), but the complete absence of IDO1 expression in tumor and host significantly increased $CD8^+$ TIL frequency on Day 57, indicating that both host- and tumor-derived IDO1 contribute to reduced TIL accumulation in the ovarian TME. Confocal microscopy of IE9mp1-mIDO1 and IE9mp1-EV tumors also confirmed that tumor-derived IDO1 inversely impacted $CD8^+$ TIL frequency (**Figure 3B**).

As IDO1 is known to induce Tregs (8, 10, 29), ovarian TME $CD4^+CD25^+FoxP3^+$ Treg frequency was examined in IDO1-sufficient C57BL/6 mice. Treg frequency was significantly elevated on Day 48 in IE9mp1-mIDO1 tumor-bearing mice (**Figure 3C**) along with increased levels of $CD11b^+Ly6Ghigh$ myeloid cells (**Figure 3D**). To address potential mechanisms regulating the influx and retention of Tregs and myeloid cells in

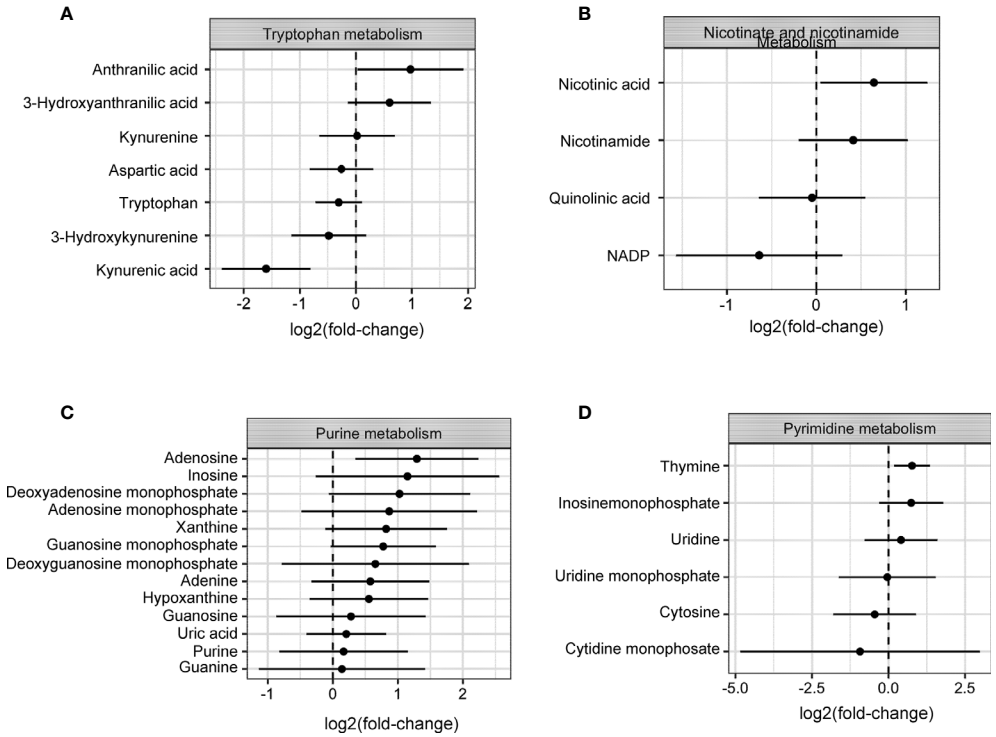

FIGURE 2 | Metabolites levels from the kynurenine, nicotinamide, purine and pyrimidine metabolic pathways are affected by IDO1 expression by the tumor. On Day 28 of tumor progression, whole tumor was harvested from IE9mp1-mIDO1 (n=4) and IE9mp1-Empty Vector control (n=4) tumor-bearing mice. On Day 47 of tumor progression, whole tumor was harvested from IE9mp1-mIDO1 (n=4) and IE9mp1-Empty Vector control (n=5) tumor-bearing mice. Mean log 2 fold changes in metabolites from **(A)** tryptophan amino acid degradation, **(B)** NAD, **(C)** purine and **(D)** pyrimidine metabolism pathways measured in IE9mp1-mIDO1 and IE9mp1-EV tumor from WT C57BL/6 mice on Days 28 and 47. These data presented are the relative abundance measurements of the metabolite level and sample t test statistical analysis reveals the 95% confidence interval of the mean log-fold change in metabolites. The p-values of all the metabolites are listed in **Supplemental Table 1**.

TABLE 1 | Impact of IDO1 on metabolism pathways.

Pathway	p-value	Impact
Tryptophan metabolism	0.003523	0.26445
Nicotinate and nicotinamide metabolism	0.029416	0.1684
Nitrogen metabolism	0.04472	0.00067
Purine metabolism	0.063504	0.20329
Pyrimidine metabolism	0.43918	0.19526

Global-ANCOVA analysis of IE9mp1-mIDO1 or IE9mp1-EV tumor from WT C57BL/6 mice. P-value indicates the significance of overall change for the metabolic pathway in IDO1-expressing tumors. Impact score measures the importance of a metabolite in the metabolic network.

the ovarian TME, chemokines were measured in cell-free tumor ascites fluid from C57BL/6 mice (30). The Treg-attractant MIP-1B/CCL4 (31) was significantly increased in IDO1-expressing tumors (**Supplemental Figure 2A**). Similarly, IDO1-expressing tumors exhibited significant increases in monocyte/macrophage attracting MCP-3/CCL7, eotaxin/CCL11, MCP-1/CCL2, and G-CSF (**Supplemental Figures 2B–E**) (32, 33). These results indicate that tumoral IDO1 expression regulates the ovarian TME chemokine signature for enhanced recruitment of immunosuppressive cells resulting in reduced $CD8^+$ TIL frequency.

Kynurenine Mediates Induction of Inhibitory Receptors on $CD8^+$ T Cells

To assess whether host- or tumor-derived IDO1 expression leads to upregulation of inhibitory receptors, we analyzed the phenotype of $CD8^+$ TILs isolated from WT and IDOKO mice bearing either IE9mp1-mIDO1 or IE9mp1-EV tumors. In both IDO1-sufficient and IDO1KO TIL, tumoral IDO1 expression significantly increased the frequency of PD-1^+ $CD8^+$ TIL on Day 48 compared with those from IE9mp1-EV challenged mice (**Figure 4A**). Notably, in the absence of host- and tumor-derived IDO1 this effect was abrogated and there was no significant upregulation of PD-1 on $CD8^+$ TIL at the same time point (Day 48) in IE9mp1-EV tumor-bearing IDOKO mice, indicating that regardless of the cellular source of IDO1 expression, presence of IDO1 enzyme activity contributes to PD-1 upregulation on ovarian $CD8^+$ TIL.

The contribution of IDO1-induced KYN generation by tumor cells on PD-1 expression was evaluated using anti-CD3/anti-CD28 activated $CD8^+$ lymphocytes. IE9mp1-mIDO1 cell culture supernatant allowed for a controlled system where IDO1-mediated Trp catabolism into KYN could be quantified (**Figure 4B**, left). $CD8^+$ T cells significantly upregulated PD-1 expression in the presence of elevated tumor-produced KYN

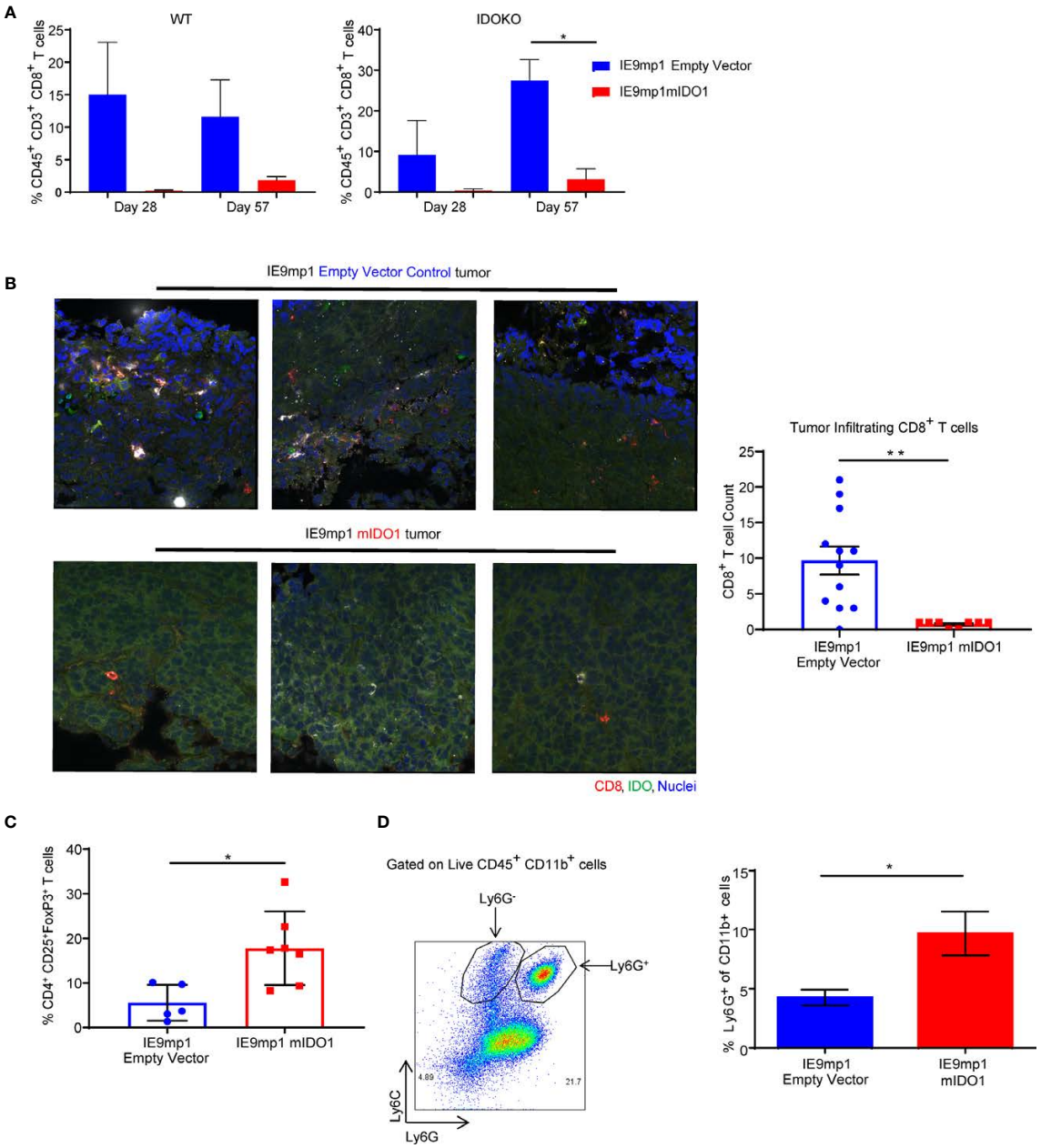

FIGURE 3 | Expression of IDO1 leads to poor tumor infiltration by CD8+ T cells and increased infiltration of suppressive immune cells in the ovarian tumor microenvironment. **(A)** Frequency of CD8+ TILs on Days 28 and 57 from WT C57BL/6 (left panel n=6) and IDOKO (right panel n=6) mice challenged i.p. with 1x10e7 IE9mp1-mIDO1 or IE9mp1-EV tumor cells. **(B)** Immuno-stained IE9mp1-mIDO1 and IE9mp1-EV tumor from WT C57BL/6 mice on Day 48 with anti-IDO1 (green), CD8+ T cell (red), and DAPI (blue). Quantification of CD8+ T cells from 3 field images per tissue slide, (n=11 IE9mp1-EV and n=8 IE9mp1-mIDO1). Total original magnification is 63x. **(C)** Flow cytometry analysis of tumor ascites for $CD4^+CD25^+FoxP3^+$ T cell frequency in IE9mp1-mIDO1 (n=7) and IE9mp1-EV (n=5) tumor-bearing WT C57BL/6 mice on Day 48. **(D)** Frequency of Ly6G+in $CD11b^+$ cell IE9mp1-EV (n=5) or IE9mp1-mIDO1 (n=5) tumor-bearing WT C57BL/6 mice on Day 28. *p < 0.05, **p < 0.01, using Student's t test **(B–D)**. The data represent means ± SEM of three independent experiments.

(**Figure 4B**, right). Activation of $CD8^+$ T cells in varying KYN concentrations resulted in upregulation of not only PD-1 (**Figure 4C**), but also additional inhibitory receptors such as *Klrg1* (**Figure 4D**) and *Tim3* (**Figure 4E**), although the effect was more pronounced at higher KYN concentrations. Taken together, these results demonstrated that kynurenine contributed to the upregulation of co-inhibitory receptors expression on CD8+ T cells *in vivo* and *in vitro*.

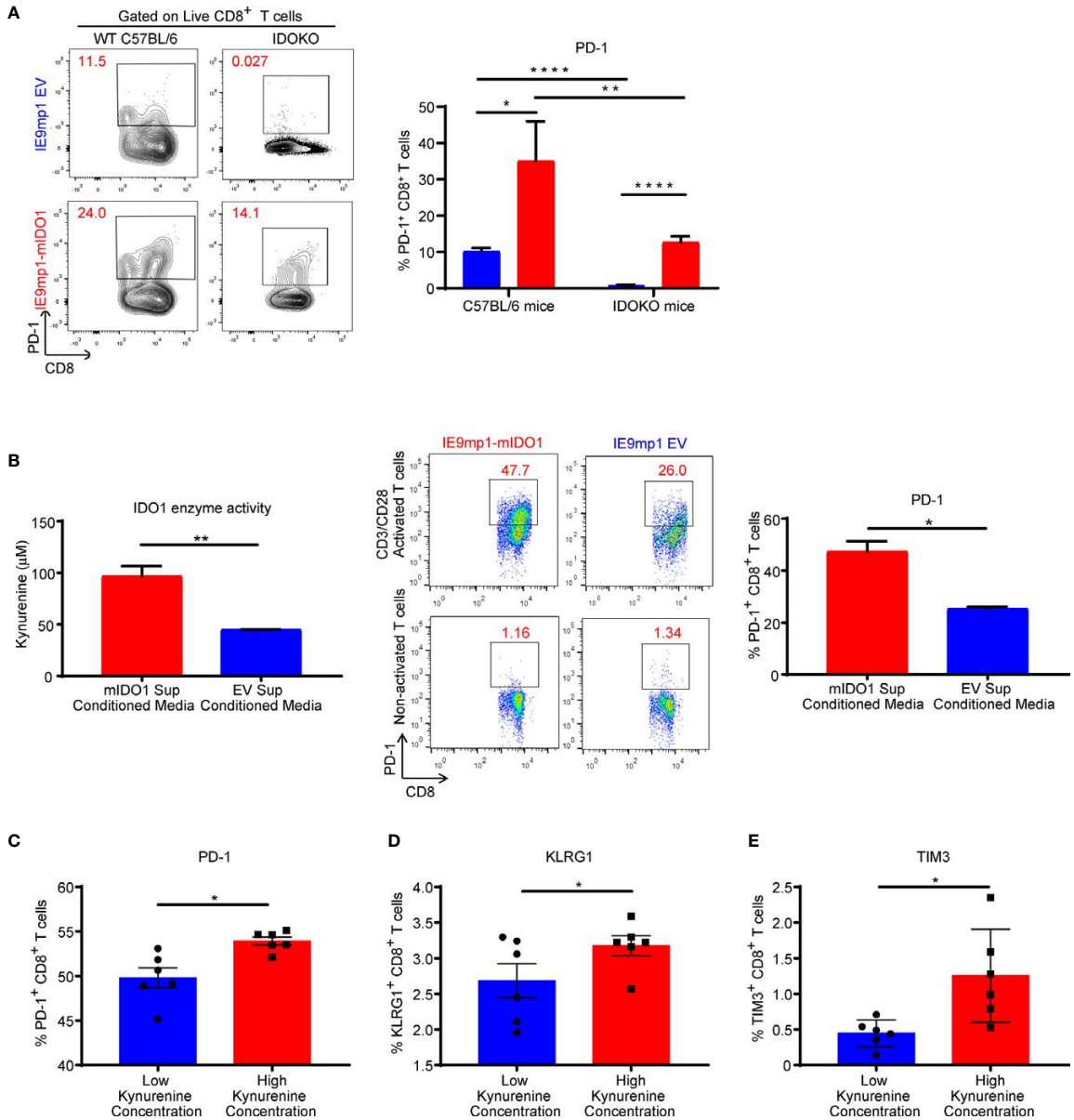

FIGURE 4 | Kynurenine mediates upregulation of inhibitory receptor on CD8+ T cells. **(A)** Frequency of PD1+CD8+ T cells in tumor ascites from WT C57BL/6 or IDOKO mice challenged i.p. with 1x10e7 IE9mp1-EV (n=5) or IE9mp1-mIDO1 (n=6) tumor cells on Day 48, as determined by flow cytometric analysis. (**B**, left) Kynurenine concentrations measured in IE9mp1-EV and IE9mp1-mIDO1 tumor cell culture supernatant by colorimetric assay. (**B**, right) Frequency of PD1+CD8+ T cells, from WT C57BL/6 mice spleens, co-cultured with 1μg/mL anti-CD3/CD28 in IE9mp1-mIDO1 or IE9mp1-EV tumor cell culture supernatant for 48 hr. PD1+CD8+ T cell frequency was determined by flow cytometric analysis. **(C)** PD-1, **(D)** KLRG1, and **(E)** TIM3 expression analyzed by flow cytometric analysis on T lymphocytes from WT C57BL/6 mice activated with 1μg/mL anti-CD3/CD28 and with treated kynurenine. *p < 0.05, **p < 0.01, ****p < 0.0001, by Student's t test **(A–E)**. The data represent means ± SEM of three independent experiments performed in triplicate.

PD-1 Gene Contains Putative AHR Binding Sites

Upon activation by its natural endogenous agonist, KYN, AHR translocates into the nucleus and regulates target gene expression in T cells (9, 10), including a tumor-promoting role *via* suppression of anti-tumor immunity (23). To account for this observation, we hypothesized that the genes encoding T cell inhibitory receptors contain AHR binding sites responsible for transcriptional regulation upon sequential KYN ligation and AHR activation. Therefore, we performed computational analysis of promoter regions of T cell inhibitory receptor genes for the consensus AHR xenobiotic response elements (XRE) binding motifs (**Figure 5A**). We identified multiple AHR binding sites in the upstream gene promoter region of murine

(**Figure 5B**) and human *Pdcd1* (PD-1) gene (**Supplemental Figures 3** and **4**). AHR binding sites were also present in the upstream promoter regions of additional inhibitory receptors such as *Lag3*, *Tim3*, *Klrg1*, *Ctla4*, *Btla*, *2B4*, *CD160* and *TIGIT* (**Supplemental Figures 3** and **4**).

To address the mechanism by which KYN mediates PD-1 expression, we next evaluated AHR expression in activated $CD8^+$ T cells. AHR gene expression in T cells was not altered by their activation in the presence of KYN or another well characterized exogenous AHR ligand, 2,3,7,8-tetrachlorodibenzo-p-dioxin (TCDD) (**Figure 5C**) (34). Although KYN ligation did not impact AHR expression in T cells, it did result in AHR target gene transcription, specifically the cytochrome P40 enzyme, *Cyp1a1* (**Figure 5D**) (35), confirming KYN-mediated AHR activation. As *Cyp1a1* expression requires nuclear translocation of the active AHR-KYN complex (36, 37), we evaluated the kinetics of KYN-mediated AHR nuclear translocation in activated $CD8^+$ T cells. At 2 hours post-activation in the presence of KYN and TCDD, AHR was observed in the nucleus (**Figure 5E**, green) and thus provides a mechanism by which AHR directly mediates PD-1 expression in $CD8^+$ T cells.

Kynurenine Permits Genome-Wide Chromatin Accessibility In Regulatory Regions of PD-1 Gene

As KYN-mediated upregulation of inhibitory receptors requires AHR interaction with XRE sequences in the promoter regions, we next evaluated how KYN treatment alters the dynamics of $CD8^+$ T cell genome-wide chromatin accessibility by ATAC-seq (38). Increases of chromatin accessibilities in KYN-treated activated $CD8^+$ T cells were observed for two regulatory elements of the *Pdcd1* (**Figure 6A**) and *Lag3* (**Supplemental Figure 5**) genes, indicating that KYN treatment mediates the extent of chromatin accessibility for key T cell inhibitory receptors leading to their upregulation. Moreover, these data also suggest an epigenetic role for IDO1 in regulating the transcriptional activity of $CD8^+$ TIL.

KYN Induces PD-1 Expression on $CD8^+$ T Cells in an AHR-Dependent Manner

Direct evidence for KYN-mediated AHR binding to XRE motifs in the PD-1 promoter was evaluated by chromatin immunoprecipitation of activated $CD8^+$ T cells (**Supplemental Figure 6**). ChIP-qPCR using anti-AHR bound to genomic DNA confirmed enrichment of AHR binding to XRE motifs within the murine *Pdcd1* gene promoter region by KYN treatment but not by TCDD (**Figure 6B**). Furthermore, ChIP-qPCR verified PD-1 gene expression was upregulated in the presence of KYN. The requirement for AHR-mediated PD-1 expression following KYN treatment was tested by utilizing the AHR antagonist CH223191 (39). In addition to inhibiting its downstream target gene *Cyp1a1*, AHR antagonism severely diminished KYN-mediated PD-1 upregulation on $CD8^+$ T cells (**Figures 6C, D**). These data confirm that AHR interaction with responsive elements in the PD-1 promoter facilitates its transcription upon treatment with KYN and suggests an approach in which AHR antagonism can be coupled with IDO1 blockade to synergistically prevent PD-1 mediated T cell dysfunction.

DISCUSSION

Tryptophan catabolism by IDO1 has been firmly established as a powerful mechanism of innate and adaptive immune tolerance in EOC and other solid tumors (13, 14, 16, 40). However, efforts to target this pathway in the clinic has met with limited success (17, 18), probably because the full biologic consequences of IDO1 on the TME remain incompletely characterized. In this study, we fill a major gap in knowledge by demonstrating that (1) the metabolic re-wiring of the TME by IDO1 is profound and goes beyond KYN accumulation by also affecting nicotinate/nicotinamide and purine metabolism; (2) KYN differentially alters frequencies of CD8 T vs regulatory T cells (Treg)/Myeloid derived suppressor cells (MDSC) cells in tumor; (3) KYN alters chromatin accessibility in regulatory regions of inhibitory receptors leading to their upregulated expression; and (4) AHR binding to consensus XRE motifs is the mechanism by which IDO1 activity mediates T cell dysfunction. These results support the design of strategies to target the IDO1 and AHR pathways for improving anti-tumor immunity in EOC. While we focused here on the impact of IDO1 on adaptive immunity, its tumor intrinsic role would need to be clarified in future studies.

To study the consequences of the metabolic microenvironment imposed by IDO1, we first investigated quantitative and qualitative changes in $CD8^+$ T cell infiltration. In addition to the effect of IDO1 in reducing intra tumoral accumulation of $CD8^+$ TIL, the cytokine milieu of the TME was noted to favor the recruitment of immunosuppressive Tregs and myeloid cells. Tumoral IDO1-induced KYN was sufficient to upregulate PD-1 on $CD8^+$ T cells *in vivo* and *in vitro*. Moreover, we established AHR activation by KYN as the mechanism by which $CD8^+$ T cells acquired an exhausted phenotype of PD-1 expression.

Although our bioinformatics analyses identified AHR XRE binding sites in the promoter region of several human and murine checkpoint receptor genes, chromatin accessibility by ATAC-seq indicated the potential for AHR transcription factor occupancy in *Pdcd1* and *Lag3* of inhibitory receptor genes. Since ATAC-seq alone cannot decide which transcription factor binds to accessible chromatin (38), we utilized ChIP-qPCR and demonstrated specific binding of AHR to DNA in the *Pdcd1* gene. Thus, KYN increased the accessibility of AHR to XRE sequences in the PD-1 gene promoter of $CD8^+$ T cells. Further support for an AHR-dependent mechanism for kynurenine upregulation of PD-1 gene expression is provided by abrogation of gene expression in the presence of the AHR antagonist CH223191. These findings establish that kynurenine activation of AHR is a critical mechanism by which IDO1 impacts the upregulation of checkpoint receptors on $CD8^+$ T cells in the ovarian TME. Although PD-1 expression was shown to be mediated by non-physiological concentrations of KYN in a recent study (41), the downstream transcriptional events that regulate this

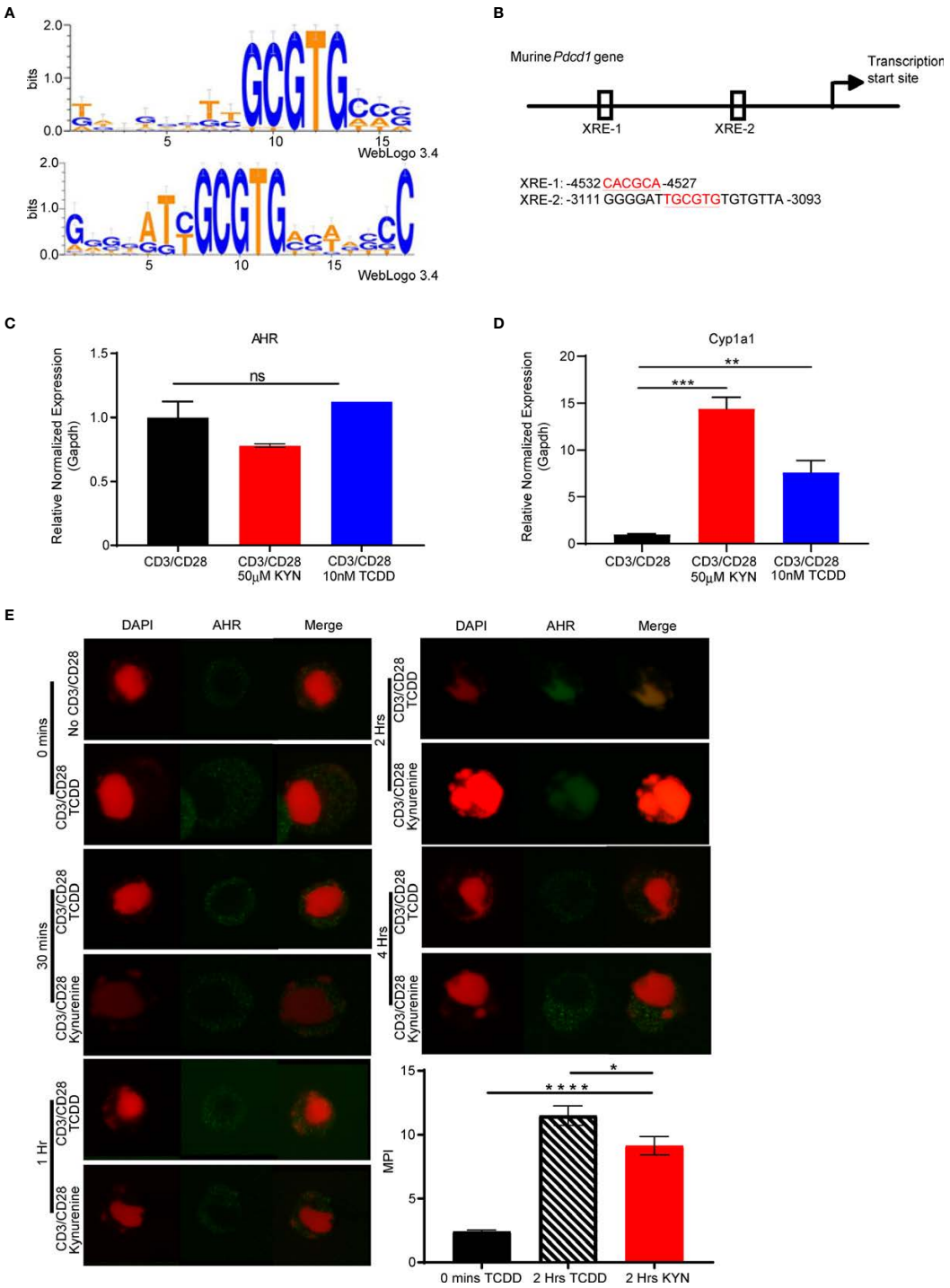

FIGURE 5 | PD-1 gene contains putative aryl hydrocarbon receptor binding sites. **(A)** Motif Logo depicting the position specific weight matrices of the AHR binding site [xenobiotic response element (XRE)]. **(B)** Schematic representation of the identified AHR binding site in the *Pdcd1* promoter. **(C)** Anti-CD3/CD28 activated CD8+ T cells from spleens of WT C57BL/6 mice were treated with IL-2 (50U/mL), KYN (50μM) or TCDD (10nM) for 6 days. AHR and **(D)** *Cyp1a1* mRNA was determined. **(E)** AHR nuclear translocation was measured in anti-CD3/CD28 bead-activated CD8+ T cells from spleens of WT C57BL/6 mice treated with KYN (50μM) or TCDD (10nM) for 0,0.5,1,2 and 4hrs as indicated. CD8+ T cells were immuno-stained for AHR (green) and DAPI (red). Mean pixel intensity (MFI) of AHR nuclear translocation was calculated (bar graph) using Image J Total original magnification is 189x. *$p < 0.05$, **$p < 0.01$, ***$p < 0.001$, ****$p < 0.0001$, ns, not significant, by Student's t test **(D, E)**. The data represent means ± SEM of three independent experiments performed in triplicate.

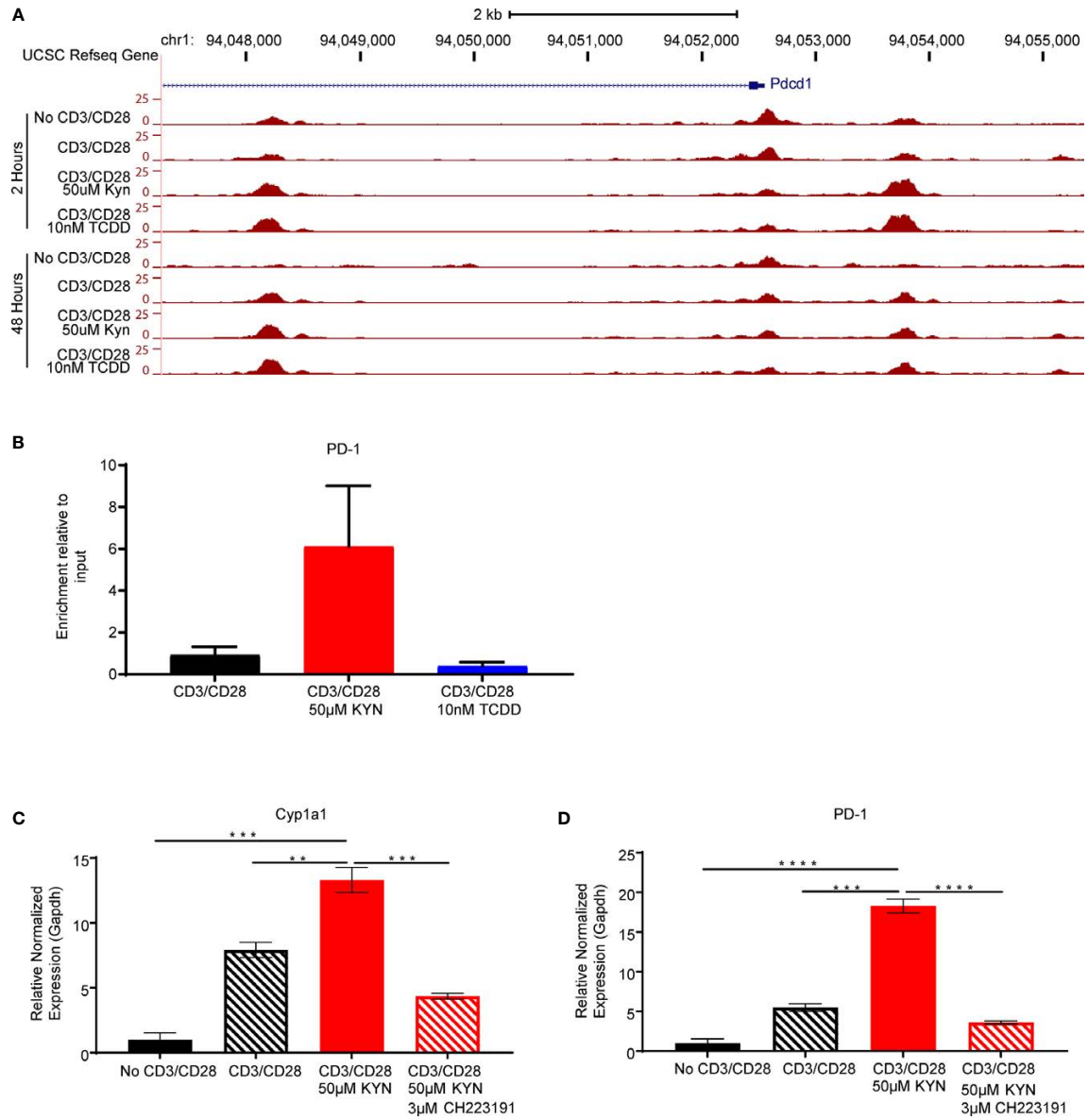

FIGURE 6 | Kynurenine induces PD-1 expression on CD8+ T cells in an AHR-dependent manner. **(A)** UCSC Genome Browser plot of open chromatin accessible regions in two DNA regulatory elements in the PD1 gene identified by ATAC-seq analysis of CD8+ T cells, from WT C57BL/6 mice, activated by anti-CD3/CD28 and treated with KYN (50μM) or TCDD (10nM) for 2 and 48 hrs. **(B)** CHIP-qPCR *Pdcd1* analysis in anti-CD3/CD28 bead-activated and KYN (50μM) treated CD8+ T cells for 2 hours from spleens of WT C57BL/6 mice with AHR antibody and *pdcd1* promoter primers. **(C)** Anti-CD3/CD28 activated CD8+ T cells from spleens of WT C57BL/6 mice were treated with KYN (50μM) and CH223191(AHR antagonist) (3μM) for 6 days. *Cyp1a1* and **(D)** PD-1 mRNA was determined. $^{**}p < 0.01$, $^{***}p < 0.001$, $^{****}p < 0.0001$ by Student's t test **(B–D)**. The data represent means ± SEM of three independent experiments performed in triplicate **(B–D)**.

dysfunctional TIL phenotype were not identified. Our study provides a targetable mechanism by which IDO1 regulates inhibitory checkpoint receptors on $CD8^+$ TIL *via* kynurenine activation of AHR.

A notable limitation of the present study is that while we have uncovered alterations in metabolic pathways beyond kynurenine, their contribution to induction of T cell inhibitory receptors or other mechanisms of immune suppression were not fully examined. For example, NAD is able to regulate CD4 T cell differentiation and promotes IL-10 and TGF-B1 production by Th1 and Th17 cells, respectively (42). In addition, it will be important to confirm whether AHR mediated upregulation of inhibitory T cell receptors is a general mechanism for other metabolites along the kynurenine pathway. Moreover, while murine studies can yield valuable insights into AHR function, there are differences between the human and mouse AHR, such as differences in the affinity to ligand activation (43) indicating that future human studies will need to be conducted with this caveat in mind. In addition, a report by

Eleftheriadis et al. (44) indicated that IDO decreased glycolysis and glutaminolysis by activating GCN2K, and IDO–induced activation of AhR increased the expression of all carnitine palmitoyltransferase I isoenzymes, leading ultimately to increased free fatty acid (FFA) oxidation and preservation of $CD4^+$ T–cell survival and proliferation. This implies that in a normal environment containing fatty acids, $CD4^+$ T–cell survival and proliferation may not be reduced since IDO-mediated supply of FFA would provide the required energy for cell survival and proliferation. Since this was not a focus of our study, future studies are warranted to examine the potential impact of any IDO-mediated effects on FFA generation on CD4+ T cells. We acknowledge that these results are described in an overexpressing IDO1 tumor model. Intrinsically, parental ID8 tumor cells do not produce appreciable levels of IDO1 (data not shown), therefore, we generated a stable IDO1-expressing EOC cell line by retroviral transduction. Also, ID8 by its nature is not a typically inflammatory tumor model, however, we show in these studies that the TILs that enter the tumor can be modulated by IDO1 and has an impact on efficacy.

Despite these limitations, our current study sheds some light on potential reasons for the limited efficacy of ECHO-301/KEYNOTE-252 (NCT02752074), the first phase 3 randomized double-blind study of epacadostat in combination with anti-PD-1 antibody pembrolizumab in patients with unresectable or metastatic melanoma (19–21). First, KYN activation of AHR may be a major resistance mechanism *via* upregulation of several immune checkpoint receptors, with the implication that PD-1 blockade monotherapy may be insufficient to derive benefit from IDO1 blockade. We demonstrate that *Lag3* gene expression on $CD8^+$ TILs are similarly impacted by KYN, and therefore *Lag3* may serve as a compensatory escape pathway when the PD-1/PD-L1 pathway is blocked. Second, the impact of tumoral IDO1 expression in ovarian cancer was not confined to the kynurenine pathway, but also mediated metabolic changes downstream of kynurenine, demonstrating a role for nicotinate, nicotinamide, purine and pyrimidine metabolic pathways. Lastly, AHR antagonists have been identified and examined as potential therapeutic tools to study the role of AHR in tumorigenesis (34). Preclinical studies in multiple myeloma, suggest that therapeutic targeting of the AHR, with an inhibitor such as the FDA-approved clofazimine (45), may improve clinical outcomes.

Altogether, this study demonstrates that IDO1-induced KYN activates AHR nuclear translocation where its direct binding to XRE motifs in the PD-1 gene promoter (**Supplemental Figure 7**) results in T cell dysfunction. Strategies to concomitantly target the IDO1 and AHR pathways may overcome immune suppression and enhance anti-tumor immunity in EOC and other solid tumors.

METHODS

The Cancer Genome Atlas (TCGA) Data Analysis

Gene expression data were downloaded from cBioportal. Immune and IDO signature scores were calculated using the sum of the gene expression selected genes (**Supplemental Table 1**) divided by the square root of the number of genes. Patients were then divided in four groups: TIL^{High}/IDO^{Low}, TIL^{Low}/IDO^{Low}, TIL^{Low}/IDO^{High}, and TIL^{High}/IDO^{High} based on immune and IDO score values. Survival analysis across groups was calculated using clinical information available on cBioportal using log rank test at a significance threshold of 0.05.

Animals. Female and male WT C57BL/6 mice and IDOKO mice (stock no. 005867) were purchased from Jackson Laboratory (Bar Harbor, ME), and bred in our facility (Roswell Park Comprehensive Cancer Center) according to an approved protocol. All animals were maintained in the Laboratory Animal Shared Resource under specific pathogen-free conditions. All animal experiments were carried out according to protocol guidelines approved by the Institute Animal Care and Use Committee (IACUC) of Roswell Park Comprehensive Cancer Center (Buffalo, NY).

Cell Lines. The murine *Ido1* (mIDO1) gene was overexpressed in mouse ovarian surface epithelial cell (MOSEC) lines by retroviral transduction. Full-length mIDO1 gene was PCR amplified from cDNA of IFNG treated ID8 cell line (25) and inserted into the first cloning site in a retrovirus backbone vector (pQCXIX, Clontech-TaKaRa). A fusion gene of codon-optimized Luciferase (Luc2) and tandem-dimeric Tomato (tdT) gene was PCR amplified from the pcDNA3.1(+)Luc2=tdT (Addgene plasmid # 32904) (a gift from Christopher Contag at Stanford University, Stanford, California) (46) and inserted into the second cloning site. The parental IE9 cell line was provided to our lab by Dr. Tahiro Shin at the University of Texas Health Sciences Center (San Antonio, Texas). A control empty vector was constructed by inserting Luc2=tdT gene alone. The retroviral transfer vector was co-transfected with pVSV-G retroviral envelope-expressing plasmid into the GP2-293 cell line (Clontech-TaKaRa) using Lipofectamine 2000 reagent (Invitrogen) to produce retrovirus supernatant. Parental ID8 (25), IE9 (47) or IE9mp1 (24) tumor cell lines were transduced by retroviral vectors in the presence of 8mg/ml polybrene (Sigma-Aldrich). Stable cell lines were established after flow cytometry cell sorting of tdT-expressing cells using a FACSAria 2 (BD Biosciences). Expression of tdT in established cell lines was periodically monitored by flow-cytometry and confirmed that >99% cells expressed tdT before experiments. All cell lines were cultured in complete culture medium: RPMI1640 (Corning Cellgro®) supplemented with 10% fetal bovine serum (VWR), 1% sodium pyruvate (100mM), 1% L-glutamine (200mM), 1% MEM nonessential amino acid (100x), 1% penicillin/streptomycin (100x), 2.5% Hepes, and 0.1% beta-2-mercaptoethanol (50mM) in an incubator at 37°C and 5% CO_2.

Tumor Challenge and Measurement

WT C57BL/6 and IDOKO mice were challenged intraperitoneally (i.p.) with $1x10^7$ IE9mp1-mIDO1 or IE9mp1-EV tumor cells in a final volume of 500µl Dulbecco's PBS (Corning Cellgro®). Tumor progression and the amount of tumor burden were monitored by measuring abdominal distension to track the accumulation of peritoneal ascites formation. Mice were euthanized by CO_2 asphyxiation and/or

cervical dislocation when the abdominal circumference of i.p. tumors reached a 50% girth increase and/or upon detection of declining health conditions as described in our standard operating procedure for Body Scoring, according to IACUC guidelines.

IDO Enzyme Activity Measurement

Kynurenine was measured in cell culture supernatants by incubating the sample with a 30% w/v Trichloroacetic acid (Sigma-Aldrich) solution prepared in water, and Ehrlich reagent (2% PDAB) prepared fresh for each assay by dissolving p-dimethylaminobenzaldehyde (PDAB) (Sigma-Aldrich) in acetic acid. The colorimetric reaction was measured using a microplate reader at OD 490nm. The OD values were measured and calculated against standard dilution curve of L-kynurenine (Sigma-Aldrich).

Flow Cytometry Antibodies and Reagents

LIVE/DEAD™ Fixable Yellow Dead Cell Stain Kit, for 405nm excitation catalog no. L34959 was purchased from Thermo Fischer Scientific. Mouse-specific FITC-anti-CD45 (clone 30-F11) catalog no.11-0451-82, eFluor 450-anti-CD11b (clone M1/70) catalog no. 48-0112-82, APC-anti-TIM3 (clone 8B.2C12) catalog no. 17-5871-80, APC-anti-CD25 (clone PC61.5) catalog no.17-0251-82, PerCP-eFluor 710-anti-CD8A (clone 53-6.7) catalog no.46-0081-82, PE-anti-Foxp3 (clone FJK-16s) catalog no. 12-5773-82, and PE-Cy7-anti-CD4 (clone GK1.5) catalog no. 25-0041-82 were purchased from eBiosciences. BV421-anti-PD-1 (clone 29F.1A12) catalog no. 135218 was purchased from BioLegend. Anti-CD16/CD32 FcBlock (clone 2.4G2) catalog no.553142, PE-Cy7-anti-Ly6G/Ly6C (clone RB6-8C5) catalog no.565033, BV450-anti-CD45 (clone 30-F11) catalog no. 560501, FITC-anti-CD8A (clone 53-6.7) catalog no. 553031, PerCP-Cy5.5-anti-Ly6G/Ly6C (clone RB6-8C5) catalog no. 561103, PerCP-anti-CD8A (clone 53-6.7) catalog no.553036, PE-anti-CD3E (clone 145-2C11) catalog no.553064, PE-anti-CD11b (M1/70) catalog no. 557397, and PerCP-anti-CD4 (clone RM4-5) catalog no. 553052 were purchased from BD Biosciences. Foxp3/Transcription Factor Fixation and Permeabilization Concentrate and Diluent kit, catalog no. 00-5523-00 (eBiosciences) was used for intracellular Foxp3 staining. Flow cytometry data were acquired using a BD Biosciences LSR 2 flow cytometer and BD FACSDiva software, and analyzed using FlowJo v10 software (TreeStar).

RNA Isolation and Quantitative Real-Time Polymerase Chain Reaction (PCR) Analysis

Total RNA was isolated using the RNeasy mini kit (Qiagen). cDNA was prepared using iScript cDNA Synthesis kit (BioRad) and reverse transcription was carried out on the T100 Thermal Cycler (BioRad). Quantitative real-time PCR was performed using iQ SYBR Green Supermix (BioRad) on the C1000 Touch Thermal Cycler, CFX96 Real-Time System (BioRad). Primer sequences used include *Ido1* forward 5'-TCTGCCTGTGC TGATTGA-3', reverse, 5'-CTGTAACCTGTGTCCTCTCA-3'; *AHR* forward 5'-CCACTGACGGATGAAGGA-3', reverse, 5'-ATCTCGTACAACACAGCCTCT-3'; *CYP1A1* forward 5'-GACACAGTGATTGGCAGAG-3', reverse, 5'-GAAGGTCTCC AGAATGAAGG-3'; *Pdcd1* forward 5'-CTCGGCCATGGGA CGTAGGG-3', reverse, 5'-GGGTCTGCAGCATGCTAATG GCTG-3'; and *Gapdh* forward 5'-GCCTTCCGTGTTCCTAC CC-3', reverse, 5'-CAGTGGGCCCTCAGATGC-3'. PCR data were analyzed using CFX Manager 3.1 (BioRad). Experiments were performed in triplicates.

Purification of $CD8^+$ T Cells From Splenocytes

$CD8^+$ T cells were isolated from spleens of WT C57BL/6 mice by negative selection using the EasySep™ Mouse $CD8^+$ T cell isolation kit (Stem Cell Technologies) according to the manufacturer's protocol and cultured in complete media. Isolated $CD8^+$ T cells were activated with either plate-bound (1μg/mL) anti-CD3 and soluble (1μg/mL) anti-CD28, or Dynabeads™ Mouse T-Activator CD3/CD28 beads (Thermo Fischer Scientific) and co-cultured in the presence or absence of 50U/mL IL2, 50μM kynurenine (Sigma Aldrich), 3μM CH223191 (Sigma-Aldrich) or 10nM 2,3,7,8-tetrachlorodibenzo-p-dioxin (TCDD, Thomas Scientific).

Tumor Tissue Processing

Liberase Thermolysin Medium Research Grade solution (Roche) was used for the digestion of IE9mp1-mIDO and IE9mp1-EV tumor tissues harvested from WT C57BL/6 and IDOKO mice. Following digestion, direct *ex vivo* analysis by flow cytometry was performed in order to phenotype immune cell infiltration into the tumor. To lyse red blood cells in hemorrhagic tumor ascites fluids in order to perform phenotypic immune cell analysis, ACK lysis buffer was used. Ammonium-Chloride-Potassium (ACK) lysing buffer was added to ascites fluid and incubated at room temperature, then washed with 1x PBS before staining for surface and intracellular markers.

Cytokine and Chemokine Analysis

Cell-free tumor ascites fluid from IE9mp1-EV or IE9mp1-mIDO1 tumor-bearing WT C57BL/6 mice on Days 28 and 48 were harvest and analyzed for cytokines and chemokine levels using the 36-Plex Mouse ProcartaPlex Panel 1A Multiplex Luminex immunoassay kit (eBioscience). Data were collected using the Luminex-100 system and analyzed using StarStation Version 1.8 software (Applied Cytometry).

Confocal Microscopy

IE9mp1-mIDO1 or IE9mp1-Empty Vector tumor excised from WT C57BL/6 mice on Day 48 of tumor progression, or naïve $CD8^+$ T cells from WT C57BL/6 mice activated with anti-CD3/anti-CD28 and treated with kynurenine (50μM) or 2,3,7,8-tetrachlorodibenzo-p-dioxin (TCDD, 10nM) alone for 0 minutes, 30 minutes, 1 hour, 2 hours and 4 hours, were embedded in Tissue Freezing Medium (Ted Pella, Inc.) containing cryomolds

and immediately frozen in 2-methyl-butane (Sigma-Aldrich). 5μm frozen sections of the tissues were made using the cryostat and layered on Superfrost™ Plus Slides (Thermo Scientific). The slides were fixed in 4% para-formaldehyde for 15 minutes, washed and blocked for 60 minutes at room temperature. The slides were then stained for 3 hours at room temperature with mouse-specific antibodies anti-IDO (D7Z7U, Cell Signaling Technologies catalog no. 68572S), anti-CD8 (clone 53-6.7, BioLegend catalog no. 100702), anti-PD-1 (clone J43, BD Biosciences, catalog no. 551892), anti-AHR (clone W16012A, BioLegend, catalog no. 694502), and Hoechst 33342 nucleic acid stain (ThermoFisher Scientific, catalog no. H3570). Confocal analyses of stained slides were performed using a TCS SP8 Laser Scanning Spectral Confocal Microscope (LEICA Microsystems). For enumeration of cells positive for the individual markers, photographs of 10 fields (at 63x magnification) of stained tumors or cells were taken and each field was counted using ImageJ 1.74v software (NIH). Mean cell counts of total 10 fields were plotted. To ascertain AHR translocation to nucleus, Mean pixel intensity of AHR within the nucleus is calculated using Image J software.

Reagents and Internal Standards for High-Performance Liquid Chromatography (HPLC)

Sources for reagents were: HPLC-grade acetonitrile and water (Burdick & Jackson); mass spectrometry-grade formic acid and ammonium acetate (Sigma-Aldrich); calibration solution containing multiple calibrants in a solution of acetonitrile, trifluroacetic acid, and water (Agilent Technologies); metabolite standards and internal standards, including N-acetyl Aspartic acid-d3, Tryptophan-15N2, Sarcosine-d3, Glutamic acid-d5, Thymine-d4, Gibberellic acid, Trans-Zeatine, Jasmonic acid, 15N Anthranilic acid, and Testosterone-d3 (Sigma-Aldrich).

Sample Preparation for Mass Spectrometry and Metabolomics Analysis

Metabolites were extracted from cell lines and the extraction procedure was previously described (48). Briefly, mouse liver tissue pool was used as quality controls in the extraction procedure. The extraction step started with the addition of 750μL ice-cold methanol:water (4:1) containing 20μL spiked internal standards to each tissue and quality control samples. Ice-cold chloroform and water were added in a 3:1 ratio for a final proportion of 2:4:3 water:methanol:chloroform. The organic (methanol and chloroform) and aqueous layers were collected, dried and resuspended with 500μL of 50:50 methanol: water. The extract was deproteinized using a 3kDa molecular filter (Millipore Corporation) and the filtrate was dried under vacuum (Gardiner). Prior to mass spectrometry, the dried extracts were re-suspended in 100μL of injection solvent composed of 1:1 water:methanol and were subjected to liquid chromatography-mass spectrometry. The injection volume was 10μL.

Liquid Chromatography–Mass Spectrometry (LC-MS) Methods

For IDO pathway metabolites, ESI positive mode was used and analyzed using a 6495B triple quadrupole mass spectrometer (Agilent Technologies) coupled to a HPLC system (Agilent Technologies) *via* single reaction monitoring (SRM). Source parameters were gas temperature-290°C; gas flow 14L/min; nebulizer 20psi; sheath gas temperature 350°C; sheath gas flow 12L/min; capillary 3000V positive and 3000V negative; nozzle voltage 1500V positive and 1500V negative. Approximately 8–11 data points were acquired per detected metabolite. The HPLC column used was Zorbax eclipse XDB C-18, 1.8μm, 4.6×100mm (Agilent Technologies). Mobile phase A and B were 0.1% formic acid in water and acetonitrile respectively. Gradient used was: 0 min at 2% B; 2 min at 10% B, 12 min at 80% B, 18 min at 2% B followed by re-equilibration till end of the gradient 25 min to the initial starting condition (2% B). Flow rate used was 0.3mL/min. For purines and pyrimidines metabolites ESI positive mode was used and analyzed using a 6495B triple quadrupole mass spectrometer (Agilent Technologies) coupled to a HPLC system (Agilent Technologies) *via* single reaction monitoring (SRM). Source parameters, flow rate, and number of data points collected for purine/pyrimidines were similar to IDO pathway metabolites. A Waters X-bridge amide 3.5μm, 4.6×100mm column was used. Gradient used was: 0 min at 2% B; 6.50 min at 30% B; 7 min at 90% B; 12 min at 95%; 13 min at 2% B followed by re-equilibration till end of the gradient 20 min to the initial starting condition (2% B). The significance differences in levels of metabolites from various pathways between the IE9mp1-EV and -mIDO1 tumors and their importance are ascertained by p value (<0.05) and by impact score. The impact scores represent the importance of the metabolites in the metabolic network. They were calculated based on the centrality measures of a metabolite in a given metabolic network. Centrality is a local quantitative measure of the position of a node relative to the other nodes and is often used to estimate a node's relative importance or role in network organization. Specifically, we used relative betweenness centrality to calculate compound importance. The pathway impact is calculated as the sum of the importance measures of the matched metabolites normalized by the sum of the importance measures of all metabolites in each pathway (49).

Assay for Transposase Accessible Chromatin Sequencing (ATAC-seq)

50,000 isolated $CD8^+$ T cells were activated with Dynabeads™ Mouse T-Activator CD3/CD28 beads (Thermo Fischer Scientific), and co-cultured in the presence of 50μM kynurenine (Sigma-Aldrich) or 10nM TCDD (Thomas Scientific) for 2 or 28 hours, and ATAC-seq DNA libraries were prepared as previously described (38, 50). The final libraries were purified using AmpureXP beads, and validated for appropriate size on a 4200 TapeStation D1000 Screentape (Agilent Technologies). The DNA libraries were quantitated using KAPA Biosystems qPCR kit, and were pooled together in an equimolar fashion, following experimental design criteria.

Each pool was denatured and diluted to 350pM with 1% PhiX control library added. The resulting pool was then loaded into the appropriate NovaSeq Reagent cartridge for 100 cycle paired-end sequencing and sequenced on a NovaSeq6000 following the manufacturer's recommended protocol (Illumina). ATAC-seq data in raw FASTQ format were processed uniformly through ENCODE ATAC-seq pipeline version 1.4.0. The sequences in FASTQ file were aligned to mouse genome version mm10 using BOWTIE2 in Paired-end mode. The mitochondria reads, the duplicated reads and the reads with mapping quality less than 30 were removed from downstream analysis. Then MACS2 (–extsize73 –shift 37) was used to call accessible regions and to generate genome-wide insertion sites profiles for visualization. The insertion sites profile shows number of insertion events found in certain genomic location normalized by sequencing depth by million reads. ATAC-seq data quality was controlled by estimating signal-to-noise ratio, transcription start sites (TSS) enrichment, and enrichment in the universal DHS regions combined by ENCODE project.

Transcription Factor Binding Site Analysis

The core xenobiotic response element (XRE) sequence recognized by the AHR is 5'-T/GCGTG-3'. Position specific weight matrices (PWM) of XRE were extracted from the database TRANSFAC 7.0. The Transcription Element Search System (TESS) was used with default setting to search for AHR binding sites in the promoter region of each inhibitory gene (51).

Chromatin Immunoprecipitation Assay

Chromatin immunoprecipitation assay was performed on $CD8^+$ T cells activated with anti-CD3/anti-CD28 in the presence of kynurenine (50μM) or TCDD (10nM), using the EpiTect ChIP kit (Qiagen) according to the manufacturer's protocol. Cells were crosslinked in 1% formaldehyde at 37°C for 10 minutes. After chromatin shearing by sonication, the sheared chromatin was precleared with Protein A beads, and then incubated overnight with a purified anti-AHR antibody clone W16012A (BioLegend, catalog no. 694502) while rotating at 4°C. After DNA isolation and purification, the IP-DNA was quantified by real-time PCR. The following primer sequences were used for analysis of AHR binding to DNA: *Pdcd1* forward 5'-TATTTGAGGAAGGCATGAGC-3', reverse, 5'-TCTTAACACACACGCAATCC-3'.

Statistics

Flow cytometry, PCR, and confocal microscopy results are expressed as mean ± SEM and analyzed by two-tailed, Student's t-test, or one- and two-way ANOVA. Kaplan-Meier curves for survival analysis were analyzed by the Log-rank Test. Statistical significance was determined by a $p<0.05$. GraphPad Prism 7 software was used to perform analyses. The Metabolomics data was log2-transformed and normalized with internal standard per-sample, per-method basis. For every metabolite in the normalized dataset, two-sample t-tests were conducted to compare expression levels between different groups. Differential metabolites were identified by adjusting the p-values for multiple testing at an FDR<0.25 and generated a heat map. The transformed and normalized levels of metabolites were visualized by heat map. Metabolites were grouped by hierarchical clustering using Euclidean distances and complete linkage. Comparison of group means was performed by independent sample t-tests and two-way ANOVA. Metabolic pathways were obtained from Kyoto Encyclopedia of Genes and Genomes (KEGG) data base (52). The overall difference of groups of metabolites between conditions was analyzed by GlobalANCOVA. The Luminex measurement of cytokines and chemokines were log-transformed before analysis. For each mice strain, the mean levels of each group were compared by two-way ANOVA, with treatment group and time as the two factors. All tests were two-sided.

Study Approval

All animal experiments were carried out according to protocol guidelines reviewed and approved by the Institute Animal Care and Use Committee (IACUC) of Roswell Park Comprehensive Cancer Center (Buffalo, NY).

DATA AVAILABILITY STATEMENT

The original contributions presented in the study are included in the article/**Supplementary Material**. Further inquiries can be directed to the corresponding author.

ETHICS STATEMENT

The animal study was reviewed and approved by Roswell Park Comprehensive Cancer Center IACUC.

AUTHOR CONTRIBUTIONS

AA-M, RM, TT, FQ, R-YH, AL, and KO designed the experiments. AA-M and KO wrote the manuscript. AA-M performed the experiments and analyzed the data. RM designed, performed experiments, wrote, edited and reviewed, and revised the manuscript. TT designed the IDO expressing Cell line. VP and NP performed the metabolomics assay. PS performed genomic assays. AA-M, RM, HY, TL, JW, SB, and SL performed computational, bioinformatics, and statistical analyses. All authors contributed to the article and approved the submitted version.

ACKNOWLEDGMENTS

This work was supported by the National Cancer Institute (NCI) funded RPCI-UPCI Ovarian Cancer SPORE P50CA159981, NIH U24 CA232979, NIH R01 CA158318, NCI Cancer Center Support Grant P30 CA016056, NCI P30CA016056, NIH/NCI R01CA220297, and NIH/NCI R01CA216426 grants, and the use of Roswell Park Comprehensive Cancer Center's shared resources including the Flow Cytometry Core, Laboratory Animal Resource, Biostatistics Shared Resource, Bioinformatics

Shared Resource, and Genomics Shared Resource. We would like to thank Cheryl Eppolito for breeding animals used in this study, and the James N. Jarvis MD Lab at the University at Buffalo Jacobs School of Medicine and Biomedical Sciences for providing their expertise with the ATAC-seq experiment.

SUPPLEMENTARY MATERIAL

The Supplementary Material for this article can be found online at: https://www.frontiersin.org/articles/10.3389/fimmu.2021.678999/full#supplementary-material

REFERENCES

1. Torre LA, Trabert B, DeSantis CE, Miller KD, Samimi G, Runowicz CD, et al. Ovarian cancer statistics, 2018. *CA Cancer J Clin* (2018) 68(4):284–96. doi: 10.3322/caac.21456
2. Marcus CS, Maxwell GL, Darcy KM, Hamilton CA, McGuire WP. Current approaches and challenges in managing and monitoring treatment response in ovarian cancer. *J Cancer* (2014) 5(1):25–30. doi: 10.7150/jca.7810
3. Secord AA. Ovarian cancer: time to move beyond one size fits all. *Lancet Oncol* (2019) 20(6):754–5. doi: 10.1016/S1470-2045(19)30285-2
4. Sato E, Olson SH, Ahn J, Bundy B, Nishikawa H, Qian F, et al. Intraepithelial CD8+ tumor-infiltrating lymphocytes and a high CD8+/regulatory T cell ratio are associated with favorable prognosis in ovarian cancer. *Proc Natl Acad Sci USA* (2005) 102(51):18538–43. doi: 10.1073/pnas.0509182102
5. Zhang L, Conejo-Garcia JR, Katsaros D, Gimotty PA, Massobrio M, Regnani G, et al. Intratumoral T cells, recurrence, and survival in epithelial ovarian cancer. *N Engl J Med* (2003) 348(3):203–13. doi: 10.1056/NEJMoa020177
6. Ovarian Tumor Tissue Analysis C, Goode EL, Block MS, Kalli KR, Vierkant RA, Chen W, et al. Dose-Response Association of CD8+ Tumor-Infiltrating Lymphocytes and Survival Time in High-Grade Serous Ovarian Cancer. *JAMA Oncol* (2017) 3(12):e173290. doi: 10.1001/jamaoncol.2017.3290
7. Mellor AL, Keskin DB, Johnson T, Chandler P, Munn DH. Cells expressing indoleamine 2,3-dioxygenase inhibit T cell responses. *J Immunol* (2002) 168 (8):3771–6. doi: 10.4049/jimmunol.168.8.3771
8. Munn DH, Sharma MD, Baban B, Harding HP, Zhang Y, Ron D, et al. GCN2 kinase in T cells mediates proliferative arrest and anergy induction in response to indoleamine 2,3-dioxygenase. *Immunity* (2005) 22(5):633–42. doi: 10.1016/j.immuni.2005.03.013
9. Gandhi R, Kumar D, Burns EJ, Nadeau M, Dake B, Laroni A, et al. Activation of the aryl hydrocarbon receptor induces human type 1 regulatory T cell-like and Foxp3(+) regulatory T cells. *Nat Immunol* (2010) 11(9):846–53. doi: 10.1038/ni.1915
10. Mezrich JD, Fechner JH, Zhang X, Johnson BP, Burlingham WJ, Bradfield CA. An interaction between kynurenine and the aryl hydrocarbon receptor can generate regulatory T cells. *J Immunol* (2010) 185(6):3190–8. doi: 10.4049/jimmunol.0903670
11. Qian F, Villella J, Wallace PK, Mhawech-Fauceglia P, Tario JDJr., Andrews C, et al. Efficacy of levo-1-methyl tryptophan and dextro-1-methyl tryptophan in reversing indoleamine-2,3-dioxygenase-mediated arrest of T-cell proliferation in human epithelial ovarian cancer. *Cancer Res* (2009) 69(13):5498–504. doi: 10.1158/0008-5472.CAN-08-2106
12. Inaba T, Ino K, Kajiyama H, Yamamoto E, Shibata K, Nawa A, et al. Role of the immunosuppressive enzyme indoleamine 2,3-dioxygenase in the progression of ovarian carcinoma. *Gynecol Oncol* (2009) 115(2):185–92. doi: 10.1016/j.ygyno.2009.07.015
13. Okamoto A, Nikaido T, Ochiai K, Takakura S, Saito M, Aoki Y, et al. Indoleamine 2,3-dioxygenase serves as a marker of poor prognosis in gene expression profiles of serous ovarian cancer cells. *Clin Cancer Res* (2005) 11 (16):6030–9. doi: 10.1158/1078-0432.CCR-04-2671
14. Takao M, Okamoto A, Nikaido T, Urashima M, Takakura S, Saito M, et al. Increased synthesis of indoleamine-2,3-dioxygenase protein is positively associated with impaired survival in patients with serous-type, but not with other types of, ovarian cancer. *Oncol Rep* (2007) 17(6):1333–9. doi: 10.3892/or.17.6.1333
15. Qian F, Liao J, Villella J, Edwards R, Kalinski P, Lele S, et al. Effects of 1-methyltryptophan stereoisomers on IDO2 enzyme activity and IDO2-mediated arrest of human T cell proliferation. *Cancer Immunol Immunother CII* (2012) 61(11):2013–20. doi: 10.1007/s00262-012-1265-x
16. Holmgaard RB, Zamarin D, Munn DH, Wolchok JD, Allison JP. Indoleamine 2,3-dioxygenase is a critical resistance mechanism in antitumor T cell immunotherapy targeting CTLA-4. *J Exp Med* (2013) 210(7):1389–402. doi: 10.1084/jem.20130066
17. Kristeleit R, Davidenko I, Shirinkin V, El-Khouly F, Bondarenko I, Goodheart MJ, et al. A randomised, open-label, phase 2 study of the IDO1 inhibitor epacadostat (INCB024360) versus tamoxifen as therapy for biochemically recurrent (CA-125 relapse)-only epithelial ovarian cancer, primary peritoneal carcinoma, or fallopian tube cancer. *Gynecol Oncol* (2017) 146(3):484–90. doi: 10.1016/j.ygyno.2017.07.005
18. ClinicalTrials.gov Identifier: NCT02752074. *A Phase 3 Study of Pembrolizumab + Epacadostat or Placebo in Subjects With Unresectable or Metastatic Melanoma (Keynote-252 / ECHO-301)*. Available at: https://clinicaltrials.gov/ct2/show/NCT02752074 (Accessed March 26, 2019).
19. Long GV, Dummer R, Hamid O, Gajewski T, Caglevic C, Dalle S, et al. Epacadostat (E) plus pembrolizumab (P) versus pembrolizumab alone in patients (pts) with unresectable or metastatic melanoma: Results of the phase 3 ECHO-301/KEYNOTE-252 study. *J Clin Oncol* (2018) 36(15_suppl):108. doi: 10.2139/ssrn.3327362
20. Mullard A. IDO takes a blow. *Nat Rev Drug Discov* (2018) 17:307. doi: 10.1038/nrd.2018.67
21. Muller AJ, Manfredi MG, Zakharia Y, Prendergast GC. Inhibiting IDO pathways to treat cancer: lessons from the ECHO-301 trial and beyond. *Semin Immunopathol* (2019) 41(1):41–8. doi: 10.1007/s00281-018-0702-0
22. Matsuzaki J, Gnjatic S, Mhawech-Fauceglia P, Beck A, Miller A, Tsuji T, et al. Tumor-infiltrating NY-ESO-1-specific CD8+ T cells are negatively regulated by LAG-3 and PD-1 in human ovarian cancer. *Proc Natl Acad Sci USA* (2010) 107(17):7875–80. doi: 10.1073/pnas.1003345107
23. Opitz CA, Litzenburger UM, Sahm F, Ott M, Tritschler I, Trump S, et al. An endogenous tumour-promoting ligand of the human aryl hydrocarbon receptor. *Nature* (2011) 478(7368):197–203. doi: 10.1038/nature10491
24. Huang RY, Eppolito C, Lele S, Shrikant P, Matsuzaki J, Odunsi K. LAG3 and PD1 co-inhibitory molecules collaborate to limit CD8+ T cell signaling and dampen antitumor immunity in a murine ovarian cancer model. *Oncotarget* (2015) 6(29):27359–77. doi: 10.18632/oncotarget.4751
25. Roby KF, Taylor CC, Sweetwood JP, Cheng Y, Pace JL, Tawfik O, et al. Development of a syngeneic mouse model for events related to ovarian cancer. *Carcinogenesis* (2000) 21(4):585–91. doi: 10.1093/carcin/21.4.585
26. Jiao L, Maity S, Coarfa C, Rajapakshe K, Chen L, Jin F, et al. A Prospective Targeted Serum Metabolomics Study of Pancreatic Cancer in Postmenopausal Women. *Cancer Prev Res (Phila)* (2019) 12(4):237–46. doi: 10.1158/1940-6207.CAPR-18-0201
27. Badawy AA. Kynurenine Pathway of Tryptophan Metabolism: Regulatory and Functional Aspects. *Int J Tryptophan Res* (2017) 10:1178646917691938. doi: 10.1177/1178646917691938
28. Ishidoh K, Kamemura N, Imagawa T, Oda M, Sakurai J, Katunuma N. Quinolinate phosphoribosyl transferase, a key enzyme in de novo NAD(+) synthesis, suppresses spontaneous cell death by inhibiting overproduction of active-caspase-3. *Biochim Biophys Acta* (2010) 1803(5):527–33. doi: 10.1016/j.bbamcr.2010.02.007
29. Fallarino F, Grohmann U, You S, McGrath BC, Cavener DR, Vacca C, et al. The combined effects of tryptophan starvation and tryptophan catabolites down-regulate T cell receptor zeta-chain and induce a regulatory phenotype in naive T cells. *J Immunol* (2006) 176(11):6752–61. doi: 10.4049/jimmunol.176.11.6752
30. Cook DB, McLucas BC, Montoya LA, Brotski CM, Das S, Miholits M, et al. Multiplexing protein and gene level measurements on a single Luminex platform. *Methods* (2019) 158:27–32. doi: 10.1016/j.ymeth.2019.01.018
31. Bystry RS, Aluvihare V, Welch KA, Kallikourdis M, Betz AG. B cells and professional APCs recruit regulatory T cells via CCL4. *Nat Immunol* (2001) 2 (12):1126–32. doi: 10.1038/ni735
32. Kumar V, Patel S, Tcyganov E, Gabrilovich DI. The Nature of Myeloid-Derived Suppressor Cells in the Tumor Microenvironment. *Trends Immunol* (2016) 37(3):208–20. doi: 10.1016/j.it.2016.01.004

33. Lesokhin AM, Hohl TM, Kitano S, Cortez C, Hirschhorn-Cymerman D, Avogadri F, et al. Monocytic CCR2(+) myeloid-derived suppressor cells promote immune escape by limiting activated CD8 T-cell infiltration into the tumor microenvironment. *Cancer Res* (2012) 72(4):876–86. doi: 10.1158/0008-5472.CAN-11-1792
34. Murray IA, Morales JL, Flaveny CA, Dinatale BC, Chiaro C, Gowdahalli K, et al. Evidence for ligand-mediated selective modulation of aryl hydrocarbon receptor activity. *Mol Pharmacol* (2010) 77(2):247–54. doi: 10.1124/mol.109.061788
35. Whitlock JP Jr. Induction of cytochrome P4501A1. *Annu Rev Pharmacol Toxicol* (1999) 39:103–25. doi: 10.1146/annurev.pharmtox.39.1.103
36. Kanno Y, Miyama Y, Takane Y, Nakahama T, Inouye Y. Identification of intracellular localization signals and of mechanisms underlining the nucleocytoplasmic shuttling of human aryl hydrocarbon receptor repressor. *Biochem Biophys Res Commun* (2007) 364(4):1026–31. doi: 10.1016/j.bbrc.2007.10.140
37. Reyes H, Reisz-Porszasz S, Hankinson O. Identification of the Ah receptor nuclear translocator protein (Arnt) as a component of the DNA binding form of the Ah receptor. *Science* (1992) 256(5060):1193–5. doi: 10.1126/science.256.5060.1193
38. Buenrostro JD, Giresi PG, Zaba LC, Chang HY, Greenleaf WJ. Transposition of native chromatin for fast and sensitive epigenomic profiling of open chromatin, DNA-binding proteins and nucleosome position. *Nat Methods* (2013) 10(12):1213–8. doi: 10.1038/nmeth.2688
39. Zhao B, Degroot DE, Hayashi A, He G, Denison MS. CH223191 is a ligand-selective antagonist of the Ah (Dioxin) receptor. *Toxicol Sci* (2010) 117 (2):393–403. doi: 10.1093/toxsci/kfq217
40. Uyttenhove C, Pilotte L, Theate I, Stroobant V, Colau D, Parmentier N, et al. Evidence for a tumoral immune resistance mechanism based on tryptophan degradation by indoleamine 2,3-dioxygenase. *Nat Med* (2003) 9(10):1269–74. doi: 10.1038/nm934
41. Liu Y, Liang X, Dong W, Fang Y, Lv J, Zhang T, et al. Tumor-Repopulating Cells Induce PD-1 Expression in CD8(+) T Cells by Transferring Kynurenine and AhR Activation. *Cancer Cell* (2018) 33(3):480–94 e7. doi: 10.1016/j.ccell.2018.02.005
42. Tullius SG, Biefer HR, Li S, Trachtenberg AJ, Edtinger K, Quante M, et al. NAD+ protects against EAE by regulating CD4+ T-cell differentiation. *Nat Commun* (2014) 5:5101. doi: 10.1038/ncomms6101
43. Zhou L. AHR Function in Lymphocytes: Emerging Concepts. *Trends Immunol* (2016) 37(1):17–31. doi: 10.1016/j.it.2015.11.007
44. Eleftheriadis T, Pissas G, Liakopoulos V, Stefanidis I. IDO decreases glycolysis and glutaminolysis by activating GCN2K, while it increases fatty acid oxidation by activating AhR, thus preserving CD4+ Tcell survival and proliferation. *Int J Mol Med* (2018) 42(1):557–68. doi: 10.3892/ijmm.2018.3624
45. Bianchi-Smiraglia A, Bagati A, Fink EE, Affronti HC, Lipchick BC, Moparthy S, et al. Inhibition of the aryl hydrocarbon receptor/polyamine biosynthesis axis suppresses multiple myeloma. *J Clin Invest* (2018) 128(10):4682–96. doi: 10.1172/JCI70712
46. Patel MR, Chang YF, Chen IY, Bachmann MH, Yan X, Contag CH, et al. Longitudinal, noninvasive imaging of T-cell effector function and proliferation in living subjects. *Cancer Res* (2010) 70(24):10141–9. doi: 10.1158/0008-5472.CAN-10-1843
47. Tomihara K, Guo M, Shin T, Sun X, Ludwig SM, Brumlik MJ, et al. Antigen-specific immunity and cross-priming by epithelial ovarian carcinoma-induced CD11b(+)Gr-1(+) cells. *J Immunol* (2010) 184(11):6151–60. doi: 10.4049/jimmunol.0903519
48. Vantaku V, Dong J, Ambati CR, Perera D, Donepudi SR, Amara CS, et al. Multi-omics Integration Analysis Robustly Predicts High-Grade Patient Survival and Identifies CPT1B Effect on Fatty Acid Metabolism in Bladder Cancer. *Clin Cancer Res* (2019) 25(12):3689–701. doi: 10.1158/1078-0432.CCR-18-1515
49. Xia J, Wishart DS. MetPA: a web-based metabolomics tool for pathway analysis and visualization. *Bioinformatics* (2010) 26(18):2342–4. doi: 10.1093/bioinformatics/btq418
50. Buenrostro JD, Wu B, Chang HY, Greenleaf WJ. ATAC-seq: A Method for Assaying Chromatin Accessibility Genome-Wide. *Curr Protoc Mol Biol* (2015) 109:21.29.1–9. doi: 10.1002/0471142727.mb2129s109
51. Schug J. Using TESS to Predict Transcription Factor Binding Sites in DNA Sequence. *Curr Protoc Bioinf* (2008) 21(1):2.6.1–15. doi: 10.1002/0471250953.bi0206s21
52. Kanehisa M, Goto S. KEGG: kyoto encyclopedia of genes and genomes. *Nucleic Acids Res* (2000) 28(1):27–30. doi: 10.1093/nar/28.1.27

Conflict of Interest: KO is a co-founder of Tactiva Therapeutics and receives research support from AstraZeneca and Tesaro.

The remaining authors declare that the research was conducted in the absence of any commercial or financial relationships that could be construed as a potential conflict of interest.

Copyright © 2021 Amobi-McCloud, Muthuswamy, Battaglia, Yu, Liu, Wang, Putluri, Singh, Qian, Huang, Putluri, Tsuji, Lugade, Liu and Odunsi. This is an open-access article distributed under the terms of the Creative Commons Attribution License (CC BY). The use, distribution or reproduction in other forums is permitted, provided the original author(s) and the copyright owner(s) are credited and that the original publication in this journal is cited, in accordance with accepted academic practice. No use, distribution or reproduction is permitted which does not comply with these terms.

frontiers in Oncology

ORIGINAL RESEARCH
published: 20 April 2021
doi: 10.3389/fonc.2021.665420

Rapamycin Promotes ROS-Mediated Cell Death *via* Functional Inhibition of xCT Expression in Melanoma Under γ-Irradiation

*Yunseo Woo[1,2], Hyo-Ji Lee[1,2], Jeongyeon Kim[1,3], Seung Goo Kang[2,4], Sungjin Moon[1,2], Jeong A. Han[5], Young Mee Jung[2,6] and Yu-Jin Jung[1,2,3]**

[1] Department of Biological Sciences, Kangwon National University, Chuncheon, South Korea, [2] Kangwon Radiation Convergence Research Support Center, Kangwon National University, Chuncheon, South Korea, [3] Graduate Program in BIT Medical Convergence, Kangwon National University, Chuncheon, South Korea, [4] Department of Systems Immunology, Kangwon National University, Chuncheon, South Korea, [5] Department of Biochemistry and Molecular Biology, Kangwon National University, Chuncheon, South Korea, [6] Department of Chemistry, Kangwon National University, Chuncheon, South Korea

OPEN ACCESS

Edited by:
Peng Qu,
National Institutes of Health (NIH), United States

Reviewed by:
Kai-Yuan Lin,
Chi Mei Medical Center, Taiwan
Likui Feng,
The Rockefeller University, United States

***Correspondence:**
Yu-Jin Jung
yjjung@kangwon.ac.kr

Specialty section:
This article was submitted to Cancer Immunity and Immunotherapy, a section of the journal Frontiers in Oncology

Received: *08 February 2021*
Accepted: *29 March 2021*
Published: *20 April 2021*

Citation:
Woo Y, Lee H-J, Kim J, Kang SG, Moon S, Han JA, Jung YM and Jung Y-J (2021) Rapamycin Promotes ROS-Mediated Cell Death via Functional Inhibition of xCT Expression in Melanoma Under γ-Irradiation. Front. Oncol. 11:665420. doi: 10.3389/fonc.2021.665420

Although many cancer patients are administered radiotherapy for their treatment, the interaction between tumor cells and macrophages in the tumor microenvironment attenuates the curative effects of radiotherapy. The enhanced activation of mTOR signaling in the tumors promotes tumor radioresistance. In this study, the effects of rapamycin on the interaction between tumor cells and macrophages were investigated. Rapamycin and 3BDO were used to regulate the mTOR pathway. *In vitro*, tumor cells cocultured with macrophages in the presence of each drug under normoxic or hypoxic conditions were irradiated with γ–rays. *In vivo*, mice were irradiated with γ–radiation after injection with DMSO, rapamycin and 3BDO into tumoral regions. Rapamycin reduced the secretion of IL-4 in tumor cells as well as YM1 in macrophages. Mouse recombinant YM1 decreased the enhanced level of ROS and the colocalized proportion of both xCT and EEA1 in irradiated tumor cells. Human recombinant YKL39 also induced results similar to those of YM1. Moreover, the colocalized proportion of both xCT and LC3 in tumor tissues was elevated by the injection of rapamycin into tumoral regions. Overall, the suppression of mTOR signaling in the tumor microenvironment might be useful for the improvement of tumor radioresistance.

Keywords: melanoma, macrophage, YM1, KEAP1, NRF2, mTOR, radiation

INTRODUCTION

Radiation therapy aims to kill cancer cells through direct damage to DNA and indirect reactive oxygen species (ROS)-induced damage to cellular organelles (1, 2). However, since tumor resistance to γ-radiation is observed in various tumor types, radioresistance factors should be considered to ensure effective radiotherapy (3). In particular, the crosstalk between tumor cells and macrophages

in the tumor microenvironment has been regarded as an important factor among the tumor radioresistance factors that make radiotherapy challenging (4). Macrophages can be polarized into antitumoral M1 or protumoral M2 populations depending on their microenvironment (5). Unlike the M1 phenotype, the M2 phenotype has been reported to have resistance against γ-irradiation (6). Therefore, functional inhibition of M2 macrophages in the tumor microenvironment may be an alternative strategy for effective radiotherapy (7).

Tumor-secreted factors, such as IL-4, IL-10, and M-CSF, can induce the polarization of macrophages into M2-like tumor-associated macrophages (M2-like TAMs) (8, 9). Among these factors, IL-4 is a typical TH2 cytokine that promotes the expression of YM1, arginase-1, PPARγ, Fizz1 and VEGF in macrophages (10). IL-4 is found in various melanoma cells, including the human SK-MEL-28 and mouse B16F10 cell lines (11). Thus, it should be investigated whether M2-like TAMs induced by IL-4 released from tumor cells enhance tumor radioresistance. YM1 is a chitinase-like protein (CLP) found in mammals (12). Most CLPs can be combined with chitin, but they are unable to decompose chitin due to a lack of chitinolytic enzymatic activity (13). Increased levels of CLPs in a host are relevant to TH2-related diseases (14). Chitinase 3-like 1 (CHI3L1, YKL40/BRP39) has been reported to accelerate the recruitment of macrophages into tumor tissues and to promote tumor angiogenesis in colorectal patients (15). CHI3L1 is also known to promote the invasion and migration of non-small cell lung cancer *via* activation of mTOR signaling (16). However, there has been little research on YM1, which is a CLP expressed only in mice.

Ionizing radiation can cause cell death in tumors through ROS-induced damage (17). However, a high antioxidant capacity is observed in various cancer types, which in tumors can be an obstacle to efficient radiotherapy (18). The mechanism of glutathione (GSH) synthesis is one of the antioxidant pathways in tumors (19). The heterodimeric glutamate-cystine transporter composed of SLC7A11 (xCT) and CD98 mediates the import of extracellular cystine into the cytoplasm during GSH biosynthesis (20). xCT expression can be controlled by the KEAP1-NRF2 pathway, and the transcriptional activity of NRF2 can depend on mTOR signaling (21). However, little is known regarding the direct control of xCT expression by mTOR signaling in tumors under γ-irradiation. In many tumor studies, inhibition of mTOR signaling has been shown to improve the efficacy of radiotherapy (22, 23). Therefore, the inhibitory effects of mTOR signaling on tumor radioresistance induced by the interaction between macrophages and tumor cells were investigated in the B16F10-derived microenvironment during γ-irradiation.

MATERIALS AND METHODS

Cell Lines and BMDM Differentiation

All cell lines were obtained from the Korean Cell Line Bank (KCLB). The following cell lines were used in this study: B16F10 (KCLB Cat# 80008, Seoul, Republic of Korea) and L929 (KCLB Cat# 10001, Seoul, Republic of Korea). B16F10 cells were cultured with DMEM supplemented with 10% FBS and 1% penicillin/streptomycin in cell culture plates at 37°C and 5% CO_2 until confluent (~90%) (24). L929 cells were maintained in complete RPMI medium for 5 days before harvesting cell supernatants (25). The supernatant, which was used as a source of M-CSF, was filtered through a 0.2-μm filter and then aliquoted for storage at -20°C until use. To differentiate BMDMs, the tibia and femur of each hind leg were obtained from C57BL/6 mice (Nara Biotech, Seoul, Republic of Korea). The whole bone marrow was flushed out using a 1-ml syringe with a 26-G needle. The cells were cultured with DMEM containing 20% FBS and 30% L929-conditioned medium in 100-mm petri dishes for 5 days.

Reagents

Rapamycin (914.18 g/mol) and 3BDO (327.33 g/mol) were purchased from Selleckchem (Houston, TX, USA). To control mTOR signaling, cells were treated with 100 nM rapamycin (mTOR inhibitor/autophagy activator) or 100 nM 3BDO (mTOR activator/autophagy inhibitor). DPI (10 μM; NADPH oxidase inhibitor; Sigma-Aldrich, St. Louis, MO, USA) was used to deplete intracellular ROS.

Animal Studies

The animal experiments in the present study were approved and confirmed by the Ethical Guidelines for Animal Experiments of Kangwon National University (KW-181214-1). B16F10 cells (5×10^5) were inoculated subcutaneously into C57BL/6 male mice (5–8 weeks old, n=5/group) (26). After 7 days, when palpable tumors (5 mm in diameter) developed, the mice were treated with intratumoral injections of DMSO, rapamycin (0.1 mg/kg/day) or 3BDO (0.036 mg/kg/day) on days 7-14. Whole-body irradiation was performed once on day 7 after drug injections at 3 h. All tumor samples were harvested on day 14. Tumor volumes were measured using calipers and calculated based on the ellipsoid formula ($a \times b \times c \times \pi \times 4/3$).

In Vitro Coculture Experiments

To understand the radioresistance roles of macrophages in the tumor microenvironment, Transwell permeable supports (0.4-μm pore size, Costar 3450, Corning Inc., Kennebunk, ME, USA) were utilized. B16F10 cells (3×10^5) were seeded in the bottom chamber, and bone marrow-derived macrophages (BMDMs) (1×10^5) were plated in the upper chamber. Each cell type was incubated separately at 37°C and 5% CO_2 for 24 h. After washing, the cells were cocultured under various experimental conditions.

Hypoxic Incubation

A hypoxia chamber (PDS-1000, COY Laboratory Products, Inc., Grass Lake, MI, USA) was filled with a mixture of 95% N_2 and 5% CO_2 gas at 2 p.s.i. for 1 h. Cells were incubated at 37°C in a humidified atmosphere containing 1% O_2 and 5% CO_2 for 24 h.

γ-Irradiation

To evaluate the effects of γ-radiation on the tumor microenvironment, each sample was irradiated with γ-rays

using a Cs-137 source (Gammacell 40 Extractor, Best Theratronics Ltd., Ottawa, Canada). Cells were irradiated with 3 Gy *in vitro*, and mice were exposed to whole-body irradiation at doses of 0, 1, 3, 5, 7 or 9 Gy *in vivo*.

Western Blot Analysis

B16F10 cells were homogenized with RIPA buffer supplemented with Halt protease and a phosphatase inhibitor cocktail (Thermo Scientific Pierce, Rockford, IL, USA). Samples were separated by SDS-PAGE (27). The membranes were incubated with specific primary and secondary antibodies, which were washed three times with TBS-T. The membranes that were activated using an ECL solution (Advansta, Menlo Park, CA, USA) were developed with AGFA X-ray film (Agfa-Gevaert NV, Mortsel, Belgium).

Confocal Microscopy

Confocal microscopy was performed as previously described (28). Briefly, B16F10 cells were plated onto coverslips (1×10^5 cells per coverslip; Paul Marienfeld GmbH & Co., KG, Lauda-Könighofen, Germany) in 12-well plates. The cells were treated with various stimuli as described in the figure legends. The cells were fixed with 4% paraformaldehyde and permeabilized with 0.2% Triton X-100 in PBS. After blocking, specific antibodies were used for intracellular staining. The samples were mounted and observed under a confocal microscope (FV1000; Olympus Corporation, Tokyo, Japan). The quantification of all images was performed by using ImageJ (version 1.48, National Institutes of Health, Bethesda, MD, USA).

ELISA

ELISA was performed as previously described (29). IL-4 and YM1 levels were measured by using the Murine IL-4 Mini ABTS ELISA Development Kit (PeproTech EC Ltd, London, UK) and the Mouse YM1/Chitinase 3-like 3 DuoSet ELISA Development Kit (R&D Systems, Minneapolis, MN, USA) according to the instructions of the manufacturer.

Determination of Cell Numbers

The number of viable cells was assessed by trypan blue exclusion assay. The trypan blue exclusion assay was performed as previously described (29). The determination of cell numbers was performed with the Countess Automated Cell Counter (Invitrogen, Carlsbad, CA, USA).

Evaluation of GEO Profiles

The Gene Expression Omnibus (GEO) database was utilized in this study. GSE29074 (https://www.ncbi.nlm.nih.gov/geo/query/acc.cgi?acc=GSE29074) data sets were used to compare the expression values of IL-4, xCT, and YM1 in wild-type mouse tissues or in melanoma tissues derived from the iMet model (metastatic melanoma, Tyr-rtTA;Tet-Met;Ink4a/Arf$^{-/-}$) and iHRAS model (non-metastatic melanoma, Tyr-rtTA;Tet-HRASV12G;Ink4a/Arf$^{-/-}$) (30). For the human study, the expression values of IL-4, xCT, and YKL39 from 70 melanoma patients (7 normal skin, 18 benign skin nevi and 45 primary malignant melanoma profiles) were obtained from GSE3189 (https://www.ncbi.nlm.nih.gov/geo/query/acc.cgi?acc=GSE3189) (31). Gene expression values are presented in a scatter plot graph created with GraphPad Prism 5 software (GraphPad Software, Inc., La Jolla, CA, USA).

Statistical Analysis

In this study, all data are presented as the mean ± standard deviation. Statistical analysis was performed with one-way or two-way analysis of variance (ANOVA) followed by the Bonferroni test to compare all pairs of columns (95% confidence intervals). Analyses were performed with GraphPad Prism 5. P values < 0.05 were considered significant. Experiments were repeated a minimum of 3 times for each condition.

RESULTS

Rapamycin Promotes Radiation-Induced Cell Death in Mouse Melanoma *In Vivo*

In radiotherapy, it is important to determine the minimum dose that delivers maximum energy to cancer cells and causes minimal damage to surrounding healthy tissues (32). B16F10 tumor-bearing mice were irradiated with γ-radiation to determine the minimum dose that could significantly affect tumor volume, and a 3-Gy dose was selected (**Supplementary Figures 1A, B**). To elucidate the roles of mTOR signaling in the tumor microenvironment during radiotherapy, rapamycin and 3BDO were used to pharmaceutically control mTOR activation in the B16F10 tumor model (**Supplementary Figure 1C**). Compared with DMSO, rapamycin reduced tumor size, whereas 3BDO increased the volume of tumors (**Supplementary Figure 1D** and **Figure 1A**). Rapamycin also promoted a reductive effect of γ-radiation on tumors (**Figure 1A**). Rapamycin and 3BDO, as pharmaceutical regulators of mTOR activation, worked effectively in tumor tissues (**Figure 1B**). These results suggest that pharmaceutical control of mTOR signaling affects tumor development and efficient radiotherapy. Tumor development is closely related to tumor proliferation and cell death in the tumor microenvironment (33). Rapamycin reduced the proportion of Ki67$^+$ cells in tumor tissues (**Figure 1C**). To determine the relationship between the difference in tumor volume and the cell death mechanism related to the mTOR pathway, the expression levels of autophagy-related (Beclin1, Atg12-5 complex, and LC3) or apoptosis-related proteins (Bcl-2, Bax, and PARP) were examined (**Figure 1D**). Compared to other groups, enhanced LC3 expression was detected in rapamycin-injected tumor tissues, and the expression levels of other autophagy-related genes, Beclin1 and Atg12-5 complex, were not changed significantly. The expression levels of Bcl2 and Bax were also enhanced in rapamycin-treated tissues, however, γ-radiation reduced the expression levels of those genes. Rapamycin also increased the ratio of cleaved PARP (cPARP) to total PARP (tPARP) in nonirradiated tumor tissues and promoted this ratio in irradiated tumors even further than other groups (**Figure 1D**). To clarify the types of regulated cell death leading to PARP cleavage in tumor tissues, autophagic (LC3$^+$PI$^+$) and apoptotic (Caspase-3$^+$PI$^+$) cell death was evaluated using confocal

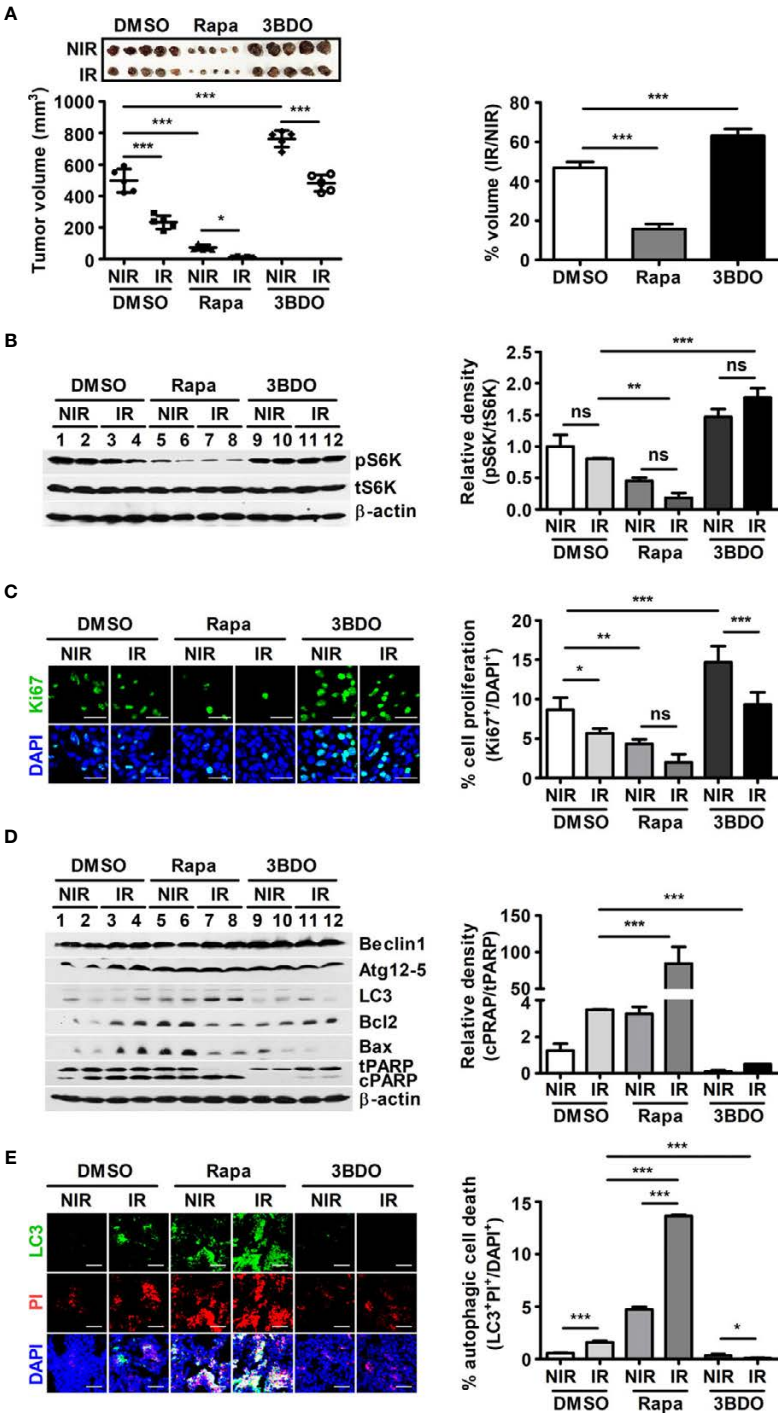

FIGURE 1 | Pharmaceutical regulation of mTOR activation affects B16F10-tumor development. **(A)** After tumor resection, all tumors were measured with calipers to calculate tumor volumes (left). To evaluate tumor radiosensitivity, percentages were calculated by dividing the volume of irradiated tumors (IR) by the volume of nonirradiated tumors (NIR) in each group (right). **(B)** The protein levels of p70 S6K, phospho-p70 S6K, and β-actin in homogenized tumor tissue samples were evaluated by western blotting. The relative density of phosphorylated forms was measured using ImageJ. **(C)** Intratumoral levels of Ki67 were analyzed by confocal microscopy. Nuclei (blue) and proliferating cells (green) were stained with DAPI and an anti-Ki67 antibody, respectively. Scale bars, 30 μm. **(D)** The protein levels of Beclin1, Atg12-5, LC3, Bcl2, Bax, PARP, and β-actin in homogenized tumor tissue samples were evaluated by western blotting. **(E)** Intratumoral levels of LC3 (green) were assessed by confocal microscopy. Nuclei (blue) and damaged cells (red) were stained with DAPI and propidium iodide, respectively. Scale bars, 100 μm. The bars and error bars represent the mean ± SD; $^{*}P < 0.05$; $^{**}P < 0.01$; $^{***}P < 0.001$; ns, not significant.

microscopy. Under γ-irradiation, the proportion of $LC3^+PI^+$ cells was significantly increased in rapamycin-injected tissues compared to other groups (**Figure 1E**). However, the patterns of apoptotic cell death induced by drugs and radiation were shown to be different from the tumor development patterns in **Figure 1A** (**Supplementary Figure 1E**). Overall, the pharmaceutical inhibition of mTOR signaling by rapamycin not only inhibits tumor development but also promotes the reductive effect of γ-radiation on tumor volumes.

Rapamycin Promotes Radiation-Induced Cell Death in Melanoma Cells Cocultured With Macrophages *In Vitro*

Macrophages in the tumor microenvironment have been reported to promote tumor development and contribute to tumor radioresistance (34). Thus, an *in vitro* coculture system was established to investigate whether macrophages in the tumor microenvironment affect the viability of tumor cells under γ-radiation during the pharmaceutical control of mTOR signaling. In addition, various oxygen conditions, such as normoxia and hypoxia, were introduced to mimic the tumor microenvironment (35). The viability of B16F10 cells cocultured with BMDMs was higher than that of single-cultured B16F10 cells, excluding the rapamycin-treated groups (**Figure 2A**). Compared to both the DMSO- and 3BDO-groups in single culture conditions, rapamycin reduced the viability of single-cultured-B16F10 cells, regardless of oxygen and radiation conditions (**Figure 2A**). These results indicate that the inhibitory effect of rapamycin on mTOR signaling could not only directly decrease the viability of B16F10 cells but also attenuate the macrophage-mediated increase in B16F10 cell viability. In **Figure 2A**, because rapamycin affected the cell viability of B16F10 cells under various culture conditions, the ratio of cPARP/tPARP was assessed in B16F10 cells under the same conditions. As a result, the effects of mTOR inhibition by rapamycin on the cleavage patterns of PARP in B16F10 cells were different between single and coculture conditions (**Figures 2B, C**). In other words, rapamycin increased the cleaved levels of PARP in B16F10 cells cocultured with BMDMs relative to those in tumor tissues, regardless of oxygen conditions during irradiation. Overall, these results indicate that macrophages may play beneficial roles in tumor survival under γ-irradiation and that rapamycin can interfere with the interaction between macrophages and tumor cells in the tumor microenvironment.

Rapamycin Attenuates the Expression and Secretion of YM1 in Macrophages Cocultured With Melanoma Cells

In the tumor microenvironment, antitumoral M1-like TAMs and protumoral M2-like TAMs are distributed according to the surrounding environmental conditions (36). First of all, the effects of tumor cells on macrophages were investigated because tumor-secreted factors can induce the polarization of macrophages. The changes in polarization markers were evaluated in BMDMs under the indicated conditions (**Supplementary Figure 2** and **Figure 3**). M1 macrophages have been reported to express *nos2 and cxcl10;* otherwise, M2 macrophages express *fizz1, arg1, pparγ,* and *ccl22*. LPS plus INF-γ induced the polarization of M0 to M1 macrophages, and IL-4 induced polarization to the M2 types (**Supplementary Figures 2A, B**). In addition, unique metabolic patterns were observed in M1 and M2 macrophages (**Supplementary Figures 2C, D**), and these results were consistent with those of a previous study (37). In M1-polarized cells, compared with DMSO treatment, rapamycin inhibited the attenuation of NOS2 expression after γ-radiation under normoxia and inhibited the increase in NOS2 expression after γ-radiation in the cells under hypoxia (**Supplementary Figure 2E**). However, 3BDO decreased the expression of NOS2 in M1 BMDMs under all conditions (**Supplementary Figure 2E**). In M2-polarized cells, compared with DMSO treatment, rapamycin attenuated the expression of M2 markers, excluding Fizz1, under all conditions (**Supplementary Figure 2F**). These results suggest that the pharmaceutical inhibition of mTOR signaling by rapamycin might attenuate the polarization of macrophages into the M2 phenotype. Meanwhile, because tumor-secreted factors could also stimulate the polarization of macrophages into an M2-like phenotype in the tumor microenvironment (38), the polarized characteristics of macrophages were investigated in BMDMs cocultured with B16F10 cells. In BMDMs cocultured with B16F10 cells, the glycolytic proton efflux rate (glycoPER) and the oxygen consumption rate (OCR) were similar to those in M2-BMDMs (**Figures 3A, B**). Although marker proteins of polarized macrophages were not detected in single-cultured BMDMs, the expression and secretion of YM1 were observed in BMDMs cocultured with B16F10 cells (**Figures 3C-F**). In addition, rapamycin attenuated the expression and secretion of YM1 in the cells (**Figures 3E, F**). To clarify the source of released YM1, the expression of YM1 was analyzed in B16F10 cells. The results showed that YM1 was not derived from B16F10 cells (**Supplementary Figures 2G, H**). Among the M2-related proteins, YM1 might be specifically expressed in macrophages stimulated by TH2 cytokines (39). To identify the prominent expression of YM1 in BMDMs cocultured with B16F10 cells, BMDMs were treated with various concentrations of IL-4. Only YM1 was expressed in BMDMs stimulated with 0.02 ng/ml IL-4 (**Supplementary Figure 2I**). These results *in vitro* were also observed *in vivo*. The proportion of $CD206^+YM1^+$ cells was reduced by rapamycin injection and was decreased by γ-irradiation even further than those in the other groups (**Figure 3G**). Overall, rapamycin attenuated the polarization of macrophages by B16F10 into YM1-producing cells with M2-like metabolism.

Rapamycin Attenuates the Expression and Secretion of IL-4 in Tumor Cells

The production of YM1 in macrophages can be induced by TH2 cytokines, such as IL-4 and IL-13 (40). In previous studies, IL-4 has been reported to be produced in various melanoma cells, including B16F10 cells (11, 41). Therefore, IL-4 expression was investigated in B16F10 cells. B16F10 cells showed considerable expression of IL-4 at the basal level, and its expression was attenuated by rapamycin (**Figure 4A**). Although various culture conditions, such as

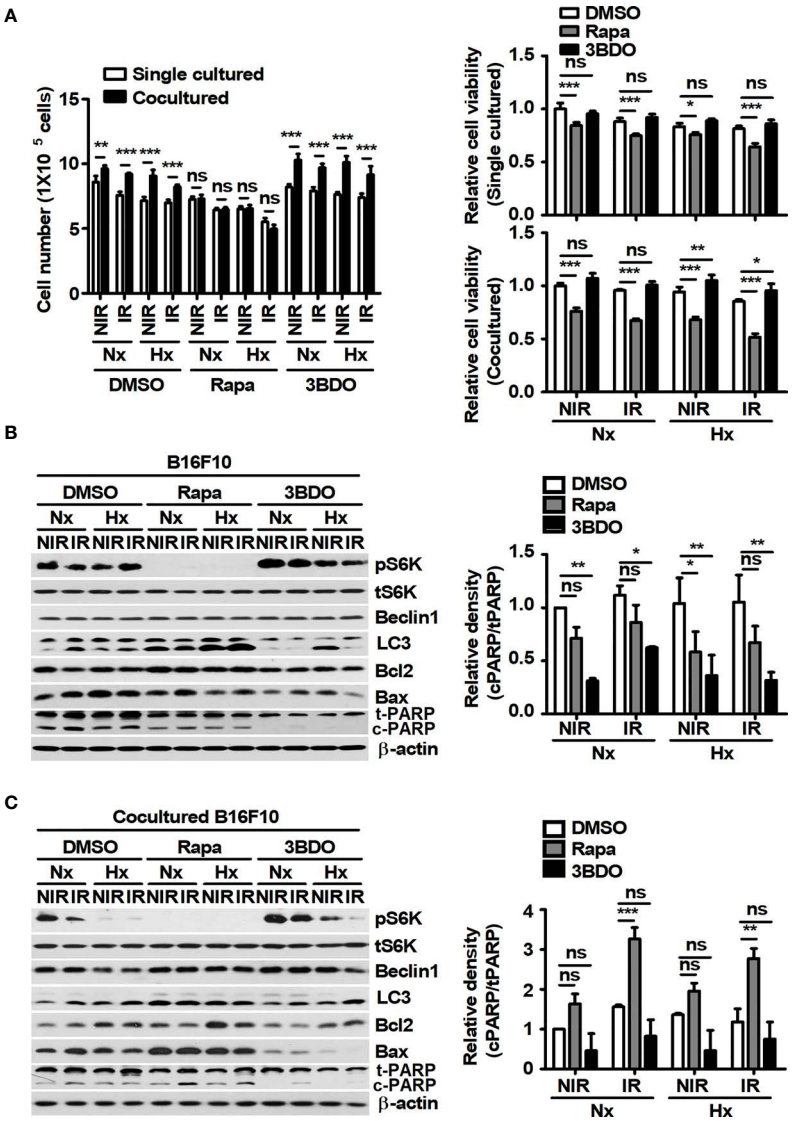

FIGURE 2 | Pharmaceutical regulation of mTOR activation affects macrophage-mediated B16F10 cell survival. B16F10 cells cultured alone or cocultured with BMDMs were incubated in the presence of 100 nM rapamycin or 100 nM 3BDO at 37°C/5% CO_2 in a normoxic (Nx) chamber or 37°C/1% O_2 in a hypoxic (Hx) chamber for 3 h. After 3-Gy γ-irradiation, B16F10 cells were incubated under the indicated conditions for 21 h. **(A)** Cell viability was measured by an automated cell counter. **(B, C)** The protein levels of p70 S6K, phospho-p70 S6K, Beclin1, LC3, Bcl2, Bax, and PARP in B16F10 cells were evaluated by western blotting. β-actin was used as an internal control. The band density of each sample was measured with ImageJ. The bars and error bars represent the mean ± SD; $^{*}P < 0.05$; $^{**}P < 0.01$; $^{***}P < 0.001$; ns, not significant.

irradiation and oxygen status, affected the expression and secretion of IL-4 in B16F10 cells, rapamycin significantly attenuated the levels of IL-4 production in the cells (**Figures 4B**–**E**). In addition, the expression and secretion of IL-4 in B16F10 cells under various culture conditions were independent of the presence or absence of macrophages (**Figures 4B**–**E**). These results suggest that IL-4 released by tumor cells may be an important factor for skewing macrophages toward the M2 population and that mTOR inhibitors may be effective drugs for blocking IL-4-mediated signaling in the tumor microenvironment.

YM1 Rescues the Decreased Viability of Melanoma *via* Attenuation of Radiation-Induced ROS

A large amount of intracellular ROS induced by γ-radiation could contribute to cell death in tumors (42). However, various cancer cells might be resistant to γ-ray-induced ROS because of high levels of antioxidant mechanisms in the cells (43). Therefore, the levels of intracellular ROS induced by a 3-Gy-dose of γ-irradiation were investigated in B16F10 cells. In addition, since B16F10 induced YM1 expression in BMDMs during coculture, the effect

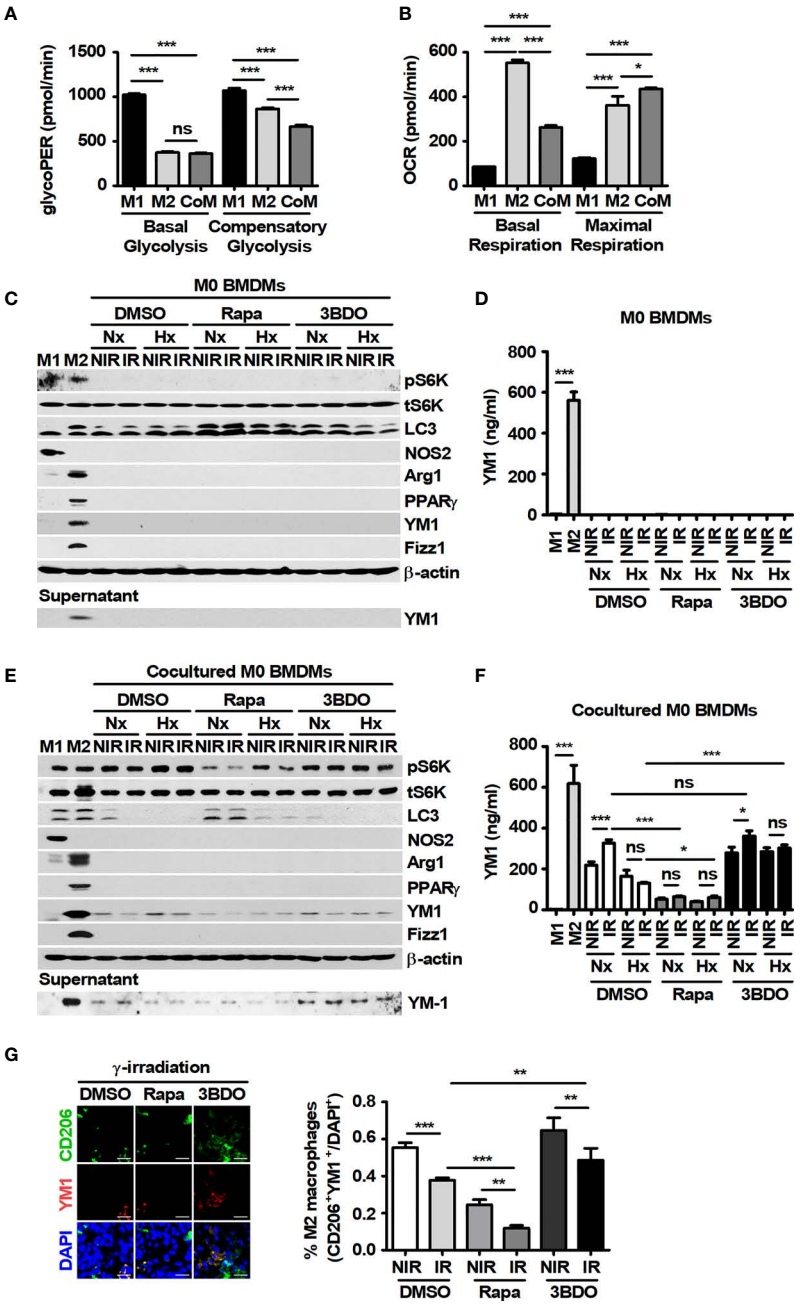

FIGURE 3 | Pharmaceutical regulation of mTOR activation affects YM1-expressing macrophages cocultured with B16F10 cells. **(A, B)** BMDMs were treated with 100 ng/ml LPS plus 20 ng/ml IFN-γ or 20 ng/ml IL-4, or were cocultured with B16F10 cells for 24 h, and then the glycolytic proton efflux rate (GlycoPER) **(A)** or the oxygen consumption rate (OCR) **(B)** in the cells was analyzed. **(C–F)** BMDMs were polarized into the M1 (LPS+IFN-γ) and M2 (IL-4) phenotypes. M1-, M2-, M0- and B16F10-cocultured BMDMs were incubated under the indicated conditions. The protein levels of p70 S6K, phospho-p70 S6K, LC3, NOS2, Arginase-1, PPAR-γ, YM-1, Fizz-1, and β-actin in BMDMs were evaluated by western blotting. Secreted YM-1 in the supernatant was detected by western blot and ELISA. **(G)** Intratumoral levels of CD206 and YM-1 were analyzed by confocal microscopy. $CD206^{+}YM1^{+}$ cells in tissue samples were assessed by ImageJ. The bars and error bars represent the mean ± SD; $^{*}P < 0.05$; $^{**}P < 0.01$; $^{***}P < 0.001$; ns, not significant.

of recombinant mouse YM1 on ROS levels was also analyzed in B16F10 cells. 3-Gy-irradiation induced intracellular ROS in B16F10 cells and the levels of γ-ray-induced ROS were attenuated by pretreatment with diphenyleneiodonium chloride (DPI), known as a ROS scavenger (**Figures 5A, C**). Recombinant YM1 diminished the levels of γ-ray-induced ROS not only in DMSO-B16F10 cells but also in rapamycin-B16F10 cells (**Figures 5B, C**). Since recombinant YM1 attenuated ROS levels in γ-

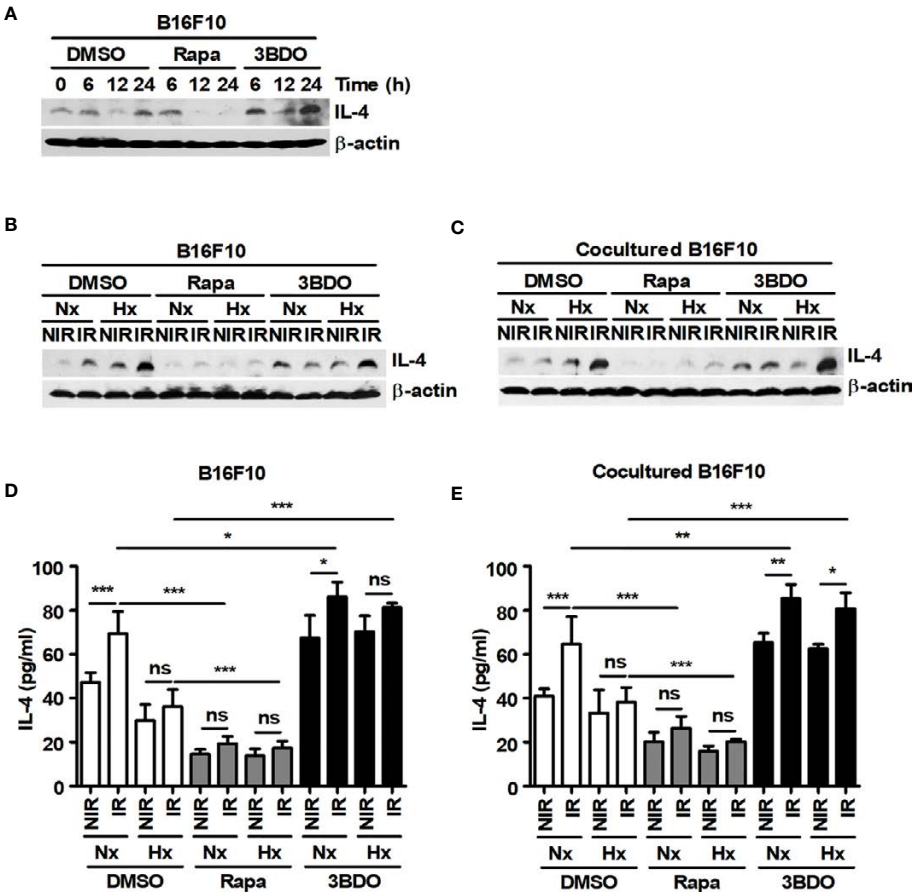

FIGURE 4 | Pharmaceutical regulation of mTOR activation affects the expression and secretion of IL-4 in B16F10 cells. **(A)** B16F10 cells were treated with DMEM containing DMSO, 100 nM rapamycin or 100 nM 3BDO for the indicated times. Intracellular IL-4 levels were detected by western blotting. **(B–E)** B16F10 cells cultured alone or cocultured with BMDMs were incubated in the presence of 100 nM rapamycin or 100 nM 3BDO under the indicated conditions for 21 h. Intracellular IL-4 levels were detected by western blotting **(B, C),** and secreted IL-4 was analyzed by ELISA **(D, E)**. The bars and error bars represent the mean ± SD; $^{*}P < 0.05$; $^{**}P < 0.01$; $^{***}P < 0.001$; ns, not significant.

irradiated B16F10 cells, the effect of YM1 on the cell viability of B16F10 cells was investigated. As a result, DPI restored the reduced viability of B16F10 cells treated with 3 Gy irradiation in DMSO- and rapamycin-B16F10 cells (**Figure 5D**). DPI also decreased the ratio of cPARP/tPARP promoted by irradiation in the same groups (**Figure 5E**). This means that a 3-Gy-dose of γ-irradiation could induce the death of B16F10 cells through the generation of intracellular ROS. Meanwhile, recombinant YM1 rescued the cell viability and reduced the increased ratio of cPARP/tPARP in the rapamycin groups during irradiation (**Figures 5D, E**). Overall, these results suggest that inhibition of mTOR signaling in tumor cells may promote their sensitivity to γ-ray-induced ROS.

Rapamycin Attenuates the Functional Expression of YM1-Induced xCT in Melanoma Cells

The intracellular ROS in tumor cells can be regulated by the xCT system, a major pathway of GSH synthesis (44). Therefore, the effect of YM1 on xCT expression was investigated because recombinant YM1 attenuated the levels of ROS in B16F10 cells during irradiation. Compared with xCT expression in single cultured DMSO-B16F10 cells, BMDMs continued to induce its expression in DMSO-B16F10 cells under various stimuli during coculture (**Figures 6A, B**). Rapamycin attenuated xCT expression in B16F10 cells under both single- and cocultured conditions but not in other groups (**Figures 6A, B**). Recombinant YM1 stimulated mTOR signaling and also promoted xCT expression in B16F10 cells (**Figure 6C**). Rapamycin can promote EEA1 expression and induce the formation of amphisomes through the fusion of autophagosomes with early endosomes (45). The degradation of CD98, a component protein in the xCT system, can be induced by EEA1-mediated capture during its recycling process (46). Therefore, the effects of recombinant YM1 on the colocalization of LC3 and EEA1 (or EEA1 and xCT) were assessed in B16F10 cells. Compared to the nonirradiated groups, γ-radiation

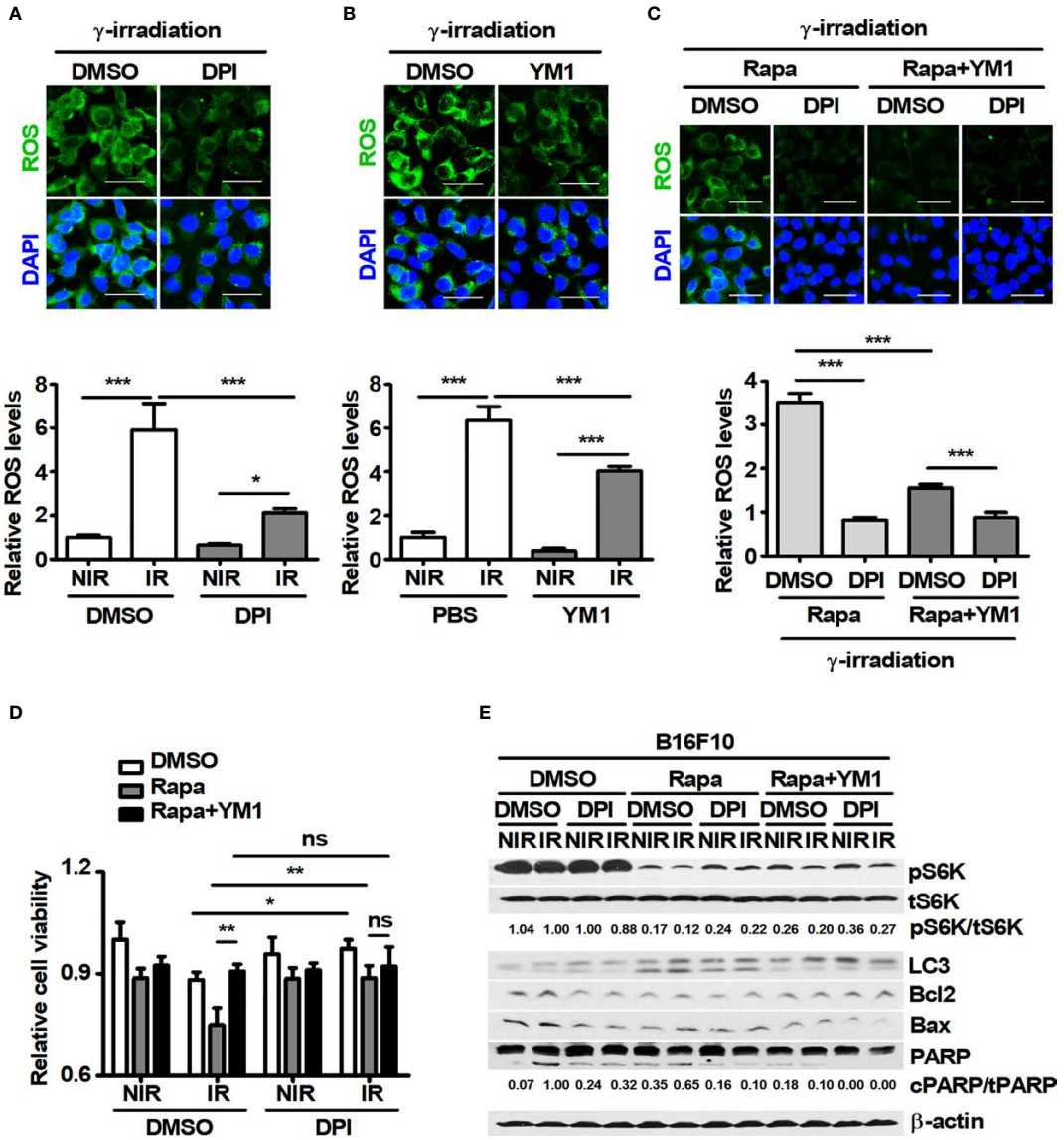

FIGURE 5 | YM1 affects ROS-induced cell death in B16F10 cells under γ-radiation. **(A–E)** After pretreatment with diphenyleneiodonium (DPI) for 1 h, B16F10 cells were treated with DMSO or 100 nM rapamycin for 3 h. B16F10 cells were washed with PBS and then incubated with DMEM and rapamycin in the presence or absence of 125 ng/ml rmYM-1 for 3 h before receiving 3-Gy γ-irradiation. After γ-irradiation, B16F10 cells were incubated with 5 μM CellROX for 30 min. **(A–C)** Intracellular ROS were assessed by confocal microscopy. Scale bars, 50 μm. **(D)** Cell viability was measured by an automated cell counter. **(E)** The protein levels of p70 S6K, phospho-p70 S6K, LC3, Bcl2, Bax, and PARP in B16F10 cells were evaluated by western blotting. β-actin was used as an internal control. The bars and error bars represent the mean ± SD; $^{*}P < 0.05$; $^{**}P < 0.01$; $^{***}P < 0.001$; ns, not significant.

increased the proportions of $LC3^{+}EEA1^{+}$ and $xCT^{+}EEA1^{+}$ cells (**Figures 6D, E**). On the other hand, YM1 significantly reduced the proportions of $LC3^{+}EEA1^{+}$ and $xCT^{+}EEA1^{+}$ cells in the irradiated groups (**Figures 6D, E**). Rapamycin enhanced the proportions of $LC3^{+}EEA1^{+}$ and $xCT^{+}EEA1^{+}$ cells in the YM1-treated groups (**Figures 6D, E**).

As mentioned in **Figure 1E**, rapamycin enhanced the proportion of $LC3^{+}PI^{+}$ cells in tumor tissues. Therefore, the relationship between $LC3^{+}$ dots induced by rapamycin and xCT expression in tumor tissues was analyzed. Rapamycin decreased the proportion of xCT^{+} cells but increased the proportion of $LC3^{+}xCT^{+}$ cells in tumor tissues (**Figure 6F**). The effect of YM1 on the expression of metastasis-related proteins in B16F10 cells was investigated. As a result, rapamycin attenuated the expression of MMP2 and MMP9, but the effects of macrophages on their expression were not observed in B16F10 cells under coculture conditions compared with those in single-culture conditions (**Supplementary Figures 3A, B**). In addition,

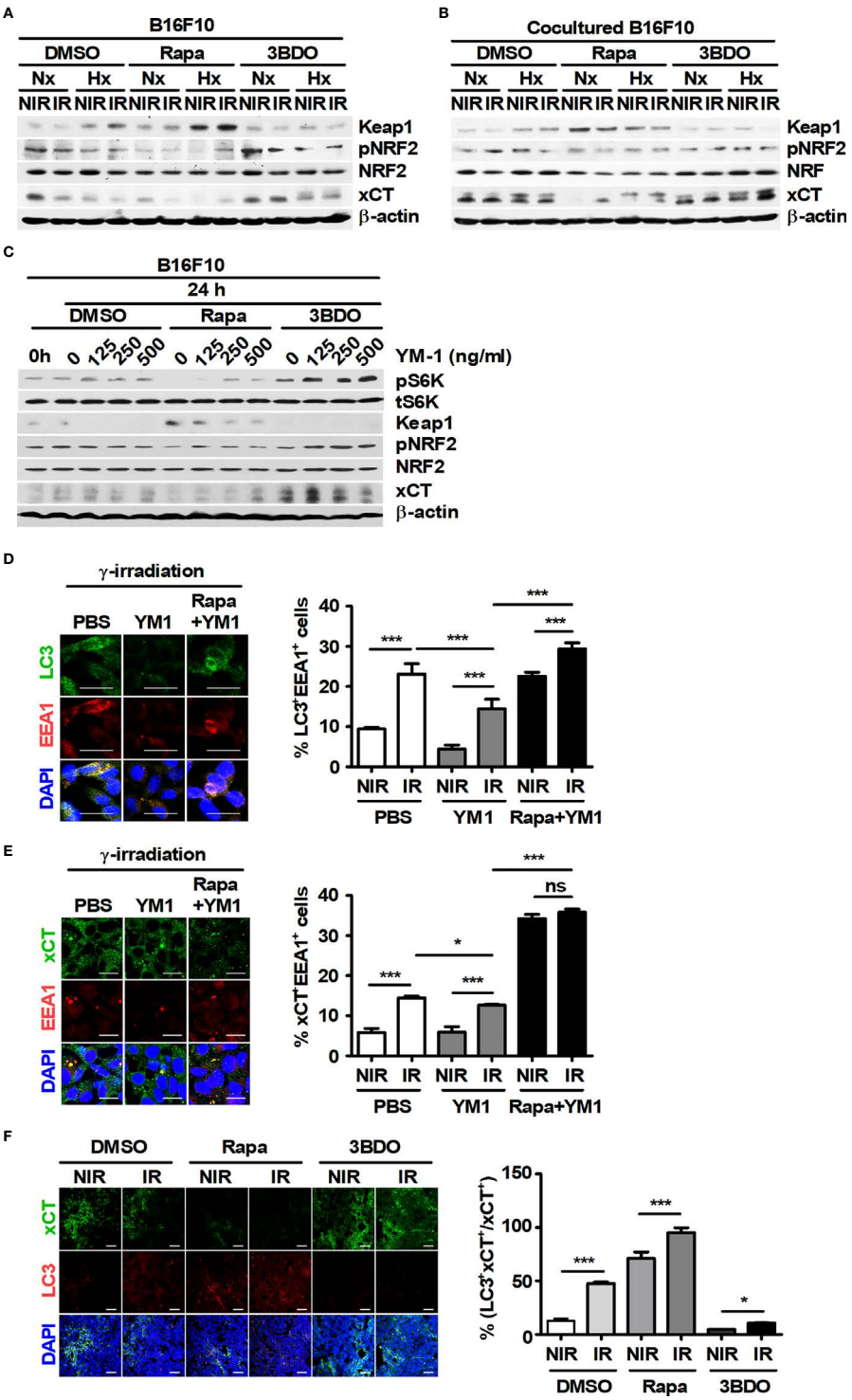

FIGURE 6 | Pharmaceutical regulation of mTOR activation affects the functional expression of xCT in B16F10 cells. **(A, B)** B16F10 cells cultured alone or cocultured with BMDMs were treated with DMSO, 100 nM rapamycin or 100 nM 3BDO under the indicated conditions. Intracellular levels of Keap1, phospho-NRF2, NRF, xCT, and β-actin in B16F10 cells were evaluated by western blotting. **(C–E)** B16F10 cells were treated with DMSO, 100 nM rapamycin or 100 nM 3BDO for 3 h and then stimulated with the indicated concentrations of recombinant mouse YM-1 for 21 h. **(C)** The expression levels of phospho-p70 S6K, p70 S6K, Keap1, phospho-NRF2, NRF, xCT, and β-actin in B16F10 cells were detected by western blotting. **(D, E)** Intracellular levels of LC3, EEA1, and xCT were assessed by confocal microscopy. Scale bars, 30 μm. **(F)** Intratumoral levels of xCT and LC3 were analyzed by confocal microscopy. All images were quantified using ImageJ. Scale bars, 200 μm. The bars and error bars represent the mean ± SD; $^{*}P < 0.05$; $^{***}P < 0.001$; ns, not significant.

YM1 also failed to affect the expression of metastasis-related proteins (**Supplementary Figure 3C**). These results mean that YM1 might not be involved in melanoma metastasis. Overall, however, these results suggested that YM1 produced by macrophages may contribute to promoting xCT expression and attenuate the EEA1-mediated capture of intracellular xCT in tumor cells during irradiation. Meanwhile, among human CLPs, YKL39 and YKL40 can promote tumor development (47, 48). To investigate the effect of CLPs on xCT expression in human melanoma cell lines, Malme-3M and SK-MEL-2 cells were treated with YKL39 and YKL40 (**Figures 7A–C**). YKL39 increased the expression of xCT in nonirradiated Malme-3M cells (**Figure 7A**). Although YKL39 did not affect the expression of xCT in γ-irradiated Malme-3M cells, it decreased the proportion of $xCT^{+}EEA1^{+}$ cells regardless of rapamycin treatment under γ-radiation (**Figures 7A, C**). The effect of YKL40 on the expression of xCT was not observed in Malme-3M cells (**Figure 7A**). Meanwhile, YKL39 and YKL40 did not affect the expression of xCT in SK-MEL-2 cells (**Figure 7B**).

Finally, the expression values of IL-4, xCT, and YM1 in control or melanoma tissues derived from metastatic (iMet model) and non-metastatic (iHRAS model) tissues were compared using Gene Expression Omnibus (GEO) data (GSE29074). Only mRNA of YM1 was significantly increased in both melanoma tissues compared with that in normal tissues (**Supplementary Figures 4A–C**). To evaluate the associations between tumorigenesis and target genes (IL-4, xCT, and YKL39) in melanoma patients, clinical data in GEO profiles (GSE3189) were used. As a result, only xCT expression was significantly associated with tumor progression (**Supplementary Figures 4D–F**). These results imply that xCT could be closely associated with melanoma malignancy in humans. The cBioPortal database (Skin Cutaneous Melanoma, TCGA, PanCancer Atlas, 448 samples) was used to analyze the correlation between xCT expression and selected genes (KEAP1, NRF2, and YKL39) in melanoma patients. Although trends of negative (KEAP1) and positive (NRF2 and YKL39) regression lines were observed, they did not appear to show a correlation between xCT and each gene (**Supplementary Figures 4G–I**).

DISCUSSION

It is important to understand the interaction between macrophages and tumor cells in the tumor microenvironment as a strategy to increase the efficiency of cancer radiotherapy (3). Moreover, finding a radiotherapy adjuvant that can reduce side effects in hosts receiving γ-irradiation is crucial. Since the contribution of mTOR signaling to tumorigenesis has been

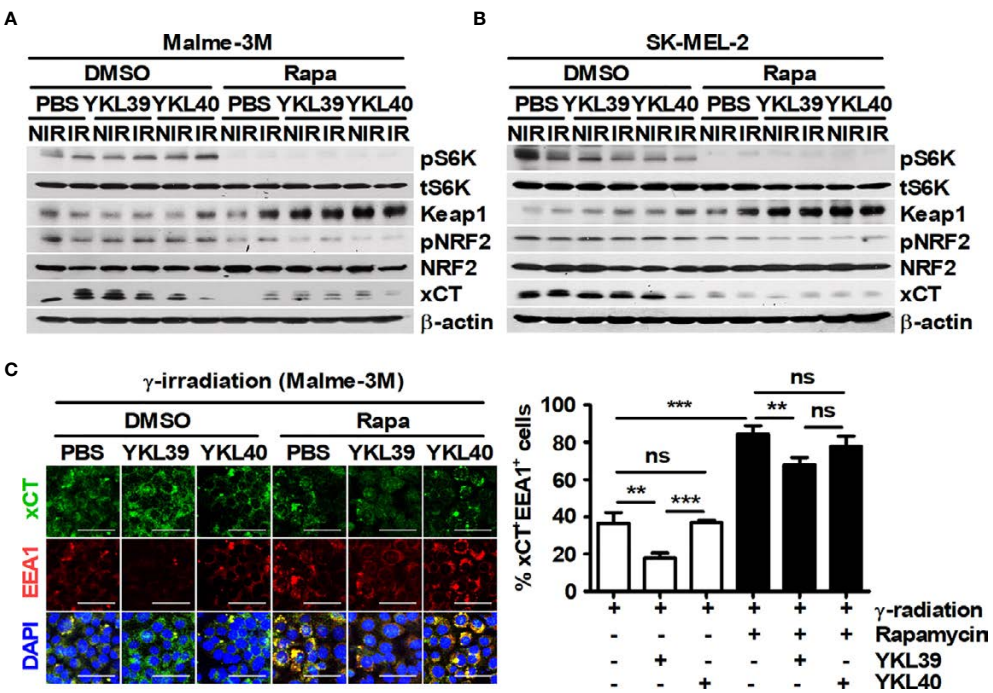

FIGURE 7 | Human YKL39 affects γ-ray-induced colocalization of xCT and EEA1 in Malme-3M, a human melanoma cell line. **(A–C)** Malme-3M and SK-MEL-2 cells were treated with DMSO or 100 nM rapamycin for 3 h. After 3-Gy γ-irradiation, each cell line was stimulated with recombinant human YKL39 and YKL40 for 21 h. **(A, B)** The expression levels of phospho-p70 S6K, p70 S6K, Keap1, phospho-NRF2, NRF, xCT, and β-actin in the cells were detected by western blotting. **(C)** Intracellular levels of xCT and EEA1 were assessed by confocal microscopy. Scale bars, 50 μm. The bars and error bars represent the mean ± SD; $^{**}P < 0.01$; $^{***}P < 0.001$; ns, not significant.

revealed in many tumor studies, targeting mTOR as a radiosensitizing strategy may be a reasonable approach.

Rapamycin is a widely used drug that can effectively block the mTOR pathway (49). Rapamycin works as an allosteric inhibitor of the FRB domain of mTORC1 through the formation of a complex with FKBP12 (also known as FKBP 1A), and it can also activate autophagy (50). 3BDO can directly activate mTOR *via* hydrogen bonding to FKBP1A and can be used as an autophagy inhibitor (51). Therefore, these two agents are suitable drugs to study the pharmaceutical effects of mTOR control on the tumor microenvironment because they can cause conflicting results by targeting the same protein. In this study, the effects of these drugs on the interaction between macrophages and tumor cells during irradiation were evaluated.

Inhibiting antioxidant activity in tumor cells during radiotherapy can be a major therapeutic strategy for increasing radiosensitivity (18). In this study, the reduction in xCT expression by mTOR inhibition was observed. In addition, the EEA1-mediated capture of intracellular xCT was newly discovered. The regulation of xCT activity in tumor cells *via* mTOR inhibition in this study can be supported by recently published studies (52, 53). Therefore, inhibiting functional xCT in tumors through the suppression of mTOR signaling might be an alternative strategy for efficient radiotherapy (21).

In this study, experiments using neutralizing antibodies against IL-4 and YM1 were not performed both *in vitro* and *in vivo*. These experimental approaches are essential for understanding the interaction between macrophages and tumor cells in the tumor microenvironment. However, the contribution of the interaction between the cells to tumor radioresistance was indirectly confirmed through recombinant proteins, such as IL-4 and YM1.

YM1 produced by macrophages may promote the expression of functional xCT *via* mTOR signaling in melanoma while mTOR inhibitors, including rapamycin, may promote the sensitivity of tumor cells to γ-ray-induced ROS *via* the functional attenuation of xCT in tumors. Although various culture conditions were utilized *in vitro* to mimic the tumor microenvironment, several ambiguous results, such as the levels of phosphorylated S6K, were observed among various conditions. These unexpected results should be clarified through further studies.

YKL40 is the human homologue for mouse breast regression protein 39 (BRP39), but there is no corresponding homologue of human YKL39 in mice (14). In addition, YM1 is expressed only in mice (39). Therefore, the effect of YKL39 on human melanoma was evaluated, as there are no alternative CLPs for YM1 in humans. In this study, human recombinant YKL39

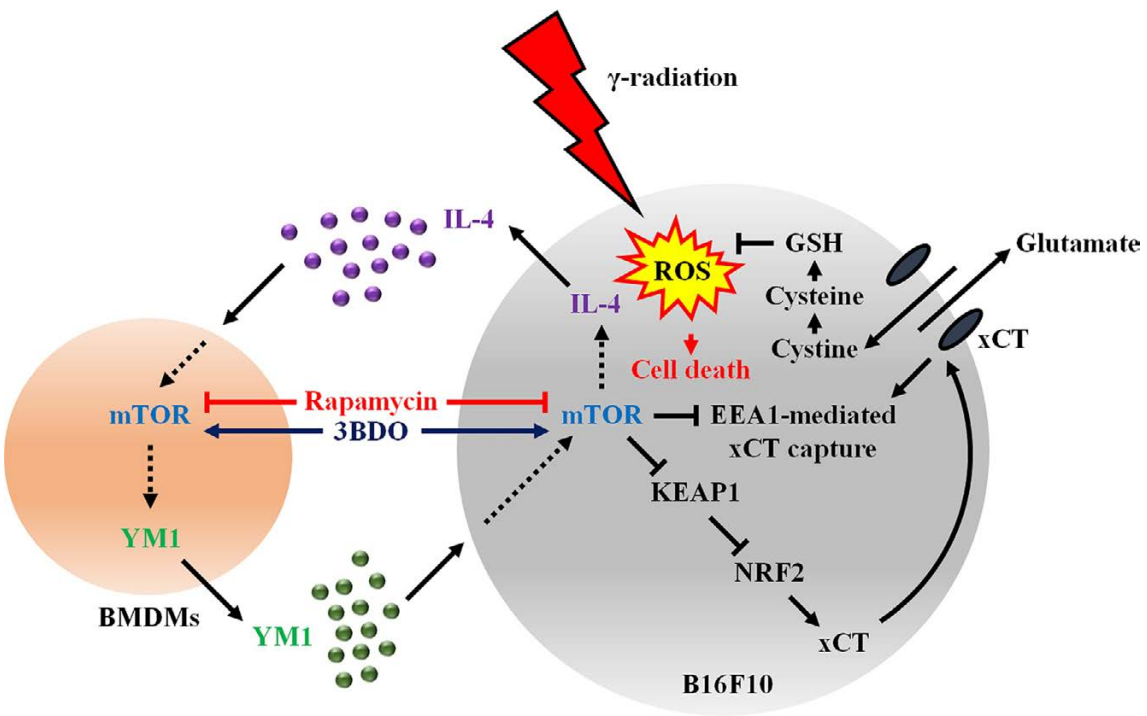

FIGURE 8 | Activated mTOR signaling induces the secretion of IL-4 in melanomas and YM1 in macrophages in the tumor microenvironment. Secreted YM-1enhances the EEA1-mediated xCT capture *via* the KEAP1/NRF2 signaling pathway to promote antioxidant mechanisms through GSH in radiotherapy. Therefore, the regulation of mTOR activity using rapamycin could increase tumor sensitivity to γ-radiation-induced ROS by inhibiting the interaction between melanoma and macrophages.

attenuated radiation-induced colocalization of xCT and EEA1 in Malme-3M, similar to mouse recombinant YM1. However, the effect of YKL39 on xCT expression was observed to be different depending on the cell line. Thus, further research is needed to determine whether YM1 and YKL39 attenuate EEA1-mediated xCT capture *via* the same mechanism in various tumor cases under γ-radiation. Our study shows that mTOR inhibition in the tumor microenvironment can attenuate the interaction between tumor cells and macrophages during radiotherapy (**Figure 8**). This study also provides a new strategy to enhance tumor radiosensitivity by blocking the system of maintaining ROS homeostasis in tumors.

DATA AVAILABILITY STATEMENT

The original contributions presented in the study are included in the article/**Supplementary Material**. Further inquiries can be directed to the corresponding author.

ETHICS STATEMENT

The animal experiments in the present study were approved and confirmed by the Ethical Guidelines for Animal Experiments of Kangwon National University (KW-181214-1).

AUTHOR CONTRIBUTIONS

YW and Y-JJ designed the study. YW performed and analyzed the *in vivo* and *in vitro* experiments together with H-JL, JK, SK, SM, YJ, and JH contributed materials and analysis tools. YW and Y-JJ wrote the paper with input from the other authors. All authors contributed to the article and approved the submitted version.

FUNDING

This research was supported by a grant from the Basic Science Research Program through the National Research Foundation of Korea (NRF), which is funded by the Ministry of Science, ICT and Future Planning of the Republic of Korea (2018R1D1A1B07049097 and 2021R1A2C1004525), and the Korea Basic Science Institute (National Research Facilities and Equipment Center) grant funded by the Ministry of Education (2020R1A6C101A195).

SUPPLEMENTARY MATERIAL

The Supplementary Material for this article can be found online at: https://www.frontiersin.org/articles/10.3389/fonc.2021.665420/full#supplementary-material

REFERENCES

1. Tang C, Wang X, Soh H, Seyedin S, Cortez MA, Krishnan S, et al. Combining radiation and immunotherapy: a new systemic therapy for solid tumors? *Cancer Immunol Res* (2014) 2(9):831–8. doi: 10.1158/2326-6066.CIR-14-0069
2. Woo Y, Lee HJ, Jung YM, Jung YJ. Regulated Necrotic Cell Death in Alternative Tumor Therapeutic Strategies. *Cells* (2020) 9(12):2709–25. doi: 10.3390/cells9122709
3. Barker HE, Paget JT, Khan AA, Harrington KJ. The tumour microenvironment after radiotherapy: mechanisms of resistance and recurrence. *Nat Rev Cancer* (2015) 15(7):409–25. doi: 10.1038/nrc3958
4. Ruffell B, Coussens LM. Macrophages and therapeutic resistance in cancer. *Cancer Cell* (2015) 27(4):462–72. doi: 10.1016/j.ccell.2015.02.015
5. Gil Del Alcazar CR, Aleckovic M, Polyak K. Immune Escape during Breast Tumor Progression. *Cancer Immunol Res* (2020) 8(4):422–7. doi: 10.1158/2326-6066.CIR-19-0786
6. Leblond MM, Peres EA, Helaine C, Gerault AN, Moulin D, Anfray C, et al. M2 macrophages are more resistant than M1 macrophages following radiation therapy in the context of glioblastoma. *Oncotarget* (2017) 8 (42):72597–612. doi: 10.18632/oncotarget.19994
7. Genard G, Lucas S, Michiels C. Reprogramming of Tumor-Associated Macrophages with Anticancer Therapies: Radiotherapy versus Chemo- and Immunotherapies. *Front Immunol* (2017) 8:828. doi: 10.3389/fimmu.2017.00828
8. Song W, Mazzieri R, Yang T, Gobe GC. Translational Significance for Tumor Metastasis of Tumor-Associated Macrophages and Epithelial-Mesenchymal Transition. *Front Immunol* (2017) 8:1106. doi: 10.3389/fimmu.2017.01106
9. Lee HJ, Woo Y, Hahn TW, Jung YM, Jung YJ. Formation and Maturation of the Phagosome: A Key Mechanism in Innate Immunity against Intracellular Bacterial Infection. *Microorganisms* (2020) 8(9). doi: 10.3390/microorganisms8091298
10. Paul WE, Zhu J. How are T(H)2-type immune responses initiated and amplified? *Nat Rev Immunol* (2010) 10(4):225–35. doi: 10.1038/nri2735
11. Lee HL, Park MH, Song JK, Jung YY, Kim Y, Kim KB, et al. Tumor growth suppressive effect of IL-4 through p21-mediated activation of STAT6 in IL-4Ralpha overexpressed melanoma models. *Oncotarget* (2016) 7 (17):23425–38. doi: 10.18632/oncotarget.8111
12. Lee CG, Da Silva CA, Dela Cruz CS, Ahangari F, Ma B, Kang MJ, et al. Role of chitin and chitinase/chitinase-like proteins in inflammation, tissue remodeling, and injury. *Annu Rev Physiol* (2011) 73:479–501. doi: 10.1146/annurev-physiol-012110-142250
13. Hamid R, Khan MA, Ahmad M, Ahmad MM, Abdin MZ, Musarrat J, et al. Chitinases: An update. *J Pharm Bioallied Sci* (2013) 5(1):21–9. doi: 10.4103/0975-7406.106559
14. Elias JA, Homer RJ, Hamid Q, Lee CG. Chitinases and chitinase-like proteins in T(H)2 inflammation and asthma. *J Allergy Clin Immunol* (2005) 116 (3):497–500. doi: 10.1016/j.jaci.2005.06.028
15. Kawada M, Seno H, Kanda K, Nakanishi Y, Akitake R, Komekado H, et al. Chitinase 3-like 1 promotes macrophage recruitment and angiogenesis in colorectal cancer. *Oncogene* (2012) 31(26):3111–23. doi: 10.1038/onc.2011.498
16. Jefri M, Huang Y-N, Huang W-C, Tai C-S, Chen W-L. YKL-40 regulated epithelial-mesenchymal transition and migration/invasion enhancement in non-small cell lung cancer. *BMC Cancer* (2015) 15(1):590. doi: 10.1186/s12885-015-1592-3
17. Lee JH, Kim SY, Kil IS, Park JW. Regulation of ionizing radiation-induced apoptosis by mitochondrial NADP+-dependent isocitrate dehydrogenase. *J Biol Chem* (2007) 282(18):13385–94. doi: 10.1074/jbc.M700303200
18. Hawk MA, McCallister C, Schafer ZT. Antioxidant Activity during Tumor Progression: A Necessity for the Survival of Cancer Cells? *Cancers (Basel)* (2016) 8(10). doi: 10.3390/cancers8100092
19. Bansal A, Simon MC. Glutathione metabolism in cancer progression and treatment resistance. *J Cell Biol* (2018) 217(7):2291–8. doi: 10.1083/jcb.201804161
20. Koppula P, Zhang Y, Zhuang L, Gan B. Amino acid transporter SLC7A11/xCT at the crossroads of regulating redox homeostasis and nutrient dependency of cancer. *Cancer Commun (Lond)* (2018) 38(1):12. doi: 10.1186/s40880-018-0288-x
21. Woo Y, Lee HJ, Jung YM, Jung YJ. mTOR-Mediated Antioxidant Activation in Solid Tumor Radioresistance. *J Oncol* (2019) 2019:5956867. doi: 10.1155/2019/5956867

22. Yu CC, Hung SK, Lin HY, Chiou WY, Lee MS, Liao HF, et al. Targeting the PI3K/AKT/mTOR signaling pathway as an effectively radiosensitizing strategy for treating human oral squamous cell carcinoma in vitro and in vivo. *Oncotarget* (2017) 8(40):68641–53. doi: 10.18632/oncotarget.19817
23. Zheng H, Wang M, Wu J, Wang ZM, Nan HJ, Sun H. Inhibition of mTOR enhances radiosensitivity of lung cancer cells and protects normal lung cells against radiation. *Biochem Cell Biol* (2016) 94(3):213–20. doi: 10.1139/bcb-2015-0139
24. Woo Y, Kim H, Kim KC, Han JA, Jung YJ. Tumor-secreted factors induce IL-1beta maturation via the glucose-mediated synergistic axis of mTOR and NF-kappaB pathways in mouse macrophages. *PloS One* (2018) 13(12): e0209653. doi: 10.1371/journal.pone.0209653
25. Lee HJ, Ko HJ, Jung YJ. Insufficient Generation of Mycobactericidal Mediators and Inadequate Level of Phagosomal Maturation Are Related with Susceptibility to Virulent Mycobacterium tuberculosis Infection in Mouse Macrophages. *Front Microbiol* (2016) 7:541. doi: 10.3389/fmicb.2016.00541
26. Cho JH, Lee HJ, Ko HJ, Yoon BI, Choe J, Kim KC, et al. The TLR7 agonist imiquimod induces anti-cancer effects via autophagic cell death and enhances anti-tumoral and systemic immunity during radiotherapy for melanoma. *Oncotarget* (2017) 8(15):24932–48. doi: 10.18632/oncotarget.15326
27. Woo Y, Jung YJ. Angiotensin II receptor blockers induce autophagy in prostate cancer cells. *Oncol Lett* (2017) 13(5):3579–85. doi: 10.3892/ol.2017.5872
28. Lee HJ, Ko HJ, Kim SH, Jung YJ. Pasakbumin A controls the growth of Mycobacterium tuberculosis by enhancing the autophagy and production of antibacterial mediators in mouse macrophages. *PloS One* (2019) 14(3): e0199799. doi: 10.1371/journal.pone.0199799
29. Lee HJ, Kang SJ, Woo Y, Hahn TW, Ko HJ, Jung YJ. TLR7 Stimulation With Imiquimod Induces Selective Autophagy and Controls Mycobacterium tuberculosis Growth in Mouse Macrophages. *Front Microbiol* (2020) 11:1684. doi: 10.3389/fmicb.2020.01684
30. Scott KL, Nogueira C, Heffernan TP, van Doorn R, Dhakal S, Hanna JA, et al. Proinvasion metastasis drivers in early-stage melanoma are oncogenes. *Cancer Cell* (2011) 20(1):92–103. doi: 10.1016/j.ccr.2011.05.025
31. Talantov D, Mazumder A, Yu JX, Briggs T, Jiang Y, Backus J, et al. Novel genes associated with malignant melanoma but not benign melanocytic lesions. *Clin Cancer Res* (2005) 11(20):7234–42. doi: 10.1158/1078-0432.CCR-05-0683
32. Barnett GC, West CM, Dunning AM, Elliott RM, Coles CE, Pharoah PD, et al. Normal tissue reactions to radiotherapy: towards tailoring treatment dose by genotype. *Nat Rev Cancer* (2009) 9(2):134–42. doi: 10.1038/nrc2587
33. Liang H, Deng L, Chmura S, Burnette B, Liadis N, Darga T, et al. Radiation-induced equilibrium is a balance between tumor cell proliferation and T cell-mediated killing. *J Immunol* (2013) 190(11):5874–81. doi: 10.4049/jimmunol.1202612
34. Shen M, Chen Y, Xu L, Zhu R, Xue X, Tsai Y, et al. Increased infiltration of macrophages to radioresistant lung cancer cells contributes to the development of the additional resistance of tumor cells to the cytotoxic effects of NK cells. *Int J Oncol* (2018) 53(1):317–28. doi: 10.3892/ijo.2018.4394
35. Baran N, Konopleva M. Molecular Pathways: Hypoxia-Activated Prodrugs in Cancer Therapy. *Clin Cancer Res* (2017) 23(10):2382–90. doi: 10.1158/1078-0432.CCR-16-0895
36. Bronte V, Murray PJ. Understanding local macrophage phenotypes in disease: modulating macrophage function to treat cancer. *Nat Med* (2015) 21(2):117–9. doi: 10.1038/nm.3794
37. Van den Bossche J, Baardman J, de Winther MP. Metabolic Characterization of Polarized M1 and M2 Bone Marrow-derived Macrophages Using Real-time Extracellular Flux Analysis. *J Vis Exp* (2015) 105). doi: 10.3791/53424
38. Colegio OR, Chu NQ, Szabo AL, Chu T, Rhebergen AM, Jairam V, et al. Functional polarization of tumour-associated macrophages by tumour-derived lactic acid. *Nature* (2014) 513(7519):559–63. doi: 10.1038/nature13490
39. Welch JS, Escoubet-Lozach L, Sykes DB, Liddiard K, Greaves DR, Glass CK. TH2 cytokines and allergic challenge induce Ym1 expression in macrophages by a STAT6-dependent mechanism. *J Biol Chem* (2002) 277(45):42821–9. doi: 10.1074/jbc.M205873200
40. Van Dyken SJ, Locksley RM. Interleukin-4- and interleukin-13-mediated alternatively activated macrophages: roles in homeostasis and disease. *Annu Rev Immunol* (2013) 31:317–43. doi: 10.1146/annurev-immunol-032712-095906
41. Son DJ, Jung YY, Park MH, Lee HL, Song MJ, Yoo HS, et al. Activated Natural Killer Cells Mediate the Suppressive Effect of Interleukin-4 on Tumor Development via STAT6 Activation in an Atopic Condition Melanoma Model. *Neoplasia* (2017) 19(7):537–48. doi: 10.1016/j.neo.2017.02.014
42. Azzam EI, Jay-Gerin JP, Pain D. Ionizing radiation-induced metabolic oxidative stress and prolonged cell injury. *Cancer Lett* (2012) 327(1-2):48–60. doi: 10.1016/j.canlet.2011.12.012
43. Tang L, Wei F, Wu Y, He Y, Shi L, Xiong F, et al. Role of metabolism in cancer cell radioresistance and radiosensitization methods. *J Exp Clin Cancer Res* (2018) 37(1):87. doi: 10.1186/s13046-018-0758-7
44. Habib E, Linher-Melville K, Lin HX, Singh G. Expression of xCT and activity of system xc(-) are regulated by NRF2 in human breast cancer cells in response to oxidative stress. *Redox Biol* (2015) 5:33–42. doi: 10.1016/j.redox.2015.03.003
45. Leiva-Rodriguez T, Romeo-Guitart D, Marmolejo-Martinez-Artesero S, Herrando-Grabulosa M, Bosch A, Fores J, et al. ATG5 overexpression is neuroprotective and attenuates cytoskeletal and vesicle-trafficking alterations in axotomized motoneurons. *Cell Death Dis* (2018) 9(6):626. doi: 10.1038/s41419-018-0682-y
46. Eyster CA, Cole NB, Petersen S, Viswanathan K, Fruh K, Donaldson JG. MARCH ubiquitin ligases alter the itinerary of clathrin-independent cargo from recycling to degradation. *Mol Biol Cell* (2011) 22(17):3218–30. doi: 10.1091/mbc.E10-11-0874
47. Pusztai C, Yusenko MV, Banyai D, Szanto A, Kovacs G. M2 Macrophage Marker Chitinase 3-Like 2 (CHI3L2) Associates With Progression of Conventional Renal Cell Carcinoma. *Anticancer Res* (2019) 39(12):6939–43. doi: 10.21873/anticanres.13915
48. Qiu QC, Wang L, Jin SS, Liu GF, Liu J, Ma L, et al. CHI3L1 promotes tumor progression by activating TGF-beta signaling pathway in hepatocellular carcinoma. *Sci Rep* (2018) 8(1):15029. doi: 10.1038/s41598-018-33239-8
49. Li J, Kim SG, Blenis J. Rapamycin: one drug, many effects. *Cell Metab* (2014) 19(3):373–9. doi: 10.1016/j.cmet.2014.01.001
50. Hausch F, Kozany C, Theodoropoulou M, Fabian AK. FKBPs and the Akt/mTOR pathway. *Cell Cycle* (2013) 12(15):2366–70. doi: 10.4161/cc.25508
51. Ge D, Han L, Huang S, Peng N, Wang P, Jiang Z, et al. Identification of a novel MTOR activator and discovery of a competing endogenous RNA regulating autophagy in vascular endothelial cells. *Autophagy* (2014) 10(6):957–71. doi: 10.4161/auto.28363
52. Nagane M, Kanai E, Shibata Y, Shimizu T, Yoshioka C, Maruo T, et al. Sulfasalazine, an inhibitor of the cystine-glutamate antiporter, reduces DNA damage repair and enhances radiosensitivity in murine B16F10 melanoma. *PloS One* (2018) 13(4):e0195151. doi: 10.1371/journal.pone.0195151
53. Li C, Chen H, Lan Z, He S, Chen R, Wang F, et al. mTOR-dependent upregulation of xCT blocks melanin synthesis and promotes tumorigenesis. *Cell Death Differ* (2019) 26(10):2015–28. doi: 10.1038/s41418-019-0274-0

Conflict of Interest: The authors declare that the research was conducted in the absence of any commercial or financial relationships that could be construed as a potential conflict of interest.

Copyright © 2021 Woo, Lee, Kim, Kang, Moon, Han, Jung and Jung. This is an open-access article distributed under the terms of the Creative Commons Attribution License (CC BY). The use, distribution or reproduction in other forums is permitted, provided the original author(s) and the copyright owner(s) are credited and that the original publication in this journal is cited, in accordance with accepted academic practice. No use, distribution or reproduction is permitted which does not comply with these terms.

frontiers in Immunology

REVIEW
published: 27 April 2021
doi: 10.3389/fimmu.2021.656908

The Role of Tumor Necrosis Factor in Manipulating the Immunological Response of Tumor Microenvironment

*Dipranjan Laha, Robert Grant, Prachi Mishra and Naris Nilubol**

Surgical Oncology Program, Center for Cancer Research, National Cancer Institute, NIH, Bethesda, MD, United States

The tumor microenvironment (TME) is an intricate system within solid neoplasms. In this review, we aim to provide an updated insight into the TME with a focus on the effects of tumor necrosis factor-α (TNF-α) on its various components and the use of TNF-α to improve the efficiency of drug delivery. The TME comprises the supporting structure of the tumor, such as its extracellular matrix and vasculature. In addition to cancer cells and cancer stem cells, the TME contains various other cell types, including pericytes, tumor-associated fibroblasts, smooth muscle cells, and immune cells. These cells produce signaling molecules such as growth factors, cytokines, hormones, and extracellular matrix proteins. This review summarizes the intricate balance between pro-oncogenic and tumor-suppressive functions that various non-tumor cells within the TME exert. We focused on the interaction between tumor cells and immune cells in the TME that plays an essential role in regulating the immune response, tumorigenesis, invasion, and metastasis. The multifunctional cytokine, TNF-α, plays essential roles in diverse cellular events within the TME. The uses of TNF-α in cancer treatment and to facilitate cancer drug delivery are discussed. The effects of TNF-α on tumor neovasculature and tumor interstitial fluid pressure that improve treatment efficacy are summarized.

Keywords: tumor microenvironment, tumor necrosis factor-α, transforming growth factor beta, extracellular matrix, interstitial fluid pressure

OPEN ACCESS

Edited by:
Peng Qu,
National Institutes of Health (NIH), United States

Reviewed by:
Guohao Wang,
National Institutes of Health (NIH), United States
Giuseppe Murdaca,
University of Genoa, Italy
Andrey Kruglov,
German Rheumatism Research Center (DRFZ), Germany

***Correspondence:**
Naris Nilubol
naris.nilubol@mail.nih.gov

Specialty section:
This article was submitted to Cancer Immunity and Immunotherapy, a section of the journal Frontiers in Immunology

Received: *21 January 2021*
Accepted: *07 April 2021*
Published: *27 April 2021*

Citation:
Laha D, Grant R, Mishra P and Nilubol N (2021) The Role of Tumor Necrosis Factor in Manipulating the Immunological Response of Tumor Microenvironment. Front. Immunol. 12:656908. doi: 10.3389/fimmu.2021.656908

INTRODUCTION

The tumor microenvironment (TME) is a complex biological ecosystem of solid tumors encompassing all the cells and structures found in healthy organ tissue (1). These include, but are not limited to, blood vessels, immune infiltrates, fibroblasts, and the extracellular matrix. Tumor cells, immune cells, fibroblasts, myofibroblasts, and microvascular structures such as vascular endothelial cells and pericytes found within the TME play various critical roles in regulating tumor initiation and progression (1–3). These cell types can control tumor growth through their normal regulatory functions. However, the dysregulation of these cells can promote tumor growth and metastasis. Recent studies demonstrate that the relationships between cancer cells and their surrounding microenvironments affect cancer cell survival, growth, proliferation, epithelial-mesenchymal transition (EMT), and metastasis (4). Thus, the modulation of the TME as a target

for clinical applications is an area of interest in cancer treatments. Communication between neoplastic cells and the TME is conducted mainly through standard mechanisms observed in communication between healthy cells in normal organ tissue: through intercellular junctions and receptor-signal pathways encased in a three-dimensional extracellular matrix (ECM). Glycoproteins, proteoglycans, cytokines, and growth factors provide structural support and information exchange (5). In both normal tissue and solid cancers, TNF-α has diverse regulatory roles in the TME depending on the type of cells.

TNF-α is, to a large degree, produced by macrophages but also by other immune cell types, including lymphoid cells, mast cells, and by non-immune cells such as endothelial cells, fibroblasts, and smooth muscle cells (6–9). The members of the TNF-α family exert their effects through two distinct receptors, TNFRSF1A (TNFR1) and TNFRSF1B (TNFR2). TNFR1 is ubiquitously expressed and found in all cell types. Among many diverse effects induced by TNF-α, the major role of TNFR1 is the initiation of apoptosis through its death domain, which is not found on TNFR2 (9). Seemingly contradictory to its apoptotic signaling function, activation of TNFR1 also can induce cell survival mechanisms (9). The determination of the final downstream activity of this receptor is based on the concentration of TNF-α in the microenvironment as well as the effects of other involved cytokines. TNFR2 is mostly found on immune cells, where its pathway activation by TNF-α assists in regulating the immune response and inflammation. TNFR2 activation on immune cells within the TME and cancer cells themselves can promote tumor growth and progression (10). Increased TNFR2 expression found on regulatory T cells within the TME can suppress the immune response and prevent activation of cytotoxic T cells, which decreases the ability of the immune response to suppress the tumor (10, 11). Myeloid-derived suppressor (MDSC) are a group of immature cells that can differentiate into several different immune cell types, but in their immature state, are potently immunosuppressive (10). TNF-α can suppress the MDSC differentiation and induce accumulation of MDSC, which enhances their immunosuppressive effects in the TME through TNFR2 signaling (10, 12, 13).

Through its roles in apoptosis, angiogenesis, and immune cell recruitment and regulation, as well as its function in assisting with the construction of the ECM, this review summarizes many roles of TNF-α and its relation to the various components of the TME. Many cell-signaling mechanisms are involved in these functions, and we attempt to explain the roles of these pathways in relation to this versatile cytokine. Through the understanding of these pathways, scientists and clinicians are finding ways to exploit them as therapeutic targets. For example, inhibition of endogenous TNF-α is a standard of care for chronic inflammatory diseases such as ulcerative colitis, Crohn's disease, rheumatoid arthritis, and several other diseases. In addition, TNF-α was previously used with good efficacy in patients with limb soft tissue sarcomas (STS) and in-transit melanoma by targeting the hap-hazard neovascular growth within the TME of these lesions (14–16). In this review, it is evident that there are many potential applications to manipulate TNF-α pathways, specifically in its role in the TME for cancer therapy.

TNF-α PATHWAY AT GLANCE

Research dating back more than twenty years has shown that the TNF-α superfamily comprises at least 19 members that signal through 29 receptors (17). It is a pleiotropic cytokine, binds two receptors – TNFR1(receptor type 1: CD120a; p55/60) and TNRFR2 (TNF receptor type 2; CD120b; p75/80) – and is produced by many different types of cells (17). Unlike the TNFR2 expression which is limited to immune cells and a few other cell types, TNFR1 expression is present in various cell types (18–20). TNF-α binds to these receptors resulting in several diverse effects, cell proliferation, survival, and apoptosis (21–23). Abnormal production of TNF-α and TNF receptor signaling has been associated with the pathogenesis of several inflammatory diseases including rheumatoid arthritis, Crohn's disease, atherosclerosis, psoriasis, and cancer (24). TNF-α has both tumor-promoting and tumor-suppressing roles in the TME. It is well reported that the tumor parenchyma and the TME continuously produce endogenous TNF-α, which induces tumor angiogenesis and promotes progression. The innate immune cells of the TME secrete various cytokines such as TNF-α and interleukin-6 (IL-6), which can promote cancer cell survival (25) and induce the expression of vascular endothelial cell adhesion molecules (CAM) that facilitate extravasation of leukocytes (26). TNF-α mediated matrix metalloproteinase (MMP) production in tumor cells or the TME also promotes tumor expansion (27, 28).

TNF-α plays an important role in tumor metastasis. It increases the expression of angiogenic factors such as basic fibroblast growth factor (bFGF), interleukin-8 (IL-8), and vascular endothelial growth factor (VEGF) in endothelial cells of the TME. TNF-α induced the expression of adhesion molecules such as intracellular adhesion molecule (ICAM)-1, E-selectin, and VCAM-1 in liver sinusoidal endothelial cells and induced tumor metastasis (29). So far, several FDA-approved TNF-α inhibitors, such as infliximab, etanercept, and adalimumab have been used to treat various human illnesses (30). We have summarized the multiple roles of TNF-α in different solid cancers based on preclinical studies (**Table 1**).

TNF-α MEDIATED SIGNALING PATHWAYS IN THE TME

Two different forms of TNF-α have been identified: (i) soluble TNF-α (sTNF-α) and (ii) transmembrane TNF-α (mTNF-α) (42). The mTNF-α is the precursor of sTNF-α. TNF-α converting enzyme (TACE) can cleave mTNF-α, releasing sTNF-α. Previous findings reported dual roles of TNF-α based

TABLE 1 | The roles of TNF-α in different cancer types.

Cancer Type	Known TNF-α target pathways
Prostate cancer	Induce pro-survival signaling in androgen-dependent prostate cancer (31) Sensitize the cells to irradiation to induced apoptosis in LNCaP cells (32) Induce apoptosis in androgen-sensitive and insensitive LNCaP and PC-3, respectively (33)
Breast Cancer	Promotes the growth of breast cancer in MDA-MB 468 and SK-BR3 cells (34) Inhibits proliferation and tumorigenesis (35)
Lung Cancer	Induce apoptosis in H292 and H1975 cell lines (36) Induce cell necrosis in H460 cells (37)
Melanoma	Inhibits apoptosis in A375, WM266.4, and Colo829 (38)
Cervical Cancer	Induce apoptotic cell death in cervical cancer cells (39)
Ovarian Cancer	Induce apoptotic cell death (40)
Hepatocellular carcinoma	Induce EMT (41)

on the exposure time and cytokine levels reached within the TME (33). Soluble TNF-α mostly binds with TNFR1 and controls the inflammatory immune response, whereas mTNF-α mostly binds with TNFR2 and controls cell proliferation, survival, and other biological activities. The interaction between mTNF-α and TNFR2 is dependent on responses to different signaling pathways. In colorectal cancer, TNFR2 modulates the expression of Ki67, influences fibroblast associated protein and α-smooth muscle actin, and increases cellular proliferation and migration (43). Anti-TNFR2 antibodies suppress tumor-associated regulatory T cells (Tregs) and inhibit ovarian cancer cell proliferation (44). Ligand binding to TNFR2 leads to the activation of NF-κB and several kinase pathways, including JNK, p38, MAPK, ERK, and PI3K (45). Apart from NF-κB and kinase pathways, other processes and signaling pathways, such as EMT and TGF-β receptor-mediated signaling, are also critically regulated through TNF-α signaling (described in detail below). We have summarized different oncogenic signaling pathways such as β-catenin, STAT3, PI3K/PTEN/AKT/mTOR, p53, which are directly or indirectly regulated by TNF-α in **Table 2**.

ROLE OF TNF-α IN TGF-β RECEPTOR MEDIATED SIGNALING PATHWAYS

The multifunctional cytokine transforming growth factor-beta (TGF-β) regulates cell growth, extracellular matrix protein synthesis, and immune cell functions (53). In normal and premalignant cells, TGF-β acts as a tumor suppressor through the induction of apoptosis. However, when cancer cells have mutations or lose tumor suppressor genes, cells become resistant TGF-β mediated growth arrest. The crucial role of the TGF-β signaling pathway in the TME has been demonstrated in several studies. Several molecules regulate the TGF-β pathway, among them, TNF-α is of significant importance. However, it is not clear whether TNF-α directly or indirectly interacts with the TGF-β pathway. Understanding the molecular mechanisms of the antagonistic activities of TNF-α against TGF-β is critical.

TABLE 2 | The roles of TNF-α in different transcription factors, cytokines, and signaling pathways by cancer type.

Cell type	Known TNF-α target genes	Effects
Breast Cancer (MDA-MB-231, MCF7, and HCC1937)	TIPE2 (35)	Induced
Lung Cancer (H292, H1299, H1975 and H460)	NF-κB (36)	Inhibited
Melanoma (A375, WM266.4, and Colo829)	BRAF (38)	Inhibited
Ovarian Cancer (SKOV-3, MDAH-2774, OVCAR-3)	AKT (46)	Induced
Human Dermal β Fibroblast	TGF-β (47)	Inhibited
Prostate carcinoma cells (LNCap)	PI3K/AKT (48)	Inhibited
Hepatocellular carcinoma (HepG2, SK-Hep-1, L02, MHCC97-H, MHCC97-L, and Huh7)	PI3K (41)	Induced
Human colon carcinoma stem cells (HT29)	WNT (49)	Induced
Hepatocellular carcinoma (HepG2, SK-Hep-1, L02, MHCC97-H, MHCC97-L, and Huh7)	GSK 3-β/β-catenin (41)	Induced
Breast Cancer (MCF-7 and MDA-MB-231)	Nur77 (50)	Induced
Breast cancer (MDA-MB-231 and MDA-MB-468)	CCL2 (51)	Induced
Gallbladder Cancer (GBC-SD and SGC-996)	ERK1/2/AP-1/VEGF-D (52)	Induced

Studies have demonstrated that TNF-α inhibits TGF-β and ECM production, such as type I collagen and elastin in cancer cells and fibroblasts (47, 54, 55). TGF-β inhibits cancer growth through the activation of tumor angiogenesis and regulates prominent compounds involved with cancer-associated fibroblasts (CAF) in TME (56). Fibroblasts have been shown to facilitate cancer progression by supporting tumor growth, extracellular matrix remodeling, angiogenesis and by mediating tumor-promoted inflammation (57). Recent research has clarified the relationship between TGF-β regulation mediated by TNF-α and CAF. In brief, TNF-α triggers the downregulation of TGF-β receptor II leading to desensitization of human dermal fibroblasts toward TGF-β. Additionally, TNF-α impaired the response of the cells to TGF-β by regulating the turnover of TRII (47). Normal fibroblasts acquire characteristics of CAFs when stimulated with TNF-α. The most widely used marker for CAFs is α-smooth muscle actin (α-SMA). TGF-β induces α-smooth muscle actin expression in fibroblasts (58).

ROLE OF TNF-α IN NF-κB PATHWAYS

The TME contains various types of cells, including tumor-associated macrophage (TAMs), dendritic cells, myeloid-derived suppressor cells, neutrophils, mast cells, natural killer T (NKT) cells, cancer-associated fibroblast (CAFs) and endothelial cells (59). The nuclear factor kappa-light chain enhancer of activated B cells (NF-κB) functions in these cell types and modulates inflammation, tumorigenesis, and metastasis. NF-κB activates several inflammatory genes in

response to cytokines like TNF-α and IL-1, as well as to bacterial endotoxin and physical stress. Whiteside reported NF-κB activation in myeloid cells enhances inflammation in the TME (60). When cells are stimulated by an extracellular signal such as TNF-α, NF-κB is activated and enters the nucleus to bind to target genes and promotes cell death or increases cell survival in a context-dependent manner (61). In lung carcinoma cells, deoxynivalenol induces dependent proteolytic cleavage of TNFR1 through the activation of ERK and p38 MAPK, and subsequently inhibits the TNF-α-induced NF-κB signaling pathway (62). Tang et al. reported that in oral squamous cell carcinoma, TNF-α activates the NF-κB pathway, which promotes invasion and metastasis (63). In addition, NF-κB is also an important player in modulating the tumor-associated macrophages (TAM). The NF- κB pathway regulates anti and pro-inflammatory signaling pathways in the TME through tumor-associated macrophage (TAM) regulation.

ROLE OF TNF-α IN THE RECEPTOR TYROSINE KINASE PATHWAY

Receptor tyrosine kinases (RTK) act as a mediator between the extracellular and intracellular compartments by transferring signals from the TME into the tumor cells (64). So far, 58 different RTKs have been discovered in humans and classified into 20 different subfamilies based on their structural features, and activation of these enzymes is well defined to regulates various cellular processes (64). Mutations in RTKs and their associated downstream signaling pathways have oncogenic roles in many solid cancers, hence the development of targeted therapy specifically for these RTKs (64). However, many cancer types often acquire treatment resistance to various RTK inhibitors such as VEGFR inhibitors (bevacizumab), EGFR inhibitors (gefitinib), and FGFR inhibitors (AZD4547) (65). The mechanism associated with RTK inhibitors to disrupt neoplastic cellular growth are (i) immunogenic modulation of the TME and (ii) immune subset conditioning (66). RTK inhibitors induce immunogenic modulation *via* tumor cell sensitivity to immune cells-mediated lysis through an alternation in tumor cell phenotype and cause immune subset conditioning by activating immune cells and suppressing the immune suppressor cells in the TME (66).

TNF-α regulates multiple RTK pathways, including mitogen-activated protein kinases (MAPK) (i) extracellular-signal-regulated kinases (ERKs); (ii) cJun NH_2-terminal kinases (JNK); and (iii) p38 MAP kinases pathways. Downregulation of MAP2K isoforms MKK4 and MKK7 in mice model prevents TNF-α mediated JNK activation (67, 68).

Apart from MAPK pathways, TNF-α signaling also controls vascular endothelial growth factor receptor (VEGFR), an RTK, which influences angiogenesis in the TME (69). This happens through TNFR1 signaling inflammatory macrophages to upregulate expression of vascular endothelial growth factor receptor 3, which causes increased production of vascular endothelial growth factor-C, and in turn, induces angiogenesis (69). The result was validated *in vivo* in mice with loss of function of TNFR1 (Tnfr1(-/-)) which reduced lymphangiogenesis and lymphatic metastasis (69). Tumor-mediated TNF-α and VEGF production is also associated with integrin receptor alpha V and beta 3 and beta 5 (αvβ3/αvβ5) mediated neovascularization, which shows an active interaction between tumor cells and endothelial cells through TNF-α (70). Another study demonstrated that a weakness of Akt/NF-κB signaling from TNF-α-mediated cross-talk signaling *via* EGFR causes the collateral sensitivity to TNF-α in a gefitinib resistant cell line (71). For instance, the over-expressions of EGFR and platelet-derived growth factor receptor α/β have been explored in tumor growth and progression (72). Sasi et al. confirmed that blocking of TNFR2/p75 with short-hairpin RNA in a Lewis Lung Carcinoma cell line induced apoptosis and decreased expression of the angiogenic growth factors VEGF, HGF, and PLGF (73). The VEGF inhibitor bevacizumab regulates a process called vessel normalization during angiogenesis through the upregulation tumor-infiltrating lymphocytes such as CD4+ and CD8+T cells in the TME (73). Below we more thoroughly discuss how TNF-α regulates T cells in the TME.

TNF-α AND EPITHELIAL-MESENCHYMAL TRANSITION REGULATORY MOLECULES

The epithelial to mesenchymal transition (EMT) is a process whereby epithelial cells lose epithelial features and acquire properties of mesenchymal cells. The EMT is classified into three main types depending upon the biological context. Type I EMT is observed during embryonic development, Type II occurs during wound healing and tissue regeneration, and Type III occurs during cancer progression. Previous findings demonstrated that TNF-α had been implicated as a major factor in EMT through cancer initiation and progression in the TME (6, 41, 74). Wang et al. showed that TNF-α induces EMT in human HCT116 cells and promotes colorectal cancer invasion and metastasis (75). The zinc finger protein *SNAI1* plays a crucial role in TNF-α induced EMT. TNF-α treatment increased the expression of *SNAI1* but not *SLUG, ZEB1*or *Twist*. Overexpression of *SNAI1*induced a switch from E-cadherin to N-cadherin expression in HCT116 cells, which is a characteristic of EMT. Recent findings from Li et al. showed that TNF-α mediated NF-κB activation upregulates EMT regulatory gene *TWIST1* expression in breast cancer cells (76). Mikesh et al. discovered the expression of molecular markers of mesenchymal phenotype in melanoma. Melanoma cells were treated with TNF-α in a 3-dimensional culture system, and the changes in the expression of E-cadherin, N-cadherin, vimentin, and fibronectin were assessed. Melanoma cells treated with TNF-α reduced the epithelial marker E-cadherin and induced mesenchymal markers N-cadherin, vimentin, fibronectin (77). The role of TNF-α in regulating the EMT in hepatocellular carcinoma cells (SMMC-7721) was studied by Chen et al. TNF-α is elevated in the supernatants of M2-tumor-associated macrophages (M2-TAMs), promoting the EMT of SMMC-7721 cells *in vitro (*78).

EXTRACELLULAR MATRIX AND TUMOR MICROENVIRONMENT

The TME comprises various cell types embedded in an altered extracellular matrix (ECM). The ECM is a major structural component of the TME and is mainly produced by cancer-associated fibroblasts (CAF) (79). It is largely composed of fibrous proteins, glycoproteins, proteoglycans and polysaccharides (79). The ECM in solid tumors differs significantly from normal organs. During cancer progression, cancer cells cross the ECM and basement membrane. MMPs are a large family of calcium-dependent, zinc-containing endopeptidases which are proteolytic enzymes capable of degrading the macromolecules of the ECM (80). Cancer cells secrete many members of the MMP family that facilitate the cellular migration into the ECM and thereby causing local invasion and can lead to metastasis (80). This process is largely regulated by TNF-α. Dilshara et al. reported that mangiferin inhibits TNF-α induced MMP9 expression and cellular invasion by suppressing the NF-κB activity in human LNCaP prostate carcinoma cells (81). An isoquinoline derivative compound, berberine inhibits TNF-α induced MMP9 and cell invasion through the inhibition of AP-1 activity in MDA-MB-231human breast cancer cells (82).

Several studies demonstrated that the biologic phenotype of cancers not only depends upon the activities of cancer cells but also tumor-infiltrating immune cells in the TME. TNF-α is produced by macrophages and other immune cells, including dendritic cells, B cells, activated natural killer cells, and activated T cells (83, 84). We summarized the effects of TNF- α on various non-cancerous cells in the TME below (**Table 3**).

MACROPHAGES

The main function of a macrophage is to engulf and digest foreign substances, cellular debris, and other components of the TME. Once macrophages are recruited into the TME, they are polarized into M1 or M2 TAMs depending on the varying concentrations of cytokines in the TME. A high density of TAMs can be found in several cancers such as pancreatic (85), breast (86), ovarian (87), and esophageal (88) and is associated with adverse prognostic features (86, 89, 90). However, the story of TAMs is more sophisticated than simply the number of cells in the TME. There are two types of mature macrophages: (i) classically activated macrophages (M1) and (ii) alternatively activated macrophages (M2). M1 and M2 macrophages play an important role in immune regulation in the TME. TAMs are a significant producer of TNF-α within the TME and interestingly are also highly responsive to TNF-α. The M1 macrophage can be stimulated to secrete a high level of TNF-α, resulting in high concentrations of superoxide, free oxygen, and nitrogen radicals (91) which promotes cell death in TME. M2 TNF-α secretion has been shown to promote EMT and induce "stemness" in an *in vitro* hepatocellular carcinoma model (78). Porta et al. reported that the p50 subunit of NF-κB plays an important role in macrophage polarization both *in vitro* and *in vivo*. They concluded that the p50 homodimer inhibited the NF-κB signaling pathway and induced macrophages to display an M2 phenotype with reduced expression of TNF-α and inducible nitric oxide synthases (iNOS) (92). M2 macrophages produce anti-inflammatory cytokines such as IL-10, IL-13, and TGF-β that may facilitate tumor development in TME. Experimental therapies to date have focused on depletion of M2 macrophages in the TME, specifically in glioblastoma through the inhibition of the colony-stimulating factor-1 receptor, which skewed macrophage polarization in the TME away from M2 and toward M1 *in vivo* (93). Data from another group using multiple different tumor models *in vitro* and *in vivo* showed higher TNFR activation shifts the balance toward the M1 phenotype and partially inhibited gene expression, specifically characteristic of M2 TAMs (94).

NEUTROPHILS

Like macrophages, two types of neutrophil populations have been identified within the TME. First described by Fridlender et al. in mesothelioma *in vitro* and xenograft model, the tumor-associated neutrophils (TAN) are polarized into a subpopulation of anti-neoplastic (N1) or, through induction by TGF-β within the TME, pro-neoplastic (N2) neutrophils (95). While TNF-α has not been directly implicated in this polarization, its role in TGF-β pathway and the other pathways in which it modulates neutrophil activity described below highlights the importance of neutrophil-neoplasm interaction. In normal vasculature *in vivo*, TNF-α increases neutrophil recruitment and endothelial adhesion *via* cytoskeletal remodeling (96, 97). TNF-α also has a "priming" effect on neutrophils, causing them to be more responsive to stimuli (98). This priming causes a respiratory burst and the generation of intracellular reactive oxygen species (ROS) and reactive nitrogen species (RNS) for neutrophils to interact with pathogens and to modulate local inflammation. In *in vitro* model of pancreatic ductal adenocarcinoma, neutrophils promoted EMT and metastasis in co-culture (99). In these experiments, cancer cells caused neutrophils to secrete large amounts of TNF-α and TGF-β in a co-culture model, indicating that the cytokines were responsible for regulating the EMT and the metastasis (99). A recent study demonstrated higher levels of circulating TNF-α in patients with breast cancer. The neutrophils from these patients exhibit more cytotoxicity against breast cancer cell lines *ex-vivo* than that of the neutrophils from patients without breast cancer (100). This work also showed that neutrophils from patients with and without breast cancer exposed to TNF-α *ex-vivo* exhibited enhanced cytotoxicity, with even further cytotoxicity seen in patients with breast cancer (100). TNF-α and TANs interact in many ways: 1) TANs are recruited into tumors partially from the influence of TNF-α 2) T cells attract and prime TANs with TNF-α 3) N1 TANs can attract cytotoxic T cells by TNF-α secretion 4) TANs can activate dendritic cells with TNF-α and assist CD4+ T cells with anti-neoplastic memory (101). In summary, neutrophil

secretion of and reaction to TNF-α causes many interactions in the TME may be exploited as potential targets in cancer therapy.

T CELLS

A heterogeneous population of tumor-infiltrating lymphocytes, $CD8^+$ cytotoxic T cells, $CD4^+$ helper T cells, and regulatory T cells (Tregs) are present in the TME. As with both TAMs and TANs, these tumor-infiltrating lymphocytes either suppress or enhance tumor growth. Previous studies demonstrated that T cell responses are regulated by TNFR activation and mediated cross-talk between T cells and other cell types. The TNFR superfamily (TNFRSF) OX40, 4-1BB, CD27, and DR3 are associated with TNFR associated factors (TRAF). In detail, TRAFs can bind with the α subunit of NF-κB and I Kappa B Kinase Beta (IkB kinase-β) to assist in the activation of both canonical and non-canonical NF-κB signaling pathways. OX40, 4-1BB, and CD27 mediated activation of signaling pathways in $CD4^+$ and $CD8^+$ T cells increase the expression of the anti-apoptotic molecule BCL-2, which correlates with the promotion of T cell survival (102). Prior work has demonstrated that the treatment with recombinant human TNF-α in a B16F10 melanoma mouse model of lung metastasis increased tumor burden and metastatic foci and was associated with increased numbers of pulmonary regulatory $CD4^+/Foxp3^+$ T cells. TNF-α activates TNFR2 on Tregs which helps expand the immunosuppressive role of the immune cell population by inducing $CD8^+$ and $CD4^+$ T cells. But the accumulation of Tregs can be prevented through dysregulation of TNF-α or TNFR2 which creates less tolerogenic environment and prevents B16F10 tumor metastasis and growth (103). Hu et al. reported that TNFR2 progranulin induced the proliferation of suppressive mouse $CD4^+/Foxp3^+$ regulatory T cells (104). Therefore, the targeting of T cell-associated mechanisms has been considered a major strategy for cancer immunotherapy.

DENDRITIC CELLS

The antigen-presenting cells (APC), dendritic cells (DC) can take up, process, and present different types of antigens, including tumor antigens, to naïve T cells. This antigen presentation can induce the creation of tumor-specific cytotoxic T cells (105). DC can also downregulate the immune response or induce immune tolerance in the TME through exposure to different stimuli. For example, when exposed to thymic stromal lymphoprotein from tumor or thymus (105), or TNF-α (106), DC express OX40 ligand, which is a member of the TNF superfamily (TNFSF4). The T cell membrane OX40 binds to OX40L on DC and induces a phenotypic subtype of $CD4^+$ T cells, promoting tumor growth (105). DC induced $CD4^+$ T cells to polarize to this subtype which highly secreted IL-13, which promoted breast cancer progression *in vivo* (107). Conversely, a subset of inflammatory DC which secrete TNF-α and produce nitric oxide are known to be tumor suppressive (108, 109). *In vivo* adjunctive use of this inflammatory DC subtype was shown to potentiate the effect of adoptive cell transfer, allowing for a more potent treatment strategy for cancer immunotherapy (108).

TABLE 3 | The effect of TNF-α on various cell types in the TME.

Cell type	Effects
Macrophages	TNF-α secreted by M1
	M2 phenotype inhibition
Neutrophils	Recruitment into the TME
	Priming and enhanced cytotoxicity
T cells	Enhances $CD4^+$ memory
	Causes Treg accumulation and immunosuppression
Dendritic cells	Induce pro-tumorigenic $CD4^+$ T cells

ROLE OF TNF-α IN CANCER STEM CELLS

The cancer stem cells (CSC) is a subpopulation within a primary cancer that have the potential to differentiate into a more mature phenotype and exhibit properties of self-renewal and immortality. CSC were first described in acute myeloid leukemia (AML) from the identification of a subset of specific surface proteins, which were found to regenerate AML *in vivo* (110). Since this initial description, they have been described in many different solid cancers in addition to hematologic malignancies and are implicated in chemotherapy resistance and progression to metastasis (111). Accumulating evidence suggests that TNF-α has a role in CSC regulation. TNF-α increased the breast CSC population through NF-κB/HIF1α/Slug (112). Zhao et al. reported that TNF-α treatment in a colon cancer cell-line (NCM460) derived spheroids induced NF-κB and Wnt/β-catenin pathways which can accelerate malignant transformation in intestinal stem cells (113). Additionally, using an osteosarcoma cell line *in vitro*, Yao et al. showed TNF-α exposure upregulated a specific microRNA (miR-155) and found that miR-155 produced a stem cell-like phenotype which promoted cancer progression (114). Suggested by these studies, the role of TNF-α in CSC may contribute to tumorigenesis and progression. However, other TNF-α-related tumor-suppressive effects may counter the effects of TNF-α on CSC.

TNF-α MEDIATED MicroRNA REGULATION

MicroRNAs (miRNA) are short non-coding RNAs that regulate gene expression at the post-transcriptional level by binding to the 3'-untranslated region of their targeted mRNA resulting in the suppression of protein production. miRNAs are dysregulated in several cancer types. Thus, understanding the role of miRNAs in the TME is crucial (115). The remodeling of miRNAs in the TME has a role in tumor growth, metastasis, and resistance to treatment. Several miRNAs are released from neoplastic cells into the TME and regulate the functions of endothelial cells, immune cells, and fibroblasts. Previous studies from several

groups reported that miR-145, miR-15a, miR-29a, miR-181A, miR-19a, miR-130a, miR-21, miR-765 are regulated by TNF-α in several cancers produced by both cancer cells and TME-related immune cells. Eleven miRNAs were shown to be differentially expressed between cancer-associated fibroblasts and healthy tissue, and 114 upregulated and 85 downregulated miRNAs have been identified in gastric cancer mesenchymal stem cells (GC-MSCs) (116). Zeng et al. showed that the tumor suppressor miR-145 is downregulated in triple-negative breast cancer cell lines MDA-MB-231, and when treated with TNF-α, this miRNA is overexpressed and induces apoptosis (117). Co-immunoprecipitation data revealed that miR-145 facilitates the formation of RIP1-FADD -caspase 8-mediated apoptotic complex with TNF-α treatment (118). Huang et al. showed that miR-19a is associated with lymph node metastasis and mediates TNF-α induced EMT in colorectal cancer (119). Furthermore, miR-19a is upregulated by TNF-α and miR-19a is required for TNF-α induced EMT and metastases in CRC cells (120). TNF-α also has a role in nuclear translocation of NF-κB followed by induction miR-130 and expression and downregulation of TNF-α (121). Higher levels of TNF-α have been observed in B-cell chronic lymphocytic leukemia (CLL) (122). Some miRNAs can regulate the TNF/TNFR gene superfamily in CLL (122). Therefore, the identification of the cross-talk between TNF-α and miRNAs could show promising effects for chemotherapeutic agents to control the TME.

CLINICAL USES OF TNF-α AND ITS IMPORTANCE IN DRUG DELIVERY

Carswell et al. discovered in 1975 TNF in the serum of bacilli Calmette-Guérin infected mice inoculated with endotoxin and found that "the substance" induced *in vivo* hemorrhagic necrosis in sarcoma. The substance was named "tumor necrosis factor" (123). Since then, the clinical utility of TNF-α is limited due to its severe systemic toxicity. To mitigate systemic toxicities, the application of TNF-α in cancer treatments became significantly more sophisticated. Its combined use with chemotherapeutic agents in isolated limb perfusion (ILP) has shown good results in tumor response and limb salvage in patients with soft tissue sarcomas (15) and regression in locoregional metastatic melanoma of a limb (14). Because ILP uses arterial and venous canulation with a closed extracorporeal circuit, high doses of TNF- α and chemotherapy can be used in the limb with minimal systemic toxicity. However, the ILP system is cumbersome and does not address its limitation to use TNF-α systemically to improve the efficacy of cancer treatments. The work by our group has shown that when attached to gold nanoparticles (CYT-6091), recombinant human TNF-α (rhTNF) can be given systemically without dose-limiting toxicities up to 3 times that of intravenously-administered unbound rhTNF in phase I clinical trial (124). Although we demonstrated the safety of gold nanomedicine carrying TNF-α in humans, the anti-cancer efficacy was limited, with only a partial response in 27 evaluable participants with advanced solid cancers (124). To prove the concept that this cytotoxic agent was needed to improve the treatment efficacy, paclitaxel analog was added to the gold nanomedicine carrying rhTNF (CYT-21625) and the treatment efficacy, drug delivery efficiency, and systemic toxicities were assessed in multiple mouse models with pancreatic neuroendocrine tumors (pNET) and metastatic aggressive thyroid cancers. We demonstrated significantly improved treatment efficacy across all mouse models treated with CYT-21625 compared to mice treated with intravenous paclitaxel or CYT-6091, with no detectable systemic toxicities or histologic evidence of normal tissue damage or vascular leakage (125). The principle behind its efficacy is related to its effect on tumor vasculature and overcoming high intratumoral interstitial fluid pressure (IFP), allowing for more efficient drug delivery and resulting in markedly increased intratumoral concentrations of paclitaxel (126).

TNF-α has a dose-dependent effect on vascular endothelial cells, inducing angiogenesis at low levels and inhibiting or disrupting it at high levels (127). Neoplasms, just as do healthy tissues, require a blood supply to provide nutrients and allow for growth. In contrast with normal healthy vasculature, neovascular growth in cancers is imperfect, exhibiting a non-continuous endothelium and a sporadically present or absent basement membrane, which increases vessel permeability (16). This increased permeability, along with high cell density, poor venous and lymphatic outflow, and an abnormal ECM contribute to high intratumoral hydrostatic and osmotic IFP (128, 129). Elevated IFP is a barrier to efficient drug delivery in solid tumors as drug cannot effectively travel against a pressure gradient to achieve local therapeutic levels. TNF-α mitigates this barrier by disrupting tumor vasculature, reducing tumor IFP, and allowing chemotherapeutic agents to diffuse into the TME. It disrupts the vasculature by inducing endothelial cell apoptosis, specifically in the tumor while having minimal effect on native healthy vessels due to the differential expression of TNF-R1 in the cancer neovascular network. Increased levels of TNF-R1 in neovascular endothelium has been shown in several tumor types, including thyroid cancer and pNET (125).

Vascular disruption leading to the reduction in intratumoral IFP is the key concept behind the therapeutic uses of TNF-α to improve drug delivery efficiency in cancer treatments. Its most common clinical application is in ILP for locoregionally metastatic melanoma or soft tissue sarcomas of the limb. In this procedure, the limb is isolated with a tourniquet and perfused with oxygenated blood from an extracorporeal circuit, similar in concept to extracorporeal membrane oxygenation for cardiopulmonary failure. Within the perfusion circuit, hyperthermic high-dose chemotherapy (typically the alkylating agent melphalan) is infused with TNF-α. TNF-α serves two functions – inducing hemorrhagic necrosis of the tumor by disrupting the vasculature and allowing the melphalan to locally accumulate in higher levels that would otherwise cause severe systemic toxicities. The limb isolation minimizes the systemic toxicity of both the chemotherapeutic agent and TNF-α –as TNF-α is an acute phase reactant and inflammatory cytokine and can lead to distributive shock –

and allows for a several-fold increase in concentration. ILP with melphalan and TNF-α was initially shown to be effective in a phase II trial, which resulted in 21 of 23 complete responses and two partial responses with no patient experiencing treatment failure (130). This cumbersome treatment strategy is only feasible in limb lesions and is not an option for primary or metastatic cancers in solid organs.

Recent work by our group has employed the concept of TNF-α as a facilitator of systemic drug delivery with a novel use of gold nanomedicine. Gold nanoparticles passively target solid tumors by the enhanced permeability and retention effect, preferentially accumulating in their tissue through a combination of highly permeable vasculature and the larger size of the particles compared to molecules dissolved in plasma (131, 132). Gold nanomedicine has a harder time passing through the tight junctions of normal vascular endothelium in non-neoplastic tissue and selectively extravasates into the TME, where it accumulates (132). In addition, the gold nanoparticles carrying rhTNF actively targets cancer neovasculature by binding to the differentially expressed TNF receptors on tumor neovascular endothelium (125). As is the case for ILP, this modality of TNF-α delivery reduces its toxic systemic effects through both active and passive tumor-specific targeting and allows for higher concentrations to be delivered. To improve treatment efficacy in cancers, we demonstrated a significantly lower tumor burden across multiple *in vivo* models using combined rhTNF and paclitaxel analog bound nanomedicine over both rhTNF nanomedicine alone and IV paclitaxel alone in anaplastic thyroid cancer and pNET with no apparent systemic toxicity, further indicating increased efficacy (125). In addition, radiographic imaging studies and histology showed the gold nanomedicine carrying rhTNF only and rhTNF with paclitaxel analog preferentially and specifically targeted tumor tissue and induced vascular leakage only in tumor tissue (125). The transgenic mouse model with pNET showed selective extravasation of MRI contrast in the pancreatic area, corresponding with 18F-FDG-avid lesions, from mice treated with rhTNF bound nanoparticles but not in mice treated with paclitaxel alone and vehicle control. We observed no evidence of extravasation in normal tissue, indicating that the TNF-α induced tumor-specific vascular damage (125). To demonstrate the applicability in a broader range of cancer, a pilot study showed 100% survival *in vivo* in mice with pancreatic ductal adenocarcinoma treated with gold nanomedicine carrying rhTNF-followed by intravenous (IV) paclitaxel compared to 50% survival in the IV paclitaxel only group and 0% in the control group at 42 days (126).

CONCLUSION

TNF-α plays a critical role in tumor signaling pathways and immune cell manipulation within the TME. Since Carswell discovered the cytokine in 1975, our understanding of its role in cancers and chronic inflammatory diseases has improved, resulting in the development of treatments that specifically target systemic and TME-related immune cellular response. However, the clinical application such as TNF receptor blockade is only limited to the treatment of chronic inflammatory diseases. Although preclinical data of TNF-α treatment in cancers to improve drug delivery is promising, the treatment efficacy in cancers is not known due to the lack of phase II clinical trials. Because TNF-α induces diverse effects in TME, both oncogenic and tumor-suppressive effects, further studies are warranted to fully understand and selectively induce the anti-tumor effect to improve treatment efficacy in patients with TNF-α sensitive cancers.

AUTHOR CONTRIBUTIONS

All authors contributed to the article and approved the submitted version.

FUNDING

The preparation of this manuscript was supported by the NIH intramural research grant (# ZIA BC 011286).

REFERENCES

1. Arneth B. Tumor Microenvironment. *Med (Kaunas)* (2019) 56(1):15. doi: 10.3390/medicina56010015
2. Chew V, Toh HC, Abastado JP. Immune Microenvironment in Tumor Progression: Characteristics and Challenges for Therapy. *J Oncol* (2012) 2012:608406. doi: 10.1155/2012/608406
3. Gajewski TF, Schreiber H, Fu YX. Innate and Adaptive Immune Cells in the Tumor Microenvironment. *Nat Immunol* (2013) 14:1014–22. doi: 10.1038/ni.2703
4. Hirata E, Ishibashi K, Kohsaka S, Shinjo K, Kojima S, Kondo Y, et al. The Brain Microenvironment Induces Dnmt1 Suppression and Indolence of Metastatic Cancer Cells. *iScience* (2020) 23:101480. doi: 10.1016/j.isci.2020.101480
5. Schwager SC, Taufalele PV, Reinhart-King CA. Cell-Cell Mechanical Communication in Cancer. *Cell Mol Bioeng* (2019) 12:1–14. doi: 10.1007/s12195-018-00564-x
6. Bates RC, Mercurio AM. Tumor Necrosis Factor-Alpha Stimulates the Epithelial-to-Mesenchymal Transition of Human Colonic Organoids. *Mol Biol Cell* (2003) 14:1790–800. doi: 10.1091/mbc.e02-09-0583
7. Ranta V, Orpana A, Carpen O, Turpeinen U, Ylikorkala O, Viinikka L. Human Vascular Endothelial Cells Produce Tumor Necrosis Factor-Alpha in Response to Proinflammatory Cytokine Stimulation. *Crit Care Med* (1999) 27:2184–7. doi: 10.1097/00003246-199910000-00019
8. Epstein Shochet G, Brook E, Israeli-Shani L, Edelstein E, Shitrit D. Fibroblast Paracrine TNF-alpha Signaling Elevates Integrin A5 Expression in Idiopathic Pulmonary Fibrosis (IPF). *Respir Res* (2017) 18:122. doi: 10.1186/s12931-017-0606-x
9. van Horssen R, Ten Hagen TL, Eggermont AM. TNF-Alpha in Cancer Treatment: Molecular Insights, Antitumor Effects, and Clinical Utility. *Oncologist* (2006) 11:397–408. doi: 10.1634/theoncologist.11-4-397
10. Sheng Y, Li F, Qin Z. Tnf Receptor 2 Makes Tumor Necrosis Factor a Friend of Tumors. *Front Immunol* (2018) 9:1170. doi: 10.3389/fimmu.2018.01170

11. Vanamee ES, Faustman DL. Tnfr2: A Novel Target for Cancer Immunotherapy. *Trends Mol Med* (2017) 23:1037–46. doi: 10.1016/j.molmed.2017.09.007
12. Sade-Feldman M, Kanterman J, Ish-Shalom E, Elnekave M, Horwitz E, Baniyash M. Tumor Necrosis Factor-Alpha Blocks Differentiation and Enhances Suppressive Activity of Immature Myeloid Cells During Chronic Inflammation. *Immunity* (2013) 38:541–54. doi: 10.1016/j.immuni.2013.02.007
13. Zhao X, Rong L, Zhao X, Li X, Liu X, Deng J, et al. TNF Signaling Drives Myeloid-Derived Suppressor Cell Accumulation. *J Clin Invest* (2012) 122:4094–104. doi: 10.1172/JCI64115
14. Deroose JP, Eggermont AM, van Geel AN, de Wilt JH, Burger JW, Verhoef C. 20 Years Experience of TNF-based Isolated Limb Perfusion for in-Transit Melanoma Metastases: TNF Dose Matters. *Ann Surg Oncol* (2012) 19:627–35. doi: 10.1245/s10434-011-2030-7
15. Neuwirth MG, Song Y, Sinnamon AJ, Fraker DL, Zager JS, Karakousis GC. Isolated Limb Perfusion and Infusion for Extremity Soft Tissue Sarcoma: A Contemporary Systematic Review and Meta-Analysis. *Ann Surg Oncol* (2017) 24:3803–10. doi: 10.1245/s10434-017-6109-7
16. Carmeliet P, Jain RK. Angiogenesis in Cancer and Other Diseases. *Nature* (2000) 407:249–57. doi: 10.1038/35025220
17. Aggarwal BB. Signalling Pathways of the TNF Superfamily: A Double-Edged Sword. *Nat Rev Immunol* (2003) 3:745–56. doi: 10.1038/nri1184
18. Speeckaert MM, Speeckaert R, Laute M, Vanholder R, Delanghe JR. Tumor Necrosis Factor Receptors: Biology and Therapeutic Potential in Kidney Diseases. *Am J Nephrol* (2012) 36:261–70. doi: 10.1159/000342333
19. Clouthier DL, Watts TH. Tnfrs and Control of Chronic Lcmv Infection: Implications for Therapy. *Trends Immunol* (2015) 36:697–708. doi: 10.1016/j.it.2015.09.005
20. Liu S, Rong L, Deng J, Zhao X, Liu X, Xu X, et al. TNFR2 Expression on non-Bone Marrow-Derived Cells is Crucial for Lipopolysaccharide-Induced Septic Shock and Downregulation of Soluble TNFR2 Level in Serum. *Cell Mol Immunol* (2011) 8:164–71. doi: 10.1038/cmi.2010.79
21. Pronk CJ, Veiby OP, Bryder D, Jacobsen SE. Tumor Necrosis Factor Restricts Hematopoietic Stem Cell Activity in Mice: Involvement of Two Distinct Receptors. *J Exp Med* (2011) 208:1563–70. doi: 10.1084/jem.20110752
22. Ghali O, Chauveau C, Hardouin P, Broux O, Devedjian JC. TNF-Alpha's Effects on Proliferation and Apoptosis in Human Mesenchymal Stem Cells Depend on RUNX2 Expression. *J Bone Miner Res* (2010) 25:1616–26. doi: 10.1002/jbmr.52
23. Chau BN, Chen TT, Wan YY, DeGregori J, Wang JY. Tumor Necrosis Factor Alpha-Induced Apoptosis Requires p73 and c-ABL Activation Downstream of RB Degradation. *Mol Cell Biol* (2004) 24:4438–47. doi: 10.1128/MCB.24.10.4438-4447.2004
24. Farrugia M, Baron B. The Role of TNF-alpha in Rheumatoid Arthritis: A Focus on Regulatory T Cells. *J Clin Transl Res* (2016) 2:84–90. doi: 10.18053/jctres.02.201603.005
25. Wu TC. The Role of Vascular Cell Adhesion Molecule-1 in Tumor Immune Evasion. *Cancer Res* (2007) 67:6003–6. doi: 10.1158/0008-5472.CAN-07-1543
26. Khatib AM, Auguste P, Fallavollita L, Wang N, Samani A, Kontogiannea M, et al. Characterization of the Host Proinflammatory Response to Tumor Cells During the Initial Stages of Liver Metastasis. *Am J Pathol* (2005) 167:749–59. doi: 10.1016/S0002-9440(10)62048-2
27. Hagemann T, Robinson SC, Schulz M, Trumper L, Balkwill FR, Binder C. Enhanced Invasiveness of Breast Cancer Cell Lines Upon Co-Cultivation With Macrophages is Due to TNF-alpha Dependent Up-Regulation of Matrix Metalloproteases. *Carcinogenesis* (2004) 25:1543–9. doi: 10.1093/carcin/bgh146
28. Stuelten CH, DaCosta Byfield S, Arany PR, Karpova TS, Stetler-Stevenson WG, Roberts AB. Breast Cancer Cells Induce Stromal Fibroblasts to Express MMP-9 Via Secretion of TNF-alpha and TGF-Beta. *J Cell Sci* (2005) 118:2143–53. doi: 10.1242/jcs.02334
29. Wagener FA, Feldman E, de Witte T, Abraham NG. Heme Induces the Expression of Adhesion Molecules ICAM-1, Vcam-1, and E Selectin in Vascular Endothelial Cells. *Proc Soc Exp Biol Med* (1997) 216:456–63. doi: 10.3181/00379727-216-44197
30. Aggarwal BB, Sethi G, Baladandayuthapani V, Krishnan S, Shishodia S. Targeting Cell Signaling Pathways for Drug Discovery: An Old Lock Needs a New Key. *J Cell Biochem* (2007) 102:580–92. doi: 10.1002/jcb.21500
31. Srinivasan S, Kumar R, Koduru S, Chandramouli A, Damodaran C. Inhibiting TNF-mediated Signaling: A Novel Therapeutic Paradigm for Androgen Independent Prostate Cancer. *Apoptosis* (2010) 15:153–61. doi: 10.1007/s10495-009-0416-9
32. Kimura K, Bowen C, Spiegel S, Gelmann EP. Tumor Necrosis Factor-Alpha Sensitizes Prostate Cancer Cells to Gamma-Irradiation-Induced Apoptosis. *Cancer Res* (1999) 59:1606–14.
33. Cruceriu D, Baldasici O, Balacescu O, Berindan-Neagoe I. The Dual Role of Tumor Necrosis Factor-Alpha (TNF-Alpha) in Breast Cancer: Molecular Insights and Therapeutic Approaches. *Cell Oncol (Dordr)* (2020) 43:1–18. doi: 10.1007/s13402-019-00489-1
34. Cai X, Cao C, Li J, Chen F, Zhang S, Liu B, et al. Inflammatory Factor TNF-alpha Promotes the Growth of Breast Cancer Via the Positive Feedback Loop of TNFR1/NF-kappaB (and/or P38)/P-STAT3/HBXIP/TNFR1. *Oncotarget* (2017) 8:58338–52. doi: 10.18632/oncotarget.16873
35. Wang K, Ren Y, Liu Y, Zhang J, He JJ. Tumor Necrosis Factor (TNF)-Alpha-Induced Protein 8-Like-2 (TIPE2) Inhibits Proliferation and Tumorigenesis in Breast Cancer Cells. *Oncol Res* (2017) 25:55–63. doi: 10.3727/096504016X14719078133320
36. Zhu J, Xin Y, Liu X, Wang Y, Liu Y. Nimotuzumab Enhances the Sensitivity of non-Small Cell Lung Cancer Cells to Tumor Necrosis Factor-Alpha by Inhibiting the Nuclear Factor-Small Ka, CyrillicB Signaling Pathway. *Exp Ther Med* (2018) 15:3345–51. doi: 10.3892/etm.2018.5856
37. Lin X, Chen Q, Huang C, Xu X. Cyld Promotes TNF-Alpha-Induced Cell Necrosis Mediated by RIP-1 in Human Lung Cancer Cells. *Mediators Inflammation* (2016) 2016:1542786. doi: 10.1155/2016/1542786
38. Gray-Schopfer VC, Karasarides M, Hayward R, Marais R. Tumor Necrosis Factor-Alpha Blocks Apoptosis in Melanoma Cells When BRAF Signaling is Inhibited. *Cancer Res* (2007) 67:122–9. doi: 10.1158/0008-5472.CAN-06-1880
39. Lee K, Lee MH, Kang YW, Rhee KJ, Kim TU, Kim YS. Parkin Induces Apoptotic Cell Death in TNF-alpha-treated Cervical Cancer Cells. *BMB Rep* (2012) 45:526–31. doi: 10.5483/BMBRep.2012.45.9.104
40. Tian X, Xu L, Wang P. MiR-191 Inhibits TNF-alpha Induced Apoptosis of Ovarian Endometriosis and Endometrioid Carcinoma Cells by Targeting DAPK1. *Int J Clin Exp Pathol* (2015) 8:4933–42.
41. Zhu Y, Cheng Y, Guo Y, Chen J, Chen F, Luo R, et al. Protein Kinase D2 Contributes to TNF-alpha-induced Epithelial Mesenchymal Transition and Invasion Via the PI3K/GSK-3beta/beta-catenin Pathway in Hepatocellular Carcinoma. *Oncotarget* (2016) 7:5327–41. doi: 10.18632/oncotarget.6633
42. Horiuchi T, Mitoma H, Harashima S, Tsukamoto H, Shimoda T. Transmembrane TNF-alpha: Structure, Function and Interaction With anti-TNF Agents. *Rheumatol (Oxford)* (2010) 49:1215–28. doi: 10.1093/rheumatology/keq031
43. Wang L, Yang D, Tian J, Gao A, Shen Y, Ren X, et al. Tumor Necrosis Factor Receptor 2/AKT and ERK Signaling Pathways Contribute to the Switch From Fibroblasts to CAFs by Progranulin in Microenvironment of Colorectal Cancer. *Oncotarget* (2017) 8:26323–33. doi: 10.18632/oncotarget.15461
44. Torrey H, Butterworth J, Mera T, Okubo Y, Wang L, Baum D, et al. Targeting TNFR2 With Antagonistic Antibodies Inhibits Proliferation of Ovarian Cancer Cells and Tumor-Associated Tregs. *Sci Signal* (2017) 10 (462):eaaf8608. doi: 10.1126/scisignal.aaf8608
45. Sughra K, Birbach A, de Martin R, Schmid JA. Interaction of the TNFR-receptor Associated Factor TRAF1 With I-Kappa B Kinase-2 and TRAF2 Indicates a Regulatory Function for NF-Kappa B Signaling. *PloS One* (2010) 5:e12683. doi: 10.1371/journal.pone.0012683
46. Cui ZY, Park SJ, Jo E, Hwang IH, Lee KB, Kim SW, et al. Cordycepin Induces Apoptosis of Human Ovarian Cancer Cells by Inhibiting CCL5-mediated Akt/NF-Kappab Signaling Pathway. *Cell Death Discovery* (2018) 4:62. doi: 10.1038/s41420-018-0063-4
47. Yamane K, Ihn H, Asano Y, Jinnin M, Tamaki K. Antagonistic Effects of TNF-alpha on TGF-beta Signaling Through Down-Regulation of TGF-beta Receptor Type II in Human Dermal Fibroblasts. *J Immunol* (2003) 171:3855–62. doi: 10.4049/jimmunol.171.7.3855

48. Jayasooriya RG, Dilshara MG, Choi YH, Moon SK, Kim WJ, Kim GY. Tianeptine Sodium Salt Suppresses TNF-alpha-induced Expression of Matrix Metalloproteinase-9 in Human Carcinoma Cells Via Suppression of the PI3K/Akt-mediated NF-Kappab Pathway. *Environ Toxicol Pharmacol* (2014) 38:502–9. doi: 10.1016/j.etap.2014.07.023
49. Wei X, Li X, Kong F, Ma L, Sui Y, Chen D, et al. TNF-Alpha Activates Wnt Signaling Pathway to Promote the Invasion of Human Colon Cancer Stem Cells. *Xi Bao Yu Fen Zi Mian Yi Xue Za Zhi* (2018) 34:982–8.
50. Xie L, Jiang F, Zhang X, Alitongbieke G, Shi X, Meng M, et al. Honokiol Sensitizes Breast Cancer Cells to TNF-alpha Induction of Apoptosis by Inhibiting Nur77 Expression. *Br J Pharmacol* (2016) 173:344–56. doi: 10.1111/bph.13375
51. Mendonca P, Horton A, Bauer D, Messeha S, Soliman KFA. The Inhibitory Effects of Butein on Cell Proliferation and TNF-alpha-induced CCL2 Release in Racially Different Triple Negative Breast Cancer Cells. *PloS One* (2019) 14: e0215269. doi: 10.1371/journal.pone.0215269
52. Hong H, Jiang L, Lin Y, He C, Zhu G, Du Q, et al. TNF-Alpha Promotes Lymphangiogenesis and Lymphatic Metastasis of Gallbladder Cancer Through the ERK1/2/AP-1/VEGF-D Pathway. *BMC Cancer* (2016) 16:240. doi: 10.1186/s12885-016-2259-4
53. Letterio JJ, Roberts AB. Regulation of Immune Responses by TGF-Beta. *Annu Rev Immunol* (1998) 16:137–61. doi: 10.1146/annurev.immunol.16.1.137
54. Chang NS. Transforming Growth Factor-Beta Protection of Cancer Cells Against Tumor Necrosis Factor Cytotoxicity is Counteracted by Hyaluronidase (Review). *Int J Mol Med* (1998) 2:653–9. doi: 10.3892/ijmm.2.6.653
55. Greenwel P, Tanaka S, Penkov D, Zhang W, Olive M, Moll J, et al. Tumor Necrosis Factor Alpha Inhibits Type I Collagen Synthesis Through Repressive CCAAT/enhancer-binding Proteins. *Mol Cell Biol* (2000) 20:912–8. doi: 10.1128/MCB.20.3.912-918.2000
56. Liu T, Han C, Wang S, Fang P, Ma Z, Xu L, et al. Cancer-Associated Fibroblasts: An Emerging Target of Anti-Cancer Immunotherapy. *J Hematol Oncol* (2019) 12:86. doi: 10.1186/s13045-019-0770-1
57. Sahai E, Astsaturov I, Cukierman E, DeNardo DG, Egeblad M, Evans RM, et al. A Framework for Advancing Our Understanding of Cancer-Associated Fibroblasts. *Nat Rev Cancer* (2020) 20:174–86. doi: 10.1038/s41568-019-0238-1
58. Desmouliere A, Geinoz A, Gabbiani F, Gabbiani G. Transforming Growth Factor-Beta 1 Induces Alpha-Smooth Muscle Actin Expression in Granulation Tissue Myofibroblasts and in Quiescent and Growing Cultured Fibroblasts. *J Cell Biol* (1993) 122:103–11. doi: 10.1083/jcb.122.1.103
59. Taniguchi K, Karin M. Nf-kappaB, Inflammation, Immunity and Cancer: Coming of Age. *Nat Rev Immunol* (2018) 18:309–24. doi: 10.1038/nri.2017.142
60. Whiteside TL. The Tumor Microenvironment and its Role in Promoting Tumor Growth. *Oncogene* (2008) 27:5904–12. doi: 10.1038/onc.2008.271
61. Lawrence T. The Nuclear Factor NF-kappaB Pathway in Inflammation. *Cold Spring Harb Perspect Biol* (2009) 1:a001651. doi: 10.1101/cshperspect.a001651
62. Hirano S, Kataoka T. Deoxynivalenol Induces Ectodomain Shedding of TNF Receptor 1 and Thereby Inhibits the TNF-alpha-induced NF-Kappab Signaling Pathway. *Eur J Pharmacol* (2013) 701:144–51. doi: 10.1016/j.ejphar.2013.01.019
63. Tang D, Tao D, Fang Y, Deng C, Xu Q, Zhou J. Tnf-Alpha Promotes Invasion and Metastasis Via NF-Kappa B Pathway in Oral Squamous Cell Carcinoma. *Med Sci Monit Basic Res* (2017) 23:141–9. doi: 10.12659/MSMBR.903910
64. Du Z, Lovly CM. Mechanisms of Receptor Tyrosine Kinase Activation in Cancer. *Mol Cancer* (2018) 17:58. doi: 10.1186/s12943-018-0782-4
65. Jia Y, Yun CH, Park E, Ercan D, Manuia M, Juarez J, et al. Overcoming EGFR(T790M) and EGFR(C797S) Resistance With Mutant-Selective Allosteric Inhibitors. *Nature* (2016) 534:129–32. doi: 10.1038/nature17960
66. Kwilas AR, Donahue RN, Tsang KY, Hodge JW. Immune Consequences of Tyrosine Kinase Inhibitors That Synergize With Cancer Immunotherapy. *Cancer Cell Microenviron* (2015) 2(1):e677. doi: 10.14800/ccm.677
67. Tournier C, Dong C, Turner TK, Jones SN, Flavell RA, Davis RJ. MKK7 is an Essential Component of the JNK Signal Transduction Pathway Activated by Proinflammatory Cytokines. *Genes Dev* (2001) 15:1419–26. doi: 10.1101/gad.888501
68. Sabio G, Davis RJ. TNF and MAP Kinase Signalling Pathways. *Semin Immunol* (2014) 26:237–45. doi: 10.1016/j.smim.2014.02.009
69. Ji H, Cao R, Yang Y, Zhang Y, Iwamoto H, Lim S, et al. TNFR1 Mediates TNF-alpha-induced Tumour Lymphangiogenesis and Metastasis by Modulating VEGF-C-VEGFR3 Signalling. *Nat Commun* (2014) 5:4944. doi: 10.1038/ncomms5944
70. Yujiao Gong YD, Cui J, Sun Q, Zhen Z, Gao Y, Su J, et al. Receptor Tyrosine Kinase Interaction With the Tumor Microenvironment in Malignant Progression of Human Glioblastoma, Glioma - Contemporary Diagnostic and Therapeutic Approaches, Ibrahim Omerhodžić and Kenan Arnautović, IntechOpen (2018). doi: 10.5772/intechopen/76873
71. Cobleigh MA, Tabesh B, Bitterman P, Baker J, Cronin M, Liu ML, et al. Tumor Gene Expression and Prognosis in Breast Cancer Patients With 10 or More Positive Lymph Nodes. *Clin Cancer Res* (2005) 11:8623–31. doi: 10.1158/1078-0432.CCR-05-0735
72. Carvalho I, Milanezi F, Martins A, Reis RM, Schmitt F. Overexpression of Platelet-Derived Growth Factor Receptor Alpha in Breast Cancer is Associated With Tumour Progression. *Breast Cancer Res* (2005) 7:R788–95. doi: 10.1186/bcr1304
73. Sasi SP, Yan X, Enderling H, Park D, Gilbert HY, Curry C, et al. Breaking the 'Harmony' of TNF-alpha Signaling for Cancer Treatment. *Oncogene* (2012) 31:4117–27. doi: 10.1038/onc.2011.567
74. Soria G, Ofri-Shahak M, Haas I, Yaal-Hahoshen N, Leider-Trejo L, Leibovich-Rivkin T, et al. Inflammatory Mediators in Breast Cancer: Coordinated Expression of TNFalpha & IL-1beta With CCL2 & CCL5 and Effects on Epithelial-to-Mesenchymal Transition. *BMC Cancer* (2011) 11:130. doi: 10.1186/1471-2407-11-130
75. Wang H, Wang HS, Zhou BH, Li CL, Zhang F, Wang XF, et al. Epithelial-Mesenchymal Transition (EMT) Induced by TNF-alpha Requires AKT/GSK-3beta-mediated Stabilization of Snail in Colorectal Cancer. *PloS One* (2013) 8:e56664. doi: 10.1371/journal.pone.0056664
76. Li CW, Xia W, Huo L, Lim SO, Wu Y, Hsu JL, et al. Epithelial-Mesenchymal Transition Induced by TNF-alpha Requires NF-kappaB-mediated Transcriptional Upregulation of Twist1. *Cancer Res* (2012) 72:1290–300. doi: 10.1158/0008-5472.CAN-11-3123
77. Mikesh LM, Kumar M, Erdag G, Hogan KT, Molhoek KR, Mayo MW, et al. Evaluation of Molecular Markers of Mesenchymal Phenotype in Melanoma. *Melanoma Res* (2010) 20:485–95. doi: 10.1097/CMR.0b013e32833fafb4
78. Chen Y, Wen H, Zhou C, Su Q, Lin Y, Xie Y, et al. TNF-Alpha Derived From M2 Tumor-Associated Macrophages Promotes Epithelial-Mesenchymal Transition and Cancer Stemness Through the Wnt/beta-catenin Pathway in SMMC-7721 Hepatocellular Carcinoma Cells. *Exp Cell Res* (2019) 378:41–50. doi: 10.1016/j.yexcr.2019.03.005
79. Theocharis AD, Skandalis SS, Gialeli C, Karamanos NK. Extracellular Matrix Structure. *Adv Drug Delivery Rev* (2016) 97:4–27. doi: 10.1016/j.addr.2015.11.001
80. Laronha H, Caldeira J. Structure and Function of Human Matrix Metalloproteinases. *Cells* (2020) 9(5):1076. doi: 10.3390/cells9051076
81. Dilshara MG, Kang CH, Choi YH, Kim GY. Mangiferin Inhibits Tumor Necrosis Factor-Alpha-Induced Matrix Metalloproteinase-9 Expression and Cellular Invasion by Suppressing Nuclear Factor-Kappab Activity. *BMB* (2015) Rep 48:559–64. doi: 10.5483/BMBRep.2015.48.10.003
82. Kim S, Choi JH, Kim JB, Nam SJ, Yang JH, Kim JH, et al. Berberine Suppresses TNF-alpha-induced MMP-9 and Cell Invasion Through Inhibition of AP-1 Activity in MDA-MB-231 Human Breast Cancer Cells. *Molecules* (2008) 13:2975–85. doi: 10.3390/molecules13122975
83. Turner M, Feldmann M. Comparison of Patterns of Expression of Tumour Necrosis Factor, Lymphotoxin and Interleukin-6 Mrna. *Biochem Biophys Res Commun* (1988) 153:1144–51. doi: 10.1016/S0006-291X(88)81347-0
84. Kelker HC, Oppenheim JD, Stone-Wolff D, Henriksen-DeStefano D, Aggarwal BB, Stevenson HC, et al. Characterization of Human Tumor Necrosis Factor Produced by Peripheral Blood Monocytes and its Separation From Lymphotoxin. *Int J Cancer* (1985) 36:69–73. doi: 10.1002/ijc.2910360112
85. Qiu SQ, Waaijer SJH, Zwager MC, de Vries EGE, van der Vegt B, Schroder CP. Tumor-Associated Macrophages in Breast Cancer: Innocent Bystander or Important Player? *Cancer Treat Rev* (2018) 70:178–89. doi: 10.1016/j.ctrv.2018.08.010

86. Zhao X, Qu J, Sun Y, Wang J, Liu X, Wang F, et al. Prognostic Significance of Tumor-Associated Macrophages in Breast Cancer: A Meta-Analysis of the Literature. *Oncotarget* (2017) 8:30576–86. doi: 10.18632/oncotarget.15736
87. Yuan X, Zhang J, Li D, Mao Y, Mo F, Du W, et al. Prognostic Significance of Tumor-Associated Macrophages in Ovarian Cancer: A Meta-Analysis. *Gynecol Oncol* (2017) 147:181–7. doi: 10.1016/j.ygyno.2017.07.007
88. Li J, Xie Y, Wang X, Li F, Li S, Li M, et al. Prognostic Impact of Tumor-Associated Macrophage Infiltration in Esophageal Cancer: A Meta-Analysis. *Future Oncol* (2019) 15:2303–17. doi: 10.2217/fon-2018-0669
89. Yu M, Guan R, Hong W, Zhou Y, Lin Y, Jin H, et al. Prognostic Value of Tumor-Associated Macrophages in Pancreatic Cancer: A Meta-Analysis. *Cancer Manag Res* (2019) 11:4041–58. doi: 10.2147/CMAR.S196951
90. Wu P, Wu D, Zhao L, Huang L, Chen G, Shen G, et al. Inverse Role of Distinct Subsets and Distribution of Macrophage in Lung Cancer Prognosis: A Meta-Analysis. *Oncotarget* (2016) 7:40451–60. doi: 10.18632/oncotarget.9625
91. Martinez FO, Helming L, Gordon S. Alternative Activation of Macrophages: An Immunologic Functional Perspective. *Annu Rev Immunol* (2009) 27:451–83. doi: 10.1146/annurev.immunol.021908.132532
92. Porta C, Rimoldi M, Raes G, Brys L, Ghezzi P, Di Liberto D, et al. Tolerance and M2 (Alternative) Macrophage Polarization are Related Processes Orchestrated by p50 Nuclear Factor Kappab. *Proc Natl Acad Sci USA* (2009) 106:14978–83. doi: 10.1073/pnas.0809784106
93. Pyonteck SM, Akkari L, Schuhmacher AJ, Bowman RL, Sevenich L, Quail DF, et al. Csf-1R Inhibition Alters Macrophage Polarization and Blocks Glioma Progression. *Nat Med* (2013) 19:1264–72. doi: 10.1038/nm.3337
94. Kratochvill F, Neale G, Haverkamp JM, Van de Velde LA, Smith AM, Kawauchi D, et al. Tnf Counterbalances the Emergence of M2 Tumor Macrophages. *Cell Rep* (2015) 12:1902–14. doi: 10.1016/j.celrep.2015.08.033
95. Fridlender ZG, Sun J, Kim S, Kapoor V, Cheng G, Ling L, et al. Polarization of Tumor-Associated Neutrophil Phenotype by TGF-beta: "N1" Versus "N2" Tan. *Cancer Cell* (2009) 16:183–94. doi: 10.1016/j.ccr.2009.06.017
96. Silveira AAA, Dominical VM, Almeida CB, Chweih H, Ferreira WA Jr, Vicente CP, et al. TNF Induces Neutrophil Adhesion Via Formin-Dependent Cytoskeletal Reorganization and Activation of Beta-Integrin Function. *J Leukoc Biol* (2018) 103:87–98. doi: 10.1189/jlb.3A0916-388RR
97. Lauterbach M, O'Donnell P, Asano K, Mayadas TN. Role of TNF Priming and Adhesion Molecules in Neutrophil Recruitment to Intravascular Immune Complexes. *J Leukoc Biol* (2008) 83:1423–30. doi: 10.1189/jlb.0607421
98. Volk AP, Barber BM, Goss KL, Ruff JG, Heise CK, Hook JS, et al. Priming of Neutrophils and Differentiated PLB-985 Cells by Pathophysiological Concentrations of TNF-alpha is Partially Oxygen Dependent. *J Innate Immun* (2011) 3:298–314. doi: 10.1159/000321439
99. Lianyuan T, Gang L, Ming T, Dianrong X, Chunhui Y, Zhaolai M, et al. Tumor Associated Neutrophils Promote the Metastasis of Pancreatic Ductal Adenocarcinoma. *Cancer Biol Ther* (2020) 21:937–45. doi: 10.1080/15384047.2020.1807250
100. Comen E, Wojnarowicz P, Seshan VE, Shah R, Coker C, Norton L, et al. TNF is a Key Cytokine Mediating Neutrophil Cytotoxic Activity in Breast Cancer Patients. *NPJ Breast Cancer* (2016) 2:16009. doi: 10.1038/npjbcancer.2016.9
101. Fridlender ZG, Albelda SM. Tumor-Associated Neutrophils: Friend or Foe? *Carcinogenesis* (2012) 33:949–55. doi: 10.1093/carcin/bgs123
102. Croft M. The Role of TNF Superfamily Members in T-cell Function and Diseases. *Nat Rev Immunol* (2009) 9:271–85. doi: 10.1038/nri2526
103. Chopra M, Riedel SS, Biehl M, Krieger S, von Krosigk V, Bauerlein CA, et al. Tumor Necrosis Factor Receptor 2-Dependent Homeostasis of Regulatory T Cells as a Player in TNF-induced Experimental Metastasis. *Carcinogenesis* (2013) 34:1296–303. doi: 10.1093/carcin/bgt038
104. Hu Y, Xiao H, Shi T, Oppenheim JJ, Chen X. Progranulin Promotes Tumour Necrosis Factor-Induced Proliferation of Suppressive Mouse CD4(+) Foxp3(+) Regulatory T Cells. *Immunology* (2014) 142:193–201. doi: 10.1111/imm.12241
105. Palucka K, Banchereau J. Cancer Immunotherapy Via Dendritic Cells. *Nat Rev Cancer* (2012) 12:265–77. doi: 10.1038/nrc3258
106. Nakae S, Suto H, Iikura M, Kakurai M, Sedgwick JD, Tsai M, et al. Mast Cells Enhance T Cell Activation: Importance of Mast Cell Costimulatory Molecules and Secreted TNF. *J Immunol* (2006) 176:2238–48. doi: 10.4049/jimmunol.176.4.2238
107. Aspord C, Pedroza-Gonzalez A, Gallegos M, Tindle S, Burton EC, Su D, et al. Breast Cancer Instructs Dendritic Cells to Prime Interleukin 13-Secreting CD4+ T Cells That Facilitate Tumor Development. *J Exp Med* (2007) 204:1037–47. doi: 10.1084/jem.20061120
108. Marigo I, Zilio S, Desantis G, Mlecnik B, Agnellini AHR, Ugel S, et al. T Cell Cancer Therapy Requires CD40-CD40L Activation of Tumor Necrosis Factor and Inducible Nitric-Oxide-Synthase-Producing Dendritic Cells. *Cancer Cell* (2016) 30:377–90. doi: 10.1016/j.ccell.2016.08.004
109. Fu C, Jiang A. Dendritic Cells and CD8 T Cell Immunity in Tumor Microenvironment. *Front Immunol* (2018) 9:3059. doi: 10.3389/fimmu.2018.03059
110. Bonnet D, Dick JE. Human Acute Myeloid Leukemia is Organized as a Hierarchy That Originates From a Primitive Hematopoietic Cell. *Nat Med* (1997) 3:730–7. doi: 10.1038/nm0797-730
111. Kusoglu A, Biray Avci C. Cancer Stem Cells: A Brief Review of the Current Status. *Gene* (2019) 681:80–5. doi: 10.1016/j.gene.2018.09.052
112. Storci G, Sansone P, Mari S, D'Uva G, Tavolari S, Guarnieri T, et al. Tnfalpha Up-Regulates SLUG Via the NF-kappaB/HIF1alpha Axis, Which Imparts Breast Cancer Cells With a Stem Cell-Like Phenotype. *J Cell Physiol* (2010) 225:682–91. doi: 10.1002/jcp.22264
113. Zhao X, Ma L, Dai L, Zuo D, Li X, Zhu H, et al. Tnfalpha Promotes the Malignant Transformation of Intestinal Stem Cells Through the NFkappaB and Wnt/betacatenin Signaling Pathways. *Oncol Rep* (2020) 44:577–88. doi: 10.3892/or.2020.7631
114. Yao J, Lin J, He L, Huang J, Liu Q. TNF-Alpha/miR-155 Axis Induces the Transformation of Osteosarcoma Cancer Stem Cells Independent of TP53INP1. *Gene* (2020) 726:144224. doi: 10.1016/j.gene.2019.144224
115. Pan Z, Tian Y, Niu G, Cao C. Role of microRNAs in Remodeling the Tumor Microenvironment (Review). *Int J Oncol* (2020) 56:407–16. doi: 10.3892/ijo.2019.4952
116. Wang M, Zhao C, Shi H, Zhang B, Zhang L, Zhang X, et al. Deregulated microRNAs in Gastric Cancer Tissue-Derived Mesenchymal Stem Cells: Novel Biomarkers and a Mechanism for Gastric Cancer. *Br J Cancer* (2014) 110:1199–210. doi: 10.1038/bjc.2014.14
117. Ding L, Gu H, Xiong X, Ao H, Cao J, Lin W, et al. Micrornas Involved in Carcinogenesis, Prognosis, Therapeutic Resistance and Applications in Human Triple-Negative Breast Cancer. *Cells* (2019) 8(12):1492. doi: 10.3390/cells8121492
118. Ranjan K, Pathak C. FADD Regulates NF-kappaB Activation and Promotes Ubiquitination of cFLIPL to Induce Apoptosis. *Sci Rep* (2016) 6:22787. doi: 10.1038/srep22787
119. Liu Y, Liu R, Yang F, Cheng R, Chen X, Cui S, et al. miR-19a Promotes Colorectal Cancer Proliferation and Migration by Targeting TIA1. *Mol Cancer* (2017) 16:53. doi: 10.1186/s12943-017-0625-8
120. Huang L, Wang X, Wen C, Yang X, Song M, Chen J, et al. Hsa-miR-19a is Associated With Lymph Metastasis and Mediates the TNF-alpha Induced Epithelial-to-Mesenchymal Transition in Colorectal Cancer. *Sci Rep* (2015) 5:13350. doi: 10.1038/srep13350
121. Zhang J, Wu H, Li P, Zhao Y, Liu M, Tang H. Nf-kappaB-modulated miR-130a Targets TNF-alpha in Cervical Cancer Cells. *J Transl Med* (2014) 12:155. doi: 10.1186/1479-5876-12-155
122. Balatti V, Pekarky Y, Croce CM. Role of microRNA in Chronic Lymphocytic Leukemia Onset and Progression. *J Hematol Oncol* (2015) 8:12. doi: 10.1186/s13045-015-0112-x
123. Carswell EA, Old LJ, Kassel RL, Green S, Fiore N, Williamson B. An Endotoxin-Induced Serum Factor That Causes Necrosis of Tumors. *Proc Natl Acad Sci USA* (1975) 72:3666–70. doi: 10.1073/pnas.72.9.3666
124. Libutti SK, Paciotti GF, Byrnes AA, Alexander HR Jr, Gannon WE, Walker M, et al. and Pharmacokinetic Studies of CYT-6091, a Novel PEGylated Colloidal gold-rhTNF Nanomedicine. *Clin Cancer Res* (2010) 16:6139–49. doi: 10.1158/1078-0432.CCR-10-0978
125. Nilubol N, Yuan Z, Paciotti GF, Tamarkin L, Sanchez C, Gaskins K, et al. Novel Dual-Action Targeted Nanomedicine in Mice With Metastatic Thyroid Cancer and Pancreatic Neuroendocrine Tumors. *J Natl Cancer Inst* (2018) 110:1019–29. doi: 10.1093/jnci/djy003
126. Libutti SK, Tamarkin L, Nilubol N. Targeting the Invincible Barrier for Drug Delivery in Solid Cancers: Interstitial Fluid Pressure. *Oncotarget* (2018) 9:35723–5. doi: 10.18632/oncotarget.26267

127. Fajardo LF, Kwan HH, Kowalski J, Prionas SD, Allison AC. Dual Role of Tumor Necrosis Factor-Alpha in Angiogenesis. *Am J Pathol* (1992) 140:539–44.
128. Cairns R, Papandreou I, Denko N. Overcoming Physiologic Barriers to Cancer Treatment by Molecularly Targeting the Tumor Microenvironment. *Mol Cancer Res* (2006) 4:61–70. doi: 10.1158/1541-7786.MCR-06-0002
129. Heldin CH, Rubin K, Pietras K, Ostman A. High Interstitial Fluid Pressure - an Obstacle in Cancer Therapy. *Nat Rev Cancer* (2004) 4:806–13. doi: 10.1038/nrc1456
130. Lienard D, Ewalenko P, Delmotte JJ, Renard N, Lejeune FJ. High-Dose Recombinant Tumor Necrosis Factor Alpha in Combination With Interferon Gamma and Melphalan in Isolation Perfusion of the Limbs for Melanoma and Sarcoma. *J Clin Oncol* (1992) 10:52–60. doi: 10.1200/JCO.1992.10.1.52
131. Gabizon A, Bradbury M, Prabhakar U, Zamboni W, Libutti S, Grodzinski P. Cancer Nanomedicines: Closing the Translational Gap. *Lancet* (2014) 384:2175–6. doi: 10.1016/S0140-6736(14)61457-4
132. Greish K. Enhanced Permeability and Retention of Macromolecular Drugs in Solid Tumors: A Royal Gate for Targeted Anticancer Nanomedicines. *J Drug Target* (2007) 15:457–64. doi: 10.1080/10611860701539584

Conflict of Interest: The authors declare that the research was conducted in the absence of any commercial or financial relationships that could be constructed as a potential conflict of interest.

The handling editor declared a shared affiliation with the authors at the time of the review.

Copyright © 2021 Laha, Grant, Mishra and Nilubol. This is an open-access article distributed under the terms of the Creative Commons Attribution License (CC BY). The use, distribution or reproduction in other forums is permitted, provided the original author(s) and the copyright owner(s) are credited and that the original publication in this journal is cited, in accordance with accepted academic practice. No use, distribution or reproduction is permitted which does not comply with these terms.

frontiers in Immunology

ORIGINAL RESEARCH
published: 06 May 2021
doi: 10.3389/fimmu.2021.663495

Tumor Immune Microenvironment Characterization Identifies Prognosis and Immunotherapy-Related Gene Signatures in Melanoma

Dan Liu[1†], *Xue Yang*[2†] *and Xiongzhi Wu*[1*]

[1] Tianjin Medical University Cancer Institute and Hospital, National Clinical Research Center for Cancer, Tianjin's Clinical Research Center for Cancer, Key Laboratory of Cancer Prevention and Therapy, Key Laboratory of Cancer Immunology and Biotherapy, National Human Genetic Resources Sharing Service Platform, Tianjin, China, [2] Department of Medical Oncology, Tianjin Medical University General Hospital, Tianjin, China

OPEN ACCESS

Edited by:
Peng Qu,
National Institutes of Health (NIH), United States

Reviewed by:
Xingping Qin,
Renmin Hospital of Wuhan University, China
Hua Jiang,
Medical University of South Carolina, United States

***Correspondence:**
Xiongzhi Wu
wxz@tmu.edu.cn

[†]These authors have contributed equally to this work

Specialty section:
This article was submitted to Cancer Immunity and Immunotherapy, a section of the journal Frontiers in Immunology

Received: 03 February 2021
Accepted: 21 April 2021
Published: 06 May 2021

Citation:
Liu D, Yang X and Wu X (2021) Tumor Immune Microenvironment Characterization Identifies Prognosis and Immunotherapy-Related Gene Signatures in Melanoma. Front. Immunol. 12:663495. doi: 10.3389/fimmu.2021.663495

Background: The tumor microenvironment (TME) involves infiltration of multiple immune cell subsets, which could influence the prognosis and clinical characteristics. The increasing evidence on the role of tumor-infiltrating lymphocytes (TILs) in primary and metastatic melanomas supports that the immune system is involved in the progression and outcomes of melanoma. However, the immune infiltration landscape in melanoma has not been systematically elucidated.

Methods: In this study, we used CIBERSORT and ESTIMATE algorithms to analyze immune infiltration pattern of 993 melanoma samples. Then we screened differential expression genes (DEGs) related to immune subtypes and survival. The immune cell infiltration (ICI) score was constructed by using principal-component analysis (PCA) based on immune signature genes from DGEs. Gene set enrichment analysis (GSEA) was applied to explore high and low ICI score related pathways. Finally, the predictive ability of ICI score was evaluated in survival prognosis and immunotherapy benefit.

Result: We identified three ICI clusters and three gene clusters associated with different immune subtypes and survival outcomes. Then the ICI score was constructed, and we found that high ICI score exhibited activated immune characteristics and better prognosis. High ICI score was significantly enriched in immune pathways and highly expressed immune signature genes. More importantly, we confirmed that melanoma patients with high ICI score had longer overall survival and rate of response to immunotherapy.

Conclusion: We presented a comprehensive immune infiltration landscape in melanoma. Our results will facilitate understanding of the melanoma tumor microenvironment and provide a new immune therapy strategy.

Keywords: melanoma, tumor microenvironment, immune cell infiltration, prognosis, immune therapy

INTRODUCTION

Malignant melanoma is one of the most severe skin cancers, with a higher risk of metastasis and mortality rates. Approximately 324,635 incident cases and 57,043 related deaths were reported worldwide in 2020 (1). In the past decades, immune checkpoint inhibitor therapy targeting cytotoxic T-lymphocyte antigen 4 (CTLA-4), programmed cell death receptor 1 (PD-1), and programmed cell death ligand 1 (PD-L1) have resulted in impressive outcomes in patients with malignant melanoma (2). However, approximately 40–65% of melanoma patients have no response to or develop relapse after anti-PD-1 therapy due to primary or acquired resistance, and over 70% of patients experience anti-CTLA-4 treatment failure (3).

Currently, PD-L1 expression, tumor mutation burden (TMB), and microsatellite instability-high (MSI-H) are the primary biomarkers for guiding the clinical practice of immune therapy and predicting survival benefit in several types of cancer (4, 5). However, neither PD-L1 expression nor TMB is a perfect biomarker for immune therapy prediction in melanoma, as responses are also observed in PD-L1-negative and low TMB patients. Despite efforts to identify new biomarkers predictive of the benefits of immune therapy, such as ARID2 and tumor MHC-I expression (6, 7), no robust biomarker has been established to drive clinical practice. Therefore, identification and characterization of potential biomarkers and their application in combination with immune therapy are urgently needed.

The tumor microenvironment (TME) involves infiltration of multiple immune cell subsets, and the pattern of immune cell infiltration (ICI) could influence the prognosis and clinical benefit of melanoma immune therapy (8, 9). TME is a vital factor that determines the efficacy of anti-tumor immune therapy (10). Studies have reported that acral and mucosal melanoma patients with a lower number of total tumor-infiltrating lymphocytes (TILs) have a poorer response to immune checkpoint inhibitors than does their cutaneous melanoma counterparts (11, 12). Primary and acquired resistance to immune checkpoint blockade commonly occurs due to a tumor immune escape mechanism regulated by the TME (13). One study proposed the degree of lymphocyte infiltration as an independent prognostic factor of disease-free survival (DFS) in melanoma patients, with a higher TIL grade associated with a lower risk of death (14). The characteristics of ICI can serve as an effective prognostic biomarker and predictive indicator of response to immune therapy (15). Therefore, it is necessary to gain a comprehensive understanding of the immune infiltrate characteristics in melanoma.

This study aimed to characterize the ICI landscape of melanoma. Toward this goal, we used two algorithms, namely, CIBERSORT and ESTIMATE, and further constructed ICI scores that can be used to predict survival prognosis and immune therapy benefit, based on the immune infiltration pattern and immune signature genes.

MATERIALS AND METHODS

Melanoma Datasets and Processing

Melanoma microarray datasets were searched and downloaded from the Cancer Genome Atlas (TCGA) (https://portal.gdc.cancer.gov/) and the Gene Expression Omnibus (GEO) (https://www.ncbi.nlm.nih.gov/geo/). The inclusion criteria were as follows: 1) human malignant melanoma sample, except mucosal and uveal melanomas; 2) mRNA expression profiling by microarray; 3) sample size ≥40; and 4) complete clinical information including overall survival time and state. After excluding repetitive samples, the following six datasets that included 993 melanoma samples were analyzed: GSE65904, GSE59455, GSE54467, GSE465517, GSE19234, and TCGA-SKCM cohorts. Detailed information on the microarray datasets is shown in **Table S1**.

The raw data from the GEO database was performed normalized including quality control, background correction, logarithmic conversion and remove batch effects, then the gene probes were annotated. The RNA-sequencing data (FPKM values) downloaded from the TCGA database were transformed into transcripts per kilobase million values, which were more similar to the microarray results facilitated to analysis.

Consensus Clustering of Tumor-Infiltrating Immune Cells

The levels of ICI for melanoma were quantified using the CIBERSORT algorithm and LM22 gene signature. CIBERSORT is a deconvolution algorithm that uses a set of reference gene expression values (a signature with 547 genes) to evaluate cell type proportions in data from bulk tumor samples with mixed cell types (16). The LM22 gene signature could discriminate 22 human immune cell phenotypes, including B cells, T cells, natural killer (NK) cells, macrophages, dendritic cells (DCs), and myeloid subsets (16). The immune and stromal scores of each melanoma sample were calculated using the ESTIMATE method (17). Unsupervised clustering was carried out to identify patterns of ICI. The analysis was performed R package "ConsensusClusterPlus," and iteration was 1,000 times to ensure classification stability.

Identification of Differentially Expressed Genes and Generation of ICI Gene Signatures

Based on the clustering results of ICI, all samples were grouped into three clusters to identify differentially expressed genes (DEGs) associated with the immune subtypes. The analysis was performed using the R package "limma", and the threshold value was an absolute fold-change >1 and an adjusted P value of <0.05.

The unsupervised clustering method was performed to group samples according to the DEG values. The DEGs that were positively and negatively correlated to the clusters were defined as the ICI signature genes A and B, respectively. Signature genes A and B have differential expressions in different gene clusters, and differential expression pattern also exits between signature genes A and B in one gene cluster.

The Boruta algorithm was applied to reduce the dimensions of the ICI gene signatures A and B. We applied principal component analysis (PCA) to construct the ICI score. The algorithm chooses best feature genes sets by a feature selection and extraction method, which has proven better statistical power. Without loss of generality, the first principal component (PC1) of matrix is selected for analysis as a signature score (18). We performed PCA to score signature genes A or B for each sample, and got two PC1 values for each sample, as PC1A and PC1B. We then used a method similar to the Gene expression grade index (19) to define each sample ICI score:

$$ICIscore = \Sigma PC1A - \Sigma PC1B$$

Functional Enrichment Analysis

ICI signature genes A and B were subjected to Gene Ontology (GO) enrichment analysis. All the samples were subjected to gene set enrichment analysis (GSEA) and were divided into the ICI high score group and the ICI low score group. The GSEA software was downloaded from the GSEA website (http://software.broadinstitute.org/gsea/index.jsp). Enrichment results were visualized using the R package "ggplot2".

Somatic Alteration Data Download and Analysis

The melanoma mutation data were downloaded from the TCGA database (https://www.cancer.gov/tcga/). The raw data were extracted and also grouped by high and low ICI scores. We evaluated the total number of non-synonymous mutations in all melanoma samples, and the somatic alterations in melanoma driver genes in the high and low ICI score groups. The R package "maftool" was used to identify driver genes.

ICI Scores and Clinical Characteristics Immune Therapy Benefit

Data from three immune therapy cohorts, that is, GSE78220, CA209308 and GSE19423 were downloaded to validate the value of the ICI score for predicting the immune therapy benefit. From the GSE78220 cohort, 27 melanoma samples treated with the anti-PD1 drug pembrolizumab were included. From the CA209038 cohort, which was downloaded from https://github.com/riazn/bms038_analysis, 68 melanoma samples treated with the anti-PD1 drug nivolumab were included. After excluding repetition or samples without clinical information, 50 samples were included in the analysis. From the GSE19423 cohort, 48 primary bladder cancer samples treated with Bacillus Calmette–Guérin (BCG) immunotherapy were included. A metastasis melanoma cohort GSE22154 was downloaded to validate the predictive value of the ICI score in metastasis, which included 22 metastatic melanoma samples.

Statistical Analyses

Between-group comparisons were performed using the Wilcoxon test, while comparisons among more than two groups were conducted using the Kruskal-Wallis test. Survival curves were generated using the Kaplan-Meier method and compared using the log-rank test. The R package "survminer" was used to evaluate the best cutoff values of dataset based on the relation between overall survival and ICI score. The heatmap was constructed using the R package "pheatmap." The correlation between the ICI score group and somatic mutation frequency was analyzed using the chi-square test, and the correlation coefficient was evaluated with Spearman analysis. All statistical analyses were performed using R (version 4.0.3) or GraphPad Prism (version 6.01), and two-tailed $P<0.05$ was considered statistically significant

RESULTS

Landscape of Immune Cells Infiltration

We searched public databases and screened microarray datasets, six melanoma microarray datasets including 993 melanoma samples were brought into analysis. Mucosal and uveal melanomas samples were excluded for significant difference from cutaneous melanoma in presentation, genetic profile, staging, response to treatment and patterns of progression (20, 21). Detailed information of the included datasets is shown in **Table S1**. We employed the CIBERSORT and ESTIMATE algorithms to calculate the levels of ICI, immune score, and stromal score of each melanoma sample (**Table S2**). The ICI pattern was analyzed using unsupervised clustering. The optimal cluster pattern was three immune subtypes, that is, ICI clusters A-C (**Figures S1B–E**). The ICI heatmap showed that the immune cells were composed of different immune clusters (**Figure 1A**). The correlation coefficient heatmap showed the landscape of immune cell interaction in melanoma TME (**Figure 1B**). Cluster A was characterized by a high immune score with increased infiltration of CD8 T cells, activated NK cells, CD4 T memory activated cells, and T follicular helper cells. Cluster B exhibited low infiltration levels for most immune cells, but with a high density of M0 macrophages, activated mast cells, and resting NK cells. ICI cluster B had minimum immune score and stromal score. ICI cluster C showed high infiltration of naive B cells, memory B cells, Tregs, M1 macrophages, and M2 macrophages.

Survival analysis to explore the prognostic value of the ICI clusters showed that ICI cluster A had better survival outcomes. Meanwhile, ICI cluster B was associated with a worse prognosis. Cluster C was characterized by an intermediate overall survival (log-rank test P=0.007, **Figure 1C**). A consistent result was observed in the boxplot of immune cell fraction for the three ICI clusters, and this was further confirmed with the Kruskal-Wallis test (**Figure 1D**). The expression of immune activity-related signature genes (CXCL9, CXCL10, TNF, IFNG, CD8A, GZMA, GZMB, and PRF1) and immune checkpoint signature genes (CTLA4, PDCD1, PDCD1LG2, and LAG3) were the highest in ICI cluster A and the lowest in ICI cluster B ($P<0.0001$, **Figures 1E, F**).

Identified Immune Gene Subtype

To identify the difference in gene expression between immune subtypes, we analyzed gene expression among the three ICI clusters using the R package "limma". Unsupervised clustering analysis was

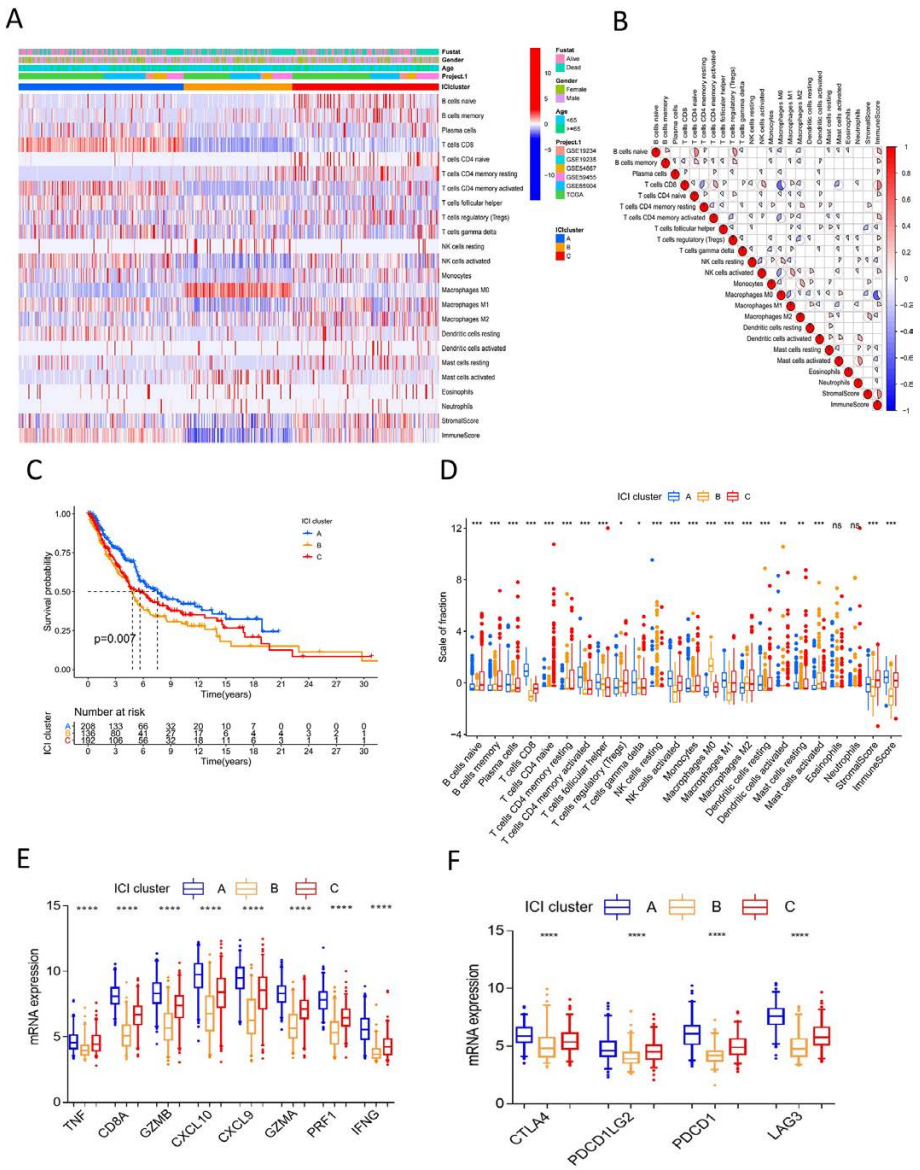

FIGURE 1 | Landscape of immune cells infiltration in melanoma. **(A)** Unsupervised clustering heatmap of immune cells infiltration for all melanoma samples. Rows represent tumor-infiltrating immune cells, and columns represent samples. **(B)** The correlation coefficient heatmap of immune cell interaction. **(C)** Kaplan-Meier curves of overall survival for ICI cluster A–C. Log rank test P = 0.007. **(D)** The box plot of immune cells fraction in ICI cluster A–C. *P<0.05; **P < 0.01; ***P<0.001; ****P<0.0001; ns: no significance. **(E)** The box plot of immune activity related signature genes expression (CXCL9, CXCL10, TNF, IFNG, CD8A, GZMA, GZMB, PRF1) between ICI cluster A–C, ****P<0.0001. **(F)** The box plot of immune checkpoint signature genes expression (CTLA4, PDCD1, PDCD1LG2, LAG3) between ICI cluster A-C, ****P<0.0001.

performed for 266 DEGs. The consensus matrix and gene cluster heatmap indicated that three gene clusters were optimal patterns (**Figures S2A–D**). Thus, DEGs were grouped into gene clusters A, B, and C (**Figure 2A**). These clusters showed significant differences in overall survival. Cluster C had better prognosis, whereas cluster A showed poor outcomes (log-rank test, P<0.001; **Figure 2B**). There was also a significant difference in ICI among gene clusters A-C (**Figure 2C**). Cluster C had a high immune score and stromal score and showed high infiltration of anti-tumor immune cells, such as CD8 T cells, NK cells, B cells, and M1 macrophages. Cluster A was characterized by low immune score and stromal score, thus showing worse prognosis. With respect to the expression of immune activity-related signature genes and immune checkpoint signature genes, Cluster C showed obvious superiority among the three groups (P<0.0001, **Figures S2E, F**).

For DEGs based on immune subtypes, genes positively and negatively associated with the gene cluster were defined as ICI gene signature A and ICI gene signature B, respectively. Gene dimension

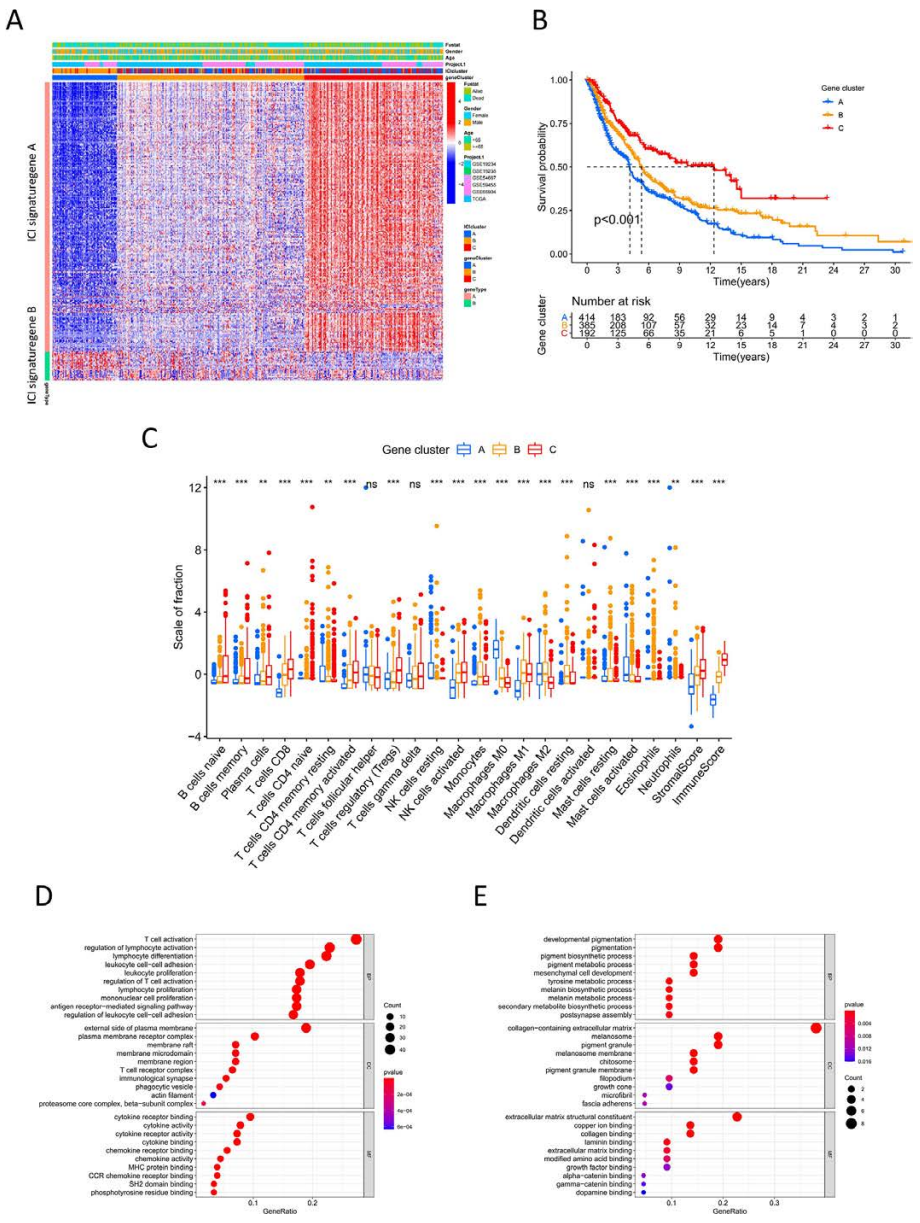

FIGURE 2 | Immune gene subtype **(A)** Unsupervised clustering heatmap of differential expression genes among three ICI cluster. **(B)** Kaplan-Meier curves of overall survival for gene cluster A-C. Log rank test P <0.001. **(C)** The box plot of immune cells fraction in gene cluster A-C. **P < 0.01; ***P<0.001; ns, no significance. **(D, E)** GO enrichment analysis for ICI signature gene A and B.

reduction using the Boruta algorithm obtained 211 signature genes (**Table S4**). In GO functional enrichment analysis, ICI gene signature A was significantly enriched in immune-related functions, while ICI gene signature B was mainly associated with biosynthesis and metabolism (**Figures 2D, E**).

Construction of ICI Score

PCA was applied to calculate two aggregate scores: ICI scores A and B from ICI gene signature A and B. We computed ICI score A and ICI score B for each melanoma sample as the sum of the relevant individual scores. The prognostic signature score was then defined as the ICI score. All samples were grouped into the high or low ICI score group based on the optimal cutoff value (**Table S5**). The alluvial diagram displayed the distribution of the ICI score groups under different gene clusters and survival outcomes (**Figure 3A**). The low ICI score group was mostly composed of gene cluster A, which had a poor prognosis. Gene cluster C, related to better outcomes, was included in the high ICI score group. Survival analysis to identify the prognostic value of the ICI score showed that for

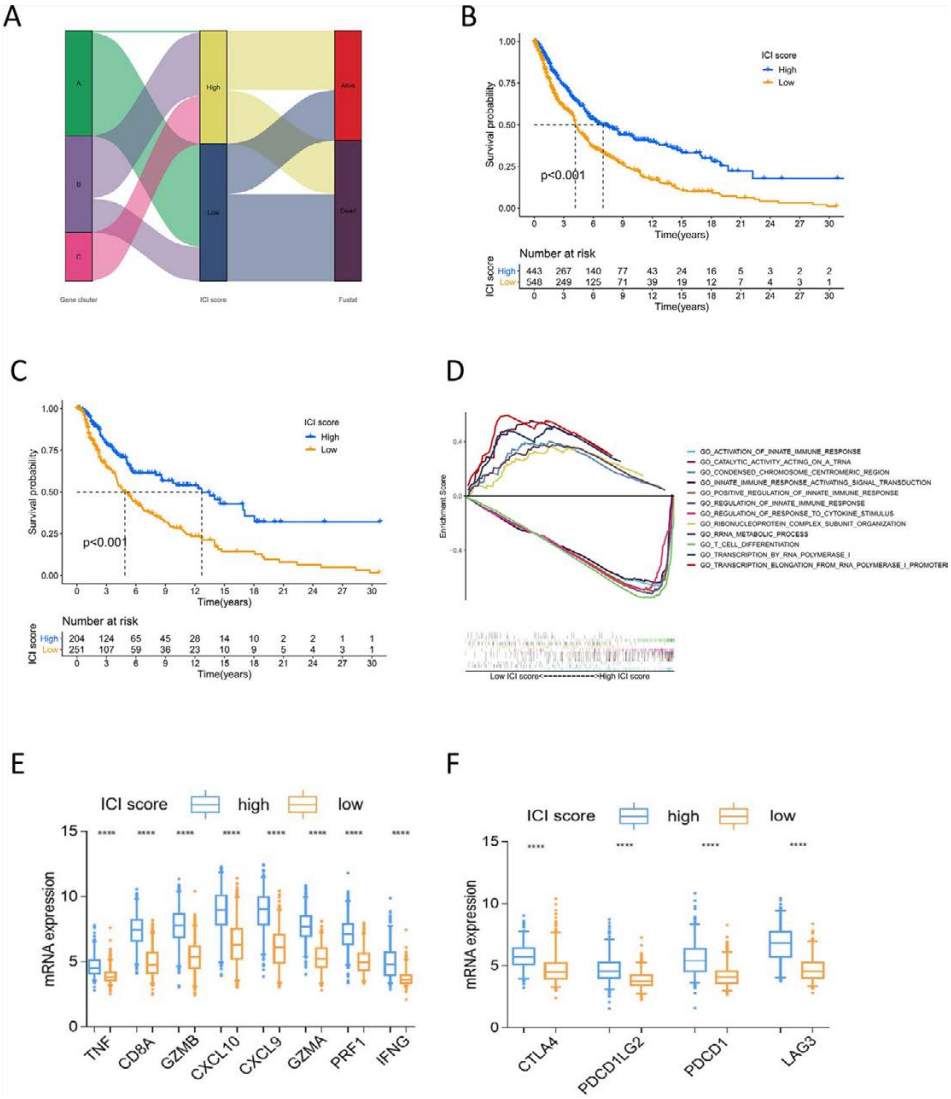

FIGURE 3 | Analysis of ICI score. **(A)** Alluvial diagram of ICI scores groups distribution in different gene cluster, and survival outcomes. **(B)** Kaplan-Meier curves of overall survival for high and low ICI score cluster in all sample. Log rank test P <0.001. **(C)** Kaplan-Meier curves of overall survival for high and low ICI score cluster in TCGA cohort. Log rank test P <0.001. **(D)** GSEA of high and low ICI score groups for all melanoma samples. **(E)** The box plot of immune activity related signature genes expression (CXCL9, CXCL10, TNF, IFNG, CD8A, GZMA, GZMB, PRF1) in high and low ICI score, ****P<0.0001. **(F)** The box plot of immune checkpoint signature genes expression (CTLA4, PDCD1, PDCD1LG2, LAG3) in high and low ICI score, ****P<0.0001.

all melanoma samples, the high-score group had superior overall survival over the low-score group (log-rank test, P<0.001; **Figure 3B**). Moreover, the prognostic value of the ICI score was validated in most datasets. The high ICI score group showed superior prognosis in the TCGA (log-rank test P<0.001, **Figure 3C**), GSE19234 (log-rank test P=0.049), GSE46517 (log-rank test P<0.001), GSE54467 (log-rank test P=0.033), and GSE65904 (log-rank test P=0.047) (**Figure S3**) datasets. These results confirm the value of the ICI score for prognostic prediction. GSEA showed that the high ICI score group had prominently enriched immune-related pathways, including innate immune response, positive regulation of innate immune response, T cell differentiation, and response to cytokine stimulus. Meanwhile, the low ICI score group mainly showed enriched biosynthesis (**Figure 3D**). The high ICI score group showed significant immune activity, with higher expression of immune activity signature genes and immune checkpoint signature genes compared with that of the low ICI score group (**Figures 3E, F**).

ICI Score and Cancer Somatic Variants

Tumor genomic mutations lead to the occurrence of neoantigens, which are favorable for immune therapy (22). TMB is a predictive factor for treatment response to immune

therapy (23). To investigate the intrinsic correlation between TMB and ICI scores, we downloaded the data of melanoma somatic variants from the TCGA database. We compared the TMB between melanoma samples with high ICI scores and those with low ICI scores. The box plot showed a difference in mutation frequency between the high and low ICI score groups, but the difference was not significant (**Figure 4A**). Correlation analyses showed that ICI scores were negatively correlated with TMB (Spearman coefficient: R=-0.11, P=0.023, **Figure 4B**). High TMB patients had better survival outcomes than did low TMB patients (log-rank test P<0.001, **Figure 4C**). We then evaluated the synergistic effect of ICI scores on prognostic stratification. Stratified survival analysis showed significant differences in survival according to the ICI scores among the TMB subgroups (log-rank P<0.001, **Figure 4D**). These results indicate that the ICI score could be a predictor of survival independent of the TMB.

The distribution of melanoma somatic variants between the low and high ICI score groups was accessed by R package "maftools." The top 20 driver genes with the highest alteration frequency are shown in **Figures 4E, F**. The alteration frequencies of FAT4, LRP1B, and ANK3 were significantly different between the low and high ICI score groups (**Table 1**).

Predictive Value of the ICI Scores for Clinical Characteristics and Immunotherapy Benefit

We then assessed the predictive value of the ICI score for the clinical characteristics and immune therapy benefit in melanoma. Combining the ICI score and clinical information, we analyzed the main clinical indicators, including age, sex, TMN stage, Breslow depth, Clark level, ulceration and tumor site. A forest plot was created for the stratified survival analysis based on ICI score, and significant differences were observed (**Figure 5A**). In all factors, except for M1, N1, and <4 mm Breslow depth, those with high scores had significantly superior overall survival to those with low scores. Breslow depth, Clark level, and ulceration are specific factors for melanoma (23). In the metastatic melanoma GSE22154 cohort, the high ICI score group had a higher survival (**Figure S4G**). Our results support that the ICI score could predict survival independent of these clinical indicators.

For the prognostic value of the ICI score with respect to the immune therapy benefit, three cohorts were evaluated. In the GSE19423 cohort, the high ICI score group had a higher overall survival after immune therapy (log rank test P=0.026, **Figures 5B, C**). In the GSE78220 cohort, the high ICI score group had

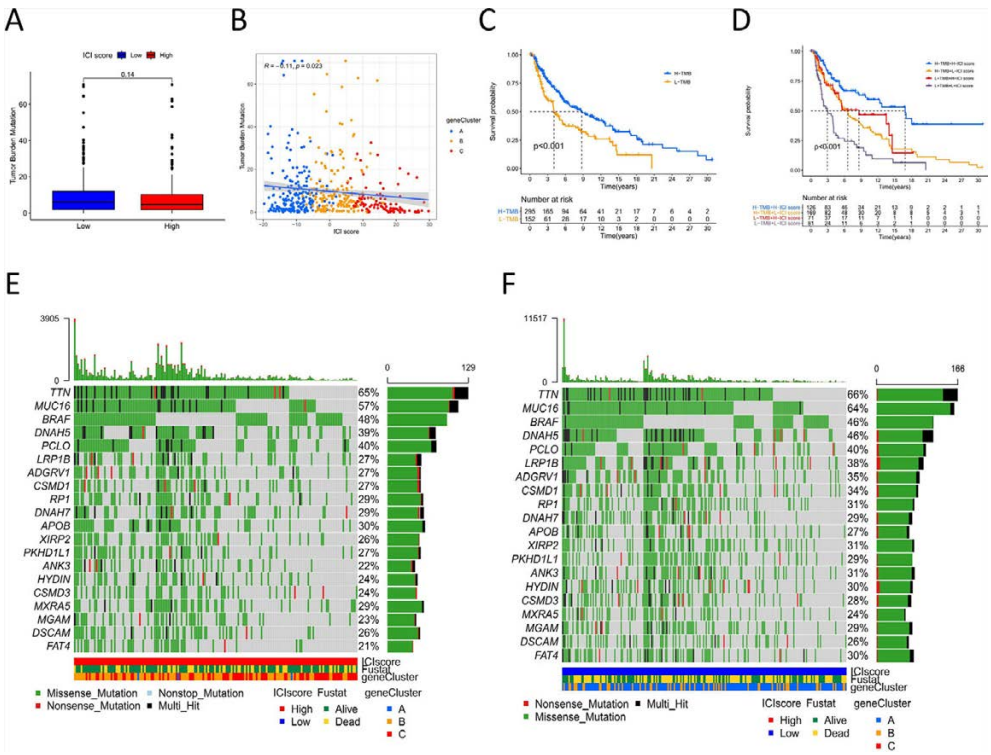

FIGURE 4 | The correlation between ICI score and cancer somatic variants. **(A)** TMB difference among the high and low ICI score groups. **(B)** The correlation Scatter plots between TMB and ICI score. **(C)** Kaplan-Meier curves of overall survival for high and low TMB group. Log rank test P <0.001. **(D)** Kaplan-Meier curves of overall survival stratified by both TMB and ICI scores. Log rank test P <0.001. **(E, F)** The oncoPrint of high (left) and low (right)ICI score. Individual patients represented in each column. Missense mutation: green; Nostop mutation: gray; Nonsense mutation: red; Multi-hit: black. The top bar plot represented TMB. The right bar plot shows the mutation frequency of each gene in separate ICI score groups. The below bar represented ICI cluster, gene cluster and survival outcome.

TABLE 1 | The Correlation between the ICI Scores and Somatic Variants.

Gene	H-wild	H-mutation	L-wild	L-mutation	P value
GLRB	192(97.46%)	5(2.54%)	221(88.4%)	29(11.6%)	0.000653446
ACSM1	192(97.46%)	5(2.54%)	226(90.4%)	24(9.6%)	0.004861082
ITGAX	194(98.48%)	3(1.52%)	231(92.4%)	19(7.6%)	0.006359613
SEL1L3	193(97.97%)	4(2.03%)	229(91.6%)	21(8.4%)	0.006885403
LRRC4C	185(93.91%)	12(6.09%)	214(85.6%)	36(14.4%)	0.007742623
CATSPERD	178(90.36%)	19(9.64%)	242(96.8%)	8(3.2%)	0.008300153
MYH4	172(87.31%)	25(12.69%)	193(77.2%)	57(22.8%)	0.008825349
PKHD1	183(92.89%)	14(7.11%)	211(84.4%)	39(15.6%)	0.009043977
ATP13A4	188(95.43%)	9(4.57%)	220(88%)	30(12%)	0.009448039
IGSF10	184(93.4%)	13(6.6%)	213(85.2%)	37(14.8%)	0.009879668
EXPH5	189(95.94%)	8(4.06%)	222(88.8%)	28(11.2%)	0.0099167
RXFP2	193(97.97%)	4(2.03%)	230(92%)	20(8%)	0.010213103
PDGFRA	192(97.46%)	5(2.54%)	228(91.2%)	22(8.8%)	0.010494566
MPP7	187(94.92%)	10(5.08%)	219(87.6%)	31(12.4%)	0.012475552
FHDC1	193(97.97%)	4(2.03%)	231(92.4%)	19(7.6%)	0.015072759
BTBD11	191(96.95%)	6(3.05%)	227(90.8%)	23(9.2%)	0.015127514
ADGRF4	192(97.46%)	5(2.54%)	229(91.6%)	21(8.4%)	0.015293351
CSF2RB	192(97.46%)	5(2.54%)	229(91.6%)	21(8.4%)	0.015293351
TGM6	182(92.39%)	15(7.61%)	244(97.6%)	6(2.4%)	0.018201576
LRP1B	143(72.59%)	54(27.41%)	154(61.6%)	96(38.4%)	0.019185781
SZT2	190(96.45%)	7(3.55%)	226(90.4%)	24(9.6%)	0.020842861
DNAH1	173(87.82%)	24(12.18%)	236(94.4%)	14(5.6%)	0.021072363
IGHM	192(97.46%)	5(2.54%)	230(92%)	20(8%)	0.022153014
PPP1R3A	176(89.34%)	21(10.66%)	203(81.2%)	47(18.8%)	0.02467418
TRPC4	184(93.4%)	13(6.6%)	216(86.4%)	34(13.6%)	0.02506211
ZNF99	184(93.4%)	13(6.6%)	216(86.4%)	34(13.6%)	0.02506211
NBEA	182(92.39%)	15(7.61%)	213(85.2%)	37(14.8%)	0.027528675
PDZD2	185(93.91%)	12(6.09%)	218(87.2%)	32(12.8%)	0.027530981
PCDHB7	189(95.94%)	8(4.06%)	225(90%)	25(10%)	0.027672056
FAT4	156(79.19%)	41(20.81%)	174(69.6%)	76(30.4%)	0.029178661
PLEKHH2	192(97.46%)	5(2.54%)	231(92.4%)	19(7.6%)	0.031882714
GRM4	193(97.97%)	4(2.03%)	233(93.2%)	17(6.8%)	0.032281736
CACNA2D4	193(97.97%)	4(2.03%)	233(93.2%)	17(6.8%)	0.032281736
PTPRB	174(88.32%)	23(11.68%)	201(80.4%)	49(19.6%)	0.032897855
FCGBP	182(92.39%)	15(7.61%)	214(85.6%)	36(14.4%)	0.03656706
SI	175(88.83%)	22(11.17%)	203(81.2%)	47(18.8%)	0.037014862
FLG	158(80.2%)	39(19.8%)	178(71.2%)	72(28.8%)	0.037794192
PCDHA12	189(95.94%)	8(4.06%)	226(90.4%)	24(9.6%)	0.038406702
HTT	189(95.94%)	8(4.06%)	226(90.4%)	24(9.6%)	0.038406702
SERPINB7	180(91.37%)	17(8.63%)	241(96.4%)	9(3.6%)	0.040168226
ACE	190(96.45%)	7(3.55%)	228(91.2%)	22(8.8%)	0.041099422
TRPM6	181(91.88%)	16(8.12%)	213(85.2%)	37(14.8%)	0.043279955
EML5	191(96.95%)	6(3.05%)	230(92%)	20(8%)	0.043557638
PRLR	187(94.92%)	10(5.08%)	223(89.2%)	27(10.8%)	0.044684979
SLITRK3	187(94.92%)	10(5.08%)	223(89.2%)	27(10.8%)	0.044684979
FSIP2	184(93.4%)	13(6.6%)	218(87.2%)	32(12.8%)	0.044972848
PLCE1	179(90.86%)	18(9.14%)	210(84%)	40(16%)	0.045282963
ANK3	153(77.66%)	44(22.34%)	172(68.8%)	78(31.2%)	0.047485414
DNAH10	169(85.79%)	28(14.21%)	195(78%)	55(22%)	0.047763319
DUOX2	188(95.43%)	9(4.57%)	225(90%)	25(10%)	0.048733515

better survival outcomes than did the low score group (log rank P=0.014, **Figures 5D, E**). The partial response rate to anti-PD-L1 therapy was also higher in the high ICI score group than that in the low score group. Further, the rate of progressive disease was significantly lower in the high ICI score group. Notably, some patients in the high ICI score group exhibited complete response, while none of the patients in the low score group achieved complete response (**Figure 5F**). The CA209038 cohort showed similar results. The high ICI score group had a greater survival benefit from immune therapy (log rank P=0.0449, **Figures 5G, H**) and a higher response rate to therapy (**Figure 5I**). The low ICI score group exhibited higher mutation frequency, consistent with our previous result (**Figure 5J**).

We compared the predictive ability of the signature genes in our study and other models in terms of the immunotherapy benefit. We selected signature genes identified by the INF model and the HNSC model (15, 24). The Kaplan-Meier curves and the ROC curves of the ICI score of the other two models are shown in Fig S4A-F. For the other two models, there were no statistically significant differences in the overall survival between those with high and low ICI scores, and the prognosis differed among the cohorts. The ROC curve showed that the predictive value was

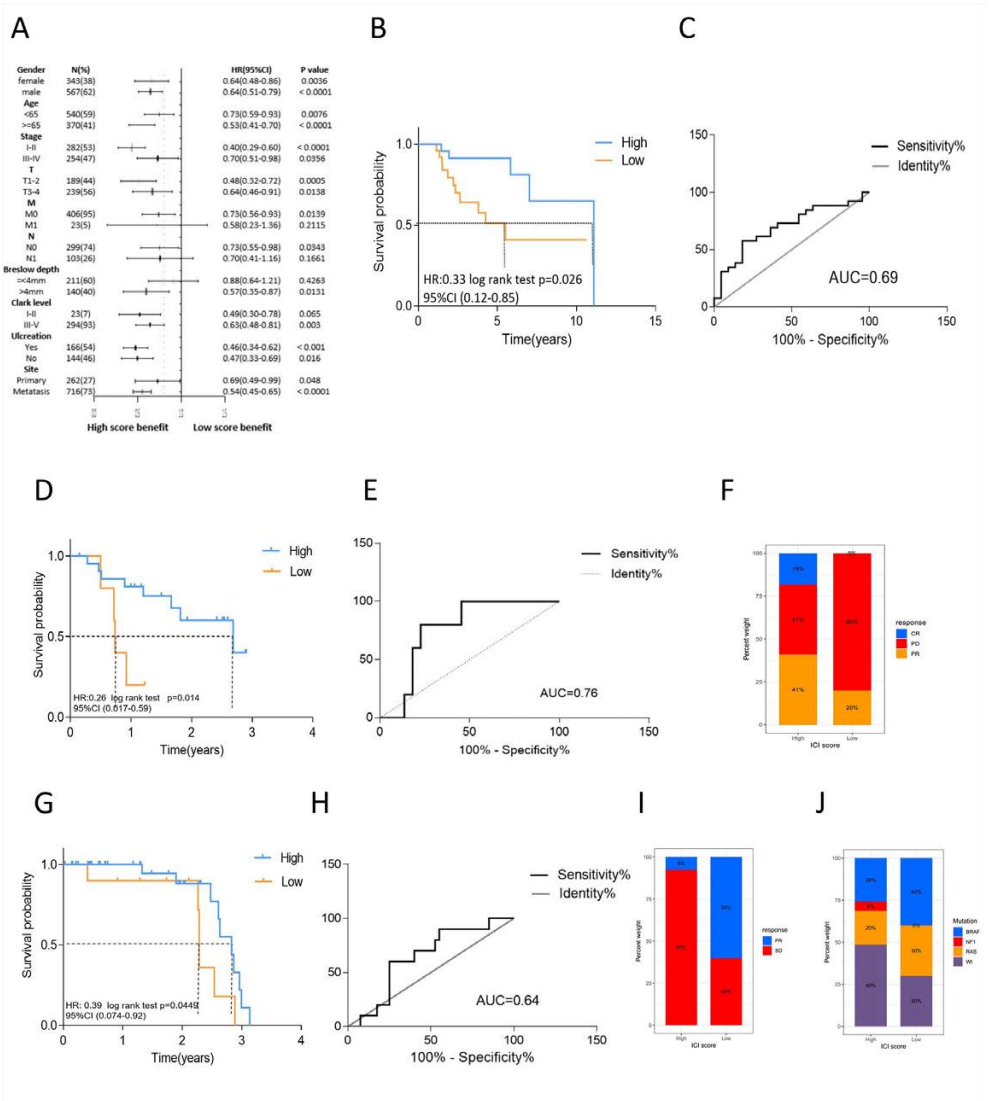

FIGURE 5 | The role of ICI scores in the evaluation of melanoma clinical characteristics and immune therapy benefit. **(A)** The forest plot of stratified survival analysis for clinical indicator based on ICI score. The length of the horizontal line represents the 95% CI for each group, the sample number, HR and 95%CI as well as P value of each group were listed. **(B)** Kaplan-Meier curves of overall survival for high and low ICI score cluster in GSE19423 cohort. Log rank test P =0.026. **(C)** The predictive value of the ICI score measured by ROC curves in GSE19423. **(D)** Kaplan-Meier curves of overall survival for high and low ICI score cluster in GSE78220. Log rank test P =0.014. **(E)** The predictive value of the ICI score measured by ROC curves in GSE78220. **(F)** Rate of clinical response to anti-PD1 treatment in high and low ICI score groups in GSE78220. **(G)** Kaplan-Meier curves of overall survival for high and low ICI score cluster in CA209038 cohort. Log rank test P =0.0449. **(H)** The predictive value of the ICI score measured by ROC curves in CA209038. **(I)** Rate of clinical response to anti-PD1 treatment in high and low ICI score groups in CA209038 cohort. **(J)** Mutation frequency between high and low ICI score group in CA209038 cohort.

low. The result indicated that the signature genes that we used had better predictive value and robustness in terms of clinical outcomes among melanoma patients.

DISCUSSION

Melanoma is one of the most immunogenic tumors because of its high genomic mutational burden, thus its great potential to respond favorably to immune therapy (25). Immune checkpoint blockade therapy, including anti-PD1, anti-PDL1, and anti-CTLA-4, has been proven to improve the overall survival of patients with advanced melanoma (26, 27). PD-L1 and TMB have been shown to be independent, not correlated, predictive variables of the benefit of immune therapy (23). However, no single factor has been validated to adequately predict the treatment benefit of immune therapy (28). The interaction between tumor cells and the microenvironment

leads to a tumor-driven immune response (9). The increasing evidence on the role of TILs in primary and metastatic melanomas supports that the immune system is involved in the progression and outcomes of melanoma (29, 30). Thus, algorithms for identifying melanoma prognosis and treatment benefit based on qualitative and quantitative characteristics of tumor and immune cells are expected (31). In this study, we analyzed the melanoma immune landscape and constructed an ICI score based on the immune microenvironment to evaluate prognosis and immune therapy benefit.

Three major immune phenotypes have been proposed in cancer, namely the immune-inflamed, immune-excluded, and immune-desert phenotypes (10, 32). In our study, ICI cluster A exhibited the immune-inflamed phenotype which is characterized by the presence of CD4 and CD8 T cells in the tumor parenchyma (33). ICI cluster B exhibited the immune-desert phenotype, which is characterized by an absence of ICI in the tumor parenchyma and stroma. This phenotype is considered to be a non-inflamed tumor (34). ICI cluster C exhibited the immune-excluded phenotype, with a high level of infiltration by B cells, naive and conventional T cells, Treg cells, and dendritic cells, as well as the highest stromal score. However, another study found that many immune cells only infiltrated the tumor margins due to the paucity of tumor stroma (35). ICI cluster C was similar to tertiary lymphoid structures (TLSs) which were present along the invasive tumor margin and stroma, and worked as sites of immune cell recruitment and activation (10). This may explain why ICI cluster C had a poorer prognosis than ICI cluster A. The results showed that the immune-inflamed phenotype had better overall survival, which is consistent with previous research which has shown that the presence of high levels of ICI is associated with favorable outcomes (29). We then analyzed the DEGs from the ICI cluster and defined three gene clusters related to immune activity. Similar to ICI clusters, gene clusters function better in distinguishing immune activity and survival outcomes. Gene clusters related with longer overall survival showed activated immune function, whereas gene clusters related to poor outcome had low levels of anti-tumor immune cells and low expression of immune signature genes. These findings on the immune landscape of melanoma warrant further studies considering the lack of independent biomarkers in this malignancy.

Some researchers have proposed the phenotype of T cell infiltration as a predictor of response to immune therapy (36). Considering the correlation between the immune subtypes of melanoma and survival, we constructed ICI scores to evaluate survival prognosis, clinical characteristics, and immune therapy benefit. The ICI score was defined by immune signature genes from gene cluster results. The high ICI score group showed prominent enrichment of immune-related pathways and high expression of immune signature genes, exhibiting a "hot" tumor phenotype. In addition, the immune phenotype was associated with better prognosis. Somatic mutations in tumors lead to neoantigens that are recognized and targeted by the immune system (22). It has been reported that low TMB conferred poor survival outcomes in melanoma and was associated with lower age and advanced pathological stage (5). Similarly, our results showed that high TMB conferred a survival benefit. Interestingly, we found that the ICI score was negatively correlated to TMB. A previous study found that a higher mutation frequency was not indicative of a higher level of ICI (37). Thus, a high TMB does not necessarily result in a high ICI score. Our stratified survival analysis showed that the ICI score could be used to evaluate prognosis. Particularly, both ICI score and TMB were independent predictors of outcome.

TMB and PD1 have been reported as predictive variables of the benefit of immune therapy (23). In our research, the ICI score was an effective factor to predict the benefit of immune therapy for melanoma patients. A clinical trial reported that the presence of CD8+ T cells was favorable for DFS in immune therapy (38). In our study, the high ICI score group benefited more from immune therapy and exhibited activated immune status than did the low ICI score group. This demonstrated that the effect of immune therapy relied on the tumor immune microenvironment. The malignant phenotypes of cancers are determined not only by the intrinsic properties of cancer cells, but also by components of the TME (39). In melanoma, tumor stage, tissue site, ulceration, thickness, and patient age and sex are associated with immune infiltration (40). Our result is in accordance with those of a previous study. Further, stratified survival analysis showed that in all primary clinical characteristics, those with high ICI scores had superior prognosis to those with low scores. In the Clark level, Breslow depth, and ulceration, three tumor-specific factors, the ICI score also robustly predicted the clinical benefit of immune therapy (41, 42). Collectively, these findings support that the ICI score is an independent prognostic biomarker. There are some limitations to the study. As the clinical information in the datasets had limited information on surgery and radiation therapy, we were unable to include these two clinical characteristics in the assessment of the predictive value of the ICI score. More clinical data was needed to support the current conclusions.

In summary, we analyzed the immune microenvironment landscape and developed an ICI score for predicting survival and immune therapy benefit in patients with melanoma, by assessing the immune microenvironment. Our results will facilitate understanding of the melanoma tumor microenvironment and provide a new immune therapy strategy.

DATA AVAILABILITY STATEMENT

The datasets presented in this study can be found in online repositories. The names of the repository/repositories and accession number(s) can be found in the article/ **Supplementary Material**.

AUTHOR CONTRIBUTIONS

Concept and Design: DL. Data collection, Analysis: DL, XY. Drafting: DL, XY. Revising: DL, XY. Supervision for the study:

XW. All authors contributed to the article and approved the submitted version.

FUNDING

This work was supported by the National Natural Science Foundation of China (81473441).

SUPPLEMENTARY MATERIAL

The Supplementary Material for this article can be found online at: https://www.frontiersin.org/articles/10.3389/fimmu.2021.663495/full#supplementary-material

Supplementary Figure 1 | (A) Overview of study design. **(B–E)** Consensus matrixes (K=3-6) of ICI cluster for all melanoma sample. **(F)** Unsupervised clustering heatmap of immune cells infiltration for TCGA cohort. Rows represent tumor-infiltrating immune cells, and columns represent samples.

Supplementary Figure 2 | (A–D) Consensus matrixes (K=3-6) of gene cluster for all melanoma sample. **(E)** The box plot of immune activity related signature genes expression (CXCL9, CXCL10, TNF, IFNG, CD8A, GZMA, GZMB, PRF1) between gene cluster A-C, ****P<0.0001. **(F)** The box plot of immune checkpoint signature genes expression (CTLA4, PDCD1, PDCD1LG2, LAG3) between gene cluster A-C, ****P<0.0001.

Supplementary Figure 3 | Kaplan-Meier curves of overall survival for high and low ICI score cluster in each datasets. **(A)**, GSE19234; **(B)**, GSE45617; **(C)**, GSE54467; **(D)**, GSE59455; **(E)**, GSE69504.

Supplementary Figure 4 | Systematic Comparision. **(A)** Kaplan-Meier curve and ROC curve of INF model in GSE19423 cohort. **(B)** Kaplan-Meier curve and ROC curve of INF model in GSE78220 cohort. **(C)** Kaplan-Meier curve and ROC curve of INF model in CA209038 cohort. **(D)** Kaplan-Meier curve and ROC curve of HNSC model in GSE19423 cohort. **(E)** Kaplan-Meier curve and ROC curve of HNSC model in GSE78220 cohort. **(F)** Kaplan-Meier curve and ROC curve of HNSC model in CA209038 cohort. **(G)** Kaplan-Meier curve and ROC curve of ICI score in GSE22154 cohort.

Supplementary Figure 5 | The box plot of immune cells fraction in ICI cluster A-C estimated by xCell Algorithm.

REFERENCES

1. Siegel RL, Miller KD, Jemal A. Cancer Statistics, 2020. *CA Cancer J Clin* (2020) 70(1):7–30. doi: 10.3322/caac.21590
2. Ballotti R, Cheli Y, Bertolotto C. The Complex Relationship Between MITF and the Immune System: A Melanoma ImmunoTherapy (Response) Factor? *Mol Cancer* (2020) 19(1):170. doi: 10.1186/s12943-020-01290-7
3. Gide TN, Wilmott JS, Scolyer RA, Long GV. Primary and Acquired Resistance to Immune Checkpoint Inhibitors in Metastatic Melanoma. *Clin Cancer Res* (2018) 24(6):1260–70. doi: 10.1158/1078-0432.CCR-17-2267
4. Pietrantonio F, Randon G, Di Bartolomeo M, Luciani A, Chao J, Smyth EC, et al. Predictive Role of Microsatellite Instability for PD-1 Blockade in Patients With Advanced Gastric Cancer: A Meta-Analysis of Randomized Clinical Trials. *ESMO Open* (2021) 6(1):100036. doi: 10.1016/j.esmoop.2020.100036
5. Yan J, Wu X, Yu J, Zhu Y, Cang S. Prognostic Role of Tumor Mutation Burden Combined With Immune Infiltrates in Skin Cutaneous Melanoma Based on Multi-Omics Analysis. *Front Oncol* (2020) 10:570654. doi: 10.3389/fonc.2020.570654
6. Fukumoto T, Lin J, Fatkhutdinov N, Liu P, Somasundaram R, Herlyn M, et al. Arid2 Deficiency Correlates With the Response to Immune Checkpoint Blockade in Melanoma. *J Invest Dermatol* (2020) S0022-202X(20)32396-4. doi: 10.1016/j.jid.2020.11.026
7. Shklovskaya E, Lee JH, Lim SY, Stewart A, Pedersen B, Ferguson P, et al. Tumor MHC Expression Guides First-Line Immunotherapy Selection in Melanoma. *Cancers (Basel)* (2020) 12(11):3374–87. doi: 10.3390/cancers12113374
8. Zeng Y, Zeng Y, Yin H, Chen F, Wang Q, Yu X, et al. Exploration of the Immune Cell Infiltration Related Gene Signature in the Prognosis of Melanoma. *Aging (Albany NY)* (2021) 13(3):3459–82. doi: 10.18632/aging.202279
9. Camisaschi C, Vallacchi V, Castelli C, Rivoltini L, Rodolfo M. Immune Cells in the Melanoma Microenvironment Hold Information for Prediction of the Risk of Recurrence and Response to Treatment. *Expert Rev Mol Diagn* (2014) 14(6):643–6. doi: 10.1586/14737159.2014.928206
10. Binnewies M, Roberts EW, Kersten K, Chan V, Fearon DF, Merad M, et al. Understanding the Tumor Immune Microenvironment (TIME) for Effective Therapy. *Nat Med* (2018) 24(5):541–50. doi: 10.1038/s41591-018-0014-x
11. Kato J, Uhara H. Immunotherapy for Advanced Melanoma: Current Situation in Japan. *Jpn J Clin Oncol* (2021) 51(1):3–9. doi: 10.1093/jjco/hyaa188
12. Nakamura Y, Zhenjie Z, Oya K, Tanaka R, Ishitsuka Y, Okiyama N, et al. Poor Lymphocyte Infiltration to Primary Tumors in Acral Lentiginous Melanoma and Mucosal Melanoma Compared to Cutaneous Melanoma. *Front Oncol* (2020) 10:524700. doi: 10.3389/fonc.2020.524700
13. de Azevedo RA, Shoshan E, Whang S, Markel G, Jaiswal AR, Liu A, et al. MIF Inhibition as a Strategy for Overcoming Resistance to Immune Checkpoint Blockade Therapy in Melanoma. *Oncoimmunology* (2020) 9(1):1846915. doi: 10.1080/2162402X.2020.1846915
14. Thomas NE, Busam KJ, From L, Kricker A, Armstrong BK, Anton-Culver H, et al. Tumor-Infiltrating Lymphocyte Grade in Primary Melanomas is Independently Associated With Melanoma-Specific Survival in the Population-Based Genes, Environment and Melanoma Study. *J Clin Oncol* (2013) 31(33):4252–9. doi: 10.1200/JCO.2013.51.3002
15. Zhang X, Shi M, Chen T, Zhang B. Characterization of the Immune Cell Infiltration Landscape in Head and Neck Squamous Cell Carcinoma to Aid Immunotherapy. *Mol Ther Nucleic Acids* (2020) 22:298–309. doi: 10.1016/j.omtn.2020.08.030
16. Newman AM, Liu CL, Green MR, Gentles AJ, Feng W, Xu Y, et al. Robust Enumeration of Cell Subsets From Tissue Expression Profiles. *Nat Methods* (2015) 12(5):453–7. doi: 10.1038/nmeth.3337
17. Yoshihara K, Shahmoradgoli M, Martinez E, Vegesna R, Kim H, Torres-Garcia W, et al. Inferring Tumour Purity and Stromal and Immune Cell Admixture From Expression Data. *Nat Commun* (2013) 4:2612. doi: 10.1038/ncomms3612
18. Zhao Y, Ning Y, Zhang F, Ding M, Wen Y, Shi L, et al. PCA-Based GRS Analysis Enhances the Effectiveness for Genetic Correlation Detection. *Brief Bioinform* (2019) 20(6):2291–8. doi: 10.1093/bib/bby075
19. Sotiriou C, Wirapati P, Loi S, Harris A, Fox S, Smeds J, et al. Gene Expression Profiling in Breast Cancer: Understanding the Molecular Basis of Histologic Grade to Improve Prognosis. *J Natl Cancer Inst* (2006) 98(4):262–72. doi: 10.1093/jnci/djj052
20. Tacastacas JD, Bray J, Cohen YK, Arbesman J, Kim J, Koon HB, et al. Update on Primary Mucosal Melanoma. *J Am Acad Dermatol* (2014) 71(2):366–75. doi: 10.1016/j.jaad.2014.03.031
21. Luke JJ, Triozzi PL, McKenna KC, Van Meir EG, Gershenwald JE, Bastian BC, et al. Biology of Advanced Uveal Melanoma and Next Steps for Clinical Therapeutics. *Pigment Cell Melanoma Res* (2015) 28(2):135–47. doi: 10.1111/pcmr.12304
22. Cohen CJ, Gartner JJ, Horovitz-Fried M, Shamalov K, Trebska-McGowan K, Bliskovsky VV, et al. Isolation of Neoantigen-Specific T Cells From Tumor and Peripheral Lymphocytes. *J Clin Invest* (2015) 125(10):3981–91. doi: 10.1172/JCI82416
23. Yarchoan M, Albacker LA, Hopkins AC, Montesion M, Murugesan K, Vithayathil TT, et al. Pd-L1 Expression and Tumor Mutational Burden are Independent Biomarkers in Most Cancers. *JCI Insight* (2019) 4(6)e126908. doi: 10.1172/jci.insight.126908
24. Ayers M, Lunceford J, Nebozhyn M, Murphy E, Loboda A, Kaufman DR, et al. IFN-Gamma-Related mRNA Profile Predicts Clinical Response to PD-1 Blockade. *J Clin Invest* (2017) 127(8):2930–40. doi: 10.1172/JCI91190

25. Marzagalli M, Ebelt ND, Manuel ER. Unraveling the Crosstalk Between Melanoma and Immune Cells in the Tumor Microenvironment. *Semin Cancer Biol* (2019) 59:236–50. doi: 10.1016/j.semcancer.2019.08.002
26. Hodi FS, O'Day SJ, McDermott DF, Weber RW, Sosman JA, Haanen JB, et al. Improved Survival With Ipilimumab in Patients With Metastatic Melanoma. *N Engl J Med* (2010) 363(8):711–23. doi: 10.1056/NEJMoa1003466
27. Wolchok JD, Kluger H, Callahan MK, Postow MA, Rizvi NA, Lesokhin AM, et al. Nivolumab Plus Ipilimumab in Advanced Melanoma. *N Engl J Med* (2013) 369(2):122–33. doi: 10.1056/NEJMoa1302369
28. Powles T, Duran I, van der Heijden MS, Loriot Y, Vogelzang NJ, De Giorgi U, et al. Atezolizumab Versus Chemotherapy in Patients With Platinum-Treated Locally Advanced or Metastatic Urothelial Carcinoma (Imvigor211): A Multicentre, Open-Label, Phase 3 Randomised Controlled Trial. *Lancet* (2018) 391(10122):748–57. doi: 10.1016/S0140-6736(17)33297-X
29. Lee N, Zakka LR, Mihm MC Jr., Schatton T. Tumour-Infiltrating Lymphocytes in Melanoma Prognosis and Cancer Immunotherapy. *Pathology* (2016) 48(2):177–87. doi: 10.1016/j.pathol.2015.12.006
30. Maibach F, Sadozai H, Seyed Jafari SM, Hunger RE, Schenk M. Tumor-Infiltrating Lymphocytes and Their Prognostic Value in Cutaneous Melanoma. *Front Immunol* (2020) 11:2105. doi: 10.3389/fimmu.2020.02105
31. Chan TA, Yarchoan M, Jaffee E, Swanton C, Quezada SA, Stenzinger A, et al. Development of Tumor Mutation Burden as an Immunotherapy Biomarker: Utility for the Oncology Clinic. *Ann Oncol* (2019) 30(1):44–56. doi: 10.1093/annonc/mdy495
32. Chen DS, Mellman I. Elements of Cancer Immunity and the Cancer-Immune Set Point. *Nature* (2017) 541(7637):321–30. doi: 10.1038/nature21349
33. Gajewski TF. The Next Hurdle in Cancer Immunotherapy: Overcoming the Non-T-Cell-Inflamed Tumor Microenvironment. *Semin Oncol* (2015) 42 (4):663–71. doi: 10.1053/j.seminoncol.2015.05.011
34. Gajewski TF, Woo SR, Zha Y, Spaapen R, Zheng Y, Corrales L, et al. Cancer Immunotherapy Strategies Based on Overcoming Barriers Within the Tumor Microenvironment. *Curr Opin Immunol* (2013) 25(2):268–76. doi: 10.1016/j.coi.2013.02.009
35. Lutz ER, Wu AA, Bigelow E, Sharma R, Mo G, Soares K, et al. Immunotherapy Converts Nonimmunogenic Pancreatic Tumors Into Immunogenic Foci of Immune Regulation. *Cancer Immunol Res* (2014) 2(7):616–31. doi: 10.1158/2326-6066.CIR-14-0027
36. Gajewski TF, Corrales L, Williams J, Horton B, Sivan A, Spranger S, et al. Cancer Immunotherapy Targets Based on Understanding the T Cell-Inflamed Versus non-T Cell-Inflamed Tumor Microenvironment. *Adv Exp Med Biol* (2017) 1036:19–31. doi: 10.1007/978-3-319-67577-0_2
37. McGranahan N, Furness AJ, Rosenthal R, Ramskov S, Lyngaa R, Saini SK, et al. Clonal Neoantigens Elicit T Cell Immunoreactivity and Sensitivity to Immune Checkpoint Blockade. *Science* (2016) 351(6280):1463–9. doi: 10.1126/science.aaf1490
38. Ascierto PA, Lewis KD, Di Giacomo AM, Demidov L, Mandala M, Bondarenko I, et al. Prognostic Impact of Baseline Tumour Immune Infiltrate on Disease-Free Survival in Patients With Completely Resected, BRAF(v600) Mutation-Positive Melanoma Receiving Adjuvant Vemurafenib. *Ann Oncol* (2020) 31(1):153–9. doi: 10.1016/j.annonc.2019.10.002
39. Pozniak J, Nsengimana J, Laye JP, O'Shea SJ, Diaz JMS, Droop AP, et al. Genetic and Environmental Determinants of Immune Response to Cutaneous Melanoma. *Cancer Res* (2019) 79(10):2684–96. doi: 10.1158/0008-5472.CAN-18-2864
40. Wang P, Zhang X, Sun N, Zhao Z, He J. Comprehensive Analysis of the Tumor Microenvironment in Cutaneous Melanoma Associated With Immune Infiltration. *J Cancer* (2020) 11(13):3858–70. doi: 10.7150/jca.44413
41. In 't Hout FE, Haydu LE, Murali R, Bonenkamp JJ, Thompson JF, Scolyer RA. Prognostic Importance of the Extent of Ulceration in Patients With Clinically Localized Cutaneous Melanoma. *Ann Surg* (2012) 255(6):1165–70. doi: 10.1097/SLA.0b013e31824c4b0b
42. Lyth J, Hansson J, Ingvar C, Mansson-Brahme E, Naredi P, Stierner U, et al. Prognostic Subclassifications of T1 Cutaneous Melanomas Based on Ulceration, Tumour Thickness and Clark's Level of Invasion: Results of a Population-Based Study From the Swedish Melanoma Register. *Br J Dermatol* (2013) 168(4):779–86. doi: 10.1111/bjd.12095

Conflict of Interest: The authors declare that the research was conducted in the absence of any commercial or financial relationships that could be construed as a potential conflict of interest.

Copyright © 2021 Liu, Yang and Wu. This is an open-access article distributed under the terms of the Creative Commons Attribution License (CC BY). The use, distribution or reproduction in other forums is permitted, provided the original author(s) and the copyright owner(s) are credited and that the original publication in this journal is cited, in accordance with accepted academic practice. No use, distribution or reproduction is permitted which does not comply with these terms.

frontiers in Immunology

ORIGINAL RESEARCH
published: 07 May 2021
doi: 10.3389/fimmu.2021.667177

CXCL8 Associated Dendritic Cell Activation Marker Expression and Recruitment as Indicators of Favorable Outcomes in Colorectal Cancer

Enhao Li[1†], Xiaobao Yang[1†], Yuzhang Du[1†], Guanzheng Wang[1], David W. Chan[2], Di Wu[1], Peiqing Xu[1], Peihua Ni[1], Dakang Xu[1] and Yiqun Hu[1*]*

[1] Faculty of Medical Laboratory Science, Ruijin Hospital, School of Medicine, Shanghai Jiao Tong University, Shanghai, China, [2] Department of Obstetrics & Gynaecology, LKS Faculty of Medicine, The University of Hong Kong, Hong Kong, Hong Kong

Accumulating evidence suggests that tumor-infiltrating immune cells (TICs) in the tumor microenvironment (TME) serve as promising therapeutic targets. CXCL8 (IL-8) may also be a potential therapeutic target in cancer. CXCL8 is a potent chemotactic factor for neutrophils, myeloid-derived suppressor cells (MDSCs) and monocytes, which are considered immunosuppressive components in cancer-bearing hosts. Here, we identified the TME-related gene CXCL8 in a high-ImmuneScore population that contributed to better survival in colorectal cancer (CRC) patients from The Cancer Genome Atlas (TCGA) database. An integrated gene profile and functional analysis of TIC proportions revealed that the dendritic cell (DC) activation markers CD80, CD83, and CD86 were positively correlated with CXCL8 expression, suggesting that CXCL8 may be functional as antitumor immune response status in the TME. The gene signature was further validated in independent GSE14333 and GSE38832 cohorts from the Gene Expression Omnibus (GEO). To test the differential contributions of immune and tumor components to progression, three CRC cell lines, CT26, MC38 and HCT116, were used. *In vitro* results suggested no significant growth or survival changes following treatment with an inhibitor of the CXCL8 receptor (CXCR1/2) such as reparixin or danirixin. *In vivo* treatment with danirixin (antagonists of CXCR2) promoted tumor progression in animal models established with CT26 cells. CXCR2 antagonism may function *via* an immune component, with CXCR2 antagonist treatment in mice resulting in reduced activated DCs and correlating with decreased Interferon gamma (IFN-γ) or Granzyme B expressed $CD8^+$ T cells. Furthermore, CXCL8 induced DC migration in transwell migration assays. Taken together, our data suggested that targeting the CXCL8-CXCR2 axis might impede DC activation or recruitment, and this axis could be considered a favorable factor rather than a target for critical antitumor effects on CRC.

Keywords: colorectal cancer, CXCL8-CXCR1/2, dendritic cell (DC), immune profiling, therapeutics

OPEN ACCESS

Edited by:
Peng Qu,
National Institutes of Health (NIH), United States

Reviewed by:
Emilie Picard,
Health Sciences North Research Institute (HSNRI), Canada
Mingxiao Feng,
Johns Hopkins University, United States
Meng Xu,
Carnegie Mellon University, United States

****Correspondence:***
Dakang Xu
dakang_xu@163.com
Yiqun Hu
ichunhu@126.com

†These authors have contributed equally to this work

Specialty section:
This article was submitted to Cancer Immunity and Immunotherapy, a section of the journal Frontiers in Immunology

Received: *12 February 2021*
Accepted: *21 April 2021*
Published: *07 May 2021*

Citation:
Li E, Yang X, Du Y, Wang G, Chan DW, Wu D, Xu P, Ni P, Xu D and Hu Y (2021) CXCL8 Associated Dendritic Cell Activation Marker Expression and Recruitment as Indicators of Favorable Outcomes in Colorectal Cancer. Front. Immunol. 12:667177. doi: 10.3389/fimmu.2021.667177

INTRODUCTION

Colorectal cancer (CRC) is the second most commonly diagnosed malignant tumor worldwide (1). CRC is usually characterized by a lengthy and very complicated process, including multiple steps leading to the normal epithelium's malignant transformation into cancer cells. It usually involves numerous genetic changes that lead to multiple phenotypic changes (2). In addition, chronic inflammation contributes significantly to tumor formation and progression. Inflammation seems to be a key process that mediates the relationship and dual functions of cancer cells and immune cells in the tumor microenvironment (TME). Current studies have evaluated the expression of various cytokines, chemokines and their receptors in CRC (3). Many studies have aimed to delineate the differential roles of cytokines, chemokines, and the TME in CRC relative to these components' antitumor status through evaluation of subsets of immune cells.

Chemokines are signaling proteins secreted by cells that are crucial for mediating the recruitment of immune cells to inflammation sites. Chemotaxis involves the coordination of cells expressing appropriate chemokine receptors that can migrate along with chemokine concentration gradient, thereby promoting the localization of individual cells to specific tissues, such as tumor sites (4). Chemokines have dual functions: in T-cell-mediated reaction with tumor cells that play as antitumor immune responses, and in recruiting neutrophils, myeloid-derived suppressor cells (MDSCs) and monocytes to play immunosuppressive roles to promote tumor progression (4). C-X-C motif chemokine 8 (CXCL8), also known as interleukin 8 (IL-8), is mainly produced by macrophages. Furthermore, it is primarily responsible for neutrophil chemotaxis during the inflammatory process (5). CXCL8 is a chemokine whose signal transduction is mediated by the extracellular binding of two G-protein coupled receptors (GPCR), acting through CXC chemokine receptor type 1 (CXCR1) and CXC chemokine receptor type 2 (CXCR2) (6). The interaction between CXCL8 and CXCR1/2 regulates the trafficking of cells for cancer progression in the TME. Tumor-associated macrophages (TAMs) also express CXCR1 and CXCR2 (6), which led the CXCL8-CXCR1/2 axis to show the critical involvement for recruiting TAM to the TME and to play a crucial role in tumor immune escape (7). The CXCL8-CXCR1/2 interaction also regulates the processes of angiogenesis, tumor growth, proliferation as well as the survival of malignant cells (5). Numerous studies have shown that CXCL8 is expressed on endothelial cells, tumor-related macrophages and cancer cells, including CRC cells (8). In the sight of the clinical significance and biological function of the CXCL8-CXCR1/2 signal transduction axis in cancer, it has been suggested that CXCL8 and its receptors are considered as attractive targets for cancer treatment (6).

Overexpression of CXCL8 promotes the proliferation, migration and invasion of CRC cells. It is also closely related to CRC angiogenesis, metastasis, poor prognosis and poor disease-free survival (9). On the other hand, high expression of CXCL8 may protect against CRC liver metastasis, producing a good prognosis (10). Objectively, the role of CXCL8 is still controversial. This study confirms that CXCL8 is related to prognosis and suggests that high CXCL8 expression is associated with a better prognosis than low expression (11). However, there is controversy regarding the relevance of CXCL8 in cancer biology, which led us to investigate further whether chemokines in the CXCL8-CXCR1/2 signaling axis have a favorable role in the antitumor immune function or promote protumor behaviors.

Dendritic cells (DCs) are specialized antigen-presenting cells responsible for activating T cells, thereby coordinating the antitumor response (12). DC activation begins with taking up the antigens and migrating from peripheral tissues to the lymph organs. During antigen presentation, DCs upregulate the costimulatory receptor molecules CD86, CD80 and CD83 on their plasma membrane. CD86 is expressed during the early stages of DC activation. Besides, CD80 and CD83 are upregulated in activated DCs. Those makers have been established as hallmarks of DC activation during immune responses (13). DC activation is a crucial factor in the effective activation of T cells (14), whose various inflammatory mediators trigger in response to immune responses. However, the differential kind of specific inflammatory mediators and cytokines and chemokines correlated with DC activation in CRC are still unknown.

The immune and stromal classification of CRC can be linked to the molecular subtypes relevant to precision immunotherapy. In the current study, using the ESTIMATE algorithm to quantify the immune and stromal cellular components in tumors, we characterized the TME-related genes in CRC by functional enrichment analysis from CRC tissue specimens in The Cancer Genome Atlas (TCGA) database. We further identified that the TME-related gene CXCL8 and a high ImmuneScore contributed to better survival in CRC patients from the TCGA database. An integrated gene profile and functional analysis of tumor-infiltrating immune cell (TIC) proportions revealed that DC activation markers (CD80, CD83, CD86) were positively correlated with CXCL8 expression. Interestingly, we also identified the TME-related gene CXCL8 as contributing to better survival in CRC patients. Then, we used a small-molecule pharmacologic CXCR1/2 antagonist to block the CXCL8 receptor in murine tumor models established with CT26 or MC38 CRC cell to determine the effect of tumor-specific CXCL8-CXCR1/2 signaling impact on tumor behavior. In addition, we also investigated the role of host immune response by the therapeutic effects mediated through CXCR1/2 antagonism.

MATERIALS AND METHODS

Gene Expression Profile Data and Clinical Parameters

The transcriptome of RNA-seq data and clinical parameters of CRC cases (normal samples, 41 cases; tumor samples, 473 cases) were downloaded from The Cancer Genome Atlas Program (TCGA) repository of the National Cancer Institute (https://cancergenome.nih.gov/). The data parameters were as follows: primary site (colon), data category with transcriptome profiling with gene expression and quantification with FPKM and counts, experimental strategy with RNA-Seq analysis and workflow type

with HTSeq-FPKM and HTSeq-Counts. Default settings were used for the other filters.

In order to test and verify the discovery in the TCGA cohort, we downloaded GSE14333 and GSE38832 from the Gene Expression Omnibus (GEO) (https://www.ncbi.nlm.nih.gov/geo/). Expression series matrix files of both datasets were based on GPL570. The former included 290 samples of primary colorectal cancer patients, while the latter had expression data of 122 human samples. To get a larger size of samples, two cohorts were combined for analyses.

Identification of Differentially Expressed Genes (DEGs) Between Tumor and Normal Tissues

The "edgeR" (15) R package (version 3.30.3) of the Bioconductor project in R software (version 4.0.2) was applied to discover the differentially expressed genes (DEGs). The genes expression with |log2 fold change (FC)| ≥3 and false discovery rate (FDR) <0.05 were considered to be significantly differentially expressed between tumor and normal tissues.

Kyoto Encyclopedia of Gene and Genomes (KEGG) Pathway Enrichment Analysis

The KEGG pathway enrichment analysis was completed by the Database for Annotation, Visualization and Integrated Discovery (DAVID) database (http://david.ncifcrf.gov, version 6.8). Pathways with p Values <0.05 were considered statistically significant.

Survival Test of Enriched KEGG Pathways Test

"GSVA" R package (16) (version 1.36.2) was applied to calculate single-sample GSEA (ssGSEA) scores of each pathway in each sample. The ssGSEA scores were used for the survival test of each pathway.

Prediction of Stromal and Immune Components in Tumor Tissues

The ESTIMATE algorithm in the "estimate" R package (version 1.0.13) of R language version 4.0.2 was used to estimate the proportions of immune and stromal cellular components in the TME for each sample. A higher score estimated by the ImmuneScore or StromalScore indicated a larger number of immune or matrix cellular components in the TME. The ESTIMATE score was calculated as the sum of combination the ImmuneScore and StromalScore, representing the combined proportions of these two components in the TME (17).

Identification of Differentially Expressed Genes (DEGs) in CRC

473 tumor tissue samples were divided into high-score and low-score groups based on separate comparison of the ImmuneScore and StromalScore to 0. The "edgeR" R package of the Bioconductor project of R software was applied to identify DEGs. The genes expression with a |log2 fold change (FC)| ≥1 and false discovery rate (FDR) <0.05 were considered to be significantly differentially expressed.

Fraction of Tumor-Infiltrating Immune Cells (TICs)

Levels of immune cells infiltrating tumors were evaluated by CIBERSORT (18) (http://cibersort.stanford.edu/). As samples with a p Value >0.05 were ignored when analyzing TICs, 208 statistically significant samples were used for analysis.

Cell Lines and Cell Culture

The colon carcinoma cell lines: MC38 Cell Line derived from C57BL6 murine colon adenocarcinoma cells, and CT26 is a murine colorectal carcinoma cell line from a BALB/c mouse. HCT116 is a human colorectal carcinoma cell line. All cells were cultured in RPMI 1640 with 10% FBS and 1% Penicillin-Streptomycin and were used within 10 generations. Mycoplasma contamination testing was performed to confirm that no mycoplasma contamination was present. Cells were cultured at 37°C with 5% CO_2 under humidified conditions.

Mice and Tumor Models

C57BL/6 and BALB/c mice were purchased from Charles River (Beijing, China). A total of 1×10^6 CT26 or MC38 cells in 200 µl of PBS were implanted subcutaneously into the right flank region of each 6- to 8-week-old Balb/c (for CT26) or C57BL/6 (for MC38) mouse on day 0, and the treatment started on the same day after injection of tumor cells. Reparixin (HY-15251) and danirixin (HY-19768) were purchased from MedChem Express (MCE, NJ, USA) and dissolved in DMSO for storage. Reparixin and danirixin were dissolved in DMSO for storage. Reparixin was injected intraperitoneally at 15 mg/kg dissolved in a mixture of PEG300, Tween 80 and saline. Danirixin dissolved in PEG400 and ddH_2O was administered by oral gavage at 15 mg/kg. All groups were treated every two days until the completion of the study. Tumor volume was measured every two days with a caliper and calculated as $width^2\times length/2$.

Cell Proliferation Assays

The proliferation of CT26, MC38 and HCT116 cells was determined with a Cell Counting Kit-8 (CCK8; Dojindo, Japan) assay. Cells were plated in 96-well plates overnight and then treated with DMSO, reparixin or danirixin for 12, 24, 36, 48, and 60 h (37°C, 5% CO2). Ten microliters of CCK-8 solution were added to each well in the 96 well plates and incubated at 37°C for 1 hour. Cell proliferation was quantified by measuring the absorbance at 450 nm.

Isolation of Immune Cells From Spleen

The mouse spleen was stripped and dipped in PBS solution. Spleen was ground to white through a nylon mesh screen in sterile PBS buffer and then filtrated. The solution was centrifuged at 300g for 5 minutes and the supernatant was discarded. 3ml of red blood cell lysis buffer (C3702, Beyotime, Shanghai, China) was used to lyse erythrocytes. Cells were washed then re-suspended in RPMI 1640 with 10% FBS and 1% Penicillin-Streptomycin. Live cells were counted using trypan blue dye exclusion (Sigma-Aldrich, St. Louis, USA) and diluted to 2×10^6 cells/50uL for further use.

DC Migration Assay

For transwell migration assays, freshly isolated mouse spleen cells were seeded in the upper well of a 24-well transwell plate (pore diameter 5 μm, Corning, NY, USA), which was pre-coated by matrigel (Corning). Lower chambers of the transwell were filled with 600 μl in the absence or presence of 10, 25, 50, 100 ng/ml of CXCL8 (200-08M, PeproTech), or 100ng/ml CXCL7 (300-14, PeproTech) as a negative control. To see whether the CXCR2 inhibitor can inhibit DC migration *in vitro*, 50 ul isolated immune cells from spleen and 25ug/ml danirixin (or vehicle control) were added in the upper chamber, while 600 ul CT26 cell culture supernatant fluids were added in the lower chamber. After 6 hours, the migrated cells were harvested from the lower chamber and further analyzed by flow cytometry.

Flow Cytometry

Tumor tissue was immediately collected on the day when mice were sacrificed. Tumors were minced and digested with collagenase IV (Sigma-Aldrich, 300 U/mL) and a hyaluronidase solution (Sigma-Aldrich, 200 U/mL) in RPMI 1640 medium (Servicebio, Wuhan, China) supplemented with penicillin and streptomycin at 37°C for 1 hour. The cell suspension was centrifuged at 1,200 rpm for 5 min and mechanically dissociated through a nylon mesh filter. The antibodies used included anti-CD45-FITC (109806), anti-CD11c-PECy7 (117318), anti-MHC-II (IA/IE)-BV510 (107635), anti-CD8-PerCP-Cy5.5 (100734), anti-CD3-PE (100220), anti-CD19-APC (152409), anti-IFN-γ-APC (505810) and anti-GzmB-Pacific Blue (515407) purchased from BioLegend (San Diego, CA, USA). The Zombie NIR Fixable Viability Kit (BioLegend) was used to discriminate live and dead cells. To identify apoptotic and necrotic tumor cells after incubated with danirixin or reparixin, a BioLegend FITC Annexin V apoptosis detection kit with propidium iodide (PI) were used according to the manufacturer's protocol. Data were acquired with an LSR-II system (BD Biosciences, Vianen, The Netherlands) and then analyzed with FlowJo software (version V10, Becton Dickinson, Ashland, OR, USA). To ensure single-cell gating, doublets were excluded with FSC-A and FSC-H linearity.

Quantitative Real-Time PCR

Total RNA was extracted by TRIzol reagent (Invitrogen, Carlsbad, CA, USA). The concentration was analyzed by Nanodrop spectrophotometer (Thermo Fisher Scientific, MA, USA). PrimeScript RT Master Mix (TaKaRa, Japan) was used for reverse transcription. Mir-X^{TM} RNA first-strand synthesis kit (TaKaRa) was used for transcribing and then for RNA expression analysis. SYBR Premix Ex Taq (TaKaRa) was used for real-time PCR in a 7900 HT Real-Time PCR system (Applied Biosystems, USA). The expression level of β-actin was used for endogenous control. The expression level was quantified using the 2-ΔΔct method. Primer information is accessible in **Supplementary Table 1**.

Statistical and Survival Analyses

Data were analyzed using R software (version 4.0.2) and GraphPad Prism 8 software. One-way ANOVA and Student t test were used to determine significant differences, and p Values <0.05 were considered significant. Survival analyses were performed to assess the prognostic value of the indexes used in the study. The Kaplan-Meier (K-M) analysis was used to plot survival curves *via* the log-rank test.

RESULTS

Identify Key Genes and Pathways in CRC

In the past few years, cancer's immune classification has provided new ideas for the treatment of patients and prognostic and predictive factors for chemotherapy and immunotherapy (19). CRC has been a paradigmatic tumor for immune classification. We intended to identify the differentially expressed genes (DEGs) between tumor and normal tissues from patients, establish clinically relevant molecular subtypes, and identify significant CRC signatures (20). First, RNA-Seq data from the TCGA database were used to identify DEGs. Eventually, 620 DEGs were found, including 384 upregulated genes and 236 downregulated genes (**Figure 1A**). To explore these genes' potential biological effects, Kyoto Encyclopedia of Genes and Genomes (KEGG) pathway analysis was then conducted using the DEGs from the dataset. KEGG analysis showed that the statistically significant 7 upregulated and 14 downregulated pathways were enriched in the CRC group (**Figures 1B, C**). Then, the total 21 pathways with their ssGSEA scores were further filtered by survival analysis, and two upregulated pathways shown in **Figure 1D** (rheumatoid arthritis and cytokine-cytokine receptor interaction) were statistically significant by survival test. These two pathways were connected by CXCL8, CXCL5, IL11, IL1A and IL23A in PPI network analysis (**Figure 1E**), which was completed by ClueGo (version 2.5.7) in Cytoscape (version 3.7.1). The above results suggested that the highly expressed cytokine and chemokine components in tumors were relevant to prolonged survival in CRC patients.

Identification of CXCL8 as a Key Regulator in Immune-Mediated CRC

To investigate the prognostic value of the estimated proportions of immune and stromal cells in tumors, the ESTIMATE algorithm was employed to estimate the proportions of immune and stromal components in the TME for each sample. Higher scores estimated by the ImmuneScore or StromalScore represented larger amounts of immune or stromal cellular components in the TME. Here, we evaluated the associations of the ImmuneScore and StromalScore with overall survival. CRC patients were split into high- and low-score groups based on the ImmuneScore and StromalScore with a cut-off of 0. A high ImmuneScore value resulted in prolonged survival (**Figure 2A**), while the StromalScore was not related to the overall survival rate (**Figure 2B**), and a total ESTIMATEScore created by combining the ImmuneScore and StromalScore did not contribute to survival rates (**Figure 2C**). Furthermore, a high ImmuneScore was correlated with subset chemokines, including

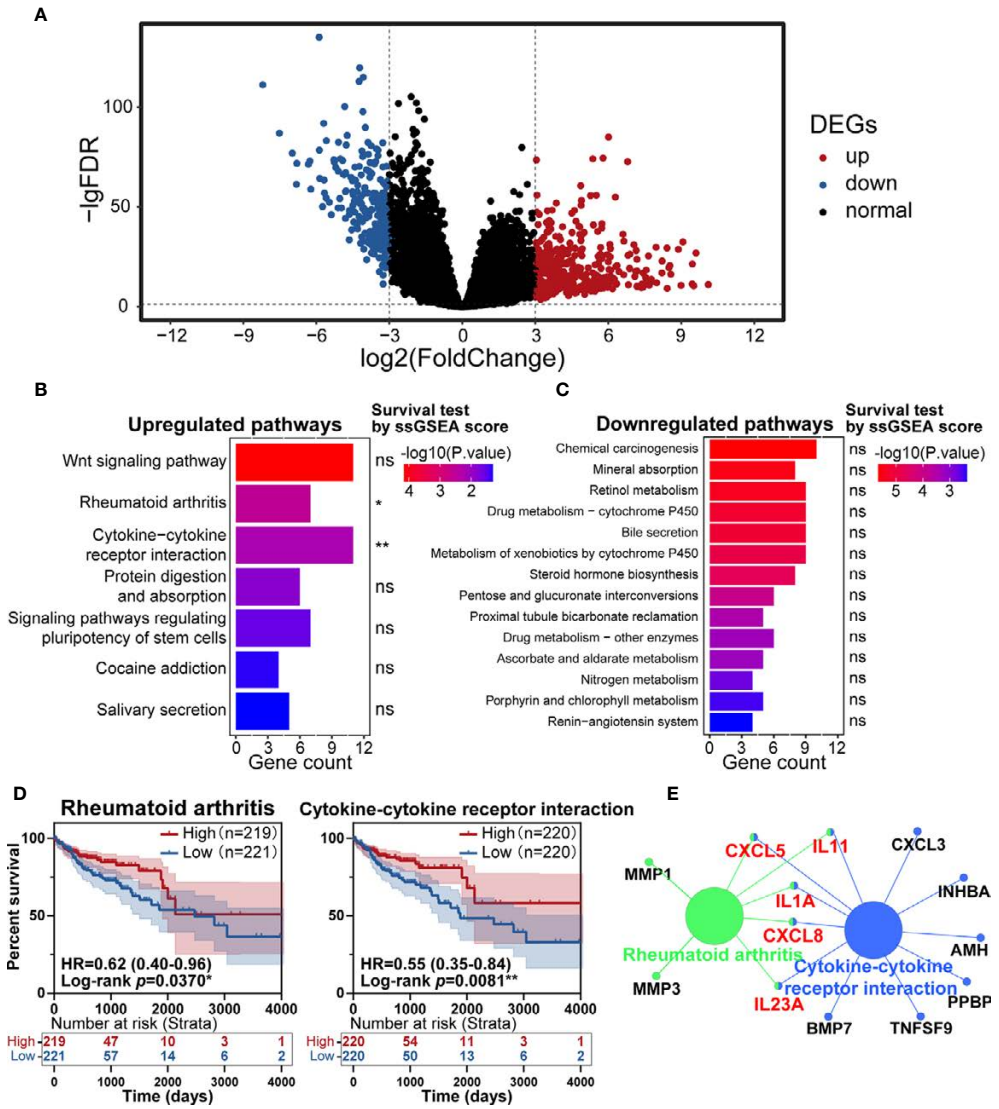

FIGURE 1 | Identification of key pathways in colorectal cancer (CRC). **(A)** Analysis of differentially expressed genes (DEGs) of transcriptome profiling from The Cancer Genome Atlas (TCGA) cohort of CRC patients. **(B, C)** Kyoto Encyclopedia of Genes and Genomes (KEGG) pathway enrichment analysis of the DEGs in the TCGA cohort, with upregulated pathways **(B)** and downregulated pathways **(C)** shown. **(D)** Patients with CRC had significant survival differences between the high and low expression groups for rheumatoid arthritis (p=0.0370) or cytokine-cytokine receptor interaction (p=0.0081) (total patients n=440). **(E)** KEGG pathway enrichment analysis of the genes in the protein-protein interaction (PPI) module. ns: $p > 0.05$, $^{*}p < 0.05$, $^{**}p < 0.01$.

CXCL8 and CXCL5 through heatmap analysis (**Figure 2D**). We further assessed the genes from the rheumatoid arthritis and cytokine-cytokine receptor interaction pathways that were identified earlier (**Figures 1D, E**) to define overlapping subset chemokines that were enriched by ImmuneScore analysis (**Figure 2D**). Interestingly, the results indicated that CXCL8 and CXCL5 were genes in the overlapping enriched pathways (**Figure 2E**). To investigate the prognostic value of CXCL8 and CXCL5, we calculated the survival rates of patients in different subgroups. All tumor samples were divided into two groups based on the median expression of CXCL8 or CXCL5 and compared. High expression of CXCL8 was associated with a better prognosis (**Figure 2F**, p=0.0103). There was no survival advantage associated with CXCL5 expression (**Figure 2G**, p=0.4188). In order to further confirm the prognostic value of CXCL8 we discovered in TCGA cohort, we picked the corresponding probes of CXCL8 (202859_x_at) for survival test in GSE14333 and GSE38832 cohorts, which also showed a better prognosis in patients with higher CXCL8 expression (**Figure 2H**, p=0.0244). These results indicated that CXCL8 in the TME had a positive correlation with CRC patients' overall survival rate.

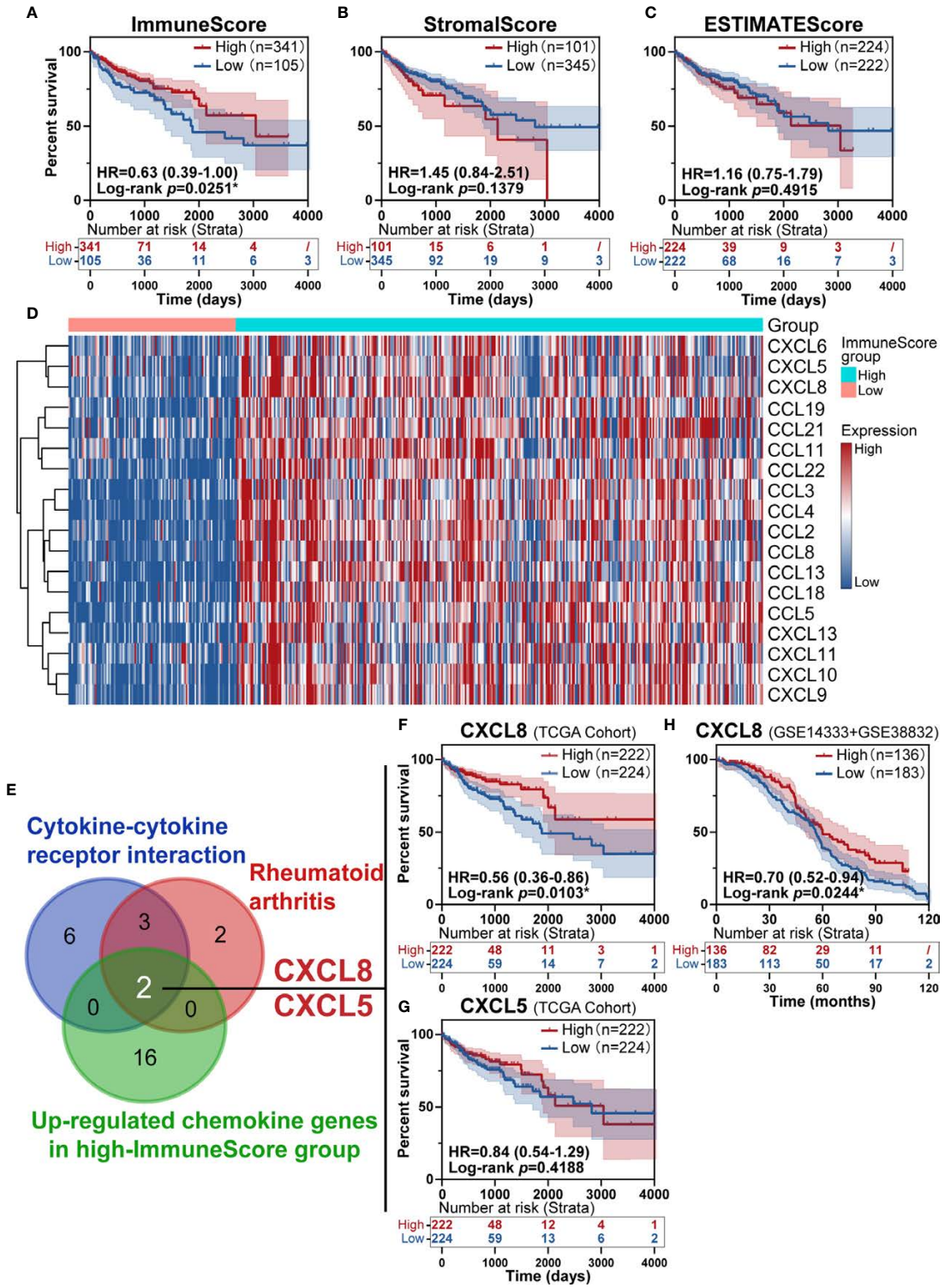

FIGURE 2 | Identification of immune subtype genes. **(A)** Survival analysis of high and low scores for the ImmuneScore. **(B)** Survival analysis of high and low scores for the StromalScore (total patients n=446). **(C)** Survival analysis of high and low ESTIMATEScores. **(D)** Heatmap showed the levels of different chemokines in CRC patients classified into the high and low ImmuneScore groups. **(E)** Venn diagrams for rheumatoid arthritis or cytokine-cytokine receptor interaction pathway after filter survival analysis showing with overlap with upregulated chemokine genes from the high-ImmuneScore group. **(F, G)** The overlapping genes CXCL8 (**F**, p=0.0103) and CXCL5 (**G**, p=0.4188) identified with a K-M survival plot (total patients n=446). **(H)** The survival test for CXCL8 in GSE14333+GSE38832 confirmed the prognostic value of CXCL8 (total patients n=319, p=0.0244). *$p < 0.05$.

Dendritic Cells (DC) Activation Gene Signatures Were Positively Associated With CXCL8 Expression

As CIBERSORT returned the result, we analyzed the difference of cell fraction between CXCL8 high and low group, whose p Value of Student t test <0.05 was considered statistically significant. As shown in **Figure 3A** samples expressing higher CXCL8 had more infiltrated M2 macrophages, activated dendritic cells, activated mast cells, eosinophils, neutrophils and less infiltrated plasma cells, T cells regulatory (Tregs), monocytes, resting dendritic cells, resting mast cells. While MDSCs are known to be recruited by CXCL8, fraction of MDSCs is inaccessible in CIBERSORT algorithm, which limited us to study the potential effect of CXCL8 attracting MDSCs in TME through bioinformatic analyses (4, 18). Furthermore, significant immune cells were further filtered by survival test, in which only activated DCs had prognostic significance (**Figure 3B** and **Supplementary Figure 1**). According to previous studies, the TME in CRC contains a rich cytokine/chemokine milieu regulating tumorigenesis (21). Strikingly, the expression of DC activation gene signatures, such as CD80, CD83, and CD86 was positively correlated with CXCL8 expression (**Figure 3C**). Additionally, the correlation tests in GSE14333 and GSE38832 cohorts showed the similar result that CD80 (1555689_at and 1554519_at), CD83 (204440_at) and CD86 (205685_at and 210895_s_at) expressed higher as CXCL8 expression rose (**Figure 3C**). The estimates of immune cell population abundance across human tumors led us to hypothesize that CXCL8 might promote the recruitment of inflammatory cells, including neutrophils, mast cells, eosinophils, M2 macrophages, and especially activated DC, and thus CXCL8 improve patients' prognosis through the recruitment of DC.

CXCL8 Contributed to DC Recruitment in *Ex Vivo* Experiments

To explore which cytokines/chemokines may contribute to the recruitment of DCs *ex vivo*, we compared the ability of CXCL8 to attract DCs among splenocytes isolated from mice. We also figured out that CXCL7 as an irrelevant chemokine didn't contribute to DC attraction (**Figure 4A**). A significant (p<0.01) enrichment of DC was observed with both low (10 ng/mL) and high doses (100 ng/mL) of CXCL8 treatment using CD11c and MHC-II gating strategies for DCs (**Figure 4A**). Additionally, the results showed a significantly increased recruitment of DCs toward dose dependent manner (**Figure 4B**). Taken together, these results implied a robust association between DC infiltration and CXCL8 expression in CRC patients from (DC) activation gene signatures with CXCL8 expression.

Antagonism of CXCR2 Promotes Tumor Progression *In Vivo*

From the above studies, we found that CXCL8 might affect antitumor activity through DCs. We further investigated whether CXCL8 could regulate tumor progression *in vivo*. Since CXCL8 is a ligand for CXCR1/CXCR2 and their expression levels are related, lack of CXCL8 (IL-8) in the mouse genome has been an essential limiting factor regarding the further investigation of targeting, so we examined the function of the chemokine receptor CXCR1/CXCR2 in two colon tumor models. To determine whether the CXCL8-CXCR1/CXCR2 axis would benefit antitumor activity, we employed a small-molecule antagonist of CXCR1/CXCR2, reparixin, and a small-molecule antagonist of CXCR2, danirixin. Danirixin were found to promote tumor growth in CT26 model, but not reparixin treated mouse in either CT26 or MC38 model (**Figure 5A**). Next, we questioned whether reparixin or danirixin treatment could affect tumor cell proliferation *in vitro*. It has been reported that inhibition of CXCL8 has been found to inhibit the migration of human colon tumor cell line (HCT116 cells) (22), so we selected HCT116 for our *in vitro* study. In CCK-8 experiments, the proliferation of reparixin- and danirixin-treated tumor cells did not change significantly (**Figure 5B**). In addition, reparixin or danirixin treatment did not obviously change the percentage of apoptotic cells (**Figure 5C**). Different immune behaviors found in CT26 and MC38 colon cancer model was mainly caused by higher immune infiltration in CT26 than MC38 (23). CT26 model also provided CXCR2 dependent mediated the trafficking and function of tumor-infiltrating immune cells in the TME (24). Taken together, these results indicated that targeting CXCR2 can promote tumor growth *in vivo* but had little or no direct effect on the proliferation of CRC tumor cells *in vitro*, which may be attributed to the difference between extracellular factors and intracellular factors in the tumor process.

Antagonism of CXCR2 and Reduces DC and $CD8^+$ T Cell Infiltration

Next, we were interested in which CXCL8 influences immune cell subsets in the regulation of antitumor immunity. It has been reported that *vivo* DC vaccine treatment on CT26 mouse, suggested that DC enhanced antitumor activities through the induction of $CD8^+$ T cell and modulation of the tumor microenvironment (25). Using CT26 tumor tissues, we analyzed the DC activation genes by qRT-PCR, and the results supported the relationship between CXCL8 and DCs activation marker in TCGA cohort. As expected, expression of DCs activation genes such as CD54, CD83 and CD86 were declined significantly in the group treated with danirixin in comparison to the untreated group (**Figure 6A**). As expected, the percentage of $CD11c^+$ and $MHC\text{-}II^+$ DCs was significantly decreased in the antagonist groups compared to the control group (**Figure 6B**). To further validate our finding on danirixin inhibit DCs infiltration, transwell migration assays were carried out. Flow cytometric analyses showed a significant decrease of DCs among total splenocytes migrating toward CT26 cell culture supernatant fluids after treated with danirixin (**Figure 6C**). In addition, CXCR2 antagonist treatment reduced the IFN-γ expressing $CD8^+$ T cells (**Figure 6D**), as well as Granzyme B-expressing $CD8^+$ T cells in the TME of tumors generated with CT26 mice (**Figure 6E**). Those subset $CD8^+$ T cells expressing IFN-γ marker associated with Cytotoxic T lymphocytes (CTL), Granzyme B expression also

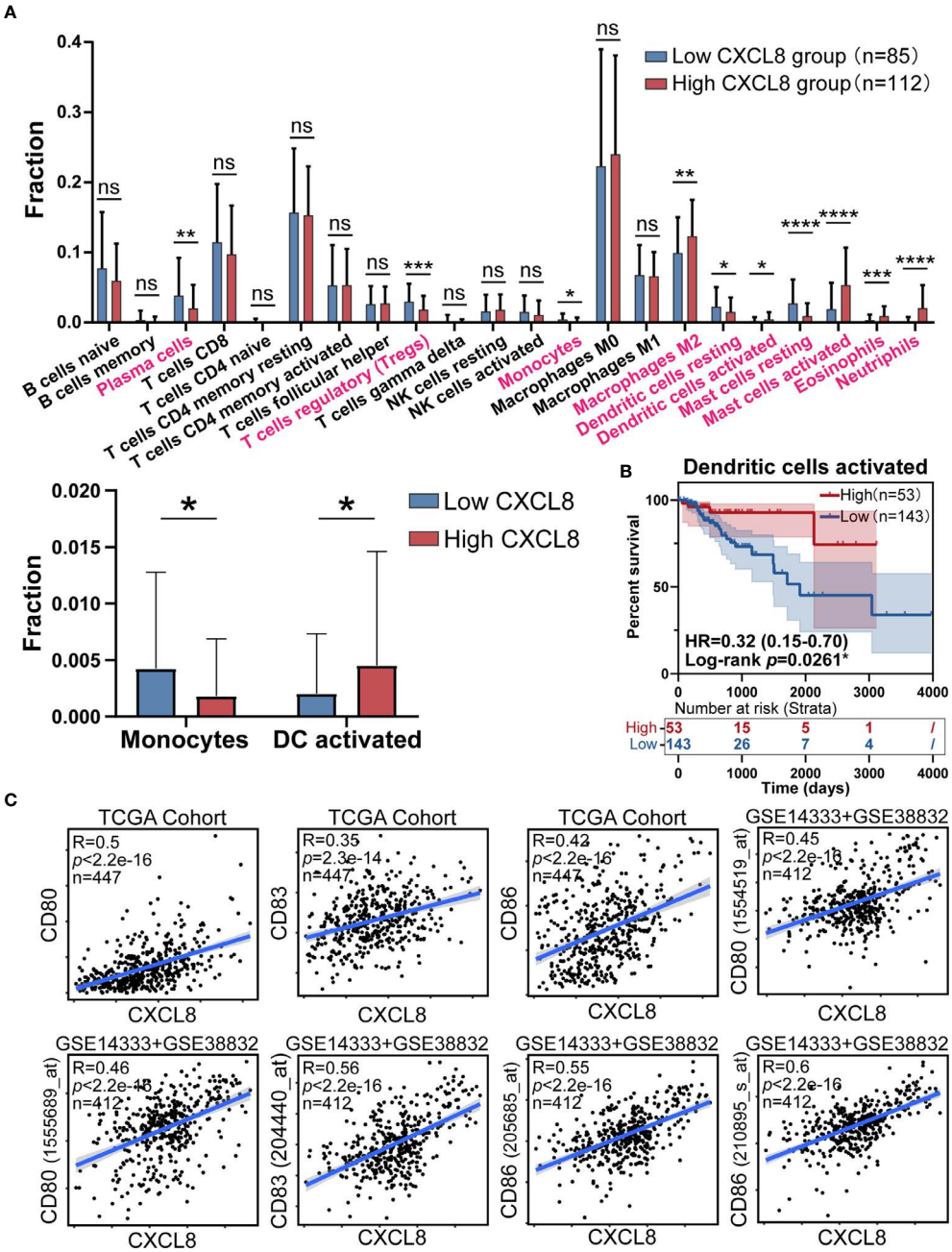

FIGURE 3 | CXCL8 expression correlates with activated dendritic cells and their gene expression. **(A)** Comparison of immune cells fraction estimated by CIBERSORT between CXCL8 high and low group. **(B)** Survival test for more infiltrated activated dendritic cells (total patients n=196) with higher CXCL8 expression **(C)** Scatterplots representing the relationships between the expression of the dendritic cell activation genes CD80, CD83, and CD86 compared with CXCL8 expression in the TCGA cohort and GSE14333 and GSE38832 cohorts. ns: $p > 0.05$, *$p < 0.05$, **$p < 0.01$, ***$p < 0.001$, ****$p < 0.0001$.

serve as a signature of CTL activation, which can directly kill tumor cells and play a very important role in antitumor immunity. Additionally, in the complex tumor micro environment, CXCL8 as a chemokine may act as an antitumor factor through other subtypes of cells. Therefore, we analyse other subtypes of cells such as NK cells and MDSCs in CT26, which didn't show any statistical difference between the treated group and the control group (**Supplementary Figure 4**). Thus, we can conclude that CXCL8-mediated antitumor effect mainly depends on activated dendritic cells instead of other types of immune cells. The results above brought us to the conclusion that antagonizing CXCL8-CXCR2 axis could inhibit the recruitment of DC in CRC tissue. All the

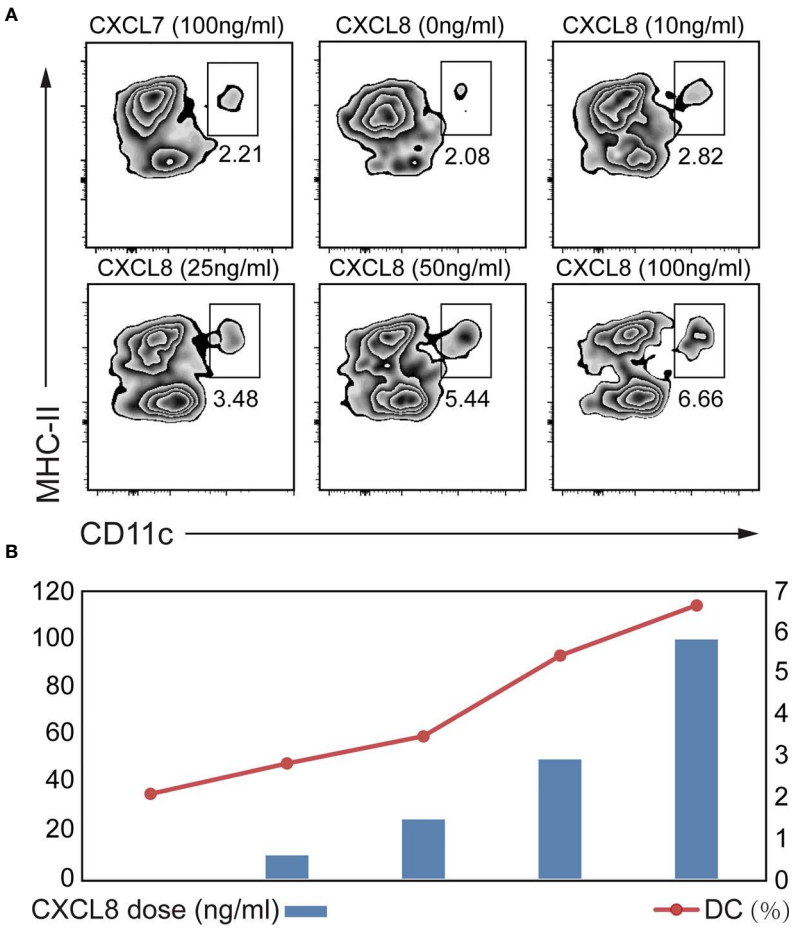

FIGURE 4 | Determination of the CXCL8 chemokine that might attract DC. A transwell migration assay was performed. Splenocytes from mice were exposed to different concentrations of CXCL8 (0, 10, 25, 50 and 100 ng/mL) for 6 hours before quantifying DCs by flow cytometric analysis. **(A, B)** Flow cytometry was performed using CD11c and MHC-II gating strategy **(A)** to quantify DC **(B)**. Significant migration of DCs was observed upon treatment with CXCL8. For each treatment, the populations of DCs in the low- and high-dose groups were compared to the untreated group population.

results collectively indicated that antagonism of CXCR2 could impacted functional $CD8^+$ T cell and DC infiltration into tumor sites in the CRC mouse model, which indicated that these treatments could change the TME in the CRC mouse model into a worse situation.

DISCUSSION

In the era of targeted therapy, especially immunotherapy that relies on the composition of the TME, we are committed to integrating the molecular and immune classification of CRC by solving the problems related to inflammation and the immune cell composition of molecular subtypes of CRC. To achieve this purpose, we applied a computational ESTIMATE algorithm to infer the abundances of immune cell populations and cytokines/chemokines from transcriptomic data. Using this method, we found that a high ImmuneScore value produced better survival. Among the chemokines upregulated in high-ImmuneScore group, CXCL8 had a prognostic value. Afterwards, We first identified that CXCL8 expression was correlated with the DC subtype compared with the other subtypes. CXCL8 was also associated with DC activation and recruitment, which indicated a favorable outcome for CRC. Treatment with a small-molecule antagonist of CXCR1/2, the receptor of CXCL8, was demonstrated to promote tumor progression in animal models established with CT26 cancer cells. Therefore, Targeting CXCL8 and the CXCR2 axis as a therapeutic strategy might impede DC activation or recruitment, which could lead to the opposite effect of antitumor immunity.

A few clinical data have indicated that the elevated levels of CXCL8 in patients' serum or tissues from a cohort study of patients with CRC related to clinical characteristics such as grade, stage and metastasis. CXCL8 is secreted by monocytes and macrophages, which exerts potent angiogenic properties on endothelial cells through interaction with CXCL8 receptors

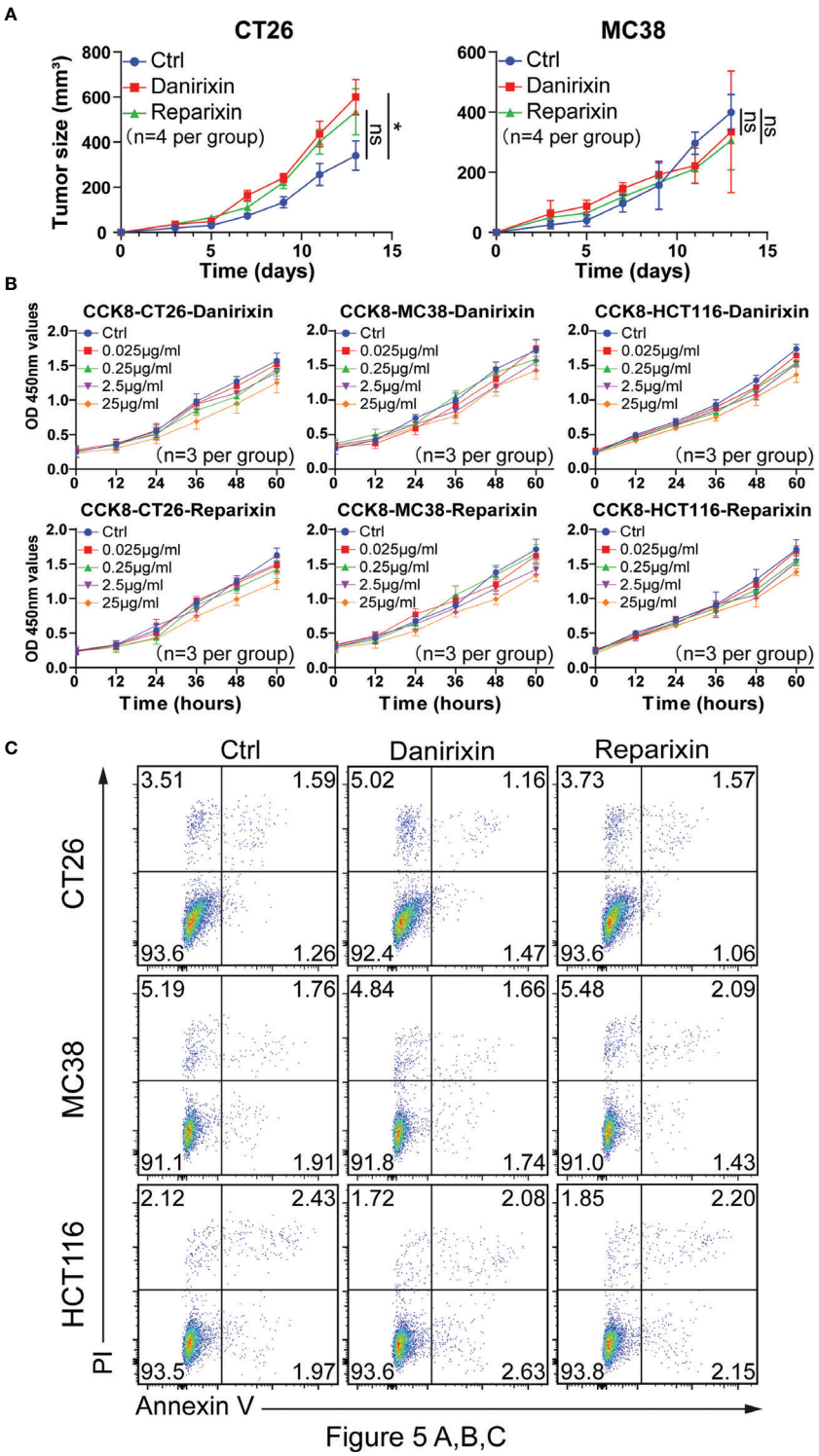

Figure 5 A,B,C

FIGURE 5 | Antagonism of CXCR2 promotes the growth of CRC *in vivo*. **(A)** BALB/c mice were inoculated with CT26 cells, and C57BL/6 mice were inoculated with MC38 cells subcutaneously. The mice had been treated with DMSO (control), reparixin or danirixin for 2 weeks since the day tumor cells were inoculated. Mean and individual tumor volumes were measured every two days (n=4 per group). Tumor growth was evaluated by measuring tumor size and compared statistically by Student t test (*$p < 0.05$, ns: $p > 0.05$). **(B)** Proliferation of CT26, MC38 and HCT116 cells after reparixin or danirixin treatment as determined using a CCK-8 assay. Data are shown as the mean ± SEM. **(C)** Apoptosis of CT26, MC38 and HCT116 cells after reparixin or danirixin treatment as determined using FACS analysis of annexin V staining. All experiments were repeated at least three times.

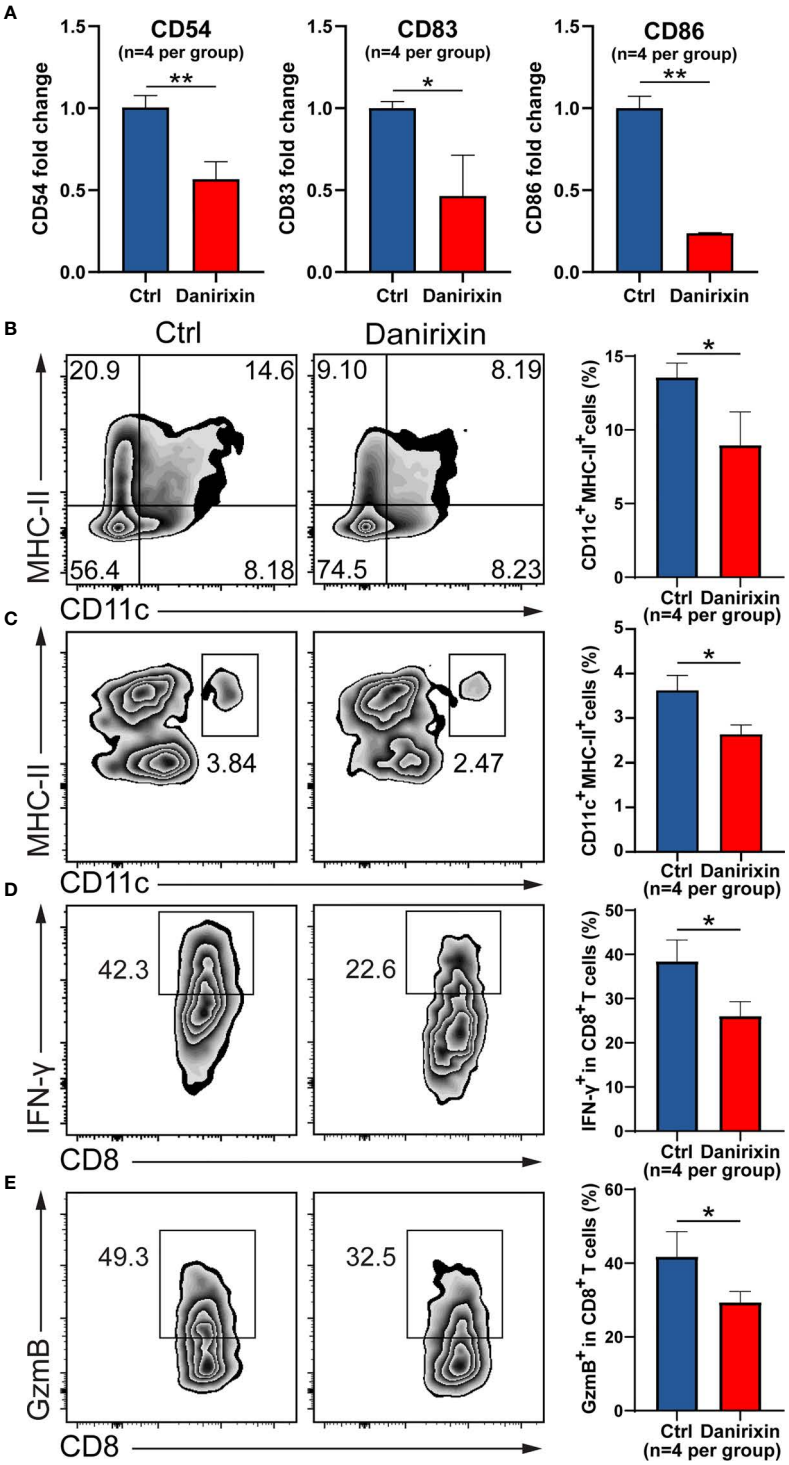

FIGURE 6 | Antagonism of CXCR2 inhibits DC activation and prevents $CD8^+$ T cell and DC infiltration in the TME. **(A–E)** CT26 murine colon tumor cells were subcutaneously injected into BALB/c mice. Since the day tumor cells were inoculated, the mice were treated with DMSO (control) and danirixin for 2 weeks. **(A)** The qRT-PCR analysis showed the statistical significance of three DC activation genes, CD54, CD83, CD86 between the group treated with danirixin and the control group. **(B)** Flow cytometric analysis of the tumor-infiltrated DC ($CD11c^+$ $MHC\text{-}II^+$) proportion in CT26 tumors after treatment with danirixin, **(C)** Flow cytometric analysis of DCs migration with or without danirixin treatment, **(D)** flow cytometry analysis of IFN-γ expressing $CD8^+$ T cell and **(E)** Granzyme B-expressing $CD8^+$ T cells in the TME of tumors generated with CT26 with or without treated with danirixin. Data are shown as the mean ± SEM. Statistical analyses were performed by a pairwise Student t test (n=4 per group). ns: $p > 0.05$, $^*p < 0.05$, $^{**}p < 0.01$.

CXCR1 and CXCR2 for regulating angiogenesis in colorectal cancer (26). Recent studies have documented that CXCL8 promoted migration, invasion, and proliferation of human cancer cells through EMT induction through the PI3K/AKT/NF-κB signaling axis (6, 27). Besides, CXCL8 is a potent chemotactic factor for neutrophils, MDSCs and monocytes, which are considered immunosuppressive components in cancer-bearing hosts (28, 29). All these data have identified CXCL8 as a poor prognostic marker that can be a promising therapeutic target.

However, little was known about the significance of CXCL8 expression correlated to the antitumor immunity induced by functional DCs. DCs are essential cells for generating antitumor immunity, but tumors can disable DCs through either to avoid immune recognition or to disable effector T-cells for escaping immune surveillance. DC activation can be induced and tested by conditioned media from number of colorectal cancer (CRC) cell lines, as reported by Michieisen AJ et al. (30). In a study, tumor conditioned medium (TCM) from a CRC line inhibited five DC markers: MHC-II, CD80, CD83, CD86 and CD54 (31). Increased expression of some activation markers on dendritic cell surface stimulates T cell activation with an antitumor immunity functional response (12). CD83 is one of the most characteristic cell surface markers of fully activated DC, which can enhance the T cell stimulation ability of DC. CD86 and CD80 are also costimulatory molecules binding to T cells while expressing a high level of MHC class II and can present antigens to the T cells (32). Altered MHC II ubiquitination reduces the ability of DC to present antigen in many types of cancer, a mechanism by which tumor cells evade T cell responses (33).

Our study revealed that CXCL8 was a good prognostic biomarker, since it contributed to DCs recruitment and related to DC activation. First, we found that a high ImmuneScore was correlated with prolonged survival, which indicated that favorable factors such as certain cytokines, chemokines and immune cell subsets played important roles in antitumor immunity. Second, CXCL8 was identified as a key regulator of immunity in CRC by many overlapping signaling pathways. Third, CXCL8 was found to have prognostic value compared with other cytokines and chemokines. Fourth, CXCL8 was associated with DC activation and recruitment. Fifth, targeting the CXCL8-CXCR1/CXCR2 axis by antagonizing CXCR2 promoted tumor progression *in vivo* by impeding DC activation or recruitment, leading to the opposite effect of antitumor immunity. Thus, CXCL8 might be considered a favorable factor for significant antitumor effects in CRC-bearing hosts, at least in our study.

Since *in vitro* DC activation experiments may not reflect a patient's tumor DC activation status, we did not perform such experiments; instead, we assessed DC activation markers in larger cohort samples. We found that CXCL8 expression was positively correlated with the expression of DC activation genes such as CD80, CD83, and CD86 (**Figure 3C**). Furthermore, higher infiltration of activated DCs was strongly linked with an increased survival rate in CRC patients, to a similar extent as elevated CXCL8 expression. In addition, DC activity and migration were analyzed by FACS in CT26 tumor tissues. In targeting the CXCL8-CXCR1/CXC2 axis, the lack of CXCL8 in the mouse genome limited us to targeting CXCL8 to antagonize CXCR1/2 instead of CXCL8. Antagonism of CXCR2 could effectively prevent functional $CD8^+$ T cells and DCs activation from infiltrating tumor sites in a CRC mouse model, which could change the CRC mouse's antitumor immunity model to promote tumor progression rather than regression.

We found that the alter of the immune behavior was only found in CT26 colon cancer model, not in MC38 mice, mainly because CT26 had the higher immune infiltration than the MC38 model (23). Additionally, antagonism of CXCR2 (danirixin) could promote tumor progression more effectively than CXCR1/2 (reparixin) in CT26 tumor model. Furthermore, main reasons why reparixin and danirixin behavior different on the antitumor role are as follows. 1) CXCL8 (IL-8) and its receptor CXCR2 in the tumor microenvironment for prompted colon cancer progression and metastasis have been reported (8), which was opposite to our findings of suppression tumor progression. However, that study have suggested that the regulation of IL-8 within the tumor and microenvironment play a critical role, but the impact of tissue microenvironment-derived CXCL8 and CXCR2 to date remains difficult to evaluate. Since they targeted the cancer cell rather than immune cells, the mouse colon carcinoma cell line CT26 and human CRC cell line HCT116 confirmed the high expression of CXCR2 in the two cell lines. 2) Interestingly, Mice bearing MC38 tumor cells treated with CXCR2-transduced pmel-1 T cells showed enhanced tumor regression and survival compared with mice receiving control, which implicated that the introduction of the CXCR2 gene into tumor-specific T cells could enhance their localization to tumors and improve antitumor immune responses, and it was correlated our results with CXCR2 mediated DC to suppression role in tumor growth (34). In addition, it has been reported that increased tumor-infiltrating DCs and upregulated their CD86 expression *in vivo* lead to increased tumor-infiltrating $CD8^+$ T cells and enhanced PD-L1 and MHC class I expression on tumor cells (35). More importantly, in CT26 colon cancer–bearing mice, the combinational use of imiquimod (TLR7) with autologous GVAX therapy displayed increased expression levels of DC marker CD86 and CD9, which led to decreased $Foxp3^+$ regulatory T cells in TDLNs and increased $CD8^+$ T cells which correlate with an antitumor phenotype (36). Collectively, these findings indicate that activate DCs as a positive regulator of T-cell priming, could enhance the immunologic antitumor effects.

As we discussed above CXCL8/CXCR2 had a role in DC-mediated anticancer immunity remains unclear, and all depend on targets specific for CXCL8, CXCR1/CXCR2, or CXCR2 alone. The different behaviors of reparixin or danirixin depend on the specific target, such as targeting CXCL8, CXCR1/CXCR2 or CXCR2, or depend on the specific target cells, such as tumor cells or different immune cell subpopulations. The efficacy of inhibition of CXCR2 has been widely investigated in preclinical experiments. Current inhibitors of CXCR is well discussed, and CXCR2 antagonists have been initially considered administrated in respiratory diseases and gradually in cancer for more insights into tumor microenvironment. Reparixin is a non-competitive

CXCR1/2 antagonist. It has shown in a phase Ib trial for HER-2-negative metastatic breast cancer. Danirixin, another oral selective CXCR2 antagonist, has been investigated in patients with virus infection disease (influenza), which had small-sample clinical trial (NCT02469298). CXCR2-mediated neutrophils play an important role in anti-infection and control pathogen invasion (37).Current evidence suggests that TICs in the TME serve as promising therapeutic targets. It has also been proposed that CXCL8 may be considered as a therapeutic target for cancer treatment. CXCL8 is a potent chemotactic factor for neutrophils, MDSCs and monocytes, leading to immunosuppression. Our data suggested that targeting the CXCL8-CXCR1/2 axis as a therapeutic strategy might impede DC activation or recruitment. This axis could be considered a favorable factor for important antitumor effects in CRC rather than a target. Considering the multiple mechanisms used by tumors to evade the immune response, the use of modified DCs for cancer immunotherapy has achieved promising results. Experiments investigating DC immunotherapy using mouse models have shown that the growth rate of tumors is reduced, and the number of metastases is diminished. The survival rate of tumor-bearing animals is increased and the tumor-specific cytotoxic T lymphocyte (CTL) response is initiated (38, 39). Despite proven immunotherapies as a favorable safety profile, antitumor DC-based treatment has not succeeded with significant objective of clinical responses in clinical trials (40). A rational reason is that the low efficacy of DC vaccines may be related to the fact that the human immune system is suppressed to a relatively great extent by tumors. We need to think about the reasons for these impacts, such as 1) the chemotactic properties of DCs in response to specific chemokines being strictly regulated during DC development, 2) MHC I/II molecules on the DC surface and the weak polarization of antitumor immune responses, and 3) DC activation markers and activation status in tumors. Generally, CXCL8-CXCR1/2 axis-associated DC activation and recruitment might indicate the modulation of the DC system at the tumor site by the cytokine and chemokine network.

CONCLUSIONS

In summary, it was previously reported that CXCL8 acts as a key multifunctional chemokine to modulate tumor cells for proliferation, invasion, migration, and as a chemotactic factor for neutrophils, MDSCs and monocytes, which served as immunosuppressive components in cancer-bearing hosts and led to a poor prognosis. CXCL8 is considered a potential attractive target for cancer treatment. However, our data suggest that CXCL8 is a key regulator of immunity in CRC that acts through associated DC activation gene expression, probably indicators of favorable outcomes of this particular subtype of CRC. Targeting the CXCL8-CXCR1/CXCR2 axis by antagonizing CXCR2 promotes tumor progression *in vivo* by impeding DC activation or recruitment, leading to the opposite effect of antitumor immunity. The CXCL8-CXCR2 axis could be considered a favorable factor for important antitumor effects on CRC rather than a target.

DATA AVAILABILITY STATEMENT

The original contributions presented in the study are included in the article/**Supplementary Material**. Further inquiries can be directed to the corresponding authors.

ETHICS STATEMENT

The animal study was reviewed and approved by Faculty of Medical Laboratory Science, Ruijin Hospital, School of Medicine, Shanghai Jiao Tong University.

AUTHOR CONTRIBUTIONS

YH and DX contributed to the concept and designed the research work. EL, XY, YD and GW performed the experiments, acquisition, analysis and interpretation of the data. EL, XY, YD, YH and DX drafted the article. PX, PN, DW, DX and YH provided critical reagents and supervised the research. All authors contributed to the article and approved the submitted version.

FUNDING

This work was supported by grants from the National Natural Science Foundation of China (NSFC) (81871274, 81871715, 82071811 and 31670905).

SUPPLEMENTARY MATERIAL

The Supplementary Material for this article can be found online at: https://www.frontiersin.org/articles/10.3389/fimmu.2021.667177/full#supplementary-material

REFERENCES

1. Torre LA, Bray F, Siegel RL, Ferlay J, Lortet-Tieulent J, Jemal A. Global Cancer Statistics, 2012. *CA: Cancer J Clin* (2015) 65(2):87–108. doi: 10.3322/caac.21262
2. Nguyen LH, Goel A, Chung DC. Pathways of Colorectal Carcinogenesis. *Gastroenterology* (2020) 158(2):291–302. doi: 10.1053/j.gastro.2019.08.059
3. Mollica Poeta V, Massara M, Capucetti A, Bonecchi R. Chemokines and Chemokine Receptors: New Targets for Cancer Immunotherapy. *Front Immunol* (2019) 10:379. doi: 10.3389/fimmu.2019.00379
4. Nagarsheth N, Wicha MS, Zou W. Chemokines in the Cancer Microenvironment and Their Relevance in Cancer Immunotherapy. *Nat Rev Immunol* (2017) 17(9):559–72. doi: 10.1038/nri.2017.49

5. Ha H, Debnath B, Neamati N. Role of the CXCL8-CXCR1/2 Axis in Cancer and Inflammatory Diseases. *Theranostics* (2017) 7(6):1543–88. doi: 10.7150/thno.15625
6. Liu Q, Li A, Tian Y, Wu JD, Liu Y, Li T, et al. The CXCL8-CXCR1/2 Pathways in Cancer. *Cytokine Growth factor Rev* (2016) 31:61–71. doi: 10.1016/j.cytogfr.2016.08.002
7. Ijichi H. Inhibition of CXCLs/CXCR2 Axis in the Tumor Microenvironment Might be a Potent Therapeutics for Pancreatic Cancer. *Oncoimmunology* (2012) 1(4):569–71. doi: 10.4161/onci.19402
8. Lee YS, Choi I, Ning Y, Kim NY, Khatchadourian V, Yang D, et al. Interleukin-8 and its Receptor CXCR2 in the Tumour Microenvironment Promote Colon Cancer Growth, Progression and Metastasis. *Br J Cancer* (2012) 106(11):1833–41. doi: 10.1038/bjc.2012.177
9. Do HTT, Lee CH, Cho J. Chemokines and Their Receptors: Multifaceted Roles in Cancer Progression and Potential Value as Cancer Prognostic Markers. *Cancers* (2020) 12(2):287. doi: 10.3390/cancers12020287
10. Wang S, Zhang C, Zhang Z, Qian W, Sun Y, Ji B, et al. Transcriptome Analysis in Primary Colorectal Cancer Tissues From Patients With and Without Liver Metastases Using Next-Generation Sequencing. *Cancer Med* (2017) 6 (8):1976–87. doi: 10.1002/cam4.1147
11. Gong B, Kao Y, Zhang C, Sun F, Gong Z, Chen J. Identification of Hub Genes Related to Carcinogenesis and Prognosis in Colorectal Cancer Based on Integrated Bioinformatics. *Mediators Inflammation* (2020) 2020:5934821. doi: 10.1155/2020/5934821
12. Mellman I, Steinman RM. Dendritic Cells: Specialized and Regulated Antigen Processing Machines. *Cell* (2001) 106(3):255–8. doi: 10.1016/s0092-8674(01)00449-4
13. Qian C, Cao X. Dendritic Cells in the Regulation of Immunity and Inflammation. *Semin Immunol* (2018) 35:3–11. doi: 10.1016/j.smim.2017.12.002
14. Eisenbarth SC. Dendritic Cell Subsets in T Cell Programming: Location Dictates Function. *Nat Rev Immunol* (2019) 19(2):89–103. doi: 10.1038/s41577-018-0088-1
15. Robinson MD, McCarthy DJ, Smyth GK. edgeR: A Bioconductor Package for Differential Expression Analysis of Digital Gene Expression Data. *Bioinformatics* (2010) 26(1):139–40. doi: 10.1093/bioinformatics/btp616
16. Hänzelmann S, Castelo R, Guinney J. GSVA: Gene Set Variation Analysis for Microarray and RNA-seq Data. *BMC Bioinf* (2013) 14:7. doi: 10.1186/1471-2105-14-7
17. Yoshihara K, Shahmoradgoli M, Martinez E, Vegesna R, Kim H, Torres-Garcia W, et al. Inferring Tumour Purity and Stromal and Immune Cell Admixture From Expression Data. *Nat Commun* (2013) 4:2612. doi: 10.1038/ncomms3612
18. Newman AM, Liu CL, Green MR, Gentles AJ, Feng W, Xu Y, et al. Robust Enumeration of Cell Subsets From Tissue Expression Profiles. *Nat Methods* (2015) 12(5):453–7. doi: 10.1038/nmeth.3337
19. Fridman WH, Pages F, Sautes-Fridman C, Galon J. The Immune Contexture in Human Tumours: Impact on Clinical Outcome. *Nat Rev Cancer* (2012) 12 (4):298–306. doi: 10.1038/nrc3245
20. Galon J, Costes A, Sanchez-Cabo F, Kirilovsky A, Mlecnik B, Lagorce-Pages C, et al. Type, Density, and Location of Immune Cells Within Human Colorectal Tumors Predict Clinical Outcome. *Science* (2006) 313(5795):1960–4. doi: 10.1126/science.1129139
21. Lukaszewicz-Zajac M, Paczek S, Mroczko P, Kulczynska-Przybik A. The Significance of CXCL1 and CXCL8 as Well as Their Specific Receptors in Colorectal Cancer. *Cancer Manage Res* (2020) 12:8435–43. doi: 10.2147/CMAR.S267176
22. Wang X, Wang Q, Ives KL, Evers BM. Curcumin Inhibits Neurotensin-Mediated Interleukin-8 Production and Migration of HCT116 Human Colon Cancer Cells. *Clin Cancer Res an Off J Am Assoc Cancer Res* (2006) 12 (18):5346–55. doi: 10.1158/1078-0432.CCR-06-0968
23. Zhong W, Myers JS, Wang F, Wang K, Lucas J, Rosfjord E, et al. Comparison of the Molecular and Cellular Phenotypes of Common Mouse Syngeneic Models With Human Tumors. *BMC Genomics* (2020) 21(1):2. doi: 10.1186/s12864-019-6344-3
24. Tannenbaum CS, Rayman PA, Pavicic PG, Kim JS, Wei W, Polefko A, et al. Mediators of Inflammation-Driven Expansion, Trafficking, and Function of Tumor-Infiltrating Mdscs. *Cancer Immunol Res* (2019) 7(10):1687–99. doi: 10.1158/2326-6066.CIR-18-0578
25. Huang FY, Wang JY, Dai SZ, Lin YY, Sun Y, Zhang L, et al. A Recombinant Oncolytic Newcastle Virus Expressing MIP-3alpha Promotes Systemic Antitumor Immunity. *J immunotherapy Cancer* (2020) 8(2):e000330. doi: 10.1136/jitc-2019-000330
26. Heidemann J, Ogawa H, Dwinell MB, Rafiee P, Maaser C, Gockel HR, et al. Angiogenic Effects of Interleukin 8 (CXCL8) in Human Intestinal Microvascular Endothelial Cells are Mediated by CXCR2. *J Biol Chem* (2003) 278(10):8508–15. doi: 10.1074/jbc.M208231200
27. Ning Y, Manegold PC, Hong YK, Zhang W, Pohl A, Lurje G, et al. Interleukin-8 is Associated With Proliferation, Migration, Angiogenesis and Chemosensitivity In Vitro and In Vivo in Colon Cancer Cell Line Models. *Int J Cancer* (2011) 128(9):2038–49. doi: 10.1002/ijc.25562
28. Alfaro C, Teijeira A, Onate C, Perez G, Sanmamed MF, Andueza MP, et al. Tumor-Produced Interleukin-8 Attracts Human Myeloid-Derived Suppressor Cells and Elicits Extrusion of Neutrophil Extracellular Traps (Nets). *Clin Cancer Res an Off J Am Assoc Cancer Res* (2016) 22(15):3924–36. doi: 10.1158/1078-0432.CCR-15-2463
29. Teijeira A, Garasa S, Gato M, Alfaro C, Migueliz I, Cirella A, et al. CXCR1 and CXCR2 Chemokine Receptor Agonists Produced by Tumors Induce Neutrophil Extracellular Traps That Interfere With Immune Cytotoxicity. *Immunity* (2020) 52(5):856–71.e8. doi: 10.1016/j.immuni.2020.03.001
30. Michielsen AJ, Noonan S, Martin P, Tosetto M, Marry J, Biniecka M, et al. Inhibition of Dendritic Cell Maturation by the Tumor Microenvironment Correlates With the Survival of Colorectal Cancer Patients Following Bevacizumab Treatment. *Mol Cancer Ther* (2012) 11(8):1829–37. doi: 10.1158/1535-7163.MCT-12-0162
31. Michielsen AJ, O'Sullivan JN, Ryan EJ. Tumor Conditioned Media From Colorectal Cancer Patients Inhibits Dendritic Cell Maturation. *Oncoimmunology* (2012) 1(5):751–3. doi: 10.4161/onci.19570
32. Flores-Romo L. In Vivo Maturation and Migration of Dendritic Cells. *Immunology* (2001) 102(3):255–62. doi: 10.1046/j.1365-2567.2001.01204.x
33. Campoli M, Ferrone S. HLA Antigen Changes in Malignant Cells: Epigenetic Mechanisms and Biologic Significance. *Oncogene* (2008) 27(45):5869–85. doi: 10.1038/onc.2008.273
34. Peng W, Ye Y, Rabinovich BA, Liu C, Lou Y, Zhang M, et al. Transduction of Tumor-Specific T Cells With CXCR2 Chemokine Receptor Improves Migration to Tumor and Antitumor Immune Responses. *Clin Cancer Res an Off J Am Assoc Cancer Res* (2010) 16(22):5458–68. doi: 10.1158/1078-0432.CCR-10-0712
35. Iwata TN, Ishii C, Ishida S, Ogitani Y, Wada T, Agatsuma T. A HER2-Targeting Antibody-Drug Conjugate, Trastuzumab Deruxtecan (DS-8201a), Enhances Antitumor Immunity in a Mouse Model. *Mol Cancer Ther* (2018) 17(7):1494–503. doi: 10.1158/1535-7163.MCT-17-0749
36. Narusawa M, Inoue H, Sakamoto C, Matsumura Y, Takahashi A, Inoue T, et al. TLR7 Ligand Augments GM-CSF-initiated Antitumor Immunity Through Activation of Plasmacytoid Dendritic Cells. *Cancer Immunol Res* (2014) 2(6):568–80. doi: 10.1158/2326-6066.CIR-13-0143
37. Cheng Y, Ma XL, Wei YQ, Wei XW. Potential Roles and Targeted Therapy of the CXCLs/CXCR2 Axis in Cancer and Inflammatory Diseases. *Biochim Biophys Acta Rev Cancer* (2019) 1871(2):289–312. doi: 10.1016/j.bbcan.2019.01.005
38. Wculek SK, Amores-Iniesta J, Conde-Garrosa R, Khouili SC, Melero I, Sancho D. Effective Cancer Immunotherapy by Natural Mouse Conventional Type-1 Dendritic Cells Bearing Dead Tumor Antigen. *J immunotherapy Cancer* (2019) 7(1):100. doi: 10.1186/s40425-019-0565-5
39. Markov O, Oshchepkova A, Mironova N. Immunotherapy Based on Dendritic Cell-Targeted/-Derived Extracellular Vesicles-a Novel Strategy for Enhancement of the Anti-tumor Immune Response. *Front Pharmacol* (2019) 10:1152. doi: 10.3389/fphar.2019.01152
40. Mastelic-Gavillet B, Balint K, Boudousquie C, Gannon PO, Kandalaft LE. Personalized Dendritic Cell Vaccines-Recent Breakthroughs and Encouraging Clinical Results. *Front Immunol* (2019) 10:766. doi: 10.3389/fimmu.2019.00766

Conflict of Interest: The authors declare that the research was conducted in the absence of any commercial or financial relationships that could be construed as a potential conflict of interest.

Copyright © 2021 Li, Yang, Du, Wang, Chan, Wu, Xu, Ni, Xu and Hu. This is an open-access article distributed under the terms of the Creative Commons Attribution License (CC BY). The use, distribution or reproduction in other forums is permitted, provided the original author(s) and the copyright owner(s) are credited and that the original publication in this journal is cited, in accordance with accepted academic practice. No use, distribution or reproduction is permitted which does not comply with these terms.

frontiers in Immunology

ORIGINAL RESEARCH
published: 13 May 2021
doi: 10.3389/fimmu.2021.651033

Immune Landscape of Gastric Carcinoma Tumor Microenvironment Identifies a Peritoneal Relapse Relevant Immune Signature

Chuang Zhang[1,2,3,4†], *Danni Li*[1,2,3,4†], *Ruoxi Yu*[5], *Ce Li*[1,2,3,4], *Yujia Song*[1,2,3,4], *Xi Chen*[1,2,3,4], *Yibo Fan*[1,2,3,4], *Yunpeng Liu*[1,2,3,4] *and Xiujuan Qu*[1,2,3,4*]

[1] *Department of Medical Oncology, The First Hospital of China Medical University, Shenyang, China,* [2] *Key Laboratory of Anticancer Drugs and Biotherapy of Liaoning Province, The First Hospital of China Medical University, Shenyang, China,* [3] *Liaoning Province Clinical Research Center for Cancer, The First Hospital of China Medical University, Shenyang, China,* [4] *Key Laboratory of Precision Diagnosis and Treatment of Gastrointestinal Tumors, Ministry of Education, The First Hospital of China Medical University, Shenyang, China,* [5] *Department of Radiation Oncology, Cancer Hospital of China Medical University, Liaoning Cancer Hospital & Institution, Shenyang, China*

OPEN ACCESS

Edited by:
Peng Qu,
National Institutes of Health (NIH), United States

Reviewed by:
Yingjie Zhang,
Wistar Institute, United States
Nikunj Satani,
University of Texas Health Science Center at Houston, United States

***Correspondence:**
Xiujuan Qu
xiujuanqu@yahoo.com

[†]*These authors have contributed equally to this work*

Specialty section:
This article was submitted to Cancer Immunity and Immunotherapy, a section of the journal Frontiers in Immunology

Received: *08 January 2021*
Accepted: *20 April 2021*
Published: *13 May 2021*

Citation:
Zhang C, Li D, Yu R, Li C, Song Y, Chen X, Fan Y, Liu Y and Qu X (2021) Immune Landscape of Gastric Carcinoma Tumor Microenvironment Identifies a Peritoneal Relapse Relevant Immune Signature. Front. Immunol. 12:651033. doi: 10.3389/fimmu.2021.651033

Background: Gastric cancer (GC) still represents the third leading cause of cancer-related death worldwide. Peritoneal relapse (PR) is the most frequent metastasis occurring among patients with advanced gastric cancer. Increasingly more evidence have clarified the tumor immune microenvironment (TIME) may predict survival and have clinical significance in GC. However, tumor-transcriptomics based immune signatures derived from immune profiling have not been established for predicting the peritoneal recurrence of the advanced GC.

Methods: In this study, we depict the immune landscape of GC by using transcriptome profiling and clinical characteristics retrieved from GSE62254 of Gene Expression Omnibus (GEO). Immune cell infiltration score was evaluated *via* single-sample gene set enrichment (ssGSEA) analysis algorithm. The least absolute shrinkage and selection operator (LASSO) Cox regression algorithm was used to select the valuable immune cells and construct the final model for the prediction of PR. The receiver operating characteristic (ROC) curve and the Kaplan-Meier curve were used to check the accuracy of PRIs. Gene Set Enrichment Analysis (GSEA) and Kyoto Encyclopedia of Genes and Genomes (KEGG) analysis were performed to explore the molecular pathways associated with PRIs.

Results: A peritoneal recurrence related immune score (PRIs) with 10 immune cells was constructed. Compared to the low-PRIs group, the high-PRIs group had a greater risk. The upregulation of the focal adhesion signaling was observed in the high-PRIs subtype by GSEA and KEGG. Multivariate analysis found that both in the internal training cohort and the internal validation cohort, PRIs was a stable and independent predictor for PR. A nomogram that integrated clinicopathological features and PRIs to predict peritoneal relapse was constructed. Subgroup analysis indicated that the PRIs could obviously distinguish peritoneal recurrence in different molecular subtypes, pathological stages and

Lauren subtypes, in which PRIs of Epithelial-Mesenchymal Transitions (EMT) subtype, III-IV stage and diffuse subtype are higher respectively.

Conclusion: Overall, we performed a comprehensive evaluation of the immune landscape of GC and constructed a predictive PR model based on the immune cell infiltration. The PRIs represents novel promising feature of predicting peritoneal recurrence of GC and sheds light on the improvement of the personalized management of GC patients after surgery.

Keywords: gastric cancer, LASSO, peritoneal relapse, TME, immune signature

INTRODUCTION

Gastric cancer (GC) ranks the fifth in prevalent lethal malignancies and the third in cancer-related death worldwide (1). Of the patients with advanced-stage GC, most of them develop liver, lymph nodes and peritoneum metastasis within 5 years after radical surgery. Among these metastases, peritoneal dissemination is the most frequent and lethal, especially in the serosa-invasive gastric cancers (2). Although the conventional clinicopathological detections such as medical imaging and cytological examination of peritoneal effusion have been applied to assess the relapse, the prediction of PR is not accurate and sensitivity enough (3). Despite optimal treatment including corrective surgery (CRS), systemic chemotherapy, intraperitoneal chemotherapy and hyperthermia intraperitoneal chemotherapy (HIPEC), they are not adopted as the first-line strategy due to the controversial outcomes after long-term follow-up (4–6). In summary, it is urgently needed to construct an individual approach or model for predicting the PR risk of GC.

The tumor immune microenvironment (TIME) is the environment of malignant tumor progression, in which the host antitumor immune response and normal tissue destruction occur (7–12). Accumulating evidence indicated the key role of immune cells infiltration in the peritoneal metastasis of different cancers including GC (13–16). It is observed that GC patients with peritoneal metastasis had increased levels of alternatively activated macrophages in the peritoneum compared to those without dissemination. The underlying mechanism is that macrophages in the peritoneum of GC patients play a supportive role in peritoneal metastasis by producing EGF and VEGF (17). Besides, Rihito Kanamaru reported that neutrophil extracellular traps (NETs) on peritoneal surface can promote the clustering and growth of free tumor cells disseminated in abdomen, which was assisted by low-density neutrophils in postoperative abdominal cavity. Although several studies have explored the relationship between immune infiltration and prognosis of GC, to date, the probable correlation between peritoneal metastasis and the landscape of immune cells infiltrating has not yet been exclusive (18–20).

With the goal of improving precise prediction of PR after curative surgery of gastric cancer, in the current study, we applied the algorithm ssGSEA, which has been deemed to be the most accurate method available (21). ssGSEA is a newly proposed computational algorithm for enumeration of immune cell subsets using RNA specimens from multiple tissue types, including solid tumors, and has outperformed other methods regarding noise, unknown mixture content and closely related cell types. This study aims to construct a novel prediction system specific to PR, showing the immune infiltration landscape of patients with or without peritoneal relapse after surgery. As a result, we established a methodology to quantify the PR related immune score (PRIs) with an integrated analysis of the infiltration status of 24 immune cells, which was found to be a robust predictor of PR. Therefore, the PRIs represents novel promising signature for predicting peritoneal recurrence of GC after surgery.

MATERIAL AND METHODS

Search and Collection of Cohort With the Pathological Data of Peritoneal Relapse

To identify gastric cancer gene expression profile data with clinical pathological data of PR, a systematic search was performed on the Gene Expression Omnibus (GEO) data set (https://www.ncbi.nlm.nih.gov/geo/). The search strategy is ((("peritoneum"[MeSH Terms] OR peritoneal[All Fields]) AND ("neoplasm metastasis"[MeSH Terms] OR metastasis [All Fields])) OR (("peritoneum"[MeSH Terms] OR peritoneal [All Fields]) AND ("recurrence"[MeSH Terms] OR relapse[All Fields])) OR (("peritoneum"[MeSH Terms] OR peritoneal[All Fields]) AND ("recurrence"[MeSH Terms] OR recurrence [All Fields]))) AND ("stomach neoplasms"[MeSH Terms] OR (((((((gastric cancer[Title] OR gastric adenocarcinoma[Title]) OR gastric tumor[Title]) OR gastric carcinoma[Title]) OR stomach cancer[Title]) OR stomach adenocarcinoma[Title]) OR stomach tumor[Title]) OR stomach carcinoma[Title])). A total of 45 items were obtained from the initial screening. After further manual identification, and under the premise that the number of cases is not less than 100, Finally, the two cohorts GSE62254 and GSE10581 passed the review and their corresponding raw data were downloaded. All 300 samples of GSE62254 and 108 samples of GSE15081 with clear clinical parameters of peritoneal relapse were selected for further analysis. The corresponding clinicopathological parameters are summarized in **Table S1**.

Analysis of Immune Cell Infiltration

The Single sample gene set enrichment analysis (ssGSEA) method is a further extension of the GSEA method (21), it can define the absolute enrichment score of a certain immune cell marker genes dataset in a particular patient. We used ssGSEA to calculate the immune infiltration score for each immune cell in each patient and normalized enrichment scores were used for subsequent analysis. The markers genes of immune cells were obtained from the work of Jérôme Galon et al. (22) (**Table S2**). The above is achieved by the R package GSVA (23).

Establishment of the Lasso-Cox Model

The process of establishing and verifying the PRIs model is displayed in **Supplement Figure 1A**. Firstly, a total of 300 patients of GSE62254 cohort included in the study were randomly assigned to a 1:1 training set and validation set. Secondly, the hazard ratio of PR of immune cells in the training set was calculated using the univariate cox proportional hazard regression model. Then Immune cells that were meaningful for univariate analysis in the training set are included in the penalized Cox regression model with least absolute shrinkage and selection operator (LASSO) Cox regression model for ten-fold cross validations to select the most significant immune cells for PR (24). Finally, a PR-related immune model was constructed based on the immune cells.

ROC Curve

Receiver operating characteristic curve (ROC), area under the curve (AUC) and calibration curve were obtained using R packages "pROC" and "rms".

KEGG Analysis Based on PRIs

Kyoto Gene and Genomic Encyclopedia (KEGG) analysis was used to determine the biological pathways in which genes associated with PRIs were significantly enriched. Pathways with adv. less than 0.5 were considered meaningful. The above is achieved by the R package clusterProfiler (25).

Gene Set Enrichment Analysis (GSEA)

GSEA v2.2.2 (http://www.broadinstitute.org/gsea) was used to investigate the biological difference between patients with high or low PRIs. C2:CP KEGG gene sets from MSigDB were used as the reference gene sets. All other parameters were set to default.

Construction and Validation of PRIs Related Nomogram

The PRIs and pStage with the stable value of predicting PR were used to construct the final nomogram. R package nomogramEx was used to calculate and plot. DCA was used to identify the clinical benefit of PRI-related nomogram.

Statistical Analysis

Continuous variables were analyzed using Student's t-tests or nonparametric tests. Categorical variables were analyzed using Chi-squared tests or Fisher's exact tests. R package survival and survminer was used for survival analysis. R package coxph was used for univariate and multivariate analyses. The ROC curve was plotted by R package survivalROC. All data were analyzed by SPSS and R software (http://www.r-project.org/). The results with $P < 0.05$ were considered statistically significant.

RESULTS

Overview of Differential Patients' Outcomes Between PR+ and PR- Patients in GSE62254 Cohort

In order to clarify the effect of PR on the overall survival (OS) and progression free survival (PFS) of gastric cancer patients after surgery, we verified it in GSE62254 cohort. 300 patients were divided into PR- and PR+ groups according to their PR status after surgery. As expected, patients in PR+ subgroup demonstrated a worse prognosis (**Figure 1A**) and a higher recurrence rate after surgery (**Figure 1B**).

Immune Landscape and the TME Characteristics in GSE62254 Cohort

Immune cells infiltration status was calculated using R package "GSVA". A total of 24 immune-related cells were included to evaluate the immune infiltration status of tumor tissues. Immune infiltration landscape and corresponding clinical parameters are shown in **Figure 2A**. As can be seen from the heatmap, patients with PR+ conducted different immune infiltration status from patients with PR-, and the infiltration abundance of different immune cells in the same patient is different. To better understand the relationship between various immune cells in gastric cancer tissues, we constructed a correlation analysis among the 24 immune cells (**Figure 2B**). The results showed that T cells, cytotoxic cells, helper T cells and CD8+T cells were highly correlated. There is also a high correlation between Th2 cells and Treg cells. Besides, Mast cells, eosinophils and IDC cells were highly correlated. Moreover, there is a high correlation between NK cells and Tem cells. Therefore, this suggests that they may be involved in the same biological behavior in the immune microenvironment of gastric cancer that promotes peritoneal recurrence of gastric cancer. In order to verify whether the immune infiltration status of patients with different PR status is different, we divided 24 immune cells into PR+ and PR- groups according to the PR status. As **Figure 2C** showed, 15 out of 24 immune cells presented different immune infiltration status between PR+ and PR- groups. Consistent with the results of **Figure 2B**, NK cell and Tem were consistently highly infiltration in PR+ patients, PR+ patients also possessed consistently lower Th2 and TReg cells infiltration, and consistently higher infiltration of mast cell, eosinophils and iDC. Then we verified the infiltration scores of 24 types of immune cells in PR+ and PR- groups in GSE15081, and the results were similarly (**Supplement Figure 1B**). This makes us realize that immune cells may play an important role in PR, and the infiltration of immune cells can reflect the PR of patients.

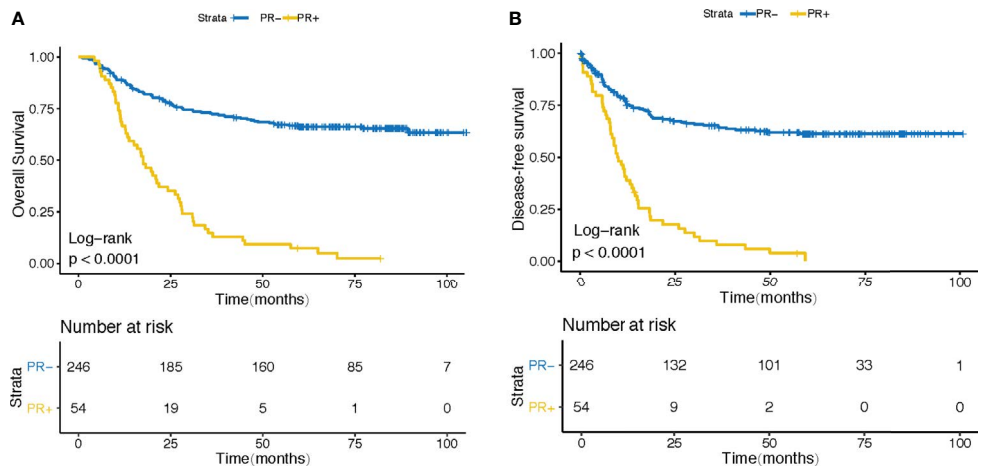

FIGURE 1 | Association between PR status and patients' outcomes. **(A)** for OS and **(B)** for PFS.

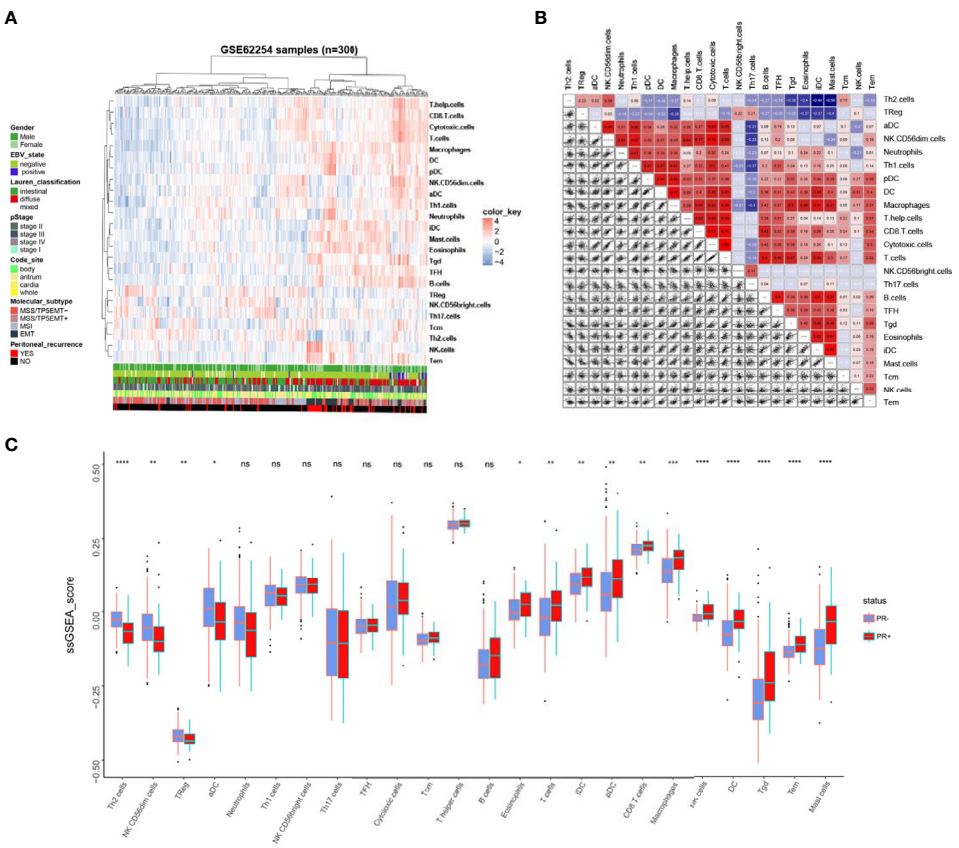

FIGURE 2 | Immune landscape of GC and the TME characteristics. **(A)** Unsupervised clustering of GC patients from the GSE62254 using ssGSEA score calculated from immune cells. **(B)** Correlation of the TME immune cells. **(C)** The Relative immune infiltration score of 24 immune cells between PR- and PR+ gastric tissues. *P < 0.05, **P < 0.01, ***P < 0.001, ****P < 0.0001, ns: no significance.

Feature Selection and Construction of PRIs Signature

First of all, all 300 patients in GSE62254 cohort were randomly divided into training cohort and validation cohort according to the ratio of 1 to 1. The survminer package in R software was used to calculate the optimal cutoff value for each immune cell in the training cohort (**Table S3**). Based on the cutoff, the Infiltration fraction score of each immune cell was valued as 0 or 1. Next, univariable analysis of the immune cells in the training cohort was performed to calculate the association between each immune cell and the risk of PR (**Figure 3A**). Finally, ten-fold cross validation LASSO Cox regression analysis was used to build a PR risk evaluation model (PRIs) in the training cohort using the immune cells associated with peritoneal recurrence (**Figures 3B, C**) and we constructed an PRIs formula:

$$\begin{aligned}\text{PRIs} = &-(0.405 \times \text{fraction level of Th2 cells}) + (0.270 \\ &\times \text{fraction level of Mast cells}) + (1.093 \times \text{fraction level of DCs}) \\ &- (0.712 \times \text{fraction level of NK . CD56dim . cells}) - (0.527 \\ &\times \text{fraction level of Tregs}) + (0.155 \times \text{fraction level of Tgd}) \\ &- (0.429 \times \text{fraction level of Th17 cells}) - (0.103 \\ &\times \text{fraction level of Neutrophils}) \\ &- (0.107 \times \text{fraction level of aDC cells}) \\ &+ (0.121 \times \text{fraction level of T helper cells})\end{aligned}$$

In the training cohort, the accuracy of PRIs was investigated at time points 2, 3, and 5 years and the AUC is 0.725,0.811,0.846 respectively (**Figure 3D**), while in the validation cohort is 0.676,0.726,0.750 respectively (**Figure 3E**). In all 300 patients, the AUC of PRIs at time points 2, 3, and 5 years is 0.689,0.762,0.793 respectively (**Figure 3F**). In addition, we further applied the obtained PRIs score formula to the external validation cohort, due to the limitation of the external validation cohort itself, we can only get the PR status at time point 3 years. ROC at time point 3 was 0.690, which shows that the PRIs has a significant stability (**Supplement Figure 1C**). According to the cutoff value (-0.508) obtained through the survminer package, the patients in the training cohort were divided into high and low PRIs groups. Patients with high PRIs accumulate more PR events and had a worse prognosis (**Figure 3G**). When applying the cutoff value to the validation cohort and all patients in GSE62254, the conclusion is consistent (**Figures 3H, I**).

Association Between PRIs and Clinicopathological Parameters

It has been reported that the specific clinical factors, including tumor size, histopathology of biopsy sample, and tumor morphology, were significantly correlated with peritoneal relapse. CA19-9, lymphocyte count and NLR were also predictive factors for peritoneal relapse (26), we further explored the association between PRIs and valuable clinicopathological parameters (**Figure 4A**). As we can see, most of the patients with EMT molecular subtype, diffuse type of Lauren classification or pSTAGE in stage III to IV were considered to be in the high PRIs group and these patients occurred PR more frequently. In the Alluvial diagram, we can more intuitively see that most EMT group patients are considered to be in high-risk group of PR (**Figure 4B** and **Supplement Figure 1D**). Moreover, patients possessed PR+ have higher PRIs in patients with EMT molecular subtype (**Figure 4C**). So more attention should be paid to patients with EMT molecular subtypes, especially these with high PRIs. Similarly, patients with pStage III, IV had a much higher proportion patients proportion that were considered to be at high risk (**Figure 4D** and **Supplement Figure 1E**). Further analysis of patients with pstage III and IV showed that patients possessed PR+ had higher PRIs (**Figure 4E**). The Log-rank text and Kaplan-Meier curves showed within pstage III (**Figure 4G**) and pstage IV (**Figure 4H**) patients, patients with high PRIs did occur more peritoneal recurrence. Patients with diffused subtype possessed higher PRIs than intestinal subtype (**Figure 4F** and **Supplement Figure 1F**). Within patients with diffused type (**Figure 4I**) and intestinal type (**Figure 4J**), peritoneal relapse did occur more frequently in patients with high PRIs. Overall, PRIs showed general applicability in different subgroups.

Pathway Enrichment Analysis Based on PRI

To elucidate the different biological characteristics between high risk and low risk patients, based on PRIs, we identified 214 genes with a spearman correlation with PRIs greater than 0.5 (**Table S4**), Further, the KEGG enrichment analysis, which was conducted by a cluster profile in R software, showed that the 214 genes were significantly enriched in MAPK signaling pathway, focal adhesion, cGMP-PKG signaling pathway, etc. (**Figure 5A**). In addition, visualized specifically enriched genes were presented in each KEGG term (**Figures 5C, D**). Next, we divided the patients into high and low groups according to PRIs for GSEA analysis, Focal adhesion and leukocyte transendothelial migration pathways were also enriched (**Figure 5B**). These results may demonstrate that focal adhesion and leukocyte transendothelial migration play a vital role in the occurrence of PR of GC. In order to explore whether immune cells can affect the activation of PR-related pathways, we further analyzed the relationship between the 10 PR-related immune cells and the 39 genes in the PR-related pathways obtained from **Figure 5D**. As shown in **Figure 5E**, DC, Mast cell, Tgd and T helper cell possessed strong positive correlation with most genes, while NK.CD56dim cells, Tregs, Th2 cells possessed strong negative correlation with these genes. This indicates that in the microenvironment of gastric cancer tumors, immune cells may regulate PR of gastric cancer by affecting the expression of these genes.

Development and Validation of PRIs-Related Nomogram

In order to provide patients with more accurate prediction of PR, we included PRIs and clinical parameters with predictive value for PR in univariate analysis into multivariate analysis. The results showed that both in the internal training cohort and the internal validation cohort, only PRIs and pStage have stable predictive effect (**Table 1** and **Table S5**). Taking the

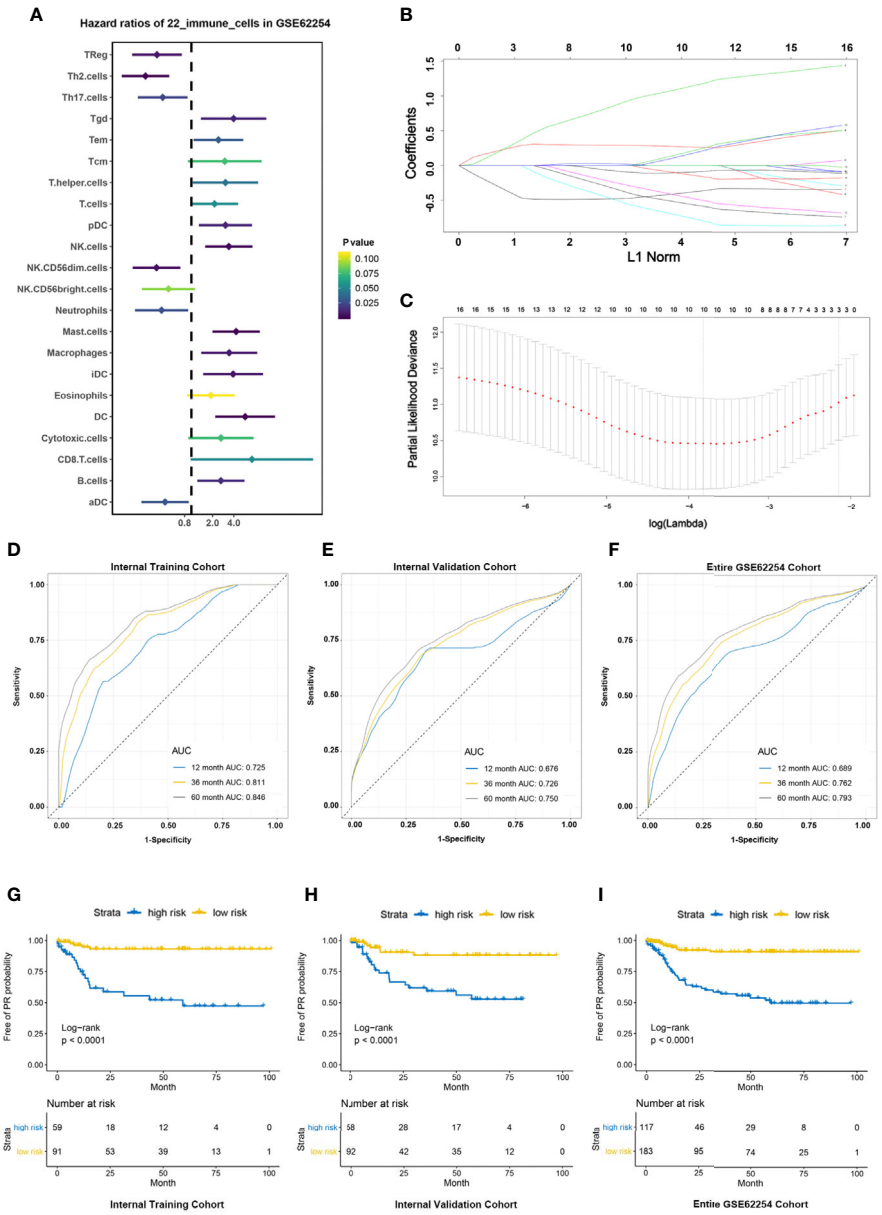

FIGURE 3 | Construction and validation of PRIs signature. **(A)** Forest plots showing associations between different immune cells and PR risk in the training cohort. **(B)** LASSO coefficient profiles of the fractions of immune cells. **(C)** Parameter selection for tuning by 10-fold cross validation in the LASSO model. **(D–F)**. PRIs measured by time-dependent receiver–operating characteristic (ROC) curves in the training cohort, validation cohort, entire cohort at 1, 3 and 5 years respectively. **(G–I)** KM-curve for patients with high and low PRIs in the training cohort, validation cohort, entire cohort respectively.

principle of simple for patient measurement into account, our subsequent studies had excluded other clinical parameters. Based on PRIs and pStage, we constructed a PR nomogram (**Figure 6A**). The calibration curve shows that nomogram has stable predictive value at the time point of 1 year, 3 years and 5 years (**Figures 6B–D**). The DCA curve showed that combining PRIs and pStage can better provide medical decisions for patients (**Figure 6E**).

Potential of PRIs as an Indicator of Immunotherapy Response in Patients With GC

Previous studies have shown that immune checkpoint inhibitory (ICI) genes and immunomodulatory genes can regulate immune infiltration. We further compared the expression patterns of ICI genes (TIM-3, PD-L1 and CTLA-4) and immunomodulatory gene (IL6, IL10, TGFB1) in patients with different PRIs

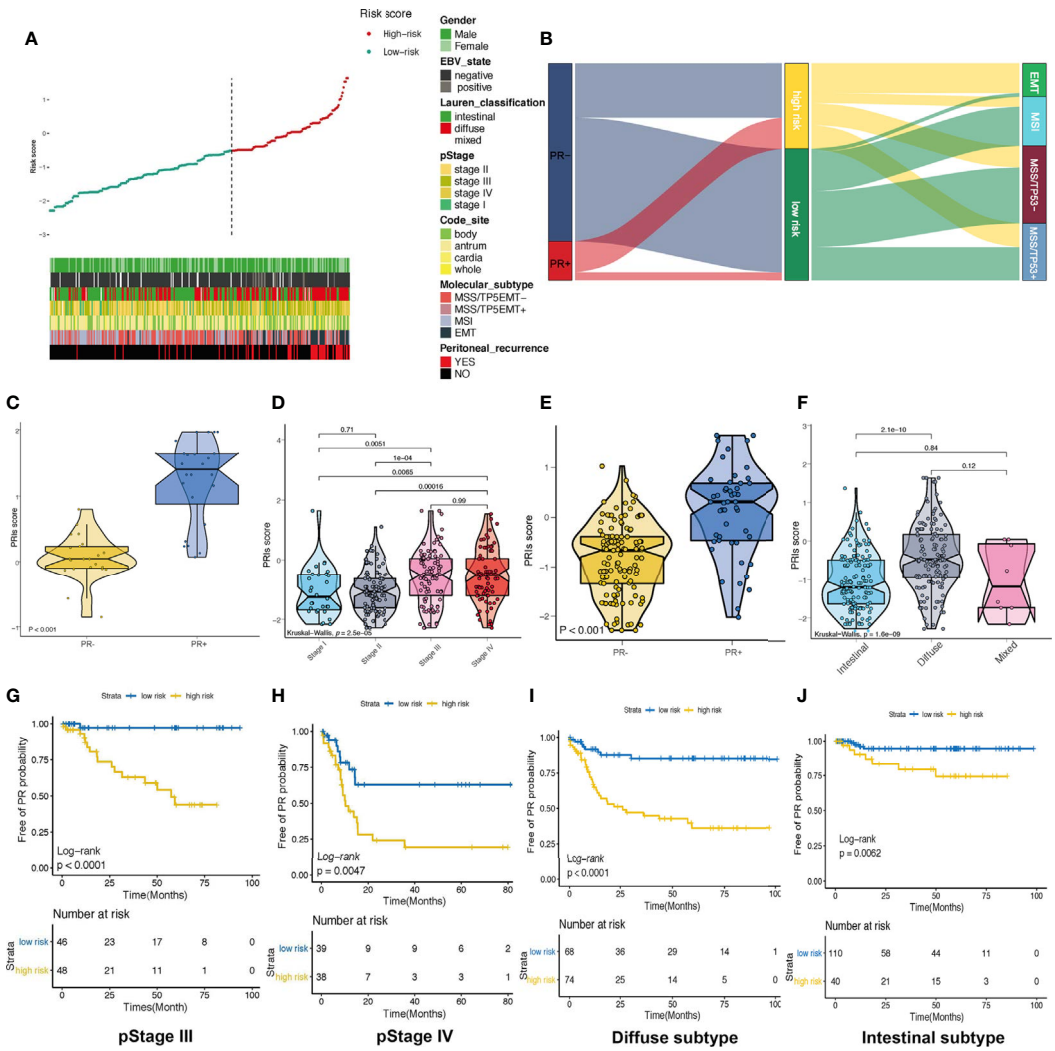

FIGURE 4 | Association between PRIs and clinicopathological parameters **(A)** Summarizing the distribution of PRIs, and clinical characteristics. **(B)** Alluvial diagram of PR status in groups with different ACRG subtypes and PRIs. **(C)** Box diagram of PRIs in PR+ and PR- crowd in patients with EMT molecular subtypes. **(D)** Box diagram of PRIs with different pStage groups. **(E)** Box diagram for the differences in PRIs among PR+ and PR- people in pStage III and IV. **(F)** Differences in PRIs among PR+ and PR- people with different lauren types. **(G)** KM-curve for patients with high and low PRIs in stage III. **(H)** KM-curve for patients with high and low PRIs in stage IV. **(I)** KM-curve for patients with high and low PRIs in diffuse subtype. **(J)** KM-curve for patients with high and low PRIs in intestinal subtype.

stratification to reveal the complex crosstalk. Compared with patients with low PRIs, patients with high PRIs tend to express high ICI genes and immunomodulatory genes (**Supplement Figure 1G**). This trend further proves that the higher expression of ICI genes and immunomodulatory genes may be associated with frequent peritoneal recurrence in patients with gastric cancer and PRIs can serve as an indicator of immunotherapy response.

DISCUSSION

The presence of PR is related to poor prognosis in patients with GC. Although conventional imaging techniques have been applied to assess the metastasis, variation of sensitivity and specificity leads to limitation. Computed tomography (CT) is currently the primary imaging modality with a relatively low sensitivity for peritoneal metastasis of GC (27). Endoscopic ultrasonography (EUS) is invasive, highly operator-dependent and has a low detection rate of distant metastasis (28). The continuous technical improvements have shown that it can enhance high contrast resolution and characteristic soft-tissue of magnetic resonance imaging (MRI), especially the diagnostic value of small liver metastases (≤10mm) and peritoneal implantation (29–31). However, MRI is usually associated with higher costs, longer acquisition time and a lower robustness with no major oncology guidelines to recommend preoperative evaluation of GC (32–35). In contrast, the predictive value of 18F FDG PET/CT was high in several metastasis from GC including peritoneal metastasis, however, its limited usability and high costs would only make PET an alternative imaging modality

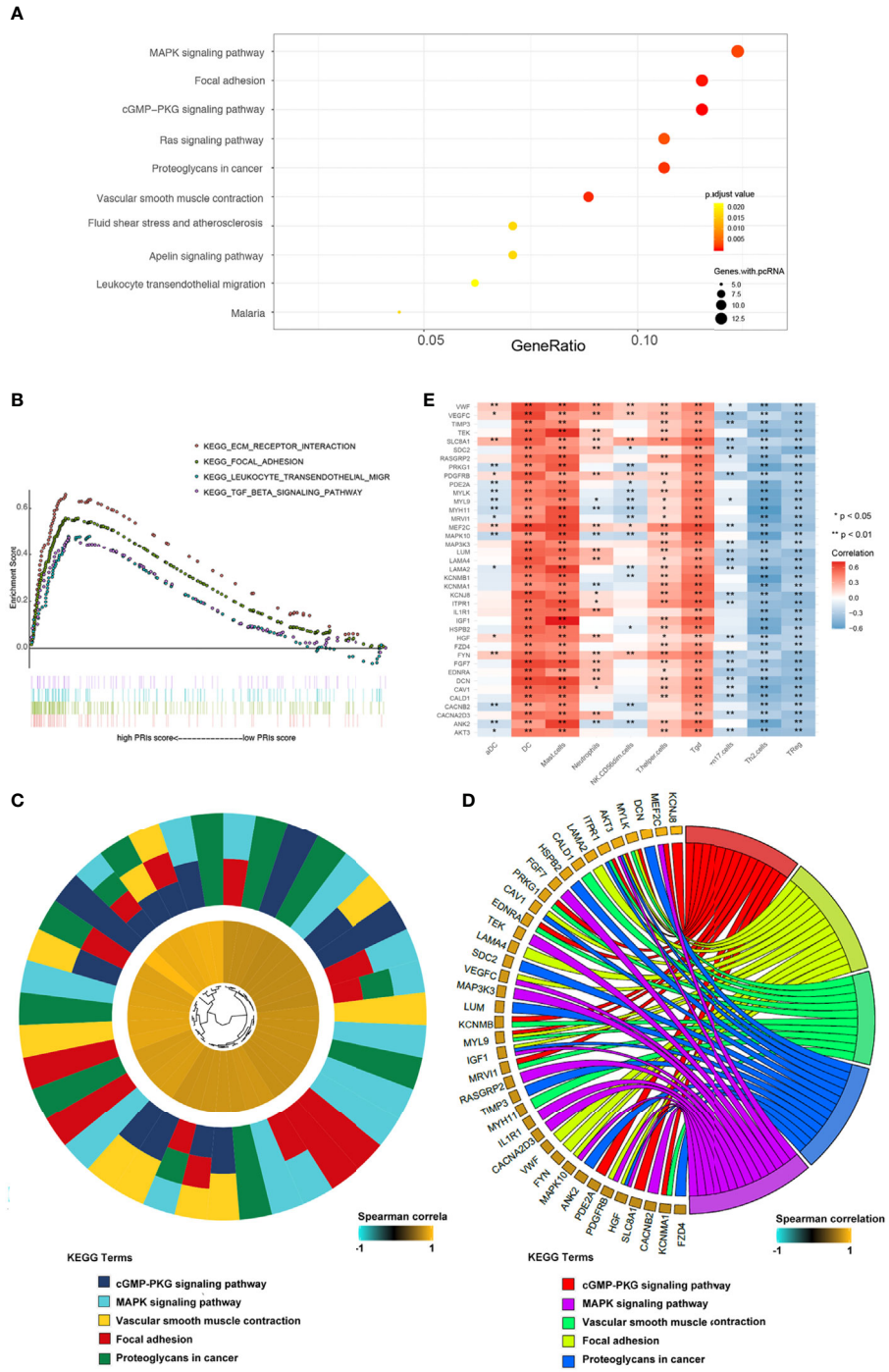

FIGURE 5 | Pathway enrichment analysis based on PRIs. **(A)** Genes with spearman correlation for PRIs greater than 0.5 were used for KEGG analysis. These genes enriched in KEGG pathways "MAPK signaling pathway," "Focal adhesion," "cGMP-PKG signaling pathway," and "Fas signaling pathway," etc. Fold enrichment of each KEGG term is indicated by the x-axis and bar color. **(B)** GSEA terms that are significantly enriched in GSE62254 cohort. "KEGG_ECM_RECEPTOR_INTERACTION","KEGG_FOCAL_ADHESION", "KEGG_LEUKOCYTE_TRANSENDOTHELIAL_MIGRATION", "KEGG_MISMATCH_REPAIR","KEGG_NOTCH_SIGNALING_PATHWAY," and "KEGG_TGB_BETA_SIGNALING_PATHWAY" was significantly enriched. **(C)** Hierarchical clustering of gene expression profiles of each KEGG pathways. **(D)** Chord plots show the relationship between genes and the KEGG pathways. **(E)** Correlation between the PR-related immune cells and genes in the KEGG pathways. *P < 0.05, **P < 0.01.

TABLE 1 | Univariate and multivariate Cox analysis among PRIs and clinical features in training cohort.

Variables	Univariate analysis			Multivariate analysis		
	HR	95%CI	*P* value	HR	95%CI	*P* value
PRIs	3.230	2.124-4.910	<0.001	2.875	1.845-4.478	<0.001
Age(years)(<60 vs. ≥60)	1.027	0.470-2.244	0.948			
Gender(Male vs. Female)	0.780	0.358-1.699	0.532			
EBV	2.535	0.753-8.398	0.134			
Lauren	2.456	1.362-4.429	0.003			
pStage	4.156	2.286-7.556	<0.001	4.468	2.266-8.811	<0.001
Molecular subtype	1.385	0.985-1.948	0.061			

(36). Besides, the peritoneal metastasis associated with serum biomarker, including CEA, CA125, CA199 and CA724 could only suggest the potential of metastasis with low specificity (37). Overall, a predictive approach or model for the PR risk after curative surgery of GC is urgently needed, making decision for the convenient scheme and dosage for GC patients with high risk of PR.

Multiple types of immune cells in TME promote tumor metastasis, either because they establish an immunosuppressive microenvironment within primary lesions or because they contribute to conditioning the pre-metastatic niche (38). These include Treg cells, myeloid-derived suppressor cells (MDSCs) (39), conventional CD11b+Ly6G+ neutrophils (40, 41) as well as macrophages (42). Instead, CD8+ T cells could directly suppress peritoneal metastasis by secreting cytokines including IFN-γ and GZMB (43–45), and Th1 CD4+ T cells T cells indirectly suppress metastasis by preventing vessel normalization (46). While Ly6G- neutrophils (47) and NK cells (48, 49) could develop innate anti-metastatic effects. Considering that recurrence and metastasis are

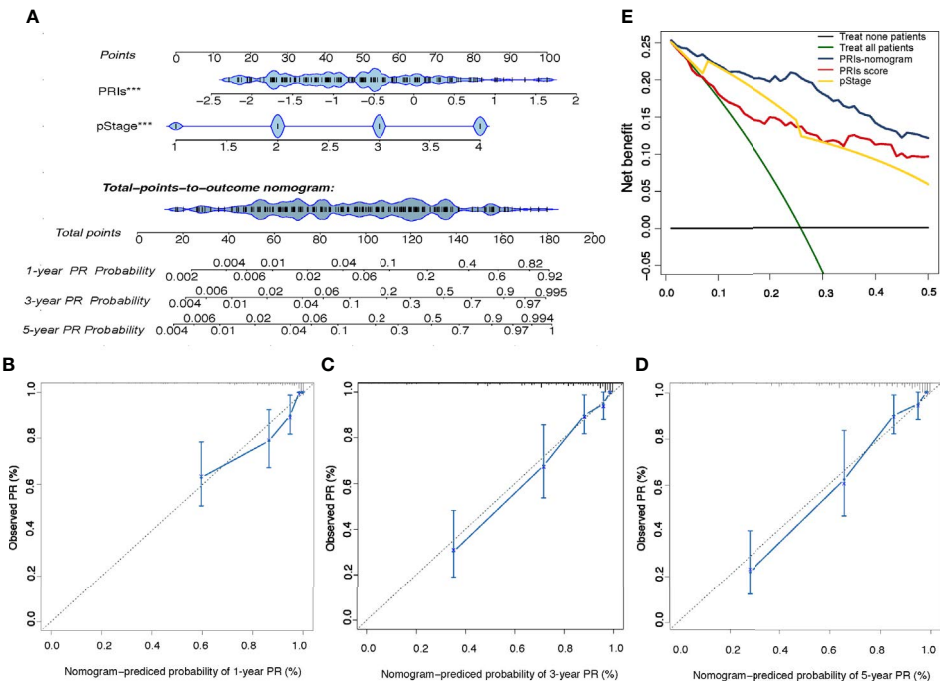

FIGURE 6 | Development and Validation of the PRIs-related Nomogram **(A)** The peritoneal relapse related nomogram based on two predictors include PRIs and pStage. Each factor corresponds to its own score, and each score is added to obtain a total score. The total scores in 1-year, 3-year, 5-year PR probability represent the peritoneal relapse possibility within 1-year, 3-year and 5-year. **(B–D)** Calibration curve at the year of 1,3,5. The calibration curve describes the calibration of the fitting model according to the consistency between the predicted peritoneal relapse risk and the actual observations. The X axis represents the predicted peritoneal relapse risk, and the y axis represents the actual peritoneal relapse rate. Solid blue lines indicate the performance of nomogram. **(E)** Decision curve analysis for the PRIs-related nomogram. The Y axis measures net benefit. The blue line, yellow line, red line represent the PRIs-nomogram, pStage and PRIs separately, green line represents the assumption that all patients occurred peritoneal relapse, and the black line at the bottom represents the assumption that no patient occurred peritoneal relapse. The proportion of all false positive patients was subtracted from the proportion of true positive patients, and the net benefit was calculated by weighting the relative harm of abandoning treatment and the negative consequences of unnecessary treatment. Relative damage is calculated in terms of $P_t/(1-P_t)$. P_t means that the expected benefit of treatment is equal to the expected benefit of avoiding treatment, at this point, the patient will choose treatment. The decision curve shows that even if the threshold probability of the patient or doctor is really small, using the PRIs nomogram in this study to predict peritoneal relapse brings more benefits than other methods.

the key factors affecting OS of patients with GC, several predictive models based on tumor- infiltration immune cells scores have been established to quantify the immune contexture and provide a statistical parameter for the prognosis of GC patients (16, 18, 19, 50). However, insufficient attention has been paid to the direct prediction of highly malignant event of PR for patients with GC.

Then, we established the PR risk immune predictive model (PRIs) of GC using LASSO-Cox regression algorithm (24). To the best of our knowledge, this study was the first bioinformatics model to predict the risk of PR for GC patients after surgical surgery. The final formula of the PRIs was composed of 10 types of immune cells including Th2 cells, mast cells, DCs, NK.CD56dim cells, Tregs, Tgd, Th17 cells, Neutrophils, αDCs and T helper cells. Similar to the previous research, CD56dim NK cells and neutrophils could directly exert the function of preventing PR (47–49, 51, 52). Besides, αDCs, as the important cells processing and presenting antigens to T cells (53), could elevate IL-1β and decreased IL-10 production to affect the metastatic ability of GC cells further (54–56). Zhao et al. reported a positive feedback that effects through TGFβ1 and IL-9 allowing cross-talk between Tregs and mast cells recently (57). The cross-talk suggests the underlying mechanism of nodes metastasis mediated by mast cells, which is in line with the findings of a previous study and ours (58). However, some inconsistency inevitably exists in this study, such as the suppressive roles of Tregs, Th2 and Th17 cells on PR (53, 59–61). The possible explanation is that CD4+ T helper cells are complex and heterogeneous at different developmental stages in GC (62). In the immune response, different subsets of CD4+ T helper cells communicate with other immune cells in TME to regulate the metastasis of GC, so the dynamic process and procedure may have effect on the multiple roles of T helper cells. Hence, to some extent, the integrated analysis of TME may better elucidate comprehensive interactions between the clinical characteristics of GC and infiltrating immune cells. With the help of ssGSEA algorithms, the results showed the PR risk of patients with high PRIs was higher than that of patients with low PRIs. Importantly, multivariate analysis demonstrated that PRIs was an independent predictor for PR, which was also verified by the nomogram integrated of PRIs, pStage and other clinical parameters. These results not only effectively certificated the efficacy and accuracy of our proposed immune predictive model, but also revealed the potential biological relationship between PR and immune infiltration landscape in GC.

We also uncovered a significant difference regarding the PRIs value in GC molecular subtypes and Lauren classification, with a higher value in the EMT subtype and diffuse type than other subtypes. Interestingly, it was also found that most patients with EMT subtype were allocated to the high risk subgroup with a higher percentage of relapse to peritoneum. Besides, the PRIs value was significantly higher in the III-IV pstage GC patients, and the PR subgroup in the III-IV pstage patients indeed had a higher PRIs. In addition, the Kaplan-Meier survival analysis showed a significantly better PR-free survival curve for patients with III stage and non-diffuse type than those with IV stage and diffuse type. Therefore, the results of biological function and clinical significance based on our PRIs value were basically consistent with the expert consensus (37). suggesting that our methodology to evaluate the risk of PR is a more predictive biomarker of gastric cancer.

Since the high-throughput sequence technology has been well improved currently, we further investigated the gene and pathway enrichment for in-depth understanding the underlying mechanism of our results. In previous researches, a large number of studies have elucidated the MAPK signaling, focal adhesion pathway, cGMP-PKG signaling pathway and etc. were closely or partially related to peritoneal metastasis of GC (63–67). Similar to the findings, the present study observed that 214 genes positively associated with PRIs enriched mainly in MAPK and focal adhesion pathway (**Figure 5A**), suggesting the major role of these two pathways taking on the peritoneal relapse of GC. Consistent with the results of our team before, several key molecules responsible for focal adhesion, including the family of integrin receptors and caveolin-1 (CAV-1) (68–70), involved in the peritoneal metastasis of GC, which were also shown in **Figure 5D**. Furthermore, by applying GSEA pathway enrichment, we also demonstrated the focal adhesion pathway, ECM receptor interaction, leukocyte transendothelial migration and TGF-β signaling pathway enriched almost in the patients with high PRIs (**Figure 5B**). In line with our findings, a previous research has indicated that peritoneal fibrosis induced by TGF-β provide a favorable environment for the dissemination of gastric cancer cells (67). In addition, the impaired cell-cell adhesion and enhanced cell-extracellular matrix (ECM) adhesion due to ECM remodeling and accumulation, has been recognized as an advancing factor of GC metastasis (71). This resource may offer mechanistic insights into the peritoneal metastasis of GC, suggesting the complex process is not only related to alteration of adhesive protein of tumors, but is also associated with microenvironment around the malignant tumor cells.

In particularly, patients with higher PRIs have higher expression levels of ICI genes (TIM-3, PD-L1 and CTLA-4). However, it is still controversial that PD-L1 expression is a favorable or adverse prognostic factor in GC according to previous researches (72–77). As illustrated before, TGF-β, IL-6, IL-10 and TIM3 could directly or indirectly promote EMT or peritoneal metastasis which was in line with our findings (78, 79), and it is reasonable to speculate that antibodies targeting these molecules may be a preferable choice for PR high risk subgroup. In fact, the experimental results have indicated the effect of anti-TIM-3 on the TME in variety tumors. A recent study illustrated the percentage of IFN-γ producing CD8+ T cells increased following anti-Tim-3 treatment to MC38 tumor bearing C57B6 mice, suggesting the enhancement of CD8+ T cell function in TME (80). Moreover, extensive data in preclinical tumor models and on-going I/II phase clinical trials in multiple tumors have shown the restoration of anti-tumor immunity by targeting Tim-3 (81), especially in combination with PD-1 blockade (82–84). Hence, based on our analysis about expression of immune related genes, emerging role of ICIs on application in the patients with GC, especially for the ones with high PR risk, are warranted to explore in the future.

Nevertheless, there are a few limitations that should be acknowledged. First, the study was based on publicly available datasets, and it was not possible to obtain the complete clinicopathologic parameters. This indicates the possibility that some patients with acute infection or immune system disorders, were inevitably included in this study. Ideally, such patients should have been excluded. Second, the public datasets in this study were based on two different platforms, though the RMA express were normalized, caution should be exerted when applying the conclusion of this study to samples tested using platforms other than GPL96 or GPL570. Finally, as all patients in the study were collected retrospectively, the potential bias due to unbalanced clinic characteristics with treatment heterogeneity could not be ignored. Thus, the results of our study should be validated in a prospective cohort of patients further.

In conclusion, this study illustrates the utility of immune cells infiltration in the prediction of PR of gastric cancer after surgery. The proposed PRIs model might provide more clinical information for shedding light on the improvement of personalized management of GC patients.

DATA AVAILABILITY STATEMENT

The datasets presented in this study can be found in online repositories. The names of the repository/repositories and accession number(s) can be found in the article/**Supplementary Material**.

AUTHOR CONTRIBUTIONS

CZ designed research and analyzed the data. DL provided clinical relevant opinions and wrote the discussion part. CL and YF Proofread the article. RY and YL helped collect data. YS and XC helped modified the discussion part. XQ supervised all works. All authors contributed to the article and approved the submitted version.

FUNDING

This work was mainly supported by National Natural Science Foundation of China (NO.82003296, 81972751, 81602098, 81972331);Natural Science Foundation of Liaoning Province (2020-bs-040); Technological Special Project of Liaoning Province of China (2019020176-JH1/103); Science and Technology Plan Project of Liaoning Province (NO.2013225585); The General Projects of Liaoning Province Colleges and Universities (LFWK201706).

SUPPLEMENTARY MATERIAL

The Supplementary Material for this article can be found online at: https://www.frontiersin.org/articles/10.3389/fimmu.2021.651033/full#supplementary-material

REFERENCES

1. Bray F, Ferlay J, Soerjomataram I, Siegel RL, Torre LA, Jemal A. Global Cancer Statistics 2018: GLOBOCAN Estimates of Incidence and Mortality Worldwide for 36 Cancers in 185 Countries. *Ca-Cancer J Clin* (2018) 68 (6):394–424. doi: 10.3322/caac.21492
2. Yoo CH, Noh SH, Shin DW, Choi SH, Min JS. Recurrence Following Curative Resection for Gastric Carcinoma. *Br J Surg* (2000) 87(2):236–42. doi: 10.1046/j.1365-2168.2000.01360.x
3. Abe S, Yoshimura H, Tabara H, Tachibana M, Monden N, Nakamura T, et al. Curative Resection of Gastric Cancer: Limitation of Peritoneal Lavage Cytology in Predicting the Outcome. *J Surg Oncol* (1995) 59(4):226–9. doi: 10.1002/jso.2930590405
4. Bonnot PE, Piessen G, Kepenekian V, Decullier E, Pocard M, Meunier B, et al. Cytoreductive Surgery With or Without Hyperthermic Intraperitoneal Chemotherapy for Gastric Cancer With Peritoneal Metastases (Cyto-CHIP Study): A Propensity Score Analysis. *J Clin Oncol* (2019) 37(23):2028–40. doi: 10.1200/JCO.18.01688
5. Yang XJ, Huang CQ, Suo T, Mei LJ, Yang GL, Cheng FL, et al. Cytoreductive Surgery and Hyperthermic Intraperitoneal Chemotherapy Improves Survival of Patients With Peritoneal Carcinomatosis From Gastric Cancer: Final Results of a Phase III Randomized Clinical Trial. *Ann Surg Oncol* (2011) 18 (6):1575–81. doi: 10.1245/s10434-011-1631-5
6. Glehen O, Gilly FN, Arvieux C, Cotte E, Boutitie F, Mansvelt B, et al. Peritoneal Carcinomatosis From Gastric Cancer: A Multi-Institutional Study of 159 Patients Treated by Cytoreductive Surgery Combined With Perioperative Intraperitoneal Chemotherapy. *Ann Surg Oncol* (2010) 17 (9):2370–7. doi: 10.1245/s10434-010-1039-7
7. Gentles AJ, Newman AM, Liu CL, Bratman SV, Feng W, Kim D, et al. The Prognostic Landscape of Genes and Infiltrating Immune Cells Across Human Cancers. *Nat Med* (2015) 21(8):938–45. doi: 10.1038/nm.3909
8. Fridman WH, Pages F, Sautes-Fridman C, Galon J. The Immune Contexture in Human Tumours: Impact on Clinical Outcome. *Nat Rev Cancer* (2012) 12 (4):298–306. doi: 10.1038/nrc3245
9. Whiteside TL. The Tumor Microenvironment and its Role in Promoting Tumor Growth. *Oncogene* (2008) 27(45):5904–12. doi: 10.1038/onc.2008.271
10. Schreiber RD, Old LJ, Smyth MJ. Cancer Immunoediting: Integrating Immunity's Roles in Cancer Suppression and Promotion. *Sci (New York NY)* (2011) 331(6024):1565–70. doi: 10.1126/science.1203486
11. Grenader T, Waddell T, Peckitt C, Oates J, Starling N, Cunningham D, et al. Prognostic Value of Neutrophil-to-Lymphocyte Ratio in Advanced Oesophago-Gastric Cancer: Exploratory Analysis of the REAL-2 Trial. *Ann Oncol* (2016) 27(4):687–92. doi: 10.1093/annonc/mdw012
12. Mori M, Shuto K, Kosugi C, Narushima K, Hayashi H, Matsubara H, et al. An Increase in the Neutrophil-to-Lymphocyte Ratio During Adjuvant Chemotherapy Indicates a Poor Prognosis in Patients With Stage II or III Gastric Cancer. *BMC Cancer* (2018) 18(1):1261. doi: 10.1186/s12885-018-5171-2
13. Hennequin A, Derangere V, Boidot R, Apetoh L, Vincent J, Orry D, et al. Tumor Infiltration by Tbet+ Effector T Cells and CD20+ B Cells is Associated With Survival in Gastric Cancer Patients. *Oncoimmunology* (2016) 5(2): e1054598. doi: 10.1080/2162402X.2015.1054598
14. Lee HE, Chae SW, Lee YJ, Kim MA, Lee HS, Lee BL, et al. Prognostic Implications of Type and Density of Tumour-Infiltrating Lymphocytes in Gastric Cancer. *Br J Cancer* (2008) 99(10):1704–11. doi: 10.1038/sj.bjc.6604738
15. Zhang R, Li F, Li H, Yu J, Ren X. The Clinical Significance of Memory T Cells and its Subsets in Gastric Cancer. *Clin Transl Oncol* (2014) 16(3):257–65. doi: 10.1007/s12094-013-1066-5
16. Zhang WJ, Zhou ZH, Guo M, Yang LQ, Xu YY, Pang TH, et al. High Infiltration of Polarized Cd163(+) Tumor-Associated Macrophages Correlates With Aberrant Expressions of CSCs Markers, and Predicts Prognosis in Patients With Recurrent Gastric Cancer. *J Cancer* (2017) 8(3):363–70. doi: 10.7150/jca.16730

17. Song H, Wang T, Tian L, Bai S, Chen L, Zuo Y, et al. Macrophages on the Peritoneum are Involved in Gastric Cancer Peritoneal Metastasis. *J Cancer* (2019) 10(22):5377–87. doi: 10.7150/jca.31787
18. Zeng D, Li M, Zhou R, Zhang J, Sun H, Shi M, et al. Tumor Microenvironment Characterization in Gastric Cancer Identifies Prognostic and Immunotherapeutically Relevant Gene Signatures. *Cancer Immunol Res* (2019) 7(5):737–50. doi: 10.1158/2326-6066.CIR-18-0436
19. Zeng D, Zhou R, Yu Y, Luo Y, Zhang J, Sun H, et al. Gene Expression Profiles for a Prognostic Immunoscore in Gastric Cancer. *Br J Surg* (2018) 105 (10):1338–48. doi: 10.1002/bjs.10871
20. Cristescu R, Lee J, Nebozhyn M, Kim KM, Ting JC, Wong SS, et al. Molecular Analysis of Gastric Cancer Identifies Subtypes Associated With Distinct Clinical Outcomes. *Nat Med* (2015) 21(5):449–56. doi: 10.1038/nm.3850
21. Subramanian A, Tamayo P, Mootha VK, Mukherjee S, Ebert BL, Gillette MA, et al. Gene Set Enrichment Analysis: A Knowledge-Based Approach for Interpreting Genome-Wide Expression Profiles. *Proc Natl Acad Sci United States America* (2005) 102(43):15545–50. doi: 10.1073/pnas.0506580102
22. Bindea G, Mlecnik B, Tosolini M, Kirilovsky A, Waldner M, Obenauf AC, et al. Spatiotemporal Dynamics of Intratumoral Immune Cells Reveal the Immune Landscape in Human Cancer. *Immunity* (2013) 39(4):782–95. doi: 10.1016/j.immuni.2013.10.003
23. Hänzelmann S, Castelo R, Guinney J. GSVA: Gene Set Variation Analysis for Microarray and RNA-seq Data. *BMC Bioinf* (2013) 14:7. doi: 10.1186/1471-2105-14-7
24. Tibshirani R. The Lasso Method for Variable Selection in the Cox Model. *Stat Med* (1997) 16(4):385–95. doi: 10.1002/(sici)1097-0258(19970228)16:4<385::aid-sim380>3.0.co;2-3
25. Yu G, Wang LG, Han Y, He QY. clusterProfiler: An R Package for Comparing Biological Themes Among Gene Clusters. *Omics J Integr Biol* (2012) 16 (5):284–7. doi: 10.1089/omi.2011.0118
26. Ohi M, Mori K, Toiyama Y, Mohri Y, Okigami M, Yasuda H, et al. Preoperative Prediction of Peritoneal Metastasis in Gastric Cancer as an Indicator for Neoadjuvant Treatment. *Anticancer Res* (2015) 35(6):3511–8.
27. Kwee RM, Kwee TC. Modern Imaging Techniques for Preoperative Detection of Distant Metastases in Gastric Cancer. *World J Gastroenterol* (2015) 21 (37):10502–9. doi: 10.3748/wjg.v21.i37.10502
28. Mocellin S, Pasquali S. Diagnostic Accuracy of Endoscopic Ultrasonography (EUS) for the Preoperative Locoregional Staging of Primary Gastric Cancer. *Cochrane Database Syst Rev* (2015) 2015(2):CD009944. doi: 10.1002/14651858.CD009944.pub2
29. Maegerlein C, Fingerle AA, Souvatzoglou M, Rummeny EJ, Holzapfel K. Detection of Liver Metastases in Patients With Adenocarcinomas of the Gastrointestinal Tract: Comparison of (18)F-FDG PET/CT and MR Imaging. *Abdom Imaging* (2015) 40(5):1213–22. doi: 10.1007/s00261-014-0283-x
30. Soussan M, Des Guetz G, Barrau V, Aflalo-Hazan V, Pop G, Mehanna Z, et al. Comparison of FDG-PET/CT and MR With Diffusion-Weighted Imaging for Assessing Peritoneal Carcinomatosis From Gastrointestinal Malignancy. *Eur Radiol* (2012) 22(7):1479–87. doi: 10.1007/s00330-012-2397-2
31. Borggreve AS, Goense L, Brenkman HJF, Mook S, Meijer GJ, Wessels FJ, et al. Imaging Strategies in the Management of Gastric Cancer: Current Role and Future Potential of MRI. *Br J Radiol* (2019) 92(1097):20181044. doi: 10.1259/bjr.20181044
32. Seevaratnam R, Cardoso R, McGregor C, Lourenco L, Mahar A, Sutradhar R, et al. How Useful is Preoperative Imaging for Tumor, Node, Metastasis (TNM) Staging of Gastric Cancer? A meta-analysis. *Gastric Cancer* (2012) 15 Suppl 1:S3–18. doi: 10.1007/s10120-011-0069-6
33. Renzulli M, Clemente A, Spinelli D, Ierardi AM, Marasco G, Farina D, et al. Gastric Cancer Staging: Is it Time for Magnetic Resonance Imaging? *Cancers (Basel)* (2020) 12(6):1402. doi: 10.3390/cancers12061402
34. Wang FH, Shen L, Li J, Zhou ZW, Liang H, Zhang XT, et al. The Chinese Society of Clinical Oncology (CSCO): Clinical Guidelines for the Diagnosis and Treatment of Gastric Cancer. *Cancer Commun (Lond)* (2019) 39(1):10. doi: 10.1186/s40880-019-0349-9
35. Smyth EC, Verheij M, Allum W, Cunningham D, Cervantes A, Arnold D, et al. Gastric Cancer: ESMO Clinical Practice Guidelines for Diagnosis, Treatment and Follow-Up. *Ann Oncol* (2016) 27(suppl 5):v38–49. doi: 10.1093/annonc/mdw350
36. Ozkan E, Araz M, Soydal C, Kucuk ON. The Role of 18F-FDG-PET/CT in the Preoperative Staging and Posttherapy Follow Up of Gastric Cancer: Comparison With Spiral CT. *World J Surg Oncol* (2011) 9:75. doi: 10.1186/1477-7819-9-75
37. 中国抗癌协会胃癌专业委员会. 胃癌腹膜转移防治中国专家共识. 中华胃肠外科杂志 (2017) 20(5):481–90. doi: 10.3760/cma.j
38. Lopez-Soto A, Gonzalez S, Smyth MJ, Galluzzi L. Control of Metastasis by NK Cells. *Cancer Cell* (2017) 32(2):135–54. doi: 10.1016/j.ccell.2017.06.009
39. Vences-Catalan F, Rajapaksa R, Srivastava MK, Marabelle A, Kuo CC, Levy R, et al. Tetraspanin CD81 Promotes Tumor Growth and Metastasis by Modulating the Functions of T Regulatory and Myeloid-Derived Suppressor Cells. *Cancer Res* (2015) 75(21):4517–26. doi: 10.1158/0008-5472.CAN-15-1021
40. Liu Y, Gu Y, Han Y, Zhang Q, Jiang Z, Zhang X, et al. Tumor Exosomal Rnas Promote Lung Pre-metastatic Niche Formation by Activating Alveolar Epithelial TLR3 to Recruit Neutrophils. *Cancer Cell* (2016) 30(2):243–56. doi: 10.1016/j.ccell.2016.06.021
41. Wculek SK, Malanchi I. Author Correction: Neutrophils Support Lung Colonization of Metastasis-Initiating Breast Cancer Cells. *Nature* (2019) 571(7763):E2. doi: 10.1038/s41586-019-1328-7
42. Georgoudaki AM, Prokopec KE, Boura VF, Hellqvist E, Sohn S, Ostling J, et al. Reprogramming Tumor-Associated Macrophages by Antibody Targeting Inhibits Cancer Progression and Metastasis. *Cell Rep* (2016) 15(9):2000–11. doi: 10.1016/j.celrep.2016.04.084
43. Senovilla L, Vacchelli E, Galon J, Adjemian S, Eggermont A, Fridman WH, et al. Trial Watch: Prognostic and Predictive Value of the Immune Infiltrate in Cancer. *Oncoimmunology* (2012) 1(8):1323–43. doi: 10.4161/onci.22009
44. Ma Z, Li W, Yoshiya S, Xu Y, Hata M, El-Darawish Y, et al. Augmentation of Immune Checkpoint Cancer Immunotherapy With IL18. *Clin Cancer Res* (2016) 22(12):2969–80. doi: 10.1158/1078-0432.CCR-15-1655
45. Fujimori D, Kinoshita J, Yamaguchi T, Nakamura Y, Gunjigake K, Ohama T, et al. Established Fibrous Peritoneal Metastasis in an Immunocompetent Mouse Model Similar to Clinical Immune Microenvironment of Gastric Cancer. *BMC Cancer* (2020) 20(1):1014. doi: 10.1186/s12885-020-07477-x
46. Tian L, Goldstein A, Wang H, Ching Lo H, Sun Kim I, Welte T, et al. Mutual Regulation of Tumour Vessel Normalization and Immunostimulatory Reprogramming. *Nature* (2017) 544(7649):250–4. doi: 10.1038/nature21724
47. Hanna RN, Cekic C, Sag D, Tacke R, Thomas GD, Nowyhed H, et al. Patrolling Monocytes Control Tumor Metastasis to the Lung. *Science* (2015) 350(6263):985–90. doi: 10.1126/science.aac9407
48. Sun JC, Lanier LL. NK Cell Development, Homeostasis and Function: Parallels With CD8(+) T Cells. *Nat Rev Immunol* (2011) 11(10):645–57. doi: 10.1038/nri3044
49. Cerwenka A, Lanier LL. Natural Killer Cell Memory in Infection, Inflammation and Cancer. *Nat Rev Immunol* (2016) 16(2):112–23. doi: 10.1038/nri.2015.9
50. Jiang Y, Zhang Q, Hu Y, Li T, Yu J, Zhao L, et al. ImmunoScore Signature: A Prognostic and Predictive Tool in Gastric Cancer. *Ann Surg* (2018) 267 (3):504–13. doi: 10.1097/SLA.0000000000002116
51. Saito H, Osaki T, Ikeguchi M. Decreased NKG2D Expression on NK Cells Correlates With Impaired NK Cell Function in Patients With Gastric Cancer. *Gastric Cancer* (2012) 15(1):27–33. doi: 10.1007/s10120-011-0059-8
52. Mao Z, Zhang J, Shi Y, Li W, Shi H, Ji R, et al. CXCL5 Promotes Gastric Cancer Metastasis by Inducing Epithelial-Mesenchymal Transition and Activating Neutrophils. *Oncogenesis* (2020) 9(7):63. doi: 10.1038/s41389-020-00249-z
53. Subhash VV, Yeo MS, Tan WL, Yong WP. Strategies and Advancements in Harnessing the Immune System for Gastric Cancer Immunotherapy. *J Immunol Res* (2015) 2015:308574. doi: 10.1155/2015/308574
54. Rhee I, Zhong MC, Reizis B, Cheong C, Veillette A. Control of Dendritic Cell Migration, T Cell-Dependent Immunity, and Autoimmunity by Protein Tyrosine Phosphatase PTPN12 Expressed in Dendritic Cells. *Mol Cell Biol* (2014) 34(5):888–99. doi: 10.1128/MCB.01369-13
55. Chang LL, Wang SW, Wu IC, Yu FJ, Su YC, Chen YP, et al. Impaired Dendritic Cell Maturation and IL-10 Production Following H. pylori stimulation in gastric cancer patients. *Appl Microbiol Biotechnol* (2012) 96 (1):211–20. doi: 10.1007/s00253-012-4034-z

56. Kim JE, Lee JY, Kang MJ, Jeong YJ, Choi JA, Oh SM, et al. Withaferin A Inhibits Helicobacter Pylori-Induced Production of IL-1beta in Dendritic Cells by Regulating NF-Kappab and NLRP3 Inflammasome Activation. *Immune Netw* (2015) 15(6):269–77. doi: 10.4110/in.2015.15.6.269
57. Zhao YB, Yang SH, Shen J, Deng K, Li Q, Wang Y, et al. Interaction Between Regulatory T Cells and Mast Cells Via IL-9 and TGF-beta Production. *Oncol Lett* (2020) 20(6):360. doi: 10.3892/ol.2020.12224
58. Ammendola M, Sacco R, Zuccala V, Luposella M, Patruno R, Gadaleta P, et al. Mast Cells Density Positive to Tryptase Correlate With Microvascular Density in Both Primary Gastric Cancer Tissue and Loco-Regional Lymph Node Metastases From Patients That Have Undergone Radical Surgery. *Int J Mol Sci* (2016) 17(11):1905. doi: 10.3390/ijms17111905
59. Su Z, Sun Y, Zhu H, Liu Y, Lin X, Shen H, et al. Th17 Cell Expansion in Gastric Cancer may Contribute to Cancer Development and Metastasis. *Immunol Res* (2014) 58(1):118–24. doi: 10.1007/s12026-013-8483-y
60. Lee K, Hwang H, Nam KT. Immune Response and the Tumor Microenvironment: How They Communicate to Regulate Gastric Cancer. *Gut Liver* (2014) 8(2):131–9. doi: 10.5009/gnl.2014.8.2.131
61. Okita Y, Ohira M, Tanaka H, Tokumoto M, Go Y, Sakurai K, et al. Alteration of CD4 T Cell Subsets in Metastatic Lymph Nodes of Human Gastric Cancer. *Oncol Rep* (2015) 34(2):639–47. doi: 10.3892/or.2015.4064
62. Speiser DE, Ho PC, Verdeil G. Regulatory Circuits of T Cell Function in Cancer. *Nat Rev Immunol* (2016) 16(10):599–611. doi: 10.1038/nri.2016.80
63. Wu S, Chen M, Huang J, Zhang F, Lv Z, Jia Y, et al. Orai2 Promotes Gastric Cancer Tumorigenicity and Metastasis Through PI3K/Akt Signaling and MAPK-dependent Focal Adhesion Disassembly. *Cancer Res* (2020) 81 (4):986–1000. doi: 10.1158/0008-5472.Can-20-0049
64. Dong H, Liu H, Zhou W, Zhang F, Li C, Chen J, et al. GLI1 Activation by non-Classical Pathway Integrin αβ/ERK1/2 Maintains Stem Cell-Like Phenotype of Multicellular Aggregates in Gastric Cancer Peritoneal Metastasis. *Cell Death Dis* (2019) 10: (8):574. doi: 10.1038/s41419-019-1776-x
65. Ichikawa T, Okugawa Y, Toiyama Y, Tanaka K, Yin C, Kitajima T, et al. Clinical Significance and Biological Role of L1 Cell Adhesion Molecule in Gastric Cancer. *Br J Cancer* (2019) 121: (12):1058–68. doi: 10.1038/s41416-019-0646-8
66. Zhang K, Yang G, Wu W, Zhang J, Xia X, Jiang T, et al. Decreased Expression of Caveolin-1 and E-Cadherin Correlates With the Clinicopathologic Features of Gastric Cancer and the EMT Process. *Recent Pat Anticancer Drug Discov* (2016) 11: (2):236–44. doi: 10.2174/1574892811666160128151437
67. Senbanjo L, Chellaiah M, Biology D. CD44: A Multifunctional Cell Surface Adhesion Receptor Is a Regulator of Progression and Metastasis of Cancer Cells. *Front Cell Dev Biol* (2017) 5:18. doi: 10.3389/fcell.2017.00018
68. Wang X, Che X, Yu Y, Cheng Y, Bai M, Yang Z, et al. Hypoxia-Autophagy Axis Induces VEGFA by Peritoneal Mesothelial Cells to Promote Gastric Cancer Peritoneal Metastasis Through an Integrin α5-Fibronectin Pathway. *J Exp Clin Cancer Res* (2020) 39: (1):221. doi: 10.1186/s13046-020-01703-x
69. Wang Y, Song Y, Che X, Zhang L, Wang Q, Zhang X, et al. Caveolin−1 Enhances RANKL−induced Gastric Cancer Cell Migration. *Oncol Rep* (2018) 40: (3):1287–96. doi: 10.3892/or.2018.6550
70. Zang D, Zhang C, Li C, Fan Y, Li Z, Hou K, et al. LPPR4 Promotes Peritoneal Metastasis Via Sp1/integrin α/FAK Signaling in Gastric Cancer. *Am J Cancer Res* (2020) 10: (3):1026–44. doi: 10.1200/jco.2016.34.4
71. Jang M, Koh I, Lee J, Lim J, Cheong J, Kim P. Increased Extracellular Matrix Density Disrupts E-Cadherin/β-Catenin Complex in Gastric Cancer Cells. *Biomater Sci* (2018) 6: (10):2704–13. doi: 10.1039/c8bm00843d
72. Shigemori T, Toiyama Y, Okugawa Y, Yamamoto A, Yin C, Narumi A, et al. Soluble PD-L1 Expression in Circulation as a Predictive Marker for Recurrence and Prognosis in Gastric Cancer: Direct Comparison of the Clinical Burden Between Tissue and Serum Pd-L1 Expression. *Ann Surg Oncol* (2019) 26(3):876–83. doi: 10.1245/s10434-018-07112-x
73. Ito S, Masuda T, Noda M, Hu Q, Shimizu D, Kuroda Y, et al. Prognostic Significance of PD-1, Pd-L1 and CD8 Gene Expression Levels in Gastric Cancer. *Oncology-Basel* (2020) 98(7):501–11. doi: 10.1159/000506075
74. Xing X, Guo J, Ding G, Li B, Dong B, Feng Q, et al. Analysis of PD1, Pdl1, PDL2 Expression and T Cells Infiltration in 1014 Gastric Cancer Patients. *Oncoimmunology* (2018) 7(3):e1356144. doi: 10.1080/2162402X.2017.1356144
75. Eto S, Yoshikawa K, Nishi M, Higashijima J, Tokunaga T, Nakao T, et al. Programmed Cell Death Protein 1 Expression is an Independent Prognostic Factor in Gastric Cancer After Curative Resection. *Gastric Cancer* (2016) 19 (2):466–71. doi: 10.1007/s10120-015-0519-7
76. Thompson ED, Zahurak M, Murphy A, Cornish T, Cuka N, Abdelfatah E, et al. Patterns of PD-L1 Expression and CD8 T Cell Infiltration in Gastric Adenocarcinomas and Associated Immune Stroma. *Gut* (2017) 66(5):794–801. doi: 10.1136/gutjnl-2015-310839
77. Wang Y, Zhu C, Song W, Li J, Zhao G, Cao H. Pd-L1 Expression and CD8(+) T Cell Infiltration Predict a Favorable Prognosis in Advanced Gastric Cancer. *J Immunol Res* (2018) 2018:4180517. doi: 10.1155/2018/4180517
78. Wu X, Tao P, Zhou Q, Li J, Yu Z, Wang X, et al. IL-6 Secreted by Cancer-Associated Fibroblasts Promotes Epithelial-Mesenchymal Transition and Metastasis of Gastric Cancer Via JAK2/STAT3 Signaling Pathway. *Oncotarget* (2017) 8 (13):20741–50. doi: 10.18632/oncotarget.15119
79. Wang R, Song S, Harada K, Ghazanfari Amlashi F, Badgwell B, Pizzi MP, et al. Multiplex Profiling of Peritoneal Metastases From Gastric Adenocarcinoma Identified Novel Targets and Molecular Subtypes That Predict Treatment Response. *Gut* (2020) 69(1):18–31. doi: 10.1136/gutjnl-2018-318070
80. Yang M, Du W, Yi L, Wu S, He C, Zhai W, et al. Checkpoint Molecules Coordinately Restrain Hyperactivated Effector T Cells in the Tumor Microenvironment. *Oncoimmunology* (2020) 9(1):1708064. doi: 10.1080/2162402x.2019.1708064
81. Acharya N, Sabatos-Peyton C, Anderson AC. Tim-3 Finds its Place in the Cancer Immunotherapy Landscape. *J Immunother Cancer* (2020) 8(1): e000911. doi: 10.1136/jitc-2020-000911
82. Sakuishi K, Apetoh L, Sullivan JM, Blazar BR, Kuchroo VK, Anderson AC. Targeting Tim-3 and PD-1 Pathways to Reverse T Cell Exhaustion and Restore Anti-Tumor Immunity. *J Exp Med* (2010) 207(10):2187–94. doi: 10.1084/jem.20100643
83. Ngiow SF, von Scheidt B, Akiba H, Yagita H, Teng MW, Smyth MJ. Anti-TIM3 Antibody Promotes T Cell IFN-γ-Mediated Antitumor Immunity and Suppresses Established Tumors. *Cancer Res* (2011) 71(10):3540–51. doi: 10.1158/0008-5472.Can-11-0096
84. Zhou Q, Munger ME, Veenstra RG, Weigel BJ, Hirashima M, Munn DH, et al. Coexpression of Tim-3 and PD-1 Identifies a CD8+ T-Cell Exhaustion Phenotype in Mice With Disseminated Acute Myelogenous Leukemia. *Blood* (2011) 117(17):4501–10. doi: 10.1182/blood-2010-10-310425

Conflict of Interest: The authors declare that the research was conducted in the absence of any commercial or financial relationships that could be construed as a potential conflict of interest.

Copyright © 2021 Zhang, Li, Yu, Li, Song, Chen, Fan, Liu and Qu. This is an open-access article distributed under the terms of the Creative Commons Attribution License (CC BY). The use, distribution or reproduction in other forums is permitted, provided the original author(s) and the copyright owner(s) are credited and that the original publication in this journal is cited, in accordance with accepted academic practice. No use, distribution or reproduction is permitted which does not comply with these terms.

frontiers in Immunology

REVIEW
published: 21 May 2021
doi: 10.3389/fimmu.2021.683332

IL-35 Regulates the Function of Immune Cells in Tumor Microenvironment

*Kewei Liu†, Ai Huang†, Jun Nie, Jun Tan, Shijie Xing, Yue Qu and Ke Jiang**

Department of Thoracic Surgery, Union Hospital, Tongji Medical College, Huazhong University of Science and Technology, Wuhan, China

OPEN ACCESS

Edited by:
Keqiang Chen, National Cancer Institute at Frederick, United States

Reviewed by:
Pablo Iribarren, CONICET Centre for Research in Clinical Biochemistry and Immunology (CIBICI), Argentina
Zhihua Kou, Fudan University, China
Peng Tang, Army Medical University, China

***Correspondence:**
Ke Jiang
kkkj_77@aliyun.com

†These authors have contributed equally to this work and share first authorship

Specialty section:
This article was submitted to Cancer Immunity and Immunotherapy, a section of the journal Frontiers in Immunology

Received: *20 March 2021*
Accepted: *11 May 2021*
Published: *21 May 2021*

Citation:
Liu K, Huang A, Nie J, Tan J, Xing S, Qu Y and Jiang K (2021) IL-35 Regulates the Function of Immune Cells in Tumor Microenvironment. Front. Immunol. 12:683332. doi: 10.3389/fimmu.2021.683332

Interleukin-35 (IL-35) is a heterodimeric cytokine composed of Epstein-Barr virus-induced gene 3 (EBI3) and IL-12p35 that has recently been shown to play diverse and important roles in the tumor microenvironment (TME). Owing to its immunosuppressive activity and ability to promote tumor growth and progression, IL-35 is widely recognized as a key mediator of TME status. Immune cells are key mediators of diverse tumor-related phenotypes, and immunosuppressive cytokines such as IL-35 can promote tumor growth and metastasis in TME. These influences should be considered together. Since tumor immunotherapy based on immune checkpoint blockade remains ineffective in many patients due to tumoral resistance, a new target or efficacy enhancing factor is urgently needed. Suppressing IL-35 production and activity has been demonstrated as an effective factor that inhibits tumor cells viability, and further investigation of this cytokine is warranted. However, the mechanistic basis for IL-35-mediated regulation of immune cells in the TME remains to be fully clarified. In the present review, we explore the roles of IL-35 in regulating immune cells within the TME. In addition, we highlight IL-35 as a specific immunological target and discuss its possible relevance in the context of immunotherapy. Lastly, we sought to summarize potential future research directions that may guide the advancement of current understanding regarding the role of this important cytokine as a regulator of oncogenesis.

Keywords: tumor microenvironment, tumor immunotherapy, regulatory immune cells, anti-tumor immunity, IL-35

INTRODUCTION

The tumor microenvironment (TME) is a primary mediator of tumor progression, and its immunosuppressive characteristics represent a significant obstacle to solid tumor immunotherapy. The TME is composed of extracellular matrix (ECM) and non-malignant stromal cells (1). Tumor cells can readily respond to external factors and interact in a dynamic fashion with other cells within the TME (2), and the cells and cytokines within this environment can profoundly impact immune cell infiltration and proliferation and reduces the anti-cancer activity of endogenous tumor-infiltrating immune cells. Tumor-infiltrating immune cells are closely linked to tumor proliferation, angiogenesis, and metastasis (3, 4), with growth factors, chemokines, and matrix-degrading enzymes derived from these cells being conducive to aggressive tumor growth and

immune responses (5–7). Immune checkpoint blockade (ICB) therapies are now used to clinically treat a range of advanced cancer types, and enhancing immune cell activation represents a novel approach to killing tumor cells (8–10). In addition, tumor cells can suppress immune responses to thereby evade detection and clearance through mechanisms including immunosuppressive regulatory cell recruitment and/or the production of inhibitory cytokines (11).

Interleukin-35 (IL-35) is an IL-12 family cytokine (12), with other members of these family consisting of heterodimeric combinations of α (p40 and EBI3) and β (p19, p28 and p35) chain subunits, including IL-12 (p35 and p40), IL-23 (p19 and p40), IL-27 (p28 and EBI3), IL-35 (p35 and EBI3), and the newly discovered member IL-39 (IL-23p19 and EBI3) (13, 14). Unlike other IL-12 family members, IL-35 has been shown to exhibit immunosuppressive activity (15). First identified by Collison et al. (16), IL-35 has since been shown to be an important regulator of tumor progression owing to its ability to drive the establishment of an immunosuppressive microenvironment (15, 17, 18). IL-35 expression within the TME can promote primary tumor cell growth and metastatic colonization at a secondary site (19, 20), signaling through a receptor composed of gp130 and IL-12Rβ2 to induce downstream Ebi3 and IL-12a transcription and the activation of a classical JAK-STAT signaling pathway (15, 21). STAT1 phosphorylation occurs upon IL-35 binding to gp130, whereas STAT4 phosphorylation occurs upon IL-35 binding to IL-12Rβ2 (22). IL-35 exert immunosuppressive action through STAT1/STAT4 in T cells and STAT1 in B cells (23, 24). IL-35 is a cytokine that is responsible for immune system maintenance and for this inhibition of immune responses, functioning by promoting the expansion of regulatory T cells (Tregs) and regulatory B cells (Bregs) while simultaneously suppressing effector T cells, Th1 cells, Th17 cells, and macrophages (25). IL-35 can control the activity of immune cells within the TME, and these cells can, in turn, regulate local IL-35 expression and function (8, 15). For example, Tregs and Bregs produce IL-35 to regulate the immune response and to facilitate tumor growth by constraining the activation of innate and adaptive immune cells (26, 27). In this review, we explore the association between IL-35 and immune cells in the TME in order to demonstrate the broad applicability of IL-35 in tumor immunology.

THE ROLE OF IL-35 IN PROMOTING TUMOR GROWTH IN THE TME

IL-35 has been shown to play an essential role in development of benign and malignant tumors, including hepatocellular carcinoma (HCC), advanced breast cancer (BRCA), pancreatic ductal adenocarcinoma (PDAC), nonsmall cell lung cancer (NSCLC), and prostate carcinoma (PCA) (19, 20, 28, 29). Previously, Collison et al. proved that IL-35 was mainly produced by Tregs, and the expression of IL-35 in tumor cells has been gradually confirmed by Western Blot (WB) and RT-PCR analysis in recent years (19, 23). Zhu et al. found that rIL-35 can enhances malignant biological behavior of RM−1 cells in vitro compared with IL-35 neutralizing antibody treatment (19). In vivo, IL-35 has been demonstrated to promote tumor growth, progression and metastasis by enhancing the secretion of other cytokines, such as IL-6 and G-CSF (granulocyte colony stimulating factor) (30). Liu et al. confirmed that IL-35 also inhibit several cytokines including IFN-γ to achieve pro-tumor effect (31). Accumulated data indicated that IL-35 can participate in the interactions between malignant tumor cells and the surrounding immune cells in the TME, inducing an immunosuppressive environment and constraining the engagement of effective anti-tumor immune responses (32). As multiple IL-35$^+$ immune cell types like M1-TAMs and DCs have been discovered and isolated, current evidence indicates that tumor-derived IL-35 has been widely implicated in pro-tumorigenic properties of different cellular contexts, likely *via* suppressing tumor-infiltrating lymphocytes (TILs) infiltration and effector cell proliferation (20, 32, 33). Overall, IL-35 produced by the malignant tumor cells as well as surrounding stromal cells contributes to immunosuppression within the tumor microenvironment thereby supports sustained tumor growth and metastasis.

IL-35 AND IMMUNE CELLS IN THE TME

TME consist of functional altered stromal cells [cancer-associated fibroblasts (CAFs), vascular endothelial cell (VEC)], myeloid populations [dendritic cells, macrophages, and myeloid-derived suppressor cells (MDSCs)], and TILs [T cells, B cells, monocytes, tumor-associated neutrophils (TANs) and natural killer (NK) cells)]. In early 2016, Pylayeva-Gupta et al. have mentioned that one of the IL-35 receptors, gp130, has been found on multiple immune cell types and the potential role of IL-35 was conceived through association involving tumor and stromal cells (34). In addition to the widespread expression of IL-35, immune cells are the main producers of IL-35 compared with tumor cells. While previous articles regarded Tregs or iTr35 cells as significant IL-35 producers (Collison et al.), IL-35 is also secreted by B cells, DCs, endothelial cells and macrophages (16, 35). In addition, NK cells, Tans, monocytes and MDSCs can also participate in bidirectional interactions between IL-35 and immune cells above (36). At the same time, IL-35 is involved in the myeloid cells recruitment and suppress differentiation of anti-tumor cytotoxic T lymphocytes (CTLs), NK cells and other effector immune cells at the tumor site (36, 37).

Interactions Between IL-35 and T Cells in the TME

T cell interactions with tumor cells in the TME has the potential to result in T cell activation and spontaneous anti-tumor immunity (38). IL-35 can influence the transcription and expression of T cell immune response-related differentially expressed genes in tumor tissues (31), but the immunosuppressive activity of this cytokine is primarily attributable to its inhibition of CD4$^+$ and CD8$^+$T cells and of anti-tumor immune responses (**Figure 1**) (39). IL-35

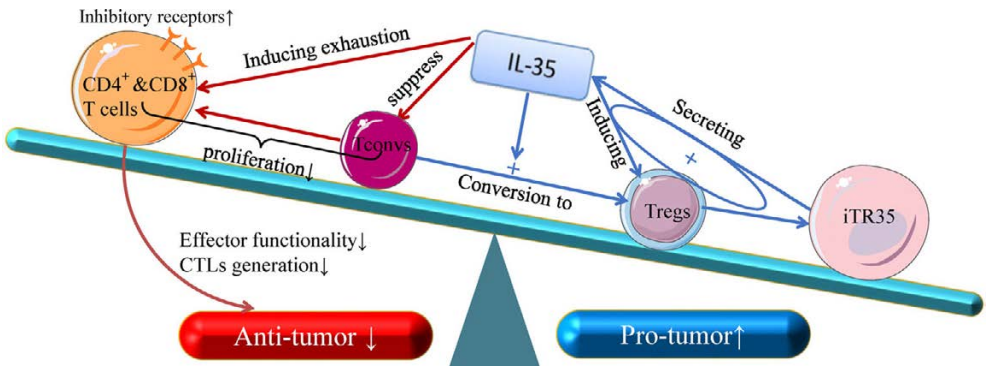

FIGURE 1 | The anti- and pro-tumor effects of T-cell subsets in response to IL-35. Recent insight into the biology of IL-35 suggests that it can both suppress naive T cells (Tconv cells) and convert these naive Tconv cells into strongly suppressive induced Treg cells (iTr35 cells). Through a positive feedback loop associated with the expression of IL-35, Treg cells can inhibit the differentiation of $CD4^+$ T cells into Th17 and Th1 cells. In addition, IL-35 is dispensable for the control of $CD8^+$ T cells, and IL-3- dependent transcription signal depletion as well as the inhibitory receptor activation of $CD8^+$ T cells play key roles in reducing CTL effector functions, which are critical for cellular anti-tumor responses. Given its broad immunoregulatory properties and its pro-tumor functions, IL-35 represents an important functional cytokine for Tregs that is secreted by multiple immunosuppressive cell subsets.

derived from Tregs within tumors can induce $CD4^+$and $CD8^+$ T cell exhaustion, reducing their effector functionality and impairing the generation of CTLs (31, 40). However, IL-35 does not directly suppress these CTLs, instead downregulating the costimulatory molecule CD28 on the surface of immature $CD8^+$ T cells and thereby interfering with their ability to differentiate into anti-tumor CTLs. IL-35 can also disrupt Th1 cell activation to suppress differentiated anti-tumor CTL activity (41). IL-35 does not alter the survival of the A549 ADC cell line or the H520 SCC cell line cultured with IL-35, suggesting that the immunosuppressive functions of IL-35 necessitate the presence of the TME *in vivo*, as this cytokine does not seem to influence tumor cells *in vitro* (39). Together, these results suggest that IL-35 can suppress the activation of tumor-infiltrating T cells and anti-tumor CTLs, specifically promoting tumor development within the TME (31, 39, 41).

Tregs are key immunomodulatory cells within the TME, wherein the control tumor growth, migration, and local immunity (42, 43). Tregs have been shown to secrete both IL-10 and IL-35 (16, 44), and are present within tumor-draining lymph nodes wherein they can be stratified into Treg subsets secreting either IL-10 or IL-35. Cooperation between these two cytokines can drive conventional T cell failure and BLIMP1 upregulation-mediated transcriptional signal depletion in tumor-infiltrating $CD8^+$T cell (45, 46). IL-35 can influence the function of T cells by modulating their expression of inhibitory cell surface receptors (IRs) and their ability to secrete effective cytokines (31). Inhibitory receptors including CTLA4 (cytotoxic T lymphocyte-associated protein 4), PD-1 (programmed cell death ligand 1 or CD279), Tim-3 (T-cell immunoglobulin and mucin-domain containing 3), and LAG-3 (lymphocyte activation 3) have been identified as hallmarks of dysfunctional T cells (47). IL-35 can specifically increase the expression of these receptors on CD4 and $CD8^+$ tumor-infiltrating lymphocytes (TILs) within the TME, thereby depleting local T cells (45, 46). Tregs can also convert between the expression of IL-10 and IL-35, enabling them to adapt to the dynamic TME (40). Conventional T cells can differentiate into Tregs in response to IL-35-mediated STAT1/STAT3 signaling, yielding so-called iTr35 cells (48), which can mediate the relationship between IL-35 and tumor cells in TME, accelerating tumor cell growth and metastasis (22, 28). In addition, iTR35-derived IL-35 can drive the differentiation of other Tregs towards an iTr35 phenotype, creating a positive feedback loop that can control TME activity over extended periods of time (48, 49). Notch signaling blockade can also alleviate the inhibitory functions of purified Tregs from gastric carcinoma patients, which can increase the secretion of IL-35, confirming the close feedback relationship between IL-35 and Tregs (50).

Intriguingly, IL-35 improve anti-tumor activity *via* the WNT/β-catenin pathway, suggesting that IL-35 plays distinct roles in different signaling pathways (51). The activation of the β-catenin pathway has recently been shown to be associated with most human tumors exhibiting spontaneous T cell infiltration (52). β-catenin maintains Treg function and contributes to regulated IL-10 production within the TME, and its expression is inhibited by IL-35 (53–55). Overexpressing IL-35 inhibits colon cancer cell migration, invasion, proliferation, and colony formation by suppressing this β-catenin pathway (51). The WNT/β-catenin pathway may thus represent a novel mechanism whereby IL-35 can influence tumor progression, highlighting this as an additional avenue for the study of IL-35 use in the context of tumor immunotherapy.

Interactions Between IL-35 and B Cells in the TME

The role of B cells within the TME remains a matter of controversy, with some evidence suggesting that these cells can promote or inhibit tumor progression *via* a range of immunomodulatory mechanisms (8, 56). B cells are known to

regulate immunity by producing specific antibodies, forming antibody-antigen complexes, secreting cytokines, and serving as antigen-presenting cells to promote cytotoxic T cell responses (57, 58). Tumor-infiltrating B cells in the TME have been shown to promote tumor progression through interactions with macrophages, MDSCs, and other immune cells by secreting cytokines such as IL-10, TGF-β, and IL-35 (56, 59). B cells also exhibit distinct phenotypes under different TME conditions, with Bregs being a recently identified B cell subtype exhibiting immunosuppressive functions (60, 61). Much like Tregs, Breg recruitment can result in the modulation of local cellular responses through the production of IL-35 and other regulatory cytokines (62). In mouse models of breast cancer, Bregs induce T cell differentiation into Tregs and thereby accelerate tumor growth and lung metastasis (63).

Several early studies of Breg-like cells that produce IL-10 (B10 cells) were conducted, underscoring the regulatory roles of these cells in a range of different tissues and immunological contexts (64, 65). However, recent evidence suggests that IL-35 is a key Breg cytokine that can drive conventional B cells and B10 cells towards an IL-35-producing B cell (i35-Breg) phenotype (57, 66). In the TME associated with gastric and pancreatic tumors, these i35-Bregs are significantly more abundant and can promote tumor progression (**Figure 2**) (37, 67). In pancreatic tumors, inhibition of the Bruton's tyrosine kinase (BTK) signaling pathway reduces IL-35 and IL-10 expression and decreases i35-Breg cell function, suppressing tumor cell growth (67). Wang et al. determined that numbers of i35-Bregs were significantly increased in those with advanced gastric cancer, and found that the amount of these cells was associated with quantities of Tregs, MDSCs, B10 cells, and $CD14^+$ monocytes in the patients (37). As a specific B cell subtype, i35-Bregs can regulate other stromal cells within the TME including effector T cells, tumor-infiltrating MDSCs, NK cells, and macrophages (35, 37). As the specific molecular markers of Bregs are unclear, however, future in-depth analyses of IL-35 and Bregs are required to understand the immunological effects of i35-Bregs (37, 62).

Interactions Between IL-35 and Dendritic Cells in the TME

Dendritic cells (DCs) are key professional antigen-presenting cells (APCs) that promote antitumor immune responses by regulating T cell activation and proliferation, modulating immunological homeostasis within the TME. The migration of activated DCs into lymphatics can efficiently present antigens to T cells (68). DCs play a critical role in the initial activation of antitumor immunity by serving as an essential interface between antigen-independent innate immunity and antigen-specific adaptive immunity (69). Restoring the antigen-presenting activity of DCs thus represents an important approach to achieving efficacious tumor immunotherapy outcomes (69, 70). Seyerl et al. were the first to show that human rhinovirus-activated DCs (R-DCs) produced IL-35, driving $CD4^+$ T cell development into ITR35 cells (33). DCs have also been shown to markedly upregulate IL-35 in response to lipopolysaccharide

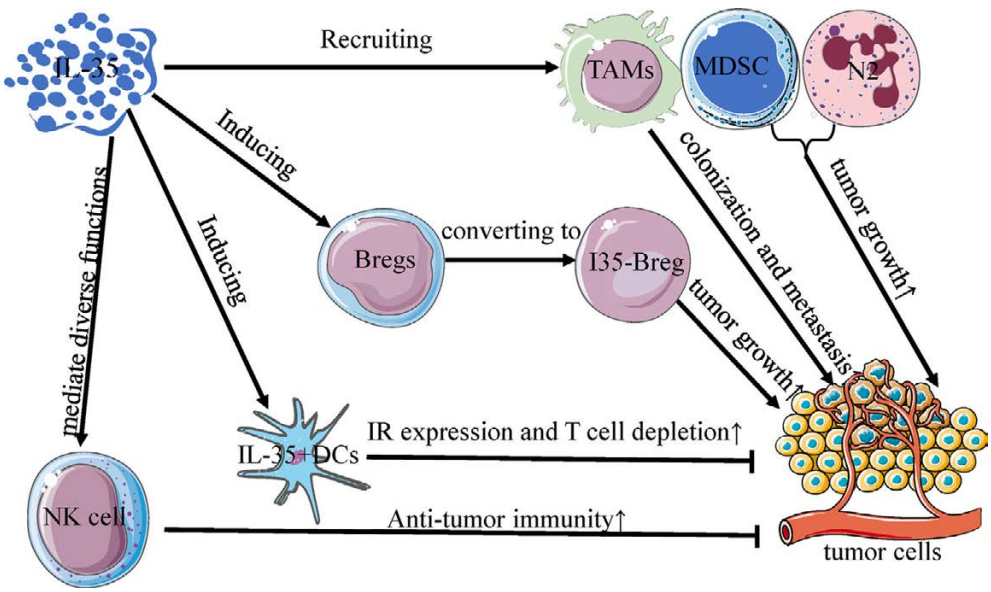

FIGURE 2 | Interactions between IL-35 and other immune cells in TME. IL-35 regulates the activity of immune cells in the tumor microenvironment, and is mainly produced by Bregs, DCs, NK cells, TAMs, MDSC, and N2 neutrophils. Much like the differentiation of Treg cells, IL-35 can convert Bregs to an active subset (I35-Bregs) which secrete IL-35 to promote tumor growth. With increased inhibitory receptor expression and T cell depletion, $IL\text{-}35^+$ DCs can slow primary tumor growth rates, unlike other $IL\text{-}35^+$ immune cells. Furthermore, IL-35 mediates diverse functions in NK cells and is obligatory for promoting the early NK cell-mediated responses to enhance primary anti-tumor immunity. TAMs, MDSCs, and N2 cells recruited by IL-35 can similarly potentiate primary tumor growth and metastatic colonization in the tumor microenvironment.

(LPS) stimulation, and there is evidence that IL-35 can suppress such LPS-triggered DC maturation and can influence the ability of DCs to produce factors including IL-10 and TGF-β (71, 72). IL-35$^+$ DCs and interacting T cells enrich P35 and Ebi3 expression, and mice vaccinated using IL-35$^+$ DCs exhibit enhanced tumor growth and reductions in T cells within the TME, consistent with the ability of this cytokine to constrain intratumoral immune responses (73, 74). Cytokine-induced killer (CIK) cells, a type of MHC-unrestricted CD3$^+$CD56$^+$ cytotoxic T lymphocytes, have also been found to exhibit anti-tumor activity as an immunotherapy target in certain malignancies (75, 76). Tregs and IL-35 levels increase in a time-dependent fashion in the context of CIK cell production, whereas DCs can inhibit such increases and enhance CIK cell cytotoxicity (77). As dendritic cell (DC)-CIK-mediated immunotherapy is an effective method for adoptive cell therapy, the potential role of IL-35 in combined CIK/DC-CIK therapy and chemotherapy warrants additional consideration (78, 79). IL-35 can also convert immunogenic CD8α-DCs into tolerogenic DCs. Such tolerance-induced DCs (TolDCs) also express IL-12p35 and Ebi3, and can upregulate Ebi3 and IL-12p35 when stimulated with IFN-γ, LPS, or CD40L (71). Such TolDCs may thus represent an important focus for future studies of interactions between IL-35 and DCs. Arginase-1 (Arg1) is a metabolic enzyme specifically expressed by DCs that functions as an immune checkpoint molecule associated with tumor immune escape, and it is also a downstream effector of IL-35 (39, 77). Downregulation of IL-35 within the TME can inhibit Arg1 expression and immunomodulatory activity, inducing immune escape and tumorigenesis (77).

Interactions Between IL-35 and Macrophages in the TME

Macrophages are among to most abundant immune cells within the TME, and they are broadly classified into the inflammatory, classically-activated M1 subtype and the pro-tumorigenic, alternatively-activated M2 subtype, which are referred to as tumor-associated macrophages (TAMs). TAMs, together with DCs, are members of APC populations in the TME and play important roles in tumor growth and progression, depending on their relative M1 or M2 polarization, respectively (80, 81). Relative to metastatic tumors, M2 markers are less abundant within primary tumors, wherein macrophages exhibit distinct activity. EBI3 and IL-12a, two subunits of IL-35, have been shown to be highly expressed in metastatic tumor-associated TAMs together. M2 cells in both humans and animal models express the IL-35 EBI3 subunit, which promotes macrophage differentiation, survival, and recruitment into the TME and maintains M2-like TAM cell functionality (20, 39, 82). Recruited by IL-35 from PDAC cells, macrophage express CXCL1 and CXCL8 to promote angiogenesis (83). Deletion of EBI3(EBI3$^{L/L\text{-}Tom}$) induced a decrease of M1-TAM population, while Sawant et al. observed a comparable advancement of it in IL-10-deficient mice (IL-10$^{L/L}$) (46). The biological interaction between IL-35 and M2 is also affected by some factors. IL-35 of M2 macrophages was suppressed by NRP1 expression in Stomach Adenocarcinoma (STAD), and the expressed cytokine was served as a major signal in the immune suppression mechanism of STAD (84). In the context of NSCLC, Heim et al. found that increased Arg1 mRNA expression was positively correlated with levels of IL-35$^+$ M2 cells and Tregs, whereas TNF-α expression fell as IL-35 expression increased. This suggests that IL-35$^+$ M2 cells produce Arg1 mRNA to induce or attract the production of iTr35 cells, thereby driving IL-35 production and associated responses (39). The number of CD68$^+$ macrophages in tumors has also been shown to decline and to be positively correlated with IL-35 levels in normal tissue, suggesting that there may be a distinct subset of macrophages expressing IL-35 within the TME (39). TAMs within primary tumors mainly secrete TNF-α to induce the process of epithelial-mesenchymal transition (EMT) which is an indispensable process that enhances the migratory and invasive abilities of tumor cells (20, 85). At metastatic sites, in contrast, TAMs produce IL-35 to reverse the EMT by activating JAK2-STAT6, GATA3, and other signaling pathways, thereby facilitating metastatic tissue colonization (20). Such TAM-mediated activity is believed to be a primary driver of NSCLC metastatic colonization of distal tissue sites (20).

Interactions Between IL-35 and Endothelial Cells/Monocytes in the TME

Angiogenesis, this process of tumor vascular growth is an inevitable program of tumor progression in the TME. It can promote the proliferation of epithelial cells by releasing several immunosuppressive cytokines and angiogenic growth factors. While secreted by endothelial cells and monocytes to less extent, the key role of IL-35 in angiogenesis should not be ignored. Wang et al. established a J558 mouse model and determined that IL-35 can induce the expression of CD31 and vascular endothelial growth factor (VEGF), inducing angiogenesis and endothelial cell activation (86).IL-35 also facilitates PDAC endothelial adhesion and transendothelial migration *in vitro via* the endothelial adhesion molecule, ICAM1 (29). With establishing a model system similar to the TME, Liao et al. confirmed that IL-35 from tumor cells, Tregs, and MDSCs promote the secretion of VEGF to attracts endothelial cells. In addition, monocytes are central players in angiogenesis and the source of pro-angiogenic cytokines. In early 2018, Huang et al. discovered that IL-35 increased the recruitment of monocytes to promote PDAC progression and monocyte-induced angiogenesis through IL-35-CXCL5 axis (C-C motif chemokine ligand 5) by RNA-seq and immunohistochemical analyses in xenograft mouse models (83). In PDAC samples from patients, they measured markers that can reflect the expression level of IL-35, such mRNA and protein. Not unexpectedly, the markers correlated with microvessel density and infiltration of monocyte lineage cells (83). Subsequently, Wang et al. identified that numbers of i35-Bregs were remarkably increased with the accumulation of CD14$^+$ monocytes (37). Moreover, IL-35 suppressed CD14$^+$ monocytes induced naive CD4$^+$ T cell activation and the production of TNF-α and granzyme B, inhibiting cytotoxicity of them, whereas this effect has not been

reported in TME (87). Further studies are needed to elucidate that function of IL-35 in the complex role of endothelial cells and monocytes during the angiogenesis in the TME.

Interactions Between IL-35 and Other Immune Cells in the TME

Prior studies have explored the interactions between IL-35 and other intratumoral immune cell populations not discussed above, such as neutrophils, MDSCs, and NK cells (88–90), although more research on these interactions is warranted. Anti-tumorigenic N1 neutrophils and pro-tumorigenic N2 neutrophils are two different subsets of neutrophils identified in previous studies (91). IL-35 has been shown to promote N2 neutrophil polarization by increasing G-CSF and IL-6 production, thereby enhancing the ability of these N2 cells to promote angiogenesis and to suppress immune responses, thereby enabling invasion of N2 cells into tumor tissue (30). MDSCs within the TME can secrete a range of immunosuppressive factors including IL-35, and in PCA model mice, high IL-35 levels were associated with increases in MDSC and Treg levels and reductions in $CD4^+$ and $CD8^+$ T cell frequencies within the spleen, blood, and TME, and with alterations in tumor growth, metastasis, and worse survival outcomes (19). Moreover, tumor-cell derived IL-35 was reported to promote tumor growth and angiogenesis through the enhancement of myeloid cell accumulation in the TME (92, 93). NK cells are important mediators of anti-tumor immune responses, and cytokines including IL-35, IL-12, IL-23, and IL-27 can modulate DC, macrophage, and NK cell functionality to directly and indirectly control NK cell immune responses (36, 94). While the mechanistic basis for these interactions remains to be clarified, there is clear evidence that IL-35 is likely to regulate a range of immune cell functions within the TME.

EXPLORATION OF IL-35 AND PD-1/PD-L1 IN CANCER IMMUNOTHERAPY

Programmed cell death protein 1 or its ligand (PD-1/PD-L1) are both important regulators of the TME (95, 96), and the emergence of antibody-based ICB therapies against PD-1/PD-L1 has led to an improved immunotherapy method of several cancer types (97). However, these treatments are effective only in a minority of cancer patients. In the present study, scholars sought to address those issues, and the interaction between IL-35 and PD-1/PD-L1 discovered by animal models or clinical samples may be a potential solution of it. Through Treg-restricted deletion of Ebi3 (subunit of IL-35), Turnis et al. originally demonstrated that IL-35 in tumor-infiltrating Treg cells can promote expression of PD-1 on the surface of the B16 tumor model T cells, leading to exhaustion of them (32). Sawant et al. similarly produced a loss of Treg cell-derived IL-10 or IL-35 model mice and observed a comparable reduction of PD-L1 expression to confirm that these cytokines can drive coordinated conventional T cell failure up regulating expression of PD-1. Yang et al. proved that IL-35 also stimulates PD-1 in peripheral $CD8^+$T cells in addition to tumor-infiltrating $CD8^+$T cells in HCC (98), and Dong et al. pointed-out that PD-L1 promotes the expansion of regulatory T cells and recruit more IL-35 in the TME, leading to AML cell proliferation (99). The connection between IL-35 and PD-1/PD-$L1^+$ non-T cells was also found beyond PD-1/PD-$L1^+$ T cells. Takahashi noticed that depletion of IL-35 decreased the number of PD-$L1^+$ B cells and constrains pancreatic tumor cell growth in the pancreata of Kc-IL-1β mice, an artificially constructed hybrid mouse overexpressing IL-1β (100).

Subsequently, the clinical samples confirm the above findings again. In NSCLC patient tumor tissues, IL-35^+ Tregs have been found to be positively correlated with TTF-1^+ (Thyroid transcription factor) PD-$L1^+$ cells confirmed by immunohistochemistry (IHC) staining (39). However, under conditions of growth factor-deprivation that yield cells sensitive to EGF (epidermal growth factor), IL-35 can inhibit expression of PD-$L1^+$ in the ADC (lung adenocarcinoma) tumor cell line without impacting EGFR (epidermal growth factor receptor) (**Figure 3**) (39). The above researchers have verified, extended and summarized the interaction between IL-35 and PD-1/PD-L1 on the surface of immune cells. However, in the DLBCL cases analyzed by Larousserie et al, a positive correlation between expression of IL-35 and PD-1 was not observed (101). This suggests that the administration of an anti-IL-35 antibody may be of value in the context of anti-PD-1 treatment, but it still needs to be further studied (39). Anti-PD-1 treatment can drive the activation of TILs that have otherwise lost their immunoreactive functionality, thereby restoring their proliferation and cytotoxicity such that the prognosis of treated treatment of NSCLC patients can be significantly improved (102, 103). Checkpoint inhibitor pneumonia (CIP) is a particularly dangerous form of immune-related adverse events (IrAE) that can arise in NSCLC patients receiving anti-PD-1/PD-L1 therapy (104, 105). Wang et al. discovered that the occurrence of CIP changes the proportion of T cell subsets in plasma, thereby promoting increased secretion of IL-35 in plasma and BALF (106). As such, measuring IL-35 levels may offer insight into the risk of developing CIP, and IL-35 may also represent a viable therapeutic target in patients undergoing tumor immunotherapy.

CONCLUSION

Undoubtedly, IL-35 is a regulator of tumor progression via the control of immune cell activities within the TME. IL-35 is primarily secreted by iTR35, and also secreted by tumor cells and other non-T immune cell subsets. IL-35 expression is evident on the surfaces of many immune cell types, potentially further influencing its ability to impact oncogenesis. Previous studies have revealed that tumors escape immune surveillance and immune attack to achieve tumor progression and metastasis by IL-35 in conjunction with regulatory immune cells (86). As discussed above, IL-35 is thought to be an important mediator of the host immune response and tumor survival which has specific immunosuppressive activity, functioning by modulating local inflammatory responses and anti-tumor immunity in the TME (32). The discovery that IL-35

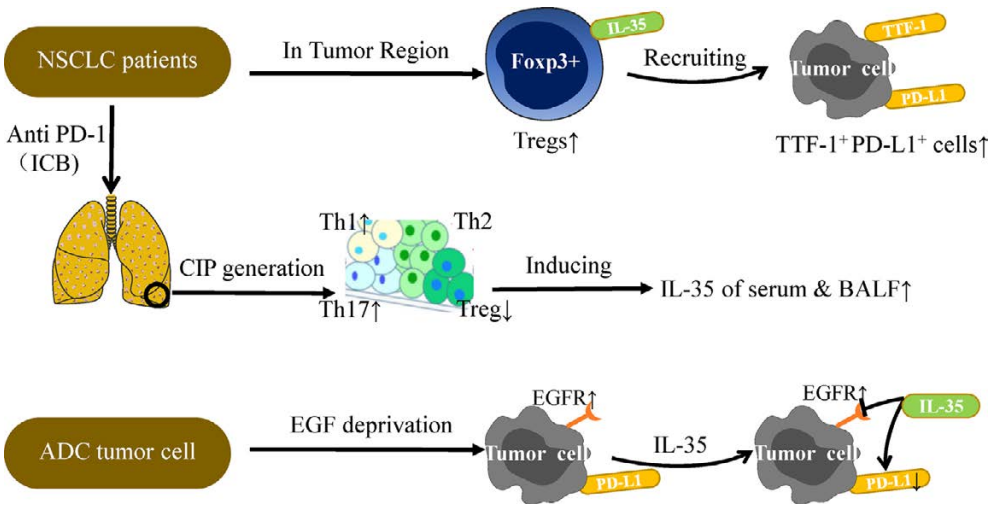

FIGURE 3 | IL-35 and PD-L1 in NSCLC immunotherapy. PD-L1 expression on tumor cells is the most studied biomarker in the context of predicting NSCLC patient immunotherapy outcomes. Further studies are needed to explore the relationship between IL-35 and PD-L1. Under conditions of EGF deprivation, IL-35 can reduce the expression of PD-L1 without impacting EGFR, which is also a target of NSCLC immunotherapy. A positive correlation between IL-35$^+$Tregs and TTF-1$^+$PD-L1$^+$ cells has been observed in the TU region, and TTF-1 is a good prognostic factor associated with survival in NSCLC. In addition, CIP generation is often observed in patients undergoing PD-1 or PD-L1 antibody therapy. CIP patients have higher mean amounts of Th1 and Th17 cells and lower levels of Tregs in serum as compared to normal subjects, thus inducing IL-35 secretion in the plasma and BALF. The levels of IL-35 in the plasma and BALF can be measured for the diagnostic evaluation of CIP patients. Overall, the complex relationship between IL-35 and PD-L1 must be considered when discussing the potential role of IL-35 in tumor immunotherapy.

can induce the angiogenesis by monocyte/macrophage which secrete this cytokine offers key insights that can guide future studies of the role of IL-35 in cancer and immunotherapeutic treatment. The expression and promoting effect of IL-35 in tumor have been described in plenty of malignant tumors, such as HCC, PDAC & PCA (19, 20, 29). As a result of the "cold" nature of these tumors, patients receive little benefit from conventional immunotherapy treatments, and by developing a more comprehensive understanding of the mechanisms governing the production and signaling activities of IL-35 it may be possible to develop better targeted anti-tumor treatment strategies for these patients. Controlling the expression of IL-35 so as to prevent it from driving tumor proliferation and metastasis thus represents a promising direction for immunotherapeutic efforts.

While we herein systematically discussed important findings pertaining to regulation of the TME or immune cells by IL-35 that have been published over the past decade, these two IL-35-dependent activities are inextricably linked to one another but the degree to which these activities influence tumor progression in different tumor types remains to be clarified. In addition, the specific roles of various immune cell types in the context of IL-35-mediated interactions within the TME remain to be fully elucidated. Studies regarding the immunosuppressive functions of IL-35 are also at a very early stage, and further preclinical research is warranted. Future studies should place more emphasis on the development of IL-35 as a therapeutic target to interfere with tumor growth and to assess the physiological impact of IL-35 on the primary tumors in human clinical trials. In this review, we systematically discussed the recent advances in our understanding of IL-35 as a regulator of immune cell regulation and proliferation, thereby highlighting a potential target for tumor immunotherapy. Given the novel role of IL-35 in creating an immunosuppressive tumor microenvironment, the tumor-related mechanisms whereby this cytokine and other IL-12 family members function warrant additional detailed research, as they may generate novel immunotherapeutic approaches and give rise to exciting clinical applications.

AUTHOR CONTRIBUTIONS

KL and AH contributed equally to this review. KJ conceptualized the review and finalized the manuscript preparation. KL and AH performed the literature search and drafted the manuscript. JN, JT, SX, and YQ modified the grammar of this review. All authors contributed to the article and approved the submitted version.

FUNDING

This work was supported by the National Natural Science Foundation of China (No. 81974038), the Hubei Provincial Natural Science Foundation of China (No. 2017CFB615).

ACKNOWLEDGMENTS

Special thanks for Dr. Huayi Li for his assistance in revising the manuscript.

REFERENCES

1. Kaymak I, Williams K, Cantor J, Jones R. Immunometabolic Interplay in the Tumor Microenvironment. *Cancer Cell* (2021) 39(1):28–37. doi: 10.1016/j.ccell.2020.09.004
2. Tanja MC. The Matrix Environmental and Cell Mechanical Properties Regulate Cell Migration and Contribute to the Invasive Phenotype of Cancer Cells. *J Rep Prog Phys* (2019) 82:064602. doi: 10.1088/1361-6633/ab1628
3. Taddei M, Giannoni E, Comito G, Chiarugi P. Microenvironment and Tumor Cell Plasticity: An Easy Way Out. *Cancer Lett* (2013) 341(1):80–96. doi: 10.1016/j.canlet.2013.01.042
4. Ge P, Wang W, Li L, Zhang G, Gao Z, Tang Z, et al. Profiles of Immune Cell Infiltration and Immune-Related Genes in the Tumor Microenvironment of Colorectal Cancer. *Biomedicine & Pharmacotherapy. Biomedecine pharmacotherapie* (2019) 118:109228. doi: 10.1016/j.biopha.2019.109228
5. Singhal M, Beyond AH. Angiogenesis: Exploiting Angiocrine Factors to Restrict Tumor Progression and Metastasis. *Cancer Res* (2020) 80(4):659–62. doi: 10.1158/0008-5472.Can-19-3351
6. Manou D, Karamanos N, Theocharis A. Tumorigenic Functions of Serglycin: Regulatory Roles in Epithelial to Mesenchymal Transition and Oncogenic Signaling. *Semin Cancer Biol* (2020) 62:108–15. doi: 10.1016/j.semcancer.2019.07.004
7. Mohan C, Rangappa S, Preetham H, Chandra Nayaka S, Gupta V, Basappa S, et al. Targeting STAT3 Signaling Pathway in Cancer by Agents Derived From Mother Nature. *Semin Cancer Biol* (2020). doi: 10.1016/j.semcancer.2020.03.016
8. Lei X, Lei Y, Li J, Du W, Li R, Yang J, et al. Immune Cells Within the Tumor Microenvironment: Biological Functions and Roles in Cancer Immunotherapy. *Cancer Lett* (2020) 470:126–33. doi: 10.1016/j.canlet.2019.11.009
9. Fraietta JA, Lacey SF, Orlando EJ, Pruteanu-Malinici I, Gohil M, Lundh S, et al. Determinants of Response and Resistance to CD19 Chimeric Antigen Receptor (CAR) T Cell Therapy of Chronic Lymphocytic Leukemia. *Nat Med* (2018) 24(5):563–71. doi: 10.1038/s41591-018-0010-1
10. Shalapour S, Font-Burgada J, Di Caro G, Zhong Z, Sanchez-Lopez E, Dhar D, et al. Immunosuppressive Plasma Cells Impede T-cell-dependent Immunogenic Chemotherapy. *Nature* (2015) 521(7550):94–8. doi: 10.1038/nature14395
11. Yazdani Z, Rafiei A, Golpour M, Zafari P, Moonesi M, Ghaffari S. Il-35, a Double-Edged Sword in Cancer. *J Cell Biochem* (2020) 121(3)2064–76. doi: 10.1002/jcb.29441
12. Chatrabnous N, Ghaderi A, Ariafar A, Razeghinia MS, Nemati M, Jafarzadeh A. Serum Concentration of interleukin-35 and its Association With Tumor Stages and FOXP3 Gene Polymorphism in Patients With Prostate Cancer. *Cytokine* (2019) 113:221–7. doi: 10.1016/j.cyto.2018.07.006
13. Lu Z, Xu K, Wang X, Li Y, Li M. Interleukin 39: A New Member of Interleukin 12 Family. *Central-European J Immunol* (2020) 45(2):214–7. doi: 10.5114/ceji.2020.97911
14. Wang X, Wei Y, Xiao H, Liu X, Zhang Y, Han G, et al. A Novel IL-23p19/Ebi3 (Il-39) Cytokine Mediates Inflammation in Lupus-like Mice. *Eur J Immunol* (2016) 46(6):1343–50. doi: 10.1002/eji.201546095
15. Teymouri M, Pirro M, Fallarino F, Gargaro M, Sahebkar A. Il-35, a Hallmark of Immune-Regulation in Cancer Progression, Chronic Infections and Inflammatory Diseases. *Int J Cancer* (2018) 143(9):2105–15. doi: 10.1002/ijc.31382
16. Collison LW, Workman CJ, Kuo TT, Boyd K, Wang Y, Vignali KM, et al. The Inhibitory Cytokine IL-35 Contributes to Regulatory T-cell Function. *Nature* (2007) 450(7169):566–9. doi: 10.1038/nature06306
17. Wang HM, Zhang XH, Feng MM, Qiao YJ, Ye LQ, Chen J, et al. Interleukin-35 Suppresses the Antitumor Activity of T Cells in Patients With Non-Small Cell Lung Cancer. *Cell Physiol Biochem* (2018) 47(6):2407–19. doi: 10.1159/000491615
18. Li X, Niu N, Sun J, Mou Y, He X, Mei L. IL35 Predicts Prognosis in Gastric Cancer and is Associated With Angiogenesis by Altering TIMP1, PAI1, and IGFBP1. *FEBS Open Bio* (2020) 10:2687–701. doi: 10.1002/2211-5463.13005
19. Zhu J, Wang Y, Li D, Zhang H, Guo Z, Yang X. Interleukin-35 Promotes Progression of Prostate Cancer and Inhibits Anti-Tumour Immunity. *Cancer Cell Int* (2020) 20(1):487. doi: 10.1186/s12935-020-01583-3
20. Lee CC, Lin JC, Hwang WL, Kuo YJ, Chen HK, Tai SK, et al. Macrophage-Secreted interleukin-35 Regulates Cancer Cell Plasticity to Facilitate Metastatic Colonization. *Nat Commun* (2018) 9(1):3763. doi: 10.1038/s41467-018-06268-0
21. Dong YJ, Li XF, Yu YY, Lv FF, Chen Y. JAK/STAT Signaling is Involved in IL-35-induced Inhibition of Hepatitis B Virus Antigen-Specific Cytotoxic T Cell Exhaustion in Chronic Hepatitis B. *Life Sci* (2020) 252:7. doi: 10.1016/j.lfs.2020.117663
22. Collison L, Delgoffe G, Guy C, Vignali K, Chaturvedi V, Fairweather D, et al. The Composition and Signaling of the IL-35 Receptor are Unconventional. *Nat Immunol* (2012) 13(3):290–9. doi: 10.1038/ni.2227
23. Zhang T, Nie J, Liu X, Han Z, Ding N, Gai K, et al. Correlation Analysis Among the Level of IL-35, Microvessel Density, Lymphatic Vessel Density, and Prognosis in Non-Small Cell Lung Cancer. *Clin Transl Sci* (2021) 14:389–94. doi: 10.1111/cts.12891
24. Guo Y, Cao W, Zhu Y. Immunoregulatory Functions of the IL-12 Family of Cytokines in Antiviral Systems. *Viruses* (2019) 11(9):772. doi: 10.3390/v11090772
25. Li X, Shao Y, Sha X, Fang P, Kuo Y, Andrews A, et al. Il-35 (Interleukin-35) Suppresses Endothelial Cell Activation by Inhibiting Mitochondrial Reactive Oxygen Species-Mediated Site-Specific Acetylation of H3K14 (Histone 3 Lysine 14). *Arterioscler thrombosis Vasc Biol* (2018) 38(3):599–609. doi: 10.1161/atvbaha.117.310626
26. Wu Q, Li B, Li J, Sun S, Yuan J, Sun S. Cancer-Associated Adipocytes as Immunomodulators in Cancer. *Biomarker Res* (2021) 9(1):2. doi: 10.1186/s40364-020-00257-6
27. Kim H, Lee M, Lee D, Min K, Koo J, Kim H, et al. The Regulatory B Cell-Mediated Peripheral Tolerance Maintained by Mast Cell IL-5 Suppresses Oxazolone-Induced Contact Hypersensitivity. *Sci Adv* (2019) 5(7):eaav8152. doi: 10.1126/sciadv.aav8152
28. Hao S, Chen X, Wang F, Shao Q, Liu J, Zhao H, et al. Breast Cancer Cell-Derived IL-35 Promotes Tumor Progression Via Induction of IL-35-producing Induced Regulatory T Cells. *Carcinogenesis* (2018) 39(12):1488–96. doi: 10.1093/carcin/bgy136
29. Huang C, Li N, Li Z, Chang A, Chen Y, Zhao T, et al. Tumour-Derived Interleukin 35 Promotes Pancreatic Ductal Adenocarcinoma Cell Extravasation and Metastasis by Inducing ICAM1 Expression. *Nat Commun* (2017) 8:14035. doi: 10.1038/ncomms14035
30. Zou J, Qin J, Li Y, Wang Y, Li D, Shu Y, et al. Il-35 Induces N2 Phenotype of Neutrophils to Promote Tumor Growth. *Oncotarget* (2017) 8(20):33501–14. doi: 10.18632/oncotarget.16819
31. Liu X, Ren H, Guo H, Wang W, Zhao N. Interleukin-35 has a Tumor-promoting Role in Hepatocellular Carcinoma. *Clin Exp Immunol* (2021) 203:219–29. doi: 10.1111/cei.13535
32. Turnis M, Sawant D, Szymczak-Workman A, Andrews L, Delgoffe G, Yano H, et al. Interleukin-35 Limits Anti-Tumor Immunity. *Immunity* (2016) 44(2):316–29. doi: 10.1016/j.immuni.2016.01.013
33. Seyerl M, Kirchberger S, Majdic O, Seipelt J, Jindra C, Schrauf C, et al. Human Rhinoviruses Induce IL-35-producing Treg Via Induction of B7-H1 (CD274) and Sialoadhesin (CD169) on DC. *Eur J Immunol* (2010) 40(2):321–9. doi: 10.1002/eji.200939527
34. Pylayeva-Gupta Y, Das S, Handler J, Hajdu C, Coffre M, Koralov S, et al. Il35-Producing B Cells Promote the Development of Pancreatic Neoplasia. *Cancer Discovery* (2016) 6(3):247–55. doi: 10.1158/2159-8290.Cd-15-0843
35. Choi JK, Egwuagu CE. Interleukin 35 Regulatory B Cells. *J Mol Biol* (2021) 433(1):166607. doi: 10.1016/j.jmb.2020.07.019
36. Abel A, Yang C, Thakar M, Malarkannan S. Natural Killer Cells: Development, Maturation, and Clinical Utilization. *Front Immunol* (2018) 9:1869. doi: 10.3389/fimmu.2018.01869
37. Wang K, Liu J, Li J. IL-35-Producing B Cells in Gastric Cancer Patients. *Medicine* (2018) 97(19):e0710. doi: 10.1097/md.0000000000010710
38. Godfrey J, Tumuluru S, Bao R, Leukam M, Venkataraman G, Phillip J, et al. Pd-L1 Gene Alterations Identify a Subset of Diffuse Large B-cell Lymphoma Harboring a T-cell-inflamed Phenotype. *Blood* (2019) 133(21):2279–90. doi: 10.1182/blood-2018-10-879015
39. Heim L, Kachler K, Siegmund R, Trufa DI, Mittler S, Geppert CI, et al. Increased Expression of the Immunosuppressive interleukin-35 in Patients With non-Small Cell Lung Cancer. *Br J Cancer* (2019) 120(9):903–12. doi: 10.1038/s41416-019-0444-3

40. Damo M, Joshi NS. Treg Cell IL-10 and IL-35 Exhaust CD8(+) T Cells in Tumors. *Nat Immunol* (2019) 20(6):674–5. doi: 10.1038/s41590-019-0389-y
41. Jiang H, Zhang T, Yan MX, Wu W. Il-35 Inhibits CD8(+) T Cells Activity by Suppressing Expression of Costimulatory Molecule CD28 and Th1 Cytokine Production. *Trans Cancer Res* (2019) 8(4):1319–25. doi: 10.21037/tcr.2019.07.30
42. Li C, Jiang P, Wei S, Xu X, Wang J. Regulatory T Cells in Tumor Microenvironment: New Mechanisms, Potential Therapeutic Strategies and Future Prospects. *Mol Cancer* (2020) 19(1):116. doi: 10.1186/s12943-020-01234-1
43. Kamada T, Togashi Y, Tay C, Ha D, Sasaki A, Nakamura Y, et al. Pd-1(+) Regulatory T Cells Amplified by PD-1 Blockade Promote Hyperprogression of Cancer. *Proc Natl Acad Sci U S A* (2019) 116(20):9999–10008. doi: 10.1073/pnas.1822001116
44. Moore K, de Waal Malefyt R, Coffman R, O'Garra A. Interleukin-10 and the interleukin-10 Receptor. *Annu Rev Immunol* (2001) 19:683–765. doi: 10.1146/annurev.immunol.19.1.683
45. McIntosh CM, Alegre M-L. Teamwork by IL-10+and Il-35(+) T-Regs. *Am J Transplant* (2019) 19(8):2147–7. doi: 10.1111/ajt.15511
46. Sawant DV, Yano H, Chikina M, Zhang Q, Liao M, Liu C, et al. Adaptive Plasticity of IL-10(+) and IL-35(+) Treg Cells Cooperatively Promotes Tumor T Cell Exhaustion. *Nat Immunol* (2019) 20(6):724–35. doi: 10.1038/s41590-019-0346-9
47. Ding Q, Chauvin J, Zarour H. Targeting Novel Inhibitory Receptors in Cancer Immunotherapy. *Semin Immunol* (2020) 49:101436. doi: 10.1016/j.smim.2020.101436
48. Ma Y, Chen L, Xie G, Zhou Y, Yue C, Yuan X, et al. Elevated Level of interleukin-35 in Colorectal Cancer Induces Conversion of T Cells Into iTr35 by Activating STAT1/STAT3. *Oncotarget* (2016) 7(45):73003–15. doi: 10.18632/oncotarget.12193
49. Collison L, Chaturvedi V, Henderson A, Giacomin P, Guy C, Bankoti J, et al. Il-35-mediated Induction of a Potent Regulatory T Cell Population. *Nat Immunol* (2010) 11(12):1093–101. doi: 10.1038/ni.1952
50. Yang L, Zhao K-L, Qin L, Ji DX, Zhang B, Zheng PF, et al. Notch Signaling Pathway Regulates CD4CD25CD127 Regulatory T Cells and T Helper 17 Cells Function in Gastric Cancer Patients. *Biosci Rep* (2019) 39(5): BSR20182044. doi: 10.1042/BSR20182044
51. Jiang Y, Ma Y, Li R, Sun J. Colon Cancer-Induced interleukin-35 Inhibits Beta-Catenin-Mediated Pro-Oncogenic Activity. *Oncotarget* (2018) 9 (15):11989–98. doi: 10.18632/oncotarget.22857
52. Li X, Xiang Y, Li F, Yin C, Li B, Ke X. WNT/Beta-Catenin Signaling Pathway Regulating T Cell-Inflammation in the Tumor Microenvironment. *Front Immunol* (2019) 10:2293. doi: 10.3389/fimmu.2019.02293
53. Sumida T, Lincoln MR, Ukeje CM, Rodriguez DM, Akazawa H, Noda T, et al. Activated Beta-Catenin in Foxp3(+) Regulatory T Cells Links Inflammatory Environments to Autoimmunity. *Nat Immunol* (2018) 19 (12):1391–402. doi: 10.1038/s41590-018-0236-6
54. Perry JM, Tao F, Roy A, Lin T, He XC, Chen S, et al. Overcoming Wnt-beta-catenin Dependent Anticancer Therapy Resistance in Leukaemia Stem Cells. *Nat Cell Biol* (2020) 22(6):689–700. doi: 10.1038/s41556-020-0507-y
55. Starling S. Mechanisms of β-Catenin-Induced Adrenal Hyperplasia. *Nat Rev Endocrinol* (2020) 16(7):345. doi: 10.1038/s41574-020-0369-1
56. Liu Z, Fu Y. Chemotherapy Induces Cancer-Fighting B Cells. *Cell* (2020) 180 (6):1037–9. doi: 10.1016/j.cell.2020.02.046
57. Hetta H, Mekky M, Zahran A, Abdel-Malek M, Ramadan H, Shafik E, et al. Regulatory B Cells and Their Cytokine Profile in HCV-Related Hepatocellular Carcinoma: Association With Regulatory T Cells and Disease Progression. *Vaccines* (2020) 8(3):380. doi: 10.3390/vaccines8030380
58. Liu M, Sun Q, Wang J, Wei F, Yang L, Ren X. A New Perspective: Exploring Future Therapeutic Strategies for Cancer by Understanding the Dual Role of B Lymphocytes in Tumor Immunity. *Int J Cancer* (2019) 144(12):2909–291714. doi: 10.1002/ijc.31850
59. Shen M, Wang J, Yu W, Zhang C, Liu M, Wang K, et al. A Novel MDSC-induced Pd-1(-)Pd-L1(+) B-cell Subset in Breast Tumor Microenvironment Possesses Immuno-Suppressive Properties. *Oncoimmunology* (2018) 7(4): e1413520. doi: 10.1080/2162402X.2017.1413520
60. Chapuy B, Stewart C, Dunford AJ, Kim J, Kamburov A, Redd RA, et al. Molecular Subtypes of Diffuse Large B Cell Lymphoma are Associated With Distinct Pathogenic Mechanisms and Outcomes. *Nat Med* (2018) 24(5):679. doi: 10.1038/s41591-018-0016-8
61. Rosser EC, Mauri C. Regulatory B Cells: Origin, Phenotype, and Function. *Immunity* (2015) 42(4):607–12. doi: 10.1016/j.immuni.2015.04.005
62. Shang J, Zha H, Phenotypes Y. Functions, and Clinical Relevance of Regulatory B Cells in Cancer. *Front Immunol* (2020) 11:582657. doi: 10.3389/fimmu.2020.582657
63. Olkhanud PB, Damdinsuren B, Bodogai M, Gress RE, Sen R, Wejksza K, et al. Tumor-Evoked Regulatory B Cells Promote Breast Cancer Metastasis by Converting Resting Cd4+ T Cells to T-Regulatory Cells. *Cancer Res* (2011) 71(10):3505–15. doi: 10.1158/0008-5472.Can-10-4316
64. Iwata Y, Matsushita T, Horikawa M, Dilillo D, Yanaba K, Venturi G, et al. Characterization of a Rare IL-10-competent B-Cell Subset in Humans That Parallels Mouse Regulatory B10 Cells. *Blood* (2011) 117(2):530–41. doi: 10.1182/blood-2010-07-294249
65. Rincón-Arévalo H, Quintero J, Fortich F, Rojas M, Vásquez G, Castaño D, et al. Low Frequency of IL-10 B Cells in Patients With Atherosclerosis is Related With Inflammatory Condition. *Heliyon* (2020) 6(3):e03441. doi: 10.1016/j.heliyon.2020.e03441
66. Horii M, Matsushita T. Regulatory B Cells and T Cell Regulation in Cancer. *J Mol Biol* (2021) 433(1):166685. doi: 10.1016/j.jmb.2020.10.019
67. Das S, Bar-Sagi D. BTK Signaling Drives CD1dCD5 Regulatory B-cell Differentiation to Promote Pancreatic Carcinogenesis. *Oncogene* (2019) 38 (17):3316–24. doi: 10.1038/s41388-018-0668-3
68. Ryu K, McGonnigal B, Moore T, Kargupta T, Mancini R, Esser-Kahn A. Light Guided in-Vivo Activation of Innate Immune Cells With Photocaged Tlr 2/6 Agonist. *Sci Rep* (2017) 7(1):8074. doi: 10.1038/s41598-017-08520-x
69. Huber A, Dammeijer F, Aerts J, Vroman H. Current State of Dendritic Cell-Based Immunotherapy: Opportunities for Antigen Loading of Different Dc Subsets? *Front Immunol* (2018) 9:2804. doi: 10.3389/fimmu.2018.02804
70. Li Y, Zhao C, Liu J, Lu Z, Lu M, Gu J, et al. CD1d Highly Expressed on DCs Reduces Lung Tumor Burden by Enhancing Antitumor Immunity. *Oncol Rep* (2019) 41(5):2679–88. doi: 10.3892/or.2019.7037
71. Dixon K, van der Kooij S, Vignali D, van Kooten C. Human Tolerogenic Dendritic Cells Produce IL-35 in the Absence of Other IL-12 Family Members. *Eur J Immunol* (2015) 45(6):1736–47. doi: 10.1002/eji.201445217
72. Liu X, Sun Y, Zheng Y, Zhang M, Jin X, Kang K, et al. Administration of Interleukin-35-Conditioned Autologous Tolerogenic Dendritic Cells Prolong Allograft Survival After Heart Transplantation. *Cell Physiol Biochem Int J Exp Cell physiol biochem Pharmacol* (2018) 49(3):1180–96. doi: 10.1159/000493298
73. Hasegawa H, Matsumoto T. In VivoMechanisms of Tolerance Induction by Dendritic Cells. *Front Immunol* (2018) 9:350. doi: 10.3389/fimmu.2018.00350
74. Haller S, Duval A, Migliorini R, Stevanin M, Mack V, Acha-Orbea H. Interleukin-35-Producing Cd8α Dendritic Cells Acquire a Tolerogenic State and Regulate T Cell Function. *Front Immunol* (2017) 8:98. doi: 10.3389/fimmu.2017.00098
75. Yang L, Du C, Wu L, Yu J, An X, Yu W, et al. Cytokine-Induced Killer Cells Modulates Resistance to Cisplatin in the A549/DDP Cell Line. *J Cancer* (2017) 8(16):3287–95. doi: 10.7150/jca.19426
76. Liu X, Zhang N, Shi H. Driving Better and Safer HER2-specific Cars for Cancer Therapy. *Oncotarget* (2017) 8(37):62730–41. doi: 10.18632/oncotarget.17528
77. Panfili E, Mondanelli G, Orabona C, Bianchi R, Gargaro M, Fallarino F, et al. Il-35Ig-expressing Dendritic Cells Induce Tolerance Via Arginase 1. *J Cell Mol Med* (2019) 23(5):3757–61. doi: 10.1111/jcmm.14215
78. Jiang N, Qiao G, Wang X, Morse M, Gwin W, Zhou L, et al. Dendritic Cell/Cytokine-Induced Killer Cell Immunotherapy Combined With S-1 in Patients With Advanced Pancreatic Cancer: A Prospective Study. *Clin Cancer Res an Off J Am Assoc Cancer Res* (2017) 23(17):5066–73. doi: 10.1158/1078-0432.Ccr-17-0492
79. Yu S, Ma C, Heinrich B, Brown Z, Sandhu M, Zhang Q, et al. Targeting the Crosstalk Between Cytokine-Induced Killer Cells and Myeloid-Derived Suppressor Cells in Hepatocellular Carcinoma. *J Hepatol* (2019) 70 (3):449–57. doi: 10.1016/j.jhep.2018.10.040
80. de Groot A, Pienta K. Epigenetic Control of Macrophage Polarization: Implications for Targeting Tumor-Associated Macrophages. *Oncotarget* (2018) 9(29):20908–27. doi: 10.18632/oncotarget.24556

81. Sun W, Lv S, Li H, Cui W, Wang L. Enhancing the Anticancer Efficacy of Immunotherapy Through Combination With Histone Modification Inhibitors. *Genes* (2018) 9(12):633. doi: 10.3390/genes9120633
82. Abolarinwa B, Ibrahim R, Huang Y. Conceptual Development of Immunotherapeutic Approaches to Gastrointestinal Cancer. *Int J Mol Sci* (2019) 20(18):4624. doi: 10.3390/ijms20184624
83. Huang CB, Li ZX, Li N, Li Y, Chang AT, Zhao TS, et al. Interleukin 35 Expression Correlates With Microvessel Density in Pancreatic Ductal Adenocarcinoma, Recruits Monocytes, and Promotes Growth and Angiogenesis of Xenograft Tumors in Mice. *Gastroenterology* (2018) 154 (3):675–88. doi: 10.1053/j.gastro.2017.09.039
84. Kang J, Gil M, Kim K. Neuropilin1 Expression Acts as a Prognostic Marker in Stomach Adenocarcinoma by Predicting the Infiltration of Treg Cells and M2 Macrophages. *J Clin Med* (2020) 9(5):1430. doi: 10.3390/jcm9051430
85. Shen S, Wang J, Zheng B, Ni X, Gao Z, Zhang D, et al. The lnc-CITED2-2:1 Inhibits Metastasis Via Inhibiting CITED2 and Epithelial-Mesenchymal Transition in Gallbladder Cancer. *Clin Trans Med* (2020) 10(2):e116. doi: 10.1002/ctm2.116
86. Wang Z, Liu JQ, Liu Z, Shen R, Zhang G, Xu J, et al. Tumor-Derived IL-35 Promotes Tumor Growth by Enhancing Myeloid Cell Accumulation and Angiogenesis. *J Immunol* (2013) 190(5):2415–23. doi: 10.4049/jimmunol.1202535
87. Xing H, Tian G. Increased Interleukin-35 Suppresses Peripheral CD14 Monocytes Function in Patients With Kawasaki Disease. *BMC Immunol* (2020) 21(1):17. doi: 10.1186/s12865-020-00348-x
88. Lian M, Zhang J, Zhao L, Chen X, Peng Y, Wang Q, et al. Interleukin-35 Regulates Immune Microenvironment of Autoimmune Hepatitis Through Inducing the Expansion of Myeloid-Derived Suppressor Cells. *Front Immunol* (2019) 10:2577. doi: 10.3389/fimmu.2019.02577
89. Frank G, Divito S, Maker D, Xu M. Hendricks, R. A Novel p40-independent Function of IL-12p35 is Required for Progression and Maintenance of Herpes Stromal Keratitis. *Invest Ophthalmol Visual Sci* (2010) 51(7):3591–8. doi: 10.1167/iovs.09-4368
90. Li W, Gao R, Xin T, Gao P. Different Expression Levels of interleukin-35 in Asthma Phenotypes. *Respir Res* (2020) 21(1):89. doi: 10.1186/s12931-020-01356-6
91. Labani-Motlagh A, Ashja-Mahdavi M, Loskog A. The Tumor Microenvironment: A Milieu Hindering and Obstructing Antitumor Immune Responses. *Front Immunol* (2020) 11:940. doi: 10.3389/fimmu.2020.00940
92. Zhou C, Zhang J, Chen Y, Wang H, Hou J. Interleukin-35 as a Predictor of Prostate Cancer in Patients Undergoing Initial Prostate Biopsy. *OncoTargets Ther* (2017) 10:3485–91. doi: 10.2147/ott.S135873
93. Fu Y, Yi Y, Cai X, Sun J, Ni X, He H, et al. Overexpression of interleukin-35 Associates With Hepatocellular Carcinoma Aggressiveness and Recurrence After Curative Resection. *Br J Cancer* (2016) 114(7):767–76. doi: 10.1038/bjc.2016.47
94. Nanbakhsh A, Srinivasamani A, Holzhauer S, Riese M, Zheng Y, Wang D, et al. Mirc11 Disrupts Inflammatory But Not Cytotoxic Responses of NK Cells. *Cancer Immunol Res* (2019) 7(10):1647–62. doi: 10.1158/2326-6066.Cir-18-0934
95. Palsson-McDermott E, Dyck L, Zasłona Z, Menon D, McGettrick A, Mills K, et al. Pyruvate Kinase M2 Is Required for the Expression of the Immune Checkpoint PD-L1 in Immune Cells and Tumors. *Front Immunol* (2017) 8:1300. doi: 10.3389/fimmu.2017.01300
96. Wang Q, Lin W, Tang X, Li S, Guo L, Lin Y, et al. The Roles of microRNAs in Regulating the Expression of PD-1/PD-L1 Immune Checkpoint. *Int J Mol Sci* (2017) 18(12):2540. doi: 10.3390/ijms18122540
97. Topalian SL, Hodi FS, Brahmer JR, Gettinger SN, Smith DC, McDermott DF, et al. Safety, Activity, and Immune Correlates of Anti-PD-1 Antibody in Cancer. *New Engl J Med* (2012) 366(26):2443–54. doi: 10.1056/NEJMoa1200690
98. Yang L, Shao X, Jia S, Zhang Q, Jin Z. Interleukin-35 Dampens Cd8 T Cells Activity in Patients With Non-viral Hepatitis-Related Hepatocellular Carcinoma. *Front Immunol* (2019) 10:1032. doi: 10.3389/fimmu.2019.01032
99. Dong Y, Han Y, Huang Y, Jiang S, Huang Z, Chen R, et al. Pd-L1 Is Expressed and Promotes the Expansion of Regulatory T Cells in Acute Myeloid Leukemia. *Front Immunol* (2020) 11:1710. doi: 10.3389/fimmu.2020.01710
100. Takahashi R, Macchini M, Sunagawa M, Jiang Z, Tanaka T, Valenti G, et al. Interleukin-1beta-induced Pancreatitis Promotes Pancreatic Ductal Adenocarcinoma Via B Lymphocyte-Mediated Immune Suppression. *Gut* (2020) 70:330–41. doi: 10.1136/gutjnl-2019-319912
101. Larousserie F, Kebe D, Huynh T, Audebourg A, Tamburini J, Terris B, et al. Evidence for IL-35 Expression in Diffuse Large B-Cell Lymphoma and Impact on the Patient's Prognosis. *Front Oncol* (2019) 9:563. doi: 10.3389/fonc.2019.00563
102. Feng M, Jiang W, Kim B, Zhang C, Fu Y, Weissman I. Phagocytosis Checkpoints as New Targets for Cancer Immunotherapy. Nature Reviews. *Cancer* (2019) 19(10):568–86. doi: 10.1038/s41568-019-0183-z
103. Xia L, Liu Y, Wang Y. Pd-1/Pd-L1 Blockade Therapy in Advanced non-Small-Cell Lung Cancer: Current Status and Future Directions. *oncologist* (2019) 24:S31–41. doi: 10.1634/theoncologist.2019-IO-S1-s05
104. Johnson DB, Chandra S, Sosman JA. Immune Checkpoint Inhibitor Toxic 2018*JAMA* (2018) 320:1702–3. doi: 10.1001/jama.2018.13995
105. Zhai X, Zhang J, Tian Y, Li J, Jing W, Guo H, et al. The Mechanism and Risk Factors for Immune Checkpoint Inhibitor Pneumonitis in non-Small Cell Lung Cancer Patients. *Cancer Biol Med* (2020) 17(3):599–611. doi: 10.20892/j.issn.2095-3941.2020.0102
106. Wang Y, Lou D, Li D, Jiang W, Dong J, Gao W, et al. Elevated Levels of IL-17A and IL-35 in Plasma and Bronchoalveolar Lavage Fluid are Associated With Checkpoint Inhibitor Pneumonitis in Patients With non-Small Cell Lung Cancer. *Oncol Lett* (2020) 20(1):611–22. doi: 10.3892/ol.2020.11618

Conflict of Interest: The authors declare that the research was conducted in the absence of any commercial or financial relationships that could be construed as a potential conflict of interest.

Copyright © 2021 Liu, Huang, Nie, Tan, Xing, Qu and Jiang. This is an open-access article distributed under the terms of the Creative Commons Attribution License (CC BY). The use, distribution or reproduction in other forums is permitted, provided the original author(s) and the copyright owner(s) are credited and that the original publication in this journal is cited, in accordance with accepted academic practice. No use, distribution or reproduction is permitted which does not comply with these terms.

frontiers in Immunology

ORIGINAL RESEARCH
published: 21 May 2021
doi: 10.3389/fimmu.2021.658681

Fusobacterium nucleatum Facilitates M2 Macrophage Polarization and Colorectal Carcinoma Progression by Activating TLR4/NF-κB/S100A9 Cascade

Lijun Hu[1†], Yan Liu[1†], Xuehua Kong[1], Rui Wu[2], Qi Peng[1], Yan Zhang[1], Lan Zhou[1] and Liang Duan[3*]*

[1] Key Laboratory of Laboratory Medical Diagnostics, Ministry of Education, Department of Laboratory Medicine, Chongqing Medical University, Chongqing, China, [2] Department of Laboratory Medicine, The First Affiliated Hospital of Chongqing Medical University, Chongqing, China, [3] Department of Laboratory Medicine, The Second Affiliated Hospital of Chongqing Medical University, Chongqing, China

Fusobacterium nucleatum (*Fn*) has been considered as a significant contributor in promoting colorectal carcinoma (CRC) development by suppressing host anti-tumor immunity. Recent studies demonstrated that the aggregation of M2 macrophage (Mφ) was involved in CRC progress driven by *Fn* infection. However, the underlying molecular mechanisms are poorly characterized. Here, we investigated the role of *Fn* in Mφ polarization as well as its effect on CRC malignancy. *Fn* infection facilitated differentiation of Mφ into the M2-like Mφ phenotype by *in vitro* study. Histological observation from *Fn*-positive CRC tissues confirmed the abundance of tumor-infiltrating M2-like Mφ. *Fn*-induced M2-like Mφ polarization was weakened once inhibiting a highly expressed damage-associated molecular pattern (DAMP) molecule S100A9 mainly derived from *Fn*-challenged Mφ and CRC cells. In addition, *Fn*-challenged M2-like Mφ conferred CRC cells a more malignant phenotype, showing stronger proliferation and migration characteristics *in vitro* and significantly enhanced tumor growth *in vivo*, all of which were partially inhibited when S100A9 was lost. Mechanistic studies further demonstrated that activation of TLR4/NF-κB signaling pathway mediated *Fn*-induced S100A9 expression and subsequent M2-like Mφ activation. Collectively, these findings indicate that elevated S100A9 in *Fn*-infected CRC microenvironment participates in M2-like Mφ polarization, thereby facilitating CRC malignancy. Furthermore, targeting TLR4/NF-κB/S100A9 cascade may serve as promising immunotherapeutic strategy for *Fn*-associated CRC.

Keywords: ***Fusobacterium nucleatum*, colorectal carcinoma, macrophage, S100A9, TLR4**

OPEN ACCESS

Edited by:
Peng Qu,
National Institutes of Health (NIH), United States

Reviewed by:
Irina V. Larionova,
Tomsk National Research Medical Center of the Russian Academy of Sciences, Russia
Fei-Ting Hsu,
China Medical University, Taiwan

***Correspondence:**
Liang Duan
duanliang@cqmu.edu.cn
Lan Zhou
zhoulan@cqmu.edu.cn

[†]These authors have contributed equally to this work

Specialty section:
This article was submitted to Cancer Immunity and Immunotherapy, a section of the journal Frontiers in Immunology

Received: *26 January 2021*
Accepted: *07 May 2021*
Published: *21 May 2021*

Citation:
Hu L, Liu Y, Kong X, Wu R, Peng Q, Zhang Y, Zhou L and Duan L (2021) Fusobacterium nucleatum Facilitates M2 Macrophage Polarization and Colorectal Carcinoma Progression by Activating TLR4/NF-κB/S100A9 Cascade. Front. Immunol. 12:658681. doi: 10.3389/fimmu.2021.658681

INTRODUCTION

Colorectal cancer (CRC) is a common digestive system neoplasm, ranking the third most common cancer worldwide and the fourth most frequent cause of cancer death following lung, liver, and stomach cancer (1). Over the past two decades, although early screening and detection have significantly reduced the incidence and mortality of adults aged 50 years with CRC, CRC still maintains a steadily rising trend in younger individuals (2, 3). Recently, accumulating evidence by metagenome-wide association studies indicated an association between gut microbiota dysbiosis and CRC, and enteropathogenic microorganism plays a role in shaping the inflammatory environment and promoting tumor initiation and progression (4, 5). Nevertheless, some key pathogenic bacteria as well as their promoting effect on CRC still need to be further clarified.

Fusobacterium nucleatum (*Fn*), a Gram-negative oral commensal anaerobe, has been found highly enriched in inflammatory bowel disease (IBD) and was regarded as a potential risk indicator of inflammation-associated CRC (6, 7). Colonization of *Fn* contributed to carcinogenesis and was associated with the poor prognosis and short-term survival of clinical CRC patients (8–10). Previous studies have reported a direct regulating effect of *Fn* on human multi-type immunocyte, including lymphocytes and NK cells, facilitating periodontitis severity (11, 12). In CRC, involvement of *Fn* in mediating tumor immune escape occurrence by regulating NK cell cytotoxicity and tumor-infiltrating T lymphocyte cell activities has also been reported (13). Recently, *Fn* infection was reported to increase tumor-associated macrophage (TAM) infiltration and participated in mediating M2-Mφ polarization, facilitating CRC progression, suggesting a crucial anti-tumor effect of tumor-associated macrophages elicited by *Fn* infection (8). Nevertheless, detailed mechanistic investigations about the presence and activation state of Mφ within *Fn*-infected CRC are scarce.

Inflammatory mediator S100A9 was secreted as a damage-associated molecular pattern (DAMP) in the tumor microenvironment (TME) of many inflammatory tumors, including gastric cancer, prostate cancer, and liver cancer (14–16). By binding its main TLR4 and RAGE receptors, S100A9 participated in regulating inflammatory-immune response and tumor progression (17). We previously found that elevated S100A9 in TME promotes CRC development by directly acting on the CRC cells and indirectly regulating myeloid-derived suppressor cell (MDSC)-mediated T cell immunosuppression (18, 19). However, the regulatory mechanism of high levels of S100A9 in TME and whether S100A9 acts on other types of cells in the microenvironment remain elusive.

Recently, S100A9 has been reported to be regulated by some pathogen infection and exerted a promoting role in several types of cancer such as Hepatitis B virus (HBV)-related hepatocellular carcinoma (HCC) and HPV-infected skin lesions and cancer (16, 20). It is well-established that TLR4, an important receptor for pathogen-associated molecular pattern (PAMP), mediated downstream NF-κB activation in Fn-infected CRC cells, and was involved in the oncogenic cascade of CRC (21). S100A9, a newly identified NF-κB target gene identified in multi-type of cancer, was also demonstrated to be involved in myeloid cell differentiation into M2-like Mφ in CRC (22, 23). Thus, these observations led us to explore whether gut microbe *Fn* is involved in Mφ activation by inducing the NF-κB/S100A9 cascade in a TLR4-dependent manner in *Fn*-infected CRC.

In the current study, we explored the impact of *Fn* on Mφ polarization in the TME of CRC and the consequences on tumor growth in subcutaneous tumor formation in nude mice. We found that activation of TLR4-mediated NF-κB/S100A9 signaling pathways is involved in *Fn*-induced M2-like Mφ polarization, which further promotes the progression of CRC. Our findings highlight the significance of S100A9 in regulating M2-like Mφ polarization in *Fn*-infected CRC and implicate that S100A9 may serve as a potential intervention target in *Fn*-associated CRC patients.

MATERIALS AND METHODS

Bacterial Strains and Culture Methods

Fn strain ATCC 25586 was purchased from the American Type Culture Collection (ATCC; Manassas, VA), and bacteria were cultured in brain heart infusion (BHI) containing hemin, K_2HPO_4, Vitamin K1, and L-Cysteine under anaerobic conditions at 37°C as previously described (24). *E. coli* was cultured for 24 h in Luria–Bertani (LB) medium overnight at 37°C in an orbital shaker incubator. Both bacteria were collected by 4°C centrifugation at 6,000×g for 8 min, and bacterial suspension was prepared after washing three times with sterile PBS. Turbidimetry was used to determine the turbidity of bacterial suspensions and adjust its concentration to 1×10^8 CFU/ml. The following experiments were all processed at a multiplicity of infection (MOI) of 100:1.

Cell Line Culture and Mφ Differentiation of THP-1

Human CRC cell lines HCT116 and SW480 and human monocyte THP-1 were presented by the Chongqing Key Laboratory of Molecular Oncology and Epigenetics, the First Affiliated Hospital of Chongqing Medical University. HCT116 and SW480 cells were cultured in Dulbecco's modified Eagle's medium (DMEM), and THP-1 cells were cultured in Roswell Park Memorial Institute (RPMI)-1640 medium. Both media were supplemented with 10% fetal bovine serum (FBS) (Gibco, USA). The final concentrations of penicillin and streptomycin (Hyclone, USA) in these two media were 100 U/ml and 100 μg/ml, respectively. Cell culture was maintained at 37°C in an incubator containing 5% CO_2, 95% air.

THP-1 cells were treated with PMA (50 ng/ml) (Sigma, USA) for 24 h to obtain differentiated Mφ as demonstrated previously (25). Successfully differentiated Mφs were washed twice with PBS and incubated in fresh medium to be used for the following experiments.

Clinical Specimens

CRC and matching distal normal tissues were collected from 16 patients who had undergone colorectal resection at the First

Affiliated Hospital of the Chongqing Medical University. The clinicopathological data of the subjects including gender, age, Dukes staging, and lymphatic metastasis at initial diagnosis are shown in **Table S1**. The patients received no chemotherapy, hormonal therapy, or radiotherapy before surgery, and written informed consent was received from all participants. This study was approved by the Ethics Committee of Chongqing Medical University (protocol number 2012-19).

Preparation of the Recombinant Proteins

Recombinant S100A9 (rS100A9) proteins used in this study have been described previously (18). Briefly, the pGST-moluc and pGST-moluc-S100A9 were transformed into BL21 bacteria following the instructions for calcium chloride transformation. Isopropylthio-β-D-galactoside was used to induce the expression of GST and GST-S100A9 proteins. The supernatant of sonicated bacteria was collected, and then incubated with glutathione-sepharose 4B beads. Then, rS100A9 and control GST on the beads were eluted using elution buffer with reduced glutathione. Finally, the two recombinant proteins were filtered with 0.22 μm membrane and stored at −80°C.

Preparation of Conditioned Medium From Cells With Various Treatments

Mφ or CRC cells were seeded in six-well plates and then infected with bacteria. After 48 h, the supernatant was harvested and clarified by centrifugation to remove the bacteria, cells and their debris, and then stored at −80°C refrigerator for later use.

Mφ or CRC cells were transfected with non-specific siRNA (siNC) or S100A9-siRNA (siS100A9) (GenePharma, China) (**Table 1**) at a final concentration of 100 pM with lipofectamine 2000 reagent (Invitrogen, USA) in serum-free medium. The medium was replaced with fresh medium containing 10% FBS after 6 h of transfection and *Fn* was added to each group. The supernatant was collected after 48 h in the same manner as before.

Mφ or CRC cells were treated with TAK-242 (5 μM) and BAY 11-7082 (10 μM) for 1 h prior to *Fn* stimulation. The supernatant was collected after 48 h in the same manner as before.

Mφ cells were treated with GST (10 μg/ml) or rS100A9 (10 μg/ml). After 24 h, we changed the media with fresh media and collected the supernatant after incubating for another 48 h in the same manner as before.

ALL mentioned conditioned medium (CM) was finally made up by mixing the supernatant with 10% FBS-supplemented fresh medium in a 1:1 ratio to make 5% FBS-containing CM.

ELISA

Concentration of S100A9, TNF-α, and IL-10 in the above-mentioned Conditioned media (CM) with different treatments was measured with specific ELISA kits (JYM, China) according to the manufacturer's instructions.

Cell Proliferation Assay

Cell proliferation was assessed by CCK-8 assay using a Cell Counting Kit (Dojindo, Japan) following the manufacturer's protocol. Briefly, HCT116 and SW480 cells were seeded in 96-well plates at 3,000 cells/well and cultured for described hours. Then CCK8 solution was added. Finally, the absorbance at 450 nm of each well was measured daily using a microplate reader. Each condition was done in quintuplicate, and the experiment was repeated thrice.

Cell Migration Assay

Cell migration assay was examined to assess the cell migratory capacity of CRC cells using 24-well Transwell cell culture chambers (pore size, 8 μm). Briefly, CRC cells were seeded at a density of 2×10^4 cells per well in serum-free medium at the upper chamber, and the corresponding CM was added in the lower chamber to establish co-culture systems. After incubating at 37°C for 24 h, the transmembrane cells were dried, fixed with methanol, and stained with commercialized crystal violet staining solution (Beyotime, China) and the migration cell number in five to eight fields of each insert was counted under an inverted microscope at a magnification of ×100. The experiment was repeated thrice.

RNA Isolation and Quantitative Real-Time PCR

Total RNA extraction from the treated cells or tumor tissues was performed with TRIzol reagents (Invitrogen). cDNA samples were synthesized using random primers from 1 mg total RNA with a Reverse Transcription kit (Takara, Japan). The mRNA levels of *S100A9*, *iNOS*, *TNF-α*, *IL-10*, *CD206*, *E-cadherin*, *N-cadherin*, *Vimentin*, *TGF-β*, *VEGF*, and *TLR4* were analyzed and normalized to the *GAPDH* with the CFX96 real-time PCR detection system (Bio-Rad, USA) using SYBR Green dye (Biomake, China) according to the manufacturer's instructions. The primers in this study were synthesized by Genscript, and the primer sequence information is shown in **Table 1**.

Western Blot

The cells of different treatment groups were collected, and total cellular protein was extracted with RIPA buffer containing phosphatase/protease inhibitor after washing three times with ice-cold PBS. The cell lysates were collected after centrifugation, and the concentration of protein was determined by BCA assay. The extraction of xenograft tumor protein was carried out with reference to the kit instructions (BestBio, China) according to the manufacturer's instructions. Samples containing equal amount of proteins were separated using SDS–PAGE according to the molecular weight of different proteins and transferred to PVDF membranes. Then the membranes were blocked with 5% non-fat dry milk and incubated with anti-S100A9 (Abcam, UK), anti-CD86 (Bioss, China), anti-CD206 (Proteintech, China), anti-total NF-κB p65 (Cell Signaling Technology, USA), anti-Phospho-NF-κB p65 (p-p65) (Ser536) (Cell Signaling Technology, USA), anti-E-cadherin (Immunoway Biotechnology, USA), anti-N-cadherin (Cell Signaling Technology, USA), anti-PCNA (Wanleibio, China), anti-VEFG (Santa Cruz Biotechnology, USA), anti-TGF-β (Abcam, UK) or anti-β-actin (Cell Signaling Technology, USA), followed by incubation with secondary antibodies conjugated with horseradish peroxidase. The proteins of interest were detected using the SuperSignal West Pico Chemiluminescent Substrate kit. The results were recorded by Bio-Rad Electrophoresis Documentation (Gel Doc 1000, Bio-Rad, USA) and Quantity One Version 4.5.0.

TABLE 1 | The primers and siRNA used in this study.

Genes		Sequences
GAPDH	Forward primer:	CAGCGACACCCACTCCTC
	Reverse primer:	TGAGGTCCACCACCCTGT
S100A9	Forward primer:	ACCCAGACACCCTGAACC
	Reverse primer:	AGCATGATGAACTCCTCGA
iNOS	Forward primer:	CAGCGGGATGACTTTCCAA
	Reverse primer:	AGGCAAGATTTGGACCTGCA
TNF-α	Forward primer:	CAGCCTCTTCTCCTTCCTGA
	Reverse primer:	GGAAGACCCCTCCCAGATAGA
IL-10	Forward primer:	CAAGACCCAGACATCAAGGCG
	Reverse primer:	GCATTCTTCACCTGCTCCACG
CD206	Forward primer:	GTCATATCGGGTTGAGCCACT
	Reverse primer:	AATCATTCCGTTCACCAGAGG
TLR4	Forward primer:	AGAATGCTAAGGTTGCCGCT
	Reverse primer:	CTATCACCGTCTGACCGAGC
E-cadherin	Forward primer:	CCCGGGACAACGTTTATTAC
	Reverse primer:	GCTGGCTCAAGTCAAAGTCC
N-cadherin	Forward primer:	CCTTTCAAACACAGCCACGG
	Reverse primer:	TGTTTGGGTCGGTCTGGATG
Vimentin	Forward primer:	CTCTGGCACGTCTTGACCTT
	Reverse primer:	ACCATTCTTCTGCCTCCTGC
VEGF	Forward primer:	TGCAGATTATGCGGATCAAACC
	Reverse primer:	TGCATTCACATTTGTTGTGCTGTAG
TGF-β	Forward primer:	CCCAGCATCTGCAAAGCTC
	Reverse primer:	GTCAATGTACAGCTGCCGCA
siS100A9	Sense	GCUUCGAGGAGUUCAUCAUTT
	Antisense	AUGAUGAACUCCUCGAAGCTT
siNC	Sense	UUCUCCGAACGUGUCACGUTT
	Antisense	ACGUGACACGUUCGGAGAATT

siNC, nonspecific siRNA; siS100A9, S100A9-siRNA.

Flow Cytometry

To investigate Mφ differentiation, M1 marker (CD86) and M2 marker (CD206) in different treatment groups were analyzed by flow cytometry. Briefly, the prepared cells were collected and washed with PBS and then stained with PE-mouse anti-human CD86 (BioLegend, USA) or PE-mouse anti-human CD206 (BioLegend, USA) for 30 min at 4°C. Cells were then washed and analyzed using FACSVantage SE flow cytometer (Becton-Dickinson, USA).

Immunofluorescence

Mφs on the climbing piece in 24-well culture plates were treated with or without bacterium infection or treated with relevant CM for 48 h. Then the cells were fixed with 4% paraformaldehyde for 20 min, washed with PBS, and permeabilized with 0.01% Triton X-100 for 10 min. After being washed with PBS, the cells were blocked with 10% goat serum for 30 min at room temperature and incubated with anti-CD86 monoclonal antibodies (Santa Cruz, USA) and anti-CD206 antibodies (Proteintech, China) at 4°C overnight. The next day, the cells were rinsed with PBS for clearing the primary antibody, and then incubated with Alexa Fluor 488-conjugated goat anti-mouse secondary antibody (Beyotime, China) or Cy3-conjugated goat anti-rabbit secondary antibody (Beyotime, China) at room temperature for 1 h in the dark, and then washed with PBS, and counterstained the nucleus with DAPI for 10 min. After washing again with PBS and mounting with antifade polyvinylpyrrolidone mounting medium (Beyotime, China), the fluorescent images were observed using confocal microscope (Lecia, Germany).

Xenograft

Four-week-old female BALB/c nude mice were purchased from Beijing Huafukang Biotechnology. For the xenograft experiments, mice were randomly divided into four groups (n = 3 in each group). HCT116 cells were mixed with equal proportion of Mφ treated with control *E. coli*, *Fn*, *Fn* + siNC or *Fn* + siS100A9 for 48 h and suspended in 100 μl PBS for the subsequent use. Then the mixed cells (1×10^7) in 100 μl PBS were injected subcutaneously into the posterior flank of each nude mouse to establish the xenograft model. The length and width of a tumor were detected using a caliper every three days. Tumor volumes were calculated according to the following formula: Volume = $(\text{width})^2 \times \text{length}/2$. The mice were sacrificed after 21 days, and the tumor tissues were removed, weighed, fixed in 4% buffered formaldehyde, embedded in paraffin, and sectioned for further immunohistochemical analysis. All the *in vivo* experiments were approved and conducted in accordance with the guidelines established by the University Animal Care and Use Committee for Laboratory Animal Research in Chongqing Medical University (protocol number 2018-003).

Microbial Fluorescence *In Situ* Hybridization Analysis

The analysis for detecting invasive *Fn* in CRC tissue used *Fn*-targeted probe, FUS664 (FITC-labeled), 5′-CTT GTA GTT CCG C(C/T) TAC CTC-3′ (26). Paraffin-embedded slides were prepared and hybridized with reference to previously described methods (26). Bacteria were counted in five random fields per

slide at a magnification of ×100 by an observer blind to the sample status, and the number of bacteria per field was calculated on average. The average number of *Fn* in each field in the case of <5, between 5 and 20, and >20 visualized FUS664 probes was defined as negative, weak, and positive *Fn* abundance, respectively.

Immunohistochemical Procedures

Indirect immunohistochemistry (IHC) analysis of formalin-fixed and paraffin-embedded tissue sections was performed. In brief, the sections were deparaffinized, dehydrated, boiled in 0.01 M citrate buffer for 10 min, and then incubated with 0.3% H_2O_2 in methanol for 10 min to block endogenous peroxidase activity. The sections were incubated with anti-S100A9 (Abcam, UK), anti-CD68 (Santa Cruz, USA), anti-CD86 (Santa Cruz, USA), anti-CD206 (Proteintech, China), anti-E-cadherin (ImmunoWay Biotechnology, USA), and anti-N-cadherin (Cell Signaling Technology, USA) following incubation with secondary antibody tagged with the peroxidase enzyme for 30 min at room temperature and were visualized with 0.05% DAB till the desired brown reaction product was obtained. All slides were counterstained with hematoxylin and then observed using Nikon E400 Light Microscope, and representative photographs were taken.

For double immunofluorescence staining, the sections were incubated with anti-S100A9 together with anti-CD68 (HUABIO, China), anti-CD86 (Santa Cruz, USA), anti-CD206 (Proteintech, China), or anti-cytokeratin 20 (Proteintech, China) antibodies, followed by incubation with secondary antibodies Alexa fluor 647-conjugated anti-mouse IgG and Alexa fluor 488-conjugated anti-rabbit IgG. These sections were also stained with 10 μg/ml DAPI. The fluorescent images were then observed and analyzed using a multi-laser confocal microscope.

Statistical Analysis

Data from the two groups were analyzed with the two-tailed Student's t-test and data from three or more groups using one-way ANOVA followed by Newman–Keuls' multiple comparison test. All experiments were independently repeated three times. The statistical analyses were carried out using SPSS version 13.0. Statistical differences are presented at probability levels of $p < 0.05$, $p < 0.01$, and $p < 0.001$.

RESULTS

Involvement of *Fn* in M2-Like Polarization of Mφ

To investigate whether the phenotypic differentiation of Mφ is affected by *Fn* infection *in vitro*, M1 markers (inducible nitric oxide synthase, iNOS; tumor necrosis factor, TNF-α; the B7-related cell surface proteins B7-2, CD86) and M2 markers (interleukin-10, IL-10; the mannose receptor, MRC/CD206) were determined. Compared to the control *E. coli*-challenged Mφ, *Fn*-challenged Mφ harbored significantly lower mRNA level of M1 markers *iNOS* and *TNF-α* but significantly higher mRNA level of M2 markers *IL-10* and *CD206* (**Figures 1A, B**). Similar tendency for protein levels of TNF-α and IL-10 in the supernatants was confirmed by ELISA (**Figure S1**). These results suggested that *Fn* may be involved in M2-like polarization. Marked CD206 expression but less CD86 expression was detected in *Fn*-challenged Mφ by western blot (**Figure 1C**). High intensity of the signal for CD206 but low intensity of signal for CD86 was also confirmed by immunofluorescence and flow cytometry analyses (**Figures 1D–F**). Collectively, these findings indicated that *Fn* might contribute to M2-like Mφ differentiation.

Elevated S100A9 Expression in *Fn*-Challenged Mφ and CRC Cells

Increased level of S100A9 is related to the infection of multiple pathogens and participates in disease progression by regulating inflammatory immunity (27, 28). Therefore, we analyzed the S100A9 level in *Fn*-challenged Mφ and CRC cells. The mRNA level of *S100A9* was significantly up-regulated in the *Fn*-challenged Mφ (**Figure 2A**). Consistently, its protein level in *Fn*-challenged Mφ as well as the supernatant was also markedly increased compared to the control groups (**Figures 2B, C**). In line with the finding, *Fn*-infected CRC cells as well as the supernatant also showed high level of S100A9 than the control group (**Figures 2D–F**). These data suggested that S100A9 may be elevated in the microenvironment of CRC with *Fn* infection. Next, we evaluated the enrichment of *Fn* and detected $CD68^+$ Mφ, $CD86^+$ M1-like Mφ, $CD206^+$ M2-like Mφ, and S100A9 expression in CRC tissues. As expected, there was more Mφ infiltration in *Fn*-positive CRC tissues compared to *Fn*-negative CRC tissues, and most of them were M2-like Mφs accompanied by higher levels of S100A9 in the TME (**Figures 2G** and **S2**). The results suggested that S100A9 expression is elevated in *Fn*-infected Mφ and CRC cells, which may be associated with M2-like Mφ polarization in CRC tissues.

S100A9 Is Involved in M2-Like Mφ Polarization in the Inflammatory Microenvironment of CRC With *Fn* Infection

The results above showed that S100A9 was highly expressed in *Fn*-infected CRC, but the direct evidence about the relation of higher S100A9 and M2-like Mφ polarization needs to be further studied. Therefore, we analyzed the Mφ polarization status in siS100A9-transfected Mφ cultured with *Fn*. As expected, S100A9 expression was successfully reduced in the supernatant of siS100A9-transfected Mφ with *Fn* infection (**Figure S3**). Knockdown of S100A9 expression obviously blocked *Fn*-induced increase of mRNA levels of M2 markers *IL-10* and *CD206* but improved *Fn*-induced decrease of mRNA levels of M1 marker *iNOS* and *TNF-α* (**Figures 3A, B**). The protein levels of TNF-α and IL-10 in the supernatants were confirmed by ELISA (**Figure S4**). Consistently, down-regulated M2 marker CD206 and up-regulated M1 marker CD86 were observed in siS100A9-transfected Mφ infection with *Fn* by western blot (**Figure 3C**). Low intensity of signal for CD206 but high signal for CD86 was also confirmed in siS100A9-transfected Mφ infection with *Fn* by immunofluorescence assay (**Figure 3D**). To better illustrate the effect of S100A9 on M2-like Mφ polarization in the *Fn*-infected

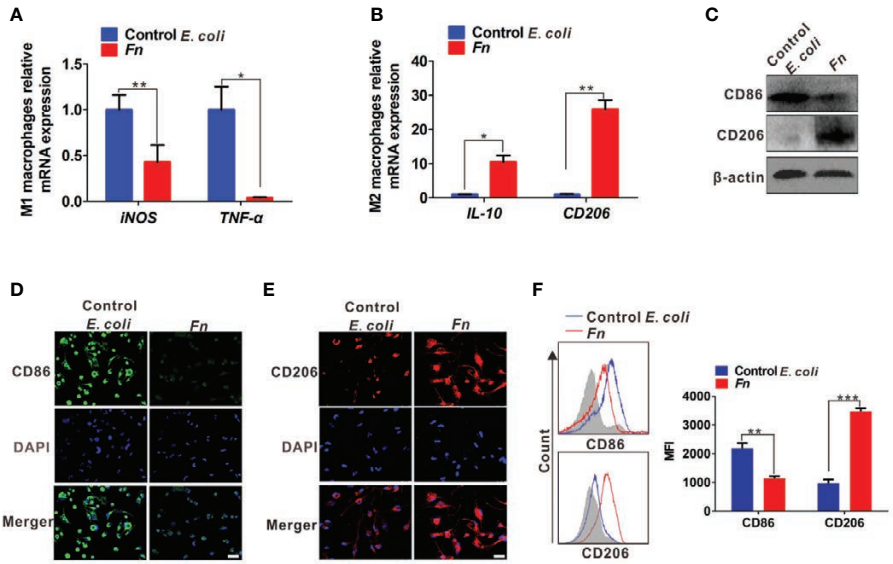

FIGURE 1 | *Fn* promotes M2-like polarization of Mφ *in vitro*. **(A, B)** qPCR analysis for mRNA levels of M1 markers (iNOS and TNF-α) and M2 markers (IL-10 and CD206) in Mφ co-cultured with control *E. coli i* or *Fn* for 24 h. **(C)** Western blot analysis of M1 marker (CD86) and M2 marker (CD206) expression in Mφ co-cultured with control *E. coli* or *Fn* for 48 h. **(D, E)** Representative immunofluorescence images of CD86$^+$ and CD206$^+$ Mφ after treatment with control *E. coli* or *Fn* for 48 h. CD86 was stained with Alexa Fluor 488 (green), CD206 was stained with Cy3 (red). Scale bars: 50 μm. **(F)** Flow cytometry analysis was performed to detect CD86$^+$ and CD206$^+$ Mφ after treatment with control *E. coli* or *Fn* for 48 h. A statistical mean fluorescence intensity (MFI) for CD86$^+$ and CD206$^+$ Mφ is shown in the right panel. Data were expressed as means ± SD in three independent experiments. *p < 0.05, **p < 0.01, ***p < 0.001.

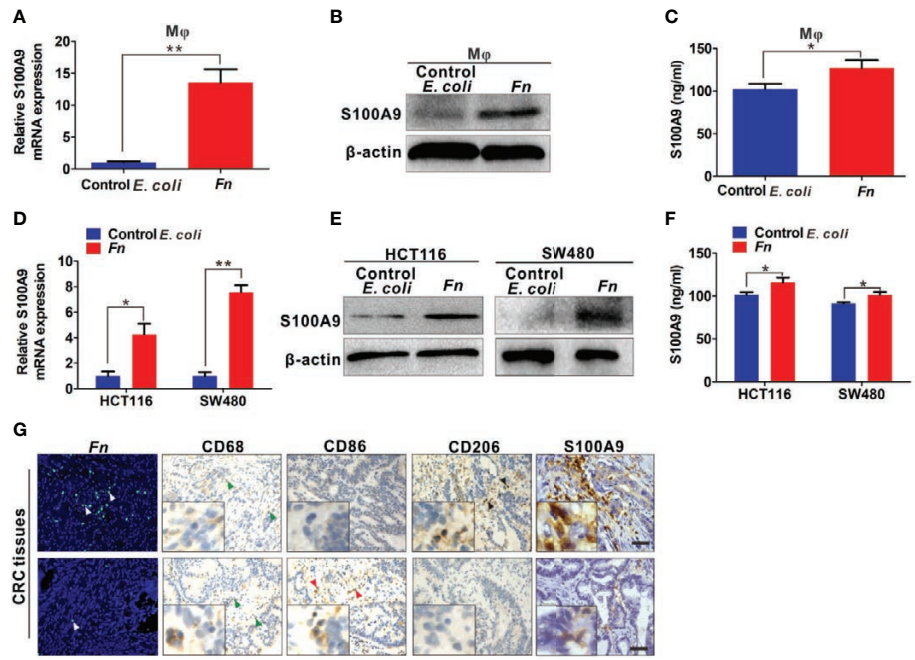

FIGURE 2 | S100A9 expression is up-regulated in *Fn*-challenged Mφ and CRC cells. **(A–F)** Mφ and CRC cells were co-cultured with control *E. coli* or *Fn*. S100A9 levels were detected by qPCR **(A, D)**, Western blot **(B, E)** and ELISA **(C, F)**. **(G)** Representative images of CD68$^+$ Mφ, CD86$^+$ Mφ, CD206$^+$ Mφ, and S100A9 expression in the TME of *Fn*-positive CRC tissues. White arrow: *Fn*; blue arrow: CD68$^+$ Mφ; red arrow: CD86$^+$ Mφ; black arrow: CD206$^+$ Mφ. Scale bars: 50 μm. Data were expressed as means ± SD in three independent experiments. *p < 0.05, **p < 0.01.

CRC inflammation microenvironment, CRC cells were transfected with siS100A9 followed by *Fn* infection, and then CM was collected for further culturing with Mφ (**Figure 3E**). siS100A9 transfection significantly inhibited the secretion of S100A9 protein in *Fn*-infected CRC cells compared to the control groups (**Figure 3F**). Moreover, Mφ tended to be polarized towards M1-like Mφ (mRNA levels: $iNOS^{high}$, $TNF\text{-}\alpha^{high}$, $IL\text{-}10^{low}$, $CD206^{low}$; protein levels: $CD86^{high}$, $CD206^{low}$) after culturing with the CM from CRC cells transfected with siS100A9 followed by *Fn* infection (**Figures 3G–I**). In contrast, after treatment with rS100A9 at a final concentration of 10 μM for 48 h, Mφs were apt to be M2 activated (mRNA levels: $iNOS^{low}$, $TNF\text{-}\alpha^{low}$; $IL\text{-}10^{high}$, $CD206^{high}$; protein levels: $CD86^{low}$, $CD206^{high}$) (**Figures 3J–L**). In conclusion, these results directly supported that elevated S100A9 favors the M2 polarization of Mφ in the TME of *Fn*-infected CRC.

Fn-Challenged M2-like Mφ, Which Is Mediated by S100A9, Promotes the Proliferation and Migration of CRC Cells

To further investigate the effects of *Fn*-challenged Mφ on the proliferation and migration ability of HCT116 and SW480 cells, CCK8 and Transwell assays were conducted after CRC cells were treated with various Mφ CM. There was a significant increase in the proliferation (**Figures 4A, B**) and migration (**Figure 4C**) abilities of HCT116 and SW480 cells cultured with *Fn*-challenged Mφ CM [(Mφ + *Fn*)-CM], while the effect would be reversed after silencing S100A9 expression in *Fn*-challenged

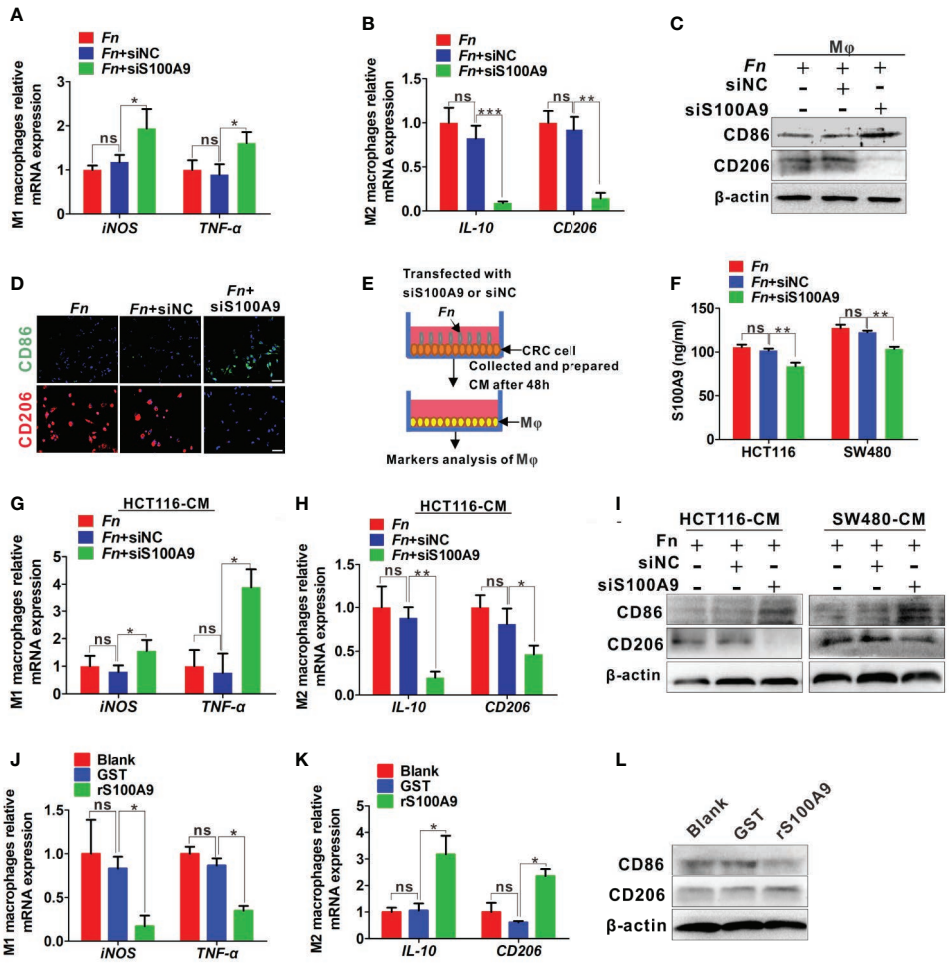

FIGURE 3 | S100A9 is involved in M2-like Mφ polarization in the presence of *Fn* in CRC. **(A–C)** Mφs were transfected with siNC or siS100A9 and subsequently co-cultured with *Fn*. The levels of M1 markers and M2 markers in Mφ were detected by qPCR **(A, B)** and Western blot **(C)**. **(D)** Representative immunofluorescence images of $CD86^+$ and $CD206^+$ in Mφ infected with *Fn* and then transfected with siNC or siS100A9. CD86 was stained with Alexa Fluor 488 (green); CD206 was stained with Cy3 (red). Scale bars: 50 μm. **(E, F)** HCT116 and SW480 cells were transfected with siNC or siS100A9 and then infected with *Fn*. After 48 h, the supernatant of each group was collected and used to culture Mφ in the next experiment **(E)**. ELISA analysis for S100A9 expression in the supernatant of HCT116 and SW480 cells **(F)**. **(G–I)** Mφs were co-cultured with the CM from CRC cells. The levels of M1 markers and M2 markers in Mφ were detected by qPCR **(G, H)** and Western blot **(I)**. **(J–L)** Mφs were treated with GST or rS100A9. The levels of M1 markers and M2 markers in Mφ were detected by qPCR **(J, K)** and Western blot **(L)**. Data were expressed as means ± SD in three independent experiments. ns, not significant. *p < 0.05; **p < 0.01; ***p < 0.001.

Mφ CM [(Mφ + siS100A9 + *Fn*)-CM)] (**Figures 4D–F**). The remarkably enhanced ability of proliferation (**Figures 4G, H**) and migration (**Figure 4I**) of HCT116 and SW480 cells was confirmed again when these cells were cultured with rS100A9-treated Mφ CM [(Mφ + rS100A9)-CM). In addition, epithelial-to-mesenchymal transition (EMT)-related genes *N-cadherin* and *Vimentin* were up-regulated, but *E-cadherin* was decreased in HCT116 cells cultured with (Mφ + *Fn*)-CM (**Figure S5**). These results, along with those aforementioned, suggested that *Fn*-challenged M2-like Mφ, which was mediated by S100A9 in the TME, confers onto CRC cells a more malignant phenotype.

Fn Up-Regulates S100A9 Expression and Promotes M2-Like Polarization *via* the TLR4/NF-κB Pathway

To further examine the mechanisms by which *Fn* engages in S100A9 expression and M2 polarization, we focused on TLR4/NF-κB pathway, which is substantially activated in CRC with *Fn* enrichment (21) and determine whether it takes part in the effect. The mRNA levels of TLR4 in Mφ, HCT116, and SW480 cells were obviously increased in response to *Fn* infection (**Figure 5A**). Phospho-NF-κB p65 (p-p65) levels in Mφ, HCT116, and SW480 cells were also increased with time and reached a peak almost at 120 min, while there was no obvious change in the total p65 (**Figure 5B**). *Fn*-induced p-p65 in the three cell lines was inhibited after TLR4 inhibitor TAK-242 stimulation (**Figure 5C**), suggesting TLR4 mediated *Fn*-mediated NF-κB activation. Especially, treatment with TLR4 inhibitor TAK-242 and NF-κB inhibitor BAY 11-7082 also inhibited S100A9 protein levels in *Fn*-challenged Mφ and CRC cells (**Figure 5D**) as well as its levels in cell supernatant (**Figures 5E–G**). Exposure of *Fn*-challenged Mφ to the TAK-242 or BAY 11-7082 failed to induce M2-like Mφ (mRNA levels: $iNOS^{high}$, $TNF\text{-}\alpha^{high}$, $IL\text{-}10^{low}$, $CD206^{low}$) (**Figures 5H, I**). Consistently, this change in Mφ phenotype was again proved when cultured with the CM from *Fn*-challenged CRC cells, which were pretreated with TAK-242 and BAY 11-7082 (**Figures 5J, K**). Altogether, these results indicated that the TLR4-mediated NF-κB pathway is partially responsible for M2-like polarization induced by S100A9 in response to *Fn* infection in CRC.

Accelerated Growth of the Subcutaneous Tumor by M2-Like Mφ Induced by *Fn*

In the xenograft nude mouse models, HCT116 and differently treated Mφ were inoculated into nude mice. The results from the

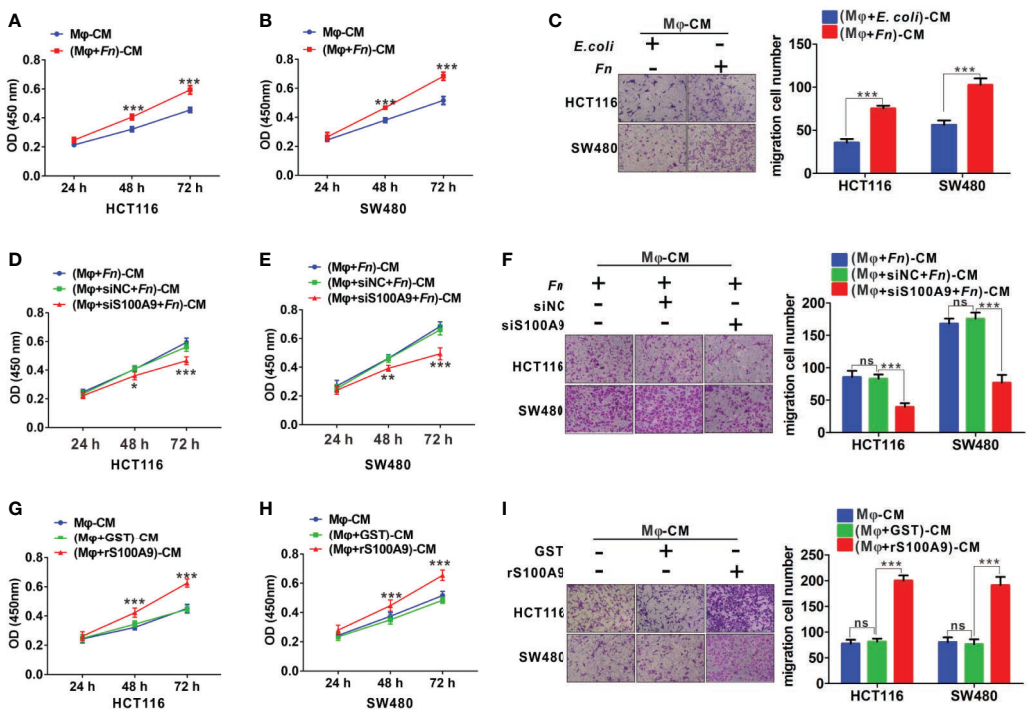

FIGURE 4 | *Fn*-challenged M2-Mφ, which was mediated by S100A9, promotes the proliferation and migration of CRC cells. **(A, B)** CCK8 assay was used to determine the proliferation ability of CRC cells co-cultured with (Mφ + *E. coli*)-CM or (Mφ + *Fn*)-CM for 24, 48, and 72 h. **(C)** Transwell assay was used to determine the migration ability of CRC cells co-cultured with (Mφ + *E. coli*)-CM or (Mφ + *Fn*)-CM for 24 h. Magnification, 100×. **(D, E)** CCK8 assay was used to determine the proliferation ability of CRC cells co-cultured with (Mφ + *Fn*)-CM, (Mφ + siNC + *Fn*)-CM, (Mφ + siS100A9 + *Fn*)-CM for 24, 48, and 72 h. **(F)** Transwell assay was used to determine the migration ability of CRC cells co-cultured with (Mφ + *Fn*)-CM, (Mφ + siNC + *Fn*)-CM, (Mφ + siS100A9 + *Fn*)-CM for 24 h. Magnification, 100×. **(G, H)** CCK8 assay was used to determine the proliferation ability of CRC cells co-cultured with untreated Mφ-CM, (Mφ + GST)-CM and (Mφ + rS100A9)-CM for 24, 48, and 72 h. **(I)** Transwell assay was used to determine the migration ability of CRC cells co-cultured with untreated Mφ-CM, (Mφ + GST)-CM and (Mφ + rS100A9)-CM for 24 h. Magnification, 100×. In **(A, B, D, E, G, H)**, data shown are mean absorbances ± SD. In **(C, F, I)**, data shown are mean migrating cells ± SD. ns, not significant. *p < 0.05, **p < 0.01, ***p < 0.001.

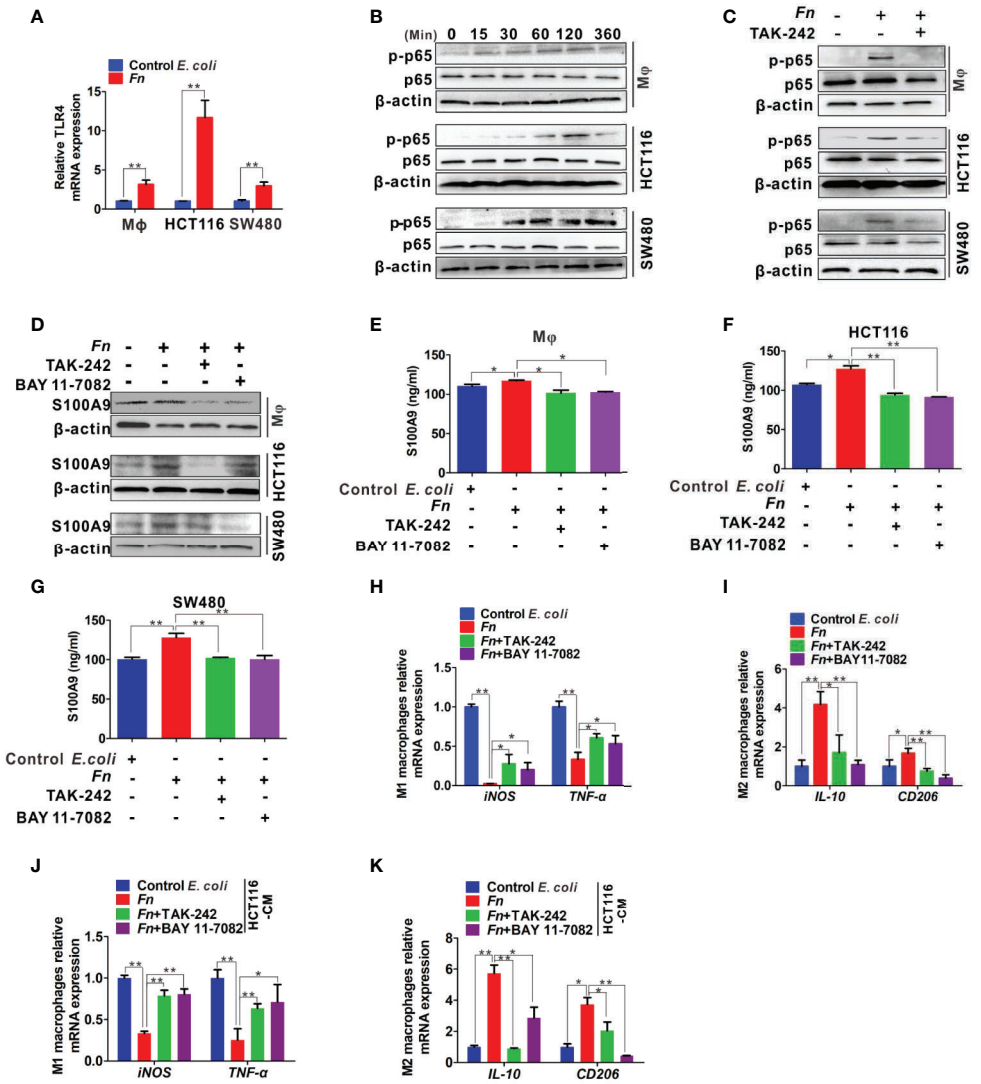

FIGURE 5 | Expression of S100A9 and M2-like Mφ polarization is regulated by TLR4/NF-κB activation caused by *Fn*. **(A)** qPCR analysis of TLR4 expression in Mφ and CRC cells co-cultured with control *E. coli* or *Fn* for 48 h. **(B)** Western blot analysis of p65 and p-p65 expression in Mφ and CRC cells co-cultured with *Fn* for 0,15, 30, 60, 120 and 360 min. **(C)** Western blot analysis of p-p65 level in Mφ and CRC cells pretreated with or without inhibitor TAK-242 for 60 min and then co-cultured with control *E. coli* or *Fn* for 120 min. **(D)** Western blot analysis of S100A9 level in Mφ and CRC cells pretreated with or without inhibitors TAK-242 and NF-κB for 60 min and then co-cultured with control *E. coli* or *Fn* for 48 h. **(E–G)** ELISA analysis of S100A9 level in the CM of Mφ and CRC cells pretreated with or without inhibitors TAK-242 and Bay 11-7082 for 60 min and then co-cultured with control *E. coli* or *Fn* for 48 h. **(H–K)** qPCR analysis for mRNA levels of M1 markers (iNOS and TNF-α) and M2 markers (IL-10 and CD206) in Mφ. The cells were pretreated with or without inhibitors TAK-242 and Bay 11-7082 for 60 min and then co-cultured with control *E. coli* or *Fn* for 24 h **(H, I)** or co-cultured with the CM of HCT116 cells for 24 h **(J, K)**. The CM of HCT116 cells were pretreated with or without inhibitors TAK-242 and Bay 11-7082 for 60 min and then co-cultured with control *E. coli* or *Fn* for 48 h. Data were expressed as means ± SD in three independent experiments. *p < 0.05, **p < 0.01.

nude mouse xenograft model showed that co-injection with HCT116/*Fn*-treated Mφ significantly accelerated the tumor growth, and this effect was partially blocked by silencing S100A9 expression in Mφ in the nude mice co-injected with HCT116/(*Fn* + siS1A00A9)-treated Mφ (**Figure 6A**). Tumor growth curve and the average weight of each group also showed the same tendency (**Figures 6B, C**). In addition, IHC results showed that the protein levels of proliferation-related marker PCNA, EMT-related marker E-cadherin and N-cadherin, and tumor-promoting molecules VEGF and TGF-β were higher in tumors of nude mice co-injected with HCT116/*Fn*-treated Mφ than those of the compared control groups, while these protein levels were decreased in the nude mice co-injected with HCT116/(*Fn* + siS1A00A9)-treated Mφ (**Figure 6D**). Western blot and qPCR results about the levels of PCNA, E-cadherin, N-cadherin, VEGF, TGF-β in each xenograft tumor were also consistent with the result of IHC (**Figures 6E–I**). These data suggested that the interaction between HCT116 and *Fn*-treated Mφ promotes

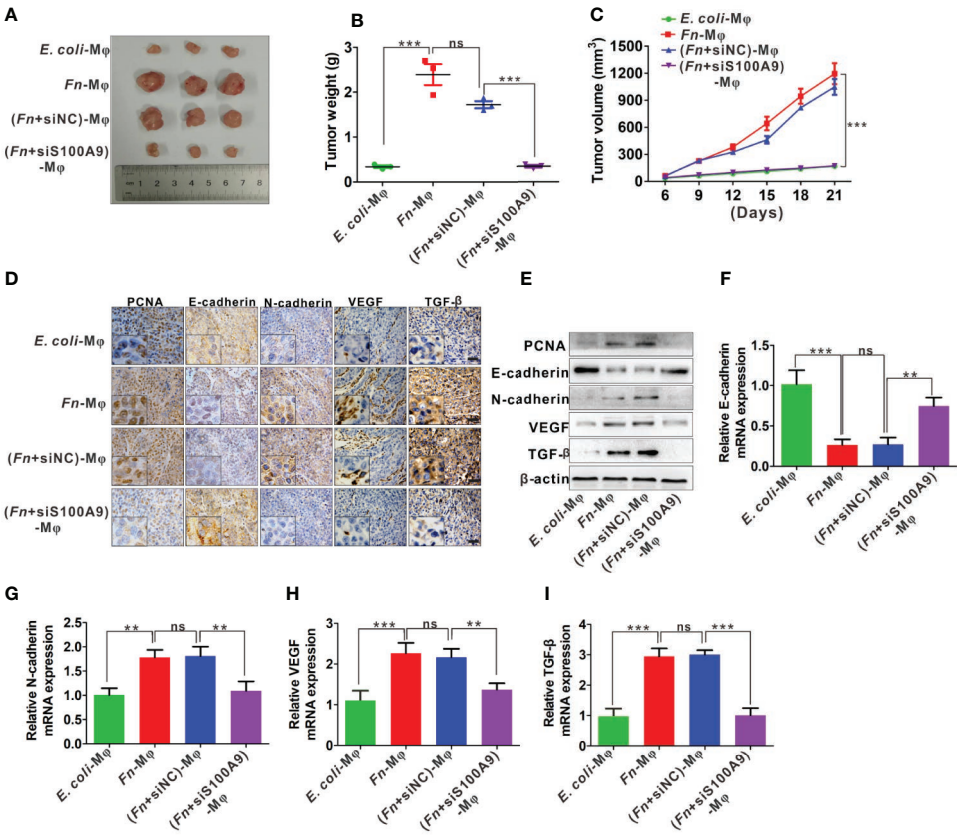

FIGURE 6 | *Fn*-caused M2 polarization mediated by S100A9 promotes the growth of subcutaneous tumor. **(A)** Representative images of tumors in mice co-injected with equal amount of HCT116 cells and control *E. coli* -treated, *Fn*-treated, (*Fn* + siNC)-treated or (*Fn* + siS100A9)-treated Mφ. **(B)** Images of tumor weights in different groups, n = 3/group. **(C)** Statistical analysis of tumor volumes in different groups, n = 3/group. **(D)** Representative immunohistochemistry images of PCNA, E-cadherin, N-cadherin, VEGF, and TFG-β proteins in representative xenograft tumor sections. Scale bars: 50 μm. **(E)** Western blot analysis of PCNA, E-cadherin, N-cadherin, VEGF, and TFG-β protein levels in representative xenograft tumor. **(F–I)** qPCR analysis of E-cadherin, N-cadherin, VEGF, and TGF-β expression in each xenograft tumor, n = 3/group. Data were expressed as means ± SD in three independent experiments. ns, not significant. $^{**}p < 0.01$, $^{***}p < 0.001$.

tumor growth in nude mice *in vivo*, which may be involved in *Fn*-induced M2-like polarization mediated by S100A9.

DISCUSSION

Identifying specific carcinogenic microorganisms remains the focus of CRC research (29). Recently, among these identified and published CRC-related gut microbes, *Fn* has attracted the most attention. Although involvement of *Fn* in immunosuppressive TME has been indicated, the detailed mechanisms by which *Fn* participated in regulating the activation of immune cells have not been well-elucidated. Here, we demonstrated a regulatory role of *Fn* in CRC TME on M2-like polarization, which is mediated by activation of TLR4-dependent NF-κB/S100A9 signaling pathway in Mφs and CRC cells (**Figure 7**).

Mφs are dynamic and heterogeneous cells whose differentiation, tissue distribution, and responsiveness to stimuli are governed by different mechanisms (30). Based on their response to different microenvironmental signaling factors, Mφs can be differentiated into two classifications, namely, M1-like Mφ sand M2-like Mφs. M1-like Mφ mainly plays a pro-inflammatory and anti-tumor role, while M2-like Mφ is often considered to be tumor-promoting (31). Viral, parasitic, fungal, and bacterial pathogens can induce M2 activation in Mφ and further promote pathogen-induced inflammatory injury and even canceration (32). Numerous studies have elucidated *Fn*, a Gram-negative oral commensal anaerobe, which is one of the most prevalent species in oral inflammation diseases and extraoral infections (33, 34). At the same time, *Fn* has been reported to be highly enriched in CRC tissues and helps tumor cells to achieve immune evasion by inhibiting immune cell activity in TME (13, 35–37). However, the presence and activation state of Mφ in *Fn*-infected CRC remain to be elucidated. In this study, we determined that *Fn*-challenged Mφs were inclined to M2-like activation, which in turn enhances the proliferation and migration of CRC cells *in vitro*. Furthermore, our results from the xenograft nude mouse also supported a positive association between *Fn*-challenged M2-like Mφ and tumor growth. Altogether, our results suggest that *Fn*-induced M2-like polarization facilitated CRC progression.

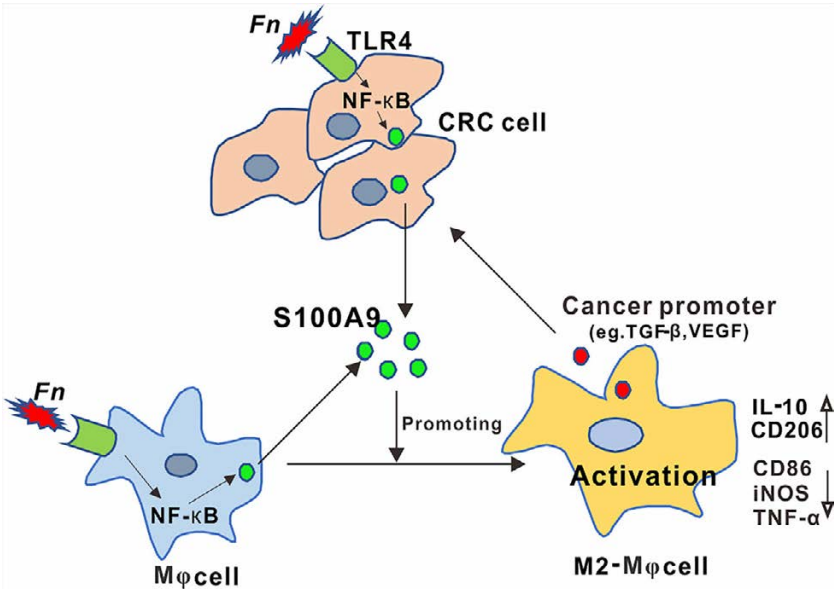

FIGURE 7 | Schematic diagram of the relationship among *Fn*, M2 polarization, and CRC progression. Activation of the TLR4/NF-κB cascade in Mφ and CRC cells by *Fusobacterium nucleatum* infection mediated high levels of S100A9 in CRC microenvironment, which led to M2-like Mφ phenotype showing increased IL-10 and CD206 levels, contributing to CRC malignance.

Compelling links are beginning to appear among bacteria, immune escape, and CRC. Base on *Fn* abundance in CRC along with weaken host anti-tumor immunity, there is a great need for further mechanistic understanding of CRC to find a novel target molecule. S100A9, originally known as immunogenic protein, is mainly expressed by bone marrow-derived cells such as mononuclear, Mφ, and neutrophils (17). Besides, S100A9 induces positive feedback and promotes further leukocyte recruitment under pathological conditions associated with inflammatory infection (38). Experimental data indicated that S100A9 presents abundant expression in various inflammation-associated human cancers, no doubt including CRC (17, 18). Our previous work confirmed elevated S100A9 levels in CRC, stimulating survival and migration of CRC cells (18). Here, we further determined that high S100A9 levels in CRC may be associated with *Fn* infection. Moreover, the number of tumor-infiltrating M2-like Mφ was more in *Fn*-positive CRC tissues accompanied by higher S100A9 expression than that in *Fn*-negative tissues with lower S100A9 expression. These results further prompt us to infer that S100A9 may play a potential role in regulating Mφ toward M2-like phenotype. Previously, tumor-infiltrating S100A9-positive inflammatory or immune cell tissues were closely related to the pathological stage of CRC (22). S100A9 was also reported to be involved in THP-1 cells differentiated into MDSCs or M2-like Mφ stimulated by myofibroblast-based CM (39). Here, our results demonstrated that up-regulation of S100A9 expression from *Fn*-infected Mφ and CRC cells in the TME was partially responsible for M2-like Mφ activation state. Not surprisingly, the proliferation and migration ability of CRC cells co-cultured with *Fn*-treated Mφ would be weakened by silencing S100A9 expression in the TME of CRC.

In this study, we attempted to uncover the mechanism for regulation of S100A9 expression and M2-like Mφ polarization by *Fn* infection. As an inflammation/immunity mediator, high levels of S100A9 have been indicated and aggravated mutiple pathogen infections, including coxsackievirus B3 (CVB3)-induced myocarditis (27), streptococcus pneumoniae (SP)-related otitis media (OM) (40), and influenza A virus-related pneumonia (28). The TLR4/NF-κB signal is often activated in pathogen infection. Influenza A virus could up-regulate S100A9 expression and synergistically activate TLR4 signaling cascade in lung Mφ and endothelial cells, exaggerating pro-inflammatory response, cell-death, and virus pathogenesis (28). Our previous study also found HBV-induced NF-κB activation enhances transcription of S100A9 by binding to its promoter, contributing to HCC malignancy (16). In human cytomegalovirus (HCMV)-related inflammatory breast cancer, NF-κB activation could result in M2-like Mφ polarization accompanied with the secretion of tumor-promoting M2-like cytokines (41, 42). Thus, we speculated that *Fn* infection may facilitate CRC malignancy involving Mφ activation, either directly or indirectly, *via* activating specific signal pathways such as that of TLR4-dependent NF-κB. Now we have shown that PAMP extracted from *Fn* and *Fn* itself could be recognized by TLR4, which further activates its downstream signaling cascade in CRC (8, 21). Also, NF-κB, as a widely acknowledged downstream effector of TLR4 signaling, is highly activated in *Fn*-associated CRC (6). Interestingly, we found a significant increase in the expression of TLR4 and time-dependent activation of NF-κB caused by *Fn* infection in Mφ and CRC cells, which was inhibited by TLR4 inhibitor TAK-242. In addition, S100A9 expression and M2 activation were also significantly suppressed when the TLR4/NF-κB pathway was blocked. All the

evidence above suggested that interference with TLR4/NF-κB/S100A9 cascade should be given enough attention in the treatment of *Fn*-associated CRC.

In conclusion, the current findings demonstrate that S100A9 plays a critical role in regulating M2-like Mφ polarization in *Fn*-infected CRC microenvironment, and targeting TLR4/NF-κB/S100A9 cascade may attenuate the immunosuppressive effect and serve as promising immunotherapy strategy for *Fn*-associated CRC.

DATA AVAILABILITY STATEMENT

The raw data supporting the conclusions of this article will be made available by the authors without undue reservation.

ETHICS STATEMENT

The studies involving human participants were reviewed and approved by the Ethics Committee of Chongqing Medical University. The patients/participants provided their written informed consent to participate in this study. The animal study was reviewed and approved by the Ethics Committee of Chongqing Medical University.

AUTHOR CONTRIBUTIONS

LH and YL performed the experiments, analyzed the data, and wrote the manuscript. XK, RW, QP, and YZ analyzed the data. LD and LZ conceived ideas, oversaw the research, and co-wrote the manuscript. All authors contributed to the article and approved the submitted version.

FUNDING

This work was supported by The National Natural Science Foundation of China (Grant No. 82072364 to LD), Natural Science Foundation of Chongqing (Grant No. cstc2019jcyj-msxmX0864 to LD), and Chongqing Health Commission (Grant No. 2020FYYX038 to LD).

SUPPLEMENTARY MATERIAL

The Supplementary Material for this article can be found online at: https://www.frontiersin.org/articles/10.3389/fimmu.2021.658681/full#supplementary-material

REFERENCES

1. Song M, Garrett WS, Chan AT. Nutrients, Foods, and Colorectal Cancer Prevention. *Gastroenterology* (2015) 148(6):1244–60.e1216. doi: 10.1053/j.gastro.2014.12.035
2. Eser S, Chang J, Charalambous H, Silverman B, Demetriou A, Yakut C, et al. Incidence Patterns of Colorectal Cancers in Four Countries of the Middle East Cancer Consortium (Cyprus, Jordan, Israel, and Izmir, Turkey) Compared With Those in the United States Surveillance, Epidemiology, and End Results Program. *Turk J Gastroenterol* (2018) 29(1):36–44. doi: 10.5152/tjg.2018.17263
3. Siegel RL, Miller KD, Goding Sauer A, Fedewa SA, Butterly LF, Anderson JC, et al. Colorectal Cancer Statistics, 2020. *CA Cancer J Clin* (2020) 70(3):145–64. doi: 10.3322/caac.21601
4. Sun J, Kato I. Gut Microbiota, Inflammation and Colorectal Cancer. *Genes Dis* (2016) 3(2):130–43. doi: 10.1016/j.gendis.2016.03.004
5. Garcia-Castillo V, Sanhueza E, McNerney E, Onate SA, Garcia A. Microbiota Dysbiosis: A New Piece in the Understanding of the Carcinogenesis Puzzle. *J Med Microbiol* (2016) 65(12):1347–62. doi: 10.1099/jmm.0.000371
6. Zhang S, Cai S, Ma Y. Association Between Fusobacterium Nucleatum and Colorectal Cancer: Progress and Future Directions. *J Cancer* (2018) 9 (9):1652–9. doi: 10.7150/jca.24048
7. Strauss J, Kaplan GG, Beck PL, Rioux K, Panaccione R, Devinney R, et al. Invasive Potential of Gut Mucosa-Derived Fusobacterium Nucleatum Positively Correlates With IBD Status of the Host. *Inflammation Bowel Dis* (2011) 17(9):1971–8. doi: 10.1002/ibd.21606
8. Chen T, Li Q, Wu J, Wu Y, Peng W, Li H, et al. Fusobacterium Nucleatum Promotes M2 Polarization of Macrophages in the Microenvironment of Colorectal Tumours Via a TLR4-Dependent Mechanism. *Cancer Immunol Immunother* (2018) 67(10):1635–46. doi: 10.1007/s00262-018-2233-x
9. Mima K, Nishihara R, Qian ZR, Cao Y, Sukawa Y, Nowak JA, et al. Fusobacterium Nucleatum in Colorectal Carcinoma Tissue and Patient Prognosis. *Gut* (2016) 65(12):1973–80. doi: 10.1136/gutjnl-2015-310101
10. Flanagan L, Schmid J, Ebert M, Soucek P, Kunicka T, Liska V, et al. Fusobacterium Nucleatum Associates With Stages of Colorectal Neoplasia Development, Colorectal Cancer and Disease Outcome. *Eur J Clin Microbiol Infect Dis* (2014) 33(8):1381–90. doi: 10.1007/s10096-014-2081-3
11. Kaplan CW, Ma X, Paranjpe A, Jewett A, Lux R, Kinder-Haake S, et al. Fusobacterium Nucleatum Outer Membrane Proteins Fap2 and RadD Induce Cell Death in Human Lymphocytes. *Infect Immun* (2010) 78(11):4773–8. doi: 10.1128/IAI.00567-10
12. Chaushu S, Wilensky A, Gur C, Shapira L, Elboim M, Halftek G, et al. Direct Recognition of Fusobacterium Nucleatum by the NK Cell Natural Cytotoxicity Receptor NKp46 Aggravates Periodontal Disease. *PLoS Pathog* (2012) 8(3):e1002601. doi: 10.1371/journal.ppat.1002601
13. Gur C, Ibrahim Y, Isaacson B, Yamin R, Abed J, Gamliel M, et al. Binding of the Fap2 Protein of Fusobacterium Nucleatum to Human Inhibitory Receptor TIGIT Protects Tumors From Immune Cell Attack. *Immunity* (2015) 42 (2):344–55. doi: 10.1016/j.immuni.2015.01.010
14. Kwon CH, Moon HJ, Park HJ, Choi JH, Park DY. S100A8 and S100A9 Promotes Invasion and Migration Through p38 Mitogen-Activated Protein Kinase-Dependent NF-kappaB Activation in Gastric Cancer Cells. *Mol Cells* (2013) 35(3):226–34. doi: 10.1007/s10059-013-2269-x
15. Srikrishna G. S100A8 and S100A9: New Insights Into Their Roles in Malignancy. *J Innate Immun* (2012) 4(1):31–40. doi: 10.1159/000330095
16. Duan L, Wu R, Zhang X, Wang D, You Y, Zhang Y, et al. Hbx-Induced S100A9 in NF-kappaB Dependent Manner Promotes Growth and Metastasis of Hepatocellular Carcinoma Cells. *Cell Death Dis* (2018) 9(6):629. doi: 10.1038/s41419-018-0512-2
17. Shabani F, Farasat A, Mahdavi M, Gheibi N. Calprotectin (S100A8/S100A9): A Key Protein Between Inflammation and Cancer. *Inflammation Res* (2018) 67(10):801–12. doi: 10.1007/s00011-018-1173-4
18. Duan L, Wu R, Ye L, Wang H, Yang X, Zhang Y, et al. S100A8 and S100A9 are Associated With Colorectal Carcinoma Progression and Contribute to Colorectal Carcinoma Cell Survival and Migration Via Wnt/beta-catenin Pathway. *PLoS One* (2013) 8(4):e62092. doi: 10.1371/journal.pone.0062092
19. Huang M, Wu R, Chen L, Peng Q, Li S, Zhang Y, et al. S100a9 Regulates Mdscs-Mediated Immune Suppression Via the RAGE and TLR4 Signaling Pathways in Colorectal Carcinoma. *Front Immunol* (2019) 10:2243. doi: 10.3389/fimmu.2019.02243
20. Podgorska M, Oldak M, Marthaler A, Fingerle A, Walch-Ruckheim B, Lohse S, et al. Chronic Inflammatory Microenvironment in Epidermodysplasia Verruciformis Skin Lesions: Role of the Synergism Between HPV8 E2 and C/EBPbeta to Induce Pro-Inflammatory S100A8/A9 Proteins. *Front Microbiol* (2018) 9:392. doi: 10.3389/fmicb.2018.00392
21. Yang Y, Weng W, Peng J, Hong L, Yang L, Toiyama Y, et al. Fusobacterium Nucleatum Increases Proliferation of Colorectal Cancer Cells and Tumor

Development in Mice by Activating Toll-Like Receptor 4 Signaling to Nuclear Factor-kappaB, and Up-Regulating Expression of Microrna-21. *Gastroenterology* (2017) 152(4):851–866 e824. doi: 10.1053/j.gastro.2016.11.018
22. Bassorgun CI, Unal B, Erin N, Ozluk A, Uzun OC, Elpek GO. S100A8 and S100A9 Positive Cells in Colorectal Carcinoma: Clinicopathological Analysis. *Gastroenterol Res Pract* (2014) 2014:943175. doi: 10.1155/2014/943175
23. Nemeth J, Stein I, Haag D, Riehl A, Longerich T, Horwitz E, et al. S100A8 and S100A9 are Novel Nuclear Factor Kappa B Target Genes During Malignant Progression of Murine and Human Liver Carcinogenesis. *Hepatology* (2009) 50(4):1251–62. doi: 10.1002/hep.23099
24. Wang Q, Zhao L, Xu C, Zhou J, Wu Y. Fusobacterium Nucleatum Stimulates Monocyte Adhesion to and Transmigration Through Endothelial Cells. *Arch Oral Biol* (2019) 100:86–92. doi: 10.1016/j.archoralbio.2019.02.013
25. Zha H, Sun H, Li X, Duan L, Li A, Gu Y, et al. S100A8 Facilitates the Migration of Colorectal Cancer Cells Through Regulating Macrophages in the Inflammatory Microenvironment. *Oncol Rep* (2016) 36(1):279–90. doi: 10.3892/or.2016.4790
26. Yu J, Chen Y, Fu X, Zhou X, Peng Y, Shi L, et al. Invasive Fusobacterium Nucleatum may Play a Role in the Carcinogenesis of Proximal Colon Cancer Through the Serrated Neoplasia Pathway. *Int J Cancer* (2016) 139(6):1318–26. doi: 10.1002/ijc.30168
27. Muller I, Vogl T, Pappritz K, Miteva K, Savvatis K, Rohde D, et al. Pathogenic Role of the Damage-Associated Molecular Patterns S100A8 and S100A9 in Coxsackievirus B3-Induced Myocarditis. *Circ Heart Fail* (2017) 10(11): e004125. doi: 10.1161/CIRCHEARTFAILURE.117.004125
28. Tsai SY, Segovia JA, Chang TH, Morris IR, Berton MT, Tessier PA, et al. DAMP Molecule S100A9 Acts as a Molecular Pattern to Enhance Inflammation During Influenza A Virus Infection: Role of DDX21-TRIF-TLR4-MyD88 Pathway. *PLoS Pathog* (2014) 10(1):e1003848. doi: 10.1371/journal.ppat.1003848
29. Hold GL, Garrett WS. Gut Microbiota. Microbiota Organization–a Key to Understanding CRC Development. *Nat Rev Gastroenterol Hepatol* (2015) 12 (3):128–9. doi: 10.1038/nrgastro.2015.25
30. Larionova I, Kazakova E, Patysheva M, Kzhyshkowska J. Transcriptional, Epigenetic and Metabolic Programming of Tumor-Associated Macrophages. *Cancers (Basel)* (2020) 12(6):1411. doi: 10.3390/cancers12061411
31. Wang J, Li D, Cang H, Guo B. Crosstalk Between Cancer and Immune Cells: Role of Tumor-Associated Macrophages in the Tumor Microenvironment. *Cancer Med* (2019) 8:4709–21. doi: 10.1002/cam4.2327
32. Labonte AC, Tosello-Trampont AC, Hahn YS. The Role of Macrophage Polarization in Infectious and Inflammatory Diseases. *Mol Cells* (2014) 37 (4):275–85. doi: 10.14348/molcells.2014.2374
33. Mitsuhashi K, Nosho K, Sukawa Y, Matsunaga Y, Ito M, Kurihara H, et al. Association of Fusobacterium Species in Pancreatic Cancer Tissues With Molecular Features and Prognosis. *Oncotarget* (2015) 6(9):7209–20. doi: 10.18632/oncotarget.3109
34. Yang NY, Zhang Q, Li JL, Yang SH, Shi Q. Progression of Periodontal Inflammation in Adolescents is Associated With Increased Number of Porphyromonas Gingivalis, Prevotella Intermedia, Tannerella Forsythensis, and Fusobacterium Nucleatum. *Int J Paediatr Dent* (2014) 24(3):226–33. doi: 10.1111/ipd.12065
35. Gur C, Maalouf N, Shhadeh A, Berhani O, Singer BB, Bachrach G, et al. Fusobacterium Nucleatum Supresses Anti-Tumor Immunity by Activating CEACAM1. *Oncoimmunology* (2019) 8(6):e1581531. doi: 10.1080/2162402X.2019.1581531
36. Kostic AD, Chun E, Robertson L, Glickman JN, Gallini CA, Michaud M, et al. Fusobacterium Nucleatum Potentiates Intestinal Tumorigenesis and Modulates the Tumor-Immune Microenvironment. *Cell Host Microbe* (2013) 14(2):207–15. doi: 10.1016/j.chom.2013.07.007
37. Hamada T, Zhang X, Mima K, Bullman S, Sukawa Y, Nowak JA, et al. Fusobacterium Nucleatum in Colorectal Cancer Relates to Immune Response Differentially by Tumor Microsatellite Instability Status. *Cancer Immunol Res* (2018) 6(11):1327–36. doi: 10.1158/2326-6066.CIR-18-0174
38. Roth J, Vogl T, Sorg C, Sunderkotter C. Phagocyte-Specific S100 Proteins: A Novel Group of Proinflammatory Molecules. *Trends Immunol* (2003) 24 (4):155–8. doi: 10.1016/s1471-4906(03)00062-0
39. Kim JH, Oh SH, Kim EJ, Park SJ, Hong SP, Cheon JH, et al. The Role of Myofibroblasts in Upregulation of S100A8 and S100A9 and the Differentiation of Myeloid Cells in the Colorectal Cancer Microenvironment. *Biochem Biophys Res Commun* (2012) 423(1):60–6. doi: 10.1016/j.bbrc.2012.05.081
40. Hong W, Khampang P, Samuels TL, Kerschner JE, Yan K, Simpson P. Expression of Calcium-Binding Proteins S100A8, S100A9 and S100A12 in Otitis Media. *Int J Pediatr Otorhinolaryngol* (2017) 101:30–6. doi: 10.1016/j.ijporl.2017.07.025
41. El-Shinawi M, Mohamed HT, El-Ghonaimy EA, Tantawy M, Younis A, Schneider RJ, et al. Human Cytomegalovirus Infection Enhances NF-kappaB/p65 Signaling in Inflammatory Breast Cancer Patients. *PLoS One* (2013) 8(2):e55755. doi: 10.1371/journal.pone.0055755
42. Chan G, Bivins-Smith ER, Smith MS, Yurochko AD. NF-Kappab and Phosphatidylinositol 3-Kinase Activity Mediates the HCMV-Induced Atypical M1/M2 Polarization of Monocytes. *Virus Res* (2009) 144(1-2):329–33. doi: 10.1016/j.virusres.2009.04.026

Conflict of Interest: The authors declare that the research was conducted in the absence of any commercial or financial relationships that could be construed as a potential conflict of interest.

Copyright © 2021 Hu, Liu, Kong, Wu, Peng, Zhang, Zhou and Duan. This is an open-access article distributed under the terms of the Creative Commons Attribution License (CC BY). The use, distribution or reproduction in other forums is permitted, provided the original author(s) and the copyright owner(s) are credited and that the original publication in this journal is cited, in accordance with accepted academic practice. No use, distribution or reproduction is permitted which does not comply with these terms.

frontiers in Immunology

ORIGINAL RESEARCH
published: 31 May 2021
doi: 10.3389/fimmu.2021.695865

Prognosis and Characterization of Immune Microenvironment in Acute Myeloid Leukemia Through Identification of an Autophagy-Related Signature

Denggang Fu[1†], Biyu Zhang[2†], Shiyong Wu[1], Yinghua Zhang[1], Jingwu Xie[1,3], Wangbin Ning[4*] and Hua Jiang[1*]*

[1] Department of Pediatrics, The Wells Center for Pediatric Research, Indiana University School of Medicine, Indianapolis, IN, United States, [2] School of Pharmacy and Life Science, Jiujiang University, Jiujiang, China, [3] The IU Simon Comprehensive Cancer Center, Indiana University, Indianapolis, IN, United States, [4] Department of Rheumatology and Immunology, Xiangya Hospital, Central South University, Changsha, China

Acute myeloid leukemia (AML) is one of the most common hematopoietic malignancies that has an unfavorable outcome and a high rate of relapse. Autophagy plays a vital role in the development of and therapeutic responses to leukemia. This study identifies a potential autophagy-related signature to monitor the prognoses of patients of AML. Transcriptomic profiles of AML patients (GSE37642) with the relevant clinical information were downloaded from Gene Expression Omnibus (GEO) as the training set while TCGA-AML and GSE12417 were used as validation cohorts. Univariate regression analyses and multivariate stepwise Cox regression analysis were respectively applied to identify the autophagy-related signature. The univariate Cox regression analysis identified 32 autophagy-related genes (ARGs) that were significantly associated with the overall survival (OS) of the patients, and were mainly rich in signaling pathways for autophagy, p53, AMPK, and TNF. A prognostic signature that comprised eight ARGs (BAG3, CALCOCO2, CAMKK2, CANX, DAPK1, P4HB, TSC2, and ULK1) and had good predictive capacity was established by LASSO–Cox stepwise regression analysis. High-risk patients were found to have significantly shorter OS than patients in low-risk group. The signature can be used as an independent prognostic predictor after adjusting for clinicopathological parameters, and was validated on two external AML sets. Differentially expressed genes analyzed in two groups were involved in inflammatory and immune signaling pathways. An analysis of tumor-infiltrating immune cells confirmed that high-risk patients had a strong immunosuppressive microenvironment. Potential druggable OS-related ARGs were then investigated through protein–drug interactions. This study

OPEN ACCESS

Edited by:
Peng Qu,
National Institutes of Health (NIH), United States

Reviewed by:
Yong Ai,
University of Maryland, United States
Xiaoguang Liu,
University of Texas MD Anderson Cancer Center, United States

***Correspondence:**
Denggang Fu
fdgszxy@163.com
Wangbin Ning
ningwb@csu.edu.cn
Hua Jiang
jianghub123@gmail.com

†These authors have contributed equally to this work

Specialty section:
This article was submitted to Cancer Immunity and Immunotherapy, a section of the journal Frontiers in Immunology

Received: *15 April 2021*
Accepted: *11 May 2021*
Published: *31 May 2021*

Citation:
Fu D, Zhang B, Wu S, Zhang Y, Xie J, Ning W and Jiang H (2021) Prognosis and Characterization of Immune Microenvironment in Acute Myeloid Leukemia Through Identification of an Autophagy-Related Signature. Front. Immunol. 12:695865. doi: 10.3389/fimmu.2021.695865

provides a systematic analysis of ARGs and develops an OS-related prognostic predictor for AML patients. Further work is needed to verify its clinical utility and identify the underlying molecular mechanisms in AML.

Keywords: acute myeloid leukemia, autophagy, signature, tumor immune microenvironment, prognosis

INTRODUCTION

AML is one of the most aggressive blood malignancies that is characterized by a heterogeneity of molecular abnormalities and the accumulation of immature myeloid progenitors in the bone marrow and peripheral blood (1, 2). An estimated 19,940 new cases of AML were diagnosed in the US in 2020, with 11,180 deaths (3). The mainstream treatment for AML patients is chemotherapy, but most patients relapse or succumb to the disease after initial remission. Although extensive efforts have been made to develop targeted therapy and/or combined therapy for it (4), the 5-year survival rate of patients of AML is still less than 30%. Thus, it is critical to identify novel prognostic biomarkers to monitor patients' prognoses and better understand the pathogenesis of AML.

Autophagy is a complex multistep self-digestive cellular process that is essential for the survival, differentiation, and homeostasis of cells (5). It sequesters damaged organelles/proteins, invading pathogens, and macromolecules in an autophagosome coated with a double membrane. Following the fusion of the autophagosome with lysosome, these materials are degraded to maintain the recycling balance between the synthesis and the consumption of the cellular components (6). In normal conditions, autophagous activity is too low to require essential nutrients of the cell by removing unfolded and excessively aged proteins, while the dysregulation of autophagy is involved in a diversity of pathologies, including tumorigenesis, infections, aging, and heart disease (7). Autophagy can be a double-edged sword for organisms in that it can prevent the formation of tumors but can also promote the survival and proliferation of cancer cells by providing them with nutrients (8). A variety of roles of autophagy have been identified in hematopoietic disease. It is required for maintaining the functions of hematopoietic stem cells (9) and T-lymphoid lineages (10, 11), and for responses to extracellular cytokine stimuli (12). Increasing evidence has shown that autophagy is a key mechanism in leukemogenesis and chemoresistance, and this has made it an attractive therapeutic target in research in recent years (13, 14). A number of autophagy-inducing agents, such as arsenic trioxide, vitamin D3, eupalinin A, APO866, and platonin, have been developed to initiate the death of leukemic cells (15). A variety of essential genes are involved in the machinery of autophagy to control the balance of catabolic processes (16). Research on the role of autophagy in the progression of AML and responses to the treatment of patients has focused on one or more autophagy-related genes (ARGs) (15), and few studies have sought to systematically clarify the potential roles of expressions of these ARGs in predicting the prognoses of AML patients.

In this study, we identified survival-related ARGs in the context of AML and develop a prognostic signature for AML patients to profile their expressions. Transcriptomic datasets of AML were downloaded from publicly accessible databases, and were divided into training and validation sets. Univariate Cox regression analysis was used to assess the prognostic effects of these ARGs for AML. Least absolute shrinkage and selection operator (LASSO) Cox regression were performed to determine the key variables and construct an ARG-related risk signature for the AML patients. The predictive accuracy of the risk signature was analyzed on the validation set, and the results suggest that it is an effective predictor of patient outcomes that is independent of the clinical parameters used to monitor them. The abundance of tumor-infiltrating immune cells defined by the signature reflected the distinct microenvironmental landscape of the tumor, and potential druggable ARGs were identified. A general analysis workflow is diagrammed in **Figure S1**.

MATERIALS AND METHODS

Data Collection and Processing

The transcriptomic profiles of three AML cohorts along with detailed clinicopathological information on them were downloaded from public databases. Raw microarray datasets of GSE37642 (17) and GSE12417 (18) were downloaded from the GEO (https://www.ncbi.nlm.nih.gov/geo/) and normalized by the robust multiarray average (RMA) algorithm using the affy package (19) between arrays. Batch effects were removed by the combat algorithm in the sva package (20). The AML RNA-seq dataset was downloaded from the UCSC Xena database (https://xenabrowser.net/datapages/). The available clinical information of samples used in this study was shown in **Table S1**.

Acquisition of ARGs

A total of 232 autophagy-related genes (ARGs) were derived from the Human Autophagy Database (HADb, http://autophagy.lu/clustering/index.html). The HADb provides a

Abbreviations: AML, Acute Myeloid Leukemia; DEGs, Differentially Expressed Genes; ARGs, Autophagy-related Genes; TCGA, The Cancer Genome Atlas; GEO, Gene Expression Omnibus; RMA, Robust Multi-array Average; HADb, Human Autophagy Database; TRRUST, Transcriptional Regulatory Relationships Unraveled by Sentence-based Text mining; PPI, Protein–Protein Interaction; MCODE. Molecular Complex Detection; AUC, Area Under Curve; ROC, The Receiver Operating Characteristics Curve; GSEA, Gene Set Enrichment Analysis; TFs, Transcription Factors; BP, Biological Process; CC, Cellular Component; MF, Molecular Function; KEGG, Kyoto Encyclopedia of Genes and Genomes; MSigDB, Molecular Signatures Databases; AIC, Akaike Information Criterion; OS, Overall Survival; PD-1, Programmed Cell Death Ligand; FLT3, FMS-like Tyrosine Kinase 3; CTLA4, Cytotoxic T-Lymphocyte-associated Protein 4.

complete and an up-to-date list of human genes and proteins involved in the biological processes of autophagy reported in the literature (21). A total of 187 ARGs were available in the expression profiles obtained from GSE37642 (**Table S2**).

Identification of Overall Survival (OS)-Related ARGs

The GSE37642 (n=553) was used as the training set to clarify the potential prognostic significance of these ARGs in the AML patients. OS-related ARGs with $P < 0.05$ were identified using univariate Cox hazard regression analysis.

Functional Enrichment Analysis of OS-Related ARGs

Functional enrichment analysis, including gene ontology (GO) and the Kyoto Encyclopedia of Genes and Genomes (KEGG), was performed to unravel the main functions of OS-related ARGs in AML by using the clusterProfiler package (22). The Benjamin–Hochberg adjusted $P < 0.05$ was regarded as statistically significant.

Molecular Characteristics of OS-Related ARGs

To investigate potential regulatory interactions among these ARGs, a protein–protein interaction (PPI) network was formulated using the STRING database (23) and displayed in Cytoscape (version 3.8.0) (24). To identify the hub modules in the network, the Molecular Complex Detection (MCODE) plugin (25) in Cytoscape was used to extract densely connected modules with the default parameters "Degree Cutoff = 2," "Node Score Cutoff = 0.2," "K-Core = 2," and "Max.Depth = 100." The CytoNCA plugin (26) was used to calculate the nodes with the highest degree scores.

The key regulatory factors (TFs) of these OS-related ARGs were identified using the Transcriptional Regulatory Relationships Unraveled by Sentence-based Text mining (TRRUST) database, which is an online tool curated to explore transcriptional regulatory interactions in humans and mice (27).

Construction and Validation of ARG-Related Prognostic Signature for AML Patients

To avoid overfitting the prognostic risk signature, we used the least absolute shrinkage and selection operator (LASSO)-based Cox regression (28) on the training dataset to identify the most significant features within the OS-related ARGs. These candidates were subjected to a multivariate Cox proportional hazards regression with the stepwise selection of variables based on the Akaike information criterion (29). The risk score of final optimized prognostic signature was calculated as follows:

$$\text{Risk score} = \sum_i^n Coefi \times \mathrm{A_i}$$

where Coef is the regression coefficient, "i" represents the ARG that comprised of the signature, A represents the relative value of the expression of the individual ARG in the signature, and n represents the number of genes in the signature. The patients were divided into high- and low-risk groups based on median risk score as cutoff value. The differences in the OS of patients were assessed by Kaplan–Meier analysis and the log-rank test. The time-dependent receiver operating characteristic (ROC) curve (30) was employed to evaluate the predictive capacity of the ARG-based signature.

To test the predictive accuracy of the signature, two external AML cohorts—TCGA-LAML (n=149) and GSE12417 (n=242)—were downloaded and used as validation sets. The risk score for each patient was calculated by using the signature, and the Kaplan–Meier curve was used to reflect its discrimination-related performance.

Identification and Enrichment Analysis of Differentially Expressed Genes (DEGs)

The differentially expressed genes (DEGs) between the high- and low-risk groups were identified using the limma package (31). To better understand the functions of the DEGs in AML, we used the clusterProfiler package (22) for enrichment analysis, including the GO terms, including biological process (BP), molecular function (MF) and cellular component (CC), and KEGG pathways. The DEGs were clustered and a heatmap for them was generated *via* ClustVis (32).

Gene Set Enrichment Analysis (GSEA)

The patients were divided into high- and low-risk groups according to the median risk score, as mentioned above. GSEA was performed to identify the primarily enriched pathways using GSEA 4.02 (http://www.broad.mit.edu/gsea/) (33). Pathway with the nominal $P < 0.05$ and FDR < 0.25 were considered statistically significant.

Development of Autophagy Clinicopathologic Nomogram

To predict the OS of each AML patient, an autophagy clinicopathologic nomogram that incorporated the prognostic signature into the clinicopathologic parameters available in the training set was conducted through the rms package (34). The final nomogram was extracted using the Akaike information criterion (AIC) for variable selection. The calibration curve was used to assess the predictive discrimination of the signature for AML patients (35).

Tumor-Immune Microenvironment Landscape and Potential Implications for Immunotherapy Defined by the Signature

CIBERSORT was used to calculate the abundance of infiltration of 22 immune cell types within a complex mixture of the gene expression data of the AML patients (36), including seven types of T cells, naïve and memory B cells, plasma cells, and NK cells, in the high- and low-risk groups. Samples with $P < 0.05$ were chosen for further analysis.

Recent years have witnessed a rise in immunotherapy and targeted therapy for AML patients. We predict the potential effect of treatment according to risk score here by analyzing the correlation between risk score and therapeutic targets in clinical trials or clinical practice using Pearson's correlation analysis (37, 38). The targets of therapy were as follows: programmed cell

death ligand (PD-1), ASXL1, BCL2, CD33, CD47, CHEK1, PLK1, DOT1L, FMS-like tyrosine kinase 3 (FLT3), Cytotoxic T-Lymphocyte-associated Protein 4 (CTLA4), IDH1, IDH2, MCL1, and MDM2.

To find potential drug targets, protein–drug interactions were analyzed in the survival-related ARGs using NetworkAnalyst 3.0 (https://www.networkanalyst.ca/). Information on the protein and drug contents of the targets were retrieved from DrugBank (version 5.0, https://go.drugbank.com/) (39).

RESULTS

Identification and Functional Enrichment Analysis of OS-Related ARGs in AML

To discover the potential prognostic significance of each available ARG in the AML training set, a univariate Cox proportional hazard regression analysis was used to screen out ARGs with a *P*-value less than 0.05. The expressions of 32 ARGs were thus found to be significantly associated with the OS of the AML patients (**Table 1**). GO functional analysis of the OS-related ARGs showed that they were primarily active in processes that utilized autophagy-related mechanisms (**Figure 1A**). These ARGs were involved in autophagy, human cytomegalovirus infection, the p53 signaling pathway, AMPK signaling pathway, and apoptosis (**Figure 1B**).

To discover interactions among these OS-related ARGs, two significant modules were identified, using PPI network analysis, with more than four nodes: CASP3 and BECN1 (**Figure 1C**). The BECN1 module contained eight nodes with 28 edges, whereas GAPDH, CDKN2A, and P4HB were the three nodes of the CASP3 module. These ARGs might have important implications for the pathogenesis of AML.

To identify the transcriptional regulators of the OS-related ARGs, 16 TFs were identified in the TRRUST database (**Table S3**), including nuclear transcription factors (NFYC, NFYB, NFYA, SP1, HSF1, E2F1), a signal transducer and an activator of transcription (STAT1, STAT3), TP53, and key members of NF-κB signaling (NFKB1, RELA). The gene expressions of several ARGs were significantly regulated, such as those of the important nodes CASP3, BECN1, ATG7, BAG3, and UKL1.

TABLE 1 | Overall survival-related ARGs in the AML patients ($P < 0.05$).

Gene symbol	HR (95% CI)	*P* value
TSC2	0.4072(0.2832 - 0.5856)	1.25E-06
CALCOCO2	0.6758(0.5680 - 0.8039)	9.69E-06
DAPK1	1.3835(1.1847 - 1.6157)	4.10E-05
BAG3	1.1503(1.0753 - 1.2305)	4.72E-05
CAMKK2	0.5397(0.3882 - 0.7504)	0.000244719
CANX	0.7301(0.6099 - 0.8739)	0.000606334
ULK1	0.7257(0.6025 - 0.8742)	0.000735293
P4HB	0.8215(0.7324 - 0.9215)	0.000790605
CCL2	1.1482(1.0510 - 1.2544)	0.002205099
GABARAP	0.7085(0.5667 - 0.8859)	0.002507313
GABARAPL1	0.8216(0.7213 - 0.9360)	0.003127288
EEF2	0.6578(0.4920 - 0.8793)	0.004684677
GAPDH	0.7715(0.6369 - 0.9345)	0.007994922
NCKAP1	1.6932(1.1345 - 2.5271)	0.009954145
CDKN1B	1.1991(1.0424 - 1.3793)	0.011027097
CAPNS1	0.8504(0.7469 - 0.9684)	0.014474617
SERPINA1	0.9062(0.8370 - 0.9811)	0.015041995
BECN1	0.7031(0.5283 - 0.9358)	0.015733367
ARSB	0.7888(0.6501 - 0.9571)	0.016217681
CDKN2A	0.7312(0.5641 - 0.9477)	0.017994775
DLC1	0.7460(0.5785 - 0.9619)	0.023876677
ERN1	0.6722(0.4728 - 0.9558)	0.026995358
CAPN1	0.8331(0.7073 - 0.9813)	0.028824089
ATG9A	0.8343(0.7059 - 0.9861)	0.03365361
EIF2AK2	1.2624(1.0181 - 1.5653)	0.03374212
WIPI2	0.7297(0.5453 - 0.9765)	0.034038805
ITGB4	0.5864(0.3552 - 0.9682)	0.036949174
CLN3	0.7788(0.6128 - 0.9897)	0.04089584
ATG7	0.8389(0.7072 - 0.9952)	0.043928123
HGS	0.8035(0.6488 - 0.9951)	0.044918193
FAS	0.8763 (0.7692 - 0.9982)	0.046832376
CASP3	0.8846(0.7838 - 0.9983)	0.046888189

Development and Validation of ARG-Related Prognostic Signature

To avoid potential overfitting, LASSO Cox regression analysis was used to select the key OS-related ARGs for modeling (**Figures S2A, B**). Eight ARGS were identified and used to develop an optimal prognostic signature for the OS of patients by multivariate Cox proportional hazards regression analysis by using forward and backward algorithms (**Figure 2A**). The patients' risk scores were defined as follows:

$$\begin{aligned}\text{Risk score} = &\left[\text{Expression level of BAG3}_{*}(0.1084)\right] + \left[\text{Expression level of CALCOCO2}_{*}(-0.3836)\right] \\ &+ \left[\text{Expression level of CAMKK2}_{*}(-0.5617)\right] + \left[\text{Expression level of CANX}_{*}(-0.2402)\right] \\ &+ \left[\text{Expression level of DAPK1}_{*}(0.5119)\right] + \left[\text{Expression level of P4HB}_{*}(0.2899)\right] \\ &+ \left[\text{Expression level of TSC2}_{*}(-0.6286)\right] + \left[\text{Expression level of ULK1}_{*}(-0.3645)\right]\end{aligned}$$

The patients were divided into high- and low-risk groups according to the median value of risk score. As the risk scores of patients increased in both groups, the number of deaths increased (**Figures 2B, C**). With regard to expressions of the eight ARGs, BAG3 and DAPK1 were highly expressed in the high-risk group (**Figures 2D**, **S3A, B**), and CALCOCO2, CAMKK2, CANX, P4HB, TSC2, and ULK1 were expressed high in the low-risk group (**Figures 2D**, **S3C–H**). This is consistent with evidence that blasts in AML show reduced expressions for most ARGs, indicating that low autophagy-related activity promotes leukemic development (40). To determine the predictive performance of the signature, the Kaplan–Meier analysis showed that patients in the high-risk group had significantly shorter OS than patients in the low-risk group ($P < 1.0E-07$, **Figure 3A**). To assess the predictive accuracy of the signature, the AUC of our signature for a 5-year OS was 0.76. In addition, the AUCs for 1-year and 3-year OS were 0.68 and 0.75, respectively, and indicated high predictive capacity of the signature (**Figure 3B**).

To calculate the predictive independence of the signature for AML patients, univariate Cox regression analysis showed that age, runx1 and runx1t1 fusion, mutations in runx1, and risk score were significantly correlated with the OS of the patients

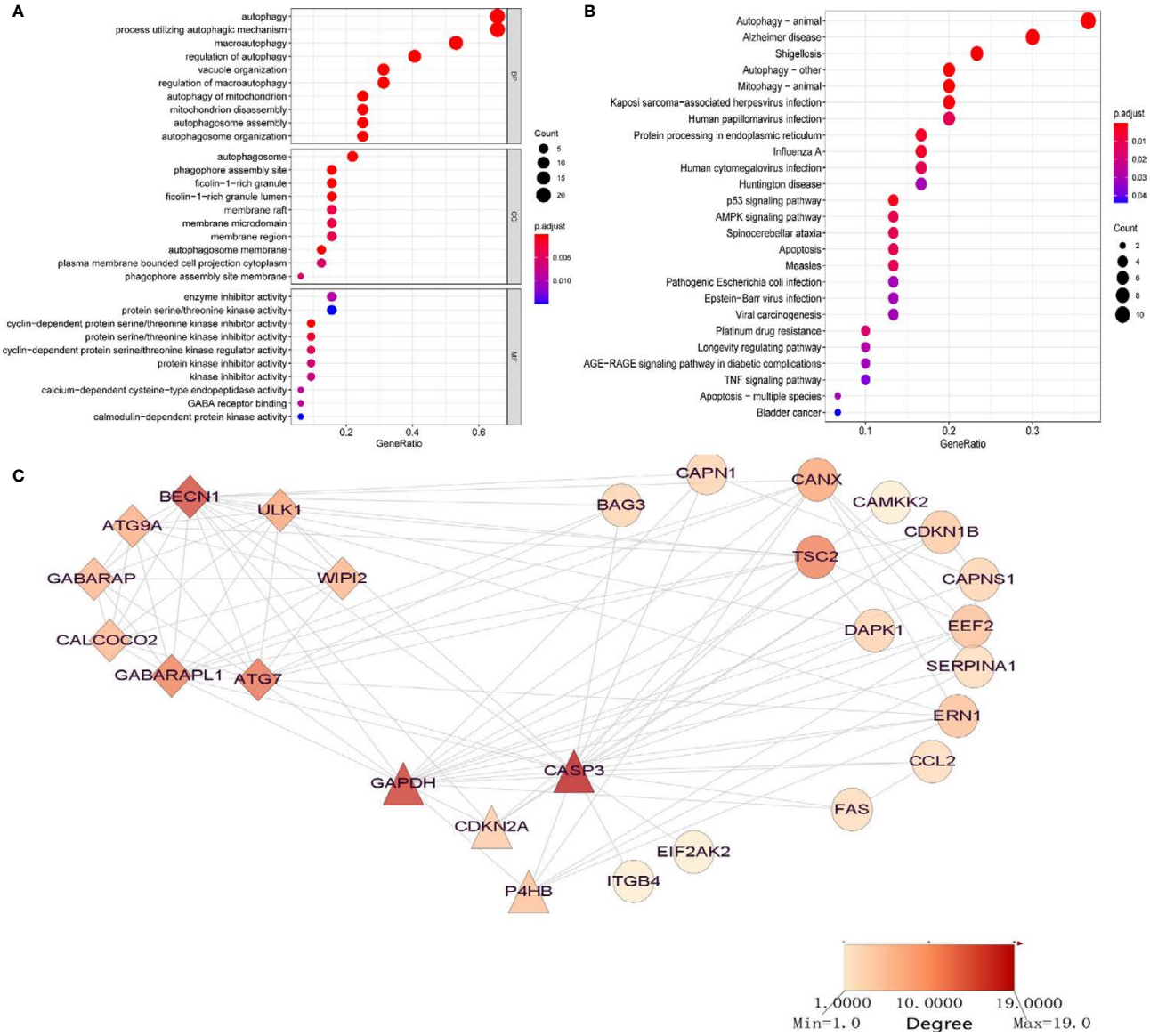

FIGURE 1 | Significantly enriched GO terms and KEGG pathways of OS-related autophagy-related genes (ARGs) (adjusted $P < 0.05$). **(A)** Significantly enriched GO terms of OS-related ARGs. **(B)** Significantly enriched pathways of OS-related ARGs. **(C)** Two modules (CASP3 and BECN1 modules) identified through protein–protein interaction network analysis of OS-related ARGs. The color of the node in each module reflects its degree score.

(**Figure 3C**). The multivariate Cox regression analysis showed that the risk score was an independent predictor for AML patients after adjusting for these clinical parameters (**Figure 3D**), although age and mutations in runx1 were also independent. A comparison of the capability of OS predictions for AML patients based on the risk score and clinical factors showed that the AUCs of 1-year, 3-year, and 5-year OS of the clinical variables were inferior to those patients of the risk scores (**Figures S4A–C**).

For a more accurate evaluation of the signature, a nomogram that integrated the risk score, age, runx1_runx1t1 fusion, and runx1 mutations, was constructed (**Figure 3E**). The calibration curves showed that it could accurately predict the utility of 1-year, 3-year, and 5-year OS for AML patients (**Figures 3F–H**). This indicates that combining our risk scores and the clinical variables can improve OS prediction.

Gene Set Enrichment Analysis

The distinct OS rates of patients in the high- and low-risk group were observed, and GSEA was used to investigate the potential molecular functional difference between them. mTOR-related

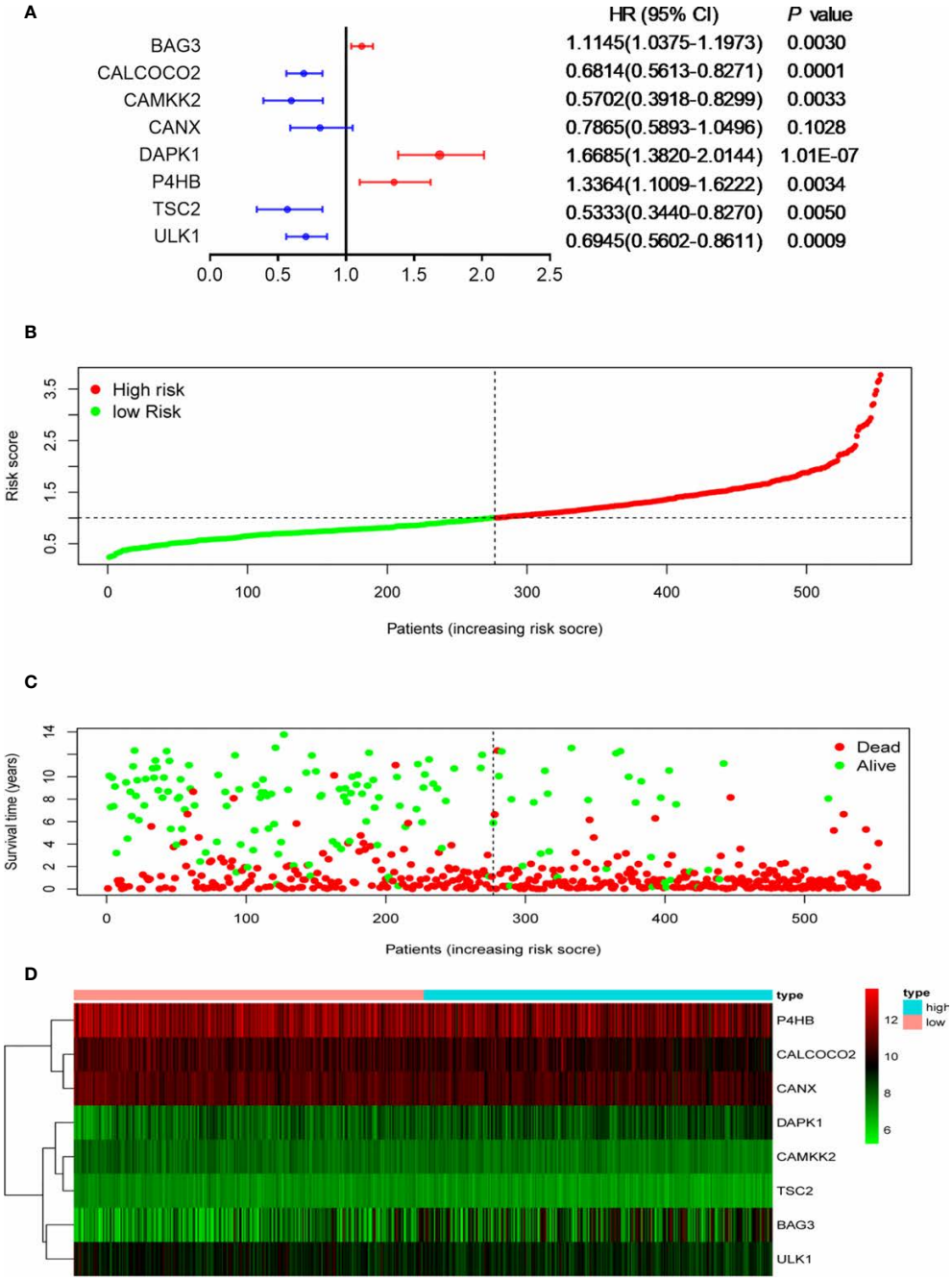

FIGURE 2 | Development of the prognostic signature based on OS-relevant ARGs. **(A)**. The hazard ratio of model genes. **(B)** Distribution of the patients' risk scores. **(C)** Patients' survival times along with their risk scores. **(D)** The expressions of the eight model genes in the high- and low-risk groups.

signaling, AKT1 signaling, and relapse prognosis for AML relapse were significantly abundant in the low-risk group (**Figure S5**). Previous studies have shown that mTOR regulates cell growth and proliferation by controlling the biological processes of mRNA translation, autophagy, and metabolism, or dual interactions with AKT family signaling to activate or deactivate mTOR-dependent processes (41). These data highlight that autophagy-related events were mainly implicated in low-risk AML patients.

Validation of Prognostic Signature in External AML Cohorts

To test the predictive utility of the prognostic signature of the patients' OS in the external AML cohorts (GSE12417 and

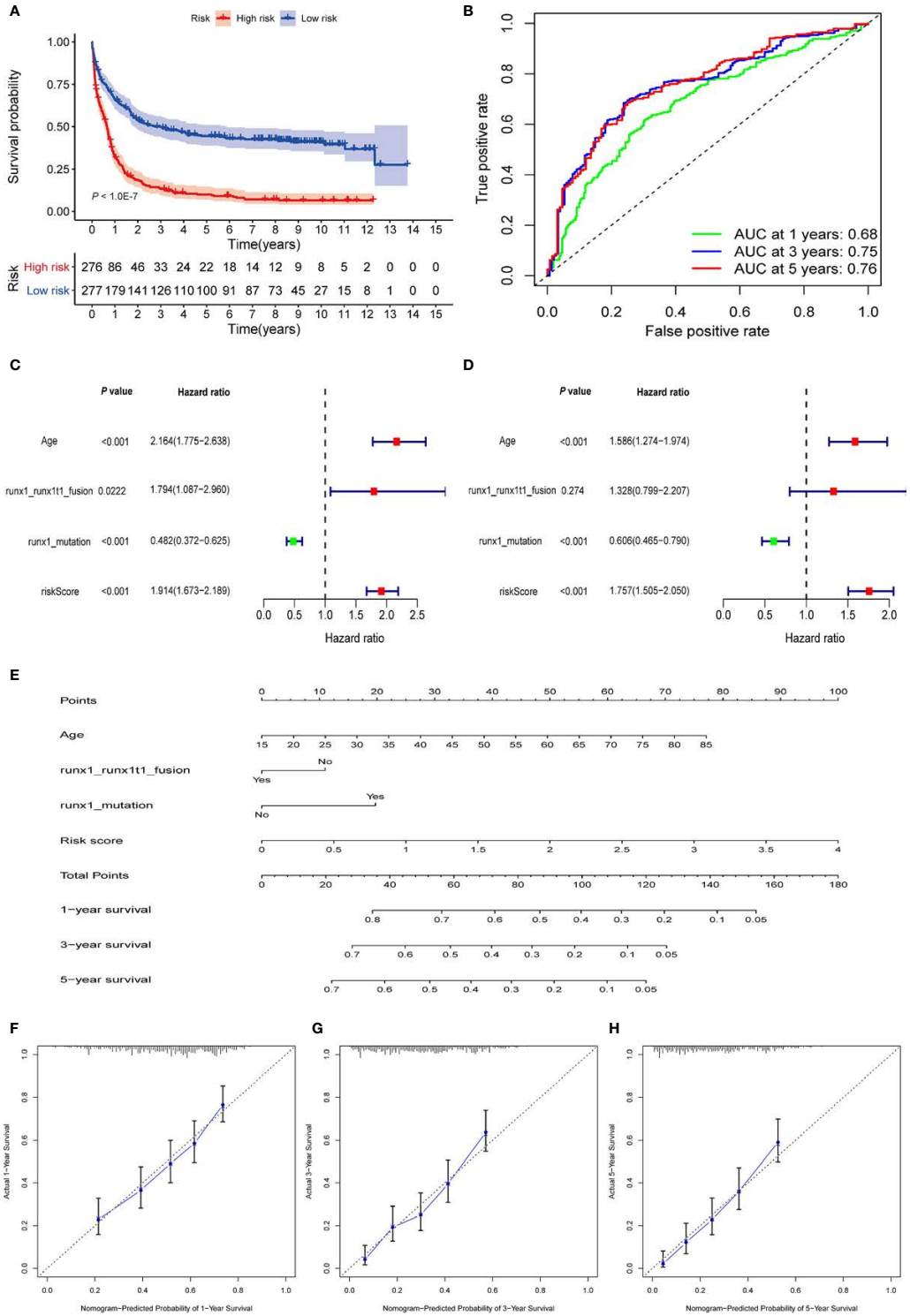

FIGURE 3 | Evaluation of prognostic signature to predict the OS of AML patients. **(A)**. Patients in the high-risk group had significantly shorter OS than those in the low-risk group. **(B)** The AUC curves of the signature for 1, 3, and 5 years. **(C)** Univariate Cox regression analysis of the risk scores and clinical parameters. **(D)** Multivariate Cox regression analysis of the risk scores and clinical parameters. **(E)** Development of autophagy clinicopathologic nomogram for predicting 1-, 3-, and 5-year OS for AML patients by incorporating risk score, age, runx1 and runx1t1 fusion, and mutations in runx1. **(F–H)** Calibration curves of the autophagy clinicopathologic nomogram-predicted and observed 1-, 3-, and 5-year survival of AML patients. The dashed line represents the ideal performance, and the actual performance of the signature is represented by the blue lines.

TCGA-LAML), the risk score for each patient was calculated based on the formula for the signature. The patients were divided into high- and low-risk groups according to median risk score. The OS times of patients in the high-risk group were significantly shorter than patients in the low-risk group (P = 3.797E-03, **Figure 4A**) in the GSE12417 cohort. The AUC of the 3-year OS for this cohort was 0.66 (**Figure 4B**). In addition, the prognosis of patients in the high-risk group was worse than that of patients in the low-risk group in the TCGA-LAML set (P = 8.864E-03, **Figure 4C**). Similarly, the AUC of the 3-year OS was 0.612 (**Figure 4D**). Overall, these data show that the signature could be used to independently predict the OS for AML patients.

Identification and Enrichment of Differentially Expressed Genes (DEGs)

We noted the differences in OS between patients in the high- and low-risk groups. To delineate the DEGs of the two groups, 34 DEGs were identified using the limma package, with 15 up-regulated genes and 19 down-regulated genes (**Figure 5A**). A distinct pattern of gene expression was observed in patients in the high- and low-risk groups (**Figure 5B**). The GO term analysis showed that these DEGs were significantly involved in the biological processes of neutrophil-related activities (activation, degranulation, and response to immunity), the cellular components that occur in secretory and cytoplasmic lumen and lysosome, and various peptidase activities (**Figure 5C**). The pathways referenced from the KEGG database showed that the DEGs highly expressed in the high-risk group were mainly involved in acute myeloid leukemia while the DEGs down-regulated in the low-risk group were markedly involved in signaling pathways for IL-17, viral protein interactions with cytokine and cytokine receptor, NF-kappa B signaling, and the TNF signaling pathway (**Figure 5D**). The data indicate that these

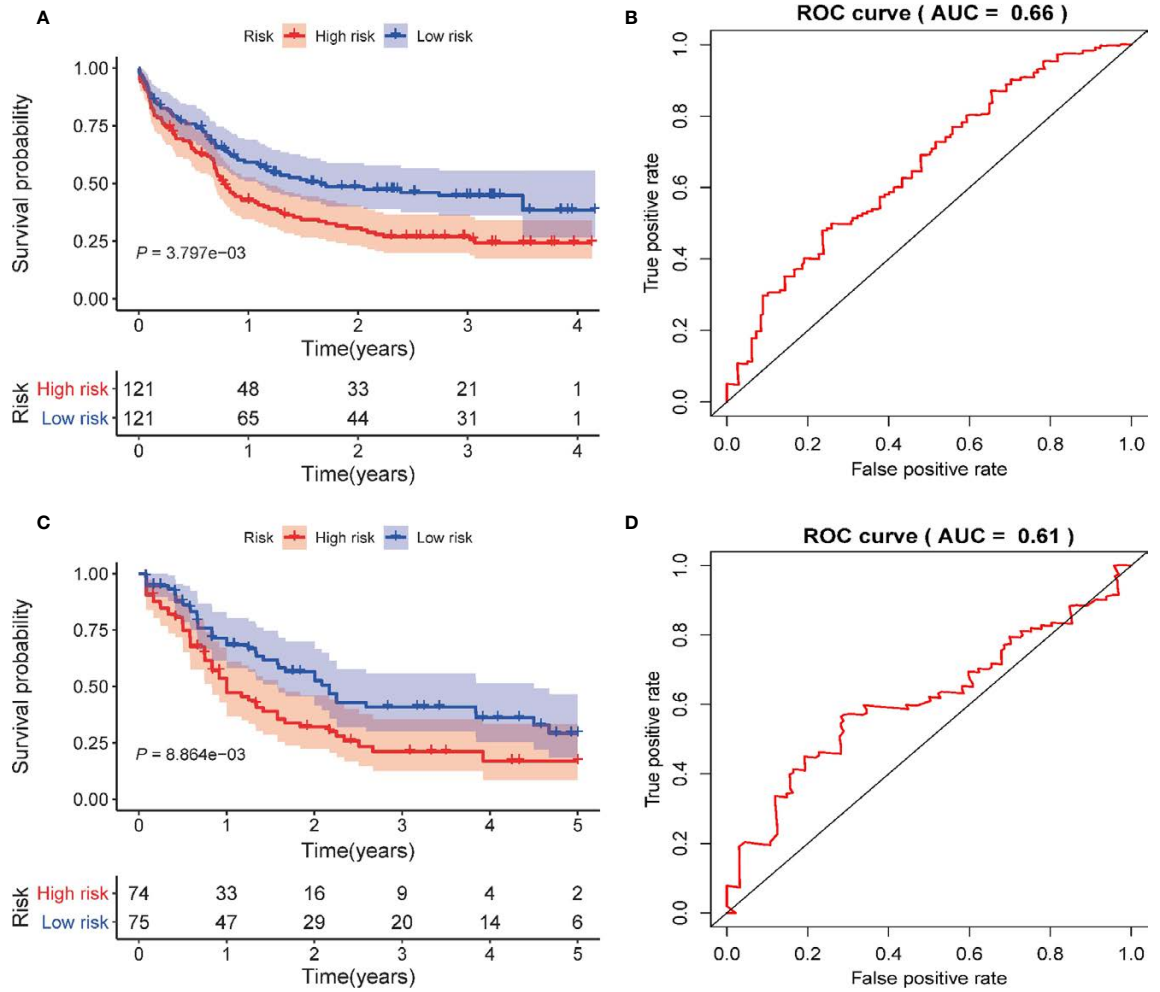

FIGURE 4 | Validation of the autophagy-related prognostic signature on external AML cohorts. **(A)** Kaplan–Meier curve of the prognostic signature in the GSE12417 cohort. **(B)** The AUC curve of the signature for 3 years in the GSE12417 cohort. **(C)** Kaplan–Meier curve of the prognostic model in the TCGA cohort. **(D)** The AUC curve of the signature for 3 years in the TCGA cohort.

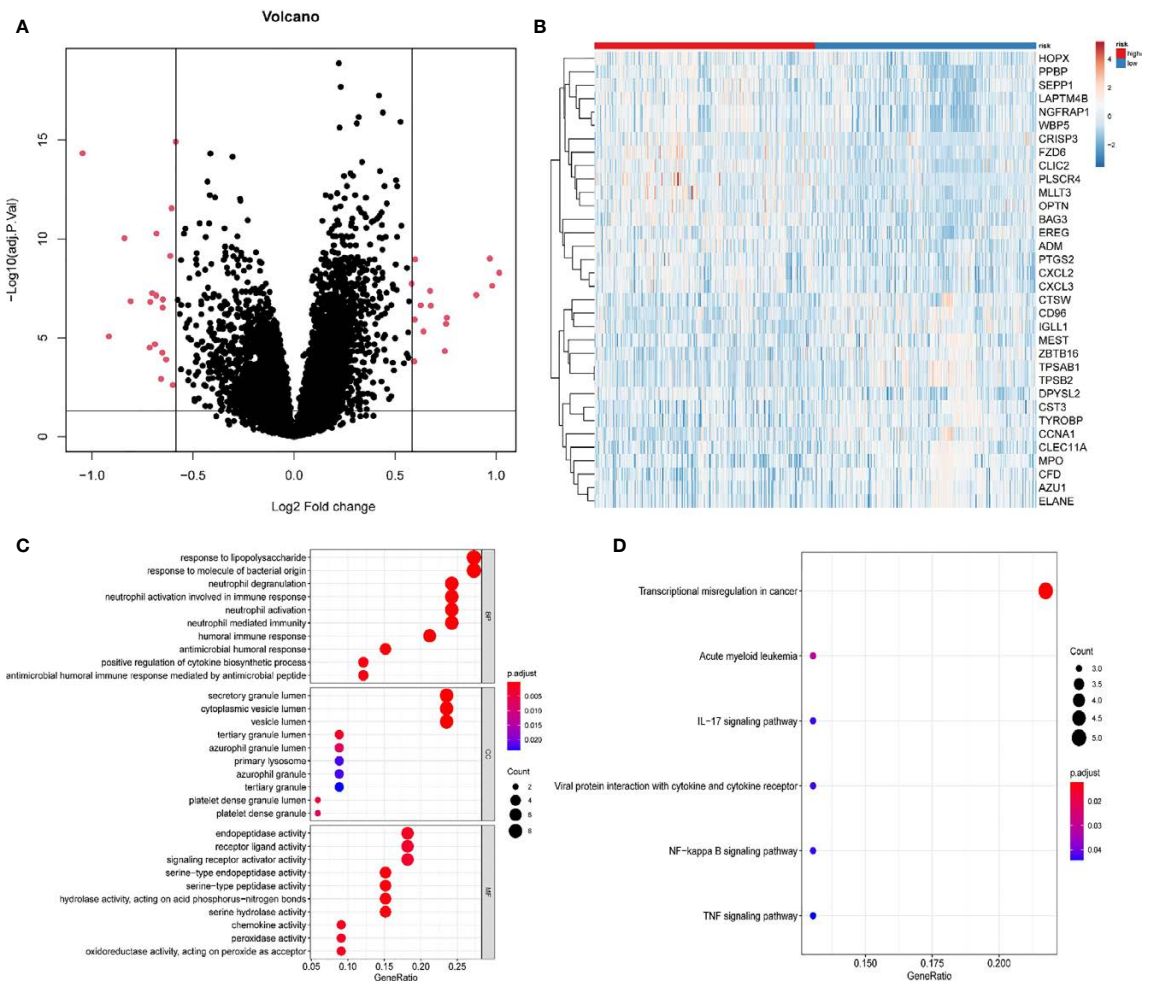

FIGURE 5 | Differentially expressed genes (DEGs) between the high-risk and the low-risk groups. **(A)** Volcano plot of the DEGs. **(B)** Heatmap of the DEGs. **(C)** Significantly enriched GO terms of the DEGs. **(D)** Significantly enriched pathways of the DEGs.

DEGs might play important roles in AML progression and immune response.

Potential Relevance of Signature in Tumor-Immune Microenvironment

Tumor-infiltrating lymphocytes (TILs) in the tumor microenvironment (TME) are involved in cancer progression, drug resistance, and clinical outcomes. As displayed in **Figure 6**, an analysis of immune cell-infiltration in the TME as defined by our signature in training set showed that CD8 T cells, resting and activated NK cells, monocytes, and mast resting cells had significantly increased in the low-risk group, while CD4 T memory resting and activated cells, T cells gamma delta, regulatory T cells, and dendritic cells had been activated at high levels in the high-risk patients. Similar trends of tumor immune infiltration have been found in the two external validation sets (**Figure S6**). In addition, the expression analysis of exhausted cytotoxicity T cells markers indicated that GZMB and Interferon gamma are significantly increased in patients in high-risk group than those patients in low-risk group (**Figure S7**). This suggests a strong immunosuppressive TME that might weaken the capacity to defend against cancer in the high-risk group.

Emerging molecules for immunotherapy and targeted therapy, such as immune checkpoint inhibitors, were recently identified and tested in pre- or clinical trials for the treatment of patients with AML. As shown in **Figure 7**, a Pearson correlation analysis showed that the risk score was significantly negatively correlated with the mRNA expressions of CD33 (cor = -0.2573, $P < 0.0001$), CD47 (cor = -0.1518, $P = 0.0003$), DOT1L (cor = -0.2451, $P < 0.0001$), and IDH2 (cor = -0.2718, $P < 0.0001$), and was positively related with those of CTLA4 (cor = 0.2222, $P < 0.0001$), FLT3 (cor = 0.1043, $P = 0.0142$), and MDM2 (cor = 0.1170, $P = 0.0059$). This suggests that patients with high risk

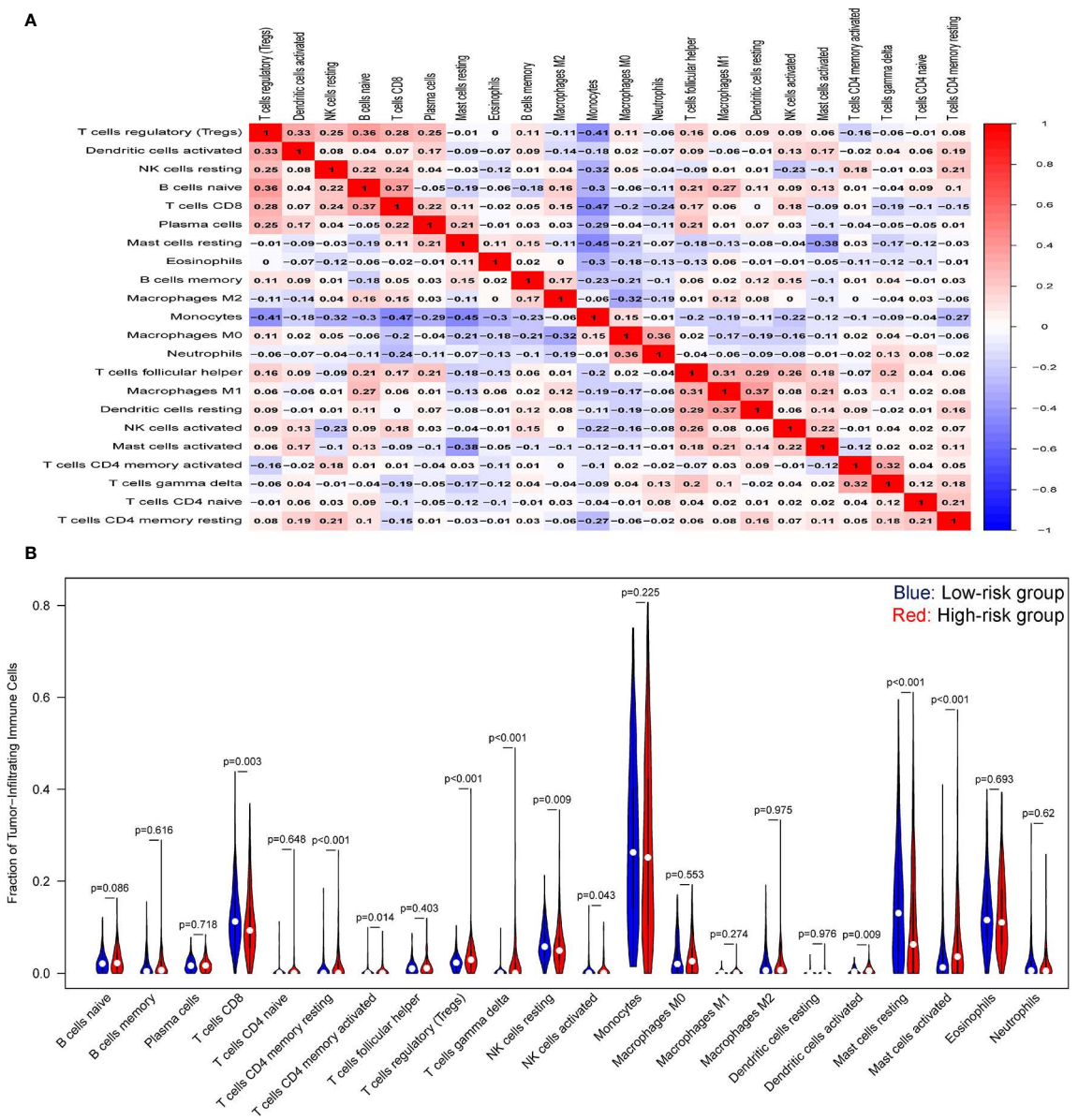

FIGURE 6 | Tumor-immune microenvironment analysis of the high- and low-risk groups. **(A)** Correlation heatmap of the ratio of tumor-infiltrating immune cells. **(B)** Difference between tumor-infiltrating immune cells. The blue violin reflects the low-risk group and the red violin represents the high-risk group.

scores might better respond to therapies targeting CTLA4, FLT3, and MDM2.

Multiple Survival-Related ARGs Are Potential Druggable Targets

To determine whether any of the available survival-related ARGs were druggable targets, a protein–drug interaction analysis of these ARGs was conducted through NetworkAnalyst 3.0, using data from the DrugBank database. The protein products of eight ARGs were identified as drug targetable (**Table 2**). A majority of these ARGs have been demonstrated to be implicated in tumorigenesis, including CASP3 (Caspase 3) (42), EEF2 (eukaryotic translation elongation factor 2) (43), GAPDH (glyceraldehyde-3-phosphate dehydrogenase) (44), CAPN1 (Calpain 1) (45), DAPK1 (death-associated protein kinase 1) (46), SERPINA1 (serpin family A member 1) (47), and CCL2 (C-C motif chemokine ligand 2) (48). Caspase-3 controlled AML1-ETO-induced leukemogenesis through autophagy modulation in a ULK1-dependent pattern, which indicates that the balance and selectivity among its substrates regulated disease

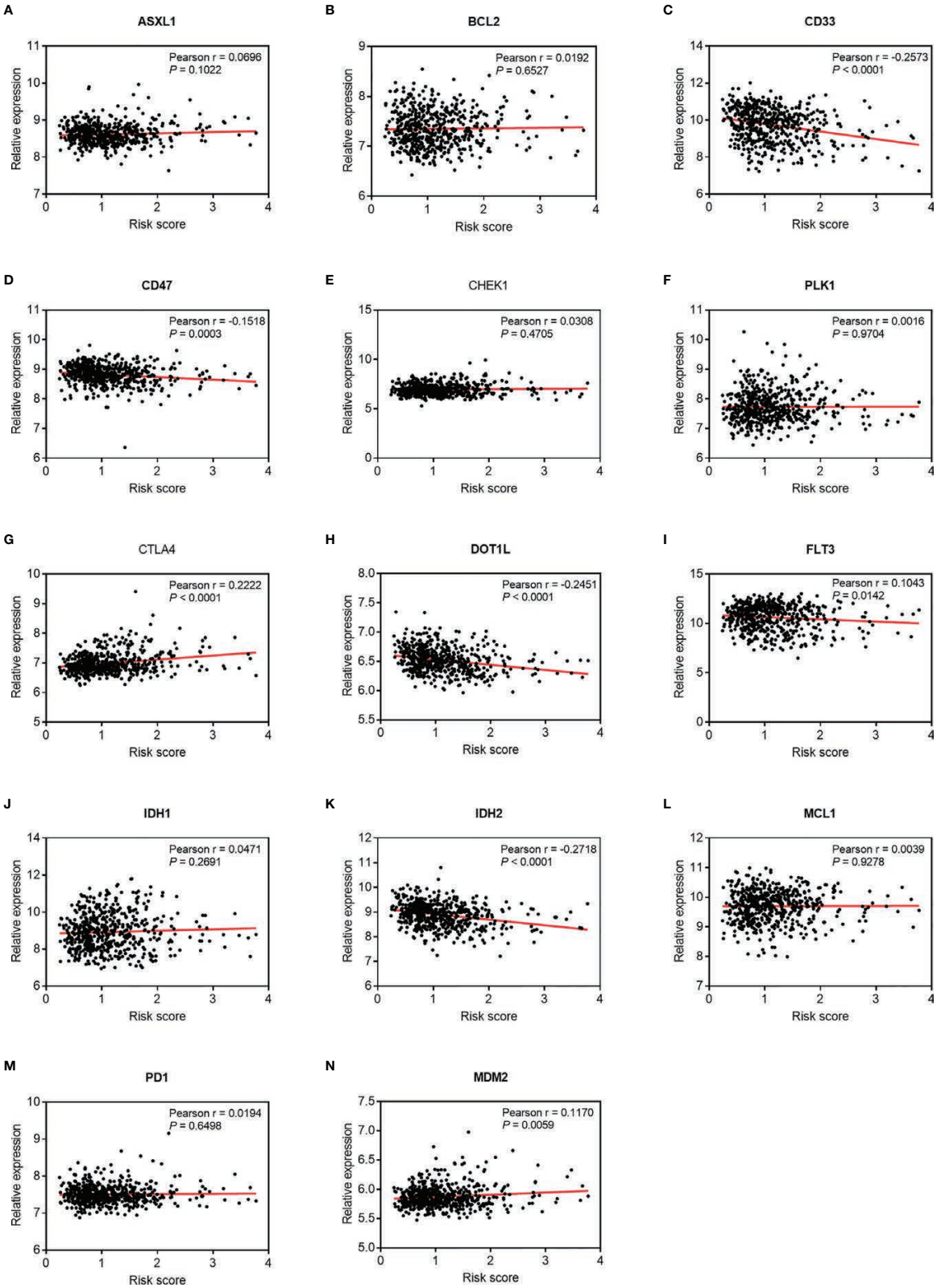

FIGURE 7 | Pearson correlation of the risk scores of the targets of immunotherapy and targeted therapy. **(A)** ASXL1. **(B)** BCL2. **(C)** CD33. **(D)** CD47. **(E)** CHEK1. **(F)** PLK1. **(G)** CTLA4. **(H)** DOT1L. **(I)** FLT3. **(J)** IDH1. **(K)** IDH2. **(L)** MCL1. **(M)** PD-1. **(N)** MDM2.

TABLE 2 | Eight OS-related ARGs targeted by the drugs available from DrugBank.

Gene Symbol	HR (95%CI)	*P*-value	Number of drugs	DrugBank ID	Drug name examples
CASP3	0.8846(0.7838-0.9983)	0.04689	11	DB08497, DB08229, DB08213, DB07696, DB01017, DB06862, DB05408, DB03124, DB08498, DB08251, DB08499	EMRICASAN, MINOCYCLINE, METHYL (3S)-3-[(TERT-BUTOXYCARBONYL]-4-OXOPENTANOATE, 2-HYDROXY-5-(2-MERCAPTO-ETHYLSUFAMOYL)-BENZOIC ACID
EEF2	0.6578(0.4920-0.8793)	0.00468	4	DB04315,DB03223,DB08348,DB02059	Diphthamide, Glycinamide, Guanosine-5'-Diphosphate, Adenosine-5-Diphosphoribose
GAPDH	0.7715(0.6369-0.9345)	0.00799	4	DB03893,DB00157,DB07347	Thionicotinamide-Adenine-Dinucleotide,NADH,4-(2-Aminoethyl)Benzenesulfonyl Fluoride
CAPN1	0.8331(0.7073-0.9813)	0.02882	3	DB07627,DB04276,DB04653	CBZ-LEU-LEU-TYR-CH2F
DAPK1	1.3835(1.1847-1.6157)	0.00004	3	DB04069,DB04395,DB07444	5,6-Dihydro-Benzo[H]Cinnolin-3-Ylamine
SERPINA1	0.9062(0.8370-0.9811)	0.01504	3	DB01998,DB05481,DB03345	Recombinant alpha 1-antitrypsin,Mercaptoethanol
CANX	0.7301(0.6099-0.8739)	0.00061	2	DB00031,DB00025	Tenecteplase, Antihemophilic factor
CCL2	1.1482(1.0510-1.2544)	0.00221	2	DB01055,DB01406	Mimosine, Danazol

progression (42). Eleven candidate drugs targeting Caspase-3 were identified. Caspase-3 inhibitors may be carboxylic acids and derivatives, such as 2-hydroxy-5-(2-mercapto-ethylsufamoyl)-benzoic acid and (1S)-2-oxo-1-phenyl-2-[(1,2,3,4-tetrahydroisoquinolin-5-yl)amino]ethyl acetate.

DISCUSSION

Acute myeloid leukemia (AML) is one of the most prevalent hematological cancers that is characterized by the accumulation of immature clones of myeloid progenitors (49). Patients with AML have benefited from advances in targeted molecular and immunotherapy, but the 5-year prognosis for AML remains unsatisfactory owing to high relapse rates. An accurately predicted prognosis improves the decision-making capacity of the physician to select personalized treatment by stratifying the patient into a high- or low-risk group based on a reliable signature. In this study, OS-related ARGs were identified by using profiles of AML patients, and a signature comprising eight ARGs that can accurately predict the OS of patients was developed. The results of external validation suggest that this signature is a steady and independent predictor for the risk stratification of AML patients. In addition, distinct tumor-immune infiltrating landscapes between the high- and low-risk patients as well as potential druggable ARGs were identified through computational biology.

The complex autophagy-related machinery assembled by dozens of known proteins plays a critical role in maintaining essential cellular homeostasis by removing unfolded, excessive, or aged proteins as well as and organelles damaged through stress (50). The dysregulation of autophagy can be a driver of oncogenic transformation (51). Increased activities related to autophagy in cancer cells, resulting from large ratios of compromised cytosol and organelles that can cause the irreversible collapse of vital cellular functions, have been used in anti-cancer therapies. Many autophagy-related genes and signaling pathways have been shown to be key regulators in tumorigenesis and progression, and have been used to target rapamycin complex 1 (mTORC1) and AMP-activated protein kinase (AMPK) signaling pathways that control the induction of phases in mammals (52). The loss of functional mutations in negative regulators, TSC1, TSC2, and PTEN, are recognized for these signaling pathways. The heterozygosity of Beclin1, a key autophagy gene, can significantly promote the possibility of canceration owing to genomic instability in the context of reduced autophagy (53). Autophagy-related processes have been highlighted in AML, and represent an attractive druggable target. Various molecular targets and chemotherapeutic inhibitors of autophagy have been identified (8). The profiling of autophagy-related genes in AML contributes to finding additional prognostic biomarkers, and stratifying high- and low-risk patients.

In this study, 32 ARGs were found to be significantly associated with the OS of patients using univariate Cox proportional hazards regression, and further protein–protein

interaction analysis showed that CASP3 and BECN1 were the leading modules correlated with the other ARGs. Previous studies have shown that some of these nodes are involved in the progression of AML through autophagy modulation (42). For example, CASP3 can control AML1-ETO-driven leukemogenesis in a ULK1-dependent pattern (42), and BECN1 plays a vital role in the initiation and progression of autophagy. Consistently with our observations, the reduced expression of BECN1 was correlated with unfavorable prognoses of AML patients (54). TSC2 has been reported to suppress mTOR signaling *via* phosphorylation and inhibition by AKT (55), while mTOR signaling is associated with neoplastic leukemic proliferation by mediating cellular energy response (56). The roles of some OS-related ARGs, such as BAG3, CANX, ERN1, EEF2, CAPN1, P4HB, CCL2, ITGB4, and FAS, in the regulation of autophagy in AML have not been reported. These ARGs may be important markers in AML as they have been implicated in different cancers (57, 58), while further work is needed to examine the underlying molecular mechanisms. Consistent with previous studies (52), we identified autophagy, p53 signaling, AMPK signaling, and apoptosis as significantly enriched pathways. As an intracellular energy sensor, multiple sites of ULK1 were directly phosphorylated by activated AMPK, and the enhanced activity of ULK1 activated the TSC2, a negative regulator of mTORC1 activity (59). This was in line with the fact that the AMPK signaling pathway plays a crucial role in the positive regulation of autophagic processes.

The identification of gene signatures based on transcriptomic profiles is a promising approach to monitor the prognostic risk of cancers (60). We developed an autophagy-related risk signature here consisting of eight OS-related ARGs to predict patients' outcomes using LASSO Cox regression analysis. Patients in the high-risk group had significantly shorter OS than those in the low-risk group, even when adjusted for clinical variables by using univariate and multivariate Cox regression analyses. In addition, the signature was validated as an independent predictor on two external AML datasets. The AUC values of the ROC curves for 3-year and 5-year OS were 0.75 and 0.76, respectively. The calibration curve also confirmed its capacity for efficient prediction of patient's outcome. A nomogram that incorporates risk scores and accessible clinical parameters provided the possibility of individual personalized utility to monitor patient's prognosis. The predictive performance of our signature is comparable to that of a signature related to six autophagies (61), although it can better reveal the potential landscape for immunoregulatory and promotes the discovery of druggable targets for AML patients.

The differentially expressed genes analyzed in the high- and low-risk groups were significantly enriched in the regulation of immune responses, including neutrophil activation, receptor ligand activity, and chemokine activity, and the main immunity-related pathways, such as acute myeloid leukemia, IL-17 signaling pathway, NF-kappa B, and TNF signaling pathways, confirmed that differentiated immune regulators were involved in these two groups. IL-17 induced the sustained production of inflammatory cytokines, such as TNF-a and IL-6, and chemokines (CXCL1, CXCL2) to promote the pathogenesis of AML (62). Furthermore, IL-17 has been shown to activate some common pro-inflammatory signaling pathways, including NF-kB, JNK/P38/ERK, and PI3K. Inflammation can cause immune cells to assemble at the site of a tumor to fight against leukemic cells. An increasing number of pre-clinical studies have shown that tumor-infiltrating lymphocytes (TILs) have a major influence on disease progression and therapeutic response in many cancers (63, 64). The increased infiltration by cytotoxic T cells, memory T cells, and T helper cells is associated with extended predicted survival (65). An analysis of the tumor-infiltrating immune cells showed significantly decreased abundance of CD8+ T cells, resting and activated NK cells, and enhanced rates of resting and activated CD4+ T cells, regulatory T cells, and gamma delta T cells in the high-risk group. This suggests that a strong immunosuppressive microenvironment, featuring immune checkpoint inhibitors, in high-risk patients might lead to a poor response to immunotherapies.

Most patients with AML exhibit resistance to conventional chemotherapy, especially older patients who cannot endure intensive chemotherapy. In such cases, targeting molecular inhibitors combined with therapy offers promising prospects for treatment (66). The levels of expression of CD47, CD33, DOT1L, and IDH2 were negatively correlated with the signature-defined risk score, and patients might respond poorly to inhibitors targeting these genes but might benefit from the blockade of CTLA4 and MDM2. Thus, the autophagy-related signature can reflect the status of immunity of patients with AML and highlight potential immunotherapeutic implications while the underlying mechanisms need to be investigated.

Drug repurposing contributes to the identification of additional uses for approved or experimental chemicals that can accelerate the development of new drugs (67). OS-related ARGs were employed here to explore potential therapeutic candidates by calculating protein-drug interactions in the DrugBank database. A total of 32 druggable chemicals were retrieved to target eight ARGs. The results showed that a Caspase-3 deficiency impairs the self-renewal of leukemic stem cells and delays AE9a-induced leukemogenesis through autophagy by regulating the cleavage of ULK1. This suggests that Caspase-3 has multiple roles in the hematopoietic development and pathogenesis of AML (40). Eleven drugs were obtained to potentially target Caspase-3. For example, minocycline has been reported to induce apoptosis in patients of acute lymphoblastic leukemia, and alleviate harm to human peripheral blood lymphocyte cells (68). This indicates that it might have an effect on AML. Resistant AML cells frequently have deficiencies in the diphthamide synthesis pathway that impairs the ability of tagraxofusp to ADP-ribosylate cellular targets. This is owing to the reduced expression of DPH1, which encodes a diphthamide pathway enzyme, through DNA CpG methylation (69). Diphthamide that targets eEF2 might be a candidate drug for AML (70). The correlation between these ARGs and drugs needed to be investigated in future work.

This study conducted a systematic analysis of autophagy-related transcriptomic profiling and developed a risk prognostic signature based on the survival-related ARGs in AML patients. There remain several limitations that should be taken into consideration when interpreting the findings, however. The enrolled ARGs were identified from the available evidence of their involvement in disease progression, but prospective data are needed to verify their clinical value. The signature was developed and validated by using retrospective, publicly accessible datasets, and requires independent external validation to assess its potential clinical relevance.

CONCLUSIONS

Our study established a prognostic autophagy-related signature comprising eight ARGs for OS prediction in AML patients. The signature was found to be independently associated with OS in the training and validation cohorts. The distinct molecular landscape defined by it, including the pathways, immune infiltration, correlation between targeted therapies, and potential druggable targets, was systematically explored. The underlying molecular mechanisms require further experimental investigation.

DATA AVAILABILITY STATEMENT

The original contributions presented in the study are included in the article/**Supplementary Material**, further inquiries can be directed to the corresponding authors.

AUTHOR CONTRIBUTIONS

Conceptualization and design: DF and HJ. Data acquisition: BZ, YZ, JX, and SW. Methodology: BZ and DF. Data analysis and interpretation: DF and BZ. Writing (original draft): BZ and DF. Writing (review and editing): DF, WN, and HJ. All authors contributed to the article and approved the submitted version.

FUNDING

This study was supported by the Science and Technology Research Project of the Jiangxi Province Department of Education (GJJ201837), and the Natural Science Foundation of Jiangxi Province (20192BAB215001).

ACKNOWLEDGMENTS

We are grateful to the contributors to the public databases used in this study.

SUPPLEMENTARY MATERIAL

The Supplementary Material for this article can be found online at: https://www.frontiersin.org/articles/10.3389/fimmu.2021.695865/full#supplementary-material

Supplementary Figure 1 | General analysis workflow of this study.

Supplementary Figure 2 | Identification of key variables *via* LASSO regression analysis. **(A)** One thousand-fold cross-validation for variable selection in LASSO regression. **(B)** LASSO coefficients of key autophagy-related genes. Each curve represents an autophagy-related gene.

Supplementary Figure 3 | Expression of the model genes in the high- and low-risk groups ($P < 0.05$). **(A)** BAG3, **(B)** DAPK1, **(C)** CALCOCO2, **(D)** CAMKK2, **(E)** CANX, **(F)** P4HB, **(G)** TSC2, **(H)** ULK1.

Supplementary Figure 4 | Multiple AUCs of risk score and clinical parameters. **(A)** Multiple AUCs for 1 year. **(B)** Multiple AUCs for 3 years. **(C)** Multiple AUCs for 5 years.

Supplementary Figure 5 | Gene set enrichment analysis of autophagy-related signature in high- and low-risk groups.

Supplementary Figure 6 | Tumor-immune microenvironment analysis of the high- and low-risk groups in two validation sets. **(A)** GSE12417. **(B)** TCGA. The blue violin reflects the low-risk group and the red violin represents the high-risk group.

Supplementary Figure 7 | The expression analysis of exhausted T cells markers in high- and low-risk group. **(A)** GZMB. **(B)** IFNG. **(C)** PRF1. **(D)** TNF.

Supplementary Table 1 | The characteristics of samples used in this study.

REFERENCES

1. Marando L, Huntly BJP. Molecular Landscape of Acute Myeloid Leukemia: Prognostic and Therapeutic Implications. *Curr Oncol Rep* (2020) 22(6):61. doi: 10.1007/s11912-020-00918-7
2. Thomas D, Majeti R. Biology and Relevance of Human Acute Myeloid Leukemia Stem Cells. *Blood* (2017) 129(12):1577–85. doi: 10.1182/blood-2016-10-696054
3. Siegel RL, Miller KD, Jemal A. Cancer Statistics, 2020. *CA Cancer J Clin* (2020) 70(1):7–30. doi: 10.3322/caac.21590
4. Tamamyan G, Kadia T, Ravandi F, Borthakur G, Cortes J, Jabbour E, et al. Frontline Treatment of Acute Myeloid Leukemia in Adults. *Crit Rev Oncol Hematol* (2017) 110:20–34. doi: 10.1016/j.critrevonc.2016.12.004
5. Mizushima N, Levine B, Cuervo AM, Klionsky DJ. Autophagy Fights Disease Through Cellular Self-Digestion. *Nature* (2008) 451(7182):1069–75. doi: 10.1038/nature06639
6. Ouyang C, You J, Xie Z. The Interplay Between Autophagy and Apoptosis in the Diabetic Heart. *J Mol Cell Cardiol* (2014) 71:71–80. doi: 10.1016/j.yjmcc.2013.10.014
7. Kim S, Eun HS, Jo EK. Roles of Autophagy-Related Genes in the Pathogenesis of Inflammatory Bowel Disease. *Cells* (2019) 8(1):77. doi: 10.3390/cells8010077
8. Evangelisti C, Evangelisti C, Chiarini F, Lonetti A, Buontempo F, Neri LM, et al. Autophagy in Acute Leukemias: A Double-Edged Sword With Important Therapeutic Implications. *Biochim Biophys Acta* (2015) 1853 (1):14–26. doi: 10.1016/j.bbamcr.2014.09.023
9. Mortensen M, Soilleux EJ, Djordjevic G, Tripp R, Lutteropp M, Sadighi-Akha E, et al. The Autophagy Protein Atg7 Is Essential for Hematopoietic Stem Cell Maintenance. *J Exp Med* (2011) 208(3):455–67. doi: 10.1084/jem.20101145
10. Xu X, Araki K, Li S, Han JH, Ye L, Tan WG, et al. Autophagy Is Essential for Effector CD8(+) T Cell Survival and Memory Formation. *Nat Immunol* (2014) 15(12):1152–61. doi: 10.1038/ni.3025

11. Le Texier L, Lineburg KE, Cao B, McDonald-Hyman C, Leveque-El Mouttie L, Nicholls J, et al. Autophagy-Dependent Regulatory T Cells Are Critical for the Control of Graft-Versus-Host Disease. *JCI Insight* (2016) 1(15):e86850. doi: 10.1172/jci.insight.86850
12. Leveque-El Mouttie L, Vu T, Lineburg KE, Kuns RD, Bagger FO, Teal BE, et al. Autophagy Is Required for Stem Cell Mobilization by G-CSF. *Blood* (2015) 125(19):2933–6. doi: 10.1182/blood-2014-03-562660
13. Auberger P, Puissant A. Autophagy, a Key Mechanism of Oncogenesis and Resistance in Leukemia. *Blood* (2017) 129(5):547–52. doi: 10.1182/blood-2016-07-692707
14. Liu Q, Chen L, Atkinson JM, Claxton DF, Wang HG. Atg5-dependent Autophagy Contributes to the Development of Acute Myeloid Leukemia in an MLL-AF9-driven Mouse Model. *Cell Death Dis* (2016) 7(9):e2361. doi: 10.1038/cddis.2016.264
15. Du W, Xu A, Huang Y, Cao J, Zhu H, Yang B, et al. The Role of Autophagy in Targeted Therapy for Acute Myeloid Leukemia. *Autophagy* (2020), 1–15. doi: 10.1080/15548627.2020.1822628
16. Yun CW, Lee SH. The Roles of Autophagy in Cancer. *Int J Mol Sci* (2018) 19 (11):3466. doi: 10.3390/ijms19113466
17. Li Z, Herold T, He C, Valk PJ, Chen P, Jurinovic V, et al. Identification of a 24-Gene Prognostic Signature That Improves the European LeukemiaNet Risk Classification of Acute Myeloid Leukemia: An International Collaborative Study. *J Clin Oncol* (2013) 31(9):1172–81. doi: 10.1200/JCO.2012.44.3184
18. Metzeler KH, Hummel M, Bloomfield CD, Spiekermann K, Braess J, Sauerland MC, et al. An 86-Probe-Set Gene-Expression Signature Predicts Survival in Cytogenetically Normal Acute Myeloid Leukemia. *Blood* (2008) 112(10):4193–201. doi: 10.1182/blood-2008-02-134411
19. Gautier L, Cope L, Bolstad BM, Irizarry RA. Affy–Analysis of Affymetrix GeneChip Data At the Probe Level. *Bioinformatics* (2004) 20(3):307–15. doi: 10.1093/bioinformatics/btg405
20. Leek JT, Johnson WE, Parker HS, Jaffe AE, Storey JD. The Sva Package for Removing Batch Effects and Other Unwanted Variation in High-Throughput Experiments. *Bioinformatics* (2012) 28(6):882–3. doi: 10.1093/bioinformatics/bts034
21. Deng Y, Zhu L, Cai H, Wang G, Liu B. Autophagic Compound Database: A Resource Connecting Autophagy-Modulating Compounds, Their Potential Targets and Relevant Diseases. *Cell Prolif* (2018) 51(3):e12403. doi: 10.1111/cpr.12403
22. Yu G, Wang LG, Han Y, He QY. clusterProfiler: An R Package for Comparing Biological Themes Among Gene Clusters. *OMICS* (2012) 16(5):284–7. doi: 10.1089/omi.2011.0118
23. Szklarczyk D, Gable AL, Lyon D, Junge A, Wyder S, Huerta-Cepas J, et al. String v11: Protein-Protein Association Networks With Increased Coverage, Supporting Functional Discovery in Genome-Wide Experimental Datasets. *Nucleic Acids Res* (2019) 47(D1):D607–13. doi: 10.1093/nar/gky1131
24. Shannon P, Markiel A, Ozier O, Baliga NS, Wang JT, Ramage D, et al. Cytoscape: A Software Environment for Integrated Models of Biomolecular Interaction Networks. *Genome Res* (2003) 13(11):2498–504. doi: 10.1101/gr.1239303
25. Bader GD, Hogue CW. An Automated Method for Finding Molecular Complexes in Large Protein Interaction Networks. *BMC Bioinf* (2003) 4:2. doi: 10.1186/1471-2105-4-2
26. Tang Y, Li M, Wang J, Pan Y, Wu FX. CytoNCA: A Cytoscape Plugin for Centrality Analysis and Evaluation of Protein Interaction Networks. *Biosystems* (2015) 127:67–72. doi: 10.1016/j.biosystems.2014.11.005
27. Han H, Cho JW, Lee S, Yun A, Kim H, Bae D, et al. Trrust v2: An Expanded Reference Database of Human and Mouse Transcriptional Regulatory Interactions. *Nucleic Acids Res* (2018) 46(D1):D380–6. doi: 10.1093/nar/gkx1013
28. Fontanarosa JB, Dai Y. Using LASSO Regression to Detect Predictive Aggregate Effects in Genetic Studies. *BMC Proc* (2011) 5(Suppl 9):S69. doi: 10.1186/1753-6561-5-S9-S69
29. Vrieze SI. Model Selection and Psychological Theory: A Discussion of the Differences Between the Akaike Information Criterion (AIC) and the Bayesian Information Criterion (BIC). *Psychol Methods* (2012) 17(2):228–43. doi: 10.1037/a0027127
30. Heagerty PJ, Lumley T, Pepe MS. Time-Dependent ROC Curves for Censored Survival Data and a Diagnostic Marker. *Biometrics* (2000) 56(2):337–44. doi: 10.1111/j.0006-341x.2000.00337.x
31. Ritchie ME, Phipson B, Wu D, Hu Y, Law CW, Shi W, et al. Limma Powers Differential Expression Analyses for RNA-sequencing and Microarray Studies. *Nucleic Acids Res* (2015) 43(7):e47. doi: 10.1093/nar/gkv007
32. Metsalu T, Vilo J. ClustVis: A Web Tool for Visualizing Clustering of Multivariate Data Using Principal Component Analysis and Heatmap. *Nucleic Acids Res* (2015) 43(W1):W566–70. doi: 10.1093/nar/gkv468
33. Subramanian A, Tamayo P, Mootha VK, Mukherjee S, Ebert BL, Gillette MA, et al. Gene Set Enrichment Analysis: A Knowledge-Based Approach for Interpreting Genome-Wide Expression Profiles. *Proc Natl Acad Sci USA* (2005) 102(43):15545–50. doi: 10.1073/pnas.0506580102
34. Zhang Z, Kattan MW. Drawing Nomograms With R: Applications to Categorical Outcome and Survival Data. *Ann Transl Med* (2017) 5(10):211. doi: 10.21037/atm.2017.04.01
35. Alba AC, Agoritsas T, Walsh M, Hanna S, Iorio A, Devereaux PJ, et al. Discrimination and Calibration of Clinical Prediction Models: Users' Guides to the Medical Literature. *JAMA* (2017) 318(14):1377–84. doi: 10.1001/jama.2017.12126
36. Newman AM, Liu CL, Green MR, Gentles AJ, Feng W, Xu Y, et al. Robust Enumeration of Cell Subsets From Tissue Expression Profiles. *Nat Methods* (2015) 12(5):453–7. doi: 10.1038/nmeth.3337
37. Valent P, Sadovnik I, Eisenwort G, Bauer K, Herrmann H, Gleixner KV, et al. Immunotherapy-Based Targeting and Elimination of Leukemic Stem Cells in AML and CML. *Int J Mol Sci* (2019) 20(17):4233. doi: 10.3390/ijms20174233
38. Winer ES, Stone RM. Novel Therapy in Acute Myeloid Leukemia (AML): Moving Toward Targeted Approaches. *Ther Adv Hematol* (2019) 10:2040620719860645. doi: 10.1177/2040620719860645
39. Wishart DS, Feunang YD, Guo AC, Lo EJ, Marcu A, Grant JR, et al. DrugBank 5.0: A Major Update to the DrugBank Database for 2018. *Nucleic Acids Res* (2018) 46(D1):D1074–D82. doi: 10.1093/nar/gkx1037
40. Staib P, Tiehen J, Strunk T, Schinkothe T. Determination of Caspase-3 Activation Fails to Predict Chemosensitivity in Primary Acute Myeloid Leukemia Blasts. *BMC Cancer* (2005) 5:60. doi: 10.1186/1471-2407-5-60
41. Guertin DA, Sabatini DM. Defining the Role of mTOR in Cancer. *Cancer Cell* (2007) 12(1):9–22. doi: 10.1016/j.ccr.2007.05.008
42. Man N, Tan Y, Sun XJ, Liu F, Cheng G, Greenblatt SM, et al. Caspase-3 Controls AML1-ETO-Driven Leukemogenesis Via Autophagy Modulation in a ULK1-Dependent Manner. *Blood* (2017) 129(20):2782–92. doi: 10.1182/blood-2016-10-745034
43. Wang RX, Xu XE, Huang L, Chen S, Shao ZM. eEF2 Kinase Mediated Autophagy as a Potential Therapeutic Target for Paclitaxel-Resistant Triple-Negative Breast Cancer. *Ann Transl Med* (2019) 7(23):783. doi: 10.21037/atm.2019.11.39
44. Xu JY, Zhang C, Wang X, Zhai L, Ma Y, Mao Y, et al. Integrative Proteomic Characterization of Human Lung Adenocarcinoma. *Cell* (2020) 182(1):245–61.e17. doi: 10.1016/j.cell.2020.05.043
45. Chen Y, Tang J, Lu T, Liu F. CAPN1 Promotes Malignant Behavior and Erlotinib Resistance Mediated by Phosphorylation of c-Met and PIK3R2 Via Degrading PTPN1 in Lung Adenocarcinoma. *Thorac Cancer* (2020) 11 (7):1848–60. doi: 10.1111/1759-7714.13465
46. Steinmann S, Kunze P, Hampel C, Eckstein M, Bertram Bramsen J, Muenzner JK, et al. DAPK1 Loss Triggers Tumor Invasion in Colorectal Tumor Cells. *Cell Death Dis* (2019) 10(12):895. doi: 10.1038/s41419-019-2122-z
47. Ercetin E, Richtmann S, Delgado BM, Gomez-Mariano G, Wrenger S, Korenbaum E, et al. Clinical Significance of SERPINA1 Gene and Its Encoded Alpha1-Antitrypsin Protein in NSCLC. *Cancers (Basel)* (2019) 11 (9):1306. doi: 10.3390/cancers11091306
48. Qian BZ, Li J, Zhang H, Kitamura T, Zhang J, Campion LR, et al. CCL2 Recruits Inflammatory Monocytes to Facilitate Breast-Tumour Metastasis. *Nature* (2011) 475(7355):222–5. doi: 10.1038/nature10138
49. Cai SF, Levine RL. Genetic and Epigenetic Determinants of AML Pathogenesis. *Semin Hematol* (2019) 56(2):84–9. doi: 10.1053/j.seminhematol.2018.08.001
50. Jin M, Klionsky DJ. Regulation of Autophagy: Modulation of the Size and Number of Autophagosomes. *FEBS Lett* (2014) 588(15):2457–63. doi: 10.1016/j.febslet.2014.06.015
51. Lalaoui N, Johnstone R, Ekert PG. Autophagy and AML–Food for Thought. *Cell Death Differ* (2016) 23(1):5–6. doi: 10.1038/cdd.2015.136

52. Yang Z, Klionsky DJ. Mammalian Autophagy: Core Molecular Machinery and Signaling Regulation. *Curr Opin Cell Biol* (2010) 22(2):124–31. doi: 10.1016/j.ceb.2009.11.014
53. Mathew R, Kongara S, Beaudoin B, Karp CM, Bray K, Degenhardt K, et al. Autophagy Suppresses Tumor Progression by Limiting Chromosomal Instability. *Genes Dev* (2007) 21(11):1367–81. doi: 10.1101/gad.1545107
54. Aasebo E, Berven FS, Bartaula-Brevik S, Stokowy T, Hovland R, Vaudel M, et al. Proteome and Phosphoproteome Changes Associated With Prognosis in Acute Myeloid Leukemia. *Cancers (Basel)* (2020) 12(3):709. doi: 10.3390/cancers12030709
55. Inoki K, Li Y, Zhu T, Wu J, Guan KL. TSC2 Is Phosphorylated and Inhibited by Akt and Suppresses mTOR Signalling. *Nat Cell Biol* (2002) 4(9):648–57. doi: 10.1038/ncb839
56. Tabe Y, Tafuri A, Sekihara K, Yang H, Konopleva M. Inhibition of mTOR Kinase as a Therapeutic Target for Acute Myeloid Leukemia. *Expert Opin Ther Targets* (2017) 21(7):705–14. doi: 10.1080/14728222.2017.1333600
57. Rapino F, Jung M, Fulda S. BAG3 Induction Is Required to Mitigate Proteotoxicity Via Selective Autophagy Following Inhibition of Constitutive Protein Degradation Pathways. *Oncogene* (2014) 33(13):1713–24. doi: 10.1038/onc.2013.110
58. Macanas-Pirard P, Quezada T, Navarrete L, Broekhuizen R, Leisewitz A, Nervi B, et al. The CCL2/CCR2 Axis Affects Transmigration and Proliferation But Not Resistance to Chemotherapy of Acute Myeloid Leukemia Cells. *PLoS One* (2017) 12(1):e0168888. doi: 10.1371/journal.pone.0168888
59. Dunlop EA, Tee AR. The Kinase Triad, AMPK, mTORC1 and ULK1, Maintains Energy and Nutrient Homoeostasis. *Biochem Soc Trans* (2013) 41(4):939–43. doi: 10.1042/BST20130030
60. Fu D, Zhang B, Yang L, Huang S, Xin W. Development of an Immune-Related Risk Signature for Predicting Prognosis in Lung Squamous Cell Carcinoma. *Front Genet* (2020) 11:978. doi: 10.3389/fgene.2020.00978
61. Chen XX, Li ZP, Zhu JH, Xia HT, Zhou H. Systematic Analysis of Autophagy-Related Signature Uncovers Prognostic Predictor for Acute Myeloid Leukemia. *DNA Cell Biol* (2020) 39(9):1595–605. doi: 10.1089/dna.2020.5667
62. Qian Y, Kang Z, Liu C, Li X. Il-17 Signaling in Host Defense and Inflammatory Diseases. *Cell Mol Immunol* (2010) 7(5):328–33. doi: 10.1038/cmi.2010.27
63. Al-Shibli KI, Donnem T, Al-Saad S, Persson M, Bremnes RM, Busund LT. Prognostic Effect of Epithelial and Stromal Lymphocyte Infiltration in Non-Small Cell Lung Cancer. *Clin Cancer Res* (2008) 14(16):5220–7. doi: 10.1158/1078-0432.CCR-08-0133
64. Takemoto N, Konishi F, Yamashita K, Kojima M, Furukawa T, Miyakura Y, et al. The Correlation of Microsatellite Instability and Tumor-Infiltrating Lymphocytes in Hereditary Non-Polyposis Colorectal Cancer (HNPCC) and Sporadic Colorectal Cancers: The Significance of Different Types of Lymphocyte Infiltration. *Jpn J Clin Oncol* (2004) 34(2):90–8. doi: 10.1093/jjco/hyh018
65. Bremnes RM, Busund LT, Kilvaer TL, Andersen S, Richardsen E, Paulsen EE, et al. The Role of Tumor-Infiltrating Lymphocytes in Development, Progression, and Prognosis of Non-Small Cell Lung Cancer. *J Thorac Oncol* (2016) 11(6):789–800. doi: 10.1016/j.jtho.2016.01.015
66. Ramos NR, Mo CC, Karp JE, Hourigan CS. Current Approaches in the Treatment of Relapsed and Refractory Acute Myeloid Leukemia. *J Clin Med* (2015) 4(4):665–95. doi: 10.3390/jcm4040665
67. Shah RR, Stonier PD. Repurposing Old Drugs in Oncology: Opportunities With Clinical and Regulatory Challenges Ahead. *J Clin Pharm Ther* (2019) 44(1):6–22. doi: 10.1111/jcpt.12759
68. Ruiz-Moreno C, Velez-Pardo C, Jimenez-Del-Rio M. Minocycline Induces Apoptosis in Acute Lymphoblastic Leukemia Jurkat Cells. *Toxicol In Vitro* (2018) 50:336–46. doi: 10.1016/j.tiv.2018.03.012
69. Togami K, Pastika T, Stephansky J, Ghandi M, Christie AL, Jones KL, et al. DNA Methyltransferase Inhibition Overcomes Diphthamide Pathway Deficiencies Underlying CD123-Targeted Treatment Resistance. *J Clin Invest* (2019) 129(11):5005–19. doi: 10.1172/JCI128571
70. Gondek LP. Hitting the Bullseye With a Nonlethal Payload: Resistance in CD123-Positive Malignancies. *J Clin Invest* (2019) 129(11):4590–2. doi: 10.1172/JCI132443

Conflict of Interest: The authors declare that the research was conducted in the absence of any commercial or financial relationships that could be construed as a potential conflict of interest.

Copyright © 2021 Fu, Zhang, Wu, Zhang, Xie, Ning and Jiang. This is an open-access article distributed under the terms of the Creative Commons Attribution License (CC BY). The use, distribution or reproduction in other forums is permitted, provided the original author(s) and the copyright owner(s) are credited and that the original publication in this journal is cited, in accordance with accepted academic practice. No use, distribution or reproduction is permitted which does not comply with these terms.

frontiers in Immunology

REVIEW
published: 08 June 2021
doi: 10.3389/fimmu.2021.705260

CD58 Immunobiology at a Glance

Yalu Zhang[†], *Qiaofei Liu*[†], *Sen Yang and Quan Liao*[*]

Department of General Surgery, State Key Laboratory of Complex Severe and Rare Diseases, Peking Union Medical College Hospital, Chinese Academy of Medical Science and Peking Union Medical College, Beijing, China

The glycoprotein CD58, also known as lymphocyte-function antigen 3 (LFA-3), is a costimulatory receptor distributed on a broad range of human tissue cells. Its natural ligand CD2 is primarily expressed on the surface of T/NK cells. The CD2-CD58 interaction is an important component of the immunological synapse (IS) that induces activation and proliferation of T/NK cells and triggers a series of intracellular signaling in T/NK cells and target cells, respectively, in addition to promoting cell adhesion and recognition. Furthermore, a soluble form of CD58 (sCD58) is also present in cellular supernatant *in vitro* and in local tissues *in vivo*. The sCD58 is involved in T/NK cell-mediated immune responses as an immunosuppressive factor by affecting CD2-CD58 interaction. Altered accumulation of sCD58 may lead to immunosuppression of T/NK cells in the tumor microenvironment, allowing sCD58 as a novel immunotherapeutic target. Recently, the crucial roles of costimulatory molecule CD58 in immunomodulation seem to be reattracting the interests of investigators. In particular, the CD2-CD58 interaction is involved in the regulation of antiviral responses, inflammatory responses in autoimmune diseases, immune rejection of transplantation, and immune evasion of tumor cells. In this review, we provide a comprehensive summary of CD58 immunobiology.

Keywords: CD58, lymphocyte functional antigen-3, LFA-3, CD2, T cell activation, immune evasion

OPEN ACCESS

Edited by:
Peng Qu,
National Institutes of Health (NIH), United States

Reviewed by:
Lucas Ferrari De Andrade,
Icahn School of Medicine at Mount Sinai, United States
Alex Michael Abel,
LEAH Labs, Inc., United States

***Correspondence:**
Quan Liao
lqpumc@126.com

[†]*These authors have contributed equally to this work*

Specialty section:
This article was submitted to Cancer Immunity and Immunotherapy, a section of the journal Frontiers in Immunology

Received: *05 May 2021*
Accepted: *24 May 2021*
Published: *08 June 2021*

Citation:
Zhang Y, Liu Q, Yang S and Liao Q (2021) CD58 Immunobiology at a Glance. Front. Immunol. 12:705260. doi: 10.3389/fimmu.2021.705260

INTRODUCTION

Intercellular adhesion is vital for a range of immunological responses, including the interaction between T lymphocytes and target cells. Conjugate formation of T cells with antigen-negative targets is nearly as efficient as with specific target cells without causing lysis of target cells. Therefore, on specific target cells, adhesion in an antigen-independent manner may occur simultaneously with or prior to antigen recognition (1).

The immune adhesion molecule CD58, also known as LFA-3, is a heavily glycosylated, distributed surface glycoprotein of 40-70 kDa and extensively expressed on hematopoietic and nonhematopoietic cells (2, 3). CD58 on the cell surface participates in potentiating effector-target adhesion during antigen-specific recognition (4). Cell-cell adhesion is crucial for leucocyte-mediated chemotaxis, phagocytosis, cytotoxicity, and induction of lymphocyte differentiation and proliferation. In terms of the antigen-presenting process, the CD58 molecule offers an effective second signal for T cell activation, thereby optimizing and replenishing the proliferative response mediated through TCR/CD3 signaling (**Figure 1A**) (5, 6).

CD2, also known as T11, LFA-2, the erythrocyte (E) rosette receptor, is the natural ligand of CD58. It is a surface glycoprotein restricted to T lymphocytes, NK cells, thymocytes, and a subset of bone marrow cells (7, 8). Both CD2 and CD58 are members of the immunoglobulin supergene family and their amino

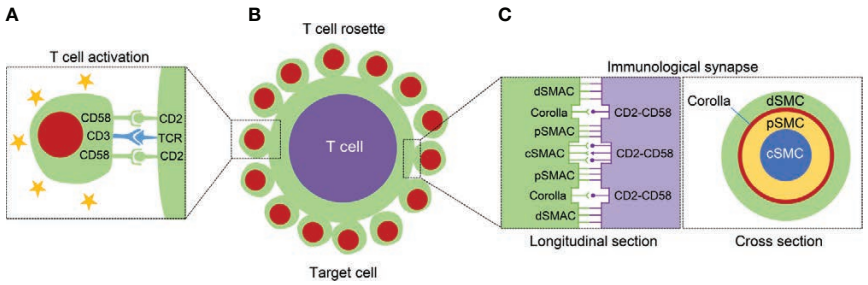

FIGURE 1 | The structure diagram with regard to T cell activation, T cell rosette, and immunological synapse (IS). **(A)** The left panel displays that the CD2-CD58 interaction facilitates the T cell activation through offering the necessary second signal and assisting TCR-mediated stimulation. **(B)** The middle panel exhibits the formation of T cell rosette mainly mediated by the binding of CD2 with CD58. **(C)** The IS can be classified into different supramolecular activation complexes (SMAC), central, peripheral, and distal SMAC (c, p and dSMAC, respectively). In addition to the cSMAC, the CD2-CD58 interactions exist between pSMAC and dSMAC, and form a ring-like structure, called "corolla". The right panel shows the longitudinal and cross section of IS.

acid sequences on the extracellular domain are significantly similar (9). The amino-terminal domain of CD2 is responsible for target cell adhesion and binds to CD58 on target cells or antigen-presenting cells (APC) with high affinity (10–12). As an important adhesion pathway between T cells and target cells, CD2-CD58 interaction is not only a crucial costimulatory signal for optimal T cell activation in response to antigens, but also induction of a series of essential signal transduction events to participate in the modulation of T cell responses (13, 14). For example, incubation of B lymphoblastoid cell with immobilized anti-CD58 mAbs causes broad tyrosine phosphorylation and increases TNF-α production (15). Accumulating evidence has demonstrated that the CD2-CD58 interaction plays a critical role in lymphocyte activation, recirculation, and effector function, e.g., cytolytic activity on neoplastic cells (16, 17).

Herein, we have collated almost all of the published literature from discovery to the present and elaborately summarized the CD58 immunobiology in a systematic and comprehensive manner, including CD58 isoforms, sCD58, IS formation, CD58 polymorphisms, CD2-CD58 interaction, their structures of interface, and related functions; simultaneously dissected the important effects of CD58 for T/NK cell-mediated immune response in tumor-related and immune-related diseases.

TWO ISOFORMS OF CD58

There are two isoforms of CD58 derived from divergent mRNA splicing: a type-I transmembrane and a glycosylphosphatidylinositol (GPI)-anchored form (**Figure 2A**) (18). The former has an extracellular domain with six N-linked glycosylation sites sequentially linked to a hydrophobic transmembrane region and a 12-amino acid cytoplasmic segment; The latter is anchored to the outer side of the cell membrane by a GPI tail without transmembrane region and cytoplasmic domain (18, 19). They are located in different membrane compartments. The GPI-anchored isoform resides in lipid raft, whereas the transmembrane isoform localizes in a non-raft microdomain (20). Despite the transmembrane CD58 outside lipid rafts, it can trigger signaling independently of the GPI-anchored isoform, such as induction of tyrosine phosphorylation of PLCγ, SYK and BLNK, and activation of AKT and ERK (20, 21). Cell adhesion is dependent on the density of CD58. At lower densities, GPI-linked isoform is crucial for enhancing adhesion, instead of the transmembrane isoform (22). Accordingly, unlike the well-accepted concept that the GPI-anchor is indispensable for signaling, the GPI-anchored CD58 is more effective in enhancing adhesion, whereas the transmembrane form is more critical for signal transduction. This kind of structural distribution is of great significance to CD58 adhesion and transmembrane signaling (23).

CD2-CD58 INTERACTION

Human peripheral blood T lymphocytes have sheep red blood cells (SRBC) receptors on their surface. Human T lymphocytes are mixed with SRBC to form a rosette centered on T cells and surrounded by SRBCs *in vitro*, known as the "E-rosette test", which reflects the immunological activity of T lymphocytes (**Figure 1B**). The formation of E-rosette is dependent on the binding of CD2 in T lymphocytes with T11 target structure (T11TS) on SRBC, which is a functionally homologous ligand for CD58 on human erythrocytes (24, 25). The anti-CD58 and anti-CD2 mAbs can inhibit rosette formation through acting on the erythrocyte and the T lymphocyte, respectively (26). In Hodgkin's lymphoma (HL) tissue, spontaneous rosette formation of T cells with Reed-Sternberg cells is also mediated *via* CD2-CD58 interaction (26).

The interaction between CD2 in T cells and CD58 in target cells is subtle and unique. Activated human T lymphocytes can form rosettes with autologous erythrocytes, while resting T cells cannot (18, 27). Moreover, the interaction of CD2-CD58 is enthalpy-driven, accompanied by adverse entropic changes and energetically remarkable conformational adjustments (28). Unlike the other adhesion, CD2-CD58 interaction does not depend on cellular metabolism and cytoskeletal involvement, insensitive to ambient temperature, and its rate constant and average affinity not influenced by variations in ionic strength such as extracellular Mg^{2+}/Ca^{2+} (26, 28).

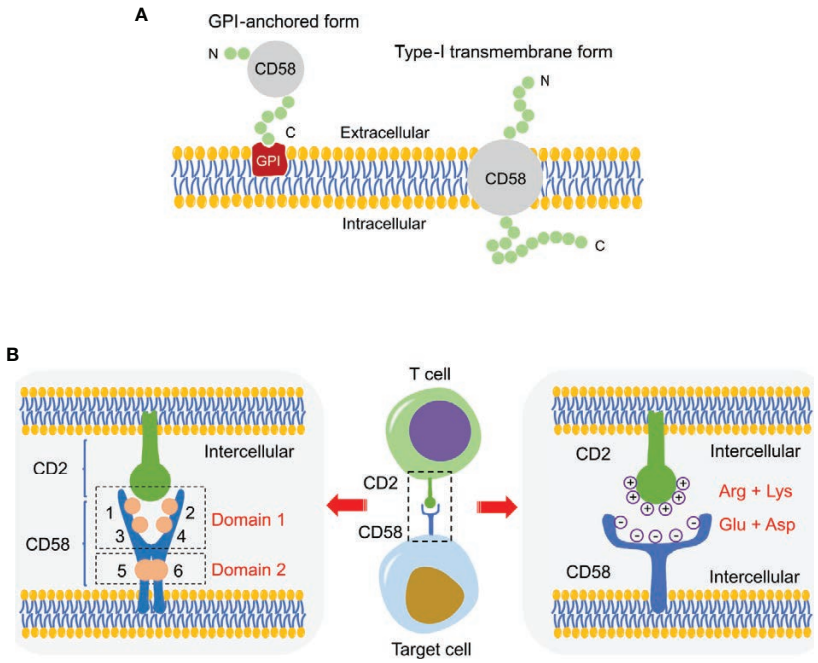

FIGURE 2 | Schematic of CD58 isoforms and CD2-CD58 interface. **(A)** Schematic diagram of two CD58 isoforms, a GPI-anchored and a type-I transmembrane form. **(B)** Structure diagram of the interface in CD2-CD58, which is mainly supported by electrostatic complementarity instead of shape matching.

STRUCTURE OF INTERFACE IN CD2-CD58

There are four discrete epitopes on the membrane-distal domain (domain 1) and two overlapping epitopes on the membrane-proximal domain (domain 2) in the CD58 molecule (**Figure 2B**) (29, 30). The N-terminus of the CD58 epitopes are functional sites involved in the interaction site with CD2, while domain 2 connects CD58 to membrane anchor independent of CD2 binding and CD58-mediated activation (29, 30). In addition, all epitopes exist in the same numbers on a wide variety of CD58-positive cells and show a uniform trend of increase/decrease after cell activation or malignant transformation (30). Protein-protein interface interactions are fundamentally supported by shape matching and electrostatic complementarity. The crystal structure between the binding interface of CD2 and CD58 is an orthogonal, asymmetric, and face-to-face interaction involving the main β-sheets of the respective N-terminal domains (31). The binding domain of CD58 is a localized and densely charged surface region on the AGFCC'C" face of the CD2 adhesion site (32). Through disrupting the highly acidic surface of the AGFCC'C" β-sheet of CD58, it was unexpectedly found that the CD2-CD58 interface lacks significant shape complementarity (33). The electrostatic potential on the CD2 surface is primarily positive because of arginine and lysine residues, whereas CD58 exhibits negative charge at the interface with CD2 due to the presence of glutamate and aspartate residues (**Figure 2B**) (34). Specifically, the CD2-CD58 binding site is composed of β-strands C and F with charged residues (34). Therefore, electrostatic attraction, rather than shape complementarity, plays a dominant role in the binding of CD2 to CD58 (35). This pattern of binding and recognition is strikingly different from the well-known interactions of other proteins, e.g., antibody-receptor or cytokine-cytokine receptor interactions (33). Under conditions of little hydrophobicity, the interlaced, charged amino acid side chains shape salt and hydrogen bonds at the interface, generating a high degree of specificity despite with low affinity that weaker than initial expectation, which satisfies the special requirements for such interaction to be easily reversible (36, 37). Selective binding, weak, reversible, these features are particularly suitable for CD2-CD58 interaction to initiate and sustain dynamic bindings between T/NK cells and target cells (36, 37). In addition, structural analysis shows that CD2-CD58 adhesion has strong conformational flexibility and some unnatural helical conformations under organic solvents or high-temperature conditions (38). The conformational state of the adhesion proteins is beneficial to the modulation of CD2 folding and cell adhesion (38).

As a costimulatory pathway, CD2-CD58 interactions provide a series of favorable conditions for signal recognition of T/NK cells with their targets. Firstly, substantial CD2-CD58 interactions contribute to overcoming intercellular charge repulsion, thereby eliminating bond strain on the interactions of TCR-ligand (39). Secondly, on account of the membrane gap of the CD2-CD58 complex is equal to that of the TCR peptide-MHC complex, numerous CD2-CD58 interactions would place the distance between T/NK cell and target cell within an optimal range for the T/NK cell receptor-ligand interaction (40). Thirdly, the cytoplasmic

domain of CD2 is large and conserved, which facilitates the recruitment of cytoskeleton and signaling molecules into the contact cap (41–43).

Additionally, glycosylation plays a crucial role in intercellular adhesion and regulates the stability and dynamics of proteins in a subtle way (44), which is likewise involved in the regulation of human CD2/CD58-mediated cell-cell adhesion by conformational adjustment (45). Fully glycosylated CD58 is more effective in suppressing the formation of E-rosette than the deglycosylated form, so the maintenance of CD58 glycosylation is essential for the exertion of its functional activity (46). The CD2-CD58 interaction is largely administrated by three hot spots forming a binding triangle, the topology of which is fundamental for the stability of CD2-CD58 binding. The topology of CD2 conformation is remarkably tuned and induced by glycosylation into a specific structure to energetically stabilizes the CD2-CD58 complex. Therefore, CD2 glycosylation facilitates CD2-CD58 binding *via* conformational adjustment (45).

According to the relevant structure epitopes, drugs or agents are designed to influence CD2/CD58-mediated intercellular adhesion to regulate the immune response. In the CD2-CD58 interface, CD58 Lys34 and CD2 Tyr86 residues are functional hot spots (47). Therefore, short peptide drugs can be constructed from the hot spot β-strand area of CD2 molecule with CD58 binding site. For example, structural constraints from CD2 are inserted into the peptides *via* the dibenzofuran moiety to nucleate β-strand conformation in the peptides, thus regulating the binding of CD2 to CD58 (48). In the collagen-induced arthritis (CIA) mouse model, a peptidomimetic designed to disrupt the interface of CD2-CD58 interaction can inhibit the T/NK cell-mediated immune response through interfering with the binding of CD2 with CD58 (49). Besides, a kind of nonimmunogenic compound 7 is successfully synthesized to act as a lead compound for immunoregulation, accompanied by a reduction of IFN-γ and anti-collagen antibody levels in the CIA model, and thus it may be an effective therapeutic drug for the autoimmune disease (50). These results indicate that peptides targeting costimulatory molecule CD2/CD58 can be used to regulate immune responses and contribute to the development of therapeutic drugs for autoimmune and inflammatory diseases.

Previously published studies have demonstrated that using the CD58 fusion protein Alefacept to disrupt the CD2-CD58 interaction can inhibit T cell activation (51). More importantly, it was found that alefacept could specifically eliminate effector memory T cells in the peripheral blood and attenuate clinical symptoms in type-I diabetes and psoriasis (52, 53). Although the constructed peptides have biological activities *in vitro* and *in vivo*, their stability *in vivo* has limitations as most other peptides (54). Sable et al. adopted a novel approach to reinforce its stability *via* integrating the CD2 adhesion domain sequence from peptide 6 into the framework of rhesus theta defensins and sunflower trypsin inhibitor (55). The constructed cyclic peptides exhibit potent resistance toward enzymatic degradation and thermal denaturation. Among them, SFTI-a possesses a strong inhibitory activity of cell adhesion in the low nanomolar range to repress T cell-mediated immune responses from humanized arthritic mice (55).

SOLUBLE CD58

It was first discovered in 1993 by Hoffmann et al. that the presence of a soluble form of CD58 in human serum, urine, and cell supernatant *in vitro* (29). At high concentrations, sCD58 can bind to CD2-positive cells and restrain rosette formation of human T cells with sheep and human erythrocytes (29). The mixed lymphocyte reaction could also be profoundly dampened by sCD58 (46). Therefore, local release of large amounts of native sCD58 may disturb cell-cell adhesion and recognition *in vivo*. Besides, similar to suppression by CD58 mAbs, sCD58 alleviates the cytotoxicity of human NK clones ($CD2^+$ $CD3^-$). In contrast, sCD58 and mitotic CD2R mAb act synergistically in the triggering of T cell activation (46). These findings reveal that sCD58 modulates intercellular adhesion and T/NK cell-mediated immune responses by acting as a biological immunoregulator.

It has been shown that sCD58 can curb the lysis of neoplastic cells through competitively suppressing the binding to CD2. The release of substantial sCD58 from melanoma cells results in their accumulation within the tumor tissue at high concentrations sufficient to inhibit cellular immune responses and immunotherapeutic sensitivity (56). Hollander et al. found sCD58 was constitutively secreted into the supernatant of human B lymphoblastoid cells and the GPI-deficient mutant cells generated more sCD58 than wild-type cells (57). A similar phenomenon can be observed in lymphocytes from patients with paroxysmal nocturnal hemoglobinuria (PNH), which is characterized by a defect in the GPI-anchoring pathway. Therefore, lymphocytes in PNH patients generate more sCD58 than normal cells as the absence of GPI anchoring (58).

Although alternative splicing, direct secretion, and proteolytic shedding have not yet been corroborated as possible mechanisms of sCD58 production, the sCD58 release is likely to be derived from enzymatic cleavage of membrane-anchored CD58, since lack of a distinct mRNA for sCD58 and the downregulation of CD58 surface expression is always accompanied by the accumulation of sCD58 in the cellular supernatant (58–60). Furthermore, subsequent studies have revealed that the expression of surface CD58 is decreased following the treatment of PI-specific phospholipase C (PI-PLC) (61). Those changes between membranous CD58 and sCD58 may significantly affect adhesion/deadhesion processes, because the CD2-CD58 axis is one of the dominant pathways to mediate the interaction between T/NK cells and other cells (62, 63). Thus, cleavage of membranous CD58 may be responsible for the production of its soluble form, which plays a crucial role in the deadhesion of T/NK cells with target cells.

Regarding the immune function of sCD58, it was found that the dimeric and multimeric forms of synthetic sCD58 have a stronger potency than the monomeric biological form. The dimeric sCD58 inhibits antigen-stimulated proliferation of T lymphocytes to exert its immunosuppressive capacities *via* inducing regulatory T cells (64). The multimeric sCD58 is more effective than the monomer in refraining the proliferation of T lymphocytes in response to allogeneic cells, tetanus toxoid, or purified protein derivative (65). This inhibitory effect is not only due to physical blockage of intercellular interactions, but may also

involve negative signaling generated *via* multimeric sCD58-CD2 interactions (65). Accordingly, it owns a strong potential as an immunomodulatory agent to suppress antigen-specific T cell responses for the treatment of inflammatory and autoimmune diseases. So far, the role of sCD58 in the tumor microenvironment has not been explored. With regard to the potential competitive inhibition of sCD58 between T/NK cells and target cells, sCD58 may be involved in cancer cell-induced immunosuppression, which has potential clinical implications and needs to be further mined and demonstrated.

EFFECTS OF CYTOKINES AND DRUGS ON CD58 EXPRESSION

The regulation of CD58 expression by cytokines is cell-dependent. In colonic epithelial cells, breast cancer cells and normal hepatocytic cells, the expression of CD58 is unresponsive to cytokine stimulation, including TNF-α, IFN-γ, IL-1, and IL-6 (66–68). There was no change in CD58 expression after stimulation of bronchial epithelial cells with TNF-α or IFN-γ (69). Similarly, TNF-α and IFN-γ do not influence the expression of CD58 in embryonic brain astrocytes (70). In contrast, the expression of CD58 was sensitively increased after incubation with IL-4 in human B-lymphoma cells and Burkitt's lymphoma cell lines (68, 71, 72). Stimulation of cultured leukemic blasts with TNF-α increases CD58 expression, in turn facilitating susceptibility to lymphocyte-mediated lysis (73). After exposure to GM-CSF, CD58 expression is significantly upregulated in acute myelogenous leukemia (AML) cells (74). Besides, ultraviolet (UV)-B irradiation decreases the expression of CD58 on Epstein-Barr virus (EBV)-transformed B cells (75).

Notably, CD58 expression is significantly affected by some exogenous stimuli or drugs. The expression of CD58 on the surface of hepatocellular carcinoma (HCC) cells is dramatically elevated after anisomycin treatment and blockade of CD58 can potently impair the anisomycin-mediated enhancement of NK cytotoxicity (76). Thus, the adhesion molecule CD58 is likely to be critical for NK-mediated immunotherapy (76). Furthermore, β-interferon can significantly enhance the proportion of CD58 positive endothelial cells (77). All-trans retinoic acid (ATRA) and dexamethasone robustly diminish the surface expression of CD58 *in vitro*, which probably explains the efficacy of these drugs in treating inflammation-related diseases *in vivo* to some extent (78, 79). Moreover, long-term lead exposure reduces the expression of the erythrocyte adhesion molecule CD58, weakening the sensitivity to IFN-γ, in preschool children (80).

The surface CD58 appears to be unresponsive to cytokines, but the production of sCD58 is relatively sensitive to cytokines such as IL-1β, IFN-γ, and TNF-α. Albeit this, the generation of sCD58 varies from cell to cell, as demonstrated by its release from some, but not all, tumor cell lines. The sCD58 is only released in 6 out of 10 melanoma cell lines. Among them, sCD58 production can be potently affected by IFN-γ in all lines and by TNF-α in one (56). The sCD58 in the adenocarcinoma cell supernatant can be detected only after IL-1β stimulation (29). Both PMA and TNF-α can augment the release of sCD58 in HCC cells, but the production of sCD58 is unaffected following IL-1β stimulation (29). Thus, different cells exhibit different susceptibility to TNF-α and IFN-γ (29, 56). This regulation is cell-specific, especially IFN-γ, which inhibits the release of sCD58 in larynx epidermoid carcinoma cells but promotes the production of the soluble form in lung epidermoid carcinoma cells (60). In fact, CD58 is also present in a cytoplasmic "pool" of each cell; meanwhile, cleavage of surface CD58 by PLC can result in an increase of intracellular CD58 (60). Therefore, the cytoplasmic, membranous, and soluble form of CD58 is likely to be interrelated and dynamic. Apart from the expression level of CD58, activation status, secretory activity, and endogenous protein sheddase levels may be the major reasons for the cell-dependent differences in the production of sCD58 (60).

CD2/CD58/CD48/CD59

CD2, CD48, CD58, and CD59 are tightly associated members of the immunoglobulin superfamily and they have similar structures in extracellular regions (81). CD58 is the primary natural ligand for human CD2; CD48 and CD59 are two additional, low-affinity ligands for human CD2, and their interactions in the human are limited and independent of glycosylation (82, 83).

The CD2 binding sites with CD58 and CD59 are overlapping, but not exactly identical (84). In murine T cell hybridomas expressing human CD2, anti-CD59 mAbs suppress CD2-mediated T cell activation, indicating that direct interaction of CD2 with CD59 likewise facilitates T cell-specific immune responses (84). Thus, CD59 is considered as the second ligand for CD2 and synergizes with CD58 to promote the adhesion and activation of T lymphocytes (85, 86). Notably, CD59 promotes CD58-mediated T cell proliferation and IL-2 production, whereas in the absence of CD2-CD58 interaction, the CD59 molecule itself cannot stimulate T cell proliferation alone even in the presence of exogenous recombinant cytokines such as IL-1, IL-6 (82).

Although CD58 is distributed on a wide range of human cells and tissues, the CD58 gene has not yet been found in murine, and the only counter-receptor for CD2 identified heretofore is CD48 (87). CD48 is considered to be a homologue of human CD58 in murine since its high similarities in distribution and structure (88). Arulanandam et al. surmise that CD58 may have evolved at the later stage of mammalian evolution due to gene duplication from CD48 to become an exclusive counter-receptor for CD2 after divergence from murine (89–91). The species-specific differences in the CD2/CD58/CD48/CD59 system are summarized in **Figure 3A** (91).

In humans, T/NK cell adhesion molecule CD2 interacts with diverse ligands, such as CD58, CD48, CD59, and even the novel carbohydrate structure (92). However, there is no additional ligand for the adhesion pair of CD2-CD48 in murine (93). The interaction affinity of mouse CD2-CD48 is lower than that of human CD2-CD58. Murine CD48 is also involved in the modulation of T cell activation, and CD48 binds to the T11 (1) region of CD2, the identical area of CD2 interacts with CD58

(94). Application of anti-CD48 mAb can effectively restrain not only weak, hapten-specific responses, but also strong, alloantigen-specific responses of cytotoxic T lymphocytes (CTLs) *in vivo* (95). Besides, anti-CD48 mAb interferes with $CD4^+$-dependent pathways *in vivo*, and the maximal effect of it concentrates on the immune efferent stage (95). Of note, combined administration of CD48 with CD2 mAbs cannot heighten the immunosuppressive effect generated by CD2 mAb alone, indicating that regulation of the CD2 receptor, rather than a disturbance of the CD2-CD48 interaction, is the primary effect of CD2-mediated immunosuppression in the murine (96).

IMMUNOLOGICAL SYNAPSE

After successful recognition of APCs by T cells, a specialized nanoscale structure is formed in the contact area through cytoskeletal remodeling and receptor rearrangement, known as the IS (97). Specifically, the IS consists of three layers of supramolecular activation complexes (SMAC), classified into central, peripheral, and distal SMAC (c, p and dSMAC, respectively) (98). The CD2-CD58 interactions are important components of the IS and contribute to the maintenance of high intracellular calcium levels (99). In addition to localizing to cSMAC together with other molecules, including CD28/CD80/86 and TCR-peptide-MHC complexes, the clusters of CD2-CD58 complexes also shape a ring-like framework between pSMAC and dSMAC at the outer edge of the mature IS, termed "corolla" (**Figure 1C**) (100). The corolla amplifies the activity of p-SFK/LAT/PLC-γ superior to TCR alone. The CD2-CD58 interactions in corollas are more signal-enhancing than central CD2-CD58 interactions. The corolla boosts CD2-dependent amplification of TCR signaling but can be buffered by PD-1 invaded the corolla (101). Chimeric antigen receptor (CAR) T-cell transfer is a novel and promising approach of adoptive T-cell immunotherapy in tumors. When in contact with the target cancer cell, CAR-T cell form an important IS with cancer cell, in turn dynamically coordinating multifarious forces to execute its cytotoxic function (102). Strategies to assist CAR-T-mediated IS with tumor cells by strengthening CD2-CD58 interaction may be beneficial for cancer immunotherapy.

CD2-CD58 IN T CELLS

T cell activation results in increased CD2 surface expression, affinity, and lateral mobility, allowing the CD2 molecules to diffuse from the lateral area into the contact interface and engage CD58 (103, 104). Afterwards, this process causes the CD2 that binds CD58 to be recognized and immobilized at the region of intercellular contact *via* CD2 conformational change, thus elevating the number of CD2-CD58 ligations and strengthening adhesion (103). This pattern combines passive diffusion with active recognition of conformational alteration to potentiate intercellular adhesion by CD2-CD58 interactions (**Figure 3B**).

In the absence of costimulatory signaling, stimulation of T cells by TCR/CD3 alone results in T cell anergy (105), thus the activation of T lymphocytes requires at least two signals. The first signal provided by ligation of the TCR with a specific MHC, and the second signal involves the ligand-receptor pair interactions of

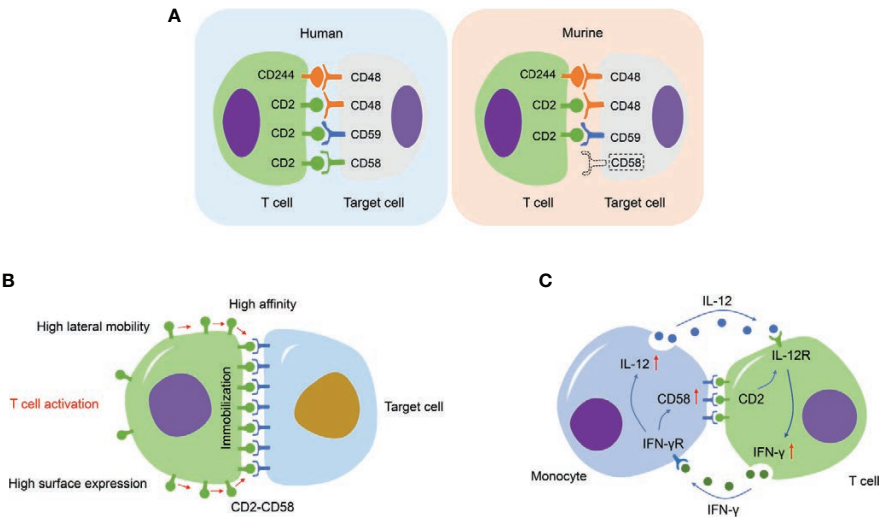

FIGURE 3 | Schematic diagram regarding CD2/CD58/CD48/CD59 system, CD2-CD58 immobilization in T cell activation, and IL-12/IFN-γ feedback loop. **(A)** Specific differences of reciprocal adhesion molecule between human and murine in the CD2/CD58/CD48/CD59 system. CD2 and CD244 (2B4) are presented at the surface of T/NK cells in human and murine. Specifically, CD2-CD58 is the principal ligand-receptor pair. CD48 and CD59 are two additional and low-affinity ligands of CD2 in human. The CD48 receptor binds both CD2 and CD244, while the CD58 gene is absent in murine. **(B)** The immobilization of CD2-CD58 following T cell activation. This process consists of three important features, increased CD2 surface expression, the high affinity of CD2-CD58, and rapidly lateral mobility; a series of conformational changes is beneficial to strengthen intercellular adhesion and aid recognition. **(C)** The important role of CD2-CD58 interaction in the IL-12/IFN-γ positive feedback loop between monocytes and activated T cells.

costimulatory adhesion (106–108). CD2 is one of the most important adhesive receptors presented on almost all of T lymphocytes and it offers costimulatory signal after interacting with CD58 on target cells (12, 109). The purified CD58 possesses a clearly mitogenic effect for human resting T lymphocytes (110). The anti-CD2 and anti-CD58 mAbs induce T cell unresponsiveness to mitogenic or antigenic stimuli and inhibit CTL-mediated killing by binding to the T cells and target cells, respectively (111). These results reveal the critical role of the CD2-CD58 interaction in T cell stimulation.

Although the CD2 engagement by CD58 alone is not sufficient for T cell activation (111–113), the CD2-CD58 interaction without other stimuli can still trigger intracellular biochemical alterations, that is, modulation of T cell function by inducing remarkable, transient upregulation of intracellular cAMP concentration (114). In the absence of TCR stimulation, CD58-bound CD2 induces signaling into microdomains *via* the actin-dependent aggregation of signaling molecules, such as LAT, Lck, and TCR-ζ chain (115). When stimulated together, TCR and CD2 were separated to different regions after transient colocalization in small microdomains; this spatial segregation is likely to allow the two receptors to synergistically strengthen signal transduction (115). Both receptors with different structures induce a fast spatial reconstruction of molecules in the cell membrane, indicating a pattern that local accumulation of signaling molecules initiates T cell signaling (115). Moreover, CD2-CD58 interaction renders the generation of a close adhesion zone between T cell and APC, in which the binding of TCR to peptide-MHC complexes is potentiated (116). TCR drives PLCγ1 phosphorylation and increases the enzymatic activity of PLCγ1, resulting in phosphoinositide cleavage and continuous $Ca2^+$ mobilization, which is necessary for T cell proliferation and cytokine production (117, 118). The CD2-CD58 interaction is able to maintain and reinforce antigen-mediated $Ca2^+$ influx in T lymphocytes interacting with APCs. CD2 and TCR is synergistic, and their signals converge to activate the PLCγ1/$Ca2^+$ pathway at the IS (99).

The costimulatory signaling of CD58 activates CTLs to proliferation, cytotoxicity, and cytokine secretion, including IFN-γ, TNF, and IL-2 (119). IL-2 is the main T cell growth factor transcribed in resting T lymphocytes (120). As an important secondary signal of T cell activation in response to CD58-positive antigen-bearing stimulator cells, CD2-CD58 signaling induces IL-2 secretion through influencing nuclear factor (NF)-mediated the transcription of the IL-2 promoter-enhancer (121, 122), which maintains autocrine T cell growth and the generation of IFN and TNF (123). Furthermore, in the presence of CD58-like signals, such as human rCD58, T cell responsiveness to both IL-6 and IL-1 is promoted by CD2-CD58 interaction, suggesting it exerts a significant function in T cell/monocyte interactions during the initial immune responses *via* increasing T cell sensitivity to monocyte-secreted cytokines (124). Costimulation of T lymphocytes by CD58 effectively facilitates IFN-γ and IL-10 secretion in a calcineurin-dependent manner, and both IFN-α and IL-12 can further increase CD58-mediated IL-10 secretion (125). In contrast, TNF-α, IL-2, IL-4, IL-5, IL-13 production is low or even absent following CD58 costimulation, which was not an inhibitory effect of endogenously produced IL-10 (125). Furthermore, T regulatory cells (Tregs) are relatively poor in terms of mediation of Th1/Th2 immune responses, secretion of IL-10, and proliferation responses *in vivo* (126). CD2-CD58 interaction can induce the of non-proliferative Tregs with the production of large quantities of IL-10. This effect is unique to CD2 signaling since it is not acquired or even suppressed *via* mobilizing other costimulatory (127).

Of note, the CD2-CD58 interaction can particularly improve the T lymphocyte response to IL-12, which possesses a series of immunoregulatory effects on activated T/NK cells, like proliferation stimulation, IFN-γ secretion, and cytotoxicity (128). IL-12 responsiveness to APC-depleted T lymphocytes is restored by the Chinese hamster ovary (CHO) cells expressing CD58 (129). More importantly, the CD2-CD58 interaction offers the central functional connection in the IL-12/IFN-γ positive feedback loop between monocytes and activated T cells (**Figure 3C**) (130). During antigen presentation, a sufficient number of CD58 molecules on monocytes bind to the amino-terminal domain of CD2 on T cells. Relating intracellular signals by CD2 subsequently generates and initiates optimal T cell responsiveness to IL-12 (131). Monocyte-secreted IL-12 induces Th1 differentiation and significantly increases cytokine secretion, including IL-2 and IFN-γ (129). In turn, T cell-derived IFN-γ motivates monocytes to produce IL-12 and boosts the expression of CD58 in monocytes, thus further strengthening CD2-mediated signaling and maintaining T cell responsiveness to IL-12 (131). Moreover, IFN-γ provokes monocyte to kill the intracellular pathogen, whereas IL-12 and IL-2 facilitate non-MHC-restricted NK cell killing. Therefore, the CD2-CD58 interaction may be regarded as an important part of innate and acquired immune responses.

One of the most important factors causing activation-induced cell death (AICD) of T cells, an essential sustainer for lymphoid homeostasis, is triggered by the ligation of Fas (Fas-L) (132). Fas-induced AICD of activated T cells is effectively protected by dendritic cells (DC) in a CD58-dependent fashion (133). More importantly, CD2-CD58 interaction potently refrains the apoptosis of T cells through blocking the CD3-mediated Fas/Fas-L upregulation (134). CD58 costimulation increases the number of effective nuclear NF-ATp and maximizes the induction of NF-AT complexes, implying CD2-CD58 signaling is implicated in the regulation of NF-AT translocation from cytosol to nucleus (122). In addition, costimulation of CD2-CD58 on primary T cells results in STAT1 phosphorylation and nuclear translocation (135). Notably, cytokine-driven STAT phosphorylation is usually transient, whereas STAT1 phosphorylation upon CD2-CD58 stimulation can sustain several days. Transcription of pivotal target genes, including c-fos and IRF1, undergoes prolonged and delayed effects after CD2 stimulation, hinting that the special model of STAT activation may incur a unique cellular response following CD2 stimulation by CD58. Interestingly, this signaling seems to be exclusive to T cells, CD2 stimulation on NK cells cannot evoke STAT1 phosphorylation (135).

A small fraction of human $CD3^+$ T cells are known to co-express CD56 (136), an antigen generally restricted to NK cell expression. It has been demonstrated that $CD3^+$ $CD56^+$ T cells have strong MHC-unrestricted cytotoxicity against neoplastic cells *in vitro* and *in vivo* (137). The CD2-CD58 interaction precisely provides the strong activation signals for expansion and differentiation of $CD3^+$ $CD56^+$ T cells (138). In adults, a considerable proportion of $CD8^+$ T lymphocytes lack the expression of CD28, which is one of the characteristics of T cell senescence, meaning a low proliferative capacity and functional impairment (139). The majority of costimulators have a low ability to activate CD28-deficient T cells, while the CD2-CD58 interaction strongly induces the proliferation and cytokine production, as well as enlarges TCR signals in $CD28^-$ $CD8^+$ T cells (140). Blocking CD58 significantly dampens the response of $CD28^-$ $CD8^+$ T cells to allogeneic DCs and viral antigens (140). These results reveal that CD2-CD58 signal is an important costimulatory pathway to facilitate the control of chronic infection by maintaining the persistent expansion of $CD28^-$ $CD8^+$ T cells.

Apart from T/NK-mediated cellular immunity, it is worth noting that CD2-CD58 interaction also participates in the immunoregulation of humoral immunity. Recently, the CD2 and CD58 homologs in the model species zebrafish have been identified, which have the same conserved structural characteristics as mammals (141). After antigen stimulation, CD2 and CD58 on $CD4^+$ T cells and APCs are increased, respectively. Loss function of CD2 and CD58 strikingly restrains the activation of $mIgM^+$ B cells and antigen-specific $CD4^+$ T cells, and subsequently suppresses the production of antibody and host defense against pathogens. The CD2-CD58 interaction offers a major costimulatory signal for the sufficient activation of $CD4^+$ Th-mediated adaptive humoral immunity in zebrafish (141). Given the absence of CD58 in rodents, zebrafish is anticipated to serve as an animal model for immunological research to make up for the shortcomings of mouse models.

CD58 IN THYMOCYTE DEVELOPMENT

During the differentiation and development of thymocytes, CD2 is one of the earliest molecules expressed; its surface density gradually reduces as thymic maturation (7). The CD2-CD58 interactions influence the affinity between TCR and peptide-MHC at the stage of positive and negative selection, which confers the ability of immature thymocytes to resist the high affinity of TCR-pMHCs to escape negative selection (100). Thymocyte proliferation needs the induction of CD58-positive L cells and phytohemagglutinin (PHA), which could be repressed by CD2 or CD58 mAb (142). Receptors for CD2 antigens situated on reticular epithelial cells, which can initiate the induction of proliferative wave of immature cortical thymocytes through interacting with the CD58 molecule (143). The anti-CD2 and anti-CD58 mAbs impede the binding of thymocyte with thymic epithelial cells, and thus suppress thymocyte activation in thymic epithelial cell-dependent manner, meaning that the natural ligand CD58 presented on human thymic epithelial cells contributes to the T cell mature and activation *via* the CD2 molecule (62, 144). Collectively, these results outline a crucial role for the CD2-CD58 pathway in T cell maturation and thymic differentiation.

CD58 IN NK CELLS

At a study of the mechanism that NK-mediated cytotoxicity to breast cancer targets, unexpectedly, anti-CD58 mAb failed to inhibit NK-mediated killing but instead mediated the enhanced cytotoxicity associated with CD58 expression, albeit CD2 blockade mildly reduced cytotoxicity (145). These results indicate NK-mediated cell lysis of breast cancer is potentiated through antibody-dependent cellular cytotoxicity (ADCC) against CD58. More importantly, CD2-CD58 interaction exerts an important function in cytotoxic function and membrane nanotube formation between NK cells and target cells (146), which is a wafery membranous protrusion physically linked two cells and able to perform substantial functions including assisting in cell-to-cell communication (147). It reveals a special role for CD2-CD58 in allowing NK cells to explore the local microenvironment through facilitating nanotube formation.

Notably, CD58 is also expressed in NK cells. Freshly isolated NK cells from human peripheral blood are consistently CD58-positive and activated NK cells with IL-2 *in vitro* results in an approximately 5-fold increase in surface expression of CD58 (148, 149). Therefore, CD58 appears to exert dual or even multiple functions. However, the exact function of CD58 on NK cells to date is still unclear. Future research should focus on this issue and investigate the functional differences of CD58 in immune cells and target cells, which is critical for therapeutic applications.

CD58 IN OTHER IMMUNE CELLS

The surface of memory T cells express high levels of CD58, which has an important role in improving their responsiveness, and the $CD58^+$ subgroup generates more IFN-γ than the $CD58^-$ subgroup following PHA stimulation (150). In terms of DCs, the significant role of the CD2-CD58 interaction in DCs is to enable immune and non-immune cells to directly interact with DCs, triggering innate and adaptive immune responses (151). Besides, CD2-CD58 interaction has been reported to participate in B cell differentiation by interacting with T cells and monocytes to some extent, but not in its proliferation (152). The binding of CD2 with CD58 located on the surface of autologous erythrocytes increases B cell responses to mitogens and antigens (153). Antibodies against CD58 can induce IgE secretion in IL-4-activated B cells (154). Thus, CD2-CD58 stimulation provides alternative signaling to modulate IgE production through intercellular contact interaction.

CD58 IN ENDOTHELIAL CELLS

CD58 molecule plays a critical role in the interactions between T cells and ECs. Early costimulation by EC facilitates lipid raft clustering in a CD2-CD58 dependent manner, resulting in the enhancement of TCR-triggered pathways (155). Human ECs increase the expression level of CD40 ligand, a vital receptor mediating T cell activation, in activated $CD4^+$ T cells *via* CD58-induced mRNA stabilization (156, 157). Furthermore, CD58 can fuel T cell adhesion to EC, facilitating the recruitment of circulating T lymphocytes into the inflammation site *in vivo* (158). The blockade of CD58 dampens T cell-mediated cytotoxicity to allogeneic EC and impairs IL-2 transcription and cytokine synthesis of EC (159–161). Activated T cells can enhance the permeability of ECs by the CD2-CD58 interaction (162).

CD58 IN INTESTINAL EPITHELIAL CELLS

It has been found that CD58 is expressed constitutively in the native IEC and IEC lines. Anti-CD58 mAb suppresses IEC-mediated proliferation of $CD4^+$ T cells (163). Specifically, CD58 molecules are highly polarized and confined to the basolateral surface of the IECs in a topological fashion at the contact area of T cells, and act as a costimulator in HLA class II-mediated antigen presentation (163). Moreover, intestinal $CD3^+$ $TCR\alpha\beta^+$ $CD8^+$ intraepithelial lymphocytes (IEL) are strongly linked to IECs and CD2-CD58 interaction participates in their crosstalking. Concretely, IELs are stimulated *via* interacting with IECs by the CD2-CD58 pathway and this process promotes the synergistic synthesis of IL-8, leading to the TNF-α release, which in turn increases IL-8 production and CD58 expression by the IECs (164).

CD58 POLYMORPHISMS

It has reported that CD58 single-nucleotide polymorphisms (SNP), including 6 variations, rs12044852A/C (SNP1), rs2300747A/G (SNP2), rs1335532C/T (SNP3), rs1016140G/T (SNP4), rs1414275C/T (SNP5) and rs11588376C/T (SNP6), related to the risk of neuromyelitis optica (NMO) (165). For instance, rs1016140 G allele can enhance T cell activity and impede the penetration of AQP4 antibody into the central nervous system (CNS), eventually causing NMO progression. The rs2300747 A allele augments NMO risk by reducing the RNA expression of CD58. Furthermore, the percentage of CD58-positive monocytes is markedly lower in healthy controls with each of these risk genotypes of autoimmune thyroid diseases (AITDs), and lower in patients with Graves' disease and Hashimoto's disease, compared to healthy individuals (166). Therefore, CD58 SNPs may participate in AITD susceptibility by decreasing CD58 expression. In a large cohort of candidemia, Kumar et al. analyzed more than 110,000 SNPs at 186 loci known to date to be related to immune-mediated diseases and showed a strong correlation between CD58 SNPs and candidemia (167). Altered level of CD58 not only modulates macrophage phagocytosis, but also indirectly affects cytokine production. For example, the SNP rs17035850 of CD58 is relevant in persistent fungemia, a positive blood culture lasted for 45 days albeit sufficient treatment, whereas the SNP rs12025416 of CD58 is linked to lower levels of Candida stimulated TNF-α and IL-6 (167).

MULTIPLE SCLEROSIS

MS is a genetically complicated autoimmune disease in the CNS. Many published studies have illustrated that CD58 SNPs such as rs12044852 and rs2300747 are tightly related to MS risk in different populations, including European Caucasian, Iranian, Russians (168–172). A recent study found that carriers of the MS risk allele rs1414273 exhibited decreased CD58 mRNA levels but elevated miR-548ac levels through analyzing diverse datasets from global populations (173). In particular, SNP rs1414273 is localized at the miR-548ac stem-loop site of CD58 first intron, which can regulate the cleavage activity of Drosha, thus propelling expression uncoupling between CD58 and miR-548ac from a common original transcript in immune cells (173). Additional evidence for the role of CD58 in MS susceptibility reveals that CD58 expression is reduced in the cerebrospinal fluid of patients with MS (174). Genome-wide association scans demonstrated that CD58 allelic variants were linked to the risk of developing MS *via* analyzing more than five thousand MS patients (170). The CD58 protective allele (rs2300747) of MS exerts its function on disease risk through elevating CD58 mRNA expression in a dose-dependent fashion in circulating mononuclear cells and lymphoblastic cells from MS patients during clinical remission (170). Mechanistically, protective allele-induced CD58 accumulation increases the expression of the transcription factor FoxP3 *via* CD2-CD58 interaction, potentiating the function of $CD4^+$ $CD25^{high}$ Tregs that are defective in MS (170). Moreover, the protective allele of rs1335532 is associated with MS and is located in the active enhancer region of the CD58 gene, generating a strong functional binding site of Ascl2, which induces activation of the CD58 promoter *via* the Wnt pathway in monocytes and lymphoblasts (175). Notably, the Alu insertion facilitates skipping of CD58 exon 3 and drives a frameshifted transcript, suggesting that Alu polymorphism is perhaps a causative factor for elevated MS risk (176).

CHRONIC HEPATITIS

The expression of CD58 in hepatocytes of chronic hepatitis exhibits cytoplasmic and membranous staining and elevated with the severity of chronic HBV infection, the degree of inflammatory activity, and liver damage (177–179). More importantly, the proportion of $CD58^+$ cells in peripheral blood mononuclear cells and the levels of sCD58 in serum of patients with HBV infection are conspicuously higher than that in the healthy individuals and positively associated with serum levels of AST and ALT (178, 179). These findings demonstrate that CD2-CD58

interactions between lymphocytes and hepatocytes exert an essential function in chronic hepatitis (177). Immune adhesion molecule CD58 may strengthen viral elimination *via* activating T/NK cells and stimulating the cytotoxic immune response. Unfortunately, this also causes the damage of hepatocytes (179).

RHEUMATOID ARTHRITIS

The level of CD58 in chondrocytes is higher in arthritic joints than in normal joints; CD58 expression is higher on synovial fluid lymphocytes of RA in comparison with peripheral blood lymphocytes from RA patients or healthy individuals (180). The expression of sCD58 in synovial fluids and serum from patients with RA are remarkably diminished in contrast with that in control subjects and patients with spondyloarthropathy (SpA) or osteoarthritis (OA) (180). Under physiological conditions, the CD2-CD58 interaction could be inhibited by local sCD58 production. Therefore, the insufficient release of sCD58 may lead to accumulation of T cells and continued inflammation in synovitis due to sCD58-mediated deadhesion (181).

CYTOMEGALOVIRUS INFECTION

CMV is the main pathogen in AIDS patients and transplant recipients, and the presence of this virus can exacerbate allograft rejection. The surface expression of CD58 augmented after CMV infection *in vitro*, caused by direct action of virus infection rather than by a secondary induction of cytokine (182). The CD2 interaction with increased CD58 on the surface of CMV-infected cells is a crucial node for antibody-induced activation and NK-mediated cytotoxicity during the antiviral response (183). Blockade of CD2-CD58 interaction causes a reduction in the secretion of TNF-α and IFN-γ by adaptive NK cells following CMV infection. As a virus-encoded downregulation factor of CD58, the CMV glycoprotein UL148 can retain CD58 within the endoplasmic reticulum without being transported to the cell surface, which weakens activation of CTLs and attenuates cell-mediated antiviral response (184). Therefore, CD2-CD58 interaction is critical for the recognition and activation between T/NK cells and CMV-infected cells.

INFLAMMATORY BOWEL DISEASE

Serum levels of sCD58 are profoundly reduced in IBD, including Crohn's disease and ulcerative colitis, relative to healthy controls. Decrease of sCD58 in sera associated with multiple clinical parameters of disease activity, including CDAI score and erythrocyte sedimentation rate (ESR) (185).

TRANSPLANTATION

Co-expression of CD58 on the stimulator cells elicits significant potentiation of the primary alloresponse and proliferative response of $CD4^+$ T cells (186). In the rat model of heart transplantation, treatment with CD2-targeting mAbs conspicuously prolong rat survival (187). Although anti-CD48 mAb alone fails to prolong graft survival, anti-CD48 mAb can synergize with anti-CD2 mAb to induce long-term survival of allograft (187, 188). Another xenograft mouse experiment shows that blocking the CD2-CD58 axis effectively prevents human skin allografts from lymphocyte infiltration and inflammation damage (189). Therefore, the CD58 molecule plays a role in lymphocyte-mediated immune rejection, and blockage of CD2-CD58 interaction contributes to alleviating allograft and xenograft responses.

HEMATOLOGICAL MALIGNANCIES

Acute Lymphoid Leukemia

In ALL, CD58 expression is negatively related to the percent of peripheral blast cells, leukocytosis, and the presence of a clinical tumoral syndrome (190). Leukemia patients with poor prognosis frequently lack the expression of CD58, while the higher expression of CD58 is strongly associated with longer survival time (191). In addition, $CD38^+$ CD58- is an independent poor prognostic factor in pediatric patients with Ph^- B-cell ALL, who have shorter survival and higher risk of relapse (192). As nonmalignant B cells differentiate from early to mature stages in the bone marrow, the expression of CD58 gradually reduces, while it is usually upregulated in pediatric and adult B-cell ALL (193). The expression of CD58 is remarkably higher in ALL blasts than that in normal B cells, whereas there is no significant difference between regenerated and normal B cells (194). More importantly, CD58 has high accuracy and stability in minimum residual disease (MRD) detection at different clinical stages, thus CD58 could be used as an effective indicator for monitoring MRD in B-cell progenitor ALL (BCP-ALL) (194, 195). Furthermore, due to the presence of hematogones, it may be difficult to distinguish leukemic lymphoblasts in the diagnosis and follow-up of BCP-ALL. The use of the CD81/CD58 ratio as the discriminating marker enhances the difference between leukemia lymphoblasts and hematogones with high sensitivity and specificity in patients with BCP-ALL (196).

Acute/chronic Myelocytic Leukemia

In AML, CD58 expression is positively correlated with complete remission rate, overall survival, and disease-free survival (191). Progenitor cells from untreated CML patients exhibit diminished CD58 expression, but surface CD58 expression could be at normal levels or even exceed normal levels after IFN-α treatment (197). CML progenitor cells lacking CD58 cannot activate normal proliferation responses of T lymphocytes, resulting in abnormal adhesion of CML progenitor cells and abnormal clonal proliferation (197). Transformed cells are generally killed by lymphokine-activated killing (LAK) cells. Anti-CD58 mAb can significantly block the LAK cell lysis, indicating the loss of CD58 in CML may be an important cause of LAK resistance (198).

LYMPHOID MALIGNANCIES

Burkitt's Lymphoma

The absence of CD58 expression is a common feature of BL, which helps tumor cells escape immunological surveillance (199). The BL cells form conjugates with EBV-specific CTLs *via* the LFA-1/CD45 pathway, but these conjugates fail to evoke target cell lysis in the absence of the CD2-CD58 interaction, suggesting the crucial effect of CD58 in activating EBV-specific CTLs (200). To some extent, the loss of CD58 in EBV-positive BL is the basis for neoplastic cells to evade virus-specific T cell control.

Hodgkin's Lymphoma

The formation of T cell rosettes in HL relied on the IS, and activation of rosetting T lymphocytes is dependent on the CD2-CD58 interaction (201). Although CD58 mutations in primary Reed/Sternberg (HRS) cells are rare, inactivating mutations in CD58 are common in HL cell lines and relapsed HL patients (202, 203). At the advanced stage of HL, CD58 inactivation of HRS cells located in pleural effusions is extremely prevalent, which provides favorable conditions for the immune escape of tumor cells (202).

Diffuse Large B Cell Lymphoma

Recently, several studies have reported that CD58 plays a key role in the pathophysiology of DLBCL. Genomic inactivation or mutation of CD58 causes loss of surface expression that is an independent adverse prognostic factor in DLBCL (204). An attenuation in T/NK-mediated cell lysis in DLBCL can be restored by re-expression of wild-type CD58 (205), indicating the absence of CD58 is beneficial to disturb recognition between DLBCL cells and T/NK cells in a CD2/CD58-dependent manner to evade immunosurveillance. Besides, EZH2 inhibitor can restore CD58 expression on the surface of lymphoma cells, which in turn increases IFN-γ secretion of T/NK cells against lymphoma cells. Mechanistically, there is a highly trimethylated H3K27 in the promoter region of CD58, which induces CD58 gene silencing and mediates immune escape of lymphoma cells, whereas EZH2 inhibitor can effectively rescue epigenetic repression of CD58 expression through boosting its demethylation and activating CD58 gene transcription (206). In addition to DLBCL, the CD58 gene is also one of the recurrent targets of genetic abnormalities in other lymphoid malignancies, such as acute adult T cell lymphoma and peripheral T cell lymphoma (207, 208). Taken together, these studies support the notion that the CD58 molecule plays a vital role in tumor cell biology and highlight that regulation of the adhesion molecule CD58 on the surface of tumor cells may be a promising immunotherapeutic strategy.

Solid Tumors

An increasing number of studies have revealed that the CD58 molecule plays the crucial roles in immune evasion of solid tumor cells. In neuroblastoma, CD58 is critical for the susceptibility of it to the cytotoxic effects of LAK and NK cells. Blocking CD58 on neuroblastoma cells could attenuate NK and LAK cytotoxicity (209). In colorectal cancer (CRC), Lorenz et al. (210) constructed a recombinant virus bearing CD58 (rv-CD58) to evaluate the role of CD58 on neoplastic cell immunogenicity. CRC cells infected by rv-CD58 were potently positive for CD58 and effectively potentiated intercellular adhesion, stimulated the T cell proliferation, and augmented CTL cytotoxicity. In the immunocompetent C57BL/6 mice model, rv-CD58-infected murine CRC cells significantly refrained tumor growth and induced antitumor immunity (210).

In addition to mediating T immune response in solid tumors, several recent reports have demonstrated that CD58 molecule can serve as stem cell marker or an oncogene in tumor initiation and progression. Xu et al. (211) found that CD58 was highly expressed in CRC, CD58-positive tumor cells were frequently present in primary specimens and CRC cell lines, and demonstrated increased tumorigenicity *in vitro* and *in vivo*. More importantly, elevated CD58 facilitated the self-renewal of CRC-initiating cells through activating the Wnt/β-catenin pathway by degradation of Dickkopf 3. Besides, CD58 silence notably dampened sphere formation and tumor growth (211). In gastric cancer (GC), high levels of CD58 are associated with cell dedifferentiation, invasion of tumor cells into lymph and blood vessels, decreased survival time, and cancer recurrence (212). Primary tumors and metastatic lymph nodes showed extensive expression of CD58. Furthermore, distant metastases, such as peritoneum and liver, have consistently high proportions of $CD58^+$ GC cells (212), indicating CD58 provides a selective advantage for GC cells to establish novel distant metastatic sites. Notably, upregulation of CD58 expression in tumors appears to contradict its role as a T cell costimulatory molecule, as high expression of CD58 on the surface of tumor cells may be more readily recognized and killed by T cells. Therefore, the function of CD58 in tumor cells is not simple and isolated, but complex and diverse, and needs to be further investigated in depth.

Although immune checkpoint blockade (ICB) therapy has exhibited unprecedented clinical efficacy in tumor treatment (213, 214), ICB still lacks efficacy in the majority of cancer patients (215). A recent study reported that the surface expression of CD58 was strongly reduced in tumor cells of melanoma patients with ICB resistance compared with that of untreated patients (216). CD58 loss induced immune evasion in different co-culture models with CTLs, and the PD-L1 expression was elevated in CD58-knockout melanoma cells (216). These data illustrated that the loss of CD58 facilitated immune evasion possibly *via* different mechanisms, including deficiency of T cell costimulation, reduction of T cell adhesion, and even synergy of the corepressor PD-L1. Thus, elevating CD58 expression is likely to contribute to the alleviation of ICB resistance in melanoma patients. In particular, the expression of CD58 was independent of the IFN-γ pathway, and the loss of CD58 led to immune escape without affecting MHC expression (216), indicating that it differs from the known mechanisms of ICB resistance.

CONCLUSION

Herein, we have comprehensively summarized CD58 isoforms, sCD58, CD2-CD58 interaction, their structure and function, IS formation, CD58 polymorphisms, meanwhile discussed the crucial roles of CD58 as a costimulatory molecule for T/NK cell-mediated immune response in tumor-related and immune-

related diseases. Regarding the roles of CD58 in tumor immunology, a looming but promising picture begins to come into sight from current studies (**Table 1**). On the one hand, loss of surface-related CD58 expression attenuates the susceptibility of tumor cells to CTL-mediated cytolysis; on the other hand, the local accumulation of sCD58 in the tumor microenvironment is likely to interfere with the adhesion and recognition of T/NK cells by serving as a natural immunosuppressor (**Figure 4**). The sCD58-mediated interference is not only for the recognition of the tumor cells themselves, but also includes T cell interaction with APCs. Only CD3/TCR-related signals alone without CD2-CD58 costimulatory signal may result in T cell anergy. Of note, the inhibitory effect incurred by sCD58 in the microenvironment is not only due to physical blockage of cell-cell interactions, but may also involve negative signaling inside T/NK cells through sCD58-CD2 interactions. These CD58-mediated possible mechanisms facilitate immune evasion and metastasis of tumor cells, although further in-depth studies are needed. The ideal clinical application model of CD58 in cancer immunology is to stimulate the surface expression of CD58 on cancer cells and to

TABLE 1 | Expression, function and clinical significance of CD58 in various malignancies.

Malignancy types	Expression	Functions	Mechanisms	Clinical characteristics	Prognosis	References
Acute lymphoid leukemia	Downregulated	NA	NA	The percent of peripheral blast cells, leucocytosis, and the presence of a clinical tumoral syndrome	Overall survival	(190, 191)
B-cell progenitor ALL	Upregulated	NA	NA	Identification marker; the detection of minimum residual disease	NA	(194–196)
Acute myelocytic leukemia	Downregulated	Evading immunosurveillance	NA	Complete remission rate	Overall survival and disease-free survival	(191)
Chronic myelocytic leukemia	Downregulated	Abnormal adhesion of CML progenitor cells and abnormal clonal proliferation of T cells	NA	NA	NA	(197)
Burkitt's Lymphoma	Downregulated	Evading immunosurveillance	NA	NA	NA	(200)
Hodgkin's lymphoma	Downregulated	Immune evasion	NA	At the advanced stage of HL, CD58 inactivation of HRS cells located in pleural effusions is extremely prevalent	Relapse of HL	(202, 203)
Diffuse large B cell lymphoma	Downregulated	Evading immunosurveillance	Inhibiting IFN-γ secretion of T/NK cells against lymphoma cells	NA	An independent adverse prognostic factor	(204–206)
Neuroblastoma	NA	Susceptibility of it to the cytotoxic effects of LAK and NK cells	NA	NA	NA	(209)
Hepatocellular carcinoma	Upregulated in anisomycin-treated HCC cells	Promotion of immune synapse formation to boost NK-mediated immunotherapeutic effects	NA	NA	NA	(76)
Gastric cancer	NA	NA	NA	Cell dedifferentiation, invasion of lymph and blood vessels, distant metastases	Overall survival and disease-free survival	(212)
Colorectal cancer	NA	Potentiation of intercellular adhesion, stimulation of the T cell proliferation, and augment of CTL cytotoxicity	NA	NA	NA	(210)
	Upregulated	Enhancement of sphere formation, EMT ability and tumor growth; Promotion of self-renewal of cancer stem cell	Activating the Wnt/β-catenin pathway by degradation of Dickkopf 3	NA	NA	(211)
Melanoma	Downregulated in patients with ICB-resistance	Immune evasion	Deficiency of T cell costimulation, reduced T cell adhesion, and even synergy of the corepressor PD-L1.	Increasing CD58 expression contributes to alleviate ICB resistance	NA	(56, 216)

NA, not available. The presence of NA in the table is due to the lack of information on related studies. ALL, acute lymphoid leukemia; CML, chronic myelocytic leukemia; HL, Hodgkin's lymphoma; HCC, hepatocellular carcinoma; LAK, lymphokine-activated killing; CTL, cytotoxic T lymphocyte; EMT, epithelial-mesenchymal transition; ICB, immune checkpoint blockade.

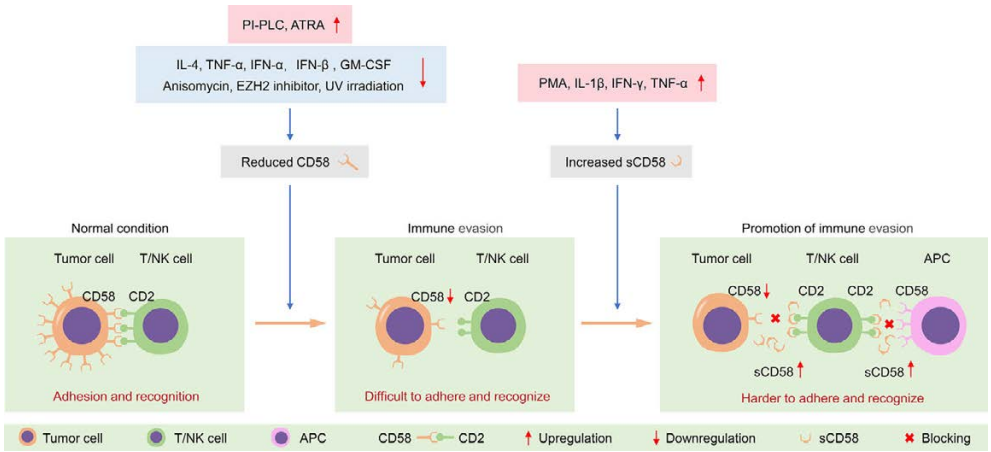

FIGURE 4 | Tumor cells evade immune surveillance by regulating the expression of CD58 on the membrane surface and sCD58 in the microenvironment. PI-PLC, phosphatidylinositol-specific phospholipase C; ATRA, all-trans retinoic acid; UV, ultraviolet; PMA, phorbol-12-myristate-13-acetate; APC, antigen-presenting cell.

inhibit the secretion of sCD58 into the tumor microenvironment, however, there still remains several pending questions (1): the molecular mechanisms of sCD58 production (2); the roles of sCD58 in varieties of cancers (3); values as a therapeutic target in autoimmune diseases and malignant tumors.

AUTHOR CONTRIBUTIONS

YZ conceived and drafted the manuscript. QFL revised the manuscript. All authors contributed to the article and approved the submitted version.

FUNDING

This work was supported by the National Natural Science Foundation of China (81872501, 81673023, 81272573, and 81502068) and the Beijing Natural Science Foundation (7172177).

ACKNOWLEDGMENTS

We thank Dr. Yunfeng Zhang and Yinuo Zhang for their encouragement and support.

REFERENCES

1. Shaw S, Luce GE, Quinones R, Gress RE, Springer TA, Sanders ME. Two Antigen-Independent Adhesion Pathways Used by Human Cytotoxic T-cell Clones. *Nature* (1986) 323(6085):262–4. doi: 10.1038/323262a0
2. Moller P, Koretz K, Schlag P, Momburg F. Frequency of Abnormal Expression of HLA-A,B,C and HLA-DR Molecules, Invariant Chain, and LFA-3 (CD58) in Colorectal Carcinoma and Its Impact on Tumor Recurrence. *Int J Cancer Suppl* (1991) 6:155–62. doi: 10.1002/ijc.2910470727
3. Krensky AM, Sanchez-Madrid F, Robbins E, Nagy JA, Springer TA, Burakoff SJ. The Functional Significance, Distribution, and Structure of LFA-1, LFA-2, and LFA-3: Cell Surface Antigens Associated With CTL-Target Interactions. *J Immunol* (1983) 131(2):611–6.
4. Krensky AM, Robbins E, Springer TA, Burakoff SJ. LFA-1, LFA-2, and LFA-3 Antigens Are Involved in CTL-Target Conjugation. *J Immunol* (1984) 132 (5):2180–2.
5. Moingeon P, Chang HC, Wallner BP, Stebbins C, Frey AZ, Reinherz EL. CD2-Mediated Adhesion Facilitates T Lymphocyte Antigen Recognition Function. *Nature* (1989) 339(6222):312–4. doi: 10.1038/339312a0
6. Koyasu S, Lawton T, Novick D, Recny MA, Siliciano RF, Wallner BP, et al. Role of Interaction of CD2 Molecules With Lymphocyte Function-Associated Antigen 3 in T-Cell Recognition of Nominal Antigen. *Proc Natl Acad Sci USA* (1990) 87(7):2603–7. doi: 10.1073/pnas.87.7.2603
7. Bierer BE, Burakoff SJ. T Cell Adhesion Molecules. *FASEB J* (1988) 2 (10):2584–90. doi: 10.1096/fasebj.2.10.2838364
8. Sanchez-Madrid F, Krensky AM, Ware CF, Robbins E, Strominger JL, Burakoff SJ, et al. Three Distinct Antigens Associated With Human T-Lymphocyte-Mediated Cytolysis: LFA-1, LFA-2, and LFA-3. *Proc Natl Acad Sci USA* (1982) 79(23):7489–93. doi: 10.1073/pnas.79.23.7489
9. Sewell WA, Palmer RW, Spurr NK, Sheer D, Brown MH, Bell Y, et al. The Human LFA-3 Gene Is Located at the Same Chromosome Band as the Gene for Its Receptor Cd2. *Immunogenetics* (1988) 28(4):278–82. doi: 10.1007/BF00345506
10. Takai Y, Reed ML, Burakoff SJ, Herrmann SH. Direct Evidence for a Receptor-Ligand Interaction Between the T-Cell Surface Antigen CD2 and Lymphocyte-Function-Associated Antigen 3. *Proc Natl Acad Sci USA* (1987) 84(19):6864–8. doi: 10.1073/pnas.84.19.6864
11. Selvaraj P, Plunkett ML, Dustin M, Sanders ME, Shaw S, Springer TA. The T Lymphocyte Glycoprotein Cd2 Binds the Cell Surface Ligand LFA-3. *Nature* (1987) 326(6111):400–3. doi: 10.1038/326400a0
12. Dustin ML, Sanders ME, Shaw S, Springer TA. Purified Lymphocyte Function-Associated Antigen 3 Binds to CD2 and Mediates T Lymphocyte Adhesion. *J Exp Med* (1987) 165(3):677–92. doi: 10.1084/jem.165.3.677
13. Bierer BE, Hahn WC. T Cell Adhesion, Avidity Regulation and Signaling: A Molecular Analysis of CD2. *Semin Immunol* (1993) 5(4):249–61. doi: 10.1006/smim.1993.1029
14. Miller GT, Hochman PS, Meier W, Tizard R, Bixler SA, Rosa MD, et al. Specific Interaction of Lymphocyte Function-Associated Antigen 3 With CD2 Can Inhibit T Cell Responses. *J Exp Med* (1993) 178(1):211–22. doi: 10.1084/jem.178.1.211
15. Itzhaky D, Raz N, Hollander N. The Glycosylphosphatidylinositol-Anchored Form and the Transmembrane Form of CD58 Associate With Protein Kinases. *J Immunol* (1998) 160(9):4361–6.

16. Schirren CA, Volpel H, Meuer SC. Adhesion Molecules on Freshly Recovered T Leukemias Promote Tumor-Directed Lympholysis. *Blood* (1992) 79(1):138–43. doi: 10.1182/blood.V79.1.138.138
17. Seed B. An LFA-3 cDNA Encodes a Phospholipid-Linked Membrane Protein Homologous to Its Receptor Cd2. *Nature* (1987) 329(6142):840–2. doi: 10.1038/329840a0
18. Springer TA. Adhesion Receptors of the Immune System. *Nature* (1990) 346 (6283):425–34. doi: 10.1038/346425a0
19. Wallner BP, Frey AZ, Tizard R, Mattaliano RJ, Hession C, Sanders ME, et al. Primary Structure of Lymphocyte Function-Associated Antigen 3 (LFA-3). The Ligand of the T Lymphocyte CD2 Glycoprotein. *J Exp Med* (1987) 166 (4):923–32. doi: 10.1084/jem.166.4.923
20. Ariel O, Kukulansky T, Raz N, Hollander N. Distinct Membrane Localization and Kinase Association of the Two Isoforms of CD58. *Cell Signal* (2004) 16(6):667–73. doi: 10.1016/j.cellsig.2003.08.015
21. Ariel O, Levi Y, Hollander N. Signal Transduction by CD58: The Transmembrane Isoform Transmits Signals Outside Lipid Rafts Independently of the GPI-Anchored Isoform. *Cell Signal* (2009) 21 (7):1100–8. doi: 10.1016/j.cellsig.2009.02.022
22. Chan PY, Lawrence MB, Dustin ML, Ferguson LM, Golan DE, Springer TA. Influence of Receptor Lateral Mobility on Adhesion Strengthening Between Membranes Containing LFA-3 and CD2. *J Cell Biol* (1991) 115(1):245–55. doi: 10.1083/jcb.115.1.245
23. Dustin ML, Selvaraj P, Mattaliano RJ, Springer TA. Anchoring Mechanisms for LFA-3 Cell Adhesion Glycoprotein at Membrane Surface. *Nature* (1987) 329(6142):846–8. doi: 10.1038/329846a0
24. Tiefenthaler G, Dustin ML, Springer TA, Hunig T. Serologic Cross-Reactivity of T11 Target Structure and Lymphocyte Function-Associated Antigen 3. Evidence for Structural Homology of the Sheep and Human Ligands of CD2. *J Immunol* (1987) 139(8):2696–701.
25. Selvaraj P, Dustin ML, Mitnacht R, Hunig T, Springer TA, Plunkett ML. Rosetting of Human T Lymphocytes With Sheep and Human Erythrocytes. Comparison of Human and Sheep Ligand Binding Using Purified E Receptor. *J Immunol* (1987) 139(8):2690–5.
26. Patarroyo M, Makgoba MW. Leucocyte Adhesion to Cells in Immune and Inflammatory Responses. *Lancet* (1989) 2(8672):1139–42. doi: 10.1016/s0140-6736(89)91498-0
27. Plunkett ML, Sanders ME, Selvaraj P, Dustin ML, Springer TA. Rosetting of Activated Human T Lymphocytes With Autologous Erythrocytes. Definition of the Receptor and Ligand Molecules as CD2 and Lymphocyte Function-Associated Antigen 3 (LFA-3). *J Exp Med* (1987) 165(3):664–76. doi: 10.1084/jem.165.3.664
28. Kearney A, Avramovic A, Castro MA, Carmo AM, Davis SJ, van der Merwe PA. The Contribution of Conformational Adjustments and Long-Range Electrostatic Forces to the CD2/CD58 Interaction. *J Biol Chem* (2007) 282 (18):13160–6. doi: 10.1074/jbc.M700829200
29. Hoffmann JC, Dengler TJ, Knolle PA, Albert-Wolf M, Roux M, Wallich R, et al. A Soluble Form of the Adhesion Receptor CD58 (LFA-3) Is Present in Human Body Fluids. *Eur J Immunol* (1993) 23(11):3003–10. doi: 10.1002/eji.1830231142
30. Dengler TJ, Hoffmann JC, Knolle P, Albert-Wolf M, Roux M, Wallich R, et al. Structural and Functional Epitopes of the Human Adhesion Receptor CD58 (LFA-3). *Eur J Immunol* (1992) 22(11):2809–17. doi: 10.1002/eji.1830221109
31. Wang JH, Smolyar A, Tan K, Liu JH, Kim M, Sun ZY, et al. Structure of a Heterophilic Adhesion Complex Between the Human CD2 and CD58 (LFA-3) Counterreceptors. *Cell* (1999) 97(6):791–803. doi: 10.1016/s0092-8674(00)80790-4
32. Arulanandam AR, Withka JM, Wyss DF, Wagner G, Kister A, Pallai P, et al. The CD58 (Lfa-3) Binding Site Is a Localized and Highly Charged Surface Area on the AGFCC'c" Face of the Human Cd2 Adhesion Domain. *Proc Natl Acad Sci USA* (1993) 90(24):11613–7. doi: 10.1073/pnas.90.24.11613
33. Ikemizu S, Sparks LM, van der Merwe PA, Harlos K, Stuart DI, Jones EY, et al. Crystal Structure of the CD2-Binding Domain of CD58 (Lymphocyte Function-Associated Antigen 3) at 1.8-A Resolution. *Proc Natl Acad Sci USA* (1999) 96(8):4289–94. doi: 10.1073/pnas.96.8.4289
34. Leherte L, Petit A, Jacquemin D, Vercauteren DP, Laurent AD. Investigating Cyclic Peptides Inhibiting Cd2-Cd58 Interactions Through Molecular Dynamics and Molecular Docking Methods. *J Comput Aided Mol Des* (2018) 32(11):1295–313. doi: 10.1007/s10822-018-0172-4
35. Wang J, Reinherz EL. Structural Basis of Cell-Cell Interactions in the Immune System. *Curr Opin Struct Biol* (2000) 10(6):656–61. doi: 10.1016/s0959-440x(00)00150-0
36. Davis SJ, Ikemizu S, Wild MK, van der Merwe PA. CD2 and the Nature of Protein Interactions Mediating Cell-Cell Recognition. *Immunol Rev* (1998) 163:217–36. doi: 10.1111/j.1600-065x.1998.tb01199.x
37. Sun ZY, Dotsch V, Kim M, Li J, Reinherz EL, Wagner G. Functional Glycan-Free Adhesion Domain of Human Cell Surface Receptor CD58: Design, Production and NMR Studies. *EMBO J* (1999) 18(11):2941–9. doi: 10.1093/emboj/18.11.2941
38. Yang JJ, Ye Y, Carroll A, Yang W, Lee HW. Structural Biology of the Cell Adhesion Protein CD2: Alternatively Folded States and Structure-Function Relation. *Curr Protein Pept Sci* (2001) 2(1):1–17. doi: 10.2174/1389203013381251
39. Dustin ML. Adhesive Bond Dynamics in Contacts Between T Lymphocytes and Glass-Supported Planar Bilayers Reconstituted With the Immunoglobulin-Related Adhesion Molecule Cd58. *J Biol Chem* (1997) 272(25):15782–8. doi: 10.1074/jbc.272.25.15782
40. Jones EY, Davis SJ, Williams AF, Harlos K, Stuart DI. Crystal Structure at 2.8 A Resolution of a Soluble Form of the Cell Adhesion Molecule Cd2. *Nature* (1992) 360(6401):232–9. doi: 10.1038/360232a0
41. He Q, Beyers AD, Barclay AN, Williams AF. A Role in Transmembrane Signaling for the Cytoplasmic Domain of the CD2 T Lymphocyte Surface Antigen. *Cell* (1988) 54(7):979–84. doi: 10.1016/0092-8674(88)90112-2
42. Hahn WC, Rosenstein Y, Calvo V, Burakoff SJ, Bierer BE. A Distinct Cytoplasmic Domain of CD2 Regulates Ligand Avidity and T-Cell Responsiveness to Antigen. *Proc Natl Acad Sci USA* (1992) 89(15):7179–83. doi: 10.1073/pnas.89.15.7179
43. Bell GM, Fargnoli J, Bolen JB, Kish L, Imboden JB. The SH3 Domain of P56lck Binds to Proline-Rich Sequences in the Cytoplasmic Domain of CD2. *J Exp Med* (1996) 183(1):169–78. doi: 10.1084/jem.183.1.169
44. Thomas D, Rathinavel AK, Radhakrishnan P. Altered Glycosylation in Cancer: A Promising Target for Biomarkers and Therapeutics. *Biochim Biophys Acta Rev Cancer* (2020) 1875(1):188464. doi: 10.1016/j.bbcan.2020.188464
45. Wang X, Ji CG, Zhang JZ. Glycosylation Modulates Human CD2-CD58 Adhesion Via Conformational Adjustment. *J Phys Chem B* (2015) 119 (22):6493–501. doi: 10.1021/jp509949b
46. Albert-Wolf M, Meuer SC, Wallich R. Dual Function of Recombinant Human CD58: Inhibition of T Cell Adhesion and Activation *Via* the CD2 Pathway. *Int Immunol* (1991) 3(12):1335–47. doi: 10.1093/intimm/3.12.1335
47. Kim M, Sun ZY, Byron O, Campbell G, Wagner G, Wang J, et al. Molecular Dissection of the CD2-CD58 Counter-Receptor Interface Identifies CD2 Tyr86 and CD58 Lys34 Residues as the Functional "Hot Spot". *J Mol Biol* (2001) 312(4):711–20. doi: 10.1006/jmbi.2001.4980
48. Gokhale A, Weldeghiorghis TK, Taneja V, Satyanarayanajois SD. Conformationally Constrained Peptides From CD2 to Modulate Protein-Protein Interactions Between CD2 and CD58. *J Med Chem* (2011) 54 (15):5307–19. doi: 10.1021/jm200004e
49. Gokhale A, Kanthala S, Latendresse J, Taneja V, Satyanarayanajois S. Immunosuppression by Co-Stimulatory Molecules: Inhibition of CD2-CD48/CD58 Interaction by Peptides From CD2 to Suppress Progression of Collagen-Induced Arthritis in Mice. *Chem Biol Drug Des* (2013) 82 (1):106–18. doi: 10.1111/cbdd.12138
50. Gokhale AS, Sable R, Walker JD, McLaughlin L, Kousoulas KG, Jois SD. Inhibition of Cell Adhesion and Immune Responses in the Mouse Model of Collagen-Induced Arthritis With a Peptidomimetic That Blocks CD2-CD58 Interface Interactions. *Biopolymers* (2015) 104(6):733–42. doi: 10.1002/bip.22692
51. Mrowietz U. Treatment Targeted to Cell Surface Epitopes. *Clin Exp Dermatol* (2002) 27(7):591–6. doi: 10.1046/j.1365-2230.2002.01171.x
52. Chamian F, Lin SL, Lee E, Kikuchi T, Gilleaudeau P, Sullivan-Whalen M, et al. Alefacept (Anti-CD2) Causes a Selective Reduction in Circulating Effector Memory T Cells (TEM) and Relative Preservation of Central Memory T Cells (Tcm) in Psoriasis. *J Transl Med* (2007) 5:27. doi: 10.1186/1479-5876-5-27
53. Rigby MR, Harris KM, Pinckney A, DiMeglio LA, Rendell MS, Felner EI, et al. Alefacept Provides Sustained Clinical and Immunological Effects in

New-Onset Type 1 Diabetes Patients. *J Clin Invest* (2015) 125(8):3285–96. doi: 10.1172/JCI81722
54. Vlieghe P, Lisowski V, Martinez J, Khrestchatisky M. Synthetic Therapeutic Peptides: Science and Market. *Drug Discovery Today* (2010) 15(1-2):40–56. doi: 10.1016/j.drudis.2009.10.009
55. Sable R, Durek T, Taneja V, Craik DJ, Pallerla S, Gauthier T, et al. Constrained Cyclic Peptides as Immunomodulatory Inhibitors of the CD2:CD58 Protein-Protein Interaction. *ACS Chem Biol* (2016) 11 (8):2366–74. doi: 10.1021/acschembio.6b00486
56. Scheibenbogen C, Keilholz U, Meuer S, Dengler T, Tilgen W, Hunstein W. Differential Expression and Release of LFA-3 and ICAM-1 in Human Melanoma Cell Lines. *Int J Cancer* (1993) 54(3):494–8. doi: 10.1002/ijc.2910540323
57. Hollander N, Selvaraj P, Springer TA. Biosynthesis and Function of LFA-3 in Human Mutant Cells Deficient in Phosphatidylinositol-Anchored Proteins. *J Immunol* (1988) 141(12):4283–90.
58. Itzhaky D, Raz N, Hollander N. The Glycosylphosphatidylinositol-Anchored Form and the Transmembrane Form of CD58 are Released From the Cell Surface Upon Antibody Binding. *Cell Immunol* (1998) 187(2):151–7. doi: 10.1006/cimm.1998.1323
59. Bazil V. Physiological Enzymatic Cleavage of Leukocyte Membrane Molecules. *Immunol Today* (1995) 16(3):135–40. doi: 10.1016/0167-5699(95)80130-8
60. Kirby AC, Cahen P, Porter SR, Olsen I. Soluble and Cell-Associated Forms of the Adhesion Molecule LFA-3 (CD58) Are Differentially Regulated by Inflammatory Cytokines. *Cell Adhes Commun* (2000) 7(6):453–64. doi: 10.3109/15419060009040303
61. Une C, Gronberg A, Axberg I, Jondal M, Orn A. Phospholipase C Treatment of Certain Human Target Cells Reduces Their Susceptibility to NK Lysis Without Affecting Binding or Sensitivity to Lytic Granules. *Cell Immunol* (1991) 133(1):127–37. doi: 10.1016/0008-8749(91)90185-e
62. Vollger LW, Tuck DT, Springer TA, Haynes BF, Singer KH. Thymocyte Binding to Human Thymic Epithelial Cells Is Inhibited by Monoclonal Antibodies to CD-2 and LFA-3 Antigens. *J Immunol* (1987) 138(2):358–63.
63. Emilie D, Wallon C, Galanaud P, Fischer A, Olive D, Delfraissy JF. Role of the LFA3-CD2 Interaction in Human Specific B Cell Differentiation. *J Immunol* (1988) 141(6):1912–8.
64. Yamashita K, Kakutani T, Ohashi T, Saibara T. A Dimeric Form of Soluble Recombinant Sheep LFA-3(CD58) Inhibits Human T-Cell Proliferation by Generating Regulatory T Cells. *Immunopharmacology* (1997) 37(2-3):209–20. doi: 10.1016/s0162-3109(97)00050-7
65. Yamashita K, Parish CR, Warren HS, Harrison LC. A Multimeric Form of Soluble Recombinant Sheep LFA-3 (CD58) Inhibits Human T-Cell Proliferation. *Immunology* (1997) 92(1):39–44. doi: 10.1046/j.1365-2567.1997.00317.x
66. Hutchins D, Steel CM. Regulation of ICAM-1 (Cd54) Expression in Human Breast Cancer Cell Lines by Interleukin 6 and Fibroblast-Derived Factors. *Int J Cancer* (1994) 58(1):80–4. doi: 10.1002/ijc.2910580114
67. Kvale D, Krajci P, Brandtzaeg P. Expression and Regulation of Adhesion Molecules ICAM-1 (CD54) and LFA-3 (CD58) in Human Intestinal Epithelial Cell Lines. *Scand J Immunol* (1992) 35(6):669–76. doi: 10.1111/j.1365-3083.1992.tb02973.x
68. Kvale D, Brandtzaeg P. Immune Modulation of Adhesion Molecules ICAM-1 (CD54) and LFA-3 (CD58) in Human Hepatocytic Cell Lines. *J Hepatol* (1993) 17(3):347–52. doi: 10.1016/s0168-8278(05)80216-8
69. Bloemen PG, van den Tweel MC, Henricks PA, Engels F, Wagenaar SS, Rutten AA, et al. Expression and Modulation of Adhesion Molecules on Human Bronchial Epithelial Cells. *Am J Respir Cell Mol Biol* (1993) 9 (6):586–93. doi: 10.1165/ajrcmb/9.6.586
70. Weber F, Meinl E, Aloisi F, Nevinny-Stickel C, Albert E, Wekerle H, et al. Human Astrocytes are Only Partially Competent Antigen Presenting Cells. Possible Implications for Lesion Development in Multiple Sclerosis. *Brain* (1994) 117(Pt 1):59–69. doi: 10.1093/brain/117.1.59
71. Shubinsky G, Schlesinger M. Kinetics of the Pleiotropic Effect of Interleukin 4 on the Surface Properties of Human B-Lymphoma Cells. *Leuk Lymphoma* (1994) 15(3-4):333–40. doi: 10.3109/10428199409049732
72. Rousset F, Billaud M, Blanchard D, Figdor C, Lenoir GM, Spits H, et al. Il-4 Induces LFA-1 and LFA-3 Expression on Burkitt's Lymphoma Cell Lines. Requirement of Additional Activation by Phorbol Myristate Acetate for Induction of Homotypic Cell Adhesions. *J Immunol* (1989) 143(5):1490–8.
73. Schirren CA, Volpel H, Hoffmann JC, Henning SW, Qiao L, Autschbach F, et al. Biological Response Modifiers Render Tumor Cells Susceptible to Autologous Effector Mechanisms by Influencing Adhesion Receptors. *Leuk Lymphoma* (1993) 10(1-2):25–33. doi: 10.3109/10428199309147353
74. Bendall LJ, Kortlepel K, Gottlieb DJ. Gm-CSF Enhances IL-2-Activated Natural Killer Cell Lysis of Clonogenic Aml Cells by Upregulating Target Cell Expression of ICAM-1. *Leukemia* (1995) 9(4):677–84.
75. Kobata T, Ikeda H, Ohnishi Y, Urushibara N, Nakata SO, Takahashi TA, et al. Ultraviolet Irradiation Inhibits Killer-Target Cell Interaction. *Vox Sang* (1993) 65(1):25–31. doi: 10.1111/j.1423-0410.1993.tb04520.x
76. Kim M, Lee SJ, Shin S, Park KS, Park SY, Lee CH. Novel Natural Killer Cell-Mediated Cancer Immunotherapeutic Activity of Anisomycin Against Hepatocellular Carcinoma Cells. *Sci Rep* (2018) 8(1):10668. doi: 10.1038/s41598-018-29048-8
77. Nakayama J, Terao H, Koga T, Furue M. Induction of CD54 and CD58 Expression in Cultured Human Endothelial Cells by Beta-Interferon With or Without Hyperthermia *In Vitro*. *J Dermatol Sci* (2001) 26(1):19–24. doi: 10.1016/s0923-1811(00)00150-x
78. Cahen P, Kirby AC, Porter SR, Olsen I. Regulation of LFA-3 (CD58) by Dexamethasone and Retinoic Acids *In Vitro*. *Inflammation Res* (2000) 49 (7):338–44. doi: 10.1007/PL00000214
79. Di Noto R, Lo Pardo C, Schiavone EM, Ferrara F, Manzo C, Vacca C, et al. All-Trans Retinoic Acid (ATRA) and the Regulation of Adhesion Molecules in Acute Myeloid Leukemia. *Leuk Lymphoma* (1996) 21(3-4):201–9. doi: 10.3109/10428199209067601
80. Huo X, Dai Y, Yang T, Zhang Y, Li M, Xu X. Decreased Erythrocyte CD44 and CD58 Expression Link E-Waste Pb Toxicity to Changes in Erythrocyte Immunity in Preschool Children. *Sci Total Environ* (2019) 664:690–7. doi: 10.1016/j.scitotenv.2019.02.040
81. van der Merwe PA, McNamee PN, Davies EA, Barclay AN, Davis SJ. Topology of the CD2-CD48 Cell-Adhesion Molecule Complex: Implications for Antigen Recognition by T Cells. *Curr Biol* (1995) 5 (1):74–84. doi: 10.1016/s0960-9822(95)00019-4
82. Menu E, Tsai BC, Bothwell AL, Sims PJ, Bierer BE. Cd59 Costimulation of T Cell Activation. CD58 Dependence and Requirement for Glycosylation. *J Immunol* (1994) 153(6):2444–56.
83. van der Merwe PA, McPherson DC, Brown MH, Barclay AN, Cyster JG, Williams AF, et al. The NH2-Terminal Domain of Rat CD2 Binds Rat CD48 With a Low Affinity and Binding Does Not Require Glycosylation of CD2. *Eur J Immunol* (1993) 23(6):1373–7. doi: 10.1002/eji.1830230628
84. Hahn WC, Menu E, Bothwell AL, Sims PJ, Bierer BE. Overlapping But Nonidentical Binding Sites on CD2 for CD58 and a Second Ligand CD59. *Science* (1992) 256(5065):1805–7. doi: 10.1126/science.1377404
85. Deckert M, Kubar J, Zoccola D, Bernard-Pomier G, Angelisova P, Horejsi V, et al. CD59 Molecule: A Second Ligand for CD2 in T Cell Adhesion. *Eur J Immunol* (1992) 22(11):2943–7. doi: 10.1002/eji.1830221128
86. Deckert M, Kubar J, Bernard A. CD58 and CD59 Molecules Exhibit Potentializing Effects in T Cell Adhesion and Activation. *J Immunol* (1992) 148(3):672–7.
87. Barbosa JA, Mentzer SJ, Kamarck ME, Hart J, Biro PA, Strominger JL, et al. Gene Mapping and Somatic Cell Hybrid Analysis of the Role of Human Lymphocyte Function-Associated Antigen-3 (LFA-3) in CTL-target Cell Interactions. *J Immunol* (1986) 136(8):3085–91.
88. Kato K, Koyanagi M, Okada H, Takanashi T, Wong YW, Williams AF, et al. CD48 Is a Counter-Receptor for Mouse CD2 and Is Involved in T Cell Activation. *J Exp Med* (1992) 176(5):1241–9. doi: 10.1084/jem.176.5.1241
89. Wong YW, Williams AF, Kingsmore SF, Seldin MF. Structure, Expression, and Genetic Linkage of the Mouse BCM1 (OX45 or Blast-1) Antigen. Evidence for Genetic Duplication Giving Rise to the BCM1 Region on Mouse Chromosome 1 and the CD2/LFA3 Region on Mouse Chromosome 3. *J Exp Med* (1990) 171(6):2115–30. doi: 10.1084/jem.171.6.2115
90. Arulanandam AR, Moingeon P, Concino MF, Recny MA, Kato K, Yagita H, et al. A Soluble Multimeric Recombinant CD2 Protein Identifies CD48 as a Low Affinity Ligand for Human Cd2: Divergence of CD2 Ligands During the Evolution of Humans and Mice. *J Exp Med* (1993) 177(5):1439–50. doi: 10.1084/jem.177.5.1439

91. Brossay A, Hube F, Moreau T, Bardos P, Watier H. Porcine CD58: Cdna Cloning and Molecular Dissection of the Porcine CD58-Human CD2 Interface. *Biochem Biophys Res Commun* (2003) 309(4):992–8. doi: 10.1016/j.bbrc.2003.08.099
92. Warren HS, Altin JG, Waldron JC, Kinnear BF, Parish CR. A Carbohydrate Structure Associated With CD15 (Lewis X) on Myeloid Cells Is a Novel Ligand for Human Cd2. *J Immunol* (1996) 156(8):2866–73.
93. Brown MH, Preston S, Barclay AN. A Sensitive Assay for Detecting Low-Affinity Interactions at the Cell Surface Reveals No Additional Ligands for the Adhesion Pair Rat CD2 and CD48. *Eur J Immunol* (1995) 25(12):3222–8. doi: 10.1002/eji.1830251204
94. Sandrin MS, Mouhtouris E, Vaughan HA, Warren HS, Parish CR. CD48 is a Low Affinity Ligand for Human CD2. *J Immunol* (1993) 151(9):4606–13.
95. Chavin KD, Qin L, Lin J, Woodward J, Baliga P, Kato K, et al. Anti-CD48 (Murine CD2 Ligand) Mabs Suppress Cell Mediated Immunity In Vivo. *Int Immunol* (1994) 6(5):701–9. doi: 10.1093/intimm/6.5.701
96. Sido B, Otto G, Zimmermann R, Muller P, Meuer SC, Dengler TJ. Modulation of the CD2 Receptor and Not Disruption of the CD2/CD48 Interaction is the Principal Action of CD2-mediated Immunosuppression in the Rat. *Cell Immunol* (1997) 182(1):57–67. doi: 10.1006/cimm.1997.1204
97. Dustin ML. The Immunological Synapse. *Cancer Immunol Res* (2014) 2 (11):1023–33. doi: 10.1158/2326-6066.CIR-14-0161
98. Freiberg BA, Kupfer H, Maslanik W, Delli J, Kappler J, Zaller DM, et al. Staging and Resetting T Cell Activation in Smacs. *Nat Immunol* (2002) 3 (10):911–7. doi: 10.1038/ni836
99. Espagnolle N, Depoil D, Zaru R, Demeur C, Champagne E, Guiraud M, et al. CD2 and TCR Synergize for the Activation of Phospholipase Cgamma1/ Calcium Pathway at the Immunological Synapse. *Int Immunol* (2007) 19 (3):239–48. doi: 10.1093/intimm/dxl141
100. Binder C, Cvetkovski F, Sellberg F, Berg S, Paternina Visbal H, Sachs DH, et al. Cd2 Immunobiology. *Front Immunol* (2020) 11:1090. doi: 10.3389/ fimmu.2020.01090
101. Demetriou P, Abu-Shah E, Valvo S, McCuaig S, Mayya V, Kvalvaag A, et al. A Dynamic CD2-Rich Compartment at the Outer Edge of the Immunological Synapse Boosts and Integrates Signals. *Nat Immunol* (2020) 21(10):1232–43. doi: 10.1038/s41590-020-0770-x
102. Li R, Ma C, Cai H, Chen W. The CAR T-Cell Mechanoimmunology at a Glance. *Adv Sci (Weinh)* (2020) 7(24):2002628. doi: 10.1002/advs.202002628
103. Zhu DM, Dustin ML, Cairo CW, Thatte HS, Golan DE. Mechanisms of Cellular Avidity Regulation in CD2-CD58-Mediated T Cell Adhesion. *ACS Chem Biol* (2006) 1(10):649–58. doi: 10.1021/cb6002515
104. van Kemenade FJ, Tellegen E, Maurice MM, Lankester AC, Kuijpers TW, Brouwer M, et al. Simultaneous Regulation of CD2 Adhesion and Signaling Functions by a Novel CD2 Monoclonal Antibody. *J Immunol* (1994) 152 (9):4425–32.
105. Boussiotis VA, Freeman GJ, Griffin JD, Gray GS, Gribben JG, Nadler LM. CD2 Is Involved in Maintenance and Reversal of Human Alloantigen-Specific Clonal Anergy. *J Exp Med* (1994) 180(5):1665–73. doi: 10.1084/ jem.180.5.1665
106. Jenkins MK, Johnson JG. Molecules Involved in T-Cell Costimulation. *Curr Opin Immunol* (1993) 5(3):361–7. doi: 10.1016/0952-7915(93)90054-v
107. Janeway CA Jr., Golstein P. Lymphocyte Activation and Effector Functions. Editorial Overview. The Role of Cell Surface Molecules. *Curr Opin Immunol* (1993) 5(3):313–23. doi: 10.1016/0952-7915(93)90048-w
108. Samelson LE. Lymphocyte Activation. *Curr Opin Immunol* (1989) 2(2):210–4. doi: 10.1016/0952-7915(89)90190-8
109. Turcovski-Corrales SM, Fenton RG, Peltz G, Taub DD. Cd28:B7 Interactions Promote T Cell Adhesion. *Eur J Immunol* (1995) 25(11):3087–93. doi: 10.1002/eji.1830251115
110. Tiefenthaler G, Hunig T, Dustin ML, Springer TA, Meuer SC. Purified Lymphocyte Function-Associated Antigen-3 and T11 Target Structure Are Active in CD2-Mediated T Cell Stimulation. *Eur J Immunol* (1987) 17 (12):1847–50. doi: 10.1002/eji.1830171227
111. Bierer BE, Peterson A, Barbosa J, Seed B, Burakoff SJ. Expression of the T-Cell Surface Molecule CD2 and An Epitope-Loss CD2 Mutant to Define the Role of Lymphocyte Function-Associated Antigen 3 (LFA-3) in T-Cell Activation. *Proc Natl Acad Sci USA* (1988) 85(4):1194–8. doi: 10.1073/pnas.85.4.1194
112. Dustin ML, Olive D, Springer TA. Correlation of CD2 Binding and Functional Properties of Multimeric and Monomeric Lymphocyte Function-Associated Antigen 3. *J Exp Med* (1989) 169(2):503–17. doi: 10.1084/jem.169.2.503
113. Moingeon PE, Lucich JL, Stebbins CC, Recny MA, Wallner BP, Koyasu S, et al. Complementary Roles for CD2 and LFA-1 Adhesion Pathways During T Cell Activation. *Eur J Immunol* (1991) 21(3):605–10. doi: 10.1002/ eji.1830210311
114. Hahn WC, Rosenstein Y, Burakoff SJ, Bierer BE. Interaction of CD2 With Its Ligand Lymphocyte Function-Associated Antigen-3 Induces Adenosine 3',5'-Cyclic Monophosphate Production in T Lymphocytes. *J Immunol* (1991) 147(1):14–21.
115. Kaizuka Y, Douglass AD, Vardhana S, Dustin ML, Vale RD. The Coreceptor Cd2 Uses Plasma Membrane Microdomains to Transduce Signals in T Cells. *J Cell Biol* (2009) 185(3):521–34. doi: 10.1083/jcb.200809136
116. Anton Van Der Merwe P, Davis SJ, Shaw AS, Dustin ML. Cytoskeletal Polarization and Redistribution of Cell-Surface Molecules During T Cell Antigen Recognition. *Semin Immunol* (2000) 12(1):5–21. doi: 10.1006/ smim.2000.0203
117. Wacholtz MC, Lipsky PE. Anti-Cd3-Stimulated Ca2+ Signal in Individual Human Peripheral T Cells. Activation Correlates With a Sustained Increase in Intracellular Ca2+1. *J Immunol* (1993) 150(12):5338–49.
118. Weiss A, Littman DR. Signal Transduction by Lymphocyte Antigen Receptors. *Cell* (1994) 76(2):263–74. doi: 10.1016/0092-8674(94)90334-4
119. Parra E, Wingren AG, Hedlund G, Kalland T, Dohlsten M. The Role of B7-1 and LFA-3 in Costimulation of CD8+ T Cells. *J Immunol* (1997) 158(2):637–42. doi: 10.1016/S0165-2478(97)85190-5
120. Durand DB, Shaw JP, Bush MR, Replogle RE, Belagaje R, Crabtree GR. Characterization of Antigen Receptor Response Elements Within the Interleukin-2 Enhancer. *Mol Cell Biol* (1988) 8(4):1715–24. doi: 10.1128/ mcb.8.4.1715
121. Halvorsen R, Leivestad T, Gaudernack G, Thorsby E. Accessory Cell-Dependent T-Cell Activation *Via* Ti-CD3. Involvement of CD2-LFA-3 Interactions. *Scand J Immunol* (1988) 28(3):277–84. doi: 10.1111/j.1365-3083.1988.tb01449.x
122. Parra E, Varga M, Hedlund G, Kalland T, Dohlsten M. Costimulation by B7-1 and LFA-3 Targets Distinct Nuclear Factors That Bind to the Interleukin-2 Promoter: B7-1 Negatively Regulates LFA-3-Induced Nf-at DNA Binding. *Mol Cell Biol* (1997) 17(3):1314–23. doi: 10.1128/mcb.17.3.1314
123. Parra E, Wingren AG, Hedlund G, Bjorklund M, Sjogren HO, Kalland T, et al. Costimulation of Human Cd4+ T Lymphocytes With B7 and Lymphocyte Function-Associated Antigen-3 Results in Distinct Cell Activation Profiles. *J Immunol* (1994) 153(6):2479–87.
124. Endler-Jobst B, Schraven B, Hutmacher B, Meuer SC. Human T Cell Responses to IL-1 and IL-6 Are Dependent on Signals Mediated Through CD2. *J Immunol* (1991) 146(6):1736–42.
125. Bullens DM, Rafiq K, Charitidou L, Peng X, Kasran A, Warmerdam PA, et al. Effects of Co-Stimulation by CD58 on Human T Cell Cytokine Production: A Selective Cytokine Pattern With Induction of High Il-10 Production. *Int Immunol* (2001) 13(2):181–91. doi: 10.1093/intimm/13.2.181
126. Cottrez F, Hurst SD, Coffman RL, Groux H. T Regulatory Cells 1 Inhibit a Th2-Specific Response In Vivo. *J Immunol* (2000) 165(9):4848–53. doi: 10.4049/jimmunol.165.9.4848
127. Wakkach A, Cottrez F, Groux H. Differentiation of Regulatory T Cells 1 Is Induced by CD2 Costimulation. *J Immunol* (2001) 167(6):3107–13. doi: 10.4049/jimmunol.167.6.3107
128. Nguyen KG, Vrabel MR, Mantooth SM, Hopkins JJ, Wagner ES, Gabaldon TA, et al. Localized Interleukin-12 for Cancer Immunotherapy. *Front Immunol* (2020) 11:575597. doi: 10.3389/fimmu.2020.575597
129. Gollob JA, Li J, Kawasaki H, Daley JF, Groves C, Reinherz EL, et al. Molecular Interaction Between CD58 and CD2 Counter-Receptors Mediates the Ability of Monocytes to Augment T Cell Activation by IL-12. *J Immunol* (1996) 157(5):1886–93.
130. Gollob JA, Li J, Reinherz EL, Ritz J. Cd2 Regulates Responsiveness of Activated T Cells to Interleukin 12. *J Exp Med* (1995) 182(3):721–31. doi: 10.1084/jem.182.3.721
131. Gollob JA, Ritz J. Cd2-CD58 Interaction and the Control of T-Cell Interleukin-12 Responsiveness. Adhesion Molecules Link Innate and Acquired Immunity. *Ann NY Acad Sci* (1996) 795:71–81. doi: 10.1111/ j.1749-6632.1996.tb52656.x

132. Dhein J, Walczak H, Baumler C, Debatin KM, Krammer PH. Autocrine T-Cell Suicide Mediated by APO-1/(Fas/CD95). *Nature* (1995) 373(6513):438–41. doi: 10.1038/373438a0
133. Daniel PT, Scholz C, Essmann F, Westermann J, Pezzutto A, Dorken B. Cd95/Fas-Triggered Apoptosis of Activated T Lymphocytes Is Prevented by Dendritic Cells Through a CD58-Dependent Mechanism. *Exp Hematol* (1999) 27(9):1402–8. doi: 10.1016/s0301-472x(99)00079-x
134. Ayroldi E, Migliorati G, Cannarile L, Moraca R, Delfino DV, Riccardi C. CD2 Rescues T Cells From T-Cell Receptor/CD3 Apoptosis: A Role for the Fas/Fas-L System. *Blood* (1997) 89(10):3717–26. doi: 10.1182/blood.V89.10.3717.3717_3717_3726
135. Mahajan S, Gollob JA, Ritz J, Frank DA. CD2 Stimulation Leads to the Delayed and Prolonged Activation of STAT1 in T Cells But Not NK Cells. *Exp Hematol* (2001) 29(2):209–20. doi: 10.1016/s0301-472x(00)00652-4
136. Ortaldo JR, Winkler-Pickett RT, Yagita H, Young HA. Comparative Studies of CD3- and CD3+ Cd56+ Cells: Examination of Morphology, Functions, T Cell Receptor Rearrangement, and Pore-Forming Protein Expression. *Cell Immunol* (1991) 136(2):486–95. doi: 10.1016/0008-8749(91)90369-m
137. Lu PH, Negrin RS. A Novel Population of Expanded Human CD3+CD56+ Cells Derived From T Cells With Potent *In Vivo* Antitumor Activity in Mice With Severe Combined Immunodeficiency. *J Immunol* (1994) 153(4):1687–96.
138. Lopez RD, Waller EK, Lu PH, Negrin RS. CD58/LFA-3 and IL-12 Provided by Activated Monocytes Are Critical in the *In Vivo* Expansion of CD56+ T Cells. *Cancer Immunol Immunother* (2001) 49(12):629–40. doi: 10.1007/s002620000148
139. Pangrazzi L, Weinberger B. T Cells, Aging and Senescence. *Exp Gerontol* (2020) 134:110887. doi: 10.1016/j.exger.2020.110887
140. Leitner J, Herndler-Brandstetter D, Zlabinger GJ, Grubeck-Loebenstein B, Steinberger P. CD58/CD2 Is the Primary Costimulatory Pathway in Human Cd28-Cd8+ T Cells. *J Immunol* (2015) 195(2):477–87. doi: 10.4049/jimmunol.1401917
141. Shao T, Shi W, Zheng JY, Xu XX, Lin AF, Xiang LX, et al. Costimulatory Function of CD58/CD2 Interaction in Adaptive Humoral Immunity in a Zebrafish Model. *Front Immunol* (2018) 9:1204. doi: 10.3389/fimmu.2018.01204
142. Bierer BE, Barbosa J, Herrmann S, Burakoff SJ. Interaction of CD2 With Its Ligand, LFA-3, in Human T Cell Proliferation. *J Immunol* (1988) 140(10):3358–63.
143. Bodey B. Development of Lymphopoiesis as a Function of the Thymic Microenvironment. Use of CD8+ Cytotoxic T Lymphocytes for Cellular Immunotherapy of Human Cancer. *In Vivo* (1994) 8(5):915–43.
144. Denning SM, Tuck DT, Vollger LW, Springer TA, Singer KH, Haynes BF. Monoclonal Antibodies to CD2 and Lymphocyte Function-Associated Antigen 3 Inhibit Human Thymic Epithelial Cell-Dependent Mature Thymocyte Activation. *J Immunol* (1987) 139(8):2573–8.
145. Cooley S, Burns LJ, Repka T, Miller JS. Natural Killer Cell Cytotoxicity of Breast Cancer Targets is Enhanced by Two Distinct Mechanisms of Antibody-Dependent Cellular Cytotoxicity Against LFA-3 and HER2/Neu. *Exp Hematol* (1999) 27(10):1533–41. doi: 10.1016/s0301-472x(99)00089-2
146. Comerci CJ, Mace EM, Banerjee PP, Orange JS. Cd2 Promotes Human Natural Killer Cell Membrane Nanotube Formation. *PloS One* (2012) 7(10):e47664. doi: 10.1371/journal.pone.0047664
147. Davis DM, Sowinski S. Membrane Nanotubes: Dynamic Long-Distance Connections Between Animal Cells. *Nat Rev Mol Cell Biol* (2008) 9(6):431–6. doi: 10.1038/nrm2399
148. Robertson MJ, Caligiuri MA, Manley TJ, Levine H, Ritz J. Human Natural Killer Cell Adhesion Molecules. Differential Expression After Activation and Participation in Cytolysis. *J Immunol* (1990) 145(10):3194–201.
149. Maenpaa A, Jaaskelainen J, Carpen O, Patarroyo M, Timonen T. Expression of Integrins and Other Adhesion Molecules on NK Cells; Impact of IL-2 on Short- and Long-Term Cultures. *Int J Cancer* (1993) 53(5):850–5. doi: 10.1002/ijc.2910530524
150. Sanders ME, Makgoba MW, Sharrow SO, Stephany D, Springer TA, Young HA, et al. Human Memory T Lymphocytes Express Increased Levels of Three Cell Adhesion Molecules (LFA-3, CD2, and LFA-1) and Three Other Molecules (Uchl1, CDw29, and Pgp-1) and Have Enhanced IFN-Gamma Production. *J Immunol* (1988) 140(5):1401–7.
151. Crawford K, Stark A, Kitchens B, Sternheim K, Pantazopoulos V, Triantafellow E, et al. CD2 Engagement Induces Dendritic Cell Activation: Implications for Immune Surveillance and T-Cell Activation. *Blood* (2003) 102(5):1745–52. doi: 10.1182/blood-2002-07-2206
152. Hoffmann JC, Kruger H, Zielen S, Bayer B, Zeidler H. Human B Cell Differentiation: Dependence on Interactions With Monocytes and T Lymphocytes *Via* CD40, CD80 (B7.1), and the CD2-Ligands CD48 and CD58 (LFA-3). *Cell Biol Int* (1998) 22(1):21–9. doi: 10.1006/cbir.1997.0208
153. Virella G, Rugeles MT, Hyman B, La Via M, Goust JM, Frankis M, et al. The Interaction of CD2 With its LFA-3 Ligand Expressed by Autologous Erythrocytes Results in Enhancement of B Cell Responses. *Cell Immunol* (1988) 116(2):308–19. doi: 10.1016/0008-8749(88)90233-x
154. Diaz-Sanchez D, Chegini S, Zhang K, Saxon A. Cd58 (LFA-3) Stimulation Provides a Signal for Human Isotype Switching and IgE Production Distinct From CD40. *J Immunol* (1994) 153(1):10–20.
155. Mestas J, Hughes CC. Endothelial Cell Costimulation of T Cell Activation Through CD58-CD2 Interactions Involves Lipid Raft Aggregation. *J Immunol* (2001) 167(8):4378–85. doi: 10.4049/jimmunol.167.8.4378
156. Karmann K, Hughes CC, Fanslow WC, Pober JS. Endothelial Cells Augment the Expression of CD40 Ligand on Newly Activated Human Cd4+ T Cells Through a CD2/LFA-3 Signaling Pathway. *Eur J Immunol* (1996) 26(3):610–7. doi: 10.1002/eji.1830260316
157. Murakami K, Ma W, Fuleihan R, Pober JS. Human Endothelial Cells Augment Early CD40 Ligand Expression in Activated Cd4+ T Cells Through LFA-3-Mediated Stabilization of mRNA. *J Immunol* (1999) 163(5):2667–73.
158. van Kooyk Y, van de Wiel-van Kemenade P, Weder P, Kuijpers TW, Figdor CG. Enhancement of LFA-1-Mediated Cell Adhesion by Triggering Through CD2 or CD3 on T Lymphocytes. *Nature* (1989) 342(6251):811–3. doi: 10.1038/342811a0
159. Collins T, Krensky AM, Clayberger C, Fiers W, Gimbrone MA Jr., Burakoff SJ, et al. Human Cytolytic T Lymphocyte Interactions With Vascular Endothelium and Fibroblasts: Role of Effector and Target Cell Molecules. *J Immunol* (1984) 133(4):1878–84.
160. Ma W, Pober JS. Human Endothelial Cells Effectively Costimulate Cytokine Production by, But Not Differentiation of, Naive Cd4+ T Cells. *J Immunol* (1998) 161(5):2158–67.
161. Hughes CC, Pober JS. Transcriptional Regulation of the Interleukin-2 Gene in Normal Human Peripheral Blood T Cells. Convergence of Costimulatory Signals and Differences From Transformed T Cells. *J Biol Chem* (1996) 271(10):5369–77. doi: 10.1074/jbc.271.10.5369
162. Damle NK, Doyle LV. Stimulation of Cloned Human T Lymphocytes Via the CD3 or CD28 Molecules Induces Enhancement in Vascular Endothelial Permeability to Macromolecules With Participation of Type-1 and Type-2 Intercellular Adhesion Pathways. *Eur J Immunol* (1990) 20(9):1995–2003. doi: 10.1002/eji.1830200918
163. Framson PE, Cho DH, Lee LY, Hershberg RM. Polarized Expression and Function of the Costimulatory Molecule CD58 on Human Intestinal Epithelial Cells. *Gastroenterology* (1999) 116(5):1054–62. doi: 10.1016/s0016-5085(99)70008-9
164. Ebert EC, Panja A, Praveen R. Human Intestinal Intraepithelial Lymphocytes and Epithelial Cells Coinduce Interleukin-8 Production Through the CD2-CD58 Interaction. *Am J Physiol Gastrointest Liver Physiol* (2009) 296(3):G671–7. doi: 10.1152/ajpgi.90497.2008
165. Kim JY, Bae JS, Kim HJ, Shin HD. Cd58 Polymorphisms Associated With the Risk of Neuromyelitis Optica in a Korean Population. *BMC Neurol* (2014) 14:57. doi: 10.1186/1471-2377-14-57
166. Yamamoto M, Watanabe M, Inoue N, Watanabe A, Ozaki H, Ohsaki M, et al. Association of CD58 Polymorphisms and Its Protein Expression With the Development and Prognosis of Autoimmune Thyroid Diseases. *Immunol Invest* (2020) 49(1-2):106–19. doi: 10.1080/08820139.2019.1659811
167. Kumar V, Cheng SC, Johnson MD, Smeekens SP, Wojtowicz A, Giamarellos-Bourboulis E, et al. Immunochip SNP Array Identifies Novel Genetic Variants Conferring Susceptibility to Candidaemia. *Nat Commun* (2014) 5:4675. doi: 10.1038/ncomms5675
168. Hoppenbrouwers IA, Aulchenko YS, Janssens AC, Ramagopalan SV, Broer L, Kayser M, et al. Replication of CD58 and CLEC16A as Genome-Wide Significant Risk Genes for Multiple Sclerosis. *J Hum Genet* (2009) 54(11):676–80. doi: 10.1038/jhg.2009.96
169. Coustet B, Agarwal SK, Gourh P, Guedj M, Mayes MD, Dieude P, et al. Association Study of ITGAM, ITGAX, and CD58 Autoimmune Risk Loci

in Systemic Sclerosis: Results From 2 Large European Caucasian Cohorts. *J Rheumatol* (2011) 38(6):1033–8. doi: 10.3899/jrheum.101053
170. De Jager PL, Baecher-Allan C, Maier LM, Arthur AT, Ottoboni L, Barcellos L, et al. The Role of the CD58 Locus in Multiple Sclerosis. *Proc Natl Acad Sci USA* (2009) 106(13):5264–9. doi: 10.1073/pnas.0813310106
171. Torbati S, Karami F, Ghaffarpour M, Zamani M. Association of CD58 Polymorphism With Multiple Sclerosis and Response to Interferon Ss Therapy in A Subset of Iranian Population. *Cell J* (2015) 16(4):506–13. doi: 10.22074/cellj.2015.505
172. Bashinskaya VV, Kulakova OG, Kiselev IS, Baulina NM, Favorov AV, Boyko AN, et al. Gwas-Identified Multiple Sclerosis Risk Loci Involved in Immune Response: Validation in Russians. *J Neuroimmunol* (2015) 282:85–91. doi: 10.1016/j.jneuroim.2015.03.015
173. Hecker M, Boxberger N, Illner N, Fitzner B, Schroder I, Winkelmann A, et al. A Genetic Variant Associated With Multiple Sclerosis Inversely Affects the Expression of CD58 and Microrna-548ac From the Same Gene. *PloS Genet* (2019) 15(2):e1007961. doi: 10.1371/journal.pgen.1007961
174. Brynedal B, Bomfim IL, Olsson T, Duvefelt K, Hillert J. Differential Expression, and Genetic Association, of CD58 in Swedish Multiple Sclerosis Patients. *Proc Natl Acad Sci USA* (2009) 106(23):E58. doi: 10.1073/pnas.0904338106
175. Mitkin NA, Muratova AM, Korneev KV, Pavshintsev VV, Rumyantsev KA, Vagida MS, et al. Protective C Allele of the Single-Nucleotide Polymorphism rs1335532 Is Associated With Strong Binding of Ascl2 Transcription Factor and Elevated CD58 Expression in B-Cells. *Biochim Biophys Acta Mol Basis Dis* (2018) 1864(10):3211–20. doi: 10.1016/j.bbadis.2018.07.008
176. Payer LM, Steranka JP, Ardeljan D, Walker J, Fitzgerald KC, Calabresi PA, et al. Alu Insertion Variants Alter mRNA Splicing. *Nucleic Acids Res* (2019) 47(1):421–31. doi: 10.1093/nar/gky1086
177. Autschbach F, Meuer SC, Moebius U, Manns M, Hess G, Meyer zum Buschenfelde KH, et al. Hepatocellular Expression of Lymphocyte Function-Associated Antigen 3 in Chronic Hepatitis. *Hepatology* (1991) 14 (2):223–30. doi: 10.1002/hep.1840140204
178. Xie M, Wang XL, Ji YQ, Li J, Meng ZJ, Shi L, et al. Study on the Relationship Between Level of CD58 Expression in Peripheral Blood Mononuclear Cell and Severity of HBV Infection. *Chin (Engl)* (2005) 118(24):2072–6.
179. Sheng L, Li J, Qi BT, Ji YQ, Meng ZJ, Xie M. Investigation on Correlation Between Expression of CD58 Molecule and Severity of Hepatitis B. *World J Gastroenterol* (2006) 12(26):4237–40. doi: 10.3748/wjg.v12.i26.4237
180. Hoffmann JC, Rauker HJ, Kruger H, Bayer B, Zeidler H. Decreased Levels of a Soluble Form of the Human Adhesion Receptor Cd58 (Lfa-3) in Sera and Synovial Fluids of Patients With Rheumatoid Arthritis. *Clin Exp Rheumatol* (1996) 14(1):23–9.
181. Hoffmann JC, Bayer B, Zeidler H. Characterization of a Soluble Form of CD58 in Synovial Fluid of Patients With Rheumatoid Arthritis (Ra). *Clin Exp Immunol* (1996) 104(3):460–6. doi: 10.1046/j.1365-2249.1996.41749.x
182. Craigen JL, Grundy JE. Cytomegalovirus Induced Up-Regulation of LFA-3 (CD58) and ICAM-1 (CD54) is a Direct Viral Effect That is Not Prevented by Ganciclovir or Foscarnet Treatment. *Transplantation* (1996) 62(8):1102–8. doi: 10.1097/00007890-199610270-00014
183. Rolle A, Halenius A, Ewen EM, Cerwenka A, Hengel H, Momburg F. Cd2-CD58 Interactions are Pivotal for the Activation and Function of Adaptive Natural Killer Cells in Human Cytomegalovirus Infection. *Eur J Immunol* (2016) 46(10):2420–5. doi: 10.1002/eji.201646492
184. Wang ECY, Pjechova M, Nightingale K, Vlahava VM, Patel M, Ruckova E, et al. Suppression of Costimulation by Human Cytomegalovirus Promotes Evasion of Cellular Immune Defenses. *Proc Natl Acad Sci USA* (2018) 115 (19):4998–5003. doi: 10.1073/pnas.1720950115
185. Hoffmann JC, Goke MN, Evers J, Rauker HJ, Bayer B, Manns MP. Reduced Serum Levels of a Soluble Form of the Human Adhesion Receptor Cd58 (LFA-3) in Patients With Inflammatory Bowel Disease. *Z Gastroenterol* (1996) 34(9):522–7.
186. Hargreaves R, Logiou V, Lechler R. The Primary Alloresponse of Human Cd4+ T Cells is Dependent on B7 (Cd80), Augmented by CD58, But Relatively Uninfluenced by CD54 Expression. *Int Immunol* (1995) 7 (9):1505–13. doi: 10.1093/intimm/7.9.1505
187. Sido B, Otto G, Zimmermann R, Muller P, Meuer S, Dengler TJ. Prolonged Allograft Survival by the Inhibition of Costimulatory Cd2 Signals But Not by Modulation of CD48 (Cd2 Ligand) in the Rat. *Transpl Int* (1996) 9 Suppl 1: S323–7. doi: 10.1007/978-3-662-00818-8_80
188. Qin L, Chavin KD, Lin J, Yagita H, Bromberg JS. Anti-CD2 Receptor and Anti-CD2 Ligand (Cd48) Antibodies Synergize to Prolong Allograft Survival. *J Exp Med* (1994) 179(1):341–6. doi: 10.1084/jem.179.1.341
189. Sultan P, Schechner JS, McNiff JM, Hochman PS, Hughes CC, Lorber MI, et al. Blockade of CD2-LFA-3 Interactions Protects Human Skin Allografts in Immunodeficient Mouse/Human Chimeras. *Nat Biotechnol* (1997) 15 (8):759–62. doi: 10.1038/nbt0897-759
190. Archimbaud E, Thomas X, Campos L, Magaud JP, Dore JF, Fiere D. Expression of Surface Adhesion Molecules Cd54 (Icam-1) and CD58 (LFA-3) in Adult Acute Leukemia: Relationship With Initial Characteristics and Prognosis. *Leukemia* (1992) 6(4):265–71.
191. Archimbaud E, Campos L, Vila L, Thomas X. Potential Role for non-HLA-Restricted Cytotoxic Cells in the Immune Surveillance of Acute Leukemia. *Immunol Lett* (1993) 39(1):13–5. doi: 10.1016/0165-2478(93)90158-x
192. Li XM, Zhang LP, Wang YZ, Lu AD, Chang Y, Zhu HH, et al. Cd38+ CD58- is an Independent Adverse Prognostic Factor in Paediatric Philadelphia Chromosome Negative B Cell Acute Lymphoblastic Leukaemia Patients. *Leuk Res* (2016) 43:33–8. doi: 10.1016/j.leukres.2015.12.015
193. Lee RV, Braylan RC, Rimsza LM. Cd58 Expression Decreases as Nonmalignant B Cells Mature in Bone Marrow and is Frequently Overexpressed in Adult and Pediatric Precursor B-cell Acute Lymphoblastic Leukemia. *Am J Clin Pathol* (2005) 123(1):119–24. doi: 10.1309/x5vv6fkjq6mublpx
194. Veltroni M, De Zen L, Sanzari MC, Maglia O, Dworzak MN, Ratei R, et al. Expression of CD58 in Normal, Regenerating and Leukemic Bone Marrow B Cells: Implications for the Detection of Minimal Residual Disease in Acute Lymphocytic Leukemia. *Haematologica* (2003) 88(11):1245–52.
195. Chen JS, Coustan-Smith E, Suzuki T, Neale GA, Mihara K, Pui CH, et al. Identification of Novel Markers for Monitoring Minimal Residual Disease in Acute Lymphoblastic Leukemia. *Blood* (2001) 97(7):2115–20. doi: 10.1182/blood.v97.7.2115
196. Nagant C, Casula D, Janssens A, Nguyen VTP, Cantinieaux B. Easy Discrimination of Hematogones From Lymphoblasts in B-Cell Progenitor Acute Lymphoblastic Leukemia Patients Using CD81/CD58 Expression Ratio. *Int J Lab Hematol* (2018) 40(6):734–9. doi: 10.1111/ijlh.12912
197. Upadhyaya G, Guba SC, Sih SA, Feinberg AP, Talpaz M, Kantarjian HM, et al. Interferon-Alpha Restores the Deficient Expression of the Cytoadhesion Molecule Lymphocyte Function Antigen-3 by Chronic Myelogenous Leukemia Progenitor Cells. *J Clin Invest* (1991) 88(6):2131–6. doi: 10.1172/JCI115543
198. Komatsu F, Kajiwara M. A Lymphokine-Activated Killer (Lak)-Resistant Cell Line, and Low Expression of Adhesion Molecules LFA-3 and VCAM-1 on its Cell Surface. *Oncol Res* (1998) 10(5):263–9.
199. Billaud M, Rousset F, Calender A, Cordier M, Aubry JP, Laisse V, et al. Low Expression of Lymphocyte Function-Associated Antigen (LFA)-1 and LFA-3 Adhesion Molecules Is a Common Trait in Burkitt's Lymphoma Associated With and Not Associated With Epstein-Barr Virus. *Blood* (1990) 75 (9):1827–33. doi: 10.1182/blood.V75.9.1827.bloodjournal7591827
200. Gregory CD, Murray RJ, Edwards CF, Rickinson AB. Downregulation of Cell Adhesion Molecules LFA-3 and ICAM-1 in Epstein-Barr Virus-Positive Burkitt's Lymphoma Underlies Tumor Cell Escape From Virus-Specific T Cell Surveillance. *J Exp Med* (1988) 167(6):1811–24. doi: 10.1084/jem.167.6.1811
201. Veldman J, Visser L, Huberts-Kregel M, Muller N, Hepkema B, van den Berg A, et al. Rosetting T Cells in Hodgkin Lymphoma Are Activated by Immunological Synapse Components Hla Class II and CD58. *Blood* (2020) 136(21):2437–41. doi: 10.1182/blood.2020005546
202. Schneider M, Schneider S, Zuhlke-Jenisch R, Klapper W, Sundstrom C, Hartmann S, et al. Alterations of the CD58 Gene in Classical Hodgkin Lymphoma. *Genes Chromosomes Cancer* (2015) 54(10):638–45. doi: 10.1002/gcc.22276
203. Abdul Razak FR, Diepstra A, Visser L, van den Berg A. CD58 Mutations Are Common in Hodgkin Lymphoma Cell Lines and Loss of CD58 Expression in Tumor Cells Occurs in Hodgkin Lymphoma Patients Who Relapse. *Genes Immun* (2016) 17(6):363–6. doi: 10.1038/gene.2016.30
204. Cao Y, Zhu T, Zhang P, Xiao M, Yi S, Yang Y, et al. Mutations or Copy Number Losses of CD58 and TP53 Genes in Diffuse Large B Cell Lymphoma are Independent Unfavorable Prognostic Factors. *Oncotarget* (2016) 7 (50):83294–307. doi: 10.18632/oncotarget.13065

205. Challa-Malladi M, Lieu YK, Califano O, Holmes AB, Bhagat G, Murty VV, et al. Combined Genetic Inactivation of Beta2-Microglobulin and CD58 Reveals Frequent Escape From Immune Recognition in Diffuse Large B Cell Lymphoma. *Cancer Cell* (2011) 20(6):728–40. doi: 10.1016/j.ccr.2011.11.006
206. Otsuka Y, Nishikori M, Arima H, Izumi K, Kitawaki T, Hishizawa M, et al. Ezh2 Inhibitors Restore Epigenetically Silenced CD58 Expression in B-Cell Lymphomas. *Mol Immunol* (2020) 119:35–45. doi: 10.1016/j.molimm.2020.01.006
207. Yoshida N, Karube K, Utsunomiya A, Tsukasaki K, Imaizumi Y, Taira N, et al. Molecular Characterization of Chronic-Type Adult T-Cell Leukemia/Lymphoma. *Cancer Res* (2014) 74(21):6129–38. doi: 10.1158/0008-5472.CAN-14-0643
208. Palomero T, Couronne L, Khiabanian H, Kim MY, Ambesi-Impiombato A, Perez-Garcia A, et al. Recurrent Mutations in Epigenetic Regulators, RHOA and FYN Kinase in Peripheral T Cell Lymphomas. *Nat Genet* (2014) 46(2):166–70. doi: 10.1038/ng.2873
209. Foreman NK, Rill DR, Coustan-Smith E, Douglass EC, Brenner MK. Mechanisms of Selective Killing of Neuroblastoma Cells by Natural Killer Cells and Lymphokine Activated Killer Cells. Potential for Residual Disease Eradication. *Br J Cancer* (1993) 67(5):933–8. doi: 10.1038/bjc.1993.173
210. Lorenz MG, Kantor JA, Schlom J, Hodge JW. Induction of Anti-Tumor Immunity Elicited by Tumor Cells Expressing a Murine LFA-3 Analog *Via* a Recombinant Vaccinia Virus. *Hum Gene Ther* (1999) 10(4):623–31. doi: 10.1089/10430349950018698
211. Xu S, Wen Z, Jiang Q, Zhu L, Feng S, Zhao Y, et al. CD58, a Novel Surface Marker, Promotes Self-Renewal of Tumor-Initiating Cells in Colorectal Cancer. *Oncogene* (2015) 34(12):1520–31. doi: 10.1038/onc.2014.95
212. Mayer B, Lorenz C, Babic R, Jauch KW, Schildberg FW, Funke I, et al. Expression of Leukocyte Cell Adhesion Molecules on Gastric Carcinomas: Possible Involvement of LFA-3 Expression in the Development of Distant Metastases. *Int J Cancer* (1995) 64(6):415–23. doi: 10.1002/ijc.2910640611
213. Cai Q, Zhang M, Li Z. Potential Strategies Against Resistance to CAR T-Cell Therapy in Haematological Malignancies. *Ther Adv Med Oncol* (2020) 12:1758835920962963. doi: 10.1177/1758835920962963
214. Zhang Y, Liu Q, Liao Q. Long Noncoding Rna: A Dazzling Dancer in Tumor Immune Microenvironment. *J Exp Clin Cancer Res* (2020) 39(1):231. doi: 10.1186/s13046-020-01727-3
215. Nagaria TS, Wang H, Wang H. Predictive Molecular Markers in the Era of Immunotherapy. *J Pancreatol* (2020) 3(3):132–8. doi: 10.1097/jp9.0000000000000043
216. Frangieh CJ, Melms JC, Thakore PI, Geiger-Schuller KR, Ho P, Luoma AM, et al. Multimodal Pooled Perturb-CITE-Seq Screens in Patient Models Define Mechanisms of Cancer Immune Evasion. *Nat Genet* (2021) 53(3):332–41. doi: 10.1038/s41588-021-00779-1

Conflict of Interest: The authors declare that the research was conducted in the absence of any commercial or financial relationships that could be construed as a potential conflict of interest.

Copyright © 2021 Zhang, Liu, Yang and Liao. This is an open-access article distributed under the terms of the Creative Commons Attribution License (CC BY). The use, distribution or reproduction in other forums is permitted, provided the original author(s) and the copyright owner(s) are credited and that the original publication in this journal is cited, in accordance with accepted academic practice. No use, distribution or reproduction is permitted which does not comply with these terms.

GLOSSARY

ADCC	antibody-dependent cellular cytotoxicity
AICD	activation-induced cell death
AITDs	autoimmune thyroid diseases
ALL	acute lymphoid leukemia
AML	acute myelogenous leukemia
APC	antigen-presenting cell
ATRA	all-trans retinoic acid
BL	Burkitt's lymphoma
CHO	Chinese hamster ovary
CIA	collagen-induced arthritis
CML	chronic myelocytic leukemia
CMV	cytomegalovirus
CNS	central nervous system
CRC	colorectal cancer
CTL	cytotoxic T lymphocyte
DC	dendritic cell
DLBCL	diffuse large B cell lymphoma
E	erythrocyte
EBV	Epstein-Barr virus
EC	endothelial cell
Fas-L	Fas ligation
GC	gastric cancer
GPI	glycosylphosphatidylinositol
HCC	hepatocellular carcinoma
HL	Hodgkin's lymphoma
HRS	Reed/Sternberg
IBD	inflammatory bowel disease
ICB	immune checkpoint blockade
IEC	intestinal epithelial cell
IEL	intraepithelial lymphocyte
IS	immunological synapse
LAK	lymphokine-activated killing
LFA-3	lymphocyte-function antigen 3
mAb	monoclonal antibody
MHC	major histocompatibility complex
MS	multiple sclerosis
NF	nuclear factor
NMO	neuromyelitis optica
PHA	phytohemagglutinin
PI-PLC	phosphatidylinositol-specific phospholipase C
PNH	paroxysmal nocturnal hemoglobinuria
RA	rheumatoid arthritis
rv-CD58	recombinant virus bearing CD58
sCD58	soluble CD58
SMAC	supramolecular activation complex
SNP	single-nucleotide polymorphism
SRBC	sheep red blood cell
T11TS	T11 target structure
TCR	T cell receptor
Tregs	T regulatory cells
UV	ultraviolet.

frontiers in Immunology

ORIGINAL RESEARCH
published: 25 June 2021
doi: 10.3389/fimmu.2021.705511

Screening and Validation of the Hypoxia-Related Signature of Evaluating Tumor Immune Microenvironment and Predicting Prognosis in Gastric Cancer

Jun-Peng Pei[1], *Chun-Dong Zhang*[1,2*], *Maimaitituusun Yusupu*[1], *Cheng Zhang*[1] *and Dong-Qiu Dai*[1,3*]

[1] Department of Gastrointestinal Surgery, The Fourth Affiliated Hospital of China Medical University, Shenyang, China, [2] Department of Gastrointestinal Surgery, Graduate School of Medicine, The University of Tokyo, Tokyo, Japan, [3] Cancer Center, The Fourth Affiliated Hospital of China Medical University, Shenyang, China

Background: Hypoxia is one driving factor of gastric cancer. It causes a series of immunosuppressive processes and malignant cell responses, leading to a poor prognosis. It is clinically important to identify the molecular markers related to hypoxia.

Methods: We screened the prognostic markers related to hypoxia in The Cancer Genome Atlas database, and a risk score model was developed based on these markers. The relationships between the risk score and tumor immune microenvironment were investigated. An independent validation cohort from Gene Expression Omnibus was applied to validate the results. A nomogram of risk score model and clinicopathological factor was developed to individually predict the prognosis.

Results: We developed a hypoxia risk score model based on SERPINE1 and EFNA3. Quantified real-time PCR was further applied to verified gene expressions of SERPINE1 and EFNA3 in gastric cancer patients and cell lines. A high-risk score is associated with a poor prognosis through the immunosuppressive microenvironment and immune escape mechanisms, including infiltration of immunosuppressive cells, expression of immune checkpoint molecules, and enrichment of signal pathways related to cancer and immunosuppression. The nomogram basing on the hypoxia-related risk score model showed a good ability to predict prognosis and high clinical net benefits.

Conclusions: The hypoxia risk score model revealed a close relationship between hypoxia and tumor immune microenvironment. The current study potentially provides new insights of how hypoxia affects the prognosis, and may provide a new therapeutic target for patients with gastric cancer.

Keywords: hypoxia, gastric cancer, nomogram, prognosis, tumor immune microenvironment

OPEN ACCESS

Edited by:
Peng Qu,
National Institutes of Health (NIH), United States

Reviewed by:
Yafeng He,
National Heart, Lung, and Blood Institute (NHLBI), United States
Likui Feng,
The Rockefeller University, United States
Yanhong Shou,
Fudan University, China

****Correspondence:***
Chun-Dong Zhang
zhangchundong2007@126.com;
cdzhang@cmu.edu.cn
Dong-Qiu Dai
daidq63@163.com

Specialty section:
This article was submitted to Cancer Immunity and Immunotherapy, a section of the journal Frontiers in Immunology

Received: *05 May 2021*
Accepted: *08 June 2021*
Published: *25 June 2021*

Citation:
Pei J-P, Zhang C-D, Yusupu M, Zhang C and Dai D-Q (2021) Screening and Validation of the Hypoxia-Related Signature of Evaluating Tumor Immune Microenvironment and Predicting Prognosis in Gastric Cancer. Front. Immunol. 12:705511. doi: 10.3389/fimmu.2021.705511

INTRODUCTION

Gastric cancer is a public health burden, ranking fifth in global incidence and fourth in mortality among all cancers (1). Therapeutic strategies are still based on the American Joint Committee on Cancer (AJCC) tumor/node/metastasis (TNM) staging system (2, 3). However, due to the high heterogeneity of gastric cancer, patients with similar clinicopathological characteristics could have different prognosis, suggesting the current TNM staging system are inadequate for predicting prognosis and risk stratification (4, 5). Therefore, it is clinically important to develop a novel biomarker to better guide clinical treatment and improve prognosis.

Tumor cells always grow faster than their blood vessels. Owing to the inadequate blood supply, the supply of oxygen and nutrients to the tumor cells is unbalanced, thereby forming a hypoxic microenvironment (6–9). Hypoxia is one of the characteristics of tumor microenvironment (TME) that can lead directly to the malignant characteristics, including tumor proliferation, migration and invasion, resulting in a poor prognosis (10–12). Previous studies have shown a significant relationship between hypoxia and poor prognosis of GC (13, 14), and hypoxia plays a key role in metastasis (15). In the hypoxic microenvironment, hypoxia-inducible factors (HIFs) are key transcription factors that allow cancer cells to survive under hypoxic conditions and promote tumor progression (16–18). Multiple genes transcribed by HIFs, including Glut1, KLF8, VEGFA, ITGβ1, etc., can promote GC metastasis and lead to poor prognosis (19).

TME is the internal environment in which tumor cells are produced and survive. It is composed of immune cells, endothelial cells, mesenchymal cells, inflammatory mediators and extracellular matrix molecules (20, 21). The immunological components of the TME can inhibit or promote tumor development (22). Recently, the significance of hypoxia in promoting tumor immunosuppression and immune escape has received increasing attentions (23, 24). It is important to understand the potential mechanisms that are involved between hypoxia and the tumor immune microenvironment. Therefore, the establishment of a hypoxia-based signature may help to identify the potential prognostic value of hypoxia, and improve the comprehension of the immunogenomic profile of gastric cancer.

Here, we established a hypoxia-related signature related to prognosis by The Cancer Genome Atlas (TCGA) data base, which was validated by the Gene Expression Omnibus (GEO) data base. Potential mechanisms of the hypoxia-related signature were further investigated.

MATERIALS AND METHODS

Patients

The Clinical data (375 cancer and 72 non-cancerous samples) and FPKM RNA-seq data from TCGA data base (https://www.cancer.gov/tcga) was applied as a screening cohort. The data of 433 cancer samples (GSE84437) from GEO data base (https://www.ncbi.nlm.nih.gov/geo/query/acc.cgi) was applied as a validation cohort (25). RNA-seq and microarray data included were transformed [$\log_2(x+1)$] and normalized by the "sva" and "limma" packages of R software. The baseline characteristics of the screening and validation cohorts are shown (**Supplementary Table S2**).

Development of a Risk Score Model

Univariate analysis was firstly applied to identify potentially hypoxia-related genes that have a statistically significant difference of prognosis in gastric cancer patients from TCGA data base. Least absolute shrinkage and selection operator (LASSO) method was then applied to shrink the scope of gene screening (26). Finally, Cox proportional hazards analysis was used to identify highly hypoxia-related genes. The risk score formula was constructed as: Risk score = ($\sum coefficient_x$ * expression of signature $gene_x$) ($gene_x$ indicated the identified genes). The regression coefficient was obtained from Cox proportional hazards analysis. The patients of gastric cancer were divided into a high-risk and a low-risk groups by the cut-off value of the median risk score.

Tumor Immune Microenvironment

To investigate the relationships between risk score and TME, the ESTIMATE algorithm was applied to determine immune score, stromal score, ESTIMATE score, and tumor purity of individual patient in the screening and validation cohorts (27). Wilcoxon test was applied to compare the differences between the high-risk and low-risk groups in terms of immune score, stromal score, ESTIMATE score, and tumor purity. The TIMER web server (http://timer.cistrome.org/) was applied to analyze the correlations between signature genes and immune cells. The TIMER algorithm was used to assess the abundances of six immune infiltration cells (B cells, $CD4^+$ T cells, $CD8^+$ T cells, neutrophils, macrophages and dendritic cells) and tumor purity (28).

The ssGSEA method was used to the transcriptome to assess immune cell infiltrations (29). We obtained a set of marker genes including immune cell types, immune-related pathways and functions (30). We used the R package called "GSVA" to perform ssGSEA to obtain the normalized enrichment score (NES) of each immune-related item.

Development and Assessment of a Predictive Nomogram

Univariate analysis and Cox proportional hazards analysis were conducted on risk score of target genes and patient clinicopathological characteristics to determine independent prognostic factors related to prognosis. The predictive nomograms were developed by including all independently prognostic factors.

GC Cell Lines and Tissue Samples

The human gastric epithelial cell line GES-1 and gastric cancer cell lines AGS, SGC-7901, HGC-27, MKN-45 and MGC-803 were purchased from the Chinese Academy of Sciences

(Shanghai, China). Cells were cultured in RPMI 1640 medium (HyClone, Logan, UT, USA) with 10% fetal bovine serum (FBS, Invitrogen) and 1% penicillin/streptomycin in a humidified atmosphere of 5% CO_2 at 37°C. Totally, 39 pairs of gastric cancer together with their adjacent non-cancerous tissues (> 5 cm away from cancer tissue) were collected. This study was approved by the Ethics Committee of the Fourth Affiliated Hospital of China Medical University (EC-2021-KS-043). All patients included in this study provided written informed consent in accordance with the Declaration of Helsinki.

Quantitative Real-Time PCR Analysis

Total RNA was extracted using Trizol reagent (Invitrogen, Eugene, OR) and was used to synthesize cDNA using Prime-Script RT Master Mix (TaKaRa, Shiga, Japan), and quantitative real-time PCR (qRT-PCR) was performed by TaKaRa SYBR® Premix Ex Taq™ (TaKaRa, Shiga, Japan). All primers of qRT-PCR were listed in **Table S1**.

Statistical Analyses

All analyses were performed by R version 4.0.2 (http://www.R-project.org). The calibration curve and area under the curve (AUC) were used to evaluate the predictive performance of the predictive nomogram. The clinical benefit was further evaluated by the decision curve analysis (DCA) (31, 32). An independent validation cohort was applied to validate these findings. All tests were two-sided, and a *P* value less than 0.05 was considered as statistically significant.

RESULTS

Patient Characteristics

The baseline characteristics of the screening and validation cohorts are shown in **Table S2**. In the screening cohort, a total of 234 (63.1%) patients were male and 137 (36.9%) were female. Among them, 17 (4.6%) patients were T1, 74 (19.9%) were T2, 177 (47.7%) were T3, and 103 (27.8%) were T4 cases. 117 (31.5%) patients were N0, 97 (26.1%) were N1, 79 (21.3%) were N2, and 78 (21.1%) were N3 cases. Accordingly, 8 (2.2%) patients were Grade I, 126 (34.0%) were Grade II, and 237 (63.8%) were Grade III. Considering the TNM staging system, 46 (12.4%) patients were stage I, 119 (32.1%) were stage II, 165 (44.4%) were stage III, 41 (11.1%) were stage IV cases.

In the validation cohort, a total of 296 (68.4%) patients were male and 137 (31.6%) were female. Among them, 11 (2.5%) patients were T1, 38 (8.8%) were T2, 92 (21.2%) were T3, and 292 (67.5%) were T4 cases. Accordingly, 80 (18.5%) patients were N0, 188 (43.4%) were N1, 132 (30.5%) were N2, and 33 (7.6%) were N3 cases.

Screening of Hypoxia-Related Risk Signature in Gastric Cancer

The hallmark hypoxia-related 200 genes, was obtained from the Molecular Signatures data base (MSigDB version 6.0). Among them, the TCGA data base contains 197 hypoxia-related genes, and 41 differentially expressed genes (DEGs) have been identified (**Table S3** and **Figures 1A–C**). To better visualize the interactions between these hypoxia genes, the STRING online data base was used to analyze the protein-protein interaction network (**Figure 1D**). We evaluated the hypoxia-related genes in the screening cohort, and identified 14 of the 41 genes that were significantly associated with prognosis (all $P < 0.05$, **Table S4**). The LASSO method was further used to analyze these 14 genes, which minimized the potential over-fitting problem and established the minimum standard. Five of the 14 genes in the model are under the optimal adjustment parameter (λ) (**Figures 1E, F**). Finally, the Cox proportional hazards analysis confirmed that two genes (*SERPINE1*, *EFNA3*) (**Figure 1G**) met the proportional hazard hypothesis and were finally used to establish the following risk score model: Risk score = (0.223 * expression level of *SERPINE1*) + (–0.165 * expression level of *EFNA3*). Of the two signature genes, *SERPINE1* was a risk DEG, and *EFNA3* was protective. The risk score of individual patient was calculated and all patients were classified into a high-risk and a low-risk groups based on the median risk score.

Prognostic Ability of Hypoxia-Related Risk Score in Gastric Cancer

Hypoxia usually promotes an aggressive tumor phenotype, so the prognostic ability of the hypoxia-related risk score was explored. In the high-risk group of the screening cohort, the heatmap showed that the expression of *SERPINE1* was up-regulated and *EFNA3* was down-regulated (**Figure 2A**). The mortality rate in the low-risk group was significantly lower than that in the high-risk group (**Figures 2B, C**). Kaplan–Meier analysis indicated that the prognosis of the low-risk group was significantly superior than that of the high-risk group (log-rank test, $P < 0.001$) (**Figure 2D**). Similar results were found in the validation cohort (**Figures 2E–H**).

Hypoxia-Related Signaling Pathways

In the screening cohort, we used GSEA to analyze the signaling pathways activated in the hypoxia-related high-risk group. In the high-risk group, the JAK-STAT signaling pathway, NOTCH signaling pathway, pathway in cancer, and TGF-β signaling pathway were activated (**Figure 3A**). These signaling pathways are related to the stimulation of tumor proliferation, migration, invasion, anti-apoptosis, Epithelial-Mesenchymal Transition (EMT), immune escape and drug resistance. These results have been confirmed in the independent validation cohort (**Figure 3B**).

The Correlation Between Risk Score and TME

The ESTIMATE analysis showed that the immune score, stromal score and ESTIMATE score were significantly positively correlated with the risk score in both the screening and validation cohorts, while tumor purity was significantly negatively correlated with the risk score (**Figures S1A–H**). It also indicated that the immune score, stromal score and ESTIMATE score of the high-risk group were significantly

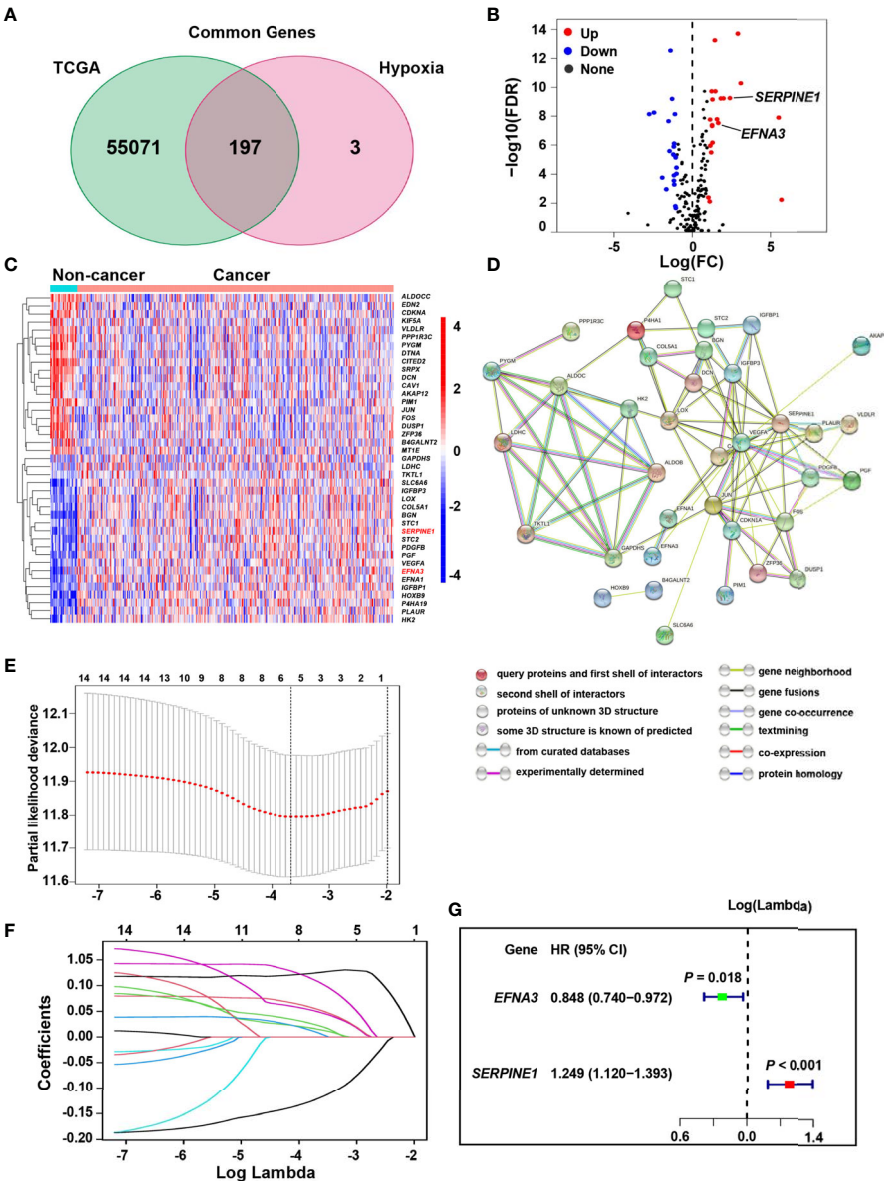

FIGURE 1 | Identification of the hypoxia risk signature. **(A)** The Venn diagram shows the hypoxia-related genes in TCGA. **(B)** The Volcano plot for differentially expressed genes (DEGs) in cancer and non-cancer tissues. **(C)** The heatmap plot for DEGs in cancer and non-cancer tissues. **(D)** The PPI network visualizes the interaction between these DEGs. **(E, F)** The LASSO method identified five genes associated with prognosis. **(G)** The Cox proportional hazards analysis identified the hypoxia risk signature.

higher than those of the low-risk group ($P < 0.001$), while the tumor purity of the high-risk group was significantly lower than that of the low-risk group ($P < 0.001$, **Figures 3C–F**).

The Correlation Between Risk Score and Immune Cell Subtypes

As the tumors of the high-risk group were proved to be infiltrated with a large number of immune cells, we further analyzed the subtypes of infiltrating immune cells. It indicated that the levels of immune cell infiltration in the high-risk group, including regulatory T cells, macrophages, neutrophils, and mast cells, were higher than those in the low-risk group ($P < 0.05$, **Figures 4A–H**). Accordingly, the high-risk group reflects the immunosuppressive tumor microenvironment, full of immunosuppressive cells, which is consistent with the poor prognosis of the high-risk group.

Then, TIMER was applied to evaluate the correlation between the expression levels of *EFNA3* and *SERPINE1* with tumor purity and infiltrating levels of immune cells (**Figures S2A, B**). It showed a correlation between immune cell infiltration and the expression levels of *EFNA3* and *SERPINE1*. It showed that the risk gene *SPERPINE1* had a significant positive correlation with

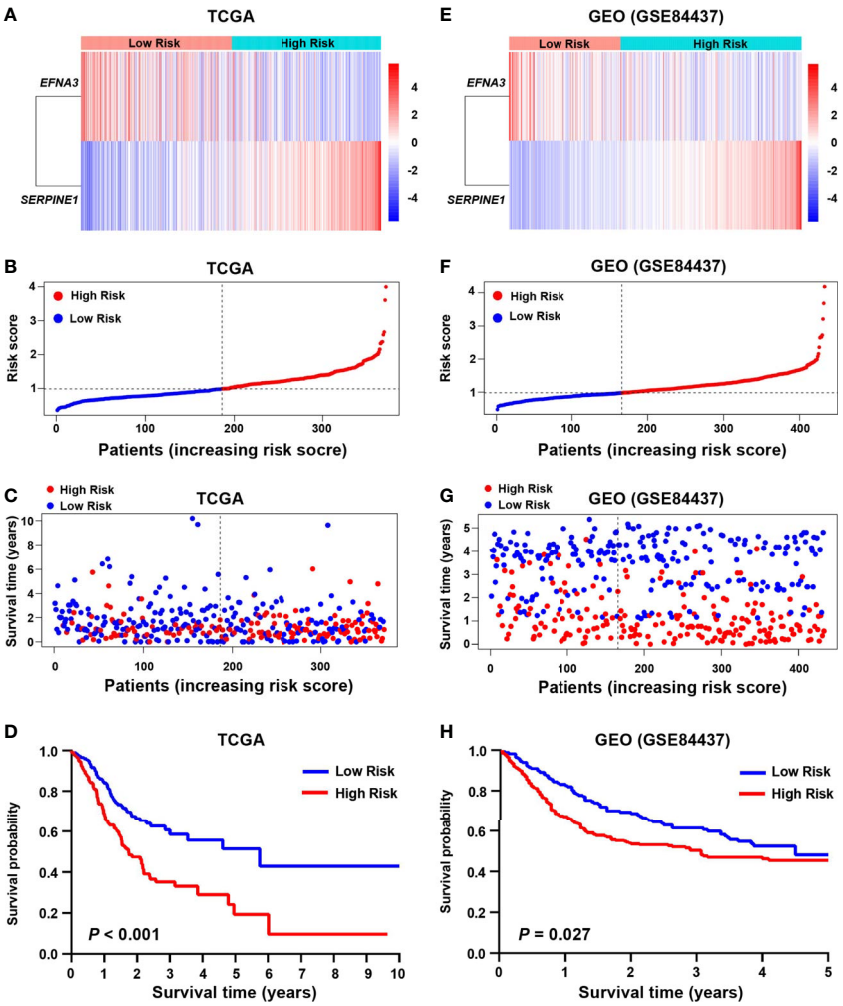

FIGURE 2 | Prognostic value of the hypoxia risk signature in gastric cancer. **(A, E)** Heatmaps of the prognostic signature in the screening (TCGA) and validation (GEO) cohorts. **(B, F)** Patient risk score in the screening and validation cohorts. **(C, G)** The status distribution of patients in the high-risk and low-risk groups in the screening and validation cohort. **(D, H)** Kaplan-Meier analysis of patients in the high-risk and low-risk groups in the screening and validation cohorts.

the infiltration of macrophages, neutrophils and dendritic cells, and a significant negative correlation with tumor purity and B cells ($P < 0.05$, **Figure S2A**). However, the prognostic protective gene *EFNA3* showed the opposite trend for most aspects except B cells (**Figure S2B**, all $P < 0.05$).

The Correlation Between Risk Score and Immune Checkpoint Molecules

We compared the immune checkpoint molecules between the high-risk and low-risk groups. The expression levels of many immune checkpoint molecules were higher in the high-risk group than those in the low-risk group (**Figures 5A, B**). In the screening cohort, the expression level of five key immune checkpoint molecules (*PD-1*, *PD-L1*, *CTLA-4*, *HAVCR2* and *TGF-β*) in the high-risk group was significantly higher than those in the low-risk group, and significantly positively correlated with risk score (**Figures 5C–G**). Similar results were obtained in the validation cohort, except that *CTLA4* and *PD-L1* showed no significant difference between the high-risk and low-risk groups (**Figures 5H–L**).

The Correlation Between Risk Score and Tumor Mutation Burden and Somatic Mutation

It showed that the risk score was significantly negatively correlated with tumor mutation burden (TMB) ($R = -0.36$, $P < 0.001$; **Figure 6A**). We further compared the TMB of patients in the low-risk and high-risk groups. It showed that the TMB of the low-risk group was significantly higher than that of the high-risk group (Wilcoxon test $P < 0.001$) (**Figure 6B**). We determined the optimal cutoff value of TMB (cutoff value = 0.68) by using the minimum *P*-value method, and divided the patients into a high

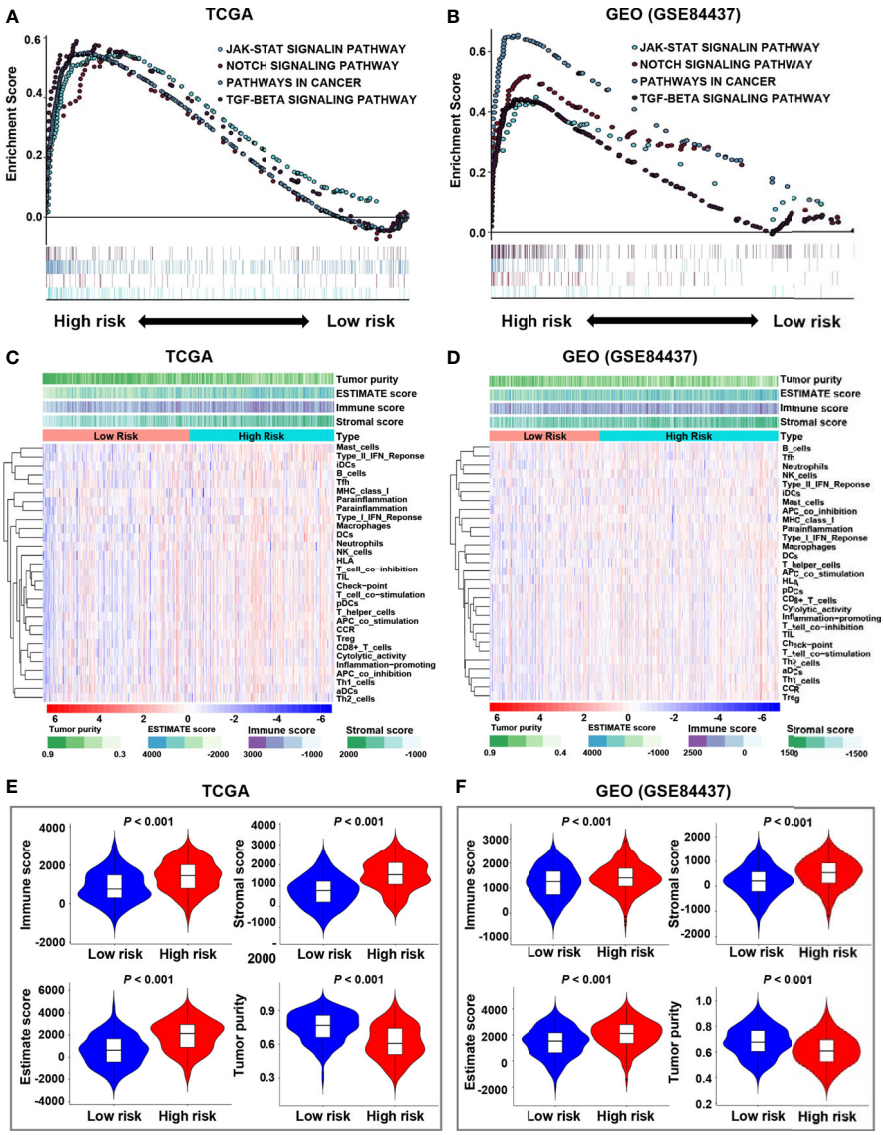

FIGURE 3 | Enrichment of pathways related to hypoxia and analysis of tumor immune microenvironment. **(A, B)** The enrichment plots show the signaling pathways related to hypoxia in the screening and validation cohorts. **(C, D)** The heatmaps show 29 immune-related gene sets, immune score, stromal score, ESTIMATE score and tumor purity in the screening and validation cohorts. **(E, F)** The relationship between risk score and immune score, stromal score, ESTIMATE score, and tumor purity in the screening and validation cohorts.

TMB group (n = 320) and a low TMB group (n = 42). It showed that patients in the high TMB group had a better survival prognosis than those in the low TMB group (log-rank test, $P < 0.001$, **Figure 6C**). We further evaluated the synergistic effect of the TMB grouping and the risk score grouping in the prognostic stratification. It showed that TMB status did not affect the survival prognosis prediction based on the risk score group. The risk score subgroup indicated significant survival differences in both the low and high TMB subgroups (log rank test, high TMB & high-risk *vs.* high TMB & low-risk, $P < 0.001$; low TMB & low-risk *vs.* low TMB & low-risk, $P < 0.001$; **Figure 6D**). Moreover, the high TMB & low-risk group had the best overall survival rate, and the low TMB & high-risk group had the worst overall survival rate.

Furthermore, we estimated somatic variations in gastric cancer driver genes between the low-risk and high-risk subgroups. We used Maftools to access gastric cancer driver genes and further analyzed the top 20 ones with the highest mutation frequency (**Figures 6E, F**). The results showed that there were significant differences in the mutation frequency of *PCLO*, *TTN*, *FLG*, *LRP1B*, *KMT2D*, *SYNE1*, *RYR2*, *OBSCN*, *CSMD1*, *FAT3*, *ARID1A*, *ZFHX4*, *FAT4* and *SPTA1* in the high-risk and low-risk groups (Chi-square test, all $P < 0.05$; **Table S5**).

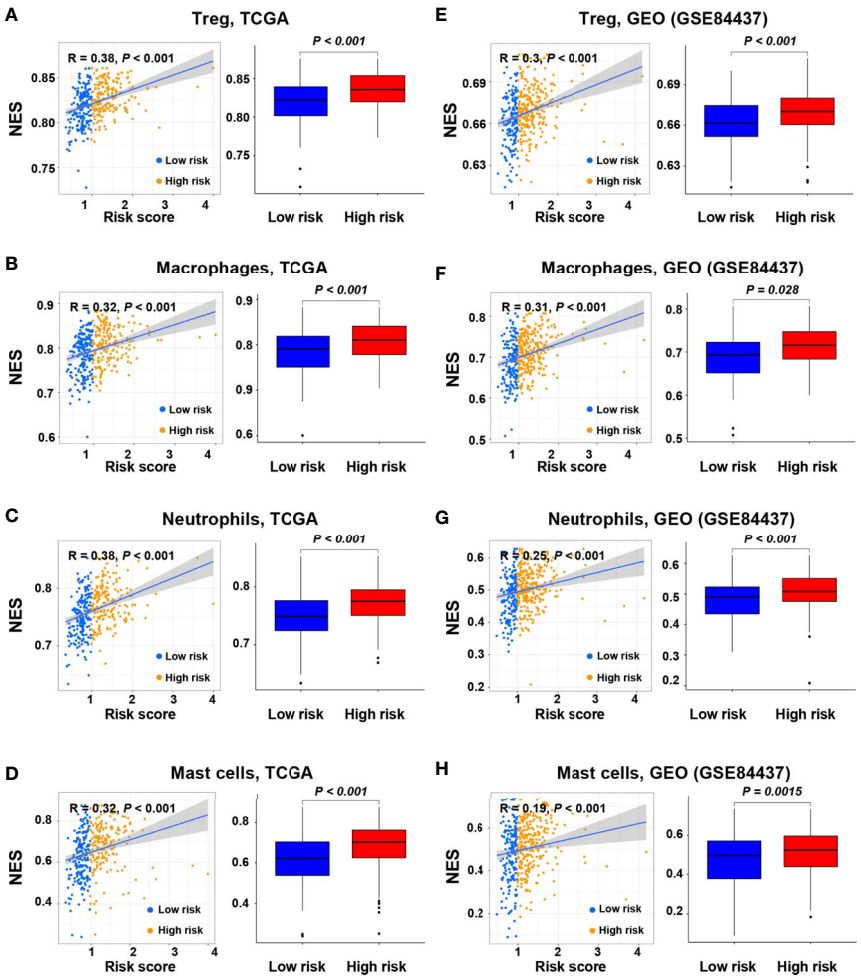

FIGURE 4 | Correlation of the risk score with immune cell subtypes in the screening and validation cohorts. **(A, E)** Regulatory T cells; **(B, F)** Macrophages; **(C, G)** Neutrophils; **(D, H)** Mast cells.

The Correlation Between Risk Score and Chemotherapeutic Drugs

We further analyzed the association between the risk score and the efficacy of chemotherapy in the treatment of gastric cancer. It showed that the high-risk group was associated with lower half inhibitory centration (IC50) of chemotherapeutic drugs, such as axitinib ($P = 0.0053$), bexarotene ($P < 0.001$), bortezomib ($P < 0.001$), bryostatin.1 ($P = 0.0067$), dasatinib ($P < 0.001$), imatinib ($P < 0.001$), midostaurin ($P < 0.001$), nilotinib ($P = 0.04$), pazopanib ($P = 0.0024$), sunitinib ($P < 0.001$), temsirolimus ($P < 0.001$), and vinblastine ($P = 0.031$), while the IC50 of methotrexate ($P = 0.019$) and mitomycin.C ($P = 0.0035$) was higher, indicating that the risk scores can be used as a potential predictor of chemical sensitivity (**Figures 7A–O**).

The Correlation Between Risk Score and Clinicopathological Characteristics

We conducted correlation analyses between clinicopathological factors and risk score in the screening cohort (**Figures S3C**), and tumor grade and T stage were significantly associated with risk score (**Figures S3C, D**). In the validation cohort, age, T stage, and N stage were significantly associated with risk score (**Figures S3H, J, K**).

Development of Nomograms to Predict Individual Survival Outcomes

We developed nomograms based on the screening cohort and further verified their predictive ability in the validation cohort. It showed that age, T stage, N stage, M stage, and risk score are significant prognostic factors (**Figure 8A**). In the first step Cox proportional hazards analysis, we incorporated age, T stage, N stage, and M stage. It showed that age, T stage, and N stage were independent prognostic factors (**Figure 8B**) and were used to construct nomogram 1 (**Figure 8D**). In the second step Cox proportional hazards analysis, we incorporated age, T stage, N stage, M stage and risk score. It showed that age, T stage, N stage and risk score were independent prognostic factors (**Figure 8C**) and were used to construct nomogram 2 (**Figure 8E**).

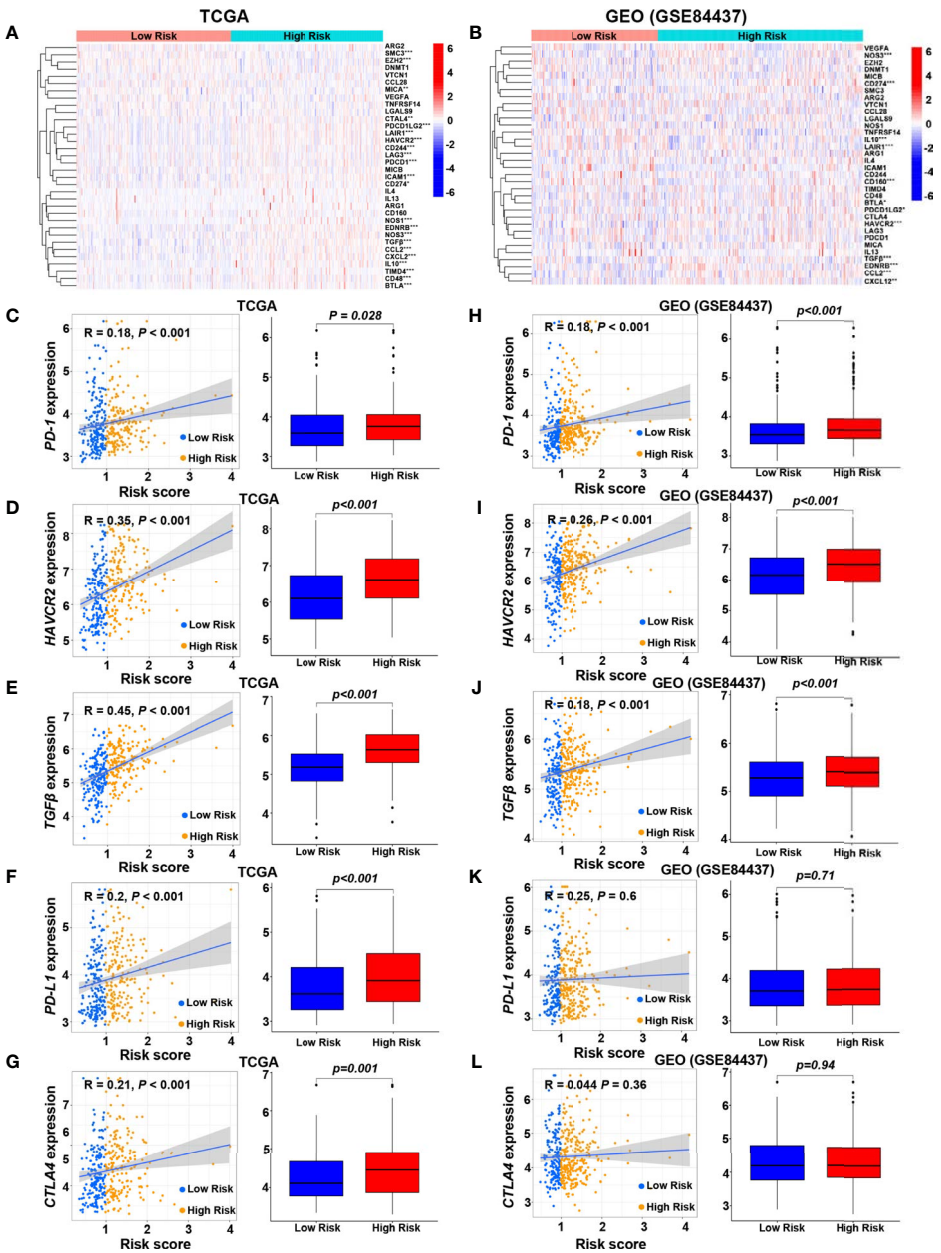

FIGURE 5 | Relationships between hypoxia risk score and immune checkpoint molecules. **(A, G)** Heatmaps show the expression level of immune checkpoint molecules in high-risk and low-risk groups in the screening and validation cohorts (*$P < 0.05$; **$P < 0.01$; ***$P < 0.001$). Scatter plots and box plots show the relationship between the risk score and the expression level of **(B, H)** *PD-1*, **(C, I)** *HAVCR2*, **(D, J)** *TGF-β*, **(E, K)** *PD-L1*, and **(F, L)** *CTLA4* in the screening and validation cohorts.

Comparison of Prognostic Performance and Clinical Usefulness Between Nomogram 1 and Nomogram 2

In the screening cohort, nomogram 2 showed superior prognostic ability [AUC 0.684, 95% confidence interval (CI), 0.630–0.735] compared with nomogram 1 (AUC 0.639, 95% CI, 0.584–0.692) (**Figure 9A**). The calibration curves of nomogram 2 at 3 years also showed better consistency between the predicted and observed survivals than that of nomogram 1 (**Figure 9B**). Nomogram 2 showed higher net benefit than nomogram 1 between the threshold probabilities of around 37–60% in predicting 3-year overall survival (**Figure 9C**). Similar results were found in the independent validation cohort (**Figures 9D–F**).

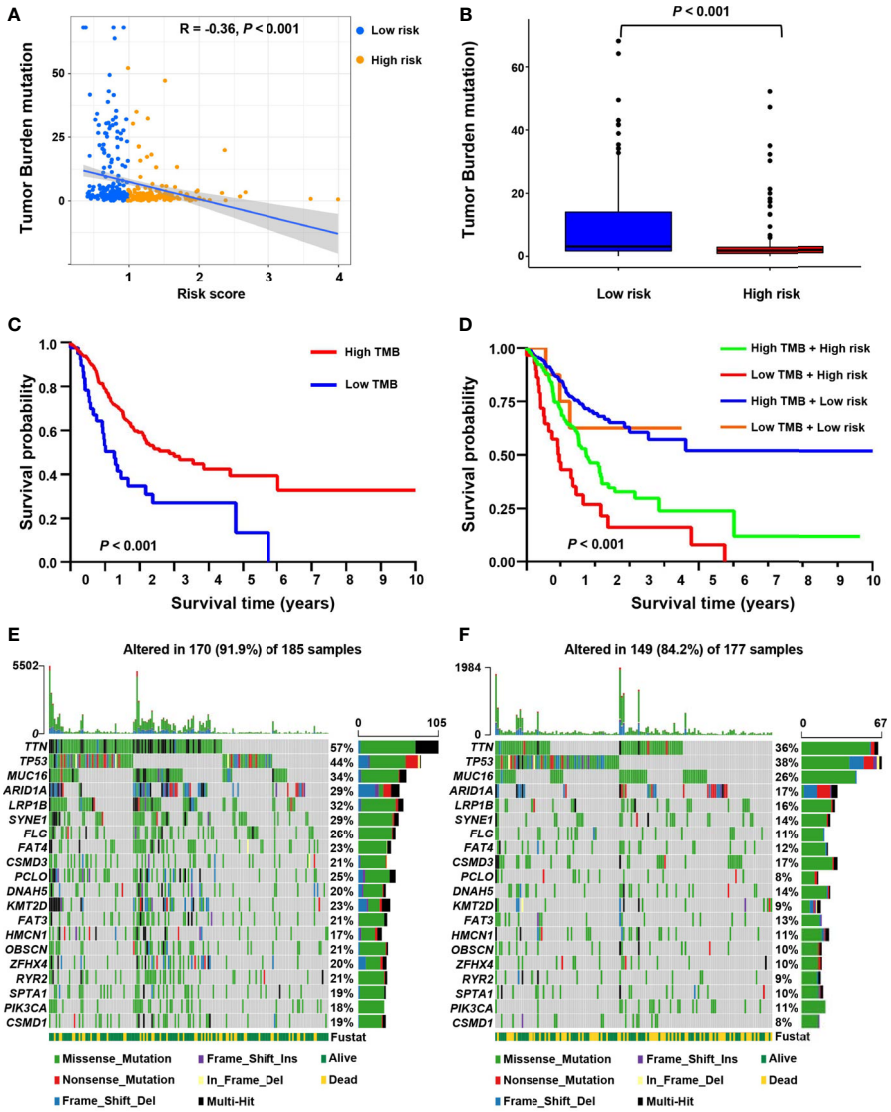

FIGURE 6 | The correlation between the risk score and somatic variants. **(A)** The scatter plot depicts the negative correlation between risk score and tumor mutation burden (TMB) in the screening cohort. **(B)** TMB difference in the high-risk and low-risk groups. **(C)** Kaplan-Meier curves for high-risk and low-TMB groups of the screening cohort. **(D)** Kaplan-Meier curves for patients in the screening cohort stratified by both risk score and TMB. **(E, F)** Waterfall plots display the frequently mutated genes in low-risk and high-risk groups in the screening cohort. The left panel shows the genes ordered by their mutation frequencies. The right panel presents different mutation types.

Expression Levels of SERPINE1 and EFNA3 in GC Cell Lines and Tissues

In the screening cohort, the expression of *SERPINE1* and *EFNA3* in tumor tissues was up-regulated when compared with adjacent non-cancerous tissues and normal tissues ($P < 0.05$, **Figures 10A–D**). To confirm the expression levels of *SERPINE1* and *EFNA3* in gastric cancer, we subsequently verified it in gastric cancer cell lines and patient tissues by qRT-PCR experiments. The results showed that, when compared with gastric normal epithelial mucosae cell line GES-1 and adjacent non-cancerous tissues, the expression of *SERPINE1* and *EFNA3* were significantly higher in gastric cancer cell lines (**Figures 10E, F**, except for *SERPINE1* in HGC-27, $P > 0.05$) and gastric cancer tissues ($P < 0.05$) (**Figures 10G, H**).

DISCUSSION

Hypoxia is caused by an imbalance between insufficient oxygen supply and increased oxygen demand (21, 33). It is also one

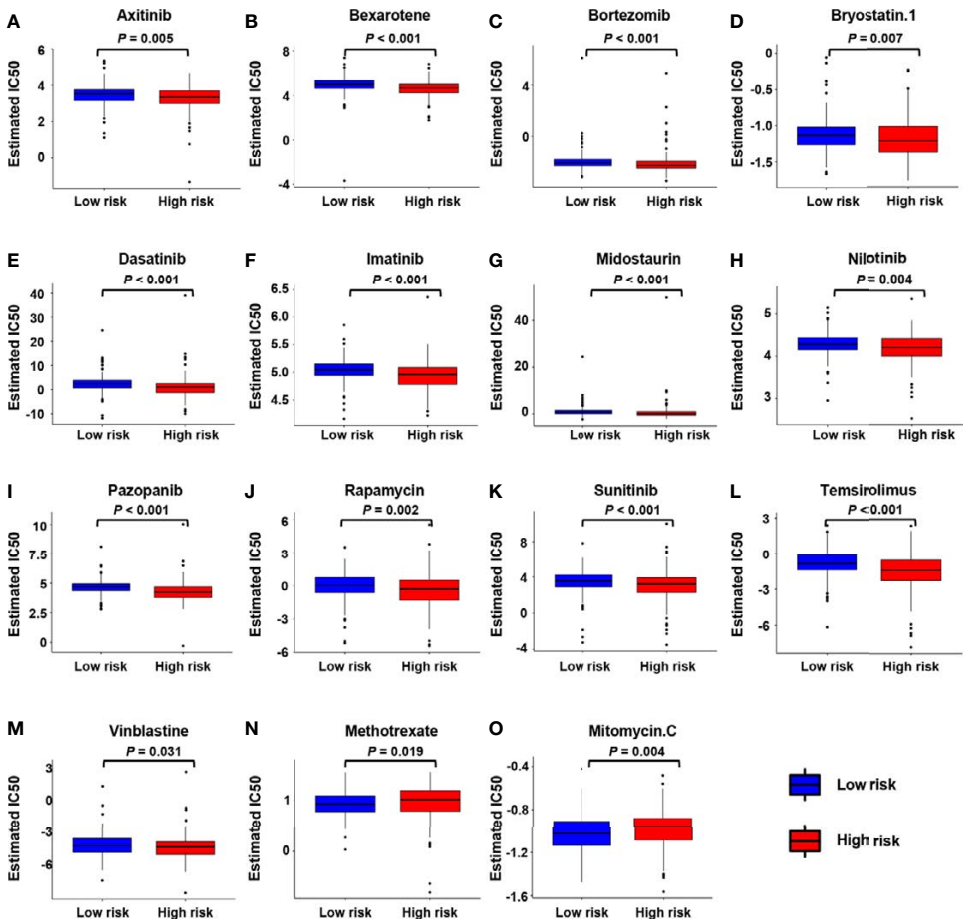

FIGURE 7 | The correlation between low-risk and high-risk groups and chemotherapeutics. Sensitivity to chemotherapeutic drugs is expressed by the half inhibitory centration (IC50) of chemotherapeutic drugs. **(A)** Axitinib; **(B)** Bexarotene; **(C)** Bortezomib; **(D)** Bryostatin.1; **(E)** Dasatinib; **(F)** Imatinib; **(G)** Midostaurin; **(H)** Nilotinib; **(I)** Pazopanib; **(J)** Rapamycin; **(K)** Sunitinib; **(L)** Temsirolimus; **(M)** Vinblastine; **(N)** Methotrexate; **(O)** Mitomycin.C.

significant characteristic of tumor microenvironment. Tumor cells adapt to and rely on tumor microenvironment, contributing to instability and diversity of gene mutations, and activating a variety of signaling pathways and cytokines, contributing to the angiogenesis, invasion, metastasis, epithelial-mesenchymal transition, cancer stem cell maintenance, immune escape and resistance to radiotherapy and chemotherapy (34, 35). Therefore, understanding the molecular mechanism of hypoxia is critical to improving the survival of cancer therapy.

In this study, we identified two prognosis-related hypoxia genes, *SERPINE1* and *EFNA3*, and establish a hypoxia risk score model based on the two genes. Subsequent survival analysis indicated that the high-risk group was associated with poorer prognosis, which was verified by an independent GEO cohort. GSEA analysis showed that the high-risk group was significantly enriched in pathways for tumor progression, such as the JAK-STAT signaling pathway (36), cancer in pathway, TGF-β signaling pathway (37, 38), and NOTCH signaling pathway (39), leading to poor prognosis. In the hypoxic microenvironment, HIFs are the main regulators of hypoxic response (18, 35). HIFs can cause the malignant phenotype of tumors by activating or enhancing JAK-STAT signaling pathway, TGF-β signaling pathway and NOTCH signaling pathway (40–43). Besides, the TCGA data base and qRT-PCR analysis confirmed the overexpression of these two hypoxia genes in tumor tissues and gastric cancer cell lines when compared with normal tissues and gastric normal epithelial cell line. Finally, the risk score model, age, T stage, and N stage were identified as independent risk factors related to OS and included in the nomogram. It showed that the nomogram was an effective tool for predicting the prognosis. The two-gene signature has a powerful ability to predict the prognosis of patients with gastric cancer, and may be helpful to guide clinical treatment decisions.

Tumor purity can reflect the characteristics of the tumor microenvironment. The risk score was significantly positively correlated with infiltrating immune cells and stromal cells, but negatively correlated with tumor purity. Previous studies showed that low tumor purity is associated with poor prognosis of

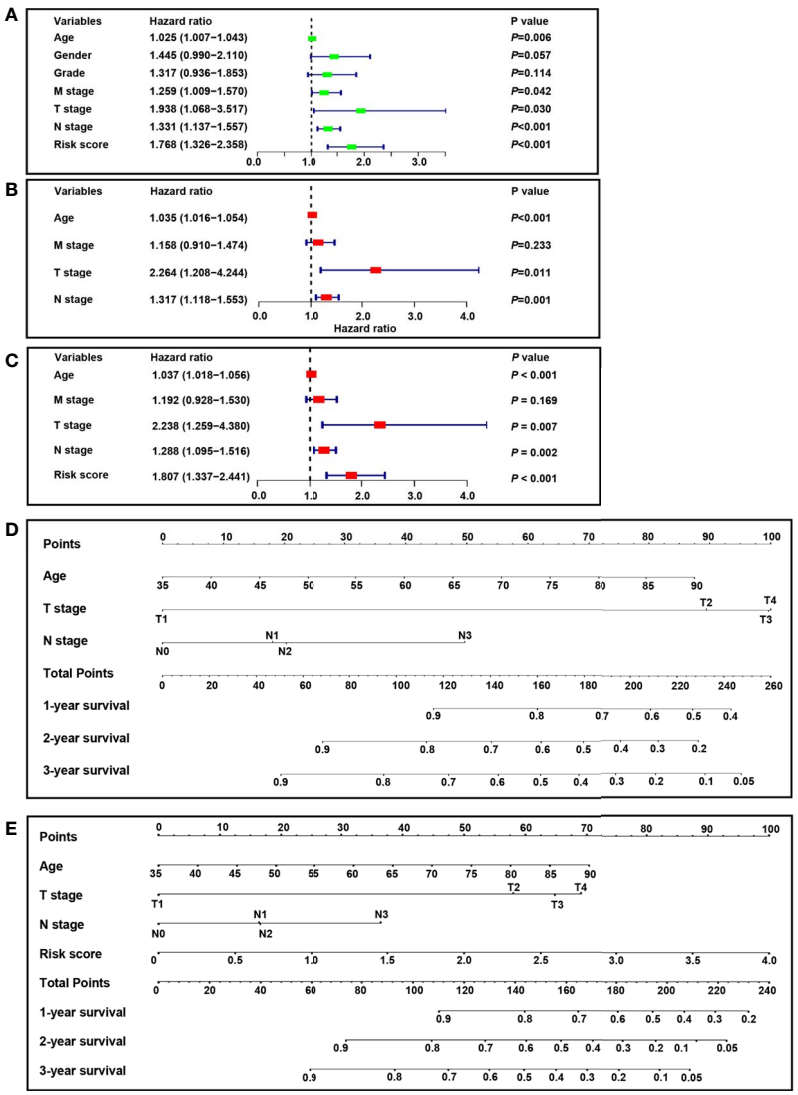

FIGURE 8 | Construction of nomograms. **(A)** Univariate analysis included risk score, age, gender, grade, M stage, T stage and N stage in the screening cohort. **(B)** Cox proportional hazards analysis included age, M stage, T stage and N stage in the screening cohort. **(C)** Cox proportional hazards analysis included risk score, age, M stage, T stage and N stage in the screening cohort. **(D)** Nomogram 1 based on the clinicopathological characteristics. **(E)** Nomogram 2 based on the risk score and clinicopathological characteristics.

multiple tumor types (44–46). We speculated that low-purity tumors may recruit more tumor immunosuppressive cells than high-purity tumors, and further studied the relationship between the risk score and the subtypes of infiltrating immune cells. We found that the tumors in the high-risk group contained more infiltrating immunosuppressive cells such as Tregs, macrophages, neutrophils, para-inflammatory and mast cells than the low-risk group. A previous study found that Tregs suppressed the anti-tumor immune response by weakening the cell-mediated immune response to tumors, thereby promoting disease progression (47). Hypoxia can protect tumors from the intrinsic anti-tumor immune response by forming an immunosuppressive microenvironment, which may explain a poor prognosis of the high-risk group.

Cytokine are important factors in regulating tumor immunity. Among them, tumor immunosuppressive cytokines are important factors inhibiting immune cell activity. Transforming growth factor-β (TGF-β) suppresses the immune system by inhibiting the maturation of dendritic cells, inhibiting the activity of NK cells, and reducing the cytotoxicity of T cells (47, 48). Interleukin 10 (IL-10) is an immunosuppressive cytokine secreted by T-helper 2 (Th2) cells, Tregs, and M2 macrophages. It has been shown to impair the proliferation, cytokine production and migration capabilities of effector T cells (49). IL-10 also promotes the stable

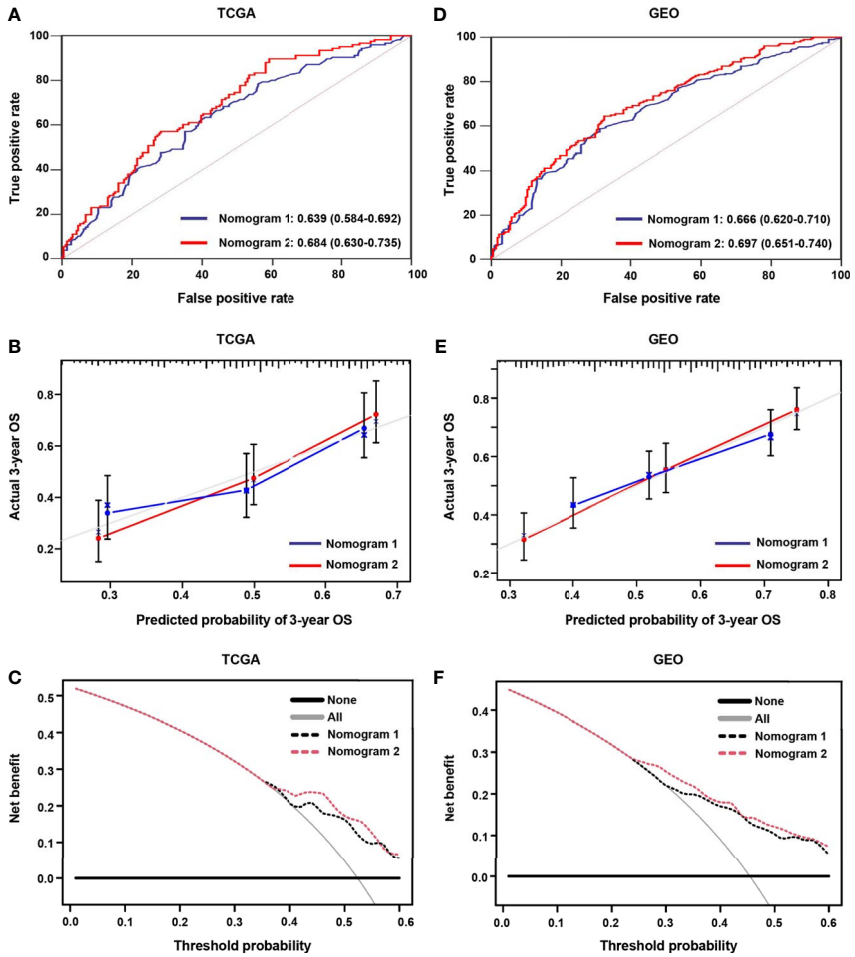

FIGURE 9 | The areas under the curve (AUC), calibration curve and decision curve analysis (DCA) for predicting patient survival. **(A, D)** The AUCs assess the accuracy of the nomograms in the screening and validation cohorts. **(B, E)** The calibration curves assess the consistency of the nomograms in the screening and validation cohorts. **(C, F)** DCAs assess the clinical usefulness of nomograms in the screening and validation cohorts.

expression of Foxp3, TGF-β-receptor 2 and TGF-β, thereby stabilizing the phenotype and functions of Treg (50). In our research, the immunosuppressive cytokines, such as IL-10 and TGF-β, were up-regulated in the high-risk group, thereby further promoting immunosuppression.

The correlation between the intrinsic escape mechanism and risk score is clinically important. The inherent immune escape of tumors demonstrates that tumor cells can mediate their own immune escape directly. Previous study has illustrated that the expression of immune check-point molecules and tumor immunogenicity are two important aspects of intrinsic immune escape (51). Immune checkpoint molecules play a key role in tumor progression and carcinogenesis by promoting tumor immunosuppression. Malignant tumors can evade immune killing by stimulating immune checkpoint target genes (such as *PD-1*, *PD-L1*, *CTLA-4*, *TGF-β*, and *HAVCR2*). In this study, immune checkpoint molecules of *PD-1*, *TGF-β*, and *HAVCR2* were up-regulated in the high-risk group. This result indicates that tumor cells in the high-risk group express immune checkpoint molecules to protect themselves from attack.

Another potentially significant intrinsic immune escape mechanism is immunogenicity. Some somatic mutations in tumor DNA produce neoantigens, and the antigens from this mutation are recognized and targeted by the immune system, especially after treatment with drugs that activate T cells (52–56). The more somatic mutations are present in a tumor, the more neoantigens it may form. TMB may represent a better estimate of tumor neoantigen burden (57). Here, we found that the high-risk group had a lower proportion of somatic mutations, and the hypoxia risk score was significantly negatively correlated with TMB. Tumor cells in the hyperoxia group produced fewer neoantigens, thus avoiding being recognized and killed by T cells.

To investigate the role of hypoxia risk in drug treatment, our research showed that, the tumors in the high-risk group were not sensitive to most chemotherapy drugs, such as axitinib, bexarotene, bortezomib, and imatinib. However, the tumors in

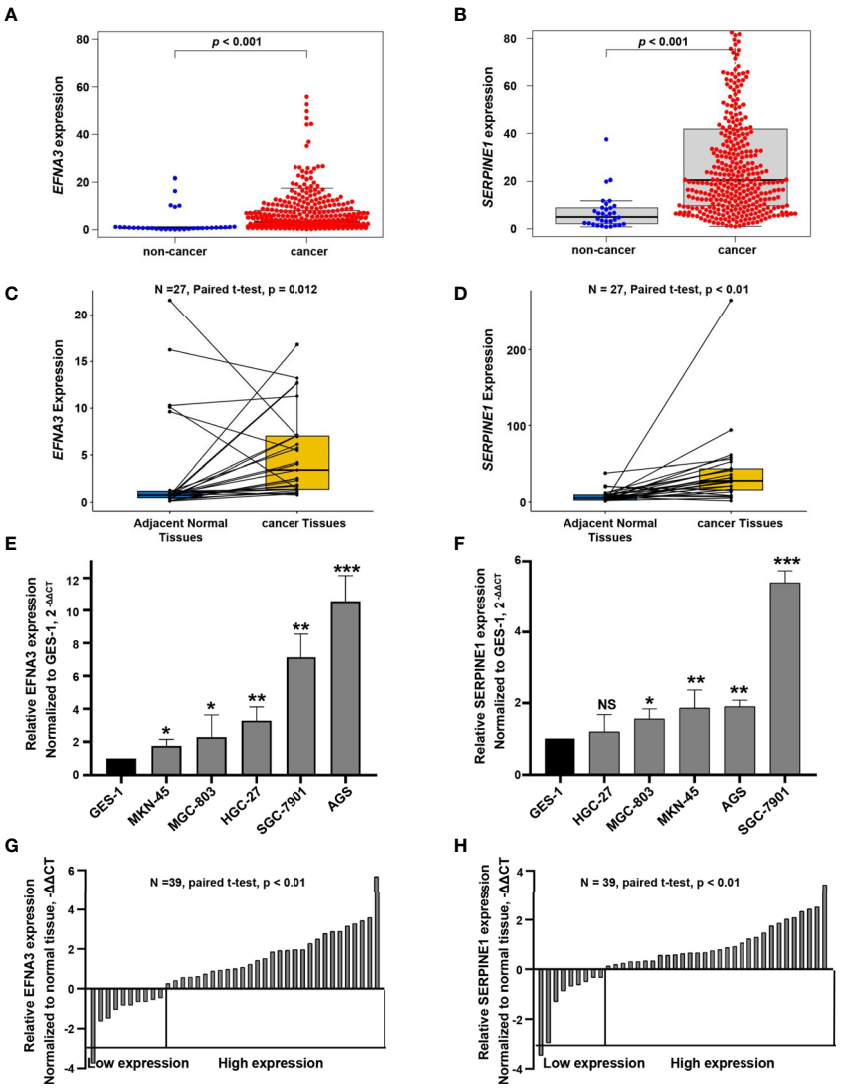

FIGURE 10 | *EFNA3* and *SERPINE1* are upregulated in gastric cancer cell lines and tissues. **(A, B)** Bioinformatics analysis of the expression of *EFNA3* and *SERPINE1* in cancer and non-cancerous tissues in TCGA. **(C, D)** Bioinformatics analysis of the expression of *EFNA3* and *SERPINE1* in 27 pairs of gastric cancer and adjacent non-cancerous tissues in TCGA. **(E, F)** qRT-PCR results of *EFNA3* and *SERPINE1* expression level in GES-1 and gastric cancer cell lines. (Data are presented as mean ± SD. NS: P ≥ 0.05, *$P < 0.05$, **$P < 0.01$, ***$P < 0.001$). **(G, H)** qRT-PCR results of *EFNA3* and *SERPINE1* expression level in 39 pairs of gastric cancer and adjacent non-cancerous tissues. (Data are shown as −ΔΔCT values).

the high-risk group were more sensitive to methotrexate and mitomycin.c and may benefit from these two chemotherapy drugs. Those in the high-risk group express higher levels of *PD-1*, *HAVCR2* and other immune checkpoint molecules to avoid the attack of anti-tumor immune cells. The high-risk group may benefit from immunotherapy, such as the use of *PD-1* and *HAVCR2* inhibitors.

Nomograms are commonly used to assess the prognosis of tumors (58, 59). In this study, we constructed two prognostic nomograms. Nomogram 1 is based on clinical characteristics, and nomogram 2 is developed by the combination of clinical characteristics and the hypoxia risk score model. It showed that the prognostic nomogram based on the combination of clinical characteristics and hypoxia risk score model has better predictive ability and higher clinical usefulness. However, owing to the lack of *in vitro* or *in vivo* experiments, the reliability of our molecular mechanism analysis may be limited.

CONCLUSIONS

In summary, we developed and validated a hypoxia risk score model based on a novel hypoxia-related gene signature revealing the relationship between hypoxia and tumor immune microenvironment. The current study may provide new

insights into how hypoxia affects the prognosis, and may be helpful in guiding targeted hypoxia therapy for gastric cancer.

DATA AVAILABILITY STATEMENT

The datasets analyzed during this current study are available in TCGA (http://cancergenome.nih.gov/) and GEO (https://www.ncbi.nlm.nih.gov/geo, GSE84437) data bases. The data are also available from the corresponding author (zhangchundong2007@126.com or daidq63@163.com) on reasonable request.

ETHICS STATEMENT

The studies involving human participants were reviewed and approved by Ethics Committee of the Medical Association of the Fourth Affiliated Hospital of China Medical University (EC-2021-KS-043). The patients/participants provided their written informed consent to participate in this study.

AUTHOR CONTRIBUTIONS

C-DZ and D-QD have contributed equally to this work as co-corresponding authors. J-PP and C-DZ wrote the main text and performed data analysis. J-PP, C-DZ, and D-QD designed the study and collected the data. All authors contributed to the article and approved the submitted version.

FUNDING

This research was funded in part by the China Scholarship Council (201908050148).

SUPPLEMENTARY MATERIAL

The Supplementary Material for this article can be found online at: https://www.frontiersin.org/articles/10.3389/fimmu.2021.705511/full#supplementary-material

REFERENCES

1. Sung H, Ferlay J L, Siegel R, Laversanne M, Soerjomataram I, Jemal A, et al. Global Cancer Statistics 2020: GLOBOCAN Estimates of Incidence and Mortality Worldwide for 36 Cancers in 185 Countries. *CA: Cancer J Clin* (2021) 71(3):209–49. doi: 10.3322/caac.21660
2. Egner JR. AJCC Cancer Staging Manual. *JAMA J Am Med Assoc* (2010) 304 (15):1726–7. doi: 10.1001/jama.2010.1525
3. Ajani JA, D'Amico TA, Almhanna K, Bentrem DJ, Chao J, Das P, et al. Gastric Cancer, Version 3.2016, NCCN Clinical Practice Guidelines in Oncology. *J Natl Compr Cancer Netw JNCCN* (2016) 14(10):1286. doi: 10.6004/jnccn.2016.0137
4. Shah MA, Ajani JA. Gastric Cancer—An Enigmatic and Heterogeneous Disease. *JAMA J Am Med Assoc* (2010) 303(17):1753–4. doi: 10.1001/jama.2010.553
5. Noh SH, Park SR, Yang HK, Chung HC, Chung IJ, Kim SW, et al. Adjuvant Capecitabine Plus Oxaliplatin for Gastric Cancer After D2 Gastrectomy (CLASSIC): 5-Year Follow-Up of an Open-Label, Randomised Phase 3 Trial. *Lancet Oncol* (2014) 15(12):1389–96. doi: 10.1016/S1470-2045(14)70473-5
6. Khouzam RA, Goutham HV, Zaarour RF, Chamseddine AN, Chouaib S. Integrating Tumor Hypoxic Stress in Novel and More Adaptable Strategies for Cancer Immunotherapy. *Semin Cancer Biol* (2020) 65:140–54. doi: 10.1016/j.semcancer.2020.01.003
7. PaiSheng C, WenTai C, PeiLing H, ShihChieh L, IChen P, ChiaYih W, et al. Pathophysiological Implications of Hypoxia in Human Diseases. *J Biomed Sci* (2020) 27(1):63. doi: 10.1186/s12929-020-00658-7
8. Vaupel P, Kelleher D, Thews O. Modulation of Tumor Oxygenation. *Int J Radiat Oncol Biol Phys* (1998) 42(4):843–8. doi: 10.1016/S0360-3016(98)00324-1
9. Petrova V, Annicchiarico-Petruzzelli M, Melino G, Amelio I. The Hypoxic Tumour Microenvironment. *Oncogenesis* (2018) 7(1):10. doi: 10.1038/s41389-017-0011-9
10. Barbara M, Pilar D, Feda A, Azab AK. The Role of Hypoxia in Cancer Progression, Angiogenesis, Metastasis, and Resistance to Therapy. *Hypoxia* (2015) 3:83–92. doi: 10.2147/HP.S93413
11. Shida M, Kitajima Y, Nakamura J, Yanagihara K, Baba K, Wakiyama K, et al. Impaired Mitophagy Activates mtROS/HIF-1 Alpha Interplay and Increases Cancer Aggressiveness in Gastric Cancer Cells Under Hypoxia. *Int J Oncol* (2016) 48(4):1379–90. doi: 10.3892/ijo.2016.3359
12. Gilkes DM, Semenza GL, Wirtz D. Hypoxia and the Extracellular Matrix: Drivers of Tumour Metastasis. *Nat Rev Cancer* (2014) 14(6):430. doi: 10.1038/nrc3726
13. Barsoum IB, Smallwood CA, Siemens DR, Graham CH. A Mechanism of Hypoxia-Mediated Escape From Adaptive Immunity in Cancer Cells. *Cancer Res* (2014) 74(3):665–74. doi: 10.1158/0008-5472.CAN-13-0992
14. Wang H, Zhao L, Zhu LT, Wang Y, Pan D, Yao J, et al. Wogonin Reverses Hypoxia Resistance of Human Colon Cancer HCT116 Cells *Via* Downregulation of HIF-1α and Glycolysis, by Inhibiting PI3K/Akt Signaling Pathway. *Mol Carcinog* (2014) 53(S1):E107–E18. doi: 10.1002/mc.22052
15. Mucaj V, Shay J, Simon MC. Effects of Hypoxia and HIFs on Cancer Metabolism. *Int J Hematol* (2012) 95(5):464–70. doi: 10.1007/s12185-012-1070-5
16. Takahashi R, Tanaka S, Hiyama T, Ito M, Kitadai Y, Sumii M, et al. Hypoxia-Inducible Factor-1 Alpha Expression and Angiogenesis in Gastrointestinal Stromal Tumor of the Stomach. *Oncol Rep* (2003) 10(4):797–802. doi: 10.3892/or.10.4.797
17. Chen WT, Huang CJ, Wu MT, Yang SF, Su YC, Chai CY. Hypoxia-Inducible Factor-1α Is Associated With Risk of Aggressive Behavior and Tumor Angiogenesis in Gastrointestinal Stromal Tumor. *JPN J Clin Oncol* (2005) 35(4):207–13. doi: 10.1093/jjco/hyi067
18. Zhang J, Xu J, Dong Y, Bo H. Down-Regulation of HIF-1α Inhibits the Proliferation, Migration, and Invasion of Gastric Cancer by Inhibiting PI3K/AKT Pathway and VEGF Expression. *Biosci Rep* (2018) 38(6):BSR20180741. doi: 10.1042/BSR20180741
19. Hao LS, Liu Q, Tian C, Zhang DX, Yuan ZX. Correlation and Expression Analysis of Hypoxiainducible Factor1α, Glucose Transporter 1 and Lactate Dehydrogenase5 in Human Gastric Cancer. *Oncol Lett* (2019) 18(2):1431–41. doi: 10.3892/ol.2019.10457
20. Hanahan D, Coussens L. Accessories to the Crime: Functions of Cells Recruited to the Tumor Microenvironment. *Cancer Cell* (2012) 21(3):309–22. doi: 10.1016/j.ccr.2012.02.022
21. Hanahan D, Weinberg RA. The Hallmarks of Cancer. *Cell* (2000) 100(1):57–70. doi: 10.1016/S0092-8674(00)81683-9
22. Lazăr D, Avram MF, Romoșan I, Cornianu M, Tăban S, Goldiș A. Prognostic Significance of Tumor Immune Microenvironment and Immunotherapy: Novel Insights and Future Perspectives in Gastric Cancer. *World J Gastroenterol* (2018) 24(32):3583–616. doi: 10.3748/wjg.v24.i32.3583
23. Lin W, Wu S, Chen X, Ye Y, Qiu S. Characterization of Hypoxia Signature to Evaluate the Tumor Immune Microenvironment and Predict Prognosis in Glioma Groups. *Front Oncol* (2020) 10:796. doi: 10.3389/fonc.2020.00796
24. Zhang B, Tang B, Gao J, Li J, Qin L. A Hypoxia-Related Signature for Clinically Predicting Diagnosis, Prognosis and Immune Microenvironment of Hepatocellular Carcinoma Patients. *J Trans Med* (2020) 18(1):342. doi: 10.21203/rs.3.rs-17783/v3
25. Yoon SJ, Park J, Shin Y, Choi Y, Huh YM. Deconvolution of Diffuse Gastric Cancer and the Suppression of CD34 on the BALB/c Nude Mice Model. *BMC Cancer* (2020) 20(1):314. doi: 10.1186/s12885-020-06814-4

26. Tibshirani R. The LASSO Method for Variable Selection in the Cox Model. *Stat Med* (1997) 16(4):385–95. doi: 10.1002/(SICI)1097-0258(19970228)16:4<385::AID-SIM380>3.0.CO;2-3
27. Yoshihara K, Shahmoradgoli M, Martínez E, Vegesna R, Kim H, Torres-Garcia W, et al. Inferring Tumour Purity and Stromal and Immune Cell Admixture From Expression Data. *Nat Commun* (2013) 4:2612. doi: 10.1038/ncomms3612
28. Taiwen L, Jingxin F, Zexian Z, David C, Jing L, Qianming C, et al. TIMER2.0 for Analysis of Tumor-Infiltrating Immune Cells. *Nucleic Acids Res* (2020) 48 (W1):W509–W14. doi: 10.1093/nar/gkaa407
29. Subramanian A, Tamayo P, Mootha VK, Mukherjee S, Ebert BL, Gillette MA, et al. Gene Set Enrichment Analysis: A Knowledge-Based Approach for Interpreting Genome-Wide Expression Profiles. *Proc Natl Acad Sci USA* (2005) 102(43):P.15545–50. doi: 10.1073/pnas.0506580102
30. Pages F, Mlecnik B, Marliot F, Bindea G, Ou FS, Bifulco C, et al. International Validation of the Consensus Immunoscore for the Classification of Colon Cancer: A Prognostic and Accuracy Study. *Lancet* (2018) 391(10135):2128–39. doi: 10.1016/S0140-6736(18)30789-X
31. Fitzgerald M, Saville BR, Lewis RJ. Decision Curve Analysis. *JAMA* (2015) 313 (4):409–10. doi: 10.1001/jama.2015.37
32. Vickers AJ, Elkin EB. Decision Curve Analysis: A Novel Method for Evaluating Prediction Models. *Med Decision Making* (2006) 26(6):565–74. doi: 10.1177/0272989X06295361
33. Brahimi-Horn MC, Chiche J, Pouysségur J. Hypoxia and Cancer. *J Mol Med* (2007) 85(12):1301–7. doi: 10.1007/s00109-007-0281-3
34. Rosella FA, Lucia C, Michela S, Veronica Z, Stefano G, Reay MA. Hypoxia-Induced Alternative Splicing: The 11th Hallmark of Cancer. *J Exp Clin Cancer Res: CR* (2020) 39(1):110. doi: 10.1186/s13046-020-01616-9
35. Schito L, Semenza GL. Hypoxia-Inducible Factors: Master Regulators of Cancer Progression. *Trends Cancer* (2016) 2(12):758–70. doi: 10.1016/j.trecan.2016.10.016
36. Owen KL, Brockwell NK, Parker BS. Jak-STAT Signaling: A Double-Edged Sword of Immune Regulation and Cancer Progression. *Cancers* (2019) 11 (12):2002. doi: 10.3390/cancers11122002
37. Yang L, Pang Y, Moses HL. TGF-Beta and Immune Cells: An Important Regulatory Axis in the Tumor Microenvironment and Progression. *Trends Immunol* (2010) 31(6):220–7. doi: 10.1016/j.it.2010.04.002
38. Ming LS, Ming O. Tgf-β Control of Adaptive Immune Tolerance: A Break From Treg Cells. *BioEssays* (2018) 40(11):e1800063. doi: 10.1002/bies.201800063
39. Goruganthu MUL, Shanker A, Dikov MM, Carbone DP. Specific Targeting of Notch Ligand-Receptor Interactions to Modulate Immune Responses: A Review of Clinical and Preclinical Findings. *Front Immunol* (2020) 11:1958. doi: 10.3389/fimmu.2020.01958
40. Tian Q, Yan X, Zheng W, Sun R, Ji W, Wang X, et al. Overexpression of Hypoxia-Inducible Factor 1α Induces Migration and Invasion Through Notch Signaling. *Int J Oncol* (2015) 47(2):728–38. doi: 10.3892/ijo.2015.3056
41. Chen J, Imanaka N, Chen J, Griffin JD. Hypoxia Potentiates Notch Signaling in Breast Cancer Leading to Decreased E-cadherin Expression and Increased Cell Migration and Invasion. *Br J Cancer* (2010) 102(2):351–60. doi: 10.1038/sj.bjc.6605486
42. Tirpe AA, Gulei D, Ciortea SM, Crivii C, Berindan-Neagoe I. Hypoxia: Overview on Hypoxia-Mediated Mechanisms With a Focus on the Role of HIF Genes. *Int J Mol Sci* (2019) 20(24):6140. doi: 10.3390/ijms20246140
43. Young LM, Hee JY, Joung LE, Jong-Hwan P, Sang-Kyu Y, Taekyu P, et al. Phosphorylation and Activation of STAT Proteins by Hypoxia in Breast Cancer Cells. *Breast* (2006) 15(2):187–95. doi: 10.1016/j.breast.2005.05.005
44. Gong Z, Zhang J, Guo W. Tumor Purity as a Prognosis and Immunotherapy Relevant Feature in Gastric Cancer. *Cancer Med* (2020) 9(23):9052–63. doi: 10.1002/cam4.3505
45. Zhang C, Cheng W, Ren X, Wang Z, Liu X, Li G, et al. Tumor Purity as an Underlying Key Factor in Glioma. *Clin Cancer Res* (2017) 23(20):6279–91. doi: 10.1158/1078-0432.CCR-16-2598
46. Mao Y, Feng Q, Zheng P, Yang L, Liu T, Xu Y, et al. Low Tumor Purity Is Associated With Poor Prognosis, Heavy Mutation Burden, and Intense Immune Phenotype in Colon Cancer. *Cancer Manage Res* (2018) 10:2569–3577. doi: 10.2147/CMAR.S171855
47. Nishikawa H, Sakaguchi S. Regulatory T Cells in Cancer Immunotherapy. *Ann New York Acad Sci* (2014) 27(1):1–7. doi: 10.1016/j.coi.2013.12.005
48. Haque S, Morris JC. Transforming Growth Factor-β: A Therapeutic Target for Cancer. *Hum Vaccines Immunotherapeutics* (2017) 13(8):1741–50. doi: 10.1080/21645515.2017.1327107
49. Dennis KL, Blatner NR, Gounari F, Khazaie K. Current Status of Interleukin-10 and Regulatory T-Cells in Cancer. *Curr Opin Oncol* (2013) 25(6):637–45. doi: 10.1097/CCO.0000000000000006
50. Barbi J, Pardoll D, Pan F. Treg Functional Stability and Its Responsiveness to the Microenvironment. *Immunol Rev* (2014) 259(1):115–39. doi: 10.1111/imr.12172
51. Schreiber RD, Old LJ, Smyth MJ. Cancer Immunoediting: Integrating Immunity's Roles in Cancer Supression and Promotion. *Science* (2011) 331 (6024):1565–70. doi: 10.1126/science.1203486
52. Snyder A, Makarov V, Merghoub T, Yuan J, Zaretsky J, Desrichard A, et al. Genetic Basis for Clinical Response to CTLA-4 Blockade in Melanoma. *N Engl J Med* (2014) 372(23):2189–99. doi: 10.1056/NEJMoa1406498
53. Matsushita H, Vesely M, Koboldt D, Rickert C, Uppaluri R, Magrini V, et al. Cancer Exome Analysis Reveals a T-Cell-Dependent Mechanism of Cancer Immunoediting. *Nature* (2012) 482(7385):400–4. doi: 10.1038/nature10755
54. Riaz N, Morris L, Havel J, Makarov V, Desrichard A, Chan T. The Role of Neoantigens in Response to Immune Checkpoint Blockade. *Int Immunol* (2016) 28(8):411–9. doi: 10.1093/intimm/dxw019
55. Ott PA, Zhuting H, Keskin DB, Shukla SA, Jing S, Bozym DJ, et al. An Immunogenic Personal Neoantigen Vaccine for Patients With Melanoma. *Nature* (2018) 547(7662):217–21. doi: 10.1038/nature22991
56. Cohen CJ, Gartner JJ, Horovitz-Fried M, Shamalov K, Robbins PF. Isolation of Neoantigen-Specific T Cells From Tumor and Peripheral Lymphocytes. *J Clin Invest* (2015) 125(10):3981–91. doi: 10.1172/JCI82416
57. Chan TA, Yarchoan M, Jaffee E, Swanton C, Quezada SA, Stenzinger A, et al. Development of Tumor Mutation Burden as an Immunotherapy Biomarker: Utility for the Oncology Clinic. *Ann Oncol* (2019) 30(1):44–56. doi: 10.1093/annonc/mdy495
58. Pei JP, Zhang CD, Liang Y, Zhang C, Dai DQ. Novel Nomograms Individually Predicting Overall Survival of Non-Metastatic Colon Cancer Patients. *Front Oncol* (2020) 10:733. doi: 10.3389/fonc.2020.00733
59. Alexia I, Deborah S, V RG, S PK. How to Build and Interpret a Nomogram for Cancer Prognosis. *J Clin Oncol* (2008) 26(8):1364–70. doi: 10.1200/JCO.2007.12.9791

Conflict of Interest: The authors declare that the research was conducted in the absence of any commercial or financial relationships that could be construed as a potential conflict of interest.

Copyright © 2021 Pei, Zhang, Yusupu, Zhang and Dai. This is an open-access article distributed under the terms of the Creative Commons Attribution License (CC BY). The use, distribution or reproduction in other forums is permitted, provided the original author(s) and the copyright owner(s) are credited and that the original publication in this journal is cited, in accordance with accepted academic practice. No use, distribution or reproduction is permitted which does not comply with these terms.

frontiers in Immunology

ORIGINAL RESEARCH
published: 16 July 2021
doi: 10.3389/fimmu.2021.717505

Follistatin-Like 3 Correlates With Lymph Node Metastasis and Serves as a Biomarker of Extracellular Matrix Remodeling in Colorectal Cancer

Chao Yang, Fengyu Cao, Shuoyang Huang and Yongbin Zheng *

Department of Gastrointestinal Surgery, Renmin Hospital of Wuhan University, Wuhan, China

OPEN ACCESS

Edited by:
Peng Qu,
National Institutes of Health (NIH), United States

Reviewed by:
Lele Song,
University of Pennsylvania, United States
Lin Jiang,
University of Cincinnati, United States

***Correspondence:**
Yongbin Zheng
yongbinzheng@whu.edu.cn

Specialty section:
This article was submitted to Cancer Immunity and Immunotherapy, a section of the journal Frontiers in Immunology

Received: *31 May 2021*
Accepted: *30 June 2021*
Published: *16 July 2021*

Citation:
Yang C, Cao F, Huang S and Zheng Y (2021) Follistatin-Like 3 Correlates With Lymph Node Metastasis and Serves as a Biomarker of Extracellular Matrix Remodeling in Colorectal Cancer. Front. Immunol. 12:717505. doi: 10.3389/fimmu.2021.717505

Background: As a heterogeneous disease, colorectal cancer (CRC) presents a great challenge to individualized treatment due to its lymph node metastasis (LNM). Existing studies have shown that immune and stromal components in extracellular matrix (ECM) act as important part in tumorigenicity and progression, while their roles in LNM have not been fully elucidated. Here, crucial ECM-related genes responsible for LNM in CRC were selected by multi-omics analysis.

Methods: Firstly, we characterized the immune infiltration landscape of CRC samples from The Cancer Genome Atlas (TCGA) and the Gene Expression Omnibus (GEO) databases by using ssGSEA algorithm. The CRC patients were divided into several immune subgroups by hierarchical clustering analyses. Then, differential genes were identified among immune subgroups and CRC *vs.* normal tissues in TCGA and GEO GSE39582 cohorts, respectively. Next, weighted correlation network analysis (WGCNA) was employed to construct a co-expression network to find LNM-related modules and hub genes. Subsequently, we evaluated the clinical value of hub gene in prognostic prediction and chemotherapy/immunotherapy. Besides, the protein level of key gene was verified in an external cohort from our center. Finally, we explored the underlying mechanism of FSTL3-mediated LNM by Gene function annotation and correlation analysis.

Results: Two immune subgroups, namely Immunity_High and Immunity_Low, were defined among the two CRC cohorts using ssGSEA algorithm, respectively. Based on the two immune subgroups, 2,635 overlapping differentially expressed genes were obtained from two cohorts, which were sequentially subjected to WGCNA and univariate Cox regression analysis. Ultimately, *FSTL3* was selected as the key gene. Here, we first confirmed that overexpression of *FSTL3* correlated with LNM and worse prognosis in CRC and was verified at the protein level in the external validation cohort. Moreover, FSTL3 expression showed strongly positive correlation with immune and stromal components in ECM. We furthermore found that FSTL3 may accelerate LNM

through the formation of inhibitory immune microenvironment *via* promoting macrophage and fibroblast polarization and T cell exhaustion. Interestingly, high FSTL3 expression is linked to chemoresistance, but immunotherapy-sensitive.

Conclusion: FSTL3 is identified as a biomarker for ECM remodeling and worse clinical outcomes for the first time in CRC and is also a potential immunotherapeutic target to block LNM for CRC.

Keywords: colorectal cancer, lymph node metastasis, extracellular matrix, tumor microenvironment, follistatin-like 3

INTRODUCTION

Colorectal cancer (CRC), the third most common gastrointestinal malignant disease around the world, ranks second in terms of cancer-related mortality (1). Lymph nodes are common metastatic site of major types of human malignancies, including CRC. Lymph node metastasis (LNM) is a crucial event of tumor cell dissemination in that the CRC cells in the primary site spread through the lymphatic vessels to the adjacent lymph nodes (2). Usually, advanced CRC is characterized by metastases to the regional lymph nodes or distant organs, which always leads to worse prognosis. The incidence of LNM in all of CRC patients has been reported ranging from 40.5 to 49.7% (3–5). Meanwhile, LNM also is one of the most important prognostic risk factor and often predicts a poor outcome. Studies have shown that the 5-year overall survival (OS) rate is as high as 56.7 to 94.8% in CRC patients without LNM, but only 16.7 to 48% in patients with LNM-positive (6–8). Moreover, a certain number of LNM represent a key risk factor strongly associated with distant metastasis and local recurrence in CRC (9, 10). Therefore, it is necessary to identify relevant genes or elucidate potential molecular mechanisms of LNM in order to develop effective prevention and treatment strategies for CRC.

In recent years, the interaction between the tumor microenvironment (TME) and tumors has become an important aspect of tumor biology research, because it is closely related to the exploration of tumor pathogenesis and the sensitivity of immunotherapy (11, 12). The success of immunotherapy in several cancer types highlights the vital role of TME. However, as a heterogeneous disease, CRC presents a great challenge to individualized treatment due to its diversity of phenotypes and dismal prognosis. A growing body of evidence shows that tumor cells acquire stronger ability to invade and metastasize through intricate bidirectional dynamical tumor–stromal interactions in CRC (13–15). It was reported that B cells, as the major tumor infiltrating immune cells (TIICs) in TME, are able to promote lymphangiogenesis *via* targeting HSPA4 and VEGF-A, suggesting that immune components have a vital role in LNM (16). Other non-tumor cells in TME, including macrophages, fibroblasts, and neutrophils, have also been reported to act a pivotal role in progression and migration of CRC (17–19). On the other side, in TME, the composition and function of TIICs can vary slightly according to tumor progression and host immune status (20). TIICs are closely related to clinicopathological characteristics and prognosis, as well as to the efficacy of immunotherapy (21, 22). In order to obtain the best outcome of immunotherapy, it is essential to identify immune-related genes in tumor-specific phenotypes and to investigate the possible mechanisms of their functions. Hence, this study aims to discern some crucial genes involved in immune microenvironment and LNM in order to obtain better treatment results for the CRC patients with LNM.

MATERIALS AND METHODS

Study Design and Data Acquisition

Flow chart of the present research is shown in **Figure 1**. Transcriptome data (level 3 data) of RNA-seq and paired clinical data were downloaded from the TCGA CRC cohort (National Cancer Institute (NCI) and National Human Genome Research Institute (NHGRI), Bethesda, Maryland, the USA, Data Release 25.0—July 22, 2020, https://portal.gdc.cancer.gov/repository). The RNA-seq transcriptome data (FPKM) were annotated using the human General Transfer Format (hunman.gtf) from the Ensembl database (https://www.ensembl.org/) with the Strawberry Perl software (*version 5.28.2.1*, https://strawberryperl.com/).

Gene expression microarray data and clinical information of GEO GSE39582 were downloaded as a series of matrix files (23, 24). Probe IDs were matched to gene symbols using the GPL570 platform (Affymetrix Human Genome U133 Plus 2.0 Array). The mean expression value of the probes is used as the expression value for the gene in question if multiple probes were mapped to a single gene.

Criteria for study exclusion were (1): patients with unknown survival status, survival time, and N_stage; and (2) patients who died within a follow-up period of 30 days (**Table S1**).

Specimens and Immunohistochemistry

Paraffin-embedded tissues of 68 primary CRC patients and corresponding clinical information were obtained from the Gastrointestinal Surgery Department of Renmin Hospital of Wuhan University. None of the patients received any radiotherapy or chemotherapy before the operation. The tissue specimens were collected from January 2016 to December 2017, and all patients have signed a prior informed consent. The last follow-up time was January 9, 2021. This study was approved by the Medical Ethics Committee of the Renmin Hospital of Wuhan University.

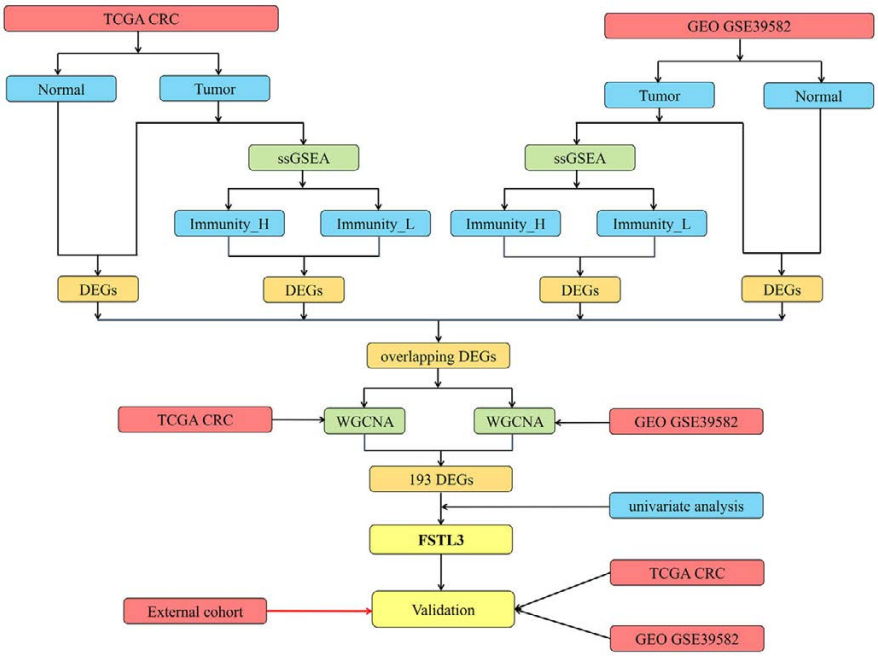

FIGURE 1 | Flow chart of the present research.

IHC staining of paraffin-embedded tissues with antibody against FSTL3 (1:25; Absin, abs101405, Shanghai, China) was performed according to standard procedures as previously described (25), and scores were recorded. The expression level of FSTL3 is evaluated according to the total histochemical score, which is calculated as the product of staining intensity and the positive cell proportion. The staining intensity is recorded as 0 (negative), 1 (weak), 2 (moderate), and 3 (strong). The positive cell proportion is scored as 0, 1, 2, 3, and 4, referring to 0, <25, 26–50, 51–75, and 76–100%.

Clustering of CRC Samples by Single-Sample Gene Set Enrichment Analysis

The 29 immune-associated gene sets, representing diverse immune cell types, cytokine/cytokine receptor, human leukocyte antigen (HLA), immune checkpoints, immune-related pathways, and functions in TME, were obtained from a previous study (**Table S2**) (26). The enrichment scores of the 29 immune-associated gene sets in each CRC sample were quantified by ssGSEA algorithm using R package *GSVA* and *GSEABase* (27). Based on the enrichment score, the CRC patients in the TCGA and GEO GSE39582 cohorts were clustered into different immune subgroups by using R package *sparcl* (https://CRAN.R-project.org/package=sparcl).

Assessment of the Effectiveness of Immune Clustering

The Immune/StromalScore, ESTIMATEScore, and TumorPurity were calculated by ESTIMATE algorithm in the TCGA and GEO cohorts to estimate the level of immune and stromal cells infiltrating in CRC (28). The relative proportion of 22 immune cells in CRC patients was calculated by the CIBERSORT deconvolution algorithm (29).

Identification Differentially Expressed Genes

The R package *limma* was used to identify the DEGs among different immune subgroups, and False Discovery Rates (FDRs) < 0.05 were considered as selection criteria (30). The intersection DEGs were yielded using Venn analysis and visualized by R package *VennDiagram* (31). Firstly, we picked up overlapping differential genes between Immunity_H and Immunity_L in the TCGA and GSE39582 cohorts. Meanwhile, we acquired common differential genes between CRC and normal tissues in the TCGA and GSE39582 cohorts. Finally, we regarded the intersection of the above-mentioned results as the ultimate gene set for subsequent analyses.

Construction of a Co-Expression Network and Recognition of the Modules Related to LNM

In this study, weighted correlation network analysis (WGCNA) algorithm is employed to construct a co-expression network to find modules associated with LNM using R package *WGCNA* (32). All of intersection genes are included into this co-expression network. Pearson correlation matrix is constructed for all gene pairs, and unsupervised hierarchical clustering analysis is performed on the basis of topological overlap matrix. Then the modules with different power values are analyzed for scale independence and average connectivity to obtain the soft

threshold parameters. The optimal power value is automatically captured by the software. In this research, we set the minimal module size as 2 and the scale-independent value as 0.9 to identify the key modules correlated with LNM. Significant modules with LNM are determined using Pearson's correlation test. A *P*-value less than 0.05 is accepted as a statistically significant difference. Venn diagram is used to select the intersection genes from WGCNA analysis among the TCGA and GEO cohorts.

Key Gene Screening

Based on results of the previous steps, univariate Cox proportional hazard analysis is used to screen the genes with prognostic value. Consequently, these selection genes are considered as key genes associated with both the immune status, prognosis value and LNM.

Statistical Analysis

Kruskal–Wallis test was used to compare gene expression in different samples. The correlation between gene expression and clinical characteristics was evaluated by Wilcoxon rank sum test or Chi-square test. The above analysis was performed in R software (version 4.0.2, https://www.r-project.org/). All statistical tests are two-tailed with a statistical significance level set at 0.05 in this study.

RESULTS

Unsupervised Cluster Analysis Identified Two CRC Subtypes

A total of 493 CRC samples from TCGA and 546 from GEO GSE39582 were included in this analyses. An unsupervised hierarchical clustering analysis was performed based on the ssGSEA scores of the 29 immune-associated gene sets (**Supplement Figures 1A, B**). The two datasets showed similar clustering results. Two immune subgroups, namely Immunity High (Immunity_H) and Immunity Low (Immunity_L) were defined among the CRC patients from two cohorts (**Figures 2A, B**).

Correlation of CRC Immune Subtypes With Tumor Immune Microenvironment

In order to verify the feasibility and effectiveness of the above grouping strategy, we compared the ImmuneScore, StromalScore, ESTIMATE Score, and TumorPurity between two subgroups. The Immunity_H subtype had a higher level of ImmuneScore, StromalScore and ESTIMATEScore than the Immunity_L subtype (**Figures 3A–C, E–G**). The changing trend of TumorPurity between two subtypes was just the opposite, indicating that Immunity_L samples contained higher number of tumor cells (**Figures 3D, H**). As shown in the box plot chart, significant differences were found in the immune checkpoint (CD274, CTLA4, and LAG3) expression levels between two immune subtypes (**Figures 3I–N**). In addition, the two groups demonstrated marked differences in the abundance of multiple of kinds of immune cells based on the CIBERSORT algorithm (**Figures 3O, P**). In summary, these results suggest that this grouping strategy is effective and can be used for subsequent study.

Identification of Differentially Expressed Genes

Firstly, 9,008 DEGs were identified by comparing the mRNA expression profiles across the Immunity_H and Immunity_L subtypes in TCGA cohort (**Figure 4A**). Similarly, 8,326 DEGs were identified in GEO GSE39582 cohort (**Figure 4B**). Secondly, 13,201 DEGs were obtained by comparing the mRNA expression profiles between tumor and normal samples in TCGA cohort (**Figure 4C**). Likewise, 11,936 DEGs were identified in GEO GSE39582 cohort (**Figure 4D**). There were 5,256 overlapping differential genes between Immunity_H and Immunity_L, and 7,631 overlapping differential genes between CRC and normal tissues in the TCGA and GSE39582 cohorts (**Figures 4E, F**). Finally, a total of 2,635 overlapping DEGs were obtained (**Figure 4G** and **Table S3**).

Identification of Modules Related to LNM by WGCNA

In this step, all 2,635 overlapping DEGs were contributed to the construction of co-expression network according to the following processes. Firstly, a sample clustering tree was drawn including all 493 CRC samples in the TCGA cohort (**Figure 5A**). Then, the scale independent value exceeded 0.9 with a low average connectivity when soft threshold power was 5 (**Figure 5B**). As shown in **Figure 5C**, WGCNA generated eight modules containing different colors after merging similar modules. Both the black, gray, and turquoise modules were

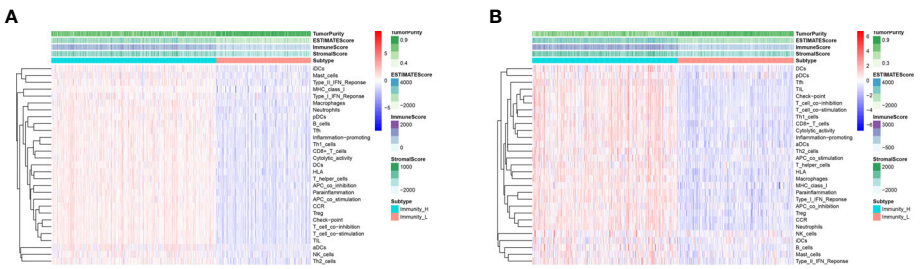

FIGURE 2 | Unsupervised Cluster Analysis Identified two CRC subtypes. **(A, B)** Two immune subtypes, namely Immunity High (Immunity_H) and Immunity Low (Immunity_L), were yielded by the hierarchical clustering from the TCGA **(A)** and GEO GSE39582 **(B)** cohorts.

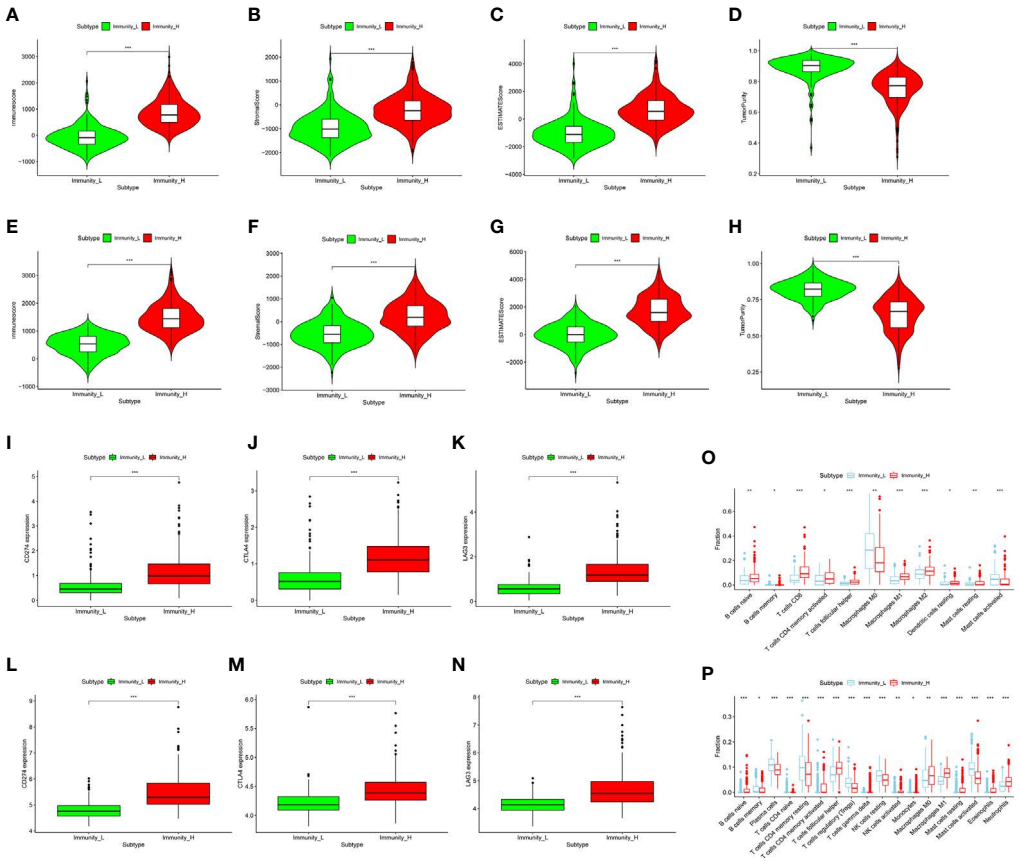

FIGURE 3 | Correlation of CRC Immune Subtypes With Tumor immune Microenvironment. **(A–D)** The violin plots showed that there were significant differences in ImmuneScore **(A)**, StromalScore **(B)**, ESTIMATE Score **(C)**, and TumorPurity **(D)** between the two subtypes in the TCGA cohort (both $P < 0.001$). **(E–H)** The same results were obtained in GEO GSE39582 cohort. **(I–K)** The expression of immune checkpoints, including CD274 **(I)**, CTLA-4 **(J)**, and LAG3 **(K)**, in Immunity_H (red) are all significantly higher than that in Immunity_L (green) in TCGA cohort (both $P < 0.001$). **(L–N)** The same results were also obtained in GEO GSE39582 cohort. **(O, P)** The boxplots showed the abundance difference of each immune cell between the Immunity_H (red) and the Immunity_L (blue) in TCGA **(O)** and GEO GSE39582 **(P)** cohorts. (*$P < 0.05$, **$P < 0.01$, ***$P < 0.001$).

closely correlated with LNM ($r \geq 0.14$, $P < 0.01$). Since gray module has only two genes, we included black and turquoise modules into further analysis.

In GEO GSE39582 cohort, a sample clustering tree, including 545 CRC samples, was drawn after removing one outlier sample (GSM972311) (**Figure 5D**). The optimal power value was still 5, which was automatically selected by the software (**Figure 5E**). A total of eight modules were obtained through average hierarchical clustering. The blue module showed the highest correlation with LNM (**Figure 5F**, $r = 0.11$, $P = 0.01$).

Key Gene Screening by Univariate Cox Proportional Hazards Analysis

Based on results of the WGCNA, 193 shared genes were extracted from modules closely related to LNM both in TCGA and GEO cohorts (**Figure 5G**, **Table S4**). Afterwards, univariate Cox proportional hazards analysis was carried out on those shared genes. Of the 193 overlapping genes evaluated, only four genes, namely CAV2, STC1, FSTL3, and FOXC1, were considered to be closely related to OS (**Figure 5H**, $P < 0.05$). Of them, FSTL3, related to both immune status and LNM, has previously hardly been reported in CRC. Hence, FSTL3 was selected as key gene of CRC to comprehensively investigate its value in TME and LNM in the current study.

Overexpression of FSTL3 mRNA Correlated With Tumor Malignancy in CRC

The mRNA expression level of FSTL3 was markedly higher in the tumor samples than that in paired adjacent normal samples ($P = 1.2e\text{-}07$, **Figure 6A**). Meanwhile, FSTL3 mRNA expression level in cancer tissues was also higher than that in normal tissues ($P = 2.1e\text{-}09$, **Figure 6B**).

The correlation between FSTL3 expression level and the clinicopathological characteristics of CRC was further investigated. The results indicated that FSTL3 expression level was in remarkable association with AJCC stage ($P = 0.0064$, **Figure 6C**) and N stage ($P = 0.004$, **Figure 6D**). Similar results were gained from GEO GSE39582 (**Figures 6E–G**). Those results

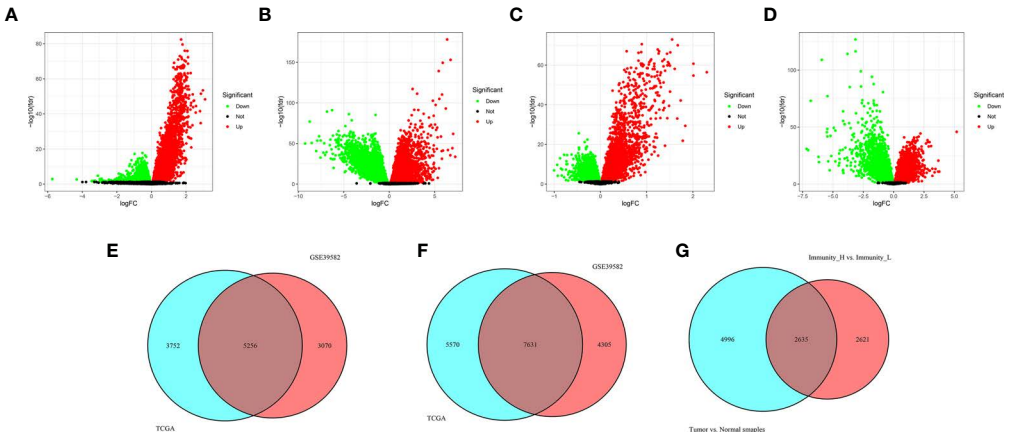

FIGURE 4 | Identification differentially expressed genes. **(A, B)** The volcano plots showed the differential genes between Immunity_H and Immunity_L **(A)**, and between CRC and normal tissues **(B)** in the TCGA cohort. Each red dot represents upregulated gene, each green dot represents upregulation gene, and each black dot represents no significant difference gene. **(C, D)** The volcano plots showed the differential genes between Immunity_H and Immunity_L **(C)**, and between CRC and normal tissues **(D)** in the GSE39582 cohorts. **(E)** Overlapping differential genes between Immunity_H and Immunity_L in the TCGA and GSE39582 cohorts. **(F)** Overlapping differential genes between CRC and normal tissues in the TCGA and GSE39582 cohorts. **(G)** A total of 2,635 overlapping DEGs were obtained.

suggested that FSTL3 is significantly overexpressed in CRC and strongly correlated with tumor malignancy.

High FSTL3 mRNA Level Indicates Worse Clinical Outcomes in CRC

Because our findings highlighted that FSTL3 correlated with tumor malignancy, we next went on to investigate its prognostic value in CRC. The CRC patients were divided into low- and high-expression groups based on optimal cutoff value of FSTL3 expression, which was determined using the 'surv_cutpoint' algorithm of the R package *survminer* (https://CRAN.R-project.org/package=survminer). The prognostic significance of FSTL3 was analyzed by Kaplan–Meier survival curves with Log-rank test. The results implied that higher FSTL3 mRNA expression was notably correlated with OS, disease-free survival (DFS), progression free survival, as well as disease-specific survival in CRC patients utilizing data from TCGA cohort (**Figures 6H–K**). Consistent results were obtained in GEO GSE39582 cohort (**Figures 6L, M**). Besides, univariate and multivariate Cox proportional hazards analysis were employed to assess whether FSTL3 could be used as an independent prognostic indicator in CRC patients. The results showed that the FSTL3 is an independent unfavorable prognostic factor both in TCGA (**Figures 6N, O**) and GEO GSE39582 (**Figures 6P, Q**) cohorts.

FSTL3 Protein Is Remarkably Upregulated in CRC and Associated With Poor Prognosis

To further verify the role of FSTL3 protein in CRC progression, IHC was conducted to evaluate the FSTL3 protein expression in 68 human CRC specimens. The results showed that compared with adjacent normal tissue, FSTL3 protein was significantly overexpressed in tumor tissues (P = 1.6e-5, **Figures 7A, B**). Further analysis revealed that the FSTL3 protein was strikingly correlated to AJCC stage (P = 0.0007, **Figure 7C**) and LNM (P < 0.05, **Figure 7D**). Additionally, we evaluated the prognostic value of FSTL3 protein expression in CRC. The cutoff value of total histochemical score in survival analysis was set according to the optimal threshold. Kaplan–Meier curve showed that CRC patients with high FSTL3 protein have shorter OS compared to those with lower FSTL3 protein (P = 1.228e-4, **Figure 7E**). The obtained results confirmed that the FSTL3 protein expression is related to LNM and always indicates worse clinical outcomes in CRC.

Functional Annotation Among the High and Low FSTL3 Expression Groups

DEGs between high and low FSTL3 groups were identified, where |log2-fold change (FC)| >1 and P <0.05 were set as the cutoff values. Differential expression analysis yielded a total of 779 upregulated and 552 downregulated genes in high FSTL3 expression group compared with the low FSTL3 expression group (**Figure 8A**). The top significant terms of GO and KEGG analysis shown in Bubble diagrams revealed that these DEGs were mainly associated with ECM, suggesting that FSTL3 might function as vital regulator in ECM of CRC (**Figures 8B, C**).

To further identify a potential function of FSTL3, the GSEA (using the Molecular Signatures Database h.all.v6.0.symbols.gmt) was conducted (**Table S5**). The GSEA showed that substantial gene sets were positively enriched in FSTL3 high-expression group including inflammatory response (NES = 2.26, *FDR* < 0.001, **Figure 8D**), epithelial–mesenchymal-transition (EMT, NES = 2.38, *FDR* < 0.001, **Figure 8E**), and TGF-β signaling (NES = 1.66, *FDR* < 0.05, **Figure 8F**). Altogether, these results suggested that FSTL3 may promote tumor progression and LNM by regulating inflammatory response and EMT *via* TGF-β signaling.

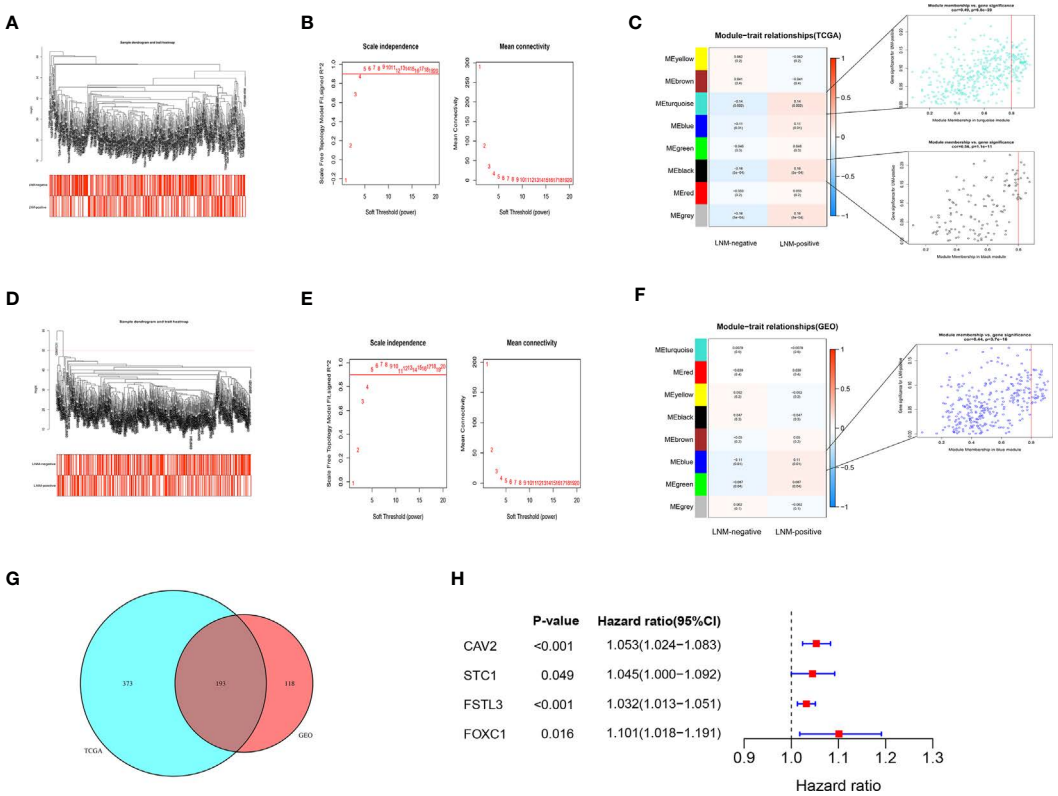

FIGURE 5 | Identification of key gene by WGCNA. **(A)** The sample clustering tree of CRC samples in the TCGA cohort, and all patients have passed the cut. The color band under the sample clustering tree presents the patients with or without LNM. Red box represents LNM-positive and white box represents LNM-negative. **(B)** The scale independent value exceeds 0.9 with a low average connectivity when soft threshold power was 5. The left image shows the relationship between the soft-threshold and scale-free R^2. The right image shows the mean connectivity for each soft-threshold. **(C)** Heatmap of the correlation between gene modules and clinical traits of CRC. The numerical value in each cell represents the correlation coefficient. Values within parentheses are *P*-values. The right images show the scatterplot of Gene Significance *vs.* Module Membership in the black and turquoise modules. **(D)** The sample clustering tree of CRC samples after removing one outlier sample (GSM972311) in the GSE39582 cohort. **(E)** The scale independent value exceeds 0.9 with a low average connectivity when soft threshold power was 5. **(F)** Heatmap of the correlation between gene modules and clinical traits of CRC. **(G)** Venn diagram showed that there were 193 overlapping genes related to LNM status in the TCGA and GSE39582 cohorts. **(H)** The forest plot showed that four genes were considered to be closely related to survival.

Correlation Between FSTL3 and TME in CRC

To better characterize the immunological role of FSTL3 plays in TME, we evaluated the relationship between FSTL3 and immune/stromal cell infiltration in CRC. Firstly, the ImmuneScore, StromalScore, and TumorPurity among the high and low FSTL3 expression groups were compared. The results showed that both the higher ImmuneScore, StromalScore, and ESTIMATE scores were found in high FSTL3 expression group (**Figure 9A**). Secondly, we found that FSTL3 expression has an observably positive association with ImmuneScore ($R = 0.37$, $P < 0.001$, **Figure 9B**), StromalScore ($R = 0.54$, $P < 0.001$, **Figure 9C**), but negative association with TumorPurity ($R = -0.49$, $P < 0.001$, **Figure 9D**) in CRC, which demonstrate that FSTL3 has a major influence on ECM remodeling.

The abundance of TILLs calculated by currently acknowledged methods, including TIMER, CIBERSORT-AB, XCELL, QUANTISEQ, MCPcounter, EPIC, and CIBERSORT algorithms, was downloaded from TIMER2.0 website to explore the relationship between the FSTL3 mRNA and immune infiltration status (33). The relationship between FSTL3 expression and immune cell infiltration is displayed in a bubble diagram (**Figure 9E**, **Table S6**). The analysis results showed that the FSTL3 expression was more positively associated with abundances of TIICs such as cancer-associated fibroblasts (CAFs), macrophages (M1- and M2-like), myeloid dendritic cell and $CD4^+$/$CD8^+$ cells, whereas it was negatively associated with B cells and NK cells. As shown in **Figure 9F**, there was obviously more immune cell infiltration in the high FSTL3 group, exhibiting a "hot" tumors phenotype (**Table S7**).

Correlation Between FSTL3 and Immune Modulators in CRC

Preliminary analyses revealed FSTL3 is more positively associated with suppressive immune cells, especially CAFs and M2-like macrophage. Therefore, we speculated that FSTL3 could be involved in inhibitory TME formation in CRC. To validate this speculation, correlation analyses were performed to explore the relationship between the FSTL3 expression and marker genes of

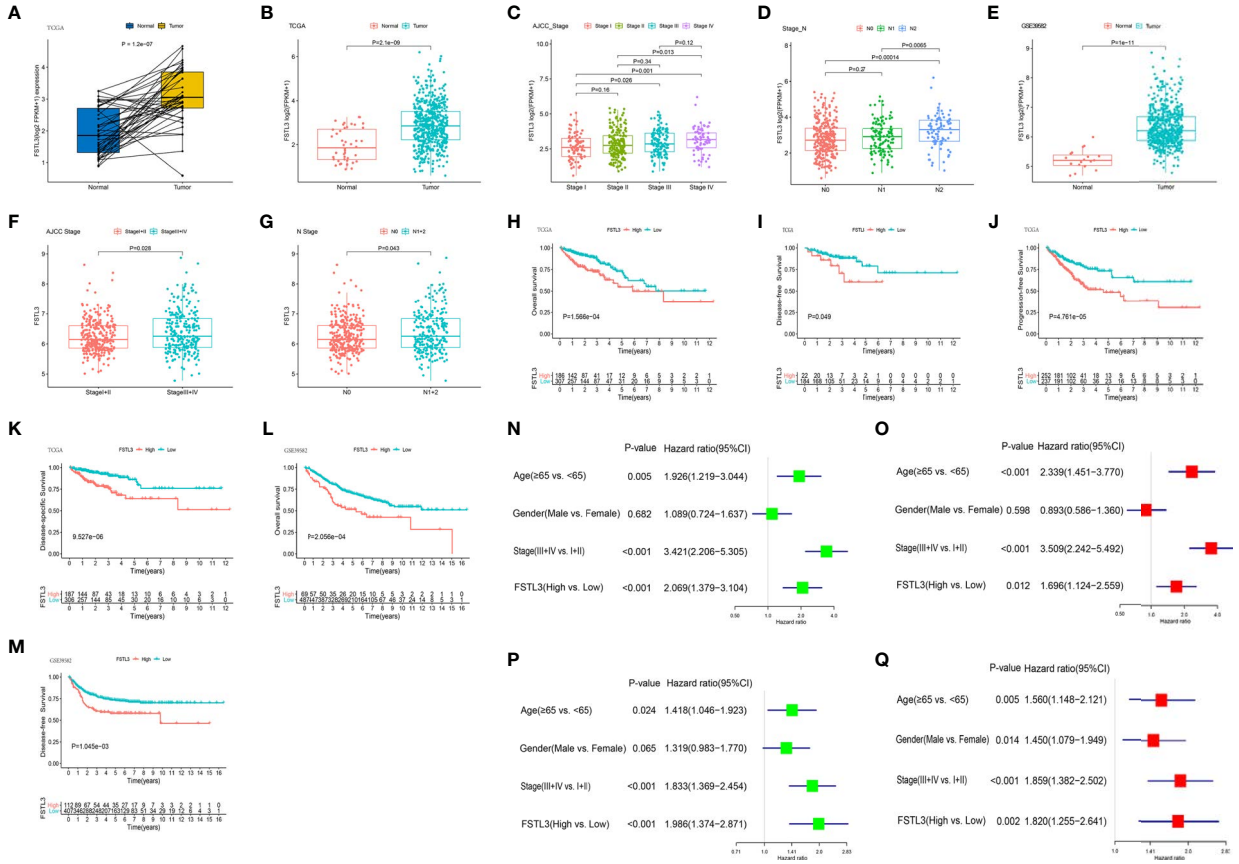

FIGURE 6 | Overexpression of FSTL3 correlated with tumor malignancy in CRC. **(A)** FSTL3 mRNA expression between normal and paired tumor samples in the TCGA cohort. **(B)** FSTL3 mRNA expression between total normal and tumor samples in the TCGA cohort. **(C, D)** FSTL3 mRNA expression is in remarkable association with AJCC stage **(C)** and N stage **(D)**. **(E–G)** Similar results were obtained in GEO GSE39582 cohort. **(H–K)** Higher FSTL3 mRNA expression was notably correlated with OS **(H)**, disease-free survival **(I)**, progression free survival **(J)**, as well as disease-specific survival **(K)** in the TCGA cohort. **(L, M)** Higher FSTL3 mRNA expression is notably correlated with OS **(L)** and disease-specific survival **(M)** in the GSE39582 cohort. **(N, O)** FSTL3 is an independent unfavorable prognostic factor in TCGA cohort by univariate **(N)** and multivariate **(O)** Cox proportional hazards analysis. **(P, Q)** FSTL3 is an independent unfavorable prognostic factor in GSE39582 cohort by univariate **(P)** and multivariate **(Q)** Cox proportional hazards analysis.

those immune cells. CAFs, also the main cellular component in TME, are known to be involved in regulating inflammatory responses, tumor cell proliferation and migration, as well as TME remodeling by secreting matrix degrading enzymes, cytokines and growth factors (34–36). Correlation heatmap showed that FSTL3 was significantly positively correlated with CAF-associated genes and had a strong positive correlation with TGFB1 (gene encoding TGF-β) (**Figure 10A**). Tumor-associated macrophages (TAMs), often characterized by M2-like macrophages, have a variety of tumor-promoting effects in the TME (37, 38). As shown in **Figure 10B**, FSTL3 was highly positively correlated with the gene set associated with M2-like macrophage, which implicated FSTL3 plays an important role in driving M2 polarization.

It is reported that suppressive TME and T cell exhaustion are critical to for the efficacy of immunotherapy, particularly immune checkpoint inhibitors (ICIs) and chimeric antigen receptor T cell therapy (39, 40). Next, the correlation between the FSTL3 expression and immunosuppressive molecules and T cell exhaustion genes was also examined. As shown in **Figure 10C**, we observed that the majority of immunosuppressive factors were correlated with FSTL3 positively. Similarly, we observed that FSTL3 was also positively correlated with T cell exhaustion genes in CRC (**Figure 10D**). These findings suggest that FSTL3 might have participated in the formation of an immunosuppressive TME *via* promoting T cell exhaustion, either directly or indirectly.

It is well known that EMT, an important hallmark of advanced cancer, is a key step for cancer cells to acquire metastasis potential (41). As the previous GSEA analysis showed that EMT-related pathway was significantly enriched in the FSTL3 high expression group, we explored the correlation between FSTL3 expression and EMT-related marker genes here. As expected, we observed that almost all EMT-related marker genes, except CDH1, which is biomarker of epithelial cells, were positively correlated with FSTL3 expression (**Figure 10E**). Collectively, these findings offer a landscape perspective in terms of the interactive relationship among FSTL3 and TME in

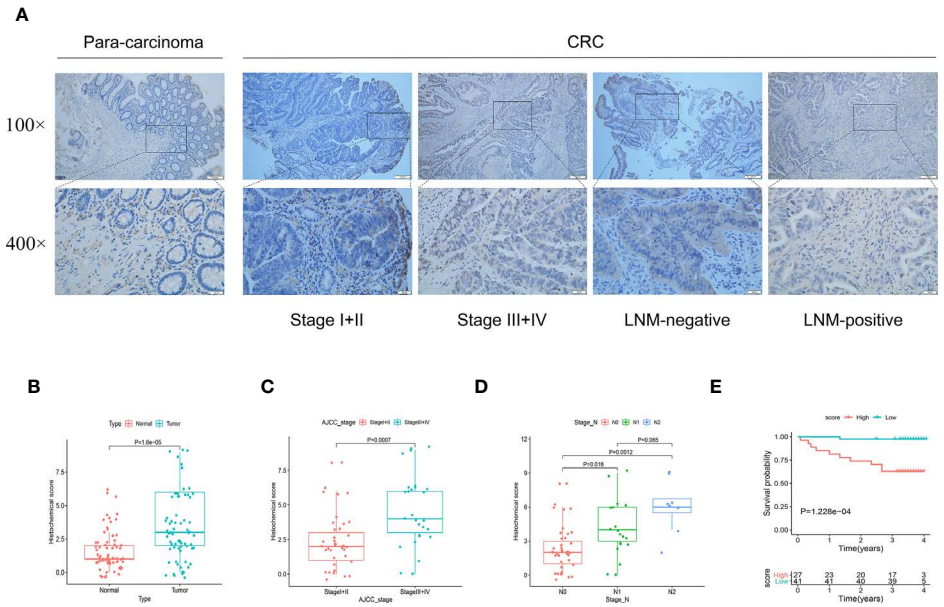

FIGURE 7 | Validation the protein function of FSTL3 by immunohistochemistry in external cohort. **(A, B)** FSTL3 protein was significantly overexpressed in tumor tissues. Scale bars, 100 and 20 μm. **(C, D)** FSTL3 protein is strikingly correlated to AJCC stage ($P = 0.0007$) and LNM ($P < 0.05$). **(E)** The survival analysis showed that CRC patients with higher FSTL3 protein has shorter OS compared with lower FSTL3 protein group ($P = 1.228e\text{-}4$).

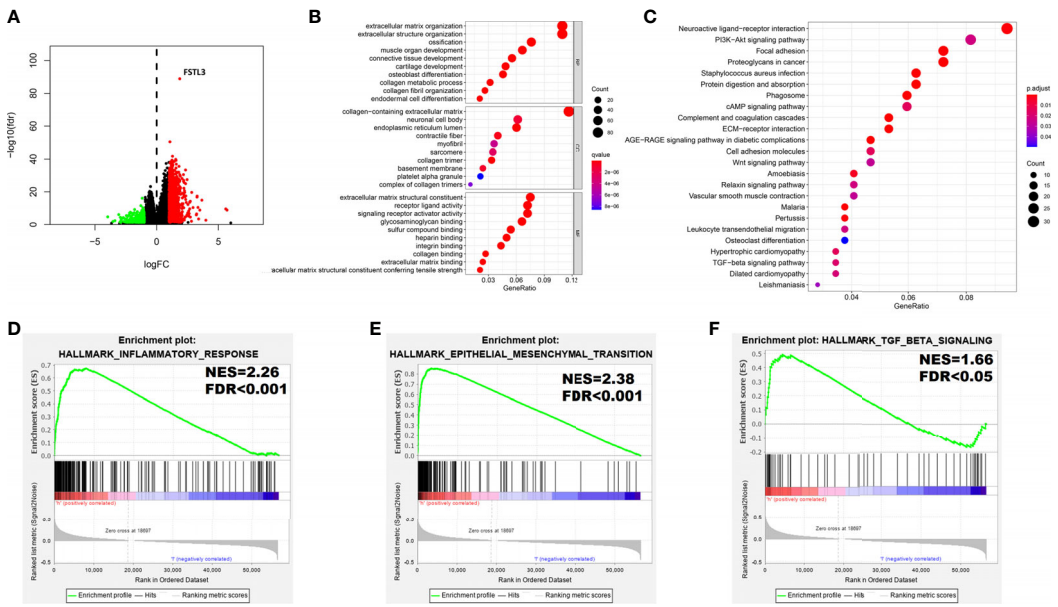

FIGURE 8 | Functional Annotation among the High and Low FSTL3 Expression Groups. **(A)** The volcano plot showed that 1,331 differential genes were identified between high and low FSTL3 groups. Each red dot represents upregulation gene, each green dot represents upregulation downregulation gene, and each black dot represents no significant difference genes. **(B)** The top 10 significant terms of GO analysis. **(C)** The top 20 significant pathways of KEGG analysis. **(D–F)** The GSEA showed that inflammatory response **(D)**, epithelial–mesenchymal-transition **(E)**, and TGF-β signaling **(F)** were positively enriched in FSTL3 high-expression group.

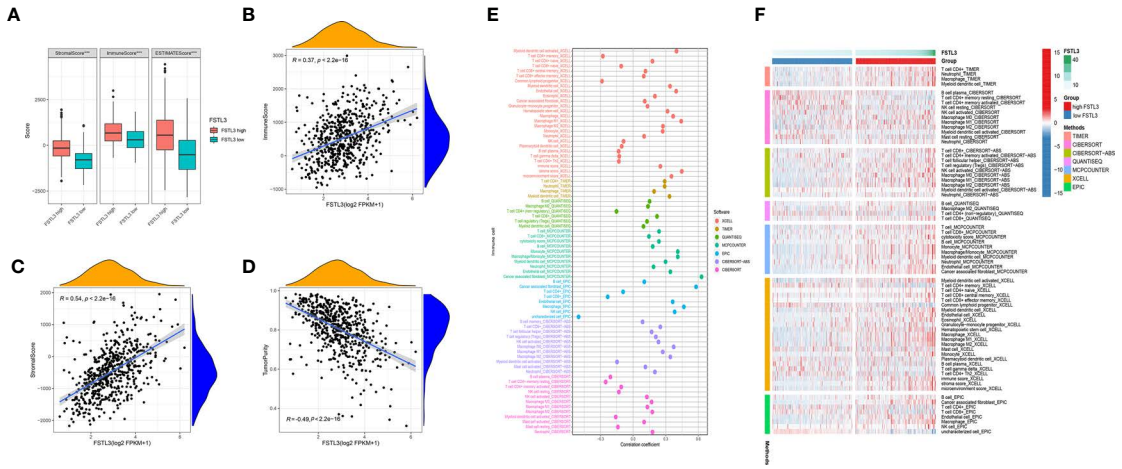

FIGURE 9 | Correlation Between FSTL3 and TME in CRC. **(A)** Both the higher ImmuneScore, StromalScore, and TumorPurity were found in high FSTL3 expression group. **(B–D)** The correlation analysis showed the FSTL3 expression has a observably positive association with ImmuneScore **(B)**, StromalScore **(C)**, but negative association with TumorPurity **(D)** in CRC. **(E, F)** The relationship between FSTL3 expression and immune cell infiltration is displayed in a bubble diagram **(E)** and heatmap **(F)**, respectively. ***$P < 0.001$.

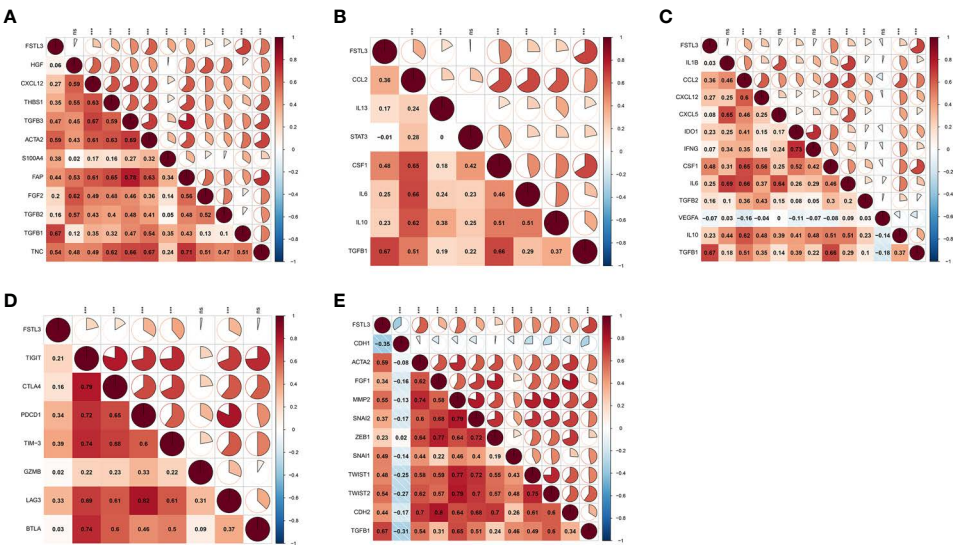

FIGURE 10 | Correlation Between FSTL3 and immune modulators in CRC. **(A, B)** FSTL3 is significantly positively correlated with CAF-associated **(A)** and M2-like macrophage **(B)** genes. **(C)** The majority of immunosuppressive factors were correlated with FSTL3 positively. **(D)** FSTL3 is positively correlated with many T cell exhaustion genes in CRC. **(E)** Almost all EMT-related marker genes, except CDH1 which is biomarker of epithelial cells, are positively correlated with FSTL3 expression. ns: non-significant; *$P < 0.05$, **$P < 0.01$, ***$P < 0.001$.

CRC, and FSTL3 might promote immune evasion and LNM, which functions by promoting T cell dysfunction and phenotypic transformation of M2 and CAFs, and mediating EMT.

FSTL3 Overexpression May Contribute to the Chemotherapy Resistance

Because complete adjuvant chemotherapy data are available in GEO GSE39582 cohort, we utilized this cohort to explore whether the FSTL3 expression level influenced the clinical outcomes of adjuvant chemotherapy in CRC. The CRC patients were separated into two groups (high and low FSTL3 expression groups) based on its median value. Overall, patients who underwent adjuvant chemotherapy had a significantly better DFS ($P = 0.001$, **Figure 11A**). The results of Kaplan–Meier survival analysis revealed that patients with lower FSTL3 could benefit from adjuvant chemotherapy ($P = 0.004$, **Figure 11B**), while high FSTL3 group showed limited benefit from chemotherapy intervention ($P = 0.107$, **Figure 11C**).

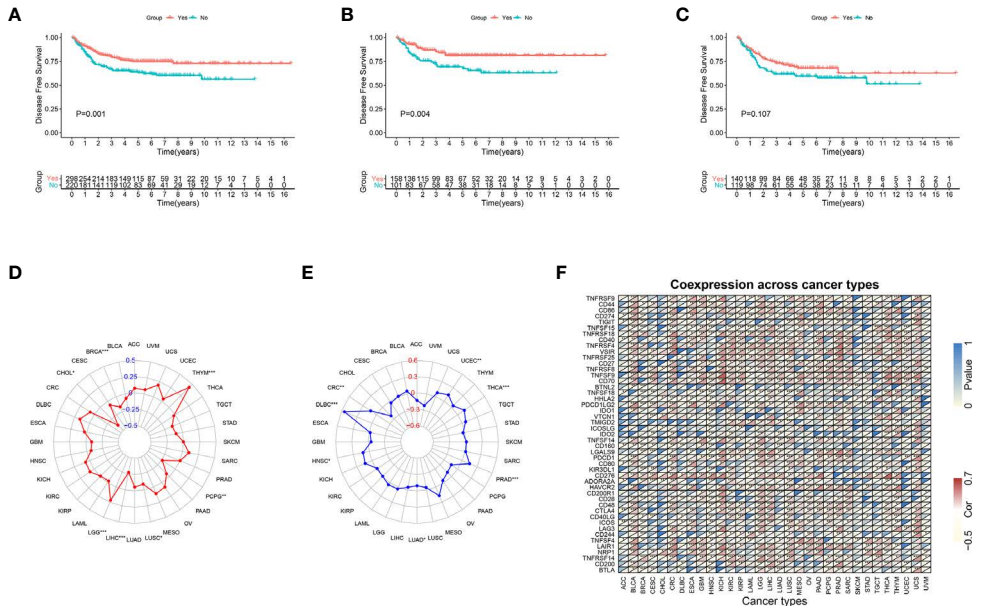

FIGURE 11 | Kaplan–Meier plots and pan-cancer analysis. **(A)** CRC patients who underwent adjuvant chemotherapy had a significantly better disease-free survival. **(B)** CRC patients with lower FSTL3 could benefit from adjuvant chemotherapy. **(C)** CRC patients with high FSTL3 would gain limited benefit from adjuvant chemotherapy. **(D)** FSTL3 expression levels are correlated with TMB among multiple types of cancers, but not including CRC. **(E)** The radar plot shown that FSTL3 expression is associated with MSI among CRC. **(F)** FSTL3 expression level is significantly correlated with the expression of immune checkpoint molecules in the vast majority of cancers. $^{*}P < 0.05$, $^{**}P < 0.01$, $^{***}P < 0.001$.

Pan-Cancer Analysis of the FSTL3

To further confirm the guidance value of FSTL3 for individualized therapy, we conducted a pan-cancer analysis. Transcriptome RNA-seq and mutation data of pan-cancer were extracted from UCSC Xena (https://xenabrowser.net/datapages/) (42). Firstly, we evaluated the relationship between FSTL3 and TMB and MSI among multiple types of cancers, which were both regarded as independent predictors of immunotherapy efficacy (43). We found that FSTL3 expression levels were correlated with TMB among multiple types of cancers, including BRCA, CHOL, LGG, LIHC, LUSC, PCPG, and THYM, but not CRC (**Figure 11D**, **Table S8**). Patients with MSI-high are always particularly responsive to immunotherapy than those with MSI-low (44). As shown in the radar plot, FSTL3 expression was associated with MSI among CRC, DLBC, HNSC, LUAD, PRAD, THCA, and UCEC (**Figure 11E**, **Table S9**). In addition, we found that FSTL3 expression level was significantly correlated with the expression of immune checkpoint molecules in the vast majority of cancers (**Figure 11F**).

DISCUSSION

LNM has a decisive role in affecting the pathological stage and clinical outcomes in many human malignancies (16). Although immunotherapy has shown promising clinical results in a variety of tumors, curing CRC patients with LNM remains a significant challenge. Therefore, the development of new immunotherapy by targeting a crucial regulator in LNM and tumor progression is a feasible therapeutic strategy. The present study aims to determine the key gene which conduced to develop cancer immunotherapy to potently blocked LNM. In this study, FSTL3 was identified as a key gene associated with TME and LNM ultimately.

FSTL3, *i.e.*, follistatin-like 3, is a secreted glycoprotein that is physiologically released by adipose tissue, reproductive, glands, liver, heart, and especially placenta. Recently, significant overexpression was also found in some malignant tumors (25, 45, 46). FSLT3 expression has been shown to be significantly associated with LNM and worse outcomes in patients with non-small cell lung cancer cell and thyroid cancer (25, 45). However, the role of FSTL3 in tumor progression and cancer immunology of CRC has been rarely studied. In this research, we have comprehensively investigated the role of FSTL3 in CRC progression, clinical outcomes, and chemotherapy resistance. Importantly, we assessed the correlation of FSTL3 expression with immune and stromal components in more depth. Besides, the protein expression level of FSTL3 was verified by IHC in an external validation cohort from our center. Collectively, the findings of this study indicate that FSTL3 is a promising biomarker of ECM remodeling and immunotherapy response in CRC patients.

LNM is one of the most important prognostic markers in many types of cancers. Research has shown that tumor cells will get a stronger ability of LMN when TGF-β-induced EMT (47). Molecularly, EMT has a crucial role in driving tumor invasion

and migration by promoting the expression of transcription factors and mesenchymal markers and inhibiting epithelial marker expression (48). The results of GSEA and correlation analysis showed EMT and TGF-β signaling pathway are significantly enriched in the high FSTL3 expression group. This suggests that FSTL3 may facilitate LNM *via* EMT and TGF-β signaling pathway in CRC. Certainly, additional experimental evidence is required to verify this conjecture.

Upregulation of immune checkpoint molecules is one of the main mechanism of immune evasion in many solid tumors (49, 50). In the present study, a strong correlation was observed between the FSTL3 expression and T cell exhaustion genes in CRC. Meanwhile, the results of the in-depth exploration show that among those TILs, the FSTL3 has the strongest correlation with CAFs and M2-macrophages, which are both immunosuppressive cells. Thus, it can be supposed that FSTL3 may contribute to format a tumor-promoting microenvironment by negatively regulating immunity. Consistent with this evidence, this study showed that FSTL3 was significantly correlated with PD1 and PD-L1, which are immune checkpoints. In consideration of the good therapeutic effect of Pembrolizumab and Nivolumab in CRC (51, 52), we speculated that ICIs may also be effective in CRC patients with high FSTL3 expression.

Macrophages have strong plasticity and functional heterogeneity, and they will be polarized as the local microenvironment changes. TAMs mediate tumor progression by secreting anti-inflammatory cytokines, angiogenic factors, and proteases (53, 54). In view of the plastic property of TAMs in TME, it is potential to develop a new therapy by repolarizing the M2-macrophages to become the tumoricidal M1-macrophages (55). Although platinum- and fluorouracil-based chemotherapy regimes effectively improve OS in CRC patients, some of them experience varying degrees of chemotherapy resistance phenomenon. Nevertheless, the molecular mechanisms of chemotherapy resistance in CRC remain largely unclear. Previous research has reported that CAF-derived exosomes might be involved in the enhanced chemoresistance by promoting cell stemness and EMT in CRC (56). Consistent with those findings, the present study has revealed that FSTL3 plays a vital role in EMT and contributes to the chemotherapy resistance in CRC. Interestingly, the study by Zhang et al. found that the TAMs and CAFs in CRC were able to synergistically inhibit the function of NK cells, which can kill tumor cells directly though innate immune signaling pathways (57). Hence, targeted therapy against FSTL3 may restore the body's own anti-tumor immunity and the chemotherapy sensitivity in CRC.

In summary, in this study, FSTL3 is considered as a key gene both associated with ECM and LMN in CRC. At first, the study thoroughly evaluated the clinical and prognostic value of FSTL3 in CRC, and was verified at the protein level *in vitro*. Then, we comprehensively explored the relationship between FSTL3 expression and immune and stromal components in TME, highlighting the crucial immunological role of FSTL3 in CRC. Besides, we confirmed that FSTL3 could serve as a predictor of sensitivity to both immunotherapy and adjuvant chemotherapy in CRC. In short, FSTL3 is first reported as a biomarker of ECM remodeling and immunotherapy, and is involved in promoting LNM in CRC.

DATA AVAILABILITY STATEMENT

The original contributions presented in the study are included in the article/**Supplementary Material**. Further inquiries can be directed to the corresponding author.

ETHICS STATEMENT

The studies involving human participants were reviewed and approved by the Medical Ethics Committee of the Renmin Hospital of Wuhan University. The patients/participants provided their written informed consent to participate in this study.

AUTHOR CONTRIBUTIONS

YZ and CY designed this study. CY, SH, and FC performed the data analyses and drafted the manuscript. CY and FC carried out data management and constructive discussions. All authors contributed to the article and approved the submitted version.

FUNDING

The study was supported by the grants of the Wu Jieping Medical Foundation (320.2710.1855).

ACKNOWLEDGMENTS

We acknowledge TCGA and GEO database and contributors for uploading their meaningful datasets.

SUPPLEMENTARY MATERIAL

The Supplementary Material for this article can be found online at: https://www.frontiersin.org/articles/10.3389/fimmu.2021.717505/full#supplementary-material

REFERENCES

1. Bray F, Ferlay J, Soerjomataram I, Siegel RL, Torre LA, Jemal A. Global Cancer Statistics 2018: GLOBOCAN Estimates of Incidence and Mortality Worldwide for 36 Cancers in 185 Countries. *CA Cancer J Clin* (2018) 68:394–424. doi: 10.3322/caac.21492

2. Zhang C, Zhang L, Xu T, Xue R, Yu L, Zhu Y, et al. Mapping the Spreading Routes of Lymphatic Metastases in Human Colorectal Cancer. *Nat Commun* (2020) 11:1993. doi: 10.1038/s41467-020-15886-6

3. Unger LW, Muckenhuber M, Riss S, Argeny S, Stift J, Mesteri I, et al. Effect of Pathologist's Dedication on Lymph Node Detection Rate and Postoperative Survival in Colorectal Cancer. *Colorectal Dis* (2018) 20:O173–80. doi: 10.1111/codi.14241

4. Huh JW, Kim HC, Kim SH, Park YA, Cho YB, Yun SH, et al. Mismatch Repair System and p53 Expression in Patients With T1 and T2 Colorectal Cancer: Predictive Role of Lymph Node Metastasis and Survival. *J Surg Oncol* (2014) 109:848–52. doi: 10.1002/jso.23592
5. Yamaoka Y, Kinugasa Y, Shiomi A, Yamaguchi T, Kagawa H, Yamakawa Y, et al. The Distribution of Lymph Node Metastases and Their Size in Colon Cancer. *Langenbecks Arch Surg* (2017) 402:1213–21. doi: 10.1007/s00423-017-1628-z
6. Huang Q, Liu E, Hu H, Zhang Q, Zhang Y, Jin Y, et al. Prognostic Significance of D3 Lymph Node for Survival in Patients With Colorectal Cancer. *J Surg Res* (2019) 239:156–65. doi: 10.1016/j.jss.2019.01.018
7. Fortea-Sanchis C, Martinez-Ramos D, Escrig-Sos J. The Lymph Node Status as a Prognostic Factor in Colon Cancer: Comparative Population Study of Classifications Using the Logarithm of the Ratio Between Metastatic and Nonmetastatic Nodes (LODDS) Versus the pN-TNM Classification and Ganglion Ratio Systems. *BMC Cancer* (2018) 18:1208. doi: 10.1186/s12885-018-5048-4
8. Sun ZQ, Ma S, Zhou QB, Yang SX, Chang Y, Zeng XY, et al. Prognostic Value of Lymph Node Metastasis in Patients With T1-Stage Colorectal Cancer From Multiple Centers in China. *World J Gastroenterol* (2017) 23:8582–90. doi: 10.3748/wjg.v23.i48.8582
9. Han EC, Kwon YH, Park KJ, Jeong SY, Kang SB, Oh JH, et al. Significance of Lymph Node Metastasis in the Survival of Stage IV Colorectal Cancer by Hematogenous Metastasis. *Ann Surg Treat Res* (2018) 95:201–12. doi: 10.4174/astr.2018.95.4.201
10. Dumont F, Munoz MA, De Franco V, Wernert R, Verriele V, Heyman MF, et al. Significance of Lymph Node Involvement in Local Recurrence of Colorectal Cancer. *J Surg Oncol* (2019) 120:722–8. doi: 10.1002/jso.25631
11. Chakravarthy A, Khan L, Bensler NP, Bose P, De Carvalho DD. TGF-Beta-Associated Extracellular Matrix Genes Link Cancer-Associated Fibroblasts to Immune Evasion and Immunotherapy Failure. *Nat Commun* (2018) 9:4692. doi: 10.1038/s41467-018-06654-8
12. Henke E, Nandigama R, Ergun S. Extracellular Matrix in the Tumor Microenvironment and Its Impact on Cancer Therapy. *Front Mol Biosci* (2019) 6:160. doi: 10.3389/fmolb.2019.00160
13. Wang M, Su Z, Amoah BP. Crosstalk Among Colon Cancer-Derived Exosomes, Fibroblast-Derived Exosomes, and Macrophage Phenotypes in Colon Cancer Metastasis. *Int Immunopharmacol* (2020) 81:106298. doi: 10.1016/j.intimp.2020.106298
14. Crotti S, Piccoli M, Rizzolio F, Giordano A, Nitti D, Agostini M. Extracellular Matrix and Colorectal Cancer: How Surrounding Microenvironment Affects Cancer Cell Behavior? *J Cell Physiol* (2017) 232:967–75. doi: 10.1002/jcp.25658
15. Machackova T, Vychytilova-Faltejskova P, Souckova K, Trachtova K, Brchnelova D, Svoboda M, et al. Mir-215-5p Reduces Liver Metastasis in an Experimental Model of Colorectal Cancer Through Regulation of ECM-Receptor Interactions and Focal Adhesion. *Cancers (Basel)* (2020) 12:3518. doi: 10.3390/cancers12123518
16. Gu Y, Liu Y, Fu L, Zhai L, Zhu J, Han Y, et al. Tumor-Educated B Cells Selectively Promote Breast Cancer Lymph Node Metastasis by HSPA4-targeting Igg. *Nat Med* (2019) 25:312–22. doi: 10.1038/s41591-018-0309-y
17. Wei C, Yang C, Wang S, Shi D, Zhang C, Lin X, et al. Crosstalk Between Cancer Cells and Tumor Associated Macrophages Is Required for Mesenchymal Circulating Tumor Cell-Mediated Colorectal Cancer Metastasis. *Mol Cancer* (2019) 18:64. doi: 10.1186/s12943-019-0976-4
18. Hu JL, Wang W, Lan XL, Zeng ZC, Liang YS, Yan YR, et al. Cafs Secreted Exosomes Promote Metastasis and Chemotherapy Resistance by Enhancing Cell Stemness and Epithelial-Mesenchymal Transition in Colorectal Cancer. *Mol Cancer* (2019) 18:91. doi: 10.1186/s12943-019-1019-x
19. Mizuno R, Kawada K, Itatani Y, Ogawa R, Kiyasu Y, Sakai Y. The Role of Tumor-Associated Neutrophils in Colorectal Cancer. *Int J Mol Sci* (2019) 20:529. doi: 10.3390/ijms20030529
20. Xiong Y, Wang K, Zhou H, Peng L, You W, Fu Z. Profiles of Immune Infiltration in Colorectal Cancer and Their Clinical Significant: A Gene Expression-Based Study. *Cancer Med* (2018) 7:4496–508. doi: 10.1002/cam4.1745
21. Saito T, Nishikawa H, Wada H, Nagano Y, Sugiyama D, Atarashi K, et al. Two FOXP3(+)CD4(+) T Cell Subpopulations Distinctly Control the Prognosis of Colorectal Cancers. *Nat Med* (2016) 22:679–84. doi: 10.1038/nm.4086
22. Passardi A, Canale M, Valgiusti M, Ulivi P. Immune Checkpoints as a Target for Colorectal Cancer Treatment. *Int J Mol Sci* (2017) 18:1324. doi: 10.3390/ijms18061324
23. Marisa L, de Reynies A, Duval A, Selves J, Gaub MP, Vescovo L, et al. Gene Expression Classification of Colon Cancer Into Molecular Subtypes: Characterization, Validation, and Prognostic Value. *PloS Med* (2013) 10: e1001453. doi: 10.1371/journal.pmed.1001453
24. Barrett T, Wilhite SE, Ledoux P, Evangelista C, Kim IF, Tomashevsky M, et al. Ncbi GEO: Archive for Functional Genomics Data Sets–Update. *Nucleic Acids Res* (2013) 41:D991–5. doi: 10.1093/nar/gks1193
25. Gao L, Chen X, Wang Y, Zhang J. Up-Regulation of FSTL3, Regulated by Lncrna DSCAM-AS1/miR-122-5p Axis, Promotes Proliferation and Migration of Non-Small Cell Lung Cancer Cells. *Onco Targets Ther* (2020) 13:2725–38. doi: 10.2147/OTT.S236359
26. He Y, Jiang Z, Chen C, Wang X. Classification of Triple-Negative Breast Cancers Based on Immunogenomic Profiling. *J Exp Clin Cancer Res* (2018) 37:327. doi: 10.1186/s13046-018-1002-1
27. Hanzelmann S, Castelo R, Guinney J. GSVA: Gene Set Variation Analysis for Microarray and RNA-seq Data. *BMC Bioinf* (2013) 14:7. doi: 10.1186/1471-2105-14-7
28. Yoshihara K, Shahmoradgoli M, Martinez E, Vegesna R, Kim H, Torres-Garcia W, et al. Inferring Tumour Purity and Stromal and Immune Cell Admixture From Expression Data. *Nat Commun* (2013) 4:2612. doi: 10.1038/ncomms3612
29. Newman AM, Liu CL, Green MR, Gentles AJ, Feng W, Xu Y, et al. Robust Enumeration of Cell Subsets From Tissue Expression Profiles. *Nat Methods* (2015) 12:453–7. doi: 10.1038/nmeth.3337
30. Ritchie ME, Phipson B, Wu D, Hu Y, Law CW, Shi W, et al. Limma Powers Differential Expression Analyses for RNA-Sequencing and Microarray Studies. *Nucleic Acids Res* (2015) 43:e47. doi: 10.1093/nar/gkv007
31. Chen H, Boutros PC. VennDiagram: A Package for the Generation of Highly-Customizable Venn and Euler Diagrams in R. *BMC Bioinf* (2011) 12:35. doi: 10.1186/1471-2105-12-35
32. Langfelder P, Horvath S. WGCNA: An R Package for Weighted Correlation Network Analysis. *BMC Bioinf* (2008) 9:559. doi: 10.1186/1471-2105-9-559
33. Li T, Fu J, Zeng Z, Cohen D, Li J, Chen Q, et al. TIMER2.0 for Analysis of Tumor-Infiltrating Immune Cells. *Nucleic Acids Res* (2020) 48:W509–14. doi: 10.1093/nar/gkaa407
34. Mosa MH, Michels BE, Menche C, Nicolas AM, Darvishi T, Greten FR, et al. A Wnt-Induced Phenotypic Switch in Cancer-Associated Fibroblasts Inhibits EMT in Colorectal Cancer. *Cancer Res* (2020) 80:5569–82. doi: 10.1158/0008-5472.CAN-20-0263
35. Aizawa T, Karasawa H, Funayama R, Shirota M, Suzuki T, Maeda S, et al. Cancer-Associated Fibroblasts Secrete Wnt2 to Promote Cancer Progression in Colorectal Cancer. *Cancer Med* (2019) 8:6370–82. doi: 10.1002/cam4.2523
36. Unterleuthner D, Neuhold P, Schwarz K, Janker L, Neuditschko B, Nivarthi H, et al. Cancer-Associated Fibroblast-Derived WNT2 Increases Tumor Angiogenesis in Colon Cancer. *Angiogenesis* (2020) 23:159–77. doi: 10.1007/s10456-019-09688-8
37. Lan J, Sun L, Xu F, Liu L, Hu F, Song D, et al. M2 Macrophage-Derived Exosomes Promote Cell Migration and Invasion in Colon Cancer. *Cancer Res* (2019) 79:146–58. doi: 10.1158/0008-5472.CAN-18-0014
38. Liu Q, Yang C, Wang S, Shi D, Wei C, Song J, et al. Wnt5a-Induced M2 Polarization of Tumor-Associated Macrophages Via IL-10 Promotes Colorectal Cancer Progression. *Cell Commun Signal* (2020) 18:51. doi: 10.1186/s12964-020-00557-2
39. Kim CG, Jang M, Kim Y, Leem G, Kim KH, Lee H, et al. VEGF-a Drives TOX-Dependent T Cell Exhaustion in Anti-PD-1-Resistant Microsatellite Stable Colorectal Cancers. *Sci Immunol* (2019) 4:eaay0555. doi: 10.1126/sciimmunol.aay0555
40. Kasakovski D, Xu L, Li Y. T Cell Senescence and CAR-T Cell Exhaustion in Hematological Malignancies. *J Hematol Oncol* (2018) 11:91. doi: 10.1186/s13045-018-0629-x
41. Yang J, Antin P, Berx G, Blanpain C, Brabletz T, Bronner M, et al. Guidelines and Definitions for Research on Epithelial-Mesenchymal Transition. *Nat Rev Mol Cell Biol* (2020) 21:341–52. doi: 10.1038/s41580-020-0237-9
42. Goldman MJ, Craft B, Hastie M, Repecka K, McDade F, Kamath A, et al. Visualizing and Interpreting Cancer Genomics Data Via the Xena Platform. *Nat Biotechnol* (2020) 38:675–8. doi: 10.1038/s41587-020-0546-8

43. Zhao P, Li L, Jiang X, Li Q. Mismatch Repair Deficiency/Microsatellite Instability-High as a Predictor for Anti-PD-1/PD-L1 Immunotherapy Efficacy. *J Hematol Oncol* (2019) 12:54. doi: 10.1186/s13045-019-0738-1
44. Li K, Luo H, Huang L, Luo H, Zhu X. Microsatellite Instability: A Review of What the Oncologist Should Know. *Cancer Cell Int* (2020) 20:16. doi: 10.1186/s12935-019-1091-8
45. Panagiotou G, Ghaly W, Upadhyay J, Pazaitou-Panayiotou K, Mantzoros CS. Serum Follistatin Is Increased in Thyroid Cancer and Is Associated With Adverse Tumor Characteristics in Humans. *J Clin Endocrinol Metab* (2021) 106:e2137–50. doi: 10.1210/clinem/dgab041
46. Du J, Yan X, Mi S, Li Y, Ji H, Hou K, et al. Identification of Prognostic Model and Biomarkers for Cancer Stem Cell Characteristics in Glioblastoma by Network Analysis of Multi-Omics Data and Stemness Indices. *Front Cell Dev Biol* (2020) 8:558961. doi: 10.3389/fcell.2020.558961
47. Karlsson MC, Gonzalez SF, Welin J, Fuxe J. Epithelial-Mesenchymal Transition in Cancer Metastasis Through the Lymphatic System. *Mol Oncol* (2017) 11:781–91. doi: 10.1002/1878-0261.12092
48. Thiery JP, Acloque H, Huang RY, Nieto MA. Epithelial-Mesenchymal Transitions in Development and Disease. *Cell* (2009) 139:871–90. doi: 10.1016/j.cell.2009.11.007
49. Bonavita E, Bromley CP, Jonsson G, Pelly VS, Sahoo S, Walwyn-Brown K, et al. Antagonistic Inflammatory Phenotypes Dictate Tumor Fate and Response to Immune Checkpoint Blockade. *Immunity* (2020) 53:1215–29. doi: 10.1016/j.immuni.2020.10.020
50. Kobayashi Y, Lim SO, Yamaguchi H. Oncogenic Signaling Pathways Associated With Immune Evasion and Resistance to Immune Checkpoint Inhibitors in Cancer. *Semin Cancer Biol* (2020) 65:51–64. doi: 10.1016/j.semcancer.2019.11.011
51. Overman MJ, McDermott R, Leach JL, Lonardi S, Lenz HJ, Morse MA, et al. Nivolumab in Patients With Metastatic DNA Mismatch Repair-Deficient or Microsatellite Instability-High Colorectal Cancer (CheckMate 142): An Open-Label, Multicentre, Phase 2 Study. *Lancet Oncol* (2017) 18:1182–91. doi: 10.1016/S1470-2045(17)30422-9
52. Le DT, Uram JN, Wang H, Bartlett B, Kemberling H, Eyring A, et al. Programmed Death-1 Blockade in Mismatch Repair Deficient Colorectal Cancer. *J Clin Oncol* (2016) 34:103. doi: 10.1200/JCO.2016.34.15_suppl.103
53. DeNardo DG, Ruffell B. Macrophages as Regulators of Tumour Immunity and Immunotherapy. *Nat Rev Immunol* (2019) 19:369–82. doi: 10.1038/s41577-019-0127-6
54. Fu LQ, Du WL, Cai MH, Yao JY, Zhao YY, Mou XZ. The Roles of Tumor-Associated Macrophages in Tumor Angiogenesis and Metastasis. *Cell Immunol* (2020) 353:104119. doi: 10.1016/j.cellimm.2020.104119
55. Yahaya M, Lila M, Ismail S, Zainol M, Afizan N. Tumour-Associated Macrophages (Tams) in Colon Cancer and How to Reeducate Them. *J Immunol Res* (2019) 2019:2368249. doi: 10.1155/2019/2368249
56. Ren J, Ding L, Zhang D, Shi G, Xu Q, Shen S, et al. Carcinoma-Associated Fibroblasts Promote the Stemness and Chemoresistance of Colorectal Cancer by Transferring Exosomal lncRNA H19. *Theranostics* (2018) 8:3932–48. doi: 10.7150/thno.25541
57. Zhang R, Qi F, Zhao F, Li G, Shao S, Zhang X, et al. Cancer-Associated Fibroblasts Enhance Tumor-Associated Macrophages Enrichment and Suppress NK Cells Function in Colorectal Cancer. *Cell Death Dis* (2019) 10:273. doi: 10.1038/s41419-019-1435-2

Conflict of Interest: The authors declare that the research was conducted in the absence of any commercial or financial relationships that could be construed as a potential conflict of interest.

Copyright © 2021 Yang, Cao, Huang and Zheng. This is an open-access article distributed under the terms of the Creative Commons Attribution License (CC BY). The use, distribution or reproduction in other forums is permitted, provided the original author(s) and the copyright owner(s) are credited and that the original publication in this journal is cited, in accordance with accepted academic practice. No use, distribution or reproduction is permitted which does not comply with these terms.

frontiers in Oncology

ORIGINAL RESEARCH
published: 26 August 2021
doi: 10.3389/fonc.2021.727605

Transferrin-Conjugated Erianin-Loaded Liposomes Suppress the Growth of Liver Cancer by Modulating Oxidative Stress

Anhui Yang[1†], *Zhen Sun*[1†], *Rui Liu*[1], *Xin Liu*[1], *Yue Zhang*[1], *Yulin Zhou*[1], *Ye Qiu*[2*] *and Xinrui Zhang*[1,2*]

[1] School of Life Sciences, Jilin University, Changchun, China, [2] Department of Pharmacy, Changchun University of Chinese Medicine, Changchun, China

OPEN ACCESS

Edited by:
Peng Qu,
National Institutes of Health (NIH), United States

Reviewed by:
Meng Xu,
Carnegie Mellon University, United States
Min Ye,
Peking University, China

***Correspondence:**
Ye Qiu
ccyeqiu@163.com
Xinrui Zhang
zhangxr17@mails.jlu.edu.cn

†These authors have contributed equally to this work and share first authorship

Specialty section:
This article was submitted to Cancer Immunity and Immunotherapy, a section of the journal Frontiers in Oncology

Received: 19 June 2021
Accepted: 06 August 2021
Published: 26 August 2021

Citation:
Yang A, Sun Z, Liu R, Liu X, Zhang Y, Zhou Y, Qiu Y and Zhang X (2021) Transferrin-Conjugated Erianin-Loaded Liposomes Suppress the Growth of Liver Cancer by Modulating Oxidative Stress. Front. Oncol. 11:727605. doi: 10.3389/fonc.2021.727605

Background: Liver cancer is one of the most malignant human cancers, with few treatments and a poor prognosis. Erianin (ERN) is a natural compound with multiple pharmacological activities that has been reported to have numerous excellent effects against liver cancer in experimental systems. However, its application *in vivo* has been limited due to its poor aqueous solubility and numerous off-target effects. This study aimed to improve the therapeutic efficacy of ERN by developing novel ERN-loaded tumor-targeting nanoparticles.

Results: In this study, ERN was loaded into liposomes by ethanol injection (LP-ERN), and the resulting LP-ERN nanoparticles were treated with transferrin to form Tf-LP-ERN to improve the solubility and enhance the tumor-targeting of ERN. LP-ERN and Tf-LP-ERN nanoparticles had smooth surfaces and a uniform particle size, with particle diameters of 62.60 nm and 88.63 nm, respectively. In HepG2 and SMMC-7721 cells, Tf-LP-ERN induced apoptosis, decreased mitochondrial membrane potentials and increased ERN uptake more effectively than free ERN and LP-ERN. In xenotransplanted mice, Tf-LP-ERN inhibited tumor growth, but had a minimal effect on body weight and organ morphology. In addition, Tf-LP-ERN nanoparticles targeted tumors more effectively than free ERN and LP-ERN nanoparticles, and in tumor tissues Tf-LP-ERN nanoparticles promoted the cleavage PARP-1, caspase-3 and caspase-9, increased the expression levels of Bax, Bad, PUMA, and reduced the expression level of Bcl-2. Moreover, in the spleen of heterotopic tumor model BALB/c mice, ERN, LP-ERN and Tf-LP-ERN nanoparticles increased the expression levels of Nrf2, HO-1, SOD-1 and SOD-2, but reduced the expression levels of P-IKKα+β and P-NF-κB, with Tf-LP-ERN nanoparticles being most effective in this regard. Tf-LP-ERN nanoparticles also regulated the expression levels of TNF-α, IL-10 and CCL11 in serum.

Conclusion: Tf-LP-ERN nanoparticles exhibited excellent anti-liver cancer activity *in vivo* and *in vitro* by inducing cellular apoptosis, exhibiting immunoregulatory actions, and targeting tumor tissues, and did so more effectively than free ERN and LP-ERN

nanoparticles. These results suggest that the clinical utility of a Tf-conjugated LP ERN-delivery system for the treatment of liver cancer warrants exploration.

Keywords: erianin, transferrin-conjugated liposomes, liver cancer, apoptosis, mitochondrial, oxidative stress

INTRODUCTION

Liver cancer is the world's third most common cause of cancer-related deaths, due to its frequent recurrence and formation of metastases, and a lack of effective treatments (1, 2). It is most prevalent in Asia and Africa; however, its incidence is increasing in Western countries (3). The primary causes of this globally rising incidence are cirrhosis and chronic hepatitis (4). Currently, radiofrequency ablation, surgery, chemotherapy, radiotherapy, and immunotherapy are the mainstays of liver cancer treatment, but their toxicity and unsatisfactory anti-cancer effects are urgent problems to be solved (5).

One of the key biochemical changes in the development of liver cancer occurs in the network of B-cell lymphoma-2 (Bcl-2) family proteins, which results in the compensatory generation of anti-apoptotic effectors (6). The activation of Bcl-2 associated X protein (Bax) and Bcl-2 homologous antagonist/killer (Bak) protein induces outer mitochondrial membrane permeability and caspase cascade activity (6). Caspase-3 is a crucial pro-apoptotic protein in caspase cascades, and is therefore considered to be a key factor of mitochondrial apoptosis (7). Specifically, caspase-3 amplifies caspase-9 initiation signals *via* the mitochondrial pathway, and also cleaves poly (ADP-ribose) polymerase (PARP), thereby amplifying the apoptotic signal (8).

Oxidative stress triggers the antioxidant response by activating the nuclear factor erythroid 2-related factor 2 (Nrf2) pathway in the liver. Nrf2 then triggers the expression of a variety of downstream cytoprotective genes to maintain cell homeostasis (9). Furthermore, an antioxidant response element in the reverse chain of the Bcl-2 promoter combines with Nrf2 to regulate expression of the *Bcl-2* gene (10). Nrf2 negatively regulates nuclear factor-κB (NF-κB), knockdown of which promotes the transcriptional activity of NF-κB (11). Over-activation of NF-κB, which is normally inactivated by binding to inhibitor of κB alpha (IκB-α). Inhibitor of κB kinase alpha + beta IκB kinase (IKKα+β) releases NF-κB, and the freed NF-κB regulates physiological processes, such as cell proliferation, invasion, and death (12).

Natural products comprise a diverse array of biologically active compounds that have been studied extensively in the field of drug development, especially for cancer therapy (13, 14). For example, erianin (ERN; 2-methoxy-5-[2-(3,4,5-trimethoxyphenyl)-ethyl]-phenol, **Figure S1**) is isolated from *Dendrobium chrysotoxum* Lindl, a widely cultivated species of orchid, and has a variety of pharmacological activities, including anti-cancer activities (15, 16). We recently confirmed that the anti-liver cancer effects of ERN are attributable to its regulation of oxidative stress-mediated mitochondrial apoptosis and the immune response (17). However, ERN has poor aqueous solubility and can only be solubilized in dimethyl sulfoxide, which limits its use *in vivo*.

LPs have similar structures to cell membranes, and are thus well absorbed by cells. Moreover, LPs are easy to modify to improve their drug-loading efficiency, therapeutic utility, and stability (18). Previous studies have successfully used LPs to encapsulate cordycepin, a derivative of adenosine, to improve its solubility and biological activity (19, 20). Transferrin (Tf), an 80-kDa glycoprotein that enables cells to absorb ferric ions (Fe^{3+}), is commonly used to actively target therapeutic drug-loaded nanoparticles (such as LPs) to cancer cells, as these cells overexpress Tf receptors on their surfaces (21, 22). In particular, relative to normal cells, liver cells highly overexpress Tf receptors (23).

Based on our previous study (17), in the present study we aimed use *in vivo* and *in vitro* experiments to determine the pro-apoptotic effect of Tf-conjugated LPs loaded with ERN (Tf-LP-ERN) on liver cancer. The resulting data confirmed that Tf-LP-ERN nanoparticles could effectively targeted tumor tissues and cells, and enhanced the immunoregulatory anti-liver cancer effects of ERN.

Abbreviations: Bad, Bcl-2 antagonist of cell death; Bak, Bcl-2 homologous antagonist/killer; Bax, Bcl-2 associated X protein; Bcl-2, B-cell lymphoma-2; Bcl-xL, B-cell lymphoma-extra large; CCL11, chemokine C-C motif ligand 11; Cou6, Coumarin 6; DiR, 1,1-dioctadecyl-3,3,3,3-tetramethylindotricarbocyanine iodide; EE, encapsulation efficiency; EPR, enhanced permeability and retention; ERN, Erianin; FESEM, field emission scanning electron microscopy; GAPDH, glyceraldehyde-3-phosphate dehydrogenase; HO-1, heme oxygenase-1; IκB-α, inhibitor of κB alpha; IKKα+β, inhibitor of κB kinase alpha + beta; IL-10, interleukin-10; LP-ERN, erianin liposomes; MMP, mitochondrial membrane potential; NF-κB, nuclear factor-κB; Nrf2, nuclear factor erythroid 2-related factor 2; P-, phospho-; PARP, poly (ADP-ribose) polymerase; PDI, polydispersity index; PUMA, p53 upregulated modulator of apoptosis; SOD, superoxide dismutase; SPF, specific-pathogen-free; T-, total-; Tf, transferrin; Tf-LP-ERN, Tf-conjugated liposomes loaded with ERN; TNF-α, tumor necrosis factor-α.

MATERIALS AND METHODS

Preparation of Liposomes

ERN liposomes (LP-ERN): 1,2-Dioleoyl-3-trimethylammonium-propane (Corden Pharma, Switzerland), egg yolk phosphatidylcholine (Kewpie Corporation, Tokyo, Japan), cholesterol (Nippon Fine Chemical Co., Ltd., Japan), and 1,2-distearoyl-*sn*-glycero-3-phosphoethanolamine-*N*-[methoxy (polyethylene glycol)-2000] (DSPE-mPEG2000) (Lipoid GmbH, Ludwigshafen, Germany) were dissolved in anhydrous ethanol at a molar ratio of 20:45:32:3 to prepare a phospholipid phase. ERN (B20844) (Source Leaf Biological Technology Co., Ltd., Shanghai, China; purity >98.0%) was dissolved in anhydrous ethanol to a concentration of 5 mg/mL. The resulting drug solution and

phospholipid phase were thoroughly mixed, and then injected into a magnetically stirred sterile solution of phosphate buffered saline, with the volume ratio of the lipid phase to the water phase=being 1:10). Stirring was continued for 10 min to afford an LP-ERN mixture.

Tf-LP-ERN: The post-insertion method was used to conjugate Tf to LP-ERN (24). A 1:10 molar ratio of a 10 mg/mL Tf (Merck KGaA, St. Louis, MO, USA) solution and a 4 mg/mL solution of Traut's reagent (2-iminothiolane; Jiamay Biotech Co., Ltd., Beijing, China) were agitated on a shaker for 1 h, and the resulting thiolated Tf was dialyzed. Then, a 1:10 molar ratio of thiolated Tf and Mal-mPEG2000-DSPE (Seebio Biotech Co., Ltd., Shanghai, China) was stirred overnight at room temperature to afford Tf-PEG-DSPE. Finally, a 100:1 molar ratio of LP-ERN and Tf-PEG-DSPE was incubated at 37°C for 30 min to form Tf-LP-ERN. Tf-LP were similarly obtained by co-incubating ERN-free LPs with Tf-DSPE-PEG.

Fluorescent-labeled LPs: A lipid-soluble fluorescent dyes [coumarin 6 (Cou6) (Merck KGaA, St. Louis, MO, USA) or 1,1-dioctadecyl-3,3,3,3-tetramethylindotricarbocyanine iodide (DiR) (Life Technologies, Carlsbad, CA, USA)] was dissolved in anhydrous ethanol, and the resulting solution was dissolved in the lipid phase during the preparation of the above LPs. These two fluorescent dyes can label plasma membranes, and are therefore commonly used to prepare fluorescent labeled LPs.

Characterization of LP-ERN and Tf-LP-ERN

Particle Size-Distribution Analysis

The particle-size distributions of LP-ERN and Tf-LP-ERN nanoparticles were measured at 25°C using a particle size analyzer (Nano ZS90, Malvern Instruments, Malvern, Worcestershire, UK) at 25°C (25).

Morphological Investigation

The surface morphologies of LP-ERN and Tf-LP-ERN nanoparticles dropped onto a silicon wafer at 3,000 V were observed by field-emission scanning electron microscopy (FESEM; JSM-6700F, JEOL, Tokyo, Japan) (25).

Encapsulation Efficiency Detection

The ERN encapsulation efficiency (EE) of LP-ERN and Tf-LP-ERN nanoparticles was determined using a previously reported procedure, with some modifications (19). Briefly, unencapsulated ERN was separated from the LPs in an ultrafiltration cell (Millipore, USA) equipped with an ultrafiltration membrane with a molecular weight cut-off of 10 kDa, which was centrifuged at 9,000 rpm for 20 min. The concentration of free ERN was recorded, and denoted as F_{ERN}. Either LP-ERN or Tf-LP-ERN were lyzed with methanol solution, and the concentrations of ERN released were measured, and denoted as T_{ERN}. ERN was quantified on a high-performance liquid chromatography system (E2695, Waters, Milford, MA, USA). The following formula was used to calculate the ERN EE of LP-ERN and Tf-LP-ERN nanoparticles:

$$EE(\%) = (T_{ERN} - F_{ERN})/T_{ERN} \times 100\,\%$$

Cell Culture, Cell Viability Assay, and Cellular Uptake Detection

Liver cancer cells [HepG2 (American Type Culture Collection, USA) or SMMC-7721 (China Center for Type Culture Collection, China)] were maintained in Dulbecco's modified Eagle's medium supplemented with 10% fetal bovine serum, 1% streptomycin and penicillin, and 0.1% plasmocin prophylactic at 37°C under 5% CO_2.

HepG2 and SMMC-7721 cells were then seeded into 96-well plates at a concentration of 5,000 cells/well, and subsequently exposed to separate concentration gradients of free ERN, LP-ERN or Tf-LP-ERN for 24 h. 3-(4,5-dimethyl-2-thiazolyl)-2,5-diphenyl-2-*H*-tetrazolium bromide assay, as per our previous study (17).

HepG2 and SMMC-7721 cells were also seeded into 35-mm-diameter glass-bottomed Petri dishes at a density of 100,000 cells/dish, and then exposed to ERN-Cou6, LP-ERN-Cou6 or Tf-LP-ERN-Cou6 nanoparticles (equivalent to 10 nM of ERN and 3 μM of Cou6) for 4 h. Then, a laser-scanning confocal microscope (710 LSMNLO, Carl Zeiss, Jena, Thuringia, Germany) was used to observe the internalization of fluorescent ERN or fluorescent ERN-containing nanoparticles by the liver cancer cells.

Cell Apoptosis and Mitochondrial Membrane Potential Analyses

HepG2 and SMMC-7721 cells were seeded into six-well plates at a concentration of 3×10^5 cells/well, and incubated for 24 h. The cells were then exposed to ERN, Tf-LP, LP-ERN or Tf-LP-ERN (to a final ERN concentration of 10 nM) for a further 24 h, and then incubated with 100 μL of Muse™ Annexin V and Dead Cell reagent (Millipore, Billerica, MA, USA) under darkness for 20 min at 25°C. Cell apoptosis was then analyzed using the Muse® Cell Analyzer (EMD Millipore, Billerica, MA, USA).

Another set of six-well plates seeded with HepG2 and SMMC-7721 cells were treated with ERN, Tf-LP, LP-ERN or Tf-LP-ERN (to a final ERN concentration of 10 nM) for 12 h, and then incubated with 10 μM of 5,5′,6,6′-tetrachloro-1,1′,3,3′ tetraethylbenzimidazolylcarbocyanine iodide (JC-1) (Calbiochem, San Diego, CA, USA) for 20 min at 37°C. The changes in the intensity of red and green fluorescence of cells were observed using a fluorescence microscope (Eclipse TE 2000-S, Nikon Corp., Tokyo, Japan).

Establishment of SMMC-7721-Xenotransplanted Mouse Model

SMMC-7721-Xenotransplanted BALB/c Nude Mouse Model

The experimental animal protocol was approved by the Animal Ethics Committee of Jilin University (SY201905019). Twenty-five specific-pathogen-free (SPF) BALB/c nude mice (male, 6 weeks old) (n = 5/group) were purchased from Wei-tongli-hua Laboratory Animal Technology Company (Beijing, China), and maintained with adaptive feeding for 1week in barrier facilities under a 12-h light-dark cycle at a temperature of 23 ± 1 °C and a humidity of 50 ± 10%. After this period, a 5×10^7/mL concentration of logarithmic growth-phase SMMC-7721 cells

were subcutaneously injected into the right flank of the mice, to generate SMMC-7721-xenotransplanted BALB/c nude mice. When the tumor volumes of these mice reached approximately 100 mm^3, they were randomly divided into five treatment groups: a control group (tail-vein injected with saline), a Tf-LP group (tail-vein injected with Tf-LP), an ERN group (tail-vein injected with 2 mg/kg of ERN), an LP-ERN group (tail-vein injected with LP-ERN containing 2 mg/kg of ERN), and a Tf-LP-ERN group (tail-vein injected with Tf-LP-ERN containing 2 mg/kg of ERN). These treatments were performed on every second for a period of 14 days. Prior to each treatment, the body weight and tumor size of each mouse were recorded. Tumor volumes were calculated in mm^3, as length × width × width× 0.5.

After the final treatment, the mice were anesthetized by intraperitoneal injection of 1.5% pentobarbital sodium, photographed, and blood was collected from the caudal vein. The mice were then euthanized, and the tumor tissues were isolated and stored at -80°C, while the organs (the liver, spleen and kidney) were preserved in 4% tissue fixative for subsequent pathological examination.

SMMC-7721-Xenotransplanted BALB/c Mice

The experimental animal protocol was approved by the Animal Ethics Committee of Jilin University (SY201905019). Thirty SPF BALB/c mice (male, 8-10 weeks old) (n = 6/group) were purchased from Liaoning Changsheng Biotechnology Company (Liaoning, China), adaptively fed for 1 week (as described above), and then intraperitoneally injected with cyclophosphamide (50 mg/kg) on 3 consecutive days. Then, they were seeded with tumors according to the methods in the literature (17). The drug treatment protocol and experimental process were the same as those used for the SMMC-7721-xenotransplanted BALB/c nude mice.

Evaluation of Distribution of Nanoparticles in SMMC-7721-Xenotransplanted BALB/c Nude Mice

When the tumor volumes of the SMMC-7721-xenotransplanted BALB/c nude mice reached 200 mm^3, LP-ERN-DiR or Tf-LP-ERN-DiR were injected into mice tail veins to give an ERN concentration of 2 mg/kg. The tissue distributions of LP-ERN-DiR and Tf-LP-ERN-DiR in the mice at 2 h, 4 h and 6 h after injection were observed using a small-animal *in vivo* imaging system (IVIS Kinetic, Caliper, Boston, MA, USA). Finally, the mice were euthanized, tissues were collected, and the fluorescence intensities of tissue types were observed and compared.

Histopathological Examination

Histopathological examination was performed as in our previous study (19). Slides of liver, spleen, and kidney tissue were stained with hematoxylin and eosin, and then observed using an optical microscope (Nikon Corp., Tokyo, Japan) to detect morphological changes in organ tissue.

Enzyme-Linked Immunosorbent Assay

The concentrations of tumor necrosis factor-α (TNF-α) (KT2132-A), interleukin-10 (IL-10) (KT2176-A), and chemokine C-C motif ligand 11 (CCL11) (KT30243-A) in blood collected from BALB/c mice were determined using commercial enzyme-linked immunosorbent assay kits (Jiangsu Kete Biotechnology Co., Ltd., Jiangsu, China), according to the manufacturer's instructions.

Western Blot Analysis

Tumor tissues obtained from BALB/c nude mice and spleen tissues obtained from BALB/c mice were lyzed and homogenized, and the protein concentrations were measured using a Bicinchoninic Acid Protein Assay Kit (Merck Millipore, Billerica, MA, USA) according to our previous study (17). Protein samples were separated by 10-12% sodium dodecyl sulfate polyacrylamide gel electrophoresis, and then transferred to 0.45 μm polyvinylidene difluoride membranes (Merck Millipore, Burlington, MA, USA). The membranes bearing tumor tissues were blocked with 5% bovine serum albumin solution at 4°C for 6 h, and then exposed to the following primary antibodies at 4°C for 12 h: Bax (ab32503), Bcl-2 antagonist of cell death (Bad) (ab129192), Bcl-2 (ab7973), PARP-1 (ab32138), cleaved PARP-1 (ab32064), cleaved caspase-3 (ab2302), cleaved caspase-9 (ab25758), total caspase-9 (ab25758) (Abcam, Cambridge, MA, USA), total caspase-3 (bs-0081R), p53 upregulated modulator of apoptosis (PUMA) (bs1573R) (Beijing Bioss Biotechnology Co., Ltd., Beijing, China), and glyceraldehyde-3-phosphate dehydrogenase (GAPDH) (E-AB-20032; Elabscience Biotechnology Co., Ltd, Wuhan, China). The membranes bearing spleen tissues were incubated with the following primary antibodies at 4°C for 12 h: Nrf2 (A1244), heme oxygenase-1 (HO-1) (A19062), superoxide dismutase (SOD)-1 (A12537), phospho (P)-NF-κB (AP0475) (Abclonal Biotechnology Co., Ltd., Wuhan, China), SOD-2 (ab13533), P-IKKα+β (ab55341), total (T)-NF-κB (ab7970) (Abcam, Cambridge, MA, USA), T-IKKα+β (bs-10123R) (Beijing Bioss Biotechnology Co., Ltd., Beijing, China), and GAPDH. After washes, the membranes were incubated with goat anti-rabbit (AS014) or goat anti-mouse secondary antibody (AS003) (Abclonal Biotechnology Co., Ltd., Wuhan, China) for 4 h at 4°C. The expression intensity of the proteins was detected using electrochemiluminescence detection kits (Merck Millipore, Billerica, MA, USA) and analyzed with Image J software (NIH, Bethesda, Rockville, MD, USA).

Statistical Analysis

All values are presented as means ± SDs. Differences were determined by one-way analysis of variance followed by Tukey's test using SPSS 16.0 software (IBM Corporation, Armonk, NY, USA). A P-value less than 0.05 was considered to be a significant difference.

RESULTS

Characterization of Tf-LP-ERN Nanoparticles

The particle size of the LP-ERN was 62.60 nm and their polydispersity index (PDI) was 0.137, whereas these parameters for the Tf-LP-ERN was 88.63 nm and 0.165, respectively (**Figure 1A** and **Table 1**). The LP-ERN and Tf-LP-ERN

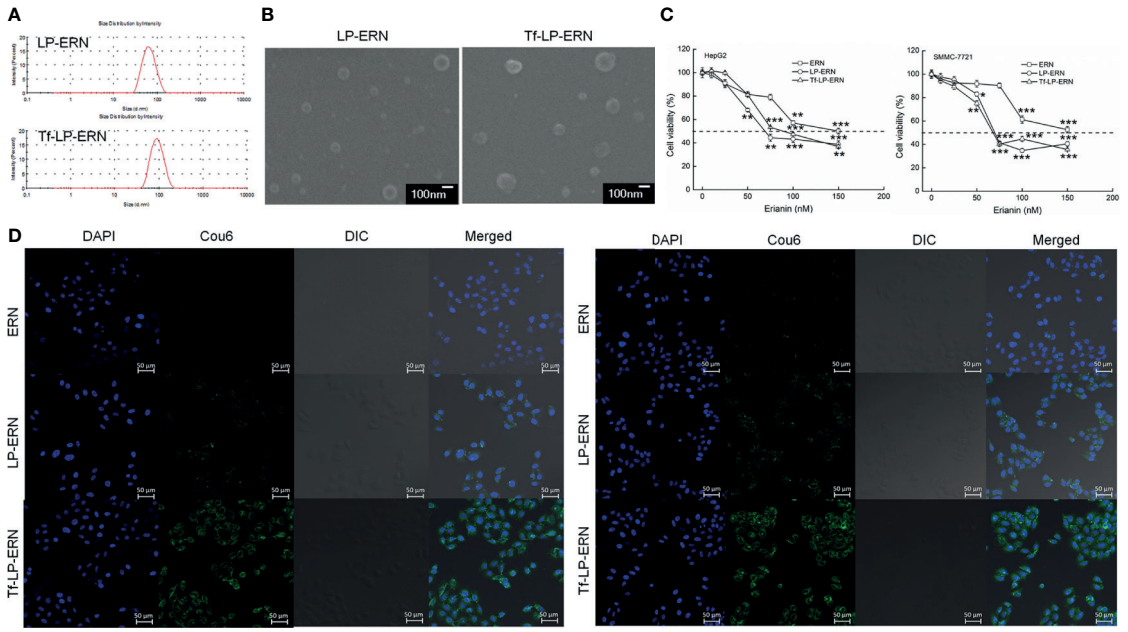

FIGURE 1 | Characterization of LP-ERN and Tf-LP-ERN. **(A)** The particle size distribution of LP-ERN and Tf-LP-ERN were uniform, both less than 100 nm (n = 3). **(B)** Field emission scanning electron microscopy (FESEM) images of LP-ERN and Tf-LP-ERN indicating their uniformly spherical (30,000 ×) (Scale bar: 100 nm) (n = 3). **(C)** ERN, LP-ERN and Tf-LP-ERN reduced the viability of HepG2 and SMMC-7721 cells in a concentration gradient (n = 6). **(D)** ERN, LP-ERN and Tf-LP-ERN can be taken up by HepG2 and SMMC-7721 cells (magnification: 200, scale bar: 50 μm) (n = 3). Liposomes were labelled with Coumarin 6 (Cou6) and the nuclei were labelled with 4',6-diamidino-2-phenylindole (DAPI). $^{*}P < 0.05$, $^{**}P < 0.01$ and $^{***}P < 0.001$ *vs*. control cells.

nanoparticles had smooth surfaces and uniform particle sizes, as shown by the FESEM results (**Figures 1A, B**). There was no significant change in the PDI of the nanoparticles, indicating that the LPs prepared by ethanol injection had good reproducibility and a uniform particle-size distribution. The EE values of the LP-ERN and Tf-LP-ERN nanoparticles were 69.5% and 68.5%, respectively (**Table 1**). The EE of the LPs modified with Tf was almost unchanged, indicating that the phospholipids effectively encapsulated ERN.

Tf-LP-ERN Induced Mitochondrial Apoptosis in Liver Cancer Cells

In HepG2 cells, the IC_{50} values of the ERN, LP-ERN, and Tf-LP-ERN were 136 nM, 99.48 nM, and 100.82 nM, respectively, whereas their IC_{50} values in SMMC-7721 cells were 147 nM, 100.23 nM, and 109.12 nM, respectively (**Figure 1C**). The Tf-modified ERN-containing nanoparticles were absorbed more effectively by liver cancer cells than the non-Tf-modified ERN-containing nanoparticles, as shown by the increased green fluorescence of the Tf-LP-ERN nanoparticle-treated cells (**Figure 1D**).

Exposure of liver cancer cells to ERN, LP-ERN and Tf-LP-ERN led to different extents of cell apoptosis: the Tf-LP-ERN caused 26.91% and 30.79% early/late apoptosis in HepG2 and SMMC-7721 cells, respectively (**Figure 2A**). Decreases in the MMP are the first indication of apoptosis (26), and treatment with ERN, LP-ERN or Tf-LP-ERN all strongly reduced the MMP in liver cancer cells. The greatest reduction was generated by Tf-LP-ERN nanoparticle treatment, as they accumulated to the greatest extent in cells, which was demonstrated by the Tf-LP-ERN nanoparticle-treated cells having the highest intensity of green fluorescence (**Figure 2B**).

Tf-LP nanoparticle treatment failed to influence liver cancer cells' apoptosis rate, and the MMPs in these cells suggested that the liposomal material was non-cytotoxic (**Figure 2**).

Tf-LP-ERN Inhibited Xenografted Tumor Growth in Nude Mice

Compared with control treatment mice, two weeks of administration of ERN, LP-ERN or Tf-LP-ERN significantly inhibited the growth of tumors in SMMC-7721-xenotransplanted

TABLE 1 | Characterization of LP-ERN and Tf-LP-ERN properties.

Sample	Particle size (nm)	PDI	EE(%)
LP-ERN	62.60 ± 3.11	0.137 ± 0.05	69.5 ± 0.8
Tf-LP-ERN	88.63 ± 4.21	0.165 ± 0.03	68.5 ± 1.3

The data were analyzed using a one-way analysis of variance and expressed as mean ± S.D. (n = 3).

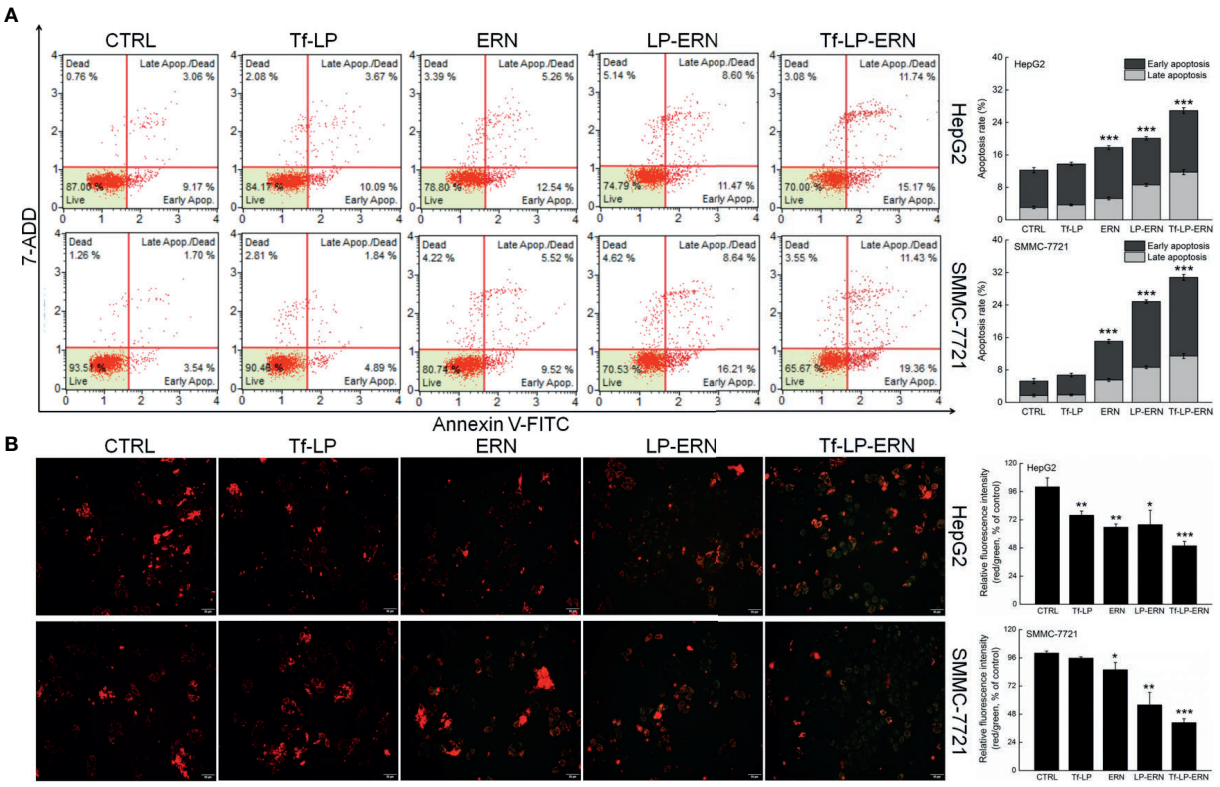

FIGURE 2 | ERN, LP-ERN and Tf-LP-ERN induced apoptosis of HepG2 and SMMC-7721 cells by reducing the mitochondrial membrane potential, among which, Tf-LP- ERN showed the best efficacy. ERN, LP-ERN and Tf-LP-ERN strongly **(A)** enhanced the apoptosis rate (n = 3) and **(B)** reduced the liver cancer cells mitochondrial membrane potential (magnification: 200, scale bar: 50 μm) (n = 3). Qualitative data of mitochondrial membrane potential are expressed as the ratio of red to green fluorescence intensity. $^{*}P < 0.05$, $^{**}P < 0.01$ and $^{***}P < 0.001$ *vs.* control cells.

BALB/c nude mice ($P < 0.05$, **Figures 3A–C**). The Tf-LP-ERN showed the best tumor volume-suppressive effects, due to the enhanced permeability and retention (EPR) effect of LPs; however, Tf-LP did not suppress tumor growth (**Figures 3A–C**).

Neither ERN nor nanoparticles (Tf-LP, LP-ERN, or Tf-LP-ERN) had significant effects on the body weight or organ morphology of SMMC-7721-xenotransplanted BALB/c nude mice (**Figures 3D, E**).

Tf-LP-ERN Targeted Tumor Tissues to Induce Mitochondrial Apoptosis

LP-ERN-DiR and Tf-LP-ERN-DiR nanoparticles were injected intravenously into SMMC-7721-xenotransplanted BALB/c nude mice to investigate their tumor-targeting abilities. Six hours after administration, the fluorescence intensity at the tumor site in the Tf-LP-ERN-DiR nanoparticle treatment group was higher than that in the LP-ERN-DiR nanoparticle treatment group, which indicated that Tf enhanced the tumor-targeting ability of the nanoparticle drug-delivery system (**Figure 4A**).

Tissues were collected 6 h after treatment to further examine the distribution of fluorescence. The liver and spleen tissue exhibited high fluorescence, due their roles in metabolism and reticuloendothelial processing (**Figure 4B**).

In the tumor tissues of SMMC-7721-xenotransplanted BALB/c nude mice, Tf-LP-ERN strongly enhanced the expression levels of Bax, Bad, PUMA, cleaved RARP-1, cleaved caspase-3 and caspase-9, and decreased the expression level of Bcl-2 (**Figure 4C**). This suggests that treatment with Tf-LP-ERN may alleviate the development of liver cancer by inducing mitochondrial apoptosis.

Tf-LP-ERN Inhibited Xenografted Tumor Growth in BALB/c Mice by Enhancing Immune Function

Treatment of SMMC-7721-xenotransplanted BALB/c mice with ERN, LP-ERN nanoparticles, or Tf-LP-ERN nanoparticles inhibited tumor growth without affecting body weight or organ morphology (**Figure 5**). Tf-LP-ERN nanoparticle treatment had the greatest suppressive effects on tumor growth, whereas Tf-LP nanoparticle treatment did not suppress tumor growth (**Figures 5A, B**).

In SMMC-7721-tumor-bearing mice, Tf-LP-ERN treatment increased the serum concentration of TNF-α ($P < 0.01$) and decreased the serum concentrations of IL-10 ($P < 0.05$) and CCL11 ($P < 0.05$) (**Figure 6A**). Nrf2 is a key transcription factor

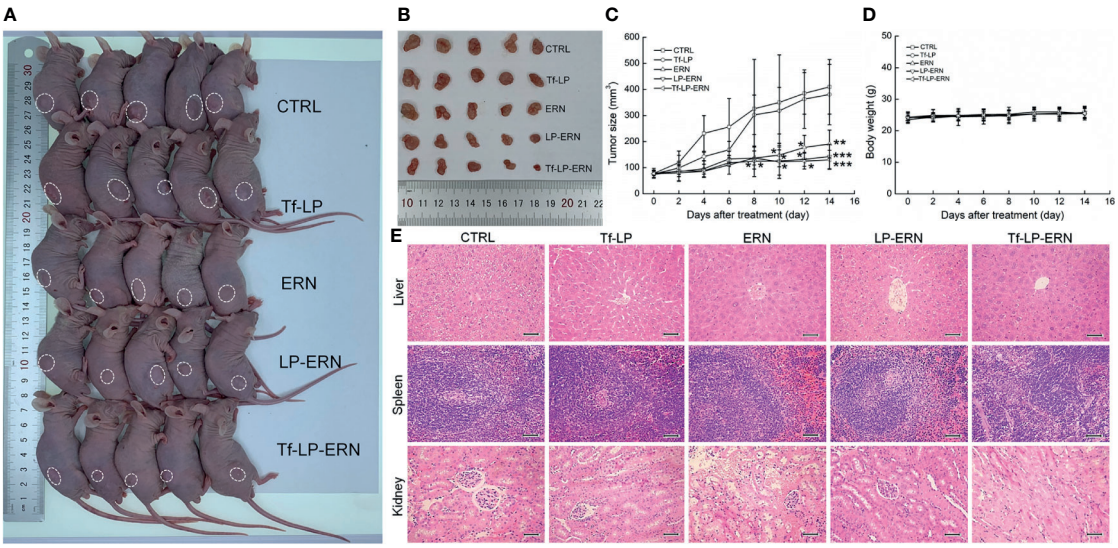

FIGURE 3 | ERN, LP-ERN and Tf-LP-ERN suppressed the tumor growth and showed biological safety in SMMC-7721-xenotransplanted BALB/c nude mice. The tumor volume comparison in **(A)** SMMC-7721-xenotransplanted BALB/c nude mice, and **(B)** their collected tumors. **(C)** Tf-LP-ERN significantly reduced the tumor volume of SMMC-7721-xenotransplanted BALB/c nude mice after 14-d administration (n = 5). Tf-LP, ERN, LP-ERN and Tf-LP-ERN showed no significant effects **(D)** on the body weight and **(E)** histopathologic changes including liver, spleen and kidney in SMMC-7721-xenotransplanted mice (magnification: 200, scale bar: 50 μm). $^{*}P < 0.05$, $^{**}P < 0.01$ and $^{***}P < 0.001$ *vs.* CTRL mice.

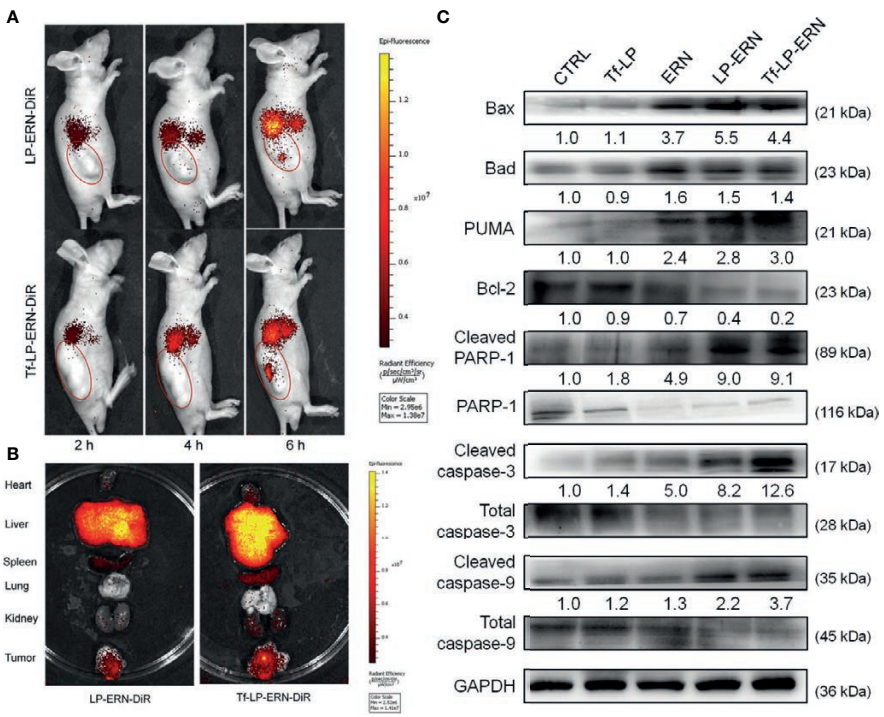

FIGURE 4 | Tf-LP-ERN alleviated cancer development by targeting tumor tissues and caused mitochondrial apoptosis. **(A)** LP-ERN and Tf-LP-ERN labelled by DiR gradually accumulate to tumor tissues in SMMC-7721-xenotransplanted BALB/c nude mice (n = 3/group). **(B)** The tissue distribution of LP-ERN and Tf-LP-ERN in heart, liver, spleen, lung, kidney and tumor after 6 h of tail vein injection in SMMC-7721-xenotransplanted BALB/c nude mice (n = 3/group). **(C)** ERN, LP-ERN and Tf-LP-ERN regulated the expressions of Bcl-2 family members and caspases in tumor tissues of SMMC-7721-xenotransplanted BALB/c nude mice. Quantification data were normalized by GAPDH or the corresponding total proteins and were reported as the folds of those from the corresponding CTRL mice (n = 3).

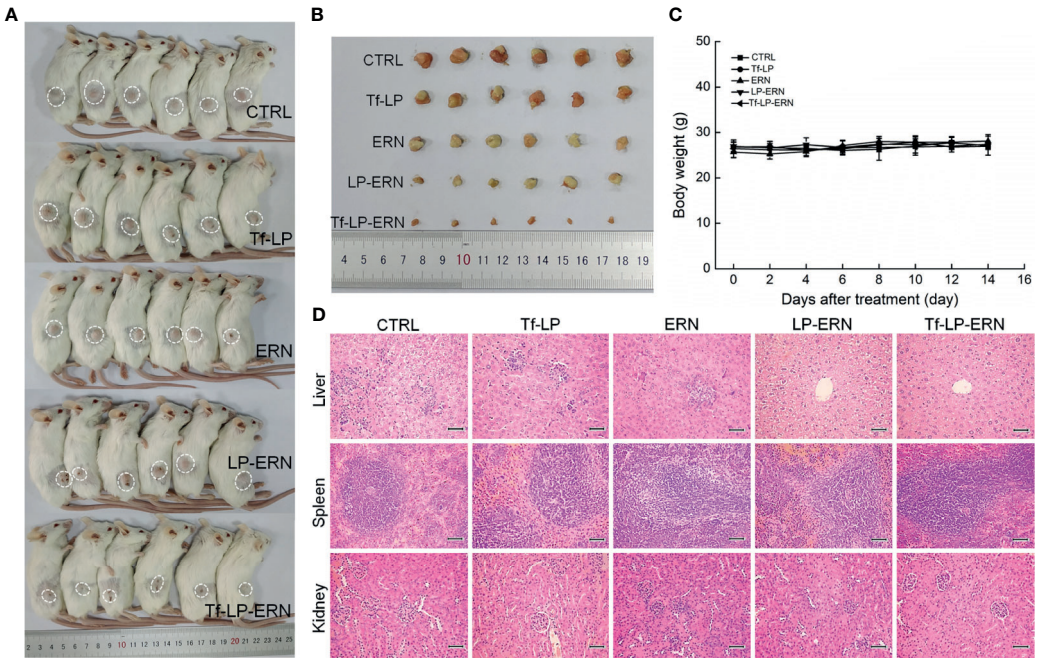

FIGURE 5 | ERN, LP-ERN and Tf-LP-ERN suppressed the tumor growth and showed biological safety in SMMC-7721-xenotransplanted BALB/c mice. The tumor volume comparison in **(A)** SMMC-7721-xenotransplanted BALB/c mice, and **(B)** their collected tumors (n = 6). Tf-LP, ERN, LP-ERN and Tf-LP-ERN showed no significant effects **(C)** on the body weight and **(D)** histopathologic changes including liver, spleen and kidney in SMMC-7721-xenotransplanted mice (magnification: 200, scale bar: 50 μm).

that regulates the expression of cytoprotective genes in various types of cells or tissues, which is crucial for defending cells against oxidative stress (27). The spleens of SMMC-7721-xenografted mice treated with ERN, LP-ERN or Tf-LP-ERN exhibited increased levels of expression of Nrf2 and its downstream proteins HO-1, SOD-1, SOD-2, and reduced the levels of expression of P-IKKα+β, and P-NF-κB. Tf-LP-ERN nanoparticle treatment had the greatest effects in this regard (**Figure 6B**).

DISCUSSION

Liver cancer is mainly caused by inflammation, such as that generated by hepatitis B and C viruses (28). Our previous study found that ERN exerts anti-liver cancer effects by regulating mitochondrial apoptosis and the immune response (17); however, its biopharmaceutical applications have been hampered due to its poor aqueous solubility and tumor-targeting ability. Therefore, in this study we aimed to develop a novel nanoparticle drug-delivery system, Tf-LP-ERN, to enhance the aqueous solubility and tumor-targeting ability of ERN. Our investigations confirmed that Tf-LP-ERN nanoparticles effectively targeted tumor tissues and exhibited increased anti-liver cancer efficacy, as they enabled ERN to strongly affect immunoregulatory pathways in liver cancer cells and in a xenografted tumor mouse model.

The penetration of drugs or drug carriers into tumor tissues, and their accumulation in such tissues, is affected by their particle size; as such, the particle size of LPs is their most practical feature (29). Drug-loaded LPs with a particle size of 60-200 nm selectively penetrate tumor blood vessels, and thereby accumulate in tumor tissues rather than normal tissues, which greatly reduces the adverse effects of drugs on normal tissues (30). The PDI is used to measure the degree of uniformity of particle sizes in a sample (31). The PDI value of Tf-LP-ERN nanoparticles, which had a particle size of 88.63 nm, was approximately 0.165, indicating that the LPs prepared by the ethanol injection method had high uniformity and stability. This accounted for their selective accumulation in tumor tissues.

A significant step in cell apoptosis is the destruction of the MMP, which largely occurs in the early stages of apoptosis. LP-ERN or Tf-LP-ERN nanoparticle treatment of HepG2 and SMMC-7721 cells suppressed cell viability, enhanced cellular apoptosis rate, reduced cell MMPs, and increased cell uptake of ERN, which are all suggestive of anti-tumor activity. Furthermore, such treatment increased the accumulation of ERN in tumor tissues, and thus LP-ERN or Tf-LP-ERN nanoparticle treatment effectively inhibited tumor growth in SMMC-7721-xenografted nude mice. Notably, this was achieved without concomitant effects on the body weight or organs structure of mice, which confirmed the safety of these treatments. Tissue distribution data confirmed these observations, and revealed that Tf-LP-ERN nanoparticles

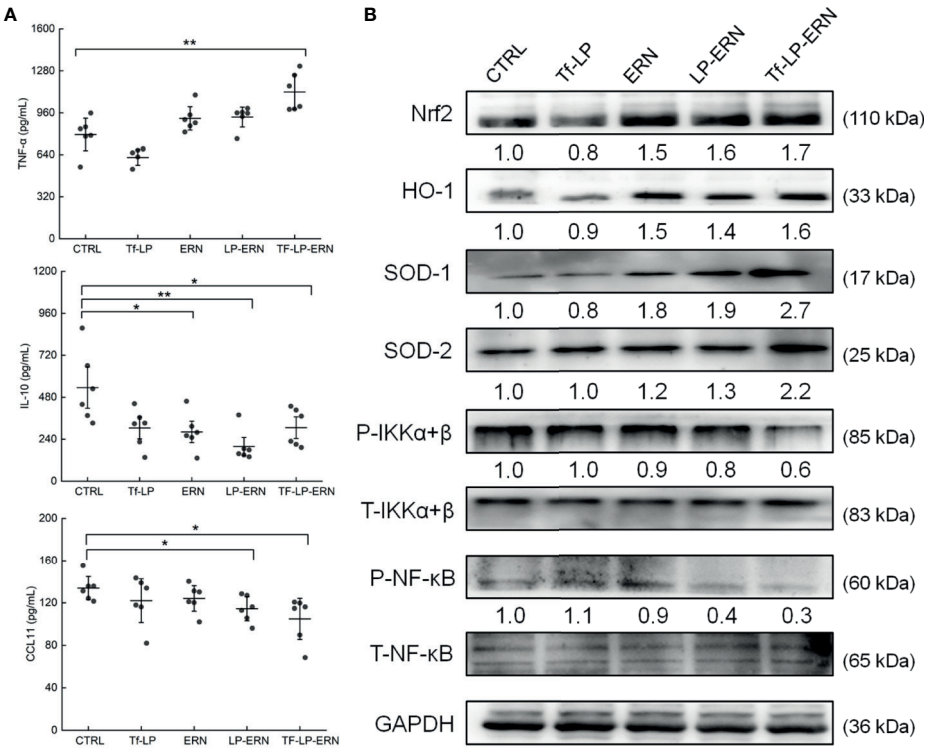

FIGURE 6 | The effects of ERN, LP-ERN and Tf-LP-ERN on inflammatory factor in serum of SMMC-7721-tumor-bearing mice. **(A)** ERN, LP-ERN and Tf-LP-ERN significantly reduced the levels of IL-10, CCL11, and enhanced the level of TNF-α (n = 6). **(B)** In spleens of SMMC-7721-xenografted mice, ERN, LP-ERN and Tf-LP-ERN increased the expression levels of Nrf2 and its downstream proteins HO-1, SOD-1, SOD-2, while reduced the expression levels of P-IKKα+β, and P-NF-κB, among which, Tf-LP-ERN showed the best efficacy. Quantification data were normalized by GAPDH or the corresponding total proteins and were reported as the folds of those from the corresponding CTRL mice (n = 3). The data were analyzed using a one-way analysis of variance and expressed as means ± S.D. (n = 3). $^{*}P < 0.05$ and $^{**}P < 0.01$ *vs*. control cells.

accumulated more in tumor tissues over time than LP-ERN nanoparticles or free ERN.

The Tf receptor has a special extracellular structure that mediates the endocytosis of Tf, enabling the cellular absorption of its Fe^{3+} cargo, and this receptor is overexpressed on the surface of tumor cells relative to normal cells (23). This is because rapidly proliferating tumor cells require high concentrations of Fe^{3+}, and accounts for the tumor-targeting ability of Tf (32). Therefore, Tf-conjugated LPs are capable of tumor targeting. For example, Tf modified paclitaxel-loaded LPs were shown to have greater tumor-inhibitory activity than paclitaxel itself (33), and the use of a Tf-LP system to deliver 1,2-Dihydroquinoline 2 increased cell uptake by approximately 3.7 times (34). Tf-conjugated LPs have negatively charged surfaces, which decreases electrostatic interactions between Tf-conjugated LPs, between Tf-conjugated LPs and cell membranes and serum proteins, thereby prolonging the presence of Tf-conjugated LPs in blood circulation and reducing their non-specific uptake by ordinary cells (35). Our results confirmed that Tf receptor-mediated endocytosis on the surface of tumor cells increased the uptake of ERN.

When an apoptotic stimulus occurs, Bad heterodimerizes with B-cell lymphoma-extra large (Bcl-xL), which releases Bax from Bcl-xL. Bax then translocates to the mitochondria and inserts its N-terminus into the outer mitochondrial membrane, which induces the mitochondrial membrane to become permeable (36, 37). Bcl-2 inhibits this process by interacting with Bax (38). The MMP is depolarized by Bax translocation and Bcl-2 dissipation, and then caspase-9 and its downstream counterpart, caspase-3, are activated, which leads to the initiation of apoptosis (39, 40). PUMA, a BH3-only protein and a pro-apoptotic member of the Bcl-2 family, indirectly inhibits anti-apoptotic Bcl-2 proteins such as Bax by inducing mitochondrial dysfunction and caspase activation (41). ERN, LP-ERN and Tf-LP-ERN enhanced the expression levels of Bax, Bad, and PUMA, promoted the cleaved caspase-3, cleaved-9 and PARP-1, and reduced the expression level of Bcl-2, which induced apoptosis and thus to inhibited tumor growth in xenotransplanted BALB/c nude mice. Tf-LP-ERN had the greatest pro-apoptotic effect, as they more effectively targeted tumors than the other treatments.

We previously confirmed that ERN inhibits the growth of liver cancer tumors due to its immunoregulatory effects (17). The spleen is the body's largest immune organ and the source of many immune cells (42). The immune response in the spleen is closely related to the development of liver cancer, which is accompanied by oxidative stress. Tf-LP-ERN improved the

anti-tumor effect of ERN without affecting its apparent mechanism of action. Moreover, Tf-LP-ERN not only accumulated in tumors and the liver but also in the spleen, which explains why splenic protein concentrations in Tf-LP-ERN-treated mice were better regulated than those in ERN-treated mice. Tf-LP-ERN also enhanced the expression levels of Nrf2 and its downstream proteins, which were responsible for the suppression of the phosphorylated activation of NF-κB. HO-1 and SOD eliminate free radicals, as part of the body's defense against diseases (43, 44). Nrf2 and NF-κB are mutually regulated. Accordingly, the downregulation of Nrf2 can increase the phosphorylation of IκB-α, resulting in the phosphorylation of NF-κB (45). TNF-α is a pleiotropic cytokine that plays an important role in the development and progression of tumors IL-10 is an anti-inflammatory and immunosuppressive cytokine that inhibits the activity of macrophages and the secretion of inflammatory cytokines, such as IL-6 and TNF-α. IL-10 therefore plays an critical role in the negative feedback regulation of the immune response and the inflammatory response (47, 48). In addition, IL-10 enables tumor cells to evade host immune-system defenses, and promotes their metastasis (49). In many inflammatory responses, NF-κB signaling is involved in the secretion of the chemokine CCL11, in coordination with other signaling mechanisms (50). CCL11 inhibits the differentiation of dendritic cells and enhances the polarization of T-helper 2 cells (51, 52). In addition, CCL11 promotes angiogenesis, and its overexpression is closely related to the occurrence and progression of cancer (53). Thus, enhancement of the body's immune response adversely affects the tumor microenvironment, which induces endogenous tumor-cell apoptosis (54).

We acknowledge that this study has some limitations. Further experiments are needed to complete the evaluation of the drug delivery system, and further investigation is needed to show how ERN interacts with the tumor microenvironment.

CONCLUSION

LP-ERN nanoparticles improved the solubility of ERN, and Tf-LP-ERN nanoparticles more effectively targeted tumor cells than LP-ERN nanoparticles, leading to better anti-liver cancer activity *in vivo*. Consistent with previous studies of ERN, we found that the enhanced anti-liver cancer effects of Tf-LP-ERN were due to immunoregulation.

Our novel Tf-conjugated nanoparticle-based ERN-delivery system was highly efficient, accurately targeted tumor cells, and had a good safety profile in a mouse model. This suggests that it warrants further exploration as a potential treatment for liver cancer.

DATA AVAILABILITY STATEMENT

The original contributions presented in the study are included in the article/**Supplementary Material**. Further inquiries can be directed to the corresponding authors.

ETHICS STATEMENT

The animal study was reviewed and approved by the Animal Ethics Committee of Jilin University.

AUTHOR CONTRIBUTIONS

YQ and XZ designed the experiments, draft and revised the manuscript. AY, ZS, RL, and XL performed the experiments and analyzed the data. YZha and YZho analyzed the data. All authors contributed to the article and approved the submitted version.

FUNDING

This study is supported by the Science and Technology Develop Project in Jilin Province of China under the grant (No. 20200201122JC and 20200201030JC) and the Science and Technology Research Project, Education Department of Jilin Province of China under the grant No. JJKH20200322KJ.

ACKNOWLEDGMENTS

Thanks to Professor Lesheng Teng for his support on the preparation of LP-ERN and Tf-LP-ERN.

SUPPLEMENTARY MATERIAL

The Supplementary Material for this article can be found online at: https://www.frontiersin.org/articles/10.3389/fonc.2021.727605/full#supplementary-material

REFERENCES

1. Yi Q, Liu Y, Cao M, Liu J, Xiang Q, Tan G, et al. Transcriptional Analysis and Differentially Expressed Gene Screening of Spontaneous Liver Tumors in CBA/CaJ Mice. *Gene* (2020) 725:144159. doi: 10.1016/j.gene.2019.144159
2. Wassef J, Xu S. Hepatocellular Carcinoma With Tumor Thrombus to the Hepatic Veins and the Right Atrium: A Case Report and Review Exploring Various Presentations and Treatment Options. *Cureus* (2020) 12(6):e8405. doi: 10.7759/cureus.8405
3. Cuestas ML. Hepatocellular Carcinoma and Multidrug Resistance: Past, Present and New Challenges for Therapy Improvement. *World J Pharmacol* (2015) 4(1):96. doi: 10.5497/wjp.v4.i1.96
4. Goossens N, Koessler T, Spahr L, Negro F. Hepatocellular Carcinoma: Updated Management Guidelines. *Rev médicale suisse* (2018) 14(616):1508–11.

5. Lei H, Wang G, Zhang J, Han Q. Inhibiting TrxR Suppresses Liver Cancer by Inducing Apoptosis and Eliciting Potent Antitumor Immunity. *Oncol Rep* (2018) 40(6):3447–57. doi: 10.3892/or.2018.6740
6. Funk K, Czauderna C, Klesse R, Becker D, Hajduk J, Oelgeklaus A, et al. BAX Redistribution Induces Apoptosis Resistance and Selective Stress Sensitivity in Human HCC. *Cancers (Basel)* (2020) 12(6):E1437. doi: 10.3390/cancers12061437
7. Lu G, Zhang G, Zheng X, Zeng Y, Xu Z, Zeng W, et al. C9, T11- Conjugated Linoleic Acid Induces HCC Cell Apoptosis and Correlation With PPAR-Gamma Signaling Pathway. *Am J Transl Res* (2015) 7(12):2752–63.
8. Jiao C, Chen W, Tan X, Liang H, Li J, Yun H, et al. Ganoderma Lucidum Spore Oil Induces Apoptosis of Breast Cancer Cells *In Vitro* and *In Vivo* by Activating Caspase-3 and Caspase-9. *J Ethnopharmacol* (2020) 247:112256. doi: 10.1016/j.jep.2019.112256
9. You XJ, Cao XZ, Lin YC. Berberine Enhances the Radiosensitivity of Hepatoma Cells by Nrf2 Pathway. *Front Biosci* (2019) 24:1190–202. doi: 10.2741/4775
10. Niture SK, Jaiswal AK. Nrf2 Protein Up-Regulates Antiapoptotic Protein Bcl-2 and Prevents Cellular Apoptosis. *J Biol Chem* (2012) 287(13):9873–86. doi: 10.1074/jbc.M111.312694
11. Li CL, Liu XH, Qiao Y, Ning LN, Li WJ, Sun YS, et al. Allicin Alleviates Inflammation of Diabetic Macroangiopathy *via* the Nrf2 and NF-kB Pathway. *Eur J Pharmacol* (2020) 876:173052. doi: 10.1016/j.ejphar.2020.173052
12. An J, Wang X, Guo P, Zhong Y, Zhang X, Yu Z. Hexabromocyclododecane and Polychlorinated Biphenyls Increase Resistance of Hepatocellular Carcinoma Cells to Cisplatin Through the Phosphatidylinositol 3-Kinase/Protein Kinase B Pathway. *Toxicol Lett* (2014) 229(1):265–72. doi: 10.1016/j.toxlet.2014.06.025
13. Pourahmad J, Salimi A, Seydi E. Natural Compounds Target Mitochondrial Alterations in Cancer Cell: New Avenue for Anticancer Research. *Iran J Pharm Res* (2014) 13(Suppl):1–2. doi: 10.9758/cpn.2013.11.3.168
14. Wu T, Dong X, Yu D, Shen Z, Yu J, Yan S. Natural Product Pectolinarigenin Inhibits Proliferation, Induces Apoptosis, and Causes G2/M Phase Arrest of HCC *via* PI3K/AKT/mTOR/ERK Signaling Pathway. *Onco Targets Ther* (2018) 11:8633–42. doi: 10.2147/OTT.S186186
15. Chen P, Wu Q, Feng J, Yan L, Sun Y, Liu S, et al. Erianin, a Novel Dibenzyl Compound in Dendrobium Extract, Inhibits Lung Cancer Cell Growth and Migration *via* Calcium/Calmodulin-Dependent Ferroptosis. *Signal Transduct Target Ther* (2020) 5(1):51. doi: 10.1038/s41392-020-0149-3
16. Chen YT, Hsieh MJ, Chen PN, Weng CJ, Yang SF, Lin CW. Erianin Induces Apoptosis and Autophagy in Oral Squamous Cell Carcinoma Cells. *Am J Chin Med* (2020) 48(1):183–200. doi: 10.1142/s0192415x2050010x
17. Zhang X, Wang Y, Li X, Yang A, Li Z, Wang D. The Anti-Carcinogenesis Properties of Erianin in the Modulation of Oxidative Stress-Mediated Apoptosis and Immune Response in Liver Cancer. *Aging (Albany NY)* (2019) 11(22):10284–300. doi: 10.18632/aging.102456
18. Li Y, Cong H, Wang S, Yu B, Shen Y. Liposomes Modified With Bio-Substances for Cancer Treatment. *Biomater Sci* (2020) 8(23):6442–68. doi: 10.1039/d0bm01531h
19. Bi YE, Zhou Y, Wang M, Li L, Lee RJ, Xie J, et al. Targeted Delivery of Cordycepin to Liver Cancer Cells Using Transferrin-Conjugated Liposomes. *Anticancer Res* (2017) 37(9):5207–14. doi: 10.21873/anticanres.11944
20. Wu PK, Tao Z, Ouyang Z, Cao JY, Geng D, Liu J, et al. The Anti-Tumor Effects of Cordycepin-Loaded Liposomes on the Growth of Hepatoma 22 Tumors in Mice and Human Hepatoma BEL-7402 Cells in Culture. *Drug Dev Ind Pharm* (2016) 42(9):1424–33. doi: 10.3109/03639045.2016.1141930
21. Saavedra-Alonso S, Zapata-Benavides P, Chavez-Escamilla AK, Manilla-Munoz E, Zamora-Avila DE, Franco-Molina MA, et al. WT1 shRNA Delivery Using Transferrin-Conjugated PEG Liposomes in an *In Vivo* Model of Melanoma. *Exp Ther Med* (2016) 12(6):3778–84. doi: 10.3892/etm.2016.3851
22. Deshpande P, Jhaveri A, Pattni B, Biswas S, Torchilin V. Transferrin and Octaarginine Modified Dual-Functional Liposomes With Improved Cancer Cell Targeting and Enhanced Intracellular Delivery for the Treatment of Ovarian Cancer. *Drug Delivery* (2018) 25(1):517–32. doi: 10.1080/10717544.2018.1435747
23. Li S, Zhao H, Mao X, Fan Y, Liang X, Wang R, et al. Transferrin Receptor Targeted Cellular Delivery of Doxorubicin *Via* a Reduction-Responsive Peptide-Drug Conjugate. *Pharm Res* (2019) 36(12):168. doi: 10.1007/s11095-019-2688-2
24. Chiu SJ, Liu S, Perrotti D, Marcucci G, Lee RJ. Efficient Delivery of a Bcl-2-Specific Antisense Oligodeoxyribonucleotide (G3139) *via* Transferrin Receptor-Targeted Liposomes. *J Control Release* (2006) 112(2):199–207. doi: 10.1016/j.jconrel.2006.02.011
25. Zhao M, Zhu T, Chen J, Cui Y, Zhang X, Lee RJ, et al. PLGA/PCADK Composite Microspheres Containing Hyaluronic Acid-Chitosan siRNA Nanoparticles: A Rational Design for Rheumatoid Arthritis Therapy. *Int J Pharm* (2021) 596:120204. doi: 10.1016/j.ijpharm.2021.120204
26. Korge P, Yang L, Yang JH, Wang Y, Qu Z, Weiss JN. Protective Role of Transient Pore Openings in Calcium Handling by Cardiac Mitochondria. *J Biol Chem* (2011) 286(40):34851–7. doi: 10.1074/jbc.M111.239921
27. Dong J, Sulik KK, Chen SY. Nrf2-Mediated Transcriptional Induction of Antioxidant Response in Mouse Embryos Exposed to Ethanol *In Vivo*: Implications for the Prevention of Fetal Alcohol Spectrum Disorders. *Antioxid Redox Signal* (2008) 10(12):2023–33. doi: 10.1089/ars.2007.2019
28. Refolo MG, Messa C, Guerra V, Carr BI, D'Alessandro R. Inflammatory Mechanisms of HCC Development. *Cancers (Basel)* (2020) 12(3):641. doi: 10.3390/cancers12030641
29. Ren H, He Y, Liang J, Cheng Z, Zhang M, Zhu Y, et al. Role of Liposome Size, Surface Charge, and PEGylation on Rheumatoid Arthritis Targeting Therapy. *ACS Appl Mater Interfaces* (2019) 11(22):20304–15. doi: 10.1021/acsami.8b22693
30. Ma JB, Shen JM, Yue T, Wu ZY, Zhang XL. Size-Shrinkable and Protein Kinase Cα-Recognizable Nanoparticles for Deep Tumor Penetration and Cellular Internalization. *Eur J Pharm Sci* (2021) 159:105693. doi: 10.1016/j.ejps.2020.105693
31. Mohamad Saimi NI, Salim N, Ahmad N, Abdulmalek E, Abdul Rahman MB. Aerosolized Niosome Formulation Containing Gemcitabine and Cisplatin for Lung Cancer Treatment: Optimization, Characterization and *In Vitro* Evaluation. *Pharmaceutics* (2021) 13(1):E59. doi: 10.3390/pharmaceutics13010059
32. Daniels TR, Bernabeu E, Rodríguez JA, Patel S, Kozman M, Chiappetta DA, et al. The Transferrin Receptor and the Targeted Delivery of Therapeutic Agents Against Cancer. *Biochim Biophys Acta* (2012) 1820(3):291–317. doi: 10.1016/j.bbagen.2011.07.016
33. Jin C, Zhao S, Zhang M, Wang Y, Kou X, Ping LU, et al. Preparation and Tumor Inhibition Effect of Transferrin Modified Paclitaxel-Loaded Liposome. *China Pharm* (2016) 27(01):44–7. doi: 10.6039/j.issn.1001-0408.2016.01.14
34. Wang M, Lee RJ, Bi Y, Li L, Yan G, Lu J, et al. Transferrin-Conjugated Liposomes Loaded With Novel Dihydroquinoline Derivatives as Potential Anticancer Agents. *PloS One* (2017) 12(10):e0186821. doi: 10.1371/journal.pone.0186821
35. Sakpakdeejaroen I, Somani S, Laskar P, Mullin M, Dufes C. Transferrin-Bearing Liposomes Entrapping Plumbagin for Targeted Cancer Therapy. *J Interdiscip Nanomed* (2019) 4(2):54–71. doi: 10.1002/jin2.56
36. Yang E, Zha J, Jockel J, Boise LH, Thompson CB, Korsmeyer SJ. Bad, a Heterodimeric Partner for Bcl-XL and Bcl-2, Displaces Bax and Promotes Cell Death. *Cell* (1995) 80(2):285–91. doi: 10.1016/0092-8674(95)90411-5
37. Teijido O, Dejean L. Upregulation of Bcl2 Inhibits Apoptosis-Driven BAX Insertion But Favors BAX Relocalization in Mitochondria. *FEBS Lett* (2010) 584(15):3305–10. doi: 10.1016/j.febslet.2010.07.002
38. Mikhailov V, Mikhailova M, Pulkrabek DJ, Dong Z, Venkatachalam MA, Saikumar P. Bcl-2 Prevents Bax Oligomerization in the Mitochondrial Outer Membrane. *J Biol Chem* (2001) 276(21):18361–74. doi: 10.1074/jbc.M100655200
39. Chatterjee S, Rhee YH, Ahn JC. Sulforaphene-Carboplatin Combination Synergistically Enhances Apoptosis by Disruption of Mitochondrial Membrane Potential and Cell Cycle Arrest in Human Non-Small Cell Lung Carcinoma. *J Med Food* (2016) 19(9):860–9. doi: 10.1089/jmf.2016.3675
40. Wang K, Lin B. Pathophysiological Significance of Hepatic Apoptosis. *ISRN Hepatol* (2013) 2013:740149. doi: 10.1155/2013/740149
41. Guan J, Liu Z, Xiao M, Hao F, Wang C, Chen Y, et al. MicroRNA-199a-3p Inhibits Tumorigenesis of Hepatocellular Carcinoma Cells by Targeting ZHX1/PUMA Signal. *Am J Transl Res* (2017) 9(5):2457–65.
42. Li BH, Jiang W, Zhang S, Huang N, Sun J, Yang J, et al. The Spleen Contributes to the Increase in PMN-MDSCs in Orthotopic H22 Hepatoma Mice. *Mol Immunol* (2020) 125:95–103. doi: 10.1016/j.molimm.2020.07.002

43. Ayaydin H, Akaltun I, Koyuncu I, CelIk H, KI A, Takatak H. High KEAP1, NRF2 and Low HO-1 Serum Levels in Children With Autism. *Noro Psikiyatr Ars* (2020) 57(4):274–9. doi: 10.29399/npa.24862
44. Jin Y, Yang J, Lin L, Lin Y, Zheng C. The Attenuation of Scutellariae Radix Extract on Oxidative Stress for Colon Injury in Lipopolysaccharide-Induced RAW264.7 Cell and 2,4,6-Trinitrobenzene Sulfonic Acid-Induced Ulcerative Colitis Rats. *Pharmacogn Mag* (2016) 12(46):153–9. doi: 10.4103/0973-1296.177913
45. Thomas NS, George K, Selvam AAA. Anticancer Mechanism of Troxerutin *via* Targeting Nrf2 and NF-kappaB Signalling Pathways in Hepatocarcinoma Cell Line. *Toxicol In Vitro* (2019) 54:317–29. doi: 10.1016/j.tiv.2018.10.018
46. Wajant H. The Role of TNF in Cancer. *Results Probl Cell Differ* (2009) 49:1–15. doi: 10.1007/400_2008_26
47. Malefyt DW R. Interleukin 10(IL-10) Inhibits Cytokine Synthesis by Human Monocytes: An Autoregulatory Role of IL-10 Produced by Monocytes. *J Exp Med* (1991) 174(5):1209–20. doi: 10.1084/jem.174.5.1209
48. Fiorentino DF, Zlotnik A, Mosmann TR, Howard MH, O'Garra A. IL-10 Inhibits Cytokine Production by Activated Macrophages. *J Immunol* (1992) 147(11):3815–22.
49. El-Emshaty HM, Nasif WA, Mohamed IE. Serum Cytokine of IL-10 and IL-12 in Chronic Liver Disease: The Immune and Inflammatory Response. *Dis Markers* (2015) 2015:707254. doi: 10.1155/2015/707254
50. Peng Y, Cordiner SB, Sawyer GM, McGhie TK, Espley RV, Allan AC, et al. Kiwifruit With High Anthocyanin Content Modulates NF-κb Activation and Reduces CCL11 Secretion in Human Alveolar Epithelial Cells. *J Funct Foods* (2020) 65:103734. doi: 10.1016/j.jff.2019.103734
51. Stevenson NJ, Addley MR, Ryan EJ, Boyd CR, Carroll HP, Paunovic V, et al. CCL11 Blocks IL-4 and GM-CSF Signaling in Hematopoietic Cells and Hinders Dendritic Cell Differentiation *via* Suppressor of Cytokine Signaling Expression. *J Leukoc Biol* (2009) 85(2):289–97. doi: 10.1189/jlb.0708394
52. Yang J, Hawkins OE, Barham W, Gilchuk P, Boothby M, Ayers GD, et al. Myeloid Ikkβ Promotes Antitumor Immunity by Modulating CCL11 and the Innate Immune Response. *Cancer Res* (2014) 74(24):7274–84. doi: 10.1158/0008-5472.Can-14-1091
53. Zheng Z, Zhang J, Liu Q, Huang S, Jin L, Pathology DO. Application of Serum CCL11,ANXA2,OPN in Gastric Cancer Patients. *Lab Med Clinic* (2017) 14 (22):3346–8.3551. doi: 10.3969/j.issn.1672-9455.2017.22.025
54. Cassim S, Pouyssegur J. Tumor Microenvironment: A Metabolic Player That Shapes the Immune Response. *Int J Mol Sci* (2019) 21(1):157. doi: 10.3390/ijms21010157

Conflict of Interest: The authors declare that the research was conducted in the absence of any commercial or financial relationships that could be construed as a potential conflict of interest.

Publisher's Note: All claims expressed in this article are solely those of the authors and do not necessarily represent those of their affiliated organizations, or those of the publisher, the editors and the reviewers. Any product that may be evaluated in this article, or claim that may be made by its manufacturer, is not guaranteed or endorsed by the publisher.

Copyright © 2021 Yang, Sun, Liu, Liu, Zhang, Zhou, Qiu and Zhang. This is an open-access article distributed under the terms of the Creative Commons Attribution License (CC BY). The use, distribution or reproduction in other forums is permitted, provided the original author(s) and the copyright owner(s) are credited and that the original publication in this journal is cited, in accordance with accepted academic practice. No use, distribution or reproduction is permitted which does not comply with these terms.

frontiers in Immunology

ORIGINAL RESEARCH
published: 20 September 2021
doi: 10.3389/fimmu.2021.739768

m^{6}A Methylation Modification Patterns and Tumor Microenvironment Infiltration Characterization in Pancreatic Cancer

Mengyu Sun[1,2], *Meng Xie*[1,2], *Tongyue Zhang*[1,2], *Yijun Wang*[1,2], *Wenjie Huang*[2,3]* and *Limin Xia*[1,2]*

[1] Department of Gastroenterology, Institute of Liver and Gastrointestinal Diseases, Tongji Hospital of Tongji Medical College, Huazhong University of Science and Technology, Wuhan, China, [2] Hubei Key Laboratory of Hepato-Pancreato Biliary Diseases, Tongji Hospital, Tongji Medical College, Huazhong University of Science and Technology, Wuhan, China, [3] Hepatic Surgery Center, Tongji Hospital, Tongji Medical College, Huazhong University of Science and Technology, Wuhan, China

Recent studies have shown that RNA N^6-methyladenosine (m^{6}A) modification plays an important part in tumorigenesis and immune-related biological processes. However, the comprehensive landscape of immune cell infiltration characteristics in the tumor microenvironment (TME) mediated by m^{6}A methylation modification in pancreatic cancer has not yet been elucidated. Based on consensus clustering algorithm, we identified two m^{6}A modification subtypes and then determined two m^{6}A-related gene subtypes among 434 pancreatic cancer samples. The TME characteristics of the identified gene subtypes were highly consistent with the immune-hot phenotype and the immune-cold phenotype respectively. According to the m^{6}A score extracted from the m^{6}A-related signature genes, patients can be divided into high and low m^{6}A score groups. The low score group displayed a better prognosis and relatively strong immune infiltration. Further analysis showed that low m^{6}A score correlated with lower tumor mutation burden and PD-L1 expression, and indicated a better response to immunotherapy. In general, m^{6}A methylation modification is closely related to the diversity and complexity of immune infiltration in TME. Evaluating the m^{6}A modification pattern and immune infiltration characteristics of individual tumors can help deepen our understanding of the tumor microenvironment landscape and promote a more effective clinical practice of immunotherapy.

Keywords: pancreatic cancer, m^{6}A, tumor microenvironment, immunotherapy, mutation burden

OPEN ACCESS

Edited by:
Peng Qu,
National Institutes of Health (NIH), United States

Reviewed by:
Chong Jin,
University of Pennsylvania, United States
Mengqi Zhang,
University of Pennsylvania, United States

***Correspondence:**
Limin Xia
xialimin@tjh.tjmu.edu.cn
Wenjie Huang
huangwenjie@tjh.tjmu.edu.cn

Specialty section:
This article was submitted to Cancer Immunity and Immunotherapy, a section of the journal Frontiers in Immunology

Received: *11 July 2021*
Accepted: *06 September 2021*
Published: *20 September 2021*

Citation:
Sun M, Xie M, Zhang T, Wang Y, Huang W and Xia L (2021) m^{6}A Methylation Modification Patterns and Tumor Microenvironment Infiltration Characterization in Pancreatic Cancer. Front. Immunol. 12:739768. doi: 10.3389/fimmu.2021.739768

INTRODUCTION

More than 160 RNA modifications including N^7-methylguanine (m^{7}G), N^6-methyladenosine (m^{6}A), and N^5-methylcytosine (m^{5}C) have been identified. These modifications play a significant role in regulating RNA fate (1). In eukaryotes, m^{6}A is regarded as the most important and abundant mRNA modification, accounting for more than 80% of all RNA methylation modifications (2). It is now clear that m^{6}A methylation exists in almost all types of RNA, including coding RNA and non-coding RNA (3). The m^{6}A modification is catalyzed by RNA methyltransferases such as METTL3, METTL14, METTL16, WTAP, VIRMA, ZC3H13, RBM15, and RBM15B (writers), while the modification is removed by demethylases such as FTO and ALKBH5 (erasers). In addition, modifications can be recognized by m^{6}A binding proteins, such as YTHDC1/2, YTHDF1/2/3, HNRNPC, FMR1, LRPPRC, HNRNPA2B1, IGFBP1/2/3, and RBMX (readers) (4–6). A growing body of evidence shows that m^{6}A regulators are involved in vital biological processes and are dynamically regulated in many physiological and pathological processes (7–9). Abnormal expression and genetic alterations of m^{6}A regulators are closely related to events such as developmental defects, metabolic disorders, abnormal immune regulation, and tumor progression (10, 11). A comprehensive understanding of potential m^{6}A regulators' expression perturbation and genetic variation under cancer heterogeneity will facilitate the identification of therapeutic targets based on RNA methylation (12, 13).

Pancreatic cancer (PC) is a highly lethal malignant tumor, which is also one of the leading causes of cancer death worldwide (14). In the past 25 years, its global burden has more than doubled (15). With the in-depth comprehending of pathology, the diversity and complexity of tumor microenvironment have been increasingly understood, and immune cell subgroups which intimately involved in tumor genesis, metastasis and treatment are gradually recognized (16–19). Tumor microenvironment (TME) has been found to play an important role in ineffective treatment and poor prognosis of pancreatic cancer. Many molecules and related signal transduction pathways in the microenvironment can promote cancer metastasis or immunosuppression. A variety of soluble immunosuppressive molecules and immunosuppressive cells can lead to the disorder of immune effector cells, thus forming a unique immunosuppressive environment for pancreatic cancer (20). Increasing research focuses on whether the components of TME (including acellular matrix, pancreatic stellate cells, immune cells and soluble factors) can be used as effective targets for PC therapy (21). Recently, immune checkpoint inhibitors and chimeric antigen receptor T (CAR-T) cell therapy have become popular immunotherapies related to TME in pancreatic cancer (22, 23). However, whether these therapies can bring clinical benefits remains to be fully studied. A comprehensive understanding of the characteristics of the tumor microenvironment in PC will make a beneficial contribution to the research of immunotherapy and provide new insights for basic and clinical applications.

An increasing number of studies have confirmed the close correlation between TME infiltrating immune cells and m^{6}A modification, which could not be completely explained by the mechanism of RNA degradation. According to the study of Liu et al. (24), FTO enhances protein expression by regulating the m^{6}A modification of JUNB and CEBPB genes, thereby promoting tumor glycolysis and inhibiting T cell effects. The FTO inhibitor Dac51 can inhibit FTO-mediated demethylation, inhibit the glycolytic ability of tumor cells, increase T cell infiltration, and have a synergistic effect with anti-PD-L1 therapy. The study of Han et al. (25) showed that YTHDF1 recognizes and binds to the transcript encoding lysosomal protein modified by m^{6}A, increases the translation of lysosomal cathepsin in dendritic cells (DC), while inhibition of cathepsin can significantly increase the ability of cross-presenting antigen of dendritic cells. The absence of YTHDF1 in DC can enhance the cross-presentation of tumor antigens and the cross-priming of CD8+ T cells, thereby increasing the anti-tumor response of CD8+ T cells and enhancing the therapeutic effect of PD-L1 checkpoint blockade. It has been reported that cytotoxic tumor-infiltrating CD8+ T cell is increased in METTL3 or METTL14 deficient tumor. Depletion of METTL3 and METTL14 can inhibit m^{6}A modification and enhance the response to anti-PD-1 therapy in colorectal cancer and melanoma (26). However, the above studies have focused on one or two m^{6}A regulators and immune cell types, while tumor formation and suppression are the results of the highly synergistic effects of multiple regulatory factors. Therefore, the comprehensive analysis of the infiltration characteristics of tumor microenvironment mediated by m^{6}A regulator is helpful to promote the cognition of tumor immune regulation.

At present, there are widely accepted molecular subtypes in pancreatic cancer, such as two tumor-specific subtypes and stromal subtypes identified by Moffitt et al. and purity Independent Subtyping of Tumors (PurIST) developed by Rashid et al. (27, 28). These classifications may mainly be concerned with the components of the tumor at the pathological level and show good clinical value. We aimed to identify new subtypes from the m^{6}A methylation modification direction and construct scores to supplement the existing clinical variable information, and correlate these analyses with the tumor microenvironment. Meng et al. have proposed an m^{6}A-related mRNA signature, which can play a good prognostic predictive effect in pancreatic cancer (29). However, their study divided groups based on the existence of alterations (mutation and/or CNV)

Abbreviations: m^{6}A, N^6-methyladenosine; TME, Tumor microenvironment; m^{7}G, N^7-methylguanine; m^{5}C, N^5-methylcytosine; PC, Pancreatic cancer; CAR-T, chimeric antigen receptor T; DC, Dendritic cells; TCGA, The Cancer Genome Atlas; GEO, Gene Expression Ominibus; TPMs, transcripts per kilobase million; CNV, copy number variation; CDF, cumulative distribution function; LM22, Leukocyte signature matrix; DEGs, differentially expressed genes; GO, Gene Ontology; MF, molecular function; BP, biological processes; CC, cellular components; KEGG, Kyoto Encyclopedia of Genes and Genomes; PCA, principal component analysis; ROC, receiver operating characteristic; TMB, tumor mutation burden; IPS, Immunophenoscore; MHC, MHC-related molecules; CP, immunomodulators; EC, effector cells; SC, suppressor cells; TCIA, The Cancer Immunome Atlas; AUC, area under curve; PurIST, purity Independent Subtyping of Tumors; MDSC, myeloid-derived suppressor cells; Tregs, regulatory T cells; TGF-β, transforming growth factor-β.

of m^{6}A-related genes, and then identified differentially expressed genes for model construction. According to previous studies (30), data including gene expression profile, somatic mutation, and DNA methylation information can be used to identify the primary sites and origins of tumors, but the accuracy of gene expression data is the highest, especially in pancreatic cancer. Since gene expression data may provide more clinical value, this study identified subtypes based on m^{6}A regulator gene expression to mine more accurate clinical subtypes and prognostic indicators.

In this study, we integrated the transcriptome information of 434 pancreatic cancer samples from five independent cohorts, comprehensively evaluated m^{6}A modification patterns, and correlated the characteristics of immune cell infiltration in TME. Through the unsupervised clustering method, we identified two different m^{6}A modification subtypes and defined two m^{6}A-related gene subtypes. We found that distinct subgroups were accompanied with different immune cell infiltration characteristics. In addition, we constructed a scoring scheme to quantify individual m^{6}A modification patterns, and predicted the prognosis and response to immunosuppressive therapy based on the score. Our findings indicate that m^{6}A modification is closely related to TME immune cell infiltration, and can be used as a favorable predictor of prognosis and immunotherapy in pancreatic cancer.

MATERIALS AND METHODS

Collection and Preprocessing of PC Public Datasets

The workflow of this study was shown in **Figure S1**. The expression profile data and clinical information of pancreatic cancer samples were obtained from the Cancer Genome Atlas (TCGA, RRID : SCR_003193, https://tcga-data.nci.nih.gov/tcga/) and Gene-Expression Omnibus (GEO, RRID : SCR_005012, https://www.ncbi.nlm.nih.gov/geo/) database. This study collected 5 independent PC cohorts (TCGA-PAAD, GSE28735, GSE57495, GSE62452, GSE85916) for further analysis. RNA sequencing data in TCGA (FPKM format) were downloaded and transformed into TPMs (transcripts per kilobase million). We download the normalized matrix file in GEO, and applied ComBat algorithm in the R package SVA to eliminate batch effects between different GEO data sets. The survival status and survival time of the samples were extracted from the clinical information of the 5 PC cohorts. Data with follow-up time less than 31 days and duplicate data were excluded. Somatic mutation data was collected from the TCGA database. The copy number variation data (CNV) of TCGA-PAAD was downloaded from the UCSC Xena database (http://xena.ucsc.edu/).

Unsupervised Clustering of 23 m^{6}A Regulators

We searched the relevant literature on m^{6}A methylation modification to identify recognized m^{6}A regulators for subsequent analysis. A total of 23 m^{6}A regulators were included, including 8 writers (METTL3, METTL14, METTL16, WTAP, VIRMA, ZC3H13, RBM15, and RBM15B), 13 readers (YTHDC1, YTHDC2, YTHDF1, YTHDF2, YTHDF3, HNRNPC, FMR1, LRPPRC, HNRNPA2B1, IGFBP1, IGFBP2, IGFBP3, and RBMX), and 2 erasers (FTO and ALKBH5). Unsupervised clustering analysis was performed to identify different m^{6}A methylation modification subtypes according to the expression of 23 m^{6}A regulators, and patients were classified for further analysis. The number of clusters (K) and their stability were determined by the consensus clustering algorithm. Li et al. (31) tested four methods for finding K: the cumulative distribution function (CDF), the proportional change in the area under the CDF curve upon an increase of K (Δ(K)), GAP-PC (32) and CLEST (33). They found that CDF was able to reveal the correct K, as the CDF curve was flat only for the true K, reflecting a perfectly or near-perfectly stable partitioning of the samples at the correct K. So we took the K corresponding to the flattest CDF curve as the determined number of clusters. The R package consusclusterplus was utilized to perform the above steps (34).

Estimation of Immune Infiltrating Cells in TME

The R package CIBERSORT was used to quantify the infiltration of different immune cells in PC samples from five cohorts. Leukocyte signature matrix (LM22) contains 547 reference genes, which can be used to distinguish 22 human immune cell phenotypes, including various types of T cells, B cells, NK cells, plasma cells, and myeloid subgroups. CIBERSORT is a deconvolution algorithm, which can calculate the proportion of different types of cells in the sample based on LM22 (35). The ESTIMATE algorithm infers the cell density and tumor purity of the tumor based on the transcriptome profile of the sample (36). Tumor tissue with rich immune cell infiltration indicates a higher immune score and lower tumor purity. The R package ESTIMATE was used to evaluate the immune and stromal content (immune and stromal score) in each sample.

Identification of Differentially Expressed Genes Between Different m^{6}A Modified Phenotypes

Previous consensus clustering algorithms divided patients into two different m^{6}A modification subtypes based on the expression of 23 m^{6}A regulators. R package Limma was used to identify DEGs between the two m^{6}A modification clusters with adjusted P value < 0.05.

Functional and Pathway Enrichment Analyses of DEGs

GO (Gene Ontology) is a crucial bioinformatics tool for annotating and analyzing the biological functions of genes, including MF (molecular function), BP (biological processes), and CC (cellular components). As a database resource, KEGG (Kyoto Encyclopedia of Genes and Genomes) is mainly used to understand the high-level functions and values of biological systems from molecular-level information. To get annotation information and explore the biological functions of the above

DEGs, GO and KEGG enrichment analyses were accomplished using clusterProfiler package with a cutoff of p-value < 0.05 and q-value < 0.05.

Construction of m^{6}A Score

To quantify the modification pattern of m^{6}A in individual PC patients, we used principal component analysis (PCA) to construct the m^{6}A scoring scheme. Firstly, univariate Cox regression model was performed on DEGs identified between different m^{6}A modification clusters, and the genes with significant prognosis effect were selected for clustering samples and constructing m^{6}A score. The patients were divided into several groups for further analysis. The number and stability of gene clusters were determined by consensus clustering algorithm. Subsequently, principal component analysis was used to construct the m^{6}A-related gene signature, and principal component 1 and principal component 2 were extracted as signature scores. This method focuses the score on the set with the largest block of strongly related or anti-related genes, while reducing the contribution of genes that are not tracked with other set members. Besides, the PCA algorithm can effectively achieve data dimensionality reduction and largely retain the information of the original data. We used a method similar to GGI (37, 38) to define the m^{6}A score: $m6Ascore = \sum(PC1_i + PC2_i)$ where i is the expression of final genes related to the m^{6}A phenotype.

Verification of the m^{6}A Score

To verify the reliability and clinical application value of m^{6}A score, the receiver operating characteristic (ROC) curves of 1-, 3-, and 5-year were drawn. We first drew the ROC curve based on all samples. Then, the ROC curve was drawn solely in the TCGA-PAAD cohort, and the prognostic prediction performance of m^{6}A score and other clinical indicators were compared. Univariate and multivariate Cox regression analyses were used to evaluate the correlation between the patient's m^{6}A score, clinical variables, and prognosis to determine whether the score can be used as an independent prognostic indicator of pancreatic cancer. P < 0.05 indicated that the difference was statistically significant. The results were shown in the forest diagram. Next, 8 indicators (age, gender, grade, stage, stage_T, stage_N, stage_M, and m^{6}A score) were used to construct a nomogram to personally predict the 1-year, 3-year, and 5-year survival rates of patients. The ROC curve was drawn to show the predictive performance of the nomogram. The R packages survival, survminer, timeROC, rms, and regplot are used for calculation and graph drawing.

Analysis of Genome Mutation Data

We calculated the copy number increase or loss frequency of 23 m^{6}A regulators in the TCGA-PAAD cohort, and used the R package Rcircos to draw a copy number variation map of m^{6}A regulators on human chromosomes. To determine the tumor mutation burden (TMB), we counted the total number of non-synonymous mutations in the TCGA-PAAD cohort. R package maftools was used to plot the oncoprint of gene mutation.

Obtain the Prediction Indicators of Immune Response

Immunophenoscore (IPS) is a favorable factor to predict the efficacy of anti-CTLA-4 and anti-PD-1 regimens, which can quantify the determinants of tumor immunogenicity and show the characteristics of tumor immune landscape (39). The score is calculated based on four categories of immune-related genes, including MHC molecules (MHC), immunomodulators (CP), effector cells (EC), and suppressor cells (SC). IPS of samples in TCGA-PAAD were downloaded from the online platform The Cancer Immunome Atlas (TCIA, RRID : SCR_014508, https://tcia.at/home) for further analysis.

Statistical Analysis

All statistical analysis and graph drawing were completed by R-4.0.3. The Wilcoxon rank-sum test was used for comparison between two groups. Kaplan-Meier survival analysis and univariate Cox regression model were performed to calculate the relationship between m^{6}A regulators and prognosis. According to the correlation between m^{6}A score and patient survival, R package Survminer was used to repeatedly test all possible cut-off points to obtain the largest rank statistic, and the patients were divided into high and low m^{6}A score groups based on the largest selected log-rank statistic. The Kaplan-Meier method was utilized to draw the survival curve for prognostic analysis, and the log-rank test was used to determine the significance of the difference. Spearman correlation analysis and distance correlation analysis were applied for the correlation test. All heat maps were generated by R package pheatmap. All statistical P value were two-tailed, and P < 0.05 was statistically significant.

RESULTS

Construction of Genetic Variation, Immune Infiltration, and Prognostic Landscape of m^{6}A Regulators

In this study, 23 m^{6}A regulators were identified, including 8 writers, 13 readers, and 2 erasers. We first calculated the incidence of somatic mutations in PC. Among 158 tumor samples, a total of 120 cases (75.95%) had genetic alterations, of which TP53 and KRAS mutations were the most frequent with more than 50% (**Figure 1A**). However, the mutation frequency of 23 m^{6}A regulators was pretty low, genetic alterations occurred in only 5 (3.16%) samples (**Figure 1B**). We further analyzed the relationship between TP53 and KRAS mutations and the expression of m^{6}A regulators. There were differences in the expression of multiple m^{6}A regulators between the wild group and mutant group (**Supplementary Figures 3, 4**). Analysis of copy number variation of 23 m^{6}A regulators showed that CNV mutations were common in PC. VIRMA, HNRNPA2B1, IGFBP1, IGFBP3, YTHDF3, and YTHDF1 had widespread CNV amplification. However, METTL16, WTAP, ALKBH5, YTHDF2, and RBM15B showed extensive CNV deletions (**Figure 1C**). The location of CNV

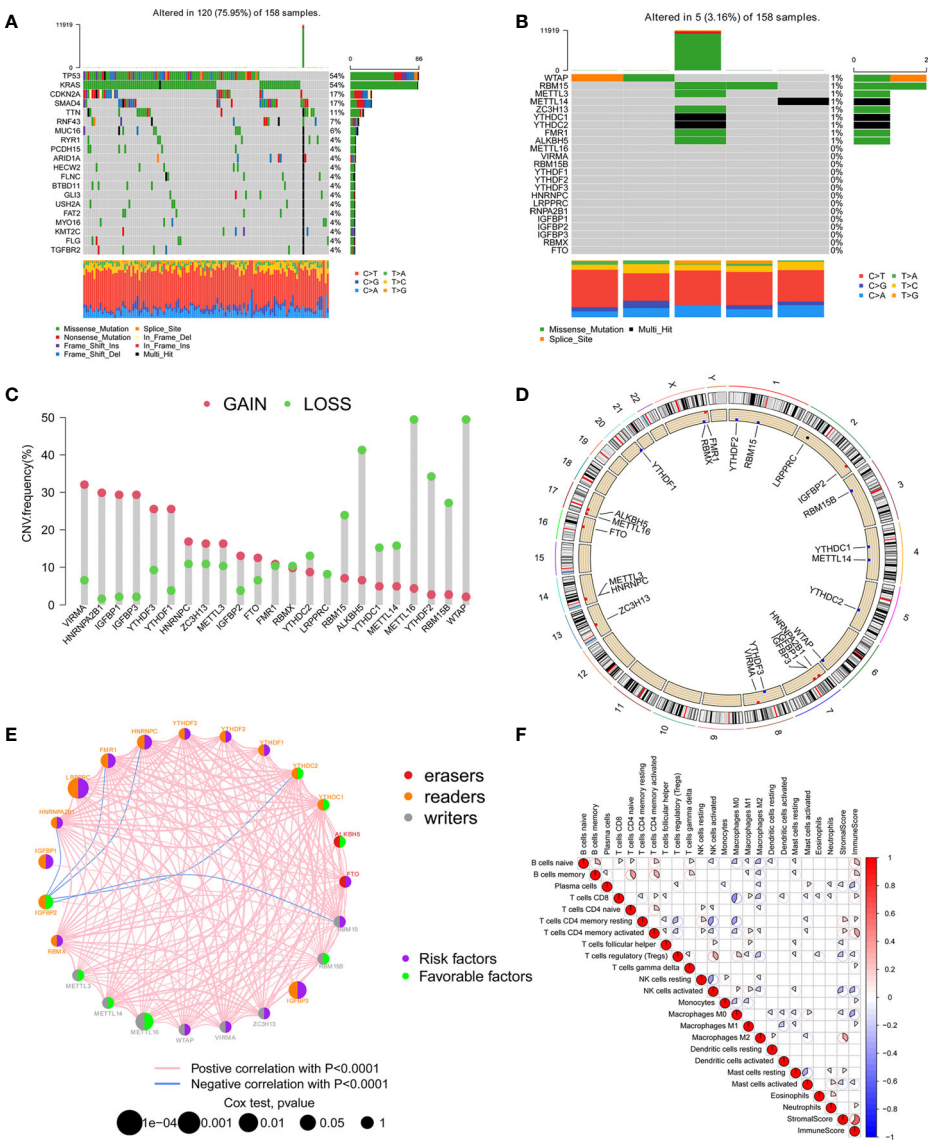

FIGURE 1 | The landscape of genetic variation, immune infiltration, and prognosis of m^{6}A regulators. **(A)** The top 20 genes with the highest mutation frequency in the TCGA-PAAD cohort. The main types of mutations were missense mutations. **(B)** Mutations of 23 m^{6}A regulators in the TCGA-PAAD cohort. **(C)** The CNV mutation frequency of 23 m^{6}A regulators in the TCGA-PAAD cohort. Each column indicated the frequency of mutations. Amplification frequency, red dot; missing frequency, green dot. **(D)** The location of CNV changes of 23 m^{6}A regulators on the chromosome. **(E)** The interaction of 23 m^{6}A regulators and their prognostic significance in 5 independent PC cohorts. The three types of m^{6}A regulatory genes were represented by different colors. Erasers, red; Readers, orange; Writers, grey. The size of the circle represented the prognostic effect of each m^{6}A regulator, and was adjusted according to the p-value. Prognostic risk factors, purple; prognostic protective factors, green. **(F)** Cellular interaction of the tumor-infiltrating immune cell types.

changes on the chromosome was illustrated in **Figure 1D**. Kaplan-Meier survival analysis showed that 15 m^{6}A regulators were correlated with the prognosis of PC patients (**Supplementary Figure 2**). Univariate Cox regression model revealed the prognostic value of 23 m^{6}A regulators in PC patients (**Supplementary Table 1**). As shown in **Figure 1E**, the network presents a comprehensive landscape of the interactions, connection, and prognostic significance of m^{6}A regulators in PC. The results indicated that writers, readers, and erasers have a significant correlation in expression. The cross-talk among them probably plays an essential role in the formation of different m^{6}A modification patterns, and might be related to the occurrence and development of cancer. In addition, we implemented CIBERSORT and ESTIMATE algorithms to quantify the activity or enrichment level of immune cells in pancreatic cancer tissues. The correlation coefficient heatmap was used to display a general landscape of immune cell interactions in the tumor microenvironment (**Figure 1F**).

23 Regulators-Mediated m^{6}A Methylation Modification Subtypes

Based on the expression of 23 m^{6}A regulators, the R package ConensusClusterPlus was used to qualitatively classify patients with different m^{6}A modification subtypes. Through the consensus clustering algorithm, two different m^{6}A modification subtypes were finally identified, including 294 cases in subtype A and 140 cases in subtype B (**Figures 2A–D** and **Supplementary Table 2**). We named these two subtypes m^{6}A cluster A and m^{6}A cluster B, showed the expression of 23 m^{6}A regulators in the two modified subtypes by heatmap (**Figure 2E**). The expression levels of 23 m^{6}A regulators between the two m^{6}A clusters were also compared and shown in **Figure 2F**. To explore the internal biological changes under different m^{6}A modification modes, we compared the composition of immune cells in TME. The result showed that m^{6}A cluster A was characterized by higher infiltration of memory B cells and activated memory CD4+ T cells. In m^{6}A cluster B, the infiltration of activated NK cells, M0 macrophages,

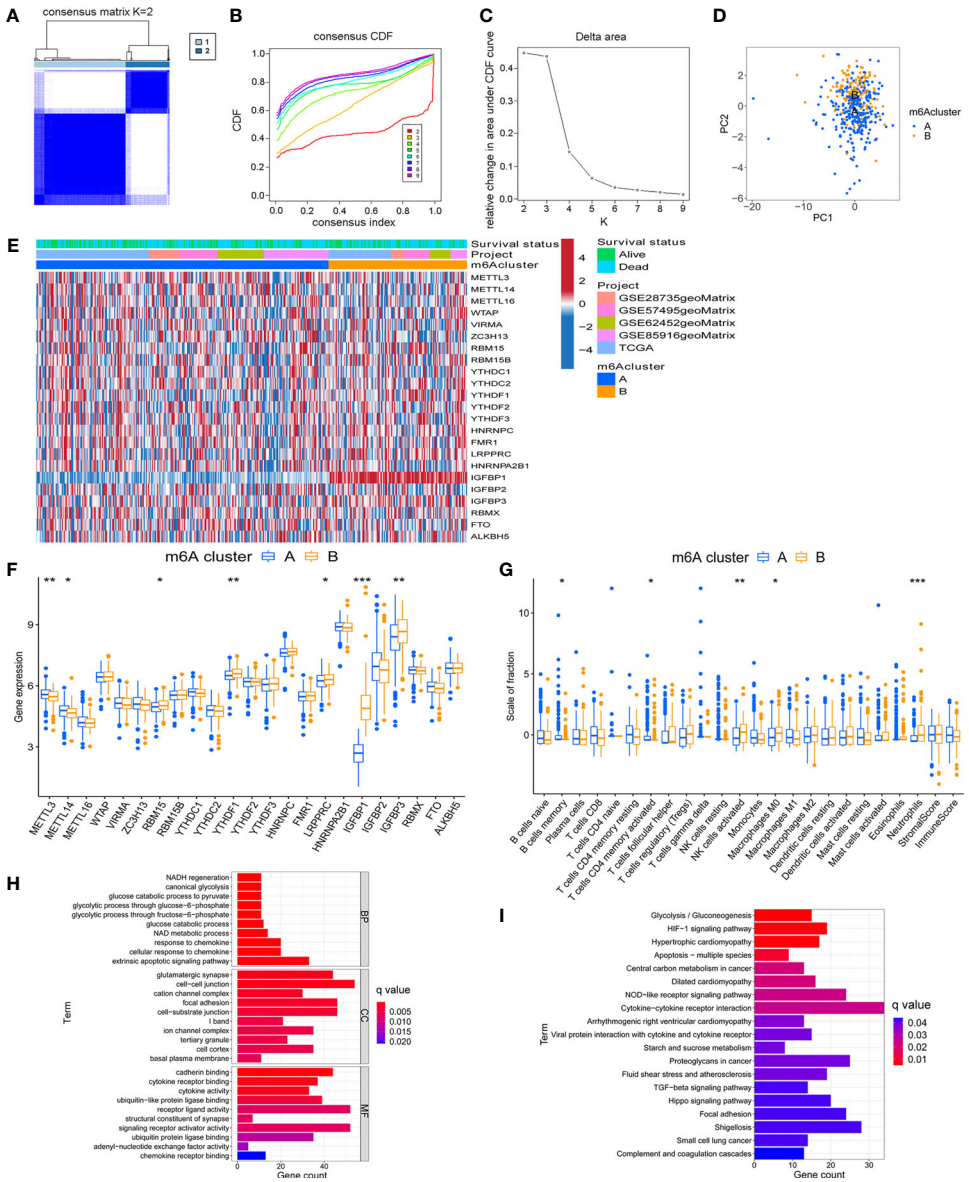

FIGURE 2 | Identification of m^{6}A methylation modification subtypes. **(A)** Heat map of sample clustering under k = 2 in 5 independent PC cohorts. **(B)** Consensus clustering cumulative distribution function (CDF) with the number of subtypes k = 2 to 9. **(C)** The relative change of the area under the CDF curve of k = 2 to 9. **(D)** Principal component analysis of the expression profiles of 23 m^{6}A regulators to distinguish two determined m^{6}A clusters. **(E)** Unsupervised clustering of 23 m^{6}A regulators in two m^{6}A clusters. **(F)** Differences in the expression of 23 m^{6}A regulators between distinct m^{6}A clusters. **(G)** TME immune-infiltrating characteristics and transcriptome traits of two m^{6}A clusters. **(H)** GO enrichment pathway of differentially expressed genes between two m^{6}A clusters. **(I)** KEGG enrichment pathway of differentially expressed genes between two m^{6}A clusters. ***P < 0.001; **P < 0.01; *P < 0.05.

and Neutrophils were significantly increased (**Figure 2G**). To reveal the potential biomolecular characteristics of different m^{6}A modified phenotypes, R package LIMMA was used for differential expression analysis to determine the transcriptome differences between two subtypes. We identified 1159 differentially expressed genes and annotated DEG with R package clusterProfiler. **Figures 2H, I** summarized the significant biological processes of DEG enrichment, such as glucose metabolism, glycolysis, HIF-1 signaling pathway, Hippo signaling pathway, and TGF-β signaling pathway. These results suggested that the m^{6}A methylation modification may involve in tumor metabolism and immune regulation, and was closely related to tumor genesis and progression. **Supplementary Tables 3, 4** provides detailed descriptions.

Identification of m^{6}A-Related Gene Subtypes

Although the consensus clustering algorithm based on 23 m^{6}A regulators classified PC patients into two subtypes, potential genetic changes and prognostic correlations in these phenotypes were not very clear. We performed univariate COX regression analysis on the 1159 DEGs between the previously identified m^{6}A clusters, and obtained 719 survival-related genes which were named m^{6}A-related signature genes (**Supplementary Table 5**). Based on representative m^{6}A-related signature genes, we adopted unsupervised cluster analysis and identified two stable transcriptome phenotypes, which were defined as gene cluster A and gene cluster B (**Figures 3A–C**). In addition, we explored the prognostic significance of gene subtypes by integrating transcriptome and survival information. Through Kaplan-Meier analysis and log-rank test, gene cluster B showed a better prognosis ($P < 0.001$, **Figure 3D**). The heatmap showed the transcriptome profile of 719 m^{6}A-related signature genes in two gene clusters (**Figure 3E**). The expression levels of 23 m^{6}A regulators between the two m^{6}A-related gene clusters were also compared. Significant differences in the expression of m^{6}A regulators were observed, which was consistent with the expected result of m^{6}A modification patterns (**Figure 3F**). Previous studies have shown that the immune system may produce favorable or unfavorable consequences, which may manifest as pro-tumor or anti-tumor activity. Monocytes and anti-tumor lymphocyte subsets such as CD8+ T cells, memory CD4+ T cells, and naive B cells had a higher level of infiltration in gene cluster B, while activated NK cells and mast cells infiltrated more abundantly in gene cluster A (**Figure 3G**). The immune and stromal score based on the ESTIMATE algorithm indicated that the infiltration of immune cells and stromal components in gene cluster B was higher. Therefore, we speculate that the abundant immune cell infiltration in gene cluster B forms an effective anti-tumor immune response.

Construction of m^{6}A Score

Although the above results demonstrated the role of m^{6}A methylation modification in the regulation of immune cell infiltration and prognosis, these analyses cannot accurately predict the m^{6}A methylation modification pattern in a single tumor patient. To obtain a quantitative index of the m^{6}A modification landscape of PC patients, we extracted the scores of principal component 1 and principal component 2 for calculating the final m^{6}A score. **Figure 4A** showed that patients' m^{6}A score in m^{6}A cluster A was lower than m^{6}A cluster B, and **Figure 4B** depicted that the m^{6}A score in gene cluster B was lower than that in gene cluster A. We drew an alluvial diagram to display the process of m^{6}A score construction (**Figure 4C**). Subsequent analysis revealed the prognostic significance of m^{6}A score. According to **Figure 4D**, the patients' survival rate (41% vs. 23%) in the m^{6}A low score group was much higher than that in the high score group. The overall average m^{6}A score of the surviving patients was lower than that of the dead patients (**Figure 4E**, $P = 0.0025$). Kaplan-Meier survival analysis showed that the prognosis of patients in the low m^{6}A score group was significantly better (**Figure 4F**, $P < 0.001$).

Validation of m^{6}A Score and Its Application in Clinical Evaluation

To verify the m^{6}A score, the 1-, 3-, and 5-year ROC curves were drawn, and the value of the area under curve (AUC) of the m^{6}A score was calculated. The results showed that the AUC values of all three curves were around 0.65 both in total samples (**Figure 5A**) and TCGA-PAAD cohort (**Figure 5B**). We also compared the 1-year ROC curve with other clinical characteristics in TCGA-PAAD cohort, and m^{6}A score had the most considerable AUC value (**Figure 5C**). Univariate Cox regression analysis showed that age (p = 0.012, HR = 1.027, 95%CI [1.006-1.049]), grade (p = 0.026, HR = 1.392, 95%CI [1.041-1.862]) and m^{6}A score (p = 0.002, HR = 1.022, 95%CI [1.008-1.037]) were considered statistically significant (**Figure 5D**). Multivariate Cox regression analysis showed age (p = 0.012, HR = 1.028, 95%CI [1.006-1.050]) and m^{6}A score (p = 0.005, HR = 1.021, 95%CI [1.006-1.036]) were independent prognostic predictors (**Figure 5E**). By integrating multiple clinical indicators, the nomogram can be an effective tool for quantitatively assessing individual risks in the clinical environment. We constructed a nomogram to predict patients' OS at 1-, 3-, and 5-year. Taking a random sample as an example, the total score of the patient was 340, the probability of survival time less than 1-, 3-, and 5-year were 0.123, 0.452, and 0.563, respectively (**Figure 5F**). The ROC curve was used to evaluate the predictive performance of the nomogram. The AUC values of 1-, 3-, and 5-year ROC curves were 0.718, 0.800, and 0.792, respectively (**Figure 5G**). The results showed that m^{6}A score could be used as a new effective clinical predictor and can be combined with other clinical variables to improve the prognosis of patients with pancreatic cancer.

Correlation Between m^{6}A Score and Somatic Variation

Previous studies have shown that tumor mutation burden may be an emerging and potential tumor marker, which can assist in the selection of patients for immune checkpoint therapy. In view of the important clinical significance of TMB, we tried to explore the inner link between TMB and m^{6}A score to clarify

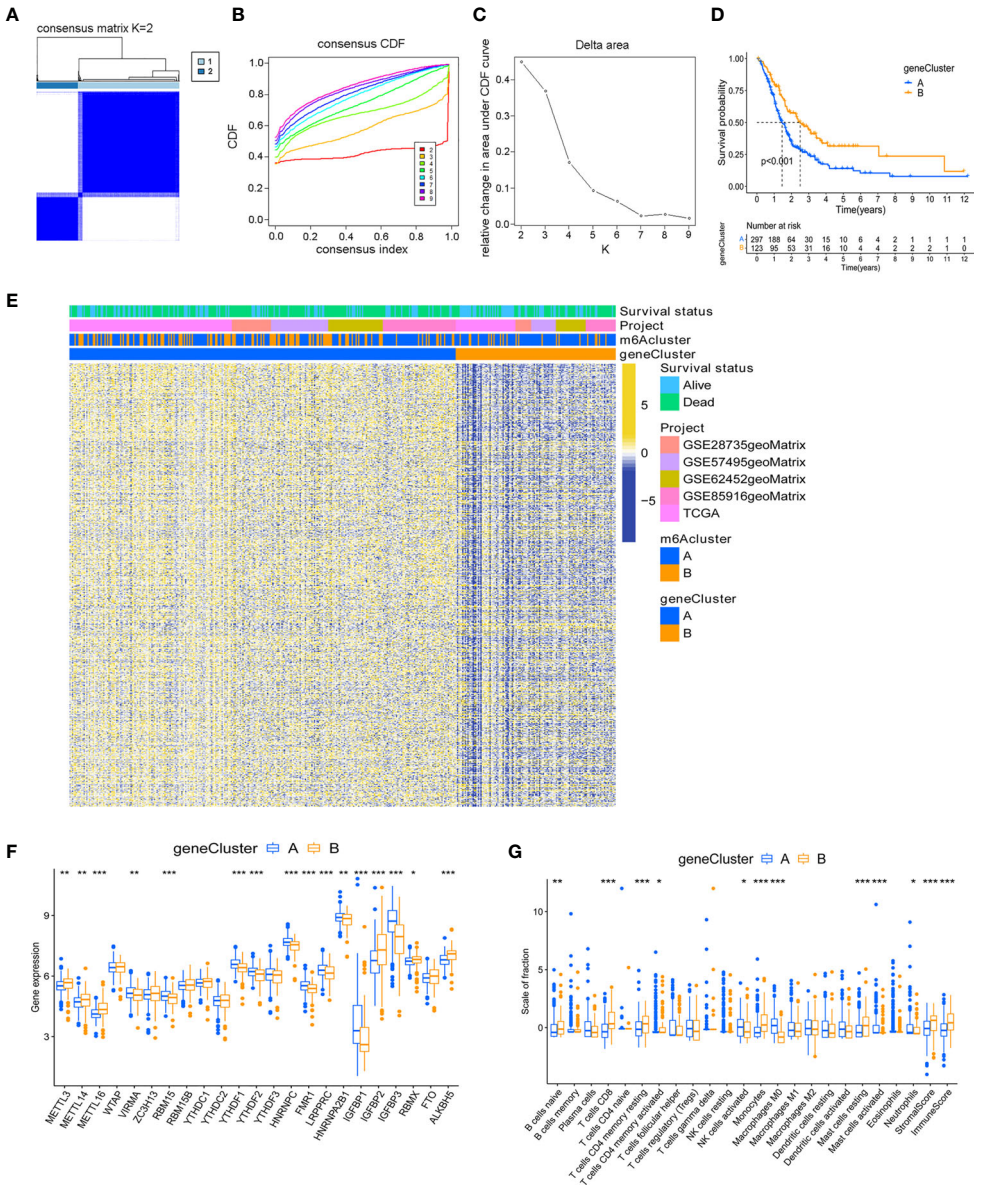

FIGURE 3 | Identification of m^{6}A-related gene subtypes. **(A)** Heat map of sample clustering under k = 2 in 5 independent PC cohorts. **(B)** Consensus clustering cumulative distribution function (CDF) with the number of subtypes k = 2 to 9. **(C)** The relative change of the area under the CDF curve of k = 2 to 9. **(D)** Survival analysis of patients in two m^{6}A-related gene clusters. **(E)** Unsupervised clustering of m^{6}A related signature genes. **(F)** Differences in the expression of 23 m^{6}A regulators between distinct gene clusters. **(G)** TME immune-infiltrating characteristics and transcriptome traits of two m^{6}A-related gene clusters. ***P < 0.001; **P < 0.01; *P < 0.05.

the genetic imprint of each m^{6}A score subgroup. Correlation analysis showed a significant and positive association between m^{6}A score and TBM (Spearman coefficient: R = 0.18, P = 0.032; **Figure 6A**). Next, we divided patients into two subgroups based on TBM. As shown in **Figure 6B**, we found that patients with low TMB showed better overall survival than patients with high TMB. Next, we evaluated the synergy of these scores in the prognostic stratification of PC. Survival analysis demonstrated that TBM status did not affect predictions based on m^{6}A score, and the low m^{6}A score group always showed a survival advantage (**Figure 6C**). In addition, we analyzed the somatic mutation landscape in the high and low m^{6}A score groups, and found that the high m^{6}A score group had a higher mutation rate (93.48%) than the low score group (70.65%). According to the results (**Figures 6D, E**), both KRAS (74% *vs.* 46%) and TP53 (78% *vs.* 43%) had a higher somatic mutation rate in the high m^{6}A score group, which may be related to the poor prognosis of high m^{6}A score group. These data can more comprehensively describe the impact of m^{6}A score on genomic variation, and may provide

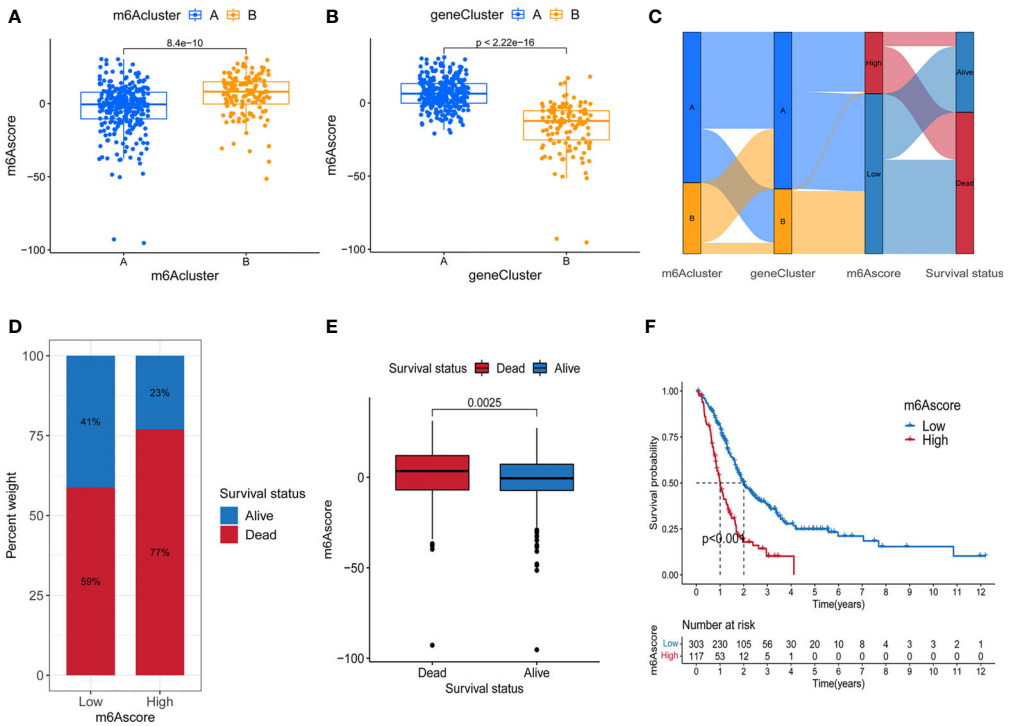

FIGURE 4 | Construction of m^{6}A score. **(A)** Difference of m^{6}A score between two m^{6}A methylation modification subtypes. **(B)** Difference of m^{6}A score between two m^{6}A-related gene subtypes. **(C)** Alluvial diagram containing m^{6}A cluster, gene cluster, m^{6}A score and survival changes. **(D)** The proportion of survival and death in high and low m^{6}A score group. **(E)** Comparison of m^{6}A scores between surviving and dead patients. **(F)** Survival analysis of high and low m^{6}A score groups.

new ideas for studying the potential interaction between m^{6}A methylation modification and somatic mutation.

The Role of m^{6}A Score in Predicting the Effect of Immunotherapy

The treatment of immune checkpoint inhibitors represented by CTLA-4/PD-1 inhibitors is undoubtedly a major progress in anti-tumor therapy. We compared the expression of common immune checkpoint genes between the high and low m^{6}A score groups, and found that PD-L1 was highly expressed in the high m^{6}A score group, PDCD1 was highly expressed in the low m^{6}A score group, while the expression of CTLA4 and IDO1 had no significant difference between the two groups (**Figures 7A–D**). As a new predictor of the immune response, IPS is widely used and recommended for evaluating the immune response of patients. Our analysis showed that the IPS of the low m^{6}A score group was higher no matter in the case of anti-PD-1/CTLA-4 therapy alone, or combination therapy (**Figures 7E–H**). These results indicated that m^{6}A methylation modification in pancreatic cancer may play an important role in mediating the immune response.

DISCUSSION

Recent studies have shown that m^{6}A methylation modification plays an indispensable role in a variety of immune-related biological processes, including innate and acquired immune response, immune recognition, immune cell dynamic balance, and anti-tumor immune response (22). Since most studies mainly focus on the regulatory relationship between single m^{6}A regulator and immune cell type, the comprehensive landscape of TME immune-infiltrating mediated by multiple m^{6}A regulators in PC has not been fully understood. Therefore, clarifying the characteristics of immune cell infiltration in different m^{6}A modification patterns will help us to improve our understanding of the anti-tumor immune response in TME, and provide new insights for the risk stratification of patients and the choice of clinical treatment strategies.

Based on 23 m^{6}A regulators, we first identified two m^{6}A modification subtypes. Differences in mRNA transcriptomes between different m^{6}A modification subtype were found to be closely related to tumor metabolism and immune-related biological processes, and differentially expressed genes (DEGs) were significantly enriched in glucose metabolism-related pathways, chemokine-related pathways, cytokine-related pathways, and TGF-β signaling pathways. DEGs correlated to the prognosis of PC were defined as m^{6}A-related signature genes. Based on the m^{6}A signature genes, we determined two m^{6}A-related gene subtypes. In the two gene clusters, we found that gene cluster A had lower immune score, stromal score and immune response-related T cell infiltration, which suggested an immune cold phenotype. In contrast, gene cluster B showed a relatively high immune score and T cell infiltration, which corresponded to the immune activation phenotype, namely hot

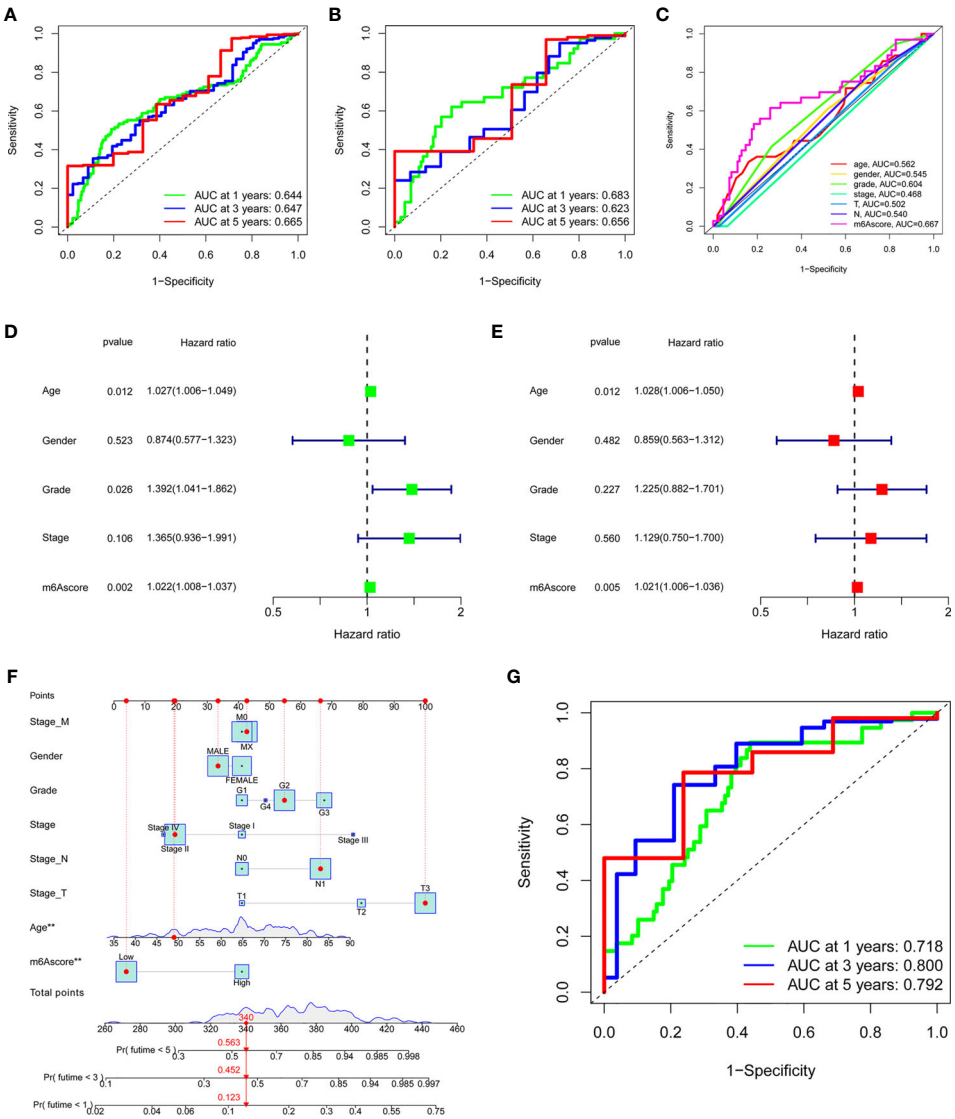

FIGURE 5 | Validation and application of the m^{6}A score in the clinical evaluation. **(A)** The AUC values of the 1-year, 3-year, and 5-year ROC curves of m^{6}A score in all samples. **(B)** The AUC values of the 1-year, 3-year, and 5-year ROC curves of m^{6}A score in the TCGA-PAAD cohort. **(C)** The comparation of 1-year ROC curve with other clinical characteristics in the TCGA-PAAD cohort. **(D)** Univariate COX regression analysis showed that age, grade, and m^{6}A score were considered statistically significant. **(E)** Multivariate Cox regression analysis showed age and m^{6}A score were independent prognostic predictors. **(F)** The nomogram to predict the probability of 1-year, 3-year, and 5-year survival rate. **(G)** The AUC values of the 1-year, 3-year, and 5-year ROC curves of the nomogram. ***P < 0.001; **P < 0.01; *P < 0.05.

tumor. Survival analysis showed that gene cluster A characterized by immune cold phenotype was associated with poor prognosis, while gene cluster B characterized by anti-tumor immune response was associated with good prognosis. We speculate that patients in gene cluster B may benefit from immunotherapy. Our results are consistent with those of previous TME studies, which also indicates that m^{6}A methylation modification is of great significance for shaping different TME immune characteristics.

In view of the individual heterogeneity of m^{6}A methylation modification, it is necessary to quantify the m^{6}A modification pattern of a single tumor sample. Scoring models based on specific biomarkers between m^{6}A modified subtypes have been well established in gastric cancer and colorectal cancer to improve the choice of clinical treatment and prognosis of patients (12, 13). Based on principal component analysis and a method similar to GGI, we established an m^{6}A scoring scheme for PC patients. Gene cluster B with immune hot phenotype showed lower m^{6}A score, while gene cluster A with immune cold phenotype indicated higher m^{6}A score. Kaplan-Meier analysis showed that the m^{6}A score had good prognostic predictive ability. The survival rate of patients in the low m^{6}A score

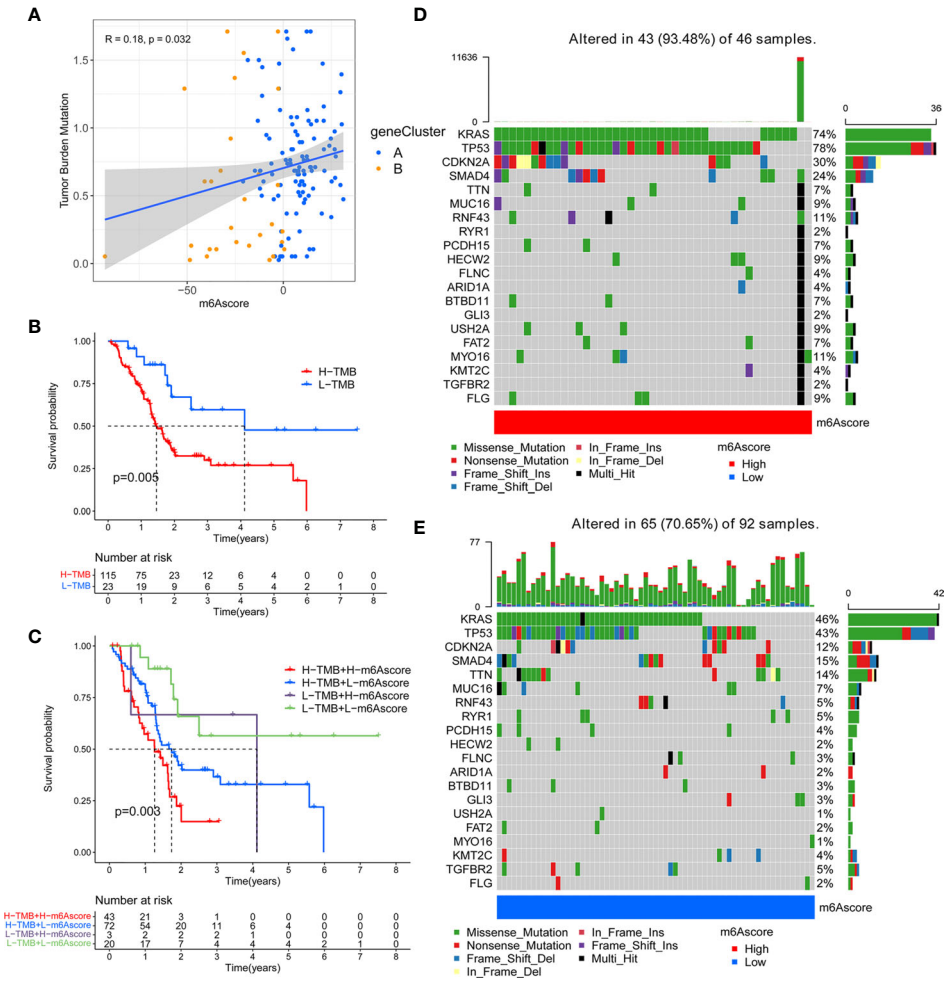

FIGURE 6 | Correlation between m^{6}A score and tumor mutation burden (TMB) in TCGA-PAAD cohort. **(A)** A scatter plot describing the positive correlation between m^{6}A score and tumor mutation burden. **(B)** Survival analysis of high TMB group and low TMB group. **(C)** Stratified survival analysis including TMB and m^{6}A scores. **(D)** OncoPrint for gene mutations in the high m^{6}A score group. **(E)** OncoPrint for gene mutations in the low m^{6}A score group.

group was higher and the prognosis was better. These results suggest that the m^{6}A score is a reliable index to comprehensively evaluate the m^{6}A modification pattern of individual tumors, and can be used to further determine the characteristics of TME immune cell infiltration, namely tumor immunophenotype. Besides, verification in the TCGA-PAAD cohort showed that m^{6}A score can be used as an independent prognostic indicator for PC patients. And the nomogram constructed by m^{6}A score combined with other clinical variables can effectively predict the prognosis of patients.

Evaluation of potential mutation driver genes in tumors is an important means to explore the potential mechanisms of cancer occurrence and development, which is conducive to cancer diagnosis and rational selection of treatment strategies. We found that the mutation rates of KRAS, TP53, CDKN2A, and AMAD4 were significantly increased in the high m^{6}A score group. An important feature of KRAS mutant tumors is the immunosuppressive state (40). KRAS signaling induces the expression of immune regulatory factors and inflammatory cytokines in tumor cells, and subsequently recruits neutrophils and myeloid-derived suppressor cells (MDSC) to form an immunosuppressive tumor microenvironment (41). Mutated KRAS in pancreatic cancer plays a central role in tumor development and growth by regulating T-cell cytokines in TME. By acting on downstream effectors, KRAS leads to impaired T-cell recognition of tumor cells, which may mediate immunity escape (22, 42). There are mutations of TP53 in most types of cancers. The deletion or mutation of TP53 in cancers will affect the recruitment and activity of T cells, leading to immune evasion and promoting cancer progression (43, 44). The loss of P53 (encoded by TP53) in pancreatic cancer leads to increased infiltration of regulatory T cells (Tregs) in the peripheral and intratumoral tissues (45). CDKN2A is a multifunctional gene that prevents the cell cycle at the G1/S

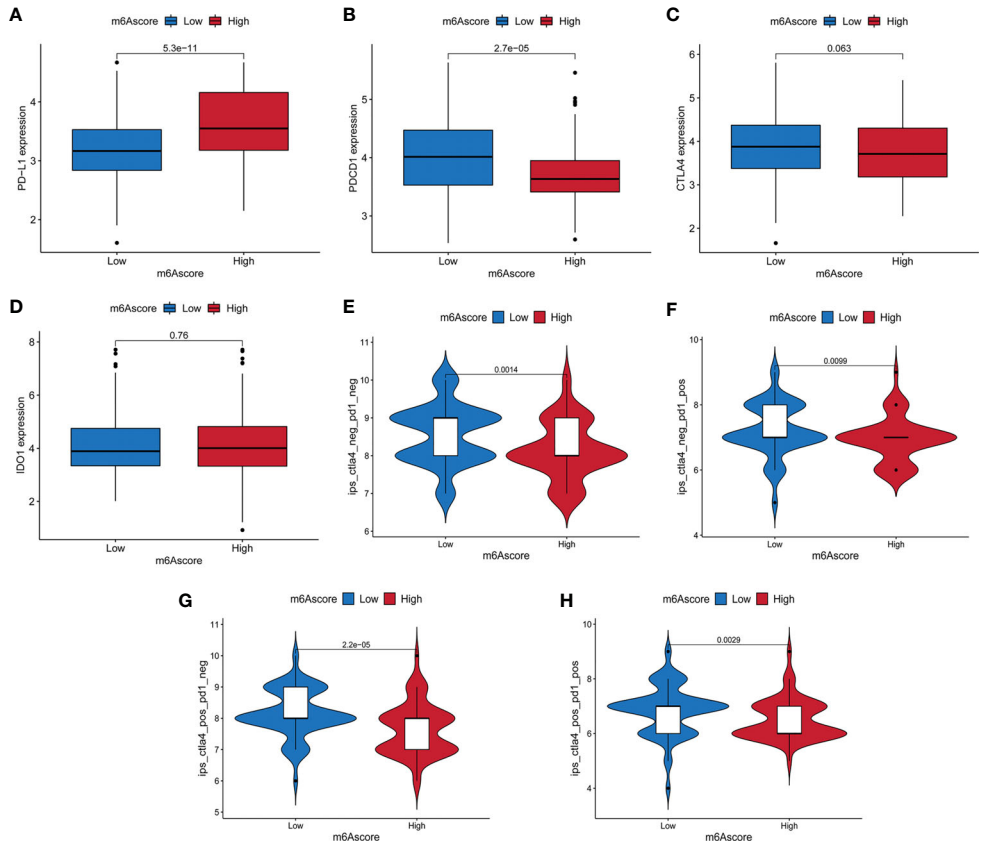

FIGURE 7 | The relationship between m^{6}A score and immune checkpoint genes and immunotherapy. **(A–D)** The expression differences of PD-L1, PDCD1, CTLA4 and IDO1 between high and low m^{6}A score groups. **(E)** The difference of Immunophenoscore (IPS) between high and low m^{6}A score groups with CTLA4 (-)/PD1 (-). **(F)** The difference of IPS between high and low m^{6}A score groups with CTLA4 (-)/PD1 (+). **(G)** The difference of IPS between high and low m^{6}A score groups with CTLA4 (+)/PD1 (-). **(H)** The difference of IPS between high and low m^{6}A score groups with CTLA4 (+)/PD1 (+).

checkpoint through the CKD4/6 regulatory mechanism. It is reported that approximately 60% of patients with pancreatic ductal adenocarcinoma carry the CDKN2A mutation, and this mutation is associated with a high risk of tumor development (46, 47). SMAD4 is a member of the SMAD family and participates in the transforming growth factor-β (TGF-β) pathway, which inhibits the activity of normal immune cells and promotes the immune escape of cancer cells (48, 49). These studies suggest that KRAS, TP53, CDKN2A, and AMAD4 mutations may be involved in the formation of immune suppression and immune escape in the high m^{6}A score group. These m^{6}A score-related gene mutations are closely related to the immune activity in TME, indicating that there may be a potential interaction between m^{6}A methylation modification and tumor immune genomics. Because the mutation data of pancreatic cancer in the TCGA database is not sufficient, and only a few genes have obvious somatic mutations, it is necessary to verify the mutation oncoprint and explore the underlying mechanism in a larger data set.

In this study, we demonstrated that m^{6}A modification patterns played an important role in the formation of different TME immune infiltration landscapes, which suggested that m^{6}A methylation modification may affect the therapeutic effect of immune checkpoint inhibitors. We found that the expression of PD-L1 was higher in the high m^{6}A score group. Previous studies suggested that pancreatic cancer had an immunosuppressive tumor microenvironment with high PD-L1 expression, which inhibited the cytotoxicity of activated T cells, and PD-L1 overexpression was associated with a poor prognosis (50, 51). We also compared the IPS that predicted the efficacy of anti-PD-1/CTLA-4 regimens in the high and low m^{6}A score groups. The low score group had higher IPS, which indicated a relatively better immunotherapy effect. However, our results do not imply causal associations of m6A score and anti-tumor immunity in PC, more clinical evidence needs to be collected in future studies to verify the relationship between m^{6}A score and immunotherapy. The above analysis suggests that m^{6}A modification characteristics combined with TME status, tumor mutation burden, neoantigen load, PD-L1 expression, IPS and other biomarkers may be a more effective predictive strategy for immunotherapy.

Our research still has some shortcomings. Although we included 23 recognized m^{6}A regulators through literature

review, newly identified regulators still need to be added into the model to improve the accuracy of the identification of m^{6}A methylation modification patterns. In addition, since not all patients with low m^{6}A scores can benefit from immunotherapy, more clinicopathological features need to be combined to improve the accuracy of prediction. Although we obtained 434 PC samples from different cohorts, the number of samples may be relatively insufficient, and our findings need to be further validated in a prospective cohort of PC patients receiving immunotherapy.

The study was done within tumor microenvironment in a whole, without distinguishing tumor component, immune component, and stromal component furthermore. This may cause some subtype information to be masked due to the mixture of the component, which is also a shortcoming of our research. We were more concerned about proposing molecular subtypes related to m^{6}A methylation in the overall tumor microenvironment and further constructing scores. Subsequent clinical analysis showed that the m^{6}A score could be used as an important supplement to existing clinical variables, and could effectively predict the prognosis of patients in combination with other clinical indicators. We may refine the differentiation of the various components of the tumor microenvironment in subsequent research work, and try to use single-cell analysis to distinguish cell types to obtain more information.

This study has provided some new insights into the clinical application of immunotherapy. By targeting m^{6}A regulators or m^{6}A-related signature genes to change the m^{6}A modification pattern and further reverse the poor infiltration of immune cells in TME, that is, the transformation of immune cold tumors to hot tumors, may contribute to the future development of new immunotherapy drugs or combination therapy strategies. In addition, the combination of therapeutic strategies for KRAS, TP53, CDKN2A, and AMAD4 mutations with immunotherapy may open up a new way for the selection of treatment options and reverse the immunosuppressive state in tumors. These findings are conducive to the identification of different immunophenotypes, thereby improving the patient's response to immunotherapy, and can promote the clinical practice of personalized immunotherapy for cancer.

In conclusion, we evaluated 23 regulators-mediated m^{6}A methylation modification landscapes based on 434 PC samples, and correlated m^{6}A modification with the TME immune-infiltrating characteristics. And we constructed the m^{6}A score, which can comprehensively evaluate the m^{6}A modification pattern and immune-infiltrating characteristics of individual tumors, and further determine the tumor immunophenotype to guide clinical application.

DATA AVAILABILITY STATEMENT

The datasets presented in this study can be found in online repositories. The names of the repository/repositories and accession number(s) can be found in the article/**Supplementary Material**.

AUTHOR CONTRIBUTIONS

LX and MS designed the work. MX, TZ, and YW collected and integrated the data. MS analyzed the data and prepared the manuscript. MS, WH, and LX edited and revised the manuscript. All authors contributed to the article and approved the submitted version.

FUNDING

This research was funded by National Natural Science Foundation of China No. 81871911 (WH), No. 81972237 (LX), and No. 81772623 (LX), and the National Key Research and Development Program of China 2018YFC1312103 (LX).

ACKNOWLEDGMENTS

The authors express gratitude to the public database TCGA and GEO.

SUPPLEMENTARY MATERIAL

The Supplementary Material for this article can be found online at: https://www.frontiersin.org/articles/10.3389/fimmu.2021.739768/full#supplementary-material

REFERENCES

1. Zheng HX, Zhang XS, Sui N. Advances in the Profiling of N(6)-Methyladenosine (M(6)a) Modifications. *Biotechnol Adv* (2020) 45:107656. doi: 10.1016/j.biotechadv.2020.107656
2. Dai F, Wu Y, Lu Y, An C, Zheng X, Dai L, et al. Crosstalk Between RNA M(6) a Modification and non-Coding RNA Contributes to Cancer Growth and Progression. *Mol Ther Nucleic Acids* (2020) 22:62–71. doi: 10.1016/j.omtn.2020.08.004
3. Huang H, Weng H, Chen J. M(6)a Modification in Coding and Non-Coding Rnas: Roles and Therapeutic Implications in Cancer. *Cancer Cell* (2020) 37:270–88. doi: 10.1016/j.ccell.2020.02.004
4. Zhao W, Qi X, Liu L, Ma S, Liu J, Wu J. Epigenetic Regulation of M(6)a Modifications in Human Cancer. *Mol Ther Nucleic Acids* (2020) 19:405–12. doi: 10.1016/j.omtn.2019.11.022
5. Huang H, Weng H, Chen J. The Biogenesis and Precise Control of RNA M(6) a Methylation. *Trends Genet* (2020) 36:44–52. doi: 10.1016/j.tig.2019.10.011
6. Yang C, Hu Y, Zhou B, Bao Y, Li Z, Gong C, et al. The Role of M(6)a Modification in Physiology and Disease. *Cell Death Dis* (2020) 11:960. doi: 10.1038/s41419-020-03143-z
7. Nombela P, Miguel-López B, Blanco S. The Role of M(6)a, M(5)C and Ψ RNA Modifications in Cancer: Novel Therapeutic Opportunities. *Mol Cancer* (2021) 20:18. doi: 10.1186/s12943-020-01263-w
8. Han SH, Choe J. Diverse Molecular Functions of M(6)a mRNA Modification in Cancer. *Exp Mol Med* (2020) 52:738–49. doi: 10.1038/s12276-020-0432-y
9. Gu J, Zhan Y, Zhuo L, Zhang Q, Li G, Li Q, et al. Biological Functions of M(6)a Methyltransferases. *Cell Biosci* (2021) 11:15. doi: 10.1186/s13578-020-00513-0
10. Jiang X, Liu B, Nie Z, Duan L, Xiong Q, Jin Z, et al. The Role of M6a Modification in the Biological Functions and Diseases. *Signal Transduct Target Ther* (2021) 6:74. doi: 10.1038/s41392-020-00450-x

11. Uddin MB, Wang Z, Yang C. The M(6)a RNA Methylation Regulates Oncogenic Signaling Pathways Driving Cell Malignant Transformation and Carcinogenesis. *Mol Cancer* (2021) 20:61. doi: 10.1186/s12943-021-01356-0
12. Zhang B, Wu Q, Li B, Wang D, Wang L, Zhou YL. M(6)a Regulator-Mediated Methylation Modification Patterns and Tumor Microenvironment Infiltration Characterization in Gastric Cancer. *Mol Cancer* (2020) 19:53. doi: 10.1186/s12943-020-01170-0
13. Chong W, Shang L, Liu J, Fang Z, Du F, Wu H, et al. M(6)a Regulator-Based Methylation Modification Patterns Characterized by Distinct Tumor Microenvironment Immune Profiles in Colon Cancer. *Theranostics* (2021) 11:2201–17. doi: 10.7150/thno.52717
14. Mizrahi JD, Surana R, Valle JW, Shroff RT. Pancreatic Cancer. *Lancet* (2020) 395:2008–20. doi: 10.1016/S0140-6736(20)30974-0
15. Klein AP. Pancreatic Cancer Epidemiology: Understanding the Role of Lifestyle and Inherited Risk Factors. *Nat Rev Gastroenterol Hepatol* (2021) 18:493–502. doi: 10.1038/s41575-021-00457-x
16. Mahajan UM, Langhoff E, Goni E, Costello E, Greenhalf W, Halloran C, et al. Immune Cell and Stromal Signature Associated With Progression-Free Survival of Patients With Resected Pancreatic Ductal Adenocarcinoma. *Gastroenterology* (2018) 155:1625–39. doi: 10.1053/j.gastro.2018.08.009
17. Fridman WH, Zitvogel L, Sautès-Fridman C, Kroemer G. The Immune Contexture in Cancer Prognosis and Treatment. *Nat Rev Clin Oncol* (2017) 14:717–34. doi: 10.1038/nrclinonc.2017.101
18. Turley SJ, Cremasco V, Astarita JL. Immunological Hallmarks of Stromal Cells in the Tumour Microenvironment. *Nat Rev Immunol* (2015) 15:669–82. doi: 10.1038/nri3902
19. Ren B, Cui M, Yang G, Wang H, Feng M, You L, et al. Tumor Microenvironment Participates in Metastasis of Pancreatic Cancer. *Mol Cancer* (2018) 17:108. doi: 10.1186/s12943-018-0858-1
20. Wang S, Li Y, Xing C, Ding C, Zhang H, Chen L, et al. Tumor Microenvironment in Chemoresistance, Metastasis and Immunotherapy of Pancreatic Cancer. *Am J Cancer Res* (2020) 10:1937–53.
21. Huang X, Ding L, Liu X, Tong R, Ding J, Qian Z, et al. Regulation of Tumor Microenvironment for Pancreatic Cancer Therapy. *Biomaterials* (2021) 270:120680. doi: 10.1016/j.biomaterials.2021.120680
22. Torphy RJ, Schulick RD, Zhu Y. Understanding the Immune Landscape and Tumor Microenvironment of Pancreatic Cancer to Improve Immunotherapy. *Mol Carcinog* (2020) 59:775–82. doi: 10.1002/mc.23179
23. Henze J, Tacke F, Hardt O, Alves F, Al RW. Enhancing the Efficacy of CAR T Cells in the Tumor Microenvironment of Pancreatic Cancer. *Cancers (Basel)* (2020) 12:1389. doi: 10.3390/cancers12061389
24. Liu Y, Liang G, Xu H, Dong W, Dong Z, Qiu Z, et al. Tumors Exploit FTO-Mediated Regulation of Glycolytic Metabolism to Evade Immune Surveillance. *Cell Metab* (2021) 33:1221–33. doi: 10.1016/j.cmet.2021.04.001
25. Han D, Liu J, Chen C, Dong L, Liu Y, Chang R, et al. Anti-Tumour Immunity Controlled Through Mrna M(6)a Methylation and YTHDF1 in Dendritic Cells. *Nature* (2019) 566:270–4. doi: 10.1038/s41586-019-0916-x
26. Wang L, Hui H, Agrawal K, Kang Y, Li N, Tang R, et al. M(6) a RNA Methyltransferases METTL3/14 Regulate Immune Responses to Anti-PD-1 Therapy. *EMBO J* (2020) 39:e104514. doi: 10.15252/embj.2020104514
27. Moffitt RA, Marayati R, Flate EL, Volmar KE, Loeza SG, Hoadley KA, et al. Virtual Microdissection Identifies Distinct Tumor- and Stroma-Specific Subtypes of Pancreatic Ductal Adenocarcinoma. *Nat Genet* (2015) 47:1168–78. doi: 10.1038/ng.3398
28. Rashid NU, Peng XL, Jin C, Moffitt RA, Volmar KE, Belt BA, et al. Purity Independent Subtyping of Tumors (Purist), A Clinically Robust, Single-Sample Classifier for Tumor Subtyping in Pancreatic Cancer. *Clin Cancer Res* (2020) 26:82–92. doi: 10.1158/1078-0432.CCR-19-1467
29. Meng Z, Yuan Q, Zhao J, Wang B, Li S, Offringa R, et al. The M(6)a-Related Mrna Signature Predicts the Prognosis of Pancreatic Cancer Patients. *Mol Ther Oncolytics* (2020) 17:460–70. doi: 10.1016/j.omto.2020.04.011
30. Liu H, Qiu C, Wang B, Bing P, Tian G, Zhang X, et al. Evaluating DNA Methylation, Gene Expression, Somatic Mutation, and Their Combinations in Inferring Tumor Tissue-of-Origin. *Front Cell Dev Biol* (2021) 9:619330. doi: 10.3389/fcell.2021.619330
31. Şenbabaoğlu Y, Michailidis G, Li JZ. Critical Limitations of Consensus Clustering in Class Discovery. *Sci Rep* (2014) 4:6207. doi: 10.1038/srep06207
32. Tibshirani R, Walther G, Hastie T. Estimating the Number of Clusters in a Data Set via the Gap Statistic. *J R Stat Soc Ser B Stat Methodol* (2001) 63:411–23. doi: 10.1111/1467-9868.00293
33. Dudoit S, Fridlyand JA. Prediction-Based Resampling Method for Estimating the Number of Clusters in a Dataset. *Genome Biol* (2002) 3:H36. doi: 10.1186/gb-2002-3-7-research0036
34. Wilkerson MD, Hayes DN. Consensusclusterplus: A Class Discovery Tool With Confidence Assessments and Item Tracking. *Bioinformatics* (2010) 26:1572–3. doi: 10.1093/bioinformatics/btq170
35. Newman AM, Steen CB, Liu CL, Gentles AJ, Chaudhuri AA, Scherer F, et al. Determining Cell Type Abundance and Expression From Bulk Tissues With Digital Cytometry. *Nat Biotechnol* (2019) 37:773–82. doi: 10.1038/s41587-019-0114-2
36. Yoshihara K, Shahmoradgoli M, Martínez E, Vegesna R, Kim H, Torres-Garcia W, et al. Inferring Tumour Purity and Stromal and Immune Cell Admixture From Expression Data. *Nat Commun* (2013) 4:2612. doi: 10.1038/ncomms3612
37. Sotiriou C, Wirapati P, Loi S, Harris A, Fox S, Smeds J, et al. Gene Expression Profiling in Breast Cancer: Understanding the Molecular Basis of Histologic Grade to Improve Prognosis. *J Natl Cancer Inst* (2006) 98:262–72. doi: 10.1093/jnci/djj052
38. Zeng D, Li M, Zhou R, Zhang J, Sun H, Shi M, et al. Tumor Microenvironment Characterization in Gastric Cancer Identifies Prognostic and Immunotherapeutically Relevant Gene Signatures. *Cancer Immunol Res* (2019) 7:737–50. doi: 10.1158/2326-6066.CIR-18-0436
39. Charoentong P, Finotello F, Angelova M, Mayer C, Efremova M, Rieder D, et al. Pan-Cancer Immunogenomic Analyses Reveal Genotype-Immunophenotype Relationships and Predictors of Response to Checkpoint Blockade. *Cell Rep* (2017) 18:248–62. doi: 10.1016/j.celrep.2016.12.019
40. Cullis J, Das S, Bar-Sagi D. Kras and Tumor Immunity: Friend or Foe? *Cold Spring Harb Perspect Med* (2018) 8:a031849. doi: 10.1101/cshperspect.a031849
41. Merz V, Gaule M, Zecchetto C, Cavaliere A, Casalino S, Pesoni C, et al. Targeting KRAS: The Elephant in the Room of Epithelial Cancers. *Front Oncol* (2021) 11:638360. doi: 10.3389/fonc.2021.638360
42. Dey P, Li J, Zhang J, Chaurasiya S, Strom A, Wang H, et al. Oncogenic KRAS-Driven Metabolic Reprogramming in Pancreatic Cancer Cells Utilizes Cytokines From the Tumor Microenvironment. *Cancer Discov* (2020) 10:608–25. doi: 10.1158/2159-8290.CD-19-0297
43. Blagih J, Buck MD, Vousden KH. P53, Cancer and the Immune Response. *J Cell Sci* (2020) 133:cs237453. doi: 10.1242/jcs.237453
44. Blagih J, Zani F, Chakravarty P, Hennequart M, Pilley S, Hobor S, et al. Cancer-Specific Loss of P53 Leads to a Modulation of Myeloid and T Cell Responses. *Cell Rep* (2020) 30:481–96. doi: 10.1016/j.celrep.2019.12.028
45. Bezzi M, Seitzer N, Ishikawa T, Reschke M, Chen M, Wang G, et al. Diverse Genetic-Driven Immune Landscapes Dictate Tumor Progression Through Distinct Mechanisms. *Nat Med* (2018) 24:165–75. doi: 10.1038/nm.4463
46. Bertoli C, Skotheim JM, de Bruin RA. Control of Cell Cycle Transcription During G1 and s Phases. *Nat Rev Mol Cell Biol* (2013) 14:518–28. doi: 10.1038/nrm3629
47. Hu C, Hart SN, Polley EC, Gnanaolivu R, Shimelis H, Lee KY, et al. Association Between Inherited Germline Mutations in Cancer Predisposition Genes and Risk of Pancreatic Cancer. *JAMA* (2018) 319:2401–9. doi: 10.1001/jama.2018.6228
48. Robert C. A Decade of Immune-Checkpoint Inhibitors in Cancer Therapy. *Nat Commun* (2020) 11:3801. doi: 10.1038/s41467-020-17670-y
49. Javadrashid D, Baghbanzadeh A, Derakhshani A, Leone P, Silvestris N, Racanelli V, et al. Pancreatic Cancer Signaling Pathways, Genetic Alterations, and Tumor Microenvironment: The Barriers Affecting the Method of Treatment. *Biomedicines* (2021) 9:373. doi: 10.3390/biomedicines9040373
50. Macherla S, Laks S, Naqash AR, Bulumulle A, Zervos E, Muzaffar M. Emerging Role of Immune Checkpoint Blockade in Pancreatic Cancer. *Int J Mol Sci* (2018) 19:3505. doi: 10.3390/ijms19113505
51. Jiang Y, Li Y, Zhu B. T-Cell Exhaustion in the Tumor Microenvironment. *Cell Death Dis* (2015) 6:e1792. doi: 10.1038/cddis.2015.162

Conflict of Interest: The authors declare that the research was conducted in the absence of any commercial or financial relationships that could be construed as a potential conflict of interest.

Publisher's Note: All claims expressed in this article are solely those of the authors and do not necessarily represent those of their affiliated organizations, or those of the publisher, the editors and the reviewers. Any product that may be evaluated in

this article, or claim that may be made by its manufacturer, is not guaranteed or endorsed by the publisher.

Copyright © 2021 Sun, Xie, Zhang, Wang, Huang and Xia. This is an open-access article distributed under the terms of the Creative Commons Attribution License (CC BY). The use, distribution or reproduction in other forums is permitted, provided the original author(s) and the copyright owner(s) are credited and that the original publication in this journal is cited, in accordance with accepted academic practice. No use, distribution or reproduction is permitted which does not comply with these terms.

frontiers in Immunology

ORIGINAL RESEARCH
published: 23 September 2021
doi: 10.3389/fimmu.2021.717688

PTP4A3 Is a Prognostic Biomarker Correlated With Immune Infiltrates in Papillary Renal Cell Carcinoma

Qian Song[1†], Yutian Zheng[2†], Junzhou Wu[3], Sheng Wang[1], Lin Meng[2], Qian Yao[4], Zhongwu Li[4] and Shenyi Lian[4*]*

[1] Department of Clinical Laboratory, The Cancer Hospital of the University of Chinese Academy of Sciences (Zhejiang Cancer Hospital); Institute of Basic Medicine and Cancer (IBMC), Chinese Academy of Sciences, Hangzhou, China, [2] Key Laboratory of Carcinogenesis and Translational Research (Ministry of Education/Beijing), Department of Biochemistry and Molecular Biology, Peking University Cancer Hospital & Institute, Beijing, China, [3] Cancer Research Institute, The Cancer Hospital of the University of Chinese Academy of Sciences (Zhejiang Cancer Hospital); Institute of Basic Medicine and Cancer (IBMC), Chinese Academy of Sciences, Hangzhou, China, [4] Key laboratory of Carcinogenesis and Translational Research (Ministry of Education/Beijing), Department of Pathology, Peking University Cancer Hospital & Institute, Beijing, China

OPEN ACCESS

Edited by:
Peng Qu,
National Institutes of Health (NIH), United States

Reviewed by:
Yafeng He,
National Heart, Lung, and Blood Institute (NHLBI), United States
Chien-Feng Li,
National Health Research Institutes, Taiwan

***Correspondence:**
Zhongwu Li
zhwuli@hotmail.com
Shenyi Lian
liansy2007@bjmu.edu.cn

[†]These authors have contributed equally to this work and share first authorship

Specialty section:
This article was submitted to Cancer Immunity and Immunotherapy, a section of the journal Frontiers in Immunology

Received: *31 May 2021*
Accepted: *31 August 2021*
Published: *23 September 2021*

Citation:
Song Q, Zheng Y, Wu J, Wang S, Meng L, Yao Q, Li Z and Lian S (2021) PTP4A3 Is a Prognostic Biomarker Correlated With Immune Infiltrates in Papillary Renal Cell Carcinoma. Front. Immunol. 12:717688. doi: 10.3389/fimmu.2021.717688

PTP4A3 plays an important role in the tumorigenesis and metastasis of multiple tumors, but its prognostic role in renal cancer is not well understood. We utilized the Oncomine and Tumor Immunoassay Resource databases to examine the differential expression of PTP4A3 in tumor tissues and normal tissues in breast, urinary tract, gastrointestinal tract and skin. Using the GEPIA and PrognoScan databases, the independent prognostic role of PTP4A3 was confirmed in clear cell renal cell cancer and papillary renal cell cancer. Expression of PTP4A3 were obviously higher in tumor tissue compare with normal tissues (P=0.028). We haven't found the associations of PTP4A3 and clinicopathological features in our IHC cohort. Ectopic expression of PTP4A3 promotes proliferation, migration and invasion and increased the mRNA level of TGFB1 in RCC cell lines. Immunohistochemical staining indicated that the expression of PTP4A3 associates with CD3+ (P =0.037)/CD8+ (P =0.037) intratumor TILs, not with invasive margins in renal cancer. Comprehensive analysis of immune infiltration in the TIMER database correlated PTP4A3 expression with the infiltration of B cells, CD8+ T cells, CD4+ T cells and neutrophils in both clear cell renal cell carcinoma and papillary renal cell carcinoma. PTP4A3 expression was associated with the infiltration of dendritic cells in papillary renal cell carcinoma. We further confirmed that the infiltration of B cells and CD8+ T cells was associated with poor prognosis in papillary renal cell carcinoma patients, consistent with the prognostic role of PTP4A3 in papillary renal cell carcinoma. PTP4A3 expression correlated genes involved in B cells, monocytes, M1 macrophages, Th2 and Treg cells in papillary renal cell carcinoma. These results suggest PTP4A3 as a prognostic factor with a role in regulating immune cell infiltration in papillary renal cell carcinoma.

Keywords: renal cancer, PTP4A3, prognosis, tumor infiltration, biomarker

INTRODUCTION

Renal cell carcinoma (RCC) is a common malignant disease expected to account for approximately 76,080 cases and 13,780 deaths in 2021 in the United States (1). RCC is divided into three major histologic subtypes: clear cell RCC (ccRCC or KIRC), papillary cell RCC (pRCC or KIRP), and chromophobe RCC (chRCC). According to The Cancer Genome Atlas (TCGA), a comprehensive database of cancer genomic profiles, these three major RCC subtypes have distinctive genetic alterations including genomic mutations, methylation status, RNA expression signatures, and immune signatures (2–4). At diagnosis, 30% of RCC patients were confirmed as distant metastatic (5). While localized RCC could be cured by surgical resection, about 40% of surgical patients eventually experienced recurrence. Recently, adjuvant therapy, and especially immune therapy, has received significant attention as an option for treating metastatic RCC (mRCC). Immune therapy combined with a tyrosine kinase inhibitor; bevacizumab, a monoclonal antibody against vascular endothelial growth factor; or ipilimumab, a monoclonal antibody against cytotoxic T-lymphocyte antigen-4 are now considered optimal treatment strategies for mRCC. The biomarkers Programmed Cell Death Protein 1 (PD1) and Programmed Death-Ligand 1 (PD-L1) exhibited higher expression in ccRCC than in chRCC or pRCC, and high expression was correlated with decreased survival in all RCC patients (P=0.02) (6, 7). Immune cell genes signatures, including those of B cells, dendritic cells, CD68, CD8, Treg cells, Th1/2 and immunoglobin G, were examined in ccRCC, pRCC and chRCC. In general, expression was higher in ccRCC than pRCC and chRCC, except for Th17, IL-8, and $CD56^{bright}$natural killer (NK) cell signatures. Th2 gene signatures were universally correlated with poor overall survival (OS) in all major histological subtypes (2). IL-8 inflammatory pathway-related genes and $CD56^{bright}$NK cell genes had higher expression in pRCC than in ccRCC and chRCC, whereas IL-17 producing T helper cells (T_H17 cells) had lower expression in pRCC than in ccRCC and chRCC. T_H17 gene signatures positively correlated with OS in ccRCC and chRCC (P=0.0021 and P=0.0362, respectively). CpG island methylator phenotype-associated RCC had increased expression of T_H2 cells and Treg cells compared with pRCC and chRCC. Therefore, immune biomarkers for different subtypes of RCC need to be explored.

Protein Tyrosine Phosphatase 4A3 (PTP4A3), also known as phosphatase of regenerating liver 3 (PRL-3), is a protein tyrosine phosphatase distributed in the cell nucleus, plasma membrane and endosome (8). It is negatively correlated with survival in colon cancer (9), breast cancer (10, 11), gastric cancer (12–14), ovarian cancer (15, 16) and acute myelogenous leukemia (AML) (17). PTP4A3 promotes the proliferation, migration, and invasion of tumor cells by activating the Rho family and matrix metalloproteinase-2. PTP4A3 has been shown to continuously activate the PI3K-AKT-ERK pathway by negatively regulating Src kinase and PTEN (18, 19). PTP4A3 is known to promote epithelial mesenchymal transition by KCNN4 channels (20), stimulate G2/M cell cycle arrest by ubiquitinating AURKA and dephosphorylating FZR1 (21), increase IL-1 alpha secretion through the NF-κB and JAK2-STAT pathway (22). Extensive data supports the deprotection role of PTP4A3 in tumorigenesis and telomere maintenance (23, 24). Studies in PTP4A3 transgenic mice have shown that high expression of PTP4A3 promotes colitis-related colon cancer, shortens telomeres, and increases expression of H3K9Me, a hallmark of genomic instability (24, 25). PTP4A3 restricts transcription in melanoma through the DDX21-MITF axis (26).

Due to the important role of PTP4A3 in cancers, a PRL-zumab was generated by the Zeng group and was shown to specifically inhibit PTP4A3-positive liver cancer cell *in vivo*, and recruit B cells, NK cells and macrophages to the PTP4A3-positive tumor microenvironment (27, 28). A DNA vaccine targeting PTP4A3 triggered high expression of interferon-γ and TNF-α in breast cancer through the CTL and T helper type 1 cells immune response and also stimulated the accumulation of PTP4A3 antibody in immunized mice (29). IL-6/8 secreted by tumor-associated macrophages (TAMs) facilitated the metastasis of colon cancer in a PTP4A3-KCNN4-dependent manner (30). Few reports have examined the role of PTP4A3 in kidney cancer, and this research has mostly focused on the correlation of clinicopathological characteristics and prognosis. The mechanism of how PTP4A3 regulates immune cells and its impact on renal cancer prognosis remains unclear.

Herein, we developed a comprehensive analysis across multiple databases to elucidate the role of PTP4A3 in ccRCC and pRCC. In addition, we analyzed the relationship of PTP4A3 and immune cell tumor infiltration (TIMER) (31, 32). This study offers new insights into the function of PTP4A3 in renal cancer and proposes a mechanism for PTP4A3 regulating tumor infiltration of immune cells.

Abbreviations: RCC, renal cell carcinoma; ccRCC or KIRC, clear cell RCC; pRCC or KIRP, papillary cell RCC; chRCC, chromophobe RCC; TCGA, the cancer genome atlas; mRCC, metastatic RCC; PD1, programmed cell death protein 1; PD-L1, programmed death-ligand 1; NK, natural killer; OS, overall survival; T_H17, T helper; PTP4A3, protein tyrosine phosphatase 4A3; PRL-3, phosphatase of regenerating liver 3; AML, acute myeloid leukemia; TAMs, tumor-associated macrophages; DFS, disease-free survival; TIMER, tumor immune estimation resource; GEPIA, gene expression profiling interactive analysis; BRCA, invasive carcinoma of the breast; CHOL, cholangiocarcinoma; COAD, adenocarcinoma of the colon; LIHC, hepatocellular carcinoma; LUAD, adenocarcinoma of the lung; PRAD, prostate adenocarcinoma; READ, adenocarcinoma of the rectum; THCA, thyroid carcinoma; STAD, gastric adenocarcinoma; BLCA, urothelial carcinoma; LUSC, squamous cell lung carcinoma; HNSC, head and neck squamous cell carcinoma; OV, ovarian serous cystadenocarcinoma; UCEC, uterine corpus endometrial carcinoma; UCS, uterine carcinosarcoma; LAML, acute myeloid leukemia; LGG, low grade glioma; UVM, uveal melanoma; INOS, inducible nitric oxide synthase.

MATERIALS AND METHODS

Oncomine Database Analysis

The Oncomine database comprises a wide range of gene expression datasets covering various cancer types. PTP4A3 expression in diverse tumor types was investigated using this database (https://www.oncomine.org/resource/login.html) (33)

with the screening thresholds set as: P-value of 0.001, fold change of 1.5 and gene rank of top 5%.

PrognoScan Database Analysis

The PrognoScan database complies accessible tumor microarray datasets, facilitating the correlation of gene expression and survival including OS and disease-free survival (DFS). We evaluated the relationship between PTP4A3 expression and prognosis in diverse tumor types using the PrognoScan database (http://www.abren.net/PrognoScan/) (34) with a threshold P-value of 0.05.

Cell Culture and Antibody

Kidney clear carcinoma cell lines 786-O and Caki-2 were obtained from the Cell Resource Center, Peking Union Medical College (which is the headquarters of National Infrastructure of Cell Line Resource, NSTI. 786-O cell were cultured in RPMI-1640 (Invitrogen, Carlsbad, CA, USA) containing 10% fetal bovine serum. Caki-2 cell were cultured in McCoys'5A (Gibco, USA) containing 10% fetal bovine serum. Anti-Myc tag (AB 103) was from TianGen Biotech (Beijing, China). Anti-GAPDH (10494-1-AP) was from Proteintech Group (Chicago, IL, USA).

Lentivirus Infection and Western Blot

To stable expression of ectopic PTP4A3 in renal cancer cell, 786-O and Caki-2 cells were infected with 50 MOI control or myc-PTP4A3 expression lentivirus for 72 hours. Cells were directly homogenized in 2 × loading buffer to get the whole cell extracts. Protein samples were separated by the SDS-polyacrylamide gel electrophoresis and transferred onto the nitrocellulose membranes, and blocked in 5% milk in PBS buffer for 1 hour. The lentivirus infection were detected by the myc-tag antibody (1μg/ml) at 4°C overnight and washed in 0.1% Tween in PBS for 3 times. After incubating with HRP-conjugated anti-mouse secondary antibody, the protein bands were visualized by the enhanced chemiluminescence detection system (Thermo Fisher Scientific, Pittsburgh, PA, USA).

Cell Proliferation Migration and Invasion

Cell Counting Kit (CCK)-8 (C0037, Beyotime, Shanghai, China) were used for cell proliferation experiments. 3 $\times 10^4$ cells of 786-O vector, 786-O-myc-PTP4A3, Caki-2 vector and Caki-2-myc-PTP4A3 cells were re-suspended in 100 μl complete medium, and seed in the 96-well plates in triplicate. At 0,24,48,72,96 hours, discarded the medium and added 100μl fresh medium containing 10 μl CCk-8 to each well, After 2 hours incubation at 37°C, the spectrophotometer (Thermo Fisher Scientific, Pittsburgh, PA, USA)was used to measure the absorbance of each well at OD450nm.

200 μl re-suspended 786-O vector, 786-O-myc-PTP4A3, Caki-2 vector and Caki-2-myc-PTP4A3 cells were seeded on the upper chamber of each transwell (Becton Dickinson, San Jose, CA, USA), 2×10^5/ml for migration and 10×10^5/ml for invasion, 800 μl medium containing 10% FBS added to the lower chamber. Cells were cultured at 37°C 24 hour for cell migration, 48 hours for cell invasions. The cells on the upper chambers were fixed in cold methanol and stained in 0.1% crystal violet for 30 mins at room temperature. The cells penetrated to the upper chamber were counted in at least 6 randomly selected field under microscope.

Quantitative Real-Time PCR

Total RNA was extracted from cells with Trizol reagent (Invitrogen, Carlsbad, CA, USA) based on the manufacturer's instruction. 1 μg of RNA was utilized to synthesize cDNA with GoScriptTM Reverse Transcription system (A5001, Promega). qRT-PCR was conducted with SYBR Green PCR master mix reagents (TOYOBO) and a StepOne Real-time PCR system (Applied Biosystems). Expression data of indicative gene was normalized to that of GAPDH. Primers used are listed in **Supplementary Table 4**.

Immunohistochemical Analysis

The kidney cancer tissue array (DC-Kid11051) were bought from Avilabio company (Shanxi). DC-Kid11051 were including 33 KIRC, 9 KIRP, 5 KICH and 6 normal kidney tissues. The sections were deparaffinized in xylene and hydrate in alcohol. Endogenous peroxidase activity was then blocked by incubation in 3% hydrogen peroxide–methanol for 10 min. For the antigen recovery, the section was heated in a citrate buffer (pH 6.0) for 15mins. Incubation with PTP4A3 antibody (11) (5μg/ml, monoclonal antibody 3B6 previous validated), CD3 antibody ((Monoclonal Rabbit Anti-Human CD3, Clone 2GV6, prediluted, Roche) and CD8 antibody (Monoclonal Mouse Anti-Human CD8, Clone C8/144B, Dako) at 4°C overnight. EnVision$^+$ TM (Dako, Carpinteria, CA, USA) was used as the secondary antibody. Antibody binding was visualized by a standard streptavidin immunoperoxidase reaction. Immunoreactivity in the cytoplasma and cytoplasmic membrane of PTP4A3 was evaluated.

Evaluation immunoreactivity was carried out independently by three experienced pathologists without any knowledge of the clinical data. The IHC score was assessed according to the percentage of positive cells and the intensity of cytoplasmic reactivity. These averaged immunoreactivity values were stratified into five scoring groups: -, not detected; ±, <10% positive cells; +, 10–20% weakly to moderately positive cells; ++, 10–20%intensely positive cells or 20–50% weakly positive cells; and +++, 20–50% positive cells with moderate to marked reactivity or >50% positive cells. In the statistical analysis, ± were considered negative, + and above were considered positive.

Quantification of CD3+ and CD8+TILs

Each entire section was evaluated for CD3+ and CD8+ TILs by two pathologists blind to PTP4A3 expression. The intratumor and invasive margins were identified by the immunohistochemistry. Each positive cell was manually counted under 40 ×magnification field in 5 independent tumor fields or invasive margins with most abundant TILs. The consecutive sections were stained for CD3 and CD8.

TIMER Database Analysis

Tumor Immune Estimation Resource (TIMER, https://cistrome.shinyapps.io/timer/) was developed to evaluate the abundance of

immune infiltrates using 10,897 cancer samples from TCGA (31, 32). TIMER gene modules were utilized to investigate PTP4A3 expression in diverse tumors and the relationship between PTP4A3 expression and the abundance of immune infiltrates. In addition, correlation modules were used to evaluate the relationship of PTP4A3 expression with gene biomarkers of tumor-infiltrating immune cells. These gene biomarkers have been previously studied (35–37).

GEPIA Database Analysis

We confirmed the correlation of PTP4A3 expression and tumor infiltration of immune cells with the Gene Expression Profiling Interactive Analysis (GEPIA, http://gepia.cancer-pku.cn/index.html) (38). We also assessed the prognostic value, including OS and DFS, of gene expression in diverse tumors with this database. Meanwhile, gene expression correlation was investigated based on TCGA expression data. Correlation analyses were conducted in both cancer and paired normal tissues. The correlation coefficient was calculated by the Spearman method. PTP4A3 was represented on the X-axis, and related biomarker genes were utilized for the Y-axis.

Statistical Analysis

Results from the Oncomine database included fold change, P-value, and gene rank. The PrognoScan and GEPIA databases produced HR and P-values or Cox P-values according to a log-rank test. The correlation between PTP4A3 expression and other related immune genes was investigated using the Spearman method and the correlation strength was categorized according to r values. R values of 0.80-1.00 were deemed very strong, r values of 0.60-0.79 were strong, r values of 0.40-0.59 were moderate, r values of 0.20-0.39 were weak, and r values of 0.00-0.19 were categorized as very weak. P-values less than 0.05 were considered statistically significant. Chi-square test and nonparametric test were utilized to analyze the Categorical data by SPSS 19.0 software (SPSS Inc., Chicago, IL, USA).

RESULTS

PTP4A3 mRNA Expression Level in Diverse Tumors and Adjacent Normal Tissues

We investigated differential PTP4A3 mRNA levels in tumor and normal tissues across various cancer types in the Oncomine database. Compared with adjacent normal tissues, PTP4A3 mRNA levels were elevated in most cancer types, including breast, colorectal, esophageal, head and neck, kidney, leukemia, liver, melanoma, myeloma, pancreatic, prostate, and sarcoma. However, PTP4A3 mRNA levels were lower in kidney and sarcoma cancer in other datasets (**Figure 1A**). PTP4A3 mRNA levels in diverse tumors are detailed in **Supplementary Table 1**.

PTP4A3 expression in diverse tumor types was further assessed using the TCGA and TIMER databases. Differential PTP4A3 expression in tumors compared with adjacent normal tissues in the TCGA datasets is presented in **Figure 1B**. Consistent with the results from the Oncomine database, PTP4A3 expression was significantly elevated in breast invasive carcinoma (BRCA) cholangiocarcinoma (CHOL), colon adenocarcinoma (COAD), kidney renal clear cell carcinoma (KIRC), liver hepatocellular carcinoma (LIHC), lung adenocarcinoma (LUAD), prostate adenocarcinoma (PRAD) rectum adenocarcinoma (READ) and

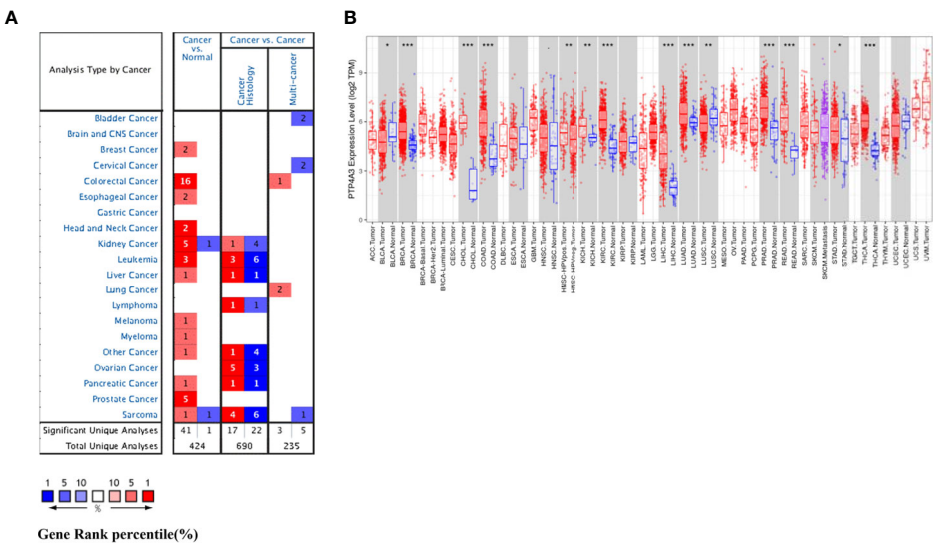

FIGURE 1 | PTP4A3 mRNA levels in various tumor tissues and adjacent normal tissues. **(A)** Differential PTP4A3 mRNA levels between tumor and adjacent normal tissues across various cancer types in the Oncomine database (threshold P-value < 0.001, fold change 1.5, gene rank top 5%). **(B)** Differential PTP4A3 expression levels between tumor and adjacent normal tissues in the TIMER datasets. Blue code represents low expression of indicated tumor. Red code represents high expression of indicated tumor (*P < 0.05, **P < 0.01, ***P < 0.001).

thyroid carcinoma (THCA) relative to adjacent normal tissues (P<0.001). PTP4A3 expression was also slightly elevated in chRCC and stomach adenocarcinoma (STAD) compared with adjacent normal tissues (P<0.01). However, PTP4A3 expression was significantly lower in urothelial carcinoma (BLCA), and squamous cell lung carcinoma (LUSC) compared with normal tissues. Notably, PTP4A3 expression was significantly higher in head and neck squamous cell carcinoma (HNSC) HPV-positive cancer tissues compared with HNSC HPV-negative cancer tissues (**Figure 1B**). Single cell RNA sequencing has shown that HNSC HPV-positive and HNSC HPV-negative patients have distinct immune gene signatures, indicating that PTP4A3 may be correlated with immune-related genes (39, 40).

Prognostic Value of PTP4A3 in Multiple Cancer Types

To better understand the impact of PTP4A3 expression on clinical outcomes, the association between PTP4A3 expression and prognosis in 33 cancer types was analyzed using the GEPIA database. OS and DFS in urothelial cancer are presented in **Figure 2**. PTP4A3 expression and OS were not correlated in BLCA, chRCC, KIRC, pRCC (KIRP), ovarian serous

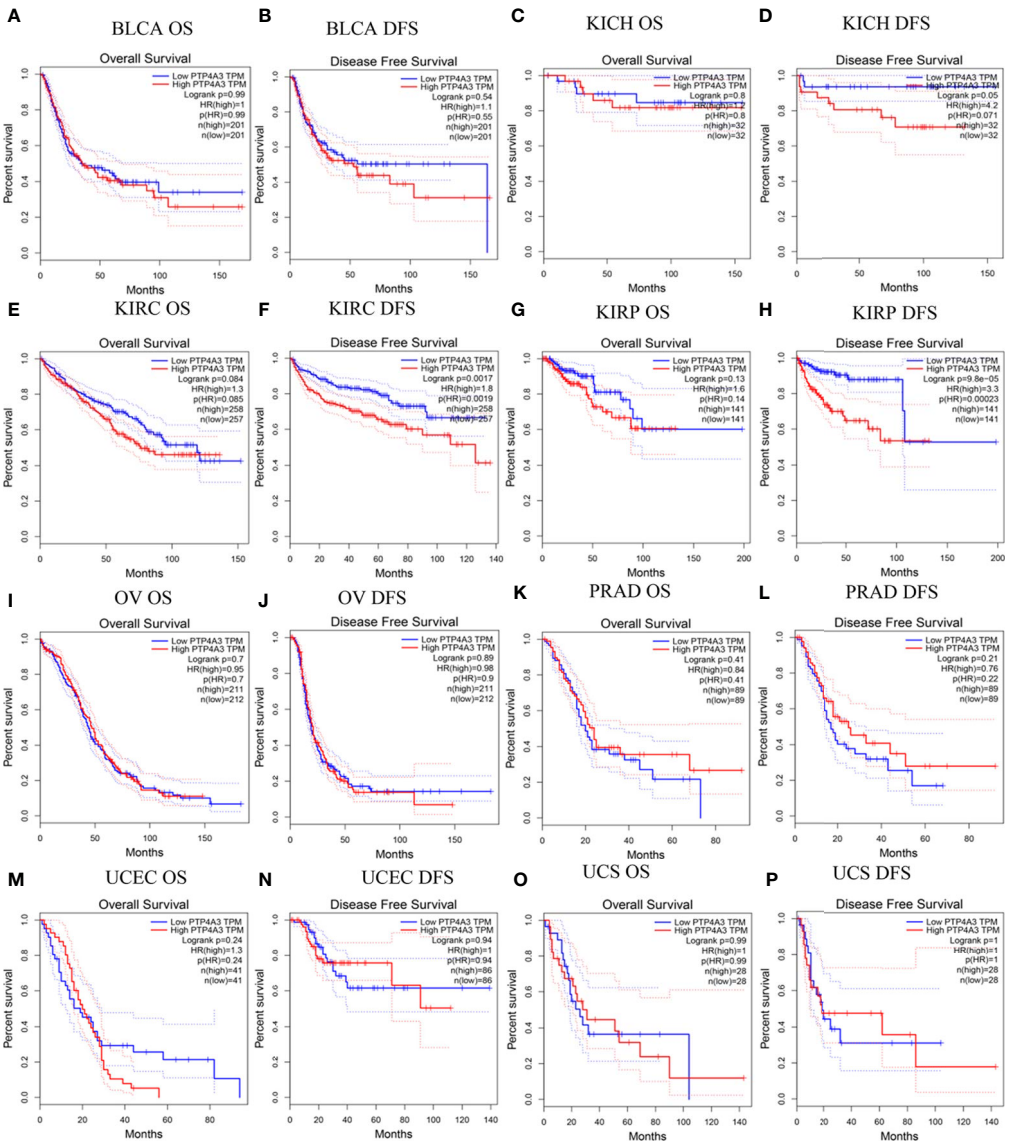

FIGURE 2 | Correlation of PTP4A3 expression level with prognosis values in urothelial tract cancer in the GEPIA database. OS and DFS in patients with differential PTP4A3 expression in bladder urothelial carcinoma (BLCA) **(A, B)**, chRCC (KICH) **(C, D)**, ccRCC(KIRC) **(E, F)**, pRCC (KIRP) **(G, H)**, ovarian serous cystadenocarcinoma (OV) **(I, J)**, prostate adenocarcinoma (PRAD) **(K, L)**, uterine corpus endometrial carcinoma (UCEC) **(M, N)**, uterine carcinosarcoma (UCS) **(O, P)**. OS, overall survival; DFS, disease free survival.

cystadenocarcinoma (OV), PRAD, uterine corpus endometrial carcinoma (UCEC) and uterine carcinosarcoma (UCS). High PTP4A3 expression was correlated with unfavorable DFS in KIRC and KIRP (HR=1.8, *P*=0.0017; HR=3.3, *P*=9.8E-05, respectively). The correlations of PTP4A3 expression and OS and DFS in 24 other types of tumors are shown in **Supplementary Figure 1**. High PTP4A3 expression was also correlated with decreased OS in acute myeloid leukemia (AML), lower grade glioma (LGG), LUSC and STAD. In addition, high PTP4A3 expression was correlated with decreased OS and DFS in uveal melanoma (UVM). Interestingly, LUAD was the only tumor type in which low PTP4A3 expression was correlated with decreased DFS.

Survival outcomes were further analyzed using the PrognoScan database. Correlations between PTP4A3 expression and clinical outcomes from 12 cancer types in 154 databases are displayed in **Supplementary Table 2**. Significant survival outcomes (Cox *P*<0.05) are shown in **Supplementary Figure 2**. PTP4A3 expression and survival outcomes were significantly correlated in AML(GSE12417-GPL96), BLCA (GSE5287 and GSE13507), glioblastoma (GSE7696), breast cancer (GSE9893, GSE9195 and GSE9195), eye cancer (GSE22138), MGH-glioma, non-small cell lung cancer (NSCLC) (GSE4716-GPL3696), ovarian cancer (GSE9891) and skin cancer (GSE19234) (**Supplementary Figures 2A–L**). These results indicated that high PTP4A3 expression is significantly associated with poorer clinical outcomes in many tumors types, including KIRC and KIRP.

PTP4A3 Plays as an Oncogene and Regulates the Cytokines in RCC

To further explore the mechanism of PTP4A3 in RCC, we stained the PTP4A3 in the kidney cancer tissue array which containing 5 different tumor histological subtypes and 6 kidney normal tissues. As shown in **Figures 3A, B**, PTP4A3 expression is obviously higher in the kidney tumor tissues (n=49) compare with the normal tissues (n=6) (*P*=0.028). The representative high expression of PTP4A3 in KIRC, KIRP and KICH, kidney squamous cancer and kidney normal tissues (**Figures 3Aa–e**). And there was no significantly difference in the various histological subtype, such as KIRC, KIRP and other types. (*P*=0.538, **Table 1**). We also calculated the association of PTP4A3 in general clinicopathological features, there was no significant difference found in gender, age, Fuhrman grade, TNM stage and lymph node metastasis (**Table 1**). Notably, PTP4A3 expression was slightly higher in the Fuhrman grade 3 compare with the expression in Grade 1 and 2(77.8% VS 40%, P=0.139). Although there was not rigorous statistic significant, PTP4A3 expression probably indicated the high grade, high recurrence and poor survival.

Results from the GEPIA and Prognoscan database also shown that PTP4A3 may play as an oncogene in the RCC. We utilized the lentivirus infection to ectopic expression of PTP4A3 in 786-O and Caki-2 cell lines. Ectopic expression of myc-PTP4A3 in 786-O and Caki-2 were detected by Myc-tagged antibody (**Figure 3E**). Overexpression of myc-PTP4A3 promoted proliferation of the 786-O and Caki-2 cell lines at 72, 96 hours in CCK-8 experiments (**Figure 3D**). Overexpression of PTP4A3 also triggered the metastasis phenotype of 786-O or Caki-2 cell lines (**Figures 3E, F**). Stable expression of PTP4A3 elevated the secretion level and mRNA level of IL-1alpha in colon cancer cell lines. And IL-1RN (IL-1 alpha inhibitor) decreased the migration and invasion of PTP4A3-stable expression cells (22). Therefore, we detected the cytokines (CD115, CCR8, IL-1 alpha, MMP-11 and TGFB1) in 786-O and Caki-2 cell lines with PTP4A3 stable expression. As shown in **Figure 3G**, ectopic expression of PTP4A3 increase the mRNA level of TGFB1 and CCR8 in 786-O and Caki-2 cells (p<0.05). But ectopic expression of PTP4A3 only elevated the CD115 (*P*=0.023) and IL-1 alpha (*P*=0.058) in 786-O cells, and slightly downregulated the CD115 (*P*=0.178) and IL-1 alpha (*P*=0.107) of Caki-2 cells. Expression of PTP4A3 downregulated the mRNA of MMP-11 in 786-O cells (*P*=0.006), and upregulated MMP-11 in Caki-2 cells (*P*=0.010). In conclusion, high expression of PTP4A3 not only promotes the cell proliferation, migration and invasion, but also increases the mRNA of cytokines TGFB1 ;and CCR8 in RCC cell lines. These results indicated the multiple roles of PTP4A3 in renal cancers, it extended the oncogene role of PTP4A3 to the regulation of cytokines and immune microenvironments.

PTP4A3 Expression Is Associated With CD3+ and CD8+ Intratumor T Cells in Renal Cancer

TGFB1 expressing and FOXP3 expressing on Treg cell is important in the maintenance of immune homeostasis. Antitumor effect of PTP4A3-target monoclonal antibody was described in gastric cancer (27). Immunotherapy combined with target therapy began the new era of malignant tumor such as lung cancer, gastric cancer (41–43). Considering tissue array is not suitable for the research of immune cell infiltration, we stained the CD3 (general T cell markers) and CD8+ T cells in KIRC surgery sections (n=10) to further explore the role of PTP4A3 in immnuo-target combined therapy. The representative IHC stains were shown in **Figure 4A**. Each count of CD3+/CD8+ intratumor and CD3/CD8+ invasive margins were shown in **Figure 4B**, divided by the PTP4A3 expression in the individual section. Compared with 8 negative PTP4A3 expression cases, the 2 positive PTP4A3 expression cases had lower CD3+ TILs intratumor counts (75.2 (57.0,182)/4 HPF VS 47.2(46.3,48.0)/4 HPF, *P*=0.037) and CD8+ TILs intratumor counts (64.2(48.0,177.3)/4 HPF VS 38.9 (34.7,43.0)/4 HPF, *P*=0.037). There were not significant differences in the counts of CD3+ (327.5(0,522.0)/4 HPF VS 157.0(0,314.0)/4 HPF, *P*=0.501) and CD8+ (153.0(0,365.0)/4 HPF VS 0(0, 0)/4 HPF, *P*=0.164) of invasion margins in the PTP4A3 negative and positive groups (**Figure 4C** and **Table 2**). Therefore, PTP4A3 associated with low CD3+/CD8+TILs and indicated poor prognosis in in renal cancers.

PTP4A3 Expression Is Associated With Immune Infiltration in Renal Cancer

Preliminary experiments in **Figure 4** showed PTP4A3 may associate with T cell infiltration in renal cancer. Renal cancer samples were not easy to collect, especially the relative low incidence subtype. Therefore, we utilized the TIMER database

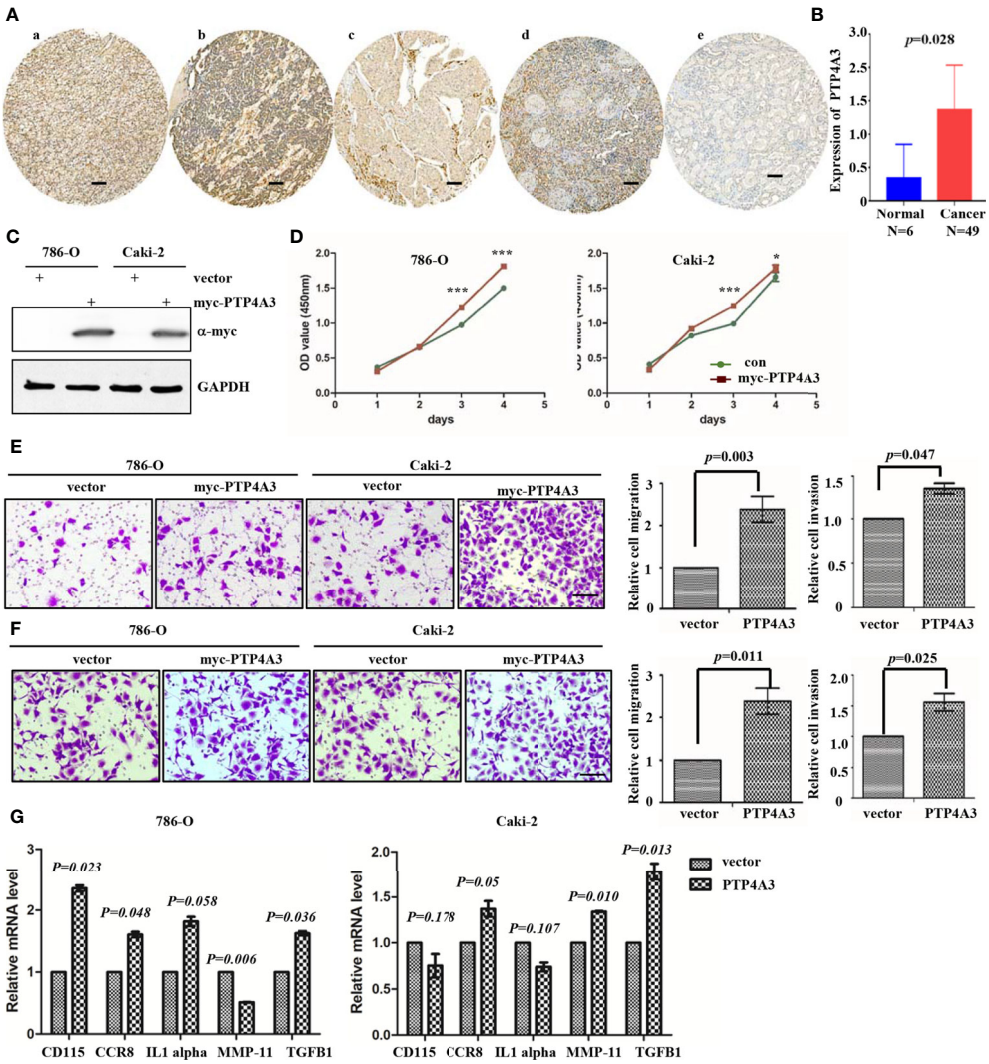

FIGURE 3 | Immunohistochemical staining of PTP4A3 in kidney cancer tissues than the normal tissues. **(A)** Representative IHC stain in kidney tumor tissue array. PTP4A3 expression in KIRC (a), KIRP (b), KICH (c), kidney squamous cancer (d) and kidney normal tissues (e). The Scale bar is 50μM. **(B)** Differential expression of PTP4A3 in kidney cancer and normal tissues. *P*=0.028. **(C)** Ectopic expression of myc-PTP4A3 in 786-O and Caki-2 cell line. GAPDH served as loading control. **(D)** Cell proliferation in 786-O and Caki-2 cells with myc-PTP4A3 and vector expression. All data are mean ± SE of three independent experiments. **P* < 0.05, ****P* < 0.001. **(E, F)** Representative cell migration and invasion in 786-O and Caki-2 with myc-PTP4A3 and control. All data are mean ± SE of three independent experiments. **P* < 0.05, ****P* < 0.001. **(G)** The mRNA level of cytokines, CD115, CCR8, IL1 alpha, MMP-11 and TGFB1 in PTP4A3 expressing 786-O and Caki-2 cells. The values are the mean and standard deviation. **P* < 0.05, n=3.

to comprehensive explore the relation of PTP4A3 and immune infiltration. Previous research has revealed that tumor-infiltrating lymphocytes could serve as an independent prognostic predictor in various cancers (44, 45). Using the databases (PrognoScan and GEPIA) and cell model, oncogene PTP4A3 expression was found to be correlated with decreased survival in KIRC and KIRP and promoted cell proliferation, migration and invasion (**Figures 2** and **3**).

Consistent with the unique immune gene profiles of renal cancer subtypes, the correlation of PTP4A3 expression with immune cell infiltration was distinct in KIRP and KIRC. In KIRC, significant correlations were observed between PTP4A3 expression and tumor purity (R=-0.231, *P*=5.2E-07), B cells (R=-0.094, *P*=4.41E-02), CD8+ T cells (R=0.116, *P*=1.53E-02), CD4+ T cells (R=0.351, *P*=9.27E-15) and neutrophils (R=0.145, *P*=1.92E-03), but not with macrophages (R=0.007, *P*=1.39E-01) or dendritic cells (R=0.072, *P*=1.26E-01). Similarly, in KIRP, PTP4A3 expression was correlated with B cells (R=0.222, *P*=3.39E-04), CD8+ T cells (R=0.148, *P*=1.78E-02), CD4+ T cells (R=0.16, *P*=1.02E-02), neutrophils (R=0.200, *P*=1.22E-03) and dendritic cells (R=0.247, *P*=6.63E-05), but not with tumor purity (R=0.015, *P*=8.06E-01) or macrophages (R=-0.009, *P*=8.83E-01) (**Figure 5A**). These results were partially accord with the CD3/CD8 staining results in real world.

TABLE 1 | PTP4A3 expression and clinical clinicopathological features in the renal cell carcinoma.

Variable		PTP4A3 Expression		*P* Value
		Negative (N = 26)	Positive (N = 23)	
Gender				
	Female	6	6	0.807
	Male	20	17	
Age,year				
	<60	19	14	0.363
	≥60	7	9	
Tumor histology				
	KIRC	13	14	0.538
	KIRP	5	2	
	Others	7	7	
Fuhrman grade				
	1	7	7	0.139
	2	8	3	
	3	2	7	
	missing	9	6	
TNM stage				
	I	7	6	0.821
	II	14	14	
	III	5	3	
lymph node metastasis				
	No	24	22	0.626
	Yes	2	1	

Kaplan-Meier curves showing immune cell infiltration and PTP4A3 expression in KIRC and KIRP were generated using the TIMER database. B cell infiltration (*P*=0.035), CD8+T cell infiltration (*P*=0.024), and PTP4A3 expression (*P*=0.017) were significantly associated with survival in KIRP (**Figure 5B**). However, there was no significant relationship between immune cell infiltration (including B cells, CD8+T cells, CD4+ T cells, neutrophils, macrophages, and dendritic cells) and survival in KIRC. Taken together, these results suggest that PTP4A3 is involved with regulating immune cell infiltration in KIRP and KIRC and, along with B cell infiltration and CD8+ T cell infiltration, influences clinical outcomes in KIRP.

Correlation Between PTP4A3 Expression and Immune Marker Sets

To further evaluate the association between PTP4A3 expression and immune cell infiltration, the TIMER and GEPIA databases were utilized to investigate the relationship between PTP4A3 and immune marker sets in KIRP and KIRC.

The association between PTP4A3 expression and immune marker sets of B cells, monocytes, TAMs, M1 macrophages, M2 macrophages, neutrophils, NK cells, dendritic cells, general T cells and CD8+ T cells were examined, both in KIRP and KIRC. Various T cells, including Th1 cells, Th2 cells, Tfh cells, Th17 cells, Tregs and exhausted T cells were also examined (**Supplementary Table 3**). The screen standard was defined as Cor>0.2, *P*<0.05 to identify PTP4A3-associated immune cell markers with or without tumor purity adjustment in KIRP and KIRC. Without tumor purity adjustment, PTP4A3 expression was correlated with CD115 in monocyte markers (Cor=0.215, *P*=2.38E-04), inducible nitric oxide synthase (INOS) in M1 macrophage markers (Cor=0.265, *P*=4.90E-06), STAT5A (Cor=0.231, *P*=7.26E-05) in Th2 markers and TGFB1 (Cor=0.421, *P*=1.72E-12) in Treg markers in KIRP (**Supplementary Table 3**). Distinct from what was observed in KIRP, PTP4A3 was associated with many immune gene markers in KIRC, including Cox2 in M1 macrophage markers (Cor=0.242, *P*=1.56E-08), CCR7 in neutrophil markers (Cor=0.271, *P*=2.10E-10), BDCA-1 (Cor=0.208, *P*=1.20E-06) and BDCA-4 (Cor=0.384, *P*=3.42E-20) in dendritic cell markers, T-bet (Cor=0.279, *P*=5.60E-11) and STAT4 (Cor=0.229, *P*=9.00E-08) in Th1 markers, BCL6 (Cor=0.249, *P*=5.55E-09) in Tfh markers, STAT3 (Cor=0.249, *P*=5.84E-09) in Th17 markers, TGFB1 (Cor=0.510, *P*=1.37E-36) in Treg markers and GZMB (Cor=0.215, *P*=5.46E-07) in T cell exhaustion markers (**Supplementary Table 3**). After adjusting for tumor purity, in both KIRP and KIRC, PTP4A3 expression was associated with M1 macrophage markers (INOS, Cor=0.297, *P*=1.14E-06, Cor=0.300, *P*=4.83E-11; COX2, Cor=0.225, *P*=2.63E-04, Cor=0.233, *P*=4.03E-07), Th17 markers (STAT3 Cor=0.225, *P*=2.74E-04, Cor=0.221, *P*=1.62E-06) and Treg markers (TGFβ Cor=0.378, *P*=3.75E-11, Cor=0.502, *P*=8.27E-31). CD79A in B cell markers (Cor=0.209, *P*=7.26E-04), CSF1R in monocyte markers (Cor=0.272, *P*=9.17E-06), VSIG4 in M2 macrophage markers (Cor=0.201, *P*=1.17E-03), CD11b in neutrophil markers(Cor=0.203, *P*=1.03E-03), HLA-DPA1 (Cor=0.210, *P*=6.99E-04) and BDCA-1 (Cor=0.225, *P*=2.65E-04)in dendritic cell markers, GATA3 (Cor=0.233, *P*=1.57E-04) and STAT5A (Cor=0.239, *P*=1.04E-04) in Th2 markersand LAG3 (Cor=0.216, *P*=4.85E-04) and GZMB (Cor=0.221, *P*=3.58E-04) in T cell exhaustion markers were correlated with PTP4A3 expression in KIRP (**Supplementary Table 3** and **Figure 6**). Weak correlations were observed between PTP4A3 expression and B cell markers (CD19), monocyte markers (CD68), NK cell markers (KIR2DL4, KIR3DL1, KIR3DL2 and KIR2DS4), dendritic cell markers (HLA-DPB1 and HLA-DRA), Th1 markers (TNF), Th2 markers (GATA3, STAT5A), Treg markers (CCR8), and exhausted T cell markers (PD1) in KIRP (*P*<0.01; **Supplementary Table 3**). TBX21 in Th1 markers was strongly correlated with PTP4A3 expression in KIRC (Cor=0.234, *P*=3.75E-07). PTP4A3 was weakly correlated with neutrophils (CCR7), NK cell markers (KIR2DL1, KIR3DL1, KIR3DL2 and KIR2DS4), dendritic cell markers (HLA-DRA and BDCA-1), Th1 (STAT4 and IFN-γ), Th2 (STAT6 and IL13), Treg (STAT5B) and T cell exhaustion (TIM-3 and GZMB) in KIRC. The correlation of PTP4A3 expression and B cell, monocyte, M1 macrophage, Th2 and Treg markers were confirmed using the GEPIA database, which compiled data from KIRP tumors and normal tissues (**Table 3**). No correlations were observed between PTP4A3 expression and M2 macrophage, neutrophil, or T cell exhaustion markers in the GEPIA database, but B cells, monocytes and Th2 markers were correlated with PTP4A3 expression in KIRP. Together, these findings confirmed the relationship of PTP4A3 to immune cell infiltration and CD79A, CSF1R, INOS, COX2, STAT5A, FOXP3 and CCR8 in KIRP, suggesting an

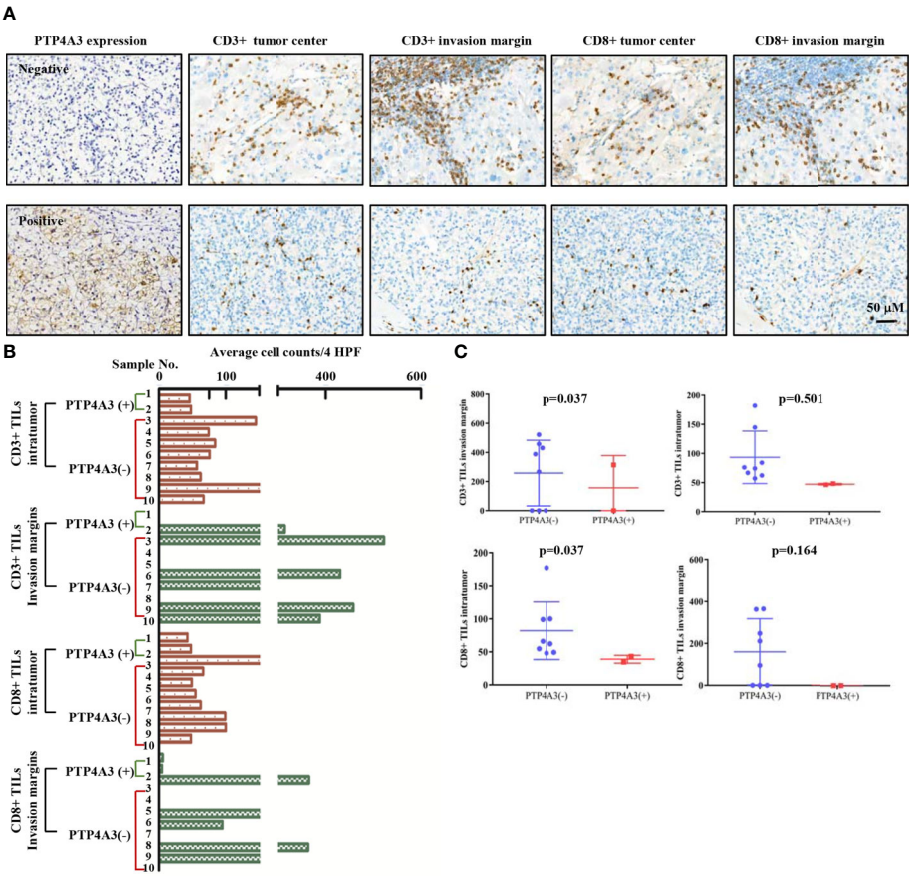

FIGURE 4 | PTP4A3 expression associates with low CD3+/CD8+ infiltration in renal cancers. **(A)** Representative IHC stain in 10 renal tumor tissues. PTP4A3 negative stains (upper panel) and positive stains (lower panel) with CD3+ intratumor stains, CD3+ invasion margins stains, CD8+ intratumor stains, CD8+ invasion margins stains, 20× magnification, scale bar, 50μM. **(B)** CD3+/CD8+ infiltration in tumor center (intratumor) and invasion margins in the PTP4A3 negative and positive tissues. All data were manually counted of positive cells in 4 HPF in each tumor field. **(C)** Histogram of the CD3+ and CD8+ intratumor and invasion margins infiltrations in renal cancers. All data are mean ± SE.

TABLE 2 | Descriptive statistics for numbers of CD3+ TILs and CD8+ TILs in patients with KIRC.

	PTP4A3(-)			PTP4A3(+)		
	Mean	**Median**	**Range**	**Mean**	**Median**	**Range**
CD3+ TILs intratumor	93.38	75.15	57-182	47.15	47.15	46.3-48
CD3+ TILs invasion margin	258.25	327.50	0-522	157.00	157.00	0-314
CD8+ TILs intratumor	82.08	64.15	48-177.3	38.85	38.85	34.7-43.0
CD8+ TILs invasion margin	160.25	153.00	0-365	0.00	0.00	0.00

important immune regulation role of PTP4A3 in the renal cancer microenvironment.

DISCUSSION

PTP4A3 is a 22kD tyrosine phosphatase and is highly homologous with PTP4A1 and PTP4A2. While PTP4A1 is expressed ubiquitously, PTP4A2 and PTP4A3 are specifically expressed in heart and skeletal muscles. PTP4A3 is a dual phosphatase and is known to act on ezrin, cytokeratin and integrin β1 (46–48). PTP4A3 is involved in the regulation of cell proliferation, migration and invasion through the PI3K-AKT-ERK pathway and destabilizes telomeres through the NFκB-RAP1-TRF2 axis (18, 23, 24, 49). Moreover, PTP4A3 contributes to the secretion of inflammatory factors, which recruit more immune cells to the tumor microenvironment. Activation of PTP4A3 expression increases IL-1 alpha secretion through the NF-κB and

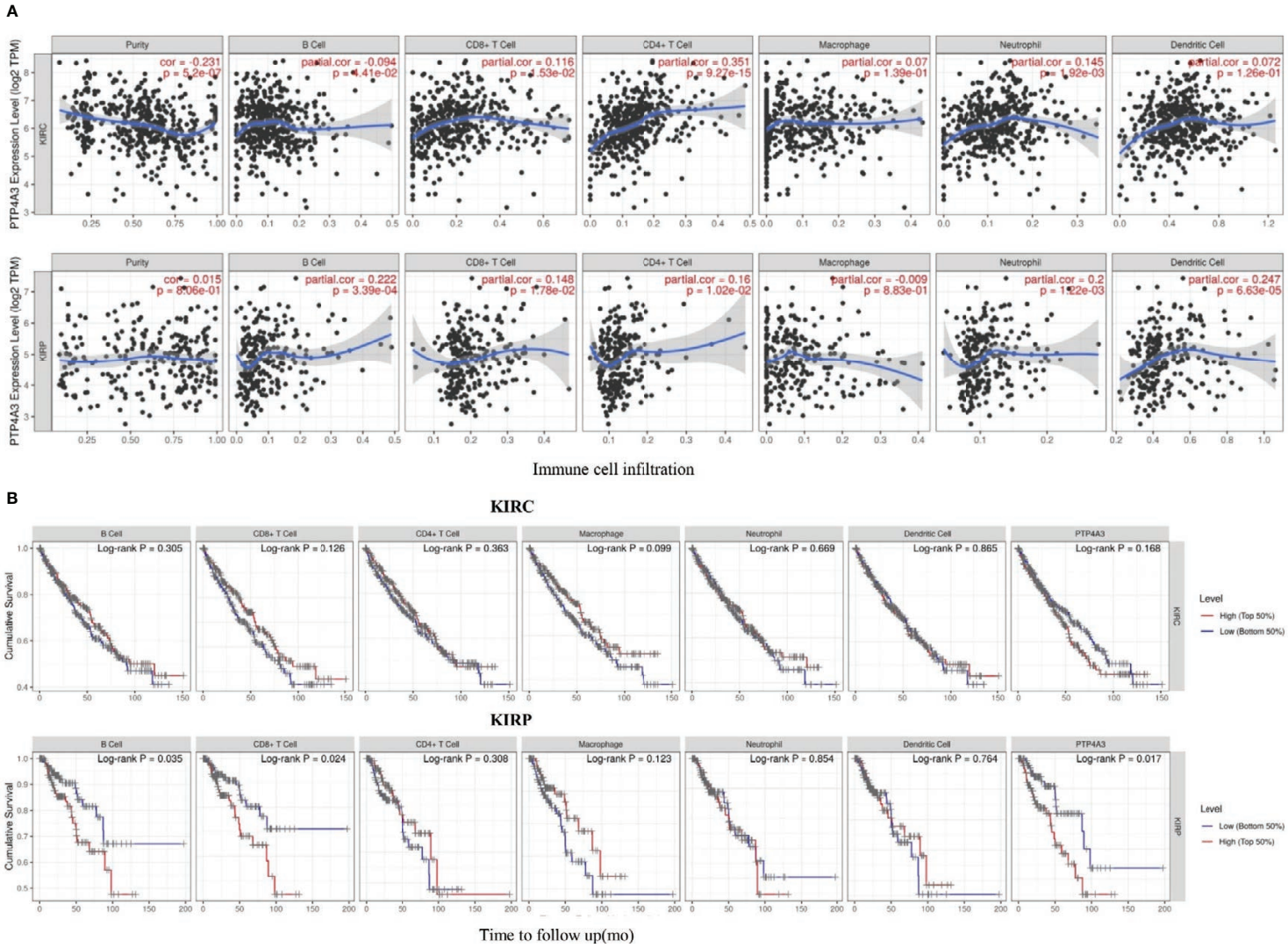

FIGURE 5 | PTP4A3 expression level is correlated with immune cell infiltration in KIRC and KIRP. **(A)** PTP4A3 expression is correlated with immune cell infiltration in KIRC and KIRP. **(B)** Kaplan-Meier plots of immune cell infiltration and PTP4A3 expression levels in KIRC and KIRP.

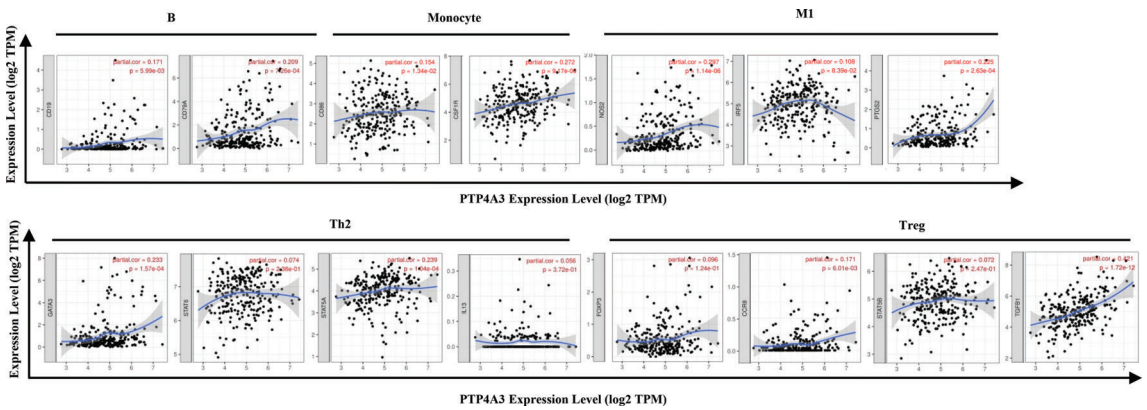

FIGURE 6 | Correlation of PTP4A3 expression levels with gene markers of immune cells in KIRP from the TIMER database. Scatterplots of relationships between PTP4A3 expression levels and gene markers of B, monocytes, M1, Th2 and Treg cells in KIRP.

TABLE 3 | Correlations between PTP4A3 expression and related gene markers in the GEPIA database.

Description	Gene markers	KIRP			
		Tumor		Normal	
		R	*P*	R	*P*
B cell	CD19	-0.039	5.10E-01	0.130	4.90E-01
	CD79A	0.210	***	0.110	5.50E-01
Monocyte	CD86	0.042	4.80E-01	0.150	4.00E-01
	CD115(CSF1R)	0.190	**	0.110	5.60E-01
M1 Macrophage	INOS(NOS2)	0.250	***	-0.390	*
	IRF5	0.047	4.30E-01	0.190	3.00E-01
	COX2(PTGS2)	0.300	***	-0.093	6.10E-01
Th2	GATA3	0.110	5.30E-02	0.410	*
	STAT6	-0.012	8.50E-01	0.430	*
	STAT5A	0.160	**	0.030	8.70E-01
	IL13	0.014	8.10E-01	0.150	4.10E-01
Treg	FOXP3	0.190	**	0.330	6.30E-02
	CCR8	0.190	**	0.220	2.20E-01
	STAT5B	-0.034	5.70E-01	-0.100	5.80E-01
	TGFβ(TGFB1)	0.370	***	0.400	*

**P < 0.05, **P < 0.01, ***P < 0.001.*
KIRP, papillary renal cell cancer.

JAK2-STAT pathway (22). On the other hand, IL-6/8 secreted by TAMs facilitated the metastasis of colon cancer in a PTP4A3-$KCNN_4$ dependent manner (30). Research with target monoclonal antibodies and DNA vaccines has indicated that PTP4A3 may collaborate with CTL and Th1 cells in the tumor microenvironment. PTP4A3-zumab recruited B cells, NK cells and macrophages to the PTP4A3+ tumor cells in an FcR-dependent manner (27, 50). Therefore, PTP4A3 could be a potential target for cancer immunotherapy. Clinical trials have shown that immunotherapy in renal cell carcinoma is superior to tyrosine kinase inhibitors, heralding a new era of renal cancer treatment.

As there is no study showing PTP4A3 expression and its potential roles in renal cancer, further experiments were conducted to evaluate whether PTP4A3 play as an oncogene in RCC. In our validation cohort, PTP4A3 expression is significantly elevated in the tumor tissues by the immunohistochemical staining of PTP4A3 in 49 kidney cancers and 6 normal tissues. As for the functional study, ectopic expression of PTP4A3 promotes proliferation, migration and invasion in RCC cell lines. Taken collectively, the above findings firstly suggested that PTP4A3 serve as an oncogene in renal cancer. The metastasis phenotype could be partially inhibited by IL-1alpha inhibitors, and MMP11 and FOXN3 were elevated in the PTP4A3 overexpressing colon cells (22). These immune related cytokines may connect the oncogene PTP4A3 with the immune infiltration. We also tried to verify the correlation of PTP4A3 and IL-1 alpha in RCC cells, but the mRNA level of IL-1 alpha showed different changes in 786-O and Caki-2 cell. Considering the possible inconsistent of mRNA level and secretion level in supernatant, the cytokines in supernatant should be detected by the ELISA to further confirm the correlations. Luckily, we found that PTP4A3 upregulated the mRNA of TGFB1 in both 786-O and Caki-2 cells. TGFB1 expressed on the Treg cell surface and maintain the immune hemostasis. The correlation of PTP4A3 and TGFB1 were also been confirmed in **Table 3** by the TIMER database (R=0.370, p<0.001). Therefore, it indicated that PTP4A3 may also regulate the immune microenvironment through cytokines TGFB1 in RCC.

In this study, we focused on the association between PTP4A3 and cytotoxic T cells, which have not been jointly reported. CD3+, CD8+ T cells represent T cells, cytotoxic T cells. Our explorations examined the immune infiltrates' density and the location of immune cell populations in intratumor and invasion margins. In KIRC, we observed negative association between PTP4A3 expression and the density of CD3+ TILs intratumor and CD8+ TILs intratumor in the tumor microenvironment. There was no significant relationship between PTP4A3 expression and the number of CD3+ TILs invasion margins and CD8+ TILs invasion margins. However, we did not assess whether the combination of PTP4A3 and CD3+ and CD8+

T cells have independent prognostic significance in renal cancer. Previous studies reported that high density of CD3+, CD8+ T cells correlated with favorable prognosis in various cancers (51, 52). These findings suggested that immune infiltrates of T cells play a protective role. The role of CD8+ T cells in renal cancer is controversial, maybe attribute to technical factors such as antibodies used to examine CD8+ T cells and different tumor location detected (intratumor vs invasion margins TILs) (52, 53).

In general, the tumor-infiltrating T cells play vital roles in renal cancer, including cytotoxic T cells, memory T cells, regulatory T cells, and so on (54, 55). In the future work, the relationship between PTP4A3 expression and B cells and other T cells including CD4+ T cells, CD45RO+ memory T cells, regulatory T cell need to be explored in renal cancer.

In this study, the role of PTP4A3 in renal cell carcinoma immune microenvironments was explored using online databases, including the Oncomine, TCGA, GEPIA, TIMER and Progscan databases. Consistent with previous findings, PTP4A3 expression was elevated in many tumor types compared with normal tissues, including renal cancer. Kaplan-Meier survival analysis suggested that PTP4A3 expression was correlated with poor DFS but not with OS in KIRC and KIRP. This may be related to the cutoff percentage setting (50% cut-off) and case numbers in the GEPIA database. PTP4A3 expression is higher in gastric cancer than in colon cancer, and the cutoff settings in various cancer types should be adjusted base on the immunohistochemistry of each cancer type. The association of PTP4A3 expression with B cells, CD8+ T cells, CD4+T cells and neutrophil infiltration was confirmed in renal cancer (**Figure 5** and **Supplementary Table 3**) using the GEPIA and TIMER databases. These results were consistent with PRL-3-zumab work from Zeng et al. (50). PTP4A3 is an oncogene related to immune cell infiltration in KIRC and KIRP.

Tumorigenesis and tumor development are complicated processes involving thousands of genes and pathways. Because of this, signal gene signatures are rarely used to predict tumor prognosis. Due to the association of PTP4A3 expression with immune cell infiltration, the relationship of immune markers and PTP4A3 expression was analyzed using the TIMER database to identify gene profile signatures that may be able to predict prognosis and immunotherapy response in KIRP. Correlations were observed between PTP4A3 expression and M1 macrophage immune markers such as INOS and COX2 in both KIRP and KIRC (**Supplementary Table 3** and **Table 3**), suggesting that PTP4A3 may regulate the polarization of M1 macrophages in renal cancer. A positive correlation was observed between PTP4A3 expression and B cell immune marker (CD79A) in KIRP only (**Supplementary Table 3** and **Table 3**), and this result was confirmed with the TIMER database. Dendritic cells can play a vital role in tumor growth and metastasis by inhibiting CD8+ T cell cytotoxicity and promoting Treg cells (56). PTP4A3 expression was correlated with HLA-DRA, BDCA-1, and BDCA-4 in dendritic cells, and with CCR8 and TGFB1 in Treg cells, indicating that PTP4A3 promoted tumor growth and metastasis through the classical PI3K-AKT-PTEN signal pathway and also by regulating the tumor immune microenvironment (18–20). Interestingly, exhausted T cell markers such as PD1, LAG3 and GZMB were also significantly correlated with PTP4A3 expression in KIRP (**Supplementary Table 3**). PD1 is the immune checkpoint receptor expressed on the activated T cells; blocking the PD1/PD-L1 interaction would release immune suppression and trigger immune clearance in tumors. This study is the first reported association of PTP4A3 and PD1 in renal cancer. The combination of PTP4A3 with immune cells is proposed as a predictor for immunotherapy response and prognosis in renal cancers, with potential applications in other cancer types such as NSCLC or gastric cancer as well (57, 58). These findings further confirm the relationship of PTP4A3 expression to immune infiltration in KIRP, suggesting that PTP4A3 influences immune escape in the renal cancer microenvironment. We are confidence in our results base on the various online datasets, therefore we are working on the collection of renal cancer samples and focusing on the immune-related role of PTP4A3 in renal cancer.

In conclusion, PTP4A3 may be a regulator in the tumor immune microenvironment and a useful biomarker for predicting prognosis and immunotherapy response in renal cancer. These results will be verified in our further workings.

DATA AVAILABILITY STATEMENT

The original contributions presented in the study are included in the article/**Supplementary Material**. Further inquiries can be directed to the corresponding authors.

ETHICS STATEMENT

The studies involving human participants were reviewed and approved by the Ethics Committee of Peking University Cancer Hospital & Institute (Beijing, China). The patients/participants provided their written informed consent to participate in this study. Written informed consent was obtained from the individual(s) for the publication of any potentially identifiable images or data included in this article.

AUTHOR CONTRIBUTIONS

QS, ZL, and SL conceived the project and wrote the manuscript. JW and SW managed data acquisition. QF, JW, and SW participated in the data analysis. QS and SL participated in the discussion and language editing. ZL reviewed the manuscript. YZ did the IHC, cell proliferation migration, and invasion experiments during the revised of the manuscript. LZ and QY counted the CD3+ and CD8+ TILs. All authors contributed to the article and approved the submitted version.

FUNDING

This research was supported by Natural Science Foundation of China [grant number 81872309], Beijing Hospitals

Authority Youth Programme [grant number QML20191109], Zhejiang Provincial Natural Science Foundation of China [grant number LQ21H200001] and General Research Program of Health Department of Zhejiang Province [grant number 2020KY480].

SUPPLEMENTARY MATERIAL

The Supplementary Material for this article can be found online at: https://www.frontiersin.org/articles/10.3389/fimmu.2021.717688/full#supplementary-material

REFERENCES

1. Siegel RL, Miller KD, Fuchs HE, Jemal A. Cancer Statistics, 2021. *CA: Cancer J Clin* (2021) 71:7–33. doi: 10.3322/caac.21654
2. Ricketts CJ, DeCubas AA, Fan H, Smith CC, Lang M, Reznik E, et al. The Cancer Genome Atlas Comprehensive Molecular Characterization of Renal Cell Carcinoma. *Cell Rep* (2018) 23:313–26.e5. doi: 10.1016/j.celrep.2018.03.075
3. Durinck S, Stawiski EW, Pavía-Jiménez A, Modrusan Z, Kapur P, Jaiswal BS, et al. Spectrum of Diverse Genomic Alterations Define Non-Clear Cell Renal Carcinoma Subtypes. *Nat Genet* (2015) 47:13–21. doi: 10.1038/ng.3146
4. Linehan WM, Ricketts CJ. The Cancer Genome Atlas of Renal Cell Carcinoma: Findings and Clinical Implications. *Nat Rev Urol* (2019) 16:539–52. doi: 10.1038/s41585-019-0211-5
5. Gupta K, Miller JD, Li JZ, Russell MW, Charbonneau C. Epidemiologic and Socioeconomic Burden of Metastatic Renal Cell Carcinoma (mRCC): A Literature Review. *Cancer Treat Rev* (2008) 34:193–205. doi: 10.1016/j.ctrv.2007.12.001
6. Chen F, Zhang Y, Şenbabaoğlu Y, Ciriello G, Yang L, Reznik E, et al. Multilevel Genomics-Based Taxonomy of Renal Cell Carcinoma. *Cell Rep* (2016) 14:2476–89. doi: 10.1016/j.celrep.2016.02.024
7. Geissler K, Fornara P, Lautenschläger C, Holzhausen HJ, Seliger B, Riemann D. Immune Signature of Tumor Infiltrating Immune Cells in Renal Cancer. *Oncoimmunology* (2015) 4:e985082. doi: 10.4161/2162402x.2014.985082
8. Rios P, Li X, Köhn M. Molecular Mechanisms of the PRL Phosphatases. *FEBS J* (2013) 280:505–24. doi: 10.1111/j.1742-4658.2012.08565.x
9. Xing X, Peng L, Qu L, Ren T, Dong B, Su X, et al. Prognostic Value of PRL-3 Overexpression in Early Stages of Colonic Cancer. *Histopathology* (2009) 54:309–18. doi: 10.1111/j.1365-2559.2009.03226.x
10. den Hollander P, Rawls K, Tsimelzon A, Shepherd J, Mazumdar A, Hill J, et al. Phosphatase PTP4A3 Promotes Triple-Negative Breast Cancer Growth and Predicts Poor Patient Survival. *Cancer Res* (2016) 76:1942–53. doi: 10.1158/0008-5472.Can-14-0673
11. Wang L, Peng L, Dong B, Kong L, Meng L, Yan L, et al. Overexpression of Phosphatase of Regenerating Liver-3 in Breast Cancer: Association With a Poor Clinical Outcome. *Ann Oncol Off J Eur Soc Med Oncol* (2006) 17:1517–22. doi: 10.1093/annonc/mdl159
12. Xing X, Lian S, Hu Y, Li Z, Zhang L, Wen X, et al. Phosphatase of Regenerating Liver-3 (PRL-3) Is Associated With Metastasis and Poor Prognosis in Gastric Carcinoma. *J Trans Med* (2013) 11:309. doi: 10.1186/1479-5876-11-309
13. Pryczynicz A, Guzińska-Ustymowicz K, Chang XJ, Kiśluk J, Kemona A. PTP4A3 (PRL-3) Expression Correlate With Lymphatic Metastases in Gastric Cancer. *Folia Histochem Cytobiol* (2010) 48:632–6. doi: 10.2478/v10042-010-0070-7
14. Dai N, Lu AP, Shou CC, Li JY. Expression of Phosphatase Regenerating Liver 3 Is an Independent Prognostic Indicator for Gastric Cancer. *World J Gastroenterol* (2009) 15:1499–505. doi: 10.3748/wjg.15.1499
15. Ren T, Jiang B, Xing X, Dong B, Peng L, Meng L, et al. Prognostic Significance of Phosphatase of Regenerating Liver-3 Expression in Ovarian Cancer. *Pathol Oncol Res POR* (2009) 15:555–60. doi: 10.1007/s12253-009-9153-1
16. Reich R, Hadar S, Davidson B. Expression and Clinical Role of Protein of Regenerating Liver (PRL) Phosphatases in Ovarian Carcinoma. *Int J Mol Sci* (2011) 12:1133–45. doi: 10.3390/ijms12021133
17. Qu S, Liu B, Guo X, Shi H, Zhou M, Li L, et al. Independent Oncogenic and Therapeutic Significance of Phosphatase PRL-3 in FLT3-ITD-Negative Acute Myeloid Leukemia. *Cancer* (2014) 120:2130–41. doi: 10.1002/cncr.28668
18. Wang H, Quah SY, Dong JM, Manser E, Tang JP, Zeng Q. PRL-3 Down-Regulates PTEN Expression and Signals Through PI3K to Promote Epithelial-Mesenchymal Transition. *Cancer Res* (2007) 67:2922–6. doi: 10.1158/0008-5472.Can-06-3598
19. Liang F, Luo Y, Dong Y, Walls CD, Liang J, Jiang HY, et al. Translational Control of C-Terminal Src Kinase (Csk) Expression by PRL3 Phosphatase. *J Biol Chem* (2008) 283:10339–46. doi: 10.1074/jbc.M708285200
20. Lai W, Liu L, Zeng Y, Wu H, Xu H, Chen S, et al. KCNN4 Channels Participate in the EMT Induced by PRL-3 in Colorectal Cancer. *Med Oncol (Northwood London England)* (2013) 30:566. doi: 10.1007/s12032-013-0566-z
21. Zhang C, Qu L, Lian S, Meng L, Min L, Liu J, et al. PRL-3 Promotes Ubiquitination and Degradation of AURKA and Colorectal Cancer Progression *via* Dephosphorylation of FZR1. *Cancer Res* (2019) 79:928–40. doi: 10.1158/0008-5472.Can-18-0520
22. Yang Y, Lian S, Meng L, Qu L, Shou C. Antibody Array Revealed PRL-3 Affects Protein Phosphorylation and Cytokine Secretion. *PloS One* (2017) 12:e0169665. doi: 10.1371/journal.pone.0169665
23. Lian S, Meng L, Liu C, Xing X, Song Q, Dong B, et al. PRL-3 Activates NF-κb Signaling Pathway by Interacting With RAP1. *Biochem Biophys Res Commun* (2013) 430:196–201. doi: 10.1016/j.bbrc.2012.11.036
24. Lian S, Meng L, Yang Y, Ma T, Xing X, Feng Q, et al. PRL-3 Promotes Telomere Deprotection and Chromosomal Instability. *Nucleic Acids Res* (2017) 45:6546–71. doi: 10.1093/nar/gkx392
25. Zimmerman MW, Homanics GE, Lazo JS. Targeted Deletion of the Metastasis-Associated Phosphatase Ptp4a3 (PRL-3) Suppresses Murine Colon Cancer. *PloS One* (2013) 8:e58300. doi: 10.1371/journal.pone.0058300
26. Johansson JA, Marie KL, Lu Y, Brombin A, Santoriello C, Zeng Z, et al. PRL3-DDX21 Transcriptional Control of Endolysosomal Genes Restricts Melanocyte Stem Cell Differentiation. *Dev Cell* (2020) 54:317–32.e9. doi: 10.1016/j.devcel.2020.06.013
27. Thura M, Al-Aidaroos AQO, Yong WP, Kono K, Gupta A, Lin YB, et al. PRL3-Zumab, a First-in-Class Humanized Antibody for Cancer Therapy. *JCI Insight* (2016) 1:e87607. doi: 10.1172/jci.insight.87607
28. Guo K, Tang JP, Jie L, Al-Aidaroos AQ, Hong CW, Tan CP, et al. Engineering the First Chimeric Antibody in Targeting Intracellular PRL-3 Oncoprotein for Cancer Therapy in Mice. *Oncotarget* (2012) 3:158–71. doi: 10.18632/oncotarget.442
29. Lv J, Liu C, Huang H, Meng L, Jiang B, Cao Y, et al. Suppression of Breast Tumor Growth by DNA Vaccination Against Phosphatase of Regenerating Liver 3. *Gene Ther* (2013) 20:834–45. doi: 10.1038/gt.2013.5
30. Xu H, Lai W, Zhang Y, Liu L, Luo X, Zeng Y, et al. Tumor-Associated Macrophage-Derived IL-6 and IL-8 Enhance Invasive Activity of LoVo Cells Induced by PRL-3 in a KCNN4 Channel-Dependent Manner. *BMC Cancer* (2014) 14:330. doi: 10.1186/1471-2407-14-330
31. Li B, Severson E, Pignon JC, Zhao H, Li T, Novak J, et al. Comprehensive Analyses of Tumor Immunity: Implications for Cancer Immunotherapy. *Genome Biol* (2016) 17:174. doi: 10.1186/s13059-016-1028-7
32. Li T, Fan J, Wang B, Traugh N, Chen Q, Liu JS, et al. TIMER: A Web Server for Comprehensive Analysis of Tumor-Infiltrating Immune Cells. *Cancer Res* (2017) 77:e108–10. doi: 10.1158/0008-5472.Can-17-0307
33. Rhodes DR, Kalyana-Sundaram S, Mahavisno V, Varambally R, Yu J, Briggs BB, et al. Oncomine 3.0: Genes, Pathways, and Networks in a Collection of 18,000cancer Gene Expression Profiles. *Neoplasia* (2007) 9:166–80. doi: 10.1593/neo.07112
34. Mizuno H, Kitada K, Nakai K, Sarai A. PrognoScan: A New Database for Meta-Analysis of the Prognostic Value of Genes. *BMC Med Genomics* (2009) 2:18. doi: 10.1186/1755-8794-2-18
35. Siemers NO, Holloway JL, Chang H, Chasalow SD, Ross-MacDonald PB, Voliva CF, et al. Genome-Wide Association Analysis Identifies Genetic Correlates of Immune Infiltrates in Solid Tumors. *PloS One* (2017) 12:e0179726. doi: 10.1371/journal.pone.0179726
36. Danaher P, Warren S, Dennis L, D'Amico L, White A, Disis ML, et al. Gene Expression Markers of Tumor Infiltrating Leukocytes. *J Immunother Cancer* (2017) 5:18. doi: 10.1186/s40425-017-0215-8

37. Sousa S, Maatta J. The Role of Tumour-Associated Macrophages in Bone Metastasis. *J Bone Oncol* (2016) 5:135–8. doi: 10.1016/j.jbo.2016.03.004
38. Tang Z, Li C, Kang B, Gao G, Li C, Zhang Z. GEPIA: A Web Server for Cancer and Normal Gene Expression Profiling and Interactive Analyses. *Nucleic Acids Res* (2017) 45:W98–102. doi: 10.1093/nar/gkx247
39. Curry JM, Johnson J, Mollaee M, Tassone P, Amin D, Knops A, et al. Metformin Clinical Trial in HPV+ and HPV- Head and Neck Squamous Cell Carcinoma: Impact on Cancer Cell Apoptosis and Immune Infiltrate. *Front Oncol* (2018) 8:436. doi: 10.3389/fonc.2018.00436
40. Cillo AR, Kürten CHL, Tabib T, Qi Z, Onkar S, Wang T, et al. Immune Landscape of Viral- and Carcinogen-Driven Head and Neck Cancer. *Immunity* (2020) 52:183–99.e9. doi: 10.1016/j.immuni.2019.11.014
41. Ruiz-Cordero R, Devine WP. Targeted Therapy and Checkpoint Immunotherapy in Lung Cancer. *Surg Pathol Clinics* (2020) 13:17–33. doi: 10.1016/j.path.2019.11.002
42. Shroff GS, deGroot PM, Papadimitrakopoulou VA, Truong MT, Carter BW. Targeted Therapy and Immunotherapy in the Treatment of Non-Small Cell Lung Cancer. *Radiol Clinics N Am* (2018) 56:485–95. doi: 10.1016/j.rcl.2018.01.012
43. Xie J, Fu L, Jin L. Immunotherapy of Gastric Cancer: Past, Future Perspective and Challenges. *Pathol Res Pract* (2021) 218:153322. doi: 10.1016/j.prp.2020.153322
44. Ohtani H. Focus on TILs: Prognostic Significance of Tumor Infiltrating Lymphocytes in Human Colorectal Cancer. *Cancer Immun* (2007) 7:4.
45. Azimi F, Scolyer RA, Rumcheva P, Moncrieff M, Murali R, McCarthy SW, et al. Tumor-Infiltrating Lymphocyte Grade Is an Independent Predictor of Sentinel Lymph Node Status and Survival in Patients With Cutaneous Melanoma. *J Clin Oncol Off J Am Soc Clin Oncol* (2012) 30:2678–83. doi: 10.1200/JCO.2011.37.8539
46. Tian W, Qu L, Meng L, Liu C, Wu J, Shou C. Phosphatase of Regenerating Liver-3 Directly Interacts With Integrin β1 and Regulates Its Phosphorylation at Tyrosine 783. *BMC Biochem* (2012) 13:22. doi: 10.1186/1471-2091-13-22
47. Forte E, Orsatti L, Talamo F, Barbato G, DeFrancesco R, Tomei L. Ezrin Is a Specific and Direct Target of Protein Tyrosine Phosphatase PRL-3. *Biochim Biophys Acta* (2008) 1783:334–44. doi: 10.1016/j.bbamcr.2007.11.004
48. Mizuuchi E, Semba S, Kodama Y, Yokozaki H. Down-Modulation of Keratin 8 Phosphorylation Levels by PRL-3 Contributes to Colorectal Carcinoma Progression. *Int J Cancer* (2009) 124:1802–10. doi: 10.1002/ijc.24111
49. Pu Y, Sun F, Sun R, Man Z, Ji S, Xu K, et al. PTP4A3, A Novel Target Gene of HIF-1alpha, Participates in Benzene-Induced Cell Proliferation Inhibition and Apoptosis Through PI3K/AKT Pathway. *Int J Environ Res Public Health* (2020) 17:910–23. doi: 10.3390/ijerph17030910
50. Thura M, Al-Aidaroos AQ, Gupta A, Chee CE, Lee SC, Hui KM, et al. PRL3-Zumab as an Immunotherapy to Inhibit Tumors Expressing PRL3 Oncoprotein. *Nat Commun* (2019) 10:2484. doi: 10.1038/s41467-019-10127-x
51. Gooden MJ, deBock GH, Leffers N, Daemen T, Nijman HW. The Prognostic Influence of Tumour-Infiltrating Lymphocytes in Cancer: A Systematic Review With Meta-Analysis. *Br J Cancer* (2011) 105:93–103. doi: 10.1038/bjc.2011.189
52. Giraldo NA, Becht E, Pages F, Skliris G, Verkarre V, Vano Y, et al. Orchestration and Prognostic Significance of Immune Checkpoints in the Microenvironment of Primary and Metastatic Renal Cell Cancer. *Clin Cancer Res An Off J Am Assoc Cancer Res* (2015) 21:3031–40. doi: 10.1158/1078-0432.CCR-14-2926
53. Bersanelli M, Gnetti L, Vaglio A, Sverzellati N, Campanini N, Incerti M, et al. Correlations Between Tumor-Infiltrating and Circulating Lymphocyte Subpopulations in Advanced Renal Cancer Patients Treated With Nivolumab. *Acta Bio-med Atenei Parmensis* (2019) 90:468–74. doi: 10.23750/abm.v90i4.7057
54. Qi Y, Xia Y, Lin Z, Qu Y, Qi Y, Chen Y, et al. Tumor-Infiltrating CD39(+)CD8(+) T Cells Determine Poor Prognosis and Immune Evasion in Clear Cell Renal Cell Carcinoma Patients. *Cancer Immunol Immunother CII* (2020) 69:1565–76. doi: 10.1007/s00262-020-02563-2
55. Ghatalia P, Gordetsky J, Kuo F, Dulaimi E, Cai KQ, Devarajan K, et al. Prognostic Impact of Immune Gene Expression Signature and Tumor Infiltrating Immune Cells in Localized Clear Cell Renal Cell Carcinoma. *J Immunother Cancer* (2019) 7:139. doi: 10.1186/s40425-019-0621-1
56. Sawant A, Hensel JA, Chanda D, Harris BA, Siegal GP, Maheshwari A, et al. Depletion of Plasmacytoid Dendritic Cells Inhibits Tumor Growth and Prevents Bone Metastasis of Breast Cancer Cells. *J Immunol* (2012) 189:4258–65. doi: 10.4049/jimmunol.1101855
57. Sengal A, Velazquez J, Hahne M, Burke TM, Abhyankar H, Reyes R, et al. Overcoming T-Cell Exhaustion in LCH: PD-1 Blockade and Targeted MAPK Inhibition Are Synergistic in a Mouse Model of LCH. *Blood* (2021) 137:1777–91. doi: 10.1182/blood.2020005867
58. Niu B, Zhou F, Su Y, Wang L, Xu Y, Yi Z, et al. Different Expression Characteristics of LAG3 and PD-1 in Sepsis and Their Synergistic Effect on T Cell Exhaustion: A New Strategy for Immune Checkpoint Blockade. *Front Immunol* (2019) 10:1888. doi: 10.3389/fimmu.2019.01888

Conflict of Interest: The authors declare that the research was conducted in the absence of any commercial or financial relationships that could be construed as a potential conflict of interest.

Publisher's Note: All claims expressed in this article are solely those of the authors and do not necessarily represent those of their affiliated organizations, or those of the publisher, the editors and the reviewers. Any product that may be evaluated in this article, or claim that may be made by its manufacturer, is not guaranteed or endorsed by the publisher.

Copyright © 2021 Song, Zheng, Wu, Wang, Meng, Yao, Li and Lian. This is an open-access article distributed under the terms of the Creative Commons Attribution License (CC BY). The use, distribution or reproduction in other forums is permitted, provided the original author(s) and the copyright owner(s) are credited and that the original publication in this journal is cited, in accordance with accepted academic practice. No use, distribution or reproduction is permitted which does not comply with these terms.

frontiers in Immunology

ORIGINAL RESEARCH
published: 04 October 2021
doi: 10.3389/fimmu.2021.751530

From Cellular Infiltration Assessment to a Functional Gene Set-Based Prognostic Model for Breast Cancer

Huamei Li[1†], Yiting Huang[1†], Amit Sharma[2,3†], Wenglong Ming[1], Kun Luo[4], Zhongze Gu[1], Xiao Sun[1] and Hongde Liu[1*]*

[1] State Key Laboratory of Bioelectronics, School of Biological Science & Medical Engineering, Southeast University, Nanjing, China, [2] Department of Neurosurgery, Center for Integrated Oncology (CIO), University Hospital Bonn, Bonn, Germany, [3] Department of Integrated Oncology, Center for Integrated Oncology (CIO), University Hospital Bonn, Bonn, Germany, [4] Department of Neurosurgery, Xinjiang Evidence-Based Medicine Research Institute, First Affiliated Hospital of Xinjiang Medical University, Urumqi, China

OPEN ACCESS

Edited by:
Peng Qu,
National Institutes of Health (NIH), United States

Reviewed by:
Shang-Qian Xie,
Hainan University, China
Meng Xu,
Carnegie Mellon University, United States

***Correspondence:**
Xiao Sun
xsun@seu.edu.cn
Hongde Liu
liuhongde@seu.edu.cn

[†]These authors have contributed equally to this work

Specialty section:
This article was submitted to Cancer Immunity and Immunotherapy, a section of the journal Frontiers in Immunology

Received: *01 August 2021*
Accepted: *15 September 2021*
Published: *04 October 2021*

Citation:
Li H, Huang Y, Sharma A, Ming W, Luo K, Gu Z, Sun X and Liu H (2021) From Cellular Infiltration Assessment to a Functional Gene Set-Based Prognostic Model for Breast Cancer. Front. Immunol. 12:751530. doi: 10.3389/fimmu.2021.751530

Background: Cancer heterogeneity is a major challenge in clinical practice, and to some extent, the varying combinations of different cell types and their cross-talk with tumor cells that modulate the tumor microenvironment (TME) are thought to be responsible. Despite recent methodological advances in cancer, a reliable and robust model that could effectively investigate heterogeneity with direct prognostic/diagnostic clinical application remained elusive.

Results: To investigate cancer heterogeneity, we took advantage of single-cell transcriptome data and constructed the first indication- and cell type-specific reference gene expression profile (RGEP) for breast cancer (BC) that can accurately predict the cellular infiltration. By utilizing the BC-specific RGEP combined with a proven deconvolution model (LinDeconSeq), we were able to determine the intrinsic gene expression of 15 cell types in BC tissues. Besides identifying significant differences in cellular proportions between molecular subtypes, we also evaluated the varying degree of immune cell infiltration (basal-like subtype: highest; Her2 subtype: lowest) across all available TCGA-BRCA cohorts. By converting the cellular proportions into functional gene sets, we further developed a 24 functional gene set-based prognostic model that can effectively discriminate the overall survival ($P = 5.9 \times 10^{-33}$, $n = 1091$, TCGA-BRCA cohort) and therapeutic response (chemotherapy and immunotherapy) ($P = 6.5 \times 10^{-3}$, $n = 348$, IMvigor210 cohort) in the tumor patients.

Conclusions: Herein, we have developed a highly reliable BC-RGEP that adequately annotates different cell types and estimates the cellular infiltration. Of importance, the functional gene set-based prognostic model that we have introduced here showed a great ability to screen patients based on their therapeutic response. On a broader perspective, we provide a perspective to generate similar models in other cancer types to identify shared factors that drives cancer heterogeneity.

Keywords: breast cancer, specific gene expression profile, cellular infiltration, prognosis, risk score, immunotherapy, cancer heterogeneity

1 INTRODUCTION

Cancer biology has now reached a point where it is well understood that cancer cells interact with their microenvironment, which ultimately determines whether it will respond to treatment, develop resistance, recur or metastasize. Therefore, it is a must to recapitulate the prevailing information on various cancer models to draw some stringent conclusions connecting the common/shared factors involved in the tumor microenvironment (TME). Considering this, herein, we focused on breast cancer (BC), which is the most common invasive disease and the leading cause of cancer death in women worldwide (1). Despite the partial success of conventional therapies (surgery, chemotherapy, radiotherapy, and targeted therapy) and other ongoing *therapeutic* advances (immunotherapy), it remains a concern why some patients eventually develop metastases and others respond poorly to treatment. Currently, the assessment of the prognostic and predictive significance of tumor-infiltrating lymphocytes (TILs) in BC is gaining quite a momentum (2, 3). Since TILs comprise a heterogeneous population of cells with different physiological/pathological effects in the tumor microenvironment (TME), therefore, new emerging technologies (e.g., single-cell RNA sequencing: scRNA-seq) have gained an advantage in resolving their functional interpretation in BC (4).

While the accuracy of predicting the cellular composition is an imperative factor to understand the heterogeneity associated with TME (5–7), the defined analysis of bulk datasets using a robust deconvolution strategy is also an considerably important parameter (5, 6, 8–11). To some extent, reference gene expression profiling (RGEP) has proven to be successful in this context, as evident from studies using RGEP either by, 1) directly using scRNA-seq data, such as the head and neck squamous cell carcinoma RGEP (called HNSCC-RGEP hereafter), or 2) using sorted bulk gene expression datasets, such as LM22 (9), ImmunoStates (12) and ABIS (13). Given that the reliability of RGEPs depends on disease-specific gene expression patterns, disease status/stage, and diversity within the tissue cell population, it is necessary to consider multiple parameters ranging from direct health/disease status to complex indicators (tissue- and disease-specific) (12, 14, 15). Interestingly in BC, a few studies have provided prognostic models based primarily on the cellular proportions (16, 17). However, when applying non-specific RGEPs to predict the cellular compositions of patients, the technical bias can be expected, therefore, the reliability of the prognostic models will come under concern. Of interest, one study suggested that the pathway-based prognostic models performed systematically better than gene-based models and proposed that by including the clinical information, the prognostic prediction of such models can be further enhanced (18).

Considering all these facts, herein, we aimed to establish BC-specific RGEP by using scRNA-seq datasets, as an initial perspective that can be used in the future to generate similar models in other cancer types to identify common factors driving cancer heterogeneity. Our work primarily focused on previously reported 15 cell types (including fibroblasts, malignant cells, and 13 immune cell types) of BC patients (19), combined with our recently published deconvolution method (LinDeconSeq) (8) and comprehensive comparisons with the preexisting RGEPs. As an extended application, we also developed 24 functional gene sets (biological processes and signaling pathways) to correlate infiltration of prognosis-related cell types, in order to obtain a robust prognostic value (risk groups, therapeutic regimens) from BC cohorts.

2 MATERIALS AND METHODS

2.1 Datasets

The BC-related datasets used in this study were retrieved from the Gene Expression Omnibus (GEO) (accession numbers: GSE114725, GSE75688, GSE5462, GSE18728, GSE41998, GSE37946, GSE25066). Similarly, the gene expression and phenotype data (an open access level 3 gene expression matrix data) of TCGA-BRCA and other 32 cancer types were obtained from The Cancer Genome Atlas Project (TCGA). Additionally, three BC datasets (Caldas, Chin, and Yao), along with their phenotype details were retrieved from the GDC Xena Hub (https://xenabrowser.net/datapages/). The Molecular Taxonomy of Breast Cancer International Consortium (METABRIC) datasets were accessed from the European Genome-Phenome Archive (EGA) using accession number EGAS00000000083. Other gene expression datasets such as NKI, Mainz, Transbig, UNT, and UPP were obtained from the R Bioconductor packages, *breastCancerNKI*, *breastCancerMAINZ*, *breastCancerTRANSBIG*, *breastCancerUNT* and *breastCancerUPP*, respectively. The scRNA-seq datasets of BC (Bassez et al.) that received anti-PD-1 were retrieved upon request from the website https://lambrechtslab.sites.vib.be/en/single-cell (20). In the absence of any published datasets of BC patients receiving immunotherapy, we utilized a urothelial cancer dataset that received anti-PD-L1 therapy (IMvigor210), and was downloaded from the R package *IMvigor210CoreBiologies* (version 1.0.0) (21). The details about all these datasets were given in **Supplementary Table S1**. To mention, all these samples were not pre-screened, but only tumor (normal samples were excluded) samples were included in the prognostic analysis. In addition, our newly establish BC-specific RGEP was compared with the external RGEPs including LM22 (9), Yu et al.'s (HNSCC-RGEP) (14), ABIS (13), immunoStates (12), which were obtained from the attachments or links given in these articles.

2.2 Methods

2.2.1 Normalization of Bulk Gene Expression Data for BC Cohorts

Particularly for microarray datasets (from NCBI-GEO), both background correction and quantile normalization were performed using the Robust Multiarray Averaging (RMA) method (22). In case of bulk RNA-Seq and scRNA-Seq datasets, the gene expression profiles were normalized as counts per million (CPM) quantifications and were then subjected to natural-log transformation.

2.2.2 Construction of BC-Specific RGEP

BC-specific RGEP is tissue and disease-specific reference matrix derived from breast tumor scRNA-seq data, where the rows represent genes and columns are cell types. It should be mentioned that each entry represents the average expression of the gene within that cell type. The details on the construction of the BC-specific RGEP have been provided below.

2.2.2.1 Pre-Processing and Clustering of BC scRNA-Seq Data

Raw UMI count matrix data of scRNA-seq obtained from eight BC patients (GEO ID, GSE114725) (19) and was analyzed using Seurat (version 4.0.1) (23). The cells with <200 or >3,000 expressed genes and those with <500 or >10,000 UMIs were discarded (**Supplementary Figure 1A**, 22,970 cells were retained). The raw UMI counts were then log-normalized with a scale of 10,000, and highly variable genes were identified using the *vst* method. In order to eliminate batch effects across samples and biological effects among normal and tumor states, the first 30 principal components tool was extracted using the integration tool Harmony (24). Cells were then clustered using the *FindCluster* function and *resolution* = 0.5. We found that both clusters 11 and 17 had highly outlier distributions of expressed genes and UMI counts and filtered out (**Supplementary Figure 2B**). Following these processing steps, there remained 12,132 cells clustered into 17 groups for the cell type annotations. We manually annotated the cell types by comparing the canonical markers with the differential expression genes identified by the *FindAllMarkers* method with *logfc.threshold* = 0.5 and *min.pct* = 0.1 (**Figure 1B** and **Supplementary Table S2**).

2.2.2.2 Selection of Cell Type-Specific Genes (Also Called Signature Genes)

An accurate deconvolution requires the selection of cell type-specific genes (i.e. the signature genes) whose expression levels must be informative enough to distinguish the cell types throughout the sample (12, 15). Hence, we combined four gene sets [750 DEGs identified by the *FindAllMarkers* (Seurat, version 4.0. 1) method at *logfc. threshold* = 0.5 and *min.pct* = 0.1 (23), 547 genes identified from LM22 (9), 317 genes from immunoStates (12), 635 genes from the Tirosh I et al. study (26)] to construct a reliable BC-specific RGEP. Following removal of duplicates, 1506 unique genes were used as signature genes for the BC-specific RGEP.

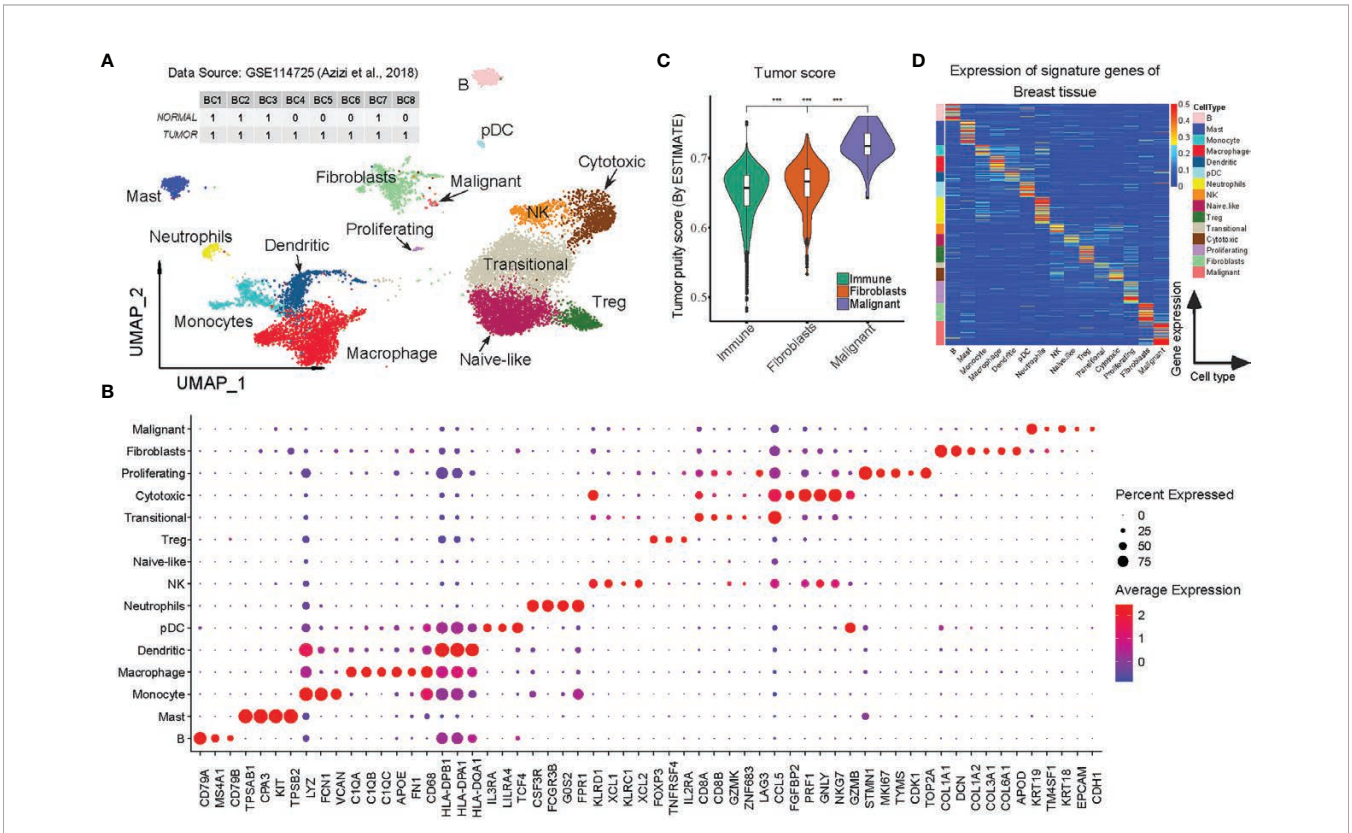

FIGURE 1 | Construction of BC-specific RGEP for cell type deconvolution using scRNA-seq data. **(A)** Two-dimensional UMAP plot of 12132 single cells from 8 breast cancer patients. Each point represents one single cell, colored according to cell cluster. **(B)** Dot-plot showed the expression of the selected DEGs in each cell cluster. **(C)** Tumor score was inferred from the stromal and immune signature using ESTIMATE algorithm (25). Each box shows the median and interquartile range (IQR 25th–75th percentiles), whiskers indicate the highest and lowest value within 1.5 times the IQR and outliers are marked as dots. *P*-value, Student's *t*-test (***$p < 0.001$). **(D)** The expression of the signature matrix of breast tissue, the expression was row-normalized (normalize each expression value by the sum over the row) across cell types. The upper bound of the color bar is 1.

2.2.3 Construction of Simulated and Realistic "Bulk" Gene Expression Data

The simulated bulk gene expression samples were generated from a random proportion of 15 cell types (provided in BC-specific RGEP) using the Dirichlet distribution, followed by replaced sampling from the GSE114725 (19) scRNA-seq dataset based on the random proportions. This resulted in a total of 100 samples, with each sample containing 10,000 cells. To validate the BC-specific RGEP, two scRNA-seq datasets (Bassez et al., and GSE75688) (20, 27), where the cellular proportions for each patient sample were known in advance, were used as realistic bulk gene expression data (by aggregating reads from all cell barcodes for each patient sample).

2.2.4 Deconvolution and Estimation Quality Assessment

To evaluate the performance of BC-specific RGEP, we used LinDeconSeq, a deconvolution toolkit that we recently developed using weighted robust linear regression (8). The accuracy of deconvolution was assessed by the Pearson correlation coefficient r and the root-mean-square error (RMSE), mainly calculated from the true and estimated cellular proportions across all the patients.

2.2.5 Functional Gene Set-Based Prognostic Model

To accurately predict the prognosis and therapeutic benefits of BC patients, we proposed a functional gene set-based prognostic model, the construction of which consisted of three main steps: converting gene expression into activation scores of functional gene sets, identifying functional gene sets significantly associated with cellular proportions, and establishing the prognostic model based on the identified functional gene sets in the previous step. The details of each step were as follows.

2.2.5.1 Calculation of Activation Score Using Gene Set Variation Analysis (GSVA) Tool

To assess the activation of 9,321 functional gene sets [the union of H (hallmark gene sets), C2 (curated gene sets) and C5 (ontology gene sets) from MSigDB (28)] for each patient in BC cohort, we exclusively used a nonparametric and unsupervised software algorithm called *GSVA* (29) in the R package with the microarray mode.

2.2.5.2 Identification of Functional Gene Sets Significantly Associated With Cellular Proportions

After estimating the activation scores (called "GSVA score" hereafter) of functional gene sets for each BC patient, we further calculated the correlations between the proportions of 11 cell types estimated from the TCGA-BRCA cohort and the GSVA scores, and subsequently performed Fisher Z-transformations by equation 1.

$$\bar{z}_g = \frac{1}{2} \sum_{C \in cellTypes} \ln\left(\frac{1 + r_{gC}}{1 - r_{gC}}\right) \quad (1)$$

Where r_{gC} is the Pearson's correlation of gene set g with cell type C. Then standardize the Fisher-transformed correlations by their median and median absolute deviation (MAD):

$$S_g = \frac{\bar{z}_g - median(z)}{1.4826 \times MAD(z)} \quad (2)$$

P-values were then calculated for *Sg* using the standard normal distribution, and functions with *P*-values less than 0.01 were considered significantly associated with cellular proportions.

2.2.5.3 Establishing the Prognostic Model (Proportion-Based Model Also Apply)

Based on the identified functional gene sets mentioned above, LASSO-Cox and multivariate Cox regression methods were applied to identify the most effective functional gene sets (or cell types for the proportion-based prognostic model) to build a prognostic model. LASSO-penalized Cox regression was used to filter out less relevant factors. Multivariate Cox regression analysis was applied to optimize the model. An optimal risk assessment model was constructed utilizing the regression coefficients derived from Cox regression multivariate analysis by multiplying the GSVA score (or cellular proportion for the proportion-based prognostic model) of each function.

2.2.6 Kaplan-Meier Survival Curve

The prognostic model was designed to provide a risk score corresponding to each patient. Kaplan-Meier (KM) survival analysis was performed in combination log-rank test to determine whether the high- and low-risk groups identified by the *surv_cutpoint* function [implemented in the R package *survminer* (version 0.4.2)] exhibit significantly different survival patterns or not. In addition, the log-rank test determined whether the estimated survival curves were the same for each group, and in the case that the *P*-value is less than 0.05, the survival curves were statistically different.

2.2.7 Differentially Expressed Genes (DEGs) Associating With the Prognostic Risk Groups

To identify DEGs between high- and low-risk groups, we corrected for the batch effects between BC cohorts using Combat (30). These DEGs were then determined using the R package *Limma* (31), and were further defined at the threshold of $|log_2FC| > 0.1$ and Benjamini-Hochberg adjusted $P\text{-}value \leq 0.01$, primarily to calculate the statistically significant differences in gene expression.

2.2.8 Functional Enrichment Analysis

Gene annotation enrichment analysis for DEGs between high- and low-risk groups was performed using the R package *clusterProfiler* (32). Gene Ontology (GO) terms and KEGG pathways were considered statistically significant according to the Benjamini-Hochberg (33), adjusted $P\text{-}value < 0.01$.

2.2.9 Immunoreactivity Characterization

Immunophenoscore (IPS) uses a number of markers of immune response or immune toleration to quantify four different immune-phenotypes in a tumor sample, including antigen presentation, effector cells, suppressor cells, and checkpoint

markers. A z-score summarizing these four categories is generated, with a higher z-score of IPS indicating a more immunogenic sample (34, 35). In addition, scores of exhaustion, cell cycle, and activation gene sets were calculated by GSVA toolkit (see **Supplementary Table S5**) (29).

2.2.10 Classification Analysis

To distinguish ER-positive/negative subtypes, a support vector machine (SVM) classifier was applied to 80% of the samples in the TCGA-BRCA cohort using parameters from five-fold cross-validation with standard parameters (using R package *e1071*). The remaining samples were used for classifier testing. A random forest model with *ntree* = 2000 (R package *randomForest*) was used to distinguish high- and low-risk BC patients. To mention, here the training set used 80% of the ten BC cohort samples, while the remaining 20% was used for testing (**Supplementary Table S1**). The receiver operating characteristic (ROC) curve was used to assess the classification performance of the model, and the area under the curve (AUC) was calculated using the *pROC* package (36).

2.2.11 Code Availability

The custom codes are available from the corresponding authors upon request.

3 RESULT

3.1 Construction of the Reliable and Robust BC-Specific RGEP

As mentioned earlier, both indication-specific (tissue and disease type) and cell type-specific reference from scRNA-seq data is a key to deconvolute the cellular composition (15). We therefore initially obtained a total of 22,970 cells (after initial quality control) from the normal and cancerous tissues of eight BC patients (GEO accession number: GSE114725) (19) (**Supplementary Figures 1A, B** and **Supplementary Table S1**). As previously suggested (12), we applied the integration toolkit Harmony (24) to simultaneously eliminate technical bias caused by the batch effects and/or biological effects in the normal and tumor samples. As a result, 19 different cell clusters were identified, of which two (clusters 11 and 17) showed excessive outliers in the distribution of expressed genes and UMI counts (possibly enriched with the duplicate cells), hence, were excluded from the analysis (**Supplementary Figures 1B, C**). The integrated visualization revealed an extensive mixing of shared cell populations among patients and between the normal and tumor states, indicating that biases were significantly reduced (**Supplementary Figure 1D**).

On the basis of canonical cell markers, we identified 15 cell types for the clusters, including BC malignant cells (mainly characterized by the expression of *KRT19*, *KRT18*, *CDH1*, *EPCAM*), fibroblasts (*COL1A1*, *COL1A2*, *DCN*), proliferating T cells (*STMN1*, *MKI67*), cytotoxic T cells (*FGFBP2*, *NKG7*, *PRF1*), Transitional T (*CD8A, CD8B, GZMK, CCL5*), Treg (*FOXP3*, *TNFRSF4*), Naive-like T cells (*IL7R*, *TCF7*), NK cells (*KLRD1*, *KLRC1*), neutrophils (*CSF3R*, *FCGR3B*, *G0S2*), pDC (*IL3RA*, *LILRA4*), dendritic cells (*HLA-DPB1*, *HLA-DPA1*), macrophages (*C1QA*, *C1QB*, *FN1*), monocytes (*LYZ*, *FCN1*, *VCAN*), mast cells (*TPSAB1*, *CPA3*), and B cells (*CD79A*, *MS4A1*, *CD79B*) (**Figures 1A, B** and **Table S2**). The high correlations ($r > 0.8$) of the aggregated expression profiles between the immune cell types that we observed were consistent with one previous study (19), confirming the reliability of our annotated cell types. It should be mentioned that the study we used for comparison also included malignant cells and fibroblasts, so we applied ESTIMATE (25) to analyze the tumor purity scores and found that malignant cells had the highest tumor purity, followed by the fibroblasts, while immune cells had the lowest, which is consistent with the findings by Chung et al. (27) (**Figure 1C**). To this end, the results clearly support the reliability and adequacy of our annotated cell types for BC scRNA-Seq data.

After the cluster annotation and validation, approximately 12,132 high-quality cells were retained of which transitional T-cells were predominant while few other cell types (proliferating T cells, pDCs, and malignant cells) accounted for a very small proportion (**Supplementary Figure 1F**). In order to create a reliable and robust BC-specific RGEP for deconvolution, we averaged the gene expression within each cell type, and only the cell type-specific genes (signature genes) were retained. In the end, a specific RGEP with 1506 genes and 15 cell types was determined for the BC. The average expression levels of the signature genes were found to be specific for each cell type (**Figure 1D** and **Supplementary Table S3**). Notably, we also specified the expression of highly correlated genes (due to close cell lineages), primarily to optimize the covariance in the deconvolution model (**Supplementary Figure 1G**).

3.2 BC-Specific RGEP Outperformed Non-BC-Specific RGEPs in Capturing the Intrinsic Heterogeneity of BC Cohorts

To evaluate the prediction performance of BC-specific RGEP, we first deconvoluted the simulated BC bulk gene expression samples using LinDeconSeq (8), and observed very high consistency ($r = 1$, P-value $< 1 \times 10^{-30}$) (**Figure 2A**, see *Materials and Methods*). To obtain realistic datasets, we extracted BC scRNA-Seq data (40 BC patients, seven broad cell types, and their proportions/patient were known in advance) from a previously published study (20) (Bassez et al.'s data, see **Supplementary Table S1**). Here again, the deconvolution showed a significantly high correlation ($r = 0.91$, $P\text{-value} < 2.1 \times 10^{-19}$) between predicted and the true proportions (**Figure 2B**). As a proof of principle, we tested another RGEP (called "HNSCC-RGEP") (14) generated from head and neck squamous cell carcinoma (HNSCC) and found that our BC-specific RGEP made the predictions closer to the true proportions (i.e., higher correlation and lower RMSE) (**Figure 2C**). A similar trend was also observed in the GSE75688 scRNA-Seq dataset (27) (**Supplementary Figures 2A, B** and **Supplementary Table S1**). These results indicate that our BC-specific RGEP can accurately predict the cellular compositions in BC-TME, and with better predictive performance compared to

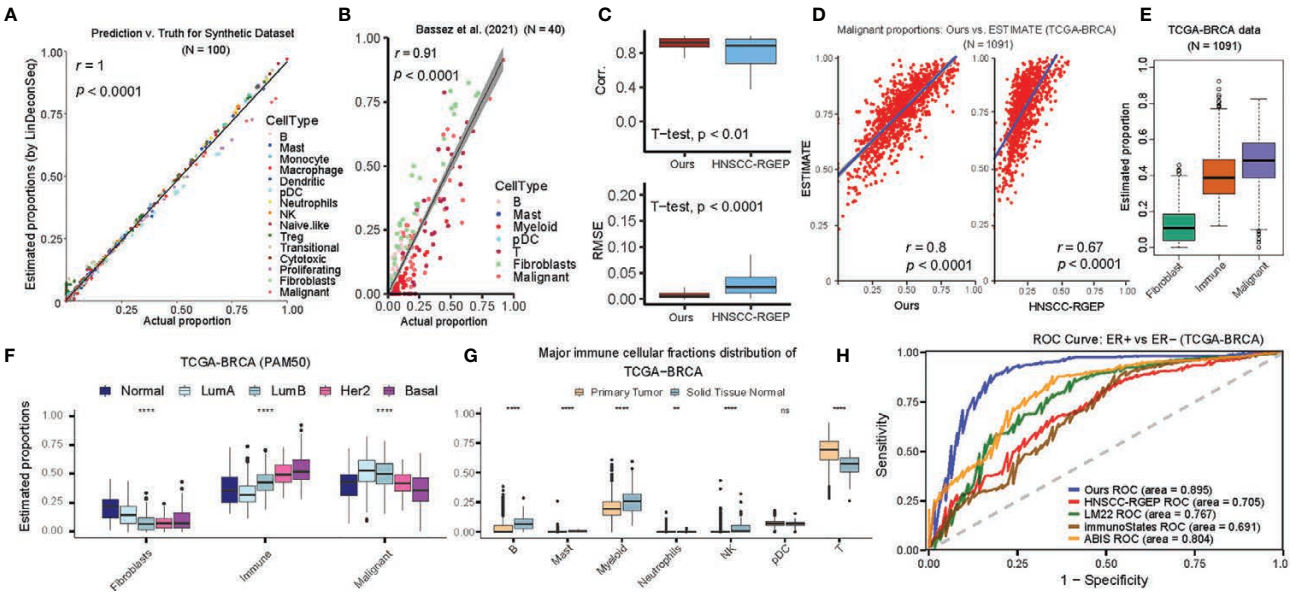

FIGURE 2 | Accuracy of cellular proportions estimated using BC-specific RGEP. **(A)** Scatter-plot of the estimated and true cellular proportions for the 100 simulated bulk breast tumor samples. Each dot represents one sample and *r* denotes the Pearson's correlation coefficient. *P*-value, Student's *t*-test. **(B)** Scatter-plot of the estimated and true cell proportions for the Bassez et al.'s scRNA-seq breast cancer data (20). Each dot represents one patient and *r* denotes the Pearson's correlation coefficient. *P* value, Student's *t*-test. The proportion of myeloid was the combined effect of monocyte, macrophage, and dendritic cell types, and T cell was the combined effect of Naïve-like, Treg, transitional, cytotoxic, and proliferating T cell types. **(C)** Side-by-side boxplot indicated the correlation (top) and RMSE (bottom) between the estimated and true cellular proportions, respectively, using BC-specific RGEP and HNSCC-RGEP (derived from HNSCC scRNA-seq data) (14) based on Bassez et al.'s dataset (20). *P*-value, Student's *t*-test. **(D)** Using the tumor purity of TCGA-BRCA patients estimated by ESTIMATE as the gold standard, scatter-plot showed the degree of consistency of the malignant proportion estimated using BC-specific RGEP (Left) and HNSCC-RGEP (14). (Right) with the gold standard purity. Each dot represents one sample and *r* denotes Pearson's correlation coefficient. *P*-value, Student's *t*-test. **(E)** Box plots showed the proportional distribution of fibroblast, immune cells and malignant cells, where the proportion of immune cells was the combined effect of B, mast, monocyte, macrophage, dendritic, pDC, neutrophils, NK, naïve-like, Treg, transitional, cytotoxic and proliferating T cells. Each box shows the median and interquartile range (IQR 25th–75th percentiles), whiskers indicate the highest and lowest value within 1.5 times the IQR and outliers are marked as dots. **(F)** Comparison of the proportions of fibroblasts, immune and malignant cell types in different cancer subtypes. Each box shows the median and interquartile range (IQR 25th–75th percentiles), whiskers indicate the highest and lowest value within 1.5 times the IQR and outliers are marked as dots. Wilcoxon rank-sum test was used for statistical analysis (****$p < 0.0001$). **(G)** Comparison of the proportions of major immune cell types between primary tumor and solid tissue normal samples. Each box shows the median and interquartile range (IQR 25th–75th percentiles), whiskers indicate the highest and lowest value within 1.5 times the IQR and outliers are marked as dots. Wilcoxon rank-sum test was used for statistical analysis (ns, "no significance", **$p < 0.01$, ****$p < 0.0001$). **(H)** ROC curve measuring the ability to distinguish ER+ and ER- of BRCA samples using cellular proportions estimated by BC-specific RGEP and non-BC-specific RGEPs in combination with the LinDeconSeq deconvolution method (8).

other non-specific references (even generated from different tissues like HNSCC).

We next assess the performance of BC-specific RGEP on traditional bulk transcriptome sequencing data (i.e. bulk RNA-seq data) by determining the proportions of 15 reference cell types in each sample. Here again, we used ESTIMATE (25) to determine the tumor purity, and found that prediction based on BC-specific RGEP showed a higher correlation compared to the one based on HNSCC-RGEP (**Figure 2D**). We also collected the malignant purity of TCGA-BRCA samples predicted by other tools, including ABSOLUTE, LUMP, IHC and CPE algorithms from the literature of Dvir Aran et al. (37). When comparing all of them, our predictions also showed a good/favorable performance (**Supplementary Figures 2C–G**). We also aggregated the predicted proportions of 15 cell types in TCGA-BRCA samples as fibroblasts, immune cells, and malignant cells and observed that the proportion of malignant cells was the highest whereas fibroblasts appeared to be the lowest (**Figure 2E**). The proportions of immune, fibroblast and malignant cells showed significant differences in the PAM50 subtypes of BC, indicating different degrees of infiltration (**Figure 2F**). Moreover, the Normal-like samples showed the highest percentage of fibroblasts, and Luminal B had the lowest number of fibroblasts. Basal-like tumors displayed the highest degree of immune cell infiltration, followed by Her2 tumors, while Luminal A tumors showed the lowest. To avoid the effect of covariance on the deconvolution, we aggregated 13 immune cell types of BC-specific RGEP into seven major lineages (B cells, mast, myeloid, neutrophil, NK, pDC, and T cells) and found that the proportions of B cells, myeloid, NK, and T-cells differed significantly between BC primary tumor and the normal tissue. These observations were consistent with previous studies (**Figures 2E–G**) (19, 38, 39).

To more systematically assess the BC-specific RGEP, we collected three additional non-BC-specific RGEPs, namely LM22 (9), immunoStates (12), and ABIS (13), and used

them with LindeconSeq to predict the cellular compositions of TCGA-cohort, respectively. To compare the accuracy and reliability of BC-specific RGEP with non-specific RGEPs for predicting cellular proportions, area under the curve (AUC) index was employed. Specifically, an SVM classifier was used to distinguish ER+ and ER- of BC patients based on the predicted cellular proportions by each RGEP, and then an AUC index was calculated (see *Materials and Methods*). Higher AUC indicates better classification ability, which suggests that this RGEP-predicted cellular composition is more capable of characterizing the intrinsic heterogeneity of BC patients with different subtypes. The result demonstrated that our BC-specific RGEP had the highest AUC (0.89) value (**Figure 2H**), suggesting that it is superior in characterizing the intrinsic heterogeneity of BC patients with different subtypes.

3.3 Construction of Functional Gene Set-Based Prognostic Model

After scaling the cellular proportions of TCGA-BRCA cohort, we focused on the TME cell network, mainly to determine the suitability of BC-specific RGEP to the tumor-immune cell interactions, cell lineages, and their effects on overall survival (OS) in BC patients (**Figure 3A**). The analysis showed significant differences (log-rank test, *P-value* < 0.05) in survival between the high and low proportion groups of these cells, with the exception of neutrophils (**Figure 3A**). Subsequently, 11 immune cell types were selected by the LASSO-Cox regression model (with minimized lambda) to build the proportion-based prediction model according to multiple Cox regression (**Supplementary Figures 3A, B**, concordance-index: 0.61). We found that the patients stratified into the high-risk score group had significantly worse overall survival compared to the low-risk score group in the TCGA-BC cohort (log-rank test, *P*-value = 7.45×10^{-7}, see *Materials and Methods*) (**Figure 3B**). Notably, since the accuracy of deconvolution can be influenced by multiple factors (including data type, e.g., microarray/RNA-seq), the accurate identification of stable signatures holds a great value for predicting the prognosis. Therefore, we specifically used gene set variation analysis (GSVA), which provides an advantage over single samples in order to perform comprehensive pathway-centric analyses in an unsupervised manner. Moreover, this strategy also helps to explore the perturbation of key functional gene sets in different patients for the prognosis prediction.

To investigate the association between these cell types and biological functions, we retrieved the H (Hallmark gene sets), C2 (curated gene sets), and C5 (ontology gene sets) collections from the MSigDB database (28), and estimated the GSVA (29) score for each sample. In this way, we retained the 964 functional gene sets with significant correlations (*P-value* < 0.01) and entered them into the LASSO-Cox regression model for features selection. In the end, we obtained 24 functional gene sets (/pathways) and used them (i.e. "GSVA score" of 24 functions) to construct a prognostic model similar to the proportion-based strategy (**Figures 3C** and **Supplementary Figures 3C–F**, concordance index: 0.782, **Table S4**, see *Materials and Methods*). The overall outcome was consistent in the proportion-based model, except that the differences between high- and low-risk groups (determined by the *surv_cutpoint* function) were more significant for the functional gene set-based prognostic model (**Figure 3D**, log-rank test, *P-value* = 5.9×10^{-33}). Interestingly, the associations with proliferating T-cells and macrophages were observed predominantly among the 24 functional gene sets (**Supplementary Figure 3D**). In particular, the association of proliferating T-cells with nucleosome localization, spindle checkpoint suggests biological processes in cell proliferation, while the associations with macrophages with MHC protein complexes, negative regulation of T-cell receptor signaling pathways suggest involvement in anti-tumor immunity.

To mention, the multivariate Cox analysis revealed that 24 functions (HR: 5.0, 95CI: 3.36-7.5) and tumor stage IV (HR: 6.4, 95CI: 2.88-14.3) were independent prognostic factors for OS in BC patients and can characterize the prognostic risk better than the proportions of 11 cell types (**Figure 3E**). In addition, the area under the curve (AUC) predictive value for the functional gene set-based model showed the highest survival rate by 3 years (**Figure 3F**). As compared to the other clinical characteristics and proportions of 11 cell types, the functional gene set-based model revealed the favourable predictive power (**Figure 3G**). Also, we found that the high-risk group had shorter survival times and more deaths (**Figure 3H**). We additionally tested nine microarray expression datasets (see **Supplementary Table S1**) and observed the significant differences between high- and low-risk groups in these validation cohorts (**Figures 3I–K** and **Supplementary Figures 4A–F**, log-rank test, *P-value* < 0.05). Overall, the analysis in multiple test cohorts suggests that our functional gene set-based prognostic model can clearly define the intrinsic characteristics of BC patients' prognosis.

3.4 Clinical and Biological Characteristics of High- and Low-Risk Groups Depicted by the Functional Gene Set-Based Prognostic Model

The relationship between prognostic risk score and clinical characteristics was further examined in the entire cohorts (10 BC cohorts, 4980 samples, **Supplementary Table S1**). It was found that the risk scores showed significant differences within the clinical characteristics, however, with the exception for age status (**Figure 4A**, Wilcoxon test, *P-value* <0.05). Of importance, each of the five molecular subtypes of PAM50 showed variations, e.g., Luminal A showed the best prognosis with the lowest risk score, whereas Her2 and Basal types were found to be more aggressive with the highest risk scores (**Figures 4A, B**). We also determined several independent factors and found that, a) histologic grading and pathologic staging of BC showed positive progression of stage and risk score, b) the patients with ER-positive showed a tendency to have a better prognosis (and lower risk) compared to ER-negative patients, c) those with or without radiotherapy showed a significant difference and had a higher risk score in the post-radiotherapy cohort. Since, the

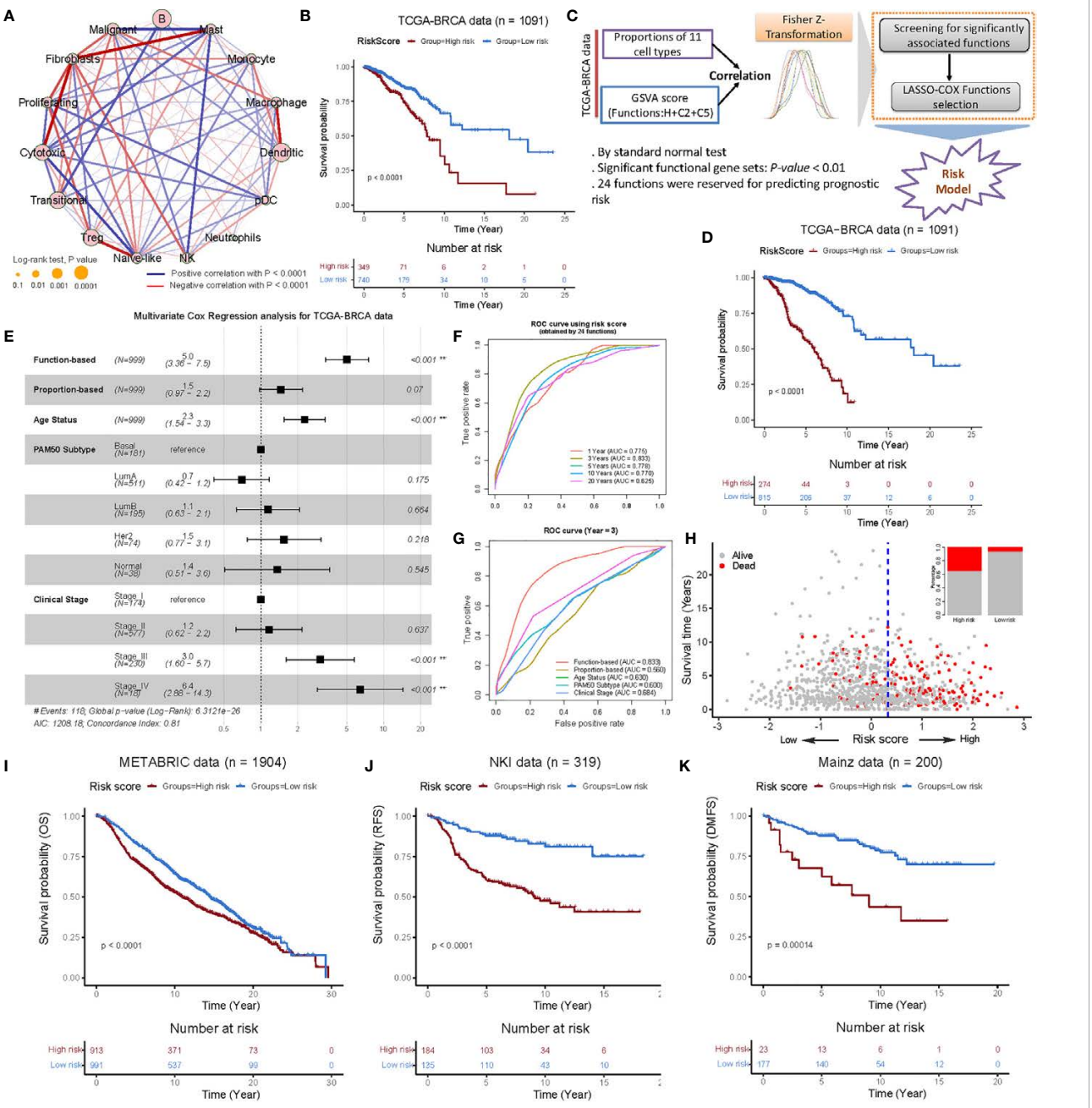

FIGURE 3 | Construction and validation of the functional gene set-based prognostic model in the BRCA cohorts. **(A)** Cellular interaction of the TME cell types. The size and filled color of each circle represent the prognosis effect of each cell type and were scaled by *P*-value. The lines connecting TME cells represent cellular interactions, where the thickness of the line represents the strength of correlation estimated by Spearman's correlation analysis. A positive correlation is indicated in red and negative correlation in blue. **(B)** Kaplan-Meier survival curves of overall survival (OS) from the TCGA-BRCA cohort using a prognostic model constructed from the proportion of 11 cell types (obtained by LASSO-COX selections) of BC patients. **(C)** Flow chart of constructing functional gene set-based prognostic mode consisted of three parts. First, correlation analysis was performed for the proportion of 11 cell types and the GSVA (29) score of 9,321 functional gene sets, respectively. Second, Fisher-Z-Transformation converted correlations into almost normally distributions, and significant functions with *P-value* < 0.01 could be retained. Third, LASSO-Cox functions selection was employed and then a functional gene set-based prognostic model was constructed. **(D)** Kaplan-Meier survival curves of OS from the TCGA-BRCA cohort using functional gene set-based prognostic model. **(E)** Multivariate analysis of the clinical characteristics, cellular proportion-based risk score and function-based risk score and functional gene set-based risk score with the OS. Log-rank test, **P < 0.01. **(F)** ROC curves of the functional gene set-based risk score at 1, 3, 5, 10 and 20 years after follow-up. **(G)** ROC curves of the clinical characteristics, cellular proportion-based risk score and functional gene set-based risk score at the year three after follow-up. **(H)** The patterns of the OS and survival status between the high- and low- groups for the TCGA-BRCA cohort. **(I-K)** Kaplan-Meier survival curves of OS, RFS and DMFS of patients in the low- and high-risk groups for the METABRIC (40) **(I)**, NKI (41) **(J)** and Mainz (42) **(K)** datasets, respectively. Relapse-free survival: RFS; Distant recurrence-free survival: DMFS.

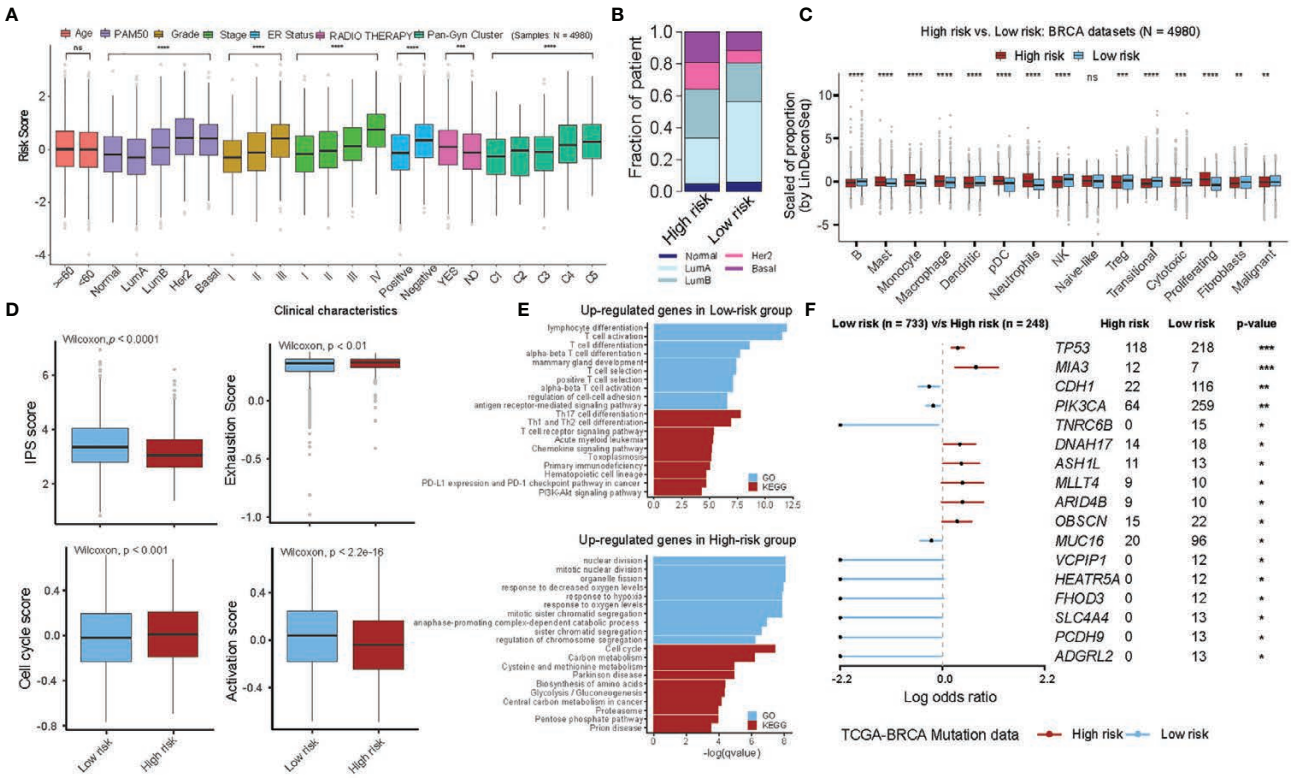

FIGURE 4 | Multi-perspective bioinformatics analysis of clinical and biological characteristics of high- and low-risk groups. **(A)** Stratified analysis of clinical characteristics for the risk score of the functional gene set-based prognostic model in ten BRCA cohorts. Each box shows the median and interquartile range (IQR 25th–75th percentiles), whiskers indicate the highest and lowest value within 1.5 times the IQR and outliers are marked as dots. The dots represent scaled risk score values. Wilcoxon rank-sum test was used for statistical analysis (ns, "no significance", *p < 0.05, **p < 0.01, ***p < 0.001, **** p < 0.0001). **(B)** The fraction of patients with PAM50 subtypes in the high- and low-risk groups. **(C)** The proportion of TME cells in high- and low-risk groups. Each box shows the median and interquartile range (IQR 25th–75th percentiles), whiskers indicate the highest and lowest value within 1.5 times the IQR and outliers are marked as dots. The dots represent the scaled fraction values of TME cells. Wilcoxon rank-sum test was used for statistical analysis (ns, "no significance", *p < 0.05, **p < 0.01, ***p < 0.001, **** p < 0.0001). **(D)** The relative distribution of immune signature gene scores was compared between high- and low-risk groups in ten BRCA cohorts. (Left-top) IPS score, (Left-bottom) Cell-cycle score, (Right-top) Exhaustion score and (Right-bottom) PI3K pathway score. **(E)** GO and KEGG analyses for differentially expressed genes in the high- and low-risk groups. Up-regulated genes in low-risk group (top) and in high-risk group (down) are shown. **(F)** Forest plot showing differentially mutated genes between the high- and low-risk groups. Only genes with more than 10 mutations in the samples in one group were included in the analysis. The statistical difference of the two groups was compared through the Fisher exact test. *P < 0.05; **P < 0.01; ***P < 0.001.

cohorts were not matched before and after the radiotherapy, thus the differences between them may vary relative to the treatment response. In addition, Pan-Gyn analysis confirmed that a positive trend increases the risk of C1 to C5 (**Figure 4A**). On the basis of deconvolution using LinDeconSeq (8) and BC-specific RGEP, TME cell infiltration of high- and low-risk groups revealed significant differences except for Naïve-like cells (**Figure 4C**). We also calculated the correlations of risk scores with genes from 24 functional sets based on the TCGA-BRCA cohort and extracted the top 10 genes each with the strongest positive and negative correlations, comparing the expression of these genes in the high- and low-risk groups showed significant differences (**Supplementary Figure 5**, *P*-value < 0.05). As shown in **Supplementary Figure 5**, genes with positive correlation have higher expression in high-risk group; conversely, genes with negative correlation have lower expression in high-risk group.

To further investigate the differences in the transcriptome between high- and low-risk groups, we additionally evaluated the number of parameters related to immune signature using the GSVA method. We observed significant differences between the high- and low-risk groups in the immunophenoscore (IPS) variable, i.e., the high-risk group showed a more severe T-cell exhaustion and cell proliferation activity, indicating a suppressed immune response with a worse prognosis (**Figure 4D**, see *Materials and Methods*). The association of risk scores with the expression of key immune checkpoint genes (including *PD-L1* (*CD247*), *PD1* (*PDCD1*), *LAG3*, and *CTLA4*) were explored and significant negative correlation were found, indicating that BC patients with high-risk scores responded poorly to immune checkpoint blockade therapy (**Supplementary Figure 6**). We further substituted the differentially expressed genes between high- and low-risk groups (see **Supplementary Table S6**) and found that the genes upregulated in the low-risk group were

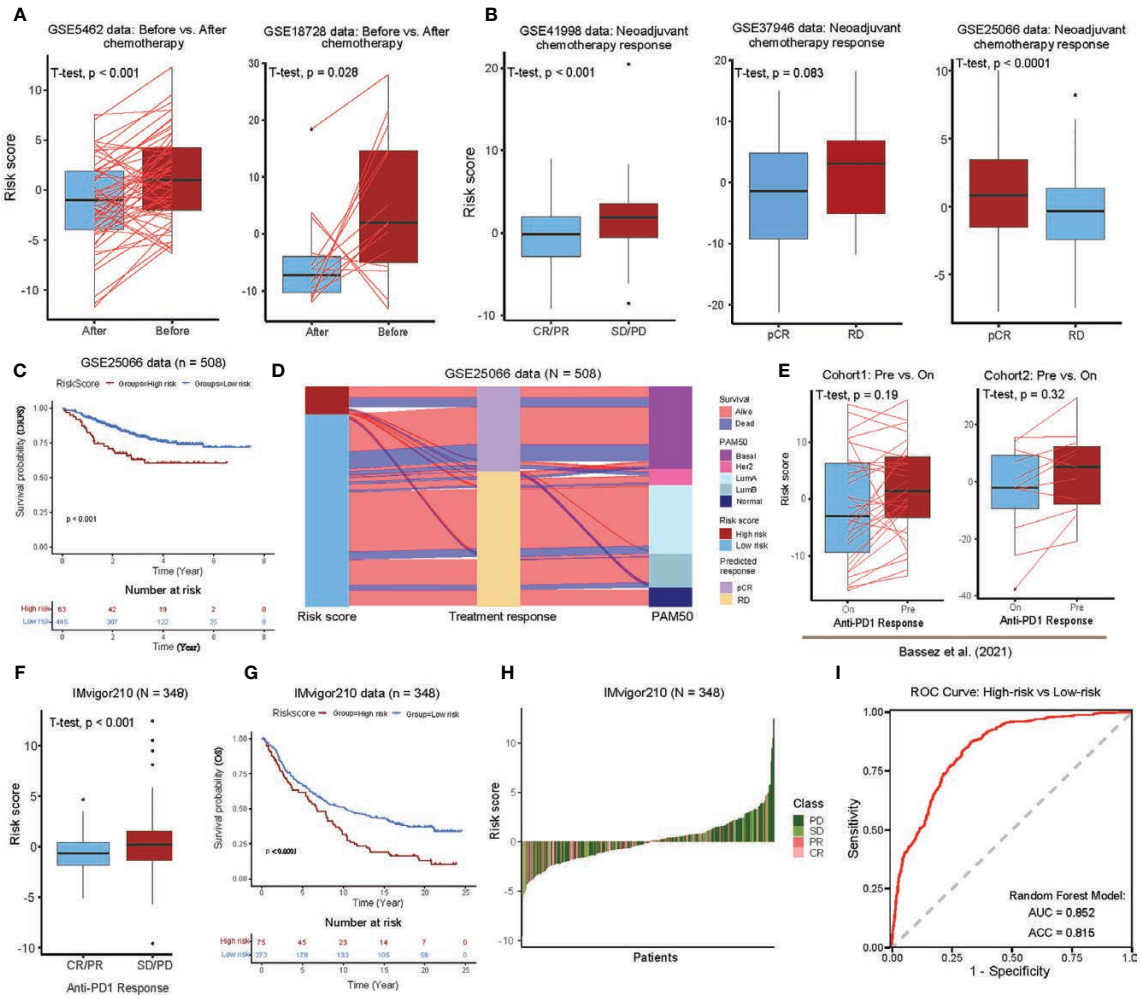

FIGURE 5 | Therapeutic benefit of the 24 functional gene set-based prognostic BC model. **(A)** Pairwise comparison of the risk scores in the patients pre- and post-chemotherapy for the GSE5462 (43) and GSE18728 (44) cohorts. Significance *P*-values were determined by pairwise Student's *t*-test. **(B)** Boxplot showing the distribution of risk scores for different neoadjuvant chemotherapy response in the GSE41998 (45), GSE37946 (46), and GSE25066 (47) cohorts. Significance *P*-value was determined by Student's *t*-test. Progressive disease (PD), stable disease (SD), partial response (PR), complete response (CR), pathologic complete response (pCR), and residual disease (RD). **(C)** Kaplan-Meier survival curves of distant recurrence-free survival (DRFS) from the GSE25066 cohort using functional gene set-based prognostic model. **(D)** Alluvial diagram of risk groups with different predicted response (pCR and RD), and molecular subtypes (Normal-like, LumA, LumB, Her2, and Basal). **(E)** Comparisons of risk scores for different status in BC scRNA-seq data provided by Bassez et al. (20). Pairwise comparison of risk scores for the cohort1 (Left) and cohort2 (Right) before and on anti-PD1 treatment. Significance *P*-values was determined by Student's *t*-test. **(F)** Boxplot showing the distribution of risk scores for different anti–PD1 response in the IMvigor210 cohort. Significance *P*-value was determined by Student's *t*-test. **(G)** Kaplan-Meier survival curves of OS from the IMvigor210 cohort using functional gene set-based prognostic model. **(H)** Waterfall plot illustrating the distribution of risk scores for patients with different anti-*CTLA4* immunotherapy responses in the IMvigor210 cohort. **(I)** ROC curve of random forest classifier for predicting high and low risk BC patients using 24 functional gene sets.

mainly enriched in immune-related categories, such as lymphocyte differentiation and Th17 cell differentiation. On the contrary, genes upregulated in the high-risk group were mainly enriched in the categories related to cell proliferation, such as nuclear division, cell cycle, and response to hypoxia (**Figure 4E** and see **Supplementary Table S7**). Interestingly, we also observed that *TP53*, *MIA3* were frequently mutated genes in the high-risk group, while *CDH1* and *PIK3CA* predominated in the low-risk group (**Figure 4F**). Overall, the high- and low-risk groups represented by the 24-functional gene sets prognostic model showed significant differences in the clinical and transcriptomic characteristics, suggesting that the prognostic model can mirror the BC prognosis.

3.5 Functional Gene Set-Based Prognostic Model Serves as a Predictive Parameter With Therapeutic Benefit in BC Cohorts

To investigate whether the risk scores predicted by our functional gene set-based prognostic model can effectively predict the tumor response in BC patients, we performed pairwise comparisons of

the risk scores (before and after treatment) with adjuvant chemotherapy, mainly in two BC cohorts (GSE5462 and GSE18728). We found significant differences in the majority of patients who responded with a lower risk score after chemotherapy (**Figure 5A**, see **Supplementary Table S1**). In accordance with patients' response to neoadjuvant chemotherapy, BC patients (in GSE41998) were further divided into four groups: progressive disease (PD), stable disease (SD), partial response (PR), and complete response (CR). Here, the analysis showed that the risk scores of BC patients with CR/PR were significantly lower than those with SD/PD. The BC patients from the GSE37946 data also showed a significantly lower risk score for pathologic complete response (pCR) compared to the residual disease (RD). To our surprise, the risk score of the pCR cohort was found to be significantly higher compared to RD in the GSE25066 data, which can be partially explained by the intrinsic association between risk score and disease-free survival (DRFS), i.e., high risk favored good prognosis in this particular data set (**Figures 5B, C**). The association between risk score, treatment response and PAM50 subtypes was further investigated, and found that the high-risk group was mainly enriched for Her2 and Basal aggressive subtypes with predominantly pCR status, while the low-risk subgroup was mainly LumA, LumB, and Normal-like with predominantly RD status. This may suggest that the difference in risk between different tumor subtypes is greater than the difference before and after treatment of the consent subtype (**Figure 5D**).

We further investigated whether the risk score could predict immunotherapeutic benefit for BC patients. For this purpose, we used scRNA-seq data from two cohorts consisting of 40 BC patients who received anti-PD1 therapy for approximately 10 days (see **Supplementary Table S1**). The pairwise comparisons of risk scores (before and after immunotherapy treatment) showed low-risk scores after the treatment in both cohorts, however, it was not significant (**Figure 5E**). In the absence of any published datasets of BC patients receiving immunotherapy, we utilized urothelial cancer dataset that received anti-PD-L1 therapy (IMvigor210), in order to test our functional gene set-based prognostic model to classify high- and low-risk groups. The boxplots further showed that the risk scores were significantly low in the patients with complete or partial response (CR/PR) compared to those with stable or progressive disease (SD/PD) (**Figure 5F**). In addition, the Kaplan-Meier curves showed that the patients in the low-risk group had a significantly better prognosis than those in the high-risk group (**Figure 5G**). In the ranking of risk scores from low to high, the low-risk side was enriched with PR/CR patients, whereas the high-risk side was predominated with SD/PD patients (**Figure 5H**). Overall, these analyses suggest that the risk scores calculated by our BC functional gene set-based prognostic model perform well for stratifying response to the immunotherapy.

In order to build the classifier that could predict the high- and low-risk group for BC patients, we applied the random forest algorithm (R package *randomForest*, version 4.6) using the GSVA scores of 24 functional gene sets as features in the training cohorts (ten BC cohorts, 80% for training and the remaining 20% for testing) (see *Materials and Methods*, see **Supplementary Table S1**). And we found the overall accuracy and AUC of the test cohorts as

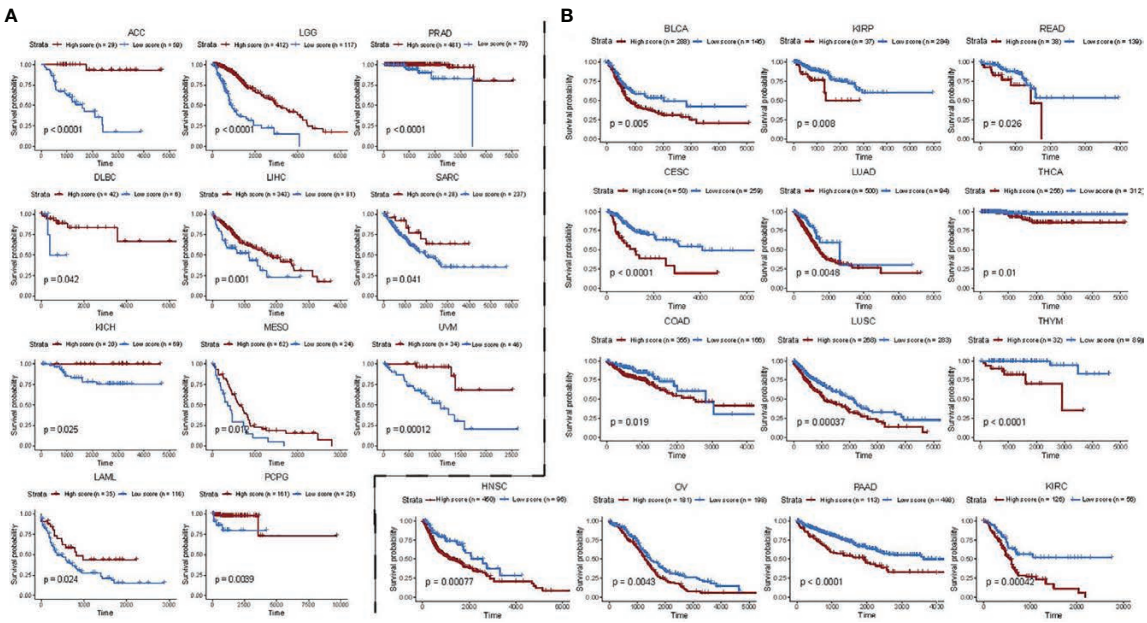

FIGURE 6 | Functional gene set-based model of BC patients as a prognostic factor for 24 other cancer types. **(A, B)** Impact of risk scores derived from BC functional gene set-based prognostic model on survival of pan-cancer patients. A high score is associated with both worse **(A)** and better **(B)** overall survival. Overall survival of patients with high score was compared with those with low score in a Kaplan–Meier survival curve analysis. Statistical significance was assessed by log-rank test. Only significant cancers with *P*-value < 0.05 were shown.

81.5% and 0.852, respectively, showing a favorable predictive power (**Figure 5I**). Of note, interleukin 21-mediated signaling and protein localization in the nucleoplasm emerged as the most important features in our analysis (**Supplementary Figure 7**).

3.6 Extending the Functional Gene Sets-Based Prognostic Model of BC to Pan-Cancer

Next, we investigated whether the association of 24 functional gene sets which we found in BC also applies to other cancers. To achieve this, we used the BC prediction model to calculate risk scores for 32 other cancers in the TCGA database (except BRCA cancers) and used the optimal cut point as an additional parameter to divide patients into two groups per cancer type. Then Kaplan–Meier survival curve analysis was performed between the high- and the low-expression groups. Among 32 cancer types, we found BC functional gene set-based prognostic model was significantly associated with overall survival in 24 cancer types (**Figures 6A, B**). In ACC, LGG, PRAD, DLBC, LIHC, SARC, KICH, MESO, UVM, LAML, and PCPG, the risk score obtained from 24 prognosis-related functional gene sets was observed as a favourable survival factor (**Figure 6A**), while the score was associated with worse survival in BLCA, KIRP, READ, CESC, LUAD, THCA, COAD, LUSC, THYM, HNSC, OV, PAAD, and KIRC (**Figure 6B**).

Taken together, our results suggest that the 24 functional genes closely associated with BC prognosis may have general prognostic significance for all other cancers.

4 DISCUSSION

Cancer is a multifactorial disease that combines yet to be known initial causative factors with the dysregulated biological pathways to reshape the genome (48, 49). In fact, cancer heterogeneity is a major challenge in the clinical setup and to some extent contributes to the treatment failure and/or acquires resistance in the cancer patients. It is also now well established that varying combinations of the different cell types and their cross-talk with tumor cells modulate TME, which further complicates the scenario. To address these challenges, advanced methods such as scRNA-seq have taken the central stage. Particularly in BC, a few scRNA-seq studies have been performed to gain better insight into the complex interactions between the immune system and tumor cells (15, 50). This in turn also raises some concerns about how to effectively explore this BC-TME heterogeneity with a direct prognostic/diagnostic clinical application. Since several studies have shown that reference-based deconvolution methods provide an important means to resolve the cellular compositions of bulk samples (5, 6, 8, 9, 11, 51), this prompted us to investigate the heterogeneity of BC-TME and patient prognosis by combining reference expression profiles (RGEPs).

Herein, we constructed a BC-specific RGEP using 15 cell types derived from scRNA-seq data of eight BC patients by considering multiple factors such as tissue and tumor types, disease status, data source (single-cell or sorted bulk data), and signature gene selection (**Figures 1A–D**). By benchmarking different gene expression reference profiles, we showed that the estimation accuracy is ultimately limited by the origin and quality of the RGEPs (**Figures 2A-H**). Moreover, we confirmed that when deconvolution algorithms are combined with scRNA-seq from tumor biopsies, the indication-specific consensus profiles of immune, stromal and malignant cells can be obtained directly from TME. Importantly, we observed that the proportions of both fibroblasts and immune cells estimated by BC-specific RGEP showed significant differences between the molecular subtypes of BC patients (**Figure 2F**), thus validating the direct clinical application of this novel tool. We observed that basal-like and Her2 tumors had the highest median degree of immune cell infiltration, whereas Luminal A tumors showed the lowest. Moreover, these differences profoundly affect the clinical treatment strategy and prognosis of BC patients, as confirmed by univariate Cox regression analysis which was based on the cellular proportions estimated with BC-specific RGEP (**Figure 3A**). Of note, even though we used the deconvolution tools similar to the previously reported non-specific RGEP studies, a slight variation in the outcome of certain variables (e.g., infiltration score of TME and patient prognosis) can be expected due to the additional clinical parameters which we have introduced in our current analysis.

We also evaluated transcriptome sequencing data and found that the cellular proportion-based on our prognostic model can well predict the prognosis of TCGA-BRCA cohorts, and confirming the previous studies (**Figure 3B**) (16, 52). Since the accuracy of deconvolution is affected by many factors (such as data type (microarray/RNA-seq)), we attempted to find stable signatures for predicting the prognosis of BC patients. Therefore, we used gene set variation analysis (GSVA) (29), which works on single samples and allows comprehensive pathway-centric analyses using statistical ranks in an unsupervised manner. Moreover, the correlations between the proportions of 11 cell types and 9,321 functional gene sets were analyzed independently to enhance the analysis. The functional gene sets that were significantly associated with cellular proportions were used in Lasso-Cox regression, and 24 functions were retained for the construction of BC prediction models (**Figures 3C, D**). The validation in ten BC cohorts demonstrated that our functional gene set-based prognostic model has good predictive power (**Figures 3I–K** and **S4A–F**). Despite the selection of features (24 functional gene sets) from different TCGA-BRCA cohorts, it was still possible to visualize the common hallmarks among BC cohorts using GSVA.

Given that prognostic risk scores provide individualized risk estimates for an outcome, the risk scores estimated by our functional gene set-based prognostic model adequately reflected the clinical characteristics of BC patients (**Figure 4A**). Also, when determined by the optimal cut-off point for the risk score, both high- and low-risk groups showed distinct transcriptional characteristics. For instance, the genes that were up-regulated in the low-risk group were mainly enriched in immune-related categories, whereas genes that were up-regulated in the high-risk group were mainly enriched in

categories related to cell proliferation (**Figures 4D, E**). Regarding the assessment of patient response to the therapy (chemotherapy and immunotherapy), the obtained risk scores also showed good discrimination between pre- and during/post-treatment (**Figures 5A–H**). Specifically, the selective 24 functions showed good predictive power in discriminating the high- and low-risk samples (**Figure 5I**). We further extended the BC functional gene set-based prognostic model to pan-cancer, and demonstrated the model is also suitable to other 24 cancers types (**Figures 6A, B**). Taken together, the functional gene set-based prognostic model that we have introduced showed a great ability to screen patients based on their therapeutic response. On a broader perspective, we provide a perspective to generate similar models in other cancer types and to identify shared factors that drives cancer heterogeneity.

It is also important to discuss the limitations of this current study, 1) some cell types that are lineage closely in the BC-specific RGEP are highly correlated, which may affect the accuracy of deconvolution, b) similar to other prognostic models, here also the difficulty of using the standardized cut-off for interpreting the risk scores remains. Nevertheless, our analysis showed that our refined BC-specific RGEP reflect the intrinsic expression of cells, and the proposed functional gene set-based prognostic model is a robust one for survival prediction and treatment guidance in BC patients. Thus, its implementation may help in stratifying BC patients to get benefit from adjuvant chemotherapy and cancer immunotherapy. Indeed, the experimental validation of our results may be highly valuable to elucidate the clinical spectrum of BC. On a broader perspective, we provide a perspective to generate similar models in other cancer types to identify shared factors that drives cancer heterogeneity.

DATA AVAILABILITY STATEMENT

The datasets presented in this study can be found in online repositories. The names of the repository/repositories and accession number(s) can be found in the article/ **Supplementary Material**.

AUTHOR CONTRIBUTIONS

HDL and XS designed the study. HML coded the algorithms. HML, HDL, and AS wrote and revised the manuscript. HML, YTH, and WLM did data analysis. HDL, KL, ZG and XS provided interpretation and discussion. All authors contributed to the article and approved the submitted version.

FUNDING

This work was supported by the National Natural Science Foundation of China (No. 61972084), the Key Research & Development Program of Jiangsu Province (BE2016002-3), "the Open Research Fund of State Key Laboratory of Bioelectronics, Southeast University" and the project of Southeast University (No. 3207032101F, and No. 3207032101C3).

ACKNOWLEDGMENTS

We thank the members in Bioinformatics Laboratory for the useful discussions.

SUPPLEMENTARY MATERIAL

The Supplementary Material for this article can be found online at: https://www.frontiersin.org/articles/10.3389/fimmu.2021.751530/full#supplementary-material

Supplementary Table S1 | Datasets and their application in this study.

Supplementary Table S7 | Gene ontology and KEGG pathway enrichment analysis.

REFERENCES

1. Siegel RL, Miller KD, Jemal A. Cancer Statistics, 2019. *CA: Cancer J Clin* (2019) 69(1):7–34. doi: 10.3322/caac.21551
2. Saltz J, Gupta R, Hou L, Kurc T, Singh P, Nguyen V, et al. Spatial Organization and Molecular Correlation of Tumor-Infiltrating Lymphocytes Using Deep Learning on Pathology Images. *Cell Rep* (2018) 23(1):181–93.e187. doi: 10.1016/j.celrep.2018.03.086
3. Dieci MV, Miglietta F, Guarneri VJC. Immune Infiltrates in Breast Cancer: Recent Updates and Clinical Implications. *Cells* (2021) 10(2):223. doi: 10.3390/cells10020223
4. Savas P, Virassamy B, Ye C, Salim A, Mintoff CP, Caramia F, et al. Single-Cell Profiling of Breast Cancer T Cells Reveals a Tissue-Resident Memory Subset Associated With Improved Prognosis. *Nat Med* (2018) 24(7):986–93. doi: 10.1038/s41591-018-0078-7
5. Tsoucas D, Dong R, Chen H, Zhu Q, Guo G, Yuan GC. Accurate Estimation of Cell-Type Composition From Gene Expression Data. *Nat Commun* (2019) 10(1):2975. doi: 10.1038/s41467-019-10802-z
6. Wang X, Park J, Susztak K, Zhang NR, Li M. Bulk Tissue Cell Type Deconvolution With Multi-Subject Single-Cell Expression Reference. *Nat Commun* (2019) 10(1):380. doi: 10.1038/s41467-018-08023-x
7. Newman AM, Steen CB, Liu CL, Gentles AJ, Chaudhuri AA, Scherer F, et al. Determining Cell Type Abundance and Expression From Bulk Tissues With Digital Cytometry. *Nat Biotechnol* (2019) 37(7):773–82. doi: 10.1038/s41587-019-0114-2
8. Li H, Sharma A, Ming W, Sun X, Liu H. A Deconvolution Method and its Application in Analyzing the Cellular Fractions in Acute Myeloid Leukemia Samples. *BMC Genom* (2020) 21(1):1–15. doi: 10.1186/s12864-020-06888-1
9. Newman AM, Liu CL, Green MR, Gentles AJ, Feng W, Xu Y, et al. Robust Enumeration of Cell Subsets From Tissue Expression Profiles. *Nat Methods* (2015) 12(5):453–7. doi: 10.1038/nmeth.3337
10. Hunt GJ, Freytag S, Bahlo M, Gagnon-Bartsch JA. Dtangle: Accurate and Fast Cell-Type Deconvolution. *bioRxiv* (2018) 290262. doi: 10.1101/290262
11. Li H, Sharma A, Luo K, Qin ZS, Sun X, Liu H. DeconPeaker, a Deconvolution Model to Identify Cell Types Based on Chromatin Accessibility in ATAC-Seq Data of Mixture Samples. *Front Genet* (2020) 11:392. doi: 10.3389/fgene.2020.00392
12. Vallania F, Tam A, Lofgren S, Schaffert S, Azad TD, Bongen E, et al. Leveraging Heterogeneity Across Multiple Datasets Increases Cell-Mixture Deconvolution Accuracy and Reduces Biological and Technical Biases. *Nat Commun* (2018) 9(1):4735. doi: 10.1038/s41467-018-07242-6

13. Monaco G, Lee B, Xu W, Mustafah S, Hwang YY, Carré C, et al. RNA-Seq Signatures Normalized by mRNA Abundance Allow Absolute Deconvolution of Human Immune Cells. *Cell Rep* (2019) 26(6):1627–40.e7. doi: 10.1016/j.celrep.2019.01.041
14. Yu X, Chen YA, Conejo-Garcia JR, Chung CH, Wang X. Estimation of Immune Cell Content in Tumor Using Single-Cell RNA-Seq Reference Data. *BMC Cancer* (2019) 19(1):715. doi: 10.1186/s12885-019-5927-3
15. Schelker M, Feau S, Du J, Ranu N, Klipp E, MacBeath G, et al. Estimation of Immune Cell Content in Tumour Tissue Using Single-Cell RNA-Seq Data. *Nat Commun* (2017) 8(1):2032. doi: 10.1038/s41467-017-02289-3
16. Sui S, An X, Xu C, Li Z, Hua Y, Huang G, et al. An Immune Cell Infiltration-Based Immune Score Model Predicts Prognosis and Chemotherapy Effects in Breast Cancer. *Theranostics* (2020) 10(26):11938–49. doi: 10.7150/thno.49451
17. Bao X, Shi R, Zhao T, Wang Y, Anastasov N, Rosemann M, et al. Immunotherapy: Integrated Analysis of Single-Cell RNA-Seq and Bulk RNA-Seq Unravels Tumour Heterogeneity Plus M2-Like Tumour-Associated Macrophage Infiltration and Aggressiveness in TNBC. *Cancer Immunol Immunother* (2021) 70(1):189–202. doi: 10.1007/s00262-020-02669-7
18. Huang S, Yee C, Ching T, Yu H, Garmire LX. A Novel Model to Combine Clinical and Pathway-Based Transcriptomic Information for the Prognosis Prediction of Breast Cancer. *PloS Comput Biol* (2014) 10(9):e1003851. doi: 10.1371/journal.pcbi.1003851
19. Azizi E, Carr AJ, Plitas G, Cornish AE, Konopacki C, Prabhakaran S, et al. Single-Cell Map of Diverse Immune Phenotypes in the Breast Tumor Microenvironment. *Cell* (2018) 174(5):1293–308.e1236. doi: 10.1016/j.cell.2018.05.060
20. Bassez A, Vos H, Van Dyck L, Floris G, Arijs I, Desmedt C, et al. A Single-Cell Map of Intratumoral Changes During Anti-PD1 Treatment of Patients With Breast Cancer. *Nat Med* (2021) 27(5):820–32. doi: 10.1038/s41591-021-01323-8
21. Mariathasan S, Turley SJ, Nickles D, Castiglioni A, Yuen K, Wang Y, et al. Tgfβ Attenuates Tumour Response to PD-L1 Blockade by Contributing to Exclusion of T Cells. *Nature* (2018) 554(7693):544–8. doi: 10.1038/nature25501
22. Hubbell E, Liu W-M, Mei R. Robust Estimators for Expression Analysis. *Bioinformatics* (2002) 18(12):1585–92. doi: 10.1093/bioinformatics/18.12.1585
23. Stuart T, Butler A, Hoffman P, Hafemeister C, Papalexi E, Mauck WM3rd, et al. Comprehensive Integration of Single-Cell Data. *Cell* (2019) 177(7):1888–902.e1821. doi: 10.1016/j.cell.2019.05.031
24. Korsunsky I, Millard N, Fan J, Slowikowski K, Zhang F, Wei K, et al. Fast, Sensitive and Accurate Integration of Single-Cell Data With Harmony. *Nat Methods* (2019) 16(12):1289–96. doi: 10.1038/s41592-019-0619-0
25. Yoshihara K, Shahmoradgoli M, Martinez E, Vegesna R, Kim H, Torres-Garcia W, et al. Inferring Tumour Purity and Stromal and Immune Cell Admixture From Expression Data. *Nat Commun* (2013) 4:2612. doi: 10.1038/ncomms3612
26. Tirosh I, Izar B, Prakadan SM, Wadsworth MH, Treacy D, Trombetta JJ, et al. Dissecting the Multicellular Ecosystem of Metastatic Melanoma by Single-Cell RNA-Seq. *Science* (2016) 352(6282):189–96. doi: 10.1126/science.aad0501
27. Chung W, Eum HH, Lee HO, Lee KM, Lee HB, Kim KT, et al. Single-Cell RNA-Seq Enables Comprehensive Tumour and Immune Cell Profiling in Primary Breast Cancer. *Nat Commun* (2017) 8:15081. doi: 10.1038/ncomms15081
28. Subramanian A, Tamayo P, Mootha VK, Mukherjee S, Ebert BL, Gillette MA, et al. Lander ESJPotNAoS: Gene Set Enrichment Analysis: A Knowledge-Based Approach for Interpreting Genome-Wide Expression Profiles. *Proc Natl Acad Sci* (2005) 102(43):15545–50. doi: 10.1073/pnas.0506580102
29. Hänzelmann S, Castelo R, Guinney J. GSVA: Gene Set Variation Analysis for Microarray and RNA-Seq Data. *BMC Bioinform* (2013) 14(1):7. doi: 10.1186/1471-2105-14-7
30. Johnson WE, Li C, Rabinovic AJB. Adjusting Batch Effects in Microarray Expression Data Using Empirical Bayes Methods. *Biostatistics* (2007) 8 (1):118–27. doi: 10.1093/biostatistics/kxj037
31. Love MI, Huber W, Anders S. Moderated Estimation of Fold Change and Dispersion for RNA-Seq Data With Deseq2. *Genome Biol* (2014) 15(12):550. doi: 10.1186/s13059-014-0550-8
32. Yu G, Wang L-G, Han Y, He Q-Y. Clusterprofiler: An R Package for Comparing Biological Themes Among Gene Clusters. *Omics: J Integr Biol* (2012) 16(5):284–7. doi: 10.1089/omi.2011.0118
33. Benjamini Y, Hochberg Y. Controlling the False Discovery Rate: A Practical and Powerful Approach to Multiple Testing. (1995) 57(1):289–300. doi: 10.1111/j.2517-6161.1995.tb02031.x
34. García-Mulero S, Alonso MH, Pardo J, Santos C, Sanjuan X, Salazar R, et al. Lung Metastases Share Common Immune Features Regardless of Primary Tumor Origin. *J Immunother Cancer* (2020) 8(1). doi: 10.1136/jitc-2019-000491
35. Charoentong P, Finotello F, Angelova M, Mayer C, Efremova M, Rieder D, et al. Pan-Cancer Immunogenomic Analyses Reveal Genotype-Immunophenotype Relationships and Predictors of Response to Checkpoint Blockade. *Cell Rep* (2017) 18(1):248–62. doi: 10.1016/j.celrep.2016.12.019
36. Robin X, Turck N, Hainard A, Tiberti N, Lisacek F, Sanchez J-C, et al. pROC: An Open-Source Package for R and S+ to Analyze and Compare ROC Curves. *BMC Bioinform* (2011) 12(1):1–8. doi: 10.1186/1471-2105-12-77
37. Aran D, Sirota M, Butte A. Systematic Pan-Cancer Analysis of Tumour Purity. *Nat Com* (2015) 6(1):1–12. doi: 10.1038/ncomms9971
38. Onuchic V, Hartmaier RJ, Boone DN, Samuels ML, Patel RY, White WM, et al. Epigenomic Deconvolution of Breast Tumors Reveals Metabolic Coupling Between Constituent Cell Types. *Cell Rep* (2016) 17(8):2075–86. doi: 10.1016/j.celrep.2016.10.057
39. Wagner J, Rapsomaniki MA, Chevrier S, Anzeneder T, Langwieder C, Dykgers A, et al. A Single-Cell Atlas of the Tumor and Immune Ecosystem of Human Breast Cancer. *Cell* (2019) 177(5):1330–45. e1318. doi: 10.1016/j.cell.2019.03.005
40. Curtis C, Shah SP, Chin S-F, Turashvili G, Rueda OM, Dunning MJ, et al. The Genomic and Transcriptomic Architecture of 2,000 Breast Tumours Reveals Novel Subgroups. *Nature* (2012) 486(7403):346–52. doi: 10.1038/nature10983
41. Van't Veer LJ, Dai H, Van De Vijver MJ, He YD, Hart AA, Mao M, et al. Gene Expression Profiling Predicts Clinical Outcome of Breast Cancer. *Nature* (2002) 415(6871):530–6. doi: 10.1038/415530a
42. Schmidt M, Böhm D, Von Törne C, Steiner E, Puhl A, Pilch H, et al. The Humoral Immune System has a Key Prognostic Impact in Node-Negative Breast Cancer. *Cancer Res* (2008) 68(13):5405–13. doi: 10.1158/0008-5472.CAN-07-5206
43. Miller WR, Larionov AA, Renshaw L, Anderson TJ, White S, Murray J, et al. Changes in Breast Cancer Transcriptional Profiles After Treatment With the Aromatase Inhibitor, Letrozole. *Pharmacogenet Genom* (2007) 17(10):813–26. doi: 10.1097/FPC.0b013e32820b853a
44. Korde LA, Lusa L, McShane L, Lebowitz PF, Lukes L, Camphausen K, et al. Gene Expression Pathway Analysis to Predict Response to Neoadjuvant Docetaxel and Capecitabine for Breast Cancer. *Breast Cancer Res Treatment* (2010) 119(3):685–99. doi: 10.1007/s10549-009-0651-3
45. Horak CE, Pusztai L, Xing G, Trifan OC, Saura C, Tseng L-M, et al. Biomarker Analysis of Neoadjuvant Doxorubicin/Cyclophosphamide Followed by Ixabepilone or Paclitaxel in Early-Stage Breast Cancer. *Clin Cancer Res* (2013) 19(6):1587–95. doi: 10.1158/1078-0432.CCR-12-1359
46. Liu JC, Voisin V, Bader GD, Deng T, Pusztai L, Symmans WF, et al. Seventeen-Gene Signature From Enriched Her2/Neu Mammary Tumor-Initiating Cells Predicts Clinical Outcome for Human HER2+: Erα– Breast Cancer. *Proc Natl Acad Sci* (2012) 109(15):5832–7. doi: 10.1073/pnas.1201105109
47. Hatzis C, Pusztai L, Valero V, Booser DJ, Esserman L, Lluch A, et al. A Genomic Predictor of Response and Survival Following Taxane-Anthracycline Chemotherapy for Invasive Breast Cancer. *Jama* (2011) 305 (18):1873–81. doi: 10.1001/jama.2011.593
48. Sharma A, Liu H, Herwig-Carl MC, Chand Dakal T, Schmidt-Wolf IGJCI. Epigenetic Regulatory Enzymes: Mutation Prevalence and Coexistence in Cancers. *Cancer Inv* (2021) 39(3):257–73. doi: 10.1080/07357907.2021.1872593
49. Sharma A, Reutter H, Ellinger JJCG. DNA Methylation and Bladder Cancer: Where Genotype Does Not Predict Phenotype. *Curr Genom* (2020) 21(1):34–6. doi: 10.2174/1389202921666200102163422
50. Berger AC, Korkut A, Kanchi RS, Hegde AM, Lenoir W, Liu W, et al. A Comprehensive Pan-Cancer Molecular Study of Gynecologic and Breast Cancers. *Cancer Cell* (2018) 33(4):690–705.e699. doi: 10.1016/j.ccell.2018.03.014

51. Qiao W, Quon G, Csaszar E, Yu M, Morris Q, Zandstra PW. PERT: A Method for Expression Deconvolution of Human Blood Samples From Varied Microenvironmental and Developmental Conditions. *PloS Comput Biol* (2012) 8(12):e1002838. doi: 10.1371/journal.pcbi.1002838
52. Wang S, Xiong Y, Zhang Q, Su D, Yu C, Cao Y, et al. Clinical Significance and Immunogenomic Landscape Analyses of the Immune Cell Signature Based Prognostic Model for Patients With Breast Cancer. *Brief Bioinform* (2021) bbaa311. doi: 10.1093/bib/bbaa311

Conflict of Interest: The authors declare that the research was conducted in the absence of any commercial or financial relationships that could be construed as a potential conflict of interest.

Publisher's Note: All claims expressed in this article are solely those of the authors and do not necessarily represent those of their affiliated organizations, or those of the publisher, the editors and the reviewers. Any product that may be evaluated in this article, or claim that may be made by its manufacturer, is not guaranteed or endorsed by the publisher.

Copyright © 2021 Li, Huang, Sharma, Ming, Luo, Gu, Sun and Liu. This is an open-access article distributed under the terms of the Creative Commons Attribution License (CC BY). The use, distribution or reproduction in other forums is permitted, provided the original author(s) and the copyright owner(s) are credited and that the original publication in this journal is cited, in accordance with accepted academic practice. No use, distribution or reproduction is permitted which does not comply with these terms.

frontiers in Immunology

ORIGINAL RESEARCH
published: 04 February 2022
doi: 10.3389/fimmu.2021.739039

Characterization of Interplay Between Autophagy and Ferroptosis and Their Synergistical Roles on Manipulating Immunological Tumor Microenvironment in Squamous Cell Carcinomas

Lijie Chen[1,2†], Xing Niu[1,2†], Xue Qiao[3], Sai Liu[2], Hongmei Ma[1], Xueqing Shi[1], Xuemei He[1] and Ming Zhong[1,2]*

[1] Department of Stomatology, Xiang'an Hospital of Xiamen University, School of Medicine, Xiamen University, Xiamen, China, [2] Department of Oral Histopathology, School and Hospital of Stomatology, China Medical University, Liaoning Province Key Laboratory of Oral Disease, Shenyang, China, [3] Department of Central Laboratory, School and Hospital of Stomatology, China Medical University, Liaoning Province Key Laboratory of Oral Disease, Shenyang, China

Objective: Squamous cell carcinomas (SCCs) with shared etiology, histological characteristics, and certain risk factors represent the most common solid cancers. This study reports the crosstalk between autophagy and ferroptosis at the molecular level in SCCs, and their roles on the immunological tumor microenvironment (TME) of SCCs.

Methods: In this study, the connections between autophagy and ferroptosis were characterized in SCCs by analyzing the associations between autophagy- and ferroptosis-related genes in mRNA expression and prognosis, protein-protein interactions and shared signaling pathways. Autophagy potential index (API) and ferroptosis potential index (FPI) of each tumor were quantified for reflecting autophagy and ferroptosis levels *via* principal-component analysis algorithm. Their synergistical roles on TME, immunity, drug resistance and survival were systematically analyzed in SCCs.

Results: There were close connections between autophagy and ferroptosis at the mRNA and protein levels and prognosis. Both shared cancer-related pathways. The API and FPI were separately developed based on prognostic autophagy- and ferroptosis-related genes. A high correlation between API and FPI was found in SCCs. Their interplay was distinctly associated with favorable prognosis, enhanced sensitivity to chemotherapy drugs (Sunitinib, Gefitinib, Vinblastine and Vorinostat), an inflamed TME and higher likelihood of response to immunotherapy in SCCs.

Conclusion: This study is the first to provide a comprehensive analysis of the interplay between autophagy and ferroptosis and their synergistical roles on manipulating the immunological TME in SCCs. These findings indicated that the induction of autophagy and

OPEN ACCESS

Edited by:
Peng Qu,
National Institutes of Health (NIH), United States

Reviewed by:
Yafeng He,
National Heart, Lung, and Blood Institute (NHLBI), United States
Weimin Zhong,
Xiamen Fifth Hospital, China

****Correspondence:***
Ming Zhong
zhongming_oral@aliyun.com

[†]These authors have contributed equally to this work

Specialty section:
This article was submitted to Cancer Immunity and Immunotherapy, a section of the journal Frontiers in Immunology

Received: *09 July 2021*
Accepted: *20 December 2021*
Published: *04 February 2022*

Citation:
Chen L, Niu X, Qiao X, Liu S, Ma H, Shi X, He X and Zhong M (2022) Characterization of Interplay Between Autophagy and Ferroptosis and Their Synergistical Roles on Manipulating Immunological Tumor Microenvironment in Squamous Cell Carcinomas. Front. Immunol. 12:739039. doi: 10.3389/fimmu.2021.739039

ferroptosis combined with immunotherapy might produce synergistically enhanced anti-SCCs activity.

Keywords: squamous cell carcinomas, ferroptosis, autophagy, crosstalk, tumor microenvironment, immunity, drug resistance, prognosis

INTRODUCTION

Squamous cell carcinomas (SCCs) represent the most common solid cancers (1). SCCs arise from epithelial tissues of the aerodigestive or genitourinary tracts, which are commonly detected in head and neck, esophagus, lung, and cervix (2). SCCs across different body sites share overlapping etiology, histopathological characteristics [such as the presence of keratin pearls, tonofilament bundles, hemidesmosomes and desmosomes (3)] and specific risk factors (such as smoking, drinking and human papillomavirus infection) (4). Previous the Cancer Genome Atlas (TCGA) research has uncovered that SCCs exhibit similar molecular patterns such as somatic mutations, copy number variations, abnormal pathways, and tumor microenvironment (TME) that differ from other cancer types (2, 5, 6). With surgery, radio- and chemotherapy as the standard of care for most SCCs, the treatment of SCCs is complex and has undergone considerable advancement in the last decade (7). Especially, treatment with immune checkpoint inhibitors (ICIs) such as anti-programmed death-1 (anti-PD-1), anti-programmed death ligand-1 (anti-PD-L1), and/or anti-cytotoxic T lymphocyte-associated antigen-4 (anti-CTLA-4) has been applied to SCCs, which can result in impressive response rates and durable disease remission in clinical trials (8–10). However, only in a subset of patients respond to ICI therapy (11).

Autophagy is an evolutionarily conserved cellular process, which may degrade various biological molecules and organelles through lysosome-dependent degradation pathway (12). Ferroptosis is a novel form of programmed cell death, which is driven by iron accumulation and lipid peroxidation (13). Recent research has revealed the role of autophagy in driving cells towards ferroptosis (14). Meanwhile, activation of autophagy is required for the induction of ferroptosis (12). The crosstalk between autophagy and ferroptosis decide cell fate through activating comprehensive signaling pathways and affecting gene expression programs (15). Growing evidence suggests that interplay of autophagy and ferroptosis exerts a key role in antitumor immunity (16), tumor suppression (17) and drug resistance (18), etc. However, the mechanism of the crosstalk between autophagy and ferroptosis in SCCs remains largely ill-defined. Uncovering when and how to modulate their interplay utilizing therapeutic strategies against SCCs depends on the in-depth understanding of the connections between autophagy and ferroptosis (18). Unraveling the interplay between autophagy and ferroptosis may not only elucidate fundamental mechanistic insights into SCCs, but also provide novel therapeutic targets for the treatment of SCCs. We hypothesize that appropriate combinations of potent drugs that specifically activate autophagy and ferroptosis with ICIs might achieve better treatment effects. Therefore, this study specifically and comprehensively characterized the interplay between ferroptosis and autophagy in SCCs and their synergistical roles on immunity, TME, drug resistance and prognosis of SCCs.

Abbreviations: TME, tumor microenvironment; SCCs, squamous cell carcinomas; TCGA, the Cancer Genome Atlas; ICIs, immune checkpoint inhibitors; HNSC, head and neck squamous cell carcinoma; LUSC, lung squamous cell carcinoma; CESC, cervical squamous cell carcinoma; ESCC, esophageal squamous cell carcinoma; CNV, copy number variation; PCA, principal component analysis; FPI, ferroptosis potential index; API, autophagy potential index; PPI, protein-protein interaction; OS, overall survival; DFI, disease-free interval; DFS, disease-free survival; DSS, disease-specific survival; PFI, progression-free interval; ROC, receiver-operating characteristic; AUC, area under the ROC curve; ESTIMATE, Estimation of STromal and Immune cells in MAlignant Tumours using Expression data; ssGSEA, single-sample gene-set enrichment analysis; HLA, human leukocyte antigen; TIDE, T cell dysfunction and exclusion; TMB, tumor mutation burden; GDSC, Genomics of Drug Sensitivity in Cancer; IC50, half-maximal inhibitory concentration; GSVA, gene set variation analysis; mRNAsi, mRNA expression-based stemness index; FDR, false discovery rate; GO, Gene Ontology; KEGG, Kyoto Encyclopedia of Genes and Genomes; CMap, Connectivity Map; MoA, mode of action; LASSO, least absolute shrinkage and selection operator; dMMR, mismatch repair deficiency; CSCs, Cancer stem cells; MTT, 3-[4,5-dimethylthiazol-2-yl]-2, 5-diphenyltetrazoliumbromide; EdU, Ethynyl-2'-deoxyuridine.

MATERIALS AND METHODS

Patients and Datasets

Figure 1 shows the workflow of this study. RNA sequencing (RNA-seq) data (fragments per kilobase of transcript per million mapped reads (FPKM) values) and clinical information of SCCs including head and neck squamous cell carcinoma (HNSC; n=500), lung squamous cell carcinoma (LUSC; n=501), cervical squamous cell carcinoma (CESC; n=241), and esophageal squamous cell carcinoma (ESCC; n=81) were acquired from TCGA (http://cancergenome.nih.gov) database *via* the Genomic Data Commons (GDC, https://portal.gdc.cancer.gov/). Then, FPKM values were converted into TPM values. Microarray datasets including gene expression profiling of GSE17710/LUSC (N=56) (19), GSE44001/CESC (N=300) (20), GSE65858/HNSC (N=270) (21) were employed from the Gene Expression Omnibus (GEO; http://www.ncbi.nlm.nih.gov/geo/) database. Batch effects from non-biological technical biases were corrected with the "ComBat" algorithm of sva package (version 3.42.0) (22). Ferroptosis- and autophagy-related genes were collected according to published literature (**Supplementary Table 1**). The locations of ferroptosis- and autophagy-related genes on human chromosomes were separately plotted by employing Rcircos package (version 1.2.1) (23). Genomic mutation data of SCCs [somatic mutation and copy number variation (CNV)] were also obtained from TCGA database. Mutation status was analyzed and visualized by maftools package (version 2.10.0) (24).

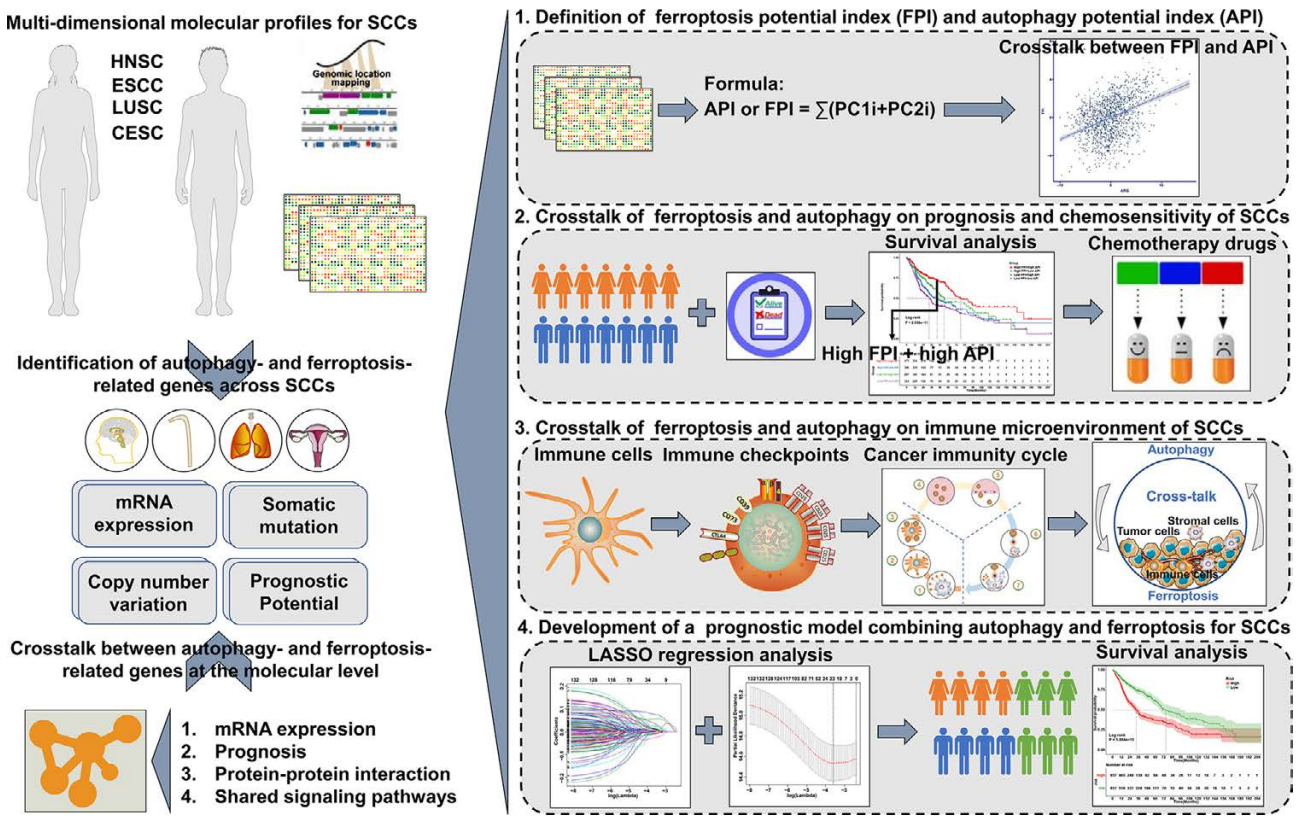

FIGURE 1 | Overview of the study design.

Computational Models of Ferroptosis and Autophagy Levels Among SCCs

A ferroptosis and autophagy scoring scheme was developed to quantify ferroptosis and autophagy levels in each specimen with principal component analysis (PCA). Survival analysis of ferroptosis- and autophagy-related genes was separately performed utilizing univariate Cox regression analysis. The expression profiles of the genes with $p<0.05$ were extracted to carried out PCA, and principal component 1 and 2 were extracted and acted as the signature score. Like previous studies (25, 26), the ferroptosis potential index (FPI) and autophagy potential index (API) were separately defined: API or FPI = $\sum(PC1_i+PC2_i)$, where i represents the expression of ferroptosis- or autophagy-related genes.

Protein-Protein Interaction (PPI) Analysis

Interactions between ferroptosis- and autophagy-related genes were analyzed through the STRING online database (version: 11.0; https://string-db.org/) (27). A PPI network was generated and displayed by Cytoscape software (version: 3.7.2) (28).

Survival Analysis

Kaplan–Meier curves for overall survival (OS), disease-free interval (DFI), disease-free survival (DFS), disease-specific survival (DSS) and progression-free interval (PFI) were plotted to compare the survival time differences. P-values were calculated with log-rank tests. Time-dependent receiver-operating characteristic (ROC) curve analysis was carried out using survivalROC package (version 1.0.3). The area under the ROC curve (AUC) was determined to assess the prognostic performance.

Estimation of Tumor Microenvironment (TME)

Estimation of STromal and Immune cells in MAlignant Tumours using Expression data (ESTIMATE) may infer the tumor cellularity and tumor purity based on unique properties of the transcriptional profiles (29). Through ESTIMATE algorithm, immune and stromal scores were determined to estimate the levels of infiltrating immune and stromal cells as well as tumor purity. Tumor tissues with abundant immune cell infiltration indicate a higher immune score and lower level of tumor purity. Through the single-sample gene-set enrichment analysis (ssGSEA) algorithm, the enrichment scores of 16 immune cells and 13 immune functions for each sample were estimated based on the expression of marker genes of tumor-infiltrating immune cells (TIICs) that were obtained from Bindea et al. utilizing gene set variation analysis (GSVA) package [version 1.42.0 (30)]. The expression of human leukocyte antigen (HLA) genes, immune checkpoints and immunomodulators (including major histocompatibility complex (MHC) molecules, receptors, chemokines, and immunostimulatory factors) (31) was also quantified in each sample (**Supplementary Table 2**).

Quantification of Immune Response Predictors

T cell dysfunction and exclusion (TIDE) (http://tide.dfci.harvard.edu/) algorithm was employed to characterize tumor immune evasion mechanism, including dysfunction of tumor infiltration cytotoxic T lymphocytes (CTLs) and exclusion of CTLs by immunosuppressors (32). Tumor mutation burden (TMB) for each sample was quantified according to mutation frequency with number of variants/the length of exons (33). The cancer immunity cycle includes release of cancer cell antigens (step 1), cancer antigen presentation (step 2), priming and activation (step 3), trafficking of immune cells to tumors (step 4), infiltration of immune cells into tumors (step 5), recognition of cancer cells by T cells (step 6), and killing of cancer cells (step 7) (**Supplementary Table 3**) (34). The activities of these steps were assessed with ssGSEA based on the gene expression of each sample (35).

Prediction of Chemosensitivity

Sensitivity to chemotherapy drugs for each specimen was predicted by the Genomics of Drug Sensitivity in Cancer (GDSC, https://www.cancerrxgene.org/) database (36). Drugs including cisplatin, paclitaxel, gemcitabine, sorafenib, sunitinib, gefitinib, vinblastine and vorinostat were selected. The half-maximal inhibitory concentration (IC50) values were determined by ridge regression analysis using pRRophetic package (37).

Gene Set Variation Analysis (GSVA)

GSVA package was employed for estimating the activity of pathways with a non-parametric and unsupervised method (38). The gene sets of "c2.cp.kegg.v7.2.symbols" were acquired from the Molecular Signatures Database (MSigDB) (39).

Acquirement of mRNA Expression-Based Stemness Index (mRNAsi)

Cancer stemness of SCCs was quantified as described by Malta et al. (40). The mRNAsi of SCCs was calculated with one-class logistic regression machine learning algorithm and expressed with β values ranging from 0 (no gene expression) to 1 (complete gene expression).

Identification of Autophagy- and Ferroptosis-Related Genes

Autophagy- and ferroptosis-related genes between high FPI + high API group and others group were screened by limma package (version 3.50.0) (41). Genes with |fold-change| >1.5 and false discovery rate (FDR) <0.05 were considered statistically significant. Gene Ontology (GO) and Kyoto Encyclopedia of Genes and Genomes (KEGG) enrichment analysis of the autophagy- and ferroptosis-related genes were performed using clusterProfiler package (version 4.2.0) (42). Terms with FDR <0.05 were significantly enriched.

Connectivity Map (CMap) Analysis

The autophagy- and ferroptosis-related genes were used to query the CMap database (https://clue.io/) (43). Compounds with p<0.05 were considered as potential therapeutic drugs for ferroptosis and autophagy based on gene expression signatures. Furthermore, the mode of action (MoA) of these compounds was analyzed.

Development of an Autophagy- and Ferroptosis-Related Prognostic Model

Univariate cox regression analysis was performed to screen prognostic autophagy- and ferroptosis-related genes with p <0.05. Least absolute shrinkage and selection operator (LASSO) regression method was applied for finding out the optimal candidate variables with glmnet package (version 4.1-3) (44). The optimal values of the penalty parameter lambda were determined by ten-fold cross-validation. The risk score of each patient was calculated based on the expression and coefficient of candidate autophagy- and ferroptosis-related genes. The formula of the risk score was as follows: risk score = $\Sigma_{i=1}^{n}$(coefi × Expri), where Expri indicates the expression of each gene for patient i, and coefi indicates the coefficient of gene i. The patients were equally stratified into high- and low-risk groups. Kaplan-Meier curves of OS were performed between two groups. Time-dependent ROC curves were plotted to determine the AUCs of OS using survivalROC package.

Cell Culture and Treatment

Human SCCs cell lines (KYSE410 and KYSE450) were purchased from ATCC (Manassas, VA, USA). Cells were maintained in RPMI-1640 (#PM150120; Procell, Wuhan, China) plus 10% fetal bovine serum (FBS; #SH30084.03; Hyclone, South Logan, UT, USA), 100 units/mL penicillin, 100 μg/mL streptomycin. Rapamycin (#ab120224; Abcam, Cambridge, MA, USA), Erastin (#ab209693; Abcam, Cambridge, MA, USA) and Gefitinib (Iressa, AstraZeneca, Macclesfield, UK) were dissolved in dimethyl sulfoxide (DMSO; Sigma, St. Louis, MO, USA) as well as stored at -20°C. To activate autophagy or ferroptosis, cells were administrated with 0.1 μM Rapamycin or Erastin for 16 h.

3-[4,5-Dimethylthiazol-2-yl]-2, 5-Diphenyltetrazoliumbromide (MTT) Assays

Cell viability was conducted with MTT assays. Cells were seeded onto 96-well plates (1×10^3 cells/well). Following 12 h of culture, cells were pre-treated with 0.1 μM Rapamycin or 10 μM Erastin for 16 h. Thereafter, cells were administrated with different concentrations of gefitinib (0, 0.01, 0.1, 1, 2, 3, 6 and 10 μM) for another 24 h. Cells were then stained with 20 μl MTT (5 mg/ml; #M5655-1G; Sigma-Aldrich, St. Louis, MO, USA) for 4 h at 37°C. Then, culture medium was removed as well as 150 μl DMSO was added. Viable cells were measured at 490 nm absorbance. Half inhibitory concentration (IC50) values were calculated with dose-response curves using GraphPad Prism software (version 8.0.1).

Western Blotting

Cell lysates were prepared with RIPA lysis buffer (#P0013B; Beyotime, Shanghai, China) plus protease inhibitors. Protein concentration was measured through BCA kit (#P0009; Beyotime, Shanghai, China) accordance with the manufacturer's instructions. Equal amount of protein was separated *via* SDS-PAGE

electrophoresis and transferred onto PVDF membrane (Millipore, Billerica, MA). Membrane was incubated with antibodies against LC3 (1:1000; #14600-1-AP; Proteintech, Wuhan, China), ATG-5 (1:500; #10181-2-AP; Proteintech, Wuhan, China), ATG-7 (1:500; #10088-2-AP; Proteintech, Wuhan, China), FTH1 (1:1000; #3998S; Cell Signaling Technology, Danvers, MA, USA), GXP4 (1:1000; #67763-1-lg; Proteintech, Wuhan, China) and β-actin (1:5000; #60008-1-lg; Proteintech, Wuhan, China) overnight at 4°C. Thereafter, horseradish peroxide-conjugated goat anti-rabbit (1:5000; #SA00001-2; Proteintech, Wuhan, China) or anti-mouse (1:5000; #SA00001-1; Proteintech, Wuhan, China) secondary antibodies were utilized for immunostaining for 1 h at room temperature, followed by exposure to ECL reagent (#K-12043-D10; Wuhan Juneng Yitong Biological Co., Ltd., Wuhan, China). Images were acquired through ChemiDoc^{TM}XRS+ Gel imaging system (Bio-Rad, Hercules, CA, USA).

5-Ethynyl-2'-Deoxyuridine (EdU) Staining

Cells were incubated with RPMI-1640 medium plus 50 μM EdU (#C0078S; Beyotime, Beijing, China) at 37°C for 2 h. After being washed twice with PBS, cells were fixed with 50 μL 4% paraformaldehyde (#E672002; Sangon Biotech, Shanghai, China) for 30 min, neutralized with 50 μL 2 mg/mL glycine solution as well as permeabilized with 100 μL 0.5% Triton X-100. Thereafter, cells were incubated with 100 μL 1 × Apollo dye at room temperature for 30 min, followed by incubation with 100 μL Hoechst 33342 for 30 min. Images were acquired under a BX53 fluorescence microscope (Olympus, Japan).

Transwell Assays

Invasion assays were conducted in 24-well transwell cell chamber coated with 30 μl Matrigel (#356234; BD Biocoat, USA). 3×10^5 indicated cells were seeded onto the coated filters while the bottom chamber was filled with 600 μl complete culture medium. Following incubation for 48 h at 37°C, invasive cells were stained with crystal violent (#C0121; Beyotime, Shanghai, China). The migration assays were performed through a similar method without coating with Matrigel.

Statistical Analysis

All the statistical analysis was executed by R software (version 4.0.1) and GraphPad Prism software (version 8.0.1). Each experiment was independently repeated three times. The Kolmogorov-Smirnov normality test was carried out to confirm if datasets followed a Gaussian distribution for each comparison. If the data were Gaussian, parametric test was carried out (unpaired student's test, one-way ANOVA or Pearson correlation). If the data were non-Gaussian, nonparametric test was performed (Wilcoxon rank test or Spearman correlation). $P < 0.05$ indicated statistical significance.

RESULTS

Landscape of Genetic Variation of Autophagy- and Ferroptosis-Related Genes in SCCs

Totally, 222 autophagy- and 60 ferroptosis-related genes were investigated in SCCs that integrated HNSC, LUSC, CESC and ESCC datasets (**Supplementary Figure 1**). We firstly determined the prevalence of CNV mutations of autophagy-related genes in SCCs. CNV mutations were less frequent in CESC while CNV amplification was prevalent in ESCC (**Figure 2A**). Particularly, CDKNA2A showed widespread CNV loss and FADD displayed widespread CNV amplification in ESCC, LUSC and HNSC. Further analysis of somatic mutation frequency displayed a prevalent somatic mutation in autophagy-related genes (**Figure 2B**). The incidence of CNV variations and somatic mutations of ferroptosis-related genes was also summarized in SCCs. The investigation of CNV mutation revealed a widespread occurrence, especially SQLE amplification in ESCC and ACSL3 loss in CESC (**Figure 2C**). Further analysis revealed a prevalent frequency of somatic mutations of ferroptosis-related genes in SCCs (**Figure 2D**). The somatic mutations of each SCC were summarized in **Supplementary Figure 2**. Collectively, we did not investigate any prominent effect on different kinds of mutations according to different tissue origins, indicating that SCCs exhibited similar CNV and somatic mutation patterns of autophagy- and ferroptosis-related genes. The locations of autophagy- and ferroptosis-related genes on chromosomes were shown in **Figures 2E, F**. The above analysis revealed that autophagy and ferroptosis were precisely regulated at multiple layers in SCCs.

Crosstalk Between Autophagy and Ferroptosis in SCCs at the Molecular Level

Univariate Cox regression analysis was applied to ascertain the relationship between the mRNA expression of autophagy- or ferroptosis-related genes and the prognosis of SCCs patients (**Figures 3A, B**; **Supplementary Figures 3–5**). Some autophagy- or ferroptosis-related genes served as protective factors of the prognosis of SCCs, others were considered risk factors. Pearson correlation analysis was employed to investigate mutual regulation between these prognostic genes in SCCs. We found that autophagy-related genes presented remarkable correlations to the ferroptosis-related genes in terms of mRNA levels (**Figure 3C**) and prognosis (**Figure 3D**). KEGG enrichment analysis of autophagy- and ferroptosis-related genes was conducted, respectively. Ferroptosis, central carbon metabolism in cancer and microRNAs in cancer were collectively enriched by two sets of genes (**Figure 3E**). The close interactions of autophagy- and ferroptosis-related genes were also illustrated in the PPI network (**Figure 3F**). The API (**Supplementary Table 4**) and FPI (**Supplementary Table 5**) were separately calculated to quantify autophagy and ferroptosis levels in individual tumors based on the autophagy- and ferroptosis-related genes that could significantly impact prognosis of SCCs patients. There was a mutual regulation between FPI and API in SCCs (**Figure 3G**). The above results indicated that the crosstalk of autophagy and ferroptosis may play critical roles in SCCs initiation and progression.

The Roles of Autophagy on Outcomes, TME, Response to Immunotherapy and Chemosensitivity in SCCs

The SCCs patients were stratified into high and low API groups based on the median value of API. Prognoses analysis for the two

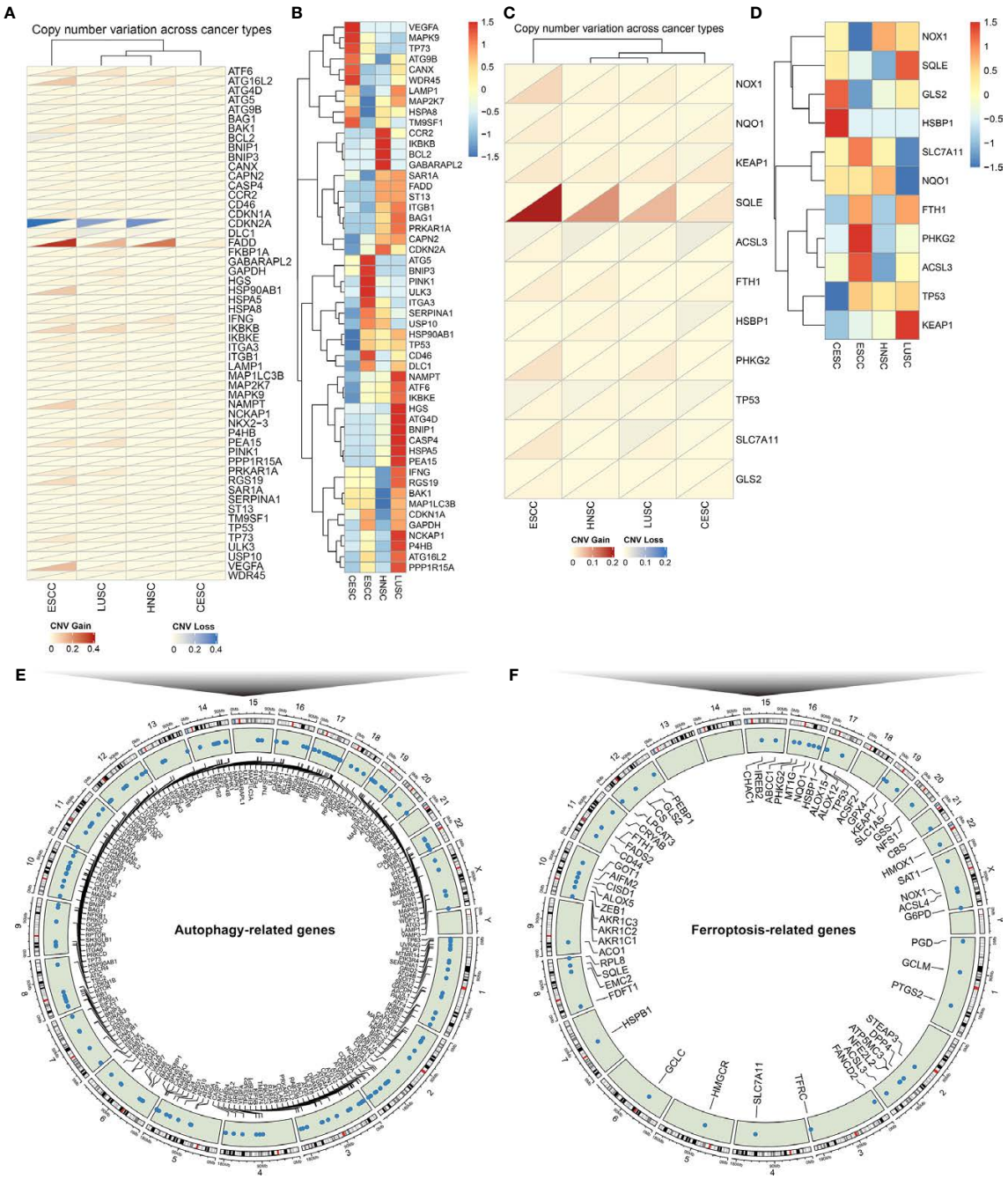

FIGURE 2 | The landscape of genetic alterations of autophagy- and ferroptosis-related genes in SCCs. **(A)** The CNV frequency of autophagy-related genes across SCCs. Red: the gain frequency; blue: the loss frequency. **(B)** The SNP frequency of autophagy-related genes across SCCs. **(C)** The CNV frequency of ferroptosis-related genes in SCCs. **(D)** The SNP frequency of ferroptosis-related genes across SCCs. **(E)** The location of autophagy-related genes on 23 chromosomes. **(F)** The location of ferroptosis-related genes on 23 chromosomes.

groups suggested the remarkably prominent survival advantage in high API (**Figure 4A**). Stromal score represents the percentage of stromal cells in the TME. High API was characterized by decreased stromal score (**Figure 4B**). Tumor purity, which reflects the proportion of cancer cells in the tumor tissue, is associated with a favorable clinical outcome of SCCs (45). High API showed the significantly increased tumor purity than low API (**Figure 4C**). Further analysis aimed at immunological role of autophagy in SCCs. We found that high API was significantly associated with low infiltration of immune cells (**Figure 4D**), low HLA expression (**Figure 4E**) and low immune checkpoint expression (**Figure 4F**). Based on the spatial distribution of

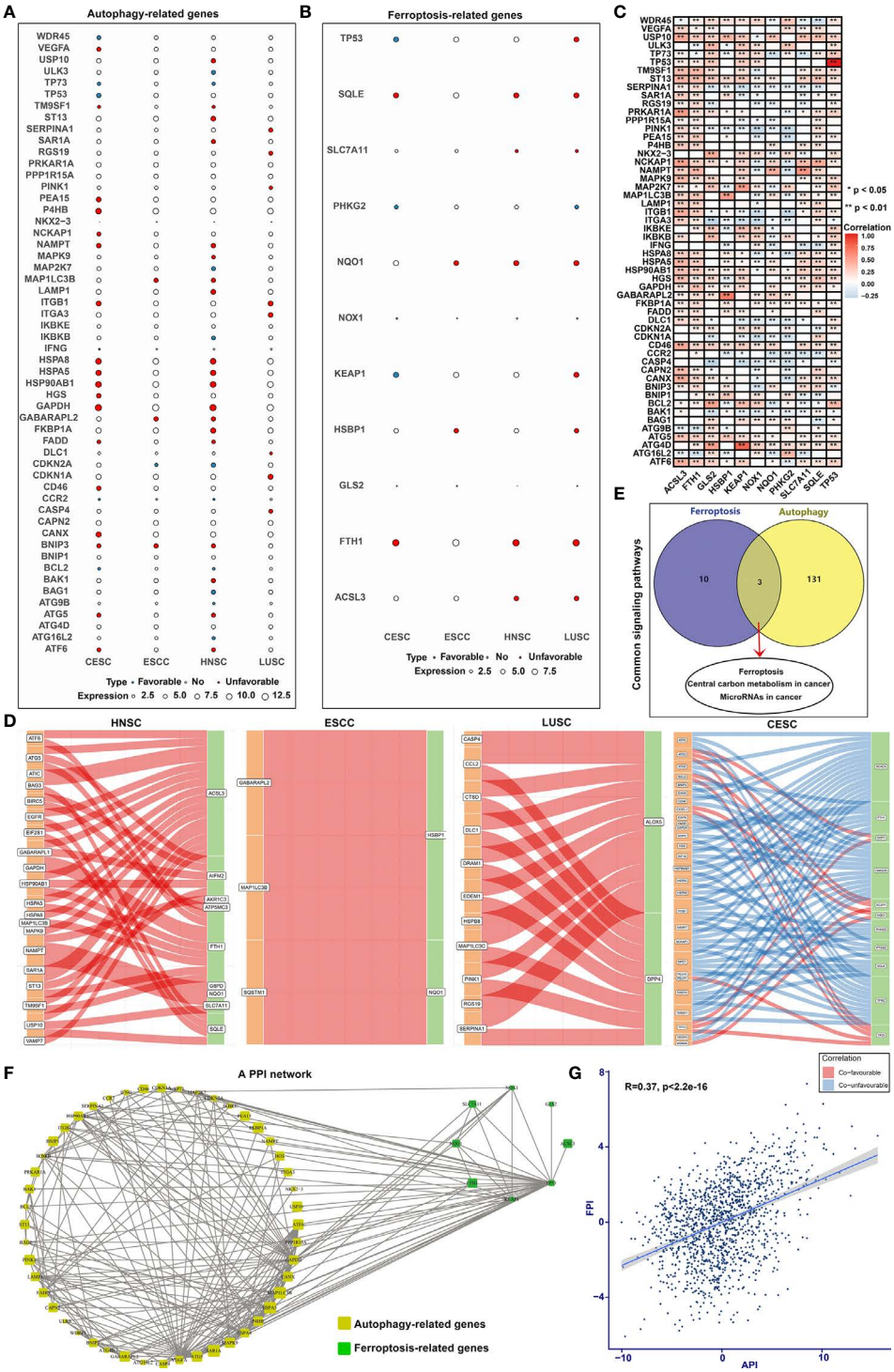

FIGURE 3 | Cross-talk between autophagy and ferroptosis in SCCs at the molecular level. **(A)** Bubble diagram showing correlations between autophagy-related genes and prognosis of SCCs using univariate cox regression analysis. Blue bubbles represented positive correlations with favorable survival outcomes and red bubbles represented positive correlations with unfavorable prognosis. The size of the bubble showed the expression level of each gene. **(B)** Correlations between ferroptosis-related genes and prognosis of SCCs. **(C)** Heatmap showing correlations between autophagy- and ferroptosis-related genes across SCCs at the mRNA level. Positive correlation was marked with red and negative correlation with blue. *p<0.05; **p<0.01. **(D)** Alluvial diagram for the shared effects of autophagy- and ferroptosis-related genes on prognosis of SCCs. **(E)** Venn diagram showing the common signals enriched by autophagy- and ferroptosis-related genes. **(F)** The PPI network of the interactions between autophagy- and ferroptosis-related genes. **(G)** Correlations between API and FPI in SCCs using Spearman test.

cytotoxic immune cells in the TME, tumors may be categorized into immune-inflamed (also described as hot tumors), immune-excluded, and immune-desert phenotypes (46). Immune-excluded and immune-desert tumors are also named as "cold tumors". These data suggested that SCCs with high API may lack innate immunity or innate antitumor immune features and autophagy could lead to "cold tumors". TIDE score exhibits the high accuracy in predicting cancer immunotherapy response (32). Our analysis showed that TIDE score was significantly decreased in high API samples (**Figure 4G**). These findings indicated that autophagy might be involved in the immunosuppression of SCCs. Chemotherapy resistance is the

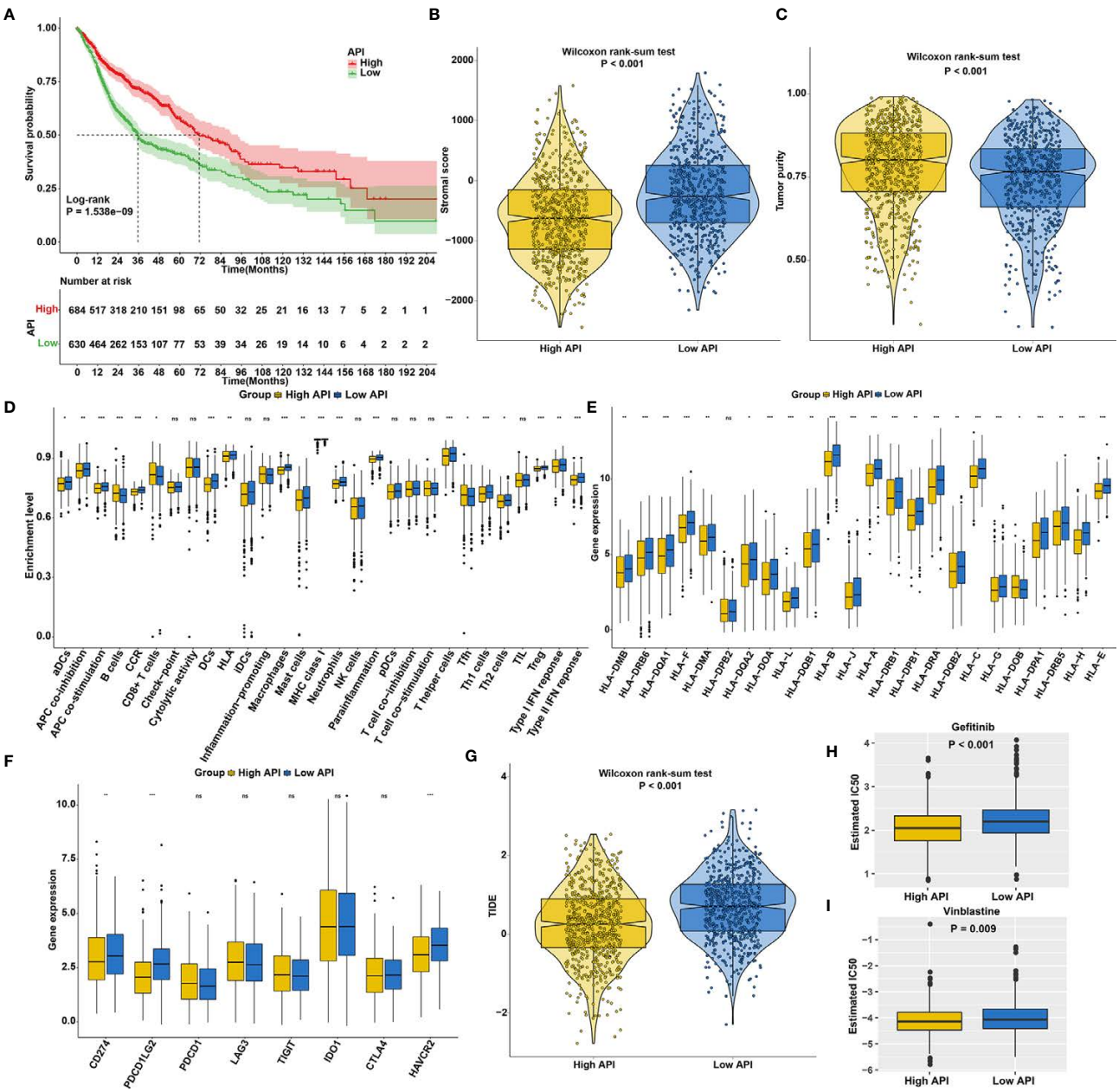

FIGURE 4 | The roles of autophagy on outcomes, TME, response to immunotherapy and chemosensitivity in SCCs. **(A)** Kaplan-Meier curves of overall survival for SCCs patients with high and low API. P value was determined with log-rank test. **(B)** Differences in stromal scores between high and low API groups in SCCs cohort. **(C)** Differences in tumor purity between high and low API groups. **(D)** Differences in the enrichment levels of immune cells and immune functions between two groups. **(E)** Differences in the expression levels of HLA genes between two groups. **(F)** Differences in the expression levels of immune checkpoints between two groups. **(G)** Differences in TIDE scores between two groups. **(H, I)** Differences in estimated IC50 values of **(H)** Gefitinib and **(I)** Vinblastine between two groups. Ns, not significant; *p<0.05; **p<0.01; ***p<0.001.

principal limitation of clinical oncology. High API samples were more sensitive to Gefitinib (**Figure 4H**) and Vinblastine (**Figure 4I**), indicating that autophagy could mediate resistance to chemotherapy drugs.

The Roles of Ferroptosis on Prognosis, TME, Response to Immunotherapy and Chemosensitivity in SCCs

We first explored the prognostic significance of ferroptosis in SCCs. As anticipated, patients with high FPI exhibited prolonged survival duration (**Figure 5A**). High FPI was characterized by increased immune score (**Figure 5B**) and lowered tumor purity (**Figure 5C**). In **Figure 5D**, high FPI was significantly correlated to increased T-cell infiltration, increased IFN-γ response and decreased immunosuppressive cells (such as macrophages), which was present in immune-inflamed phenotype. Also, high FPI was characterized by increased HLA expression (**Figure 5E**) and increased immune checkpoint expression (**Figure 5F**). TMB is a predictive biomarker for identifying patients most likely to respond to immunotherapy (47). Low TMB was found in high FPI samples (**Figure 5G**). Further analysis revealed that high FPI patients were more sensitive to Gemcitabine (**Figure 5H**), Sunitinib (**Figure 5I**), Vinblastine (**Figure 5J**) and Vorinostat (**Figure 5K**).

Synergistical Roles of Autophagy and Ferroptosis on Prognosis and Chemosensitivity of SCCs

According to FPI and API scores, SCCs patients were stratified into four molecular patterns: high FPI + high API; high FPI + low API; low FPI + high API; low FPI + low API. Prognosis analysis revealed that patients with high FPI in concert with high API exhibited a prominent survival benefit (**Figure 6A**), indicating that autophagy and ferroptosis synergistically contributed to a favorable prognosis. GSVA was performed to better illustrate the biological behaviors of autophagy and ferroptosis. Surprisingly, carcinogenic pathways and immunity were remarkably enriched in high FPI and high API, indicating that the crosstalk of autophagy and ferroptosis played a nonnegligible role in ornamenting tumor immune microenvironment (**Figure 6B**; **Supplementary Table 6**). Further analysis showed that high FPI in concert with high API was linked to a better DFI, DFS, DSS and PFI of SCCs (**Figure 6C**). Moreover, we sought to determine the performance of the crosstalk of autophagy and ferroptosis in predicting OS outcomes in HNSC, ESCC, LUSC and CESC. As expected, patients with high FPI in concert with high API were remarkably correlated to a better prognosis in each SCC type (**Figure 6D**). We also observed that patients with high FPI in concert with high API were more sensitive to Sunitinib, Gefitinib, Vinblastine and Vorinostat (**Figure 6E**). Therefore, the crosstalk of autophagy and ferroptosis was significantly relevant to SCCs progression, recurrence, and chemotherapy resistance.

Synergistical Roles of Autophagy and Ferroptosis Shape an Inflamed TME

High FPI and high API SCCs samples showed increased T-cell infiltrations (such as $CD8^+$ T cell, Tfh cell, Th2 cell and TIL) and low immunosuppressive cell populations (such as macrophages; **Figure 7A**), indicating that crosstalk between autophagy and ferroptosis might be involved in modulating immune cell infiltration. Most immune checkpoints (LAG3, IDO1, CTLA4, PD-1, TIGIT, CD200R1, CEACAM1, BTLA and ADORA2A) were found to be up-regulated in high FPI and high API samples (**Figure 7B**). Furthermore, our findings revealed that high FPI in concert with high API was positively associated with a majority of immunomodulators in SCCs (**Figure 7C**). Thus, synergistical roles of autophagy and ferroptosis might shape an inflamed TME of SCCs. Antitumor immunity is mediated to a large extent by $CD8^+$ T cells. Emerging evidence suggests that autophagy and ferroptosis changes in $CD8^+$ T cell metabolism directly modulate anti-tumor immunity (48, 49). Hence, it is of significance to comprehensively analyze the synergistical roles of autophagy, ferroptosis and $CD8^+$ T cell infiltration on SCC prognosis. Combining $CD8^+$ T cells, we found that patients with low infiltration of $CD8^+$ T cells and "others" experienced the worst clinical outcomes (**Figure 7D**). The predictive efficacy of $CD8^+$ T cell, API, FPI and their combinations was evaluated by ROC analysis. In **Figure 7E**, combination of $CD8^+$ T cells, API, FPI exhibited the best performance on predicting SCCs prognosis (**Supplementary Figure 6**).

ESTIMATE algorithm was employed to quantify the overall infiltration of immune cells and stromal cells in SCCs tissue. Our results showed high FPI and high API samples were characterized by increased immune score (**Figure 8A**) and low stromal score (**Figure 8B**), which also confirmed that the crosstalk of autophagy and ferroptosis was linked to immune cell infiltrations. Furthermore, we found that tumors with high FPI in concert with high API exhibited low TIDE scores (**Figure 8C**). This indicated that the crosstalk of autophagy and ferroptosis might influence response to immune checkpoint blockade for SCCs patients. High expression of HLAs (HLA-DMA, HLA-DPB2, HLA-DPB1, HLA-DQB2 and HLA-DOB) was found in SCCs with high FPI in concert with high API (**Figure 8D**). The activities of the cancer immunity cycle are the direct comprehensive performance of the functions of the chemokine system and other immunomodulators (**Figure 8E**). For specimens with high FPI in concert with high API, activities of most of the steps in the cycle were found to be up-regulated, including priming and activation (step 3), B cell recruiting (step 4), CD4+ T cell recruiting (step 4), $CD8^+$ T cell recruiting (step 4), dendritic cell recruiting (step 4), NK cell recruiting (step 4), T cell recruiting (step 4), Th1 cell recruiting (step 4), Th2 cell recruiting (step 4), Treg cell recruiting (step 4) and killing of cancer cells (step 7; **Figures 8F, G**). These data indicated that synergistical roles of autophagy and ferroptosis might shape an inflamed TME in SCCs.

Bioactive Compounds for SCCs Treatment Based on Autophagy- and Ferroptosis-Related Genes

Mismatch repair deficiency (dMMR) leads to microsatellite instability (MSI), which is in relation to response to immune- and chemotherapies (50). We found that there was a distinct difference in MSI status between high FPI + high API group and "others" group (**Figure 9A**). Cancer stem cells (CSCs) are characterized by differentiation, self-renewal, and homeostatic control, which allowing tumor maintenance and spread. Increasing evidence has

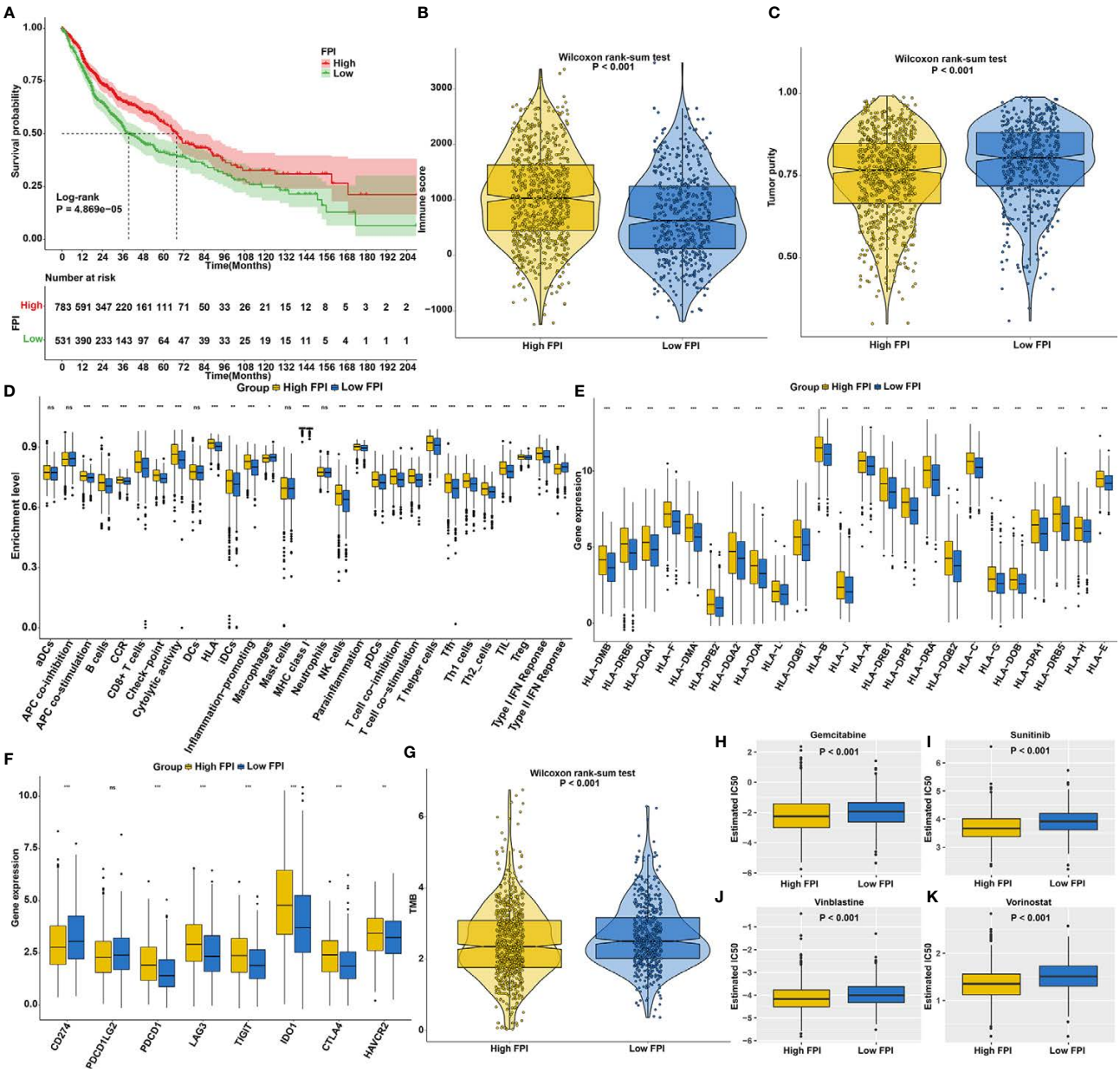

FIGURE 5 | The roles of ferroptosis on prognosis, TME, response to immunotherapy and chemosensitivity in SCCs. **(A)** Kaplan-Meier curves of overall survival for SCCs patients with high and low FPI. P value was determined with log-rank test. **(B)** Differences in immune scores between high and low FPI groups. **(C)** Differences in tumor purity between high and low API groups. **(D)** Differences in the enrichment levels of immune cells and immune functions between two groups. **(E)** Differences in the expression levels of HLA genes between two groups. **(F)** Differences in the expression levels of immune checkpoints between two groups. **(G)** Differences in TMB scores between two groups. **(H–K)** Differences in estimated IC50 values of **(H)** Gemcitabine, **(I)** Sunitinib, **(J)** vinblastine and **(K)** vorinostat between two groups. Ns, not significant; *p<0.05; **p<0.01; ***p<0.001.

demonstrated that recurrence and therapeutic resistance of SCCs are attributed to CSCs (51). Here, this study quantified cancer stemness by mRNAsi in SCCs. Increased mRNAsi was found in SCCs specimens with high FPI in concert with high API (**Figure 9B**). To further observe the potential biological behaviors of the crosstalk between autophagy and ferroptosis, we identified 154 down- and 538 up-regulated genes in high FPI + high API group compared to "others" group (**Figure 9C**; **Supplementary Table 7**). Potential drugs for SCCs treatment were predicted by CMap based on these up and down-regulated tags, respectively. Following the signature query, arecoline, ketotifen and viomycin with the highest positive enrichment score were determined as potential bioactive compounds for specifically activating autophagy and ferroptosis (**Supplementary Table 8**). MoA analysis of

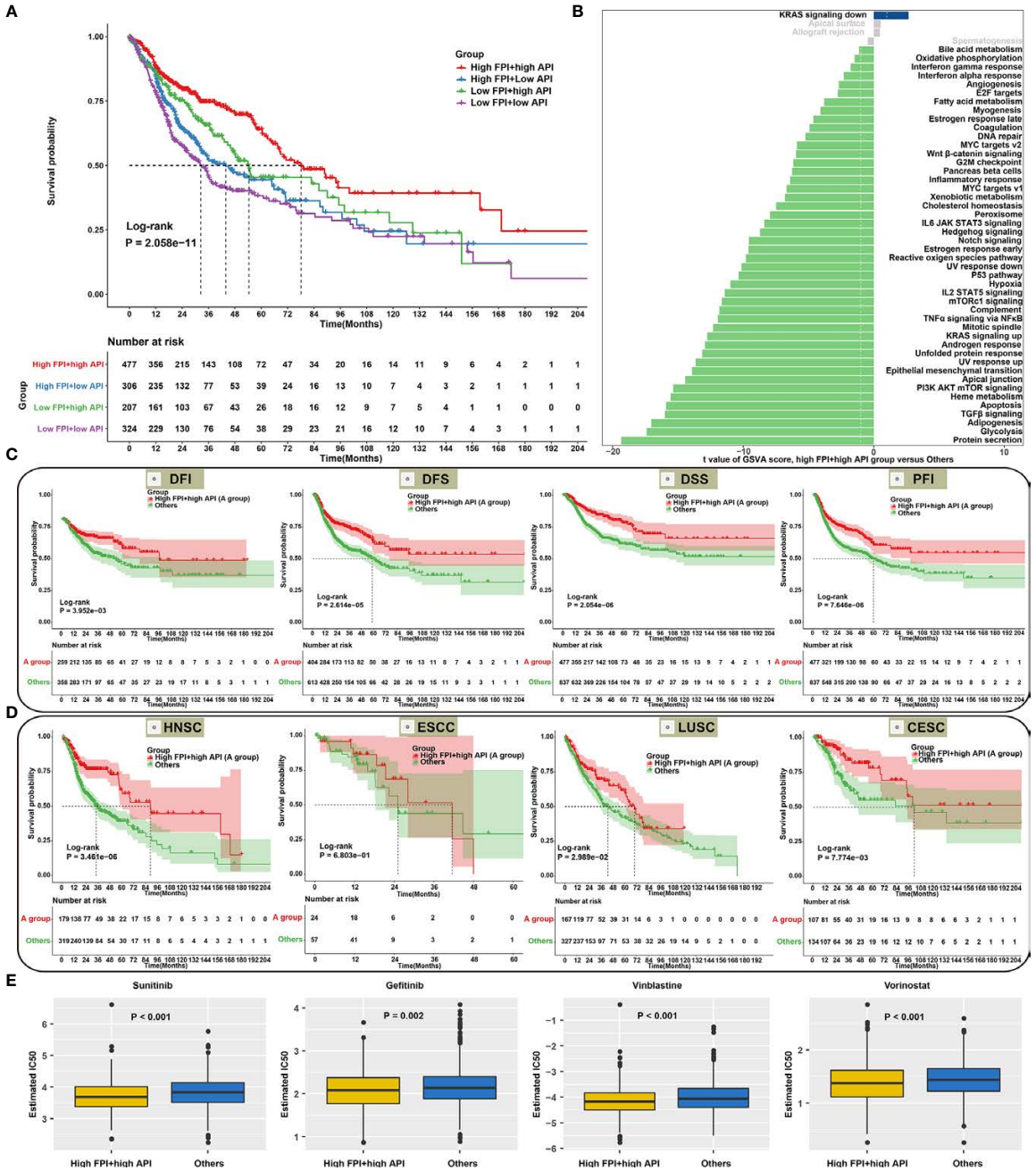

FIGURE 6 | Synergistical roles of autophagy and ferroptosis on prognosis and chemosensitivity of SCCs. **(A)** Overall survival analysis for SCCs patients stratified by both API and FPI using Kaplan-Meier curves. P value was calculated with log-rank test. **(B)** Differences in signaling pathways between high FPI + high API group and "others" group in SCCs cohort. The "others" indicated the remaining patients with SCCs except for those with high FPI + high API. **(C)** Kaplan-Meier curves of DFI, DFS, DSS and PFI in patients with high FPI + high API and "others". **(D)** Overall survival analysis for HNSC, ESCC, LUSC and CESC patients with high FPI + high API and "others". **(E)** Differences in estimated IC50 values of Sunitinib, Gefitinib, Vinblastine and Vorinostat between two groups.

predicted compounds demonstrated mechanisms of action shared by the compounds (**Figure 9D**). Three compounds (orciprenaline, oxymetazoline and terbutaline) shared the MoA of adrenergic receptor agonist and three compounds (oxprenolol, labetalol and tolazoline) shared adrenergic receptor antagonist.

Generation of a Prognostic Model Combining Autophagy and Ferroptosis

Our functional enrichment analysis showed that autophagy- and ferroptosis-related genes were significantly enriched in

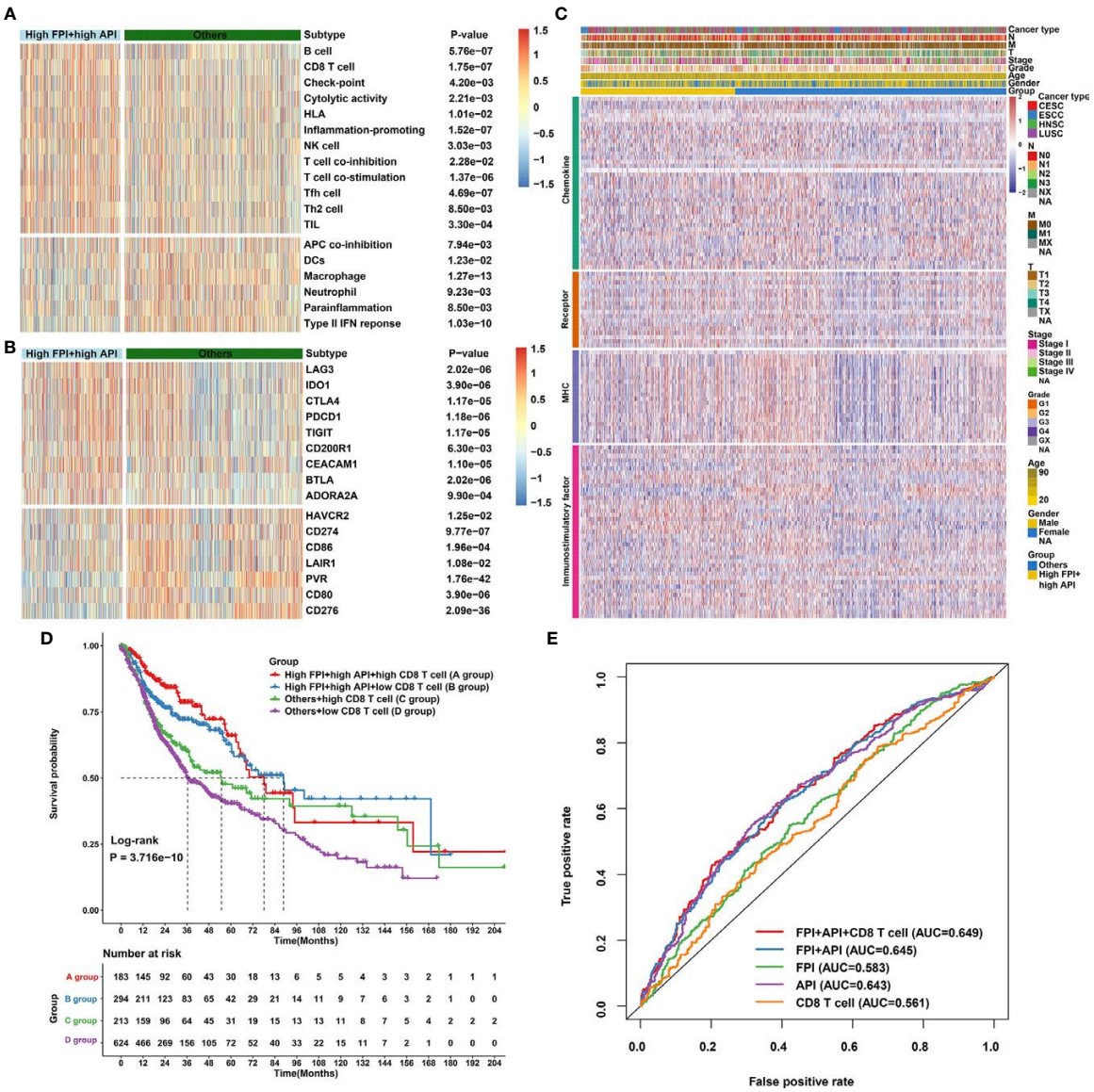

FIGURE 7 | Synergistical roles of autophagy and ferroptosis on immunity and survival outcomes of SCCs. **(A)** Heatmap showing the differences in immune cell infiltrations and immune functions in patients with high FPI + high API group and "others" group. The "others" indicated the remaining patients with SCCs except for those with high FPI + high API. **(B)** Heatmap of the expression levels of immune checkpoints in patients with high FPI + high API group and "others". **(C)** Differences in the expression levels of 122 immunomodulators (chemokines, receptors, MHC, and immunostimulatory factors) between high FPI + high API and "others" groups in SCCs. **(D)** Overall survival analysis for SCCs patients stratified by API, FPI and CD8$^+$ T cells using Kaplan-Meier curves. P value was determined with log-rank test. **(E)** Predictive accuracy of API, FPI, CD8$^+$ T cells or combinations according to the area under the ROC curves.

extracellular matrix (ECM), cancer-related pathways (PI3K-Akt signaling pathway, MAPK signaling pathway, EGFR tyrosine kinase inhibitor resistance, transcriptional misregulation in cancer and estrogen signaling pathway) and ferroptosis (**Figure 10A**), indicating the potential clinical implications of these genes. Among all autophagy- and ferroptosis-related genes, 138 were significantly associated with prognosis of SCCs patients using univariate Cox regression analysis (**Supplementary Table 9**). With the LASSO Cox regression method, 22 optimal candidate genes were selected with the minimum lambda (**Figures 10B, C**). A risk score model was created based on the expression and coefficients of the candidate genes (**Supplementary Table 10**). In TCGA cohort, SCCs patients were stratified into high-risk group (n=657) and low-risk group (n=657) with the median risk score as the cutoff value. In **Figure 10D**, patients with high risk indicated worse OS time compared to those with low risk. The AUC of the risk score was 0.677 (**Figure 10E**). We further investigated the prognostic value of the risk score in each SCC type. High risk scores were distinctly correlated to poorer prognosis for HNSC

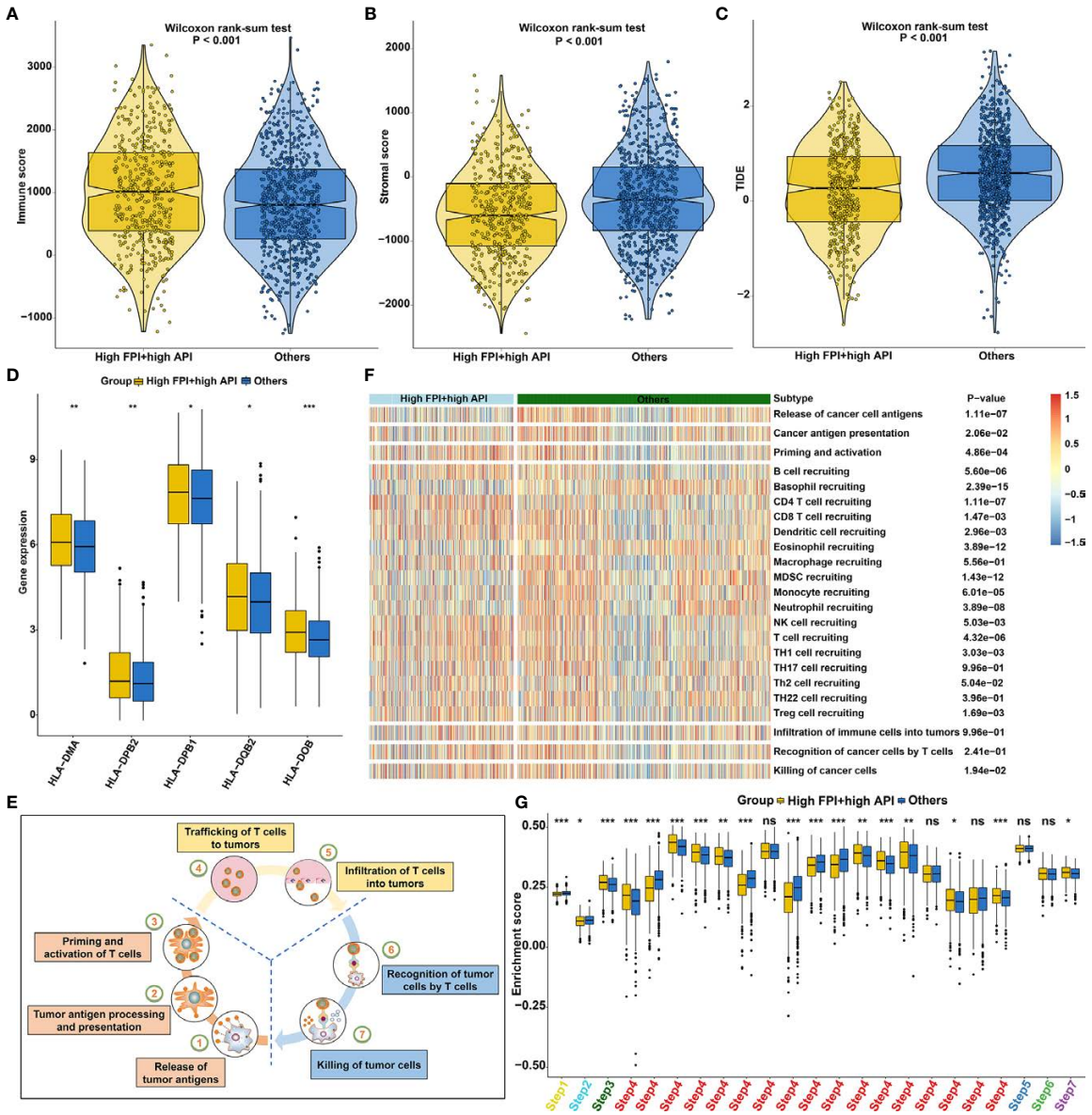

FIGURE 8 | Synergistical roles of autophagy and ferroptosis shape an inflamed TME of SCCs. **(A–C)** Differences in **(A)** immune score, **(B)** stromal score and **(C)** tumor purity between high FPI + high API and "others" groups in SCCs. The "others" indicated the remaining patients with SCCs except for those with high FPI + high API. **(D)** Differences in the expression of HLA genes between patients with high FPI + high API and "others". **(E)** Schematic diagram of the cancer immunity cycle. **(F, G)** Differences in the activity of the steps of the cancer immunity cycle between high FPI + high API and "others" groups in SCCs. Ns, not significant; *p<0.05; **p<0.01; ***p<0.001.

(**Figure 10F**), ESCC (**Figure 10G**), LUSC (**Figure 10H**) and CESC (**Figure 10I**). The well predictive performance was also observed in each SCC type (**Figures 10J–M**). After removing batch effects (**Figure 11A**), three external datasets (GSE17710, GSE44001 and GSE65858) were employed to confirm the excellent predictive accuracy of the risk score in SCCs prognosis (**Figures 11B, C**). Furthermore, we found that the risk score was a promising prognostic panel for each SCC type (**Figures 11D–I**).

Synergistical Roles of Autophagy and Ferroptosis on Gefitinib Sensitivity and Tumor Progression in SCCs

We further validated the synergistical roles of autophagy and ferroptosis on gefitinib resistance and tumor progression in SCCs through *in vitro* experiments. Two SCC cell lines KYSE410 and KYSE450 were exposed to ferroptosis agonist Erastin and autophagy agonist Rapamycin to confirm the crosstalk between autophagy and ferroptosis in SCCs. Our western blotting results

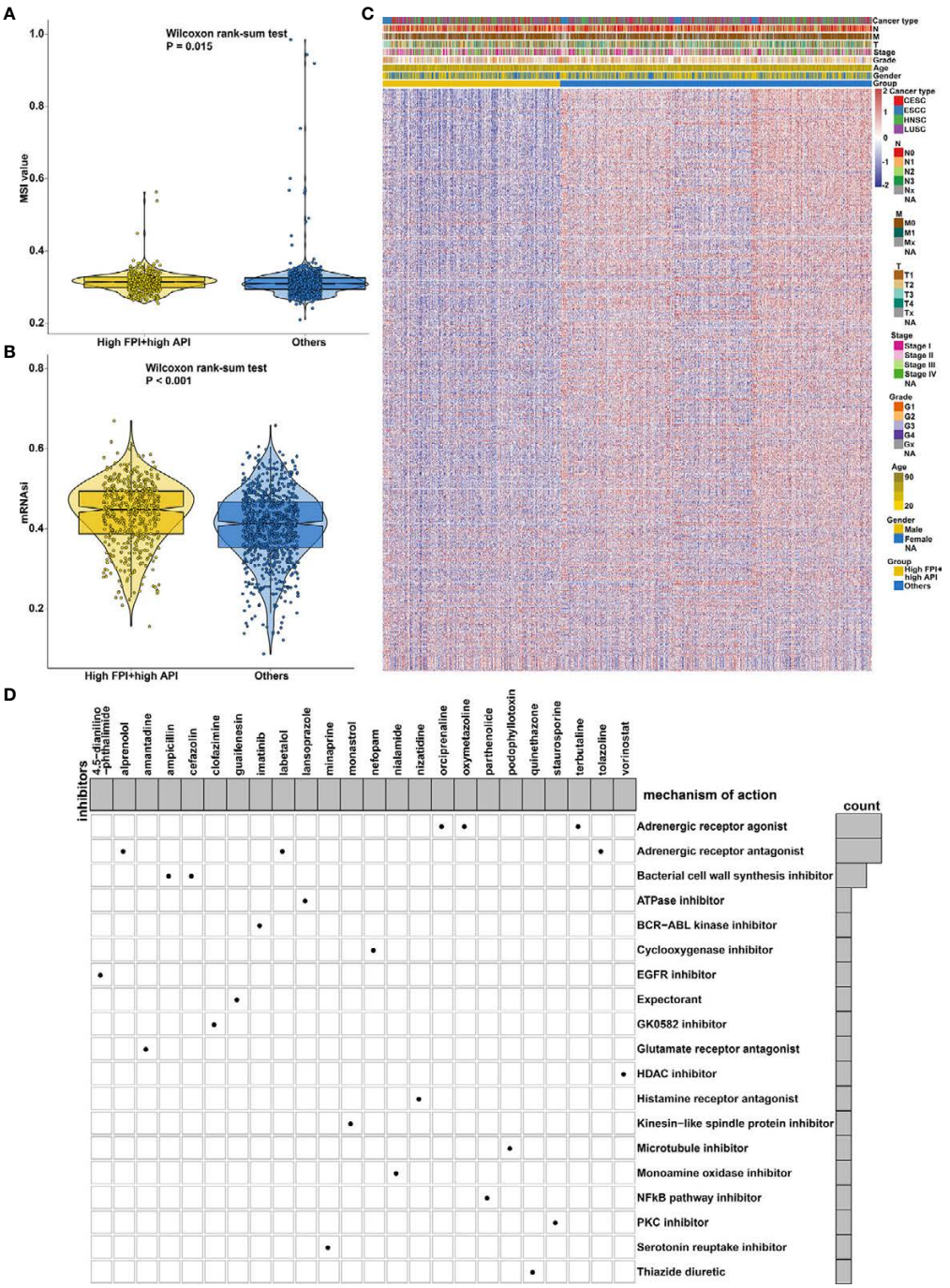

FIGURE 9 | Synergistical roles of autophagy and ferroptosis on MSI status and cancer stemness and prediction of potential bioactive compounds for SCCs treatment. **(A)** Differences in MSI status between high FPI + high API and "others" groups in SCCs. **(B)** Differences in mRNAsi between groups in SCCs. **(C)** Heatmap of the expression of DEGs between high FPI + high API and "others" groups. Red indicated high expression and blue indicated low expression. The gender, age, grade, stage, T, N, M and SCCs type were used as patient annotations. **(D)** Heatmap for each compound (perturbagen) from the CMap that shared a MoA (rows) based on autophagy- and ferroptosis-related genes, ranked by descending number of compounds with a shared MoA.

showed that both Erastin and Rapamycin significantly enhanced the expression of autophagy-related proteins including LC3II/I (**Figures 12A–C**), ATG-3 (**Figures 12D, E**) and ATG-3 (**Figures 12F, G**). Additionally, both Erastin and Rapamycin significantly increased the expression of ferroptosis-related protein FTG1 (**Figures 12H, I**) but reduced the expression of ferroptosis inhibitor GPX4 (**Figures 12J, K**). As expected, co-treatment of Erastin and Rapamycin synergistically prominently

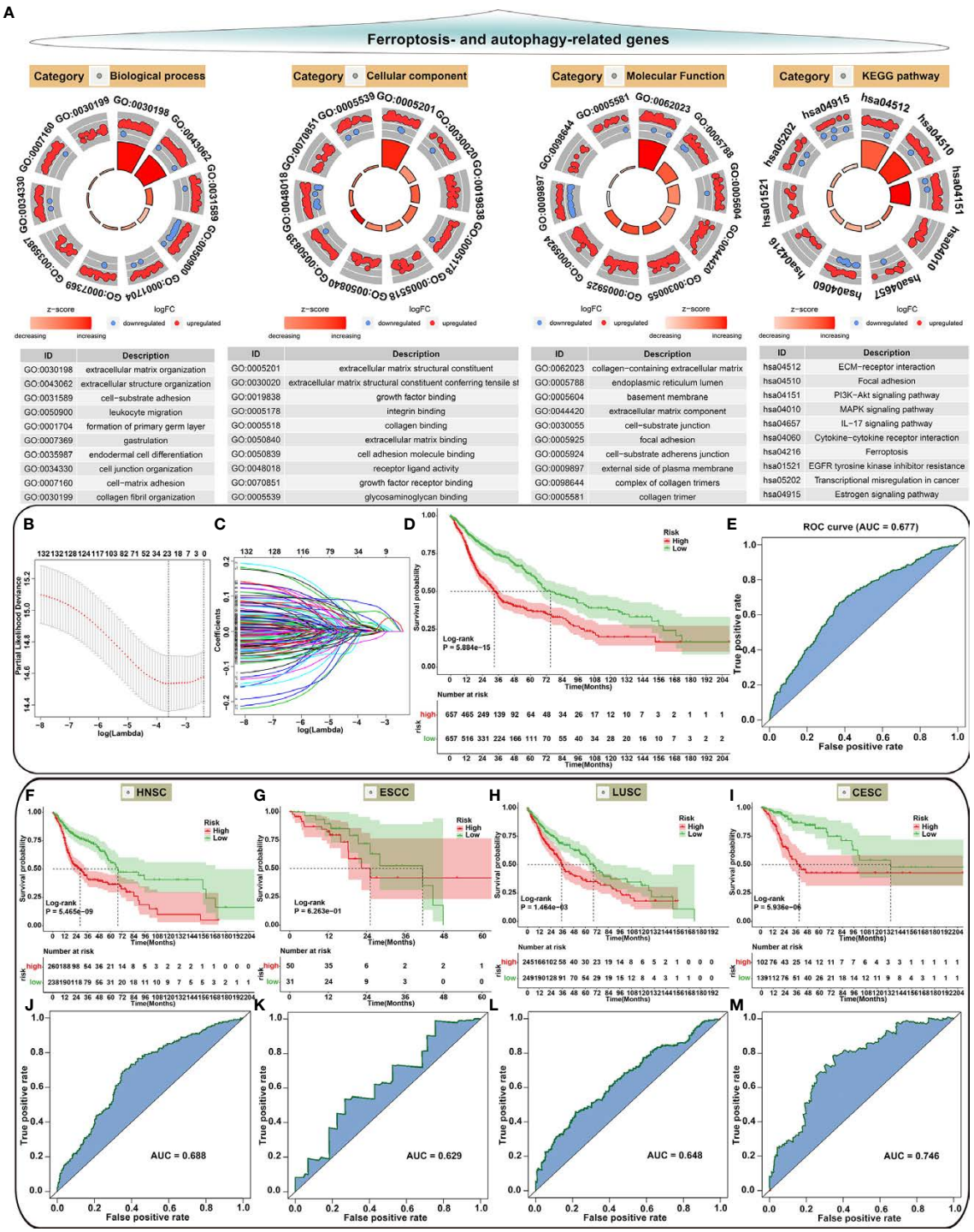

FIGURE 10 | Biological functions of autophagy- and ferroptosis-related genes and development of a prognostic model for SCCs. **(A)** Functional annotation analysis showing the biological functions and pathways involving autophagy- and ferroptosis-related genes. **(B)** Cross-validation for turning parameter selection by the minimum criteria in the LASSO regression model. Two dotted vertical lines were depicted at the optimal values based on the minimum criteria. Totally, 22 optimal DEGs with the best discriminative ability were selected for establishing the model. **(C)** LASSO coefficient profiles of 138 prognostic DEGs in SCCs. The coefficient profiles were plotted according to the log (Lambda) values. **(D)** Kaplan-Meier curves of overall survival for patients with high and low risk. P value was determined with log-rank test. **(E)** Assessment of the predictive accuracy of the model for survival of SCCs patients from TCGA cohort according to the area under ROC curves. **(F–I)** Survival analysis for the two groups in **(F)** HNSC, **(G)** ESCC, **(H)** LUSC and **(I)** CESC patients from TCGA cohort. **(J–M)** Predictive accuracy of the model for survival of **(J)** HNSC, **(K)** ESCC, **(L)** LUSC and **(M)** CESC patients.

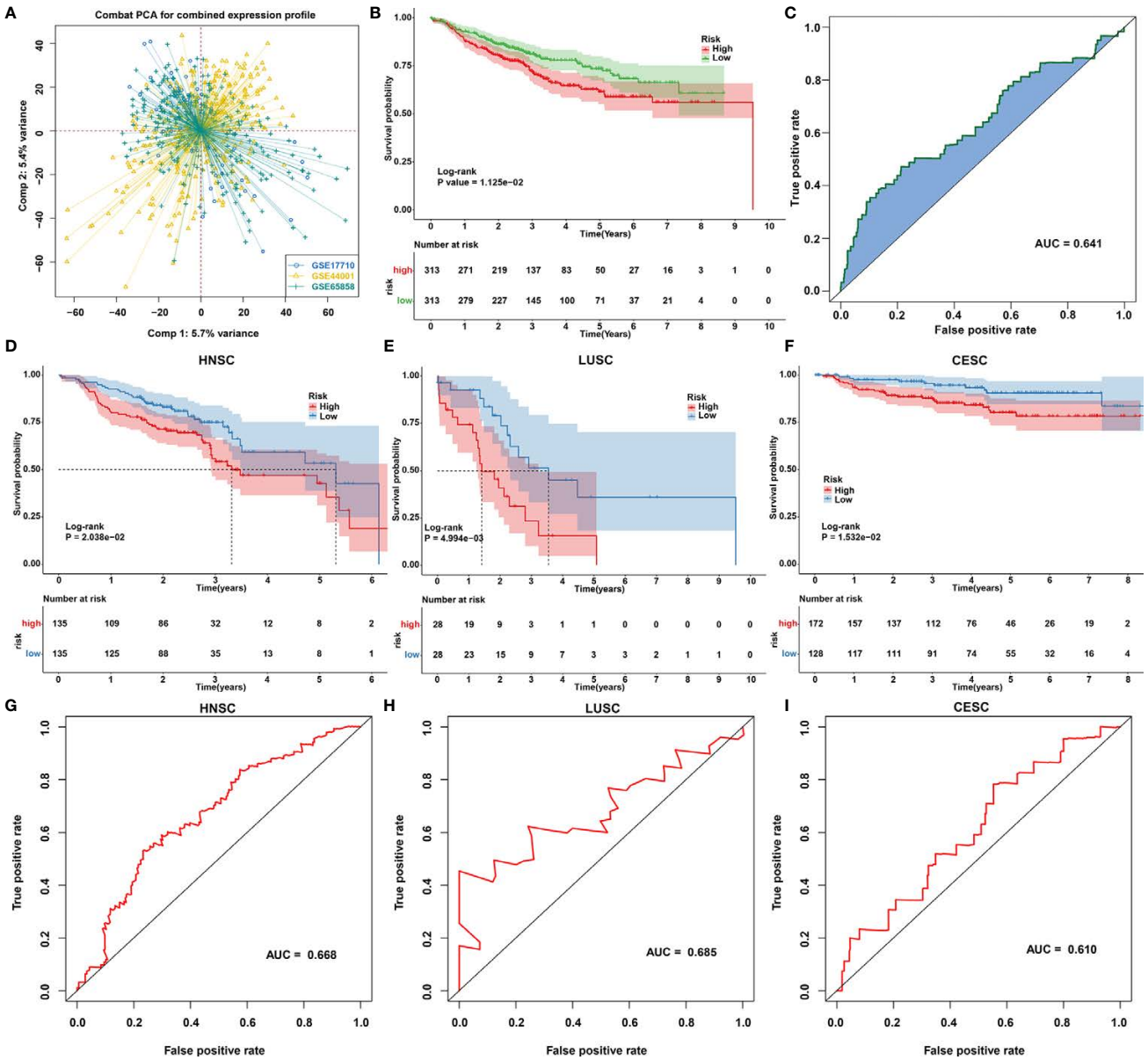

FIGURE 11 | Validation of the autophagy- and ferroptosis-related prognostic model for SCCs in external cohorts. **(A)** Principal component analysis showing the batch effects removed for three external cohorts: GSE17710, GSE44001 and GSE65858. **(B, C)** Validation of the predictive accuracy of the model for SCCs prognosis using integrated three datasets. **(D–F)** Validation of the overall survival of **(D)** HNSC, **(E)** LUSC and **(F)** CESC patients with high and low risk using Kaplan-Meier curves. **(G–I)** Validation of the predictive efficacy of the model for **(G)** HNSC, **(H)** LUSC and **(I)** CESC patients based on the area under ROC curves.

enhanced autophagy and ferroptosis in KYSE410 and KYSE450 cells. Our cell viability assays demonstrated that both Erastin and Rapamycin reduced the gefitinib IC50 values than control cells (**Figures 12L, M**). Additionally, we observed the synergistical roles of Erastin in concert with Rapamycin on gefitinib sensitivity. EdU staining (**Figures 12N–P**) and transwell (**Figures 12Q–U**) assays demonstrated that proliferation, migration and invasion were remarkedly suppressed by Erastin or Rapamycin in KYSE410 and KYSE450 cells. Also, there were synergistical roles of Erastin and Rapamycin on inhibiting proliferation, migration and invasion of KYSE410 and KYSE450 cells. Above evidence confirmed the synergistical roles of autophagy and ferroptosis on gefitinib sensitivity and tumor progression in SCCs.

DISCUSSION

Autophagy, a lysosome-dependent catabolic process, promotes cell survival and accelerates cellular demise (12). Ferroptosis, an iron-

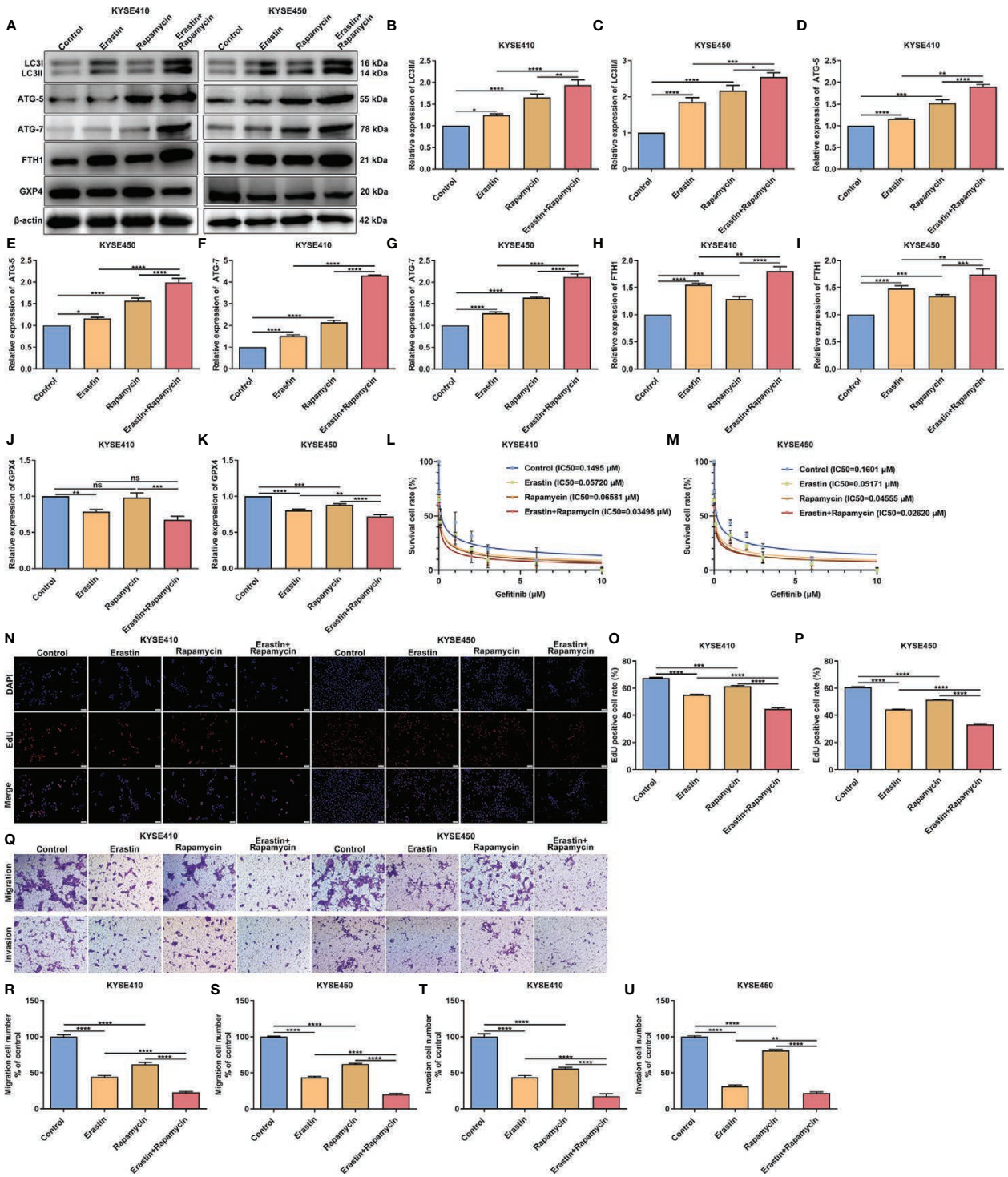

FIGURE 12 | Synergistical roles of autophagy and ferroptosis on gefitinib sensitivity and tumor progression in SCCs. **(A–K)** Detection of the expression of autophagy-related proteins including LC3II/I, ATG-5 and ATG-7 as well as ferroptosis-related proteins including FTH1 and GPX4 in KYSE410 and KYSE450 SCC cells exposed to Erastin and/or Rapamycin through western blotting. **(L, M)** Cell viability of KYSE410 and KYSE450 cells under treatment with Erastin and/or Rapamycin by MTT assay. **(N–P)** Measurement of proliferation of KYSE410 and KYSE450 cells treated with Erastin and/or Rapamycin by EdU staining. Scale bar, 50 μm and magnification, 200×. **(Q–U)** Detection of migration and invasion of KYSE410 and KYSE450 cells following administration with Erastin and/or Rapamycin using transwell assay. Scale bar, 50 μm and magnification, 200×. Ns, not significant; *p<0.05; **p<0.01; ***p<0.001; ****p<0.0001.

dependent cell death type, is in relation to the accumulation of lethal reactive lipid species (52). Recent experiment findings indicate that ferroptosis could occur while sharing common pathways or regulators with autophagy (15). Consistent with published research, this study comprehensively uncovered the close crosstalk between autophagy and ferroptosis at the molecular level (18). Moreover, their interplay was closely related to TME, immunity, chemotherapy resistance and survival outcomes of SCCs.

Herein, we quantified FPI and API for reflecting ferroptosis and autophagy levels in SCCs *via* PCA method. Their synergistical roles contributed to favorable survival outcomes of SCCs. The TME that is mainly composed of cancer cells, immune cells, and other components may mediate SCCs development and therapeutic response (53). Novel anticancer therapeutic strategies are required to target the pathways and molecular communications between cancer cells and the surrounding immune cells in the TME (54). Although previous experiment findings have reported the interplay between autophagy, ferroptosis and anti-tumor immunity, there is still lack of evidence from human SCCs specimens that may hinder the clinical translation (16). We found that autophagy in concert with ferroptosis participated in shaping an inflamed TME in human SCCs. Immune cells such as $CD8^+$ T cells are related to favorable prognosis of patients and increased curative effects of immunotherapy (55). Herein, we found that high $CD8^+$ T cell infiltration in concert with high FPI and high API indicated undesirable survival outcomes of SCCs and their combination displayed the well predictive efficacy in SCCs prognosis. Recent experiments have reported that $CD8^+$ T cells may inhibit tumor growth through inducing ferroptosis and autophagy (48). ICI therapy may be combined with other strategies that transform "cold tumors" to "hot tumors", which may increase sensitivity to ICI therapy. Tumors usually induce immune checkpoint expression for avoid being detected and killed by the host immune system (56). Therapies with anti-PD-1, anti-PD-L1, or anti-CTLA-4 reinvigorate T cells as well as allow the adaptive immune system thereby targeting cancer cells. Our data indicated that the induction of ferroptosis and autophagy combined with ICIs might produce synergistically enhanced antitumor activity for SCCs. Resistance to chemotherapy and molecular targeted therapies is a major problem facing current cancer research, which severely limits the effectiveness of cancer therapies. We found that synergistical roles of autophagy and ferroptosis may improve the sensitivity to sunitinib, gefitinib, vinblastine and vorinostat for SCCs patients. Taken together, the induction of autophagy and ferroptosis combined with immune- or chemotherapies might produce synergistically enhanced anti-SCCs activity. By CMap database, this study predicted arecoline, ketotifen and viomycin with the highest positive enrichment score as potential small molecule compounds for specifically activating autophagy and ferroptosis. Our *in vitro* experiments showed that ferroptosis agonist Erastin and autophagy agonist Rapamycin synergistically enhanced the sensitivity to gefitinib and suppressed cell proliferation, migration and invasion in SCCs cells, indicating the synergistical roles of autophagy and ferroptosis on gefitinib sensitivity and tumor progression in SCCs.

To facilitate personalized prediction of the prognosis of SCCs patients, we established a prognostic model based on 22 autophagy- and ferroptosis-related genes utilizing the LASSO algorithm to improve predictive accuracy for SCCs. Following external verification, this prognostic model possessed the well performance in predicting patients' prognosis. Nevertheless, this model will be validated in a prospective cohort.

CONCLUSION

Collectively, our bioinformatic analysis uncovered the interplay between autophagy and ferroptosis and their synergistical roles on prognosis, TME, immunity, and chemotherapy resistance in SCCs. The concomitant induction of autophagy and ferroptosis may be a promising strategy for treating SCCs. Although we predicted several bioactive compounds, potent drugs that function in activating autophagy and ferroptosis should be designed in future studies. Furthermore, clinical trials that treat patients with approved drugs that specifically activate autophagy and ferroptosis with the concomitant utilization of ICIs will be carried out in the future.

DATA AVAILABILITY STATEMENT

The datasets presented in this study can be found in online repositories. The names of the repository/repositories and accession number(s) can be found in the article/**Supplementary Material**.

AUTHOR CONTRIBUTIONS

MZ conceived and designed the study. LC, XN, and XQ conducted most of the experiments and data analysis, and wrote the manuscript. SL, HM, XS, and XH participated in collecting data and helped to draft the manuscript. All authors contributed to the article and approved the submitted version.

FUNDING

This work was funded by the National Natural Science Foundation of China (81072197, 81470758).

SUPPLEMENTARY MATERIAL

The Supplementary Material for this article can be found online at: https://www.frontiersin.org/articles/10.3389/fimmu.2021.739039/full#supplementary-material

Supplementary Table 1 | Summary of autophagy- and ferroptosis-related genes.

Supplementary Table 2 | The list of HLA genes, immune checkpoints and immunomodulators.

Supplementary Table 3 | The cancer immunity cycle.

Supplementary Table 4 | The API scores of SCCs samples.

Supplementary Table 5 | The FPI scores of SCCs samples.

Supplementary Table 6 | The activated signaling pathways in high FPI and high API SCCs samples by GSVA.

Supplementary Table 7 | Differentially expressed genes associated with high FPI and high API SCCs.

Supplementary Table 8 | Bioactive compounds for SCCs treatment based on autophagy- and ferroptosis-related genes.

Supplementary Table 9 | Autophagy- and ferroptosis-related genes that could impact survival of SCCs patients using univariate cox regression analysis.

Supplementary Table 10 | Coefficients of 22 autophagy- and ferroptosis-related genes in the risk score model for SCCs.

Supplementary Figure 1 | Correction of batch effects of HNSC, LUSC, CESC and ESCC datasets from TCGA database.

Supplementary Figure 2 | The somatic mutations of **(A)** autophagy- and **(B)** ferroptosis-related genes in HNSC, ESCC, LUSC and CESC samples.

Supplementary Figure 3 | The autophagy-related genes that could significantly impact the survival of **(A)** HNSC, **(B)** ESCC, **(C)** LUSC and **(D)** CESC patients.

Supplementary Figure 4 | The ferroptosis-related genes that could significantly impact the survival of **(A)** HNSC, **(B)** ESCC, **(C)** LUSC and **(D)** CESC patients.

Supplementary Figure 5 | (A) The autophagy- and **(B)** ferroptosis-related genes that could significantly impact the survival of SCCs patients.

Supplementary Figure 6 | Predictive accuracy of API, FPI, $CD8^+$ T cells or combination for **(A)** HNSC, **(B)** ESCC, **(C)** LUSC and **(D)** CESC prognosis according to the area under the ROC curves.

REFERENCES

1. Dotto GP, Rustgi AK. Squamous Cell Cancers: A Unified Perspective on Biology and Genetics. *Cancer Cell* (2016) 29(5):622–37. doi: 10.1016/j.ccell.2016.04.004
2. Li B, Cui Y, Nambiar DK, Sunwoo JB, Li R. The Immune Subtypes and Landscape of Squamous Cell Carcinoma. *Clin Cancer Res* (2019) 25 (12):3528–37. doi: 10.1158/1078-0432.Ccr-18-4085
3. Guan Y, Wang G, Fails D, Nagarajan P, Ge Y. Unraveling Cancer Lineage Drivers in Squamous Cell Carcinomas. *Pharmacol Ther* (2020) 206:107448. doi: 10.1016/j.pharmthera.2019.107448
4. Sánchez-Danés A, Blanpain C. Deciphering the Cells of Origin of Squamous Cell Carcinomas. *Nat Rev Cancer* (2018) 18(9):549–61. doi: 10.1038/s41568-018-0024-5
5. Hoadley KA, Yau C, Hinoue T, Wolf DM, Lazar AJ, Drill E, et al. Cell-of-Origin Patterns Dominate the Molecular Classification of 10,000 Tumors From 33 Types of Cancer. *Cell* (2018) 173(2):291–304.e6. doi: 10.1016/j.cell.2018.03.022
6. Campbell JD, Yau C, Bowlby R, Liu Y, Brennan K, Fan H, et al. Genomic, Pathway Network, and Immunologic Features Distinguishing Squamous Carcinomas. *Cell Rep* (2018) 23(1):194–212.e6. doi: 10.1016/j.celrep.2018.03.063
7. Kaidar-Person O, Gil Z, Billan S. Precision Medicine in Head and Neck Cancer. *Drug Resist Update* (2018) 40:13–6. doi: 10.1016/j.drup.2018.09.001
8. Brahmer J, Reckamp KL, Baas P, Crinò L, Eberhardt WE, Poddubskaya E, et al. Nivolumab Versus Docetaxel in Advanced Squamous-Cell Non-Small-Cell Lung Cancer. *N Engl J Med* (2015) 373(2):123–35. doi: 10.1056/NEJMoa1504627
9. Ferris RL, Haddad R, Even C, Tahara M, Dvorkin M, Ciuleanu TE, et al. Durvalumab With or Without Tremelimumab in Patients With Recurrent or Metastatic Head and Neck Squamous Cell Carcinoma: EAGLE, a Randomized, Open-Label Phase III Study. *Ann Oncol* (2020) 31(7):942–50. doi: 10.1016/j.annonc.2020.04.001
10. Jiang T, Shi J, Dong Z, Hou L, Zhao C, Li X, et al. Genomic Landscape and Its Correlations With Tumor Mutational Burden, PD-L1 Expression, and Immune Cells Infiltration in Chinese Lung Squamous Cell Carcinoma. *J Hematol Oncol* (2019) 12(1):75. doi: 10.1186/s13045-019-0762-1
11. Saâda-Bouzid E, Defaucheux C, Karabajakian A, Coloma VP, Servois V, Paoletti X, et al. Hyperprogression During Anti-PD-1/PD-L1 Therapy in Patients With Recurrent and/or Metastatic Head and Neck Squamous Cell Carcinoma. *Ann Oncol* (2017) 28(7):1605–11. doi: 10.1093/annonc/mdx178
12. Park E, Chung SW. ROS-Mediated Autophagy Increases Intracellular Iron Levels and Ferroptosis by Ferritin and Transferrin Receptor Regulation. *Cell Death Dis* (2019) 10(11):822. doi: 10.1038/s41419-019-2064-5
13. Dixon SJ, Lemberg KM, Lamprecht MR, Skouta R, Zaitsev EM, Gleason CE, et al. Ferroptosis: An Iron-Dependent Form of Nonapoptotic Cell Death. *Cell* (2012) 149(5):1060–72. doi: 10.1016/j.cell.2012.03.042
14. Hou W, Xie Y, Song X, Sun X, Lotze MT, Zeh HJ3rd, et al. Autophagy Promotes Ferroptosis by Degradation of Ferritin. *Autophagy* (2016) 12 (8):1425–8. doi: 10.1080/15548627.2016.1187366
15. Liu J, Kuang F, Kroemer G, Klionsky DJ, Kang R, Tang D. Autophagy-Dependent Ferroptosis: Machinery and Regulation. *Cell Chem Biol* (2020) 27 (4):420–35. doi: 10.1016/j.chembiol.2020.02.005
16. Tang R, Xu J, Zhang B, Liu J, Liang C, Hua J, et al. Ferroptosis, Necroptosis, and Pyroptosis in Anticancer Immunity. *J Hematol Oncol* (2020) 13(1):110. doi: 10.1186/s13045-020-00946-7
17. Dai E, Han L, Liu J, Xie Y, Kroemer G, Klionsky DJ, et al. Autophagy-Dependent Ferroptosis Drives Tumor-Associated Macrophage Polarization *via* Release and Uptake of Oncogenic KRAS Protein. *Autophagy* (2020) 16 (11):2069–83. doi: 10.1080/15548627.2020.1714209
18. Zhou Y, Shen Y, Chen C, Sui X, Yang J, Wang L, et al. The Crosstalk Between Autophagy and Ferroptosis: What Can We Learn to Target Drug Resistance in Cancer? *Cancer Biol Med* (2019) 16(4):630–46. doi: 10.20892/j.issn.2095-3941.2019.0158
19. Wilkerson MD, Yin X, Hoadley KA, Liu Y, Hayward MC, Cabanski CR, et al. Lung Squamous Cell Carcinoma mRNA Expression Subtypes Are Reproducible, Clinically Important, and Correspond to Normal Cell Types. *Clin Cancer Res* (2010) 16(19):4864–75. doi: 10.1158/1078-0432.Ccr-10-0199
20. Lee YY, Kim TJ, Kim JY, Choi CH, Do IG, Song SY, et al. Genetic Profiling to Predict Recurrence of Early Cervical Cancer. *Gynecol Oncol* (2013) 131 (3):650–4. doi: 10.1016/j.ygyno.2013.10.003
21. Wichmann G, Rosolowski M, Krohn K, Kreuz M, Boehm A, Reiche A, et al. The Role of HPV RNA Transcription, Immune Response-Related Gene Expression and Disruptive TP53 Mutations in Diagnostic and Prognostic Profiling of Head and Neck Cancer. *Int J Cancer* (2015) 137(12):2846–57. doi: 10.1002/ijc.29649
22. Leek JT, Johnson WE, Parker HS, Jaffe AE, Storey JD. The Sva Package for Removing Batch Effects and Other Unwanted Variation in High-Throughput Experiments. *Bioinformatics* (2012) 28(6):882–3. doi: 10.1093/bioinformatics/bts034
23. Zhang H, Meltzer P, Davis S. RCircos: An R Package for Circos 2D Track Plots. *BMC Bioinf* (2013) 14:244. doi: 10.1186/1471-2105-14-244
24. Mayakonda A, Lin DC, Assenov Y, Plass C, Koeffler HP. Maftools: Efficient and Comprehensive Analysis of Somatic Variants in Cancer. *Genome Res* (2018) 28(11):1747–56. doi: 10.1101/gr.239244.118
25. Zhang B, Wu Q, Li B, Wang D, Wang L, Zhou YL. m(6)A Regulator-Mediated Methylation Modification Patterns and Tumor Microenvironment Infiltration Characterization in Gastric Cancer. *Mol Cancer* (2020) 19(1):53. doi: 10.1186/s12943-020-01170-0
26. Chong W, Shang L, Liu J, Fang Z, Du F, Wu H, et al. m(6)A Regulator-Based Methylation Modification Patterns Characterized by Distinct Tumor Microenvironment Immune Profiles in Colon Cancer. *Theranostics* (2021) 11(5):2201–17. doi: 10.7150/thno.52717

27. Szklarczyk D, Morris JH, Cook H, Kuhn M, Wyder S, Simonovic M, et al. The STRING Database in 2017: Quality-Controlled Protein-Protein Association Networks, Made Broadly Accessible. *Nucleic Acids Res* (2017) 45(D1):D362–d8. doi: 10.1093/nar/gkw937
28. Shannon P, Markiel A, Ozier O, Baliga NS, Wang JT, Ramage D, et al. Cytoscape: A Software Environment for Integrated Models of Biomolecular Interaction Networks. *Genome Res* (2003) 13(11):2498–504. doi: 10.1101/gr.1239303
29. Yoshihara K, Shahmoradgoli M, Martínez E, Vegesna R, Kim H, Torres-Garcia W, et al. Inferring Tumour Purity and Stromal and Immune Cell Admixture From Expression Data. *Nat Commun* (2013) 4:2612. doi: 10.1038/ncomms3612
30. Bindea G, Mlecnik B, Tosolini M, Kirilovsky A, Waldner M, Obenauf AC, et al. Spatiotemporal Dynamics of Intratumoral Immune Cells Reveal the Immune Landscape in Human Cancer. *Immunity* (2013) 39(4):782–95. doi: 10.1016/j.immuni.2013.10.003
31. Charoentong P, Finotello F, Angelova M, Mayer C, Efremova M, Rieder D, et al. Pan-Cancer Immunogenomic Analyses Reveal Genotype-Immunophenotype Relationships and Predictors of Response to Checkpoint Blockade. *Cell Rep* (2017) 18(1):248–62. doi: 10.1016/j.celrep.2016.12.019
32. Jiang P, Gu S, Pan D, Fu J, Sahu A, Hu X, et al. Signatures of T Cell Dysfunction and Exclusion Predict Cancer Immunotherapy Response. *Nat Med* (2018) 24(10):1550–8. doi: 10.1038/s41591-018-0136-1
33. Sha D, Jin Z, Budczies J, Kluck K, Stenzinger A, Sinicrope FA. Tumor Mutational Burden as a Predictive Biomarker in Solid Tumors. *Cancer Discov* (2020) 10(12):1808–25. doi: 10.1158/2159-8290.Cd-20-0522
34. Chen DS, Mellman I. Oncology Meets Immunology: The Cancer-Immunity Cycle. *Immunity* (2013) 39(1):1–10. doi: 10.1016/j.immuni.2013.07.012
35. Xu L, Deng C, Pang B, Zhang X, Liu W, Liao G, et al. TIP: A Web Server for Resolving Tumor Immunophenotype Profiling. *Cancer Res* (2018) 78 (23):6575–80. doi: 10.1158/0008-5472.Can-18-0689
36. Yang W, Soares J, Greninger P, Edelman EJ, Lightfoot H, Forbes S, et al. Genomics of Drug Sensitivity in Cancer (GDSC): A Resource for Therapeutic Biomarker Discovery in Cancer Cells. *Nucleic Acids Res* (2013) 41(Database issue):D955–61. doi: 10.1093/nar/gks1111
37. Geeleher P, Cox N, Huang RS. Prrophetic: An R Package for Prediction of Clinical Chemotherapeutic Response From Tumor Gene Expression Levels. *PloS One* (2014) 9(9):e107468. doi: 10.1371/journal.pone.0107468
38. Hänzelmann S, Castelo R, Guinney J. GSVA: Gene Set Variation Analysis for Microarray and RNA-Seq Data. *BMC Bioinf* (2013) 14:7. doi: 10.1186/1471-2105-14-7
39. Liberzon A, Birger C, Thorvaldsdóttir H, Ghandi M, Mesirov JP, Tamayo P. The Molecular Signatures Database (MSigDB) Hallmark Gene Set Collection. *Cell Syst* (2015) 1(6):417–25. doi: 10.1016/j.cels.2015.12.004
40. Malta TM, Sokolov A, Gentles AJ, Burzykowski T, Poisson L, Weinstein JN, et al. Machine Learning Identifies Stemness Features Associated With Oncogenic Dedifferentiation. *Cell* (2018) 173(2):338–54.e15. doi: 10.1016/j.cell.2018.03.034
41. Ritchie ME, Phipson B, Wu D, Hu Y, Law CW, Shi W, et al. Limma Powers Differential Expression Analyses for RNA-Sequencing and Microarray Studies. *Nucleic Acids Res* (2015) 43(7):e47. doi: 10.1093/nar/gkv007
42. Yu G, Wang LG, Han Y, He QY. Clusterprofiler: An R Package for Comparing Biological Themes Among Gene Clusters. *Omics* (2012) 16(5):284–7. doi: 10.1089/omi.2011.0118
43. Lamb J, Crawford ED, Peck D, Modell JW, Blat IC, Wrobel MJ, et al. The Connectivity Map: Using Gene-Expression Signatures to Connect Small Molecules, Genes, and Disease. *Science* (2006) 313(5795):1929–35. doi: 10.1126/science.1132939
44. Engebretsen S, Bohlin J. Statistical Predictions With Glmnet. *Clin Epigenet* (2019) 11(1):123. doi: 10.1186/s13148-019-0730-1
45. Liu J, Wu Z, Wang Y, Nie S, Sun R, Yang J, et al. A Prognostic Signature Based on Immune-Related Genes for Cervical Squamous Cell Carcinoma and Endocervical Adenocarcinoma. *Int Immunopharmacol* (2020) 88:106884. doi: 10.1016/j.intimp.2020.106884
46. Galon J, Bruni D. Approaches to Treat Immune Hot, Altered and Cold Tumours With Combination Immunotherapies. *Nat Rev Drug Discov* (2019) 18(3):197–218. doi: 10.1038/s41573-018-0007-y
47. Merino DM, McShane LM, Fabrizio D, Funari V, Chen SJ, White JR, et al. Establishing Guidelines to Harmonize Tumor Mutational Burden (TMB): *In Silico* Assessment of Variation in TMB Quantification Across Diagnostic Platforms: Phase I of the Friends of Cancer Research TMB Harmonization Project. *J Immunother Cancer* (2020) 8(1):e000147. doi: 10.1136/jitc-2019-000147
48. Wang W, Green M, Choi JE, Gijón M, Kennedy PD, Johnson JK, et al. CD8(+) T Cells Regulate Tumour Ferroptosis During Cancer Immunotherapy. *Nature* (2019) 569(7755):270–4. doi: 10.1038/s41586-019-1170-y
49. DeVorkin L, Pavey N, Carleton G, Comber A, Ho C, Lim J, et al. Autophagy Regulation of Metabolism Is Required for CD8(+) T Cell Anti-Tumor Immunity. *Cell Rep* (2019) 27(2):502–13.e5. doi: 10.1016/j.celrep.2019.03.037
50. Baretti M, Le DT. DNA Mismatch Repair in Cancer. *Pharmacol Ther* (2018) 189:45–62. doi: 10.1016/j.pharmthera.2018.04.004
51. Tian Y, Wang J, Qin C, Zhu G, Chen X, Chen Z, et al. Identifying 8-Mrnasi Based Signature for Predicting Survival in Patients With Head and Neck Squamous Cell Carcinoma *via* Machine Learning. *Front Genet* (2020) 11:566159. doi: 10.3389/fgene.2020.566159
52. Tang D, Chen X, Kang R, Kroemer G. Ferroptosis: Molecular Mechanisms and Health Implications. *Cell Res* (2021) 31(2):107–25. doi: 10.1038/s41422-020-00441-1
53. Miyauchi S, Kim SS, Pang J, Gold KA, Gutkind JS, Califano JA, et al. Immune Modulation of Head and Neck Squamous Cell Carcinoma and the Tumor Microenvironment by Conventional Therapeutics. *Clin Cancer Res* (2019) 25 (14):4211–23. doi: 10.1158/1078-0432.Ccr-18-0871
54. Binnewies M, Roberts EW, Kersten K, Chan V, Fearon DF, Merad M, et al. Understanding the Tumor Immune Microenvironment (TIME) for Effective Therapy. *Nat Med* (2018) 24(5):541–50. doi: 10.1038/s41591-018-0014-x
55. Yost KE, Satpathy AT, Wells DK, Qi Y, Wang C, Kageyama R, et al. Clonal Replacement of Tumor-Specific T Cells Following PD-1 Blockade. *Nat Med* (2019) 25(8):1251–9. doi: 10.1038/s41591-019-0522-3
56. Chan TA, Yarchoan M, Jaffee E, Swanton C, Quezada SA, Stenzinger A, et al. Development of Tumor Mutation Burden as an Immunotherapy Biomarker: Utility for the Oncology Clinic. *Ann Oncol* (2019) 30(1):44–56. doi: 10.1093/annonc/mdy495

Conflict of Interest: The authors declare that the research was conducted in the absence of any commercial or financial relationships that could be construed as a potential conflict of interest.

Publisher's Note: All claims expressed in this article are solely those of the authors and do not necessarily represent those of their affiliated organizations, or those of the publisher, the editors and the reviewers. Any product that may be evaluated in this article, or claim that may be made by its manufacturer, is not guaranteed or endorsed by the publisher.

Copyright © 2022 Chen, Niu, Qiao, Liu, Ma, Shi, He and Zhong. This is an open-access article distributed under the terms of the Creative Commons Attribution License (CC BY). The use, distribution or reproduction in other forums is permitted, provided the original author(s) and the copyright owner(s) are credited and that the original publication in this journal is cited, in accordance with accepted academic practice. No use, distribution or reproduction is permitted which does not comply with these terms.

Advantages of publishing in Frontiers

OPEN ACCESS
Articles are free to read for greatest visibility and readership

FAST PUBLICATION
Around 90 days from submission to decision

HIGH QUALITY PEER-REVIEW
Rigorous, collaborative, and constructive peer-review

TRANSPARENT PEER-REVIEW
Editors and reviewers acknowledged by name on published articles

Frontiers
Avenue du Tribunal-Fédéral 34
1005 Lausanne | Switzerland

Visit us: www.frontiersin.org
Contact us: frontiersin.org/about/contact

REPRODUCIBILITY OF RESEARCH
Support open data and methods to enhance research reproducibility

DIGITAL PUBLISHING
Articles designed for optimal readership across devices

FOLLOW US
@frontiersin

IMPACT METRICS
Advanced article metrics track visibility across digital media

EXTENSIVE PROMOTION
Marketing and promotion of impactful research

LOOP RESEARCH NETWORK
Our network increases your article's readership